Digitized by Arya Samaj Foundation Chennai and eGangotri

CC-0. In Public Domain. Gurukul Kangri Collection, Haridwar

Digitized by Arya Samaj Foundation Chennai and eGangotri

112441

गुरुकुल कांगड़ी विश्वविद्यालय, हरिद्वार
पुस्तकालय

R
विषय संख्या 530.5
पुस्तक संख्या AM3R V.38
आगत पंजिका संख्या 8203 S

पुस्तक पर किसी प्रकार का निशान लगाना वर्जित है। कृपया १५ दिन से अधिक समय तक पुस्तक अपने पास न रखें।

CC-0. In Public Domain. Gurukul Kangri Collection, Haridwar

Digitized by Arya Samaj Foundation Chennai and eGangotri

8203 s

स्थान प्रमाणीकरण १९८४-१९८५

सन्दर्भ ग्रन्थ
REFRENCE BOOK

यह पुस्तक वितरित न की जाय
NOT TO BE ISSUED

CC-0. In Public Domain. Gurukul Kangri Collection, Haridwar

Digitized by Arya Samaj Foundation Chennai and eGangotri

CC-0. In Public Domain. Gurukul Kangri Collection, Haridwar

112441 Digitized by Arya Samaj Foundation Chennai and eGangotri

REVIEWS OF MODERN PHYSICS

CHECKED 1973

BOARD OF EDITORS

S. A. GOUDSMIT, *Managing Editor* E. U. CONDON, *Editor*

Associate Editors

E. A. UEHLING
C. P. SLICHTER
W. M. FAIRBANK
E. FEENBERG
H. PRIMAOFF
W. A. FOWLER

VOLUME 38

1966

Published for

THE AMERICAN PHYSICAL SOCIETY

by the

AMERICAN INSTITUTE OF PHYSICS

NEW YORK, NEW YORK

CC-0. In Public Domain. Gurukul Kangri Collection, Haridwar

Digitized by Arya Samaj Foundation Chennai and eGangotri

Reviews of Modern Physics

Reviews of Modern Physics is published quarterly to provide those interested in developments in physics with comprehensive and timely discussions of the problems that are of especial interest and importance.

It is hoped that the studies in this journal will give to the specialist the benefit of the viewpoint of other specialists; to the student, a background of critical knowledge and an adequate bibliography of source material; to those whose time is absorbed in the teaching of physics, a stimulating account of the forward movement of their science.

Published by the
American Institute of Physics
for

The American Physical Society

OFFICERS

President
FELIX BLOCH
Stanford University
Stanford, California

Vice President
JOHN A. WHEELER
Princeton University
Princeton, New Jersey

Vice-President Elect
C. H. TOWNES
Massachusetts Institute of Technology
Cambridge, Massachusetts

Secretary
K. K. DARROW
Bell Telephone Laboratories, Inc. (*retired*)
Office: Columbia University
New York, New York 10027

Treasurer
S. L. QUIMBY
Columbia University
New York, New York 10027

Deputy Secretary
W. H. HAVENS, JR.
Columbia University
New York, New York 10027

Regional Secretaries
Central States
R. G. SACHS
University of Wisconsin
Western States
WARD WHALING
California Institute of Technology

Managing Editor
S. A. GOUDSMIT
Brookhaven National Laboratory
Upton, Long Island, New York 11973

Board of Editors

Managing Editor
S. A. GOUDSMIT

Editor
E. U. CONDON

Associate Editors

1963–1965	*1964–1966*	*1967–1969*
E. A. UEHLING	W. M. FAIRBANK	H. PRIMAKOFF
C. P. SLICHTER	E. FEENBERG	W. A. FOWLER

Manuscripts for publication should be submitted to E. U. CONDON, Editor, *Reviews of Modern Physics,* Joint Institute for Laboratory Astrophysics, University of Colorado, Boulder, Colorado 80304.

Manuscripts and copy for figures must be prepared in the style of the American Institute of Physics Style Manual. Preferably two copies of each manuscript should be submitted for convenience in reviewing. Advance correspondence with the editor concerning prospective review articles is sometimes advisable to avoid duplication of effort.

Proof and all correspondence concerning papers in the process of publication should be addressed to the Supervisor, Editorial Department, American Institute of Physics, 335 East 45 Street, New York, New York 10017. Reference must be made to title, author, Journal, and scheduled date of issue.

Subscription Price

	U.S.A., Canada, and Mexico	Elsewhere
Members of The American Physical Society	$6.00	$6.50
Nonmembers	8.00	8.50

Back Numbers

Yearly rate when complete year is available: $12.00
Single copies: $3.50 each. *Double number:* $7.00

Subscriptions, renewals, orders for back numbers, and change of address should be addressed to the American Institute of Physics, 335 East 45 Street, New York, New York 10017. For change of address, allow at least six weeks' advance notice; send both old and new addresses and, if possible, please include an address stencil imprint from the mailing envelope of a recent issue.

Permission is granted to quote from this journal in scientific articles, with the customary acknowledgment of the source. Reproduction of figures and tables is permitted provided that the author's consent be obtained and that the editorial office be notified. Reproduction of whole articles for commercial purposes requires written permission of both Editor and author.

Reviews of Modern Physics is published quarterly in January, April, July, and October at Prince & Lemon Streets, Lancaster, Pa. 17604

Second-class postage paid at Lancaster, Pennsylvania.

CC-0. In Public Domain. Gurukul Kangri Collection, Haridwar

Digitized by Arya Samaj Foundation Chennai and eGangotri

गुरुकुल कांगड़ी विश्वविद्यालय
हरिद्वार

REVIEWS OF
MODERN PHYSICS

VOLUME 38, NUMBER 1 JANUARY 1966

Electron Impact Ionization Cross-Section Data for Atoms, Atomic Ions, and Diatomic Molecules: I. Experimental Data

L. J. KIEFFER,* GORDON H. DUNN*
Joint Institute for Laboratory Astrophysics,† Boulder, Colorado

This review includes a compilation and critical evaluation of absolute cross sections for ionization of atoms and diatomic molecules by electron impact. Experimental techniques used for ionization are surveyed. Selected relative cross sections for production of multiply charged ions and a brief discussion of relative cross-section data near threshold are presented. Absolute limits are not set on the size of probable systematic errors in the various experiments.

I. INTRODUCTION

Ionization of atoms and molecules by electron impact is a subject of great practical interest for predicting the properties of nonequilibrium plasmas. This interest is represented in diverse fields of research such as stellar atmospheres, low- and high-temperature laboratory plasmas, atmospheric physics, and mass spectrometry. The experimental data are also of interest for comparison with theoretical predictions. The validity of various necessary approximations in the theories can thus be tested.

This review is an attempt to assemble and to evaluate the experimental cross-section data for electron-impact ionization of atoms, atomic ions, and diatomic molecules. More complicated molecules are not considered here. A subsequent review will include a summary of the theoretical methods and results and a comparison of these results with the experimental data. (This review and evaluation of the theoretical techniques for calculating electron-impact ionization cross sections is being prepared by Alan Burgess. This review is being supported by the University of Colorado under contract with the National Bureau of Standards through the National Standard Reference Data Program.)

The relevant data fall into two main classes: (1) "Gross" or "total" ionization cross sections, i.e., the cross sections for producing a single positive charge of any atomic or molecular species regardless of the mass or multiplicity of charge on the ions produced. These measurements are important for practical reasons as well as being important in evaluating cross sections for individual processes as discussed in later sections. (2) Cross sections for individual ionization processes, including dissociative ionization, ionization to a particular final state of an ion, and multiple ionization.

A general discussion of the various experimental techniques used to obtain the data is given in Sec. II. Table I in this section lists the criteria by which the data have been selected. Section III contains the cross-section data together with a discussion comparing the individual experiments.

Table II is a classification of the experiments according to the criteria in Table I. Section IV contains a brief discussion of some of the high-resolution, relative cross-section data and some interpretations thereof.

II. EXPERIMENTAL TECHNIQUES FOR DETERMINATION OF IONIZATION CROSS SECTIONS

A measurement of an ionization cross section usually involves the determination of the quantities in the relation

$$I_i(E)/I_e(E)=\rho L\sum_n n\sigma_n(E)=\rho L\sigma_T(E). \qquad (1)$$

Here $I_i(E)$ is the ion current generated by single electron impact, $I_e(E)$ is the current of bombarding electrons of energy E, ρ is the number density of the target gas, L is the collision path length over which the measured ion current is collected, and $\sigma_n(E)$ is the

* Staff members, Laboratory Astrophysics Division, National Bureau of Standards.
† Of the National Bureau of Standards and the University of Colorado.

Copyright © 1966 by the American Physical Society
CC-0. In Public Domain. Gurukul Kangri Collection, Haridwar

Digitized by Arya Samaj Foundation Chennai and eGangotri

TABLE I. Necessary conditions in order to obtain accurate ionization cross sections.

Measured quantity	Necessary conditions
I_i	1. Collection of a known fraction of the ions. 2. No secondary electron current from ions hitting the collector. 3. No ions reflected from the collector. 4. No spurious ion or electron current. 5. Separation into final state components.
I_e	1. Total collection of electron current producing the ions. 2. No secondary electron current from electrons hitting the collector. 3. No reflection of electrons from the collector. 4. No collection of electrons ejected in the ionizing collision. 5. No collection of secondary electrons ejected from electron beam defining apertures.
ρ	1. Accurate number density standard for experiments done in static gas samples. 2. Temperatures of pressure gauge and ionization region known. 3. Accurate vapor pressure when a gas from a volatile liquid or solid is used. 4. Velocity of target known in beam experiments. 5. Accurate technique for measuring total target beam flux. 6. Measurement of inhomogeneities in target and electron beams.
L	1. Path length known for electron orbits when a confining magnetic field is used. A. Transverse velocity components due to electric or magnetic field effects. B. Transverse velocity components due to background gas scattering. 2. Path length known for electron orbits when no confining magnetic field is used. A. Transverse velocity components due to electron optical effects or space charge spreading. B. Transverse velocity components due to gas scattering.

cross section for producing an ion of nth degree of ionization in the collision. The summation is over the charge states which contribute to the collected current of ions. When all charge states are included, the summation is denoted by $\sigma_T(E)$, the total or gross cross section.

In spite of the conceptual simplicity of such an experiment and in spite of the large number of experiments done, the practical problems involved in obtaining accurate determinations of *all* the above quantities are severe.

Table I lists the most important conditions necessary for obtaining accurate measurements of the quantities needed to calculate $\sigma_n(E)$ from Eq. (1). These conditions are tabulated for use in discussing specific experiments, although, of course, one cannot include in such a general listing all the subtle difficulties which may be inherent in an individual experiment. In a similar way the magnitude of the various systematic errors is difficult to assess quantitatively. It is obviously incumbent upon all experimentors using Eq. (1) and its variations to *demonstrate* the functional dependences there and to *show* that systematic errors implied from Table I are absent or to estimate *realistically* their magnitude.

There are many types of apparatus for ionization studies, but most of them can be classified as one of the following:

A. Total ionization apparatus,
B. Total ionization tube with q/M discrimination,
C. Mass spectrometer,
D. Crossed-beam apparatus.

The problem of accurately defining electron energy is discussed in a separate paragraph as is the application of these methods to measuring ionization cross sections of molecules.

A. Total Ionization Apparatus

Early investigators (Ref. 1) of ionization tried many forms of apparatus, but it now appears that the most satisfactory type is that introduced by Jones (2) and used for the classic measurements of Smith (3) and Tate and Smith (4). The technique has recently been used by others (Refs. 5–8).

A schematic illustration of Tate and Smith's tube is shown in Fig. 1. Electrons from the differentially pumped filament F are accelerated through apertures S_1, S_2, and S_3 by an electric field maintained by a constant potential difference. A variable potential difference between S_3 and S_4 is used to give the electrons their final energy, and a longitudinal magnetic field B serves to confine the electrons in a beam. They are collected by the trap T, and their current is monitored with appropriate instruments. In determing $I_e(E)$, it is necessary to ascertain that reflected and secondary electrons in T do not escape, that electrons formed from ionizing the gas are small in number compared to the primary electron current, that photoelectrons do not constitute an appreciable fraction of the current, and that the number of secondary electrons formed on aperture edges is inappreciable. An electric field between P_3 and P_4 can ensure adequate trapping, and operation at low enough pressures can eliminate the problem of volume electrons and photoelectrons. The importance of secondary electrons which come from slit edges is best evaluated by examining the currents to and from all electrodes in the absence of a gas, and by performing

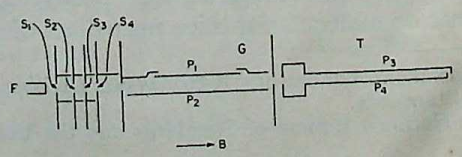

FIG. 1. Schematic illustration of typical total ionization tube.

CC-0. In Public Domain. Gurukul Kangri Collection, Haridwar

Digitized by Arya Samaj Foundation Chennai and eGangotri

a differential retarding analysis on the collected electrons to demonstrate the absence of a lower energy component.

Ions formed are accelerated by a uniform electric field between P_2 and P_1 and G. With a sufficiently strong field, the current measured to P_1 should be the ion current formed over a path length L. Secondary electrons ejected from P_1 by the ions or by photons do not escape because of the magnetic field. The determination of $I_i(E)$ must account for ions formed in the trap region or in the region prior to the space between P_2 and P_1 and G. Ions formed in these places by electrons of energy different from E may be accelerated into the collision region and collected on P_1. It is also necessary to demonstrate that the ion current to P_1 is independent of the applied ion collection field. This independence is necessary for complete collection of all ions, including ions formed with kinetic energy from dissociative ionization of molecules. At low electron energies—on the rising side of the cross-section curve—the ion drawout field may affect the collected ion current due to the spreading of the electron energy distribution by the electric field.

The path length L is nominally just the length l of p_1. However, because the electrons have a helical path in the magnetic field and a trochoidal drift in the crossed electric and magnetic fields, L is greater than l. The increase in length due to crossed field drift (Ref. 8) is a small fraction of a percent under typical conditions and may usually be neglected. If one assumes that the diameter of helices described by the electron paths is limited by an aperture of diameter d, then the maximum path length is given by

$$L=l[1-(v_\perp^2/v^2)]^{-\frac{1}{2}}, \qquad (2)$$

where $v_\perp$ is the transverse electron velocity (limited by d) and v is the total velocity. [Massey and Burhop (9) give an approximate expression for this formula.]

For the condition $v_\perp=v$, L becomes infinite. For a fixed helix diameter d, there is a minimum energy for which this equation has meaning. Electrons with energies smaller than this minimum value clearly have helical paths with diameters smaller than d. However, this should be an absolute upper limit, assuming that there is no trochoidal drift. Asundi (10) noted that the transverse velocity components imparted to the electrons by the lens system of apertures may more reasonably fix the helix diameter. He made a simple estimate based upon electrostatic lenses, ignoring the magnetic field, and found $(v_\perp/v)^2\simeq 0.001$ for geometries such as Tate and Smith used. Craggs *et al.* (11) pointed out that another possible cause of transverse velocity components is gas scattering of the electrons. Rapp and Golden (7a) concluded that transverse velocities introduced by lens effects are even smaller than estimated by Asundi, primarily because of the confining effect of the magnetic field. They estimated the effect of gas scattering in H_2 near ionization threshold and found that $L\simeq 1.0014l$ with an H_2 pressure of about 5×10^{-5} Torr. The effect on cross section measurements due to transverse velocities imparted by lenses or gas scattering should be independent of magnetic field (as long as the crossed-field drift velocity is small compared to the longitudinal velocity). The presence of an effect from these sources should be detectable by noting systematic changes of the apparent cross section when lens-operating conditions or gas pressure are changed.

Assuming an ideal gas, the target density ρ can be computed from

$$\rho=(3.535\times 10^{16})P_c(273/T_c),$$

where P_c and T_c are the pressure in mm Hg and temperature in °K, respectively, in the collision chamber and 3.535×10^{16} is the number of particles per cc at 1 mm pressure at 273 °K. If the gauge at temperature T_G used to determine P_c is connected to the chamber with tubing with a diameter small compared to the mean free path of the gas particles, then (Ref. 12) at equilibrium, $P_c/P_G=(T_c/T_G)^{\frac{1}{2}}$; and the equation for the density becomes

$$\rho=(3.535\times 10^{16})\ 273\ P_G\ (T_cT_G)^{-\frac{1}{2}}. \qquad (3)$$

It is not apparent whether all authors have properly accounted for temperature differences (see Table II, Sec. III), although the corrections can typically amount to 10%. Rapp and Golden pointed out that when different temperature and density regions are between the gauge and ionization chamber, the simple one-half power thermal transpiration law may not apply. Deviations from the ideal $(T)^{\frac{1}{2}}$ relation have been considered by other authors (13).

Gauge pressure P_G is typically obtained by using a McLeod gauge, an absolute device which has been assumed to be accurate to a conservative 2 or 3%. Quite recently, Ishii and Nakayama (14) found that McLeod gauge readings strongly depended on temperature. This effect has since been observed by others (15), and within the accuracy of the techniques used, it has been found that the effect seems to agree with the prediction of Gaede (16). He suggested that the mercury stream from the gauge to the cold trap should act like a diffusion pump. Apparent errors at room temperatures have been found ranging from 1 or 2% for H_2 to 20 to 40% for xenon. Cooling the McLeod gauge cutoff (Refs. 14, 15) or refrigerating the whole gauge are techniques which have been used to diminish this systematic effect. Further definitive tests are certainly desirable, and better theoretical understanding is needed of all possible mechanisms which could cause the McLeod gauge to behave in such a manner. A dynamic technique for measuring pressure has been used in ionization measurements by Rapp and Golden

CC-0. In Public Domain. Gurukul Kangri Collection, Haridwar

Digitized by Arya Samaj Foundation Chennai and eGangotri

(7a). This technique requires effusive flow through a leak between a volume with a high pressure and the ionization chamber and out of the ionization chamber through another aperture leading to pumps. The technique has not been used nor tested enough to demonstrate whether it is free of systematic effects which may be as large as those encountered in using the McLeod gauge. At present ionization gauges are secondary standards and depend ultimately upon a primary standard such as the McLeod gauge. It appears that measurement of system pressure gives rise to one of the largest uncertainties in the determination of total ionization cross sections by this method.

Total ionization measurements have been recently made in a Lozier tube (Refs. 6, 11) and in a cylindrical tube which has grids (Ref. 17) instead of vanes as does the Lozier tube. These measurements depend upon Tate and Smith's (3, 4) measurements for calibration, and there are too few data to evaluate completely the method for absolute measurements. Except for the different problems of ion collection with these tubes, the same problems exist as for the parallel-plate method described above.

B. Total Ionization Tube with q/M Discrimination

The method discussed in Sec. IIA does not separate ionization components of different charge q and mass M that contribute to the summation in Eq. (1). To accomplish this, q/M analysis of the ions must be introduced. This was done by Bleakney (18) and by Tate and Smith (19), who made a narrow slit longitudinally in P_1, and who used a ribbon beam of electrons wider than the slit. Ions passing through the slit entered a q/M analyzer, were collected, and their current measured. By scanning the analyzer fields ion currents due to different q/M components could be measured. A simultaneous measurement of $\sigma_T(E)$ as described in Sec. IIA above could be made, and Eq. (1) could be solved for $\sigma_n(E)$. The same problems that were discussed above in Sec. IIA pertain to this device. In addition, q/M analysis has inherent problems which are discussed in the next paragraph.

C. Mass Spectrometer

The term mass spectrometer is used here generically to include any device which separates ions of different q/M. Standard techniques with these instruments and apparatus descriptions are widely discussed in the literature (Ref. 20). Because of the difficulty in ascertaining their collection efficiency, their primary value in ionization cross-section studies has been in determining *relative* cross sections as a function of electron energy, i.e., $C\sigma_n(E)$, where it is hoped and is usually assumed that C is constant. If C is a constant for each ionic species, the ratios $\sigma_{n_1}(E)/\sigma_{n_2}(E)$ can be determined. The mass spectrometer has been used very extensively in recent years to examine detailed variations of $\sigma_n(E)$ with E.

For measurements of this type to be deemed reliable, the experimentor must show that C is constant, i.e., that the ion collection efficiency is independent of q/M and of the electron energy E. He must show that ion source operating conditions—magnetic field, pressure, electron current—do not change the shape of the observed relative cross section.

Most ion sources contain various combinations (which stay relatively fixed during a q/M scan) of electric and magnetic fields for the purpose of ion extraction and focusing into the mass analyzer. Ions of different q/M will not necessarily behave in the same way in these fields, and the instruments will discriminate in detection of them. Discrimination may also occur at the detector if sufficient care is not taken to eliminate effects from secondary electron emission and from ion reflection, since these effects depend strongly on ion species and energy. An extreme example of this is encountered when an electron multiplier is used as detector, since the multiplier response depends (Ref. 21) quite strongly on q/M.

When a focusing mass spectrometer of the usual sector magnetic field variety is used, the collection efficiency of the instrument may change with electron energy if the electron beam changes size, shape, or position with energy. These changes can occur if all fields involved with the electron gun, including fields due to space charge, are not carefully scaled with the final accelerating field.

D. Crossed-Beam Apparatus

Many atomic species are not stable at normal temperatures, and techniques must be used which will produce the species in adequate abundance and in an environment where its ionization can be studied. This is the case, for example, with atomic hydrogen, oxygen, and nitrogen and with alkali metals, ions, and metastable atoms and molecules. The study of ionization of sodium in crossed beams of atoms and electrons was undertaken by Funk (22), and relative ionization cross sections of some alkali metals as a function of energy were measured by Tate and Smith (19) using an apparatus held at a high temperature to allow vaporization of the metal such as discussed in B. The most significant technique for study of such species is, however, the modulated crossed-beam technique which was apparently first used for ionization studies by Boyd and Green (23) and by Fite and Brackmann (24).

The application of this technique has resulted in apparatus which varies significantly in detail and in problems encountered, so a discussion of particular problems is deferred to a discussion of individual experiments.

The general technique can be understood in terms of

CC-0. In Public Domain. Gurukul Kangri Collection, Haridwar

Digitized by Arya Samaj Foundation Chennai and eGangotri

the block diagram in Fig. 2. A beam of target particles is crossed with a beam of electrons in high vacuum, and ions resulting from the collision are detected. Usually particles of either one beam or the other collide with the background gas to produce unwanted ions of the type which one desires to detect. The number of ions from this source is often much greater than that from the intended target–electron collision; thus long sampling times are required to keep the statistical fluctuations in the background from being large compared to the signal. These long times, however, impose impractical stability limitations upon such variables as background pressure, beam magnitude, amplifier gains, etc. These limitations are overcome by chopping one or both of the beams and observing the resultant modulated ion signal in the proper phase with the modulated primary beam. [It is usual to modulate the beam that is least likely to give rise to a background ion current in the collector. Dolder *et al.* (25) in measuring ionization of ions chopped both beams with varying phases.] Required sampling times to achieve a given signal to statistical noise ratio are still comparable to the times needed in nonchopped cases, but extreme stability of parameters mentioned must now be maintained only over the chopping period.

Some changes in Eq. (1) are necessary, since the beams may not be homogeneous in space and since the target beam may have an appreciable velocity compared to that of the electrons. The equation becomes (Ref. 25):

$$I_i/I_e=\sigma(E)R[(v_e^2+v_t^2)^{\frac{1}{2}}/v_tv_e]F, \qquad (4)$$

where v_e and v_t are velocities of the electrons and target particles, respectively (assumed to be perpendicular), R is the number of target particles per second arriving at the target detector, E is the relative energy of target and electron which is or order $E_e+(M_e/M_i)E_t$, and $\sigma(E)$ may be either $\sigma_T(E)$ or $\sigma_n(E)$ as defined in Eq. (1). The factor F is a measure of the overlap of the two beams; and if the beams are individually parallel (i.e., do not diverge or converge) over the length of the interaction region, F may be calculated from

$$F=\int j_e(z)j_t(z)dz[\int j_t(z)dz\int j_e(z)dz]^{-1}. \qquad (5)$$

Here $j_e(z)$ and $j_t(z)$ are the spatial distributions of the electron and target beams, respectively, which are usually measured by scanning each beam with a fine slit movable in the dimension z (Refs. 25–27). The integrations are practically over the real extents of the beams. Since it is difficult to estimate systematic errors in F, it is necessary to demonstrate experimentally the independence of $\sigma(E)$ on F.

When the target particles are neutral and in the ground state, R is difficult to measure. Some experimentors (Refs. 24, 28–31) normalize the signal from a beam of atoms to measurements on a beam of the stable parent diatomic molecules which in turn have been measured with techniques described above, e.g., ionization of H atoms is compared with ionization of H_2. In this way, if mass flow from the source is kept constant, the cross sections can be normalized to the measured molecular cross sections without knowing R absolutely. Experiments on alkali metals (Refs. 32, 33) make use of the surface ionization detector to measure R. For its absolute calibration, however, this detector depends upon the assumption (Ref. 34) that the reflection coefficient of incident atoms and of the resultant ions is zero and that the number of ions evaporated from the surface, for those beam atoms that are absorbed, is the same as the number evaporated under steady-state conditions. There do not seem to be any measurements at very low energies, but experiments on ions at higher energies (Ref. 35) show reflection coefficients 10–30% and rising with decreasing energy. The recent experiment of Schroen (36) indicates that the reflection coefficient for potassium atoms on pure tungsten and platinum surfaces is probably zero. The assumption is also made that the ionization efficiency for all alkali atoms on oxidized tungsten is 100%. Absolute calibration in such experiments thus seems open to some question. R. H. McFarland [Abstracts of Papers presented at *IV International Conference on the Physics of Electronic and Atomic Collisions* (Science Bookcrafters, Inc., Hastings-on-Hudson, New York, 1965), p. 416] has used a known amount of alkali beam material and monitored the beam over many hours until the known oven load was completely depleted. With a knowledge of geometry R could be calculated. This method gave cross sections slightly higher than are obtained by using a surface ionization detector. Calorimetry was used by Peterson (26) to measure R for a fast nitrogen atom beam formed by charge exchange of N^+. The absolute calibration of this technique depends upon the assumption that the accomodation coefficients of fast N^+ and N on a surface are the same. Here again there does not seem to be any

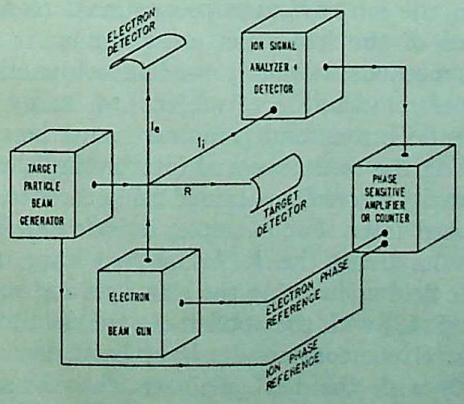

FIG. 2. Block diagram of a typical crossed-beam apparatus for measuring ionization cross sections by electron impact.

CC-0. In Public Domain. Gurukul Kangri Collection, Haridwar

Digitized by Arya Samaj Foundation Chennai and eGangotri

direct experimental evidence that this assumption is justified.

Collection and detection of ions formed in these experiments are done in a variety of ways which are not all described here. When q/M analysis is employed the usual assumption is that negligible momentum is transferred by the electron to the atom in the collision. This assumption is easily justified when the target beam is energetic. When the target is a thermal beam, however, the momentum transferred (at ionization threshold all the electron momentum is transferred to the atom) can be a significant part of the total momentum. This implies that sizable deviations of resultant ion trajectories may take place. The assumption of negligible momentum transfer would thus appear questionable—contrary to rather convincing indirect evidence of Fite and Brackmann (24) that the assumption is good. It is important that collection and detection efficiency be carefully analyzed and described by authors using crossed-beam techniques, since obscure effects such as momentum transfer, space charge deflection of the primary beam, and unknown or variable dispersion of the analyzer may give rise to systematic errors.

E. Determination and Definition of Electron Energy, E

Due to potential drop across the filament, contact potential differences between electrodes, and surface potential differences of the electrodes, the electron energy E may be quite different from the nominal voltage difference applied between the cathode and collision region. The difference between the actual electron energy and the "nominal energy" may amount to a volt or more. This may not be important at high energies where the cross section varies relatively slowly, but may make a large difference in the apparent cross section at low energies where the cross section rises steeply. Absolute calibration of energy is normally done by introducing a gas sample for which the ionization energy is known spectroscopically. The appearance of singly charged ions of this gas is observed, and "the straight line portion" of the ionization efficiency curve is extrapolated to the abscissa. The intercept is taken as the spectroscopic ionization energy, and the energy scale is shifted to agree. Asundi and Kurepa (37) have shown that when the electron beam has a thermal energy distribution the intercept is shifted by $2kT$ toward lower energies from the actual critical potential. Energy distributions distorted by nonuniform surface potentials, by electric fields in the interaction region, etc., gives rise to different shifts. The extrapolation procedure above is valid only for comparing differences in appearance potential, i.e., it does not set the absolute scale of energy unless the shift in the intercept is taken into account. If the calibration gas and sample gas are introduced into the chamber separately, it is possible that surface potentials will change enough from one gas to the other to render this procedure useless. It is thus desirable where possible to mix sample and calibration gases for comparison. Even in this case, there may be a shift in the energy scale because of altered surface potentials caused by ions from the gas with the lower ionization potential. Straight line extrapolation may not always be justified if the ion has low-lying excited states or if there are autoionizing levels in the vicinity of threshold. If the shape of the electron energy distribution is grossly distorted, these simple techniques cannot be used. The cross section should be unfolded using knowledge of the electron energy distribution.

The observed ion signal for any setting of the nominal electron energy is proportional to the integral over energy of the product of the cross section and the electron energy distribution. Fine details occurring in an energy range comparable to or less than the width of the electron energy distribution may thus be obscured or distorted, and it is important in order to observe these details to have the energy distribution be as narrow as possible.

Nottingham (38) used magnetic selection of electron energies to study ionization of mercury, but little more was done with the technique. Perhaps the next advance in energy selection was the introduction of the ingenious retarding potential difference (RPD) technique by Fox *et al.* (39) in 1951. Other techniques used effectively for ionization work in recent years include energy analysis with uniform electric fields (Ref. 40) and cylindrical fields varying as the inverse distance from the center (Ref. 41). Morrison (42) has recently used energy analysis from a 127° analyzer and a sophisticated unfolding technique to resolve details in the cross section.

Morrison (43) has used another technique to observe details in ionization cross sections. This involves a small amplitude modulation of the electron accelerating voltage. The ion current will be modulated at frequencies which are harmonics of the electron modulation frequency, and the amplitude of the Mth harmonic in the ion current is proportional to the Mth derivative of the ionization cross section.

These methods, normally used in conjunction with mass spectrometers, are subject to many serious instrumental errors, and great care must be exercised in applying the technique and interpreting the results. The disparity in results obtained using these techniques is discussed later. For example, it is found (Ref. 44) that results using the RPD method vary with the magnetic field collimating the electrons and sometimes vary (Ref. 45) with the applied electric field extracting the ions. Extraneous results have been demonstrated (Ref. 46) with the 127° analyzer when ions are apparently formed by bombardment of gas adsorbed on the ion-source walls. Because of interactions with the lattice, these ions are formed with an energy dependence

CC-0. In Public Domain. Gurukul Kangri Collection, Haridwar

Digitized by Arya Samaj Foundation Chennai and eGangotri

different than that for free molecules. Marmet (47) has recently analyzed some of the systematic errors which can be present with the devices noted here. He also emphasized that an appreciable spread in effective interaction energy is introduced from the target gas energy—especially for light gases. This latter effect is not negligible when a claim of 0.050-V resolution and better is made.

F. Ionization of Diatomic Molecules

Little reference has been made thus far to the specific problems encountered in measuring ionization cross sections of molecules. The distinguishing feature in molecular ionization is that some fraction of ionizing collisions result in atomic ions with kinetic energies in the range 1–15 eV, i.e., dissociative ionization occurs. In addition, the velocities of the ions may not be isotropically oriented in space, but will instead have some definite distribution of directions relative to the impacting electron beam (Refs. 48, 49).

Presence of these ions necessitates the use of higher collection fields in total ionization apparatus as discussed in Sec. IIA but does not introduce any other apparent difficulties in measuring $\sigma_T(E)$. However, these energetic particles are represented by one or more of the summation terms in Eq. (1), and severe difficulties are encountered in trying to arrive at individual terms. It appears that no ion sources for mass spectrometers have been devised which do not strongly discriminate against these energetic particles as compared to the thermal molecular ions formed, and reliable ratios of the individual cross sections have not been obtained with such devices.

Apparatus such as the one shown in Fig. 1 can be used to obtain approximate absolute values (Refs. 7b, 7c, 50) for the energetic ion cross sections. The voltage on P_1, G is made positive by an amount ΔV above the mean potential along which the electrons travel. Those ions with kinetic energies greater than ΔV reach P_1, and their current is measured. By applying a correction for the solid angle subtended by P_1, the cross section can be deduced. When making this correction one should also take into account the angular distribution of velocities of the dissociating particles as a function of electron energy. Unfortunately, this distribution is known only for hydrogen (Ref. 49), so an isotropic distribution has been assumed (Ref. 7b, 7c, 50). Reflection of ions from P_1 is not accounted for and may introduce some error.

Cook and Peterson (51) have applied a fast beam technique to look at ionizing processes in N_2 which include dissociative ionization, but comparison of some of their results with what appear to be reliable total ionization data (Refs. 4, 7a) leads one to conclude that further development of this difficult technique is needed.

A further complication arises in molecular ionization when one tries to separate the summation components in Eq. (1). This is due to the fact that a twice ionized, homonuclear, diatomic molecule has the same q/M as the atomic ion resulting from dissociative ionization. Isotopic substitution so that the molecule is no longer exactly homonuclear has been used by Morrison (52) to observe multiple ionization in some homonuclear molecules.

G. Fluorescence Measurements

Those who must know ionization cross sections for understanding plasma phenomena and those who want to test theoretical predictions of ionization need to know the final states of the ions observed in experiments purporting to measure ionization cross sections. It is apparent that the methods mentioned in the preceding paragraphs do little to determine final states of ions.

One technique which can be applied in a limited number of cases is to measure the light emitted from excited ions formed by electrons of known energy. The problems of measuring the quantities appearing in the obvious variation of Eq. (1) are present as in the methods above. In addition the method has the difficult problem of absolute radiometry. This fluorescence technique has been used to observe ionization to the $n=4$ level (Ref. 53) of He^+ and to the $v=0$ level (Ref. 54–56) of the $B\ ^2\Sigma_u^+$ state of N_2^+.

III. EXPERIMENTAL RESULTS

A. Introduction

The first step in selection of the data was a survey of the literature which purported to contain experimental electron impact ionization cross-section data (Ref. 57).

The question of what are valid sources, published or unpublished, is, of course, a matter of opinion. In general we have selected data from recognized journals. In one case data have been included from an unpublished thesis. In several cases information has been included from the published proceedings of conferences which were not reviewed. Original data has been obtained from the authors which in some cases was not presented in publications. In all cases the actual source of the data as distinct from the general reference is identified. The method of obtaining data from figures is discussed below.

Regardless of the source, all of the experiments for which data are presented in this section were compared with criteria given in Table I to determine whether they may have been subject to the systematic errors discussed in Sec. II. To make this comparison we used the published material available and correspondence or personal contact with the authors when possible.

All of the experiments for which data are presented were subject to many of the systematic errors discussed in Sec. II (see Table II). Experiments for which data

CC-0. In Public Domain. Gurukul Kangri Collection, Haridwar

Digitized by Arya Samaj Foundation Chennai and eGangotri

TABLE II. Classification of experiments and their probable systematic errors. Only experiments for which results are presented in Secs. IIIB(1), IIIB(2), and IIIB(3) are listed here. The experiment of Fite (66) is not included because not enough information was available to compare it with the criteria given in Table I. The experiment is discussed in Sec. IIIB(3). The column headings and numbers in the columns refer to the criteria of Table I. "The Type" of data is either absolute A or relative R. All of the relative results were normalized, and the footnotes describe the method used by the authors to do so.

Author (year)	Species	Type of apparatus	Type of data	I_i	I_e	ρ	L
1. T. J. Jones (2) *1927*	Hg	Parallel plate total ion collection	A	4[a], 5	4, 5	2[b], 3[c]	1 A, 1B
2. W. Bleakney (59) *1930*	Hg	Parallel plate, total ion collection with mass spectrometer	A[d]	4[e]	2, 3, 5		1 A
3. P. T. Smith (3) *1930*	He, Ne, Ar	Parallel plate total ion collection	A	5		1	1 A, 1 B
4. P. T. Smith (60) *1931*	Hg	Parallel plate total ion collection	A	5	4, 5	3[f]	1 A, 1B
5. J. T. Tate, P. T. Smith (4) *1932*	H_2, N_2, O_2, NO, CO	Parallel plate total ion collection	A	3, 1, 5	4	1	1 A, 1 B
6. J. W. Liska (61) *1934*	He, Hg	Parallel plate geometry, small solid angle for collection of ions	R[g]	1, 5	1, 2, 3, 4, 5		1 A, 1 B
7. H. Harrison (62) *1956*	He, Hg, H_2	Parallel plate total collection and rf mass spectrometer	A[h]	1[i,j], 3, 4[k]		1[l], 2	1 A, 1 B
8. W. L. Fite, R. T. Brackmann (24) *1958*	H	Crossed beam with mass spectrometer	R[m]	1[n]			2 A
9. W. L. Fite, R. T. Brackmann (28)° *1959*	O	Crossed beam with mass spectrometer and total ion collector	R[p]	1[q]	3	6	2 B
10. B. A. Tozer, J. D. Craggs (65) *1960*	Ar, Kr, Xe	Lozier tube with cylindrical drawout field	R[r]	1, 3, 5	1, 2, 3, 4, 5	1, 2	1 A, 1 B
11. A. Boksenberg (31) *1961*	H, O	Mass spectrometer (H): mass spectrometer with total ion collector (O)	R[s]	1[t]	3, 5	6	1 A[u]
12. K. T. Dolder, M. F. A. Harrison, P. C. Thonemann (25) *1961*	He^+	Crossed beam with mass spectrometer and total ion collection	A	1, 3, 4			2 A
13. E. W. Rothe, L. L. Marino, R. H. Neynaber, S. M. Trujillo (29) *1962*	H, O	Crossed beam with total ion collection	R[v]	1[w], 3, 5	1, 2, 3, 5	6	2 A
14. G. J. Schulz (17) *1962*	O_2	Total ion collection with cylindrical drawout field	A	1, 3, 5	1, 2, 3, 4, 5	2	1 A, 1 B
15. A. C. H. Smith, E. Caplinger, R. H. Neynaber, E. W. Rothe, S. M. Trujillo (30) *1962*	N	Crossed beam with total ion collection	R[x]	3, 4[y], 5		4[z], 6	1 A, 1 B
16. R. K. Asundi, M. V. Kurepa (5) *1963*	He, Ne, Ar, Kr, Xe	Parallel plate total ion collection[aa]	A[aa]	5	4, 5	1, 2	1 A, 1 B
17 R. K. Asundi, J. D. Craggs, M. V. Kurepa (6) *1963*	CO, O_2	Parallel plate total ion collection	A	3, 4[bb], 5	2, 3, 4, 5	1, 2	1 A, 1 B
18. K. T. Dolder, M. F. A. Harrison, P. C. Thonemann (63) *1963*	Ne^+	Crossed beam with mass spectrometer and total ion collection	A	1, 3			2 A
19. M. F. A. Harrison, K. T. Dolder, P. C. Thonemann (64) *1963*	N^+	Crossed beam with mass spectrometer and total ion collection	A	1, 3, 4			2 A

CC-0. In Public Domain. Gurukul Kangri Collection, Haridwar

Digitized by Arya Samaj Foundation Chennai and eGangotri

TABLE II. (*Continued*)

20. J. R. Peterson (26) *1963*	N	Fast crossed beam with mass spectrometer and total ion collection	*A*	1, 3, 4	1, 2, 3, 5	5[ee]	1 A
21. D. Rapp, P. Englander-Golden (7a) *1965*	He, Ne, Ar, Kr, Xe, H_2, D_2, N_2, O_2, CO, NO	Parallel plate total ion collection	*A*	5, 3	5	1	1 A, 1 B
22. R. H. McFarland, J. D. Kinney (33) *1965*	Li, Na, K, Rb, Cs	Crossed-beam total ion collection	*A*	3, 5	1[dd]	5[ee], 6	2 A
23. B. L. Schram, F. J. de Heer, M. J. van der Wiel, J. Kistemaker (8) *1965*	He, Ne, Ar, Kr, Xe, H_2, D_2, N_2, O_2	Parallel plate total ion collection	*A*	3, 5	5	2	
24. J. W. Hooper, W. C. Lineberger, E. W. McDaniel, F. M. Bacon (27) *1966*	Li^+, Na^+, K^+	Crossed-beam total ion collection	*A*	1, 3			2 A

[a] Ions formed in the electron collector may have gotten back to the ion collector.
[b] Efficiency data presented was for an ionization chamber temperature of 70°C.
[c] Vapor pressure at 0°C from A. Smith and A. W. C. Menzies [Ann. Phys. (Paris) 33, 979 (1910)] now considered incorrect.
[d] Relative numbers of multiply charged ions also given.
[e] Ions formed in the electron collector may have gotten back to the ion collector.
[f] No mention of vapor pressure data used.
[g] Relative values normalized to P. T. Smith's (3, 60) at maximum of cross section for Hg and at 2500 V for He.
[h] Relative numbers of multiply charged ions were also measured using rf mass spectrometer.
[i] A grid was in front of the ion collector. No discussion was given to indicate a correction was made for its finite transmission. The potential difference between the parallel plates was only 9 V. This is insufficient to collect all the energetic protons from dissociative ionization of H_2.
[j] It was assumed that the rf mass spectrometer had the same collection efficiency for all multiply charged ions.
[k] Ions formed in the electron collector may have gotten back to the ion collector.
[l] A calibrated ion gauge was used to make pressure measurements.
[m] Cross sections normalized to Tate and Smith's (4) total ionization cross sections for H_2. The procedure used neglected ion current from dissociatively ionized H_2 molecules.
[n] Possible sideways momentum imparted to ions by electron impact.
[o] See ASTIA Document No. AD 208599 for more details about this experiment.
[p] Relative cross sections normalized to Tate and Smith's (4) total ionization cross sections for O_2.
[q] Technique for collecting all ions does not appear to yield saturation under any conditions. See Boyd and Green (23).
[r] Relative cross sections normalized to Smith's (3) cross section for argon at 80 eV.
[s] Atomic hydrogen cross sections normalized to Born approximation calculation at 300 V. Atomic oxygen cross sections normalized using Tate and Smith's (4) total ionization cross sections for molecular oxygen.
[t] No data were presented to show saturation of ion current for oxygen.
[u] Path length corrections were made using Tate and Smith's (4) total ion cross sections and a weighted sum of mass analyzed currents.
[v] Relative cross sections normalized to Tate and Smith's (4) total ionization cross sections.
[w] Inadequate evidence for saturation of ion current was presented.
[x] Relative cross sections normalized to Tate and Smith's (4) total ionization cross sections for molecular nitrogen.
[y] Neutral beam may have had metastable species in it.
[z] Particle velocities in neutral beam may have been different for discharge on and off conditions.
[aa] Data were also taken with a Lozier tube apparatus, but these data have not been given in the figures.
[bb] Ions formed in the electron collector may have gotten back to the ion collector.
[cc] Calorimetric beam detector efficiencies are uncertain.
[dd] No details of electron gun and collector were given.
[ee] Hot wire beam detector efficiencies are uncertain (see discussion Sec. II).

are not presented were rejected for one of the following reasons:

(1) The experimental technique used had been demonstrated to be unreliable.

(2) Systematic effects were observed by the authors while taking the data, for which no correction was applied, or it appeared that in our judgment the correction was not properly made. The data are presented whenever there is reasonable doubt about rejection.

(3) The data are only of historical interest and have been superseded.

Some mass spectrometer data on the relative abundance of multiply charged atomic ions and on ionization threshold behavior are presented in Sec. IIIB(5) and IV, respectively.

Table II lists the authors whose data are presented in Sec. IIIB(1), B(2), and B(3). The table also classifies the experiments and lists the "likely" systematic errors implied when the conditions given in Table I were not satisfied. Systematic errors are listed as "likely" if the experimental technique used was subject to an error implied in Table I and if: (1) the author did not discuss it; (2) the author gave inadequate evidence for the

CC-0. In Public Domain. Gurukul Kangri Collection, Haridwar

Digitized by Arya Samaj Foundation Chennai and eGangotri

absence of the error; or (3) the author indicated its presence but did not adequately correct for it. The latter cases are discussed in the Comments in Table II. The numbers listed in Table II under columns I_i, I_e, ρ, and L refer to the designations in Table I.

There is some evidence that some data should be preferred over others, but in no case was the evidence unequivocal. These cases are discussed specifically.

All of the absolute or normalized data points presented are either taken directly from tables given by the authors or read from their graphs. In no case is interpolated data given. The data of Sheridan, Oldenberg, and Carleton (55) on the ionization of N_2 to an excited state of N_2^+ and the data of Stanton and Monahan on the relative yield of He^+ to He^{2+} were originally presented as line drawings in a graph. These results are presented here in the same form. For data which were only available graphically, enlarged photographs were made, and the cross section and electron energy values for each data point were determined by measuring the positions of the points relative to the scale given on the graph. Although this technique might seem questionable, it appears to be quite accurate. One set of data compiled in this manner was compared with a set of tables supplied later by the author; all cross section and energy values agreed to within 1% or better. Any tabular data supplied by the authors which were not included in their published paper or circulated report are noted.

Most of the absolute and normalized data are "total" cross sections σ_T, as defined by Eq. (1). In some cases, where mass spectrometer analysis of the ions was done, the cross sections given are for the production of ion species of specific charge/mass ratio. Such cases are specifically noted. In all cases use of the term "total cross section" implies that no charge, or mass analysis, was made.

The relative cross sections for the production of multiply charged atomic ions from atoms [Sec. IIIB(5)] are expressed as σ_{n+}/σ_T. All data points on the figures in Sec. IIIB(5) indicate a measurement of either i_{n+} or σ_{n+}, where

$$i_{n+} \propto n\sigma_{n+}. \tag{6}$$

All of these data are relative, and in some cases a measurement of i_{n+} or σ_{n+} was not made for each ion species at every electron energy. In order to evaluate σ_{n+}/σ_T at such electron energies, it was assumed that

$$\sigma_{n+}/\sigma_T = n^{-1}[i_{n+}/(i_{1+}+i_{2+}+i_{3+}\ldots)], \tag{7}$$

in which some of the ion currents in the denominator of the right-hand side of the equation may have been interpolated from the graph or table presented by the author. As stated above, the relative ion currents [or cross sections, since they are simply related by Eq. (6)] in the numerator of Eq. (7) are data points given in the graph or table presented by the author and are not interpolated.

The electron energy scale for each of the cross sections should be called "nominal" in the sense that the origin is uncertain. No attempt was made to correct the energy scale given by the author, and in no case, did the authors present an energy profile of the electron beam and unfold the cross section. Because of this and because of the uncertainty of the threshold behavior of ionization cross sections, it is likely that the absolute energy scale may differ from the "nominal" by ± 1.0 eV.

Much of the older data in the literature were given as efficiency versus electron energy. Ionization efficiency is defined as the number of unit positive charges produced in a 1-cm path at 1-mm pressure and 0 °C per electron. To convert ionization efficiency to cross section, the number of molecules/cm^3 at 1 mm of pressure and 0°C was taken to be 3.53490×10^{16}. This number was derived by using the following constants (Ref. 58): volume of a g-mole, 22420.7 cm^3; 1 atm, 76.0000 cm Hg; Avogadro's number, 6.02338×10^{23} molecules/g-mole. To convert ionization efficiency to cross section in πa_0^2 units (assuming single impact), efficiency was multiplied by 0.321573. To convert cross sections in 10^{-16} cm^2 units to πa_0^2 units, cross sections in 10^{-16} cm^2 units were multiplied by 1.13673.

In spite of the fact that the total cross-section data appear to be more accurately known (based on comparison of independent absolute experiments), one might question their usefulness, since one would really like to know the charge, mass, and state of the various ions created by electron impact. There are three reasons why we consider these cross sections to be important.

First, total cross sections are very intimately connected with the measurement of number density of atomic scatterers at low pressure ($<10^{-3}$ Torr). The uncertainty of number density in gases at low pressure is probably responsible for the largest systematic errors in most of the total ionization cross-section measurements. In other words, if the atomic and molecular total ionization cross sections were known, one could, in principle, construct an absolute ion gauge.

Second, these cross sections are in general more accurately known than those for creating a specific ion species, since their determination only requires a measurement of the total ion current. Because the total ionization cross section is a weighted sum of all cross sections for producing ions, it provides, if accurately known, an upper limit on this sum.

Finally, in many experiments the total absolute cross sections for stable species are used to normalize the relative cross sections for unstable species such as H, N, and O. From one point of view the total cross sections can be regarded as most fundamental, since most of our knowledge of the absolute cross sections for creating ions of specific charge and mass rest on these measurements.

CC-0. In Public Domain. Gurukul Kangri Collection, Haridwar

B. Cross-Section Data

Digitized by Arya Samaj Foundation Chennai and eGangotri

(1) *Absolute and Normalized Cross Sections for Ionization of Atoms*

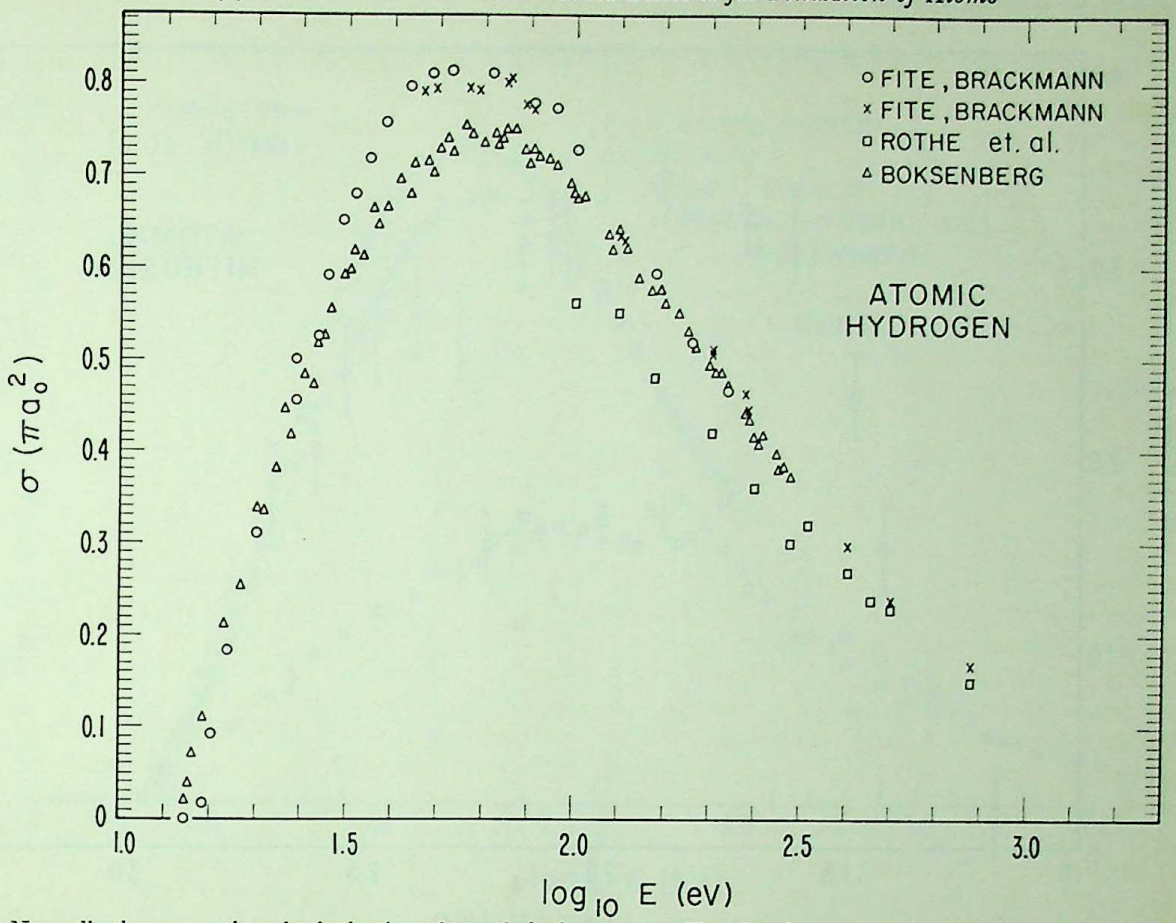

FIG. 3. Normalized cross sections for ionization of atomic hydrogen. ○—Fite, Brackmann are the data referred to by the authors as "relative"; they were normalized to Born approximation calculations at 500 eV. ×—Fite, Brackmann are the data referred to by the authors as "absolute"; they were normalized using the total absolute cross sections measured by Tate and Smith (4) for molecular hydrogen. References: Fite (24); Rothe (29); Boksenberg (31).

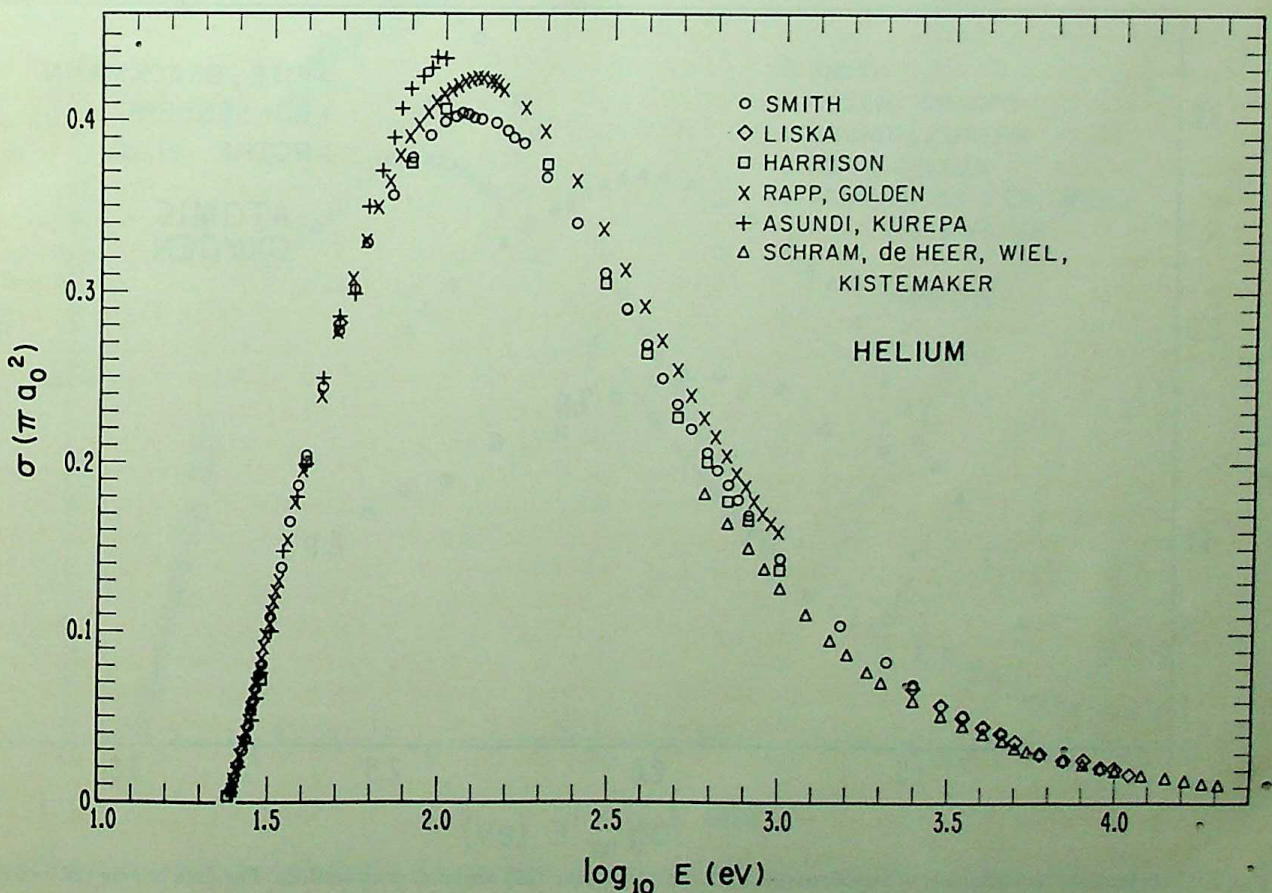

CC-0. In Public Domain. Gurukul Kangri Collection, Haridwar

FIG. 4. Total cross sections for the ionization of atomic helium. References: Smith (3); Liska (61); Harrison (62); Rapp (7a); Asundi (5); Schram (8).

Digitized by Arya Samaj Foundation Chennai and eGangotri

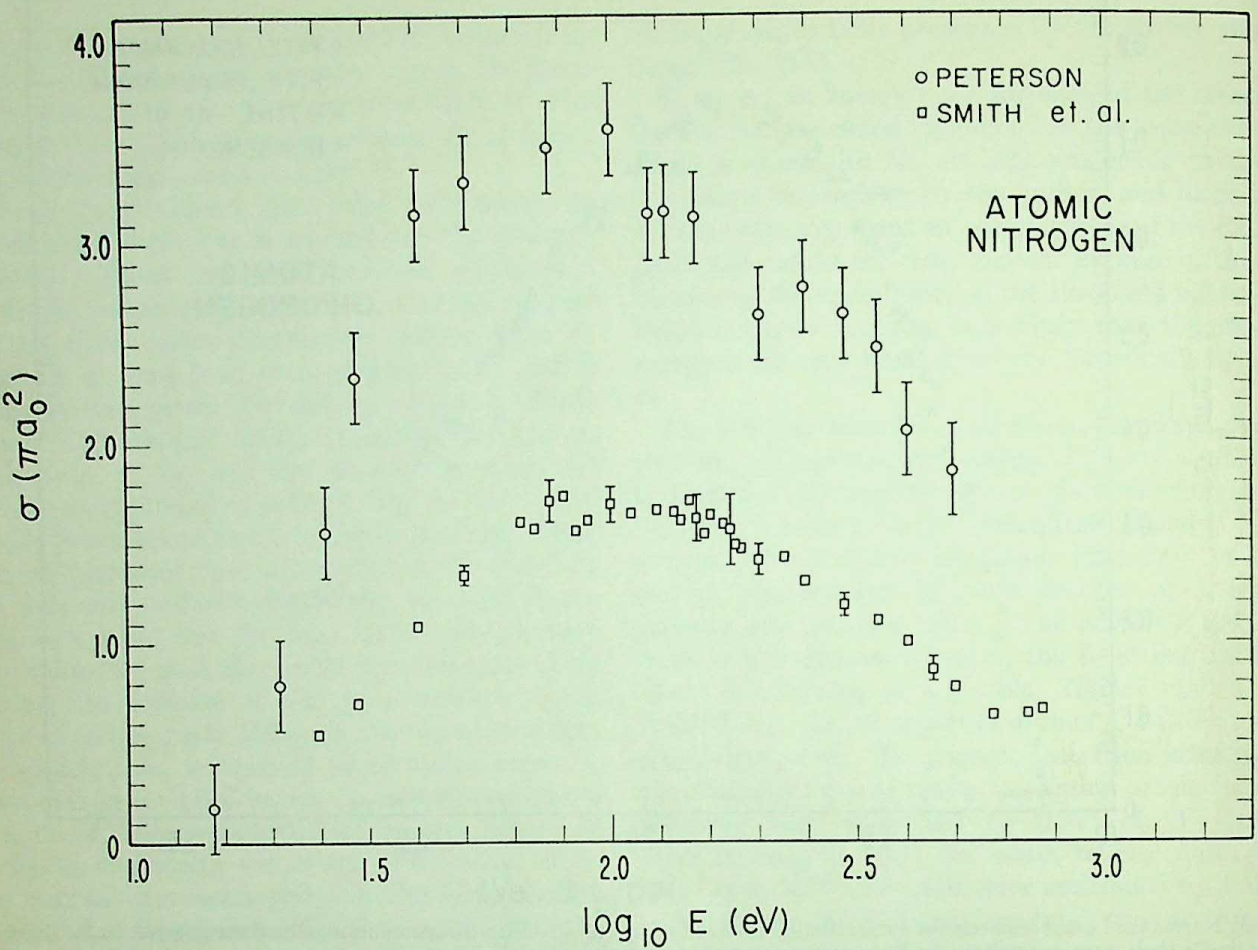

FIG. 5. Cross sections for ionization of atomic nitrogen. The data of Smith (30) are total cross sections. The data of Peterson (26) because of mass analysis are cross sections for the production of N^+ from N.

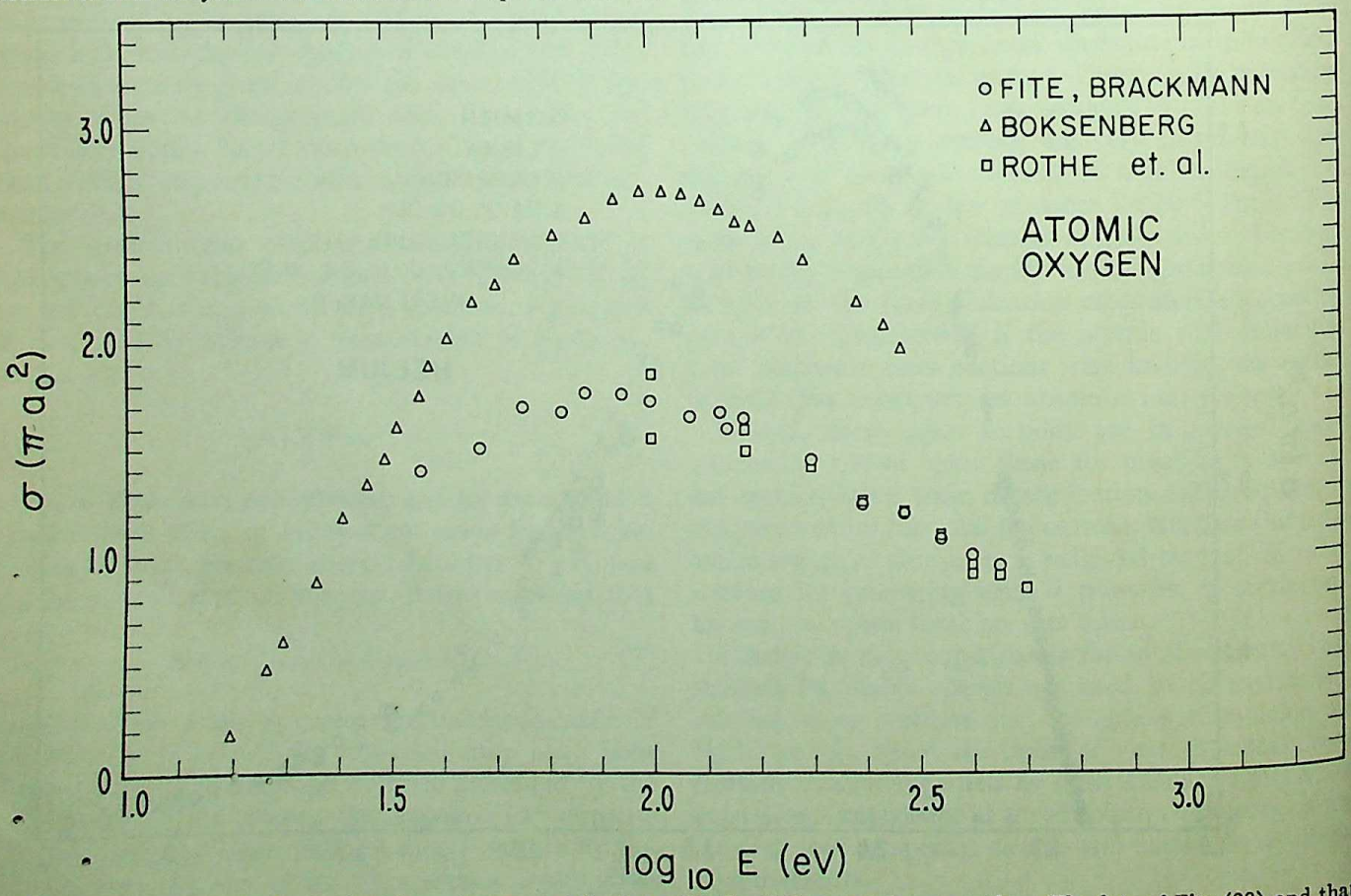

FIG. 6. Cross sections for ionization of atomic oxygen. The data of Rothe (29) are total cross sections. The data of Fite (28) and that of Boksenberg (31) because of mass analysis are cross sections for the production of O^+ from O.

CC-0. In Public Domain. Gurukul Kangri Collection, Haridwar

Digitized by Arya Samaj Foundation Chennai and eGangotri

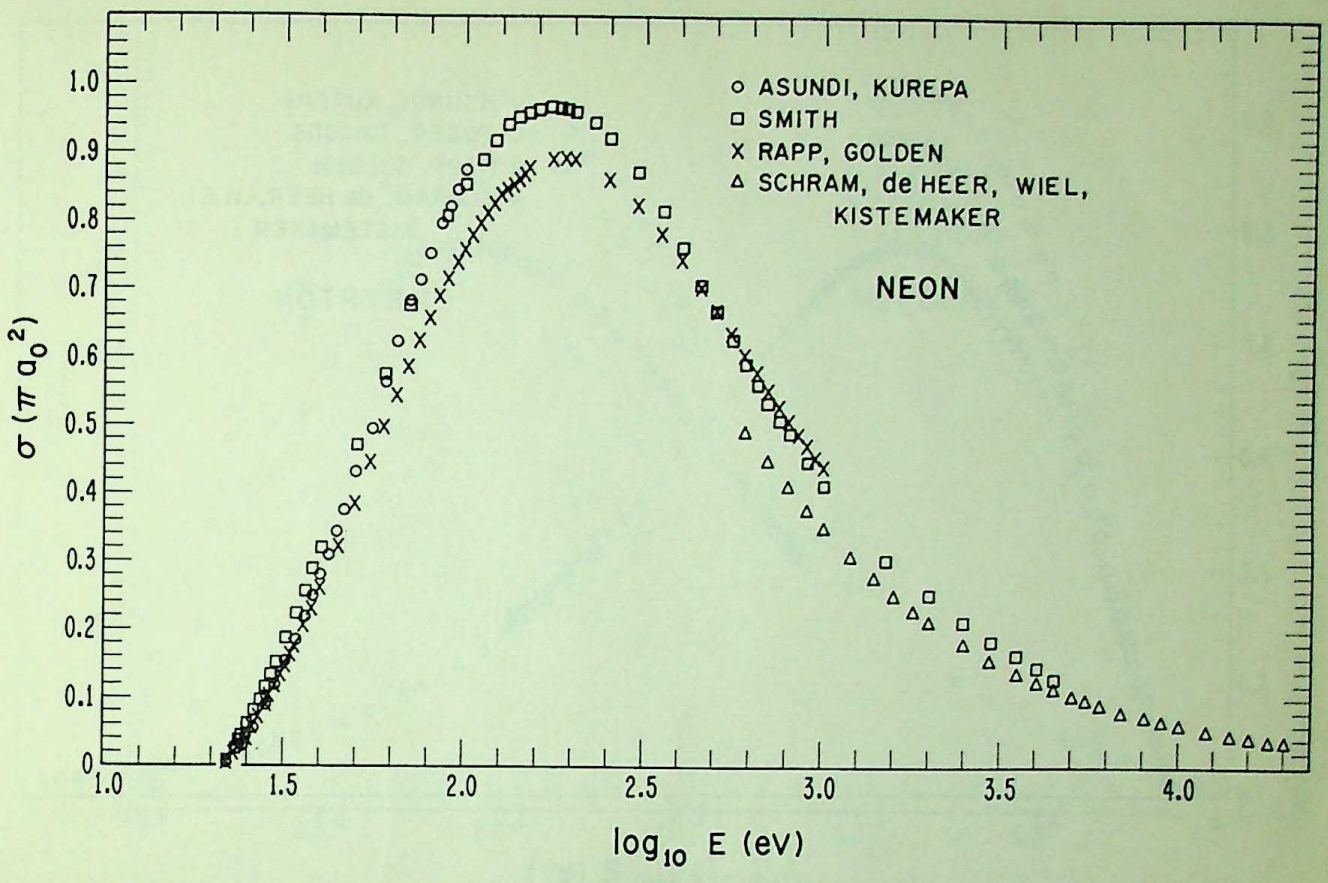

FIG. 7. Total cross sections for the ionization of atomic neon. References: Asundi (5); Smith (3); Rapp (7a); Schram (8).

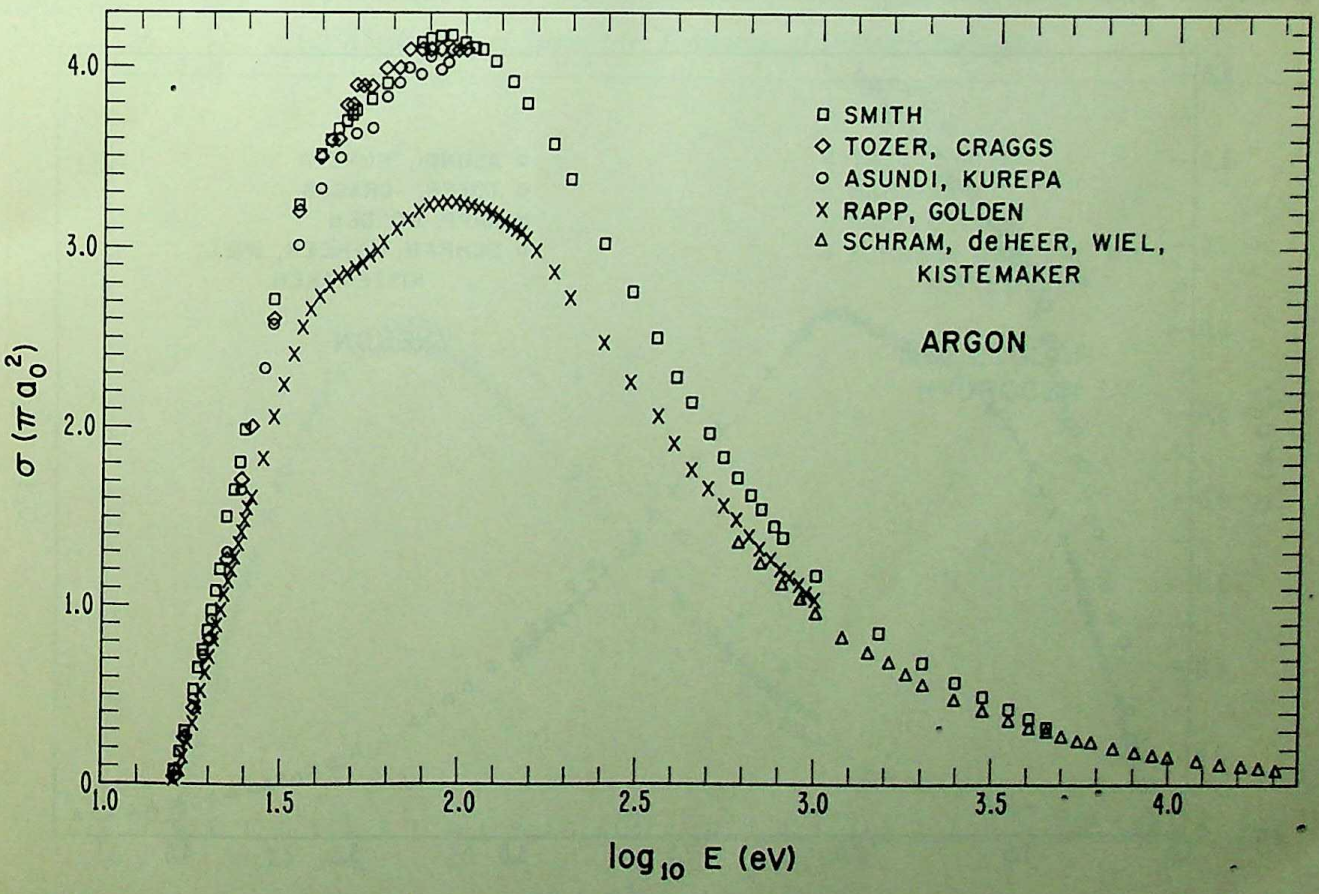

FIG. 8. Total cross sections for the ionization of atomic argon. References: Smith (3); Tozer (65); Asundi (5); Rapp (7a); Schram (8).

CC-0. In Public Domain. Gurukul Kangri Collection, Haridwar

Digitized by Arya Samaj Foundation Chennai and eGangotri

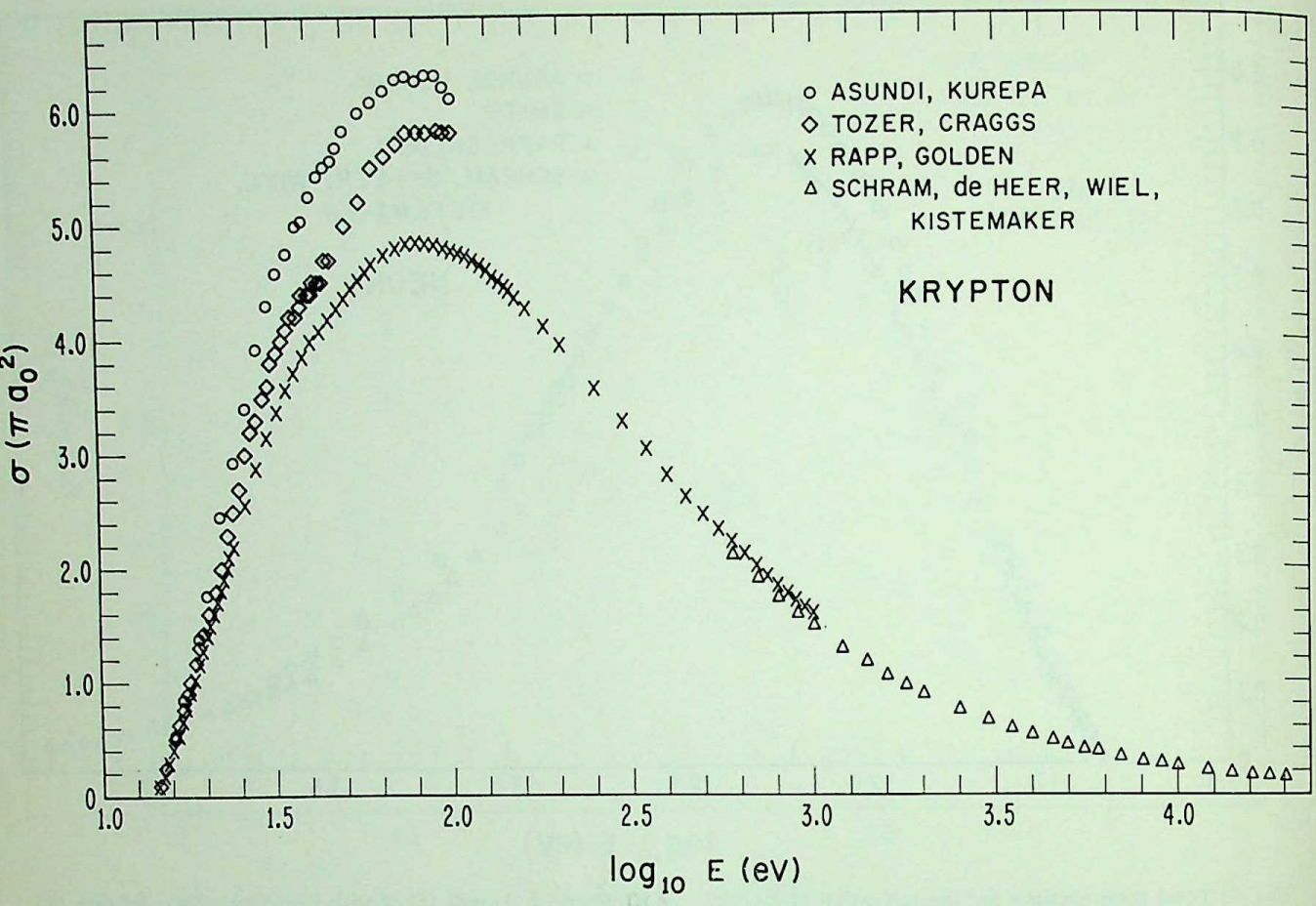

FIG. 9. Total cross sections for the ionization of atomic krypton. References: Asundi (5); Tozer (65); Rapp (7a); Schram (8).

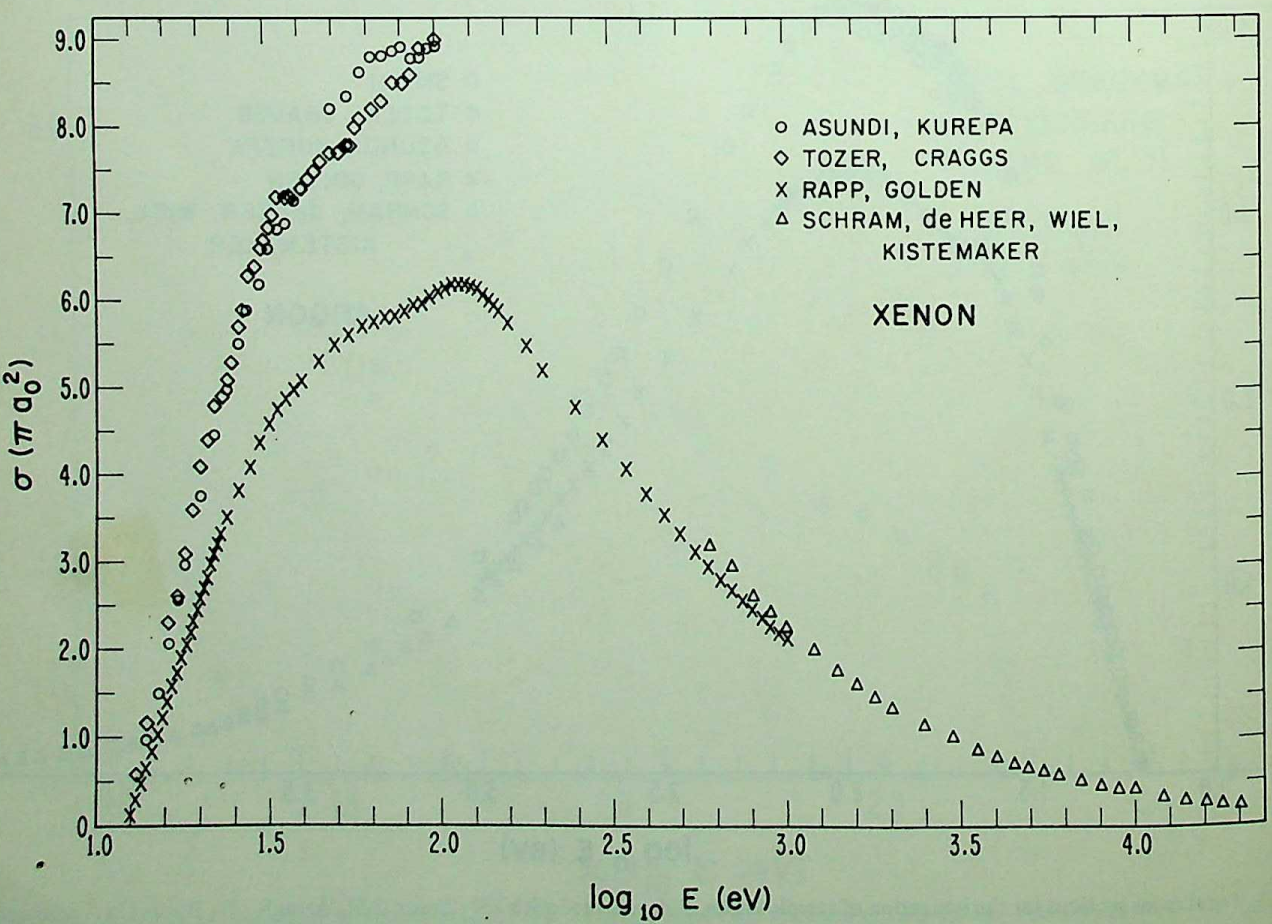

FIG. 10. Total cross sections for the ionization of atomic xenon. References: Asundi (5); Tozer (65); Rapp (7a); Schram (8).

CC-0. In Public Domain. Gurukul Kangri Collection, Haridwar

Digitized by Arya Samaj Foundation Chennai and eGangotri

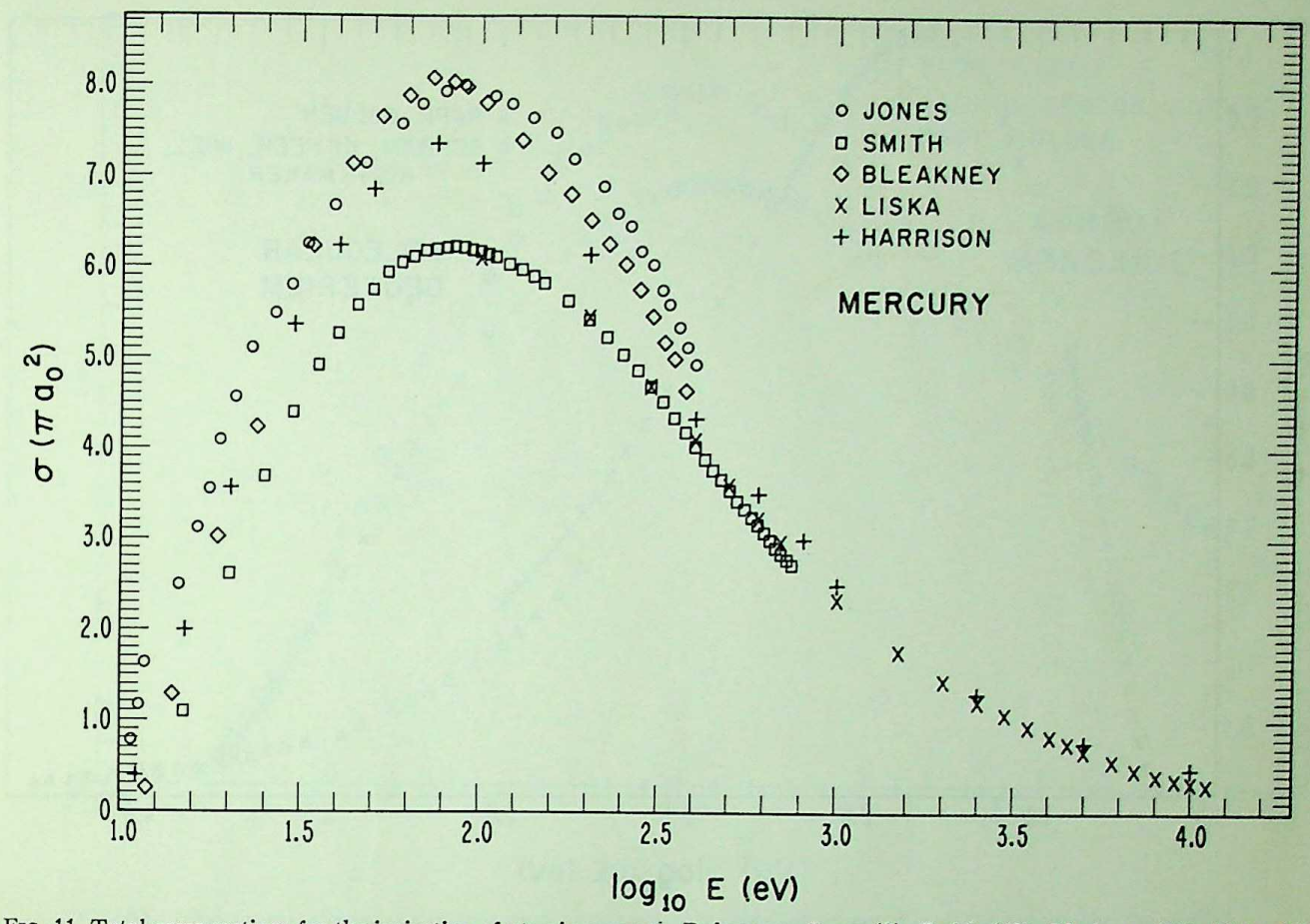

FIG. 11. Total cross sections for the ionization of atomic mercury. References: Jones (2); Smith (60); Bleakney (59); Liska (61); Harrison (62).

(2) Absolute Cross Sections for Ionization of Diatomic Molecules

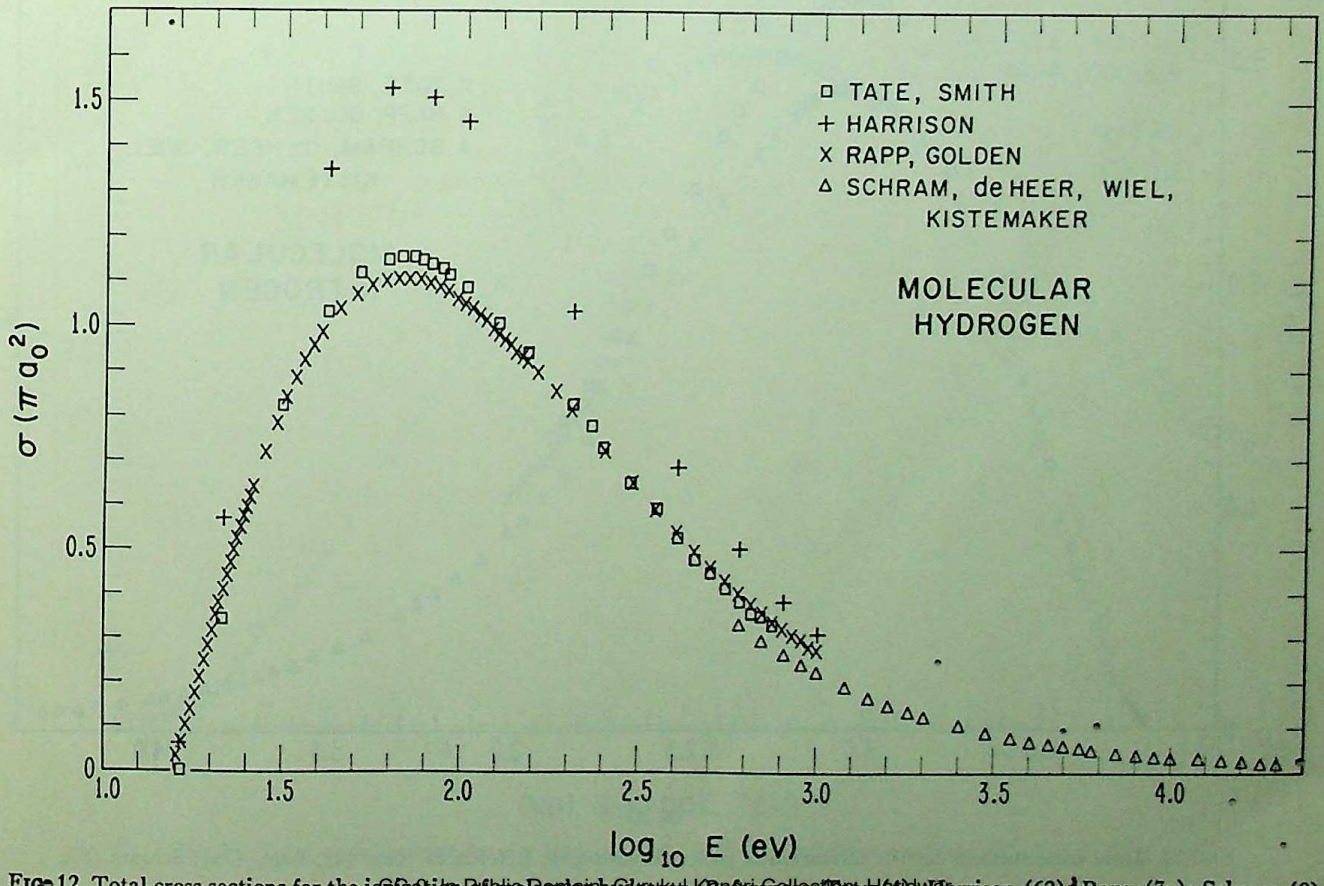

FIG. 12. Total cross sections for the ionization of molecular hydrogen. References: Tate (4); Harrison (62); Rapp (7a); Schram (8).

CC-0. In Public Domain. Panini Kanad Collection. Haridwar

Digitized by Arya Samaj Foundation Chennai and eGangotri

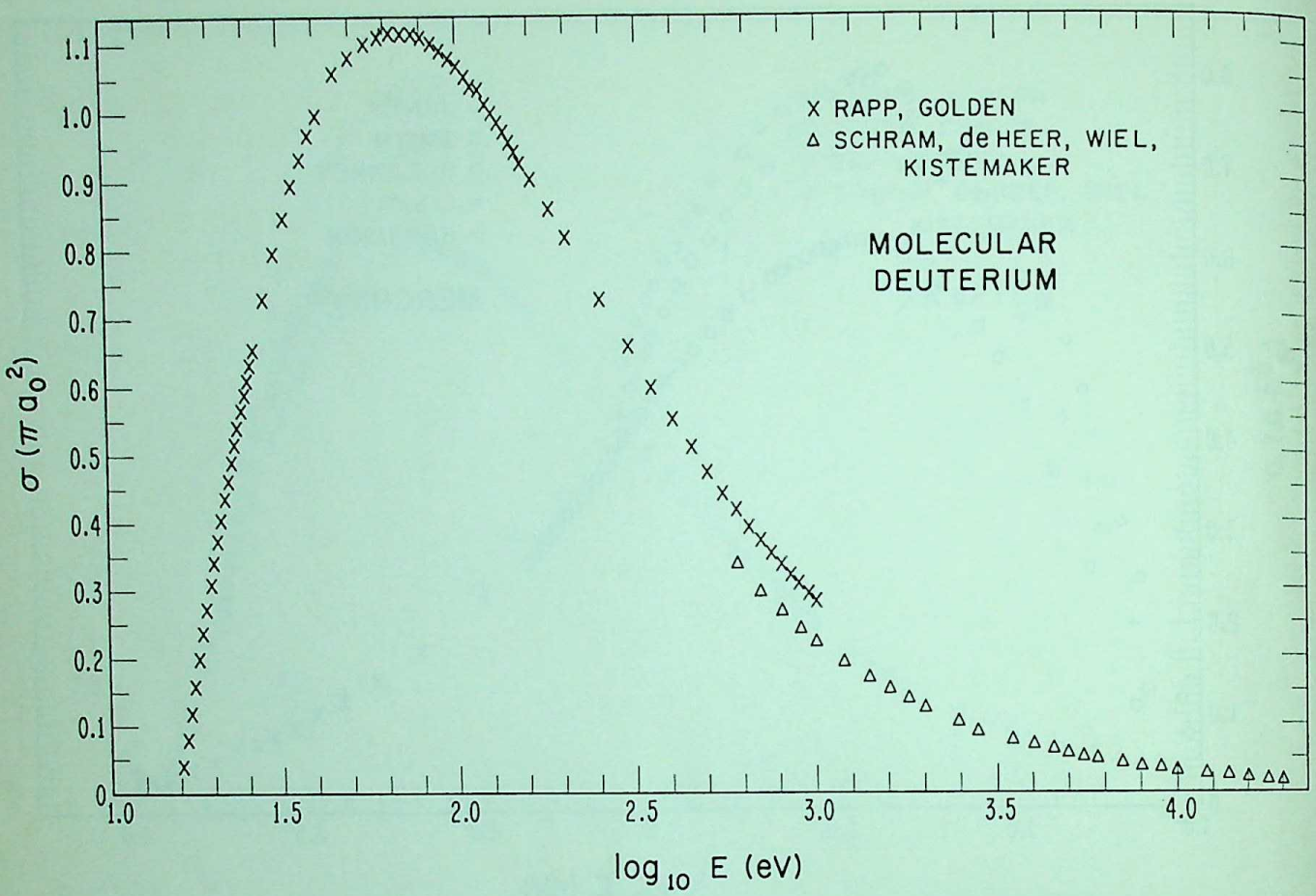

FIG. 13. Total cross sections for the ionization of molecular deuterium. References: Rapp (7a); Schram (8).

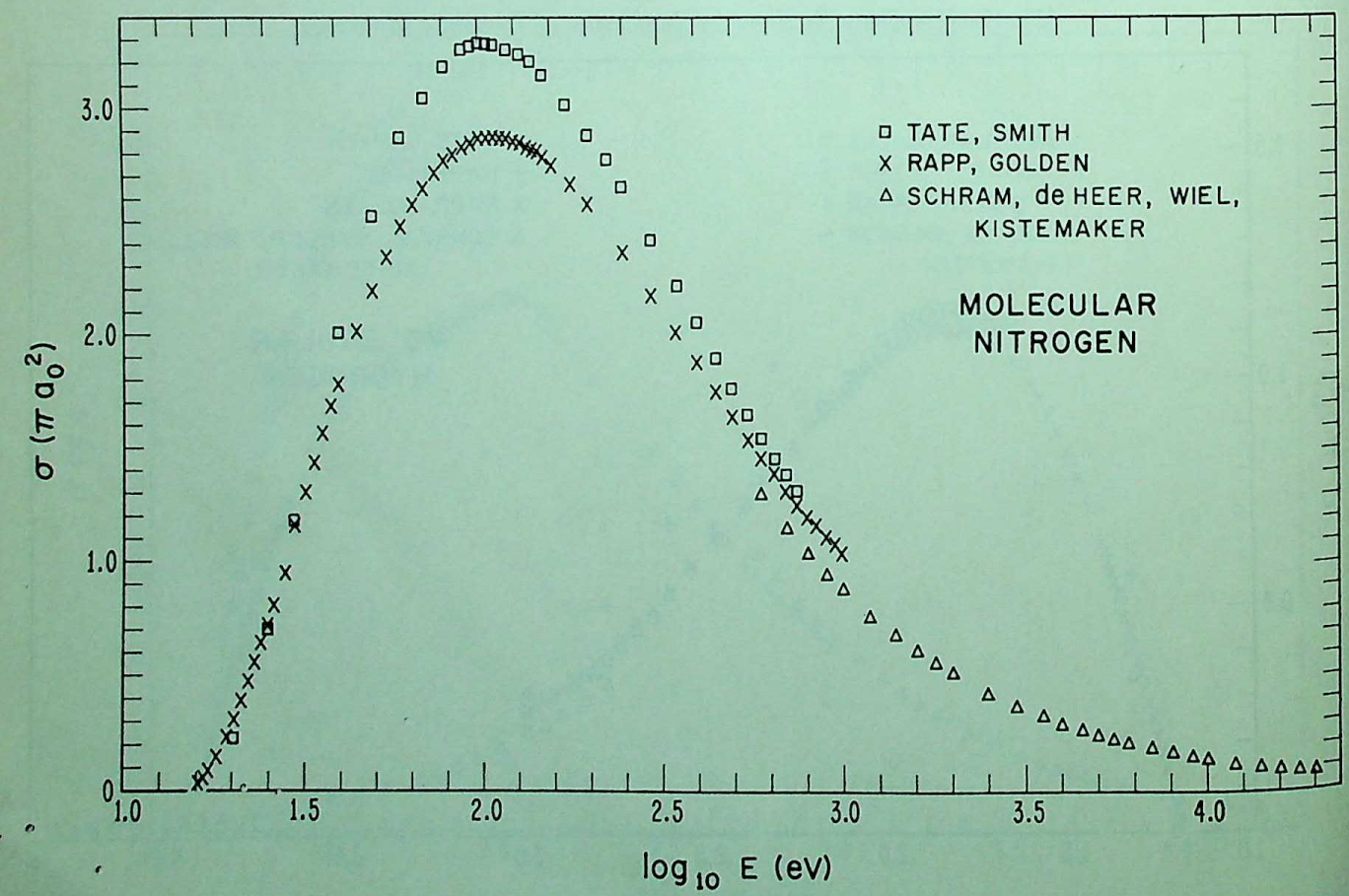

FIG. 14. Total cross sections for the ionization of molecular nitrogen. References: Tate (4); Rapp (7a); Schram (8).

CC-0. In Public Domain. Gurukul Kangri Collection, Haridwar

Digitized by Arya Samaj Foundation Chennai and eGangotri

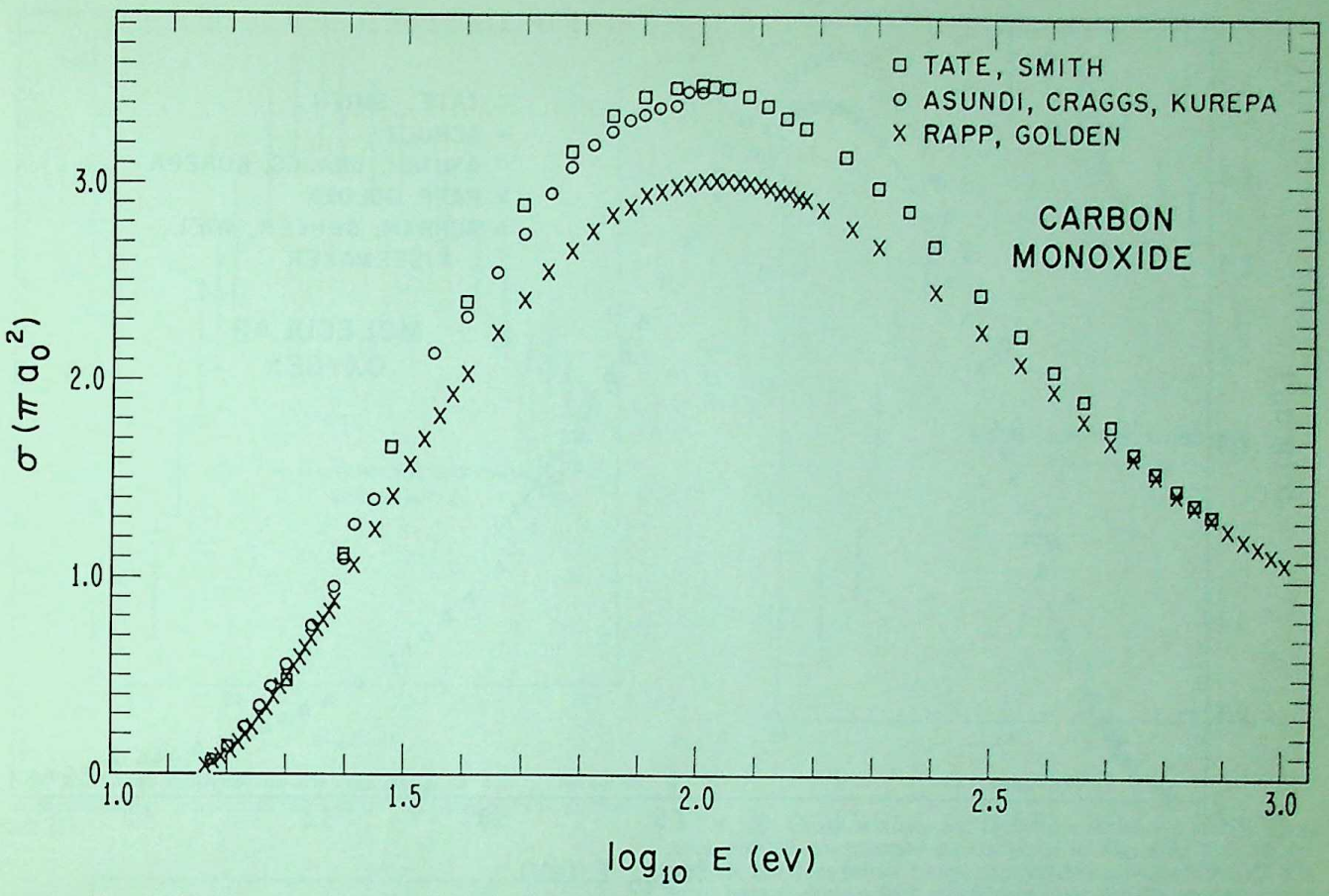

FIG. 15. Total cross sections for the ionization of carbon monoxide. References: Tate (4); Asundi (6); Rapp (7a).

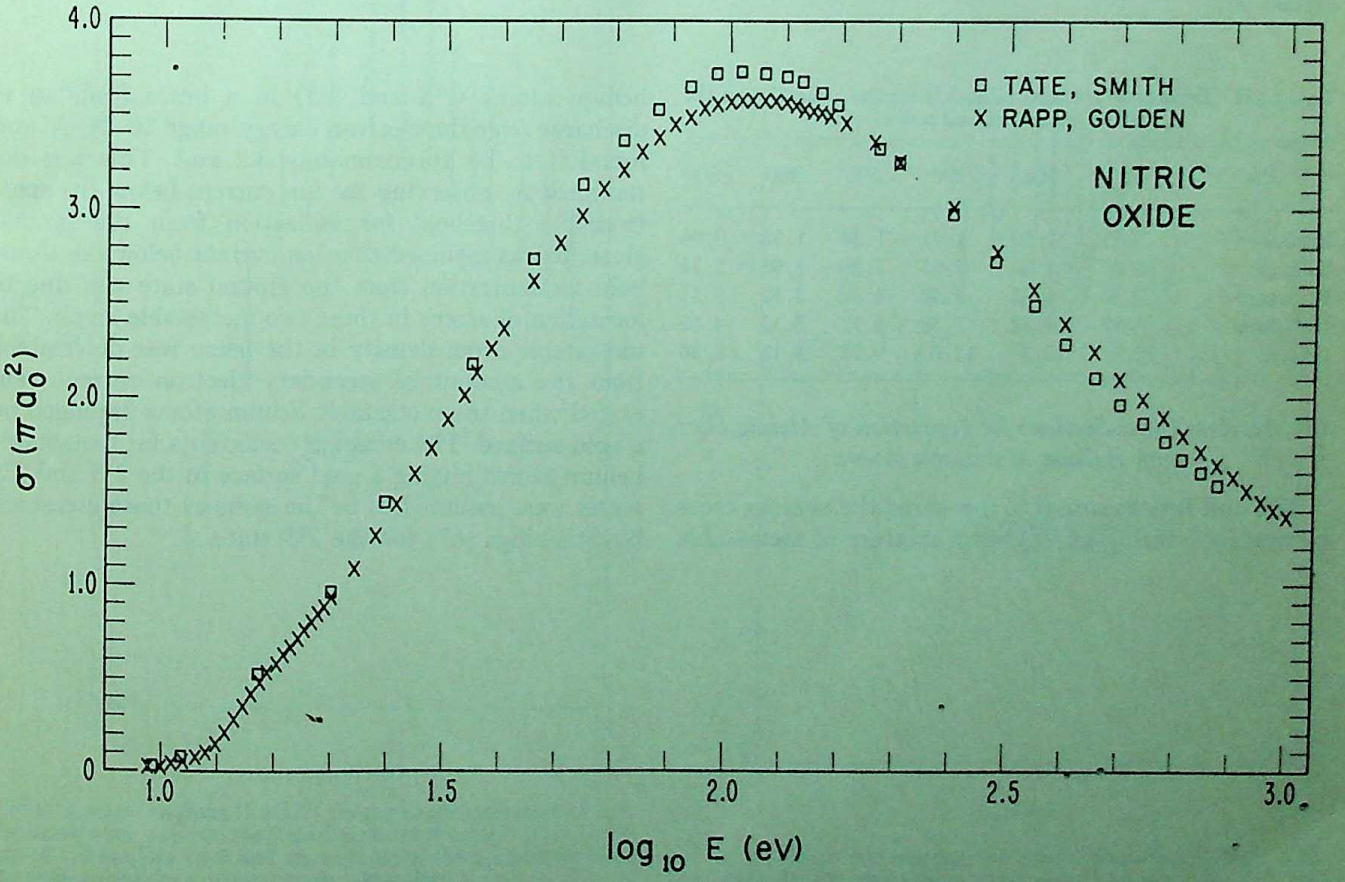

FIG. 16. Total cross sections for the ionization of nitric oxide. References: Tate (4); Rapp (7a).

CC-0. In Public Domain. Gurukul Kangri Collection, Haridwar

Digitized by Arya Samaj Foundation Chennai and eGangotri

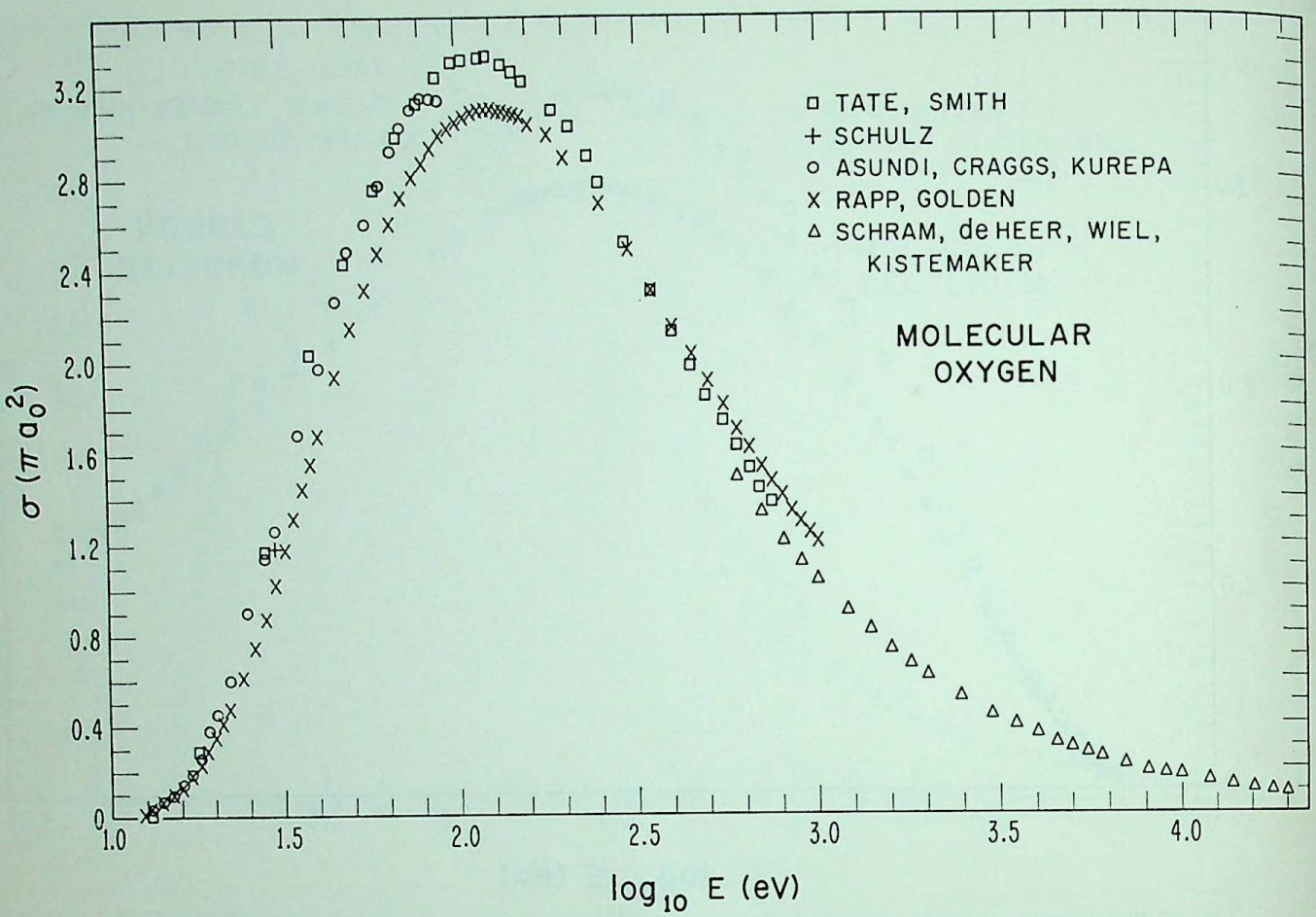

FIG. 17. Total cross sections for the ionization of molecular oxygen. References: Tate (4); Schulz (17); Asundi (6); Rapp (7a); Schram (8).

TABLE III. Total cross sections (Ref. 33) for the ionization of the alkali metals in πa_0^2 units.

E(eV)	50	100	200	300	400	500
Lithium	3.52	2.50	1.71	1.36	1.13	0.94
Sodium	4.68	3.60	2.85	2.29	1.95	1.71
Potassium	7.30	6.82	5.46	4.22	3.52	3.11
Rubidium	9.57	9.32	7.58	6.11	5.13	4.62
Cesium	12.9	12.3	11.0	9.78	8.18	7.10

(3) *Absolute Cross Sections for Ionization of Atomic Ions and Helium Metastable Atoms*

Fite and Brackmann (66) measured the average cross section for ionizing an unknown mixture of metastable helium atoms (2^1S and 2^3S) in a beam from an rf discharge over the electron energy range 10–24 eV and found it to be approximately 3.2 πa_0^2. This was determined by observing the ion current below the spectroscopic threshold for ionization from the ground state. It was assumed that ion current below the threshold for ionization from the ground state was due to ionization of atoms in these two metastable levels. The metastable atom density in the beam was determined from the amount of secondary electron current generated when the metastable helium atoms impinged on a gold surface. The emission coefficients for metastable helium atoms hitting a gold surface in the 2^1S and 2^3S states were assumed to be the same as those measured by Stebbings (67) for the 2^3S state.

CC-0. In Public Domain. Gurukul Kangri Collection, Haridwar

Digitized by Arya Samaj Foundation Chennai and eGangotri

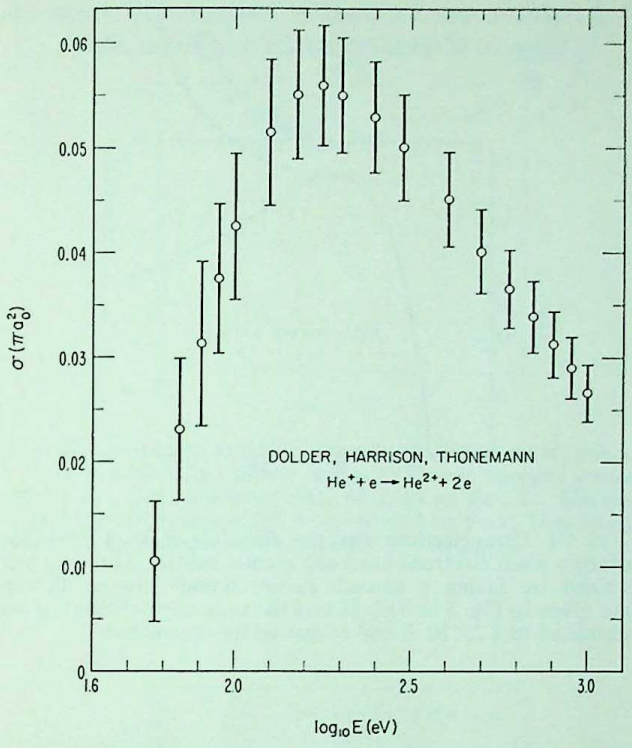

FIG. 18. Cross sections for the ionization of He^+. The error bars indicate the "maximum total error" as listed by the authors (Ref. 25).

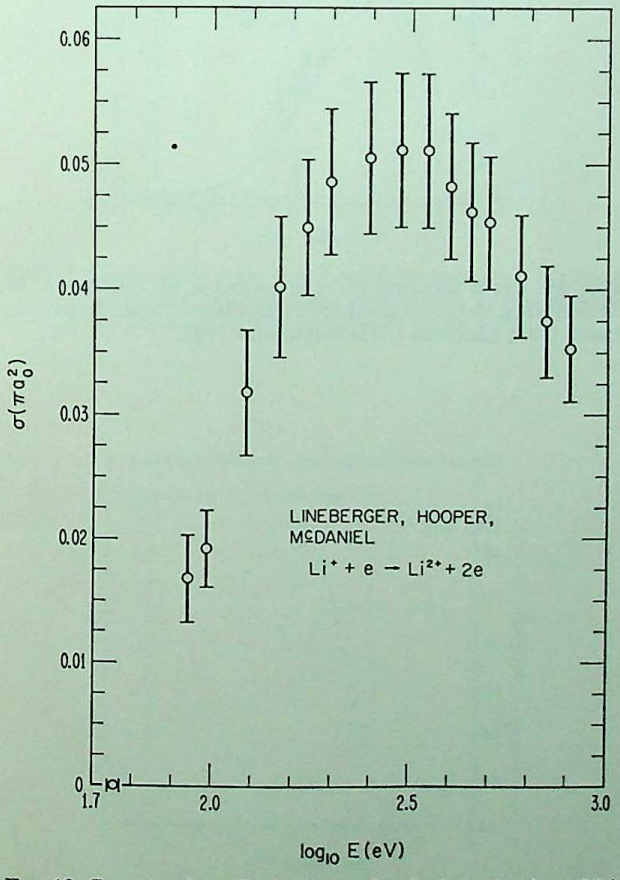

FIG. 19. Cross sections (Ref. 27) for the single ionization of Li^+. The error bars indicate the "maximum total error." This is the sum of the random error and an estimate of the systematic error due to an uncertainty in instrument calibration.

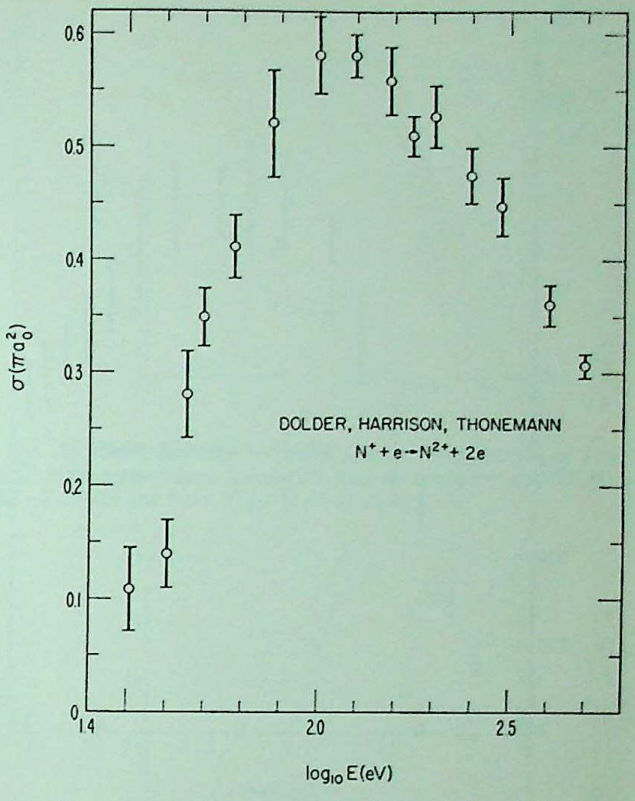

FIG. 20. Cross sections for the single ionization of N^+. These data are the uncorrected points given in Fig. 1 in Ref. 64 and exclude the data below the spectroscopic threshold of 29.6 eV. The error bars indicate a 95% confidence limit for the random errors.

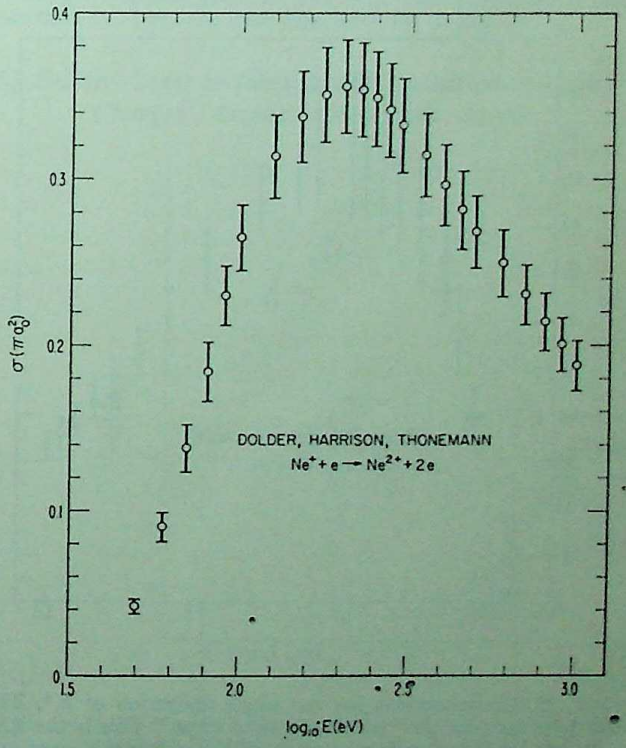

FIG. 21. Cross sections for the single ionization of Ne^+. The bars indicate the "maximum total error" as listed in Ref. 63.

CC-0. In Public Domain. Gurukul Kangri Collection, Haridwar

Digitized by Arya Samaj Foundation Chennai and eGangotri

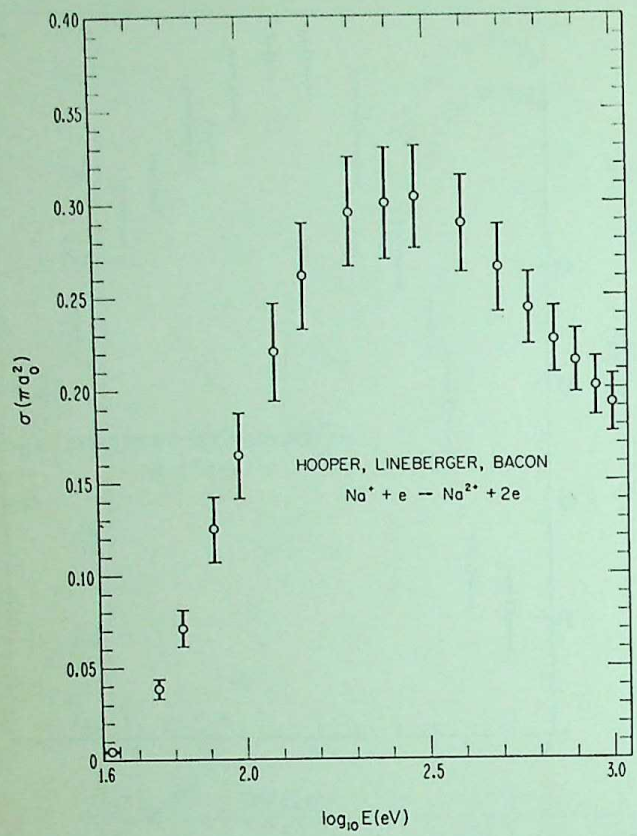

FIG. 22. Cross sections for the single ionization of Na^+. The error bars indicate the "maximum total error." This is the sum of the random error and a estimate of the systematic error due to uncertainty in instrument calibration. The reference for these data is (27).

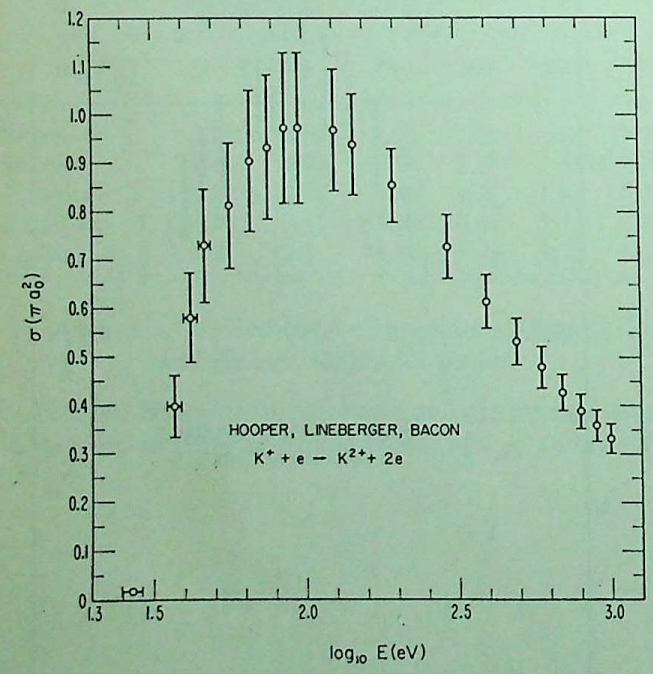

FIG. 23. Cross sections for the single ionization of K^+. The error bars indicate the "maximum total error." This is the sum of the random error and an estimate of the systematic error due to uncertainty in instrument calibration. The reference for these data is (27).

(4) *Absolute Cross Sections for Ionization of Atoms and Diatomic Molecules into Excited Final States*

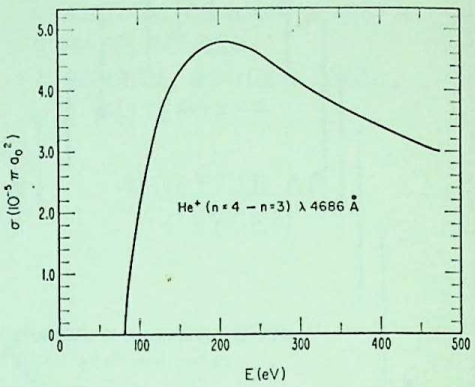

FIG. 24. Cross sections for the emission of λ=4686-Å He^+ radiation when electrons bombard atomic helium. The data were obtained by fitting a smooth curve through the oscilloscope trace given in Fig. 3 in Ref. 53 and the maximum of this line was normalized to 4.2×10^{-21} cm² as quoted by the authors.

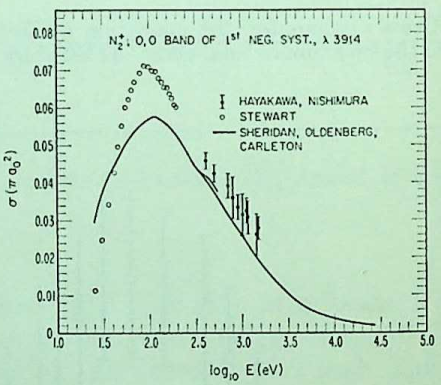

FIG. 25. Cross sections for the emission of λ=3914-Å N_2^+ radiation when electrons bombard molecular nitrogen. References: Stewart (54); Sheridan (55); Hayakawa (56).

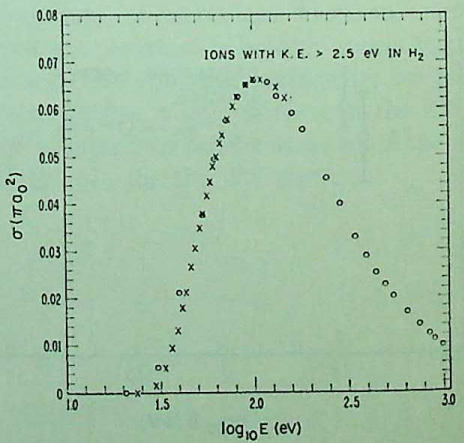

FIG. 26. Cross sections for the dissociative ionization of molecular hydrogen yielding product ions with kinetic energies greater than 2.5 eV. These data were taken from Figs. 43(c, d) in Ref. 7c.

CC-0. In Public Domain. Gurukul Kangri Collection, Haridwar

Digitized by Arya Samaj Foundation Chennai and eGangotri

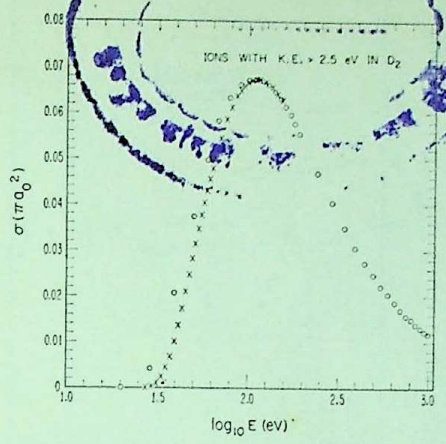

FIG. 27. Cross sections for the dissociative ionization of molecular deuterium yielding product ions with kinetic energies greater than 2.5 eV. Data are from Figs. 43(f, g) in Ref. 7c. Electron energy values from Fig. 43(g) were reduced by 9 eV. This correction was communicated to us privately by Dr. Rapp.

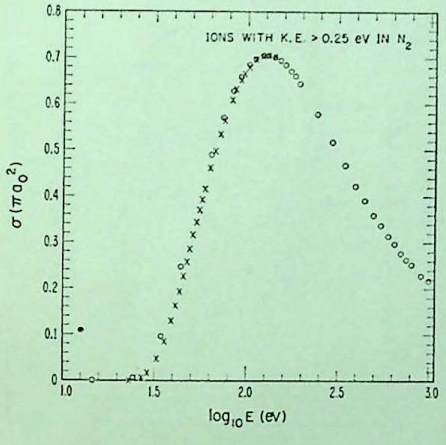

FIG. 28. Cross sections for the dissociative ionization of molecular nitrogen yielding product ions with kinetic energies greater than 0.25 eV. Data are from Figs. 43(i, j) in Ref. 7c.

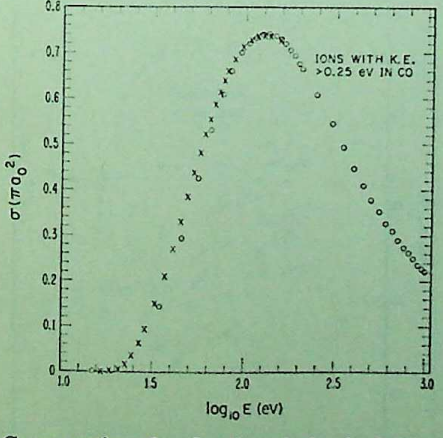

FIG. 29. Cross sections for the dissociative ionization of carbon monoxide yielding product ions with kinetic energies greater than 0.25 eV. Data are from Figs. 43(o, p) in Ref. 7c.

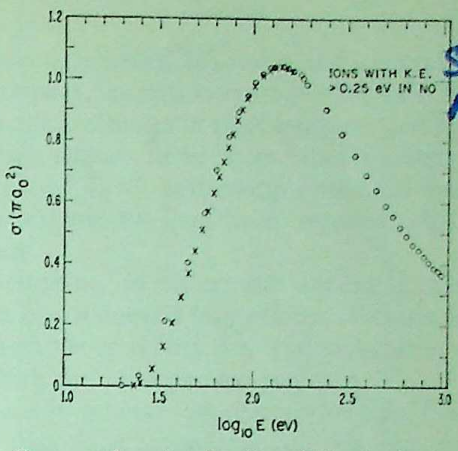

FIG. 30. Cross sections for the dissociative ionization of nitric oxide yielding product ions with kinetic energies greater than 0.25 eV. Data are from Figs. 43(r, s) in Ref. 7c.

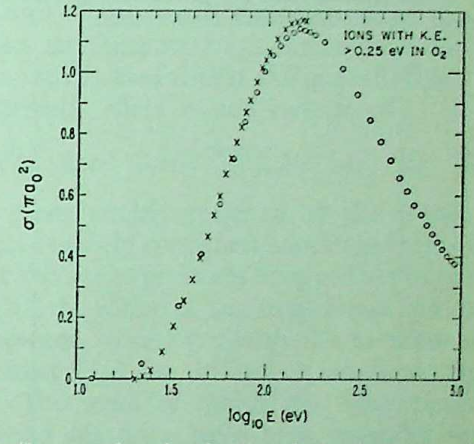

FIG. 31. Cross sections for the dissociative ionization of molecular oxygen yielding product ions with kinetic energies greater than 0.25 eV. Data are from Figs. 43(l, m) in Ref. 7c.

(5) *Relative Cross Sections for the Production of Multiply Charged Atomic Ions from Atoms*

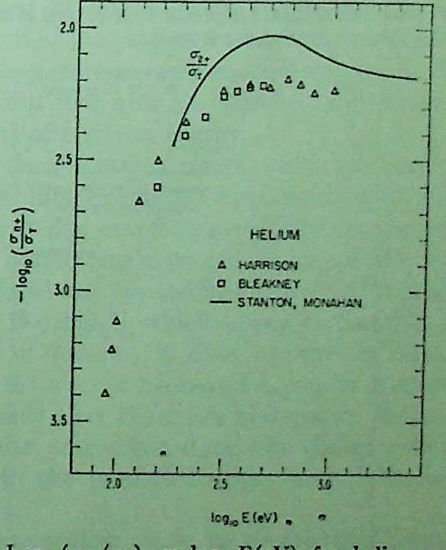

FIG. 32. $\text{Log}_{10}(\sigma_{2+}/\sigma_T)$ vs $\log_{10}E$(eV) for helium, where σ_{2+} is the cross section for production of ions of charge $+2$, and σ_T is the total ionization cross section. References: Harrison (62); Bleakney (68); Stanton (69).

CC-0. In Public Domain. Gurukul Kangri Collection, Haridwar

Digitized by Arya Samaj Foundation Chennai and eGangotri

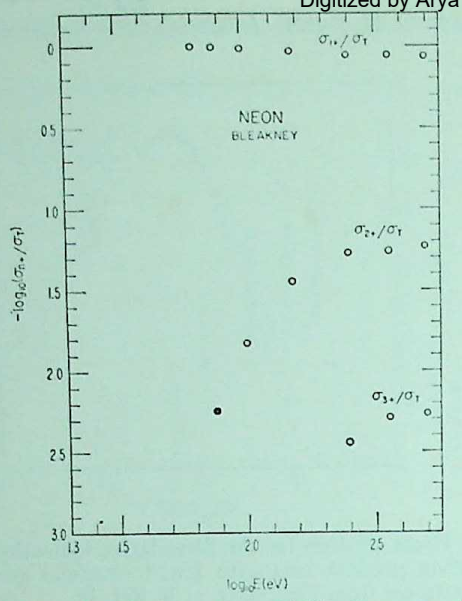

FIG. 33. $\text{Log}_{10}(\sigma_{n+}/\sigma_T)$ vs $\log_{10}E(\text{eV})$ for neon (Ref. 70), where σ_{n+} is the cross section for production of ions of charge $+n$, and σ_T is the total ionization cross section.

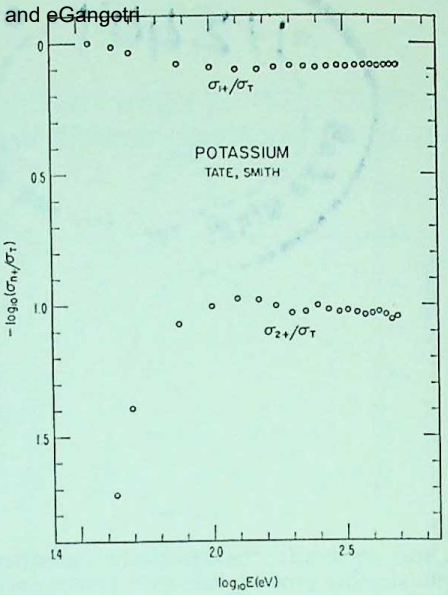

FIG. 36. $\text{Log}_{10}(\sigma_{n+}/\sigma_T)$ vs $\log_{10}E(\text{eV})$ for potassium (Ref. 19), where σ_{n+} is the cross section for production of ions of charge $+n$, and σ_T is the total ionization cross section.

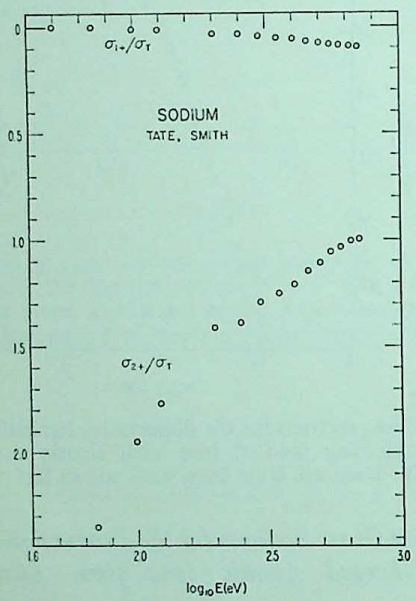

FIG. 34. $\text{Log}_{10}(\sigma_{n+}/\sigma_T)$ vs $\log_{10}E(\text{eV})$ for sodium (Ref. 19), where σ_{n+} is the cross section for production of ions of charge $+n$, and σ_T is the total ionization cross section.

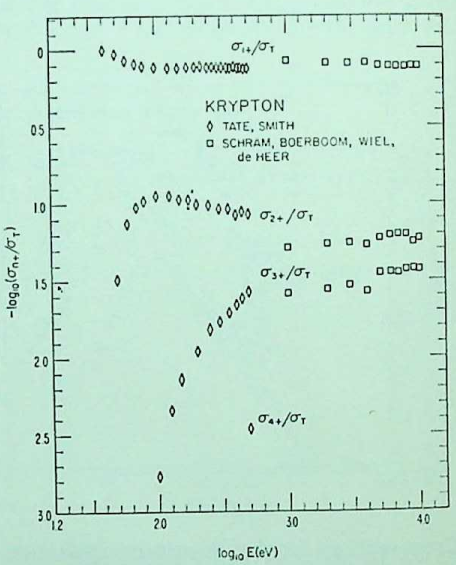

FIG. 37. $\text{Log}_{10}(\sigma_{n+}/\sigma_T)$ vs $\log_{10}E(\text{eV})$ for krypton, where σ_{n+} is the cross section for production of ions of charge $+n$, and σ_T is the total ionization cross section. References: Tate (19); Schram (71).

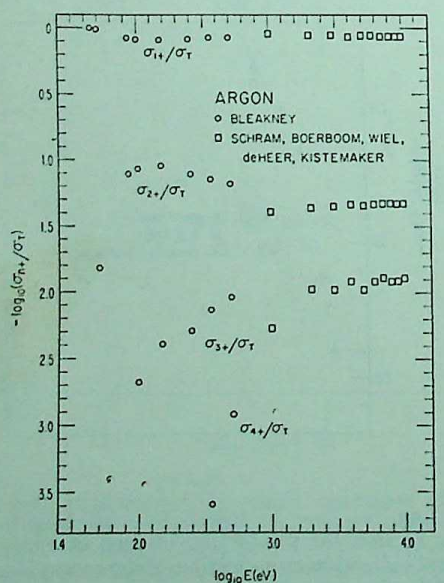

FIG. 35. $\text{Log}_{10}(\sigma_{n+}/\sigma_T)$ vs $\log_{10}E(\text{eV})$ for argon, where σ_{n+} is the cross section for production of ions of charge $+n$, and σ_T is the total ionization cross section. References: Bleakney (70); Schram (71).

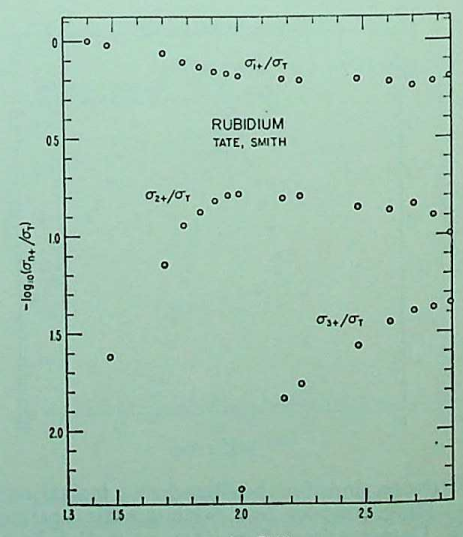

FIG. 38. $\text{Log}_{10}(\sigma_{n+}/\sigma_T)$ vs $\log_{10}E(\text{eV})$ for rubidium (Ref. 19), where σ_{n+} is the cross section for production of ions of charge $+n$ and σ_T is the total ionization cross section.

CC-0. In Public Domain. Gurukul Kangri Collection, Haridwar

Digitized by Arya Samaj Foundation Chennai and eGangotri

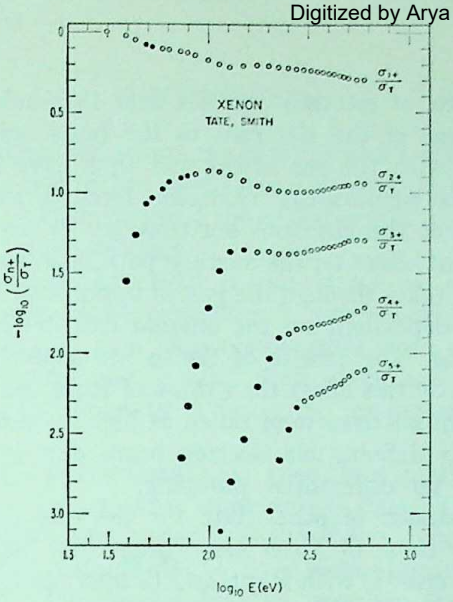

FIG. 39. $\text{Log}_{10}(\sigma_{n+}/\sigma_T)$ vs $\log_{10}E(\text{eV})$ for xenon (Ref. 19), where σ_{n+} is the cross section for production of ions of charge $+n$, and σ_T is the total ionization cross section.

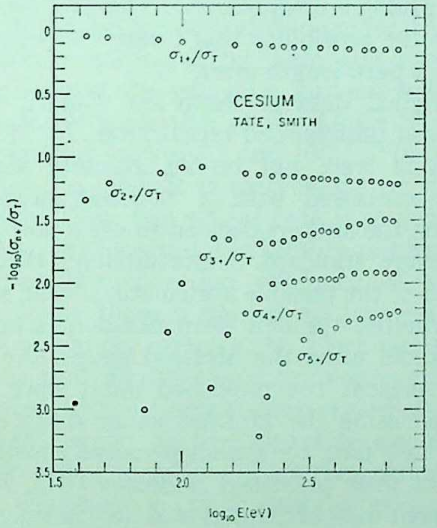

FIG. 40. $\text{Log}_{10}(\sigma_{n+}/\sigma_T)$ vs $\log_{10}E(\text{eV})$ for cesium (Ref. 19), where σ_{n+} is the cross section for production of ions of charge $+n$, and σ_T is the total ionization cross section.

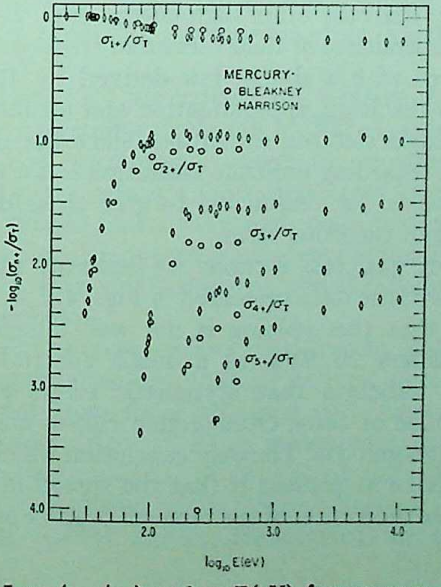

FIG. 41. $\text{Log}_{10}(\sigma_{n+}/\sigma_T)$ vs $\log_{10}E(\text{eV})$ for mercury, where σ_{n+} is the cross section for production of ions of charge $+n$, and σ_T is the total ionization cross section. Reference: Bleakney (59), Harrison (62).

B. Discussion of Experiments

General

We have attempted to assess the accuracy of the electron impact, ionization cross-section data for atoms and diatomic molecules in the literature, and to present those which appear to be most reliable based on conclusions about likely systematic errors. In some cases only one experiment has been reported and is presented here.

In attempting to determine accuracy, systematic errors are of paramount importance. Authors reporting data almost never report limits of possible systematic errors which are later proved realistic.

There are in general two reasons for this: (1) Experimentors may lack knowledge of the existence of a significant systematic error, possibly because certain parameters cannot be controlled in the experimental arrangement. (2) Empirical tests used to demonstrate the absence of systematic errors are often inadequate. Such tests are necessary but not sufficient, and reliance on them usually means that the quantitative nature of the systematic effect is not understood.

The Rare Gases: He, Ne, Ar, Kr, Xe

Rare gases would appear to be the atomic species most likely to yield consistent measurements, since they are inert and at the pressures involved act as ideal gases. In Fig. 42 the ratios of the total ionization cross sections reported by P. T. Smith (3) to those of Rapp and Golden (7a) for helium, neon, and argon are plotted. The work of Smith has been considered a classic, and his data have been used by numerous authors as a standard for comparing their relative measurements, and also for normalizing their relative data. The experiment of Rapp and Golden is an attempt to repeat the experiments of Smith and to verify his results. The design of the experimental apparatus used by Rapp and Golden is essentially the same as the design used by Smith. Some improvements have been made, such as longer guard plates, differential pumping for the electron gun, and smaller apertures. The trend of the ratios indicates a systematic difference which is a function of electron energy.

One of the systematic errors, which has been discussed as a possibility in Smith's apparatus, is an increase in path length due to off-axis velocity components (Ref. 9). The maximum expected value of the error (see Sec. II) has been plotted in all three figures for $d=1.5$ mm and $B=250$ G which apply to Smith's work. In the case of helium, it does appear to be an upper limit; in the case of neon and argon, it does not. Since it is possible that there are systematic pressure errors in the neon and argon data, the disagreement of the ratios with the predicted upper limit is probably not significant.

The assumption made to derive this formula [see Eq. (2)] is that all the electrons have helical paths of diameter d, which is determined by the apertures in the electron gun. Asundi (10) tried to obtain a more realistic limit to the possible error in Smith's data by calculating an "effective" d, using two separate models for the

CC-0. In Public Domain. Gurukul Kangri Collection, Haridwar

Digitized by Arya Samaj Foundation Chennai and eGangotri

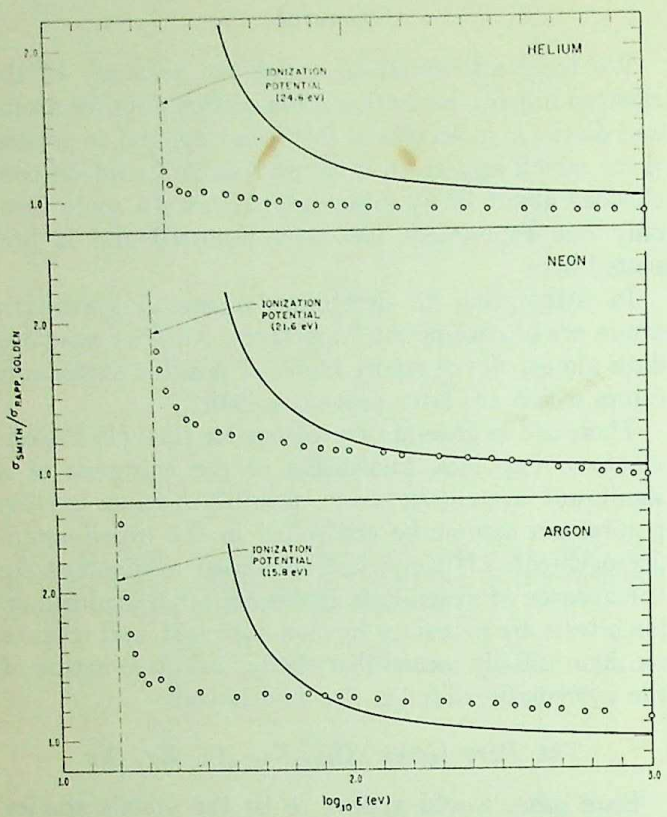

FIG. 42. Comparison of the total cross-section data of Smith (3) and Rapp, Golden (7a) for helium, neon, argon. The line represents the maximum ratio expected [Eq. (2)] if the only systematic error in either experiment was a path length error in Smith's.

mechanism whereby the electrons acquire off-axis velocity components. Both models were based upon geometrical considerations and not on the gas used. An attempt was made to fit this formula to the ratios given in Fig. 42 in order to obtain an "effective" d. There was no "effective" d which would give a reasonable fit to the ratios. This applies to each of the gases separately. The large ratios, particularly in neon and argon, which are very near threshold can be altered considerably by assuming a difference in the energy scale of the two experiments of a few tenths eV. Since both experimentors used essentially the same value for the ionization potential (within 0.1 eV), it is unlikely that this can completely explain the rather rapid rise in the ratios below 50 eV. It does mean, though, that there is considerable uncertainty in the ratios within 1.0 eV of the ionization potential.

Although the general trend of these ratios for the three gases is the same, the slopes above 100 eV are quite different. This suggests that the effect probably has something to do with the properties of the gases involved.

At their maxima (which are below their respective ionization potentials), the momentum transfer cross sections for He, Ne, and Ar are about a factor of five larger than the ionization cross sections *at their maxima.* Therefore, at electron energies near threshold a small percentage of the electrons in the beam might have collided with the gas atoms and thus have had their momenta significantly changed. Even a very small fraction of the electrons scattered at 90° can have a significant effect on the average path length which the electron takes through the gas. If important, this effect is very dependent on the angular distribution of the scattering. The results of Smith are somewhat more affected by this effect than those of Rapp and Golden; since Smith's data were taken at higher pressures, the apertures defining his electron beam were larger, and he had no differential pumping.

Comparison of other data for the rare gases, particularly those of Tozer and Craggs (65), and Asundi and Kurepa (5) with Rapp and Golden does not reveal any systematic differences of this type. In most cases the data for these experiments differ by a constant percentage which probably results from systematic errors in pressure measurement. This fact tends to add weight to the possibility that Smith's experiment may have had a path-length error.

The original data of Rapp and Golden were presented in an unpublished report (Ref. 7c). These cross section data were put on an absolute scale, using pressures measured with a McLeod gauge. Before publication the authors decided to use a flow technique as a pressure standard. Unfortunately, they did not explore all of the possible systematic effects, so it is not certain whether the new normalization is better than that obtained using the McLeod gauge. We have decided to present the published data, since the data normalized using the McLeod gauge differ essentially from the new data by a multiplicative constant which is given in their published reference (Ref. 7a).

The recent data of Schram *et al.* (8), in the range 0.6–20 KeV, is in general lower than that of the other experiments at the same energies. As they point out, their data also have a significantly different dependence on energy than the other high energy data. In fact, the energy dependence of their measured cross sections is in accordance with a simple law derived by Bethe (72) based on the Born approximation and on the assumption of single electron excitation. Since the theoretical situation regarding multiple ionization is not clear, it is on this basis not reasonable to give these data more weight than the other data.

The rare gas cross sections are generally regarded as well known; the data presented in Figs. 4, 7, 8, 9, and 10 indicate that this opinion is not well founded unless one considers 20–30% as a small uncertainty. The evidence indicates that systematic errors exist both in the shape of these cross-section curves and in their absolute magnitude. The only conclusion which it seems safe to make at present is that the spread in the data gives some indication of the range of possible systematic errors.

CC-0. In Public Domain. Gurukul Kangri Collection, Haridwar

Digitized by Arya Samaj Foundation Chennai and eGangotri

Atomic Hydrogen

The three experiments, the data for which are plotted in Fig. 3, are in rather good agreement considering their difficulty and the fact that the experimental techniques used were quite different.

Since atomic hydrogen is not stable at ordinary temperatures, these experiments were done using a beam generated in a high temperature oven or radio frequency discharge. All of these data are relative because of the difficulty in measuring the neutral beam density.

Fite and Brackmann (24) used two methods to normalize their relative cross-section data. The first method, which they called "relative," was to normalize their relative data at 500 eV to a Born approximation calculation. The second was to compare signals of proton current and H_2^+ current from their mass spectrometer, taking into account the amount of dissociation in the neutral beam. They then assumed that the corrected H^{2+} signal corresponded to the total ionization cross section as measured by Tate and Smith. This procedure neglects the energetic protons which result from dissociative ionization of H_2. Above 50 eV these protons represent between 5 and 10% of the total ion current [see Fig. 26]. It is surprising that the agreement between these two sets of data is so good.

The elaborate procedure used by Fite and Brackmann to determine the collection efficiency of the mass spectrometer for thermal ions at all temperatures involved use of a heavy rare gas, Ar. The conclusion they reached was that no detectable transverse momentum was imparted to the thermal ions regardless of their mass and the energy of the impacting electron. This result is somewhat surprising, since they claim that the collection efficiency of their spectrometer was extremely sensitive to very small changes in its position, and since at threshold essentially all of the momentum of the incoming electron is imparted to the ion. An average hydrogen atom from a 1000°C source has only about three times the momentum of an electron with an energy of 13 eV.

Boksenberg (31) normalized his relative data to a Born approximation calculation at 300 eV (his highest energy). The spectrometer used by Boksenberg in determining the relative ionization cross sections for atomic hydrogen had a very high collection efficiency for thermal ions. He presented evidence which indicated it probably was 100% efficient for the collection of thermal protons.

Other relative cross sections measured by Boksenberg with this apparatus, e.g., that for helium, were drastically different from those obtained with total ion collection devices (Ref. 3). After extensive experimental and theoretical analysis, he concluded that the effect resulted from a change in the average electron path due to electron optical effects. He applied an empirical correction to his data by comparing the relative cross section data observed for H_2^+ with the total ionization cross sections observed by Tate and Smith (4). The contribution of dissociative ionization to the shape of the total ionization cross section was ignored.

The work of Rothe *et al.* (29) was different from the two previous experiments in that it was designed to collect all of the ions, including the energetic protons from dissociative ionization. The normalization of these data to those of Tate and Smith would have been correct if both groups had collected all ions. There is considerable doubt that this was so since Tate and Smith (4, 7a) apparently did not have high enough fields to collect all of the energetic ions. In a private communication R. H. Neynaber indicated that in the experiment of Rothe *et al.*, saturation of ion current was achieved. This is somewhat inconsistent with the discussion in their paper, since the fields used to collect the ions were based upon their very low estimate of the maximum energy of the energetic H^+ ions (Refs. 29, 49).

The degree of agreement among these result is, as has been stated, somewhat surprising considering the rather poor agreement among results for the rare gases.

Atomic Nitrogen

The experiment of Smith *et al.* (30), is a relative experiment, and that of Peterson (26) is an absolute experiment. Technically these results should not be compared, since Peterson's apparatus had a mass spectrometer to select the ions, and since he measured the cross section for producing the singly charged atomic nitrogen ion, whereas Smith *et al.* measured the total ion cross section. In any case, the cross section measured by Peterson should have been smaller than that measured by Smith *et al.* Both of these experiments might have had excited atomic species in the neutral atomic beam. The atomic nitrogen used by Smith *et al* was formed in a pulsed dc discharge. Peterson formed his neutral atomic beam by charge exchange of fast N^+ ions with O_2 and Ar.

Peterson also measured cross sections for N_2, Ar, and Ne with this same apparatus. The sum of his partial cross sections should have been very close to the total cross sections measured by Smith (3), and Tate and Smith (4), but was considerably larger except below 60 eV in argon. It is therefore probable that the cross sections that he measured for atomic nitrogen are too large. The measurements are absolute however and do not depend on knowledge of any other cross sections. The assumption that the efficiency of a calorimetric detector is the same for ions as for neutral atoms of the same velocity and mass has never been verified and could lead to large systematic errors.

In the experiment by Smith *et al.* (30), the cross section is obtained from the difference of two ion currents when the beam is completely molecular and

CC-0. In Public Domain. Gurukul Kangri Collection, Haridwar

Digitized by Arya Samaj Foundation Chennai and eGangotri

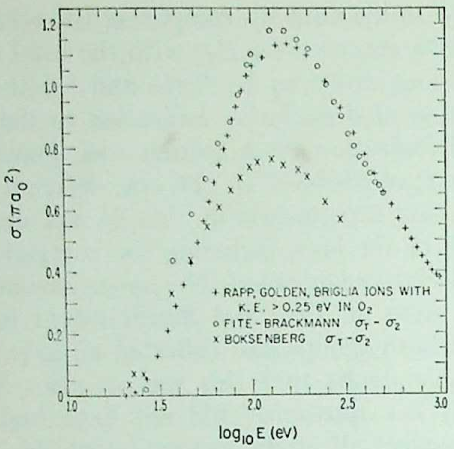

FIG. 43. Comparison of the partial cross sections for dissociative ionization of O_2 measured by Rapp (7c) with approximate cross sections for dissociative ionization deduced from the data of Fite (28) and Boksenberg (31).

when it is partially dissociated. The data were normalized by using the absolute cross sections for molecular nitrogen measured by Tate and Smith (4). Since the dissociation fraction was quite small, about 20%, and the cross section measured for the atom was one half that measured for the molecule, this technique was not very sensitive.

Atomic Oxygen

The experiments of Fite and Brackmann (28), and Rothe *et al.* (29) agree quite well in view of the fact that there is considerable doubt that they had 100% collection efficiency for all ions (see Table II). There is some evidence that the cross sections measured by Boksenberg (31) are too large. All of these experiments were relative and were normalized to the total cross section measurements of Tate and Smith for O_2.

Rapp, Golden, and Briglia (7b) have measured the cross sections for the production of energetic ions from O_2. In Fig. 43 these cross sections as measured by Rapp, Golden, and Briglia, $(\sigma_T-\sigma_2)$ as measured by Fite and Brackmann, and $(\sigma_T-\sigma_2)$ as measured by Boksenberg are plotted. Here σ_2 is the cross section for producing thermal O_2^+ by single electron impact on O_2. Since $(\sigma_T-\sigma_2)$ contains contributions from O_2^{2+}, the close agreement between Fite and Brackmann and Rapp, Golden, and Briglia is possibly fortuitous, but the evidence does indicate that the ratio (σ_2/σ_T) as measured by Boksenberg is probably too large. The total cross sections reported for molecular oxygen by Tate and Smith and by Rapp *et al.* differ by about 10%. This does not affect the agreement between Rapp *et al.* and Fite and Brackmann for the energetic ion cross sections; nor does this affect the discrepancy with the Boksenberg data, since the Rapp, Golden, and Briglia data on dissociative ionization were normalized using a McLeod gauge standard.

If Boksenberg's value for $(\sigma_T-\sigma_2)$ is too small, then his measured cross sections for the ionization of atomic oxygen would be too large (ignoring other possible systematic errors).

Atomic Mercury

All of the data presented in Fig. 9 except that of Liska (61) are absolute and were taken with parallel plate geometry and collection of all ions. The data of Nottingham (38) are not presented because the collection efficiency for positive ions as a function of the electron energy in his apparatus was uncertain and because the data were not corrected for a large number of secondary effects which appear to be systematic.

The data of Jones (2) are here corrected for obsolete mercury vapor pressure data, and for diffusion. [The mercury reservoir and ionization chamber were at 0°C and 70°C, respectively. Bleakney (59) noted these errors.] The vapor pressure data from the International Critical Tables were used instead of those of Smith and Menzies (see Table II).

Harrison (62) had two possible systematic pressure errors. First, he used a secondary standard, an ion gauge, to determine the mercury pressure; and second, he assumed that the temperature of the ionization region was that of room temperature, 27°C. This assumption is probably incorrect. If the temperature of the ionization region were higher than room temperature, which is likely, correcting for this would have the effect of slightly increasing his cross sections. Making this correction would tend to bring his data into better agreement with Bleakney and Jones. Since Liska's data were normalized to that of Smith (60), these are not independent measurements.

Although the cross-section data of Smith are considerably smaller than those of Jones, Bleakney, and Harrison, there appears to be no reason for rejecting Smith's results or giving them less weight.

One of the uncertainties in all of these experiments is the purity of the gas. The mercury vapor was introduced through the pumping line by regulating the temperature of the trap.

Alkali Metals: Li, Na, K, Rb, Cs

The absolute, total ionization, cross-section data for the alkali metals are presented in a small table, since only one set of experimental results, that of McFarland and Kinney (33), was selected for presentation.

The data of Brink (32) are not presented, since only cross sections for production of the single ion were presented, and since these were derived from his total cross-section data, using relative cross sections for the production of multiply charged ions that were not defined. His total cross-section data were not available.

McFarland and Kinney did a crossed-beam experi-

CC-0. In Public Domain. Gurukul Kangri Collection, Haridwar

Digitized by Arya Samaj Foundation Chennai and eGangotri

ment. The intensity of the neutral atomic beam was determined, using a surface ionization detector. The efficiency of this detector has not been clearly established for the alkalis (see Sec. II) and is probably the source of the largest systematic error in the experiment.

Molecular Cross Sections: H_2, D_2 N_2, O_2, CO, NO

The cross sections reported by Tate and Smith (4) decrease more rapidly with energy than those of Rapp and Golden (7a) above 100 eV. The cause of this decrease may be the same as that which produced a similar effect in the comparisons of the cross sections for He, Ne, and Ar. The data of Schram *et al.* (8) are again lower than the other available results at the same energies.

In the case of these diatomic molecules, dissociative ionization can make it difficult to collect all of the ions. Rapp, Golden, and Briglia (7b) have estimated [see Sec. III, B(4)] the percentage of total ion current due to energetic ions from dissociative ionization and found it to range at maximum from 36% for O_2 to 7% for H_2. If these ions were not efficiently collected, a significant underestimate of the total ionization cross section would be made. Both Rapp *et al.* (7b) and Schram *et al.* (8) were careful to assure saturation of their collected ion current, and it seems unlikely that their experiments had this systematic error. Tate and Smith may not have used high enough collecting voltages to assure complete collection of the energetic ion current.

The data of Harrison (62) for molecular hydrogen are considerably higher than those of all the other results presented. Harrison may not have collected all of the ion current because the voltage used for collecting the ions, nine volts, was only sufficient to assure total collection of ions with energies less than 4.5 eV. Harrison noted that his cross sections were considerably larger than those reported by Smith. He rechecked the calibration of his ion gauge and found it to be essentially unchanged. Another possible pressure error in this experiment is noted in the discussion of the mercury cross-section data. The likely systematic errors in this experiment would probably tend to increase the cross sections, but there appears to be no valid reason for rejecting Harrison's results.

Ion Cross Sections: He^+, Li^+, N^+, Ne^+, Na^+, K^+

Since each of these experiments was done with mass analysis, the data are cross sections for single ionization of the ions involved. The recent data of Latypov *et al.* (73) are not included because, as they demonstrated, their measured cross sections are so dependent on conditions in their ion source as to be practically meaningless. Only in the case of neon this was not so, which provides strong evidence that their Ne^+ beam was not contaminated with excited species. Dolder *et al.* (63) came to this same conclusion about their own work, when they observed no Ne^{2+} current below the threshold for the appearance of these ions from the ground state of Ne^+. The one data point for Ne^+ from the experiment of Latypov *et al.* was not considered of comparable reliability to the data of Dolder *et al.* and hence is not presented.

Because only one set of data is available for each of these atomic ions, it is difficult to estimate what the magnitude of possible systematic errors might be. For He^+, comparison of the experimental values of Dolder *et al.* (25) with the scaled atomic hydrogen cross sections measured by Fite and Brackmann shows good agreement, i.e., they differ by less than 10% at energies greater than 10 times threshold. At energies less than five times threshold, the agreement is rather poor.

For N^+ it is possible that the beam was contaminated by metastable nitrogen atomic ions, but the evidence presented by Harrison *et al.* (64) seems to indicate that the contamination was quite small. This conclusion was based on an assumed cross section shape for the dissociative ionization of N_2^{2+}, a probable constituent which could give rise to an observed signal below the expected ionization potential. Since their ion beam was mass analyzed, using magnetic deflection, they could not separate N^+ from N_2^{2+} in their primary beam. This possible contamination obviously introduces very large uncertainties in their reported cross sections near threshold.

The experiments of Hooper, Lineberger, McDaniel, and Bacon (27) on the ionization of the singly charged alkali metal ions are significantly different from those of Dolder, Harrison, and Thonemann. The former differ in two ways which tend to reduce systematic errors: First, the experiments were done at much lower background pressure ($\approx 10^{-8}$ Torr) which tended to reduce stripping of the ions on the background gas. Second, the source of ions was thermal emission from a surface, which does not populate metastable excited states.

Again in this case because only one experiment has been reported for each ionic species, it is difficult to predict the magnitude of the systematic errors. The authors have estimated their maximum systematic errors resulting from uncertainties in instrument calibration as $\pm 6\%$. It is probable that this is a lower limit to the total possible systematic errors.

Absolute Cross Sections for Ionization of Atoms and Diatomic Molecules into Excited Final States

The data of Rapp, Golden, and Briglia (7b, 7c) on the approximate cross sections for production of energetic ions (Figs. 26–31), i.e., dissociative ionization, are the only absolute measurements of these cross

CC-0. In Public Domain. Gurukul Kangri Collection, Haridwar

Digitized by Arya Samaj Foundation Chennai and eGangotri

sections. These data are quite uncertain for the following reasons:

(1) Because dissociation is not necessarily an isotropic process, an uncertain fraction of the ions was collected.

(2) Since ions of thermal energy were eliminated by retarding, this technique may eliminate some fraction of ions resulting from dissociation.

(3) Under the conditions used, reflection of low energy ions from the collector could be serious.

Rapp *et al.* do not claim that their data are accurate, but these are the only absolute results presently available.

Bleakney in 1930 (59) used this same experimental technique with H_2 to estimate the percentage of total ion current resulting from energetic ions with an appearance potential greater than 30 eV. His estimated percentage rises from threshold to an almost constant 7% at higher energies. Considering the nature of the experiments, this result is in good agreement with the results of Rapp.

Experiments to measure approximate cross sections for ionization into excited electronic states which radiate have been done by St. John and Lin on He (53), by Stewart (54), Sheridan *et al.* (55), and by Hayakawa *et al.* on N_2 (56). The detection mechanism must measure absolutely the intensity of this radiation. These experiments are difficult to evaluate, but since they are the only ones available and are done absolutely, they are presented. They are not cross sections for ionization into a single excited ion state but for the production of radiation of a certain wave length. Cascading and branching ratios were not taken into account in analyzing the data.

Relative Cross Sections for Production of Multiply Charged Atomic Ions

Most of the data in the literature on the relative abundances of multiply charged ions were collected using electron multipliers as detectors. In most cases authors did not take proper account of the fact that the gain (i.e., the number of secondary electrons per ion) is quite different for ions of different charge and mass which have been accelerated through the same potential.

Secondary emission coefficients for ions having the same kinetic energy but having different charge or mass can differ by factors of two or three. We compared data collected using uncalibrated multipliers and those using Faraday cups as collectors. The differences in relative cross sections were typically of the order of two for data taken in these two ways. We concluded that data collected with uncalibrated multipliers could not be considered as reliable as measurements of ion current directly. None of the data presented here except that of Stanton and Monahan (69) were taken using a multiplier as a detector. Stanton and Monahan obtained their helium data by counting ions, which, if properly done, effectively calibrates the multiplier. It is probable that in none of these experiments were there the same collection efficiencies for the different ions. The magnitude of these collection efficiency errors is difficult to estimate, but some idea of it can be obtained by noting the differences between the results of independent experiments. The data on multiple ions are presented as the logarithm of the ratio of the cross section for the production of the ion in question to σ_T. In order to obtain normalized cross sections for the production of an ion per atom and electron, one multiplies the σ_T given in Sec. IIIB(1) by the ratios given in Figs. 32–41.

These relative cross sections are presented as ratios; we decided that the accuracy of these cross sections was so uncertain that it would have been unreasonable to present them in absolute units. The crux of this problem is obvious from the total cross sections given in Sec. IIIB(1). The disparity in the data makes it impossible to decide which σ_T to use, even if one has confidence in the ratios σ_{n+}/σ_T.

IV. STRUCTURE IN AND THRESHOLD BEHAVIOR OF IONIZATION EFFICIENCY

In recent years most of the research in the study of ionization of atoms and molecules by electron impact has been directed at discovering structure in and determining the threshold shape of the ionization efficiency function. Ideally, its shape should be identical to that of the cross-section curve if single collisions are predominant. Unfortunately, observation of the detailed structure of the ionization efficiency has yielded conflicting results. Review of the techniques, as described in the literature, reveals that they all require very careful adjustment of instrumental parameters. Many of these adjustments rely on reproducing results of other investigators using similar techniques. It appears that these techniques cannot in general be compared with the criteria given in Table I which could be considered minimum criteria for assuring reliability. Therefore we have not included data in this section because the experiments compare favorably with the criteria in Table I. The data were selected because they illustrate major points of agreement or conflict.

The focus of attention on structure and threshold may in large part be attributed to the development of techniques for diminishing the effects of the electron energy distribution in obscuring details of the observed ionization efficiencies. Added incentive to threshold ionization studies was given by the theoretical predictions of Wannier (74) and of Geltman (75) and more

CC-0. In Public Domain. Gurukul Kangri Collection, Haridwar

Digitized by Arya Samaj Foundation Chennai and eGangotri

recently by Rudge and Seaton (76) for the variation of ionization cross sections near threshold. Existence of mechanisms of ionization other than direct transitions of electrons to the first continuum have been demonstrated, although the relative importance of these mechanisms has not been fully demonstrated. Some investigators have correlated structure in the ionization efficiency curves with energy levels of the neutrals or ions under study and thus a form of spectroscopy has developed in ionization studies. This "spectroscopy" will not be discussed here except when it is pertinent to the discussion of threshold laws and ionization mechanisms.

We emphasize, before discussing some of the experimental results, that instrumental effects such as mentioned in Sec. II and such as analyzed by Marmet (47) may play a large role here in the results. The only apparent theoretical basis for interpreting structure in ionization curves near threshold are the threshold laws noted above. The energy range of validity of these laws is not predicted. However, it is natural (and sometimes apparently irresistible) for the experimentor to try to interpret structure which he observes, and thus a large literature has grown up, demonstrating and interpreting structure in ionization efficiency curves.

There are several experimental results that seem to indicate that the ionization cross section varies with the nth power of the excess energy above threshold of the

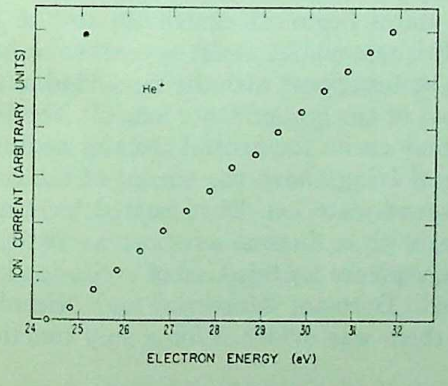

FIG. 44. Data of Hickam *et al.* (77) showing the linear rise with energy of ion current for single ionization of He.

impacting electron where n times ionized ions are being formed. The results of Hickam, Fox, and Kjeldaas (77) using the RPD method mentioned in Sec. II for single ionization of He are shown in Fig. 44. A straight line as predicted by Geltman, Rudge, and Seaton can be readily fitted to the points, and these authors show that there are large deviations from a fitted 1.1-power law, the dependence which is predicted by Wannier. Others (78, 79) have confirmed that the first ionization of He is consistent with a first-power law. Fite and

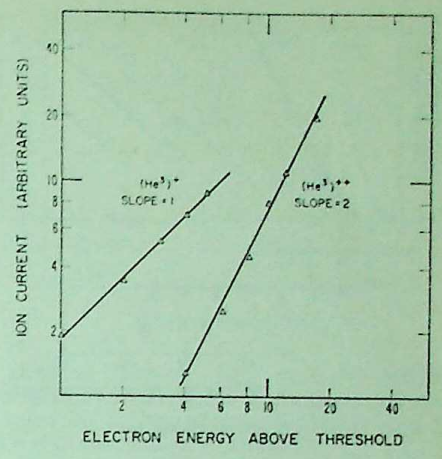

FIG. 45. Data of Fox (81) demonstrating the linear and quadratic threshold laws of single and double ionization, respectively of He.

Brackmann (24) observe that the ionization cross section for H atoms increases linearly with excess energy with a slope of 0.078 πa_0^2/eV. McGowan and Fineman (80) have recently done the experiment with high energy resolution; and they confirm the linearity, finding a slope of 0.064 πa_0^2/eV.

Double ionization of He has been shown by Fox (81) and by Krauss, Reese, and Dibeler (82) to be consistent with a threshold law varying as the square of excess energy above threshold. Figure 45 shows Fox's results. Fox used He^3 to avoid complications from H_1^+, while Krauss *et al.* used a high resolution, mass spectrograph to separate H_2^+ from He^{++}. Both groups used the full energy spectrum of electrons emitted from a filament. Dibeler and Reese (83), using the full electron energy width from a filament, showed that the

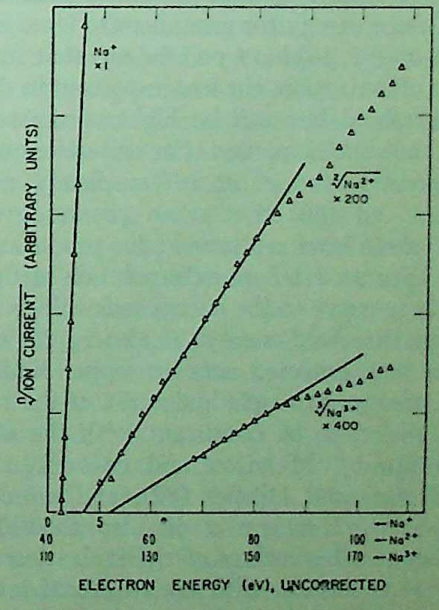

FIG. 46. Data of Dibeler and Reese (83) demonstrating threshold behavior for one, two, and three times ionized sodium.

CC-0. In Public Domain. Gurukul Kangri Collection, Haridwar

Digitized by Arya Samaj Foundation Chennai and eGangotri

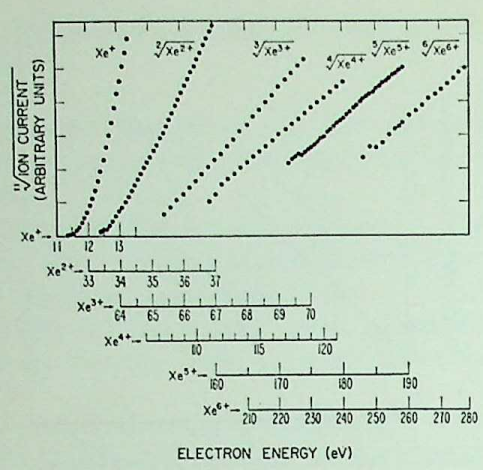

FIG. 47. Data of Dorman *et al.* (85) demonstrating threshold behavior for up to six times ionized xenon.

appearance behavior of one, two, and three times ionized sodium is consistent, respectively, with a linear, square, and cubic dependence on energy above threshold. Their results are shown in Fig. 46. The linear and square laws for single and double ionization, respectively, of sodium and potassium have been demonstrated by Kaneko (84), using the RPD method.

The unique feature of all of these systems studied is the absence of excited states lying near the ground state of the ion. Fortuitously, the use of the natural spread in electron energies in some of the above work does not seem to be a great disadvantage, since the threshold law seems to be obeyed over an energy range which is large compared to the spread.

More severe difficulties of interpretation in terms of threshold laws have occurred for other than the systems mentioned above, and some controversy over these interpretations still exists. This is often attributed to the onsets of other ionization processes relatively near the appearance energy for ground-state ions. However, Dorman *et al.* (85, 86) have pointed out that the greater the degree of ionization, the less important in determining the threshold law will be higher processes *having the same threshold law*, and for ionization of degree four or greater, the effect is completely negligible. They point out (86) that when processes with different threshold laws are present for producing ions of charge n, then an nth root extrapolation of the ionization efficiency curve to the energy axis will give a lower limit to the threshold energy. The energy at which ion current is first detected sets an upper limit on the threshold energy. Multiple ionization of the rare gases has been shown to be consistent with the nth power threshold law by Morrison and co-workers (85–87), Krauss, Reese, and Dibeler (82), and more recently by Kiser (88). Morrison *et al.* also showed that in many cases the derivatives of the ionization efficiency curves were consistent with the threshold laws. All of these workers used the full energy spread of electrons from a filament. Representative results of Morrison are shown in Fig. 47. Clarke (41), using an electrostatic electron energy selector, found that the threshold law for Xe^{++} is consistent with a square-law dependence on excess energy. In contrast to this, Fox (81, 89) and Hickam, Fox, and Kjeldaas (77) found that a series of straight-line segments fits their data most satisfactorily. Although an nth root plot of these data yields reasonable straight lines, extrapolations of such plots do not give threshold energies in agreement with spectroscopic values, in contrast to extrapolation of straight-line segments fitted directly. Similarly, Blais and Mann (90) fitted straight-line segments to double ionization of Au, but Dorman and Morrison (52) pointed out that a plot of the square root of ionization efficiency against energy is also a straight line within experimental error over a range of at least 10 eV. Within the limitations set by higher processes as discussed by Dorman and Morrison (86) and mentioned above, the data of other workers seem to be consistent both with the form of the threshold law and the nth root extrapolated threshold energy. A comparison of threshold energies as found by various workers is given by Kiser (88). Dorman and Morrison (52) have also found that double ionization of NO, CO, N_2, and of some polyatomic molecules increases in a way that is consistent with dependence on the square of the energy above threshold.

Fine structural variation observed in ionization efficiency curves may be interpreted in terms of at least three kinds of mechanisms: (1) Higher lying states of the ion become energetically accessible, and ions formed in these states begin to contribute to the observed current. It is reasonable, and it appears to be borne out, that such states appear with the same kind of threshold law as that of the ground-state ion. (2) The impacting electron may excite the neutral atom or molecule to an energy level lying above the energy of the continuum of the ground-state ion. This excited level may then autoionize with a lifetime as short as 10^{-14} sec. The energy dependence for this kind of excitation is not well established. Dorman, Morrison, and Nicholson (91) had felt there was evidence for a step function thres-

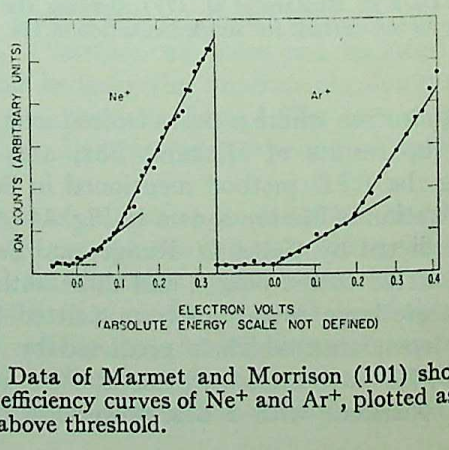

FIG. 48. Data of Marmet and Morrison (101) showing direct ionization efficiency curves of Ne^+ and Ar^+, plotted as a function of energy above threshold.

CC-0. In Public Domain. Gurukul Kangri Collection, Haridwar

Digitized by Arya Samaj Foundation Chennai and eGangotri

hold, but in more recent work Morrison (42) notes that there may be pronounced effects due to configuration interaction. (3) Auger processes also account for some observations of structure. In these an inner shell electron is knocked out by the impacting electron; and an outer electron, in transferring into the vacancy, gives the transition energy to another outer electron. If this energy is high enough, the outer electron is ejected, thus leaving the atom ionized to one higher degree.

The first mechanism leading to structure—that of forming ions in excited states—has perhaps been most observed in ionizing noble gases where the ion ground state is a doublet, with $^2P_{\frac{1}{2}}$ higher than $^2P_{\frac{3}{2}}$. This doublet separation is 1.31 eV in xenon, 0.67 eV in krypton, 0.18 eV in argon, and 0.10 eV in neon. Structure which has been attributed to these doublets has been observed many times (Refs. 77, 78, 92–103). Results of Marmet and Morrision (101) for Ne and Ar are shown in Fig. 48. One might expect that with no other ionizing mechanisms present, the ratio of the slopes of lines fitted to the data might be the same as the ratio of the statistical weights of the two states. The various data referenced above, however, do not show consistent results for the ratios of these slopes. That the ratio may not be as predicted can perhaps be explained in terms of autoionization as discussed below. The technique of observing "breaks" in straight-line fits to data has also been applied to some molecules, and interpretation of the results has been made in terms of excited electronic states of the ion (Refs. 41, 93–96, 98, 99, 104–109) and in terms of vibrationally excited states of the ion (Refs. 41, 95, 109, 110). Here again the role of autoionization has probably not been thoroughly accounted for in interpreting the shapes of these ionization efficiency curves.

The ionization efficiency curve of H_2 near threshold is an interesting case in point. Figure 49 shows the data of Marmet and Kerwin (110) who used a 127° selector and a volume gas sample in conjunction with a mass spectrometer, the data of Briglia and Rapp (111) who used

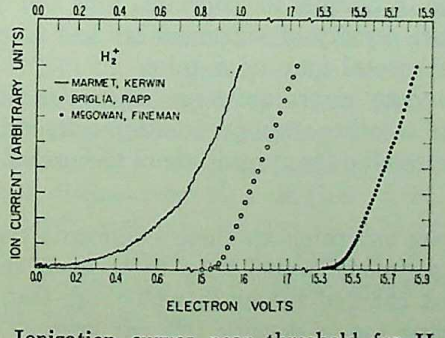

FIG. 49. Ionization curves near threshold for H_2. Data of Marmet and Kerwin (110) are plotted on an energy scale with an arbitrary zero reference. Data of Briglia and Rapp (111) and McGowan and Fineman (80) are plotted on absolute energy scales.

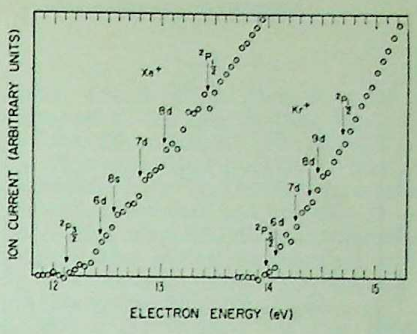

FIG. 50. Data of Morrison (103) on ionization efficiency of Xe and Kr near threshold, reduced by an analytical method. The $^2P_{\frac{1}{2}}$ and $^2P_{\frac{3}{2}}$ ionization limits and some excited neutral levels lying between these states are shown by arrows.

the RPD method in a total ionization tube, and the data of McGowan and Finemann (80) who used a 127° selector and a molecular beam in conjunction with a mass spectrometer. Marmet and Kerwin interpret their curve in terms of breaks at the thresholds for individual vibrational states of H_2^+. They compare the slopes at the breaks and find reasonable agreement with the Franck–Condon factors between H_2 and H_2^+. Briglia and Rapp observe a nearly straight line and conclude that a direct ionization model of H_2 for which the Franck–Condon factors predict the relative populations of vibrational levels is not valid. McGowan and Fineman also observe a nearly straight line, but look at the first and second derivative of the ionization efficiency curve as well as the curve itself. Comparison of the derivative curve (see below) with photoionization data (Refs. 112, 113) on H_2 shows many similarities. Many peaks which can be traced to autoionization occur in the photoionization data. Similar peaks occur in the derivative of the electron impact curve. The disagreements (Fig. 49) demonstrate and emphasize the extreme difficulties faced in measuring and interpreting ionization efficiency curves near threshold.

The mechanism of autoionization has long been known from interpretation of spectra (Refs. 114), but it appears that Fox, Hickah, and Kjeldaas (92) were the first to use the process to explain structure in ionization efficiency curves. They invoked the mechanism to explain their inability to fit two straight lines as above to the ionization efficiency curves of krypton and xenon. This mechanism has since been suggested as an explanation of features in the ionization efficiency curves of Zn, Cd, Hg (Ref. 115), of O_2 (Refs. 91, 116) and N_2 (Refs. 41, 91, 98, 99) of Mg (Ref. 84) and Ca (Ref. 44), of K, Rb, and Cs (Ref. 117), and of Cu, Ag, and Au (Ref. 90). Recent data of Morrison (103) and of Burns (102) show more clearly the apparent effects of autoionization in the ionization of Kr and Xe. The data of Morrison (103) are shown in Fig. 50. He has pointed out a great similarity between the ionization efficiency curve for Xe and the integral over energy

CC-0. In Public Domain. Gurukul Kangri Collection, Haridwar

Digitized by Arya Samaj Foundation Chennai and eGangotri

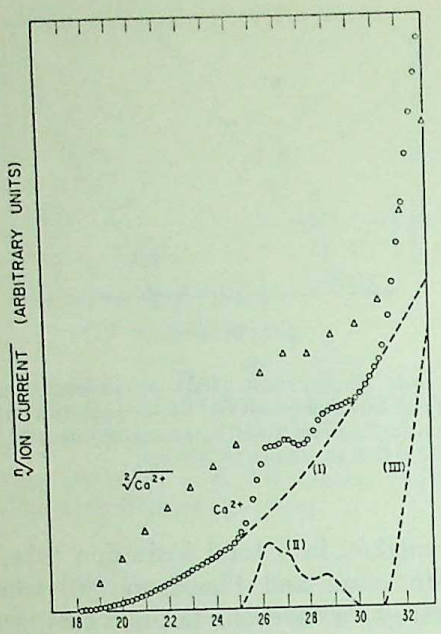

FIG. 51. Data of Kaneko and Kanomata (44) showing double ionization of Ca near threshold. Circles represent the ion current directly, and triangles represent the square root of this current. Dashed curves II and III are the difference between a curve through the circles and a quadratic curve I deduced from a straight line fit to the triangles below 25 eV.

of the photoionization curve. An equivalent similarity has been noted in recent high resolution data (Ref. 116) for O_2 and in H_2 as noted above (Ref. 80). There seems to be no theoretical basis at present upon which such comparisons can be made, so the meaning of the comparisons is doubtful.

Autoionizing lifetimes are usually thought to be of the order of 10^{-13}–10^{-14} sec. However, lifetimes of nearly 10^{-4} sec have been observed (Ref. 118) for some autoionizing levels of alkaline metals. Such a spread in lifetimes can contribute to difficulties in getting consistent results in ionization efficiency curves. Thus it has been observed (Ref. 45) that the shapes of some curves are very sensitive to the ion-source, drawout field; and reasonably long-lived autoionizing levels are suggested as an explanation.

Fox (81) suggested the Auger process as a means of explaining the anomalous shape of his multiple ionization data. It has since been observed more conclusively (Refs. 44, 45, 119), and data of Kaneko (44) for double ionization of Ca are shown in Fig. 51. A portion of the curve shows a quadratic energy dependence, followed by an irregular portion between 25 eV and 30 eV, and a linearly increasing portion starting at 31 eV. This latter portion has been attributed according to a suggestion by Fayard *et al.* (45) to Auger ejection caused by ionization of a $3p$ electron. The Auger process results in a probability for creating Ca^{++} which is comparable to that for Ca^{+}. The threshold law appears to be linear, even though the resultant ion is Ca^{++} because the electron collision produces $(Ca^{+})^{*}$.

V. CONCLUSIONS

The conceptual simplicity of ionization measurements by no means implies that such measurements will be reliable. Although in many of the experiments (particularly total ionization) random errors are small, systematic errors seem often to be serious. There are two main observations leading to this conclusion:

(1) There are large systematic differences in the number density standards used in the various experiments to obtain absolute cross sections. Several recent efforts (see Sec. II) have been made to eliminate temperature effects observed when using McLeod gauges as standards. Although various procedures have been developed based on empirical tests, these tests are necessary, but not sufficient, to define a reliable standard. There thus seems to be an inadequate basis for strongly recommending some of the more recent results in which attempts to improve the pressure standards were made.

(2) Large systematic differences exist in the cross section shapes as a function of electron energy. The causes of these differences have not as yet been identified with certainty, nor are they quantitatively understood.

Rare gases being nonreactive should behave like "ideal" gases. Even for the rare gases, however, systematic differences among the experimentally measured cross sections range from about 10% in helium to 30% in xenon (excluding the threshold region). At this point one must accept these differences as a reasonable measure of the possible range of systematic errors.

Crossed-beam experiments for neutral ground-state species are probably less accurate than the total ionization experiments for the following reasons:

(1) Crossed-beam experiments rely for normalization on the cross sections measured which use the Tate and Smith technique.

(2) The techniques for collecting ions and determining number density of scatterers are less reliable than that of the total ionization tube.

(3) Random errors are large, and it is difficult to determine whether any systematic errors exist, much less to determine the magnitude of the errors.

A strong exception to these comments on crossed-beam experiments would have to be made in the case of crossed charged beams in which the standards for determining target density (electric current and distance) are accurate and easily accessible. However, in these experiments the random errors are quite large and systematic errors of a subtle nature may be ob

CC-0. In Public Domain. Gurukul Kangri Collection, Haridwar

Digitized by Arya Samaj Foundation Chennai and eGangotri

scured. Reliable independent experiments have never been performed using crossed charged beams, and it is thus not reasonable to speculate about the probable range of systematic errors.

There is a very decided lack of cross-section measurements for individual processes, i.e., cross sections from a known initial state to a single known final state. Fluorescence techniques have been applied in only a small number of experiments on ionization, and it is not yet clear what role is played by structure near the ionization threshold in determining the relative magnitudes of cross sections to individual final states. Mass spectrometers have been used to determine the relative cross sections for going to different final charge states, but in general the assumption of a constant collection efficiency of a mass spectrometer for different charge states has not been demonstrated, and one cannot look upon the relative cross-section data as more than approximate. Clearly, these measurements await new techniques, or imaginative use and interpretation of old techniques.

One final comment which, although it may appear obvious, is worth emphasizing. Consideration of all the data shows that none of the cross sections discussed are reliable to within 10% at best; therefore, any comparison of theoretical calculation with the data should take this uncertainty into account.

ACKNOWLEDGMENTS

This critical review was supported by the National Bureau of Standards through the National Standard Reference Data Program. The authors would also like to acknowledge the use of the facilities of the JILA Information Center. The Information Center is supported by the Advanced Research Projects Agency (Project DEFENDER), which is monitored by the U.S. Army Research Office-Durham, and the National Bureau of Standards, through the National Standard Reference Data Program. One of us, Gordon H. Dunn, is grateful for partial support to the Controlled Thermonuclear Branch of the U. S. Atomic Energy Commission.

We would like to thank Donald Rapp and Robert H. McFarland for the generous use of their time in discussing their respective experiments. Also, we would like to acknowledge the following individuals who supplied tabular data not given in their publications or preprints: A. Boksenberg, F. J. de Heer, J. W. Hooper, R. H. Neynaber, and B. L. Schram. Helpful correspondence from G. O. Brink, W. L. Fite, R. E. Fox, Y. Kaneko, J. R. Peterson, G. J. Schulz, and P. T. Smith is gratefully acknowledged.

Finally, we would like to thank John Conroy for his very careful and accurate work in compiling the experimental results which are presented here.

REFERENCES

[1] A. Ll. Hughes and E. Klein, Phys. Rev. **23**, 450 (1924); K. T. Compton and C. C. Van Voorhis, Phys. Rev. **26**, 436 (1925); W. P. Jesse, Phys. Rev. **26**, 208 (1925).

[2] T. J. Jones, Phys. Rev. **29**, 822 (1927). These absolute data (Fig. 11) were obtained from Fig. 2 in this reference and corrected for obsolete vapor pressure data and for diffusion (i.e., the trap and ionization regions were at different temperatures) before converting them to cross sections as described in Sec. III. See Bleakney (51) for a discussion of these corrections.

[3] P. T. Smith, Phys. Rev. **36**, 1293 (1930).

[4] J. T. Tate and P. T. Smith, Phys. Rev. **39**, 270 (1932).

[5] R. K. Asundi and M. V. Kurepa, J. Electron. Control **15**, 41 (1963). All of the data presented from this reference are those listed by the authors as "absolute (Tate and Smith)." The helium data (Fig. 4) are taken from Table 1. The neon data (Fig. 7) were taken from Table 2. The argon data (Fig. 8) were taken from Table 3. The krypton data (Fig. 9) were taken from Table 4. The xenon data (Fig. 10) were taken from Table 5.

[6] R. K. Asundi, J. D. Craggs, and M. V. Kurepa, Proc. Phys. Soc. (London) **82**, 967 (1963).

[7] (a) D. Rapp and P. Englander-Golden, J. Chem. Phys. **43**, 1464 (1965); (b) D. Rapp, P. Englander-Golden, and D. D. Briglia, J. Chem. Phys. **42**, 4081 (1965); (c) P. Englander-Golden and D. Rapp, *Total Cross Sections for Ionization of Atoms and Molecules by Electron Impact*, No. LMSC-6-74-64-12 (Lockheed Missiles and Space Company, Palo Alto, California, 1964).

[8] B. L. Schram, F. J. de Heer, M. J. van der Wiel, and J. Kistemaker, Physica **31**, 94 (1964).

[9] H. S. W. Massey and E. H. S. Burhop, *Electronic and Ionic Impact Phenomena* (Oxford University Press, London, 1952), p. 34.

[10] R. K. Asundi, Proc. Phys. Soc. (London) **82**, 372 (1963).

[11] J. D. Craggs, R. Thorburn, and B. A. Tozer, Proc. Roy. Soc. (London) **A240**, 473 (1957).

[12] S. Dushman, *Scientific Foundations of Vacuum Technique* (John Wiley & Sons, Inc., New York, 1962), 2nd ed., pp. 14, 58.

[13] J. P. Hobson, J. Edmonds, and R. Verreault, Can. J. Phys. **41**, 983 (1963); G. A. Miller, J. Phys. Chem. **67**, 1359 (1963).

[14] H. Ishii and K. Nakayama, Proc. 8th Natl. Vac. Symp. 519 (1961).

[15] Ch. Meinke and G. Reich, Vacuum **13**, 579 (1963); A. E. de Vries and P. K. Rol, Vacuum (to be published); E. W. Rothe, J. Vac. Sci. Technol. **1**, 66 (1964).

[16] W. Gaede, Ann. Physik **46**, 354 (1915).

[17] G. J. Schulz, Phys. Rev. **128**, 178 (1962).

[18] W. Bleakney, Phys. Rev. **34**, 157 (1929).

[19] J. T. Tate and P. T. Smith, Phys. Rev. **46**, 773 (1934).

[20] *Mass Spectrometry*, edited by C. A. McDowell (McGraw-Hill Book Company, Inc., New York, 1963).

[21] M. G. Inghram and R. J. Hayden, *A Handbook on Mass Spectroscopy*, Publication 311 (National Academy of Sciences–National Research Council, Washington, D.C., 1954).

[22] H. Funk, Ann. Physik **4**, 149 (1930).

[23] R. L. F. Boyd and G. W. Green, Proc. Phys. Soc. (London) **71**, 351 (1958).

[24] W. L. Fite and R. T. Brackmann, Phys. Rev. **112**, 1141 (1958). The data (Fig. 3) were taken from Figs. 4 and 5 in this reference. The details of the procedures for normalizing the data are discussed in the reference.

[25] K. T. Dolder, M. F. A. Harrison, and P. C. Thonemann, Proc. Roy. Soc. (London) **A264**, 367 (1961).

[26] J. R. Peterson, in *Atomic Collision Processes*, edited by M. R. C. McDowell (North-Holland Publishing Company, Amsterdam, 1964), pp. 465–473. [Proceedings of the Third International Conference on the Physics of Electronic and Atomic Collisions (London), 22–26 July 1963].

[27] W. C. Lineberger, J. W. Hooper, and E. W. McDaniel, Phys. Rev. **141**, 151 (1966); data for Li^+; J. W. Hooper, W. C. Lineberger, and F. M. Bacon, Phys. Rev. **141**, 165 (1966); data for Na^+ and K^+.

[28] W. L. Fite and R. T. Brackmann, Phys. Rev. **113**, 815 (1959). These relative cross-section data (Fig. 6) were taken from Fig. 1 in this reference. They were normalized by the authors using the absolute total ionization cross-section data of Tate and Smith (Fig. 15) for the oxygen molecule. Since the ion current

CC-0. In Public Domain. Gurukul Kangri Collection, Haridwar

Digitized by Arya Samaj Foundation Chennai and eGangotri

was mass analyzed, these are not total cross sections but cross sections for the production of O^+ from O.

[29] E. W. Rothe, L. L. Marino, R. H. Neynaber, and S. M. Trujillo, Phys. Rev. **125**, 582 (1962). These data (Figs. 3 and 6) were supplied in tabular form by Dr. R. H. Neynaber of General Dynamics/Astronautics, San Diego, California. The relative cross-section data for atomic hydrogen and oxygen were normalized using the absolute total ionization cross-section data of Tate and Smith (Figs. 12 and 15) for molecular hydrogen and oxygen, respectively.

[30] A. C. H. Smith, E. Caplinger, R. H. Neynaber, E. W. Rothe, and S. M. Trujillo, Phys. Rev. **127**, 1647 (1962). The data (Fig. 5) were supplied in tabular form by Dr. R. H. Neynaber of General Dynamics/Astronautics, San Diego, California. The data were used to plot Fig. 4 in this reference. The relative cross sections were normalized, using the absolute total ionization cross-section data of Tate and Smith (Fig. 14) for molecular nitrogen.

[31] A. Boksenberg, thesis, University of London (1961). The hydrogen data (Fig. 3) were supplied in tabular form by Dr. A. Boksenberg, University of London. The data were normalized to a Born calculation at 300 eV. The oxygen data (Fig. 6) were taken from Fig. V3 in this reference. The data were normalized using the total ionization cross-section data of Tate and Smith (Fig. 15) for the oxygen molecule. Since the ion current was mass analyzed, these are not total cross sections but cross sections for the production of O^+ from O.

[32] G. O. Brink, Phys. Rev. **134**, A345 (1964).

[33] R. H. McFarland and J. D. Kinney, Phys. Rev. **137**, A1058 (1965). The cross-section data given in Table III were privately communicated by Dr. McFarland. They are not found in the reference.

[34] S. Datz and E. H. Taylor, J. Chem. Phys. **25**, 389 (1956).

[35] N. N. Petrov, Fiz. Tver. Tela **2**, 940, 949 (1960) [English transl.: Soviet Phys.—Solid State **2**, 857, 865 (1960)]; C. Brunnee, Z. Physik **147**, 161 (1957).

[36] W. Schroen, Z. Physik **176**, 237 (1963).

[37] R. K. Asundi and M. V. Kurepa, J. Sci. Instr. **40**, 183 (1963).

[38] W. B. Nottingham. Phys. Rev. **55**, 203 (1939).

[39] R. E. Fox, W. M. Hickam, D. Grove, and T. Kjeldaas, Rev. Sci. Instr. **26**, 1101 (1955); Phys. Rev. **84**, 859 (1951).

[40] D. A. Hutchinson, in *Advances in Mass Spectrometry*, edited by R. M. Elliott (Pergamon Press, Inc., New York, 1962), Vol. II, p. 527.

[41] E. M. Clarke, Can. J. Phys. **32**, 764 (1954).

[42] J. D. Morrison, J. Chem. Phys. **40**, 2488 (1964).

[43] J. D. Morrison, J. Chem. Phys. **22**, 1219 (1954).

[44] Y. Kaneko and I. Kanomata, J. Phys. Soc. Japan **18**, 1822 (1963).

[45] F. Fiquet-Fayard and M. Lahmani, J. Chim. Phys. **59**, 1050 (1962).

[46] P. Marmet and J. D. Morrison, J. Chem. Phys. **36**, 1238 (1962).

[47] P. Marmet, Can. J. Phys. **42**, 2102 (1964).

[48] G. H. Dunn, Phys. Rev. Letters **8**, 62 (1962).

[49] G. H. Dunn and L. J. Kieffer, Phys. Rev. **132**, 2109 (1963).

[50] W. Bleakney, Phys. Rev. **35**, 1180 (1930).

[51] C. J. Cook and J. R. Peterson, Phys. Rev. Letters **9**, 164 (1962).

[52] F. H. Dorman and J. D. Morrison, J. Chem. Phys. **35**, 575 (1961).

[53] R. M. St. John and C. C. Lin, J. Chem. Phys. **41**, 195 (1964).

[54] D. T. Stewart, Proc. Phys. Soc. (London) **A69**, 437 (1956). These data (Fig. 25) on N_2^+ were obtained from Fig. 2 in this reference.

[55] W. F. Sheridan, O. Oldenberg, and N. P. Carleton, in *Second International Conference on the Physics of Electronic and Atomic Collisions* (W. A. Benjamin, Inc., New York, 1961), p. 159. [Conference held at the University of Colorado Boulder, 12–15 June 1961].

[56] S. Hayakawa and N. Nishimur, J. Geomagnetism and Geoelectricity (Japan) **16**, 72 (1964).

[57] Our original bibliographic source was JILA Report No. 4, which has subsequently been revised and issued as JILA Report No. 34.

[58] E. R. Cohen, K. M. Crowe and J. W. Dumond, *The Fundamental Constants of Physics* (Interscience Publishers, Inc., New York, 1957).

[59] W. Bleakney, Phys. Rev. **35**, 139 (1930). The absolute mercury data (Fig. 11) were obtained from Fig. 8 in this reference. The relative mercury data (Fig. 41) were obtained from Fig. 6.

[60] P. T. Smith, Phys. Rev. **37**, 808 (1931).

[61] J. W. Liska, Phys. Rev. **46**, 169 (1934). The helium data presented in Fig. 4 were taken from Table I in this reference. The author normalized his data by matching ionization efficiency he obtained at 2500 eV to that measured by P. T. Smith(3). The mercury data (Fig. 11) were taken from Table I in this reference. The author normalized his data by matching the maximum efficiency he obtanied to that measured absolutely by P. T. Smith(60).

[62] H. Harrison, *The Experimental Determination of Ionization Cross Sections of Gases under Electron Impact*, thesis (The Catholic University of America Press, Inc., Washington, D.C., 1956). The helium data (Fig. 4) were taken from Table 6. The mercury data (Fig. 11) were taken from Table 1. The molecular hydrogen data (Fig. 12) were taken from Table 4. The relative helium data (Fig. 32) were computed from "Probability of Ionization" data, Table 7, because they are consistent with the ionization efficiency data given in Table 6. The cross section data given in Table 7 are inconsistent and assumed to be incorrect. The relative mercury data (Fig. 41) were taken from Table 3.

[63] K. T. Dolder, M. F. A. Harrison, and P. C. Thonemann, Proc. Roy. Soc. (London) **A274**, 546 (1963).

[64] M. F. A. Harrison, K. T. Dolder, and P. C. Thonemann, Proc. Phys. Soc. (London) **82**, 368 (1963).

[65] B. A. Tozer and J. D. Craggs, J. Electron. Control **8**, 103 (1960).

[66] W. L. Fite, and R. T. Brackmann, in *Proceedings of the Sixth International Conference on Ionization Phenomena in Gases* edited by P. Hubert and E. Cremieu-Alcan (S.E.R.M.A., Paris, 1965), Vol. I, p. 21.

[67] R. F. Stebbings, Proc. Roy. Soc. (London) **A241**, 270 (1957).

[68] W. Bleakney and L. G. Smith, Phys. Rev. **49**, 402 (1936).

[69] H. E. Stanton and J. E. Monahan, Phys. Rev. **119**, 711 (1960). The data on helium (Fig. 32) is a reconstruction of the "average" ratio of He^+ yield to He^{2+} yield which is represented as a line in Fig. 4 of this reference.

[70] W. Bleakney, Phys. Rev. **36**, 1303 (1930). The relative neon data (Fig. 33) were taken from Fig. 2 in this reference; the relative argon data (Fig. 35) were taken from Fig. 5 in this reference.

[71] These data were presented at the Institute of Petroleum ASTM Mass Spectrometry Symposium, Paris, September 14–18, 1964. A manuscript of this presentation was privately communicated by Dr. B. L. Schram.

[72] H. A. Bethe, Ann. Physik **5**, 325 (1930).

[73] Z. Z. Latypov, S. E. Kupriyanov, and N. N. Tunitskiĭ, Zh. Eksperim. i Teor. Fiz. **46**, 833 (1964) [English transl.: Soviet Phys.—JETP **19**, 570 (1964)].

[74] G. H. Wannier, Phys. Rev. **90**, 817 (1953).

[75] S. Geltman, Phys. Rev. **102**, 171 (1956).

[76] M. R. H. Rudge and M. J. Seaton, Proc. Phys. Soc. (London) **83**, 680 (1964).

[77] W. M. Hickam, R. E. Fox, and I. Kjeldaas, Jr., Phys. Rev. **96**, 63 (1954).

[78] J. D. Morrison, J. Chem. Phys. **21**, 1767 (1953).

[79] D. A. Hutchinson, in *Atomic Collision Processes*, edited by M. R. C. McDowell (North-Holland Publishing Company, Amsterdam, 1964), p. 443.

[80] J. W. McGowan and M. A. Fineman, Phys. Rev. Letters **15**, 179 (1965); and Abstracts of Papers presented at *IV International Conference on the Physics of Electronic and Atomic Collisions* (Science Bookcrafters, Inc., Hastings-on-Hudson, New York, 1965).

[81] R. E. Fox, *Advances in Mass Spectrometry* (Pergamon Press, Inc., London, 1959), pp. 397–412.

[82] M. Krauss, R. M. Reese, and V. H. Dibeler, J. Res. Natl. Bur. Std. (U.S.) **63A**, 201 (1959).

[83] V. H. Dibeler and R. M. Reese, J. Chem. Phys. **31**, 282 (1959).

[84] Y. Kaneko, Proc. Phys. Soc. Japan **16**, 2288 (1961).

[85] F. H. Dorman, J. D. Morrison, and A. J. C. Nicholson, J. Chem. Phys. **31**, 1335 (1959).

CC-0. In Public Domain. Gurukul Kangri Collection, Haridwar

Digitized by Arya Samaj Foundation Chennai and eGangotri

[86] F. H. Dorman and J. D. Morrison, J. Chem. Phys. **34**, 1407 (1961).
[87] J. D. Morrison and A. J. C. Nicholson, J. Chem. Phys. **31**, 1320 (1959).
[88] R. W. Kiser, J. Chem. Phys. **36**, 2964 (1962).
[89] R. E. Fox, J. Chem. Phys. **33**, 200 (1960).
[90] N. C. Blais and J. B. Mann, J. Chem. Phys. **33**, 100 (1960).
[91] F. H. Dorman, J. D. Morrison, and A. J. C. Nicholson, J. Chem. Phys. **32**, 378 (1960).
[92] R. E. Fox, W. M. Hickam, and T. Kjeldaas, Jr., Phys. Rev. **89**, 555 (1953).
[93] D. C. Frost and C. A. McDowell, Proc. Roy. Soc. (London) **A232**, 227 (1955).
[94] D. C. Frost and C. A. McDowell, *Advances in Mass Spectrometry* (Pergamon Press, Inc., London, 1959), pp. 413–430.
[95] G. G. Cloutier and H. I. Schiff, J. Chem. Phys. **31**, 793 (1959).
[96] R. E. Fox, J. Chem. Phys. **32**, 385 (1960).
[97] P. Marmet and L. Kerwin, Can. J. Phys. **38**, 787 (1960).
[98] R. E. Fox, J. Chem. Phys. **35**, 1379 (1961).
[99] Y. Kaneko, J. Phys. Soc. Japan **16**, 1587 (1961).
[100] S. N. Foner and B. H. Nall, Phys. Rev. **122**, 512 (1961).
[101] P. Marmet and J. D. Morrison, J. Chem. Phys. **35**, 746 (1961).
[102] J. F. Burns, in *Atomic Collision Processes*, edited by M. R. C. McDowell (North-Holland Publishing Company, Amsterdam, 1964), p. 451.
[103] J. D. Morrison, J. Chem. Phys. **40**, 2488 (1964).
[104] R. E. Fox and W. M. Hickam, J. Chem. Phys. **22**, 2059 (1954).
[105] J. D. Morrison, J. Chem. Phys. **22**, 1219 (1954).
[106] D. C. Frost and C. A. McDowell, J. Am. Chem. Soc. **80**, 6183 (1958).
[107] D. C. Frost and C. A. McDowell, Can. J. Chem. **38**, 407 (1960).
[108] C. E. Melton and W. H. Hamill, J. Chem. Phys. **41**, 546 (1964).
[109] C. E. Brion, J. Chem. Phys. **40**, 2995 (1964).
[110] P. Marmet and L. Kerwin, Can. J. Phys. **38**, 972 (1960).
[111] D. D. Briglia and D. Rapp, Phys. Rev. Letters **14**, 245 (1965).
[112] V. H. Dibeler, R. M. Reese, and M. Krauss, J. Chem. Phys. **42**, 2045 (1965).
[113] G. R. Cook and P. H. Metzger, J. Opt. Soc. Am. **54**, 968 (1964).
[114] H. E. White, Phys. Rev. **38**, 2016 (1931).
[115] W. M. Hickam, Phys. Rev. **95**, 703 (1954).
[116] J. W. McGowan, E. M. Clarke, H. P. Hanson, and R. F. Stebbings, Phys. Rev. Letters **13**, 620 (1964).
[117] G. O. Brink, Phys. Rev. **127**, 1204 (1962).
[118] P. Feldman and R. Novick, Phys. Rev. Letters **11**, 278 (1963).
[119] F. Fiquet-Fayard and J. Ziesel, in *Proceedings of the VI International Conference on the Phenomena of Ionization in Gases*, edited by P. Hubert and E. Cremieu-Alsan (S.E.R.M.A., Paris, 1963), Vol. I., p. 37.

CC-0. In Public Domain. Gurukul Kangri Collection, Haridwar

Digitized by Arya Samaj Foundation Chennai and eGangotri

Complex Coordinates and Quantum Mechanics

F. STROCCHI*
Laboratoire de Physique Théorique et Hautes Energies, Orsay, Seine et Oise, France†

By introducing complex canonical coordinates, classical and quantum mechanics may be embedded in the same formulation. In such a way, the connection between Poisson brackets and commutators, canonical transformations and unitary transformations, etc., become apparent. This formulation is also particularly suitable for discussing the classical limit of quantum mechanics and for quantum-statistical mechanics.

I. INTRODUCTION

The general structures of classical and quantum mechanics are usually regarded as essentially different and the relation between them has been the subject of several investigations.[1] As a matter of fact, the connection between the usual formulation of classical mechanics and quantum mechanics is not immediate. The classical limit of quantum mechanics, which is usually identified with the limit $\hbar \to 0$, is rather obscure; the connection between commutators and Poisson brackets is difficult to explain in that limit. Neither is the connection between the theory of canonical transformations and unitary transformations in quantum mechanics apparent, and one has to rely on analogy arguments.

A better understanding of the relation between the two theories may be obtained by a formal theory of generalized dynamics which includes classical and quantum mechanics as special cases. This is realized by a more general formulation of Hamiltonian mechanics, with the introduction of complex canonical variables. Hamilton's equations, Poisson brackets, and canonical transformations exhibit an elegant and compact form, when written in terms of the new variables. In particular the analysis of canonical transformations reduces to the study of the analytical properties of the generating functions as functions of the new variables.

Quantum mechanics may be regarded as a special case of the above formulation. The Schrödinger equation may in fact be written as Hamilton equations for complex canonical coordinates, the Hamiltonian function being the mean value of the Hamiltonian operator. In this formulation the analogy between classical and quantum mechanics goes beyond the formal structure of the equations of motion. In the same way as for the Hamiltonian, a "classical" phase function of complex variables may be introduced for any other observable and for them the Poisson brackets may be defined as in the classical case. Thus, the quantum problem takes a form similar to that of a classical problem; for example the Poisson bracket of two conjugate variables has the same value 1 in both the classical and quantum cases.

Most of the assumptions of quantum mechanics have a natural explanation in the framework of complex classical mechanics, in which they have a strictly related analog. For example, the correspondence between Poisson brackets and commutators is not arbitrary: the Poisson bracket of two "classical" phase functions is in fact the mean value of the commutator between the corresponding operators. Similarly, the hermiticity of observables has its analogue in the fact that the phase functions of complex variables must satisfy a reality condition, and the unitarity condition is nothing but the canonicity condition for generating functions in the case of complex canonical coordinates.

Thus, classical and quantum mechanics may be embedded in the same formulation, the "classical" form of quantum mechanics being obtained by taking the mean values of the corresponding operators. The difference between the two theories does not lie in their mathematical structures, but rather in the way a physical problem is schematized and reduced to a mathematical problem. For example, the system of one single particle is completely described by *six* variables in classical mechanics, whereas an *infinite* number of canonical variables is needed in quantum mechanics. In particular, as we show below, a quantum particle is equivalent to a set of infinite classical harmonic oscillators. This aspect of the theory is emphasized by second quantization or field theory. As a matter of fact, both classical and quantum mechanics have the structure of a Lie group of transformations associated with a Lie algebra of functions of the canonical variables. The two formulations may be regarded as different representations of the same algebraic structure, the difference being in the number of dimensions of the space in which the representation is realized.

Thus, the classical limit of quantum mechanics may be understood as an approximation in which the dynamical variables are described by average values: $q_{\text{class}} = \langle \Psi \mid q \mid \Psi \rangle$, $p_{\text{class}} = \langle \Psi \mid p \mid \Psi \rangle$ etc., in which the "hidden" quantum structure of the state is neglected.

---

* On leave from Scuola Normale Superiore, Pisa, and Istituto Nazionale di Fisica Nucleare, Sezione di Pisa, Italy.

† Present address: Laboratoire de Physique Théorique et Hautes Energies, Faculté des Sciences, Bât. 211, Orsay, Seine et Oise, France.

[1] J. Von Neumann, Ann. Math. **33**, 587, (1932); U. Uhlhorn, Arch. Phys. **11**, 87 (1956); H. J. Groenewold, Physica **12**, 405 (1946); E. Wigner, Phys. Rev. **40**, 749 (1932); T. F. Jordan and E. C. Sudarshan, Rev. Mod. Phys. **33**, 515 (1961); etc.

CC-0. In Public Domain. Gurukul Kangri Collection, Haridwar

Digitized by Arya Samaj Foundation Chennai and eGangotri

The limit $\hbar \to 0$ should be better understood as a condition on the magnitude of the dynamical variables involved in a specific problem in order that the above approximation is valid (Ehrenfest theorem).

II. COMPLEX VARIABLES AND CLASSICAL MECHANICS

The state of a classical system is completely described by the real canonical coordinates q_k, p_k, $k=1, \cdots, N$ (N being the number of degrees of freedom) and the time evolution is governed by the Hamilton equations

$$\dot{q}_k = \partial H/\partial p_k, \qquad \dot{p}_k = -\partial H/\partial q_k. \tag{1}$$

In the place of the variables q_k, p_k, which play a non-symmetric role in Eqs. (1), we introduce the variables z_k and $z_k,^*$ so defined[2]

$$z_k = (q_k + ip_k)/\sqrt{2}, \qquad z_k{}^* = (q_k - ip_k)/\sqrt{2}.$$

In terms of the new variables, the Hamilton equations take the compact form:

$$i\dot{z}_k = \partial H/\partial z_k{}^*, \qquad -i\dot{z}_k{}^* = \partial H/\partial z_k. \tag{2}$$

The second set of equations may be obtained from the first by complex conjugation, and it is therefore superfluous. In Eqs. (2), the Hamiltonian has to be regarded as a function of z_k and $z_k{}^*$, satisfying the reality condition:

$$H(z, z^*) = [H(z, z^*)]^* \equiv H^*(z^*, z). \tag{3}$$

Like the Hamiltonian, any other phase function $f(q, p)$, may be written in terms of the variables z, z^* and the analogue of Eq. (3) is satisfied by definition:

$$f(z, z^*) = [f(z, z^*)]^*. \tag{3'}$$

For any two phase functions $f(z, z^*)$ and $g(z, z^*)$, the Poisson bracket is given by:

$$\{f, g\} \equiv \frac{\partial f}{\partial q_k}\frac{\partial g}{\partial p_k} - \frac{\partial f}{\partial p_k}\frac{\partial g}{\partial q_k} = -i\left(\frac{\partial f}{\partial z_k}\frac{\partial g}{\partial z_k{}^*} - \frac{\partial f}{\partial z_k{}^*}\frac{\partial g}{\partial z_k}\right)$$

$$\equiv -i[f, g]. \tag{4}$$

The sum over repeated indices is implied. The bracket $[\ ,\ ]$, defined before may be regarded as a definition of the Poisson bracket in the new variables. As is evident from Eqs. (2) and (4), the variables z_k and $z_k{}^*$ play the role of canonical *conjugate* variables, just as the old q's and p's.

III. CANONICAL TRANSFORMATIONS

We are now in the position of characterizing the canonical transformations in terms of the new variables. They are implicitly defined by the property of leaving the Poisson brackets invariant. However, as far as the study of canonical transformations is concerned, it is useful to give a differential characterization.

In the usual formulation, a transformation from the variables q, p to the variables Q, P is canonical if the following condition is satisfied:

$$p_k\dot{q}_k - P_k\dot{Q}_k - H + K = dF/dt,$$

where $H = H(q, p)$ and $K = K(Q, P)$ are the Hamiltonians in the two systems of coordinates and F is an arbitrary function. When the complex variables are used, the above equation is equivalent to:

$$K(Z, Z^*) - H(z, z^*)$$

$$+\tfrac{1}{2}i[Z_k\dot{Z}_k{}^* - \dot{Z}_kZ_k{}^* - z_k\dot{z}_k{}^* + z_k{}^*\dot{z}_k] = dF/dt.$$

The above condition may be transformed into a set of differential equations. For this purpose, a system of independent variables has to be chosen, with the prescription that part of them belong to the old system and part to the new one. In the usual formulation, one may choose either p, Q or P, q or p, P or q, Q. Now one may choose either z, Z or z^*, Z^* or z, Z^* or z^*, Z. Then one has, e.g., in the first case:

$$K(z, Z) - H(z, Z)$$

$$+\tfrac{1}{2}i[Z_k\dot{Z}_k{}^* + \dot{Z}_kZ_k{}^* - 2\dot{Z}_kZ_k{}^* - (z_k\dot{z}_k{}^* + \dot{z}_kz_k{}^*) + 2\dot{z}_kz_k{}^*]$$

$$= dF/dt$$

or

$$K - H + i[\dot{z}_kz_k{}^* - \dot{Z}_kZ_k{}^*] = \frac{\partial F^{(1)}}{\partial z_k}\dot{z}_k + \frac{\partial F^{(1)}}{\partial Z_k}\dot{Z}_k + \frac{\partial F^{(1)}}{\partial t}.$$

The above condition is equivalent to the set of differential equations:

$$iz_k{}^* = \partial F^{(1)}/\partial z_k, \quad -iZ_k{}^* = \partial F^{(1)}/\partial Z_k, \quad K - H = \partial F^{(1)}/\partial t. \tag{5}$$

Similarly, one has, in the other cases,

$$-iz_k = \partial F^{(2)}/\partial z_k{}^*, \qquad iZ_k = \partial F^{(2)}/\partial Z_k{}^*, \tag{6}$$

$$iz_k{}^* = \partial F^{(3)}/\partial z_k, \qquad iZ_k = \partial F^{(3)}/\partial Z_k{}^*, \tag{7}$$

[2] By a suitable choice of the system of units or by a simple similarity transformation, the variables q and p may be made to have the same dimensions.

CC-0. In Public Domain. Gurukul Kangri Collection, Haridwar

Digitized by Arya Samaj Foundation Chennai and eGangotri

and

$$-iz_k=\partial F^{(4)}/\partial z_k^*, \qquad -iZ_k^*=\partial F^{(4)}/\partial Z_k. \tag{8}$$

Here, $F^{(1)}=F^{(1)}(z,\ Z)$, $F^{(2)}=F^{(2)}(z^*,\ Z^*)$, $F^{(3)}=F^{(3)}(z,\ Z^*)$, and $F^{(4)}=F^{(4)}(z^*,\ Z)$ may be regarded as the generating functions of the transformations. It is not difficult to see that there are only two independent sets of generating functions. Equations (6) and (8) may in fact be obtained by (5) and (7) by complex conjugation. Therefore,

$$F^{(2)}(z^*,\ Z^*)=[F^{(1)}(z,\ Z)]^*,$$

$$F^{(4)}(z^*,\ Z)=[F^{(3)}(z,\ Z^*)]^*.$$

Thus, of the four types of generating functions of the usual theory, only two are really different, in each pair the two functions being the real and imaginary part of the same analytic function. Apart from a greater elegance and simplicity, the reduction from four to two is in agreement with what one would expect from a group theoretical point of view. The two types of generating functions classify, in fact, the transformations which are connected with the identity and those which are not.

The integrability conditions for Eqs. (7) and (8) are:

$$\frac{\partial^2 F}{\partial z_i \partial Z_k^*}\frac{\partial^2 F^*}{\partial z_i^* \partial Z_l}+\frac{\partial^2 F}{\partial Z_k^* \partial Z_i^*}\frac{\partial^2 F^*}{\partial Z_i \partial Z_l}=\delta_{kl},$$

$$\frac{\partial^2 F}{\partial z_i \partial z_k}\frac{\partial^2 F^*}{\partial z_i^* \partial z_l^*}+\frac{\partial^2 F}{\partial z_k \partial Z_i^*}\frac{\partial^2 F^*}{\partial z_l^* \partial Z_i}=\delta_{kl}, \tag{9}$$

Hence, defining

$$F_{ik}=F_{ki}\equiv\partial^2 F/\partial Z_i^* \partial Z_k^*, \qquad F_{ki}^\dagger\equiv F_{ik}^*,$$

$$f_{ik}=f_{ki}\equiv\partial^2 F/\partial z_i \partial z_k, \qquad f_{ki}^\dagger\equiv f_{ik}^*,$$

$$g_{ik}\equiv\partial^2 F/\partial z_i \partial Z_k^*, \qquad (g^\dagger)_{ki}\equiv g_{ik}^*,$$

Eqs. (9) and (10) take the form of matrix equations

$$g^\dagger g+F^\dagger F=I, \tag{10}$$

$$gg^\dagger+ff^\dagger=I. \tag{11}$$

Here I denotes the unit matrix. The set of Eqs. (7), (10), and (11) define a canonical transformation connected with the identity.

Similarly, from Eqs. (5) and (6) one has

$$\frac{\partial^2 F'}{\partial z_i \partial z_k}\frac{\partial^2 F'^*}{\partial z_i^* \partial z_l^*}-\frac{\partial^2 F'}{\partial z_k \partial Z_i}\frac{\partial^2 F'^*}{\partial z_l^* \partial Z_i^*}=\delta_{kl},$$

$$\frac{\partial^2 F'}{\partial Z_i \partial Z_k}\frac{\partial^2 F'^*}{\partial Z_i^* \partial Z_l^*}-\frac{\partial^2 F'}{\partial z_i \partial Z_k}\frac{\partial^2 F'^*}{\partial Z_l^* \partial z_i^*}=\delta_{kl},$$

or, with obvious notations,

$$f'f'^\dagger-hh^\dagger=I, \tag{12}$$

$$F'^\dagger F-h^\dagger h=I. \tag{13}$$

In this formulation, canonical transformations may be studied by investigating the analytic properties of the generating functions. For example, conformal transformations of phase space, i.e., transformations which preserve the angles, are characterized by analytic functions[3]

$$Z_k=Z_k(z), \qquad Z_k^*=Z_k^*(z^*).$$

On the other hand, the conditions (10), (11) require

$$g^\dagger g=gg^\dagger=I,$$

F_{ik} and f_{ik} vanishing in this case. Thus, one has

$$Z_k=a_{ki}z_i, \qquad Z_k^*=a_{ki}^* z_i^*,$$

$$a_{ik}a_{il}^*=a_{ik}^* a_{il}=\delta_{kl},$$

i.e., the only canonical transformations preserving the angles in phase space are the linear orthogonal transformations. In a similar way, the transformations that preserve angles except for their sign, are the inverse conformal transformations. By conditions (12), (13) they are restricted to linear "orthogonal" transformations with determinant -1:

$$Z_k=Z_k(z^*)=a_{ki}z_i^*, \qquad Z_k^*=Z_k^*(z)=a_{ki}^* z_i,$$

$$a_{ki}a_{li}^*=a_{ik}a_{il}^*=-\delta_{kl}.$$

We list now some cases of canonical transformations that take a simple expression in the above formulations. We restrict ourselves to rotations in the planes q_k, p_k:

$$Z_k=z^{i\alpha}kz_k, \qquad Z_k^*=\exp(-i\alpha_k)z_k^*,$$

The above transformation is equivalent to the following transformation of the real canonical coordinates:

$$Q_k=(\cos\alpha_k)q_k-(\sin\alpha_k)p_k,$$

$$P_k=(\sin\alpha_k)q_k+(\cos\alpha_k)p_k,$$

Thus for $\alpha_k=\frac{1}{2}\pi$, the exchange of p and q is obtained,

$$Q_k=-p_k, \qquad P_k=q_k,$$

[3] H. Cartan, *Théorie élémentaire des fonctions analytiques d'une ou plusieurs variables complexes* (Hermann & Cie., Paris, 1961).

CC-0. In Public Domain. Gurukul Kangri Collection, Haridwar

Digitized by Arya Samaj Foundation Chennai and eGangotri

whereas for $\alpha_k=\pi$, the space inversion is obtained,

$$Q_k=-q_k, \qquad P_k=-p_k.$$

(Note that it is continuously connected with the identity.) The generating function is

$$F=-i\exp(-i\alpha_k)z_k^*Z_k.$$

therefore if the Hamiltonian is invariant under the above transformation, the quantity

$$2z_k^*Z_k\exp(-i\alpha_k)=2z_kz_k^*=q_k^2+p_k^2$$

is a constant of motion. This means that the modulus of the two-dimensional vector $(q_k,\ p_k)$ is conserved. This is the case of the harmonic oscillator, when the variables

$$q_k=(m\omega_k)^{\frac{1}{2}}x_k, \qquad p_k=m\dot{x}_k/(m\omega_k)^{\frac{1}{2}}$$

are chosen as canonical variables. (The transformation from $q_k'=x_k$, $p_k'=m\dot{x}_k$ to q_k, p_k is obviously a canonical transformation.)

IV. "CLASSICAL" FORM OF QUANTUM MECHANICS

An interesting application of the above formulation is given by quantum mechanics.[4] To this purpose we consider a system of particles, contained in a box of finite volume Ω. The Hilbert space $\mathcal{H}$ of the states of the system has infinite but numerable dimensions. For example, one may take as basic states the eigenstates of the momentum, spin, etc. of each particle; because of the finite volume Ω, the eigenvalues of the components of the momentum of each particle are discrete and numerable. For simplicity sake, we further assume that the energy spectrum is bounded, i.e., the energy of the system cannot exceed a definite, arbitrary large value $\bar{E}$. Then, we may restrict ourselves to a subspace $\mathcal{H}'\subseteq\mathcal{H}$ of finite dimensions. The above assumptions are not restrictive since one may make $\Omega\to\infty$ and $\bar{E}\to\infty$ at the end of calculations, then making $\mathcal{H}'$ go to $\mathcal{H}$.

The generic state $|\Psi\rangle$ may be written as a superposition of the basic states $|\alpha_k\rangle$, $k=1,\cdots,N$, which form a complete orthonormal set

$$|\Psi\rangle=u_k|\alpha_k\rangle$$

(sum over k is implied), where u_k are complex coefficients which completely determine the state $|\Psi\rangle$, once the basic states $|\alpha_k\rangle$ are fixed. As we see below, the coefficients u_k may be regarded as a sort of canonical coordinates and the complex $2N$-dimensional euclidean space of the u_k's may be regarded as the phase space of our quantum system.[4]

On using the Schrödinger picture for the state vectors, and taking the basic states as time-independent, the Schrödinger equation may be written as ($\hbar=c=1$)

$$i(d|\Psi\rangle/dt)=i(du_i/dt)|\alpha_i\rangle=H|\alpha_i\rangle u_i$$

or

$$i(du_k/dt)=\partial\mathcal{H}/\partial u_k^*=\langle\alpha_k|H|\alpha_i\rangle u_i,$$

where

$$\mathcal{H}\equiv H_{ki}u_k^*u_i\equiv\langle\alpha_k|H|\alpha_i\rangle u_iu_k^*=\langle\Psi|H|\Psi\rangle.$$

In that form the Schrödinger equation is nothing but the Hamilton equations in complex canonical coordinates for a classical system whose Hamiltonian function is the mean value of the quantum Hamiltonian operator. We shall call $\mathcal{H}$ the "classical" Hamiltonian.

Introducing the real coordinates

$$q_k\equiv(1/\sqrt{2})(u_k+u_k^*), \qquad p_k\equiv(i/\sqrt{2})(u_k^*-u_k),$$

the "classical" Hamiltonian becomes

$$\mathcal{H}=\tfrac{1}{2}H_{ki}(q_iq_k+p_ip_k+iq_kp_i-iq_ip_k).$$

This is the Hamiltonian for N coupled harmonic oscillators. An interesting case is when the Hamiltonian is one of the basic observables. Then

$$H_{ki}=E_k\delta_{ki}$$

(because of a possible degeneracy not all the E_k are different, i.e., it may be $E_k=E_l$ even if $k\neq l$). In this case, one has

$$\mathcal{H}=\tfrac{1}{2}E_k(q_k^2+p_k^2).$$

This is equivalent to using *normal* canonical coordinates for describing a system of classical harmonic oscillators.

The above-shown analogy between quantum and classical mechanics goes beyond a formal structure of the equations of motion. All the physical quantities may be expressed as bilinear functions of the variables u_k, u_k^*:

$$\langle\Psi|B|\Psi\rangle=\langle k|B|i\rangle u_k^*u_i\equiv b_{ki}u_k^*u_i\equiv\mathfrak{B}(u,u^*).$$

The hermiticity condition for observables requires

$$b_{ki}=\langle k|B|i\rangle=\langle i|B^\dagger|k\rangle^*=\langle i|B|k\rangle^*=b_{ik}^*.$$

[4] This formulation is particularly suitable in quantum statistical mechanics, see: F. Strocchi, "An Axiomatic Approach to Statistical Mechanics" (to be published).

CC-0. In Public Domain. Gurukul Kangri Collection, Haridwar

Digitized by Arya Samaj Foundation Chennai and eGangotri

Therefore,

$$\mathfrak{B}(u, u^*) = [\mathfrak{B}(u, u^*)]^*;$$

this is just condition (3′). Thus, with any observable, one may associate a real phase function of the complex variables u, u^*.

One of the basic quantities in classical mechanics is the Poisson bracket. Then, given any two Hermitian operators A and B, we may define the Poisson bracket between the corresponding phase functions $\mathfrak{A}$ and $\mathfrak{B}$, as in classical mechanics:

$$[\mathfrak{A}, \mathfrak{B}] \equiv \frac{\partial \mathfrak{A}}{\partial u_k}\frac{\partial \mathfrak{B}}{\partial u_k^*} - \frac{\partial \mathfrak{A}}{\partial u_k^*}\frac{\partial \mathfrak{B}}{\partial u_k}$$

$$= a_{ik}u_i^* b_{kl}u_l - a_{ki}u_i b_{lk}u_l^*$$

$$= \langle i \mid AB - BA \mid l \rangle u_i^* u_l = \langle [A, B] \rangle,$$

i.e., the classical Poisson bracket $[\mathfrak{A}, \mathfrak{B}]$ between the quantities $\mathfrak{A}$ and $\mathfrak{B}$ is the mean value of the commutator $[A, B]$ between the corresponding operators. Thus, the "classical" form of quantum mechanics leads necessarily to the usual correspondence between classical Poisson brackets and quantum commutators.

V. CANONICAL OR UNITARY TRANSFORMATION IN QUANTUM MECHANICS

A transformation of the Hilbert space into itself may be regarded as generated by a linear operator U, thus yielding

$$U \mid \Psi \rangle = u_k' \mid \alpha_k \rangle = U_{ki}u_i \mid \alpha_k \rangle,$$

where

$$U_{ki} \equiv \langle k \mid U \mid i \rangle \equiv \langle i \mid U^\dagger \mid k \rangle^*.$$

Hence, on defining

$$U_{ki}^\dagger = \langle k \mid U^\dagger \mid i \rangle,$$

one has

$$U_{ki} = (U_{ik}^\dagger)^*.$$

If the operator U has an inverse U^{-1}, one gets

$$u_k = (U^{-1})_{ki}u_i', \qquad U_{ki}^{-1} \equiv \langle k \mid U^{-1} \mid i \rangle.$$

The above transformation of the Hilbert space is therefore equivalent to a transformation of the complex canonical variables according to:

$$u_k' = U_{ki}u_i.$$

On requiring that the above transformation is canonical, one obtains as generating functions

$$F = iU_{ki}u_k'^* u_i,$$

and conditions (10) and (11) imply

$$U_{ki}U_{li}^* = U_{ik}U_{il}^* = \delta_{kl},$$

i.e.,

$$U^\dagger U = UU^\dagger = I.$$

Thus, unitary transformation in quantum mechanics are canonical transformations in the sense of classical mechanics.

From the generating function F, it is easy to see that

$$U_{ki}u_k'^* u_i = u_k^* u_k = u_k'^* u_k'$$

is a constant of motion, i.e., the norm of state vectors is conserved.

It is interesting to note that a large class of canonical transformations, corresponding to the classical transformations of Eqs. (5), (6), (12), and (13) have not been considered in quantum mechanics. For them, one has:

$$U^\dagger U = UU^\dagger = -I,$$

i.e., they change the sign of the metric in Hilbert space. However, from a physical point of view, an Hilbert space with negative definite metric is acceptable just as one with positive definite metric. Then, one should expect that transformations of kind (1), (2) should be used in quantum mechanics, e.g., for representing discontinuous transformations such as, e.g., charge conjugation etc.

CC-0. In Public Domain. Gurukul Kangri Collection, Haridwar

Digitized by Arya Samaj Foundation Chennai and eGangotri

Survey of Some Systematic Properties of the Nuclear *E*1 Transition Probability

CHARLES F. PERDRISAT

Department of Physics, University of Illinois, Urbana, Illinois

A survey of the experimental data for *E*1 transitions between levels below nucleon emission threshold in medium and heavy nuclei is presented. A general classification of these transitions is proposed and it is shown that, within most of the classes defined, the experimental "reduced" *E*1 transition probabilities differ by less than a factor 10^4. The data are compared with specific nuclear model predictions. Precise theoretical descriptions of the anomalous parity states involved in *E*1 transitions exist in a few cases only. However it is often possible to link the observed behavior of *E*1 transition rates as a function of different parameters, with qualitative model predictions.

The data available before 1 January 1965 are presented in tables including level lifetimes, quantum numbers, branching ratios, internal-conversion data, and deduced transition probabilities.

CONTENTS

1. Introduction 41
2. Single-Particle Transition Probability 42
3. Classes of *E*1 Transitions 44
4. Experimental Data and Nuclear Models 45
4.1. Odd-*A* Nuclei with Spherical Shape 45
4.1.1. Introduction 45
4.1.2. Discussion of the Experimental Data 46
4.2. Even-*A* Nuclei with Spherical Shape 47
4.2.1. Introduction 47
4.2.2. Transitions of the $(3^-\rightarrow 2^+)$ Type 47
4.2.3. Transitions of the $(5^-\rightarrow 4^+)$ Type 48
4.2.4. Transitions of the $(1^-\rightarrow 0^+$ g.s.) or $(1^-\rightarrow 2^+)$ Type 49
4.2.5. Transitions in odd-odd Nuclei 51
4.3. Odd-*A* Nuclei with Large Deformation 51
4.3.1. Introduction 51
4.3.2. Independent-Particle Model for Deformed Nuclei 51
4.3.3. *E*1 Transitions in the Nilsson Model 52
4.3.4. Comparison of the Experimental Data with the Weisskopf Estimate 53
4.3.5. Comparison of the Experimental Data with the Nilsson Estimate 54
4.3.6. Effect of a Rotation–Particle Interaction 55
4.3.7. Effect of the Pairing Correlation 57
4.4. Even-*A* Nuclei with Large Deformation 57
4.4.1. Models for Negative Parity Levels 57
4.4.2. Discussion of the Data for Rare-Earth Nuclei 58
4.4.3. Discussion of the Data for Actinide Nuclei 59
Acknowledgments 59
Appendix A
Single-Particle Estimate for Spherical Nuclei 59
Single-Particle Estimate for Deformed Nuclei 60
Bibliography 60
Appendix B. Tables of Experimental Data for *E*1 Transitions 62
Tables B-I–B-IV 63
Bibliography of Tables B-I–B-IV 91

1. INTRODUCTION

The first comprehensive survey of isomeric transitions was given by Goldhaber and Sunyar in 1951 (Go 51); it included about 100 transitions. Of these, only 15 were of low multipolarity (magnetic dipole, electric and magnetic quadrupoles). Four years later, the same authors discussed a much larger number of low-multipolarity transitions (Go 55). Nine of these were electric dipole. Since then the number of electric-dipole transitions with measured transition probability has constantly increased. Some classes of electric-dipole transitions have already been reviewed. At the Rehovoth meeting, Wilkinson (Wi 58) discussed about 70 electric-dipole transitions in light nuclei. The higher energy electric-dipole transitions following thermal-neutron capture reactions have been examined by Bartholomew (Ba 61). Electric-dipole transitions observed in photonuclear reactions have been surveyed by Levinger (Le 60). However, the experimental data for electric-dipole transitions in medium and heavy nuclei between levels stable against nucleon emission have not yet been reviewed. As the number of transitions of this kind with measured transition probability is currently around 150, it seems profitable to look for some common properties among them and to compare them to the predictions of nuclear models.

Electric-dipole transitions (called in the following *E*1) between an initial state $|J_i, \pi_i\rangle$ of spin J_i and parity π_i and a final state $|J_f, \pi_f\rangle$ are allowed provided the following selection rules are satisfied:

$$|J_i - J_f| \leq 1 \leq J_i + J_f$$

$$\pi_i = -\pi_f, \qquad (\text{no } 0\rightarrow 0).$$

Therefore *E*1 transitions are observed in nuclei where levels with spin differing by 1 or 0 unit and with different parity are present.

The single-particle version of the shell model does not predict levels with a spin difference of 1 or 0 and opposite parity within one shell, if a shell is supposed to include the orbitals between two magic nucleon numbers. Hence, either the initial or the final level (or both) of a *E*1 transition must contain many-particle configurations. The introduction into the shell model of residual interactions between the nucleons results in mixings of shell-model states. The *E*1 transition probability is expected to be particularly sensitive to configuration mixings. The number of configurations contributing to a given *E*1 transition can be large, but the amplitudes of these configurations are usually small. The hindrances observed for almost all the *E*1 transitions between levels stable against nucleon emission are due in part to these small admixture ampli-

CC-0. In Public Domain. Gurukul Kangri Collection, Haridwar

Digitized by Arya Samaj Foundation Chennai and eGangotri

tudes and in part to their destructive interference. The giant-resonance dipole states, however, are a coherent combination of a large number of configurations. As a result the $E1$ radiation width of the dipole states is large, and does not depend so sensitively on the nature of the individual configurations. It is also a coherent participation of several configurations which is at the origin of the collective properties of specific low-energy states like the first 2^+ and the 3^- levels in spherical even-A nuclei. In this discussion the distinction between intrinsic (or particle) and collective (or coherent) states is made with the following criteria:

(a) The intrinsic states are those whose properties (electric-multipole moments and transition probabilities) are close to the values obtained with the independent single-particle model.

(b) The levels for which the electric moments and transition probabilities are significantly larger than the single-particle estimate will be referred to as collective states.

This survey is organized as follows:

Section 2: The single-particle estimate for the electromagnetic transition probabilities is summarized.

Section 3: A classification of the $E1$ transitions with measured rates is proposed, as a function of the kind of nucleus and levels involved. As shown in Table I, the spread of the reduced transition probabilities within a number of classes is small.

Section 4: A detailed discussion of the experimental data and of the relevant nuclear models is given. It is divided into four subsections:

Sec. 4.1, transitions in odd-A spherical nuclei;
Sec. 4.2, transitions in even-A spherical nuclei;
Sec. 4.3, transitions in odd-A deformed nuclei; and finally
Sec. 4.4, transitions in even-A deformed nuclei.

In each subsection a further partition is made according to the kind of levels between which $E1$ transitions proceed. The possible theoretical descriptions of the levels not predicted by the simple shell model are emphasized.

In Sec. 4.1 several descriptions of the anomalous parity states in odd-A nuclei are mentioned. The $E1$ transitions observed in these nuclei all involve many-particle configurations.

In Sec. 4.2 the discussion of the $(3^-\rightarrow 2^+)$ transitions in even-A nuclei is related to the structure of the 3^- states. The $E1$ transitions of this kind are poorly known. The 5^- levels in tin isotopes are discussed together with the two-quasiparticle states calculated by Arvieu and Veneroni (Ar 60 and Ar 62). The 1^- levels in the region between the closed neutron shell $N=82$ and the onset of strong deformations at $N=88$ are tentitatively interpreted as two-quasiparticle excitations in a weakly deformed potential.

In Sec. 4.3 the Nilsson model is shown to give a straightforward description of the $E1$ transitions in the odd-A deformed nuclei. $E1$ transitions proceeding with $\Delta K=0$ agree more closely with the Nilsson estimate than those with $|\Delta K|=1$. The disagreement with the Nilsson estimate noted for some of the transitions can be attributed to a different deformation in the initial and final states. An alternative explanation for the strong hindrance of the transitions with $|\Delta K|=1$ is possible when a rotation–particle interaction is taken into account. The rotation–particle interaction term proposed by Kerman (Ke 56) has a strong effect on the $E1$ transition probabilities. Finally, attempts to evaluate $E1$ transition probabilities and branching ratios to the ground-state rotational band with pairing-model wave functions are reviewed. These calculations do not remove the disagreement observed in a number of cases when Nilsson wave functions are used.

In Sec. 4.4 the transitions in even-A deformed nuclei are understood as single-particle transitions between two-quasiparticle configurations of Nilsson states (Ga 62 and So 64). Except for the fast transitions in $_{62}Sm^{152}$, the order of magnitude of the hindrance factors observed are compatible with the ones for transitions in odd-A deformed nuclei. An estimate of the hindrance factors for $E1$ transitions using a pairing Hamiltonian with octupole-force term has been given by Zaretskii and Urin (Za 62). The hindrance factor observed for the $_{62}Sm^{152}$ $(1^-\rightarrow 2^+)$ transition can be calculated for characteristic values of a few parameters.

The discussion of the experimental data shows that these are still scarce outside the regions of strong nuclear deformations. Fifty percent of the measured $E1$ transitions occur in odd-A deformed nuclei. Reproducing the $E1$ transition probabilities requires a very precise description of the nuclear states and is a challenging test for models. Some of the calculations reviewed in this survey have already given promising results. However, numerous improvements will be needed until a detailed agreement with the experimental data can be obtained.

2. SINGLE-PARTICLE TRANSITION PROBABILITY

Calculations of electromagnetic-transition probabilities in nuclei have been discussed by Weisskopf (We 51), Moszkowski (Mo 51, Mo 53), Stech (St 52), Bohr and Mottelson (Bo 53), and Wilkinson (Wi 53, Wi 56, Wi 60). Details about the assumptions and results of these calculations can be found in various textbooks (Bl 52, Mo 55, Sh 63). Calculations with different coupling schemes for the transitions in light nuclei have been done by Lane and Radicati (La 54) and many others.

Some of the expressions relevant for electric-multipole transitions will be written down with an indication of the essential assumptions. When the wavelength condition $\omega R/c \ll 1$ is satisfied (ω is the frequency corre-

CC-0. In Public Domain. Gurukul Kangri Collection, Haridwar

Digitized by Arya Samaj Foundation Chennai and eGangotri

sponding to the transition energy $E_\gamma = E_i - E_f$ and R is the radius of the emitting system of nucleons), the transition probability for an electric transition of multipole order L is

$$T_{e1}(L) = \frac{8\pi(L+1)}{\hbar L[(2L+1)!!]^2}\left(\frac{\omega}{c}\right)^{2L+1} \times \sum_{M,Mf} |\langle \pi_f; J_f, M_f | M_{e1}^{\pi}(L, M) | \pi_i; J_i, M_i \rangle|^2, \quad (1)$$

where

$$M_{e1}^{\pi}(L, M) = \int \rho(\mathbf{r}) r^L Y_{LM}(\theta, \phi)\, dx^3. \quad (2)$$

π_f, J_f, M_f and π_i, J_i, M_i are the quantum numbers for the parity, the total angular momentum and the z component of the angular momentum operators, in the final and initial states, respectively. $\rho(\mathbf{r})$ is the operator for the charge density. It is assumed that the nucleons are nonrelativistic, and the spin part of the interaction is neglected.

Matrix elements of $M_{e1}^{\pi}(L, M)$ vanish unless the triangular condition is satisfied and the parity is conserved in the transition:

$$|J_i - J_f| \leq L \leq J_i + J_f,$$
$$\pi_f = \pi \cdot \pi_i. \quad (3)$$

For electric transitions, by definition $\pi = (-1)^L$, whereas for magnetic ones $\pi = (-1)^{L+1}$. Hence, $E1$ transitions occur only between states of opposite parity and with a change of the resulting angular momentum for the nucleus of 0 or 1 unit. The vector character of the $E1$ transition operator forbids $0 \rightarrow 0$ transitions absolutely.

The transition matrix element for the total transition rate can be written as a function of a reduced matrix element $\langle \| \| \rangle$:

$$\sum_{M,Mf} |\langle \pi_f; J_f, M_f | M_{e1}^{\pi}(L, M) | \pi_i, J_i, M_i \rangle|^2 = (2J_i+1)^{-1} |\langle J_f \| \int \rho(s) r^L Y_L\, dx^3 \| J_i \rangle|^2. \quad (4)$$

This expression is identical to the reduced transition rate $B_{e1}(L)$ introduced by Bohr and Mottelson (Bo 53). The reduced matrix element, as well as the charge-density operator, depend on the nucleus structure through the initial- and final-state wave functions. A comparison of an experimentally determined reduced transition rate with its value calculated with the wave functions of a given model allows a test of these wave functions. Such a test is expected to be particularly sensitive in the case of $E1$ transitions, as well as for all observables depending on an order-1 operator (the magnetic-dipole moments and transition rates or the matrix elements $\int 1$ and $\int \sigma$ in beta decay).

In the single-particle picture of the nucleus, electromagnetic transitions are caused by the jump of a single proton between two states of the model. In a central potential the transition rate $T_{e1}(L)$ in formula (1) can be calculated as the integrals over the radial part and the angular and spin parts can be separated. If the former integral is written $\langle r^L \rangle$ and the latter $[S_{e1}(L)]^{\frac{1}{2}}$, one gets:

$$T_{e1}(L) = \frac{8\pi(L+1)e^2}{\hbar L[(2L+1)!!]^2}\left(\frac{\omega}{c}\right)^{2L+1} \langle r^L \rangle^2 S_{e1}(L). \quad (5)$$

A strongly simplified form of the single-proton estimate is frequently used for the purpose of comparing various transitions. This is the Weisskopf (We 51) estimate in which a maximum value for the overlap of the radial wave functions $\langle r^L \rangle$ is used. With this simplication, one gets for the $E1$ transition probability

$$T_W(E1) = 0.72 E_\gamma^2 r_0^2 S(E1)\, 10^{14}\ \text{sec}^{-1}, \quad (6)$$

where E_γ is in MeV and r_0 is the nuclear radius in F. With $|r_0| = 1.2A^{\frac{1}{3}}$ F, one gets

$$T_W(E1) = 1.04 E_\gamma^3 A^{\frac{2}{3}} S(E1)\, 10^{14}\ \text{sec}^{-1}. \quad (7)$$

In the following, it is not the reduced rate given by Eq. (4) that is used, but a slightly different one, defined by

$$T(E1) = B(E1) E_\gamma^3 A^{\frac{2}{3}}\ \text{sec}^{-1}. \quad (8)$$

Supposing for the moment $S(E1) = 1$, the reduced transition probability defined by Eq. (8) is proportional to the radial overlap integral squared, $|\langle r \rangle|^2$. The Weisskopf estimate for $B(E1)$ can be deduced from Eqs. (7) and (8); it is

$$B_W(E1) = 1.04 \times 10^{14}\ \text{MeV}^{-3}\ \text{sec}^{-1}. \quad (9)$$

The hindrance factor of a transition, relative to the Weisskopf estimate, is defined as

$$H_W(E1) = B(E1)/B_W(E1) \cong B(E1)\, 10^{14}. \quad (10)$$

As will be shown in Appendix A, the true value of $S(E1)$ is indeed close to 1 when the transition occurs with $|J_i - J_f| = 1$. However, there is another reason to take $S(E1) = 1$ for all the $E1$ transitions discussed below. Apart from the light nuclei, the single-particle model simply does not predict within one shell two levels with a spin difference of 0 or 1 unit and different parities.[1] Therefore it makes little sense to use the precise values of $S(E1)$. That a comparison of the experimental data with the single-particle estimate is still meaningful will be justified in the next section.

[1] This statement is not in contradiction with the known fact that in the simplest shell-model $E1$ transitions can occur from one shell to another. However, in the kind of nuclei considered here, such transitions have energies larger than the binding energy of one nucleon.

CC-0. In Public Domain. Gurukul Kangri Collection, Haridwar

Digitized by Arya Samaj Foundation Chennai and eGangotri

TABLE I. Statistical analysis of the $E1$ transitions discussed in this survey. The solid lines define the range of $B(E1)$ observed within one class. The nine transitions that do not fit in these classes are given individually. A total of six transitions are not shown in this table, as indicated in text.

Class	Nucleus	Transition	Number	$\rightarrow B(E1)$
1	odd, spherical	all	10	
2	even, spherical	$3^- \rightarrow 2^+$	5	
3	even, spherical	$5^- \rightarrow 4^+$, $1^- \rightarrow 0^+$	8	
4	odd–odd, spherical	$72 < A < 152$	3	
5	odd, deformed lanthanide	$\Delta K = 0$	10	
6	odd, deformed lanthanide	$\Delta K = +1$	5	
7	odd, deformed lanthanide	$\Delta K = -1$	19	
8	odd, deformed lanthanide	K-forbidden	11	
9	odd, deformed actinides	$\Delta K = 0$	9	
10	odd, deformed actinides	$\lvert \Delta K \rvert = 1$	5	
11	odd, deformed actinides	K-forbidden	6	
12	even, deformed lanthanides and actinides	K-allowed	25	
13	even, deformed lanthanides and actinides	K-forbidden	12	

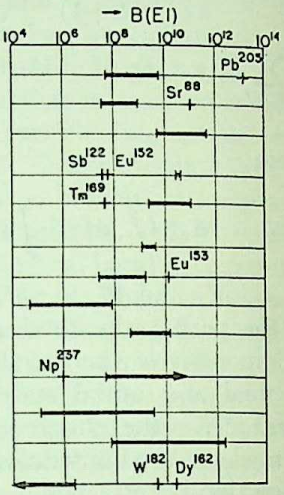

3. CLASSES OF $E1$ TRANSITIONS

The $E1$-transition matrix elements are sensitive functions of the nuclear structure; the experimental reduced transition probabilities $B(E1)$ as defined by Eq. (8) are scattered over about 15 orders of magnitude.

As far as $E1$ transitions are concerned, in many cases selection rules additional to the absolute one given by Eq. (3) are the only predictions one can get out of models. Examples of such additional selection rules are: a limitation on the change of the seniority quantum number in odd- and even-A nuclei; a maximum value for the variation of the z component K of the total angular momentum or of the asymptotic quantum numbers in deformed nuclei; a condition for the number of vibrational phonons annihilated or created in a transition. The finite transition rates observed for transitions forbidden by the selection rules of a given model are indications of the validity of this model.

The $E1$ transitions to be discussed here are all slower than the single-particle estimates as given by Eq. (7). They have furthermore a second feature in common: one of the levels between which they proceed is not predicted by the simple shell model for spherical nuclei. However, for the deformed nuclei, an independent-particle model (Ni 54) describes well both the initial and the final levels of $E1$ transitions. For spherical nuclei, as is discussed in Sec. 4, descriptions of the anomalous parity levels in terms of many-particle configurations or collective excitations are possible. These remarks suggest that one should determine whether $E1$ transitions involving levels of a given spin and parity in *similar nuclei* do have $B(E1)$ values of the same order of magnitude. A division of the nuclei into four families, according to the number of nucleons (odd or even) and the shape of the nuclei (approximately spherical or deformed) will be used. The different classes defined in this way will be discussed in detail in Secs. 4.1–4.4. A simple statistical analysis of this classification is given below.

Out of a total of 143 transitions with measured transition probability (see Tables B-I–B-IV in Appendix B), 128 can be classified in 13 different classes. The minimum number of transitions in one class is 3, the maximum 25. Of the 15 transitions that do not fit into any of these 13 classes, 4 observed in odd-A deformed nuclei involve one level not identified in the Nilsson model and 2 are observed in the deformed odd–odd nucleus $_{91}Pa^{234}$. The remaining 9 are shown in Table I.

Table I shows how the 13 classes are defined, how the 128 transitions are distributed among them and the range of $B(E1)$ values observed in each class. In most of these classes the range of experimental $B(E1)$ values is small. In some cases a prediction of the kind of transition can be made from this $B(E1)$ value. As an example, in the even-A spherical nuclei a definite difference is observed for the reduced rates of $(3^- \rightarrow 2^+)$ and $(5^- \rightarrow 4^+)$ or $(1^- \rightarrow 0^+)$ transitions. Also for the odd-A lanthanide nuclei it is possible to make an identification of the ΔK value involved. Finally, the K-forbiddenness of transitions in even-A deformed nuclei can also be determined from the $B(E1)$ values in most cases. In the following, these facts are considered as sufficient to justify the use of the single-particle

CC-0. In Public Domain. Gurukul Kangri Collection, Haridwar

Digitized by Arya Samaj Foundation Chennai and eGangotri

estimate of Eq. (7) for the comparison of $E1$ transition rates. Therefore the transitions will be discussed in terms of the hindrance factor defined by Eq. (10).

4. EXPERIMENTAL DATA AND NUCLEAR MODELS

4.1. Odd-A Nuclei with Spherical Shape

4.1.1. Introduction

Many properties of odd-A spherical nuclei are successfully explained on the basis of the single-particle shell model. The basic assumption in this highly simplified model is that the odd nucleon is responsible for all the properties of the nucleus. Refinements of this model have been discussed in which residual interactions between the nucleons are taken into account. Recent developments of the shell model take into account two-body residual interactions between the nucleons using approximation techniques introduced in the theory of superconductivity [Bohr, Mottelson, and Pines (Bo 58a), Belyaev (Be 59), Baranger (Bar 60), Arvieu and Veneroni (Ar 60)]. The works of these authors have shown that it may be sufficient to approximate the residual interaction by taking into account the pairing and the long-range parts of the correlation between nucleons. Along this line, considerable progress towards an understanding of the ground-state and the low-energy properties of spherical nuclei has been made. A method often used for the approximate diagonalization of the pairing Hamiltonian is the transformation to quasiparticles. The states of nucleons interacting by a pairing force are transformed into quasiparticle states, the energy of which includes the pairing interaction. In the first approximation the quasiparticles can be considered as independent. The ground states of a nucleus contains no quasiparticle (vacuum state). Excited states in odd-A nuclei are obtained by the creation of an odd number of quasiparticles. The addition of long-range force terms to the pairing Hamiltonian manifests itself as an interaction between the quasiparticles. Kisslinger and Sorensen (Ki 60) have discussed the application to even-A nuclei of a pairing Hamiltonian with a schematic multipole force added. Sorensen (Sor 61) has performed calculations for odd-A nuclei including a coupling of the odd nucleon to the collective core excitations (see also Ki 63). The results of Sorenson can be summarized in the following way[2]:

(a) The low-lying levels of odd-A spherical nuclei are predominantly mixture of one-quasiparticle states and, to a smaller extend, three-quasiparticle states. The broken pair of the three-quasiparticle states is the one corresponding to the 2^+ vibrational state.[3]

(b) At energies higher than the gap energy the levels are predominantly mixtures of three-quasiparticle states and states of one quasiparticle plus n vibrational phonons ($n=1, 2, \cdots$).

No $E1$ transitions are allowed within a given shell of the single-particle model without spin–orbit coupling as in such a shell all the levels have the same parity. $E1$ transitions from one shell to another are, of course, predicated by the single-particle shell model, but are of higher energy than the ones considered here. They contribute to the 1^- dipole states of isospin $T=1$ Interacting-particle shell-model studies of the dipole states in magic nuclei have shown the need for traiting the excited states and the ground state symmetrically. The importance of collective correlations in the ground state has been demonstrated by several authors [Brown *et al.* (Bro 61), Sawicki *et al.* (Ni 62)]. However, for the $T=0$ collective states (2^+ quadrupole, 3^- octupole, etc.) models with collective correlations between shell-model states of particle excitations seem to give a good approximation.

Levels with anomalous parity within one shell are indeed observed. A number of these levels are responsible for the systematic occurrence of isomeric states. These levels are explained in the independent-particle model as originating in the next shell, from which they are lowered by a spin–orbit interaction. However, the large number of anomalous parity states revealed by the existence of $E1$ transitions cannot be explained within the single-particle model with spin–orbit interaction. The models in which the interaction between quasiparticles is represented in terms of multipole forces, include states with seniority larger than one as well as states with one or several vibrational phonons. The spins and parities of these levels can often be compared with those of the anomalous states (anomalous refers here only to the prediction of the independent-particle shell model).

The possibility of describing some of the excited states of odd-A nuclei in terms of a collective excitation of the even–even core has been discussed by Lawson and Uretsky (Law 57), Bayman and Silverberg (Bay 60) and de-Shalit (Sh 61). This simplified model has achieved some success, as discussed, i.e., by Braunstein and de-Shalit (Br 62). Anomalous parity states are produced when octupole-core excitation takes place.

Finally, small deformation regions are known to exist besides the ones of large deformation [Okamoto (Ok 58) and Popov (Po 62)]. $E1$ transitions of the kind observed in the strongly deformed nuclei are expected in weakly deformed nuclei, too.

[2] The calculations of Sorensen (Sor 61) are in fact limited to single-closed-shell nuclei.

[3] The seniority conception is generalized to the quasiparticles. The seniority quantum number simply numerates the number of (unpaired) quasiparticles. In the approximation used by Sorensen, one-phonon quadrupole states correspond to a seniority 2.

CC-0. In Public Domain. Gurukul Kangri Collection, Haridwar

Digitized by Arya Samaj Foundation Chennai and eGangotri

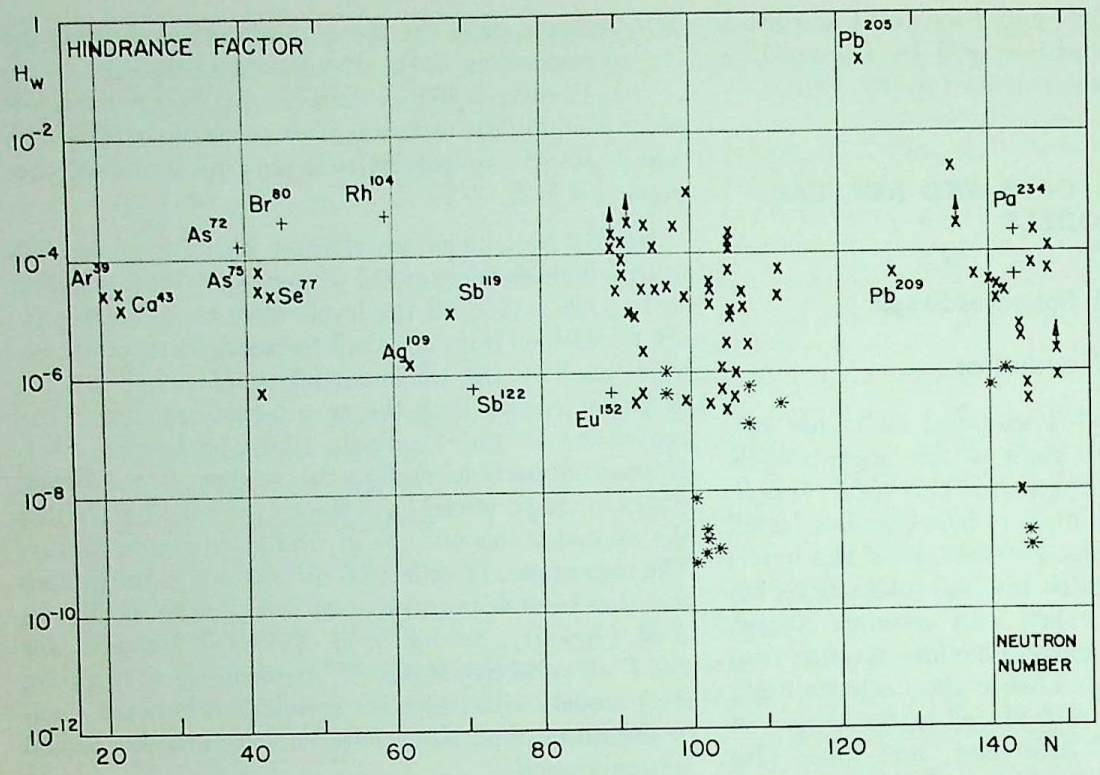

FIG. 1. Medium and heavy odd-A and odd-odd nuclei: Experimental hindrance factors $H_W(E1)$ relative to the Weisskopf estimate, as a function of the neutron number N. ×, odd-A nuclei; +, odd-odd nuclei; *K-forbidden transitions in deformed nuclei.

Within the single-particle model, electromagnetic transitions are induced by a single-particle multipole operator; transitions of more than one particle are absolutely forbidden. The selection rule of Eq. (3) can be rewritten as a function of j, the total angular momentum of the odd nucleon:

$$|j_i - j_f| \leq L \leq j_i + j_f$$
$$\pi_f = \pi \cdot \pi_i. \qquad (3')$$

If, instead of a single-particle transition operator, a many-particle one is considered, each of the individual nucleon transitions has to satisfy the selection rule [formula (3′)] in order to have a nonvanishing matrix element. This condition may be satisfied for some of the components of levels which are mixtures of shell-model states. In the independent-particle model with spheroidal average potential, j is not a good quantum number. The selection rule of formula (3′) has to be replaced by a condition on Ω, the z component of the nucleonic momentum (see Sec. 4.3).

4.1.2. Discussion of the Experimental Data

As can be seen in Table B-I (also Fig. 1), 10 of the 11 transitions measured in odd-A spherical nuclei have hindrance factors H_W in the range 5×10^{-7} to 6×10^{-5} when compared with the Weisskopf estimate. Except for the transition in $_{82}Pb^{205}$, the other $E1$ transitions occur in nuclei with open shell for which no detailed calculations with the model of interacting quasiparticles have been done. For this reason the following discussion is based primarily on shell-model arguments.

The odd neutron of the nuclei $_{18}Ar^{39}$ and $_{20}Ca^{43}$ is in the $(1f_{7/2})$ shell. The levels of normal parity are expected to be $(1f_{7/2})_j{}^n$ configurations. Direct-reaction data (Kas 64) have shown that the levels of anomalous parity in the calcium isotopes are core excitations $(1d_{3/2})$ and $(1d_{5/2})$.

In $_{33}As^{75}$ a $\frac{5}{2}^+$ level is observed to decay with three $E1$ transitions. This anomalous parity state may be a mixture of $(1g_{9/2})_{5/2}{}^n$ configurations ($n\geq3$). The $E1$ branching to the ground state is 100 times smaller than the branchings to the first and second excited states. This fact suggests that the latter are, like the initial level, largely seniority-3 states. The ground-state transition occurring with a seniority change of 2 is forbidden.

In $_{34}Se^{77}$ and $_{47}Ag^{109}$ the $\frac{7}{2}^+$ final state of the $E1$ transition has anomalous parity. For this level the dominant configuration is possibly $(1g_{9/2})_{7/2}{}^{-3}$. The systematic occurrence of anomalous parity levels of this kind in nuclei with Z or $N=43$, 45, and 47 has been known for a long time [Mayer and Jensen (Ma 55)]. A comparison with the level schemes for Ag^{107} and Ag^{111} [see Lark *et al.* (Lar 62) and Eccles (E 62)] suggests that the $\frac{5}{2}^-$ initial state of the $E1$ transition in Ag^{109} can be described as a one-quasiparticle and one-phonon quadrupole state.

The $\frac{3}{2}^+$ assignment proposed by Svedberg and Andersson (Sv 63) for the final level of the $E1$ transition in $_{51}Sb^{119}$ cannot be understood as a seniority-1 state, neither with a spherical nor with a spheroidal average potential. Small deformations have been recognized in several antimony isotopes. Sb^{121} and Sb^{123} have probably an oblate shape in the ground state [Osborn and

CC-0. In Public Domain. Gurukul Kangri Collection, Haridwar

Digitized by Arya Samaj Foundation Chennai and eGangotri

Klema (Os 56), Ciuffolotti and Demichelis (Ci 63)]. However, Kantele and Fink (Ka 63) have proposed a level scheme with all positive parity levels, i.e., without $E1$ transition.

The 1.863-MeV $E1$ transition in $_{82}Pb^{205}$ is weakly hindered ($H_W=0.15$). Begstrom *et al.* (Ber 62) have proposed that the $\frac{9}{2}^+$ anomalous parity levels found in odd-A lead isotopes around 2.6 MeV are indications for collective octupole vibrational states of the even–even core of these nuclei. This assumption is supported by the analogy between the energy of these levels and that of the 3^- states observed in several even-A lead isotopes. Evidences for core-octupole excitations in $_{82}Pb^{207}$ and $_{83}Bi^{209}$ have been reported also by Alster (Als 64). In Pb^{205} two $\frac{9}{2}^+$ levels are excited in the beta decay of Bi^{205} around 2.6 MeV. One of these levels is probably the three-particle state predicted at 2.56 MeV by True (Tr 61). A similar description has been proposed by Hamburger (Ha 62) and Shafroth *et al.* (Sha 63) for the $\frac{5}{2}^+$ and $\frac{7}{2}^+$ anomalous parity levels at 2.22 and 2.53 MeV, respectively, in $_{39}Y^{89}$. Y^{89}, like the lead isotopes, is a single closed-shell nucleus. In Y^{89} the $\frac{3}{2}^-$ and $\frac{5}{2}^-$ levels at 1.506 and 1.745, respectively, are probably results of the coupling of the $p_{1/2}$ proton in the ground state to the first 2^+ vibrational state of the even–even core $_{38}Sr^{88}$. The $(\frac{7}{2}^+\rightarrow\frac{5}{2}^-)$ and $(\frac{5}{2}^+\rightarrow\frac{3}{2}^-)$ are then $(3^-\rightarrow2^+)$ core transitions and their $E1$ components are expected to have hindrances similar to the $(3^-\rightarrow2^+)$ transition in Sr^{88} (see Sec. 4.2.2). The $(\frac{5}{2}^+\rightarrow\frac{5}{2}^-)$ transition should be slower as it corresponds to a spin–flip of the odd proton.

The similarity between these descriptions for the anomalous parity levels in $_{82}Pb^{205}$ and $_{39}Y^{89}$ may be, however, superficial because the one has a closed neutron whereas the other has a closed proton shell. In the quasiparticle model the 3^- levels in even-A nuclei are described with an octupole-force term added to the pairing Hamiltonian (see Sec. 4.2.2). If one assumes that the electric transitions are attributable to the protons, then a different situation occurs depending on the kind of nucleons filling a shell completely. With a closed proton shell, the proton energy gap vanishes. Furthermore, from the two-quasiparticle configurations which are admixed in the 3^- and 2^+ states, respectively, those which contribute to the $(3^-\rightarrow2^+)$ transition with an allowed $E1$ matrix element are deep in the core. This fact has the result that the proton contribution to the $(3^-\rightarrow2^+)$ $E1$ transitions must be small in a nucleus with filled proton shell. With a filled neutron shell, however, the proton energy gap is finite. This different type of proton level occupancy near the Fermi surface results in nonvanishing $E1$ transitions between two-quasiparticle configurations contributing to the 3^- and 2^+ states, respectively. In this simplified picture, however, the fact that because of the nuclear recoil, neutron $E1$ transitions can proceed with an "effective" charge $\sim Z/A$, is ignored (see also Appendix A).

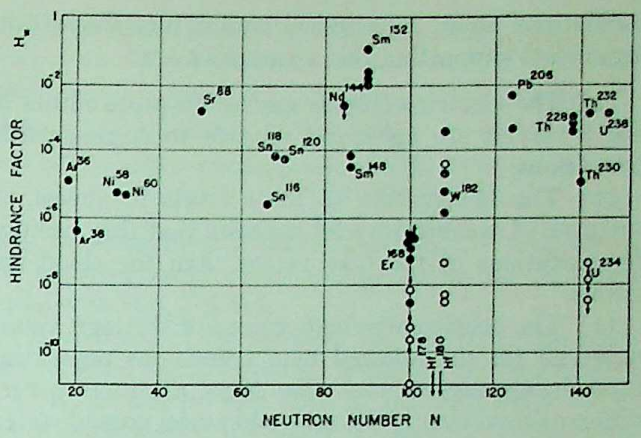

FIG. 2. Even-A nuclei: Experimental hindrance factors $H_W(E1)$ relative to the Weisskopf estimate, as a function of the neutron number N. ○, K-forbidden transitions in deformed nuclei; ●, other transitions.

The conclusion is that in $_{82}Pb^{205}$ the very fast $E1$ transition observed from the $\frac{9}{2}^+$ level at 2.556 MeV indicates that this level is not necessarily a collective core excitation but can be a seniority-3 state. In $_{39}Y^{89}$, however, the anomalous parity levels at 2.22 and 2.53 MeV are very likely octupole core excitations. The life times of these two levels are now known.

This discussion shows that in odd-A spherical nuclei all the $E1$ transitions observed are many-particle transitions. Calculations of the rate for these transitions are not possible as no detailed wave functions for the levels involved are available.

4.2. Even-A Nuclei with Spherical Shape

4.2.1. Introduction

In the following, several nuclear models are discussed in relation to the $E1$ transitions measured in the even-A spherical nuclei. Recent developments of the interacting quasiparticle model give interesting results for the 3^- levels. The 5^- levels observed in the tin isotopes have also been calculated in this model. Finally, the 1^- levels found in nuclei with $82\leq N\leq88$ are tentatively interpreted as two-quasiparticle excitations in a weakly deformed potential.

This section is divided into three subsections, according to the spins (3, 5, and 1) of the states deexcited by $E1$ transitions. The experimental data discussed are in Tables B-IIA, B-IIB, and B-IIC of Appendix B, and are displayed in Fig. 2.

4.2.2. Transitions of the $(3^-\rightarrow2^+)$ Type

A large number of 3^- levels is observed in the even-A spherical nuclei. Several attempts to describe them within the framework of different models have been published. Lane and Pendlebury (La 60) have shown that the 3^- levels can be described as collective octupole

CC-0. In Public Domain. Gurukul Kangri Collection, Haridwar

Digitized by Arya Samaj Foundation Chennai and eGangotri

oscillations about a spherical equilibrium shape. The arguments supporting this assumption are:

(a) The electric-octupole excitation probabilities of the 3^- levels are enhanced relative to single-particle transitions,

(b) The observation of these levels in almost all the even-A spherical nuclei suggests that they are due to excitations of the core rather than the cloud nucleons,

(c) The consistently high values of the logft values observed for the allowed beta transitions populating these levels suggest that they have a structure very different from that of the odd-odd nuclei ground states.

Calculations of the 3^- states with a pairing and multipole-force Hamiltonian have been presented by S. Yoshida (Yo 62) and Lombard (Lo 64). Both were able to reproduce the behavior of the 3^--level excitation energy in single-magic-shell nuclei. These computations show the importance of the core configurations for the construction of the 3^- states. Some of the core configurations give nonvanishing $E1$ matrix elements for transitions between two-quasiparticle states like the 3^- and the first 2^+ levels. Calculations of the $(3^-\rightarrow 2^+)$ $E1$ and $M2$ and of the $(3^-\rightarrow 0^+$ g.s.) $E3$ transition probabilities are in progress (Lo 64a). As discussed in Sec. 4.1.2, one can anticipate different results for the $E1$ transition probabilities, depending on the kind of nucleons which complete the filling of a shell. The conclusion of this discussion was that $(3^-\rightarrow 2^+)$ $E1$ transitions should be strongly hindered in nuclei with a magic number of protons, and only weakly hindered in nuclei with a magic number of neutrons. The experimental data support this prediction.

Before discussing the experimental data a few remarks will point out that these are in fact not as reliable as one would like. First, there are no *direct* lifetime measurements for any 3^- levels (the lifetime of the 3.75-MeV level in $_{18}Ar^{38}$ is a limit only!). The transition probabilities given in Table B-IIA (Appendix B) are calculated from the $B(E3)$ values measured in inelastic-scattering experiments and are model-dependent. Furthermore, the $M2/E1$ mixing ratios are measured for 2 out of 6 transitions only. The $(3^-\rightarrow 2^+)$ transition energies are larger than 1 MeV, and therefore the $M2$ component as calculated from the Weisskopf estimate[4] (We 51) is of the order of magnitude of the transition probabilities deduced from the experimental data. No reliable data exist for the M2 transition probability of this type of transitions. From a systematic survey of experimental data by Foucher and de Pinho (Fo 62), (Pi 63), one may conclude that the M2 transition probability can be 100 times faster than the Weisskopf estimate, yet in some cases it is possibly 10^8 times slower than this estimate. On the other hand, on $E3$ contribution of the order of the $M2$ one could be present in the transitions of $_{18}Ar^{38}$ and $_{50}Sn^{116}$, provided the $E3$ component proceeds about 100 times faster than predicted by the Weisskopf estimate.[5] Such a contribution is very unlikely for the other transitions as it would indicate an $E3$ enhancement of the order of 10^4 or more.

In Table II a hypothetical $M2/E1$ branching ratio is calculated, assuming the $M2$ contribution given by the Weisskopf estimate, but small relative to the $E1$ transition probability

$$\delta^2\left(\frac{M2}{E1}\right)=\frac{T(M2)}{T(E1)}=\frac{T(M2)}{T(3^-\rightarrow 2^+)-T(M2)}\cong\frac{T(M2)}{T(3^-\rightarrow 2^+)}.$$

Except for the case of $_{38}Sr^{88}$, it can be concluded that if the $M2$ component of these transitions is unhindered it is of the same order of magnitude as the $E1$ component. Therefore the $E1$ transition probabilities given in Table B-IIA (Appendix B) are upper limits.

A discussion of the data of Table B-IIA allows the following conclusions. The nuclei $_{28}Ni^{58}$, $_{28}Ni^{60}$, and $_{50}Sn^{116}$ have a magic number of protons; the $B(E1)$ values observed in these three nuclei correspond to hindrance factors $2.2\times10^{-6}\leq H_W(E1)\leq 7.8\times10^{-6}$. In $_{38}Sr_{50}^{88}$, with a magic number of neutrons, the hindrance factor is $H_W\sim 1.2\times10^{-3}$. Although no quantitative evaluation is available, the strong hindrances found in magic-proton-number nuclei are compatible with the pairing-model prediction discussed above and in Sec. 4.1.2, as is the weak hindrance observed in $_{38}Sr^{88}$. That the transitions in magic proton nuclei are not totally forbidden but only strongly hindered may be attributable to several causes. It is compatible with the assumption of a neutron "effective" charge for $E1$ transitions. A hindrance factor of about 10^{-6} is of the order of the magnetic-dipole-moment contribution to the electric-transition operator, which is expected to allow neutron $E1$ transitions with a rate of order $(v/c)^2$ relative to the charge contribution for protons.

4.2.3. *Transitions of the* $(5^-\rightarrow 4^+)$ *Type*

$(5^-\rightarrow 4^+)$ transitions with a measured transition probability are known in $_{50}Sn^{118}$, Sn^{120}, and $_{82}Pb^{206}$. The properties of these three single-closed-shell nuclei have been extensively studied, both from the experimental and from the theoretical points of view.

The 5^- level at 3.404 MeV in Pb^{206} is unfortunately too high in energy to be discussed in terms of current nuclear models. According to True and Ford (Tr 58), several high-lying levels observed in the decay of Bi^{206} are probably excitations of core protons along with the two neutron holes. Since a more detailed descrip-

[4] The Weisskopf estimate gives $T(M2)=8.25\times10^7\,E_\gamma^5A^{\frac{2}{3}}$ sec^{-1}, where E_γ is the transition energy in MeV. The nuclear radius is assumed to be given by $r_0=1.2A^{\frac{1}{3}}$ F.

[5] The Weisskopf estimate gives $T(E3)=4.1\times10\,E_\gamma^7A^2$ sec^{-1} with a nuclear radius $r_0=1.2A^{\frac{1}{3}}$ F.

CC-0. In Public Domain. Gurukul Kangri Collection, Haridwar

Digitized by Arya Samaj Foundation Chennai and eGangotri

TABLE II. Calculated $M2/E1$ branching ratios assuming the $M2$ component given by the Weisskopf estimate.

Nucleus	$_{18}Ar^{36}$	$_{18}Ar^{38}$	$_{28}Ni^{58}$	$_{28}Ni^{60}$	$_{38}Sr^{88}$	$_{50}Sn^{116}$
$T(M2)/T(3^-\rightarrow 2^+)$	0.35	≤ 5.6	1 ± 0.5	1.2 ± 0.6	0.0056	0.34 ± 0.17

tion of these levels is lacking, the following discussion is limited to the better understood tin isotopes.

Levels with negative parity occur regularly in the even-A tin isotopes. 3^-, 5^-, and 7^- levels are known in $_{50}Sn^{116,118,120}$. These nuclei have been studied by Arvieu, Baranger, Veneroni, Baranger, and Gillet (Ar 63) [see also Arvieu and Veneroni (Ar 60) and Arvieu (Ar 62)] on the basis of the pairing model. According to these calculations, the initial 5^- and the final 4^+ levels of the $E1$ transitions in Sn^{118} and Sn^{120} are predominantly mixings of two-quasiparticle configurations. $E1$ transitions between the two-quasiparticle configurations of the Arvieu's states are all j-forbidden. The $(5^-\rightarrow 4^+)$ $E1$ transitions in Sn^{118} and Sn^{120} are 30 times faster than the $(3^-\rightarrow 2^+)$ transition in Sn^{116}. This different behavior suggests that unlike the 3^- levels, the 5^- and possibly also the 4^+ levels contain four-quasiparticle excitations. Four-quasiparticle contributions are indeed more likely to be important for the 5^- and 4^+ than for the 3^- states. The 5^- and 4^+ states are observed in the region where two-phonon excitations are important. The 3^- state, however, is a pure one-phonon octupole state. One-phonon states are known to be well described in terms of two-quasiparticle configurations, whereas two-phonon states contain probably some admixture of four-quasiparticle excitations. The hindrances found for the $(5^-\rightarrow 4^+)$ transitions ($H_W\sim 6\times 10^{-5}$) suggest that the relative amplitudes of the four-quasiparticle configurations admixed in these states is small.

4.2.4. Transitions of the $(1^-\rightarrow 0^+$ g.s.) or $(1^-\rightarrow 2^+)$ Type

Although only two $(1^-\rightarrow 0^+)$ transitions have been measured until now, the very existence of 1^- levels in the region between the magic neutron number $N=82$ and the onset of strong nuclear deformations at $N=88$–90 raises an interesting problem. In this region of the periodic table it is not possible to construct 1^- levels with excitations of two independent nucleons in spherical-shell-model states. Proton–neutron configurations are not expected to contribute in an important way to $E1$ transitions. Other possible origins of the observed 1^- levels are four-particle excitations. The ground-state transition from such a level involves four nucleons, and is expected to be extremely hindered. A small admixture in the initial-level wave function of the giant-dipole state ($J=1^-$, $T=1$) would be sufficient to explain the measured $E1$ transition rates. Sakai (Sa 63) has proposed that a relationship may exist between these 1^- levels and the 1^- member of the negative-parity rotational bands in the deformed nuclei with $90\leq N\leq 114$.

Figure 3 shows the behavior for the excitation energies of some negative-parity levels in the region $80\leq N\leq 114$. It can be seen that if, for each value of N, one considers only the lower 1^- and 3^- levels, these behave similarly for $82\leq N\leq 108$.

Another quantity sensitive to the nature of the 1^- levels is the ratio of the reduced transition probabilities to the first 2^+ level and to the ground state. In deformed nuclei the branching ratio for transitions between a vibrational state and the members of the ground-state rotational band is given by [see Alder *et al.* (Al 56)]:

$$\frac{B(E1; I_iK_i\rightarrow 2, 0)}{B(E1; I_iK_i\rightarrow 0, 0)}=\left|\frac{\langle I_i, 1, K_i, -K_i \mid 2, 0\rangle}{\langle I_i, 1, K_i, -K_i \mid 0, 0\rangle}\right|^2, \quad (11)$$

where $\langle \mid \rangle$ stands for vector addition coefficients. When $I_i=1$, this ratio is equal to 2 and 0.5, for $K_i=0$ and $K_i=1$, respectively.

As shown in Table III, this ratio does not change dramatically at the deformation limit. Evidently the large scattering of this ratio around the theoretical possible values of 2 and 0.5 does not allow one to consider these data as the best pieces of evidence for the validity of the vibrational model for the 1^- levels observed in the region $84\leq N\leq 108$.

The nuclei with $82\leq N\leq 90$ have a small ground-state deformation, but do not have the typical level structure of an axially symmetric rotator. However,

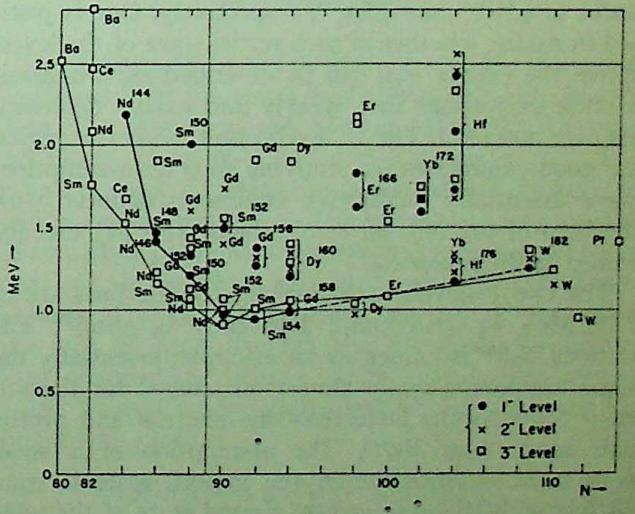

FIG. 3. Excitation energies for the negative-parity levels in even-A nuclei, near the deformation limit at $N\sim 88$–90. The solid lines are arbitrary fits to the lowest level of a given spin.

CC-0. In Public Domain. Gurukul Kangri Collection, Haridwar

Digitized by Arya Samaj Foundation Chennai and eGangotri

TABLE III. Branching ratios $B(E1;\ 1^-\rightarrow 2^+)/B(E1;\ 1^-\rightarrow 0^+)$ in nuclei $82\leq N\leq 114$.

Nucleus	Energy of the initial 1^- level (MeV)	Branching ratio	Comments	References
$_{60}Nd^{144}$	2.18	1.03		
$_{62}Sm^{148}$	1.465	2.6±0.5		(B 63)
Sm^{150}	2.00	1.58		(Ko 64)
Sm^{152}	0.963	1.83		(Na 59)
$_{64}Gd^{152}$	1.317	1.24	from Eu^{152} decay	
		2.98	from Tb^{152} decay	
Gd^{156}	1.242	1.25		(Pe 64)
	1.366	2.07		
Gd^{158}	0.978	2.04		(Gro 62)
$_{66}Dy^{160}$	1.200	0.82		(Gri 59)
$_{68}Er^{166}$	1.654	1.7±0.7		(Cl 62)
$_{70}Yb^{172}$	1.60	1.48		(Hel 61)
$_{72}Hf^{176}$	1.159	≤0.62		(Sta 64)
	1.722	2.23		(Sta 64)
$_{74}W^{182}$	1.257	1.14±0.33		(Ry 61)

as pointed out by Popov (Po 62), this is not necessarily a proof of sphericity. These weakly deformed nuclei have, in fact, mean deformations of the order of magnitude of the quadrupole oscillation amplitudes. Strong differences with the excitation spectrum of a rigid rotator are thus expected in this region. These differences can be clearly seen, i.e., in the positive parity levels of $_{62}Sm^{148}$.

The data from isotopic-shift measurements indicate effective deformations β of 0.17 and 0.16 for the ground states of $_{60}Nd^{144}$ and $_{62}Sm^{148}$, respectively. One is justified in asking whether in such nuclei some of the levels above the energy gap can be described as two-quasiparticle excitations in a weakly and axially deformed average potential. The 1^- levels observed in this region are good candidates for studying such an assumption. Some essentially qualitative arguments deduced with the help of the Nilsson level scheme (Ni 54) are discussed in the following.

The two 1^- levels with investigated lifetimes are at 2.18 MeV in $_{60}Nd^{144}$ and 1.46 MeV in $_{62}Sm^{148}$. The nucleus Nd^{144} is chosen as an example; essentially the same arguments apply almost unchanged for the nucleus Sm^{148} as the latter has one neutron and proton pair more than Nd^{144}. The assumption of a small permanent deformation in the ground state is compatible with the observed 0^- ground state of the odd–odd $_{59}Pr^{144}$ nucleus. If this nucleus has a ground-state deformation $\eta\sim 2$ ($\beta\sim 0.10$ to 0.12) the Nilsson orbitals available for the last proton and neutron are

$$\text{proton:}\quad |\,411\,|\,\tfrac{3}{2}$$

$$\text{neutron:}\quad |\,532\,|\,\tfrac{3}{2},\ \text{respectively.}$$

(See Sec. 4.3.2 for a definition of the deformation parameter η and of the asymptotic state $|\,N,\ n_z,\ \Lambda\,|\,\Omega$.)

The empirical law of Gallagher and Moszkowski (Ga 58) for the coupling of angular momenta in deformed odd–odd nuclei predicts that the ground state must have a resulting intrinsic spin equal to 1. Hence the ground state of $_{59}Pr^{144}$ must be

$$\{p\,|\,411\,|\,\tfrac{3}{2}-n\,|\,532\,|\,\tfrac{3}{2}\}_{J^\pi=0^-}$$

in agreement with recent experimental data [see Raghaven and Steffen (Ra 63) and many others].

For $_{60}Nd^{144}$ a large number of two-proton and two-neutron Nilsson-state excited configurations with spin 1 and negative parity can be found. Gallagher (Ga 62a) has proposed an empirical coupling law for the even-A deformed nuclei. This law predicts that the state with antiparallel intrinsic spin must be lower in energy. A tentative classification of the possible Nilsson configurations can be made assuming the Nilsson states to be unperturbed. The two following 1^- configurations are expected to be the lowest in energy for a deformation $\eta\sim 2$:

$$\{p\,|\,420\,|\,\tfrac{1}{2}-p\,|\,541\,|\,\tfrac{3}{2}\}_{1^-}$$

$$\{n\,|\,521\,|\,\tfrac{3}{2}-n\,|\,660\,|\,\tfrac{1}{2}\}_{1^-}.$$

The pairing interaction produces configuration mixing in the ground state. However, none of the numerous configurations contributing to the ground-state wave function can be the final state of an $E1$ transition allowed by the asymptotic selection rules (the asymptotic selection rules are defined in Sec. 4.3.3). If this description is correct, the $E1$ transitions in the $82\leq N\leq 90$ and in the strong permanent deformation regions must be closely related.

The strong hindrances observed recently by Metzger (Me 64) for the $E1$ transitions de-exciting the lower 1^- level in $_{62}Sm^{148}$ seems therefore normal. The reduced transition probability $B(E1)=4\times 10^9$ sec^{-1} MeV^{-3} for the ground-state transition in $_{62}Sm^{148}$ compares well with the $B(E1)$ values found in odd-A deformed nuclei. However, this description of the 1^- levels in the region $82\leq N\leq 90$ makes it difficult to find any explanation for the very fast $E1$ transitions observed in the deformed nucleus $_{62}Sm^{152}$. This difficulty will be discussed in more detail in Sec. 4.4.

Another description of the 1^- levels has been proposed by Alder *et al.* (Al 56). In spherical nuclei the coupling of a quadrupole and an octupole vibration gives rise, in first order, to a degenerate quintuplet with $J^\pi=1^-,\ 2^-,\ \cdots,\ 5^-$. Assuming that the observed 1^- levels are the first members of such quintuplets, their

CC-0. In Public Domain. Gurukul Kangri Collection, Haridwar

Digitized by Arya Samaj Foundation Chennai and eGangotri

energy should roughly be equal to the sum of the one-phonon quadrupole and octupole states. Table IV shows the observed 1^- level energies and the sums of the 2^+ and 3^- level energies for a few nuclei with $N \leq 88$.

As expected, the discrepancy between these two quantities increases as one comes closer to the deformation limit. However, this interpretation of the 1^- levels seems hard to reconcile with the measured branching ratios to the first 2^+ and to the ground state (see Table III). A transition between the two-phonon 1^- state (one quadrupole plus one octupole phonon) and the zero-phonon ground state should be much more hindered than the transition to the 2^+ state; the former annihilates two phonons, whereas the latter only one. The same prediction is obtained when the levels involved are described as quasiparticle states. The 1^- level would have probably a large four-quasiparticle component, whereas the one-phonon quadrupole state is described by two-quasiparticle configurations. A transition like the ground state one involves the annihilation of four quasiparticles and is expected to be strongly hindered.

4.2.5. Transitions in Odd–Odd Nuclei

A few $E1$ transitions are measured in odd–odd nuclei. Four are observed in the nuclei $_{33}As^{72}$, $_{35}Br^{80}$, $_{45}Rh^{104}$, and $_{51}Sb^{122}$. In the first three, the observed hindrance factors are $H_W \sim 10^{-4}$, whereas in the fourth one $H_W \sim 10^{-7}$. The two transitions measured in the deformed odd–odd nuclei $_{63}Eu^{152}$ and $_{91}Pa^{234}$ are discussed in Secs. 4.4.2 and 4.4.3, respectively. The hindrance found for the transitions of this type can be understood within the framework of the shell model. In the simple shell model no j-allowed $E1$ transitions are possible within a shell, neither for the odd proton nor for the odd neutron. In the shell model with pairing interaction, the quasiparticle states have components resulting from deeper core configurations. Some of these components can contribute to $E1$ transitions by an allowed partial transition amplitude. The hindrances observed are then explained by the small amplitudes of the core configurations. However, no detailed calculations have been done for the excited states of the spherical odd–odd nuclei.

TABLE IV. Energy of the 1^- levels in the nuclei $82 \leq N \leq 88$.

Nucleus	Energy of the observed 1^- level (MeV)	Sum of the energies of the 2^+ and 3^- levels (MeV)
$_{60}Nd^{144}$	2.18 (MeV)	2.13 (MeV)
$_{60}Nd^{146}$	1.37 (Dan 64)	1.66 (Dan 64)
$_{62}Sm^{148}$	1.464	1.62
$_{64}Gd^{152}$	1.317	1.47

4.3. Odd-A Nuclei with Large Deformation

4.3.1. Introduction

Two families of strongly deformed nuclei are known. The first one comprises the rare-earth nuclei and Ta, W, and Os ($90 \leq N \leq 114$). The second one begins with uranium and contains the actinides nuclei ($N \leq 134$). The existence of several $E1$ transitions in both regions has been recognized for a long time. Discussions of the experimental and theoretical data already exist (Strominger and Rasmussen (Stro 57), Asaro, Stephens, Hollander, and Perlman (As 60)]. In the following a summary of these early discussions is presented. Recent attempts to predict the $E1$ transition probabilities in deformed nuclei are reviewed. The experimental data in Table B-IIA, B-IIB, B-IIC, and B-IID of Appendix B are discussed. Some earlier conclusions on possible systematic features for these transitions are confirmed by new experimental results but others do not hold.

The question of internal conversion anomaly for $E1$ transitions in deformed nuclei has been discussed elsewhere [see Nilsson and Rasmussen (Ni 58) and Kramer and Nilsson (Kr 62)]. These authors have shown that the experimental data for $E1$, L-shell internal conversion are compatible with the theory of Church and Weneser (Ch 60). Whereas the L_{III}-shell conversion is never anomalous, the conversion coefficients for the L_I and L_{II} shells show an anomaly that is an increasing function of the gamma transition hindrance. The theory predicts that K-forbidden transitions should display no conversion anomaly (see further in text for a definition of the K selection rule), in accord with all the experimental data until now.

4.3.2. The Independent-Particle Model for Deformed Nuclei

The independent-particle model for odd-A deformed nuclei has been discussed by Nilsson (Ni 54), Rassey (Ras 58), Mottelson and Nilsson (Mot 59), Lemmer and Green (Lem 60), and Liu Yüan (LY 62). The wave functions of Nilsson are tabulated and the formula for the electromagnetic matrix element is easy to use. $E1$ transition probabilities calculated with Nilsson wave functions are in overall agreement with the experimental data. The Nilsson estimate for the $E1$ transition rate will be used through the discussion to follow. Some points of the Nilsson model will be given here.

The Nilsson model single-particle Hamiltonian has the following form:

$$H = H_0 + \hbar\omega_0{}^0\kappa[\eta U - 2\mathbf{l}\cdot\mathbf{s} - \mu l^2], \qquad (12)$$

where $H_0{}^0$ is the isotropic harmonic oscillator potential, $\mathbf{l}$ is the nucleon orbital momentum, and $\mathbf{s}$ the intrinsic

CC-0. In Public Domain. Gurukul Kangri Collection, Haridwar

Digitized by Arya Samaj Foundation Chennai and eGangotri

spin in a nondeformed potential. $\mathbf{l}\cdot\mathbf{s}$ is the usual spin–orbit term, l^2 is a correction to the oscillator potential, and U is a perturbation proportional to (r^2Y_{20}). U describes the coupling of the odd particle to the deformation axis. The parameters κ and μ are, respectively, an energy scale factor and a constant fixing the importance of the spin–orbit term. The deformation parameter η is proportional to the parameter β defined by Bohr and Mottelson (Bo 53) ($\eta\sim\beta/\kappa$). Finally, $\hbar\omega_0{}^0$ is the oscillator quantum of the isotropic oscillator ($\hbar\omega_0{}^0=41A^{-\frac{1}{3}}$ MeV).

In the unified model discussed by Bohr and Mottelson (Bo 53) and Bohr (Bo 54) the internal as well as collective modes of motion are considered. This model has a simple form when the nuclear deformation is large. For large deformations, the frequencies associated to collective excitations are expected to be small compared with the frequencies of the internal motion. Provided the latter condition—often called adiabaticity condition—is fulfilled, one expects the nuclear shape to be stable, i.e., not affected by collective modes of motion. The nuclear wavefunctions can hence be written as a product of an internal (or intrinsic) part χ_Ω determined by the Hamiltonian of Eq. (12), and of a collective part. As far as an axially symmetric potential is considered, the intrinsic motion is characterized by Ω, the projection on the nuclear symmetry axis z of the resulting nucleonic angular momentum. The resulting motion is characterized by the total angular momentum $\mathbf{I}$ and its projection $\mathbf{K}$ on the nuclear z axis. The total angular momentum $\mathbf{I}$ is built up from the resulting angular momentum $\boldsymbol{\Omega}$ and the rotation angular momentum $\mathbf{R}$. It is usually assumed that in the ground state for vibrational excitations, the rotational motion occurs around an axis perpendicular to z. When $\mathbf{R}$ is perpendicular to the z axis, $\mathbf{K}$ is identical to $\boldsymbol{\Omega}$.[6] Hence the different levels of a rotational band have the same intrinsic structure, characterized by $K=\Omega$.

The adiabaticity condition is fairly well satisfied for deformed even-A nuclei. However, for odd-A deformed nuclei the rotational energies are often of the same order or smaller than the single-particle excitations. The effect on the intrinsic structure of a rotation–particle interaction has been studied and is discussed in Sec. 4.3.6.

Nilsson has diagonalized the Hamiltonian Eq. (12) with the spherical oscillator eigenstates $|N, l, \Lambda, \Sigma\rangle$ as basis vectors. Here N is the total number of oscillator quanta, and l, Λ, Σ are the quantum numbers of the orbital angular momentum operators l^2 and l_z and of the intrinsic spin operator s_z, respectively. The sum of Λ and Σ is equal to Ω. For finite deformations the eigenstates are represented by a sum over several eigenstates of the spherical harmonic oscillator:

$$\chi_\Omega \propto |N, \Omega\rangle=\sum_l[A_{l,\Omega-\frac{1}{2}}|N, l, \Omega-\tfrac{1}{2}, +\tfrac{1}{2}\rangle + A_{l,\Omega+\frac{1}{2}}|N, l, \Omega+\tfrac{1}{2}, -\tfrac{1}{2}\rangle]. \quad (13)$$

The amplitudes $A_{l,\Lambda}$ as well as the eigenvalues are given in (Ni 54) and (Mot 59). In the notation of Nilsson, the energy eigenvalues $E^{N\Omega}(\eta)$ are obtained from the dimensionless eigenvalues $r^{N\Omega}(\eta)$ by the formula

$$E^{N\Omega}(\eta)=(N+\tfrac{3}{2})\hbar\omega_0(\eta)+\kappa\hbar\omega_0{}^0r^{N\Omega}(\eta). \quad (14)$$

The parameters κ and μ have been chosen by Nilsson in order to reproduce the level sequence of the shell model for zero deformation. The Nilsson state wave functions are admixtures of spherical states with different j and different l. These configuration mixings give rise to finite $E1$ matrix elements in a way similar to the situation in the pairing-force model with multipole-force term.

For large deformations it is convenient to use the vector basis $|N, n_z, \Lambda, \Omega\rangle$, where n_z is the number of oscillator quanta in the z direction for the anisotropic oscillator potential.[7] The asymptotic states give good approximations for the electromagnetic multipole moments and transition probabilities. However, as shall be emphasized below, the $E1$ transitions are an exception to this rule.

4.3.3. E1 Transitions in the Nilsson Model

The Nilsson model allows a direct explanation for the occurrence of low-energy $E1$ transitions in the deformed nuclei. The isotropic-shell-model states are $(2j+1)$-fold degenerate. If only cylindrical symmetry is retained, the state degeneracy decreases. Each j state splits into $(j+1)$ new states with z projection of the total angular momentum $\Omega=j, j-1, \cdots, \frac{1}{2}$. The states $(+\Omega)$ and $(-\Omega)$ are still degenerate. The splitting of the Nilsson states is an increasing function of the deformation. This behavior results eventually in the crossing of levels with N values differing by ±1, and therefore with different parities. This fact explains why many $E1$ transitions, some with an energy of a few keV are predicted by the Nilsson model.

The equations for the one-particle electromagnetic transition probabilities are given in the original paper (Ni 54). The one relevant for $E1$ transitions can also be found in Appendix A, at the end of this survey. One can easily understand why the $E1$ transition probabilities calculated with Nilsson states are smaller than the Weisskopf estimate. On one hand, the characteristic level splitting disappears for vanishing deforma-

[6] In this picture a rotation around the symmetry axis does not affect the nucleonic motion; therefore the corresponding moment of inertia is zero.

[7] A representation with the basis vectors $|N, n_z, \Lambda, \Omega\rangle$ has been used by Rassey (Ras 58) and Liu Yüan (LY 62) for the diagonalization of a Nilsson type Hamiltonian. The solutions obtained by these authors show less admixture of different angular momentum states than the Nilsson ones.

CC-0. In Public Domain. Gurukul Kangri Collection, Haridwar

Digitized by Arya Samaj Foundation Chennai and eGangotri

tion. The Nilsson states tend to the spherical ones. As pointed out in Sec. 4.1, no $E1$ transitions are possible within one shell of the isotropic shell model outside the light nuclei region. On the other hand, for large deformations ($\eta \rightarrow \infty$) the Nilsson states are represented by the asymptotic states $|N, n_z, \Lambda, \Sigma\rangle$. The $E1$ matrix element between asymptotic states vanishes unless the conditions on the asymptotic quantum numbers given in Table V are satisfied. To these *asymptotic selection rules*, first given by Alaga (A 57), the conservation of angular momentum adds the condition $\Delta\Omega = \Delta\Lambda + \Delta\Sigma$. Finally the conservation of angular momentum requires also that in a transition of multipole order L, the variation of the z component of the total angular momentum satisfies the K-selection rule $\Delta K = |K_i - K_f| \leq L$. Strominger and Rasmussen (Stro 57) have pointed out that all the low-energy $E1$ transitions observed so far in the deformed nuclei occur with violation of the asymptotic selection on n_z. In fact, an examination of the level scheme of Nilsson shows that no low-energy

TABLE V. Asymptotic selection rules for $E1$ transitions.

Operator	$\Delta\Omega$	ΔN	Δn_z	$\Delta\Lambda$
$x \pm iy$	± 1	± 1	0	± 1
z	0	$\begin{cases} +1 \\ -1 \end{cases}$	$\begin{cases} +1 \\ -1 \end{cases}$	0

$E1$ transitions can occur without violation of the n_z selection rule.

For the average values of the deformation parameters found in the lanthanide and actinide nuclei ($3 \leq \eta \leq 6$), the $E1$ transition rates calculated with the states given by Eq. (13) are finite, but smaller than the Weisskopf estimate by a factor 10^4 to 10^6. This slowing down of the $E1$ transition rates in the Nilsson model is due to a cancellation of the different partial transition amplitudes between the components of different l [see Eqs. (A1) and (A7) in Appendix A].

In the following subsections (4.3.4–4.3.7) the experimental data are discussed and compared to the Weisskopf and Nilsson estimates. Similar analyses have been presented by Hauser, Runge, and Knissel (Hau 61), Vergnes (Ve 62), and Perdrisat (Per 62).

4.3.4. Comparison of the Experimental Data with the Weisskopf Estimate

Such a comparison may seem superfluous since for deformed nuclei the Nilsson model is expected to give a better estimate of the $E1$ transition rate than the Weisskopf estimate. However the comparison indicates different trends for the reduced transition probabilities for different values of ΔK. As shown by Fig. 4, four

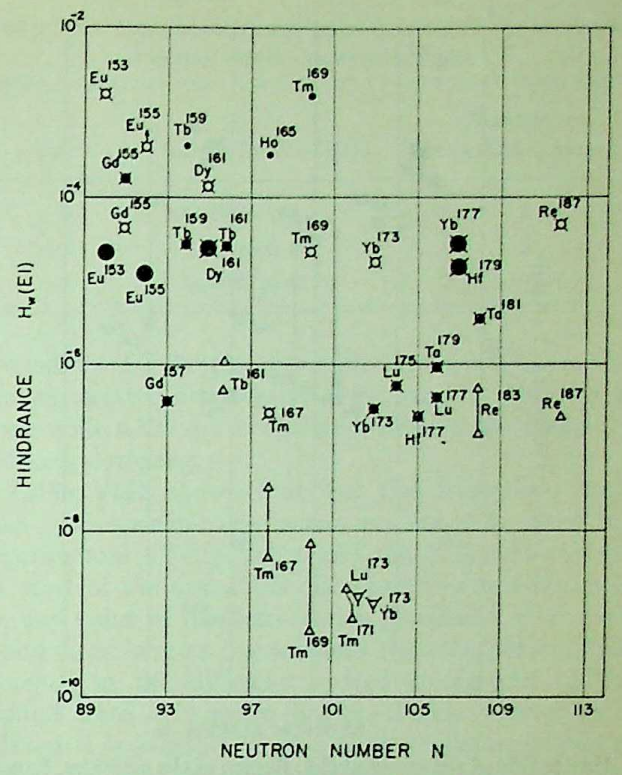

FIG. 4. Odd-A deformed nuclei: region of the rare earths. Experimental hindrance factors $H_W(E1)$ for $E1$ transitions, as a function of the neutron number N. ○, transitions with $\Delta K = 0$; ●, transitions with $\Delta K = +1$; ●, transitions with $\Delta K = -1$; △, K-forbidden transitions. The crosses × indicate a transition between two intrinsic states. (The transitions to rotational levels have been omitted, except for the K-forbidden ones.)

classes of transitions can be defined, with $\Delta K = 0, -1, +1$, and $|\Delta K| \geq 2$. A determination of the ΔK value of a transition between intrinsic states from its reduced transition probability is possible. For the rare-earth nuclei, Table VI can be used for such a determination. For the $E1$ transitions in actinide nuclei the situation is unfortunately not so clear, as shown in Fig. 5. The experimental data are still too scarce for these nuclei to allow a discussion. Diamond, Elbeck, and Stephens (Di 63) have proposed that the initial levels of three $E1$ transitions in $_{65}Tb^{159}$, $_{67}Ho^{165}$, and $_{69}Tm^{169}$ are not Nilsson states (these transitions are not included in

TABLE VI. Reduced transition probabilities $B(E1)$ for transitions between intrinsic states in rare-earth nuclei.

ΔK	Range of $B(E1)$	Number of transitions observed
0	2×10^{9}–1.6×10^{11}	7
+1	1×10^{9}–2.6×10^{9}	5
−1	2×10^{7}–4×10^{9}	10
≥2	6×10^{4}–5×10^{7}	11[a]

[a] None of the measured K-forbidden transitions occurs between intrinsic levels.

CC-0. In Public Domain. Gurukul Kangri Collection, Haridwar

Digitized by Arya Samaj Foundation Chennai and eGangotri

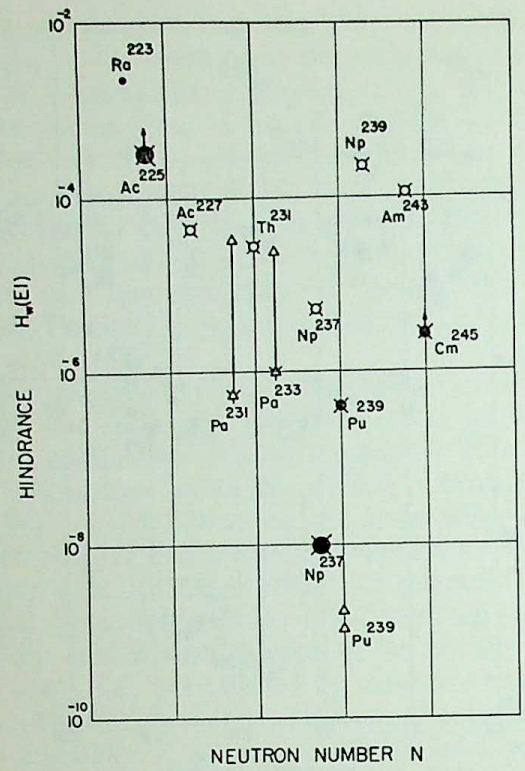

FIG. 5. Odd-A deformed nuclei: Region of the actinides. Experimental transition hindrance factors $H_W(E1)$, as a function of the neutron number N. Same symbols as in Fig. 4.

Table IV), but γ-vibrational states built on intrinsic configurations. They identify these levels as one of the $K=\Omega\pm2$ states resulting from such a coupling. Incidentally, all three transitions have very high $B(E1)$ values (larger than 3×10^{10}). Gallagher and Edwards (Ga 60) have proposed that the 686-keV level in $_{75}Re^{187}$ is also a γ-vibrational state. However this assumption implies Ω-forbiddenness for the $E1$ transitions depopulating this level. The $B(E1)$ values observed suggest that this transition is allowed and occur with $\Delta\Omega=0$ (see also Table B-IIIA, Appendix B).

Figure 4, as well as Table I, shows that in the rare-earth nuclei the K-forbiddenness results in a strong hindrance allowing an identification of these transitions. In the actinides region, however, a clear cut between K-allowed and K-forbidden transitions is not observed. An empirical law has been proposed by Rusinov (Ru 61) which connects the hindrance factor to the degree of K-forbiddenness by the relation, $\log H_W=2(\Delta K-L)$, where L is the transition multipolarity. This empirical law is roughly compatible with K-forbidden $E1$ transitions measured in odd- and even-A nuclei. However, it does not allow a unique determination of ΔK from the hindrance H_W. Only $E1$ transitions with $(\Delta K-L)=1$, 2, and 7 have been measured until now. An attempt to evaluate the hindrance of K-forbidden $E1$ transitions has been presented by Rouhaninejad (Ro 63). He used a method of projecting the Nilsson eigenfunctions on the eigenstates of the total angular momentum. A good agreement has been found for the transitions in Tm^{169}, Lu^{173}, and Re^{183}.

As proposed by Bohr and Mottelson (reference in Ax 63), the transition probabilities for K-forbidden transitions between levels of different rotational bands can be calculated when the effect of a rotation–particle interaction is taken into account. A coupling of the initial and final levels K_i and K_f with states having K values between K_i and K_f results in a finite transition probability. The matrix elements characterizing the level admixtures produced by this coupling can be calculated from the experimental branching ratio of interband transitions. However, no prediction for these level admixtures have been presented until now. A further discussion of the rotation–particle interaction is in Sec. 4.3.6.

4.3.5. *Comparison of the Experimental Data with the Nilsson Estimate*

The Nilsson asymptotic states identified with the levels involved in $E1$ transitions are given in the Tables B-IIIA and B-IIIC. The corresponding transition probabilities $T_N(E1)$ have been calculated with formula (A5), (A6), and (A7) of Appendix A, for several values of the deformation parameter η. The corresponding hindrance factors $H_N=T(E1)/T_N(E1)$ are given in the tables.

TABLE VII. Values of η_i and η_f for which the Nilsson estimate fits the experimental data in the rare-earth nuclei.

Nucleus	Transition	ΔK	η_f	η_i	Hindrance H_W with $\eta_i=\eta_f$
$_{63}Eu^{153}$	$\lvert 532\rvert\frac{3}{2}\rightarrow\lvert 413\rvert\frac{3}{2}$	0	6	4.0 to 4.8	90
	$\lvert 411\rvert\frac{3}{2}\rightarrow\lvert 532\rvert\frac{5}{2}$	+1	6	4.3 or 5.4	0.17
$_{63}Eu^{155}$	$\lvert 532\rvert\frac{3}{2}\rightarrow\lvert 413\rvert\frac{3}{2}$	0	6	≤4.25	≥20
	$\lvert 411\rvert\frac{3}{2}\rightarrow\lvert 532\rvert\frac{5}{2}$	+1	6	4.7 or 5.2	0.030
$_{65}Tb^{159}$	$\lvert 532\rvert\frac{5}{2}\rightarrow\lvert 411\rvert\frac{3}{2}$	−1	6	4.4 or 5.3	0.097
$_{64}Gd^{155}$	$\lvert 651\rvert\frac{3}{2}\rightarrow\lvert 521\rvert\frac{3}{2}$	0	6	6.1	0.6
	$\lvert 642\rvert\frac{5}{2}\rightarrow\lvert 521\rvert\frac{3}{2}$	−1	6	6.1 or ∼8	0.74
$_{64}Gd^{157}$	$\lvert 642\rvert\frac{5}{2}\rightarrow\lvert 521\rvert\frac{3}{2}$	−1	6	∼8	0.00175
$_{65}Tb^{161}$	$\lvert 523\rvert\frac{7}{2}\rightarrow\lvert 413\rvert\frac{5}{2}$	−1	5	5.7 or 6.3	0.11
$_{66}Dy^{161}$	$\lvert 521\rvert\frac{3}{2}\rightarrow\lvert 642\rvert\frac{5}{2}$	+1	4	4.7 or 5.3	0.15
	$\lvert 523\rvert\frac{5}{2}\rightarrow\lvert 642\rvert\frac{5}{2}$	0	6	6.3	2.10
$_{69}Tm^{169}$	$\lvert 523\rvert\frac{7}{2}\rightarrow\lvert 404\rvert\frac{7}{2}$	0	6	5.9	1.60
$_{70}Yb^{173}$	$\lvert 514\rvert\frac{7}{2}\rightarrow\lvert 633\rvert\frac{7}{2}$	0	6	6.1	1.35
	$\lvert 633\rvert\frac{7}{2}\rightarrow\lvert 512\rvert\frac{5}{2}$	−1	5	5.7 or 5.8	0.0057
Yb^{177}	$\lvert 514\rvert\frac{7}{2}\rightarrow\lvert 624\rvert\frac{9}{2}$	+1	5	5.4 or 6.6	0.30
$_{71}Lu^{175}$	$\lvert 514\rvert\frac{9}{2}\rightarrow\lvert 404\rvert\frac{7}{2}$	−1	5	∼6	0.0055
Lu^{177}	$\lvert 514\rvert\frac{9}{2}\rightarrow\lvert 404\rvert\frac{7}{2}$	−1	5	∼6	0.0040
$_{72}Hf^{177}$	$\lvert 624\rvert\frac{9}{2}\rightarrow\lvert 514\rvert\frac{7}{2}$	−1	5	∼6	0.0034
Hf^{179}	$\lvert 514\rvert\frac{7}{2}\rightarrow\lvert 624\rvert\frac{9}{2}$	+1	5	5.6 or 6.4	0.15
$_{73}Ta^{179}$	$\lvert 514\rvert\frac{9}{2}\rightarrow\lvert 404\rvert\frac{7}{2}$	−1	4	4.9	0.012
Ta^{181}	$\lvert 514\rvert\frac{9}{2}\rightarrow\lvert 404\rvert\frac{7}{2}$	−1	4	4.9	0.035
$_{75}Re^{187}$	$\lvert 532\rvert\frac{5}{2}\rightarrow\lvert 402\rvert\frac{5}{2}$	0	4.5	6.6	7.1

CC-0. In Public Domain. Gurukul Kangri Collection, Haridwar

Digitized by Arya Samaj Foundation Chennai and eGangotri

As long as one assumes that, for a given nucleus, the deformation in the initial state is the same as in the final state, one finds that the Nilsson estimate of the transition rate is weakly sensitive to the deformation η. For most of the transitions concerned here, the Nilsson estimate $T_N(E1)$ changes by a factor less than 5 when the deformation varies from $\eta=2$ to $\eta=6$. The requirement of equal deformation in the initial state and in the final state can be relaxed. The initial-state deformation can be calculated as a function of the final-state deformation for a given value of $T(E1)$. The values of η_i and η_f needed to reproduce the experimental transition probabilities are given in Table VII. This table shows that for the transitions in $_{63}$Eu and $_{65}$Tb^{159} the experimental $T(E1)$ values are obtained with a smaller deformation for the initial state than for the final state. The reverse holds for almost all the other transitions. The difference in deformation is as large as 50% in the former nuclei, whereas it is smaller than 20% in the latter group.

A smaller deformation for the $|532|\frac{3}{2}$ excited state than for the ground state in the $_{63}$Eu isotopes has been proposed in Mot 59. The nuclear deformation is known to suffer a sharp rise at $N=90$ when the neutron orbital $|660|\frac{1}{2}$ is filled. The possibility that smaller deformations are energetically more favorable in some excited states can be understood. There is no experimental evidence against the assumption of a different deformation for different nuclear states. Furthermore, it is likely that the Nilsson model in its original form (Ni 54) is not reliable for the prediction of excited-state deformations.

When only the transitions between intrinsic states are considered, some interesting conclusions can be drawn from a study of Fig. 6 (see also Table VIII). (a) Transitions with $\Delta K=0$ have hindrances $H_N(E1)$ around 1. (b) Transitions with $|\Delta K|=1$ have hindrances scattered between 3×10^{-3} and 1. The transitions with $\Delta K=+1$ considered alone show a greatly reduced scattering.

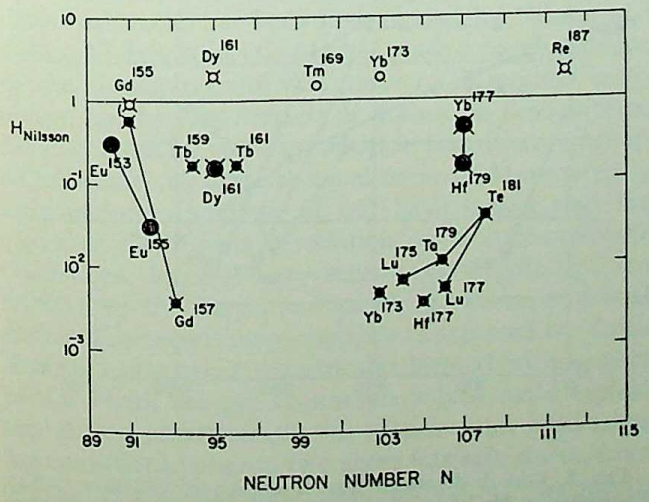

FIG. 6. Odd-A deformed nuclei: Region of the rare earths. Experimental hindrance factor $H_N(E1)$ relative to the Nilsson estimate, as a function of the neutron number N. The transitions with $\Delta K=0$, $+1$ and -1 are shown with the symbols used in Figs. 4 and 5. Transitions involving similar Nilsson states are bound by a solid line.

TABLE VIII. Hindrance H_N for equal deformation in the initial and final states. Rare-earth nuclei.

ΔK	Range for $H_N(E1)$	Number of transitions observed
0	0.18 to 14	7
+1	0.03 to 0.20	5
−1	0.0032 to 0.74	10

Table VIII shows that for the transitions with $|\Delta K|=1$ a definitive discrepancy exists between the experimental $T(E1)$ value and the Nilsson estimate. In most of the cases this discrepancy is not removed for any value of the deformation parameter η between 2 and 6, as long as one assumes that the deformation is equal in the different excited states and in the ground state of a given nuclei. If this restriction is relaxed it is possible to find a set of deformations η_i and η_f such that the experimental transition probability is reproduced by the Nilsson estimate (see Table VII).

For $\Delta K=0$ transitions the good agreement between the experimental data and the Nilsson estimate (except for the two transitions in $_{63}$Eu^{153,155}) make such an assumption superfluous.

This difference in behavior for $\Delta K=0$ and $|\Delta K|=1$ transition has been pointed out by Vergnes (Ve 62). Vergnes (Ve 62) has discussed the effect of changing the value of the parameter defined by Eq. (12). In the $N=4$ shell one can use the eigenstates calculated by Nilsson for $\mu=0.45$ and 0.55. As a rule such a change does not affect the Nilsson estimate by more than a factor 5.

The hindrance factors $H_N(E1)$ for the transitions between intrinsic states are plotted as a function of the transition energy in Fig. 7 ($\Delta K=0$ transitions have been left out). $H_N(E1)$ would be energy independent if the Nilsson estimate gave a correct energy dependence for $T_N(E1)$. For transitions of the types $|514|\frac{9}{2}\rightleftarrows|404|\frac{7}{2}$ and $|411|\frac{3}{2}\rightleftarrows|532|\frac{5}{2}$ a smooth energy behavior is observed. Transitions of the types $|642|\frac{5}{2}\rightleftarrows|521|\frac{3}{2}$ and $|624|\frac{9}{2}\rightleftarrows|514|\frac{7}{2}$ show strong variations of $H_N(E1)$ for small changes in the transition energy.

4.3.6. Effect of a Rotation–Particle Interaction

For odd-A nuclei the rotational energies are frequently of the same order of magnitude as the single-particle excitations. The conditions for an adiabaticity assumption no longer exist. A correction to the adiabatic approximation taking into account a rotation–particle interaction was first proposed by Bohr (Bo 54). The effect of this perturbation is demonstrated by deviations

CC-0. In Public Domain. Gurukul Kangri Collection, Haridwar

Digitized by Arya Samaj Foundation Chennai and eGangotri

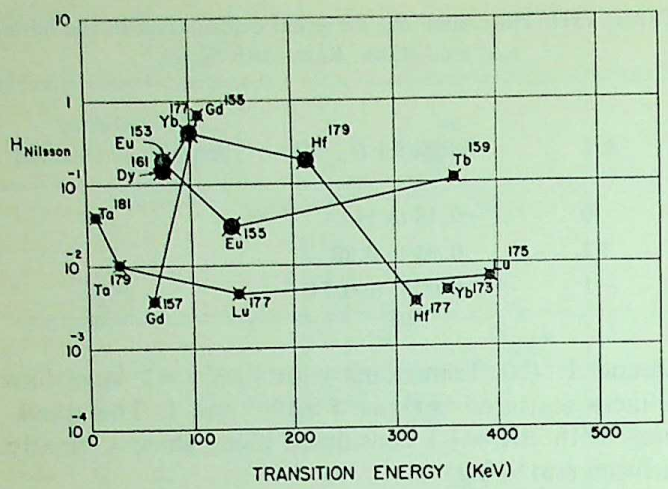

FIG. 7. Odd-A deformed nuclei: Region of the rare earths. Experimental hindrance factors $H_N(E1)$ relative to the Nilsson estimate, as a function of the transition energy in keV. Only transitions with $\Delta K=\pm 1$ are shown in this figure.

from the normal rotational spectra in odd-A nuclei. It is known to excite higher energy modes and is found to be small for nuclei far from closed shells.

The rotation–particle interaction has been discussed in detail by Kerman (Ke 56). He proposed to add to the single-particle Hamiltonian a term of the form $(\hbar^2/2\tau)(I_+j_-+I_-j_+)$, where $I_\pm, j_\pm$ are raising and lowering operators defined for the total angular momentum and the angular momentum of the last particle, respectively. This form of the perturbation term implies that only states will be mixed that have z components (K) of the total intrinsic angular momentum differing by ± 1 and have identical spins and parities. In the perturbation limit, such an interaction term will induce the mixing of the levels of close-lying rotational bands. For large deformations, the perturbation matrix elements vanish unless the asymptotic quantum numbers of the states to be mixed satisfy asymptotic selection rules. For strongly deformed nuclei, the perturbing states are very high in energy. Within the framework of the Nilsson model they can be found as a rule in the next, next-plus-one, or next-minus-one N shell. This implies that the admixture amplitudes are always small compared to unity, as expected from the experimental evidences of such perturbations. The admixture normally results in a small change of the transition probabilities. However, if the transition between the unperturbed levels is hindered, a small admixture can result in a large change of the total transition probability. Such a situation occurs whenever the perturbation matrix elements are unhindered, and there are furthermore unhindered transition amplitudes for the admixed components of the states involved in the transitions. The effect of the rotation–particle interaction on $E1$ transition probabilities in odd-A deformed nuclei is demonstrated in Fig. 8. In this picture the hindrance factor $H_N(E1)$ is again plotted as a function of the transition energy. But in contrast to Fig. 7, here the three transitions from a given intrinsic level to the ground-state rotational band are shown; this selection limits the transitions displayed to those occurring with $\Delta K=-1$. The solid lines drawn between the transitions with common initial state in a given nucleus emphasize a decrease of the hindrance as a final state is higher in the rotational band. It appears that the rotation–particle interaction affects the different levels of a rotational band differently.

A qualitative discussion is possible if one considers only the asymptotic states with unhindered coupling matrix elements. Using the admixture amplitudes given by Kerman (Ke 56) one finds that for three of the five identified transitions with $\Delta K=-1$ between intrinsic states the admixture produced by the rotation-particle interaction must result in a hindrance of the transition. For the two others ($|624|\frac{9}{2}\rightarrow|514|\frac{7}{2}$ and $|514|\frac{9}{2}\rightarrow|404|\frac{7}{2}$ identified in Hf_{105}^{177} and $_{71}Lu^{175}$, respectively) the admixture produces an enhancement. However, these two transitions have the strongest hindrances known ($H_N\sim 4\times 10^{-3}$); they are also the two only ones known occurring with $\Delta n_z=-1$. All the other $\Delta K=-1$ transitions occur with $\Delta n_z=-2$.

Grin and Pavlichenkow (Gr 64 and Gr 64a) have pointed out that the different hindrances observed for $\Delta K=0$ and $|\Delta K|=1$ transitions can be predicted. However, they assume that only the allowed coupling matrix element must be taken into account. For $\Delta K=0$ transitions the coupling matrix elements are always hindered by the asymptotic selection rules. For the $|\Delta K|=1$ transitions either the initial or the final states are perturbed by the rotation–particle interaction. The same authors have discussed an evaluation (Gr 64) which explains some of the facts discussed

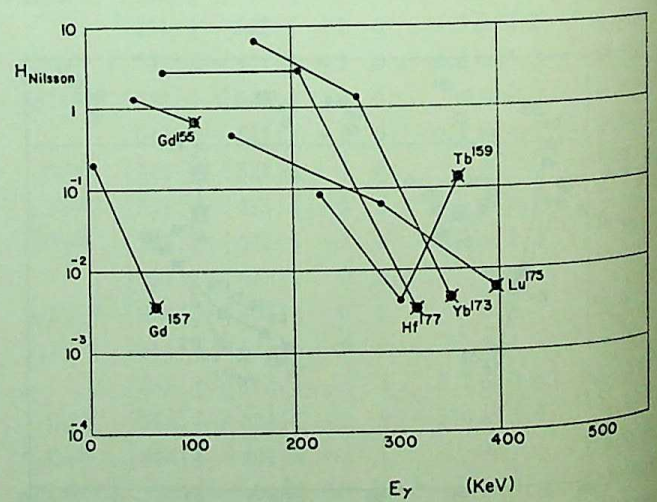

FIG. 8. Odd-A deformed nuclei: Region of the rare earths. Experimental hindrance factors $H_N(E1)$ relative to the Nilsson estimate, as a function of the transition energy in keV. Transitions to the successive levels of the ground state rotational bands are bound by a solid line. Only transitions with $\Delta K=-1$ are shown in this figure.

CC-0. In Public Domain. Gurukul Kangri Collection, Haridwar

Digitized by Arya Samaj Foundation Chennai and eGangotri

above for the transitions with $\Delta K=-1$. They evaluate the two branching ratios

$$B(E1; K, I\to K-1, I-1)/B(E1; K, I\to K-1, I)$$

and

$$B(E1; K, I\to K-1, I-1)/B(E1; K-1\to I+1).$$

These two ratios depend on one parameter only; this parameter is a function of the intrinsic state wave functions. The parameter can be evaluated from one of the two experimental branching ratio as the root of a quadratic equations, and subsequently used to predict the second one. For one of the solutions of the quadratic equation the agreement with the experimental data is good. Unfortunately, the model does not predict which solution is correct.

As far as $E1$ transitions in nuclei with finite deformation are concerned, the asymptotic states are not a precise enough approximation. Hence, the rotation–particle interaction is expected to produce important admixtures not only between the states with asymptotically allowed coupling matrix elements, but also for a much larger number of states. The $E1$ branching ratios to the ground-state rotational band of a given nucleus are precisely reproduced when all the relevant perturbing states are taken into account. Calculations of this type have been made by Berlovich (Berl 64) for $_{70}Yb^{173}$ and $_{72}Hf^{177}$. He finds an impressive agreement with the experimental data in these two cases.

Finally, an evaluation of the absolute transition probability for some $E1$ transitions with $\Delta K=-1$, based on considerations of the same type, has been proposed by Yoshida and Lin (Yos 62).

4.3.7. Effect of the Pairing Correlation

The effect of the pairing correlation on the moment of inertia and the collective gyromagnetic ratio for deformed nuclei has been investigated by Nilsson and Prior (Ni 59). Grin (Gr 61) has made a rough estimate of the consequence of this part of the residual interaction on the electromagnetic transition probabilities. He estimated for electric-multipole transitions an overall hindrance by a factor equal to $\sim A^{\frac{1}{3}}$. More recently Ikegami and Udagawa (I 64) have shown that the effect of the pairing correlation on electric-multipole transitions depends very sensitively on the position relative to the Fermi surface of the initial and final states. The transition probability is expected to vanish if both levels are symmetrically located with respect to the Fermi energy. This result indeed could explain the strong variations of the experimental hindrances for transitions between two given intrinsic states, from one nucleus to the other (see Sec. 4.3.5). Monsonego and Piebenbring (Mon 64) have calculated the hindrances for most of the $E1$ transitions in odd-A deformed nuclei (rare-earths region) with the wave functions of the pairing model. They found no definitive improvement as compared with the Nilsson estimate. The results of a similar calculation by Pyatov (Py 64) are compatible with most of the conclusions of Monsonego *et al.* (Mon 64). The question remains open whether better wave functions could be obtained if the pairing and the rotation–particle interactions were taken into account simultaneously. However, evaluations of the branching ratios to the ground-state rotational band of $\Delta K=-1$ transitions have been made by Berlovich (Berl 64) with both corrections. The results are closer to the experimental data when only the rotation–particle interaction is taken into account. They deteriorate markedly as the pairing correction is added, a result compatible with the conclusion of Monsonego *et al.* (Mon 64).

4.4. Even-A Nuclei with Large Deformation

4.4.1. Models for Negative-Parity Levels

A large number of negative-parity levels with excitation energies smaller than $\sim$2.5 MeV is observed in even-A deformed nuclei. The systematic occurrence of odd-parity levels between 0.2 and 1 MeV in the region of the actinide nuclei has been discussed by Sheline (She 60) and Leper (Lep 64). These levels have been interpreted as octupole vibrations by Alder *et al.* (Al 56) who pointed out that the $E1$ branching ratios to the ground-state rotational band characterize these states as $K=0$ collective excitations, with levels of spin $I=1, 3, 5, \cdots$.

The octupole vibration of a spheroidal nucleus produces a nuclear polarization. The static dipole moment of a nucleus vanishes since the center of mass coincides with the center of charge. The polarization associated with an odd-multipole vibration of a spheroidal nucleus results in a nonvanishing dynamical dipole moment. Evaluations of this dynamical dipole moment and of the related $E1$ transition probability have been discussed by Bohr and Mottelson (Bo 57, Bo 58), Strutinsky (Str 56, Str 57) and Lipas (Li 63). Bohr and Mottelson have estimated the mean induced dipole moment in terms of the symmetry energy constant of the semiempirical mass formula. They found the corresponding $E1$ transition probability proportional to a product of the squares of the quadrupole deformation and of the mean octupole oscillation amplitude. Bohr and Mottelson observed that the use of this result for the fast $(1^-\to 0^+)$ $E1$ transition from the 0.963-MeV level in $_{62}Sm^{152}$ leads to a calculated mean octupole oscillation amplitude of 0.18. They suggested that this value is considerably larger than one would expect.

Lipas and Davidson (Li 61) have discussed a Hamiltonian consisting of the conventional Bohr and Mottelson Hamiltonian (Bo 53) with two octupole degrees of freedom added. Beside the normal $K=0$ and $K=2$

CC-0. In Public Domain. Gurukul Kangri Collection, Haridwar

Digitized by Arya Samaj Foundation Chennai and eGangotri

quadrupole vibrational states (the β- and γ-vibrational states with positive parity), two octupole vibrational states with $K=0$ and $K=2$ (the b- and g-vibrational states with negative parity) are found. The corresponding rotational bands have the spin sequences $J=1, 3, 5, \cdots$ and $J=2, 3, 4, \cdots$, respectively. This model seems to explain successfully some of the negative-parity levels in the region of the actinide nuclei. The situation is less clear for the rare-earth nuclei in which the negative-parity levels are not so low in energy as in the actinides nuclei.

The electric-transition probabilities from vibrational states of the kind discussed in Li 61 have subsequently been calculated by Lipas (Li 63). He re-evaluates the nonconstant charge density on the basis of the semi-empirical mass formula. His result is quite similar to that of Bo 57 or Str 56. Two different kinds of $E1$ transitions can occur in the model: between states of the b band and the ground-state band, and between states of the g band and the γ band. The corresponding formula for the $E1$ transition probabilities can be found in Li 63. Lipas has calculated a few applications of this model. One of these is concerned with the 1^- level at 0.963 MeV in $_{62}Sm^{152}$. The 1^- level and the 3^- level at 1.070 MeV are expected to be the lower members of the $K=0$ b-band. The calculation of Lipas gives a hindrance factor of 4.8×10^{-4} for the $(1^-\rightarrow2^+)$ transition to the ground state. The experimental hindrance factor is 10^{-2}. Lipas calculated also a theoretical hindrance factor of $\sim2\times10^{-4}$ for the two $(3^-\rightarrow2^+)$ transitions in $_{90}Th^{232}$ and $_{92}U^{238}$. The experimental hindrance factors are $\sim10^{-3}$.

An application of the pairing model with multipole-force term to the $K=0$ negative-parity states has been discussed by Zaretskii and Urin (Za 62). They replace the usual quadrupole by an octupole-force term. The 1^- level energy is proportional to the octupole-force strength and can be determined empirically. The $E1$ transition probability depends on this strength constant and not on the octupole-vibration amplitude. Zaretskii and Urin derive an approximate formula for the $E1$ transition probability from a 1^- level, assuming as usual that the single-particle distances are much smaller than the energy gap and that the 1^- level is inside the gap. The parameters entering in this approximate formula are the quadrupole deformation β_0, the mean single-particle level density ρ_0 and the 1^--level excitation energy E_1^-. For values of the parameters $\beta_0=0.27$, $\rho_0=5$ level per MeV and $E_1^-=0.963$ MeV one finds a hindrance factor of 2.5×10^{-2} for the $_{62}Sm^{152}$ $(1^-\rightarrow0^+)$ transition in good agreement with the observed hindrance factor of 10^{-2}. This agreement may, however, be accidental; the approximate formula of Zaretskii *et al.* does not predict the observed variation of the $E1$ hindrance factor as a function of the neutron number in even-A rare-earth nuclei. Calculations of the levels in rare-earth nuclei by Gallagher and Soloviev (Ga 62), using the pairing model Hamiltonian, show that the intrinsic states in these nuclei can be described as two-quasiparticle excitations. Only a few levels have properties definitively different from the two-quasiparticle states. The first 2^+ level in all these nuclei is probably better described as a collective state. Most of the negative-parity levels are also interpreted by Gallagher and Soloviev as two-quasiparticle states. However, the 1^- levels in $_{62}Sm^{152}$ and $_{68}Er^{166}$ (at 0.963 and 1.654 MeV, respectively) are observed at energies somewhat smaller than calculated. Soloviev (So 63) has suggested that four-quasiparticle states should also be observed at relatively low energy, typically around 3 MeV. The data available do not allow an identification of such levels with confidence. The collective descriptions of the negative-parity levels identify them as rotational bands of octupole vibrational states. The 1^- levels, as an example, can be either in a $K=0$ and $J=1^-, 3^-, 5^-, \cdots$, or in a $K=1$ and $J=1^-, 2^-, 3^-, \cdots$ rotational band. The determination of the K value of the negative-parity states is not obvious. The spin succession in a rotational band is often guessed from the observed branching ratios to lower states of known K value. These data are not very conclusive for the 1^- states, as discussed in Sec. 4.2.4 (see Table III).

4.4.2. Discussion of the Data for Rare-Earth Nuclei

$E1$ transitions are measured in the $_{62}Sm^{152}$, $_{68}Er^{168}$, $_{72}Hf^{178,180}$, and $_{74}W^{182}$ nuclei. The observed transitions rates for the very fast $E1$ depopulating the 1^- and 2^- levels are different from the other negative-parity levels in rare earth nuclei. The characteristic hindrance factors for the K-allowed transitions in Er^{168} is 10^{-7} (3^- level), the ones in W^{182} are $10^{-4}\geq H_W\geq10^{-6}$, to be compared with $H_W\sim10^{-2}$ in Sm^{152}.

In $_{62}Sm^{152}$ the 1^- level at 0.963 MeV probably has $K=0$. Gallagher and Soloviev (Ga 62) suggest that this level has a collective nature. However, Kenefick and Sheline (Ken 64) have observed two levels at 0.939 and 0.988 MeV, and discuss the possibility of a $K=0$ intrinsic configuration with rotational states $J=0^-, 1^-, 2^-, \cdots$, the moment of inertia of this rotational band would be $\tau/\hbar^2=62.5$ MeV^{-1}. This value compares well with the one associate with the second negative-parity rotational band starting in this nucleus at 1.510 MeV. The 2^- level at 1.531 MeV has probably $K=1$. The 1^- (at 1.510 MeV) and the 3^- levels of this rotational band are identified and the corresponding moment of inertia is about four times larger than that of the ground state. Two quasiparticle configurations with $K=1$ are expected at this energy (Ga 62). For both rotational bands the moment of inertia is much larger than one would expect. A description of the two rotational ground states as $K=0$ and $K=1$ two-quasiparticle excitations in the pure pairing model is hardly compatible with the observed hindrance factors.

In $_{68}Er^{168}$ the 3^- level at 1.543 MeV can probably be identified with the proton $\{|411|\frac{1}{2}-|523|\frac{7}{2}\}$ two-quasiparticle state calculated at 1.3 MeV in Ga 62.

CC-0. In Public Domain. Gurukul Kangri Collection, Haridwar

Digitized by Arya Samaj Foundation Chennai and eGangotri

The 3^- level at 1.095 MeV can be compared to the neutron $\{ \mid 521 \mid \frac{1}{2}- \mid 633 \mid \frac{7}{2}\}$ state calculated at 1.1 MeV. In both cases the $E1$ are expected to be one-particle transitions forbidden by the asymptotic selection rules. The observed hindrance factors are compatible with those observed in odd-A deformed nuclei (Sec. 4.3).

In $_{72}Hf^{178,180}$ the K-forbidden transitions have the strongest hindrances observed for $E1$ transitions ($H_W = 10^{-14}$ and 10^{-16}, respectively). They are supposed to proceed from a $K=8$ negative parity level to the 8^+ member of the ground-state rotational band. Incidentally, these transitions dominate a determination of the slope of the linear empirical law for the transition rate of K-forbidden transitions suggested by Rusinov (Ru 61) and discussed shortly in Sec. 4.3.4.

In $_{74}W^{182}$ the 2^- level at 1.290 MeV is expected to be a proton two-quasiparticle state, and the 3^-, 4^- levels are the associate rotational states. The configuration proposed by Gallagher and Soloview (Ga 62) is $p\{ \mid 514 \mid \frac{9}{2}- \mid 402 \mid \frac{5}{2}\}$. The $\mid 514 \mid \frac{9}{2}$ state is observed to decay to a $\mid 404 \mid \frac{7}{2}$ $_{71}Lu^{175,177}$ and $_{73}Ta^{179,181}$, with hindrance factors between 5×10^{-7} and 10^{-6}. The hindrance factor measured for the $(2^-\rightarrow 2^+)$ transition in W^{182} is 3×10^{-4}. However, the nature of the final state ($J=2^+$; $K=2$) at 1.222 MeV is uncertain. If this 2^+ state is the $K=2$ γ-vibrational state, the weak hindrance is not compatible with the two-quasiparticle assignment of the 2^- level.

A $(4^+\rightarrow 3^-)$ transition has been measured in the odd-odd deformed nucleus $_{63}Eu^{152}$. From the Nilsson states available for the odd proton and neutron in the initial and final states a few can contribute to a asymptotically forbidden $E1$ transition. The hindrance factor of 6.3×10^{-7} is similar to the ones observed for $E1$ transitions with $\mid \Delta K \mid = 1$ in odd-A deformed nuclei.

4.4.3. Discussion of the Data for Actinide Nuclei

The lifetimes of a few negative-parity levels have been measured in $_{90}Th^{228}$ (5^-; $K=0$), Th^{230} (1^-), Th^{232} (3^-; $K=0$), $_{92}U^{234}$ (5^-; $K=5$), and U^{238} (3^-; $K=0$). The three K-forbidden transitions in U^{234} have hindrance factors H_w smaller than 6×10^{-8}. The other transitions are K-allowed and have hindrance factors $10^{-5} \leq H_w \leq 10^{-3}$.

Experimental data on the two-quasiparticle levels in these nuclei are poor. Except for the $(5^-; K=5)$ level in U^{234}, the levels concerned here are probably of collective nature. Soloviev and Siklos (So 64) have calculated these collective states within the framework of the pairing model. They give the dominant configurations of these levels. The pairing model describes the collective states as mixtures of two-quasiparticle excitations. The $E1$ transitions between levels of this kind and levels of the ground-state rotational band are expected to be described as single-nucleon transitions forbidden by the asymptotic selection rules. In odd-A actinide nuclei (see Sec. 4.3.4) such transitions are hindered by factors between 2×10^{-3} and 10^{-8}. The very limited amount of data for the $E1$ transitions in even-A nuclei does not allow a more detailed discussion for the moment.

The two $E1$ transitions de-exciting a $(1^+; K=1)$ level in the deformed odd-odd nucleus $_{91}Pa^{234}$ are hindered by factors $H_w=4\times10^{-5}$ and 2.5×10^{-4}. These hindrance factors are also of the order of magnitude expected for single-particle transitions in nuclei of this kind.

ACKNOWLEDGMENTS

I wish to thank Dr. Konrad Bleuler for his interest in this work. Dr. Roland Lombard at Orsay has contributed to many parts of the discussion by numerous comments for which the author is very grateful. Furthermore, I wish to express my acknowledgments to Dr. Dieter Zeh, Dr. Peter Debrunner, and Dr. Hans Frauenfelder, the former for an interesting discussion and the latters for a critical reading of the manuscript and several suggestions and comments. This work was supported by the U.S. Air Force Office of Scientific Research under Contract AF49(638)-1048.

APPENDIX A

Single-Particle Estimate for Spherical Nuclei

For a one-proton electric transition of multipole order L, the reduced matrix element $B_{el}(L)$ introduced in formula (8) of Sec. 2 has the form:

$$B_{el}(L) = (2j_i+1)^{-1} \mid \langle j_f l_f \mid\mid r^L Y_L(\theta, \phi) \mid\mid j_i l_i \rangle \mid^2$$

$$= (2j_f+1)\langle r^L \rangle^2 \langle l_f \mid\mid Y_L \mid\mid l_i \rangle^2 \begin{Bmatrix} l_f & j_f & \frac{1}{2} \\ j_i & l_i & L \end{Bmatrix}^2, \quad (1A)$$

where the eigenstates of the isotropic potential are now labeled $l_i j_i$ and $l_f j_f$ instead of J_i and J_f. $\{\ \}$ stands for the 6-j Wigner coefficient. The factor $S_{el}(L)$ introduced in formula (5) of Sec. 2 is then given by:

$$S_{el}(L) = S_{el}(j_i, L, j_f) = (4\pi)^{-1}(2j_p+1)(2l_f+1)$$

$$\times(2L+1)(2l_i+1)\begin{pmatrix} l_f & L & l_i \\ 0 & 0 & 0 \end{pmatrix}^2 \begin{Bmatrix} l_f & j_f & \frac{1}{2} \\ j_i & l_i & L \end{Bmatrix}^2 \quad (A2)$$

if the matrix element $\langle l_f \mid Y_L \mid l_i \rangle$ is reduced according to the Wigner–Eckart theorem. The factor $S_{el}(j_i, L, j_f)$ has a very simple form in the particular case of a single-particle $E1$ transition:

when $j_f = j_i - 1$,

$$S(E1) = \tfrac{3}{2}[(j_i - \tfrac{1}{2})/j_i];$$

when $j_f = j_i + 1$,

$$S(E1) = \tfrac{3}{4}[(2j_i+3)/(j_i+1)];$$

CC-0. In Public Domain. Gurukul Kangri Collection, Haridwar

Digitized by Arya Samaj Foundation Chennai and eGangotri

when $j_f=j_i$,

$$S(E1)=[4j_i(j_i+1)]^{-1}. \quad \text{(A3)}$$

As pointed out in Wi 56, the actual value of the factor S is meaningless when it cannot be assumed that the total nuclear spin of the two levels of a transition is due entirely to the spin of the transiting nucleon. It has been shown throughout this paper that at least one of the two levels in a $E1$ transition does not fulfill this condition; this particular level has been denoted the anomalous parity state. Hence, a comparison with the single-particle estimate for $E1$ transitions should be done with the assumption $S(E1)=1$, as proposed in Sec. 2.

The electric-multipole transition probability of Eq. (5) in Sec. 2 is valid for a proton transition only. The contribution of the nucleon magnetic moment has been neglected. Single-neutron transitions can only happen by the interaction of the neutron magnetic moment with the radiation field. The predicted transition rate is of the order $(v/c)^2$ relative to the rate for a proton transition. The recoil of the nucleus can be taken into account by using an "effective" electric charge instead of the elementary charge e. For a proton $E1$ transition the effective charge produces a reduction of the transition rate by a factor

$$(1-Z/a)^2\sim(N/A)^2. \quad \text{(A4)}$$

Single-Particle Estimate for Deformed Nuclei

The transition probability for an electric-multipole single-particle transition between the Nilsson states $|N_i, l_i, \Lambda_i, \Sigma_i\rangle\Omega_i$ and $|N_f, l_f, \Lambda_f, \Sigma_f\rangle\Omega_f$ is given in Ni 54 as:

$$T_N(EL)=\frac{8\pi(L+1)}{L[(2L+1)!!]^2}\hbar^{-1}\left(\frac{\omega}{c}\right)^{2L+1}B_N(EL), \quad \text{(A5)}$$

with the reduced matrix element $B_N(EL)$ given by (neglecting the case $L\geq\Omega_i+\Omega_f$):

$$B_N(EL)=e_{\text{eff}}^2\left(\frac{\hbar}{M\omega_0}\right)^L\frac{2L+1}{4\pi}\times\langle I_iL,\ \Omega_i,\ \Omega_f-\Omega_i\mid I_f\Omega_f\rangle^2G^2(EL) \quad \text{(A6)}$$

where:

$$G(EL)=\sum_{l_il_f}\langle N_fl_f\mid r^L\mid N_il_i\rangle\left(\frac{2l_i+1}{2l_f+1}\right)^{\frac{1}{2}}\langle l_fL,\ 0,\ 0\mid l_i\,0\rangle\times\sum_{\Lambda_i\Lambda_f}\sum_{\Sigma_i\Sigma_f}\delta_{\Sigma_i\Sigma_f}a_{l_f\Lambda_f}a_{l_i\Lambda_i}\langle l_iL,\ \Lambda_i,\ \Omega_f-\Omega_i\mid l_f\Lambda_f\rangle. \quad \text{(A7)}$$

$\langle N_fl_f\mid r^L\mid N_il_i\rangle$ are the radial matrix elements between isotropic harmonic oscillator states. The coefficients $a_{i\Lambda}$ are normalized amplitudes defined form the $A_{i\Lambda}$'s of formula (13) in Sec. 4.3.2 by

$$a_{l\Lambda}^2=A_{l\Lambda}^2/\sum_{l\Lambda}(A_{l\Lambda})^2. \quad \text{(A8)}$$

Numerically, if one takes, as suggested in Ni 54, $\hbar\omega_0=41A^{-\frac{1}{3}}$ MeV, one gets for $E1$ proton transitions (see, e.g., Al 56, page 500):

$$T_N(E1)=3.85\times10^{14}A^{\frac{1}{3}}(N/A)^2E_\gamma^3\times\langle I_i1,\ \Omega_i,\ \Omega_f-\Omega_i\mid I_f\Omega_f\rangle^2G^2(E1)[\text{sec}^{-1}]. \quad \text{(A9)}$$

In the calculation of the neutron transition hindrance factors of the Tables B-IIIA and B-IIIC, the proton effective electric charge (N/A) has been replaced by a neutron effective charge (Z/A).[8] The A dependence in $T_N(E1)$ is not the same as in the Weisskopf estimate for spherical nuclei. The hindrance factor $H_N(E1)$ has been defined in Sec. 4.3.5 as the ratio of the transition probabilities and not of the reduced transition probabilities.

BIBLIOGRAPHY

A 57 G. Alaga, Nucl. Phys. **4**, 625 (1957).
Al 56 K. Alder, A. Bohr, T. Huus, B. Mottelson, and A. Winther, Rev. Mod. Phys. **28**, 432 (1956).
Als 64 J. Alster, *Abstracts of the Congrès International Physique Nucléaire* (Paris, 1964), p. 51.
Ar 60 R. Arvieu and M. Veneroni, Compt. Rend. (Paris) **250**, 992, 2155 (1960).
Ar 62 R. Arvieu, thesis, University of Paris, 1962 (unpublished).
Ar 63 R. Arvieu, E. Baranger, M. Veneroni, M. Baranger, and V. Gillet, Phys. Letters **4**, 118 (1963).
As 60 F. Asaro, F. S. Stephens, J. M. Hollander, and I. Perlman, Phys. Rev. **117**, 492 (1960).
Ax 63 P. Alexander and F. Boehm, Nucl. Phys. **46**, 108 (1963).
B 63 C. V. K. Baba, G. T. Ewan, and J. F. Suarez, Nucl. Phys. **43**, 264, 285 (1963).
Ba 61 G. A. Bartholomew, Ann. Rev. Nucl. Sci. **11**, 259 (1961).
Bar 60 M. Baranger, Phys. Rev. **120**, 957 (1960).
Bay 60 B. F. Bayman and L. Silverberg, Nucl. Phys. **16**, 625 (1960).

[8] As pointed out above, strictly speaking the single-particle model predicts that electric-multipole neutron-transition rates must be of the order of $(v/c)^2$ relative to proton transitions. However, the experimental results in odd-A deformed nuclei show no definite difference between the $E1$ rates of proton and neutron transitions. Although the use of an effective charge for the neutron is meaningless in the single-particle model, the term $(Z/A)^2$ describes the fact that a neutron electric transition is a result of the recoil of the whole nucleus minus the transiting neutron.

CC-0. In Public Domain. Gurukul Kangri Collection, Haridwar

Digitized by Arya Samaj Foundation Chennai and eGangotri

Be 59 S. T. Belyaev, Kgl. Danske Videnskab. Selskab, Mat. Fys. Medd. **31**, No. 11 (1959).
Ber 62 I. Bergström, E.C.O. Bonacalza, and P. Thieberger, Arkiv Fysik **22**, 95 (1962).
Berl 64 E. Ye. Berlovich, Phys. Letters **13**, 161 (1964); and erratum, **14**, 72 (1965).
Bl 52 J. M. Blatt and V. F. Weisskopf, *Theoretical Nuclear Physics* (John Wiley & Sons, Inc., New York, 1952).
Bo 53 A. Bohr and B. R. Mottelson, Kgl. Danske Videnskab. Selskab. Mat. Fys. Medd. **27**, No. 16 (1953).
Bo 54 A. Bohr, *Rotational States in Atomic Nuclei* (E. Munksgaard, Copenhagen, 1954).
Bo 57 A. Bohr and B. R. Mottelson, Nucl. Phys. **4**, 529 (1957).
Bo 58 A. Bohr and B. R. Mottelson, Nucl. Phys. **9**, 689 (1958).
Bo 58a A. Bohr, B. R. Mottelson, and D. Pines, Phys. Rev. **110**, 936 (1958).
Boe 63 F. Boehm and J. Rogers, Nucl. Phys. **41**, 553 (1963).
Br 62 A. Braunstein and A. de Shalit, Phys. Letters **1**, 264 (1962).
Bro 61 G. A. Brown, J. A. Ewans, and D. J. Thouless, Nucl. Phys. **24**, 1 (1961).
Ch 60 E. L. Church and J. Weneser, Ann. Rev. Nucl. Sci. **10**, 193 (1960).
Ci 63 L. Ciuffolotti and F. Demichelis, Nucl. Phys. **48**, 305 (1963).
Cl 62 J. E. Cline, E. C. Yates, and E. H. Turk, Nucl. Phys. **30**, 154 (1962).
Dan 64 W. R. Daniels and D. C. Hoffman, Bull. Am. Phys. Soc. **9**, 562 (1964) and private communication, 1965.
Di 63 R. M. Diamond, B. Elbeck, and F. S. Stephens, Nucl. Phys. **43**, 560 (1963).
E 62 S. F. Eccles, Physica **28**, 251 (1962).
Fo 62 G. Foucher and A. de Pinho, J. Phys. Radium **23**, 22 (1962).
Ga 58 C. J. Gallagher, Jr., and S. A. Moskowski, Phys. Rev. **111**, 1282 (1968).
Ga 60 C. J. Gallagher, Jr., and W. F. Edwards, Nucl. Phys. **19**, 18 (1960).
Ga 62 C. J. Gallagher, Jr., and V. G. Soloviev, Kgl. Danske Videnskab. Selskab, Mat. Fys. Skrifter **2**, No. 2 (1962).
Ga 62a C. J. Gallagher, Jr., Phys. Rev. **126**, 1525 (1962).
Go 51 M. Goldhaber and A. W. Sunyar, Phys. Rev. **83**, 906 (1951).
Go 55 M. Goldhaber and A. W. Sunyar, *Beta and Gamma Ray Spectroscopy* (North-Holland Publishing Company, Amsterdam, 1955), p. 453.
Gr 61 Yu. T. Grin, Zh. Eksperim. i Teor. Fiz. **39**, 138 (1960) [English transl.: Soviet Phys.—JETP **12**, 100 (1961)].
Gr 64 Yu. T. Grin and I. M. Pavlichenkow, Phys. Letters **9**, 249 (1964).
Gr 64a Yu. T. Grin (private communication, 1964).
Gri 59 E. P. Grigorev, B. S. Dzhelepov and A. V. Zolotavin, Bull. Acad. Sci. USSR **23**, 183, 859 (1959).
Gro 62 L. V. Groshev, A. M. Demidov, V. A. Ivanov, V. N. Lutsenko, and V. I. Pelekhov, Bull. Acad. Sci. USSR **26**, 1127 (1962).
Ham 62 E. W. Hamburger, Nucl. Phys. **39**, 139 (1962).
Hau 61 U. Hauser, K. Runge, and G. Knissel, Nucl. Phys. **27**, 632 (1961).
Hel 61 R. G. Helmer and S. B. Burson, Phys. Rev. **123**, 978 (1961).
I 64 H. Ikegami and T. Udagawa, Phys. Rev. **133B**, 1388 (1964).
Ka 63 J. Kantele and R. W. Fink, Nucl. Phys. **43**, 187 (1963).
Kas 64 E. Kashy and T. W. Coulomb, Bull. Am. Phys. Soc. **9**, 457 (1964).
Ke 56 A. K. Kerman, Kgl. Danske Videnskab. Selskab, Mat. Fys. Medd. **30**, No. 15 (1956).
Ken 64 R. A. Kenefik and R. K. Sheline, Phys. Rev. **135B**, 934 (1964).
Ki 60 L. S. Kisslinger and R. A. Sorensen, Kgl. Danske Videnskab. Selskab, Mat, Fys. Medd. **32**, No. 9 (1960).
Ki 63 L. S. Kisslinger and R. A. Sorensen, Rev. Mod. Phys. **35**, 853 (1963).
Ko 64 G. A. Kotel'nikov and N. Shadiev, Bull. Acad. Sci. USSR **27**, 295 (1964).
Kr 62 G. Kramer and S. G. Nilsson, Nucl. Phys. **35**, 273 (1962).
La 54 A. M. Lane and L. A. Radicati, Proc. Phys. Soc. (London) **67A**, 167 (1954).
La 60 A. M. Lane and E. D. Pendlebury, Nucl. Phys. **15**, 39 (1960).
Lar 62 N. L. Lark, P. F. A. Goudsmit, J. F. W. Jansen, J. E. J. Oberstei, and A. H. Wapstra, Nucl. Phys. **35**, 582 (1962).
Law 57 R. D. Lawson and J. L. Uretsky, Phys. Rev. **108**, 1300 (1957).
Le 60 J. S. Levinger, *Nuclear Photo-Disintegration* (Oxford University Press, London, 1960).
Lem 60 R. H. Lemmer and A. E. S. Green, Phys. Rev. **119**, 1043 (1960).
Lep 64 D. P. Leper, Nucl. Phys. **50**, 234 (1964).
Li 61 P. O. Lipas and J. P. Davidson, Nucl. Phys. **26**, 80 (1961).
Li 63 P. O. Lipas, Nucl. Phys. **40**, 629 (1963).
Lo 64 R. J. Lombard, Helv. Phys. Acta **37**, 160 (1964).
Lo 64a R. J. Lombard, to be published (private communication, 1964).
LY 62 Liu Yüan, N. I. Pyatov, V. G. Soloviev, I. N. Silin, and V. I. Furman, Zh. Eksperim. i Teor. Fiz. **42**, 1219 (1962) [English transl.: Soviet Phys.—JETP **15**, 845 (1962)].
Ma 55 M. G. Mayer and J. H. D. Jensen, *Elementary Theory of Nuclear Shell Structure* (John Wiley & Sons, Inc., New York, 1955).
Me 64 F. Metzger, Bull. Am. Phys. Soc. **9**, 496 (1964).
Mo 51 S. A. Moszkowski, Phys. Rev. **83**, 1071 (1951).
Mo 53 S. A. Moszkowski, Phys. Rev. **89**, 474 (1953).
Mo 55 S. A. Moszkowski, *Beta and Gamma Ray Spectroscopy* (North-Holland Publishing Company, Amsterdam, 1955), p. 373.
Mot 59 B. R. Mottelson and S. G. Nilsson, Kgl. Danske Videnskab. Selskab, Mat. Fys. Skrifter **1**, No. 8 (1959).

CC-0. In Public Domain. Gurukul Kangri Collection, Haridwar

Digitized by Arya Samaj Foundation Chennai and eGangotri

Mon 64 G. Monsonego and R. Piepenbring, Nucl. Phys. **58**, 593 (1964) and J. Phys. **25**, 690 (1964).
Na 59 O. Nathan and S. Hultberg, Nucl. Phys. **10**, 118 (1959).
Ni 54 S. G. Nilsson, Kgl. Danske Videnskab. Selskab, Mat. Fys. Medd. **29**, No. 16 (1954).
Ni 58 S. G. Nilsson and J. O. Rasmussen, Nucl. Phys. **35**, 273 (1962).
Ni 59 S. G. Nilsson and O. Prior, Kgl. Danske Videnskab. Selskab, Mat. Fys. Medd. **32**, No. 16 (1960).
Ni 62 S. G. Nilsson, J. Sawicki, and N. K. Glendenning, Nucl. Phys. **33**, 239 (1962).
No 50 L. W. Nordheim, Phys. Rev. **78**, 294 (1950).
Ok 58 K. Okamoto, Phys. Rev. **100**, 143 (1958).
Os 56 R. K. Osborn and E. D. Klema, Nucl. Phys. **2**, 454 (1956).
Pe 64 N. F. Peek, J. A. Jungerman, and C. G. Patten, Phys. Rev. **136B**, 330 (1964).
Per 62 Chs. F. Perdrisat, *Comptes-Rendus Colloque Physique Nucléaire des Basses Energies à Bruxelles* (L. Wouters, Louvain, 1962), p. 68.
Pi 63 A. de Pinho, 1963 (unpublished).
Po 62 V. I. Popov, Bull. Acad. Sci. USSR **26**, 149 (1962).
Py 64 N. I. Pyatov, Acta Phys. Polon. **25**, 21 (1964).
Ra 63 R. S. Raghavan and R. M. Steffen, Phys. Letters **5**, 198 (1963).
Ras 58 A. J. Rassey, Phys. Rev. **109**, 949 (1958).
Ro 63 H. Rouhaninejad, J. Phys. **24**, 705 (1963).
Ru 61 L. I. Rusinov, Usp. Fiz. Nauk **73**, 615 (1961) [English transl.: Soviet Phys.—Usp. **4**, 282 (1961)].
Ry 61 H. Ryde and Z. Sujkowski, Arkiv Fysik **20**, 289 (1961).
Sa 63 M. Sakai, Phys. Letters **3**, 338 (1963).
Sh 61 A. de Shalit, Phys. Rev. **122**, 1530 (1961).
Sh 63 A. de Shalit and J. Talmi, *Nuclear Shell Theory* (Academic Press Inc., New York, 1963), p. 158.
Sha 64 S. M. Shafroth, P. N. Trehan, and D. M. Van Patter, Phys. Rev. **129**, 704 (1963).
She 60 R. K. Sheline, Rev. Mod. Phys. **32**, 1 (1960).
So 63 V. G. Soloviev, Zh. Eksperim. i Teor. Fiz. **43**, 246 (1962) [English transl.: Soviet Phys.—JETP **16**, 176 (1963)].
So 64 V. G. Soloviev and T. Siklos, Nucl. Phys. **59**, 145 (1964).
Sor 61 R. A. Sorensen, Nucl. Phys. **25**, 674 (1961).
St 52 B. Stech, Z. Naturforsch. **7a**, 401 (1952).
Sta 64 G. G. Staehle and M. L. Pool, Bull. Am. Phys. Soc. **9**, 718 (1964) and private communication, 1965.
Str 56 V. Strutinsky, Physica **22**, 1166 (1956).
Str 57 V. Strutinsky, Nucl. Energy **4**, 523 (1957).
Stro 57 D. Strominger and J. O. Rasmussen, Nucl. Phys. **3**, 197 (1957).
Sv 63 J. Svedberg and G. Anderson, Nucl. Phys. **48**, 313 (1963).
Tr 58 W. W. True and K. W. Ford, Phys. Rev. **109**, 1675 (1958).
Tr 61 W. W. True, Nucl. Phys. **25**, 155 (1961).
Ve 62 M. N. Vergnes, Nucl. Phys. **39**, 273 (1962).
We 51 V. Weisskopf, Phys. Rev. **83**, 1073 (1951).
Wi 53 D. H. Wilkinson, Phil. Mag. **44**, 450 (1953).
Wi 56 D. H. Wilkinson, Phil. Mag. **1**, 127 (1956).
Wi 58 D. H. Wilkinson, *Proceeding of the Rehovoth Conference on Nuclear Structure* (North-Holland Publishing Company, Amsterdam, 1958), p. 175.
Wi 60 D. H. Wilkinson, *Nuclear Spectroscopy*, edited by F. Ajzenberg-Selove (Academic Press Inc., New York, 1960), p. 852.
Yo 62 S. Yoshida, Nucl. Phys. **38**, 380 (1962).
Yos 62 H. Yoshida and C. L. Lin, Phys. Letters **3**, 107 (1962).
Za 62 D. F. Zaretskii and M. G. Urin, Zh. Eksperim. i Teor. Fiz. **42**, 304 (1962) [English transl.: Soviet Phys.—JETP **15**, 211 (1962)].

APPENDIX B: TABLES OF EXPERIMENTAL DATA FOR $E1$ TRANSITIONS

The data concerned with $E1$ transitions between bound states in medium and heavy nuclei ($A \geq 36$) are collected in four groups of tables. Each one of these groups B-I to B-IV is related with Secs. 4.1 to 4.4, respectively, in text. The literature references are given at the end of the tables. The literature survey includes the paper available before 1 March 1956. (Data received after 1 January 1965 are not discussed in the text.)

Values of level lifetimes or transition probabilities given between square brackets [ ] have not been measured but deduced from systematic trends for transitions with multipolarity other than $E1$. The reference to the paper in which such deductions have been proposed is given at the point (6) of the reference lists for each transition.

The notation used in the tables has been introduced in the text.

CC-0. In Public Domain. Gurukul Kangri Collection, Haridwar

Digitized by Arya Samaj Foundation Chennai and eGangotri

TABLE B–I. Odd spherical nuclei.

Nucleus	$_{18}Ar^{39}$	$_{20}Ca^{43}$	$_{20}Ca^{43}$	$_{33}As^{75}$	$_{33}As^{75}$	$_{33}As^{75}$
$J_i\pi_i$	$\frac{3}{2}^+$	$(\frac{3}{2}, \frac{5}{2})^+$		$\frac{5}{2}^+$		
E(initial level)	1.516 MeV	0.993 MeV		0.40065 MeV		
τ_i (level) [sec^{-1}]	9.5×10^{-10}	1.3×10^{-10}		1.5×10^{-9}		
$J_f\pi_f$	$(\frac{3}{2}, \frac{5}{2})^-$	$\frac{3}{2}^-$	$\frac{5}{2}^-$	$\frac{3}{2}^-$	$\frac{3}{2}^-$	$\frac{5}{2}^-$
E (final level)	1.27 MeV	0.593 MeV	0.374 MeV	g.s.	0.2646 MeV	0.2796 MeV
E (transition)	246 keV	394 keV	619 keV	401 keV	136 keV	121 keV
Experimental internal-conversion coefficient	$\alpha_t \leq 0.021$			$\alpha_K = 1.2\times10^{-3}$	$\alpha_K = 0.026$	$\alpha_K = 0.027$
Theoretical internal conv. coef. for pure $E1$	[a]					
Mixing ratio $M2/E1$	~ 0			≤ 0.028	0.012	
Relative gamma intensity	52%	11.7%	86.2%	13%	64%	19%
$(TE1)$ [sec^{-1}]	3.8×10^{8}	9.0×10^{8}	6.6×10^{9}	5.9×10^{7}	2.8×10^{8}	8.5×10^{7}
Hindrance H_W	2.2×10^{-5}	1.4×10^{-5}	2.6×10^{-5}	5.2×10^{-7}	6.25×10^{-5}	2.7×10^{-5}
References						
Level identif.						
τ_i	Pen 56	We 62		Me 58; La 59		
Int. conv. coef.	Pen 56			Me 59	Me 59	Gri 59
$M2/E1$						
Relat. intens.	En 62	We 62	We 62	Boe 60	Boe 60	Boe 60
Discussion				Boe 60	Boe 60	Boe 60

[a] For the theoretical internal conversion coefficients see Ros 58 and Sl 56.

CC-0. In Public Domain. Gurukul Kangri Collection, Haridwar

Digitized by Arya Samaj Foundation Chennai and eGangotri

TABLE B–I (*Continued*)

Nucleus	$_{34}Se^{77}$	$_{47}Ag^{109}$	$_{51}Sb^{119}$	$_{82}Pb^{205}$	$_{82}Pb^{209}$
$J_i\pi_i$	$\frac{5}{2}^-$	$\frac{5}{2}^-$	$\frac{11}{2}^-$	$\frac{9}{2}^+$	$\frac{1}{2}^-$
E (initial level)	0.248 MeV	0.414 MeV	1.37 MeV	2.566 MeV	2.13 MeV
$\tau_{\frac{1}{2}}$ (level) [sec^{-1}]	9.7×10^{-9}	3.3×10^{-11}	[$\sim10^{-8}$]	1.25×10^{-16}	3.1×10^{-9}
$J_f\pi_f$	$\frac{7}{2}^+$	$\frac{7}{2}^+$	$\frac{9}{2}^+$	$\frac{7}{2}^-$	$\frac{1}{2}^+$
E (final level)	0.161 MeV	0.088 MeV	1.22 MeV	0.703 MeV	2.01 MeV
E (transition)	87 keV	325 keV	153 keV	1863 keV	120 keV
Experimental internal conversion coefficient				$\alpha_K=7.1\times10^{-4}$	
Theoretical internal conv. coef. for pure $E1$	$\alpha_K=0.096$		$\alpha_K=0.049$		$\alpha_K=0.215$
Mixing Ratio $M2/E1$				~0	
Relative gamma intensity	38%	0.5%	92%	60%	100%
$T(E1)$ [sec^{-1}]	2.7×10^{7}	9.7×10^{7}	[8.6×10^{7}]	3.4×10^{15}	2.2×10^{8}
Hindrance H_W	2.3×10^{-5}	1.4×10^{-6}	[$\sim10^{-5}$]	1.5×10^{-1}	3.7×10^{-5}
References					
Level identif.			Sv 63	Ber 62	Muk 62
$\tau_{\frac{1}{2}}$	Mo 63; N 61	Mc 58	Sv 63	Per 62; Per 62a	Str 56
Int. conv. coef.	Sl 56		Sl 56	Sto 59	Sl 56
$M2/E1$				Per 62a	
Relat. intens.	Mo 63	Hu 54		Sto 59	
Discussion	Ro 62	A 54	Sv 63; Bh 63		

CC-0. In Public Domain. Gurukul Kangri Collection, Haridwar

Digitized by Arya Samaj Foundation Chennai and eGangotri

TABLE B–IIA. $(3^- \rightarrow 2^+)$ transitions in even spherical nuclei.

Nucleus	$_{18}Ar^{36}$	$_{18}Ar^{38}$	$_{28}Ni^{58}$	$_{28}Ni^{60}$	$_{38}Sr^{88}$	$_{50}Sn^{116}$
$J_i\pi_i$	3^-	3^-	3^-	3^-	3^-	3^-
E (initial level)	4.17 MeV	3.75 MeV	4.50 MeV	4.05 MeV	2.74 MeV	2.23 MeV
τ_i (level) [sec^{-1}]		$\leq 4\times10^{-10}$				
$J_f\pi_f$	2^+	2^+	2^+	2^+	2^+	2^+
E (final level)	1.97 MeV	2.16 MeV	1.45 MeV	1.33 MeV	1.835 MeV	1.27 MeV
E (transition)	2.20 MeV	1.59 MeV	3.05 MeV	2.72 MeV	899 keV	970 keV
Experimental internal conversion coefficient						$\alpha_t=(6.0\pm0.6)\times10^{-4}$
Theoretical internal conv. coef. for pure $E1$				$\alpha_K=1.5\times10^{-5}$	$\alpha_K=2.7\times10^{-4}$	$\alpha_K=5.1\times10^{-4}$
Mixing Ratio $M2/E1$		$\sim10^{-3}$			5.5×10^{-3}	
Relative gamma intensity	90%	100%				89%
$T(E1)$ [sec^{-1}]	$[1.3\times10^{11}]$	$\geq1.7\times10^{9}$	$(3.3\pm1.7)\times10^{11}$	$(1.6\pm0.8)\pm10^{11}$	1.7×10^{12}	5.0×10^{9}
Hindrance H_W	$[1.1\times10^{-5}]$	$\geq3.8\times10^{-7}$	$\sim8\times10^{-6}$	5.3×10^{-6}	1.2×10^{-3}	2.2×10^{-6}
References						
Level identif.						
τ_i		Kr 54; Sun				
Int. conv. coef.				Sl 56	Sl 56	Sl 56; Bol 64
$M2/E1$		Bra 58				
Relat. intens.	Li 60					St 55
Discussion	Li 60	Mey 49	Cr 61	Cr 61	He 56; Pee 60	Han 61

CC-0. In Public Domain. Gurukul Kangri Collection, Haridwar

Digitized by Arya Samaj Foundation Chennai and eGangotri

TABLE B-IIB. $(5^- \rightarrow 4^+)$ and $(1^- \rightarrow 0^+, 2^+)$ transitions in even spherical nuclei.

Nucleus	$_{50}Sn^{118}$	$_{50}Sn^{120}$	$_{60}Nd^{144}$	$_{60}Nd^{144}$	$_{62}Sm^{148}$	$_{62}Sm^{148}$
$J_i\pi_i$	5^-	5^-	1^-		1^-	
E (initial level)	2.32 MeV	2.30 MeV	2.18 MeV		1.46 MeV	
$\tau_{\frac{1}{2}}$ (level) [sec^{-1}]	2.0×10^{-8}	5.2×10^{-9} 5.7×10^{-9} 6.05×10^{-9}	$\geq1.0\times10^{-14}$		$(1.4\pm0.7)\times10^{-13}$	
$J_f\pi_f$	4^+	4^+	0^+	2^+	0^+	2^+
E (final level)	2.28 MeV	2.21 MeV	g.s.	0.69 MeV	g.s.	0.55 MeV
E(transition)	40.7 keV	90 keV	2.18 MeV	1.49 MeV	1.46 MeV	0.91 MeV
Experimental internal conversion coefficient	$\alpha_t=2.4\pm0.25$				$\alpha_K=(4.7\pm1.4)\times10^{-4}$	$\alpha_K=(6.8\pm1.9)\times10^{-4}$
Theoretical internal conv. coef. for pure $E1$		$\alpha_K=0.25$	$\alpha_K=2.2\times10^{-4}$	$\alpha_K=3.9\times10^{-4}$	$\alpha_K=4.4\times10^{-4}$	$\alpha_K=1.05\times10^{-3}$
Mixing Ratio $M2/E1$	97.6%	100%	75%	25%	66%	34%
$T(E1)$ [sec^{-1}]	1.0×10^{7}	1.07×10^{8}	$\leq5.25\times10^{13}$	$\leq1.75\times10^{13}$	3.3×10^{12}	1.7×10^{12}
Hindrance H_W	6.0×10^{-5}	5.8×10^{-5}	$\leq1.85\times10^{-3}$	$\leq1.9\times10^{-3}$	3.8×10^{-5}	8.1×10^{-5}
References						
Level identif.			Ba 62	Ba 62	H 64	H 64
$\tau_{\frac{1}{2}}$	Bol 61	*Bol 61*[a]; Cur 63; I 60; I 61	Bl 63		Me 64	
Int. conv. coef.	Bol 61	Sl 56	Sl 56	Sl 56	B 63; Sl 56	B 63; Sl 56
$M2/E1$						
Relat. intens.	Bol. 61				Sch 62	Sch 62
Discussion	Bod 62	Bod 62				

[a] The data of the italicized reference are used for the calculation of $T(E1)$ and $B(E1)$.

CC-0. In Public Domain. Gurukul Kangri Collection, Haridwar

Digitized by Arya Samaj Foundation Chennai and eGangotri

TABLE B-IIB (*Continued*)

Nucleus	$_{82}Pb^{206}$	$_{82}Pb^{206}$
$J_i\pi_i$	5^-	
E (initial level)	3.404 MeV	
τ_i (level) [sec^{-1}]	6.4×10^{-15} 1.5×10^{-14}	
$J_f\pi_f$	4^+	4^+
E (final level)	1.684 MeV	1.988 MeV
E (transition)	1.720 MeV	1.405 MeV
Experimental internal conversion coefficient		
Theoretical internal conv. coef. for pure $E1$	$\alpha_K=8.4\times10^4$	$\alpha_K=1.15\times10^{-3}$
Mixing Ratio $M2/E1$		
Relative gamma intensity	68%	3.4%
$T(E1)$ [sec^{-1}]	7.3×10^{13}	3.7×10^{12}
Hindrance H_W	4.1×10^{-3}	3.7×10^{-4}
References		
Level identif.		
τ_i	Br 59; Le 61; *Per 62a;* Wi 63	
Int. conv. coef.	Sl 56	Sl 56
$M2/E1$		
Relat. intens.	Sto 59	Sto 59
Discussion	Per 62a; Wi 63	

CC-0. In Public Domain. Gurukul Kangri Collection, Haridwar

Digitized by Arya Samaj Foundation Chennai and eGangotri

TABLE B-IIC. Spherical odd-odd nuclei.

Nucleus	$_{33}As^{72}$	$_{35}Br^{80}$	$_{45}Rh^{100}$	$_{45}Rh^{100}$	$_{45}Rh^{104}$	$_{51}Sb^{122}$
$J_i\pi_i$	1^+	2^-	2^+		2^-	(3^+)
E (initial level)	46 keV	37 keV	74.8 keV		51 keV	61 keV
$\tau_{\frac{1}{2}}$(level)[sec^{-1}]	$(1.07\pm0.03)\times10^{-8}$	$(7.4\pm0.2)\times10^{-9}$	2.35×10^{-7}		2.6×10^{-9}	1.8×10^{-6}
$J_f\pi_f$	2^-	1^+	1^-	2^-	1^+	2^-
E (final level)	g.s.	g.s.	g.s.	32.7 keV	g.s.	g.s.
E (transition)	46 keV	37 keV	74.77 keV	42.10 keV	51 keV	61 keV
Experimental internal conversion coefficient	$\alpha_K=0.63\pm0.06$	$\alpha\sim1.3$			$\alpha_K=0.89$ $\alpha_K=1.0\pm0.2$ $\alpha_t=1.6\pm0.5$	$\alpha_K=0.65\pm0.03$
Theoretical internal conv. coef. for pure $E1$	$\alpha_K=0.6$		$\alpha_t\sim0.5$	$\alpha_t\sim2$	$\alpha_K=0.93$	$\alpha_K=0.63$
Mixing Ratio $M2/E1$						
Relative gamma intensity	100%	100%	~80%	~20%	100%	100%
$T(E1)$[sec^{-1}]	4.0×10^7	4.1×10^7	1.9×10^6	5×10^5	1.4×10^8	2.0×10^5
Hindrance H_W	1.6×10^{-4}	4.3×10^{-4}	2.1×10^{-6}	3.1×10^{-6}	4.7×10^{-4}	3.7×10^{-7}
References						
Level identif.						
$\tau_{\frac{1}{2}}$	Hue 64	Fla 64	Ev 64		To 61	Mat 62
Int. conv. coef.	Cu 58; Sl 56				Gre 62; Es 64	Ci 63; Sl 56
$M2/E1$						
Relat. intens.						
Discussion						

CC-0. In Public Domain. Gurukul Kangri Collection, Haridwar

Digitized by Arya Samaj Foundation Chennai and eGangotri

TABLE B–IIIA. *K*-allowed transitions for odd-*A* deformed nuclei with $90 \leq N \leq 114$.

Nucleus	$_{63}Eu^{153}$	$_{63}Eu^{153}$	$_{63}Eu^{153}$	$_{63}Eu^{155}$	$_{63}Eu^{155}$
$J_i\pi_i\Omega_i[N, n_z, \Lambda]_i$	$(\frac{5}{2})^-$; $\frac{5}{2}$ [532]		$(\frac{5}{2}^+)$; $\frac{3}{2}$ [411]	$(\frac{5}{2})^-$; $\frac{5}{2}$[532]	$(\frac{3}{2})^+$; $\frac{3}{2}$[411]
E (initial level)	97 keV		173 keV	105 keV	246 keV
$\tau_{\frac{1}{2}}$(level) [sec^{-1}]	$\leq 1\times10^{-9}$ $\geq 3\times10^{-10}$ $(1.6\pm0.13)\times10^{-10}$		1.4×10^{-10}	$\leq 4\times10^{-10}$	1.2×10^{-9}
$J_f\pi_f\Omega_f[N, n_z, \Lambda]_f$	$\frac{5}{2}^+$; $\frac{5}{2}$[413]	$\frac{7}{2}^+$; $\frac{5}{2}$[413]	$(\frac{5}{2})^-$; $\frac{5}{2}$[532]	$\frac{5}{2}^+$; $\frac{5}{2}$[413]	$(\frac{5}{2})^-$; $\frac{5}{2}$[532]
E (final level)	g.s.	84 keV	97 keV	g.s.	105 keV
E (transition)	97 keV	14.1 keV	75.4 keV	105 keV	141 keV
Experimental internal conversion coefficient	$\alpha_K = 0.36^{+0.03}_{-0.07}$ $\alpha_t = 0.41$	$\alpha_t = 1.5$	$\alpha_t = 0.4\pm0.07$	$\alpha_t = 0.27$	$\alpha_K = 0.16$
Theoretical internal conv. coef. for pure $E1$	$\alpha_K = 0.24$		$\alpha_K = 0.48$	$\alpha_K = 0.20$	$\alpha_K = 0.093$
Mixing Ratio $M2/E1$	0.08			≤ 0.01	0.03
Relative gamma intensity	100%	$(3.5\pm1.5)\times10^{-3}$	5.5×10^{-3}	100%	17.6%
$T(E1)$ [sec^{-1}]	4.4×10^{9}	1.5×10^{7}	2.7×10^{7}	$\geq 1.25\times10^{9}$	1.0×10^{8}
Hindrance H_W	1.65×10^{-3}	1.9×10^{-3}	2.2×10^{-5}	$\geq 3.75\times10^{-4}$	1.25×10^{-5}
Hindrance H_N for η_i and η_f	$\eta=2$: 14 $\eta=4$: 42 $\eta=6$: 90 $\eta_i=4, \eta_f=6$: 3	5.7 17 31 1.25	$\eta=3$: 0.23 $\eta=4$: 0.20 $\eta=5$: 0.23	$\eta=2$: ≥ 3.0 $\eta=4$: ≥ 9.1 $\eta=6$: ≥ 20 $\eta_i=4, \eta_f=6$: ≥ 0.66	$\eta=3$: 3.8×10^{-2} $\eta=4$: 3.2×10^{-2} $\eta=5$: 3.8×10^{-2}
References					
Level identif.					
$\tau_{\frac{1}{2}}$	Ve 60; D 64; *Ham 64*		G 54	Ve 61	Ve 61
Int. conv. coef.	Su 60		Sut 62	Sc 59	Sc 59
$M2/E1$				Sc 59	Sc 59
Relat. intens.		Su 60	Sut 62		Sc 59
Discussion				Su 60a	

CC-0. In Public Domain. Gurukul Kangri Collection, Haridwar

Digitized by Arya Samaj Foundation Chennai and eGangotri

TABLE B–IIIA (*Continued*)

Nucleus	$_{61}Gd^{155}$	$_{64}Gd^{155}$	$_{64}Gd^{155}$	$_{64}Gd^{155}$	$_{64}Gd^{157}$	$_{64}Gd^{157}$
$J_i\pi_i\Omega_i[N, n_z, \Lambda]_i$	$(\frac{3}{2})^+$; $\frac{3}{2}[651]$		$(\frac{5}{2})^+$; $\frac{5}{2}[642]$		$\frac{5}{2}^+$; $\frac{5}{2}[642]$	
E (initial level)	86.5 keV		105 keV		64 keV	
τ_i(level)[sec^{-1}]	5×10^{-9}		1.05×10^{-9}		4.6×10^{-7}	
$J_f\pi_f\Omega_f[N, n_z, \Lambda]_f$	$\frac{3}{2}^-$; $\frac{3}{2}[521]$	$\frac{5}{2}^-$; $\frac{3}{2}[521]$	$\frac{3}{2}^-$; $\frac{3}{2}[521]$	$\frac{5}{2}^-$; $\frac{3}{2}[521]$	$\frac{3}{2}^-$; $\frac{3}{2}[521]$	$\frac{5}{2}^-$; $\frac{3}{2}[521]$
E (final level)	g.s.	60 keV	g.s.	60 keV	g.s.	54.5 keV
E (transition)	86.5 keV	26.5 keV	105 keV	45 keV	64.0 keV	9.5 keV
Experimental internal conversion coefficient	$\alpha_K=0.49\pm0.07$	$\alpha_L=1.2$	$\alpha_K=0.29\pm0.05$		$\alpha_K\sim0.8$	$\alpha_t\sim32$
Theoretical internal conv. coef. for pure $E1$	$\alpha_K=0.32$		$\alpha_K=0.20$			
Mixing Ratio $M2/E1$	≤0.04		≤0.07			
Relative gamma intensity	96%	4%	96.5%	3.5%	(50±15)%	(50±15)%
$T(E1)$[sec^{-1}]	8.0×10^{7}	3.2×10^{6}	5.2×10^{8}	1.9×10^{7}	2.7×10^{6}	2.25×10^{4}
Hindrance H_W	4.3×10^{-5}	6.1×10^{-5}	1.55×10^{-4}	7.2×10^{-5}	3.5×10^{-7}	9.1×10^{-6}
Hindrance H_N for η_i and η_f	$\eta=3$: 1.03 $\eta=4$: 0.62 $\eta=5$: 1.25	2.2 1.3 2.7	$\eta=3$: 1.6 $\eta=4$: 1.2 $\eta=5$: 1.2	1.6 1.2 1.2	$\eta=3$: 3.6×10^{-3} $\eta=4$: 2.8×10^{-3} $\eta=5$: 2.8×10^{-3}	0.21 0.17 0.17
References						
Level identif.						
τ_i	Ve 60; Hau 62		Hau 62		K 63	
Int. conv. coef.	Sub 62		Sub 62			
$M2/E1$	Sub 62		Sub 62			
Relat. intens.		Hat 59	Hat 62	Hat 62	K 63	K 63
Discussion	Sub 62		De 60			

CC-0. In Public Domain. Gurukul Kangri Collection, Haridwar

Digitized by Arya Samaj Foundation Chennai and eGangotri

TABLE B-IIIA (*Continued*)

Nucleus	$_{65}Tb^{159}$	$_{65}Tb^{159}$	$_{65}Tb^{159}$	$_{65}Tb^{159}$	$_{65}Tb^{161}$
$J_i\pi_i\Omega_i[N, n_z, \Lambda]_i$	$(\frac{5}{2})^-$; $\frac{5}{2}[532]$			$(\frac{3}{2}, \frac{5}{2}, \frac{7}{2})^+$	$\frac{7}{2}^-$; $\frac{7}{2}[523]$
E (initial level)	362 keV			560 keV	418 keV
τ_i(level)[sec^{-1}]	2×10^{-10} 1.7×10^{-10}			$B(E2)=0.03$	$(8.7\pm0.4)\times10^{-10}$
$J_f\pi_f\Omega_f[N, n_z, \Lambda]_f$	$\frac{3}{2}^+$; $\frac{3}{2}[411]$	$\frac{5}{2}^+$; $\frac{3}{2}[411]$	$\frac{7}{2}^+$; $\frac{3}{2}[411]$	$(\frac{5}{2})^-$; $\frac{5}{2}[532]$	$\frac{5}{2}^+$; $\frac{5}{2}[413]$
E (final level)	g.s.	58 keV	137 keV	362 keV	315 keV
E (transition)	362 keV	305 keV	225 keV	198 keV	102 keV
Experimental internal conversion coefficient	$\alpha_K=0.008$	$\alpha_K\leq0.04$			
Theoretical internal conv. coef. for pure $E1$	$\alpha_K=0.009$	$\alpha_K=0.014$	$\alpha_K=0.030$		$\alpha_t=0.275$
Mixing Ratio $M2/E1$	~0				~0
Relative gamma intensity	97%	8.3×10^{-3} 7.3×10^{-3}	1.8%	40%	13.2%
$T(E1)$[sec^{-1}]	4.0×10^{9}	3.5×10^{7}	7.0×10^{7}	9.0×10^{9}	8.3×10^{7}
Hindrance H_W	2.9×10^{-5}	4.2×10^{-7}	2.1×10^{-6}	4.1×10^{-4}	2.6×10^{-5}
Hindrance H_N for η_i and η_f	$\eta=3$: 0.13 $\eta=4$: 0.11 $\eta=5$: 0.13	4.6×10^{-3} 3.9×10^{-3} 4.6×10^{-3}	0.13 0.11 0.13		$\eta=3$: 0.18 $\eta=4$: 0.13 $\eta=5$: 0.095
References					
Level identif.				Na 60	
τ_i	Me 59a; *Va 62*			Na 60	Lo 64
Int. conv. coef.	Me 59a	Pe 64			
$M2/E1$	Me 59a				Sc 59a
Relat. intens.	Sub 62	*Sub 62*; Ew 64	Sub 62	Na 60	Sc 59a
Discussion				Di 63	

CC-0. In Public Domain. Gurukul Kangri Collection, Haridwar

Digitized by Arya Samaj Foundation Chennai and eGangotri

TABLE B-IIIA (*Continued*)

Nucleus	$_{66}Dy^{161}$	$_{66}Dy^{161}$	$_{67}Ho^{165}$	$_{69}Tm^{167}$	$_{69}Tm^{169}$	$_{69}Tm^{169}$
$J_i\pi_i\Omega_i[N, n_z, \Lambda]_i$	$(\frac{5}{2})^-$; $\frac{5}{2}[523]$	$(\frac{3}{2})^-$; $\frac{3}{2}[521]$	$(\frac{3}{2}, \frac{5}{2})^-$	$\frac{7}{2}^-$; $\frac{7}{2}[523]$	$\frac{7}{2}^-$; $\frac{7}{2}[523]$	$\frac{9}{2}^-$; $\frac{7}{2}[523]$
E (initial level)	25.7 keV	74.5 keV	515 keV	292.7 keV	379.3 keV	472.9 keV
τ_i(level) [sec^{-1}]	2.7×10^{-8}	$(3.0\pm0.3)\times10^{-9}$ $(2.3\pm0.7)\times10^{-9}$	$B(E2)=0.016$ $<10^{-9}$	$(0.9\pm0.1)\times10^{-6}$	4.5×10^{-8} 3.6×10^{-8}	1.4×10^{-10}
$J_f\pi_f\Omega_f[N, n_z, \Lambda]_f$	$\frac{5}{2}^+$; $\frac{5}{2}[642]$	$\frac{5}{2}^+$; $\frac{5}{2}[642]$	$\frac{3}{2}^+$; $\frac{3}{2}[411]$	$\frac{7}{2}^+$; $\frac{7}{2}[404]$	$\frac{7}{2}^+$; $\frac{7}{2}[404]$	$\frac{7}{2}^+$; $\frac{7}{2}[404]$
E (final level)	g.s.	g.s.	360 keV	179.4 keV	316.2 keV	316.2 keV
E (transition)	25.7 keV	74.5 keV	155 keV	113.3 keV	63.1 keV	156.7 keV
Experimental internal conversion coefficient					$\alpha_L=0.019\pm0.04$	$\alpha_t=0.089$
Theoretical internal conv. coef. for pure $E1$	$\alpha_L=1.8$	$\alpha_K=0.52$			$\alpha_t\cong1.05$	$\alpha_K=0.076$
Mixing Ratio $M2/E1$					<0.001	0.0001
Relative gamma intensity	100%	11%	20% 16%	1.03×10^6	96%	7.2%
$T(E1)$ [sec^{-1}]	7.6×10^6	3.2×10^7	3.6×10^9	2.3×10^{-7}	1.5×10^7	3.7×10^6
Hindrance H_W	1.3×10^{-4}	2.6×10^{-5}	3.2×10^{-4}		2.1×10^{-5}	3.2×10^{-7}
Hindrance H_N for η_i and η_f	$\eta=3.5$: 2.5 $\eta=4.5$: 2.3 $\eta=6$: 2.1	$\eta=4$: 0.15 $\eta=5$: 0.15 $\eta=6$: 0.085		$\eta=3.5$: 0.015 $\eta=4.5$: 0.018 $\eta=6$: 0.015	$\eta=3.5$: 1.3 $\eta=4.5$: 1.35 $\eta=6$: 1.6	$\eta=3.5$: 0.087 $\eta=4.5$: 0.090 $\eta=6$: 0.11
References						
Level identif.				Har 59; Tam 65		
τ_i	Ve 60; Han 58	Han 58; *Ve 57*	*Na 60*; Ha 64	Tam 65	*Mih 56*; Ax 63; Bak	Ax 63
Int. conv. coef.						Ax 63
$M2/E1$						Ax 63
Relat. intens.			*Po 61*; Cra	Tam 65	Ax 63; Hat 56	
Discussion			Di 63	Tam 65; Wil 60	Ni 58	

CC-0. In Public Domain. Gurukul Kangri Collection, Haridwar

Digitized by Arya Samaj Foundation Chennai and eGangotri

TABLE B-IIIA (*Continued*)

Nucleus	$_{69}Tm^{169}$	$_{70}Yb^{173}$	$_{70}Yb^{173}$	$_{70}Yb^{173}$	$_{70}Yb^{173}$	$_{70}Yb^{177}$
$J_i\pi_i\Omega_i[N, n_z, \Lambda]_i$	$(\frac{3}{2}, \frac{5}{2})^+$	$\frac{7}{2}^+$; $\frac{7}{2}$[633]			$\frac{7}{2}^-$; $\frac{7}{2}$[514]	$\frac{7}{2}^-$; $\frac{7}{2}$[514]
E (initial level)	565 keV	351 keV			637 keV	104 keV
$\tau_{\frac{1}{2}}$(level) [sec^{-1}]	$B(E2)=0.05$	4.2×10^{-10}			$B(E2)=0.070$	
		$(4.7\pm0.3)\times10^{-10}$			$(1.9\pm0.2)\times10^{-10}$	$(5.0\pm0.4)\times10^{-9}$
						$(4.48\pm0.08)\times10^{-9}$
$J_f\pi_f\Omega_f[N, n_z, \Lambda]_f$	$(\frac{5}{2}, \frac{7}{2})^-$; $\frac{7}{2}$[523]	$\frac{5}{2}^-$; $\frac{5}{2}$[512]	$\frac{7}{2}^-$; $\frac{5}{2}$[512]	$\frac{9}{2}^-$; $\frac{5}{2}$[512]	$\frac{7}{2}^+$; $\frac{7}{2}$[633]	$\frac{9}{2}^+$; $\frac{9}{2}$[624]
E (final level)	334 keV	g.s.	78.7 keV	179.5 keV	351 keV	g.s.
E (transition)	231 keV	351 keV	272 keV	171 keV	286 keV	104 keV
Experimental internal conversion coefficient		$\alpha=0.02$	$\alpha=0.05$	$\alpha=0.06$	$\alpha_t=0.014$	
Theoretical internal conv. coef. for pure $E1$		$\alpha_K=0.0115$	$\alpha_K=0.0215$	$\alpha_K=0.070$	$\alpha_K=0.019$	$\alpha_t=0.49$
Mixing Ratio $M2/E1$					≤0.05	~0
Relative gamma intensity		2.3%	82%	15.6%	45%	100%
$T(E1)$ [sec^{-1}]	80%	3.7×10^{7}	1.3×10^{9}	2.4×10^{8}	1.6×10^{9}	9.3×10^{7}
Hindrance H_W	7.0×10^{10}	2.8×10^{-7}	2.1×10^{-5}	1.55×10^{-5}	2.25×10^{-5}	2.26×10^{-5}
Hindrance H_N for η_i and η_f		$\eta=4$: 3.9×10^{-3}	0.98	5.7	1.45	$\eta=3.5$: 0.41
		$\eta=5$: 5.7×10^{-3}	1.4	7.8	1.45	$\eta=4.5$: 0.35
		$\eta=6$: 2.8×10^{-3}	0.52	3.1	1.45	$\eta=6$: 0.26
References						
Level identif.	1.6×10^{-3}					
$\tau_{\frac{1}{2}}$	Po 61	*Va 62*; Berl 61			Alk 63; *Berl 61*	*Lo 64*; Mal 65
Int. conv. coef.		Bi 59	Bi 59	Bi 59	Bi 59	
$M2/E1$					Bi 59	Hof 60
Relat. intens.	Po 61		Wil 60	Wil 60	Bi 59	Hof 60
Discussion	Di 63					

CC-0. In Public Domain. Gurukul Kangri Collection, Haridwar

Digitized by Arya Samaj Foundation Chennai and eGangotri

TABLE B–IIIA (*Continued*)

Nucleus	$_{71}Lu^{175}$	$_{71}Lu^{175}$	$_{71}Lu^{175}$	$_{71}Lu^{177}$	$_{72}Hf^{177}$	$_{72}Hf^{177}$
$J_i\pi_i\Omega_i[N, n_z, \Lambda]_i$	$\frac{9}{2}^-$; $\frac{9}{2}$[514]			$\frac{9}{2}^-$; $\frac{9}{2}$[514]	$\frac{9}{2}^+$; $\frac{9}{2}$[624]	
E (initial level)	396.3 keV			147 keV	321 keV	
$\tau_{\frac{1}{2}}$(level)[sec^{-1}]	3.1×10^{-9} $(3.4\pm0.3)\times10^{-9}$			1.22×10^{-7}	6.47×10^{-10} 5.2×10^{-10}	
$J_f\pi_f\Omega_f[N, n_z, \Lambda]_f$	$\frac{7}{2}^+$; $\frac{7}{2}$[404]	$\frac{9}{2}^+$; $\frac{7}{2}$[404]	$\frac{11}{2}^+$; $\frac{7}{2}$[404]	$\frac{7}{2}^+$; $\frac{7}{2}$[404]	$\frac{7}{2}^-$; $\frac{7}{2}$[514]	$\frac{9}{2}^-$; $\frac{7}{2}$[514]
E (final level)	g.s.	113.8 keV	251.5 keV	g.s.	g.s.	113 keV
E (transition)	396.1 keV	282.6 keV	144.8 keV	147 keV	321 keV	208 keV
Experimental internal conversion coefficient	$\alpha_t=0.075$	$\alpha=0.034$	$\alpha=0.12$	$\alpha_K<0.4$ $\alpha_t=0.63\pm0.08$	$\alpha=0.1$	$\alpha=0.044$
Theoretical internal conv. coef. for pure $E1$	$\alpha_K=0.0085$	$\alpha_K=0.0195$	$\alpha_K=0.11$	$\alpha_K=0.10$	$\alpha_K=0.015$	$\alpha_K=0.0445$
Mixing Ratio $M2/E1$	0.25	0.05 0.02	~0	0.09 <0.04	0.18	~0.001
Relative gamma intensity	60%	36%	4%	100%	2.2%	97.5%
$T(E1)$[sec^{-1}]	1.0×10^{8}	7.7×10^{7}	7.5×10^{6}	3.6×10^{6}	2.5×10^{7}	1.3×10^{9}
Hindrance H_W	5.05×10^{-7}	1.1×10^{-6}	7.9×10^{-7}	3.7×10^{-7}	2.3×10^{-7}	4.6×10^{-5}
Hindrance H_N for η_i and η_f	$\eta=3.5$: 8.9×10^{-3} $\eta=4.5$: 5.5×10^{-3} $\eta=6$: 2.8×10^{-3}	8.6×10^{-2} 5.2×10^{-2} 2.7×10^{-2}	6.2×10^{-1} 3.8×10^{-1} 1.9×10^{-1}	$\eta=3.5$: 6.5×10^{-3} $\eta=4.5$: 4.0×10^{-3} $\eta=6$: 2.0×10^{-3}	$\eta=3.5$: 6.5×10^{-3} $\eta=4.5$: 3.6×10^{-3} $\eta=6$: 2.7×10^{-3}	3.8 3.3 2.6
References						
Level identif.						
$\tau_{\frac{1}{2}}$	Hau 61; Va 57			W 55	Hau 62a; *Wes 61*	
Int. conv. coef.	Hat 56	Hat 56	Hat 56	Mi 56a; W 55	Wes 61	Ma 55
$M2/E1$	Hat 56	Cl 61; Hat 56	Hat 56	W 55; Mi 56a	Wes 61	Ma 55
Relat. intens.	Hat 56	Hat 56	Hat 56		Wes 61	Wes 61
Discussion					Ax 64	Ax 64

CC-0. In Public Domain. Gurukul Kangri Collection, Haridwar

Digitized by Arya Samaj Foundation Chennai and eGangotri

TABLE B-IIIA (*Continued*)

Nucleus	$_{72}Hf^{177}$	$_{72}Hf^{177}$	$_{72}Hf^{177}$	$_{72}Hf^{177}$	$_{72}Hf^{177}$	$_{72}Hf^{177}$
$J_i\pi_i\Omega_i[N, n_z, \Lambda]_i$		$\frac{11}{2}^+$; $\frac{9}{2}[624]$		$\frac{13}{2}^+$; $\frac{9}{2}[624]$		$\frac{15}{2}^+$; $\frac{9}{2}[624]$
E (initial level)		426.8 keV		555.2 keV		708.5 keV
τ_i(level)[sec^{-1}]						
$J_f\pi_f\Omega_f[N, n_z, \Lambda]_f$	$\frac{11}{2}^-$; $\frac{7}{2}[514]$	$\frac{9}{2}^-$; $\frac{7}{2}[514]$	$\frac{11}{2}^-$; $\frac{7}{2}[514]$	$\frac{11}{2}^-$; $\frac{7}{2}[514]$	$\frac{13}{2}^-$; $\frac{7}{2}[514]$	$\frac{13}{2}^-$; $\frac{7}{2}[514]$
E (final level)	250 keV	113 keV	250 keV	250 keV	409.1 keV	409.1 keV
E (transition)	71 keV	313.5 keV	177.0 keV	306.0 keV	145.6 keV	299.1 keV
Experimental internal conversion coefficient	$\alpha=1.0$					
Theoretical internal conv. coef. for pure $E1$	$\alpha_K=0.74$					
Mixing Ratio $M2/E1$						
Relative gamma intensity	0.3%	8.2%	23.5%	8.7%	7.4%	6.4%
$T(E1)$[sec^{-1}]	4.0×10^6					
Hindrance H_W	3.6×10^{-6}	[8×10^{-6}]	[1.1×10^{-4}]	[1.4×10^{-4}]	[1.1×10^{-4}]	[9.5×10^{-6}]
Hindrance H_N for η_i and η_f	$\eta=3.5:3.0$	0.175	5.9	3.5	4.9	
	$\eta=4.5:2.6$	0.15	5.0	3.0	4.2	
	$\eta=6:\ 2.0$	0.11	3.8	2.3	3.2	
References						
Level identif.						
τ_i						
Int. conv. coef.	Ma 55					
$M2/E1$						
Relat. intens.	Wes 61	Ax 64	Ax 64	Ax 64	Ax 64	Ax 64
Discussion	Ax 64	Ax 64	Ax 64	Ax 64	Ax 64	Ax 64

CC-0. In Public Domain. Gurukul Kangri Collection, Haridwar

Digitized by Arya Samaj Foundation Chennai and eGangotri

TABLE B–IIIA (*Continued*)

Nucleus	$_{72}Hf^{177}$	$_{72}Hf^{179}$	$_{73}Ta^{179}$	$_{73}Ta^{181}$	$_{75}Re^{187}$	$_{75}Re^{187}$
$J_i\pi_i\Omega_i[N, n_z, \Lambda]_i$		$\frac{7}{2}^-$; $\frac{7}{2}$[514]	$\frac{9}{2}^-$; $\frac{9}{2}$[514]	$\frac{9}{2}^-$; $\frac{9}{2}$[514]	$\frac{5}{2}^-$; $\frac{5}{2}$[532]	
E (initial level)		217 keV	30.7 keV	6.25 keV	686.1 keV	
$\tau_{\frac{1}{2}}$(level)[sec^{-1}]		$(1.5\pm0.15)\times10^{-9}$ $(1.86\pm0.05)\times10^{-9}$	$(1.5\pm0.2)\times10^{-6}$	6.8×10^{-6}	$(2\pm0.7)\times10^{-10}$ 5.9×10^{-12} $(2.8\pm1.9)\times10^{-10}$	
$J_f\pi_f\Omega_f[N, n_z, \Lambda]_f$	$\frac{1}{2}^-$; $\frac{7}{2}$[514]	$\frac{9}{2}^+$; $\frac{9}{2}$[624]	$\frac{7}{2}^+$; $\frac{7}{2}$[404]	$\frac{7}{2}^+$; $\frac{7}{2}$[404]	$\frac{5}{2}^+$; $\frac{5}{2}$[402]	$\frac{7}{2}^+$; $\frac{5}{2}$[402]
E (final level)	591.5 keV	g.s.	g.s.	g.s.	g.s.	134.25 keV
E (transition)	117.0 keV	217 keV	30.7 keV	6.25 keV	686 keV	551.7 keV
Experimental internal conversion coefficient		$\alpha_t=0.055$	$\alpha_t=3.5$	$\alpha_t=44\pm7$	$\alpha_t=0.0048$	
Theoretical internal conv. coef. for pure $E1$		$\alpha_K=0.042$			$\alpha_K=0.0033$	$\alpha_K=0.0052$
Mixing Ratio $M2/E1$		~0	~0			
Relative gamma intensity	7.7%	100%	100%	100%	46%	12%
$T(E1)$[sec^{-1}]		4.4×10^{8}	1.03×10^{5}	2.5×10^{3}	5.4×10^{10}	1.4×10^{10}
Hindrance H_W	$[1.9\times10^{-4}]$	1.35×10^{-5}	1.12×10^{-6}	3.25×10^{-6}	5.1×10^{-5}	2.5×10^{-5}
Hindrance H_N for η_i and η_f		$\eta=3.5$: 0.21 $\eta=4.5$: 0.17 $\eta=6$: 0.13	$\eta=3.5$: 2.0×10^{-2} $\eta=4.5$: 1.2×10^{-2} $\eta=6$: 7.1×10^{-3}	$\eta=3.5$: 2.0×10^{-2} $\eta=4.5$: 3.5×10^{-2} $\eta=6$: 1.8×10^{-2}	$\eta=3$: 1.8 $\eta=3.5$: 1.6 $\eta=4$: 2.6	2.2 2.0 3.2
References						
Level identif.						
$\tau_{\frac{1}{2}}$		*Ve 63*; Mal 65	P 64	Cl 61	Var 62a; *Lan 64*; Shu 65	
Int. conv. coef.		Hof 59	Va 63	Mu 59	Bis 62	
$M2/E1$		Hof 59	P 64			
Relat. intens.	Ax 64				Ne 60	Ne 60
Discussion	Ax 64		Va 63		Ga 60	Ga 60

CC-0. In Public Domain. Gurukul Kangri Collection, Haridwar

Digitized by Arya Samaj Foundation Chennai and eGangotri

TABLE B–IIIB. *K*-forbidden transitions for odd-A deformed nuclei with $90 \leq N \leq 114$.

Nucleus	$_{65}Tb^{161}$	$_{65}Tb^{161}$	$_{69}Tm^{167}$	$_{69}Tm^{167}$	$_{69}Tm^{169}$	$_{69}Tm^{169}$
$J_i\pi_i\Omega_i[N, n_z, \Lambda]_i$	$\frac{7}{2}^-$; $\frac{7}{2}[523]$		$\frac{7}{2}^-$; $\frac{7}{2}[523]$		$\frac{7}{2}^-$; $\frac{7}{2}[523]$	
E (initial level)	418 keV		292.7 keV		379.3 keV	
τ_i(level) [sec^{-1}]	$(8.7\pm0.5)\times10^{-10}$		$(0.9\pm0.1)\times10^{-6}$		3.6×10^{-8}	
$J_f\pi_f\Omega_f[N, n_z, \Lambda]_f$	$\frac{5}{2}^+$; $\frac{3}{2}[411]$	$\frac{7}{2}^+$; $\frac{3}{2}[411]$	$\frac{5}{2}^+$; $\frac{1}{2}[411]$	$\frac{7}{2}^+$; $\frac{1}{2}[411]$	$\frac{5}{2}^+$; $\frac{1}{2}[411]$	$\frac{7}{2}^+$; $\frac{1}{2}[411]$
E(final level)	57 keV	134 keV	116.5 keV	142.3 keV	118.2 keV	139.0 keV
E(transition)	361 keV	284 keV	176.2 keV	150.3 keV	261 keV	241 keV
Experimental internal conversion coefficient						
Theoretical internal conv. coef. for pure $E1$	$\alpha_t=0.011$	$\alpha_t=0.020$			$\alpha_t=0.03$	$\alpha_t=0.03$
Mixing Ratio $M2/E1$	~0	~0				
Relative gamma intensity	77.5%	9.5%			3.7%	0.27%
$T(E1)$ [sec^{-1}]	5.9×10^{8}	7.3×10^{7}	3.8×10^{5}	4.8×10^{4}	3.65×10^{5}	2.55×10^{4}
Hindrance H_W	4.2×10^{-7}	1.1×10^{-6}	2.2×10^{-8}	4.5×10^{-9}	6.75×10^{-9}	6.0×10^{-10}
Hindrance H_N for η_i and η_f						
References						
Level identif.			Har 59			
τ_i	Lo 64		Tam 65		Ax 62	
Int. conv. coef.						
$M2/E1$	Sc 59a	Sc 59a				
Relat. intens.	Sc 59a	Sc 59a	Tam 65	Tam 65	Ax 62	Ax 62
Discussion						

CC-0. In Public Domain. Gurukul Kangri Collection, Haridwar

Digitized by Arya Samaj Foundation Chennai and eGangotri

TABLE B–IIIB (*Continued*)

Nucleus	$_{69}Tm^{171}$	$_{69}Tm^{171}$	$_{70}Yb^{173}$	$_{71}Lu^{173}$	$_{75}Re^{183}$	$_{75}Re^{183}$
$J_i\pi_i\Omega_i[N, n_z, \Lambda]_i$	$\frac{7}{2}^-$; $\frac{7}{2}[523]$		$\frac{3}{2}^+$; $\frac{1}{2}[651]$	$\frac{5}{2}^-$; $\frac{1}{2}[541]$	$\frac{9}{2}^-$; $\frac{9}{2}[514]$	
E(initial level)	425.1 keV		395 keV	123.6 keV	496 keV	
$\tau_{\frac{1}{2}}$(level)[sec^{-1}]	2.6×10^{-6}		2.9×10^{-6}	7.0×10^{-5} $(7.7\pm0.5)\times10^{-5}$	7.7×10^{-9}	
$J_f\pi_f\Omega_f[N, n_z, \Lambda]_f$	$\frac{5}{2}^+$; $\frac{1}{2}[411]$	$\frac{7}{2}^+$; $\frac{1}{2}[411]$	$\frac{5}{2}^-$; $\frac{5}{2}[512]$	$\frac{7}{2}^+$; $\frac{7}{2}[404]$	$\frac{7}{2}^+$; $\frac{5}{2}[402]$	$\frac{9}{2}^+$; $\frac{5}{2}[402]$
E(final level)	116.7 keV	129.1 keV	g.s.	g.s.	114 keV	260 keV
E(transition)	308.4 keV	296 keV	395 keV	123.6 keV	382 keV	236 keV
Experimental internal conversion coefficient	$\alpha_K=0.017$	$\alpha_K=0.35$	$\alpha_t=0.0085$	$\alpha_K=0.145\pm0.02$	$\alpha_K=0.011$	
Theoretical internal conv. coef. for pure $E1$	$\alpha_K=0.016$	$\alpha_L=0.017$				
Mixing Ratio $M2/E1$	~0	0.034 ± 0.020	~0		0.005	~0
Relative gamma	75%	25%	100%	100%	90%	6.2%
$T(E1)$[sec^{-1}]	2.0×10^5	6.7×10^4	2.4×10^5	1.0×10^4	8.0×10^7	5.5×10^6
Hindrance H_W	2.3×10^{-9}	8.4×10^{-10}	1.25×10^{-9}	1.7×10^{-9}	4.47×10^{-7}	1.3×10^{-7}
Hindrance H_N for η_i and η_f						
References						
Level identif.				V 62	Mot 59; Ga 62a	
$\tau_{\frac{1}{2}}$	Cra 58		Ku 63	*V 62*; P 64a	Ne 60	
Int. conv. coef.	Cra 58	Cra 58	Ku 63	P 64a	Ni 58	
$M2/E1$	Cra 58	Cra 58	Ku 63		Hey 56	Hey 56
Relat. intens.	Cra 58	Cra 58	Ku 63		Hey 56	Hey 56
Discussion				Har 59	Ni 58	

CC-0. In Public Domain. Gurukul Kangri Collection, Haridwar

Digitized by Arya Samaj Foundation Chennai and eGangotri

TABLE B-IIIB (*Continued*)

Nucleus	$_{75}Re^{187}$
$J_i\pi_i\Omega_i[N, n_z, \Lambda]_i$	$\frac{9}{2}^-$; $\frac{9}{2}[514]$
E(initial level)	206 keV
$\tau_{\frac{1}{2}}$(level) [sec^{-1}]	5.5×10^{-7}
$J_f\pi_f\Omega_f[N, n_z, \Lambda]_f$	$\frac{7}{2}^+$; $\frac{5}{2}[402]$
E(final level)	134 keV
E(transition)	72 keV
Experimental internal conversion coefficient	$\alpha_K\sim2$
Theoretical internal conv. coef. for pure $E1$	
Mixing Ratio $M2/E1$	0.01
Relative gamma intensity	96%
$T(E1)$ [sec^{-1}]	4.0×10^5
Hindrance H_W	3.3×10^{-7}
Hindrance H_N for η_i and η_f	
References	
Level identif.	
$\tau_{\frac{1}{2}}$	Mc 49
Int. conv. coef.	Ga 60
$M2/E1$	Mic 63
Relat. intens.	Mic 63
Discussion	K 63

CC-0. In Public Domain. Gurukul Kangri Collection, Haridwar

Digitized by Arya Samaj Foundation Chennai and eGangotri

TABLE B–IIIC. K-allowed transitions for nuclei with $N \geq 134$ (odd A).

Nucleus	$_{88}Ra^{223}$	$_{89}Ac^{225}$	$_{89}Ac^{227}$	$_{90}Th^{231}$	$_{90}Th^{231}$	$_{93}Np^{237}$
$J_i\pi_i\Omega_i[N, n_z, \Lambda]_i$		$(\frac{1}{2}^-)$; $\frac{1}{2}[530]$	$\frac{3}{2}^+$; $\frac{3}{2}[651]$	$(\frac{5}{2})^-$; $\frac{5}{2}[752]$		$\frac{5}{2}^-$; $\frac{5}{2}[523]$
E(initial level)	50 keV	40.5 keV	27.5 keV	185 keV		59.6 keV
$\tau_{\frac{1}{2}}$(level) [sec^{-1}]	6.3×10^{-10}	$\leq 4\times10^{-9}$	3.7×10^{-8} 4.2×10^{-8}	7.7×10^{-10}		6.3×10^{-8}
$J_f\pi_f\Omega_f[N, n_z, \Lambda]_f$	$\frac{1}{2}^+$	$(\frac{3}{2})^+$; $\frac{3}{2}[651]$	$\frac{3}{2}^-$; $\frac{3}{2}[532]$	$(\frac{5}{2})^+$; $\frac{5}{2}[633]$	$(\frac{7}{2})^+$; $\frac{5}{2}[633]$	$\frac{5}{2}^+$; $\frac{5}{2}[642]$
E(final level)	g.s.	g.s.	g.s.	g.s.	41 keV	g.s.
E(transition)	49.8 keV	40.5 keV	27.5 keV	185 keV	144 keV	59.6 keV
Experimental internal conversion coefficient	$\alpha = 0.7\pm0.2$	$\alpha = 1.29$	$\alpha_t = 4.0$			$\alpha_t = 1.0\pm0.1$ $\alpha_{LI} = 1.6\alpha_{th}$ $\alpha_{LI} = 2.7\alpha_{th}$
Theoretical internal conv. coef. for pure $E1$						
Mixing Ratio $M2/E1$			$\leq 3\times10^{-3}$			
Relative gamma intensity	100%	100%	100%	82%	18%	93.5%
$T(E1)$ [sec^{-1}]	7.4×10^{8}	$\geq 7.5\times10^{7}$	3.5×10^{6}	6.8×10^{8}	1.5×10^{8}	4.0×10^{6}
Hindrance H_W	2.2×10^{-3}	$\geq 3.1\times10^{-4}$	4.5×10^{-5}	2.9×10^{-5}	1.3×10^{-5}	4.9×10^{-6}
Hindrance H_N for η_i and η_f		$\eta=2$: ≥ 1.4 $\eta=3$: ≥ 0.80 $\eta=4$: ≥ 0.70	$\eta=2$: 0.31 $\eta=3$: 0.21 $\eta=4$: 0.16	$\eta=2$: 9.3 $\eta=3$: 2.4 $\eta=4$: 3.2	$\eta=2$: 12 $\eta=3$: 3.1 $\eta=4$: 4.2	$\eta=2.5$: 3.5×10^{-1} $\eta=4.5$: 3.1×10^{-1} $\eta=6.0$: 2.9×10^{-1}
References						
Level identif.			Fo 64			
$\tau_{\frac{1}{2}}$	Va 59	Ste 55	T 53 and Fo 56	Ra 54		Be 52
Int. conv. coef.	Pi 57a	Ste 55	As 60			M 57
$M2/E1$			As 60			
Relat. intens.				Pi 57	Pi 57	M 57
Discussion			Ni 58			

CC-0. In Public Domain. Gurukul Kangri Collection, Haridwar

Digitized by Arya Samaj Foundation Chennai and eGangotri

TABLE B-IIIC (*Continued*)

Nucleus	$_{93}Np^{237}$	$_{93}Np^{237}$	$_{93}Np^{239}$	$_{93}Np^{239}$	$_{94}Pu^{239}$	$_{94}Pu^{239}$
$J_i\pi_i\Omega_i[N, n_z, \Lambda]_i$		$\frac{3}{2}^-$; $\frac{3}{2}$[521]	$\frac{5}{2}^-$; $\frac{5}{2}$[523]		$\frac{7}{2}^-$; $\frac{7}{2}$[743]	
E(initial level)		267 keV	74.6 keV		392 keV	
$\tau_{\frac{1}{2}}$(level) [sec^{-1}]		5.4×10^{-9}	1.4×10^{-9} 1.2×10^{-9}		1.9×10^{-7}	
$J_f\pi_f\Omega_f[N, n_z, \Lambda]_f$	$\frac{7}{2}^+$; $\frac{5}{2}$[642]	$\frac{5}{2}^+$; $\frac{5}{2}$[642]	$\frac{5}{2}^+$; $\frac{5}{2}$[642]	$\frac{7}{2}^+$; $\frac{5}{2}$[642]	$\frac{5}{2}^+$; $\frac{5}{2}$[622]	$\frac{7}{2}^+$; $\frac{5}{2}$[622]
E(final level)	33.2 keV	g.s.	g.s.	31.5 keV	286 keV	330 keV
E(transition)	26.4 keV	267 keV	74.6 keV	43 keV	106.1 keV	61.5 keV
Experimental internal conversion coefficient	$\alpha_t=10\pm2$ $\alpha_L=2\,\alpha_{th}$	$\alpha_K=0.63$ $\alpha_t=0.82$	$\alpha_t=0.27$	$\alpha_t=1.1$	$\alpha_L=0.23$	$\alpha_{LI}=0.04$
Theoretical internal conv. coef. for pure $E1$		$\alpha_K=0.06$		$\alpha_L=0.83$		
Mixing Ratio $M2/E1$						
Relative gamma intensity	6.5%	1.0%	91.5%	8.5%	80%	9.8%
$T(E1)$ [sec^{-1}]	2.75×10^{5}	7.0×10^{5}	3.6×10^{8}	2.0×10^{7}	2.9×10^{6}	3.2×10^{5}
Hindrance H_W	3.9×10^{-6}	9.7×10^{-9}	2.3×10^{-4}	6.5×10^{-5}	6.3×10^{-7}	3.6×10^{-7}
Hindrance H_N for η_i and η_f	8.7×10^{-2} 7.8×10^{-2} 7.2×10^{-2}	$\eta=2$: 1.2×10^{-4} $\eta=3$: 3.4×10^{-5} $\eta=4$: 2.8×10^{-5}	$\eta=2.5$: 2.1 $\eta=4.5$: 1.85 $\eta=6.0$: 1.7	1.45 1.3 1.2	$\eta=4$: 0.51 $\eta=6$: 0.15	0.13 3.7×10^{-2}
References						
Level identif.						
$\tau_{\frac{1}{2}}$		Bu 57	Ch 63; Fl 63		Eng 55	
Int. conv. coef.	M 57	Ra 57	As 60	As 60	Eng 55	Hol 57
$M2/E1$						
Relat. intens.	M 57	Dz 61		Ch 63	Ew 57	Ew 57
Discussion		Ni 58				

CC-0. In Public Domain. Gurukul Kangri Collection, Haridwar

Digitized by Arya Samaj Foundation Chennai and eGangotri

TABLE B–IIIC (*Continued*)

Nucleus	$_{95}Am^{243}$	$_{95}Am^{243}$	$_{96}Cm^{245}$	$_{96}Cm^{245}$
$J_i\pi_i\Omega_i[N, n_z, \Lambda]_i$	$\frac{5}{2}^+$; $\frac{5}{2}$[642]		$\frac{9}{2}^-$; $\frac{9}{2}$[734]	
E(initial level)	84 keV		394 keV	
$\tau_{\frac{1}{2}}$(level)[sec^{-1}]	2.0×10^{-9}		$\leq 8.0\times10^{-10}$	
$J_f\pi_f\Omega_f[N, n_z, \Lambda]_f$	$\frac{5}{2}^-$; $\frac{5}{2}$[523]	$\frac{7}{2}^-$; $\frac{5}{2}$[523]	$\frac{7}{2}^+$; $\frac{7}{2}$[624]	$\frac{9}{2}^+$; $\frac{7}{2}$[624]
E(final level)	g.s.	42 keV	g.s.	55 keV
E(transition)	84 keV	42 keV	394 keV	339 keV
Experimental internal conversion coefficient	$\alpha_t=0.20$			
Theoretical internal conv. coef. for pure $E1$				
Mixing Ratio $M2/E1$				
Relative gamma intensity	95.5%	4.5%	72%	15%
$T(E1)$[sec^{-1}]	2.7×10^{8}	1.4×10^{7}	$\geq 6.2\times10^{8}$	$\geq 1.3\times10^{8}$
Hindrance H_W	1.15×10^{-4}	4.8×10^{-5}	$\geq 2.6\times10^{-6}$	$\geq 8.5\times10^{-7}$
Hindrance H_N for η_i and η_f	$\eta=2.5$: 1.0 $\eta=4.5$: 0.92 $\eta=6.0$: 0.85	1.1 0.96 0.89	$\eta=2$: ≥ 2.4 $\eta=4$: ≥ 1.9	≥ 0.35 ≥ 0.27
References				
Level identif.				
$\tau_{\frac{1}{2}}$	Eng		Ste 57	
Int. conv. coef.	Eng 53			
$M2/E1$				
Relat. intens.	Fr 57	Fr 57	L 61	L 61
Discussion	Ni 58		M 56	

CC-0. In Public Domain. Gurukul Kangri Collection, Haridwar

Digitized by Arya Samaj Foundation Chennai and eGangotri

TABLE B–IIID. *K*-forbidden transitions for nuclei with $N \geq 134$ (odd A).

Nucleus	$_{91}Pa^{231}$	$_{91}Pa^{231}$	$_{91}Pa^{233}$	$_{91}Pa^{233}$	$_{94}Pu^{239}$	$_{94}Pu^{233}$
$J_i\pi_i\Omega_i[N, n_z, \Lambda]_i$	$\frac{5}{2}^+$; $\frac{5}{2}[642]$		$\frac{5}{2}^+$; $\frac{5}{2}[642]$		$\frac{7}{2}^-$; $\frac{7}{2}[743]$	
E(initial level)	84.1 keV		86.3 keV		392 keV	
τ_i(level) [sec^{-1}]	3.7×10^{-8} 4.5×10^{-8} 4.1×10^{-8}		3.7×10^{-8}		1.9×10^{-7}	
$J_f\pi_f\Omega_f[N, n_z, \Lambda]_f$	$\frac{3}{2}^-$; $\frac{1}{2}[530]$	$\frac{7}{2}^-$; $\frac{1}{2}[530]$	$\frac{3}{2}^-$; $\frac{1}{2}[530]$	$\frac{7}{2}^-$; $\frac{1}{2}[530]$	$\frac{5}{2}^+$; $\frac{1}{2}[631]$	$\frac{7}{2}^+$; $\frac{1}{2}[631]$
E(final level)	g.s.	58.5 keV	g.s.	57 keV	57 keV	76 keV
E (transition)	84.1 keV	25.6 keV	86.3 keV	29.2 keV	334.5 keV	316.1 keV
Experimental internal conversion coefficient	$\alpha_t = 2.8\pm0.4$	$\alpha_t = 4.8\pm1.2$	$\alpha_t = 1.9\pm0.7$	$\alpha_t = 3.0\pm0.8$		
Theoretical internal conv. coef. for pure $E1$					$\alpha_K \cong 0.03$	$\alpha_K \cong 0.03$
Mixing Ratio $M2/E1$	$\leq 2\times10^{-4}$					
Relative gamma intensity	36%	53.5%	53%	47%	5.8%	4.4%
$T(E1)$ [sec^{-1}]	1.25×10^{6}	2.1×10^{6}	2.7×10^{6}	2.3×10^{6}	1.9×10^{5}	1.45×10^{5}
Hindrance H_W	5.6×10^{-7}	3.3×10^{-5}	1.1×10^{-6}	2.5×10^{-5}	1.8×10^{-9}	1.15×10^{-9}
Hindrance H_N for η_i and η_f						
References						
Level identif.	Mot 59	Mot 59	Mot 59	Mot 59		
τ_i	Ho 56; *As 60* Mi 56; *Str 55*		Eng 54		Eng 55	
Int. conv. coef.	As 60	As 60	As 60	As 60		
$M2/E1$	As 60					
Relat. intens.			Ste 55			
Discussion	Ni 58				Ni 58	Ni 58

CC-0. In Public Domain. Gurukul Kangri Collection, Haridwar

Digitized by Arya Samaj Foundation Chennai and eGangotri

TABLE B-IVA. Transitions in even-A deformed nuclei with $90 \leq N \leq 114$ (odd-odd nuclei included).

Nucleus	$_{62}Sm^{152}$	$_{62}Sm^{152}$	$_{62}Sm^{152}$	$_{62}Sm^{152}$	$_{63}Eu_{89}^{152}$	$_{66}Dy^{160}$
$J_i\pi_i k_i$	1^-; 0		2^-; (1)		4^+	3^-; 1
E(initial level)	0.963 MeV		1.531 MeV		89.83 keV	1.399 MeV
τ_i(level) [sec^{-1}]	1.2×10^{-14}		$\geq 7\times10^{-15}$ $\geq 4.9\times10^{-15}$		$(4\pm1)\times10^{-7}$	
	2.5×10^{-14}		$(4.0\pm1.6)\times10^{-15}$			
$J_f\pi_f k_f$	0^+; 0	2^+; 0	2^+; 0	2^+; 2	3^-	2^+; 0
E(final level)	g.s.	0.122 MeV	0.122 MeV	1.087 MeV	g.s.	0.0867 MeV
E(transition)	963 keV	841 keV	1409 keV	444 keV	90 keV	1312 keV
Experimental internal conversion coefficient					$\alpha_K=0.30\pm0.05$ $\alpha_t\cong0.34$	
Theoretical internal conv. coef. for pure $E1$					$\alpha_K=0.31$	
Mixing Ratio $M2/E1$			~0	~0		~0
Relative gamma intensity	45%	55%	84%	16%	100%	
$T(E1)$ [sec^{-1}]	2.6×10^{13}	3.2×10^{13}	1.5×10^{14}	2.8×10^{13}	1.3×10^{6}	$\geq[1.3\times10^{14}]$
Hindrance H_W	1.0×10^{-2}	1.9×10^{-2}	1.9×10^{-2}	2.15×10^{-1}	6.3×10^{-7}	$\geq[2.0\times10^{-2}]$
References						
Level identif.					Ki 63	
τ_i	*Gr 58*; Sh 60		Vas 61; Per 62b; *S 64*		Ta 64	
Int. conv. coef.						
$M2/E1$					Ki 63	
Relat. intens.			Na 59	Na 59		Ew 61
Discussion					Ta 64	Boe 63

CC-0. In Public Domain. Gurukul Kangri Collection, Haridwar

Digitized by Arya Samaj Foundation Chennai and eGangotri

TABLE B–IV A (*Continued*)

Nucleus	$_{66}Dy^{160}$	$_{66}Dy^{160}$	$_{66}Dy^{160}$	$_{66}Dy^{160}$	$_{68}Er^{168}$	$_{68}Er^{168}$
$J_i\pi_i k_i$		$3^-; 2$			$3^-; 3$	
E (initial level)		1.358 MeV			1.095 MeV	
τ_i(level) [sec^{-1}]					1.2×10^{-7}	
$J_f\pi_f k_f$	$4^+; 0$	$2^+; 0$	$2^+; 0$	$(3^+); 2$	$2^+; 0$	$4^+; 0$
E(final level)	0.284 MeV	0.0867 MeV	0.966 MeV	1.094 MeV	0.080 MeV	0.264 MeV
E(transition)	1115 keV	1272 keV	392 keV	310 keV	1016 keV	831 keV
Experimental internal conversion coefficient						
Theoretical internal conv. coef. for pure $E1$						
Mixing Ratio $M2/E1$	~0					
Relative gamma intensity					0.5%	≤12%
$T(E1)$[sec^{-1}]	$\geq[8.6\times10^{13}]$	$[4.1\times10^{12}]$	$[7.1\times10^{11}]$	$[4.4\times10^{11}]$	2.9×10^{4}	$\leq7\times10^{5}$
Hindrance H_W	$\geq[2.1\times10^{-2}]$	$[6.7\times10^{-4}]$	$[4.0\times10^{-3}]$	$[5.0\times10^{-3}]$	9.1×10^{-12}	$\leq2.7\times10^{-10}$
References						
Level identif.						
τ_i					J 60	
Int. conv. coef.						
$M2/E1$						
Relat. intens.	Ew 61	Ew 61	Ew 61	Ew 61	Re 64	Re 64
Discussion	Boe 63	Boe 63	Boe 63	Boe 63		

CC-0. In Public Domain. Gurukul Kangri Collection, Haridwar

Digitized by Arya Samaj Foundation Chennai and eGangotri

TABLE B–IVA (*Continued*)

Nucleus	$_{68}Er^{168}$	$_{68}Er^{168}$	$_{68}Er^{168}$	$_{68}Er^{168}$	$_{68}Er^{168}$	$_{68}Er^{168}$
$J_i\pi_i k_i$				3^-; 3		
E(initial level)				1.543 MeV		
τ_i(level) [sec^{-1}]				$\leq 8\times10^{-10}$		
$J_f\pi_f k_f$	2^+; 2	3^+; 2	4^+; 2	2^+; 0	4^+; 0	2^+; 2
E(final level)	0.822 MeV	0.897 MeV	0.996 MeV	0.080 MeV	0.264 MeV	0.822 MeV
E(transition)	273 keV	198 keV	99 keV	1464 keV	1280 keV	721 keV
Experimental internal conversion coefficient						
Theoretical internal conv. coef. for pure $E1$						
Mixing Ratio $M2/E1$					$<8\times10^{-4}$	$<5\times10^{-4}$
Relative gamma intensity	$\leq 2.7\%$	80%	$\sim 5\%$	weak	5%	32%
$T(E1)$ [sec^{-1}]	$\leq 1.5\times10^{5}$	3.9×10^{6}	$\sim 3\times10^{5}$		$\geq 4.3\times10^{7}$	$\geq 2.6\times10^{8}$
Hindrance H_W	$\leq 2.7\times10^{-9}$	2.0×10^{-7}	$\sim 1\times10^{-7}$	$\geq 6.3\times10^{-10}$	$\geq 6.7\times10^{-9}$	$\geq 2.3\times10^{-7}$
References						
Level identif.						
τ_i				Bod 62a		
Int. conv. coef.						
$M2/E1$					Re 64	Re 64
Relat. intens.	Re 64	Re 64	Re 64	Re 64	Re 64	Re 64
Discussion				Re 64	Re 64	Re 64

CC-0. In Public Domain. Gurukul Kangri Collection, Haridwar

Digitized by Arya Samaj Foundation Chennai and eGangotri

TABLE B-IVA (*Continued*)

Nucleus	$_{68}Er^{163}$	$_{68}Er^{168}$	$_{72}Hf^{178}$	$_{72}Hf^{180}$	$_{74}W^{182}$	$_{74}W^{182}$
$J_i\pi_i k_i$			8^-; 8	8^-; 8	2^-; 2	
E(initial level)			1.1485 MeV	1.1428 MeV	1.289 MeV	
$\tau_{\frac{1}{2}}$(level) [sec^{-1}]			4.8	5.5 h	1.04×10^{-9} $(1.4\pm0.1)\times10^{-9}$ $(1.03\pm0.03)\times10^{-9}$	
$J_f\pi_f k_f$	3^+; 2	4^+; 2	8^+; 0	8^+; 0	2^+; 0	2^+; 2
E(final level)	0.897 MeV	0.996 MeV	1.0597 MeV	1.0858 MeV	0.100 MeV	1.222 MeV
E(transition)	646 keV	547 keV	88 keV	58 keV	1189 keV	67.9 keV
Experimental internal conversion coefficient			$\alpha_K=0.69$	$\alpha_L=0.33$	$\alpha_K=(4.2\pm0.35)\times10^{-3}$	$\alpha_t=0.31$ $\alpha_{LI}=0.17$ $\alpha_{LII}=\alpha_{LIII}=0.07$
Theoretical internal conv. coef. for pure $E1$					$\alpha_K=1.1\times10^{-3}$	
Mixing Ratio $M2/E1$			$(7\pm7)\times10^{-2}$	$\leq5\times10^{-2}$	~0.26	~0
Relative gamma intensity	(5%)	9%	100%	83%	~27%	~62%
$T(E1)$ [sec^{-1}]	$\geq4.3\times10^{7}$	$\geq7.8\times10^{7}$	8.1×10^{-2}	3.0×10^{-5}	1.8×10^{8}	3.15×10^{8}
Hindrance H_W	$\geq5.3\times10^{-8}$	$\geq1.6\times10^{-7}$	3.8×10^{-14}	4.8×10^{-17}	3.3×10^{-8}	3.0×10^{-4}
References						
Level identif.					Sta 64	
$\tau_{\frac{1}{2}}$			F 58	Bur 51	*Sun 61*; Dor 65; *Bas 63*; Berl 64	
Int. conv. coef.			Ga 62b	Gro 58	Sta 64	Mur 55
$M2/E1$			Deu 60	Deu 60	Sta 64	Hi 60
Relat. intens.	Re 64	Re 64			Mur 55	Mur 55
Discussion	Re 64	Re 64				

CC-0. In Public Domain. Gurukul Kangri Collection, Haridwar

Digitized by Arya Samaj Foundation Chennai and eGangotri

TABLE B–IVA (*Continued*)

Nucleus	$_{74}W^{182}$	$_{74}W^{182}$	$_{74}W^{182}$	$_{74}W^{182}$	$_{74}W^{182}$	$_{74}W^{182}$
$J_i\pi_i k_i$		$3^-; 2$				$4^-; 2$
E(initial level)		1.374 MeV				1.554 MeV
$\tau_{\frac{1}{2}}$(level) [sec^{-1}]		2.25×10^{-9}				4.7×10^{-9}
$J_f\pi_f k_f$	$2^+; 0$	$2^+; 0$	$4^+; 0$	$2^+; 2$	$3^+; 2$	$3^+; 2$
E(final level)	1.258 MeV	0.100 MeV	0.329 MeV	1.222 MeV	1.332 MeV	1.332 MeV
E(transition)	31.7 keV	1273 keV	1044.7 keV	152.5 keV	42.7 keV	222 keV
Experimental internal conversion coefficient	$\alpha\sim1.9$			$\alpha_K=0.068$	$\alpha\sim0.8$	$\alpha_K=0.044$ $K/L=6.3$
Theoretical internal conv. coef. for pure $E1$				$\alpha_K=0.105$		$\alpha_K=0.041$ $K/L=6.3$
Mixing Ratio $M2/E1$		~0.2		$\leq5\times10^{-3}$		~0
Relative gamma intensity	$\sim0.6\%$	7.6%	$\leq4.8\%$	20.5%	$\leq2\%$	31%
$T(E1)$ [sec^{-1}]	4.2×10^{6}	2.3×10^{7}	$\leq1.5\times10^{7}$	6.3×10^{7}	$\leq6.2\times10^{6}$	4.6×10^{7}
Hindrance H_W	4.1×10^{-5}	3.5×10^{-9}	$\leq4.1\times10^{-9}$	5.5×10^{-6}	$\leq2.5\times10^{-5}$	1.4×10^{-6}
References						
Level identif.		Hi 60				Hi 60
$\tau_{\frac{1}{2}}$		Bas 62				Bas 63
Int. conv. coef.				Ry 61		Ry 61
$M2/E1$		Har 61	Har 61	Hi 60		Ry 61
Relat. intens.		Har 61	Har 61	Har 61	Har 61	Mur 55
Discussion						

CC-0. In Public Domain. Gurukul Kangri Collection, Haridwar

Digitized by Arya Samaj Foundation Chennai and eGangotri

TABLE B-IVB. Transitions in even-A deformed nuclei with $N \geq 134$ (odd-odd nuclei included).

Nucleus	$_{90}Th^{230}$	$_{90}Th^{230}$	$_{90}Th^{230}$	$_{90}Th^{230}$	$_{90}Th^{230}$	$_{90}Th^{232}$
$J_i\pi_i k_i$	$3^-; 0$		$5^-; 0$	$1^-;$		$3^-; 0$
E(initial level)	0.396 MeV		0.514 MeV	0.508 MeV		1.060 MeV
τ_j(level)[sec^{-1}]			$\leq 8\times10^{-12}$	$\leq 1.0\times10^{-10}$		
$J_f\pi_f k_f$	$2^+; 0$	$4^+; 0$	$4^+; 0$	$0^+; 0$	$2^+; 0$	$2^+; 0$
E(final level)	0.058 MeV	0.1866 MeV	0.1866 MeV	g.s.	0.052 MeV	0.050 MeV
E(transition)	338 keV	208 keV	327.5 keV	508 keV	456 MeV	1010 keV
Experimental internal conversion coefficient						
Theoretical internal conv. coef. for pure $E1$	$\alpha_K=0.022$	$\alpha_K=0.063$	$\alpha_K=0.024$	$\alpha_K=9.5\times10^{-3}$	$\alpha_K=0.012$	
Mixing Ratio $M2/E1$						
Relative gamma intensity	70%	30%	62%			
$T(E1)$[sec^{-1}]	[1.0×10^{11}]		$\geq 5.4\times10^{10}$			
Hindrance H_W	[4.3×10^{-4}]	[7.7×10^{-4}]	$\geq 4.1\times10^{-4}$	$>10^{-5}$	$>10^{-5}$	$\sim10^{-3}$
References						
Level identif.						
τ_j	Bo 57	Bj 57; Bo 57	Ar 61	Bel 60		E 60
Int. conv. coef.						
$M2/E1$						
Relat. intens.	Bj 57	Bj 57	Ar 61			
Discussion	Bo 57			Bel 60	Bel 60	E 60

CC-0. In Public Domain. Gurukul Kangri Collection, Haridwar

Digitized by Arya Samaj Foundation Chennai and eGangotri

TABLE B-IVB (*Continued*)

Nucleus	$_{91}Pa_{143}^{234}$	$_{91}Pa_{143}^{234}$	$_{92}U^{234}$	$_{92}U^{231}$	$_{92}U^{234}$	$_{92}U^{238}$
$J_i\pi_i k_i$	1^+; 1		(5^-); (5)			3^-; 0
E(initial level)	0.1633 MeV		1.374 MeV			0.660 MeV
τ_i(level)[sec^{-1}]	$(1.8\pm0.3)\times10^{-9}$		$\geq1.4\times10^{-7}$			
$J_f\pi_f k_f$	0^-; 0	2^-; 0	4^+; 2	5^+; 2	6^+; 2	2^+; 0
E(final level)	0.0698 MeV	0.0997 MeV	1.020 MeV	1.087 MeV	1.167 MeV	0.045 MeV
E(transition)	93.52 keV	63.64 keV	355 keV	287 keV	208 keV	615 keV
Experimental internal conversion coefficient	$\alpha_t\sim0.14$					
Theoretical internal conv. coef. for pure $E1$			$\alpha_K=0.020$	$\alpha_K=0.033$	$\alpha_K=0.064$	
Mixing Ratio $M2/E1$						
Relative gamma intensity	34%	66%	18%	36%	45%	
$T(E1)$[sec^{-1}]	1.3×10^8	2.5×10^8	$\leq9.0\times10^5$	$\leq1.75\times10^6$	$\leq2.1\times10^6$	
Hindrance H_W	4.2×10^{-5}	2.6×10^{-4}	$\leq5.9\times10^{-9}$	$\leq1.95\times10^{-8}$	$\leq6.2\times10^{-8}$	$\sim10^{-3}$
References						
Level identif.	V 62a	V 62a				
τ_i	Va 56		Bj 62			E 60
Int. conv. coef.	Fo 60					
$M2/E1$						
Relat. intens.				Bj 62	Bj 62	
Discussion	V 62a; Pin 63	V 62a; Pin 63				E 60

CC-0. In Public Domain. Gurukul Kangri Collection, Haridwar

Digitized by Arya Samaj Foundation Chennai and eGangotri

BIBLIOGRAPHY (TABLES B-I TO B-IV)

A 55 G. Alaga, K. Alder, A. Bohr, and B. R. Mottelson, Kgl. Danske. Videnskab. Selskab, Mat. Fys. Medd. **29**, No. 9 (1955).
Alk 63 D. G. Alkazov, K. I. Erokhima, and I. Kh. Lemberg, Bull. Acad. Sci. USSR **27**, 1339 (1963).
Ar 61 E. Arbman, S. Bjørnholm, and O. B. Nielsen, Nucl. Phys. **21**, 406 (1961).
As 60 F. Asaro, F. S. Stephens, J. M. Hollander, and I. Perlman, Phys. Rev. **117**, 492 (1960).
Ax 63 P. Alexander and F. Boehm, Nucl. Phys. **46**, 108 (1963).
Ax 64 P. Alexander, F. Boehm, and E. Kankeleit, Phys. Rev. **133B**, 284 (1964).
B 64 C. V. K. Baba, G. T. Ewan, and J. F. Suarez, Nucl. Phys. **43**, 264 (1964).
Ba 62 J. F. Bakker, R. Hess, and J. W. Sunier, Helv. Phys. Acta **35**, 555 (1962).
Bak D. M. Baker and J. D. Rogers (unpublished report).
Bas 62 E. Bashandy and M. S. El-Nesr, Physica **28**, 1015 (1962).
Bas 63 E. Bashandy, M. S. El-Nesr, and S. C. Pancholi, Nucl. Phys. **41**, 436 (1963).
Bel 60 R. E. Bell, S. Bjørnholm, and J. C. Severiens, Kgl. Danske. Videnskab. Selskab, Mat. Fys. Medd. **32**, No. 12 (1960).
Beli 52 J. K. Beling, J. O. Newton, and B. Rose, Phys. Rev. **87**, 670 (1952), and **86**, 797 (1952).
Ber 62 I. Bergstrøm, E. C. O. Bonacalza, and P. Thieberger, Arkiv Fysik **22**, 95 (1962).
Berl 61 E. E. Berlovich, M. P. Bonitz, Yu. K. Gusev, and M. K. Nikitin, Bull. Acad. Sci. USSR **25**, 1286 (1961).
Berl 64 E. E. Berlovich, Yu. K. Gusev, D. M. Khai, and I. Shenaikh, Bull. Acad. Sci. USSR **28**, 77 (1964).
Bh 63 R. Bhattacharyya and S. Shastry, Nucl. Phys. **48**, 313 (1963).
Bi 59 J. W. Bichard, J. W. Mihelich, and B. Harmatz, Phys. Rev. **116**, 720 (1959).
Bis 62 K. M. Bisgard, K. Olesen, and P. Østergard, Nucl. Phys. **33**, 126 (1962).
Bj 57 S. Bjørnholm, O. Nathan, O. B. Nielsen, and A. K. Sheline, Nucl. Phys. **4**, 313 (1957).
Bj 62 S. Bjørnholm and O. B. Nielsen, Nucl. Phys. **30**, 488 (1962).
Bla 63 J. P. Blanc, M. Lambert, and C. F. Perdrisat, Helv. Phys. Acta **36**, 820 (1963).
Bo 57 A. Bohr and B. R. Mottelson, Nucl. Phys. **4**, 528 (1957).
Bod 62 E. Bodenstedt, H. J. Körner, E. Gerdau, J. Radeloff, K. Auerbach, L. Meyer, and A. Roggenbach, Z. Physik **168**, 370 (1962).
Bod 62a E. Bodenstedt, H. J. Körner, E. Gerdau, J. Radeloff, L. Meyer, K. Auerbach, J. Braunsfurth, and G. Mielken, Z. Physik **170**, 355 (1962).
Boe 60 F. Boehm and C. J. Gallagher, Jr., Phys. Rev. **119**, 258 (1960).
Boe 63 F. Boehm and J. Rogers, Nucl. Phys. **41**, 553 (1963).
Bol 61 H. H. Bolotin, A. C. Li, and A. Schwarzschild, Phys. Rev. **124**, 213 (1961).
Bol 64 H. H. Bolotin, Phys. Rev. **136B**, 1566 (1964).
Br 59 J. H. Brunner, H. J. Leisi, C. F. Perdrisat, and P. Scherrer, Phys. Rev. Letters **2**, 207 (1959).
Bra 58 J. N. Brazos, AECU–3696 (1958) (unpublished).
Bu 57 M. E. Bunker, J. P. Mize, and J. W. Starner, Bull. Am. Phys. Soc. **2**, 104 (1957).
Bur 51 S. B. Burson, K. W. Blair, H. B. Keller, and S. Wexler, Phys. Rev. **83**, 62 (1951).
Ch 63 P. R. Christensen, Nucl. Phys. **41**, 17 (1963).
Ci 63 L. Ciuffolotti and F. Demichelis, Nucl. Phys. **48**, 305 (1963).
Cl 61 M. A. Clark, Can. J. Phys. **39**, 1092 (1961).
Cr 61 H. Crannel, R. Helm, H. Kendall, J. Deser, and M. Yearian, Phys. Rev. **123**, 923 (1961).
Cra M. E. Cranston *et al.* (private communication given in Di 63).
Cra 58 M. E. Cranston, Jr., M. E. Bunker, and J. W. Starner, Phys. Rev. **110**, 1427 (1958).
Cu 58 J. B. Cumming and N. R. Johnson, Phys. Rev. **110**, 1104 (1958).
Cur 63 W. M. Currie, Nucl. Phys. **48**, 561 (1963).
D 64 P. Debrunner (private communication, 1964).
De 60 B. I. Deutch, F. R. Metzger, and F. J. Wilhelm, Nucl. Phys. **16**, 81 (1960).
Deu 60 M. Deutsch and R. W. Bauer, Nucl. Phys. **21**, 128 (1960).
Di 63 R. M. Diamond, B. Elbeck, and F. S. Stephens, Nucl. Phys. **43**, 560 (1963).
Do 65 M. Dorikens, O. Segaert, J. Demuynek, and L. Dorikens-Vaupraer, Nucl. Phys. **61**, 33 (1965).
Dz 61 B. S. Dzhelepov and L. K. Peker, *Decay Schemes of Radio Nuclei* (Pergamon Press, Inc., New York, 1961).
E 60 B. Elbeck, *Proceedings of the International Conference on Nuclear Structure* (in Kingston) (University of Toronto Press, Toronto, Canada, 1960), p. 563.
En 62 P. M. Endt and C. van der Leun, Nucl. Phys. **34**, 238 (1962).
Eng D. W. Engelkemeir (private communication given in As 60).
Eng 53 D. W. Engelkemeir, P. R. Fields, and J. R. Huizenga, Phys. Rev. **90**, 6 (1953).
Eng 54 D. W. Engelkemeir and L. B. Magnusson, Phys. Rev. **94**, 1395 (1954).
Eng 55 D. W. Engelkemeir and L. B. Magnusson, Phys. Rev. **99**, 135 (1955).
Es 64 I. V. Estulin, L. F. Kalinkin and A. S. Melioranskii, Bull. Acad. Sci. USSR **28**, 89 (1964).
Ev 64 J. S. Evans and R. A. Naumann, Bull. Am. Phys. Soc. **10**, 82 (1964) and private communication, 1965.
Ew 57 G. T. Ewan, J. W. Knowles, and D. R. MacKenzie, Phys. Rev. **108**, 1308 (1957).
Ew 61 G. T. Ewan, R. L. Graham, and J. S. Geiger, Nucl. Phys. **22**, 610 (1961).
Ew 64 G. T. Ewan and A. G. Tavendale, Can. J. Phys. **42**, 2286 (1964).

CC-0. In Public Domain. Gurukul Kangri Collection, Haridwar

Digitized by Arya Samaj Foundation Chennai and eGangotri

F 58 F. F. Felber, F. S. Stephens, and F. Asaro, J. Inorg. Nucl. Chem. **7**, 153 (1958).
Fl 63 E. Flamm and F. Asaro, Phys. Rev. **129**, 290 (1963).
Fla 64 W. Flauger and H. Schneider, Nucl. Phys. **55**, 207 (1964).
Fo 56 R. Foucher, L. Dick, N. Perrin, and H. Vartapétian, J. Phys. Radium **17**, 581 (1956).
Fo 62 R. Foucher, J. Mérinis, A. de Pinho, and M. Valadares, Compt. Rend. **255**, 886 (1962).
Fo 64 R. Foucher, A. G. de Pinho, and M. Valadares, *Abstracts of the Congrès International de Physique Nucléaire* (Paris, 1964).
Fr 57 M. S. Freedman, F. T. Porter, F. Wagner, Jr., P. Day, and D. W. Engelkmeir, private communication to J. M. Hollander, 1957.
G 54 R. L. Graham and J. Walker, Phys. Rev. **94**, 794A (1954).
Ga 60 C. J. Gallagher, Jr., W. F. Edwards, and G. Manning, Nucl. Phys. **19**, 18 (1960).
Ga 62a C. J. Gallagher, Jr., Phys. Rev. **126**, 1525 (1962).
Ga 62b C. J. Gallagher, Jr., and H. L. Nielsen, Phys. Rev. **126**, 1520 (1962).
Gr 58 L. Grodzins, Phys. Rev. **109**, 1014 (1958).
Gre 62 R. C. Greenwood and J. H. Reed, Bull. Am. Phys. Soc. **7**, 316MB8 (1962).
Gri 59 E. P. Grigorev, A. V. Zolotavin, V. Ia. Klementer, and R. V. Sinitzin, Bull. Acad. Sci. USSR **23**, 181 (1959).
Gro 58 V. S. Grodzev, L. I. Rusinov, Yu. L. Filimonov, and Yu. L. Khazov, Nucl. Phys. **6**, 561 (1958).
H 64 J. W. Harpster and K. J. Casper, Nucl. Phys. **52**, 497 (1964).
Ha 64 R. Hardell, S. Malmskog, and L. Persson, Arkiv Fysik **25**, 333 (1964).
Ham 64 W. D. Hamilton and K. E. Davies, Nucl. Phys. **58**, 407 (1964).
Han 58 P. G. Hansen, O. Nathan, O. B. Nielsen, and R. K. Sheline, Nucl. Phys. **6**, 630 (1958).
Han 61 O. Hansen and O. Nathan, *Proceedings of the 1961 Rutherford Conference* (Heywood and Company, Ltd., London, 1961), p. 267.
Han 61a O. Hansen and O. Nathan, Nucl. Phys. **42**, 197 (1963).
Har 59 B. Harmatz, T. H. Handley, and J. W. Mihelich, Phys. Rev. **114**, 1082 (1959).
Har 61 B. Harmatz, T. H. Handley, and J. W. Mihelich, Phys. Rev. **123**, 1758 (1961).
Hat 56 E. N. Hatch, F. Boehm, P. Marmier, and J. W. M. Dumond, Phys. Rev. **104**, 745 (1956).
Hat 59 E. N. Hatch and F. Boehm, Z. Physik **155**, 609 (1959).
Hau 61 U. Hauser, K. Runge, and G. Knissel, Nucl. Phys. **27**, 632 (1961).
Hau 62 U. Hauser, E. N. Hatch, K. Runge, G. Knissel, and W. Schneider in Proceedings of the Gatlinburg Conference on *Electromagnetic Lifetimes and Properties of Nuclear States* (National Academy of Sciences Council, Nuclear Science Series, Report No. 37, 1962), p. 230.
Hau 62a U. Hauser, Nucl. Phys. **35**, 342 (1962).
He 56 R. H. Helm, Phys. Rev. **104**, 1466 (1956).
Hey 56 N. P. Heydenburg and G. M. Temmer, Phys. Rev. **104**, 981 (1956).
Hi 60 G. D. Hickman and M. L. Wiedenbeck, Phys. Rev. **118**, 1049 (1960).
Ho 56 R. W. Hoff, J. L. Olsen, and L. G. Mann, Phys. Rev. **102**, 805 (1956).
Hof 59 K. W. Hoffman, I. Y. Krause, W. D. Schmidt-Ott, and A. Flammersfeld, Z. Physik **154**, 408 (1959).
Hof 60 K. W. Hoffman, I. Y. Krause, W. D. Schmidt-Ott, and A. Flammersfeld, Z. Physik **160**, 201 (1960).
Hol 56 J. M. Hollander, W. G. Smith, and J. O. Rasmussen, Phys. Rev. **102**, 1372 (1956).
Hu 54 T. Huus and A. Lunden, Phil. Mag. **45**, 966 (1954).
Hue 64 A. Huebner and H. Schneider, Z. Naturforsch. **19a**, 809 (1964).
I 60 H. Ikegami, Phys. Rev. **120**, 2185 (1960).
I 61 H. Ikegami and T. Udagawa, Phys. Rev. **124**, 1519 (1961).
J 60 K. P. Jacob, J. W. Mihelich, B. Harmatz, and T. H. Handley, Phys. Rev. **117**, 1102 (1960).
K 63 S. Koicki, A. Koicki, and G. T. Wood, Nucl. Phys. **49**, 161 (1963).
Kr 54 J. J. Kraushaar, J. W. Mihelich, and A. W. Sunyar, Phys. Rev. **95**, 456 (1954).
Ku 63 T. Kuroyanagi and T. Tamura, Nucl. Phys. **48**, 675 (1963).
L 61 Landolt-Börnstein, "Zahlenwerte und Funktionen," in *Energie-Niveaus der Kerne* (Springer-Verlag, Berlin, 1961), Group I Vol. 1.
La 58 H. Langevin-Joliot and M. Langevin, J. Phys. Radium **19**, 765 (1958).
Lan 64 H. Langhoff, Bull. Am. Phys. Soc. **9**, 9, AB9 (1964).
Lan 64a H. Langhoff, Phys. Rev. **135B**, 1 (1964).
Le 61 H. J. Leisi, J. H. Brunner, C. F. Perdrisat, and P. Scherrer, Helv. Phys. Acta **34**, 161 (1961).
Li 60 J. C. Lisle and P. F. D. Shaw, Proc. Phys. Soc. (London) **76**, 926 (1960).
Lo 64 K. E. G. Löbner and S. A. de Witt, Phys. Letters **12**, 238 (1964).
M 56 L. B. Magnusson, A. M. Friedman, D. Engelkemeir, P. R. Fields, and F. Wagner, Jr., Phys. Rev. **102**, 1097 (1956).
M 57 L. B. Magnusson, Phys. Rev. **107**, 161 (1957).
Ma 55 P. Marmier and F. Boehm, Phys. Rev. **97**, 103 (1955).
Mal 65 S. G. Malmskog, Nucl. Phys. **62**, 37 (1965).
Man 61 R. Manquenouille, Ann. Physik **6**, 1121 (1961).
Mat 62 E. der Mateosian and M. L. Sehgal, Phys. Rev. **125**, 1615 (1962).
Mc 49 F. K. McGowan, S. de Benedetti, and J. E. Francis, Phys. Rev. **75**, 1761 (1949).

CC-0. In Public Domain. Gurukul Kangri Collection, Haridwar

Digitized by Arya Samaj Foundation Chennai and eGangotri

Mc 54 F. K. McGowan and P. H. Stelson, Phys. Rev. **109**, 901 (1958).
Me 58 F. R. Metzger, Phys. Rev. **110**, 123 (1958).
Me 59 F. R. Metzger and W. B. Todd, Nucl. Phys. **10**, 220 (1959).
Me 59a F. R. Metzger and W. B. Todd, Nucl. Phys. **13**, 177 (1959).
Me 64 F. R. Metzger, Bull. Am. Phys. Soc. **9**, 496 (1964).
Mey 49 V. Meyers and A. Wattenberg, Phys. Rev. **75**, 992 (1949).
Mi 56 J. P. Mize and J. W. Starner, Bull. Am. Phys. Soc. **1**, 171, E6 (1956).
Mi 56a J. P. Mize, M. E. Bunker, and J. W. Starner, Phys. Rev. **103**, 182 (1956).
Mic 63 W. Michaelis, Nucl. Phys. **48**, 422 (1963).
Mih 56 J. W. Mihelich, T. J. Ward, and K. P. Jacob, Phys. Rev. **103**, 1285 (1956).
Mo 63 S. Monaro, Nuovo Cimento **30**, 1379 (1963).
Mot 59 B. R. Mottelson and S. G. Nilsson, Kgl. Danske Videnskab. Selskab, Mat. Fys. Skrifter **1**, No. 8 (1959).
Mu 59 A. H. Muir and F. Boehm, Bull. Am. Phys. Soc. **4**, 367, Q8 (1959).
Muk 62 P. Mukherjee and B. L. Cohen, Phys. Rev. **127**, 1284 (1962).
Mur 55 J. J. Murray, F. Boehm, P. Marmier, and J. W. M. Dumond, Phys. Rev. **97**, 1007 (1955).
N 61 T. D. Nainan, Phys. Rev. **123**, 1751 (1961).
Na 59 O. Nathan and S. Hultberg, Nucl. Phys. **10**, 118 (1959).
Na 60 O. Nathan and V. I. Popov, Nucl. Phys. **21**, 631 (1960).
Ne 60 J. D. Newton, Phys. Rev. **117**, 1510, 1520 (1960).
Ni 54 S. G. Nilsson, Kgl. Danske Videnskab. Selskab, Mat. Fys. Medd. **29**, No. 16 (1954–55).
P 64 N. Perrin and J. Valentin, Phys. Letters **8**, 338 (1964).
P 64a N. Perrin, Compt. Rend. (Paris) **258**, 1475 (1964).
Pe 64 L. Persson, Arkiv Fysik **25**, 307 (1964).
Pee 60 R. W. Peele, Oak Ridge National Laboratory, Report No. 3016, p. 110, 1960 (unpublished).
Pen 56 J. R. Penninger, H. R. Maltrud, J. C. Hopkins, and F. M. Schmidt, Phys. Rev. **104**, 740 (1956).
Per 62 Chs. F. Perdrisat, H. J. Leisi, and J. H. Brunner, Nucl. Phys. **31**, 157 (1962).
Per 62a Chs. F. Perdrisat, J. H. Brunner, and J. H. Leisi, Helv. Phys. Acta **35**, 175 (1962).
Per 62b Chs. F. Perdrisat, H. J. Leisi, J. H. Brunner, and L. Piaggio, Nucl. Phys. **31**, 160 (1962).
Pi 57 R. C. Pilger, F. S. Stephens, Jr., F. Asaro, and I. Perlman, Bull. Am. Phys. Soc. **2**, 394, R3 (1957).
Pi 57a R. C. Pilger, University of California Radiation Laboratory, Report No. 3877, 1957 (unpublished).
Pin 63 A. G. de Pinho, J. Physik **24**, 861 (1963).
Po 61 V. I. Popov, Bull. Acad. Sci. USSR **25**, 1160 (1961).
Ra 54 J. Rasmussen and F. Stephens, 1954 (unpublished data).
Ra 57 J. Rasmussen, F. L. Canavan, and J. M. Hollander, Phys. Rev. **107**, 141 (1957).
Re 64 J. J. Reidy, E. G. Funk, and J. W. Mihelich, Phys. Rev. **133B**, 556 (1964).
Ro 62 R. L. Robinson and F. K. McGowan, Phys. Rev. **125**, 1753 (1962).
Ros 58 M. E. Rose, *Internal Conversion Coefficient* (North-Holland Publishing Company, Amsterdam, 1958).
Ry 61 H. Ryde and Z. Sujkowski, Arkiv Fysik **20**, 289 (1961).
S 64 S. Shimizu, Y. Nakayama, H. Hirata, and H. Mazaki, Nucl. Phys. **54**, 265 (1964).
Sc 59 L. C. Schmidt and S. B. Burson, Phys. Rev. **115**, 447 (1959).
Sc 59a L. C. Schmidt, S. B. Burson, and J. M. Cork, Phys. Rev. **115**, 174 (1959).
Sch 62 C. F. Schwerdtfeger, E. G. Funk, and J. W. Mihelich, Phys. Rev. **125**, 1641 (1962).
Sh 60 G. G. Shute and B. S. Sood, Proc. Roy. Soc. (London) **A257**, 52 (1960).
Shu 65 Yu. K. Shubnyi, D. K. Kaipov, and R. B. Begzhanov, Zh. Eksperim. i Teor. Fiz. **47**, 16 (1965) [English transl.: Soviet Phys.—JETP **20**, 11 (1965)].
Sl 56 L. A. Sliv and I. M. Band, *Coefficient of Internal Conversion of Gamma Radiations* (Academy of Sciences USSR, Moscow, 1956).
Su 60 R. E. Sund and M. L. Wiedenbeck, Phys. Rev. **120**, 1792 (1960).
Su 60a R. E. Sund, R. G. Arns, and M. L. Wiedenbeck, Phys. Rev. **118**, 776 (1960).
Sub 60 B. N. Subba Rao, Nuovo Cimento **16**, 286 (1960).
Sub 62 B. N. Subba Rao and W. B. Todd, Nucl. Phys. **13**, 177 (1959).
Sun A. W. Sunyar, unpublished (reference in Kr 54).
Sun 61 A. W. Sunyar, Phys. Rev. **93**, 1122 (1954).
Sut 62 T. Suter, P. Reyes, S. Gustafson, and I. Marklund, Nucl. Phys. **29**, 33 (1962).
Sv 63 J. Svedberg and G. Anderson, Nucl. Phys. **48**, 313 (1963).
St 55 P. Stähelin, D. Maeder, and M. Pochon, Z. Physik **140**, 498 (1955).
Sta 64 S. V. Starodubtsev, R. B. Begzhanov and S. L. Rakovitskii, Zh. Eksperim. i Teor. Fiz. **45**, 921 (1963) [English transl.: Soviet Phys.—JETP **18**, 635 (1964)].
St 55 F. S. Stephens, University of California Radiation Laboratory, Report No. 2970, 1955 (unpublished).
St 57 F. S. Stephens, Jr., F. Asaro, S. G. Thompson, and I. Perlman, Bull. Am. Phys. Soc. **2**, 394, R2 (1957).
Sto 59 R. Stockendal and S. Hultberg, Arkiv Fysik **15**, 33 (1959).
Str 55 D. Strominger and J. O. Rasmussen, Phys. Rev. **100**, 844 (1955).

CC-0. In Public Domain. Gurukul Kangri Collection, Haridwar

Digitized by Arya Samaj Foundation Chennai and eGangotri

Str 56 D. Strominger, F. S. Stephens, Jr., and J. O. Rasmussen, Phys. Rev. **103**, 748 (1956).
T 53 J. Teillac, M. Riou, and P. Desneiges, Compt. Rend. (Paris) **237**, 41 (1953).
Ta 64 K. Takahashi, M. McKeown, and G. Scharff-Goldhaber, Bull. Am. Phys. Soc. **9**, 718 (1964) and Phys. Rev. **137B**, 763 (1965).
Tam 65 T. Tamura, Nucl. Phys. **62**, 305 (1965).
To 61 S. J. du Toit and L. M. Bollinger, Phys. Rev. **123**, 629 (1961).
V 62 J. Valentin, D. H. Horen, and J. M. Hollander, Nucl. Phys. **31**, 353 (1962).
V 62a J. Valentin, *Comptes-rendus du Colloque de Physique des Basses Energies à Bruxelles* (L. Wouters, Louvain, 1962), p. 246.
V 63 J. Valentin and A. Santoni, J. Physik **24**, 648 (1963).
Va 56 H. Vartapétian, L. Dick, R. Foucher, and N. Perrin, J. Phys. Radium **17**, 537 (1956).
Va 57 H. Vartapétian, Compt. Rend. (Paris) **244**, 65 (1957).
Va 59 H. Vartapétian, Compt. Rend. (Paris) **246**, 1109 (1959).
Var 62 G. A. Vartapetyan *et al.*, Zh. Eksperim. i Teor. Fiz. **41**, 1704 (1961) [English transl.: Soviet Phys.—JETP **14**, 1213 (1962)].
Var 62a G. A. Vartapetyan *et al.*, Zh. Eksperim. i Teor. Fiz. **41**, 1710 (1961) [English transl.: Soviet Phys.—JETP **14**, 1217 (1962)].
Vas 61 S. S. Vasilenko, M. S. Kagangskii, D. L. Kaminskii, and S. F. Koksharova, Zh. Eksperim. i Teor. Fiz. **39**, 970 (1960) [English transl.: Soviet Phys.—JETP **12**, 672 (1961)].
Ve 57 M. Vergnes, J. Phys. Radium **18**, 579 (1957).
Ve 60 M. Vergnes, Ann. Phys. (Paris) **5**, 11 (1960).
Ve 61 M. Vergnes and J. Jartrzebski, J. Phys. Radium **22**, 669 (1961).
Ve 63 M. Vergnes, J. Phys. Radium **24**, 131 (1963).
W 55 H. de Waard, Phil. Mag. **46**, 445 (1955).
We 62 R. S. Weaver and R. Barton, Can. J. Phys. **40**, 660 (1962).
Wes 61 H. I. West, Jr., L. G. Mann, and R. G. Nagle, Phys. Rev. **124**, 527 (1961).
Wi 63 R. Wiener, C. Chasman, P. Harihar, and C. S. Wu, Phys. Rev. **130**, 1069 (1963).
Wil 60 R. G. Wilson and M. L. Pool, Phys. Rev. **117**, 807 (1960).

CC-0. In Public Domain. Gurukul Kangri Collection, Haridwar

Digitized by Arya Samaj Foundation Chennai and eGangotri

Unitary Groups: Representations and Decompositions

C. ITZYKSON*
Stanford Linear Accelerator Center, Stanford University, Stanford, California
M. NAUENBERG†
Department of Physics, Stanford University, Stanford, California

An elementary account is given of the representation theory for unitary groups. We review the basic definitions and the construction of irreducible representations using tensor methods, and indicate the connection to the infinitesimal approach. Special attention has been given to the detailed procedure to obtain Clebsch–Gordan series and to the problem of finding the (SU_m, SU_n) content of an irreducible representation of SU_{mn} or SU_{m+n}. An appendix summarizes the properties of the Young operators used in constructing the tensor representations; this provides the link with the representation theory of the symmetric groups. We include a tabulation of various decompositions which appear in the text and of Weyl's dimension formula for tensor representation.

CONTENTS

I. Introduction 95
II. Review of Unitary Groups 95
III. Description of the Irreducible Representations of SU_n 97
IV. The Generators of SU_n 101
V. Decomposition of the Product of Two Representations of SU_n 104
VI. The (SU_m, SU_n) Content of Irreducible Representations of SU_{mn} and SU_{m+n} 106
VII. Tables 108
Appendix: The Symmetric Group and Properties of the Young Symmetry Operators 119

I. INTRODUCTION

In these notes we describe some fundamental properties of the irreducible representations of SU_n, the special unitary group in n dimensions. We use, as basis for these representations, tensors which satisfy certain symmetry properties with respect to permutations of their indices, and discuss briefly in this connection the symmetric group. We also relate this global analysis of the representations to the method based on the infinitesimal transformations of continuous groups: the Lie algebra of SU_n.

The unitary groups are very important in physics. The best-known example is SU_2 which describes the spin and isospin of particles. Recently unitary groups in higher dimensions have been applied with success to study the properties of elementary particles. Although the mathematical theory of these groups and their representations has been developed for a long time, useful results are somewhat scattered in the literature. We therefore have attempted to collect here some formulas and tricks, and have computed several tables that are useful in the application of unitary groups to particle physics.

Throughout the text we have tried to give some idea of how one derives the more important results; this should help the reader to remember them and also serve to explain our notation. Some topics which we have left out of our discussion include the construction of explicit basis in each representation space in terms of which to express the analogs of Clebsch–Gordan coefficients, and formulas for the elements of the representation matrices. There is no special reason for such omissions which are useful in practical applications. However, for low dimensional representations the tensor methods which are described here can be successfully used. The discussion of SU_n can be extended with minor modifications to the special linear groups $SL(n, R)$ and $SL(n, C)$, the groups of $n \times n$ matrices of determinant one with real and complex entries, respectively.[1–7]

We have included a short list of books to which we refer for omitted proofs, and some recent articles on the subject.

The preparation of this report was supported by the Atomic Energy Commission and the U.S. Air Force Office of Scientific Research under contract AF 49(638)-1389.

II. REVIEW OF UNITARY GROUPS

When dealing with symmetries in particle physics, one is led to study the representations of some simple

* On leave from Service de Physique Theorique, CEN Saclay, BP No. 2, Gif sur Yvette (S. et O.), France.
† A. P. Sloan Fellow.

[1] H. Weyl, *Classical Groups* (Princeton University Press, Princeton, New Jersey, 1946); *The Theory of Groups and Quantum Mechanics* (Dover Publications, Inc., New York, 1950).
[2] F. D. Murnaghan, *The Theory of Group Representations* (Dover Publications, Inc., New York, 1963).
[3] D. Littlewood, *Theory of Group Characters and Matrix Representations of Groups* (Oxford University Press, New York, 1950).
[4] M. Hamermesh, *Group Theory and Its Application to Physical Processes* (Addison-Wesley Publishing Company, Reading, Massachusetts, 1962).
[5] G. Racah, *Group Theory and Spectroscopy* (Princeton University Press, Princeton, New Jersey, 1951).
[6] M. L. Whippman, "Branching Rules for Simple Lie Groups," University of Pennsylvania preprint (1964).
[7] C. R. Hagen and A. J. MacFarlane, "Reduction of Representations of SU_{mn} and SU_{m+n} with Respect to the Subgroup SU_m, SU_n," Syracuse University preprint (1965).

CC-0. In Public Domain. Gurukul Kangri Collection, Haridwar

Digitized by Arya Samaj Foundation Chennai and eGangotri

groups. Here we are concerned mainly with the special unitary groups in n dimensions, denoted by SU_n. To be precise, our group is the set of $n\times n$ matrices with complex entries which are unitary and of determinant equal to one. A typical such matrix will be denoted by g. By a unitary transformation (which can be chosen to be of determinant one) such a matrix can be diagonalized; hence, for a given g there always exists a g' in the group such that

$$g'gg'^{-1}=\begin{pmatrix}\epsilon_1 & & & \\ & \cdot & & \\ & & \cdot & \\ & & & \epsilon_n\end{pmatrix}, \qquad \text{(II.1)}$$

where the ϵ_l are just the eigenvalues of g of modulus one, and $\epsilon_1\epsilon_2\cdots\epsilon_n=1$. Any unitary matrix can be written

$$g=e^{ih}, \qquad \text{(II.2)}$$

where h is a Hermitian matrix. This is an immediate consequence of Eq. (II.1). Moreover, for g to have determinant one, it is sufficient that h be traceless. Now an arbitrary Hermitian matrix is given in terms of the n diagonal elements which are necessarily real, and the $n(n-1)/2$ complex elements above the main diagonal; hence, this matrix depends on n^2 real parameters. If we impose the condition that the trace be zero, we are left with n^2-1 independent parameters.

The group SU_n has three fundamental properties:

(1) *It is compact.* The precise meaning of this word in this context is the following: If we are given an infinite sequence of elements $g_1, \cdots, g_i, \cdots$, we can always extract a subsequence which converges to an element of the group.

We shall not investigate further the topological properties, but mainly remark that the compactness property has the important consequence that the irreducible representations to be introduced below enjoy the following properties: (i) They are all finite dimensional. (ii) They are all equivalent to unitary representations. (iii) Any representation can be split in a direct sum of irreducible representations.

(2) SU_n is a *Lie group.* This means that certain differentiability conditions (obvious in this case) are satisfied. This reduces the study of such a group to the study of the so-called infinitesimal elements, i.e., those close to unity. We discuss briefly this approach in Sec. IV; however, we shall not emphasize this point of view.

(3) Finally, SU_n is a *simply connected group.* Connected means that, given an arbitrary element g, one can find a continuous set of elements in the group $g(t)$, where $0\leq t\leq 1$ such that $g(0)$ is the identity e, and $g(1)=g$. In a simply connected group two such "paths" leading from e to g can be continuously transformed in one another. In summary: *SU_n is a simply connected compact Lie group depending on n^2-1 real parameters.*

In view of what has been said we need only define representations in finite dimensional spaces. This is always understood here. By *representation* of a group G one means a correspondence which assigns to every element g a linear operator $A(g)$ (i.e., a matrix once a basis has been chosen) in some vector space, the carrier of representation, such that the image of e is the identity operator I, and the group law is preserved; i.e.,

$$A(g)A(g')=A(gg').$$

The carrier space is assumed to be a *complex* vector space, i.e., the matrices $A(g)$ have complex entries.

Two representations are *equivalent* if the carrier spaces can be put in a one-to-one *linear* correspondence $x\leftrightarrow x'$ with the property that $A(g)x\leftrightarrow A'(g)x'$. In the following we shall be concerned with representations *up to equivalence*; i.e., we shall identify equivalent representations. If a basis has been chosen in the two equivalent carrier spaces, and if A and A' denote the matrices of the representations, the statement of equivalence can be rephrased by saying that there exists a nonsingular matrix B such that for every g in the group

$$A'(g)=BA(g)B^{-1}.$$

A subspace of the carrier space is said to be *invariant* if it is left unchanged by all operators $A(g)$. The representation is said to be reducible if such a proper invariant subspace exists; otherwise, it is called *irreducible.* In our case, $[G=SU_n]$ reducibility implies, in fact, a little more, namely, if there exists a proper invariant subspace, then one can find a complementary subspace which is also invariant. In other words, the representation splits. In pictures, if all the matrices $A(g)$ have the form

$$\left(\begin{array}{c|c} X & X \\ \hline O & X \end{array}\right),$$

there exists a basis in which $A(g)$ takes the form

$$\left(\begin{array}{c|c} X & O \\ \hline O & X \end{array}\right),$$

we say that the representation is completely reducible. Given a representation we can thus split it again and again until we reach irreducible parts.

Given an irreducible representation $A(g)$, the only linear operators C which commute with every $A(g)$, i.e., $CA(g)=A(g)C$ for all g, are multiples of the identity $C=\lambda I$ (Schur's Lemma). The converse is also true.

Our first task will be to describe all the irreducible representations of SU_n up to equivalence. This construction is entirely algebraic in nature and is carried

CC-0. In Public Domain. Gurukul Kangri Collection, Haridwar

Digitized by Arya Samaj Foundation Chennai and eGangotri

out in the next section. However, since the results are often given an interesting meaning using some analytic tools, we say a word on characters and integration on the group.

Given a representation $A(g)$, we can compute the trace $x(g)\equiv\sum_i A_{ii}(g)$ which is basis-independent. The (complex-valued) function $x(g)$ is the *character* of the representation. Immediate properties are[8]

$$x(g'gg'^{-1})=x(g),$$
$$x(g^{-1})=\bar{x}(g). \tag{II.3}$$

The second property stems from the fact that every representation of the compact group SU_n is equivalent to a unitary representation. The importance of the *character* lies in the fact that it determines the representation up to equivalence: i.e., two representations with the same characters are equivalent. Using Eqs. (II.1) and (II.3), one obtains the result that $x(g)$ is in fact a *symmetric function* of $\epsilon_1\cdots\epsilon_n$, where $\epsilon_1\cdots\epsilon_n$ are the eigenvalues of g. Stated in an equivalent manner, $x(g)$ is a function of the coefficients $(a_1\cdots a_n)$ of the characteristic polynomial of g:

$$\det(1-\lambda g)=\sum_{p=1}^{n}(-1)^p a_p\lambda^p \qquad a_0\equiv 1.$$

(In fact a_n is also equal to one, since $\det g=1$.) Now it is possible to introduce an invariant integration on $G\equiv SU_n$. By this we mean the following: parametrize in some way the group (in our case with n^2-1 real parameters); then there exists a measure $d\mu(g)$ on the group, such that if g' is a fixed element in the group,

$$d\mu(g'g)=d\mu(g)$$

and

$$d\mu(gg')=d\mu(g).$$

The measure $d\mu$ is essentially unique up to a scale factor. We use this freedom and the compactness of SU_n to normalize $\mu(g)$,

$$\int_G d\mu(g)=1.$$

In the case of SU_n it turns out that a particular choice of parameters is indicated. Let us go back to Eq. (II.1) and put $\epsilon_i=\exp(i2\pi\phi_i)$. Then it is possible to make the parametrization in such a way that

$$d\mu(g)=[\delta(\textstyle\sum\phi_i)/\Omega]\times\displaystyle\prod_{i\neq j}|(\epsilon_i-\epsilon_j)|\,d\phi_1 d\phi_2\cdots d\phi_n d\omega_g, \tag{II.4}$$

where $d\omega_g$ depends essentially on the matrix which diagonalizes g and need not be considered further here, and Ω is a normalization constant.

[8] A bar over a number means complex conjugation.

Note that

$$\prod_{i\neq j}|(\epsilon_i-\epsilon_j)|=\Delta(\epsilon)\bar{\Delta}(\epsilon)$$

with

$$\Delta(\epsilon)=\prod_{i<j}(\epsilon_i-\epsilon_j).$$

We shall denote the invariant measure $d\mu(\epsilon)$,

$$d\mu(\epsilon)=(\Delta\bar{\Delta}/\Omega)\,\delta(\textstyle\sum\phi_i)\,d\phi_i\cdots d\phi_n, \tag{II.5}$$

with Ω determined by the condition

$$\int_{0\leq\phi_1\leq 1,0\leq\phi_2\leq 1\cdots} d\mu(\epsilon)=1.$$

The following important orthogonality relations hold: If $x^i(\epsilon)$ is the character of an *irreducible* representation of SU_n, then

$$\int\bar{x}(\epsilon)x(\epsilon)\,d\mu(\epsilon)=1.$$

If $x(\epsilon)$ and $x'(\epsilon)$ correspond to inequivalent irreducible representations,

$$\int\bar{x}(\epsilon)x'(\epsilon)\,d\mu(\epsilon)=0.$$

Applications of these formulas will be found in Sec. III.

III. DESCRIPTION OF THE IRREDUCIBLE REPRESENTATIONS OF SU_n

We consider the set of tensors, $T_{i_1 i_2\cdots i_f}$, where the indices $i_1, i_2, \cdots, i_f$, run from 1 to n. To each unitary matrix g, we associate a linear transformation $A(g)$ in the space of tensors

$$T_{i_1\cdots i_f}\rightarrow T'_{i_1\cdots i_f}=A(g)_{i_1\cdots i_f;i'_1\cdots i'_f}T_{i'_1\cdots i'_f}, \tag{III.1}$$

where a sum over repeated indices is implied, and

$$A(g)_{i_1\cdots i_f;i'_1\cdots i'_f}\equiv g_{i_1 i'_1}\cdots g_{i_f i'_f}.$$

In a more compact notation,

$$A(g)=g\times g\times\cdots\times g, \tag{III.2}$$

which defines $A(g)$ as the Kronecker or direct product of matrices g.

The matrices $A(g)$ build a unitary, but in general, reducible representation of SU_n. They satisfy the important property that they are *bisymmetric*, that is, invariant under a permutation of the indices $i_1\cdots i_f$ and the *same* permutation on the indices $i'_1\cdots i'_f$. A permutation p on f integers is denoted by

$$p=\begin{pmatrix}1 & 2 & \cdots & f\\ p_1 & p_2 & \cdots & p_f\end{pmatrix},$$

where $p_1 p_2\cdots p_f$ is a rearrangement of the ordered f integers, and the permutation p of the indices is indi-

CC-0. In Public Domain. Gurukul Kangri Collection, Haridwar

Digitized by Arya Samaj Foundation Chennai and eGangotri

cated by

$$p(i_1\cdots i_f)=(i_{p_1}i_{p_2}\cdots i_{p_f})$$

or more briefly $p(i)=(i_p)$. The property of bisymmetry of $A(g)$ is then expressed by the relation

$$A(g)_{(i_p,i'_p)}=A(g)_{(i,i')}. \tag{III.3}$$

It can be readily seen that if we take a linear combination of tensors satisfying some symmetry condition with respect to the permutation of their indices, this property is preserved under the transformations generated by $A(g)$. In general, these symmetrized tensors span a subspace of the tensor space which is then invariant under SU_n, and therefore gives a representation of the group. The *fundamental theorem* on representations of unitary groups states that there exists *maximal symmetry conditions* which can be imposed on the tensors, such that the resulting invariant subspaces generate all the irreducible representations of SU_n.[9]

We begin by giving a description of these maximal symmetry conditions by means of Young tableaux. A Young tableau consists of an array of f boxes with f_1 boxes in the first row, f_2 boxes in the second row, and f_{n-1} boxes in the $(n-1)$-th row, where the integers $f_1, f_2\cdots f_{n-1}$ satisfy the relations

$$f_1\geq f_2\geq f_3\geq\cdots\geq f_{n-1}$$

and

$$f=f_1+f_2+\cdots f_{n-1}. \tag{III.4}$$

For convenience of notation we include in some formulas $f_n=0$. In pictures, a tableau is usually drawn as follows:

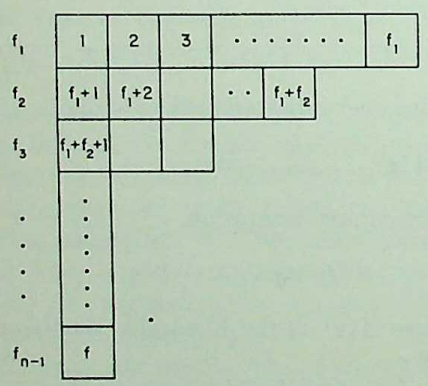

To this tableau corresponds the following symmetry operation on a tensor $T_{i_1\cdots i_f}$.

(i) Symmetrize completely with respect to the first f_1 indices $i_1\cdots i_{f_1}$, the following f_2 indices $i_{f_1+1}\cdots i_{f_1+f_2}$, and so on, thus getting a tensor

$$T'_{i_1\cdots i_{f_1},i_{f_1+1}\cdots i_{f_1+f_2},\cdots}$$

(ii) Then antisymmetrize the tensor T' with respect to the indices i_1, i_{f_1+1}, $i_{f_1+f_2+1}\cdots$, the indices i_2, i_{f_1+2}, $i_{f_1+f_2+2}\cdots$, and so on. The resulting set of tensors T'' form the basis of an invariant subspace which generates an irreducible representation of SU_n.

We can write in compact notation

$$T''_{i_1\cdots i_f}=YT_{i_1\cdots i_f},$$

where

$$Y=\sum\delta_q qp \tag{III.5}$$

is the Young symmetry operator associated with the Young tableau. The sum in Y [Eq. (III.5)] is carried over all permutations p of integers in the same row, and all permutations q of integers in the same column of the Young tableau, while δ_q is the signature of the permutation q; $\delta_q=+1(-1)$ for q even (odd). The tableau has no more than $n-1$ rows. This is a result of two facts: first, that it is impossible to antisymmetrize more than n indices each running from 1 to n, and, second, that we restrict our attention to transformations of determinant 1.[10] To different tableaux corresponds inequivalent representations. *There is a one-to-one correspondence between the Young tableaux of no more than $n-1$ rows and the irreducible representations of the group SU_n.* The tableau with zero box corresponds to the identity representation, i.e., to the representation which assigns to every element of the group the unit operator in a one dimensional space, and will be denoted by a dot. The tableau with one box corresponds to the representation by the group itself. Among other interesting representation, let us point out the following:

(i) Representations with one row only, $f_1=f$. They correspond, according to what we have seen, to a carrier space of totally symmetric tensors. The dimension of this representation is easily computed as the number of ways one can choose f objects among n objects allowing repetitions, namely,

$$N=\binom{n+f-1}{f}\equiv\frac{(n+f-1)!}{f!(n-1)!}, \tag{III.6}$$

(the familiar counting problem for an Einstein–Bose gas).

There is an infinite number of such representations.

(ii) Representations corresponding to rows of length 1 or 0. In other words, the tableau is reduced to its first column. Excluding the identity representation, there are $n-1$ such representations

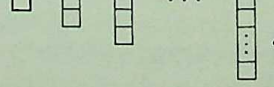

[9] See Ref. 1, Chaps. III and IV for the full development of this duality between the linear groups and the symmetric groups.

[10] It is convenient to use the following convention. In some cases we add to a Young tableau of no more than $n-1$ rows columns of n boxes on the left. These new tableaux will be considered as equivalent to those where these extra columns are dropped. The dimension formula [see Eq. (III. 10)] is invariant under that transformation.

CC-0. In Public Domain. Gurukul Kangri Collection, Haridwar

Digitized by Arya Samaj Foundation Chennai and eGangotri

They correspond to carrier spaces built up of totally antisymmetric tensors. If $\bar{y}$ is the length of the column, the representation is of dimension

$$N=\binom{n}{\bar{y}}=\frac{n!}{\bar{y}!(n-\bar{y})!}$$ (the counting problem for a Fermi–Dirac gas). (III.7)

We shall give below a formula which gives the dimension of a general representation.

(iii) The representation with $f_1=2, f_2=1, f_3=1,\cdots, f_{n-1}=1$. This is called the adjoint representation and is very important, because its basis transforms like the generators of the group. Let us briefly outline how one gets this representation. Let h be an arbitrary, traceless, $n\times n$ Hermitian matrix. The set of these matrices is closed with respect to addition and multiplication by real numbers; hence, they build up a vector space whose dimension we have already computed to be n^2-1. The transformation

$$h\rightarrow h'=ghg^{-1},$$

where g is an element of SU_n, is obviously a linear transformation of our set of Hermitian matrices. We thus get a representation of SU_n in this space which can be shown to be irreducible. This is the adjoint representation. Its dimension is

$$N=n^2-1,$$ (III.8)

and with our choice of basis the representation consists of real matrices only.

(iv) Finally, let us discuss *contragradient* representations. Given any representation of a group by the correspondence

$$g\rightarrow A(g),$$

one can define the contragradient representation[11]

$$g\rightarrow A^{\mathrm{T}}(g^{-1})=A^{-1\mathrm{T}}(g).$$

One verifies that it is a representation, and also that it is reducible or not according to whether A is reducible or not. If the representation A is unitary, so is the contragradient representation which in fact is simply the complex conjugate of A, i.e., $g\rightarrow\bar{A}(g)$ in that case. Note in this connection that $\bar{T}_{i_1\cdots i_f}$, the complex conjugate of a tensor $T_{i_1\cdots i_f}$, transforms according to the rule $\bar{T}'=(\bar{g}\times\bar{g}\cdots\times\bar{g})\,\bar{T}$ which is used to define contravariant tensors by setting the indices as superscripts, $T^{i_1\cdots i_f}$. The relation to covariant tensors is obtained through the Levi-Civita symbol $\epsilon_{i_1\cdots i_n}$, which is totally antisymmetric in its n indices, and equals $+1$ of -1 according to whether $i_1 i_2\cdots i_n$ is an even or odd permutation of the integers $1, 2,\cdots n$. It can readily be seen that it is invariant under any unimodular transformations. For each contravariant index i, we multiply the contravariant tensor by $\epsilon_{i_1 i_2\cdots i_{n-1} i}$ and sum over i giving rise to $n-1$ covariant indices. For example, if T^i is a contravariant tensor, of rank 1, then

$$T_{i_1\cdots i_{n-1}}=\epsilon_{i_1\cdots i_{n-1} i}T^i$$

is a covariant antisymmetric tensor of rank $n-1$. Naturally, we can equally well construct contravariant indices from any covariant tensor which contains $n-1$ antisymmetric indices. For example, if $A_{i_1\cdots i_{n-1}}$ is totally antisymmetric in $i_1\cdots i_{n-1}$,

$$y^i=\epsilon_{i i_1\cdots i_{n-1}}A_{i_1\cdots i_{n-1}}$$

is a contravariant tensor. The raising and lowering of tensor indices by $\epsilon_{i_1\cdots i_n}$ makes it possible to contract these indices, e.g., the sum $\sum_i x_i y^i$ is an invariant.

If a representation is equivalent to a representation by real matrices, then it follows that it is equivalent to its contragradient. For a given tableau of SU_n corresponding to a representation A, one obtains the contragradient representation by the following process:

(i) Draw the initial Young tableau.

(ii) Complete the drawing to obtain a rectangle of horizontal dimension f_1 and vertical dimension n.

(iii) The complementary part is the desired Young tableau if one rotates it by π. It is seen that the procedure is equivalent to saying that if $f'_1\geq\cdots\geq f'_{n-1}$ are the rows of the Young tableau corresponding to the contragradient representation, then

$$f'_1=f_1-f_n=f_1$$

$$f'_2=f_1-f_{n-1}$$

$$f'_p=f_1-f_{n-p+1}$$

$$\vdots$$

In particular, representations equivalent to their contragradient are such that

$$f_p=f'_p=f_1-f_{n-p+1}$$

or

$$f_p+f_{n-p+1}=f_1 \qquad p=1\cdots n.$$

As an example we see that the adjoint representation has this property. Obviously, a representation and its contragradient have the same dimensions; thence, the dimension formula has to be invariant with respect to the transformation $f_p\rightarrow f'_p$.

Digressing, we note that all the finite dimensional

[11] The superscript T on A denotes the transpose of A.

CC-0. In Public Domain. Gurukul Kangri Collection, Haridwar

Digitized by Arya Samaj Foundation Chennai and eGangotri

irreducible representations of the special linear group on real numbers $SL(n, R)$ can similarly be described in terms of the tensor spaces used for SU_n. The matrix elements of these representations are polynomials in the matrix elements of the element $g \epsilon SL(n, R)$. If we extend these polynomials to complex values, we get a representation of the special linear group on complex numbers $SL(n, C)$. The most general finite dimensional irreducible representations of this group are obtained by forming Kronecker products $D' \times \bar{D}''$, where D' and D'' are representations of the type just discussed, and $\bar{D}''$ is the complex conjugate of D''.

As an example, the finite dimensional representations of $SL(2, C)$ which is in two-to-one correspondence with the Lorentz group, can be labeled by *two* Young tableaux consisting of one row of $2j_1$ and $2j_2$ boxes, respectively.

It must be emphasized that $SL(nR)$ and $SL(nC)$ are *not compact* and that the finite dimensional representations are *not unitary*. In order to find unitary representations one has to introduce infinite dimensional Hilbert spaces, which we shall not discuss here.

We return to SU_n and discuss the characters and dimensions of the representations.

We have already quoted the fact that a representation is completely determined by its character. The following formula[12] gives the character for the presentation belonging to the Young tableau $f_1, f_2, \cdots, f_n (=0)$ as a symmetric function of the eigenvalues $\epsilon_1 \cdots \epsilon_n$ of the general element g in SU_n (Weyl's character formula)

$$x_{f_1,\cdots,f_n} = \frac{\begin{vmatrix} \epsilon_1^{f_1+n-1} & \epsilon_1^{f_2+n-2} & \cdots & \epsilon_1^{0} \\ \epsilon_2^{f_1+n-1} & \epsilon_2^{f_2+n-2} & \cdots & \\ \vdots & & & \\ \epsilon_n^{f_1+n-1} & & & \epsilon_n^{0} \end{vmatrix}}{\begin{vmatrix} \epsilon_1^{n-1} & \epsilon_1^{n-2} & \cdots & \epsilon_1^{0} \\ \epsilon_2^{n-1} & \epsilon_2^{n-2} & \cdots & \epsilon_2^{0} \\ \epsilon_n^{n-1} & \epsilon_n^{n-2} & \cdots & \epsilon_n^{0} \end{vmatrix}} . \quad \text{(III.9)}$$

From this formula one gets the dimension N by letting $\epsilon_1, \cdots, \epsilon_n$ go to one, i.e., N is the character of the identity. The calculation must be made carefully because the denominator and the numerator vanish in this limit.

We set $l_1 = f_1 + n - 1$, $l_2 = f_2 + n - 2$, $\cdots$. In order to take a proper limit we first relax the condition $\epsilon_1 \cdots \epsilon_n = 1$ and choose

$$\epsilon_1 = \epsilon^{n-1}, \quad \epsilon_2 = \epsilon^{n-2} \cdots, \quad \epsilon_n = \epsilon^0 .$$

With $\epsilon \to e^{i\Phi}$, and $\Phi \to 0$, we have

$$N = \lim_{\Phi \to 0} \frac{\begin{vmatrix} (\epsilon^{l_1})^{n-1} & (\epsilon^{l_1})^{n-2} & \cdots & (\epsilon^{l_n})^{n-1} \\ (\epsilon^{l_1})^{n-2} & (\epsilon^{l_2})^{n-2} & & \vdots \\ \vdots & \vdots & & \\ (\epsilon^{l_1})^{0} & (\epsilon^{l_2})^{0} & & (\epsilon^{l_n})^{0} \end{vmatrix}}{\begin{vmatrix} (\epsilon^{n-1})^{n-1} & \cdots & (\epsilon^{0})^{n-1} \\ (\epsilon^{n-1})^{n-2} & & \vdots \\ (\epsilon^{n-1})^{0} & & (\epsilon^{0})^{0} \end{vmatrix}} .$$

We now use the classical result that

$$\Delta(x_1, \cdots, x_n) \equiv \begin{vmatrix} x_1^{n-1} & x_2^{n-1} & \cdots & x_n^{n-1} \\ x_1^{n-2} & x_2^{n-2} & & x_n^{n-2} \\ x_1^{0} & \vdots & & x_n^{0} \end{vmatrix}$$

$$= (x_1 - x_2)(x_1 - x_3) \cdots (x_1 - x_n)(x_2 - x_3) \cdots$$

$$= \prod_{i<j} (x_i - x_j) .$$

Hence, taking into account that

$$(\epsilon^{l_i} - \epsilon^{l_j}) \underset{\Phi \to 0}{\approx} i\Phi(l_i - l_j) ,$$

we obtain

$$\boxed{N = \frac{\Delta(l_1, l_2, \cdots, l_n = 0)}{\Delta(n-1, n-2, \cdots, 0)}} . \quad \text{(III.10)}$$

Note that $\Delta(n-1, n-2, \cdots, 0) = (n-1)!(n-2)! \cdots 1!$

We illustrate, as an example, the calculation of the dimension of the regular representation of SU_6 which we know already to be of dimension $6^2 - 1 = 35$.

f	l	n
2	7	5
1	5	4
1	4	3
1	3	2
1	2	1
0	0	0

$$N = \frac{(23457)(1\,2\,3\,5)(124)(13)(2)}{(1\,2\,3\,4\,5)(1\,2\,3\,4)(123)(12)(1)} ,$$

$$N = 35 .$$

It is sometimes convenient to label differently the

[12] See, for instance, Ref. 1, p. 201.

CC-0. In Public Domain. Gurukul Kangri Collection, Haridwar

Digitized by Arya Samaj Foundation Chennai and eGangotri

representation. Let λ_1 be the number of *columns* of length one, λ_2 of length two, etc., of a Young tableau. Then

$$\begin{aligned} l_1&=\lambda_1+\lambda_2+\cdots+\lambda_{n-1}+n-1\\ l_2&=\lambda_2+\cdots+\lambda_{n-1}+n-2\\ &\vdots\\ l_{n-1}&=\lambda_{n-1}+1\\ l_n&=0 \end{aligned}$$

and

$$\begin{aligned} l_1-l_2&=\lambda_1+1,\\ l_1-l_3&=\lambda_1+\lambda_2+2,\\ l_1-l_n&=\lambda_1+\cdots+\lambda_{n-1}+n-1\\ l_2-l_3&=\lambda_2+1,\\ l_2-l_4&=\lambda_2+\lambda_3+2\\ &\vdots \end{aligned}$$

Hence,

$$N=\frac{(\lambda_1+1)(\lambda_2+1)\cdots(\lambda_{n-1}+1)(\lambda_1+\lambda_2+2)\cdots(\lambda_{n-2}+\lambda_{n-1}+2)\cdots(\lambda_1+\lambda_2\cdots+\lambda_{n-1}+n-1)}{1!\,2!\cdots(n-1)!}.$$

Finally, if n is much larger than the number of rows r of a Young tableau, we write

$$N=\frac{\Delta(\nu_1,\nu_2,\cdots,\nu_r)}{\nu_1!\nu_2!\cdots\nu_r!}\times\frac{(\nu_1+n-r)!(\nu_2+n-r)!\cdots(\nu_r+n-r)!}{(n-1)!(n-2)!\cdots(n-r)!},$$

where $\nu_i=f_i+r-i$ and i runs from 1 to r only. Asymptotically

$$N\cong\frac{\Delta(\nu_1,\nu_2,\cdots,\nu_r)}{\nu_1!\nu_2!\cdots\nu_r!}n^f,$$

which gives a quick estimate of N.

IV. THE GENERATORS OF SU_n

We have already noted that any g belonging to SU_n can be written in the form

$$g=e^{ih}, \tag{IV.1}$$

where h is a Hermitian traceless $n\times n$ matrix. It will be convenient, in order to get a parametrization of the group, to choose a basis of n^2-1 linearly independent such matrices called the generators of the group. For SU_2 these are the famous Pauli matrices corresponding to spin. Of fundamental importance are the commutation relations satisfied by the generators; a matrix representation of the generators which satisfies these relations yields a representation of the unitary group.

A convenient choice of basis introduces n^2 traceless Hermitian matrices with one constraint. We define first n diagonal matrices $H_1, H_2, \cdots, H_n$ such that H_i has diagonal elements $-1/n$ except for the ith element which is equal to $(n-1)/n$,

$$H_i=\begin{pmatrix} -n^{-1} & & & & & \\ & -n^{-1} & & & & \\ & & \ddots & & & \\ & & & (n-1)n^{-1} & & \\ & & & & \ddots & \\ & & & & & -n^{-1} \end{pmatrix}=\begin{pmatrix} 0 & & & & & \\ & 0 & & & & \\ & & \ddots & & & \\ & & & 1 & & \\ & & & & \ddots & \\ & & & & & 0 \end{pmatrix}-n^{-1}I \tag{IV.2}$$

with

$$\sum_{i=1}^{n}H_i=0. \tag{IV.3}$$

Next we introduce matrices $E_{jk}^{(1)}$ and $E_{jk}^{(2)}$ for all $j<k$, which are generalizations of the Pauli matrices

$$\sigma_1=\begin{pmatrix} 0 & 1\\ 1 & 0 \end{pmatrix} \quad \text{and} \quad \sigma_2=\begin{pmatrix} 0 & -i\\ i & 0 \end{pmatrix};$$

$E_{jk}^{(1)}$ ($E_{jk}^{(2)}$) has zero entries except at the intersection

CC-0. In Public Domain. Gurukul Kangri Collection, Haridwar

Digitized by Arya Samaj Foundation Chennai and eGangotri

of the jth row and the kth column where it is $1(-i)$, and the kth row and the jth column where it is $1(+i)$,

$$E_{jk}^{(1)}=\begin{array}{c} \\ j- \\ k- \end{array}\begin{array}{c} \begin{array}{ccccc} & & j & & k \end{array} \\ \begin{pmatrix} - & - & \vdots & - & - & - & 1 & - & - \\ - & - & 1 & - & - & - & \vdots & - & - \end{pmatrix} \end{array}-,$$

$$E_{jk}^{(2)}=\begin{array}{c} \\ j- \\ k- \end{array}\begin{array}{c} \begin{array}{ccccc} & & j & & k \end{array} \\ \begin{pmatrix} - & - & \vdots & - & - & - & (-i) & \\ - & - & i & - & - & - & \vdots & \\ \end{pmatrix} \end{array}-. \quad \text{(IV.4)}$$

The set of matrices H_i, $E_{jk}^{(1)}$, and $E_{jk}^{(2)}$ together with the constraint (IV.3), form a basis in terms of which we can expand an arbitrary traceless Hermitian matrix h.

Let us compute the commutation relations of these matrices. For that purpose, we introduce column vectors $e^{(1)}\cdots e^{(n)}$ such that the only nonvanishing component of $e^{(i)}$ is the ith componet equal to 1. Then one obtains

$$\begin{aligned}
&[H_i, H_j]=0,\\
&[H_i, E_{jk}^{(1)}]=i(e^{(j)}-e^{(k)})_i E_{jk}^{(2)}=i(\delta_{ij}-\delta_{ki})E_{jk}^{(2)},\\
&[H_i, E_{jk}^{(2)}]=-i(e^{(j)}-e^{(k)})_i E_{jk}^{(1)}\\
&\qquad\qquad =-i(\delta_{ji}-\delta_{ki})E_{jk}^{(1)},\\
&[E_{jk}^{(1)}, E_{mn}^{(1)}]=-i(\delta_{km}E_{jn}^{(2)}+\delta_{jn}E_{km}^{(2)}+\delta_{kn}E_{jm}^{(2)}\\
&\qquad\qquad +\delta_{jm}E_{kn}^{(2)}),\\
&[E_{jk}^{(1)}, E_{mn}^{(2)}]=i(\delta_{km}E_{jn}^{(1)}-\delta_{jn}E_{km}^{(1)}-\delta_{kn}E_{jm}^{(1)}\\
&\qquad\qquad +\delta_{jm}E_{kn}^{(1)}),\\
&[E_{jk}^{(2)}, E_{mn}^{(2)}]=i(\delta_{km}E_{jn}^{(2)}+\delta_{jn}E_{km}^{(2)}-\delta_{kn}E_{jm}^{(2)}\\
&\qquad\qquad -\delta_{jm}E_{kn}^{(2)}), \quad \text{(IV.5)}
\end{aligned}$$

where for convenience of notation we have set

$$E_{jj}^{(1)}\equiv 2H_j, \quad E_{jk}^{(1)}=E_{kj}^{(1)},$$

and

$$E_{jk}^{(2)}=-E_{kj}^{(2)} \quad \text{for} \quad j>k. \quad \text{(IV.6)}$$

This set of commutation rules constitutes the "Lie algebra" of the group SU_n. The elements of this algebra are the generators of the group. Actually the relations (IV.5) can be written in a simpler form due to Cartan. Introduce the *non-Hermitian* matrices E_{jk} for $j\neq k$ with zeroes everywhere except at the intersection of the jth row and the kth column,

$$E_{jk}=\begin{array}{c} \\ j \end{array}\begin{array}{c} \begin{array}{c} k \end{array} \\ \begin{pmatrix} - & - & - & - & - & \vdots \\ & & & & 1 & \vdots \end{pmatrix} \end{array}. \quad \text{(IV.7)}$$

In terms of E_{jk}, we have

$$\begin{aligned}
E_{jk}^{(1)}&=E_{jk}+E_{kj},\\
E_{jk}^{(2)}&=-i(E_{jk}-E_{kj}). \quad \text{(IV.8)}
\end{aligned}$$

Note that E_{jk} is no longer Hermitian. Then the commutation relations take the canonical form

$$\begin{aligned}
&[H_i, H_j]=0,\\
&[H_i, E_{jk}]=[e^{(j)}-e^{(k)}]_i E_{jk}=(\delta_{ij}-\delta_{ik})E_{jk},\\
&[E_{jk}, E_{mn}]=E_{jn}\delta_{km}-E_{mk}\delta_{jn}, \text{ where } E_{ii}=H_i. \quad \text{(IV.9)}
\end{aligned}$$

The vectors $[e^{(i)}-e^{(j)}]$ are the *roots* of the algebra. If we denote in n-dimensional space the components of a vector by $x_i,\cdots, x_n$, the roots are seen to satisfy the equation $x_1+x_2\cdots+x_n=0$. Hence the roots are n^2-n vectors in an $(n-1)$-dimensional space. For $n=3$ we get the following six roots $\pm(e^{(1)}-e^{(2)})$, $\pm(e^{(2)}-e^{(3)})$, $\pm(e^{(3)}-e^{(1)})$. These are all of length $\sqrt{2}$, and they subtend among themselves angles which are multiples of $\pi/3$ since the cosine of this angle is ±1 or $\pm\frac{1}{2}$. The over-all scale factor is irrelevant. The resulting diagram

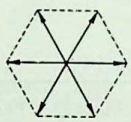

is well known from the eightfold way of Gell-Mann and Ne'eman. Generally, cosines of the angles between roots will take only the values ±1, $\pm\frac{1}{2}$, 0. This is illustrated in the root diagram for SU_4 which is drawn in the 3-dimensional hyperplane $x_1+x_2+x_3+x_4=0$ [the roots join the center of a cube to the midpoints of its 12 edges in agreement with the fact that there are $n^2-n=(4)^2-4=12$ roots].

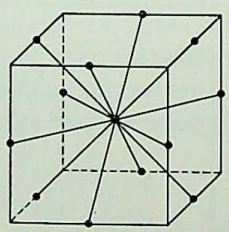

It is straightforward to show that the representations of the unitary group obtained from transformations in the tensor space can also be expressed in terms of generators satisfying the commutation relations (IV.5) and (IV.9). We note simply that the reducible Kronecker product is given by

$$e^{ih}\times e^{ih}\times\cdots\times e^{ih}=e^{iH},$$

where

$$H=h\times 1\times\cdots\times 1\oplus 1\times h\times 1\times\cdots \times 1\oplus\cdots\oplus 1\times 1\times\cdots\times h.$$

CC-0. In Public Domain. Gurukul Kangri Collection, Haridwar

Digitized by Arya Samaj Foundation Chennai and eGangotri

An important point is that the representations of H obtained from the irreducible representations of the group are clearly irreducible representations of the Lie algebra, and that the converse is true. This is the basis, for example, of the well-known method in quantum mechanics to obtain the irreducible representation of SU_2 by constructing the representations of the spin operators satisfying the "angular momentum commutation relations."

The H_i commute among themselves; hence, they can be simultaneously diagonalized. The set of n eigenvalues $H_i u = m_i u$ (with vanishing sum) is called a weight of the representation. *The irreducible representations are uniquely characterized by their highest weight.* The adjective highest refers to an ordering of the weights in which $(m_1 \cdots m_n)$ is said to be higher than $(m'_1 \cdots m'_n)$ if the first nonvanishing difference $m_i - m'_i$ is greater than zero. To each weight we can associate a vector $m_1 e_1 + \cdots + m_n e_n$ in the $(n-1)$-dimensional space which already was used for the roots. One can show that in our case, apart from the condition

$$\sum_1^n m_i = 0,$$

we must also have $m_i - m_k =$ integer. In fact, the m_i's are at most fractions with denominator n which differ by integers. The highest weight appears as a linear combination with nonnegative integral coefficients of $n-1$ fundamental ones[5]

$$M^{(1)} = \left(\frac{n-1}{n}, \frac{-1}{n}, \cdots, \frac{-1}{n}\right),$$

$$M^{(2)} = \left(\frac{n-2}{n}, \frac{n-2}{n}, \frac{-2}{n}, \cdots, \frac{-2}{n}\right),$$

$$M^{(3)} = \left(\frac{n-3}{n}, \frac{n-3}{n}, \frac{n-3}{n}, \frac{-3}{n}, \cdots, \frac{-3}{n}\right),$$

$$\vdots$$

$$M^{(p)} = \left(\frac{n-p}{n}, \cdots, \frac{-p}{n}, \cdots, \frac{-p}{n}\right),$$

$$\vdots$$

$$M^{(n-1)} = \left(n^{-1}, \cdots, n^{-1}, \frac{-(n-1)}{n}\right).$$

First we recognize in the weight $M^{(1)}$ the set of eigenvalues of the operators $H_1, \cdots, H_n$ corresponding to the eigenvector

$$y_1 = \begin{pmatrix} 1 \\ 0 \\ 0 \\ \vdots \end{pmatrix}$$

in the defining n-dimensional representation of the group. (We define analogously the coordinate vectors $y_2 \cdots y_n$.) It is clearly the highest possible weight and corresponds to the Young tableau $\square$. We shall use the compact notations of exterior calculus to denote antisymmetric tensors. Then consider the second-rank antisymmetric tensors and examine the result of H_i acting on $y_1 \Lambda y_2$. If g acts as

$$g(y_1 \Lambda y_2) = (g y_1) \Lambda (g y_2),$$

then with $g \simeq 1 + i\epsilon H$ (ϵ small) H acts as

$$H(y_1 \Lambda y_2) = (H y_1) \Lambda y_2 + y_1 \Lambda H(y_2).$$

Using the explicit form of H_i given above, one finds

$$H_1(y_1 \Lambda y_2) = \frac{n-1}{n} y_1 \Lambda y_2 + \left(\frac{-1}{n}\right) y_1 \Lambda y_2 = \frac{n-2}{n} y_1 \Lambda y_2,$$

$$H_2(y_1 \Lambda y_2) = \frac{-1}{n} y_1 \Lambda y_2 + \frac{(n-1)}{n} y_1 \Lambda y_2 = \frac{n-2}{n} y_1 \Lambda y_2,$$

$$H_i(y_1 \Lambda y_2) = \frac{-1}{n} y_1 \Lambda y_2 + \frac{-1}{n} y_1 \Lambda y_2 = \frac{-2}{n} y_1 \Lambda y_2, \quad i > 2.$$

The weight just obtained is in fact the highest weight of the representation. Hence the second weight $M^{(2)}$ corresponds to the representation previously described in terms of antisymmetric second rank tensors or $\square\!\!\square$. There is obviously no difficulty in using the previous technique to prove that $M^{(p)}$ corresponds to the representation in terms of antisymmetric tensors of rank p:

$\left.\begin{matrix}\square \\ \vdots \\ \square\end{matrix}\right\}$ p boxes.

Accordingly, the $n-1$ representations of SU_n obtained in terms of antisymmetric tensors of rank 1, $2, 3, \cdots, n-1$ are the $n-1$ fundamental representations of the group. Once these representations are known it is possible to form direct products of representations (see below) in such a way that at each step one gets only one new representation.

We recall that to each Young tableau (that is, to each representation) we attached two series of $n-1$ numbers, (i) $f_1, f_2 \cdots f_{n-1}$ (f_n is always identically zero), giving the number of boxes in each row $f_1 \geq f_2 \cdots \geq f_{n-1}$, and (ii) $\lambda_1, \lambda_2 \cdots \lambda_{n-1}$, λ_1 being the number of columns of length one, and so on $\cdots$. This second set is in direct relation to the highest weight of the representation which is equal to

$$M = \lambda_1 M^{(1)} + \lambda_2 M^{(2)} + \cdots + \lambda_{n-1} M^{(n-1)}.$$

Before leaving the subject of infinitesimal transformations, it is interesting to notice that among the

CC-0. In Public Domain. Gurukul Kangri Collection, Haridwar

Digitized by Arya Samaj Foundation Chennai and eGangotri

special unitary groups, SU_2 and SU_4, turn out to be "isomorphic in the small" to the rotation groups in 3 and 6 dimensions. This means they have the same Lie algebra. The first fact is of constant use in the study of the 3-dimensional rotation group. In terms of group theory, the second homomorphism $SU_4 \rightarrow R_6$ can be understood as follows: both SU_4 and R_6 depend on 15 (real) parameters. If we look at the representation of SU_4 in terms of antisymmetric tensors of rank two, we find the representation to be of dimension 6, equivalent to its complex conjugate (see above). A little algebra shows that indeed in that case one can find a basis in terms of which the representative matrices are real so that they correspond to rotations. It is then a simple matter to show that one gets all six dimensional rotations in that manner.

More generally, it can be shown that all groups having the same Lie algebra as SU_n are isomorphic to SU_n divided by a subgroup of its center. The center of SU_n is the discrete abelian group which consists of multiples of the identity with determinant one, u:

$$u_r = \exp[2i\pi(r/n)]I,$$

where $r = 1, 2 \cdots n$.

V. DECOMPOSITION OF THE PRODUCT OF TWO REPRESENTATIONS OF SU_n

Let $\mathfrak{V}^{(1)}$ and $\mathfrak{V}^{(2)}$ be the carrier spaces of two irreducible representations of a group G, $A^{(1)}(g)$, and $A^{(2)}(g)$. Then the Kronecker product $\mathfrak{V}^{(1)} \otimes \mathfrak{V}^{(2)}$ is the carrier space of the product $A^{(1)}(g) \otimes A^{(2)}(g)$ which is generally a reducible representation of the group. In many applications the question arises to decompose $A^{(1)} \otimes A^{(2)}$ in its irreducible parts.

There exist various ways to solve this problem. We will concentrate here on the description of a particularly simple method adapted to the case of SU_n. In this case the carrier spaces $\mathfrak{V}^{(1)}$ and $\mathfrak{V}^{(2)}$ are composed of of tensors S and T with certain symmetry properties. Consider a typical element of the product

$$S_{i_1 \cdots i_{f_1}} T_{j_1 \cdots j_{f_2}}.$$

It may be considered as a tensor with f_1+f_2 indices. As such we have a universal procedure to decompose it into parts of maximal symmetry (see Sec. II). If S and T were not already satisfying certain symmetry conditions, we would thus get each representation with a Young tableau of f_1+f_2 boxes a certain number of times (in fact, a number of times equal to the dimension of the representation of the symmetric group in f_1+f_2 objects which corresponds also to the same tableau). However, we must take into account the conditions imposed on S and T. It is clear that the following statement will be true in any case. The only representations of SU_n which appear in the decomposition of the product of two representations corresponding to Young tableaux with f_1 and f_2 boxes are those corresponding to tableaux with f_1+f_2, f_1+f_2-n, f_1+f_2-2n, $\cdots$ boxes.

The possibility of subtracting the columns of n boxes explains the statement of the previous proposition. Following Hamermesh,[4] we now give the recipe for solving the decomposition problem. (The reader might find it useful before using the general method to solve the problem for the simple case of the product of an arbitrary representation with $\square$ and then compare.)

General Recipe

(i) Let

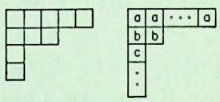

be the two representations. Choose one of those as the trunk on which the representations contained in the product will be built. Then label the boxes in the first row of the second tableau a, the boxes in the second row b, the boxes in the third row c, and so on.

(ii) Add one box labeled a to the first tableau in all possible ways so that it remains a *tableau*, i.e., the first row of length greater than or equal to the second row, etc. Then add a second box labeled a (if any) always requiring that the resultant object be a tableau. When the "a's" are exhausted, use the "b's," then the "c's," and so on.

(iii) In the process described in (ii) never let two boxes with the same label stand in the same column.

(iv) At the end of the process keep only those tableaux with no more than n rows. (Later on the columns of n boxes will be dropped; as we have already mentioned, for SU_n the columns of n boxes are irrelevant and can be added or omitted without destroying the meaning of the tableau.)

(v) Among the tableaux with no more than n rows some will be dropped and some others will be kept. In order to decide which are the relevant ones (which correspond to irreducible representations contained in the decomposition of the product), the following device is used. Take some resultant tableau. Reading from right to left and from the upper end to the lower collect the labels of the boxes. In the process of recollecting, one should always find a number of "a's" greater or equal to the number of "b's," a number of "b's" greater or equal to the number of "c's," and so on. Hence, only certain tableaux satisfying the previous criteria survive—they give the desired decomposition.

It is worthwhile to note that at the end some of the tableaux obtained might be identical (i.e., the corresponding representation appears several times); how-

CC-0. In Public Domain. Gurukul Kangri Collection, Haridwar

Digitized by Arya Samaj Foundation Chennai and eGangotri

ever, with attached labels some identical tableaux must differ by the disposition of the letters. For instance,

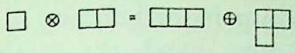

and not

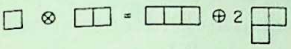

as one could at first have thought. For following the process described above, we label the tableau with two boxes

then attach an "a" to $\square$, thus obtaining

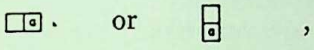

then a second "a"

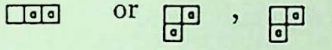

while

is forbidden by the rules. However, the two tableaux

 differ neither by the tableau nor by the labels

and therefore must be treated as a single tableau. This illustrates a second point: that a check on the dimensions is generally useful. If N_1 and N_2 are the dimensions of $A^{(1)}$ and $A^{(2)}$, and if $N^{(\lambda)}$ denotes the dimension of the irreducible constituents of $A^{(1)} \times A^{(2)}$, we must have

$$N_1 N_2 = \sum_{(\lambda)} N^{(\lambda)}.$$

A last comment before turning to an example—it concerns the case when a diagram contains two rows of the same length, then one must label the two rows *differently* and proceed as before. As an example, consider the problem of decomposing the product of two adjoint representations of SU_6;

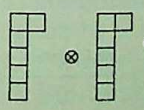

We follow the rules, and label the boxes of one tableau,

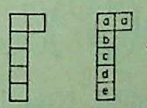

First Stage

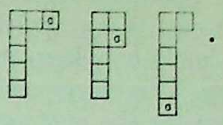

Second Stage

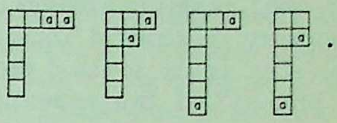

Third Stage

It is impossible to put a "b" before all "a's" or "c" before "b" [see (v)], and we do not want columns longer than 6, so the only possibilities are

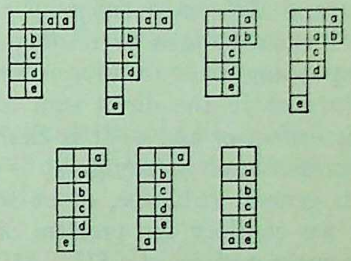

This is the desired decomposition. The final seven representations (with their attached labels) satisfy all the desired criteria. Writing for the symbol of a representation $D^N(\lambda_1, \lambda_2, \lambda_3, \lambda_4, \lambda_5)$, we have obtained the result:

$$D^{35}(1,0,0,0,1) \times D^{35}(1,0,0,0,1) = D^{1}(0,0,0,0,0) + 2D^{35}(1,0,0,0,1) + D^{189}(0,1,0,1,0) + D^{280}(2,0,0,1,0) + D^{280}(0,1,0,0,2) + D^{405}(2,0,0,0,2).$$

Indeed, one verifies that

$$35 \times 35 = 1 + 35 + 35 + 189 + 280 + \overline{280} + 405.$$

The bar recalls the fact that the two representations $(2,0,0,1,0)$ and $(0,1,0,0,2)$ are contragradient to each other,

It is clear that in some sense one could have kept the tableaux with more than 6 rows if, instead of dealing with SU_6, one were dealing with some SU_n, $n>6$. Part of the result previously obtained would still be valid.

CC-0. In Public Domain. Gurukul Kangri Collection, Haridwar

Digitized by Arya Samaj Foundation Chennai and eGangotri

Hence, it seems desirable to tabulate once and for all the result of the operation relaxing the condition on the number of rows. When applying the result to a given SU_n one should only keep the tableaux with no more than n rows. This corresponds in fact to solving a related problem for the symmetric group on f_1+f_2 objects: namely, the decomposition of the product of two tensors with given symmetries (described by Young tableaux of f_1 and f_2 boxes) into tensors (of rank f_1+f_2) of given symmetry (in terms of Young tableaux with f_1+f_2 boxes). This is the so-called decomposition of the "outer product" of two representations of the permutation groups on f_1 and f_2 objects. Some tables are given in Sec. VII.

VI. THE (SU_m, SU_n) CONTENT OF IRREDUCIBLE REPRESENTATIONS OF SU_{mn} AND SU_{m+n}

The direct product (SU_m, SU_n) of two unitary groups SU_m and SU_n in a subgroup of SU_{mn} and of SU_{m+n}. This can be seen by relating (SU_m, SU_n) to the corresponding linear transformation in the Kronecker product or in the direct sum of two vector spaces of dimension m and n. It is clear than an irreducible representation of any group is also a representation, in general reducible, of its subgroups. In this section we consider the problem of finding the irreducible representations of (SU_m, SU_n) which are contained in an irreducible representation of SU_{mn} or of SU_{m+n}, that is, its (SU_m, SU_n) content. This has become an important question in applications of groups to the study of elementary particles; for example, we are interested in the (SU_2, SU_1) or isospin content of $SU_3=SU_{2+1}$ and in the (SU_2, SU_3) or spin-unitary spin content of $SU_6=SU_{2\times3}$. We shall discuss these two decompositions separately.

To obtain the (SU_m, SU_n) content of an irreducible representation of SU_{mn} we consider two vector spaces $V^{(m)}$ and $V^{(n)}$ of dimensions m and n, respectively, in which SU_m and SU_n operate. The group (SU_m, SU_n) corresponds to unitary transformations in the tensor product space $V^{(m)}\times V^{(n)}$, with the scalar product defined by

$$(w^{(m)}\times w^{(n)}, v^{(m)}\times v^{(n)})=(w^{(m)}, v^{(m)})\,(w^{(n)}, v^{(n)}),$$

which leave (w^m, v^m) and (w^n, v^n) invariant, where $w^{(i)}$ and $v^{(i)}$ are vectors in $V^{(i)}$, $i=m, n$, and $(w^{(i)}, v^{(i)})$ is the scalar product of $w^{(i)}$ and $v^{(i)}$. It is then clear that (SU_m, SU_n) is a subgroup of SU_{mn} which operates in $V^{(m)}\times V^{(n)}$.

The components of a vector in $V^{(m)}\times V^{(n)}$ can be written in the form $V_{(i,\alpha)}$, where i runs from 1 to m and α from 1 to n. Hence a tensor of rank f has the form

$$T_{(i_1\alpha_1),(i_2\alpha_2),\cdots,(i_f\alpha_f)}.$$

To obtain the carrier space of an irreducible representation of SU_{mn} we have to impose a "maximal symmetry condition" on the indices of T (see Sec. III). In applying this symmetry condition to T we have to permute pairs of indices (i_j, α_j) at the same time. On the other hand, the carrier space for the irreducible representations of (SU_m, SU_n) is obtained by imposing a maximal symmetry condition on the indices i and α separately. Hence to get the (SU_m, SU_n) content of an irreducible representation of SU_{mn} we have to decompose the tensors which satisfy symmetry conditions with respect to the permutation of pairs of indices (i, α) into the sum of tensor which satisfy such conditions for separate permutation of the indices i and α.

Consider as an example the representation of SU_{mn}, corresponding to the Young tableau:

It is described in terms of tensors

$$T_{i_1\alpha_1,i_2\alpha_2}=T_{i_2\alpha_2,i_1\alpha_1}.$$

One can obviously write

$$T_{i_1\alpha_1,i_2\alpha_2}=\tfrac{1}{2}(T_{i_1\alpha_1,i_2\alpha_2}+T_{i_2\alpha_1,i_1\alpha_2})+\tfrac{1}{2}(T_{i_1\alpha_1,i_2\alpha_2}-T_{i_2\alpha_1,i_1\alpha_2}).$$

The first parenthesis is symmetric in the interchange of of i_1 and i_2; it is also invariant with respect to the interchange of α_1, α_2. The second is antisymmetric in the interchange of i_1, i_2, and separately in the interchange of α_1, α_2. The symbolic notation for the decomposition is

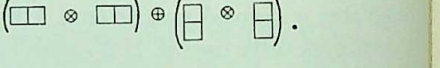

We can make a check on the dimensions. On the left we have a representation of SU_{mn} [and hence of (SU_m, SU_n)] of dimension

$$\binom{mn+1}{2}=\frac{(mn+1)mn}{2}.$$

On the right we have a representation of dimension

$$\binom{m+1}{2}\binom{n+1}{2}=\frac{(m+1)m}{2}\,\frac{(n+1)n}{2}$$

and another one of dimension

$$\binom{m}{2}\binom{n}{2}=\frac{m(m-1)}{2}\,\frac{n(n-1)}{2}.$$

Hence we should have

$$\binom{mn+1}{2}=\binom{m+1}{2}\binom{n+1}{2}+\binom{m}{2}\binom{n}{2},$$

which is indeed satisfied. Now it is apparent that the

CC-0. In Public Domain. Gurukul Kangri Collection, Haridwar

Digitized by Arya Samaj Foundation Chennai and eGangotri

following general statement is true: "Given an irreducible representation of SU_{mn} whose Young tableau contains f boxes, the only irreducible representations of (SU_m, SU_n) it contains are those with $f-\lambda m$ and $f-\lambda' n$ boxes, respectively, where λ and λ' are integers." Again this stems from the irrelevance of columns with p boxes added to the Young tableaux of an irreducible representative of SU_p.

The decomposition of tensors of high rank involves a considerable amount of labor. If we are mainly interested in finding the (SU_m, SU_n) content of SU_{mn} we can use a simpler method based on the observation that this decomposition is directly related to the reduction of the Kronecker product of two representations of the symmetric group Σ_f. We note that for fixed values of the indices i and α, the tensors $T_{(i_1\alpha_1),(i_2\alpha_2)\cdots}$ with maximal symmetry conditions for permutations on i and α *separately*, are also basis for the Kronecker product of two representations of Σ_f. The decomposition of these tensors into tensors with maximal symmetry conditions under *simultaneous* permutations of i and α leads to the reduction of the corresponding Kronecker product into irreducible parts according to Σ_f. This leads to the following procedure:

Suppose we want to know whether a representation $(D_m \times D_n)$ is contained in a given representation D_{mn} of SU_{mn} symbolized by a Young tableau with f boxes. First, as explained above, one can add to the Young tableau of D_m (D_n) a certain number[13] of columns of length m (n) on the left in order to bring them to a form where it contains f boxes. The Young tableaux obtained in that fashion describe also two irreducible representations of the symmetric group Σ_f. Then the given representation D_{mn} of SU_{mn} contains the representation (D_m, D_n) of (SU_m, SU_n) as many times as the corresponding representation of Σ_f appears in the decomposition of the product of the representations of Σ_f corresponding to the Young tableaux of D_m and D_n. In other words, what one has to do is to obtain the *Clebsch–Gordan series* of the corresponding representations of Σ_f. An important advantage of this method is that it allows us to forget essentially the subscripts m and n. The tabulation of the Clebsch–Gordan series can in fact be made only with reference to the symmetric group. To use the tables for specific m, n, one only has to disregard Young tableaux of more than m (n) rows, and columns of length m (n) (see Sec. VII).

We now turn our attention to the problem of finding the (SU_m, SU_n) content of a representation of SU_{m+n}. For this purpose we form the vector space sum $V^{(m)}+V^{(n)}$ in which the scalar product is now defined by

$$(w^{(m)}+w^{(n)}, v^{(m)}+v^{(n)}) = (w^{(m)}, v^{(m)})+(w^{(n)}, v^{(n)}).$$

The transformations (SU_m, SU_n) in this space form a subgroup of $SU_{(m+n)}$ which leaves $(w^{(m)}, v^{(m)})$ and $(w^{(n)}, v^{(n)})$ separately invariant. The components of a vector in $V^{(m)}+V^{(n)}$ are now written in the form V_i, where i runs from 1 to $m+n$ with the convention that for $i=1\cdots m (i=m+1,\cdots,m+n)$ these components belong to V^m (V^n). Then for a tensor of rank f we write $T_{i_1\cdots i_f}$. Now if we want to build irreducible representations of (SU_m, SU_n) we need to consider only tensors in which the index i_j runs *either* from 1 to m *or* from $m+1$ to $m+n$ and impose maximal symmetry conditions among indices of the same kind. These symmetrized tensors can also serve to induce a representation of SU_{m+n} if we adopt the convention that they have zero components for the absent values of the indices. The representation obtained in this way is reducible and corresponds to the Kronecker product of the two representations of SU_{m+n} labeled by the two Young tableaux which previously referred to SU_m and SU_n. The decomposition problem has been solved in Sec. V. This is the basis for the method of obtaining the (SU_m, SU_n) content of SU_{m+n} which we now describe.

Given a representation of (SU_m, SU_n) we can associate with it two Young tableaux, one for SU_m and one for SU_n, for instance,

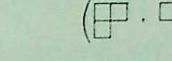

Then we know from Sec. V how to decompose the "outer" product of the corresponding regresentations of the symmetric groups, namely,

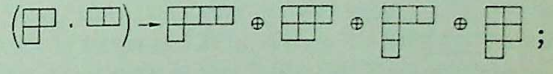

we refer the tableaux of the right-hand side to representations of SU_{m+n}. Then the given representation of (SU_m, SU_n) appears in the decomposition of the representations of SU_{m+n} which appear on the right-hand side as many times as their multiplicity indicate (in our example 0 or 1).

Note that to the Young tableaux for the given representation of (SU_m, SU_n) we can add α columns of length m, and β columns of length n, respectively. In our example we have

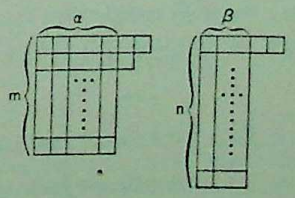

Hence this representation of (SU_m, SU_n) will also appear in the decomposition of representations of SU_{m+n} with $\alpha m+\beta n$ extra boxes. In general a given representa-

[13] This number can of course be zero.

CC-0. In Public Domain. Gurukul Kangri Collection, Haridwar

Digitized by Arya Samaj Foundation Chennai and eGangotri

tion of SU_{m+n} with a Young tableau of f boxes contains only those representations of (SU_m, SU_n) for which the number of boxes of the two Young tableaux, call them f_1 and f_2, are such that

$$f_1+f_2+\alpha m+\beta n=f.$$

A special case of this decomposition is Weyl's branching law which gives the SU_{n-1} content of a representation of SU_n. Indeed, it corresponds to the (SU_{n-1}, SU_1) content of SU_n, where SU_1 is a trivial group reduced to one element. Its representations are all the unity matrix, but may be represented by arbitrary Young tableaux with one row. Suppose we are given a representation $(f_1', f_2', \cdots, f'_{n-2})$ of SU_{n-1}. First we allow for an arbitrary number of extra columns of length $n-1$ by writing it

$$(f'_1+\alpha, f'_2+\alpha, \cdots, f'_{n-2}+\alpha, \alpha).$$

Then consider a "representation" of SU_1 (β) and decompose the outer product

$$(f'_1+\alpha, f'_2+\alpha, \cdots f'_{n-2}+\alpha, \alpha)\ (\beta)$$

according to the rules of Sec. V; α and β are chosen in order to find $(f_1, \cdots, f_{n-1})$ in the decomposition. Clearly a necessary condition is that

$$f'_1+\cdots+f'_{n-2}+\alpha(n-1)+\beta=f_1+f_2+\cdots+f_{n-1}.$$

Then we shall have in the process of decomposition tableaux with rows of length

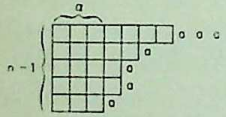

$$f'_1+\alpha+\beta_1$$
$$f'_2+\alpha+\beta_2$$
$$\vdots$$
$$f'_{n-2}+\alpha+\beta_{n-2}$$
$$\alpha+\beta_{n-1}$$

with $\beta_1+\cdots+\beta_{n-1}=\beta$, and due to the process of construction ("two a's cannot be in the same column")

$$f'_2+\alpha+\beta_2\leq f'_1+\alpha$$
$$f'_3+\alpha+\beta_3\leq f'_2+\alpha$$
$$\cdots$$
$$\alpha+\beta_{n-1}\leq f'_{n-2}+\alpha.$$

We also want

$$f'_1+\alpha+\beta_1=f_1$$
$$f'_2+\alpha+\beta_2=f_2$$
$$\cdots$$
$$f'_{n-2}+\alpha+\beta_{n-2}=f_{n-2}$$
$$\alpha+\beta_{n-1}=f_{n-1}.$$

So

$$\alpha+f_1'=f_1-\beta_1\leq f_1,$$
$$f_2=f_2'+\alpha+\beta_2\leq f'_1+\alpha,$$

and analogous inequalities for f'_3, $f'_4\cdots$. The result reads:

$$f_2\leq\alpha+f'_1\leq f_1$$
$$\cdots$$
$$f_{l+1}\leq\alpha+f'_l\leq f_l$$
$$\cdots$$
$$0\equiv f_n\leq\alpha\leq f_{n-1}.$$

This set of inequalities is the content of Weyl's branching law: the representations $(f'_1\cdots f'_{n-2})$ of SU_{n-1} contained in a representation $(f_1\cdots f_{n-1})$ of SU_n are those for which there exists a positive integer (or zero) α such that the previous inequalities are satisfied. It appears as a special case of the general method outlined above.

In practice it is better to tabulate the decomposition of "outer" products of representations of the symmetric groups. We are thus able to use these tables to solve two *different* problems pertaining to the unitary groups. The details are discussed in the next section.

VII. TABLES

We give below tables which are useful for the various decomposition problems of both the symmetric group Σ_f and the unitary group SU_n (see Secs. V and VI). We shall next discuss their use.

A. Dimension of representations.

From SU_3 to SU_{12} we give the value of the dimension of the representations up to Young tableaux with 8 boxes. The first column gives the dimension of the corresponding representation for the symmetric group Σ_f.

B. Decomposition of the "outer product" of two representations of Σ_{f_1} and Σ_{f_2} with respect to $\Sigma_{f_1+f_2}$ and Clebsch–Gordan series for the product of two representations of SU_n.

The tables first refer to the decomposition of the "outer product" of two representations of Σ_{f_1} and Σ_{f_2} or, what is equivalent, to the decomposition of the product of two tensors with given "maximal" symmetries in the f_1 and f_2 indices, respectively, into tensors with "maximal" symmetries in the f_1+f_2 indices. Hence, they also solve the problem of decomposing the product of two representations of SU_n (see Sec. V). As an example, the following representations of Σ_2 and Σ_5 induce the following representations of Σ_7 as read in the tables

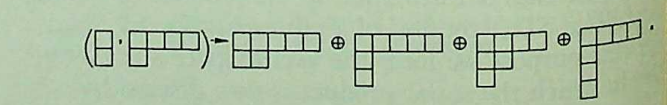

Notice that reading from Table A the dimensions of the corresponding representations of the symmetric groups, one finds,

$$1\times 4\rightarrow 14+15+35+20=84.$$

CC-0. In Public Domain. Gurukul Kangri Collection, Haridwar

Digitized by Arya Samaj Foundation Chennai and eGangotri

The dimensions on both sides are not equal, but the left-hand side always divides the right-hand side.[14]

When *labeling* the representations we have used $f_1 \geq f_2 \geq \cdots \geq f_{n-1}$; "$f$'s" equal to zero are omitted and when

$$f_{p+1} = \cdots = f_{p+r} = s$$

instead of repeating "s" r times, we have written s^r.

In using the tables to decompose the Kronecker product of two representations of SU_n, it is necessary (i) to ignore Young tableaux with more than n rows (ii) to consider as equivalent two Young tableaux when they differ only in the fact that one has extra columns of n boxes.

Example: Using the tables for SU_3 one gets

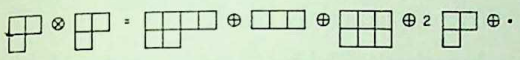

(The dot indicates the one-dimensional representation.) This also reads in familiar language

$$(8) \times (8) = (27) + (10) + (\overline{10}) + 2(8) + (1).$$

The dimensions are equal on both sides.

If we turn to SU_6 the same decomposition problem now leads to

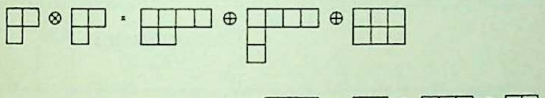

or in terms of the dimensions

$$(70) \times (70) = (1134) + (840) + (490) + 2(896) + (175) + (280) + (189).$$

Finally, the tables are also used "vertically" to find the (SU_m, SU_n) content of an irreducible representation SU_{m+n} (Sec. VI). In order to do this, select the column of the given representation of SU_{m+n} corresponding to a Young tableau with f boxes in the table $f_1+f_2=f$.

Each entry in the column is equal to the number of times the representation of (SU_m, SU_n) appearing on the left occurs in the given representation of SU_{m+n}. The two partitions corresponding to the Young tableaux appearing on the side of the table correspond to representations of (SU_m, SU_n) in two ways: (i) the first partition refers to SU_m and the second to SU_n, and (ii) the first partition refers to SU_n and the second partition refers to SU_m.[15] The only exception to this rule is when the two partitions are identical in which case one reads them only once. The table for $f_1+f_2=f$ must be trivially completed by extra rows corresponding to $0+f=f$, that is, the outer products of the representations of Σ_f by those of a group reduced to the identity thus inducing the same representation of Σ_f.[16] As customary we disregard tableaux of more than m (n) rows for SU_m (SU_n) and columns of length m (n). As an example, consider the representation of SU_6 and let us find its (SU_2, SU_4) content. Using the table for $f_1+f_2=3$ we find[17]

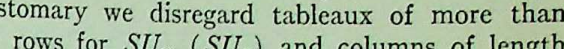

$$(SU_6) \rightarrow (SU_2, SU_4),$$

or

$$(56) = (1, 20) + (4, 1) + (2, 10) + (3, 4).$$

C. These tables give the Clebsch–Gordan series for the symmetric group, and the content of an irreducible representation of SU_{mn} in terms of its (SU_m, SU_n) subgroup (Sec. VI) up to Young tableaux with eight boxes.

Reading "horizontally" one finds the Clebsch–Gordan series of the product of two representations of Σ_f. Example for Σ_4:

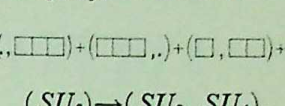

One can also read them "vertically" for a representation of SU_{mn}, thus collecting on the sides of the table its content in terms of (SU_m, SU_n). To do this, first select in the upper part of the table the Young tableau of a given representation of SU_{mn}. This same tableau reappears in the lower part of the table. Each entry is the number of times the representations of (SU_n, SU_m) appearing on the left (right) of a corresponding row occurs in the representation of SU_{nm} indicated in the top (bottom) of the column. The two partitions corresponding to the Young tableaux appearing on each side of the table, correspond to representations of (SU_m, SU_n) in two ways: (i) the first partition refers to SU_m and the second to SU_n; (ii) the first partition refers to SU_n, the second to SU_m.[18] However, as usual, Young tableaux with more than m (n) rows referring to SU_m (SU_n) are disregarded as well as columns of length m (n).

---

[14] This is due to the following fact. The representation of $(\Sigma_{f_1}, \Sigma_{f_2})$ of dimension $n_1 n_2$ induces a representation of $\Sigma_{f_1+f_2}$ of dimension equal to $n_1 n_2$ times the number of cosets of $(\Sigma_{f_1} + \Sigma_{f_2})$ in $\Sigma_{f_1+f_2}$, i.e., $(f_1+f_2)!/f_1!f_2!$. In our example this is $1 \times 4 \times (7!/2!5!) = 84$.

[15] Even if $m=n$.

[16] In the preceding problem of Clebsch–Gordan series for group SU_n this corresponds to the trivial decomposition of the product of an identity representation $(f_1' = \cdots = f_{n-1}' = 0)$ by a representation $(f_1, \cdots, f_{n-1})$ thus reducing to $(f_1, \cdots, f_{n-1}) \times (0, \cdots, 0) = (f_1, \cdots, f_{n-1})$.

[17] Note that the two first terms correspond precisely to the extra rows to be added to the tables.

[18] Except in the case when the two partitions are identical.

CC-0. In Public Domain. Gurukul Kangri Collection, Haridwar

Digitized by Arya Samaj Foundation Chennai and eGangotri

Example for SU_6: Reading the table one obtains the (SU_2, SU_3) content of the following representation (interesting in the case of baryon number two states),

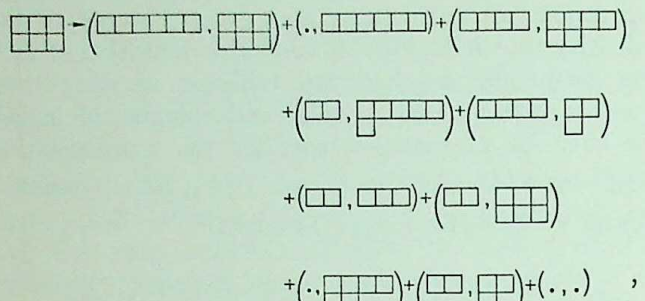

$$(SU_6)\rightarrow(SU_2,\ SU_3),$$

or in terms of dimensions

$$(490)\rightarrow(7,\ \overline{10})+(1,\ 28)+(5,\ 27)+(3,\ 35)+(5,\ 8)$$
$$+(3,\ 10)+(3,\ \overline{10})+(1,\ 27)+(3,\ 8)+(1,\ 1).$$

Of course the sum of the dimensions on the right adds up to the dimension on the left.

In general, when the two representations have the same Young tableau they should not be duplicated (as explained above). To illustrate this remark, consider for instance the (SU_3, SU_4) content of the following representation of SU_{12},

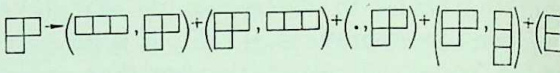

or

$$(572)\rightarrow(10,\ 20')+(8,\ 20)+(1,\ 20')+(8,\ 4)+(8,\ 20').$$

Notice that the representation 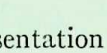 of (SU_3, SU_4) appears only once.

The tabulation of Table C requires long calculations.[19] For higher orders we have used a computer.

We summarize the various applications of the tables in the following diagram:

Table	Symmetric group Σ_f	Unitary group SU_n
A	Dimension	Dimension
B	Decomposition of outer product Σ_{f_1}, $\Sigma_{f_2}\rightarrow\Sigma_{f_1+f_2}$	(SU_m, SU_n) content of SU_{m+n} Clebsch-Gordan series for SU_n
C	Clebsch-Gordan series of Σ_f	(SU_m, SU_n) content of SU_{mn}

[19] Some explicit formulas can be found, for instance, in Ref. 4 or can be computed using Frobenius' formula for the characters of the symmetric group. The most straightforward method uses the orthogonality of characters.

CC-0. In Public Domain. Gurukul Kangri Collection, Haridwar

TABLE A

	$\sum$	SU_3	SU_4	SU_5	SU_6	SU_7	SU_8	SU_9	SU_{10}	SU_{11}	SU_{12}
(1)	1	3	4	5	6	7	8	9	10	11	12
(2)	1	6	10	15	21	28	36	45	55	66	78
(1^2)	1	3	6	10	15	21	28	36	45	55	66
(3)	1	10	20	35	56	84	120	165	220	286	364
(2,1)	2	8	20	40	70	112	168	240	330	440	572
(1^3)	1	1	4	10	20	35	56	84	120	165	220
(4)	1	15	35	70	126	210	330	495	715	1001	1365
(3,1)	3	15	45	105	210	378	630	990	1485	2145	3003
(2^2)	2	6	20	50	105	196	336	540	825	1210	1716
$(2,1^2)$	3	3	15	45	105	210	378	630	990	1485	2145
(1^4)	1	*	1	5	15	35	70	126	210	330	495
(5)	1	21	56	126	252	462	792	1287	2002	3003	4368
(4,1)	4	24	84	224	504	1008	1848	3168	5148	8008	12012
(3,2)	5	15	60	175	420	882	1680	2970	4950	7865	12012
$(3,1^2)$	6	6	36	126	336	756	1512	2772	4752	7722	12012
(2^21)	5	3	20	75	210	490	1008	1890	3300	5445	8580
$(2,1^3)$	4	*	4	24	84	224	504	1008	1848	3168	5148
(1^5)	1	*	*	1	6	21	56	126	252	462	792
(6)	1	28	84	210	462	924	1716	3003	5005	8008	12376
(5,1)	5	35	140	420	1050	2310	4620	8580	15015	25025	40040
(4,2)	9	27	126	420	1134	2646	5544	10692	19305	33033	54054
$(4,1^2)$	10	10	70	280	840	2100	4620	9240	17160	30030	50050
(3^2)	5	10	50	175	490	1176	2520	4950	9075	15730	26026
(3,2,1)	16	8	64	280	896	2352	5376	11088	21120	37752	64064
$(3,1^3)$	10	*	10	70	280	840	2100	4620	9240	17160	30030
(2^3)	5	1	10	50	175	490	1176	2520	4950	9075	15730
(2^21^2)	9	*	6	45	189	588	1512	3402	6930	13068	23166
$(2,1^4)$	5	*	*	5	35	140	420	1050	2310	4620	8580
(1^6)	1	*	*	*	1	7	28	84	210	462	924
(7)	1	36	120	330	792	1716	3432	6435	11440	19448	31824
(6,1)	6	48	216	720	1980	4752	10296	20592	38610	68640	116688
(5,2)	14	42	224	840	2520	6468	14784	30888	60060	110110	192192
$(5,1^2)$	15	15	120	540	1800	4950	11880	25740	51480	96525	171600

TABLE A (Continued)

	$\sum$	SU_3	SU_4	SU_5	SU_6	SU_7	SU_8	SU_9	SU_{10}	SU_{11}	SU_{12}
(4,3)	14	24	140	560	1764	4704	11088	23760	47190	88088	156156
(4,2,1)	35	15	140	700	2520	7350	18480	41580	85800	165165	300300
$(4,1^3)$	20	*	20	160	720	2400	6600	15840	34320	68640	128700
$(3^2,1)$	21	6	60	315	1176	3528	9072	20790	43560	84942	156156
$(3,2^2)$	21	3	36	210	840	2646	7056	16632	35640	70785	132132
$(3,2,1^2)$	35	*	20	175	840	2940	8400	20790	46200	94380	180180
$(3,1^4)$	15	*	*	15	120	540	1800	4950	11880	25740	51480
$(2^3,1)$	14	*	4	40	210	784	2352	6048	13860	29040	56628
(2^21^3)	14	*	*	10	84	392	1344	3780	9240	20328	41184
$(2,1^5)$	6	*	*	*	6	48	216	720	1980	4752	10296
(1^7)	1	*	*	*	*	1	8	36	120	330	792
(8)	1	45	165	495	1287	3003	6435	12870	24310	43758	75582
(7,1)	7	63	315	1155	3465	9009	21021	45045	90090	170170	306306
(6,2)	20	60	360	1500	4950	13860	34320	77220	160875	314600	583440
$(6,1^2)$	21	21	189	945	3465	10395	27027	63063	135135	270270	510510
(5,3)	28	42	280	1260	4410	12936	33264	77220	165165	330330	624624
(5,2,1)	64	24	256	1440	5760	18480	50688	123552	274560	566280	1098240
$(5,1^3)$	35	*	35	315	1575	5775	17325	45045	105105	225225	450450
(4^2)	14	15	105	490	1764	5292	13860	32670	70785	143143	273273
(4,3,1)	70	15	175	1050	4410	14700	41580	103950	235950	495495	975975
$(4,2^2)$	56	6	84	560	2520	8820	25872	66528	154440	330330	660660
$(4,2,1^2)$	90	*	45	450	2430	9450	29700	80190	193050	424710	868725
$(4,1^4)$	35	*	*	35	315	1575	5775	17325	45045	105105	225225
(3^21^2)	42	3	45	315	1470	5292	15876	41580	98010	212355	429429
(3^21^2)	56	*	20	210	1176	4704	15120	41580	101640	226512	468468
$(3,2^21)$	70	*	15	175	1050	4410	14700	41580	103950	235950	495495
$(3,2,1^3)$	64	*	*	40	384	2016	7680	23760	63360	151008	329472
$(3,1^5)$	21	*	*	*	21	189	945	3465	10395	27027	63063
(2^4)	14	*	1	15	105	490	1764	5292	13860	32670	70785
(2^31^2)	28	*	*	10	105	588	2352	7560	20790	50820	113256
(2^21^4)	20	*	*	*	15	140	720	2700	8250	21780	51480
$(2,1^6)$	7	*	*	*	*	7	63	315	1155	3465	9009
(1^8)	1	*	*	*	*	*	1	9	45	165	495

Digitized by Arya Samaj Foundation Chennai and eGangotri

CC-0. In Public Domain. Gurukul Kangri Collection, Haridwar

Digitized by Arya Samaj Foundation Chennai and eGangotri

TABLE B

$f_1+f_2=2$	(2)	(1^2)
(1) (1)	1	1

$f_1+f_2=3$	(3)	(2,1)	(1^3)
(1) (2)	1	1	
(1) (1^2)		1	1

	$f_1+f_2=4$	(4)	(3,1)	(2^2)	$(2,1^2)$	(1^4)
1+3	(1) (3)	1	1			
	(1) (2,1)		1	1	1	
	(1) (1^3)				1	1
2+2	(2) (2)	1	1	1		
	(2) (1^2)		1		1	
	(1^2) (1^2)			1	1	1

	$f_1+f_2=5$	(5)	(4,1)	(3,2)	$(3,1^2)$	$(2^2,1)$	$(2,1^3)$	(1^5)
1+4	(1) (4)	1	1					
	(1) (3,1)		1	1	1			
	(1) (2^2)			1		1		
	(1) $(2,1^2)$				1	1	1	
	(1) (1^4)						1	1
2+3	(2) (3)	1	1	1				
	(2) (2,1)		1	1	1	1		
	(2) (1^3)				1		1	
	(1^2) (3)		1		1			
	(1^2) (2,1)			1	1	1	1	
	(1^2) (1^3)					1	1	1

	$f_1+f_2=6$	(6)	(5,1)	(4,2)	$(4,1^2)$	(3^2)	(3,2,1)	(2^3)	$(3,1^3)$	$(2^2,1^2)$	$(2,1^4)$	(1^6)
1+5	(1)(5)	1	1									
	(1)(4,1)		1	1	1							
	(1)(3,2)			1		1	1					
	(1)$(3,1^2)$				1		1		1			
	(1)$(2^2,1)$						1	1		1		
	(1)$(2,1^3)$								1	1	1	
	(1)(1^5)										1	1
2+4	(2)(4)	1	1	1								
	(2)(3,1)		1	1	1	1	1					
	(2)(2^2)			1			1	1				
	(2)$(2,1^2)$				1		1		1	1		
	(2)(1^4)								1		1	
	(1^2)(4)		1		1							
	(1^2)(3,1)			1	1		1		1			
	$(1^2)$$(2^2)$					1	1			1		
	$(1^2)$$(2,1^2)$						1	1	1	1	1	
	$(1^2)$$(1^4)$									1	1	1

	$f_1+f_2=6$	(6)	(5,1)	(4,2)	$(4,1^2)$	(3^2)	(3,2,1)	(2^3)	$(3,1^3)$	$(2^2,1^2)$	$(2,1^4)$	(1^6)
3+3	(3)(3)	1	1	1		1						
	(3)(2,1)		1	1	1		1					
	(3)(1^3)				1				1			
	(2,1)(2,1)			1	1	1	2	1	1	1		
	(2,1)(1^3)						1		1	1	1	
	(1^3) (1^3)									1	1	1

CC-0. In Public Domain. Gurukul Kangri Collection, Haridwar

Digitized by Arya Samaj Foundation Chennai and eGangotri

TABLE B (Continued)

1 + 6

$f_1+f_2=7$	(7)	(6,1)	(5,2)	$(5,1^2)$	(4,3)	(4,2,1)	$(3^2,1)$	$(4,1^3)$	$(3,2^2)$	$(3,2,1^2)$	$(2^3,1)$	$(3,1^4)$	$(2^2,1^3)$	$(2,1^5)$	(1^7)
(1)(6)	1	1													
(1)(5,1)		1	1	1											
(1)(4,2)			1		1	1									
$(1)(4,1^2)$				1		1		1							
$(1)(3^2)$					1		1								
(1)(3,2,1)						1	1		1	1					
$(1)(2^3)$									1		1				
$(1)(3,1^3)$								1		1		1			
$(1)(2^2,1^2)$										1	1		1		
$(1)(2,1^4)$												1	1	1	
$(1)(1^6)$														1	1

2 + 5

$f_1+f_2=7$	(7)	(6,1)	(5,2)	$(5,1^2)$	(4,3)	(4,2,1)	$(3^2,1)$	$(4,1^3)$	$(3,2^2)$	$(3,2,1^2)$	$(2^3,1)$	$(3,1^4)$	$(2^2,1^3)$	$(2,1^5)$	(1^7)
(2)(5)	1	1	1												
(2)(4,1)		1	1	1	1	1									
(2)(3,2)			1		1	1	1		1						
(2) $(3,1^2)$				1		1	1	1		1					
$(2)(2^2,1)$						1			1	1	1				
$(2)(2,1^3)$								1		1		1	1		
$(2)(1^5)$												1		1	
$(1^2)(5)$		1		1											
$(1^2)(4,1)$			1	1		1		1							
$(1^2)(3,2)$					1	1	1			1					
$(1^2)(3,1^2)$						1		1	1	1		1			
$(1^2)(2^2,1)$							1		1	1	1		1		
$(1^2)(2,1^3)$										1	1	1	1	1	
$(1^2)(1^5)$													1	1	1

3 + 4

$f_1+f_2=7$	(7)	(6,1)	(5,2)	$(5,1^2)$	(4,3)	(4,2,1)	$(3^2,1)$	$(4,1^3)$	$(3,2^2)$	$(3,2,1^2)$	$(2^3,1)$	$(3,1^4)$	$(2^2,1^3)$	$(2,1^5)$	(1^7)
(3)(4)	1	1	1		1										
(3)(3,1)		1	1	1	1	1	1								
$(3)(2^2)$			1			1			1						
$(3)(2,1^2)$				1		1		1		1					
$(3)(1^4)$								1			1				
(2,1)(4)		1	1	1		1									
(2,1)(3,1)			1	1	1	1	1	1	1	1					
$(2,1)(2^2)$					1	1	1		1	1	1				
$(2,1)(2,1^2$						1	1	1	1	1	1	1	1		
$(2,1)(1^4)$										1		1	1	1	
$(1^3)(4)$				1				1							
$(1^3)(3,1)$						1		1		1		1			
$(1^3)(2^2)$							1			1			1		
$(1^3)(2,1^2)$									1	1	1	1	1	1	
$(1^3)(1^4)$											1		1	1	1

CC-0. In Public Domain. Gurukul Kangri Collection, Haridwar

Digitized by Arya Samaj Foundation Chennai and eGangotri

TABLE B (Continued)

	$f_1+f_2=8$	(8)	(7,1)	(6,2)	(6,1²)	(5,3)	(5,2,1)	(5,1³)	(4²)	(4,3,1)	(4,2²)	(4,2,1²)	(3²,2)	(3²,1²)	(3,2²,1)	(2⁴)	(4,1⁴)	(3,2,1³)	(2³,1²)	(3,1⁵)	(2²,1⁴)	(2,1⁶)	(1⁸)
1+7	(1)(7)	1	1																				
	(1)(6,1)		1	1	1																		
	(1)(5,2)			1		1	1																
	(1)(5,1²)				1		1	1															
	(1)(4,3)					1			1	1													
	(1)(4,2,1)						1			1	1	1											
	(1)(3²,1)									1			1	1									
	(1)(4,1³)							1				1				1							
	(1)(3,2²)										1		1		1								
	(1)(3,2,1²)											1		1	1			1					
	(1)(2³1)														1	1			1				
	(1)(3,1⁴)																1	1		1			
	(1)(2²,1³)																	1	1		1		
	(1)(2,1⁵)																			1	1	1	
	(1)(1⁷)																					1	1
2+6	(2)(6)	1	1	1																			
	(2)(5,1)		1	1	1	1	1																
	(2)(4,2)			1		1	1		1	1	1												
	(2)(4,1²)				1		1	1		1		1											
2+6	(2) (3²)					1			1			1											
	(2) (3,2,1)						1			1	1	1	1	1	1								
	(2) (2³)									1					1	1							
	(2) (3,1³)							1				1		1			1	1					
	(2) (2²,1²)											1			1			1	1				
	(2) (2,1⁴)																1	1		1			
	(2) (1⁶)																			1		1	
	(1²) (6)		1		1																		
	(1²) (5,1)			1	1		1	1															
	(1²) (4,2)					1	1			1		1											
	(1²) (4,1²)						1	1			1	1					1						
	(1²) (3²)								1	1					1								
	(1²) (3,2,1)									1	1	1	1	1	1			1					
	(1²) (2³)											1		1					1				
	(1²) (3,1³)											1			1		1	1		1			
	(1²) (2²,1²)													1	1	1		1	1		1		
	(1²) (2,1⁴)																	1	1	1	1	1	
	(1²) (1⁶)																				1	1	1

TABLE B (Continued)

	$f_1+f_2=8$	(8)	(7,1)	(6,2)	(6,1²)	(5,3)	(5,2,1)	(5,1³)	(4²)	(4,3,1)	(4,2²)	(4,2,1²)	(3²,2)	(3²,1²)	(3,2²,1)	(2⁴)	(4,1⁴)	(3,2,1³)	(2³,1²)	(3,1⁵)	(2²,1⁴)	(2,1⁶)	(1⁸)
3+5	(3) (5)	1	1	1		1																	
	(3) (4,1)		1	1	1	1	1		1	1													
	(3) (3,2)			1		1	1			1	1		1										
	(3) (3,1²)				1		1	1		1		1		1									
	(3) (2²,1)						1				1	1			1								
	(3) (2,1³)							1				1					1	1					
	(3) (1⁵)																1			1			
	(2,1) (5)		1	1	1		1																
	(2,1) (4,1)			1	1	1	2	1		1	1	1											
	(2,1) (3,2)					1	1		1	2	1	1	1	1									
	(2,1) (3,1²)						1	1		1	1	2	1	1	1		1	1					
	(2,1) (2²1)									1	1	1	1	1	2	1		1	1				
	(2,1) (2,1³)											1		1	1		1	2	1	1	1		
	(2,1) (1⁵)																	1		1	1	1	
	(1³) (5)				1		1																
	(1³) (4,1)					1	1				1						1						
	(1³) (3,2)								1		1		1					1					
	(1³) (3,1²)									1	1			1			1	1		1			
	(1³) (2²1)											1	1	1				1	1		1		
	(1³) (2,1³)													1	1		1	1	1	1	1		
	(1³) (1⁵)																			1	1	1	1

	$f_1+f_2=8$	(8)	(7,1)	(6,2)	(6,1²)	(5,3)	(5,2,1)	(5,1³)	(4²)	(4,3,1)	(4,2²)	(4,2,1²)	(3²2)	(3²,1²)	(3,2²,1)	(2⁴)	(4,1⁴)	(3,2,1³)	(2³,1²)	(3,1⁵)	(2²,1⁴)	(2,1⁶)	(1⁸)
4+4	(4) (4)	1	1	1		1			1														
	(4) (3,1)		1	1	1	1	1			1													
	(4) (2²)			1			1				1												
	(4) (2,1²)				1		1	1				1											
	(4) (1⁴)							1								1							
	(3,1) (3,1)			1	1	1	2	1	1	2	1	1	1	1									
	(3,1) (2²)					1	1			1	1	1	1		1								
	(3,1) (2,1²)						1	1		1	1	2		1	1		1	1					
	(3,1) (1⁴)											1				1	1			1			
	(2²) (2²)								1	1	1			1	1	1							
	(2²) (2,1²)									1		1	1	1	1			1	1				
	(2²) (1⁴)													1				1		1			
	(2,1²) (2,1²)										1	1	1	1	2	1	1	2	1	1	1		
	(2,1²) (1⁴)														1			1	1	1	1	1	
	(1⁴) (1⁴)															1			1		1	1	1

CC-0. In Public Domain. Gurukul Kangri Collection, Haridwar

Digitized by Arya Samaj Foundation Chennai and eGangotri

TABLE C

$\sum_2$		1	1	
$(2)\otimes(2)$	$(1^2)\otimes(1^2)$	(2)	(1^2)	$(1^2)\otimes(2)$
		1		
		(1^2)	(2)	

$\sum_3$		1 (3)	2 $(2,1)$	1 (1^3)	
$(3)\otimes(3)$	$(1^3)\otimes(1^3)$	1			$(3)\otimes(1^3)$
$(3)\otimes(2,1)$	$(1^3)\otimes(2,1)$		1		
$(2,1)\otimes(2,1)$		1	1	1	
		(1^3)	$(2,1)$	(3)	

$\sum_4$	1 (4)	3 $(3,1)$	2 (2^2)	3 $(2,1^2)$	1 (1^4)	
$(4)\otimes(4)$ $(1^4)\otimes(1^4)$	1					$(4)\otimes(1^4)$
$(4)\otimes(3,1)$ $(1^4)\otimes(2,1^2)$		1				$(1^4)\otimes(3,1)$ $(4)\otimes(2,1^2)$
$(4)\otimes(2^2)$ $(1^4)\otimes(2^2)$			1			
$(3,1)\otimes(3,1)(2,1^2)\otimes(2,1^2)$	1	1	1	1		$(3,1)\otimes(2,1^2)$
$(3,1)\otimes(2^2)$ $(2,1^2)\otimes(2^2)$		1		1		
$(2^2)\otimes(2^2)$	1		1		1	
	(1^4)	$(2,1^2)$	(2^2)	$(3,1)$	(4)	

$\sum_5$	1 (5)	4 $(4,1)$	5 $(3,2)$	6 $(3,1^2)$	5 $(2^2,1)$	4 $(2,1^3)$	1 (1^5)	
$(5)\otimes(5)$ $(1^5)\otimes(1^5)$	1							$(5)\otimes(1^5)$
$(5)\otimes(4,1)$ $(1^5)\otimes(2,1^3)$		1						$(1^5)\otimes(4,1)$ $(5)\otimes(2,1^3)$
$(5)\otimes(3,2)$ $(1^5)\otimes(2^2,1)$			1					$(1^5)\otimes(3,2)$ $(5)\otimes(2^2,1)$
$(5)\otimes(3,1^2)$ $(1^5)\otimes(3,1^2)$				1				
$(4,1)\otimes(4,1)$ $(2,1^3)\otimes(2,1^3)$	1	1	1	1				$(4,1)\otimes(2,1^3)$
$(4,1)\otimes(3,2)$ $(2,1^3)\otimes(2^2,1)$		1	1	1	1			$(2,1^3)\otimes(3,2)$ $(4,1)\otimes(2^2,1)$
$(4,1)\otimes(3,1^2)$ $(2,1^3)\otimes(3,1^2)$		1	1	1	1	1		
$(3,2)\otimes(3,2)$ $(2^2,1)\otimes(2^2,1)$	1	1	1	1	1	1		$(3,2)\otimes(2^2,1)$
$(3,2)\otimes(3,1^2)$ $(2^2,1)\otimes(3,1^2)$		1	1	2	1	1		
$(3,1^2)\otimes(3,1^2)$	1	1	2	1	2	1	1	
	(1^5)	$(2,1^3)$	$(2^2,1)$	$(3,1^2)$	$(3,2)$	$(4,1)$	(5)	

CC-0. In Public Domain. Gurukul Kangri Collection, Haridwar

Digitized by Arya Samaj Foundation Chennai and eGangotri

TABLE C (Continued)

$\sum_6$		1 (6)	5 (5,1)	9 (4,2)	10 $(4,1^2)$	5 (3^2)	16 (3,2,1)	5 (2^3)	10 $(3,1^3)$	9 $(2^2,1^2)$	5 $(2,1^4)$	1 (1^6)	
$(6)\otimes(6)$	$(1^6)\otimes(1^6)$	1											$(6)\otimes(1^6)$
$(6)\otimes(5,1)$	$(1^6)\otimes(2,1^4)$		1										$(1^6)\otimes(5,1)$ $(6)\otimes(2,1^4)$
$(6)\otimes(4,2)$	$(1^6)\otimes(2^2,1^2)$			1									$(1^6)\otimes(4,2)$ $(6)\otimes(2^2,1^2)$
$(6)\otimes(4,1^2)$	$(1^6)\otimes(3,1^3)$				1								$(1^6)\otimes(4,1^2)$ $(6)\otimes(3,1^3)$
$(6)\otimes(3^2)$	$(1^6)\otimes(2^3)$					1							$(1^6)\otimes(3^2)$ $(6)\otimes(2^3)$
$(6)\otimes(3,2,1)$	$(1^6)\otimes(3,2,1)$						1						
$(5,1)\otimes(5,1)$	$(2,1^4)\otimes(2,1^4)$	1	1	1	1								$(5,1)\otimes(2,1^4)$
$(5,1)\otimes(4,2)$	$(2,1^4)\otimes(2^2,1^2)$		1	1	1	1	1						$(2,1^4)\otimes(4,2)$ $(5,1)\otimes(2^2,1^2)$
$(5,1)\otimes(4,1^2)$	$(2,1^4)\otimes(3,1^3)$		1	1	1		1		1				$(2,1^4)\otimes(4,1^2)$ $(5,1)\otimes(3,1^3)$
$(5,1)\otimes(3^2)$	$(2,1^4)\otimes(2^3)$			1			1						$(2,1^4)\otimes(3^2)$ $(5,1)\otimes(2^3)$
$(5,1)\otimes(3,2,1)$	$(2,1^4)\otimes(3,2,1)$			1	1	1	2	1	1	1			
$(4,2)\otimes(4,2)$	$(2^2,1^2)\otimes(2^2,1^2)$	1	1	2	1		2	1	1				$(2^2,1^2)\otimes(4,2)$
$(4,2)\otimes(4,1^2)$	$(2^2,1^2)\otimes(3,1^3)$		1	1	2	1	2		1	1			$(2^2,1^2)\otimes(4,1^2)$ $(4,2)\otimes(3,1^3)$
$(4,2)\otimes(3^2)$	$(2^2,1^2)\otimes(2^3)$		1		1	1	1			1			$(2^2,1^2)\otimes(3^2)$ $(4,2)\otimes(2^3)$
$(4,2)\otimes(3,2,1)$	$(2^2,1^2)\otimes(3,2,1)$		1	2	2	1	3	1	2	2	1		
$(4,1^2)\otimes(4,1^2)$	$(3,1^3)\otimes(3,1^3)$	1	1	2	1	1	2	1	1	1	1		$(3,1^3)\otimes(4,1^2)$
$(4,1^2)\otimes(3^2)$	$(3,1^3)\otimes(2^3)$			1	1		1	1	1				$(3,1^3)\otimes(3^2)$ $(4,1^2)\otimes(2^3)$
$(4,1^2)\otimes(3,2,1)$	$(3,1^3)\otimes(3,2,1)$		1	2	2	1	4	1	2	2	1		
$(3^2)\otimes(3^2)$	$(2^3)\otimes(2^3)$	1		1				1	1				$(2^3)\otimes(3^2)$
$(3^2)\otimes(3,2,1)$	$(2^3)\otimes(3,2,1)$		1	1	1	1	2		3	1	1		
$(3,2,1)\otimes(3,2,1)$		1	2	3	4	2	5	2	4	3	2	1	
		(1^6)	$(2,1^4)$	$(2^2,1^2)$	$(3,1^3)$	(2^3)	(3,2,1)	(3^2)	$(4,1^2)$	(4,2)	(5,1)	(6)	

CC-0. In Public Domain. Gurukul Kangri Collection, Haridwar

Digitized by Arya Samaj Foundation Chennai and eGangotri

TABLE C (Continued)

$\sum_7$		1	6	14	15	14	35	21	20	21	35	14	15	14	6	1	
		(7)	(6,1)	(5,2)	$(5,1^2)$	(4,3)	(4,2,1)	$(3^2,1)$	$(4,1^3)$	$(3,2^2)$	$(3,2,1^2)$	$(2^3,1)$	$(3,1^4)$	$(2^2,1^3)$	$(2,1^5)$	(1^7)	
(7)⊗(7)	$(1^7)\otimes(1^7)$	1															(7)⊗ (1^7)
(7)⊗(6,1)	$(1^7)\otimes(2,1^5)$		1														(7)⊗$(2,1^5)$ $(1^7)\otimes(6,1)$
(7)⊗(5,2)	$(1^7)\otimes(2^2,1^3)$			1													(7)⊗$(2^2,1^3)$ $(1^7)\otimes(5,2)$
$(7)\otimes(5,1^2)$	$(1^7)\otimes(3,1^4)$				1												(7)⊗$(3,1^4)$ $(1^7)\otimes(5,1^2)$
(7)⊗(4,3)	$(1^7)\otimes(2^3,1)$					1											(7)⊗$(2^3,1)$ $(1^7)\otimes(4,3)$
(7)⊗(4,2,1)	$(1^7)\otimes(3,2,1^2)$						1										(7)⊗$(3,2,1^2)$ $(1^7)\otimes(4,2,1)$
$(7)\otimes(3^2,1)$	$(1^7)\otimes(3,2^2)$							1									(7)⊗$(3,2^2)$ $(1^7)\otimes(3^2,1)$
$(7)\otimes(4,1^3)$	$(1^7)\otimes(4,1^3)$								1								
(6,1)⊗(6,1)	$(2,1^5)\otimes(2,1^5)$	1	1	1	1												(6,1)⊗$(2,1^5)$
(6,1)⊗(5,2)	$(2,1^5)\otimes(2^2,1^3)$		1	1	1	1	1										(6,1)⊗$(2^2,1^3)$ $(2,1^5)\otimes(5,2)$
$(6,1)\otimes(5,1^2)$	$(2,1^5)\otimes(3,1^4)$		1	1	1		1		1								(6,1)⊗$(3,1^4)$ $(2,1^5)\otimes(5,1^2)$
(6,1)⊗(4,3)	$(2,1^5)\otimes(2^3,1)$			1		1	1	1									(6,1)⊗$(2^3,1)$ $(2,1^5)\otimes(4,3)$
(6,1)⊗(4,2,1)	$(2,1^5)\otimes(3,2,1^2)$			1	1	1	2	1	1	1	1						(6,1)⊗$(3,2,1^2)$ $(2,1^5)\otimes(4,2,1)$
$(6,1)\otimes(3^2,1)$	$(2,1^5)\otimes(3,2^2)$					1	1	1		1	1						(6,1)⊗$(3,2^2)$ $(2,1^5)\otimes(3^2,1)$
$(6,1)\otimes(4,1^3)$	$(2,1^5)\otimes(4,1^3)$				1		1		1		1		1				
(5,2)⊗(5,2)	$(2^2,1^3)\otimes(2^2,1^3)$	1	1	2	1	1	2	1	1	1							(5,2)⊗$(2^2,1^3)$
$(5,2)\otimes(5,1^2)$	$(2^2,1^3)\otimes(3,1^4)$		1	1	2	1	2	1	1		1						(5,2)⊗$(3,1^4)$ $(2^2,1^3)\otimes(5,1^2)$
(5,2)⊗(4,3)	$(2^2,1^3)\otimes(2^3,1)$		1	1	1	1	2	1		1	1						(5,2)⊗$(2^3,1)$ $(2^2,1^3)\otimes(4,3)$
(5,2)⊗(4,2,1)	$(2^2,1^3)\otimes(3,2,1^2)$		1	2	2	2	4	2	2	2	3	1	1				(5,2)⊗$(3,2,1^2)$ $(2^2,1^3)\otimes(4,2,1)$
$(5,2)\otimes(3^2,1)$	$(2^2,1^3)\otimes(3,2^2)$			1	1	1	2	2	1	1	2	1		1			(5,2)⊗$(3,2^2)$ $(2^2,1^3)\otimes(3^2,1)$
$(5,2)\otimes(4,1^3)$	$(2^2,1^2)\otimes(4,1^3)$			1	1		2	1	2	1	2		1	1			
$(5,1^2)\otimes(5,1^2)$	$(3,1^4)\otimes(3,1^4)$	1	1	2	1	1	2		1	1	1		1				$(5,1^2)\otimes(3,1^4)$
$(5,1^2)\otimes(4,3)$	$(3,1^4)\otimes(2^3,1)$			1	1	1	2	1	1	1	1						$(5,1^2)\otimes(2^3,1)$ $(3,1^4)\otimes(4,3)$
$(5,1^2)\otimes(4,2,1)$	$(3^4)\otimes(3,2,1^2)$		1	2	2	2	4	3	2	2	3	1	1	1			$(5,1^2)\otimes(3,2,1^2)$ $(3,1^4)\otimes(4,2,1)$
$(5,1^2)\otimes(3^2,1)$	$(3,1^4)\otimes(3,2^2)$			1		1	3	1	1	2	2	1	1				$(5,1^2)\otimes(3,2^2)$ $(3,1^4)\otimes(3^2,1)$
$(5,1^2)\otimes(4,1^3)$	$(3,1^4)\otimes(4,1^3)$		1	1	1	1	2	1	1	1	2	1	1	1	1		
(4,3)⊗(4,3)	$(2^3,1)\otimes(2^3,1)$	1	1	1	1	1	1	1	1	1	1	1					(4,3)⊗$(2^3,1)$
(4,3)⊗(4,2,1)	$(2^3,1)\otimes(3,2,1^2)$		1	2	2	1	4	2	2	2	3	1	1	1			(4,3)⊗$(3,2,1^2)$ $(2^3,1)\otimes(4,2,1)$
$(4,3)\otimes(3^2,1)$	$(2^3,1)\otimes(3,2^2)$		1	1	1	1	2	1	1	1	2	1	1	1			(4,3)⊗$(3,2^2)$ $(2^3,1)\otimes(3^2,1)$
$(4,3)\otimes(4,1^3)$	$(2^3,1)\otimes(4,1^3)$				1	1	2	1	2	1	2	1	1				
(4,2,1)⊗(4,2,1)	$(3,2,1^2)\otimes(3,2,1^2)$	1	2	4	4	4	9	5	5	5	8	3	3	3	1		(4,2,1)⊗$(3,2,1^2)$
$(4,2,1)\otimes(3^2,1)$	$(3,2,1^2)\otimes(3,2^2)$		1	2	3	2	5	3	3	3	5	2	2	2	1		(4,2,1)⊗$(3,2^2)$ $(3,2,1^2)\otimes(3^2,1)$
$(4,2,1)\otimes(4,1^3)$	$(3,2,1^2)\otimes(4,1^3)$		1	2	2	2	5	3	2	3	5	2	2	2	1		
$(3^2,1)\otimes(3^2,1)$	$(3,2^2)\otimes(3,2^2)$	1	1	2	1	1	3	1	2	2	3	1	2	1	1		$(3^2,1)\otimes(3,2^2)$
$(3^2,1)\otimes(4,1^3)$	$(3,2^2)\otimes(4,1^3)$			1	1	1	3	2	2	2	3	1	1	1			
$(4,1^3)\otimes(4,1^3)$		1	1	2	1	2	2	2	1	2	2	2	1	2	1	1	
		(1^7)	$(2,1^5)$	$(2^2,1^3)$	$(3,1^4)$	$(2^3,1)$	$(3,2,1^2)$	$(3,2^2)$	$(4,1^3)$	$(3^2,1)$	$(4,2,1)$	$(4,3)$	$(5,1^2)$	$(5,2)$	$(6,1)$	(7)	

CC-0. In Public Domain. Gurukul Kangri Collection, Haridwar

Digitized by Arya Samaj Foundation Chennai and eGangotri

TABLE C (Continued)

Σ_8		1 (8)	7 (7,1)	20 (5,2)	21 (6,1²)	28 (5,3)	64 (5,2,1)	35 (5,1³)	14 (4²)	70 (4,3,1)	56 (4,2²)	90 (4,2,1²)	42 (3²,2)	56 (3²,1²)	70 (3,2²1)	14 (2⁴)	35 (4,1⁴)	64 (3,2,1³)	28 (2³,1²)	21 (3,1⁵)	20 (2²,1⁴)	7 (2,1⁶)	1 (1⁸)		
(8)⊗(8)	(1⁸)⊗(1⁸)	1																					(8)⊗(1⁸)	
(8)⊗(7,1)	(1⁸)⊗(2,1⁶)		1																				(8)⊗(2,1⁶)	(1⁸)⊗(7,1)
(8)⊗(6,2)	(1⁸)⊗(2²,1⁴)			1																			(8)⊗(2²,1⁴)	(1⁸)⊗(6,2)
(8)⊗(6,1²)	(1⁸)⊗(3,1⁵)				1																		(8)⊗(3,1⁵)	(1⁸)⊗(6,1²)
(8)⊗(5,3)	(1⁸)⊗(2³,1²)					1																	(8)⊗(2³,1²)	(1⁸)⊗(5,3)
(8)⊗(5,2,1)	(1⁸)⊗(3,2,1³)						1																(8)⊗(3,2,1³)	(1⁸)⊗(5,2,1)
(8)⊗(5,1³)	(1⁸)⊗(4,1⁴)							1															(8)⊗(4,1⁴)	(1⁸)⊗(5,1³)
(8)⊗(4²)	(1⁸)⊗(2⁴)								1														(8)⊗(2⁴)	(1⁸)⊗(4²)
(8)⊗(4,3,1)	(1⁸)⊗(3,2²,1)									1													(8)⊗(3,2²,1)	(1⁸)⊗(4,3,1)
(8)⊗(4,2²)	(1⁸)⊗(3²,1²)										1												(8)⊗(3²,1²)	(1⁸)⊗(4,2²)
(8)⊗(4,2,1²)	(1⁸)⊗(4,2,1²)											1												
(8)⊗(3²,2)	(1⁸)⊗(3²,2)												1											
(7,1)⊗(7,1)	(2,1⁶)⊗(2,1⁶)	1	1	1	1																		(7,1)⊗(2,1⁶)	
(7,1)⊗(6,2)	(2,1⁶)⊗(2²,1⁴)		1	1	1	1	1																(7,1)⊗(2²,1⁴)	(2,1⁶)⊗(6,2)
(7,1)⊗(6,1²)	(2,1⁶)⊗(3,1⁵)		1	1	1		1	1															(7,1)⊗(3,1⁵)	(2,1⁶)⊗(6,1²)
(7,1)⊗(5,3)	(2,1⁶)⊗(2³,1²)			1		1	1		1	1													(7,1)⊗(2³, 1²)	(2,1⁶)⊗(5,3)
(7,1)⊗(5,2,1)	(2,1⁶)⊗(3,2,1³)			1	1	1	2	1		1	1	1											(7,1)⊗(3,2,1³)	(2,1⁶)⊗(5,2,1)
(7,1)⊗(5,1³)	(2,1⁶)⊗(4,1⁴)				1		1	1				1					1						(7,1)⊗(4,1⁴)	(2,1⁶)⊗(5,1³)
(7,1)⊗(4²)	(2,1⁶)⊗(2⁴)					1				1													(7,1)⊗(2⁴)	(2,1⁶)⊗(4²)
(7,1)⊗(4,3,1)	(2,1⁶)⊗(3,2²,1)					1	1		1	2	1	1	1	1									(7,1)⊗(3,2²,1)	(2,1⁶)⊗(4,3,1)
(7,1)⊗(4,2²)	(2,1⁶)⊗(3²,1²)						1			1	1	1	1		1								(7,1)⊗(3²,1²)	(2,1⁶)⊗(4,2²)
(7,1)⊗(4,2,1²)	(2,1⁶)⊗(4,2,1²)						1	1		1	1	2		1	1		1	1						
(7,1)⊗(3²,2)	(2,1⁶)⊗(3²,2)									1	1		1	1	1									
(6,2)⊗(6,2)	(2²,1⁴)⊗(2²,1⁴)	1	1	2	1	1	2	1	1	1	1												(6,2)⊗(2²,1⁴)	
(6,2)⊗(6,1²)	(2²,1⁴)⊗(3,1⁵)		1	1	2	1	2	1		1		1											(6,2)⊗(3,1⁵)	(2²,1⁴)⊗(6,1²)
(6,2)⊗(5,3)	(2²,1⁴)⊗(2³,1²)		1	1	1	2	2			2	1	1	1										(6,2)⊗(2³,1²)	(2²,1⁴)⊗(5,3)
(6,2)⊗(5,2,1)	(2²,1⁴)⊗(3,2,1³)		1	2	2	2	4	2	1	3	2	3	1	1	1		1						(6,2)⊗(3,2,1³)	(2²,1⁴)⊗(5,2,1)
(6,2)⊗(5,1³)	(2²,1⁴)⊗(4,1⁴)			1	1		2	2		1	1	2		1			1	1					(6,2)⊗(4,1⁴)	(2²,1⁴)⊗(5,1³)
(6,2)⊗(4²)	(2²,1⁴)⊗(2⁴)			1			1		1	1	1			1									(6, 2)⊗(2⁴)	(2²,1⁴)⊗(4²)
(6,2)⊗(4,3,1)	(2²,1⁴)⊗(3,2²1)			1	1	2	3	1	1	4	2	3	2	2	2			1					(6,2)⊗(3,2²1)	(2²,1⁴)⊗(4,3,1)
(6,2)⊗(4,2²)	(2²,1⁴)⊗(3²1²)			1		1	2	1	1	2	3	2	1	2	2	1	1	1					(6,2)⊗(4,2²)	(2²,1⁴)⊗(4,3²)
(6,2)⊗(4,2,1²)	(2²,1⁴)⊗(4,2,1²)				1	1	3	2		3	2	5	2	2	3		2	3	1	1				
(6,2)⊗(3²,2)	(2²,1⁴)⊗(3²,2)					1	1			2	1	2	2	1	2			1	1					
(6,1²)⊗(6,1²)	(3,1⁵)⊗(3,1⁵)	1	1	2	1	1	2	1			1	1					1						(6,1²)⊗(3,1⁵)	
(6,1²)⊗(5,3)	(3,1⁵)⊗(2³,1²)			1	1	1	2	1	1	2	1	1		1									(6,1²)⊗(2³,1²)	(3,1⁵)⊗(5,3)
(6,1²)⊗(5,2,1)	(3,1⁵)⊗(3,2,1³)		1	2	2	2	4	2	1	3	2	3	1	1	1		1	1					(6,1,2)⊗(3,2,1³)	(3,1⁵)⊗(5,2,1)
(6,1²)⊗(5,1³)	(3,1⁵)⊗(4,1⁴)		1	1	1	1	2	1		1	1	2			1		1	1		1			(6,1²)⊗(4,1⁴)	(3,1⁵)⊗(5,1³)
(6,1²)⊗(4²)	(3,1⁵)⊗(2⁴)					1	1			1		1	1										(6,1²)⊗(2⁴)	(3,1⁵)⊗(4²)
(6,1²)⊗(4,3,1)	(3,1⁵)⊗(3,2²,1)			1		2	3	1	1	4	3	3	2	2	2		1	1					(6,1²)⊗(3,2²1)	(3,1⁵)⊗(4,3,1)
(6,1²)⊗(4,2²)	(3,1⁵)⊗(3²,1²)				1	1	2	1		3	1	3	2	2	2			1	1				(6,1²)⊗(3²,1²)	(3,1⁵)⊗(4,2²)
(6,1²)⊗(4,2,1²)	(3,1⁵)⊗(4,2,1²)			1	1	1	3	2	1	3	3	4	2	3	3	1	2	3	1	1	1			
(6,1²)⊗(3²,2)	(3,1⁵)⊗(3²,2)						1		1	2	2	2	1	2	2	1		1						
(5,3)⊗(5,3)	(2³,1²)⊗(2³,1²)	1	1	2	1	1	2	1	1	2	2	1	1	1	1								(5,3)⊗(2³,1²)	
(5,3)⊗(5,2,1)	(2³,1²)⊗(3,2,1³)		1	2	2	2	5	2	1	4	3	4	2	2	2		1	1					(5,3)⊗(3,2,1³)	(3²,1²)⊗(5,2,1)
(5,3)⊗(5,1³)	(2³,1²)⊗(4,1⁴)				1	1	2	2		2	1	3	1	1	1		1	1					(5,3)⊗(4,1⁴)	(2³,1²)⊗(5,1³)
(5,3)⊗(4²)	(2³,1²)⊗(2⁴)		1		1	1	1			1		1	1		1								(5,3)⊗(2⁴)	(2³,1²)⊗(4²)
(5,3)⊗(4,3,1)	(2³,1²)⊗(3,2²,1)		1	2	2	2	4	2	1	4	3	4	2	3	3	1	1	2	1				(5,3)⊗ (3,2²,1)	(2³,1²)⊗(4,3,1)
		(1⁸)	(2,1⁶)	(2²,1⁴)	(3,1⁵)	(2³,1²)	(3,2,1³)	(4,1⁴)	(2⁴)	(3,2²,1)	(3²,1²)	(4,2,1²)	(3²,2)	(4,2²)	(4,3,1)	(4²)	(5,1³)	(5,2,1)	(5,3)	(6,1²)	(6,2)	(7,1)	(8)	

CC-0. In Public Domain. Gurukul Kangri Collection, Haridwar

Digitized by Arya Samaj Foundation Chennai and eGangotri

TABLE C (Continued)

Σ_s		1 (8)	7 (7,1)	20 (6,2)	21 (6,1²)	28 (5,3)	64 (5,2,1)	35 (5,1³)	14 (4²)	70 (4,3,1)	56 (4,2²)	90 (4,2,1²)	42 (3³,2)	56 (3²,1²)	70 (3,2³,1)	14 (2⁴)	35 (4,1⁴)	64 (3,2,1³)	28 (2³,1²)	21 (3,1⁵)	20 (2²,1⁴)	7 (2,1⁶)	1 (1⁸)	
(5,3)⊗(4,2²)	(2³,1²)⊗(3²,1²)			1	1	2	3	1		3	2	4	2	1	3		1	2	1	1				(5,3)⊗(3²,1²) (2³,1²)⊗(4,2²)
(5,3)⊗(4,2,1²)	(2³,1²)⊗(4,2,1²)			1	1	1	4	3	1	4	4	6	2	4	4	1	3	4	1	1	1			
(5,3)⊗(3²,2)	(2³,1²)⊗(3²,2)			1		1	2	1	1	2	2	2	1	2	2	1	1	2	1		1			
(5,2,1)⊗(5,2,1)	(3,2,1³)⊗(3,2,1³)	1	2	4	4	5	9	5	2	9	6	9	4	5	5	1	3	4	1	1				(5,2,1)⊗(3,2,1³)
(5,2,1)⊗(5,1³)	(3,2,1³)⊗(4,1⁴)		1	2	2	2	5	2	1	4	3	5	2	3	3		2	3	1	1	1			(5,2,1)⊗(4,1⁴) (3,2,1³)⊗(5,1³)
(5,2,1)⊗(4²)	(3,2,1³)⊗(2⁴)			1	1	1	2	1		2	2	2	1	1	1			1						(5,2,1)⊗(2⁴) (3,2,1³)⊗(4²)
(5,2,1)⊗(4,3,1)	(3,2,1³)⊗(3,2²,1)		1	3	3	4	9	4	2	9	7	10	5	6	7	1	3	5	2	1	1			(5,2,1)⊗(3,2²,1) (3,2,1³)⊗(4,3,1)
(5,2,1)⊗(4,2²)	(3,2,1³)⊗(3²,1²)		1	2	2	3	6	3	2	7	5	8	4	5	6	1	3	5	2	1	1			(5,2,1)⊗(3²,1²) (3,2,1³)⊗(4,2²)
(5,2,1)⊗(4,2,1²)	(3,2,1³)⊗(4,2,1²)		1	3	3	4	9	5	2	10	8	13	6	8	10	2	5	9	4	3	3	1		
(5,2,1)⊗(3²,2)	(3,2,1³)⊗(3²,2)			1	1	2	4	2	1	5	4	6	3	4	5	1	2	4	2	1	1			
(5,1³)⊗(5,1³)	(4,1⁴)⊗(4,1⁴)	1	1	2	1	2	2	1	1	2	2	2	1	1	2	1	1	2	1	1	1	1		(5,1³)⊗(4,1⁴)
(5,1³)⊗(4²)	(4,1⁴)⊗(2⁴)						1	1	1	1	1	1		1	1		1							(5,1³)⊗(2⁴) (4,1⁴)⊗(4²)
(5,1³)⊗(4,3,1)	(4,1⁴)⊗(3,2²,1)			1	1	2	4	2	1	5	4	6	3	3	4	1	2	3	1	1				(5,1³)⊗(3,2²,1) (4,1⁴)⊗(4,3,1)
(5,1³)⊗(4,2²)	(4,1⁴)⊗(3²,1²)			1	1	1	3	2	1	4	3	4	2	4	3	1	1	3	1		1			(5,1³)⊗(3²,1²) (4,1⁴)⊗(4,2²)
(5,1³)⊗(4,2,1²)	(4,1⁴)⊗(4,2,1²)		1	2	2	3	5	2	1	6	4	6	4	4	6	1	2	5	3	2	2	1		
(5,1³)⊗(3²,2)	(4,1⁴)⊗(3²,2)					1	2	1		3	2	4	2	2	3		1	2	1					
(4²)⊗(4²)	(2⁴)⊗(2⁴)	1		1				1	1		1			1		1							(4²)⊗(2⁴)
(4²)⊗(4,3,1)	(2⁴)⊗(3,2²,1)		1	1	1	1	2	1		2	1	2	1	1	2		1	1	1					(4²)⊗(3,2²,1) (2⁴)⊗(4,3,1)
(4²)⊗(4,2²)	(2⁴)⊗(3²,1²)			1			2	1	1	1	2	1		2	1	1	1	1			1			(4²)⊗(3²,1²) (2⁴)⊗(4,2²)
(4²)⊗(4,2,1²)	(2⁴)⊗(4,2,1²)				1	1	2	1		2	1	4	2	1	2		1	2	1	1				
(4²)⊗(3²,2)	(2⁴)⊗(3²,2)				1	1	1			1		2	1		1			1	1	1				
(4,3,1)⊗(4,3,1)	(3,2²,1)⊗(3,2²,1)	1	2	4	4	4	9	5	2	8	7	11	5	6	8	2	4	7	3	2	2			(4,3,1)⊗(3,2²,1)
(4,3,1)⊗(4,2²)	(3,2²,1)⊗(3²,1²)		1	2	3	3	7	4	1	7	5	9	4	5	6	1	3	6	3	2	2	1		(4,3,1)⊗(3²,1²) (3,2²,1)⊗(4,2²)
(4,3,1)⊗(4,2,1²)	(3,2²,1)⊗(4,2,1²)		1	3	3	4	10	6	2	11	9	14	6	9	11	2	6	10	4	3	3	1		
(4,3,1)⊗(3²,2)	(3,2²,1)⊗(3²,2)		1	2	2	2	5	3	1	5	4	6	2	4	5	1	3	5	2	2	2	1		
(4,2²)⊗(4,2²)	(3²,1²)⊗(3²,1²)	1	1	3	1	2	5	3	2	5	6	6	2	5	5	2	4	5	1	2	2			(4,2²)⊗(3²1²)
(4,2²)⊗(4,2,1²)	(3²1²)⊗(4,2,1²)		1	2	3	4	8	4	1	9	6	12	6	6	9	1	4	8	4	3	2	1		
(4,2²)⊗(3²,2)	(3²1²)⊗(3²,2)		1	1	2	2	4	2		4	2	6	3	2	4		2	4	2	2	1	1		
(4,2,1²)⊗(4,2,1²)		1	2	5	4	6	13	6	4	14	12	17	8	12	14	4	6	13	6	4	5	2	1	
(4,2,1²)⊗(3²,2)				2	2	2	6	4	2	6	6	8	4	6	6	2	4	6	2	2	2			
(3²,2)⊗(3²,2)		1	1	2	1	1	3	2	1	2	3	4	1	3	2	1	2	3	1	1	2	1	1	
		(1⁸)	(2,1⁶)	(2³,1²)	(3,1⁵)	(2²1²)	(3,2,1³)	(4,1⁴)	(2⁴)	(3,2²,1)	(3²1²)	(4,2,1²)	(3²,2)	(4,2²)	(4,3,1)	(4²)	(5,1³)	(5,2,1)	(5,3)	(6,1²)	(6,2)	(7,1)	(8)	

APPENDIX: THE SYMMETRIC GROUP AND PROPERTIES OF THE YOUNG SYMMETRY OPERATORS

The theory of linear groups is intimately linked with the study of the symmetric group Σ_f, the permutation group of f objects. We have given in Sec. III rules for obtaining the irreducible representations of SU_n by imposing certain maximal symmetry conditions on the indices of tensors. These symmetry conditions are completely described by the Young tableau. We want to discuss now the fundamental properties of the corresponding Young symmetry operators of the symmetric group Σ_f, following the treatment of Weyl.[1-4]

A useful technique for obtaining the irreducible representations of discrete groups is based on the construction of a finite vector space in which the group elements can be chosen as a basis. Such a vector space, in which there exists a natural law of vector multiplication, has the properties of a *ring*; it is called the group ring. The subspaces of the ring which are left invariant under this multiplication are called left *ideals*, and provide representations of the group.

Let $p_1 p_2 \cdots p_g$ be the elements of a discrete group of g elements. The group ring R is defined by the set of vectors

$$x = x_1 p_1 + x_2 p_2 + \cdots + x_g p_g, \qquad \text{(A1)}$$

CC-0. In Public Domain. Gurukul Kangri Collection, Haridwar

Digitized by Arya Samaj Foundation Chennai and eGangotri

where $(x_1x_2\cdots xj)$ is a g-uple of complex number, which satisfies the following law of multiplication based on the group multiplication law:

$$xy\equiv\sum_{i,j}x_ix_j(p_ip_j)=\sum_h(xy)_kp_k, \qquad \text{(A2)}$$

where

$$(xy)_k=\sum x_iy_j \qquad \text{(A3)}$$

and the sum is carried over all i, j for which $p_ip_j=p_k$. A left (right) *ideal* I is then defined by the condition that if $x\in I$, then $yx\in I$ $(xy\in I)$, for every $y\in R$. A trivial example of an ideal is the ring R itself.

Due to the associativity of the group multiplication law, it is clear that a left ideal gives rise to a representation of the group. To obtain the irreducible representations we require the *minimal ideals*, which are those ideals which contain no proper invariant subspaces. A very important element of an ideal I is its *idempotent* element e, which has the property that $e^2=e$, i.e., it is a projection of the ring on the ideal. Suppose that $x\in R$; then $xe\in I$, and if $x\in I$, then $xe=x$. For the permutation group, we want to show that the idempotents of its minimal ideals can be chosen to be precisely the Young symmetry operators Y described earlier in Sec. III (apart from normalization). The two crucial properties which we have to demonstrate are:

(1) $Y^2=\mu Y$, where μ is a constant;

(2) If $Y=\mu(e_1+e_2)$, where $e_1^2=e_1, e_2^2=e_2$, and $e_1e_2=0$, then either e_1 or $e_2=0$; in other words, the corresponding ideal is *minimal*.

First we show that if an element x of the permutation ring has the property

$$xp=x \quad \text{and} \quad qx=\delta_qx,$$

where p and q are elements of the Young symmetry Y [see Sec. III, formula (5)], then $x=cY$, where c is a constant. Any element YzY where z belongs to the ring R, naturally has this property. Hence Y^2 must be a multiple of Y. To prove property (1) we also have to show that the proportionality constant does not vanish. Finally, the minimal property (2) follows immediately since it also implies that

$$Ye_iY=e_i, \qquad i=1, 2.$$

Hence, by (A1), either $\mu e_1=Y$, $e_2=0$ or $e_1=0$ and $\mu e_2=Y$.

Expanding $x=\Sigma x(t)t$, we find the conditions $xp^{-1}=x$ and $q^{-1}x=\delta_qx$ imply that $x(tp)=x(t)$ and $x(qt)=\delta_qx(t)$, respectively. In particular, substituting for t the identity $t=1$, we obtain $x(p)=x(1)$ and $x(qp)=\delta_qx(1)$. These are precisely the expansion coefficients of Y [apart from the constant $x(1)$]. It remains to demonstrate that $x(t)=0$ when t is not a permutation element contained in Y. A bit of reflection will show that all permutations which do not belong to Y are characterized by the property that, if they are applied to the integers 1 to f occupying the boxes of a Young tableau at least two integers in the same row, end up in the same column. It follows that if u is the transposition of these integers in the initial row and v is the corresponding transposition in the final column,

$$vt=tu.$$

But we have the property that

$$x(tu)=x(t) \quad \text{and} \quad x(vt)=-x(t)$$

which implies

$$x(t)=0.$$

Finally, we evaluate the coefficient μ. For this purpose we introduce a reducible representation for the group generated by the linear transformations induced by the group elements when they act on R, the so-called regular representation. The only property of the regular representation which we require here is that the trace of all matrices corresponding to elements other than the identity vanish, hence trace $Y=f!$ (recall that $f!$ is the dimension of the regular representation, i.e., the order of the symmetric group Σ_f). On the other hand if we introduce as basis a set of vectors belonging to the ideal generated by Y of dimension l, Y must be a multiple of the $l\times l$ unit matrix in the corresponding representation. Hence, trace $Y=\mu l$, and $\mu=f!/l$.

We have shown that the Young symmetry operator Y is an idempotent or projection in the ring of the symmetric group Σ_f. It generates a minimal ideal, that is, an invariant subspace under group multiplication which does not contain any smaller invariant subspaces. Hence, it gives an irreducible representation of Σ_f. In fact, all the irreducible representations of Σ_f are given by the possible Young tableaux of f boxes. The proof is quite simple and will not be given here. In conclusion, we note that the ideals corresponding to different Young tableaux are carrier spaces for unequivalent representations.

ACKNOWLEDGMENTS

We would like to thank Professor L. Schiff and Professor W. K. H. Panofsky for their hospitality at Stanford University.

CC-0. In Public Domain. Gurukul Kangri Collection, Haridwar

Digitized by Arya Samaj Foundation Chennai and eGangotri

Quasi-Free Scattering and Nuclear Structure*

GERHARD JACOB, TH. A. J. MARIS

Instituto de Física and Faculdade de Filosofia, Universidade do Rio Grande do Sul, Pôrto Alegre, Brasil

Quasi-free processes in nuclei are reviewed both from a theoretical and an experimental point of view. The discussion is limited to nuclei with mass number ≥ 4 and to incident energies larger than 100 MeV for quasi-free proton–proton and 300 MeV for electron–proton scattering. The reactions are discussed qualitatively, and their relevance for the investigation of nuclear shells, in particular of the strongly bound ones, is shown. The cross section for quasi-free scattering is then derived in the distorted wave impulse approximation, and some special cases are considered. Through a few examples the main features of the experimental results are presented and compared with calculated ones. Measurements on several $1p$, $2s$–$1d$, and $2p$–$1f$ shell nuclei are discussed.

CONTENTS

I. Introduction 121
II. Qualitative Description 123
III. Quantitative Considerations 125
A. The Cross Section in the Impulse Approximation .. 126
B. The Distorted Wave Impulse Approximation 129
C. Special Cases 130
IV. Some Examples and Survey of Results 132
A. Experimental Results 132
B. Calculated Results 138
V. Results for Other Nuclei 139
VI. Concluding Remarks 140
Acknowledgments 142

I. INTRODUCTION

In the last fifteen years the shell model[1] has been successful in the explanation of numerous properties of the nucleus. With respect to the domain of validity of the model, it should, however, be remarked that although the existence of strongly bound shells in nuclei seems to be implied, nearly all experiments performed until recently have been restricted to investigations of the least bound and of the unoccupied shells. To test the shell model predictions for the more strongly bound shells, these have to be broken up, and consequently a relatively high energy is needed; for decay experiments and scattering at low energies the core of the nucleus somewhat resembles an elementary particle of which only over-all properties are relevant and can be determined.

As the energy differences between neighboring shells vary from about 25 MeV for light nuclei to probably less than 10 MeV for heavy ones, one could expect that experiments with nucleons of a medium energy, larger than these differences but substantially smaller than 100 MeV might be suitable for investigations of inner shells. This is not the case because the mean free path of nucleons for those energies is relatively small and surface reactions occur almost exclusively. The nuclear surface, however, consists predominantly of upper shell particles because of the sloping edges of the shell model potential and, also, due to the dependence of the exponential tail of a single-particle wave function on its separation energy. (We use the term separation energy in a generalized sense, defining it as the energy necessary to lift any bound nucleon, not only the least bound one, to zero energy). When photons are used as projectiles, only the lower energy limitation exists because gammas have a long mean free path in nuclear matter. Actually, the giant dipole gamma resonance was the first excitation for which it became clear that particles from a closed inner shell (namely, the next to the upper one) can be involved.[2] However, medium energy gammas have a wavelength which is considerably larger than the average internucleon distance and, therefore, excite almost exclusively collective modes.[3] In fact, another reason for the use of a high bombarding energy is that a high momentum transfer results in a localized interaction which emphasizes single-particle properties.

Experiments which are particularly suited to investigate the inner nuclear shell structure are the quasi-free (also called quasi-elastic) scattering experiments. Qualitatively speaking, by quasi-free scattering a process is meant in which a high energy (100–1000 MeV) particle knocks a nucleon out of a nucleus and no further violent interaction occurs between the nucleus and the incident or the two outgoing particles. Because the mean free path of high energy nucleons in nuclear matter is of the same order of magnitude as the nuclear radius such events are expected to be reasonably probable.[4]

The first experiments demonstrating the existence of such processes were performed at Berkeley[5] in 1952 by the bombardment of light nuclei with 340-MeV protons and the observation of coincident proton pairs emerging from the target with a strong angular correlation. Semiquantitatively,[4,6] these events can be described

---

* This review is based on a paper submitted by one of us (G.J.) to the Faculdade de Filosofia, Universidade do Rio Grande do Sul, in partial fulfillment of the requirements for the Chair of Theoretical Physics.

[1] M. G. Mayer and J. H. D. Jensen, *Elementary Theory of Nuclear Shell Structure* (John Wiley & Sons, Inc., New York, 1955).

[2] D. H. Wilkinson, Physica **22**, 1039 (1956).

[3] G. E. Brown and M. Bolsterli, Phys. Rev. Letters **3**, 472 (1959).

[4] R. Serber, Phys. Rev. **72**, 1114 (1947); M. L. Goldberger, Phys. Rev. **74**, 1269 (1948).

[5] O. Chamberlain and E. Segrè, Phys. Rev. **87**, 81 (1952); J. B. Cladis, W. N. Hess, and B. J. Moyer, Phys. Rev. **87**, 425 (1952).

[6] G. F. Chew, Phys. Rev. **80**, 196 (1950); G. F. Chew and M. L. Goldberger, Phys. Rev. **87**, 778 (1952).

CC-0. In Public Domain. Gurukul Kangri Collection, Haridwar

Digitized by Arya Samaj Foundation Chennai and eGangotri

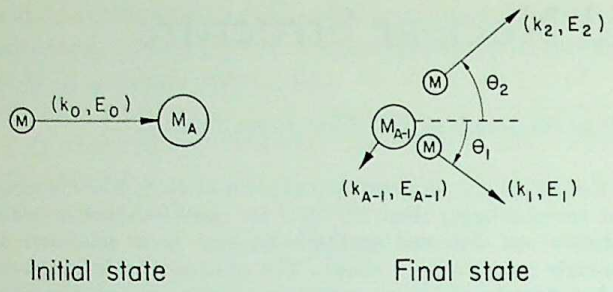

FIG. 1. The notation used in the text.

by assuming that the incoming proton collides with a single proton in the nucleus as if both particles were free. The observed angular correlation of the outgoing proton pairs differs from the one in free scattering (where the protons emerge under a definite angle which is nonrelativistically 90°) due to the fact that the nuclear protons are not at rest in the nucleus but have a momentum distribution. The momentum distributions estimated[7] on this basis from the Berkeley experiments are of a reasonable order of magnitude (see also Ref. 8).

After the development of the shell model, it became clear that not only the momentum distribution of the nuclear protons but also their separation energy distribution is an interesting quantity which is measurable by quasi-free scattering.[9] For a definite energy of the incoming particle, the summed energy spectrum of the emerging particle pairs is expected to show peaks at the separation energies corresponding to the various nuclear shells from which the protons can be ejected. Furthermore, the width of such a peak is related by the uncertainty principle to the lifetime of the hole left in the corresponding shell. Finally, by combined energy and angular selection of the outcoming particles, information on the momentum distributions of the protons in individual shells might be obtained. Experiments started in 1957 at Uppsala[10] indeed show these expected features.

Above 100 MeV, which is the lower incident energy limit considered in this paper, $(p, 2p)$ reactions of the type mentioned above have been performed at Chicago[11–13] using 460-MeV incident energy, at Harvard[14–16] with 160 MeV, at Harwell[17] with 155 MeV, at Orsay[18–20] with 150 MeV, and at Uppsala[10,11,21,22] with 185 MeV. Mainly, nuclei up to ^{40}Ca have been investigated. For heavier nuclei there exists as yet little information[13,15,20]; in this region both the energy differences between the shells and the cross sections become relatively small.

Until recently only experiments with incoming protons were considered. In principle the large mean free path of electrons in nuclear matter makes these particles preferable as projectiles.[23] Although these experiments are difficult to perform because of the smallness of electromagnetic cross sections, the shell structure in ^{12}C and ^{27}Al has recently been resolved by the Istituto Superiore di Sanità group working at Frascati[24]; quasi-free electron–proton scattering in ^{2}H, ^{3}H, and ^{3}He has been performed at Stanford[25,26] and Orsay.[27] In all these measurements the incident electrons had energies between 500 and 600 MeV.

The present article reviews the theory and the experimental results of the mentioned quasi-free processes. We show how to extract information on the nucleus from the measurements, but we do not go into experimental details nor into a systematic investigation of the meaning of the obtainable nuclear data. The discussion is in general limited to nuclei with $A \geq 4$.

In the next section the quasi-free scattering process is considered in more detail but still qualitatively; the various types of experiments which have been performed are briefly discussed, and a comparison with deuteron pick-up is made. The third section contains a quantitative formulation of the reaction problem and a discussion of the methods used for the evaluation

[7] P. A. Wolff, Phys. Rev. **87**, 434 (1952).
[8] J. M. Wilcox and B. J. Moyer, Phys. Rev. **99**, 875 (1955); J. G. McEwen, W. M. Gibson, and P. J. Duke, Phil. Mag. **2**, 231 (1957); L. S. Azhgirey, I. K. Vzorov, V. P. Zrelov, M. G. Mescheryakov, B. S. Neganov, R. M. Ryndin, and A. F. Shabudin, Nucl. Phys. **13**, 258 (1959).
[9] Th. A. J. Maris, P. Hillman, and H. Tyrén, Nucl. Phys. **7**, 1 (1958).
[10] H. Tyrén, Th. A. J. Maris, and P. Hillman, Nuovo Cimento **6**, 1507 (1957); H. Tyrén, P. Hillman, and Th. A. J. Maris, Nucl. Phys. **7**, 10 (1958); P. Hillman, H. Tyrén, and Th. A. J. Maris, Phys. Rev. Letters **5**, 107 (1960).
[11] H. Tyrén, P. Hillman, P. Isacsson, and Th. A. J. Maris, Proc. Intern. Conf. Nucl. Struct., Kingston (1960), p. 429.
[12] H. Tyrén, S. Kullander, and R. Ramachandran, Proc. Conf. Direct Interactions Nucl. Reaction Mech., Padua (1962), p. 1109.
[13] H. Tyrén, S. Kullander, O. Sundberg, R. Ramachandran, and P. Isaacson (private communication); see also Ref. 66.
[14] B. Gottschalk and K. Strauch, Phys. Rev. **120**, 1005 (1960).
[15] B. Gottschalk, K. Strauch, and K. H. Wang, Compt. Rend. Congr. Intern. Phys. Nucl., Paris (1964), Vol. 2, p. 324.
[16] B. Gottschalk, Ph.D. thesis, Harvard University (1962); B. Gottschalk, K. Strauch, and K. H. Wang (private communication).
[17] T. J. Gooding and H. G. Pugh, Nucl. Phys. **18**, 46 (1960); H. G. Pugh and K. F. Riley, Proc. Rutherford Jubilee Intern. Conf., Manchester (1961), p. 195.
[18] J. P. Garron, J. C. Jacmart, M. Riou, and C. Ruhla, J. Phys. Radium **22**, 622 (1961); J. P. Garron, J. C. Jacmart, M. Riou, C. Ruhla, J. Teillac, and K. Strauch, Nucl. Phys. **37**, 126 (1962).
[19] J. P. Garron, Ann. Phys. (Paris) **7**, 301 (1962).
[20] C. Ruhla, M. Riou, R. A. Ricci, M. Arditi, H. Doubre, J. C. Jacmart, M. Liu, and L. Valentin, Phys. Letters **10**, 326 (1964).
[21] G. Tibell, O. Sundberg, and U. Miklavžič, Phys. Letters **1**, 172 (1962); **2**, 100 (1962); G. Tibell, O. Sundberg, and U. Miklavžič, Proc. Conf. Direct Interaction Nucl. Reaction Mech., Padua (1962) 1134.
[22] G. Tibell, O. Sundberg, and P. U. Renberg, Arkiv Fysik **25**, 433 (1963).
[23] G. Jacob and Th. A. J. Maris, Proc. Rutherford Jubilee Intern. Conf., Manchester (1961), p. 153; G. Jacob and Th. A. J. Maris, Nucl. Phys. **31**, 139 (1962); **31**, 152 (1962).
[24] U. Almaldi, Jr., G. Campos Venuti, G. Cortellessa, G. Fronterotta, A. Reale, P. Salvadori, and P. Hillman, Phys. Rev. Letters **13**, 341 (1964); Compt. Rend. Congr. Intern. Phys. Nucl., Paris (1964), Vol. 2, p. 341; Atti Accad. Nazl. Lincei, Rend. Classe Sci. Fis. Mat. Nat. **38**, 499 (1965); and private communication.
[25] M. Croissiaux, Phys. Rev. **127**, 613 (1962).
[26] A. Johansson, Phys. Rev. **136**, B1030 (1964).
[27] P. Bounin, Ann. Phys. (Paris) **10**, 475 (1965).

CC-0. In Public Domain. Gurukul Kangri Collection, Haridwar

Digitized by Arya Samaj Foundation Chennai and eGangotri

of the expression found for the cross section. The fourth section gives some typical experimental and theoretical results and reviews the most interesting information so far obtained. In the fifth section more results for individual nuclei are given, and finally some concluding remarks are made.

Without an appreciable loss of continuity Secs. IIIA, IIIB, and V may be omitted, except for formulas (3.23) and (3.27) and the immediately following discussions. In order not to obscure the basic simplicity of the matter, we have tried to avoid those questions of formal or technical nature which up to now have not been fruitful for the subject.

II. QUALITATIVE DESCRIPTION

When a 200-MeV proton is scattered at an angle of the order of 45°, the transferred momentum corresponds to a reduced de Broglie wavelength of about 0.5 F. This is a rather small quantity compared to the average distance of 2 F between two neighboring nucleons in the nucleus. Taking also into account that very small momentum transfers to a nucleon in the nucleus are unlikely to cause excitation because of the exclusion principle, one may expect that the inelastic interaction of a high energy nucleon with a nucleus can crudely be described as a sequence of independent nucleon–nucleon collisions.[4] A quasi-free event corresponds in this picture to the case in which only one such collision has taken place.

In the following we denote the incoming proton, the nuclear proton to be knocked out and the two outgoing protons by the indices 0, 3, 1, and 2. The index A denotes the initial nucleus, and $(A-1)$ refers to the state of the final nucleus, which may have an energy located in the continuous part of the spectrum. The remaining notation used is shown in Fig. 1; $(\hbar\mathbf{k}_j, E_j/c)$ are energy momentum four vectors.

From its definition the separation energy of the ejected proton for a certain final state of the nucleus is

$$S = T_0 - (T_1 + T_2 + T_{A-1}), \tag{2.1}$$

where T_j stands for a kinetic energy; the initial nucleus is supposed to be at rest. Energy momentum conservation gives

$$E_0 + M_A c^2 = E_1 + E_2 + E_{A-1}, \tag{2.2}$$

$$\mathbf{k}_0 = \mathbf{k}_1 + \mathbf{k}_2 + \mathbf{k}_{A-1}, \tag{2.3}$$

where

$$E_{A-1} = M_{A-1}c^2 + E_{\text{exc}} + T_{A-1}, \tag{2.4}$$

E_{exc} being the excitation energy of the residual nucleus. From Eqs. (2.1), (2.2), and (2.4), it follows that this excitation energy equals the difference between the separation energies of the least bound proton and the ejected one.

We consider first the idealized situation in which the incoming proton interacts with only one nucleon which is moving in an ideal shell model nucleus. It is not difficult to see which corrections have to be applied to this model in order to make it more realistic; the application to electron scattering is also an easy matter. In this idealized case the separation energy of application to electron scattering is also a simple matter. In this idealized case the separation energy of the ejected proton and the recoil momentum of the residual nucleus have a simple physical meaning. The final nucleus has evidently a hole in the shell from which the proton was ejected, and the separation energy equals the (negative) energy of its single-particle state. Because the initial nucleus was at rest, the nuclear recoil momentum $\hbar\mathbf{k}_{A-1}$ equals $-\hbar\mathbf{k}_3$, i.e., minus the momentum the knocked out nucleon had in the nucleus. Consequently, the energy spectrum and recoil momentum distribution of the residual nucleus will directly correspond to the possible energies and momentum distributions of the single-particle states in the individual shells. These may therefore be determined from a measurement of the dependence of the number of proton pairs emerging from quasi-free collisions on the momenta $\hbar\mathbf{k}_1$ and $\hbar\mathbf{k}_2$.

Although several important modifications are necessary, the simple picture just given contains, in our opinion, the essential physics of the quasi-free process and motivates the use of these reactions for the investigation of nuclear structure.

In fact, the experimental energy spectra show peaks corresponding to the knocking out of nuclear protons from different shells and subshells, and the qualitative features of the momentum correlations of protons ejected from a shell agree well with the expected behavior of the corresponding wave function in momentum space.

Now the main corrections which have to be made to the above mentioned model will be discussed.[9] First we still consider the nucleus as having a perfect single-particle structure, but take into account the multiple collisions which the incoming and the two outgoing protons suffer in the nucleus. Then deviations from the single-particle structure are included.

A quasi-free event can be "spoiled" because the incoming particle or the two outgoing ones have inelastic interactions with other nucleons in the nucleus before, during, or after the quasi-free collision. By such multiple collisions either additional particles are ejected or at least extra excitations of the nucleus are caused. These events tend to blur the simple picture from which we started.

The cases in which the incoming proton interacts during the quasi-free collision with a third particle will be relatively rare if the de Broglie wavelength corresponding to the momentum transfer is sufficiently small and strong short-range correlations between nuclear nucleons are absent.[6] However, the multiple

CC-0. In Public Domain. Gurukul Kangri Collection, Haridwar

Digitized by Arya Samaj Foundation Chennai and eGangotri

collisions before and after the quasi-free event are important. As seen in the next section one may take these into account by introducing complex optical potentials for the incoming and outgoing protons. Either from experimental proton–nucleon total cross sections or from the optical potential obtained from elastic proton–nucleus scattering, the mean free path of a 150–400-MeV proton in nuclear matter may be estimated to be smaller than the radius of even a very light nucleus; it is therefore clear that in general multiple collisions will not be rare but will in fact occur more frequently than quasi-free ones. Thus one might fear that the measured energy spectrum and the correlation pattern of the outcoming proton pair mainly stem from protons which have suffered multiple collisions and therefore no longer reflect the single particle structure of the nucleus. The following circumstance saves the situation. Because of the large number of degrees of freedom available in the final states resulting from multiple collisions, the measured energies and momenta of a proton pair are distributed over the whole available energy and angular range and should therefore result in a rather smooth background in the measured energy spectrum of the residual nucleus. This background starts at the energy corresponding to the ground state of the residual nucleus and rises with excitation energy and atomic number. Superimposed on it one may expect to see the peaks caused by clean knock out collisions as long as any structure in the background does not become comparable with these peaks. This is also the general reason why the expected spectra are not very sensitively dependent on the perfect applicability of the Serber–Chew model[4,6] for quasi-free collisions.

Nevertheless, for the study of quasi-free scattering the multiple collisions are an unfavorable effect, decreasing the peak heights, increasing the background, and distorting the momentum correlation distributions. From the expected values of the mean free path of the incoming and outgoing protons, one may estimate that in this respect the optimum bombarding energy is about 400 MeV. The great advantage of $(e, e'p)$ over $(p, 2p)$ experiments is that in the former case only the absorption of one outgoing proton is of importance. The effect of multiple collisions on the experimental results, and the calculated corrections for specific nuclei are found in the following sections.

The extreme single-particle model is only a very approximate description of the nucleus; it predicts an energy spectrum with a small number of sharp peaks, whereas observed spectra are often rather complex and contain peaks of considerable width. We now discuss how these features may be qualitatively understood by taking deviations from the single-particle model into account.

A considerable amount of short-range nucleon–nucleon correlations would frequently lead to rearrangements in the residual nucleus[23,29] and, consequently, depress the number of quasi-free collisions. This effect has hardly been studied and should probably be taken into account by a momentum- and shell-dependent reduction factor to be applied to calculated cross sections. In practice, at present one is only able to obtain information on the low momentum part of the momentum distributions; for this region one would not expect the effect of short-range correlations and the resulting rearrangements to be very important, except perhaps for a nearly constant normalization factor.

The structure of the long-range nucleon–nucleon correlations, for example those described by configuration mixing and by a deformation of the nucleus, may, however, considerably influence the spectra obtained from quasi-free scattering processes in the upper shell. These spectra become less simple because of the splittings of the upper shell states and the complicated overlap of these states in the initial and final nucleus. In favorable cases fractional parentage coefficients might be estimated from experimental results[9,30,31]; the effect of deformations on the experimental results will be seen in ^{9}Be and in the $2s$–$1d$ shell nuclei.

Of special interest is the investigation of inner shell states, which up to now has been exclusively performed by quasi-free scattering experiments. The width of a peak in the energy spectrum corresponding to those states may be understood by considering the lifetime of the resulting hole state of the (highly excited) residual nucleus. If a proton has been ejected from an inner shell, the exclusion principle is no longer effective[32,33] in forbidding collisions which fill up the hole. The hole state may therefore have a short lifetime, and this causes a broadening of the peaks in the spectrum corresponding to inner shell states. The lifetimes of these states are expected to decrease with increasing number of particles in the shell above the one containing the hole.[34] If the lifetime becomes very small, the simple shell model description ceases to be useful for these states. The broadening effect has been clearly observed in the quasi-free spectra of inner shells and may constitute a limitation of the number of shells which can be investigated. For example, we see that the full width at half-height of the energy peak corresponding to the ejection of a proton out of the $1s$ shell rises from 3 MeV or less for ^{6}Li [as obtained from

[28] Discussion remarks of K. A. Brueckner and V. F. Weisskopf, Proc. Intern. Conf. Nucl. Optical Model, Tallahassee (1959), p. 143.
[29] D. R. Inglis, Nucl. Phys. **30**, 1 (1962).
[30] V. V. Balashov and A. N. Boyarkina, Nucl. Phys. **38**, 629 (1962); V. V. Balashov, A. N. Boyarkina, and I. Rotter, Nucl. Phys. **59**, 417 (1964).
[31] K. Dietrich, Phys. Letters **2**, 139 (1962).
[32] V. F. Weisskopf, Helv. Phys. Acta **23**, 187 (1950).
[33] L. C. Gomes, J. D. Walecka, and V. F. Weisskopf, Ann. Phys. (N.Y.) **3**, 241 (1958).
[34] Th. A. J. Maris, Proc. Conf. Direct Interaction Nucl. Reaction Mech., Padua (1962), p. 31.

CC-0. In Public Domain. Gurukul Kangri Collection, Haridwar

Digitized by Arya Samaj Foundation Chennai and eGangotri

(p, $2p$) experiments] to about 20 MeV for ^{27}Al [from (e, $e'p$) experiments].

A state with a hole in the inner shell of a nucleus with nonzero total angular momentum (or isospin) should be split because of the coupling of the angular momenta (isospins) of the inner shell and the upper one. We will meet an indication of this splitting in the spectrum of ^{6}Li.

Turning now to the experimental side, we briefly comment on the types of quasi-free measurements which have been performed up to date. It is apparent from the discussion above that one must determine the momenta (i.e., energies and directions) of both outgoing particles, which therefore have to be detected in coincidence. The energies are measured by range telescopes, total energy absorbing crystals or magnets.

For a fixed energy of the incoming particle there are in the quasi-free experiment not less than five parameters which can be continuously varied, even disregarding polarizations; this should be compared with the two parameters in inelastic scattering. It is therefore essential to select measurements which are favorable from an experimental or theoretical point of view.

Until now the following types of experiments have been performed (see also Table I in Sec. IV):

Coplanar (p, $2p$) experiments,

(a) Experiments with no further restriction on the outgoing angles and energies.[17]

(b) Symmetric experiments, in which the two outgoing protons are selected to have equal energies and to emerge at equal angles with respect to the incoming beam.[10] The high symmetry makes the theoretical analysis of these experiments particularly simple.[35]

(c) Energy sharing experiments, in which the directions of the outgoing protons are kept fixed and the outgoing energies are varied.[14] Because, in contradistinction to case (b), a large part of the number of particle pairs entering the counters is used, these measurements are attractive from an experimental point of view.

Coplanar (e, $e'p$) experiments,

(d) In the only experiments which have been performed at present for nuclei with $A \geq 4$, the incoming energy has been varied, with all other parameters fixed.[24]

Closing this section we compare the quasi-free scattering with the high energy deuteron pick-up reaction[36] in which also a nucleon is taken out of the nucleus. The following reasons lead one to expect that, compared with appropriately chosen quasi-free scattering at the same energy, deuteron pick-up emphasizes the upper shell more strongly.

(a) In deuteron pick-up, especially at higher energies, high momentum nucleons are snatched out of the nucleus,[37] and the nucleons of the upper shell have the largest average kinetic energy. In symmetric quasi-free scattering at about 45°, one is selecting low momentum nucleons which belong more to the inner nuclear shells.

(b) A strong absorption tends to locate the interactions at the nuclear surface, which consists predominantly of upper shell nucleons. The choice of equal energies of the two outgoing particles, as obtainable in quasi-free scattering, results in the smallest total absorption. In deuteron pick-up the distorted deuteron wave function in the nucleus corresponds to a neutron and a proton of greatly differing absolute momenta, resulting in an increase of absorption and reflection.[38]

For these reasons we think that at a given bombarding energy quasi-free scattering offers better possibilities than deuteron pick-up for the study of inner shells. The optimum energy for the investigation of these shells with quasi-free scattering is probably about 400 MeV. At such energies the nucleon to be picked up in deuteron pick-up must have a very high momentum, so that the cross section for this reaction becomes very small, and secondary processes become important. At present there seems to exist only one experiment[39] in which there is an indication of a pick-up from an inner shell, namely from the $1p$ shell in ^{19}F. In this case there are only three particles in the upper shell.

Although quasi-free scattering holds at present a near monopoly for inner shell investigations, this is of course in no way the case with respect to the upper shell. For this shell pick-up (and other) reactions, though accentuating different properties of the wave-functions than the quasi-free experiments, are in general more practical because they do not require a coincidence technique and allow for higher resolutions.

III. QUANTITATIVE CONSIDERATIONS

In this section we give a somewhat naive but simple derivation of the relativistic cross section formula in the Distorted Wave Impulse Approximation (DWIA).[9,35,40] Although the same result may be obtained in a slightly more sophisticated manner, drastic approximations are anyhow unavoidable in order to reduce the number of degrees of freedom of the many-body problem under

[35] Th. A. J. Maris, Nucl. Phys. **9**, 577 (1958/59).

[36] K. Brueckner and W. Powell, Phys. Rev. **75**, 1274 (1949); J. Hadley and H. York, Phys. Rev. **80**, 345 (1950); W. Selove, Phys. Rev. **101**, 231 (1956); P. Radvanyi, J. Genin, and C. Detraz, Phys. Rev. **125**, 295 (1962); D. Bachelier, M. Bernas, I. Brissaud, C. Detraz, N. K. Ganguly, and P. Radvanyi, Phys. Letters **8**, 56 (1964).

[37] G. F. Chew and M. L. Goldberger, Phys. Rev. **77**, 470 (1950).

[38] L. R. B. Elton and L. C. Gomes, Phys. Rev. **105**, 1027 (1957).

[39] P. Radvanyi (private communication).

[40] T. Berggren and G. Jacob, Phys. Letters **1**, 258 (1962); T. Berggren and G. Jacob, Proc. Conf. Direct Interaction Nucl. Reaction Mech., Padua (1962), p. 33; T. Berggren and G. Jacob, Nucl. Phys. **47**, 481 (1963).

CC-0. In Public Domain. Gurukul Kangri Collection, Haridwar

Digitized by Arya Samaj Foundation Chennai and eGangotri

investigation to a manageable one (see the Introduction of Ref. 41). These approximations do not have a mathematical basis but only a physical one, and therefore, it seems natural to try to keep the derivation transparent from a physical point of view.

We first calculate the cross section in the Born approximation, in this way obtaining the general structure of the relevant matrix element with the correct kinematical factors, without being troubled by other complications. The improvement of the resulting expression to the DWIA is then a relatively simple matter; in the last part of this section, applications to some special cases are made.

Although our treatment is in general relativistic where fast particles are involved, for simplicity we use two-component wave functions for the nucleons. At the end it will be clear that a four-component description would not affect the derivation and the result appreciably.

A. The Cross Section in the Impulse Approximation

We start by listing some results from the theory of scattering.[42]

The process of interest is the transition from an initial state $|i\rangle$ consisting of a nucleus A and an incoming proton, to a final state $|f\rangle$ with a recoiling nucleus $(A-1)$ and two outgoing protons; for the symbols used see Fig. 1.

The general expression for the cross section is

$$\frac{d^9\sigma}{d^3k_1 d^3k_2 d^3k_{A-1}}=\frac{4\pi^2}{\hbar}\frac{E_0E_A}{F}|t_{fi}|^2\,\delta^3(\mathbf{k}_1+\mathbf{k}_2+\mathbf{k}_{A-1}-\mathbf{k}_0-\mathbf{k}_A)\,\delta(E_1+E_2+E_{A-1}-E_0-E_A), \tag{3.1}$$

where

$$F=c[(E_0E_A-\hbar^2c^2\mathbf{k}_0\cdot\mathbf{k}_A)^2-c^8M^2M_A{}^2]^{\frac{1}{2}}. \tag{3.2}$$

The matrix element t_{fi} is defined by

$$T_{fi}=\tfrac{1}{2}\pi^{-1}\delta^3(\mathbf{k}_1+\mathbf{k}_2+\mathbf{k}_{A-1}-\mathbf{k}_0-\mathbf{k}_A)\,t_{fi}, \tag{3.3}$$

with T_{fi} being related to the S matrix element by

$$S_{fi}=\delta_{fi}-2\pi i\delta(E_f-E_i)\,T_{fi}. \tag{3.4}$$

A perturbation expansion of T_{fi} is given by

$$T_{fi}=\langle f|\,V+V(E_i-H_0+i\epsilon)^{-1}V+\cdots|\,i\rangle. \tag{3.5}$$

In the first Born approximation, which we use as a starting point, one has for the quasi-free scattering process

$$T_{fi}=\langle f|\,V\,|i\rangle=\sum_{\alpha\neq\beta=0}^{A}\int\mathfrak{A}\{\exp(-i\mathbf{k}_2\cdot\mathbf{r}_0)s_2{}^+(0)t_p{}^+(0)\exp(-i\mathbf{k}_1\cdot\mathbf{r}_1)s_1{}^+(1)t_p{}^+(1)\psi^*_{A-1}(\mathbf{r},m,\mu)\}$$

$$\times V(\alpha,\beta)\mathfrak{A}\{\exp(i\mathbf{k}_0\cdot\mathbf{r}_0)s_0(0)t_p(0)\psi_A(\mathbf{r}_1,m_1,\mu_1;\mathbf{r},m,\mu)\}\,d^3r_0\,d^3r_1\,d^3r. \tag{3.6}$$

The symbols have the following meaning: $\mathfrak{A}\{\ \}$ is the antisymmetrization and normalization operator, $s(j)$ and $t(j)$ are spin and isospin wave functions of particle j, and m_j, μ_j are the corresponding variables in the nuclear wave functions; $V(\alpha,\beta)$ is the nucleon–nucleon interaction which is of course symmetric under the exchange of α and β. In scalar products summations over spin and isospin variables are understood.

Because of the antisymmetry of the wave functions, the terms under the sum of the right-hand side of Eq. (3.6) for different values of α and β are all equal and one may write

$$T_{fi}=\tfrac{1}{2}A(A+1)\int\mathfrak{A}\{\exp(-i\mathbf{k}_2\cdot\mathbf{r}_0)s_2{}^+(0)t_p{}^+(0)\exp(-i\mathbf{k}_1\cdot\mathbf{r}_1)s_1{}^+(1)t_p{}^+(1)\psi^*_{A-1}(\mathbf{r},m,\mu)\}$$

$$\times V(0,1)\mathfrak{A}\{\exp(i\mathbf{k}_0\cdot\mathbf{r}_0)s_0(0)t_p(0)\psi_A(\mathbf{r}_1,m_1,\mu_1;\mathbf{r},m,\mu)\}\,d^3r_0\,d^3r_1\,d^3r. \tag{3.7}$$

In practice the magnitudes of the momenta $\hbar\mathbf{k}_1$ and $\hbar\mathbf{k}_2$ are so large that they very seldom occur in the momentum distribution of the nuclear protons; thus each of the antisymmetrization operations will give rise to only two terms in the integrand of Eq. (3.7). Mathematically this follows from the fact that the rapidly oscillating functions $\exp(i\mathbf{k}_1\cdot\mathbf{r}_j)$ and $\exp(i\mathbf{k}_2\cdot\mathbf{r}_j)$ are practically orthogonal to the nuclear wave function with respect to integration over $\mathbf{r}_j$, and physically it is also clear that a nucleon pair can only obtain the very large momenta $\hbar\mathbf{k}_1$ and $\hbar\mathbf{k}_2$ through a direct interaction with a particle of high momentum. With the antisymmetric wave functions ψ_A and

[41] D. R. Hartree, Rept. Progr. Phys. 11, 113 (1946/47).

[42] C. Møller, Kgl. Danske Videnskab. Selskab., Mat.-Fys. Medd. 23, Nr. 1 (1945); W. Brenig and R. Haag, Fortschr. Physik 7, 183 (1959); K. Nishijima, *Fundamental Particles* (W. A. Benjamin, Inc., New York, 1963); M. L. Goldberger and K. M. Watson, *Collision Theory* (John Wiley & Sons, Inc., New York, 1964).

CC-0. In Public Domain. Gurukul Kangri Collection, Haridwar

Digitized by Arya Samaj Foundation Chennai and eGangotri

ψ_{A-1} normalized to unity, one has thus

$$T_{fi}=\frac{A^{1/2}}{2(2\pi)^{9/2}}\int[\exp(-i\mathbf{k}_2\cdot\mathbf{r}_0)s_2^+(0)t_p^+(0)\exp(-i\mathbf{k}_1\cdot\mathbf{r}_1)s_1^+(1)t_p^+(1)$$
$$-\exp(-i\mathbf{k}_2\cdot\mathbf{r}_1)s_2^+(1)t_p^+(1)\exp(-i\mathbf{k}_1\cdot\mathbf{r}_0)s_1^+(0)t_p^+(0)]\psi^*_{A-1}(\mathbf{r},m,\mu)V(0,1)$$
$$\times[\exp(i\mathbf{k}_0\cdot\mathbf{r}_0)s_0(0)t_p(0)\psi_A(\mathbf{r}_1,m_1,\mu_1;\mathbf{r},m,\mu)-\exp(i\mathbf{k}_0\cdot\mathbf{r}_1)s_0(1)t_p(1)\psi_A(\mathbf{r}_0,m_0,\mu_0;\mathbf{r},m,\mu)]d^3r_0\,d^3r_1\,d^3r. \quad (3.8)$$

Because of charge conservation, μ_0 and μ_1 in ψ_A have the value corresponding to a proton. It is convenient to expand ψ_A in the following manner:

$$\psi_A(\mathbf{r}_1,m_1,\mu_1;\mathbf{r},m,\mu)=\frac{1}{(2\pi)^{\frac{3}{2}}}\sum_{n,j}\int\exp(i\mathbf{k}\cdot\mathbf{r}_1)s_n(1)t_j(1)g_A^{(n,j)}(\mathbf{k};\mathbf{r},m,\mu)\,d^3k. \quad (3.9)$$

Inserting (3.9) in (3.8), we obtain

$$T_{fi}=\int d^3k\sum_n A^{\frac{1}{2}}\int d^3r\psi^*_{A-1}(\mathbf{r},m,\mu)g^{(n)}{}_A(\mathbf{k};\mathbf{r},m,\mu)$$
$$\int d^3r_0\,d^3r_1\mathfrak{A}\{\exp(-i\mathbf{k}_2\cdot\mathbf{r}_0)s_2^+(0)t_p^+(0)\exp(-i\mathbf{k}_1\cdot\mathbf{r}_1)s_1^+(1)t_p^+(1)\}$$
$$\times V(0,1)\mathfrak{A}\{\exp(i\mathbf{k}_0\cdot\mathbf{r}_0)s_0(0)t_p(0)\exp(i\mathbf{k}\cdot\mathbf{r}_1)s_n(1)t_p(1)\}$$
$$=\sum_n\int d^3kA^{\frac{1}{2}}\int\psi^*_{A-1}(\mathbf{r},m,\mu)g_A^{(n)}(\mathbf{k};\mathbf{r},m,\mu)\,d^3r\langle\mathbf{k}_1,m_1;\mathbf{k}_2,m_2\,|\,V_{pp}\,|\,\mathbf{k}_0,m_0;\mathbf{k},n\rangle, \quad (3.10)$$

where $g_A^{(n)}=g_A^{(n,p)}$, t_p being a proton isospin function. Defining the function $M(1,2;0,3)$ by

$$M(1,2;0,3)\,\delta^3(\mathbf{k}_1+\mathbf{k}_2-\mathbf{k}_0-\mathbf{k}_3)=(E_1E_2)^{\frac{1}{2}}\langle\mathbf{k}_1,m_1;\mathbf{k}_2,m_2\,|\,V_{pp}\,|\,\mathbf{k}_0,m_0;\mathbf{k}_3,m_3\rangle(E_0E_3)^{\frac{1}{2}}, \quad (3.11)$$

we obtain, with $\mathbf{k}_3=\mathbf{k}_1+\mathbf{k}_2-\mathbf{k}_0$ and $E_3=(\hbar^2c^2k_3^2+M^2c^4)^{\frac{1}{2}}$,

$$T_{fi}=\sum_n A^{\frac{1}{2}}\int\psi^*_{A-1}(\mathbf{r},m,\mu)g_A^{(n)}(\mathbf{k}_3;\mathbf{r},m,\mu)d^3r(E_0E_1E_2E_3)^{-\frac{1}{2}}M(1,2;0,(\mathbf{k}_3,n)). \quad (3.12)$$

The total momentum conserving δ function which, according to Eq. (3.3), should occur in T_{fi} is contained in the integral of expression (3.12). To extract this δ function, we write the integral again in configuration space

$$\int\psi^*_{A-1}(\mathbf{r},m,\mu)g_A^{(n)}(\mathbf{k}_3;\mathbf{r},m,\mu)d^3r=\frac{1}{(2\pi)^{\frac{3}{2}}}s_n^+(1)t_p^+(1)\int\exp(-i\mathbf{k}_3\cdot\mathbf{r}_1)\psi^*_{A-1}(\mathbf{r},m,\mu)\psi_A(\mathbf{r}_1,m_1,\mu_1;\mathbf{r},m,\mu)\,d^3r_1\,d^3r. \quad (3.13)$$

Introducing as new variables the center of mass coordinates of the final nucleus $\mathbf{R}_{A-1}$ and the relative coordinates $\mathbf{x}_j=\mathbf{r}_j-\mathbf{R}_{A-1}$ ($j=1,2,\cdots,A-1$), one may write for the nuclear wave functions, assuming the initial nucleus to be at rest,

and
$$\psi^*_{A-1}(\mathbf{r},m,\mu)=[(A-1)^{\frac{1}{2}}/(2\pi)^{\frac{3}{2}}]\exp(-i\mathbf{k}_{A-1}\cdot\mathbf{R}_{A-1})\varphi^*_{A-1}(\mathbf{x},m,\mu)$$
$$\psi_A(\mathbf{r}_1,m_1,\mu_1;\mathbf{r},m,\mu)=[(A-1)^{\frac{1}{2}}/(2\pi)^{\frac{3}{2}}]\varphi_A(\mathbf{x}_1,m_1,\mu_1;\mathbf{x},m,\mu). \quad (3.14)$$

The so defined internal nuclear wave functions φ_A and φ_{A-1} contain, respectively, $(A-1)$ and $(A-2)$ space coordinates $\mathbf{x}_j$, with respect to which they are normalized to one.

Inserting Eqs. (3.14) in Eq. (3.13), we obtain after integration over $\mathbf{R}_{A-1}$

$$A^{\frac{1}{2}}\int\psi^*_{A-1}(\mathbf{r},m,\mu)g_A^{(n)}(\mathbf{k}_3;\mathbf{r},m,\mu)\,d^3r=g^{(n)}{}_{A-1,A}(\mathbf{k}_1+\mathbf{k}_2-\mathbf{k}_0)\,\delta^3(\mathbf{k}_1+\mathbf{k}_2-\mathbf{k}_0+\mathbf{k}_{A-1}), \quad (3.15)$$

where we have defined $g^{(n)}{}_{A-1,A}(\mathbf{k})$ by

$$g^{(n)}{}_{A-1,A}(\mathbf{k})=\frac{A^{\frac{1}{2}}}{(2\pi)^{\frac{3}{2}}}\int\exp(i\mathbf{k}\cdot\mathbf{x})\varphi^*_{A-1}(\mathbf{x},m,\mu)\varphi_A(\mathbf{x}_1,m_1,\mu_1;\mathbf{x},m,\mu)\,d^3x_1\,d^3x\,s_n^+(1)t_p^+(1). \quad (3.16)$$

In the case of a pure single-particle model, where the conservation of the center of mass momentum is neglected,

CC-0. In Public Domain. Gurukul Kangri Collection, Haridwar

Digitized by Arya Samaj Foundation Chennai and eGangotri

$|\, g^{(n)}{}_{A-1,A}(\mathbf{k})\,|^2$ is the momentum distribution the knocked-out proton had in the nucleus; in general it is the probability of finding a proton in a state of momentum $\hbar\mathbf{k}$ and spin state s_n, the rest of the initial nucleus being in the state ψ_{A-1}, i.e., in the internal state φ_{A-1} with momentum $-\hbar\mathbf{k}$.

From Eqs. (3.12), (3.15), and (3.3) we have

$$t_{fi}=2\pi\sum_n g^{(n)}{}_{A-1,A}(\mathbf{k}_3)\,(E_0E_1E_2E_3)^{-\frac{1}{2}}M(1,\,2;\,0,\,(\mathbf{k}_3,\,n)), \tag{3.17}$$

and consequently, for the cross section (3.1), after integrating over the coordinates of the undetected recoiling nucleus,

$$\frac{d^6\sigma}{d^3k_1d^3k_2}=\frac{(2\pi)^4}{\hbar}\frac{E_A}{F}(E_1E_2E_3)^{-1}\sum_n |\, M(1,\,2;\,0,\,(\mathbf{k}_3,\,n))\,|^2\,|\, g^{(n)}{}_{A-1,A}(\mathbf{k}_3)\,|^2\,\delta(E_1+E_2+E_{A-1}-E_0-E_A). \tag{3.18}$$

Using the relation

$$d^6\sigma/dE_1d\Omega_1dE_2d\Omega_2=[E_1E_2k_1k_2/(\hbar c)^4](d^6\sigma/d^3k_1d^3k_2) \tag{3.19}$$

and the value of F obtained from Eq. (3.2),

$$F=\hbar c^2k_0E_A, \tag{3.20}$$

Equation (3.18) may be written

$$\frac{d^6\sigma}{dE_1d\Omega_1dE_2d\Omega_2}=\left(\frac{2\pi}{\hbar c}\right)^4\frac{k_1k_2}{\hbar^2c^2k_0E_3}\sum_n |\, M(1,\,2;\,0,\,(\mathbf{k}_3,\,n))\,|^2\,|\, g^{(n)}{}_{A-1,A}(\mathbf{k}_3)\,|^2\,\delta(E_1+E_2+E_{A-1}-E_0-E_A). \tag{3.21}$$

Neglecting for the moment all off-energy shell effects, we can relate the function M of Eq. (3.21) to a cross section for the scattering process of free protons with initial momenta $\hbar\mathbf{k}_0$, $\hbar\mathbf{k}_3$ to the momenta $\hbar\mathbf{k}_1$, $\hbar\mathbf{k}_2$. Starting from the analog of Eq. (3.1) for this case, one finds for this cross section in the center of mass system, again using the Born approximation,

$$\frac{d\sigma^{fr}}{d\bar{\Omega}}(\bar{1},\,\bar{2};\,\bar{0},\,(\bar{\mathbf{k}}_3,\,n))=\frac{1}{4}\left(\frac{2\pi}{\hbar c}\right)^4\frac{1}{\bar{E}_0{}^2}\,|\, M(1,\,2;\,0,\,(\mathbf{k}_3,\,n))\,|^2, \tag{3.22}$$

where barred quantities are taken in the center of mass system. Eliminating M from Eqs. (3.21) and (3.22), we obtain

$$\frac{d^6\sigma}{dE_1d\Omega_1dE_2d\Omega_2}=\frac{4}{(\hbar c)^2}\frac{k_1k_2\bar{E}_0{}^2}{k_0E_3}\sum_n |\, g^{(n)}{}_{A-1,A}(\mathbf{k}_3)\,|^2\frac{d\sigma^{fr}}{d\bar{\Omega}}(\bar{1},\,\bar{2};\,\bar{0},\,(\bar{\mathbf{k}}_3,\,n))\,\delta(E_1+E_2+E_{A-1}-E_0-E_A). \tag{3.23}$$

In expressing the quasi-free proton–proton scattering matrix element by the free proton–proton cross section, we have neglected the fact that the momenta of the quasi-free matrix element do not occur in the free scattering because of the difference in energy conservation between the two cases. This difference is caused by the nonzero value of the separation energy in the quasi-free scattering and by the fact that in this case the recoiling nucleus has a smaller kinetic energy than the recoiling proton with the same momentum in the free scattering. This results in a certain arbitrariness; instead of eliminating the function M from Eqs. (3.21) and (3.22) one could, for instance, also have directly eliminated the matrix element of V_{pp} occurring in expression (3.11). Furthermore, there is an uncertainty for which momentum values to take the free cross section. Fortunately, these uncertainties, and therefore probably also the associated errors, amount only to a few percent as long as one considers quasi-free processes for which the equivalent free proton–proton scattering corresponds to a bombarding energy in the laboratory system between 150 and 400 MeV, where the cross section is nearly energy and angle independent.[43] In our expressions we have defined the equivalent free scattering by the two outgoing momenta $\hbar\mathbf{k}_1$ and $\hbar\mathbf{k}_2$; slightly different formulae are obtained for other definitions.

Expression (3.23) has a very simple interpretation. Except for some kinematical factors, the cross section for a process in which the two final protons have momenta $\hbar\mathbf{k}_1$ and $\hbar\mathbf{k}_2$ and the final nucleus is in the state ψ_{A-1} is given by the product of a free proton-proton cross section with the probability to find a proton in the initial nucleus in a state with the momentum demanded by momentum conservation, the rest of the nucleus being in the required final state. If the initial and final nuclei are polarized, the free cross sections for polarized protons will in general enter in Eq. (3.23). For unpolarized nuclei, averaging over the initial spin states m_A and summing over the final

[43] V. S. Barashenkov and V. M. Maltsev, Fortschr. Physik 9, 549 (1961).

CC-0. In Public Domain. Gurukul Kangri Collection, Haridwar

Digitized by Arya Samaj Foundation Chennai and eGangotri

ones m_{A-1}, one may make the replacement[9]

$$\sum_{m_{A-1},m_A}\sum_{n}|\,g^{(n)}{}_{m_{A-1},m_A}(\mathbf{k}_3)\,|^2\frac{d\sigma^{fr}}{d\bar{\Omega}}(\bar{1},\bar{2};\bar{0},(\bar{\mathbf{k}}_3,n))$$

$$=\frac{d\sigma^{fr}}{d\bar{\Omega}}(\bar{1},\bar{2};\bar{0},\bar{3}_u)\sum_{m_{A-1},m_A}|\,g_{m_{A-1},m_A}(\mathbf{k}_3)\,|^2,$$

where $(d\sigma^{fr}/d\bar{\Omega})(\bar{1},\bar{2};\bar{0},\bar{3}_u)$ is the cross section for the case in which proton 3 is unpolarized, the remaining ones having the spin orientation selected by the experiment. As is seen later this does not hold anymore when distortion is taken into account.

Up to now we have used the Born approximation both for the quasi-free and for the free scattering. In reality our final formula is more accurate than this approximation would suggest. The Born approximation in the quasi-free scattering introduces two types of errors. It neglects the possibility of obtaining the final state through various intermediate nuclear states, and it gives the proton–proton matrix element badly even for free scattering. At the present energies the last error is by far the most serious one. In the present so-called impulse approximation,[6] we have largely eliminated this error by expressing the proton–proton matrix element directly in terms of an experimental quantity; in this matrix element we have still neglected off energy shell effects. In contradistinction to the Born approximation, however, the impulse approximation gives the exact cross section for the limiting case of a shell model nucleus with a common potential which is negligible compared to the kinetic energies of the incoming and emerging protons.

B. The Distorted Wave Impulse Approximation

In order to take the multiple scattering of the incoming and the two outgoing protons into account, we consider the corresponding plane waves to be distorted by optical potentials which are taken as spin independent for simplicity. In general different potentials have to be taken for each of these protons, mainly because they have different energies. Neglecting the contribution of the knocked out particle to the optical potential for the incoming proton, we write the distorted plane waves as

$$\exp(i\mathbf{k}_0\cdot\mathbf{r}_j)D_0(\mathbf{r}_j-\mathbf{R}_{A-1}),$$

$$\exp(-i\mathbf{k}_1\cdot\mathbf{r}_j)D_1(\mathbf{r}_j-\mathbf{R}_{A-1}),$$

and

$$\exp(-i\mathbf{k}_2\cdot\mathbf{r}_j)D_2(\mathbf{r}_j-\mathbf{R}_{A-1})\qquad(j=0,1),\quad(3.24)$$

respectively; the D's are slowly varying functions compared to the plane waves and go to unity for values of the argument larger than the nuclear radius.

As in the preceding subsection we start using the Born approximation. In formula (3.6) the plane waves are to be replaced by the functions (3.24), and Eq. (3.8) becomes

$$T_{fi}=\frac{A^{1/2}}{2(2\pi)^{9/2}}\int\!\Big[\exp(-i\mathbf{k}_2\cdot\mathbf{r}_0)D_2(\mathbf{r}_0-\mathbf{R}_{A-1})s_2{}^+(0)t_p{}^+(0)\exp(-i\mathbf{k}_1\cdot\mathbf{r}_1)D_1(\mathbf{r}_1-\mathbf{R}_{A-1})s_1{}^+(1)t_p{}^+(1)$$

$$-\exp(-i\mathbf{k}_2\cdot\mathbf{r}_1)D_2(\mathbf{r}_1-\mathbf{R}_{A-1})s_2{}^+(1)t_p{}^+(1)\exp(-i\mathbf{k}_1\cdot\mathbf{r}_0)D_1(\mathbf{r}_0-\mathbf{R}_{A-1})s_1{}^+(0)t_p{}^+(0)\Big]\psi^*{}_{A-1}(\mathbf{r},m,\mu)V(0,1)$$

$$\times\Big[\exp(i\mathbf{k}_0\cdot\mathbf{r}_0)D_0(\mathbf{r}_0-\mathbf{R}_{A-1})s_0(0)t_p(0)\psi_A(\mathbf{r}_1,m_1,\mu_1;\mathbf{r},m,\mu)$$

$$-\exp(i\mathbf{k}_0\cdot\mathbf{r}_1)D_0(\mathbf{r}_1-\mathbf{R}_{A-1})s_0(1)t_p(1)\psi_A(\mathbf{r}_0,m_0,\mu_0;\mathbf{r},m,\mu)\Big]\,d^3r_0\,d^3r_1\,d^3r.\qquad(3.25)$$

We now assume that the relative change of the distorting functions is small over a distance of the order of the range of the potential $V(0,1)$; we may then suitably replace $\mathbf{r}_0$ by $\mathbf{r}_1$ and vice-versa in the D's to obtain formula (3.8) with the replacement of ψ_A by the function

$$\psi'_A(\mathbf{r}_j,m_j,\mu_j;\mathbf{r},m,\mu)=D_0(\mathbf{r}_j-\mathbf{R}_{A-1})D_1(\mathbf{r}_j-\mathbf{R}_{A-1})D_2(\mathbf{r}_j-\mathbf{R}_{A-1})\psi_A(\mathbf{r}_j,m_j,\mu_j;\mathbf{r},m,\mu)\qquad(j=0,1).\quad(3.26)$$

From here on the treatment leading from Eq. (3.8) to Eq. (3.23) is completely applicable if the replacement $\psi_A\to\psi'_A$ is made everywhere. Finally we obtain instead of Eq. (3.23)

$$\frac{d^6\sigma}{dE_1d\Omega_1dE_2d\Omega_2}=\frac{4}{(\hbar c)^2}\frac{k_1k_2\bar{E}_0{}^2}{k_0E_3}\sum_n|\,g'^{(n)}{}_{A-1,A}(\mathbf{k}_3)\,|^2\frac{d\sigma^{fr}}{d\bar{\Omega}}(\bar{1},\bar{2};0,(\bar{\mathbf{k}}_3,n))\delta(E_1+E_2+E_{A-1}-E_0-E_A),\quad(3.27)$$

with

$$g'^{(n)}{}_{A-1,A}(\mathbf{k})=\frac{A^{\frac{1}{2}}}{(2\pi)^{\frac{3}{2}}}\int\exp(i\mathbf{k}\cdot\mathbf{x}_1)\varphi^*{}_{A-1}(\mathbf{x},m,\mu)\varphi_A(\mathbf{x}_1,m_1,\mu_1;\mathbf{x},m,\mu)D_0(\mathbf{x}_1)D_1(\mathbf{x}_1)D_2(\mathbf{x}_1)\,d^3x_1\,d^3x\,s_n{}^+(1)t_p{}^+(1).$$

We refer to the quantity $|\,g'^{(n)}{}_{A-1,A}\,|^2$ as the "distorted momentum distribution," having in mind that the momentum distribution $|\,g^{(n)}{}_{A-1,A}\,|^2$ as defined in Eq. (3.16) is modified by the distortions D of the plane waves of the incoming and emerging protons. This corresponds to the fact that the protons before and after the collision are scattered in the nucleus and that therefore the momentum distribution, naively deduced with the help of momentum conservation from the asymptotic momenta of the protons, does not corre-

CC-0. In Public Domain. Gurukul Kangri Collection, Haridwar

Digitized by Arya Samaj Foundation Chennai and eGangotri

spond exactly to the actual momentum distribution the knocked out proton had in the nucleus.

From this picture it is also clear that the matrix element of $V(0, 1)$ which contributes in the actual scattering is not only the one between proton states with the asymptotic momenta. If, however, the momentum dependence of $V(0, 1)$ is not very strong, one may neglect this momentum spread and calculate the matrix element with the asymptotic values. This corresponds partly to our assumption in the derivation that the distortion does not change much over the range of $V(0, 1)$. In expressing an off energy shell matrix element of $V(0, 1)$ in terms of an experimental cross section, we introduce anyhow a certain arbitrariness in the choice of this cross section, which again demands a smooth momentum dependence of $V(0, 1)$.

In the case of $(p, 2p)$ scattering, the above mentioned uncertainties are probably unimportant, as the proton–proton cross section varies very little[43] with energy and angle in the 150–400-MeV region. For quasi-free electron–proton scattering this is no longer true, and a simple approximation of the type discussed above, in which a measurable free cross section is directly used, may be good only for special choices of the geometry in the experiment.[23]

Exhibiting the nuclear magnetic quantum numbers, the term

$$\sum_n |\, g'^{(n)}{}_{A-1,A}\,|^2\,(d\sigma^{fr}/d\bar{\Omega})\,(\bar{1},\,\bar{2};\,\bar{0},\,(\bar{\mathbf{k}}_3,\,n))$$

in Eq. (3.27) is equal to

$$\sum_n |\, g'^{(n)}{}_{m_{A-1},m_A}\,|^2$$

times the corresponding matrix element for free scattering on a proton with the normalized spin wave function

$$\sum_n g'^{(n)}{}_{m_{A-1},m_A} s_n \Big(\sum_n |\, g'^{(n)}{}_{m_{A-1},m_A}\,|^2\Big)^{-\frac{1}{2}}. \tag{3.28}$$

Quantizing the spin in the z direction, the polarization vector of such a proton is given by[35]

$$\mathbf{P}_{m_{A-1},m_A}=\frac{\mathrm{Re}\,(g'^{*(+)}{}_{m_{A-1},m_A}g'^{(-)}{}_{m_{A-1},m_A});\,\mathrm{Im}\,(g'^{*(+)}{}_{m_{A-1},m_A}g'^{(-)}{}_{m_{A-1},m_A});\,(|\,g'^{(+)}{}_{m_{A-1},m_A}\,|^2-|\,g'^{(-)}{}_{m_{A-1},m_A}\,|^2)}{\sum_n |\,g'^{(n)}{}_{m_{A-1},m_A}\,|^2}. \tag{3.29}$$

Likewise in the case of unpolarized nuclei, averaging over initial nuclear spin orientations and summing over the final ones shows that the equivalent free proton–proton cross section is the one for scattering on protons with the polarization vector

$$\mathbf{P}=\frac{\mathrm{Re}\,(\sum_{m_{A-1},m_A} g'^{*(+)}{}_{m_{A-1},m_A}g'^{(-)}{}_{m_{A-1},m_A});\,\mathrm{Im}\,(\sum_{m_{A-1},m_A} g'^{*(+)}{}_{m_{A-1},m_A}g'^{(-)}{}_{m_{A-1},m_A});\,\sum_{m_{A-1},m_A}(|\,g'^{(+)}{}_{m_{A-1},m_A}\,|^2-|\,g'^{(-)}{}_{m_{A-1},m_A}\,|^2)}{\sum_{m_{A-1},m_A}\sum_n |\,g'^{(n)}{}_{m_{A-1},m_A}\,|^2} \tag{3.30}$$

In case there exists a plane of mirror symmetry, $\mathbf{P}$ is perpendicular to it.

For unpolarized nuclei the cross section may therefore be written

$$\frac{d^6\sigma}{dE_1 d\Omega_1 dE_2 d\Omega_2}=\frac{4}{(\hbar c)^2}\frac{k_1 k_2 \bar{E}_0^2}{k_0 E_3}\frac{d\sigma^{fr}}{d\bar{\Omega}}(\bar{1},\,\bar{2};\,\bar{0},\,\bar{3}_p)\frac{1}{2J_A+1}\sum_{m_{A-1},m_A}\sum_n |\,g'^{(n)}{}_{m_{A-1},m_A}(\mathbf{k}_3)\,|^2\,\delta(E_1+E_2+E_{A-1}-E_0-E_A), \tag{3.31}$$

in which $(d\sigma^{fr}/d\bar{\Omega})\,(\bar{1},\,\bar{2};\,\bar{0},\,\bar{3}_p)$ is the experimental cross section in the center of mass system for scattering of protons on protons with the polarization vector $\mathbf{P}$.

C. Special Cases

As the kinematical factors and the proton–proton cross sections occurring in expression (3.27) are slowly varying functions of $\mathbf{k}_3$, the shape of the correlation cross sections is governed by the value of the distorted momentum distribution

$$\sum |\,g'\,|^2=(2J_A+1)^{-1}\sum_{m_{A-1},m_A}\sum_n |\,g'^{(n)}{}_{m_{A-1},m_A}(\mathbf{k}_3)\,|^2,$$

which is investigated in the present subsection.

To obtain an idea of this function one may first neglect the distortion. In the single-particle shell model, which is a good approximation for quasi-free scattering on a filled shell, $\sum |\,g'\,|^2$ is simply the momentum density distribution of this shell. For a harmonic oscillator potential the momentum density distribution of a shell differs only by a scale transformation from its density distribution in space. For other potentials both distributions have still several characteristics in common. Only s shells have nonvanishing zero momentum components, and in fact their densities are peaked at the origin, where the densities of the other shells have a minimum. The higher is the angular momentum in a shell, the further away from the origin the first maximum tends to be located. For any other model of the nucleus, as for example for the cluster model,[44]

[44] K. Wildermuth and Th. Kanellopoulos, Nucl. Phys. 7, 150 (1958); K. Wildermuth and Th. Kanellopoulos, CERN Report 59-23 (1959).

CC-0. In Public Domain. Gurukul Kangri Collection, Haridwar

Digitized by Arya Samaj Foundation Chennai and eGangotri

one may easily show from the definition (3.16) that the undistorted momentum distributions can still only have nonvanishing values at the origin for angular momenta of the initial and final nucleus differing by $\frac{1}{2}$. All other distributions have a minimum at the origin, which is also true for the case of a different parity of the initial and final nuclei.[45] The distortion will more or less fill in these minima; it turns out in practice that a minimum resulting from a parity difference is more stable than one caused only by a nonzero angular momentum; for instance, the minimum for a p-state under similar circumstances will tend to be less filled in by the distortion than the one for a d-state.

Another instructive extreme is the case of very large absorption.[46] In this case the region in the nucleus where interactions leading to quasi-free scattering can occur is very limited and depends on the geometry of the experiment. If, for example, one considers approximately coplanar scattering with not too small an angle between the two outgoing proton momenta, the effective interaction region consists of two pole caps at the end of the nuclear diameter orthogonal to the scattering plane. One has now a situation analogous to the one in classical optics in which there are two coherent light sources. An interference pattern orthogonal to the scattering plane is expected; in the scattering plane a maximum or minimum should occur depending on the mirror-parity of the single-particle overlap integral. Comparing these distributions with the undistorted ones, one finds that the remark made at the end of the preceding paragraph applies. Experimentally, noncoplanar quasi-free scattering has not yet systematically been investigated.

For more general cases in which the absorption is neither extremely strong nor negligible, g'_{m_A-1,m_A} may be found from Eq. (3.27). In this general case the distorting functions D have been determined using a complex optical potential, calculated from elastic scattering or from the nucleon–nucleon forward scattering amplitude.[47]

At the energies being considered in this paper, it seems to be most practical to calculate the distorted waves with the WKB (semiclassical) method (see, for example, Ref. 48). An elaborate phase-shift analysis[49,50] is not in the spirit of the present experiments, in which approximately sharp momenta but many angular momenta of the particles are involved. Already the error made in the phase-shift analysis by the necessary cutoff of the angular momentum value is of the same order of magnitude as the error of the WKB method.[51]

In the relativistic semiclassical method, the expressions for the D's are given by

$$D_0(\mathbf{r}) = \exp\left(-i\frac{E_0}{\hbar^2c^2k_0}\int_{-\infty}^{\mathbf{r}} V_0(\mathbf{r}')\,ds_0\right)$$

$$D_j(\mathbf{r}) = \exp\left(-i\frac{E_j}{\hbar^2c^2k_j}\int_{\mathbf{r}}^{\infty} V_j(\mathbf{r}')\,ds_j\right) \qquad (j=1,2), \tag{3.32}$$

where the V's are the complex optical potentials for the three particles and the integrations have to be performed along their classical paths.

Even for simple final and initial wavefunctions, the calculations of the distortions and the subsequent integrations necessary to calculate g' are not easy to do by hand. The general effect of the distorting exponentials (3.32) is to introduce additional real and imaginary momentum components. The former mainly smear out the angular distributions, and the latter decrease the intensity. This decrease may be by a considerable factor and can be crudely estimated for a specific nucleus and shell by mean free path considerations, as was already indicated in Sec. II.

With one exception[52] all detailed calculations of Eq. (3.31) have been performed for the symmetric coplanar scattering of unpolarized nucleons on unpolarized nuclei not observing final polarizations (see Table II in Sec. IV). For this case expression (3.27) simplifies to[35,40]

$$\frac{d^6\sigma}{dE_1d\Omega_1dE_2d\Omega_2} = \frac{4}{(\hbar c)^2}\frac{k^2}{k_0}\frac{\hbar^2c^2k^2\sin^2\theta+M^2c^4}{[\hbar^2c^2(2k\cos\theta-k_0)^2+M^2c^4]^{\frac{1}{2}}}\frac{d\sigma^{fr}}{d\bar{\Omega}}\frac{1}{2J_A+1}$$
$$\times\sum_{m_{A-1},m_A}\sum_n |g'^{(n)}_{m_{A-1},m_A}(\mathbf{k}_1+\mathbf{k}_2-\mathbf{k}_0)|^2\,\delta(2E+E_{A-1}-E_0-E_A). \tag{3.33}$$

Because there are two planes of mirror symmetry to which the effective polarization vector (3.30) of the knocked out nucleon has to be orthogonal, this vector vanishes and accordingly the cross section $d\sigma^{fr}/d\bar{\Omega}$ in Eq (3.33) is for unpolarized nucleons. This center of

[45] T. Berggren, G. E. Brown, and G. Jacob, Phys. Letters 1, 88 (1962).
[46] G. Jacob and Th. A. J. Maris, Proc. Intern. Conf. Nucl. Struct., Kingston (1960), p. 433; G. Jacob and Th. A. J. Maris, Nucl. Phys. 20, 440 (1960).
[47] K. M. Watson, Phys. Rev. 89, 575 (1953); A. K. Kerman, H. McManus, and R. M. Thaler, Ann. Phys. (N.Y.) 8, 551 (1959).
[48] L. D. Landau and E. M. Lifshitz, *Quantum Mechanics* (Pergamon Press, Inc., New York, 1958), p. 181; G. P. McCauley and G. E. Brown, Proc. Phys. Soc. (London) 71, 893 (1958).
[49] K. L. Lim and I. E. McCarthy, Phys. Rev. Letters 10, 529 (1963); K. L. Lim and I. E. McCarthy, Phys. Rev. 133, B1006 (1964).
[50] D. F. Jackson and T. Berggren, Nucl. Phys. 62, 353 (1965).
[51] T. Berggren (private communication).
[52] K. F. Riley, Nucl. Phys. 13, 407 (1959); K. F. Riley, H. G. Pugh, and T. J. Gooding, Nucl. Phys. 18, 65 (1960).

CC-0. In Public Domain. Gurukul Kangri Collection, Haridwar

Digitized by Arya Samaj Foundation Chennai and eGangotri

TABLE I. Quasi-free scattering experiments with incident energies larger than 100 MeV on nuclei with $A \geqslant 4$.

Group	Type of experiment	Energies	Nuclei investigated
Chicago (Refs. 11–13)	symmetric $(p, 2p)$	460 MeV	He, ^{6}Li, ^{7}Li, Be, ^{10}B, ^{11}B, C, N, O, Al, Si, P, S, A, Ca, V, Co
Rome (Ref. 24)	asymmetric $(e, e'p)$	500–600 MeV	Be, C, Al, S
Harvard (Refs. 14–16)	energy sharing $(p, 2p)$	160 MeV	^{6}Li, ^{7}Li, Be, ^{10}B, ^{11}B, C, N, O, F, Na, Mg, Al, Si, S, Cl, K, Ca, Sc, V, Co, Ni
Harwell (Ref. 17)	coplanar $(p, 2p)$	155 MeV	C; preliminary but not confirmed results on Li, Be, O, F, Na, Al, Si, P, S, Cl, Ca
Orsay (Refs. 18–20)	symmetric $(p, 2p)$	150 MeV	^{6}Li, ^{7}Li, Be, ^{10}B, ^{11}B, C, Ca, Sc, Ti, V, Cr, Mn, Fe, Ni, As
Uppsala (Refs. 10, 11, 21, 22)	symmetric $(p, 2p)$	185 MeV	He, ^{6}Li, ^{7}Li, Be, ^{10}B, ^{11}B, C, N, O, Na, Mg, Al, Si, P, Ca

mass cross section has to be taken at an angle of 90° and at an energy

$$\bar{E}_0 = (\hbar^2 c^2 k^2 \sin^2\theta + M^2 c^4)^{\frac{1}{2}};$$

$$k^2 = k_1^2 = k_2^2, \qquad \theta = \theta_1 = \theta_2, \qquad E = E_1 = E_2.$$

Finally, a few words on quasi-free electron–proton scattering,[23] which has recently been performed on complex nuclei.[24] To avoid the problems introduced by the fast variation of the Coulomb-scattering matrix element with the momenta of the particles involved [see the discussion following expression (3.27)], the calculations are performed for fixed momenta of the electron, taking the variation of the momentum of the emerging proton approximately orthogonal to the scattering plane (for coplanar scattering see Ref. 53). The cross section for this process is given by[23]

$$\frac{d^6\sigma}{dE_e d\Omega_e dE_p d\Omega_p}$$

$$= (E_p^2-1)^{\frac{1}{2}}(1+2E_0\sin^2\tfrac{1}{2}\theta_e)\frac{d\sigma^{fr}}{d\Omega_e}\frac{1}{2J_A+1}$$

$$\times \sum_{m_{A-1},m_A}\sum_{n} |\, g'^{(n)}_{m_{A-1},m_A}(\mathbf{k}_e+\mathbf{k}_p-\mathbf{k}_0)\,|^2$$

$$\times \delta(E_e+E_p+E_{A-1}-E_0-E_A), \qquad (3.34)$$

where the indices 0, e, and p refer, respectively, to the incoming and outgoing electrons and to the outgoing proton; the rest mass of the electron has been neglected and all quantities have been expressed in units of $\hbar$, c and the proton mass M. The distorted momentum distribution $\sum |\, g' \,|^2$ has been evaluated for incoming and outgoing electrons of at least several hundred MeV and outgoing protons of an energy between 150 and 400 MeV. The general result is that the shape of the angular correlations is practically unchanged by the multiple scattering of the emerging proton, but that its magnitude is reduced by a factor of order one (see Fig. 14 of the next section). This is in agreement with the qualitative expectation of Sec. II.

IV. SOME EXAMPLES AND SURVEY OF RESULTS

In this section we discuss a few examples showing the main features of the experimental results and make a comparison with calculations.

A. Experimental Results

The experimental work which has been done up to now is summarized in Table I; for more experimental details see Table 1.3 in Ref. 22. Up to now virtually all of the quasi-free experiments have been performed with incident protons. The few existing electron experiments seem however to show their potential advantage for the investigation of inner shells, as expected from the large mean free path of electrons in nuclear matter.

The energy spectrum and angular correlation obtained in the symmetric quasi-free proton–proton scattering of 460-MeV protons on ^{4}He is shown in Fig. 2.

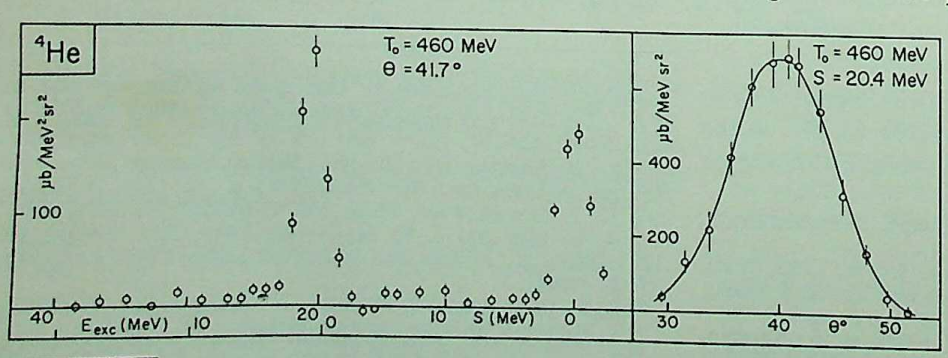

FIG. 2. Energy spectrum and angular correlation[13] for the ^{4}He$(p, 2p)^3$H reaction (symmetric case). The peak at zero separation energy results from scattering on free target protons.

[53] J. Potter, Nucl. Phys. 45, 33 (1963).

CC-0. In Public Domain. Gurukul Kangri Collection, Haridwar

Digitized by Arya Samaj Foundation Chennai and eGangotri

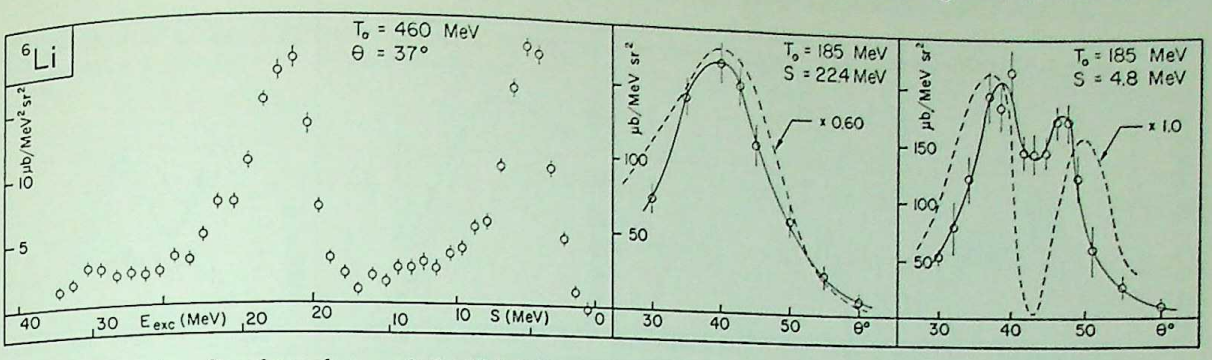

FIG. 3. Energy spectrum[13] and angular correlations[22] for the reaction ^{6}Li$(p, 2p)^5$He (symmetric case). The dotted lines are calculated results[67] multiplied by the indicated factors.

(At the cost of some uniformity we have tried to represent the experimental results in a way similar to the one of the original publications; absolute values for the cross section of the energy sharing experiments are given in the references 14–16.) At zero separation energy one sees the peak corresponding to the scattering on free protons which were present in the target; because these protons are at rest, they cause a relatively high contribution for certain angles. Only one group of protons is knocked out of the ^{4}He nucleus, and the angular correlation with its maximum at the angle for scattering on free protons at rest, corrected for the separation energy (which from now on is called the "free" scattering angle), clearly corresponds to the momentum distribution of an s proton. The width of the peak in the energy spectrum equals the experimental energy resolution. The separation energy is about 20 MeV, which means that the residual ^{3}H nucleus is left in its ground state or in a slightly excited state. For this very light nucleus, it is surprising that the results are, at least qualitatively, the ones predicted by the shell model. The measurements clearly support the soundness of the general interpretation described in the preceding sections.

Figures 3–6 show the energy spectra and angular correlation curves for quasi-free scattering experiments [symmetric $(p, 2p)$ and nonsymmetric $(e, e'p)$] on some $1p$ shell nuclei at the energies indicated in the figures. The dotted lines in the angular correlation curves represent calculated results, to which we will come back later.

In the framework of the shell model, the ^{6}Li nucleus is an alpha-particle with one proton–neutron pair added in the $1p$ shell; this picture is clearly in agreement with the energy spectrum and the angular correlations given in Fig. 3. The two added particles have increased the separation energy of the $1s$ proton to 22 MeV and decreased the cross section for the quasi-free process because of the absorption. The spectrum also shows the group of protons from the $1p$ shell with 4.8-MeV separation energy.

The angular correlation curves confirm the above assignments. Compared to other cases, the two maxima in the $1p$ correlation curve are relatively high and rather close to each other, which causes the minimum at about 42° to be shallow. This is qualitatively understandable from the low separation energy of the $1p$ proton, which causes a long exponential tail in its single particle wave function, thus reducing the absorption and also introducing additional low momentum components.

Because the ground state of ^{6}Li has $J=1$, one would expect the hole in the $1s$ shell to couple with the $1p$ shell to give states with $J=\frac{3}{2}$ and $J=\frac{1}{2}$, occurring with a probability ratio of 2:1. Speculating that the deformation of the $1s$ peak in Fig. 3 is caused by this splitting, one would find that the state with an antiparallel coupling of the two angular momenta has an energy of about 2 MeV lower than the state with a parallel coupling.

Also the energy spectrum and angular correlations for ^{12}C, given in Fig. 4, agree qualitatively with the shell model expectations. The $1s$ proton is bound by 36 MeV, and the hole state has a width of about 13 MeV, evidently being already quite short lived. The knocking out of a $1p$ proton is expected to lead to the $\frac{1}{2}^-$ ground state and to the $\frac{3}{2}^-$, 2.13-MeV first excited state[54] of ^{11}B. The intensity ratio for intermediate coupling is expected to lie between 0:1 and 1:2, the extreme values being the ones for pure j–j and L–S coupling. The splitting is clearly indicated in Fig. 4, the mentioned ratio being about 1:3.

For comparison Fig. 5 shows the spectrum of ^{12}C from electron scattering with the geometry indicated in the figure. This is the first experiment of this type on a complex nucleus; the resolution is not yet high, but the qualitative agreement with the $(p, 2p)$ result is evident. Also the number of events agrees well with the expected one,[55] assuming the quasi-free scattering model.

Basically the same features as in ^{12}C are shown by the $(p, 2p)$ results for ^{16}O in Fig. 6. The separation energy and the width of the $1s$ peak have increased still more, as expected. The spin–orbit splitting in the

[54] F. Ajzenberg-Selove and T. Lauritsen, Nucl. Phys. 11, 1 (1959).
[55] Private communication from the Istituto Superiore di Sanità (Rome) group.[24]

CC-0. In Public Domain. Gurukul Kangri Collection, Haridwar

Digitized by Arya Samaj Foundation Chennai and eGangotri

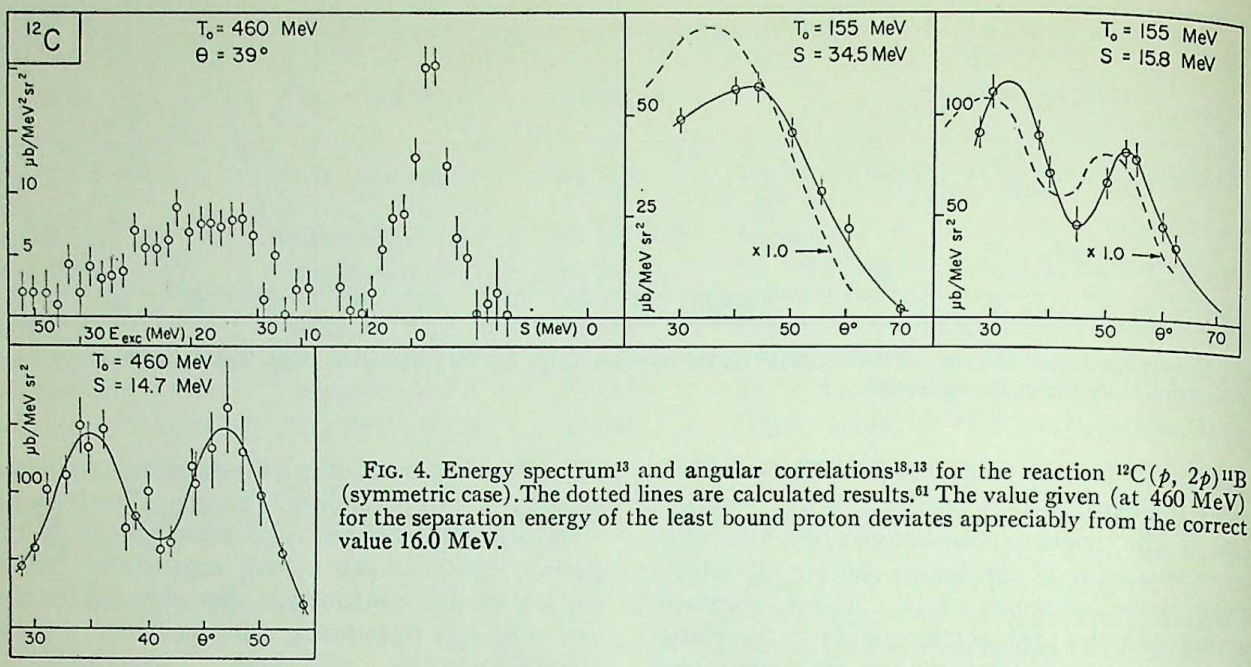

FIG. 4. Energy spectrum[13] and angular correlations[18,13] for the reaction $^{12}C(p, 2p)^{11}B$ (symmetric case). The dotted lines are calculated results.[61] The value given (at 460 MeV) for the separation energy of the least bound proton deviates appreciably from the correct value 16.0 MeV.

$1p$ shell is well resolved; the energies of the two maxima correspond within the experimental accuracy to the $\frac{1}{2}^-$ ground state and to the 6.3 MeV, $\leq\frac{5}{2}^-$ excited state[54] of ^{15}N. The intensity ratio of the two $1p$ shell peaks gives a clear experimental indication of the considerable absorption which already takes place in this light nucleus. Independently of the coupling scheme, one would for this closed shell nucleus expect the $\frac{3}{2}^-$ and $\frac{1}{2}^-$ states of ^{15}N to occur in the ratio 2:1 for all angles. Figure 6 shows that in reality the first excited state results at most angles with about the same probability as the ground state. We shall see below that this difference is naturally explained by the difference in separation energy of the two states.

In each of the investigated $1p$ shell nuclei (see next section) the predicted $1s$ and $1p$ shells have both been observed. For the $2s$–$1d$ shell nuclei the situation is not yet as favorable for the $(p, 2p)$ scattering; besides the upper shell the $1p$ shell has clearly been observed in only one case (^{19}F).

A serious difficulty for the detection of the inner shells is the intensity reduction due to the absorption.

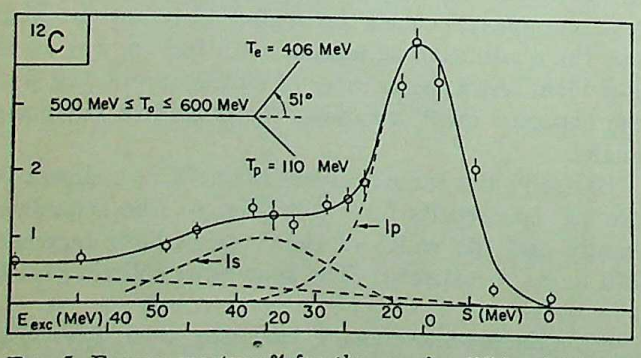

FIG. 5. Energy spectrum[24] for the reaction $^{12}C(e, e'p)^{11}B$ performed in the indicated geometry. The dotted curves give a decomposition in shell contributions and background.

This effect reduces not only the absolute cross sections but also the ratio of the cross sections for inner shells to the ones for upper shells because the last ones predominantly contribute to the nuclear surface. It is therefore perhaps not surprising that in the published investigations by quasi-free electron–proton scattering (on ^{12}C and ^{27}Al) all shells seem to have been observed in both nuclei. As mentioned earlier, another effect which adds to the difficulty of the investigation of inner shells is the increase of the width of a hole state with the number of particles in less bound shells and with the excitation energy of the residual nucleus. This is valid for both the $(p, 2p)$ and the $(e, e'p)$ experiments, and at present it is not known how far the various shells can be followed up.

As examples for the $2s$–$1d$ shell nuclei Figs. 7–10 show the results for ^{19}F, ^{27}Al, and ^{40}Ca. The spectrum of ^{19}F, obtained by the energy sharing experiment, shows three peaks. The distorted momentum distributions in Fig. 7, calculated from the experimental cross section dependence on the energy ratio of the two outgoing particles, agree with the interpretation of an ejection of $2s_{\frac{1}{2}}$, $1p_{\frac{1}{2}}$, and $1p_{\frac{3}{2}}$ protons. The resolution does not seem to be sufficient to observe the energy splittings of each of the two last mentioned groups, expected because of the angular momentum coupling of the hole state with the upper shell. The spin–orbit splitting of the inner $1p$ shell is 8 MeV.

The symmetric $(p, 2p)$ spectrum of ^{27}Al (Fig. 8) shows a maximum, with an only partially resolved structure, leading to an excited state of the residual nucleus ^{26}Mg. The ground state of this nucleus does not seem to be populated. A similar result is found for some other nuclei of the $2s$–$1d$ shell. This may be due to a strong difference in the ground state deformations of the initial and final nucleus but also energy inversions

CC-0. In Public Domain. Gurukul Kangri Collection, Haridwar

Digitized by Arya Samaj Foundation Chennai and eGangotri

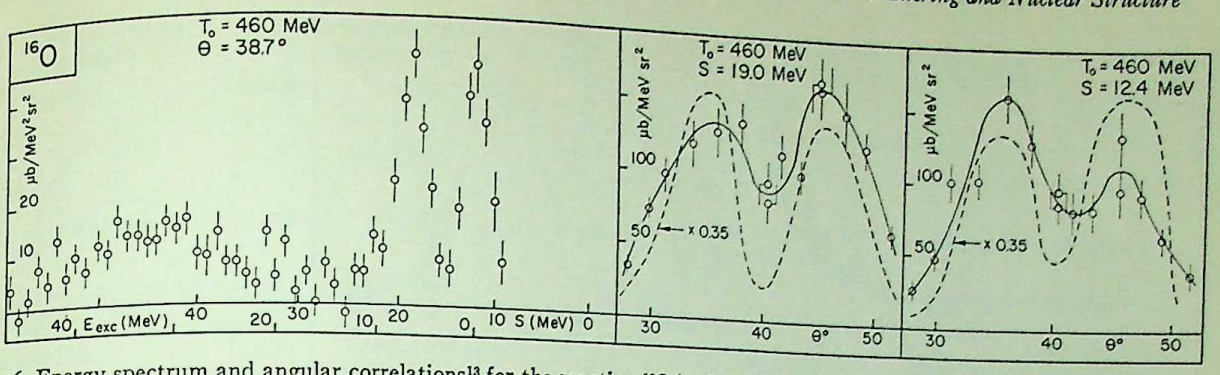

FIG. 6. Energy spectrum and angular correlations[13] for the reaction $^{16}O(p, 2p)^{15}N$ (symmetric case). The dotted lines are calculated results[40] multiplied by the indicated factor.

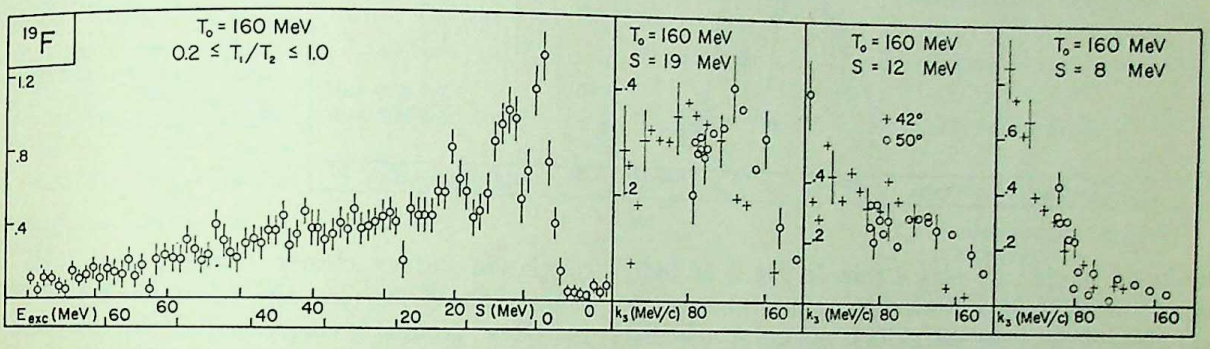

FIG. 7. Energy spectrum and deduced momentum correlations[15] for the reaction $^{19}F(p, 2p)^{18}O$ (energy sharing).

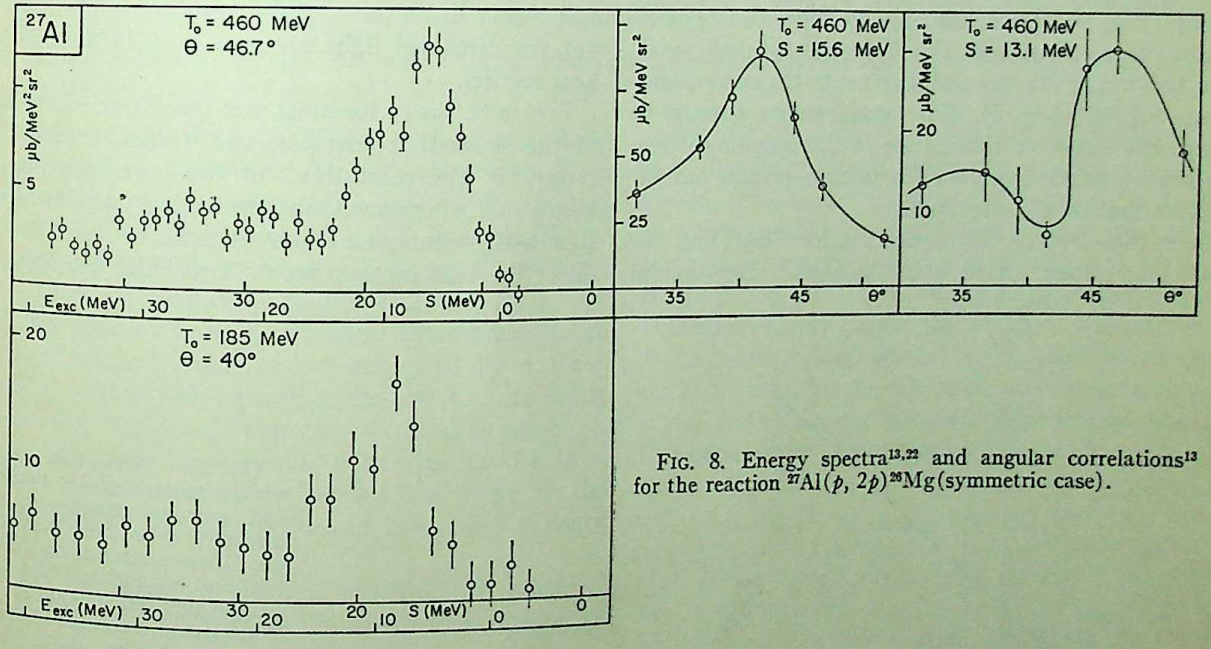

FIG. 8. Energy spectra[13,22] and angular correlations[13] for the reaction $^{27}Al(p, 2p)^{26}Mg$ (symmetric case).

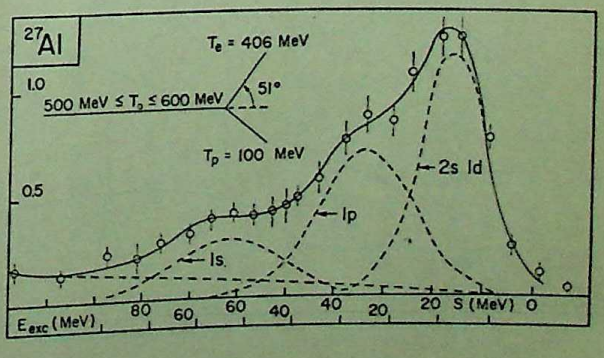

FIG. 9. Energy spectrum[24] for the reaction $^{27}Al(e, e'p)^{26}Mg$ performed in the indicated geometry. The dotted curves give a decomposition in shell contributions and background.

CC-0. In Public Domain. Gurukul Kangri Collection, Haridwar

Digitized by Arya Samaj Foundation Chennai and eGangotri

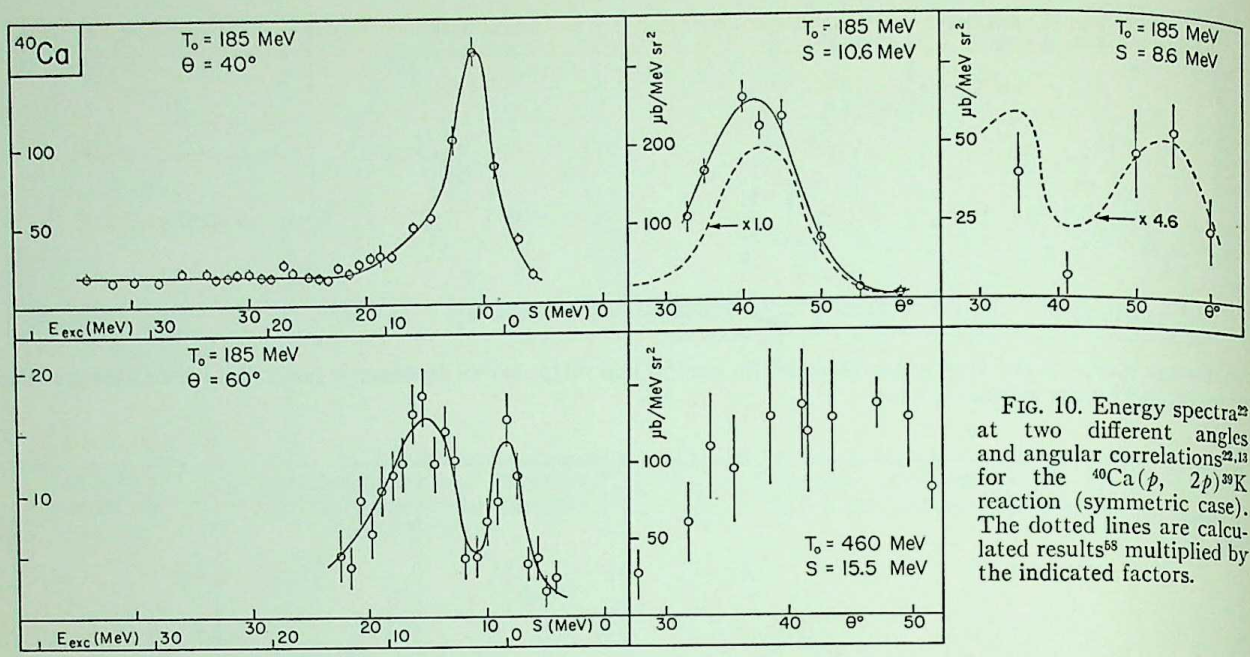

FIG. 10. Energy spectra[22] at two different angles and angular correlations[22,13] for the $^{40}Ca(p, 2p)^{39}K$ reaction (symmetric case). The dotted lines are calculated results[58] multiplied by the indicated factors.

of the $2s$–$1d$ levels may play a role. In Fig. 8 an indication of the $1p$ shell protons may be present between 30 and 40 MeV, but the statistics is not quite sufficient to make this certain.

The spectrum from electron scattering on the same nucleus (Fig. 9) seems not only to show the $1p$ shell protons clearly, but probably also the $1s$ shell maximum; this figure may be compared with the corresponding one for ^{12}C (Fig. 5). The measurement appears to confirm the expected advantage of the quasi-free electron–proton scattering over the proton–proton one for the investigation of inner shells.

The symmetric $(p, 2p)$ spectrum for ^{40}Ca (Fig. 10) shows only upper shell contributions. The angular correlation curves clearly support the shell model assignments of $1d_{\frac{3}{2}}$, $2s_{\frac{1}{2}}$, and $1d_{\frac{5}{2}}$ to the 8.4-, 11.1-, and 14.5-MeV groups, giving 6.1 MeV for the spin–orbit splitting between the $1d_{\frac{3}{2}}$ and $1d_{\frac{5}{2}}$ states.

For nuclei heavier than ^{40}Ca, the measurements are still rather incomplete; these results and the ones for not yet discussed lighter nuclei may be found in the next section.

Figure 11 shows for most measured nuclei the values of the separation energies, the natural widths (corrected for the resolution) of the corresponding hole states and, where available, the orbital angular momentum assignments; for each nucleus we have tried to select the best measurements available. The figure es-

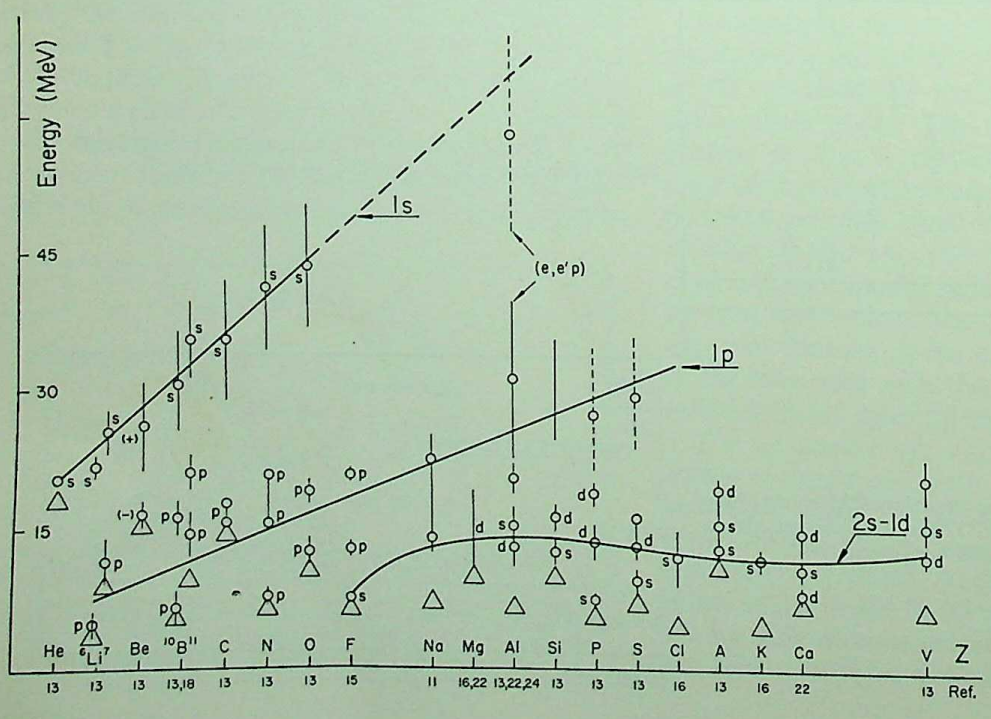

FIG. 11. Separation energies, widths (corrected for resolution) and angular momentum assignments of the hole states from quasi-free scattering as function of the atomic number. The angular momentum assignments are given if unique on the basis of a correlation distribution assuming the validity of the shell model. The position of a clear maximum is indicated by a circle; uncertain levels are dotted. The triangles indicate the separation energy of the least bound proton; references are given under the abscissa. The full lines are meant as guides for the eye to crudely follow the shells.

CC-0. In Public Domain. Gurukul Kangri Collection, Haridwar

Digitized by Arya Samaj Foundation Chennai and eGangotri

TABLE II. Distorted wave calculations for quasi-free scattering with incoming energies larger than 100 MeV.

Authors	Reaction	Energies	Nuclei	Remarks
Berggren (Ref. 66)	$(p, 2p)$	460 MeV	^{4}He, ^{6}Li, ^{7}Li, ^{8}Be, ^{12}C, ^{14}N, ^{16}O	semiclassical calculation
Berggren and Jacob (Ref. 40)	$(p, 2p)$	170 MeV	^{6}Li, ^{7}Li, ^{9}Be, ^{10}B, ^{11}B, ^{12}C, ^{16}O (also 450 MeV) ^{6}Li	semiclassical calculation
Jackson and Berggren (Ref. 48)	$(p, 2p)$	185 MeV	^{6}Li	phase shift analysis
Jacob and Maris (Ref. 23)	$(e, e'p)$	300–1000 MeV	^{12}C, ^{40}Ca, and interpolation graph for nuclei with $4 \leqslant A \leqslant 60$	semiclassical calculation
Johansson and Sakamoto (Ref. 57)	$(p, 2p)$	180 MeV	^{6}Li, ^{7}Li	semiclassical calculation
Johansson and Tibell (Ref. 58)	$(p, 2p)$	180 MeV	^{27}Al, ^{31}P, ^{40}Ca	semiclassical calculation
Lim and McCarthy (Ref. 47)	$(p, 2p)$	155 MeV	^{6}Li, ^{7}Li, ^{10}B, ^{11}B, ^{12}C	phase shift analysis
Maris (Ref. 35)	$(p, 2p)$	180 and 400 MeV	^{7}Li	semiclassical calculation
Riley, Pugh, and Gooding (Ref. 52)	$(p, 2p)$	153 MeV	^{12}C	asymmetric; semiclassical calculation
Rosenblum (Ref. 59)	$(p, 2p)$	100, 180 and 400 MeV	^{7}Li	semiclassical calculation
Sakamoto (Refs. 60, 61)	$(p, 2p)$	185 and 155 MeV	^{6}Li, ^{12}C	semiclassical calculation
Strnad (Ref. 62)	$(p, 2p)$	155 MeV	^{12}C	semiclassical calculation
Takemiya (Ref. 63)	$(p, 2p)$	155 MeV	^{6}Li, ^{7}Li	distortion calculated from double scattering

sentially contains the only direct experimental information which is known at the time of writing (June 1965) on the separation energies and widths of inner shell states in light nuclei. The full lines are drawn to guide the eye along levels belonging to the same shell. Towards increasing values of Z there is a clear tendency of the curves to diverge. For separation energies of single-particle states generated by a static potential which only increases in size for increasing values of A, one would expect the curves to converge. A comparison of these results with expectations from nuclear theory is however beyond the scope of the present review; for calculations of inner shell energies see Ref. 56.

Figure 12 shows the natural width of the measured $1s$ states as a function of A. Evidently it is a strongly increasing function. This is understandable from the fact that in the shell model the mechanism which in lowest order causes the decay of these states is the one in which the hole is filled by an interaction (collision) between a proton of the $1p$ shell with another nucleon in the same shell. For the $1p$ shell nuclei one would therefore crudely expect the width of the $1s$ hole state to be directly proportional to the number of proton–nucleon pairs in the $1p$ shell and inversely proportional to the nuclear volume.[34] The dotted line shows this dependence, normalized at ^{14}N.

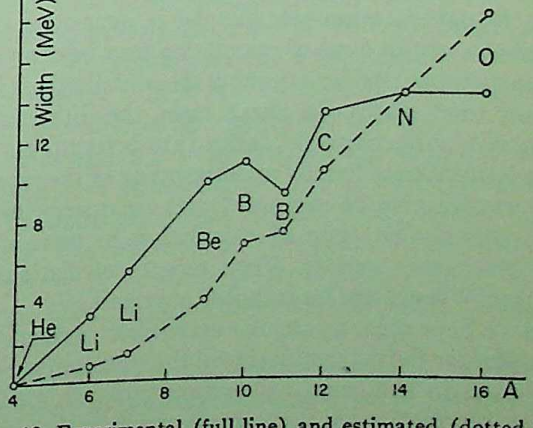

FIG. 12. Experimental (full line) and estimated (dotted line) widths of the $1s$ hole states for the $1p$ shell nuclei.

[56] W. E. Frahn and R. H. Lemmer, Nuovo Cimento 6, 1221 (1957); K. A. Brueckner, A. M. Lockett, and M. Rotenberg, Phys. Rev. 121, 255 (1961); D. M. Brink and N. Sherman, Phys. Rev. Letters 11, 393 (1965); H. S. Köhler, Phys. Rev. 138, B831 (1965).
[57] A. Johansson and Y. Sakamoto, Nucl. Phys. 42, 625 (1963).
[58] A. Johansson and G. Tibell, quoted in Ref. 22.
[59] W. M. Rosenblum, master thesis, Florida State University (1960).
[60] Y. Sakamoto, Phys. Letters 1, 256 (1962); Y. Sakamoto, Nuovo Cimento 26, 461 (1962).
[61] Y. Sakamoto, Progr. Theoret. Phys. (Kyoto) 28, 803 (1962).
[62] J. Strnad, Glasnik Mat.-Fiz. Astron. 17, 89 (1962).
[63] T. Takemiya, Progr. Theoret. Phys. (Kyoto) 30, 191 (1963).

CC-0. In Public Domain. Gurukul Kangri Collection, Haridwar

Digitized by Arya Samaj Foundation Chennai and eGangotri

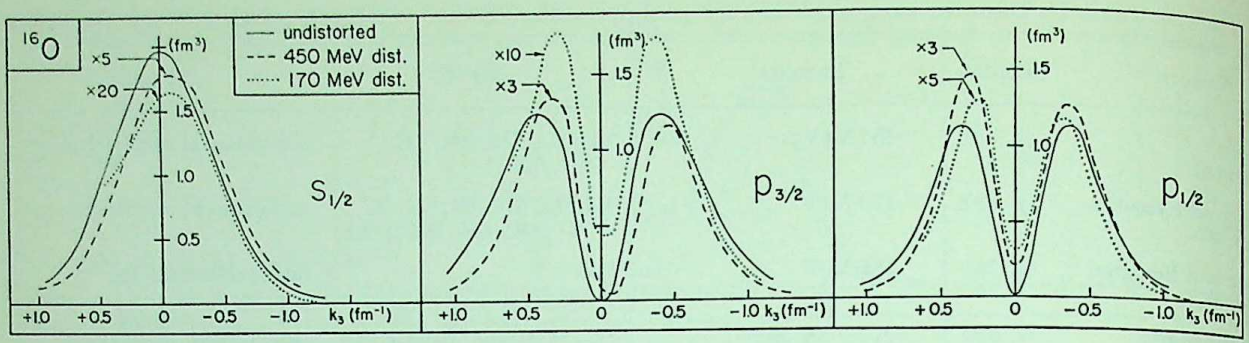

FIG. 13. Calculated undistorted and distorted (multiplied by the indicated factors) momentum distributions,[40] for the reaction $^{16}O(p,2p)^{15}N$ (symmetric case) at 450 and 170 MeV.

B. Calculated Results

The determination of the cross section Eq. (3.33) amounts to a computation of the distorted momentum distribution

$$\sum_{m_{A-1},m_A} \sum_{n} |\, g'^{(n)}_{m_{A-1},m_A}(\mathbf{k}_1+\mathbf{k}_2-\mathbf{k}_0)\,|^2$$

defined in Eq. (3.27). Up to now this function has been determined in two quite different approximations, namely, either by neglecting the distortion or by assuming a j–j coupled extreme single-particle model.

In the first mentioned type of work,[30,31] the one-particle fractional parentages of the states excited in the residual nucleus with respect to the ground state of the initial nucleus are determined using some model. The results predict which final nuclear states are expected to occur with an appreciable probability. Neglect of the distortion is, however, serious. It affects the cross section for different states by different angle-dependent factors, and therefore, it is not possible to derive reliable values for the fractional parentage coefficients from the experimental results without taking distortion into account. The dependence of the distortion on the properties of the overlap integral are clearly shown below for ^{16}O (see Fig. 13).

A considerable amount of work (see Table II) has been done simply using j–j coupled single-particle wave functions but taking the distortion of the plane proton waves into account. For closed shells this seems to be the natural approach; but also in some other cases the results of this type of calculation may be compared with experiments after summing the contributions from certain final states. In these cases the distortion is again not quite correctly taken into account. As this work is of interest for the understanding of the reaction and may directly be compared with measurements, we now discuss this type of calculation in more detail and give some results. Very recent calculations by Berggren[64] could not be included anymore.

As we have seen, an angular correlation measurement is helpful for the determination of the quantum numbers of a peak in the energy spectrum; however, more detailed information on the wave function in momentum space, though in principle contained in an angular correlation curve, is in practice not yet obtainable. Mainly due to the uncertainty in the distortion of the plane proton waves, comparisons of the results of calculations with measurements are still in a somewhat exploratory stage. The analysis however shows that the shapes and the orders of magnitude of the correlation distributions are in agreement with the basic model for this reaction.

The most extensive calculations have been performed for ^6Li. The results (dotted lines) in Fig. 3, taken from Ref. 57, show that the agreement with the experimental data is promising though the filling in of the minimum for the $1p$ correlation is insufficient.[65] In this calculation numerical wave functions, obtained from a truncated harmonic oscillator potential with an exponential tail, have been used and the distortion has been taken into account in the semiclassical way using square well potentials. In Ref. 57 it is also shown how seemingly small variations in the shape of the wave functions may have a relatively large influence on the cross section.

The results[61] for ^{12}C in Fig. 4 are in a surprising agreement[65] with the experimental ones, considering the simplicity of the calculations, in which infinite harmonic oscillator wave functions and purely imaginary square well potentials in a semiclassical approximation for the distortions have been used.

For ^{16}O the dotted curves shown in Fig. 6 have been calculated[40] with exponential wave functions and with Gaussian complex potentials in a semiclassical approximation for the distortion. The calculated results are about three times larger than the experimental ones, but the ratio of the magnitudes of the calculated $1p_{\frac{1}{2}}$ and $1p_{\frac{3}{2}}$ distributions is approximately correct. The deviation of the experimental result from the expected ratio of two can be traced to the effect of the separation energy on the absorption and on the momentum distribution, which has already been discussed for the case of ^6Li in the preceding subsection. The asymmetries in the calculated and the experimental curves are just opposite, a result for which we do not have a simple explanation.

[64] H. Tyrén, S. Kullander, O. Sundberg, R. Ramachandran, P. I. Isaacson, and T. Berggren, preprint (to be published).

[65] Recent measurements[16] on ^{12}C indicate, however, that the depth of the measured minimum is very sensitively dependent on the angular resolution.

CC-0. In Public Domain. Gurukul Kangri Collection, Haridwar

Digitized by Arya Samaj Foundation Chennai and eGangotri

The calculated curves[58] shown in Fig. 10 for ^{40}Ca have been obtained in a similar way as the ones for ^{6}Li. Except for the magnitude of the $1d_{\frac{3}{2}}$ state the agreement is good, showing that even for a relatively heavy nucleus the simple model used still works rather well.

In order to compare the influence of absorption at different energies, we give in Fig. 13 the undistorted and the distorted momentum distributions for ^{16}O at 170 and 450 MeV calculated in the same way as the previous results for this nucleus; the $1s$ wave function has been taken of the harmonic oscillator type. One sees that the influence of distortion is larger for smaller bombarding energies and for states with higher binding energies; this result was anticipated in Sec. II and seems to imply an advantage of experiments at higher energies.

Figure 14 shows the calculated results of the distorted and undistorted momentum distributions for an $(e, e'p)$ reaction on ^{40}Ca. The wave functions have been obtained from a harmonic oscillator potential, and the plane proton wave has been distorted by an imaginary Gaussian potential in the semiclassical approximation; the electron wave functions have been taken as plane waves. One clearly sees that the expected effect of multiple collisions is not very important; the distorted distributions have nearly the shape of the undistorted ones and the reduction of the size of the cross section is orders of magnitude smaller than in the case of $(p, 2p)$ scattering, in agreement with the qualitative discussion of Sec. II.

V. RESULTS FOR OTHER NUCLEI

This section is meant for readers who are interested in detailed data for nuclei other than those which have been considered as examples in the preceding section. As in the other sections, we do not go into the implications which the experimental results may have for the detailed structure of the individual nuclei.

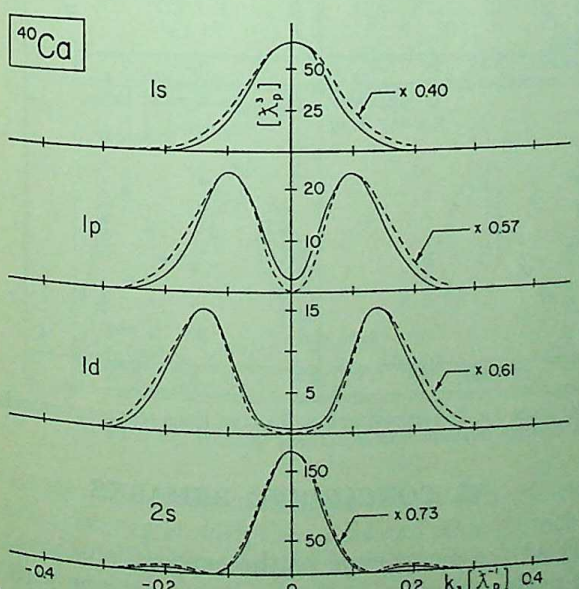

FIG. 14. Calculated undistorted (multiplied by the indicated factors) and distorted momentum distributions,[23] for the reaction ^{40}Ca$(e, e'p)^{39}$K; incident electron energy between 300 and 1000 MeV, proton energy between 150 and 400 MeV; the unit of length is the reduced proton Compton wavelength.

Typical measurements for the $1p$ shell nuclei are shown in Fig. 15. In all nuclei one sees the $1s$ and $1p$ maxima in the energy spectrum; these assignments are supported by the angular correlations.

In some cases the upper shell peaks clearly show a structure, which should be understandable from a fractional parentage analysis[9]; as remarked earlier, calculations neglecting distortion[30,31] should however be considered with caution. The spin–orbit splitting of the $1p$ shell and the increase of the width of the $1s$ shell with A are clearly seen in the figure. Probably in all cases (except ^{11}B) the residual nucleus remains rather frequently in its ground state, which shows that this state has a considerable overlap with the ground state of the initial nucleus.

In general the separation energies (see Fig. 11 of the preceding section) vary smoothly from nucleus to nucleus, except in the case of ^{9}Be. This exception is not quite unexpected as this nucleus is generally assumed in the shell model to be strongly deformed and is probably more naturally described by a cluster model.[44] The angular correlations indicate that the parity assignments of the two energy maxima in the ^{9}Be spectrum are still the ones suggested by the extreme single-particle model.

The effect of the extra neutron in ^{11}B as compared to ^{10}B is an increase of the separation energy by about 3 MeV and of the absorption by a factor of about 1.5.

The calculated angular correlation curves (dotted in the figures) show a semiquantitative agreement with the measuremenrs[66]; in general the minimum in the $1p$ distribution is not sufficiently filled (see, however, footnote 65). In contradistinction to the earlier case of ^{16}O, the asymmetry in this distribution around the "free" scattering angle is in general reasonably well reproduced.

Figure 16 shows a selection of energy spectra and angular correlations for several of the $2s$–$1d$ shell nuclei. The information available in this case is less extensive than for the $1p$ shell nuclei. The transition to the ground state of the residual nucleus is absent in several spectra as already discussed in the last section. (Note also the discrepancy in the energy scales of the two ^{24}Mg spectra.) In a few nuclei indications of the $1p$ shell are visible in the energy spectrum.

If momentum correlations of the peaks in an energy spectrum are measured, a $2s$ level is easily recognizable by its sharp maximum at the "free" scattering momenta. The minimum at this point in the correlation curves for $1d$ protons (positive parity!) may be completely filled, but the curves are still much flatter than the $2s$ ones.

The information available for nuclei heavier than ^{40}Ca is still very incomplete. Because of the larger absorption

[66] The absolute cross sections of some $1p$ shell nuclei determined by the Orsay[18,19] (155 MeV) and Uppsala[22] (185 MeV) groups differ by a factor of about three.

CC-0. In Public Domain. Gurukul Kangri Collection, Haridwar

Digitized by Arya Samaj Foundation Chennai and eGangotri

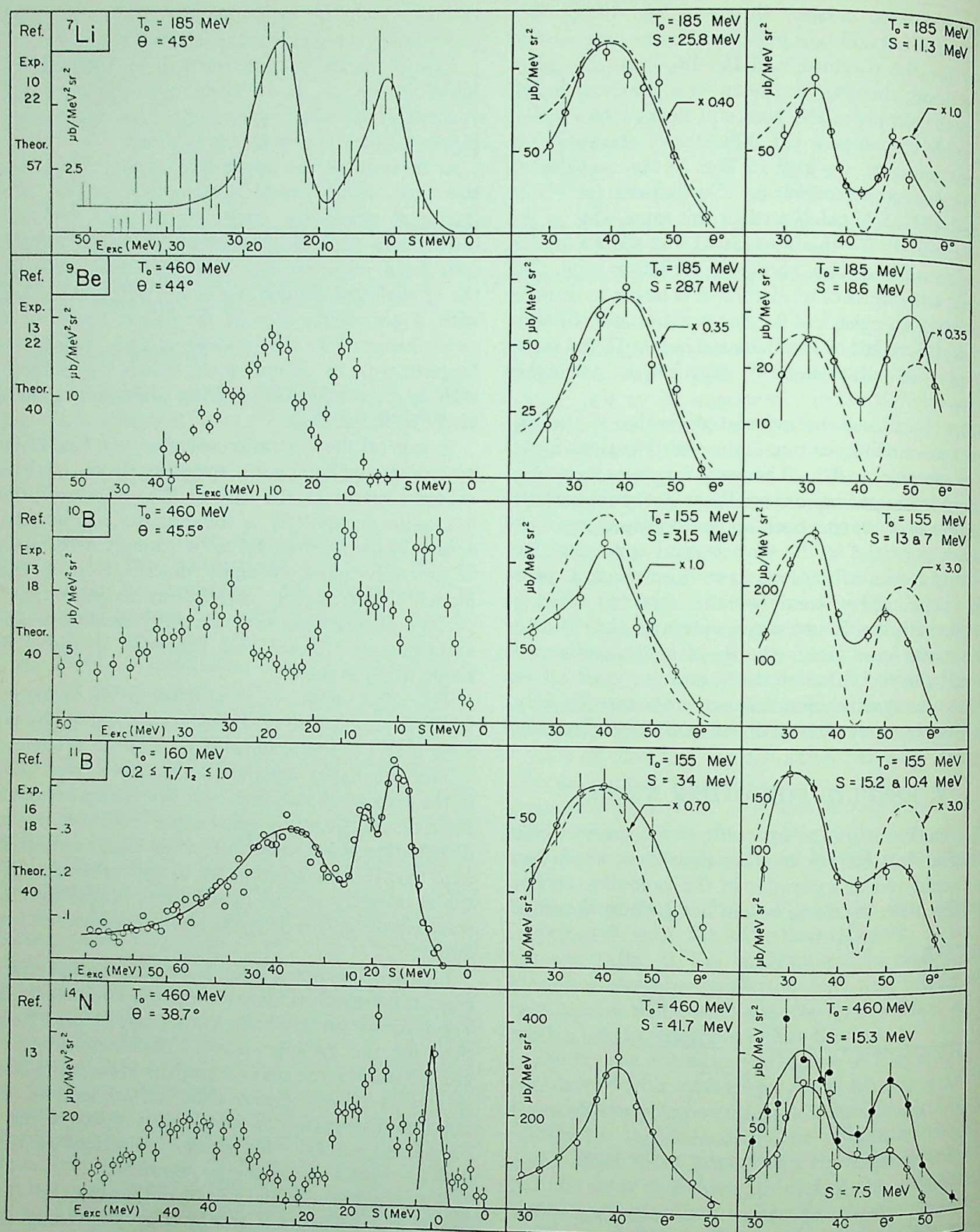

FIG. 15. Energy spectra and angular correlations for some $1p$ shell nuclei from $(p, 2p)$ experiments. Dotted lines represent calculated results multiplied by the indicated factors.

and smaller energy differences between the shells the experimental difficulties tend to increase with increasing atomic number. The most extensive measurements have been reported in Ref. 20. Figure 17 shows the examples of ^{51}V and ^{52}Cr. As in previous cases a $2s$ state is easily recognizable by its large contribution at zero momentum transfer, but not much can be said before more detailed results are available.

VI. CONCLUDING REMARKS

From the comparison of the expectations based on the model described in the preceding sections with the experimental results, it seems fair to conclude that our interpretation of the quasi-free reaction is essentially correct. The general structure of the energy spectra and the shapes of the correlation curves are under-

CC-0. In Public Domain. Gurukul Kangri Collection, Haridwar

Digitized by Arya Samaj Foundation Chennai and eGangotri

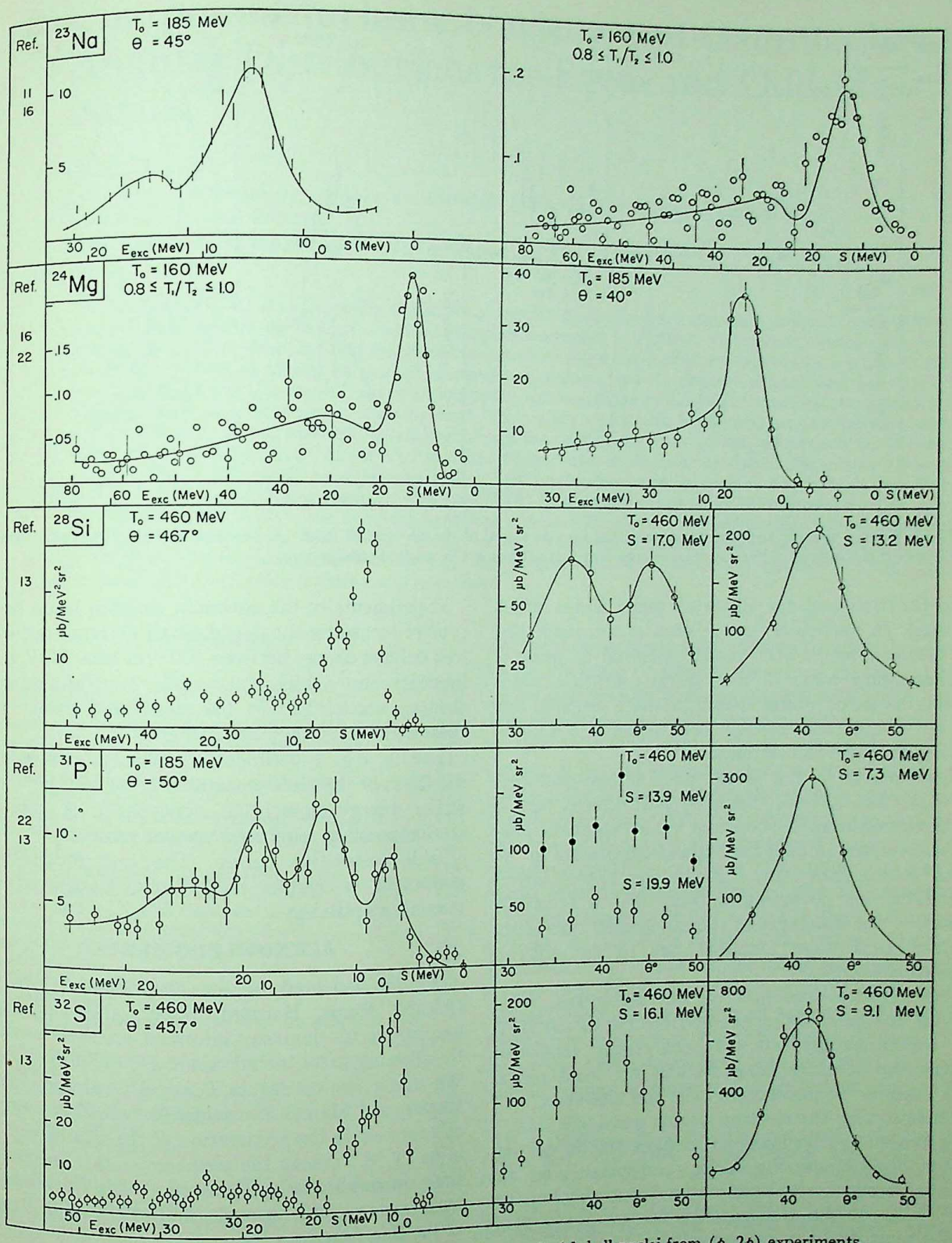

FIG. 16. Energy spectrum and angular correlations for some 2*s*–1*d* shell nuclei from (*p*, 2*p*) experiments.

stood; also, the orders of magnitude of the experimental cross sections agree with the calculated ones. At present the graph of the separation energies and hole state widths for the various shells (Fig. 11) seems to be the most interesting information supplied by the reaction under discussion.

Though one might hope ultimately to obtain detailed information on the low momentum region of the momentum distributions of the various shells, at the present time we seem to be still distant from this aim. In fact, the agreement between the calculated and measured correlation cross sections is only a very crude one, both with respect to absolute magnitudes and to relative ones for different angles, energies and nuclei. This is not surprising if one observes how sensitively the calculated cross sections depend on the nuclear

CC-0. In Public Domain. Gurukul Kangri Collection, Haridwar

Digitized by Arya Samaj Foundation Chennai and eGangotri

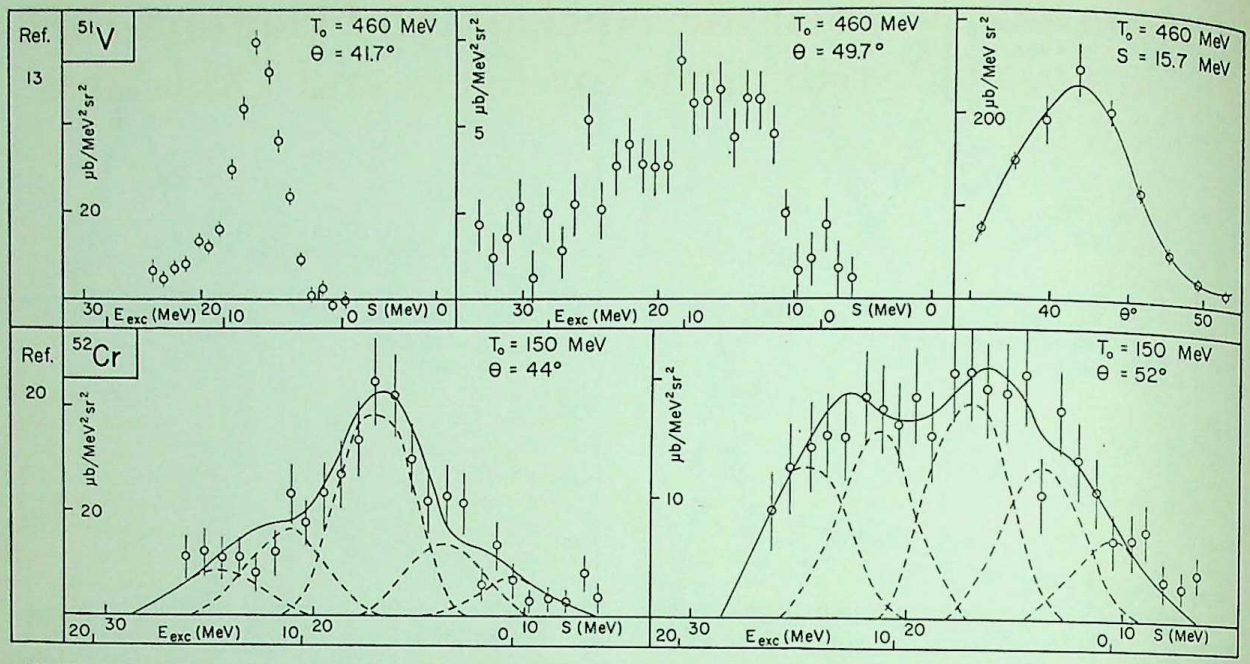

FIG. 17. Energy spectra and angular correlations for two nuclei of the $2p$–$1f$ shell from $(p, 2p)$ experiments. The dotted lines are tentative decompositions of the spectra performed by the authors of the original publication.

wave function and the distorted plane waves which are used. In particular, the relation of the shape and size of the selected shell model potential to those of the imaginary parts of the optical potentials which distort the plane waves should be quite essential and has up to now only crudely been taken into account in the performed calculations.

How details in the wave function may influence the experimental result has been most directly seen in the deviation from the constant value two of the ratio of the cross sections for the $1p_{\frac{3}{2}}$ and $1p_{\frac{1}{2}}$ protons in ^{16}O. It is encouraging that calculations approximately reproduce this deviation, showing that it is mainly caused by the difference in the exponential tails of the single-particle wave functions due to the differing separation energies.

The expected decrease of the absorption, when varying the bombarding energy from 150 to 450 MeV, has experimentally not yet been clearly confirmed. Where the absolute cross sections are measured at both energies no calculations exist and vice-versa.

Theoretically the electron–proton quasi-free scattering promises to have many advantages over the proton–proton one because the nuclear transparency for the former process is expected to be about equal to the third root of the transparency for the latter. This would seem to offer an opportunity to observe more inner shells, and the distortion of the momentum distributions is expected to be much smaller.

Experimentally the optimum electron beam for this type of measurement would be an external one with a well defined energy between 500 and 1000 MeV, a high intensity and a high duty cycle. In planning future electron accelerators in the considered energy range these conditions could be of interest.

The $(e, e'p)$ experiment is difficult because of the smallness of the electromagnetic cross section, and the strong energy–momentum dependence of this cross section possibly requires a special geometry to obtain reliable correlation curves. The first measurements performed on complex nuclei seem, however, to give reason for optimism.

ACKNOWLEDGMENTS

We are indebted to the experimental groups of Chicago, Rome, Harvard, Orsay, and Uppsala for keeping us continuously informed on their work and for allowing us to include several unpublished results. We thank our colleagues Darcy Dillenburg, John D. Rogers, and Marcus Zwanziger for valuable comments and for help in the preparation of the manuscript. One of us (T.M.) thanks the members of this Institute for their warm hospitality; his stay at this University has been made possible through the Professorship Program of the Pan American Union.

This work has been supported by the Pan American Union, by the U. S. Army Research Office, and by the Conselho Nacional de Pesquisas, Brazil.

CC-0. In Public Domain. Gurukul Kangri Collection, Haridwar

Digitized by Arya Samaj Foundation Chennai and eGangotri

REVIEWS OF MODERN PHYSICS VOLUME 38, NUMBER 1 JANUARY 1966

Compound Inelastic Nucleon and Gamma-Ray Angular Distributions for Even- and Odd-Mass Nuclei

ERIC SHELDON
Laboratorium für Kernphysik, Eidgenössische Technische Hochschule, 8049 Zürich, Switzerland
DOUGLAS M. VAN PATTER
Bartol Research Foundation, Swarthmore, Pennsylvania

The current theoretical and experimental status of angular distributions of inelastically scattered nucleons and succeeding γ radiations on the basis of a compound-nucleus mechanism is reviewed, with special reference to symmetry, isotropy, and identity characteristics. Results of investigations using a fast computer to ascertain the influence of higher partial waves, multipole mixing, unobserved intermediate transitions, and the presence of additional exit channels are presented, together with an over-all survey of distribution systematics and tabulations of numerical parameters to assist in evaluation of differential cross sections by hand. The predictions for both proton and neutron inelastic scattering are discussed in detail and illustrated by analyses of experimental data for many nuclear spin sequences. In particular, it is shown for γ distributions that the effect of cascades from higher levels upon the distribution structure and magnitude can be very appreciable. Also, the examination of the predicted behavior of $(n, n'\gamma)$ distributions near threshold has disclosed features deserving of further experimental and theoretical study. A set of recently measured $(n, n'\gamma)$ distributions for several heavy nuclei involving transitions between nuclear states of relatively high integer or half-integer spin is shown to compare well with the theoretical predictions when suitable account is taken of cascade and exit-channel contributions. It is concluded that there is a wide range of application of this theoretical approach to energy-averaged distributions, much of which remains yet to be exploited.

CONTENTS

1. Introduction 143
2. Underlying Theory 144
3. Isotropy and Identity of Gamma-Ray Distributions 146
4. Numerical Evaluation of Angular Distributions 147
   A. Introduction 147
   B. Restricted Legendre Expansion Coefficients $\alpha_{i\nu}$ 148
   C. Conversion Factors c_ν and C_ν 148
   D. Automatic Computation of Angular Distributions 149
5. Influence of Higher Partial Waves upon Angular Distributions 150
6. Influence of Multipole Mixing Ratios 150
7. Limiting Angular Distributions 155
8. Effect of Extra CN Exit Channels 158
9. Influence of Cascades from Higher Levels 162
10. Systematics of Angular Distributions 163
    A. Introduction 163
    B. Nucleon Distributions 163
    C. Gamma Distributions 164
11. Analysis of Experimental Gamma Distributions for Heavy Nuclei 166
12. Concluding Remarks 172
    A. General 172
    B. Inelastic Proton Distributions 172
    C. Inelastic Neutron Distributions 172
    D. $(p, p'\gamma)$ Distributions 174
    E. $(n, n'\gamma)$ Distributions 174
    F. Other Reactions 175
Appendix A: Tabulation of Restricted Legendre Expansion Coefficients $\alpha_{i\nu}$ 176
Appendix B: Distribution Symmetry about 90° 184

1. INTRODUCTION

Availability of fast computers conjoined with improvements in experimental techniques has opened the way to increasingly wide-ranging studies of the angular distributions of reaction products from such processes as inelastic scattering of nucleons and heavier particles. In the case of compound inelastic scattering of relatively low-energy nucleons, the means are now at hand to measure and analyze absolute nucleon and γ distributions for odd- as well as even-mass target nuclei and thereby to extend greatly the variety of nuclear spin sequences beyond those involving a ground-state spin-parity of 0^+. The numerical analysis can take cognizance of spin–orbit interaction, the presence of competing exit channels in decay of the compound nucleus (CN), *mixed* multipolarity in the γ transitions, and the existence of intermediate unobserved (mixed) transitions.

Except that it does not take CN fluctuations into account, as has been done in the recent Moldauer formalism,[1] the familiar theory due to Wolfenstein,[2] Hauser and Feshbach,[3] and Satchler[4] (with emendations) continues to furnish an appropriate basis for distribution analyses of the type presented here. The fundamental expressions have been embodied in a very general computer program (described in Sec. 4D),

[1] P. A. Moldauer, Phys. Rev. **123**, 968 (1961); and **129**, 754 (1963); Rev. Mod. Phys. **36**, 1079 (1964); Phys. Rev. **135**, B642 (1964). An automatic code for the evaluation of total cross sections from Moldauer's formulae has been described by P. A. Moldauer, C. A. Engelbrecht, and G. J. Duffy, "NEARREX, A Computer Code for Nuclear Reaction Calculations," Argonne National Laboratory Report ANL-6978, 1964 (unpublished). Other programs which take account of level width fluctuations have been compiled by R. S. Caswell at the National Bureau of Standards [J. Res. Natl. Bur. Std. (U.S.) **A66**, 389 (1962) and Bull. Am. Phys. Soc. **10**, 12 (1965)], and by L. Cranberg and T. A. Oliphant at Los Alamos.

[2] L. Wolfenstein, Phys. Rev. **82**, 690 (1951).

[3] W. Hauser and H. Feshbach, Phys. Rev. **87**, 366 (1952).

[4] G. R. Satchler, Phys. Rev. **94**, 1304 (1954); and **104**, 1198 (1956); erratum, Phys. Rev. **111**, 1747 (1958).

CC-0. In Public Domain. Gurukul Kangri Collection, Haridwar

Digitized by Arya Samaj Foundation Chennai and eGangotri

which goes somewhat beyond the capabilities of other[5] commensurate codes and makes possible the evaluation of differential cross sections for a number of recently measured inelastic-scattering processes, as well as permitting an over-all survey of distribution behavior for an extensive range of nuclear spin sequences. The calculations can include arbitrarily many partial waves in nucleon entrance and exit channels.

2. UNDERLYING THEORY

In order to pave the way for a description of the computer program and calculations, we commence with an outline of the familiar statistical continuum approach.

The general expression for a differential cross section[6] as a Legendre-polynomial expansion of even order,

$$d\sigma/d\Omega = \sum a_\nu P_\nu(\cos\theta), \tag{1}$$

in which the summation extends over angular momenta entering into the over-all process and over the index ν ($\nu=0, 2, 4, \cdots$) whose range is prescribed by vector momentum coupling conditions, contains coefficients a_ν that weight the angular-dependent Legendre terms and that can be decomposed into a product of energy-dependent and of momentum-dependent terms. The latter are just appropriate "transition parameters," one for each constituent step of the over-all process. Their values are dictated by the nature and angular momentum of the particle effecting the transition, as well as by the initial and final nuclear spins involved; for example, in the case of a γ transition of pure multipolarity L linking nuclear levels of spin J_i and J_f, the appropriate parameter, as tabulated by Ferentz and Rosenzweig,[7] is[8]

$$F_\nu(LLJ_fJ_i) \equiv (-)^{J_f-J_i-1}\hat{J}_i(\hat{L})^2 \times \langle \nu 0 \mid LL1-1\rangle W(LLJ_iJ_i;\nu J_f). \tag{2a}$$

F_ν must be written with the *intermediate* state J_i at the end of its argument.

For mixed multipolarity L, L' having a mixing ratio[9]

$$\delta \equiv \langle J_f \| L' \| J_i\rangle / \langle J_f \| L \| J_i\rangle, \tag{3}$$

the requisite γ-transition parameter expressed in terms of generalized F_ν as defined by Biedenharn,[10]

$$F_\nu(LL'J_fJ_i) \equiv (-)^{J_f-J_i-1}\hat{J}_i\hat{L}\hat{L}' \times \langle \nu 0 \mid LL'1-1\rangle W(LL'J_iJ_i;\nu J_f) \tag{2b}$$

is

$$A_\nu(LL'J_fJ_i) = (1+\delta^2)^{-1} \times [F_\nu(LLJ_fJ_i) + 2\delta F_\nu(LL'J_fJ_i) + \delta^2 F_\nu(L'L'J_fJ_i)] \tag{4}$$

When the transition is effected by particles other than photons, the appropriate linking term results on multiplying the commensurate γ-transition parameter by a "particle parameter" b_ν $(ij';\, x)$ for particles x of total angular momentum j, j'. The b_ν have been defined by Biedenharn and Rose [following Eq. (41d) and Eq. (79) of Ref. 11] and later, more explicitly, by Devons and Goldfarb [Eqs. (15.9), (13.10), (13.11), (13.12), (14.12), (14.13), (14.14) of Ref. 12.]. A nucleon transition from J_i to J_f is accordingly represented by a term of the form

$$\eta_\nu(jj'J_fJ_i) \equiv b_\nu(jj';N)F_\nu(LL'J_fJ_i) = (-)^{J_f-J_i-\frac{1}{2}}\hat{J}_i\hat{j}\hat{j}'\langle \nu 0 \mid jj'\tfrac{1}{2}-\tfrac{1}{2}\rangle \times W(jj'J_iJ_i;\nu J_f), \tag{5}$$

some principal values of which have been tabulated by Satchler.[13] Since $(\hat{s})^2/2=1$ for nucleons, the η_ν are the same for emission as for absorption of nucleons.

In the case of one or more *unobserved* transitions intervening between the observed steps, the linking parameter for radiation of total angular momentum L, L' is

$$U_\nu(LL'J_iJ_f) = (1+\delta^2)^{-1}[\hat{J}_i\hat{J}_f(-)^{J_i+J_f}] \times [(-)^L W(J_iJ_iJ_fJ_f;\nu L) + \delta^2(-)^{L'}W(J_iJ_iJ_fJ_f;\nu L')] \tag{6}$$

for each unobserved transition $J_i \longrightarrow J_f$.[14] This expression is independent of the nature of the unobserved radiation $(\gamma, N, d, \alpha, \cdots)$ and is an *incoherent* sum for nonzero values of the mixing ratio δ. The normalization is

$$F_0 = A_0 = \eta_0 = U_0 = b_0 = 1. \tag{7}$$

An alternative formalism used by Satchler[4] employs a parameter I_ν such that[15]

$$I_\nu \equiv (\hat{J}_i/\hat{J}_f)U_\nu \tag{8}$$

---

[5] Commensurate Hauser–Feshbach programs have been compiled in FORTRAN by several groups. For a listing of the code assembled by J. G. Wills we are indebted to G. R. Satchler, and for a more recent modified, extended version in use at Los Alamos, to L. Cranberg and T. A. Oliphant. Control calculations comparing results of our program with these two codes yielded perfect numerical agreement. Also recently made available to us is the ABACUS code of E. H. Auerbach, which performs compatible calculations and supplies substantially the same results.

[6] We make a distinction between a cross section $d\sigma/d\Omega$, expressed in absolute units (mb sr^{-1}), and a distribution $W(\theta)$, expressed in arbitrary units, which in general is normalized to $W(90°)=1$, or alternatively to $a_0=1$.

[7] M. Ferentz and N. Rosenzweig, Argonne National Laboratory Report ANL-5324, 1955 (unpublished).

[8] For brevity, we employ the notation $\hat{k} \equiv (2k+1)^{\frac{1}{2}}$.

[9] M. Sakai and T. Yamazaki, Institute for Nuclear Study, Tokyo, Report INSJ-66, 1964 (unpublished).

[10] L. C. Biedenharn, in *Nuclear Spectroscopy*, edited by F. Ajzenberg-Selove (Academic Press Inc., New York, 1960) Part B, p. 732.

[11] L. C. Biedenharn and M. E. Rose, Rev. Mod. Phys. 25, 729 (1953).

[12] S. Devons and L. J. B. Goldfarb, in *Handbuch der Physik*, Vol. 42, edited by S. Flügge (Springer-Verlag, Berlin, 1957), p. 362.

[13] G. R. Satchler, Proc. Roy. Soc. (London) 66A, 1081 (1953).

[14] The phase factor has been corrected from that quoted by Satchler (Ref. 4).

[15] The argument of the phase factor should read $(J_1'+J_2-j-\cdots$

CC-0. In Public Domain. Gurukul Kangri Collection, Haridwar

Digitized by Arya Samaj Foundation Chennai and eGangotri

for an unobserved transition from J_i to J_f. This Racah function has the disadvantage of not being normalized to unity when $\nu=0$.

For inelastic nucleon scattering $(N, N'\gamma)$ involving the spin sequence [Fig. 1(a)]

$$J_0(j_1=l_1\pm\tfrac{1}{2})\,J_1(j_2=l_2\pm\tfrac{1}{2})\,J_2(L, L')\,J_3,$$

the set of transition parameters appropriate to the N' distribution is, accordingly,

$$\eta_\nu(j_1j_1J_0J_1)\cdot\eta_\nu(j_2j_2J_2J_1), \tag{9}$$

wherein mixed-j interferences of the type j_1, j_1' and j_2, j_2' are absent. For the γ distributions, the parameter product is

$$\eta_\nu(j_1j_1J_0J_1)\,U_\nu(j_2j_2J_2J_1)\,A_\nu(LL'J_3J_2), \tag{10}$$

since the scattered nucleons are not observed.

This can readily be extended to include additional unobserved intermediate transitions, as in $(N, N'\gamma-\gamma)$ processes characterized by the spin sequence [Fig. 1(b)]

$$J_0(j_1=l_1\pm\tfrac{1}{2})\,J_1(j_2=l_2\pm\tfrac{1}{2})$$
$$\rightarrow J_2(L_2+\delta_2{}^2L_2')\,J_3(L_3+\delta_3{}^2L_3')\,J_4,$$

where the radiation L_2, L_2' is unobserved and L_3, L_3' observed. The product of transition parameters now becomes

$$\eta_\nu(j_1j_1J_0J_1)\,U_\nu(j_2j_2J_2J_1)\,U_\nu(L_2L_2'J_2J_3)$$
$$\times A_\nu(L_3L_3'J_4J_3). \tag{11}$$

To arrive at the over-all distribution coefficients a_ν that weight the Legendre polynomials, the respective transition-parameter product must be multiplied by a statistical spin factor

$$g=\hat{J}_1{}^2/(\hat{s}\cdot\hat{J}_0)^2, \tag{12}$$

which takes account of the probability that the incident particles of spin s have the right orientation for resonance capture,[16] and by a Hauser–Feshbach penetrability term

$$\tau\equiv T_{l_1}(E_1)\cdot T_{l_2}(E_2)/\sum_{ljE}T_l(E), \tag{13}$$

which takes account of CN barrier penetrabilities for incident particles of energy E_1 and emergent particles of energy E_2 in the c.m. system. The summation in the denominator runs over all possible decay channels of the compound nucleus. If, for simplicity, this is confined to just the elastic channels to J_0 and inelastic channels to J_2 it is termed the "two-channel approximation." In general, however, additional exit channels are open, which should be taken into account, since they can exert a radical influence upon the magnitude of the angular distribution.

The theoretical expressions can be extended to take account of spin–orbit interaction by using "generalized" transmission coefficients[17] $T_l{}^{(\pm)}$, wherein the superscript $(\pm)$ refers to the vector composition of spin and orbital angular momenta to a resultant $j=l\pm\frac{1}{2}$. The relationship between generalized and normal transmission coefficients is simply[17]

$$T_l=[(l+1)\,T_l{}^{(+)}+lT_l{}^{(-)}]/(2l+1). \tag{14}$$

In absolute magnitude (e.g., mb sr^{-1}) the differential cross section ensues on multiplying the above terms by $\frac{1}{4}\lambda\!\!\!^{-2}$, where $\lambda\!\!\!^{-}$ is the rationalized wavelength of the incident particle in the center-of-mass system [for low energies, $\lambda\!\!\!^{-2}=\hbar^2/(2ME_1)=207.3963/E_1{}^{(\mathrm{MeV})}$ mb].

For the *nucleon distribution* we obtain

$$d\sigma/d\Omega_1=\tfrac{1}{4}\lambda\!\!\!^{-2}\textstyle\sum g\eta_\nu(j_1j_1J_0J_1)\eta_\nu(j_2j_2J_2J_1)\tau P_\nu(\cos\theta_1) \tag{15}$$

as a function of the scattering angle θ_1 referred to the incident beam direction. Substitution of the requisite Racah functions reduces this to

$$d\sigma/d\Omega_1=\tfrac{1}{8}\lambda\!\!\!^{-2}\textstyle\sum NCW\tau P_\nu(\cos\theta_1), \tag{16}$$

with summation over j_1, j_2, ν and with

$$N\equiv(-)^{J_0-2J_1+J_2-1}(\hat{J}_1)^4(\hat{j}_1)^2(\hat{j}_2)^2/(\hat{J}_0)^2, \tag{17}$$

$$C\equiv\langle\nu0\,|\,j_1j_1\tfrac{1}{2}-\tfrac{1}{2}\rangle\langle\nu0\,|\,j_2j_2\tfrac{1}{2}-\tfrac{1}{2}\rangle, \tag{18}$$

$$W\equiv W(J_1J_1j_1j_1;\nu J_0)\,W(J_1J_1j_2j_2;\nu J_2). \tag{19}$$

The Racah coefficients vanish unless ν is restricted to the range $0\leq\nu\leq 2j_1, 2J_1, 2j_2$.

For the $(N, N'\gamma)$ process, the γ distribution is[18]

$$d\sigma/d\Omega_2=\tfrac{1}{4}\lambda\!\!\!^{-2}\textstyle\sum g\eta_\nu(j_1j_1J_0J_1)\,U_\nu(j_2j_2J_1J_2)$$
$$\times A_\nu(LL'J_3J_2)\tau P_\nu(\cos\theta_2) \tag{20}$$

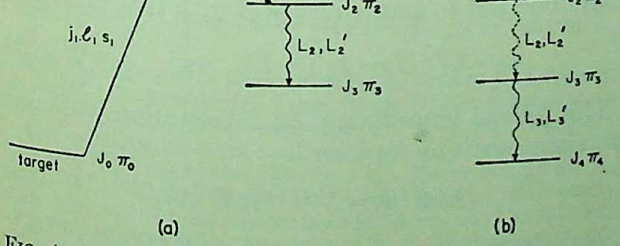

FIG. 1. Spin and angular momentum nomenclature employed for various types of transition sequences.

[16] E. Fermi, *Nuclear Physics*, notes compiled by J. Orear, A. H. Rosenfeld, and R. A. Schluter (University of Chicago Press, Chicago, 1950), revised ed., p. 157.

[17] E. Sheldon, Rev. Mod. Phys. **35**, 795 (1963).

[18] As mentioned by R. B. Day and M. Walt [Phys. Rev. **117**, 1330 (1960)], Satchler's expression in Ref. 4 for the γ distribution $W(\theta)$ should be multiplied by $\hat{J}_2/\hat{J}_1$. In the numerical formula that follows for $J_0=0$, $J_2=2$, $J_3=0$, the coefficient of the third term should read $[4+P_2(\cos\theta)]$, that of the fourth term, $[5+2.714\,P_2(\cos\theta)-1.714\,P_4(\cos\theta)]$, and that of the final term, $[10-0.714P_2(\cos\theta)+0.857P_4(\cos\theta)]$.

CC-0. In Public Domain. Gurukul Kangri Collection, Haridwar

Digitized by Arya Samaj Foundation Chennai and eGangotri

in terms of the angle of emergence θ_2 referred to the incident beam direction. This in turn reduces to

$$d\sigma/d\Omega_2=\tfrac{1}{8}\lambda^2\sum N'C'W'M(\delta)\tau P_\nu(\cos\theta_2), \quad (21)$$

with summation over j_1, j_2, and ν (now restricted to $0\leq\nu\leq 2j_1, 2J_1, 2J_2, 2L'$),

and

$$N'\equiv(-)^{J_0+J_3-j_2+\frac{1}{2}}(\hat{J}_1)^4(\hat{j}_1)^2(\hat{J}_2)^2/(\hat{J}_0)^2, \quad (22)$$

$$C'\equiv\langle\nu 0\,|\,j_1 j_1\tfrac{1}{2}-\tfrac{1}{2}\rangle, \quad (23)$$

$$W'\equiv W(J_1J_1j_1j_1;\nu J_0)W(J_1J_1J_2J_2;\nu j_2), \quad (24)$$

$$M(\delta)\equiv(1+\delta^2)^{-1}[M(LL)+2\delta M(LL')+\delta^2M(L'L')], \quad (25)$$

where

$$M(LL')\equiv\hat{L}\hat{L}'\langle\nu 0\,|\,LL'1-1\rangle W(J_2J_2LL';\nu J_3). \quad (26)$$

For an $(N, N'\gamma-\gamma)$ process in which the second gamma transition (from J_3 to J_4) is observed, its distribution is given by

$$d\sigma/d\Omega_{2'}=\tfrac{1}{4}\lambda^2\sum g\eta_\nu(j_1j_1J_0J_1)U_\nu(j_2j_2J_1J_2)$$
$$\times U_\nu(L_2L_2'J_2J_3)A_\nu(L_3L_3'J_4J_3)\tau P_\nu(\cos\theta_{2'}), \quad (27)$$

or, in reduced form, by

$$d\sigma/d\Omega_{2'}=\tfrac{1}{8}\lambda^2\sum N''C'W'U(\delta_2)M'(\delta_3)\tau P_\nu(\cos\theta_{2'}), \quad (28)$$

where the summation extends over j_1, j_2, ν (with $0\leqq\nu\leqq 2j_1, 2J_1, 2J_2, 2J_3, 2L_3'$) and

$$N''\equiv(-)^{J_0-J_4-j_2+\frac{1}{2}}(\hat{J}_1)^4(\hat{J}_2)^2(\hat{J}_3)^2(\hat{j}_1)^2/(\hat{J}_0)^2, \quad (29)$$

$$U(\delta_2)\equiv(1+\delta_2^2)^{-1}[U(L_2L_2)+\delta_2^2U(L_2'L_2')], \quad (30)$$

$$U(L_2L_2)=(-)^{L_2}W(J_2J_2J_3J_3;\nu L_2), \quad (31)$$

$$M'(\delta_3)\equiv(1+\delta_3^2)^{-1}$$
$$\times[M(L_3L_3)+2\delta_3M(L_3L_3')+\delta_3^2M(L_3'L_3')], \quad (32)$$

$$M(L_3L_3')\equiv\hat{L}_3\hat{L}_3'\langle\nu 0\,|\,L_3L_3'1-1\rangle$$
$$\times W(J_3J_3L_3L_3';\nu J_4). \quad (33)$$

When $\delta_2=\delta_3=0$, we arrive at the simpler form

$$d\sigma/d\Omega_{2'}=\tfrac{1}{8}\lambda^2\sum N'''C'''W'''\tau P_\nu(\cos\theta_{2'}), \quad (34)$$

where

$$N'''\equiv(-)^{J_0-J_4-j_2+L_2+\frac{1}{2}}(J_1)^4(J_2)^2$$
$$\times(J_3)^2(\hat{j}_1)^2(\hat{L}_3)^2/(\hat{J}_0)^2, \quad (35)$$

$$C'''\equiv\langle\nu 0\,|\,j_1j_1\tfrac{1}{2}-\tfrac{1}{2}\rangle\langle\nu 0\,|\,L_3L_31-1\rangle, \quad (36)$$

$$W'''\equiv W(J_1J_1j_1j_1;\nu J_0)W(J_1J_1J_2J_2;\nu j_2)$$
$$\times W(J_2J_2J_3J_3;\nu L_2)W(J_3J_3L_3L_3;\nu J_4). \quad (37)$$

It is a characteristic of the angular distributions in all the above cases that they are exactly symmetrical about 90°. In the mathematical formalism, this is expressed by the fact that throughout, the angular dependence is given by Legendre polynomial expansions of *even* order (P_0, P_2, P_4, $\cdots$, each of which is symmetrical about 90°). A brief discussion of the factors underlying this symmetry property is given in Appendix B, where it is shown that unless there is a preferred spin direction, as in the case of aligned nuclei or polarized particles, the angular distributions of the products of reactions proceeding by way of CN formation display this basic symmetry exactly. For a direct interaction this is not the case with particle distributions—though it must be stressed that, contrary to widespread belief, DI particle distributions *can* in particular instances evince a form indistinguishable from that of a symmetrical CN distribution (the respective absolute magnitudes differ appreciably, however, and the peak-to-valley ratios appear to be considerably higher than those for CN distributions)—the subsequent γ transitions have, of course, symmetrical distributions.

We relegate discussion of these points to Appendix B, and proceed to a consideration of conditions which bring about isotropy or identity of γ distributions.

3. ISOTROPY AND IDENTITY OF γ DISTRIBUTIONS

When the summation index is restricted to the single value $\nu=0$, the distribution is isotropic, as is well known, and has the value

$$(d\sigma/d\Omega_1)_{\nu=0}=(d\sigma/d\Omega_2)_{\nu=0}=\sigma/(4\pi)=\tfrac{1}{8}\lambda^2\textstyle\sum_s(\hat{J}_1/\hat{J}_0)^2\tau. \quad (38)$$

Thus the γ distribution from an $(N, N'\gamma)$ process is isotropic when $J_2=0$ or $\frac{1}{2}$, and that from an $(N, N'\gamma-\gamma)$ process is isotropic when J_2 *or* $J_3=0$ or $\frac{1}{2}$. Apart from this trivial instance of equality of γ distributions in a cascade, more general conditions leading to distribution identity can be established. Of various possibilities, all involving *pure* multipolarity (or alternatively the same values of mixing ratios δ for corresponding γ transitions), the first is familiar, viz., (a) in an $(N, N'\gamma_1-\gamma_2)$ process, the distribution of γ_1 is in magnitude and structure identical with that of γ_2 when

$$L_2=L_2'=L_3=L_3'(=L) \quad \text{and} \quad J_4=0. \quad (39)$$

This follows immediately on substitution in the appropriate condition for identity,

$$N'M(0)=N''U(0)M'(0), \quad (40)$$

derived from the expressions (21) and (28).

We note that the above depends only on J_2, J_3, J_4, and L, and hence on the nature of the transitions preceding the γ decay. If, however, more than a single unobserved γ transition precedes the observed γ decay

CC-0. In Public Domain. Gurukul Kangri Collection, Haridwar

Digitized by Arya Samaj Foundation Chennai and eGangotri

to a spin-zero level, as in an $(N, N'\gamma_1-\gamma_2-\gamma_3)$ process, the distributions of γ_1 and γ_3 are not in general identical even if the γ radiations are of the same pure multipolarity. Only in the special case of a regular monotonic level sequence (e.g., 0^+, 2^+, 4^+, 6^+) does equality obtain.

For the consideration of basic γ transitions[19] cascading through nuclear levels whose spins form a regular monotonic sequence, it is useful[20] to invoke an identity which can readily be verified from first principles:

$$\frac{W(J-L,\ J-L,\ L,\ L;\ \nu J)}{W(J-L,\ J-L,\ J,\ J;\ \nu L)} \equiv (-)^{2J}(\hat{J})^2 W(JJLL;\ \nu,\ J+L). \quad (41)$$

The condition (40) can upon substitution and use of the Racah identity (41) be shown to be satisfied in the more general situation when (b)

$$L_2=L_2'=L_3=L_3'\ (=L)$$

and

$$L=|\ J_2-J_3\ |=|\ J_3-J_4\ |. \quad (42)$$

This situation is encountered not only in the case of a rotational band of levels with spins 0^+, 2^+, 4^+, but in several odd-mass nuclei having half-integer spins which would appear to be amenable to experimental investigation (e.g., P^{31}, Tb^{159}, Lu^{175}, Hf^{177}, $Tl^{203,205}$).

In point of fact, an even less restrictive condition than this has been formulated by Raboy and Krohn[21] who extended the work of Weneser and Hamilton[22] and Biedenharn, Arfken, and Rose,[23] considering multiple γ cascades. The decay scheme is symbolized in Fig. 2. Raboy and Krohn showed that with respect to a transition (A) between levels of arbitrary spin (irrespective of the multipolarity, mixing ratio or, indeed, the particle nature of the radiation effecting the transition), the individual distributions of either of two preceding or following transitions (B, C) are equal when they entail pure, basic decay between levels whose spins form a regular monotonic sequence. No restrictions on L, δ, and J obtain for unobserved transitions common to both the AB, AC sequences, but any unobserved transitions intervening between B and C must be basic as well as of pure multipolarity, and at the same time involve a monotonic sequence of nuclear spins which join regularly to those for the transitions B and C.

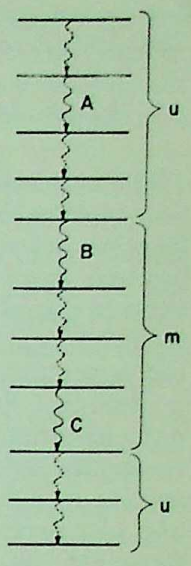

FIG. 2. Symbolic representation of the requisite level-spin conditions for validity of the Raboy–Krohn theorem (Ref. 21). When referred to the direction of A as quantization direction, the distribution of radiation B is identical with that of C when the intervening nuclear levels in the region marked "m" form a regular monotonic sequence. The spins of the levels in the regions labeled "u" are unrestricted in value. No parity restriction applies beyond that necessary to ensure that all the radiations in the regions AB and AC are of the same pure multipolarity L.

A subsidiary remark in the first sentence of the paper by Weneser and Hamilton[22] to the effect that the distributions are unaltered on adding a constant to all the level spins has to be qualified, however. Only when the constant is a multiple of the basic pure multipolarity L is this statement valid (for example, increasing the level spins by $\frac{1}{2}$ throughout drastically changes the distributions from their previous form and magnitude; similarly for unit spin increase throughout when $L=2$).

4. NUMERICAL EVALUATION OF ANGULAR DISTRIBUTIONS

A. Introduction

The expressions (15), (21), (28), and (34) furnish differential cross sections for such processes as $(n, n'\gamma)$, $(p, p'\gamma)$, $(n, p\gamma)$, $(p, n\gamma)$, $(t, p\gamma)$, $(He^3, p\gamma)$, etc., of the type $(N, N'\gamma)$ or $(N, N'\gamma-\gamma)$, but can involve lengthy summations which render hand calculations both tedious and liable to error.

In the present section, we define and discuss weighting coefficients $\alpha_{i\nu}$ in the expansion

$$d\sigma/d\Omega=\tfrac{1}{8}\lambda\!\!\!^{-2}\sum_{i,\nu}\alpha_{i\nu}\tau_i P_\nu(\cos\theta)\equiv\tfrac{1}{8}\lambda\!\!\!^{-2}\sum_{\nu}a_\nu P_\nu(\cos\theta). \quad (43)$$

Numerical values of the $\alpha_{i\nu}$ for some commonly occurring spin sequences have been tabulated in Appendix A. Next, we present expressions for the coefficients c_ν and C_ν used in converting given numerical expansions for a certain nuclear spin transition sequence to those for other spin sequences. Finally, details of the flexible

[19] Unmixed radiation of pure multipolarity L between levels J_i and J_f such that $L=|\ J_i-J_f\ |$.

[20] Also useful for effecting the reduction is the sum rule due to G. Racah [Phys. Rev. 62, 438 (1942)], which is most conveniently represented as

$$W(abcd;\ ef)=\sum_g(-)^{a+b+c+d+e+f+g}(\hat{g})^2 W(adbc;\ ge)W(adcb;\ gf).$$

Although the alternative form given by A. Simon, J. H. Vander Sluis, and L. C. Biedenharn [Oak Ridge National Laboratory Report ORNL-1679, 1954 (unpublished)] is correct, there are erroneous versions in other publications, e.g., the argument of the phase in Eq. (16) of the paper by L. C. Biedenharn [J. Math. Phys. 31, 287 (1952–3)] should read $(j_1+j_2-J_a)$ and the recursion relation (28) in the above paper should be emended to $W(avcd;\ ad)W(a\bar{v}cd;\ ad)=\cdots$. In the paper of L. C. Biedenharn, J. M. Blatt, and M. E. Rose [Rev. Mod. Phys. 24, 249 (1952)], the left-hand side of Eq. (16) should read $W(afgb;\ cd)$.

[21] S. Raboy and V. E. Krohn, Phys. Rev. 98, 24 (1955).

[22] J. Weneser and D. R. Hamilton, Phys. Rev. 92, 321 (1953).

[23] L. C. Biedenharn, G. B. Arfken, and M. E. Rose, Phys. Rev. 83, 586 (1951).

CC-0. In Public Domain. Gurukul Kangri Collection, Haridwar

Digitized by Arya Samaj Foundation Chennai and eGangotri

distribution code "MANDY," written in ALGOL for a CDC 1604-A computer, are outlined.

B. Restricted Legendre Expansion Coefficients $\alpha_{i\nu}$

The evaluation of CN angular distributions follows from building products of requisite numerical and Racah functions for each permitted permutation of the momentum ensemble l_1, j_1, J_1, l_2, j_2 and for each even value of ν, to obtain the respective restricted expansion coefficients $\alpha_{i\nu}$, where i is a running index characterizing the permutation. The permutation range is restricted by setting a limit to the orbital momenta l_1, l_2 taken into consideration; under present physical conditions a reasonable limit is $l_{\max}=4$, as discussed in Sec. 5. The ensuing $\alpha_{i\nu}$ refer to a given sequence of nuclear spins and to observation of radiation in a given transition step (e.g., N', γ_1, γ_2, or γ_3, etc.), but can in many instances be converted from those for a certain "basic" sequence to those for related spin sequences, as discussed later. The $\alpha_{i\nu}$ for N' distributions, dictated essentially only by the nuclear spins J_0 and J_2, can readily be transformed from those for a J_0/J_2 sequence to those for a J_0/J_2' combination involving a new value J_2' of the residual nuclear spin. For γ-transitions, the $\alpha_{i\nu}$ are governed additionally by further spins, such as J_3, J_4, etc. and by multipole mixing ratios, which renders conversion more difficult and tabulation more involved. The policy adopted has been to choose a set of "basic" spin sequences and list the $\alpha_{i\nu}$ together with respective momenta $l_1, j_1, J_1\pi_1, l_2, j_2$.

C. Conversion Factors c_ν and C_ν

It is possible to define simple numerical conversion coefficients that generate the $\alpha_{i\nu}$ for a new transition sequence from known α's for a different given sequence. These conversion factors eliminate the labor of evaluating the $\alpha_{i\nu}$ afresh from first principles. They can be applied to nucleon transitions wherever the total particle angular momenta j_1 or j_2 are the same in the new as in the old transition. From the $\alpha_{i\nu}$ for observed N' radiation in a $J_0\pi_0\rightarrow J_1\pi_1\rightarrow J_2\pi_2$ reaction sequence, those for a new sequence in which J_2 is replaced by J_2' (but π_2 unchanged, and the new j_2 numerically equal to the old) are obtained by multiplying by

$$c_{i\nu}=\eta_\nu(j_2j_2J_2'J_1)/\eta_\nu(j_2j_2J_2J_1) \tag{44}$$

$$=(-)^{J_2'-J_2}W(j_2j_2J_1J_1;\,\nu J_2')/W(j_2j_2J_1J_1;\,\nu J_2), \tag{45}$$

where $c_{i0}\equiv 1$ for all i. Alternatively, the $\alpha_{i\nu}$ for a sequence in which J_0 is replaced by J_0' (but π_0 and j_1 unchanged), are generated by the similarly normalized conversion factor

$$c_{i\nu}=\eta_\nu(j_1j_1J_0'J_1)/\eta_\nu(j_1j_1J_0J_1) \tag{46}$$

$$=(-)^{J_0'-J_0}W(j_1j_1J_1J_1;\,\nu J_0')/W(j_1j_1J_1J_1;\,\nu J_0). \tag{47}$$

Any additional terms in the basic tabulation where j_2 or j_1 do not coincide with the old values have to be evaluated afresh or alternatively necessitate construction of an appropriately modified numerical conversion factor.

In the case of observed γ distributions, the factors C_ν represent a more powerful approach in that the basic tabulation now involves no new combination of momenta and $\alpha_{i\nu}$. Accordingly, instead of using c_ν's to convert individual $\alpha_{i\nu}$'s, it suffices to multiply the summed coefficients $a_\nu\equiv\sum_i \alpha_{i\nu}\tau_i$ by an over-all factor C_ν. (These factors are identical with those employed in β–γ and γ–γ angular-correlation calculations.) From the a_ν determined for a standard sequence, $J_0\pi_0\text{—}J_1\pi_1\cdots\!\rightarrow J_2\pi_2\rightarrow J_3\pi_3$, those for a sequence (i) $J_0\pi_0\text{—}J_1\pi_1\cdots\!\rightarrow J_2\pi_2\rightarrow J_3'\pi_3'$ and others involving unobserved intermediate γ transitions ($\cdots\!\rightarrow$), such as (ii) $J_0\pi_0\text{—}J_1\pi_1\cdots\!\rightarrow J_2\pi_2\cdots\!\rightarrow J_3\pi_3\rightarrow J_4\pi_4$, or (iii) $\cdots\!\rightarrow J_3\pi_3\text{—}J_4\pi_4\rightarrow J_5\pi_5$, etc. can be generated by use of the C_j. The situation is, however, complicated if γ transitions involve mixed multipolarity. For simplicity, the standard sequence should involve pure γ radiation of multipolarity $L_2=L_2'$ effecting the transition from J_2 to J_3. The appropriate γ transition parameter then reduces from $A_\nu(L_2L_2'J_3J_2)$ to $F_\nu(L_2L_2J_3J_2)$, so that the conversion factor for case (i) above becomes

$$C_\nu=A_\nu(L_2^{\text{new}}L_2'^{\text{new}}J_3'J_2)/F_\nu(L_2L_2J_3J_2), \tag{48}$$

and if $L_2^{\text{new}}=L_2'^{\text{new}}$, this reduces further to

$$C_\nu=F_\nu(L_2^{\text{new}}L_2^{\text{new}}J_3'J_2)/F_\nu(L_2L_2J_3J_2) \tag{49}$$

$$=(-)^{J_3'-J_3}\left(\frac{\hat{L}_2^{\text{new}}}{\hat{L}_2}\right)^2\frac{\langle\nu0\mid L_2^{\text{new}}L_2^{\text{new}}1-1\rangle}{\langle\nu0\mid L_2L_21-1\rangle}$$

$$\times\frac{W(L_2^{\text{new}}L_2^{\text{new}}J_2J_2;\,\nu J_3')}{W(L_2L_2J_2J_2;\,\nu J_3)}, \tag{50}$$

which becomes particularly simple if $L_2^{\text{new}}=L_2$.

For case (ii), in which one unobserved intermediate γ transition is involved, the general expression for the conversion factor is

$$C_\nu=U_\nu(L_2L_2'J_2J_3)\,A_\nu(L_3L_3'J_4J_3)/A_\nu(L_2L_2'J_3J_2), \tag{51}$$

and if the standard transition is of pure multipolarity

CC-0. In Public Domain. Gurukul Kangri Collection, Haridwar

Digitized by Arya Samaj Foundation Chennai and eGangotri

$L_2=L_2'$ then

$$C_\nu=U_\nu(L_2L_2'J_2J_3)A_\nu(L_3L_3'J_4J_3)/F_\nu(L_2L_2J_3J_2) \quad (52)$$

$$=N''U(\delta_2)M'(\delta_3)/N'M(0), \quad (53)$$

allowing for the unobserved new transition to be of mixed multipolarity L_2, L_2' and the observed radiation to be of multipolarity L_3, L_3'.

Analogously, for case (iii), which involves two unobserved intermediate steps, the conversion factor is

$$C_\nu=U_\nu(L_2L_2'J_2J_3)U_\nu(L_3L_3'J_3J_4)$$
$$\times A_\nu(L_4L_4'J_5J_4)/A_\nu(L_2L_2'J_3J_2), \quad (54)$$

and so on for higher numbers of successive intervening transition steps involving unobserved cascade radiation. Numerical results for cases (i), (ii), and (iii) have been given by Benjamin,[24] and also by Mathur and Tucker.[25]

The above expressions can be combined when it is, for example, desired to establish conversion factors taking the a_ν for the standard sequence $J_0\pi_0\rightarrow J_1\pi_1\cdots\rightarrow J_2\pi_2\rightarrow J_3\pi_3$ into those for a sequence such as $J_0\pi_0\rightarrow J_1\pi_1\cdots\rightarrow J_2\pi_2\cdots\rightarrow J_3'\pi_3'\rightarrow J_4\pi_4$, where we have an intermediate unobserved step leading to a new level of spin-parity $J_3'\pi_3'$. In this instance, the conversion factor ensues from combination of (48) and (51):

$$C_\nu=U_\nu(L_2^{\text{new}}L_2'^{\text{new}}J_2J_3')$$
$$\times A_\nu(L_3L_3'J_4J_3')/A_\nu(L_2L_2'J_3J_2). \quad (55)$$

A similar approach applied to an observed γ transition of pure multipolarity leads to conversion factors of the type C_ν' which transform the a_ν from those for a given spin sequence involving pure multipolarity L to those for the same sequence but different pure multipolarity L'. Such factors, which we distinguish from the normal C_ν by the superscript $(L\rightarrow L')$, take the form

$$C_\nu^{(L\rightarrow L')}=\frac{F_\nu(L'L'J_fJ_i)}{F_\nu(LLJ_fJ_i)}=\frac{M(L'L')}{M(LL)}$$

$$=\frac{(\hat{L}')^2}{(\hat{L})^2}\cdot\frac{\langle\nu0\mid L'L'1-1\rangle}{\langle\nu0\mid LL1-1\rangle}\cdot\frac{W(L'L'J_iJ_i;\nu J_f)}{W(LLJ_iJ_i;\nu J_f)}. \quad (56)$$

These $C_\nu^{(L\rightarrow L')}$ do not depend upon the spins of levels other than those between which the transition is observed. However, the range of ν is dictated by selection rules which involve extraneous spins. The $C_\nu^{(L\rightarrow L')}$ are normalized to unity for $\nu=0$; when $\nu>0$, they can take on numerically simple values. An instance is furnished by the spin sequence $\frac{1}{2}^+\rightarrow J_1\pi_1\cdots\rightarrow\frac{3}{2}^+\rightarrow\frac{1}{2}^+$, for which the $\alpha_{i\nu}$ are listed in Table X of Appendix A. The values of the latter are given for pure $M1$ multipolarity, since those for $E2$ γ radiation are numerically the same: with ν curbed to $\nu=0$, 2 we find that

$$C_0^{(M1\rightarrow E2)}=1; \qquad C_2^{(M1\rightarrow E2)}=\frac{F_2(22\frac{1}{2}\frac{3}{2})}{F_2(11\frac{1}{2}\frac{3}{2})}=-1. \quad (57)$$

Thus the $E2$ distribution has identically the same form as the $M1$ except that it is inverted about the line $d\sigma/d\Omega_2=a_0$. On the other hand, for an observed $\frac{3}{2}^+\rightarrow\frac{3}{2}^+$ γ transition, with the same restriction upon the range of ν, we obtain multipole conversion factors from $M1$ to $E2$ radiation which have the values $C_0^{(M1\rightarrow E2)}=1$, $C_2^{(M1\rightarrow E2)}=0$. It accordingly follows that the distribution of pure $E2$ radiation effecting the transition $\frac{3}{2}^+\rightarrow\frac{3}{2}^+$ or $\frac{3}{2}^-\rightarrow\frac{3}{2}^-$ is isotropic. However, for an observed $\frac{5}{2}^+\rightarrow\frac{3}{2}^+$ γ transition, the appropriate $M1\rightarrow E2$ multipole conversion factors are $C_0^{(M1\rightarrow E2)}=1$, $C_2^{(M1\rightarrow E2)}=-0.51020$ and terms with $\nu=4$ now have to be evaluated. Similarly, for an observed $3^+\rightarrow2^+$ transition, we have $C_0^{(M1\rightarrow E2)}=1$, $C_2^{(M1\rightarrow E2)}=-0.35714$ and new $\nu=4$ terms.

In the case of multipolarity conversion $L\rightarrow L'$ in an *unobserved* transition (followed by a given observed γ transition), the factors are

$$C_\nu^{(L\rightarrow L')}=\frac{U_\nu(L'L'J_iJ_i')}{U_\nu(LLJ_iJ_i')}=\frac{U(L'L')}{U(LL)}$$

$$=(-)^{L-L'}\frac{W(J_iJ_iJ_i'J_i';\nu L')}{W(J_iJ_iJ_i'J_i';\nu L)}, \quad (58)$$

with $C_0^{(L-L')}=1$ again.

D. Automatic Computation of Angular Distributions

The ALGOL code "MANDY" for a fast computer (e.g., CDC 1604-A) was compiled independently of existing Hauser–Feshbach programs (such as that of Wills, and its modifications[5]) to attain the widest degree of flexibility in application and to serve thereafter as a basis for a general CN *correlation* code "BARBARA" of greater complexity, going beyond the confines of the present publication. Both programs are designed to handle arbitrarily high angular momenta, arbitrary values of nuclear spin (integer and half-integer), and γ radiation (at will, preceded by an unobserved mixed transition) of mixed multipolarity. Results are automatically furnished not only for a specified multipole mixture (using δ from input data) but also for $\delta=0$.

The input data for "MANDY," apart from specification of various options which steer the course of calculation, is in the simplest instance confined to statement of nuclear spins and parities, $J_0\pi_0$, $J_2\pi_2$, $J_3\pi_3$ (and $J_4\pi_4$ if relevant), the γ multipolarities L_2, L_2' with requisite mixing ratio δ_2 (and L_3, L_3', δ_3 if needed), and the nucleon orbital momentum cutoff limits $l_{1\,\max}$, $l_{2\,\max}$. In this instance the code will effect automatic tabulation

[24] R. W. Benjamin, Ph.D. thesis, University of Texas, 1965 (unpublished), and private communication.

[25] I. L. Morgan, J. B. Ashe, D. O. Nellis, R. W. Benjamin, S. C. Mathur, W. E. Tucker, O. M. Hudson, and P. S. Buchanan, Annual Progress Report, Nuclear Physics Laboratory, Texas Nuclear Corporation, August 1964 (unpublished).

CC-0. In Public Domain. Gurukul Kangri Collection, Haridwar

Digitized by Arya Samaj Foundation Chennai and eGangotri

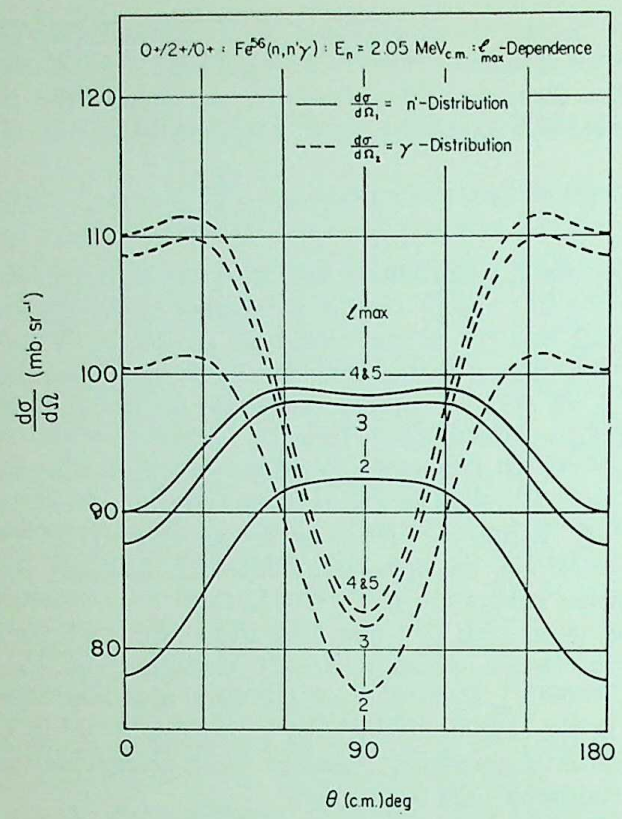

FIG. 3. Dependence of the absolute nucleon and γ distributions upon the orbital momentum cutoff l_{max}, illustrated by inelastic neutron scattering on Fe^{56} at 2.05 MeV. In this case, the distribution *structure* experiences no appreciable change as the number of partial waves is increased, and the magnitude attains its ultimum value at $l_{max}=4$.

(bearing in mind Racah and conservation restrictions) and evaluation of the Legendre polynomial series restricted expansion coefficients $\alpha_{i\nu}$, as relevant to the species of distribution under consideration (viz., N', γ, γ–γ or, at will, both nucleon *and* γ distributions consecutively). In each instance the Racah functions which make up the appropriate distribution expressions are evaluated in subroutines.

The above is usually extended to proceed further to numerical evaluation of absolute and normalized angular distributions, together with print-out of absolute and normalized expansion coefficients a_ν and $a_\nu{}^* \equiv a_\nu/a_0$, respectively. Since $a_\nu = \sum_i \alpha_{i\nu}\tau_i$, the latter Legendre expansion coefficients depend through the τ_i upon the transmission coefficients $T_l^{(\pm)}$ and thus upon the choice of optical potential, unlike the potential-independent restricted coefficients $\alpha_{i\nu}$. Apart from necessary changes in options, additional input data has to be supplied for subroutine automatic evaluation of the τ_i and thence of the differential cross sections $d\sigma/d\Omega_1$ or $d\sigma/d\Omega_2$ (or both) in mb sr^{-1}, and normalized distributions $W(\theta_1)$ or $W(\theta_2)$ (or both) such that $W(90°)\equiv 1$. These additional input data comprise incident and emergent particle energies E_1 and E_2 in the center-of-mass system, the angular interval $\Delta\theta$ for which the distribution is to be evaluated [because of symmetry about 90°, the CN distribution is evaluated over the range $0°(\Delta\theta)90°$] and four sets of transmission coefficients, the first pair of sets, $T_0, \cdots, T_{l_1max}{}^{(-)}$, $T_0, \cdots, T_{l_1max}{}^{(+)}$ referring to the incident channel $J_0 \rightarrow J_1$ and the second pair, $T_0', \cdots, T_{l_2max}{}^{(-)'}$, $T_0', \cdots, T_{l_2max}{}^{(+)'}$ to the emergent channel $J_1 \rightarrow J_2$. If spin–orbit interaction is neglected, the $T_l{}^{(-)}$ and $T_l{}^{(+)}$ are mutually identical. If the possibility of CN decay through additional exit channels is to be taken into account (resulting in a marked influence upon the τ_i values and thence upon the cross section), the number of extra channels has to be specified through a final option, and the relevant sets of transmission coefficients appended to the input data.

5. INFLUENCE OF HIGHER PARTIAL WAVES UPON ANGULAR DISTRIBUTIONS

Computer calculations in which the orbital momentum limit l_{max} was increased stepwise have confirmed that the partial-wave cutoff at $l_{max}=2$ adopted by some authors in order to curb the complexity of their hand calculations represents too restrictive a condition. Incorporation of the influence of higher partial waves not only results in an increase in the magnitude of the differential cross section, as illustrated in Fig. 3, but can perceptibly change the distribution structure.

Figure 3 shows results[26] for the Fe^{56} $(n, n'\gamma)$ reaction at 2.05 $MeV_{c.m.}$ using a partial wave cutoff l_{max}, which ranges from 2 to 5. Each curve, as computed using generalized Perey–Buck transmission coefficients $T_l{}^{(\pm)}$, is indistinguishable from that for the averaged coefficients T_l. The figure indicates that at low energies partial waves having momenta $l>4$ exert no appreciable influence upon the magnitude or structure of angular distributions. The slight dip in the neutron distribution around 90°, as occasioned by the influence of the a_4 Legendre expansion coefficient, becomes evident only when orbital momenta higher than $l=2$ are taken into account.

This effect is illustrated still more vividly in the proton distributions to the first 2^+ level of Ni^{60} in Fig. 4. Here the higher partial waves induce relative augmentation of the a_4 with the result that the dip around 90° becomes progressively more apparent.

6. INFLUENCE OF MULTIPOLE MIXING RATIOS

Quantitative evaluation of the effect upon the γ distribution on varying the mixing ratio δ for various different spin sequences, using the code "MANDY," has indicated that marked sensitiveness may be found

[26] In Ref. 17, the left-hand scale of Fig. 43 is numerically wrong; it should be multiplied by 25. The curve for $l\leqq 4$ in the figure should be displaced to tally with that for $l\leqq 5$. An unfortunate error in Fig. 18 of Ref. 17 has also come to light: the experimental points for $\theta_2=30°$ should be interchanged with those for $\theta_2=90°$, thereby yielding somewhat better agreement with the theoretical correlation curves, which have been correctly drawn and captioned. Also, in Eq. (153), the factor $(8\pi)^{\frac{1}{2}}\sigma^3$ should be deleted.

CC-0. In Public Domain. Gurukul Kangri Collection, Haridwar

Digitized by Arya Samaj Foundation Chennai and eGangotri

among odd-mass as well as even-mass nuclei. Figure 5 depicts the case of a

$$\tfrac{1}{2}+\longrightarrow J_1\pi_1\longrightarrow\tfrac{3}{2}+\xrightarrow[M1+E2]{}\tfrac{1}{2}+$$

transition sequence as evaluated for the inelastic scattering of 2-MeV neutrons on Si^{29}. The striking inversion of structure for $\delta=+3.4$ (a value taken from Ref. 27) is immediately evident upon comparison with curves for alternative values proposed in the past. The intersection of all γ distributions around $\theta_2=55°$ and 125° is a consequence of their structure being of the form

$$d\sigma/d\Omega_2=a_0+a_2P_2(\cos\theta_2), \qquad (59)$$

since higher orders in ν are ruled out by the condition $\nu\leq 2J_2=2\times\frac{3}{2}$. The δ-dependence, which thus reposes solely in the coefficient a_2 (the term a_0 is simply a constant), is rendered ineffective at the two angles for which the second-order Legendre polynomial P_2 is zero. In the case of comparison with relative, rather than absolute, measurements these special angles would represent suitable points for normalization. That the *neutron* distribution, whose form is given by

$$d\sigma/d\Omega_1=a_0+a_2P_2(\cos\theta_1)+a_4P_4(\cos\theta_1), \qquad (60)$$

also appears to pass through the points of coincidence is because of the negligibly small value of a_4 which obtains in this case and the equality of the terms a_0 for nucleon and γ distributions in the same spin sequence.

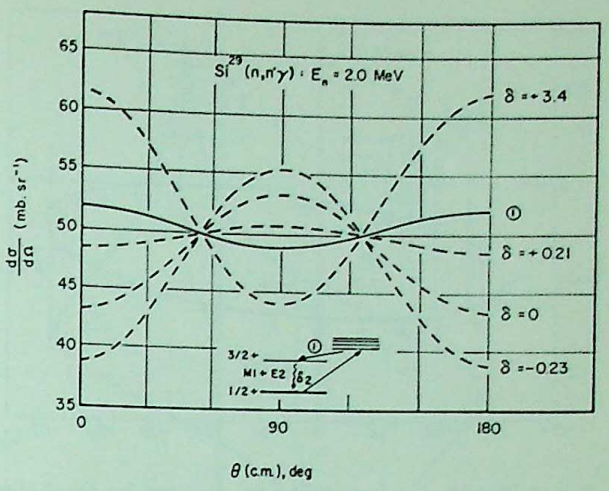

FIG. 5. Different distributions associated with different values of the mixing ratio δ in the case of de-excitation radiation of mixed $M1+E2$ multipolarity following inelastic scattering of 2-MeV neutrons on Si^{29}. The curves intersect around 55° and 125° because the δ dependence in the weighting coefficient a_2 of the second-order Legendre polynomial $P_2(\cos\theta)$ is suppressed by the vanishing of P_2 at the above angles. The intersection of the neutron distribution ① also approximately coincides with these angles because the value of a_4 is here too small to exert any appreciable influence. Of the numerical values of δ depicted in the figure, which were taken from various publications, the most likely are −0.23 or +3.4 (Ref. 27).

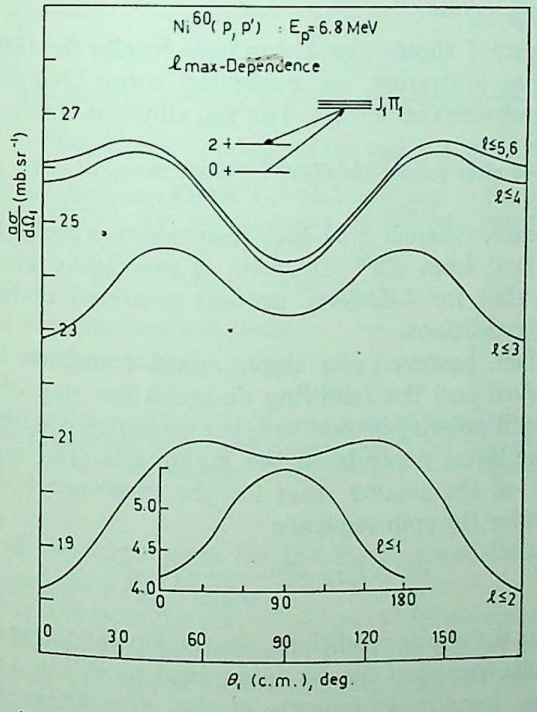

FIG. 4. An analogous orbital momentum dependence to that of Fig. 3, and for the same spin sequence, but for inelastic proton scattering on Ni^{60} at 6.8 MeV. Attention is drawn to the change in structure as higher partial waves are taken into consideration, causing the dip at 90° to become progressively more pronounced. The figure in the insert shows that the distribution for the unrealistically low momentum cutoff at $l_{max}=1$ displays no indication of a dip, since terms with ν higher than 2 are absent.

Radioactive decay processes have provided the main basis for experimental elucidation of a γ transition's multipole character through studies of γ–γ angular correlations, whose sensitivity to the multipole mixing ratio generally enables the latter to be established within fairly narrow limits. Since statistical reaction theory makes definite predictions for an $(N, N'\gamma)$ angular distribution as a function of δ, comparison of experimental least-squares-fit values of a_2^* and a_4^* (where $a_\nu^*\equiv a_\nu/a_0$) with the range of values given by theory enables δ to be established together with its (fairly narrow) error limits. For an $(N, N'\gamma)$ process in which no unobserved γ transitions intervene before the observed γ distribution, the locus of points associated with δ's ranging from 0 to ∞ and of positive or negative phase is an ellipse in which points for δ's of the same magnitude but opposite sign have the same ordinate. The zone within this representation described by the values and error limits of a_2^* and a_4^* which give the least-squares fit to the experimental γ distribution defines the value of δ for the observed transition.

It has recently been shown that γ distributions from inelastic nucleon scattering can also be utilized. Sen Gupta and Van Patter have investigated $(p, p'\gamma)$

[27] D. A. Bromley, H. E. Gove, E. B. Paul, A. E. Litherland, and E. Almqvist, Can. J. Phys. **35**, 1042 (1957); G. J. McCallum and A. E. Litherland, Bull. Am. Phys. Soc. **5**, 56 (1960).

CC-0. In Public Domain. Gurukul Kangri Collection, Haridwar

Digitized by Arya Samaj Foundation Chennai and eGangotri

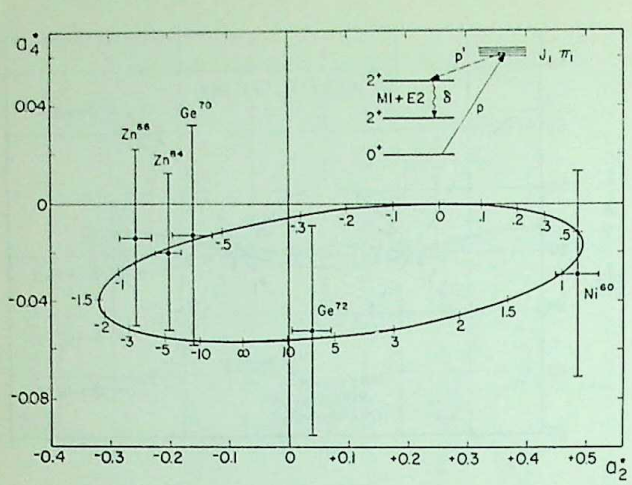

FIG. 6. Experimental results for $(p, p'\gamma)$ angular distributions of $2_2^+ \rightarrow 2_1^+$ transitions compared with the theoretical δ ellipse plotted in a_4^* vs a_2^* space. The theoretical predictions for the various nuclei do not differ by more than 3% from the average δ ellipse shown. The points for Ni^{60}, Zn^{66}, and Zn^{68} are the average of four measurements with $E_p = 4.42$ to 5.42 MeV (Ref. 28), while the points for Ge^{70} and Ge^{72} are the averages of two measurements at 5 and 6 MeV (Ref. 29).

reactions on Ni^{60}, Zn^{64}, and Zn^{66} involving the $2_2^+(M1+E2)2_1^+(E2)0_1^+$ transitions.[28] Their results, together with more recent measurements[29] for Ge^{70} and Ge^{72}, are summarized in Fig. 6. Each point represents the average of two or more angular distributions, which have been averaged to reduce effects due to level density fluctuations.

In Fig. 6, the a_4^* scale is expanded by a factor of 4 relative to the a_2^* scale in order to separate the two branches $(\pm)$ of δ values. The present accuracy of the experimental measurements is not sufficient to distinguish between these branches, since these a_4^* values have a typical uncertainty of about ± 0.04, which is comparable with the separation of the two branches of the ellipse. In fact, the precision of these present measurements may well be limited by the presence of fluctuations in level densities.

From presently available knowledge of measured δ values for $2_2^+ \rightarrow 2_1^+$ transitions in medium-weight nuclei, values roughly within the region $-3 < \delta < 3$ are expected. Accordingly, it is assumed that values of δ from the lower side of the δ-ellipse should be taken in accord with the experimental limits for a_2^*. This procedure yields δ values for Zn^{66} and Ge^{72} in reasonable agreement with those measured in radioactivity studies,[30] while in the case of Zn^{64} and Ge^{70}, no previous determinations have been made. The Ni^{60} value indicates an anomalously large $M1$ component, in distinct disagreement with one earlier radioactivity measurement, but probably in good agreement with new preliminary results[31] for the Cu^{60} decay.

At higher proton bombarding energies, the possibility arises that the second 2^+ level may be fed by transitions from higher levels: e.g., in the case of Ni^{60}, there is a feeding from the 2.63-MeV 3_1^+ state to the 2.16-MeV 2_2^+ state. Unless an appropriate correction is applied, this could cause a systematic error in the δ determination by this method. If the $2_2^+ \rightarrow 0_1^+$ transition is sufficiently prominent to permit an accurate angular distribution measurement, then a second procedure may be employed. This involves the measurement of the ratio $a_2^*(2_2^+ \rightarrow 2_1^+)/a_2^*(2_2^+ \rightarrow 0_1^+)$, which is independent of the magnetic substate populations for this 2_2^+ state and hence avoids our usual assumption of compound nucleus formation. This method is equivalent to taking the ratio of a_2^* values from two γ–γ angular correlations in a radioactive decay, which is ordinarily not necessary since in this case each correlation may be used independently. Using this second procedure, Mohindra and Van Patter[29] have recently determined δ values for Ni^{60}, Ge^{70} and Ge^{72}. This procedure was implied in the discussion of ellipse II in the paper of Sen Gupta and Van Patter.[28]

Figure 7 shows new theoretical results for inelastic neutron scattering, as evaluated using Perey-Buck transmission coefficients. The top ellipse is that for a

$$0^+ \rightarrow J_1\pi_1 \rightarrow 2^+ \xrightarrow[M1+E2]{} 2^+$$

sequence, wherein 2.37-MeV neutrons are inelastically scattered from Zn^{66}. Its form is practically identical with that for 4.82-MeV protons scattered under the same conditions.

When, however, the above mixed transition is unobserved and the following de-excitation step of pure $E2$ multipolarity is observed, the measured distribution of the latter depends on the magnitude (but not the sign) of the mixing ratio for the unobserved decay. Thus for the spin sequence

$$0^+ \rightarrow J_1\pi_1 \rightarrow 2^+ \xrightarrow[M1+E2]{} 2^+ \xrightarrow[E2]{} 0^+$$

under the above conditions, the multipole mixing of the penultimate step can be determined to within a phase factor from measurements of the distribution of the final $E2$ γ radiation. Results for different δ's now lie on a line in the a_2^*/a_4^* representation, points for δ's of equal magnitude but opposite sign being coincident since the U_ν term for the unobserved step involves only δ^2 [see Eq. (30)]. For a process in which not only the intermediate (unobserved) step but also the fina

[28] A. K. Sen Gupta and D. M. Van Patter, Phys. Letters **3**, 355 (1963); Nucl. Phys. **50**, 17 (1964); A. K. Sen Gupta, P. N. Trehan, and D. M. Van Patter, Bull. Am. Phys. Soc. **7**, 81 (1962).

[29] R. K. Mohindra and D. M. Van Patter, Bull. Am. Phys. Soc. **10**, 38 (1965); Phys. Rev. **139**, B274 (1965).

[30] A. Schwarzschild and L. Grodzins, Phys. Rev. **119**, 276 (1960); R. B. Arns and M. L. Wiedenbeck, Phys. Rev. **112**, 229 (1958).

[31] G. T. Wood and S. M. Shafroth, Topical Conference on *Bases for Nuclear Spin Parity Assignments*, Gatlinburg, abstract B10 (1965).

CC-0. In Public Domain. Gurukul Kangri Collection, Haridwar

Digitized by Arya Samaj Foundation Chennai and eGangotri

(observed) transition are of mixed multipolarity, the locus of points for different values of δ_2 but a fixed value of δ_2 again becomes an ellipse.

Though the δ ellipse representation offers a large amount of information in compact form, particularly when ellipses (and point "ellipses") for several sequences are depicted conjointly for comparison, as has been done by Van Patter and Mohindra,[32] certain features are brought out more clearly by the alternative representation of $|\delta|$ separately against a_2^* and a_4^* (a representation employed in studies of radioactive γ decay). By way of contrast with the preceding, direct

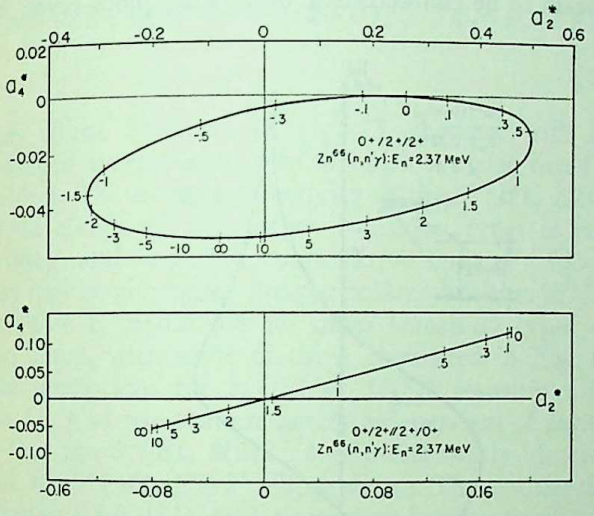

FIG. 7. Theoretical predictions for the variation of a_4^* vs a_2^* for the entire range of values of multipole mixing ratio δ in the case of inelastic scattering of 2.37-MeV neutrons to the second level (2^+) of Zn^{66}. The loci of points for different values of δ form an ellipse for the spin sequence

$$0^+ \longrightarrow J_1\pi_1 - - - \rightarrow 2_2^+ \xrightarrow[M1+E2]{} 2_1^+,$$

but a straight line for the sequence

$$0^+ \longrightarrow J_1\pi_1 - - - \rightarrow 2_2^+ - - - \rightarrow 2_1^+ \xrightarrow[E2]{} 0^+,$$

since in the latter instance only even-powered terms in ν enter into the calculation which also causes points for positive and negative δ phases to coincide. The symbol $- - - \rightarrow$ denotes an unobserved transition.

plots of the latter type for the above transitions are given in Figs. 8 and 9.

Figure 8 depicts the plot of $|\delta|$ vs a_2^* for an observed mixed transition (curves No. 1) from the second to the first level, contrasted with the curve (No. 2) for the same transition, but now unobserved, followed by a pure observed ground-state transition. The latter curve is of altogether different character, symmetric about the δ origin, where a_2^* is maximal (positive). The symmetry ensues from the fact that the second transition is pure quadrupole, and δ for the first transition is of even order in the distribution expression. In the plots of $|\delta|$ vs a_4^*, as depicted in Fig. 9, this symmetry about

[32] D. M. Van Patter and R. K. Mohindra, Phys. Letters 12, 223 (1964).

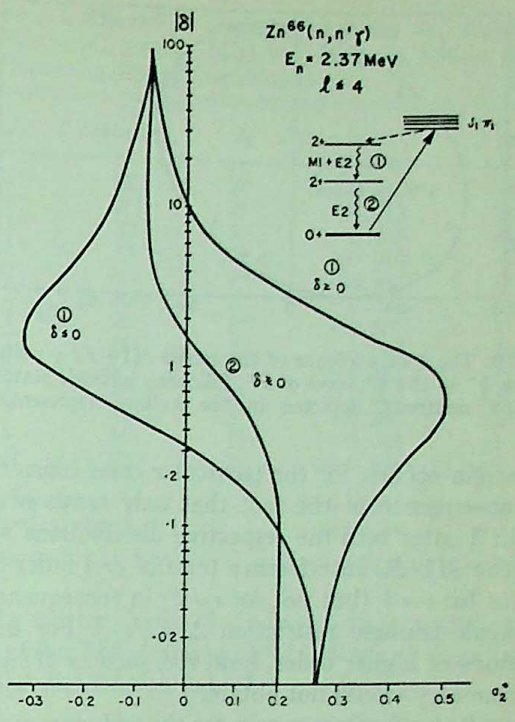

FIG. 8. The same data as contained in Fig. 7, but depicted in the alternative representation of δ vs a_2^*, showing characteristic symmetry with respect to positive and negative phases of δ.

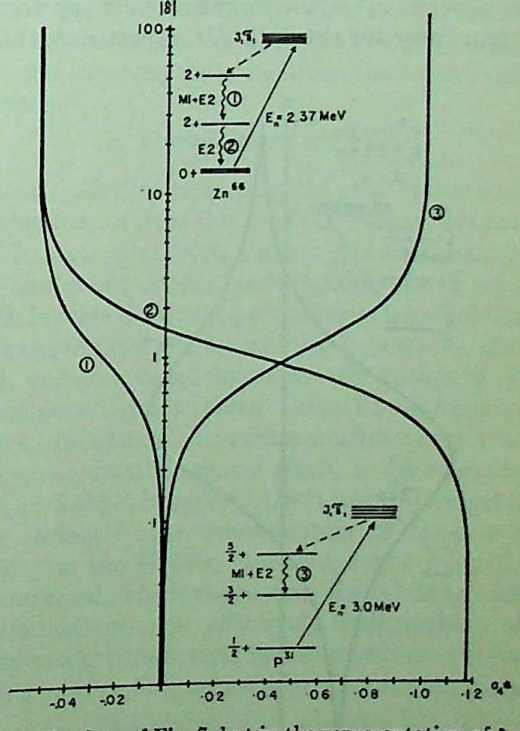

FIG. 9. The data of Fig. 7, but in the representation of δ vs a_4^*, which complements Fig. 8. Also shown is the theoretical result for the half-integer spin sequence

$$\tfrac{1}{2}^+ \longrightarrow J_1\pi_1 - - - \rightarrow \tfrac{5}{2}^+ \xrightarrow[M1+E2]{} \tfrac{3}{2}^+$$

as exemplified by inelastic scattering of 3-MeV neutrons on P^{31}.

CC-0. In Public Domain. Gurukul Kangri Collection, Haridwar

Digitized by Arya Samaj Foundation Chennai and eGangotri

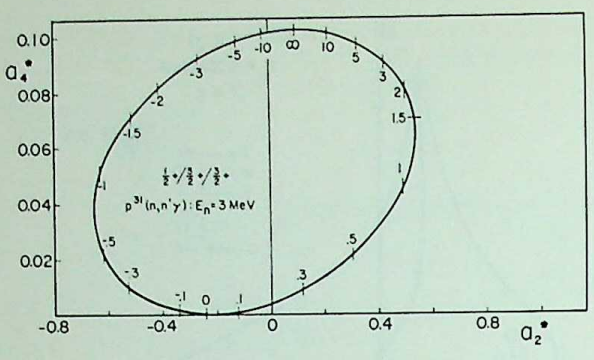

FIG. 10. The δ dependence of the mixed $M1+E2$ γ radiation from the $\frac{5}{2}^+$ to the $\frac{3}{2}^+$ level of P^{31}, following inelastic scattering of 3-MeV neutrons, depicted in the δ-ellipse representation.

the δ origin occurs, for the particular cases considered, as a consequence of the fact that only terms of *even* order in δ enter into the respective distributions when $\nu=4$ [the $M1$–$E2$ interference term of *first* order in δ_2 vanishes for $\nu=4$ (but not for $\nu=2$) in consequence of the Racah triangle restriction $\Delta(LL'\nu)$]. For mixed transitions of higher order, however, such as $M2+E3$, this symmetry would not obtain.

Figure 9 also displays results for the odd-mass nucleus P^{31}, which involves the half-integer spin sequence

$$\tfrac{1}{2}^+ \longrightarrow J_1\pi_1 \longrightarrow \tfrac{5}{2}^+ \xrightarrow[M1+E2]{} \tfrac{3}{2}^+.$$

This differs from that above by being confined to *positive* values of a_4^* whose magnitudes are appreciably larger than those for the $0^+/2^+/2^+$ sequence. Again, as

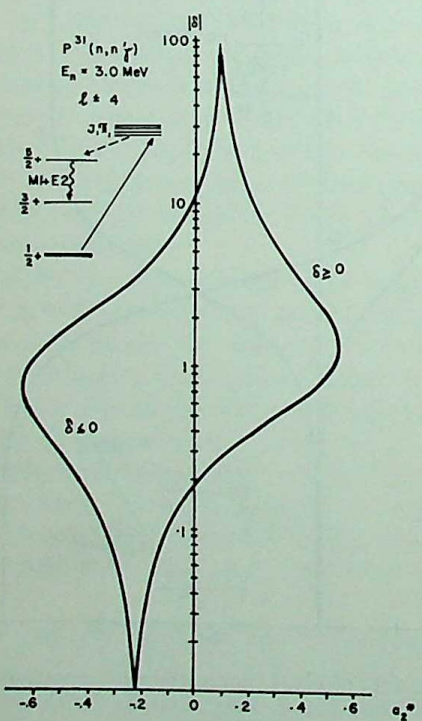

FIG. 11. Plot of δ vs a_2^* for a mixed $M1+E2$ γ transition from the second level ($\frac{5}{2}^+$) to the first level ($\frac{3}{2}^+$) of P^{31} at E_n=3.0 MeV. This complements curve No. 3 shown in Fig. 9 and presents the data of Fig. 10 in alternative form.

follows from symmetry considerations, the points for $\delta=0$ and ∞ correspond with extremal values of a_4^*. Figure 10 shows the δ dependence for this half-integral spin sequence in the elliptical representation, while Fig. 11 depicts the same data plotted directly against a_2^*, for comparison with Fig. 8.

In the case of a sequence such as $\frac{1}{2}^+ \longrightarrow J_1\pi_1 \cdots\cdots\longrightarrow \frac{3}{2}^+ \longrightarrow \frac{1}{2}^+$, for which $a_4^*=0$, the δ ellipse representation cannot be employed. Hence direct plots of δ vs a_2^* for Si^{29} are shown in Fig. 12.

This latter representation truly comes into its own when nuclear states of spin 1 or $\frac{3}{2}$ experience mixed multipole γ decay. The slightly asymmetric structure appears to be characteristic of δ vs a_2^* plots (even for

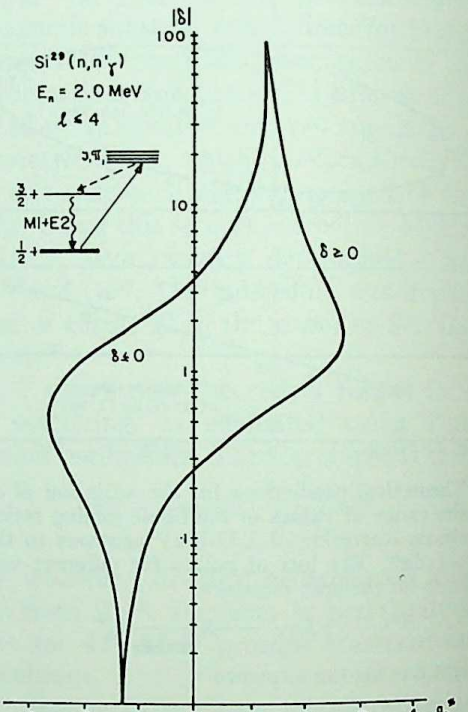

FIG. 12. Plot of δ vs a_2^* for a $\frac{3}{2}^+ \longrightarrow \frac{1}{2}^+$ γ transition of mixed $M1+E2$ multipolarity following inelastic scattering of 2-MeV neutrons to the first level of Si^{29}.

sequences when the a_4^* are nonzero), as follows from comparison with Figs. 8 and 11, and a further common feature is revealed on examining the δ values for which a_2^* is maximal, a situation which corresponds with the distributions essentially having maximal amplitude. Throughout, one finds maximal positive a_2^* when $\delta\approx 1.4$, indicating distributions to have maximal amplitude (forming a dip at 90°) when the $E2$ intensity admixture in mixed radiation is double that of $M1$ (with the relative phase positive). Maximal *negative* values of a_2^* (distributions peaking at 90°) occur at negative δ's varying between -0.56 and -1.45, and accordingly do not display so striking a uniformity as that for positive $(a_2^*)_{max}$. Whereas Fig. 12 refers to de-excitation of the first level, Figs. 8 and 11 are concerned with transitions from the second to the first level.

CC-0. In Public Domain. Gurukul Kangri Collection, Haridwar

Digitized by Arya Samaj Foundation Chennai and eGangotri

In general, levels of even nuclei with $J_2 \leqq 4$ have a substantial decay to the first 2^+ state. Recent calculations have revealed that in such instances transitions of the type $3(D, Q)2$ have the largest sensitivity to the $E2/M1$ mixing ratio.[32] In the case of (p, p') excitation of a 2.63-MeV state in Ni^{60} with 5.92-MeV protons, the calculated $3^+(E2)2^+$ angular distribution is given by

$$W(\theta_2)=1+0.092P_2(\cos\theta_2)+0.225P_4(\cos\theta_2). \quad (61)$$

A substantial contribution (43%) still originates from the $l_1=2$, $l_2=0$ term. The δ ellipse for a $3^+(M1, E2)2^+$ transition is generated by the conversion factors:

$$C_2=(-2.8+15.336\delta+\delta^2)/(1+\delta^2); \qquad C_4=\delta^2/(1+\delta^2). \quad (62)$$

This ellipse is shown in Fig. 13, together with the averaged experimental results which are also listed in Table I. The extreme sensitivity of the $3^+(M1, E2)2^+$ ellipse compared with other transition types is very striking, and in fact a conservative limit of $|\delta|>30$ may now be given[29] for this particular transition in Ni^{60}. In Table I, predictions for other transition types are also given, with some of them illustrated in Fig. 13. The predictions for $3(D)2$ or $3(Q)2$ transitions for this $(p, p'\gamma)$ reaction are nearly independent of parity, so that the $3^-(E1, M2)2^+$ δ ellipse is nearly identical with the $3^+(M1, E2)2^+$ ellipse shown. The angular distributions for $1(D, Q)2$ transitions are confined to a small region on the a_2* axis, all corresponding to near isotropy. It may thus be very difficult to identify transitions of this type by this method. Fortunately, as Day and Walt[18] have pointed out, spin-1 levels can be recognized on the basis of angular distributions of their $1(D)0$ ground-state transitions, which differ markedly from those for levels of spins 2 or 3. Transitions of this $1(D)0$ type have been recently identified in Fe^{56} (3.45 MeV) on the basis of $(n, n'\gamma)$ angular-distribution data of Benjamin[24] and in Ni^{60} (3.19 MeV) from $(p, p'\gamma)$ angular-distribution data.[29]

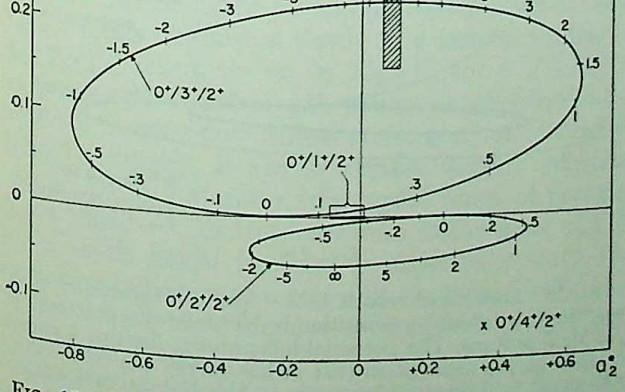

FIG. 13. Theoretical predictions for various transition types for the $(p, p'\gamma)$ angular distribution of a 2.63→2.16-MeV transition in Ni^{60}. The average result of three angular distribution measurements (Ref. 32) is represented by the cross-hatched area.

TABLE I. Theoretical predictions for the $(p, p'\gamma)$ angular distribution of a 2.63→2.16-MeV transition in Ni^{60} at $\bar{E}_p=5.92$ MeV, assuming different transition types.

J_2	Transition	J_3	a_2*	a_4*
0^+	$E2$	2^+	0	0
1^+	$M1$	2^+	−0.013	0
1^+	$E2$	2^+	−0.063	0
1^-	$E1$	2^+	−0.010	0
2^+	$M1$	2^+	+0.245	0
2^+	$E2$	2^+	−0.075	−0.052
2^-	$E1$	2^+	+0.201	0
2^-	$M2$	2^+	−0.062	−0.008
3^+	$M1$	2^+	−0.257	0
3^+	$E2$	2^+	+0.092	+0.225
3^-	$E1$	2^+	−0.246	0
3^-	$M2$	2^+	+0.088	+0.183
4^+	$E2$	2^+	+0.366	−0.120
Experimental weighted average			+0.084 ±0.024	+0.191 ±0.036

7. LIMITING ANGULAR DISTRIBUTIONS

It is possible to make some general predictions regarding the behavior of $(n, n'\gamma)$ angular distributions near the threshold for excitation of a particular level. These are based on the expectation that for incident neutron energies sufficiently close to threshold, the (n, n') cross section for that level will be dominated by terms involving penetrabilities for s-wave outgoing neutrons.

a. Transitions from 2^+ Levels

A particularly simple example of a limiting angular distribution involves the $2^+(E2)0^+$ transition from the first 2^+ state of an even nucleus. We shall focus attention on the properties of terms of the type τ [Eq. (13)], which involve dominant partial-wave combinations. In this case, the two τ terms with $l_2=0$ (s wave) also have $l_1=2$, and correspond to d-wave excitation of $\frac{3}{2}^+$ and $\frac{5}{2}^+$ compound states. From Table VI of Appendix A, the contributions of these compound states to the overall angular distribution are given by $[4+2P_2(\cos\theta)]$ and $[6+3.428P_2(\cos\theta)-3.428P_4(\cos\theta)]$, respectively. Near threshold, the denominators of these τ terms [which are the Hauser–Feshbach sums $\sum_{lJE} T_l(E)$] are also equal, which means that the predicted angular distributions become effectively independent of the optical-model parameters. The sum of these two contributions yields a limiting angular distribution given by

$$W(\theta_2)=1+0.5428P_2(\cos\theta_2)-0.3428P_4(\cos\theta_2), \quad (63)$$

which has an angular asymmetry $W(0°)/W(90°)$ of 2, as shown on the right of Fig. 14. We therefore expect experimental $(n, n'\gamma)$ angular distributions to approach this model-independent limit near threshold.

CC-0. In Public Domain. Gurukul Kangri Collection, Haridwar

Digitized by Arya Samaj Foundation Chennai and eGangotri

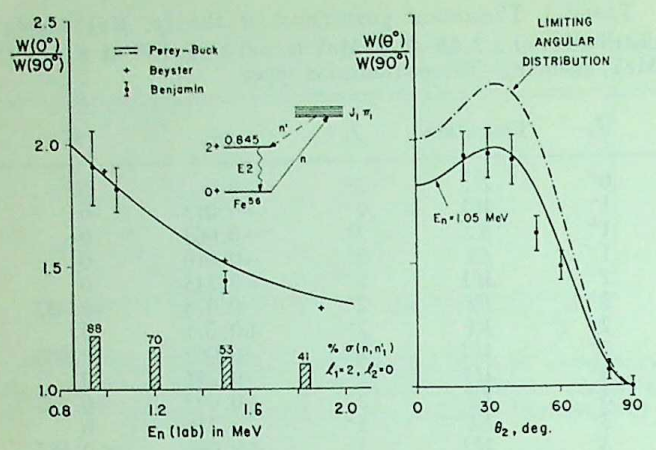

FIG. 14. Variation of the asymmetry in the distributions of γ rays following scattering of neutrons to the first level (2^+) of Fe^{56} as the incident neutron energy is increased from the threshold value of 0.85 to 2 MeV. Results of calculations employing Perey–Buck and Beyster penetrabilities are compared with recent measurements by Benjamin (Refs. 24, 25). On the lower left, the percentage contribution to the (n, n_1') cross section is shown for the partial wave combination which dominates at threshold. On the right, Benjamin's angular distribution data is shown to be slightly less anisotropic than the predicted limit, in accord with calculation for an energy slightly above threshold.

Despite the present paucity of relevant experimental data, this prediction has now been clearly verified by recent measurements of Benjamin[24,25] which included some $(n, n'\gamma)$ angular distributions near the threshold for the 0.845-MeV first 2^+ state of Fe^{56}. The experimental conditions (neutron energy spread of 70 keV) were evidently satisfactory for adequate statistical averaging. The observed distributions for $E_n(\text{lab})=0.95$ and 1.05 MeV were nearly identical to the limiting case (63), with asymmetries only slightly less than 2. The experimental asymmetries shown on the left of Fig. 14 have been estimated by extrapolating the forward angle data ($\theta \leqq 40°$) to 0° in a manner consistent with theory. An alternative procedure would be to employ least-squares analyses, which should yield asymmetries lying within the range of the indicated error bars.

Calculations using Perey–Buck penetrabilities predict a rapid decrease in the angular asymmetry above threshold, despite the fact that the percentage contribution to the inelastic cross section of the two $T_2 \cdot T_0'$ terms decreases rather slowly. (For brevity, we add a prime to penetrabilities that refer to outgoing channels.) This dropoff is primarily caused by the increased influence of τ terms of the types $T_1 \cdot T_1'$ and $T_2 \cdot T_2'$, both of which are associated with much smaller asymmetries. The form of this dropoff is very nearly model-independent for Fe^{56}, as revealed in Fig. 14 by the similarity in predicted asymmetries using Beyster penetrabilities, and therefore should be insensitive to effects due to fluctuations of level widths. At $E_n=1.05$ MeV (roughly 0.2 MeV above threshold), the extent of this dropoff is clearly revealed by the angular distribution data shown on the right of Fig. 14, which is less anisotropic than the limiting case. At higher energies, the asymmetry is expected to level off gradually, in agreement with Benjamin's data for $E_n=1.5$ MeV, as well as with the earlier results of Day and Walt[18] at 2.56 MeV, in which an asymmetry close to 1.3 was observed.

This limiting angular distribution (63) has in fact a wider application. It should also be approached near threshold for ground-state transitions from second 2^+ states, since the denominators of the $J_1=\frac{3}{2}^+$ and $\frac{5}{2}^+$ terms will still remain equal (if terms involving $l_2=4$ to the first 2^+ state are negligible). A lower-lying 4^+ state should not appreciably influence this equality. For higher 2^+ states, one expects in general that contributions from final states with different J, π will effect an inequality in the denominators of these two τ terms, thereby altering the limiting angular distribution to some extent. However, the limiting angular asymmetry *will remain* 2, since each of the angular contributions from $J_1=\frac{3}{2}^+$ or $\frac{5}{2}^+$ has $W(0°)/W(90°)=2$. This statement applies equally well to the two contributions from $J_1=\frac{3}{2}^-$ or $\frac{5}{2}^-$ for a 2^- level. One therefore expects that every spin-2 level will exhibit a similar behavior of the $2^+(E2)0^+$ angular asymmetry near threshold, which should approach a limiting value of 2, and decrease rapidly above, the rate being accentuated for nuclei near a p-wave resonance of the optical model.

Another transition of general interest is the $2^+(M1, E2)2^+$ γ decay, particularly from the second 2^+ level. By application of the appropriate conversion factor C_ν as given by Eq. (48), the limiting angular distribution for this mixed transition is

$$W(\theta_2)=1+(1+\delta^2)^{-1}(0.38+1.112\delta-0.1163\delta^2)P_2(\cos\theta_2) - (1+\delta^2)^{-1}\times 0.0979 P_4(\cos\theta_2). \quad (64)$$

As indicated in Fig. 15, this limiting expression yields an elongated ellipse with a narrow range of negative a_2'

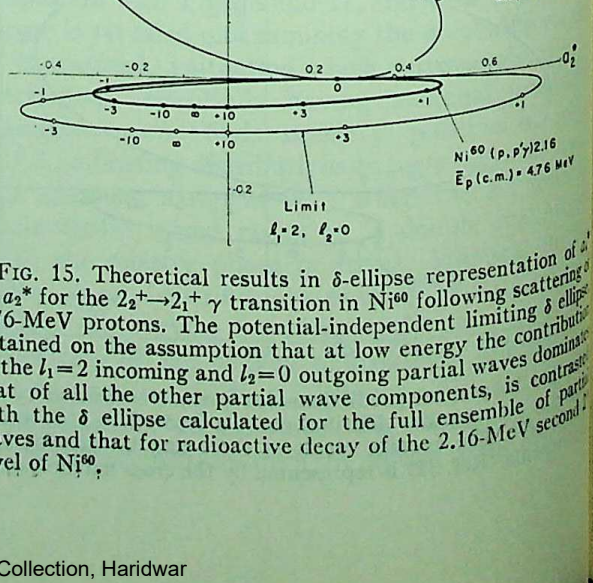

FIG. 15. Theoretical results in δ-ellipse representation of a_4' vs a_2' for the $2_2^+ \rightarrow 2_1^+$ γ transition in Ni^{60} following scattering of 4.76-MeV protons. The potential-independent limiting δ ellipse obtained on the assumption that at low energy the contribution of the $l_1=2$ incoming and $l_2=0$ outgoing partial waves dominates that of all the other partial wave components, is contrasted with the δ ellipse calculated for the full ensemble of partial waves and that for radioactive decay of the 2.16-MeV second 2^+ level of Ni^{60}.

CC-0. In Public Domain. Gurukul Kangri Collection, Haridwar

Digitized by Arya Samaj Foundation Chennai and eGangotri

values. This limiting ellipse should be approached near threshold for an $(n, n'\gamma)$ reaction under the same conditions as has been outlined above for $2^+(E2)0^+$ transitions. By way of contrast, the familiar $2(D, Q)2(Q)0$ ellipse for a γ–γ angular correlation in radioactivity has a much wider range of $a_4{}^*$ values (positive), together with a slightly reduced range of $a_2{}^*$ values. Because the mixed transition occurs first in this radioactivity decay, the sign of δ measured will be opposite to that determined from an $(N, N'\gamma)$ angular distribution measurement. As is illustrated in Fig. 15 for a typical case in Ni^{60}, the predicted ellipse for a $(p, p'\gamma)$ reaction is substantially smaller than the limit (64). This diminution is mainly caused by the presence of dominating τ terms involving $l_1=1$, $l_2=1$. In the case of inelastic proton scattering, the basic condition for the limit is not fulfilled, i.e., one does not have

$$T_2(E_1)\,T_0'(E_2) \gg T_1(E_1)\,T_1'(E_2), \text{ etc.} \qquad (65)$$

b. Ground-State Transitions from Spin-3 Levels

A study of the behavior of theoretical $(n, n'\gamma)$ angular patterns for octupole $(3\rightarrow 0)$ transitions has revealed some unexpected facets near threshold. First let us consider the rare but interesting case where the first excited state has $J^\pi=3^-$. Near threshold, the two dominating τ terms [Eq. (13)] have $l_1=3$, $l_2=0$, corresponding to f-wave excitation of $\frac{5}{2}^-$ and $\frac{7}{2}^-$ compound states, whose contributions to the overall angular distribution are proportional to $[6+5.143P_2(\cos\theta)+0.857P_4(\cos\theta)]$ and $[8+7.143P_2(\cos\theta)+1.403P_4(\cos\theta)-4.545P_6(\cos\theta)]$, respectively. In this instance, since the denominators of these τ terms are equal, the sum of their contributions yields a model-independent limit

$$W(\theta_2)=1+0.8776P_2(\cos\theta_2)+0.1614P_4(\cos\theta_2) -0.3247P_6(\cos\theta_2), \qquad (66)$$

which has an angular asymmetry of 2.37, as indicated in Fig. 16.

Above threshold, the percentage contribution of these $T_3\cdot T_0'$ terms diminishes slowly in a fashion similar to the $T_2\cdot T_0'$ terms shown in Fig. 14 for a $2^+(E2)0^+$ transition. Nevertheless, the predicted behavior of the $3^-(E3)0^+$ asymmetry differs strikingly, for instead of dropping rapidly, it should remain roughly constant (about 2.3 to 2.5) for a substantial range of energies above threshold. In fact, as shown in the inset of Fig. 16, a small initial increase is expected due to the increasing influence of τ terms of the type $T_2\cdot T_1'$ and $T_4\cdot T_1'$, which have angular asymmetries of 2.44 and 2.73, respectively.

The presence of other open exit channels (excepting 0^+ states) will generally cause some minor changes in these predictions. Figure 16 illustrates the effect of open (n, p) channels on the angular asymmetry of the

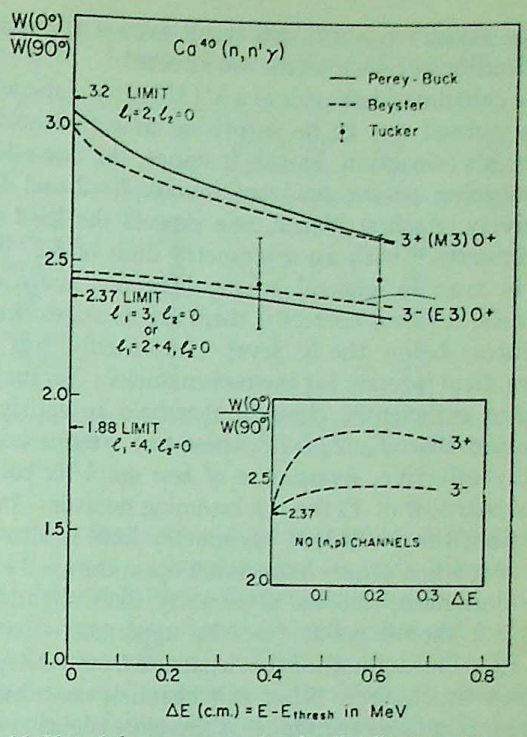

FIG. 16. Plot of the asymmetry for the distribution of de-excitation γ radiation from the second level of Ca^{40} against the energy above threshold of incident neutrons inelastically scattered to the second level. For spin–parity assignments of $3^\pm$ for this level, the theoretical curves evaluated from Perey–Buck and Beyster transmission coefficients are compared with the values derived from the experimental results of Tucker (Refs. 25, 33, 37). Also shown are the potential-independent limiting values of the asymmetry at threshold for different dominant partial-wave combinations. The calculations, which take account of four neutron and four proton exit channels for decay of the compound nucleus, show the transition multipolarity to be $E3$, and the parity of the spin-3 level to be negative. The inset shows the theoretical curves of asymmetry vs energy above threshold when no account is taken of proton decay channels.

3.73-MeV $3^-(E3)0^+$ transition in the Ca^{40} $(n, n'\gamma)$ reaction. For these calculations, we have adopted proton transmission coefficients corresponding to a Woods–Saxon potential with a surface-derivative absorptive term having the same parameters as used previously.[28,29] These open (n, p) channels go to low-lying negative-parity states in K^{40}, and their inclusion causes the denominator of the $J_1=\frac{7}{2}^-$ τ term to become larger than the $J_1=\frac{5}{2}^-$ τ term. The net result is a slightly increased asymmetry limit, which is no longer model-independent, together with a gradually decreasing asymmetry above threshold (Fig. 16). For the more general case of an $(n, n'\gamma)$ reaction for a 3^- state lying above one or more 2^+ states, the denominator of the $J_1=\frac{5}{2}^-$ τ term will be larger than that of the $\frac{7}{2}^-$ term, causing the limiting asymmetry to be less than 2.37. Nevertheless, the presence of other τ terms with larger asymmetries should still maintain the overall asymmetry for such a 3^- state to a value near 2.5 for a considerable energy range above threshold. Any influence due to fluctuations in level widths on the asymmetry should be relatively unimportant in this instance, since

CC-0. In Public Domain. Gurukul Kangri Collection, Haridwar

Digitized by Arya Samaj Foundation Chennai and eGangotri

a large asymmetry will still result even if the relative contributions of such terms are affected.

The calculated behavior of a $3^+(M3)0^+$ angular asymmetry turned out to be surprising near threshold for an $(n, n'\gamma)$ reaction. In this instance, the two τ-terms for outgoing s-wave neutrons involve $l_1=2$ and 4, respectively. At first glance, one expects the $l_1=2$ term to dominate,[32] with an asymmetry limit of 3.2. While this is true in general when there are many open channels, it is not correct if there are no states (except 0^+ states) below the 3^+ level. (Admittedly, this is of no practical interest for even–even nuclei.) For incident energies sufficiently close to threshold to satisfy the condition that T_2, $T_4 \gg T_0'$, these two τ-terms become equally effective, *irrespective of how much the value of* T_2 *exceeds that of* T_4 for the incoming neutrons. In this situation, the $3^+(M3)0^+$ asymmetry limit is also 2.37. However when other channels are open, the $l_1=2$ τ term does dominate, and an asymmetry limit slightly less than 3.2 should result (see the uppermost curves of Fig. 16). The amount of the departure from 3.2 depends on how much these other exit channels contribute to the reaction cross section. It is therefore slightly model-dependent, as illustrated by the small difference in the predicted limits using either Perey–Buck or Beyster neutron T_l values.

The net outcome of this theoretical study is the discovery of an appreciable parity dependence for the angular distributions of $(3\rightarrow 0)$ transitions near threshold of an $(n, n'\gamma)$ reaction. It is of interest to compare these predictions with Tucker's recent Ca^{40} $(n, n'\gamma)$ results for $E_n=4.20$ and 4.43 MeV.[25,33] We have extrapolated his forward-angle data ($\theta=30°$, 40°) to 0° in accord with the expected theoretical shape in order to extract values for the angular asymmetry. This procedure seems to be reasonable since his data fit the theoretical shapes very well, as is described at the end of Sec. 8. Although his measurements do not begin as close to threshold as might be desired, they appear to favor the known $3^-(E3)0^+$ assignment for this 3.73-MeV transition in Ca^{40}. If the $(n, n'\gamma)$ angular distributions of ground-state transitions from other spin-3 levels could be measured with comparable accuracy near threshold, it is likely that they could be uniquely identified.

8. EFFECT OF EXTRA CN EXIT CHANNELS

Further physical factors influence markedly the magnitude of the differential cross section, and thus need to be taken into account in comparison of absolute experimental results with theoretical data, even though the distribution *structure* may hardly be affected. Having already dealt with the *increase* in the cross section that ensues upon including higher partial waves in the reaction channels, we now examine the *decrease* in the cross section that results from taking additional CN decay channels into account. The "two-channel approximation," in which the exit channels are confined solely to those leading to the ground state (elastic channel) and a single excited state (inelastic channel) of the target nucleus, represents an approach which is not meaningful under most experimental conditions. A valid treatment must take into account each of the additional open exit channels by which the CN can decay—this involves simply a modification of the transmission term τ in evaluation of the numerical cross section. The presence of appropriate additional transmission coefficients in the denominator of the τ term occasioned by each extra open decay channel results in a reduction of the overall cross section by an amount which depends upon the channel spin and energy but is of the order of 20% per extra channel. The reduction affects nucleon and γ distributions alike, as is evident from examples in this section and in Sec. 10.

As examples, we have chosen instances of spin sequences that yield distributions characterized by particularly large anisotropy, since these are of especial interest in their own right. It is fortunate that absolute experimental results have recently become available for comparison with theoretical predictions, since a purely structural comparison would be relatively insensitive to the influence of extra decay channels.

To illustrate the quantitative effect upon a *neutron distribution*, measurements taken by Cranberg *et al.*[34] are especially well suited. Inelastic scattering distributions for 2.5-MeV neutrons on Pb^{206} were measured by the Los Alamos group absolutely for seven low-lying states of the target nucleus. Of this data, the differential cross section for scattering to the first 0^+ level at 1.18-MeV excitation is particularly striking because of the large anisotropy associated with a $0^+\rightarrow J_1\pi_1\rightarrow 0^+$ spin sequence. The theoretical distribution also features this pronounced structure, but is in marked quantitative disagreement with experimental absolute cross sections unless adequate provision is made for the many open decay channels of the compound nucleus Pb^{207*}. Use of the two-channel approximation furnishes a theoretical cross section whose magnitude is more than 10-fold that measured experimentally, and even incorporation of all the eight levels (comprising the ground state and seven excited levels) for which data are shown by the authors does not suffice to bring the calculated cross sections down to the observed values. However, when 13 levels lying below an excitation energy of 2.5 MeV are considered (in some instances, by allocating tentative spin assignments) excellent numerical agreement

[33] W. E. Tucker, Ph.D. thesis, University of Texas, 1964 (unpublished).

[34] L. Cranberg, C. D. Zafiratos, J. S. Levin, and T. A. Oliphant, Phys. Rev. Letters 11, 341 (1963); L. Cranberg, in *Progress in Fast Neutron Physics*, edited by G. C. Phillips, J. B. Marion, and J. R. Risser (University of Chicago Press, Chicago, 1963) p. 89.

CC-0. In Public Domain. Gurukul Kangri Collection, Haridwar

Digitized by Arya Samaj Foundation Chennai and eGangotri

ensues on using transmission coefficients derived by the authors from an optical potential of the derivative Woods–Saxon type which had been found to give good fits to elastic and inelastic scattering data for bismuth. These transmission coefficients, which are appreciably lower than corresponding tabulated values[35] for a Perey–Buck or a Bjorklund–Fernbach potential, yield commensurately lower cross sections, even when the number of partial waves (corresponding to $l \leqq 6$) exceeds that ($l \leqq 4$) for which Perey–Buck penetrabilities are listed.

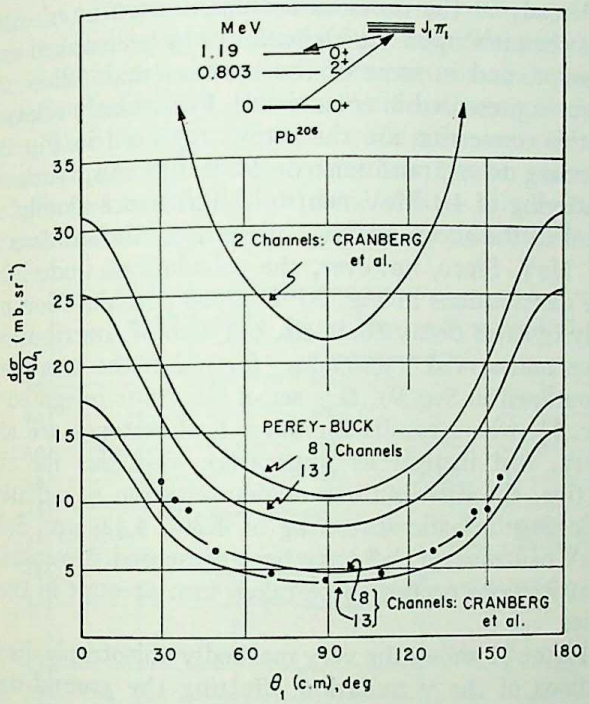

FIG. 17. Comparison of the experimentally determined differential cross sections for scattering of 2.5-MeV neutrons to the second 0^+ level of Pb^{206} (Ref. 34) with theoretical curves evaluated for various numbers of open neutron channels for decay of the compound nucleus. The calculations have been based upon two distinct, but formally similar, optical potentials, namely the nonlocal "global" potential of Perey and Buck, and a local derivative potential of Woods–Saxon type derived by Cranberg *et al.* from analysis of elastic and inelastic neutron distributions at 2.5 MeV on Bi^{209}. The parameters of the equivalent local Perey–Buck potential applicable to this case, namely $V=47.25$ MeV, $W'=10$ MeV, $r_0=1.25$ F, $a=0.65$ F, $V_{so}=8$ MeV, may be compared with those for the potential of Cranberg *et al.* when expressed in the same nomenclature: $V=41.9$ MeV, $W'=14.4$ MeV, $r_0=1.32$ F, $a=0.635$ F, $V_{so}=6$ MeV. The higher transmission coefficients furnished by the potential of Perey and Buck account for the higher differential cross sections derived therefrom. The curve in the two-channel approximation for a Perey–Buck potential dips from 191 mb sr^{-1} at 0° to 50 mb sr^{-1} at 90°, whereas that for the potential of Cranberg *et al.* drops from 89 mb sr^{-1} at 0° to the values indicated in the figure (which shows only the lower values for reasons of space). The eight levels employed in the next order of approximation are those which feature in the papers of Cranberg *et al.* (Ref. 34): 0 (0^+), 0.803 (2^+), 1.175 (0^+), 1.341 (3^+), 1.462 (2^+), 1.720 (4^+), 1.762 (2^+), and 1.998 MeV (4^+). The thirteen levels in the highest order are those actually used in the calculations of Cranberg *et al.* (see footnote 36); in addition to the above, they comprise the following levels (with tentative spin assignments): 1.720 (1^+), 2.155 (2^+), 2.20 (2^+), 2.20 (7^-), and 2.384 MeV (6^-). A still closer fit to the experimental points can be achieved when level-width fluctuations are taken into account (Ref. 36).

[35] E. H. Auerbach and F. G. J. Perey, Brookhaven National Laboratory Report No. 765 (T-286), July 1962 (unpublished).

TABLE II. Computed values of the differential cross section for scattering of 2.5-MeV neutrons to the 1.18-MeV (0^+) level of Pb^{206}.

Potential	l_{max}	No. of exit channels	$d\sigma(0°)$ (mb sr^{-1})	$d\sigma(90°)$ (mb sr^{-1})
Perey–Buck	3	2	184	49
Perey–Buck	4	2	191	50
Cranberg	6	2	89	22
Cranberg	6	8	17	5
Perey–Buck	4	8	31	10
Perey–Buck	2	13	15	7
Perey–Buck	4	13	25	8
Cranberg	6	13[a]	15	4

[a] Also computed by Cranberg *et al.* (Refs. 34, 36), who obtained identically the same results.

Calculations have been effected using not only the transmission coefficients ($T_l^{(\pm)}$ up to $l \leqq 6$) and spin assignments of Cranberg *et al.* for 13 decay channels of the compound nucleus,[36] but also for the 8 channels mentioned above, and for simply 2 channels in order to elucidate the effect of open exit channels. The results have in Fig. 17 been compared with those derived using penetrabilities ($T_l^{(\pm)}$ up to $l \leqq 4$) for a Perey–Buck nonlocal potential. In all cases the distribution *structure* was found to be essentially the same, but the magnitudes differ markedly with change in the number of channels, as shown in Table II. We add two remarks concerning the above results. Firstly, the computations with the code "MANDY" were throughout in perfect numerical agreement with those obtained from the *correlation* code "BARBARA" (since de-excitation γ radiation from a 0^+ state has an isotropic distribution, the N'–γ correlation is basically the same as the N' distribution, albeit lower by a factor 4π), and with those undertaken by Cranberg *et al.* using a completely independent program. Secondly, additional (as yet unpublished) calculations by Cranberg, Oliphant, and Levin that take level-width fluctuations into account evidently yield a still closer measure of agreement with the experimental data as regards structure and magnitude [the improvement applies not only to the scattering distribution of neutrons to the second (0^+) level, but of those to other levels, especially to the first (2^+) level].

The dependence of theoretical *proton distributions* on the number of open CN channels is essentially similar. For example, consider the theoretical calculations shown in Fig. 18 for the Ni^{58} (p, p') reaction at $E_p=9.35$ MeV. These were obtained using an optical potential of the

[36] We are indebted to T. A. Oliphant of Los Alamos for several private communications on this subject, as also to L. Cranberg for stimulating discussions on the most recent aspects of this work, now being prepared for publication.

CC-0. In Public Domain. Gurukul Kangri Collection, Haridwar

Digitized by Arya Samaj Foundation Chennai and eGangotri

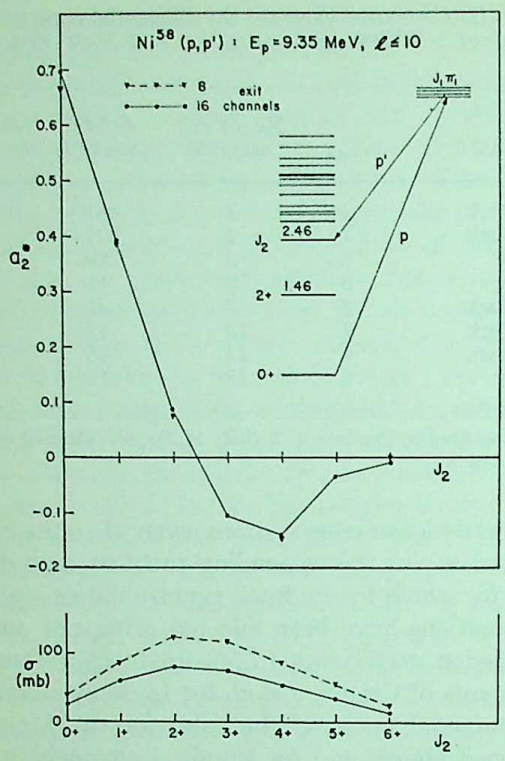

FIG. 18. Systematic variation of the values of a_2^* and inelastic cross section with the spin assignment J_2 of the 2.46-MeV level of Ni^{58} populated by scattering of 9.35-MeV protons. The calculations have included the effect of either 8 or 16 exit channels and orbital momenta with $l \leqq 10$, and have been based upon an optical potential of the derivative Woods–Saxon type (see text).

derivative Woods–Saxon type:

$$V = -V_0/(e^x+1) + iW'(d/dx')\{1/(e^{x'}+1)\}, \quad (67)$$

where $x=(r-r_0A^{\frac{1}{3}})/a$ and $x'=(r-r_0'A^{\frac{1}{3}})/a'$. The same parametric choices were made as for earlier comparisons with $(p, p'\gamma)$ cross sections,[28,29] i.e., $V_0=52$ MeV, $W'=44$ MeV, $r_0=r_0'=1.25$ F, $a=0.65$ F, and $a'=0.47$ F.

Figure 18 shows the predicted a_2^* variation of the distribution structure with spin J_2 (2.46-MeV level), taking 16 exit channels (with tentative spin choices) into account. (A similar variation of differential cross sections is shown in Fig. 36, Sec. 12, for the 2.78-MeV level of Ni^{58}.) Halving this number of exit channels does not affect appreciably either the structure of these distributions, or the relative cross sections for different spin-value assignments to a particular level. Nevertheless, each calculated (p, p') cross section is increased by roughly 50% with this reduction of exit channels, as illustrated at the bottom of Fig. 18.

Such an effect is not only important for reliable estimates of CN cross sections for inelastic proton channels, but cannot be disregarded in calculations of elastic scattering from a zero-spin target, particularly at back angles where the compound elastic-scattering contribution becomes comparable to the shape elastic cross section. Even for nuclei where reliable spin determinations for most of the low-lying levels are not yet available, it is better to include many exit channels using reasonable spin choices rather than to omit them entirely. At lower proton bombarding energies ($\lesssim 5$ MeV), the number of effective exit channels is considerably reduced, and in the case of a nucleus such as Ni^{58}, only levels with excitation energies $\lesssim 3$ MeV need to be considered. The systematic variations of (p, p') distributions and their comparison with experimental data are discussed in Sec. 12.

Already in the previous section, the effect of extra exit channels upon γ *distributions* has been taken into account, and in some of the sections that follow the effect is presented in some detail. Particularly relevant in this connection are the results depicted in Fig. 30, referring to γ transitions in Pb^{206} following inelastic scattering of 4.1-MeV neutrons, and hence closely related to the above analysis of the Los Alamos data at 2.5 MeV. Since, however, the calculations underlying the distributions in Fig. 30 involved consideration not only of extra decay channels, but also of contributions from unobserved γ cascades (for which the treatment is outlined in Sec. 9), this set of results is relegated to Sec. 11, where results for other lead isotopes are also given, and instead as illustrative examples for this section, the distributions of de-excitation γ radiation following inelastic scattering of 4.20-, 4.43- and 5.00-MeV neutrons on Ca^{40} have been presented. No cascade contributions needed to be taken into account in these cases.

Figure 19 shows the very markedly anisotropic distributions of the γ radiation effecting the ground-state transition from the second level of Ca^{40} ($3^- \rightarrow 0^+$, pure $E3$). The γ-distributions for de-excitation of the 0^+ first level are, of course, isotropic. The experimental data is that of Tucker,[25,33,37] to which reference has already been made in Sec. 7.2 (see Fig. 16). The calculations that yielded the curves in Fig. 19 differ from those of Tucker in that they solely employed Perey-Buck penetrabilities for the neutron transitions (whereas Tucker used Perey–Buck, Bjorklund–Fernbach, and Beyster penetrabilities, of which the last-named were found to provide the best fits to experimental data, since there was an appreciable progressive decrease in the cross sections furnished by the above sequence of potentials) and included higher partial waves ($l \leqq 5$ as against Tucker's limits $l_1 \leqq 3$, $l_2 \leqq 2$). The proton penetrabilities (up to $l \leqq 3$) for the extra CN decay channels to K^{40} were the same as those used by Tucker (derived from "black nucleus" parameters of Feshbach, Shapiro, and Weisskopf[38]). Although Tucker further took account of an extra α-decay channel

[37] I. L. Morgan, J. B. Ashe, R. W. Benjamin, O. M. Hudson, S. C. Mathur, D. O. Nellis, C. V. Parker, and W. E. Tucker, Annual Progress Report, Nuclear Physics Division, Texas Nuclear Corporation, Sept. 1963 and Status Report, June 1964 (unpublished).

[38] H. Feshbach, M. M. Shapiro, and V. F. Weisskopf, New York Operations Office, U. S. Atomic Energy Commission, NYO-3077, 1953 (unpublished).

CC-0. In Public Domain. Gurukul Kangri Collection, Haridwar

Digitized by Arya Samaj Foundation Chennai and eGangotri

to the ground state of Ar^{37} in his hand calculations, using penetrabilities derived from the formulae of Feshbach, Shapiro, and Weisskopf, this has been omitted from the present computations because, firstly, the spin assignment is ambiguous; secondly, the code "MANDY" treats spin-$\frac{1}{2}$ particles only; and thirdly, the use of the above penetrabilities is open to criticism in the present case. The large numerical discrepancy between theoretical and experimental absolute cross sections in the two-channel approximation is greatly diminished on inclusion of the additional open neutron and proton decay channels, but nevertheless remains appreciable even when full provision is made (the considerable reduction brought about by the four proton channels is indicated in the 5-MeV data of Fig. 19). Such an overestimate of the inelastic cross section for a low-

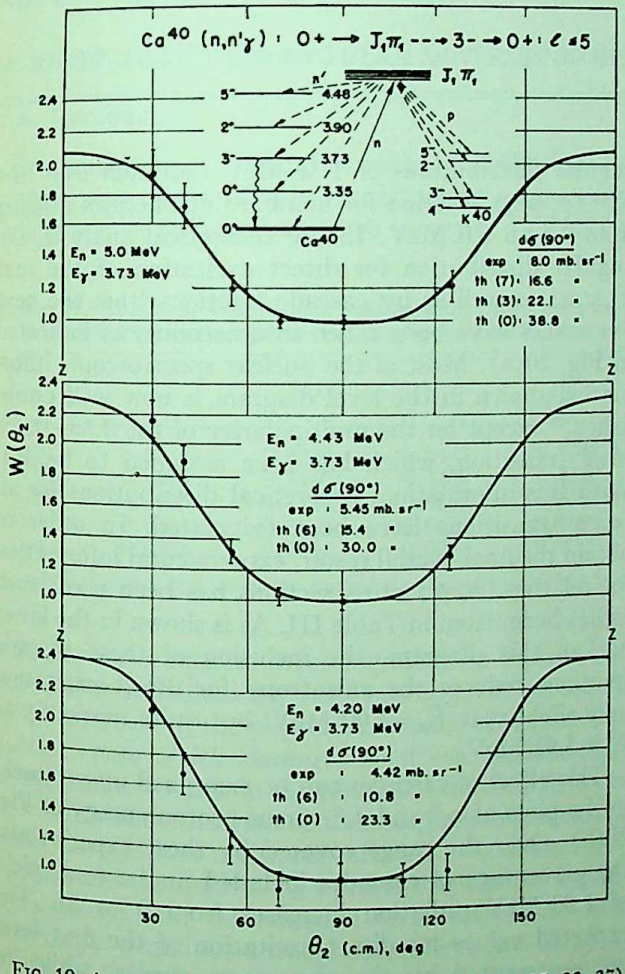

FIG. 19. Angular distribution data of Tucker (Refs. 25, 33, 37) for $E3$ de-excitation γ radiation from the $Ca^{40}(n, n'\gamma)$ reaction at three incident energies, compared with theoretical curves based on Perey–Buck penetrabilities, as in Fig. 16. The absolute cross sections show discrepancies which may be ascribed to level-width fluctuations near threshold. The calculated numerical results are labelled according to the number of *extra* exit channels taken into consideration, so that *th*(0) denotes the value derived in the two-channel approximation. Even with 7 extra channels at the highest incident energy, theoretical values derived from Perey–Buck penetrabilities appreciably exceed those determined experimentally, but with a Beyster potential the agreement is much closer.

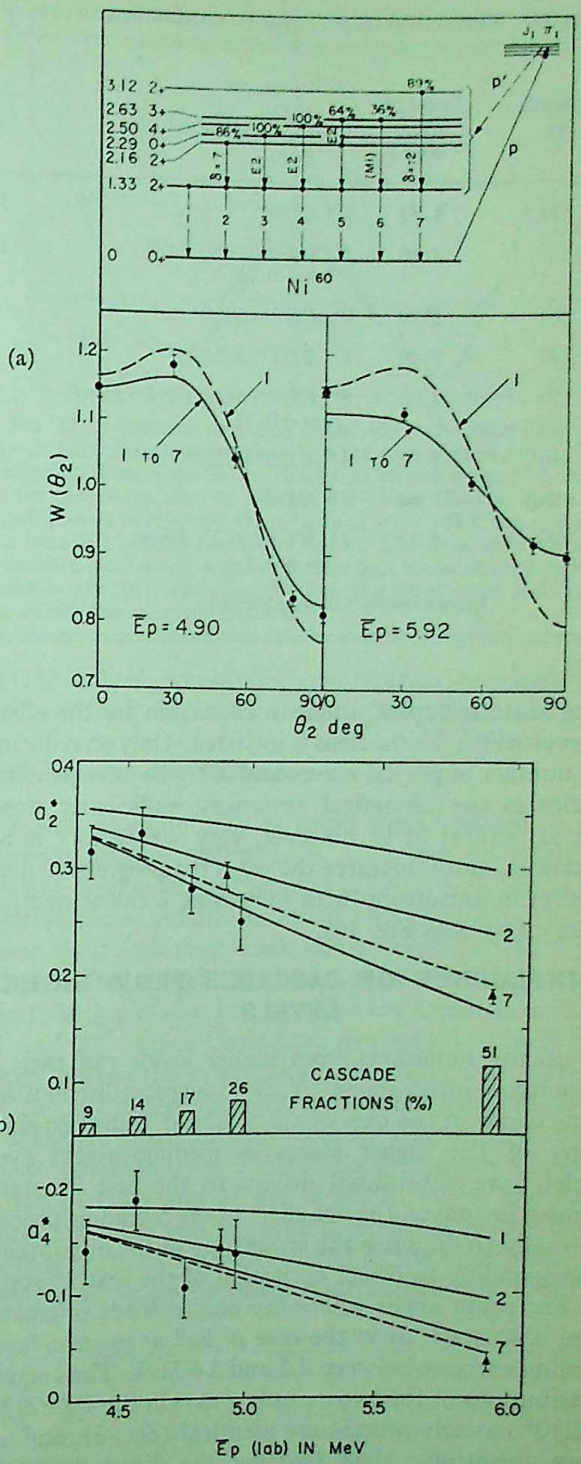

FIG. 20. (a) Experimental angular distributions (Ref. 29) for 1.33-MeV γ radiation from the $Ni^{60}(p, p'\gamma)$ reaction, compared with theoretical predictions for direct excitation [curve (1)], and for the sum of cascade radiations from the first six levels, using the nuclear spectroscopic information listed in the level diagram. (b) A comparison of the same results as in (a), but in more detail, with values of both a_2* and a_4* vs incident proton energy. For the upper two curves in each plot, γ rays from the first one and two levels have been taken into account. For the lower two curves, two different multipolarities have been assumed for the 2.63→1.33-MeV transition: $M1$ (solid line) and $E2$ (dashed line). Experimental data (Refs. 28 and 29) refer to two different targets with thicknesses of 120 keV (circles) and 260 keV (triangles) at E_p=5 MeV.

CC-0. In Public Domain. Gurukul Kangri Collection, Haridwar

Digitized by Arya Samaj Foundation Chennai and eGangotri

TABLE III. Theoretical $(p, p'\gamma)$ angular distributions for cascade fractions of 1.33-MeV radiation originating from first six levels of Ni^{60}.

Cascade No.	Level of origin (MeV)	Transition type	$\bar{E}_p$=4.90 MeV			$\bar{E}_p$=5.92 MeV		
			% σ_{in}	a_2*	a_4*	% σ_{in}	a_2*	a_4*
(1)	1.33	$2^+(E2)0^+$	74.8	0.340	−0.178	46.2	0.300	−0.152
(2)	2.16	$2^+(M1+E2)2^+(E2)0^+$ $\delta=+0.75$	14.0	0.086	0.058	17.8	0.082	0.056
(3)	2.29	$0^+(E2)2^+(E2)0^+$	4.6	0	0	9.8	0	0
(4)	2.50	$4^+(E2)2^+(E2)0^+$	2.1	0.390	−0.153	4.6	0.366	−0.120
(5)	2.63	$3^+(E2)2^+(M1+E2)2^+(E2)0^+$ $\delta=+0.75$	1.7	−0.035	0.127	4.8	−0.034	0.113
(6)	2.63	$3^+(M1)2^+(E2)0^+$	1.2	−0.386	0.169	3.2	−0.367	0.150
(6a)	2.63	$3^+(M1)2^+$	1.2	−0.270	0	3.2	−0.257	0
(7)	3.12	$2^+(M1+E2)2^+(E2)0^+$ $\delta=+0.2$	0.4	0.167	0.104	3.6	0.167	0.111
	higher levels	not established	...	...	...	6.8	...	...

lying state is typical unless a correction for the effect of level-width fluctuations is included.[1] Only on reducing the number of partial waves and using Beyster penetrabilities is the numerical agreement sufficiently close. The structural fit is, however, very satisfactory in all instances, and illustrates the expected progressive diminution in anisotropy with increasing incident neutron energy (see also Fig. 16).

9. INFLUENCE OF CASCADES FROM HIGHER LEVELS

Cascade radiations from higher levels can exert a pronounced effect on an $(N, N'\gamma)$ angular distribution, particularly in the case of a $2_1^+(E2)0_1^+$ transition since many of the higher states in medium-weight even nuclei have substantial decays to the first 2^+ state. In most instances, the net effect of the cascading process is usually to diminish the anisotropy of the distribution corresponding to direct excitation of the first 2^+ state. An exception arises where the only cascade originates from a 4^+ state, as in the case of Fe^{56} at neutron bombarding energies between 2.1 and 2.6 MeV. The angular distributions of the two cascade γ rays in the $4^+(E2)2^+$-$(E2)0^+$ cascade process are identical (Sec. 3), and are more anisotropic than that for the direct $2^+(E2)0^+$ transition. Day and Walt[18] assumed isotropy when subtracting such a cascade contribution from their experimental angular distribution for 0.845-MeV γ radiation for the Fe^{56} $(n, n'\gamma)$ reaction at $\bar{E}_n$=2.56 MeV. This correction affected its anisotropy in the wrong direction (0.08 of the a_2* value), but was of no consequence because of the limited accuracy of their angular distribution measurement.

A clear demonstration of the effect of cascade fractions is possible in the case of recent measurements[28,29] of angular distributions of 1.33-MeV radiation from the Ni^{60} $(p, p'\gamma)$ reaction for bombarding energies ranging from 4.4 to 6.0 MeV. In the theoretical analysis, the angular distribution for direct excitation of the first 2^+ state as well as for cascade fractions from the next five states have been taken into account, as indicated in Fig. 20(a). Most of the nuclear spectroscopic information shown in the level diagram is now well established,[29] except for the multipolarity of the 2.63→1.33-MeV transition, which has been assumed to be $M1$. With this information, theoretical distributions for all seven transitions have been calculated. In order to obtain the final overall result, experimental information for relative (p, p') cross sections has been used, such as has been listed in Table III. As is shown in the lower half of this diagram, the inclusion of these cascade fractions reduces the anisotropy for direct excitation only slightly at $\bar{E}_p$=4.90 MeV, but quite markedly at $\bar{E}_p$=5.92 MeV.

This effect of cascades can be examined more closely in the plots of a_2* and a_4* versus proton energy of Fig. 20(b). Over the range covered by these experiments, the percentage of cascades included in the total yield of 1.33-MeV radiation increases from 9 to 51. The expected values for direct excitation of the first level are represented by the uppermost curves, while inclusion of the cascade from the second level causes a substantial reduction in the absolute a_2* and a_4* values. The assumption of $M1$ multipolarity for the 2.63→1.33-MeV transition does introduce some uncertainty, since a choice of $E2$ multipolarity for this radiation would alter the overall prediction perceptibly, as shown by the dashed curves. The influence of this transition is unfortunately enhanced because the upper cascade (1.29 MeV) was not resolved from 1.33-MeV radiation in

CC-0. In Public Domain. Gurukul Kangri Collection, Haridwar

Digitized by Arya Samaj Foundation Chennai and eGangotri

the scintillator spectrum,[29] and its effect had to be included.

It is evident that the influence of cascade radiations from the first six levels is quite substantial, and that the experimental results are in excellent agreement with these calculations using statistical reaction theory at least up to 6-MeV proton bombarding energy. The data points with smaller error bars were obtained using a thinner target (factor of 2), with consequently less averaging over compound states. The small fluctuations in a_2^* and a_4^* values (of the order of ± 0.04) could be caused by fluctuations in the density of levels with large (p, p_1') reduced widths. Nevertheless, the agreement of these $(p, p'\gamma)$ angular distributions with the assumption of simple compound-nucleus formation is quite striking, once the contributions of cascade radiations have been taken into account.

10. SYSTEMATICS OF ANGULAR DISTRIBUTIONS

A. Introduction

In addition to evaluating numerical distributions for an extensive range of spin combinations encountered in practice, we have undertaken a survey of distribution behavior for sequences involving stepwise variation in the various individual spins and parities, without regard to the question of the physical existence of appropriate nuclei. These *Spielrechnungen* shed considerable light on systematic trends in distribution behavior. In order to secure standardization of all input parameters except spins, parities and multipole mixtures, the orbital momenta were confined to $l \leqq 4$ and a single set of Perey–Buck generalized transmission coefficients $T_l^{(\pm)}$ was arbitrarily employed throughout. These are listed in Table IV. In point of fact, these correspond to penetrabilities for scattering of 3-MeV neutrons to the ground state and first level of Fe^{56}. In the calculations the "two-channel approximation" was used. In the case of nucleon distributions 138 different sequences were considered, as against 822 sequences (omitting forbidden $0 \to 0$ transitions) for γ distributions *without* intermediate unobserved transitions. For instance, the following spin combinations for J_0/J_2 were investigated with permutation of positive and negative parities: $0(1)5/0(1)5$, $\frac{1}{2}(1)\frac{11}{2}/\frac{1}{2}(1)\frac{11}{2}$, wherein for computational reasons, the six cases involving 0^- levels had to be omitted.

TABLE IV. Values of Perey–Buck transmission coefficients used for calculation of the systematics of angular distributions.

l	$T_l^{(-)}$	$T_l^{(+)}$	$T_l^{(-)'}$	$T_l^{(+)'}$
0	0.9239	0.9239	0.9442	0.9442
1	0.4979	0.5160	0.4400	0.4540
2	0.8925	0.7184	0.7852	0.6431
3	0.0984	0.1638	0.0423	0.0648
4	0.0328	0.0231	0.0092	0.0075

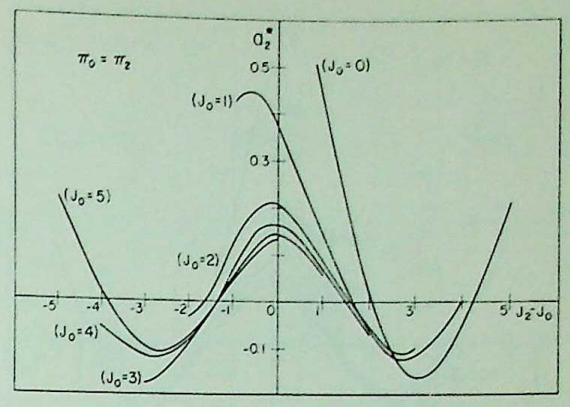

FIG. 21. Systematic variation of a_2^* with the spin difference $J_2 - J_0$ for various integer spins J_0 in the case of inelastic nucleon scattering, when there is no change in parity from the initial to the final state ($\pi_0 = \pi_2$, whence $l_1 + l_2 =$ even). The curve for $J_0 = 0$ goes on to intercept the a_2^* axis at $a_2^* = 0.853$, but this part has been left out for reasons of space. The data indicate that transitions with small angular momentum transfer evince large anisotropy in the nucleon distribution. The parameters underlying the calculation are given in the text.

B. Nucleon Distributions

A striking uniformity in trend was observed in the inelastic nucleon distributions. This can be rendered evident on plotting a_2^* against $\Delta J \equiv J_2 - J_0$, since the distribution structure is essentially dictated by the value of a_2^* (the very much smaller terms a_4^*, a_6^*, $\cdots$ simply effect a slight modification of the basic structure). Such plots for integer spins are depicted in Figs. 21 and 22 (which distinguish between instances for which the parities π_0 and π_2 are the same, and those in which they differ). The curves display vindication of Wolfenstein's expectation[2,34] that the distribution anisotropy (governed by a_2^*) should be large when the spins of the particles and of the target in initial and final states are small and the orbital momenta of the bombarding particles are unrestricted to the lowest values. Positive a_2^* values represent distributions which dip at

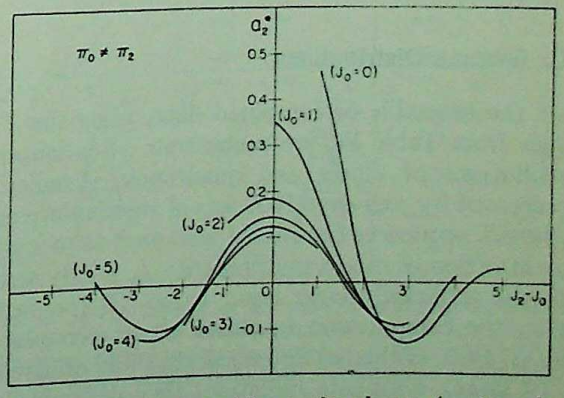

FIG. 22. As Fig. 21, but with a parity change ($\pi_0 \neq \pi_2$, whence $l_1 + l_2 =$ odd).

CC-0. In Public Domain. Gurukul Kangri Collection, Haridwar

Digitized by Arya Samaj Foundation Chennai and eGangotri

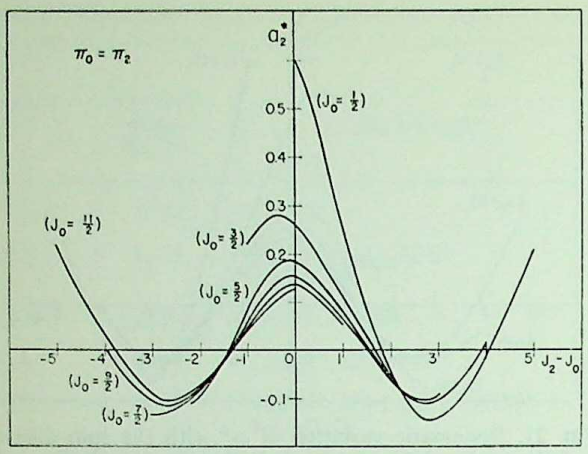

FIG. 23. As Fig. 21, but for half-integer spins, with no parity change.

90°, and negative a_2^* values, distributions which peak at 90°. The over-all trend toward reversal of behavior as ΔJ increases beyond 1 and again beyond 4 is paralleled by the corresponding curves for half-integer spins, Figs. 23 and 24. Isolated exceptions to this tendency occur when the influence of an exceptionally large a_4^* dominates over the a_2^*, as occurs for the sequences $0^+/2^\pm$, $2^+/0^+$, $\frac{1}{2}^+/\frac{5}{2}^+$.

In Fig. 18, the calculated variation of a_2^* with J_2 for inelastic proton distributions (corresponding to the 2.46-MeV level in Ni^{58}) has the same general trend for low nuclear spins as the $J_0=0$ curve of Fig. 21. However, the reversal in the sign of a_2^* for $\Delta J=5$ (Figs. 21–24) does not occur. The source of this difference could be the partial-wave cutoff ($l\leqq 4$) taken for the systematic calculations shown in Figs. 21–24, although the a_2^* value for such a high spin does depend somewhat on the spin choices for other low-lying states. The (p, p') calculations were made using the ABACUS-2 Code[5] with orbital momenta of $l\leqq 10$ included, so that for these the predicted behavior for high nuclear spins should be more reliable. For levels with higher excitations, the magnitude of each a_2^* value diminishes slowly, but the large fore–aft anisotropies for low spins ($J_0=0$, 1) still persist as a distinguishing feature.

C. Gamma Distributions

Of the ensemble of computed data, using the $T_l^{(\pm)}$ values from Table IV, we concentrate attention upon distributions of dipole and quadrupole γ radiation, represented by well over 1000 sets of results since most of the 822 sequences considered were such as to involve a γ transition of mixed multipolarity L, L'. By setting δ to the arbitrarily large input value 100 (or, better, 1000), the computation furnished separate results for pure $L(\delta=0$, evaluated automatically) and nearly pure L' (δ large) multipole radiation, thus delivering two sets of results per sequence. First we present some theoretical considerations that have a bearing upon distribution characteristics.

We first consider dipole radiation (pure $M1$ or $E1$). The index ν is restricted to the values 0 and 2, and the distribution takes the form

$$W(\theta_2)=1+a_2^*P_2(y)=1+a_2^*(\tfrac{3}{2}y^2-\tfrac{1}{2}), \quad (68)$$

with $y\equiv\cos\theta_2$. On differentiation one sees that the plot of $W(\theta_2)$ vs θ_2 has turning points at 0°, 90°, 180°, with the one at 90° corresponding to a *dip if* $a_2^*>0$ and a *peak if* $a_2^*<0$. Here and throughout, we note that $|a_\nu^*|<1$. The zero values of $P_2(y)$ at $\theta\approx 55°$ and 125° cause W to be unity at these angles in this normalized representation. Similarly it follows that

$$a_2^*=W(0°)-1=\tfrac{2}{3}[W(0°)-W(90°)]. \quad (69)$$

Analogous considerations apply to quadrupole radiation (pure $M2$ or $E2$), for which ν takes the values 0, 2, 4 and the distribution assumes the form

$$W(\theta_2)=1+a_2^*P_2(y)+a_4^*P_4(y)$$
$$=1+a_2^*(\tfrac{3}{2}y^2-\tfrac{1}{2})+a_4^*(\tfrac{35}{8}y^4-\tfrac{30}{8}y^2+\tfrac{3}{8}). \quad (70)$$

Differentiation now indicates the presence of turning points not only at $\theta_2=0°$, 90°, 180° but also at the two intermediate angles given by the condition that

$$y\equiv\cos\theta_2=\pm[(15a_4^*-6a_2^*)/35a_4^*]^{\frac{1}{2}} \quad (71)$$

be real. This is satisfied (i) for *positive* a_4^* when $a_2^*<\frac{5}{2}a_4^*$ (including the entire negative region of a_2^*); (ii) for *negative* a_4^* when a_2^* is positive, or when a_2^* is negative but $|a_2^*|<\frac{5}{2}|a_4^*|$. Under these circumstances, subsidiary turning points modify the structure of the distribution (symmetrically about 90°) in a manner which will next be examined. We study the ratio

$$r=\frac{W(0°)}{W(90°)}-1=\frac{5a_4^*+12a_2^*}{3a_4^*-4a_2^*+8} \qquad (|a_2^*|, |a_4^*|<1). \quad (72)$$

Then (i) for *positive* a_4^* this is positive when a_2^* is

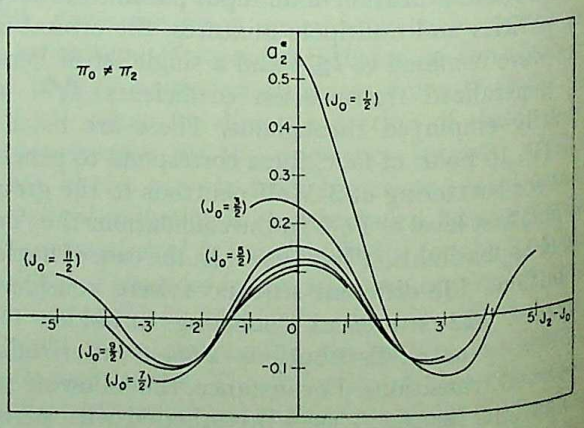

FIG. 24. As Fig. 23, but with a parity change.

CC-0. In Public Domain. Gurukul Kangri Collection, Haridwar

Digitized by Arya Samaj Foundation Chennai and eGangotri

positive, or when a_2^* is negative but $|a_2^*| < \frac{5}{12}|a_4^*|$: for numerically larger negative values of a_2^*, the ratio is negative, indicating that marked peaking occurs at 90°; (ii) for *negative* a_4^* the ratio r is positive for positive a_2^* which have a magnitude exceeding $\frac{5}{12}|a_4^*|$, whereas r is negative for all negative values of a_2^* and for those positive values below $\frac{5}{12}|a_4^*|$. From these results, a schematic of distribution structure from 0° to 180° has been drawn up which shows the changes in appearance as a_2^* is varied (Fig. 25).

In the case of sequences where $|a_2^*|$ happens to be vanishingly small compared with $|a_4^*|$ these γ distributions take on the forms shown at the bottom of Fig. 25, corresponding to displaced P_4 curves. The normalized distributions have the value unity at the angles 31°, 70°, 120°, and 149° at which $P_4(y)$ vanishes, and have subsidiary maxima or minima at 49° and 131°, the angles at which the value of $[1 \mp |a_4^*| P_4(y)]$ peaks or dips, respectively.

These overall predictions have been borne out by scrutiny of the structures of computed γ distributions. Since the basis of these predictions is furnished by values of a_2^* and a_4^* but not by the basic data, namely nuclear spins and γ multipolarities, their relevance to γ distribution systematics is only indirect. In an attempt

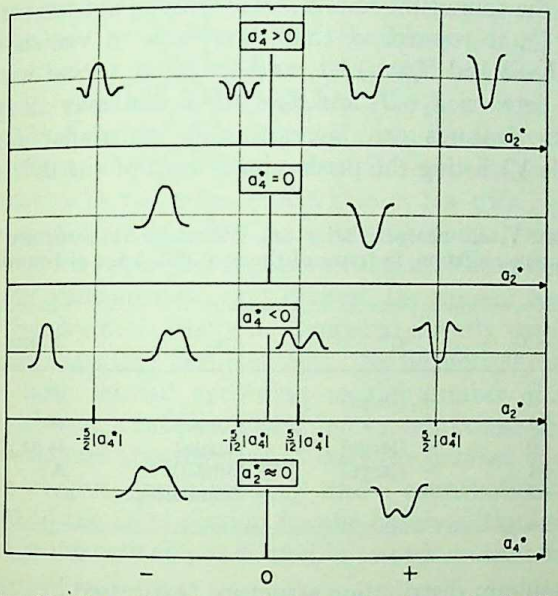

FIG. 25. Symbolic scheme depicting the change in distribution structure with change in a_2^* and a_4^*. Each curve is understood to represent the shape of the distribution from 0° to 180°, as given by the expression $W(\theta) = 1 + a_2^* P_2(\cos\theta) + a_4^* P_4(\cos\theta)$. When $a_4^* > 0$, the peak at 90° diminishes as a_2^* becomes less negative, until $W(90°) = W(0°)$ at $a_2^* = -(5/12)a_4^*$; for increasing a_2^*, the 90° value lies below that for 0°, and when $a_2^* > \frac{5}{2}a_4^*$ the effect of a_4^* becomes imperceptible. When $a_4^* = 0$, the curves are of pure Λ or V form according as $a_2^* < 0$ or $a_2^* > 0$. When $a_4^* < 0$, the form is pure Λ for large negative values of a_2^*, whereas the dip at 90° becomes increasingly pronounced between $a_2^* = -\frac{5}{2}|a_4^*|$ and $a_2^* > 0$; the 90° value equals that at 0° when $a_2^* = (5/12)|a_4^*|$, and thereafter falls below the 0° value. In the special case when $a_2^* \approx 0$, the distributions take the form M or W according as $a_4^* < 0$ or $a_4^* > 0$.

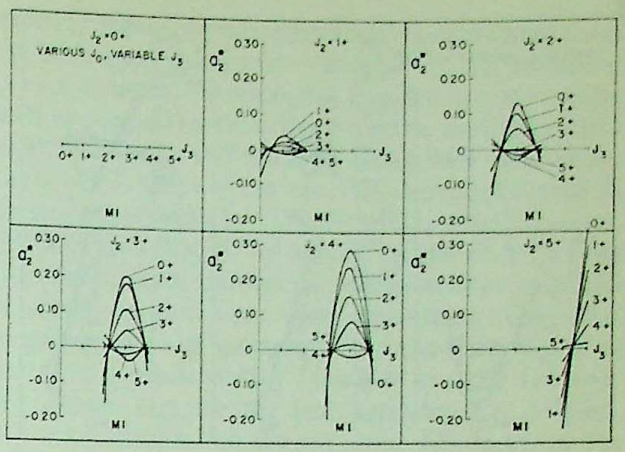

FIG. 26. Systematics of γ distributions. The curves show plots of a_2^* vs J_3 for $M1$ radiation in the transition sequence

$$J_0 \longrightarrow J_1 \overset{M1}{\dashrightarrow} J_2 \longrightarrow J_3.$$

In each case a set of curves for different values of J_0 is collated for a given value of J_2.

to link the a_2^* values systematically to spin sequences and multipolarities, the set of *Spielrechnung* computations embodying permutation of commonly-encountered nuclear spins was undertaken. The results are conveniently expressed in graphical form: we here confine ourselves to data for a_2^*, presented in Figs. 26–29, whereas systematic results for a_4^* are given in Table V.

Within the diversity of data, some overall features are apparent which may be regarded to have universal validity. The variation in values of a_2^*, and thus essentially of the distribution structure, for different nuclear spins depends sensitively upon the multipole order L (and hence upon $|J_2 - J_3|$) but not markedly upon the multipole character (E or M) of the radiation effecting the observed transition (compare Figs. 26 and

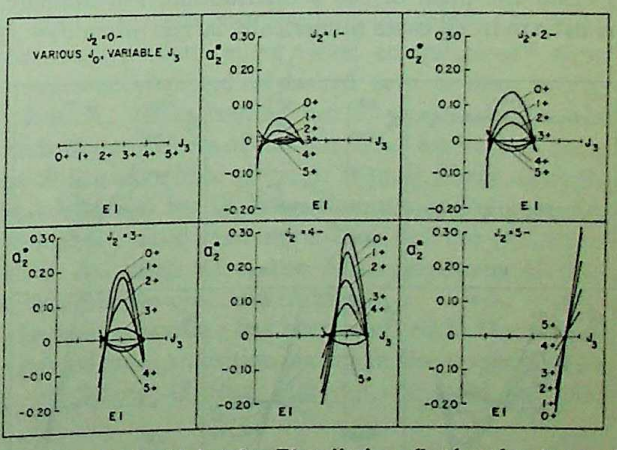

FIG. 27. As Fig. 26, but for $E1$ radiation effecting the observed transition $J_2 \rightarrow J_3$. The distribution systematics are practically uninfluenced by the multipole character of the dipole radiation (M or E). A very similar systematic trend applies in the case of a transition sequence involving half-integer spins (results are not shown for reasons of space).

CC-0. In Public Domain. Gurukul Kangri Collection, Haridwar

Digitized by Arya Samaj Foundation Chennai and eGangotri

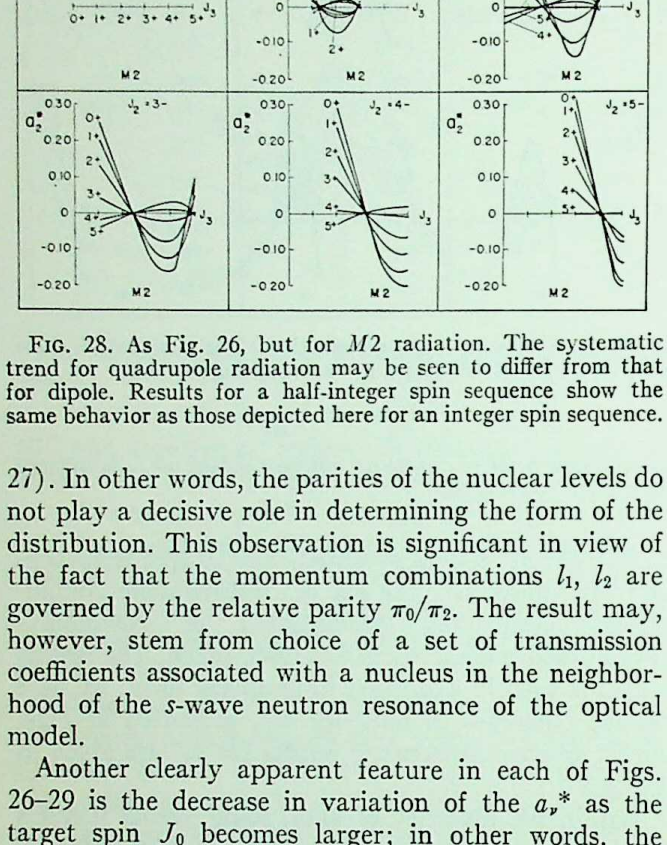

FIG. 28. As Fig. 26, but for $M2$ radiation. The systematic trend for quadrupole radiation may be seen to differ from that for dipole. Results for a half-integer spin sequence show the same behavior as those depicted here for an integer spin sequence.

27). In other words, the parities of the nuclear levels do not play a decisive role in determining the form of the distribution. This observation is significant in view of the fact that the momentum combinations l_1, l_2 are governed by the relative parity π_0/π_2. The result may, however, stem from choice of a set of transmission coefficients associated with a nucleus in the neighborhood of the s-wave neutron resonance of the optical model.

Another clearly apparent feature in each of Figs. 26–29 is the decrease in variation of the a_ν^* as the target spin J_0 becomes larger; in other words, the distributions have larger amplitude and are more acutely influenced by the residual nuclear spins J_2 and J_3 when the initial spin J_0 is low, as has long been known. In this sense, J_0 exerts a more crucial influence upon distribution structure than do J_2 or J_3.

We begin by discussing the results for *dipole radiation*. No disparity was found between the influences of J_2 and J_3 upon the form of the γ distribution. Furthermore, the a_2^* are in all cases numerically largest when $J_2 = J_3$ and smallest when $|J_3 - J_2| = 1$. It was found that a_2^* is predominantly negative when $|J_3 - J_2| = 1 = L$ (distributions peak at 90°) and positive when $J_3 - J_2 = 0 = L - 1$ (distributions dip). To this rule of systematics, only the curves for large numerical values of $J_0 (\gtrsim 4)$ appear to constitute an exception—and this may be a specious deviation resulting from too low a limit upon the partial waves taken into consideration ($l \leq 4$) when high nuclear spins are involved.

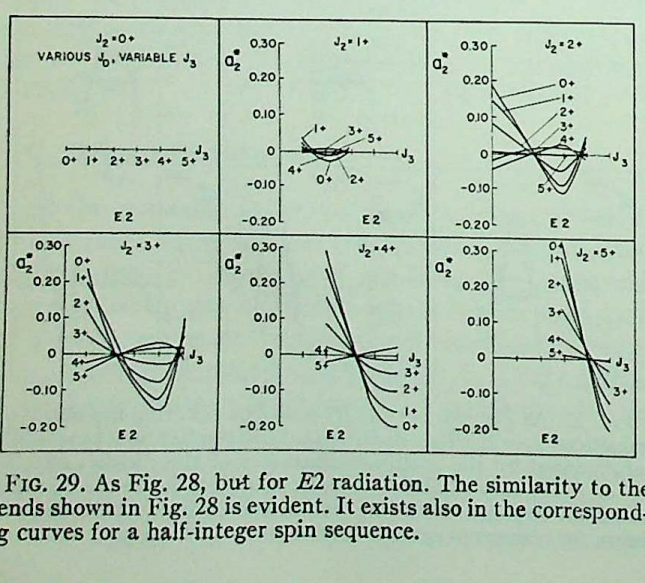

FIG. 29. As Fig. 28, but for $E2$ radiation. The similarity to the trends shown in Fig. 28 is evident. It exists also in the corresponding curves for a half-integer spin sequence.

The character of the a_2^* curves for *quadrupole radiation*, Figs. 28 and 29, is altogether different from the preceding, and of rather more complicated structure. As a general rule applicable to quadrupole transitions when the spin of the final nuclear state is not too small ($J_3 \gtrsim \frac{3}{2}$), it was found that a_2^* tends to vanish for $J_2 = J_3 - 2$ and $J_2 = J_3 + 1$, and to reach a local maximum between $J_2 = J_3$ and $J_2 = J_3 - 1$. The over-all systematic features can be expressed in tabular form (Table V) listing the predominant sign of the a_ν^* and the resultant distribution structure (expressed in a self-evident symbolic form: Λ, M, W, V, corresponding to the distribution curves shown in Fig. 25).

TABLE V. a_ν^* characteristics and distributional structure for quadrupole radiation, in terms of the spin difference of transition levels.

$J_3 - J_2$	a_2^*	a_1^*	Form
−2	+ (large)	−	V
−1	+	+ (large)	W
0	− (large)	− (large)	M or Λ
+1	− (large)	+ (small)	Λ
+2	+	− (vanishing)	V

11. ANALYSIS OF EXPERIMENTAL γ DISTRIBUTIONS FOR HEAVY NUCLEI

We here confine attention to a portion of the extensive set of measurements undertaken by the Texas group under I. L. Morgan, who determined γ distributions over a wide range of angles for $(n, G\gamma)$ processes on nuclei ranging from those of low mass[25] (C^{12}, N^{14}, O^{16}) and medium mass (see Refs. 24, 25, 33, 39–41) (Mg^{24}, Al^{27}, Si^{29}, Ca^{40}, Fe^{56}) to the heavy nuclei[25,37,42] $Pb^{206,207,208}$ and Bi^{209}. Absolute γ-distributions from inelastic scattering of 4.1- and 2.5-MeV neutrons on these latter heavy nuclei form the subject of analysis in this section, since they involve a large variety of spin sequences, satisfy the requirements of the statistical

[39] R. W. Benjamin, D. O. Nellis, and I. L. Morgan, Bull. Am. Phys. Soc. 8, 478 (1963).
[40] R. W. Benjamin, D. O. Nellis, I. L. Morgan, and W. E. Tucker, Bull. Am. Phys. Soc. 9, 153 (1964).
[41] I. L. Morgan, Bull. Am. Phys. Soc. 9, 154 (1964).
[42] D. O. Nellis, I. L. Morgan, and R. W. Benjamin, Bull. Am. Phys. Soc. 8, 478 (1963).

CC-0. In Public Domain. Gurukul Kangri Collection, Haridwar

Digitized by Arya Samaj Foundation Chennai and eGangotri

continuum assumption, and up to the present have only in part been compared with theoretical predictions.[43–49] The application of theory not only illustrates several of the facets covered in preceding sections and raises fresh points of interest, but in the case of Pb^{206} complements the discussion of inelastic neutron distributions presented in Sec. 8.

In each instance, we have employed the maximum number of partial waves for which Perey–Buck transmission coefficients $T_l^{(\pm)}$ have been listed ($l \leq 5$), and taken account of extra exit channels to states of known (or assigned) spin, of γ-cascade contributions and of mixed multipolarity in observed and unobserved γ transitions. The results are depicted in a representation similar to that adopted by the Texas group, who normalized all data to unity at $\theta_2 = 90°$ and cited numerical cross sections separately. We have used this normalization here (even though it can adversely affect the extent of over-all agreement if the point for 90° appears to be either flagrantly high or low with regard to the distribution of the remaining points) simply because the experimenters gave particular attention to the 90° measurement and because the present results can thereby more easily be compared directly with the original data (see also Ref. 50). The theoretical curves have been labeled according to the number of exit channels taken into consideration extra to those of the "two-channel approximation" and the number of cascades of given multipolarity whose contribution was added to the cross section for the observed transition. Since in the case of γ radiation in cascade transitions of mixed multipolarity no information was available about the mixing ratios, separate cases had to be considered in each instance; the respective transitions were treated as if of pure magnetic or pure electric multipole character. The numerical result in either case was almost the same[50] at 90°, but the structure depended markedly upon the multipolarity. The 90° differential cross section was then derived by adding all the contributions from *pure* cascade transitions (irrespective of multipole character) to those from *mixed* transitions taken as of pure magnetic multipolarity (Cascade case M) or of pure electric multipolarity (Cascade case E) throughout. Hence, e.g., for the four cascades $E2$, $M1/E2$, $M1/E2$, $E1$ added to the observed $E2$ decay of the first excited state of Pb^{206} we depict the cross section for the combination $E2$, $M1$, $M1$, $E1$ as 4CaM and for the combination $E2$, $E2$, $E2$, $E1$ as 4CaE. In absence of detailed knowledge concerning the individual cascade fractions, the respective contributions have been summed directly without introducing the weighting factors employed in Sec. 9.

Results for Pb^{206} at $E_n = 4.1$ MeV are shown in Fig. 30, the upper portion of which refers to the decay of the first excited state and the lower portion to the $3^+ \rightarrow 2^+$ transition from the third to the first level. In both instances, not only the experimental magnitude but also the distribution amplitude exceed the theoretical values. The specious numerical agreement in the two-channel approximation is lost as soon as extra exit channels are taken into account, and only up to a point redeemed by the inclusion of cascade contributions. The situation is complicated by the fact that only 10 of the 18 extra levels shown in the level scheme in Fig. 30 have been observed by nuclear bombardment (these are depicted as full lines, whereas the others are shown dashed). This results in an ambiguity not only as to the number of extra channels which should be taken into consideration, but also as to the inclusion or exclusion of cascade contributions to the $3^+ \rightarrow 2^+$ differential cross section (energy-level compilations[51] show two cascades, depicted as dashed vertical lines in Fig. 30, from 4^+ states feeding the 3^+ level). Under the circumstances, results of computations for both of these possibilities have been given. It is more likely, though, that the results for 18 extra channels and 2 cascades represent the more meaningful choice of the two alternatives. In either case, the $M1$ component is preponderant in the observed transition.

The same procedure has been adopted in the case of the ground-state transition shown in the upper part of Fig. 30, where all four cascades, depicted as solid

---

[43] Beyster penetrabilities (Refs. 44, 45) for $l_1 \leqq 4$, $l_2 \leqq 3$ have been used by Nellis (Ref. 37 and private communication) to derive theoretical distribution curves for the $2^+ \rightarrow 0^+$ γ transition in Pb^{206}, using emended Hosoe–Suzuki formulae (Refs. 47, 48) and for the $3^- \rightarrow 0^+$ γ transition in Pb^{208}, using hand-calculated expressions (Ref. 37) which check against those furnished by the code "MANDY."

[44] R. G. Schrandt, J. R. Beyster, M. Walt, and E. W. Salmi, Los Alamos Report LA-2099 (1957) (unpublished).

[45] For a discussion concerning the present status of the transmission coefficients tabulated by R. G. Schrandt, J. R. Beyster, M. Walt, and E. W. Salmi (Ref. 44), see the comments of R. B. Day in Ref. 46.

[46] R. B. Day, in *Progress in Fast Neutron Physics*, edited by G. C. Phillips, J. B. Marion, and J. R. Risser (University of Chicago Press, Chicago, 1963), pp. 111 and 268.

[47] In the appendix to the paper of M. Hosoe and S. Suzuki (Ref. 48), the last three curly brackets of Eq. (8) should read, respectively, $\{3+1.714P_2(\cos\theta)\}$, $\{4-0.7143P_2(\cos\theta)\}$, $\{6+0.8571P_4(\cos\theta)\}$, and the second curly bracket of Eq. (9) should read $\{6+1.6837P_2(\cos\theta)\}$. The expression for the γ distribution given in the appendix to the paper of F. D. Seward (Ref. 49) has an error in the penultimate bracket, which should read $(10+4.762P_2-2.857P_4)$.

[48] M. Hosoe and S. Suzuki, J. Phys. Soc. Japan **14**, 699 (1959).

[49] F. D. Seward, Phys. Rev. **114**, 514 (1959).

[50] The differential cross section at 90° is given by the expression $d\sigma(90°) = a_0 - (1/2)a_2 + (3/8)a_4 - (5/16)a_6 + (35/128)a_8 - \cdots$, in which the δ-independent term a_0 is numerically predominant. Hence the influence of δ through the higher-order terms $a_2, a_4, \cdots$ is slight. We have already drawn attention to the vanishing of the δ-dependence at 55° and 125° when terms higher than a_0 and a_2 are vanishingly small. In the general case, the influence of the mixing ratio δ is most perceptible at 0°, where $d\sigma(0°) = \Sigma_\nu a_\nu$.

[51] K. Way, N. B. Gove, C. L. McGinnis, and R. Nakasima, in *Energy Levels of Nuclei* (Springer-Verlag, Berlin, 1961), Group I, Vol. 1 of Landolt-Börnstein, *Nuclear Physics and Technology*, New Series. See also, *Nuclear Data Sheets*, compiled by the Nuclear Data Group, under K. Way, at the Oak Ridge National Laboratory.

CC-0. In Public Domain. Gurukul Kangri Collection, Haridwar

Digitized by Arya Samaj Foundation Chennai and eGangotri

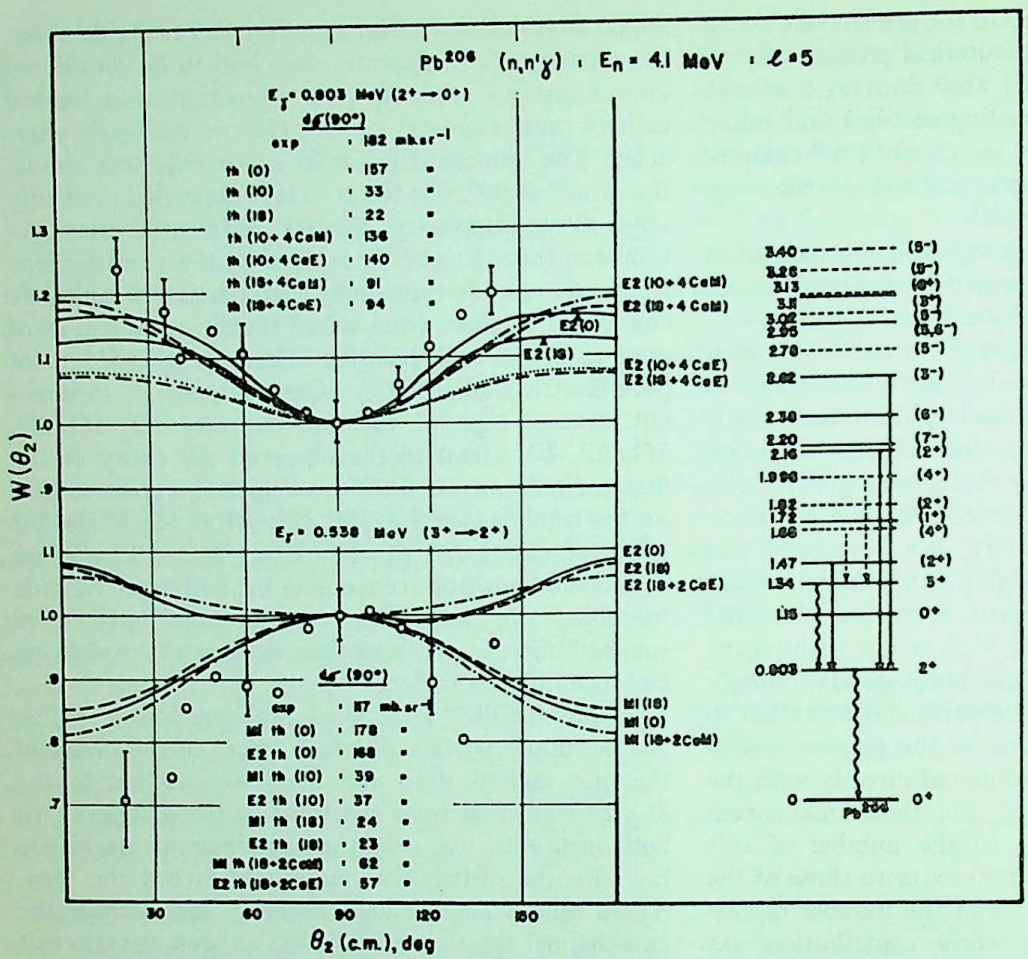

FIG. 30. Comparison of the experimental data of Morgan *et al.* (Refs. 25, 37, 42) with theoretical curves for two γ distributions following inelastic scattering of 4.1-MeV neutrons on Pb^{206}. The theoretical functions have been calculated with Perey–Buck transmission coefficients $T_l^{(\pm)}$ up to $l_{max}=5$. The nomenclature and the level scheme (which differs very slightly from that adopted for Fig. 17, with which the present results should be compared) are explained in the text. The rather poor structural and numerical agreement may be a result of insufficient consideration of cascade contributions to the cross section for the observed radiation or, in the case of the 0.538-MeV $3^+ \rightarrow ?^+$ transition, to a consideration of pure radiation only, rather than an $M1+E2$ mixture with $0>\delta\gtrsim-0.5$.

vertical lines, stem from levels observed in nuclear bombardment.

The unacceptably poor agreement between theory and experiment can most likely be ascribed to inadequate recognition of additional cascade contributions, whose influence upon the magnitude and structure of the distributions would suffice to reduce the discrepancies very appreciably. Only those cascade contributions involving a single unobserved γ transition have been included in our calculations.

Note added in proof. On the other hand, some improvement in fit would, as in the cases to follow, result for the 0.538-MeV $(3^+\rightarrow 2^+)$ γ distribution on admitting an $E2$ admixture with $0>\delta\gtrsim-0.5$ to the observed preponderantly $M1$ radiation.

We next discuss each of the results for Pb^{207} at $E_n=4.1$ MeV, shown in Figs. 31 and 32. The experimental data in the upper part of Fig. 31 are distributed too discontinuously for any conclusion to be drawn as regards the multipole mixture from a comparison with the theoretical curves. Even though a *structural* comparison is precluded, the right numerical magnitudes are obtained when three extra exit channels are taken into account. The ground-state transition treated in the lower part of Fig. 31 has a more regular distribution, which in form and magnitude is well fitted by theoretical curves for predominantly $M1$ radiation when three extra exit channels are included in the calculation. The best fit ensues when the de-excitation radiation is taken to contain a 25% admixture of $E2$ multipolarity ($\delta=-0.5$). This is evident in the figure, and so is the fact that distribution curves for pure multipolarity do not represent bounds between which those for mixed multipolarity must invariably lie. In this instance, the $\delta=-0.5$ curve would roughly represent a lower bound and a $\delta=+1.7$ curve an upper bound, as is explained later. If account is taken of a γ cascade from the $\frac{7}{2}^-$ level (pure $E2$ multipolarity), the structural agreement remains excellent, the best fit being attained with $\delta=$ rather than $\delta=-0.5$ for the observed transition. The cascade, however, contributes a large cross section which somewhat impairs the numerical agreement.

For the nucleus Pb^{207} at $E_n=4.1$ MeV, the Texas group also measured the angular distribution of 2.64-MeV γ radiation which they tentatively attributed to de-excitation of a level at 2.635 MeV of unknown spin-parity recently observed by Cranberg[52] in the course of inelastic neutron scattering investigations. A least-squares-fit analysis to establish the values of the normalized Legendre weighting coefficients a_ν^* appropriate to this distribution gave the result $a_2^*=+0.188$, $a_4^*=$ -0.009. The small value of a_4^* led the authors to suggest a dipole assignment to the radiation and thence a spin assignment of $\frac{3}{2}^\pm$ to the 2.635-MeV level. C

[52] L. Cranberg (private communication).

CC-0. In Public Domain. Gurukul Kangri Collection, Haridwar

Digitized by Arya Samaj Foundation Chennai and eGangotri

these two possibilities, the present more detailed analysis rules out the spin $\frac{3}{2}^+$, and in its stead suggests the further alternatives $\frac{5}{2}^{\pm}$. A set of computations has been carried out with J_2 set to $\frac{3}{2}^{\pm}$, $\frac{5}{2}^{\pm}$, $\frac{7}{2}^{\pm}$, noting that the anisotropy of the observed distribution eliminates a $\frac{1}{2}^{\pm}$ spin assignment. Four extra exit channels were taken into consideration, leading to levels of Pb^{207} shown in Fig. 31, and the values of a_2^* and a_4^* so determined were compared with those established empirically. To this end, it was necessary to allow for multipole mixing in the case of $\frac{3}{2}^-$, $\frac{5}{2}^+$, and $\frac{7}{2}^-$ assignments and to plot the results in a form amenable to comparison with the experimental values. The δ ellipse representation which, in general, would be well suited to this purpose is in the present case precluded by the fact that the loci of points for different values of δ in δ-dependent distributions lie along straight lines of mutually differing slope in a plot of a_4^* vs a_2^*, and not along ellipses. The extremum values of δ characterizing the ends of each of the lines can readily be derived from a knowledge of the multipole terms $M(L_2L_2)$, $M(L_2L_2')$, $M(L_2'L_2')$ [see Eq. (26)]. When the a_2^* for a given value of δ (for instance, $\delta=0$) is known, that for any other value of δ can be generated[53] from the expression

$$a_2^*(\delta)=a_2^*(0)[M(L_2L_2)+2\delta M(L_2L_2')+\delta^2M(L_2'L_2')]\times[(1+\delta^2)M(L_2L_2)]^{-1}. \quad (73)$$

In order that $a_2^*(\delta)$ be an extremum, its derivative with respect to δ must vanish. This provides the condition

$$\delta^2[M(L_2L_2')]-\delta[M(L_2'L_2')-M(L_2L_2)]-M(L_2L_2')=0, \quad (74)$$

whence

$$\delta_{\text{lim}}=\{M(L_2'L_2')-M(L_2L_2)\pm[M^2(L_2'L_2')-2M(L_2L_2)M(L_2'L_2')+M^2(L_2L_2)+4M^2(L_2L_2')]^{\frac{1}{2}}\}/[2M(L_2L_2')]. \quad (75)$$

Substitution of the numerical values of the M terms as listed in the computer output furnishes the limiting δ values. (E.g., the values $\delta=-0.577$ and $\delta=+1.732$ in the case of $M1+E2$ radiation effecting a $\frac{3}{2}^-\rightarrow\frac{1}{2}^-$ transition, already cited in connection with the lower part of Fig. 31. For $M2+E3$ radiation effecting a $\frac{5}{2}^+\rightarrow\frac{1}{2}^-$ transition, the limiting δ values are -0.707 and $+1.414$, and for $M3+E4$ radiation in the case of a $\frac{7}{2}^-\rightarrow\frac{1}{2}^-$ transition the limiting δ values are -0.775 and $+1.291$.) Thence the extremum values of a_2^* can easily be determined and bounds to the straight lines in the a_4^* vs a_2^* representation established.

Accordingly, the alternative representation of $|\delta|$ vs a_2^* was adopted for comparison with the experimental value; this is shown at the top of Fig. 32. Since calculations showed that for each of the possible spin assignments the value of a_4^* is so small compared with a_2^* that its influence upon the distribution structure is negligible, it suffices to compare the a_2^* values alone. Fig. 32 clearly indicates that a spin $\frac{3}{2}^+$ assignment is unacceptable, but that the data are compatible with the assignments $\frac{3}{2}^-$ (for $M1+E2$ mixed radiation with $\delta=\delta_{\text{lim}}=+1.732$), $\frac{5}{2}^-$ (pure $E2$), or $\frac{5}{2}^+$ (for $M2+E3$ radiation with $\delta\approx 0$ or $\delta\simeq -2.4$). For each of these possibilities, it was confirmed that not only the distribution structure, but also the absolute magnitudes agree well with the experimental data. A reduction of the error limits in the latter would assist in discriminating between the remaining alternatives.

In Fig. 33 are depicted results for the ground-state transition from the first level (3^-) of Pb^{208} at various incident neutron energies, when account is taken of

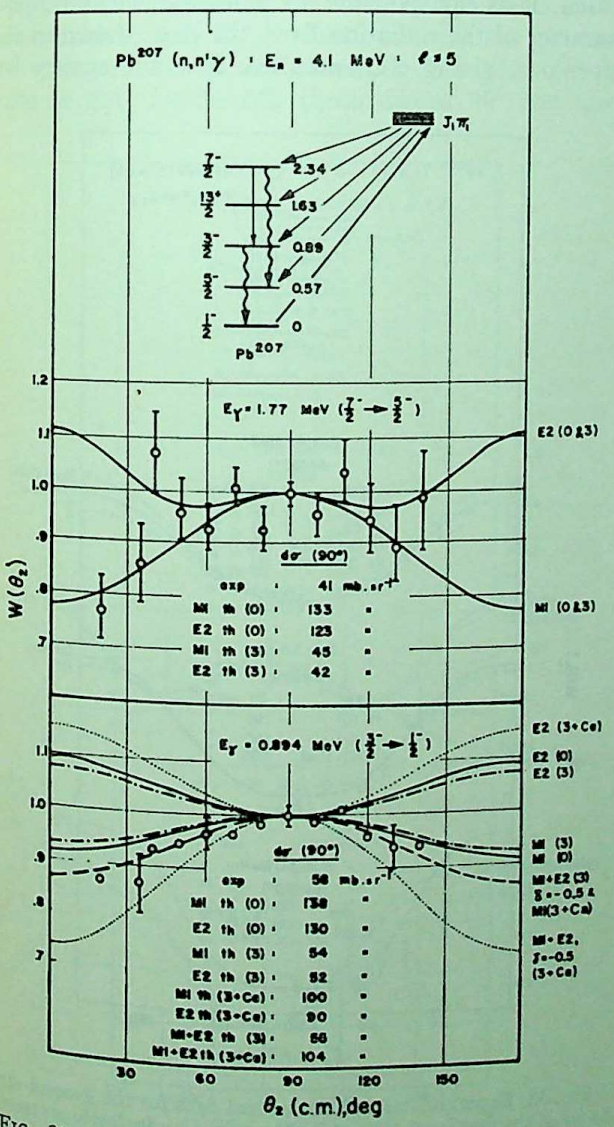

FIG. 31. Preliminary measurements by the Texas group of two γ-distributions following inelastic scattering of 4.1-MeV neutrons on Pb^{207}, compared with theoretical predictions based on Perey–Buck penetrabilities for $l\leqq 5$.

[53] For generating the $a_\nu^*(\delta)$ in general, it may be better to commence from those for $\delta=1$ or $\delta=\infty$ (pure L_2' radiation), since the range of ν for pure L_2 radiation may be lower than for L_2'.

CC-0. In Public Domain. Gurukul Kangri Collection, Haridwar

Digitized by Arya Samaj Foundation Chennai and eGangotri

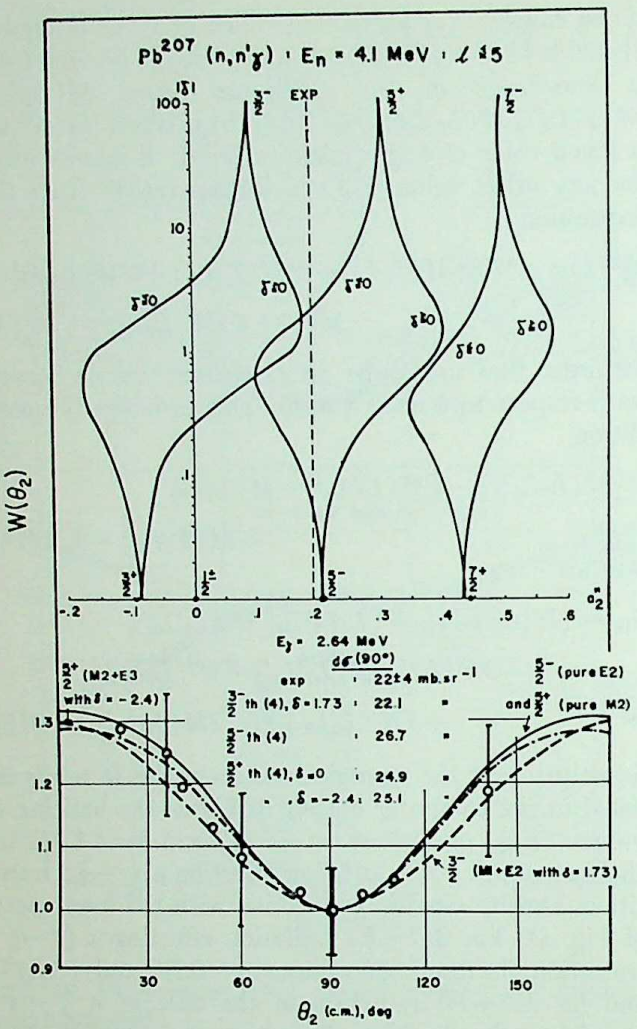

FIG. 32. Experimental distribution of a 2.64-MeV γ-ray transition observed by the Texas group and ascribed to de-excitation of a level at 2.635 MeV recently detected by Cranberg (Ref. 52), compared with theoretical predictions for various assignments of spin and parity for this level. The experimental data are commensurate with the possible assignments $\frac{3}{2}^-(M1+E2$ radiation with $\delta=+1.73)$, $\frac{5}{2}^-$(pure $E2$ radiation), or $\frac{5}{2}^+(M2+E3$ radiation with $\delta\approx 0$ or $\delta\cong -2.4)$.

several extra exit channels and cascade contributions. As expected, the agreement in magnitude and structure improves with increasing energy (threshold effects clearly persist at 3 MeV), and at the highest energy may be regarded as satisfactory. Although only three cascade transitions to the 3^- level are shown in Nuclear Data Sheets,[51] the 1.36-MeV γ transition observed by Nellis[25,42] has tentatively been ascribed to γ decay from the 3.961-MeV (6^-) state to the 3^- level at 2.615 MeV, and its contribution to the de-excitation cross section of the 3^- state was therefore included in the calculation —it is in any case very small compared with the other three cascade contributions. Independent calculations by Nellis[54] using Beyster penetrabilities up to $l_1\leq 4$, $l_2\leq 3$ have yielded good fits to the distribution structure as well as good numerical agreement with the experimental results. At $E_n=4.1$ MeV, the value of $d\sigma(90°)$ was 84 mb sr^{-1} on considering only three extra exit channels (up to the 3.709-MeV level) and two cascades (from the 3.198-MeV and the 3.475-MeV levels), of which the second was taken to be of pure $M1$ multipolarity. At $E_n=3.5$ MeV, Nellis obtained the result $d\sigma(90°)=60$ mb sr^{-1} on including two extra channels (to the 3.198- and the 3.475-MeV levels) and one cascade (from the 3.198-MeV level), whereas at $E_n=3.0$ MeV, the cross section was determined as $d\sigma(90°)=34$ mb sr^{-1} on the basis of the two-channel approximation which is valid in this latter case. The use of fewer partial waves and of Beyster penetrabilities is responsible for the cross sections being lower throughout than those given in the present paper, and hence in better agreement with the values established experimentally.

The data shown in Fig. 34 for two γ transitions going to the 3^- first level of Pb^{208} following inelastic scattering of 4.1-MeV neutrons represent preliminary measurements, which have rather large error limits. For this reason, it is not possible to elucidate the multipole character of the radiation from the data shown in the upper part of Fig. 34, and there is a discrepancy be-

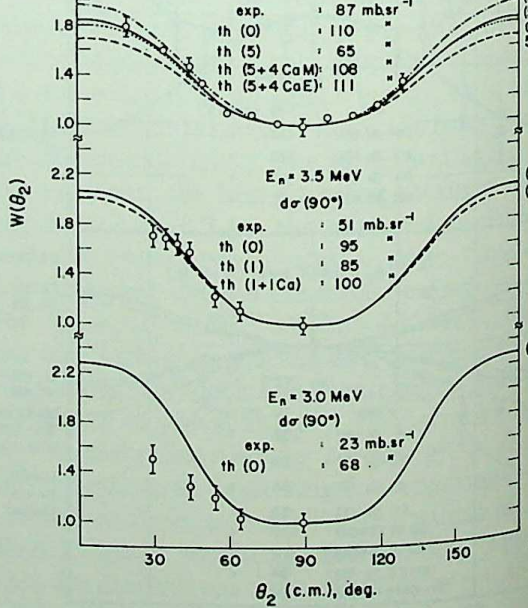

FIG. 33. Experimental and theoretical data for the ground-state decay of the first level (3^-) of Pb^{208}, excited by inelastic scattering of 3-, 3.5-, and 4.1-MeV neutrons. With increasing energy the degree of agreement improves, which could be an indication that threshold fluctuation effects are playing an ever diminishing role.

[54] D. O. Nellis and I. L. Morgan (private communication).

CC-0. In Public Domain. Gurukul Kangri Collection, Haridwar

Digitized by Arya Samaj Foundation Chennai and eGangotri

tween the rather small experimental cross section and those calculated theoretically. Since measurements of the K-conversion coefficient α_K yield a value consistent with $M1$ or $E3$ multipolarity, we infer that the $M1$ curve is more likely to apply to this situation.

The set of results in the lower part of Fig. 34 is not symmetrical about 90° and hence cannot be fitted adequately by any theoretical curve, but the numerical cross section at 90° agrees well with the calculated values when three cascades are taken into consideration. The cascades shown as dashed vertical lines in Fig. 34 have been taken over nuclear level schemes,[51] whereas those shown as full vertical lines correspond with those observed by Nellis *et al.*[37]

The results for the $\frac{1}{2}3+\rightarrow\frac{9}{2}-$ γ transition in Bi^{209} at the two incident neutron energies $E_n=2.55$ MeV and $E_n=4.1$ MeV shown in Fig. 35 illustrate the almost isotropic distribution for a transition which takes place between levels of high spin (the vertical scale in the distribution function is therefore very extended). A noteworthy feature of the distributions is the fact that the structure for an $E3$ transition is practically the same as that for an $M2$ (both dip at 90° and have

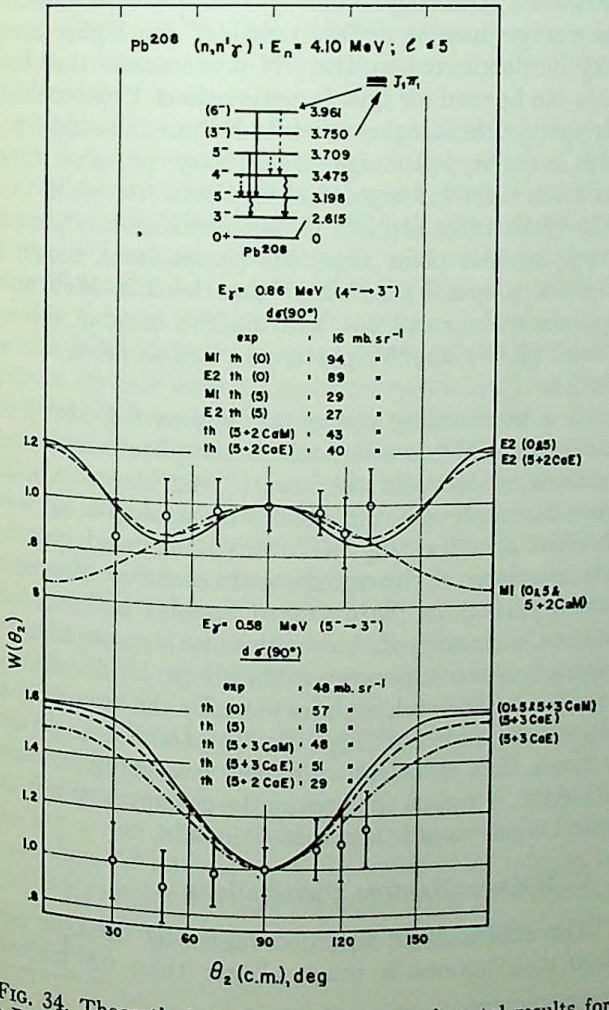

FIG. 34. Theoretical and preliminary experimental results for the Pb^{208} $(n, n'\gamma)$ reaction at $E_n=4.1$ MeV, including the effect of extra exit channels and cascade contributions.

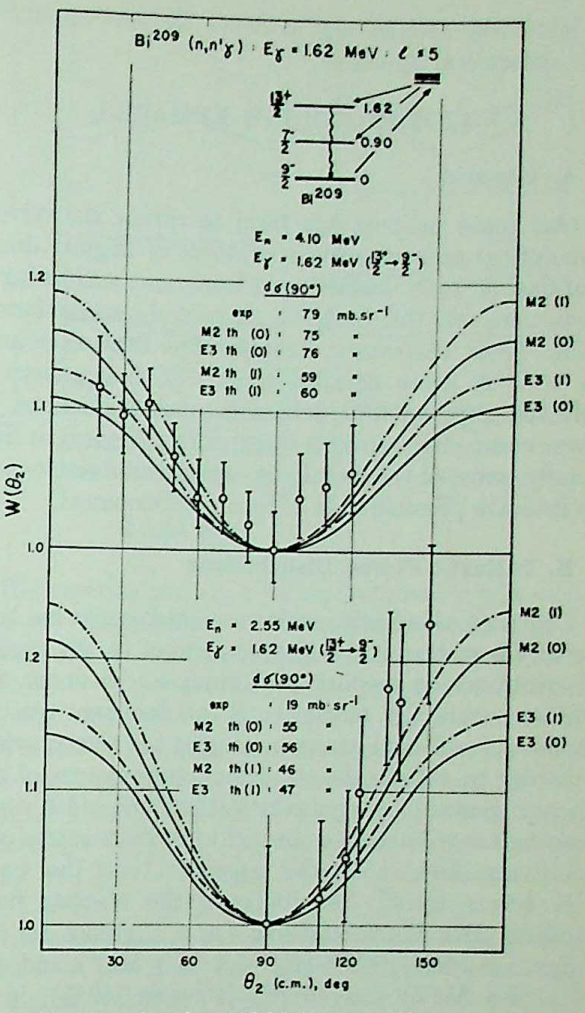

FIG. 35. Data for the 1.62-MeV γ-ray distribution in the transition $13/2^+\rightarrow 9/2^-$ in Bi^{209}, initiated by inelastic neutron scattering at $E_n=2.55$ MeV and $E_n=4.1$ MeV. The distribution between levels of such high nuclear spin is almost isotropic, for which reason the vertical scale has been exaggerated.

roughly the same small amplitude), unlike results for other spin sequences, which displayed the tendency for curves of opposite multipole character to be roughly mutual inversions of one another. Comparatively little is known of the level scheme of Bi^{209}, and hence the calculations could take only one extra channel into account, namely that to the intermediate $\frac{7}{2}-$ level at 0.90 MeV. The numerical agreement can accordingly be classed as but fair (at the lower energy, threshold effects play a decisive role), yet the structural agreement is good. Because of the special characteristics of the distribution functions, no conclusion as regards the multipole mixing in the observed radiation could be drawn. It might be mentioned in conclusion that the evaluation of the distribution for a high-spin sequence such as the above was made possible only through the existence of an automatic code for a high-speed computer, since the very large number of terms which figure in the tabulation preclude hand calculation (there are 800 terms to be built and summed over for $l\leq 5$). The results may therefore be considered to provide

CC-0. In Public Domain. Gurukul Kangri Collection, Haridwar

Digitized by Arya Samaj Foundation Chennai and eGangotri

particularly satisfactory evidence for the validity of the theoretical approach.

12. CONCLUDING REMARKS

A. General

Our main purpose has been to review the current theoretical and experimental status of angular distributions of both inelastic nucleons and succeeding γ radiations on the basis of compound-nucleus formation. Their systematic behavior has been examined, as well as some detailed aspects of comparisons of selected experimental data with such predictions. In these concluding remarks we attempt to review, at least briefly, some of the remaining experimental results, and to indicate possible lines of future development.

B. Inelastic Proton Distributions

One area of inelastic nucleon scattering that has been greatly neglected is the measurement of (p, p') angular distributions in medium and heavy nuclei under conditions where CN formation is the dominant reaction mode and sufficient energy averaging has been provided in order to satisfy the statistical requirements of this theory. Seward's early investigations[49] provided a pioneering contribution to this field. He deliberately used relatively thick (150-keV) targets, in order that many CN levels would contribute to the reaction being studied. His distributions of (p, p_1') groups for Ti^{48} ($E_p<5.5$ MeV), Cr^{52} ($E_p=5.4-7.0$ MeV) and Fe^{56} ($E_p=5.5$ MeV) were nearly isotropic (10%), in essential agreement with the theoretical predictions for such 2^+ states. One exception was seen for Ti^{48} ($E_p=7.02$ MeV), with a distinct forward peaking typical of a direct interaction contribution. His excitation curves ($E_p=3.5-7$ MeV, $\theta_1=90°$) did reveal some "intermediate" structure, which he attributed to fluctuations in the number or properties of the several CN levels included in his energy spread of 150 keV. Since his angular distributions were taken at only a few scattered incident energies, any possible effect of this intermediate structure on such distributions was not investigated.

Recently, two more exhaustive investigations concerning the excitation curves[55] and angular distributions[56] of many Ni^{58} (p, p') groups have been initiated, the basic impetus being a search for possible intermediate resonances or at least structure. The excitation curves (taken in 25-keV steps from 8 to 11 MeV with a 25-keV target) show small fluctuations (±15%) as well as some broader structure.[55] The angular distribution data (taken in 25-keV steps from 9.12 to 9.5 MeV with a 18-keV target) for most of the (p, p') groups reveal many rapid fluctuations. In addition, in the case of the (p, p_1') group some intermediate structure is also apparent.[56] These fluctuating distributions emphasize the importance of sufficient energy averaging if comparisons with CN theory are contemplated.

Energy averages of these data (corresponding to an energy spread of ≈300 keV) are shown in Fig. 36. Since the experimental points represent relative cross sections, they have been normalized [by the same factor for all (p, p') groups] for purposes of comparison with the theoretical differential cross sections. The forward peaking for the Ni^{58} (p, p_1') group (1.33-MeV first 2^+ state) reveals a substantial DI contribution; in addition, part of the $\theta_1=90°$ peaking for the 2.46-MeV (4^+) group could have a similar origin. The remaining (p, p') distributions of Fig. 36 are essentially symmetric about 90°, with only that for the 2.90-MeV state having any appreciable fore–aft asymmetry. In the latter case the experimental distribution has an asymmetry closely resembling the prediction (dashed curve) for a 1^+ level which includes a contribution for an unresolved 2.94-MeV state (assumed to be 6^+). It is quite possible that these experimental distributions for the higher levels may be dominated by the CN process, and that such data can be used for spin determinations. Unfortunately, the spins of these higher states in Ni^{58} are not established with certainty, although preliminary $(p, p'\gamma)$ data[57] favors a spin-2 assignment for both the 3.04- and 3.26-MeV states of Ni^{58}. If any conclusions are to be drawn at this point from the comparisons shown in Fig. 36, a spin-0 possibility[57] for the 2.78-MeV state appears to be ruled out both on the basis of the observed (p, p') angular pattern as well as relative cross section.

At a bombarding energy as high as 9.5 MeV, one can expect DI contributions to complicate such comparisons, at least for the lowest-lying states. A much more favorable situation should be attainable at lower incident energies (say, 4–7 MeV), although possible contributions of intermediate resonances (including analog states) to the averaged angular patterns may have to be considered. An obvious first step would be the measurement of an energy-averaged (p, p') distribution for a known 0^+ level, in order to verify the large fore–aft asymmetry expected (Figs. 18, 36) as well as to provide a check that sufficient statistical averaging has been achieved. A search for previously unknown spin-0 and spin-1 levels would then be worthwhile.

C. Inelastic Neutron Distributions

The experimental situation regarding inelastic neutron distributions is much clearer than for inelastic

[55] J. E. Monahan, A. J. Elwyn, R. E. Segel, L. L. Lee, Jr., L. Meyer-Schützmeister, Z. Vager, and P. P. Singh, Bull. Am. Phys. Soc. 10, 495 (1965); A. Elwyn, L. L. Lee, Jr., L. Meyer-Schützmeister, J. E. Monahan, R. E. Segel, P. P. Singh, and Z. Vager, *ibid.* 10, 104 (1965).

[56] R. K. Mohindra and L. W. Swenson, Bull. Am. Phys. Soc. 10, 496 (1965); L. W. Swenson, R. K. Mohindra, and D. M. Van Patter, *ibid.* 10, 104 (1965).

[57] S. M. Shafroth, A. K. Sen Gupta, and G. T. Wood, Bull. Am. Phys. Soc. 9, 93 (1964); and private communication.

CC-0. In Public Domain. Gurukul Kangri Collection, Haridwar

Digitized by Arya Samaj Foundation Chennai and eGangotri

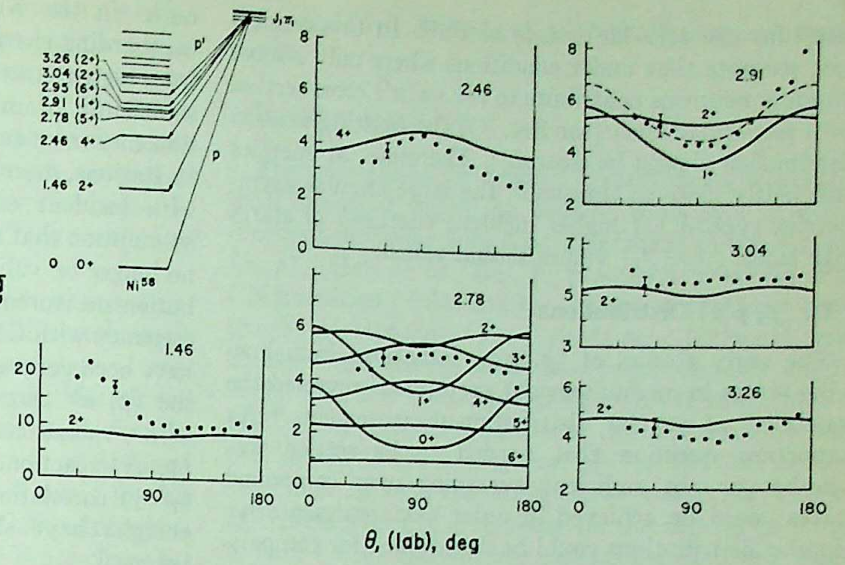

FIG. 36. Comparison of the averaged angular distribution results of Mohindra and Swenson (Ref. 56) for six $Ni^{58}(p, p')$ groups with theoretical predictions for $E_p=9.35$ MeV based on an optical model of the derivative Woods–Saxon type (see Sec. 8). The data represent the average of 16 distributions taken in the range $E_p=9.12-9.55$ MeV, using a 18-keV target. They have been subjected to a single over-all normalization in order to fit them to the theoretical region of values.

proton distributions as far as comparisons with CN theory are concerned. A key factor is the fact that substantial CN cross sections are attainable for most levels ($J_2<5$) for neutron energies not much (a few hundred keV) above threshold, irrespective of the nuclear mass. Auerbach and Moore[58] have recently reviewed the comparisons between theory and experiment for heavy nuclei (Ta^{181}, W^{184}, Th^{232}, Pb^{208}), while Cranberg included a discussion of his preliminary data for Pb^{206}, Pb^{207} and Bi^{209} in his earlier review.[34]

Angular distributions having large anisotropies typical of spin-0 states have thus far been reported only for 0^+ levels in Pb^{206} (1.19 MeV) and Ce^{140} (1.90 MeV).[34] The angular distributions for low-lying 2^+ states (W^{184}, Th^{232}, U^{238}) are nearly isotropic, and consistent with theoretical calculations,[58] which predict only a slight peaking (about 10%) at 90°. Cranberg's distribution for the 0.80-MeV 2^+ level of Pb^{206} ($E_n=2.50$ MeV) shows a distinct fore–aft asymmetry ($\approx$25%) which is considerably less than that predicted unless level-width fluctuations are taken into account.[36] For levels of higher spins (3^+, 4^+), the experimental distributions are typically nearly isotropic as expected, although recent data of Gilboy and Towle[59] for the 2.085-MeV 4^+ state in Fe^{56} indicate a slightly larger peaking at 90° than predicted for $E_n=3.99$ MeV. Another possible disagreement exists in the case of their data for the 2.62-MeV 3^- state of Pb^{208} for $E_n=3.96$ MeV, since the least-squares fit indicates a minimum ($\approx$30 %) rather than the predicted peaking ($\approx$10%) at 90°. There is a puzzling discrepancy (see Fig. 33) in the Pb^{208} $(n, n'\gamma)$ distribution results[54] for an incident energy of 3.0 MeV, which is closer to threshold, but there are satisfactory fits at $E_n=3.5$ and 4.1 MeV. It would be of interest to see if this possible discrepancy in the (n, n') distribution persists or perhaps increases for neutron energies closer to threshold.

The experimental (n, n') distributions for odd nuclei bear out the systematic predictions shown in Figs. 23 and 24. For example, the angular distributions for states in Pb^{207} ($J_0=\frac{1}{2}^-$) should be roughly comparable with the ($J_0=\frac{1}{2}$) curve of Fig. 23, i.e., one should expect low spin states to have the most asymmetric (n, n') distributions. Cranberg's angular distributions[34] for the 0.89-MeV ($\frac{3}{2}^-$) and 0.57-MeV ($\frac{5}{2}^-$) states have large asymmetries $[W(0°)/W(90°)]$ decreasing from about 1.7 to 1.2 as (J_2-J_0) changes from 1 to 2, while that for the 1.63-MeV ($\frac{1}{2}^+$) state with $(J_2-J_0)=6$ is essentially isotropic. The systematic predictions of Figs. 23 and 24 also show that the distribution anisotropy for a given value of (J_2-J_0) should be reduced for a larger target spin J_0. This is borne out in Cranberg's data for Bi^{209} ($J_0=\frac{9}{2}^-$), since the observed asymmetry for the 0.90-MeV ($\frac{7}{2}^-$) state is much smaller (1.1–1.2) than that for the 0.89-MeV state in Pb^{207} which also has $|J_2-J_0|=1$. Recently, Gilboy and Towle[60] have reported preliminary data for Y^{89} ($J_0=\frac{1}{2}^-$) that include some anisotropic as well as isotropic distributions for various levels, some of which appear to be in conflict with tentative spin assignments made earlier by Shafroth *et al.*,[61] provided that the systematic trends of Figs. 23 and 24 remain valid.

The effect of level-width fluctuations on the (n, n') *cross section* near threshold for low-lying states has been clearly demonstrated by the recent work of Tucker, Wells, and Meyerhof.[62] Similar detailed examinations of the effect near threshold on the inelastic neutron *distributions* should be of interest, particularly for low spin states with large predicted asymmetries at higher energies, such as is indicated by Cranberg's preliminary

[58] E. H. Auerbach and S. O. Moore, Phys. Rev. **135**, B895 (1964).
[59] W. B. Gilboy and J. H. Towle, Nucl. Phys. **64**, 130 (1965).
[60] W. B. Gilboy and J. H. Towle, *Comptes Rendus du Congrès International de Physique Nucléaire*, edited by P. Gugenberger (Centre National de la Recherche Scientifique, Paris, 1964), Vol. II, p. 690.
[61] S. M. Shafroth, P. N. Trehan, and D. M. Van Patter, Phys. Rev. **129**, 704 (1963).
[62] A. B. Tucker, J. T. Wells, and W. E. Meyerhof, Phys. Rev. **137**, B1181 (1965).

CC-0. In Public Domain. Gurukul Kangri Collection, Haridwar

Digitized by Arya Samaj Foundation Chennai and eGangotri

data[34] for the 1.19-MeV state of Pb^{206}. In this connection, we note that under conditions where only *s*-wave outgoing neutrons contribute to the (n, n') cross section for a particular level (see Sec. 7), the limiting *neutron* distribution should be isotropic. Therefore, at energies sufficiently close to threshold, the large angular asymmetries typical (at higher incident energies) of states with small $(J_2 - J_0)$ values should vanish.

D. $(p, p'\gamma)$ Distributions

The early studies of $(p, p'\gamma)$ radiations from low-lying states in medium-weight even nuclei revealed the feasibility of angular distribution measurements.[63] An important question that needed to be settled was whether or not sufficient averaging over compound states could be achieved in order that representative angular distributions could be determined for comparison with statistical theory. An average over a rather large number of compound states is required, since it is not the total number which is of concern, but rather the number of states with a small range of J_1 values that have large reduced widths for the (p, p_1') channel of interest. For example, in the case of inelastic excitation of a first 2^+ state at a low bombarding energy, one is mainly concerned with the statistical average of $\frac{3}{2}^+$ and $\frac{5}{2}^+$ states with large (p, p_1') reduced widths. Therefore, the number of compound states (of all J, π) that need to be averaged may be of the order of 10^3 rather than 10^2. For this reason, the first measurements of $(p, p'\gamma)$ distributions were carried out for a series of different bombarding energies to see if any large fluctuations were detected.[28] An example of such measurements is the series shown for Ni^{60} in Fig. 20(b) for $\bar{E}_p = 4.36$–4.96 MeV (solid circles).[28] Since the theoretical predictions vary slowly within this energy interval, it is reasonable to average the four measurements together to improve the statistical averaging. In this example, the average extends over an energy spread of nearly 0.5 MeV and includes an estimated total number of compound states (all J, π) of approximately 2500. While some fluctuations in the individual measurements of $(p, p'\gamma)$ distributions were observed, particularly for the second 2^+ states, the results indicate that adequate statistical averaging was achieved if the energy average included at least 1000 compound states. Obviously, this could be done equally well by making only one distribution measurement with a sufficiently thick target.

The first measurements of such energy-averaged $(p, p'\gamma)$ distributions confirmed the expectation that transitions of the types $4^+(E2)2^+$, $2^+(M1, E2)2^+$ and $0^+(E2)2^+$ could be distinguished for sufficiently prominent γ radiations in the $(p, p'\gamma)$ spectra.[28] These measurements have provided the primary evidence for the identification of $(0^+, 2^+, 4^+)$ triplets for even nuclei in the Ni, Zn region. Unfortunately, for the bombarding energies used (4.4–5.0 MeV), γ radiations from higher states above about 3 MeV are usually not sufficiently prominent to allow good angular distribution measurements. In order to study levels at higher excitations, more recent investigations have been made with incident energies up to 7 or 8 MeV.[29,57] The assumption that DI contributions can be neglected may no longer be valid. Nevertheless, these $(p, p'\gamma)$ distribution measurements have revealed no detectable discrepancy with CN theory to date. These measurements have been generally confined to incident energies below the (p, n) threshold in order to eliminate problems with γ radiations from induced activities as well as the $(p, n\gamma)$ reaction. It is just under these conditions that $(p'-\gamma)$ correlation measurements for such bombarding energies have shown the best agreement with CN theory.[17]

Use of these higher bombarding energies permits the investigation of the complicated nuclear structure typically lying above 3-MeV excitation in such medium-weight nuclei. An interesting problem would be the determination of the $(E1, M2)$ admixture in the decay of the collective 3^- octupole levels, since the sensitivity of a $3^-(E1, M2)2^+$ distribution to the (D, Q) admixture is as large as shown in Fig. 13 for a $3^+(M1, E2)2^+$ transition.

While the use of incident energies in the range of about 5–7 MeV permits the study of higher level structure, it does have the major disadvantage that the $(p, p'\gamma)$ spectra observed with NaI scintillation detectors are typically quite complex.[29,57] With the advent of high-resolution Ge (Li-drifted) detectors, studies of such complicated $(p, p'\gamma)$ spectra have become much more attractive. Using these new detectors, the advantage of the simplicity of the energy-averaged angular distribution measurements will still be maintained, as compared with the more general approach[64] of angular correlation measurements to elucidate magnetic substate populations independently of reaction mechanism.

E. $(n, n'\gamma)$ Distributions

Early measurements of $(n, n'\gamma)$ angular distributions using sodium iodide detectors were subject to technical limitations, particularly low counting rates and large backgrounds. While most of these data were in reasonably good agreement with CN theory, unexplained discrepancies did remain, as pointed out by Van Patter *et al.*[65] in the case of the Fe^{56} $(n, n_1'\gamma)$ reaction. In his recent review of $(n, n'\gamma)$ measurements, Day[46] noted that systematic errors may have been present in some of these earlier measurements. A major advance in this field has been accomplished by the Texas nuclear group who have carried out an extensive program using a tota

[63] D. M. Van Patter, R. Rikmenspoel, and P. N. Trehan, Nucl. Phys. **27**, 467 (1961).

[64] A. E. Litherland and A. J. Ferguson, Can. J. Phys. 39, 788 (1961).

[65] D. M. Van Patter, N. Nath, S. M. Shafroth, S. S. Malik, and M. A. Rothman, Phys. Rev. 128, 1246 (1962).

CC-0. In Public Domain. Gurukul Kangri Collection, Haridwar

Digitized by Arya Samaj Foundation Chennai and eGangotri

absorption γ-spectrometer system for pulsed $(n, n'\gamma)$ measurements, eliminating many of the technical difficulties of previous investigations. From comparisons with theory such as are shown in Figs. 14, 19, 30–34, their results using this system appear to be quite reliable. For this reason, we have chosen samples of only their $(n, n'\gamma)$ distribution data for discussion. In their most recent report, Morgan *et al.*[25] give a detailed summary of their present results.

For target nuclei with $J_0=0^+$, the $(n, n'\gamma)$ angular patterns for levels with spins 1, 2, or 3 differ sufficiently to permit spin assignments if the ground-state γ transitions are prominent enough. For example, Mathur and Morgan[25] have found a $2(Q)0$ distribution for the ground-state decay of the 2.53-MeV state of Ar^{40}, and have clearly eliminated a possibility [66] of spin 1 for this level. They have also identified a $4^+(E2)2^+$ pattern for a 3.22→1.45 MeV transition, although it is not clear that a $2^+(M1, E2)2^+$ possibility has been eliminated. For transitions of mixed multipolarity, the present accuracy of $(n, n'\gamma)$ distribution measurements is usually only sufficient to identify the major multipole. Examples of such mixed transitions in heavy nuclei have been described in Sec. 11, and in some instances even the dominant multipole is uncertain due to the limited experimental accuracy. By way of contrast, the determination of multipole admixtures for $2^+(M1, E2)2^+$ and $3(D, Q)2$ transitions from $(p, p'\gamma)$ distributions (Figs. 6 and 13) reveal the present higher precision which can be achieved by this alternative approach.

Future developments in $(n, n'\gamma)$ distribution measurements will very likely involve the use of lithium-drifted germanium detectors. Chasman *et al.*[67] have examined the response of such a detector (3 cm^3) bombarded with neutrons with energies of 1.2, 2.2, 4.7, and 16.3 MeV. They point out that background effects due to neutron activation should be less important (roughly an order of magnitude) than for NaI detectors, while background contributions from $(n, n'\gamma)$ and $(n,$ charged particle) reactions are comparable per unit volume. They were able to see an enhancement of $(n, n'\gamma)$ radiations from samples of aluminum and lead. While discrete background γ peaks were observed, particularly from $(n, n'\gamma)$ processes in the germanium isotopes, these detectors may well prove to be quite valuable for $(n, n'\gamma)$ distribution measurements, particularly if such prompt $(n, n'\gamma)$ background events can be removed using a sufficiently large detector in conjunction with a time-of-flight system.

Note added in proof. A recent investigation by J. M. Daniels and J. Felsteiner [Bull. Am. Phys. Soc. **10**, 1116 (1965)] of $(n, n'\gamma)$ spectra from Co^{59} and Cu^{63} using a Li–Ge detector has revealed new γ radiations. They have not attempted any distribution measurements.

F. Other Reactions

The predictions for angular distributions which we have discussed should be equally applicable to other reactions involving spin-$\frac{1}{2}$ particles such as the (p, n), (n, p), (He^3, n) or (He^3, p) processes, provided that CN formation predominates. Johnson *et al.*[68] have compared their absolute (p, n) yields near threshold with Hauser–Feshbach calculations for many medium-weight nuclei with low thresholds, mainly in the range of 1–3 MeV. They have concluded that this CN theory works well for an interval of a few keV to 500 keV above threshold. At such low energies, we would also expect agreement with CN predictions for the angular patterns of both (p, n) and $(p, n\gamma)$ radiations; however, there appears to be very little experimental information of this type available.

At somewhat higher incident energies of 4.7–5.5 MeV, Lightbody *et al.*[69] have recently reported angular distributions for the (p, n_0) and (p, n_1) groups from Y^{89} $(J_0=\frac{1}{2}^-)$, corresponding to excitation of states with $J_2=\frac{9}{2}^+$ and $\frac{1}{2}^-$, respectively. On the basis of the systematics presented in Figs. 23 and 24, we would expect near isotropy for the n_0 group, and substantial fore–aft peaking for the n_1 group. Qualitatively, these predictions are borne out, although some fluctuations in the n_0 distributions are observed, which could result from insufficient statistical averaging ($\Delta E=25$ keV). The presence of CN analog states[70] in Zr^{90} complicates these results, and affects the angular distributions measured at $E_p=4.68$ and 5.02 MeV.

Iyengar *et al.*[71] have measured distributions of the Cl^{37} (p, n_0) group at incident energies (5.1, 5.3, and 5.5 MeV) considerably above threshold (1.64 MeV) with a target thickness of 150 keV. Since their results appear to be inconsistent with CN predictions, they conclude that direct interactions are contributing to the reaction yield. We would recommend more extensive measurements of (p, n) and $(p, n\gamma)$ distributions at lower incident energies and for heavier nuclei. The relatively high yield of $(p, n\gamma)$ radiations and the typically complex low-energy spectrum favors the use of high-resolution germanium detectors, as illustrated by the recent investigation of the Ca^{48} $(p, n\gamma)$ reaction by Chasman *et al.*,[72] which included γ–γ coincidence measurements between the Li–Ge detector and a NaI counter.

[66] T. Wakatsuki, Y. Hirao, and I. Miura, Nucl. Phys. **39**, 335 (1962).
[67] C. Chasman, K. W. Jones, and R. A. Ristinen, Brookhaven National Laboratory Report 9157, April 1965 (unpublished); R. A. Ristinen, C. Chasman, and K. W. Jones, Bull. Am. Phys. Soc. **10**, 36 (1965).
[68] C. H. Johnson, C. C. Trail, and A. Galonsky, Phys. Rev. **136**, B1719 (1964); C. H. Johnson, A. Galonsky, and J. P. Ulrich, *ibid.* **109**, 1243 (1958).
[69] D. B. Lightbody, G. E. Mitchell, and A. Sayres, Phys. Letters **15**, 155 (1965).
[70] J. D. Fox, C. F. Moore, and D. Robson, Phys. Rev. Letters **12**, 198 (1964).
[71] K. V. K. Iyengar, S. K. Gupta, B. Lal, and D. Kondaiah (to be published).
[72] C. Chasman, K. W. Jones, and R. A. Ristinen, Bull. Am. Phys. Soc. **10**, 26 (1965).

CC-0. In Public Domain. Gurukul Kangri Collection, Haridwar

Digitized by Arya Samaj Foundation Chennai and eGangotri

While the number of experimentally favorable (n, p) reactions may be much more limited than that of (p, n) reactions, it is possible for the CN mechanism to predominate in some instances. The production cross section and angular distribution of a 0.767-MeV γ ray arising from a 0.797→0.030 MeV $(2^-\rightarrow 3^-)$ transition in the $Ca^{40}(n, p\gamma)K^{40}$ reaction has been found by Tucker[25,33] to be consistent with CN predictions for $E_n=3.5$ to 5.0 MeV, although some systematic background problems were present. However, as also in the case of He^3-induced reactions, DI contributions may be more important for many (n, p) studies.

We conclude from this present survey of experimental information that there is a wide range of application of CN theory to energy-averaged distributions which merits attention, both now and in the future as improved experimental techniques become available.

APPENDIX A: TABULATION OF RESTRICTED LEGENDRE EXPANSION COEFFICIENTS $\alpha_{i\nu}$

The Tables (VI to X) which follow for various nuclear spin sequences list in each instance the momentum combination l_1, j_1, J_1, l_2, j_2, followed by the expansion coefficients $\alpha_{i\nu}$ for different radiations (see Secs. 4A and 4B). For each momentum ensemble the $\alpha_{i\nu}$ for outgoing nucleons and subsequent γ radiation [of pure multipolarity $L=|J_2-J_3|$ (or $|J_2-J_3|+1$ when $J_2-J_3=0$) and, when relevant, $L'=|J_2-J_3|+1$ (or $|J_2-J_3|+2$)] have been tabulated. The reason for listing coefficients for such multipole combinations as *E1 or M2*, and *E2 or M3*, although in practice the alternative multipolarity would be precluded by rules governing the transition probability, lies in the usefulness of such a full tabulation for hand conversion of the $\alpha_{i\nu}$ to those for other spin sequences.

TABLE VI. $0^+\rightarrow J_1\pi_1\rightarrow 2^+\rightarrow 0^+$ transition sequence.

l_1	j_1	J_1	l_2	j_2	Rad.	α_{i0}	α_{i2}	α_{i4}	α_{i6}	α_{i8}
0	$\frac{1}{2}$	$\frac{1}{2}^+$	2	$\frac{3}{2}$	N'	2				
					$\gamma: E2$	2				
				$\frac{5}{2}$	N'	2				
					$\gamma: E2$	2				
1	$\frac{1}{2}$	$\frac{1}{2}^-$	1	$\frac{3}{2}$	N'	2				
					$\gamma: E2$	2				
			3	$\frac{5}{2}$	N'	2				
					$\gamma: E2$	2				
	$\frac{3}{2}$	$\frac{3}{2}^-$	1	$\frac{1}{2}$	N'	4				
					$\gamma: E2$	4	2			
				$\frac{3}{2}$	N'	4	−2.4			
					$\gamma: E2$	4				
			3	$\frac{5}{2}$	N'	4	−0.45714			
					$\gamma: E2$	4	−1.42857			
				$\frac{7}{2}$	N'	4	2.85714			
					$\gamma: E2$	4	0.57143			
2	$\frac{3}{2}$	$\frac{3}{2}^+$	0	$\frac{1}{2}$	N'	4				
					$\gamma: E2$	4	2			
			2	$\frac{3}{2}$	N'	4	−2.4			
					$\gamma: E2$	4				
				$\frac{5}{2}$	N'	4	−0.45714			
					$\gamma: E2$	4	−1.42857			
			4	$\frac{7}{2}$	N'	4	2.85714			
					$\gamma: E2$	4	0.57143			
	$\frac{5}{2}$	$\frac{5}{2}^+$	0	$\frac{1}{2}$	N'	6				
					$\gamma: E2$	6	3.42857	−3.42857		
			2	$\frac{3}{2}$	N'	6	−0.68571			
					$\gamma: E2$	6	1.22449	3.91837		
				$\frac{5}{2}$	N'	6	0.68571	−2.57143		
					$\gamma: E2$	6	−1.22449	−2.20408		
			4	$\frac{7}{2}$	N'	6	2.85714	−2.57143		
					$\gamma: E2$	6	−2.08163	0.65306		
				$\frac{9}{2}$	N'	6	5.71429	2.57143		
					$\gamma: E2$	6	1.22449	−0.08163		

CC-0. In Public Domain. Gurukul Kangri Collection, Haridwar

Digitized by Arya Samaj Foundation Chennai and eGangotri

TABLE VI. (*Continued*)

l_1	j_1	J_1	l_2	j_2	Rad.	α_{i0}	α_{i2}	α_{i4}	α_{i6}	α_{i8}
3	$\frac{5}{2}$	$\frac{5}{2}^-$	1	$\frac{1}{2}$	N'	6				
					$\gamma: E2$	6	3.42857	−3.42857		
				$\frac{3}{2}$	N'	6	−0.68571			
					$\gamma: E2$	6	1.22449	3.91837		
			3	$\frac{5}{2}$	N'	6	0.68571	−2.57143		
					$\gamma: E2$	6	−1.22449	−2.20408		
				$\frac{7}{2}$	N'	6	2.85714	−2.57143		
					$\gamma: E2$	6	−2.08163	0.65306		
	$\frac{7}{2}$	$\frac{7}{2}^-$	1	$\frac{3}{2}$	N'	8	5.71429			
					$\gamma: E2$	8	4.08163	−2.93878		
			3	$\frac{5}{2}$	N'	8	3.80952	−3.42857		
					$\gamma: E2$	8	0.68027	5.22449		
				$\frac{7}{2}$	N'	8	4.44444	−2.80520	−2.02020	
					$\gamma: E2$	8	−2.17687	−3.91837		
4	$\frac{7}{2}$	$\frac{7}{2}^+$	2	$\frac{3}{2}$	N'	8	5.71429			
					$\gamma: E2$	8	4.08163	−2.93878		
				$\frac{5}{2}$	N'	8	3.80952	−3.42857		
					$\gamma: E2$	8	0.68027	5.22449		
			4	$\frac{7}{2}$	N'	8	4.44444	−2.80520	−2.02020	
					$\gamma: E2$	8	−2.17687	−3.91837		
				$\frac{9}{2}$	N'	8	6.11833	−0.25502	−3.82002	
					$\gamma: E2$	8	−2.58503	1.42486		
	$\frac{9}{2}$	$\frac{9}{2}^+$	2	$\frac{5}{2}$	N'	10	9.52381	4.28571		
					$\gamma: E2$	10	4.76191	−2.85714		
			4	$\frac{7}{2}$	N'	10	7.64791	−0.31877	−4.77502	
					$\gamma: E2$	10	0.21645	6.23377		
				$\frac{9}{2}$	N'	10	7.89715	0.17165	−4.70156	−1.24603
					$\gamma: E2$	10	−3.03030	−5.45455		

TABLE VII. $0^+ \rightarrow J_{1\pi 1} \rightarrow 2^+ \rightarrow 2^+$ transition sequence.

l_1	j_1	J_1	l_2	j_2	Rad.	α_{i0}	α_{i2}	α_{i4}	α_{i6}	α_{i8}
0	$\frac{1}{2}$	$\frac{1}{2}^+$	2	$\frac{3}{2}$	N'	2				
					$\gamma: M1$	2				
					$\gamma: E2$	2				
				$\frac{5}{2}$	N'	2				
					$\gamma: M1$	2				
					$\gamma: E2$	2				
1	$\frac{1}{2}$	$\frac{1}{2}^-$	1	$\frac{3}{2}$	N'	2				
					$\gamma: M1$	2				
					$\gamma: E2$	2				
			3	$\frac{5}{2}$	N'	2				
					$\gamma: M1$	2				
					$\gamma: E2$	2				
	$\frac{3}{2}$	$\frac{3}{2}^-$	1	$\frac{1}{2}$	N'	4				
					$\gamma: M1$	4	1.4			
					$\gamma: E2$	4	−0.42857			
				$\frac{3}{2}$	N'	4	−2.4			
					$\gamma: M1$	4				
					$\gamma: E2$	4				
			3	$\frac{5}{2}$	N'	4	−0.45714			
					$\gamma: M1$	4	−1			
					$\gamma: E2$	4	0.30612			
				$\frac{7}{2}$	N'	4	2.85714			
					$\gamma: M1$	4	0.4			
					$\gamma: E2$	4	−0.12245			

CC-0. In Public Domain. Gurukul Kangri Collection, Haridwar

Digitized by Arya Samaj Foundation Chennai and eGangotri

TABLE VII. (*Continued*)

l_1	j_1	J_1	l_2	j_2	Rad.	α_{i0}	α_{i2}	α_{i4}	α_{i6}	α_{i8}
2	$\frac{3}{2}$	$\frac{3}{2}^+$	0	$\frac{1}{2}$	N'	4				
					$\gamma:M1$	4	1.4			
					$\gamma:E2$	4	−0.42857			
			2	$\frac{3}{2}$	N'	4	−2.4			
					$\gamma:M1$	4				
					$\gamma:E2$	4				
				$\frac{5}{2}$	N'	4	−0.45714			
					$\gamma:M1$	4	−1			
					$\gamma:E2$	4	0.30612			
			4	$\frac{7}{2}$	N'	4	2.85714			
					$\gamma:M1$	4	0.4			
					$\gamma:E2$	4	−0.12245			
	$\frac{5}{2}$	$\frac{5}{2}^+$	0	$\frac{1}{2}$	N'	6				
					$\gamma:M1$	6	2.4			
					$\gamma:E2$	6	−0.73469	−0.97959		
			2	$\frac{3}{2}$	N'	6	−0.68571			
					$\gamma:M1$	6	0.85714			
					$\gamma:E2$	6	−0.26239	1.11953		
				$\frac{5}{2}$	N'	6	0.68571	−2.57143		
					$\gamma:M1$	6	−0.85714			
					$\gamma:E2$	6	0.26239	−0.62974		
			4	$\frac{7}{2}$	N'	6	2.85714	−2.57143		
					$\gamma:M1$	6	−1.45714			
					$\gamma:E2$	6	0.44606	0.18659		
				$\frac{9}{2}$	N'	6	5.71429	2.57143		
					$\gamma:M1$	6	0.85714			
					$\gamma:E2$	6	−0.26239	−0.02332		
3	$\frac{5}{2}$	$\frac{5}{2}^-$	1	$\frac{1}{2}$	N'	6				
					$\gamma:M1$	6	2.4			
					$\gamma:E2$	6	−0.73469	−0.97959		
				$\frac{3}{2}$	N'	6	−0.68571			
					$\gamma:M1$	6	0.85714			
					$\gamma:E2$	6	−0.26239	1.11953		
			3	$\frac{5}{2}$	N'	6	0.68571	−2.57143		
					$\gamma:M1$	6	−0.85714			
					$\gamma:E2$	6	0.26239	−0.62974		
				$\frac{7}{2}$	N'	6	2.85714	−2.57143		
					$\gamma:M1$	6	−1.45714			
					$\gamma:E2$	6	0.44606	0.18659		
	$\frac{7}{2}$	$\frac{7}{2}^-$	1	$\frac{3}{2}$	N'	8	5.71429			
					$\gamma:M1$	8	2.85714			
					$\gamma:E2$	8	−0.87464	−0.83965		
			3	$\frac{5}{2}$	N'	8	3.80952	−3.42857		
					$\gamma:M1$	8	0.47619			
					$\gamma:E2$	8	−0.14577	1.49271		
				$\frac{7}{2}$	N'	8	4.44444	−2.80520	−2.02020	
					$\gamma:M1$	8	−1.52381			
					$\gamma:E2$	8	0.46647	−1.11953		
4	$\frac{7}{2}$	$\frac{7}{2}^+$	2	$\frac{3}{2}$	N'	8	5.71429			
					$\gamma:M1$	8	2.85714			
					$\gamma:E2$	8	−0.87464	−0.83965		
				$\frac{5}{2}$	N'	8	3.80952	−3.42857		
					$\gamma:M1$	8	0.47619			
					$\gamma:E2$	8	−0.14577	1.49271		
			4	$\frac{7}{2}$	N'	8	4.44444	−2.80520	−2.02020	
					$\gamma:M1$	8	−1.52381			
					$\gamma:E2$	8	0.46647	−1.11953		
				$\frac{9}{2}$	N'	8	6.11833	−0.25502	−3.82002	
					$\gamma:M1$	8	−1.80952			
					$\gamma:E2$	8	0.55394	0.40710		

CC-0. In Public Domain. Gurukul Kangri Collection, Haridwar

Digitized by Arya Samaj Foundation Chennai and eGangotri

TABLE VII. (*Continued*)

l_1	j_1	J_1	l_2	j_2	Rad.	α_{i0}	α_{i2}	α_{i4}	α_{i6}	α_{i8}
4	$\frac{9}{2}$	$\frac{9}{2}^+$	2	$\frac{5}{2}$	N'	10	9.52381	4.28571		
					$\gamma:M1$	10	3.33333			
					$\gamma:E2$	10	−1.02041	−0.81633		
			4	$\frac{7}{2}$	N'	10	7.64791	−0.31877	−4.77502	
					$\gamma:M1$	10	0.15152			
					$\gamma:E2$	10	−0.04638	1.78108		
				$\frac{9}{2}$	N'	10	7.89715	0.17165	−4.70156	−1.24603
					$\gamma:M1$	10	−2.12121			
					$\gamma:E2$	10	0.64935	−1.55844		

TABLE VIII. $0^+ \rightarrow J_1\pi_1 \rightarrow 3^- \rightarrow 2^+$ transition sequence.

l_1	j_1	J_1	l_2	j_2	Rad.	α_{i0}	α_{i2}	α_{i4}	α_{i6}
0	$\frac{1}{2}$	$\frac{1}{2}^+$	3	$\frac{5}{2}$	N'	2			
					$\gamma:E1$	2			
					$\gamma:M2$	2			
				$\frac{7}{2}$	N'	2			
					$\gamma:E1$	2			
					$\gamma:M2$	2			
1	$\frac{1}{2}$	$\frac{1}{2}^-$	2	$\frac{5}{2}$	N'	2			
					$\gamma:E1$	2			
					$\gamma:M2$	2			
			4	$\frac{7}{2}$	N'	2			
					$\gamma:E1$	2			
					$\gamma:M2$	2			
	$\frac{3}{2}$	$\frac{3}{2}^-$	2	$\frac{3}{2}$	N'	4	0.8		
					$\gamma:E1$	4	−0.96		
					$\gamma:M2$	4	0.34286		
				$\frac{5}{2}$	N'	4	−2.51429		
					$\gamma:E1$	4	0.24		
					$\gamma:M2$	4	−0.08571		
			4	$\frac{7}{2}$	N'	4	−0.95238		
					$\gamma:E1$	4	0.8		
					$\gamma:M2$	4	−0.28571		
				$\frac{9}{2}$	N'	4	2.66667		
					$\gamma:E1$	4	−0.4		
					$\gamma:M2$	4	0.14286		
2	$\frac{3}{2}$	$\frac{3}{2}^+$	1	$\frac{3}{2}$	N'	4	0.8		
					$\gamma:E1$	4	−0.96		
					$\gamma:M2$	4	0.34286		
			3	$\frac{5}{2}$	N'	4	−2.51429		
					$\gamma:E1$	4	0.24		
					$\gamma:M2$	4	−0.08571		
				$\frac{7}{2}$	N'	4	−0.95238		
					$\gamma:E1$	4	0.8		
					$\gamma:M2$	4	−0.28571		
	$\frac{5}{2}$	$\frac{5}{2}^+$	1	$\frac{1}{2}$	N'	6			
					$\gamma:E1$	6	−2.05714		
					$\gamma:M2$	6	0.73469	2.69388	
				$\frac{3}{2}$	N'	6	−3.77143		
					$\gamma:E1$	6	−1.13143		
					$\gamma:M2$	6	0.40408	−1.34694	
			3	$\frac{5}{2}$	N'	6	−2.84082		
					$\gamma:E1$	6	0.06857		
					$\gamma:M2$	6	−0.02449	−1.34694	
				$\frac{7}{2}$	N'	6	−0.81633	−1.46939	
					$\gamma:E1$	6	1.02857		
					$\gamma:M2$	6	−0.36735	1.79592	

CC-0. In Public Domain. Gurukul Kangri Collection, Haridwar

Digitized by Arya Samaj Foundation Chennai and eGangotri

TABLE VIII. (*Continued*)

l_1	j_1	J_1	l_2	j_2	Rad.	α_{i0}	α_{i2}	α_{i4}	α_{i6}
3	$\frac{5}{2}$	$\frac{5}{2}^-$	0	$\frac{1}{2}$	N'	6			
					$\gamma:E1$	6	−2.05714		
					$\gamma:M2$	6	0.73469	2.69388	
			2	$\frac{3}{2}$	N'	6	−3.77143		
					$\gamma:E1$	6	−1.13143		
					$\gamma:M2$	6	0.40408	−1.34694	
				$\frac{5}{2}$	N'	6	−2.84082	2.32653	
					$\gamma:E1$	6	0.06857		
					$\gamma:M2$	6	−0.02449	−1.34694	
			4	$\frac{7}{2}$	N'	6	−0.81633	−1.46939	
					$\gamma:E1$	6	1.02857		
					$\gamma:M2$	6	−0.36735	1.79592	
				$\frac{9}{2}$	N'	6	1.97403	−3.03869	
					$\gamma:E1$	6	1.02857		
					$\gamma:M2$	6	−0.36735	−0.77551	
	$\frac{7}{2}$	$\frac{7}{2}^-$	0	$\frac{1}{2}$	N'	8			
					$\gamma:E1$	8	−2.85714		
					$\gamma:M2$	8	1.02041	4.40816	
			2	$\frac{3}{2}$	N'	8	−1.90476		
					$\gamma:E1$	8	−1.90476		
					$\gamma:M2$	8	0.68027	−0.48980	
				$\frac{5}{2}$	N'	8	−1.08844	−1.95918	
					$\gamma:E1$	8	−0.57143		
					$\gamma:M2$	8	0.20408	−2.77551	
			4	$\frac{7}{2}$	N'	8	0.45352	−3.67954	3.12213
					$\gamma:E1$	8	0.76190		
					$\gamma:M2$	8	−0.27211	−0.17811	
				$\frac{9}{2}$	N'	8	2.53968	−4.08028	0.29385
					$\gamma:E1$	8	1.56190		
					$\gamma:M2$	8	−0.55782	2.62709	
4	$\frac{7}{2}$	$\frac{7}{2}^+$	1	$\frac{1}{2}$	N'	8			
					$\gamma:E1$	8	−2.85714		
					$\gamma:M2$	8	1.02041	4.40816	
				$\frac{3}{2}$	N'	8	−1.90476		
					$\gamma:E1$	8	−1.90476		
					$\gamma:M2$	8	0.68027	−0.48980	
			3	$\frac{5}{2}$	N'	8	−1.08844	−1.95918	
					$\gamma:E1$	8	−0.57143		
					$\gamma:M2$	8	0.20408	−2.77551	
				$\frac{7}{2}$	N'	8	0.45352	−3.67954	3.12213
					$\gamma:E1$	8	0.76190		
					$\gamma:M2$	8	−0.27211	−0.17811	
	$\frac{9}{2}$	$\frac{9}{2}^+$	1	$\frac{3}{2}$	N'	10	6.66667		
					$\gamma:E1$	10	−3.33333		
					$\gamma:M2$	10	1.19048	4.28571	
			3	$\frac{5}{2}$	N'	10	3.29004	−5.06494	
					$\gamma:E1$	10	−1.81818		
					$\gamma:M2$	10	0.64935	−2.20779	
				$\frac{7}{2}$	N'	10	3.17460	−5.10035	0.36731
					$\gamma:E1$	10	−0.12121		
					$\gamma:M2$	10	0.04329	−3.11688	

CC-0. In Public Domain. Gurukul Kangri Collection, Haridwar

Digitized by Arya Samaj Foundation Chennai and eGangotri

TABLE IX. $0^+ \rightarrow J_1\pi_1 \rightarrow 4^+ \rightarrow 2^+$ transition sequence.

l_1	j_1	J_1	l_2	j_2	Rad.	α_{i0}	α_{i2}	α_{i4}	α_{i6}	α_{i8}
0	$\frac{1}{2}$	$\frac{1}{2}^+$	4	$\frac{7}{2}$	N'	2				
					$\gamma:E2$	2				
					$\gamma:M3$	2				
				$\frac{9}{2}$	N'	2				
					$\gamma:E2$	2				
					$\gamma:M3$	2				
1	$\frac{1}{2}$	$\frac{1}{2}^-$	3	$\frac{7}{2}$	N'	2				
					$\gamma:E2$	2				
					$\gamma:M3$	2				
	$\frac{3}{2}$	$\frac{3}{2}^-$	3	$\frac{5}{2}$	N'	4	1.14286			
					$\gamma:E2$	4	1.12245			
					$\gamma:M3$	4	1.17857			
				$\frac{7}{2}$	N'	4	−2.47619			
					$\gamma:E2$	4	−0.44898			
					$\gamma:M3$	4	−0.47143			
2	$\frac{3}{2}$	$\frac{3}{2}^+$	2	$\frac{5}{2}$	N'	4	1.14286			
					$\gamma:E2$	4	1.12245			
					$\gamma:M3$	4	1.17857			
			4	$\frac{7}{2}$	N'	4	−2.47619			
					$\gamma:E2$	4	−0.44898			
					$\gamma:M3$	4	−0.47143			
				$\frac{9}{2}$	N'	4	−1.21212			
					$\gamma:E2$	4	−1			
					$\gamma:M3$	4	−1.05			
	$\frac{5}{2}$	$\frac{5}{2}^+$	2	$\frac{3}{2}$	N'	6	1.71429			
					$\gamma:E2$	6	2.40525	−0.83382		
					$\gamma:M3$	6	2.52551	−0.13265		
				$\frac{5}{2}$	N'	6	−3.42857	−0.85714		
					$\gamma:E2$	6	0.96210	0.83382		
					$\gamma:M3$	6	1.01020	0.13265		
			4	$\frac{7}{2}$	N'	6	−3.42857	2.80519		
					$\gamma:E2$	6	−0.50729	0.30321		
					$\gamma:M3$	6	−0.53265	0.04824		
				$\frac{9}{2}$	N'	6	−1.55844	−0.70130		
					$\gamma:E2$	6	−1.45190	−0.83382		
					$\gamma:M3$	6	−1.52449	−0.13265		
3	$\frac{5}{2}$	$\frac{5}{2}^-$	1	$\frac{3}{2}$	N'	6	1.71429			
					$\gamma:E2$	6	2.40525	−0.83382		
					$\gamma:M3$	6	2.52551	−0.13265		
			3	$\frac{5}{2}$	N'	6	−3.42857	−0.85714		
					$\gamma:E2$	6	0.96210	0.83382		
					$\gamma:M3$	6	1.01020	0.13265		
				$\frac{7}{2}$	N'	6	−3.42857	2.80519		
					$\gamma:E2$	6	−0.50729	0.30321		
					$\gamma:M3$	6	−0.53265	0.04824		
	$\frac{7}{2}$	$\frac{7}{2}^-$	1	$\frac{1}{2}$	N'	8				
					$\gamma:E2$	8	3.74150	−2.12245		
					$\gamma:M3$	8	3.92857	−0.33766	3.40909	
				$\frac{3}{2}$	N'	8	−4.95238			
					$\gamma:E2$	8	2.77940	−0.30321		
					$\gamma:M3$	8	2.91837	−0.04824	−2.72727	
			3	$\frac{5}{2}$	N'	8	−4.57143	3.74026		
					$\gamma:E2$	8	1.37026	1.07501		
					$\gamma:M3$	8	1.43878	0.17102	−0.55785	
				$\frac{7}{2}$	N'	8	−3.17460	0.93506	−2.02020	
					$\gamma:E2$	8	−0.19436	0.88206		
					$\gamma:M3$	8	−0.20408	0.14033	2.47934	

CC-0. In Public Domain. Gurukul Kangri Collection, Haridwar

Digitized by Arya Samaj Foundation Chennai and eGangotri

TABLE IX. (*Continued*)

l_1	j_1	J_1	l_2	j_2	Rad.	α_{i0}	α_{i2}	α_{i4}	α_{i6}	α_{i8}
4	$\frac{7}{2}$	$\frac{7}{2}^+$	0	$\frac{1}{2}$	N'	8				
					$\gamma:E2$	8	3.74150	−2.12245		
					$\gamma:M3$	8	3.92857	−0.33766	3.40909	
			2	$\frac{3}{2}$	N'	8	−4.95238			
					$\gamma:E2$	8	2.77940	−0.30321		
					$\gamma:M3$	8	2.91837	−0.04824	−2.72727	
			2	$\frac{5}{2}$	N'	8	−4.57143	3.74026		
					$\gamma:E2$	8	1.37026	1.07501		
					$\gamma:M3$	8	1.43878	0.17102	−0.55785	
			4	$\frac{7}{2}$	N'	8	−3.17460	0.93506	−2.02020	
					$\gamma:E2$	8	−0.19436	0.88206		
					$\gamma:M3$	8	−0.20408	0.14033	2.47934	
				$\frac{9}{2}$	N'	8	−1.15440	−2.40632	2.82546	
					$\gamma:E2$	8	−1.50632	−0.51100		
					$\gamma:M3$	8	−1.58163	−0.08130	−2.02638	
	$\frac{9}{2}$	$\frac{9}{2}^+$	0	$\frac{1}{2}$	N'	10				
					$\gamma:E2$	10	4.76190	−2.85714		
					$\gamma:M3$	10	5	−0.45455	5.45455	
			2	$\frac{3}{2}$	N'	10	−3.03030			
					$\gamma:E2$	10	3.78788	−0.90909		
					$\gamma:M3$	10	3.97727	−0.14463	−2.35537	
				$\frac{5}{2}$	N'	10	−2.59740	−1.16883		
					$\gamma:E2$	10	2.31911	0.94620		
					$\gamma:M3$	10	2.43506	0.15053	−2.97521	
			4	$\frac{7}{2}$	N'	10	−1.44300	−3.00790	3.53182	
					$\gamma:E2$	10	0.58751	1.49565		
					$\gamma:M3$	10	0.61688	0.23794	2.16465	
				$\frac{9}{2}$	N'	10	0.18365	−4.62565	3.70700	−2.97129
					$\gamma:E2$	10	−1.08225	0.42957		
					$\gamma:M3$	10	−1.13636	0.06834	1.90718	

TABLE X. $\frac{1}{2}^+\to J_1\pi_1\to\frac{3}{2}^+\to\frac{1}{2}^+$ transition sequence. *Note*: For brevity, the $\alpha_{i\nu}$ for $E2$ radiation have not been listed, since numerically they are identical to those for $M1$ radiation. The sign of the α_{i0} is, of course, the same, but that for the α_{i2} is opposite (higher values of ν than $\nu=2$ are excluded by the Racah rule $\nu\leqq 2J_2$). As discussed in Sec. 4C, the conversion factors from $M1$ to $E2$ radiation for this spin sequence are $C_0=c_{i0}=+1$, $C_2=c_{i2}=-1$.

l_1	j_1	J_1	l_2	j_2	Rad.	α_{i0}	α_{i2}	α_{i4}	α_{i6}	α_{i8}
0	$\frac{1}{2}$	0^+	2	$\frac{3}{2}$	N'	0.5				
					$\gamma:M1$	0.5				
		1^+	0	$\frac{1}{2}$	N'	1.5				
					$\gamma:M1$	1.5				
			2	$\frac{3}{2}$	N'	1.5				
					$\gamma\ M1$	1.5				
				$\frac{5}{2}$	N'	1.5				
					$\gamma:M1$	1.5				
1	$\frac{1}{2}$	0^-	1	$\frac{3}{2}$	N'	0.5				
					$\gamma:M1$	0.5				
		1^-	1	$\frac{1}{2}$	N'	1.5				
					$\gamma:M1$	1.5				
				$\frac{3}{2}$	N'	1.5				
					$\gamma:M1$	1.5				
			3	$\frac{5}{2}$	N'	1.5				
					$\gamma:M1$	1.5				

CC-0. In Public Domain. Gurukul Kangri Collection, Haridwar

Digitized by Arya Samaj Foundation Chennai and eGangotri

TABLE X. (*Continued*)

l_1	j_1	J_1	l_2	j_2	Rad.	α_{i0}	α_{i2}	α_{i4}	α_{i6}	α_{i8}
1	$\frac{3}{2}$	1^-	1	$\frac{1}{2}$	N'	1.5				
					$\gamma:M1$	1.5	−0.375			
				$\frac{3}{2}$	N'	1.5	−0.6			
					$\gamma:M1$	1.5	0.3			
			3	$\frac{5}{2}$	N'	1.5	0.6			
					$\gamma:M1$	1.5	−0.075			
		2^-	1	$\frac{1}{2}$	N'	2.5				
					$\gamma:M1$	2.5	−0.875			
				$\frac{3}{2}$	N'	2.5				
					$\gamma:M1$	2.5				
			3	$\frac{5}{2}$	N'	2.5	0.71429			
					$\gamma:M1$	2.5	0.625			
				$\frac{7}{2}$	N'	2.5	1.78571			
					$\gamma:M1$	2.5	−0.25			
2	$\frac{3}{2}$	1^+	0	$\frac{1}{2}$	N'	1.5				
					$\gamma:M1$	1.5	−0.375			
			2	$\frac{3}{2}$	N'	1.5	−0.6			
					$\gamma:M1$	1.5	0.3			
				$\frac{5}{2}$	N'	1.5	0.6			
					$\gamma:M1$	1.5	−0.075			
		2^+	0	$\frac{1}{2}$	N'	2.5				
					$\gamma:M1$	2.5	−0.875			
			2	$\frac{3}{2}$	N'	2.5				
					$\gamma:M1$	2.5				
				$\frac{5}{2}$	N'	2.5	0.71429			
					$\gamma:M1$	2.5	0.625			
			4	$\frac{7}{2}$	N'	2.5	1.78571			
					$\gamma:M1$	2.5	−0.25			
	$\frac{5}{2}$	2^+	0	$\frac{1}{2}$	N'	2.5				
					$\gamma:M1$	2.5	−1			
			2	$\frac{3}{2}$	N'	2.5				
					$\gamma:M1$	2.5				
				$\frac{5}{2}$	N'	2.5	0.81633			
					$\gamma:M1$	2.5	0.71429			
			4	$\frac{7}{2}$	N'	2.5	2.04082	0.45918		
					$\gamma:M1$	2.5	−0.28571			
		3^+	2	$\frac{3}{2}$	N'	3.5	2.4			
					$\gamma:M1$	3.5	−1.2			
				$\frac{5}{2}$	N'	3.5	1.88571	−0.78571		
					$\gamma:M1$	3.5	0.3			
			4	$\frac{7}{2}$	N'	3.5	2.38095	−0.21429		
					$\gamma:M1$	3.5	1			
				$\frac{9}{2}$	N'	3.5	3.33333	1.5		
					$\gamma:M1$	3.5	−0.5			
3	$\frac{5}{2}$	2^-	1	$\frac{1}{2}$	N'	2.5				
					$\gamma:M1$	2.5	−1			
				$\frac{3}{2}$	N'	2.5				
					$\gamma:M1$	2.5				
			3	$\frac{5}{2}$	N'	2.5	0.81633	−0.81633		
					$\gamma:M1$	2.5	0.71429			
				$\frac{7}{2}$	N'	2.5	2.04082	0.45918		
					$\gamma:M1$	2.5	−0.28571			

CC-0. In Public Domain. Gurukul Kangri Collection, Haridwar

Digitized by Arya Samaj Foundation Chennai and eGangotri

TABLE X. (*Continued*)

l_1	j_1	J_1	l_2	j_2	Rad.	α_{i0}	α_{i2}	α_{i4}	α_{i6}	α_{i8}
3		3^-	1	$\frac{3}{2}$	N'	3.5	2.4			
					$\gamma:M1$	3.5	−1.2			
			3	$\frac{5}{2}$	N'	3.5	1.88571	−0.78571		
					$\gamma:M1$	3.5	0.3			
				$\frac{7}{2}$	N'	3.5	2.38095	−0.21429		
					$\gamma:M1$	3.5	1			
	$\frac{7}{2}$	3^-	1	$\frac{3}{2}$	N'	3.5	2.5			
					$\gamma:M1$	3.5	−1.25			
			3	$\frac{5}{2}$	N'	3.5	1.96429	−0.96429		
					$\gamma:M1$	3.5	0.3125			
				$\frac{7}{2}$	N'	3.5	2.48016	−0.26299	−0.88384	
					$\gamma:M1$	3.5	1.04167			
		4^-	3	$\frac{5}{2}$	N'	4.5	4.20918	1.79082		
					$\gamma:M1$	4.5	−1.47321			
				$\frac{7}{2}$	N'	4.5	3.64796	0.48840	−1.13636	
					$\gamma:M1$	4.5	0.58929			
4	$\frac{7}{2}$	3^+	2	$\frac{3}{2}$	N'	3.5	2.5			
					$\gamma:M1$	3.5	−1.25			
				$\frac{5}{2}$	N'	3.5	1.96429	−0.96429		
					$\gamma:M1$	3.5	0.3125			
			4	$\frac{7}{2}$	N'	3.5	2.48016	−0.26299	−0.88384	
					$\gamma:M1$	3.5	1.04167			
				$\frac{9}{2}$	N'	3.5	3.47222	1.84091	0.35354	
					$\gamma:M1$	3.5	−0.52083			
		4^+	2	$\frac{5}{2}$	N'	4.5	4.20918	1.79081		
					$\gamma:M1$	4.5	−1.47321			
			4	$\frac{7}{2}$	N'	4.5	3.64796	0.48840	−1.13636	
					$\gamma:M1$	4.5	0.58929			
				$\frac{9}{2}$	N'	4.5	3.97727	1.17149	−0.78512	
					$\gamma:M1$	4.5	1.31250			
	$\frac{9}{2}$	4^+	2	$\frac{5}{2}$	N'	4.5	4.28571	1.92857		
					$\gamma:M1$	4.5	−1.5			
			4	$\frac{7}{2}$	N'	4.5	3.71429	0.52597	−1.45455	
					$\gamma:M1$	4.5	0.6			
				$\frac{9}{2}$	N'	4.5	4.04959	1.26160	−1.00496	−0.89714
					$\gamma:M1$	4.5	1.33636			
		5^+	4	$\frac{7}{2}$	N'	5.5	5.77778	3.68182	1.37374	
					$\gamma:M1$	5.5	−1.73333			
				$\frac{9}{2}$	N'	5.5	5.25253	2.26573	−0.54949	−1.30210
					$\gamma:M1$	5.5	0.86667			

APPENDIX B: DISTRIBUTION SYMMETRY ABOUT 90°

As has been shown by Blatt and Weisskopf,[73] and discussed by Sheldon,[74] angular distributions of nuclear reaction products are symmetric about 90° if (i) parity is conserved in the reaction, (ii) the measurement of the distribution is effected in a system which makes no distinctions between right- and left-hand coordinate systems, and (iii) the parity of the wave function describing the reaction (hence, essentially, the parity of the intermediate state) is definite. Before going on to comment upon these requirements in turn, we recall the Blatt–Weisskopf derivation of distribution symmetry about 90° when the above conditions are fulfilled.

The differential cross section for a reaction $A(a,b)B$ may be expressed as

$$d\sigma = (\hat{s}_a)^{-2}(\hat{s}_A)^{-2}\sum_s |\, q_s(\theta,\phi)\,|^2\, d\Omega \qquad (7b$$

in terms of reaction amplitudes q which depend not only upon the angle θ of emergence of b but, in the general case, also upon the azimuthal angle ϕ referred

[73] J. M. Blatt and V. F. Weisskopf, *Theoretical Nuclear Physics* (John Wiley & Sons, Inc., New York, and Chapman & Hall, Ltd., London, 1952), 1st ed., Chap. X.3, pp. 533–535.

[74] E. Sheldon, in *Les Mécanismes des Réactions Nucléaires* VIe Cours de Perfectionnement de l'Association des Chercheurs en Physique, Grächen/Saint-Nicolas, April 1964 (Bureau d'impression MRP, Rue de Bourg 11, Lousanne, 1965), p. 155 (especially p. 164).

CC-0. In Public Domain. Gurukul Kangri Collection, Haridwar

Digitized by Arya Samaj Foundation Chennai and eGangotri

to a plane defined by the quantization axis and a spin axis. The individual amplitudes q_s additionally depend upon the spin states of the reaction partners in the initial and final systems, viz., s_A, s_a, s_b, s_B, collectively described by the single index s. In the outgoing channel the parity operation corresponds to the transformation

$$\theta \rightarrow \pi - \theta, \qquad \phi \rightarrow \pi + \phi, \tag{77}$$

and hence, on the assumption of definite, conserved parity [conditions (i) and (iii)], since then

$$q_s(\pi-\theta, \pi+\phi) = \pm q_s(\theta, \phi), \tag{78}$$

it follows that

$$\frac{d\sigma}{d\Omega}(\pi-\theta, \pi+\phi) = \frac{d\sigma}{d\Omega}(\theta, \phi). \tag{79}$$

Now, condition (ii) is tantamount to averaging over spins, as in the case of unaligned targets or polarization-insensitive radiation detectors, which restores symmetry about the quantization axis and removes the ϕ dependence. In consequence,

$$\frac{d\sigma}{d\Omega}(\pi-\theta) = \frac{d\sigma}{d\Omega}(\theta), \tag{80}$$

and the distribution is, in the center-of-mass system, symmetric about 90°.

Conversely, it is evident on the one hand that under conditions that satisfy requirement (ii), the distribution of γ radiation depends on the multipolarity L (and on the mixing ratio δ for multipolarities L, L') but *not* upon the parity of the radiation and hence *not* upon the multipole character (E or M), so that it cannot of itself yield information on the parities of the nuclear states between which the γ transition takes place. On the other hand, it follows that distributions from aligned nuclei, or distributions measured by counters sensitive to polarization (e.g., to linear polarization in the case of fermions, or to circular polarization in the case of γ rays), cease to display symmetry about 90°. This feature, dealt with in earlier reviews[11,12,75] and discussed in detail by a number of authors,[76–80] provides the underlying reason for CN angular *correlations* to be devoid of precise symmetry about 90°, since they essentially correspond to a determination of distributions from nuclei aligned in a selected direction (for a discussion of correlation symmetries, see Ref. 81).

[75] H. Feshbach, in *Nuclear Spectroscopy*, edited by F. Ajzenberg-Selove (Academic Press Inc., New York, 1960), Part B, p. 625.
[76] G. R. Satchler, Proc. Phys. Soc. (London) **68A**, 1041 (1955); Nucl. Phys. **8**, 65 (1958).
[77] E. G. Beltrametti, Nucl. Phys. **8**, 445 (1958).
[78] L. W. Fagg and S. S. Hanna, Rev. Mod. Phys. **31**, 711 (1959).
[79] L. J. B. Goldfarb and R. C. Johnson, Nucl. Phys. **18**, 353 (1960).
[80] T. A. Welton, in *Fast Neutron Physics*, edited by J. B. Marion and J. L. Fowler (Interscience Publishers, Inc., New York, 1963), Part II, Chap. V.F., p. 1317.
[81] E. Sheldon, Phys. Letters **2**, 178 (1962).

Whereas under the experimental conditions examined in this paper, the requirements (i) and (ii) are satisfied irrespective of whether we deal with a CN or a DI mechanism, the circumstances under which (iii) is satisfied have no such independence, and merit further consideration.

The condition (iii) is clearly not satisfied in the case of DI processes, since these do not involve an explicit intermediate state associated with incoming and outgoing reaction channels, and hence cannot entail a definite parity. Accordingly, DI particle distributions lack precise symmetry about 90°, and can, especially in the case of elastic nucleon scattering, evince strong forward peaking (backward peaking has also been discerned in heavy-ion reactions). To a lesser extent, this is featured also in inelastic nucleon distributions but, as has already been stressed in Sec. 2, exceptions to such behavior exist, in that the DI distributions can in certain instances take on a form which is almost perfectly symmetrical about 90° and closely resembles the type of structure characteristic of a CN mechanism, albeit with a much larger peak-to-valley ratio and a totally different order of absolute magnitude. An example of such a situation has been given by Satchler *et al.*[82] for the $Cr^{52}(p, p')_{1.43\ MeV}$ reaction at $E_p = 5.54$ MeV. The DI distribution dips smoothly from 2.6 mb sr^{-1} at $\theta_{p'} = 0°$ to 0.9 mb sr^{-1} at 90° and rises symmetrically to 2.7 mb sr^{-1} at 180°. It thus has a fore–aft asymmetry of only 3.6% and a peak-to-valley ratio of 2.9. The CN distribution evaluated in the two-channel approximation with $l \leq 2$ rises from 17.0 mb sr^{-1} at 0° to 19.6 mb sr^{-1} at 90°, and accordingly has opposite structure, with the much smaller ratio $d\sigma(0°)/d\sigma(90°)$ of 0.9. Another such case has been found for the $Fe^{56}(p, p')_{0.845\ MeV}$ distribution at $E_p = 4.3$ MeV, where the inelastic proton differential cross section for a DI (CN) mechanism changes from 0.26 (1.50) mb sr^{-1} at 0° to 0.06 (1.61) mb sr^{-1} at 90° and thence to 0.22 (1.50) mb sr^{-1} at 180°, corresponding to a fore–aft asymmetry of 16% (0%) and a ratio $d\sigma(0°)/d\sigma(90°)$ of 4.18 (0.93). For comparison, it may be mentioned that the fore–aft asymmetry for the DI *elastic* distribution in the above case was computed to be

$$\frac{d\sigma(4°)}{d\sigma(176°)} = \frac{3.31\times10^{7}\ \text{mb sr}^{-1}}{42.67\ \text{mb sr}^{-1}} = 7.76\times10^{5}.$$

The CN distribution symmetry about 90° which ensues when (iii) is satisfied breaks down in the case of nonresonant processes or interferences between nuclear levels. It may accordingly be deemed to apply exactly only for the case of a resonance reaction involving but a single intermediate state, or, at the opposite extreme, for a reaction involving a statistically distributed continuum of states in the compound nu-

[82] G. R. Satchler, R. M. Drisko, and R. H. Bassel, Bull. Am. Phys. Soc. **6**, 66 (1961) and preprint; E. Sheldon (unpublished).

CC-0. In Public Domain. Gurukul Kangri Collection, Haridwar

Digitized by Arya Samaj Foundation Chennai and eGangotri

cleus. Although general group-theoretical methods[83] (see also Ref. 73) suffice to show that symmetry must invariably result under these conditions, the departure from symmetry is not always to be taken as indicative of the intrusion of a non-CN mechanism, but rather as a disturbance of the above conditions, such as might arise when there is an incomplete statistical mixture of states in the compound nucleus. In such a situation, one would expect to observe fluctuations in the total reaction cross section. Only if the asymmetry does not fluctuate with incident energy, but remains a smooth and persistent function of energy does this constitute evidence for the intrusion of a foreign mechanism.

It remains but to mention that the isotropic emission of reaction products from a compound nucleus as given by statistical reaction theory is bound up with two further requirements, namely, (a) that the transmission coefficients are not spin-dependent, and (b) that the nuclear spin dependence of the level density is of the form

$$\rho(E, J) = (2J+1)\rho(E, 0). \tag{81}$$

Clearly, this is inapplicable to states of high nuclear spin; on replacing this by the more valid relationship[84,85]

$$\rho(E, J) = (2J+1)\exp\left[-J(J+1)/2\sigma^2\right]\rho(E, 0), \tag{82}$$

the distributions become anisotropic, while remaining symmetric about 90°. A more detailed discussion of this has been given by Feshbach[75] and Goldstein.[86]

ACKNOWLEDGMENTS

Support of the U.S. Air Force Office of Scientific Research (AF-AFOSR-401-63) and the National Science Foundation (GP-3745) are gratefully acknowledged by one of the authors (D. M. V. P).

One of the authors (E.S.) desires to express his indebtedness to Professor P. Marmier for providing the facilities and the Swiss Nationalfonds for providing the financial support without which this project could not have been realized. Appreciation is expressed for calculational and coding assistance rendered by J. Costandi, R. Corfu, P. Gantenbein, J. L. Léger, and the staff of the E. T. H. Rechenzentrum. It is a pleasure to acknowledge the generous spirit displayed by Dr. I. L. Morgan and members of his group at the Texas Nuclear Corporation, as also by Professor B. Kinsey and his colleagues at the University of Texas, Austin, in making it possible during the concluding stages of this work for the authors to engage in personal discussions covering many of the points raised therein, to participate in an informal inelastic-scattering symposium at the University of Texas, and to use experimental results prior to publication. We are indebted to Dr. L. W. Swenson and Dr. R. K. Mohindra of the Bartol Research Foundation for the use of their experimental data and theoretical calculations in advance of publication.

[83] C. N. Yang, Phys. Rev. **74**, 764 (1948).
[84] H. A. Bethe, Rev. Mod. Phys. **50**, 332 (1936); **9**, 69 (1937).
[85] T. Ericson, Phil. Mag. Suppl. **9**, No. 36, 425 (1960).
[86] H. Goldstein, in *Fast Neutron Physics*, edited by J. B. Marion and J. L. Fowler (Interscience Publishers, Inc., New York, 1963), Part II, Chap. V.J., p. 1525.

CC-0. In Public Domain. Gurukul Kangri Collection, Haridwar

Digitized by Arya Samaj Foundation Chennai and eGangotri

The Role of Boltzmann Factors in Line Shape

D. L. HUBER*
Department of Physics, University of Wisconsin, Madison, Wisconsin
J. H. VAN VLECK
Lyman Laboratory of Physics, Harvard University, Cambridge, Massachusetts

A study is made of the effect of temperature and environment on the absorption spectra of simple systems. In part I the longitudinal and transverse susceptibilities of a two-level system are analyzed in terms of simple stochastic models. Particular attention is paid to the different roles played by the phase-interruption and frequency-modulation mechanisms. A calculation is given of the susceptibility of a harmonic oscillator perturbed by interaction with other oscillators. In part II the same systems are studied using Green's function methods. It is assumed that the two-level system is coupled to a crystal lattice by an isotropic interaction that is linear in the lattice displacement. Expressions are obtained for the longitudinal and transverse susceptibilities and comparison is made with the results of part I. The susceptibility of the harmonic oscillator is calculated and found to be identical to the susceptibility obtained by more elementary methods.

INTRODUCTION

Although there are innumerable papers on the subject of line shape, there has been very little written on one particular aspect of this subject, viz., how the temperature affects the line contour in case the Boltzmann factor cannot be treated as constant over the profile. With the increasing amount of spectroscopic work at exceedingly low temperatures, this aspect is no longer academic, and so an article on the subject seems in order. Many of our results are not new, but the existing presentations are rather fragmentary and sometimes not entirely correct. Also, quite irrespective of the role of Boltzmann factors, we discuss and contrast how one calculates line shapes for rapid interactions both without (part I) and with (part II) the use of Green's functions.

If N_r and N_s denote the number of atoms in the upper state and lower states, respectively (both supposed nondegenerate), then the rate of spontaneous radiation is $A(\omega, T)=N_rA_{r\to s}$ and that of absorption is

$$B(\omega, T)=B_{r\to s}(N_s-N_r)\rho(\omega),$$

where $\rho(\omega)$ is the radiation energy density. If the atoms are in thermal equilibrium at a temperature T, then $N_r/N_s=\exp(-\hbar\omega/kT)$ and the absorption coefficient $B(\omega, T)$ is connected with $A(\omega, T)$ by the relation[1]

$$A(\omega, T)=F(\omega)B(\omega, T)/[\exp(\hbar\omega/kT)-1], \quad (0.1)$$

with[2]

$$F(\omega)=2\hbar\omega^3/\pi c^3 \quad (0.2)$$

since then absorption and emission balance when $\rho(\omega)$ has the Planck form. In Einstein's classic derivation of (0.1), and for most practical purposes, the distinction between the impressed frequency ω (measured in angular units) and the atomic resonance frequency ω_0 is disregarded. In other words, $A(\omega, T)$ and $B(\omega, T)$ are considered to be delta functions of $(\omega-\omega_0)$. The present article, however, is concerned with situations where this procedure is not allowable In problems of line structure, what is sometimes done is to calculate a shape $f(\omega)$ that is independent of temperature, and assume that the net absorption is proportional to $f(\omega)N_s[1-\exp(\hbar\omega_0/kT)]$ and the emission to $f(\omega)N_s\exp(-\hbar\omega_0/kT)$. Then a relation of the type (0.1) is not satisfied, since a factor $[\exp(\hbar\omega_0/kT)-1]^{-1}$ occurs in place of $[\exp(\hbar\omega/kT)-1]^{-1}$ which is required in order for there to be equilibrium between absorption and emission over the entire line profile when $\rho(\omega)$ has the Planck form. The anomaly has arisen because when the line shape is not ideally monochromatic, the atomic levels are "fuzzed out," be it by interaction with other molecules through collision, phonon coupling, or even coupling to the radiation field itself. Consequently $A(\omega, T)$ and $B(\omega, T)$ are not simply decomposable into thermal and line-shape factors, or in other words, ω and T are scrambled together so that the problem ceases to be an elementary one. In principle it should be possible to treat the entire system, i.e., the given atom plus other molecules, phonons, etc., as one big glorified atom, and then each line should be monochromatic, since all disturbances have been incorporated in the "inner" system. Actually, however, the

---

* Alfred P. Sloan Fellow.

[1] A. Einstein, Phys. Z. 18, 121 (1917).

[2] The absorption coefficient $B(\omega)$ as we use it is defined as the quotient of rate of absorption of energy to field energy, both computed per unit volume. The value of $F(\omega)$ given in (0.2) is on the assumption of an isotropic radiation field. The appropriate value of $F(\omega)$ for other cases can be deduced from purely geometrical considerations as long as the field can be described by harmonic oscillators, as then generally $F(\omega)=2\pi\hbar\omega K_\omega$, where $K_\omega V$ is the density of these oscillator states in ω space. This general formula for $F(\omega)$ applies regardless of whether the transitions are caused by interactions of our atomic system with radiation, magnons, or phonons, since any of these can be described by the oscillator model. With longitudinal isotropic phonons, for example, $F(\omega)$ has half the value given in (0.2) (with c now an acoustic velocity) as there are not two directions of polarization. The fact that electromagnetic fields carry equal amounts of electric and magnetic energies is the counterpart of the fact that the kinetic and potential energies are equal for a harmonic oscillator. Oftentimes one has situations where there is only an alternating magnetic field without an appreciable electric one or vice versa, rather than both equal as in the radiation "wave zone." Then the harmonic-oscillator model is inapplicable, and the factor $F(\omega)$ has double the value (0.2) since the energy density is halved.

CC-0. In Public Domain. Gurukul Kangri Collection, Haridwar

Digitized by Arya Samaj Foundation Chennai and eGangotri

internal dynamics are so complicated that this procedure is usually not feasible.

Fortunately, other methods are available in particular the Green's function technique which has come into vogue in recent years. It is possible to give satisfactory answers to the problem for special cases, viz., the two-level system (especially the spin system $S=\frac{1}{2}$) and the harmonic oscillator, to the extent that essentially the Lorentzian or stochastic model is used. In the extreme wings of the line this model fails completely, yielding even an infinite second moment, i.e., an infinite mean square of the deviation of the frequency from its average value. In this region one should instead use the so-called statistical model, in which the perturbations are regarded as static, and one averages over all possible distributions weighted with the proper probability of occurrence.[3] This procedure is equivalent to treating collisions as infinitely slow, rather than infinitely short as in the stochastic model. Since the statistical model is essentially static in character, the role of temperature poses no additional problem, as each static configuration is weighted according to its appropriate Boltzmann factor.

Although Green's functions furnish the most refined approach, they do not provide the most intuitive one, and so in the first part of the paper (Secs. I.1–I.6) we derive most of the results in a less rigorous fashion based essentially on rudimentary examination of the correlation function for the two level system, and of the work done in the case of the harmonic oscillator. In the second part (Secs. II.1–II.8) we use the Green's function formalism. In part I the accent is on the stochastic model, equivalent to taking the Fourier components of the broadening mechanism as independent of frequency. In part II this specialization is not made, and instead the calculation is pointed particularly towards spin–lattice coupling, where the phonon spectrum is not flat.

PART I. ELEMENTARY METHODS

1. Relation between the Complex Susceptibility, the Correlation Function, and Absorption

In calculating line shapes or absorption, it is convenient and customary to introduce a complex, frequency-dependent atomic susceptibility tensor, defined by

$$\langle P_\beta \rangle = \chi_{\beta\alpha} F_\alpha \exp(i\omega t) \qquad (\alpha, \beta = x, y, z), \quad \text{(I.1)}$$

where the real part (Re) of $F_\alpha \exp(i\omega t)$ is the impressed rf field, and the real parts of P_x, P_y, P_z are the components of moment, electrical or magnetic, as appropriate to the problem. The symbol $\langle\ \rangle$ denotes the statistical average over the ensemble of atoms. If we write $\chi=\chi'-i\chi''$, then if there are N atoms/cc, the absorption coefficient per unit volume is

$$B(\omega) = 4\pi\omega\chi''(\omega) N \quad \text{(I.2)}$$

since this expression is[4] the time average of the product $(\mathrm{Re}\ \dot{P}_\alpha)\cdot[\mathrm{Re}\ F_\alpha \exp(i\omega t)]N$ divided by the energy density $|F_\alpha|^2/8\pi$.

The starting point of practically all modern calculations of line shape is a formula, apparently first given by Kubo,[5] relating the imaginary part of the diagonal components of the susceptibility tensor to the transform of the correlation function. This formula is

$$\chi_{\alpha\alpha}''(\omega) = \frac{1}{2\hbar} \tanh\left(\frac{\hbar\omega}{2kT}\right) \times \int_{-\infty}^{\infty} \cos(\omega t) \langle P_\alpha(0) P_\alpha(t) + P_\alpha(t) P_\alpha(0) \rangle\, dt. \quad \text{(I.3)}$$

Here and elsewhere, $\langle\ \rangle$ denotes the thermodynamic average or expectation value, i.e.,

$$\langle P_\alpha(0) P_\alpha(t) \rangle = \frac{\mathrm{Tr}\,[P_\alpha(0) P_\alpha(t) \exp(-\mathcal{H}/kT)]}{\mathrm{Tr} \exp(-\mathcal{H}/kT)}. \quad \text{(I.4)}$$

The Heisenberg representation is to be understood throughout, so that

$$P_\alpha(t) = \exp(i\mathcal{H}t/\hbar) P_\alpha(0) \exp(-\mathcal{H}t/\hbar). \quad \text{(I.5)}$$

The Boltzmann factors entering in (I.4) are to be evaluated at $t=0$. It is not necessary to include the impressed field $F_\alpha \exp(i\omega t)$ to evaluate the correlation function (I.4) involved in (I.3). Consequently, the Hamiltonian $\mathcal{H}$ entering in (I.5) is to be taken as exclusive of this field, but inclusive of the atomic system's interaction with the collision agency (e.g., phonons or colliding gas molecules) responsible for the line broadening, and also this agency's self-energy, so that $\mathcal{H}$ is a constant of the motion when $F_\alpha=0$. If this self energy is omitted, then time-dependent perturbation theory must be used, and $\mathcal{H}t$ replaced by

---

[3] For references on the statistical model, as well as to the literature of line breadths generally, see the review article by R. G. Breene, Jr., Rev. Mod. Phys. **29**, 94 (1957).

[4] In (I.2) we have assumed the radiation case, where the electric and magnetic energy densities are equal. If the incident field is purely electrical or magnetic, the factor in the right-hand side of (I.2) is 8 instead of 4. Cf. end of footnote 2.

[5] R. Kubo, *Lectures in Theoretical Physics*, edited by W. E. Britten and L. G. Dunham (Interscience Publishers, Inc., New York, 1959), Vol. I, p. 151. The relation (I.3) is also implicitly contained in an earlier paper by R. Kudo and K. Tomita, Proc. Phys. Soc. Japan **9**, 888 (1954). For a good discussion of the Heisenberg representation used in connection with (I.3) see Chap. VIII, especially sections 10, 14, 19 of A. Messiah's *Quantum Mechanics* (English transl.) (North-Holland Publishing Co., Amsterdam, 1961).

CC-0. In Public Domain. Gurukul Kangri Collection, Haridwar

Digitized by Arya Samaj Foundation Chennai and eGangotri

$\int \mathcal{H} dt$ in (I.5), making the exponentials become time-development operators.

The derivation of (I.3), which is now fairly standard and best achieved by use of the density matrix, is given in Appendix A.

2. Longitudinal Susceptibility of a Two-Level System

We will now restrict our calculations to a two-level system. Without any essential loss of generality we may suppose this to be a spin system $S=\frac{1}{2}$. We then have $P_\alpha=-g\beta S_\alpha$, where β is the Bohr magneton, and in order to allow the spin to be real or fictitious, we do not specialize the g factor to the value 2. We assume that there is a large constant magnetic field along the z axis. We examine separately the longitudinal and the transverse susceptibilities as they must be handled in somewhat different fashions. With obvious, appropriate changes in notation, our calculations apply to any two-level system if we understand by *longitudinal* and *transverse* the absorption stemming from the part of the moment, respectively, diagonal and nondiagonal in the index specifying the two energy levels.

We first consider the longitudinal case $\alpha=z$, i.e., the aperiodic absorption studied so extensively by Gorter and his school at Leiden.

At $t=0$ the eigenvalues of S_z are $\pm\frac{1}{2}$, with probabilities

$$p_-=\tfrac{1}{2}+\tfrac{1}{2}\tanh(\hbar\omega_0/2kT), \quad p_+=1-p_-, \quad (\hbar\omega_0=g\beta H_0) \tag{I.6}$$

and the thermodynamic mean of the two eigenvalues is

$$\langle S_z\rangle=\tfrac{1}{2}(p_+-p_-)=-\tfrac{1}{2}\tanh(\hbar\omega_0/2kT).$$

We now assume that the transition between the two eigenvalues of S_z occurs by a purely random, stochastic process. If τ is the mean free time between switches between the two eigenvalues, the mean lives τ_-, τ_+ in the states $S_z=-\frac{1}{2}$, $+\frac{1}{2}$ are, respectively,

$$\tau_-=2p_-\tau, \qquad \tau_+=2p_+\tau. \tag{I.7}$$

[The factor 2 occurs in (I.7) because half of the collisions end life in a given state.] One cannot disregard correlations after a switch, as the product of the two eigenvalues of S_z before and after a switch is $-\frac{1}{4}$. However, one can avoid the necessity of following through the correlations by imagining partially dummy collisions to take place such that in the + state a fraction p_+ remain in the +, and a fraction p_- change over into the − state. Similarly in the − state a fraction p_- of the imaginary collisions do nothing and a fraction p_+ are real. The frequency of occurrence $1/\tau_1$ of such artificially defined collisions is the same in either state since

$$\tau_1^{-1}=[(p_-+p_+)/p_+]\tau_-^{-1}=[(p_-+p_+)/p_-]\tau_+^{-1}=(2\tau p_-p_+)^{-1} \tag{I.8}$$

by (I.6) and (I.7). After such an artificially defined collision the mean value of $S_z-\langle S_z\rangle$ is zero regardless of whether one is starting from $+\frac{1}{2}$ or $-\frac{1}{2}$. Thus one has a simple decay of $S_z-\langle S_z\rangle$ to zero with time constant τ_1. We can write

$$4\int_{-\infty}^{\infty}\langle S_z(0)S_z(t)\rangle\cos\omega t\,dt=\int_{-\infty}^{\infty}p_+(1-\bar\sigma)(2S_+(t)-\bar\sigma)\cos\omega t\,dt+\int_{-\infty}^{\infty}p_-(-1-\bar\sigma)[2S_-(t)-\bar\sigma]\cos\omega t\,dt$$
$$+\int_{-\infty}^{\infty}\bar\sigma^2\cos\omega t\,dt, \tag{I.9}$$

where $\bar\sigma=2\langle S_z\rangle=p_+-p_-$ and $S_+(t)$, $S_-(t)$ are the values of $S_z(t)$ emanating, respectively, from $S_z=\frac{1}{2}$ and $S_z=-\frac{1}{2}$ at $t=0$. In virtue of what has been said above, the first two integrals on the right-hand side of (I.9) involve a simple exponential decay with the same constant, and so the right-hand side of (I.7) is

$$[p_+(1-\bar\sigma)^2+p_-(-1-\bar\sigma)^2]\int_{-\infty}^{\infty}\exp(-|t|/\tau_1)\cos\omega t\,dt+\bar\sigma^2\int_{-\infty}^{\infty}\cos\omega t\,dt=[1-\bar\sigma^2]\frac{2\tau_1}{1+\tau_1^2\omega^2}+2\bar\sigma^2\pi^{-1}\delta(\omega). \tag{I.10}$$

Because of the factor $\tanh(\hbar\omega/2kT)$ in (I.3) we can safely drop the term involving the Dirac delta function $\delta(\omega)$ (really a limiting operator) with singularity at $\omega=0$. Since our calculation is a semiclassical one, we do not need[6] to distinguish between $S_z(0)S_z(t)$ and $S_z(t)S_z(0)$, and so we can identify the integral in (I.3) with $\frac{1}{2}g^2\beta^2/\hbar$ times the expression (I.10). Thus (I.3) becomes

$$\chi_z''(\omega)=\frac{g^2\beta^2}{2\hbar}\tanh\left(\frac{\hbar\omega}{2kT}\right)\frac{\tau_1}{1+\tau_1^2\omega^2}\operatorname{sech}^2\left(\frac{\hbar\omega_0}{2kT}\right), \tag{I.11}$$

where $\hbar\omega_0=g\beta H_0$.

This equation is to be compared with the equation for the nonresonant susceptibility obtained by Casimir

[6] In adapting semiclassically quantum-mechanical formulas involving the correlation function one must select a form which is symmetric in $P_\alpha(0)$ and $P_\alpha(t)$. If one were naively to use the alternative form, for instance, which involves the antisymmetric combination one would get zero. The proper transcription of the antisymmetric form would involve a complicated consideration of Poisson brackets.

CC-0. In Public Domain. Gurukul Kangri Collection, Haridwar

Digitized by Arya Samaj Foundation Chennai and eGangotri

and du Pré,[7] viz.,

$$\chi_z''(\omega)=\tfrac{1}{4}(g^2\beta^2/kT)\{\tau_1\omega/[1+(\tau_1\omega)^2]\}. \quad \text{(I.12)}$$

Equation (I.12) differs from (I.11) in two respects. The first of these is the factor of $\frac{1}{2}\omega/kT$ as compared to $\hbar^{-1}\tanh(\hbar\omega/2kT)$. This difference is indicative of the fact that the Casimir–du Pré analysis is valid only in the quantum-mechanical adiabatic limit $\omega=0$. It is usually of little importance in conventional experiments.

Of greater significance is the factor $\mathrm{sech}^2(\hbar\omega_0/2kT)$. Its existence apparently was explicitly pointed out for the first time by Van Vleck and Orbach.[8] It is intimately connected with the fact that in the limit of zero temperature, the population of the spin system remains entirely in the ground state, and so is unaffected by the alternating field. As a consequence, $\chi_z''(\omega)$ becomes exponentially small as $T\to 0$. The same factor could have been obtained from a thermodynamic analysis if the Curie susceptibility $g^2\beta^2/4kT$ is replaced by the static susceptibility evaluated in a finite field:

$$\chi_{H_0}=\frac{d}{dH}M(H)\bigg|_{H=H_0}=\tfrac{1}{2}g\beta\frac{d}{dH}\tanh\left(\frac{g\beta H}{2kT}\right)$$
$$=\frac{g^2\beta^2}{4kT}\,\mathrm{sech}^2\left(\frac{\hbar\omega_0}{2kT}\right).$$

A more or less equivalent procedure was used by Van Vleck and Orbach to obtain the sech^2 factor, though in connection with a somewhat different problem, viz., the effect of anisotropy in the aperiodic susceptibility of rare earth impurities on the ferrimagnetic resonance of iron garnets.

3. Effect of Phase Interruptions on the Resonant Absorption of a Two-Level System

We now proceed to treat the case that the rf field is perpendicular to the dc field that splits the energy levels. This is the case involved in the usual experiments in magnetic resonance of a system $S=\frac{1}{2}$. Also the analysis applies more generally to any two-level system, or system with two singled-out "effective levels" if the broadening due to interaction with other levels is not important, and if by N in (I.2) we understand the sum total of atoms in the two particular levels under consideration.

We note first of all that in the transverse case the matrix elements of, say, S_x for the transition $\frac{1}{2}\to-\frac{1}{2}$ are of the form

$$(\tfrac{1}{2}\mid S_x\mid -\tfrac{1}{2})=\int\psi_{\frac{1}{2}}^{*}S_x\psi_{-\frac{1}{2}}\,d\tau, \quad \text{(I.13)}$$

where the wave function is inclusive of spin. The wave function ψ has a phase factor ϵ in the sense that $\psi=|\psi|\exp(-iEt/\hbar)\exp(-i\epsilon)$. There is no question of persistence of phase at collision, as the new phases are random. The situation is different from the longitudinal or diagonal case, where the same phase enters fore and, with reversed sign, aft in the formula for the matrix element, so that the phase cancels out in the expression for the matrix element. Consequently in treating longitudinal absorption, correlation could not be ignored when one switches from one eigenvalue to another, and only by introducing the artifice of fake collisions were we able to disregard correlations.

If there were no interruptions caused by collisions the product of spin operators involved in the integrand of (I.3) for the transverse case would be simply

$$[P_x(0)\,P_x(t)+P_x(t)\,P_x(0)]=\tfrac{1}{2}g^2\beta^2\cos\omega_0 t \quad \text{(I.14)}$$

regardless of the initial conditions, inasmuch as

$$(\tfrac{1}{2}\mid P_x(t)\mid -\tfrac{1}{2})=(-\tfrac{1}{2}\mid P_x(t)\mid \tfrac{1}{2})^{*}=\tfrac{1}{2}g\beta\exp[i(\omega_0 t+\epsilon)]$$

The value of ω_0 is $g\beta H_0/\hbar$ for the particular case that the decomposition is due to an applied magnetic field.

Since in the transverse case there is no "hang-over effect" and the coherence is lost whenever there is an interruption of either the initial or final state, at first sight, it appears that allowance can be made for the gradual loss of correlation by multiplying (I.14) by $\exp(-|t|/\tau_2')$ with $1/\tau_2'=(1/\tau_-)+(1/\tau_+)$, where τ_- τ_+ are the mean lifetimes in the initial and final states associated with (I.13). However, a little reflection will convince one that the proper value of the constant in the exponent is instead

$$1/\tau_2'=\tfrac{1}{2}(\tau_-^{-1}+\tau_+^{-1}). \quad \text{(I.15)}$$

The appropriateness of the additional factor $\frac{1}{2}$ involved in (I.15) can be seen in a variety of ways. In the first place, in classical theory the appropriate decay factor associated with a mean life τ is $\exp(-t/\tau)$, and considerations of symmetry require that in quantum mechanics $1/\tau$ be apportioned symmetrically between the initial and final states. Alternatively or essentially equivalently, one can say that in quantum mechanics the life time of a state is determined by the rate of decay of the squared modulus of its probability amplitude (i.e., $|c_i|^2$ in an expansion of the form $\sum_i c_i\psi_i$), whereas a matrix element is represented by $c_i c_j^{*}$, and c_i, of course, decays half as fast as $|c_i|^2$. All this is rather heuristic, but for more rigorous confirmation of the factor $\frac{1}{2}$, appeal can be made to the results of Wigner and Weisskopf,[9] or to our calculation by means of Green's functions in part II. In virtue of (I.7) and

[7] H. B. G. Casimir and F. K. du Pré, Physica 5, 507 (1938).
[8] J. H. Van Vleck and R. Orbach, Phys. Rev. Letters 11, 65, 303 (E) (1963).
[9] V. Weisskopf and E. Wigner, Z. Physik 63, 54 (1930); 65, 18 (1930).

CC-0. In Public Domain. Gurukul Kangri Collection, Haridwar

Digitized by Arya Samaj Foundation Chennai and eGangotri

(I.8), Eq. (I.15) reduces to

$$1/\tau_2' = \tfrac{1}{2}\tau_1^{-1}. \tag{I.16}$$

When we multiply (I.14) by the exponential factor to allow for the loss of correlation and substitute in (I.3) we obtain for the transverse absorptive susceptibility the expression

$$\chi_{xx}''(\omega) = \tfrac{1}{4}g^2\beta^2\int_{-\infty}^{\infty}\cos(\omega_0 t)\cos(\omega t)\exp(-|t|/\tau_2')\,dt \times\hbar^{-1}\tanh(\hbar\omega/2kT). \tag{I.17}$$

Evaluation of the integral in (I.17) gives

$$\chi_{xx}''(\omega) = \tfrac{1}{4}g^2\beta^2\hbar\tanh\left(\frac{\hbar\omega}{2kT}\right) \times\left[\frac{1/\tau_2}{(\omega-\omega_0)^2+(1/\tau_2)^2}\quad\frac{1/\tau_2}{(\omega+\omega_0)^2+(1/\tau_2)^2}\right] \tag{I.18}$$

if we take $\tau_2=\tau_2'$. We use different notations τ_2, τ_2' because it will later turn out that (I.16) is not really the correct value of the transverse damping constant $1/\tau_2$ which should be used in (I.18).

4. Effect of Frequency Modulation on the Resonant Absorption of a Two-Level System

If we identify the damping constant $1/\tau_2$ in (I.18) with the expression $1/\tau_2'$ given in (I.16) the line-breadth constant $1/\tau_2$ for transverse resonance is half as large as that $1/\tau_1$ entering in the longitudinal case [Eq. (I.11)]. It is clear that something is wrong or incomplete, since it is well known that under certain circumstances the transverse relaxation time τ_2 is equal to the longitudinal one τ_1. In fact, if the collision mechanism is an isotropic one, then in the limit $\omega_0\to 0$ there is no possible way of distinguishing between the transverse and longitudinal situations, and this, of course, demands equal relaxation times or line-breadth constants for the two cases.

The difficulty is due to the fact that there are two mechanisms responsible for broadening in the transverse case, viz., phase interruption and frequency modulation, and we have considered only the first of these. The existence of the two mechanisms was recognized in the early work of Bloembergen, Purcell, and Pound,[10] and to distinguish between the two of them, they introduced the notation $1/\tau_2'$ and $1/\tau_2''$, which we follow, for the two corresponding line-breadth constants, with a combined total

$$1/\tau_2 = (1/\tau_2') + (1/\tau_2''). \tag{I.19}$$

The phase interruptions are caused by the involvement of S_x, S_y in the perturbing mechanism, and the frequency modulations by that of S_z. The reason is that for a system of spin $\frac{1}{2}$, the most general Hamiltonian is a linear function of S_x, S_y, S_z. The terms in S_x, S_y in the collision Hamiltonian are nondiagonal in the magnetic quantum number, and so induce collisions, with attendant phase interruptions, whereas the terms in S_z represent, so to speak, a noise field and merely alter the precession in a wobbly fashion. The term noise field is a catch-all for any kind of disturbance which adds to the Hamiltonian function a term linear in S_z, and may represent interactions with magnons, phonons, forces present at collision in gases, or even coupling to radiation. Our analysis is general, since we simply incorporate any of these effects in a time-dependent perturbation theory.

Because of the noise field, the time-dependent phase factor associated with, say, S_x+iS_y is $\exp[i\omega_0 t+i\phi(t)]$ instead of $\exp(i\omega_0 t)$. The excursion in phase $\phi(t)$ caused by the wobbles in the precession rate can be either positive or negative. We suppose that the longitudinal noise field is the sum

$$H_{nz} = \sum_k A_{kz}\exp(i\omega_k t) \tag{I.20}$$

of Fourier components without correlation except for the reality condition $A_{-k}^* = A_k$. Note that since the phase factor ϵ_k in $A_k = |A_k|\exp(i\epsilon_k)$ is random we have

$$\langle A_{kz}A_{k'z}\rangle_{Av} = |A_{kz}|^2\delta_k^{-k}. \tag{I.21}$$

Because the noise field is random, the addition of the various Fourier components is a random-walk affair, and, in accordance with rudimentary statistical theory, the excursion in phase after a sufficiently long time t has a Gaussian disturbation[11]

$$P(\phi) = (1/2\pi)^{\frac{1}{2}}\exp(-\phi^2/2\Delta)$$

with the mean-square excursion Δ a linear function of time. To compute Δ we note that

$$\phi(t) = g\beta\hbar^{-1}\int_0^t H_{nz}\,dt$$

so that

$$\Delta = g^2\beta^2\hbar^{-2}\{\sum_k[\exp(i\omega_k t)-1]A_{kz}/i\omega_k\}^2{}_{Av}. \tag{I.22}$$

If we use (I.21) and replace the sum by an integral (I.22) becomes

$$\Delta = 2g^2\beta^2\hbar^{-2}\int_{-\infty}^{\infty}\rho_\omega|A_z(\omega)|^2\left(\frac{1-\cos\omega t}{\omega^2}\right)d\omega,$$

[10] N. Bloembergen, E. M. Purcell, and R. V. Pound, Phys. Rev. 73, 679 (1948).

[11] The present treatment of the broadening due to frequency modulation as a random-walk process parallels closely that previously given by J. H. Van Vleck in a review article on nuclear relaxation times in Ned. T. Natuurk. 27, 1 (1961). This previous treatment, however, was primarily for high temperatures.

CC-0. In Public Domain. Gurukul Kangri Collection, Haridwar

Digitized by Arya Samaj Foundation Chennai and eGangotri

where ρ_ω is the density of k values in ω space and we now use the notation $A_z(\omega)$ rather than A_{kz}. For large t, all the contribution to the integral comes from the vicinity of the origin, so that $A_z(\omega)$ may be replaced by $A_z(0)$ and taken outside the integration sign, giving

$$\Delta = 2\pi g^2\beta^2 t\hbar^{-2}\rho_0 \mid A_z(0)\mid^2. \tag{I.23}$$

The extra factor in the integrand of the correlation function because of the frequency modulation effect is thus

$$\left(\frac{1}{2\pi}\right)^{\frac{1}{2}}\int_{-\infty}^{\infty}\exp\,(i\phi)\,\exp\,(-\phi^2/2\Delta)\,d\phi = \exp\,(-\mid t\mid/\tau_2''), \tag{I.24}$$

where

$$1/\tau_2'' = \pi\hbar^{-2}g^2\beta^2\rho_0 \mid A_z(0)\mid^2. \tag{I.25}$$

When now the extra factor (I.24) is inserted in the integrand of (I.17) the absorptive susceptibility is still given by (I.18), but now τ_2 is given by (I.19).

We must now examine the conditions under which $\tau_2''=\tau_2'$ so as to make $(1/\tau_2')+(1/\tau_2'')=1/\tau_1$ [of (I.16)], i.e., the longitudinal and transverse relaxation times equal to each other.

Let us first consider the case of high temperatures, so that the mean lives τ_+, τ_- in the upper and lower states are equal. Then by (I.15) the part $1/\tau_2'$ of the transverse relaxation rate is the mean decay rate out of either state. By the "golden rule," if the perturbation is

$$g\beta\sum_k[A_{kx}S_x+A_{ky}S_y]\exp\,(i\omega t), \tag{I.26}$$

this rate is

$$\frac{1}{\tau_2'}=\frac{1}{2}\left(\frac{1}{\tau_-}+\frac{1}{\tau_+}\right)$$
$$=2\pi\hbar^{-2}g^2\beta^2(\tfrac{1}{4})[\mid A_x(\omega_0)\mid^2+\mid A_y(\omega_0)\mid^2]\rho_{\omega_0}. \tag{I.27}$$

For an isotropic milieu, the averages for the x, y, and z components will all be the same. Also if, in addition, the broadening and frequency modulation are ideally stochastic, in other words if the spectrum of the disturbance is independent of frequency, corresponding to infinitely rapid collision times, then

$$\mid A_z(0)\mid^2\rho_0 = \mid A_x(\omega_0)\mid^2\rho_{\omega_0} = \mid A_y(\omega_0)\mid^2\rho_{\omega_0}, \tag{I.28}$$

and one does indeed have $\tau_2'=\tau_2''$ and $\tau_1=\tau_2$, so that the longitudinal and transverse relaxation times are equal. Of course, the Fourier spectrum cannot extend to infinity, as supposed in the ideally stochastic model, but the cutoff may be well above ω_0, in which case no harm is done in assuming that it extends to infinity.

To extend the proof to the case that ω_0 is not small compared to $kT/\hbar$, i.e., that $\tau_-\neq\tau_+$ in (I.15) requires some more quantum theory. The square modulus of an x-Fourier component in (I.26) as applied to the spin state $-\frac{1}{2}$ corresponds in quantum mechanics to a factor of the form $\langle\mid(j\mid A_x\mid j')\mid^2 N_j\rangle_{\text{Av}}$, where N_j is the population factor for the perturbing agency: phonons, magnons, or what-have-you, before it is changed by interaction with the spin system. The corresponding square for the state $\frac{1}{2}$ is $\langle\mid(j'\mid A_x\mid j)\mid^2 N_{j'}\rangle_{\text{Av}}$. The state j exceeds j' in energy by an amount $\hbar\omega_0$ in order to ensure conservation and a thermal average is to be understood over the various states of the perturbing agency. The Hermitian property and detailed balancing require that

$$(j\mid A_x\mid j')=(j'\mid A_x\mid j)^*, \qquad N_{j'}/N_j = p_-/p_+,$$

where p_-, p_+ are the thermal or probability factors defined in (I.5). Hence, using (I.15), we see that (I.27) is replaced by

$$\tfrac{1}{4}g^2\beta^2\hbar^{-2}\pi\{[\mid(j\mid A_x\mid j')\mid^2+\mid(j\mid A_y\mid j')\mid^2](N_j+N_{j'})\}_{\text{Av}}\rho_{\omega_0}$$

Similarly Eq. (I.25) transcribes quantum mechanically into

$$1/\tau_2'' = \tfrac{1}{2}\pi\hbar^{-2}g^2\beta^2\{\mid(j\mid A_z\mid j')\mid^2(N_j+N_{j'})\}_{\text{Av}}\rho_{\omega_0},$$

where the energy difference between the states j and j' is negligible. The isotropic and stochastic assumptions means that $\{\mid(j\mid A_q\mid j')\mid^2(N_j+N_{j'})\}_{\text{Av}}$ is independent of q or of the energy difference between the states j and j', also that $\rho_0=\rho_{\omega_0}$ giving us again $\tau_1=\tau_2$. This proof can be criticized on grounds of rigor, and skeptics can refer to the treatment by means of Green's functions in part II. It is doubtful, anyway, if the stochastic model has much meaning except when $\hbar\omega_0\ll kT$ and then we do not need to worry about the distinction between τ_- and τ_+.

5. Discussion of the Final Formula for the Transverse Absorptive Susceptibility

The final bracketed factor in (I.18), our expression for the transverse absorptive susceptibility, yields the same line shape as that given by Kronig,[12] Van Vleck and Weisskopf,[13] Fröhlich,[14] Karplus and Schwinger,[15] Garstens,[16] and others. It can be derived in a variety of ways, among them transitions between smeared out initial and final energy levels,[12] or Fourier analysis of spontaneous emission with absorption obtained from detailed balancing.[17] If the absorption is calculated directly[13,15] from the equations of motion without use

[12] R. de L. Kronig, Physica **5**, 65 (1938).
[13] J. H. Van Vleck and V. F. Weisskopf, Rev. Mod. Phys. **17**, 227 (1945).
[14] H. Frohlich, Nature **157**, 478 (1946).
[15] R. Karplus and J. Schwinger, Phys. Rev. **73**, 1020 (1948).
[16] M. A. Garstens, Phys. Rev. **93**, 1228 (1954).
[17] J. H. Van Vleck and H. Margenau, Phys. Rev. **76**, 1 (1949).

CC-0. In Public Domain. Gurukul Kangri Collection, Haridwar

Digitized by Arya Samaj Foundation Chennai and eGangotri

of correlation functions, it is necessary to take into account the fact that after collisions the assumed spatial distribution conforms to the Boltzmann law appropriate to the instantaneous value of the rf field, rather than being random.[18] Otherwise an expression is obtained which is correct only near resonance—in fact the antiresonant term—that in $\omega+\omega_0$ even has the wrong sign. In Lorentz's[19] original work he was interested only in the behavior near resonance, and so his assumption of randomness was warranted.

Our primary interest, however, is the way that the temperature enters. If one refers to the papers by Van Vleck,[20] Karplus and Schwinger,[15] etc., it is found that they used a factor

$$(\omega/\omega_0)\tanh(\hbar\omega_0/2kT)$$

in place of $\tanh(\hbar\omega/2kT)$ in (I.18). If one has both

$$(\hbar\omega/kT)\ll 1, \qquad (\hbar\omega_0/kT)\ll 1 \qquad \text{(I.29)}$$

then there is no distinction between the two expressions. This is also true near resonance, where

$$\hbar\,|\,\omega-\omega_0\,|/kT\ll 1, \qquad |\,\omega-\omega_0\,|/\omega\ll 1 \qquad \text{(I.30)}$$

even though $\hbar\omega$ may not be negligible compared with kT. Fortunately, in most cases one of the conditions (I.29) or (I.30) is satisfied, e.g., (I.30) is well-tuned resonance experiments and (I.29) in the propagation of radar or far-infrared waves, or in conventional studies of nuclear magnetization. However, with the modern techniques of very low temperatures achieved by adiabatic demagnetization, one can think of situations where the distinction is important. Also, from the sheer logic of the situation, it is desirable to know which form is correct, and there is no doubt that the proper factor is $\tanh(\hbar\omega/2kT)$. This conclusion is not a new one, since the correct factor has long been used in the fluctuation dissipation theorem, as adapted from Nyquist to the quantum-mechanical case by Callen and Welton[21] in connection with the study of the Johnson noise in circuits. This theorem is frequently used by workers on many-body problems.

It should be emphasized that the relation $\tau_1=\tau_2$ holds only under the particular condition that the perturbations responsible for the broadening are isotropic and the noise spectrum is independent of frequency. If one uses for a solid instead of the stochastic model a more realistic mechanism in which the perturbations are due to interaction with either phonons or magnons, then the spectral density ρ_0 at zero frequency is zero (i.e., $\rho\sim\omega^2$ for the well-known Debye law). In such cases we expect that $1/\tau_2''=0$ and $1/\tau_2=\frac{1}{2}(1/\tau_1)$, as already emphasized by McCumber.[22] The other extreme is where the noise spectrum is so narrow that it is largely cut off for the $1/\tau_1$ and $1/\tau_2'$ effects, which depend on perturbations being able to bridge the gap between $S_z=-\frac{1}{2}$ and $S_z=\frac{1}{2}$. Then the broadening is caused almost entirely by the FM effect, and we expect $1/\tau_2''\gg 1/\tau_1$. Under such circumstances the line shape must be calculated by the statistical rather than stochastic model. The classic experiments of Bloembergen, Purcell, and Pound[10] on nuclear resonance in liquid mixtures reveal vividly how $1/\tau_2$ begins to deviate from and exceed $1/\tau_1$ as the viscosity is increased and the perturbations by collisions become slower and more nearly static.

Finally it should be noted that as long as the surroundings are isotropic even if the noise spectrum is not flat, the formulas for the transverse and longitudinal susceptibilities should become identical when the static applied field is made to approach zero and the resonance frequency ω_0 hence is small compared to the impressed frequency ω. This is an obvious consequence of symmetry, for in the limit $\omega_0=0$ there can be no distinction between the longitudinal and transverse situations. This requirement is fulfilled by our formulas, for in the limit $\omega\rightarrow 0$ there can be no distinction between τ_1 and τ_2 inasmuch as $A_x(\omega)\rightarrow A_z(0)$ if there is isotropy, and if $\tau_1=\tau_2$, $\omega_0=0$, the longitudinal and transverse expressions (I.11) and (I.18) both reduce to a common expression

$$\chi''=\tfrac{1}{2}g^2\beta^2\hbar^{-1}\tanh(\hbar\omega/2kT)[\tau_1/(1+\tau_1^2\omega^2)]. \qquad \text{(I.31)}$$

[18] It is an advantage of the Kubo approach based on correlation functions that it gives the spectral shape without the necessity of investigating how the rf field affects the distribution after collision as it is a little hard to see what is implied in the assumption that the collisions readjust themselves to conform to the instantaneous value of a rapidly oscillating field. It should, however, be mentioned that if it assumed that such adjustment takes place, it is possible to show that for the stochastic model one has $\tau_1=\tau_2$ without the need of isolating the two kinds of contribution to τ_2. This was done by one of the present authors (V.V.) in J. Appl. Phys. **35**, 882 (1964), footnote 13. He assumed following Van Vleck and Weisskopf, or Karplus and Schwinger, that each collision restores the distribution to that appropriate to the instantaneous value of the total field. If τ' be the interval between such collisions, then the work of Karplus and Schwinger (Ref. 15) shows that τ_2 is the same as the transverse damping constant τ'. Elementary considerations such as given in our Sec. I.2, and not elaborated in the original article of Van Vleck, show that the τ_1 is the same as τ'. It is at first sight rather surprising that with this approach one obtains the full value of $1/\tau_2$ without ostensibly invoking the frequency modulation effect. The explanation is a rather subtle one. Adjustment to the proper orientation relative to the applied transverse field can be obtained by rephasing without changing the eigenvalues of s_z. Thus what looks like a "do-nothing" collision as far as s_z is concerned is a real one as regards s_x, s_y and such rephasing is another way of looking at the FM effect.

[19] H. A. Lorentz, Proc. Amst. Akad. Sci. **8**, 591 (1906), or *The Theory of Electrons* (Teubner, Leipzig, 1909, or Dover Publications, New York, 1952, note 57).

[20] J. H. Van Vleck, Phys. Rev. **71**, 413 (1947); an attempt by the same author [Conference on the Broadening of Spectral Lines, Pittsburgh, (1955)] to improve on the thermal factor he originally used is not satisfactory.

[21] H. B. Callen and T. A. Welton, Phys. Rev. **83**, 34 (1951).

[22] D. E. McCumber, Phys. Rev. **133**, A163 (1964).

CC-0. In Public Domain. Gurukul Kangri Collection, Haridwar

Digitized by Arya Samaj Foundation Chennai and eGangotri

6. Line Shape for a Perturbed Harmonic Oscillator

We now turn to a completely different problem—a harmonic oscillator X perturbed by interactions with other systems $x_1, x_2, \cdots$. We assume that these other systems are themselves harmonic oscillators, and that the interaction is linear in the coordinates which it couples. These conditions are met if, for example, the perturbing systems are phonons, magnons, or even photons. We assume that the applied field E acts only on x, so that the Hamiltonian function is

$$\mathfrak{IC}_E=\tfrac{1}{2}m[(p_X/m)^2+\omega_0^2X^2]+\sum_k\tfrac{1}{2}\mu_k[(p_k/\mu_k)^2+\omega_k^2x_k^2]$$
$$+X\sum_k c_kx_k-eXE_0\cos\omega t. \quad \text{(I.32)}$$

We attach a subscript E to $\mathfrak{IC}$ in order to emphasize that the Hamiltonian (I.32) is inclusive of the interaction $-eXE_0\cos\omega t$ with the impressed rf field, and in order to distinguish it clearly from the Hamiltonian exclusive thereof which we throughout denote by $\mathfrak{IC}$ and which we use generally in evaluating the correlation function [cf. e.g., Eqs. (I.3)–(I.5)].

We suppose we are dealing with a one-dimensional problem, but the extension to the isotropic three-dimensional problem occasions no difficulty. For concreteness we assume that we are dealing with a harmonically bound electric charge e of mass m. Without resorting to any mathematical analysis, one can immediately conclude how the temperature enters in absorption and emission. If we take $E_0=0$, the dynamical problem is simply that of a system of coupled harmonic oscillators whose Hamiltonian is a quadratic form. In either classical or quantum mechanics, it is possible to introduce normal coordinates ξ_j such that the Hamiltonian is reduced to a sum of squares $\frac{1}{2}\sum_j(\alpha_jp_j^2+\beta_j\xi_j^2)$. The extra term from the perturbing field acquires the form $\sum_j\gamma_j\xi_jE_0\cos\omega t$. In other words a fraction of the perturbing field acts on each of the new, uncoupled harmonic oscillators that correspond to the normal coordinates. The absorption by a harmonic oscillator in thermal equilibrium is independent of temperature in both classical and quantum mechanics. Its emission is proportional to $1/[\exp(\hbar\omega/kT)-1]$ in quantum theory and to kT classically. The absorption coefficient $B(\omega)$ for our system is thus independent of temperature and the corresponding coefficient associated with spontaneous radiation is

$$A(\omega)=F(\omega)B(\omega)/[\exp(\hbar\omega/kT)-1], \quad \text{(I.33)}$$

where $F(\omega)$ has the value $2\hbar\omega^3/\pi c^3$ if the electric field arises from isotropic radiation. The form of the temperature-independent function $F(\omega)$ for other cases is discussed in footnote 2.

The absorption $B(\omega)$ is the net difference between the true upwards absorption $B_+(\omega, T)$ and the stimulated emission $B_-(\omega, T)$, which are connected with $B(\omega)$ by the relations

$$B_+(\omega, T)=\frac{\exp(\hbar\omega/kT)}{\exp(\hbar\omega/kT)-1}B(\omega),$$

$$B_-(\omega, T)=\frac{B(\omega)}{\exp(\hbar\omega/kT)-1}.$$

Only the difference B_+-B_- is independent of temperature. It is particularly to be noted that the thermal factor for the spontaneous emission is

$$[\exp(\hbar\omega/kT)-1]^{-1}$$

and not

$$[\exp(\hbar\omega_0/kT)-1]^{-1}.$$

Consequently the low frequency tail of the line can be emitted when $\hbar\omega/kT\sim1$ even though $\hbar\omega_0/kT\ll1$ provided only that $F(\omega)B(\omega)$ is not negligible. If the oscillator X was uncoupled to other oscillators, the absorption coefficient would be a line-strength factor times a delta function located at $\omega=\omega_0$. Because of the interaction terms $X\sum_kc_kx_k$ the myriads of other oscillators $x_1, x_2, \cdots$ steal a fraction of the line strength otherwise associated purely with X, and it is this stealing effect which is responsible for the line shape. We allow the ensemble of perturbing oscillators to become more and more closely spaced, and in the limit the absorption becomes a continuum rather a discrete set of closely spaced delta functions. The original oscillator X has then lost its identity and contributed all its line strength to the ensemble, as some of the oscillators x_k fall so close to X in frequency that in this region there is complete scrambling.

Our problem is now to determine how the absorption intensity is distributed among the various new eigenfrequencies. It turns out to be remarkably easy to solve.

Instead of using correlation functions, it is easiest to compute directly the work done by the impressed field $E_0\cos\omega t$. All the coordinates will oscillate in phase with the field, i.e., have time factors $\cos\omega t$. The equation of motion

$$\mu_k(\ddot{x}_k+\omega_k^2x_k)+c_kX=0$$

for the coordinate x_k gives immediately

$$x_k=[c_k/\mu_k(\omega^2-\omega_k^2)]X \quad \text{(I.34)}$$

and substitution of (I.34) into the equation for X yields

$$X=eE_0\cos\omega t/f(\omega), \quad \text{(I.35)}$$

where

$$f(\omega)=m(\omega_0^2-\omega^2)+\sum_k[c_k^2/\mu_k(\omega^2-\omega_k^2)]. \quad \text{(I.36)}$$

CC-0. In Public Domain. Gurukul Kangri Collection, Haridwar

Digitized by Arya Samaj Foundation Chennai and eGangotri

We now assume that the values of ω_k, the original frequencies of the perturbing oscillators, are closely spaced at intervals ϵ_k which are small compared with ω, and which vary only slowly with the region of the spectrum so that they can be regarded as sensibly constant in the vicinity of a given ω_k. The denominator (I.36) of (I.35) has one simple zero ω_k' in the interval ω_k+0 to $\omega_{k+1}-0$ as it seings from $+\infty$ to $-\infty$ in this interval. (There are no higher order zeros, as we will later find a non-vanishing derivative at each root.) The expression (I.35) can thus be written in the form

$$X=\sum_k[g_k(\omega)/(\omega_k'-\omega)], \tag{I.37}$$

where ω_k' is not quite the same as ω_k, and $g_k(\omega)$ is finite at $\omega=\omega_k'$. There is absorption only if the impressed frequency is accurately tuned to one of the poles ω_k'. Actually, however, any impressed field is not strictly monochromatic, and will have a practically uniform intensity over the small region separating two roots, which in the limit becomes negligible as they finally contract together to make the perturbing agency (magnons, phonons, etc.) have a continuous spectrum. If instead of being monochromatic, the electric energy has a spectral distribution described by

$$\tfrac{1}{2}E_0^2=\int K(\omega)\,d\omega \tag{I.38}$$

the absorption arising from a given term of (I.37) is proportional to $g(\omega_k')K(\omega_k')$. The proportionality factor is most readily determined by comparison with the time-honored and familiar result that an undamped harmonic oscillator of frequency ω_0 absorbs radiation from a field of the form (I.38) at a rate[23]

$$dW/dt=(e^2/4m)\cdot 2\pi K(\omega_0). \tag{I.39}$$

The response of a harmonic oscillator near resonance is

$$X=\frac{eE_0\cos\omega t}{m(\omega_0^2-\omega^2)}\sim\frac{eE_0\cos\omega t}{2m\omega_0(\omega_0-\omega)}. \tag{I.40}$$

Each member of (I.37) is evidently equivalent to a fictitious harmonic oscillator having an apparent e/m value $2\omega_k'g_k(\omega_k')$. Any one term of (I.37) therefore absorbs energy at a rate

$$dW/dt=\pi e\omega_k'g_k(\omega_k')K(\omega_k'). \tag{I.41}$$

If, instead of being strictly monochromatic, the intensity in (I.35) is spread uniformly over a band wide enough to include n roots of (I.36), then $K(\omega_k')=\frac{1}{2}E_0^2/\epsilon_k n$. The factor n cancels out of the formula for dW/dt, in terms of E_0, since an extra factor n must be inserted in the right side of (I.41) to allow for the fact that there is now absorption from n resonances of approximately equal strength. The absorptive susceptibility χ'' is $(dW/dt)/\frac{1}{2}E_0^2\omega$ and is consequently

$$\chi_\omega''=\pi g_k(\omega)\rho_k e, \tag{I.42}$$

where $\rho_k=1/\epsilon_k$ is the density of the roots of (I.36) in ω space and we use a value of k such that ω_k is near ω. Since the coefficients c_k are very small, and the roots crowd very close together, we do not need to distinguish between the spacing between consecutive infinities (the ω_k) and that between consecutive zeros (the ω_k') of (I.36).

Our problem is now to compute the pole strength $g_k(\omega)$, which by (I.35), (I.36), and (I.37) is

$$g_k=-e/[df/d\omega]_{\omega=\omega_k'}. \tag{I.43}$$

To evaluate the derivative needed in (I.43) we write the function f defined in (I.36) near some particular root ω_k' in the form

$$f(\omega)=m(\omega_0^2-\omega^2)+\Delta+Q, \tag{I.44}$$

where

$$\Delta=\sum_k[c_k^2/\mu_k(\omega^2-\omega_k^2)]-Q, \tag{I.45}$$

$$Q=\frac{c_k^2}{\mu_k'}\frac{\Omega}{\omega_k'}\left[\frac{1}{\Omega^2-(\frac{1}{2}\epsilon)^2}+\frac{1}{\Omega^2-(\frac{3}{2}\epsilon)^2}+\frac{1}{\Omega^2-(\frac{5}{2}\epsilon)^2}+\cdots\right], \tag{I.46}$$

where $\epsilon=\epsilon_k'$ and where $\Omega=\omega-\frac{1}{2}(\omega_k+\omega_{k+1})$ is the frequency measured relative to the midpoint of the interval which is bounded by two adjacent infinities of $f(\omega)$ and which contains the particular zero of $f(\omega)$ that is being studied. If we let ϵ_k gradually contract towards zero, we can ultimately replace the sum in (I.45) [but not in (I.46)] by an integral that can be written in the convenient form

$$\Delta=\mathcal{P}\int_0^\infty\frac{c_k^2}{\mu_k(\omega^2-\omega_k^2)}\rho_k\,d\omega_k, \tag{I.47}$$

where $\mathcal{P}$ denotes the principal part. The validity of the expression (I.47) for Δ is a consequence of the fact that the pole of the second term of (I.45) just cancels that of the first one, and the principal part of the integral associated with the second (Q) term is zero. (Strictly speaking this is true only if the lower limit of integration is $-\infty$, but the resulting error is inconsequential.) Were it not for the fact that c_k, μ_k, ρ_k are

[23] Cf., for instance, M. Planck, *Vorlesungen Uber die Theorie der Warmestrahlung* (Barth, Leipzig, 1921), 4th ed., part IV, Chap. 1.

CC-0. In Public Domain. Gurukul Kangri Collection, Haridwar

Digitized by Arya Samaj Foundation Chennai and eGangotri

slowly varying functions of k, the entire expression (I.45) could also be set equal to zero. The displacement of the resonance maximum which will later turn out to be a consequence of the nonvanishing Δ is thus an expression of the nonuniformity of the perturbing spectrum.

Thanks to a mathematical formula[24] tailor-made for our purposes, the series in brackets in (I.46) can be summed exactly, and has the value

$$-(\pi/2\epsilon\Omega)\tan(\pi\Omega/\epsilon).$$

The expression (I.44) is consequently

$$f(\omega)=m(\omega_0^2-\omega^2)+\Delta-(c_{k'}{}^2\pi/2\mu_{k'}\omega_{k'}\epsilon)\tan(\pi\Omega/\epsilon). \tag{I.48}$$

In evaluating $df/d\omega$, we need only consider the term coming from the differentiation of the tangent, as this throws down a factor $1/\epsilon$, which is large compared to $1/\omega$. Hence

$$\left.\frac{df}{d\omega}\right|_{\omega=\omega_{k'}}=-\frac{c_{k'}{}^2\pi^2}{2\mu_{k'}\omega_{k'}\epsilon^2}\left[1+\tan^2\left(\frac{\pi\Omega}{\epsilon}\right)\right]. \tag{I.49}$$

Since (I.49) is to be evaluated at a root of (I.48) we see, using (I.43), that formula (I.42) becomes

$$\chi_\omega''=\frac{2\pi e^2\rho_{k'}(c_{k'}{}^2/\omega_{k'}\mu_k)}{4[m(\omega_0^2-\omega^2)+\Delta]^2+(c_{k'}{}^2\pi\rho_{k'}/\mu_{k'}\omega_{k'})^2}, \tag{I.50}$$

where $\rho_{k'}=1/\epsilon$ and k' is determined by $\omega_{k'}=\omega$. Equation (I.50) is also obtained in part II by a different method. The contrast between the two approaches yielding the same result is quite striking.

In conclusion we should mention that the model that we have used, in which the perturbing mechanism is an ensemble of harmonic oscillators, is somewhat specialized, and does not portray the most general stochastic or collision process. Since even after the coupling our system remained harmonic, any light scattered from incident monochromatic radiation should be coherent and have the same frequency as the latter. On the other hand, Holstein[25] and Towne[26] have shown that an oscillator excited by a monochromatic beam interrupted by strong collisions can reradiate part of the energy absorbed from the beam as light which is not monochromatic or coherent, and is centered around the resonance rather than the impressed frequency. To yield this effect, essentially a Raman process involving the states of the atomic + colliding system, something more general than a completely harmonic total system is required.

II. GREEN'S FUNCTION APPROACH

1. Preliminaries

In this and the following sections we attack the line-shape problem using powerful, but more formal, Green's function techniques. Seven of the remaining eight sections are devoted to the treatment of a two-level (spin-$\frac{1}{2}$) system interacting with a crystal lattice. In the final section we discuss the behavior of a harmonic oscillator which is also coupled to a lattice.

To a certain extent our treatment of the two-level system parallels the recent work of McCumber.[27] He discusses the influence of the spin–phonon coupling on the optical spectrum. There are, however, important differences between optical- and magnetic-resonance phenomena which are relevant to the line shape analysis. First, because of the enormous separation between optical levels, population effects arising from thermal excitation can usually be neglected. Second, there is no optical analog of the longitudinal susceptibility, where the absorption is measured with the alternating field parallel to the static field. Our analysis also overlaps somewhat with a study of the influence of the spin–phonon coupling on the magnetic-resonance spectrum that has been made by Aminov and Kochelaev.[28] They, however, were mainly interested in determining the magnitude of the shifts arising from the interaction.

Prior to introducing the Hamiltonian appropriate to the spin problem it will be convenient to rewrite (I.3) in terms of the Fourier transforms of the spin–spin correlation functions. The Fourier transform (or spectral intensity function) associated with $\langle S_z S_z\rangle$ is defined by

$$\langle S_z(t)\,S_z(t')\rangle=\int_{-\infty}^{\infty}J^{zz}(\omega)\exp[-i\omega(t-t')]\,d\omega. \tag{II.1}$$

By making use of (II.1) we can rewrite $\chi_{zz}''(\omega)$ in the following fashion (specializing to the magnetic dipole):

$$\chi_{zz}''(\omega)=(\pi g^2\beta^2/\hbar)\tanh(\hbar\omega/2kT)(J^{zz}(\omega)+J^{zz}(-\omega)). \tag{II.2}$$

In the case of the xx and yy components of χ'' we introduce the spectral functions associated with the operators $S_+=S_x+iS_y$ and $S_-=S_x-iS_y$ by means of

[24] Knopp, *Unendliche Reihen* (Springer-Verlag, Berlin, 1922), p. 197; quoted by O. K. Rice in Phys. Rev. **33**, 755 (1929).
[25] T. Holstein, Phys. Rev. **72**, 1212 (1947), Appendix IA.
[26] D. Towne, Ph.D. thesis, Harvard, 1954 (unpublished).
[27] D. E. McCumber, J. Math. Phys. **5**, 222 (1964); **5**, 508 (1964).
[28] L. K. Aminov and B. I. Kochelaev, Fiz. Tverd. Tela **4**, 1604 (1962) [English transl.: Soviet Phys.—Solid State **4**, 1175 (1962)].

CC-0. In Public Domain. Gurukul Kangri Collection, Haridwar

Digitized by Arya Samaj Foundation Chennai and eGangotri

the equations

$$\langle S_-(t)S_+(t')\rangle = \int_{-\infty}^{\infty} J^{-+}(\omega)\exp(\hbar\omega/kT)\exp[-i\omega(t-t')]\,d\omega, \tag{II.3}$$

$$\langle S_+(t')S_-(t)\rangle = \int_{-\infty}^{\infty} J^{-+}(\omega)\exp[-i\omega(t-t')]\,d\omega, \tag{II.4}$$

$$\langle S_+(t)S_+(t')\rangle = \int_{-\infty}^{\infty} J^{++}(\omega)\exp[-i\omega(t-t')]\,d\omega, \tag{II.5}$$

$$\langle S_-(t)S_-(t')\rangle = \int_{-\infty}^{\infty} J^{--}(\omega)\exp[-i\omega(t-t')]\,d\omega. \tag{II.6}$$

It should be noted that Eqs. (II.3) and (II.4) showing the interdependence of $\langle S_+S_-\rangle$ and $\langle S_-S_+\rangle$ follow from the definition of the correlation function and the cyclic properties of the trace.[29]

Upon inserting (II.3)–(II.6) into (I.3) we obtain the result

$$\begin{aligned}\chi''_{xx,yy}(\omega) = (\pi g^2\beta^2/4\hbar)\tanh(\hbar\omega/2kT)\\ \times\{[1+\exp(\hbar\omega/kT)]J^{-+}(\omega)\\ +[1+\exp(-\hbar\omega/kT)]J^{-+}(-\omega)\pm J^{++}(\omega)\\ \pm J^{++}(-\omega)\pm J^{--}(\omega)\pm J^{--}(-\omega)\},\end{aligned} \tag{II.7}$$

where the plus and minus signs refer to the xx and yy components, respectively. Equations (II.2) and (II.7) from the basis for our subsequent discussion. We emphasize that the expressions for χ''_{zz} and $\chi''_{xx,yy}$ are completely general. No assumptions have been made about the nature of the interaction of the spin with its environment.

2. Hamiltonian

We consider a system having spin $\frac{1}{2}$ that is coupled to the crystal lattice by terms that are linear in the lattice displacement. If we take the direction of the static magnetic field to define the z axis, then the Hamiltonian, in its general form, is written

$$\begin{aligned}\mathcal{H} = \hbar\omega_0 S_z + \sum_{\mathbf{k}p}\hbar\omega_{\mathbf{k}p}a_{\mathbf{k}p}^{+}a_{\mathbf{k}p} + \sum_{\mathbf{k}p}(A_x(\mathbf{k}p)S_x\\ + A_y(\mathbf{k}p)S_y + A_z(\mathbf{k}p)S_z)(a_{\mathbf{k}p}^{+} + a_{-\mathbf{k}p}).\end{aligned} \tag{II.8}$$

[29] D. N. Zubarev, Usp. Fiz. Nauk **71**, 71 (1960) [English transl.: Soviet Phys.—Uspekhi **3**, 320 (1960)].

Here $\hbar\omega_0(=g\beta H)$ is the splitting between the upper and lower spin levels, and $\hbar\omega_{\mathbf{k}p}$ is the energy of a phonon having wave vector $\mathbf{k}$ and polarization p. The $a_{\mathbf{k}p}$ and $a_{\mathbf{k}p}^{+}$ are phonon annihilation and creation operators with the commutation relations

$$\begin{aligned}[a_{\mathbf{k}p}, a_{\mathbf{k}'p'}]&=0;\\ [a_{\mathbf{k}p}^{+}, a_{\mathbf{k}'p'}^{+}]&=0;\\ [a_{\mathbf{k}p}, a_{\mathbf{k}'p'}^{+}]&=\delta_{\mathbf{k}\mathbf{k}'}\delta_{pp'}.\end{aligned} \tag{II.9}$$

The $A_\alpha(\mathbf{k}p)$ are coupling constants which depend on the detailed properties of the magnetic ion and its crystalline environment.

Rather than work with the general Hamiltonian we will find it convenient to consider a simplified isotropic approximation to (II.8) which we write in the form

$$\begin{aligned}\mathcal{H}_{\text{iso}} = \hbar\omega_0 S_z + \sum_{\mathbf{k}p}\hbar\omega_{\mathbf{k}}a_{\mathbf{k}p}^{+}a_{\mathbf{k}p}\\ + \sum_{\mathbf{k}p}A_{\mathbf{k}}\mathbf{S}\cdot\boldsymbol{\varepsilon}(\mathbf{k}p)(a_{\mathbf{k}p}^{+} + a_{-\mathbf{k}p}),\end{aligned} \tag{II.10}$$

where we assume $\omega_{\mathbf{k}}=\omega_{-\mathbf{k}}$ and $A_{\mathbf{k}}=A_{-\mathbf{k}}$. Here $\boldsymbol{\varepsilon}(\mathbf{k}p)$ is the polarization vector associated with the mode designated by $\mathbf{k}$ and p. Our reasons for choosing to work with the model interaction are twofold. First, the isotropic nature of the coupling makes possible a direct comparison of the effects of the spin–lattice interaction with the effects of analogous broadening mechanisms in liquids and gases. Second, the use of an interaction involving the scalar product of the polarization and spin vectors leads to a considerable simplification in the calculation of the spectral functions. Although there is an accompanying loss in generality, we will relate the results obtained with $\mathcal{H}_{\text{iso}}$ to what would have been obtained with a more general Hamiltonian in the situations which are of experimental interest.

3. Green's Function Formalism

Having specified the Hamiltonian we are left with the problem of calculating the correlation functions. A convenient way of doing this is to make use of the double-time thermodynamic Green's functions introduced by Zubarev.[29] We define the Green's function $\langle\langle A(t);B(t')\rangle\rangle_{\pm}$ associated with the operators A and B by means of equation

$$\langle\langle A(t);B(t')\rangle\rangle_{\pm} = -i\theta(t-t')[\langle A(t)B(t')\rangle \pm \langle B(t')A(t)\rangle]. \tag{II.11}$$

Here $\theta(t-t')$ is the unit step function with the property

$$\theta(t-t')=1,\quad t>t';\qquad \theta(t-t')=0,\quad t<t'. \tag{II.12}$$

It is shown in Ref. 29 that $\langle\langle A(t);B(t')\rangle\rangle_{\pm}$ satisfies

CC-0. In Public Domain. Gurukul Kangri Collection, Haridwar

Digitized by Arya Samaj Foundation Chennai and eGangotri

the equation of motion

$$i\hbar(d/dt)\langle\langle A(t);B(t')\rangle\rangle_{\pm} = \hbar\delta(t-t')[\langle A(t)B(t)\pm B(t)A(t)\rangle] + \langle\langle(A(t)\mathfrak{IC}(t)-\mathfrak{IC}(t)A(t));\ B(t')\rangle\rangle_{\pm}, \quad \text{(II.13)}$$

where $\mathfrak{IC}(t)$ is the Hamiltonian.

For the most part we will work with the Fourier transform of $\langle\langle A(t);B(t')\rangle\rangle_{\pm}$ which we define by the integral

$$\langle\langle A;B\rangle\rangle_{\pm}(E)=\frac{1}{2\pi}\int_{-\infty}^{\infty}\exp\left(\frac{iEt}{\hbar}\right)\langle\langle A(t);B(0)\rangle\rangle_{\pm}\,dt. \quad \text{(II.14)}$$

The transform of (II.13) is then written

$$E\langle\langle A;B\rangle\rangle_{\pm}(E)=(1/2\pi)[\langle AB\pm BA\rangle] + \langle\langle[A,\mathfrak{IC}];B\rangle\rangle_{\pm}(E). \quad \text{(II.13')}$$

In Ref. 29 it is demonstrated that the correlation functions $\langle A(t)B(t')\rangle$ and $\langle B(t')A(t)\rangle$ can be expressed in the following form

$$\langle A(t)B(t')\rangle=\int_{-\infty}^{\infty}\exp\left(\frac{\hbar\omega}{kT}\right)J_{\pm}^{AB}(\omega)\exp[-i\omega(t-t')]\,d\omega, \quad \text{(II.15)}$$

$$\langle B(t')A(t)\rangle=\int_{-\infty}^{\infty}J_{\pm}^{AB}(\omega)\exp[-i\omega(t-t')]\,d\omega, \quad \text{(II.16)}$$

where the spectral function $J_{\pm}^{AB}(\omega)$ is defined in terms of the limiting values of $\langle\langle A;B\rangle\rangle_{\pm}(E)$ as E approaches the real axis. That is, we have

$$J_{\pm}^{AB}(\omega)=\frac{i\hbar}{\exp(\hbar\omega/kT)\pm 1}[\langle\langle A;B\rangle\rangle_{\pm}(\hbar\omega+i\epsilon)-\langle\langle A;B\rangle\rangle_{\pm}(\hbar\omega-i\epsilon)], \quad \text{(II.17)}$$

where the limit $\epsilon\to 0+$ is understood.

In the spin-$\frac{1}{2}$ problem we are led to consider the Green's functions $\langle\langle S_-;S_+\rangle\rangle_+$ and $\langle\langle S_z;S_z\rangle\rangle_+$. In the subsequent sections we will solve equations for these functions. With the aid of (II.17) we will obtain expressions for the spectral functions which appear in the formal definitions of the susceptibility. In order to obtain closed expressions for the Green's functions it is necessary to employ a simple decoupling approximation similar to that used in Ref. 29. The details and significance of this approximation are discussed at appropriate places in the calculation.

4. Calculation of χ_{zz}''

From the analysis given in the preceding sections it is evident that the Fourier transform of the Green's function $\langle\langle S_z(t);S_z(t')\rangle\rangle_+$ can be directly related to the longitudinal susceptibility. In this section we will outline the calculation of $\langle\langle S_z;S_z\rangle\rangle_+$. The application of (II.13') together with the Hamiltonian (II.10) leads to the equation

$$E\langle\langle S_z;S_z\rangle\rangle_+(E)=1/4\pi+\tfrac{1}{2}\sum_{\mathbf{k}p}A_{\mathbf{k}}(\epsilon_x(\mathbf{k}p)-i\epsilon_y(\mathbf{k}p))(\langle\langle S_+a_{\mathbf{k}p}{}^+;S_z\rangle\rangle_+(E)+\langle\langle S_+a_{-\mathbf{k}p};S_z\rangle\rangle_+(E)) - \tfrac{1}{2}\sum_{\mathbf{k}p}A_{\mathbf{k}}(\epsilon_x(\mathbf{k}p)+i\epsilon_y(\mathbf{k}p))(\langle\langle S_-a_{\mathbf{k}p}{}^+;S_z\rangle\rangle_+(E)+\langle\langle S_-a_{-\mathbf{k}p};S_z\rangle\rangle_+(E)). \quad \text{(II.18)}$$

It is evident that the equation for $\langle\langle S_z;S_z\rangle\rangle_+$ involves the Green's functions $\langle\langle S_{\pm}a_{\mathbf{k}p}{}^+;S_z\rangle\rangle_+$ and $\langle\langle S_{\pm}a_{-\mathbf{k}p};S_z\rangle\rangle_+$. Following Zubarev[29] we are led to consider the equations of motion for these higher-order functions. We will discuss in detail only $\langle\langle S_+a_{\mathbf{k}p}{}^+;S_z\rangle\rangle_+$ since a nearly identical analysis can be made for the other functions. The equation of motion for $\langle\langle S_+a_{\mathbf{k}p}{}^+;S_z\rangle\rangle_+$ is written

$$(E+\hbar\omega_0+\hbar\omega_{\mathbf{k}})\langle\langle S_+a_{\mathbf{k}p}{}^+;S_z\rangle\rangle_+(E)=\sum_{\mathbf{k}'p'}A_{\mathbf{k}'}(\epsilon_x(\mathbf{k}'p')+i\epsilon_y(\mathbf{k}'p'))\langle\langle S_z(a_{\mathbf{k}'p'}{}^++a_{-\mathbf{k}'p'})a_{\mathbf{k}p}{}^+;S_z\rangle\rangle_+(E) - \sum_{\mathbf{k}'p'}A_{\mathbf{k}'}\epsilon_z(\mathbf{k}'p')\langle\langle S_+(a_{\mathbf{k}'p'}{}^++a_{-\mathbf{k}'p'})a_{\mathbf{k}p}{}^+;S_z\rangle\rangle_+(E)-\tfrac{1}{2}A_{\mathbf{k}}(\epsilon_x(\mathbf{k}p)+i\epsilon_y(\mathbf{k}p)) \times(\langle\langle S_z;S_z\rangle\rangle_+(E)+\tfrac{1}{2}\langle\langle 1;S_z\rangle\rangle_+(E))+\tfrac{1}{2}A_{\mathbf{k}}\epsilon_z(\mathbf{k}p)\langle\langle S_+;S_z\rangle\rangle_+(E). \quad \text{(II.19)}$$

We see that the equation for $\langle\langle S_+a_{\mathbf{k}p}{}^+;S_z\rangle\rangle_+$ has in it still higher order Green's functions. It follows that an exact expression for $\langle\langle S_z;S_z\rangle\rangle_+$ can only be obtained by solving an infinite set of coupled equations. In order to reduce the problem to manageable size we introduce an approximate decoupling scheme. We replace the products of phonon operators appearing on the right-hand side of (II.19) by their thermal averages taken in the absence of a spin–phonon interaction

$$(a_{\mathbf{k}'p'}{}^+(t)+a_{-\mathbf{k}'p'}(t))a_{\mathbf{k}p}{}^+(t)\to\langle(a_{\mathbf{k}'p'}{}^++a_{-\mathbf{k}'p'})a_{\mathbf{k}p}{}^+\rangle=\delta_{\mathbf{k}-\mathbf{k}'}\delta_{pp'}(n_{\mathbf{k}}+1). \quad \text{(II.20)}$$

CC-0. In Public Domain. Gurukul Kangri Collection, Haridwar

Digitized by Arya Samaj Foundation Chennai and eGangotri

Here $n_k[=[\exp(\hbar\omega_k/kT)-1]^{-1}]$ is the Bose–Einstein occupation number. The significance of the approximation will become more clear in the subsequent discussion. At present it suffices to say that the approximation takes into account only one-phonon processes in which a single lattice mode is created or destroyed. Making use of (II.20) Eq. (II.19) is written

$$(E+\hbar\omega_0+\hbar\omega_k)\langle\langle S_+a_{kp}^+;\ S_z\rangle\rangle_+(E)=\tfrac{1}{2}A_k(\epsilon_x(\mathbf{k}p)+i\epsilon_y(\mathbf{k}p))(2n_k+1)\langle\langle S_z;\ S_z\rangle\rangle_+(E)$$
$$-\tfrac{1}{4}A_k(\epsilon_x(\mathbf{k}p)+i\epsilon_y(\mathbf{k}p))\langle\langle 1;\ S_z\rangle\rangle_+(E)-\tfrac{1}{2}A_k\epsilon_z(\mathbf{k}p)(2n_k+1)\langle\langle S_+;\ S_z\rangle\rangle_+(E). \quad \text{(II.19')}$$

Analogous equations for the functions $\langle\langle S_-a_{kp}^+;\ S_z\rangle\rangle_+$ and $\langle\langle S_\pm a_{-kp};\ S_z\rangle\rangle_+$ can also be derived in a straightforward fashion with the help of the decoupling approximation. Insertion of the expressions thus obtained into (II.18) leads to an inhomogeneous equation for $\langle\langle S_z;\ S_z\rangle\rangle_+$. The algebra is especially simplified when the orthogonality properties of the polarization vectors are taken into account

$$\sum_p \epsilon_\alpha(\mathbf{k}p)\epsilon_\beta(\mathbf{k}p)=\delta_{\alpha\beta}. \quad \text{(II.21)}$$

For this reason the terms involving $\epsilon_z(\mathbf{k}p)$ in the equations for the higher order functions do not appear in the equation for $\langle\langle S_z;\ S_z\rangle\rangle_+$. This simplification is a particular feature of the isotropic interaction and the assumption that the phonon energies are independent of polarization. The resulting expression for the longitudinal Green's function is written

$$E\langle\langle S_z;\ S_z\rangle\rangle_+(E)=1/4\pi+\tfrac{1}{2}\sum_k A_k^2(2n_k+1)$$
$$\times[(E+\hbar\omega_0+\hbar\omega_k)^{-1}+(E+\hbar\omega_0-\hbar\omega_k)^{-1}+(E-\hbar\omega_0+\hbar\omega_k)^{-1}+(E-\hbar\omega_0-\hbar\omega_k)^{-1}]\langle\langle S_z;\ S_z\rangle\rangle_+(E)$$
$$+\tfrac{1}{4}\sum_k A_k^2[(E-\hbar\omega_0+\hbar\omega_k)^{-1}+(E+\hbar\omega_0-\hbar\omega_k)^{-1}-(E+\hbar\omega_0+\hbar\omega_k)^{-1}-(E-\hbar\omega_0-\hbar\omega_k)^{-1}]\langle\langle 1;\ S_z\rangle\rangle_+(E). \quad \text{(II.22)}$$

The function $\langle\langle 1;\ S_z\rangle\rangle_+$ can be evaluated from its equation of motion

$$\langle\langle 1;\ S_z\rangle\rangle_+(E)=\langle S_z\rangle/\pi E=-(1/2\pi E)\tanh(\hbar\omega_0/2kT). \quad \text{(II.23)}$$

Here we have made the approximation of replacing $\langle S_z\rangle$ by its value in the absence of a spin–phonon coupling, $-\tfrac{1}{2}\tanh(\hbar\omega_0/2kT)$.

The spectral function $J^{zz}(\omega)$ is obtained from Eqs. (II.22) and (II.23) and the defining equation, (II.17). Insertion of the expression for $J^{zz}(\omega)$ into (II.2) leads to an equation for $\chi_{zz}''(\omega)$. Omitting a number of intermediate steps we arrive at the result

$$\chi_{zz}''(\omega)=\frac{1}{2\hbar}g^2\beta^2\tanh\frac{\hbar\omega}{2kT}$$
$$\times\frac{[(\Gamma(\omega+\omega_0)+\Gamma(\omega-\omega_0))(1-[\Lambda(\omega)/\omega]\tanh(\hbar\omega_0/2kT))-[\Psi(\omega)/\omega]\tanh(\hbar\omega_0/2kT)(\omega-\mathrm{K}(\omega-\omega_0)-\mathrm{K}(\omega+\omega_0))]}{(\omega-\mathrm{K}(\omega-\omega_0)-\mathrm{K}(\omega+\omega_0))^2+(\Gamma(\omega-\omega_0)+\Gamma(\omega+\omega_0))^2}, \quad \text{(II.24)}$$

where[30]

$$\Gamma(\omega)=(\pi/2\hbar)\sum_k A_k^2\coth(\hbar\omega_k/2kT)(\delta(\hbar\omega_k+\hbar\omega)+\delta(\hbar\omega_k-\hbar\omega)), \quad \text{(II.25)}$$

$$\mathrm{K}(\omega)=(\mathcal{P}/2\hbar)\sum_k A_k^2\coth(\hbar\omega_k/2kT)[(\hbar\omega_k+\hbar\omega)^{-1}-(\hbar\omega_k-\hbar\omega)^{-1}], \quad \text{(II.26)}$$

since

$$2n_k+1=\coth(\hbar\omega_k/2kT). \quad \text{(II.27)}$$

Also, we have

$$\Psi(\omega)=(\pi/2\hbar)\sum_k A_k^2(\delta(\hbar\omega-\hbar\omega_k+\hbar\omega_0)+\delta(\hbar\omega+\hbar\omega_k-\hbar\omega_0)-\delta(\hbar\omega-\hbar\omega_k-\hbar\omega_0)-\delta(\hbar\omega+\hbar\omega_k+\hbar\omega_0)), \quad \text{(II.28)}$$

$$\Lambda(\omega)=(\mathcal{P}/2\hbar)\sum_k A_k^2[(\hbar\omega-\hbar\omega_k+\hbar\omega_0)^{-1}+(\hbar\omega+\hbar\omega_k-\hbar\omega_0)^{-1}-(\hbar\omega-\hbar\omega_k-\hbar\omega_0)^{-1}-(\hbar\omega+\hbar\omega_k+\hbar\omega_0)^{-1}]. \quad \text{(II.29)}$$

We defer discussion of these rather formidable expressions to the following section.

[30] In obtaining (II.25)–(II.29) we have made use of the symbolic identity $(\omega+i\epsilon)^{-1}=\mathcal{P}/\omega-i\pi\delta(\omega)$, where $\mathcal{P}$ denotes the principal part [Ref. 29, Eq. (3.29)].

CC-0. In Public Domain. Gurukul Kangri Collection, Haridwar

Digitized by Arya Samaj Foundation Chennai and eGangotri

5. Discussion of the Longitudinal Susceptibility

In typical experiments measuring $\chi_{zz}''(\omega)$ the frequency of the alternating field is much less than the precession frequency. Thus in evaluating (II.24) we are justified in neglecting ω in comparison with ω_0. In which case we have

$$\Gamma(\omega_0)+\Gamma(-\omega_0) = (\pi/\hbar)\sum_{\mathbf{k}} A_{\mathbf{k}}{}^2\delta(\hbar\omega_{\mathbf{k}}-\hbar\omega_0)\coth(\hbar\omega_{\mathbf{k}}/2kT)=\tau_1{}^{-1}, \tag{II.30}$$

$$\mathrm{K}(\omega_0)+\mathrm{K}(-\omega_0)=0, \tag{II.31}$$

$$\Psi(0)=(\pi/\hbar)\sum_{\mathbf{k}} A_{\mathbf{k}}{}^2\delta(\hbar\omega_{\mathbf{k}}-\hbar\omega_0)=\tau_1{}^{-1}\tanh(\hbar\omega_0/2kT), \tag{II.32}$$

$$\Lambda(0)=0, \tag{II.33}$$

where τ_1 is the spin–lattice relaxation time for the direct process.[31] With the help of (II.30)–(II.33) we obtain the following equation for $\chi_{zz}''(\omega)$ $(\omega\ll\omega_0)$

$$\chi_{zz}''(\omega)=\frac{g^2\beta^2}{2\hbar}\tanh\frac{\hbar\omega}{2kT}\frac{\tau_1}{1+(\omega\tau_1)^2}\operatorname{sech}^2\frac{\hbar\omega_0}{2kT}, \tag{II.34}$$

which is identical to Eq. (I.11). Although our expression for $\chi_{zz}''(\omega)$ was obtained from a particularly simple Hamiltonian, a similar but more lengthy analysis based on (II.8) shows that (II.34) is still valid in the limit $\omega\ll\omega_0$ provided the value of τ_1 appropriate to the more general interaction is used.

Examination of the steps in the calculation of $\chi_{zz}''(\omega)$ indicates that the terms in the interaction which couple the z component of the spin to the lattice make no contribution to the susceptibility. The linewidth arises solely from the phase-interrupting (S_x and S_y) terms. This last result is rigorously true for the model Hamiltonian. In the case of a more general Hamiltonian it is valid to the extent to which Green's functions of the form $\langle\langle S_\pm;\ S_z\rangle\rangle_+$ can be neglected in the equation for $\langle\langle S_z;\ S_z\rangle\rangle_+$. A rough calculation shows that $\langle\langle S_+;\ S_z\rangle\rangle_+\approx(1/\omega_0\tau_1)\langle\langle S_z;\ S_z\rangle\rangle_+$ in the region of interest. The dropping of these terms is justified as long as $\omega_0\tau_1\gg1$, a condition which is nearly always satisfied.

The presence of the relaxation time for the direct process in the expression for $\chi_{zz}''(\omega)$ reflects the fact that the decoupling approximation takes into account only one-phonon transitions. Transitions involving multiple phonon emission are neglected. General phase-space considerations show that these higher order effects are negligible in comparison with the direct process as long as there are lattice modes with energies comparable to $\hbar\omega_0$.

6. Calculation of the Transverse Susceptibility

The spectral functions for the transverse susceptibilities are obtained from Green's functions associated with the operators S_+ and S_-. From the symmetry of the model Hamiltonian it is evident that $\chi_{xx}''=\chi_{yy}''$ so that we need solve only for $\langle\langle S_-;\ S_+\rangle\rangle_+$. The terms in (II.7) involving $J^{--}(\omega)$ and $J^{++}(\omega)$ make no contribution as long as the two transverse susceptibilities are equal. The equation of motion for $\langle\langle S_-;\ S_+\rangle\rangle_+$ is written

$$(E-\hbar\omega_0)\langle\langle S_-;\ S_+\rangle\rangle_+(E)=1/2\pi-\sum_{kp}A_{\mathbf{k}}(\epsilon_x(\mathbf{kp})-i\epsilon_y(\mathbf{kp}))(\langle\langle S_z a_{kp}{}^+;\ S_+\rangle\rangle_+(E)+\langle\langle S_z a_{-kp};\ S_+\rangle\rangle_+(E)) +\sum_{kp}A_{\mathbf{k}}\epsilon_z(\mathbf{kp})(\langle\langle S_- a_{kp}{}^+;\ S_+\rangle\rangle_+(E)+\langle\langle S_- a_{-kp};\ S_+\rangle\rangle_+(E)). \tag{II.35}$$

As before we are faced with the problem of calculating higher order Green's functions involving products of spin and lattice operators. In order to do this we make use of the decoupling approximation introduced previously. Because of the orthogonality of the polarization vectors we need keep only terms having the factor $\epsilon_x(\mathbf{kp})+i\epsilon_y(\mathbf{kp})$ in the equations for $\langle\langle S_z a_{kp}{}^+;\ S_+\rangle\rangle_+$ and $\langle\langle S_z a_{-kp};\ S_+\rangle\rangle_+$. By the same token we keep only terms proportional to $\epsilon_z(\mathbf{kp})$ in the equations for $\langle\langle S_- a_{kp}{}^+;\ S_+\rangle\rangle_+$ and $\langle\langle S_- a_{-kp};\ S_+\rangle\rangle_+$. The results of the calculation are as follows:

$$(E+\hbar\omega_{\mathbf{k}})\langle\langle S_z a_{kp}{}^+;\ S_+\rangle\rangle_+(E)=-\tfrac{1}{4}A_{\mathbf{k}}(\epsilon_x(\mathbf{kp})+i\epsilon_y(\mathbf{kp}))(2n_{\mathbf{k}}+1)\langle\langle S_-;\ S_+\rangle\rangle_+(E), \tag{II.36}$$

$$=(E-\hbar\omega_{\mathbf{k}})\langle\langle S_z a_{-kp};\ S_+\rangle\rangle_+(E), \tag{II.37}$$

$$(E-\hbar\omega_0+\hbar\omega_{\mathbf{k}})\langle\langle S_- a_{kp}{}^+;\ S_+\rangle\rangle_+(E)=(1/2\pi)\langle a_{kp}{}^+\rangle+\tfrac{1}{2}A_{\mathbf{k}}\epsilon_z(\mathbf{kp})(2n_{\mathbf{k}}+1)\langle\langle S_-;\ S_+\rangle\rangle_+(E), \tag{II.38}$$

$$(E-\hbar\omega_0-\hbar\omega_{\mathbf{k}})\langle\langle S_- a_{-kp};\ S_+\rangle\rangle_+(E)=(1/2\pi)\langle a_{-kp}\rangle+\tfrac{1}{2}A_{\mathbf{k}}\epsilon_z(\mathbf{kp})(2n_{\mathbf{k}}+1)\langle\langle S_-;\ S_+\rangle\rangle_+(E). \tag{II.39}$$

The functions $\langle a_{kp}{}^+\rangle$ and $\langle a_{-kp}\rangle$ can be calculated by making use of the time-independence of the expectation value[29]

$$i\hbar(d/dt)\langle\cdots\rangle=0=\langle[\cdots,\ \mathcal{H}]\rangle. \tag{II.40}$$

[31] R. Orbach, Proc. Roy. Soc. (London) **A264**, 458 (1961).

CC-0. In Public Domain. Gurukul Kangri Collection, Haridwar

Digitized by Arya Samaj Foundation Chennai and eGangotri

We have

$$i\hbar(d/dt)\langle a_{kp}^{+}\rangle = 0 = -\hbar\omega_k\langle a_{kp}^{+}\rangle + \tfrac{1}{2}\tanh(\hbar\omega_0/2kT)\epsilon_z(\mathbf{k}p)A_k, \tag{II.40}$$

$$i\hbar(d/dt)\langle a_{-kp}\rangle = 0 = \hbar\omega_k\langle a_{-kp}\rangle - \tfrac{1}{2}\tanh(\hbar\omega_0/2kT)\epsilon_z(\mathbf{k}p)A_k, \tag{II.41}$$

where we have kept only terms proportional to $\epsilon_z(\mathbf{k}p)$.

With the help of (II.36)–(II.41) we obtain the following equation for $\langle\langle S_-; S_+\rangle\rangle_+$:

$$(E-\hbar\omega_0)\langle\langle S_-; S_+\rangle\rangle_+(E) = (2\pi)^{-1} + \tfrac{1}{2}\sum_k A_k^2(2n_k+1)$$
$$\times[(E-\hbar\omega_k)^{-1}+(E+\hbar\omega_k)^{-1}+(E-\hbar\omega_0-\hbar\omega_k)^{-1}+(E-\hbar\omega_0+\hbar\omega_k)^{-1}]\langle\langle S_-; S_+\rangle\rangle_+(E)$$
$$+\frac{\tanh(\hbar\omega_0/2kT)}{4\pi}\sum_k(A_k^2/\hbar\omega_k)[(E-\hbar\omega_0-\hbar\omega_k)^{-1}+(E-\hbar\omega_0+\hbar\omega_k)^{-1}]. \tag{II.42}$$

From (II.42) we obtain the spectral function $J^{-+}(\omega)$ by means of the limiting procedure described in Sec. II.3. Inserting the expression thus obtained into (II.7) leads to the following equation for the transverse susceptibility

$$\chi_{xx}''(\omega) = \chi_{yy}''(\omega) = \frac{g^2\beta^2}{4\hbar}\tanh\frac{\hbar\omega}{2kT}\Bigg[\frac{(\Gamma(\omega)+\Gamma(\omega-\omega_0))(1+\frac{1}{2}\tanh(\hbar\omega_0/2kT)\Theta(\omega-\omega_0))}{(\omega-\omega_0-\mathrm{K}(\omega)-\mathrm{K}(\omega-\omega_0))^2+\Gamma((\omega)+\Gamma(\omega-\omega_0))^2}$$
$$+\frac{\frac{1}{2}\tanh(\hbar\omega_0/2kT)(\omega-\omega_0-\mathrm{K}(\omega)-\mathrm{K}(\omega-\omega_0))\Phi(\omega-\omega_0)}{(\omega-\omega_0-\mathrm{K}(\omega)-\mathrm{K}(\omega-\omega_0))^2+(\Gamma(\omega)+\Gamma(\omega-\omega_0))^2}$$
$$+\frac{(\Gamma(\omega)+\Gamma(\omega+\omega_0))(1-\frac{1}{2}\tanh(\hbar\omega_0/2kT)\Theta(\omega+\omega_0))}{(\omega+\omega_0-\mathrm{K}(\omega)-\mathrm{K}(\omega+\omega_0))^2+(\Gamma(\omega)+\Gamma(\omega+\omega_0))^2}$$
$$-\frac{\frac{1}{2}\tanh(\hbar\omega_0/2kT)(\omega+\omega_0-\mathrm{K}(\omega)-\mathrm{K}(\omega+\omega_0))\Phi(\omega+\omega_0)}{(\omega+\omega_0-\mathrm{K}(\omega)-\mathrm{K}(\omega+\omega_0))^2+(\Gamma(\omega)+\Gamma(\omega+\omega_0))^2}\Bigg], \tag{II.43}$$

where $\Gamma(\omega)$ and $\mathrm{K}(\omega)$ are defined by Eqs. (II.25) and (II.26), respectively. The functions $\Theta(\omega)$ and $\Phi(\omega)$ have as their defining equations

$$\Theta(\omega) = (\mathcal{P}/\hbar)\sum_k(A_k^2/\hbar\omega_k)[(\hbar\omega+\hbar\omega_k)^{-1}+(\hbar\omega-\hbar\omega_k)^{-1}], \tag{II.44}$$

$$\Phi(\omega) = (\pi/\hbar)\sum_k(A_k^2/\hbar\omega_k)[\delta(\hbar\omega+\hbar\omega_k)+\delta(\hbar\omega-\hbar\omega_k)]. \tag{II.45}$$

We postpone discussion of (II.43) until the following section.

7. Discussion of the Transverse Susceptibility

In typical paramagnetic resonance experiments only the values of $\chi_{xx}''(\omega)$ in the neighborhood of $\omega=\omega_0$ are of interest. In this region the equation for χ_{xx}'' simplifies considerably. Because of the vanishing volume of phase space accessible to phonons of zero energy we have

$$\Gamma(0) = (\pi/\hbar)\sum_k A_k^2\delta(\hbar\omega_k)\coth(\hbar\omega_k/2kT) = 0, \tag{II.46}$$

$$\Phi(0) = (2\pi/\hbar)\sum(A_k^2/\hbar\omega_k)\delta(\hbar\omega_k) = 0, \tag{II.47}$$

as well as

$$\Theta(0) = \mathrm{K}(0) = 0. \tag{II.48}$$

Neglecting the second-order shift, $\mathrm{K}(\omega_0)$, in comparison with ω_0 we obtain the result $(\omega\approx\omega_0)$

$$\chi_{xx}''(\omega) = \frac{g^2\beta^2}{4\hbar}\tanh\frac{\hbar\omega}{2kT}\left(\frac{1/2\tau_1}{(\omega-\omega_0)^2+(1/2\tau_1)^2}\right). \tag{II.49}$$

We note that the susceptibility has a Lorentzian profile with a width $1/2\tau_1$. As was pointed out in part I, this width reflects the absence of a contribution from the frequency modulation terms in the Hamiltonian. Indeed such terms are represented in the factor $\Gamma(\omega-\omega_0)$ in (II.43) which vanishes at resonance in virtue of (II.46). [In the stochastic case, where the spectrum is flat, one has $\Gamma(\omega)=\Gamma(\omega-\omega_0)$ and $1/\tau_1$ appears in place of $1/2\tau_1$ in (II.49) and the transverse and longitudinal relaxation times become equal, in agreement with Sec. I.6, where the situation is discussed more fully.] Our expression for $\chi_{xx}''(\omega)$ in the vicinity of the resonance is easily modified to include the effects of an anisotropic interaction. As in the case of χ_{xx}'' it is only necessary to replace the expression for τ_1 by the corresponding relaxation time calculated from the more general Hamiltonian.

An interesting limiting case of (II.43) is obtained when we take the doublet splitting to be much greater than the maximum phonon energy. Since there are no

CC-0. In Public Domain. Gurukul Kangri Collection, Haridwar

Digitized by Arya Samaj Foundation Chennai and eGangotri

phonons "on speaking terms" with the spins we have $\Gamma(\omega_0)=0$. The resulting expression for the susceptibility has the approximate form

$$\chi_{xx}''(\omega)\approx\frac{g^2\beta^2}{4\hbar}\tanh\frac{\hbar\omega}{2kT}\frac{\Gamma(x)+\frac{1}{2}x\tanh(\hbar\omega_0/2kT)\Phi(x)}{x^2}$$

$$=\frac{g^2\beta^2}{4\hbar x^2}\tanh\frac{\hbar\omega}{2kT}$$

$$\times\left\{\frac{\pi}{\hbar}\sum_k A_k^2\left[(n_k+\tfrac{1}{2})+\tfrac{1}{2}\tanh\left(\frac{\hbar\omega_0}{2kT}\right)\right]\delta(\hbar\omega_k-\hbar x)\right.$$

$$\left.+\frac{\pi}{\hbar}\sum_k A_k^2\left[(n_k+\tfrac{1}{2})-\tfrac{1}{2}\tanh\left(\frac{\hbar\omega_0}{2kT}\right)\right]\delta(\hbar\omega_k+\hbar x)\right\},\quad(\text{II.50})$$

where $x=\omega-\omega_0$. The terms in the numerator of (II.50) arise from the FM part of the interaction. They characterize vibrational sidebands associated with the simultaneous creation or destruction of phonon–photon pairs. In the zero-temperature limit $n_k=0$ and $\tanh(\hbar\omega_0/2kT)=1$ so that χ_{xx}'' differs from zero only for $\omega>\omega_0$. These sidebands have been extensively studied in recent years in connection with the optical spectra of magnetic ions imbedded in insulating crystals.[32]

A check on the consistency of our analysis can be made by setting ω_0 equal to zero. We then find

$$\chi_{xx}''(\omega)=\frac{g^2\beta^2}{2\hbar}\tanh\frac{\hbar\omega}{2kT}\frac{2\Gamma(\omega)}{(\omega-2K(\omega))^2+(2\Gamma(\omega))^2},\quad(\text{II.51})$$

$$=\chi_{zz}''(\omega),$$

as can be seen from (II.24). The equality of χ_{xx}'' and χ_{zz}'' in the limit of zero field is to be expected in view of the isotropy of the model interaction.

Finally we would like to point out that although we have explicitly considered a system having $S=\frac{1}{2}$ the Green's function techniques can be applied equally well to a system having arbitrary spin. However for $S>\frac{1}{2}$ the analysis becomes complicated. One encounters Green's functions of the form $\langle\langle S_\alpha S_\beta; S_\gamma\rangle\rangle_+$ which do not appear in the spin $\frac{1}{2}$ problem. The simplification for $S=\frac{1}{2}$ results from there being only three linearly independent spin operators. Any product $S_\alpha S_\beta S_\gamma\cdots$ can be expressed in terms of the operators S_x, S_y, S_z and the unit operator.

8. Harmonic Oscillator

In this section we use the Green's function formalism to calculate the susceptibility of a harmonic oscillator coupled to the lattice by a term linear in the lattice displacement. We take as the Hamiltonian [cf. (I.32)]

$$\mathcal{H}=\tfrac{1}{2}m[(P_x/m)^2+\omega_0^2X^2]+\sum_k\tfrac{1}{2}\mu_k[(P_k/\mu_k)^2+\omega_k^2x_k^2]$$

$$+X\sum_k c_k x_k.\quad(\text{II.52})$$

The imaginary part of the susceptibility, $\chi''(\omega)$, can be written in terms of the Fourier transform of the electric dipole-moment correlation function

$$\chi=\frac{e^2}{2\hbar}\tanh\frac{\hbar\omega}{2kT}\int_{-\infty}^{\infty}\cos\omega t[\langle X(t)X(0)+X(0)X(t)\rangle]dt.\quad(\text{II.53})$$

We introduce the spectral function $J_{xx}(\omega)$ through the equation

$$\langle X(t)X(t')\rangle=\int_{-\infty}^{\infty}J_{xx}(\omega)\exp[-i\omega(t-t')]\,d\omega,\quad(\text{II.54})$$

so that $\chi''(\omega)$ is expressed as

$$\chi''(\omega)=(\pi e^2/\hbar)\tanh(\hbar\omega/2kT)(J_{xx}(\omega)+J_{xx}(-\omega)).\quad(\text{II.55})$$

The spectral function can be obtained from the Green's function $\langle\langle X(t); X(0)\rangle\rangle_-$. By making use of the commutation relations $[X, P_x]=i\hbar$, $[x_k, P_{k'}]=i\hbar\delta_{kk'}$ we find the following equations for $\langle\langle X; X\rangle\rangle_-$.

$$-(d^2/dt^2)\langle\langle X(t); X(0)\rangle\rangle_-=$$

$$[\hbar\delta(t)/m]+\omega_0^2\langle\langle X(t); X(0)\rangle\rangle_-$$

$$+m^{-1}\sum_k c_k\langle\langle x_k(t); X(0)\rangle\rangle_-,\quad(\text{II.56})$$

$$-(d^2/dt^2)\langle\langle x_k(t); X(0)\rangle\rangle_-=\omega_k^2\langle\langle x_k(t); X(0)\rangle\rangle_-$$

$$+c_k\langle\langle X(t); X(0)\rangle\rangle_-/\mu_k.\quad(\text{II.57})$$

The equations are readily solved without approximation for the transformed functions $\langle\langle X; X\rangle\rangle_-(E)$ and $\langle\langle x_k; X\rangle\rangle_-(E)$. In particular we have

$$\langle\langle X; X\rangle\rangle_-(E)$$

$$=\frac{(1/2\pi m)}{(E/\hbar)^2-\omega_0^2-\sum(c_k^2/m\mu_k)((E/\hbar)^2-\omega_k^2)^{-1}}.\quad(\text{II.58})$$

The spectral function can be obtained from (II.58) with the help of (II.17). Omitting several intermediate steps we arrive at the result

$$\chi''(\omega)=\frac{e^2}{m}\frac{\mathrm{Im}\,G(\omega)}{[\omega_0^2-\omega^2+\mathrm{Re}\,G(\omega)]^2+[\mathrm{Im}\,G(\omega)]^2},\quad(\text{II.59})$$

[32] For example, G. F. Imbusch, W. M. Yen, A. L. Schawlow, D. E. McCumber, and M. D. Sturge, Phys. Rev. **133**, A1029 (1964).

CC-0. In Public Domain. Gurukul Kangri Collection, Haridwar

Digitized by Arya Samaj Foundation Chennai and eGangotri

where

$$\mathrm{Re}\,G(\omega)=(\mathcal{P}/m\mu_k)\sum_k c_k^2(\omega^2-\omega_k^2)^{-1},$$

$$=\frac{\mathcal{P}}{m\mu_k}\int_0^\infty \rho_k c_k^2(\omega^2-\omega_k^2)^{-1}\,d\omega_k=\frac{\Delta}{m}, \qquad \text{(II.60)}$$

with the symbols ρ_k and Δ having the same meaning as in Sec. I.6. Also, we have

$$\mathrm{Im}\,G(\omega)=(\pi/m\mu_k)\sum_k (c_k^2/2\omega_k)[\delta(\omega-\omega_k)-\delta(\omega+\omega_k)],$$

$$=(\pi/m\mu_{k'})(c_{k'}^2\rho_{k'}/2\omega_{k'}), \qquad \text{(II.61)}$$

where k' is fixed by the equation $\omega_{k'}=\omega$. If we rewrite (II.59) using (II.60) and (II.61) we obtain the expression

$$\chi''(\omega)=\frac{e^2(\pi c_{k'}^2\rho_{k'})/2\omega_{k'}\mu_{k'}}{(m(\omega_0^2-\omega^2)+\Delta)^2+(\pi c_{k'}^2\rho_{k'}/2\omega_{k'}\mu_{k'})^2}, \qquad \text{(II.62)}$$

in agreement with (I.50).

ACKNOWLEDGMENT

The authors would like to express their thanks to Paul C. Martin who introduced one of them (DLH) to Green's function methods and contributed to the understanding of the other through illuminating discussions.

APPENDIX A: RELATIONS BETWEEN THE CORRELATION FUNCTION AND THE SUSCEPTIBILITY

The change in the component of moment P_α along the αth direction, which arises from the interaction $-P_\alpha F_\alpha \exp(i\omega t)$, is given by

$$\delta P_\alpha(t)=(i/\hbar)$$

$$\times\int_{-\infty}^{t}\langle P_\alpha(t)\,P_\alpha(t')-P_\alpha(t')\,P_\alpha(t)\rangle F_\alpha\exp(i\omega t')\,dt'. \qquad \text{(A1)}$$

This formula can be established as follows by a method slightly different from that of Kubo,[5] or of Kadanoff and Martin,[33] whose procedure we follow in the main in this appendix. Let us imagine the field F_α to be first applied at a large negative time $-t_A$. Since there is no outstanding polarization prior to the application of the field, one has

$$\delta P_\alpha(t)=\int_{-t_B}^{t}\mathrm{Tr}\left[\rho\frac{dP_\alpha(t'')}{dt''}\right]dt'',$$

where $-t_B$ is some time prior to $-t_A$, and the Boltzmann factor or density matrix

$$\rho=\exp[-\mathcal{H}_0/kT]/\mathrm{Tr}\,(\exp[-\mathcal{H}_0/kT])$$

is to be evaluated at $t=-t_A$ and so involves only the Hamiltonian function $\mathcal{H}$ exclusive of the field. The equation of motion for P_α is

$$dP_\alpha/dt=i\hbar^{-1}[\mathcal{H}P_\alpha-P_\alpha\mathcal{H}]$$

inasmuch as P_α commutes with the part $-P_\alpha F_\alpha \exp(i\omega t)$ of the Hamiltonian that arises from the applied field. From the fact that the change in inner energy just equals the work done by the applied field, we have

$$d\mathcal{H}/dt=(dP_\alpha/dt)\,F_\alpha\exp(i\omega t).$$

Since $\delta P_\alpha=0$ for $t<-t_A$, we can write

$$\delta P_\alpha=i\hbar^{-1}\int_{-t_B}^{t}dt''\int_{-t_A}^{t''}\Theta(t',t'')\,F_\alpha\exp(i\omega t')\,dt', \qquad \text{(A2)}$$

where

$$\Theta(t',t'')=\mathrm{Tr}\,\rho\left[\frac{dP_\alpha(t')}{dt'}P_\alpha(t'')-P_\alpha(t'')\frac{dP_\alpha(t')}{dt'}\right].$$

We now utilize the fact that we wish an expression for δP_α that is correct only to the first power of F_α. This means that the factor $\Theta(t',t'')$ can be evaluated as though the field were not there, and $\mathcal{H}$ treated as a constant. In the unperturbed condition, any expression of the form $\langle A(t')B(t'')\rangle$ is a function only of the argument $t'-t''$ since the equilibrium distribution is a stationary one. This permits us to replace $\Theta(t',t'')$ by $\Theta(t'',t')$, and after this permutation, the integration over t'' in (A2) can immediately be performed. (It is really a partial integration, but the portion coming from the fact that the upper limit of the t' integral involves t'' makes no contribution because of a cancellation of terms when $t'=t''$.) Such terms as $\langle P_\alpha(-t_B)\,P_\alpha(t)\rangle$ resulting from the integration can be dropped since $-t_B$ can be taken an arbitrarily long time before $-t_A$, and $\lim_{-t_B\to-\infty}\langle P_\alpha(-t_B)\,P_\alpha(t)\rangle=0$ if there is no mean polarization in the absence of the applied field—in other words, all correlation is lost if the time interval is sufficiently long. The integration over t'' when $t_B\longrightarrow-\infty$ thus reduces (A2) to (A1), which we wished to establish.

On introducing the integral representation of the unit step function $\theta(t-t')$, by means of the equation

$$\theta(t-t')=\frac{i}{2\pi}\int_{-\infty}^{\infty}\frac{\exp[-i\omega(t-t')]\,d\omega}{\omega+i\epsilon},$$

[33] L. P. Kadanoff and P. C. Martin, Ann. Phys. (N.Y.) **24**, 419 (1963), particularly Secs. I and II and Appendix A.

CC-0. In Public Domain. Gurukul Kangri Collection, Haridwar

Digitized by Arya Samaj Foundation Chennai and eGangotri

(with $\epsilon \to 0+$) we can rewrite (A1) as follows:

$$\delta P_\alpha(t) = \left(-\frac{1}{2\pi\hbar}\right)\int_{-\infty}^{\infty}\int_{-\infty}^{\infty}\frac{d\omega' dt'}{\omega'+i\epsilon}\exp\left[-i(\omega'+\omega)(t-t')\right]\langle P_\alpha(t)P_\alpha(t') - P_\alpha(t')P_\alpha(t)\rangle F_\alpha \exp(i\omega t). \tag{A3}$$

In view of the definition of $\chi_{\alpha\beta}$, (I.1), we have

$$\chi_{\alpha\alpha}(\omega) = \frac{1}{2\pi\hbar}\int_{-\infty}^{\infty}\int_{-\infty}^{\infty}\frac{d\omega' dt \exp(i\omega' t)}{\omega'-\omega+i\epsilon}\langle P_\alpha(t)P_\alpha(0) - P_\alpha(0)P_\alpha(t)\rangle. \tag{A4}$$

In obtaining (A4) we have made use of the fact that $\chi_{\alpha\alpha}$ is independent of t so that we can set t equal to zero in the bracketed factor of (A3). Noting that

$$\int_{-\infty}^{\infty}\exp(i\omega t)\langle P_\alpha(0)P_\alpha(t)\rangle dt = \mathrm{Tr}\int_{-\infty}^{\infty}\exp\left[-\mathfrak{IC}/kT\right]P_\alpha \exp\left[i\mathfrak{IC}t/\hbar\right]P_\alpha \exp\left[-i\mathfrak{IC}t/\hbar\right]\exp\left[i\omega t\right]dt, \tag{A5}$$

and making use of the cyclic property of the trace, $\mathrm{Tr}\,ABC = \mathrm{Tr}\,BCA = \mathrm{Tr}\,CAB$, we see that the right-hand side of (A5) can be written as follows:

$$\int_{-\infty}^{\infty}\exp(i\omega t)\langle P_\alpha(0)P_\alpha(t)\rangle dt = \mathrm{Tr}\int_{-\infty}^{\infty}\exp\left[-\mathfrak{IC}/kT\right]\exp\left[i\mathfrak{IC}(t-(i\hbar/kT))/\hbar\right]P_\alpha$$
$$\times \exp\left[-i\mathfrak{IC}(t-(i\hbar/kT))/\hbar\right]P_\alpha \exp(i\omega t)\,dt$$
$$= \exp\left(-\frac{\hbar\omega}{kT}\right)\int_{-\infty}^{\infty}\exp(i\omega t)\langle P_\alpha(t)P_\alpha(0)\rangle dt. \tag{A6}$$

With the help of (A6) $\chi_{\alpha\alpha}$ becomes

$$\chi_{\alpha\alpha}(\omega) = \frac{1}{2\pi\hbar}\int_{-\infty}^{\infty}\int_{-\infty}^{\infty}\frac{d\omega'\,dt\exp(i\omega' t)}{\omega'-\omega+i\epsilon}\tanh\frac{\hbar\omega'}{2kT}\langle P_\alpha(0)P_\alpha(t)+P_\alpha(t)P_\alpha(0)\rangle. \tag{A7}$$

Upon expanding $\langle P_\alpha(0)P_\alpha(t)+P_\alpha(t)P_\alpha(0)\rangle$ in terms of the eigenstates of $\mathfrak{IC}$

$$\langle P_\alpha(0)P_\alpha(t)+P_\alpha(t)P_\alpha(0)\rangle = 2\sum_{n,n'}\exp(-E_n/kT)\,|\langle n\mid P_\alpha\mid n'\rangle|^2\cos\left[(E_n-E_{n'})t/\hbar\right], \tag{A8}$$

it is evident that the bracketed expression in (A7) is both real and an even function of t. Utilizing these properties together with the symbolic identity, $(\omega+i\epsilon)^{-1} = \mathcal{P}/\omega - i\pi\delta(\omega)$, we infer that the real and imaginary parts of the susceptibility, $\chi_{\alpha\alpha} = \chi_{\alpha\alpha}' - i\chi_{\alpha\alpha}''$, can be written

$$\chi_{\alpha\alpha}'(\omega) = \frac{1}{2\pi\hbar}\mathcal{P}\int_{-\infty}^{\infty}\int_{-\infty}^{\infty}\frac{d\omega'\,dt\cos\omega' t}{\omega'-\omega}\tanh\frac{\hbar\omega'}{2kT}\langle P_\alpha(0)P_\alpha(t)+P_\alpha(t)P_\alpha(0)\rangle, \tag{A9}$$

$$\chi_{\alpha\alpha}''(\omega) = \frac{1}{2\hbar}\tanh\frac{\hbar\omega}{2kT}\int_{-\infty}^{\infty}\cos\omega t\,\langle P_\alpha(0)P_\alpha(t)+P_\alpha(t)P_\alpha(0)\rangle dt. \tag{A10}$$

Comparing (A10) with (A9) we immediately deduce the Kramers–Kronig relation

$$\chi_{\alpha\alpha}'(\omega) = \frac{\mathcal{P}}{\pi}\int_{-\infty}^{\infty}\frac{\chi_{\alpha\alpha}''(\omega')\,d\omega'}{\omega'-\omega}, \tag{A11}$$

relating the real and imaginary parts of the susceptibility.

CC-0. In Public Domain. Gurukul Kangri Collection, Haridwar

Digitized by Arya Samaj Foundation Chennai and eGangotri

Spectral Distribution of Scattered Light in a Simple Fluid

RAYMOND D. MOUNTAIN*
National Bureau of Standards, Washington, D.C.

The spectral distribution of light scattered by density fluctuations in a dense, monatomic, one-component fluid is calculated from the time dependence of the density fluctuations predicted by the linearized hydrodynamic equations of irreversible thermodynamics. The results of Landau and Placzek are verified and a procedure for deriving correction terms is discussed with the dispersion in the velocity of thermal sound waves obtained as an illustration. Particular attention is paid to the critical region. The properties of carbon dioxide are used to estimate the spectral distribution of critical opalescence. A comparison is made between light-scattering and sound-propagation experiments. Space dispersion near the critical point in the pressure and the thermal conductivity is examined briefly. Finally, some of the experimental problems involved in measuring the spectral distribution of the scattered light are discussed.

I. INTRODUCTION

When a beam of monochromatic light is passed through a dense, transparent medium, some of the light is scattered since the density is not uniform. There would be no shift in frequency of the scattered light if the density nonuniformities were static. As frozen-in nonuniformities are not possible in a fluid, density fluctuations in a fluid are time-dependent. This means that the frequency of light scattered by density fluctuations in a dense fluid exhibits a spectrum characteristic of the time dependence of the density fluctuations.[1]

In the past it has not been possible to study experimentally, in any detail, the spectral distribution of the scattered light.[2–12] The changes in frequency are very small, too small to be resolved fully by the optical detection systems which were available. This situation is changing. The gas laser has made possible the development of optical heterodyne systems which are capable of detecting exceedingly small changes in frequency.[13] Laser research has inspired the development of very high resolution interferometers.[14] These developments have increased the interest in the spectrum of light scattered by density fluctuations.

This article describes the type of information which can be obtained by determining the spectrum of the light scattered by density fluctuations in a dense fluid. To accomplish this we calculate the spectrum of light scattered by density fluctuations in a dense, one component, classical fluid of spherically symmetric molecules. The linearized hydrodynamic equations of irreversible thermodynamics are used to compute the relaxation in time of the spontaneous density fluctuations in the fluid.[15] This phenomenological theory is valid for low frequencies and long wavelengths. Although the frequencies we consider are much higher than those usually encountered in hydrodynamics, it is hoped that the results will be of use in understanding the properties of fluids.

This approach is essentially that of Landau and Placzek.[16] The lowest order solutions of these equations are well known in the sense that they are quoted in the literature. We also obtain higher order terms in the solutions which are of interest to anyone trying to interpret light-scattering experiments of this type.

This study was undertaken with the hope that the spectrum of critical opalescence would contain useful information about the critical point of the liquid–vapor transition. Sections 5 and 7 are concerned with the spectrum of critical opalescence.

Section 6 is devoted to a comparison of what can be learned from a light-scattering experiment as opposed to a sound-propagation and absorption experiment. As is shown, the two types of measurements are not identical.

---

* NAS–NRC Postdoctoral Fellow at the National Bureau of Standards.

[1] I. L. Fabelinskiĭ, Usp. Fiz. Nauk **63**, 355 (1957). [English transl.: Advan. Phys. Sci. **63**, 474 (1957)]. This broad review of light scattering in liquids contains a good discussion of the attempts to measure the spectrum of light scattered by fluctuations.

[2] E. Gross, Nature **126**, 201, 400, 603 (1930); **129**, 722 (1932).

[3] E. H. L. Meyer and W. Ramm, Physik. Z. **33**, 270 (1932).

[4] Karl Birus, Physik. Z. **39**, 80 (1938).

[5] K. Sunanda Bai, Proc. Indian Acad. Sci. **A15**, 338, 349, 357 (1942).

[6] C. S. Venkateswaran, Proc. Indian Acad. Sci. **A15**, 316, 322, 362, 371 (1942).

[7] D. H. Rank, J. S. McCartney, and G. J. Szasz, J. Opt. Soc. Am. **38**, 287 (1948).

[8] I. L. Fabelinskiĭ, Dokl. Akad. Nauk SSSR **106**, 882 (1955) [English transl.: Soviet Phys. —Dokl. **1**, 115 (1956)].

[9] M. S. Pesin and I. L. Fabelinskiĭ, Dokl. Akad. Nauk SSSR **122**, 575 (1958); **129**, 299 (1959); **135**, 1114 (1960) [English transls.: Soviet Phys.—Dokl. **3**, 974 (1958); **4**, 1264 (1960); **5**, 1290 (1960)].

[10] I. L. Fabelinskiĭ, Usp. Fiz. Nauk **77**, 644 (1962) [English transl.: Soviet Phys.—Usp. **5**, 667 (1963)].

[11] G. B. Bendek, J. B. Lastovka, K. Fritsch, and T. Greytak, J. Opt. Soc. Am. **54**, 1284 (1964).

[12] R. Y. Chiao and B. P. Stoicheff, J. Opt. Soc. Am. **54**, 1286 (1964).

[13] H. Z. Cummins, N. Kable, and Y. Yeh, Phys. Rev. Letters **12**, 150 (1964).

[14] Donald R. Herriot, Appl. Opt. **2**, 865 (1963).

[15] F. V. Hunt in *AIP Handbook*, edited by D. E. Gray (McGraw-Hill Book Company, Inc., New York, 1957), Chap. 3c, p. 3-33.

[16] L. Landau and G. Placzek, Physik. Z. Sowjetunion **5**, 172 (1934). This note suggests the method used in this article. No calculations are presented in support of their conclusions.

CC-0. In Public Domain. Gurukul Kangri Collection, Haridwar

Digitized by Arya Samaj Foundation Chennai and eGangotri

In the final section, we summarize the information one could expect to obtain from the spectrum of the scattered light. We also discuss the experimental problem of resolution and the detectors one might use in such light-scattering experiments.

2. THERMODYNAMIC APPROACH

A qualitative picture of the scattering of light by density fluctuations can be obtained by separating density fluctuations into two types, those relieved by mechanical processes and those relieved by thermal processes. This separation occurs naturally in the thermodynamic theory of fluctuations where density fluctuations can be described in terms of pressure fluctuations and temperature or entropy fluctuations. Brillouin has suggested that light is scattered by thermal sound waves in the fluid.[17] These waves are analogous to Debye waves in a crystal. Because sound propagation is an adiabatic process, density fluctuations should be decomposed into pressure fluctuations at constant entropy and entropy fluctuations at constant pressure. This decomposition is discussed in detail by Frenkel.[18] We quote his conclusions only.

The frequency of the light scattered by the fluctuations at constant entropy (thermal sound waves or phonons) is shifted by an amount proportional to the velocity of the phonons. Energy and momentum considerations require that the proportionality constant be the magnitude of the change in the wave vector of the scattered light. Two lines are observed because scattering can occur from waves traveling in opposite directions but at the same speed. These lines are broadened somewhat because of the dissipative processes which damp out the waves. These lines are known as the Mandelshtam-Brillouin doublet or more simply as the Brillouin lines.

The light scattered by the fluctuations at constant pressure is not shifted in frequency although it is broadened somewhat due to the thermal dissipative processes which damp out these fluctuations.

We see that the fine structure of the scattered light consists of three lines. The ratio of the intensity of the central line I_0 to that of the two shifted lines $2I_1$ is determined by thermodynamic fluctuation theory to be

$$I_0/2I_1=(c_p-c_v)/c_v, \tag{1}$$

where c_p and c_v are the specific heats at constant pressure and constant volume. Landau and Placzek have observed that the widths of these lines are determined by the lifetimes of the density fluctuations described by the linearized hydrodynamic equations of irreversible thermodynamics.[16]

There have been numerous attempts to observe the spectrum of the light scattered by density fluctuations.[2–12] It has been possible to detect the presence of the Brillouin lines in liquids using the conventional techniques of high resolution spectroscopy. The details such as line widths and shapes have not been measured with any precision.[19] Only one study of the spectrum of the central line has been reported.[20]

In the next few sections the Landau–Placzek theory is developed in detail. First we point out the relationship between the fluctuations in the density and the intensity of scattered light. Then we obtain the time dependence of the kth Fourier component of the density fluctuation. Finally, we determine the fine structure implied by this time dependence.

3. HYDRODYNAMIC THEORY OF FLUCTUATIONS

Komarov and Fisher[21] have shown, by adapting Van Hove's[22] neutron-scattering results to light scattering, that the intensity I' of light scattered from a fluid is

$$I'(\mathbf{R},\omega)=(\alpha^2\Omega^4N/2\pi c^4R^2)I_0\sin^2\phi\,\mathcal{S}(\mathbf{k},\omega). \tag{2}$$

The light, scattered at the origin, is observed at R. The angular frequency of the scattered light is Ω, ω is the *shift* in the angular frequency and $\mathbf{k}$ is the *change* in the wave vector of the scattered light from that of the incident light in the medium, $\mathbf{k}_1$;

$$k=k_1 2\sin(\theta/2), \tag{3}$$

where θ is the scattering angle. There are N spherically symmetric molecules of polarizability α in the scattering volume. The incident light is assumed to be in the form of a plane, polarized, monochromatic wave.

The angle between $\mathbf{R}$ and the electric vector of the incident wave is denoted by ϕ. The polarization of the scattered light depends only on ϕ because the molecules are isotropic. The intensity of the incident light is I_0. R. Pecora has derived an equation equivalent to Eq. (2).[23]

The information about the density fluctuations is contained in the generalized structure factor $\mathcal{S}(\mathbf{k},\omega)$, which is the space and time Fourier transform of the two-body correlation function of the medium. It is defined by Van Hove[22] to be

$$G(\mathbf{r},t)=N^{-1}\langle\sum_{l,j=1}^{N}\int d\mathbf{r}'\,\delta[\mathbf{r}+\mathbf{r}_l(0)-\mathbf{r}']\,\delta[\mathbf{r}'-\mathbf{r}_j(t)]\rangle, \tag{4}$$

[17] Leon Brillouin, Ann. Phys. (Paris) **17**, 88 (1922).
[18] J. Frenkel, *Kinetic Theory of Liquids* (Oxford University Press, London, 1946), pp. 235–46.
[19] The first measurements of the width of Brillouin lines in liquids were reported recently by D. I. Mash, V. S. Starunov, and I. L. Fabelinskiĭ, Zh. Eksperim. i Teor. Fiz. **47**, 783 (1964) [English transl.: Soviet Phys.—JETP **20**, 523 (1965)].
[20] G. B. Benedek and N. C. Ford, reported at the Conference on Phenomena in the Neighborhood of Critical Points held at the National Bureau of Standards, 5–8 April 1965 (to be published).
[21] L. I. Komarov and I. Z. Fisher, Zh. Eksperim. i Teor. Fiz. **43**, 1927 (1962) [English transl.: Soviet Phys.—JETP **16**, 1358 (1963)].
[22] Leon Van Hove, Phys. Rev. **95**, 249 (1954).
[23] R. Pecora, J. Chem. Phys. **40**, 1604 (1964).

CC-0. In Public Domain. Gurukul Kangri Collection, Haridwar

Digitized by Arya Samaj Foundation Chennai and eGangotri

where the sums are carried out over all molecules in the system. The angular brackets $\langle \cdots \rangle$ indicate an ensemble average over the initial states of the system. For long times and sufficiently large r, the form of $G(\mathbf{r}, t)$ reduces to the autocorrelated density

$$G(\mathbf{r}, t) = N^{-1} \int d\mathbf{r}' \langle \rho[\mathbf{r}'-\mathbf{r}, 0]\rho(\mathbf{r}', t) \rangle. \quad (5)$$

Here we consider only this latter form of $G(\mathbf{r}, t)$.

Our main concern is with the frequency dependence of $S(\mathbf{k}, \omega)$. We determine this by implementing the Landau–Placzek observation that the decay in time of density fluctuations is described by the linearized hydrodynamic equations of irreversible thermodynamics. First we obtain the time dependence of the kth Fourier component of the density. From this, we construct the time-dependent density–density correlation function and the generalized structure factor.

This way of constructing $S(\mathbf{k}, \omega)$ has been discussed by Van Hove and shown to be a long-time approximation. As defined, $S(\mathbf{k}, \omega)$ is the transform of a density-density correlation function. Since we are making a long-time approximation, our results are valid only at "low" frequencies. This should not lead to any difficulties, because the time constants involved in the hydrodynamic small-oscillation problem are long compared to the time intervals characteristic of molecular scattering processes. This method has been quite useful in describing the magnetic scattering of neutrons near the Curie point in iron.[24–26]

The linearized hydrodynamic equations[15] are: the continuity equation

$$\partial\rho_1/\partial t + \rho_0 \operatorname{div} \mathbf{v} = 0; \quad (6)$$

the Navier–Stokes equation

$$\rho_0 \frac{\partial \mathbf{v}}{\partial t} + \frac{C_0^2}{\gamma} \operatorname{grad} \rho_1 + \frac{C_0^2 \beta \rho_0}{\gamma} \operatorname{grad} T_1 - (\tfrac{4}{3}\eta_S + \eta_B) \operatorname{grad} \operatorname{div} \mathbf{v} = 0; \quad (7)$$

and the energy-transport equation

$$\rho_0 c_v \frac{\partial T_1}{\partial t} - \frac{c_v(\gamma-1)}{\beta} \frac{\partial \rho_1}{\partial t} - \lambda \nabla^2 T_1 = 0. \quad (8)$$

In these equations, $\rho = \rho_0 + \rho_1$ is the number density, $T = T_0 + T_1$ is the temperature; ρ_0 and T_0 being the equilibrium values. The ratio of the specific heat at constant pressure to the specific heat at constant volume is denoted by $\gamma = c_p/c_v$. The shear and bulk viscosities are η_S and η_B, λ is the thermal conductivity, β is the thermal expansion coefficient, and C_0 is the low-frequency limit of the sound velocity.

In this linearized theory of small oscillations about equilibrium, the transverse part of the velocity is not coupled to the density. For this reason we neglect the transverse part of the Navier–Stokes equation in our considerations. This limits the applicability of this theory to fluids in which angular correlations between the molecules are not important. Also, we made use of the concept of local thermodynamic equilibrium when we replaced the pressure and entropy deviations which usually appear in the Navier–Stokes and energy equations by the corresponding density and temperature deviations. Thermodynamic relationships were used to to this. The choice of density and temperature over entropy and pressure as independent variables is an arbitrary one. The final expression for the density–density correlation function is, of course, independent of this choice as long as local thermodynamic equilibrium obtains. The labor involved is less when the density is an independent variable.

The procedure used is to first eliminate the velocity by taking the divergence of each term in Eq. (7) and then substitute for div $\mathbf{v}$ from Eq. (6). Next we obtain the Fourier (space) and Laplace (time) transforms of these equations. Then we solve the resulting equations for $n(\mathbf{k}, s)$, the Fourier–Laplace transform of the density. The inverse Laplace transform of $n(\mathbf{k}, s)$ is the time-dependent, kth Fourier component of the density, $n(\mathbf{k}, t)$:

$$n(\mathbf{k}, s) = \int_v d\mathbf{r} \int_0^\infty dt \exp(-i\mathbf{k}\cdot\mathbf{r}) \exp(-st) \rho_1(\mathbf{r}, t),$$

$$T(\mathbf{k}, s) = \int_v d\mathbf{r} \int_0^\infty dt \exp(-i\mathbf{k}\cdot\mathbf{r}) \exp(-st) T_1(\mathbf{r}, t). \quad (9)$$

The elimination of the velocity (longitudinal component) and the transformation of the density and temperature leads to two simultaneous linear equations for $n(\mathbf{k}, s)$ and $T(\mathbf{k}, s)$ in terms of the initial values

$$n(\mathbf{k}) = \int_v d\mathbf{r} \exp(-i\mathbf{k}\cdot\mathbf{r}) \rho_1(\mathbf{r}, 0)$$

and

$$T(\mathbf{k}) = \int_v d\mathbf{r} \exp(-i\mathbf{k}\cdot\mathbf{r}) T_1(\mathbf{r}, 0). \quad (10)$$

These equations are

$$n(\mathbf{k}, s)[s^2 + C_0^2 k^2/\gamma + (\tfrac{4}{3}\eta_S + \eta_B) k^2 s/\rho_0] + (C_0^2 \beta \rho_0 k^2/\gamma) T(\mathbf{k}, s) = n(\mathbf{k})[s + (\tfrac{4}{3}\eta_S + \eta_B) k^2/\rho_0] \quad (11)$$

and

$$n(\mathbf{k}, s)[-sc_v(\gamma-1)/\beta] + T(\mathbf{k}, s)[\rho_0 c_v s + \lambda k^2] = -n(\mathbf{k}) c_v(\gamma-1)/\beta + \rho_0 c_v T(\mathbf{k}). \quad (12)$$

[24] Leon Van Hove, Phys. Rev. 95, 1374 (1954).
[25] B. Jacrot, J. Konstantinovic, G. Parette, and D. Cribier, Symposium on Inelastic Scattering of Neutrons in Solids and Liquids, Chalk River, 1962.
[26] L. Passell, K. Blinowski, T. Brun, and P. Nielsen, J. Appl. Phys. 35, 933 (1964).

CC-0. In Public Domain. Gurukul Kangri Collection, Haridwar

Digitized by Arya Samaj Foundation Chennai and eGangotri

Only the magnitude of **k** is important so the vector notation is no longer used. Because the density and temperature are thermodynamically independent, it is unnecessary to include terms involving $T(k)$ in the solution for $n(k, s)$.

The solution of Eqs. (11) and (12) for $n(k, s)$ is

$$n(k,s)=n(k)\frac{s^2+(a+b)k^2s+abk^4+C_0^2(1-1/\gamma)k^2}{s^3+(a+b)k^2s^2+(C_0^2k^2+abk^4)s+aC_0^2k^4/\gamma}. \tag{13}$$

We have introduced the notation

$$a=\lambda/\rho_0 c_v$$

and

$$b=(\tfrac{4}{3}\eta_s+\eta_B)/\rho_0. \tag{14}$$

The next step is to compute the inverse Laplace transform of $n(k, s)$. This inversion requires that we find the roots of the denominator of Eq. (13) set equal to zero,

$$s^3+(a+b)k^2s^2+(C_0^2k^2+abk^4)s+aC_0^2k^4/\gamma=0. \tag{15}$$

While an exact algebraic solution of a cubic equation is always possible, it is not particularly useful in this case because of its algebraic complexity.

It is more convenient to develop a convergent scheme for approximating the solutions to the dispersion equation, Eq. (15), in a power series of the coefficients. To do this, we first note that $k=10^5$ cm^{-1} is typical of the changes in the wave vector which occur in light scattering. (This corresponds to a scattering angle of approximately 60° when a 6328-Å He–Ne laser is used as the light source). With $k=10^5$ cm^{-1}, the ratio of ak^2 to C_0k and of bk^2 to C_0k is commonly on the order of $\frac{1}{100}$. The parameters to use are ak^2/C_0k and bk^2/C_0k.

The solutions to Eq. (15) to lowest order in ak^2 and bk^2 are

$$\begin{aligned} s&=\pm iCk_0-\tfrac{1}{2}(a+b-a/\gamma)k^2,\\ s&=-(a/\gamma)k^2; \end{aligned} \tag{16}$$

or, in terms of the original parameters,

$$\begin{aligned} s&=\pm iC_0k-\tfrac{1}{2}\left[\frac{\frac{4}{3}\eta_s+\eta_B}{\rho_0}+\frac{1}{\rho_0}\left(\frac{\lambda}{c_v}-\frac{\lambda}{c_p}\right)\right]k^2\\ s&=-\lambda k^2/\rho_0 c_p. \end{aligned} \tag{17}$$

These are the predictions of the Landau–Placzek theory. The real part of the first two solutions is effectively the low-frequency sound-absorption coefficient. In the rest of this paper, it is denoted by Γk^2; i.e.,

$$\frac{1}{2}\left[\frac{\frac{4}{3}\eta_s+\eta_B}{\rho_0}+\frac{1}{\rho_0}\left(\frac{\lambda}{c_v}-\frac{\lambda}{c_p}\right)\right]k^2=\Gamma k^2. \tag{18}$$

Higher order corrections to the usual solutions, Eq. (17), can be generated by the same procedure. The first correction to the low-frequency sound velocity is found to be quadratic in k:

$$s=\pm i(C_0k+C_2k^3)-\Gamma k^2, \tag{19}$$

where

$$C_2=[3\Gamma^2+ab-2\Gamma(a+b)]/2C_0. \tag{20}$$

The velocity of a thermal sound wave, $v_{\rm th}$, exhibits dispersion when k is large enough;

$$v_{\rm th}=C_0\left[1+\frac{3\Gamma^2+ab-2\Gamma(a+b)}{2C_0^2}k^2+\cdots\right]. \tag{21}$$

The significance of this dispersion and its relationship to the sound propagation problem are discussed in Sec. 6.

Using the first-order solutions, Eq. (17), the lowest order terms of the inverse Laplace transform of $n(k, s)$ are

$$n(k,t)=n(k)\left\{\frac{c_p-c_v}{c_p}\exp\left[-(\lambda k^2/\rho_0 c_p)t\right]+\frac{c_v}{c_p}\exp\left(-\Gamma k^2t\right)\cos C_0kt\right\}. \tag{22}$$

The kth component of the density–density correlation function $F(k, t)$ is

$$\begin{aligned} F(k,t)&=\langle n(-k)n(k,t)\rangle\\ &=\langle n(-k)n(k)\rangle\left\{\frac{c_p-c_v}{c_p}\exp\left[-(\lambda k^2/\rho_0 c_p)t\right]+\frac{c_v}{c_p}\exp\left(-\Gamma k^2t\right)\cos C_0kt\right\}. \end{aligned} \tag{23}$$

The angular brackets $\langle\cdots\rangle$ indicate an ensemble average over the initial values of the variables.

The quantity which is of direct interest in a light-scattering experiment is the generalized structure factor $\mathcal{S}(k, \omega)$;

$$\mathcal{S}(k,\omega)=2\,\mathrm{Re}\int_0^\infty dt\,\exp(i\omega t)F(k,t). \tag{24}$$

It follows from Eq. (23) that

$$\mathcal{S}(k,\omega)=S(k)\sigma(k,\omega), \tag{25}$$

where

$$S(k)=\langle n(-k)n(k)\rangle \tag{26}$$

is the ordinary structure factor and

$$\sigma(k,\omega)=\frac{c_p-c_v}{c_p}\frac{2\lambda k^2/\rho_0 c_p}{(\lambda k^2/\rho_0 c_p)^2+\omega^2}+\frac{c_v}{c_p}\left[\frac{\Gamma k^2}{(\Gamma k^2)^2+(\omega+C_0k)^2}+\frac{\Gamma k^2}{(\Gamma k^2)^2+(\omega-C_0k)^2}\right]. \tag{27}$$

This way of constructing the density–density correlation function, Eq. (23), is essentially a convolution approximation. It is not the same as the "convolution

CC-0. In Public Domain. Gurukul Kangri Collection, Haridwar

Digitized by Arya Samaj Foundation Chennai and eGangotri

approximation" introduced by Vineyard[27] in the analysis of neutron-scattering experiments. This distinction has been discussed by Singwi and Sjölander.[28]

The method used to obtain Eq. (23) is the same as that used by Kadanoff and Martin.[29] Their results differ in that they used the density and the heat energy density as the independent variables. Because the heat energy density is linear in the density, it is difficult to obtain a direct evaluation of the generalized structure factor from their equations. Leontovich[30,31] and Rytov[32] also have used this approach to study time-dependent fluctuations.

Away from the critical point, the structure factor

$$S(k)=\langle n(-k)n(k)\rangle$$

is proportional to the compressibility and is independent of k. As the critical point is approached, k dependence develops reflecting the long range of the correlation between two particles. The Ornstein–Zernicke[33] expression for the two-body, time-independent correlation function is

$$g(r)-1=A\exp(-\kappa r)/r, \tag{28}$$

where κ^{-1} is the two-body correlation length. The quantity A has been shown by Fixman to be on the order of the range of intermolecular forces.[34] The structure factor associated with Eq. (28) is

$$S(k)=A/(k^2+\kappa^2). \tag{29}$$

Equation (29) is commonly used to describe scattering of light and x rays in the critical region.[35,36] The appropriateness of Eq. (29) has been questioned by some authors.[37–39] Since the exact form of $S(k)$ is not really important for this discussion, we do not examine these interesting questions. The recent review by M. E. Fisher is particularly recommended for that purpose.[40]

4. ACCURACY OF THE APPROXIMATE SOLUTIONS

The approximation procedure used to solve Eq. (15) is valid when ak^2 and bk^2 are sufficiently small in comparison with C_0k. To obtain some idea of the usefulness of the approximate solutions, Eq. (17), we solve the dispersion equation numerically, Eq. (15), when the parameters a, b, C_0, and γ are given numerical values appropriate to water at 22.9°C and 1 atm pressure.[41] Under these conditions $a=1.46\times10^{-3}$ cm²/sec, $b=4.47\times10^{-2}$ cm²/sec, $C_0=1.49\times10^{5}$ cm/sec,[42] and $\gamma=1.009$. With $k=10^5$ cm^{-1}, the dispersion equation is

$$s^3+(4.62\times10^8)s^2+(2.22\times10^{20}+9.92\times10^{15})s+3.14\times10^{27}=0. \tag{30}$$

The roots of Eq. (30) obtained numerically are

$$s=-1.46\times10^7/\text{sec}$$

$$s=-2.24\times10^8\pm1.49\times10^{10}i/\text{sec}.$$

The approximate solutions, Eqs. (16) and (17), yield the same results to three significant figures. Increasing k to 10^6 cm^{-1} does not alter the agreement significantly.

The value of the bulk viscosity used to compute b was inferred from ultrasonic absorption data and found to be about three times as large as the shear viscosity.[43] Recent measurements of Brillouin scattering in water[11,12] have found a small amount (on the order of three percent) of negative dispersion in the phonon velocity. In order to have Eq. (21) account for this shift in the phonon velocity it is necessary that the absorption coefficient, Γ, be about one order of magnitude larger than required by the ultrasonic measurements. The approximate solutions give good estimates even if bk^2/C_0 is as large as $\frac{1}{10}$. If larger values of this ratio occur it probably would be worthwhile to solve the dispersion equation by a procedure which takes the large value of b into account.

5. CRITICAL OPALESCENCE

As stated earlier, a primary reason for this review was an interest in critical opalescence. In this section we examine the structure predicted by $\sigma(k,\omega)$, Eq. (27), of the light scattered in the supercritical region of carbon dioxide.

Figures 1, 2, and 3 contain most of the relevant parameters for carbon dioxide in the supercritical region. [$T_c=31.04$°C, $P_c=72.85$ atm, $\rho_c=236$ amagat. (For

---

[27] G. H. Vineyard, Phys. Rev. **110**, 999 (1958).
[28] K. S. Singwi and A. Sjölander, Phys. Letters **9**, 120 (1964).
[29] L. P. Kadanoff and P. C. Martin, Ann. Phys. (N.Y.) **24**, 419 (1963).
[30] M. Leontovich, Z. Physik **72**, 247 (1931).
[31] M. Leontovich, J. Phys. (USSR) **4**, 499 (1941).
[32] S. M. Rytov, Zh. Eksperim. i Teor. Fiz. **33**, 166, 514, 671 (1957) [English transl.: Soviet Phys.—JETP **6**, 130, 401, 513 (1958)]. These papers are concerned mainly with viscoelastic fluids.
[33] L. S. Ornstein and F. Zernike, Physik. Z. **19**, 134 (1918); **27**, 761 (1926).
[34] Marshall Fixman, J. Chem. Phys. **33**, 1357 (1960); V. L. Ginsburg, Compt. Rend. URSS **36**, 8 (1942). A term similar to Eq. (32) was discussed in connection with early measurements of Brillouin scattering.
[35] J. E. Thomas and Paul W. Schmidt, J. Chem. Phys. **39**, 2509 (1963). A brief discussion of other experiments is contained in this paper.
[36] J. E. Thomas and Paul W. Schmidt, J. Am. Chem. Soc. **86**, 3554 (1964).
[37] M. S. Green, J. Chem. Phys. **33**, 1403 (1960).
[38] H. L. Frisch and G. W. Brady, J. Chem. Phys. **37**, 1514 (1962).
[39] I. Z. Fisher, *Statistical Theory of Liquids* (University of Chicago Press, Chicago, 1964), pp. 202–205.
[40] Michael E. Fisher, J. Math. Phys. **5**, 944 (1964).
[41] M. Greenspan and C. E. Tschiegg, J. Res. Natl. Bur. Std. (U.S.) **59**, 249 (1957).
[42] N. E. Dorsey, *Properties of Ordinary Water Substance* (Reinhold Publishing Corporation, New York, 1940).
[43] J. J. Markam, R. T. Beyer, and R. B. L. Lindsay, Rev. Mod. Phys. **23**, 353 (1951).

CC-0. In Public Domain. Gurukul Kangri Collection, Haridwar

Digitized by Arya Samaj Foundation Chennai and eGangotri

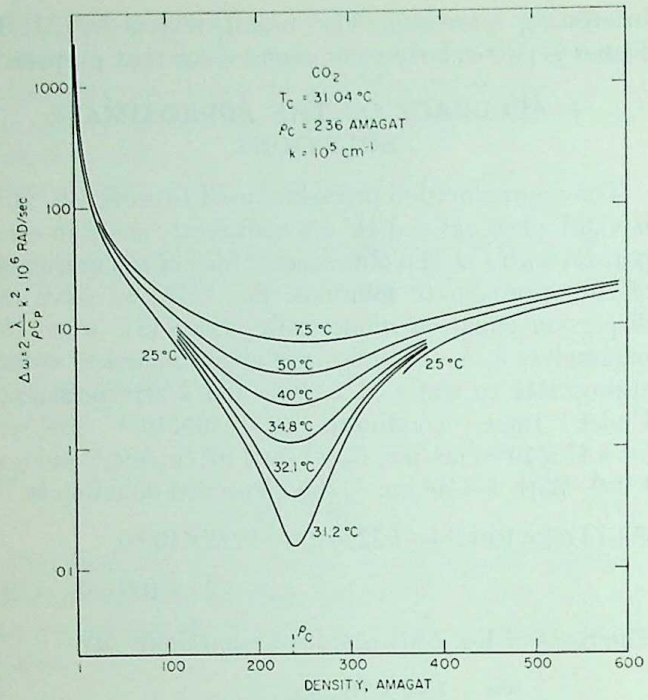

FIG. 1. The half-width of the undisplaced line in the supercritical region of carbon dioxide for $k=10^5$ cm^{-1}.

carbon dioxide, 1 amagat$=0.0019764$ g/cm^3.)][44-51] Figure 1 is the width of the central line; twice the thermal diffusivity times $k^2=10^{10}$ cm^{-2}. The shift of the Brillouin lines, C_0k with $k=10^5$ cm^{-1}, is shown in Fig. 2. The fraction of the light contained in the central line, $(1-\gamma^{-1})$, is indicated in Fig. 3.

Estimates of the width of the Brillouin lines, $2\Gamma k^2$, are not reliable near the critical point of carbon dioxide because the bulk viscosity, η_B, is not known as a function of density and temperature. There is reason to believe that Γk^2 is on the order of $C_0k/10$. This is based on the large sound absorption observed near the critical point.[52] In any case the Brillouin lines are much broader than the central lines. If $\Gamma k^2/C_0k\sim\frac{1}{10}$, there is also a small ($\sim$1%) amount of negative dispersion in the phonon velocity. This would result in a corresponding decrease in the separation of the Brillouin lines. This small effect has not been included in Fig. 2.

Figure 4 gives the relative intensity per unit solid angle of the scattered light for a 1-cm^3 scattering volume as predicted by Eq. (29) of Ref. 21. No attempt has been made to correct for the angular dissymmetry indicated by Eq. (29). Estimates of this effect based on the available PVT data and Fixman's[34] expression for κ^{-1}, the correlation length, indicate that the anisotropy is less than 10 percent for the indicated isotherms. These estimates are in agreement with the measurements of Skripov and Kopalakov.[53]

In Fig. 5, $\sigma(k,\omega)$ defined by Eq. (27) is plotted as a function of frequency, ω, for carbon dioxide at $T=32.1$°C, $\rho=230$ amagat, and $k=10^5$ cm^{-1}. Near the critical point, the central line of $\sigma(k,\omega)$ is dominant because of the large value of the ratio of the specific heats, γ. As the scattering angle is decreased, the width of the central line is strongly reduced since k is proportional to $\sin\theta/2$, where θ is the scattering angle.

In Fig. 6, $\sigma(k,\omega)$ is plotted for the same density and wave vector but for $T=75$°C. While the spacing between the lines is not to scale, the lines themselves are. The width of the Brillouin lines was computed under the unverified assumption that the shear and bulk viscosities are equal.

Fixman[34] has modified the basic equations, Eqs. (6), (7), and (8), slightly by including a term which describes the effects of the long-range density correlations on the pressure. If this term were included in Eq. (7) the term

$$(\partial p/\partial\rho)_T \text{ grad } \rho_1 \qquad (3$$

would be replaced by

$$(\partial p/\partial\rho)_T \text{ grad } [\rho_1-\kappa^{-2}\nabla^2\rho_1], \qquad (3$$

where κ^{-1} is the Ornstein–Zernicke[33] two-body corr

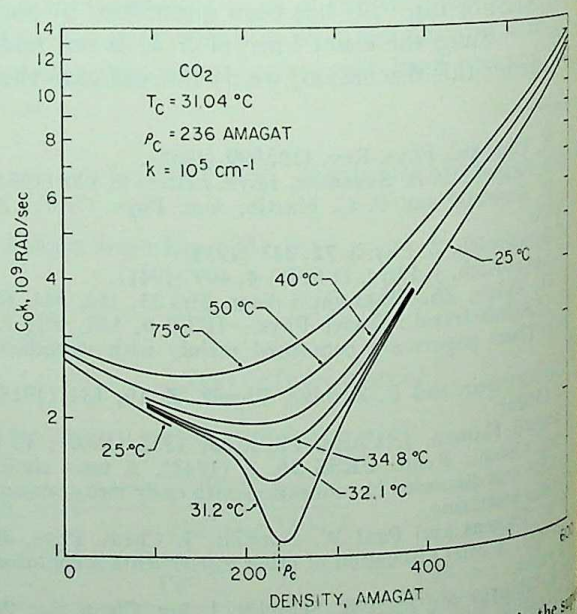

FIG. 2. The frequency shift of the Brillouin lines in the s critical region of carbon dioxide for $k=10^5$ cm^{-1}.

[44] Figures 1–4 have been constructed from a compilation of the properties of carbon dioxide prepared by J. V. Sengers. The author wishes to thank Dr. Sengers for his aid and encouragement in preparing this section. References 45–51 are the sources of the data.

[45] A. Michels and H. Wouters, Proc. Roy. Soc. (London) **A153**, 214 (1935).

[46] A. Michels and C. Michels, Proc. Roy. Soc. (London) **A153**, 201 (1935); **A160**, 348 (1937).

[47] A. Michels, B. Blaisse, and C. Michels, Proc. Roy. Soc. (London) **A160**, 358 (1937).

[48] A. Michels and S. R. deGroot, Appl. Sci. Res. Sec. A **94** (1948).

[49] A. Michels and J. C. Strijland, Physica **18**, 613 (1952).

[50] A. Michels, J. V. Sengers, and P. S. Van der Gulik, Physica **28**, 1216 (1962).

[51] J. Kestin, J. H. Whitelaw, and T. F. Zien, Physica **30**, 161 (1964).

[52] N. S. Anderson and L. P. Delsasso, J. Acoust. Soc. Am. **23**, 423 (1951).

[53] V. P. Skripov and Yu. D. Kopalakov, Tr. Soveshch. Kriticheskin Yaveleniyam: Flyuktuatsii v Rastvorakh, Akad. Nauk USSSR, Otd. Khim. Nauk, Moscow **1960**, 126 (19

CC-0. In Public Domain. Gurukul Kangri Collection, Haridwar

Digitized by Arya Samaj Foundation Chennai and eGangotri

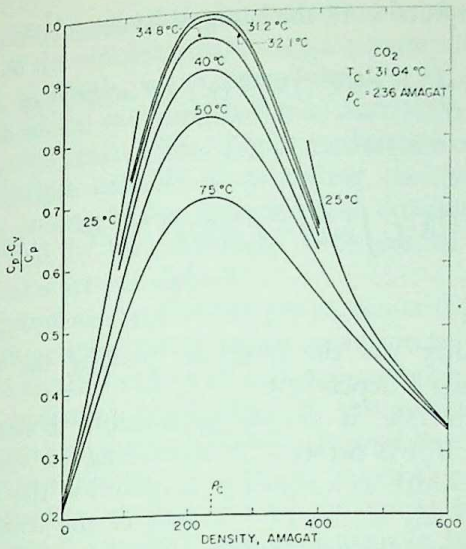

FIG. 3. The fraction of the scattered light contained in the undisplaced line for carbon dioxide in the supercritical regon.

lation length. The argument used to introduce this term is somewhat involved and the reader is referred to Fixman's papers for the details. We shall examine the significance of this term after we examine the consequences of the term.

The dispersion equation is changed by the inclusion of Fixman's term in Eq. (7). This new dispersion equation can be solved using the method of Sec. III.

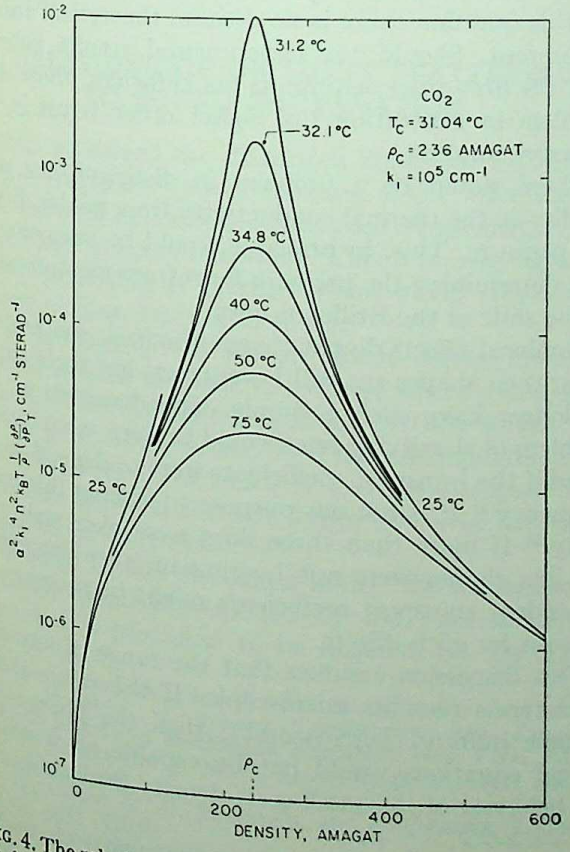

FIG. 4. The relative intensity per unit solid angle of the scattered light for a 1-cm³ sample of carbon dioxide in the supercritical region. The number density is indicated by n.

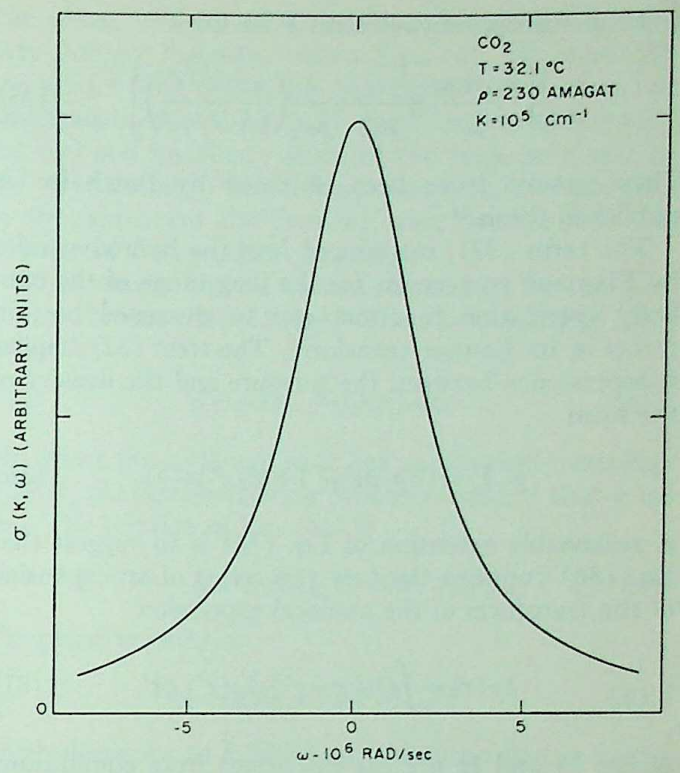

FIG. 5. The distribution in frequency of the scattered light near the critical point. The Brillouin doublet does not show up on this scale.

As expected, there are no important changes unless the two-body correlation length of Eq. (25), κ^{-1}, is of the order of k^{-1} or larger. The half-width of the central line is changed from

$$2\lambda k^2/\rho_0 c_p.$$

to

$$\frac{2\lambda k^2}{\rho_0 c_p}\left(\frac{1+k^2/\kappa^2}{1+k^2/\gamma\kappa^2}\right). \tag{33}$$

The velocity of the low-frequency phonons is

$$C_0(1+k^2/\gamma\kappa^2)^{\frac{1}{2}}, \tag{34}$$

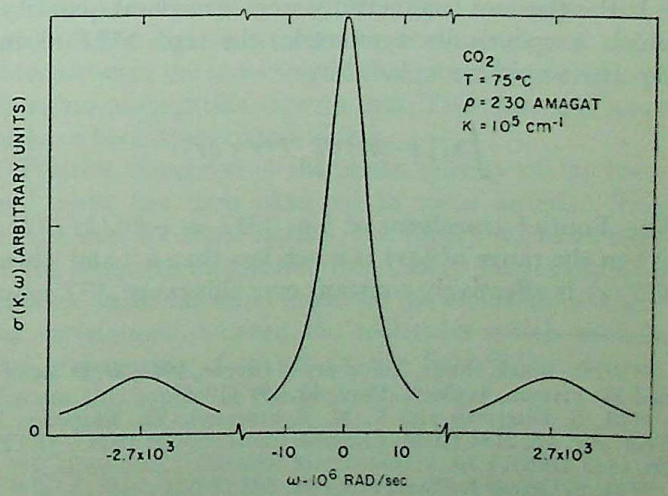

FIG. 6. The distribution in frequency of the scattered light away from the critical point.

CC-0. In Public Domain. Gurukul Kangri Collection, Haridwar

Digitized by Arya Samaj Foundation Chennai and eGangotri

and the absorption coefficient Γ becomes

$$\frac{1}{2}\left[\frac{\frac{4}{3}\eta_s+\eta_B}{\rho_0}+\frac{\lambda}{\rho_0 c_v}-\frac{\lambda}{\rho_0 c_p}\left(\frac{1+k^2/\kappa^2}{1+k^2/\gamma\kappa^2}\right)\right]. \tag{35}$$

These results have been obtained by Botch in his published thesis.[54]

The term (32), introduced into the hydrodynamics by Fixman[34] to account for the long range of the two-body correlation function, can be discussed best in terms of its Fourier transform. The term (32) implies k dependence between the pressure and the density of the form

$$p(k)=(\partial p/\partial\rho)_T[1+k^2/\kappa^2]n(k). \tag{36}$$

A reasonable extension of Eq. (36) is to suggest that Eq. (36) contains the first two terms of an expansion of the transform of the nonlocal expression

$$\delta p(\mathbf{r})=\int Q(|\mathbf{r}-\mathbf{r}'|)\,\delta\rho(\mathbf{r}')\,d\mathbf{r}', \tag{37}$$

where δp and $\delta\rho$ are the deviations from equilibrium. Some of the consequences of Eq. (37) for both light scattering and sound propagation have been investigated by Giterman and Kontorovich.[55] Because the functional form of $Q(r)$ is not known, their results are formal.

Some of the transport coefficients also may be nonlocal near the critical point. In the "derivation" of hydrodynamics, the transport coefficients appear as integrals of current–current correlation functions.[56,57] The macroscopic coefficients are the $k\to 0$ and $\omega\to 0$ limits of these integrals. In Mori's Markoffian, nonlocal theory of fluctuations, the "transport coefficients" may be k-dependent; i.e., the $k\to 0$ limit need not be taken.[57]

Near the critical point, the current–current correlation functions *may* have a range which is comparable with the reciprocal of the change in the wave vector of the scattered light. This is suggested by the long range of the two-body correlation function.

If the thermal conductivity were a nonlocal quantity which is spherically symmetric, the term $\lambda\nabla^2T(r)$ in Eq. (6) would be replaced by

$$\int\lambda(|\mathbf{r}-\mathbf{r}'|)\nabla'^2T(r')\,d\mathbf{r}'. \tag{38}$$

The Fourier transform of Eq. (38) is $-k^2\lambda(k)T(k)$. When the range of $\lambda(r)$ is much less than k^{-1} and when $\nabla^2T(r)$ is effectively constant over this range, ∇^2T may be taken outside of the integral so that

$$\int\lambda(|\mathbf{r}-\mathbf{r}'|)\nabla'^2T(r')\,d\mathbf{r}'=\lambda\nabla^2T(r) \tag{39}$$

and

$$\int\exp(i\mathbf{k}\cdot\mathbf{r})\int\lambda(|\mathbf{r}-\mathbf{r}'|)\nabla^2T(r')\,d\mathbf{r}'=-k^2\lambda T(k). \tag{40}$$

Nonlocality has the effect of making the transport coefficients k-dependent.

In principle, it should be possible to detect nonlocality, if it is present, by measuring the variation of the line width as k changes. In practice, this would be possible only if the $k=0$ values of the transport coefficients and the values of the thermodynamic functions are known quite accurately. To illustrate this, we discuss the effect of a k-dependent thermal conductivity on the width of the central line.

If the thermal conductivity is k-dependent, care must be exercised in using the solution to the dispersion equation which produces the unshifted line, Eq. (17). If $\lambda(r)$ is always nonnegative, there is no problem because $\lambda(k)\leq\lambda$ for all values of k and the approximation scheme we have used will converge rapidly. However, if $\lambda(r)<0$ for some range of values of r, it is possible that $\lambda(k)$ may be appreciably greater than λ for some values of k and the first-order solution, Eq. (17), with λ replaced by $\lambda(k)$, may not be adequate. To this question there is no definite theoretical answer at present. Should the experimental results indicate that the first-order solution is not sufficient, there is no problem in generating the higher order terms in the diffusive solution.

There would be a problem in distinguishing nonlocality in the thermal conductivity from nonlocality in the pressure. This, in principle, could be overcome by first determining the pressure term from measurements of the shift of the Brillouin lines.

Nonlocal effects do not change the basic shape of the lines; their shapes are still Lorentzian, but their widths no longer have such a simple dependence on k. The problem of classifying lines would be even more complicated if the transport coefficients were to depend on the frequency.[32] It is not our purpose to discuss this possibility.[58] If more than three lines were observed, or if the line shapes were not Lorentzian, then frequency-dependent transport coefficients might be necessary to account for such effects.

This discussion assumes that the range of any nonlocal terms remains microscopic. If the range should become infinite (macroscopic), then the phenomenological equations would not be capable of describing the behavior of the small-scale density fluctuations.

---

[54] W. D. Botch, thesis, University of Oregon, 1963; W. D. Botch and M. Fixman, J. Chem. Phys. **42**, 199 (1965).

[55] M. S. Giterman and V. M. Kontorovich, Zh. Eksperim. i Teor. Fiz. **47**, 2134 (1964) [English transl.: Soviet Phys.—JETP **20**, 1433 (1965)].

[56] M. S. Green, J. Chem. Phys. **22**, 398 (1954).

[57] H. Mori, Progr. Theoret. Phys. (Kyoto) **28**, 763 (1962).

[58] Robert Zwanzig, Phys. Rev. **124**, 983 (1961). The origin of frequency-dependent transport coefficients is discussed.

CC-0. In Public Domain. Gurukul Kangri Collection, Haridwar

Digitized by Arya Samaj Foundation Chennai and eGangotri

The resolution needed to measure the frequency spectrum of the scattered light is much higher than the resolution available with conventional optical techniques. An optical resolving power $\omega/\Delta\omega \approx 10^9$ is needed to resolve the central line. Light modulation systems are in principle capable of providing the necessary resolution, although the experimental difficulties are increased due to the relatively wide spread in the frequency of scattered light.[13]

Light-scattering experiments are particularly appealing near the critical point where experiments are notoriously difficult, because in a light-scattering experiment no gradients are imposed on the system. This makes it much easier to maintain thermal equilibrium during the experiment. In fact, it is possible to determine optically whether or not true equilibrium has been achieved.[59] Density measurements can be made precisely if optical methods are used.[60,61] (It may be that only optical methods are suitable for accurate density determinations near the critical point.)

Light-scattering experiments are also of value in probing the very high frequency properties of materials. In the next section, we compare the information obtained by light-scattering and the information obtained by sound-propagation and absorption measurements.

It is important to keep in mind that *light-scattering experiments are only as good as the PVT data used to specify the thermodynamic state of the scattering system.* In this respect, light-scattering measurements are no different from conventional determinations of transport properties.

6. RELATIONSHIP OF LIGHT SCATTERING TO SOUND PROPAGATION

When we solved the dispersion equation, Eq. (15), for the "frequency" s as a function of the wave vector k, we assumed that k was a real, positive quantity. The result was a complex frequency. This is in keeping with the representation of thermal sound waves (phonons) damped in time, but not in space.

The propagation of driven sound waves involves waves of a fixed frequency, $s=2\pi i\nu$, where ν is a real quantity. The dispersion equation is then solved for the complex wave vector k. This corresponds to a stationary wave train which is spatially damped. The distinction between the two types of waves has been recognized for may years.[43,62]

The point of this discussion is that the dispersion in the phase velocity measured by the light-scattering experiment is predicted to be negative by Eq. (21). The phase velocity of driven sound waves can only have positive dispersion when Eqs. (6), (7), and (8) are valid.[63] The reason for this difference is that the dispersion equation, Eq. (15), contains four unknowns, the real and imaginary parts of the frequency and of the wave vector. Two of these quantities are specified by the experiment and then the other two are obtained in terms of the specified quantities.

This situation can be worked out exactly for the case of zero thermal conductivity.[30] Then $a=0$ and Eq. (15) becomes

$$s[s^2+bk^2s+C_0^2k^2]=0. \tag{41}$$

We ignore the $s=0$ root as it has no physical meaning.

First, the light-scattering problem requires that k be real. The solution of Eq. (41) is

$$s=-\tfrac{1}{2}bk^2\pm iC_0k[1-b^2k^2/4C_0^2]^{\frac{1}{2}}. \tag{42}$$

The phase velocity is

$$v_{\text{th}}=\pm C_0[1-b^2k^2/4C_0^2]^{\frac{1}{2}}, \tag{43}$$

which decreases as k increases; the dispersion is negative.

The sound problem requires that $s=i\omega$, where ω is the angular frequency (real) of the sound generator. The dispersion equation is

$$k^2(C_0^2+ib\omega)-\omega^2=0$$

$$k^2=[\omega^2(C_0^2-ib\omega)]/(C_0^4+b^2\omega^2). \tag{44}$$

The phase velocity for the driven sound wave is

$$v_s=\omega/Rek$$

$$=\frac{\pm\sqrt{2}C_0(1+b^2\omega^2/C_0^4)^{\frac{1}{2}}}{[1+(1+b^2\omega^2/C_0^4)^{\frac{1}{2}}]^{\frac{1}{2}}}. \tag{45}$$

This phase velocity is an increasing function of frequency; the dispersion is positive. A discussion of why the two-phase velocities are different may be found in Sec. 10 of Ref. 43.

From this example, it is clear that the information contained in light-scattering experiments is not to be interpreted in the same way as the information obtained in sound-propagation experiments. This does not seem to have been appreciated widely.

Positive dispersion in the phase velocity of the thermal wave has been observed in some liquids.[1] This means that for those liquids, the theory we have used is not adequate to describe the density fluctuations. A reasonable modification might be the inclusion of angular correlations between the molecules which modify the propagation of waves in the fluid.[64] We do not discuss this aspect of the problem further.

[59] E. M. N. Schmidt and K. Traube, *Advances in Thermophysical Properties at Extreme Temperatures and Pressures* (American Society of Mechanical Engineers, New York, 1962).
[60] S. Y. Larsen and J. M. H. Levelt-Sengers, Progr. Therm. Transp. Prop. 1965.
[61] S. Y. Larsen, R. D. Mountain, and R. Zwanzig, J. Chem. Phys. 42, 2187 (1965).
[62] R. B. Lindsay, Koninkl. Vl. Acad. Wetenschap. Letter. Schone Kunst, Belg., p. 86 (1951).
[63] C. Truesdell, J. Rational Mech. Anal. 2, 643 (1953).
[64] W. A. Steele and R. Pecora, J. Chem. Phys. 42, 1872 (1965). Ref. 18, pp. 294–302.

CC-0. In Public Domain. Gurukul Kangri Collection, Haridwar

Digitized by Arya Samaj Foundation Chennai and eGangotri

7. SUMMARY

A measurement of the spectrum of the light scattered by density fluctuations contains four pieces of information. The Brillouin doublet contains two of these. The separation of the doublets is determined by the speed of the *thermal* sound wave while the width of these lines is proportional to Γ, the sound absorption coefficient. By measuring the speed and lifetime of the phonons, it is possible to examine the high-frequency properties of the fluid. A precise measurement of Γ would be very useful in inferring the value of the bulk viscosity, η_B. Direct measurement of η_B has not been possible, and sound absorption measurements, which also measure Γ, are often difficult to make with sufficient precision to determine accurately the bulk viscosity.

The width of the central line is proportional to the thermal diffusivity, $\lambda/\rho_0 c_p$. Interest in this quantity is greatest near the critical point where conventional measurements of the thermal conductivity are difficult.[50]

Finally, the ratio of the intensity of the central line to that of the doublet lines is

$$I_0/2I_1=(c_p-c_v)/c_v. \quad (1)$$

The integrated intensity of each of the lines can be used to determine γ, the ratio of the specific heats. The intensity of the central line, I_0, increases rapidly as the critical point is approached. The intensity of the doublet, $2I_1$, remains more or less constant because their total intensity is proportional to the isothermal compressibility divided by c_p, the specific heat at constant pressure. This ratio is not varying rapidly in the critical region. Of course, to utilize this information as efficiently as possible, measurements should be made for several values of k (scattering angle).

So far, we have examined only the theoretical side of the problem. What is possible experimentally? As in all scattering problems, what is possible depends on the intensity of the scattered light and the resolving power of the detector. To date, only the intensity of the three lines and the position of the Brillouin lines have been measured in liquids.[19,20]

A resolving power on the order of 10^8 is needed to measure the widths of the Brillouin lines. Resolving powers as large as 3×10^8 have been obtained, using a spherical-mirror interferometer of the type invented by Connes.[14,65,66] It may be quite difficult to detect the Brillouin lines in the critical region. These lines are broad and, in comparison with the central line, very weak.

The central line is much narrower than the doublets and probably will require another type of detector. Optical heterodyne detection techniques have been used to obtain extremely large resolving powers.[13] It should be possible for this technique to operate in the range of frequencies appropriate to the width of the central line. However, because this system requires a large amount of scattered light in order to work, its usefulness may be limited to the scattering in the critical region. Since this is the region where the central line is most interesting, this is not a serious limitation.

In conclusion, it is now possible to study the spectral distribution of light scattered by density fluctuations. Such experiments are of interest because they provide a means of probing the dynamical behavior of a fluid on a scale which is not available by other means. Also they are a way to measure transport properties of the fluid without imposing some sort of gradient on the system. This is particularly desirable near the critical point. The inference of the bulk viscosity from the width of the Brillouin lines and the possibility of studying nonlocal effects near the critical point are two examples of what can be examined in this way.

ACKNOWLEDGMENTS

I wish to thank my colleagues at the National Bureau of Standards for many helpful discussions. Special thanks are due M. S. Green and J. V. Sengers for their interest and encouragement.

---

[65] P. Connes, J. Phys. Radium **19**, 262 (1958).
[66] R. L. Fork, D. R. Herriott, and H. Kogelnik, Appl. Opt. **3**, 1471 (1964).

CC-0. In Public Domain. Gurukul Kangri Collection, Haridwar

Digitized by Arya Samaj Foundation Chennai and eGangotri

REVIEWS OF
MODERN PHYSICS

VOLUME 38, NUMBER 2 APRIL 1966

Dynamical Symmetry in Particle Physics*

A. PAIS
Rockefeller Institute, New York, New York

A review is given of recent applications of symmetry arguments in particle physics. It deals with the developments which start with $SU(6)$.

I. INTRODUCTION

The purpose of this paper is to give an account of recent applications of symmetry arguments in particle physics. It deals with the developments which start with $SU(6)$. The properties of $SU(3)$ [G 1] and those of Pauli and Dirac spinors and matrices are supposed known. It has been attempted to make this paper fairly self-contained otherwise, though it is certainly not complete in many mathematical details.

In order to explain the plan of the paper we begin by giving the table of contents.

II. Some Physical Applications of Unitary Groups
  A. A Few Definitions
  B. Kinematical and Dynamical Unitary Symmetries
III. Some Mathematical Tools
  A. Representations of $SU(N)$
  B. Representations of $U(N)$
  C. Reduction of Product Representations
  D. Reduction of $SU(MN)$ with respect to $SU(M)\times SU(N)$
  E. Generators, Labeling Problems, Currents
  F. Reduction of $SU(M+N)$ with Respect to $SU(M)\times SU(N)$
  G. Pseudo-Unitary Groups
IV. $SU(6)$
  A. Introduction
  B. Some Specific Supermultiplets
  C. Mass Formulae
  D. Magnetic Moments
  E. Electromagnetic Mass Differences
  F. The Semi-Leptonic Vertex
  G. S-Wave Nucleon–Nucleon Scattering
  H. Non-Leptonic Decays
  I. The Master Problem
  J. Triplets: Formal Tool or Reality?
V. Relativistic Explorations
  A. Introduction
  B. The Boosted *6*, *36*, *56*; the Group $U(6, 6)$
  C. The Meson–Baryon Vertex
  D. Groups Related to $U(6, 6)$
  E. Unitarity; other Implications
  F. W-Spin
  G. Conclusion
VI. Current Algebras
VII. No-Go Theorems for Certain Kinematic Symmetries
VIII. Questions

Section III can be skipped by readers familiar with the algebra of unitary tensors. In that section, Lie groups and Lie algebras are only touched on lightly, as their treatment is well accessible elsewhere [B 1, H 1].

During the period covered in this paper, intense work went on concerning three main and distinct problems. (The Babylonian confusion of this period was largely due to the fact that their distinct nature was not always stated.)

(A) Investigations of approximate dynamical symmetries such as static $SU(6)$ and of larger ones, in which the latter is contained.

(B) Explorations of dynamical equations which yield $SU(6)$ or related groups as a symmetry of some of their approximate solutions.

(C) Limitations on approximate kinematic symmetries imposed by the rules of quantum theory and relativity theory.

It seems possible at this time, and it is tried in this paper, to assess the success and limitations of work related to (A); to state what preliminary steps have

*The present paper contains an enlarged version of lectures given by the author in Erice and in Dubna in the fall of 1965. It will be attempted to outline the main ideas in this field up till December 1965.

Copyright © 1966 by the American Physical Society
CC-0. In Public Domain. Gurukul Kangri Collection, Haridwar

Digitized by Arya Samaj Foundation Chennai and eGangotri

been taken and what questions have arisen in regard to (B), which thus far is an open problem; and to illustrate the nature of theorems that bear on (C).

The purpose of Sec. II is to make the distinction between kinematical and dynamical symmetry. Section IV deals with the properties of static $SU(6)$. In Sec. V, relativistic explorations are discussed which fall mainly under the heading of problem (A). Section VI contains a brief account of what is known about current algebras; here one deals with questions of type (B). Some results concerning (C) are summarized in Sec. VII.

Numerous discussions with many colleagues are gratefully acknowledged, especially with M. A. B. Bég, B. W. Lee, S. Meshkov, and R. Oehme. Also, I want to thank M. A. B. Bég for his help in the writing of Sec. VI; M. A. B. Bég, O. W. Greenberg, and S. B. Treiman for helpful criticism of the manuscript; and A. Q. Sarker for his assistance in compiling the published literature up till early December 1965.

II. SOME PHYSICAL APPLICATIONS OF UNITARY GROUPS

A. A Few Definitions

Notation. Matrices will be written as $A_\beta{}^\alpha$ where the upper and lower indices denote rows and columns, respectively. x^α, $\alpha = 1, \cdots, N$ denotes a complex vector, represented as a one-column matrix x. The vector with complex conjugate components is conveniently written as $x_\alpha{}^*$ and as such it is represented as a one-row matrix $x^\dagger$. († stands for Hermitian conjugate).

Consider a transformation

$$x' = Ax \quad \text{or} \quad x'^\alpha = A_\beta{}^\alpha x^\beta. \tag{2.1}$$

The complex conjugate of x transforms as

$$x^{\dagger\prime} = x^\dagger A^\dagger \quad \text{or} \quad x_\alpha{}'^* = x_\beta{}^* A_\beta{}^{*\alpha} = x_\beta{}^* (A^\dagger)_\alpha{}^\beta. \tag{2.2}$$

(Summations over β are understood.) The unitary length of x is defined by

$$x^\dagger x = x_\alpha{}^* x^\alpha. \tag{2.3}$$

The unitary group $U(N)$ may be defined as the group of all transformations (2.1) which leave $x^\dagger x$ invariant. This implies that the matrices A satisfy

$$A^\dagger A = 1. \tag{2.4}$$

The further restriction

$$\det A = 1 \tag{2.5}$$

corresponds to the unimodular subgroup $SU(N)$ of $U(N)$.

The vector x is a particular representation of $U(N)$, or $SU(N)$, called the defining representation and often denoted by its dimension: N. The complex conjugate vector $x^\dagger$ gives a representation with the same dimension but which is in general inequivalent to N [for the special case $N=2$ see the discussion of Eq. (3.6) below]. We denote it by N^* and call it the representation conjugate to N.

The set of all A acting on an x generates an N-dimensional complex vector space. In this space we can choose a base of N linearly independent vectors x_j, $j=1, \cdots, N$. Thus $x_j{}^\alpha$ is the αth component of the jth base vector. In physical language, a particular choice of the x_j corresponds to the choice of "axes of quantization." We read the transformation (2.1) on x_j as

$$x_j{}'^\alpha = A_\beta{}^\alpha x_j{}^\beta, \tag{2.6}$$

that is, we let A act on the *components* for fixed axes of quantization, so that A changes the direction of a vector in a fixed coordinate system. Cf. the discussion in [F 1]. In what follows, x^α will mean the αth component of a vector, regardless of choice of axes. In the later discussion of boost matrices (Sec. V), the more fully specified notation used in Eq. (2.6) will be needed again.

B. Kinematical and Dynamical Unitary Symmetries

There are a variety of groups $SU(N)$ which play a role in physics. As an introduction to our subject, it is useful to give some examples of these physically interesting cases. They have in common that conserved quantities for physical systems are defined in terms of the generators of the group at hand. They are distinct in the way the region of validity of the conservation is defined.

(I) Strict kinematical group $SU(2)$: angular momentum. We shall call this strict symmetry kinematical to indicate that the corresponding conservation laws are valid independently of what may be the detailed dynamics of the system. The defining representation 2 is "the spinor."

(II) Approximate kinematic group $SU(2)$: isospin. The group applies in an approximate way, namely, only in the limit $e \to 0$. This restriction is expressed in terms of a parameter which is independent of the dynamical variables (positions, momenta, etc.) of the system. For this reason the approximate group will be called an approximate kinematic group. The defining representation 2 is the nucleon.

Of course one can use isospin in practice also when $e \neq 0$, for example when we say: isospin works well in hadron–hadron scattering for energies large compared with the isomultiplet splittings and for angles large compared with the region of Coulomb interference. However, we like to think that the size of these "bad" regions tends to zero as $e \to 0$. This is probably not a very physical way of putting things. The only reason this $e \to 0$ limit is discussed here is to contrast the approximate nature of isospin, as it is thought of presently, with approximate symmetries of a different kind.

(III) Approximate dynamical group $SU(2)$: normal

CC-0. In Public Domain. Gurukul Kangri Collection, Haridwar

Digitized by Arya Samaj Foundation Chennai and eGangotri

coupling in atomic spectra [C 1]. Write the Hamiltonian for an atom as

$$H = H_0 + H' \tag{2.7}$$

$$H_0 = \sum \frac{p_i^2}{2m} - \sum \frac{Ze^2}{r_i} + \sum_{i>j} \frac{e^2}{r_{ij}}. \tag{2.8}$$

H' contains all nonstatic effects, for example, spin-orbit coupling. Whenever it is legitimate to neglect H' to a good approximation, the orbital angular momentum L and the spin angular momentum S are separately conserved and we have S-multiplets $^{2S+1}L_J$ (normal or Russell–Saunders coupling). The group $SU(2)$ is now the spin group, the defining representation *2* is the electron with spin.

Take the ^3P and ^1P levels in helium as an example. Even though (2.8) is explicitly spin independent, a ^3P–^1P split arises due to the exclusion principle, (Austausch effect). On the other hand, we have a "supermultiplet" in the H_0 approximation, as $^3P_{2,1,0}$ are degenerate. This degeneracy is lifted by spin-orbit coupling.

The spin-orbit coupling is proportional to e and also proportional to v/c via the momentum. Yet we cannot define the H_0 approximation by $e \to 0$, for then we lose the atom. The normal coupling approximation is thus to be defined as the neglect of v/c effects, that is in terms of the small expectation value in specific states of certain dynamical variables.

Normal coupling may be better in one part of the spectrum than in another; for heavy atoms it is bad for the Roentgen part of the spectrum, it is better in the outer shells provided that there is not too much excitation. All these effects which make the spin group $SU(2)$ to an approximate one are not (as for isospin) expressable in terms of a nondynamical parameter. Thus we speak of an approximate dynamical group.

With the Hamiltonian (2.7) in hand, the dynamical nature of the approximation is of course obvious from the start, and there is no need to discuss trouble with $SU(2)$. There would be trouble indeed if one would think of the spin group as approximately kinematical in nature. This is so because taking a limit of the kinematical type "coupling constant"$\to 0$ *is itself a relativistically invariant procedure.* In the zero limit we would then have a strict symmetry in which spin and total angular momentum would be separately strictly conserved. We would then have a theory of finite multiplets with more integrals of the motion than the Poincaré group allows which is absurd. This is at the root of many no-go theorems for certain approximate kinematical symmetries [W 1]. These theorems will be briefly reviewed in Sec. VII.

(IV) Approximate group $SU(3)$: strong interaction symmetry [G 1]. It is not impossible, as far as is known, that this is an approximate kinematical group, that there is a symmetry breaking interaction which is characterized by one (or more) nondynamical parameters which in their zero limit define a strict $SU(3)$. However, some bootstrap ideas favor a more dynamical view (which could perhaps also be applied to isospin.) The defining representation *3* is the triplet.

Regarding the experimental status of $SU(3)$, it seems that the predictions are best for mass relations and for semileptonic and electromagnetic vertices. On the other hand, from the analysis of scattering and production amplitudes alone one would not be very clear about this symmetry [H 2, A 1].

(V) Approximate dynamical group $SU(4)$: nuclear supermultiplets [W 2]. This symmetry was suggested to apply as a dynamical approximation for low-lying nuclear levels only [W 2]. In that region the theory works well [F 2]. The defining representation *4* is the nucleon with spin. This $SU(4)$ has much in common with the $SU(2)$ of (III). But of course we do not know as much about the Hamiltonian in this case as we do for (2.7). All the success of $SU(4)$ really says about the fundamental dynamics is that there is a regime in which a spin- and isospin-independent H_0 is a a good approximation. It is not part of the $SU(4)$ theory per se to *derive* an H_0 and an H' from first dynamical principles, as in (2.7, 8).

This brief discussion of some aspects of the foregoing unitary symmetries is given in order to set the stage for the main topic of this paper.

(VI) Approximate dynamical group $SU(6)$ in particle physics [S 1, G 3, P 1, G 4]. The fundamental representation *6* is the sextet, an $SU(3)$ triplet of spin $\frac{1}{2}$ particles. Thus (as will be explained more fully in Sec. IV) this group contains the unitary spin group $SU(3)$ and the ordinary spin group $SU(2)$. By the argument given for the case of Russell–Saunders coupling, $SU(6)$ must be an approximate dynamical group because it *contains* the spin group. Indeed, what is often referred to as the difficulties of $SU(6)$ has nothing to do with the fact that $SU(6)$ contains the internal symmetry group $SU(3)$. It is instructive to read the pertinent literature as if it had reference to atomic Russell–Saunders coupling, where the internal symmetry group is shrunk to the identity.

For the nuclear $SU(4)$, it was mentioned how one may refer back from the validity of that supermultiplet theory to the structure of a leading part of the Hamiltonian. The analog for $SU(6)$ would be to ask for the "inner" dynamics of a baryon (for example) built up out of sextets (see Sec. IV J). But this is only one facet of what has been attempted with $SU(6)$ and its descendants. Beyond that, there arise questions in particle physics which have had no analogous treatments elsewhere. For example, can one say anything new about the scattering of two particles each of which is assigned to an $SU(6)$ supermultiplet? The analog would be the scattering of two nuclei on each other where the state of each one separately is (approximately) described in terms of the nuclear $SU(4)$. This clearly must involve questions of recoupling with

CC-0. In Public Domain. Gurukul Kangri Collection, Haridwar

Digitized by Arya Samaj Foundation Chennai and eGangotri

orbital angular momentum (except for S-wave scattering see Sec. IV G).

There is another type of problem which arises in the context of $SU(6)$, namely the off-the mass shell problems as they appear for example in the study of vertices. In this context belong also many questions related to the possible existence of a field theory. Attempts in this direction must go well beyond the phenomenological level as it was sketched for $SU(4)$. These problems, which seem particularly pressing as the principal encouragements for $SU(6)$ theory come from vertices, are taken up again in Sec. IV I, V, and VI.

III. SOME MATHEMATICAL TOOLS

A. Representations of $SU(N)$

(1) Following a procedure familiar from the ordinary rotation group, one can obtain general representations from the defining representation by the construction of tensors. A tensor $T_{\beta_1\cdots\beta_n}{}^{\alpha_1\cdots\alpha_m}$ is defined by

$$T_{\beta_1\cdots\beta_n}{}^{\alpha_1\cdots\alpha_m}\sim x^{\alpha_1}(1)\cdots x^{\alpha_m}(m)x_{\beta_1}(1')\cdots x_{\beta_n}(n'), \tag{3.1}$$

where $\sim$ means: transforms like. This definition of a tensor holds for $U(N)$ and $SU(N)$ alike. Thus unitary tensors have two kinds of indices, upper and lower ones. Apart from the component labels the x's are marked with " configuration labels" (i), or (i') to distinguish one unitary vector from another. x^α transforms with A, x_β with $A^\dagger$, as in Eqs. (2.1) and (2.2), respectively.

For the case of $SU(N)$ only one can, without loss of generality, consider tensors which have only upper (or only lower) indices by introducing the Levi-Civita symbols $\epsilon^{\lambda_1\cdots\lambda_N}$. ϵ is totally antisymmetric in its N indices and $\epsilon^{123\cdots N}=1$; $\epsilon_{\lambda_1\cdots\lambda_N}$ has similar properties. Under a transformation of $U(N)$, these symbols transform as follows:

$$\epsilon'^{\lambda_1\cdots\lambda_N}=D^{-1}a_{\mu_1}{}^{\lambda_1}\cdots a_{\mu_N}{}^{\lambda_N}\epsilon^{\mu_1\cdots\mu_N}, \tag{3.2}$$

$$\epsilon'_{\lambda_1\cdots\lambda_N}=D^{*-1}a_{\lambda_1}{}^{\dagger\mu_1}\cdots a_{\lambda_N}{}^{\dagger\mu_N}\epsilon_{\mu_1\cdots\mu_N}, \tag{3.3}$$

$$D=\det\|a\|, \qquad D^*=\det\|a^*\|. \tag{3.4}$$

The transformations (3.2, 3) preserve the total antisymmetry, while also $\epsilon'^{1\cdots N}=\epsilon'_{1\cdots N}=1$, as is easily checked. It is in order to preserve these unit values that the factors D^{-1} (or D^{*-1}) had to be introduced. Thus the ϵ symbols do *not* behave as tensors under $U(N)$. But for $SU(N)$ where $D=D^*=1$, the ϵ's are true tensors. One may call the ϵ's pseudo-tensors under $U(N)$, in straight generalization of the terminology for the rotation group, where ϵ^{ijk} is a constant tensor under $SO(3)$ but changes sign under the reflections included in $O(3)$.

Confining ourselves now to $SU(N)$, we can raise all lower tensor indices to upper ones. Thus to x_i we can associate a totally antisymmetric tensor y:

$$x_i=\epsilon_{il_2\cdots l_N}y^{l_2\cdots l_N},$$
$$y^{l_2\cdots l_N}=[1/(N-1)!]\epsilon^{il_2\cdots l_N}x_i. \tag{3.5}$$

Note the familiar case $N=2$:

$$x_i=\epsilon_{ij}y^j, \qquad y^j=\epsilon^{ij}x_j, \tag{3.6}$$

where one may associate a spinor y^j to a conjugate spinor x_i.

Let us return to the tensor T of Eq. (3.1) with both upper and lower indices. This T corresponds in general to a reducible representation, for two reasons.

(a) If its trace with respect to α_i and β_j is unequal to zero, then the original T contains a nonvanishing tensor of lower rank which is itself a representation [as $x^\alpha(i)x_\alpha(i')$ is a scalar].

(b) Consider

$$T^{\alpha_1\alpha_2}=\tfrac{1}{2}(T^{\alpha_1\alpha_2}+T^{\alpha_2\alpha_1})+\tfrac{1}{2}(T^{\alpha_1\alpha_2}-T^{\alpha_2\alpha_1}).$$

Each of the two terms in brackets separately forms a representation of $SU(N)$: the unitary transformations commute with permutations on the indices, they preserve the (anti-)symmetry. It is true in general for tensors of any rank that if there exists a permutational symmetry or antisymmetry of the indices then this is respected by the unitary transformations, [H 1]. Thus one step toward getting irreducible representations is to find "tensors with permutational symmetry."

Moreover, the tracelessness condition itself can be expressed as a particular kind of permutational symmetry. Consider for example the tensor

$$t_\beta{}^\alpha,\ t_\alpha{}^\alpha=0. \tag{3.7}$$

This is a (N^2-1)-dimensional representation, the adjoint representation. The condition $t_\alpha{}^\alpha=0$ can also be expressed as follows.

$$\epsilon^{\beta\alpha_1\cdots\alpha_{N-1}}t_\beta{}^{\alpha_N}\pm\epsilon^{\beta\alpha_2\cdots\alpha_N}t_\beta{}^{\alpha_1}+\epsilon^{\beta\alpha_3\cdots\alpha_N\alpha_1}t_\beta{}^{\alpha_2}$$
$$\pm\cdots\pm\epsilon^{\beta\alpha_N\alpha_1\cdots\alpha_{N-2}}t_\beta{}^{\alpha_{N-1}}=0, \tag{3.8}$$

where all signs are $+$ for N odd, while signs alternate for N even. It is easily checked that (3.8) is tantamount to the one condition $t_\alpha{}^\alpha=0$. We can therefore associate to $t_\beta{}^\alpha$ a new tensor:

$$T^{[\alpha_1\alpha_2\cdots\alpha_{N-1}]\alpha_N}=\epsilon^{\beta\alpha_1\cdots\alpha_{N-1}}t_\beta{}^{\alpha_N}, \tag{3.9}$$

where T is totally antisymmetric in its first $N-1$ indices and where the symmetrization condition

$$T^{[\alpha_1\cdots\alpha_{N-1}]\alpha_N}\pm T^{[\alpha_2\cdots\alpha_N]\alpha_1}$$
$$+\cdots\pm T^{[\alpha_N\alpha_1\cdots\alpha_{N-2}]\alpha_{N-1}}=0 \tag{3.10}$$

is imposed in addition. It is therefore clear that to any irreducible tensor $T_{\beta_1\cdots\beta_n}{}^{\alpha_1\cdots\alpha_m}$ can be associated a tensor with upper indices *only*. For this new tensor there must then exist mixed symmetry–antisymmetry

CC-0. In Public Domain. Gurukul Kangri Collection, Haridwar

Digitized by Arya Samaj Foundation Chennai and eGangotri

conditions between these upper indices. Unless specified otherwise, we mean in the following by tensor always this latter kind with upper indices only.

According to a general theorem [H 1] we can find *all* irreducible representations of $SU(N)$ by classifying all tensors with permutational symmetry and with one kind of index (say upper) only.

(2) There are other standard forms for the tensors which can be arrived at by the use of the ϵ's. For example, in the case of $SU(3)$ one can make all tensors totally symmetric in upper and likewise in lower indices and furthermore require tracelessness [B 1]. The form chosen here is perhaps most easily suited for the application of Young tableau rules, which give a quick and exhaustive way of treating all possible symmetry/antisymmetry situations. The rules are the following [H 1, L 1].

To an irreducible tensor of rank n of the group $SU(N)$ there corresponds an "allowed" partition

$$(n_1, n_2, \cdots, n_N), \ \sum_i n_i = n,$$
$$n_1 \geq n_2 \geq \cdots \geq n_N. \quad (3.11)$$

Some of the n_i at the back end may be zeros in which case we do not write them explicitly. In evident shorthand then, for example for $N=6$, the partition (31^2) stands for (311000). If all $n_i=0$ we write (0). This is the identity representation. The partition can be pictured by a "tableau" like

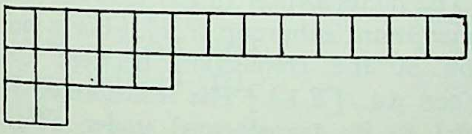

with N rows of successive length $n_1, \cdots, n_N$. The structure of this tableau is meant to prescribe symmetrizations and antisymmetrizations as follows. Fill each square of the tableau with one of the configuration labels, as they occur for example in (3.1). For a given filling, antisymmetrize in the labels occurring in the columns; then symmetrize in the labels occurring in the rows. Thus a Young tableau stands for a permutation operator. When these operators act on $T^{\alpha_1 \cdots \alpha_r} \sim x^{\alpha_1}(1) \cdots x^{\alpha_r}(r)$, many of the N^r (r=rank of the tensor) combinations of tensor indices get annihilated. The remaining combinations are $D_N(n_1, \cdots, n_N)$ in number. D_N is the dimension of the representation.

Remarks. (1) Alternatively, we can first symmetrize, then antisymmetrize, or follow more complex procedures of ordering symmetrizations and antisymmetrizations. Each order gives a set of D_N vectors spanning the representation space. Different orders give different sets. Nor are these sets in general orthogonal sets. For procedures to get orthogonal sets see [Y 1, J 1, T 1].

(2) Except for purely symmetric or purely antisymmetric tensors there are more (independent) ways than one to distribute the configuration labels over the squares. The various independent ways yield *equivalent* representations of $SU(N)$, for an example see [B 1, p. 22]. [The number of equivalent representations is equal to the number of times the tensor $(n_1, \cdots, n_N)$ occurs in the direct product of $1 \otimes 1 \otimes \cdots \otimes 1$; n factors).

Proceeding as in (3.11) for all n and all allowed partitions of n one obtains all irreducible representations of $SU(N)$. The association: tensor$\leftrightarrow$Young tableau is unique.

(3) Formula for D_N.

$$D_N(n_1, \cdots, n_N) = [(n_1-n_2+1)/1!] \cdot (n_1-n_3+2) \cdots (n_1-n_N+N-1) \cdot$$
$$\cdot (n_2-n_3+1)/2! \cdots (n_2-n_N+N-2) \cdot$$
$$\cdot \quad \cdot$$
$$\cdot \quad \cdot$$
$$\cdot \quad \cdot$$
$$(n_{N-1}-n_N+1)/(N-1)\,! \quad (3.12)$$

This formula gives the dimension for any N. For $N=2$ take only the first column on the right-hand side of (3.12); for $N=3$, take both first and second columns, etc. Note that

$$D_N(n_1, \cdots, n_N) = D_N(n_1-n_N, n_2-n_N, \cdots, n_{N-1}-n_N, 0) \quad (3.13)$$

so we always may strike off the columns of length N. This corresponds to the fact that $\epsilon_{\lambda_1 \ldots \lambda_N} x^{\lambda_1}(1) \cdots x^{\lambda_N}(N)$ is a scalar under $SU(N)$.

The case $N=2$:

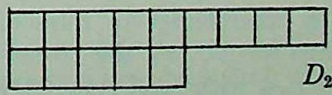

$$D_2(n_1, n_2) = n_1-n_2+1 \quad (3.14)$$

is quite familiar. The n_2 pairs of "spins" are each paired off to zero resultant. The residual n_1-n_2 spins are in a totally symmetric state, and therefore correspond to a total spin $(n_1-n_2)/2=S$. Hence $D_2=2S+1$. Thus given the total spin of an n spin $\frac{1}{2}$ system its symmetry

CC-0. In Public Domain. Gurukul Kangri Collection, Haridwar

Digitized by Arya Samaj Foundation Chennai and eGangotri

is determined. That is why for $SU(2)$ problems like normal atomic coupling there is not such a great advantage to use tableaux.

Examples.

(a)

$$D_N(1) = D_N(1^{N-1}) = N. \tag{3.15}$$

(1) is the defining representation, (1^{N-1}) its conjugate. (1^{N-1}) corresponds to the y tensor in (3.5). The representation (1) is self-conjugate if and only if $N=2$, cf. (3.6).

(b)

$$D_N(21^{N-2}) = N^2-1, \tag{3.16}$$

this is the adjoint representation.

(c)

$$D_N(n_1) = \binom{N+n_1-1}{n_1}, \tag{3.17}$$

these are the totally symmetric representations. Thus $D_3(3)=10$, $D_6(3)=56$, etc.

(d)

$$D_N(1^k) = \binom{N}{k}, \tag{3.18}$$

the totally antisymmetric representations; $D_6(1^3)=20$, etc.

(4) Conjugate representations. We have the identity

$$D_N(n_1, \cdots, n_N) = D_N(n_1-n_N, n_1-n_{N-1}, \cdots, n_1-n_2, 0). \tag{3.19}$$

The partition on the right-hand side (which is an allowed one if the one on the left-hand side is) corresponds to a representation called the conjugate representation of $(n_1, \cdots, n_N)$. The special case (1) versus (1^{N-1}) has been met already. Other examples: (3^2) is the *10** of $SU(3)$, (3^5) is the *56** of $SU(6)$.

These are examples of inequivalent representations with the same dimensions. However, conjugation does not exhaust the possible equality of dimensions. Example: $D_4(3)=D_4(21)=D_4(22)=20$. Where possible, representations will often be referred to by their dimensions (in italics), with the understanding that this is not adequate in general. [For $SU(2)$ it is always adequate.]

Using the language of upper and lower indices as in (3.1), the connection between a representation and its conjugate amounts to an interchange of roles of upper and lower indices. Thus for $SU(3)$, the *10* corresponds to $T^{\alpha\beta\gamma}$, the *10** to $T_{\alpha\beta\gamma}$ with total symmetry in the 3 indices in each case. In $SU(6)$, $D_6(31^3)=D_6(3^22^3)=280$. To each representation belongs a traceless tensor $T_{\gamma\delta}{}^{\alpha\beta}$. For (31^3), the *280*, we have symmetry in (α, β), antisymmetry in (γ, δ). For $(3^2, 2^3)$, the *280**, we have antisymmetry in (α, β), symmetry in (γ, δ).

If the conjugate representation is identical with the original one, we have a self-conjugate case. In tensor language, we have equivalent properties of upper and lower indices. Thus (21^{N-2}), the adjoint representation, is the self conjugate tensor $T_\beta{}^\alpha$. Other examples: $D_6(42^4)=405$, $D_6(2^21^2)=189$ are each self-conjugate and correspond to a tensor $T_{\gamma\delta}{}^{\alpha\beta}$, symmetric (*405*), antisymmetric (*189*), both in the lower and in the upper indices.

Whether a tensor is self-conjugate depends both on the partition and on the dimension. Thus $D_3(21)=8$ is self-conjugate, but $D_6(21)=70$ is not. In either case we can represent the tensor by $T^{[\alpha\beta]\gamma}$, antisymmetric in $[\alpha, \beta]$ which satisfies in addition $T^{[\alpha\beta]\gamma}+T^{[\gamma\alpha]\beta}+T^{[\beta\gamma]\alpha}=0$. For $N=3$ we can revert from $T^{[\alpha\beta]\gamma}$ to l_δ, see (3.9); for $N=6$ we cannot do so.

Finally, we recall that a familiar way to construct explicit representations for the rotation group is to find the spherical harmonics. One can in principle construct analogous "harmonic functions" for all unitary groups [M 1, B 4, K 2, I 2].

B. Representations of $U(N)$

Let us return to the tensor T, Eq. (3.1), defined as a tensor under $U(N)$. By definition a transformation of T involves a product of m factors A, n factors $A^\dagger$ where A is an element of $U(N)$. Now generally

$$A = (e^{i\phi}\cdot 1)\cdot a, \tag{3.20}$$

where a is an element of $SU(N)$, 1 is the $N\times N$ unit matrix. The factorization (3.20) says that $U(N)$ contains an invariant subgroup $U(1)$. [For a more refined discussion of the connection between $U(N)$ and $SU(N)$ see, e.g., [E 1].] The transformed T is therefore equal to its transformed under $SU(N)$ times a "gauge" factor $\exp[i(m-n)\phi]$. As $\det A = \exp(iN\phi)$ we may therefore put

$$D^{-1} = \exp(-iN\phi) \tag{3.21}$$

in Eq. (3.2).

Even though, as noted above, the Levi-Civita symbol is not a tensor under $U(N)$ we may nevertheless apply the entire apparatus of Sec. III A also to the case of $U(N)$, with one additional stipulation. All we have to do is to assign to the general tensor T of Eq. (3.1) a "baryon number" $B=\lambda(m-n)$, where λ is a number independent of m and n. For the defining representation $B=\lambda$. Note that B is independent of any possible symmetry between upper or between lower tensor indices. After B has been assigned the problem is reduced to $SU(N)$ and we may again consider tensors with only upper (or only lower) indices.

Example. Consider $SU(3)$. Let x^α be a "quark" [G 2, Z 1] with baryon number $B=\frac{1}{3}$. Then $x_\alpha{}^*$ is an "anti-quark", $B=-\frac{1}{3}$. $M_\beta{}^\alpha$ has $B=0$ and may represent a meson octet. Its Young tableau is (21). Consider the tensor $T^{[\alpha\beta]\gamma}$ with

$$T^{[\alpha\beta]\gamma}+T^{[\gamma\alpha]\beta}+T^{[\beta\gamma]\alpha}=0. \tag{3.22}$$

CC-0. In Public Domain. Gurukul Kangri Collection, Haridwar

Digitized by Arya Samaj Foundation Chennai and eGangotri

T has $B=1$. After having established the value of B, we now put

$$T^{[\alpha\beta]\gamma}=\epsilon^{\alpha\beta\delta}B_\delta{}^\gamma$$

as in Eq. (3.9). Then $B_\delta{}^\gamma$ is traceless. It may represent the baryon octet. Its Young tableau is also (21). Thus the same (21) describes a quark–antiquark set and a three-quark set. There is no source of confusion as long as the assignment of a B value is separately established.

Once this point is out of the way we can restrict the rest of Sec. III to $SU(N)$. The generalizations to $U(N)$ will be obvious.

C. Reduction of Product Representation

Tableaux are also useful for the decomposition of $(n_1, \cdots, n_N)\otimes(n_1', \cdots, n_N')$ into irreducible representations. The general procedure is best arrived at as follows [L 1].

(I). $(n_1, \cdots, n_N)\times(1)$, product of the general tableau with $\square$. Add $\square$ to the original tableau in all possible ways such that one still has an allowed partition (3.11) (of $n+1$) as a result. Each of these ways corresponds to an irreducible representation in the product.

Examples.

$$\begin{aligned}
(1)\times(1)&=(2)+(1^2)\\
(21)\times(1)&=(31)+(22)+(21^2), && N\geq 3,\\
&=(31)+(22)+(1), && N=3,\\
&=(2)+(0), && N=2,\\
(2^2)\times(1)&=(32)+(2^21), && N\geq 3,\\
&=(32)+(1^2), && N=3.
\end{aligned}$$

(II). $(n_1, \cdots, n_2)\times(m)$. We now multiply with a totally symmetric representation $\square\square\square\square\square\square$ of m squares. Proceed successively square by square of this set of m as under (I). But never add two or more squares of the set of m to the same column.

Examples.

(1) $SU(2)$. Let $m\geq n$, then

$$\begin{aligned}
(m)\times(n)&=(m+n)+(m+n-1,\,1)+(m+n-2,\,2)\\
&\quad+\cdots+(m,\,n),\\
&=(m+n)+(m+n-2)+(m+n-4)\\
&\quad+\cdots+(m-n) \qquad (3.23)
\end{aligned}$$

where columns of length 2 have been struck away, see (3.13). Put $m=2S$, $n=2S'$, then the dimension check for Eq. (3.23) reads

$$(2S+1)\times(2S'+1)$$
$$=[2(S+S')+1]+\cdots+[2(S-S')+1].$$

Thus with the tableau rules we have the reduction for angular momentum as a special case.

Equation (3.23) provides an example of simple reducibility. We say that a product representation is simply reducible if any representation which occurs in the product appears only once. Equation (3.23) is a special case of a slightly more general situation.

Lemma 1. For any $SU(N)$ the product $(m,\ m,\ m,\ \cdots,\ m)\times(n)$ (where the number of m's is $\leq N$) is simply reducible.

The following special case of Lemma 1 will be important for later purposes.

Lemma 2. The conjugate representation of (n) is $(n, n, \cdots, n)$ where the number of n's is equal to $N-1$. The product of (n) and its conjugate is simply reducible; in particular it contains the adjoint representation (21^{N-2}) once and only once.

(2) $SU(3)$.

$$\begin{aligned}
(3^2)\times(3)&=(63)+(531)+(432)+(333)\\
&=(63)+(42)+(21)+(0).
\end{aligned}$$

Dimension check [use (3.12)],

$$10^*\times 10=64+27+8+1.$$

Also

$$\begin{aligned}
(21)\times(3)&=(51)+(42)+(41^2)+(321),\\
&=(51)+(42)+(3)+(21),\\
8\times 10&=35+27+10+8.
\end{aligned}$$

(3) $SU(6)$.

$$\begin{aligned}
(3^5)\times(3)&=(3^6)+(43^42)+(53^41)+(63^4)\\
&=(0)+(21^4)+(42^4)+(63^4).
\end{aligned}$$

(Strike columns of length 6). Check:

$$56^*\times 56=1+35+405+2695. \qquad (3.24)$$

Also

$$\begin{aligned}
(21^4)\times(3)&=(41^5)+(321^4)+(421^3)+(51^4),\\
&=(3)+(21)+(421^3)+(51^4),\\
35\times 56&=56+70+1134+700. \qquad (3.25)
\end{aligned}$$

(III). $(n_1, \cdots, n_N)\times(n_1', \cdots, n_N')$. First proceed with the top row of length n_1' as under (II); then add on the next row of length n_2' as under (II); $\cdots$, etc. But now mark one last additional rule.

Put a 1 in each of the n_1' squares of the top row in $(n_1', \cdots, n_N')$, put a 2 in each of the n_2' squares of the second row, $\cdots$, an N in each of the n_N' squares of the last row. Now look at one of the product tableaux obtained as per previous instructions *with* the markings 1, or 2, $\cdots$ or N in the various squares inserted. Read from right to left the numbers found in the first row; continue to read from right to left what is marked in the second row, $\cdots$, from right to left in the last row. This gives one total sequence of numbers which should obey the rule: up to any point within the sequence the

CC-0. In Public Domain. Gurukul Kangri Collection, Haridwar

Digitized by Arya Samaj Foundation Chennai and eGangotri

number of 1's ≥ number of 2's ⋯ ≥ number of n's. (This is known as a lattice permutation [L 1]).

Examples.

(1) $SU(3)$

$$(2^2)\times(2^2)=(4^2)+(431)+(42^2),$$
$$=(4^2)+(32)+(2),$$
$$6^*\times 6^*=15+15'+6.$$

(Note the two distinct representations of dimension *15*).

$$(21)\times(21)=(42)+(41^2)+(3^2)+(321)+(321)+(2^3)$$
$$=(42)+(3)+(3^2)+(21)+(21)+(0)$$
$$8\otimes 8=27+10+10^*+8+8+1.$$

(2) $SU(6)$.

$$(21^4)\times(21^4)=(2^6)+(32^41)+(32^41)+(3^22^21^2)$$
$$+(3^22^3)+(42^31^2)+(42^4)$$
$$=(0)+(21^4)+(21^4)+(2^21^2)+(3^22^3)$$
$$+(31^3)+(42^4).$$

Check:

$$35\times 35=1+35+35+189+280^*+280+405. \quad (3.26)$$

Exercise. (21) is the *70*, (2^41) the 70^*. Show that

$$70^*\times 70=1+2\times 35+189+280$$
$$+280^*+405+3675. \quad (3.27)$$

It is important not only to know which representations occur in the product of two representations. Also one wants to know what is the structure of the transformation which expresses the product of any tensor component of one representation times any component of the other as a sum of components contained in the irreducible parts of the product. This is the problem of the Clebsch–Gordan coefficients. For a number of cases this has been discussed in the literature. For $SU(6)$ see [C 2, C 3, S 8].

D. Reduction of $SU(MN)$ with Respect to $SU(M)\times SU(N)$

Consider the invariant quadratic form $x_\alpha{}^*x^\alpha$ of $SU(MN)$, where x^α is the defining representation, $\alpha=1, \cdots, MN$. We can replace each index value α by an index pair Ai, $A=1, \cdots, M$; $i=1, \cdots, N$, so

$$x_\alpha{}^*x^\alpha=x_{Ai}{}^*x^{Ai}. \quad (3.28)$$

For fixed i (or A) we recognize within (3.28) an invariant form of $SU(M)$ [or $SU(N)$]. In other words, for fixed i (or A) but running A (or i), x^{Ai} is a fundamental representation of $SU(M)$ [or $SU(N)$]. We can represent this content of Eq. (3.28) in tableau language as follows.

$$\square=(\square;\square). \quad (3.29)$$

where the left-hand side is the (1) of $SU(MN)$ while on the right-hand side the first $\square$ is the (1) of $SU(M)$, the second $\square$ is the (1) of $SU(N)$. Thus, equivalently to (3.29):

$$1=(1;1). \quad (3.30)$$

Still a third way of representing the contents of (3.28) is by dimensions

$$MN=(M;N). \quad (3.31)$$

For the conjugate to the defining representation,

$$(1^{MN-1})=(1^{M-1};1^{N-1}), \quad (3.32)$$
$$(MN)^*=(M^*,N^*). \quad (3.33)$$

Another obvious example for this kind of notation is

$$(0)=(0;0), \quad \text{(tableaux)} \quad (3.34)$$
$$1=(1;1), \quad \text{(dimensions)} \quad (3.35)$$

linking the respective identity representations.

We have now three examples where to an irreducible representation of $SU(MN)$ there belongs *one* irreducible representation pair of $SU(M)$; $SU(N)$. For all other representations of $SU(MN)$ we will have more than one pair. We can find all such pairs by operating separately with the tableau rules for each of the three groups as will be clear from the following examples.

(1) $(1)\times(1)=(2)+(1^2)=(1,1)\times(1,1)$
$$=(2+1^2;2+1^2),$$

or

$$(2)+(1^2)=(2;2)+(1^2;2)+(2;1^2)+(1^2;1^2). \quad (3.36)$$

From (3.17, 18) this has the dimension check

$$\tfrac{1}{2}MN(MN+1)+\tfrac{1}{2}MN(MN-1)$$
$$=(\tfrac{1}{2}M(M+1);\tfrac{1}{2}N(N+1))$$
$$+(\tfrac{1}{2}M(M-1);\tfrac{1}{2}(N(N+1))$$
$$+(\tfrac{1}{2}M(M+1);\tfrac{1}{2}N(N-1))$$
$$+(\tfrac{1}{2}M(M-1);\tfrac{1}{2}N(N-1)), \quad (3.37)$$

with the observation that a dimension pair $(a;b)$ counts for ab. We want of course to know the separate content of the (2) and the (1^2) of $SU(MN)$. This also follows uniquely from the dimension check (3.12):

$$(2)=(2;2)+(1^2;1^2), \quad (3.38)$$
$$(1^2)=(1^2;2)+(2;1^2).$$

For $SU(6)$, $M=3$, $N=2$ (3.38) corresponds to (in dimensions)

$$21=(6;3)+(3^*;1), \quad (3.39)$$
$$15=(3^*;3)+(6;1).$$

CC-0. In Public Domain. Gurukul Kangri Collection, Haridwar

Digitized by Arya Samaj Foundation Chennai and eGangotri

Of course (3.38) could also have been found from the observation that the symmetric tensor (2) of $SU(MN)$ corresponds either to symmetry in both the tensor indices of $SU(M)$ and $SU(N)$ or to anti-symmetry in both these cases.

$$(2)\quad (1^{MN-1})\times(1) = (21^{MN-2})+(0)$$
$$= (1^{M-1}, 1^{N-1})\times(1, 1)$$
$$= (21^{M-2}+0, 21^{N-2}+0).$$

Using (3.35) we therefore have at once for the adjoint representation (21^{MN-2}):

$$(21^{MN-2}) = (21^{M-2}, 21^{N-2}) + (21^{M-2}, 0)+(0, 21^{N-2}), \quad (3.40)$$

corresponding to

$$(MN)^2-1 = (M^2-1, N^2-1) + (M^2-1, 1)+(1, N^2-1). \quad (3.41)$$

For $M=3$, $N=2$:

$$35 = (8; 3)+(8, 1)+(1, 3). \quad (3.42)$$

The general procedure will now be clear and we give some further results for $SU(6)\supset SU(3)\otimes SU(2)$. Multiply both (2) and (1^2) with (1). This gives, in dimensions:

$$56 = (8; 2)+(10; 4), \quad (3.43)$$

$$70 = (1; 2)+(8; 2)+(10; 2)+(8; 4), \quad (3.44)$$

$$20 = (1; 4)+(8; 2), \quad (3.45)$$

for the three (three-sextet) tableaux (3), (21), (1^3), respectively.

Conjugate tableaux have conjugate content. Thus from (3.39):

$$21^* = (6^*; 3)+(3; 1), \quad (3.46)$$

$$15^* = (3; 3)+(6^*, 1), \quad (3.47)$$

for the $SU(6)$ tableaux (2^5) and (1^4), respectively. Now

$$21^*\times 21 = 405+35+1, \quad (3.48)$$

$$15^*\times 15 = 189+35+1. \quad (3.49)$$

Thus with the help of (3.35) and (3.42)

$$189 = (8+1; 5)+(8+8+10+10^*; 3) + (27+8+1; 1), \quad (3.50)$$

$$405 = (27+8+1; 5)+(27+8+8+10+10^*; 3) + (27+8+1; 1). \quad (3.51)$$

Likewise, $15^*\times 21$ gives

$$280 = (10+8; 5)+(27+8+8+10+1; 3) + (10+10^*+8, 1) \quad (3.52)$$

while 280^* has the conjugate content.

More details and examples are found in [H 3].

In equations such as (3.39–47) we find examples where the contents of an $SU(6)$ representation is completely specified in terms of labels provided by the subgroup $SU(3)\otimes SU(2)$. On the other hand, Eqs. (3.50–52) show that this specification is not adequate in general, as $(8; 3)$ occurs twice in each instance. This raises the general problem of a full labeling of the D_N states which span a given representation of $SU(N)$. This question is discussed in the next section.

E. Generators; Labeling Problems; Currents

A unitary transformation acting on a tensor with D_N linearly independent components is a linear transformation in the D_N-dimensional space spanned by these components. The transformation can be represented by a $D_N\times D_N$ matrix U which itself is unitary and which can be represented by [H1, B1]

$$U = \exp(i\epsilon_B F_B), \quad (3.53)$$

where a summation over B is implied. For $U(N)$, $B=1, \cdots, N^2$; for $SU(N)$, $B=1, \cdots, N^2-1$. The ϵ_B are parameters which may be chosen to be real. Thus $SU(N)$ is an (N^2-1)-parameter group. Like U, the *generators* F_B can be represented by $D_N\times D_N$ matrices which are hermitian for real ϵ_B. Moreover, for $SU(N)$ we have the trace condition

$$(F_B)_i{}^i = 0. \quad (3.54)$$

The F_B satisfy commutation relations

$$[F_B, F_C] = if_{BCD}F_D. \quad (3.55)$$

Here the totally antisymmetric real f_{BCD} are the so called structure constants of the Lie algebra of the F's. The f_{BCD} have the all-important property to be independent of the particular representation on which the F's act. The f's are therefore fully specified by what will be called the defining generators (DG). The DG are defined as the representation of the generators by $N\times N$ sized matrices in as far as they act on the defining representation.

Example. For $SU(2)$ the three generators are the angular momentum operators; $f_{BCD}=\epsilon_{BCD}$, the 3-dimensional Levi-Civita symbol. The DG are $\sigma_B/2$ where the σ's are the three Pauli matrices.

It is easy to write down the DG for $SU(N)$. Put $F_B=(C_\beta{}^\alpha, C'_\beta{}^\alpha, H_k)$. Here $\alpha>\beta=1, \cdots, N$ so there are $N(N-1)/2$ C and the same number of C' matrices; $k=1, \cdots, N-1$. We may put

$$(C_\beta{}^\alpha)_j{}^i = \tfrac{1}{2}(\delta^{\alpha i}\delta_{\beta j}+\delta^{\alpha j}\delta_{\beta i}),$$
$$(C'_\beta{}^\alpha)_j{}^i = (i/2)(\delta^{\alpha i}\delta_{\beta j}-\delta^{\alpha j}\delta_{\beta i}), \quad (3.56)$$

while the H_k are diagonal matrices whose elements

CC-0. In Public Domain. Gurukul Kangri Collection, Haridwar

Digitized by Arya Samaj Foundation Chennai and eGangotri

along the diagonal may be chosen as follows:
For H_k:

$$[2k(k+1)]^{-\frac{1}{2}}(\underbrace{1, 1, \cdots, 1}_{k}, -k, 0, \cdots, 0),$$

$$k=1, \cdots, N-1. \tag{3.57}$$

It is very convenient to normalize such that Tr $F_B{}^2$ is independent of B, as has been done here. From this realization of the F_B, the f_{BCD} can be computed. For $SU(3)$ this is done in [G 1].

The H_k are a set of commuting matrices. From the main property of the f's it follows then that for any representation there is such a commuting subset of $(N-1)$ generators. It is known that this is the maximal commuting subset. Thus for $SU(N)$ a partial labeling is provided by $N-1$ additive quantum numbers. (The number $N-1$ of H_k is the "rank" of the group.)

The important question arises to find the matrix respresentation of the F's acting on any representation of $SU(N)$. This problem has been solved explicitly [B 2].

We now turn to the question of a complete labeling of the D_N "vectors" spanning the representation space for a tensor in $SU(N)$. For $SU(2)$ the answer is familiar. The representation is characterized by the angular momentum squared, which we write as

$$\sum_{B=1}^{3} F_B{}^2$$

in the present language and for which we introduce the symbol $C_2{}^{(2)}$:

$$C_2{}^{(2)}=\sum_{B=1}^{3} F_B{}^2. \tag{3.58}$$

Furthermore the individual vectors in the representation space are labeled by the magnetic quantum number, which we now call H_1. The labeling by $C_2{}^{(2)}$ and H_1 is complete. How is this for $SU(N)$?

(1) The number of commuting operators whose eigenvalues are sufficient for the specification of a state is $(N-1)(N+2)/2$, see [R 1, B 2].

(2) $N-1$ such operators are given by the H_k.

(3) A further set of $N-1$ operators is given by the "Casimir operators" $C_i{}^{(N)}$, $i=2, \cdots, N$. $C_i{}^{(N)}$ is a polynomial of degree i in the F_B. It is known [R 2, B 3] that there are just $N-1$ independent nonlinear expressions in the F_B which commute with all F_B.

The $C_2{}^{(N)}$ are easy:

$$C_2{}^{(N)}=\sum_{1}^{N} F_B{}^2. \tag{3.59}$$

The other $C_i{}^{(N)}$ have been explicitly constructed, see [B 2] (also for the earlier literature on the subject) and [K 1]. The answer is as follows (sum over repeated labels from 1 to N).

$$C_3{}^{(N)}=d_{ABC}F_AF_BF_C,$$

$$C_4{}^{(N)}=d_{ABE}d_{ECD}F_AF_BF_CF_D,$$

$$C_5{}^{(N)}=d_{ABP}d_{PQC}d_{QDE}F_AF_BF_CF_DF_E, \quad \text{etc.}$$

where the d's are defined by the anticommutator of the DG which can generally be written as

$$F_AF_B+F_BF_A=2C\delta_{AB}F_0+d_{ABC}F_C, \tag{3.60}$$

where the real d_{ABC} are totally symmetric, C is a number depending on the choice of normalization for the F_B and F_0 is the unit matrix.

A perhaps simpler way of writing the C operators is as follows [O 1]. Go to $U(N)$ and write the N^2 generators as $A_\beta{}^\alpha$, $\alpha, \beta=1, \cdots, N$. Then a (non-Hermitian) representation of the DG is

$$(A_\beta{}^\alpha)_j{}^i=\delta^{\alpha i}\delta_{\beta j}, \tag{3.61}$$

so that

$$[A_\beta{}^\alpha, A_\delta{}^\gamma]=f_{\beta\delta\sigma}{}^{\alpha\gamma\rho}A_\rho{}^\sigma, \tag{3.62}$$

$$f_{\beta\delta\sigma}{}^{\alpha\gamma\rho}=\delta_\sigma{}^\alpha\delta_\beta{}^\gamma\delta_\delta{}^\rho-\delta_\delta{}^\alpha\delta_\sigma{}^\gamma\delta_\beta{}^\rho. \tag{3.63}$$

These f's are again the structure constants (in a slightly different guise). The C operators are simply traces of powers of A:

$$C_i{}^{(N)}=\text{Tr}\,(A^i)\equiv A_{\alpha_2}{}^{\alpha_1}A_{\alpha_3}{}^{\alpha_2}\cdots A_{\alpha_1}{}^{\alpha_i}, \tag{3.64}$$

where now i runs from 1 to N (rather than from 2). $C_1{}^{(N)}=A_\alpha{}^\alpha$ (summed over α) commutes with all A. Hence $(A_\alpha{}^\alpha)_j{}^i=c\delta_j{}^i$. The restriction $U(N)\to SU(N)$ amounts to the condition that on any representation $C_1{}^{(N)}=0$.

The $C_i{}^{(N)}$ label fully a representation of $SU(N)$. We found a previous labeling, namely the partition numbers $(n_1, \cdots, n_N)$ of which only $N-1$ are independent for $SU(N)$ see Eq. (3.13). These two ways of labeling are equivalent; $C_i{}^{(N)}$ is a polynomial of degree i in the n_j.

Examples. For $SU(3)$, [B 3], partition (pq):

$$C_2{}^{(3)}=\tfrac{1}{3}(p^2+q^2-pq+3p), \tag{3.65}$$

$$C_3{}^{(3)}=\tfrac{1}{18}(p-2q)(2p+3-q)(p+q+3). \tag{3.66}$$

For $SU(4)$, partition (pqr), [B 5],

$$C_2{}^{(4)}=\tfrac{3}{8}(p^2+q^2+r^2)-\tfrac{1}{4}(pq+qr+rp)+\tfrac{1}{2}(3p+q-r). \tag{3.67}$$

{There are always constant cofactors to be fixed by a normalization convention. The present ones correspond to the normalizations in (3.56–57). See further [W 6].}

(4) We have now found $2(N-1)$ of the desired commuting operators which is not yet enough (except for $N=2$). One way to get a complete set is to consider

CC-0. In Public Domain. Gurukul Kangri Collection, Haridwar

Digitized by Arya Samaj Foundation Chennai and eGangotri

the factorization [W 3, B 3]

$$SU(N) \supset U(1) \otimes SU(N-1),$$

where $U(1)$ is generated by a linear combination of the $N-1$ H_i and where the generators of $SU(N-1)$ commute with the generator of $U(1)$. For example, the DG of $U(1)$ can be given by H_{N-1} of Eq. (3.57) and the DG of $SU(N-1)$ by Eqs. (3.56–57) with $N \to N-1$. We may then further label by the $C_i^{(N-1)}$. Continue next likewise: $SU(N-1) \supset U(1) \otimes SU(N-2)$ which yields the $C_i^{(N-2)}$, etc. A full labeling is then obtained by: $N-1$ H_i (or linear combinations thereof) and the $C_i^{(k)}$, $k=2, 3, \cdots, N$; $i=2, 3, \cdots, k$ which yields the desired total number.

Example. $SU(3) \supset U(1) \otimes SU(2)$. The 5 labels are: $C_2^{(3)}$, $C_3^{(3)}$ or equivalently the partition (pq); $C_2^{(2)}$: isospin; the hypercharge [generator of $U(1)$]; and the z component of isospin.

While this procedure is sufficient for any N, it is not the only one and in fact it is not the one commonly used. To conclude this section, we discuss the method followed [B 5] in the discussion of $SU(6)$.

For a full labeling in $SU(6)$ one needs 20 operators. The following have been used:

(I) The partition numbers $(n_1, \cdots, n_5)$ of the $SU(6)$-Young tableau, equivalent to the $C_i^{(6)}$: five in number.

(II) The contents classification by the chain

$$SU(6) \supset SU(3) \otimes SU(2) \tag{3.68}$$

where the two subgroups are commuting ones. This gives: 5 labels from $SU(3)$, 2 from $SU(2)$, thus seven in total.

From (I) and (II) we get 12 labels. These are sufficient to label fully the representations *35*, *56*, *70*, *20* as was already seen in Eqs. (3.42–45).

(III) The labeling by a second chain [B 5]

$$SU(6) \supset U(1) \otimes SU(2) \otimes SU(4) \tag{3.69}$$

$$\hookrightarrow SU(4) \supset SU(2) \otimes SU(2). \tag{3.70}$$

The subgroup in the first link (3.69) was introduced in [G 4]. In (3.69) we pick up: three labels from the $SU(4)$-tableau plus two labels from $SU(2)$ (the "strange quark spin"): the $U(1)$ chosen in this particular case (hypercharge) is already contained in the $SU(3)$ of the chain (3.68). Finally the subgroup labeling (3.69) yields two more labels from one of the $SU(2)$ ("nonstrange quark spin") while the other $SU(2)$ (isospin) is identical with the $SU(2)$ used in the first chain.

Thus under (III) we find seven new labels and we have now 19 in all. This is ample to classify the contents of *189*, *405*, *280*, Eqs. (3.50–52). A 20th label has not so far been necessary. It would suffice to take one of those H_k of $SU(6)$ that have not been explicitly used till now.

It should be stressed [B 5] that the operators of the first chain (3.68) do not all commute with those of the second one (3.69–70). This, however, is not an objection of principle, and such a situation has been met before [M 1]. The use of noncommuting chains is dictated by physical arguments to be discussed below [Sec. IV]. It necessitates additional recoupling transformations to which correspond such phenomena as $\omega-\phi$ mixing.

We conclude this section by recalling the well-known properties of the operators F_A under the transformation

$$F_A' = U^\dagger F_A U, \tag{3.71}$$

where U is given by Eq. (3.53). This transformation can also be written as

$$F_A' = C_{AB}(\epsilon)\, F_B, \tag{3.72}$$

where C is an $N \times N$-sized matrix which is unitary. In fact, with a hermitian choice for the generators, C is orthogonal. C depends on the values of the parameters ϵ_A. These properties of C are easily verified when the ϵ_A are infinitesimal. From Eqs. (3.55), (3.71) we have in this case

$$C_{AB}(\epsilon) = \delta_{AB} + \epsilon_C f_{CAB} \tag{3.73}$$

so that C is orthogonal as the f's are antisymmetric.

Thus the set of operators F_A themselves form an (N^2-1)-dimensional representation of $SU(N)$ ("angular momentum is a vector"); and if we add the identity operator we have a representation of $U(N)$.

Consider two unitary vectors x, y and construct the quantity

$$J_A^{(N)}(x, y) \equiv x^\dagger F_A y = x_\alpha^* (F_A)_\beta{}^\alpha y^\beta, \tag{3.74}$$

where $(F_A)_\beta{}^\alpha$ are the DG matrices. From Eqs. (2.1–2) and (3.71–72) the $J_A^{(N)}$ behave as follows under a transformation of $U(N)$:

$$J_A'^{(N)}(x, y) = C_{AB}(\epsilon)\, J_B^{(N)}(x, y). \tag{3.75}$$

Thus they transform as a representation of $U(N)$. We shall call the $J_A^{(N)}(x, y)$ the currents of $U(N)$. Note in particular that

$$J_A^{(N)\dagger}(x, x) = J_A^{(N)}(x, x) \tag{3.76}$$

if we choose a Hermitian set F_A. Finally

$$\sum_A J_A^{(N)}(x, y)\, J_A^{(N)}(u, v) = \text{invariant under } U(N). \tag{3.77}$$

F. Contents of $SU(M+N)$ with Respect to $SU(M) \times SU(N)$

In Eq. (3.69) we met the chain $SU(6) \supset SU(4) \otimes SU(2)$. This raises the question stated in the title of

CC-0. In Public Domain. Gurukul Kangri Collection, Haridwar

Digitized by Arya Samaj Foundation Chennai and eGangotri

this section. Once again we start with the quadratic invariant in terms of the defining representation, now for $SU(M+N)$ and write

$$\sum_{1}^{M+N} x_\alpha^* x^\alpha = \sum_{1}^{M} x_\alpha^* x^\alpha + \sum_{M+1}^{M+N} x_\alpha^* x^\alpha. \tag{3.78}$$

The first term on the right-hand side is the corresponding quadratic invariant for an $SU(M)$, the second one for an $SU(N)$. In terms of Young tableaux the following identification is evident.

$$\square = (\square, 0) + (0, \square), \tag{3.79}$$

where 0 stands for the identity tableau. Equivalently

$$1 = (1, 0) + (0, 1), \tag{3.80}$$

or in dimensions

$$M+N = (M; 1) + (1; N).$$

In a similar (but of course not identical) way to $SU(MN) \supset SU(M) \otimes SU(N)$ one now starts building up higher representations of $SU(M+N)$ in terms of sums of representation pairs. Full details are found in [H 4]. Some examples are given at the end of Sec. IV B.

G. Pseudo-Unitary Groups

Following the notations of Sec. IIA, let x denote a complex vector in an $(M+N)$-dimensional space and $x^\dagger$ its Hermitian conjugate. We define an adjoint $\bar{x}$ as

$$\bar{x} = x^\dagger \Gamma, \quad \text{or} \quad \bar{x}_\alpha = x_\beta^* \Gamma_\alpha{}^\beta, \tag{3.81}$$

where

$$\begin{aligned} \Gamma_\beta{}^\alpha &= \delta_\beta{}^\alpha, && 1 \leq \alpha, \beta \leq M \\ &= -\delta_\beta{}^\alpha, && M+1 \leq \alpha, \beta \leq M+N \\ &= 0, && \text{otherwise.} \end{aligned} \tag{3.82}$$

Under the transformation

$$x' = Ax, \tag{3.83}$$

$\bar{x}$ becomes

$$\bar{x}' = \bar{x}\bar{A}, \tag{3.84}$$

$$\bar{A} = \Gamma A^\dagger \Gamma, \tag{3.85}$$

as $\Gamma^2 = 1$. The transformations (3.83–84) which leave invariant the "pseudo-unitary length"

$$\bar{x}x = \sum_{1}^{M} x_\alpha^* x^\alpha - \sum_{M+1}^{M+N} x_\alpha^* x^\alpha \tag{3.86}$$

form a "pseudo-unitary" group denoted [H 5] by $U(M, N)$ and defined by the matrices A for which

$$\bar{A}A = 1. \tag{3.87}$$

[One may restrict oneself to $M \geq N$; $U(M, 0) \equiv U(M)$.]

The further restriction

$$\det A = 1$$

corresponds to the subgroup $SU(M, N)$.

[The restriction: A real, would lead to the pseudo-orthogonal group $O(M, N)$ of which the Lorentz group $O(3, 1)$ is an example.]

Also for $SU(M, N)$ we can start to build tensors T, again defined as in Eq. (3.1), but where now "transforms like" means that an upper index transforms with A as in Eq. (3.83) and a lower index with $\bar{A}$ as in (3.84). It is therefore clear that there exists a one-to-one correspondence between the representations of $SU(M+N)$ and the finite dimensional representations of $SU(M, N)$. Therefore we have at once a full classification of these latter tensors in terms of $SU(M+N)$. Moreover the product reduction $(n_1, \cdots, n_{M+N}) \otimes (n'_1, \cdots, n'_{M+N})$ in $SU(M, N)$ is one-to-one to the same reduction in $SU(M+N)$. Also the considerations of Sec. IIB, D, F adapt at once to the pseudo-unitary case.

In regard to the question of generators of $U(M, N)$ one has to be careful with questions of Hermiticity. The action of a transformation in $U(M, N)$ on a D_R-dimensional representation may again be represented as in Eq. (3.53). (We consider only finite dimensional representations.) However, for real ϵ_B, not all the generators are Hermitian. In fact the Hermiticity condition

$$F_A{}^\dagger = F_A \quad \text{(unitary case)} \tag{3.88}$$

is replaced by

$$\bar{G}_A \equiv \Gamma G_A{}^\dagger \Gamma = G_A \quad (ps\text{-unitary case}), \tag{3.89}$$

where we denote the generators of $U(M, N)$ by G_A. Note that Γ itself may be taken as one of the G_A.

Using the DG it is easy to establish a one-to-one correspondence between the G_A and the F_A of $U(M+N)$. As Γ is Hermitian it may also be taken as one of the DG of $U(M+N)$. We have for the DG

$$\Gamma F_A + \eta_A F_A \Gamma = 0 \tag{3.90}$$

where

$$\eta_A = -1 \text{ for } M^2+N^2 \text{ of the } F_A, \tag{3.91}$$

$$= +1 \text{ for the other } 2MN \ F_A, \tag{3.92}$$

and we have [by verifying that (3.87) is satisfied]

$$\begin{aligned} G_A &= F_A && \text{if } \eta_A = -1, \\ &= iF_A && \text{if } \eta_A = +1. \end{aligned} \tag{3.93}$$

[The subset of G_A which satisfy (3.93) generate a subgroup $U(M) \otimes U(N)$ of $U(M, N)$. This is the "maximal compact subgroup" of $U(M, N)$.]

Example: $U(2)$ for which $x_1^* x^1 + x_2^* x^2 = \text{invariant}$, has DG: σ_1, σ_2, σ_3, and 1. For $U(1, 1)$: $x_1^* x^1 - x_2^* x^2 = \text{invariant}$. $\Gamma = \sigma_3$ and the DG are $i\sigma_1$, $i\sigma_2$, σ_3, and 1.

CC-0. In Public Domain. Gurukul Kangri Collection, Haridwar

Digitized by Arya Samaj Foundation Chennai and eGangotri

Finally we define a set of currents for $U(M, N)$ by

$$J_A^{(M,N)}(x, y) = \exp\{(i\pi/4)(1+\eta_A)\}\cdot\bar{x}G_A y. \quad (3.94)$$

The phase factor is introduced so that [see (3.90)]

$$J_A^{(M,N)}(x, x)^\dagger = J_A^{(M,N)}(x, x). \quad (3.95)$$

As we shall see in Sec. VI [see the remark after Eq. (6.14)] for SU(2, 2) these phase factors are quite familiar from relativistic theory. Now $\bar{x}G_A y = x^\dagger \Gamma G_A y$ and $\Gamma G_A = \exp\{(i\pi/4)(1+\eta_A)\}\cdot\Gamma F_A$. As we have remarked before, Γ may be considered as one of the DG of $SU(M+N)$, thus for some fixed X we may put $\Gamma = F_X$. Now from Eqs. (3.55) and (3.60)

$$F_X F_A = \sum_C \rho_{XAC} F_C,$$

$$\rho_{XAC} = C\delta_{XA}\delta_{C0} + \tfrac{1}{2}(d_{XAC} + if_{XAC}), \quad (3.96)$$

and where F_0 is the identity. If we insert (3.96) into (3.94) and compare with (3.74) we get (sum over C, but keep X final!)

$$J_A^{(M,N)}(x, y) = \exp\{(i\pi/2)(1+\eta_A)\}\cdot\sum_C \rho_{XAC} J_C^{(M+N)}(x, y) \quad (3.97)$$

so that the currents $J_A^{(M,N)}$ are linear combinations of the currents $J_A^{(M+N)}$ belonging to the compact group $U(M+N)$. It is this connection which plays a role in the algebra of currents, see Sec. VI, Appendix.

IV. $SU(6)$

A. Introduction

Consider the fundamental triplet u^A of $U(3)$, $A=1, 2, 3$. Name them: $u^1=p$, $u^2=n$, $u^3=\lambda$. (p, n) is the isodoublet, λ the isosinglet. (To avoid confusion, we denote proton and neutron by P, N, respectively, in this paper.) I_3, the charge Q, the hypercharge Y, and the baryon number B are as follows.

	p	n	λ
I_3	$\frac{1}{2}$	$-\frac{1}{2}$	0
Q	q_0	q_0-1	q_0-1
Y	y_0	y_0	y_0-1
B	b	b	b.

(4.1)

There are well-known degrees of freedom of choice for q_0, y_0, b [G 1, B 7, G 5, N 1]. Until further notice [in Sec. IV J] we shall take

$$q_0=\tfrac{2}{3}, \quad y_0=\tfrac{1}{3}, \quad b=\tfrac{1}{3}. \quad (4.2)$$

Correspondingly,

$$Q = I_3 + Y/2. \quad (4.3)$$

More specifically, let the triplet have spin $\frac{1}{2}$. We write the one particle wave function for zero three-momentum as

$$u^\alpha = u^{Ai}, \quad \alpha=1, \cdots, 6; \quad i=1, 2, \quad (4.4)$$

with the following correspondence between α and (Ai):

$$\begin{array}{llllllll} \alpha= & 1, & 2, & 3, & 4, & 5, & 6 \\ A= & 1, & 2, & 3, & 1, & 2, & 3 \\ i= & 1, & 1, & 1, & 2, & 2, & 2 \end{array} \quad (4.5)$$

where the spin index $i=1, 2$, corresponds to spin "up," "down." For any dynamical situation where $SU(3)$ invariance holds and where, in the *static* limit, no spin dependence appears, the physical wave functions u^α satisfy the property that

$$u_\alpha^* u^\alpha = \text{invariant under } SU(6). \quad (4.6)$$

Thus the u^α may be considered as the defining representation of that group. Call X_n the DG of $SU(6)$. The X_n can be expressed in terms of the DG of $SU(2)$: S_a and the DG of $SU(3)$: F_P as follows.

$$X_n: S_a\otimes 1, 1\otimes F_P, S_a\otimes F_P; \quad a=1, 2, 3, P=1, \cdots, 8, \quad (4.7)$$

so $n=1, \cdots, 35$. The $\otimes$ means the following. The X_n are 6×6 matrices and

$$(X_n)_\alpha^\beta: (S_a)_i^j\delta_A^B, \delta_i^j(F_P)_A^B, (S_a)_i^j(F_P)_A^B; \quad \alpha=(Ai), \beta=(Bj). \quad (4.8)$$

Having explained the $\otimes$ notation, we now go to the customary shorthand:

$$X_n: X_a = S_a, \quad X_P = F_P, \quad X_{aP} = S_a F_P, \quad (4.9)$$

with the commutation relations

$$\begin{aligned} &[X_a, X_b] = i\epsilon_{abc}X_c, \\ &[X_a, X_P] = 0, \\ &[X_P, X_Q] = if_{PQR}X_R, \\ &[X_a, X_{bP}] = i\epsilon_{abc}X_{cP}, \\ &[X_P, X_{bQ}] = if_{PQR}X_{bR}, \\ &[X_{aP}, X_{bQ}] = (i/2)\delta_{ab}f_{PQR}X_R + i\epsilon_{abc}(\tfrac{1}{3}\delta_{PQ}X_c + d_{PQR}X_{cR}). \end{aligned} \quad (4.10)$$

Here the f_{PQR}, d_{PQR} refer to $SU(3)$, cf. Eqs. (3.55,60). [We have used the normalization $c=\frac{1}{6}$ in (3.60).] They are tabulated in [G 1]. Equation (4.10) specifies the structure constants of $SU(6)$. (Note that X_{aP} is a simple direct product only in the defining representation of the generators.)

CC-0. In Public Domain. Gurukul Kangri Collection, Haridwar

Digitized by Arya Samaj Foundation Chennai and eGangotri

We are now going to discuss the consequences of the assumption that static phenomena involving hadrons are approximately described by the dynamical group $SU(6)$. We are not yet going to raise questions about the meaning of such an assumption as regards the underlying dynamics. To this question we return in Sec. IV I. The order of business is here reversed as compared with for example the discussion of Russell–Saunders coupling where we could start with the secure underpinning of the Hamiltonian (2.7). For the present it cannot be otherwise. The exciting thing about $SU(6)$ is that, if there is anything to it, it must give stronger clues to the almost totally unsolved problem of strong dynamics than can be gotten from kinematical symmetries.

The following items will be discussed. In Sec. IVB we treat the question of $SU(6)$ representations for hadron states. It may at once be noted that, whereas all generators of $SU(6)$ commute with parity, all states within a $SU(6)$ supermultiplet should have the same parity. In Sec. IVC, mass formulae are discussed. Then we turn to the static electromagnetic and semi-leptonic vertices, Sec. IVD, E, F, non-leptonic decays, IVH, and the S-wave nucleon–nucleon scattering Sec. IVG. Questions about the structure of the dynamics lead us into the discussion of the reality of triplets Sec. IVJ. Up till there we will often use triplets u^α as a good mathematical tool, but without prejudice as to their actual existence.

Concerning the interpretation of $SU(6)$ symmetry, the early papers contain the following comments. The nonrelativistic nature of $SU(6)$ is stated in [S 1]. A possible kinematic origin of the symmetry is contemplated in [G 3]. Limitations on $SU(6)$ due to recoupling of spin to orbital angular momentum are stated in [P 1]. The study of baryon–meson interaction then begins with the analysis of effective vertices [G 4]. Here one is already one step beyond the static limit, however, as will be further discussed in Secs. VA and C. The survey in this section is in part an elaboration of an earlier review of $SU(6)$ as a dynamical group [B 8].

B. Some Specific Supermultiplets

The first kind of clue to $SU(6)$ stems from a simple counting problem. Can one fill representations of this group with known hadrons?

(I) The *56*.+ This is the dimension of the representation (3), corresponding to the tensor structure $B^{\alpha\beta\gamma}$, with total symmetry in (α, β, γ). Its $SU(3)\otimes SU(2)$ content is given in Eq. (3.43). Thus it can be filled with the usual baryon octet and decuplet which have indeed the same parity [G 3]. There are other baryon resonances inside the *56*-mass range. Thus closeness in mass alone is not a sufficient ground for this symmetry.

Next we construct $B^{\alpha\beta\gamma}$, at first using quarks (q) as a tool. Thus we put

$$B^{\alpha\beta\gamma}\sim\tfrac{1}{6}\sum_P u^\alpha(1)u^\beta(2)u^\gamma(3). \tag{4.11}$$

The summation is over all permutations of the configuration labels 1, 2, 3. Otherwise the notations are as in Eq. (3.1). Let $\|u^\alpha\|$, the norm of u^α for fixed α be unity. Then

$$\begin{aligned}\|B^{\alpha\beta\gamma}\|&=1, &&\alpha=\beta=\gamma,\\ &=\tfrac{1}{3}, &&\alpha=\beta\neq\gamma,\\ &=\tfrac{1}{6}, &&\alpha,\beta,\gamma \text{ distinct.}\end{aligned} \tag{4.12}$$

Consider now as an example the state $|N^{*+\frac{1}{2}}\rangle$, where $\frac{1}{2}$ is the S_z value. From (4.1, 4, 5, 11) we see that it is a mixture of B^{115} and B^{124}. The mixture is determined from the fact that this state is totally symmetric in spin and in unitary spin *separately*. Hence

$$\begin{aligned}|N^{*+\frac{1}{2}}\rangle=\tfrac{1}{3}[&u^1(1)u^1(2)u^5(3)+u^1(1)u^5(2)u^1(3)\\ &+u^5(1)u^1(2)u^1(3)+u^1(1)u^4(2)u^2(3)\\ &+u^1(1)u^2(2)u^4(3)+u^2(1)u^1(2)u^4(3)\\ &+u^4(1)u^1(2)u^2(3)+u^4(1)u^2(2)u^1(3)\\ &+u^2(1)u^4(2)u^1(3)]\\ =B^{115}&+2B^{124},\end{aligned} \tag{4.13}$$

where the over-all norm is such that $\|N^{*+\frac{1}{2}}\|=1$, see (4.12). Also $|P^{\frac{1}{2}}_{\frac{1}{2}}\rangle$ is a normed mixture of B^{115} and B^{124} and it must be orthogonal to $|N^{*+\frac{1}{2}}\rangle$, hence we may put $|P^{\frac{1}{2}}_{\frac{1}{2}}\rangle=2^{\frac{1}{2}}(B^{115}-B^{124})$.

Note. One does not need to keep track of the I-spin in such derivations. The reason for this is that for $SU(2)$ the tensor symmetry itself determines I, see (3.14).

One can construct likewise by hand the other members of the *56*. However there is a quicker way. From Eq. (3.43) we know the content of *56* with respect to spin and unitary spin. One knows the tensor structure of the individual $SU(3)$ and $SU(2)$ representations involved. This makes it possible to write down the answer almost at once [B9].

$$\begin{aligned}B^{\alpha\beta\gamma}=\chi^{ijk}d^{ABC}&+(1/3\sqrt{2})[\epsilon^{ij}\chi^k\epsilon^{ABD}b_D{}^C\\ &+\epsilon^{jk}\chi^i\epsilon^{BCD}b_D{}^A+\epsilon^{ki}\chi^j\epsilon^{CAD}b_D{}^B],\end{aligned} \tag{4.14}$$

where the following definitions have been used:

$$\begin{aligned}(1)\quad &\chi^{111}=\psi^{\frac{3}{2}}, &&\chi^{112}=(1/\sqrt{3})\psi^{\frac{1}{2}},\\ &\chi^{122}=(1/\sqrt{3})\psi^{-\frac{1}{2}}, &&\chi^{222}=\psi^{-\frac{3}{2}},\end{aligned} \tag{4.15}$$

where ψ^a is a normed wave function for $S=\frac{3}{2}$, $S_z=a$. The χ^i are normed spin-$\frac{1}{2}$ wave functions.

CC-0. In Public Domain. Gurukul Kangri Collection, Haridwar

Digitized by Arya Samaj Foundation Chennai and eGangotri

(2) d^{ABC} is the decuplet tensor:

$$d^{111}=N^{*++},\quad d^{112}=(1/\sqrt{3})N^{*+},\quad d^{122}=(1/\sqrt{3})N^{*0},\quad d^{222}=N^{*-},$$
$$d^{113}=(1/\sqrt{3})Y^{*+},\quad d^{123}=(1/6^{\frac{1}{2}})Y^{*0},\quad d^{223}=(1/\sqrt{3})Y^{*-},$$
$$d^{133}=(1/\sqrt{3})\Xi^{*0},\quad d^{233}=(1/\sqrt{3})\Xi^{*-},\quad d^{333}=\Omega^{-}. \tag{4.16}$$

[The numerical coefficients are of course derived in a way similar to the derivation of Eq. (4.13).]

(3) ϵ^{ij} and ϵ^{ABC} are the Levi–Civita symbols for $SU(2)$ and $SU(3)$, respectively.

(4) $b_B{}^A$ is the baryon octet

$$b_1{}^1=(\Sigma^0/\sqrt{2})+(\Lambda/6^{\frac{1}{2}}),\qquad b_2{}^2=-(\Sigma^0/\sqrt{2})+(\Lambda/6^{\frac{1}{2}}),\qquad b_3{}^3=-(2\Lambda/6^{\frac{1}{2}}),$$
$$b_2{}^1=\Sigma^+,\qquad b_3{}^1=P,\qquad b_1{}^2=\Sigma^-,\qquad b_3{}^2=N,$$
$$b_1{}^3=\Xi^-,\qquad b_2{}^3=-\Xi^0. \tag{4.17}$$

The coefficient $(3\sqrt{2})^{-1}$ in Eq. (4.14) follows from the condition:

$$\sum_{\alpha\beta\gamma}\|B^{\alpha\beta\gamma}\| = \text{sum of norms of the individual particle states, each with norm 1.} \tag{4.18}$$

The following two identities are often useful.

$$\epsilon^{ij}\chi^k+\epsilon^{jk}\chi^i+\epsilon^{ki}\chi^j=0, \tag{4.19}$$

$$\epsilon^{ABD}b_D{}^C+\epsilon^{BCD}b_D{}^A+\epsilon^{CAD}b_D{}^B=0. \tag{4.20}$$

(4.20) is a special case of (3.8).

(II) The 35^-. This is the dimension of (21^4), the tensor is $M_\beta{}^\alpha$ with $M_\alpha{}^\alpha=0$. Its content is given by Eq. (3.42). Choosing odd parity, it is filled by a nonet of vector mesons and octet of pseudoscalar mesons [S 1, G 3].

However, it is now well established that there exists a ninth pseudoscalar meson as well with a mass $\simeq$960 MeV which is inside the *35*-mass range [G 6, G 7, K 3, K 4, L 2]. It is called X^0 (also η' or η^*). The mixing with the η appears to be rather small, $\simeq 12^0$ [L 2]. We shall see later on in Sec. V that a set of $9V$ and $9P$ mesons comes in naturally from relativistic considerations.

The structure of $M_\beta{}^\alpha$ can be determined as for the *56*, either by building up from a $\bar{q}q$ system or directly from the tensor structure read off from (3.42), [G 4].

$$M_\beta{}^\alpha=-i\delta_j{}^iP_B{}^A-(\delta\varepsilon)_j{}^iV_B{}^A, \tag{4.21}$$

$$P_1{}^1=(\pi^0/\sqrt{2})+(\eta/6^{\frac{1}{2}}),\qquad P_2{}^2=-(\pi^0/\sqrt{2})+(\eta/6^{\frac{1}{2}}),\qquad P_3{}^3=-2\eta/6^{\frac{1}{2}},$$
$$P_1{}^2=\pi^-,\qquad P_1{}^3=K^-,\qquad P_2{}^1=\pi^+,\qquad P_3{}^1=K^+,\qquad P_3{}^2=K^0,\qquad P_2{}^3=\bar{K}^0; \tag{4.22}$$

$$V_1{}^1=(\rho^0/\sqrt{2})+(\omega^0/6^{\frac{1}{2}})+(\phi^0/\sqrt{3}),\qquad V_2{}^2=-(\rho^0/\sqrt{2})+(\omega^0/6^{\frac{1}{2}})+(\phi^0/\sqrt{3}),\qquad V_3{}^3=-(2\omega^0/6^{\frac{1}{2}})+(\phi^0/\sqrt{3}),$$
$$V_1{}^2=\rho^-,\qquad V_1{}^3=K^{-*},\qquad V_2{}^1=\rho^+,\qquad V_3{}^1=K^{+*},\qquad V_3{}^2=K^{0*},\qquad V_2{}^3=\bar{K}^{0*}. \tag{4.23}$$

$\|M_\beta{}^\alpha\|=M_\alpha{}^{*\beta}M_\beta{}^\alpha$ satisfies again a relation like (4.18). In (4.23) ω^0 is the isosinglet member of the vector *8*. ϕ^0 is the unitary singlet vector meson.

(III) The 70^-. The $SU(6)$ multiplets contained in the product of $35^-\times 56^+$ are given in Eq. (3.25). With the parity assignments chosen for *35* and *56*, the specific product considered reduces to a sum of representations with odd parity.

It has been suggested [P 1] that the 70^- might perhaps be useful for the classification of some higher baryon resonances which decay strongly into baryon (in the *8*)+meson (in the *35*). From the content formula (3.44) the 70^- could accomodate a $(\frac{3}{2})^-$ octet. This "γ octet" has often been suggested, but its status is presently quite unclear. Another candidate for the 70^- would be the $Y_0{}^*(1405)$. A recent analysis [K 5] indicates that this is a $(\frac{1}{2})^-$ state, as was often supposed. For a detailed discussion of the 70^- see [G 8, G 9].

The tensor structure of the *70* is $T^{[\alpha\beta]\gamma}$, antisymmetric in (α,β) and subject to the constraint equation (3.22). $T^{[\alpha\beta]\gamma}$ has been constructed explicitly, [B 10, Eq. (4.2)].

The *70* with odd parity provides a good starting point for a very preliminary discussion of strong vertices. As 35×56 contains *70* only once, Eq. (3.25), the "decay vertex" of the *70* is unique, namely,

$$T^*{}_{[\alpha\beta]\gamma}B^{\alpha\gamma\delta}M_\delta{}^\gamma. \tag{4.24}$$

Equation (4.24) is $SU(6)$ invariant and parity-conserving. One may now discuss relative decay rates in a way often done in a discussion of higher symmetries:

CC-0. In Public Domain. Gurukul Kangri Collection, Haridwar

Digitized by Arya Samaj Foundation Chennai and eGangotri

compute matrix elements from (4.24) and correct for mass differences within a multiplet by adjusting the phase space. Regardless of whether this is a reliable procedure, it should be stressed that for $SU(6)$ there arise new questions as compared to a purely internal symmetry group like $SU(3)$, for the following connected reasons. (1) In an actual decay we cannot have all particles with zero momentum; but we have not yet given meaning to "an $SU(6)$ multiplet with finite momentum." (2) The *70* contains $S=\frac{3}{2}$ states. These cannot decay into baryon ($S=\frac{1}{2}$)+pseudoscalar meson unless orbital angular momentum appears. Correspondingly, (4.24) gives zero for this particular kind of decay, as one can readily verify from Eqs. (4.14, 20) and [B 10, Eq. (4.2)]. Again the question of including (angular) momentum appears.

We shall discuss in Sec. V the attempts which have been made to include momentum in a systematic way in vertex structures. Other examples of the urgent need do so are given by decays like $V\to 2P$, $N^*\to N\pi$, etc.

(IV) A discussion has been given recently of static baryon resonances in a 70^+ [G 10].

(V) "Recoupled" multiplets. By way of model, let us consider the *35* as given by Eq. (4.21) to be a $\bar{q}q$ system in an orbital S state. We can imagine that this system has "higher excited states" with $L>0$. Take for example P states. The contents of these states is given by 35×3, where the *3* denotes the dimension of the $L=1$ representation of $O(3)$. Coupling L to S one gets from Eq. (3.42)

$$35\otimes 3=(8+1;\,5)+(8+8+1;\,3)+(8+1;\,1), \quad (4.25)$$

where the number following the semicolon is $2J+1$, J being the *total* angular momentum of the system. For a *35* with odd parity, the multiplets on the right-hand side of Eq. (4.25) all have even parity.

One can phrase this procedure without necessarily talking of quarks. The formal question then is to discuss supermultiplets which correspond to the group $SU(6)\times O(3)$, [M 2].

Possible assignments of meson resonances to the states given in Eq. (4.25) have been discussed [B 11]. These "P-state mesons" may indeed be of interest in view of the recent evidence for a 2^+ nonet of vector mesons [B 12]; for a theoretical discussion of their decay rates see [G 11]. *Added note:* see also [A 19].

As the coupling with orbital angular momentum does not of course affect $SU(3)$, one can generate in this way only unitary octets and singlets from the *35*. In this respect the situation is different if one asks, on the other hand, whether spin 2 mesons should be accomodated in higher $SU(6)$ multiplets without recoupling to L. To get spin 2 one needs at least systems which transform like $\bar{q}\bar{q}qq$. These are found in Eqs. (3.50, 51, 52). In particular the spin 2 content of the *189* is a nonet only, while *280*, *280** do not contain a nonet of this kind. As the f^*–f^0 mixing [B 12] appears to be comparable to the ω–ϕ mixing, the latter is perhaps a more plausible subject for further study than the *405*. At any rate, the main qualitative distinction between these $SU(6)$ multiplets and the recoupled *35* is the appearance of the *27* of $SU(3)$. For this reason it would be of great interest to know if further experiments will confirm the indication of a $Y=2$ meson resonance [F 3], in the same mass range as the 2^+ states. For the $Y=2$ state one needs at least a *27*. Either picture, the recoupled *35*, or a new $SU(6)$ multiplet, leads to a quite complex set of resonant states. The region of resonances above the *35* may well give further dynamical clues.

We conclude this section with a few examples of the decomposition of $SU(6)$ multiplets under the subgroup given in Eq. (3.69). Specifically, $U(1)$ corresponds to hypercharge, $SU(2)$ to λ-spin and $SU(4)$ to the union of (p, n)-spin and isospin. With the help of Eqs. (4.4, 5, 14, 21) one finds

$$56=(20,\,1)_1+(10,\,2)_0+(4,\,3)_{-1}+(1,\,4)_{-2}$$
$$=(N,\,N^*)+(\Lambda,\,\Sigma,\,Y_1^*)+(\Xi,\,\Xi^*)+(\Omega^-).$$

The first (second) number in brackets is the dimension of the $SU(4)$ [$SU(2)$] representation, the subscript is the Y value. [The *20* of $SU(4)$ corresponds to the tableau (3).] Likewise

$$35=(15,\,1)_0+(1,\,1)_0+(1,\,3)_0+(4,\,2)_1+(4^*,\,2)_{-1}$$
$$=(\pi\rho\omega)+(\eta)+(\phi)+(K,\,K^*)+(\bar{K},\,\bar{K}^*),$$

where the ω and ϕ are the physical states given in Eq. (4.31) below.

C. Mass Formulae

As an introduction to the discussion of $SU(6)$-mass formulae, the following two remarks on the $SU(3)$ case may be helpful.

(1) As is well known [G 1], in $SU(3)$ one assumes that the mass split operator transforms like the hypercharge operator F_8, which is a member of the octet of $SU(3)$ generators. There are two operators of this kind which may be written as

$$\partial C_2^{(3)}/\partial F_8\sim F_8, \qquad \partial C_3^{(3)}/\partial F_8\sim d_{8AB}F_AF_B, \quad (4.26)$$

see Eqs. (3.59, 60). Thus from two independent "scalar operators," the Casimir operators, one gets two "vector operators" by formal differentiation. A procedure of this kind holds for all $SU(N)$ (and more generally) [G 12]. The effective mass operator is therefore generally of the form

$$m+aF_8+bd_{8AB}F_AF_B, \quad (4.27)$$

which is equivalent to the usual $SU(3)$ mass formula.

The number of vector operators determines the *maximum* number of parameters in the mass formula. For a specific representation R, the actual number is

CC-0. In Public Domain. Gurukul Kangri Collection, Haridwar

Digitized by Arya Samaj Foundation Chennai and eGangotri

equal to the number of times that *8* appears in the reduction $R^*\times R$, where R^* is conjugate to R. For $R=8$, *8* occurs twice and we have a three-parameter formula. For $R=10$, *8* occurs *once* and a two-parameter formula results (equal spacing). Correspondingly, for the *10*, the expectation values of the second operator in (4.26) is itself of the form $\langle m+aF_8\rangle$.

(2) Call dynamical mass split operator the part of a Hamiltonian which induces the effective mass split. If we say that the dynamical mass operator transforms like *8*, then this is equivalent to the statement under (1) only in first-order perturbation theory. Because the $SU(3)$ breaking effects are not obviously small in any known scale it is a much discussed puzzle how to understand the simple structure of the effective mass operator from a simple structure of a dynamical mechanism.

Now let us turn to $SU(6)$. At least two mechanisms for effective mass splits are involved. (1) A spin-dependent effect to separate different spins within the supermultiplet. (2) $SU(3)$ breaking effects. It is not obvious *a priori* that these effects should be linearly independent. For example the $SU(3)$ theory does not preclude that the two mass parameters in (4.27) should be spin-dependent. Nor is there a known ground to exclude that the spin dependent terms should have $SU(3)$-dependent coefficients.

Let us nevertheless consider an additivity assumption [P 1]: (1) $SU(3)$ breaking transforms like F_8 but with spin-independent coefficients [at least within an $SU(6)$ multiplet], (2) a spin-dependent effect independent of $SU(3)$ [at least within an $SU(6)$ multiplet]. This leads to the following results. For the *56*, the mass operator is

$$M+aY+b[I(I+1)-Y^2]+c(S), \qquad (4.28)$$

where a, b are constants and c depends in some way on $S(S+1)$. M is the "central mass," the value to which all masses collapse in the absence of $SU(6)$ breaking. Equation (4.28) enables one to calculate from the *8* an equidistance $\simeq 130$ MeV for the *10* which compares rather well with the experimental value $\simeq 145$ MeV [P 1]. It may be noted that this result is independent of the way c depends on S.

For the *35* we use Eq. (4.21) and write the mass operator as

$$\alpha M_\beta{}^{*\alpha} M_\alpha{}^\beta+\beta[\delta M^*]_B{}^A[\delta M]_A{}^B+\gamma M_\beta{}^{*i3} M_{i3}{}^\beta, \qquad (4.29)$$

where the α term corresponds to the central mass, β gives the $SU(3)$-independent and spin-dependent effect. [ ] denotes spin trace. In the internal symmetry breaking γ term, the summation over $i=1, 2$ guarantees spin independence; the singling out of the unitary index value "3" corresponds to the proper hypercharge dependence. Equation (4.29) has the following consequences.

(1) For P:

$$4K^2-\pi^2=3\eta^2. \qquad (4.30)$$

(2) Mixing between ω^0 and ϕ^0 such that the physical states are

$$\omega=(1/\sqrt{3})(\omega^0+\phi^0\sqrt{2}),$$
$$\phi=(1/\sqrt{3})(\omega^0\sqrt{2}-\phi^0). \qquad (4.31)$$

These are the mixtures proposed before [O 2, S 2]. They appear here in a rather natural way because of the (8+1)-vector meson degeneracy in the strict $SU(6)$ limit.

Remark. $\omega-\phi$ mixing was introduced to explain deviations from an octet mass formula for vector mesons. It also serves to explain the suppression of such modes as $\phi\rightarrow\rho\pi$ compared to $\phi\rightarrow K\bar{K}$. From phase space, barrier factors, and spin–isospin weights one estimates a rate ratio [L 2]

$$(\phi\rightarrow\rho\pi)/(\phi\rightarrow K\bar{K})\simeq 4,$$

in the absence of any other inhibitions. Recent experimental results for this ratio are: 0.22 ± 0.09 [L 3]; 0.3 ± 0.15 [L 2] which indicate a $\rho\pi$ supression by one order of magnitude. This fits well with the mixing given by Eq. (4.31) which forbids $\phi\rightarrow\rho\pi$. On the other hand, another recent measurement [B 13] gives a quite high relative rate for $\phi\rightarrow\pi$ mesons which appears to be in confiict with the other two measurements. For other discussions of $\omega-\phi$ mixing see [K 6, C 7]. For the connection between $\omega-\phi$ mixing and a subgroup of $SU(6)$ see [G 4].

(3) For V:

$$\rho^2=\omega^2,$$
$$2K^{*2}-\phi^2=\rho^2. \qquad (4.32)$$

(4) The P–V relation

$$K^{*2}-\rho^2=K^2-\pi^2 \qquad (4.33)$$

which is well satisfied [P 1].

Thus for the *56* and the *35* the simple further assumption of additivity seems to work rather well. This may indicate that spin-dependent effects appear dynamically in a different mass scale than $SU(3)$ breaking effects.

A different starting point is to assign definite tensor properties under $SU(6)$ to the $SU(6)$-breaking effective mass operator. A first attempt was to assign this operator to a representation *35*. By an argument similar to the derivation of Eq. (4.26) there are 5 such operators [K 7]. But by Lemma 2 (Sec. IIIC), $56^*\times 56$ contains *35* only once. Hence one gets a one parameter mass formula for the *56*. In particular no spin dependence is introduced: *35* does not contain (*1*; *1*). Also Σ and Λ remain degenerate.

A more systematic approach in this direction then developed [B 6]. For a representation R of $SU(6)$,

CC-0. In Public Domain. Gurukul Kangri Collection, Haridwar

Digitized by Arya Samaj Foundation Chennai and eGangotri

project out from all representations in $R^* \otimes R$ the parts which transform like $(8;1)$. These give each a candidate for $SU(6)$ breaking with the desired $SU(3)$ properties. In addition project out all parts which transform like $(1;1)$. These do not break $SU(3)$ but may give $S(S+1)$ terms.

The detailed application of this program [B 5] necessitates a further labeling of the representations *189*, *405* as briefly discussed in Sec. IIIE. More details are given in [B 6] and we state the results.

(1) For the *56* one obtains Eq. (4.28). The central mass M is found to be

$$M \simeq 1065 \text{ MeV}. \tag{4.34}$$

(2) For the *35* one finds Eq. (4.30), but no other relations, unless more restrictive assumptions are made. The central mass of the *35* is found to be

$$\mu \simeq 615 \text{ MeV}. \tag{4.35}$$

(3) A detailed discussion of the *70*-mass formula has also been given [B 5]. Here several mixing problems have to be resolved. These mass formulae are analyzed further in [G 8, G 9].

In conclusion, there are several quite suggestive indications from mass parameters and $\omega-\phi$ mixing which fit in with $SU(6)$ in a natural way. Relations like (4.32, 33) are compatible with the tensor analysis of mass splits under special conditions [B 8]. It appears that the tensor method is too general.

The foregoing discussion refers to the effective mass split operator in $SU(6)$. As for $SU(3)$, we must also ask the deeper question of the dynamical mechanism for this effective split. It is at this point that the distinction between kinematical and dynamical symmetry plays an important role. As was discussed in Sec. IIB, the $SU(3)$ breaking could well be characterized by nondynamical parameters while for $SU(6)$ this is impossible. As will be discussed further in Sec. V, the kinetic energy terms in the free part of a Hamiltonian must give rise to spin-dependent mass terms in the presence of interaction. Thus there is a natural mechanism for the breakdown $SU(6) \to SU(3) \otimes SU(2)$.

Further remarks. (1) It has been noted [H 6] that the coefficients of tensors which appear in the general tensor method must be baryon number-dependent. (2) A more specific model for mass breaking is found in [D 1]. (3) It has been attempted to unify the *56*- and the *70*-mass formulae in terms of a higher symmetry [B 17].

D. Magnetic Moments

The electric charge and the magnetic moment of particles are static limits of effective vertices. Their discussion within the static $SU(6)$ picture is therefore appropriate. We recall first some $SU(3)$ results.

(1) The electric charge operator Q is supposed to transform like the component of an octet operator, in accordance with equation (4.3) which can also be written as $Q = F_3 + F_8/\sqrt{3}$. In the defining representation Q is the 3×3 matrix

$$Q_A{}^B = \tfrac{1}{3}\begin{pmatrix} 2 & 0 & 0 \\ 0 & -1 & 0 \\ 0 & 0 & -1 \end{pmatrix}. \tag{4.36}$$

(In Sec. IVJ a more general form of the charge operator is discussed.) Charge conservation implies the F-coupling

$$e\bar{b}_A{}^B(Qb - bQ)_B{}^A \tag{4.37}$$

for the baryon *8*, where e is the proton charge. For the *10*, the coupling is $3e\bar{d}_{ABD}d^{ABC}Q_C{}^D$, etc.

(2) The magnetic moment operator is also supposed to transform like an *8*. The most general form for the baryon *8* magnetic moments,

$$\mu_8 = \mu_D \bar{b}_A{}^B(Qb + bQ)_B{}^A + \mu_F \bar{b}_A{}^B(Qb - bQ)_B{}^A, \tag{4.38}$$

contains an arbitrary mixture of D and F coupling. From (4.38):

$$\mu(P) = \mu_F + \tfrac{1}{3}\mu_D, \tag{4.39}$$

$$\mu(N) = -\tfrac{2}{3}\mu_D, \text{ etc.} \tag{4.40}$$

For the *10*, Lemma 2 of Sec. IIIC implies that there can be only one type of magnetic coupling. Hence for the members of the *10* their respective magnetic moments are proportional to the charge:

$$\mu_{10} = \text{const. } Q_{10}. \tag{4.41}$$

(3) If one assumes in $SU(3)$ that the electromagnetic form factors transform like an *8* for all momentum transfers q, then one has generally a D and an F contribution for all q which may be different for different q.

We now turn to the $SU(6)$ theory.

(1) The charge operator is assumed to transform like an $(8;1)$ member of a *35*. The $SU(6)$ analog of (4.36) is

$$q_\alpha{}^\beta = \delta_i{}^j Q_A{}^B. \tag{4.42}$$

The static electric charge of the *56* is

$$3eB^*{}_{\alpha\beta\gamma}q_\delta{}^\gamma B^{\alpha\beta\delta} \tag{4.43}$$

which gives the respective charges of the *56* members, as is verified by inserting Eqs. (4.14–17). The electrostatic interaction is equal to (4.43) times an external Coulomb potential.

(2) The magnetic moment operator $\mathbf{m}$ is assumed to transform like an $(8;3)$ member of a *35*:

$$\mathbf{m}_\alpha{}^\beta = (\boldsymbol{\delta})_i{}^j Q_A{}^B. \tag{4.44}$$

The crucial consequence of this straightforward assump-

CC-0. In Public Domain. Gurukul Kangri Collection, Haridwar

Digitized by Arya Samaj Foundation Chennai and eGangotri

tion is that the D/F ratio in (4.38) becomes unique because, by Lemma 2, the *35* can be coupled in only one way to the *56*. The magnetic moments for the *56* are given by

$$3\mu(P)B^*_{\alpha\beta\gamma}(\mathrm{m})_\delta{}^\gamma B^{\alpha\beta\delta}, \tag{4.45}$$

where $3\mu(P)$ ensures proper normalization. The magnetic interaction is equal to the scalar product of the 3-vector (4.45) and the magnetic field [which is a 3-vector external to $SU(6)$]. The consequences of (4.45) which go beyond $SU(3)$ are the following.

(a) Baryon-*8* magnetic moments [B 9; S 3]. The ratio of μ_D and μ_F in Eq. (4.38) is now fixed and is given by

$$\mu_D/\mu_F=\tfrac{3}{2}. \tag{4.46}$$

Hence from Eqs. (4.39, 40)

$$\mu(N)/\mu(P)=-\tfrac{2}{3}, \tag{4.47}$$

in good agreement with the experimental ratio -0.68. The *8*-magnetic moments are discussed further in Sec. IVJ.

(b) Baryon-*10* magnetic moments [B 9]. In Eq. (4.45) the *56*-wave function in the $SU(6)$ limit is used. Hence the constant in (4.41) is expressible in terms of $\mu(P)$:

$$\mu_{10}=\mu(P)Q_{10}. \tag{4.48}$$

In particular

$$\mu(\Omega^-)=-\mu(P). \tag{4.49}$$

See further Sec. IVJ for remarks on mass corrected magnetic moments.

(c) Transition moments between *10* and *8*. By Lemma 1, 8×10 is simply reducible. Hence $SU(3)$ says that all transition moments ($8\to10$) are expressible in one of them. We denote the M_1-transition moment between states with $S_z=\frac{1}{2}$ by $\langle P\,|\,\mu\,|\,N^{*+}\rangle$, etc. Then [B 9]

$$\begin{aligned}\langle P\,|\,\mu\,|\,N^{*+}\rangle&=-\langle\Sigma^+\,|\,\mu\,|\,Y^{*+}\rangle=\langle N\,|\,\mu\,|\,N^{*0}\rangle\\&=2\langle\Sigma^0\,|\,\mu\,|\,Y_0{}^*\rangle=(2/\sqrt{3})\langle\Lambda\,|\,\mu\,|\,Y_0{}^*\rangle\\&=\langle\Xi^0\,|\,\mu\,|\,\Xi^{*0}\rangle.\end{aligned} \tag{4.50}$$

According to (4.45) these moments can be expressed in terms of $\mu(P)$. One finds [B 9]

$$\langle P\,|\,\mu\,|\,N^{*+}\rangle=(2\sqrt{2}/3)\mu(P). \tag{4.51}$$

Comparisons of (4.51) have been made with photo- and electroproduction data at the *33*-resonance. This involves the assumption that transition form factors do not vary much from their $SU(6)$-limit value to the region of physical interest. While such an assumption is open to question, it is nevertheless interesting that the $E2$ transition at resonance is much smaller than $M1$ [G 13]; in the static limit there is of course no room for $E2$ [B 18]. Regarding $M1$, an earlier analysis of photoproduction [G 13] gives a value 1.6 times the right-hand side of (4.51) [B 9]; while a much closer agreement is claimed with electro production [G 14, G 15]. I am indebted to R. H. Dalitz for the communication of a re-analysis of photoproduction and electroproduction by him and D. Sutherland, which continues to indicate an effective discrepancy by a factor ~1.6.

Further remarks. (1) The same assumptions applied to the *35* yield one additional $SU(6)$ relation: $\mu(\rho^+)=3(\pi^+\,|\,\mu\,|\,\rho^+)$ [B 9].

(2) Magnetic moments have been calculated for the baryon *20* [S 3].

(3) The magnetic moments of the baryon *70* can be related to those of the *56* by a symmetry stronger than $SU(6)$ [R 3].

(4) It has been observed [A 2] that Eq. (4.47) is more stable against symmetry breaking than are $SU(3)$ relations like $\mu(\Lambda)=\mu(N)/2$. This is perhaps not surprising as the neutron and proton belong to the same isomultiplet.

(5) Several attempts have been made to relate Eq. (4.47) to the weaker assumption of invariance under the subgroup $SU(4)$ discussed in [G 4]. This author finds himself in agreement with the conclusions on this subject in [B 14].

(6) Several authors have discussed radiative decays $\rho^0,\ \omega,\ \phi\to\pi^0\gamma$ [B 15, T 2, A 3, R 4, S 4, B 20].

E. Electromagnetic Mass Differences

There have been several investigations of these mass differences. The starting point is to consider to second (and higher) order the effects of the charge operator and of the magnetic moment operator which have been discussed to first order in the previous section. We shall discuss the various attempts in increasing order of generality.

(1) Charge operator to second order [S 3]. The charge operator is assumed to be in the $(8;\ 1)$, part of a *35*, as in Eq. (4.42). Consider the electromagnetic mass splits as second-order effects in $q_\alpha{}^\beta$. For the *56* this amounts first to finding the independent $SU(6)$ invariants contained in $56^*\times56\times35\times35$ and secondly to project out those terms in the *35*'s which transform like $q_\alpha{}^\beta$. With the help of Eqs. (3.24) and (3.26) it is easily seen [S 3] that there are only two such invariants, corresponding to one tensor *35* and a *405* contained in the product of $56^*\times56$ as well as in 35×35. A two-parameter mass split operator results which leads to the following relations.

$$N^{*+}-N^{*0}=Y_1{}^{*+}-Y_1{}^{*0}=P-N=\Sigma^+-\Sigma^0, \tag{4.52}$$

$$\Xi^{*-}-\Xi^{*0}=N^{*-}-N^{*0}=Y_1{}^{*-}-Y_1{}^{*0}=\Xi^--\Xi^0=\Sigma^--\Sigma^0, \tag{4.53}$$

$$N^{*++}-N^{*-}=3(N^{*+}-N^{*0}). \tag{4.54}$$

CC-0. In Public Domain. Gurukul Kangri Collection, Haridwar

Digitized by Arya Samaj Foundation Chennai and eGangotri

(2) Charge operator to all orders [C 4]. This leads to only one additional parameter in the mass split operator. This is so because if $Q_\beta{}^\alpha$ is a *35*, then for arbitrary powers of Q we can at most have the following three distinct baryon contractions:

$$B^*{}_{\alpha\beta\gamma}B^{\alpha\beta\delta}Q_\delta{}^\gamma; \quad B^*{}_{\alpha\beta\gamma}B^{\alpha\delta\epsilon}Q_\delta{}^\beta Q_\epsilon{}^\gamma; \quad B^*{}_{\alpha\beta\gamma}B^{\delta\epsilon\zeta}Q_\delta{}^\alpha Q_\epsilon{}^\beta Q_\zeta{}^\gamma. \tag{4.55}$$

The first two terms correspond to the *35* and *405* mentioned above; the third one is a contraction of Q's with the *2695* in $56^*\times 56$. The inclusion of higher powers of Q can no longer give any new baryon density structure.

The consequence of the inclusion of the *2695* density is [C 4] that the relation (4.54) no longer follows. On the other hand, the relations (4.52, 53) both survive.

(3) Charge operator and magnetic moment operator to second order [K 8, D 2, V 1]. One includes here to second order not only the effects of $q_\beta{}^\alpha$ but also of $\mathbf{m}_\beta{}^\alpha$, Eq. (4.44). The resulting mass relations are as follows.

$$\Xi^- - \Xi^0 = \Sigma^- - \Sigma^+ - N + P, \tag{4.56}$$

$$N^{*0} - N^{*+} = Y_1{}^{*0} - Y_1{}^{*+} = N - P, \tag{4.57}$$

$$N^{*-} - N^{*0} = Y_1{}^{*-} - Y_1{}^{*0} = \Xi^{*-} - \Xi^0 = N - P + (\Sigma^- + \Sigma^+ - 2\Sigma^0), \tag{4.58}$$

$$N^{*-} - N^{*++} = 3(N - P). \tag{4.59}$$

These relations are weaker than (but of course compatible with) Eqs. (4.52–54).

The agreement of the strong relations (4.52, 53) with experiment is not too impressive [S 3, C 4]. The weaker relations (4.56–59) involve first of all the $SU(3)$ relation (4.56) [C 5] which is well satisfied [K 8]:

$$\Sigma^- - \Sigma^+ - N + P = 6.38 \text{ MeV}$$

$$\Xi^- - \Xi^0 = 6.5 \pm 1.0 \text{ MeV}.$$

Furthermore one derives [K 4] a predicted value $Y_1{}^{*-} - Y_1{}^{*+} = 4.47$ MeV. This is to be compared with two experimental results for this difference: 17 ± 7 MeV [C 6] and 4.3 ± 2.2 MeV [H 7]. One can therefore not yet judge the agreement with experiment, but the third approach outlined above seems so far the more reasonable one.

The last method has also been applied to the *35* mesons. Three relations are obtained which for the present are not very useful [K 4]. For applications to the baryon *70* see [D 11].

F. The Semi-Leptonic Vertex

Some of the most interesting results obtained with $SU(3)$ follow from the assumption that the effective hadron currents associated with semi-leptonic processes transform like the adjoint representation of $SU(3)$ [C 8]. The simplest extension of this idea to $SU(6)$ is to assume that these currents transform like members of a *35* [B 19]. This incorporates the $SU(3)$ results and in addition gives rise to new predictions. As has been stressed several times now, we may only use $SU(6)$, as so far defined, provided we neglect hadron recoil. On the other hand, the lepton current which is an external probe may carry any momentum. This makes it possible to include such nonstatic effects as weak magnetism.

To begin with, we write the vertex for the *56* in the following form

$$3B^*{}_{\alpha\beta\gamma}C_\delta{}^\gamma(q)\,B^{\alpha\beta\delta} \tag{4.60}$$

and put

$$C_\delta{}^\gamma(q) = (G_V/\sqrt{2})\left[\delta_i{}^j(L_0)_A{}^B + i\mu_W(\boldsymbol{\sigma}\cdot\mathbf{q}\times\mathbf{L}_A{}^B)_i{}^j\right] + (3G_A/\sqrt{2})\,(\boldsymbol{\sigma}\mathbf{L}_A{}^B)_i{}^j, \tag{4.61}$$

$$\mu_W = \tfrac{3}{5}[\mu(N) - \mu(P)]/e. \tag{4.62}$$

The lepton currents are defined as follows.

$$(L_\mu)_A{}^B = \sqrt{2}\begin{pmatrix} 0 & l_\mu \cos\theta & l_\mu \sin\theta \\ l_\mu{}^+ \cos\theta & 0 & 0 \\ l_\mu{}^+ \sin\theta & 0 & 0 \end{pmatrix},$$

$$-il_\mu = \bar{\mu}(p)\gamma_\mu(1+\gamma_5)\nu_\mu(p+q) + \bar{e}(p)\gamma_\mu(1+\gamma_5)\nu_e(p+q). \tag{4.63}$$

θ is the Cabibbo angle. Normalizations are such that

$$[N\tfrac{1}{2} \longrightarrow P\tfrac{1}{2}]_V = G_V/\sqrt{2}; \qquad [N\tfrac{1}{2} \longrightarrow P\tfrac{1}{2}]_A = G_A/\sqrt{2}. \tag{4.64}$$

Individual transition elements are computed with the help of (4.14–17). From $SU(3)$ only one finds the amplitude relations

$$(\Omega^- \longrightarrow \Xi)\,\cot\theta = (N^{*-} \longrightarrow N) = -(N^{*+} \longrightarrow N)\sqrt{3} \tag{4.65}$$

while the specific $SU(6)$ predictions are as follows.

(1) The semi-leptonic D/F ratio is

$$D/F = \tfrac{3}{2} \tag{4.66}$$

which agrees within the error with the best experimental value 1.7 ± 0.35 [W 4]. See also [R 5].

Remark. The D/F value given in (4.66) was first obtained in [G 4] for a somewhat different, but closely related, situation namely the pseudo-vector baryon-meson vertex. If in the latter instance one neglects the baryon recoil and treats the pseudo-vector coupling P as an "external field" the value (4.66) follows also in that case. We return in Sec. V to a more systematic exposé of the strong vertex.

(2)

$$(N^{*+\frac{1}{2}} \longrightarrow N\tfrac{1}{2})_V = -(2\sqrt{2}/5)\,(N\tfrac{1}{2} \longrightarrow P\tfrac{1}{2})_{V,\text{magn}}, \tag{4.67}$$

$$(N^{*+\frac{1}{2}} \longrightarrow N\tfrac{1}{2})_A = -\tfrac{2}{5}G_A. \tag{4.68}$$

In Eq. (4.67) the subscript "V, magn" refers to the contribution from the μ_W term in Eq. (4.61) only.

CC-0. In Public Domain. Gurukul Kangri Collection, Haridwar

Digitized by Arya Samaj Foundation Chennai and eGangotri

With a similar warning as was made for the electromagnetic transition elements, one may attempt to compare (4.67, 68) with experiments on N^* production by neutrinos. Given the present rough data, the comparison is not discouraging [A 4, P 2, A 5]. Added note. See further [A20].

(3) Ω^- decays should be strongly dominated by the axial vector contribution, as is discussed in more detail in [M 3].

The foregoing discussion is independent of the ratio G_A/G_V in (4.61). It is a natural further assumption that the A and V currents belong to the *same 35*- representation of $SU(6)$. From this condition it follows that in Eq. (4.61):

$$G_A/G_V=1. \tag{4.69}$$

In physical terms, Eq. (4.69) means that the (effective) *coupling of the fundamental sextet, but not of the nucleon, is of the V–A type in the $SU(6)$ limit.* In fact from (4.60) and (4.69) one can compute the corresponding ratio for nucleons:

$$(G_A/G_V)_{\text{nucleon}}=\tfrac{5}{3}. \tag{4.70}$$

Remarks. (1) With the same comment as was made after Eq. (4.66), it should be noted that Eq. (4.70) also appears in [G 4].

(2) For a connection between generalized Goldberger–Treiman relations and the ratio G_A/G_V see [B 19], and also [S 5, L 4].

(3) It has recently been shown [V 2] that many of the consequences of the static $U(6)$ actually follow from the weaker requirement of invariance under the subgroup $U(3)\times U(3)$ generated by 1, S_3, F_P, S_3F_P [notations as in Eq. (4.7)]. For a different (chiral) $U(3)\times U(3)$ see [H 11].

(4) For the question of the renormalization of V- and A-coupling constants see [A 12, G 25].

G. S-Wave Nucleon–Nucleon Scattering

Within the static theory, only $L=0$ scattering channels are amenable to treatment. For the nucleon–nucleon scattering $1+2\to3+4$ this has been discussed in detail in [B 21]. We summarize their argument.

As [D 3]

$$56\times56=462+1050+1134'+490, \tag{4.71}$$

there can be only four independent amplitudes. Moreover, the Pauli principle allows the *490* and *1050* only [D 3], so that only two parameters remain. The scattering amplitude can be written as follows.

$$\begin{aligned}
&aB^*_{\alpha\beta\gamma}(3)B^{\alpha\beta\gamma}(1)\cdot B^*_{\lambda\mu\nu}(4)B^{\lambda\mu\nu}(2)\\
&+bB^*_{\alpha\beta\gamma}(3)B^{\alpha\beta\nu}(1)\cdot B^*_{\lambda\mu\nu}(4)B^{\lambda\mu\gamma}(2)\\
&+cB^*_{\alpha\beta\gamma}(3)B^{\alpha\mu\nu}(1)\cdot B^*_{\lambda\mu\nu}(4)B^{\lambda\beta\gamma}(2)\\
&+dB^*_{\alpha\beta\gamma}(3)B^{\lambda\mu\nu}(1)\cdot B^*_{\lambda\mu\nu}(4)B^{\alpha\beta\gamma}(2),
\end{aligned} \tag{4.72}$$

with the additional constraint

$$c=-b, \qquad d=-a. \tag{4.73}$$

Equations (4.72, 73) are then applied only to nucleons. In terms of the usual exchange operators, the nucleon–nucleon scattering matrix becomes

$$[a-(b/27)](1-P_\sigma P_\tau) \tag{4.74}$$

which is bad in the sense that equal scattering lengths are predicted for ^1S and ^3S [K 9, A 6]. The reasonable suggestion is made [B 21] to apply the theory only at energies large compared to the $^3S-{}^1S$ mass split.

It is then seen that the curves for phase shifts $\delta(^1S)$ and $\delta(^3S)$ are close in the region of 100–400 MeV [B 21]. Of course this is necessarily a qualitative statement. Perhaps the main thing we learn is that there appears nothing untoward from the comparison of an $SU(6)$ four-point function with experiment.

Further remarks. (1) An attempt has been made to classify two-baryon resonances by means of the *490* representation. It appears that such an assignment to a single $SU(6)$ multiplet does not work well [D 3].

(2) Λ- and Σ-nucleon scattering is discussed in [C 9].

Addendum. S-wave scattering is also discussed in [B 48].

H. Non-Leptonic Decays

In $SU(3)$ one commonly assumes that the non-leptonic decay interaction transforms like an 8-component. Under more stringent conditions the following amplitude equality was derived [L 4, S 6]

$$\sqrt{3}\langle\Sigma^+\mid p\pi^0\rangle+\langle\Lambda\mid p\pi^-\rangle-2\langle\Xi^-\mid\Lambda\pi^-\rangle=0. \tag{4.75}$$

for both the S and the P wave. For the variety of the additional conditions, see, e.g. [L 5, P 3]. Experimentally these relations appear to hold well [S 7].

S-wave hyperon decay is a natural case for treatment with $SU(6)$. For this channel the simplest extension of the $SU(3)$ discussion to $SU(6)$ is to assume that the interaction transforms like a 35 component. The S-wave problem can then be treated as follows.

Let $P_\alpha{}^\beta=\delta_i{}^j P_A{}^B$ be the pseudoscalar part of the meson *35*, see (4.22). Introduce a corresponding spurion $S_\alpha{}^\beta=\delta_i{}^j s_A{}^B$ with $K^0(s)\equiv s_3{}^2=1$; $\bar K^0(s)\equiv s_2{}^3=1$, all other $s_A{}^B=0$. The $K^0(s)$ are the spurions for $|\Delta I|=\frac{1}{2}$ transitions. For example write $\Lambda\to P+\pi^-$ as $K^0(s)+\Lambda\to P+\pi^-$. The amplitude for this and similar processes can then be obtained by taking a linear combination of all fully $SU(6)$-contracted Hermitian scalars made from B^*, B, P, and S. These are

$$B^*_{\alpha\beta\gamma}B^{\alpha\beta\gamma}P_\sigma{}^\rho S_\rho{}^\sigma; \qquad B^*_{\alpha\beta\gamma}B^{\alpha\beta\delta}(PS+SP)_\delta{}^\gamma;$$

$$B^*_{\alpha\beta\gamma}B^{\alpha\delta\epsilon}P_\delta{}^\beta S_\epsilon{}^\gamma,$$

of which the first one does not contribute to the processes of interest. Thus we get a two parameter expres-

CC-0. In Public Domain. Gurukul Kangri Collection, Haridwar

Digitized by Arya Samaj Foundation Chennai and eGangotri

sion for the set of all S-wave decays. As a result, Eq. (4.75) follows at once for S waves, without any additional assumptions. See [R 5, S 9, A 7] and [K 10, B 22, I 1, M 4]. These papers deal also with other amplitude relations. For example, $\langle \Sigma^+ \mid N\pi^+ \rangle_S = 0$ from $SU(6)$, a current×current interaction and $|\nabla I| = \frac{1}{2}$ [A 8].

This concludes the survey of consequences of the static $SU(6)$. Non-leptonic P wave relations belong properly to the subject of Sec. V, but they will be reviewed briefly at this point. There have been many discussions of the P-wave situation. The common feature is a much greater theoretical complexity and less transparent predictions. The methods used are to introduce a further spurion (*1*; *3*) to describe one unit of orbital angular momentum; or alternatively to use dynamical groups of the kind mentioned in Sec. V. There appears to be a consensus that the P-wave relation (4.75) does not appear in any natural way. However, a rather straightforward analysis gives the P-wave relation (4.75) but with the rhs equal to $2\langle \Omega^- \mid \Lambda K^- \rangle_P/\sqrt{3}$, so that the validity of the P-wave triangle gets linked with a presumed smallness of this Ω^--decay amplitude [A 9, I 1]. For further literature see [A 10, G 19, H 8, I 3, K 11, K 12, O 4, R 6, R 7, S 19]. Finally, it may be recalled [P 3] that non-leptonic asymmetry parameters depend very sensitively on the way mass split effects are introduced.

I. The Master Problem

We have now learned that $SU(6)$ gives interesting results for counting states, for mass regularities and particle mixing, for magnetic moments and semi-leptonic vertices, for S-wave non-leptonic decays, and that the S-wave nucleon scattering results, though not compelling, are not unreasonable or paradoxical either. Faced with this situation, we must consider a much more difficult question.

The master problem: to find the structure of *dynamical equations* such that $SU(6)$ appears as a symmetry *of some of their approximate solutions*; and to state the dynamical nature of what is meant by "approximate."

If one assumes that the answer to this question lies within the framework of present-day theory, the following comments and further questions are in order.

(1) The dynamics should be relativistically invariant.

(2) The question before us is

$$\text{dynamics?} \rightarrow SU(6). \tag{4.76}$$

It may be good to emphasize once more [B 10] that this question is distinct from the one to be discussed in Sec. V:

$$SU(6) \rightarrow \text{larger or other dynamical groups?} \tag{4.77}$$

In Sec. VA the motivation is discussed for this question, to ask for larger dynamical groups which contain $SU(6)$. These groups appear in connection with the so-called relativistic completion procedures, to be discussed below. The question whether there is such a useful group is evidently not identical with the question of the underlying dynamics. In fact, a group which contains $SU(6)$ is a group which contains spin. Hence by the argument sketched in Sec. II, such a larger group must itself be of approximate dynamical character.

(3) Consider as an example the magnetic moment result (4.47). We have all learned in school that the "anomalous" values of the nucleon moments are due to the virtual meson cloud. In the cloud virtual scatterings take place and many-particle virtual states appear, involving arbitrarily high virtual momenta. Is this picture correct? If so by what mechanism do spin-orbit interactions in the cloud average out to give the $SU(6)$ answer?

(4) For dynamical approaches involving bootstrap methods see for example [B 25, C 10]. A short discussion of the algebra of currents is deferred till Sec. VI.

(5) An interesting dynamical question is the connection between the nuclear physics $SU(4)$ [W 2] in which the nucleon is the representation *4* with that subgroup $SU(4)$ of $SU(6)$ in which the nucleon is in the *20* [G 4]. For a discussion see [C 11].

(6) In the nuclear $SU(4)$ case, the dynamics is divided in two stages. First, it should be shown that the (mean) potential between nucleons (in a many nucleon system) is spin- and isospin-independent. Secondly, one discusses energy levels in such a potential.

Is there a similar adiabatic approximation in $SU(6)$? Should one understand the $SU(6)$ dynamics in terms of spin-unitary spin-independent properties of real triplets? The concluding part of Sec. IV is devoted to some aspects of this question.

J. Triplets: Formal Tool or Reality?

In Sec. IVB we started to construct baryon states "as if" they were three triplet configurations. This was a mathematical illustration and we switched soon to a tensorial method. Likewise, certain selection rules can be expressed vividly in terms of triplet properties [L 6, L 7], but equally well as a property of tensor products. Added note: see also [L 14].

The question is whether one can make any predictions from properties of the *35*, *56* or higher representations of $SU(6)$ which are predicated on the real existence of triplets. Thus we must ask for the dynamics of multi-triplet systems.

It has been suggested that the internal dynamics of these systems might be nonrelativistic [N 6, M 5]. Consider a two-triplet (or triplet–antitriplet) system bound by a square well. If the range is a, the velocities are $\sim h/M_t a$, where M_t is the triplet mass. Thus for $v \sim h/M_t a$, $h/M_{\text{nucleon}} c$, $v/c \sim M_{\text{nucleon}}/M_t$ which is ~ 0.1 for $M \sim$ BeV. However, such estimates depend very importantly on the potential shape. They may not be applied to

CC-0. In Public Domain. Gurukul Kangri Collection, Haridwar

Digitized by Arya Samaj Foundation Chennai and eGangotri

Yukawa potential for example [M 5]. This point will be discussed in a forthcoming paper by O. W. Greenberg, to whom I am indebted for an illuminating discussion. At any rate, a potential in which nonrelativistic dynamics can be justified is just what lends itself to an $SU(6)$ picture. With its help an analysis of higher meson resonances has recently been attempted [D 4].

The baryon *56*, viewed as a genuine three-body problem raises interesting questions. As the *56* is symmetric in the internal variables, the generalized Pauli principle requires that the space part be totally antisymmetric, if the triplets satisfy Fermi–Dirac statistics. In the nonrelativistic picture under consideration, this is a puzzlement, at least if we suppose that simple (non-exchange) two-body forces are responsible for the binding. Several suggestions have been made for a way out of this dilemma.

(1) The baryon is not just a three-triplet structure but has a "core" in addition; attractive core–triplet forces overcome repulsive triplet–triplet forces [G 3].

(2) Attractive three-body forces overcome repulsive two-body forces [K 13].

(3) There exists more than one kind of $SU(3)$ triplet, see for example [H 9], and the *56* is made up out of triplet members belonging to different kinds. The internal part of the wave function is then not necessarily totally symmetric in *all* internal variables—which now further include a variable specifying which triplet we use. We come back to this point below.

(4) The triplets do not obey Fermi–Dirac statistics but follow para-statistics [G 16]. Because of the distinction between triplet and antitriplet this assumption does not affect the interpretation of the *35*. Higher para-states have been constructed which may possibly accomodate higher resonances [G 16]. For a survey of parafield theory see [G 17].

Let us see next what realistic triplet models can say about electromagnetic properties.

(α) Assume one set of triplets only, embedded in an internal symmetry not larger than $SU(3)$. For definiteness one may imagine a baryon model of the kind (1) or (2). Instead of using the tensor method described in Sec. IVD, one can (equivalently) use vector addition of triplet magnetic moments [B 9, S 10], very much as in nuclear physics calculations [B 26]. We do this next, but use the general charge assignments of Eq. (4.1) instead of Eq. (4.2). The corresponding charge operator is given by $Q=I_3+Y/2+(q_0-\frac{2}{3})t$. t is the triality, see, e.g. [B 7] and q_0 is defined in Eq. (4.1). The corresponding static magnetic moment operator $\mathbf{M}$ is assumed to be proportional to Q, as in (4.44). Hence for a set of triplets and anti-triplets

$$\mathbf{M}=\mu\{[q_0\mathfrak{d}^{(p)}+(q_0-1)(\mathfrak{d}^{(n)}+\mathfrak{d}^{(\lambda)})] - [q_0\mathfrak{d}^{(\bar{p})}+(q_0-1)(\mathfrak{d}^{(\bar{n})}+\mathfrak{d}^{(\bar{\lambda})})]\}. \quad (4.78)$$

Take the expectation value of M in the composite three-body states of the *56*. Then [B 8]

$$\mu(P):\mu(N):\mu(\Lambda)=(3q_0-4):(3q_0+1):(3q_0-3). \quad (4.79)$$

For $q_0=\frac{2}{3}$ we recover the results of Sec. IVD. The "nuclear physics' calculation described here rests on the additional assumption that "internal exchange currents" between the triplets, which may give additional terms in (4.78) do not play an appreciable role. (Such additional assumptions cannot appear in the formal method of Sec. IVD.)

Equation (4.79) shows that $q_0\neq\frac{2}{3}$ will spoil the good relation (4.47). Thus if only one set of triplets exists [and the internal symmetry is not larger than $SU(3)$], then it is indicated that they should be fractionally charged. Note that $SU(6)$ considerations play an essential role at this point. For example in an $SU(3)$ model with a core, the core should be an $SU(3)$ singlet but may carry spin. According to $SU(6)$ a possible core should be an $SU(6)$ singlet, hence spinless. Thus in $SU(3)$ but not in $SU(6)$ could the core give an additional magnetic moment itself.

It has been noted [N 1] that for general q_0 the hyperon magnetic moments need not take on the values predicted [C 5] on the basis of Eq. (4.3). This would give two independent sources for deviations from a relation like $\mu(\Lambda)=\mu(N)/2$: (a) because of the q_0 effect, (b) because of breakdown of $SU(3)$. Let us now exclude cause (a) on the grounds just mentioned. Then cause (b) only remains. As an extension of the successful description of mass splits as first-order effects, the assumption is plausible that the $SU(6)$ magnetic moment ratios for the *56* should be corrected by the inverse of the true mass ratios [B 8]. The resulting magnetic moment values are found in the "Mass-corrected" column of [Table I, B 8]. In particular

$$\mu(\Lambda)=-0.78\mu(P)$$

which agrees within the error with the weighted average of available experiments [H 10]

$$\mu(\Lambda)=(-0.73\pm0.17)\mu(P).$$

Remarks. (1) If one takes Eq. (4.78) seriously, then one can express the magnetic moment of $\mu(p)$ in terms of $\mu(P)$. For $q_0=\frac{2}{3}$: $\mu(p)=2\mu(P)/3$. At first sight it seems curious that the triplet moment should be of the order of the nucleon moment, if the triplet mass is quite high ($\gtrsim$10 BeV). It has been noted, however [B 27], that triplet magnetic moments can be enhanced by strong binding in an external field of the scalar type. The Dirac equation in a scalar potential is

$$[M+V+\beta\boldsymbol{\alpha}(\mathbf{p}-e\mathbf{A})]u=\beta Eu.$$

In a region where V is constant, the effective mass is $M+V$ [L 8]. Applied to triplets, a large M can be compensated by a large V. The situation is distinct for external fields other than the scalar kind [L 8, G 18].

CC-0. In Public Domain. Gurukul Kangri Collection, Haridwar

Digitized by Arya Samaj Foundation Chennai and eGangotri

(2) For attempts to deduce radiative vector meson decay rates from a realistic triplet model see [T 2, B 20]. The importance of these calculations lies in the fact that the $M1$-transition element for $\omega\to\pi^0+\gamma$ is expressed in terms of the *nucleon* magnetic moment via Eq. (4.78). The method appears to depend more decisively on the real existence of quarks than in any of the problems mentioned earlier, as is also evident from the fact that the results obtained *cannot* be deduced from $SU(6)$-algebra alone.

(β) The case of three triplets [H 10, B 27]. The introduction of more triplets allows one to retain Eq. (4.47) in a theory with integrally charged triplets. I am indebted to Professor A. Tavkhelidze for an illuminating discussion of this point. The argument is as follows.

Consider a second group $SU(3)'$ with corresponding tensor indices A', B', $\cdots$. Let $u^{A,A'}$ denote a three triplet set, where A is the usual $SU(3)$ index. Define a charge operator as follows

$$Q_{B,B'}{}^{A,A'}=Q_B{}^A\delta_{B'}{}^{A'}+\delta_B{}^A\tilde{Q}_{B'}{}^{A'}, \tag{4.80}$$

where $Q_B{}^A$ is given by (4.36) and

$$\tilde{Q}_{B'}{}^{A'}=\tfrac{1}{3}\begin{pmatrix}1&&\\&1&\\&&-2\end{pmatrix}. \tag{4.81}$$

This corresponds to three $SU(3)$ triplets with respective charges: (1, 0, 0); (1, 0, 0); (0, −1, −1). The 56 is supposed to be made up of one triplet member of each kind and instead of $B^{\alpha\beta\gamma}$, Eq. (4.14), the baryon tensor is taken to be

$$B^{\alpha\beta\gamma}\to\epsilon^{A'B'C'}B^{\alpha\beta\gamma} \tag{4.82}$$

which is now totally *anti*symmetric in the internal variables.

Next define a magnetic moment operator as in (4.44) but with $Q_A{}^B$ replaced by (4.80). The baryon moments are computed by replacing $B^{\alpha\beta\gamma}$ in (4.45) by (4.82).

Observe the identity

$$\epsilon_{A'B'D'}\tilde{Q}_{C'}{}^{D'}\epsilon^{A'B'C'}=0 \tag{4.83}$$

from which it follows that the second term in (4.80) does not contribute to the magnetic moments. Hence Eq. (4.47) has recovered.

Much more experimental information is needed before one can know which if any of these preliminary models of multi-triplet systems will survive. Nor are more complex models excluded [F 5]. The possibility may finally be noted that $SU(3)$ is perhaps not the full group of internal symmetry and that there are larger groups (see, e.g. [N 2]) in which there is room for the *8*- and *10*-representations of $SU(3)$; but not for triplets.

In summary, $SU(6)$ results obtained from quark models are often suggestive, yet they do not appear to be compelling for the reality of quarks. On the other hand, such stronger than $SU(6)$ results as, for example, the $\omega\to\pi^0+\gamma$ decay rate seem more difficult to understand without a real structure of the nucleon with three quarks in its "outer shell."

V. RELATIVISTIC EXPLORATIONS

A. Introduction

In parallel with the sorting out of the consequences of the static $SU(6)$, discussed in the previous section, several distinct attempts began to develop to embed the static $SU(6)$ in a relativistic description. Up till now there does not exist a satisfactory solution to this question. The main approaches to the question stated in Eq. (4.77) will be outlined in this Introduction.

(A) It was realized from the start [G 3] that it is possible to give a classification of supermultiplet states also for $\mathbf{p}\neq 0$. To see this, recall that for spin $\frac{1}{2}$ a relativistic spin $S(\mathbf{p})$ can be defined [F 6] which commutes with the free Hamiltonian $\boldsymbol{\alpha}\mathbf{p}+\beta m$. For each $\mathbf{p}$ it is possible to define a group by DG as in Eq. (4.7) but with S replaced by $S(\mathbf{p})$. This is the group called $SU(6)_p$, see [G 20].

It is possible to generalize the Foldy–Wouthuysen spin description [and hence $SU(6)_p$] to a relativistic N-body system with interaction. More precisely, one can construct for such a system a corresponding representation of the Poincaré group [F 7]. One must next ask whether a system so described is necessarily a physically reasonable system, in particular whether it is separable [F 7]. In a concrete instance, one means the following by separability. Consider a three-body system with its assigned representation. Move one of the particles to infinity. Do we approach in this way a system of two interacting particles plus a free particle in all frames? This is a far from trivial question. In particular separability in the center-of-mass frame does not guarantee separability in all other frames [F 7]. The question is clearly of interest if one wishes to find connections with local dynamical theories, because of creation and annihilation processes.

In the context of such theories, $SU(6)_p$ runs into difficulties. For specific examples it has been shown that local interaction violates the symmetry [M 6, R 8], and it has been proved, more generally, that this symmetry implies a unit S-matrix [J 2]. This approach will not be discussed further in this paper.

(B) The starting point for a second approach is to seek for an approximate dynamical symmetry which in the language of a Lagrangian field theory, is broken by free kinetic energy terms [B 8, B 16]. This new symmetry is supposed to contain the static $SU(6)$ and to be of use for $\mathbf{p}\neq 0$.

It may be helpful to illustrate the idea by an example

CC-0. In Public Domain. Gurukul Kangri Collection, Haridwar

Digitized by Arya Samaj Foundation Chennai and eGangotri

[B 8]. Consider a 12×12 matrix

$$^{(1)}\mathfrak{M}_b{}^a(q)=if_V(q^2)\,(\gamma\epsilon(q)\,)_\mu{}^\lambda V_B{}^A - f_A(q^2)\,\{\gamma_5[(\gamma q)/\mu]\}_\mu{}^\lambda P_B{}^A, \quad (5.1)$$

where V and P are given by Eqs. (4.22, 23). $q=(\mathbf{q}, iq_0)$. $(\gamma q)=\gamma_s=(\boldsymbol{\gamma}, \gamma_4)$ are Hermitian Dirac matrices, $(\gamma q)=(\gamma_\mu q_\mu)$, etc. The polarization four-vector $\epsilon_\mu(q)=(\boldsymbol{\epsilon}(q), i\epsilon_0(q))$ is related to the $\boldsymbol{\epsilon}$ in Eq. (4.21) as follows

$$\boldsymbol{\epsilon}(q)=\boldsymbol{\epsilon}+[\mathbf{q}(\mathbf{q}\boldsymbol{\epsilon})/\mu(q_0+\mu)\,], \qquad \epsilon_0(q)=\mathbf{q}\boldsymbol{\epsilon}/\mu, \quad (5.2)$$

so that

$$q\epsilon(q)=0. \quad (5.3)$$

In regard to indices, the ranges for α, i, A will be maintained as in Sec. IVA. In addition we shall use from here on the following conventions. The early letters a, b, $\cdots$ of the Latin alphabet run from 1–12. The middle letters λ, μ, $\cdots$ of the Greek alphabet run from 1–4.

Unless otherwise specified, we use the representation

$$\boldsymbol{\gamma}=\rho_2\boldsymbol{\sigma}, \qquad \gamma_4=\rho_3, \qquad \gamma_5=\rho_1. \quad (5.4)$$

Then $^{(1)}\mathfrak{M}_b{}^a$ can be written as

$$^{(1)}\mathfrak{M}_b{}^a(q)=\begin{pmatrix} N_\beta{}^\alpha(q), & -M_\beta{}^\alpha(q) \\ M_\beta{}^\alpha(q), & -N_\beta{}^\alpha(q)\end{pmatrix}, \quad (5.5)$$

$$M_\beta{}^\alpha(q)=-f_V(q^2)\,(\boldsymbol{\sigma}\boldsymbol{\epsilon}(q)\,)_j{}^i V_B{}^A - if_A(q^2)\,(q_0/\mu)\,P_B{}^A\delta_i{}^j, \quad (5.6)$$

$$N_\beta{}^\alpha(q)=-f_V(q^2)\,\epsilon_0(q)\,\delta_j{}^i V_B{}^A - if_A(q^2)[(\boldsymbol{\sigma}\mathbf{q})_j{}^i/\mu]P_B{}^A. \quad (5.7)$$

Define the static limit q^0 of q by $q^0=(0, i\mu)$. Then

$$\text{while} \qquad N_\beta{}^\alpha(q^0)=0, \quad (5.8)$$

$$M_\beta{}^\alpha(q^0)=M_\beta{}^\alpha, \quad (5.9)$$

provided that

$$f_V(-\mu^2)=f_A(-\mu^2). \quad (5.10)$$

The right-hand side of Eq. (5.9) is just the static $SU(6)$ matrix of Eq. (4.21) and Eq. (5.10) may therefore be regarded as the *static* $SU(6)$ form factor condition.

Note that

$$^{(1)}\mathfrak{M}_b{}^a(q^0)=\begin{pmatrix} 0, & -M_\beta{}^\alpha \\ M_\beta{}^\alpha, & 0\end{pmatrix}. \quad (5.11)$$

This doubling of the matrix is well known from the treatment of the $\mathfrak{D}^{[\frac{1}{2},\frac{1}{2}]}$ representation (four-vector) of the orthochronous Lorentz group in the $SL(2, C)$ language [S 11]. The doubling is necessary in order to assign a definite parity to the representation.

$M_\alpha{}^\beta$ is odd, $N_\alpha{}^\beta$ is even under space reflection. We now define the baryon–meson vertex in the no-baryon recoil limit to be [B 8]

$$B^*{}_{\alpha\beta\gamma}N_\delta{}^\gamma(q)\,B^{\alpha\beta\delta}.$$

The vertex depends on the single three-momentum $\mathbf{q}$. To order v/c (P-wave vertex) one should retain only terms of the first power in $|\mathbf{q}|$. This means that to this order Eq. (5.10) is valid.

Using the methods of Sec. IVD, one obtains from Eq. (5.12) all the nonrelativistic vertex results first given in [G 4] and reviewed in [B 8]. The use of Eq. (5.10) is essential. It follows that such strong interaction relations as

$$D/F=\tfrac{3}{2}, \qquad g_A/g_V=\tfrac{5}{3} \text{ (strong int.)}$$

do not involve any further relation between form factors than those implied by the static $SU(6)$. It has been shown in [B 10] and will be discussed further in Sec. VC that under the same conditions the inclusion of baryon recoil to order v/c is also possible. (It may be noted incidentally that up to this order the Foldy–Wouthuysen spin is identical with the nonrelativistic spin.) See further the derivation of Eqs. (5.63) and (5.76) below.

The prescription just described amounts to associating to the static meson tensor its "relativistic completion" Eq. (5.1), the even parity part of which is coupled to the baryon current. The general theme to be discussed in several variations may now be stated as follows.

(a) To associate to any static $SU(6)$ representation their relativistic completion or completions. This is done by "boosting," a procedure described in Sec. VB. It will be shown there that there are in general more than one completions to a given static $SU(6)$ tensor.

(b) To give rules for the coupling of the completed $SU(6)$ tensors to each other in the form of effective vertices which are covariant. This can be done in more than one way and the variety of these ways can be classified by means of a "booster group" which is $U(6, 6)$ [S 13, B 28].

$U(6, 6)$ is a special case of the pseudo-unitary groups discussed in Sec. IIIG. It was seen there that the transformations of such groups leave invariant pseudo-unitary quadratic forms, Eq. (3.86). What is this form for $U(6, 6)$? Let $u^\lambda(p)$ be a four-component Dirac spinor, $\lambda=1$–4, and let $u^{\lambda A}(p)$ be a triple of such spinors describing the relativistic $SU(3)$ triplet. $U(6, 6)$ is the group of transformations for which the "relativistic mass term"

$$\bar{u}_{\lambda A}(p)u^{\lambda A}(p)=\text{invariant}, \quad (5.12)$$

where $\bar{u}=u^\dagger\gamma_4$. Using the representation (5.4) one sees that this quadratic form has six $+$, and six $-$ signs, whence $U(6, 6)$. The structure of this group is explained in more detail in Sec. VB.

CC-0. In Public Domain. Gurukul Kangri Collection, Haridwar

Digitized by Arya Samaj Foundation Chennai and eGangotri

Equation (5.12) may be looked upon as a covariant generalization of the invariance requirement (4.6) for $SU(6)$. As $SU(6)$ is an approximate dynamical symmetry, the same is true therefore for $U(6, 6)$, as the latter contains $SU(6)$. Moreover, one knows *explicitly* at least one mechanism by which $U(6, 6)$ is broken: As will be seen in Sec. VB, $U(6, 6)$ does not leave invariant the "kinetic energy term" $\bar{u}_{\lambda A}(p)(\gamma p)_{\mu}{}^{\lambda} u^{\mu A}(p)$. Thus *in the presence of interactions* [where the identity $\bar{u}(\gamma p)u = im\bar{u}u$ is not valid], $U(6, 6)$ is intrinsically broken by the spin-orbit couplings inherent in (γp) terms. While the intrinsically broken character of $U(6, 6)$ was often well appreciated, the applications of $U(6, 6)$ and some of its subgroups was nevertheless pursued further, motivated by the idea (see Sec. IVI) that, where the static $SU(6)$ is successful, an *effective* damping out of these symmetry breaking spin-orbit couplings must be at work. However, it was soon realized that no systematic application of such invariance ideas is possible for all n-point functions. This is because of the unitarity problem, as is explained in Sec. VE.

The approach just sketched is only one of several which were followed in the fall of 1964 in order to find approximate dynamical symmetries which contain $SU(6)$. For example, others took the structure of four quark interactions as a starting point. Independently, the following groups were suggested: the chiral group $U(6)\otimes U(6)$ [F 4, D 5, B 16]; the nonchiral group $U(6)\otimes U(6)$ [O 3, B 16]: $SL(6, C)$ [F 8, R 9, S 12]; $U(6, 6)$ [S 13, B 28, B 16, R 10]. [The latter group went for a while under a variety of names: $\tilde{U}(12)$, $U(12)_{\mathfrak{L}}$, $M(12)$, $V(12)$.] These groups will be discussed in Sec. VD. As they are all related to $U(6, 6)$ it is convenient to take the latter as a starting point.

It may directly be noted that the matrix ${}^{(1)}\mathfrak{M}_b{}^a(q)$ has a vanishing 12-trace:

$$ {}^{(1)}\mathfrak{M}_a{}^a(q) = 0. \tag{5.13} $$

This is true for all q and therefore in particular in the static limit $q = q_0$ see Eq. (5.11). Observe an important difference between the $SU(6)$ condition $M_{\alpha}{}^{\alpha} = 0$ and Eq. (5.13). The former implies that $P_A{}^A = 0$, corresponding to 8 pesudoscalar mesons. On the other hand, Eq. (5.13) is also true if $P_A{}^A \neq 0$. It will be shown more systematically below that in fact all the larger groups mentioned above accomodate a 36th meson along with the 35 of $SU(6)$. It is natural to identify this extra meson with the X^0 mentioned in Sec. IVB. Accordingly we shall from now on redefine $P_B{}^A$ as follows.

$$ P_B{}^A = [P_B{}^A \text{ of Eq. (4.22)}] + (X^0/\sqrt{3})\,\delta_B{}^A. \tag{5.14} $$

(c) Closely related to the methods of (B) are attempts to embed $SU(6)$ in a kinematical symmetry by means of the formal introduction of more than the four usual translation operators p_{μ}. The idea, first mention dine [S 1], is the following. Consider the kinetic energy $\gamma_{\mu} p_{\mu}$ for a free relativistic quark. In the notation of Eq. (5.1) this term can be written as a 12×12 matrix $(\gamma_{\mu} p_{\mu})_b{}^a \delta_B{}^A$. Thus the kinetic energy can be brought in formal correspondence with the ϕ^0-meson part of the meson matrix and the fact that the kinetic energy breaks all of the symmetries mentioned above can be expressed as the formal statement that $(\gamma_{\mu} p_{\mu})_b{}^a \delta_B{}^A$ is not a full representation of any of these groups. In essence, the idea is now to enlarge the set of 4 translations to a set of 36 (or a multiple thereof). In this way one can obtain descriptions which are invariant inclusive of these generalized translations which contain the four usual ones. See [F 8, B 29, B 30, R 11, N 3, K 14, N 4, R 12, Z 2]; also [N 5]. *Added note.* See further [B 49].

For physical applications it is necessary, however, to introduce the boundary condition that the operators of the theory act on such states which depend on the four translational variables p_{μ} only. Thus till now the extra translations have not led to physical predictions that cannot be obtained as well without their introduction. In practice, we are back to some of the methods included in (B). Extra translations will not be discussed further in what follows.

(D) Another line of development finds its origin in the observation [B 31] that for a vertex in the brick wall system one can define a conserved "spin" W:

$$ \mathbf{W} = \tfrac{1}{2}\gamma_4\sigma_1,\ \tfrac{1}{2}\gamma_4\sigma_2,\ \tfrac{1}{2}\sigma_3, \tag{5.15} $$

(where all vertex momenta are in the 3-direction) which has the same commutation relations as $\frac{1}{2}\mathfrak{d}$. Thus one can define a group isomorphic to $SU(6)$ by replacing $\mathbf{S}$ by $\mathbf{W}$ in Eq. (4.7). This group is called $SU(6)_W$. It can be applied to any collinear configuration [L 9]. It is a subgroup of $U(6, 6)$ see Sec. VD.

The W-spin will be discussed in more detail in Sec. VF, but we state some of its main consequences right here. (A detailed survey of W-spin predictions is given in [H 12].)

(1) When applied to baryon vertices it leads to the relations [B 31]

$$ G_m{}^N(q^2)/G_m{}^P(q^2) = -\tfrac{2}{3}, \qquad G_e{}^N(q^2) = 0 \tag{5.16} $$

for all q^2 where G_m, G_e are the magnetic and electric Sachs form factors, respectively. Slightly more generally it gives [B 31, P 4]

$$ G_m(q^2)/G_m{}^P(q^2) \quad \text{and} \quad G_e(q^2)/G_e{}^P(q^2) \quad \text{are independent of } q^2, \tag{5.17} $$

where the respective numerators refer to any member of the baryon octet or to the $(\Sigma^0 \mid \Lambda)$-transition form factors.

$G_e{}^N(q^2)$ is known to have a nonzero slope near $q^2 = 0$ but $G_e{}^P(q^2)/G_e{}^N(q^2) < 0.2$ in the known region. Within such $\sim 20\%$ margins the relations (5.16) appear to be reasonable up to $q^2 \sim (1\ \text{BeV}/c)^2$, see, e.g. [D 6].

CC-0. In Public Domain. Gurukul Kangri Collection, Haridwar

Digitized by Arya Samaj Foundation Chennai and eGangotri

(2) Applied to the forward meson–baryon scattering amplitudes one obtains the Johnson–Treiman relations [J 3]

$$\tfrac{1}{2}[f(K^+)-f(K^-)]=[f(K^0)-f(\bar{K}^0)]=[f(\pi^+)-f(\pi^-)] \tag{5.18}$$

for scattering off protons. Of the many ways in which this relation has been derived, the one using W-spin seems to be the most transparent. The J–T relations appear to be well satisfied for not too low energies [G 21, L 10] (especially for the K-particle equalities). There are many puzzles why these relations work, in the face of $SU(3)$ breaking effects [H 2], but these relations are currently regarded as one of the more promising consequences of W spin. It has been noted, however, [S 14], that the J–T relations may perhaps be understood by dynamical approximations which do not invoke W-spin or other symmetries.

$SU(6)_W$ is necessarily an approximate symmetry of the dynamical kind, as collinear and noncollinear configurations are dynamically coupled. It is interesting that at least some noncollinear diagrams do not violate the J-T relations [H 13].

(E) Finally we mention the kinetic spurion approach [A 11, G 22, F 10, B 32, O 5, F 9]. One introduces in all possible ways spurions $(\gamma p)_\mu{}^\lambda \delta_B{}^A$ into $U(6, 6)$ vertices or other effective matrix elements. Here p can be any 4-momentum characteristic for the problem at hand. This implies the breakdown of $U(6, 6)$ to a lower symmetry (see Sec. VD). One finds the following symmetry survives: (a) $U(6)\otimes U(6)$ (nonchiral) for one-particle states. (b) $SU(6)_W$ for collinear configurations. (c) $U(3)\otimes U(3)$ for coplanar configurations (d) $SU(3)$ only for more complicated situations. This hierarchy has been noticed by several authors [O 6, D 7, H 14].

The remainder of Sec. V is devoted to the discussion of techniques, consequences, and difficulties for the approximate dynamical symmetries mentioned above. In VB, boost matrices are defined, boosts are performed on the *6*, *36*, *56* and the group $U(6, 6)$ is introduced. In VC the meson–baryon coupling is discussed under the weakest conditions which give the "good" results for the phenomenological vertex. In VD some subgroups of $U(6, 6)$ are treated. Section VE deals with the implications of the higher symmetries in the nonstatic domain; in particular the unitarity difficulties are discussed. Finally in VF more details about W spin are given.

B. The Boosted 6, 36, 56; the Group $U(6, 6)$

1. Boost Matrices

We return briefly to the labeling explained in Eq. (2.6) by means of components and base vectors. For $SU(2)$ we consider the two-base vectors $u_{(1)}{}^i$, $u_{(2)}{}^i$:

$$u_{(1)}{}^i=\begin{pmatrix}1\\0\end{pmatrix}, \qquad u_{(2)}{}^i=\begin{pmatrix}0\\1\end{pmatrix}. \tag{5.19}$$

These u's, enlarged as follows,

$$u_{(1)}{}^\lambda=\begin{bmatrix}1\\0\\0\\0\end{bmatrix}, \qquad u_{(2)}{}^\lambda=\begin{bmatrix}0\\1\\0\\0\end{bmatrix} \tag{5.20}$$

represent Dirac spinors for $p=0$, $p_0>0$. The number of *components* for given state has doubled. In addition we introduce the $\mathbf{p}=0$ negative energy spinors

$$v_{(1)}{}^\lambda=\begin{bmatrix}0\\0\\1\\0\end{bmatrix}, \qquad v_{(2)}{}^\lambda=\begin{bmatrix}0\\0\\0\\1\end{bmatrix}. \tag{5.21}$$

Note. In the nonrelativistic two-component language, u^i (upper two u^λ) and v^i (lower two v^λ) may both be considered as *6*-representations of one and the same $U(6)$. Even at $\mathbf{p}=0$, this is no longer true in the four component language, as is shown by the distinct structure of (5.20) and (5.21). The four-component quantities u^λ and v^λ are actually representations of a group $U(6)\otimes U(6)$, as will be seen in more detail after Eq. (5.88) below.

We have now an array $D_{(\mu)}{}^\lambda(0)$ defined as

$$D_{(\mu)}{}^\lambda(0)=(u_{(1)}{}^\lambda, u_{(2)}{}^\lambda, v_{(1)}{}^\lambda, v_{(2)}{}^\lambda)=\delta_{(\mu)}{}^\lambda, \tag{5.22}$$

where the index λ numbers components, and the bracketed index (μ) labels states. In the representation (5.4) we have correspondingly for $\mathbf{p}\neq 0$ (and mass m)

$$D_{(\mu)}{}^\lambda(p)=\left[\frac{m-i(\gamma p)\gamma_4}{\{2m(p_0+m)\}^{\frac{1}{2}}}\right]^\lambda_{(\mu)}, \tag{5.23}$$

where to $(\mu)=1, 2$ correspond solutions of the Dirac equation for $\mathbf{p}$, p_0 and to $(\mu)=3, 4$ the solutions for $-\mathbf{p}$, $-p_0$ $(p_0>0)$. From (5.22):

$$D_{(\mu)}{}^\lambda(p)=D_\nu{}^\lambda(p)D_{(\mu)}{}^\nu(0). \tag{5.24}$$

$D_{(\mu)}{}^\lambda$ is a matrix with one index in component space, and one in base vector (state) space. $D_\nu{}^\lambda(p)$ is the *same* matrix but with both indices in component space. $D_\nu{}^\lambda(p)$ is called the boost matrix [W 5].

Define as usual

$$\bar{D}_\lambda{}^{(\mu)}(p)=D_\nu{}^{*(\mu)}(p)(\gamma_4)_\lambda{}^\nu \tag{5.25}$$

CC-0. In Public Domain. Gurukul Kangri Collection, Haridwar

Digitized by Arya Samaj Foundation Chennai and eGangotri

for all p. Hence (5.24) gives

$$\bar{D}_\lambda{}^{(\mu)}(p)=\bar{D}_\nu{}^{(\mu)}(0)\bar{D}_\lambda{}^\nu(p), \tag{5.26}$$

where

$$\bar{D}_\lambda{}^\nu(p)=(\gamma_4 D^\dagger(p)\gamma_4)_\lambda{}^\nu. \tag{5.27}$$

From now on the matrices D, $\bar{D}$ defined by Eqs. (5.23, 24, 27) will always be meant to be the boost matrices. We list some of their properties.

$$D\bar{D}=1, \tag{5.29}$$

$$D\gamma_5\bar{D}=\gamma_5, \tag{5.30}$$

$$D\gamma_4\bar{D}=-i(\gamma p)/m, \tag{5.31}$$

$$D\boldsymbol{\gamma}\boldsymbol{\varepsilon}\bar{D}=\boldsymbol{\gamma}\epsilon(p), \tag{5.32}$$

$$D\gamma_4\boldsymbol{\gamma}\boldsymbol{\varepsilon}\bar{D}=\sigma_{\mu\nu}p_\mu\epsilon_\nu(p)/m,$$

$$\sigma_{\mu\nu}=-i[\gamma_\mu,\gamma_\nu]/2,$$

where $\epsilon_\mu(p)$ is defined in Eq. (5.2). Let C be the charge conjugation matrix, $C^{-1}\gamma_\mu C=-\gamma_\mu{}^t$, $C^t=-C$; t=transpose. In the representation (5.4) C may be taken as

$$C=i\gamma_5\sigma_2. \tag{5.33}$$

We have

$$CD^t=\bar{D}C, \qquad \bar{D}^tC^{-1}=C^{-1}D. \tag{5.34}$$

2. The Boosted 6

We go from the static sextet u^{iA} defined in Eq. (4.4) to the corresponding $u^{\lambda A}=u^a$ by using the transition (5.19)→(5.20). The boosted sextet $u^a(p)$ is

$$u^a(p)=u^{\lambda A}(p)=D_\mu{}^\lambda(p)u^{\mu A}, \tag{5.35}$$

and likewise

$$v^a(p)=v^{\lambda A}(p)=D_\mu{}^\lambda(p)v^{\mu A}. \tag{5.36}$$

u and v are associated to the sextet and antisextet, respectively, in the sense of the canonical expansion

$$\psi^a(x)=\sum_{(i)=1,2}(m/E)^{\frac{1}{2}}$$

$$\times[a_{(i)}u_{(i)}{}^a(p)\exp(ipx)+b_{(i)}{}^\dagger v_{(i)}{}^a(p)\exp(-ipx)].$$

The particle–antiparticle conjugation operation is not part of $SU(6)$, but it can be implemented as an additional rule. In Eqs. (5.35, 36) we have reverted to the dropping of state labels and will continue to do so from now on.

3. The Boosted 36

Start from Eqs. (4.21) and (5.14). The static $SU(6)$ matrix $M_{jB}{}^{iA}$ has first to be "enlarged" in a similar way as was done for the 6 in going from (5.19) to (5.20). This can be done as follows.

$$M_{jB}{}^{iA}\longrightarrow\mathfrak{M}_b{}^a(0)=\mathfrak{M}_{\mu B}{}^{\lambda A}(0)=[\tfrac{1}{2}\gamma_5(1+\gamma_4)M]_{\mu B}{}^{\lambda A},$$

that is,

$$\mathfrak{M}_b{}^a(0)=\begin{pmatrix}0 & 0\\ M_{\beta}{}^{\alpha} & 0\end{pmatrix}.$$

Next we boost the static matrix to momentum q with the help of $D(q)$ and $\bar{D}(q)$ (for mass μ):

$$\mathfrak{M}_b{}^a(q)=\mathfrak{M}_{\mu B}{}^{\lambda A}(q)=D_\nu{}^\lambda(q)\mathfrak{M}_{\rho B}{}^{\nu A}(0)\bar{D}_\mu{}^\rho(q), \tag{5.37}$$

and find with the help of Eqs. (5.29–32):

$$\mathfrak{M}_b{}^a(q)={}^{(1)}\mathfrak{M}_b{}^a(q)+{}^{(2)}\mathfrak{M}_b{}^a(q), \tag{5.38}$$

$${}^{(1)}\mathfrak{M}_b{}^a(q)=i(\gamma\epsilon(q))_\mu{}^\lambda V_B{}^A-\{\gamma_5[(\gamma q)/\mu]\}_\mu{}^\lambda P_B{}^A, \tag{5.39}$$

$${}^{(2)}\mathfrak{M}_b{}^a(q)=-(i/\mu)\{\sigma_{\mu\nu}q_\mu\epsilon_\nu(q)\}_\mu{}^\lambda V_B{}^A-i(\gamma_5)_\mu{}^\lambda P_B{}^A. \tag{5.40}$$

Dropping indices, one notes that

$$\gamma_5\mathfrak{M}(q)\gamma_5=-{}^{(1)}\mathfrak{M}(q)+{}^{(2)}\mathfrak{M}(q). \tag{5.41}$$

Remarks. (1) Equation (5.39) is proportional to the expression (5.1) *provided that* $f_V(q^2)=f_A(q^2)$ *for all* q^2. (2) ${}^{(2)}\mathfrak{M}$ is a second matrix which has static $SU(6)$ limit properties in the sense described in Sec. V.A. (3) We could have started from $\gamma_5\mathfrak{M}(0)\gamma_5$ instead of from Eq. (5.39) and would have obtained (5.41) directly by boosting because of Eq. (5.30). (4) $\mathfrak{M}$ and $\gamma_5\mathfrak{M}\gamma_5$ obviously have the same parity.

4. The Boosted 56

Once again we enlarge the zero momentum $SU(6)$ tensor $B^{\alpha\beta\gamma}$, Eq. (4.14).

$$B^{iA,jB,kC}\longrightarrow B^{\lambda A,\mu B,\nu C}(0)=B^{abc}(0),$$

$$B^{abc}(0)=u^{(\lambda\mu\nu)}(0)d^{ABC}+(1/3\sqrt{2})[\epsilon^{\lambda\mu}u^\nu(0)X^{ABC}$$

$$+\epsilon^{\mu\nu}u^\lambda(0)X^{BCA}+\epsilon^{\nu\lambda}u^\mu(0)X^{CAB}], \tag{5.42}$$

where $u^\mu(0)$ is given by Eq. (5.20) and $X^{ABC}=\epsilon^{ABD}b_D{}^C$. $u^{\lambda\mu\nu}(0)$ is the correspondingly enlarged spin-$\frac{3}{2}$ wave function [We may construct $u^{(\lambda\mu\nu)}(0)$ as a totally symmetric direct product of three functions $u^\lambda(0)$.] We have to enlarge ϵ^{ij} of Eq. (4.14) as follows.

$$\epsilon^{ij}\longrightarrow\epsilon^{\lambda\mu}=\begin{bmatrix}0&1&0&0\\-1&0&0&0\\0&0&0&0\\0&0&0&0\end{bmatrix}=\left[\frac{1+\gamma_4}{2}\gamma_5 C\right]^{\lambda\mu} \tag{5.43}$$

see Eq. (5.33). [Note that $\epsilon^{\lambda\mu}$ represents a spin-zero state constructed out of two *four*-component spin-$\frac{1}{2}$ states given by Eq. (5.20).] We now define the *totally symmetric boost* to momentum p (for mass M):

$$B^{abc}(p)=D_\rho{}^\lambda(p)D_\sigma{}^\mu(p)D_\tau{}^\nu(p)B^{\rho A,\sigma B,\tau C}(0). \tag{5.44}$$

CC-0. In Public Domain. Gurukul Kangri Collection, Haridwar

Digitized by Arya Samaj Foundation Chennai and eGangotri

Note in particular that

$$\epsilon^{\lambda\mu}u^{\nu}(0)\to\tfrac{1}{2}\{[1-(i\gamma p/M)]\gamma_5 C\}^{\lambda\mu}u^{\nu}(p). \quad (5.45)$$

By means of Eq. (5.44) we have obtained a boosted *56* which is totally symmetric in (a, b, c). By means of γ_5-insertion we can obtain alternative boosts, in a similar way as was described for the *36*. For example we can start from $(\gamma_5)_\rho{}^\lambda(\gamma_5)_\sigma{}^\mu B^{\rho A,\sigma B,\nu C}(0)$ instead of from Eq. (5.43), and we can insert γ_5 pairs in a variety of ways, always ending up with a boosted *56* which has the same parity as does $B^{abc}(p)$. This is the variety of boosts discussed in [B 28] (where a γ-representation was chosen in which γ_5 is diagonal). These asymmetric boosts will not be used explicitly in what follows, but we shall comment further on them in Sec. VC and D.

The totally symmetric boosted anti-*56* is given by

$$C^{abc}(p)=D_\rho{}^\lambda(p)D_\sigma{}^\mu(p)D_\tau{}^\nu(p)C^{\rho A,\sigma B,\tau C}(0), \quad (5.46)$$

where $C(0)$ is obtained from $B(0)$, Eq. (5.42) by the replacement

$$u^{(\lambda\mu\nu)}(0)\to v^{(\lambda\mu\nu)}(0), \qquad u^{\lambda}(0)\to v^{\lambda}(0), \quad (5.47)$$

where $v^\lambda(0)$ is given in (5.21) and $v^{(\lambda\mu\nu)}(0)$ is the negative energy function which corresponds similarly to $u^{(\lambda\mu\nu)}(0)$.

Remarks. (a) The enlargment of the number of components which we have met several times is always necessary in order to have boosted super multiplets with a definite parity [S 11]. (b) The wave equations satisfied by the boosted functions are the Bargmann–Wigner equations [B 32, S 13, S 15].

5. *The Group* $U(6, 6)$

Consider the set Γ^X of 16 Hermitian matrices defined by

$$\Gamma^X\colon \rho^\lambda\otimes\sigma^\mu \qquad X=1,\cdots,16.$$

$$\rho^\lambda=(\varrho, 1), \qquad \sigma^\mu=(\sigma, 1). \quad (5.48)$$

The ρ and the σ sets are each made up of the 2×2 Pauli matrices and a 2×2 unit matrix. The direct product notation in (5.48) is explained after Eq. (4.7), we write briefly $\Gamma^X\colon(\rho^\lambda\sigma^\mu)$. The Γ^X may be considered as the DG of a $U(4)$. Equivalent to (5.48) is the set

$$\Gamma^X\colon (1, \gamma_\mu, \sigma_{\mu\nu}, i\gamma_\mu\gamma_5, \gamma_5) \quad (5.49)$$

of 4×4 Hermitian Dirac matrices. In analogy with Eq. (4.7) we can define a 144 set of 12×12 matrices

$$T^K\colon \Gamma^X F^P; \qquad (T^K)_b{}^a=(\Gamma^X)_\mu{}^\lambda(F^P)_B{}^A, \quad (5.50)$$

$$P=0, 1, \cdots, 8, \qquad K=1, \cdots, 144.$$

The F^P are the DG of $U(3)$, and the T^K are those of a group $U(12)$.

It has been explained in Eq. (3.89) how one can associate the DG of pseudo-unitary groups to the DG of a unitary group. Following the prescriptions given there we define a set $\tilde{T}^K$ by

$$\tilde{T}^K=\tfrac{1}{2}(1+i)T^K+\tfrac{1}{2}(1-i)\Gamma T^K\Gamma, \quad (5.51)$$

where the 12×12 matrix Γ is given by

$$\Gamma_b{}^a=(\gamma_4)_\mu{}^\lambda\delta_B{}^A, \qquad a=(\lambda A), \qquad b=(\mu B). \quad (5.52)$$

Thus Γ is the direct product of γ_4 and the unit DG of $U(3)$. Γ is of the form (3.82) with $M=N=6$. Hence the $\tilde{T}^K$ are the DG of $U(6, 6)$.

For any p the $u^a(p)$ defined in (5.24) may be regarded as a fundamental representation of $U(6, 6)$. Indeed, the infinitesimal transformation (with real ϵ^K)

$$u^a(p)\to(1+i\epsilon^K\tilde{T}^K)_b{}^a u^b(p) \quad (5.53)$$

satisfies

$$\bar{u}_a(p)u^a(p)=\text{invariant}; \qquad \bar{u}_a=u_a{}^*\Gamma_b{}^a \quad (5.54)$$

where we have a special case of Eqs. (3.81–86). Here we have used Eq. (3.89), namely $\tilde{T}^K=\Gamma\tilde{T}^{K\dagger}\Gamma$. $\bar{u}_a(p)u^a(p)$ is "the mass term" and $U(6, 6)$ is the group which leaves the mass term invariant. But it does not leave invariant "the kinetic energy term" $\bar{u}_a(p)(\gamma p)_b{}^a u^b(p)$ as is evident from Eq. (5.53). (At this point we recognize the formal device of introducing more translations as a means to get an "invariant generalized kinetic energy term," as discussed in Sec. VA.)

The quadratic form (5.54) is also a scalar density with respect to the Poincaré group, as is seen by the application [S 11] of an inhomogeneous Lorentz transformation (a, Λ):

$$u^{\lambda A}(p)\to e^{ipa}S_\mu{}^\lambda u^{\mu A}(\Lambda^{-1}p). \quad (5.55)$$

It is important to note that the matrix

$$(S_\mu{}^\lambda\delta_B{}^A) \text{ is contained in the } (\tilde{T}^K)_b{}^a. \quad (5.56)$$

One can build a tensor calculus for $U(6, 6)$. For example $\bar{u}_a(p_1)u^b(p_2)$ is a (reducible) $U(6, 6)$ tensor *for any* p_1, p_2. In particular we meet the following finite dimensional, and therefore nonunitary, representations.

(a) $\mathfrak{M}_b{}^a(q)$ given in Eq. (5.37) is the *143* of $U(6, 6)$.

(b) $B^{abc}(p)$ given in Eq. (5.44) is also a $U(6, 6)$ tensor. [It belongs to the representation with partition (3) and dimension $D_{12}(3)=364$ of $U(6, 6)$ see Eq. (3.12). For more details on $U(6, 6)$ tensor calculus see [D 8].]

Once one has a tensor calculus one can build interactions. Consider as a simple example

$$g(q^2)\bar{u}_a(p_1)\mathfrak{M}_b{}^a(q)u^b(p_2), \qquad q=p_2-p_1 \quad (5.57)$$

where $g(q^2)$ is a form factor. For definiteness we consider the sextet to be on the mass shell. (5.57) is an $U(6, 6)$ scalar. It also has the right covariance structure because of (5.56). Equation (5.57) involves an assumption of analytic continuation. By boosting, $\mathfrak{M}(q)$ was obtained for q's for which $q^2=-\mu^2$. It is assumed that

CC-0. In Public Domain. Gurukul Kangri Collection, Haridwar

Digitized by Arya Samaj Foundation Chennai and eGangotri

this expression may be continued off the mass shell, as in (5.57).

Crossing symmetry is not part of $U(6,6)$ but is not at variance with the latter symmetry. For example [B 28] the substitution rules $u^\mu(p_2)\to v^\mu(-p_2)$; $q=(p_2-p_1)\to q=-p_2-p_1$ applied to Eq. (5.57) bring us to a crossed channel.

The baryon–meson vertex proposed for $U(6,6)$ is $f(q^2)\bar{B}_{abc}(p_1)\mathfrak{M}_d{}^c(q)B^{abd}(p_2)$, [S 13, B 28, S 15]. This form implies a common form factor for all values of q^2.

This is a far stronger assumption than the one given in Eq. (5.10) in connection with a preliminary discussion of the P-wave vertex. It has become clear in the intervening period that the strong $f(q^2)$-assumption is by no means necessary to derive any of the vertex predictions that are considered "good." In Sec. VC we turn to a discussion of the vertex under what appear to be minimal conditions for obtaining the good results.

Remarks. (1) Concerning mass formulae for $U(6,6)$ and related groups see [R 13, C 12]. (2) Trilinear meson couplings are discussed in [B 32, G 23, H 15, G 24]. (3) Other boosted supermultiplets and their vertices are discussed in [S 16, D 9, D 10, D 12, H 18]. Note in particular that in the U(6, 6) limit many decay modes of higher resonances are forbidden [H 16]. (4) For parity assignments to $U(6,6)$ representations see [C 13]. (5) Instead of considering the vertices mentioned above to be of the effective kind, one can also try to think of them as a Lagrangian interaction. Then the free kinetic energy terms are explicit symmetry breaking terms. In this way one formulates at least in principle a dynamical theory. See the survey [D 8] and also [O 6]. In this approach the boosted *36*, *56*, etc., are considered as primitive fields. The frustrating thing is that one does not know how to calculate reliably with such a scheme. (6) *Added note.* For a relativistic version of the "recoupled" multiplets discussed in Sec. IVB, see [G 28].

C. The Baryon–Meson Vertex

We consider the covariant coupling of the baryon octet to pseudoscalar and to vector mesons in the $SU(3)$-symmetry limit and make only one additional assumption [P 4].

(A) The baryon octet is part of the totally symmetrical boosted *56*.

The vertex then has the following form

$$\bar{B}_{abc}(p_1)\mathfrak{M}_d{}^c(q)B^{abd}(p_2), \qquad q=p_2-p_1, \quad (5.58)$$

where we mean by B^{abd} the octet part of Eq. (5.44) and where

$$\mathfrak{M}_d{}^c(q)=\{f_V(q^2)i\gamma\epsilon(q)V-f_A(q^2)\gamma_5[(\gamma q)/\mu]P$$
$$-f_T(q^2)[i\sigma_{\mu\nu}q_\mu\epsilon_\nu(q)/\mu]V-if_P(q^2)\gamma_5P\}_d{}^c. \quad (5.59)$$

The form factors f_V, f_A, f_T, f_P are considered to be four independent functions of q^2. We take the baryons to be on the mass shell, so no questions arise of analytic continuation of boosted functions.

$SU(3)$ contractions reduce (5.58) to

$$4(D+F)\bar{u}\mathfrak{N}u[1+(q^2/4M^2)]$$
$$-\tfrac{1}{4}(D-F-2T)\bar{u}\{Z_2Z_1\mathfrak{N}\}u$$
$$-\tfrac{1}{2}(D-T)\bar{u}Z_2\mathfrak{N}'Z_1u, \quad (5.60)$$

where

$$Z_i=1-(i\gamma p_i/M), \qquad \mathfrak{N}'=\gamma_5C\mathfrak{N}{}^tC^{-1}\gamma_5.$$

{ } denotes a trace with respect to the Dirac matrices. The following definitions have also been used:

$$D\bar{u}\mathfrak{N}u=\bar{u}_B{}^A(\mathfrak{N}u+u\mathfrak{N})_A{}^B,$$
$$F\bar{u}\mathfrak{N}u=\bar{u}_B{}^A(\mathfrak{N}u-u\mathfrak{N})_A{}^B,$$
$$T\bar{u}\mathfrak{N}u=\bar{u}_B{}^A\mathfrak{N}_C{}^Cu_A{}^B. \quad (5.61)$$

Equation (5.60) yields the following results (divide by 6 and drop the $\bar{u}$, u symbols).

1. Pseudoscalar Vertex

$$-i[D+(2F/3)-T/3][1+(q^2/4M^2)]\gamma_5$$
$$\times[(2M/\mu)f_A(q^2)+f_P(q^2)], \quad (5.62)$$

so that

$$D/F=\tfrac{3}{2} \text{ for all } q^2. \quad (5.63)$$

Remarks. (1) From $SU(3)$ alone it follows in general that the D/F ratio may be a function of q^2. (2) The alternative boosts of the *56* with γ_5-insertions as described in Sec. VB give different values for D/F [B 28, R 9]. I learned from N. Cabibbo and M. Veltman the following elegant way to obtain these various alternative vertices from the $\bar{B}\mathfrak{M}B$ vertex, where $\mathfrak{M}$ is given by Eq. (5.38): insert in this vertex in all possible ways pairs of "γ_5 spurions" $(\gamma_5)_\mu{}^\lambda\delta_B{}^A$. This gives the various D/F ratios including the "regular" as well as the "irregular" couplings [R 9]. In Sec. VD the connection between these γ_5 insertions and the group $SL(6,C)$ will be explained. The preceding remarks make clear the necessity of assumption (A) to obtain (5.63).

2. Vector Vertex

$$i[\gamma_\mu F_1(q^2)+\sigma_{\mu\nu}q_\nu F_2(q^2)]\epsilon_\mu(q), \quad (5.64)$$

$$F_1(q^2)=\left\{F+T+\frac{q^2}{4M^2}\left(D+\frac{2F}{3}-\frac{T}{3}\right)\right\}f_V(q^2)$$
$$+\frac{q^2}{2M\mu}\left(D-\frac{F}{3}-\frac{4T}{3}\right)f_T(q^2), \quad (5.65)$$

$$2MF_2(q^2)=\left(D-\frac{F}{3}-\frac{4T}{3}\right)f_V(q^2)$$
$$+\frac{2M}{\mu}\left\{D+\frac{2F}{3}-\frac{T}{3}+\frac{q^2}{4M^2}(F+T)\right\}f_T(q^2). \quad (5.66)$$

CC-0. In Public Domain. Gurukul Kangri Collection, Haridwar

Digitized by Arya Samaj Foundation Chennai and eGangotri

The Sachs-type form factors are defined by

$$G_e = F_1 - (q^2/2M)F_2, \qquad G_m = (F_1/2M) + F_2, \quad (5.67)$$

so that

$$G_e(q^2) = (F+T)[1+(q^2/4M^2)] \times [f_V(q^2) - (q^2/2M\mu)f_T(q^2)], \quad (5.68)$$

$$2MG_m(q^2) = \left(D + \frac{2F}{3} - \frac{T}{3}\right)\left(1+\frac{q^2}{4M^2}\right) \times [f_V(q^2) + (2M/\mu)f_T(q^2).] \quad (5.69)$$

Note that the $D/F/T$ ratios factor out for G_e, G_m but not for the Dirac–Pauli form factors F_1, F_2.

(1) Equation (5.17) follows from (5.68, 69) and the $SU(3)$ assumption that the electromagnetic couplings are proportional to the strong $(\rho^0 + \omega^0/\sqrt{3})$ coupling.

(2) The relation [B 34]

$$G_e^P(q^2) = \text{const.}\ G_m^P(q^2) \quad (5.70)$$

which appears to be in good agreement with experiment [D 6] does not follow from the present considerations. It demands an additional constraint between f_V and f_T [B 35, P 4]. In this connection it is worth while to ask "how relativistic" the Eqs. (5.16, 70) really are and the following remark is perhaps instructive [F 11]. Consider the proton as a rigid sphere which bounces off a brick wall with a momentum transfer of say 500 MeV/c. We have neglected the Lorentz contraction, but $(1-v^2/c^2)^{\frac{1}{2}} \simeq 0.97$ so we make only a 3% error. Thus the "experimental" relations (5.16, 70) may be approximately described as a property of the *static* charge and magnetic moment distributions. In this connection it is of interest that these relations have been derived from an essentially static quark model for the region $q^2/M^2 \lesssim 1$ [B 27]. From this point of view it is of considerable interest to know how good the relations (5.17, 70) are in the truly relativistic region.

(3) The $U(6, 6)$ limit corresponds to

$$f_V(q^2) = f_A(q^2) = f_P(q^2) = f_T(q^2). \quad (5.71)$$

This does give a connection between G_e and G_m [see also the preceding remark (1)], namely [S 13, S 15] $G_e^P/G_m^P = 1 + q^2/2M\mu$. This relation can be modified, however, by arguments about how to continue analytically to $q^2 = 0$ [F 12].

(4) Returning to the strong vertex, we make one additional assumption.

(B) The form factors in (5.59) satisfy the *static* $SU(6)$ limit conditions [B 10]

$$f_V(-\mu^2) = f_A(-\mu^2); \qquad f_P(-\mu^2) = f_T(-\mu^2), \quad (5.72)$$

one of which was already encountered, Eq. (5.10). Put [B 10]

$$f_V(-\mu^2)/f_T(-\mu^2) = \xi, \quad (5.73)$$

where ξ is a free parameter. From Eqs. (5.62–66) one finds the following results for g_A, g_V defined by the P-wave vertex part $g_V P^\dagger P \rho_0^0 + g_A P^\dagger \mathfrak{d} P \nabla \pi^0/\mu$ (ρ_0^0 is the longitudinal component of ρ^0):

$$g_A = \tfrac{5}{3}[f_A(-\mu^2) + (\mu/2M)f_P(-\mu^2)], \quad (5.74)$$

$$g_V = f_V(-\mu^2) + (\mu/2M)f_T(-\mu^2). \quad (5.75)$$

Thus

$$g_A/g_V = \tfrac{5}{3} \text{ independent of } \xi. \quad (5.76)$$

This concludes the discussion of the octet vertex under minimal conditions. For more details see [S 13, S 15]. The closely related vertex for semi-leptonic processes is discussed in [R 15, A 13, K 15].

D. Groups Related to $U(6, 6)$

Equations (5.48–52) imply that the group $U(2, 2)$ has the DG

$$\tilde{\Gamma}^X = \tfrac{1}{2}(1+i)\Gamma^X + \tfrac{1}{2}(1-i)\gamma_4\Gamma^X\gamma_4. \quad (5.77)$$

A subgroup of $U(4)$ has as DG a subset of the Γ^X, call it the set $\Gamma^{(X)}$. The corresponding subgroup of $U(2, 2)$ has the DG

$$\tilde{\Gamma}^{(X)} = \tfrac{1}{2}(1+i)\Gamma^{(X)} + \tfrac{1}{2}(1-i)\gamma_4\Gamma^{(X)}\gamma_4. \quad (5.78)$$

We are interested in such sub groups of $U(6, 6)$ which have as DG those matrices obtained by substituting $\Gamma^{(X)}$ for Γ^X in Eqs. (5.50, 51):

$$\tilde{T}^{(K)}: \tilde{\Gamma}^{(X)} F^P. \quad (5.79)$$

(a)

$$U(6, 6) \supset GL(6, C). \quad (5.80)$$

The corresponding $\Gamma^{(X)}$ and $\tilde{\Gamma}^{(X)}$ are

$$\Gamma^{(X)}: 1, \gamma_5, \sigma_{\mu\nu}; \quad \tilde{\Gamma}^{(X)}: 1, i\gamma_5, \mathfrak{d}, i\gamma_5\mathfrak{d}. \quad (5.81)$$

The corresponding group (5.79) is homomorphic with $GL(6, C)$.

This group has two bilinear invariant forms, namely,

$$\bar{u}_a u^a; \quad i\bar{u}_{\lambda A}(\gamma_5)_\mu{}^\lambda u^{\mu A}. \quad (5.82)$$

Corresponding to this doubling there are more higher rank tensors in this group than in $U(6, 6)$ (for given number of indices). Thus of the set

$$\mathfrak{M}, \gamma_5\mathfrak{M}\gamma_5, \quad (5.83)$$

with $\mathfrak{M}$ defined by Eqs. (5.37–40) only one is a $U(6, 6)$ tensor while both are $GL(6, C)$ tensors. The "γ_5 insertions" discussed in Eq. (5.41) and after Eq. (5.47) just correspond to the breakdown Eq. (5.80). For more details about the tensors of $SL(6, C)$ see [H 17].

(a′)

$$GL(6, C) \to GL(6, C) \otimes GL(6, C) \quad (5.84)$$

by means of the following procedure. Use Eq. (5.81)

CC-0. In Public Domain. Gurukul Kangri Collection, Haridwar

Digitized by Arya Samaj Foundation Chennai and eGangotri

and define

$$\tilde{\Gamma}_{\pm}^{(X)}=\tfrac{1}{2}(1\pm\gamma_5)\tilde{\Gamma}^{(X)}. \tag{5.85}$$

(This is a "complexification" because the γ_5 appears without an i.) $\tilde{\Gamma}_{\pm}^{(X)}F^P$ generate $GL(6, C)\otimes GL(6, C)$. (The subgroup $SL(2, C)\otimes SL(2, C)$ is associated with the proper complex Lorentz group [S 11].)

(b)

$$GL(6, C)\otimes GL(6, C)\supset U(6)\otimes U(6), \text{ chiral} \tag{5.86}$$

is achieved by contracting $\tilde{\Gamma}_{\pm}^{(X)}$ such that $\tilde{\Gamma}^{(X)}$ is restricted to $(1, \mathfrak{d})$. For details on this group see [F 4, D 5, B 16].

(c)

$$U(6, 6)\supset U(6)\otimes U(6)\text{; nonchiral.} \tag{5.87}$$

In this case

$$\Gamma^{(X)}\colon 1, \gamma_4, \mathfrak{d}=\tilde{\Gamma}^{(X)}. \tag{5.88}$$

Consider a one quark state with its $U(6, 6)$ breaking kinetic energy operator. In its rest frame $\gamma p=i\gamma_4 p_0$. In this situation only that subgroup of $U(6, 6)$ survives generated by those DG of $U(6, 6)$ which commute with γ_4. This leads to the set (5.88) [O 6, D 7, H 14].

The determination of the particle content of $U(6, 6)$ multiplets by means of this compact subgroup $U(6)\otimes U(6)$ proceeds as follows. The factors of the $SU(2)\otimes SU(2)$ subgroup of $U(6)\otimes U(6)$ with respective DG $(1\pm\gamma_4)\mathfrak{d}/2$ correspond to quark spin ($\gamma_4=1$) and antiquark spin ($\gamma_4=-1$), respectively (in the rest frame). Correspondingly, the $U(6)$ factors refer to particles and anti particles, respectively. The sextet is $(6, 1)$, the anti sextet is $(1, 6^*)$. See also the note after Eq. (5.21). The meson *35* corresponds to $(6, 6^*)$ and the *56* to $(56, 1)$, the anti-*56* to $(1, 56^*)$, etc.

(d) $SU(6)_W$. Consider two Lorentz-orthogonal unit vectors $\epsilon_\mu{}^1$, $\epsilon_\mu{}^2$: $(\epsilon_\mu{}^i\epsilon_\mu{}^j)=(\epsilon^i\epsilon^j)=\delta^{ij}$. Define

$$W_1=\tfrac{1}{2}i(\gamma\epsilon^1)\gamma_5, \qquad W_2=\tfrac{1}{2}i(\gamma\epsilon^2)\gamma_5, \qquad W_3=\tfrac{1}{2}i(\gamma\epsilon^1)(\gamma\epsilon^2). \tag{5.89}$$

W satisfies the same algebra as does $\mathbf{S}=\mathfrak{d}/2$. Choose the $\epsilon_\mu{}^i$ to be orthogonal to a four-vector p_μ: $(\epsilon^i p)=0$. Then

$$[W, (\gamma p)]=0 \tag{5.90}$$

so W commutes with "the kinetic energy." Choose $p_\mu=(0, 0, p, ip_0)$; $\epsilon_\mu{}^1=(1, 0, 0, 0)$: $\epsilon_\mu{}^2=(0, 1, 0, 0)$, then W reduces to the expression (5.15).

One also arrives at (5.15) as follows [O 6, D 7, H 14]. Consider the kinetic energy operator (γp). For p in the 3-direction this becomes $\gamma_3 p_3+i\gamma_4 p_0$. Let p represent any of the four-vectors which may occur in a collinear configuration. The breakdown of $U(6, 6)$ to a lower symmetry then amounts to finding the subset of the Γ^X, Eq. (5.49) which commute with γ_3, γ_4. This is the W-spin set (5.15). The consequences of $SU(6)_W$-symmetry are discussed further in Sec. VF.

(e) $U(3)\otimes U(3)$. Consider a coplanar configuration with "3" the direction normal to the plane. The corresponding surviving set $\Gamma^{(X)}$ is

$$\Gamma^{(X)}=\tilde{\Gamma}^{(X)}\colon 1, \gamma_4\sigma_3, \tag{5.91}$$

and the group in question has DG $(1\pm\gamma_4\sigma_3)F^P/2$.

$U(6)$ representations are reducible under this group, for example [D 7]: $56=(3, 6)+(6, 3)+(1, 10)+(10, 1)$. The decuplets are the $S_3=\pm\frac{3}{2}$ components of the *56*. The remainder corresponds to the $S_3=\pm\frac{1}{2}$ parts.

Equation (5.91) implies spin conservation normal to the plane. From this symmetry alone nucleon-nucleon scattering predictions have been derived [D 7] which were found and are further discussed in [K 9, A 6].

E. Unitarity; Other Implications

For any of the groups discussed in Sec. VD one can by tensor contraction construct scalars which (wherever applicable) can represent effective matrix elements. This is true not only for vertices but also for scattering, annihilation processes etc. $SU(3)$-violating effects must play a quite important role for many of these processes [A 1, H 2] and a systematic method for dealing with such violations is not available at present. This is to be compounded with violations of the higher symmetries under discussion.

1. The Unitarity Problem

Soon after the examination of the consequences of $U(6, 6)$ and related groups had begun, it was realized that these symmetries are not compatible in general with the unitarity conditions [B 36, B 37, G 26]. An example will clarify the point.

Consider an $SU(6, 6)$ invariant scattering amplitude

$$f(s, t)\sum_K \bar{u}_a(p_4)(\tilde{T}^K)_b{}^a u^b(p_1)\cdot\bar{v}_c(p_2)(\tilde{T}^K)_d{}^c v^d(p_3) \tag{5.92}$$

for the scattering $S(p_1)+\bar{S}(p_2)\to\bar{S}(p_3)+S(p_4)$ (S=sextet, $\bar{S}$=antisextet). The summation over K ranges over the 143 DG of $SU(6, 6)$, see Eq. (5.51). Equation (5.92) is $SU(6, 6)$ invariant for any set of values p_1-p_4. Strict $SU(6, 6)$ implies a common form factor $f(s, t)$ for all the 143 terms in the sum. But this is in conflict with unitarity in the elastic region, as a simple calculation shows [B 36]. Briefly stated, the closure in the unitarity sum is effected by the introduction of projection operators which behave like the kinetic energy terms often referred to, and which almost always break the invariance. The unitarity conflict exists independently of any details regarding a possible underlying local field theory. A few technical comments follow.

(a) Stripped of its inessential $SU(3)$ details, the mentioned example amounts to saying that a four-fermion interaction cannot be an equal mixture of P, V, A, and T for all s, t without violating unitarity.

CC-0. In Public Domain. Gurukul Kangri Collection, Haridwar

Digitized by Arya Samaj Foundation Chennai and eGangotri

(b) It was noted in [B 36] that the unitarity conflict is not confined to $U(6, 6)$ but holds true for more general relativistic completions. This aspect is discussed in more detail in [A 14, B 39], where it is shown that the same problem arises also for $SL(6, C)$ and also if one allows for the introduction of all possible $(\gamma\dot{p})$ spurions.

(c) The unitarity condition is satisfied "asymptotically" as we go to zero velocities [B 36]. The unitarity violations are of the characteristic order $(v/c)^2$. In the nonrelativistic limit one can implement one-particle unitarity for meson–baryon scattering. This leads to $SU(6)$-coupling constant sum rules [B 36] which are closely related to the J–T relations. Sum rules of this kind for broken $SU(6)$ are considered in [C 14].

(d) For some cases unitarity can be saved at the price of crossing symmetry [B 38]. *Added note.* See also [B 49].

(e) As far as I understand it, it is a matter of language whether or not the collinear group $SU(6)_W$ is compatible with unitarity. The group makes no claims concerning nonforward directions which are coupled to the forward direction in the unitarity sum. One may say that this coupling is not comprehended by $SU(6)_W$.

(f) A formal unitarity condition can be satisfied if extra translations are introduced [H 19].

The unitarity conflict would be a violation of our physical principles if an approximate kinematical symmetry were involved. From the present phenomenological point of view it means a most severe restriction: the two sides of a unitarity relation cannot both be right. This circumstance together with the $SU(3)$-breaking problem mentioned earlier makes it no great surprise that not many encouraging phenomenological clues have emerged in the subsequent investigation of specific processes.

2. *Meson–Baryon Scattering*

Static $SU(6)$-type studies have been made along the lines of Sec. IVG [C 2, B 40, B 41]. However, no S-wave projection has been studied separately as was done for the nucleon–nucleon case. It is therefore not easy to interpret the results. Relativistic calculations [R 16, C 15, B 37, M 7] give several bad predictions in the symmetry limit such as no Ξ polarization in $K^-p\to\Xi^-K^+$.

3. *Baryon–Baryon Scattering* [K 9, A 6, S 17, F 13]

No suggestive regularities are found. Some disagreeable features remain also in the presence of spurions. The most detailed numerical comparisons are in [K 9]. For $B\bar{B}$-scattering see [A 6, B 42].

4. *Nucleon–Antinucleon Annihilation at Rest*

The following discussion is for annihilation purely from the S state. First consider the case of $U(6, 6)$ symmetry. Then the nucleon is in $B^{abc}(0)$, Eq. (5.44) and the antinucleon in $C^{abc}(0)$, Eq. (5.46).

(a) The following property of the once contracted product is important

$$\bar{C}_{abc}(0)\,B^{ade}(0)=0. \tag{5.93}$$

This is a direct consequence of $\bar{v}_a(0)\,w^a(0)=0$, Eqs. (5.20, 21). This type of orthogonality can be expressed in terms of a selection rule [H 23]. Equation (5.93) applied to the $\bar{C}B$-current gives [H 21]

$$\bar{p}+p\to e^+e^-\text{: forbidden.} \tag{5.94}$$

(b) *2-meson annihilation.* Equation (5.93) gives

$$\text{nucleon}+\text{antinucleon}\to 2\text{ mesons: forbidden,} \tag{5.95}$$

not only for PP channels (P=pseudoscalar meson) [H 20, H 21] but also for PV combinations [D 13, C 16]. There are some models which involve some PP suppression, but in any case (5.95) is not good for the $\rho\pi$ mode which is appreciable. Its rate is $\sim$10 times the 2π rate [B 43].

Several investigations have been made about 2-meson annihilation using lower symmetry. First, a single spurion of the type $(\delta\mathbf{q})$ was introduced but this leads to a new difficulty. It predicts (R=rate)

$$\frac{R(K^+K^-)}{R(K_1^0K_2^0)}=\frac{16}{1} \tag{5.96}$$

see [H 20, D 14, A 15]. (The result of [K 16] does not agree with this answer.) This is to be compared with an experimental ratio $(1.1\pm0.1)/(0.61\pm0.09)$, [B 43]. Other attempts to treat 2-meson annihilation proceed by the introduction of a pair of (γq) or of γ_5 spurions [H 22, L 11]. This leads to better results for the ratio in Eq. (5.96). Also the result $R(\rho\pi)/R(\pi\pi)\cong 6$ was obtained [M 8]. It appears that so far no compelling conclusion can be drawn from 2-meson annihilation.

(c) *3-meson annihilation.* Returning to $U(6, 6)$, the identity Eq. (5.93) implies a unique coupling in this case. A main consequence is that annihilations involving a ϕ or strange mesons are forbidden [D 13, C 16]. In $\bar{p}p$ annihilation, ϕ production is rare and the $KK\pi$ to 3π ratio is small [B 44, B 45]. (Note that $KK\pi$ means a true three-body channel, not K^*K.) The predictions also hold for $\bar{n}p$ annihilation for which no detailed data are yet available.

More detailed predictions in the 3-meson case include the following [C 16]. [Note that these allow for the inclusion of the parameter ξ defined in Eq. (5.73).]

(α) The $3P$ annihilations should be in the ^1S state. This is in agreement with an experiment [B 45] on nonresonant 3π annihilation.

(β) The ratio $R(\pi^+\pi^-\pi^0)/R(\pi^+\pi^-\eta^0)$ should be $\simeq 3$. The experimental ratio is $(3.3\pm0.5)/(1.2\pm0.3)$ [F 14].

(γ) The PPV annihilation should be in the ^3S state. This is in agreement with an experiment on $\omega\pi\pi$ annihilation [B 46].

CC-0. In Public Domain. Gurukul Kangri Collection, Haridwar

Digitized by Arya Samaj Foundation Chennai and eGangotri

(δ) The ratio $R(\pi^+\pi^-\rho^0)/R(\pi^+\pi^-\omega)$ should be $\simeq 1$. This is to be compared with an experimental ratio $(5.8\pm1.0)/(3.9\pm0.5)$ [F 14].

The $U(6, 6)$ predictions therefore reproduce some of the striking experimental regularities about preferred angular momentum states. Moreover the predicted $(3\pi/2\pi\eta)$ and $(2\pi\rho/2\pi\omega)$ ratios are not in disagreement with the present experimental information. All these results do *not* depend on a prescribed relative strength of pseudoscalar meson/vector meson coupling. They do depend on the totally symmetric boosted structure for baryons and antibaryons. It will be very interesting to see how the $\bar{p}n$ predictions [C 16] will fare.

(d) *4-meson annihilation.* $U(6, 6)$ forbids $\bar{p}p\rightarrow K^+K^-\pi^+\pi^-$ [H 23]; for more details on these channels see [L 12].

Added note. The reactions $\bar{P}P\rightarrow\bar{B}B$ are discussed in [B 50].

F. W-Spin

We now continue the discussion of $SU(6)_W$ started in Sec. VC. It was noted there that **W**, Eq. (5.15), acts in the same way on a sextet (but not on an antisextet) state at rest as does **S**. The same is therefore true for a multi-sextet state. It follows that the baryon *56*, looked upon as a representation of static $SU(6)$ is likewise a representation *56* of $SU(6)_W$. In addition, W commutes with the DG $\gamma_5\sigma_3$ for Lorentz transformations in the 3-direction of motion. Thus also for $p_3\neq0$ we may assign the baryon to the same $SU(6)_W$ representation *56* as for $p_3=0$; and likewise for other baryon representations. This is sometimes called the boost-free property (in the direction of motion) of $SU(6)_W$ representations [L 9].

For mesons we have a *35* (not *36*) of $SU(6)_W$ which is $\neq$*35* of static $SU(6)$ (even for $p_3=0$), because mesons are like a sextet–antisextet system. To see what happens, let $V_{1,0,-1}$ and P be a degenerate quartet of vector mesons (with helicities 1, 0, -1) and a pseudoscalar meson which are (for illustration purposes only) written as fermion pairs as follows.

$$V_1=\bar{f}_\uparrow f_\uparrow,\qquad V_0=(1/\sqrt{2})(\bar{f}_\uparrow f_\downarrow-\bar{f}_\downarrow f_\uparrow),\qquad V_{-1}=-\bar{f}_\downarrow f_\downarrow,$$
$$P=(1/\sqrt{2})(\bar{f}_\uparrow f_\downarrow+\bar{f}_\downarrow f_\uparrow).$$

f is the fermion, $\bar{f}$ its antiparticle, the indices denote S_3 values. Let S_- be the spin lowering operator: $S_-V_1=V_0$, $S_-V_0=V_{-1}$, $S_-V_{-1}=0$. There is a corresponding W-spin operator W_- which acts the same on f but with different phases on $\bar{f}$ [for which $\gamma_4=-1$ in Eq. (5.15)]. We now have $W_-V_1=P$, $W_-P=V_{-1}$, $W_-V_{-1}=0$. Going from a single f to the $SU(3)$ triplets we therefore get the following multiplets for $SU(6)_W$ [C 17].

$$35=(8, 3)+(8, 1)+(1, 3);\ (W),$$

where (a) $(8, 3)$ is an $SU(3)$ octet with W-spin 1. It contains the vector octet with $S_3=\pm1$ and the pseudoscalar octet. (b) $(8, 1)$: W-spin 0. This is the vector octet with $S_3=0$. (c) $(1, 3)$: unitary singlet, W-spin 1. Its members are $\phi_1{}^0$, X^0, $\phi_{-1}{}^0$. Note how the inclusion of X^0 in a $U(6, 6)$ multiplet remains necessary in the $SU(6)_W$ subgroup.

In addition one has the representation $1=(1, 1)$ to which the $\phi_0{}^0$ is assigned.

Furthermore a photon $\gamma_{\pm1}$ with helicity ±1 may be considered as a W-spin 1 (and U-spin zero) member of an $(8, 3)_W$, while a virtual photon γ_0 is like a member of an $(8, 1)_W$ [C 17]. Such assignments enable the analysis of photo- and electroproduction by means of W-spin methods.

The following are some applications of $SU(6)_W$.

(a) Recalling that $W=S$, $W_3=S_3$ for baryons, one easily verifies that $\rho\rightarrow2\pi$; $N^*\rightarrow N\pi$ are W-spin allowed decays.

(b) MB$\rightarrow$MB, elastic and inelastic. From Eq. (3.25) applied to 35_W and 56_W, it follows that there are four independent amplitudes. This leads to many relations [C 17] *always for forward or backward configurations.*

(α) The J–T relation. It should be noted that this relation had been shown to be independent of any particular form of relativistic completion [B 36, C 18].

(β) A number of reactions are forbidden, like $K^-P\rightarrow K^-N^{*+}$, $K^+P\rightarrow K^0N^{*++}$ etc.

(γ) Relations for $Y=2$ systems:

$$d\sigma(K^+P\rightarrow K^{*+}P)=2/3d\sigma(K^+P\rightarrow K^0N^{*++})$$
$$=16d\sigma(K^0P\rightarrow K^{0*}P)$$
$$=16/3d\sigma(K^0P\rightarrow K^+N).$$

(δ) Many relations for $Y=1$ and 0 amplitudes. Note in particular:

$$d\sigma(\pi^-P\rightarrow\pi^-N^{*+}):d\sigma(\pi^-P=\pi^0N^{*0}):d\sigma(\pi^-P\rightarrow\pi^+N^{*-})$$
$$=2:9:24.$$

See [O 7]. Several MB-scattering predictions are in disagreement with experiment [C 19, J 4].

(ϵ) For photoproduction see [C 17] and also [D 15].

Added note. See further [J 5, K 18].

(c) For the application of non-leptonic decays see [H 8].

(d) For the vertex one obtains the results stated in [B 31].

G. Conclusion

From the phenomenological study of approximate dynamical symmetries which contain static $SU(6)$ we have so far learned the following. Regarding the main motivation, the inclusion of the baryon–meson vertex, the treatment of the vertex to order v/c is possible with the only additional nonstatic assumption that the boosted *56* remains totally symmetric, Sec. VD. Phenomenologically I regard this vertex to be neither better nor worse understood to v/c than the static vertices discussed in Sec. IV. From the order $(v/c)^2$ on, the unitarity troubles set in which make illusory as a matter of principle any systematic phenomenological comparison.

CC-0. In Public Domain. Gurukul Kangri Collection, Haridwar

Digitized by Arya Samaj Foundation Chennai and eGangotri

Those that have been made give many bad results along with a few interesting ones, such as the J-T relations which emerge as the result of whatever relativistic completion one chooses. Annihilation processes into two mesons have not led to very constructive conclusions so far. There appear to be a number of regularities for $\bar{P}P \to 3$ mesons (in which the number of triplets and of anti-triplets are separately conserved!). Whether these will be of further interest will perhaps be clearer after the corresponding $\bar{P}N$ experiments will be available. Regarding the form factor relations like Eq. (5.17), one may question the extent to which they are truly relativistic for $q^2 < (1\ \mathrm{BeV}/c)^2$, Sec. VC. A number of new and interesting methods have emerged, notably the W spin. No compelling directions have emerged so far from asking the question stated in Eq. (4.77).

VI. CURRENT ALGEBRAS

This section was written in collaboration with M. A. B. Bég.

A. Introduction

This section deals with some of the applications of current commutator algebras [G 27] to dynamical problems involving hadrons. These applications have so far gone in two rather distinct directions.

(I) Current commutation relations supplemented by external information (such as the experimental values of scattering cross sections) have been used for the derivation of strict sum rules. This direction is very promising. In particular an approximately quantitative evaluation of the absolute value of $|C_A/C_V|$ has been achieved in this way [A 16, W 7].

(II) It has been attempted to derive $SU(6)$ and related results as internal consistency properties of some of the approximate solutions of sets of current commutation relations. This approach is aimed at the master problem (B), Sec. I (see also Sec. IVJ). Its status is presently unclear. In particular it is not yet understood in what sense the solutions are approximate.

This survey would not be complete without a discussion of current algebras, but for two reasons this section must be very brief. First, because it is restricted to such applications only which bear on the interpretation of the symmetries discussed in this paper. Secondly, because of the many still open questions which are met in this connection.

B. The Current Algebra $U(12)$

In Eq. (5.50) quantities T^K were defined ($K=1, \cdots, 144$) which are the DG of $U(12)$. In the language of Eq. (3.55) the generators T^K satisfy

$$[T^K, T^L]_- = if^{KLM} T^M, \tag{6.1}$$

where f^{KLM} are the structure constants of $U(12)$. Acting on the defining representation, Eq. (6.1) is a matrix relation between the $(T^K)_b{}^a$, $a, b=1, \cdots, 12$. The $(T^K)_b{}^a$ are Hermitian matrices.

Let $\psi^a(\mathbf{x}, t) = \psi^{\lambda A}(\mathbf{x}, t)$, ($\lambda = 1$–$4$, $A = 1$–3) denote the bare field operator for an $SU(3)$ triplet of spin-$\frac{1}{2}$ particles. $\psi_a{}^\dagger(\mathbf{x}, t)$ is its Hermitian conjugate. They satisfy the equal time anticommutation relations

$$[\psi_a{}^\dagger(\mathbf{x}, t), \psi^b(\mathbf{y}, t)]_+ = \delta_a{}^b \delta(\mathbf{x}-\mathbf{y}). \tag{6.2}$$

Define 144 Hermitian current densities

$$J^K(\mathbf{x}, t) = \psi_a{}^\dagger(\mathbf{x}, t)\,(T^K)_b{}^a \psi^b(\mathbf{x}, t). \tag{6.3}$$

From an uncritical application of Eq. (6.2) and with the help of Eq. (6.1) one obtains

$$[J^K(\mathbf{x}, t),\ J^L(\mathbf{y}, t)]_- = if^{KLM} J^M(\mathbf{x}, t)\,\delta(\mathbf{x}-\mathbf{y}). \tag{6.4}$$

Define

$$Q^K = \int d^3x\, J^K(\mathbf{x}, t). \tag{6.5}$$

Then

$$[J^K(\mathbf{x}, t), Q^L] = if^{KLM} J^M(\mathbf{x}, t). \tag{6.6}$$

$$[Q^K, Q^L] = if^{KLM} Q^M. \tag{6.7}$$

However, it is well known [S 18] that the above "derivation" of Eq. (6.4) is open to serious objection. More strongly singular terms may appear in the right-hand side of Eq. (6.4) because of the singular nature of bilinear products of $\psi^\dagger$ and ψ taken at the same space–time point. Concrete counter examples to special cases of Eq. (6.4) have been given [S 18]. At this stage the study of current commutators branches out in two directions.

(a) For such cases where the converse has not been proved, one introduces relations of the kind (6.4) as an explicit new postulate [G 27]. Furthermore one abstracts from the fact that the relations (6.4) are initially suggested by a representative quark model and makes the additional assumption [G 27] that the relations (6.4) hold (qualified as above) for the set of full (rather than quark) current densities which we shall continue to call $J^K(\mathbf{x}, t)$. Which particular current density one has in mind is specified by the nature of the corresponding representative T^K.

Example. T^K: $\tau^3/2$, (τ^i = isospin). J^K is the isocharge density. Call I^3 the corresponding Q^K, Eq. (6.5). From T^K: $\gamma_5\tau^i/2$ one obtains the isocharge raising and lowering axial densities $\gamma_5\tau^\pm = \gamma_5(\tau^1 \pm i\tau^2)/2$. Denote the corresponding Q^K by $Q_a{}^\pm$. Then

$$[Q_a{}^+, Q_a{}^-] = 2I^3. \tag{6.8}$$

This is the relation which has been applied successfully in the calculation of $|C_A/C_V|$, [A 16, W 7].

(b) One asks for specific dynamical conditions under which at least some of the Eq. (6.4) can be guaranteed to have no extra singular terms on the right-hand side. See for example [A 17] where in particular Eq. (6.8) is justified for some models. Also, nonforward neutrino reactions have been studied with the inclusion of such extra terms in those current commutators for which their existence has not been disproved [A 18].

CC-0. In Public Domain. Gurukul Kangri Collection, Haridwar

Digitized by Arya Samaj Foundation Chennai and eGangotri

Remarks. (α) Because integrations as in Eqs. (6.6, 7) may average out some extra singularities [such as for example a constant times a $\delta'(\mathbf{x}-\mathbf{y})$-function], Eq. (6.6) may be safer than Eq. (6.4) and Eq. (6.7) may be still safer.

(β) The circumstance that Eq. (6.2) does not depend on mass (because of its *equal time* character) has led to the view [G 27] that the validity of the generalized Eq. (6.4) may persist in the presence of symmetry breaking.

(γ) The density corresponding to I^3 is the 4th component of the isovector 4-vector. Likewise $Q_a^{\pm}$ corresponds to the 4th component of the isovector axial vector. As the Γ^x run through the set defined in Eq. (5.49), we meet *all* the invariant S, V, T, A, P densities with factors i automatically included to guarantee Hermiticity. For example, $\psi^\dagger\delta F^P\psi=-i\bar{\Psi}\gamma_5\gamma F^P\psi$, the space part of the axial vector unitary nonet density. The group $U(12)$ of Eq. (6.4) [D 7] is therefore the group of the *Hermitian* current densities. See also subsection D) below.

(δ) Subgroups of $U(12)$ can be recognized by the same method as was used in Sec. VD for $U(6, 6)$, see for example [F 4]. In fact, $U(6, 6)$ and $U(12)$ have such subgroups in common which are less than or equal to the maximal compact subgroups $U(6)\otimes U(6)$ of $U(6, 6)$. Thus the recognition of the role of the chiral or nonchiral $U(6)\otimes U(6)$, of $SU(6)_W$ and of $U(3)\otimes U(3)$ is no unique property of the current algebras per se.

(ϵ) The group $U(12)$ has also been recognized [O 8] in a different physical context as the maximal compact unitary symmetry of quark–antiquark systems. This symmetry group $U(12)$ has quite distinct implications such as the inclusion within a given supermultiplet of states with different baryon numbers.

C. Applications

Take Eq. (6.8) as an example. From this equation:

$$\sum\{\langle P_q\,|\,Q_a^+\,|\,\nu\rangle\cdot\langle\nu\,|\,Q_a^-\,|\,P_{q'}\rangle-\text{“}Q_a^+\leftrightarrow Q_a^-\text{”}\}$$
$$=\langle P_q\,|\,I^3\,|\,P_{q'}\rangle, \quad (6.9)$$

P is a proton state with 4-momentum q_μ (or q_μ'), ν is a complete set of intermediate states. The $|\,C_A/C_V\,|$ calculation proceeds by separating out the neutron from ν and relating the full remaining ν-set to off mass-shell nucleon cross sections via $PCAC$. For the present purpose the following is relevant.

(a) Sum rules are obtained for each value of $q_0(=q_0')$. In the $|\,C_A/C_V\,|$-calculation the limit $q_0\to\infty$ is sometimes taken, but this is not essential [W 7].

(b) Treating the ν-set in full gives $|\,C_A/C_V\,|\simeq 1.2$ [A 16, W 7].

(c) Truncating the scattering cross section integral so as to take only the 33-region into account gives $|\,C_A/C_V\,|\simeq 1.44$, [A 16]. The mentioned results are for a calculation of the type (I) mentioned above.

In order to go to type (II), consider the set of Eqs. (6.7), or a subset thereof. As in (6.9), put these relations between baryon octet states (for example) and consider a further approximation of the ν set, in which one takes out not only the possible baryon octet states, but also decuplet states of zero width, degenerate (or approximately degenerate) with the octet, in the spirit of approximate $SU(6)$ symmetry.

The input of scattering information is now lost. Instead, one asks [L 13, D 7] if there are self-consistent solutions of such sets of equations (not identities) obtained from (6.7) by truncating the ν-set to *56* states only ("one-particle saturation" of intermediate states).

The subset chosen for this purpose is the group of currents corresponding to the chiral group $U(6)\otimes U(6)$, [L 13, D 7] but one may also consider smaller sets, see further [B 47, O 9, R 18]. In this way self-consistent solutions $|\,C_A/C_V\,|=\frac{5}{3}$, $|\,D/F\,|=\frac{3}{2}$ were obtained. These include the $SU(6)$ answers $g_A/g_V=\frac{5}{3}$, $D/F=\frac{3}{2}$. No explicit N^*-N mass degeneracy need be used. (This was also true for the initial derivation, Sec. IVF).

This result raises the general question whether all $SU(6)$ results can be obtained from sum rules like (6.4) and related ones by truncating the intermediate ν set. This seems possible. For example, the characteristic *56* results for the magnetic moments can be obtained by taking matrix elements of magnetic moment operators between *56* states only. In fact, such matrix elements are just the Clebsch–Gordan coefficients [F 15] of the group $U(12)$, or of a specific subgroup such as $SU(6)_W$ which is of interest for vertex calculations.

The question arises if we have learned anything really new from this one particle saturation. In this connection the following theorem [C 20] is important. If one assumes [D 7] that matrix elements are strictly saturated by states which belong to the same $SU(6)_W$ representation then $SU(6)_W$ would be a group of the Hamiltonian. Thus the saturation assumption is equivalent to earlier results and difficulties, but in another language, and the master problem remains open. See also [S 21]. Also, the notion of "approximate saturation" leads to complications [C 20]. Moreover, the uniform application of one-particle saturation for all q_μ appears to lead to difficulties [K 17].

Alternatively one may proceed without the explicit assumption of saturation, but hope that higher states in the ν set cancel in the *commutator* so as to produce the $SU(6)$ results wherever desired [L 13]. Now the burden of proof changes to the demonstration that this cancelation indeed takes place.

There are many other interesting predictions from commutator algebras, combined with the restriction to one-particle ν states only, such as for the charge radius of the proton [L 13, D 7]. But also new questions are raised. Under what dynamical conditions is the algebra consistent (question of extra singularities)? What is the extent to which the algebra exhausts dynamical information? Can the approximate sense of one particle state calculations be justified by a degree of cancelation of higher states in the commutator?

CC-0. In Public Domain. Gurukul Kangri Collection, Haridwar

Digitized by Arya Samaj Foundation Chennai and eGangotri

D. Appendix. Symmetry Group $U(6, 6)$, Current Group $U(12)$ and $GL(12, C)$

The following mathematical remark may perhaps help to make clear how such distinct 12-dimensional unitary groups as the noncompact $U(6, 6)$ and the compact $U(12)$ have both put in an appearance in the discussion of strongly interacting particles.

Consider the four 2×2 matrices $\sigma^\mu=(\mathfrak{o}, 1)$ with matrix elements $\sigma_{mn}{}^\mu$. One sees that

$$\sum_\mu \sigma_{mn}{}^\mu \sigma_{rs}{}^\mu = 2\delta_{ms}\delta_{nr}. \tag{6.10}$$

With the help of this relation and of Eq. (5.48) one obtains a similar relation for the 16 Dirac matrices. It is in fact easy to show the following [for example with the help of Eqs. (3.56, 57]].

Let the Γ^X be the Hermitian DG of a unitary group $U(N)$, represented by matrices $(\Gamma^X)_{mn}$; $X=1, \cdots, N^2$; $m, n=1, \cdots, N$. Norm the matrices so that $\mathrm{Tr}(\Gamma^X)^2$ is independent of X. Then

$$\sum_X \Gamma_{mn}{}^X \Gamma_{rs}{}^X = \text{const.}\,\delta_{ms}\delta_{rn}, \tag{6.11}$$

where the constant depends on the scale set by $\mathrm{Tr}(\Gamma^X)^2$.

Equation (6.11) is invariant under the similarity transformations

$$\Gamma^X \longrightarrow S^{-1}\Gamma^X S, \tag{6.12}$$

where S is any nonsingular complex valued matrix. Thus the group of Eq. (6.11) is $GL(N, C)$. Of course the transformed Γ^X remain Hermitian only for those S which are in $U(N)$.

For $N=12$, consider the following special choices for S.

(α) S satisfies the $U(6, 6)$ condition

$$\bar{S}S=1, \qquad \bar{S}=\gamma_4 S^\dagger \gamma_4. \tag{6.13}$$

Multiply Eq. (6.11) by $\bar{\psi}_m(x)\psi_n(y)\bar{\psi}_r(u)\psi_s(v)$, where ψ_n is a relativistic quark field operator and $\bar{\psi}_n=\psi_n{}^\dagger\gamma_4$. One gets

$$\sum_X \bar{\psi}(x)\Gamma^X\psi(y)\cdot\bar{\psi}(u)\Gamma^X\psi(v)=\bar{\psi}(x)[\psi^t(y)\bar{\psi}^t(u)]\psi(v) \tag{6.14}$$

which is a $U(6, 6)$ current identity in the restricted (quark) sense. The corresponding bilinear invariant $\bar{\psi}(x)\psi(x)$ is "the mass term." Note that $\bar{\psi}(y)\Gamma^X\psi(y)$ is not generally a Hermitian density. Shrinking $SU(3)$ to the identity one obtains $U(2, 2)$ relations of a kind that have long been known [P 5].

(β) S satisfies the $U(12)$ condition

$$S^\dagger S=1. \tag{6.15}$$

Multiply Eq. (6.11) by $\psi_m{}^\dagger(x)\psi_n(y)\psi_r{}^\dagger(u)\psi_s(v)$:

$$\sum_X \psi^\dagger(x)\Gamma^X\psi(y)\cdot\psi^\dagger(u)\Gamma^X\psi(v) = \psi^\dagger(x)[\psi^t(y)\psi^{\dagger t}(u)]\psi(v) \tag{6.16}$$

which is a $U(12)$ identity for non local current densities. The corresponding bilinear invariant $\psi^\dagger(x)\psi(x)$ plays no special role. The connection between unitary and pseudo-unitary currents was referred to before in Eqs. (3.93, 94).

Note that $U(12)$ is a group acting on tensor indices only [like $U(6, 6)$] and not on the arguments like x of the fields (or field operators).

VII. NO-GO THEOREMS FOR CERTAIN APPROXIMATE KINEMATIC SYMMETRIES

At the time that the $SU(6)$ theory began to develop, several theorems were known already which showed that, under a number of rather general conditions, a union of the Poincaré group and an internal symmetry group can only be achieved in the trivial sense of a direct product, unless violence is done to some generally accepted physical principles.

In the language of Sec. IIB, these theorems are applicable to approximate kinematic symmetries. As was noted there, it is a relativistically invariant operation to take the limit "coupling constant→zero." Hence the no go theorems may be applied to this limit world. If inconsistencies appear in the limit world then, in the kinematic case, it is no excuse that the symmetry is broken in the real world. The inconsistency would apply to the real world as well.

The no-go theorems have no bearing on approximate symmetries of the dynamical kind. In this case the symmetry appears in an approximation which itself is not defined in a covariant way. Then it has no meaning to apply to the limit world a symmetry which contains the full Poincaré group. In this class belong static $SU(6)$ and the dynamical groups discussed in Sec. V which contain the static $SU(6)$.

Neither the scope of this paper nor the competence of this author permit a detailed discussion of what has been achieved in the study of no go theorems. However, as they have added so much to the hilarity and confusion in recent discussions of the symmetries at hand, and as they are quite important for the future use of symmetry arguments, it may not be out of place to mention just a few examples. For detailed references, see, e.g. [J 2, S 20, O 10]. For these rigorous theorems, the rigorous definition of a symmetry operation applies: a one-to-one correspondence which associates to any physically realizable state another such state in such a way that all transition probabilities are preserved [S 11].

A number of no-go theorems were derived in response to the following question. In the conventional way of dealing with internal symmetries, one assumes that the over-all symmetry is the direct product $T\otimes P$ (T=internal symmetry group, P=Poincaré group) in the kinematic limit in which T is exact. As a result, all particles in a T multiplet have the same mass. Is it possible to have a symmetry group G which (in the kinematical limit) contains T and P, but not as a direct product, so that the imposition of G would allow

CC-0. In Public Domain. Gurukul Kangri Collection, Haridwar

Digitized by Arya Samaj Foundation Chennai and eGangotri

for the possibility of a unified description of particles with different mass?

Consider first the case: T is any semi-simple Lie group, with generators T_A; the set of generators of G is neither less nor more than the combined set T_A and the ten generators L_i of P. One can next proceed in either of two ways.

(α) Assume in addition that $[T_A, J_{\mu\nu}]=0$ where the six $J_{\mu\nu}$ are the subset of L_i corresponding to the homogeneous Lorentz group. It follows from these assumptions [M 9] that also $[T_A, P_\mu]=0$, where the four P_μ are the translation operators, so that $G=T\otimes P$ again.

(β) Assume in addition that $[H_a, L_i]=0$. Here the H_a are the maximal commuting subset of the T_A in terms of which the (additive) quantum numbers of T are defined, see Eq. (3.57). It follows also from these assumptions that $G=T\otimes P$ [C 22]. See also [T 3].

Thus, in physical terms, the Lorentz invariance of the internal quantum numbers is sufficient to prove that all members of multiplets must have the same mass and spin. The two theorems just mentioned can also be applied to the case that T is any compact group. Their proofs do not exclude [M 9, C 22] the possibility that something new might happen if the number of generators of G is larger than was specified above.

The next important step in weakening the conditions on G is contained in the following theorem [O 11]. Let G be a Lie group of finite order which contains P as a subgroup. The irreducible representations of G define a Hilbert space. The mass operator P_μ^2 and any power of P_μ^2 are assumed to be self-adjoint over this Hilbert space. Then the spectrum of P_μ^2 is either a single point or else it is continuous. (It was not shown that the continuous case is actually realizable.)

Subsequently, this theorem was still further strengthened as follows [R 17]. Let G again be a Lie group of finite order, the Lie algebra of which contains the Lie algebra of P as a subalgebra. Then in any irreducible representation of G, P_μ^2 cannot have more than one eigenvalue.

Thus for finite order Lie groups there is no way known to escape from the $T\otimes P$ structure. There are no general theorems known for infinite parameter groups, but such groups do not seem too attractive for other reasons. One special no go theorem in this category is the result [J 2] mentioned in Sec. IVA.

Finally, a conjecture should be noted [C 23] which has been stated for the case that the kinematic group G is a connected Lie group which is "particle finite." This means that (a) $G\supset P$, (b) G has at least one locally faithful unitary representation which under P decomposes into the direct sum of a finite number of positive-mass representations of P with mass $<M$ (where M is any finite positive mass). The conjecture says that any connected particle finite Lie group is locally isomorphic to $T\otimes P'$, where T is a compact Lie group, and P' is a trivial extension of P. The conjecture has been proved for the case that G is locally isomorphic to the semi direct product of a semi-simple Lie group and an Abelian group (the latter containing the P_μ); no counter examples to the conjecture are known.

VIII. QUESTIONS

Many of the questions collected in this concluding section were met in the previous parts of this survey.

(a) In explaining the distinction between kinematical and dynamical symmetry, atomic analogies may have been helpful. It is clear, however, that this distinction can be fully abstracted from the question of a possible substructure of baryons or mesons. Nevertheless, the question remains: is there such a substructure in terms of prime matter? Could such matter have unusual properties (such as parastatistics) which "average out" for the usual hadrons? As to whether or not triplets are the answer, it has been seen that one must further ask: is $SU(3)$ the biggest internal symmetry group?

(b) Is it at all true that $SU(3)$ is an approximate symmetry of the kinematic type? There is a perhaps related technical question: why have all higher symmetries that have had some measure of success been more manifest for masses and vertices while scatterings etc. are much less transparent? Higher symmetry means: higher than the direct product of isospin and hypercharge. Are even the latter two of the kinematical kind?

(c) Are there other ways to think of symmetry in particle physics than the approximate ways discussed before? (Lorentz invariance is globally an approximate kinematic symmetry in the presence of gravitational coupling. Yet it is a strict symmetry in local inertial frames!)

(d) The master problem (B), Sec. I is so far still open. In spite of its successes for the derivation of sum rules, it has not been shown that the algebra of currents provides the answer. Is it possible to show, where desired, that the contributions of higher intermediate states inserted in the commutators cancel out, sometimes to a very high degree?

(e) The intrinsic breaking of some of the symmetries discussed here by kinetic energy terms is reminiscent of strong coupling approximations [P 1, B 9] where the interaction terms are diagonalized first. In the old-fashioned strong coupling calculations some masses are put equal to infinity from the start. Can one obtain some dynamical symmetries in strong coupling approximations with masses kept finite? [C 21].

(f) To what extent are dynamical symmetries other than static $SU(6)$ useful for a phenomenological description? Is the independence of q^2 of a number of form factor ratios an indication for the approximate validity of W-spin, or should this approximate q^2-independence [for $q^2\lesssim(1\ \mathrm{BeV}/c)^2$] be explained as a property of static charge and magnetic moment distributions?

Are noncompact spectrum generating algebras a useful tool in particle physics [D 16, C 21]?

(g) Are there any alternatives left to the internal

CC-0. In Public Domain. Gurukul Kangri Collection, Haridwar

Digitized by Arya Samaj Foundation Chennai and eGangotri

symmetry⊗Poincaré group picture in the face of the no-go theorems?

REFERENCES

A 1. Abarbanel, H., and C. Callan, Phys. Letters **16,** 191 (1965).
A 2. Akhizer, A. I., and M. P. Rekalo, JETP Letters **1,** 29 (1965).
A 3. Anisovich, V. V., *et al.*, Phys. Letters **16,** 194 (1965).
A 4. Albright, C. H., and L. S. Liu, Phys. Rev. Letters **13,** 673 (1964); **14,** 324, 532(E) (1965).
A 5. Albright, C. H., and L. S. Liu, Phys. Rev. **140,** B748 (1965).
A 6. Akyeampong, D. A., and R. Delbourgo, Phys. Rev. **140,** B1013 (1965).
A 7. Altarelli, G., F. Buccella, and R. Gatto, Phys. Letters **14,** 70 (1965).
A 8. Alles, W., Phys. Letters **16,** 359 (1965).
A 9. Alles, W., and G. Segre, Phys. Letters **15,** 94 (1965).
A 10. Ademollo, M., G. Altarelli, and R. Gatto, Phys. Rev. Letters **14,** 420 (1965).
A 11. Alfaro, V. de, and Y. Tomozawa, Phys. Rev. **138,** B1193 (1965).
A 12. Altarelli, G., F. Buccella, G. Preparata, and R. Gatto, Phys. Letters **16,** 174 (1965).
A 13. Altarelli, G., G. Preparata, and R. Gatto, Nuovo Cimento **37,** 1817 (1965).
A 14. Alles, W., and D. Amati, Nuovo Cimento **39,** 758 (1965).
A 15. Alles, W., E. Borchi, G. Martucci, and R. Gatto, Phys. Letters **17,** 328 (1965).
A 16. Zdler, S., Phys. Rev. Letters **14,** 1051 (1965); Phys. Rev. **140,** B736 (1965).
A 17. Adler, S., and C. G. Callan, Cern Report Th587 (1965).
A 18. Adler, S., Phys. Rev. **143,** 1144 (1966).
A 19. Azimov, Ya., V. Anisovich, A. Anselm, G. Danilov, and I. Dyatlov, JETP Letters **2,** 68 (1965).
A 20. Albright, C. H., and L. S. Liu, Phys. Rev. **140,** B1611 (1965).
B 1. Behrends, R. E., J. Dreitlein, C. Fronsdal, and B. W. Lee, Rev. Mod. Phys. **34,** 1 (1962).
B 2. Baird, G. E., and L. C. Biedenharn, J. Math. Phys. **4,** 1449 (1963).
B 3. Biedenharn, L. C., J. Math. Phys. **4,** 436 (1963).
B 4. Bég, M. A. B., and H. Ruegg, J. Math. Phys. **6,** 677 (1965).
B 5. Bég, M. A. B., and V. Singh, Phys. Rev. Letters **13,** 509 (1964).
B 6. Bég, M. A. B., and V. Singh, Phys. Rev. Letters **13,** 418, 601(E) (1964).
B 7. Baird, G. E., and L. C. Biedenharn, *Proceedings of the Coral Gables Conference* (W. H. Freeman and Co., San Francisco, 1964), p. 58.
B 8. Bég, M. A. B., and A. Pais, Phys. Rev. **137,** B1514 (1965).
B 9. Bég, M. A. B., B. W. Lee, and A. Pais, Phys. Rev. Letters **13,** 514, 650(E) (1964).
B 10. Bég, M. A. B., and A. Pais, Phys. Rev. **138,** B692 (1965).
B 11. Borchi, E., and R. Gatto, Phys. Letters **14,** 352 (1965).
B 12. Barnes, V. E., *et al.*, Phys. Rev. Letters **15,** 322 (1965).
B 13. Badier, J., *et al.*, Phys. Letters **17,** 337 (1965).
B 14. Biedenharn, L. C., J. Nuyts, and N. Straumann, Phys. Letters **16,** 92 (1965).
B 15. Badier, S., and C. Bouchiat, Phys. Letters **15,** 96 (1965).
B 16. Bardakci, K., J. Cornwall, P. Freund, and B. W. Lee, Phys. Rev. Letters **13,** 698 (1964); **14,** 48 (1965).
B 17. Bardakci, K., J. Cornwall, P. Freund, and B. W. Lee, Phys. Letters **15,** 79 (1965).
B 18. Becchi, C., and G. Morpurgo, Phys. Letters **17,** 352 (1965).
B 19. Bég, M. A. B., and A. Pais, Phys. Rev. Letters **14,** 51 (1965).
B 20. Becchi, C., and G. Morpurgo, Phys. **140,** B687 (1965).
B 21. Bilenky, S. M., *et al.*, Dubna Report E-2156 (1965).
B 22. Babu, P., Phys. Rev. Letters **14,** 166 (1965).
B 23. Borchi, E., F. Buccella, and R. Gatto, Phys. Rev. Letters **14,** 507 (1965).
B 24. Buccella, F., G. Martucci, and R. Gatto, Nuovo Cimento **37,** 782 (1965).
B 25. Belinfante, J. G., and R. E. Cutcosky, Phys. Rev. Letters **14,** 33 (1965).
B 26. Blatt, J., and V. Weisskopf, *Theoretical Nuclear Physics* (John Wiley & Sons, Inc., New York, 1952), p. 30.
B 27. Bogoliubov, N. N., *et al.*, Dubna Reports D 1968, D 2015, D 2141 (1965).
B 28. Bég, M. A. B., and A. Pais, Phys. Rev. Letters **14,** 267 (1965).
B 29. Bose, S. K., and Yu. M. Shirkov, Phys. Rev. Letters **14,** 398 (1965).
B 30. Bacry, H., and J. Nuyts, Nuovo Cimento **37,** 1702 (1965).
B 31. Barnes, K., P. Carruthers, and F. von Hippel. Phys. Rev. Letters **16,** 92 (1965).
B 32. Bardakci, K., J. Cornwall, P. Freund, and B. W. Lee, Phys. Rev. Letters **14,** 264 (1965).
B 33. Bargmann, V., and E. P. Wigner, Proc. Natl. Acad. Sci. **34,** 211 (1948).
B 34. Barnes, K., Phys. Letters **1,** 166 (1962).
B 35. Barnes, K., Phys. Rev. Letters **14,** 798 (1965); Phys. Rev. **140,** B1355 (1965).
B 36. Bég, M. A. B., and A. Pais, Phys. Rev. Letters **14,** 509, 577(E) (1965).
B 37. Blankenbecler, R., M. Goldberger, K. Johnson, and S. Treiman, Phys. Rev. Letters **14,** 515 (1965).
B 38. Bell, J. S. Cern Report Th. 573 (1965).
B 39. Bokov, O., N. V. Hieu, K. Rerikli, and A. Khelashvili, Dubna Report P2283 (1965).
B 40. Barger, V., and M. H. Rubin Phys. Rev. Letters **14,** 713 (1965)
B 41. Binford, T., D. Cline, and M. Olsson, Phys. Rev. Letters **14,** 715 (1965).
B 42. Buccella, F., G. Martucci, and R. Gatto, Phys. Letters **17,** 333 (1965).
B 43. Baltay, C., *et al.*, Phys. Rev. Letters **15,** 532 (1965).
B 44. Barash, N., *et al.*, Phys. Rev. **139,** B1659 (1965).
B 45. Baltay, C., *et al.*, Phys. Rev. **140,** B1039 (1965).
B 46. Baltay, C., *et al.*, Phys. Rev. **140,** B1042 (1965).
B 47. Bergia, S., and F. G. Lannoy, Cern Report Th623 (1965).
B 48. Barger, V., and M. H. Rubin, Phys. Rev. **140,** B1366 (1965).
B 49. Bell, J. S., and H. Ruegg, Nuovo Cimento **39,** 1166 (1965).
B 50. Badier, S., and C. Bouchiat, Nuovo Cimento **39,** 1183 (1965).
C 1. Condon, E. U., and G. H. Shortley, *The Theory of Atomic Spectra* (Cambridge University Press, New York, 1951).
C 2. Carter, J. C., J. J. Coyne, and S. Meshkov, Phys. Rev. Letters **14,** 523, 580(E) (1965).
C 3. Cook, C. L., and G. Murtaza, Nuovo Cimento **39,** 531 (1965).
C 4. Chan, C. H., and A. Q. Sarker, Phys. Rev. Letters **13,** 731 (1964).
C 5. Coleman, S., and S. Glashow, Phys. Rev. Letters **6,** 423 (1961).
C 6. Cooper, W. A., *et al.*, Phys. Letters **8,** 365 (1964).
C 7. Capps, R. H., and J. Koerner, Phys. Rev. Letters **15,** 320 (1965).
C 8. Cabibbo, N., Phys. Rev. Letters **10,** 531 (1963).
C 9. Cline, D., and M. Olsson, Phys. Letters **17,** 340 (1965).
C 10. Capps, R. H., Phys. Rev. Letters **14,** 31, 456 (1965).
C 11. Cicogna, G., E. Fabri, and L. Picasso, Nuovo Cimento **37,** 765 (1965).
C 12. Castell, L., Phys. Rev. Letters **14,** 753 (1965).
C 13. Charap, J., P. Matthews, A. Salam, and J. Strathdee, Phys. Letters **15,** 184 (1965).
C 14. Chan, C. H., and A. Q. Sarker, Phys. Rev. **139,** B626 (1965).
C 15. Cornwall, J., P. Freund, and K. Mahanthappa, Phys. Rev. Letters **14,** 515 (1965).
C 16. Chang, N. P., and J. M. Shpiz, Phys. Rev. Letters **14,** 617 (1965)
C 17. Carter, J. C., *et al.*, Phys. Rev. Letters **15,** 373, 768(E). (1965).
C 18. Charap, J. M., and P. T. Matthews, Phys. Letters **16,** 95 (1965).
C 19. Cini, M., Phys. Letters **19,** 251 (1965).
C 20. Coleman, S., Phys. Letters **19,** 144 (1965).
C 21. Cook, T., C. J. Goebel, and B. Sakita, Phys. Rev. Letters **15,** 35 (1965).

CC-0. In Public Domain. Gurukul Kangri Collection, Haridwar

Digitized by Arya Samaj Foundation Chennai and eGangotri

C 22. Coester, F., M. Hamermesh, and W. D. McGlinn, Phys. Rev. **135,** B451 (1964).
C 23. Coleman, S., Phys. Rev. **138,** B1262 (1965).
D 1. Duimio, F., and A. Scotti, Phys. Rev. Letters **14,** 926 (1965).
D 2. Dolgov, A. D., L. B. Okun, I. Pomeranchuck, and V. V. Soloviev, Phys. Letters **15,** 84 (1965).
D 3. Dyson, F. J., and N. H. Xuong, Phys. Rev. Letters **13,** 815 (1964); **14,** 339(E) (1965).
D 4. Dalitz, R. H., Report to the Oxford Conference (September 1965).
D 5. Delbourgo, R., A. Salam, and J. Strathdee, Phys. Rev. **138,** B420 (1965).
D 6. Dunning, J. R., *et al.*, Phys. Rev. Letters **13,** 631 (1964).
D 7. Dashen, R. F., and M. Gell-Mann, Phys. Letters **17,** 142, 145 (1965).
D 8. Delbourgo, R., M. Rashid, A. Salam, and J. Strathdee, in *High Energy Physics and Elementary Particles* (International Atomic Energy Agency, Vienna, 1965), p. 455.
D 9. Delbourgo, R., Phys. Letters **15,** 347 (1965).
D 10. Delbourgo, R., M. Rashid, and J. Strathdee, Phys. Rev. Letters **14,** 719 (1965).
D 11. Dao Wong Duc, and Cao Chi, Dubna Report P-2208 (1965).
D 12. Delbourgo, R., and M. Rashid, Proc. Roy. Soc. (London) 286A, 412 (1965).
D 13. Delbourgo, R., Y. Leung, M. Rashid, and J. Strathdee, Phys. Rev. Letters **14,** 609 (1965).
D 14. Dyson, F. J., and N. H. Xuong, Phys. Rev. Letters **14,** 655 (1965).
D 15. Dietz, K., and W. Drechsler, Nuovo Cimento **40,** 634 (1965).
D 16. Dothan, Y., M. Gell-Mann, and Y. Ne'eman, Phys. Letters **17,** 148 (1965).
E 1. Englert, F., and R. Brout, Phys. Rev. Letters **12,** 682 (1964).
F 1. Fano, U., and G. Racah, *Irreducible Tensorial Sets* (Academic Press Inc., New York, 1959), Chap. 2.
F 2. Franzini, P., and L. A. Radicati, Phys. Letters **6,** 322 (1962).
F 3. Ferro-Luzzi, M., *et al.*, Phys. Letters **17,** 155 (1965).
F 4. Feynman, R. P., M. Gell-Mann, and G. Zweig, Phys. Rev. Letters **13,** 678 (1964).
F 5. Freund, P. G. O., and B. W. Lee, Phys. Rev. Letters **13,** 592 (1964).
F 6. Foldy, L., and S. Wouthuysen, Phys. Rev. **78,** 29 (1950).
F 7. Foldy, L., Phys. Rev. **122,** 275 (1961).
F 8. Fulton, T., and G. Wess, Phys. Letters **14,** 57, 334 (1965); **15,** 177 (1965).
F 9. Freund, P. G. O., Phys. Rev. Letters **14,** 803 (1965).
F 10. Ferrari, R., and M. Konuma, Phys. Rev. Letters **14,** 378 (1965).
F 11. Foldy, L. L. (private communication).
F 12. Freund, P. G. O., and R. Oehme, Phys. Rev. Letters **14,** 1085 (1965).
F 13. Freund, P. G. O., and S. Y. Lo, Phys. Rev. **140,** B927 (1965).
F 14. Franzini, P., Lectures at Erice (September 1965).
F 15. Fubini, S., G. Furlan, and D. Rossetti, Nuovo Cimento **40,** 1171 (1965).
G 1. Gell-Mann, M., and Y. Ne'eman, *The Eightfold Way* (W. A. Benjamin, Inc., New York, 1964).
G 2. Gell-Mann, M., Phys. Letters **8,** 214 (1964).
G 3. Gürsey, F., and L. A. Radicati, Phys. Rev. Letters **13,** 173 (1964)
G 4. Gürsey, F., A. Pais, and L. A. Radicati, Phys. Rev. Letters **13,** 299 (1964).
G 5. Gürsey, F., T. D. Lee, and M. Nauenberg, Phys. Rev. **135,** 467 (1964).
G 6. Goldberg, M., *et al.*, Phys. Rev. Letters **12,** 546 (1964).
G 7. Goldberg, M., *et al.*, Phys. Rev. Letters **13,** 249 (1964).
G 8. Gyuk, I. P., and S. F. Tuan, Phys. Rev. Letters **14,** 121 (1965).
G 9. Gyuk, I. P., and S. F. Tuan, Phys. Rev. **140,** B164 (1965).
G 10. Griffith, R. W., Phys. Rev. **139,** B667 (1965).
G 11. Glashow, S., and R. Socolow, Phys. Rev. Letters **15,** 329 (1965).
G 12. Ginibre, J., J. Math. Phys. **4,** 720 (1963).
G 13. Gourdin, M., and Ph. Salin, Nuovo Cimento **27,** 193 (1963).
G 14. Geshkenbein, B. V., Phys. Letters **16,** 323 (1965).
G 15. Geshkenbein, B. V., JETP Letters **1,** 127 (1965).
G 16. Greenberg, O. W., Phys. Rev. Letters **13,** 598 (1964).
G 17. Greenberg, O. W., *Proceedings of the Conference on Mathematical Theory of Elementary Particles*, Dedham, Mass., 1965 (to be published).
G 18. Greenberg, O. W., Phys. Letters **19,** 423 (1965).
G 19. Gedalin, E. V., O. Kancheli, and S. Matinyan, JETP Letters **1,** 131 (1965).
G 20. Gürsey, F., Phys. Letters **14,** 330 (1965).
G 21. Galbraith, W. *et al.*, Phys. Rev. **138,** B913 (1965).
G 22. Gell-Mann, M., Phys. Rev. Letters **14,** 334 (1965).
G 23. Gerstein, I. S., Phys. Rev. Letters **14,** 453 (1965).
G 24. Griffiths, D., and D. Welling, Phys. Rev. Letters **14,** 874 (1965)
G 25. Gedalin, E., O. Kancheli, and S. Matinyan, JETP Letters **1,** 93 (1965).
G 26. Geshkenbein, B., B. Ioffe, M. Marinov, and V. Roginsky, Phys. Letters **16,** 347 (1965).
G 27. Gell-Mann, M., Phys. Rev. **125,** 1064 (1962); Physics **1,** 63 (1964).
G 28. Gatto, R., L. Maiani, and G. Preparata, Phys. Rev. **140,** B1579 (1965); Nuovo Cimento **39,** 1192 (1965); Phys. Rev. **142,** 1135 (1966).
H 1. Hamermesh, M., *Group Theory* (Addison-Wesley Publishing Co., Reading, Mass., 1962).
H 2. Harari, H., in *High Energy Physics and Elementary Particles* (International Atomic Energy Agency, Vienna, 1965), p. 353.
H 3. Hagen, C. R., and A. J. Macfarlane, J. Math. Phys. **6,** 1355 (1965).
H 4. Hagen, C. R., and A. J. Macfarlane, J. Math. Phys. **6,** 1366 (1965).
H 5. Helgason, S. *Differential Geometry and Symmetric Spaces* (Academic Press Inc., New York, 1962).
H 6. Harari, H., and H. J. Lipkin, Phys. Rev. Letters **14,** 570, 850(E) (1965).
H 7. Huwe, D. O., UCRL-11291 (1964).
H 8. Horn, D., *et al.*, Phys. Rev. Letters **14,** 717 (1965).
H 9. Han, M. Y., and Y. Nambu, Phys. Rev. **139,** B1006 (1965).
H 10. Hill, D. A., *et al.*, Phys. Rev. Letters **15,** 85 (1965).
H 11. Hara, Y., Phys. Rev. **139,** B134 (1965).
H 12. Harari, H., SLAC-PUB-148 (1965).
H 13. Harari, H., and H. J. Lipkin, Phys. Rev. Letters **15,** 983 (1965).
H 14. Harari, H., and H. J. Lipkin, Phys. Rev. **140,** B1617 (1965).
H 15. Hussain, F., Phys. Letters **15,** 78 (1965).
H 16. Harari, H., Phys. Rev. Letters **14,** 1100 (1965).
H 17. Hieu, N. V., and F. K. Tu, Dubna Reports P1991, P-2338 (1965).
H 18. Harari, H., D. Horn, M. Kugler, H. Lipkin, and S. Meshkov, Phys. Rev. **140,** B431, B1003 (1965).
H 19. Hieu, N. V., and A. Tavkhelidze, Dubna Report E-2247 (1965).
H 20. Harari, H., and H. Lipkin, Phys. Letters **15,** 286 (1965).
H 21. Hara, Y., Phys. Rev. Letters **14,** 603 (1965).
H 22. Hussain, F., and P. Rotelli, Phys. Rev. Letters **16,** 183 (1965); Phys. Rev. **142,** 1013 (1966).
H 23. Harari, H., H. Lipkin, and S. Meshkov, Phys. Rev. Letters **14,** 845 (1965).
I 1. Iso, C., and M. Kato, Nuovo Cimento **37,** 1734 (1965).
I 2. Ikeda, M., Prog. Theoret. Phys. (Kyoto) **32,** 178 (1964).
I 3. Itoh, C., Prog. Theoret. Phys. (Kyoto) **34,** 318 (1965).
J 1. Jahn, H., and H. van Wieringen, Proc. Roy. Soc. (London) **A209,** 502 (1951).
J 2. Jordan, T. F., Phys. Rev. **139,** B149 (1965).
J 3. Johnson, K., and S. B. Treiman, Phys. Rev. Letters **14,** 189 (1965).
J 4. Jackson, J. D., Phys. Rev. Letters **15,** 990 (1965).
J 5. Jengo, R., and R. Odorico, Nuovo Cimento **39,** 1184 (1965).
K 1. Klein, A., J. Math. Phys. **4,** 1283 (1963).
K 2. Kleima, D., thesis, Groningen (1965).
K 3. Kalbfleisch, G. R., *et al.*, Phys. Rev. Letters **12,** 527 (1964).
K 4. Kalbfleisch, G. R., *et al.*, Phys. Rev. Letters **13,** 349 (1964).
K 5. Kim. J. K., thesis, Columbia University (1965).
K 6. Kim, Y. S., S. Oneda, and J. C. Pati, Phys. Rev. **135,** B1076 (1964).

CC-0. In Public Domain. Gurukul Kangri Collection, Haridwar

Digitized by Arya Samaj Foundation Chennai and eGangotri

K 7. Kuo, T. K., and T. Yao, Phys. Rev. Letters **13,** 418 (1964).
K 8. Kuo, T. K., and T. Yao, Phys. Rev. Letters **14,** 79 (1965).
K 9. Kantor, P., T. K. Kuo, R. Peierls, and L. Trueman, Phys. Rev. **140,** B1008 (1965).
K 10. Kawarabayashi, K., Phys. Rev. Letters **14,** 86, 169(E) (1965).
K 11. Kawarabayashi, K., and R. White, Phys. Rev. Letters **14,** 527 (1965).
K 12. Khanna, M. P., Phys. Rev. Letters **14,** 711 (1965).
K 13. Kuo, T. K., and L. A. Radicati, Phys. Rev. **139,** B746 (1965).
K 14. Kadyshevsky, V. G., *et al.*, Phys. Letters **15,** 180 (1965).
K 15. Ketley, I. J., Phys. Letters **16,** 340 (1965).
K 16. Konuma, M., and E. Remiddi, Phys. Rev. Letters **14,** 1082 (1965); **15,** 89(E) (1965).
K 17. Khanna, M. P., S. Okubo, and N. Mukunda, University of Rochester Report UR 875-96 (1965).
K 18. Kupsch, J., Nuovo Cimento **40,** 287, 640 (1965).
L 1. Littlewood, D. E., *Theory of Group Characters* (Oxford University Press, Oxford, England, 1950).
L 2. London, G. W., *et al.*, Phys. Rev. **143,** 952 (1966).
L 3. Lindsay, J. S., and G. A. Smith, Bull. Am. Phys. Soc. **10,** 502 (1965), Abstract GD7.
L 4. Lee, B. W., Phys. Rev. Letters **12,** 83 (1964).
L 5. Lee, B. W., Phys. Rev. **140,** B152 (1965).
L 6. Lipkin, H. J., Phys. Rev. Letters **13,** 590 (1964).
L 7. Lipkin, H. J., Phys. Rev. Letters **14,** 513 (1965).
L 8. Lipkin, H. J., and A. Tavkhelidze, Phys. Letters **17,** 331 (1965).
L 9. Lipkin, H. J., and S. Meshkov, Phys. Rev. Letters **14,** 670 (1965).
L 10. Lindenbaum, S., Report to the Oxford Conference (September 1965).
L 11. Lai, C. S., Phys. Rev. Letters **15,** 563 (1965).
L 12. Leung, Y. C., and M. Rashid, Phys. Rev. Letters **15,** 424 (1965).
L 13. Lee, B. W., Phys. Rev. Letters **14,** 676, 850(E) (1965).
L 14. Levin, E. M., and L. L. Frankfurt, JETP Letters **2,** 65 (1965).
M 1. Moshinsky, M., J. Math. Phys. **4,** 1128 (1963).
M 2. Mahanthappa, K. T., and E. C. G. Sudarshan, Phys. Rev. Letters **14,** 163 (1965).
M 3. Muzinich, I. J., Phys. Letters **14,** 252 (1965).
M 4. Matinyan, S. G., JETP Letters **1,** 57 (1965).
M 5. Morpurgo, G., Physics **2,** 95 (1965).
M 6. Mahanthappa, K. T., and E. Sudarshan, Phys. Rev. Letters **14,** 458 (1958).
M 7. Marinov, M., Phys. Letters **16,** 320 (1965).
M 8. Meshkov, S. (private communication).
M 9. McGlinn, W. D., Phys. Rev. Letters **12,** 467 (1964).
N 1. Nauenberg, M., Phys. Rev. **135,** B1047 (1964).
N 2. Ne'eman, Y., Phys. Rev. **138,** B1474 (1965).
N 3. Novozhilov, Yu., and I. Terentjev, Phys. Letters **15,** 86 (1965).
N 4. Novozhilov, Yu., Phys. Letters **16,** 348 (1965).
N 5. Ne'eman, Y., Phys. Letters **14,** 327 (1965).
N 6. Nambu, Y., *Proceedings of the 2nd Coral Gables Conference* (W. H. Freeman and Co., San Francisco, 1965), p. 274.
O 1. Okubo, S., Prog. Theoret. Phys. (Kyoto) **27,** 949 (1962).
O 2. Okubo, S., Phys. Letters **5,** 165 (1963).
O 3. Okubo, S., and R. E. Marshak, Phys. Rev. Letters **13,** 818 (1964).
O 4. Oehme, R., Phys. Letters **15,** 284 (1965).
O 5. Oehme, R., Phys. Rev. Letters **14,** 664, 866 (1965); **15,** 286 (1965).
O 6. Oehme, R., in *Preludes* (Interscience Publishers, Inc., New York, 1966), p. 143.
O 7. Olsson, M. G., Phys. Rev. Letters **15,** 710, 768(E) (1965).
O 8. Okubo, S., and R. E. Marshak, Phys. Rev. Letters **14,** 156 (1965).
O 9. Oehme, R., University of Chicago Report EFINS 65-90 (1965).
O 10. O'Raifeartaigh, L., Phys. Rev. Letters **14,** 332 (1965).
O 11. O'Raifeartaigh, L., Phys. Rev. Letters **14,** 575 (1965).
P 1. Pais, A., Phys. Rev. Letters **13,** 175 (1964).
P 2. Papastemiou, N. J., and D. G. Sutherland, Phys. Letters **14,** 246 (1965).
P 3. Pais, A., and S. B. Treiman, *Proceedings of the 1964 Dubna Conference.*
P 4. Pais, A., in *Preludes* (Interscience Publishers, Inc., New York, 1966), p. 302.
P 5. Pauli, W., *Handbuch der Physik* (Verlag Julius Springer, Berlin, 1933), Vol. XXIV/1.
R 1. Racah, G., "Group Theory and Spectroscopy," Princeton Lectures, 1951.
R 2. Racah, G., Rend. Atti Accad. Lincei **8,** 108 (1950).
R 3. Rashid, M. A., Phys. Rev. Letters **14,** 272 (1965.)
R 4. Rekalo, M. P., JETP Letters **1,** 91 (1965).
R 5. Rosen, S. P., and S. Pakvasa, Phys. Rev. Letters **13,** 773 (1964)
R 6. Rosen, S. P., Phys. Rev. Letters **14,** 758 (1965).
R 7. Rosen, S. P., Phys. Rev. **140,** B326 (1965).
R 8. Riazuddin, and L. K. Pandit, Phys. Rev. Letters **14,** 462 (1965).
R 9. Rühl, W., Phys. Letters **14,** 346 (1965).
R 10. Roman, P., and J. J. Aghassi, Phys. Letters **14,** 68 (1965).
R 11. Rühl, W., Nuovo Cimento **37,** 301, 320 (1965).
R 12. Rothleitner, J., and B. Stech, Z. Physik **186,** 399 (1965).
R 13. Roman, P., and J. J. Aghassi, Nuovo Cimento **36,** 1062 (1965).
R 14. Rühl, W., Phys. Letters **15,** 101 (1965).
R 15. Rühl, W., Phys. Letters **15,** 99 (1965).
R 16. Rühl, W., Phys. Letters **15,** 340 (1965).
R 17. Roman, P., and C. J. Koh, Nuovo Cimento **39,** 1015 (1965).
R 18. Ryan, C., Phys. Rev. **140,** B480 (1965).
S 1. Sakita, B., Phys. Rev. **136,** 1756 (1964).
S 2. Sakurai, J., Phys. Rev. **132,** 434 (1963).
S 3. Sakita, B., Phys. Rev. Letters **13,** 643 (1964).
S 4. Soloviev, L. D., Phys. Letters **16,** 345 (1965).
S 5. Sakurai, J. Phys. Rev. Letters **12,** 79 (1964).
S 6. Sugawara, H., Prog. Theoret. Phys. (Kyoto) **31,** 213 (1964).
S 7. Samios, N., Rapporteurs Talk at Argonne Conference, ANL-7130, p. 189, 1965.
S 8. Schulke, L., Z. Physik **183,** 424 (1965).
S 9. Suzuki, M., Phys. Letters **14,** 64 (1965).
S 10. Struminsky, B., Dubna Report (1965).
S 11. Streater, R. F., and A. S. Wightman, *TCP, Spin and Statistics and all that* (W. A. Benjamin, Inc., New York, 1964).
S 12. Sakita, B., and K. Wali, Phys. Rev. Letters **14,** 404 (1965).
S 13. Salam, A., R. Delbourgo, and J. Strathdee, Proc. Roy. Soc. (London) **A284,** 146 (1965).
S 14. Sawyer, R. F., Phys. Rev. Letters **14,** 471 (1965).
S 15. Sakita, B., and K. Wali, Phys. Rev. **139,** B1355 (1965).
S 16. Salam, A., R. Delbourgo, M. Rashid, and J. Strathdee, Proc. Roy. Soc. (London) **A285,** 312 (1965).
S 17. Suzuki, M., Nuovo Cimento **38,** 368 (1965).
S 18. Schwinger, J., Phys. Rev. Letters **3,** 296 (1959).
S 19. Suzuki, M., Phys. Rev. **140,** B1405 (1965).
S 20. Sudarshan, E. C. G., *Proceedings Second Coral Gables Conference* (W. H. Freeman and Co., San Francisco, 1965), p. 160.
S 21. Sudarshan, E. C. G., Phys. Rev. Letters **14,** 1083 (1965).
T 1. Thrall, R., Duke Math. J. **8,** 611 (1941).
T 2. Thirring, W., Phys. Letters **16,** 335 (1965).
T 3. Tomozawa, Y., Prog. Theoret. Phys. (Kyoto) **33,** 319 (1965).
V 1. Volkov, D. V., JETP Letters **1,** 32 (1965).
V 2. Volkov, D. V., JETP Letters **1,** 129 (1965); D. V. Volkov and H. Ruegg (to be published).
W 1. Weinberg, S., Phys. Rev. **139,** B597 (1965).
W 2. Wigner, E. P., Phys. Rev. **51,** 106 (1937).
W 3. Weyl, H., *The Theory of Groups and Quantum Mechanics* (Dover Publications, Inc., New York, 1960), p. 390.
W 4. Willis, W., *et al.*, Phys. Rev. Letters **13,** 291 (1964); (and private communication).
W 5. Weinberg, S., Phys. Rev. **133,** B1318 (1964).
W 6. Whipman, M. L., Nuovo Cimento **37,** 824 (1965).
W 7. Weisberger, W. I., Phys. Rev. Letters **14,** 1047 (1965); Phys. Rev. **143,** 1302 (1966).
Y 1. Yamanouchi, T., Proc. Math. Soc. Japan **18,** 623 (1936).
Z 1. Zweig, G., CERN Reports Th. 401, Th. 412 (1964).
Z 2. Zimmerman, W., Ann. Phys. (N.Y.) (to be published).

CC-0. In Public Domain. Gurukul Kangri Collection, Haridwar

Digitized by Arya Samaj Foundation Chennai and eGangotri

Recent Work on the Interstellar Medium*

NANNIELOU H. DIETER AND W. MILLER GOSS
Radio Astronomy Laboratory, University of California, Berkeley, California

Emphasis in this review of current problems in the study of the interstellar medium is on a few specialized topics. The first treated is the problem of the cloud structures and the velocity fields in the interstellar gas. Another section deals with the observations suggesting the presence of dust as well as gas in the medium and with the proposed nature of the dust grains. These grains were the first indicators of the presence of a general galactic magnetic field and are believed to be catalytic agents in the formation of molecules in the gas. The status of current observational investigations of the magnetic field and of current theoretical studies of the formation of interstellar molecules is described. Finally, very recent observations in the microwave spectrum of the hydroxyl radical are outlined. These suggest the availability of new and surprising information about conditions in the interstellar medium.

I. Introduction 256
A. Outline 256
B. What's There 258
C. Observational Techniques 259
II. The Velocity Field 262
A. Cloud Structure and Velocities 262
B. Internal Motions in Interstellar Clouds 265
C. Theories of the Velocity Field 267
III. Interstellar Grains 270
A. Introduction 270
B. Observations of Extinction 271
C. Theories of the Grains 273
1. Dielectric Particles 273
2. "Platt Particles" 276
3. Graphite Particles 277
D. Further Observations 279
1. Optical Polarization 279
2. HII Regions and Interstellar Grains 282
3. The Unidentified Diffuse Lines 282
IV. Galactic Magnetic Fields 283
V. Formation of Interstellar Molecules 287
VI. Recent Observations of OH 291

I. INTRODUCTION

A. Outline

The space between the stars in our galaxy is not an empty wasteland, but a region filled with gas and dust. This interstellar material is not distributed uniformly, nor are its chemical and physical properties homogeneous throughout the galaxy. Local concentrations of matter seem to be the rule rather than the exception. The particle density in the interstellar medium is everywhere very small compared with that in stars. The mean concentration is about 0.1 atoms/cm^3, and the maximum is about 100 atoms/cm^3 in some large complexes of interstellar clouds, while the most tenuous observable regions of the outer solar atmosphere, for example, contain 10^6 to 10^8 atoms/cm^3.

Yet the total amount of this gas is very great, from one to ten percent of the galaxy, and a study of this gaseous component of the galaxy is critical to the understanding of the distribution and physical condition of matter in our, or any other, galaxy. The study of the physics of the interstellar medium is beset by enormous difficulty because of the low concentration of matter (which requires observing over a great volume to obtain detectable results), and because of the associated great deviations from local thermodynamic equilibrium. To illustrate the problem, so diffuse is the gas that the mean free path of a hydrogen atom is about 10^{14} cm, and so varied is the environment that material sometimes freezes into dust grains a thousand Ångstroms (10^{-5} cm) in size, and sometimes is completely ionized by the light of a nearby star. Local concentrations of ionized gas gave the first indication of the presence of interstellar gas because they radiate as emission nebulae in the visible spectrum when excited by a nearby hot star. Evidence of the presence of a more general distribution of gas came first from the study of spectra of distant, hot stars. These spectra contain peculiar, narrow absorption lines, which are not related to the stars but are superposed on the spectra by the intervening interstellar gas. The constituents observed are sodium, calcium, potassium, titanium, and iron, along with CH and CN—all absorption lines arising from the ground state. The following Table I of Herbig (1963) shows the observed interstellar constituents. Not included in the entries are the so-called diffuse bands which remain unidentified but are observed as interstellar features in stellar spectra. By far the most abundant element is neutral hydrogen, which produces no absorption lines in the visible spectrum. The use of the optical interstellar absorption lines to study the gas is handicapped by the low abundance of the ions, by the uncertainty in theoretical knowledge of the ionization equilibrium, and by the small number of stars in which the lines can be observed. The situation is rather like trying to investigate the composition and motions of the earth's atmosphere by looking only at aurorae and at the absorption lines superposed on the solar spectrum by, say, CO_2 and neon.

A great step forward in the study of the interstellar gas was made when van de Hulst (1945) predicted, and Ewen and Purcell (1951) observed, the 21 cm line of neutral hydrogen arising from hyperfine levels in the $n=1$ level. Thus, for the first time use was made of this most abundant element in the study of the interstellar medium. Further steps are currently being made in the search for molecular and atomic constituents in the radio frequency spectrum. OH radicals and excited hydrogen atoms have been detected. The observed transition in OH arises from Λ-doubling in the ground state at 18-cm wavelength, and those in the excited

* Support of this work by the U.S. Office of Naval Research under contract Nonr. 222 (66) is gratefully acknowledged.

CC-0. In Public Domain. Gurukul Kangri Collection, Haridwar

Digitized by Arya Samaj Foundation Chennai and eGangotri

Table I. Sharp interstellar lines.

Å	Identification	Classification
3072.97	Ti II	$a^4F_{\frac{3}{2}}-z^4D^\circ_{\frac{3}{2}}$
3137.53	CH	$C\,^2\Sigma^+-X\,^2\Pi$, $R_2(1)$ of 0, 0
3143.15	CH	$C\,^2\Sigma^+-X\,^2\Pi$, $Q_2(1)+{}^QR_{12}(1)$ of 0, 0
3146.01	CH	$C\,^2\Sigma^+-X\,^2\Pi$, ${}^PQ_{12}(1)$ of 0, 0
3229.19	Ti II	$a^4F_{\frac{3}{2}}-z^4F^\circ_{5/2}$
3241.99	Ti II	$a^4F_{\frac{3}{2}}-z^4F^\circ_{\frac{3}{2}}$
3302.38	Na I	$3^2S_{\frac{1}{2}}-4^2P^\circ_{\frac{3}{2}}$
3302.99	Na I	$3^2S_{\frac{1}{2}}-4^2P^\circ_{\frac{1}{2}}$
3383.76	Ti II	$a^4F_{\frac{3}{2}}-z^4G^\circ_{5/2}$
3440.61	Fe I	$a^5D_4-z^5P^\circ_3$
3447.08	CH^+	$A\,^1\Pi-X\,^1\Sigma$, $R(0)$ of 4, 0
3579.02	CH^+	$A\,^1\Pi-X\,^1\Sigma$, $R(0)$ of 3, 0
3719.94	Fe I	$a^5D_4-z^5F^\circ_5$
3745.31	CH^+	$A\,^1\Pi-X\,^1\Sigma$, $R(0)$ of 2, 0
3859.91	Fe I	$a^5D_4-z^5D^\circ_4$
3874.00	CN	$B\,^2\Sigma^+-X\,^2\Sigma^+$, $R(1)$ of 0, 0
3874.61	CN	$B\,^2\Sigma^+-X\,^2\Sigma^+$, $R(0)$ of 0, 0
3875.76	CN	$B\,^2\Sigma^+-X\,^2\Sigma^+$, $P(1)$ of 0, 0
3878.77	CH	$B\,^2\Sigma^--X\,^2\Pi$, $R_2(1)$ of 0, 0
3886.41	CH	$B\,^2\Sigma^--X\,^2\Pi$, $Q_2(1)+{}^QR_{12}(1)$ of 0, 0
3890.21	CH	$B\,^2\Sigma^--X\,^2\Pi$, ${}^PQ_{12}(1)$ of 0, 0
3933.66	Ca II	$4^2S_{\frac{1}{2}}-4^2P^\circ_{\frac{3}{2}}$
3957.70	CH^+	$A\,^1\Pi-X\,^1\Sigma$, $R(0)$ of 1, 0
3968.47	Ca II	$4^2S_{\frac{1}{2}}-4^2P^\circ_{\frac{1}{2}}$
4226.73	Ca I	$4^1S-4^1P^\circ$
4232.54	CH^+	$A\,^1\Pi-X\,^1\Sigma$, $R(0)$ of 0, 0
4300.32	CH	$A\,^2\Delta-X\,^2\Pi$, $R_2(1)$ of 0, 0
5889.95	Na I	$3^2S_{\frac{1}{2}}-3^2P^\circ_{\frac{3}{2}}$
5895.92	Na I	$3^2S_{\frac{1}{2}}-3^2P^\circ_{\frac{1}{2}}$
7664.91	K I	$4^2S_{\frac{1}{2}}-4^2P^\circ_{\frac{3}{2}}$
7698.98	K I	$4^2S_{\frac{1}{2}}-4^2P^\circ_{\frac{1}{2}}$

hydrogen from high quantum jumps ($n>109$) at various centimeter wavelengths (Höglund and Mezger 1965; Lilley, Menzel, Penfield, Zuckerman 1966). The combination of information from the optical absorption and from the emission lines in both the optical and the radio-frequency regions should provide the means to attack both the problem of the distribution and of the behavior of matter in interstellar space.

In trying to review our present knowledge of this material which lies between the stars, we face the problem of limiting the subjects to be included. The problem arises not so much from the quantity of facts which are known as from the complexity and fascination of the currently unsolved problems. Our guide in the choice of problems to be included has been primarily a personal one—based on our own current interests and plans. This is, then, in no sense a complete digest of the whole problem of the interstellar medium; to attempt such a statement would be dangerous at a moment when the subject is in an explosive state of change.

We have included some description of the observational techniques available for studying the interstellar medium and where appropriate, a bit of the history of developments. The rapidity with which advances are being made in our understanding of the interstellar medium makes it essential to emphasize the transitory nature of any conclusions. This paper states very few such conclusions; it is full of statements of unsolved problems. Such a dynamic field is exciting to work in but difficult to describe coherently.

We begin with a general and largely qualitative description of what is known about the material which lies between the stars. The next section is one containing a brief description of the techniques available for observing the gas and dust, including their special applications and limitations. The remaining sections deal with the problems facing us in understanding the interstellar medium from the point of view of the physical conditions within it. Until recently the gas has been studied primarily as a tool for investigating the structure of our galaxy—at least in the radio-frequency portion of its spectrum. In particular, the hydrogen line has been used as a primary tool for investigating the large-scale kinematics of the galaxy and its spiral structure. Recently we have been able for the first time to study the nature of the gas itself as a

CC-0. In Public Domain. Gurukul Kangri Collection, Haridwar

Digitized by Arya Samaj Foundation Chennai and eGangotri

major constituent of our environment (on an astronomical scale). We deal first, in Sec. II, with the velocity field of the gas, both in terms of motions of clouds and in terms of the motions within a single cloud. Section III is a description of the interstellar grains and the information they yield on the interstellar conditions. We then discuss, in Sec. IV, the deductions made about the galactic magnetic field from studies of the interstellar medium. The problem of the formation of molecules in the gas forms the subject of Sec. V. The last section, VI, deals with the very recent discoveries in the microwave spectrum of the interstellar gas.

With regard to references, we aim at making it possible to locate all original work on the subject by including in the bibliography primarily the review papers which will lead the reader back to the original papers. There are, of course, references to the original work directly, but they are by no means complete.

B. What's There

The interstellar medium consists of all matter which is not contained in the stars. In this section we present a brief description of the gaseous constituents of the medium. The detailed study of the majority of the kinds of objects has been made in the Milky Way; moreover, examination of the nearby galaxies (primarily the Magellanic Clouds and M31 and M33) shows evidence for the same types of interstellar objects.

As we have pointed out, a relatively large percentage of the mass of the Milky Way is contributed by the interstellar gas. Our galaxy consists of spiral arms similar to those in the nearly spiral galaxies such as the Andromeda Nebula (M31). The Galaxy (Milky Way) has a diameter of about 30 kparsecs (1 parsec$=3\times10^{18}$ cm) and a relatively small thickness; thus, the over-all form is that of flattened disk. The sun is located 10 kparsecs from the galactic center, where the interstellar gas has a total thickness which is about 200 parsecs.

Emission nebulae and reflection nebulae are very prominent regions in the interstellar medium. The emission nebulae are regions of high excitation (kinetic temperatures of $\sim10^4$ °K) surrounding hot, luminous stars (O stars); the nebular spectra consist of the recombination lines of hydrogen and other elements, and the forbidden lines of oxygen, sulfur, and nitrogen, which are excited by electron collision. Further observations of hydrogen in the emission nebulae are now possible using the high quantum number "jumps" whose frequencies lie in the microwave spectrum.

The emission nebulae are of great importance for abundance determinations in the interstellar gas. The high excitation produces numerous lines of various elements, thus providing an opportunity for a fairly complete abundance analysis. These results indicate that the abundances of the elements in the interstellar medium are quite similar to those found in stellar atmospheres.

The reflection nebulae are regions of nebulosity with a continuous spectrum surrounding cooler stars (type B1 and cooler). As we will point out in Sec. III, this nebulosity is due to scattered light from interstellar dust grains in the vicinity of the star. It appears that the type of nebulosity depends not on the type of interstellar material (either gas or dust) but on the temperature of the exciting star. The consensus is that the composition of the clouds in the case of the two types of nebulae is the same; the interstellar matter accommodates itself to the radiation field near the star.

As we will show in Sec. IIA, most of the interstellar gas seems to be concentrated in discrete clouds of sizes 2–6 parsecs which occupy 10% of the volume in the galactic plane. Strömgren (1939, 1948) has shown that the interstellar gas is divided into two types of regions: HI (neutral hydrogen) and HII (ionized hydrogen) regions. The latter are the emission nebulae surrounding hot, luminous stars. This distinction is made for hydrogen since this element is by far the most abundant gas in the interstellar medium.

The HI regions have a kinetic temperature of ~125°K (see Sec. IIB), while the HII regions are characterized by kinetic temperatures of $\sim10^4$ °K. The HII regions contain only a small fraction (about 10% in a spiral arm) of the interstellar gas, due to the fact that the O stars are relatively rare. The interesting property of the HII regions is the sharp transition between them and the surrounding neutral gas. Near the exciting star practically all the hydrogen is ionized (HII)—the density of HI being about 10^{-2} times the density of HII. As the distance r from the star increases, the energy density beyond the Lyman limit falls off as r^2; more important, the opacity due to HI between r and the star increases exponentially ($\propto e^{-\tau}$, where τ is optical depth at Lyman limit 912 Å) as the number of neutrals increases. Using the Saha ionization equation with the above two effects included, Strömgren showed that the feedback between the two effects causes a very sharp transition region between HI and HII. The radius of the so-called "Strömgren sphere" is given by

$$r_0=R_0 n_{\mathrm{H}}^{-\frac{2}{3}},$$

where n_{H} is the total number density of H atoms and R_0 equals $(3L/4\pi\alpha)^{\frac{1}{3}}$, where L is the luminosity of the star and α is the recombination coefficient. Within r_0 practically all the hydrogen is HII; for $r>r_0$, the hydrogen is almost completely HI. For $n_{\mathrm{H}}=10$ cm^{-3}, $r_0=30$ parsecs for an O5 star; for a cooler B5 star $r_0=0.8$ parsec. For stars as cool as the sun, $r_0\approx10^{-4}$ parsec. Thus, only for stars hotter than B0 are the emission nebulae prevalent objects.

As a consequence of the "Strömgren spheres" the radiation field in HI regions has a sharp cut-off at the Lyman limit—the photons of higher energy are absorbed in the HII regions. A knowledge of the spectrum of the

CC-0. In Public Domain. Gurukul Kangri Collection, Haridwar

Digitized by Arya Samaj Foundation Chennai and eGangotri

interstellar radiation field is important in two respects: (1) The calculation of the ionization equilibrium in the interstellar medium requires the shape of the interstellar radiation field at and beyond certain ionization limits. The ionization equilibrium is needed to calculate the total abundance of a particular nuclear species from the observed concentrations of one of its ions, e.g., we observe Na° in the interstellar medium; since most of the sodium present is Na^{+}, we must use the ionization equation to calculate the interstellar sodium abundance. (2) As we point out in Sec. V, molecular formation in the interstellar medium depends critically on the radiation field. Various authors (Dunham, 1939; Lambrecht and Zimmerman, 1955; Stecher and Milligan, 1962; and Zimmerman, 1965) have attempted to calculate the interstellar radiation field using the observed numbers of different types of stars. This calculation is extremely difficult due to our lack of knowledge of stellar radiation below the earth's atmospheric cut-off at 3000 A. Furthermore, a correction must be made for the ultraviolet interstellar extinction (see Sec. IIIB)—again unobservable from the earth's surface. The early estimates (Dunham, and Lambrecht and Zimmerman) approximated the stellar radiation in the ultraviolet by a blackbody approximation, while the later calculations by Lambrecht and Zimmerman have utilized model atmospheres to calculate the ultraviolet contributions of the stars. The Stecher and Milligan calculation is based on observations of the stars in the region 2600–1600 Å by rockets; these observations indicated that the model atmospheres had grossly overestimated the ultraviolet contributions. The Zimmerman (1964) calculation utilizes improved model atmospheres.

Figure 1 illustrates the comparison between the five calculated radiation fields in the region 3800 Å to the Lyman limit at 912 Å. If the Stecher and Milligan field is correct, the ionization of those elements whose ionization energies lie in the region 5–13 eV would be greatly reduced. The great disparity between the recent calculations is indeed discouraging. Nevertheless, it is obvious that the interstellar radiation field leads to great deviations from thermodynamic equilibrium.

In the interstellar medium, many of the objects which appear as major structural features are regions of exceptional states of excitation or regions of unusual interaction with certain types of stars. These features contain a very small percentage of the mass of the interstellar medium. They are important, however, since they exhibit various degrees of excitation, densities, and ages. The quasi-attached shells and envelopes of certain objects such as novae, emission stars, and planetary nebulae are examples of these types of features. The supernovae and their remnants (the explosion of certain types of stars and the interaction with the interstellar gas) are of great importance because of the vast amount of energy involved in these

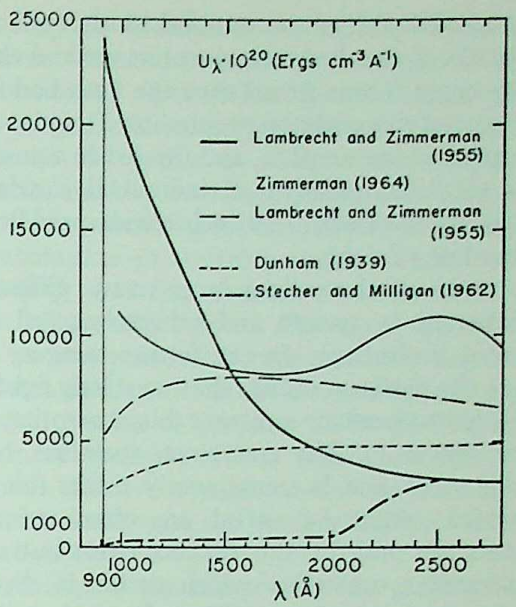

Fig. 1. The interstellar ultraviolet radiation field in HI regions according to various authors (Stecher and Milligan 1962). The Lyman continuum cut-off at 912 Å is indicated. The solid line curve for L–Z refers to model atmospheres for the stars and the dashed line for L–Z refers to a blackbody approximation for the atmospheres.

events. In Sec. IIC, we mention the possible importance of supernovae as energy sources for the whole interstellar medium.

C. Observational Techniques

We wish now to describe the techniques used to study the interstellar medium. They may be classified by the wavelength range studied, that is, into optical and radio-frequency approaches. Each approach deals in its own way with the absorption by the interstellar medium of the continuous radiation from distant sources—in the optical case from starlight and in the radio case from radio sources. Each approach also deals with the emission of the interstellar gas itself, the visible emission arising only from excited regions of the galactic gas, the microwave emission originating throughout the galaxy in the case of neutral hydrogen and from excited regions in the case of OH.

The presence of an absorbing material in interstellar space is apparent from photographs of the Milky Way. This material absorbs the light of distant stars in a way dependent on wavelength, and it polarizes the light which penetrates it. These observations provide important clues to the nature of this interstellar dust.

Observations of the interstellar gas by means of its selective absorption of the light of distant stars was, until 1951, the only way this component of the diffuse, pervading material could be detected. It was found that the spectra of some hot stars showed very sharp absorption lines of atoms and molecules quite uncharacteristic of the rest of the spectrum. The observation that they did not share the stellar motion, especially

CC-0. In Public Domain. Gurukul Kangri Collection, Haridwar

Digitized by Arya Samaj Foundation Chennai and eGangotri

in the case of double stars, established that they originated in the space between the observer and the star. In many cases it was found that the lines had several closely spaced components, presumably Doppler-shifted with respect to one another, and this led to a model of a gaseous medium made up of individual clouds. This model consisted of about 10 such clouds per kiloparsec along the line of sight.

The study of these lines faces many difficulties—some inherent in nature and others imposed by instrumental limitations. In the former category is the fact that the gas is so diffuse that very long light paths are required to produce a measurable absorption line in a stellar spectrum. The star must, therefore, be at a great distance—and is consequently rather faint. The stars which might be useful are often reduced in brightness not only by the distance effect but also by the interstellar extinction which occurs in directions likely also to contain the gas. These factors have limited the maximum distance of stars in whose spectra are observed interstellar lines to about 2.5 kparsecs (about 8×10^{21} cm), and thus, on the average, the distance of the observed interstellar gas to about one-half this distance. This restriction on the region of the galaxy which we can study by this technique is a severe one when one remembers that the center of the galaxy is 10 kparsecs away from the sun. Another natural difficulty arises from the fact that in order to detect an interstellar line, measure its wavelength (and hence radial velocity), and intensity one must find it in a stellar spectrum which does not have strong stellar lines of the interstellar atoms sought for—usually Na° and Ca^{+}. This means we need to study "early-type" stars—young, hot, massive stars, which are much rarer than the cooler ones. This further restricts the observational material—especially if one wishes to look at regions out of the plane of the galaxy, where young, hot stars are rare.

Measurement of the precise wavelength of an interstellar line is hampered by the difficulty of obtaining the spectra at high dispersion. The faintness of the stars requires the average spectrum to be taken with a 5-h exposure with a 100-in. telescope, for example. Consequently, the accumulation of data is limited by the observing time available on large telescopes. The use of image tubes to increase the sensitivity of such instruments (by an order of magnitude) may well soon make possible a great increase in the amount of data. With spectra now available obtained with conventional techniques, errors in wavelength measures and hence, in radial velocity estimates, are likely to be 1 to 3 km/sec. This is far less accuracy than can be attained easily by radio-frequency techniques. With two new and sophisticated techniques higher resolution has been obtained: use of a high resolution solar telescope on stars by Livingston and Lynds (1964) gives velocities within $\frac{1}{2}$ km/sec, and use of a Fabry–Perot interferometer by Hobbs (1965) gives them to within $\frac{1}{4}$ km/sec. Both techniques are difficult and are limited to use with bright objects, but they do equal the highest radio-frequency resolution now routinely available.

In terms of detection of a small concentration of an element, however, the optical techniques far out-do the radio ones. This is primarily due to the higher transition probabilities in the spectral lines studied. A typical optical line is formed by about 3×10^{11} atoms/cm^2 along the line of sight, while the weakest observed neutral hydrogen (1420 Mc/sec) lines are formed by of the order of 10^{19} atoms/cm^2. Actually, nature works for us in this case, because the hydrogen is so abundant compared to the sodium and calcium (by a factor of 10^6) that a high transition probability in this radio-frequency transition would mean we would reach high optical depths for a small length of absorbing gas, and thus be unable to observe the gas far away. So, if we could choose, this combination of circumstances would be our choice. (In this regard molecules provide an intermediate case; that is, the detection possibility for a given number of molecules is about the same in the two spectral regions.) Interpretation of the optical results in terms of the abundance of calcium and sodium is, however, hampered by a peculiar circumstance. In the visible spectrum the lines of Ca^{+} and Na° are those observable, but in the interstellar medium most calcium is in the form of Ca^{++} and most sodium is Na^{+}. What is required, then, is a knowledge of the ionization equilibrium in interstellar space, which depends on the atomic ionization cross sections and the radiation field, neither of which is well known, as we pointed out in Part B of the introduction.

Optical observations suffer from one further natural limitation which will soon be overcome by the newest instrumental advances. The limitation is that the earth's atmosphere cuts off the radiation below 3000 Å and above 20 000 Å. The advance is, of course, the instrumented satellite. The primary contribution of the satellite observations to the problem will be the extension of our knowledge of the spectrum of the interstellar gas both into the ultraviolet and the far infrared. In the ultraviolet lie strong lines of abundant atoms like carbon, nitrogen, oxygen, and iron. In addition, from these lines we get a far clearer picture of the composition of the gas and possibly a measure of the ionization equilibrium and electron density. A particularly important advance may be made because the hydrogen molecule produces bands in both the ultraviolet and infrared. This molecule could well be a major constituent of the interstellar gas which has until now completely escaped detection. A full discussion of the possibilities of observations in the ultraviolet has been made by Spitzer and Zabriskie (1959).

All these optical methods suffer a serious limitation compared to some radio-frequency ones and in turn

CC-0. In Public Domain. Gurukul Kangri Collection, Haridwar

Digitized by Arya Samaj Foundation Chennai and eGangotri

have an important advantage over them. The limitation is that all the measurements depend on the presence of a star as a background source of radiation. This prevents a mapping of the sky on an extensive and detailed scale and limits our understanding of the structure and dynamics of the gas derived in this way. The advantage is that an upper limit to the distance of the intervening material is available from the distance of the star. In only a few cases is such an estimate available in the studies of the microwave spectra of the gas—the most notable case being the OH emission from bright, diffuse nebulae. The velocity of the hydrogen emission has been used to estimate its distance, but this depends on the adoption of an uncertain model for the rotation of the galaxy.

Observations of the interstellar medium by radio-frequency techniques has its own set of problems and potentialities. The very large difference in wavelength from the visible radiation (of the order of 10^6) leads to greatly different observational methods. For example, the angular resolution of the largest radio telescope used in studies of interstellar microwave lines is about 10 min of arc, a far cry from the seconds of arc obtainable optically. On the other hand, the frequency resolution of a radio astronomy receiver can easily be a few kilocycles/sec—equivalent to less than half a kilometer/sec in terms of Doppler shifts, while the optical resolution is usually not greater than 1 km/sec. The technique in optical spectroscopy is to photograph the spectrum of a star (covering the whole visible range) and to search in it for lines of interstellar gas of known atoms and molecules. This is, if not impractical, at least much more difficult in the radio-frequency range. An observation there covers at most a small fraction of the spectrum, of the order of 10^{-3} times the average frequency of the line. It has therefore been possible to study only one interstellar constituent at a time, with a consequent cry from observers for better values of the frequencies of lines to be expected from materials in the interstellar gas.

One aspect of radio observations of the interstellar gas is similar to optical observations. This is the technique of observing the absorption lines superposed on spectra of distant sources by the intervening gas. The situation is in some ways better and in some ways worse than in the optical case. On the positive side, the radio sources are not dimmed by interstellar dust and so in a few cases permit observations over very long path lengths. In addition, the sources have no observable intrinsic spectral lines to complicate the measurement of the interstellar ones. However, only a handful are bright enough to permit observation of absorption lines of even the strongest microwave line—the 1420-Mc/sec line of neutral hydrogen. A further problem arises from the low angular resolution of the antennas. An observation in the direction of a source includes also radiation from a considerable solid angle around the source. Only clouds in the line of sight between observer and source will absorb radiation from the source, but all other lines of sight within the solid angle will contribute to the measured profile. They will in general add emission to the profile at about the absorption line frequencies and hence weaken the apparent absorption. Study of the absorbing clouds therefore requires that the contribution of emitting regions be removed by constructing what this emission would look like in the absence of a radio source. The usual procedure involves an interpolation between nearby regions, and contributes significantly to the uncertainties in measurement of intensities of the lines. Nevertheless, the observation of absorption lines makes possible a large increase in effective angular resolution since the principal factor is no longer the beam width but the angular size of the source.

Observation of the microwave line at 1420 Mc/sec of neutral atomic hydrogen in the interstellar medium has special advantages over any other available technique for studying the gas. In the first place, hydrogen is by far the most abundant element in the gas. The properties of the transition are very accurately known—the frequency, transition probability, and excitation mechanism. Recent work on other microwave lines originating in the interstellar medium has shown the importance of these factors; for example, the uncertainty in the excitation mechanism for OH is a real problem. In the case of the HI hyperfine transition, however, the excitation is known to be collisional and the brightness temperature[1] of an optically thick cloud therefore represents the kinetic temperature of the gas. In addition the kinetic temperature derived from the thermal Doppler broadening of observed lines is a direct measure of the excitation temperature, if there is no turbulence.

Absorption measurements offer a way of detecting weaker HI lines than is possible in emission. For an individual interstellar cloud lying in the same line of of sight as a radio source, the brightness temperature

$$T_B = T_L - T_C,$$

where T_L is the brightness temperature in the spectral line, and T_C is the brightness temperature of the continuous source. Integration of the equation of transfer along the line of sight gives

$$T_L = T_C e^{-\tau} + T_{ex}(1 - e^{-\tau}),$$

where T_{ex} is the excitation temperature of the gas, and

[1] In the radio spectrum intensities are measured in terms of a brightness temperature. This follows from the Rayleigh–Jeans approximation to the Planck function:

$$B = (2kT\nu^2/c^2) \text{ (ergs/sec cm}^2 \text{ cpc sr)}.$$

Hence, all intensities can be expressed in terms of an equivalent brightness temperature.

CC-0. In Public Domain. Gurukul Kangri Collection, Haridwar

Digitized by Arya Samaj Foundation Chennai and eGangotri

τ is its optical depth. The equation for the brightness temperature is then

$$T_B = -T_C(1-e^{-\tau})+T_{ex}(1-e^{-\tau}).$$

When $T_{ex}<T_C$, we observe an absorption line; when $T_C<T_{ex}$, we observe an emission line. The brightness temperature of many sources is much greater than the excitation temperature of the interstellar hydrogen, and these sources offer the possibility of observing clouds with very small optical depths.

The second advantage in observing the hydrogen line is that it is detectable in emission over the whole sky. An observer is not limited to directions containing background sources and can therefore map the distribution of the gas over the sky. He has then a three-dimensional view of the interstellar gas, two dimensions on the celestial sphere and one in the frequency or velocity domain because of Doppler shifts of the observed lines. In one case—that of observations made in the galactic plane—this third dimension can be converted into distance. Here the dominant radial velocity shifts are due to differential galactic rotation and can be related to distance from the galactic center through the assumption of a model of this rotation. In other directions, however, there is no estimate possible of the distance of the emitting material without observations made in some other way.

This problem suggests the importance of the combination of radio and optical techniques. If, for example, a cloud of interstellar gas can be observed both in the microwave radiation from its hydrogen atoms and in the optical radiation of others of its constituents, the first dividend is an upper limit on the distance of the cloud (the distance of the star). This, in combination with the angular size of the cloud, yields the linear size and hence the density and mass of the cloud. Another piece of valuable information derivable from the combined observation is the abundance of the trace elements in the gas in relation to the hydrogen. Another area in which the combined optical and radio techniques should yield large dividends in our understanding lies in the study of the HII regions, the diffuse nebulae. Observations of the emission of the OH molecule from these clouds and the optical radiation from the other elements present will surely open new avenues for understanding the complex mechanisms operating in these excited regions. Further progress in the development of each of the techniques will soon make possible significant progress in many areas of study of the interstellar medium.

II. THE VELOCITY FIELD

A. Cloud Structure and Velocities

We shall now discuss the kinds of specific information about this interstellar medium which we can deduce from use of the various techniques—to begin with, the nature and velocities of interstellar gas clouds. The stars in our galaxy move quite independently of one another, each under the influence of the force field of the galaxy, but each affected in only a minor way by nearby stars. The gas between the stars, however, interacts significantly with nearby material so that it can be said to have a definable pressure, density, and temperature at each point. The investigation of these thermodynamic quantities is intimately tied to studies of the velocity fields in the gas, which can be made, to a limited extent, with present techniques.

We can measure the position in space, central wavelength, and frequency profile of a spectral line—absorption or emission—which we identify as coming from the interstellar gas. The measure of the wavelength gives us two things: an identification of the constituent producing the line; and a measure of the velocity of the "object" along the line-of-sight. The profile of the line measures for us two kinds of things: the dispersion in velocity along the line-of-sight of all the infinitestimal elements of gas producing the line; and the number of atoms along the line-of-sight. With respect to the interstellar medium, there is usually little ambiguity in the interpretation of the wavelength measures. In studying the optical spectra, it was noticed very early that the spectral lines coming from a single element were often split into several components, whose widths were small compared with their separations. Such a result suggested the presence of condensations of matter, moving with differing velocities. The number of these components was found to increase in number with the distance from the sun to the star in whose spectrum the interstellar line was observed. Thus the suggestion arose that the interstellar medium actually consists of "clouds", rather than of a homogeneous layer. These clouds occupy only about 10% of the total volume, and their densities are several orders of magnitude greater than the surrounding medium. Presumably, if there were indeed a substratum in which there were differential velocity fields, the various components of the spectral lines would not be so clearly separated, but would blend more. So this picture of an interstellar medium concentrated into clouds, with any residual substratum being only a small fraction of the whole, has gained acceptance. (For a review of the subject, see Spitzer, 1966.)

More recent observations have supported the model and have led to a more quantitative description of a typical cloud. The great observational difficulty has been to be certain that one is looking at the velocity profile of a single cloud and not a blend of many clouds along the line of sight. One piece of evidence that earlier data on clouds was distorted by this effect comes from an examination of the interstellar lines in the bright star α Cygni. Adams (1949), with a resolution of 8 to 16 km/sec, found two components in the interstellar calcium lines in the spectrum of this star. In 1964, Livingston and Lynds, using a solar telescope with

CC-0. In Public Domain. Gurukul Kangri Collection, Haridwar

Digitized by Arya Samaj Foundation Chennai and eGangotri

a resolution of 0.5 km/sec, found five components in the same lines. Application of radio techniques to the problem of cloud structure was made by means of a survey with high-frequency resolution (2 kc/sec or 0.4 km/sec) in the 21-cm hydrogen line in the area around the north galactic pole (Dieter, 1965). In this direction we are observing along the shortest path length in the interstellar medium where we might expect to see clouds separately. Four clouds are, in fact, individually observable in this area. On the reasonable assumption that the clouds are about 100 pc away, the average diameter is 10 pc; the average density, 2 atoms/cc; and the average mass, 15 solar masses. The diameter is similar to that deduced from more indirect evidence, but the densities and masses are both lower than previously found.

A typical cloud will have within it a small quantity (1/100 of the gas by weight) of grains. The observations which support this statement are not entirely unambiguous, but do suggest it to be true on the average. The radii and number density of the gas clouds and the dust clouds are found to be the same, although they are observed by quite different techniques. Interstellar extinction is high in directions in which the Ca^+ absorption is large, and on a large scale it correlates also with the neutral hydrogen emission. Attempts to derive the gas-to-dust ratio as a constant throughout the interstellar medium have, however, not proved successful when they have dealt in detail with small volumes of space.

This picture of the interstellar gas existing in the form of discrete clouds is, however, not without difficulty. In the first place we do not know what maintains the cloud as a unit. A typical cloud would not be held together by self-gravitation, but would dissipate into the intercloud medium in a time of the order of 10^7 years—a time short compared to the age of the galaxy. Either clouds are continually being formed or something holds them together.

Two proposals have been made for the nature of an external pressure acting to stabilize these interstellar clouds (in addition to a controversial magnetic pressure). Although each is plausible, neither is susceptible to an obvious quantitative test. The first, due to Spitzer (1954), depends on the balance of pressure between the cloud and intercloud material. He proposes that the clouds are cool, relatively dense condensations in a hot, very tenuous medium. The pressure within a cloud, which is proportional to the product of its density and temperature, is balanced by that of the intercloud gas where the temperature is high ($\sim 10^6$ °K) and the density low. The density is so low that the intercloud gas is essentially unobservable. The second suggestion for the source of the external pressure, due to Kahn (1955a), is the collision of the cloud with other clouds. Such cloud–cloud collisions will be mentioned as a means of limiting grain size (Sec. III) and discussed as a means of heating the interstellar gas. Here an average cloud is described as having a mean free collision time of 10^7 years. A collision compresses the cloud and the pressure resulting from such collisions depends on the random cloud motions. Both the specific details of the compression mechanism and the parameters which govern it are poorly understood. Thus, we can only accept that the clouds exist and speculate on their persistence.

In order to discuss the velocity fields associated with these clouds we shall describe the hierarchy of motions, as we think we understand them. When we measure the radial velocity of a component in the profile of an interstellar absorption or emission line, we can identify it with various motions of the gas. In general, the measured velocity is affected by

(a) differential galactic rotation on the basis of circular orbits,

(b) systematic group motion of many clouds deviating from circular orbits,

(c) random motions of individual clouds in the group.

Two further velocity fields affect the line by broadening it—gas streaming in one cloud and thermal motions of individual atoms in the cloud. By gas streaming, we mean mass motions within the cloud which are not dependent on the mass of particles within it. It is useful to make this arrangement of effects because we want to understand the details of the rotation of the galaxy, to find the forces which drive the additional systematic motions, and to calculate the dissipation of energy, partly due to the collisions of individual clouds. We have, however, two problems in making and using the arrangement. One is a conceptual one, in that we cannot really justify treating an "individual cloud" like a self-contained unit if we first give it motion in common with other such units and then say it has streaming motion within itself. We are not sure what is a cloud and what is not. So, conceptually, the arrangement has flaws. The second problem is that it is not possible, except in unusual cases, to observe the effects separately. We measure, after all, a single radial velocity for a component of interstellar absorption or emission. This velocity is affected more or less by all these motions. We can make a reasonable attempt to separate the differential galactic rotation contribution to the radial velocity because we understand the rotation fairly well. The galaxy rotates as a whole—stars and gas together—in such a way that the velocity increases roughly linearly with distance from the center, up to just short of the sun's distance. Beyond that it rotates in a way which is thought to approach a Keplerian form. We cannot, however, distinguish in general between systematic motions of groups of clouds and individual cloud random motions within the group. This probably does not affect our interpretation of the group motions very much, but it does affect in a devastating way our

CC-0. In Public Domain. Gurukul Kangri Collection, Haridwar

Digitized by Arya Samaj Foundation Chennai and eGangotri

interpretation of random cloud velocities, because they are not truly random but partially systematic.

The conceptual problem does not seem susceptible to solution at the moment. The observational problem holds out greater hope because of the increasing precision of 21-cm hydrogen emission line measurements.

These measurements have given us some insight into the systematic group motions, although explanations only for those in the galactic plane. Surveys of the neutral hydrogen emission in the plane have indicated the structure of the galactic system, including the spiral arms, and have delineated the rotation of the system, an example of the group (a) motions. Surveys of neutral hydrogen emission out of the plane (McGee and Murray, 1961; McGee, Murray, and Milton, 1963; Dieter, 1964–5) have shown that there is great asymmetry in these motions in the sense that most of the material is approaching the sun, an example of group (b) motions. What is more, there are large-scale features observable in this approaching gas, especially at high galactic latitudes. (Galactic latitudes are measured with the sun as center and the galactic plane as zero point.) On the average, if one observes at high latitudes one is seeing gas closer to the sun than at low latitudes, because the layer of gas is highly flattened. The survey by Oort, Blaauw, Hulsbosch, Muller, Raimond, and Tolbert (1966) covers with a coarse grid of observations the area of the sky from 40° to the north galactic pole. There is at all positions some gas nearly at rest with respect to the region about the sun, but all departures from this quiescent gas are in the negative velocity sense. In particular, over about half the total longitude range there is more of this approaching gas than there is gas at rest. The highest velocities and greatest densities occur at all latitudes at about a longitude of 120°, and near this same longitude there is very little zero velocity material. (Longitude is measured with the sun as center and the galactic center as zero point.) These authors suggest that the explanation may lie in a flow of gas which has disturbed the quiescent hydrogen layer near the sun. Results of a similar survey by van Woerden, Takakubo, and Braes (1962) at intermediate latitudes (15° to 40°) show an excess of negative velocity components also centered at a longitude of 120°, suggesting that the flow extends over a very large volume near the sun.

A natural question which arises is—just how much material is involved in such a local disturbance? It is one which is impossible to answer directly except in special cases, because we do not normally know the distance to the emitting HI. We therefore have no measure of the volume of the gas and hence no way to translate our measure of the number of hydrogen atoms per cm^2 along the line of sight to a total mass of material. It is clear, however, that this "disturbance" contains a significant fraction of the interstellar gas near the sun at these latitudes.

A more detailed survey near the galactic poles (Dieter, 1964) shows another case of a large-scale systematic motion of a group of clouds. Near the poles, looking directly out of the galactic plane at the sun's distance from the center, one observes the shortest path length through the interstellar gas and one along which differential galactic rotation should have no effect (since the local gas shares the same rotational velocity). In neither polar cap does the expected simple velocity picture appear; there is again gas approaching the sun. In the case of the polar observations, one is observing as radial velocity the true velocity of the gas with respect to the galactic plane. At other latitudes one is unable to determine how much of the observed radial velocity is attributable to this so-called z-motion. In both polar caps there is some gas at rest and some approaching the plane with rather high velocities. In the north the two components are clearly separable—one near zero velocity and the other with velocities ranging from −20 to −55 km/sec. The approaching gas shows a very complex pattern of velocities with no apparent systematic effects. Areas over which similar velocities appear are several degrees in extent, suggesting that the gas is relatively nearby. In the case of the polar observations one can make a somewhat more quantitative estimate of the distance from the fact that the layer of gas around the galactic plane is known to have a total thickness of about 200 pc. If one assumes that the zero velocity and the negative velocity gas exist at the same mean distance from the sun, the approaching gas contains 0.4 of the total amount of hydrogen in the region. If this distance is 100 pc, this gas has a mass 400 times the mass of the sun. A larger assumed distance for this component will increase both its percentage and its mass. If one now assumes that at the sun we are observing a flux of material approaching the plane which is typical of the whole galaxy, we can calculate how much material is "falling in" to the plane from both north and south. This assumption has very little validity since we have only a small sample area—10^{-4} times the total—and we know that conditions near the center are markedly different from those in the solar neighborhood. As an indication only, then, this assumption leads to the conclusion that 100 solar masses reach the galactic plane each year.

One naturally asks where all this material comes from. One logical assumption is that it is part of a large-scale flow of material from one part of the galaxy to another, perhaps up out of the center and down onto the plane farther out. The absence of any observed positive velocities requires either that the flow is oriented so that none of the gas is receding from us or that this gas is unobservable—low density, ionized hydrogen, for example. All this is believable enough but can scarcely be said to be based on anything but conjecture. Two possibilities are that this is a continuing, normal flow of interstellar gas occurring throughout the lifetime of the

CC-0. In Public Domain. Gurukul Kangri Collection, Haridwar

Digitized by Arya Samaj Foundation Chennai and eGangotri

galaxy or is a result of a catastrophic event (perhaps at the nucleus of the galaxy), which occurs over a period short compared to the lifetime of the system.

In optical observations of interstellar absorption lines at positions all over the sky, components of rather high velocity are found, and a large percentage of them are approaching the sun. A survey of interstellar lines in the spectra of stars high above the plane by Münch and Zirin (1961) shows, in fact, that 32 out of 46 components have negative radial velocities, and hence a component in the direction of the galactic plane. Comparison of these high velocity clouds with the low velocity ones turns up a curious difference in the abundance of elements within them. The two principal lines measured are those of neutral sodium and singly ionized calcium. In the low velocity clouds the ratio of calcium to sodium atoms is lower than that in the high velocity clouds by a factor of about 6. Implicit in the determination of the relative abundance is the calculation of the ionization equilibrium of each of the elements, which depends on the radiation field in which the material finds itself. The most likely supposition is that the radiation field is different on the average in the low and high velocity clouds. This is, however, only supposition and mainly serves to throw doubt on our calculations of all abundances in the interstellar gas. An ingenious explanation due to Spitzer (1954) is that the high velocity clouds have recently been accelerated by being in the neighborhood of a bright, hot star. The high radiation field near the star may also have served to evaporate more calcium atoms from interstellar grains (described in Sec. III) and hence leave more in the gaseous state.

A somewhat rarer phenomenon, but one fully as difficult to explain, is the group of so-called "high velocity clouds" found first by Oort, Blaauw, Hulsbosch, Muller, Raimond, and Tolbert (1966). These are condensations of neutral hydrogen with very large radial velocities, from 60 to 175 km/sec, and all negative in sign. They have so far been found in two general areas, one between 70° and 165° longitude and between +15° and +50° latitude (where there are 11 clouds or agglomerations of clouds) and in the south galactic polar cap (where there are 3 or 4). In both areas it is apparent that the clouds are several degrees in angular extent and that they have a complex structure. It is very difficult to say anything about the nature of the clouds beyond this, because we have no idea at all of their distance. Our observations tell us only the number of atoms along the line of sight (between 10^{19} and $10^{20}/cm^2$) and the dispersion in velocity, 10 to 15 km/sec, which is rather high. Any further deductions depend on the distance—and we do not even know whether the objects are inside our galaxy or beyond it.

We should like to know also the velocities of individual clouds within a group, in particular, the form of the random velocity distribution of the clouds, in other words, motions described as group (c). The problem was first of interest in order to aid in estimating the number of clouds along the line of sight, in the face of incomplete velocity resolution of individual clouds. Different authors have used the form proposed by Blaauw (1952),

$$\exp(-|v|/\eta),$$

v being the mean speed of the clouds, and have derived values of η from their own observations. Results have ranged from 2 to 8 km/sec, depending on methods and places in the galaxy observed. The situation is hopelessly complicated by the presence of the large-scale systematic motions of groups of clouds already described. There are great differences in the form of the velocity distribution of the clouds at different places, which quite mask any "average" random motions. Blaauw's treatment of Adams' (1949) observations of optical interstellar lines in the galactic plane certainly shows a distribution of the exponential form indicated with $\eta = 2$ km/sec. More general surveys at both poles, however, indicated a very much flatter distribution with a large excess of high velocities (one quarter of the total are greater than 24 km/sec). In Münch and Zirin's (1961) optical study at high latitudes a very similar distribution is found, including the percentage of components above 24 km/sec. The procedure of treating only the absolute value of the velocity of course masks the fact of the great asymmetry toward negative values. Thus, a single function with a single determining parameter does not describe the observed cloud motions. One might hope that knowledge of such a function would provide an estimate of the energy in the form of individual cloud motions and hence a boundary condition on the choice of mechanism for the acceleration of clouds. It appears, however, that so many large-scale, unexplained motions of groups of clouds are present that we cannot find a clear description of the random ones within the groups.

B. Internal Motions in Interstellar Clouds

We turn now to the velocity fields which broaden the line profile produced by an interstellar cloud—gas streaming within the cloud and thermal motions. One of the central problems is to separate these two effects so as to deduce the amount of mass motion within a cloud and the kinetic temperature of the material within it. In the case of the 21-cm neutral hydrogen radiation, the kinetic temperature is also the excitation temperature because the excitation of the line is collisional (Purcell and Field, 1956). This is the case because the natural lifetime of the atoms in the upper level of this hyperfine transition is extremely long (about 10^6 years—this is due to the magnetic dipole character of the hyperfine transition). This time is

CC-0. In Public Domain. Gurukul Kangri Collection, Haridwar

Digitized by Arya Samaj Foundation Chennai and eGangotri

long compared with the rate of collisions of the atoms, so that these collisions determine the populations of the atomic levels. In addition to its importance from this point of view there is the fact that this kinetic temperature depends on the balance of heating and cooling mechanisms in the interstellar gas and therefore its observed value provides a limit on requirements for these mechanisms.

An estimate of T_K for the neutral hydrogen has also been made on the basis of other considerations than line broadening. The estimate is based on the difference in brightness temperature along paths of different lengths in the galactic plane. The accepted value from this technique is 125°K, but this is only an upper limit because the measured brightness temperature is actually the harmonic mean of the temperatures of all the clouds along the line of sight (Kahn, 1955a). This means that the clouds with lower temperatures are weighted more heavily in this average, and the value derived is therefore not even a proper upper limit for the temperature in a single cloud. The most direct way to derive the kinetic temperature of the interstellar gas is to measure the dispersion in velocity of a spectral line produced by a single cloud. There are two problems in doing so; one is to eliminate the contribution to the broadening of the line by gas streaming in the cloud, and the other is to observe the profile from a single cloud, not a superposition of many along the line of sight. We shall discuss the first problem later in this section. No solution to the second problem is possible with presently existing radio telescopes when one is looking at neutral hydrogen emission along the galactic plane. The blending of radiation from the many clouds along the line of sight is too severe to be resolved by even very high-frequency resolution techniques. The greater angular resolution available by use of the absorption features in the spectra of continuum sources mitigates the problem somewhat, but one is still not quite sure that any feature in the spectrum is indeed a single cloud. Another possibility for observing single clouds along the line of sight is that of looking at high galactic latitudes where the path length through the dense gas in the plane is small. In this case one can in some places isolate individual clouds.

Two surveys of hydrogen emission have been carried out at positions out of the galactic plane, one at intermediate latitudes (van Woerden, Takakubo, and Braes, 1962; Takakubo and van Woerden, 1966) and one near the north galactic pole by Dieter (1965). Each of the surveys was carried out with rather low angular resolution but with very high resolution in velocity, equivalent to 0.4 km/sec in the intermediate latitude survey and 0.2 km/sec in the polar one. The results of the velocity dispersions measured can in no way be considered representative, since profiles which appeared to have narrow features were chosen for study with the high resolution. In fact, the higher velocity components in the profiles were not included since they, in general, have larger dispersions. The principal object of these studies was to find the narrowest possible components—those which were most likely not be blends. The dispersion of such a narrow component would of course still not be a direct measure of the temperature because of the possible presence of gas streaming in the cloud, but would be an upper limit to the temperature in that cloud. The hope was to find some which were narrower than the Doppler width corresponding to a temperature of 125 °K and hence evidence for cooler clouds. This dispersion is 1.0 km/sec for HI. No such clouds were found. The median dispersion in the polar survey was 2.5 km/sec, and the intermediate latitude values were similar. More significant is the fact that the narrowest line observed in each survey was 1.1 km/sec wide, even though the instrumental broadening was far below this level.

One may also use the technique of absorption measurements in the hydrogen line to measure dispersions. The primary advantage in this technique is the very much higher effective angular resolution. If the reason for the absence of narrow features in the emission observations is that the antenna beam is accepting many overlapping features which are not resolved, there should be a pronounced difference in the absorption and emission linewidths. The results are, at the moment, inconclusive. Clark, Radhakrishnan, and Wilson (1962) in a survey of 15 sources found a median dispersion of 2 km/sec, in agreement with emission results. Shuter and Verschuur (1964), however, found much narrower lines in their study of four bright sources. The narrow widths found are a direct result of the large number of separate Gaussian functions used to fit each spectrum, and the choice of the number of such functions is arbitrary. A better comparison with emission measurements may be possible with the use of large antennas to allow observation of weaker absorption lines at high latitudes.

On other grounds, however, the observed emission and absorption linewidths may not be strictly comparable, because we may not be observing on the average the same sort of cloud. In emission the brightness temperature:

$$T_B = T_m(1-e^{-\tau}),$$

where T_m is the harmonic mean of the T_{ex} of all the clouds along the line of sight, while in absorption

$$T_B = -T_c(1-e^{-\tau}),$$

where T_c is the brightness temperature of the continuum source. (For a fuller discussion see Sec. II.) Suppose we are observing a source with T_c larger than T_m; then a cloud of fixed low optical depth which might not contribute significantly to an emission profile could contribute to the absorption in this source. Conversely, if T_c were less than T_m, such a cloud (of the same optical depth) seen in emission could be quite

CC-0. In Public Domain. Gurukul Kangri Collection, Haridwar

Digitized by Arya Samaj Foundation Chennai and eGangotri

invisible in absorption. Furthermore, in a given cloud, since $\tau \propto N_{\rm H}/T_{\rm ex}$, an optically thin cloud would be expected to have a low density. In addition, since the cooling processes in interstellar clouds operate more slowly in low density clouds, the equilibrium $T_{\rm ex}$ in such a cloud would be expected to be relatively high. Thus a cloud of low optical depth would be hotter than the over-all average of all clouds. As we have seen, the average optical depth of clouds observed depends not only on properties of nature but on our observing methods—on the use of an emission or absorption technique and on the size of the antenna. Any interpretation of linewidths seen by different techniques is, therefore, influenced by a subtle, but important, selection effect.

The possibility of observing absorption and emission from a cloud extended enough to be visible in both is an interesting one, because one could then find the optical depth from the absorption and solve for the excitation temperature using the emission. The velocity dispersion in the lines would probably be larger than the pure thermal width expected from the measured $T_{\rm ex}$ ($T_{\rm ex}=T_K$), and the remainder could be attributed to gas streaming in the cloud.

Another avenue for studying the velocity dispersion lies in the microwave spectrum of the OH radical (to be described in detail in Sec. VI). Absorption from interstellar OH clouds has been observed in the spectra of several sources. Barrett, Meeks, and Weinreb (1964) used high resolution observations of the OH lines in Cas A, which occur at the same velocity as HI clouds in this direction, to separate thermal and turbulent contributions to line broadening. Because the streaming motions do not depend on molecular weight, the contribution to the linewidths of this effect are the same for the two lines, while the thermal effects are different—the linewidths due to the latter effect are inversely proportional to the square root of the mass. Thus the OH lines are narrower than the HI lines. Barrett *et al.* found for two clouds kinetic temperatures of 90° and 120°K and turbulent velocities of 0.24 and 0.27 km/sec. If we assume that the turbulent velocities of these clouds are representative of clouds near the galactic pole, we can derive the kinetic temperature in this region as well. The result for the narrowest features ($\sigma=1.1$ km/sec) observed is 125°K, in agreement with the clouds in the direction of Cas A. However, if one considers from this point of view the dispersions in the four individual clouds mapped over angular extents of several degrees in this region (and described earlier in this section), one finds that the average thermal width is 2.2 km/sec and the kinetic temperature therefore 570°K.

We cannot at the present time conclude that we know the kinetic temperature in the interstellar gas, or even that there is a uniform value for this parameter over the whole galaxy. The solution to these problems is vital to our understanding of the heat balance in the gas.

C. Theories of the Velocity Field

We are now confronted with the problem of the dynamics of the interstellar gas. Any theory related to this problem must satisfy several observed conditions: (1) the gas occurs in the form of clouds; (2) these clouds are in motion partially in a systematic way; (3) the clouds have also a superposed random motion; and (4) the clouds have internal motions and a kinetic temperature which must in some way be related to the dynamics of the system as a whole. We shall deal first with theories for the maintenance of the random cloud motions and then with theories dealing with the establishment of the kinetic temperature of the gas.

It is clear that the random motions of interstellar clouds would soon die out if there were no kinetic energy added to the medium to sustain them. The clouds collide with each other rather frequently, about every 10^7 years, and the motions would soon be lost in these probably highly inelastic collisions. Attempts to find sources for the kinetic energy are hampered not only by the great uncertainties in the mechanisms of generation of such energy but by the unknown efficiency of conversion of this energy to motions of interstellar material. In addition, as we have pointed out, we do not know with any accuracy the average amount of random motion of the interstellar clouds. Several possibilities for accelerating mechanisms have been suggested (reviewed by Kahn and Dyson, 1965), and we take as a rough estimate of the energy dissipated in the cloud-cloud collisions a value of 5×10^{39} ergs/sec.

One possible source of the kinetic energy is the violent explosition of stars—the supernovae. The explosion injects into the interstellar medium a portion of the material of the star at high velocity. The amount of kinetic energy available from each such explosion is extremely difficult to estimate since only four have been observed in our galaxy (in 1006, 1054, 1574, and 1604), where estimates of the amount and velocity of the material are possible. Minkowski (1964) finds an average kinetic energy of about 10^{50} ergs from each supernova on the basis of the small amount of information available. An even greater source of uncertainty in discussing supernovae as a source of kinetic energy lies in the attempt to estimate the rate at which these events occur. The most recent estimate, which is a lower limit, is that one supernova explosion occurs every one thousand years (Minkowski, private communication). This leads to an input of kinetic energy into the interstellar medium of 3×10^{39} ergs/sec, about the amount required. The uncertainty in this estimate is obviously enormous, and the details of the communication of the motion of the ejected shells of gas to the interstellar medium are unknown. Obviously, this theory requires that the efficiency of conversion of the supernova energy into translation energy of the clouds must be high.

Another source of energy is the acceleration of

CC-0. In Public Domain. Gurukul Kangri Collection, Haridwar

Digitized by Arya Samaj Foundation Chennai and eGangotri

clouds in the neighborhood of HII regions (Oort, 1954). One expects the gas in HII regions to acquire velocities of 10 km/sec, or energies of the order of 5×10^{11} ergs/g. If the HII region lies in a dense HI cloud, a shock wave can develop which accelerates a much larger amount of neutral gas, up to about 40 times the mass of the HII region. This would then come to 2×10^{12} ergs/g for each occurrence of an HII region. If each part of the interstellar gas becomes involved in such a situation once in 10^8 years, over the whole system a kinetic energy of 6×10^{39} ergs/sec is available. The numbers used in making this estimate, which again turns out to be adequate, are obviously very uncertain.

This mechanism of interaction between HII regions and the interstellar gas has been suggested as an important factor in a cycle of the growth and fragmentation of clouds (Oort, 1954; Field and Saslaw, 1965). It is suggested that a cloud starts in this cycle by the acceleration of a small region of high density near an expanding HII region. The cloud grows in size by processes of coalescence in cloud–cloud collisions until it reaches a mass great enough (~6000 solar masses) to make self-gravitation dominant and gravitational fragmentation a possibility (discussed by Spitzer, 1966). The result is a group of young stars which ionize the surrounding gas and thus begin the cycle again.

A more violent energy source related to HII regions is the rocket effect proposed by Oort and Spitzer (1955), which could accelerate a few clouds to quite high velocities by the sudden heating by a hot star of one side of a large dense cloud of hydrogen at some distance from the star. In this case, the outward acceleration of the cloud is determined by the reaction of the ionized gases which shoot out towards the star, exactly as in an ordinary rocket. The cloud must be very large, some thousands of times the mass of the sun, in order that a part of it can remain neutral and react to the motion of the ionized part. The simplified picture described by Oort and Spitzer has raised many questions concerning the details of such an intrinsically complex problem. Twenty-one centimeter observations of HI may be able to contribute to their solution because some of the clouds accelerated by the mechanism may be directly observable. One likely case is that of the California Nebula (NGC 1499), which is an ionized hydrogen cloud with a velocity of about 59 km/sec with respect to a nearby group of stars (the Zeta Persei association). The proposed sequence of events is that a neutral cloud was shot off from the association and in it there subsequently was formed a new star. The star ionized part of the cloud, making it visible optically. If some neutral hydrogen remains, it should be observable around the ionized region and should have the same velocity. We would then deduce the total amount of momentum imparted to this particular cloud in this particular "rocket."

We turn now to a problem intimately related to that of finding the driving force for the motions of interstellar clouds—finding the sources of heating and cooling of the gas. The path followed in this search has been a somewhat zig-zag one with the ultimate goal being the production of the observed kinetic temperature. Following the comprehensive study of the problem by Spitzer (1954), new mechanisms for each of the processes were sought, each to balance the heat generated or lost by the processes so far suggested. This is, of course, a perfectly legitimate procedure, but two kinds of problems interfere with it. One is the appalling number of assumptions necessary to calculate the heating and cooling rates for each mechanism. The other is the difficulty, described earlier, of establishing the goal of the search—the observed kinetic temperature of the gas.

We first describe the proposed heating mechanisms, then the cooling processes and finally the temperatures derived from the combination. Several articles reviewing the subject in detail are available (Takayanagi, 1964; Takayanagi and Nishimura, 1960; Kahn and Dyson, 1965) so that this will be only a brief résumé.

Among the possible heating agents the two that are most likely to be effective are cloud–cloud collisions and ionization by low-energy cosmic rays. In discussions of both these processes a large number of unknown quantities limit severely the calculation of the rates with which they proceed. The cloud–cloud collision theory (Kahn, 1955a) depends on the conversion of random cloud motions into heat at the time of collisions. In order to estimate the gain in thermal energy due to such collisions one must use a mean velocity of random motion of the clouds as a whole, which is hard to find even in a restricted region and impossible over the galaxy as a whole (see Sec. IIA). In addition, one must estimate the time interval between collisions, which also depends, of course, on cloud sizes and the number of clouds per unit volume. Finally, one must estimate the degree of inelasticity of the collisions. This last point illustrates the interrelation of the theories for motions of the interstellar gas, because if the collisions are completely inelastic and the heating mechanism efficient, the random motions will die out in about 10^7 years. In which case we are forced to say either that the clouds are young or are being continually fed energy from elsewhere, or that the collisions are nearly elastic and the postulated mechanism for heating the gas is ineffective. On the assumption of a random velocity of 7 km/sec, a density of ten hydrogen and 1.5 helium atoms per cm^3, time between collisions of 7×10^6 years, and completely inelastic collisions, the gain due to the process of cloud–cloud collisions is

$$\Gamma_{\infty}\cong3\times10^{-26}\ \text{erg cm}^{-3}\ \text{sec}^{-1}.$$

This process depends linearly on the density of the clouds. The second heating process is the ionization

CC-0. In Public Domain. Gurukul Kangri Collection, Haridwar

Digitized by Arya Samaj Foundation Chennai and eGangotri

atoms in the interstellar clouds by low energy cosmic rays, called suprathermal particles by the proponents of the theory (Hayakawa, 1960; Takayanagi and Nishimura 1960; Hayakawa, Nishimura, and Takayanagi, 1961; Takayanagi, 1964). The proposal is that these low-energy cosmic rays (between 10 and 100 MeV) ionize the hydrogen atoms (the cross sections for ionization increase rapidly at these low energies), thus adding electrons with considerable velocities to the medium. The principal unknown in this mechanism is the flux of the low-energy particles. There is no direct evidence for the cosmic-ray energy spectrum in this low-energy range, because only high-energy galactic cosmic rays can penetrate the solar system's magnetic field. Thus, the low-energy cosmic-ray spectrum must be extrapolated from the 1-BeV range—a very dubious process. On the basis of an assumed flux of 40 particles/cm² sec (and for a cloud with a number density of 10 hydrogen atoms/cm³) the gain in energy by this mechanism is

$$\Gamma_{CR} \cong 1.6 \times 10^{-26} \text{ erg cm}^{-3} \text{ sec}^{-1}.$$

[This rate is, like Γ_{cc}, also linearly dependent on n(H).] This is comparable to the heating by cloud–cloud collisions. It should be noted that both heating processes are more efficient in high density clouds than in low.

There are other possible heating mechanisms, each with its own set of assumptions, but they are thought to be less important than the two described. One is the ionization of various other atoms in the gas by ultraviolet radiation, rendered less efficient by the low abundance of the atoms. Other possibilities are the photodetachment of electrons from grains and the degeneration of turbulent energy into heat.

For the cooling of the interstellar gas once it has been heated by one or both of these agents there are three reactions which are probably important. The first one suggested was the excitation of low-lying levels of the positive ions, especially C^+, Si^+, and Fe^+, by electron impact, followed by the emission of radiation (Seaton, 1958). The rate of this cooling depends critically on the excitation cross sections and on the abundance of the ions. The latter factor is very uncertain not only because of the difficulty in estimating relative abundances throughout the galaxy but of the unknown amount of these elements which is tied up in grains and not contributing to the cooling. Since these elements contribute also to heating at the time of their ionization by ultraviolet radiation, the difference in loss and gain must be evaluated. The rate also depends on the temperature and the square of the absolute number density of hydrogen atoms. The loss in energy by this process at 100°K and for Seaton's estimate of relative abundance is

$$\Lambda_{ei} \cong 3.6 \times 10^{-25} \, n(\text{H}) n(e).$$

The second important cooling mechanism is probably the excitation of low-lying rotational levels of molecular hydrogen by collision with hydrogen atoms followed by emission of infrared radiation. The dependence of this mechanism on the kinetic temperature makes it a candidate for a primary role in cooling only above about 500°K (if the density is as low as is expected). Aside from the problems associated with the details of the excitation and radiation, this mechanism is uncertain because of its dependence on the abundance of H_2 in the interstellar gas. No observational evidence for the presence of H_2 has ever been found, much less a basis for estimating the density. The cooling rates have been calculated on the basis of a number density of $10^{-4}n$(H), a number by no means in agreement with the density suggested by possible formation mechanisms described in Sec. V. The value derived there is between three and five orders of magnitude greater. To complicate the problem further, the cooling rate is dependent on the square of the number density of hydrogen atoms. For a temperature of 500°K, the assumed H_2 abundance, and n(H) = 10, the cooling rate is 2.75×10^{-28} ergs/sec, of the same order as the electron–ion-impact cooling rate; at 100° the rate is only 2.80×10^{-30} ergs/sec. A possible observational check on the mechanism would be observations above the earth's atmosphere in the 10- to 100-μ wavelength region where the radiation from this cooling process appears.

A third possible cooling mechanism is the excitation of oxygen by collisions with hydrogen atoms rather than with electrons (Burgess, Field, and Michie, 1960; Field, 1962). The rate of energy loss again depends on the abundance of the ion and on the square of the number density of HI, and in addition on the probability of de-excitation per collision. If this probability is about 0.1, the cooling rate is comparable with that for electron–ion cooling at 100°K.

Two other presumably less important cooling mechanisms are the collisions of atoms with grains and the collisional excitation of molecules such as CH, CN, and OH. In both cases the low number density of the particles makes the process of no importance in ordinary HI clouds. Clouds with either an abnormally high dust content or an unusually great abundance of these molecules (and there is evidence for the existence of each) could well be cooled more effectively by these mechanisms.

The processes for heating and cooling the gas can be seen to be extremely uncertain both in concept and in detail. If we try, nevertheless, to see what sort of equilibrium temperature is established with several alternatives for the parameters, we can gain some insight into the problem. If first we assume the cloud-cloud collision process to be the principal source of heating, we can describe the cooling which occurs after a collision which heats the gas to several thousand degrees. Figure 2 (Takayanagi and Nishimura, 1960)

CC-0. In Public Domain. Gurukul Kangri Collection, Haridwar

Digitized by Arya Samaj Foundation Chennai and eGangotri

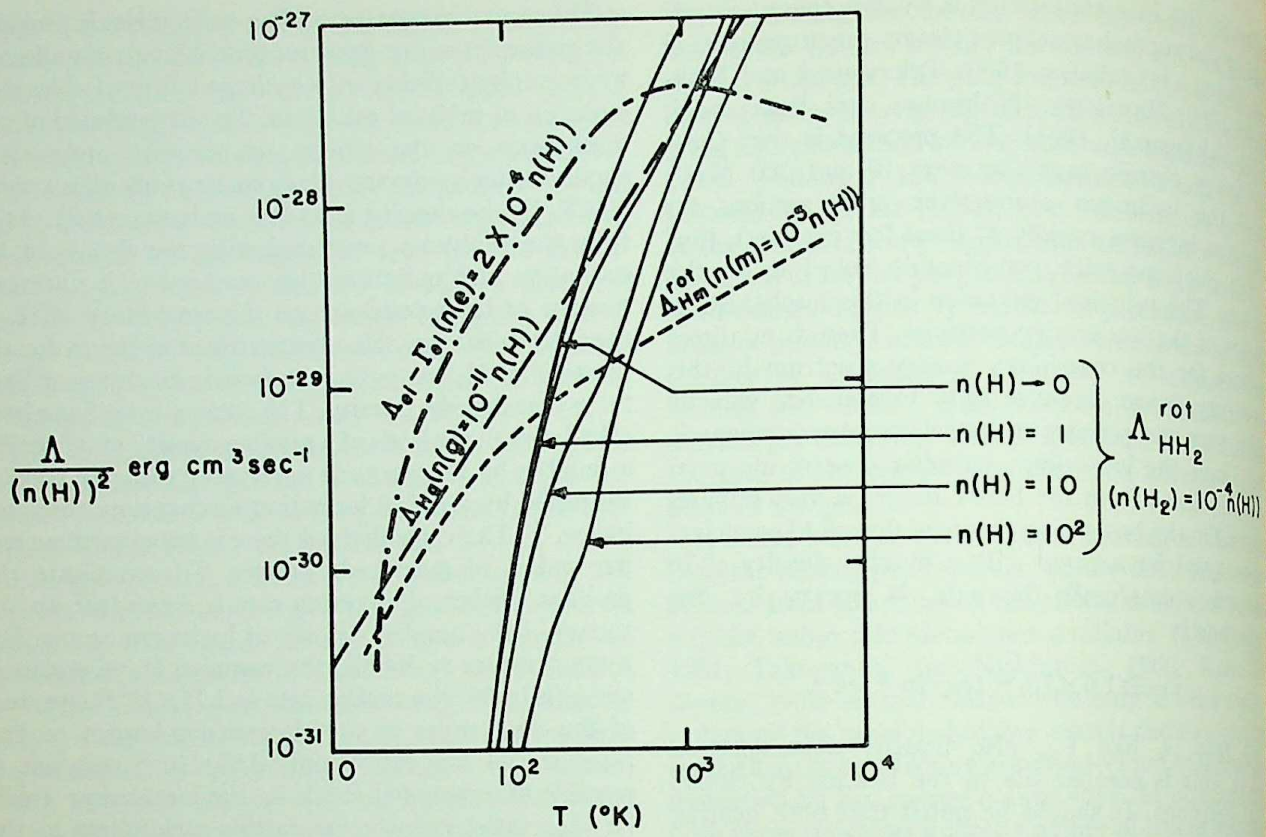

FIG. 2. Cooling rates as a function of temperature and composition of interstellar clouds (Takayanagi and Nishimura 1960). excitation of low-lying levels of positive ions: $\Lambda_{ei}-\Gamma_{ei}$. By rotational excitation of H_2 by collisions with H: $\Lambda_{HH_2}^{rot}$. By rotational ex tation of other molecules: Λ_{Hm}^{rot}. By collisions of H atoms with grains: Λ_{Hg}.

shows these cooling rates as a function of the temperature and of the density and the abundance of various constituents. For several combinations of these processes harmonic mean temperatures have been calculated. If, for instance, the cloud collision frequency is once in 5×10^6 years, and the initial temperature (after collision) is 3000°K, the harmonic mean temperature will be 60°K for a cloud with $n(H_2)=10^{-3}$ and $n(e)=2\times10^{-3}$. Each of these values may well be larger and the temperature consequently lower; in addition, the cooling by collisions of hydrogen and oxygen atoms (about equal in effect to electron collisions) has not been included. A similar analysis of the situation with cosmic-ray heating leads to about the same temperature—much lower than the usually quoted 125°K.

The uncertainty in the harmonic mean temperature from an observational point of view makes it impossible to say that any combination of the theories is totally inadequate. This is suggested by the fact that the equilibrium temperature depends on the density of the cloud. The two principal heating mechanisms proposed depend on $n(H)$ while all the cooling mechanisms depend on $[n(H)]^2$. A low density cloud will therefore on the average be hotter, and hence of lower optical depth.

It is perhaps appropriate to quote a paragraph from E. N. Parker (1958) in relation to problems of interstellar dynamics:

"Most of the interesting theoretical problems i interstellar dynamics are entirely nonlinear, involvi the simultaneous and coordinated functioning o several physical processes. Hence we cannot constru a rigorous, general, quantitative theoretical treatme of the interstellar problem. . . . Someday our unde standing of compressible, radiating, supersonic, hydr magnetic motions in a tenuous gas may develop to t point where most of the contemporary uncertaintie can be decided on a more rigorous basis."

III. INTERSTELLAR GRAINS

A. Introduction

The dark patches that exist in the Milky Way w the first indication that the interstellar medium co tains obscuring matter. Although these regions co be due to a lack of stars, the fact is that dark patch are in reality globules of obscuring matter. The co centration of this matter to the plane of the Mil Way gives rise to the so-called "zone of avoidance Furthermore, the spectra of reflection nebulae w found to be very similar to that of the central sta suggesting that obscuring matter in the nebulae scattering light from the stars.

Further investigations have shown that the

CC-0. In Public Domain. Gurukul Kangri Collection, Haridwar

Digitized by Arya Samaj Foundation Chennai and eGangotri

parently clear regions of space also contain the interstellar obscuring matter. In 1930 Trumpler (1930a, b) showed that the apparent diameters of galactic clusters increased with distance. Since this seemed unreasonable it implied that the distances estimated from apparent and absolute magnitudes of the stars in the clusters were wrong, probably overestimated due to interstellar extinction of the starlight.

The interpretation of the extinction agents as interstellar grains follows from a consideration of "Oort's limit" and the extinction properties of various atomic, molecular, and dust-like particles. "Oort's limit" (Oort, 1932, 1960) refers to the total density in the solar neighborhood. This quantity is derived by considering the observed acceleration law of the stars in a direction perpendicular to the galactic plane, which measures the total accelerating mass in the plane. From the velocity statistics of certain groups of stars, Oort derives a value for the total density of 10.2×10^{-24} g/cm^3. Thus, the extinction agents must have a density consistent with this limit.

The extinction observed is about 1 magnitude per kiloparsec. To explain the extinction by electron scattering requires about 500 electrons/cm^3, a totally unreasonable value in HI regions. The density of neutral atoms required to give the observed amount of extinction by Rayleigh scattering would also violate "Oort's limit." Thus, the atomic and molecular constituents of the interstellar medium cannot explain the observations.

The early observations (Trumpler, 1930c) showed that the extinction (defined as the sum of absorption and scattering) increases approximately monotonically with $1/\lambda$. We thus speak of interstellar reddening since the radiation from a star is "reddened" as it passes through the interstellar medium. This fact implies that the obscuring matter consists of some type of composite particles—the interstellar dust or grains, since individual atoms or molecules cannot give such a λ^{-1} law. Furthermore, this dust component can give the required extinction with a density several orders of magnitude below "Oort's limit."

Further verification that the obscuring agents are grains came from polarization observations. Hiltner (1949) and Hall (1949) attempted to detect polarization in hot, luminous stars following a suggestion by Chandrasekhar (1946) that the light from the edges of these stars would be polarized due to electron scattering. To isolate the limb of the star, eclipsing binary systems were used, in which a large cool star periodically occults the edge of the hot star. It was found, however, that occultation was not necessary to detect polarization. A constant amount of polarization was found throughout all phases of the binary system.

The polarization was found in other types of stars and the position angles of the electric vector were practically parallel for each of the stars in any region of the galaxy. The effect decreased with latitude and was found to be positively correlated with the distance of the star. Finally, it was noted that interstellar extinction was a necessary but not sufficient condition for polarization. Thus, we conclude that polarization is due to the grains which lie between the earth and the stars. To explain the polarization effect, preferential alignment of the particles was postulated. The mechanism generally accepted is magnetic alignment of slightly asymmetric grains.

Thus, we see the great importance of observations of interstellar extinction and polarization and of theories relating to the grains. The grains are an important constituent of the interstellar medium. They probably exert an influence on molecule formation in the regions between the stars, as we shall see in Sec. V, and are probably involved in the formation of new stars. The grains may exert an influence on energy exchange in HI regions; the temperature of the gas is effected by inelastic collisions with the grains. One method of inferring the magnetic field of the galaxy consists in using the observed polarization in conjunction with a suitable theory. In general, we use the grains as a tracer for conditions in the interstellar medium. Finally, the grains play the important negative role of extinction agents. The astonomer is thus faced with the operational problem of determining the amount of extinction in order to determine astronomical distances from the measured apparent brightness and the known absolute brightness of different objects.

The next sections summarize present knowledge regarding the interstellar grains. The observations of extinction will be treated first since the grain models are based primarily on these observations. After the three major theories are discussed, we shall show how the theories influence the interpretation of the polarization data. Next, we consider the interaction of HII regions and grains. Finally, the problem of the interstellar diffuse lines is discussed.

B. Observations of Extinction

The observations of extinction are important in two respects: (1) evaluation of the correction to observed magnitudes and colors to translate these quantities into intrinsic magnitudes and colors, and (2) providing a discrimination between differing theories of the grains. Figure 3 shows a schematic reddening curve as taken from Greenberg (1963). U, B, V, R are the ultraviolet, blue, visual, and red magnitudes on the Johnson and Morgan (1953) magnitude system. We see that in the visible portion of the spectrum $A \propto 1/\lambda$ (A is the normalized extinction in magnitudes). At small λ^{-1} the curve behaves as if the wavelength is greater than the particle size, producing a situation analogous to Rayleigh scattering ($A \propto \lambda^{-4}$). At large λ^{-1}'s the curve looks as if the particle size is much greater than the wavelength and geometrical ($A \propto 1/\lambda^{0}$) blocking is

CC-0. In Public Domain. Gurukul Kangri Collection, Haridwar

Digitized by Arya Samaj Foundation Chennai and eGangotri

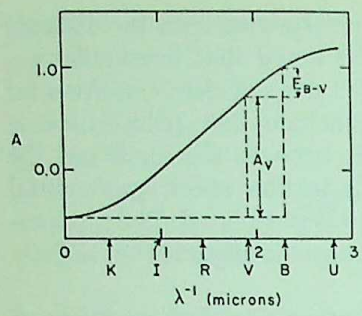

FIG. 3. Schematic extinction curve (Greenberg 1963). A is the normalized extinction in magnitudes. The inverse wavelengths corresponding to the U (ultraviolet), B (blue), V (visual), R (red), I, and K magnitudes are indicated. The color excess $E_{B-V}=A_B-A_V$.

occurring. Thus, the reddening curve indicates that the grains are approximately of the same size as the wavelength in the visible region—an important clue to the theories of the grains.

To correct the observations for extinction it is convenient to define R as

$$R=A_V/(A_B-A_V)=A_V/E_{B-V},$$

where E_{B-V} is called the color excess; this quantity is the easily determined difference between the measured B-V color and the B-V for an unreddened star. The color excess is a measure of the slope of the reddening curve in the visible region. It is important to consider R for three reasons: (1) As will be shown, A_V is hard to determine for one particular star. Thus, if R is known for the particular region, A_V can be obtained from the directly obtainable E_{B-V}. (2) Up to the present, astronomers have generally assumed that R is a constant of the interstellar medium. All corrections for extinction and hence distance determinations have been based on a constant value of R. (3) The fact that R will be shown to vary from region to region indicates that previous distance determinations may be in error. The variations in R also indicate that the distribution and possibly types of grains are not uniform throughout the interstellar medium. The value of R in a particular region gives some information on the grain distribution in that region.

Two methods of determining R and testing its constancy over the galactic plane are available. The first is the color-difference method. This method utilizes multicolor broadband photometry or spectrophotometry (evaluating the reddening in the star's continuum by a dispersing element) to compare the colors of unreddened and reddened stars of the same spectral type. The color difference method yields the extinction curve up to a small λ^{-1}. To obtain the zero point, an extrapolation must be made to $\lambda^{-1}=0$. Then one measures A_V/E_{B-V} from the curve. To be successful, observations in the far infrared must be used in order to achieve the best possible extrapolations. This method is the only method available outside of clusters to obtain R.

The second method, the variable extinction method, enables us to test for neutral absorption; i.e., extinction independent of λ. With this method R is determined directly from observations of distant clusters in which the color excesses vary across the cluster; we tacitly assume that R is the same throughout the cluster and that all the stars are at the same distance. The difference in apparent visual magnitude and absolute visual magnitude is plotted versus E_{B-V}. The slope of the linear relation is R. The major problem here is determining the star's absolute magnitude from its spectrum and the setting up of an accurate absolute magnitude calibration.

The most thorough investigations of the extinction curve have been published in the past few years. Johnson (1965) has used both methods to compute R in several regions. He uses the variable extinction method in six clusters to compute R. His results indicate the range of R from region to region is $3\leq R\leq 6.6$. He also obtains regional mean reddening curves by the color-difference method using broadband photometry from the ultraviolet to 10.45 μ. He then extrapolates to $\lambda^{-1}=0$ to obtain the zero point of the reddening curve. Five of the regions have zero points determined by the two methods. The zero points agree reasonably well. Johnson has proved that the extrapolation in the color-difference method is meaningful only if observations extend to the 10-μ region. The agreement of the two zero points implies that neutral absorption must be quite small. However, two stars (ι Aurigae and α Leonis) are quite anomalous and can be explained in terms of neutral absorption by particles 3–5 μ in diameter. Johnson has also proved that $R=3$ is a minimum value. Since astronomers in the past have generally assumed $R=3$, distances have been overestimated.

In addition, Johnson has shown that the detailed shapes of the reddening curve differ from region to region. Figure 4 shows his regional extinction curves. The NGC 2244 and Cepheus curves show sinuous variation at large wavelengths. According to Johnson, these can be explained by particles with a bimodal size distribution, with peaks near 0.3 μ and 3 μ. It is quite obvious that the reddening law is different in various regions of the Galaxy.

Johnson and Borgman (1963) determined R for stars at different longitudes by the variable color method from broadband photometric methods (ultraviolet to 3.5 μ). They found that R varies as a function of galactic longitude l and goes through a minimum at $l=110°$. The spread in R at certain longitudes is quite large. Furthermore, at a fixed l, as we move away from the plane the spread in R becomes quite pronounced for regions away from the galactic plane. As Johnson (1965) points out, the variation of R with l seriously distorts the true picture of the galactic spiral structure. The determination of accurate distances is quite a subtle problem.

Nandy (1964, 1965) has recently reported on very accurate spectrophotometric extinction measurements

CC-0. In Public Domain. Gurukul Kangri Collection, Haridwar

Digitized by Arya Samaj Foundation Chennai and eGangotri

in Cygnus and Perseus in the wavelength range 8000 Å to 3400 A. He obtains the extinction curve at many more points than the broadband measures and thus is able to detect small changes in the slope of the curve. The extinction curves for Cygnus and Perseus differ significantly and each has a change in slope for $\lambda^{-1}>2.3$—it appears that two straight lines intersect at $\lambda^{-1}=2.3$; the change in slope in the Perseus curve is greater, however, than in the Cygnus curve. This observation is quite significant for the graphite grain theory.

A recent series of observations of extinction of six stars in the rocket ultraviolet at 2600 Å and 2200 Å has been reported by Boggess and Borgman (1964). (In Fig. 5 the two far ultraviolet points are shown). These observations may be quite significant in deciding between the various grain models since the different types of grains have different behaviors in the ultraviolet. Of the six stars only two of the stars' extinction curves could be determined accurately at the ultraviolet wavelengths. Furthermore, the interpretation of the observations is hindered by uncertainties in the intrinsic colors of the stars at these wavelengths. The consensus is, however, that the qualitative features of these observations are correct. The surprising result is that the extinction is found to be much greater than the theories would predict. We comment later on this discrepancy and the attempts to explain it.

The observations clearly show that the extinction curve differs greatly from region to region. It appears that grains have different properties and distribution laws throughout the galaxy. As Wickramasinghe and Guillaume (1965) point out, the existence of the so-

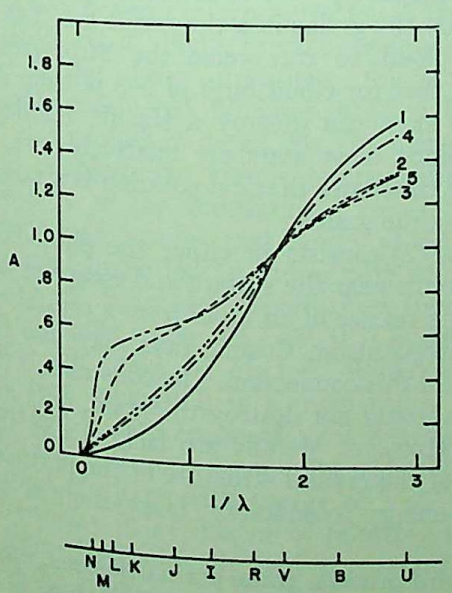

Fig. 4. The regional extinction curves of Johnson (1965). The data have been normalized to $A_V=1.00$ mag. The regions are identified as follows: (1) Perseus, (2) Orion Belt, (3) NGC 2244, (4) Cygnus, and (5) Cepheus.

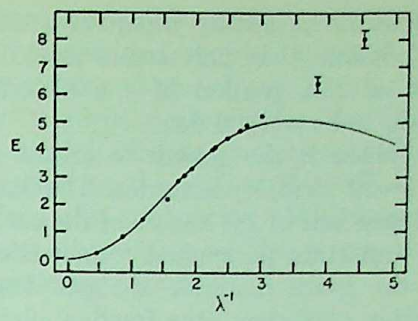

Fig. 5. Normalized extinction curve (Boggess and Borgman 1964). The two ultraviolet points of Boggess and Borgman at 2600 Å and 2200 Å are shown with error bars. The remaining observational points are taken from Johnson and Borgman (1963). The solid curve is van de Hulst's (1949) curve No. 15, based on the dielectric grain model.

called "uniform extinction law" prior to 1960 raised a very serious theoretical problem. This law implied that the mean particle size had to be specified to within a few percent in order to fit the observations. Thus, it was difficult to comprehend how this precise size could be established throughout the Galaxy. The new observations remove this difficulty.

C. Theories of the Grains

1. Dielectric Particles

To understand the complexity in the observations, several theories of the interstellar grains have been proposed. The first objective of the theories is to reproduce the observed extinction curve and secondly to predict optical properties, temperature, and composition of the grains. The observations yield limitations on the size, form, and numbers of any type of grains proposed in each of the theories. We consider first the dielectric grain model developed primarily by van de Hulst and Oort. Next, we consider the "Platt particle" theory and finally the graphite grain theory as developed by Wickramasinghe and Hoyle.

The dielectric grain or "dirty ice" model as developed by van de Hulst (1946, 1949) and Oort and van de Hulst (1946) considers that the grains grow from the interstellar gas by accretion. This hypothesis is based on the fact that where there is a large amount of gas, as revealed by interstellar lines, there is also a large amount of extinction—hence grains. On this theory the formation of the dielectric grains follows in three steps: (1) condensation nuclei of large molecules form out of the gas, (2) the abundant gases strike the nuclei and adhere (except H and He), and (3) the grains strike each other in cloud–cloud collisions and vaporize, thus leading to a steady-state distribution of grain sizes.

Step (1) is the weakest point of the theory. Following the work of ter Haar and Kramers (1946), it is supposed that diatomic molecules such as CH, and CH^+ are formed by radiative capture (more is said of this in

CC-0. In Public Domain. Gurukul Kangri Collection, Haridwar

Digitized by Arya Samaj Foundation Chennai and eGangotri

Sec. V on molecule formation) when two atoms collide. It is then possible that polyatomic molecules form. The details of this portion of the dielectric grain theory remain to be worked out.

The next phase is the growth to several thousand Ångstroms ($\sim 10^{-5}$ cm) by accretion. The final composition is independent of the nature of the condensation nuclei. The important parameters for accretion are the density of the grain material, the gas density, the accommodation coefficient (the fraction sticking), the kinetic temperature of the gas, and the temperature T_g of the grains. The T_g determines to a great extent what atoms will condense onto the grains. This temperature is determined by radiative processes; the kinetic energy exchange due to impinging atoms has a negligible effect on the grains. The equation of energy balance is

$$\int_0^\infty C_{ab}(\lambda, a)R(\lambda)\, d\lambda = \int_0^\infty C_{ab}(\lambda, a)B(\lambda_0, T_g)\, d\lambda.$$

The left-hand side gives the energy absorbed; C_{ab} is the absorption cross section; $R(\lambda)$ is the intensity of the interstellar radiation field. The right hand side gives the energy emitted; $B(\lambda_0, T_g)$ is the Planck function for T_g. The C's are computed using the Mie theory.

If the particle radiated as a blackbody, its temperature would be ~ 3°K. The particle at this temperature absorbs the visible and ultraviolet light of stars and emits infrared light with a wavelength exceeding its size. (We have seen that the particle size is of the order of several thousand Ångstroms.) These particles have a low emissivity compared to a blackbody in the infrared and the particle thus attains the higher temperature of 10°–20°K. The actual value is unknown, and it is found that T_g apparently increases with decreasing size of the grain (Greenberg, 1963).

The temperature of 10°–20°K means that H and He does not condense permanently since these atoms quickly evaporate at this T_g. Heavier atoms do, however, remain. In particular, van de Hulst considers that most of the oxygen atoms impinging on the grain remain permanently. They eventually become part of a water molecule after being bombarded by hydrogen atoms. The water molecule is quite stable and becomes the major constituent of the grain. Other molecules which contain the less abundant metallic elements exist in smaller proportions. Based on the above T_g and cosmic abundances, van de Hulst gives the following model for the grains: Each particle has 100 molecules of H_2O, 30 molecules of H_2, 20 molecules of CH_4, 10 molecules of NH_3, 5 molecules of MgH, etc. The resultant particle has a complex index of refraction: $m \approx 1.3\text{–}0.05i$. The nature of the electrical charge of the particle is still unclear; this charge, as we will see, is important in considering the motion of the grains with respect to a magnetic field and in considering the interaction of positive ions with the grains in the process of molecule formation. The general consensus is that the grains have a slight negative charge due to the higher velocities of electrons than positive ions. An equilibrium is reached when the electrostatic repulsion of the electrons and the attraction of the ions offsets the difference in the number of collisions due to the higher velocities of the electrons (van de Hulst, 1948).

We turn now to a discussion of the third process in the Oort–van de Hulst theory: the establishment of an equilibrium size distribution of grains. Van de Hulst and Oort computed that a particle would reach a size of 10^3 Å in about 3×10^7 years. Since this is appreciably less than the time scale of the Galaxy (10^{10} years), some process must be considered which prevents the particles from growing beyond the several thousand Ångstrom range. Furthermore, the process of reaching an equilibrium distribution must be fairly uniform since variations in the extinction law indicate that effective particle sizes differ at most by a factor of two. It is quite obvious that the exhaustion of the gas cannot be the limiting factor in the grains' growth since gas is observed in the same place as grains. Four processes to limit growth will be considered: (1) evaporation of the grains, (2) photodissociation of the atoms and molecules in the grains, (3) destruction during grain-grain collisions, and (4) sputtering by atoms in cloud-cloud collisions.

Process (1) has already been mentioned; most of the H and He evaporates since the vapor pressure of these two gases exceeds the partial pressure in the gas. In order to test the idea that the grains are completely evaporated, Wickramasinghe (1965) has made detailed calculations of the process of an encounter of a gas-grain cloud with a Strömgren sphere of a young, hot star. He adopts $T_g = 100$°K as the temperature required to vaporize the grains in a time scale less than the time for the cloud to transverse the Strömgren sphere. He finds that for cloud radii of 2–3 pc only extremely bright O stars can destroy a sizable fraction of the grains. Since these stars are relatively rare, Wickramasinghe concludes that evaporation is a rare event in destroying the grains.

Process (2) consists in either the photodissociation of a molecule near the surface and escape of one of the atoms or a release of an atom from a crystal by means of a light-quantum. Cosmic rays may also be of importance in this connection. The consensus is that these processes would not destroy the grain, only modify its surface. However, details are lacking due to our ignorance of the crystal structure of the particles and of the low-energy cosmic-ray (suprathermal particles) density.

The third process, grain–grain collisions, was initially proposed by Oort and van de Hulst (1946) to limit the growth of the particles. The basic mechanism here is that in cloud–cloud collisions two grains will collide and the energy will be sufficient to vaporize the particles. These collisions take place with a mean time of one pa

CC-0. In Public Domain. Gurukul Kangri Collection, Haridwar

Digitized by Arya Samaj Foundation Chennai and eGangotri

10^7 years. Using the properties of the dielectric grains, Oort and van de Hulst conclude that a head-on collision with $v > 2.8$ km/sec will lead to vaporization. Using the estimated properties for the clouds and grains, they derive the probability p per unit time that an ice grain of radius r is removed by the collision process:

$$p = 8.7(r/10^{-5})^3 10^{-9} \text{yr}^{-1}.$$

For $r = 10^{-5}$ cm we have an average lifetime of $\sim 10^8$ years. Since this is about 10^{-2} times the life of the galaxy, we may conclude that an equilibrium situation exists between growth and destruction. Oort and van de Hulst then derive the distribution function $n(r)$ of sizes of the particles. The final result may be represented by

$$n(r) = n(0) \exp\{-0.69(r/r_{\frac{1}{2}})^{2.6}\},$$

where $r_{\frac{1}{2}}$ is the radius at which $n(r)/n(0) = \frac{1}{2}$. The form of the distribution does not depend on the shapes or distribution of the interstellar clouds. This picture has many uncertainties about it. The data on the frequencies, sizes, and motions of interstellar clouds are quite uncertain. There are no clear-cut observational tests for cloud-cloud collisions, although Oort (1946) and van de Hulst (1948) have suggested that the energy freed by the collision can provide an explanation for the luminous rims of dark nebulae.

Recently, the cloud–cloud destruction mechanism has been criticized. Cloud collisions may not be completely inelastic due to the presence of large magnetic fields which prevent free penetration of the colliding clouds (Takayanagi and Nishimura, 1960). Also from a microscopic point of view, the charge of the grains may cause the grains to move in circular orbits about the magnetic field with gyroscopic radii of $10^{12}-10^{13}$ cm and this may prevent interpenetration of the grains from two clouds (G. B. Field, private communication).

In view of the above objections, the sputtering process must be considered. Wickramasinghe (1965) has considered this process in detail. He considers that in cloud–cloud collisions the kinetic temperature builds up to ~ 3000°K as the translational velocity of the clouds is converted into internal energy of the clouds. The grains are bombarded by atoms with an average energy of 0.3 eV. Since the vaporization energy of a water molecule from ice is ~ 0.2 eV, it is possible that some of the ice could be ejected. Wickramasinghe points out that sputtering is a momentum transfer process and not a mechanism of local heating of the irradiated surface. Using a semi-empirical relation, he concludes that H atoms with energy of 2 eV or more have a probability of at least $\frac{1}{4}$ of releasing a lattice molecule from the grain. He derives the rate of diminution of the grain:

$$dr/dt = -2\times 10^{-9} \exp\{-2/kT\} \text{cm yr}^{-1}$$

(k in eV deg^{-1}).

The probability per unit time that an ice grain will be destroyed by sputtering is $p \cong 10^{-8}$ yr^{-1}; this holds for all radii not greater than several thousand Angstroms. In contrast to the Oort–van de Hulst theory, this probability is independent of size. The Oort–van de Hulst process is less efficient than the sputtering process for removing ice mantles with radii $\leq 10^3$ Å.

Next, given this probability, Wickramasinghe derives the size distribution of the grains that results from the sputtering process:

$$n(r) = n(0)e^{-r/a},$$

where $\bar{a}$ is the mean size. Thus, the two processes give different types of distribution laws.

Given these two types of particle distributions, we next discuss the attempts to reproduce the observed extinction curve. We will investigate the possibility of choosing between the two, thus arriving at conclusions regarding the grain destruction process. All theoretical and observational results are normalized to some convenient scale. The calculated extinction is then proportional to:

$$Q(\lambda) = \int_0^\infty Q_{\text{ext}}(r, \lambda)\pi r^2 n(r)\, dr.$$

$Q_{\text{ext}}(r, \lambda)$ is the efficiency factor for extinction (cross section/area) for a particle of radius r at wavelength λ. Van de Hulst (1949) attempted to fit the observations of extinction using the Oort–van de Hulst distribution function. He chose $m = 1.25 - 0.03i$ for the complex index of refraction. Using the Mie theory for Q_{ext}, he found the best fit with the extinction curve with his curve number 15, reproduced as a solid line in Fig. 5. For this particular fit, $r_{\frac{1}{2}}$ (the radius at which $n(r)/n(0) = 0.5$) is ~ 3000 Å. Unfortunately, there is no unique solution for $r_{\frac{1}{2}}$ and for m. We must make an estimate for m from the composition of the particle.

As Fig. 5 indicates, the Oort–van de Hulst theory does not give agreement with the ultraviolet points of Boggess and Borgman; the change in the character of the theoretical curve indicates the importance of ultraviolet observations. Krishna Swamy (1965) has attempted to fit the ultraviolet observations by including the wavelength dependence of the real part of the index of refraction (van de Hulst assumed this was constant). Krishna Swamy found that with a smaller $r_{\frac{1}{2}}$ (~ 2000 Å) the theoretical curve constructed with the Oort–van de Hulst particle distribution agrees well up to the 2600-Å observation; however, the theoretical curve begins to flatten and falls well below the 2200-Å point. Wickramasinghe, Ray, and Wyld (1966) attempt to explain the observed extinction curve, including the two ultraviolet points at 2600 Å and 2200 Å, by the sputtering distribution function. They find that they can get a very good fit to the observations up to $\lambda \simeq 3000$ Å if $\bar{a} = 750$ Å and a reasonably good fit at 2600 Å. Again, the 2200-Å point falls well above the theoretical curve. Thus, we cannot make

CC-0. In Public Domain. Gurukul Kangri Collection, Haridwar

Digitized by Arya Samaj Foundation Chennai and eGangotri

a direct test of the Oort–van de Hulst particle distribution versus the sputtering particle distribution due to the fact that a reasonably good fit to the observations (excluding the two ultraviolet points) can be attained with both distributions. We are forced to agree with van de Hulst (1964): "Fitting a theoretical curve to these data . . . is (unfortunately) rather easy."

One further observation may be of significance in accepting or rejecting the dielectric grain model. In the second flight of Stratoscope II (infrared observations from high altitudes by means of a balloon), a reddened late-type supergiant was investigated in the far infrared. Danielson, Wolf, and Gaustad (1965) have attempted to locate an absorption band in the spectrum of the star due to ice in the region of 3.1 μ. They use van de Hulst's curve number 15 and the observed A_v as the basis for the expected strength of the band, assuming that the grains are entirely ice. No band is found. These authors conclude that no more than 25% of the interstellar grains can be ice. Although the exact interpretation of these results is not clear, they may well be an argument in favor of other types of particles.

2. *"Platt Particles"*

One of the various problems in the dielectric grain theory is the formation of the grains. Van de Hulst assumed that all possible reactions involving abundant atoms which satisfy energy considerations would occur. Since the chemical composition of the grains determines the optical properties, it is necessary that we understand, in addition, the condensation and adsorption processes which take place on the surface of the grains. Donn (1955) has criticized the van de Hulst formation process. He cites several experimental studies which indicate that the surface reactions would be very inefficient at the temperatures of interstellar space. In particular, he considers the formation of H_2O molecules by surface reactions of H_2 and O; there is some experimental evidence that this reaction is quite inhibited at low temperatures. The formation of H_2O is, of course, central to the Oort–van de Hulst theory. However, very little is known about surface reactions at low temperatures and extrapolation from higher temperatures to 10°–20°K is far from satisfactory.

Following these criticisms, Platt (1956) made a proposal for a new type of interstellar dust particle; this type of particle has subsequently been known as a "Platt particle." Platt's basic premise is that the particles grown by accretion from a gas containing ions or molecules and subjected to constant radiation damage will not have filled electronic bands. They will not be any more chemically stable or electrically neutral than the ions and radicals of which they are formed. Even if a system were to reach a situation where all of its energy bands were full, there are more ways of losing this property than preserving it. Platt proposes that a large free radical of size 1–10 Å is formed by accretion. He then uses theoretical and experimental arguments to assert that the longest wavelength of absorption in a particle of radius r caused by a one-electron jump between free electron levels is about 800 r. Finally, on the basis of crude experimental data, Platt proposes that the absorption cross section of the particles is approximately constant with wavelength and equal to the geometrical cross section down into the ultraviolet.

Due to the lack of a suitable theory, the detailed wavelength dependence of extinction caused by this sort of grain remains unknown up to the present. No really significant observational test using the extinction curve is possible, since the optics of these particles are unknown. The only definite conclusions we obtain from this rudimentary theory are that the particles will be small (1−10 Å), that the total mass of absorbing material will be about 1/200 that of the dielectric grains, and that the extinction curve will not have a strong dependence on the exact size of the particles.

An interesting attempt to treat the "Platt particles" in detail has been made by Kimura (1962). His proposal is based on the hypothesis due to Hayakawa (1960) that the cosmic-ray flux (the suprathermal particles) in the region 0.1 to 100 MeV is substantial. (See Sec. II.C for further discussion of the suprathemal particles.)

Kimura states that dielectric grains would initially form as in the Oort–van de Hulst theory. After detailed calculations concerning the interaction of the cosmic-ray protons and alpha particles with the grains, he derives the probability per unit time that a particle of radius r is destroyed:

$$p = 3\times 10^{-6}\ \mathrm{yr}^{-1}.$$

Thus, in comparison with the p given by the cloud-cloud collision in the Oort–van de Hulst theory, the cosmic-ray destruction process will be quite effective in limiting the growth of grains with radii less than 100 Å.

Using the above p, Kimura derives the size distribution function for the particles as $n(r)=n(0)\exp\{-r/\bar{a}\}$, the same function that Wickramasinghe derives for the sputtering process. Kimura then attempts to calculate a theoretical extinction curve for these particles. Since no detailed information on the wavelength dependence of the extinction to be expected is available, he uses two simplified types of absorption coefficients as suggested by Platt.

Case A:	$Q_{\mathrm{ext}}=\pi r^2$	$\lambda\leq\lambda_m$
	$Q_{\mathrm{ext}}=0$	$\lambda>\lambda_m$
Case B:	$Q_{\mathrm{ext}}=\pi r^2(\lambda/\lambda_m)$	$\lambda\leq\lambda_m$
	$Q_{\mathrm{ext}}=0$	$\lambda>\lambda_m$,

where λ_m is the longest wavelength of strong allowed absorptions ($\lambda_m=800r$). With $\bar{a}=2$ Å, he is able to

CC-0. In Public Domain. Gurukul Kangri Collection, Haridwar

Digitized by Arya Samaj Foundation Chennai and eGangotri

the observed extinction curve with Case B from the far infrared to 4000 Å. The ultraviolet points ($\lambda \leq 3500$ Å) which are a crucial test for any theory, show a great disparity between observations and theory. Since the Q_{ext} is only a crude approximation, even the partial agreement between theory and observation must be considered to be fortuitous. We again see how easy it is to fit the observed extinction curve with widely different theories. The imperfections in our knowledge of the optics of these particles thus prevent a detailed study of the "Platt particle" theory.

3. *Graphite Grains*

In 1954, Cayrel and Schatzman (1954) proposed that a component of the interstellar dust consists of graphite grains. Since 1962 Hoyle, Wickramasinghe, and others have investigated in detail the possibility of explaining interstellar extinction by graphite particles. We will consider the work of the latter authors in three parts: (1) the formation of the graphite particles, (2) the formation of the ice mantles over the graphite cores as proposed by Wickramasinghe, and (3) the attempts to explain extinction by these particles.

As we have pointed out, the major problem with the dielectric grain theory is the formation process; the low densities in the interstellar medium imply that the formation of condensation nuclei is a very slow process. Hoyle and Wickramasinghe (1962) attempted to overcome this problem by proposing that the graphite grains form in a high density environment—the atmospheres of C (carbon) stars. These are cool, luminous stars which have an abundance of carbon much greater than that of oxygen, in contrast to the sun where carbon is about half as abundant as oxygen. In the C stars' atmospheres the densities of monatomic and polyatomic carbon are appreciable. Among the C stars is one group, the N stars, which have large radii; these would contribute most of the interstellar graphite. Most of the C stars are variable; they pulsate with periods of $\sim$100 days. At minimum phase the surface temperature is $\sim$2000°K, and at maximum phase $\sim$2700°K. In contrast, the atmosphere of the sun is $\sim$6000°K.

Hoyle and Wickramasinghe consider in detail the manner in which graphite is formed in the atmospheres of the *N* stars and the method by which the graphite leaves the star and moves into the interstellar medium. They consider the concentrations of monatomic and polyatomic carbon; most of the carbon is in the form C_1, C_2, and C_3. The fact that a larger number of species (C_4, C_5, etc.) is not present in large concentrations means that fairly sizable grains will form, rather than a much larger number of small nuclei.

As the star cools below 2700°K when it goes from maximum to minimum phase, graphite begins to form as the partial pressure of carbon exceeds the vapor pressure of graphite. Once the graphite is formed, radiation pressure begins to act on the particles, which are shown to be less than 10^{-5} cm. This force exceeds the gravitational force and the particles begin moving away from the star. The escape of the grains is, however, hindered by the viscous drag produced as the grains encounter the gases in the star's atmosphere. The grains formed near minimum phase must escape before maximum phase since they all will be evaporated as the star heats up again. Approximately 10^7 sec is the time allowed for escape. Hoyle and Wickramasinghe show that the escape can take place if the gas density in the star's atmosphere remains below a certain upper limit for $\sim 10^7$ sec. This in turn implies that the temperature must remain below 2300°K for $\sim 10^7$ sec.

Once the grains leave the star no further condensation of carbon takes place. The grains are exposed to the star's radiation field and evaporation will take place unless the grains move several stellar radii in a relatively short time. Hoyle and Wickramasinghe show that the grains move at a high velocity and are at two stellar radii in $\sim 3 \times 10^5$ sec. Thus, the grains escape quite easily once they leave the stellar atmosphere.

A substantial fraction of the carbon in the atmosphere is said to escape during each cycle. Then the carbon is resupplied to the atmosphere by convection from the star's interior.

Finally, Hoyle and Wickramasinghe consider the amount of graphite interjected into the interstellar medium per year. Using the fact that there are 10^4–10^5 N stars in the galaxy and estimating the mass loss of graphite by these stars per cycle, they conclude that the present grain density of $\sim 10^{-27}$–10^{-26}g/cm^3 can be attained in $\sim 10^{10}$ years—the lifetime of the Milky Way.

As in the other grain theories, the formation of the graphite particles is the weakest point in the theory; although the general features seem reasonable, a more detailed analysis is needed. Furthermore, there are at present no observations that directly relate to graphite formation in the N stars' atmospheres. Tsuji (1964), in an investigation of molecular abundances in cool stars, has criticized the Hoyle and Wickramasinghe theory on two points: (1) the carbon is depleted as polyatomic molecules of carbon, hydrogen, and nitrogen form; thus, the amount of free carbon available for forming graphite is severely limited. (2) Tsuji states that Hoyle and Wickramasinghe adopt a value of the saturated vapor pressure of graphite which is too small. Hence, the graphite will begin to form at $\sim$2200°K and not at 2700°K; this effect also results in a reduction of the amount of graphite which will form.

The final step in the growth process is the formation of ice mantles in the interstellar medium. Since graphite is strongly chemisorbent, practically all the heavy atoms will be adsorbed. Hydrogen can then combine with the oxygen and a mantle of predominantly ice will grow.

CC-0. In Public Domain. Gurukul Kangri Collection, Haridwar

Digitized by Arya Samaj Foundation Chennai and eGangotri

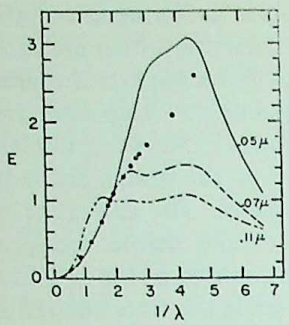

FIG. 6. Normalized extinction E versus $1/\lambda$ (λ in microns) for graphite spheres of various radii (Wickramasinghe and Guillaume 1965). $E=1$ at 5470 Å. The closed circles represent the observational extinction curve of Boggess and Borgman (1964, see Fig. 5).

Since the graphite grain of size ~100 Å will acquire a mantle with radius ~1000 Å in 10^8 years, Wickramasinghe (1965) considers processes which are effective in mantle removal; if these processes are not efficient, the composite grains will acquire the optical properties of the dirty ice grains. Wickramasinghe considers the three major processes mentioned in the section on dielectric grains: (1) evaporation in grain–grain impacts during cloud–cloud collisions, (2) sputtering by H atoms in cloud–cloud collisions, and (3) thermal evaporation by encounters with O and B stars. The graphite is not affected by any of these processes since the heat of vaporization is 170 kcal/mole, as contrasted with 250 cal/mole for ice. For process (1) to be effective, the relative cloud velocities would have to be >20 km/sec—a totally unreasonable value. Since the composite grains are generally $<10^3$ Å, process (2) dominates as we have seen in the section on dielectric grains. An exponential distribution of mantle sizes results:

$$n(r)=n(r_0)\ \exp\{-(r-r_0)/(\bar{a}-r_0)\},$$

where r_0 is the graphite core radius and $\bar{a}$ is the mean mantle radius. Since the destruction process is so efficient, the mantle growth will increase the total radius by only two to three times. This will ensure that the optical properties of the composite particle are still determined primarily by the graphite cores.

Several attempts have been made to compare the extinction observations with the graphite theory. As in the other types of grain theories, the observations in the visible region are quite easy to fit with theoretically constructed curves. In order to explain differences in extinction, Wickramasinghe has proposed that in some regions graphite grains of size 200–1000 Å predominate, while in other areas the composite particles dominate. In either case, accurate extinction cross sections for various size particles as a function of wavelength are needed. Wickramasinghe *et al.* (Wickramasinghe 1966, Krishna Swamy and Wickramasinghe 1966, Guillaume and Wickramasinghe 1966) have used new experimental data on the wavelength dependence of the index of refraction of graphite from 1100 Å to the far infrared to calculate these cross sections for pure graphite grains.

Two significant results were found: (1) the absorptive index $k(m=n-ik)$ reaches a sharp maximum near 2600 Å. This feature may explain the large extinction measured by Boggess and Borgman (Fig. 5), which we have described in Sec. IIIB. However, as shown in Fig. 6, attempts to explain the observations in detail have not been successful. This figure shows three theoretical curves for $r_0=500$ Å, 700 Å, and 1100 Å; the observations of Boggess and Borgman are indicated by circles. It is evident, nevertheless, that the graphite grains are much more promising as an explanation for the 2600 Å and 2200 Å observations than the dielectric grains. (2) For $r_0<700$ Å, the extinction is approximately linear as a function of λ^{-1} in the region from 12 000 Å to 4300 Å. Below the latter limit, the extinction curves vary considerably depending on particle size. The linear part arises from Rayleigh scattering in the range of constant m and the variable portion arises from the fact that m ceases to be constant below ~4300 Å. This set of circumstances may well explain the break at 4300 Å in the observed extinction curve that Nandy has detected for Cygnus and Perseus. The theory predicts a nonlinear extinction for $\lambda<4300$ Å in contradiction to observation; however, Nandy and Wickramasinghe (1965) suggest that a collection of different mean particle sizes could give an approximately linear curve for $\lambda<4300$ Å.

Wickramasinghe, Dharmawardhana, and Wyl... (1966) extend the above results by calculating extinction cross sections for graphite-core ice mantle grains. Three major effects are found. (1) The extinction at infrared wavelengths comes almost entirely from absorption arising in the graphite cores. For a core of radius 200 Å and with a mantle twice this size, 75% of the extinction at 6000 Å is due to absorption by the graphite core; in the blue and ultraviolet, scattering from the ice mantle contributes about 50% of the extinction. (2) the ratio $R=A_V/E_{B-V}$ is increased relative to a pure graphite grain. (3) Using various values of $\bar{a}-r_0$ in the mantle distribution law:

$$n(r)=n(r_0)\ \exp\{-(r-r_0)/(\bar{a}-r_0)\},$$

Wickramasinghe *et al.* show that practically identical extinction curves result provided the cores' radii are less than 600 Å. This effect is caused by the fact that the extinction due to the graphite cores is approximately linear in the region 12 500 A to 5000 Å and is independent of core radius. Hence, knowledge of exact values of core sizes is not necessary to predict extinction. To further test the theory Wickramasinghe and Nandy (1965) have attempted to fit Nandy's detailed observations of Perseus and Cygnus. For the former they adopt a model of pure graphite grains, with a Gaussian distribution of radii with a dispersion of 100 Å centered at $\bar{a}=600$ Å. For the Cygnus observations they choose a composite grain model with a sputtering distribution function of mantle sizes: $r_0=200$ Å, $\bar{a}-r_0=300$ Å. Since there are so many free parameters

CC-0. In Public Domain. Gurukul Kangri Collection, Haridwar

Digitized by Arya Samaj Foundation Chennai and eGangotri

these two models can scarcely be unique. Furthermore, it is very difficult to explain the existence of composite particles in one extended region of the Galaxy, while pure graphite grains exist in another. *A priori* the graphite grains would be expected to grow mantles unless very special conditions existed. In many respects, nevertheless, the graphite grain theory is very promising for explaining interstellar extinction. In the section on optical polarization (Sec. IIID1) we will express a further difficulty that the graphite grain theory encounters.

D. Further Observations

1. Optical Polarization

We next consider the question of interstellar polarization. Polarization does not provide the fundamental data on which the above theories of the grains are based. In a few cases however, as we will point out, the characteristics of the polarization have implications for the theories of the grains. In general, we must first have a theory for the grains in order to infer properties of the interstellar medium from the polarization data.

Two conditions are necessary to explain polarization: (1) asymmetric particles and (2) an alignment mechanism. The former is slightly different for each grain model while the latter is the same for all models. We shall first discuss the alignment mechanism and then investigate its operation on each of the three types of grains proposed. We turn then to a further discussion of the uniformity of the grains.

The theory of alignment in a weak magnetic field is due to Davis and Greenstein (1951). The grains are set spinning by the interstellar gas; angular velocities of 10^5–10^6 rad/sec build up. Since the smallest kinetic energy of rotation for a given angular momentum corresponds to rotation about the shortest axis of the ellipsoid of inertia, the grain tends to rotate about its smallest axis (Hall and Serkowski, 1963). The effect of paramagnetic relaxation then comes into play. For those volume elements which experience a changing magnetic field due to the orientation of the field with respect to the axis of rotation, paramagnetic absorption takes place. The energy in this mode of rotation goes partially into the internal energy of the grain. Therefore, these motions are damped out, and the particle tends to rotate with its axis of rotation parallel to the field; in the limit of complete alignment, the field in each part of the grain remains constant if the transverse gradient of the field is larger than the long dimension of the grain.

Davis and Greenstein are not able to solve the problem of the alignment exactly since the torques acting on the grain due to paramagnetic absorption are not conservative. An approximate solution for the size of the magnetic field is given by comparing the relaxation time for orientation with that for disorientation due to collisions with gas atoms. Two limiting cases are discussed: (1) the alignment is practically complete, and (2) the alignment is small. In case (1) they obtain

$$B > [a n_H T^{\frac{1}{2}} \omega / (7.5 \times 10^{18} \chi'')]^{\frac{1}{2}}, \qquad (1)$$

where χ'' is the imaginary part of the magnetic susceptibility, ω is the angular velocity of the grain, a is the average radius of a grain, n_H is the number of gas atoms per cm^3, T is the kinetic temperature of the gas. The lower limit exists because of the obvious saturation effect in the alignment. This, then, is a measure of the magnetic field necessary to align the particles completely.

For slight alignment:

$$B = [a n_H T^{\frac{1}{2}} \omega F / (2.5 \times 10^{18} \chi'')]^{\frac{1}{2}}, \qquad (2)$$

where F is the distribution parameter which is a measure of how well the particles are aligned. In order to estimate the magnetic field in this case we must find the degree of alignment by some other means. The quantity F can be determined by observing the ratio of polarization to extinction. This is related to F by

$$p/A_v = 4.5 \frac{(\sigma_E/\sigma_H - 1)}{(2\sigma_E/\sigma_H + 1)} F \sin^2 \theta, \qquad (3)$$

where p is the amount of polarization in magnitudes, θ is the angle between the field and the direction of the line of sight, σ_E and σ_H are the cross sections that correspond to the axes of symmetry of the grain parallel to the electric and magnetic vectors of the incident light, respectively. Thus, the measured quantity p/A_v depends both on the degree of alignment F and on the degree of asymmetry of the particles. In order to find F from this equation we must have some independent idea of the degree of the asymmetry from the grain models.

To obtain B, F is calculated from (3) if θ and σ_E/σ_H can be estimated. If $F \cong \frac{1}{3}$ (complete alignment), Eq. (1) is used to obtain a lower limit to B. If $F \ll \frac{1}{3}$, Eq. (2) is used to obtain B.

The observations of polarization indicate that the plane of vibration is generally in the galactic plane. The Davis–Greenstein theory predicts that the long axis of the grain lies perpendicular to the field. Hence, we conclude that the field lies in the plane. If, in addition, one assumes that the field is along the spiral arms, the theory is also successful in explaining the longitude dependence of polarization. When we look along a spiral arm we look parallel to the field and the amount of polarization, p, should be zero. If we look across the spiral arm, the field is perpendicular to the line of sight and the polarization is maximized. The polarization goes to zero at $l = 50°$ and 230°. The direction of the galactic field as derived from polarization agrees quite well with the spiral arms as delineated by young clusters and associations. (In Sec. IV we will

CC-0. In Public Domain. Gurukul Kangri Collection, Haridwar

Digitized by Arya Samaj Foundation Chennai and eGangotri

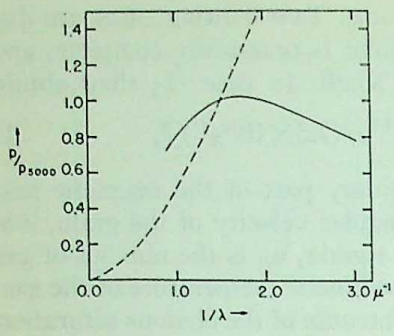

Fig. 7. Wavelength dependence of polarization. The solid curve is a theoretical fit (Greenberg, Lind, Wang, and Libels 1963) to Gehrel's (1960) observations. The dashed line represents Greenberg's (1966) calculations for small graphite spheroids. This curve is normalized to unity at $\lambda^{-1}=1.5$.

point out objections to this interpretation.) The theory also explains the correlation in filamentary nebulae that exists between the directions of the filaments and the position angles of the transmitted starlight.

We shall first describe the application of the Davis–Greenstein theory to dielectric (dirty ice) particles, where it was initially used. The problems of formation, comparison with extinction observations, and the determination of B will be considered. The anisotropy of the particles must be explained since the Oort–van de Hulst particles supposedly grow by random accretions. Two methods of explaining the anisotropy have been proposed. The first is that grain–grain collisions not energetic enough to vaporize the grains give rise to melting and the grains fuse to form elongated grains. Secondly, Kahn (1952) has suggested that the growth of ice particles is strongly influenced by the electrostatic potential due to the electric dipole moment of the H_2O molecule. He envisions the formation of H_2O on the surface of the grains, which then line up with existing molecules, thus giving rise to elongated particles. This theory does, of course, raise many unresolved questions.

The paramagnetic nature is attributed to small quantities of iron and iron compounds which the grain obtains in the random accretion process. We now examine these particles to see if they can produce both the observations of *extinction* and the color dependence of polarization. We cannot compare the situation analytically because no exact expressions are available for extinction cross sections for spheroids as a function of orientation. Approximate expressions have been developed by Greenberg (1960b), and he and his associates (Greenberg, Pedersen, and Pedersen 1961) have conducted microwave analogue experiments at 3 cm to measure cross sections of spheroids. The general conclusion is that the wavelength dependence of polarization of spinning particles is similar to that produced by perfectly aligned particles. Greenberg, Ling, Wong, and Libels (1963) considered the polarization due to long cylinders with an index of refraction of 1.3 and an Oort–van de Hulst distribution of radii. The wavelength dependence for perfect alignment is quite similar to the dependence found in the observations of eight stars by Gehrels (1960). The polarization reaches a maximum at about 6500 Å; it falls off rapidly to the infrared and gradually to the shorter wavelengths (see Fig. 7).

Next, we consider the determination of B for the dielectric grain model. Reasonable values of σ_E/σ_S are not much larger than one; if $\theta=90°$, the maximum value of (p/A) is observed and F is found to be about $\frac{1}{3}$, i.e., practically complete alignment. Using the theory of paramagnetic relaxation (1), Davis and Greenstein obtain $\chi''/\omega \simeq 2.5\times10^{-12}/T_g$. Since $a \gtrsim 2000$ Å, $n_H = 10/\text{cm}^3$, $T=100°$, and $T_g=10°$, they find $B>3\times10^{-6}$ G.

Two obvious problems arise from the above considerations. (1) The mechanism giving rise to the asymmetry of the dielectric grains remains to be fully explained. (2) The lower limit obtained for the general galactic field B is quite different from the value obtained from other considerations ($\approx10^{-6}$ G or less). (See Sec. IV.)

Henry (1958) proposed a solution for the second objection by considering the particles to be ferromagnetic. The particles attain a large residue of iron and iron compounds after selective evaporation in collisions. In this case, $\chi''/\omega \simeq 3\times10^{-7}$ and $B>1.2\times10^{-4}$ G. However, the details of selective evaporation have not been considered.

The "Platt particles," or large free radicals, represent an attempt to overcome the first objection. Since the particles are so small, they are said to have aspherical shapes because of statistical fluctuations in the arrangements of molecules or atoms. The degree of asymmetry required can be estimated and compared with the expected size of such variations. If the particles are elongated with length/width$=1+\epsilon$, the maximum ratio of polarization to extinction is $\epsilon/2$ (Hall and Serkowski, 1963). Since the observed value for $(p/A)_{max}$ is 0.06, $\epsilon=0.12$. As Greenberg (1960a) points out, this value is two or three times larger than the value obtained from random growth. Thus, we see that the problem of asymmetry is not entirely solved by invoking "Platt particles." However, these particles are highly paramagnetic and it is possible that the Davis–Greenstein effect could apply. However, no estimate for χ''/ω is available and hence no information on the magnetic field can be obtained.

We turn now to graphite grains which are able to overcome both objections to the dielectric grain model in a very effective way. First, the asymmetry required can be attributed to the intrinsic structure of graphite. The graphite has a conductivity perpendicular to the basal planes two orders of magnitude less than in the planes. Thus for light with the electric vector in the of the planes the grain produces metallic absorption while for light with the electric vector perpendicular to the plane, the graphite has dielectric properties. The extinction cross section for the latter component is the smaller of the two. Second, the magnetic field required

CC-0. In Public Domain. Gurukul Kangri Collection, Haridwar

Digitized by Arya Samaj Foundation Chennai and eGangotri

to produce the observed polarization is much smaller. Wickramasinghe (1962) gives a detailed discussion of polarization due to graphite particles. Since $\sigma_E/\sigma_H \gg 1$, we obtain $p/A = 2.25\ F \sin^2\theta$. When $\theta = 90°$ the maximum p/A is obtained and we find $F = 0.02$, a very slight alignment. Then from a discussion of the magnetic properties of graphite, we obtain $\chi''/\omega = 1.2\times10^{-10}/T_g$; leading to an estimate of the field from Equation (2) of $B = 1.1\times10^{-6}$ G, more in line with the results from other considerations. In this model, the polarization is due primarily to the anisotropic conductivity of graphite rather than to a strong magnetic field.

One of the reasons the graphite theory was initially proposed was the ease with which the observed amount of polarization can be explained by these particles. Ironically, Greenberg (1966) has pointed out that the wavelength dependence of polarization may well rule out graphite particles as constituents of the interstellar medium. He considers the wavelength dependence of the polarization which would be expected from small oblate spheroids with major axes of 500 Å (a size which, as we have seen, will roughly reproduce the observed extinction curve). Greenberg finds that polarization rises monotonically from the far infrared to the ultraviolet [see the dashed curve in Fig. 7. The solid line represents the observations of Gehrels (1960).] If the graphite becomes covered with an ice mantle of moderate dimensions, the polarization would hardly be altered in the infrared; in the visible and ultraviolet, Greenberg proposes that the polarization would continue to increase as a function of λ^{-1} with a smaller slope. This result is in clear contradiction to the observations. Although the graphite grain model has several very attractive features, as we have mentioned in Sec. IIIC3, the above result is obviously a serious objection to this theory.

Up to now, we have not considered the relationship between extinction and polarization and the information available from the various models from this relationship. Several authors (Wilson 1959, Greenberg and Meltzer 1960, and Greenberg 1963) have attempted to show that changes in the wavelength dependence of extinction were due to orientation effects: when viewed along the lines of force all grains present themselves sideways; when viewed perpendicular to the lines of force they present themselves both sideways and edge-on. Greenberg (1960) then suggested an observational test to distinguish between dielectric particles and "Platt particles." He shows that the extinction curve due to the latter particles should be independent of orientation.

However, it now seems evident that any change in the extinction curve due to orientation is masked by differences in the particle size distribution and intrinsic properties from place to place. Wampler (1962) has looked for a correlation between fluctuations in the polarization (hence alignment) and deviations from a mean reddening law. He found that this effect does not exist; this conclusion is supported by Serkowski's results (1963). In fact, near $l = 130°$, where polarization is quite large, Wampler found the lowest value of the reddening slope.

A most important recent development in our understanding of the nonuniformity of the grains has been presented by Gehrels and Silvester (1965). They have made polarization measurements which give further evidence that the properties of the grains change from cloud to cloud; in some places not only the amount but also the position angle of polarization changes with wavelength. The nearby stars show no change as a function of wavelength, while the distant stars show a decided change with wavelength. The interpretation is as follows: The light from the star traverses several clouds. Each cloud has different size grains and hence a different distribution parameter r_1; thus the polarization due to each cloud will predominate at a particular wavelength, i.e., the clouds with small particles dominate the polarization in the ultraviolet. Finally, the magnetic field orientation changes slightly from cloud to cloud. Thus, the position angle changes as a function of wavelength. Again, we come to the conclusion that the grains are far from uniform throughout the interstellar medium.

We can also use the polarization data to answer a question which has long plagued studies of the interstellar medium: is the ratio of grains to gas (n_g/n_H) constant throughout the galaxy? Lilley's (1955) 21-cm investigation of the Taurus–Orion Dark Nebulae Complex indicates that on a large scale n_g/n_H is constant with position. In general, the ratio of the mass densities of dust to gas is found to be about 10^{-2}. On the other hand, Bok, Lawrence, and Menon (1955) show that on a small scale (in certain dark nebulae) n_g increases without an increase in n_H. As Hall and Serkowski (1963) have shown, a new method of attacking this question is provided by polarization measurements in open clusters. Since polarization and extinction have the same dependence on distance and galactic latitude (both depend on the grains), the stars at a given longitude normally show a strong correlation of polarization and extinction. However, the strange thing is that if the stars are grouped together at the same galactic coordinates and the same distance, as in a cluster, the observations indicate that the correlation between polarization and extinction is quite small. This lack of correlation can be explained if n_g/n_H is constant between the sun and the cluster. We have seen that polarization is directly proportional to n_g and to F. But F is inversely proportional to n_H for a fixed B [see Eq. (2)]. Hence, p is proportional to the ratio of n_g and n_H. If p is constant, the ratio n_g/n_H is constant. Thus, if the grain density in front of a particular star is larger than the average density, A_v

CC-0. In Public Domain. Gurukul Kangri Collection, Haridwar

Digitized by Arya Samaj Foundation Chennai and eGangotri

will increase for this star. The polarization will, however, remain constant since n_H increases in the same proportion as n_g. Thus, the polarization is not correlated with extinction for stars in open clusters, and this test indicates a constant n_g/n_H.

2. HII *Regions and Interstellar Grains*

Recently, the important problem of the relationship between HII regions and grains has been considered. As we will point out, these considerations may have important implications for molecule formation in HII regions.

The grains in the direction of the Orion Nebula were noted, in 1937, to have peculiar properties when Baade and Minkowski (1937) determined that the ratio of extinction to color excess was quite large in this direction. Recent measurements indicate that R is $\sim$7.5. Krishna Swamy (1965) has applied the Oort–van de Hulst distribution for "dirty ice" and attained a good fit to the observations with $r_{\frac{1}{2}} \simeq 4000$ Å, i.e., a relative depletion of the small grain sizes has occurred.

O'Dell and Hubbard (1965) have recently shown that part of the interstellar extinction in the direction of Orion occurs in the HII region. They have investigated the ratio of the brightness in the continuum to that in the second Balmer line (H_β) as a function of distance from the center of Orion at five wavelengths. They calculate the amount of scattering due to atomic processes and conclude that the major portion of the brightness in the continuum is due to scattering from dust particles in the HII region. $N_{dust}\, Q/N_{gas}$ is found to increase by a factor of ten from the inner to outer regions (Q is the effective scattering cross section for the particles). Hence, the cross section and/or number of particles is quite a bit smaller near the young, hot stars in Orion. O'Dell and Hubbard suggest two possible mechanisms to explain the apparent increase in dust in the outer regions and the anomalous reddening law: (1) radiation pressure drives the smaller particles out at a faster rate than the larger ones, and (2) the smaller grains are evaporated by the intense radiation field. The details of these mechanisms are not now known; the over-all effect depends on the lifetime of the nebula, which is given as 2×10^4 years by Vandervoort (1964) on the basis of the expansion of the gas due to ionization.

Finally, Herbig (1958) has shown that for the nebula IC 405 dust and gas coexist in space in a unique set of circumstances. The exciting star for this nebula is AE Aurigae, an O 9.5 (high luminosity and temperature) star moving away from the association of stars I Orionis. The star differs in radial velocity from that of the nebula by 37 km/sec. The nebula consists of two parts: (1) an emission nebula whose presence is indicated by hydrogen emission lines and (2) a reflection nebula of different shape and size, whose presence is indicated by a purely continuous spectrum. The first component shows up in photographs taken in the light of Hα (the first Balmer line). The second component shows in the blue regions of the spectrum which are free from emission lines. Herbig shows that the second component is probably due to scattered light from interstellar grains, since the nebula which has the continuous spectrum is coincident with dark lanes in the emission nebula. It seems that the dust does not share the motion of the star since obscuring lanes of dust are visible for some distance from the star. As we have seen (in Sec. IB), the presence of a reflection nebula or an emission nebula usually depends on the type of exciting star. The hot luminous stars give rise to emission nebulae and the cooler less luminous stars produce reflection nebulae. In the case of IC 405, both types are present. Herbig proposes that this situation is due to the large velocity of AE Aurigae; the dust has not had enough time to accommodate itself to the properties of the star. Presumably, if the star did not have the large space motion, only an emission nebula would be produced. In support of this contention is the fact that none of the dust lies directly to the south of AE Aurigae; this is the direction from which the star has come and there has probably been enough time for the grains in this region to have been evaporated by the star's radiation. The HII region is due to the encounter of the star with a low density gas cloud. Thus, we find the anomalous result that the material associated with the reflection nebula has little free gas associated with it. As Herbig points out, this conclusion is contrary to the idea that the grains "... are only trace condensates from gas, and hence should have a large amount of gas still associated with them since no efficient separation processes are known."

3. *The Unidentified Diffuse Lines*

As a conclusion to the section on interstellar grains we briefly consider another observational component of the interstellar medium which seems to be related to the grains—the group of "diffuse unidentified lines." About twenty of these discrete spectral features in a very high frequency should [have been] used since absorption have been presently discovered in the range 4000–6800 Å (Herbig, private communication). These features have half-widths of up to 10 Å as contrasted with several hundredths of an Ångstrom for the atomic and molecular lines, as indicated in Table I. The diffuse absorption lines remove about six times as much light from the spectra of background stars as do the atomic and molecular lines. These lines always appear at the same wavelengths but the shape of the line profiles and the ratios of strengths vary from star to star.

Observations of diffuse lines have established three boundary conditions (Herbig 1963):

(1) The strength of the lines is more strongly correlated with the amount of interstellar extinction than

CC-0. In Public Domain. Gurukul Kangri Collection, Haridwar

Digitized by Arya Samaj Foundation Chennai and eGangotri

with the number of Ca^+ atoms in the line of sight. Wampler (1963) has also shown that the strength of the strongest diffuse line at 4430 Å is strongly correlated with the slope of the reddening curve determined in the same region of space. It seems that extinction and the strength of 4430 vary as a function of galactic longitude in the same manner. These facts indicate that the carrier of the diffuse lines is in some way closely associated with the interstellar grains.

(2) The carrier seems to be disrupted by the presence of an HII region since the diffuse lines are weakest in these regions. This fact may be connected with the anomalies in extinction near HII regions.

(3) The strength of the diffuse features implies that the carrier consists of abundant elements.

As Herbig (1963) points out, one of the most surprising things about the diffuse lines is that they have yet to be explained. The lines were actually discovered in 1921; their interstellar origin was shown 15 years later. There have been numerous attempts at explanation—the main problem being the explanation of the large widths of the lines. The first attempts involved diatomic and polyatomic molecules. Recent attempts by Unsöld (1964) (plasma oscillations in solids) and by Herbig (1963) (metastable H_2 molecules on interstellar grains) have not been successful in providing a full explanation. Quite probably, the solution to the problem of the diffuse lines will come after we attain a more complete understanding of the nature of the interstellar grains.

IV. GALACTIC MAGNETIC FIELDS

The interstellar grains were the first observed tracer of a galactic magnetic field and are believed to be a catalyst in the formation of molecules. The next two sections deal with these aspects of the interstellar medium.

For many years astronomers have accepted the idea that the galaxy is influenced by magnetic forces in addition to the gravitational ones. The presence of ionized gases in motion which would produce a magnetic field, and of cosmic rays distributed isotropically as seen from the earth, which would result from the existence of such a field, have contributed to this acceptance. However, the strength and topography of this field remain uncertain. Since the influence of the field is likely to be important, a lack of knowledge of its size and direction spawns a variety of theories based solely on guesses of these quantities. The intriguing thing about the problem of the magnetic field at this moment is that the crucial question of the importance of its influence on motions of the interstellar gas requires for its answer observations lying at the limit of sensitivity of current instruments. If the field is of the order of 10^{-5} G, it dominates the motion of the gas, and if it is of the order of 10^{-6} G, it exerts very little influence on the motion. These limits arise because the balance of the kinetic energy of the gas clouds and the magnetic energy associated with the field changes radically between these two values of the field strength; that is, if $B \geq 10^{-5}$ G, the magnetic pressure is larger than the pressure due to cloud–cloud collisions. It is also just in the range of 10^{-5} to 10^{-6} G that the observational techniques reach their sensitivity limit.

There are several different avenues for investigating the galactic magnetic field; investigation of the alignment of interstellar grains, the intensity and polarization of the galactic background radiation at radio frequencies, the rotation of the plane of polarization of distant discrete radio sources, and the Zeeman splitting in spectral lines. None of these is entirely satisfactory. In all cases but one there is a significant piece of the puzzle missing in the attempt to deduce the nature of the field from the observations. In that one case, the Zeeman splitting of the interstellar neutral hydrogen line at 1420 Mc/sec, observations refer to conditions in individual clouds, which may not give a valid picture of a general galactic field, if any. Although all the techniques are ambiguous and extremely difficult from an observational point of view, serious attempts to study the magnetic field continue because of its importance to the structure of the galaxy and to the physical condition of the interstellar material.

The first observation to be interpreted as direct evidence of the presence of a galactic magnetic field was that of the polarization of starlight. As we have stated in Sec. IIID1, this observation, although of fundamental importance, is not sufficient in itself to establish the size of the magnetic field. The missing piece of the puzzle in this case is the vital one—knowledge of the nature of the grains producing the polarization. The range in possible fields, depending on the model of the grains adopted, is 10^{-5} to 10^{-7} G—just too large to contribute definitively to a resolution of the current dilemma.

There are then very great difficulties in relating the observed interstellar polarization of starlight to a quantitative discussion of the strength of the magnetic field. The polarization does tell us, however, the average orientation of the field along the line of sight to the star. It must be perpendicular to the line of sight in the directions in which we observe the effect. In addition, the predominant appearance of the electric vectors parallel to the galactic plane indicates that the field is preferentially also parallel to the plane. The field so defined can not, however, be said to be a general galactic magnetic field. The polarization must be quite a local phenomenon since it must occur between the star and us, and distant stars which might show distant conditions are obscured by the very dust which would outline the field for us. In addition, a very interesting correlation with the polarization of nonthermal radio radiation further suggests that the effect has a very

CC-0. In Public Domain. Gurukul Kangri Collection, Haridwar

Digitized by Arya Samaj Foundation Chennai and eGangotri

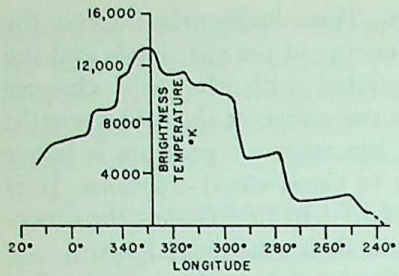

FIG 8. Longitude distribution of 85.5-Mc/sec radiation in the galactic plane (Mills 1964). Location of the steps is approximately coincident with directions tangential to spiral arms.

local origin, and this point will be discussed in a later part of this section.

We have further evidence on the strength and topography of the magnetic field from quite another kind of observation. This is the measurement of the intensity of the galactic background radiation at long radio wavelengths. This was, in fact, the first observation made in radio astronomy, and remains an area of active interest both because of its implications for the structure of the galaxy and because the problems associated with it are by no means solved. The early history of the problem is described by Grote Reber (1958), the man whose capacity for wonder led him to begin the serious exploration of radio astronomy. He describes the two fundamental problems as "How does the cosmic static, at any given frequency, change in intensity with position in the sky; and how does cosmic static, at any given position in the sky, change in intensity with frequency?" In broad terms we know the answers to these questions, but by no means in the detail which would give us real physical insight into the conditions in the interstellar medium which influence their answers. We know, for example, that the intensity of radiation increases in the direction of the galactic plane, and in particular in the direction of the center, but we do not yet understand its relation to spiral structure nor the degree to which its origin lies in individual sources. Concerning the frequency dependence, we have improved on the situation facing Reber, who writes, "Thus, on the face of the prevailing ignorance, a very high frequency should [have been] used since much better resolution would be secured and very much more energy would be available for measurement." The second of these reasons was based on the assumption that the radiation had a dependence on frequency given by the Planck function, increasing in intensity in the radio region as the frequency squared, the so-called thermal emission. Reber himself discovered before long that the frequency dependence is quite the opposite, and the radiation, therefore, is nonthermal. It is now believed to be the result of the synchrotron radiation of relativistic electrons spiraling in the galactic magnetic field. A measurement of vital importance is the frequency dependence of this radiation. It is, however, very difficult to obtain because of the presence of thermal radiation in unknown amounts in just the directions in the galaxy where the nonthermal radiation also appears. (See Mills, 1964, for a comprehensive review of the subject.)

The importance of the frequency dependence lies in the interpretation of the synchrotron mechanism in terms of the conditions in the galaxy. If we assume that the relativistic electrons have an energy spectrum of the form

$$N(E)dE = KE^{-\beta}\,dE,$$

the synchrotron energy radiated per electron is

$$I_\nu = f(e, m, \beta) H_\perp^{(1+\beta)/2} \nu^{(1-\beta)/2},$$

where $H_\perp$ is the field perpendicular to the line of sight. If we wish to use this equation to estimate the galactic magnetic field, we must know the parameters in the electron energy spectrum, and we can only get at these indirectly. The exponent, β, in the energy distribution appears also in the exponent of the frequency in the equation for the radiated energy, and is therefore observable. The accepted value of β, with recognition of its uncertainty, is 2.2. In order to use this radiation as a measure of the galactic magnetic field, we must know, in addition, the electron energy flux, represented by the parameter K. Measurements of the electron flux in the high atmosphere of the earth give a value for this flux which is not at all certain to be representative of the flux in the galaxy in general, principally because of the probable influence of the sun on the flux in our neighborhood. If the value measured by Earl (1961), of 1.5×10^{-1} electrons cm^{-2} sec^{-1} sr^{-1} with energies greater than 10^9 eV, is taken to be representative, the measured intensity of the radiation by Mills lead to a value for the magnetic field in the plane of about 3×10^{-4} G.

One must, however, be careful to notice the fact that this deduced field is actually only the component of the field perpendicular to the direction of motion of the electrons and depends also on the direction of the line of sight to the observer. If α is the angle between the magnetic field vector and the direction of observation, the intensity of the observed radiation detected is

$$I_\nu \propto (\sin \alpha)^{(1+\beta)/2}.$$

The degree of angular dependence of the radiation thus, also depends on the characteristics of the electron energy spectrum. In any case one would expect that in directions parallel to the magnetic field vector one should see no radiation at all. A test of one of the theories of the structure of the galactic field is therefore possible. This particular theory states that the field is aligned along the spiral arms. The observation by Mills (1959), shown in Fig. 8, of an increase in long wavelength radiation in directions along which one is looking tangentially at a spiral arm, and where one is therefore looking parallel to the field, devastating as it may seem, has not entirely ruled out the theory. It has been suggested that one needs only to allow the field lines to be "tangled" somewhat with root mean square irregularities of about 20° (Brown and Hazard, 1960; Field, 1960). In order to interpret observations of the intensity of the nonthermal radiation in terms

CC-0. In Public Domain. Gurukul Kangri Collection, Haridwar

Digitized by Arya Samaj Foundation Chennai and eGangotri

the size of a galactic field, one must know in detail the nature of this tangling, because only the lines intersecting the line of sight close to the perpendicular direction will contribute to the measured intensity. That the lines cannot be strictly parallel to the arms is clear from the observations, but whether the irregularities are random or systematic, in or out of the plane, is not known. One possible model is that in which the lines of force spiral about the arms to give this effect. Hoyle and Ireland (1961) and Ireland (1961) have developed this theory, and Ireland has described the effect of a tightly wound spiral in terms of interstellar polarization of starlight. Since the polarization of starlight is a highly local phenomenon, the predictions of the theory might better be compared with the intensity of the nonthermal radio emission.

Observation of the intensity of the galactic background as a function of position and frequency cannot alone give us a description of the galactic magnetic field. Our interpretation of the measurements depends on our estimates of the electron energy spectrum at a place quite inaccessible to us and on our models for the topography of the field itself.

The synchrotron emission has inherent in it another clue concerning the fields in the region in which it originates. That is, the radiation is known to be polarized in a direction perpendicular to the lines of force of the magnetic field. This would be an ideal property to use to separate the effects of orientation and strength of the field, but for the fact that we look through a long path length to observe the polarization. It is very likely that the integrated radiation along the line of sight is effectively depolarized for two reasons. One is the tangling of the field in the region of production of the radiation and the other is the irregularity of this field along the line of sight to the region of production. As a consequence, we observe polarization of the background nonthermal radiation only from regions very close to us in the galaxy; that is, from the same sort of volume as is observed in observations of the interstellar polarization of starlight. The causes of the polarization are quite different but the effectively limited field of view is the same.

Indications from the measurements of polarization of long wavelength radio emission over the whole sky are that, indeed, the phenomenon is a local one. Mathewson and Milne (1965) find that the areas of intense amounts of polarization are not correlated with intense amounts of radiation. In fact, the regions of high polarization are quite localized and lie in a band about 60° wide along a great circle coming high out of the plane. One of the places of intersection of this circle with the plane is at $l^{II}=160°$—just where the most intense interstellar polarization of starlight occurs. In addition, the intrinsic direction of the plane of polarization of this radiation lies parallel to this great circle (Mathewson, Broten, and Cole 1966). (It should be emphasized that the optical polarization is an effect which can accumulate along the line of sight, while the radio effect can only be destroyed by Faraday rotation.) The magnetic field is indicated by the radio observations to be parallel to the plane, but the polarization effects are not confined to the plane—even reaching the galactic pole. Mathewson and Milne (1965) interpret the large scale distribution of polarization as indicating that the sun lies almost at the center of a spiral arm which has a magnetic field directed along it towards $l^{II}=70°$ and 250°. They also derive a value for the strength of the field of 5×10^{-5} G, but this is based on a number of assumptions, especially with regard to the distance and cross section of the radiating regions.

We have still another indication that there is a galactic magnetic field, one which is again, however, dependent on unknown factors. This is the observation that the emission from some distant radio sources which are intrinsically polarized show the effects of traversing a medium with free electrons and magnetic fields. The position angle of the electric vector of this radiation varies with the square of the wavelength in just the way characteristic of Faraday rotation (Gardner and Whiteoak 1963). This rotation is described in terms of a rotation measure, the slope of the line showing this wavelength dependence. This rotation measure can be written

$$\text{R.M.} = \int_0^s n_e B_{||} ds,$$

where n_e is the electronic density, $B_{||}$ the strength of the magnetic field parallel to the line of sight, and s the distance over which the radiation encounters the rotating medium. A fundamental unknown is the amount of Faraday rotation which occurs in the source itself. Any dependence of the rotation measure on galactic coordinates indicates that some of the effect occurs in our galaxy. There is apparently a correlation of rotation measure with latitude, at least in the sense that the scatter of values is larger near the plane than far from it. We would expect this from the greater complexity along the path length in the plane, both in terms of magnetic field strength and direction and in terms of variations in electron density. The total amount of Faraday rotation is a cumulative effect of the medium along the line of sight and hence is an indication of average conditions along that line. There appears also to be a weak correlation with galactic longitude, in the sense that some regions tend to have positive rotation measures and others negative, the sign being determined by the direction of the field. The suggestion of Morris and Berge (1964) is that the local field is aligned along the nearby spiral arms since they find maxima in the rotation measures near the longitudes at which this arm is tangential to the line of sight.

An interesting comparison of the rotation measures with the polarization of the long-wavelength background was made by Mathewson and Milne (1965).

CC-0. In Public Domain. Gurukul Kangri Collection, Haridwar

Digitized by Arya Samaj Foundation Chennai and eGangotri

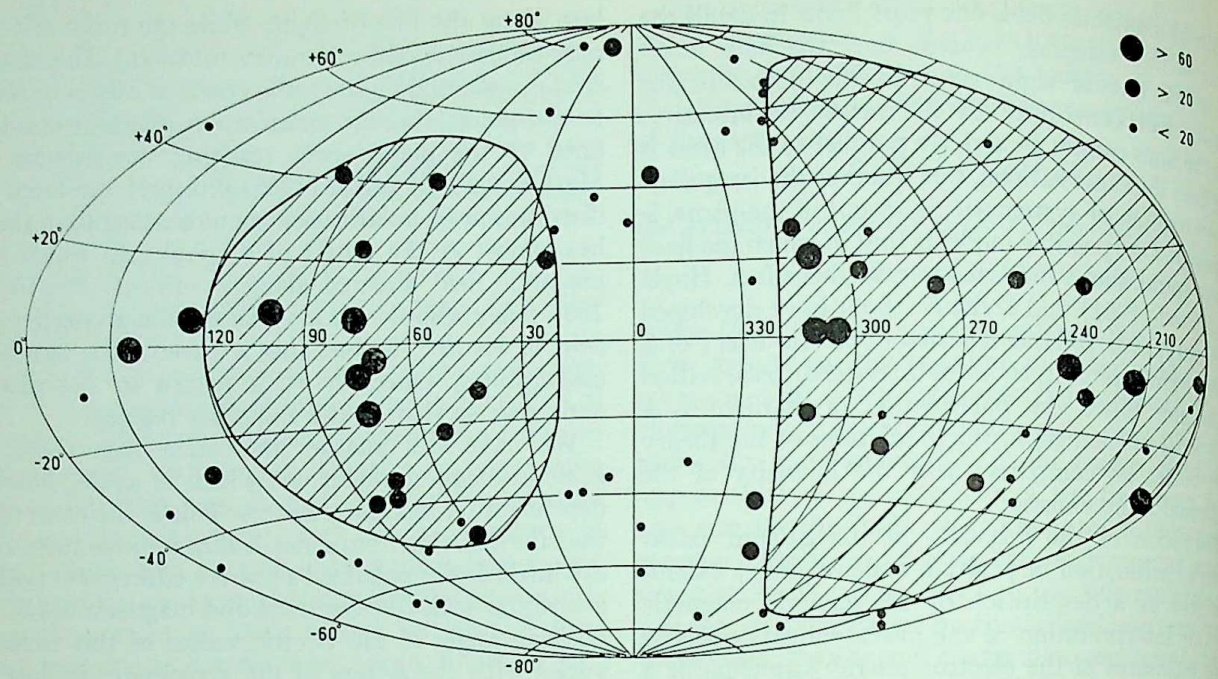

FIG. 9. Comparison of polarization and rotation measure as a function of galactic coordinates (Mathewson and Milne 1965). Area maximum polarization of 408-Mc/sec radiation is unshaded. The points are the rotation measures of the discrete sources.

They showed that the regions of high polarization are regions of low rotation measure—especially if one looks at the latitude and longitude dependence together. This is consistent with the fact that (1) the degree of Faraday rotation of the plane of polarization of a source depends on the component of a magnetic field which lies along the line of sight, and (2) the amount of polarization of radio emission produced by the synchrotron mechanism depends on the component of the field which is perpendicular to the line of sight. Figure 9 shows the rotation measures of Gardner and Davies (1965) (separated into three groups, >60, >20, <20) and the areas of polarization. The unshaded area is the 60° band which contains most of the long-wavelength polarization. This suggests that the amount of rotation of the plane of polarization of distant sources is also very dependent on local conditions.

In investigating Faraday rotation we are dealing with a phenomenon which depends on the parallel field component, not the perpendicular, as in the intensity of the nonthermal radio emission. Here we are confronted with having to imagine the field lines tangled in such a way as to lead to the presence of enough lines perpendicular to the field for production of the radiation, and enough remaining undisturbed to produce rotation which depends on those parallel to the line of sight. Without knowing the degree and nature of this tangling we are at a loss to use these observations to determine the strength of the magnetic field from them. In addition there is another unknown factor, the electron density. In the equation for the rotation measure we have two factors which can vary by large amounts. The electron density in a region where hydrogen is not ionized at all is of the order of 10^{-4}/cm^3 or less, while regions where hydrogen is partially ionized it may as high as 1/cm^3 and still not be obvious on photographs as an emission region. The path length, s, can be anything from a few tens of parsecs, if the rotation occurs in an isolated cloud, to thousands of parsecs if the rotation occurs all along the path length and the source lies close to the direction of the galactic plane. This leaves $B_{\parallel}$ practically indeterminate.

Faraday rotation in the galaxy probably contributes to another observed effect. The percentage of linear polarization in some sources is much smaller than would be expected for radiation produced by the synchrotron mechanism, and the percentage varies with the wavelength of observation. It is possible that this "depolarization" (so-called because the percentage of polarization usually decreases with increasing wavelength) is due to differential Faraday rotation of different parts of the source due to the medium between us and the source. If there are regions small in angular size compared to the source and with differing densities or fields, each will rotate the plane of polarization at any wavelength by different amounts and, hence, reduce the integrated amount of polarization. If one now observes at a longer wavelength, the amount of rotation for each small region will be greater and the difference between them also greater, so that the integrated effect will be to reduce the degree of polarization. If this depolarization could be related to irregularities in the magnetic field in the galaxy, we would have some indication of the scale of such irregularities. The problem is that we do not know the percentage polarization of the radiation as it emerges from

CC-0. In Public Domain. Gurukul Kangri Collection, Haridwar

Digitized by Arya Samaj Foundation Chennai and eGangotri

Table II. Characteristics of methods of measuring galactic magnetic fields.

Observation	Location of effect	Predominant field orientation to line of sight	Estimated field (gauss)	Other influencing unknowns
Polarization of starlight	Along path	$\perp$	10^{-5} to 10^{-7}	Size, composition of grains
Nonthermal radio emission	At source	$\perp$	10^{-5}	Electron energy spectrum, field orientation
Polarization of non-thermal background	At source Along path	$\perp$ $\parallel$	10^{-5}	Distance of emitting regions
Faraday rotation of sources	Along path	$\parallel$	10^{-3} to 10^{-8}	Electron density, field orientation, path length
Zeeman effect	At source	$\parallel$	10^{-5} to 10^{-6}	Relation of individual cloud to general field

source. Some depolarization certainly could occur within the source from internal differential Faraday rotation or variation in the electron energy spectrum.

There is one method for measuring the magnetic field which does not depend on other unknown factors. That is the observation of the Zeeman splitting of the neutral hydrogen line at 21-cm wavelength. The presence of a magnetic field with a component along the observer's line of sight within a cloud of hydrogen causes the radiation from the cloud to be split into two components circularly polarized in opposite senses and with a separation in frequency of 2.8 cps per 10^{-6} G. This is an extremely small separation and very difficult to measure. The best hope is to find a hydrogen profile which is broadened as little as possible by Doppler effects and to look for a difference in intensity in the two senses of polarization. The sharpest lines to be found are in the absorption spectra of discrete sources and even they are about 10 to 20 kc/sec wide. Weinreb (1962), in his description of an attempt at measuring the field in this way describes the procedure in terms of the difference profile which is obtained when the signals received at the two different polarizations are compared. This difference profile, $\Delta T(f)$ is related to the observed (either polarization) profile $T(f)$ by the following relation, which holds if the frequency splitting Δf is small compared with the width of the observed line:

$$\Delta T(f)=\Delta f T'(f)=2.8\times 10^6 B_{11} T'(f),$$

where B_{11} is the line of sight component of the magnetic field and the prime denotes derivative with respect to frequency. Thus, only the profiles showing a steep slope at the edges have any hope of yielding a measurable Zeeman splitting. The method is therefore very limited in the sense that only a few clouds, at the present time at least, can be considered. The danger is that these clouds may not be typical of the general situation. They may happen to have a significant amount of the field directed away from the line of sight, and individual small clouds may not be intimately connected in a magnetic sense with the more general background.

The difficulty of the measurement is reflected in the fact that the separate recent attempts at observing the splitting are in disagreement. Davies reports the measurement of a field of 1.4×10^{-5} G in the spectrum of the Crab nebula (1964), while Weinreb (1962) and Morris, Clark, and Wilson (1963) each indicate that the upper limit for the field is approximately 5×10^{-6}. Most recently Verschuur (1965) has described measurements which lead to a field of less than 10^{-6} G in this source. The situation is complicated by the fact that the line in this source is complex in structure due to the presence of unresolved clouds, and the interpretation is therefore somewhat ambiguous. In the case of the spectrum of Cas A, the authors all agree that the field has an upper limit 10^{-6} G. It is thus apparent that a significant improvement in instrumental techniques is likely to produce a very important result; that is, a decision between 10^{-5} and 10^{-6} as the order of magnitude of the field. It is possible that the OH lines at 18-cm wavelength offer as least as good a chance to observe the Zeeman effect. The line is intrinsically narrower because of the larger mass of the molecule, and in fact some very narrow emission lines have been observed in the direction of several distant thermal sources. The separation of Zeeman components should be about the same as in hydrogen, so that we may be able to observe the magnetic field in two different sorts of areas in the galaxy, near or in HII regions, and in the cold, undisturbed general medium. This hope is contingent upon our understanding of the mechanism producing the very peculiar OH results, and the enormity of that problem will be indicated in the last section.

Table II gives a summary of our sources of information about the galactic magnetic field. Column 4, which gives values for the strength of the field estimated from each method, suggests strongly that the degree of influence of the magnetic field on interstellar conditions remains virtually unknown.

V. FORMATION OF INTERSTELLAR MOLECULES

The existence of molecules in the interstellar medium was realized in the early 1940's (McKellar 1941). Three constituents were apparent from the optical absorption lines: CH, CH^+, and CN (see Table I). In 1963 the first non-carbon molecule, OH, was de-

CC-0. In Public Domain. Gurukul Kangri Collection, Haridwar

Digitized by Arya Samaj Foundation Chennai and eGangotri

tected in the interstellar medium by its microwave transition at 18 cm (Weinreb, Barrett, Meeks, Henry 1963). Several attempts to find the OH optical transitions (Gaustad and van Woerden 1966, Goss and Spinrad 1966) at 3080 Å, have not, however, been successful, due to the opacity of the earth's atmosphere at this wavelength and to a low transition probability for the optical transition. The interstellar nature of CH, CH^+, and CN was shown conclusively by the observations of Adams (1949), thus dispelling earlier suggestions by Merrill (1946) that the lines are circumstellar. Adams showed that the velocities of the molecular features generally agree with those found for the atomic interstellar lines. Furthermore, Bates and Spitzer (1951) have shown that the intensities of the molecular lines are usually correlated with interstellar extinction. (Later on we will mention the one exception to this correlation.)

With several important exceptions all of the molecular lines arise from ground levels. This is caused by the fact that the kinetic temperatures in HI regions are so low that collisional excitations above the ground level are not important. The exceptions are two lines of CN which originate in a rotational level 4 cm^{-1} above ground level; the relative strengths of these lines correspond to a rotational temperature of $\sim 3°K$. The possible cosmological significance of this result has recently been pointed out by Field, Herbig, and Hitchcock (1965), who propose that the radiation temperature of the interstellar radiation field at 2.54 mm (the wavelength corresponding to 4 cm^{-1}) is $\sim 3°K$. (See Penzias and Wilson 1965, and Dicke, Peebles, Roll, and Wilkinson 1965 for a discussion of this problem.)

The observations of molecules present three fundamental problems: (1) The continual formation of molecules in the interstellar medium must be explained since the molecules are rapidly dissociated by the interstellar radiation field. (The mean life of CH against dissociation is 4×10^3 years—a short time compared with the age of the Galaxy.) Thus, we cannot say that the molecules are left over from some primeval stage of the Galaxy. (2) The observations indicate immense variation in intensity with position and also with respect to the atomic interstellar lines. In some cases, CH is stronger, in other cases CH^+. Furthermore, in a few striking examples, CN is much stronger than the other molecular lines. (3) Finally, we are faced with a fundamental problem of the interstellar medium: In which direction does the interstellar medium evolve? Does it go from simple entities (atoms, diatomic molecules) to complicated forms (polyatomic molecules, grains) or *vice versa*? Obviously, the three questions are not independent; in particular (1) and (3) may well be closely interconnected. Since our understanding of (2) and (3) is quite limited, we will discuss in some detail the problem of molecule formation in relation to CH, CH^+, CN, and OH—the molecules which are observed.

Three methods for forming diatomic molecules have been considered: (1) radiative association, (2) formation on grains, and (3) formation from polyatomic molecules. Radiative association was the first method proposed (Swings 1941, Kramers and ter Haar 1946). The excess energy of the colliding pair of atoms must be carried off by the emission of a photon since the collision of three atoms in the interstellar medium would occur at a rate of 10^{-24} yr^{-1} cm^{-3} and could only account for a negligible number of molecules. Thus, two-body radiative association is efficient only for molecules which satisfy two conditions: (1) an excited electronic state of the molecule must arise from ground-state atoms (the incoming atoms will be in the ground-state) and (2) a permitted transition must connect the above excited state with the ground state in order to rid the molecule of the excess energy. H_2 violates condition (2) while OH violates condition (1); CH, CH^+, and CN satisfy both conditions.

Bates and Spitzer (1951) have attempted to explain the observed densities of CH and CH^+ by means of radiative association. They consider practically all possible reactions governing the abundances of CH and CH^+: radiative association leading to CH and CH^+, photodissociation, photoionization, recombination ($CH^+ + e \rightarrow CH + h\nu$) and dissociative recombination ($CH^+ + e \rightarrow C + H$). (They neglect exothermic chemical exchange reactions of the form $CH + H \rightarrow C + H_2$. The rate coefficients for these reactions are much smaller than the other processes, however.) The values for the various rate coefficients involve the transition probabilities, the value of the radiation density at the dissociation and ionization limits, and various cross sections. Some of these values are known rather well and others can only be estimated. In particular, the rate constant for dissociative recombination is completely unknown. Bates and Spitzer then calculate the expected number densities of CH and CH^+ within a cloud. They concluded that the observed densities are about 100 times the values predicted by their theory of the order of 10^3 H atoms cm^{-3} would be required by their theory to give the observed densities of CH and CH^+. This value is one to two orders of magnitude greater than the observed cloud density.

Radiative association is an inherently inefficient process as the following rough example indicates: The time for the two atoms to travel the intranuclear distance is about 10^{-14} sec. The half-life of the transition from the excited electronic state to the ground level is about 10^{-8} sec. Hence, the probability of radiative capture is $10^{-14}/10^{-8} = 10^{-6}$. Another major problem is that the molecules are dissociated quite rapidly by the interstellar radiation field—the lifetime for the destruction of CH is 4×10^3 years.

The radiative association process has not been appli-

CC-0. In Public Domain. Gurukul Kangri Collection, Haridwar

Digitized by Arya Samaj Foundation Chennai and eGangotri

to the formation of CN—primarily since CN^+ is not observed. This latter fact in itself argues against the radiative association, since CN^+ would be expected in analogy to CH^+. [Since $n(C^+)/n(C) \sim 10^4 - 10^5$, $C^+ + N \rightarrow CN^+ + h\nu$, and $C^+ + H \rightarrow CH^+ + h\nu$ would be the predominant reactions followed by electron capture.] The major problem, however, for this test is that the ground state of CN^+ may not be the state determined experimentally by Douglas and Routly (1954) and tentatively assumed to be the ground state.

Before the 1963 observations of OH, the fact that all the observed free radicals (CH, CH^+, CN) could be formed by radiative association was taken as partial support for this method. The OH observations, along with the difficulties found by Bates and Spitzer force us to consider other formation mechanisms.

As an alternative, Bates and Spitzer (1951) suggested that the grains might be the third bodies which take up the excess in the kinetic energy. Details of this procedure have been dealt with by McCrea and McNally (1960), McNally (1962), and Gould and Salpeter (1963). Since the grain properties enter into these considerations, a model for the interstellar dust must be adopted. The dielectric grain theory has usually been used. An obvious logical difficulty is immediately encountered: in the dielectric grain theory, diatomic molecules are the basis of the condensation process. On the other hand, we need to invoke grains in order to explain the densities of CH and CH^+. No suitable solution to this paradox has been proposed.

The proposed method of forming CH and CH^+ is as follows (McNally 1962): the grain has a slight negative charge, as we have pointed out. Since most of the interstellar carbon is C^+, the collision cross section of the carbon gas with the grains is increased by an order of magnitude. Although H evaporates rapidly from the grain at a $T_0 \sim 15°K$, the outside of the grain is thought to be covered with a layer of H atoms due to the great number of collisions of H atoms with the grains. McNally proposes that a C^+ ion hits the grain, neutralizes, and forms CH—the excess energy being taken up by the grain. Since the binding energy between molecules and solids is less than that between atoms and solids and since energy (3–4 eV) is liberated in the formation of CH, the molecule is freed from the grain surface and injected into the interstellar medium. CH^+ is subsequently formed by photoionization of CH. In computing the rate coefficient for this formation process, McNally uses the dielectric grain model of van de Hulst. The most uncertain parameter is $\tilde{\omega}$—the probability that an atom of C striking the grain will leave as part of a molecule. McNally quotes experimental and theoretical evidence which indicates that this probability is approximately unity. There is, however, a great deal of uncertainty on this point. The final rate coefficient γ[number of CH molecules formed per cm^3 per sec$=\gamma n(C)n(H)$] is found to be 1.6×10^{-16} cm^3 sec^{-1}—approximately two orders of magnitude greater than the value for radiative association. McNally then sets up the equations of equilbrium for CH and CH^+, using the various processes of dissociation and ionization considered by Bates and Spitzer. Finally, he computes $n(CH)/n(H)$ for several assumed radiation fields in the interstellar medium. If the Lambrecht–Zimmerman field (see Sec. IB and Fig. 1) is correct, the above ratio is less than the observed value ($\sim 10^{-8}$) by an order of magnitude. If, however, the Lambrecht–Zimmerman field contains too much ultraviolet (as is expected), then the McNally theory can account for the observed number density of molecules.

As in the case of radiative association, the grain formation theory is not applicable to CN: an incident C atom has a very small probability of hitting a N atom ($[n(N)/n(H)]_{gas} \sim 10^{-4}$). Again, we cannot explain the fact that the density of CN is not negligible with respect to the density of CH.

The above theory is based on the dielectric grain model; if instead the graphite grain model is correct this could very well have important consequences for molecule formations. Indeed, pure graphite surfaces are not suitable for the formation of CH—graphite bombarded with neutral hydrogen will not yield CH; the carbon must be in gaseous form before formation can take place.

One further method for forming molecules has been proposed—the break-up of polyatomic molecules. Two methods of break-up have been proposed: (1) the ejection of polyatomic molecules from cool stars and the subsequent formation of diatomic molecules by the interstellar radiation field, and (2) the break-up of grains by low-energy cosmic rays or by evaporation near hot stars. Tsuji (1964) proposes that cool, luminous stars, which are known to eject mass at the rate of $\sim 10^{-6}$ solar masses per year, eject polyatomic molecules such as C_2H_2, CH_4, HCN, H_2O, NH_3, etc. After interaction with the interstellar radiation field, the observed free radicals are produced.

Process (2) was initially proposed by Bates and Spitzer to explain the observations of CH^+ in the Pleiades. The interstellar CH^+ lines seen in the late B type (fairly luminous) stars in this cluster are very strong with respect to other molecular and atomic lines. Two further peculiarities are found: (1) the number of molecules per cm^2 in the line of sight is not correlated with extinction in the cluster and (2) the velocities in all cases of the CH^+ molecule are such that the relative motion is in the sense of the star moving towards the gas. (The Pleiades are not unique, however; other unreddened B stars have CH^+ lines which are strong with respect to atomic lines.) To explain these unusual circumstances, Bates and Spitzer proposed that sublimation of solid CH_4 takes place from the grains; then the CH_4 is broken down in steps by the intense radiation field and subsequently passes through the CH^+

CC-0. In Public Domain. Gurukul Kangri Collection, Haridwar

Digitized by Arya Samaj Foundation Chennai and eGangotri

stage. The CH molecule is not seen since the radiative dissociation and ionization rates of CH near a star with a surface temperature of $\sim 2\times 10^4$ °K are much more rapid than CH^+. As the star moves into an interstellar cloud (the single cloud will produce a very small amount of extinction), the CH_4 begins to sublime as the grain temperature reaches 30°K. After the formation of the CH^+, this molecule is dissociated by the radiation field of the star. A hemispherical shell (centered on the star) of CH^+ is thus formed; the CH^+ that originally existed on the other side of the shell (i.e., behind the star as it moved through the cloud) has been dissociated by the radiation field of the star. This explains the fact that the CH^+ is found to be always moving towards the star. Again, this method is not successful in explaining the presence of interstellar CN which is occasionally seen in absorption in the late B stars. C_2N_2, if it exists in the grains at all, sublimates at $\sim$100°K—a much higher temperature than the CH_4 value (Herbig 1963).

Based on the high density of cosmic rays in the region 1–100 MeV (the suprathermal particles) proposed by Hayakawa (1960), Kimura (1962) and Takayanagi (1964) have proposed that diatomic molecules are produced by the interaction of these cosmic rays with the interstellar grains. They propose that the H_2O, CH_4, NH_3 molecules in the grains are broken down by the cosmic rays into OH, CH, CH^+, H_2, NH, CN, etc. This method can be efficient in forming molecules only if many radicals are formed for each incident proton. This method suffers from our ignorance of the suprathermal particle density; the existence of these particles is, indeed, not substantiated. However, one advantage to this method is that $n(CN)/n(CH)$ would be $\sim[n(N)/n(H)]_{dust}$ (about 0.1 if the grains are dielectric) and not $[n(N)/n(H)]_{gas}$ ($\sim 10^{-4}$). As we have seen, the previous methods of molecule formation cannot explain the observed numbers of CN molecules.

In the discussion of interstellar grains, we noticed several cases where anomalous phenomena are associated with HII regions. Recently, observations of CN at 3875 A and of OH at 18 cm in the microwave spectrum have shown peculiarities which seem to be associated with HII regions. The OH observations will be described in a later section. The anomalous excitation mechanism found in some of the OH observations operates only in the direction of the HII regions. At present no quantitative theory regarding the formation of OH is available. As we have seen, radiative association cannot account for the formation of OH. The scanty evidence available at this time indicates that the OH is formed near or inside the HII region. Might it not be that the OH is formed when dielectric or ice mantles of H_2O, CH_4, NH_3 grains are sputtered by colliding atoms?

The hydroxyl radical is not unique in showing peculiarities near HII regions. Münch (1964) has found two HII regions (NGC 7822 and IC 1396) whose ex citing O stars contain very strong interstellar CN lines which are an order of magnitude stronger than a which had previously been detected. In NGC 78 three of the associated O stars have CN lines bes CH and Ca^+ lines. One of the stars has a He° abso tion line which arises inside the nebula. The veloci of the He°, CN, and CH are approximately eq (It is possible, however, that there is a small ference in the velocities of the CH and CN lines, s gesting that the two molecules are not coexiste The Ca^+ lines usually originate in regions roug midway between the sun and the background s this appears to be the case in NGC 7822 since t Ca^+ lines differ in velocity from the molecular lines 3–4 km/sec. On this basis, Münch has proposed t the CN molecules arise in rich dust complexes in t immediate neighborhood of the HII region—they a somehow related to the interaction process betwe the HII and HI regions. The Bates–Spitzer hypothe for sublimation is not applicable to CN since C_2N_2 probably not a major constituent of the grains. Mün has instead proposed that CN is formed as the gra are "flashed" by an ionization-pressure front a vancing into the cool HI region from the HII regi This interesting proposal should be tested by laborat experiments.

In the above considerations, we have only dealt w the formation of the four molecules which are o served in the interstellar medium. Several authors h also suggested the presence of H_2 in the interste medium. Unfortunately, the presence of H_2 cannot ascertained from the earth's surface–the ultravio and far infrared contain the strong lines of H_2. T amount of H_2 is important in two respects: (1) T amount of molecular hydrogen may be a substan component of the interstellar gas. (2) H_2 is an effect cooling agent, as we have pointed out elsewhere. Th the percentage of molecular hydrogen must be kno to determine cooling rates in HI regions.

The direct radiative association of two hydro atoms in the ground state to form H_2 is a very i probable process since the photon emitted arises fro forbidden transition between $^3\Sigma$ and $^1\Sigma$ states. Th various authors (Kahn 1955b, McCrea and McN 1960, Gould and Salpeter 1963, Gould, Gold, a Salpeter 1963) have considered the formation of H the surfaces of the interstellar grains in the man which we have described above. Kahn, using t harmonic mean temperature of approximately 100 and the fact that cloud–cloud collisions heat up clouds to $3\text{–}4\times 10^3$ °K once in 10^7 years, proposed th 0.5% of the hydrogen present is in molecular form order to give the proper cooling rate. The Gould a papers treat in considerable detail the formation dissociation of H_2—they start from first princip and attempt to predict the density of H_2. The for

CC-0. In Public Domain. Gurukul Kangri Collection, Haridwar

Digitized by Arya Samaj Foundation Chennai and eGangotri

tion on grains is found to have a characteristic time of $\sim 10^8$ years. They also propose that dissociation of the H_2 takes place in encounters of gas clouds with the Strömgren spheres of O and B stars with a characteristic time of $\sim 10^8$ years. On this basis they propose that the equilibrium ratio of the densities of H_2 to H is in the range 0.1 to 10. A density of H_2 in this range will insure that molecular hydrogen is a major cooling agent in the HI regions. [However, van der Meyderberg, Knapp, Beenakker, and van de Hulst (1965) have reconsidered the formation of H_2 on grains and find that the process is much more inefficient than proposed by Gould *et al.* Clearly, additional work is needed to clarify these points.] The observations of H_2 will indeed be a significant breakthrough in our knowledge of the interstellar medium.

We have seen that the observations of molecules from one region to another are far from uniform. It seems quite reasonable to suppose that different formation processes would operate depending on the local conditions. However, many more observations and theoretical studies will be needed before we are capable of presenting a unified picture of molecule formation in the interstellar medium.

VI. RECENT OBSERVATIONS OF OH

The hope that another constituent of the interstellar gas could be studied in the microwave spectrum arose immediately after the discovery of the 21-cm hydrogen line. The search for the 18-cm lines of the OH radical was begun within five years after the discovery of the hydrogen line (Barrett and Lilley 1957). In the fall of 1963 two of the four lines in the multiplet formed by Λ doubling (hyperfine structure splits each of the Λ doublets) in the ground state were discovered as absorption lines in the spectrum of the strong radio source Cas A (Weinreb, Barrett, Meeks, and Henry 1963). These four lines occur at 1720, 1667, 1665, and 1612 Mc/sec with an expected intensity ratio of 1:9:5:1 (see Fig. 10) so that it is not surprising that 1667 and 1665 were observed first. The developments since this discovery have been extremely rapid and have led to such a new view of processes in the interstellar medium that, despite the great danger of this review's being outdated before it is printed, we wish to conclude with this current report on the developments.

The particular usefulness of OH in a study of the interstellar gas arises from several factors. One is the obvious measure of the abundance of oxygen compared to hydrogen. Another is the different molecular weight which, under certain conditions, allows separation of thermal and turbulent effects in line broadening (as described in Sec. IIB). From the point of view of excitation conditions in the interstellar medium, OH is an invaluable tool—on well-known grounds and on newly discovered ones. The former relate to the fact

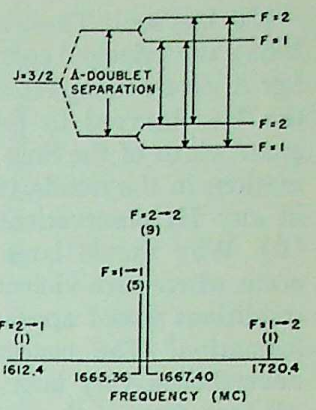

FIG. 10. The complete energy level diagram for the $^2\Pi_{\frac{3}{2}}$, $J=\frac{3}{2}$ ground level of OH showing the hyperfine structure and the related microwave spectrum with theoretical relative intensities indicated in parentheses.

that the OH excitation mechanism is quite different from that of hydrogen. The excitation of the hyperfine line in the hydrogen spectrum is collisional, and the excitation temperature is therefore the kinetic temperature (Purcell and Field 1956). The excitation of the OH lines is not collisional, due to the fact that they arise from electric dipole transitions with much higher transition probabilities than the magnetic dipole transition producing the 21-cm hydrogen line. The excitation temperature of these lines is therefore more closely coupled to the radiation temperature in the medium. This fact led to the search for OH first in absorption, since the radiation temperature is certain to be very low in HI regions. More recent observations have suggested the existence of a totally unexpected excitation mechanism for the OH radical, the complexity of which defies theoretical explanation at the present time. The early observations did not suggest such peculiarities, for in the spectrum of Cas A the lines at 1667 and 1665 Mc/sec were both observed, in about the expected intensity ratio of 9 to 5. In addition, each of the components of the multiplet was split into several lines because of the presence of several clouds of OH along the line of sight each with its differential Doppler shift. Each of these clouds could be directly associated with similar HI clouds which had been observed long before in the spectrum of Cas A.

Following the discovery of OH in Cas A, it was found also by several groups in the spectrum of Sgr A, the source at the galactic center. The situation there was not so simple. The line was at first reported to have an optical depth of a few percent and to have a velocity nearly the same as the velocity of an HI cloud in this direction (nearly at rest with respect to the sun). The Australian group (Robinson, Gardner, van Damme, and Bolton 1964) was the first one to find that the line which had previously been observed was actually only a small dip on the side of an enormous feature with optical depth of 0.9 and width of 50 km/sec centered at a frequency corresponding to a Doppler shift of +40 km/sec. The group at Harvard (Goldstein, Gundermann, Penzias, and Lilley 1964) subsequently found a similar line displaced to negative velocity (at

CC-0. In Public Domain. Gurukul Kangri Collection, Haridwar

Digitized by Arya Samaj Foundation Chennai and eGangotri

−120 km/sec). Thus, as shown in Fig. 11 (Williams 1965), the principal components of the OH spectrum in Sgr A were a complete surprise and bore no relation to the HI observed in this direction. In addition, the great width of the lines indicated tremendous internal motions in the clouds, internal motions quite unknown in any HI observations and certainly unexpected in OH. Why should large concentrations of a molecule occur where such violent motions were going on, where conditions would appear so unfavorable for molecular formation? The concentration of OH molecules is nevertheless very large, as shown by the line ratios. All four lines of the multiplet were observed, but not in the predicted ratio of intensity; that is, they appear in the ratio 1:2.7:2.2:1 rather than 1:9:5:1. These anomalous intensities could be attributed to an effect long known by astronomers in their study of stellar atmospheres—that is, the variation of the intensity ratio in a multiplet due to great optical depth and the saturation of one or more of the lines, the so-called "curve-of-growth" effect. (See also McGee, Robinson, Gardner, and Bolton 1965).

The next important contribution was the observation of OH absorption in regions near the direction of the galactic center, but not at the position of Sgr A. The galactic background continuum radiation is strong enough in these regions to permit observation of OH in absorption. This observation provides several very important additions to our store of knowledge of OH. The important factor is that the background source is an extended one, many degrees in extent. Thus, it provides an opportunity to study the angular distribution of the radiation and to make models of the structure of a great complex of OH clouds. The region is full of broad, high velocity components bearing little or no relation to the HI observations in the same directions. The extended background makes possible another conclusion because the source fills the beam of the antenna. In this case the measured antenna temperature at frequencies outside the OH line is equal to the brightness temperature of the continuum background at these frequencies. Since the OH appears in absorption, it must be cooler than the background, which has a brightness temperature of about 10°K. By cooler, of course, we mean a lower excitation temperature of the molecule, which is not the kinetic temperature, but is the factor which determines the population of the levels in the molecule and, hence, its absorbing properties.

This discovery of a 10° limit on the excitation temperature was something of a blow to the search for OH in emission. If the excitation temperature were, indeed, so low, the chances of finding the line in emission would be very small. It should be remembered that in the case of absorption the measured brightness temperature for a fixed amount of material depends on the temperature of the background source, and in the case of emission it depends on the excitation temperature of the material. This decrease in the chance of finding OH in emission was also a blow to the hope that OH would become an important tool in studying the interstellar medium. If its study were limited to absorption lines in the spectra of a few bright sources, to be seen at only isolated places in the sky, its usefulness would certainly be limited. Searches for OH in emission were nevertheless carried out in all the likely places in the anticenter, in the midst of dark clouds of dust and at random places in the galactic plane, all without notable success.

With the advent of improved receivers, attempts to find OH absorption in weaker sources were begun. It was not found in the next three brightest sources, the Crab Nebula, the Orion Nebula, and Cyg A. The next most likely candidates at this frequency were to be found in the Westerhout catalogue of radio sources at 1390 Mc/sec (Westerhout 1958). These sources are largely thermal emitters, and mostly identified with optically observed HII regions, clouds of gas radiating in the radio region by free–free emission (*bremsstrahlung* of electrons at a temperature of about 10^4°K. They have an advantage from the observational point of view in that they are relatively extended in angular size, of the order of a degree. Rather quickly a few of these sources were found to have measurable absorption lines at 1667 Mc/sec, the strongest line of the multiplet (Williams 1965). The search was then extended to fainter continuum sources, in particular to the source W49. This is a relatively bright thermal source at this frequency but shows no optical radiation whatever. The region does, however, have many heavy obscuring clouds which probably hide from our view a large HII region beyond. The dust does not obscure the radio radiation, and so we observe a bright thermal radio source. The first observations of this source provided the greatest surprise since the discovery of OH (Weaver, Williams, Dieter, and Lum 1965). The 1667-Mc/sec line was not in absorption *but in emission*! These observations were made with an instrumental resolution of 10 kc/sec, or about 2 km/sec. Very considerable structure was visible in the profile and indicated that still greater resolution would be desirable. The next step was observation with 2-kc/sec resolution (0.4 km/sec). The profile was indeed further resolved and showed lines as narrow as 1 km/sec and antenna temperatures as high as 9°K, as shown in Fig. 12. Therefore, the excitation temperature of OH near this HII region must be higher than in regions of the galaxy far from the sources of intense radiation. But still further surprises lay in store. The profile of the 1665-Mc/sec line in the same source did indeed have components resembling what was expected (several clouds rather like the 1667-Mc/sec ones with reduced intensity), but the surprise was that at a place in the spectrum where only a small amount of 1667-Mc/sec radiation appeared there were several very strong sharp peaks of emission at 1665 Mc/sec. They were, in fact, as bright as 20° and as narrow as 0.4 km/sec—

CC-0. In Public Domain. Gurukul Kangri Collection, Haridwar

Digitized by Arya Samaj Foundation Chennai and eGangotri

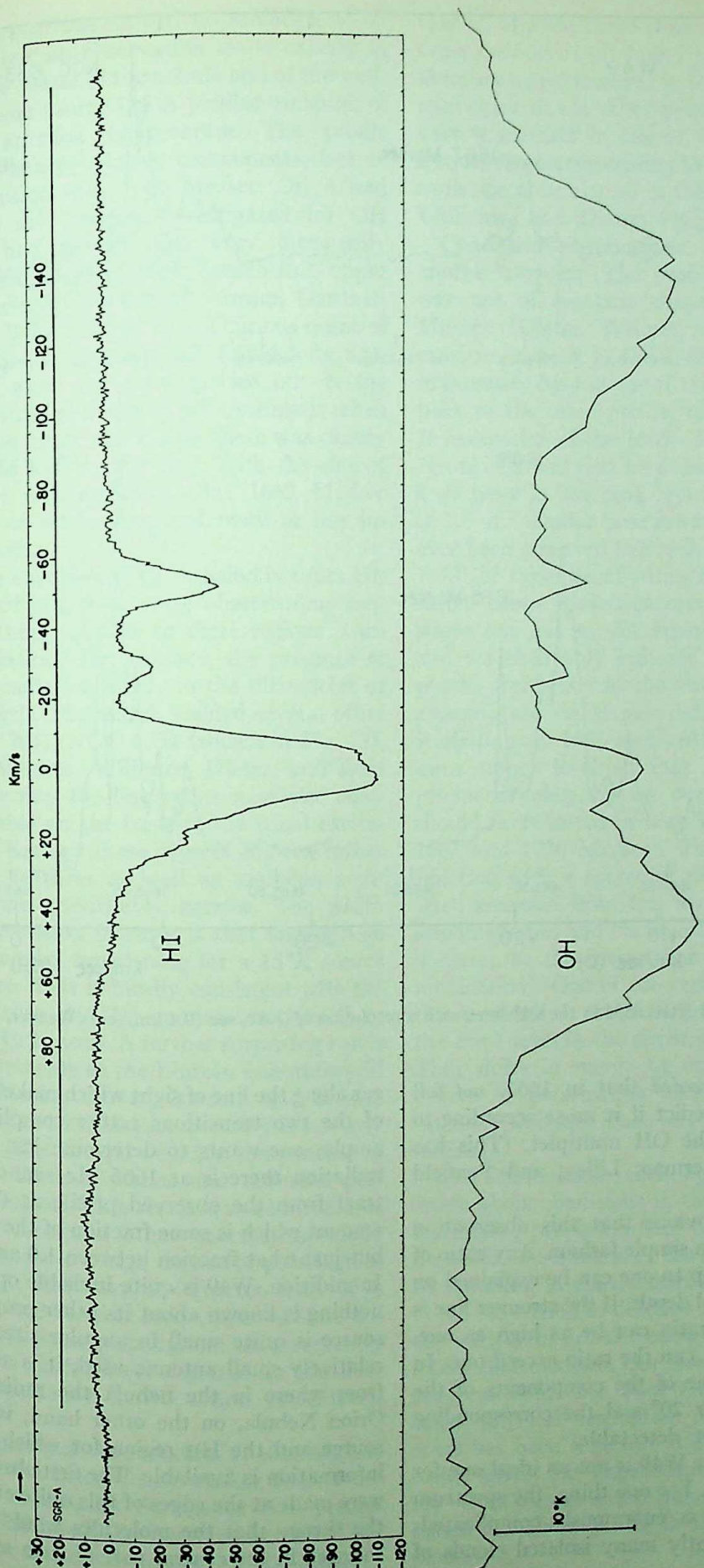

FIG. 11. Profiles of HI and OH (1667 Mc/sec) in the direction of the galactic center (Williams 1965). Velocities are with respect to the local standard of rest, the average velocity in the vicinity of the sun.

CC-0. In Public Domain. Gurukul Kangri Collection, Haridwar

Digitized by Arya Samaj Foundation Chennai and eGangotri

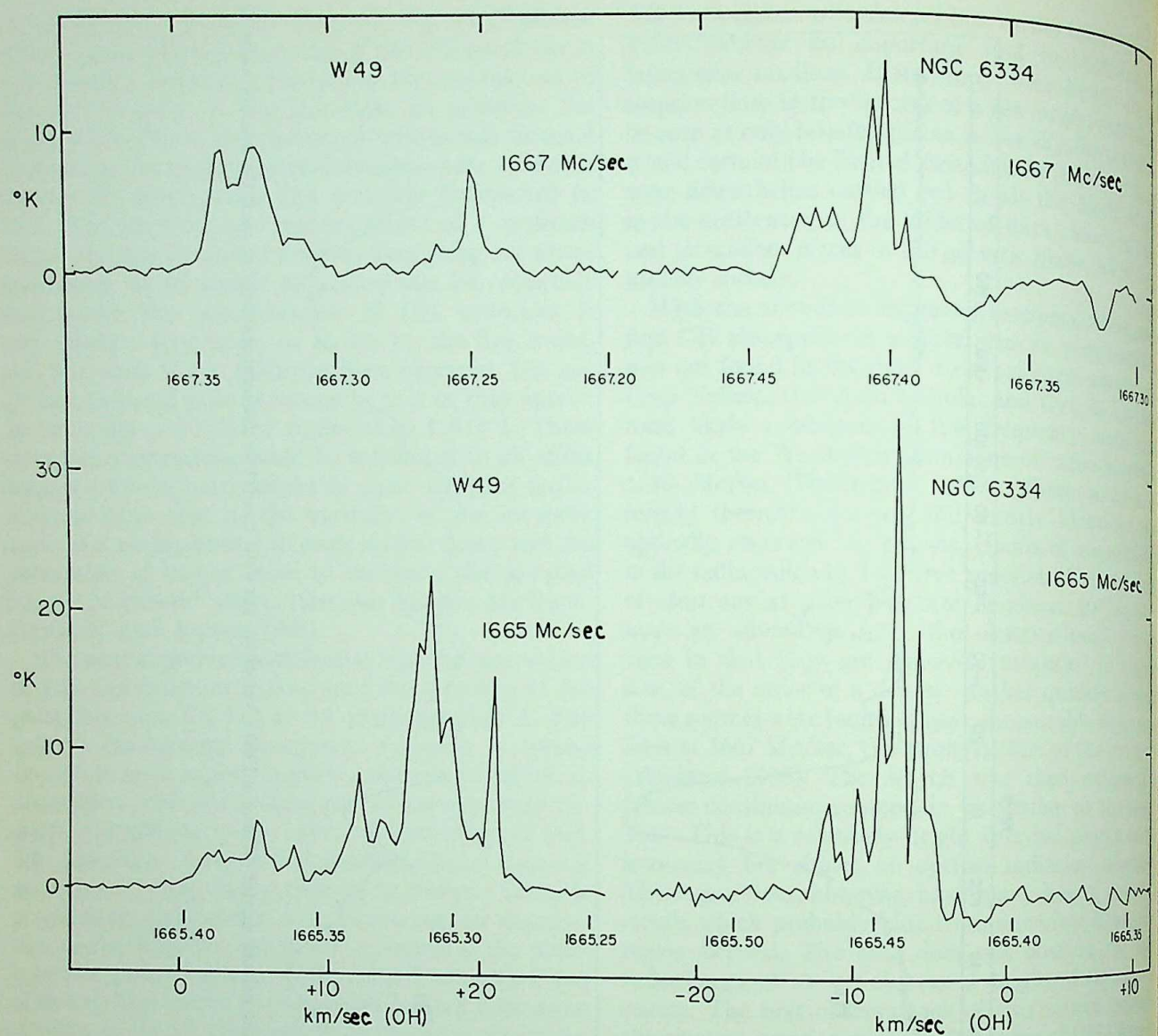

FIG. 12. Spectra of W49 and NGC 6334 in the OH lines with a resolution of 2 kc/sec (0.4 km/sec) (Weaver, Williams, Dieter, and Lum 1965).

the emission in 1665 *exceeded* that in 1667, *not* fell below it, as we would predict if it arose according to normal expectation for the OH multiplet. (This has been confirmed by Zuckerman, Lilley, and Penfield 1965.)

It was immediately obvious that this observation could not be explained in a simple fashion. Any ratio of intensities of 1665/1667 up to one can be explained on the grounds of high optical depth. If the stronger line is saturated, the apparent ratio can be as high as one. In no such way, however, can the ratio exceed one. In W49 the intensity in some of the components of the 1665 line profile are near 20° and the corresponding 1667 components are not detectable.

In some ways the source W49 is not an ideal one for investigating the problem. For one thing, the spectrum in the region of interest is enormously complicated; that is, there are apparently many isolated clouds of gas along the line of sight which make direct comparison of the two transitions rather complicated. If, for example, one wants to determine just how much extra radiation there is at 1665 Mc/sec, one needs to subtract from the observed profile at that frequency an amount which is some fraction of the intensity at 1667, but just what fraction between 1.0 and 1.8 is not clear. In addition, W49 is quite invisible optically and hence nothing is known about its other properties. The radio source is quite small in angular size so that with the relatively small antenna used, it is not possible to tell from where in the nebula the radiation comes. The Orion Nebula, on the other hand, is a bright nearby source and the HII region for which the most optical information is available. The first observations of Orion were made at the edges of this quite extended nebula on the theory that the molecules would probably be dissociated in the central part of such an enormously hot

CC-0. In Public Domain. Gurukul Kangri Collection, Haridwar

Digitized by Arya Samaj Foundation Chennai and eGangotri

region. These observations showed no radiation at all at 1665 Mc/sec; but an observation made exactly in the direction of the center of the nebula and of the well-known thermal radio source Ori A yielded emission of several degrees antenna temperature. The profile again has several sharp velocity components, but in this case no confusion with 1667 Mc/sec. Ori A had been one of the first sources investigated for OH absorption, and had indeed been very thoroughly observed near 1667 Mc/sec, with consequent upper limits on optical depth of 0.005 (Robinson, Gardner, van Damme, and Bolton 1964). It is a curious quirk of fate that this emission line was not found long ago. Searches for OH were obviously carried out in the frequency of the strongest line of the multiplet; when no radiation in this range was found, there was clearly no point in looking at a weaker line. With the clue of W49, however, it was apparent that 1665 Mc/sec should from now on be investigated more or less independently of 1667.

A search for the anomalous OH emission in other HII regions was carried out since these observations suggested that something peculiar to these regions is influencing the radiation—for instance, the presence of large amounts of radiation either in the ultraviolet or at 18-cm wavelength. The search yielded several other sources: IC 1795 (W3), NGC 6334 (shown in Fig. 12), W51, and W75 (Weaver, Williams, Dieter, and Lum 1965). In these sources the line ratios were also completely unexplainable on the basis of the usual excitation mechanisms. Each of these sources showed rather broad absorption features as well as emission components which were remarkably narrow. The width of some of these emission features is that appropriate to the thermal Doppler broadening for a 13°K source with no turbulence. This is hardly consistent with the observed temperature (10^4 °K) or mass motions (5 or more km/sec) in HII regions. A further surprising result came from measurements at the Lincoln Laboratory of MIT (Weinreb, Meeks, Carter, Barrett, and Rogers 1965); the emission at 1665 Mc/sec from W3 is strongly linearly polarized. The several velocity components of the profile show different planes and different percentages of polarization. This result was confirmed at Berkeley and extended to other sources, especially NGC 6334, which shows a high degree of polarization at both 1667 and 1665 Mc/sec—greater than 35% (Williams, Dieter, and Weaver 1965). (One of the components shows 100% linear polarization.) Most recently Barrett and Rogers (1966) have detected, in addition, strong circular polarization in W3, Orion, NGC 6334, W49, and Sgr B_2.

Careful investigation of the radiation at 1612 Mc/sec and 1720 Mc/sec, the theoretically weaker lines of the multiplet, showed a complete divergence from prediction. The shape of thejprofile as measured in each of the lines appears to be quite independent of the others—that is, a given cloud does not seem to radiate in the same fashion at all four frequencies. In some sources there are broad features at 1612 and 1720, where narrow ones occur at the other frequencies; in others there are narrow features in one or the other of these lines at frequencies corresponding to Doppler shifts at which no radiation occurs at all in the "stronger" lines (Weaver, Williams, and Dieter 1965).

Continued observations presented observers with another surprise. The profile observed in NGC 6334 was not of constant shape at either 1667 or 1665 Mc/sec (Dieter, Weaver, and Williams 1965). For example, a peak in the 1665-Mc/sec profile decreased in intensity by a factor of three with respect to another peak in the same profile, in a period of two months. Investigation of the 1665—Mc/sec profile of the Orion Nebula showed that here also were secular variations—a decrease in one peak relative to another by a factor of 1.5 in a similar time interval. No such variation has ever been observed before in the interstellar medium.

All of these peculiarities have led to suggestions of rather exotic excitation mechanisms for the lines. No single one has as yet explained all the observations, and we shall only indicate roughly the current proposals. Reference to the energy level diagram in the ground state Fig. 10 may indicate some of the problems. Radiation at 1665 and 1612 Mc/sec arises from the same upper level so that any anomalous intensity produced solely by an overpopulation of this level should be reflected in both lines (the same is true for 1667 and 1720 Mc/sec). This overpopulation in conjunction with a source of radiation to provide stimulated emission from this level could produce peculiar line intensities and "artificially" narrow lines; in effect, a maser in the interstellar gas (Field, private communication). One of the central unsolved problems in this proposal is the question of how to overpopulate the $F=1$ level in the upper state with respect to $F=2$. They differ in energy by only about 1 μV. The high degree of polarization and the rapid variations in intensity also still elude any credible theoretical explanation.

The OH molecule, then, opens a new realm of speculation about conditions in the interstellar medium. Its fascinating properties lend new impetus to the search for other constituents of the interstellar gas which may be radiating in the microwave spectrum.

We have tried to describe the complex problems and the variety of attacks upon them in the study of the interstellar medium. Our intention was to describe the progress which has been made in building up a detailed physical description of this medium. The outcome has been a picture full of uncertainties, but one which gives the impression that the discovery of a few vital pieces of the puzzle will clarify it all. The search for these pieces is likely to be a fascinating pursuit.

CC-0. In Public Domain. Gurukul Kangri Collection, Haridwar

Digitized by Arya Samaj Foundation Chennai and eGangotri

BIBLIOGRAPHY

Adams, W. S., Astrophys. J. **109**, 354 (1949).
Baade, W., and R. Minkowski, Astrophys. J. **86**, 123 (1937).
Barrett, A. H., and A. E. Lilley, Astron. J. **62**, 5 (1957).
Barrett, A. H., M. L. Meeks, and S. Weinreb, Nature **202**, 475 (1964).
Barrett, A. H., and A. G. E. Rogers, Nature (to be published in 1966).
Bates, D. R., and L. Spitzer, Jr., Astrophys. J. **113**, 441 (1951).
Blaauw, A., Bull. Astron. Inst. Netherlands **11**, 459 (1952).
Boggess, A., and J. Borgman, Astrophys. J. **140**, 1636 (1964).
Bok, B. J., T. K. Menon, and R. S. Lawrence, Publ. Astron. Soc. Pacific **67**, 108 (1955).
Brown, R. H., and C. Hazard, Observatory **80**, 137 (1960).
Burgess, A., G. B. Field, and R. W. Michie, Astrophys. J. **131**, 529 (1960).
Cayrel, R., and E. Schatzman, Ann. d'Astrophys. **17**, 555 (1954).
Chandrasekhar, S., Astrophys. J. **103**, 350 (1946).
Clark, B. G., V. Radhakrishnan, and R. W. Wilson, Astrophys. J. **135**, 151 (1962).
Danielson, R. E., N. J. Woolf, and J. E. Gaustad, Astrophys. J. **141**, 116 (1965).
Davies, R. D., *The Galaxy and the Magellanic Clouds*, edited by F. J. Kerr and A. W. Rodgers (Australian Academy of Science, Canberra, Australia, 1964), p. 134.
Davis, L. Jr., and J. L. Greenstein, Astrophys. J. **114**, 206 (1951).
Dicke, R. H., P. J. E. Peebles, P. G. Roll, and D. T. Wilkinson, Astrophys. J. **142**, 414 (1965).
Dieter, N. H., Astron. J. **69**, 288 (1964).
Dieter, N. H., Astron. J. **70**, 552 (1965).
Dieter, N. H., H. F. Weaver, and D. R. W. Williams, Paper given at Am. Astron. Soc., Dec. 1965 at Berkeley, Calif.
Donn, B., "Les Particles Solid dans les Astres," Liège Sym. (4) **15**, 571 (1955).
Douglas, A. E., and P. M. Routly, Astrophys. J. **119**, 303 (1954).
Dunham, T., Proc. Am. Phil. Soc. **81**, 277 (1939).
Earl, J. A., Phys. Rev. Letters **6**, 125 (1961).
Ewen, H. I., and E. M. Purcell, Nature **168**, 356 (1951).
Field, G. B., Publ. Astron. Soc. Pacific **72**, 303 (1960).
Field, G. B., *Interstellar Matter in Galaxies*, edited by L. Woltjer (W. A. Benjamin, Inc., New York, 1962), p. 183.
Field, G. B., G. Herbig, and J. Hitchcock, Paper given at Am. Astron. Soc., Dec. 1965 at Berkeley, Calif.
Field, G. B., and W. C. Saslaw, Astrophys. J. **142**, 568 (1965).
Gardner, F. F., and R. D. Davies, Australian J. Phys. (to be published 1965).
Gardner, F. F., and J. B. Whiteoak, Nature **197**, 1162 (1963).
Gaustad, J. E., and H. van Woerden (to be published 1966).
Gehrels, T., Astron. J. **65**, 69 (1960).
Gehrels, T., and A. B. Silvester, Astron. J. **70**, 579 (1965).
Goldstein, S. J., E. J. Gundermann, A. A. Penzias, and A. E. Lilley, Nature **203**, 65 (1964).
Goss, W. M., and H. Spinrad, Astrophys. J. (to be published in 1966).
Gould, R. J., and E. E. Salpeter, Astrophys. J. **138**, 408 (1963).
Greenberg, J. M., Astrophys. J. **132**, 672 (1960).
Greenberg, J. M., J. Appl. Phys. **31**, 82 (1960).
Greenberg, J. M., *Annual Reviews of Astronomy and Astrophysics* (Annual Reviews, Inc., Palo Alto, Calif. 1963), Vol. I, p. 267.
Greenberg, J. M., Astrophys. J. (to be published in 1966).
Greenberg, J. M., A. Lind, R. T. Wang, and L. Libels, *Interdisciplinary Conf. on Electromagnetic Scattering* (Pergamon Press, Oxford, England, 1963).
Greenberg, J. M., and A. S. Meltzer, Astrophys. J. **132**, 667 (1960).
Greenberg, J. M., N. E. Pedersen, and J. C. Pedersen, J. Appl. Phys. **32**, 233 (1961).
Guillaume, C., and N. C. Wickramasinghe (to be published 1966).
Hall, J. S., Science **109**, 166 (1949).
Hall, J. S., and K. Serkowski, in *Basic Astronomical Data*, edited by K. Aa. Strand (University of Chicago Press, Chicago, 1963), p. 293.
ter Haar, D., and H. A. Kramers, Bull. Astron. Inst. Netherlands **10**, 137 (1946).
Hayakawa, S., Publ. Astron. Soc. Japan **12**, 110 (1960).
Hayakawa, S., S. Nishimura, and K. Takayanagi, Publ. Astron. Soc. Japan **13**, 184 (1961).
Henry, J., Astrophys. J. **128**, 497 (1958).
Herbig, G. H., Publ. Astron. Soc. Pacific **70**, 468 (1958).
Herbig, G. H., J. Quant. Spectry. Rad. Transfer **3**, 529 (1963).
Herbig, G. H., Astrophys. J. **137**, 200 (1963).
Hiltner, W. A., Science **109**, 165 (1949).
Hobbs, L. M., Astrophys. J. **142**, 160 (1965).
Höglund, B., and P. G. Mezger, Science **150**, 339 (1965).
Hoyle, F., and N. C. Wickramasinghe, Monthly Notices Roy. Astron. Soc. **124**, 417 (1962).
Hoyle, F., and J. G. Ireland, Monthly Notices Roy. Astron. Soc. **122**, 35 (1961).
van de Hulst, H. C., Nederl. Tij. Natuurkunde **11**, 201 (1945).
van de Hulst, H. C., Rech. Astron. Obs. Utrecht **11**, Part 1 (1946).
van de Hulst, H. C., Harvard Obs. Monographs No. 7, 75 (1949).
van de Hulst, H. C., Rech. Astron. Obs. Utrecht **11**, Part 2 (1949).
Ireland, J. G., Monthly Notices Roy. Astron. Soc. **122**, 461 (1961).
Johnson, H. L., Astrophys. J. **141**, 923 (1965).
Johnson, H. L., and J. Borgman, Bull. Astron. Inst. Netherlands **17**, 115 (1963).
Johnson, H. L., and W. W. Morgan, Astrophys. J. **117**, 313 (1953).
Kahn, F. D., Monthly Notices Roy. Astron. Soc. **112**, 518 (1952).
Kahn, F. D., in *Gas Dynamics of Cosmic Clouds*, edited by H. C. van de Hulst and J. M. Burgers (North-Holland Publishing Co., Amsterdam, 1955a), p. 115.
Kahn, F. D., *Les Particles Solid dans les Astres*, Liège Sym. (4) **15**, 578 (1955b).
Kahn, F. D., and J. E. Dyson, *Annual Reviews of Astronomy and Astrophysics* (Annual Reviews, Inc., Palo Alto, Calif. 1965), Vol. III, p. 47.
Kimura, H., Publ. Astron. Soc. Japan **14**, 374 (1962).
Kramers, H. A., and D. ter Haar, Bull. Astron. Inst. Netherlands **10**, 137 (1946).
Krishna Swamy, K. S., Publ. Astron. Soc. Pacific **77**, 164 (1965).
Krishna Swamy, K. S., and N. C. Wickramasinghe (to be published in 1966).
Lambrecht, H., and H. Zimmerman, Wiss. Z. Schiller Univ. (Jena) **5**, 217 (1955).
Lilley, A. E., Astrophys. J. **121**, 559 (1955).
Lilley, A. E., D. H. Menzel, H. Penfield, and B. Zuckerman, Nature (to be published in 1966).
Livingston, W. C., and C. R. Lynds, Astrophys. J. **140**, 810 (1964).
Mathewson, D. S., and D. K. Milne, Australian J. Phys. **18**, 635 (1965).
Mathewson, D. S., N. W. Broten, and D. J. Cole, Australian J. Phys. (to be published, in 1966).
McCrea, W. H., and D. McNally, Monthly Notices Roy. Astron. Soc. **121**, 283 (1960).
McGee, R. X., and J. D. Murray, Australian J. Phys. **14**, 204 (1961).
McGee, R. X., J. D. Murray, and J. A. Milton, Australian J. Phys. **16**, 136 (1963).
McGee, R. X., B. J. Robinson, F. F. Gardner, and J. G. Bolton, Nature **208**, 1193 (1965).
McKellar, A., Publ. Dominion Astrophys. Obs. **7**, 251 (1941).
McNally, D., Monthly Notices Roy. Astron. Soc. **124**, 155 (1962).
Merrill, P. W., Publ. Astron. Soc. Pacific **58**, 354 (1946).
van der Meyderberg, C. J. N., H. F. P. Knapp, J. J. M. Beenakker, and H. C. van de Hulst, Paper given at I.A.U. Colloquium on Interstellar Grains, Troy, N.Y. (1965).
Mills, B. Y., *Annual Reviews of Astronomy and Astrophysics* (Annual Reviews Inc., Palo Alto, Calif. 1964), Vol. II, p. 165.
Mills, B. Y., *Paris Symposium on Radio Astronomy*, Paris 1958, edited by R. N. Bracewell (Stanford University Press, Stanford, Calif., 1959), p. 498.
Minkowski, R., *Annual Reviews of Astronomy and Astrophysics* (Annual Reviews Inc., Palo Alto, Calif. 1964), Vol. II, p. 247.
Münch, G., Astrophys. J. **140**, 107 (1964).
Münch, G., and H. Zirin, Astrophys. J. **133**, 11 (1961).
Morris, D., and G. L. Berge, Astrophys. J. **139**, 1388 (1964).
Morris, D., B. G. Clark, and R. W. Wilson, Astrophys. J. **138**, 889 (1963).
Nandy, K., Publ. Roy. Obs. Edinburgh **4**, 57 (1964).
Nandy, K., Publ. Roy. Obs. Edinburgh **5**, 13 (1965).
Nandy, K., and N. C. Wickramasinghe, Publ. Roy. Obs. Edinburgh **5**, 29 (1965).
O'Dell, C. R., and W. B. Hubbard, Astrophys. J. **142**, 591 (1965).
Oort, J. H., Bull. Astron. Inst. Netherlands **6**, 249 (1932).

CC-0. In Public Domain. Gurukul Kangri Collection, Haridwar

Digitized by Arya Samaj Foundation Chennai and eGangotri

Oort, J. H., Monthly Notices Roy. Astron. Soc. **106,** 159 (1946).
Oort, J. H., Bull. Astron. Inst. Netherlands **12,** 177 (1954).
Oort, J. H., Bull. Astron. Inst. Netherlands **15,** 45 (1960).
Oort, J. H., A. Blaauw, A. N. M. Hulsbosch, C. A. Muller, E. Raimond, and C. M. Tolbert, Bull. Astron. Inst. Netherlands (to be published 1966).
Oort, J. H., and L. Spitzer, Jr., Astrophys. J. **121,** 6 (1955).
Oort, J. H., and H. C. van de Hulst, Bull. Astron. Inst. Netherlands **10,** 187 (1946).
Parker, E. N., Rev. Mod. Phys. **30,** 955 (1958).
Penzias, A. A., and R. W. Wilson, Astrophys. J. **142,** 419 (1965).
Platt, J. R., Astrophys. J. **123,** 486 (1956).
Purcell, E. M., and G. B. Field, Astrophys. J. **124,** 542 (1956).
Reber, G., Proc. Inst. Radio Eng. **46,** 15 (1958).
Robinson, B. J., F. F. Gardner, K. J. van Damme, and J. G. Bolton, Nature **202,** 989 (1964).
Shuter, L. H., and G. L. Verschuur, Monthly Notices Roy. Astron. Soc. **127,** 387 (1964).
Seaton, M. J., Rev. Mod. Phys. **30,** 979 (1958).
Serkowski, K., private communication to J. M. Greenberg (1963).
Spitzer, L. Jr., Astrophys. J. **120,** 1 (1954).
Spitzer, L. Jr., *Stars and Stellar Systems* (University of Chicago Press, Chicago, 1966), Vol. 7, Chap. IX.
Spitzer, L. Jr., and F. R. Zabriskie, Publ. Astron. Soc. Pacific **71,** 412 (1959).
Stecher, T. P., and J. E. Milligan, Ann. d'Astrophys. **25,** 268 (1962).
Strömgren, B., Astrophys. J. **89,** 526 (1939).
Strömgren, B., Astrophys. J. **108,** 242 (1948).
Swings, P., Astrophys. J. **95,** 270 (1941).
Takakubo, K., and H. van Woerden, Bull. Astron. Inst. Netherlands (to be published in 1966).
Takayanagi, K., Joint Inst. Lab. Astrophys. Pub. No. 19 (1964).
Takayanagi, K., and S. Nishimura, Publ. Astron. Soc. Japan **12,** 77 (1960).
Trumpler, R. J., Lick Obs. Bull. **14,** 54 (1930a).
Trumpler, R. J., Publ. Astron. Soc. Pacific **42,** 214 (1930b).
Trumpler, R. J., Publ. Astron. Soc. Pacific **42,** 267 (1930c).
Tsuji, T., Ann. Tokyo Obs. 2nd Ser. **9,** No. 1 (1964).
Unsöld, A., Publ. Roy. Obs. Edinburgh **4,** 35 (1964).
Vandervoort, P. O., Astrophys. J. **139,** 869 (1964).
Verschuur, G. L., thesis, University of Manchester (1965).
Wampler, E. J., Astrophys. J. **136,** 100 (1963).
Wampler, E. J., Astrophys. J. **137,** 1071 (1963).
Weaver, H. F., D. R. W. Williams, and N. H. Dieter, Paper given at Am. Astron. Soc., Dec. 1965 at Berkeley, Calif.
Weaver, H. F., D. R. W. Williams, N. H. Dieter, and W. T. Lum, Nature **208,** 29 (1965).
Weinreb, S., Astrophys. J. **136,** 1149 (1962).
Weinreb, S., A. H. Barrett, M. L. Meeks, and J. C. Henry, Nature **200,** 829 (1963).
Weinreb, S., M. L. Meeks, J. C. Carter, A. H. Barrett, and A. G. E. Rogers, Nature **208,** 440 (1965).
Westerhout, G., Bull. Astron. Inst. Netherlands **14,** 215 (1958).
Wickramasinghe, N. C., Monthly Notices Roy. Astron. Soc. **125,** 87 (1962).
Wickramasinghe, N. C., Monthly Notices Roy. Astron. Soc. **126,** 99 (1963).
Wickramasinghe, N. C., and C. Guillaume, Nature **207,** 366 (1965).
Wickramasinghe, N. C., Monthly Notices Roy. Astron. Soc. **131,** 177 (1965).
Wickramasinghe, N. C., Monthly Notices Roy. Astron. Soc. (to be published in 1966).
Wickramasinghe, N. C., W. D. Ray, and C. Wyld, Monthly Notices Roy. Astron. Soc. (to be published in 1966).
Wickramasinghe, N. C., M. W. C. Dharmawardhana, and C. Wyld (to be published in 1966).
Williams, D. R. W., N. H. Dieter, and H. F. Weaver, Paper given at Am. Astron. Soc., December 1965 at Berkeley, Calif.
Williams, D. R. W., Paper presented at U.R.S.I.–I.E.E.E. Meeting, April 1965 at Washington, D.C.
van Woerden, H., K. Takakubo, and L. L. E. Braes, Bull. Astron. Inst. Netherlands **16,** 321 (1962).
Zimmerman, H., Astron. Nach. **288,** 95 (1964).
Zuckerman, B., Nature **208,** 441 (1965).

CC-0. In Public Domain. Gurukul Kangri Collection, Haridwar

Digitized by Arya Samaj Foundation Chennai and eGangotri

Considerations on the Flow of Superfluid Helium*

P. W. ANDERSON
Bell Telephone Laboratories, Murray Hill, New Jersey

First, we show that the most important equations of the dynamics of the two types of superfluids, He II and superconductors, follow quite directly from the simple assumption that the quantum field of the particles has a mean value which may be treated as a macroscopic variable. The background of this ansatz is also discussed. Second, we apply these equations to various physical situations in He II, notably the orifice geometry and the superfluid film, and show how the and particularly the idea of phase slippage accompanying all dissipative processes, can be applied and what kinds of macroscopic interference phenomena may be expected. The effect of synchronization in the ac interference experiment is discussed.

I. INTRODUCTION

The material of the first part of this article covers really much the same areas of basic physics which are treated by Martin and by Nozieres in their articles at the same conference at which this was presented. Nonetheless the reader will find that the emphasis is sharply different. The striking macroscopic interference phenomena, the observation of which has been stimulated by Josephson's remarkable discovery,[1] call out for a description in terms of a definite wave function with a definable phase ϕ in every part of the system, while quantum hydrodynamics as pioneered by Landau[2] has tended to emphasize the superfluid velocity v_s and its equations of motion. The identification of $v_s = (\hbar/m)\nabla\phi$ has its limitations in relating these points of view, especially in Josephson junctions; while the opposite point of view, that ϕ exists, makes theorists uncomfortable because it breaks the gauge symmetry. Nonetheless I shall choose to take the latter path, assuming either that the reader has read such a discussion as Ref. 3 which gives the reason why this broken symmetry is possible, or that he will understand that the superfluid system is to be attached at some point to a large superfluid reservoir, with respect to which the phase is to be measured.

The idea of off-diagonal long-range order was introduced by Penrose and Onsager.[4] They suggested that superfluidity be described as a state in which the density matrix

$$\rho(r, r') = \langle \psi^*(r)\psi(r') \rangle$$

could be factorized:

$$\rho(r, r') = \psi^*(r)\psi(r') + \text{small terms.} \quad (1)$$

Beliaev[5] extended this for helium to a Green's function theory in which ψ was explicitly time-dependent, and first observed that the chemical potential determines the time dependence. Sortly thereafter Gor'kov[6] observed that superconductivity theory could be cast into the same form by substituting electron pair field operators $\psi\psi$ for the He atom bose field. In superconductivity there already existed a set of phenomenological equations proposed by Ginzburg and Landau[7] which dealt with an "order parameter" η, and it was soon recognized that this order parameter was the same as the factorized ψ of the Gor'kov theory.[8] It was only much later that Gross[9] and Pitaevskii[10] proposed similar sets of equations for liquid helium.

The notion that it was possible to regard the function which appears in these treatments as essentially the mean value of the quantum particle field has long been accepted in both helium[5] and superconductivity (there the first explicit discussion of the transformation between the "ODLRO" and mean field points of view was given by Anderson[11]) but only in the case of a homogeneous system; apparently the general case has not been discussed until recently even for superconductivity.[3] The basic idea is that it is as legitimate to treat the quantum field amplitude as a macroscopic dynamical variable as it is the position of a solid body; both represent a broken symmetry which, however, cannot be conveniently repaired until one gets to the stage of quantizing and studying the quantum fluctuations of the macroscopic behavior of the system.

Here we are going to discuss less the microscopic background of this ansatz than a number of its most important consequences for He II, many of which follow without further microscopic assumptions and are therefore of fundamental interest. Only some of what we will have to say is new, in the sense that many of the

---

* This paper was presented at the Brighton Symposium on Quantum Fluids at the University of Sussex, England, 18 August 1965. The full proceedings of this Conference will be published by the North-Holland Publishing Company in 1966, including the present article as well as those referred to above, in which a more conventional approach to superfluid dynamics is employed. Many of the other contributions have of course also been published in various journals.

[1] B. D. Josephson, Phys. Letters **1**, 251 (1962).

[2] L. D. Landau, J. Phys. USSR **5**, 71 (1941).

[3] P. W. Anderson, in *Lectures on the Many-Body Problem*, edited by E. R. Caianello (Academic Press Inc., New York, 1964), Vol. 2, p. 113.

[4] O. Penrose and L. Onsager, Phys. Rev. **104**, 576 (1956); see also O. Penrose, Phil. Mag. **42**, 1373 (1951).

[5] S. T. Beliaev, Zh. Eksperim. i Teor. Fiz. **34**, 417 (1958) [English transl.: Soviet Phys.—JETP **7**, 289 (1958)]. 735 (1958)

[6] L. P. Gor'kov, Zh. Eksperim. i Teor. Fiz. **34**, [English transl.: Soviet Phys.—JETP **7**, 505 (1958)].

[7] V. L. Ginsburg and L. D. Landau, Zh. Eksperim. i Teor. Fiz. **20**, 1064 (1950).

[8] L. P. Gor'kov, Zh. Eksperim. i Teor. Fiz. **36**, 1918 (1959) [English transl.: Soviet Phys.—JETP **9**, 1364 (1958)].

[9] E. P. Gross, Nuovo Cimento **20**, 454 (1951).

[10] L. P. Pitaevskii, Zh. Eksperim. i Teor. Fiz. **40**, 646 (1961) [English transl.: Soviet Phys.—JETP **13**, 451 (1961)].

[11] P. W. Anderson, Phys. Rev. **112**, 1900 (1958).

CC-0. In Public Domain. Gurukul Kangri Collection, Haridwar

Digitized by Arya Samaj Foundation Chennai and eGangotri

appropriate equations have been written down (see the papers of Martin and Nozieres). The basic idea was previously stated in a Letter,[12] and some of the consequences have been explored in subsequent Letters by Donnelly[13] and by Zimmerman.[14] We will first discuss a particularly simple point of view on the derivation of the basic equations, following more closely than usually the corresponding ideas in superconductivity.[3,15] The emphasis will be on what can be shown to follow more or less rigorously from using this ansatz as a general semimicroscopic definition of superfluidity. Only the parameter values in the resulting equations require any other knowledge of the microscopic system. Then we will discuss the dynamical consequences for the orifice experimental geometry, as well as some more general situations such as film flow. In Appendix B we discuss briefly the interesting connection with classical ideal fluid hydrodynamics, where the basic "Josephson" theorem turns out to have a classical analogue which has not to our knowledge been clearly stated previously.

II. BASIC EQUATIONS

We take as our definition of a superfluid that it is a fluid in which the particle field operator ψ has a macroscopic mean value, in a sense which is defined shortly.

$$\langle\psi(r,t)\rangle = f(r,t)\exp[i\phi(r,t)]. \tag{2}$$

Here we allow slow (on the atomic scale) space and time variations; the essential point is that $\langle\psi\rangle$ has a mean value in the thermodynamic, quasi-equilibrium sense. One may think of the situation here as completely analogous to the definition of temperature in a nonequilibrium state; it is possible if there are equilibrating processes of shorter range in time or space than the coarse-grained scale of our averaging, which in turn is to occur over regions smaller than the macroscopic scale of physical measurements. Of course, in every system one can define a temperature and entropy if the average is allowed to extend over a long enough time, while only certain special systems will give a stable limiting value to $\langle\psi\rangle$. More explicitly, we visualize averaging ψ over some small region of space–time; if the region is small enough compared to the rates and ranges of microscopic fluctuations, we will obtain some finite value. As we increase the size ΔV of the region $\langle\psi\rangle$ will decrease to zero in a normal system very rapidly, in times of the order $h/$(mean kinetic energy) and ranges of order interparticle distances. In a superfluid system, on the other hand, we assume that at an intermediate, "coarse-grained" scale $\langle\psi\rangle$ approaches a limiting finite value, not changing until we reach a scale on which it varies because of the presence of macroscopic perturbations such as macroscopic fields and flows. (In Appendix A we discuss this definition a little more deeply.)

The whole problem of superfluid dynamics, then, reduces to the question of how to deal with $\langle\psi\rangle$ (often denoted the superfluid order parameter) as a thermodynamical variable. It is quite important that $\langle\psi\rangle$ is a *complex* order parameter; it has both an amplitude f and a phase ϕ. There is actually rather a sharp distinction between the two real thermodynamic variables f and ϕ, and it is the behavior with respect to ϕ which is responsible for specific superfluid properties. The distinction is that ϕ is coupled, like a polarization or a strain, to external forces, where f is merely an internal order parameter in the sense, for instance, of the original long-range order parameter of order–disorder systems, or of the antiferromagnetic sublattice magnetization. In principle a corresponding force might exist but in practice it does not, so f simply manifests itself as a convenient tool by which to describe the condensation process.

The point of ϕ, then, is that it is not only a thermodynamic but also a dynamical variable. The latter fact comes from its being the dynamically (not thermodynamically) canonically conjugate variable to N, the total number of particles in the system described by ϕ. (The limitations of this statement for systems of few particles[16] are irrelevant here.)

We illustrate this fact by forming wave packets in many-body wave-function space, just as in discussing the relationship of p and q it is useful to form wave packets. Let us write the wave function of one of our coarse-grained cells of volume ΔV as

$$\Psi(\Delta V) = \sum_N a_N \Psi_N(\Delta V) \tag{3}$$

where, since our cell is only a part of the superfluid, it is essential to realize that the state is a superposition of states Ψ_N with different numbers of particles N, with coefficients a_N large in some range of values $\Delta N \sim N^{\frac{1}{2}}$. An important simplifying assumption concealed in (3) is that the cell may be made big enough so that a_N and Ψ_N do not depend very much parametrically on the variables of the rest of the system: this is what is meant (see Appendix A) by a "satisfactory" local description.

We postulate that $\langle\psi\rangle$ has a limiting mean value, which must be of order $(N/\Delta V)^{\frac{1}{2}}$; we calculate this value from (3):

$$\frac{1}{\Delta V}\int_{\Delta V} d\tau\,\langle\psi(r)\rangle = \frac{1}{\Delta V}\sum_{N,N'} a_{N'}{}^* a_N \int (\Psi_{N'}, \psi(r)\Psi_N)\, d\tau$$

$$= \sum_N a_{N-1}{}^* a_N \int \frac{(\Psi_{N-1}, \psi(r)\Psi_N)\, d\tau}{\Delta V}. \tag{4}$$

[12] P. L. Richards and P. W. Anderson, Phys. Rev. Letters **14**, 540 (1965).
[13] R. J. Donnelley, Phys. Rev. Letters **14**, 939 (1965).
[14] W. Zimmermann, Phys. Rev. Letters **14**, 976 (1965).
[15] P. W. Anderson, N. R. Werthamer, and J. M. Luttinger, Phys. Rev. **138**, A1157 (1965).
[16] W. H. Louisell, Phys. Letters **7**, 60 (1963); L. Susskind and J. Glogower, Physics **1**, 49 (1964).

CC-0. In Public Domain. Gurukul Kangri Collection, Haridwar

Digitized by Arya Samaj Foundation Chennai and eGangotri

In the case of the Bose-condensed perfect gas, one may take

$$\Psi_N = (c_0^+)^N \Psi_{\text{vac}}, \tag{5}$$

where

$$c_0 = \frac{1}{(\Delta V)^{\frac{1}{2}}} \int \psi(r)\, d\tau$$

$$c_0 \Psi_N = N^{\frac{1}{2}} \Psi_{N-1}, \tag{6}$$

so that

$$\langle \psi \rangle = \sum_N a_{N-1}^* a_N (N/\Delta V)^{\frac{1}{2}}. \tag{7}$$

This is the maximum possible value of the matrix element. (Here we have taken advantage, as we will always, of our freedom to choose the phase of Ψ_N to make the matrix element real in order to keep the phase factors—which of course are *not* irrelevant—in the a_N's.) In real superfluid systems and at finite temperatures (the case of superconductivity is of course quite similar if for a single Bose ψ or c we read Fermion pair operators) the matrix element does not take on its maximum possible value—in He, for instance, as McMillan has shown,[17] the value is about 11% of the maximum when ΔV is reasonably large. Even if

$$M = (\Psi_{N-1}, \bar{\psi} \Psi_N) \tag{8}$$

is large, however, $\langle \psi \rangle$ will not be large unless the a_N preserve phase coherence. For example, we may form a wave packet using

$$a_N = (2\pi \Delta N)^{-\frac{1}{2}} \exp\left[-\tfrac{1}{2}(N-\bar{N})^2/(\Delta N)^2\right] \exp(i\phi N). \tag{9}$$

In this case if $\Delta N \gg 1$,

$$\langle \psi \rangle \cong |M| \exp(i\phi) \tag{10}$$

whereas if the phase factors are arbitrary $\langle \psi \rangle$ will be very much smaller, even if every individual Ψ_N represents a pure Bose-condensed state of the volume element ΔV. We will very shortly discuss the reason why wave packets like (9) actually occur in superfluid systems; first, however, let us dispose of a few formal preliminaries.

Any linear combination of the set of fixed-number states Ψ_N may be written as a linear combination of our basic wave packets (3)–(9) [which we will call $\Psi(\phi)$]. In particular, the number eigenfunction Ψ_{N_0} may itself be written

$$\Psi_{N_0} \propto \int_0^{2\pi} d\phi \exp(-i\phi N_0) \Psi(\phi) \tag{11}$$

$$\left(= \sum_N a_N\, \delta(N, N_0) \Psi_N\right).$$

The operator $-i\partial/\partial\phi$ acting on $\Psi(\phi)$ has the same effect as multiplying Ψ_{N_0} by N_0:

$$\int_0^{2\pi} d\phi \exp(-i\phi N_0)\left(-i\frac{\partial}{\partial\phi}\right)\Psi(\phi)$$

$$= N_0 \int_0^{2\pi} d\phi \exp(-i\phi N_0)\Psi(\phi) = N_0 \Psi_{N_0},$$

so that we may take

$$N \leftrightarrow -i(\partial/\partial\phi) \tag{12a}$$

and correspondingly it may be shown that

$$i(\partial/\partial N) \leftrightarrow \phi \tag{12b}$$

in the limit that N may be considered a continuous variable. Thus, as we stated, N and ϕ are conjugate dynamical variables.

In general, also, N and ΔN are sufficiently large that the system's dynamics may be treated reasonably well classically and the uncertainty in ϕ is not excessive—of course (12) implies $\Delta N \Delta\phi \sim 1$.

In any case the equations of motion of N and ϕ are

$$i\hbar \dot{N} = [\mathcal{H}, N] = i(\partial \mathcal{H}/\partial\phi)$$

$$i\hbar \dot{\Phi} = [\mathcal{H}, \phi] = -i(\partial \mathcal{H}/\partial N).$$

Taking the mean values of these two equations and assuming that the wave packets are such that $\Delta N/N$ and $\Delta\phi$ are both small (quasi-classical case) is the source of the two equations which essentially characterize superfluidity: the equation for superfluid flow, corresponding to London's equation or the Ginsburg-Landau current equation in superconductivity, and the "Josephson" frequency equation, which is related to the acceleration equation for superfluid flow in both He and superconductivity. The second is somewhat simpler though less generally known: it is just

$$\hbar(d\phi/dt) = \partial E/\partial N = \mu. \tag{13}$$

Here we have used the standard definition of the chemical potential μ; if the fluid is in motion so that the particles have kinetic energy $\frac{1}{2}mv_s^2$ that is to be included in μ as well as the internal energy and any external forces. Obviously the partial derivative holds S fixed. In an isothermal, assumed incompressible bath of liquid helium, with free surface at height h in a gravitational field g,

$$\mu = m(p/\rho) + mgh + \tfrac{1}{2}mv_s^2. \tag{14}$$

In the nonisothermal case (14) should contain the thermomechanical term.

Equation (13) is of the utmost importance in understanding superfluidity. It says two things: first, that if the state of the superfluid is constant in time, because ϕ is a thermodynamic variable it will be constant and μ must be constant everywhere: there can be no potential differences in the truly steady state. Second, if there

[17] W. L. McMillan, Phys. Rev. **138**, A442 (1965).

CC-0. In Public Domain. Gurukul Kangri Collection, Haridwar

Digitized by Arya Samaj Foundation Chennai and eGangotri

is any potential difference $\mu_1-\mu_2$ between two elements in the superfluid $\phi_1-\phi_2$ must change in time. This can happen in two ways. The simplest is acceleration. If we take the gradient of (13), we obtain

$$(d/dt)(\hbar\nabla\phi)=\mathbf{F}, \tag{15}$$

where $\mathbf{F}$ is the total force on the particles, and making the identification (which we shall discuss shortly) of

$$\hbar\nabla\phi=p_s=mv_s, \tag{16}$$

this is the statement that the superfluid may undergo acceleration without frictional damping by whatever external forces act upon it. A potential difference may lead to continuous acceleration, then.

Slightly more subtle and much more physically important is the concept of phase slippage by quantized vortex motion. As we have emphasized, ϕ is the phase of the thermodynamic variable $\langle\psi\rangle$, which is of course necessarily single-valued. ϕ, however, being a phase, need not be single-valued in a multiply connected system such as a toroid; it need merely return to its original value $\pm 2n\pi$ on traversing a path around a nonsuperfluid obstacle:

$$\oint\nabla\phi\cdot d\mathbf{s}=2n\pi. \tag{17}$$

In terms of the superfluid momentum p_s this expresses the idea of the quantization of angular momentum in units of $\hbar$ or of vorticity $\boldsymbol{\omega}=\frac{1}{2}\nabla\times v_s$ through a closed curve in units of $h/2m$. As we shall see, however, the quantity v_s is not necessarily a measurable particle velocity and so (17) is somewhat more fundamental than the usual concept of vorticity quantization.

A bucket of superfluid may be made multiply connected not only by the presence of actual solid obstacles but by the introduction of one-dimensional regions of nonsuperfluidity within the liquid itself: lines where $\langle\psi(r)\rangle=0$. These are "vortex cores" and may of course move according to the usual laws of hydrodynamics along with the surrounding fluid. Around such a line there can be a circulation of one or, less usually, an integral number of quanta, according to (17).

Equation (17) shows that the integral of $\nabla\phi$ along a path on one side of a vortex core differs from that on the other by 2π (see Fig. 1). Thus when a vortex core moves across the line between points 1 and 2, this may cause a time rate of change of $\phi_1-\phi_2$. Mathematically, we may write

$$\langle\mu_1-\mu_2\rangle_{Av}=T^{-1}\int_0^T dt\hbar\frac{d(\phi_1-\phi_2)}{dt}=\frac{\hbar}{T}\int_0^T dt\frac{d}{dt}\int_1^2\nabla\phi\cdot dl, \tag{C}$$

where $\langle\ \rangle_{Av}$ denotes time average, where we consider the limit T very long, and C is any path from 1 to 2. If the liquid is assumed to be in a reasonably steady

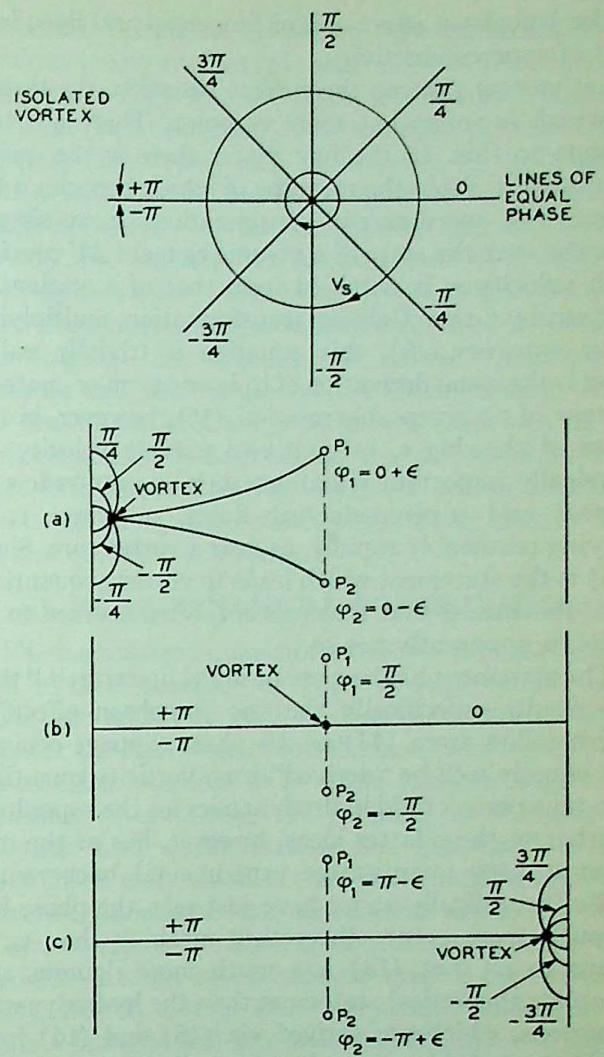

FIG. 1. Illustration of phase changes at two points P_1 and P_2 in a channel as a vortex moves between them. From a to b to c the vortex moves across from left to right; as it moves from one wall to the other the relative phase changes by 2π.

state, so that at 0 and T the positions of the various vortices do not differ very much, the integral is just equal to 2π times the number of vortices which have crossed C in this time interval. Thus we have

$$\langle\mu_1-\mu_2\rangle_{Av}=h\langle dn/dt\rangle_{Av}, \tag{18}$$

where $\langle dn/dt\rangle_{Av}$ is the average rate of motion of vortices across a path from 1 to 2. This is the "phase slippage" concept which is used to explain the various "ac Josephson"-like experiments.[18,19] Of course, this is not incompatible with the acceleration equation (15), so in a sense this phenomenon too is merely a manifestation of the fact that potential differences occur only in an accelerated superfluid; but it is a point of view which had not previous to Ref. 12 found its way into the He literature, nor until recently, with the discovery

[18] S. Shapiro, Phys. Rev. Letters **11**, 80 (1963).
[19] P. W. Anderson and A. H. Dayem, Phys. Rev. Letters **13**, 195 (1964).

CC-0. In Public Domain. Gurukul Kangri Collection, Haridwar

Digitized by Arya Samaj Foundation Chennai and eGangotri

of the Josephson effect and of flux creep and flow, into that of superconductivity.

Let us now take up the current equation, the theory of which is somewhat more complex. There are two aspects to this. In the first place there is the quasi-rigorous Eq. (16) the meaning of which becomes a bit vague with more careful consideration. If we simply suppose that the state of a volume element ΔV moving with velocity v_s is obtained from that of a stationary element by a pure Galilean transformation, multiplying ψ by $\exp(imv_s x/\hbar)$, this equation is trivially valid. That is the usual derivation of it, in one form or another. I know of no acceptable proof of (16), however, in the sense of showing v_s to be a real particle velocity, in physically important situations such as counterflow of normal and superconducting fluids, or where v_s is varying reasonably rapidly, as near a vortex core. Since (16) is the statement which leads to vorticity quantization, this means that that concept, often claimed to be exact, is apparently not so.

The statement has been made in the literature[13,14] that the results—specifically the "ac Josephson effect"—which follow from (13) or the phase slippage concept can equally well be "derived" from vorticity quantization plus perfect fluid hydrodynamics for the superfluid. Neither of these latter ideas, however, has at the moment a very quantitative experimental background, while theoretically as we have just seen the phase has a much more secure theoretical meaning than v_s; it seems to us that (13) is a much more rigorous and complete theoretical statement than the hydrodynamic equations, which are derived via (15) and (16) from it. Normal fluid counterflow and dissipation do not affect it. In a perfect classical fluid, for instance, the vortices cannot move across stream lines, so clearly He II is not such a fluid.

Perhaps a more rigorous general reason for using (16) at least as a *definition* for v_s (other than that it allows us to use ϕ as a velocity potential for the superfluid flow) is (15), which shows that mdv_s/dt does then give the rate of exchange of momentum per superfluid particle with external forces, an excellent operational definition of v_s.

The superflow, however, is best determined not from the expression for v_s but from the other of the two Hamilton equations for the conjugate variables N and ϕ:

$$\hbar(dN/dt)=\partial E/\partial\phi. \tag{19}$$

Gauge invariance assures us that in fact the energy of an isolated bit of superfluid is independent of ϕ, so that in the absence of a coupling to its neighbors $dN/dt=0$. Consider, on the other hand, a pair of neighboring volume elements ΔV_1 and ΔV_2. Our definition of superfluid implies that $\langle\psi\rangle$ has a tendency to constancy, so that the mean phases ϕ_1 and ϕ_2 of the two neighboring elements will be coupled by some energy which is a minimum when $\phi_1-\phi_2=0$:

$$E=U(\phi_1-\phi_2).$$

Assuming the effects of other neighboring elements can be treated independently (suitable arguments can be found for this step) we see that the flow across the boundary between ΔV_1 and ΔV_2 is given by

$$J_{\text{tot}}=\frac{dN_1}{dt}=-\frac{dN_2}{dt}=\frac{1}{\hbar}\frac{\partial U(\phi_1-\phi_2)}{\partial(\phi_1-\phi_2)}. \tag{20}$$

This is the expression used in the theory of the Josephson current[1,3] across a barrier between two macroscopic pieces of superconductor; at this point we are carrying the same reasoning over to the continuous interior of a superfluid or superconductor. As in that case, we may pause now to point out that it is this coupling energy which enforces the phase coherence of each individual volume element of the superfluid. The kinetic energy matrix element which transfers particles across the boundary can cause transitions like

$$\{\Psi_1{}^N\rightarrow\Psi_1{}^{N-1};\ \Psi_2{}^{N'}\rightarrow\Psi_2{}^{N'+1}\}, \tag{21}$$

with a matrix element we may call M_{12}. (Here $\Psi_{1,2}$ is the many-body wave function of $\Delta V_{1,2}$.) If the wave packets (3) have coefficients a_N which, like (9), have coherent phase relationships, all transitions $N'\rightarrow N'+1$ can occur coherently with all transitions $N\rightarrow N-1$. Mathematically, the energy due to transitions like (21), inserting wave packets like (3), is

$$(\Psi_1\Psi_2,\ (\text{K.E.})\Psi_1\Psi_2)=\Big(\sum_N a_N{}^* a_{N-1}\Big)\Big(\sum_{N'} a_{N'}{}^* a_{N'+1}\Big)M_{12}. \tag{22}$$

As we see, this energy is orders of magnitude larger for coherent wave packets like (9), for which ϕ is determinate, than in the incoherent case.

In the interior of the superfluid, it is more convenient to go over to a continuum representation of the coupling energy which maintains phase coherence. We write U as a functional of the gradient of ϕ (as well as f, of course)

$$U=\int U[(f),\nabla\phi]\,d\tau$$
$$\simeq\int E(f,S)(\nabla\phi)^2\,d\tau \tag{23}$$

and then by considering a cell of wall area A and thickness d we find

$$\frac{J}{\text{unit area}}=\frac{dN_1}{dt}\Big/A=\frac{\delta U}{\hbar\delta\nabla\phi}=\hbar^{-1}E\nabla\phi. \tag{24}$$

If we use the pseudo-identity

$$v_s=\hbar\nabla\phi/m,$$

CC-0. In Public Domain. Gurukul Kangri Collection, Haridwar

Digitized by Arya Samaj Foundation Chennai and eGangotri

we may write

$$J_s = n_s(f, S)v_s = [\hbar n_s(T)/m]\nabla\phi, \tag{25a}$$

so that we can identify the parameter E of (24):

$$E = \delta^2 U/\delta(\nabla\phi)^2 = \hbar^2 n_s(T)/m. \tag{25b}$$

Thus the current equation contains a completely arbitrary parameter n_s. In pure, homogeneous systems at absolute zero Galilean invariance can be used to show that $n_s = n$, the total number of particles; but in impure systems at $T=0$, or any system at $T\neq 0$, no such identity holds, though in general n_s is of the same order of magnitude as n.

The supercurrent (24) exists even if the phase ϕ is completely stationary in time, which as we have shown implies the absence of accelerating forces. In fact, in the presence of accelerating forces and time-dependent ϕ we must expect additional quasi-particle currents, in general; the system will exhibit a two-fluid hydrodynamics, the complexities of which need not concern us here. So far as I know their proper treatment requires more knowledge of the actual physical system than we are assuming here.

One very important point about (24) taken together with (15) is that it makes it at least highly probable that there is both a necessary and a sufficient connection between the existence of supercurrents and our definition of superfluidity (1) (which is essentially equivalent to what Yang[20] has named ODLRO). Namely, $\langle\psi\rangle$ and therefore ϕ will not exist if the energy is not such as to maintain spatial coherence of ϕ, so $\delta^2 U/\delta(\nabla\phi)^2$ must exist and be positive in a superfluid in this sense, meaning necessarily supercurrents by (24). (15) shows that they flow with zero forces and are therefore supercurrents. Hypothetical phases with $\langle\psi\rangle$ but no supercurrents (Cohen[21]) seem to ignore this half of the argument.

Conversely, the only dynamically conjugate variable to N is the phase as we have defined it, so that the existence of a dN/dt in a stationary state implies a $\delta U/\delta\phi$, which implies that ϕ is a meaningful variable. Various hypothetical superconducting phases (e.g., Frohlich[22]) do not satisfy *this* half of the argument.

This concludes our general discussion of the basic equations of superfluidity. We restate the conclusions: the phase equation (13) and the corresponding equation of phase slippage are exact in the "integrated" sense that they give the phase difference between two distant points in undisturbed regions of superfluid. The existence of the order parameter alone guarantees the existence of quantized vortices, and according to (24) these are indeed vortices in that they contain a superfluid circulation. However, the quantization of vorticity in any true sense is dependent on the imprecise assumption (15) that the phase is the velocity potential with fixed coefficient. This need not be true unless we treat (15) merely as a definition of v_s, for instance near a vortex core, just as the quantization of flux in superconductivity is not necessarily precise. Operationally, for example, the measurement of h/e by the ac Josephson effect, or of h/mg by the helium counterpart, is more precise in principle than by flux or vorticity quantization. In practice, of course, present-day methods are not capable yet of distinguishing these niceties, but it is of value to have a clear idea of the theoretical assumptions behind the various equations, since it is foreseeable that the most precise measurements of many important physical quantities will involve quantum coherence.

[20] C. N. Yang, Rev. Mod. Phys. **34**, 694 (1962).
[21] M. H. Cohen, Phys. Rev. Letters **12**, 664 (1964).
[22] H. Frohlich and C. Terreaux, Proc. Phys. Soc. (London) **86**, 233 (1965).

III. SOME DYNAMICAL CONSEQUENCES

The macroscopic quantum interference effects promised by the existence of $\langle\psi\psi\rangle$ in superconductivity have been relatively easy to observe for a number of reasons: the light mass of the electron, permitting weak superfluid connections to be made easily by use of the tunneling phenomenon, the coupling to the electromagnetic field which leads to flux quantization, and most particularly the fact that that coupling provides a second parameter, the penetration depth λ, which in screening out the current and magnetic field from the interior of the superconductor creates the Meissner effect, that is ensures that every superconductor exhibits a finite critical magnetic field H_{c_1} below which it contains no vortices and thus essentially exhibits constant ϕ. In He, $\lambda\to\infty$ so that the corresponding $\omega_{c_1}=0$; no rotation of a sufficiently large He sample is too small for vortices to be energetically favorable. Indeed, experiments show that few samples are ever free of vorticity. Even worse, the coherence length—the length given by the ratio of $\delta U/\delta|\psi|^2$ to $\delta U/\delta|\nabla\psi|^2$, which determines how rapidly the order parameter can vary and thus how large a vortex core is—is of order a few Å, so that no channel through which He can flow is too small to contain a vortex. All this means that the useful idealization in superconductivity of the "ideal Josephson junction," a weak link between two reservoirs having constant phase, is probably not relevant to the helium case. Any barrier in which the flow occurred only by quantum-mechanical tunneling would have to be of subatomic dimensions, especially in thickness, to permit any measurable current to flow, and could not be supported mechanically. Any attempt to replace the ideal junction by a thin channel, on the other hand, runs into exactly the same difficulties that are encountered with long thin bridges in the case of superconductivity,[23,19] namely, that the device acts like a

[23] R. D. Parks and J. M. Mochel, Rev. Mod. Phys. **36**, 284 (1964).

CC-0. In Public Domain. Gurukul Kangri Collection, Haridwar

Digitized by Arya Samaj Foundation Chennai and eGangotri

sequence of weak links in series and one is never sure exactly where the phase rigidity is breaking down. The closest approximation we could imagine to a single definable "weak superfluid junction" was the orifice geometry, which is analogous to the "short" thin film bridge of Anderson and Dayem[19] in superconductivity.

Let us analyze this system in some detail, as we did the Josephson junction previously.[3] First, a note as to the driving term to be inserted to represent any externally applied conditions. In the case of normal systems it is natural to place the ends of a specimen in contact with reservoirs at different chemical potential levels μ_1, μ_2, giving an "applied" potential gradient $\nabla\mu$, and to describe any situation in terms of solutions of the resulting applied field problem; we calculate J as a function of the pressure gradient or field, even though actually we may be driving the system with a constant current generator. The microscopic theory is done by inserting μN terms into the Hamiltonian, as is well-understood in the calculation of resistance, for instance, or thermoelectric power.

It is precisely the nature of superfluids that they cannot assume a stationary state under a field or pressure gradient, but will, as explained by Anderson, Werthamer, and Luttinger,[15] have to be described by phases with a time dependence obeying (13). This condition follows when we insert the appropriate μN terms, as there described; but that does not lead to a way to discuss the equally interesting case of an imposed current. One obvious technique is to impose a fixed phase difference by postulating an infinitely tight coupling to reservoirs consisting of large superfluids of fixed phase, but that is often quite unphysical. We have used without discussion[3] the technique of inserting a term

$$\Delta E = J_{12}(\phi_1 - \phi_2)$$

in the energy to describe the effect of a fixed supercurrent J_{12} between regions 1 and 2. In superconductivity a rather rough physical derivation of this can be given in terms of the electromagnetic interaction between J and the magnetic flux of a vortex line. It is analogous to, but more general than, the technique of inserting a $p\cdot v_s$ term sometimes used to derive the hydrodynamic equations.

In the case of He we may return very simply to Eq. (19). We showed that the particle accumulation rate dN_1/dt in a volume element ΔV_1 is given by:

$$dN_1/dt = \hbar^{-1}(\partial U/\partial\phi_1).$$

If no net accumulation is to occur, and if the current leaving ΔV_1 to neighboring elements is given in terms of the coupling energy between them by

$$J_{12} = dN_1/dt)_{\text{into superfluid}} = \hbar^{-1}(\partial U_{\text{coupling}}/\partial\phi_1)$$

there must be a compensating term

$$dN_1/dt)_{\text{current generator}} = -\hbar J_{12}\phi_1.$$

Similarly, to make the corresponding current leave element (2) we must have $dN_2/dt)_{\text{c.g.}} = \hbar J_{12}\phi_2$ so we may represent a constant current generator by

$$\mathcal{H}_{\text{gen}} = \hbar J_{12}(\phi_2 - \phi_1). \tag{26}$$

Using this let us discuss the orifice problem in the presence of a constant driving current. Current acceleration can be important only on the time-scale of the U-tube oscillations, which is usually longer than the time necessary to create a vortex or otherwise change the phase but can be included if desired. Also, it will greatly simplify one's thinking without falsifying any important physical features to assume $T\to 0$; i.e., only incompressible, superfluid flows.

Under these conditions $\hbar/m\nabla\phi = v_s$ and

$$\nabla\cdot v_s = 0$$

so

$$\nabla^2\phi = 0.$$

Thus we can solve for the flow in the absence of vortices by a simple potential calculation. Let the radius of the orifice be a. The equipotentials and streamlines are along coordinate surfaces in a set of oblate spheroidal coordinates, defined in terms of cylindrical coordinates r, θ, z through the axis of the orifice by

$$\begin{gathered}(r^2/a^2\cosh^2 u) + (z^2/a^2\sinh^2 u) = 1;\\ (r^2/a^2\sin^2 v) - (z^2/a^2\cos^2 v) = 1;\\ \theta = \theta;\\ -\infty \le u \le \infty, \qquad 0 \le v \le \pi/2, \qquad 0 \le \theta < 2\pi;\end{gathered} \tag{27}$$

or

$$\begin{aligned} r &= a\cosh u \sin v\\ z &= a\sinh u\cos v. \end{aligned} \tag{28}$$

The potential (i.e., phase) is

$$\phi(r, z) = C\int\frac{du}{\cosh u} = 2C\tan^{-1}e^u, \tag{29}$$

so that the total phase difference between the two large reservoirs separated by the orifice is

$$\phi_1 - \phi_2 = \pi C = \phi(+\infty) - \phi(-\infty). \tag{30}$$

The velocity is in the "u" direction and is

$$v_s = \frac{\hbar}{ma}\frac{C}{\cosh u(\sinh^2 u + \cos^2 v)^{\frac{1}{2}}}. \tag{31}$$

Some special values of the velocity field are:

Along the axis:

$$r = 0, \qquad \sin v = 0, \qquad z = a\sinh u$$

$$v_s = \frac{\hbar C}{ma}(\cosh u)^{-2} = \frac{\hbar C}{m}\frac{a}{a^2 + z^2}. \tag{32a}$$

CC-0. In Public Domain. Gurukul Kangri Collection, Haridwar

Digitized by Arya Samaj Foundation Chennai and eGangotri

In the orifice:

$$z=0, \qquad r=a\sin v, \qquad u=0$$

$$v_s=(\hbar/m)[C/(a^2-r^2)^{\frac{1}{2}}]. \tag{32b}$$

On the plane:

$$r=\pm a\cosh u, \qquad \cos v=0$$

$$v_s=(\hbar C/mr)[a/(r^2-a^2)^{\frac{1}{2}}]. \tag{32c}$$

The total particle flow is

$$J=\frac{\rho}{m}\int v_s\cdot dS=\frac{2\pi\hbar Ca\rho}{m^2}=\frac{2\hbar a\rho}{m^2}(\phi_1-\phi_2), \tag{33}$$

[using (30)] and the total kinetic energy is

$$K=\tfrac{1}{2}\rho\int v_s^2\,d\tau$$

$$=\tfrac{1}{2}\rho\frac{\hbar^2}{m^2}\int(\nabla\phi)^2\,d\tau$$

$$=\tfrac{1}{2}\rho\frac{\hbar^2}{m^2}\left(\int dS_{+\infty}\cdot-\int dS_{-\infty}\cdot\right)\phi\nabla\phi$$

$$K=\tfrac{1}{2}J\hbar(\phi_1-\phi_2)=(\rho a/m)[\hbar^2(\phi_1-\phi_2)^2/m]. \tag{34}$$

Thus this energy is a quadratic function of the phase difference $(\phi_1-\phi_2)$. However, it is essential to realize that this is only one branch of a multiple-valued function, because by gauge invariance K must be a periodic function of $\phi_1-\phi_2$ with period 2π. That is, if we were to pin down the phases in the two reservoirs by coupling to reservoirs of fixed relative phase $(\phi_1-\phi_2)_0$ we could satisfy the boundary conditions by any flow

$$J=(2\hbar a\rho/m^2)[(\phi_1-\phi_2)_0\pm 2n\pi]$$

and the corresponding kinetic energy

$$K=(\rho a/m)(\hbar^2/m)[(\phi_1-\phi_2)_0\pm 2n\pi]^2. \tag{34}$$

Equation (34) must also be used, then, in the presence of a current generator (27); thus the total energy is

$$E=(\rho a\hbar^2/m^2)[(\phi_1-\phi_2)\pm 2n\pi]^2-\hbar J_{12}(\phi_1-\phi_2). \tag{35}$$

This energy considered as a function of $\phi_1-\phi_2$ has an infinity of points of metastable equilibrium where

$$J=J_{12}$$

$$(\phi_1-\phi_2)=2n\pi+(m^2J_{12}/2\hbar a\rho).$$

$$E=-J_{12}[nh+(m^2J_{12}/4a\rho)]. \tag{36}$$

The situation is diagrammed in Fig. 2. The first drawing assumes a small current generator, $J_{12}<h a\rho/m^2$, which is the current value when $\phi_1-\phi_2=\pi$, the value at which the parabolas cross. For this current, although none of the energy minima are truly stable each is at least the lowest energy state for a given fixed phase difference (this has not been proved but seems obvious).

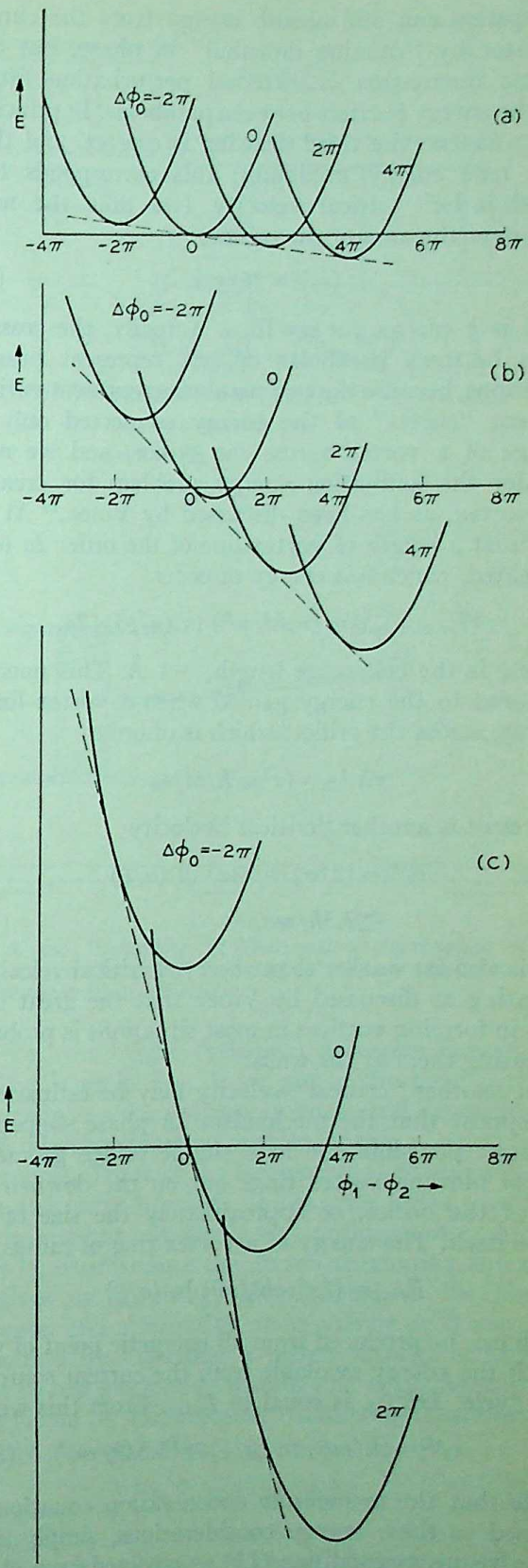

FIG. 2. Energy parabolas for potential flow in an orifice as a function of relative phase for different constant current generators J_{12}. $(\Delta\phi)_0$ is the relative phase "slippage" defined by $E(\Delta\phi_0)=J_{12}\Delta\phi_0$. (a) Low current; (b) $J_{12}\simeq v_c^0$; (c) J_{12} approaching observed critical current.

CC-0. In Public Domain. Gurukul Kangri Collection, Haridwar

Digitized by Arya Samaj Foundation Chennai and eGangotri

The system can still absorb energy from the current generator by "running downhill" in phase, but only if some fluctuation or external perturbation lifts it over the energy barriers between parabolas. In principle, if $J_{12}>h a\rho/m^2$ the third drawing is correct, and there is no true energy minimum; this corresponds to a "zeroth-order" critical velocity (we take the mean value over the area of the orifice)

$$(v_s)^0=2\hbar/ma \tag{37}$$

which is $\frac{1}{3}$ cm/sec for $a=10$ μ. Actually, the crossing points between parabolas do not represent possible transitions, because the two parabolas represent entirely different "sheets" of the energy connected only by passage of a vortex across the orifice, and we must consider the activation energy problem for creation of a vortex, as has been discussed by Vinen.[24] At the very least a length of vortex line of the order $2a$ must be created, which has energy of order

$$(E_{\text{vortex}})_{\min}=(\pi\rho\hbar^2/m^2)\ln(a/\xi)\times 2a,$$

where ξ is the coherence length, ~ 1 Å. This must be compared to the energy gained when a vortex line is halfway across the orifice, which is of order

$$\pi\hbar J_{12}=(\pi^2\rho a^2\hbar/m)v_s.$$

The result is another "critical" velocity

$$v_s^{(1)}=(2/\pi)(\hbar/ma)\ln(a/\xi)$$
$$\cong 7.5\hbar/ma. \tag{37'}$$

This is also far smaller than observed critical velocities, indicating as discussed by Vinen that the great difficulty in forming vortices in most situations is probably nucleating them at the walls.

Yet another "critical" velocity may be estimated if we suppose that the mechanism for phase slippage is the most plausible one in a simple orifice geometry, that of blowing vortex rings out on the downstream side of the orifice, of approximately the size of the orifice itself. The energy of a vortex ring of radius a is

$$E_{\text{ring}}=(2\pi^2\rho a\hbar^2/m^2)\ln(a/\xi)$$

which can be produced from an energetic point of view only if the energy available from the current source in each cycle, $2\pi\hbar J_{12}$, is equal to E_{ring}. From this we get

$$v_s^{(2)}=(\hbar/ma)\ln(a/\xi)\cong 11.5(\hbar/ma). \tag{37''}$$

[Note that the momentum conservation equation, as opposed to these energy considerations, simply gives us the frequency condition (13) as expected from (15)].

The essential physical point here is that all of these "critical" velocities are much less than real observed superflow velocities, indicating that in all cases the generation and motion of vortices is controlled by large random fluctuations, presumably either in the generation near the walls or in the motion of vortices already present. In general, the working point of an orifice is found to be not near the lowest intersection of two energy curves, where

$$v_s=2\hbar/ma \quad \text{and} \quad (\phi_2-\phi_1)_0=\pi,$$

but at a phase-difference of the order of 10π, where the energy available is much greater than that necessary to form a vortex and thus we may expect rather irregular and unstable behavior. When vortices are created under such conditions they are accelerated rather strongly and give up considerable energy to the normal excitations.

It is because of this large value of the phase difference that the orifice geometry—and, correspondingly, to a lesser extent superconducting thin film bridges—are more difficult to demonstrate spacial interference effects with than the Josephson tunnel junction, for which the system moves adiabatically from one energy minimum to the next, 2π away, whenever that is energetically possible. Incidentally, it is clear that since v_c is not very dependent on channel length, the total phase difference for a long channel at v_c is even greater than for a short one, and as a result even more randomness in the creation of vortices and even less sensitivity to the precise value of phase difference is to be expected for long channels.

It is probably for these reasons that of all the macroscopic quantum interference effects, only the driven ac experiment has as yet succeeded in He. This experiment depends on the principle of synchronization, in which a strong external ac signal is introduced which can override the internal fluctuations.

First let us consider a free-running orifice connecting two reservoirs with a height difference Z. This height difference will decrease at a rate

$$\frac{dZ}{dt}\equiv\frac{J\rho}{mA}=v_s\left(\frac{\pi a^2}{A}\right), \tag{38}$$

where A is the area of the surface in the smaller reservoir. J also determines the rate of generation of vortices; if J is greater than the observed J_c, vortices will be generated very rapidly, and conversely; but actually of course there is a functional dependence of the rate on the current:

$$dn/dt=f(v_s) \tag{39}$$

which will be rather steep, as shown in Fig. 3(a), but at least finite at very low v_s. Finally, we have the Josephson relation (13):

$$mgZ=-h(dn/dt)=-hf[(A/\pi a^2)(dZ/dt)]. \tag{40}$$

Equation (40) neglects the possibility of phase change by acceleration, i.e., it really contains a term in dJ/dt or d^2Z/dt^2, which will have no effect in the mean but does lead to the U-tube oscillations. If f were a step

[24] W. F. Vinen, *Proceedings of the International School of Physics "Fermi" (Varenna) 1961*, edited by G. Careri (Academic Press Inc., New York, 1963), p. 336.

CC-0. In Public Domain. Gurukul Kangri Collection, Haridwar

Digitized by Arya Samaj Foundation Chennai and eGangotri

function, dZ/dt would be fixed and the height difference would decay linearly, but presumably f is somewhat "soft," and as Z decreases the decay rate will do so also, but perhaps less slowly. Figure 3(b) shows a hypothetical decay curve which fits qualitatively with the vortex generation rate shown in 3(a).

Now suppose that as the height difference drops, we are causing an ac flow to be superimposed on the dc. During half the cycle we will be increasing the tendency to form vortices, during the other half decreasing it. When the height difference is such that $dn/dt = h\nu$, one vortex per cycle will be formed—presumably in the positive half-cycle, with quite high probability. When formed it uses up some considerable fraction of the available energy so another cannot be formed immediately; thus there will be a strong tendency for exactly one vortex per cycle to be formed, since the second half-cycle is not available. Because of (40) this will mean a tendency to fixed Z, i.e., a plateau in dn/dt [Fig. 3(a)] and thus in Z. Another way of putting it is that when the vortex formation is in a definite phase relationship with the ac signal, power can be transferred from the ac generator to the system as a whole, enough power to appreciably change the flow rate. If the alternating current is larger than the dc—as in our experiment[12]—clearly it is quite possible to stop the dc flow entirely, because we can control vortex formation wholly with the ac.

I have found a very simple mechanical analogy useful for understanding the ac Josephson effect. (See Fig. 4.) The relative phase of the two reservoirs I think of as the angular position coordinate ϕ of a set of locomotive wheels, and the velocity of the locomotive is the height difference Z; the ratio of position to phase is then the radius of the wheels corresponding to h/mg. The equation (40) for the rate of generation of vortices as a function of the flow (acceleration) may be inverted to give an effective nonlinear frictional force on the "locomotive"

$$\frac{A}{\pi a^2}\frac{dZ}{dt} = -f^{-1}\frac{mgZ}{h} = -f^{-1}\left(\frac{dn}{dt}\right). \qquad (41)$$

If f is a step function, this gives a constant frictional force—i.e., the height (velocity) decreases linearly to zero. If f is as in Fig. 3, we get a "braking" action which leads to a decay between linear and exponential. It is an oversimplification to think of this as a constant force in time. Think of the locomotive as having square wheels and rusty bearings, so that the losses occur in some definite but not simple way during each cycle.

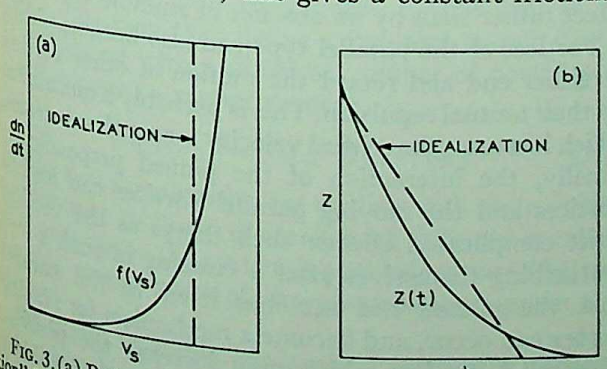

FIG. 3. (a) Rate of vortex formation as a function of v_s. "idealization" is the sharp critical current assumption; reality is probably more like $f(v_s)$ shown. (b) Decay of a helium head through an orifice or channel for critical current idealization and real situation.

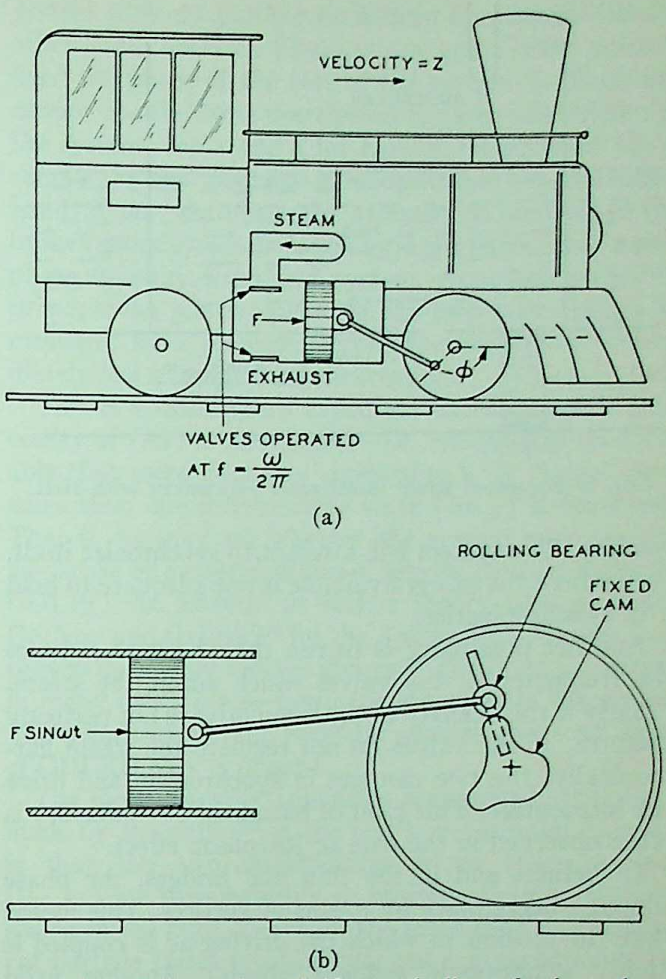

FIG. 4. (a) Illustration of "locomotive" mechanism of ac Josephson-type effect. (b) "Locomotive" system which could be driven at submultiple velocities.

Now let us introduce the driven alternating current. This gives us an energy proportional to the phase coordinate, and alternating at frequency ω; it may be schematized by attaching a piston through a simple linkage to our locomotive wheels, and applying a force on the piston by (for instance) admitting steam intermittently at a rate $\omega/2\pi$:

$$F = F_0 \cos(\omega t + \phi_0). \qquad (42)$$

(See Fig. 4.)

As we very well know, such an alternating force is capable of keeping the locomotive going at a steady velocity Z if it is large enough, and if

$$\omega = 2\pi(dn/dt),$$

i.e., the force is applied once per revolution of the wheels. Also, as is less well-known but obvious, this mechanism can act as a brake or an accelerator at this

CC-0. In Public Domain. Gurukul Kangri Collection, Haridwar

Digitized by Arya Samaj Foundation Chennai and eGangotri

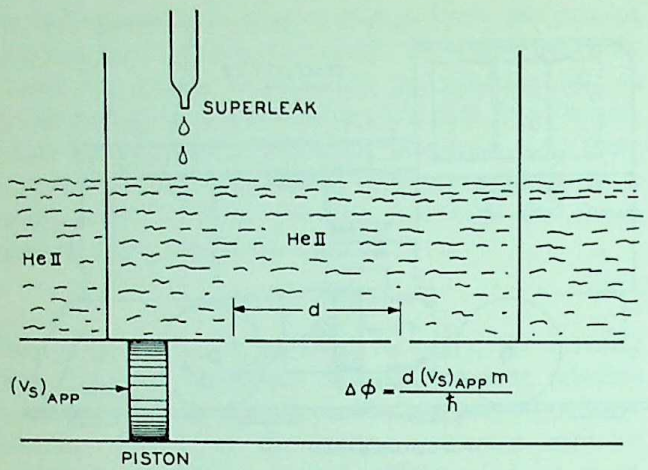

FIG. 5. Suggested space interference experiment with HeII.

velocity. The system will attempt to synchronize itself, even where the power available is not adequate to hold it in synchronization.

Another possibility is to run the wheels at n times the frequency of the valves which admit the steam. Clearly if the velocity of the locomotive is not perfectly uniform, or the valves do not regulate the steam harmonically, the two can run in synchronism and drive the locomotive. This kind of harmonic ($V=n\hbar\omega/2e$) is often observed in the true ac Josephson effect.

In helium and in the thin film bridges, the phase slippage takes place by means of vortices. This means that the motion to which the driving ac is coupled is highly anharmonic (square wheels). Another valid schematization of this is to make the piston linkage highly anharmonic—let it roll on a queer-shaped cam, for instance [see Fig. 4(b)]. Then not only can the wheels be driven faster than the frequency of the force, but also they can be driven at subharmonics, since, for example, the vortex may be formed only every nth cycle of the driving current. Thus we expect and observe both harmonics and subharmonics, in the Anderson–Dayem and Richards–Anderson experiments.[12,19]

Both of these experiments, for final quantitative description, must wait for quantitative theoretical treatments of the generation and motion of vortices. But the basic principle of phase synchronization of the external signal with the relative phase of the order parameter in the reservoirs is independent of detailed mechanism.

As for spacial interference experiments, the most promising seems to be the orifice analog of the Mercereau "current" experiment.[25] Here one drives a supercurrent through two orifices in parallel, and at the same time causes a superflow past the orifices on one side (see Fig. 5).

The second superflow enforces a phase difference $\Delta\phi$ at the two orifices on one side so that both orifices cannot simultaneously be at metastable minima of their energy curves (see Fig. 2), unless that phase difference is $2n\pi$. Another way of putting it is that the circulation through the two orifices must be quantized, leading to an additional circulating current which may aid breakdown (vortex creation) at one or both orifices. This effect would be periodic in the phase. Unfortunately it is very sensitive to fluctuations and instabilities.

A phenomenon in which the idea of phase slippage must play an important role is the superfluid creep of films. It has been suggested that vortices form at the critical velocity with axes parallel to the film and perpendicular to the flow.[13] That is almost certainly correct—it gives dimensionally the correct critical velocity, which again is of order $\sim 10\hbar/md$. However I would speculate somewhat differently on certain details.

First, the motion of the vortices. Examination of typical estimates indicates that the frictional forces on He vortices allow them to move with a velocity component parallel to the Magnus force of about 10^{-5} of the flow velocity. Thus vortices of the type postulated above will be generated at the solid surface and move out of the film into the free surface only a few thousand Å downstream (or vice versa, but this seems less likely). This will be the predominant dissipative mechanism if it occurs. It is hard to believe that vortex flow into the bulk fluids at either end can play an important role in a direct fashion.

There is, however, a somewhat more subtle question to be considered. If we are to take seriously the usual vortex creation critical velocity expression, h/md, it is not obvious that the smaller dimension of the film is really the value of d which must be considered. Why do not vortices form perpendicular to the film and move across it from one edge to the other? While at velocities $\sim h/mW$, where W is the width of the film ~ 1 cm (velocities $\sim 10^{-3}$ cm/sec) one would expect the formation of such vortices to be difficult dynamically, at velocities of 10^2–10^3 times that, still small compared with critical film velocities, there appears to be no such process at work.

It is suggested here that the predominant mechanism in film flow is the *pinning* of such vortices by surface flaws and thin spots in the film. Thus the film is a "hard superfluid": its flow is maintained by a pinning effect rather than by an absence of suitable vortices.

Vortices of the parallel type can also become pinned at either end and retard the motion of other vortices by their mutual repulsion. This is probably a mechanism which increases the critical velocity for rough substrates. Finally, the interaction of the pinned perpendicular vortices and the moving parallel vortices can lead to quite complicated effects: such things as the vortices reattaching themselves after a crossing in such a way that the pinned end attaches itself to the parallel vortex can occur, and become a mechanism for pinning of parallel vortices which may increase the pinning and thus the critical velocity, as a function of the vorticity flowing into the film from the bulk liquid. Another mechanism which may play a role is motion of the free end of a pinned perpendicular vortex under

[25] R. C. Jaklevic, J. Lambe, J. E. Mercereau, and A. H. Silver, Phys. Rev. **140**, A1628 (1965).

CC-0. In Public Domain. Gurukul Kangri Collection, Haridwar

Digitized by Arya Samaj Foundation Chennai and eGangotri

the Magnus force until it becomes a pinned parallel vortex. This could be a copious source of vorticity.

In conclusion, then, the fundamental point made here is that in helium II, as in superconductivity, the Josephson equation and the associated concept of phase slippage are the most fundamental and exact consequences of our present theoretical understanding of superfluidity. Where phase slippage in superconductivity can occur in the absence of identifiable flux quanta, in helium with present technology it will always involve vortex lines because their core size is only a few Å, and no tunneling medium is available. Thus the crucial problem in helium flow is to find the vortex lines and study how they move across the flow path into the walls or disappear into the bulk. The complicated dynamics of vorticity is beyond the scope of this paper; we have merely speculated, with little quantitative study, in order to present concrete examples of the central ideas.

ACKNOWLEDGMENTS

I have benefitted throughout from the close collaboration of P. L. Richards. Discussions with P. C. Hohenberg, J. M. Luttinger, and W. L. McMillan were of value. A suggestion of D. J. Scalapino was reworked into the form of the space-interference experiment using orifices suggested in Sec. III. Questions asked by F. Reif and P. A. Wolff stimulated the first part of the work.

APPENDIX A. ODLRO VS MACROSCOPIC PARTICLE FIELDS

As explained in the introduction, Penrose's initial definition of the order parameter[4] in terms of a large eigenvalue of the density matrix was later extended by Beliaev,[5] by Gor'kov[6] (in terms of Green's functions), and a generalization conveniently named "off-diagonal long-range order" (ODLRO) by Yang.[20] That is, one writes

$$\langle 0_N \mid \psi^*(x)\psi(x') \mid 0_N \rangle = \sum_n \lambda_n f_n^*(x) f_n(x') \quad \text{(A1)}$$

and "ODLRO" is present when $\lambda_1 \sim N$, giving a contribution to the sum comparable to the sum of all others. One may then define a "ground state" $\langle 0_{N-1} \mid$ of the system with a different number of particles so that f_1 becomes a matrix element

$$[\lambda_1 f_1(x)]^{\frac{1}{2}} = \langle 0_{N-1} \mid \psi(x) \mid 0_N \rangle. \quad \text{(A2)}$$

In this way the necessity for dealing with states which are coherent mixtures of states with different numbers N of particles in the system is avoided, apparently, and for this reason most of the above authors prefer this scheme.

We argue that this approach is physically unnecessary, though valid, and occasionally inconvenient. For one, this definition does not permit convenient subdivision of a system. The over-all phase of f_1 is quite arbitrary—as it correctly should be for an isolated system with no particle exchanges permitted. On the other hand, once the phase at any space–time point is fixed the phase of the rest of the system is. Thus one cannot use the same description for any subdivision of the system; the λ and f for half of a bucket of He II simply do not describe it adequately. On the other hand, if one abandons the attempt to hold on to the broken gauge symmetry and ascribes a fixed, measurable phase to every superfluid system, recognizing that in principle the relative phase of any two may always be measured by a Josephson-type experiment, one immediately has a usable local description.

This is a satisfactory expedient unless the full generality of (A1) is meaningful—i.e., unless it is conceivable that more than one eigenvalue λ_1 is "large" and more than one intermediate state $\mid 0_{N-1} \rangle$ is involved. That is, we may ask whether the system may ever in any sense be a superposition of several distinct types of ODLRO. An attempt at such a theory was made by Gor'kov and Galitskii[26] for the d-state BCS theory, and proven invalid by various groups.[27] The question enters in many other cases—even, for example, in discussing flux quantization, one must be assured that one type of ODLRO only is present.

The most generally applicable argument here is that made by the author[28] in the Gor'kov–Galitskii case. It is that the two intermediate states $\mid 0_{N-1,1} \rangle$ and $\mid 0_{N-1,2} \rangle$ are demonstrably in entirely distinct Hilbert spaces in the limit $N \to \infty$, in the sense that $\sim N$ different particle states must be changed a finite amount to get from one to the other. Thus the $\mid 0_N \rangle$ state must be simply a superposition of a $\mid 0_{N,1} \rangle$ state communicating with $\mid 0_{N-1,1} \rangle$ and a $\mid 0_{N,2} \rangle$ state, and no interference effects whatever can connect the two types of states. In particular, every measurable quantity—energy, current, etc.—is the simple linear superposition of the two values. Then such a state is no more meaningful than Schrödinger's famous superposition of the quantum states of a dead cat and a live cat: a possible mathematical description of a physical absurdity.

APPENDIX B. A "NEW" COROLLARY IN CLASSICAL HYDRODYNAMICS?

Euler's equation of motion in a classical ideal fluid is

$$(\partial v/\partial t) + \nabla[(v^2/2) + \mu] = v \times \nabla \times v. \quad \text{(B1)}$$

μ is an appropriately defined chemical potential per unit mass. We now consider a general flow and draw a path C entirely inside the fluid—otherwise general—between two points P_1 and P_2 in the fluid. Points P_1 and P_2 are to be thought of eventually as being in reasonably quiet regions where the flow is steady over a long time T.

---

[26] L. P. Gor'kov and V. M. Galitskii, Zh. Eksperim. i Teor. Fiz. **40**, 1124 (1961) [English transl.: Soviet Phys.—JETP **13**, 792 (1961)].

[27] D. Hone, Phys. Rev. Letters **8**, 370 (1963); R. Balian, L. H. Nosanow, and N. R. Werthamer, *ibid.* **8**, 372 (1962).

[28] P. W. Anderson, Bull. Am. Phys. Soc. **7**, 465 (1962).

CC-0. In Public Domain. Gurukul Kangri Collection, Haridwar

Digitized by Arya Samaj Foundation Chennai and eGangotri

Let us now perform two integrations on (B1): first, along C from P_1 to P_2

$$\int_{P_1(C)}^{P_2} \frac{\partial v}{\partial t}\, d\mathbf{l} + (\tfrac{1}{2}v^2+\mu)_{P_1}^{P_2} = \int_C (v \times \nabla \times v)\, d\mathbf{l}. \quad \text{(B2)}$$

[It was brought out in the discussions of the conference that (B2) is even more general than I had thought, in that most types of viscosity terms which might be added to (B1) involve gradients, so that if viscosity is not acting at P_1 and P_2 they cancel out.]

Second, we integrate over a very long time interval T and divide by T, thus taking a time mean value as is done in the virial theorem:

$$\int_{P_1}^{P_2} d\mathbf{l}\, T^{-1} \int_0^T \frac{\partial v}{\partial t}\, dt + \left\langle \left(\frac{v^2}{2}+\mu\right)_{P_2} \right\rangle_{\text{Av}} - \left\langle \left(\frac{v^2}{2}+\mu\right)_{P_1} \right\rangle_{\text{Av}}$$
$$= T^{-1} \int_0^T 2 \int d\mathbf{l} \cdot (v \times \omega). \quad \text{(B3)}$$

We have defined ω, the vorticity, as $\frac{1}{2}\nabla \times v$ and written the time mean value at the points of steady flow in an obvious notation. The first term on the left-hand side is

$$T^{-1}\left[\left(\int_C v \cdot d\mathbf{l}\right)_T - \left(\int_C v \cdot d\mathbf{l}\right)_0\right].$$

We define a "quasi-steady" flow as one in which this difference increases less rapidly than T; almost any turbulent flow one wishes to consider, or periodic flow, etc. will satisfy this condition. Then as far as time mean values are concerned we arrive at the basic corollary of Euler's equation:

$$\langle (\tfrac{1}{2}v^2+\mu)_{P_2} \rangle_{\text{Av}} - \langle (\tfrac{1}{2}v^2+\mu)_{P_1} \rangle_{\text{Av}} = \left\langle 2 \int_{P_1}^{P_2} d\mathbf{l} \cdot (v \times \omega) \right\rangle_{\text{Av}}. \quad \text{(B4)}$$

It is easy to interpret the quantity on the right-hand side. Writing v as dr/dt, the particle velocity, this is

$$2 \int_{P_1}^{P_2} (d\mathbf{l} \times d\mathbf{r}/dt) \cdot \omega,$$

which is the *rate at which vorticity is being carried across the curve* C by the particle motion. Thus

$$\langle \Delta[(v^2/2)+\mu] \rangle_{\text{Av}} = \langle 2\text{“}(d\omega/dt)\text{”} \rangle_{\text{Av}}. \quad \text{(B5)}$$

We see immediately that this equation is far more important in a superfluid, where vorticity is conserved and quantized, than it is in ordinary fluids, where in a laminar flow, for instance, the right-hand side has little or no special significance. In helium, in fact, by turning to the integrated form of (B1) involving the potential we get the detailed Josephson equation without the special assumptions necessary here.

A number of somewhat surprising consequences immediately appear. One example is that the Pitot tube,[29] for instance, must involve transport of vorticity and thus motion of vortex lines in liquid He II. Ordinary aerodynamic lift and drag also would do so if the surface condition were $v=0$, but of course it is not; the vorticity there can be thought of as all in the surface layer outside the superfluid and thus not quantized.

I have tried at length to find a clear statement of (B4–5) in the classical literature, including the voluminous works of Rayleigh and Lamb, but have so far failed to find anything but corollaries and lemmas related to it. I will be pleased to hear from any reader who can find the theorem stated in this form; one can only assume that it was understood by the "classics" but is of no value in classical hydrodynamics so was never stated.

[29] J. R. Pellam, Phys. Rev. **78**, 818 (1950).

CC-0. In Public Domain. Gurukul Kangri Collection, Haridwar

Digitized by Arya Samaj Foundation Chennai and eGangotri

REVIEWS OF MODERN PHYSICS VOLUME 38, NUMBER 2 APRIL 1966

Magnetic Electron Scattering from Nuclei

J. GOLDEMBERG
École Normale Supérieure, Laboratoire de l'Accelérateur Linéaire, Orsay (78), France

R. H. PRATT
Department of Physics, University of Pittsburgh, Pittsburgh, Pennsylvania

In this article we review the calculations and experimental information available in the studies of electron scattering (elastic and inelastic) from the magnetic-moment distribution of nuclei. The corresponding information on the properties of nucleons has been reviewed previously and is not discussed here. As usual in electron-scattering investigations we are concerned mostly with the determination of two functions of the momentum transfer, the charge and magnetic form factors or linear combinations of them, which are closely related to the spatial structure of the charge and magnetic-moment distributions. We specialize the discussion to the magnetic form factor and the nuclear properties connected with it.

I. Introduction 311
II. Structure of Cross Sections for Electron Scattering from Nuclear Targets 311
A. General Form 311
B. Proof 312
C. Interpretation 313
D. Connection with Photoabsorption 313
E. Extensions and Limitations 314
F. The Measurement of Magnetic Scattering 314
III. Extracting Information on Nuclear Structure 316
A. Bremsstrahlung at Large Angles 316
B. Radiative Corrections 319
IV. Interpreting Information on Nuclear Structure 319
A. General Remarks 319
B. Elastic Scattering 321
1. The Deuteron 322
2. H^3 and He^3 323
3. He^4 323
4. F^{19} 324
C. Inelastic Scattering in Levels 324
1. $M1$ Levels 325
2. $E1$ Levels 326
D. Quasielastic (Incoherent) Scattering 328

I. INTRODUCTION

In this article we review the calculations and experimental information available in the studies of electron scattering (elastic and inelastic) from the magnetic-moment distribution of nuclei. The corresponding information on the properties of nucleons has been reviewed previously (Refs. 1–3) and is not discussed here. As usual in electron-scattering investigations we are concerned mostly with the determination of two functions of the momentum transfer, the charge and magnetic form factors or linear combinations of them, which are closely related to the spatial structure of the charge and magnetic-moment distributions. We specialize the discussion to the magnetic form factor and the nuclear properties connected with it.

In Sec. II we discuss the general structure of scattering formulas and methods of measuring the magnetic cross section. The approximations of the theory and possible extensions are discussed briefly. In Sec. III methods of extracting information on nuclear structure are presented ("radiation tail" problems). In Sec. IV the connection between the information extracted in Sec. III and the nuclear properties (such as nuclear currents, nuclear magnetization, and exchange currents) are discussed separately for elastic, inelastic, and quasielastic scattering.[4]

[1] R. Hofstadter, Ann. Rev. Nucl. Sci. **7**, 231 (1957).
[2] R. Hofstadter, *Electron Scattering and Nuclear and Nucleon Structure*, a collection of reprints with an introduction (W. A. Benjamin, Inc., New York, 1963); R. Herman and R. Hofstadter, *High Energy Electron Scattering Tables* (Stanford University Press, Stanford, 1960). See also, T. A. Griffy and L. I. Schiff, "Electromagnetic Form Factors," to be published in the book *High Energy Physics*.
[3] L. N. Hand, D. G. Miller, and R. Wilson, Rev. Mod. Phys. **35**, 335 (1963).

II. STRUCTURE OF CROSS SECTIONS FOR ELECTRON SCATTERING FROM NUCLEAR TARGETS

A. General Form

For any process in which a single (virtual) photon interacts with a nucleus, as in the electron–nucleus scattering diagram of Fig. 1, the entire dependence of the cross section on nuclear properties can be described by two form factors, W_1 and W_2, which are functions of the invariant momentum transfer q^2 and the energy transfer[5] (or of q^2 and $q\cdot P$). This follows from the vector nature of the photons and electromagnetic current conservation; it also assumes an experimental situation in which the target is initially unoriented and all final nuclear states P' consistent with specified P, q are summed over (i.e., in the electron scattering process of Fig. 1 only the final electron p' would be detected).

Further, neglecting the mass of the electron, the cross section for electron scattering from a nuclear target can be given explicitly in the laboratory frame in terms of these form factors as[6]

$$\frac{d\sigma}{d\Omega' d\epsilon'}=\frac{4Z^2\alpha^2}{q^4}\frac{\epsilon'^2}{M_T}\cos^2\tfrac{1}{2}\theta[W_2+2W_1\tan^2\tfrac{1}{2}\theta], \quad (1)$$

where θ is the scattering angle, M_T the mass of the

[4] For a more detailed review of nuclear structure and inelastic electron scattering see T. de Forest and J. D. Walecka, Advan. Phys. (to be published).
[5] S. D. Drell and J. D. Walecka, Ann. Phys. (N.Y.) **28**, 18 (1964).
[6] We use the notation $\hbar=c=m=1$, with m the rest mass of the electron.

CC-0. In Public Domain. Gurukul Kangri Collection, Haridwar

Digitized by Arya Samaj Foundation Chennai and eGangotri

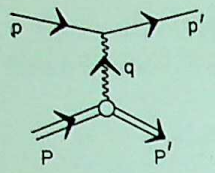

FIG. 1. Diagram for an electron–nucleus interaction. p and p' are the initial and final momentum of the electron, P and P' the initial and final momentum of the nucleus, and q the momentum transfer.

target, ϵ and ϵ' the initial and final electron enegies, and the 4-momentum transfer $q^2=4\epsilon\epsilon'\sin^2\frac{1}{2}\theta$, $q\cdot P=M_T(\epsilon-\epsilon')$. The objective of such experiments is the determination of these form factors, W_1 and W_2, and their theoretical interpretation in terms of nuclear models.

If one does not neglect the electron mass, the factors that multiply the form factors in Eq. (1) become slightly more complicated (see below). If one considers a process in which the electron lines of Fig. 1 may be virtual, as in bremsstrahlung or pair production, the factors become appreciably more complex (Sec. IIIA), but the cross section is still of the form AW_1+BW_2, where the factors A and B can be given explicitly and all information on nuclear structure continues to reside in W_1 and W_2. Equation (1) is equally applicable to electron, positron, and muon scattering from a nucleus; for a given nucleus the *same* form factors W_1 and W_2 should be used in all three cases.

B. Proof

For completeness we indicate here the proof of the foregoing statements, following the treatment of Drell and Walecka.[5] We adopt the following notations[7]: P denotes the initial 4-momentum of the target, $P^2=-M_T^2$. q is the 4-momentum of the virtual photon, and $P'=P+q$ is the final 4-momentum of the target. We assume that the target is initially unoriented and that experimentally *all final nuclear states* consistent with the given kinematic conditions (given q and P) are summed over. In this case, the contribution of the nuclear part of the process indicated in Fig. 1 is given by

$$W_{\mu\nu}=\frac{(2\pi)^3\Omega}{(Ze)^2}\bar{\sum_{\text{initial states}}}\sum_{\text{final states}}\delta^{(4)}(P-P'+q)\langle P\mid J_\nu(0)\mid P'\rangle \times\langle P'\mid J_\mu(0)\mid P\rangle(E), \quad (2)$$

where Ω is the normalization volume, E is the initial energy of the target, $\bar{\Sigma}$ indicates an average over the initial target states (i.e., M_J of the target), $\mid P\rangle$ and $\mid P'\rangle$ are the Heisenberg state vectors of the initial and final nuclear states (that is they are eigenstates of the nuclear 4-momentum operator P_μ), and $J_\mu(0)$ is the electromagnetic current operator of the nucleus at the space–time point $x_\mu=0$. The four-dimensional delta function summarizes the translation invariance of the theory. Lorentz invariance tells us that $W_{\mu\nu}$ must be a second-rank tensor since the current operator is a 4-vector. Because of the sum over initial and final states, there are only two 4-vectors on which this tensor can depend, P and q. Since $P^2=-M_T^2$, there are only two independent scalars which can be formed from these 4-vectors, q^2 and $q\cdot P$. Thus the most general form of the tensor $W_{\mu\nu}$ is

$$W_{\mu\nu}=A(q^2,q\cdot P)\delta_{\mu\nu}+B(q^2,q\cdot P)q_\mu q_\nu+C(q^2,q\cdot P)P_\mu P_\nu +D(q^2,q\cdot P)(q_\mu P_\nu+q_\nu P_\mu)+E(q^2,q\cdot P)(q_\mu P_\nu-q_\nu P_\mu). \quad (3)$$

No term in $\epsilon_{\mu\nu\rho\sigma}P_\rho q_\sigma$ can appear since the current operator is a polar vector under spatial reflections. We know further that the nuclear current operator must satisfy the continuity equation

$$(\partial/\partial x_\mu)J_\mu(x)=0, \quad (4)$$

which implies that $q_\mu W_{\mu\nu}=W_{\mu\nu}q_\nu=0$. These relations are sufficient to eliminate three of the invariant functions and one can thus write a symmetric tensor, with W_1 and W_2 both ≥ 0 according to the definition in Eq. (1)

$$W_{\mu\nu}=W_1(q^2,q\cdot P)\left(\delta_{\mu\nu}-\frac{q_\mu q_\nu}{q^2}\right) +W_2(q^2,q\cdot P)\frac{1}{M_T^2}\left(P_\mu-\frac{P\cdot q}{q^2}q_\mu\right)\left(P_\nu-\frac{P\cdot q}{q^2}q_\nu\right). \quad (5)$$

This theorem is due to Bjorken,[8] von Gehlen,[9] and Gourdin.[10]

In terms of W_1 and W_2 the electron or muon scattering cross section for fixed electron energy and angle but summing over all else can be computed in standard fashion:

$$d\sigma=2Z^2\alpha^2\frac{d\mathbf{p}'}{2\epsilon'}\frac{1}{q^4}W_{\mu\nu}N_{\mu\nu}\frac{1}{[(p\cdot P)^2-m^2M_T^2]^{\frac{1}{2}}}, \quad (6)$$

where

$$N_{\mu\nu}=-\tfrac{1}{2}\,\mathrm{Tr}\,\gamma_\mu(m-i\gamma\cdot p)\gamma_\nu(m-i\gamma\cdot p') =2[p_\mu p_\nu'+p_\nu p_\mu'-\delta_{\mu\nu}(p\cdot p'+m^2)]. \quad (7)$$

Combining gives

$$d\sigma=2Z^2\alpha\frac{d\mathbf{p}'}{2\epsilon'}\frac{1}{q^4}\frac{1}{[(p\cdot P)^2-m^2M_T^2]^{\frac{1}{2}}} \times\left\{2(q^2-2m^2)W_1+2\left[\frac{2(p\cdot P)[(p-q)\cdot P]}{M_T^2}-\tfrac{1}{2}q^2\right]W_2\right\}. \quad (8)$$

The three independent scalar functions in electron scattering can be taken as ϵ, ϵ', θ in the laboratory system or as the three scalar variables q^2, $p\cdot P$, and $q\cdot P$. Measurements at fixed q^2 and $q\cdot P$ can separate W_1 and W_2 and check the one-photon-exchange form.

[7] We use a metric such that $a_u=(\boldsymbol{a}, ia_0)$ and $a\cdot b=\boldsymbol{a}\cdot\boldsymbol{b}-a_0b_0$. In this metric $q^2>0$ for both scattering and pair production.

[8] J. D. Bjorken (unpublished).
[9] R. von Gehlen, Phys. Rev. **118**, 1455 (1960).
[10] M. Gourdin, Nuovo Cimento **21**, 1094 (1961).

CC-0. In Public Domain. Gurukul Kangri Collection, Haridwar

Digitized by Arya Samaj Foundation Chennai and eGangotri

The cross section can be written in the laboratory frame as

$$\frac{d\sigma}{d\Omega' d\,|\mathbf{p}'|}=\frac{2Z^2\alpha^2}{q^4}\left(\frac{\mathbf{p}'^2}{\epsilon'\,|\,\mathbf{p}\,|}\right)\frac{1}{M_T}\times[2(\epsilon\epsilon'-|\,\mathbf{p}\,||\,\mathbf{p}'\,|\cos\theta-2m^2)W_1+(\epsilon\epsilon'+|\,\mathbf{p}\,||\,\mathbf{p}'\,|\cos\theta+m^2)W_2],$$

where

$$-q\cdot P/M_T=\epsilon-\epsilon',$$
$$q^2=2\epsilon\epsilon'-2\,|\,\mathbf{p}\,||\,\mathbf{p}'\,|\cos\theta-2m^2. \quad (9)$$

These formulas simplify if one can neglect the mass of the electron

$$\frac{d\sigma}{d\Omega' d\epsilon'}=\frac{4Z^2\alpha^2}{q^4}\frac{\epsilon'^2}{M_T}\cos^2\tfrac{1}{2}\theta\times[W_2(q^2,q\cdot P)+2W_1(q^2,q\cdot P)\tan^2\tfrac{1}{2}\theta],$$
$$q^2=4\epsilon\epsilon'\sin^2\tfrac{1}{2}\theta. \quad (10)$$

C. Interpretation

Considering the electron–nucleus scattering cross section as a function of q^2, $q\cdot P$, and θ, it is clear that for fixed energy and momentum transfer to the nucleus an experiment at small electron-scattering angles is sensitive to the form factor W_2 and an experiment at large scattering angles is sensitive to W_1. Theoretical predictions for these form factors depend on a model for the nucleus. However, it is easy to see that W_1, measurable at large angles, is connected with the magnetic properties of the nucleus. Thus, in the case that we have only elastic scattering from the nucleus, $P'^2=-M_T^2$ and $2q\cdot P=q^2$, and a spin-zero target we have with the aid of Eq. (4)

$$(\Omega^2EE')^{\frac{1}{2}}\langle P'=p+q\,|\,J_\mu(0)/Ze\,|\,P\rangle=F(q^2)[P_\mu-(P\cdot q/q^2)q_\mu] \quad (11)$$

with $F(0)=1$. By substituting in the equation for $W_{\mu\nu}$ one finds

$$W_1=0,$$
$$W_2=|\,F(q^2)\,|^2(M_T^2/E')\,\delta(E-E'-q_0), \quad (12)$$

i.e., for a spin-zero nucleus (no magnetic moment) W_1 vanishes for elastic scattering. Similarly (Sec. IVA) one can show in the elastic scattering from a fixed nucleus that, for small momentum transfer q^2, W_1 is proportional to the magnetic moment of the nucleus. In elastic scattering from a fixed nucleus $F(q^2)$ is simply the Fourier transform of the charge distribution of the nucleus.

The Rosenbluth cross section for elastic scattering from a spin-$\frac{1}{2}$ target is also a special case of Eq. (9)

$$(\Omega^2EE')^{\frac{1}{2}}\langle P',\lambda'\,|\,J_\mu(0)/Ze\,|\,P,\lambda\rangle=iM_T\bar{u}_{\lambda'}(\mathbf{p}')[F_1(q^2)\gamma_\mu+F_2(q^2)\sigma_{\mu\nu}q_\nu]u_\lambda(\mathbf{p}) \quad (13)$$

in the usual Dirac notation with $F_1(0)=1$, $F_2(0)=\frac{1}{2}\lambda/M_T$ the anomalous magnetic moment. Inserting this in the equation for $W_{\mu\nu}$ one finds

$$W_1=q^2\,|\,\tfrac{1}{2}F_1(q^2)+M_TF_2(q^2)\,|^2\delta(E-E'-q_0)\,(E')^{-1}, \quad (14)$$

$$W_2=M_T^2[|\,F_1(q^2)\,|^2+q^2\,|\,F_2(q^2)\,|^2]\delta(E-E'-q_0)\,(E')^{-1}. \quad (15)$$

Inserting in Eq. (9) yields (integrating over ϵ')

$$\frac{d\sigma}{d\Omega'}=\frac{Z^2\alpha^2}{4\epsilon^2\sin^4\frac{1}{2}\theta}\cos^2\tfrac{1}{2}\theta\left[\frac{1}{1+(2\epsilon/M_T)\sin^2\frac{1}{2}\theta}\right]\times\{[|\,F_1\,|^2+q^2\,|\,F_2\,|^2]+(q^2/2M_T^2)\,|\,F_1+2M_TF_2\,|^2\tan^2\tfrac{1}{2}\theta\}, \quad (16)$$

which is the Rosenbluth result.[11]

Another method of analysis of electron scattering involves the separation of the cross section into contributions from longitudinal and transverse currents.[12] From $q_\mu W_{\mu\nu}=W_{\mu\nu}q_\nu=0$ and the similar relation for $N_{\mu\nu}$ one can eliminate all scalar terms in $N_{\mu\nu}W_{\mu\nu}$. In the laboratory frame there is no interference between longitudinal terms (along $\mathbf{q}$) and transverse terms:

$$N_{\mu\nu}W_{\mu\nu}=[1-(q_3/q_0)^2]^2N_{33}W_{33}+N_{tt'}W_{tt'}. \quad (17)$$

D. Connection with Photoabsorption

If the photon of Fig. 1 were real (and we dispense with the electron) we would be concerned with the total cross section σ_γ for absorption of a real photon. Our previous analysis of $W_{\mu\nu}$ in terms of form factors W_1 and W_2 would still be valid, except that here we would now have the condition $q^2=0$. The cross section is

$$\sigma_\gamma=\{(2\pi)^2Z^2\alpha[(q\cdot P)^2]^{-\frac{1}{2}}\}\tfrac{1}{2}W_{\mu\mu}\,|_{q^2=0}. \quad (18)$$

We can thus relate W_1 and W_2 evaluated at $q^2=0$ to σ_γ.

The expression Eq. (5) for $W_{\mu\nu}$ has no singularities when one sets $q^2=0$, as can be seen from Eq. (2), since the matrix elements are just the physical amplitudes for photoabsorption to individual final states. The apparent singularities in Eq. (5) hence must cancel as $q^2\to0$, whence one deduces

$$W_2\underset{q^2\to0}{=}O(q^2),\qquad W_1-[(P\cdot q)^2/q^2]W_2\underset{q^2\to0}{=}O(q^2);\qquad (W_{\mu\mu}=2W_1)_{q^2=0} \quad (19)$$

and hence

$$\sigma_\gamma=\{(2\pi)^2Z^2\alpha[(q\cdot P)^2]^{-\frac{1}{2}}\}W_1\,|_{q^2=0}. \quad (20)$$

For fixed energy transfer and small q^2 we can thus write the form factors W_1 and W_2 for electron–nucleus scattering in terms of the total photoabsorption cross section at the same energy transfer as

$$W_1=[(2\pi)^2Z^2\alpha]^{-1}[(q\cdot P)^2]^{\frac{1}{2}}\sigma_\gamma,$$
$$W_2=[(2\pi)^2Z^2\alpha]^{-1}\{q^2[(q\cdot P)^2]^{-\frac{1}{2}}\}\sigma_\gamma. \quad (21)$$

[11] M. N. Rosenbluth, Phys. Rev. 79, 615 (1950).
[12] R. H. Dalitz and D. Yennie, Phys. Rev. 105, 1598 (1957).

CC-0. In Public Domain. Gurukul Kangri Collection, Haridwar

Digitized by Arya Samaj Foundation Chennai and eGangotri

E. Extensions and Limitations

From the derivation of the form for $W_{\mu\nu}$ it is apparent where the assumption of an experimental situation appropriate to an average over initial and a sum over final nuclear states enters: without these requirements there would be more independent 4-vectors on which the tensor $W_{\mu\nu}$ could depend and consequently more independent form factors. Hence one can expect to measure additional nuclear properties, (1) by polarizing or aligning the target, or (2) by measuring independent properties of the nuclear final state in addition to detecting the electron. Effects of nuclear orientation have been discussed recently by Wiegert and Rose[13]; some general results for the amplitudes for two- and three-body final states have been given by Berman.[14]

On the other hand, the entire method of analysis we have presented depends on the assumption of one-photon exchange only; this corresponds to neglecting higher Born-approximation corrections of $O(Z\alpha)$ and can only be appropriate for light nuclei. Deviations from Born approximation (one-photon exchange) can be tested by observing differences between electron and positron scattering cross sections, or by detecting violation of the two form-factor parameterization of electron scattering. Experimental results on the difference between electron and positron scattering from nuclei at small angles, both elastic and inelastic, have been obtained by Goldemberg, Pine, and Yount.[15] When many-photon exchange effects must be considered, no correspondingly simple theoretical analysis of experimental results has yet been developed. Three approaches have been used in calculation of both elastic and inelastic scattering: (1) Second Born approximation,[16] (2) numerical partial-wave calculations for scattering in a potential,[17] and (3) replacement of the free electron of Fig. 1 with a modified plane wave.[18] When applied to inelastic scattering these methods generally correspond to the use of a distorted-wave Born approximation in Fig. 1: the excitation of the nucleus treated only in lowest order, but the incoming and outgoing wave function treated more exactly. Both theory and experiment agree that in light nuclei for small momentum transfers (within the first zero of the form factors) the one-photon exchange analysis is adequate.

[13] L. J. Wiegert and M. E. Rose, Nucl. Phys. **51**, 529 (1964); D. Schildknecht, Phys. Letters **10**, 254 (1964). Some time ago R. G. Newton [Phys. Rev. **103**, 385 (1956); **109**, 2213 (1958); and **110**, 1483 (1958)] discussed the use of electron scattering for aligned nuclei for obtaining information on magnetic moment distributions.

[14] S. M. Berman, Phys. Rev. **135**, B1249 (1964).

[15] J. Goldemberg, J. Pine, and D. Yount, Phys. Rev. **132**, 406 (1953).

[16] S. D. Drell and R. H. Pratt, Phys. Rev. **125**, 1394 (1962).

[17] T. A. Griffy, D. S. Onley, J. T. Reynolds, and L. C. Biedenharn, Phys. Rev. **128**, 833 (1962); D. S. Onley, T. A. Griffy, and J. T. Reynolds, *ibid.* **129**, 1689 (1963); D. S. Onley, J. T. Reynolds, and L. E. Wright, *ibid.* **134**, B945 (1964).

[18] D. R. Yennie, F. L. Boos, Jr., and D. G. Ravenhall, Phys. Rev. **137**, B882 (1965); A. Baker, Phys. Rev. **134**, B240 (1964); H. Greenstein (to be published).

F. The Measurement of Magnetic Scattering

As seen above [Eq. (10)] all the processes considered in this paper have a differential cross section which can be written in the form

$$d\sigma/d\Omega=\sigma_{NS}[A(q)+B(q)\tan^2\tfrac{1}{2}\theta],$$
$$\sigma_{NS}=\left(\frac{Z\alpha}{2\epsilon}\right)^2\frac{\cos^2\theta}{\sin^4\tfrac{1}{2}\theta}\frac{E}{E'}, \tag{22}$$

where $A(q)$ and $B(q)$ are functions of the momentum and energy transfer, related to the charge and magnetic form factors. Consequently if one has two measurements of $d\sigma/d\Omega$ at two angles but at the same momentum and energy transfer, one can obtain $A(q)$ and $B(q)$. Better yet, in a linear plot of $d\sigma/d\Omega\,\sigma_{NS}$ as ordinate against $\tan^2\frac{1}{2}\theta$ as abcissa, $A(q)$ is the intercept with the ordinate axis and $B(q)$ the slope of the resulting straight line. An example is shown in Fig. 2. If the magnetic contribution to the scattering is not insignificant compared to the charge scattering, this method permits the determination of $F_{\rm mag}$ with a precision comparable to $F_{\rm ch}$.

The relative order of the magnetic to charge elastic scattering cross sections, for example, can be simply estimated as the ratio of the strength of the magnetic $q\mu$ and Coulomb interactions eZ

$$\left(\frac{q\mu}{eZ}\right)^2\left(\frac{1}{2}\frac{q}{Mc}\frac{\mu/\mu_N}{Z}\right)^2, \tag{23}$$

where Z is the nuclear charge, μ the magnetic moment of the scatterer, μ_N the nuclear magneton, and M the nucleon mass. This ratio is small for large Z and small magnetic moments, which is the case of medium and heavy nuclei; however, it increases with the momentum transfer. For the case of the nucleons it has been feasible to use Eq. (22) and separate $F_{\rm ch}$ and $F_{\rm mag}$ with high accuracy.[19,20] In other elements however conditions are not favorable; the slope of the straight line is small and the precision in its determination poor.

An obvious solution is to extend the measurement to such large angles that the increase in $\tan^2\frac{1}{2}\theta$ compensates the smallness of $B(q)$. In particular, if one makes measurements at exactly $\theta=180°$ one has from (22)

$$\left(\frac{d\sigma}{d\Omega}\right)_{180°}=B(q)\left(\frac{Z\alpha}{2\epsilon}\right)^2\frac{E}{E'}. \tag{24}$$

The cross section is then purely magnetic and although small can be measured without the usually dominating contribution from charge scattering.

[19] See, for example, D. Aitken, R. Hofstadter, E. B. Hughes, T. Janssens, and M. R. Yearian, in *Proceedings of the 1962 International Conference on High Energy Physics* (CERN, Geneva, 1962), p. 185.

[20] The Mott cross section is really proportional to

$$[1-(v/c)^2\sin^2\tfrac{1}{2}\theta],$$

which for $v\to c$ becomes $\cos^2\theta/2$.

CC-0. In Public Domain. Gurukul Kangri Collection, Haridwar

Digitized by Arya Samaj Foundation Chennai and eGangotri

A special method is necessary to measure cross sections at 180°; the reason is that the detection of the scattered electrons is usually made in magnetic spectrometers which for structural reasons cannot swing to angles larger than ~150° without the incident beam of electrons hitting the spectrometer pole faces or mount. In the method developed at Stanford University by Peterson and Barber[21] electrons are deflected ~10° by an auxiliary magnet before striking the target and the ones scattered at 180° are deflected again approximately 10° (in the opposite direction) before entering a magnetic spectrometer located at 160° with respect to the incident beam. A sketch of this experimental setup is given in Fig. 3. Other arrangements are possible and are in use at Stanford, Orsay, and other laboratories.

In general what one measures in magnetic scattering experiments is the complete spectrum of electrons scattered by a target at some large angle ($\theta \sim 180°$) when

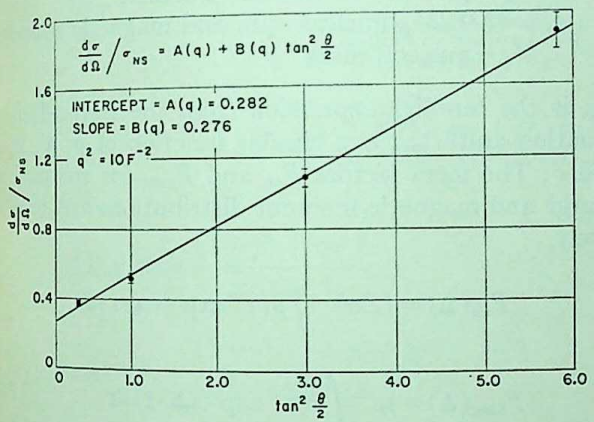

FIG. 2. Typical plot of the differential cross section for scattering as a function of $\tan^2 \frac{1}{2}\theta$. This corresponds to electron–proton scattering data at a $q^2 = 10$ F^{-2}.

electrons of incident energy E_0 are incident upon it. Figure 4 shows a sketch of the expected features of this spectrum. This sketch shows six regions in the spectrum which we discuss separately:

1. In region "a" one has magnetic elastic scattering by the magnetic moment of the nucleus, as well as a contribution from electrons that are scattered by the charge of the nucleus but enter the detector for reasons discussed below.

2. In region "b" discrete nuclear energy levels are excited. It is shown later that they correspond mainly to magnetic multipole transitions; at low incident electron energies they constitute what one could call a "giant magnetic-dipole resonance."

3. In region "c" electric-dipole transitions resulting from the transverse terms in the electromagnetic interactions of the electrons are outstanding; they correspond to the "giant electric-dipole resonance," which is generally studied with real photons.

[21] G. A. Peterson and W. C. Barber, Phys. Rev. **128**, 812 (1962).

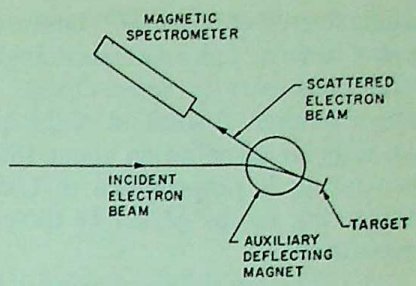

FIG. 3. Sketch of the experimental arrangement for 180° scattering in use at the Mark II Stanford Accelerator.

4. Region "d" corresponds to quasielastic scattering, i.e., scattering of electrons by the many individual nucleons; the shape of this broad "peak" is determined by the momentum distribution of the nucleons inside the nucleus.

5. Region "e" corresponds to the high-energy tail of the momentum distribution where short-range correlations are expected to appear.

6. In region "f" electrons that have lost energy through radiation are dominant; these can be attributed to the basic process of bremsstrahlung at very large angles or to such processes as radiation by an electron that was already degraded in energy by a previous scattering. Electrons of this origin are present also in the other regions and are represented by the dotted line in Fig. 4. The "nuclear physics" features of the spectrum are therefore superimposed on a continuous spectrum of electrons that have a basically different origin. Furthermore the radiative corrections (Schwinger correction) contributes in an important way to this continuous spectrum. These contributions make up what is generally called the "radiation tail," which must be subtracted before any interpretation of the nuclear physics can be made.

Measurements of cross sections at 180° have special problems associated with them. The basic ones are:

(a) The cross section at 180° is a minimum and it increases very rapidly because of the charge-scattering contributions (which goes as $\cos^2 \frac{1}{2}\theta / \sin^4 \frac{1}{2}\theta$) as the

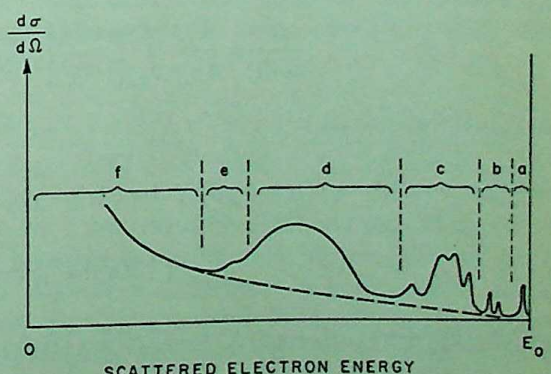

FIG. 4. Regions of the spectrum of high-energy electrons scattered at large angles by a nucleus: Region "a"—magnetic elastic scattering; region "b"—magnetic dipole transitions; region "c"—electric dipole transitions; region "d"—quasielastic scattering; region "e"—tail of quasielastic peak; region "f"—radiation tail. The dotted line represents the radiation tail in regions "b", "c", "d", and "e".

CC-0. In Public Domain. Gurukul Kangri Collection, Haridwar

Digitized by Arya Samaj Foundation Chennai and eGangotri

angle decreases from 180°; on the other hand, spectrometers have a finite entrance angle (typically 0.01 sr) and consequently some charge scattering enters the spectrometer. A solution of this problem is to measure an angular distribution about 180°; since the magnetic scattering is proportional to $1/\sin^4\frac{1}{2}\theta$ and the charge scattering to $\cos^2\frac{1}{2}\theta/\sin^4\frac{1}{2}\theta$ these contributions can be separated.

(b) The multiple scattering of electrons in the target either before or after scattering can represent a considerable complication to the experiment since it effectively increases the entrance angle of the spectrometer in an energy dependent way; at low energies and for thick targets considerable care must be taken with this effect.

(c) The radiation tail at 180° cannot be calculated using the usual approximate formulas which deal only with bremsstrahlung by the nuclear charge. Not only a better expression for this spectrum has to be used but in addition the bremsstrahlung resulting from the magnetic moment of the nucleus (if it has one) has to be considered. This point is discussed in greater detail in Sec. III.

III. EXTRACTING INFORMATION ON NUCLEAR STRUCTURE

A. Bremsstrahlung at Large Angles

The spectrum of electrons scattered at a given angle, regardless of the direction of the accompanying photon in the bremsstrahlung process, has been calculated by Parzen *et al.*[22] for point nuclei with no magnetic moment. We are interested here in finite-size nuclei with magnetic moments. Calculations have been made for this problem by Ginsberg and Pratt[23] in Born approximation, neglecting nuclear recoil and processes in which the nucleus is left in excited states.

The differential cross section for bremsstrahlung from a nucleus with a charge and magnetic moment, after summing over final electron and nuclear spins, photon polarizations, and averaging over initial electron and nuclear spins, was found to be

$$\frac{d\sigma}{d\Omega_{p'}d\Omega_k}=\frac{\Phi}{(2\pi)^2}\frac{p'}{p}\frac{dk}{k}\frac{1}{\Delta^4}$$

$$\times\left\{|F_{\rm ch}|^2T_{\rm ch}+\left(\frac{\mu}{Ze}\right)^2\left(\frac{I+1}{3I}\right)\Delta^2|F_{\rm mag}|^2T_{\rm mag}\right\},\quad(25)$$

with the notation:

$\Phi=Z^2r_0^2/137$,
$\hbar=c=m_e=1$,
$\mathbf{p}$, ϵ initial electron momentum and energy,
$\mathbf{p}'$, ϵ' scattered electron momentum and energy,
$\mathbf{k}$, $k=\epsilon-\epsilon'$ photon momentum and energy,
$\boldsymbol{\Delta}=\mathbf{p}-\mathbf{p}'-\mathbf{k}$ 3-momentum transfer,
I, $\mu=\lambda e/2M_p$ nuclear spin and magnetic moment,
M_p—nucleon mass.

$T_{\rm ch}$ is the familiar expression from the Bethe-Heitler equation and $T_{\rm mag}$ is a similar function of $\mathbf{p}$, $\mathbf{p}'$, $\mathbf{k}$, ϵ and ϵ'. The form factors $F_{\rm ch}$ and $F_{\rm mag}$ for the nuclear charge and magnetic-moment distributions are, respectively,

$$F_{\rm ch}(\Delta)=(Z\alpha)^{-1}\int\rho(\mathbf{r})\exp(i\boldsymbol{\Delta}\cdot\mathbf{r})d\mathbf{r},$$

$$F_{\rm mag}(\Delta)=i\mu^{-1}\int\mu(\mathbf{r})\exp(i\boldsymbol{\Delta}\cdot\mathbf{r})d\mathbf{r}.\quad(26)$$

These are exactly the same form factors that enter in the elastic scattering cross sections, as we see later.

The spectrum of the electrons that constitutes part of the radiation tail can be obtained from Eq. (25) by integrating over the photon angles $d\Omega_k$. The result is

$$\frac{d\sigma}{d\epsilon'd\Omega}=\frac{\Phi}{4\pi}\frac{p'}{p}\int_{\chi_{\min}}^{\chi_{\max}}\frac{d\chi}{\chi^2}\left\{|F_{\rm ch}|^2R_{\rm ch}+\left(\frac{\mu}{Ze}\right)^2\left(\frac{I+1}{3I}\right)2\chi|F_{\rm mag}|^2R_{\rm mag}\right\},\quad(27)$$

where

$$R_{\rm ch}=-2a^{-1}-(2\epsilon^2-\chi)(\alpha\beta_0+\chi\beta)X^{-\frac{1}{2}}-(2\epsilon'^2-\chi)(\alpha\beta+\chi\beta_0)X_0^{-\frac{1}{2}}$$
$$+\{2(\epsilon^2+\epsilon'^2)+\alpha-\chi-2[(1+\alpha)(\epsilon^2+\epsilon'^2-\chi)-k^2](\alpha-\chi)^{-1}\}(X^{-\frac{1}{2}}-X_0^{-\frac{1}{2}}),\quad(28)$$

$$R_{\rm mag}=2a^{-1}(2p^2+\chi)(\alpha\beta_0+\chi\beta)X^{-\frac{1}{2}}-(2p'^2+\chi)(\alpha\beta+\chi\beta_0)X_0^{-\frac{1}{2}}$$
$$+\{2(\epsilon^2+\epsilon'^2)-\alpha+\chi-2[(1+\alpha)(p^2+p'^2+\chi)-k^2](\alpha-\chi)^{-1}\}X^{-\frac{1}{2}}-X_0^{-\frac{1}{2}},\quad(29)$$

[22] P. T. McCormick, D. G. Keiffer, and G. Parzen, Phys. Rev. **103**, 29 (1956).
[23] Edward S. Ginsberg and R. H. Pratt, Phys. Rev. **134**, B773 (1964); **137**, B1500 (1965).

CC-0. In Public Domain. Gurukul Kangri Collection, Haridwar

Digitized by Arya Samaj Foundation Chennai and eGangotri

and where

$$\mathbf{q}=\mathbf{p}-\mathbf{p}', \qquad a=|\mathbf{q}|,$$
$$\chi_{\min}=\tfrac{1}{2}\Delta^2_{\min}=\tfrac{1}{2}(a-k)^2,$$
$$\chi_{\max}=\tfrac{1}{2}\Delta^2_{\max}=\tfrac{1}{2}(a+k)^2,$$
$$\alpha=\epsilon\epsilon'-\mathbf{p}'\cdot\mathbf{p}-1,$$
$$\beta_0=\mathbf{q}\cdot\mathbf{p}=p^2-\mathbf{p}\cdot\mathbf{p}',$$
$$\beta=\mathbf{q}\cdot\mathbf{p}'=\mathbf{p}\cdot\mathbf{p}'-p'^2,$$
$$X_0=p^2\chi^2+2\chi[k^2-\alpha(\epsilon'\epsilon_0-1)]+p'^2\alpha^2,$$
$$X=p'^2\chi^2+2\chi[k^2-\alpha(\epsilon'\epsilon-1)]+p^2\alpha^2. \tag{30}$$

Equation (27) is the exact Born-approximation result for the spectrum of scattered electrons due to bremsstrahlung from a static spherically symmetric distribution of charge and magnetic moment.

In the limit of point nuclei, high incident energies and large scattering angles one obtains

$$d\sigma=d\sigma_{\rm ch}+d\sigma_{\rm mag},$$

with

$$d\sigma_{\rm ch}=\frac{\Phi}{2\pi}\frac{p'}{p}\frac{d\epsilon'}{k}\frac{d\Omega_{p'}}{\epsilon^2}[A_{\rm ch}(\gamma,\theta)\log 2\epsilon+B_{\rm ch}(\gamma,\theta)], \tag{31}$$

$$d\sigma_{\rm mag}=\frac{\Phi}{2\pi}\frac{p'}{p}\frac{d\epsilon'}{k}d\Omega_{p'}\left(\frac{2\mu}{Ze}\right)^2\left(\frac{I+1}{3I}\right)[A_{\rm mag}(\gamma,\theta)\log 2\epsilon+B_{\rm mag}(\gamma,\theta)], \tag{32}$$

and

$$A_{\rm ch}(\gamma,\theta)=\frac{(1+\gamma^2)^2\cos^2\frac{1}{2}\theta}{2\gamma^3\sin^4\frac{1}{2}\theta},$$

$$A_{\rm mag}(\gamma,\theta)=\frac{(1+\gamma^2)(1+\sin^2\frac{1}{2}\theta)}{\gamma\sin^2\frac{1}{2}\theta},$$

$$B_{\rm ch}(\gamma,\theta)=\frac{1+\gamma^2}{2\gamma^3}\left\{\frac{\cos^2\frac{1}{2}\theta}{\sin^4\frac{1}{2}\theta}-\log\gamma-\frac{1+\gamma^2}{2\sin^4\frac{1}{2}\theta}+\frac{1-\gamma+\gamma^2}{\sin^2\frac{1}{2}\theta}+\left(\frac{\gamma}{\sin^4\frac{1}{2}\theta}-\frac{2\gamma^2}{(1+\gamma^2)\sin^2\frac{1}{2}\theta}\right)\log(\sin^2\tfrac{1}{2}\theta)\right\},$$

$$B_{\rm mag}(\gamma,\theta)=\frac{1-\gamma}{\gamma}\log\gamma-\frac{1+\sin^2\frac{1}{2}\theta}{\sin^2\frac{1}{2}\theta}+\sigma\log\left(\frac{1+\sigma}{1-\sigma}\right)+\left(1+\frac{1+\gamma^2}{2\gamma\sin^2\frac{1}{2}\theta}\right)\log(\gamma\sin^2\tfrac{1}{2}\theta). \tag{33}$$

In these expressions, $\gamma=\epsilon'/\epsilon$ and

$$\sigma=(1-\gamma)[(1-\gamma)^2+4\gamma\sin^2\tfrac{1}{2}\theta]^{-\frac{1}{2}}.$$

The result for $d\sigma_{\rm ch}$ was obtained by Parzen *et al.*[22] The structure of Eq. (31) is interesting since the term $A_{\rm ch}(\gamma,\theta)$, which is dominant at all angles except near 180°, has the familiar $\cos^2\frac{1}{2}\theta/\sin^4\frac{1}{2}\theta$ and thus is important where the charge scattering cross section is. The approximate formulas used at forward angles consider only this first term. However, $B_{\rm ch}$ contains terms which do not vanish with $\cos^2\frac{1}{2}\theta$ and so dominates the large-angle charge bremsstrahlung. [In Eqs. (31)–(33) the electron mass has been neglected in comparison to the energy. As usual it is due to this approximation that charge scattering vanishes at 180°; the corrections due to finite m_e must in some circumstances be considered.]

The ratio of the magnetic to the charge elastic bremsstrahlung for the point case [Eq. (32) divided by Eq. (31)] is

$$\frac{d\sigma_{\rm mag}}{d\sigma_{\rm ch}}=\left(\frac{\lambda}{Z}\right)^2\left(\frac{I+1}{3I}\right)\left(\frac{\epsilon}{M}\right)^2\frac{A_{\rm mag}\log 2\epsilon+B_{\rm mag}}{A_{\rm ch}\log 2\epsilon+B_{\rm ch}}, \tag{34}$$

where we have put $\mu=\lambda e/2M$. As expected, the magnetic bremsstrahlung is most appreciable at $\theta=180°$, where $A_{\rm ch}=0$, and becomes less important as Z increases. For fixed γ and θ as $E\to\infty$ the magnetic bremsstrahlung becomes relatively more and more important. In Fig. 5, we illustrate the relative contributions of the point charge and point magnetic moment for $E=54$ MeV and $\theta=180°$ using Eqs. (3) and (4). The contribution of the magnetic bremsstrahlung is large for scattered electrons undergoing small energy

CC-0. In Public Domain. Gurukul Kangri Collection, Haridwar

Digitized by Arya Samaj Foundation Chennai and eGangotri

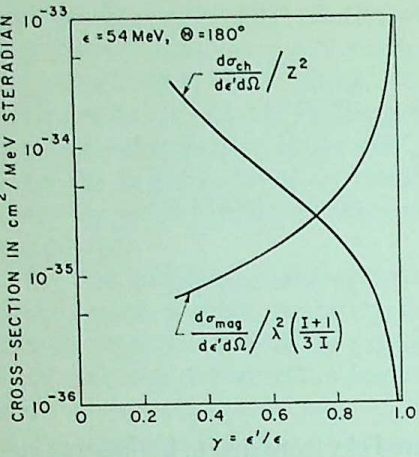

FIG. 5. Relative contributions to the radiative tail of the elastic peak from a point charge (Ze) and point magnetic moment ($\lambda e/2M_p$) in the limit $\epsilon, \epsilon' \gg 1$, $\theta \gg \epsilon^{-1}$.

loss, i.e., near the elastic peak from magnetic scattering. The relative importance of the magnetic bremsstrahlung can be inferred from Fig. 5 by multiplying the ratio of the two curves by the factor $(\lambda/Z)^2(I+1)/3I$, which in the case of Al^{27} is ≈ 0.037 yielding a ratio of $d\sigma_{mag}/d\sigma_{ch} \approx 0.026$ for $\gamma = 0.7$ and ≈ 1.75 at $\gamma = 0.95$. (For Cu these percentages are reduced by a factor of 10.)

Recently magnetic bremsstrahlung in electron–proton scattering has been observed for the first time. This constitutes an interesting problem in itself. Figure 6 shows the results of a measurement of the elastic peak in hydrogen for an incident energy of 54 MeV and a scattering angle of 180°.[24] The experimental points have not been corrected for magnetic bremsstrahlung. The dashed curve represents our approximate theoretical result for the elastic magnetic bremsstrahlung given by Eq. (32). (At these energies effects of the finite size of the proton are small.) We have interpreted γ as the fraction of the peak energy, i.e., we replace E_0 by the peak energy (the effects of recoil are about 10%). It is encouraging that Eq. (32) agrees fairly well with the data.[25]

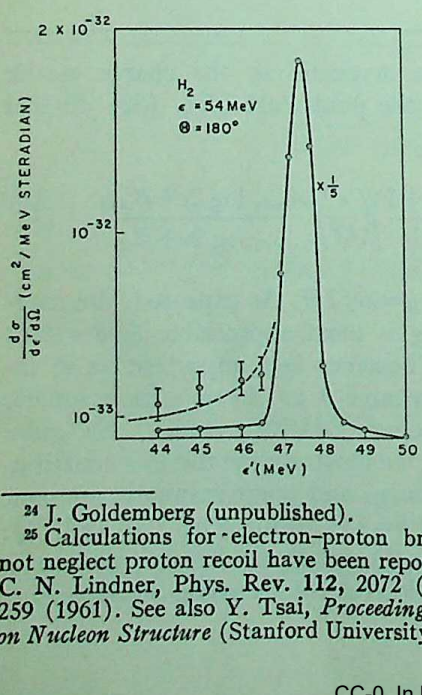

FIG. 6. Elastic peak in electron scattering from hydrogen (J. Goldemberg, unpublished). The dashed curve is the approximate analytic result for a point magnetic moment given by Eq. (32).

[24] J. Goldemberg (unpublished).

[25] Calculations for electron–proton bremmstrahlung that do not neglect proton recoil have been reported by R. A. Berg and C. N. Lindner, Phys. Rev. **112**, 2072 (1958); Nucl. Phys. **26**, 259 (1961). See also Y. Tsai, *Proceedings of the 1963 Conference on Nucleon Structure* (Stanford University Press, Stanford, 1964).

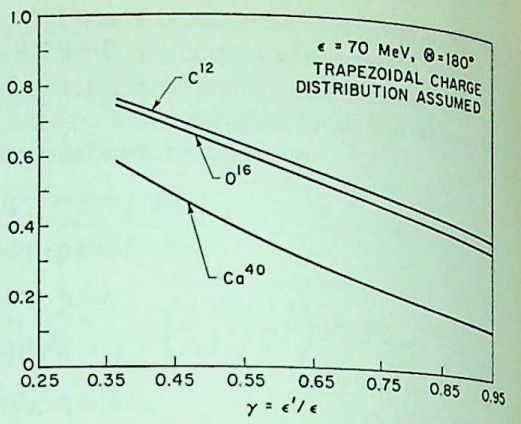

FIG. 7. Ratio of the cross section for scattered electrons after bremsstrahlung calculated with form factors (determined from elastic scattering) to the point charge result, for some spinless nuclei.

In the case of finite nuclei the integral in Eq. (27) can be evaluated numerically. The effect of finite nuclear extension in reducing the radiative tail is clearly shown in Fig. 7, where we have plotted the ratio of cross sections given by Eq. (27), to the point cross section, for some spinless nuclei (the situation is not complicated by the presence of magnetic bremsstrahlung). For simplicity we have chosen a form factor corresponding to a trapezoidal charge distribution for all three nuclei, with values of the half radius and skin thickness taken from Table 3 of Herman and Hofstadter.[2]

Finally, in Fig. 8, we illustrate the effect of the contribution of magnetic bremsstrahlung. Inelastic scattering experiments have been performed on Li^7 at 180° using 41.5-MeV incident electrons.[26] This nucleus

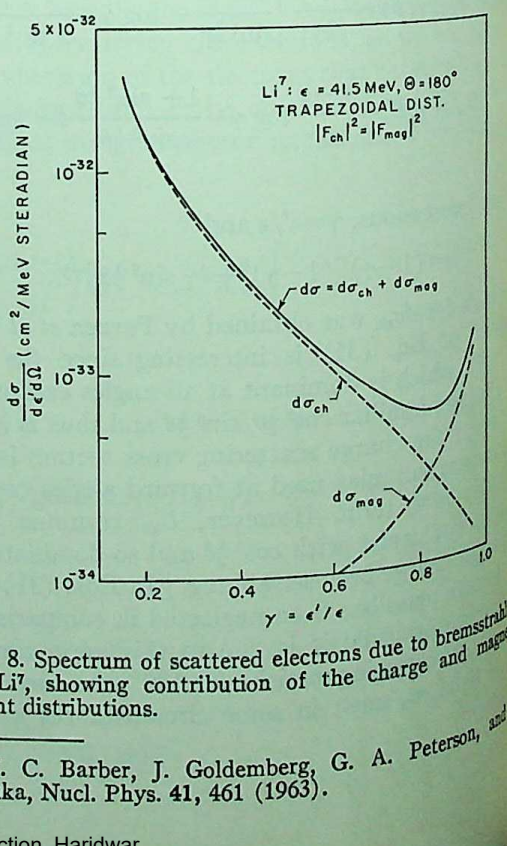

FIG. 8. Spectrum of scattered electrons due to bremsstrahlung from Li^7, showing contribution of the charge and magnetic moment distributions.

[26] W. C. Barber, J. Goldemberg, G. A. Peterson, and Y. Torizuka, Nucl. Phys. **41**, 461 (1963).

CC-0. In Public Domain. Gurukul Kangri Collection, Haridwar

Digitized by Arya Samaj Foundation Chennai and eGangotri

has a large magnetic moment and a low Z [the factor $(\lambda/Z)^2(I+1)/3I$ is approximately 0.65] so we expect magnetic effects to be important. As a first approximation we may set $|F_{ch}|^2 = |F_{mag}|^2$ and assume a trapezoidal form factor with parameters taken from Herman and Hofstadter.[2] Besides the differential cross section, the separate contributions of $d\sigma_{ch}$ and $d\sigma_{mag}$ are also shown in Fig. 6. The ratio $d\sigma_{mag}/d\sigma_{ch}$ is about 0.24 at $\gamma=0.7$ and rises up to 8.0 at $\gamma=0.95$. [This compares with ratios for the point case from Eq. (22) of 0.25 and 17.4, respectively.]

Maximon and Isabelle[27] have extended these calculations in order to include inelastic scattering; in their integration of the Bethe–Heitler formula they separate terms of order $\ln E/mc^2$ ("peak contribution") which are dominant at most angles and terms of order unity ("background contribution") which are in general neglected at forward angles,[28] but which become dominant at angles near 180°.

B. Radiative Corrections

These corrections are well known and have been used extensively in the literature; they account for the fact that in a scattering event there are higher order corrections (such as emission and absorption of virtual photons and emission of many low energy photons) which are responsible for the removal of electrons from a peak to a continuous spectrum that extends down to lower energies.

To obtain the real cross section of the peak it is then necessary to multiply the observed cross section by a correction factor. If one divides the spectrum of electrons in bins of width $\delta\epsilon$ starting at the highest energy at which electrons are present (ϵ') then the cross section in the highest energy bin is given by

$$(d\sigma/d\Omega)_{\text{real}} = (d\sigma/d\Omega)_{\text{observed}} \exp[y(\delta\epsilon)] \quad (35)$$

where y is given by Tsai[29] as

$$y(\delta\epsilon) = (2\alpha/\pi) \times\{[\ln(\epsilon/\eta^2\delta\epsilon)+\tfrac{1}{2}\ln(\epsilon/\delta\epsilon)-\tfrac{13}{12}][2m(q^2/M^2)-1]+\tfrac{17}{36}\}, \quad (36)$$

where α is the fine-structure constant, M is the nucleon mass, and

$$\eta = 1+(2\epsilon\sin^2\tfrac{1}{2}\theta/Mc^2). \quad (37)$$

In the case of a spectrum of electrons such as the one in Fig. 4 in which one has not only an elastic peak but others as well, the radiative correction is applied using an iterative procedure that treats all the scattered electrons (elastic and inelastic) in a similar way[30]: the cross section of the second bin [between the energies $(\epsilon-2\delta\epsilon)$ and $(\epsilon-\delta\epsilon)$] is reduced by the amount that comes from electrons that would have been at higher energies had there been no radiative corrections and then multiplied by its own e^y factor to correct for the electrons that were removed from it. A similar procedure is applied to the third bin and so on. This iterative procedure can be programmed in a computer and other corrections such as energy loss, electron–electron collisions, etc., incorporated. Alternatively the radiation tail can be computed using analytical expressions instead of being extracted by the procedure described above.[31] These problems have also recently been discussed by Nguyen-Ngoc and Perez-y-Jorba.[32]

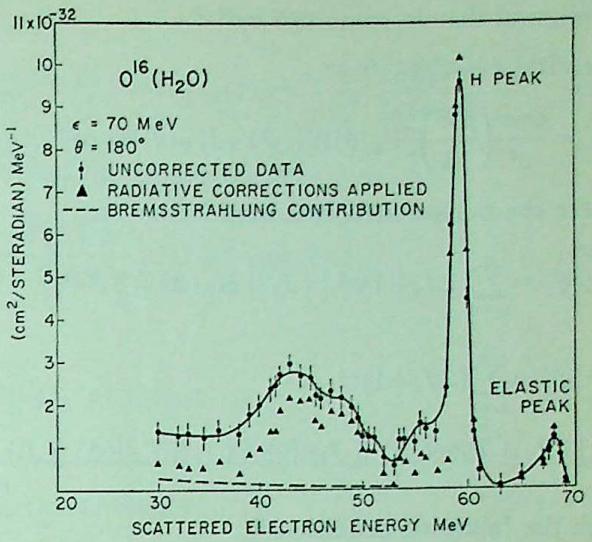

FIG. 9. Spectrum of electrons, initially 70 MeV, after scattering 180° from a water target. Shown also are the experimental points after the radiative correction (Schwinger correction) has been applied. The dotted line represents the bremmsstrahlung contribution.

As an example of the application of the methods discussed in this section, Fig. 9 shows the uncorrected data obtained from the scattering of 70-MeV electrons in a H_2O (water) target at a scattering angle of ~180°, and the importance of the corrections.

IV. INTERPRETING INFORMATION ON NUCLEAR STRUCTURE

A. General Remarks[33]

In agreement with our general result, the formula for the differential cross section for an unpolarized electron beam to scatter through an angle θ and at the same time take an unoriented nucleus from the state $J_i \to J_f$ is given in Born approximation (which should be good if Z is not too large), and with the neglect of nuclear

[27] L. C. Maximon and D. B. Isabelle, Phys. Rev. **133**, B1344 (1964); **136**, B674 (1964).
[28] L. I. Schiff, Phys. Rev. **87**, 750 (1952).
[29] Y. S. Tsai, Phys. Rev. **122**, 1898 (1961); see also N. T. Meister and D. R. Yennie, *ibid.* **130**, 1210 (1963), and N. T. Meister and T. A. Griffy, *ibid.* **133**, 1032 (1964).
[30] H. Crannell (private communication).
[31] D. B. Isabelle and G. R. Bishop, Nucl. Phys. **45**, 209 (1963).
[32] H. Ngugen-Ngoc and J. P. Perez-y-Jorba, Phys. Rev. **136**, B1036 (1964).
[33] R. H. Pratt, J. D. Walecka, and T. A. Griffy, Nucl. Phys. **64**, 677 (1965).

CC-0. In Public Domain. Gurukul Kangri Collection, Haridwar

Digitized by Arya Samaj Foundation Chennai and eGangotri

recoil, and the electron mass by[34–36]

$$(d\sigma/d\Omega)(J_i \rightarrow J_f) = \frac{8\pi\alpha^2}{q^4}\left(\frac{p'k'}{pk}\right)[V_L(\theta)W_L(q^2)+W_T(\theta)W_T(q^2)], \quad (38)$$

where the nuclear structure form factors are

$$W_L(q^2)=\sum_{L=0}^{\infty}(2J_i+1)^{-1}\,|\,(J_f\,||\,M_L(\Delta)\,||\,J_i)\,|^2,$$

$$W_T(q^2)=\sum_{L=1}^{\infty}(2J_i+1)^{-1}$$
$$\times\{|\,(J_f\,||\,T_J^{\rm mag}(\Delta)\,||\,J_i)\,|^2+|\,(J_f\,||\,T_J^{\rm el}(\Delta)\,||\,J_i)\,|^2\}, \quad (39)$$

with the following definitions[37]:

$$V_L(\theta)=(q^4/\Delta^4)2p\,p'\cos^2\tfrac{1}{2}\theta \xrightarrow[p=p']{} 2P^2\cos^2\tfrac{1}{2}\theta,$$

$$V_T(\theta)=(2p\,p'/\Delta^2)\sin^2\tfrac{1}{2}\theta$$
$$\times[(p+p')^2-2pp'\cos^2\tfrac{1}{2}\theta] \xrightarrow[p=p']{} p^2(1+\sin^2\tfrac{1}{2}\theta), \quad (40)$$

$\mathbf{p}(\mathbf{p}')$ = initial (final) electron wave numbers, $\boldsymbol{\Delta}^2=(\mathbf{p}-\mathbf{p}')^2$ is the 3-momentum transfer, $q^2=\boldsymbol{\Delta}^2-(p-p')^2$ is the relativistic invariant 4-momentum transfer. $M_{LM}(\Delta)$ is the Lth multipole moment of the nuclear charge density,

$$M_{LM}(\Delta)=\int d\mathbf{x}\rho_N(\mathbf{x})\,Y_{LM}(\Omega_x)j_L(\Delta x), \quad (41)$$

and the operators $T_{LM}^{\rm mag}$ and $T_{LM}^{\rm el}$ are the transverse multipole operators

$$T_{LM}^{\rm el}(\Delta)=\Delta^{-1}\int d\mathbf{x}\{\mathbf{j}_N(\mathbf{x})\cdot[\nabla_\Delta j_L(\Delta x)\mathbf{Y}_{LL1}^M(\Omega_x)]$$
$$+\boldsymbol{\Delta}^2 j_L(\Delta x)\mathbf{Y}_{LL1}^M(\Omega_x)\cdot\boldsymbol{\mu}_N(\mathbf{x})\} \quad (42)$$

$$T_{LM}^{\rm mag}(\Delta)=\int d\mathbf{x}\{\boldsymbol{\mu}_N(\mathbf{x})\cdot[\nabla_\Delta j_L(\Delta x)\mathbf{Y}_{LL1}^M(\Omega_x)]$$
$$+j_L(\Delta x)\mathbf{Y}_{LL1}^M(\Omega_x)\cdot\mathbf{j}_N(\mathbf{x})\}, \quad (43)$$

where $\mathbf{j}_N(\mathbf{x})$ is the nuclear convection current density and $\boldsymbol{\mu}_N(\mathbf{x})$ is the spin magnetization density. The $\mathbf{Y}_{LL1}^M$ are the vector spherical harmonics as defined by Edmonds.[38] The transverse multiple operators are *exactly the same as those governing radiative γ transitions in nuclei.*[39] The only difference in the latter case is that there $|\boldsymbol{\Delta}|=E_f-E_i$ (E_f and E_i are the initial and final energies of the nucleus) while here it is the momentum transferred by the electron.

We note the following important feature of the differential cross section. If we fix Δ, and then look in the backward direction, $\theta/2=\pi/2$, only the *transverse multipole terms* contribute. If we further restrict to elastic scattering as in the experiments of Goldemberg and Torizuka,[40] then $J_f=J_i\equiv J$, and there is no parity change since the final and initial states are just the nuclear ground state. In this case the selection rules are

$$1\leq L\leq 2J$$
$$\Delta\pi=N0.$$

This means we can have $M1$, $E2$, $M3$, $E4$, $M5$, $E6$ multipoles, etc. Time-reversal invariance eliminates the even electric multipoles.[33,41] Thus only the odd magnetic transverse multipoles remain, $M1$, $M3$, $M5$, etc.

In the limit as the momentum transfer Δ goes to zero, we can make use of the fact that the transverse multipole operators are just those of γ decay, and use the results of Blatt and Weisskopf[39] for the ordering of the magnitude of the contributions of the various multipoles. [The expansion parameters are essentially $\Delta c/Mc^2$ and ΔR divided by the various factors that come into the expansions of the spherical Bessel functions $j_L(\Delta R)$.] The dominant multipole will be the $M1$. If we now use the fact that

$$T_{1M}^{\rm mag}(\Delta)\xrightarrow[\Delta\to 0]{}\frac{iq\sqrt{2}}{3}\int d\mathbf{x}[\boldsymbol{\mu}_N(\mathbf{x})+\tfrac{1}{2}\mathbf{x}_\Delta\,\mathbf{j}_N(\mathbf{x})]$$
$$\cdot[\nabla\times Y_{1M}(\Omega_x)]=[iq/(6\pi)^{\frac{1}{2}}]\mu_{1M}, \quad (44)$$

where μ_{1M} is just the magnetic-dipole operator, then we can relate the transverse $M1$ matrix element to the static magnetic moment by

$$(JJ\,|\,\mu_{10}\,|\,JJ)\equiv\mu$$
$$(2J+1)^{-1}\,|\,(J\,||\,\mu_1\,||\,J)\,|^2$$
$$=\left[\mu^2\begin{pmatrix} J & 1 & J \\ -J & 0 & J\end{pmatrix}^{-2}\right](2J+1)^{-1}(J+1)\,J^{-1}\mu^2. \quad (45)$$

---

[34] L. I. Schiff, Phys. Rev. **96**, 765 (1954).

[35] K. Alder, A. Bohr, T. Huus, B. Mottelson, and A. W. Winther, Rev. Mod. Phys. **28**, 476 (1956).

[36] The main effect of including nuclear recoil is to add a phase-space factor

$$[dW_f/dP_f]^{-1}=\{1+[(P'-P\cos\theta)/E_f]\}^{-1},$$

where E_f is the final *total* energy of the target.

[37] The use of the 3-momentum transfer Δ in the form factors that appear in electron-scattering formulae indicates that the target is treated nonrelativistically (no recoil). For the case of elastic scattering in this approximation one has $q^2=\Delta^2$. Since a relativistic generalization would probably contain the 4- instead of the 3-momentum transfer this substitution is made usually. For inelastic scattering in general $p\approx p'$, and consequently again $q^2\simeq\Delta^2$. In the case of excitation by real photons, on the other hand, $q^2\equiv 0$ and $\Delta=E_f-E_i$ (excitation energy).

[38] A. R. Edmonds, *Angular Momentum in Quantum Mechanics* (Princeton University Press, Princeton, New Jersey, 1957).

[39] J. M. Blatt and V. F. Weisskopf, *Theoretical Nuclear Physics* (John Wiley & Sons, Inc., New York, 1952). This ordering does not remain valid for higher momentum transfers.

[40] J. Goldemberg and Y. Torizuka, Phys. Rev. **129**, 312 (1963).

[41] L. Durand, P. DeCelles, and R. Marr, Phys. Rev. **126**, 1882 (1962).

CC-0. In Public Domain. Gurukul Kangri Collection, Haridwar

Digitized by Arya Samaj Foundation Chennai and eGangotri

Therefore,

$$\left(\frac{d\sigma}{d\Omega}\right)_{el} \xrightarrow[\Delta\to 0]{} \frac{8\pi\alpha^2}{q^4}\left(\frac{k'}{k}\right)\left[V_L(\theta)\sum_{L=0}^{\infty}(2J+1)^{-1}\,|\,(J\,||\,M_L(\Delta)\,||\,J)\,|^2+V_T(\theta)(2\pi)^{-1}\left(\frac{J+1}{3J}\right)\frac{\lambda^2\hbar^2\Delta^2}{4M^2c^2}\right], \tag{46}$$

where $\mu\equiv\lambda\hbar/2Mc$ (M is the nucleon mass). If we set $p'=p$ we find the simpler form[33]

$$\left(\frac{d\sigma}{d\Omega}\right)_{el} \xrightarrow[p'=p]{\Delta\to 0} \left[\frac{\alpha^2\cos^2\tfrac{1}{2}\theta}{4k^2\sin^4\tfrac{1}{2}\theta}\right]\left[|\,F_{ch}(\Delta)\,|^2+\left(\frac{J+1}{3J}\right)\left(\frac{\hbar^2\Delta^2}{4M^2c^2}\right)\lambda^2(1+2\tan^2\tfrac{1}{2}\theta)\right], \tag{47}$$

where

$$|\,F_{ch}(\Delta)\,|^2=\frac{4\pi}{2J+1}\sum_{L=0}^{\infty}|\,(J\,||\,M_L(\Delta)\,||\,J)\,|^2. \tag{48}$$

In the backward direction, as $\Delta\to 0$, one sees just the *static magnetic moment*. The above formula (if one sets $|\,F_{ch}(\Delta)\,|^2=Z^2$) is identical with the formula originally derived by Jauch[42] and independently by Scofield[43] for the scattering of an electron by a point system with a charge Z and magnetic moment λ.[44] The present derivation has the advantage that it holds for an extended target with arbitrary charge and current distribution and with any spin.

B. Elastic Scattering

As seen in the discussion above the magnetic scattering cross section given by Eq. (47) has a very simple structure that can be compared with experiment by measuring the scattering cross section at 180° as a function of Z at a given (small) momentum transfer. The form factors simplify in this case to $F_{ch}=Z^2$ and $F_{mag}=\lambda$ and we get

$$\frac{1}{Z^2}\frac{d\sigma}{d\Omega}=\sigma_{\text{Mott}^p}\left\{1+\frac{J+1}{3J}\frac{K^2}{Z^2}\frac{\hbar^2\Delta^2}{4m^2c^2}(1+2\tan^2\tfrac{1}{2}\theta)\right\}$$

$$\sigma_{\text{Mott}^p}=\left(\frac{e^2}{2\epsilon_0}\right)^2\frac{\cos^2\tfrac{1}{2}\theta}{\sin^4\tfrac{1}{2}\theta}\,;\qquad K=\mu/(e\hbar/mc). \tag{49}$$

At 180° there should not be any charge scattering but the finite solid angle of the spectrometer and scattering in the target (which is particularly important at low energies) gives an appreciable contribution to the cross section; the proper subtraction of this background constitutes an important part of this type of experiment (at low momentum transfers).

Figure 10 shows the data obtained for a number of elements by Goldemberg and Torizuka[40] using incident electrons of 41.5 MeV. The data are presented as the cross section divided by Z^2. For spin-zero nuclei, $K=0$, and the cross section reduces to

$$(1/Z^2)(d\sigma/d\Omega)=\sigma_{\text{Mott}^p}=\text{constant}. \tag{50}$$

This is then a base line above which the magnetic scattering contribution appears. The solid line of Fig. 10 was obtained using Eq. (49) and the known static magnetic moments. Except for a few anomalies (B^{10} and B^{11}) agreement between theory and experiment is reasonable and one of the main features of the problem becomes clear: since the magnetic moment is attributable always (according to the shell model) to one or a few unpaired nucleons, it does not change much as Z increases; the Mott cross section however increases with Z^2 and thus the relative contribution of magnetic scattering decreases.

There are two ways in which the magnetic scattering can differ from that determined by the static limit of the magnetic moment, Eq. (49):

(i) The magnetic moment can have a structure and hence a form factor for elastic scattering. This is contained in the Δ dependence of $|\,(J\,||\,T_1^{\text{mag}}(\Delta)\,||\,J)\,|^2$. In particular, if the system has $J\leq 1$, and if Born

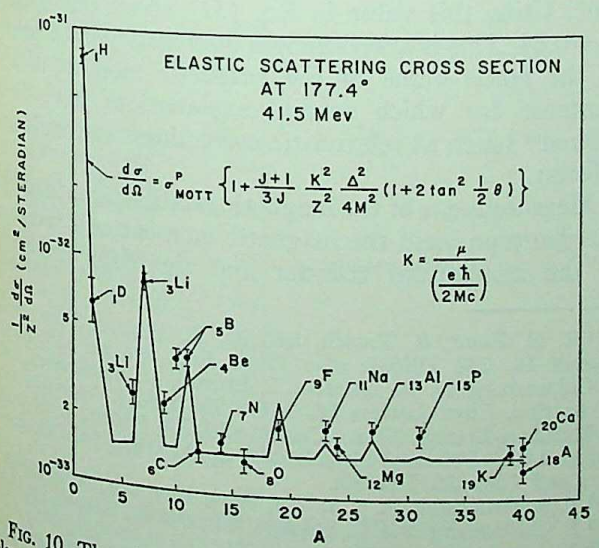

FIG. 10. The elastic magnetic cross section at 180° for light elements.

[42] J. M. Jauch, Helv. Phys. Acta **13**, 451 (1940).
[43] J. Scofield (private communication).
[44] A similar result was obtained by R. Gatto, Nuovo Cimento **12**, 613 (1954), in a calculation of the scattering of muons by nuclei.

CC-0. In Public Domain. Gurukul Kangri Collection, Haridwar

Digitized by Arya Samaj Foundation Chennai and eGangotri

approximation is valid, this is *the only way* the scattering can differ.

(ii) The cross section will always be *increased* by the contributions of the higher multipoles which can contribute. Thus one might expect that the higher the spin J, the faster one will see a *positive* deviation from the cross section containing just the static moment. This is probably the case for B^{10}, which has an anomalously large magnetic scattering cross section.

The two effects above tend to compensate each other if the magnetic-moment form factor is a decreasing function of Δ as is usually true (but does not *have* to be true). The second effect is only seen for $J \geq \frac{3}{2}$.

In order to learn about the spatial distribution of the magnetic moment one has to make measurements at a variety of momentum transfers. In the shell model the orbits are expected to be fairly well defined in space and consequently pronounced maxima and minima might be expected in the differential cross section for magnetic scattering; while the charge scattering probes the nuclear charge as a whole, magnetic scattering probes in general the part of the nucleus responsible for the nuclear magnetic moment.

Furthermore exchange currents contribute to the magnetic scattering although they do not contribute to charge scattering. As is well known, electric multipole moment operators are independent of exchange effects[45] (Siegert's theorem)[46]; the reason is that the electric multipoles depend on the charge distribution only while the magnetic moments are determined by both the charge and current distribution. In other words, in making predictions concerning electric moments or electric-multipole transitions one can feel reasonably secure even if one does not have a full knowledge of the exchange effects. However, the wavefunctions are needed (and might be affected by the exchange currents) but in general either they are known by other methods (as in the deuteron) or can be calculated according to some model. The study of electric multipoles constitutes then a test of how good they are.

In the study of magnetic-multipole transitions or moments one can only test the adequacy of the wave functions if all the exchange contributions are known at the outset. Consequently, if one knows the wave function (as in the case of the deuteron), one can obtain information on the exchange contributions.

Somewhat detailed studies of elastic magnetic scattering have been made for the deuteron, tritium and helium-3 and helium-4; we discuss them briefly. Very few measurements have been made of the form factors of nuclei heavier than He^4. Results have recently been reported for Li^6, Li^7, Be^9, B^{10}, B^{11}, and N^{14};[47] magnetic octupole moment effects have been observed. As an example of the form factor one can expect from a typical shell-model magnetic-moment distribution we give also in this section the calculation of the form factor for the magnetic scattering of F^{19}. Further shell-model calculations have been made by Griffy and Yu[48]

1. *The Deuteron*

The magnetic elastic-scattering cross section of the deuteron was measured at 180° at low momentum transfers (0.26 and 0.41 inverse fermis) by Goldemberg and Schaerf.[49] The measurements were made relative to the photon cross section. From the data, the magnetic moment of the deuteron at the q values mentioned above can be obtained (Fig. 11). Also available in the literature is the static magnetic moment of the deuteron which is known very precisely ($\mu_D = 0.857$ nm).

In the impulse approximation and neglecting exchange effects a simple nonrelativistic expression can be written for the static moment of the deuteron

$$\mu_D = \mu_S - \tfrac{3}{2}(\mu_S - \tfrac{1}{2}) P_D, \qquad (51)$$

where $\mu_S = \mu_P + \mu_N$; μ_P and μ_N are the static magnetic moments of the proton and neutron, respectively, and P_D is the D state probability in the deuteron ground state. This equation has been used in the past to determine P_D which comes out to be $\cong 0.04$.

Using the latest information on P_D obtained by analysis of the quadrupole moment of the deuteron,[5] of the photodesintegration studies[51] and the coherent photoproduction of pions[52] one obtains however $P_D \cong 0.07$. Using this value in Eq. (51) above one obtains $\mu_D = 0.84$. This is a well-known discrepancy in the value of the static value of the magnetic moment of the deuteron for which several explanations have been offered[53] (such as relativistic corrections, and exchange effects).

Measurements of the magnetic elastic scattering from the deuteron yield the magnetic moment as a function of the momentum transfer and therefore offer two

---

[45] R. G. Sachs, *Nuclear Theory* (Addison-Wesley Publishing Co., Inc., New York, 1953), mainly pp. 241–258.

[46] The conditions for the validity of Siegert's theorem in electron scattering have been investigated recently by J. M. Eisenberg and M. E. Rose, Phys. Rev. **131**, 848 (1963).

[47] R. E. Rand, R. Frosch, and M. R. Yearian, Phys. Rev. Letters **14**, 234 (1965); also Phys. Rev. (to be published); J. Goldemberg, D. B. Isabelle, T. Stovall, D. Vincigverra, and A. Bottino, Phys. Letters **16**, 141 (1965); G. J. Vanpraet and P. Kussanyi-Demay, Nuovo Cimento **39**, 388 (1965). Early work is due to G. A. Peterson, Phys. Letters **2**, 162 (1962); and Goldemberg and Torizuka, Ref. 40.

[48] T. A. Griffy and D. U. L. Yu, Phys. Rev. **139**, B880 (1965).

[49] J. Goldemberg and C. Schaerf, Phys. Rev. Letters **12**, 304 (1964).

[50] R. Wilson, *The Nucleon-Nucleon Interaction* (Interscience Publishers, Inc., New York, 1963).

[51] M. L. Rustgi, W. Zernik, G. Breit, and D. L. Andrews, Phys. Rev. **120**, 1881 (1960); M. Matsumoto, *ibid.* **129**, 1351 (1963); F. Partovi, Ann. Phys. (N.Y.) **27**, 79 (1964).

[52] F. T. Hadjioannou, Phys. Rev. **125**, 1414 (1962); E. Erickson, Friedman and H. W. Kendall, *ibid.* **129**, 2802 (1963). and C. Schaerf, Phys. Rev. Letters **11**, 432 (1963).

[53] G. Breit and R. M. Thaler, Phys. Rev. **89**, 1177 (1953).

CC-0. In Public Domain. Gurukul Kangri Collection, Haridwar

Digitized by Arya Samaj Foundation Chennai and eGangotri

additional pieces of information:

(a) An independent check on the absolute value of the magnetic moment of the deuteron can be obtained by extrapolation of the measurements to low momentum transfers. This is the information which may be obtained from the Goldemberg–Schaerf experiment, and as can be seen in Fig. 11 corroborates what is known for the static value of μ_D.

(b) The q dependence of the form factor can be calculated from theory and compared with experiments. Calculations were made using Gourdin's[54] formulae and the wave functions given by Breit *et al.*[51] and $P_D=0.07$ (Fig. 11). The experiments described in Ref. 49 cover a rather limited region of momentum transfers to be very useful for this kind of comparison.[55]

Calculations have been made recently by Harrington[56] and by Adler and Drell[57] on the contribution of 3-meson exchanges to the magnetic moment of the deuteron and the results are of the order of magnitude necessary to explain the experimental results.[58]

The relativistic corrections to the magnetic moment of the deuteron have not been calculated yet in detail.

2. *Tritium and Helium-3*

After the deuteron, the simplest nuclear systems are the three-body mirror-nuclei H^3 (3 protons) and He^3 (2 protons, 1 neutron). Naively, one can think of these systems as formed by a pair of protons with spins up and down, thereby canceling their magnetic moments,

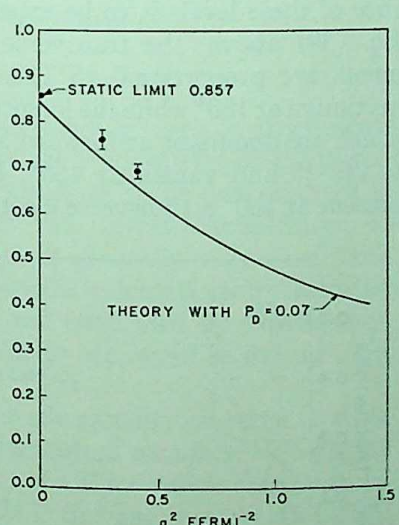

FIG. 11. The deuteron magnetic moment as function of the momentum transfer. The theoretical curve has been calculated with a D-wave contribution of 0.07.

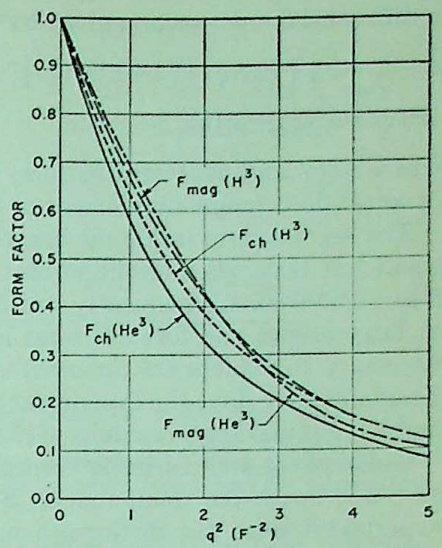

FIG. 12. H^3 and He^3 form factors as a function of momentum transfer.

so that the magnetic properties of the systems are then determined by the remaining nucleon (proton in H^3 and neutron in He^3). A detailed analysis of the magnetic moments of these nuclei in the light of the mirror theorem for nuclear moments[45] gives a clear indication of the existence of exchange currents in He^3.

These nuclei have been recently investigated by electron scattering (both charge and magnetic) by Hofstadter and collaborators[59]; the form factors obtained are shown in Fig. 12 where it is seen that they are approximately equal except for F_{ch} of He^3 which is appreciably larger than the others. The rms radius (R) that can be obtained are the following:

$$R_{ch}(H^3)=1.64\text{ F} \qquad R_{mag}(H^3)=1.64\text{ F}$$
$$R_{ch}(He^3)=1.80\text{ F} \qquad R_{mag}(He^3)=1.64\text{ F}.$$

Thus there is a concentration of the magnetism of He^3 as compared to its charge distribution.

Schiff *et al.*[60] have made a detailed analysis of the data of Hofstadter *et al.* and derived among other things the form factor for the exchange part of the magnetic moment of He^3.

3. *Helium-4*

Since He^4 has spin 0 and no static magnetic moment, Eq. (47) predicts that no magnetic scattering should be observed in this case. However the presence of a nonvanishing electric-dipole moment (edm) or "anomallous" magnetic moment for the electron (not the anomalous magnetic moment which has origin in electromagnetic corrections and can be shown to be unimportant at the momentum transfers at which the scattering experiments are performed[61]) would lead to

[54] M. Gourdin, Nuovo Cimento **28**, 533 (1963).
[55] This experiment was extended to higher momentum transfers (up to $q^2=5$) recently by D. Drickey, D. Frerejacque, and D. Benaksas, Phys. Rev. Letters **13**, 353 (1964), and the q-dependence of the form factor effectively agrees with the theoretical predictions of the impulse approximation with no relativistic or exchange effects (Jankus formula).
[56] D. R. Harrington, Phys. Rev. **133**, B142 (1964).
[57] R. Adler and S. D. Drell, Phys. Rev. Letters **13**, 349 (1964). See also, D. J. Drickey and L. N. Hand, Phys. Rev. Letters **9**, 521 (1962).
[59] H. Collard, R. Hofstadter, A. Johansson, R. Parks, M. Rynewel, A. Walker, M. R. Yearian, R. B. Day, and R. T. Wagner, Phys. Rev. Letters **11**, 387 (1963).
[60] L. I. Schiff, H. Collard, R. Hofstadter, A. Johansson, and M. R. Yearian, Phys. Rev. Letters **11**, 387 (1963).
[61] S. D. Drell and F. Zachariasen, Phys. Rev. **111**, 1727 (1958).

CC-0. In Public Domain. Gurukul Kangri Collection, Haridwar

Digitized by Arya Samaj Foundation Chennai and eGangotri

a differential cross section given by[62]

$$d\sigma/d\Omega=\sigma_M \mid F_{\rm ch}(q) \mid^2[1+\alpha^2(q)\,(\hbar q/m_0c)^2(\cos^2\theta)^{-1}],$$
$$\alpha^2(q)=\lambda^2(q)+\mu^2(q), \qquad (52)$$

where $\lambda(q)$ and $\mu(q)$ are the form factors of the edm or anomalous magnetic moment of the electron.

The second term inside the bracket is generally very small but becomes more important as q increases and also as $\theta\rightarrow 180$. Consequently one can measure $d\sigma/d\Omega$ at large angles and find out what is the value of $\alpha(q)$ necessary to explain the observed value. Burleson and Kendall[63] have done the experiment at angles up to 135° and have found that α in units of $e\hbar/m_0c$ was $<2\times10^{-4}$.

Goldemberg and Torizuka[64] repeated the experiment at ~180° with the result that $\alpha\lesssim 3\times10^{-5}\ e\hbar/m_0c$. The experiment does not distinguish between an electric-dipole moment and an anomalous magnetic moment. Attributing the upper limit above to an edm one can say that the dipole moment of the electron is smaller than 10^{-15} e-cm. The limit placed on the same number by other methods such as an analysis of the Lamb-shift experiments are ~3 times larger. Rand[65] subsequently used 180° scattering from C^{12} at higher momentum transfers and obtained $\alpha\lesssim 6\times10^{-6}\ e\hbar/m_0c$.

4. *Fluorine-19*

As an example of the calculation of the form factors to be expected for large nuclei we reproduce here the calculation[33] of the magnetic elastic scattering form factor for F^{19}. We assign F^{19} as an odd proton in the $s_{\frac{1}{2}}$ state; since the known magnetic moment $\mu_F=+2.629$ agrees so well with the Schmidt value $\mu(\text{Schmidt})=2.79$, the single-particle shell model may be applied with some confidence. We have

$$T_{1M}^{\rm mag}(\Delta)=\int d\mathbf{x}\, j_1(\Delta x)\,\mathbf{Y}_{111}{}^{M}(\Omega_x)\cdot[\mathbf{j}_N(\mathbf{x})+\nabla_\Delta \mathbf{u}_N(\mathbf{x})], \qquad (53)$$

and we want to calculate $[(0\tfrac{1}{2})\tfrac{1}{2} \mid\mid T_1^{\rm mag}(\Delta) \mid\mid (0\tfrac{1}{2})\tfrac{1}{2}]$ where the notation is $\mid (ls)j)$. The first term can be written (for a single particle)

$$(i/\sqrt{2})[\nabla j_1(\Delta x_i)\,Y_{1M}(\Omega_{x_i})]\cdot \boldsymbol{l}_i \qquad (54)$$

and since $\boldsymbol{l}\mid(0\tfrac{1}{2})\tfrac{1}{2})=0$ this term makes no contribution. The second term can be written

$$\int d\mathbf{x}\,\mathbf{u}_N(\mathbf{x})\cdot[\nabla_\Delta j_1(\Delta x)\,\mathbf{Y}_{111}{}^{M}(\Omega_x)], \qquad (55)$$

where $\mathbf{u}_N(\mathbf{x})=\lambda\mu_0\boldsymbol{\delta}_i\delta(\mathbf{x}-\mathbf{x}_i)$ (for a single particle). With the aid of identities on the vector spherical harmonies in Edmonds[38] and using the fact that only the $l=0$ part of the operator contributes, we find

$$T_{1M}^{\rm mag}(\Delta)\rightarrow i\lambda\Delta\mu_0(\tfrac{2}{3})^{\frac{1}{2}}j_0(\Delta x_i)[\boldsymbol{\delta}_i\cdot\mathbf{Y}_{101}{}^{M}(\Omega_{x_i})]. \qquad (56)$$

The only difference from the static case is the radial function $j_0(\Delta x)$. We can thus compute the form factor for the transition as

$$F(\Delta)=(N_{2s}/\sqrt{\pi})\int \mid u_2{}^{s}(x) \mid^2 x^2\,dx\, j_0(\bar{\Delta}x), \qquad (57)$$

in the notation of Elliott and Lane[66] and the oscillator wave functions are

$$u_{2s}(x)=(x^2-\tfrac{3}{2})\,\exp(-\tfrac{1}{2}x^2),$$
$$N_{2s}=\tfrac{8}{3},$$
$$\bar{\Delta}\equiv\Delta\left(\frac{\hbar}{MW_{\rm osc}}\right)^{\frac{1}{2}}=\left(\frac{\hbar^2\Delta^2}{M}\Big/\hbar W_{\rm osc}\right)^{\frac{1}{2}}. \qquad (58)$$

Computation of the integral gives

$$F(\Delta)=[1-\tfrac{1}{3}\bar{\Delta}^2+\tfrac{1}{24}\bar{\Delta}^4]\exp(-\tfrac{1}{4}\bar{\Delta}^2). \qquad (59)$$

C. Inelastic Scattering in Levels

As one measures the energy spectrum of scattered electrons down from the elastic peak (region "b" of Fig. 4) some outstanding levels such as the one at 3.56 MeV in Li^6 are seen[26] (Fig. 13). This is a well-known 0^+ state and since the ground state of Li^6 is a 1^+ state its excitation involves a magnetic-dipole transition. The same is the case for other levels of light nuclei such as the 15.1-MeV 1^+ level in C^{12}; these are in general bound levels of nuclei and therefore quite narrow.[67] The presence of these levels is to be expected as one can see in Eq. (39) above; the transverse magnetic matrix elements are proportional to $(1+\sin^2\tfrac{1}{2}\theta)$ which has a maximum at 180° while the longitudinal matrix elements which are dominant at forward angles are proportional to $\cos^2\tfrac{1}{2}\theta$ and vanish at 180°. However there is also present at 180° a transverse electric term which has the

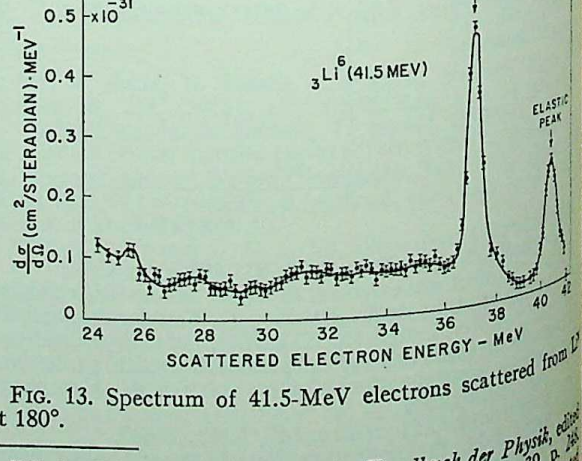

FIG. 13. Spectrum of 41.5-MeV electrons scattered from Li^6 at 180°.

[62] B. Margolis, S. Rosendorff, and A. Sirlin, Phys. Rev. **114**, 1530 (1959).
[63] G. R. Burleson and H. W. Kendall, Nucl. Phys. **19**, 68 (1960).
[64] J. Goldemberg and Y. Torizuka, Phys. Rev. **129**, 2580 (1963).
[65] R. E. Rand, Phys. Rev. **140**, B1605 (1965).
[66] J. P. Elliot and A. M. Lane, in *Handbuch der Physik*, edited by S. Flügge (Springer-Verlag, Berlin, 1957), Vol. 39, p. 241.
[67] Further experiments on Na^{23} have recently been reported by W. C. Barber and G. J. Vanpraet, Nucl. Phys. **72**, 63 (1965).

CC-0. In Public Domain. Gurukul Kangri Collection, Haridwar

Digitized by Arya Samaj Foundation Chennai and eGangotri

same angular dependence as the magnetic transitions; distinction between them has to be made from independent information on their spins. In the limit of low momentum transfers the ordering of the different terms of the multipole expansion is the same as the one used in photon excitation so the dominant multipoles are electric dipole ($E1$) and magnetic dipole ($M1$).

The identification of transitions as $E1$ or $M1$ is not easy because they have the same angular distribution; information from other sources helps to establish their character but whenever this is not available the comparison of the q dependence of the form factor with models helps in making the distinction.

In comparing the measured cross sections with calculated matrix elements there is one important piece of information which can be included. That is the cross section for photoabsorption in the level considered. In this case the operators $T_J^{\rm el}$ and $T_J^{\rm mag}$ are *exactly* the same ones that describe emission and absorption of real photons but the relation between the momentum transfer and the energy of the photon is

$$E_f - E_i = E_{\rm excit} = |\,\mathbf{\Delta}_{\rm ph}\,|. \tag{60}$$

Lewis and Walecka[68] have shown that the integrated absorption cross section in one level is given by

$$\int_{\rm level}\sigma(\epsilon)\,d\epsilon = (2\pi)^3\alpha E_{\rm excit}^{-1}(J+1)^{-1} \times\sum\{\langle J_f\|\,T_J^{\rm el}(\Delta_{\rm ph})\,\|\,J_i\rangle^2+\langle J_f\|\,T_J^{\rm mag}(\Delta_{\rm ph})\,\|\,J_i\rangle^2\} \tag{61}$$

In general, the parity of the transition allows only one of the matrix elements to contribute.

1. *M1 Levels*

These are the most outstanding levels in experiments at large angles because of the tendency for all the transition strength of $M1$ transitions to be concentrated in a few, generally one or two, levels. Furthermore, as bound levels their width is generally very small; this was predicted by shell-model calculations by Kurath[69] in $1p$ and $2s$–$1d$ shells and confirmed by experiments. The most outstanding levels are found in Be^9, Li^6, C^{12}, Mg^{24}, and Si^{28}.

Measurements were made recently on some of these levels for a number of momentum transfers.[70] We discuss only the 15.1-MeV level of C^{12} for which many experiments exist[71] (Fig. 14).[72] If one assumes the 15.1-MeV

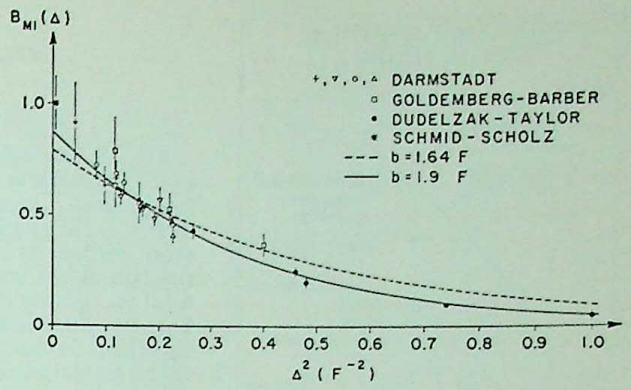

FIG. 14. The reduced transition probability $B_{M1}(1\to0)$ for the 15.1-MeV level in C^{12} as a function of the momentum transfer. The curves are calculated for different values of the harmonic oscillator parameter. The data are from various experiments.

level is due to single-particle transitions from the $(1p_{\frac{1}{2}})$ to the $(1p_{\frac{3}{2}})$ shell, and uses j–j coupling,[70] one obtains for the reduced matrix element

$$\langle(1p_{\frac{1}{2}})(1p_{\frac{3}{2}})^{-1},\ J^\pi=1^+,\ T=0\mid T_1^{\rm mag}(\Delta)\mid J=0,\ T=0\rangle^2 = (9\pi)^{-1}(g/M)^2\{[(\mu_P-\mu_N)-\tfrac{1}{2}]F_0^2(\Delta) +[\tfrac{1}{4}(\mu_P-\mu_N)-\tfrac{1}{2}]F_2^2(\Delta)\}, \tag{62}$$

where M is the proton mass, μ_P and μ_N the proton and neutron magnetic moments, and

$$F_l(\Delta)=\int_0^\infty[R_{1p}(r)]^2 j_l(\Delta r)r^2\,dr, \tag{63}$$

where R_{1p} is the radial wave function for a particle in the $1p$ shell. Calculation of $F_0(\Delta)$ and $F_2(\Delta)$ using harmonic oscillator wave functions gives

$$F_0(\Delta)=\exp(-\tfrac{1}{4}x^2)[1-\tfrac{1}{6}x^2], \tag{64}$$

$$F_2(\Delta)=\exp(-\tfrac{1}{4}x^2)[\tfrac{1}{6}x^2], \tag{65}$$

where $x=\Delta b$, b being the oscillator length parameter.

As seen in Eq. (62) the Δ dependence of the reduced matrix element is all contained in $F_0(\Delta)$ and $F_2(\Delta)$. Its absolute value depends on a coefficient related to the magnetic moments of the nucleons. It turns out that the absolute value depends sensitively on the assumed amount of spin–orbit coupling; however this choice has little effect on the radial dependence.[73] Two independent pieces of information can be obtained from experiments. The curves of Fig. 14 were drawn for a spin–orbit coupling ratio of $a/K=4.6$ and two oscillator strengths; the best fit is obtained with an oscillator parameter $b=1.9$ F, which is larger than the one obtained in the analysis of charge scattering experiments[74] ($b=1.64$ F).

Calculations and measurements for other transitions were also made by Bishop.[75]

---

[68] F. H. Lewis and J. D. Walecka, Phys. Rev. **133**, 849 (1964).
[69] D. Kurath, Phys. Rev. **130**, 1525 (1963).
[70] J. Goldemberg, W. C. Barber, F. H. Lewis, and J. D. Walecka, Phys. Rev. **134**, B1022 (1964).
[71] F. Gudden, Phys. Letters **10**, 313 (1964); B. Dudelzak and R. E. Taylor, J. Phys. Radium **22**, 544 (1961); H. Schmid and W. Scholz, Z. Physik **175**, 430 (1963).
[72] In analyzing data of this kind one usually plots reduced transition probabilities B_{M1} which are related to the reduced matrix elements that appear in the formulae of this paper by the relation

$$(xc\Delta)^2 B_{M1}(1\to0,\Delta)=5.28\times10^8\langle1\,\|\,T^{\rm mag}(\Delta)\,\|\,0\rangle^2.$$

[73] D. Kurath, Phys. Rev. **134**, B1025 (1964).
[74] U. Meyer-Berkhout, K. W. Ford, and A. E. S. Green, Ann. Phys. (N.Y.) **8**, 119 (1959).
[75] G. R. Bishop, Phys. Letters **8**, 128 (1964).

CC-0. In Public Domain. Gurukul Kangri Collection, Haridwar

Digitized by Arya Samaj Foundation Chennai and eGangotri

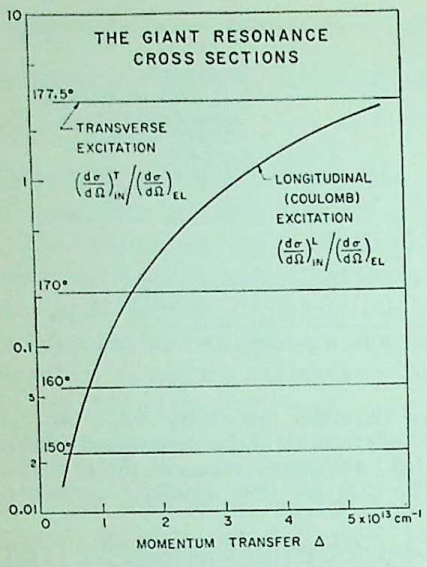

FIG. 15. The ratio of the transverse and longitudinal cross section to the elastic cross section as a function of the momentum transfer. For the transverse part this ratio is plotted for several angles of scattering.

2. *E1* Levels

Electric-dipole transitions of low energy (≤ 10 MeV) are strongly suppressed in nuclei due to the existence of correlations between the neutrons and protons.[39] This can be understood simply by considering a system consisting of protons only; in such a system the electric center is the same as the center of mass; for every charge moving to the left there is an equal one moving to the right since the center of mass stays at rest; hence the dipole moment is always zero. In fact few electric-dipole transitions of low energy are known to exist. For higher excitation energies, however, more complicated motions of the neutrons and protons are possible[76] (such as moving all the neutrons against all the protons) and a strong electric-dipole transition may occur. These have been studied extensively by photon excitation, although experimental difficulties have prevented measurements of the detailed shape and absolute magnitude of most cross sections. The general name of "giant dipole resonance" is given to the group of levels (or continuum) in which strong electric-dipole absorption is observed; these occur in general between energies of 15 and 25 MeV and are not bound, so their widths are expected to be large enough to cause overlapping.

Inspection of Eq. (39) shows that these transitions can be investigated by inelastic electron scattering either at forward angles (through the longitudinal operators) or at large angles where only the transverse operators are present. An analysis of the most favorable conditions for the observation of the *E*1 "giant resonance" in electron scattering was made by Goldemberg *et al.*[77] using a simple model for the nucleus: protons oscillating as a unit against the neutrons—this is referred to sometimes as the Goldhaber–Teller model.[76]

In this model one obtains

$$\left(\frac{d\sigma}{d\Omega}\right)^L_{\text{in}} \Big/ \left(\frac{d\sigma}{d\Omega}\right)_{\text{el}} = \left(\frac{N}{A}\right)^2 \left(\frac{\Delta^2}{2\mu}\right) \omega^{-1} \tag{66}$$

for the longitudinal part,

$$\left(\frac{d\sigma}{d\Omega}\right)^T_{\text{in}} \Big/ \left(\frac{d\sigma}{d\Omega}\right)_{\text{el}} = \frac{1}{2}\left(\frac{N}{A}\right)^2 \frac{\omega}{\mu c^2} \frac{(1+\sin^2\frac{1}{2}\theta)}{\cos^2\frac{1}{2}\theta} \tag{67}$$

for the transverse part, where $(d\sigma/d\Omega)_{\text{el}}$ is the elastic cross section, N and A are the neutron and mass number, respectively; $\mu = \frac{1}{4}AM$, M being the nucleon mass, ω is the peak energy of the resonance. These expressions are valid under the assumption of $\hbar\omega \ll \epsilon$.

Figure 15 shows the ratio of the transverse and longitudinal cross sections to the elastic one as a function of the momentum transfer. For the longitudinal part this ratio is independent of the angle and depends only on Δ. For the transverse part the ratio is independent of the momentum transfer and depends only on the angle of scattering. Large angles ($\theta \to 180°$) are more favorable for the observation of the transverse part of the cross section.

Other models were used by Lewis and Walecka[48] to compute the reduced matrix elements ("inelastic form factors") of the transverse part of the cross section. For the case of C^{12}, which we will discuss here, these were the hydrodynamical model of Steinwedel-Jensen[78] and the Brown model[79] (independent-particle model

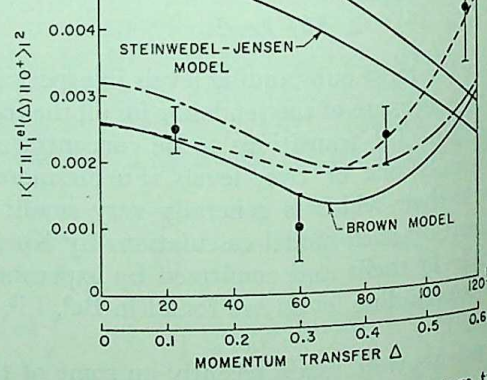

FIG. 16. Inelastic form factor versus momentum transfer for the giant electric-dipole resonance in O^{12}. The solid curve is calculated using a spin-dependent force with zero range for the residual interaction. The dashed curve is calculated using an ordinary force with zero range and leaving the high-lying states in C^{12} out of the calculation. The long-dash short-dash curve is calculated using a Serber force with a Yukawa potential for the residual interaction. We also show the curves for the collective models and the data of Goldemberg and Barber. But see discussion in Ref. 4.

[76] M. Goldhaber and E. Teller, Phys. Rev. **74**, 1046 (1948).
[77] J. Goldemberg, Y. Torizuka, W. C. Barber, and J. D. Walecka, Nucl. Phys. **43**, 242 (1963).
[78] H. Steinwedel and J. H. D. Jensen, Z. Naturforsch. **5a**, 413 (1950).
[79] G. E. Brown and M. Bolsterli, Phys. Rev. Letters **3**, 472 (1959).

CC-0. In Public Domain. Gurukul Kangri Collection, Haridwar

Digitized by Arya Samaj Foundation Chennai and eGangotri

with particle–hole interactions). The important result of these calculations is that they give *widely different form factors*, both in absolute magnitude and in their q-dependence. One has, therefore, a sensitive method of testing nuclear models.

Figure 16 shows the "inelastic form factor" for the giant resonance in C^{12} as a function of momentum transfer for the different models. Figure 17 extends the calculations to higher momentum transfers and includes also the longitudinal form factors. The data of Goldemberg and Barber[80] shown also in these figures are in reasonable agreement with the Brown model. For a more recent discussion of this problem see Ref. 4 and references cited therein.

The choice of the two-particle residual interaction is an important parameter which can affect the results;

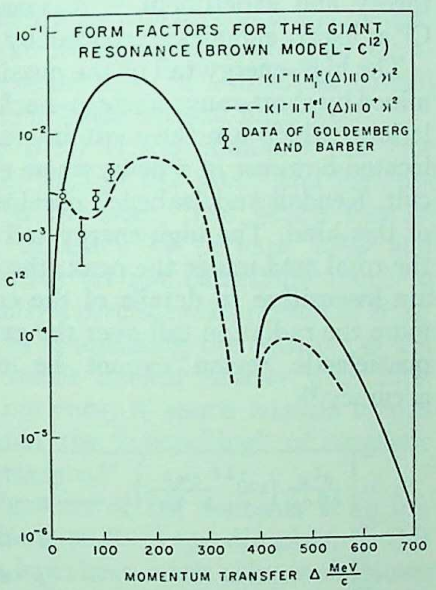

FIG. 17. Longitudinal and transverse form factors versus momentum transfer for the giant dipole resonance in C^{12}. The curves are calculated using a spin-dependent force with zero range for the residual interaction.

in general, one chooses a Serber force with a Yukawa potential well or an ordinary force with zero range. An experimental study of the form factors then gives information on the adequacy of one choice over the other. This was done in detail[80] for one of the $E1$ levels of C^{12} and Figure 18 shows that a Serber force fits the data considerably better than an ordinary force.

In the independent-particle model the "giant resonance" consists of a number of closely spaced levels which are located in the region of 20–30 MeV below the elastic peak. Each one of these levels corresponds to transitions from the ground state to one of the particle–hole final states; since these may have a different spatial distribution a measurement of the Δ-dependence of the form factors which "probes" this structure might give a result that is typical of each level. This was predicted by Lewis and Walecka[68] and confirmed by experiment; it explains why the shape of

[80] J. Goldemberg and W. C. Barber, Phys. Rev. **134**, B963 (1964).

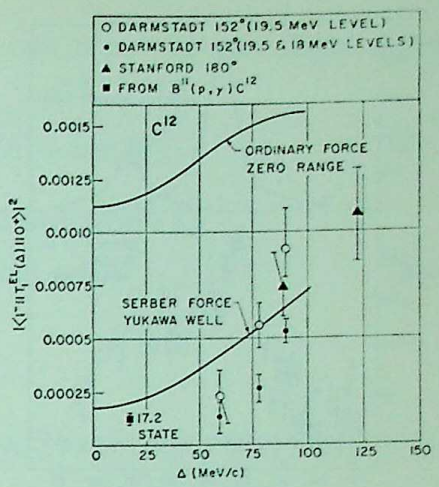

FIG. 18. Form factor for the lowest 1^- state in C^{12} plotted as a function of the momentum transfer. The two curves are for independent-particle-model calculations with two different assumptions for the two-particle residual interaction.

the giant resonance may be different for photon and for electron scattering excitation.

Figure 19 shows the relative transition probabilities for transverse excitation of the 1^-, $T=1$ states of O^{16}.[81] The height of each line is proportional to the square of the form factor corresponding to excitation of that state. The relative magnitudes change with the momentum transfer. Figure 20 shows the experimental data obtained for O^{16} by Burgov *et al.*[82] (photon absorption) and by Goldemberg and Barber[80] (for electron excitation at $h\Delta \cong 120$ MeV/c). This shows clearly the inversion in strength of the two main levels at the two momentum transfers. This figure also shows the shell-model calculations of Elliot and Flowers[83] for photon excitation in the two main levels of O^{16}.

A considerable amount of detailed, high-resolution work of this type remains to be done; it is expected that

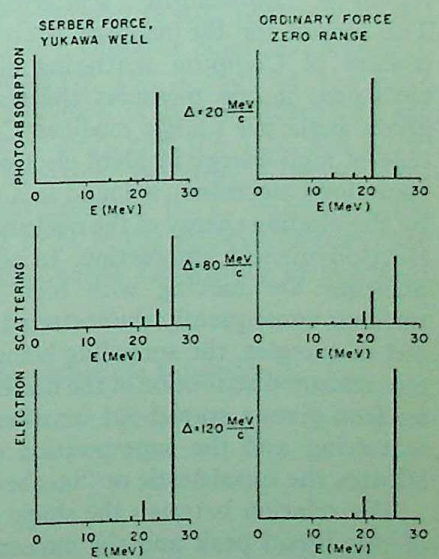

FIG. 19. Relative transition probabilities for transverse excitation of the 1^-, $T=1$ states in O^{16}. The height of each line is proportional to the square of the form factor for excitation of the corresponding state at the given energy and momentum transfer. Two types of residual interaction were used.

[81] F. H. Lewis, Phys. Rev. **134**, B331 (1964).

[82] N. A. Burgov, G. V. Danilyan, B. S. Dolbilkin, E. Lazareva, and F. A. Nikolaev, Zh. Eksperim. i Teor. Fiz. **43**, 70 (1962) [English transl.: Soviet Phys.—JETP **16**, 50 (1963)].

[83] J. P. Elliot and B. H. Flowers, Proc. Roy. Soc. (London) **242A**, 57 (1957).

CC-0. In Public Domain. Gurukul Kangri Collection, Haridwar

Digitized by Arya Samaj Foundation Chennai and eGangotri

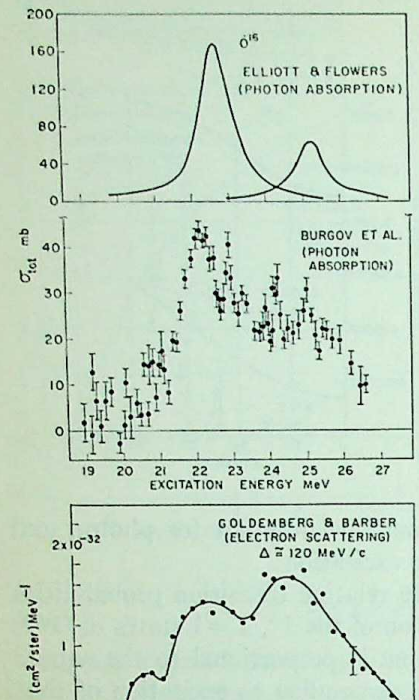

FIG. 20. A comparison of the photon-absorption cross-section measurements of Burgov *et al.* in O^{16} with the electron scattering cross - section measurements of Goldemberg and Barber at a Δ of 120 MeV/c and 180°. The top graph shows the results of the calculation of Elliot and Flowers.

inelastic electron scattering in levels will prove to be an important tool for nuclear structure studies. Experimental[84] and theoretical[85] studies are proceeding rapidly.

D. Quasielastic (Incoherent) Scattering

Extending the measurement of inelastic scattered electrons to include large energy losses, one finds the region of "quasielastic" scattering ("d" in Fig. 4). The reason for the name is related to the analogous process of Compton scattering of x rays by bound electrons; if one measures the scattered x rays at a given angle one finds a modified Compton line. In the case of high-energy incident electrons the modified line (scattered electrons) is found in a position determined by the binding energy of the nucleus and the recoil in the electron–nucleon interaction. In addition however the nucleons are moving with high energies inside the nucleus; consequently the scattered electrons are spread out in energies, the spreading being determined by the momentum distribution of the nucleons. Each individual nucleon gives a spread-out contribution to the inelastic scattering and the superposition of all of them constitutes the quasielastic or "incoherent" peak.

The relation between the shape and integrated area of this broad peak and the momentum distribution of the nucleons has been studied extensively by Drell and Schwartz,[86] McVoy and van Hove,[87] Gottfried and Czyz,[88] and recently Czyz.[89] These calculations show that the main part of the quasielastic peak is determined by the Pauli principle correlations and the results are rather model insensitive, to the point that even a free degenerate Fermi gas gives roughly the right shape and position.

Figure 21 shows measurements of Leiss and Taylor[90] with 148.5-MeV incident electrons at 135° in C^{12}, and the calculations of Czyz considering all single-particle excitations compatible with the Pauli principle. The momentum distribution for the C^{12} nucleus was taken as

$$n(p) = [1 + \tfrac{4}{3}(p/p_0)^2] \exp[-(p/p_0)^2]. \quad (6)$$

Several values of the effective mass M_{eff} of the nucleons inside nuclear matter were tried. Agreement between theory and experiment is reasonable. Other data for C^{12} at higher energies is reported by Bounin and Bishop.[91]

The high-energy tail of the quasielastic peak is determined by short-range nucleon–nucleon dynamical correlations, which are the most interesting to study; it is located however in a place where experiments are difficult. Kendall and Isabelle[92] obtained some information of this kind. The high-energy tail contributes little to the total area under the peak; the calculated sum-rules are insensitive to details of the correlations. Furthermore the radiation tail over the extended region of the quasielastic region cannot be obtained with high accuracy.[91]

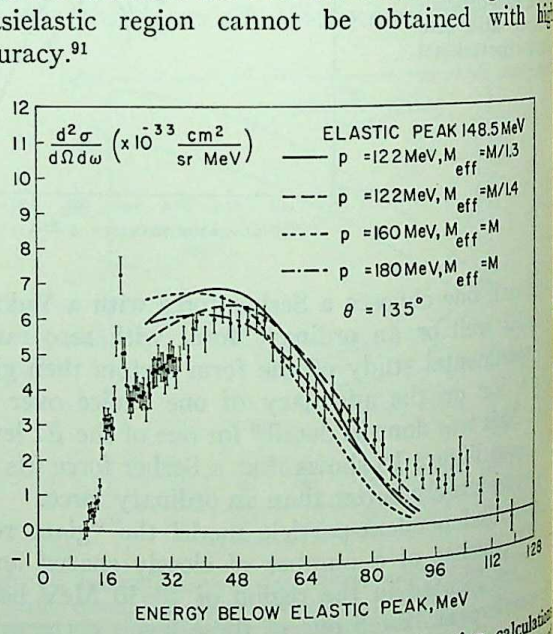

FIG. 21. Comparison of impulse approximation calculation for C^{12} with measurements of Leiss and Taylor. The energy of the incident electrons is 148.5 MeV and the spectrum was measured at 135°.

[84] G. Vanpraet, Phys. Letters **17**, 120 (1965); G. Vanpraet, Nucl. Phys. **74**, 219 (1965); G. J. Vanpraet, W. C. Barber, P. Kessanyi-Demay, and G. J. Vanpraet (to be published).

[85] T. deForest Phys. Rev. **139**, B1217 (1965); T. deForest, J. D. Walecka, G. Vanpraet, and W. C. Barber, Phys. Letters **16**, 311 (1965); J. L. Frian (to be published).

[86] S. D. Drell and C. L. Schwartz, Phys. Rev. **112**, 568 (1958).

[87] K. W. McVoy and L. Van Hove, Phys. Rev. **125**, 1034 (1962).

[88] W. Czyz and K. Gottfried, Ann. Phys. (N.Y.) **21**, 47 (1963).

[89] W. Czyz, Phys. Rev. **131**, 2141 (1963).

[90] J. E. Leiss and R. E. Taylor (quoted in Ref. 66).

[91] J. I. Friedman, Phys. Rev. **116**, 1257 (1959); P. Bounin and G. R. Bishop, J. Phys. Radium **29**, 974 (1963).

[92] D. B. Isabelle and H. W. Kendall, Bull. Am. Phys. Soc. **9**, 95 (1964).

CC-0. In Public Domain. Gurukul Kangri Collection, Haridwar

Digitized by Arya Samaj Foundation Chennai and eGangotri

However it has been pointed out recently by Czyz[93] that an interesting case occurs at very large angles ($\theta \sim 180°$). The sum-rule of McVoy and van Hove[87] is

$$\int_0^\infty \frac{d\sigma}{d\omega\, d\Omega}(\Delta, \omega, \theta)\, d\omega = |f(\Delta)|^2 \left(\frac{e}{2p_1}\right) \frac{\cos^2 \tfrac{1}{2}\theta}{\sin^2 \tfrac{1}{2}\theta} [A(\Delta) + B(\Delta) + \tan^2 \tfrac{1}{2}\theta], \tag{69}$$

where ω is the energy loss of the electrons. $f(\Delta)$ is related to the conventional form factors by

$$f(\Delta) = F_{1p}(\Delta) = F_{2p}(\Delta) = F_{2n}(\Delta); \qquad F_{1n}(\Delta) \text{ (assumed zero)}. \tag{70}$$

At 180° one can measure $B(\Delta)$, which is given (to second order in Δ/M) by

$$B(\Delta) = (\Delta^2/M^2)(Z^2\mu_p^2 + N^2\mu_n^2) + \tfrac{4}{3} Z(\langle p^2 \rangle_{\mathrm{Av}}/M^2)$$
$$+ \langle 0 | \sum_{j \neq k}^{A} \sum^{A} \exp[i\boldsymbol{\Delta} \cdot (\mathbf{r}_j - \mathbf{r}_k)] \{\mu_j \mu_k (2M^2)^{-1} [\Delta^2 \boldsymbol{\sigma}_j \cdot \boldsymbol{\sigma}_k - (\boldsymbol{\Delta} \cdot \boldsymbol{\sigma}_j)(\boldsymbol{\Delta} \cdot \boldsymbol{\sigma}_k)] + \mu e_j e_k (p_{xj} p_{xk}/M^2)\} | 0 \rangle, \tag{71}$$

where Z and N are the number of protons and neutrons, μ_p and μ_n their magnetic moments *inside* nuclear matter, e_j=1 for protons and 0 for neutrons; $\boldsymbol{\sigma}_j$ are spin operators; p_{xj} is the component of $\mathbf{p}_j$ in a direction normal to $\boldsymbol{\Delta}$. The summation extends over all nucleons.

The first term of $B(\Delta)$ is the dominant one (for Δ=1 F) it makes up 90% of the total) and becomes more dominant as Δ increases. The others can be evaluated with an accuracy of perhaps 25% and although model-sensitive do not contribute much in the result. Consequently a precise measurement of $B(\Delta)$ could be important in establishing the equality of the magnetic moments inside nuclear matter with their values for the free nucleons; it seems feasible in this way to find out about the "quenching" of magnetic moments inside the nucleus.[94]

The electrodisintegration of the deuteron is an important special problem of the type discussed in this section. Calculations have been made using well-known wave functions due to Yankus.[95] The deuteron has no bound excited states and it disintegrates at 2.23 MeV so there are no levels in the spectrum but only a broad peak that extends down to lower energies. Measurements have been made at forward angles by many authors.[1,2] Peterson and Barber[21] and Barber *et al.*[18] measured the spectrum of electrons inelastically scattered from the deuteron at 180° using 41.5-MeV electrons and compared their results with the Yankus theory,[95] neglecting exchange currents. All multipole order transitions were taken into account although the magnetic dipole ($M1$) process is predominant; final-state interactions were not taken into account. Agreement with theory was obtained with little evidence for effects due to exchange currents although they are expected to contribute. These experiments have been recently extended to higher energies by Goldemberg and Schaerf[96] and some disagreement with theory is apparent from the data.

[93] W. Czyz (private communication).
[94] B. Bremond, Nucl. Phys. **35**, 49 (1962).
[95] V. Z. Jankus, Phys. Rev. **102**, 1586 (1956).

ACKNOWLEDGMENTS

We are pleased to acknowledge useful discussions with Professor W. C. Barber, Professor J. D. Walecka, Dr. F. H. Lewis, Dr. E. Ginsberg, Dr. W. Czyz, and Professor S. D. Drell. This review was begun at Stanford University and supported in part by the U.S. Air Force through Air Force Office of Scientific Research Contract AF 49(638)-1389, and in part by the joint program of the U.S. Office of Naval Research, the Atomic Energy Commission, and the U.S. Air Force Office of Scientific Research. We wish to thank Professor L. I. Schiff and Professor W. C. Barber for the hospitality extended to us in the Physics Department and the High Energy Physics Laboratory at Stanford University.

[96] C. Schaerf and J. Goldemberg (to be published).

CC-0. In Public Domain. Gurukul Kangri Collection, Haridwar

Digitized by Arya Samaj Foundation Chennai and eGangotri

REVIEWS OF MODERN PHYSICS VOLUME 38, NUMBER 2 APRIL 1966

Group Theory and the Hydrogen Atom (I)

M. BANDER, C. ITZYKSON*

Stanford Linear Accelerator Center, Stanford University, Stanford, California

The internal 0(4) symmetry group of the nonrelativistic hydrogen atom is discussed and used to relate the various approaches to the bound-state problems. A more general group 0(1, 4) of transformations is shown to connect the various levels, which appear as basis vectors for a continuous set of unitary representations of this noncompact group.

I. INTRODUCTION

There has been great interest recently in the possible application of group theory to the strongly interacting particles. Not only do certain systems possess obvious symmetries which allow a classification of their spectra, but it has also been suggested[1] that one look for certain transformations which allow passing from one level to another and thus get new insight into the structure of the system.

In nonrelativistic quantum mechanics, several examples of such behavior are known and it may be worthwhile to investigate in detail a specific one. We have chosen to undertake such a study for the Coulomb potential which seems very well suited for such an investigation.

The classical treatment of the subject consists of solving explicitly the Schrödinger equation in coordinate space by means of hypergeometric functions. In 1926 W. Pauli,[2] found the spectrum of the Kepler problem in a very elegant way by the use of the conservation of a second vector besides the angular momentum. A few years later, V. Fock[3] explained the degeneracy of the levels in terms of a symmetry group isomorphic to the one of rotations in a four-dimensional space 0_4, and a few months later V. Bargmann[4] related the two approaches explaining further how, in the Coulomb case, the separation of variables in parabolic coordinates was linked with the new, conserved vector —a relation well known in classical mechanics. Later on the rotational invariance was used, for instance, by J. Schwinger[5] to construct the Green function of the problem.

Thus the Coulomb problem is interesting for its 0_4 invariance, but it has been recently remarked that one can operate in the Hilbert space of bound states with a still larger group, isomorphic to the de-Sitter group, 0(1, 4), in such a way that one thus gets an irreducible infinite dimensional unitary representation of this noncompact group.

Our aim has thus been twofold. We first review the symmetry group of the system, describing succinctly the methods discussed above. We note some further relations which were implicit in the works quoted. Actually, following a remark of Alliluev,[6] we shall even generalize the problem to an arbitrary number of dimensions. The larger group, 0(1, 4), is then introduced in an heuristic way. The new terminology suggested for this kind of superstructure is "Physical Transformation Group." We shall write the explicit realization of this group as a set of unitary operations in the Hilbert space of bound states and prove irreducibility using the infinitesimal generators. Finally it is suggested that the type of considerations used can be generalized to obtain special types of unitary representations for noncompact groups. This paper is mainly concerned with the problem of bound states. We hope to consider in the future the case of scattering states.

Several recent lectures given at Stanford by Professor Y. Ne'eman were the inspiration for this work. It is a pleasure to thank him for his stimulation. It is clear that many of the results were known to him and certainly to many other physicists. We apologize in advance for giving only a very sketchy bibliography.

II. THE SYMMETRY GROUP

A. The Infinitesimal Method[2]

We want to solve the Schrödinger equation for the Coulomb potential.

$$[-(\hbar^2\Delta/2\mu)-(k/r)]\Psi(x)=E\Psi(x) \tag{1}$$

with Δ the Laplacian

$$\Delta=\frac{\partial^2}{\partial x_1^2}+\frac{\partial^2}{\partial x_2^2}+\frac{\partial^2}{\partial x_3^2}, \qquad r=(x_1^2+x_2^2+x_3^2)^{\frac{1}{2}},$$

μ is the reduced mass and, in the case of an hydrogen-like atom, $k=Ze^2$. Let $p_i=(\hbar/i)(\partial/\partial x_i)$, then due

---

* On leave of absence from Service de Physique Théorique, CEN Saclay, B.P. No. 2, Gif-sur-Yvette (Seine et Oise), France.

[1] Y. Dothan, M. Gell-Mann, and Y. Ne'eman, Phys. Letters **17**, 148 (1965).

[2] W. Pauli, Z. Physik **36**, 336 (1926).

[3] V. Fock, Z. Physik **98**, 145 (1935).

[4] V. Bargmann, Z. Physik **99**, 576 (1936).

[5] J. Schwinger, J. Math. Phys. **5**, 1606 (1964).

[6] The first relation in Eq. (5) has an obvious geometrical meaning in the Kepler problem where L is orthogonal to the elliptic orbit and M is along the main axis with a length given by the excentricity of the ellipse times k. The expression for the energy differs from the classical one only by the $\hbar^2$ term.

CC-0. In Public Domain. Gurukul Kangri Collection, Haridwar

Digitized by Arya Samaj Foundation Chennai and eGangotri

the invariance of Eq. (1) under spatial rotation the angular momentum

$$L_{ij}=x_ip_j-x_jp_i \qquad L_k=\epsilon_{kij}L_{ij}/2 \tag{2}$$

is conserved, and it is possible to separate the equation using polar coordinates. However, it is known that in the Kepler problem, the following three-vector

$$\mathbf{v}\times\mathbf{L}-k(\mathbf{r}/r)$$

is also a constant of the motion, $\mathbf{v}$ is the velocity, $\mathbf{L}$ the angular momentum, and $\mathbf{r}$ the position vector, $\mathbf{r}=(x_1, x_2, x_3)$. Pauli simply used the correspondence principle and investigated the commutation relations of the Hermitian part of the previous vector, i.e.,

$$\mathbf{M}=(2\mu)^{-1}\mathbf{p}\times\mathbf{L}-(2\mu)^{-1}\mathbf{L}\times\mathbf{p}-k(\mathbf{r}/r). \tag{3}$$

The commutation relations of $\mathbf{L}$, $\mathbf{M}$ and the Hamiltonian H are

$$[H, L_i]=0,$$

$$[H, M_i]=0,$$

$$[L_j, L_k]=i\hbar\epsilon_{jkl}L_l,$$

$$[L_j, M_k]=i\hbar\epsilon_{jkl}M_l,$$

$$[M_j, M_k]=(\hbar/i)\epsilon_{jkl}L_l(2/\mu)H, \tag{4}$$

and[6]

$$L\cdot M=M\cdot L=0 \qquad (M^2-k^2)=(2/\mu)H(L^2+\hbar^2). \tag{5}$$

Relations (4) suggest the consideration of a subspace belonging to the eigenvalue E $(E<0)$ of the Hamiltonian as L and M commute with it. In this subspace it is meaningful to introduce the operator

$$\tilde{M}_i=(\mu/-2E)^{\frac{1}{2}}M_i.$$

Then, as a result, $(L+\tilde{M})/2$ and $(L-\tilde{M})/2$ build up two commuting sets of operators, each one satisfying the commutation relations of ordinary angular momentum; hence $[(L+\tilde{M})/2]^2=\hbar^2j_1(j_1+1)$ and

$$[(L-\tilde{M})/2]^2=\hbar^2j_2(j_2+1).$$

But according to Eq. (5), $L\cdot\tilde{M}=\tilde{M}\cdot L=0$ so that

$$[(L+\tilde{M})/2]^2=[(L-\tilde{M})/2]^2,$$

i.e., $j_1=j_2$. It is not clear at this point whether $j=j_1=j_2$ has to be limited to integer values or can also take half-integer values. Assuming for a moment that $2j$ can take any integer value, we derive from Eq. (5), that

$$(2E/\mu)(\tilde{M}^2+L^2+\hbar^2)=-k^2$$

but

$$\tilde{M}^2+L^2+\hbar^2=4[(\tilde{M}\pm L)/2]^2+\hbar^2$$

$$=\hbar^2[4j(j+1)+1]$$

$$=\hbar^2(2j+1)^2$$

and

$$E=-(\mu k^2/2\hbar^2)[1/(2j+1)^2]$$

or with $k=Ze^2$

$$E=-(Ze^2/\hbar)^2\tfrac{1}{2}\mu[1/(2j+1)^2]. \tag{6}$$

If we identify $2j+1$ with the principal quantum number n, we recognize the familiar expression for the levels in a Coulomb potential. With n taking every integer value from 1 to ∞, we see that j is allowed to take the values $0, \frac{1}{2}, 1, \frac{3}{2}, \cdots$. Moreover, as $L=(L+\tilde{M})/2+(L-\tilde{M})/2$, the familiar addition theorem for angular momenta shows that for a given $n=2j+1$ the possible values of L are $0, 1, 2, \cdots, 2j$. This procedure shows that the degeneracy of the levels is equal to

$$\sum_{l=0}^{2j}(2l+1)=(2j+1)^2=n^2.$$

It is tempting to assume that some group with the Lie algebra of $0_3\times0_3$ is acting (0_3 is the three-dimensional rotational group). A good candidate is 0_4, but when contemplating the actual form of M [Eq. (3)] it is seen that it is essentially a second-order differential operator in coordinate space. However, since the main part is linear in x, there might be some suspicion that it would be interesting to look in p-space for we know that properly parametrized infinitesimal generators are linear differential operators. This explains the second approach to the symmetry due to Fock.

B. The Global Method[3]

We make a Fourier transformation and write the equation in momentum space. The $1/r$ term gives rise to a convolution integral and we find

$$\left(\frac{p^2}{2\mu}-E\right)\Phi(p)=\frac{k}{2\pi^2\hbar}\int\frac{d^3q\Phi(q)}{|\mathbf{q}-\mathbf{p}|^2}. \tag{7}$$

In fact, it will be of interest to follow the remark of Alliluev[7] that the method can be generalized to any

[7] S. P. Alliluev, Zh. Eksperim. i Teor. Fiz. **33**, 200 (1957) [English transl.: Soviet Phys.—JETP **6**, 156 (1958)].

CC-0. In Public Domain. Gurukul Kangri Collection, Haridwar

Digitized by Arya Samaj Foundation Chennai and eGangotri

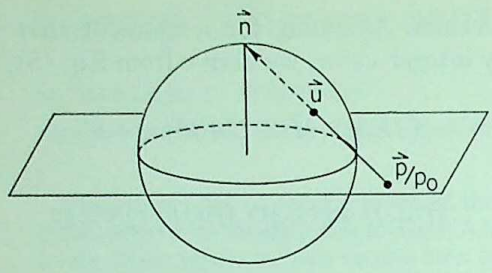

FIG. 1. Stereographic projection of the f-dimensional space to the unit sphere in $f+1$ dimensions.

number of dimensions greater than or equal to 2. The dimension will be denoted by f. We have

$$r^{-1}=(\pi\omega_{f-1})^{-1}\int\frac{d^fq}{|\mathbf{q}|^{f-1}}\exp(-i\mathbf{q}\cdot\mathbf{r}),$$

where ω_n is the area of the unit hypersphere in an n-dimensional space

$$\omega_n=2\pi^{n/2}/\Gamma(\tfrac{1}{2}n).$$

For dimension f, Eq. (7) generalizes to

$$\left(\frac{p^2}{2\mu}-E\right)\Phi(p)=\frac{k}{\pi\omega_{f-1}\hbar}\int\frac{d^fq\Phi(q)}{|\mathbf{q}-\mathbf{p}|^{f-1}}. \qquad (7')$$

Let us remark that, in the case of bound states, E is negative. We introduce the quantity

$$p_0^2=-2mE>0, \qquad (8)$$

and the equation now reads

$$(p^2+p_0^2)\Phi(p)=\frac{k}{\hbar}\frac{\Gamma[\frac{1}{2}(f-1)]}{\pi^{\frac{1}{2}}(f+1)}\int d^fq\frac{\Phi(q)}{|\mathbf{q}-\mathbf{p}|^{f-1}}. \qquad (9)$$

In this form the equation seems to exhibit nothing more than the usual f-dimensional rotational invariance. We now perform a change of variable. First, we replace $\mathbf{p}$ by $\mathbf{p}/p_0$, then imbed the f-dimensional space in an $f+1$ dimensional one and perform a stereographic projection on the unit sphere (Fig. 1). Let $\mathbf{u}$ be the point on the unit sphere corresponding to $\mathbf{p}$ and let $\mathbf{n}$ denote the unit vector from the origin to the north pole of the sphere; we have

$$\mathbf{u}=\frac{p^2-p_0^2}{p^2+p_0^2}\mathbf{n}+\frac{2p_0}{p^2+p_0^2}\mathbf{p}. \qquad (10)$$

An immediate calculation shows that

$$\begin{cases} d^{f+1}\Omega_u=2\delta(u^2-1)d^{f+1}u=[(2p_0)^f/(p_0^2+p^2)^f]d^fp \\ |\mathbf{p}-\mathbf{q}|^2=[(p^2+p_0^2)(q^2+p_0^2)/(2p_0)^2]\,|\mathbf{u}-\mathbf{v}|^2 \end{cases} \qquad (11)$$

if $\mathbf{v}$ corresponds to $\mathbf{q}$. Let us also change the wave function by defining

$$\hat{\Phi}(u)=(p_0)^{-\frac{1}{2}}[(p_0^2+p^2)/2p_0]^{(f+1)/2}\Phi(p). \qquad (12)$$

Inserting these values in Eq. (9) we get

$$\Phi(u)=\frac{\mu k}{2p_0\hbar}\frac{\Gamma[(f-1)/2]}{\pi(f+1)/2}\int\frac{d^{f+1}\Omega_v\hat{\Phi}(v)}{|\mathbf{v}-\mathbf{u}|^{f-1}}. \qquad (13)$$

The great interest of Eq. (13) is to show that the problem is rotationally invariant in an $(f+1)$-dimensional space, which in the case of $f=3$ implies an O_4 symmetry group. Before solving Eq. (13) it is interesting to compare the normalization of $\hat{\Phi}$ and Φ. We have

$$\int|\hat{\Phi}(u)|^2\,d\Omega_u=\int\frac{p_0^2+p^2}{2p_0^2}|\Phi(p)|^2\,d^fp.$$

We can now use the virial theorem which states

$$E\int|\Phi(p)|^2\,d^fp=-\int\frac{p^2}{2\mu}|\Phi(p)|^2\,d^fp$$

to obtain the result that [for a solution of Eq. (13)]

$$\int d^{f+1}\Omega_u|\hat{\Phi}(u)|^2=\int d^fp\,|\hat{\Phi}(p)|^2. \qquad (15)$$

Hence the mapping: $\Phi(p)$, belonging to the eigenvalue E, $\leftrightarrow\hat{\Phi}(u)$ satisfying Eq. (13) as given by conditions (10) and (12) preserves the scalar products. The mapping can be extended on one side to the Hilbert space of L^2 functions on the sphere—call it $\mathcal{H}_{f+1}$—the other to the Hilbert space of linear combinations of eigenfunctions (and their limits) corresponding to the discrete spectrum of the Hamiltonian. As the functions corresponding to different eigenvalues of the Hamiltonian are orthogonal and as the same property holds on the sphere for solutions of Eq. (13) corresponding to different eigenvalues of p_0, the extended mapping obtained in that way is one-to-one and isometric that is unitary. Note that it cannot be given through a geometric transformation of the type (14) which clearly depends on p_0.[8] We now solve Eq. (13) using the following remark. In the $(f+1)$-dimensional space, the kernel $(|\mathbf{u}-\mathbf{v}|^{f-1})^{-1}$ is essentially the Green function of the Laplace operator. More precisely,

$$\Delta_u{}^{f+1}(|\mathbf{u}-\mathbf{v}|^{f-1})^{-1}=-(f-1)\omega_{f+1}\delta^{f+1}(\mathbf{u}-\mathbf{v}). \qquad (16)$$

Moreover, the spherical harmonics defined on the sphere form a complete system of functions in $\mathcal{H}$. They are labeled by an integer λ taking the values

[8] If we vary p_0 in Eq. (10) we obtain a mapping of the sphere onto itself of a type which will be of interest in the next section. It can be geometrically described as follows. First perform an inversion of radius $\sqrt{2}$ with center at the north pole of Fig. 1); this sphere (this projects the sphere on the plane of Fig. 1); then "scale" transformation ($\mathbf{u}\to\lambda\mathbf{u}$), finally the inversion again. The whole operation leaves the sphere invariant and the north and south poles do not move. It turns out that we can get the same result as the product of two inversions with respect to two spheres orthogonal to the unit one with centers on the north-south axis.

CC-0. In Public Domain. Gurukul Kangri Collection, Haridwar

Digitized by Arya Samaj Foundation Chennai and eGangotri

0, 1, 2, ... and an index α whose meaning will be specified in a moment, such that if $Y_{\lambda,\alpha}$ is the spherical harmonic

$$|\mathbf{u}|^{\lambda} Y_{\lambda,\alpha}(\mathbf{u}/|\mathbf{u}|) = \mathcal{Y}_{\lambda,\alpha}(\mathbf{u})$$

is an homogeneous polynomial of degree λ in $\mathbf{u}$ constrained by the condition

$$\Delta^{f+1} \mathcal{Y}_{\lambda,\alpha}(\mathbf{u}) = 0. \tag{16}$$

The index α allows us to classify the set of solutions of Eq. (16) properly orthonormalized. An arbitrary homogeneous polynomial in $f+1$ variables of degree λ depends on

$$\binom{\lambda+f}{\lambda}$$

constants. Equation (16) gives

$$\binom{\lambda+f-2}{\lambda-2}$$

homogeneous conditions; hence the number of independent spherical harmonics belonging to the same λ, N_λ, is

$$N_\lambda = \binom{\lambda+f}{\lambda} - \binom{\lambda+f-2}{\lambda-2} = \frac{(\lambda+f-2)!(2\lambda+f-1)}{(f-1)!\lambda!} \tag{17}$$

(indeed, for $f=2$ we find $2\lambda+1$ and for $f=3$ $(\lambda+1)^2$, a result which we will use in a moment). Taking into account the fact that $\mathcal{Y}_{\lambda,\alpha}(\mathbf{v})$ and $(|\mathbf{v}-\mathbf{u}|^{f-1})^{-1}$ are harmonic in $\mathbf{v}$ everywhere except at the point $\mathbf{v}=\mathbf{u}$, we write Green's formula for $\mathbf{u}$ on the unit sphere and a surface S_ϵ as shown in Fig. 2:

$$S_\epsilon \equiv \{V\colon v^2=1, |\mathbf{v}-\mathbf{u}|^2 \geq \epsilon\}$$

$$\mathbf{U}\{v\colon v^2 \leq 1, |\mathbf{v}-\mathbf{u}|^2 = \epsilon\}.$$

We have

$$0 = \int_{S_\epsilon} \left[\mathcal{Y}_{\lambda,\alpha}(\mathbf{v}) \frac{d}{dn} \frac{1}{|\mathbf{v}-\mathbf{u}|^{f-1}} - \frac{1}{|\mathbf{v}-\mathbf{u}|^{f-1}} \frac{d}{dn} \mathcal{Y}_{\lambda,\alpha}(\mathbf{v}) \right] d\sigma.$$

The integral splits into two parts. The first one tends smoothly when ϵ goes to zero to an integral evaluated on the whole sphere. The second part taken over a small hemisphere around the point u tends to

$$[(f-1)/2]\omega_{f+1} \mathcal{Y}_{\lambda,\alpha}(\mathbf{u})$$

and since $\mathbf{u}$ is on the unit sphere $\mathcal{Y} \equiv Y$. Moreover, due to the homogeneity of $\mathcal{Y}$, we have

$$(d/dn)\mathcal{Y}_{\lambda,\alpha}(\mathbf{v})\,|_{v^2=1} = \lambda Y_{\lambda,\alpha}(\mathbf{v})$$

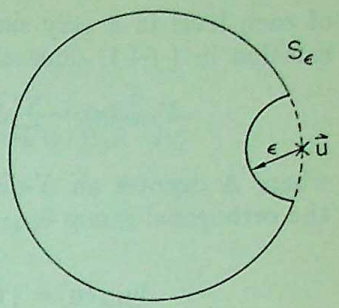

FIG. 2. The surface of integration in Green's formula.

and on the sphere $v^2=1$ (with $u^2=1$)

$$\frac{d}{dn} \frac{1}{|\mathbf{v}-\mathbf{u}|^{f-1}}\bigg|_{v^2=u^2=1} = -\frac{f-1}{2} \frac{1}{|\mathbf{v}-\mathbf{u}|^{f-1}}\bigg|_{v^2=u^2=1}.$$

Hence

$$0 = \frac{f-1}{2} \omega_{f+1} Y_{\lambda,\alpha}(\hat{u}) + \int \frac{d^{f+1}\Omega_v}{|\hat{v}-\hat{u}|^{f-1}} Y_{\lambda,\alpha}(\hat{u}) [-\tfrac{1}{2}(f-1)-\lambda].$$

Using again the formula for the area of the sphere, we get

$$Y_{\lambda,\alpha}(\hat{u}) = \frac{(f-1+2\lambda)}{4\pi^{\frac{1}{2}}(f+1)} \Gamma\left(\frac{f-1}{2}\right) \int \frac{d^{f+1}\Omega_v}{|\hat{v}-\hat{u}|^{f-1}} Y_{\lambda,\alpha}(\hat{u}). \tag{18}$$

Equation (13) is now to be compared with Eq. (18). Obviously, due to the completeness of spherical harmonics, we have thus found all the possible levels given by

$$\mu k/p_0\hbar = (f-1+2\lambda)/2$$

thus

$$E = -(p_0^2/2\mu) \equiv \tfrac{1}{2}\mu(k^2/\hbar^2)\tfrac{1}{2}(f-1+2\lambda)^{-2}. \tag{19}$$

If we now set $f=3$, then $\frac{1}{2}(f-1+2\lambda) = \lambda+1$ and we again get formula (6) with λ now identified with $2j$. The energy levels do not depend on the index α, and thus there are N_λ orthogonal states belonging to the same eigenvalue of the energy. Equation (17) gives the degeneracy in that case, $N_\lambda = (\lambda+1)^2$.

At the same time we have obtained the eigenfunctions which are to be identified with a set of spherical harmonics on the four-dimensional sphere [or more generally on an $(f+1)$-dimensional sphere]. There are several possible ways to label the additional quantum numbers in one level and this will be discussed in the next paragraph. For the moment let us observe that the 0(4) symmetry group acts on the eigenfunctions

CC-0. In Public Domain. Gurukul Kangri Collection, Haridwar

Digitized by Arya Samaj Foundation Chennai and eGangotri

of each level in a very simple way for if 0 denotes a rotation in $(f+1)$-dimensional space

$$Y_{\lambda,\alpha}(0\hat{u}) = \sum_{\alpha'} \Delta_{\alpha,\alpha'}{}^{\lambda}(0)\, Y_{\lambda,\alpha}(\hat{u}),$$

where Δ denotes an N-dimensional representation of the orthogonal group $0_{(f+1)}$. Remembering that

$$\mathcal{Y}_{\lambda,\alpha}(\mathbf{u}) = |\,\mathbf{u}\,|^{\lambda} Y_{\lambda,\alpha}\left(\frac{\mathbf{u}}{|\,\mathbf{u}\,|}\right)$$

the representation just written is, in fact, obtained by letting the matrix 0 transform the coordinates of $\mathbf{u}$ in the form $(0u)_i = \sum_j 0_{ij} u_j$ and looking for the corresponding transformation of the symmetric polynomial $\mathcal{Y}_{\lambda,\alpha}$. In fact, $\mathcal{Y}_{\lambda,\alpha}$ is not an arbitrary symmetric polynomial and the corresponding representation of $0_{(f+1)}$ is the one which, in the language of Young tableaux, is made of a single row of λ boxes. (A harmonic polynomial can essentially be written as

$$\sum_{i_1,i_2,\ldots,i_\lambda} t_{i_1,i_2,\ldots,i_\lambda}\, x_{i_1} x_{i_2} \cdots x_{i_\lambda},$$

with t symmetric in its indices and of zero trace in each pair of term.) In particular, for 0(4) these representations when described in terms of two angular momenta are labeled $\mathfrak{D}^{j,j}$ with $\lambda = 2j$. Using the classical branching law for the orthogonal group, one readily sees that they split according to the 0(3) subgroup in a direct sum of representations with $l = 0, 1, \cdots, 2j$. This gives us the allowed values of the ordinary angular momentum for a level with principal quantum number $n = \lambda+1 = 2j+1$. It is even intuitive that an homogeneous polynomial of degree λ in $f+1$ variables can be written as a sum of homogeneous polynomials of degrees $0, 1, \cdots, 2j$ in the first f variables. By choosing them harmonic, one has thus a procedure to compute the wave function. We shall obtain explicitly the wave functions in another way.

Let us finally use Eq. (18) to write an expansion of the Green kernel. For $\mathbf{v}$ and $\mathbf{u}$, not of equal length, one deduces immediately from the fact that in a p-dimensional space

$$|\,\mathbf{u}\,|^{\lambda} Y_{\lambda,\alpha}(\mathbf{u}/|\,\mathbf{u}\,|) \quad \text{and} \quad (1/|\,\mathbf{u}\,|)^{\lambda+p-2} Y_{\lambda,\alpha}(\mathbf{u}/|\,\mathbf{u}\,|)$$

are both harmonic

$$\frac{\Gamma[\frac{1}{2}(p-2)]}{4\pi^{p6/2}} \frac{1}{|\,\mathbf{u}-\mathbf{v}\,|^{p-2}}$$

$$= \sum_{\lambda} \frac{W_<{}^{\lambda}}{W_>{}^{l+p-2}} \frac{\sum_\alpha Y_{\lambda,\alpha}{}^{(p)}(\mathbf{u}/u)\, Y_{\lambda,\alpha}{}^{(p)}(\mathbf{u}/u)}{p-2+2\lambda}, \quad (20)$$

where $W_<(W_>)$ denotes the smaller (greater) of the two quantities $|\,\mathbf{u}\,|$, and $|\,\mathbf{v}\,|$. The superscript on the spherical harmonics recalls the dimension of the space. In this formula they are assumed orthonormalized.

C. Calculation of Wave Functions

We shall now compute the wave functions using another possibility afforded by group theory. We recall the remark that the four-dimensional sphere is homomorphic with the space of parameters of the group SU_2, the uni-modular unitary group in two dimensions (which is the covering group of the ordinary three-dimensional rotation group). Moreover, we know a complete set of functions on this space,[9] namely, the matrix elements of the various representations $\mathfrak{D}_{m,m'}$ labeled by j, taking the values $0, \frac{1}{2}, 1, \cdots$ and $-j \leq m \leq j$, $-j \leq m' \leq j$. The $\mathfrak{D}$ functions were computed by Wigner and are given below. They seem to be good candidates for being spherical harmonics on the sphere if we notice further that, corresponding to a "spin" j, they are $(2j+1)^2$ in number—precisely the number of spherical harmonics of degree $\lambda = 2j$. We shall prove that this is, indeed, the case. This kind of coincidence is very peculiar to the dimension we are precisely interested in.

Let us first recall the correspondence between the sphere and SU_2. The most general unitary unimodular two-by-two matrix can be written:

$$A = u_0 + i\boldsymbol{\sigma}\cdot\mathbf{u}, \quad (21)$$

with $(u_0, \mathbf{u})$ real, $u_0{}^2+\mathbf{u}^2 = 1$, and $\sigma_1, \sigma_2, \sigma_3$ are the usual Pauli matrices. This parametrization sets a one-to-one correspondence between the two spaces and hence between the functions defined on the two spaces.

Writing the previous matrix A as

$$A = \begin{pmatrix} a & b \\ -\bar{b} & \bar{a} \end{pmatrix}, \qquad a\bar{a}+b\bar{b} = 1$$

$$a = u_0 + iu_3, \qquad b = iu_1 + u_2. \quad (22)$$

An invariant measure on SU_2 is

$$\delta(a\bar{a}+b\bar{b}-1)\tfrac{1}{2}(da\,d\bar{a}\,db\,d\bar{b}),$$

but up to a constant factor we know that invariant measures are unique on a compact group; hence, this measure is the usual one (up to a factor). It also results

$$2\delta(u^2-1)\,d^4u = \delta(a\bar{a}+b\bar{b}-1)\tfrac{1}{2}(da\,d\bar{a}\,db\,d\bar{b}). \quad (23)$$

Consequently, the measure on SU_2 coincides with the usual measure on the sphere and we have

$$\int 2\delta(u^2-1)\, diu = \int_{SU_2} \delta(a\bar{a}+b\bar{b}-1)\tfrac{1}{2}(da\,d\bar{a}\,db\,d\bar{b}) = 2\pi^2. \quad (24)$$

Moreover, we can extend SU_2 to a group $\{R_+\}$ X

[9] This is the content of Peter–Weyl theorem. C. Chevalley, *Theory of Lie Groups* (Princeton University Press, Princeton, N.J., 1946), p. 203.

CC-0. In Public Domain. Gurukul Kangri Collection, Haridwar

Digitized by Arya Samaj Foundation Chennai and eGangotri

where R_+ is the multiplicative group of real positive numbers and make it in one-to-one correspondence with the four-dimensional space without the origin. This means that we multiply the matrix A by a real positive factor. Including the value 0 extends the correspondence to the whole space. Now let us recall the definition of Wigner's $\mathfrak{D}$ functions. Let B be the most general two-by-two matrix

$$B=\begin{pmatrix} a & b \\ c & d \end{pmatrix}.$$

Consider polynomials in two variables of degree $2j$ of which a basis is given by

$$P_{j,m}(\xi,\eta)=\frac{\xi^{j+m}}{[(j+m)!]^{\frac{1}{2}}}\frac{\eta^{j-m}}{[(j+m)!]^{\frac{1}{2}}}$$

$$m=j, j-1, \cdots, -j. \tag{25}$$

$$P_{j,m}(a\xi+b\eta, c\xi+d\eta)=\frac{(a\xi+b\eta)^{j+m}}{[(j+m)!]^{\frac{1}{2}}}\frac{(c\xi+d\eta)^{j-m}}{[(j-m)!]^{\frac{1}{2}}}$$

$$=\sum_{m'=-j}^{j}\mathfrak{D}_{m,m'}{}^{j}(B)\,P_{j,m'}(\xi,\eta) \tag{26}$$

with

$$\mathfrak{D}_{m,m'}{}^{j}(B)=[(j+m)!(j-m)!(j+m')!(j-m')!]^{\frac{1}{2}}$$

$$\times\sum_{n_i>0}\frac{a^{n_1}\cdot b^{n_2}\cdot c^{n_3}\cdot d^{n_4}}{n_1!\cdot n_2!n_3!\cdot n_4!} \tag{27}$$

$$n_1+n_2=j+m, \qquad n_3+n_4=j-m$$

$$n_1+n_3=j+m', \qquad n_2+n_4=j-m'.$$

The ordinary matrix elements of the irreducible representations of SU_2 corresponding to spin j are obtained by putting in Eq. (27) for B the general element $A\in SU_2$. Formula (27) is suited for computing $\mathfrak{D}_{m,m'}{}^{j}\times(sA)$ when $s\geq 0$. Now $\mathfrak{D}_{m,m'}{}^{j}(sA)$ can be considered as a function in the four-dimensional (real) space, and obviously it is homogeneous of degree $2j$; that is,

$$\mathfrak{D}_{m,m'}{}^{j}(sA)=s^{2j}\mathfrak{D}_{m,m'}{}^{j}(A). \tag{28}$$

Moreover, we will now show that it satisfies the Laplace equation. Since we obtain for each integer $2j$ a set of $(2j+1)^2$ linearly independent homogeneous polynomials satisfying the Laplace equation, the $\mathfrak{D}_{m,m'}{}^{j}(A)$ form a complete set of spherical harmonics on the four-dimensional sphere. The Laplace operator is

$$\Delta_u{}^4=\frac{\partial^2}{\partial u_0{}^2}+\frac{\partial^2}{\partial u_1{}^2}+\frac{\partial^2}{\partial u_2{}^2}+\frac{\partial^3}{\partial u_3{}^2}.$$

We now use the relation

$$\frac{\partial^2}{\partial x^2}+\frac{\partial^2}{\partial y^2}=4\frac{\partial}{\partial(x+iy)}\frac{\partial}{\partial(x-iy)}$$

hence

$$\Delta_u{}^4=4\left[\frac{\partial}{\partial(u_0+iu_3)}\frac{\partial}{\partial(u_0-iu_3)}+\frac{\partial}{\partial(iu_1+u_2)}\frac{\partial}{\partial(-iu_1+u_2)}\right]$$

$$=4\left[\frac{\partial}{\partial(sa)}\frac{\partial}{\partial(s\bar{a})}+\frac{\partial}{\partial(sb)}\frac{\partial}{\partial(s\bar{b})}\right]. \tag{29}$$

In order to prove that $\Delta^4\mathfrak{D}_{m,m'}{}^{j}=0$, it is sufficient to prove that

$$\sum_{m'=-j}^{j}\Delta^4\mathfrak{D}_{m,m'}{}^{j}(sA)\frac{\xi^{j+m'}}{(j+m')!}\frac{\eta^{j-m'}}{(j-m')!}=0 \tag{30}$$

since the $P_{j,m'}(\xi,\eta)$ are linearly independent polynomials; hence we have to compute

$$\Delta^4(sa\xi+sb\eta)^{j+m}(-s\bar{b}\xi+s\bar{a}\eta)^{j-m}.$$

Using Eq. (29) we easily find that this quantity is zero. More generally, we can check that

$$\left(\frac{\partial^2}{\partial a\partial d}-\frac{\partial^2}{\partial b\partial c}\right)\mathfrak{D}_{m,m'}{}^{j}(B)=0.$$

Next we study the normalization. We have

$$\int(\mathfrak{D}_{m_1m_2}{}^{j}(A))^*\mathfrak{D}_{m_1'm_2'}{}^{j'}(A)\,d^4\Omega_u$$

$$=\frac{2\pi^2}{2j+1}\delta_{jj'}\delta_{m_1m_1'}\delta_{m_2m_2'}$$

$$A=u_0+i\boldsymbol{\sigma}\cdot\mathbf{u} \qquad u_0{}^2+\mathbf{u}^2=1. \tag{31}$$

The only point to be verified is the factor $2\pi^2/(2j+1)$, otherwise the orthogonality stems from Schur's lemma. For that purpose we note that

$$\sum_{\mu}\mathfrak{D}_{m_1\mu}{}^{j}(A)\mathfrak{D}_{\mu m_2}{}^{j}(A)=\delta_{m_1m_2}.$$

Hence

$$\int\sum_{\mu}(\mathfrak{D}_{\mu m_1}{}^{j})^*(A)\mathfrak{D}_{\mu m_2}{}^{j}(A)\,d^4\Omega_\mu=\delta_{m_1m_2}2\pi^2,$$

where $2\pi^2$ is the surface of the sphere. On the other hand, Eq. (31) gives

$$\frac{2\pi^2}{2j+1}\sum_{n=-j}^{+j}\delta_{m_1m_2}=2\pi^2\delta_{m_1m_2}.$$

CC-0. In Public Domain. Gurukul Kangri Collection, Haridwar

Digitized by Arya Samaj Foundation Chennai and eGangotri

A complete set of spherical harmonics properly normalized on the four-dimensional sphere is thus

$$Y_{2j;m_1,m_2}{}^{(4)}(u)=[(2j+1)/2\pi^2]^{\frac{1}{2}}\mathfrak{D}_{m_1,m_2}{}^{j}(u_0+iu\cdot\sigma)$$
$$2j=0,1,\cdots,\quad -j\leq m_i\leq j. \tag{32}$$

The $\mathfrak{D}_{m_1,m_2}{}^{j}$ also afford very quickly the representation of $0(4)$ in the following way. First let U be a generic element of SU_2. Then if we select V and W belonging to SU_2, the correspondence

$$U\rightarrow U'=VUW^{+}$$

is a mapping of SU_2 on itself. It is clear that if we write $U=u_0+i\sigma\mathbf{u}$ the mapping $u\rightarrow u'$ is linear; hence, we have obtained an orthogonal transformation. The set of pairs (V, W) with the law of multiplication (V', W') $(V, W)=(V'V, W'W)$ forms a group—namely $(SU_2\times SU_2)$ and we have an homomorphism $(SU_2, SU_2)\rightarrow 0(4)$ which can readily be seen to cover $0(4)$. This is, of course, well known. The kernel of the mapping consists of the two elements (I, I) and $(-I, -I)$. The diagonal subgroup of pairs of the form (U, U) corresponds to three-dimensional rotations of $\mathbf{u}$, and we are going to use it in the following.

The transformations of the type (U, U^{+}), on the other hand {where $U=\exp[(i\theta/2)\sigma\cdot\mathbf{n}]$}, correspond to rotations (through angle θ) in the two-plane passing through the 0 axis and the axis $\mathbf{n}$ (in the three-dimensional subspace $u_0=0$). Now we write the general orthogonal transformation as:

$$Y_{\lambda,\alpha}{}^{(4)}(u)\rightarrow Y_{\lambda,\alpha}{}^{(4)}(0^{-1}u)=\sum\Delta_{\alpha'\alpha}(0)\,Y_{\lambda,\alpha'}{}^{(4)}(u)\,0\in 0_4.$$

If $(V, W)\rightarrow 0$, then $(V, W)^{-1}=(V^{+}, W^{+})\rightarrow 0^{-1}$; with the set of spherical harmonics given by Eq. (32), we have as a result of the properties of $\mathfrak{D}$ functions

$$Y_{2j;m_1,m_2}{}^{(4)}(0^{-1}u)$$
$$=\mathfrak{D}_{m_1m_1'}{}^{j}(V^{+})\mathfrak{D}_{m_2'm_2}{}^{j}(W)\,Y_{2j;m_1'm_2'}{}^{(4)}(u).$$

Hence

$$\Delta_{m_1',m_2';m_1,m_2}{}^{2j}[(V, W)]=\mathfrak{D}_{m_1',m_1}{}^{j}(W). \tag{33}$$

Of course, (V, W) and $(-V, -W)$ give rise to the same matrix. In particular, since we are to make use of it, we find easily the representation of a rotation through angle θ in the $(0, 3)$ plane, namely,

$$\Delta_{m_1'm_2';m_1m_2}{}^{2j}(\{\exp[i(\theta/2)\sigma_3],\exp[-(\theta/2)\sigma_3]\})$$
$$=\exp[-i(m_1+m_2)\theta]\delta_{m_1'm_1}\delta_{m_2'm_2}. \tag{33'}$$

Before giving further interpretation of formula (32) we shall construct the set corresponding to the diagonalization in angular momentum. We remark that rotating $\mathbf{p}$, the three-dimensional momentum, amounts to submitting $\mathbf{u}$, the projection of the 4-vector $\{u_0, \mathbf{u}\}$, to the same rotation.

If $A(u)=u_0+i\sigma\mathbf{u}$, then

$$A(u_0, R\mathbf{u})=RAR^{-1},$$

where for simplicity of the notation, R stands on the right-hand side for the 2×2 unitary matrix which corresponds to the rotation. Our second remark is that Γ is the two-by-two unitary unimodular matrix

$$\Gamma=\begin{pmatrix}0 & 1\\ -1 & 0\end{pmatrix}.$$

Then for any 2×2 unitary unimodular matrix

$$R^{-1}\Gamma=\Gamma R^{T}.$$

Consider $\mathfrak{D}_{m,m'}{}^{j}[A(u)\Gamma]$; then

$$\mathfrak{D}_{m,m'}{}^{j}[A(u_0, R\mathbf{u})\Gamma]=\mathfrak{D}_{m,m'}{}^{j}[RA(u)\Gamma R^{T}]$$
$$=\mathfrak{D}_{m,m_1}{}^{j}(R)\mathfrak{D}_{m_1'm'}{}^{j}(R^{T})$$
$$\times\mathfrak{D}_{m_1m_1'}{}^{j}[A(u)\Gamma]$$

But, as is immediate from formula (27), $\mathfrak{D}^{j}(R^{T})=\mathfrak{D}^{jT}(R)$ so that

$$\mathfrak{D}_{m,m'}{}^{j}[A(u_0, R\mathbf{u})\Gamma]$$
$$=\mathfrak{D}_{m,m_1}{}^{j}(R)\mathfrak{D}_{m',m_1'}{}^{j}(R)\mathfrak{D}_{m_1,m_1'}{}^{j}[A(u)\Gamma].$$

This last formula shows that the spherical harmonics of degree $2j$ form the carrier space of a reducible representation of the three-dimensional rotation group and this representation can be reduced to a sum corresponding to angular momenta $L=0, 1, 2, \cdots, 2j$. $(j, m; j, m' \mid LM)$ denotes the usual Clebsch-Gordan coefficient,[10] we recall that

$$\sum_{-L\leq M'\leq L}(jm; jm' \mid LM')\mathfrak{D}_{MM'}{}^{L}(R)$$
$$=\sum_{\substack{-j\leq m_1\leq +j\\ -j\leq m_1'\leq +j}}(jm_1; jm_1' \mid LM)\mathfrak{D}_{m_1m}{}^{j}(R)\mathfrak{D}_{m_1'm'}{}^{j}(R).$$

With the help of Eq. (37) we obtain immediately in space the properly normalized eigenfunctions of the problem with principal quantum number $n=2j+1$, angular momentum L, and magnetic quantum number M as

$$Y_{\substack{n;L,M\\ n=2j+1}}{}^{(4)}(u)=\left(\frac{2j+1}{2\pi^2}\right)^{\frac{1}{2}}\sum_{\substack{-j\leq m\leq +j\\ -j\leq m'\leq +j}}(j, m; jm' \mid LM)$$
$$\times\mathfrak{D}_{m,m'}{}^{j}[(u_0+i\sigma\cdot\mathbf{u})\Gamma]$$

such that

$$Y_{n,L,M}{}^{(4)}(u_0, R^{-1}\mathbf{u})=Y_{n,LM'}{}^{(4)}(u_0, \mathbf{u})\mathfrak{D}_{M'M}{}^{j}(R).$$

[10] See for instance, A. Messiah, *Quantum Mechanics* (North-Holland Publishing Company, Amsterdam, 1964), especially Vol. II, Appendix C.

CC-0. In Public Domain. Gurukul Kangri Collection, Haridwar

Digitized by Arya Samaj Foundation Chennai and eGangotri

Using the properties of C. G. coefficient one shows that

$$Y_{n;LM}{}^{(4)}(u)=\left(\frac{2}{\pi}\right)^{\frac{1}{2}}\frac{i^L\sin\delta^L}{[(n^2-1^2)\cdots(n^2-L^2)]^{\frac{1}{2}}}\frac{d^L}{d(\cos\delta)^L}\times\left(\frac{\sin n\delta}{\sin\delta}\right)Y_{LM}{}^{(3)}\left(\frac{\mathbf{u}}{|\mathbf{u}|}\right),\quad(40)$$

where δ is defined through $u_0+i\mathbf{u}=e^{i\delta}$. The derivation of this formula is given in the appendix.

We can easily derive from Eq. (32) or (38) the projection operator on to the space corresponding to principal quantum number $n=2j+1$ which appears in several formulas, as for instance in Eq. (20). We have $\mathcal{P}$ standing for this projection operator:

$$\begin{aligned}\mathcal{P}_{n=2j}{}^{(4)}(u,v)&=\sum_{L,M}Y_{2j;L,M}(u)\,\bar{Y}_{2j;L,M}(v)\\&=\sum_{m,m'}[(2j+1)/2\pi^2]\mathfrak{D}_{m,m'}{}^{j}[A(u)]\times(\mathfrak{D}_{m,m'}{}^{j}[A(v)])^*,\\&=\sum_{m,m'}[(2j+1)/2\pi^2]\mathfrak{D}_{m,m'}{}^{j}[A(u)]\times\mathfrak{D}_{m,m'}{}^{j}[A^{-1}(v)],\\&=[(2j+1)/2\pi^2]\sum_{m}\mathfrak{D}_{m,m}{}^{j}[A(u)A^{-1}(v)],\\&=[(2j+1)/2\pi^2]\,\mathrm{Tr}\,\mathfrak{D}^{j}[A(u)A^{-1}(v)].\end{aligned}\quad(41)$$

Now we want to compute $A(u)A^{-1}(v)$. We have

$$\begin{aligned}A(u)A^{-1}(v)&=(u_0+i\boldsymbol{\sigma}\cdot\mathbf{u})(v_0-i\boldsymbol{\sigma}\mathbf{v})\\&=u_0v_0+\mathbf{u}\cdot\mathbf{v}+i\boldsymbol{\sigma}\cdot(v_0\mathbf{u}-u_0\mathbf{v}+\mathbf{u}\times\mathbf{v})\end{aligned}$$

the unitary unimodular matrix can also be written

$$\begin{aligned}A(u)A^{-1}(v)&=\cos(\phi/2)-i\sin(\phi/2)\,\boldsymbol{\sigma}\cdot\mathbf{n}\\&=\exp[-i(\phi/2)\,\boldsymbol{\sigma}\cdot\mathbf{n}].\end{aligned}$$

If θ is the angle between u and v on the 4-sphere, we have

$$\cos\theta=u_0v_0+\mathbf{u}\cdot\mathbf{v}=\cos(\phi/2)$$

hence, $\phi=2\theta$ (the sign is irrelevant). Since we compute a trace, we can choose our coordinate system as we please. In particular, "quantizing" along the axis $\mathbf{n}$, we have

$$\mathrm{Tr}\,\mathfrak{D}^{j}[A(u)A^{-1}(v)]=\sum_{m=-j}^{+j}\exp(2im\theta)=\frac{\sin(2j+1)\theta}{\sin\theta}$$

(we recognize the Chebichev polynomials if $\sin(2j+1)\theta/\sin\theta$ is expressed as a polynomial of degree $2j$ in $\cos\theta$). The answer is thus

$$\begin{aligned}\mathcal{P}_n{}^{(4)}(u,v)&=\frac{n}{2\pi^2}\frac{\sin n\theta}{\sin\theta}\\&=\frac{1}{2\pi^2}\frac{d}{d\cos\theta}(\cos n\theta)\end{aligned}$$

$$\begin{aligned}u\cdot v&=\cos\theta,\\u^2&=v^2=1.\end{aligned}\quad(42)$$

Using this result, we can rewrite formula (20) for $f+1=4$ as

$$\frac{1}{4\pi^2}\frac{1}{|\mathbf{u}-\mathbf{v}|^2}=\frac{1}{4\pi^2}w_>{}^{-2}\left(1+\left(\frac{w_<}{w_>}\right)^2-\left(\frac{2w_<}{w_>}\right)\cos\theta\right)^{-1}$$

$$=\frac{1}{w_>{}^2}\sum_{2j=0,1,\ldots}\left(\frac{w_<}{w_>}\right)^{2j}\frac{1}{2(2j+1)}\times\frac{(2j+1)}{2\pi^2}\frac{\sin(2j+1)\theta}{\sin\theta}.$$

Thus with $t=(w_</w_>)<1$, we find the classical generating functions for Chebichev polynomials

$$(1+t^2-2t\cos\theta)^{-1}=\sum_{\lambda=0}^{\infty}t^\lambda\frac{\sin(\lambda+1)\theta}{\sin\theta}.\quad(43)$$

Comparing this result with the generating function for Legendre polynomials (which arises in our case for $f=2$ from the Green function corresponding to the Laplace equation in three dimensions):

$$(1+t^2-2t\cos\theta)^{-\frac{1}{2}}=\sum_{l=0}^{\infty}t^\lambda P_\lambda(\cos\theta)$$

we deduce the relation

$$[\sin(\lambda+1)\theta/\sin\theta]=\sum_{\lambda_1+\lambda_2=\lambda}P_{\lambda_1}(\cos\theta)\,P_{\lambda_2}(\cos\theta).\quad(44)$$

More generally, we can compute similar projectors in arbitrary dimensions. Our examples suggest that we distinguish between odd and even dimensions. We have in even dimension $p=2r$, according to formula (20)

$$\frac{1}{(1+t^2-2t\cos\theta)^{r-1}}=\sum_{0}^{\infty}t^\lambda\frac{4(\pi)^r}{2\Gamma(r-1)}\frac{\mathcal{P}_\lambda{}^{(2r)}(\cos\theta)}{r+\lambda-1}.$$

Where $\mathcal{P}_\lambda{}^{(2r)}$ is the projector, i.e., a polynomial of degree λ in $\cos\theta$ which can be obtained simply by differentiating Eq. (43) to give

$$\frac{1}{(1+t^2-2t\cos\theta)^{r-1}}=\frac{1}{2^{r-2}\Gamma(r-1)}\times\sum_{\lambda=0}^{\infty}t^\lambda\left(\frac{d}{d\cos\lambda}\right)^{r-2}\frac{\sin(\lambda+r-1)\theta}{\sin\theta}$$

CC-0. In Public Domain. Gurukul Kangri Collection, Haridwar

Digitized by Arya Samaj Foundation Chennai and eGangotri

and

$$\mathcal{P}_\lambda^{(2r)}(\cos\theta)=\frac{2(r+\lambda-1)}{(2\pi)^r}\left(\frac{d}{d\cos\theta}\right)^{r-2}\frac{\sin(\lambda+r-1)\theta}{\sin\theta}$$
$$\equiv\sum_\alpha Y_{\lambda,\alpha}^{(2r)}(u)\,\bar{Y}_{\lambda,\alpha}^{(2r)}(v);\qquad r\geq 2. \quad (45)$$

In the odd case the calculation is completely similar and yields:

$$\mathcal{P}_\lambda^{(2r+1)}(\cos\theta)=\frac{(r+\lambda-\frac{1}{2})}{(2\pi)^r}\left(\frac{d}{d\cos\theta}\right)^{r-1}P_{\lambda+r-1}(\cos\theta)$$
$$\equiv\sum_\alpha Y_{\lambda,\alpha}^{(2r+1)}(u)\,\bar{Y}_{\lambda,\alpha}^{(2r+1)}(v);$$
$$r\geq 1. \quad (46)$$

Of course, one can express these polynomials in terms of products of Legendre polynomials.

D. Connection Between the Two Approaches; Parabolic Coordinates[4]

In this paragraph we want to show that the generators of the group of symmetry found in the global method coincide essentially with the two vectors, L and M, introduced in Sec. IIA, as should be expected. We will also show that the two sets of spherical harmonics that we have found (connected one to another by a unitary fixed transformation), equations (32) and (38), correspond indeed, with the possibility already present in the classical problem, of separating variables into two different systems of coordinates. Classically it is also known that the "accidental degeneracy" is related to this fact.

To generate our group, $0(4)$, we can use six infinitesimal operators—the first three correspond to ordinary rotations in $\mathbf{p}$-space and lead to the conservation of angular momentum. The next three correspond in u-space to infinitesimal rotations in the (u_0u_1), (u_0u_2), and (u_0u_3) planes. We shall compute the generator in that case. For that purpose let $\Phi(p)$ be a solution of Eq. (7); then the transformation, corresponding to an infinitesimal rotation in the (u_0u_3) plane is

$$\frac{p'^2-p^2}{p'^2+p_0^2}=\frac{p^2-p_0^2}{p^2+p_0^2}-\epsilon_{03}\frac{2p_0p_3}{p^2+p_0^2}$$
$$\frac{2p_0p_3'}{p'^2+p_0^2}=\epsilon_{03}\frac{p^2-p_0^2}{p^2+p_0^2}+\frac{2p_0p_3}{p^2+p_0^2}$$
$$\frac{2p_0p_i'}{p'^2+p_0^2}=\frac{2p_0p_i}{p^2+p_0^2};\qquad i=1,2$$

or

$$\delta p_3=\epsilon_{03}[(p^2-p_0^2-2p_3^2)/2p_0],$$
$$\delta p_2=-\epsilon_{03}(p_3p_2/p_0),$$
$$\delta p_1=-\epsilon_{03}(p_3p_1/p_0). \quad (47)$$

Using Eq. (12) this gives the infinitesimal transformation $\Phi(p)\to\Phi'(p)=\Phi(p)+\delta\Phi(p)$

$$\delta\Phi(p)=\frac{\epsilon_{03}}{(p^2+p_0^2)^2}$$
$$\times\left[\frac{p^2-p_0^2-2p_3}{2p_0}\frac{\partial}{\partial p_3}-\frac{p_3p_1}{p_0}\frac{\partial}{\partial p_0}-\frac{p_3p_2}{p_0}\frac{\partial}{\partial p_2}\right]$$
$$\times(p^2+p_0^2)^2\Phi(p). \quad (4$$

The infinitesimal generator when written as

$$\delta\Phi(p)=(-i\mu/\hbar p_0)\,\epsilon_{03}M_{03}\Phi(p) \quad (4$$

is [with $x_i=i\hbar(\partial/\partial p_i)$]

$$M_{03}=\frac{1}{(p^2+p_0^2)^2}\left[\frac{p^2-p_0^2}{2\mu}x_3-\frac{p_3}{\mu}(\mathbf{p}\cdot\mathbf{r})\right](p^2+p_0^2)^2$$
$$=\frac{p^2-p_0^2}{2\mu}x_3-\frac{p_3}{\mu}(\mathbf{p}\cdot\mathbf{r})-2i\frac{\hbar p_1}{\mu}.$$

At this point we recall that M_{0i} acts on an eigenfu tion of the Hamiltonian—corresponding to the eige value $E=-p_0^2/2m$. Moving p_0^2 to the right, we c replace it by $-2mH=-2m[(p^2/2m)-(k/r)]$ so th M can now act on any linear combination of eige functions. Clearly the calculation of M_{02} and M_{0} completely analogous. We introduce the vector whose components are M_{01}, M_{02}, M_{03}

$$\mathbf{M}=\frac{p^2}{2\mu}\mathbf{r}+\mathbf{r}\left(\frac{p^2}{2\mu}-\frac{k}{r}\right)-\frac{\mathbf{p}}{\mu}(\mathbf{p}\cdot\mathbf{r})-2i\hbar\frac{\mathbf{p}}{\mu}$$

$$\mathbf{M}=\left(\frac{p^2}{\mu}\mathbf{r}-\frac{\mathbf{p}}{\mu}(\mathbf{p}\cdot\mathbf{r})-i\hbar\frac{\mathbf{p}}{\mu}\right)-\frac{k}{r}\mathbf{r}. \quad (5$$

Equation (50) can also be written

$$\mathbf{M}=(\mathbf{p}/2\mu)\times\mathbf{L}-\mathbf{L}\times(\mathbf{p}/2\mu)-(k/r)\mathbf{r}$$

which is seen to coincide with Eq. (3) and leads to t interpretation of the second vector. It merely cor sponds to the three generators of rotations in the planes passing through the fourth axis introduced the stereographic projection.

Our second remark has to do with the two systems spherical harmonics we have used on the sphere The first one $\{Y_{n;L,M}\}$ clearly corresponds to usual separation of variables in polar coordinates. natural to ask if the second system

$$\{Y_{n:m,m'}=(2j+1/2\pi^2)^{\frac{1}{2}}\mathfrak{D}_{m,m'}^{j};\qquad n=2j+1\}$$

corresponds to another natural system of coordina which allow separation of variables. As expected, will show that this is related to parabolic coordinat For that purpose we write in the p space

$$\Phi_{n;m,m'}(\mathbf{p})=(2j+1/\pi^2)^{\frac{1}{2}}[2p_0/(p^2+p_0^2)]^2$$
$$\times(p_0)\,\epsilon\mathfrak{D}_{m,m'}^{j}[A(\mathbf{p})] \quad (5$$

with

$$A(\mathbf{p})=\frac{p^2-p_0^2}{p^2+p_0^2}+i\frac{2p_0}{p^2+p_0^2}\boldsymbol{\delta}\cdot\mathbf{p}.$$

CC-0. In Public Domain. Gurukul Kangri Collection, Haridwar

Digitized by Arya Samaj Foundation Chennai and eGangotri

According to Eq. (36)

$$\Phi_{n;m,m_1'}(R\mathbf{p}) = \mathfrak{D}_{m,m_1}{}^{j}(R)\,\mathfrak{D}_{m',m_1'}{}^{j}(R^{-1})\,\Phi_{n;m_1m_1'}(\mathbf{p}).$$

In particular, if R is a rotation of angle ψ around the z axis

$$\mathfrak{D}_{m,m_1}{}^{j}(R_\psi) = \exp(-im\psi)\,\delta_{m,m_1}$$

so that

$$\Phi_{n;m,m'}(R_\psi) = \exp[-i(m-m')\psi]\Phi_{n;m,m'}(p).$$

Hence, $\Phi_{n;m,m'}$ is an eigenfunction of the third component of the angular momentum L_3 corresponding to the eigenvalue $\hbar(m'-m)$. Now, L_3 commutes with $M_3 \equiv M_{03}$ according to Eq. (4). We thus investigate the effect of an infinitesimal "rotation" in the (03) u-plane. For that purpose we use Eq. (33′)

$$\mathfrak{D}_{m,m'}{}^{j}(R_{-\epsilon_{03}u}) = \exp[-i(m_1+m_2)\epsilon_{03}]\mathfrak{D}_{m,m'}{}^{j}(u),$$

where $R_{-\epsilon_{03}}$ indicates a rotation through angle $-\epsilon_{03}$ in the (03) plane. Changing from $-\epsilon_{03}$ to $+\epsilon_{03}$ and comparing with Eq. (49), we have immediately the action of M_3. We now have

$$L_3\Phi_{n_1,m,m'}(p) = \hbar(m'-m)\,\Phi_{n;m,m'}(p)$$

$$M_3\Phi_{n_1m_1m'}(p) = -(\hbar p_0/u)(m+m')\,\Phi_{n;m,m'}(p). \quad (52)$$

On the other hand, we may introduce parabolic coordinates to separate variables in the original Schrödinger Eq. (1). Those are defined in terms of the parameters of two systems of paraboloids with focus at the origin and an azimuthal angle ϕ in the (x_1, x_2) plane (Fig. 3). Analytically

$$x_1 = (\lambda_1\lambda_2)^{\frac{1}{2}}\cos\phi \qquad \lambda_1 \geq 0, \quad \lambda_2 \geq 0, \quad 0 \leq \phi \leq 2\pi$$

$$x_2 = (\lambda_1\lambda_2)^{\frac{1}{2}}\sin\phi$$

$$x_3 = (\lambda_1-\lambda_2)/2. \quad (53)$$

One has $r = (x_1^2+x_2^2+x_3^2)^{\frac{1}{2}} = (\lambda_1+\lambda_2)/2$ so that

$$\lambda_1 = r+x_3$$

$$\lambda_2 = r-x_3. \quad (54)$$

The Laplacian takes the form:

$$\Delta = \frac{2}{\lambda_1+\lambda_2}\left[2\frac{\partial}{\partial\lambda_1}\lambda_1\frac{\partial}{\partial\lambda_1} + 2\frac{\partial}{\partial\lambda_2}\lambda_2\frac{\partial}{\partial\lambda_2} + \frac{1}{2}\left(\frac{1}{\lambda_1}+\frac{1}{\lambda_2}\right)\frac{\partial^2}{\partial\phi^2}\right].$$

The Schrödinger equation now reads

$$[A_1+A_2+(2\mu k/\hbar^2)]\psi(\lambda_1,\lambda_2,\phi) = 0, \quad (55)$$

with

$$A_i = 2\frac{\partial}{\partial\lambda_i}\lambda_i\frac{\partial}{\partial\lambda_i} + \frac{1}{2\lambda_i}\frac{\partial}{\partial\phi^2} - \frac{p_0^2}{2\hbar^2}\lambda_i,$$

$$i = 1, 2, \quad (p_0^2/2\mu) = -E.$$

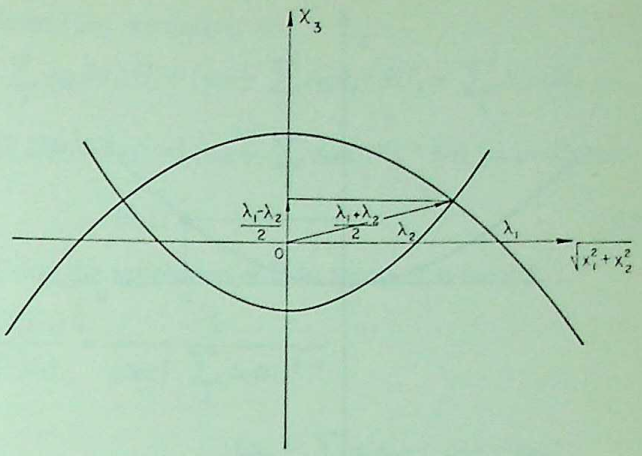

FIG. 3. Parabolic coordinates.

We have also written above the third component of the operator $\mathbf{M}$ as

$$M_3 = \frac{p^2-p_0^2}{2\mu}x_3 - \frac{p_3}{\mu}(\mathbf{p}\cdot\mathbf{r}) - \frac{2i\hbar}{\mu}p_3.$$

Using $p_j = (\hbar/i)(\partial/\partial x_j)$ and Eq. (54), we easily find

$$M_3 = -\frac{\hbar^2}{2\mu}\frac{\lambda_1-\lambda_2}{\lambda_1+\lambda_2}\left(2\frac{\partial}{\partial\lambda_1}\lambda_1\frac{\partial}{\partial\lambda_1} + 2\frac{\partial}{\partial\lambda_2}\lambda_2\frac{\partial}{\partial\lambda_2} + \frac{1}{2}\frac{1}{\lambda_1} + \frac{1}{\lambda_2}\frac{\partial^2}{\partial\phi^2}\right) - \frac{\lambda_1-\lambda_2}{4\mu}p_0^2 + \frac{2\hbar^2}{\mu}\left(\lambda_1\frac{\partial}{\partial\lambda_1} + \lambda_2\frac{\partial}{\partial\lambda_2}\right) \times \frac{1}{(\lambda_1+\lambda_2)}\left(\lambda_1\frac{\partial}{\partial\lambda_1} - \lambda_2\frac{\partial}{\partial\lambda_2}\right) + 2\frac{\hbar^2}{\mu}\frac{1}{\lambda_1+\lambda_2} \times \left(\lambda_1\frac{\partial}{\partial\lambda_1} - \lambda_2\frac{\partial}{\partial\lambda_2}\right),$$

that is, simplifying and comparing with Eq. (55),

$$M_3 = (\hbar/2\mu)(A_1-A_2). \quad (56)$$

Hence, parabolic coordinates where the natural operators to diagonalize are $L_3 = (\hbar/i)(\partial/\partial\phi)$, A_1 and A_2 lead naturally to M_3 and changing the axis of coordinates (or through commutation with $\mathbf{L}$) to the other components of M as constants of the motion. It is also in this way that V. Bargmann[4] was naturally led to wave functions on the sphere S_4, essentially identical with the $\mathfrak{D}^j$ functions of Wigner.

III. THE LARGER GROUP

We have remarked that the Hilbert space generated by the eigenfunctions of the Schrödinger equation corresponding to bound states is mapped unitarily on the Hilbert space of square-integrable functions on the unit sphere of a four-dimensional space, which we cal.

CC-0. In Public Domain. Gurukul Kangri Collection, Haridwar

Digitized by Arya Samaj Foundation Chennai and eGangotri

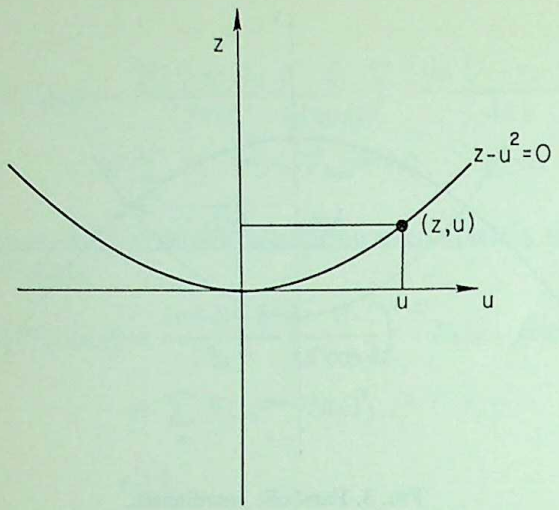

FIG. 4. Projection of a p-dimensional space on a paraboloid in $p+1$ dimensions.

$\mathfrak{C}_4$. We now want to find a larger group G for which the following conditions are satisfied.

(i) G contains 0_p as a maximal compact subgroup $p \geq 2$;
(ii) G acts on the sphere S_p.
(iii) $\mathfrak{C}_p$ is an irreducible space for a unitary representation of G;

$\mathfrak{C}_p$ is the space of L^2 functions on a unit sphere in a p-dimensional real space. Instead of giving the answer and verify the previous conditions we indicate a heuristic derivation. Discussing the Fock transformation [Eq. (10)] mapping the three-dimensional space on the sphere we have casually remarked that the transformation depended on the energy (or equivalently on p_0) and we have investigated the effect of varying the energy. The result was a combination of operations which could be described geometrically in terms of inversions and "scale" transformations. Since we are now looking for operations which eventually will help us to relate subspaces corresponding to various energy levels it seems appropriate to investigate the general class of transformations to which the particular ones just mentioned belong. For that purpose, consider the following set of transformations in a p-dimensional space ($\mathbf{u}$ now stands for the complete p-dimensional vector):

(a) orthogonal transformations	$\mathbf{u} \to 0\mathbf{u}$
(b) translations	$\mathbf{u} \to \mathbf{u}+\mathbf{a}$
(c) scale transformations	$\mathbf{u} \to \lambda\mathbf{u}$
(d) inversions	$\mathbf{u} \to \mathbf{u}/\lvert\mathbf{u}\rvert^2$.

When combined in all possible manners these transformations generate a group: the conformal group. All these transformations leave the angle between two curves invariant. We can describe this group more precisely as follows[11]: imbed the p-dimensional space in an $(p+1)$-dimensional space. We call z the extra component. Consider the paraboloid $z=\mathbf{u}^2$; its points are in one to one correspondence with those of the hyperplane $z=0$ (Fig. 4). The set of projective transformations which leave the paraboloid invariant, when translated into the $\mathbf{u}$ space is the conformal group. We obtain it by taking homogeneous coordinates z/l, $\mathbf{u}$, so that this group is the homogeneous linear group which leaves invariant the quadratic form $zl-\mathbf{u}^2$.

It is a pseudo orthogonal group $0(1, p+1)$ since $zl=\frac{1}{4}[(z+l)^2-(z-l)^2]$. It contains the transformations (i) to (iv) which appear as

(a) $\mathbf{u} \to 0\mathbf{u}$, $\quad z \to z,\ l \to l$
(b) $\mathbf{u} \to \mathbf{u}+\mathbf{a}l$, $\quad z \to z+2\mathbf{a}\cdot\mathbf{u}+\mathbf{a}^2 l,\ l \to l$
(c) $\mathbf{u} \to \mathbf{u}$, $\quad z \to \lambda z,\ l \to \frac{1}{\lambda} l$
(d) $\mathbf{u} \to \mathbf{u}$, $\quad z \to l,\ l \to z$.

The general transformation in p-dimensional space is then[12]

$$u_i \to u_i' = \frac{\alpha_{ij}u_j+\alpha_{iz}\mathbf{u}^2+\alpha_{it}}{[\alpha_{ij}u_j+\alpha_{iz}\mathbf{u}^2+\alpha_{it}]}, \tag{57}$$

where the matrix

$$\alpha = \begin{bmatrix} \alpha_{tt} & \cdots & \alpha_{tz} & \cdots & \alpha_{ti} \\ \cdot & & \cdot & & \cdot \\ \cdot & & \cdot & & \cdot \\ \cdot & & \cdot & & \cdot \\ \alpha_{zt} & \cdots & \alpha_{zz} & \cdots & \alpha_{zj} \\ \cdot & & \cdot & & \cdot \\ \cdot & & \cdot & & \cdot \\ \cdot & & \cdot & & \cdot \\ \alpha_{it} & \cdots & \alpha_{iz} & \cdots & \alpha_{ij} \end{bmatrix}$$

leaves the form $zl-\mathbf{u}^2$ invariant, that is $\alpha^T\gamma\alpha=\gamma$ with

$$\gamma \equiv \begin{bmatrix} 0 & \frac{1}{2} & 0 & \cdot & \cdot & \cdots \\ \frac{1}{2} & 0 & 0 & \cdot & \cdot & \cdots \\ 0 & 0 & -1 & 0 & & \\ & & 0 & -1 & 0 & \\ & & 0 & 0 & -1 & \cdots \\ & & & & & \cdot \\ & & & & & \cdot \\ & & & & & \cdot \\ & & & & & -1 \end{bmatrix}.$$

[11] This is a familar device when using the conformal group and has been used also for nondefinite metric. We learned it from Dr. R. Stora.

[12] The conformal group is a general invariance group for the Laplace equation in the following sense. If $f(u')$ is a solution of $\Delta'^p f(u')=0$ then $g(u)=(\alpha_{tt}+\alpha_{tz}u^2+\sum_j \alpha_{tj}u_j)^{(2-p)/2} f(u')$ with u' given by Eq. (57) satisfies also Laplace equation $\Delta^p g(u)=0$. This result can be quickly obtained by checking it for the four types of transformations. The only nonstraightforward case gives rise to the fact that if $Y_\lambda^{(p)}$ is a spherical harmonic both $r^\lambda Y_\lambda^{(p)}$ and $r^{-(\lambda+p-2)} Y_\lambda^{(p)}$ are solutions of the Laplace equation; a property which we have already used.

CC-0. In Public Domain. Gurukul Kangri Collection, Haridwar

Digitized by Arya Samaj Foundation Chennai and eGangotri

We can now ask the following question: what is the subgroup of the conformal group which leaves the unit sphere invariant? In other words, we want $z-t$ to remain invariant. Since

$$zt-u^2\equiv\tfrac{1}{2}(z+t)^2-\tfrac{1}{2}(z-t)^2-u^2$$

we see that the remaining subgroup is also a pseudo orthogonal group $0(1, p)$. We will how prove that this group indeed satisfies our criteria. Conditions (i) and (ii) are verified by construction. In order to examine (iii) we will construct explicitly the representations in $\mathcal{K}_p$. Let Λ be an element of $0(1, p)$ that is

$$\Lambda=\begin{bmatrix} a_{00} & \cdots & a_{0j} & \cdots \\ \vdots & & \vdots & \\ a_{i0} & \cdots & a_{ij} & \cdots \\ \vdots & & \vdots & \end{bmatrix}$$

with

$$\Lambda^T G\Lambda=G=\begin{bmatrix} 1 & & & \\ & -1 & & \\ & & \ddots & \\ & & & -1 \end{bmatrix}. \tag{58}$$

Then the transformation on $\mathbf{u}$, z, t is

$$\tfrac{1}{2}(z'+t')=a_{00}\tfrac{1}{2}(z+t)+\sum_j a_{0j}u_j,$$

$$\tfrac{1}{2}(z'-t')=\tfrac{1}{2}(z-t),$$

$$u_i'=a_{i0}\tfrac{1}{2}(z+t)+\sum_j a_{ij}u_j,$$

or if the initial point $(z=1,\ t=1,\ \mathbf{u})$ belongs to the unit sphere then

$$u_i'=a_{i0}+\sum_j a_{ij}u_j$$

$$t'=a_{00}+\sum a_{0j}u_j.$$

Hence on the sphere the transformation induced by Λ is

$$\Lambda: u\to U: U_i=u_i'/t'=(a_{i0}+\sum_j a_{ij}u_j)/(a_{00}+\sum_j a_{0j}u_j). \tag{59}$$

One verifies that

$$U^2-1=(u^2-1)/(a_{00}+\sum_j a_{0j}u_j)^2. \tag{60}$$

We now compute the Jacobian of the transformation. For that purpose we extend the transformation (59) to the whole u-space and write the element of area on the unit-sphere as

$$d^p\Omega_U=2\delta(U^2-1)\,d^pU. \tag{61}$$

From (56) we derive

$$(\sum_j a_{0j}\,du_j)\,U_i+(a_{00}+\sum_j a_{0j}u_j)\,dU_i=\sum_j a_{ij}\,du_j$$

$$D(U_i)/D(u_j)=[(a_{00}+\sum_j a_{0j}u_j)^p]^{-1}\det(a_{ij}-U_ia_{0j}). \tag{62}$$

Using the expression of $\mathbf{U}$ in terms of $\mathbf{u}$ we get

$$\frac{D(U_i)}{D(u_j)}=\frac{1}{(a_{00}+\sum_j a_{0j}u_j)^{p+1}}$$

$$\times\det\begin{bmatrix} a_{00}+\sum_j a_{0j}u_j & \cdots & a_{01} & \cdots & a_{0p} \\ \vdots & & \vdots & & \vdots \\ a_{0i}+\sum_j a_{ij}u_j & \cdots & a_{i1} & \cdots & a_{ip} \\ \vdots & & \vdots & & \vdots \end{bmatrix} \tag{63}$$

$$\frac{D(U_i)}{D(u_j)}=\frac{1}{(a_{00}+\sum_j a_{0j}u_j)^{p+1}}\det\Lambda.$$

We know that $\det\Lambda=\pm1$. Further we remark that

$$(\sum_j a_{0j}u_j)^2\le(\sum_j a_{0j}^2)(\sum_j u_j^2).$$

We shall only use the preceding expression for $u^2=\sum_j u_j^2=1$. Then

$$(\sum_j a_{0j}u_j)^2\le(\sum_j a_{0j}^2)=a_{00}^2-1.$$

Hence for $\mathbf{u}^2=1$ we have $|a_{00}+\sum_j a_{0j}u_j|\ge|a_{00}|-(a_{00}^2-1)^{\frac{1}{2}}>0$ and the Jacobian never vanishes. From (57) and (60) we get

$$d^p\Omega_u=2\delta(U^2-1)\,d^pU=\frac{1}{|(a_{00}+\sum_j a_{0j}u_j)|^{p-1}}\,d^p\Omega_u. \tag{64}$$

Let $f(U)$ and $g(U)$ be L^2-functions on the sphere S_p. The previous calculation shows that

$$\int_{S_p}\bar f(U)g(U)\,d^p\Omega_U$$

$$=\int_{S_p}\left[\frac{\bar f(U(u))}{|a_{00}+\sum_j a_{0j}u_j|^{(p-1)/2}}\right]$$

$$\times\left[\frac{g(U(u))}{|a_{00}+\sum_j a_{0j}u_j|^{(p-1)/2}}\right]d^p\Omega_u \tag{65}$$

with $u\to U$ given by (59).

We are now ready to describe the representation of

CC-0. In Public Domain. Gurukul Kangri Collection, Haridwar

Digitized by Arya Samaj Foundation Chennai and eGangotri

$0(1, p)$ afforded by $\mathfrak{K}_p$.[13] Given a $\Lambda \in 0(1, p)$ and an element $f \in \mathfrak{K}_p$ we set

$$f \to T^\Lambda f$$

$$[T^\Lambda \cdot f](u) = \frac{f(\Lambda^{-1}u)}{|\, a_{00}(\Lambda^{-1}) + \sum_j a_{0j}(\Lambda^{-1})\, u_j \,|^{(p-1)/2}}$$

$$(\Lambda^{-1}u)_i = \frac{a_{i0}(\Lambda^{-1}) + \sum_j a_{ij}(\Lambda^{-1})\, u_j}{a_{00}(\Lambda^{-1}) + \sum_j a_{0j}(\Lambda^{-1})\, u_j}. \tag{66}$$

The operator T^Λ is obviously a linear operator from $\mathfrak{K}_p$ to $\mathfrak{K}_p$. Equation (62) shows that it is an isometric operator. All that remains to be verified is that the correspondence $\Lambda \to T^\Lambda$ is a representation of $0(1, p)$; in other words we want to show

$$T^{\Lambda_1} \cdot T^{\Lambda_2} = T^{\Lambda_1 \Lambda_2}. \tag{67}$$

Since obviously $T^I = I$ (the identity operator) Eq. (67) will also show that T^Λ has an inverse (and hence is unitary). We will thus get a unitary representation of $0(1, p)$. For that purpose consider

$$[(T^{\Lambda_1} T^{\Lambda_2}) f](u) = \frac{f(\Lambda_2^{-}\, \Lambda_1^{-} \cdot u)}{|\, (a_{00}(\Lambda_2^{-1}) + \sum_j a_{0j}(\Lambda_2^{-1})\, (\Lambda_1^{-1}u)_j)\, (a_{00}(\Lambda_1^{-1}) + \sum_j a_{0j}(\Lambda_1^{-1})\, u_j) \,|^{(p-1)/2}}. \tag{68}$$

Clearly as $\Lambda_2^{-1}\Lambda_1^{-1} = (\Lambda_1\Lambda_2)^{-1}$ all we have to show is that the denominator in the preceding equation is

$$a_{00}(\Lambda_2^{-1}\Lambda_1^{-1}) + \sum_j a_{0j}(\Lambda_2^{-1}\Lambda_1^{-1})\, u_j, \tag{69}$$

This can be shown by a direct calculation but it is easier to remark that (69) stems from the properties of Jacobians [compare with Eq. (64)]. The group law (67) is satisfied. Hence, we have constructed a unitary representation (infinite dimensional) of $0(1, p)$ in the space of L^2 functions on the sphere S_p. In view of the explicit equations of transformations our representation satisfies all the usual continuity requirements. We recall that $0(1, p)$ has four sheets and our representation is a representation of the full-group. However, in the sequel we might as well assume that we deal with the connected part, which allows us to derive the form of the infinitesimal generators. If the representation of the connected subgroup is irreducible the representation of the whole group is *a fortiori* irreducible.

For the sake of simplicity let us first examine the case where $p = 2$. Our construction leads to a unitary representation of the (real) Lorentz group in three dimensions $0(1, 2)$. Restricting ourselves to the connected part of the group, it is generated by three types of transformations:

rotation in the (1, 2) plane: generator L
"pure" Lorentz transformation in the (0, 1) plane; generator P_1
"pure" Lorentz transformation in the (0, 2) plane; generator P_2.

The corresponding infinitesimal transformations are [$(\alpha_1\alpha_2\beta)$ infinitesimal]

$$1 + \alpha_1 P_1 + \alpha_2 P_2 + \beta L$$

$$L = \begin{pmatrix} 0 & 0 & 0 \\ 0 & 0 & -1 \\ 0 & 1 & 0 \end{pmatrix}$$

$$P_1 = \begin{pmatrix} 0 & 1 & 0 \\ 1 & 0 & 0 \\ 0 & 0 & 0 \end{pmatrix}. \tag{70}$$

$$P_2 = \begin{pmatrix} 0 & 0 & 1 \\ 0 & 0 & 0 \\ 1 & 0 & 0 \end{pmatrix}$$

The commutation relations are

$$[L, P_1] = P_2 \quad [L, P_2] = -P_1 \quad [P_1, P_2] = -L. \tag{71}$$

The sphere S_2 is a unit circle on which the spherical harmonics

$$Y_m^{(1)}(\phi) = \frac{e^{im\phi}}{(2\pi)^{\frac{1}{2}}}$$

constitute a complete basis for $\mathfrak{K}_2$ (classical result from the theory of Fourier series); m takes all integer values from $-\infty$ to $+\infty$. In the following we drop the index (1) of $Y_m^{(1)}$. For $\Lambda \simeq 1 + \beta L$ we write $T^\Lambda \simeq I + \beta T(L)$ then

$$T(L)\, Y_m = -im Y_m. \tag{72}$$

[13] The quantity $|\, a_{00} + \Sigma a_{0j} u_j \,|$ is real positive; it is clear that to satisfy the unitarity condition we can more generally set

$$[T^\gamma f](u) = [f(\Lambda^{-1}u)/|\, a_{00}(\Lambda^{-1}) + \textstyle\sum_j a_{0j}(\Lambda^{-1})\, u_j \,|^{[(p-1)/2] + i\gamma}],$$

where γ is real and say nonnegative. Different γ define inequivalent representations. This shows that the representation of the group G is not uniquely defined. The minor changes in adding λ are all very simple and we do not include them in the text. The only formula for which this does not go through as simply is Eq. (80) which is the basis of the introduction of "noncompact" operators in Ref. 1.

CC-0. In Public Domain. Gurukul Kangri Collection, Haridwar

Digitized by Arya Samaj Foundation Chennai and eGangotri

Let ψ be equal to $\Lambda^{-1}\phi$ with $\Lambda \simeq 1+\alpha_1 P_1$, we get from Eq. (59)

$$\cos\psi \simeq (-\beta+\cos\phi)/(1-\beta\cos\phi),$$

$$\sin\psi \simeq [\sin\phi/(1-\beta\cos\phi)],$$

$$\tan\psi = [\sin\phi/(-\beta+\cos\phi)],$$

and

$$(T^{\Lambda}f)(\phi) \approx \frac{1}{(1-\beta\cos\phi)^{\frac{1}{2}}} f\left(\arctan\frac{\sin\phi}{\cos\phi-\beta}\right),$$

$$\approx f(\phi)+\beta\left((\cos\phi/2)f(\phi)+\sin\phi(\partial/\partial\phi)f(\phi)\right),$$

$$T(P_1)Y_m = \tfrac{1}{4}(Y_{m+1}+Y_{m-1})+\tfrac{1}{2}m(Y_{m+1}-Y_{m-1})$$

$$= \tfrac{1}{4}(1+2m)Y_{m+1}+\tfrac{1}{4}(1-2m)Y_{m-1}. \qquad (73)$$

An analogous calculation yields

$$T(P_2)Y_m = \frac{1}{4i}(Y_{m+1}-Y_{m-1})+\frac{m}{2i}(Y_{m+1}+Y_{m-1})$$

$$= \frac{1+2m}{4i}Y_{m+1}-\frac{1-2m}{4i}Y_{m-1}. \qquad (74)$$

The formulas (72), (73), and (74) give us the representation of the Lie algebra of 0(1, 2) afforded by our construction. One verifies of course the commutation relations (71). Moreover the generators are anti-Hermitian as a consequence of the unitarity of the representation. We can prove the irreducibility using the Lie algebra. Indeed constructing $T_{\pm}=T(P_1)\pm iT(P_2)$ we find

$$T_{\pm}Y_m = [(1\pm 2m)/2]Y_{m\pm 1}. \qquad (75)$$

Since m is an integer $(1\pm 2m)/2$ can never vanish and starting from one vector Y_m by successive application of $T(L_1)\pm iT(L_2)$ we generate all the others. Hence, the representation is irreducible.

The proof of irreducibility in the general case can be made along similar lines. Let us denote by $L_1, \cdots, L_p$ the generators of "pure Lorentz transformations" in the two-planes $(0, 1), (0, 2), \cdots, (0, p)$. We calculate $T(P_i)$. Let

$$\Lambda_i \simeq I+\beta P_i = \begin{bmatrix} 1 & 0 & \cdots & \beta & & \cdots \\ 0 & 1 & & & & \\ \cdot & & \cdot & & & \\ \cdot & & & \cdot & & \\ \cdot & & & & \cdot & \\ \beta & & & 1 & & \\ & & & & & \\ 0 & & & & 1 & \\ \cdot & & & & & \cdot \\ \cdot & & & & & \cdot \\ & & & & & \cdot \end{bmatrix}.$$

We have

$$(T^{\Lambda_i}f)(u) \simeq \frac{1}{(1-\beta u_i)^{(p-1)/2}} f$$

$$\times\left(\frac{u_1}{1-\beta u_i}, \frac{u_2}{1-\beta u_i}, \cdots, \frac{-\beta+u_i}{1-\beta u_i}, \cdots, \frac{u_p}{1-\beta u_i}\right).$$

Writing $T^{\Lambda_i}=I+\beta T(P_i)$

$$T(P_i) = \tfrac{1}{2}(p-1)u_i + u_i\sum_j u_j(\partial/\partial u_j) - (\partial/\partial u_i). \qquad (76)$$

This expression can be given an interesting meaning. Let us introduce the generators L_{ij} of rotations in the (ij) planes—according to (66) we have

$$T(L_{ij}) = u_i(\partial/\partial u_j) - u_j(\partial/\partial u_i). \qquad (77)$$

Let us now commute the Casimir operator

$$L^2 = -\sum_{i<j} T(L_{ij})^2 \qquad (78)$$

with the operators u_i [as an operator u_i means $f(u)\to u_i f(u)$]. We easily find

$$[L^2, u_i] = -2u^2(\partial/\partial u_i) + 2u_i\sum_j u_j(\partial/\partial u_j) + (p-1)u_i. \qquad (79)$$

But $u^2=1$ on the unit sphere hence comparing (76) and (79) we have

$$T(P_i) = \tfrac{1}{2}[L^2, u_i]. \qquad (80)$$

This last equation gives in essence the procedure described by Dothan, Gell-Mann, and Ne'eman[1] to generate the "noncompact" operators, as commutators between a Casimir operator of the compact subgroup and a set of abelian operators submitted to auxiliary conditions invariant under the compact subgroup and which transform among themselves under commutation with generators of the subgroup.

We will now prove irreducibility in a fashion similar to the case $p=2$. It is clear that if by combining linearly the operators $T(P_i)$ we can find two operators which acting on a spherical harmonic of degree λ generate one of degree $\lambda+1$ and another of degree $\lambda-1$ the proof of irreducibility will be complete since the set of spherical harmonics of a given degree is the carrier space of an irreducible representation the subgroup of rotations 0_p. Now we recall that

$$|\mathbf{u}|^{\lambda}Y_{\lambda\alpha}^{(p)}(\hat{u})$$

satisfies the Laplace equation

$$\Delta^p(|\mathbf{u}|^{\lambda}Y_{\lambda\alpha}^{(p)}(\hat{u})) = 0.$$

But

$$\Delta_p = \frac{p-1}{|\mathbf{u}|}\frac{\partial}{\partial|\mathbf{u}|} + \frac{\partial^2}{\partial|\mathbf{u}|^2} - \frac{1}{|\mathbf{u}|^2}L^2 \qquad (81)$$

CC-0. In Public Domain. Gurukul Kangri Collection, Haridwar

Digitized by Arya Samaj Foundation Chennai and eGangotri

with L^2 given above. Hence

$$L^2 Y_{\lambda\alpha}{}^{(p)} = +\lambda(\lambda+p-2)\, Y_{\lambda\alpha}{}^{(p)}.$$

Now consider the special set of spherical harmonics

$$Y_\lambda{}^{(p)} = (u_1+iu_2)^\lambda. \tag{82}$$

These are not normalized but this is irrelevant here. For each λ they provide us with one spherical harmonic, the other ones being simply generated by rotations. Now

$$\begin{aligned}&[T(P_1)+iT(P_2)]Y_\lambda{}^{(p)}(u)\\ &\quad = +\tfrac{1}{2}L^2 Y_{\lambda+1}{}^{(p)}\tfrac{1}{2}(u+iu_2)\, L^2 Y_\lambda{}^{(p)},\\ &\quad = \tfrac{1}{2}[(\lambda+1)(\lambda+p-1)-\lambda(\lambda+p-2)\, Y_{\lambda+1}{}^{(p)}],\\ &\quad = [\lambda+\tfrac{1}{2}(p-1)]Y_{\lambda+1}{}^{(p)}.\end{aligned} \tag{83}$$

Hence

$$\begin{aligned}&[T(P_1)+iT(P_2)]^\lambda Y_0{}^{(p)} = \tfrac{1}{2}(p-1)\\ &\qquad \times[1+\tfrac{1}{2}(p-1)]\cdots(\lambda-1+\tfrac{1}{2}(p-1)]Y_\lambda{}^{(p)}.\end{aligned} \tag{84}$$

$Y_0{}^{(p)}$ is the unit function, $[T(P_1)+iT(P_2)]$ is a "step"-operator. Repeated application of this operator generates, starting from the spherical harmonic of degree zero, a spherical harmonic of degree λ. Combining the action of this operator with the generators of rotations we obtain all spherical harmonics. Hence the representation is irreducible.

IV. CONCLUSION

The construction of unitary representations of noncompact groups which have the property that the irreducible representation of their maximal subgroup appear at most with multiplicity one is of certain interest for physical applications. The method of construction used here in the Coulomb potential case can be extended to various other cases. The geometrical emphasis may help to visualize things and provide a global form of the transformations.

We hope to develop this approach.

ACKNOWLEDGMENTS

We wish to thank Professor W. Panofsky for the hospitality extended to us at SLAC. This work was supported by the U. S. Atomic Energy Commission.

APPENDIX

We want to derive formula (40) from (38). We have

$$\begin{aligned}&Y_{n;L;M}{}^{(4)}(u)\\ &\quad = \left(\frac{n}{2\pi^2}\right)^{\frac{1}{2}} \sum_{m,m'} (jm;jm' \mid LM)\, (\mathfrak{D}_{mm'}{}^j[(u_0+i\partial\mathbf{u})\,\Gamma])^*\end{aligned}$$

$$u \equiv (u_0, \mathbf{u}) \qquad 2j+1=n.$$

Let us first remark that from Eq. (27)

$$(\mathfrak{D}_{mm'}{}^j[(u_0+i\partial\mathbf{v})\,\Gamma])^*,$$

where $\mathbf{v}$ is a vector along the z axis, vanishes unless $m+m'=0$. Now any $\mathbf{u}$ can be written $R_{\alpha,\beta,0}\mathbf{v}$ with α,β the polar angles of $\mathbf{u}$. From the very construction of $Y^{(4)}$ [Eq. (39)] we have

$$\begin{aligned}Y_{n,L,M}{}^{(4)}(u_0, \mathbf{u}) &= Y_{n,LM}{}^{(4)}(u_0, R_{\alpha,\beta,0}\mathbf{v})\\ &= Y_{n,L,0}{}^{(4)}(u_0, \mathbf{v})\, \mathfrak{D}_{0M}{}^L(R_{\alpha\beta}{}^{-1}),\end{aligned}$$

$$Y_{n,LM}{}^{(4)}(u_0, \mathbf{u}) = Y_{n,L,0}{}^{(4)}(u_0, \mathbf{v})\, (\mathfrak{D}_{M0}{}^L(R_{\alpha\beta}))^*.$$

In this last equality the second factor is, except for a factor $[4\pi/(2L+1)]^{\frac{1}{2}}$, the usual three-dimensional spherical harmonic; hence

$$Y_{n,L,M}{}^{(4)}(u_0) = [4\pi/(2L+1)]^{\frac{1}{2}} Y_{n,L,0}{}^{(4)}(u_0, \mathbf{v})$$

$$Y_{LM}{}^{(3)}(\mathbf{u}/|\mathbf{u}|). \quad \text{(A1}$$

The vector $\mathbf{v}$ is along the z axis and its length is given by $|\mathbf{v}| = |\mathbf{u}| = (1-u_0{}^2)^{\frac{1}{2}}$. We shall write $u_0 = \cos\delta$, $|\mathbf{v}| = \sin\delta$. It remains to study the first factor on the right-hand side of this equation. For convenience we write

$$Y_{n;L,0}{}^{(4)}(u_0, \mathbf{v}) = i^L[(2L+1)/2\pi^2]^{\frac{1}{2}} T_{n,L}(\delta). \quad \text{(A1}$$

From Eq. (38) and (27) it now follows that

$$\begin{aligned}T_{n,L}(\delta) &= \left(\frac{2j+1}{2L+1}\right)^{\frac{1}{2}} \frac{1}{i^L}\\ &\quad \times \sum_m (j, m; j, -m \mid L, 0)\, (\mathfrak{D}_{m,-m}{}^j(u_0+iv\partial)\Gamma)^*\end{aligned}$$

$$\begin{aligned}T_{n,L}(\delta) &= \left(\frac{2j+1}{2L+1}\right)^{\frac{1}{2}} \frac{1}{i^L}\\ &\quad \times \sum_m (j, m; j, -m \mid L, 0)\, (-1)^{j-m} \exp(-2im\end{aligned}$$

We shall now simply use known properties of the Clebsch–Gordan coefficients in order to express $T_{n,L}$ in a simpler way. First we note that

$$(j, m; j, -m \mid L, 0) = (-1)^{2j-L}(j, -m; j, m \mid L, 0$$

Hence

$$(T_{nL}(\delta))^* = T_{nL}(\delta)$$

$$T_{nL}(-\delta) = (-1)^L T_{nL}(\delta).$$

That was the reason for introducing the factor i^L.

CC-0. In Public Domain. Gurukul Kangri Collection, Haridwar

Digitized by Arya Samaj Foundation Chennai and eGangotri

Then using $(j, m; j, -m \mid 0, 0) = (-1)^{j-m}(2j+1)^{\frac{1}{2}}$ we find

$$T_{n,0}(\delta) = \sum_{m=-(n-1)/2}^{m=+(n-1)/2} \exp(-2im\delta) = \frac{\sin n\delta}{\sin \delta}. \quad \text{(A3)}$$

Furthermore

$$2m(j, m; j, -m \mid L0) = (L+1)\left[\frac{n^2-(L+1)^2}{(2L+1)(2L+3)}\right]^{\frac{1}{2}} \times (j, m; j, -m \mid L+1, 0) + L\left[\frac{n^2-L^2}{(2L-1)(2L+1)}\right]^{\frac{1}{2}} (j, m; j, -m \mid L-1, 0).$$

Hence

$$\frac{d}{d\delta} T_{n,L}(\delta) = \frac{L+1}{2L+1}[n^2-(L+1)^2]^{\frac{1}{2}} T_{n,L+1}(\delta) + \frac{L}{2L+1}(n^2-L^2)^{\frac{1}{2}} T_{n,L-1}. \quad \text{(A4)}$$

Using a similar technique we find, with the help of

$$(j, m; j, -m \mid L, 0) + (j, m+1, j, -m-1 \mid L, 0) = \left[\frac{L(L+1)}{j(j+1)-m(m+1)}\right]^{\frac{1}{2}} (j, m+1, j, -m \mid L, 1)$$

and

$$(2m+1)(j, m+1; j, -m \mid L, 1) = \left[\frac{L(L+2)(n^2-(L+1)^2)}{(2L+1)(2L+3)}\right]^{\frac{1}{2}} \times (j, m+1; j, -m \mid L+1, 1) + \left[\frac{(L+1)(L-1)(n^2-L^2)}{(2L+1)(2L-1)}\right]^{\frac{1}{2}} \times (j, m+1; j, -m \mid L-1, 1,)$$

that

$$\frac{d}{d\delta}\sin\delta T_{n,L}(\delta) = \sin\delta\left\{-\frac{L}{2L+1}[n^2-(L+1)^2]^{\frac{1}{2}} \times T_{n,L+1}(\delta) + \frac{L+1}{2L+1}(n^2-L^2)^{\frac{1}{2}} T_{n,L-1}(\delta)\right\}. \quad \text{(A5)}$$

Relations (A4) and (A5) are equivalent to

$$\begin{cases} [(d/d\delta)+L\cot\delta]T_{n,L}(\delta) = [n^2-(L+1)^2]^{\frac{1}{2}} T_{n,L+1} \\ [(d/d\delta)+(L+1)\cot\delta]T_{n,L}(\delta) = [n^2-(L)^2]^{\frac{1}{2}} T_{n,L-1}. \end{cases} \quad \text{(A6)}$$

Using the fact that

$$-(d/d\delta)+L\cot\delta \equiv \sin\delta^{L+1}(d/d\cos\delta)(1/\sin^L\delta),$$

we deduce from (A3) that

$$T_{n,L}(\delta) = \frac{1}{[(n^2-1^2)(n^2-2^2)\cdots(n^2-L^2)]^{\frac{1}{2}}} \times \sin\delta^L\left(\frac{d}{d\cos\delta}\right)^L \frac{\sin n\delta}{\sin\delta}. \quad \text{(A7)}$$

Putting this expression in (A2) we get the desired result. The functions $T_{n,L}(\delta)$ are, of course, well known.[4] Our calculation relates them in a very simple way to the Clebsch–Gordan coefficients through

$$T_{nL}(\delta) = \frac{1}{[(n^2-1^2)(n^2-2^2)\cdots(n^2-L^2)]^{\frac{1}{2}}} \times \sin\delta^L\left(\frac{d}{d\cos\delta}\right)^L \frac{\sin(n\delta)}{\sin\delta} \equiv \left(\frac{n}{2L+1}\right)^{\frac{1}{2}} \frac{1}{i^L} \sum_{m=-j}^{+j} (j, m; j, -m \mid L0)(-1)^{j-m} \times \exp(-2im\delta)$$

$2j+1 \equiv n.$

CC-0. In Public Domain. Gurukul Kangri Collection, Haridwar

Digitized by Arya Samaj Foundation Chennai and eGangotri

Group Theory and the Hydrogen Atom (II)

M. BANDER, C. ITZYKSON*
Stanford Linear Accelerator Center, Stanford University, Stanford, California

A previous work dealing with bound states in a Coulomb potential is extended to the case of scattering states. T symmetry of the problem under the Lorentz group 0(1, 3) is used to construct wave functions. Harmonic analysis on t sheeted hyperboloids is briefly discussed in arbitrary dimension. The set of scattering states for both an attractive a repulsive potential is shown to provide a unitary representation of the group 0(1, 4).

I. INTRODUCTION

In a previous article, hereafter denoted by I, we have reviewed the symmetries of the Schrödinger equation for a Coulomb potential and discussed the use of a noncompact group isomorphic to the pseudo-orthogonal group 0(1, 4) to relate the bound state levels.[1] It is of some interest to pursue the analysis further to the scattering states. This is the goal of this work. The "hidden symmetry" is now an invariance under the homogeneous Lorentz group 0(1, 3) and the space of scattering states can be written as a direct integral of infinite dimensional Hilbert spaces, which are carrier spaces of unitary representations of the Lorentz group. This is a frequent occurrence when dealing with a noncompact group, the simplest example being Fourier analysis for the group of translations in one dimension. We shall follow the usual device of introducing nonnormalizable scattering states in order to achieve the decomposition. Physically, of course, the direct integral is related to the continuous spectrum of the Hamiltonian. As in the bound state case, there exists a larger group, isomorphic to 0(1, 4) which connects the scattering states, but we have to introduce wave functions for both attractive and repulsive potentials. We shall show that the representation of this group, obtained in this way, is equivalent with the one previously discussed in I. This representation is in fact not unique and the ambiguity which arises is the same as the one already encountered.

We shall slightly generalize the discussion by taking an arbitrary dimension f for the configuration space. In order to construct the wave functions it will be necessary to use harmonic analysis on a two-sheeted hyperboloid. This has been developed in four dimensions in a series of papers by Dolginov and collabrators[2] but we shall briefly recall the main features including orthogonality and completeness of the "spherical functions." This part can perhaps be used for other purp in a different context.

In an appendix we have performed the necess transformations in order to show that the wave fu tions coincide with their ordinary expressions in c figuration space, both for scattering and bound stat

We will have to use repeatedly the follow notations:

S_p: unit sphere in a p-dimensional real Euclid space, the measure on the sphere being $d^{p-1}\Omega$ with

$$\int_{S_p} d^{p-1}\Omega = \omega_p = \frac{2\pi^{p/2}}{\Gamma(p/2)}.$$

$\delta_{\rm sph}(n_1, n_2)$ will stand for the "δ function" on S_p, i.e.,

$$\int_{S_p} d^{p-1}\Omega(n_1)\, g(n_1)\, \delta_{\rm sph}(n_1, n_2) = g(n_2).$$

T_p: unit hyperboloid in a p-dimensional real Euclid space,

$$u: u_0^2 - \sum_{i=1}^{p-1} u_i^2 = 1.$$

$T_p^{\pm}$ will denote, respectively, the upper $(u_0 \geq 1)$ lower $(u_0 \leq -1)$ sheet of this hyperboloid. Our consta parameterization of T_p^+ will be: $u_0 = \cosh\theta$, u_i $\sinh\theta n_i$, with $\theta \geq 0$ and n_i on S_{p-1}. The measure T_p^+ will be written as $d^{p-1}\mu$ with $d^{p-1}\mu = \sinh\theta^{p-2} d\theta d^{p-1}$ The measure on T_p^- will be related to the one T_p^+ by the transformation $u \epsilon T_p^- \to u\epsilon T_p^+$. Fina $\delta_{\rm hyp}(u_1, u_2)$ will stand for the "δ function" on T_p^+.

II. THE SYMMETRY GROUP

A. Infinitesimal Method

We study the scattering states in a Coulomb pote tial. As in I, we introduce the following two ve operators:

The angular momentum,

$$\mathbf{L} = \tfrac{1}{2}(\mathbf{r}\times\mathbf{p} - \mathbf{p}\times\mathbf{r})$$

The Runge–Lenz vector,

$$\mathbf{M} = (1/2\mu)(\mathbf{p}\times\mathbf{L} - \mathbf{L}\times\mathbf{p}) - k\hat{r}$$

with $\hat{r}$ standing for $\mathbf{r}/|\mathbf{r}|$; $\mathbf{p}$ is the linear momentu

---

* On leave from Service de Physique Theorique, CEN Saclay, BP No. 2, Gif-sur-Yvette (Seine et Oise), France.

[1] M. Bander and C. Itzykson, Rev. Mod. Phys. **38**, 330 (1966), preceding paper.

[2] A. Z. Dolginov, Zh. Eksperim. i Teor. Fiz. **30**, 746 (1956) [English transl.: Soviet Phys.—JETP **3**, 589 (1956)]; A. Z. Dolginov and I. N. Toptygin, Zh. Eksperim. i Teor. Fiz. **37**, 1441 (1959) [English transl.: Soviet Phys.—JETP **10**, 1022 (1960)]; A. Z. Dolginov and A. N. Moskalev, Zh. Eksperim. i Teor. Fiz. **37**, 1967 (1959)] [English transl.: Soviet Phys.—JETP **10**, 1202 (1960)].

CC-0. In Public Domain. Gurukul Kangri Collection, Haridwar

Digitized by Arya Samaj Foundation Chennai and eGangotri

μ the reduced mass; k denotes the strength of the potential.

The Hamiltonian

$$H=(p^2/2\mu)-(k/|\,\mathbf{r}\,|)$$

commutes with both these vectors. They also satisfy the following commutation relations:

$$[L_i, L_j]=i\hbar\epsilon_{ijk}L_k, \qquad [M_i, M_j]=-(2i\hbar H/\mu)\epsilon_{ijk}L_k$$
$$[L_i, M_j]=i\hbar\epsilon_{ijk}M_k. \tag{2}$$

Consider the subspace corresponding to the positive spectrum of H. In this subspace let $\tilde{M}_i=(\mu/2H)^{\frac{1}{2}}M_i$, where the square root of H is defined by the condition of positiveness. Then L_i and $\tilde{M}_i$ build up the Lie algebra of the homogeneous Lorentz group $0(1, 3)$ [our notation implies that $0(p, q)$ is the pseudo-orthogonal real group leaving the metric with p plus signs and q minus signs invariant]. In terms of L and $\tilde{M}$ the Hamiltonian reads:

$$H=-(k^2\mu/2)[L^2-\tilde{M}^2+\hbar^2]^{-1}.$$

The requirement that H be Hermitian restricts L and $\tilde{M}$ to be likewise Hermitian, and hence we are interested in unitary representations of the Lorentz group.[3] These representations are labeled by two numbers (l_0, c) with l_0 a nonnegative integer and c pure imaginary, $c=i\rho$ (the principal series) or $l_0=0, 0\leq c\leq 1$ (the supplementary series). $(L^2-\tilde{M}^2)/\hbar^2$ is a Casimir operator equal for each representation to $l_0^2+c^2-1$. From Eq. (1) it follows that we have one further relation among L and $\tilde{M}$, namely,

$$L\tilde{M}+\tilde{M}L=0=2il_0c. \tag{3}$$

Equation (3) thus restricts us to the representations with $l_0=0$. Thus

$$E=-(k^2\mu/2\hbar^2)(1/c^2), \tag{4}$$

where E is the energy; and as we have assumed H to be positive $c=i\rho$ and we are only concerned with representations of the principal series.

B. Global Method—The Fock Transformation

As mentioned above, we shall now generalize the problem to an arbitrary dimension $f\geq 2$. The Schrödinger equation in momentum space takes the form

$$(p^2-2\mu E)\Phi(\mathbf{p})=\frac{2\mu k}{\pi\omega_{f-1}\hbar}\int d^fq\,\frac{\Phi(\mathbf{q})}{|\,\mathbf{p}-\mathbf{q}\,|^{f-1}} \tag{5}$$

with $E>0$. Changing variables from $\mathbf{p}$ to $(2\mu E)^{-\frac{1}{2}}\mathbf{p}$ and letting

$$\Phi(\mathbf{p})=\Psi[(2\mu E)^{-\frac{1}{2}}\mathbf{p}]$$

[3] M. A. Naimark, *Linear Representations of the Lorentz Group*, American Mathematical Society Translations (American Mathematical Society, Providence, R.I., 1957), Series 2, Vol. 6.

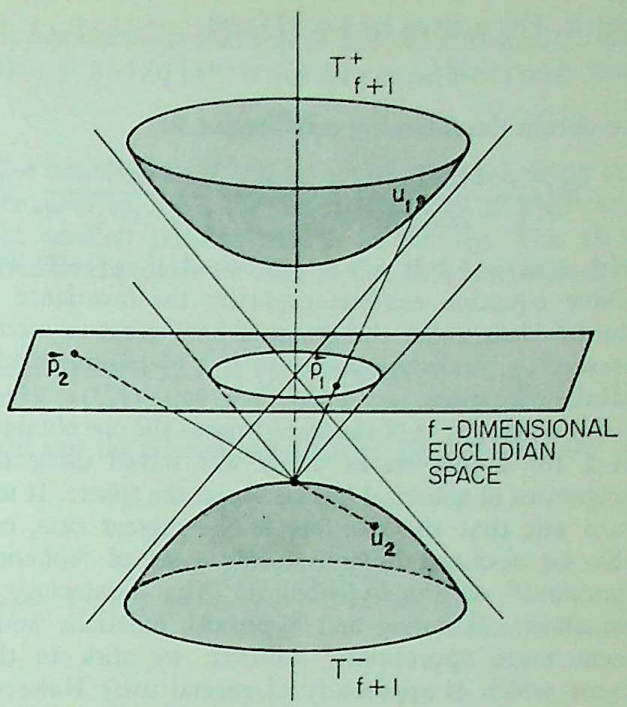

FIG. 1. Stereographic projection of an f-dimensional space to the unit hyperboloid in $f+1$ dimensions.

Eq. (5) becomes

$$(p^2-1)\Psi(\mathbf{p})=\frac{k(2\mu)^{\frac{1}{2}}}{\pi\omega_{f-1}\hbar E^{\frac{1}{2}}}\int d^fq\,\frac{\Psi(\mathbf{q})}{|\,\mathbf{p}-\mathbf{q}\,|^{f-1}}. \tag{6}$$

We now imbed the f-dimensional space into one of $f+1$ dimensions and perform a projection of the original momentum space onto a two-sheeted hyperboloid, T_{f+1} (the Fock transformation, see Fig. 1). Let u be an arbitrary point in the $(f+1)$-dimensional space with component u_0 along the $f+1$ direction and $\mathbf{u}$ its ordinary projection in the original space. We introduce a Minkowski metric into this space, i.e., $u^2=u_0^2-\mathbf{u}^2$. The hyperboloid is given by the equation $u^2=1$ and the point $\mathbf{p}$ corresponds to a point on this hyperboloid with coordinates:

$$\mathbf{p}\to u=\left(\frac{1+p^2}{1-p^2}, \frac{2\mathbf{p}}{1-p^2}\right). \tag{7}$$

The region $p^2<1$ is mapped on the upper sheet while $p^2>1$ is mapped on the lower one. We shall need the following relations. If $\mathbf{p}$ and $\mathbf{q}$ correspond to u and v, respectively, then

$$|\,\mathbf{p}-\mathbf{q}\,|^2=-\frac{(u-v)^2}{(1+u_0)(1+v_0)}=\frac{|\,(u-v)\,|^2}{|\,1+u_0\,|\,|\,1+v_0\,|}$$

$$d^fp=\frac{2\delta(u^2-1)d^{f+1}u}{|\,1+u_0\,|^f}=\frac{d^f\mu(u)}{|\,1+u_0\,|^f},$$

where we remind ourselves that all scalar products involving u and v must be taken with the Minkowski

CC-0. In Public Domain. Gurukul Kangri Collection, Haridwar

Digitized by Arya Samaj Foundation Chennai and eGangotri

metric. For u given by Eq. (7) and

$$\hat{\Phi}(u) = |1+u_0|^{-\frac{1}{2}(f+1)}\Psi(\mathbf{p}) \tag{8}$$

we obtain the following equation for $\hat{\Phi}$:

$$\hat{\Phi}(u) = \frac{k(2\mu)^{\frac{1}{2}}\epsilon(u_0)}{2\pi\omega_{f-1}\hbar E^{\frac{1}{2}}}\int_{T_{f+1}} d^f\mu(v)\,\frac{\hat{\Phi}(v)}{|(u-v)^2|^{\frac{1}{2}(f-1)}} \tag{9}$$

with $\epsilon(u_0)=+1$ if $u_0>1$, $\epsilon(u_0)=-1$ if $u_0\leq -1$. The above equation exhibits explicitly the invariance of the problem under the group of homogeneous, metric preserving, transformations in a $(f+1)$-dimensional Minkowski space, i.e., under the group $0(1,f)$.

Equation (9) is of the same type as the one obtained in I for bound states which was solved using the properties of spherical harmonics on the sphere. It will turn out that the solution, in the present case, can also be obtained by introducing a set of "spherical functions" on the hyperboloid. (The terminology is somehow misleading and hyperbolic functions would seem more appropriate; however, we stick to this name which is apparently of general use.) However, while the spherical harmonics are well known, the corresponding functions for the "Lorentz group" $0(1,f)$ enjoy less popularity. As mentioned in the introduction, they were studied in particular for $f=3$ by Dolginov and collaborators.[2] The case of $f=2$ was also used in the context of Regge poles but dates back in the mathematical literature to Mehler. We shall for the moment interrupt our discussion of the Coulomb problem to give a description of these functions in order to apply them to the solution of Eq. (9). However, they certainly deserve some study for their own sake and, while exhibiting some results with lots of "δ-functions," we shall be careful to present the proofs in such a way that they can, hopefully, be made rigorous.

C. Definition of Spherical Functions on Hyperboloids

Let T_{f+1}^+ be the upper sheet, $u_0\geq 1$, of the hyperboloid T_{f+1},

$$u: u_0^2 - \sum_{i=1}^{f} u_i^2 = 1.$$

Given two points on T_{f+1}^+, u_1 and u_2, there always exists a transformation $\Lambda\in 0^{(+,+)}(1,f)$ such that $u_1=\Lambda u_2$. $0^{(+,+)}(1,f)$ is the component of the identity of $0(1,f)$. The set of transformations which leave a point invariant is isomorphic to a proper rotation group $0^{(+)}(f)$ so that $T_{f+1}^+\approx 0^{(+,+)}(1,f)/0^{(+)}(f)$. The measure of $d^f\mu$ is invariant under $0^{(+,+)}(1,f)$. Hence the Hilbert space $\mathcal{H}_{f+1}$ of square integrable functions defined on T_{f+1}^+,

$$\mathcal{H}_{f+1} = \left\{ g: \int_{T_{f+1}^+} |g|^2\, d^f\mu < \infty \right\},$$

is the carrier space of a unitary representation of the noncompact group $0^{(+,+)}(1,f)$

$$g\to U_\Lambda g \quad \text{with} \quad (U_\Lambda g)(u) = g(\Lambda^{-1}u).$$

This representation is not irreducible and decomposes into a direct integral of irreducible ones:

$$U_\Lambda = \int_0^\infty dN\, U_\Lambda^N.$$

Each U_Λ^N is itself a unitary irreducible representation of the group but again the noncompactness results in the fact that it is infinite dimensional. Different N corresponds to inequivalent representations. Correspondingly, the space $\mathcal{H}_{f+1}$ will be split as a direct integral of infinite dimensional Hilbert spaces and any function in $\mathcal{H}_{f+1}$ will have a representation

$$g(u) = \int_0^\infty dN \sum_\nu g_{N,\nu}(u), \tag{10}$$

where ν is a discrete index which distinguishes the components in the space of the representation U_Λ^N. The function $g_{N,\nu}(u)$ will not belong to $\mathcal{H}_{f+1}$ but will satisfy a certain partial differential equation in terms of the Casimir operator of the group. Having properly chosen the indices, $g_{N,\nu}$ will be proportional to a spherical function. We shall now derive the equation satisfied by these functions. Let $u\equiv(\cosh\theta, \sinh\theta\mathbf{n})$ we shall investigate functions of the type

$$H_{N,\alpha,\beta^{(f+1)}}(u) = Z_{N,\alpha^{(f)}}(\theta)\, Y_{\alpha,\beta^{(f)}}(\mathbf{n}), \tag{11}$$

where $Y_{\alpha,\beta^{(f)}}(\mathbf{n})$ is a spherical harmonic on the sphere S_f. The discrete index α takes the values $\alpha=0,1,2,\cdots$. If $\mathbf{x}=r\mathbf{n}$ is a point in an f-dimensional Euclidian space, $r^\alpha Y_{\alpha,\beta^{(f)}}(\mathbf{n})$ is a homogeneous polynomial of degree α in the components of $\mathbf{x}$ and

$$\Delta_f[(r^\alpha Y_{\alpha,\beta^{(f)}})(\mathbf{n})] = 0$$

with the Laplace operator given in polar coordinates by

$$\Delta_f \equiv \frac{\partial^2}{\partial r^2} + \frac{f-1}{r}\frac{\partial}{\partial r} - \frac{\mathfrak{L}^2}{r^2}$$

and $\mathfrak{L}^2$ is the generalization of the angular momentum and operates only on the angular variables. Hence

$$\mathfrak{L}^2 Y_{\alpha,\beta^{(f)}}(\mathbf{n}) = \alpha(\alpha+f-2)\, Y_{\alpha,\beta^{(f)}}(\mathbf{n}).$$

The index β distinguishes the finitely many, linearly independent, solutions of this equation. Once normalized, the spherical harmonics satisfy:

$$\sum_{\alpha,\beta} Y_{\alpha,\beta^{(f)}}(n_1)\,(Y_{\alpha,\beta^{(f)}}(n_2))^* = \delta_{\text{sph}}(n_1,n_2) \tag{12}$$

$$\int_{S_f} d^{f-1}\Omega(n)\, Y_{\alpha_1,\beta_1^{(f)}}(n)\,(Y_{\alpha_2,\beta_2^{(f)}}(n))^* = \delta_{\alpha_1,\alpha_2}\delta_{\beta_1,\beta_2} \tag{13}$$

In $f+1$ dimensions we write the wave equation in

CC-0. In Public Domain. Gurukul Kangri Collection, Haridwar

Digitized by Arya Samaj Foundation Chennai and eGangotri

neighborhood of $T_{f+1}{}^{+}$:

$$\Box_{f+1}\equiv\frac{\partial^2}{\partial w_0{}^2}-\sum_{i=1}^{f}\frac{\partial^2}{\partial w_i{}^2}=\frac{\partial^2}{\partial\rho^2}+\frac{f}{\rho}\frac{\partial}{\partial\rho}-\frac{\mathcal{C}}{\rho^2}, \tag{14}$$

where $\mathcal{C}$ is the Casimir operator on the hyperboloid and $w_0=\rho\cosh\theta$, $w_i=\rho\sinh\theta n_i$, ρ close to $+1$. Then $H_{N,\alpha,\beta}(u)$ is required to be an eigenfunction of $\mathcal{C}$, or $\rho^{\lambda}H_{N,\alpha,\beta}(u)$ defined in the neighborhood of $T_{f+1}{}^{+}$ to be an homogeneous function of $w=\rho u$, of degree λ, with $\lambda=-\frac{1}{2}(f-1)+iN$ (N will turn to be real) such that

$$\Box_{f+1}[\rho^{\lambda}H_{N,\alpha,\beta}(u)]=0.$$

The condition on N will be obtained by requiring that $H_{N,\alpha,\beta}{}^{(f+1)}(u)$ be a continuous function of $T_{f+1}{}^{+}$ with the smallest possible growth at infinity. The above conditions provide for $Z_{N,\alpha}(\theta)$ the following equation:

$$\left\{\sinh^2\theta\frac{d^2}{d\cosh\theta^2}+f\cosh\theta\frac{d}{d\cosh\theta}-\frac{\alpha(\alpha+f-2)}{\sinh^2\theta}+N^2+\left(\frac{f-1}{2}\right)^2\right\}Z_{N,\alpha}{}^{(f)}(\theta)=0. \tag{15}$$

The boundary conditions just mentioned require N to be real and the relevant solutions of Eq. (15) are for our purpose—including a normalization to be discussed later:

For $f_{f\geq 3}$ odd;

$$Z_{N,\alpha}{}^{(f)}(\theta)=\{\tfrac{1}{2}\pi N^2(N^2+1^2)\cdots[N^2+(f-1+\alpha)^2]\}^{-\frac{1}{2}}\times\sinh\theta^{\alpha}\left(\frac{d}{d\cosh\theta}\right)^{\frac{1}{2}(f-1)+\alpha}\cos N\theta, \tag{16}$$

For $f_{f\geq 2}$ even;

$$Z_{N,\alpha}{}^{(f)}(\theta)=\left[\frac{[N^2+(\frac{1}{2})^2][N^2+(\frac{3}{2})^2]\cdots\{N^2+\frac{1}{2}[(f-2)+\alpha-\frac{1}{2}]^2\}}{N\tanh\pi N}\right]^{-\frac{1}{2}}\times\sinh\theta^{\alpha}\left(\frac{d}{d\cosh\theta}\right)^{\frac{1}{2}(f-2)+\alpha}P_{iN-\frac{1}{2}}(\cosh\theta), \tag{17}$$

where it is understood in Eq. (17) that the factor on the right-hand side reduces to $(N\tanh\pi N)^{\frac{1}{2}}$ for $f=2$; $P_{iN-\frac{1}{2}}(\cosh\theta)$ is the Legendre function, and we shall follow throughout and use Chap. III of Ref. 4 for these functions which in this context are called conical functions. In both cases we have an even function of N; in the following it is assumed that N is positive. With $Z_{N,\alpha}{}^{(f)}(\theta)$ given by Eq. (16) or (17), we have the following basic three relations for spherical functions:

Orthogonality relations, N_1 and N_2 are positive:

$$\int_{T_{f+1}+}d^f\mu(u)H_{N_1,\alpha_1,\beta_1}{}^{(f+1)}(u)\bar{H}_{N_2,\alpha_2,\beta_2}{}^{(f+1)}(u)$$

$$=\delta_{\alpha_1,\alpha_2}\delta_{\beta_1,\beta_2}\,\delta(N_1-N_2), \tag{18}$$

completeness relations in $\mathcal{H}_{f+1}$:

$$\int_0^{\infty}dN\sum_{\alpha,\beta}H_{N,\alpha,\beta}{}^{(f+1)}(u_1)H_{N,\alpha,\beta}{}^{(f+1)}(u_2)=\delta_{\text{hyp}}(u_1,u_2), \tag{19}$$

integral equation

$$\int_{T_{f+1}+}d^f\mu(v)\frac{H_{N,\alpha,\beta}{}^{(f+1)}(v)}{(1+t^2+2tuv)^{\frac{1}{2}(f-1)}}=\frac{2\pi^{\frac{1}{2}(f+1)}}{\Gamma\frac{1}{2}(f-1)}$$

$$\times\frac{t^{-\frac{1}{2}(f-1)}\cos(N\log t)}{N\sinh\pi N}H_{N,\alpha,\beta}{}^{(f+1)}(u). \tag{20}$$

In Eq. (20) t is a complex variable in a cut plane from $-\infty$ to 0; $\log t$ is real for t real positive and the argument of the expression $(1+t^2+2tuv)$ which appears in the integrand is 0 for t real positive. As is apparent from their definition [Eqs. (16) and (17)], the spherical functions are somehow different according to whether f is even or odd. This again reflects the fact that the kernel in Eq. (20) has a square root singularity for even f. Hence, we shall distinguish between the two cases to prove our basic three relations.

D. Proof of the Three Relations in the Case f Odd

We start with the orthogonality relations. According to Eqs. (11) and (13) one has

$$\int_{T_{f+1}+}d^f\mu(u)H_{N_1,\alpha_1,\beta_1}{}^{(f+1)}(u)H_{N_2,\alpha_2,\beta_2}{}^{(f+1)}(u)=\delta_{\alpha_1,\alpha_2}\delta_{\beta_1\beta_2}$$

$$\times\int_0^{\infty}\sinh\theta^{f-1}Z_{N_1,\alpha_1}{}^{(f)}(\theta)Z_{N_2,\alpha_1}{}^{(f)}(\theta)\,d\theta.$$

Using the definition of $Z_{N,\alpha}{}^{(f)}$ [Eq. (16)], this reduces to the study of the integral:

$$\int_0^{\infty}d\theta\sinh\theta^{f-1+2\alpha_1}\left[\left(\frac{d}{d\cosh\theta}\right)^{\frac{1}{2}(f-1)+\alpha_1}\cos N_1\theta\right]$$

$$\times\left[\left(\frac{d}{d\cosh\theta}\right)^{\frac{1}{2}(f-1)+\alpha_1}\cos N_2\theta\right],$$

Let us introduce the notation

$$q_p(N,\Omega)=\sinh\theta^p(d/d\cosh\theta)^p\cos N\theta.$$

We want to evaluate

$$\int_0^{\infty}d\theta q_p(N_1,\theta)q_p(N_2,\theta).$$

CC-0. In Public Domain. Gurukul Kangri Collection, Haridwar

Digitized by Arya Samaj Foundation Chennai and eGangotri

It is understood that N_1 and N_2 are positive. The auxiliary functions $q_p(N,\theta)$ enjoy the following properties which are easily eatablished:

$$q_{p+1}(N,\theta)=[(d/d\theta)-p\coth\theta]q_p(N,\theta)$$

$$[N^2+(p-1)^2]q_{p-1}(N,\theta)$$
$$=-[(d/d\theta)+(p-1)\coth\theta]q_p(N,\theta)$$

$$\left\{\frac{d^2}{d\theta^2}+N^2-\frac{p(p-1)}{\sinh^2\theta}\right\}q_p(N,\theta)=0.$$

$q_p(N,0)=0$ if $p\geq 1$ and $q_p(N,\theta)$ has an oscillatory behavior at infinity. Using the recurrence relations given above we find by using integration by parts that for $p\geq 1$:

$$\int_0^\infty d\theta q_p(N_1,\theta)q_p(N_2,\theta)$$

$$=\int_0^\infty d\theta q_p(N_1,\theta)\left(\frac{d}{d\theta}-(p-1)\coth\theta\right)q_{p-1}(N_2,\theta)$$

$$=\int_0^\infty d\theta q_{p-1}(N_2,\theta)\left(-\frac{d}{d\theta}-(p-1)\coth\theta\right)q_p(N_1,\theta)$$

$$=[N^2+(p-1)^2]\int_0^\infty d\theta q_{p-1}(N_1,\theta)q_{p-1}(N_2,\theta).$$

Since for $p=0$, $q_p(N,\theta)$ reduces to $\cos N\theta$ and

$$\int_0^\infty d\theta\cos N_1\theta\cos N_2\theta=\tfrac{1}{2}(\pi)\,\delta(N_1-N_2)$$

we find for $p\geq 1$

$$\int_0^\infty d\theta q_p(N_1,\theta)q_p(N_2,\theta)$$
$$=[N_1^2(N_1^2+1^2)\cdots(N_1^2+(p-1)^2]\tfrac{1}{2}(\pi)\,\delta(N_1-N_2).$$

Let now $p=\alpha_1+\frac{1}{2}(f-1)$ and introduce the proper normalization for $Z_{N,\alpha}{}^{(f)}$. One sees that we have just proved Eq. (18).

We turn to the completeness relation. For that purpose we use the following addition theorem (see Ref. 4):

$$\sum_{\alpha,\beta}H_{N,\alpha,\beta}{}^{(f+1)}(u_1)\,(H_{N,\alpha,\beta}{}^{(f+1)}(u_2))^*$$
$$=\frac{(-1)^{\frac{1}{2}(f-1)}}{(2\pi)^{\frac{1}{2}(f-1)}\pi}\left(\frac{d}{d\cosh\theta}\right)^{\frac{1}{2}(f-1)}\cos N\theta,\quad(21)$$

f off ≥ 3, $u_1u_2=\cosh\theta$.

Integrating this result over N requires a little attention, since in interpreting the result as $\delta_{\rm hyp}(u_1,u_2)$ we shall naturally want to adapt the coordinate system on the hyperboloid in order that, say, u_1 be the point $(1,0,0,\cdots,0)$. Integration of Eq. (21) over N will introduce "δ functions" of θ. However, with this special system of coordinates, $\theta=0$ will be an end point of the integration interval in θ. Hence we use the following procedure. We multiply Eq. (21) by $\cos(N\epsilon)$, with $\epsilon>0$, ϵ will be allowed to go to zero at the end of the calculation (the same device will later be used without comment in the case of f even). With this in mind we find:

$$\int_0^\infty dN\sum_{\alpha,\beta}H_{N,\alpha,\beta}{}^{(f+1)}(u_1)\,(H_{N,\alpha,\beta}{}^{(f+1)}(u_2))^*$$
$$=\lim_{\epsilon\to+0}\frac{(-1)^{\frac{1}{2}(f-1)}}{(2\pi)^{\frac{1}{2}(f-1)}}\left(\frac{d}{d\cosh\theta_{12}}\right)^{\frac{1}{2}(f-1)}\delta(\theta_{12}-\epsilon)$$

The right-hand side does not appear at first sight to be equal to $\delta_{\rm hyp}(u_1,u_2)$, but is indeed equal to it. To see that, recall that $d^f\mu=\sinh\theta^{f-1}d\theta d^{f-1}\Omega$. Adapting the coordinate system as explained above, we compute with a test function ψ:

$$\lim_{\epsilon\to+0}\frac{(-1)^{\frac{1}{2}(f-1)}}{(2\pi)^{\frac{1}{2}(f-1)}2}\int_0^\infty d\theta\int_{S_f}d^{f-1}\Omega(n)\,\sinh\theta^{f-1}\psi(\theta,\mathbf{n})\left(\frac{d}{d\cosh\theta}\right)^{\frac{1}{2}(f-1)}\delta(\theta-\epsilon)$$
$$=\lim_{\epsilon\to+0}\frac{1}{2(2\pi)^{\frac{1}{2}(f-1)}}\int_0^\infty d\theta\int_{S_f}d^{f-1}\Omega(n)\delta(\theta-\epsilon)\,\sinh\theta\left(\frac{d}{d\cosh\theta}\right)^{\frac{1}{2}(f-1)}\sinh\theta^{f-2}\psi(\theta,\mathbf{n}).$$

We now use the fact that $\sinh\theta(d/d\cosh\theta)^q\sinh\theta^{f-2}$ goes to zero for $\theta\to+0$ as long as $q<\frac{1}{2}(f-1)$ (recall that f is odd and greater or equal to 3), while

$$\lim_{\theta\to+0}\sinh\theta\left(\frac{d}{d\cosh\theta}\right)^{\frac{1}{2}(f-1)}\sinh\theta^{f-2}=\frac{\Gamma(f-1)}{2^{\frac{1}{2}(f-1)-1}\Gamma\frac{1}{2}(f-1)}.$$

Our integral is thus $\psi(0)$ (which stands for $\psi(0,\mathbf{n})$, $\mathbf{n}$ arbitrary, the value being the same for all $(\mathbf{n})$ times $\Gamma(f-1)/(4\pi)^{\frac{1}{2}(f-1)}\Gamma[\frac{1}{2}(f-1)]\omega_f$ which is in fact equal to 1, using the area of the sphere given in the introduction $2\pi^{f/2}/\Gamma(f/2)$. In short, Eq. (19) is proved.

It remains to prove Eq. (20). Let t be for the moment a real positive variable with $\log t$ real and compute the following absolutely convergent integral:

$$t^{-1}\int_0^\infty\frac{dN}{\sinh\pi N}\cos(N\log t)\,\frac{\sin N\theta}{\sin\theta}=(2\sinh\theta t)^{-1}$$
$$\times\int_0^\infty dN\left(\frac{\sin N(\theta+\log t)}{\sinh\pi N}+\frac{\sin N(\theta-\log t)}{\sinh\pi N}\right)$$

It is easy to show that

$$\int_{-\infty}^{+\infty}dx\,\frac{\sin yx}{\sinh x}=\pi\tanh\pi\tfrac{1}{2}y.$$

CC-0. In Public Domain. Gurukul Kangri Collection, Haridwar

Digitized by Arya Samaj Foundation Chennai and eGangotri

Hence our integral is equal to

$$\frac{1}{4t\sinh\theta}\times\left\{\tanh\frac{\theta+\log t}{2}+\tanh\frac{\theta-\log t}{2}\right\}=\frac{1}{1+t^2+2t\cosh\theta}.$$

The integral is absolutely convergent for complex t as long as t varies in a plane cut from $-\infty$ to 0, such that $\log t$ is real for real positive t. For these values of t we get by analytic continuation:

$$\frac{1}{1+t^2+2t\cosh\theta}=\frac{-1}{t}\int_0^\infty\frac{dN}{N\sinh\pi N}\cos(N\log t)\frac{d}{d\cosh\theta}(\cos N\theta). \quad (22)$$

The addition theorem (21) together with Eq. (22) yields with the same restrictions on t

$$\frac{1}{(1+t^2+2tu_1u_2)^{\frac{1}{2}(f-1)}}=\frac{2\pi^{\frac{1}{2}(f+1)}}{[\frac{1}{2}(f-1)-1]!}\frac{1}{t^{\frac{1}{2}(f-1)}}\int_0^\infty\frac{dN}{N\sinh\pi N}\cos(N\log t)\times\sum_{\alpha,\beta}H_{N,\alpha,\beta}{}^{(f+1)}(u_1)\,(H_{N,\alpha,\beta}{}^{(f+1)}(u_2))^*.$$

Hence, using the orthogonality relations Eq. (18), we get the desired result Eq. (20)

E. Proof of the Three Relations in the Case of f Even

We first must give some properties of the Legendre functions which will be used in the following, principally the Mehler's transformation formulas. $P_{iN-\frac{1}{2}}(z)$ is the solution of the Legendre equation:

$$[(d/dz)(z^2-1)(d/dz)+N^2+\tfrac{1}{4}]P_{iN-\frac{1}{2}}(z)=0 \quad (23)$$

with the property that it is regular at the point $+1$ where it takes the value $+1$. For z real greater than one, N real, which is the domain in which we are interested, $P_{iN-\frac{1}{2}}$ is real and is even in N. For θ real positive, the following two integral representations hold[4]:

$$P_{iN-\frac{1}{2}}(\cosh\theta)=\frac{\sqrt{2}}{\pi\tanh\pi N}\int_\theta^\infty\frac{\sin N\psi d\psi}{(\cosh\psi-\cosh\theta)^{\frac{1}{2}}}=\frac{\sqrt{2}}{\pi}\int_0^\theta\frac{\cos N\psi}{(\cosh\theta-\cosh\psi)^{\frac{1}{2}}}d\psi. \quad (24)$$

These two integrals are reminiscent of the theory of Abel's integral equation. We propose to show that it leads us to the theory of Mehler's transforms. Let $g(\psi)$ be a function defined for $\psi\geq 0$ vanishing for $\psi=0$, square integrable between 0 and ∞ and sufficiently regular for the following integrals to be well defined. One has the couple of equations:

$$g(\psi)=\frac{2}{\pi}\int_0^\infty\sin N\psi G(N)\,dN$$

$$G(N)=\int_0^\infty\sin N\psi g(\psi)\,d\psi. \quad (25)$$

Consider the linear transformation:

$$g(\psi)\to f(\theta)=\int_0^\infty\frac{g(\psi)}{(\cosh\psi-\cosh\theta)^{\frac{1}{2}}}d\psi, \quad (26)$$

where $\theta\geq 0$. The inverse formula of this Abel equation is defined, if say $g(\psi)<A\psi$ for small ψ, and gives us

$$g(\psi)=-\frac{1}{\pi}\frac{d}{d\psi}\int_\psi^\infty\frac{f(\theta)\sinh\theta d\theta}{(\cosh\psi-\cosh\theta)^{\frac{1}{2}}}. \quad (27)$$

Combining Eqs. (26) and (25) we find

$$f(\theta)=\frac{2}{\pi}\int_0^\infty dN\,G(N)\int_\theta^\infty\frac{\sin N\psi}{(\cosh\psi-\cosh\theta)^{\frac{1}{2}}}d\psi=\int_0^\infty dN\,P_{iN-\frac{1}{2}}(\cosh\theta)\sqrt{2}(\tanh\pi N)G(N) \quad (28)$$

where we have used the first integral representation in Eq. (24) for the Legendre function. Similarly combining Eqs. (27) and (25) we find:

$$G(N)=\int_0^\infty d\psi(\sin N\psi)g(\psi)$$

$$=-\int_0^\infty d\psi\sin N\psi\pi^{-1}\frac{d}{d\psi}\int_\psi^\infty\frac{f(\theta)\sinh\theta}{(\cosh\theta-\cosh\psi)^{\frac{1}{2}}}d\theta$$

$$=\left[-\frac{\sin\psi}{\pi}\int_\psi^\infty\frac{f(\theta)\sinh\theta}{(\cosh\theta-\cosh\psi)^{\frac{1}{2}}}d\theta\right]_0^\infty+\pi^{-1}\int_0^\infty d\psi N\cos N\psi\int_\psi^\infty\frac{f(\theta)\sinh\theta}{(\cosh\theta-\cosh\psi)^{\frac{1}{2}}}d\theta.$$

Assuming that $g(\psi)$ is the derivative of a function which vanishes at infinity, we can drop the integrated term and we find, using the second integral representation in Eq. (24):

$$G(N)=\frac{N}{2^{\frac{1}{2}}}\int_0^\infty\sinh\theta d\theta f(\theta)P_{iN-\frac{1}{2}}(\cosh\theta)\,d\theta. \quad (29)$$

If we call $F(N)=G(N)\sqrt{2}\tanh\pi N$ we deduce from Eqs. (28) and (29) the couple of Mehler transforms:

$$f(\theta)=\int_0^\infty F(N)P_{iN-\frac{1}{2}}(\cosh\theta)\,dN$$

$$F(N)=N\tanh\pi N\int_0^\infty d\theta\sinh\theta f(\theta)P_{iN-\frac{1}{2}}(\cosh\theta). \quad (30)$$

We can express Eq. (30) in a different language with

[4] A. Erdelyi, W. Magnus, F. Oberhettinger, and F. Tricomi, *Higher Transcendental Functions* (McGraw-Hill Book Company, Inc., New York, 1953), Vol. 1.

CC-0. In Public Domain. Gurukul Kangri Collection, Haridwar

Digitized by Arya Samaj Foundation Chennai and eGangotri

x_1, x_2 real and greater than one, N_1 and N_2 positive;

$$\int_0^\infty dN P_{iN-\frac{1}{2}}(x_1) P_{i-N\frac{1}{2}}(x_2) N \tanh \pi N = \delta(x_1 - x_2)$$

$$\int_1^\infty dx P_{iN_1-\frac{1}{2}}(x) P_{iN_2-\frac{1}{2}}(x) = \frac{\delta(N_1 - N_2)}{N_1 \tanh \pi N_1}. \tag{31}$$

We are now in a position to derive formulas (18), (19), and (20) in the case of f even ≥ 2. From Eqs. (11) and (13) we get as before

$$\int_{T_{f+1+}} d^f\mu(u) H_{N_1,\alpha_1,\beta_1}(u) (H_{N_2,\alpha_2,\beta_2}(u))^* = \delta_{\alpha_1,\alpha_2}\, \delta_{\beta_1,\beta_2} \times \int_0^\infty \sinh \theta^{f-1} d\theta Z_{N_1,\alpha_1}{}^{(f)}(\theta) Z_{N_2,\alpha_1}{}^{(f)}(\theta).$$

Using the definition of $Z_{N,\alpha}{}^{(f)}$, Eq. (17), leads us to study the integral:

$$\int_0^\infty r_{\frac{1}{2}(f-2)+\alpha_1}(N_1, \theta) r_{\frac{1}{2}(f-2)+\alpha_1}(N_2, \theta) \sinh \theta d\theta$$

where the auxiliary function $r_p(N, \theta)$ (equal up to a factor to the associated Legendre function) is defined through:

$$r_p(N, \theta) = (\sinh \theta)^p (d/d \cosh \theta)^p P_{iN-\frac{1}{2}}(\cosh \theta).$$

This function satisfies the following relations deduced from the analogous ones valid for the Legendre functions:

$$r_{p+1}(N, \theta) = [(d/d\theta) - p \coth \theta] r_p(N, \theta),$$

$$[N^2 + (p-\tfrac{1}{2})^2] r_{p-1}(N, \theta) = -[(d/d\theta) + p \coth \theta] r_p(N, \theta),$$

$$\left[\sinh^2 \theta \left(\frac{d}{d \cosh \theta}\right)^2 + 2 \cosh \theta \frac{d}{d \cosh \theta} + N^2 + \tfrac{1}{4} - \frac{p^2}{\sinh^2 \theta}\right] r_p(N, \theta) = 0.$$

Hence, by integration by parts using the fact that $r_p(N, \theta)$ is bounded at infinity by $A(\cosh \theta)^{-\frac{1}{2}}$:

$$\int_0^\infty d\theta \sinh \theta r_p(N_1, \theta) r_p(N_2, \theta) = \int_0^\infty d\theta \sinh \theta r_p(N_1, \theta) \left(\frac{d}{d\theta} - (p-1) \coth \theta\right) r_{p-1}(N_2, \theta)$$

$$= -\int_0^\infty d\theta \sinh \theta r_{p-1}(N_2, \theta) \left(\frac{d}{d\theta} + p \coth \theta\right) r_p(N_1, \theta)$$

$$= [N^2 + (p-\tfrac{1}{2})^2] \int_0^\infty d\theta \sinh \theta r_{p-1}(N_1, \theta) r_{p-1}(N_2, \theta).$$

Since for $p=0$, $r_p(N, \theta)$ reduces to the Legendre function for which Eq. (31) holds, we get

$$\int_0^\infty d\theta \sinh \theta r_p(N_1, \theta) r_p(N_2, \theta) = \{[N_1^2 + (p-\tfrac{1}{2})^2] \cdots (N^2 + \tfrac{1}{4})\} (N_1 \tanh \pi N_1)^{-1} \delta(N_1 - N_2).$$

The coefficient in front of the δ-function is to be understood as $(N_1 \tanh \pi N_1)^{-1}$ if $p=0$. Comparing this result with the normalization of $Z_{N,\alpha}{}^{(f)}(\theta)$ we see that we have proved Eq. (18).

For the completeness relations we use the addition theorem[4]:

$$\sum_{\alpha,\beta} H_{N,\alpha,\beta}{}^{(f+1)}(u_1) (H_{N,\alpha,\beta}{}^{(f+1)}(u_2))^* = \frac{n \tanh \pi N}{(2\pi)^{f/2}} (-1)^{\frac{1}{2}(f-2)} \left(\frac{d}{d \cosh \theta}\right)^{\frac{1}{2}(f-2)} P_{iN-\frac{1}{2}}(\cosh \theta). \tag{32}$$

$$\cosh \theta = \mu_1 u^2$$

To prove Eq. (19) it remains to integrate Eq. (32) over N. With the same trick as in the previous section, we find with the help of Eq. (31):

$$\int_0^\infty dN \sum_{\alpha,\beta} H_{N,\alpha,\beta}{}^{(f+1)}(u_1) (H_{N,\alpha,\beta}{}^{(f+1)}(u_2))^* = \lim_{\epsilon \to +0} \frac{(-1)^{\frac{1}{2}(f-2)}}{(2\pi)^{f/2}} \left(\frac{d}{d \cosh \theta}\right)^{\frac{1}{2}(f-2)} \delta(\cosh \theta - 1 - \epsilon).$$

Again, this is indeed $\delta_{\text{hyp}}(u_1, u_2)$ since with the test function ψ

$$\lim_{\epsilon \to +0} \int_0^\infty d^f\mu(u) \psi(u) \frac{(-1)^{\frac{1}{2}(f-2)}}{(2\pi)^{f/2}} \left(\frac{d}{d \cosh \theta}\right)^{\frac{1}{2}(f-2)} \delta(\cosh \theta - 1 - \epsilon)$$

$$= \lim_{\epsilon \to +0} \int_0^\infty \sinh \theta d\theta \delta(\cosh \theta - 1 - \epsilon) \frac{1}{(2\pi)^{f/2}} \left(\frac{d}{d \cosh \theta}\right)^{\frac{1}{2}(f-2)} \sinh \theta^{\frac{1}{2}(f-2)} \int_{S_f} \psi(\theta, n)^{f-1} d\Omega(n)$$

CC-0. In Public Domain. Gurukul Kangri Collection, Haridwar

Digitized by Arya Samaj Foundation Chennai and eGangotri

Again

$$\lim_{\theta\to+0}(d/d\cosh\theta)^q \sinh\theta^{f-2}=\begin{cases}0 & \text{if } q<\tfrac{1}{2}(f-2)\\ \tfrac{1}{2}(f-2)!2^{\frac{1}{2}(f-2)} & \text{if } q=\tfrac{1}{2}(f-2)\end{cases}$$

so that the integral reduces by Leibniz rule to $\psi(0)$ times $\omega_f[(f-2)/2]!2^{(f-2)/2}(2\pi)^{f/2}=1$. The completeness relations, Eq. (19), are thus proved.

It remains to obtain the integral equation (20). For this we use the alternative integral representation of $P_{iN-\frac{1}{2}}(\cosh\theta)$:

$$P_{iN-\frac{1}{2}}(\cosh\theta)=\frac{\cosh\pi N}{N}\int_0^\infty \frac{t^{-\frac{1}{2}-iN}}{(1+2t\cosh\theta+t^2)^{\frac{1}{2}}}\,dt. \tag{33}$$

By Fourier transformation Eq. (33) gives

$$t^{-\frac{1}{2}}\int_0^\infty \cos(N\log t)\,P_{iN-\frac{1}{2}}(\cosh\theta)\frac{dN}{\cosh\pi N}=\frac{1}{(1+2t\cosh\theta+t^2)^{\frac{1}{2}}}. \tag{34}$$

This result can again be continued analytically in the complex t plane cut from $-\infty$ to 0, with the principal determination of the logarithm in the left-hand side and the square root on the right-hand side such that it will be positive for real positive t.

Combining Eqs. (32) and (34) we get

$$\int_0^\infty \frac{dN}{N\sinh\pi N}\cos(N\log t)\sum_{\alpha,\beta}H_{N,\alpha,\beta}^{(f+1)}(u_1)\,(H_{N,\alpha,\beta}^{(f+1)}(u_2))^*=\frac{t^{\frac{1}{2}(f-1)}}{(2\pi)^{f/2}}\frac{1\cdot3\cdots(f-3)}{(1+2tu_1\cdot u_2+t^2)^{\frac{1}{2}(f-1)}} \tag{35}$$

with $1\cdot3\cdots(f-3)$ replaced by 1 if $f=2$ and the same restrictions on t as before. With the help of the orthogonality relation, Eq. (18), we deduce from Eq. (35) the desired integral equation (20).

F. Solution of the Integral Equation for the Coulomb Potential

Having now the required tools, we compare Eqs. (9) and (20). If we let t go to 1 in Eq. (20) the expression is well defined. If we approach -1, either by the upper or lower imaginary plane, we again find a unique limit. Using these facts, let $g(u)$ be a function defined on the whole hyperboloid $T_{f+1}=T_{f+1}^{+}+T_{f+1}^{-}$, by

$$u\in T_{f+1}^{+},\qquad g(u)=N_{N,\alpha,\beta}(u)$$

$$u\in T_{f+1}^{-},\qquad g(u)=aH_{N,\alpha,\beta}(-u).$$

One deduces from Eq. (20) that

$$\int_{T_{f+1}} d^f\mu(v)\,\frac{g(v)}{|(u-v)^2|^{(f-1)}}=\frac{2\pi^{\frac{1}{2}(f+1)}}{\Gamma\frac{1}{2}(f-1)N\sinh\pi N}\times g(u)\begin{cases}a+\cosh N\pi & \text{if } u\in T_{f+1}^{+}\\ a^{-1}+\cosh N\pi & \text{if } u\in T_{f+1}^{-}.\end{cases}$$

In order that $g(u)$ be a solution of Eq. (9), it is thus necessary that $(a+\cosh\pi N)=-(a^{-1}+\cosh\pi N)$, in which case $a=-e^{\mp\pi N}$. Correspondingly we have two solutions (up to a normalization):

$$\hat{\Phi}_{N,\alpha,\beta}^{(\pm)}(u)=\begin{cases}H_{N,\alpha,\beta}(u) & \text{if } u\in T_{f+1}^{+}\\ -e^{\mp\pi N}H_{N,\alpha,\beta}(-u) & \text{if } u\in T_{f+1}^{-}\end{cases} \tag{36}$$

which satisfy

$$\hat{\Phi}_{N,\alpha,\beta}^{(\pm)}(u)=\pm N\frac{\Gamma^{\frac{1}{2}(f-1)}}{2\pi^{\frac{1}{2}(f+1)}}\in(u)\times\int_{T_{f+1}} d^f\mu(v)\,\frac{\hat{\Phi}_{N,\alpha,\beta}^{\pm}(v)}{|(u-v)^2|^{\frac{1}{2}(f-1)}}. \tag{37}$$

Because of the completeness relations, Eq. (19), one can convince oneself that the functions, Eq. (36), exhaust the solutions of Eq. (9). The fact that for given N, α, β there exist two solutions is a natural consequence from the fact that choosing N positive was a matter of indifference; indeed $\hat{\Phi}_{N,\alpha,\beta}^{(+)}(u)=\hat{\Phi}_{-N,\alpha,\beta}^{(-)}(u)$. On the other hand, this double solution reflects the fact that we can as well treat attractive or repulsive potentials. $\hat{\Phi}^{(+)}$ corresponds to the attractive case ($k>0$), $\hat{\Phi}^{(-)}$ to the repulsive case ($k<0$). Comparing Eqs. (9) and (37) we get the following relation between the energy E and N:

$$E=(\mu k^2/2\hbar^2)\,(1/N^2) \tag{38}$$

independently of the dimension f. Equation (38) is the analytic continuation in the index λ of the equation corresponding to bound states [Eq. (19) in I] from real integer values to complex values of the form $\lambda=-\frac{1}{2}(f-1)+iN$. So, in fact, are the eigenfunctions. We observe also in the case $f=3$, from the Lie-algebra

CC-0. In Public Domain. Gurukul Kangri Collection, Haridwar

Digitized by Arya Samaj Foundation Chennai and eGangotri

analysis, that the eigenvalue c which characterizes our representations of $0(1,3)$ is equal to iN.

Each set of functions $H_{N,\alpha,\beta}{}^{(f+1)}(u)$ for fixed N provides a basis for an irreducible unitary representation of $0^{(+,+)}(1,f)$ through

$$H_{N,\alpha,\beta}{}^{(f+1)}(\Lambda^{-1}u)=D_{\alpha',\beta';\alpha,\beta}{}^{N}(\Lambda)H_{N,\alpha',\beta'}{}^{(f+1)}(u). \quad (39)$$

This is clear since the equation satisfied by this function for fixed N is invariant under the group. We shall not exhibit explicitly the matrix elements of these representations; it would require too lengthy calculations. We return to this question in the following section.

III. TRANSFORMATION GROUP

We shall discuss briefly the introduction of a larger group of transformations. The motivation is the same as in I: We want to find a group which relates the various scattering states corresponding to different energies but we have to mix solutions for attractive and repulsive potentials. Consider the space $\mathfrak{K}_{f+1}$ of square integrable functions on T_{f+1} with the measure $d^f\mu$. It is spanned by our scattering states $\tilde{\Phi}_{N,\alpha,\beta}{}^{(\pm)}(u)$. We are looking for a group which contains $0(1,f)$ as subgroup and has a unitary representation in $\mathfrak{K}_{f+1}$ which reduces to the ones described above when restricted to $0(1,f)$. Again, the answer is in terms of projective transformations.

We recall the construction of this group. Let us denote for the moment by u an arbitrary point in Euclidian $(f+1)$-dimensional space. Introduce the quantity $z=u^2$ (where u^2 denotes the Minkowski square). In the (z,u) space we are restricted to the previous "paraboloid." Consider the projective transformations which leave this paraboloid invariant. Introducing the homogenity variable t we find the homogeneous group, leaving

$$zt-u^2\equiv\tfrac{1}{2}(z+t)^2-\tfrac{1}{2}(z-t)^2-u_0{}^2+\sum_{i=1}^{f}u_i{}^2$$

invariant. That is the "conformal Lorentz group" $0(2,f+1)$. Going back to our $f+1$, Euclidian space we ask for the subgroup of $0(2,f+1)$ which leaves the initial hyperboloid T_{f+1} invariant. The condition is $z-t=0$. Hence the required group is $G\equiv 0(1,f+1)$. The result turns out to be the same as for the bound state case. This will appear clear at the end of this section. Going through the previous transformations, the action of G on the hyperboloid is found to be

$$u\to\Lambda u=u'; \qquad u,u'\in T_{f+1}$$

$$u'_\alpha=(\sum_\beta a_{\alpha\beta}u_\beta+a_{\alpha t})/(\sum_\beta a_{t\beta}u_\beta+a_{tt}). \quad (40)$$

The Greek indices run from 0 to f, the Latin ones from 1 to f. The real matrix Λ belongs to G; that is

$$\Lambda=\begin{pmatrix} a_{\alpha\beta} & a_{\alpha t} \\ a_{t\alpha} & a_{tt}\end{pmatrix}$$

$$\gamma=\begin{bmatrix} 1 & & & & & \\ & -1 & & & & \\ & & -1 & & & \\ & & & \cdot & & \\ & & & & -1 & \\ & & & & & -1 \end{bmatrix},$$

$$\Lambda^T\gamma\Lambda=\gamma. \quad (41)$$

The hyperboloid is clearly invariant since one finds

$$u'^2-1=(u^2-1)/(\sum_\alpha a_{t\alpha}u_\alpha+a_{tt})^2=0. \quad (42)$$

It is to be remarked that in Eqs. (40) and (42) the denominator may vanish for certain transformations. This means in fact that in order to consider the action of G on T_{f+1} we have to add to the hyperboloid extra points "at infinity." In other words, T_{f+1} has been compactified by the adjunction of a surface at infinity.

We build the following unitary representations of G in $\mathfrak{K}_{f+1}$ which depend on the index ρ:

$$\Phi(u)\to T_\rho{}^\Lambda\Phi(u)=\frac{\Phi(\Lambda^{-1}u)}{|\sum a_{t\alpha}(\Lambda^{-1})u_\alpha+a_{tt}(\Lambda^{-1})|^{(f/2)+i\rho}}. \quad (43)$$

Using Eq. (42) one checks the unitarity of these representations:

$$\int_{T_{f+1}}d^f\mu\bar{\Phi}\psi=\int_{T_{f+1}}d^f\mu([T_\rho{}^\Lambda\Phi])^*[T_\rho{}^\Lambda\psi]. \quad (44)$$

We have studied in I similar representations of $0(1,f+1)$ realized in the Hilbert space of square integrable functions on the sphere S_{f+1}; denote it by $\mathfrak{K}_{f+1}$. It may be interesting to know whether we have constructed equivalent or inequivalent representations of the same group. The remainder of this section will be devoted to the proof of the unitary equivalence of the two sets of representations. All the properties investigated before, such as irreducibility, will then hold true in the present case.

For that purpose we first define a transformation which maps the sphere

$$S_{f+1}=\{v: v_0{}^2+\sum_{i=1}^{f}u_i{}^2=1\}$$

CC-0. In Public Domain. Gurukul Kangri Collection, Haridwar

Digitized by Arya Samaj Foundation Chennai and eGangotri

on the hyperboloid

$$T_{f+1}=\{u: u_0^2-\sum_{i=1}^{f}u_1^2=1\}.$$

It is the following mapping [see Fig. 2(a)]

$$v\in S_{f+1}\to u=\tau v\in T_{f+1}; \qquad u=[v_0^{-1},\ (-v_i/v_0)]$$
$$u\in T_{f+1}\to v=\tau^{-1}u\in S_{f+1}; \qquad v=[u_0^{-1},\ (-u_i/u_0)]. \quad (45)$$

Let $v\to\Lambda v=v'$ be a conformal transformation of S_{f+1}; $\Lambda\in O(1,f+1)$ and

$$v'_0=(a_{00}v_0+\sum_j a_{0j}v_j+a_{0t})/(a_{t0}v_0+\sum_j a_{tj}v_j+a_{tt}),$$
$$v'_i=(a_{i0}v_0+\sum_j a_{ij}v_j+a_{it})/(a_{t0}v_0+\sum_j a_{tj}v_j+a_{tt}), \quad (46)$$

with

$$\Lambda=\begin{pmatrix} a_{tt} & a_{t\beta} \\ a_{\alpha t} & a_{\alpha\beta}\end{pmatrix}; \qquad \Lambda^T\gamma\Lambda=\gamma, \quad (47)$$

γ being as in Eq. (41). Performing the projection τ we find that the corresponding point on T_{f+1} undergoes the following transformation:

$$u\to\Lambda_\tau u=u'$$
$$u_0=(a_{tt}u_0-\sum_j a_{tj}u_j+a_{t0})/(a_{0t}u_0-\sum_j a_{0j}u_j+a_{00}),$$
$$u_i=(-a_{it}u_0+\sum_j a_{ij}u_j-a_{i0})/(a_{0t}u_0-\sum_j a_{0j}u_j+a_{00}). \quad (48)$$

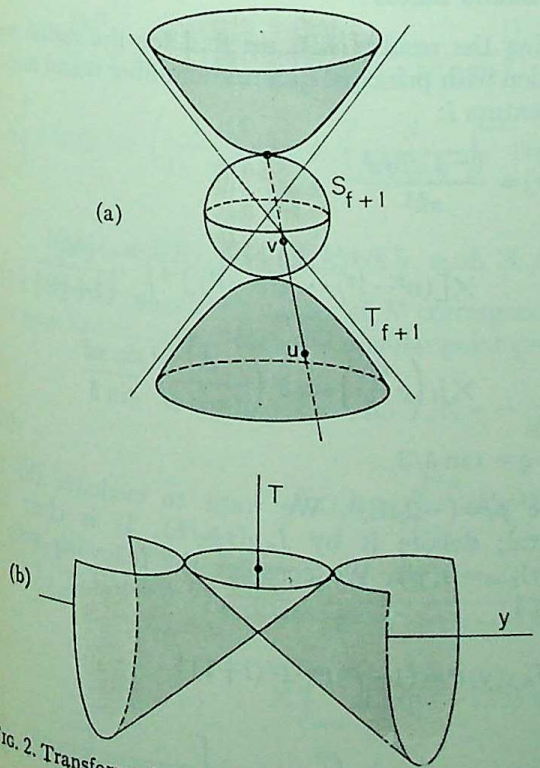

FIG. 2. Transformations between a sphere and a hyperboloid.

That is, with

$$\Lambda_\tau=\begin{pmatrix}1&0&0\\0&0&-I_f\\0&1&0\end{pmatrix} \qquad \Lambda_0^{-1}=\begin{pmatrix}1&0&0\\0&0&1\\0&-I_f&0\end{pmatrix}$$

one has

$$\Lambda_0\Lambda\Lambda_0^{-1}=\begin{pmatrix} a_{tt} & -a_{tj} & a_{t0} \\ -a_{it} & a_{ij} & -a_{i0} \\ a_{0t} & -a_{0j} & a_{00}\end{pmatrix}. \quad (49)$$

I_f is a unit $f\times f$ matrix. The correspondence $\Lambda\to\Lambda_\tau$ is an inner automorphism of $O(1,f+1)$ and one even remarks that Λ_0 always belongs to the component of the identity.

If $u=\tau v$ one also finds, using Eq. (45), that

$$d^f\Omega(v) \quad d^f\mu(u)/|u_0|^f; \qquad u=\tau v. \quad (50)$$

Hence, if $\psi(v)$ is a function defined on S_{f+1} and belongs to $\mathcal{K}_{f+1}$;

$$\int_{S_{f+1}}|\psi(v)|^2\,d^f\Omega(v)=\int_{T_{f+1}}\frac{|\psi(\tau^{-1}u)|^2}{|u_0|^{f/2}}\,d^f\mu(u). \quad (51)$$

Using Eq. (51) we define a unitary mapping U_ρ from $\mathcal{K}_{f+1}$ to $\mathcal{K}_{f+1}$ by

$$\psi(v)\in\mathcal{K}_{f+1}\to[U_\rho\psi](u)=[\psi(\tau^{-1}u)/|u_0|^{(f/2)+i\rho}]\in\mathcal{K}_{f+1}$$
$$\Phi(u)\in\mathcal{K}_{f+1}\to[U_\rho^{-1}\Phi](v)=[\Phi(\tau v)/|v_0|^{(f/2)+i\rho}]\in\mathcal{K}_{f+1}. \quad (52)$$

The unitary representation of $O(1,f+1)$ that we investigated in I for $\mathcal{K}_{f+1}$ was defined through

$$\psi(v)\to[R_\rho^\Lambda\psi](v)=\frac{\psi(\Lambda^{-1}v)}{|\sum_\alpha a_{t\alpha}(\Lambda^{-1})v_\alpha+a_{tt}(\Lambda^{-1})|^{(f/2)+i\rho}} \quad (53)$$

with Λv given by Eq. (46). Similarly, Eq. (43) defines a unitary representation T_ρ^Λ of the same group in $\mathcal{K}_{f+1}$. We will now prove that

$$U_\rho R_\rho^\Lambda=T_\rho^{\Lambda_\tau}U_\rho. \quad (54)$$

Since in virtue of Eq. (49)

$$T_\rho^{\Lambda_\tau}=T_\rho^{\Lambda_0}T_\rho^\Lambda(T_\rho^{\Lambda_0})^{-1} \quad (55)$$

and all operators are unitary, Eq. (54) is indeed a statement of unitary equivalence. The proof of this equality is rather straightforward. Consider for instance $[U_\rho R_\rho^\Lambda\psi](u)$

$$=\frac{\psi(\Lambda^{-1}\tau^{-1}u)}{|a_{tt}(\Lambda^{-1})u_0-\sum_j a_{tj}(\Lambda^{-1})u_j+a_{t0}(\Lambda^{-1})|^{(f/2)+i\rho}};$$

CC-0. In Public Domain. Gurukul Kangri Collection, Haridwar

Digitized by Arya Samaj Foundation Chennai and eGangotri

on the other hand,

$$[T_\rho^{\Lambda_\tau} U_\rho \psi](u)$$

$$= \frac{\psi(\tau^{-1}\Lambda_\tau^{-1}u)}{|\, a_{00}(\Lambda^{-1})u_0 - \sum_j a_{0j}(\Lambda^{-1})u_j + a_{0t}(\Lambda^{-1})\,|^{(f/2)+i\rho}}$$

$$\times \left| \frac{a_{00}(\Lambda^{-1})u_0 - \sum_j a_{0j}(\Lambda^{-1})u_j + a_{0t}(\Lambda^{-1})}{a_{tt}(\Lambda^{-1})u_0 - \sum_j a_{tj}(\Lambda^{-1})u_j + a_{t0}(\Lambda^{-1})} \right|^{(f/2)+i\rho},$$

and since by definition of the automorphism t, $\tau^{-1}\Lambda_\tau^{-1} = \Lambda_\tau^{-1}\tau^{-1}$, Eq. (54) is easily obtained and the unitary equivalence established. The geometric transformation (45) which was at the basis of our proof is best understood by adding an homogeneous coordinate such that $u_0 = Y/T$, $u_i = X_i/T$ and the same for v. The sphere and the hyperboloid appear as cones centered respectively around the T and the Y axis; the abstract group $0(1, f+1)$ is realized in two different ways as homogeneous linear group which leave one of these cones invariant. A rotation of 180 degrees around the line $X_i = 0$, $Y = T$ which is tangent to both cones is the substitute for the transformation τ. This is pictured in Fig. 2(b).

As a matter of fact, one can prove that the unitary representations of $0(1, f)$ constructed in Sec. II with the help of spherical functions and those obtained in the section by means of conformal transformations on a sphere or an hyperboloid are equivalent. The proof is an extension of the one given in the case of $f = 3$ in the third paper of Ref. 2.

Before concluding this section we shall briefly mention the case of zero energy. From the commutation relations, Eq. (2), we note that $[M_i, M_j] = 0$ and the operators $\mathbf{L}$, $\mathbf{M}$, build the algebra of the Euclidian group in three dimensions, $E(3)$. In f dimensions this may likewise be realized globally. We project the f-dimensional momentum space onto a paraboloid in $f+1$ dimensions, P_{f+1}. If u is a point on the paraboloid $u_0 = \mathbf{u}^2/2$, with u_0 in the $f+1$ direction and $\mathbf{u}$ in the original f-dimensional subspace, we let $p \to u = [1/(2p^2), \mathbf{p}/p^2]$. Performing this transformation on Eq. (5) we obtain, with $\hat{\Phi}(u) = \Phi(\mathbf{p}/p^2)\,1/p^{f+1}$.

$$\hat{\Phi}(u) = \frac{2uk}{\pi\omega_{f-1}\hbar} \int \frac{d^{f+1}f\,\delta(v_0 - \frac{1}{2}\mathbf{v}^2)\,\hat{\Phi}(v)}{|\, \mathbf{u} - \mathbf{v}\,|^{f-1}},$$

which exhibits the invariance of the problem under the Euclidian group in f dimensions, E_f. It may also be noted that the group of conformal transformations in $f+1$ dimensions which leaves P_{f+1} invariant is again $0(1, f+1)$. The action of the group on functions defined on P_{f+1} may be obtained from its action on S_{f+1} or T_{f+1} by noting that in Fig. 2(b), if we make a rotation of 45° in the (T, Y) plane, we transform S_{f+1} and T_{f+1} into P_{f+1}. It is amusing to note that the large group of transformations in all cases is $0(1, f+1)$, the subgroups which are symmetries of the problem in the cases $E<0$, $E=0$, $E>0$ are $0(f+1)$, $E(f)$, $0(1, f)$ respectively, which are the little groups of the Poincaré group in an $(1, f+1)$-dimensional Minkowski space.

IV. CONCLUSION

The hydrogen atom illustrates several aspects of the use of group theory, and especially noncompact groups in quantum mechanics. The theory of infinite dimensional representations can be of interest in various problems. We hope to have shown in this work that it can be used beyond the realm of Lie algebras.

ACKNOWLEDGMENTS

It is a pleasure to thank Professor Panofsky for his hospitality at SLAC. Thanks are due Dr. R. Stora for discussions on the necessity of including both attractive and repulsive solutions. The work was supported by the U. S. Atomic Energy Commission.

APPENDIX

In Sec. II, Eq. (36), and Ref. 1, Eqs. (12) and (45), we obtained representations of the wave function in momentum spaces, in the scattering and bound-state cases, respectively. We shall explicitly transform both to configuration space and show that we obtain the usual expressions. We set, of course, $f = 3$.

1. Bound States

Using the results of I, we find for the radial wave function with principal quantum number n and angular momentum l:

$$\psi_{n,l}(r) = \frac{(-1)^l 8 p_0^{\frac{3}{2}}}{\pi\hbar^{\frac{3}{2}}} \times [(n^2-1^2)\cdots(n^2-l^2)]^{-\frac{1}{2}} \int_0^\infty \frac{q^2 dq}{(1+q^2)^2} \times j_l\left(q\frac{rp_0}{\hbar}\right) \sin\delta^l \left(\frac{d}{d\cos\delta}\right)^l \frac{\sin n\delta}{\sin\delta} \tag{A1}$$

$$q = \tan\delta/2,$$

where $p_0 = (-2\mu E)^{\frac{1}{2}}$. We want to evaluate the last integral; denote it by $I_{n,l}(rp_0/\hbar)$. It is clear that $I_{n,l}(y)_{y\to 0} = 0(y^l)$. We consider the following sum for $|t| < 1$

$$\sum_1^\infty n I_{n,l}(y)\, t^n = (1-t^2)\, t^{l+1} 2^{2l} (l+1)! \times \int_0^\infty dq j_l(qy) \left[\frac{q}{q^2(1+t)^2 + (1-t)^2}\right]$$

CC-0. In Public Domain. Gurukul Kangri Collection, Haridwar

Digitized by Arya Samaj Foundation Chennai and eGangotri

The integrand is even; we can extend the integration from $-\infty$ to $+\infty$ and use

$$j_l(z)=(1/2i)\{h_l^{(+)}(z)-h_l^{(-)}(z)\}.$$

The Hankel functions satisfy:[5]

$$h_l^{(+)}(-z)=(-1)^{l+1}h^{(-1)}(z), \qquad h_l^{(\pm)}(z)_{z\to 0}=0(z^{-l-1}).$$

Hence we can write

$$\sum nI_{n,l}(y)\,t^n$$

$$=\frac{(1-t^2)}{2i}\,t^{l+1}2^{2l}(l+1)!$$

$$\times\int_{-\infty}^{+\infty}dqh^{(+)}(qy)\left(\frac{q}{q^2(1+t)^2+(1-t)^2}\right)^{l+2}$$

$$=\frac{(1-t^2)}{2i}\,t^{l+1}2^{2l}\,\frac{2\pi i}{(1+t)^{l+2}}\left(\frac{d}{dq}\right)^{l+1}$$

$$\times\left\{h_l^{(+)}(qy)\left(\frac{q}{q(1+t)+i(1-t)}\right)^{l+2}\right\}_{q=i[(1-t)/(1+t)]}$$

where the integral was performed by closing the contour in the upper half q plane. Since the sum behaves like y^l for $y\to 0$ we can drop in the derivative all the terms which are of smaller power in y. We use explicit form of the Hankel function[5] and obtain:

$$\sum_1^\infty nI_{n,l}(y)\,t^n=\pi t^{l+1}2^{l2}y^le^{-y}\,\frac{e^{y[2t/(1+t)]}}{(1+t)^{2l+2}}.$$

On the right-hand side we recognize the generating function of associated Laguerre polynomials:

$$\frac{e^{y[t/(1+t)]}}{(1+t)^{1+k}}=\sum_{p=0}^{\infty}\frac{(-1)^p t^p}{(p+k)!}L_p^k(y) \qquad |t|<1$$

and thus get

$$I_{n,l}(y)$$

$$=\int_0^\infty\frac{q^2dq}{(1+q^2)}j_l(qy)\,\sin\delta^l\left(\frac{d}{d\cos\delta}\right)^l\left(\frac{\sin n\delta}{\sin\delta}\right)_{\delta=2\arctan}$$

$$=\frac{(-1)^{n-l-1}}{n(n+l)!}\,\pi 2^{l-2}y^le^{-y}L_{n-l-1}^{2l+1}(2y). \qquad \text{(A2)}$$

Introducing the Bohr radius

$$a=\hbar^2/k\mu, \qquad \text{(A3)}$$

we obtain by combining Eqs. (A1) and (A2) the radial wave function:

$$\psi_{n,l}(r)=\frac{(-1)^{n-1}}{a^{\frac{3}{2}}}\,\frac{2}{n^2}\left[\frac{(n-l-1)!}{[(n+l)!]^3}\right]^{\frac{1}{2}}\rho^le^{-\rho/2}L_{n-l-1}^{2l+1}(\rho);$$

$$\rho=(2r/na). \qquad \text{(A4)}$$

2. Scattering Case

With the necessary adjustments for normalization we find for the radial wave function with angular momentum l and energy

$$\psi_{N,l}(r)=\frac{4\pi i^l}{(2\pi)^{\frac{3}{2}}}\left\{\frac{N}{(1-e^{-2\pi N})N^2(N^2+1^2)(N^2+l^2)}\right\}^{\frac{1}{2}}$$

$$\times\left[\int_0 dqq^2j_l(q\rho)\left(\frac{2}{1-q^2}\right)^2\sinh\theta_-{}^l\left(\frac{d}{d\cosh\theta_-}\right)^{l+1}\cos N\theta_- - e^{-\pi N}\int_1^\infty dqq^2j_l(q\rho)\left(\frac{2}{1-q^2}\right)^2\sinh\theta_+{}^l\left(\frac{d}{d\cosh\theta_+}\right)^{l+1}\cos N\theta_+\right], \qquad \text{(A5)}$$

$$N=k(\mu/2\hbar^2E)^{\frac{1}{2}},\ \rho=[(2\mu E)^{\frac{1}{2}}/\hbar]r,\ \tanh(\theta_-/2)=q \quad \text{for} \quad 0<q<1,\ \tanh(\theta_+/2)=(1/q) \quad \text{for} \quad q>1.$$

The positive (negative) values of N correspond to attractive (repulsive) potentials. Of course we must give some prescription to deal with the singular point $q=1$. We introduce

$$F_l(N,\theta)=-\frac{1}{\sinh\pi N}\left(\frac{d}{d\cosh\theta}\right)^{l+1}\frac{\cos N\theta}{\sinh\theta},$$

$$\tilde F_l(t,\theta)=\int_{-\infty}^{+\infty}dNe^{iNt}F_l(N,\theta)=\frac{i\sinh t(-1)^l(l+1)!}{(\cosh\theta+\cosh t)^{l+2}},$$

$$\psi_{N,l}=\frac{4\pi i^{l-1}}{(2\pi)^{\frac{1}{2}}}\sinh\pi N\left[\frac{N}{(1-e^{-2\pi N})N^2(N^2+1^2)\cdots(N^2+l^2)}\right]^{\frac{1}{2}}(-1)^l(l+1)!2^{l+1}$$

$$\times\int_{-\infty}^{+\infty}dt\,\exp(-iNt)\sinh t\int_{-\infty}^{+\infty}dqj_l(q\rho)\left(\frac{q}{q^2[1-\cosh(t-i\epsilon)]+[1+\cosh(t-i\epsilon)]}\right)^{l+2}.$$

[5] A. Messiah, *Quantum Mechanics* (North-Holland Publ. Co., Amsterdam, 1964), Vol. I.

CC-0. In Public Domain. Gurukul Kangri Collection, Haridwar

Digitized by Arya Samaj Foundation Chennai and eGangotri

The prescription cosh $(t-i\epsilon)$ takes care of the singularity at $q=1$. We replace again j_l by $(1/2i)$ $(h_l^{(+)}-h_l^{(-)})$, close the contour in the upper half of the q plane and use the explicit form of the Hankel function to calculate the derivative which occurs at the point $q=\coth[(t-i\epsilon)/2]$. The result is

$$\psi_{N,l}=\frac{8\pi^2 i^l}{(2\pi)^{\frac{1}{2}}}\sinh\pi N \times\left[\frac{N}{(1-e^{-2\pi N})N^2(N^2+1^2)\cdots(N^2+l^2)}\right]^{\frac{1}{2}}2^{-l-2}\rho^l \times\int_{-\infty}^{+\infty}\frac{dt}{[\sinh^2(t/2)]^{l+1}}\exp[i\cosh(t/2)\rho-iNt].$$

We take $x=\cosh(t/2)$ as a variable, the region of integration being the real axis except the segment $(-1, +1)$. We can close the contour in the upper half-plane (ρ is positive) and move it to $(-1, +1)$. Taking into account changes of arguments in the integrand we get

$$\psi_{N,l}=\sinh\pi N\left(\frac{N}{2\pi 1-e^{-2\pi N}}\right)^{\frac{1}{2}}\left(\frac{-i\rho}{2}\right)^l\frac{e^{\pi N}}{[N^2\cdots(N^2+l^2)]^{\frac{1}{2}}} \times\int_{-1}^{+1}dx e^{i\rho x}(1-x)^{l-iN}(x+1)^{iN}$$

with Arg $(x+1)=$ Arg $(1-x)=0$. Apart from a proportionality factor and an exponential, the integral is a classical representation of the hypergeometric function. Taking this factor into account and

$$[\pi N^2(N^2+1)\cdots(N^2+l^2)]^{\frac{1}{2}}=(N\sinh\pi N)^{\frac{1}{2}}\,|\,\Gamma(l+iN+1$$

our result reads

$$\psi_{N,l}(r)=\exp(\pi N/2)\frac{|\,\Gamma(l+iN+1)\,|}{(2l+1)!}\left(\frac{2\rho}{i}\right)^l e^{-i\rho} \times F(l+iN+1\,|\,2l+2\,|\,2i\rho)$$

with ρ as in (A5).

CC-0. In Public Domain. Gurukul Kangri Collection, Haridwar

Digitized by Arya Samaj Foundation Chennai and eGangotri

REVIEWS OF MODERN PHYSICS VOLUME 38, NUMBER 2 APRIL 1966

Classical Noise III: Nonlinear Markoff Processes

MELVIN LAX
Bell Telephone Laboratories, Murray Hill, New Jersey

Our previous treatment of noise in the nonequilibrium steady state is extended to include nonstationary processes, and processes for which the quasilinear approximation is inadequate. By use of backward-equation methods, we show that

$$M_0(\mathbf{a}_0, t, t_0) = \left\langle \exp\left[-\int_{t_0}^{t} Q(\mathbf{a}(s), t-s)\, ds\right] \right\rangle$$

subject to $\mathbf{a}(t_0)=\mathbf{a}_0$ obeys the differential (integral) equation:

$$\frac{\partial M_0(\mathbf{a}_0, t, t_0)}{\partial t_0} = [Q(\mathbf{a}_0, t-t_0) - \sum_{n=1}^{\infty} \mathbf{D}_n(\mathbf{a}_0, t_0) : (\partial/\partial \mathbf{a}_0)^n] M_0,$$

where the $\mathbf{D}_n$ are the nth-order diffusion coefficients of the $\mathbf{a}(s)$ process, and $Q(\mathbf{a}(s), s)$ is an arbitrary function of $\mathbf{a}$ and s. The choice $D_n=0$, $n>2$, $D_2=D$. $D_1(a)=-\Lambda a$ makes $a(s)$ an Ornstein–Uhlenbeck (O.U.) process, i.e., white noise that has been filtered through an RC network with time constant $1/\Lambda$. The choice $Q(a(s), s)=k(t-s)[a(s)]^2$ squares the output and applies the time smoothing $k(t-s)$. For $k(s)=\exp(-2\beta s)$ [time smoothing through an RC network with time constant $(1/2\beta)$], an explicit solution is obtained for the characteristic function M_0. For arbitrary positive $k(s)$, we show that M_0 becomes independent of a_0 as $t\to\infty$ if $k(\infty)=0$, and M_0 becomes stationary if $\Lambda>0$ and

$$\int_0^{\infty} k(u)\, du < \infty.$$

CONTENTS

1. Introduction and Summary 359
2. Properties of Markoff Processes in the Large 361
3. A Class of Problems to be Solved 362
A. Adiabatic Line Broadening 362
B. Free Induction and Spin-Echo Experiments 363
C. Nonlinear Transformations on Noise 363
D. Domain Probabilities 364
E. Random Walk with Absorbing Barriers 364
F. Distribution of Spectral Components 364
4. Reduction of the Path Integral 364
5. Markoff Processes in the Small 365
6. Characteristic Functions and Linked Averages 366
7. Examples of Markoff Processes 368
A. The Weiner Process 368
B. The Fokker–Planck Process 368
C. The Ornstein–Uhlenbeck (O.U.) Process 369
D. The Poisson Process (Shot Noise) 371
E. The Homogeneous Process 372
F. Homogeneous Noise Plus Linear Decay 373
8. Smoothed Square-Law Response 374
Forward-Equation Method 374
Backward-Equation Method 375
Case 1. Linearly Smoothed Weiner Process 377
Case 2. Linearly Smoothed O.U. Process 377
Case 3. Exponentially Smoothed O.U. Process 377
Case 4. Exponentially Smoothed Weiner Process 378
Case 5. Arbitrary Positive Smoothing Function 378

1. INTRODUCTION AND SUMMARY

Our previous treatment of fluctuations from the nonequilibrium steady state[1,2] was more general than previous work in that it did not assume linearity of the system, time reversibility of the system, Gaussian character of the random variables, Langevin forces, the Fokker–Planck approximation, or that fluctuations are from an equilibrium state.

We found that the assumptions[1] that the system is *Markoffian*, *stationary*, and *quasilinear* were sufficient to compute all autocorrelations $\langle \boldsymbol{\alpha}(t)\, \boldsymbol{\alpha}(u) \rangle$ of the deviations $\boldsymbol{\alpha}=\mathbf{a}-\mathbf{a}_0$ of a set of random variables $\mathbf{a}=[a_1, a_2, \cdots, a_n]$ from their steady-state values. The essential idea is that if one knows the solution $\langle \boldsymbol{\alpha}(t) \rangle_{\boldsymbol{\alpha}(u)}$ of the mean motion subject to the initial condition $\boldsymbol{\alpha}=\boldsymbol{\alpha}(u)$ at time u, one can compute the autocorrelation, and hence the fluctuations from

$$\langle \boldsymbol{\alpha}(t)\, \boldsymbol{\alpha}(u) \rangle = \langle \langle \boldsymbol{\alpha}(t) \rangle_{\boldsymbol{\alpha}(u)} \boldsymbol{\alpha}(u) \rangle_{\text{av}} \text{ over } \boldsymbol{\alpha}(u) \quad (1.1)$$

as proven in I(2.13). Thus the regression of a fluctuation obeys the "macroscopic" equations of motion for $\langle \boldsymbol{\alpha}(t) \rangle$, and the spectrum of the noise, is given by the Fourier transform of the time-dependent decay exhibited by $\langle \boldsymbol{\alpha}(t) \rangle_{\boldsymbol{\alpha}(u)}$. For a quasilinear system, this time dependence obeys a matrix equation I(3.6):

$$d\langle \boldsymbol{\alpha}(t) \rangle / dt = -\boldsymbol{\Lambda} \langle \boldsymbol{\alpha}(t) \rangle, \quad (1.2)$$

leading to an exponential time dependence. The spectrum is thus known, but the magnitude of the noise requires a knowledge of $\langle \boldsymbol{\alpha}(u)\, \boldsymbol{\alpha}(u) \rangle$, i.e., of the fluctuations at one time. These can then be computed from the generalized Einstein relation I(5.18):

$$\boldsymbol{\Lambda}\langle \boldsymbol{\alpha}\boldsymbol{\alpha} \rangle + \langle \boldsymbol{\alpha}\boldsymbol{\alpha} \rangle \boldsymbol{\Lambda}^{\dagger} = 2\mathbf{D}, \quad (1.3)$$

where $\boldsymbol{\Lambda}^{\dagger}$ is the transpose of $\boldsymbol{\Lambda}$ and the diffusion matrix $\mathbf{D}$ can be computed from I(5.7),

$$2\mathbf{D} = \lim_{\Delta t \to 0} (\Delta t)^{-1} \langle [\boldsymbol{\alpha}(t+\Delta t) - \boldsymbol{\alpha}(t)][\boldsymbol{\alpha}(t+\Delta t) - \boldsymbol{\alpha}(t)] \rangle \quad (1.4a)$$

[1] M. Lax, Rev. Mod. Phys. **32**, 25 (1960). This paper contains an extensive bibliography that will not be duplicated here. This paper will be referred to as I in our series of papers on noise in classical systems. It treats Markoffian noise in the stationary state by quasilinear methods.

[2] M. Lax, Phys. Chem. Solids **14**, 248 (1960). This is Classical Noise II. It applies the methods of I on continuous parameters to trapping, diffusion, and carrier concentration noise.

CC-0. In Public Domain. Gurukul Kangri Collection, Haridwar

Digitized by Arya Samaj Foundation Chennai and eGangotri

or from the transition probabilities in the form[3] I(5.6),

$$2\mathbf{D}(\mathbf{a}) = (\Delta t)^{-1}\int (\mathbf{a}'-\mathbf{a})\,(\mathbf{a}'-\mathbf{a})\,P(\mathbf{a}'t+\Delta t \mid \mathbf{a}t)\,d\mathbf{a}' \tag{1.4b}$$

and $\mathbf{D}=\mathbf{D}(\mathbf{a}_0)$. [The conditional probabilities P are defined in Sec. 2.] Similarly, the drift vector is defined by I(5.5):

$$\mathbf{A}(\mathbf{a}) = \lim\,(\Delta t)^{-1}\int (\mathbf{a}'-\mathbf{a})\,P(\mathbf{a}',\, t+\Delta t \mid \mathbf{a}t)\,d\mathbf{a}' \tag{1.5}$$

and

$$(d/dt)\,\langle \mathbf{a}\rangle = \langle \mathbf{A}(\mathbf{a})\rangle \approx -\boldsymbol{\Lambda}\cdot(\mathbf{a}-\mathbf{a}_0), \tag{1.6}$$

where $\mathbf{a}_0$ is determined by $\mathbf{A}(\mathbf{a}_0)=0$.

In summary, if one is concerned with the frequency spectrum (or alternatively the autocorrelation $\langle \boldsymbol{\alpha}(t)\,\boldsymbol{\alpha}(u)\rangle$) of the noise of a classical, stationary nonlinear Markoffian process, then this problem is already solved in Eqs. (1.1)–(1.6) as long as *over the range of fluctuation* one can replace the system by a quasilinear one. In this case, we need not evaluate the complete conditional probability $P(\mathbf{a}'t' \mid \mathbf{a}t)$, but have simplified the problem of showing that the first and second moments $\langle \mathbf{a}(t)\rangle$; $\langle \mathbf{a}(t)\mathbf{a}(u)\rangle$ obey a closed system of equations that can be solved exactly.

The present paper, III, is written to cover some of the techniques available when the stationarity and quasilinearity approximations are no longer valid.[4–7] In particular we wish to be able to discuss cases when:

(1) the transition probabilities and/or the solution is nonstationary;

(2) the nonlinearity over the range of the fluctuations is large enough, that quasilinear approximations are invalid;

(3) the signal is passed through a nonlinear device, so that a knowledge of the complete distribution $P(\mathbf{a}'t' \mid \mathbf{a}t)$ is needed;

(4) the results depend on the random variables $\mathbf{a}(t)$ at more than two times. In particular, if the output of a nonlinear device is time-smoothed the distribution of outputs depends on the random variables over a continuum of times—all the past history!

Most of the problems we wish to solve can be reduced to an evaluation of the average

$$M = \left\langle \exp\left[-\int_{t_0}^{t} Q(\mathbf{a}(s),\, s)\,ds\right]\right\rangle, \tag{1.7}$$

which can be thought of as the characteristic function of the random variable in the exponent. The latter involves an arbitrary time smoothing, over an arbitrary nonlinear function Q of the $\mathbf{a}(s)$ over the history from t_0 to t. We shall use the label M_0, if we wish the average conditional on $\mathbf{a}(t_0)=\mathbf{a}_0$. By introducing a new unnormalized Markoff process $\hat{P}$ whose transition probability for small times is related to that for P by

$$\hat{P}(\mathbf{a}'t+\Delta t \mid \mathbf{a}t) = [1-Q(\mathbf{a},\, t)\,\Delta t]P(\mathbf{a}',\, t+\Delta t \mid \mathbf{a},\, t), \tag{1.8}$$

we show that

$$M_0 = \int \hat{P}(\mathbf{a}t \mid \mathbf{a}_0,\, t_0)\,d\mathbf{a} = \hat{\phi}(0,\, t), \tag{1.9}$$

where

$$\hat{\phi}(\mathbf{y},\, t) = \int \exp\,(i\mathbf{y}\cdot\mathbf{a})\,\hat{P}(\mathbf{a}t \mid \mathbf{a}_0t_0)\,d\mathbf{a} \tag{1.10}$$

is the characteristic function associated with unnormalized probability $\hat{P}$. [It could be written more explicitly as $\hat{\phi}(\mathbf{y}t \mid \mathbf{a}_0t_0)$ to emphasize the initial condition.]

We then define the *characteristic function* associated with (unmodified) transitions in a small time interval by

$$\exp\,[-L(\mathbf{y},\, \mathbf{a},\, t)\,\Delta t] = \langle \exp\,(i\mathbf{y}\cdot\Delta\mathbf{a})\rangle$$

$$= \int d\Delta\mathbf{a}\,\exp\,(i\mathbf{y}\cdot\Delta\mathbf{a})\,P(\mathbf{a}+\Delta\mathbf{a},\, t+\Delta t \mid \mathbf{a},\, t). \tag{1.11}$$

In particular

$$-L(\mathbf{y},\, \mathbf{a},\, t) = \sum_{n=1}^{\infty} (i\mathbf{y})^n : \mathbf{D}_n(\mathbf{a},\, t), \tag{1.12}$$

where

$$n!\mathbf{D}_n(\mathbf{a},\, t) = (\Delta t)^{-1}\int (\mathbf{a}'-\mathbf{a})^n P(\mathbf{a}',\, t+\Delta t \mid a,\, t)\,d\mathbf{a}' \tag{1.13}$$

and

$$\mathbf{y}^3 : \mathbf{D}_3 \equiv \sum y_i y_j y_k D_{ijk3} \tag{1.14}$$

displays the use of the colon : to imply the contraction of the product of two tensors on all their indices. With L understood to have all $\mathbf{y}$'s to the left of all $\mathbf{a}$'s as in (1.12), we show that $\hat{P}$ and $\hat{\phi}$ obey[8] (5.15)

---

[3] To comform with the mathematical literature, the times in our probability functions increase as one moves from right to left. The opposite convention was used in I.

[4] A review of the literature on nonlinear random processes with extensive bibliography is given by Ralph Deutsch, *Nonlinear Transformations of Random Processes* (Prentice-Hall, Inc., Englewood Cliffs, New Jersey, 1962). See also Refs. 5–7, and the references contained therein.

[5] David Middleton, *Introduction To Statistical Communication Theory* (McGraw-Hill Book Company, Inc., New York, 1960).

[6] R. L. Stratonovich, *Topics in the Theory of Random Noise* (Gordon and Breach, Inc., New York, 1963), Vol. I.

[7] *Fluctuation Phenomena in Solids*, edited by R. E. Burgess (Academic Press Inc., New York, 1965).

[8] Such forward equations have been obtained by A. J. F. Siegert, IRE Trans. Inform. Theory **3**, 4 (1954). See also, Ref. 4, Chap. and R. Kubo in *Fluctuation, Dissipation and Resonance in Stochastic Systems*, edited by D. ter Haar (Plenum Press, Inc., New York, 1962).

CC-0. In Public Domain. Gurukul Kangri Collection, Haridwar

Digitized by Arya Samaj Foundation Chennai and eGangotri

(6.18):

$$\partial\hat{P}/\partial t=-[Q(\mathbf{a},t)+L(\mathbf{y}_{op},\mathbf{a},t)]\hat{P}(\mathbf{a},t) \quad (1.15)$$

$$\partial\hat{\phi}/\partial t=-[Q(\mathbf{a}_{op},t)+L(\mathbf{y},\mathbf{a}_{op},t)]\hat{\phi}(\mathbf{y},t) \quad (1.16)$$

with

$$\mathbf{y}_{op}=i\partial/\partial\mathbf{a}; \qquad \mathbf{a}_{op}=-i\partial/\partial\mathbf{y}. \quad (1.17)$$

We also show that $\hat{P}(\mathbf{a}t\mid\mathbf{a}_0t_0)$ obeys the "backward equation," (5.19),

$$\partial P/\partial t_0=[Q(\mathbf{a}_0,t_0)+L^\dagger(\mathbf{y}_{op},\mathbf{a}_0)]\hat{P}(\mathbf{a}t\mid\mathbf{a}_0t_0) \quad (1.18)$$

or

$$\frac{\partial\hat{P}}{\partial t_0}=\left[Q(\mathbf{a}_0,t_0)-\sum_{n=1}^{\infty}\mathbf{D}_n(\mathbf{a}_0,t_0):\left(\frac{\partial}{\partial\mathbf{a}_0}\right)^n\right]\hat{P}. \quad (1.19)$$

Since $\mathbf{a}$ is now only a parameter, an integration over $\mathbf{a}$ commutes with the operations in (1.18) and (1.19). Thus M_0 of (1.9) obeys (1.18) and (1.19) in its dependence on $\mathbf{a}_0$ and t_0.

If we are interested in $M_0(\mathbf{a}_0,t,t_0)$, (1.7), it is *much simpler to compute it directly* by the use of (1.19) with the initial condition $M_0(\mathbf{a}_0,t,t)=1$ than to calculate the more detailed $\hat{P}(at\mid a_0t_0)$ or $\hat{\phi}(\mathbf{y}t\mid\mathbf{a}_0t_0)$. When the $\mathbf{D}_n$ do not depend explicitly in t_0, and $Q=Q(a(s),t-s)$ then $M_0(\mathbf{a}_0,t,t_0)=M_0(\mathbf{a}_0,t-t_0)$ which obeys[9]

$$\frac{\partial M_0(\mathbf{a}_0,u)}{\partial u}$$

$$=\left[Q(\mathbf{a}_0,u)-\sum_{n=1}^{\infty}D_n(\mathbf{a}_0):\left(\frac{\partial}{\partial\mathbf{a}_0}\right)^n\right]M_0(\mathbf{a}_0,u). \quad (1.20)$$

Section 7 reviews our knowledge of linear processes: the Weiner process, the Ornstein–Uhlenbeck process, the Poisson process, the homogeneous process, and a process that includes all the preceding: homogeneous noise plus linear damping,[10] for a *set* of random variables $\mathbf{a}$. For this most general linear case, we determine the multitime property:

$$M_0=\left\langle \exp i\int_{t_0}^{t}\mathbf{q}(s)\cdot\mathbf{a}(s)\,ds\right\rangle, \quad (1.21)$$

where $\mathbf{q}(s)$ is an *arbitrary* (vector) function of the time.

Section 7B discusses the multidimensional Fokker–Planck process (i.e., $\mathbf{D}_n=0$ for $n>2$) as an example of a nonlinear process.

When the $\mathbf{D}_n$'s or Q depend nonlinearly on $\mathbf{a}$, there are, of course, no general methods of solution. A *pièce de résistance* of the present paper is the reduction of

$$M_0=\left\langle \exp\left[i\int_{t_0}^{t}\mathbf{q}(s)\cdot\mathbf{a}(s)\,ds\right]\right.$$

$$\left.\times\exp\left[-\lambda\int_{t_0}^{t}\mathbf{a}(s)\cdot\mathbf{k}(t-s)\cdot\mathbf{a}(s)\,ds\right\rangle\right] \quad (1.22)$$

to the solution of a set of coupled *ordinary* differential equations of Riccati form when $\mathbf{a}(s)$ is an Ornstein–Uhlenbeck process, and $\mathbf{q}(s)$ and $\mathbf{k}(t-s)$ are arbitrary functions of the time.

For the one-dimensional case, in particular, we show that

$$M_0=\left\langle \exp\left[-\lambda\int_{t_0}^{t}k(t-s)\,a(s)^2\,ds\right]\right\rangle \quad (1.23)$$

$$=[Y(t-t_0)]^{-\frac{1}{2}}\exp[-a_0^2R(t-t_0)], \quad (1.24)$$

$$Y(t-t_0)=\exp\left[4D\int_0^{t-t_0}R(u)\,du\right], \quad (1.25)$$

$$dR/du=\lambda k(u)-2\Lambda R-4DR^2, \quad (1.26)$$

where Λ is the decay constant and D the diffusion constant of the Ornstein–Uhlenbeck process. For the case of exponential smoothing, $k(u)=\exp(-2\beta u)$, we find an exact solution to the differential equation (1.26). Thus we have found the answer to a hitherto unsolved problem: *RC*-smoothed white noise (time constant $1/\Lambda$) is passed through a square-law device and the output is again *RC*-smoothed (time constant $1/2\beta$). Then M_0 is the characteristic function of the output.

The special cases $\beta=\Lambda=0$; $\beta=0$, $\Lambda>0$; $\beta>0$, $\Lambda>0$; $\beta>0$, $\Lambda=0$ all yield different answers as to (1) whether M_0 forgets $a_0=a(t_0)$ and (2) whether M_0 becomes stationary, i.e., independent of t. For *any* $k(u)>0$, we show that M_0 forgets a_0 if and only if $k(u)\to 0$ as $u\to\infty$. Moreover, M_0 becomes stationary, if and only if $\Lambda\neq 0$ and

$$\int_0^{\infty}k(u)\,du$$

converges.

We intend in paper IV of this series to discuss nonlinear random processes from the Langevin point of view. We shall show how Langevin processes can often be reduced to Markoff processes and thus made amenable to the techniques of the present paper.

2. PROPERTIES OF MARKOFF PROCESSES IN THE LARGE

Let $\mathbf{a}(t)\equiv[a_1(t),a_2(t),\cdots,a_N(t)]$ be an N-dimensional random process, and

$$P[\mathbf{a}(t_n)\mid\mathbf{a}(t_{n-1}),\cdots,\mathbf{a}(t_2),\mathbf{a}(t_1)]$$

$$\equiv\frac{P[\mathbf{a}(t_n),\cdots,\mathbf{a}(t_1)]}{P[\mathbf{a}(t_{n-1}),\cdots,\mathbf{a}(t_1)]} \quad (2.1)$$

[9] This paper may be the first to make explicit use of backward equations as a means of dealing directly with the characteristic function $M_0(\mathbf{a}_0,t-t_0)$.

[10] This terminology is explained in the body of this paper. For definitions see also Refs. 1–8 or the collection of papers in N. Wax, *Noise and Stochastic Processes* (Dover Publications, Inc., New York, 1954).

CC-0. In Public Domain. Gurukul Kangri Collection, Haridwar

Digitized by Arya Samaj Foundation Chennai and eGangotri

be the conditional probability density[6] that $\mathbf{a}(t)$ take the value $\mathbf{a}(t_n)$ at time t_n given the values $\mathbf{a}(t_j)$ at the earlier times $t_n \geq t_{n-1} \geq t_{n-2} \geq \cdots \geq t_2 \geq t_1$. The random process $\mathbf{a}(t)$ is Markoffian if

$$P[\mathbf{a}(t_n) \mid \mathbf{a}(t_{n-1}), \cdots, \mathbf{a}(t_1)] = P[\mathbf{a}(t_n) \mid \mathbf{a}(t_{n-1})], \tag{2.2}$$

i.e., if the probability of any event depends *only* on the latest piece of information available. A Markoff process has no memory of earlier events.

If we now write briefly $\mathbf{a}(t_j) = \mathbf{a}_j$, the repeated use of the definition (2.1) of conditional probability density in terms of the full probability densities permits one to write

$$P(\mathbf{a}_n, \mathbf{a}_{n-1}, \cdots, \mathbf{a}_1) = P(\mathbf{a}_n \mid \mathbf{a}_{n-1}, \cdots, \mathbf{a}_1) P(\mathbf{a}_{n-1} \mid \mathbf{a}_{n-2}, \cdots, \mathbf{a}_1), \cdots, P(\mathbf{a}_2 \mid \mathbf{a}_1) P(\mathbf{a}_1), \tag{2.3}$$

which for Markoff processes reduces to

$$P(\mathbf{a}_n, \cdots, \mathbf{a}_1) = P(\mathbf{a}_n \mid \mathbf{a}_{n-1}) P(\mathbf{a}_{n-1} \mid \mathbf{a}_{n-2}) \cdots P(\mathbf{a}_2 \mid \mathbf{a}_1) P(\mathbf{a}_1). \tag{2.4}$$

The factorization (2.4) permits the probability of a compound event occurring at many times to be expressed entirely in terms of the transition probability $P(\mathbf{a}_n \mid \mathbf{a}_{n-1})$ and the initial distribution $P(\mathbf{a}_1)$. For example, if $V(t)$, a one-dimensional Markoff process (e.g., a noise voltage) is passed through a square-law rectifier:

$$I(t) = V(t)^2, \qquad V(t) > 0;$$
$$I(t) = 0, \qquad V(t) < 0. \tag{2.5}$$

The triple correlation is given by

$$\langle I(t_3) I(t_2) I(t_1) \rangle = \int_0^\infty \int_0^\infty \int_0^\infty dV_1\, dV_2\, dV_3 \times V_3^2 P(V_3 \mid V_2) V_2^2 P(V_2 \mid V_1) V_1^2 P(V_1). \tag{2.6}$$

Strictly speaking, P depends not only on $\mathbf{a}(t_n)$, but also on t_n. Processes will be called *stationary* if

$$P(\mathbf{a}, t_n, \mathbf{a}_{n-1} t_{n-1}, \cdots, \mathbf{a}_1, t_1) = P(\mathbf{a}_n, t_n + \tau, \mathbf{a}_{n-1}, t_{n-1} + \tau, \cdots, \mathbf{a}_1, t_1 + \tau), \tag{2.7}$$

i.e., if all probabilities are functions only of the time differences. In particular, stationarity implies that

$$P(\mathbf{a}_2 t_2 \mid \mathbf{a}_1 t_1) = P(\mathbf{a}_2, t_2 - t_1 \mid \mathbf{a}_1 0), \tag{2.8}$$
$$P(\mathbf{a}, t) = P(\mathbf{a}, 0) = P(\mathbf{a}), \tag{2.9}$$
$$\lim t \to \infty \qquad P(\mathbf{a}, t \mid \mathbf{a}_0 t_0) = P(\mathbf{a}). \tag{2.10}$$

Whereas a stationary process has transition probabilities that are functions only of the time difference, the converse follows from (2.4) only if $P(\mathbf{a}_1, t_1)$ is not time-dependent. Even if $P(\mathbf{a}_2 \mid \mathbf{a}_1)$ is a function only of $t_2 - t_1$, no time-independent solution may exist for $P(\mathbf{a}_1, t_1)$ if the process possesses some instability, or even neutral stability. A simple example of neutral stability is Brownian motion in an infinite domain.

If we set $n = 3$ in (2.4) and divide by $P(\mathbf{a}_1)$ we obtain

$$P(\mathbf{a}_3 \mathbf{a}_2 \mid \mathbf{a}_1) = P(\mathbf{a}_3 \mid \mathbf{a}_2) P(\mathbf{a}_2 \mid \mathbf{a}_1). \tag{2.11}$$

Integrating over $\mathbf{a}_2$ we obtain the Chapman-Kolmogoroff condition

$$P(\mathbf{a}_3 \mid \mathbf{a}_1) = \int P(\mathbf{a}_3 \mid \mathbf{a}_2)\, d\mathbf{a}_2 P(\mathbf{a}_2 \mid \mathbf{a}_1) \tag{2.12}$$

on the transition probabilities.

Our equations are written in a form appropriate to continuous variables. They remain valid for the discrete case if integrals over $\mathbf{a}$ are replaced by sums.

It is customary to take all probabilities to be normalized. In particular this leads to the requirement that the transition probability obey

$$\int d\mathbf{a}_2 P(\mathbf{a}_2 \mid \mathbf{a}_1) = 1. \tag{2.13}$$

However, we shall carry through our analysis without imposing this condition, since processes *violating* (2.13) can be used to analyze nonlinear time-smoothing of processes that *do* obey (2.13) [see Sec. 4].

We shall call a process that obeys

$$P(\mathbf{a}_2 t_2 \mid \mathbf{a}_2, t_1) = P(\mathbf{a}_2 - \mathbf{a}_1, t_2 \mid 0 t_1) \tag{2.14}$$

a *homogeneous Markoff process* since it has no preference for origin in $\mathbf{a}$ space.

3. A CLASS OF PROBLEMS TO BE SOLVED

A number of important problems in the theory of random processes can be reduced to an expectation value of the form[11]

$$M = \left\langle \exp\left[-\int_{t_0}^{t} Q(\mathbf{a}(s), s)\, ds \right] \right\rangle \tag{3.1}$$

or to a Fourier transform of such an expression.

A. Adiabatic Line Broadening

The absorption of radiation at frequency ω by a system with electric (or magnetic) dipole moment μ is given by

$$I(\omega) \propto T^{-1} \int_{-T/2}^{T/2} \mu(t'') \times \exp(-i\omega t'')\, dt'' \int_{-T/2}^{T/2} \mu(t')^* \exp(i\omega t')\, dt' \tag{3.2}$$

[11] See Ref. 4, Chap. 7.

CC-0. In Public Domain. Gurukul Kangri Collection, Haridwar

Digitized by Arya Samaj Foundation Chennai and eGangotri

or with $t''=t'+t$ and $\langle\ \rangle$ representing an ensemble average

$$I(\omega)=\int_{-\infty}^{\infty}\exp(-i\omega t)M(t)\,dt, \tag{3.3}$$

$$M(t)=\lim_{T\to\infty}T^{-1}\int_{-T/2}^{T/2}dt'\langle\mu(t+t')\mu(t')^*\rangle. \tag{3.4}$$

In the usual "adiabatic" theory of line broadening[12] (say of absorption by one gas atom in a background of foreign atoms) the influence of collisions on the dipole matrix element $\mu=\mu_{fi}$

$$\mu_{fi}(t)=(\psi_f(t),\,\mu\psi_i(t))$$
$$=\left(\exp\left[-i\int_{-\infty}^{t}H(s)\,ds\right]\psi_f,\,\mu\exp\left[-i\int_{-\infty}^{t}H(s)\,ds\right]\psi_i\right)$$
$$=\mu_{fi}\exp\left[i\int_{-\infty}^{t}\omega(s)\,ds\right], \tag{3.5}$$

$$\omega(s)=H_{ii}(s)-H_{ff}(s), \tag{3.6}$$

is taken to be purely that of a phase shift induced in the initial and final states (i and f) with no off-diagonal elements in the Hamiltonian H to correspond to "nonadiabatic" transitions. (The nonadiabatic modification of this theory has been given by Anderson[13] and by Byron and Foley.[14])

In the adiabatic theory, $\omega(s)$ is regarded as a random variable subject to jumps introduced by the reservoir of foreign atoms. For *spin diffusion*[15] the same model has been assumed with the atom in question being a "spin," and the foreign atoms other spins that interact with the first.

With (3.5), Eq. (3.4) can be rewritten in the form

$$M(t)=\text{average over } t' \text{ of } \left\langle\exp\left[i\int_{t'}^{t'+t}\omega(s)\,ds\right]\right\rangle \tag{3.7}$$

or

$$M(t)=\left\langle\exp\left[i\int_{0}^{t}\omega(s)\,ds\right]\right\rangle \tag{3.8}$$

where the last form is valid when $\omega(s)$ is a stationary random variable so that the previous average is independent of t'. Our result (3.8) has the form (3.1). See the evaluation of $M(t)$ in Secs. 7E and 7F.

[12] For a review of line broadening see R. G. Breene, Jr., *The Shift and Shape of Spectral Lines* (Pergamon Press, Inc., New York, 1961).
[13] P. W. Anderson, Phys. Rev. **76**, 647 (1949).
[14] F. W. Byron, Jr., and H. M. Foley, Phys. Rev. **134**, A625 (1964).
[15] J. R. Klauder and P. W. Anderson, Phys. Rev. **125**, 912 (1962).

B. Free-Induction and Spin-Echo Experiments

In a free-induction experiment[15] a short rf pulse at time $t\approx 0$ rotates the resonant spins from the z direction onto the x axis. Thus all spins start with the same phase at $t=0$. The resulting free-induction signal is proportional to $\mu(t)$ or

$$M(t)=\langle\mu(t)\rangle=\left\langle\exp\left[i\int_0^t\omega(s)\,ds\right]\right\rangle. \tag{3.9}$$

Thus the free-induction experiment measures directly the Fourier transform of the line shape $I(\omega)$.

A disadvantage of the free-induction experiment is that the signal $M(t)$ will decay rapidly if there is a spread of initial frequencies $\omega(0)$ because of a distribution of dc magnetic fields at the various sites. This inhomogeneous broadening which makes the phases $\omega(0)t$ differ from one another, is overcome in a spin-echo experiment in which a 180° pulse is applied at time τ to reverse the direction of each spin. This reverses the phase acquired up to time τ. For $t>\tau$ the phase is then

$$\int_\tau^t\omega(s)\,ds-\int_0^\tau\omega(s)\,ds. \tag{3.10}$$

If the frequencies have a spread but are not random in time, the phase distribution associated with this spread cancels at $t=2\tau$. Thus a peak is seen in the induced signal at $t=2\tau$, that is less than that at $t=0$ only if dynamic random fluctuations occur in ω. The observed signal at any time t is given by[15]

$$M(t)=\left\langle\exp\left[i\int_0^t m(s)\omega(s)\,ds\right]\right\rangle, \tag{3.11}$$

where

$$m(s)=-1,\qquad 0<s<\tau;$$
$$m(s)=+1,\qquad \tau<s<t.$$

More general spin-echo experiments, with more than two pulses can be described using more complicated functions $m(s)$. In general the echo occurs at the time t for which

$$\int_0^t m(s)\,ds=0 \tag{3.12}$$

and the effect of the initial frequency distribution cancels. For this general case, $a=\omega$, $Q=-im(s)a$ in Eq. (3.1)

C. Nonlinear Transformations on Noise

If a signal a is passed through a nonlinear device, and the result passed through a linear filter, the output signal takes the form[8]

$$S(t)=\int_{-\infty}^{t}k(t-s)V[a(s)]\,ds. \tag{3.13}$$

CC-0. In Public Domain. Gurukul Kangri Collection, Haridwar

Digitized by Arya Samaj Foundation Chennai and eGangotri

The characteristic function whose Fourier transform (on z) gives the probability distribution of S is

$$\langle \exp(izS) \rangle = \left\langle \exp\left\{ iz \int_{-\infty}^{t} k(t-s)\, V[a(s)]\, ds \right\} \right\rangle, \tag{3.14}$$

a result that also has the form (3.1). Special cases such as

$$S(t) = \int_0^t k(s)\, a^2(s)\, ds, \tag{3.15}$$

$$S(t) = \int_0^1 |\, a(s)\, |\, ds, \tag{3.16}$$

have been studied by Kac and Siegert,[16] by Kac,[17] by Siegert,[18] and others.[19]

D. Domain Probabilities

If we set[17]

$$Q(\mathbf{a}(s), s) = \begin{cases} 1 & \text{if } \mathbf{a}(s) \text{ in } D \\ 0 & \text{if } \mathbf{a}(s) \text{ not in } D \end{cases} \tag{3.17}$$

where D is some domain, e.g., $\sum [a_i(s)]^2 < R$ and

$$S(t, t_0) = \int_{t_0}^{t} Q(\mathbf{a}(s), s)\, ds, \tag{3.18}$$

then $S(t, t_0)/(t-t_0)$ is the fraction of time spent in the domain D, and $\langle \exp(izS) \rangle$ gives the characteristic function whose Fourier transform gives the probability distribution of S. As remarked by Deutsch,[11] the fluctuations in S measure the reliability with which a finite measurement time $t-t_0$ can be used to estimate the distribution of $\mathbf{a}(s)$.

E. Random Walk With Absorbing Barriers

The probability that $\mathbf{a}(s)$ never leaves domain D in the time interval (t_0, t) is given by[11,17]

$$\text{Prob}\{\mathbf{a}(s) \text{ in } D,\ t_0 < s < t\} = \lim_{z \to \infty} \left\langle \exp\left[-z \int_{t_0}^{t} V_D[\mathbf{a}(s)]\, ds \right] \right\rangle, \tag{3.19}$$

$$V_D(\mathbf{a}(s)) = \begin{cases} 0 & \mathbf{a}(s) \text{ in } D \\ 1 & \mathbf{a}(s) \text{ outside } D. \end{cases}$$

Equation (3.19) corresponds to a random walk with an absorbing barrier at the boundary of the domain D.

F. Distribution of Spectral Components

The components of a one-dimensional random variable $a(s)$ in some orthogonal basis $\phi_n(s)$ (e.g., the terms of a Fourier series) are given by $\int \phi_n(s) a(s)$ and the joint characteristic function of a number of such components is given by[11]

$$M = \left\langle \exp\left[i \sum z_n \int_{t_0}^{t} \phi_n(s)\, a(s)\, ds \right] \right\rangle, \tag{3.2}$$

which also has the standard form (3.1).

4. REDUCTION OF THE PATH INTEGRAL

Our average of a functional (3.1) can be written in the form

$$M = \left\langle \exp\left[-\sum_{j=0}^{n-1} Q(\mathbf{a}_j, s_j)\, \Delta s_j \right] \right\rangle$$

$$= \int \exp\left[-\sum_{j=0}^{n-1} Q(\mathbf{a}_j, s_j)\, \Delta s_j \right] P(\mathbf{a}_n, \mathbf{a}_{n-1}, \cdots, \mathbf{a}_1, \mathbf{a}_0)\, d\mathbf{a}_n, \cdots, d\mathbf{a}_0, \tag{4.1}$$

where $s_n = t$, $\Delta s_j = s_{j+1} - s_j$. For a Markoff process, the factorization (2.4) permits us to rewrite this result in the form

$$M = \int M_0 P(\mathbf{a}_0)\, d\mathbf{a}_0, \tag{4.}$$

where $P(\mathbf{a}_0)$ is the probability density at $t = t_0$ and M_0 is the conditional average with $\mathbf{a}(t_0) = \mathbf{a}_0$:

$$M_0 = \prod_{j=0}^{n-1} \int \exp[-Q(\mathbf{a}_j, s_j)\, \Delta s_j] P(\mathbf{a}_{j+1} \mid \mathbf{a}_j)\, d\mathbf{a}_{j+1}. \tag{4.}$$

Direct evaluation of M_0 by such functional ("path") integrations has only been performed[20] for Weiner processes, i.e., the special case in which

$$P(\mathbf{a}'t' \mid \mathbf{a}t) = [4\pi(t'-t)]^{-N/2} (\det \mathbf{D})^{-\frac{1}{2}} \times \exp[-(\mathbf{a}'-\mathbf{a}) \cdot \mathbf{D}^{-1} \cdot (\mathbf{a}'-\mathbf{a})/4(t'-t)] \tag{4.}$$

and for homogeneous processes and slight generalizations thereof.[15] All such results, and many others, can be obtained by the following procedure which reduces the problem to one for which standard analytical techniques are available: Define (for sufficiently small Δs_j)

$$\hat{P}(\mathbf{a}_{j+1}, s_{j+1} \mid \mathbf{a}_j, s_j) = [1 - Q(\mathbf{a}_j, s_j)\, \Delta s_j] P(\mathbf{a}_{j+1}, s_{j+1} \mid \mathbf{a}_j, s_j). \tag{4.}$$

[16] M. Kac and A. J. F. Siegert, Phys. Rev. **70**, 449 (1946); J. Appl. Phys. **18**, 383 (1947); Ann. Math. Stat. **18**, 38 (1947).

[17] M. Kac, Trans. Am. Math. Soc. **59**, 401 (1946); *Berkeley Symposium on Mathematics, Statistics and Probability* (University of California Press, Berkeley, 1951), Vol. 2, p. 189.

[18] A. J. F. Siegert, Phys. Rev. **81**, 617 (1951); IRE Trans. Inform. Theory **3**, 38 (1957); **4**, 4 (1958).

[19] R. C. Emerson, J. Appl. Phys. **24**, 1168 (1953); A. Rosenbloom, J. Heilfron, and D. C. Trautman, IRE Natl. Conv. Record Part 4, 106 (1955); M. A. Meyer and D. Middleton, J. Appl. Phys. **25**, 1037 (1954); P. Erdos and M. Kac, Bull. Am. Math. Soc. **52**, 292 (1946); W. Feller, Ann. Math. Stat. **2**, 427 (1951); D. A. Darling and A. J. F. Siegert, IRE Trans. Inform. Theory **3**, 32 (1957); Ann Math. Stat. **24**, 624 (1953).

[20] R. H. Cameron and W. T. Martin, Trans. Am. Math. Soc. **58**, 184 (1945); Ann. Math. **45**, 386 (1944); J. Math. Phys. **195** (1944); Bull. Am. Math. Soc. **51**, 73 (1945); Am. J. Math. **66**, 281 (1944); E. W. Montroll, Commun. Pure Appl. Math. 415 (1952).

CC-0. In Public Domain. Gurukul Kangri Collection, Haridwar

Digitized by Arya Samaj Foundation Chennai and eGangotri

We may regard $P(\mathbf{a}_{j+1} \mid \mathbf{a}_j)$ as the transition probability of a new Markoffian process. It obeys the usual properties of transition probabilities except for a change in normalization:

$$\int \hat{P}(\mathbf{a}', t+\Delta t \mid \mathbf{a}, t)\, d\mathbf{a}' = 1 - Q(\mathbf{a}, t)\, \Delta t \quad (4.6)$$

to first order in Δt. Thus if we regard $\hat{P}(\mathbf{a}, t)$ as a density of systems, then $Q(\mathbf{a}, t)$ can be regarded as the rate at which they disappear.

The transition probability $\hat{P}(\mathbf{a}, t \mid \mathbf{a}_0 t_0)$ over a finite time interval can be decomposed into transition probabilities over "infinitesimal" intervals by integrating (2.4) over the intermediate values $\mathbf{a}_2, \cdots, \mathbf{a}_{n-1}$ or by repeated use of the Chapman–Kolmogoroff relation:

$$\hat{P}(\mathbf{a}_n \mid \mathbf{a}_0) = \int d\mathbf{a}_{n-1}, \cdots, d\mathbf{a}_1 \hat{P}(\mathbf{a}_n \mid \mathbf{a}_{n-1}), \cdots, \hat{P}(\mathbf{a}_2 \mid \mathbf{a}_1) \hat{P}(\mathbf{a}_1 \mid \mathbf{a}_0) \quad (4.7)$$

on the P probabilities. Comparison with (4.3) now yields the result

$$M_0 = \int \hat{P}(\mathbf{a}_n \mid \mathbf{a}_0)\, d\mathbf{a}_n = \int \hat{P}(\mathbf{a}, t \mid \mathbf{a}_0, t_0)\, d\mathbf{a}, \quad (4.8)$$

i.e., $\hat{P}(\mathbf{a} \mid \mathbf{a}_0)$ is the probability density that a system starting at system $\mathbf{a}_0$ at t_0 will arrive at $\mathbf{a}$ at time t taking into account the loss rate $Q(\mathbf{a}, t)$, and M_0 is the fraction of systems starting at $\mathbf{a}_0$ that survive *anywhere* when losses are included. Our problem has thus been reduced, in the Markoff case, to the determination of the transition probability $\hat{P}(\mathbf{a}t \mid \mathbf{a}_0 t_0)$ over finite time intervals.

5. MARKOFF PROCESSES IN THE SMALL

To obtain a differential equation for $\hat{P}(\mathbf{a}t \mid \mathbf{a}_0 t_0)$ we can write the Chapman–Kolmogoroff equation in the form

$$\hat{P}(\mathbf{a}, t+\Delta t) = \int \hat{P}(\mathbf{a}, t+\Delta t \mid \mathbf{a}', t)\, d\mathbf{a}' \hat{P}(\mathbf{a}', t), \quad (5.1)$$

where $\hat{P}(\mathbf{a}, t)$ reduces to $\hat{P}(\mathbf{a}t \mid \mathbf{a}_0 t_0)$ if we adopt the initial condition

$$\hat{P}(\mathbf{a}, t_0) = \delta(\mathbf{a} - \mathbf{a}_0). \quad (5.2)$$

For small Δt, we shall assume that the moments of the transition probability are expandable in powers of Δt. To first order in Δt, we shall write

$$\int \hat{P}(\mathbf{a}, t+\Delta t \mid \mathbf{a}', t)\, d\mathbf{a} = 1 - Q(\mathbf{a}', t)\, \Delta t \quad (5.3)$$

and for $n \geq 1$ there is no distinction between the moments of the $\hat{P}$ and P transition probabilities:

$$\int \hat{P}(\mathbf{a}, t+\Delta t \mid \mathbf{a}', t)\, (\mathbf{a} - \mathbf{a}')^n\, d\mathbf{a} = n! \mathbf{D}_n(\mathbf{a}', t)\, \Delta t$$

and

$$\int P(\mathbf{a}, t+\Delta t \mid \mathbf{a}', t)\, (\mathbf{a} - \mathbf{a}')^n\, d\mathbf{a} = n! \mathbf{D}_n(\mathbf{a}', t)\, \Delta t, \quad (5.4)$$

where boldface $\mathbf{D}_n$ has n (suppressed) subscripts, e.g., the moment of $(a_1 - a_1')^2 (a_2 - a_2')$ would be written D_{112} in expanded notation rather than $\mathbf{D}_3$.

The Taylor expansion of an arbitrary function $f(\mathbf{a})$ can also be written in a condensed notation

$$f(\mathbf{a}) = f(\mathbf{a}') + \sum_{n=1}^{\infty} (\mathbf{a} - \mathbf{a}')^n : \mathbf{f}^{(n)}(\mathbf{a}')/n! \quad (5.5)$$

where the : is a shorthand notation that tells us to multiply corresponding terms and add. The second-order term is, for example,

$$(1/2!) \sum_{i,j=1}^{N} (a_i - a_i')(a_j - a_j') \partial^{(2)} f / \partial a_i' \partial a_j'.$$

Let us now multiply Eq. (5.1) by $f(\mathbf{a})$ and integrate over $\mathbf{a}$. On the right-hand side, $f(\mathbf{a})$ can be placed under the $\int d\mathbf{a}'$ and then replaced by the right-hand side of Eq. (5.5). Making use of (5.3), (5.4) we obtain

$$\langle f(a) \rangle_{t+\Delta t} = \langle [1 - Q(a, t)\Delta t] f(a) \rangle_t + \Delta t \sum_{n=1}^{\infty} \int d\mathbf{a}' P(\mathbf{a}', t) \mathbf{f}^{(n)}(\mathbf{a}') : \mathbf{D}_n(\mathbf{a}', t)$$

or

$$(\partial/\partial t) \langle f(\mathbf{a}) \rangle = -\langle Q(\mathbf{a}, t) f(\mathbf{a}) \rangle + \sum_{n=1}^{\infty} \langle \mathbf{D}_n(\mathbf{a}, t) : (\partial/\partial \mathbf{a})^n f(\mathbf{a}) \rangle \quad (5.6)$$

$$= -\langle (Q + L^\dagger) f(\mathbf{a}) \rangle, \quad (5.7)$$

where

$$\langle f(\mathbf{a}) \rangle = \int f(\mathbf{a}) \hat{P}(\mathbf{a}, t)\, d\mathbf{a} \quad (5.8)$$

$$L^\dagger = -\sum_{n=1}^{\infty} \mathbf{D}_n(\mathbf{a}, t) : (\partial/\partial \mathbf{a})^n. \quad (5.9)$$

Using $\mathbf{A}$ as an abbreviation for $\mathbf{D}_1(\mathbf{a}, t)$ (the drift vector) and $\mathbf{D}$ as an abbreviation for $\mathbf{D}_2(\mathbf{a}, t)$ (the diffusion matrix) let us set $f(\mathbf{a}) = 1, \mathbf{a}, \mathbf{a}^2, \mathbf{a}^3, \cdots$ in Eq. (5.6) to obtain the useful moment relations,

$$\begin{aligned}
\partial \langle 1 \rangle / \partial t &= -\langle Q \rangle, \\
\partial \langle \mathbf{a} \rangle / \partial t &= -\langle Q\mathbf{a} \rangle + \langle \mathbf{A} \rangle, \\
\partial \langle \mathbf{a}^2 \rangle / \partial t &= -\langle Q\mathbf{a}^2 \rangle + 2\langle \mathbf{aA} \rangle + 2\langle \mathbf{D} \rangle, \\
\partial \langle \mathbf{a}^3 \rangle / \partial t &= -\langle Q\mathbf{a}^3 \rangle + 3\langle \mathbf{a}^2\mathbf{A} \rangle + 6\langle \mathbf{aD} \rangle + 6\langle \mathbf{D}_3 \rangle. \quad (5.10)
\end{aligned}$$

When $\mathbf{a}$ is a set of variables, the right-hand side is

CC-0. In Public Domain. Gurukul Kangri Collection, Haridwar

Digitized by Arya Samaj Foundation Chennai and eGangotri

understood to be completely symmetrized. Thus

$$\partial\langle a_i a_j a_k\rangle/\partial t=\langle a_i a_j a_k Q\rangle+\langle a_i a_j A_k\rangle+\langle A_i a_j a_k\rangle$$
$$+\langle a_i A_j a_k\rangle+2\langle a_i D_{jk}\rangle+2\langle a_j D_{ik}\rangle+2\langle a_k D_{ij}\rangle+6\langle D_{ijk}\rangle. \tag{5.11}$$

[The second-moment equations for a set of variables were derived directly in I(5.12), and higher moment equations for one variable written out explicitly in I(14.29).]

If in (5.8) we set $f(\mathbf{a})=\delta(\mathbf{a}-\mathbf{x})$ we find that

$$\hat{P}(\mathbf{x}, t)=\langle\delta(\mathbf{a}-\mathbf{x})\rangle. \tag{5.12}$$

Inserting this choice for $f(\mathbf{a})$ into (5.6) and integrating by parts we obtain

$$\partial\hat{P}(\mathbf{x}, t)/\partial t=-Q(\mathbf{x})\hat{P}$$
$$+\sum_{n=1}^{\infty}(-1)^n(\partial/\partial\mathbf{x})^n:[D_n(\mathbf{x}, t)\hat{P}(\mathbf{x}, t)] \tag{5.13}$$

or

$$\partial\hat{P}(\mathbf{a}, t)/\partial t=-[Q(\mathbf{a})+L]\hat{P}(\mathbf{a}, t),$$

where L is the Hermitian adjoint of $L^\dagger$:

$$-L=\sum_{n=1}^{\infty}(-1)^n(\partial/\partial\mathbf{a})^n:\mathbf{D}_n(\mathbf{a}, t). \tag{5.14}$$

Associated with the operator L, we shall define a numerical function

$$-L(\mathbf{y}, \mathbf{a}, t)=\sum_{n=1}^{\infty}(i\mathbf{y})^n:\mathbf{D}_n(\mathbf{a}, t). \tag{5.15}$$

With the understanding that the $\mathbf{y}$'s are always to the left of the $\mathbf{a}$'s, we can write the operator as

$$L=L(\mathbf{y}_{op}, \mathbf{a}, t); \qquad \mathbf{y}_{op}=i\partial/\partial\mathbf{a}. \tag{5.16}$$

Equation (5.13) is customarily referred to as a forward equation, since it refers to $\partial\hat{P}/\partial t$. We can rewrite the Chapman–Kolmogoroff equations in a form

$$\hat{P}(\mathbf{a}t\mid\mathbf{a}_0, t-\Delta t)=\int\hat{P}(\mathbf{a}t\mid\mathbf{a}'t_0)\,d\mathbf{a}'\hat{P}(\mathbf{a}'t_0\mid\mathbf{a}_0, t_0-\Delta t) \tag{5.17}$$

suitable to derive an equation for $\partial\hat{P}/\partial t_0$, i.e., a backward equation. In (5.17) we insert

$$\hat{P}(\mathbf{a}, t\mid\mathbf{a}', t_0)=\hat{P}(\mathbf{a}t\mid\mathbf{a}_0t_0)$$
$$+\sum[(\mathbf{a}'-\mathbf{a}_0)^n/n!]:(\partial/\partial\mathbf{a}_0)^n\hat{P}(\mathbf{a}t\mid\mathbf{a}_0t_0) \tag{5.18}$$

and use (5.3), (5.4) to obtain the backward equation

$$[\partial\hat{P}(\mathbf{a}t\mid\mathbf{a}_0t_0)/\partial t_0]=Q(\mathbf{a}_0, t_0)\hat{P}$$
$$-\sum\mathbf{D}_n(a_0, t_0):(\partial/\partial\mathbf{a}_0)^n\hat{P}. \tag{5.19}$$

If the random variable whose properties we wish to discuss has the form

$$\int_{t_0}^{t}Q(\mathbf{a}(s), t-s)\,ds, \tag{5.2}$$

rather than depending on $Q(\mathbf{a}(s), s)$, then Eq. (5.1) remains valid when t regarded as a parameter, and $Q(\mathbf{a}(s), t-s)$ enters the equation as $Q(\mathbf{a}(t_0), t-t_0)$, i.e.,

$$[\partial\hat{P}(\mathbf{a}t\mid\mathbf{a}_0t_0)/\partial t_0]=Q(\mathbf{a}_0, t-t_0)\hat{P}$$
$$-\sum_{n=1}^{\infty}\mathbf{D}_n(\mathbf{a}_0, t_0):(\partial/\partial\mathbf{a}_0)^n\hat{P}. \tag{5.2}$$

Moreover if the transition probabilities are time-independent, $\mathbf{D}_n$ is independent of t_0 and we may expect our solution to be a function only if $u=t-t_0$:

$$-\partial\hat{P}/\partial u=[Q(\mathbf{a}_0, u)-\sum_{1}^{\infty}\mathbf{D}_n(\mathbf{a}_0):(\partial/\partial\mathbf{a}_0)^n]\hat{P}. \tag{5.2}$$

6. CHARACTERISTIC FUNCTIONS AND LINKED AVERAGES

The characteristic function ϕ of a *normalized* probability density function P is defined by

$$\phi(\mathbf{y}, t)=\langle\exp(i\mathbf{y}\cdot\mathbf{a})\rangle=\int\exp(i\mathbf{y}\cdot\mathbf{a})P(\mathbf{a}, t)d\mathbf{a}. \tag{6.1}$$

The moments $\langle\mathbf{a}^n\rangle$ are determined by the nth derivatives of ϕ at $\mathbf{y}=0$ since

$$\phi(\mathbf{y}, t)=\sum_{n=0}^{\infty}(i\mathbf{y})^n:\langle\mathbf{a}^n\rangle/n!. \tag{6.2}$$

If $\mathbf{a}$ and $\mathbf{b}$ are two independent sets of random variables,

$$\langle\exp i\mathbf{y}\cdot(\mathbf{a}+\mathbf{b})\rangle=\langle\exp i\mathbf{y}\cdot\mathbf{a}\rangle\langle\exp i\mathbf{y}\cdot\mathbf{b}\rangle \tag{6.3}$$

or

$$\phi_{a+b}(\mathbf{y})=\phi_a(\mathbf{y})\phi_b(\mathbf{y}),$$

i.e., the ln of ϕ_{a+b} is an additive function. If we define

$$\langle\exp(i\mathbf{y}\cdot\mathbf{a})\rangle=\exp\sum_{n=1}^{\infty}(1/n!)(i\mathbf{y})^n:\mathfrak{y}_n, \tag{6.4}$$

then for independent variables,

$$\mathfrak{y}_n(\mathbf{a}+\mathbf{b})=\mathfrak{y}_n(\mathbf{a})+\mathfrak{y}_n(\mathbf{b}). \tag{6.5}$$

The $\mathfrak{y}_n(\mathbf{a})$ are referred to as Thiele semi-invariants or cumulants,[22] or linked (L) moments and can be written symbolically as

$$\mathfrak{y}_n(\mathbf{a})\equiv\langle\mathbf{a}^n\rangle^L. \tag{6.6}$$

---

[21] H. Cramer, *Mathematical Methods of Statistics* (Princeton University Press, Princeton, New Jersey, 1946), Sec. 15.8; M. Kendall and A. Stuart, *The Advanced Theory of Statistics* (Charles Griffin and Company, Ltd., London, 1958), Chap. 3.

[22] R. Kubo, J. Phys. Soc. Japan **17**, 1100 (1962).

CC-0. In Public Domain. Gurukul Kangri Collection, Haridwar

Digitized by Arya Samaj Foundation Chennai and eGangotri

The value of these moments must of course be obtained by expanding both sides of (6.4) and comparing coefficients of $\mathbf{y}^n$. For a single random variable a, we find, for example, that

$$\langle a\rangle^L=\langle a\rangle,$$
$$\langle a^2\rangle^L=\langle a^2\rangle-(\langle a\rangle)^2,$$
$$\langle a^3\rangle^L=\langle(a-\langle a\rangle)^3\rangle,$$
$$\langle a^4\rangle^L=\langle(a-\langle a\rangle)^4\rangle-3[\langle(a-\langle a\rangle)^2\rangle]^2, \quad (6.7)$$

so that $\langle a^n\rangle^L$ represents intrinsic correlations of nth order, i.e., those that do not arise from lower order correlations. If $\langle a^n\rangle^L=0$ for $n>m$ then all moments $\langle a^n\rangle$ for $n>m$ can be expressed in terms of the lower order correlations $\langle a^s\rangle$ for $s\leq m$.

With the notation (6.6), Eq. (6.4) can be rewritten in the elegant symbolic form

$$\langle\exp(i\mathbf{y}\cdot\mathbf{a})\rangle=\exp\{\langle[\exp(i\mathbf{y}\cdot\mathbf{a})-1]\rangle^L\}. \quad (6.8)$$

Although our diffusion coefficients are originally defined in terms of ordinary moments

$$n!\mathbf{D}_n(\mathbf{a},t)=\lim_{\Delta t\to 0}\langle[\mathbf{a}(t+\Delta t\rangle-\mathbf{a}(t)]^n\rangle/\Delta t, \quad (6.9)$$

we can also use a linked-moment definition

$$n!\mathbf{D}_n(\mathbf{a},t)=\lim_{\Delta t\to 0}\langle[\mathbf{a}(t+\Delta t)-\mathbf{a}(t)]^n\rangle^L/\Delta t, \quad (6.10)$$

since the lower order moments to be subtracted off, yield higher powers of Δt. In both cases averages are taken subject to $\mathbf{a}(t)=\mathbf{a}$ as initial condition. With the notation $\Delta\mathbf{a}=\mathbf{a}(t+\Delta t)-\mathbf{a}(t)$ and (6.10) we can rewrite (5.15) for $L(\mathbf{y},\mathbf{a},t)$ in the form:

$$-L(\mathbf{y},\mathbf{a},t)=\langle[\exp(i\mathbf{y}\cdot\Delta\mathbf{a})-1]\rangle^L/\Delta t. \quad (6.11)$$

Thus the characteristic function of the transition probability

$$\langle\exp(i\mathbf{y}\cdot\Delta\mathbf{a})\rangle$$
$$\equiv\int d\,\Delta\mathbf{a}\exp(i\mathbf{y}\cdot\Delta\mathbf{a})\,P(\mathbf{a}+\Delta\mathbf{a},t+\Delta t\mid\mathbf{a},t) \quad (6.12)$$

can be rewritten using (6.8) and (6.11) in the form

$$\langle\exp(i\mathbf{y}\cdot\Delta\mathbf{a})\rangle=\exp[-L(\mathbf{y},\mathbf{a},t)\Delta t]. \quad (6.13)$$

If the average (6.12) is taken against the unnormalized transition probability $\hat{P}(\mathbf{a}+\Delta\mathbf{a},t+\Delta t\mid\mathbf{a},t)$, the result is simply multiplied by the normalization:

$$\langle\exp(i\mathbf{y}\cdot\Delta\mathbf{a})\rangle$$
$$=\exp[-Q(\mathbf{a},t)\Delta t]\exp[-L(\mathbf{y},\mathbf{a},t)\Delta t]. \quad (6.14)$$

These results are correct to order Δt, and permit the transition probability to be represented in the form

$$\hat{P}(\mathbf{a}+\Delta\mathbf{a},t+\Delta t\mid\mathbf{a},t)$$
$$=(2\pi)^{-N}\int d\mathbf{y}\exp\{-i\mathbf{y}\cdot\Delta\mathbf{a}-[Q(\mathbf{a})+L(\mathbf{y},\mathbf{a})]\Delta t\}. \quad (6.15)$$

If this integral representation is inserted for $\hat{P}(\mathbf{a}_j\mid\mathbf{a}_{j-1})$ with an integration variable $\mathbf{y}_j$, the path integral (4.7) is converted into an integral over paths in the phase space $\mathbf{a}_j,\mathbf{y}_j$. If $\mathbf{a}$ is a position, then $\mathbf{y}$ can be thought of as a "momentum" and $L(\mathbf{y},\mathbf{a})$ as a kind of Hamiltonian operator. We found that $\mathbf{y}$ must be replaced by $i\partial/\partial\mathbf{a}$ when acting on P, just as the momentum operator in quantum mechanics is replaced when acting on the Schrödinger wave function.[23]

If we define the unnormalized characteristic function as

$$\hat{\phi}(\mathbf{y},t)=\langle\exp(i\mathbf{y}\cdot\mathbf{a})\rangle=\int\exp(i\mathbf{y}\cdot\mathbf{a})\hat{P}(\mathbf{a},t)\,d\mathbf{a} \quad (6.16)$$

then by (5.6) we obtain

$$\partial\hat{\phi}/\partial t=-\langle Q(\mathbf{a},t)\exp(i\mathbf{y}\cdot\mathbf{a})\rangle$$
$$-\sum_{n=1}^{\infty}(i\mathbf{y})^n:\langle D_n(\mathbf{a},t)\exp(i\mathbf{y}\cdot\mathbf{a})\rangle. \quad (6.17)$$

Now $\mathbf{a}$ can be brought down from the exponent by acting with $-i\partial/\partial\mathbf{y}$ so that

$$\partial\hat{\phi}(\mathbf{y},t)/\partial t=-[Q(\mathbf{a}_{op},t)+L(\mathbf{y},\mathbf{a}_{op},t)]\hat{\phi}(y,t) \quad (6.18)$$

or

$$\partial\hat{\phi}/\partial t=[-Q(\mathbf{a}_{op})+\sum_{n=1}^{\infty}(i\mathbf{y})^n:D_n(\mathbf{a}_{op})]\hat{\phi}$$

where

$$\mathbf{a}_{op}=-i\partial/\partial\mathbf{y}.$$

If $\hat{P}$ is the analog of the Schrödinger wave function of quantum mechanics, then $\hat{\phi}$ is the analog of the corresponding momentum wave function,[23] and $L(\mathbf{y}_{op},\mathbf{a}_{op})$ is the analog of the Hamiltonian operator.

If $\hat{P}(\mathbf{a},t)$ is to be determined subject to the initial condition

$$\hat{P}(\mathbf{a},t_0)=\delta(\mathbf{a}-\mathbf{a}_0), \quad (6.19)$$

i.e., $\hat{P}(\mathbf{a},t)\equiv\hat{P}(\mathbf{a},t\mid\mathbf{a}_0,t_0)$ then the corresponding initial condition on $\hat{\phi}$ is

$$\hat{\phi}(\mathbf{y},t_0)=\exp(i\mathbf{y}\cdot\mathbf{a}_0), \quad (6.20)$$

and a comparison with (4.8) shows that the functional average (4.3) is simply given by

$$M_0=\hat{\phi}(0,t) \quad (6.21)$$

---

[23] A. Messiah, *Quantum Mechanics* (John Wiley & Sons, Inc., New York, 1961).

CC-0. In Public Domain. Gurukul Kangri Collection, Haridwar

Digitized by Arya Samaj Foundation Chennai and eGangotri

which depends on $\mathbf{a}_0$. The complete average M can be obtained by multiplying by $P(\mathbf{a}_0)$ and integrating over $\mathbf{a}_0$ as in (4.2), or using

$$M=\hat{\phi}(0,t) \quad \text{where} \quad \hat{\phi}(\mathbf{y},t_0)\equiv\int \exp(i\mathbf{y}\cdot\mathbf{a}_0)P(\mathbf{a}_0)\,d\mathbf{a}_0 \tag{6.22}$$

is the initial condition.

7. EXAMPLES OF MARKOFF PROCESSES

A. The Weiner Process

This is a one-dimensional process in which $D_2=D$, a constant, and all other $D_n=0$. Thus the characteristic function obeys

$$\partial\phi/\partial t=-Dy^2\phi. \tag{7A.1}$$

The solution subject to the initial condition $\phi(y,0)=\exp(iya_0)$ of (6.20) is

$$\phi(y,t)=\exp(-Dy^2t)\exp(iya_0). \tag{7A.2}$$

Taking the inverse Fourier transform

$$P(at\mid a_0 0)=(4\pi Dt)^{-\frac{1}{2}}\exp[-(a-a_0)^2/4Dt]. \tag{7A.3}$$

Thus a is a Gaussian random variable with

$$\langle a\rangle=a_0,$$
$$\langle(a-a_0)^2\rangle=2Dt, \tag{7A.4}$$

so that D is the diffusion coefficient of this simple "Brownian-motion" process in which a is usually interpreted as a distance x.

The generalization of this result to a many dimensional process is immediate. The conditional probability already stated in Eq. (4.4) can be written down immediately from the knowledge that the process is Gaussian with

$$\langle\mathbf{a}\rangle=\mathbf{a}_0,$$
$$\langle(\mathbf{a}-\mathbf{a}_0)(\mathbf{a}-\mathbf{a}_0)\rangle=2\mathbf{D}t, \tag{7A.5}$$

where $\mathbf{D}$ is an $N\times N$ matrix.

B. The Fokker–Planck Process

This is a random process for which $\mathbf{D}_n=0$ for $n>2$ so that the probability density obeys the "Fokker–Planck" equation:

$$\frac{\partial P}{\partial t}=-\frac{\partial}{\partial a_i}[A_iP]+\frac{\partial}{\partial a_i}\frac{\partial}{\partial a_j}[D_{ij}P]\equiv-\frac{\partial}{\partial a_i}J_i, \tag{7B.1}$$

in which repeated indices are summed over, and A_i, D_{ij} can be functions of $\mathbf{a}$. If we regard

$$J_i\equiv A_iP-(\partial/\partial a_j)(D_{ij}P) \tag{7B.2}$$

as a probability current, then (7B.1) describes a conservation of probability. Steady-state solutions ob... $\partial P/\partial t=0$ but need not have $J_i=0$. The condit... $J_i=0$ is a detailed balance (D.B.) condition that ... be obeyed in many problems. When it is, one can w...

(D.B.): $\partial\ln P/\partial a_k=U_k\equiv-(D^{-1})_{ki}[\partial D_{ij}/\partial a_j-A_i]$ (7B.

In this case, one can express $\ln P$ in terms of the ... integral

$$\ln P=\int_{a_0}^{a}U_k\,da_k, \tag{7B.}$$

a result that is meaningful and independent of ... path only if the integrability conditions curl $U_k=0$ ... obeyed:

$$\partial U_k/\partial a_l=\partial U_l/\partial a_k. \tag{7B.}$$

This is a condition on the coefficients D_{ij}, A_i that ... permit such a detailed balance solution in the ste... state.

For the special case of a linear Fokker–Planck pr... ess in which

$$D_{ij}=\text{const.}, \qquad A_i=-\Lambda_{ij}a_j,$$

the integrability condition takes a form

$$(\mathbf{D}^{-1}\mathbf{\Lambda})_{kl}=(\mathbf{D}^{-1}\mathbf{\Lambda})_{lk}, \tag{7B.}$$

equivalent to our previously described condition ... time reversibility.[24] A close connection between ... tailed balance and time reversibility has been deri... in another way by van Vliet.[25] The steady-state s... tion of the linear Fokker–Planck process is well kno... Section 5 of Ref. 1, for example, presents the solu... without assuming detailed balance or time reversibi... The general time-dependent solution will be obta... in our discussion of the Ornstein–Uhlenbeck pro... which follows in example C.

The one-dimensional Fokker–Planck process ha... special simplicity in the steady state, because then

$$\partial J/\partial a=0 \quad \text{or} \quad J=\text{const.} \tag{7B.}$$

The general solution of (7B.2) can then be wri... down in the well-known form[6]

$$P(a)=-\frac{J}{D(a)}\int_{a_1}^{a}da'\exp\int_{a'}^{a}\frac{A(b)}{D(b)}db + \frac{C}{D(a)}\exp\int_{a_1}^{a}\frac{A(b)}{D(b)}db, \tag{7B.}$$

where (for any a_1) the integration constant C is ... by normalization. The boundary conditions ... (but not always) require P (and J) to vanish

[24] See II, Ref. 2, last paragraph of Appendix A.
[25] K. M. van Vliet, Phys. Rev. **133**, A1182 (1964); ... **138**, AB3 (1965).

CC-0. In Public Domain. Gurukul Kangri Collection, Haridwar

Digitized by Arya Samaj Foundation Chennai and eGangotri

infinity thus forcing J to be zero in this one-dimensional case.

The time-dependent problem is usually attacked[26] by seeking the eigenfunctions of the operator L

$$\partial P_n/\partial t = -LP_n = -\lambda_n P_n \tag{7B.9}$$

whether L has the Fokker–Planck, or a more general form.

For the one-dimensional Fokker–Planck case, these eigenfunctions obey an orthogonality condition

$$\int P_m(a)\, P_n(a)\, da/W(a) = \delta_{mn}, \tag{7B.10}$$

where the weight factor

$$W(a) = \frac{C}{D(a)} \exp \int^a \frac{A(b)}{D(b)}\, db \tag{7B.11}$$

is the steady solution when $J=0$ is imposed. To prove (7B.10) we make the transformation

$$P = \exp\left(\int f\, da\right) Q, \tag{7B.12}$$

$$\exp\left(-\int f\, da\right)\partial/\partial a \exp \int f\, da = \partial/\partial a + f, \tag{7B.13}$$

$$L' \equiv \exp\left(-\int f\, da\right) L \exp\left(\int f\, da\right)$$

$$= -\frac{\partial}{\partial a}\left(D\frac{\partial}{\partial a}\right) + \left[A - \left(2fD + \frac{\partial D}{\partial a}\right)\right]\frac{\partial}{\partial a} + m(a) \tag{7B.14}$$

$$m(a) = \left(\frac{\partial}{\partial a} + f\right)A - \left(\frac{\partial}{\partial a} + f\right)\left(\frac{\partial}{\partial a} + f\right)D. \tag{7B.15}$$

Then L' will be Hermitian (of Sturm–Liouville type) if the coefficient of $\partial/\partial a$ vanishes, i.e., if

$$\text{or} \qquad 2f = [A - \partial D/\partial a]/D \tag{7B.16}$$

$$\exp 2\int f\, da = D^{-1} \exp \int (A/D)\, da \equiv W(a). \tag{7B.17}$$

Thus $P = W^{\frac{1}{2}}Q$ and the Hermiticity of L' guarantees that its eigenfunctions Q_n obey the unweighted orthogonality condition

$$\int Q_m(a) Q_n(a)\, da = \delta_{mn} \tag{7B.18}$$

which demonstrates (7B.10). We shall assume completeness[27]:

$$\sum_n Q_n(a) Q_n(a') = \delta(a - a'). \tag{7B.19}$$

[26] N. G. van Kampen, Phys. Rev. **110**, 319 (1958); also Ref. 6.

[27] See, e.g., P. M. Morse and H. Feshbach, *Methods of Theoretical Physics* (McGraw-Hill Book Company, Inc., New York, 1953), Sec. 6.3, Eq. (6.3.11), and p. 729.

The general time-dependent solution using (7B.9) and (7B.19) can be written in the form

$$P(at \mid a_0 t_0) = \sum_n \exp\left[-\lambda_n(t - t_0)\right] P_n(a)\, P_n(a_0)/W(a_0). \tag{7B.20}$$

The lowest eigenvalue is $\lambda_0 = 0$ with $P_0(a)$ the steady-state solution, which is equal to $W(a)$ when $J=0$, so that in this case

$$P(at, a_0 t_0) \equiv P(at \mid a_0 t_0)\, P_0(a_0)$$
$$= \sum_n \exp\left[-\lambda_n(t - t_0)\right] P_n(a)\, P_n(a_0). \tag{7B.21}$$

For $V = V(a) =$ any function of a,

$$\langle V(t)\, V(0)\rangle = \sum_n \exp(-\lambda_n t)\left[\int V(a)\, P_n(a)\, da\right]^2. \tag{7B.22}$$

Continuity Theorem (7B.1): Almost all sample functions of a one-dimensional Fokker–Planck process with bounded $D(a) \leq D_m$ are continuous. We shall make this theorem plausible by using (6.15) to obtain

$$P(a + \Delta a, t + \Delta t \mid a, t)$$
$$= (4\pi \Delta t D)^{-\frac{1}{2}} \exp\left[-(\Delta a - A\Delta t)^2/4D\Delta t\right] \tag{7B.23}$$

for the transition probability. The drift term $A(a)\Delta t$ causes a differentiable change in a so that we shall ignore $A(a)$ and concentrate on $D(a)$. Over the time interval $0 \leq t \leq T$, choose $\Delta t = T/N$. Using the inequality[28]

$$\int_\lambda^\infty \exp(-\tfrac{1}{2}\xi^2)\, d\xi \leq \int_\lambda^\infty \frac{\xi}{\lambda} \exp(-\tfrac{1}{2}\xi^2)\, d\xi = \frac{\exp(-\frac{1}{2}\lambda^2)}{\lambda},$$

$$P(\Delta a > (4D_0 T)^{\frac{1}{2}} N^{-\frac{1}{2}})$$
$$\leq \pi^{-\frac{1}{2}} (D_m/D_0) N^{-\frac{1}{2}} \exp\left[-D_0 N^{\frac{1}{2}}/D_m\right]. \tag{7B.24}$$

Thus for all N intervals Δt, the probability for the largest Δa obeys

$$P((\Delta a)_{\text{largest}} > (4D_0 T)^{\frac{1}{2}} N^{-\frac{1}{2}})$$
$$\leq N \pi^{-\frac{1}{2}} (D_m/D_0) N^{-\frac{1}{2}} \exp(-D_0 N^{\frac{1}{2}}/D_m) \tag{7B.25}$$

so that as $N \to \infty$, even the largest Δa goes to zero with probability one.

C. The Ornstein–Uhlenbeck (O.U.) Process

The O.U. process[29] is originally defined as a velocity $a = u$ subject to a damping linear in the velocity plus a random force (see the Langevin noise source de-

[28] Our proof is a slight generalization of that given by J. L. Doob, *Stochastic Processes* (John Wiley & Sons, Inc., New York, 1953), Sec. VIII.2.

[29] G. E. Uhlenbeck and L. S. Ornstein, Phys. Rev. **36**, 823 (1930).

CC-0. In Public Domain. Gurukul Kangri Collection, Haridwar

Digitized by Arya Samaj Foundation Chennai and eGangotri

scription in I, Sec. 8). In our present language, the linear damping [see Eq. (5.10)] means

$$\mathbf{D}_1(\mathbf{a}) \equiv \mathbf{A}(\mathbf{a}) = -\boldsymbol{\Lambda}\cdot\mathbf{a}, \tag{7C.1}$$

where we have generalized to the multivariable case at the minor expense of using a matrix decay constant $\boldsymbol{\Lambda}$. The "Brownian motion" random force results in simple diffusion with

$$\mathbf{D}_2(\mathbf{a}) = \mathbf{D} = \text{a constant matrix}; \qquad \mathbf{D}_n = 0 \text{ for } n > 2. \tag{7C.2}$$

(The relation between the Langevin and Markoff descriptions of random processes will be developed in paper IV of this series.)

Thus our "Hamiltonian" (5.16) has the form

$$L(\mathbf{y}, \mathbf{a}, t) = i\mathbf{y}\cdot\boldsymbol{\Lambda}\cdot\mathbf{a} + \mathbf{y}\cdot\mathbf{D}\cdot\mathbf{y}; \qquad \mathbf{a} = -i\partial/\partial\mathbf{y} \tag{7C.3}$$

so that by (6.18), the characteristic function $\phi(\mathbf{y}, t)$ obeys

$$\partial\phi/\partial t = -\mathbf{y}\cdot\boldsymbol{\Lambda}\cdot\partial\phi/\partial\mathbf{y} - \mathbf{y}\cdot\mathbf{D}\cdot\mathbf{y}\phi \tag{7C.4}$$

subject to

$$\phi(\mathbf{y}, 0) = \exp(i\mathbf{y}\cdot\mathbf{a}_0), \tag{7C.5}$$

the initial condition (6.20).

This partial differential equation can be solved by first eliminating the "drift terms" (those proportional to $\boldsymbol{\Lambda}$). The transformation that does this leads to an exact solution of the case in which $\mathbf{D}=0$. For this special case, it is well known that such a linear partial differential equation of the first order is equivalent to the set of ordinary differential equations:

$$dt = (\mathbf{y}\cdot\boldsymbol{\Lambda})^{-1}\cdot d\mathbf{y} \tag{7C.6}$$

or

$$d\mathbf{y}/dt = \mathbf{y}\cdot\boldsymbol{\Lambda}.$$

[A physicist's way of arriving at this drift equation would be to write a "material" derivative in the form

$$\frac{d\phi}{dt} \equiv \frac{\partial\phi}{\partial t} + \frac{d\mathbf{y}}{dt}\frac{\partial\phi}{\partial\mathbf{y}}.$$

Comparison with (7C.4) then yields $d\mathbf{y}/dt$.] The general solution of the ordinary differential equations is

$$\mathbf{y}(t) = \mathbf{y}(0)\exp(\boldsymbol{\Lambda}t)$$

or

$$\mathbf{y}(t)\exp(-\boldsymbol{\Lambda}t) = \mathbf{y}(0) = \text{const.} \tag{7C.7}$$

Thus the general solution for ϕ is

$$\phi = \text{arbitrary function of } \mathbf{y}\exp(-\boldsymbol{\Lambda}t). \tag{7C.8}$$

The solution obeying the initial condition (7C.5) is then

$$\phi(\mathbf{y}, t) = \exp[i\mathbf{y}\cdot\exp(-\boldsymbol{\Lambda}t)\cdot\mathbf{a}_0] \tag{7C.9}$$

and the corresponding density is

$$P(\mathbf{a}, t) = \delta(\mathbf{a} - [\exp(-\boldsymbol{\Lambda}t)]\cdot\mathbf{a}_0). \tag{7C.10}$$

Thus

$$\langle\mathbf{a}(t)\rangle = \exp(-\boldsymbol{\Lambda}t)\mathbf{a}_0 \tag{7C.11}$$

in agreement with the first moment equation of (5.16) when $Q=0$, and, when $\mathbf{D}=0$, no fluctuations are present.

The results suggest, that when $\mathbf{D}\neq 0$ we make the transformation

$$\mathbf{y} = \mathbf{z}\cdot\exp(\boldsymbol{\Lambda}t) \tag{7C.12}$$

$$\phi(\mathbf{y}, t) = \phi(\mathbf{z}\exp(\boldsymbol{\Lambda}t), t) \equiv \psi(\mathbf{z}, t) \tag{7C.13}$$

with

$$\psi(\mathbf{z}, 0) = \phi(\mathbf{z}, 0) = \exp(i\mathbf{z}\cdot\mathbf{a}_0) \tag{7C.14}$$

as the initial condition. Since

$$\left.\frac{\partial\psi}{\partial t}\right|_z = \frac{\partial\phi}{\partial t} + \left.\frac{d\mathbf{y}}{dt}\right|_z \frac{\partial\phi}{\partial\mathbf{y}} = \frac{\partial\phi}{\partial t} + \mathbf{z}\exp(\boldsymbol{\Lambda}t)\boldsymbol{\Lambda}\frac{\partial\phi}{\partial\mathbf{y}}$$

$$= (\partial\phi/\partial t) + \mathbf{y}\cdot\boldsymbol{\Lambda}(\partial\phi/\partial\mathbf{y}) = -\mathbf{y}\cdot\mathbf{D}\cdot\mathbf{y}\phi, \tag{7C.15}$$

the drift terms disappear and

$$\partial\psi/\partial t = -\mathbf{z}\exp(\boldsymbol{\Lambda}t)\mathbf{D}\exp(\boldsymbol{\Lambda}^\dagger t)\mathbf{z}\psi(\mathbf{z}, t), \tag{7C.16}$$

where $\boldsymbol{\Lambda}^\dagger$ is the transpose of $\boldsymbol{\Lambda}$. The solution of this equation with the initial condition (7C.14) is then

$$\psi(\mathbf{z}, t) = \exp\left[-\mathbf{z}\cdot\int_0^t \exp(\boldsymbol{\Lambda}s)\mathbf{D}\exp(\boldsymbol{\Lambda}^\dagger s)\,ds\cdot\mathbf{z}\right] \times\exp(i\mathbf{z}\cdot\mathbf{a}_0), \tag{7C.17}$$

or in terms of the original variable $\mathbf{y}$,

$$\phi(\mathbf{y}, t) = \exp[i\mathbf{y}\cdot\langle\mathbf{a}\rangle^L - (1/2!)\mathbf{y}\cdot\langle\mathbf{aa}\rangle^L\cdot\mathbf{y}], \tag{7C.18}$$

using (6.8) where the linked averages are given by

$$\langle\mathbf{a}\rangle^L = \langle\mathbf{a}(t)\rangle = \exp(-\boldsymbol{\Lambda}t)\mathbf{a}_0, \tag{7C.19}$$

$$\langle\mathbf{aa}\rangle^L = \langle[\mathbf{a}(t) - \langle\mathbf{a}(t)\rangle][\mathbf{a}(t) - \langle\mathbf{a}(t)\rangle]\rangle$$

$$= 2\int_0^t \exp(-\boldsymbol{\Lambda}u)\mathbf{D}\exp(-\boldsymbol{\Lambda}^\dagger u)\,du, \tag{7C.20}$$

where $u = t - s$. The stationary result can be obtained by taking the limit as $t\to\infty$. Thus $\langle\mathbf{a}\rangle\to 0$, and writing $\langle\boldsymbol{\alpha\alpha}\rangle$ for the second moment fluctuation in the stationary case:

$$\langle\boldsymbol{\alpha\alpha}\rangle = 2\int_0^\infty \exp(-\boldsymbol{\Lambda}t)\mathbf{D}\exp(-\boldsymbol{\Lambda}^\dagger t)\,dt. \tag{7C.21}$$

We have previously obtained this result (I, Sec. 5) by solving the Einstein relation

$$2\mathbf{D} = \boldsymbol{\Lambda}\langle\boldsymbol{\alpha\alpha}\rangle + \langle\boldsymbol{\alpha\alpha}\rangle\boldsymbol{\Lambda}^\dagger, \tag{7C.22}$$

which is a consequence of stationarity of the second

CC-0. In Public Domain. Gurukul Kangri Collection, Haridwar

Digitized by Arya Samaj Foundation Chennai and eGangotri

moments. In the presence of underlying time reversibility, I, Sec. 6, or if $\mathbf{\Lambda}^{-1}\mathbf{D}$ is symmetric,[24]

$$\langle \boldsymbol{\alpha}\boldsymbol{\alpha} \rangle = \mathbf{\Lambda}^{-1}\mathbf{D}. \tag{7C.23}$$

If (7C.22) is inserted into (7C.20), the integrand is found to be a perfect differential so that

$$\langle \mathbf{a}\mathbf{a} \rangle^{L} = \langle \boldsymbol{\alpha}\boldsymbol{\alpha} \rangle - \exp(-\mathbf{\Lambda}t)\langle \boldsymbol{\alpha}\boldsymbol{\alpha} \rangle \exp(-\mathbf{\Lambda}^{\dagger}t), \tag{7C.24}$$

which explicitly displays the approach to the stationary case. Equation (7C.24) is in turn a special case of our earlier result

$$\langle [\mathbf{a}(t) - \langle \mathbf{a}(t) \rangle][\mathbf{a}(u) - \langle \mathbf{a}(u) \rangle] \rangle_{\mathbf{a}_0} = \exp(-\mathbf{\Lambda} \mid t-u \mid) \langle \boldsymbol{\alpha}\boldsymbol{\alpha} \rangle - \exp(-\mathbf{\Lambda}t) \langle \boldsymbol{\alpha}\boldsymbol{\alpha} \rangle \exp(-\mathbf{\Lambda}^{\dagger}u), \tag{7C.25}$$

I(8.18), obtained by Langevin techniques.

The O.U. process and the Weiner process are *quasi-stationary* in the sense that their transition probabilities or "Hamiltonians" $L(\mathbf{y}, \mathbf{a}, t) = L(\mathbf{y}, \mathbf{a})$ do not depend explicitly on the time. The Weiner process possesses no stationary limit in the sense of (2.10) whereas the linear decay causes the O.U. process to possess such a stationary limit.

The O.U. process is linear and Gaussian as well as stationary. Thus it illustrates

Doob's Theorem: A random process that is stationary, Gaussian and Markoffian possesses an autocorrelation of the form

$$\langle \mathbf{a}(t)\mathbf{a}(0) \rangle = \exp(-\mathbf{\Lambda}t) \langle \mathbf{a}(0)\mathbf{a}(0) \rangle. \tag{7C.26}$$

Doob[30] states this theorem for a one-dimensional random process. It was extended to the many-dimensional case by Kac.[31] The proofs are based on the Chapman-Kolmogoroff relation (2.12) and are manipulative rather than informative. Let us therefore state the

Generalized Doob Theorem: A random process that is Gaussian and Markoffian must be a linear, Fokker-Planck process, i.e., $\mathbf{D}_n = 0$ for $n > 2$, $\mathbf{D}_2 = \mathbf{D} =$ independent of $\mathbf{a}$, $\mathbf{D}_1 = -\mathbf{\Lambda}\cdot\mathbf{a}$, where $\mathbf{D}$ and $\mathbf{\Lambda}$ can be time-dependent.

Proof: If the $\mathbf{a}$ process is Gaussian, then the transition probability has the form

$$P(\mathbf{a}+\Delta\mathbf{a}, t+\Delta t \mid \mathbf{a}, t) \propto \exp[\mathbf{a}\cdot\mathbf{\mu}\cdot\mathbf{a} + \mathbf{a}\cdot\mathbf{\nu}\cdot\Delta\mathbf{a} + \Delta\mathbf{a}\cdot\mathbf{\lambda}\cdot\Delta\mathbf{a}], \tag{7C.27}$$

where $\mathbf{\mu}$, $\mathbf{\nu}$, and $\mathbf{\lambda}$ may depend on time, but not on $\mathbf{a}$ or $\Delta\mathbf{a}$. The characteristic function (6.12) of the transition probability then necessarily has the form

$$\exp[-L(\mathbf{y}, \mathbf{a}, t)\Delta t] \sim \exp[(i\mathbf{y}\cdot\mathbf{\Lambda}\cdot\mathbf{a} + \mathbf{y}\cdot\mathbf{D}\cdot\mathbf{y})\Delta t] \tag{7C.28}$$

since the Fourier transform of a Gaussian in $\Delta\mathbf{a}$ is a Gaussian in $\mathbf{y}$. Moreover, the form of (7C.27) requires that $\mathbf{D}$ be independent of $\mathbf{a}$, and the coefficient of $\mathbf{y}$ be linear in $\mathbf{a}$. With a suitable (possibly time-dependent) choice of origin, this coefficient can be written $\mathbf{\Lambda}\cdot\mathbf{a}$. This completes our proof. The original Doob theorem then follows if we note that stationarity forces $\mathbf{\Lambda}$ and $\mathbf{D}$ to be independent of time, reducing the process to an O.U. process. Then

$$\langle \mathbf{a}(t)\mathbf{a}(0) \rangle = \int \mathbf{a}\, d\mathbf{a} P(\mathbf{a}t \mid \mathbf{a}_0 0)\, d\mathbf{a}_0 \mathbf{a}_0 P(\mathbf{a}_0)$$

$$= \int \langle \mathbf{a}(t) \rangle_{\mathbf{a}_0} \mathbf{a}_0\, d\mathbf{a}_0 P(\mathbf{a}_0),$$

which reduces to the desired form (7C.26) when the conditional mean $\langle \mathbf{a}(t) \rangle_{\mathbf{a}(0)}$ is given the appropriate value $\exp(-\mathbf{\Lambda}t)\mathbf{a}(0)$ for an O.U. process (7C.29).

D. The Poisson Process (Shot Noise)

This is a discrete process with $a(0) = 0$ and $a(t) =$ an integer $=$ the number of events that have occurred in the time interval $(0, t)$. Then events are assumed to occur at random at a rate ν per unit time. Thus

$$\partial P(a, t)/\partial t = \nu[P(a-1, t) - P(a, t)], \tag{7D.1}$$

where the first term represents transitions into state a from $a-1$, and the second term represents transitions out of a (into $a+1$). For the case $a=0$,

$$\partial P(0, t)/\partial t = -\nu P(0, t). \tag{7D.2}$$

Thus

$$P(0, t) = \exp(-\nu t). \tag{7D.3}$$

Setting

$$P(a, t) = \exp(-\nu t) Q(a, t), \tag{7D.4}$$

Eq. (7D.1) reduces to

$$\partial Q(a, t)/\partial t = \nu Q(a-1, t). \tag{7D.5}$$

Using $Q(0, t) = 1$ and iterating we get

$$Q(a, t) = (\nu t)^a/a!, \qquad P(a, t) = (\nu t)^a \exp(-\nu t)/a!. \tag{7D.6}$$

All of these results are standard, and the moments $\langle a^n \rangle$ can be computed from $P(a, t)$. It is more instructive, however, to rewrite (7D.1) as

$$\partial P(a, t)/\partial t = \nu[\exp(-\partial/\partial a) - 1]P(a, t)$$

$$= \nu \sum_{1}^{\infty} [(-1)^n/n!](\partial/\partial a)^n P(a, t)$$

$$= \sum (-1)^n (\partial/\partial a)^n D_n P(a, t) \tag{7D.7}$$

so that

$$D_n = \nu/n!, \tag{7D.8}$$

[30] J. L. Doob, Ann. Math. **43**, 351 (1942).
[31] See M. C. Wang and G. E. Uhlenbeck, Rev. Mod. Phys. **17**, 323 (1945), Appendix II.

CC-0. In Public Domain. Gurukul Kangri Collection, Haridwar

Digitized by Arya Samaj Foundation Chennai and eGangotri

and

$$-L(y, a, t)=\sum_1^\infty (iy)^n D_n=\nu[\exp(iy)-1]. \quad (7D.9)$$

Thus

$$\partial\phi/\partial t=\nu(e^{iy}-1)\phi. \quad (7D.10)$$

With the initial condition $P(a, 0)=\delta(a)$ or $\phi(y, 0)=1$ we have

$$\langle \exp iya(t)\rangle=\phi(y, t)=\exp[\nu t(e^{iy}-1)] \quad (7D.11)$$

or

$$\exp\langle e^{iya}-1\rangle^L=\exp[\nu t(e^{iy}-1)], \quad (7D.12)$$

and

$$\langle a^n\rangle^L=\nu t; \qquad n\geq 1 \quad (7D.13)$$

so that all linked moments, $n\geq 1$, in a Poisson process take the same value!

E. The Homogeneous Process

A homogeneous process is a random process that is independent of the choice of origin of **a**. Thus all higher order probability densities $P(\mathbf{a}_n, \mathbf{a}_{n-1}, \cdots, \mathbf{a}_1)$ are functions only of the differences $\mathbf{a}_i-\mathbf{a}_j$. A homogeneous Markoff process can be defined most succintly by the requirement that

$$L(\mathbf{y}, \mathbf{a}, t)=L(\mathbf{y}, t) \quad (7E.1)$$

independent of **a**. (If the process is also stationary, L will be independent of t.)

As a simple example of a homogeneous process, we note the one-dimensional Poisson process with jump η:

$$\partial P/\partial t=\nu[P(a-\eta, t)-P(a, t)], \quad (7E.2)$$

which may be immediately generalized to a normalized distribution $g(\eta)$ of possible jumps

$$\int g(\eta)\,d\eta=1,$$

$$\partial P/\partial t=\nu\int g(\eta)\,d\eta[\exp(-\eta\partial/\partial a)-1]P(a, t)$$

$$=\sum_{n=1}^\infty (-1)^n(\partial/\partial a)^n D_n P(a, t), \quad (7E.3)$$

where

$$D_n=(\nu/n!)\int g(\eta)\,d\eta\eta^n.$$

Thus

$$-L(y, t)=\sum_1^\infty (iy)^n D_n=\nu\int g(\eta)\,d\eta[\exp(iy\eta)-1]. \quad (7E.4)$$

This process will be stationary or not, according as $g(\eta)$ does or does not depend explicitly on t. In a case

$$\partial\phi/\partial t=-L(y, t)\phi(y, t) \quad (7E.5)$$

has the explicit solution

$$\phi(y, t)=\exp\left[-\int_0^t L(y, s)\,ds\right]\exp(iya_0) \quad (7E.6)$$

if we take $\phi(y, 0)=\exp(iya_0)$ appropriate to $a(0)=a_0$. Thus

$$P(a, t\mid a_0, 0)=\frac{1}{2\pi}\int \exp[-iy(a-a_0)]\,dy \times\exp\left[-\int_0^t L(y, s)\,ds\right] \quad (7E.7)$$

In the adiabatic theory of line broadening discussed in Sec. 3A, we are concerned with

$$M(t)=\left\langle \exp\left(i\int_0^t \omega(s)\,ds\right)\right\rangle. \quad (7E.8)$$

If we interpret

$$a(t)-a(0)=\int_0^t \omega(s)\,ds \quad (7E.9)$$

and η as the phase shift $\int\omega\,ds$ induced in each collision and write

$$L(y)=\nu\int g(\eta)\,d\eta[1-\exp(iy\eta)], \quad (7E.10)$$

then with $g(\eta)$ independent of the time,

$$M(t)=\langle\exp[i(a-a_0)]\rangle$$

$$=\phi(1, t)\exp(-ia_0)=\exp[-L(1)t]$$

$$=\exp[-\nu t\int g(\eta)\,d\eta(1-e^{i\eta})]. \quad (7E.11)$$

If now we write

$$\nu=nv\sigma, \quad (7E.12)$$

where n is the density of foreign atoms producing the collision broadening, v a typical relative velocity, and σ the total cross section for collision, then $\sigma g(\eta)d\eta$ is the cross section for collision with phase shift in $\eta+d\eta$. If we define

$$\sigma_r+i\sigma_i=\sigma\int g(\eta)\,d\eta(1-e^{i\eta}), \quad (7E.13)$$

then

$$M(t)=\exp[-nvt(\sigma_r+i\sigma_i)], \quad t>0,$$

$$=\exp[-nv\sigma_r\mid t\mid -inv\sigma_i t], \quad \text{all } t, \quad (7E.14)$$

where the last form has used $M(-t)=M(t)^*$ in accor

CC-0. In Public Domain. Gurukul Kangri Collection, Haridwar

Digitized by Arya Samaj Foundation Chennai and eGangotri

that the spectral distribution

$$I(\omega)=\int \exp\left[-i(\omega-\omega_{if})t\right]dtM(t) \quad (7E.15)$$

$$=\frac{2n\nu\sigma_r}{(n\nu\sigma_r)^2+(\omega-\omega_{if}+n\nu\sigma_i)^2} \quad (7E.16)$$

be real. The usual Lorentz line shape,[13] with width $n\nu\sigma_r$ and frequency shift $n\nu\sigma_i$ is thus seen to be a simple consequence of the (generalized) Poisson matrix of the collisions, i.e., the assumption that the duration of each collision is so short that we have a succession of independent phase shifts occurring at a certain rate, and with a certain distribution.

F. Homogeneous Noise Plus Linear Damping

We can always decompose L into a drift part and a noise or diffusion part:

$$L(\mathbf{y}, \mathbf{a}, t)=-i\mathbf{y}\cdot\mathbf{A}+K(\mathbf{y}, \mathbf{a}, t), \quad (7F.1)$$

where

$$-K(\mathbf{y}, \mathbf{a}, t)=\sum_{n=2}^{\infty}(i\mathbf{y})^n:\mathbf{D}_n(\mathbf{a}, t). \quad (7F.2)$$

The process we wish to consider in this subsection involves linear damping and homogeneous noise, i.e.,

$$L(\mathbf{y}, \mathbf{a}, t)=i\mathbf{y}\cdot\mathbf{\Lambda}(t)\cdot\mathbf{a}+K(\mathbf{y}, t). \quad (7F.3)$$

Except for the nonlinear Fokker–Planck case, this process includes all previous cases A to E. Moreover, we shall ask a more general question,

$$M_0=\left\langle \exp i\int_0^t \mathbf{q}(s)\cdot\mathbf{a}(s)\,ds \right\rangle, \quad (7F.4)$$

than solved in the previous cases. [The most important applications will be stationary, i.e., $\mathbf{\Lambda}(t)=\mathbf{\Lambda}$; $K(\mathbf{y}, t)=K(\mathbf{y})$.] It follows from (6.21) and (6.18) with $Q=-i\mathbf{q}(t)\cdot\mathbf{a}$ that

where $$M_0=\hat{\phi}(0, t), \quad (7F.5)$$

$$\left[\partial\hat{\phi}(\mathbf{y}, t)\right]/\partial t=(\mathbf{q}-\mathbf{y}\cdot\mathbf{\Lambda})\cdot(\partial\hat{\phi}/\partial\mathbf{y})-K(\mathbf{y}, t)\hat{\phi}. \quad (7F.6)$$

We now follow our procedure in treating the O.U. process. The solution of the "dynamical" equation

$$d\mathbf{y}/dt=\mathbf{y}\cdot\mathbf{\Lambda}(t)-\mathbf{q}(t) \quad (7F.7)$$

can be written

$$\mathbf{y}(t)=\mathbf{y}(0)\cdot\mathbf{m}(t)+\mathbf{y}_0(t), \quad (7F.8)$$

where $\mathbf{m}(t)$ obeys

$$d\mathbf{m}/dt=\mathbf{m}\cdot\mathbf{\Lambda}(t). \quad (7F.9)$$

If Λ does not depend explicitly on the time

$$\mathbf{m}(t)=\exp(\mathbf{\Lambda}t). \quad (7F.10)$$

Otherwise,

$$\mathbf{m}(t)=1+\int_0^t\mathbf{\Lambda}(s_1)\,ds_1+\int_0^t ds_2\int_0^{s_2} ds_1\mathbf{\Lambda}(s_1)\mathbf{\Lambda}(s_2)+\cdots$$

$$+\int_0^t ds_n\int_0^{s_n} ds_{n-1}\cdots\int_0^{s_2} ds_1\mathbf{\Lambda}(s_1)\mathbf{\Lambda}(s_2)\cdots\mathbf{\Lambda}(s_n)+\cdots$$

$$=\sum_{n=0}^{\infty}\frac{1}{n!}\int_0^t\int_0^t\cdots\int_0^t ds_n \cdots ds_1 T_{\rightarrow}[\mathbf{\Lambda}(s_1)\mathbf{\Lambda}(s_2)\cdots\mathbf{\Lambda}(s_n)]$$

$$=T_{\rightarrow}\left[\exp\int_0^t ds\mathbf{\Lambda}(s)\right], \quad (7F.11)$$

where $T_{\rightarrow}$ is the usual time-ordering symbol[32] that places the matrices from left to right in order of increasing time. The other term in (7F.8) obeys

$$d\mathbf{y}_0/dt=-\mathbf{q}(t)+\mathbf{y}_0(t)\cdot\mathbf{\Lambda}(t), \quad (7F.12)$$

and is given explicitly by

$$\mathbf{y}_0(t)=-\int_0^t du\mathbf{q}(u)\mathbf{m}(u, t), \quad (7F.13)$$

where

$$\mathbf{m}(u, t)\equiv\mathbf{m}(u)^{-1}\mathbf{m}(t)=T_{\rightarrow}\left[\exp\int_u^t ds\Lambda(s)\right]. \quad (7F.14)$$

Equation (7F.8) suggests the transformation

$$\mathbf{y}=\mathbf{z}\cdot\mathbf{m}(t)+\mathbf{y}_0(t) \quad (7F.15)$$

$$\psi(\mathbf{z}, t)=\hat{\phi}(\mathbf{y}, t)=\hat{\phi}(\mathbf{z}\cdot\mathbf{m}(t)+\mathbf{y}_0(t), t) \quad (7F.16)$$

with

$$\psi(\mathbf{z}, 0)=\hat{\phi}(\mathbf{z}, 0)=\exp(i\mathbf{z}\cdot\mathbf{a}_0). \quad (7F.17)$$

As in the O.U. case, the first-derivative terms have been made to disappear:

$$\partial\psi(\mathbf{z}, t)/\partial t=-K((\mathbf{z}\cdot\mathbf{m}(t)+\mathbf{y}_0(t), t)\psi(\mathbf{z}, t) \quad (7F.18)$$

or

$$\psi(\mathbf{z}, t)=\exp\left[-\int_0^t K(\mathbf{z}\cdot\mathbf{m}(s)+\mathbf{y}_0(s), s)\,ds\right] \times\exp(i\mathbf{z}\cdot\mathbf{a}_0). \quad (7F.19)$$

Inserting $\mathbf{z}=[\mathbf{y}-\mathbf{y}_0(t)]\cdot\mathbf{m}(t)^{-1}$ we obtain

$$\hat{\phi}(\mathbf{y}, t)=\exp\left[-\int_0^t K\left(\mathbf{y}\cdot\mathbf{m}(t, s) +\int_s^t du\mathbf{q}(u)\cdot\mathbf{m}(u, s), s\right)ds\right]$$

$$\times\exp\left[i\mathbf{y}\cdot\mathbf{m}(t)^{-1}\cdot\mathbf{a}_0+i\int_0^t du\mathbf{q}(u)\mathbf{m}^{-1}(u)\cdot\mathbf{a}_0\right]. \quad (7F.20)$$

[32] See, e.g., F. J. Dyson, Phys. Rev. **75**, 486, 1736 (1949); R. P. Feynman, *ibid.* **84**, 108 (1951); M. L. Goldberger and E. N. Adams, J. Chem. Phys. **20**, 240 (1952). Also Ref. 22, S. S. Schweber, H. Bethe, and F. de Hoffman, *Mesons and Fields* (Row, Peterson and Company, New York, 1956), Vol. I, Sec. 16.

CC-0. In Public Domain. Gurukul Kangri Collection, Haridwar

Digitized by Arya Samaj Foundation Chennai and eGangotri

Thus

$$M_0=\hat{\phi}(0,t)=\exp\left(i\int_0^t ds\mathbf{q}(s)\cdot\langle\mathbf{a}(s)\rangle\right)$$
$$\times\exp\left[-\int_0^t K\left(\int_s^t du\mathbf{q}(u)\cdot\mathbf{m}(u,s),s\right)ds\right], \quad (7F.21)$$

where

$$\langle\mathbf{a}(s)\rangle=\mathbf{m}(s)^{-1}\cdot\mathbf{a}_0 \quad (7F.22)$$

is the mean "position" in the original random process (with $\mathbf{q}=0$) in the sense that

$$d\langle\mathbf{a}(s)\rangle/ds=\mathbf{\Lambda}(s)\langle\mathbf{a}(s)\rangle. \quad (7F.23)$$

If we set $\mathbf{q}(s)=\mathbf{y}\delta(t-s)$, we obtain

$$\left\langle\exp\left[i\int_0^t\mathbf{q}(s)\cdot\mathbf{a}(s)\,ds\right]\right\rangle=\langle\exp[i\mathbf{y}\cdot\mathbf{a}(t)]\rangle$$
$$=\exp[i\mathbf{y}\cdot\langle\mathbf{a}(t)\rangle]$$
$$\times\exp\left[-\int_0^t K(\mathbf{y}\cdot\mathbf{m}(t,s),s)\,ds\right]. \quad (7F.24)$$

But this result is just $\phi(\mathbf{y},t)$ which can also be obtained by setting $\mathbf{q}=0$ in $\hat{\phi}(\mathbf{y},t)$. Finally,

$$P(\mathbf{a}t\mid\mathbf{a}_0,0)=\frac{1}{(2\pi)^N}\int d\mathbf{y}\exp[-i\mathbf{y}\cdot(\mathbf{a}-\langle\mathbf{a}(t)\rangle_{\mathbf{a}_0})]$$
$$\times\exp\left[-\int_0^t K(\mathbf{y}\cdot\mathbf{m}(t,s),s)\,ds\right]. \quad (7F.25)$$

If we set

$$K(\mathbf{y},s)=\mathbf{y}\cdot\mathbf{D}\cdot\mathbf{y},$$
$$\mathbf{\Lambda}(s)=\mathbf{\Lambda},$$
$$\mathbf{m}(t,s)=\exp[(s-t)\mathbf{\Lambda}], \quad (7F.26)$$

and set $u=t-s$, our results (7F.24) specialized immediately to the O.U. process results (7C.18)–(7C.20).

8. SMOOTHED SQUARE-LAW RESPONSE

If a nonlinear device produces an output signal $\mathbf{b}$ that is nonlinearly related to the corresponding input signal $\mathbf{a}$ at the same instant of time then the probability distribution of the output is immediately determined by that of the input through the nonlinear transformation, e.g.,

$$P_{\text{out}}(\mathbf{b}'t'\mid\mathbf{b}t)d\mathbf{b}'=P_{\text{in}}(\mathbf{a}'t'\mid\mathbf{a}t)d\mathbf{a}'$$

or

$$P_{\text{out}}(\mathbf{b}',t'\mid\mathbf{b}t)=P_{\text{in}}(\mathbf{a}'(\mathbf{b}'),t'\mid\mathbf{a}(\mathbf{b}),t)J(\mathbf{a}'/\mathbf{b}'), \quad (8.1)$$

where $\mathbf{a}=\mathbf{a}(\mathbf{b})$ is the inverse of the nonlinear transformation $\mathbf{b}=\mathbf{b}(\mathbf{a})$ performed by the device and $J(\mathbf{a}'/\mathbf{b}')$ is the Jacobian of this (inverse) transformation.

A much more complicated problem arises if a time-smoothing operation is then performed on the output signal, since the new random variable is then a function of the original variables at many (a continuum of) time points. It is simplest to deal with the nonlinearity and time smoothing together. For example, we might be interested in the statistical behavior of

$$S=\int^t k(t-s)V(\mathbf{a}(s))\,ds \quad (8.2)$$

which we can ascertain by investigating $\langle\exp(-\lambda S)\rangle$. The procedure for solving such a problem is already given by (6.18) with $Q(\mathbf{a},s)=\lambda k(t-s)V(\mathbf{a})$ with λ regarded as a parameter. To have a specific problem in mind, let us attempt to evaluate

$$M_0=\left\langle\exp\left[i\int_{t_0}^t\mathbf{q}(s)\mathbf{a}(s)\,ds\right]\right.$$
$$\left.\times\exp\left[-\lambda\int_{t_0}^t\mathbf{a}(s)\cdot\mathbf{k}(t-s)\cdot\mathbf{a}(s)\,ds\right]\right\rangle. \quad (8.3)$$

With $\mathbf{q}=0$, our nonlinear device is "square law," but with $\mathbf{q}\neq0$ it is a general quadratic device. Moreover $\mathbf{k}$ is a matrix that combines different components of $\mathbf{a}$.

Forward-Equation Method

If the original random process is described by the function $L(\mathbf{y},\mathbf{a},t)$ of (6.13) then we must solve the problem

$$\frac{\partial\hat{\phi}}{\partial s}=\mathbf{q}\cdot\frac{\partial\hat{\phi}}{\partial\mathbf{y}}+\lambda\frac{\partial}{\partial\mathbf{y}}\cdot\mathbf{k}(t-s)\cdot\frac{\partial\hat{\phi}}{\partial\mathbf{y}}-L\left(\mathbf{y},-i\frac{\partial}{\partial\mathbf{y}},s\right)\hat{\phi}, \quad (8.4)$$

where

$$\hat{\phi}=\hat{\phi}(\mathbf{y},s)=\hat{\phi}(\mathbf{y},s,t) \quad (8.5)$$

depends on t as a parameter, and our desired result is

$$M_0=\phi(0,t,t), \quad (8.6)$$
$$\hat{\phi}(\mathbf{y},t_0,t)=\exp(i\mathbf{y}\cdot\mathbf{a}_0). \quad (8.7)$$

A subsequent average over the equilibrium distribution of $\mathbf{a}_0$ can be performed if desired.

For homogeneous noise with linear decay (Sec. 7F) our equation simplifies to

$$\frac{\partial\hat{\phi}}{\partial s}=(\mathbf{q}-\mathbf{y}\cdot\mathbf{\Lambda})\frac{\partial\hat{\phi}}{\partial\mathbf{y}}+\lambda\frac{\partial}{\partial\mathbf{y}}\cdot\mathbf{k}\cdot\frac{\partial\hat{\phi}}{\partial\mathbf{y}}-K(\mathbf{y},s)\hat{\phi}. \quad (8.8)$$

This is equivalent to solving the Schrödinger equation for a (multidimensional) oscillator with time-varying mass moving in an arbitrary potential $K(\mathbf{y})$. Exact solutions are, of course, only possible with selected forms of the potential. The most important case, corresponding to *Gaussian noise* is

$$K(\mathbf{y},s)=\mathbf{y}\cdot\mathbf{D}\cdot\mathbf{y}, \quad (8.9)$$

i.e., the Ornstein–Uhlenbeck process.

CC-0. In Public Domain. Gurukul Kangri Collection, Haridwar

Digitized by Arya Samaj Foundation Chennai and eGangotri

We now make the *ansatz*

$$\hat{\phi}=[X(s)]^{-\frac{1}{2}}\exp\{-[\mathbf{y}\cdot\mathbf{C}(s)\cdot\mathbf{y}+\mathbf{B}(s)\cdot\mathbf{y}]\}, \quad (8.10)$$

subject to the initial conditions

$$X(0)=1, \qquad \mathbf{C}(0)=0, \qquad \mathbf{B}(0)=-i\mathbf{a}_0. \quad (8.11)$$

Remembering that $X(s)=X(s,t)$ depends on t as a parameter, our answer is determined once we know X:

$$M_0=[X(t,t)]^{-\frac{1}{2}}, \quad (8.12)$$

and X, $\mathbf{B}$, and $\mathbf{C}$ are determined by

$$\begin{aligned} X^{-1}dX/ds&=4\lambda\,\mathrm{Tr}\,(\mathbf{k}\cdot\mathbf{C})+2\mathbf{q}\cdot\mathbf{B}-2\lambda\mathbf{B}\cdot\mathbf{k}\cdot\mathbf{B},\\ d\mathbf{B}/ds&=2\mathbf{q}\cdot\mathbf{C}-(\mathbf{\Lambda}+4\lambda\mathbf{k}\cdot\mathbf{C})\mathbf{B},\\ d\mathbf{C}/ds&=-[\mathbf{\Lambda}\cdot\mathbf{C}+\mathbf{C}\cdot\mathbf{\Lambda}^{\dagger}]-4\lambda\mathbf{C}\cdot\mathbf{k}\cdot\mathbf{C}+\mathbf{D}, \end{aligned} \quad (8.13)$$

where $\mathbf{\Lambda}^{\dagger}$ is the transpose of $\mathbf{\Lambda}$. These equations are valid even for the nonstationary case in which $\mathbf{\Lambda}$ and $\mathbf{D}$ depend explicitly on s. For the remainder of this section, we restrict ourselves to the stationary case, however.

The equations for $\mathbf{C}$ (a set of coupled Riccati equations) are not coupled to those for $\mathbf{B}$ and X. Thus these equations must be solved first. The equations for $\mathbf{B}$ and X can then be integrated immediately. To illustrate the procedure, we shall develop in detail the solution for the *one-dimensional case*—a not entirely trivial problem.

The transformation

$$4\lambda kC=Y'/Y \quad (8.14)$$

reduces

$$dC/ds=D-2\Lambda C-4\lambda k\cdot C^2 \quad (8.15)$$

to the simple form

$$Y''+[2\Lambda-(k'/k)]Y'=4\lambda DkY, \quad (8.16)$$

where primes are derivatives with respect to s and $k=k(t-s)$ is now a scalar function of s. Since the normalization of Y clearly has no effect on C, we shall take our initial conditions in the form

$$Y(t_0)=1, \qquad Y'(t_0)=0. \quad (8.17)$$

The exact solution for $B(s)$ is then given by

$$\begin{aligned} Y(s)B(s)&=-ia_0\exp[-\Lambda(s-t_0)]\\ &+2\int_{t_0}^{s}ds'\exp[-\Lambda(s-s')]q(s')C(s')Y(s')\,ds', \end{aligned} \quad (8.18)$$

and the solution for X yields our answer in the form

$$\begin{aligned} M_0=[X(t,t)]^{-\frac{1}{2}}&=[Y(t,t)]^{-\frac{1}{2}}\exp\left[-\int_{t_0}^{t}q(s)B(s)\,ds\right]\\ &\times\exp\left[\lambda\int_{t_0}^{t}k(t-s)B(s)^2\,ds\right]. \end{aligned} \quad (8.19)$$

Note that $Y^{-\frac{1}{2}}$ is already the solution to the square-law problem ($q=0$) with the initial condition $\mathbf{a}_0=0$. If $q=0$, but $a_0\neq 0$, we have

$$M_0=[Y(t,t)]^{-\frac{1}{2}}\exp[-R(t)a_0^2], \quad (8.20)$$

$$R(t)=\lambda\int_{t_0}^{t}k(t-s)\exp[-2\Lambda(s-t_0)]\,ds/[Y(s,t)]^2. \quad (8.21)$$

[As a check on our arithmetic, we set $\lambda=0$ and $Y=1$ in (8.15), (8.18), and (8.19) to obtain

$$\begin{aligned} &\left\langle\exp i\int_{t_0}^{t}q(s)a(s)\,ds\right\rangle\\ &=\exp\left[i\int_{t_0}^{t}q(s)\,ds a_0\exp[-\Lambda(s-t_0)]\right]\\ &\times\exp\left\{-\frac{D}{\Lambda}\int_{t_0}^{t}\int_{t_0}^{t}q(s)q(s')\{\exp[-\Lambda(s-s')]\right.\\ &\left.-\exp[\Lambda(2t_0-s-s')]\}\,ds\,ds'\right\}, \end{aligned} \quad (8.22)$$

a result which may be compared with (7F.21) on setting $K=Dy^2$ in the latter.]

For the special case of exponential smoothing $k(t-s)=\exp[-2\beta(t-s)]$ Eq. (8.16) for $Y(s,t)$ can be solved exactly. Indeed, our first calculations were performed in this way. But we were not always able to perform the integration in (8.21) to obtain $R(t)$. Moreover, the procedure was cumbersome because one solves for $Y(s,t)$ when one is only interested in $Y(t,t)\equiv Y(t)$. Both of these difficulties are immediately removed by the use of the backward Eq. (5.22) since that procedure leads directly to an equation for the desired object $Y(t)\equiv Y(t,t)$ and moreover, we shall show that

$$R(t)=(4D)^{-1}Y'(t)/Y(t). \quad (8.23)$$

Backward-Equation Method

According to (4.8), $M_0(t,t_0)$ can be obtained by integrating $\hat{P}(\mathbf{a}t\,|\,\mathbf{a}_0t_0)$ over $\mathbf{a}$. Since $\mathbf{a}$ is only a parameter in the backward Eq. (5.21), we may integrate this equation over $\mathbf{a}$ without changing its form:

$$\begin{aligned} \frac{\partial M_0(\mathbf{a}_0,t,t_0)}{\partial t_0}&=[Q(\mathbf{a}_0,t-t_0)\\ &-\sum_{n=1}^{\infty}\mathbf{D}_n(\mathbf{a}_0,t_0):(\partial/\partial\mathbf{a}_0)^n]M_0. \end{aligned} \quad (8.24)$$

For the case of time-independent transition probabilities $\mathbf{D}_n(\mathbf{a}_0,t_0)=\mathbf{D}_n)\mathbf{a}_0)$, we expect that $M_0=M_0(\mathbf{a}_0,u)$

CC-0. In Public Domain. Gurukul Kangri Collection, Haridwar

Digitized by Arya Samaj Foundation Chennai and eGangotri

where $u=t-t_0$ and

$$-\frac{\partial M_0(\mathbf{a}_0,u)}{\partial u}=\left[Q(\mathbf{a}_0,u)-\sum_{n=1}^{\infty}\mathbf{D}_n(\mathbf{a}_0):\left(\frac{\partial}{\partial \mathbf{a}_0}\right)^n\right]M_0. \tag{8.25}$$

For a (multidimensional) Ornstein–Uhlenbeck process

$$-\frac{\partial M_0}{\partial u}=\left[Q(\mathbf{a}_0,u)+(\mathbf{\Lambda a}_0)\cdot\frac{\partial}{\partial \mathbf{a}_0}-\frac{\partial}{\partial \mathbf{a}_0}\cdot\mathbf{D}\cdot\frac{\partial}{\partial \mathbf{a}_0}\right]M_0. \tag{8.26}$$

If, moreover, we are concerned with the average

$$M_0=\left\langle \exp i\int_{t_0}^{t}\mathbf{q}(t-s)\cdot\mathbf{a}(s)\,ds \times\exp-\lambda\int_{t_0}^{t}\mathbf{a}(s)\cdot\mathbf{k}(t-s)\cdot\mathbf{a}(s)\,ds\right\rangle, \tag{8.27}$$

then comparing with (5.20) and (5.21),

$$Q(\mathbf{a}_0,u)=-i\mathbf{q}(u)\cdot\mathbf{a}_0+\lambda\mathbf{a}_0\cdot\mathbf{k}(u)\cdot\mathbf{a}_0. \tag{8.28}$$

We can now assume a solution of the form

$$M_0(\mathbf{a}_0,u)=[Y(u)]^{-\frac{1}{2}}\exp\left[-\mathbf{a}_0\cdot\mathbf{R}(u)\cdot\mathbf{a}_0-\mathbf{S}(u)\cdot\mathbf{a}_0\right], \tag{8.29}$$

explicitly displaying the $\mathbf{a}_0$ dependence. The coefficients then obey

$$Y'(u)/Y(u)=4\mathbf{R}(u):\mathbf{D}+\mathbf{S}(u)\cdot\mathbf{D}\cdot\mathbf{S}(u), \tag{8.30}$$

$$\mathbf{S}'(u)=\mathbf{S}\cdot[\mathbf{\Lambda}-4\mathbf{D}\cdot\mathbf{R}]-\mathbf{q}(u), \tag{8.31}$$

$$\mathbf{R}'(u)=\lambda\mathbf{k}(u)-4\mathbf{R}\cdot\mathbf{D}\cdot\mathbf{R}-(\mathbf{R}\cdot\mathbf{\Lambda}+\mathbf{\Lambda}^{\dagger}\cdot\mathbf{R}), \tag{8.32}$$

where $\mathbf{\Lambda}^{\dagger}$ is the transpose of $\mathbf{\Lambda}$. Thus $\mathbf{S}$ is expressible in terms of $\mathbf{R}$ using (7F.7), (7F.13):

$$\mathbf{S}(u)=-\int_0^u\mathbf{q}(u')\,du' \times T_{-}\exp\int_{u'}^{u}ds\,[\mathbf{\Lambda}-4\mathbf{D}\cdot\mathbf{R}(s)] \tag{8.33}$$

and Y can be obtained if both $\mathbf{S}$ and $\mathbf{R}$ are known:

$$Y(u)=\exp 4\int_0^u\mathbf{R}(u'):\mathbf{D}\,du'\exp\int_0^u\mathbf{S}(u')\cdot\mathbf{D}\cdot\mathbf{S}(u')\,du'. \tag{8.34}$$

The problem is thus reduced to obtaining $\mathbf{R}$ by solving Eq. (8.32) which is an equation for $\mathbf{R}$ alone.

It is easier to solve for $\mathbf{R}$ if we transform to new coordinates

$$\mathbf{a}_0=\mathbf{U}\cdot\mathbf{b}_0; \tag{8.35}$$

$$\mathbf{a}_0\cdot\mathbf{R}\cdot\mathbf{a}_0=\mathbf{b}_0\cdot\mathbf{V}\cdot\mathbf{b}_0, \qquad \mathbf{R}=\mathbf{U}^{\dagger}\mathbf{V}\mathbf{U}; \tag{8.36}$$

$$\mathbf{R}\cdot\mathbf{D}\cdot\mathbf{R}=\mathbf{U}^{\dagger}\mathbf{V}\mathbf{U}\mathbf{D}\mathbf{U}^{\dagger}\mathbf{V}\mathbf{U}; \tag{8.37}$$

in such a way that the new $\mathbf{D}$ is proportional to the unit matrix

$$\mathbf{D}'=\mathbf{U}\cdot\mathbf{D}\cdot\mathbf{U}^{\dagger}=\tfrac{1}{4}\mathbf{1}, \tag{8.38}$$

which is accomplished by the choice

$$\mathbf{U}=\tfrac{1}{2}(\mathbf{D})^{-\frac{1}{2}}=\mathbf{U}^{\dagger}, \tag{8.39}$$

where the symmetric (inverse) square root is understood ($\mathbf{U}^{\dagger}$ is the transpose of $\mathbf{U}$). Then

$$d\mathbf{V}/du=\mathbf{K}+\mathbf{\Gamma}^{\dagger}\mathbf{\Gamma}-(\mathbf{V}+\mathbf{\Gamma}^{\dagger})\cdot(\mathbf{V}+\mathbf{\Gamma}); \tag{8.40}$$

$$\mathbf{K}=(\mathbf{U}^{\dagger})^{-1}\cdot\lambda\mathbf{k}\cdot\mathbf{U}^{-1}; \tag{8.41}$$

$$\mathbf{\Gamma}=\mathbf{U}\cdot\mathbf{\Lambda}\cdot\mathbf{U}^{-1},$$

$$\mathbf{\Gamma}^{\dagger}=(\mathbf{U}^{\dagger})^{-1}\cdot\mathbf{\Lambda}^{\dagger}\cdot\mathbf{U}^{\dagger}. \tag{8.42}$$

The further transformation

$$\mathbf{V}=\mathbf{Z}^{-1}\cdot d\mathbf{Z}/du-\mathbf{\Gamma}^{\dagger} \tag{8.43}$$

transforms our coupled Riccati equations into a set of linear (coupled) second-order differential equations:

$$d^2\mathbf{Z}/du^2+(d\mathbf{Z}/du)(\mathbf{\Gamma}-\mathbf{\Gamma}^{\dagger})=\mathbf{Z}\cdot(\mathbf{K}+\mathbf{\Gamma}^{\dagger}\mathbf{\Gamma}). \tag{8.44}$$

Equation (8.34) can now be simplified to

$$Y(u)=\exp\int_0^u[\mathrm{Tr}\,\mathbf{V}(u')]\,du' \times\exp\int_0^u\mathbf{S}(u')\cdot\mathbf{D}\cdot\mathbf{S}(u')\,du'. \tag{8.45}$$

The initial condition $M_0(\mathbf{a}_0,0)=1$ implies

$$\mathbf{R}(0)=\mathbf{S}(0)=Y'(0)=0, \qquad Y(0)=1. \tag{8.46}$$

For the *one-dimensional case* our equations reduce to

$$dR/du=\lambda k(u)-2\Lambda R-4R^2D, \tag{8.47}$$

$$dV/du=4\lambda Dk(u)-2\Lambda V-V^2, \tag{8.48}$$

$$d^2Z/du^2=[4\lambda Dk(-u)+\Lambda^2]Z(u), \tag{8.49}$$

$$4DR(u)=V(u)=Z^{-1}dZ/du-\Lambda,$$

$$Y(u)=\exp(-\Lambda u)Z(u)\exp D\int_0^u[S(u')]^2\,du'. \tag{8.50}$$

The combination $Z\exp(-\Lambda u)$ obeys the simple equation

$$[Z\exp(-\Lambda u)]''+2\Lambda[Z\exp(-\Lambda u)]' =4\lambda Dk(u)[Z\exp(-\Lambda u)]$$

For the case in which $q=S=0$, we can write this as

$$Y''(u)+2\Lambda Y'(u)=4\lambda Dk(u)Y(u), \tag{8.51}$$

$$4DR(u)=Y'(u)/Y(u).$$

CC-0. In Public Domain. Gurukul Kangri Collection, Haridwar

Digitized by Arya Samaj Foundation Chennai and eGangotri

Exponential smoothing then leads to the differential equation

$$Y''(u)+2\Lambda Y'(u)=4\lambda D\exp(-2\beta u)\,Y(u), \quad (8.54)$$

an equation similar to but not identical to Eq. (8.10) obeyed by $Y(s,t)$. Our initial conditions are:

$$Y(0)=1, \qquad Y'(0)=0 \quad (8.55)$$

Case 1. $\Lambda=\beta=0$, *Linearly Smoothed, Squared Weiner Process*

$$Y''(u)=4\lambda DY(u), \quad (8.56)$$

$$Y(u)=\cosh\left[(4\lambda D)^{\frac{1}{2}}u\right], \quad (8.57)$$

$$R(u)=(4D)^{-1}(4\lambda D)^{\frac{1}{2}}\tanh\left[(4\lambda D)^{\frac{1}{2}}u\right], \quad (8.58)$$

$$M_0=\left\langle \exp\left[-\lambda\int_{t_0}^{t}a(s)^2\,ds\right]\right\rangle = M_0(t-t_0),$$

$$M_0(u)=\cosh\left[(4\lambda D)^{\frac{1}{2}}u\right]$$

$$\times\exp\left\{-\lambda a_0^2(4\lambda D)^{-\frac{1}{2}}\tanh\left[(4\lambda D)^{\frac{1}{2}}u\right]\right\}, \quad (8.59)$$

with $u=t-t_0$. Thus we find that as $u=t-t_0\to\infty$, $Y(u)$ continues to depend on u, i.e., our output random variable never becomes stationary. Moreover, $R(u)$ does not vanish as $u\to\infty$, so that *memory of* a_0 *is retained forever*. Cameron and Martin,[20] have previously evaluated $M_0(a)$ for this special case by nontrivial path integral techniques.

Case 2. $\beta=0$, $\Lambda\neq 0$, *Linearly Smoothed Squared O.U. Process*

$$Y''+2\Lambda Y=4\lambda DY, \quad (8.60)$$

$$Y(u)=(2\Gamma)^{-1}\exp(-\Lambda u)\left[(\Gamma+\Lambda)\exp(\Gamma u)+(\Gamma-\Lambda)\exp(-\Gamma u)\right],$$

$$=\Gamma^{-1}(4\lambda D)^{\frac{1}{2}}e^{-\Lambda u}\cosh(\Gamma u+\theta], \quad (8.61)$$

where

$$\Gamma=(\Lambda^2+4\lambda D)^{\frac{1}{2}},$$

$$e^{\theta}=(\Gamma+\Lambda)/(\Gamma^2-\Lambda^2)^{\frac{1}{2}},$$

$$\tanh\theta=\Lambda/\Gamma,$$

$$R(u)=(4D)^{-1}Y'/Y=\Gamma\left[\tanh(\Gamma u+\theta)-(\Lambda/\Gamma)\right], \quad (8.62)$$

$$M_0(u)=\left[Y(u)\right]^{-\frac{1}{2}}$$

$$\times\exp\left\{-\lambda a_0^2(\Gamma/4\lambda D)\left[\tanh(\Gamma u+\theta)-\tanh\theta\right]\right\}. \quad (8.63)$$

Thus the linearly smoothed squared O.U. process remains nonstationary as $u=t-t_0\to\infty$, and moreover it always remembers the starting value $a(t_0)=a_0$ even though the O.U. process with $\Lambda>0$ has a built in mechanism for forgetting this value.

Case 3. $\beta\neq 0$, $\Lambda\neq 0$, *Exponentially Smoothed O.U. Process*

$$Y''+2\Lambda Y'=4\lambda D\exp(-2\beta u)\,Y. \quad (8.64)$$

Let

$$x=\left[4\lambda D/\beta^2\right]^{\frac{1}{2}}e^{-\beta u}, \qquad \frac{d}{du}=\frac{dx}{du}\frac{d}{dx}=-\beta x\frac{d}{dx}, \quad (8.65)$$

$$\frac{d^2Y}{dx^2}+\frac{1-2p}{x}\frac{dY}{dx}-Y=0, \qquad p\equiv\Lambda/\beta, \quad (8.66)$$

from which we can conclude[33]

$$Y=x^p\left[AI_p(x)+BK_p(x)\right],$$

where I_p and K_p are the modified Bessel functions. With $x_0=\left[4\lambda D/\beta^2\right]$, we can make $dY/dx=0$ at $u=0$, i.e., $x=x_0$ by choosing

$$Y(x)=C\{-(d/dx_0)\left[x_0^pK_p(x_0)\right]x^pI_p(x)+(d/dx_0)\left[x_0^pI_p(x_0)\right]x^pK_p(x)\}$$

$$=Cx_0^{p-1}x^p\left[K_{p-1}(x_0)I_p(x)+I_{p-1}(x_0)K_p(x)\right],$$

where we have used the relations[33]

$$(x^{-1}\,d/dx)^m x^pI_p(x)=x^{p-m}I_{p-m}(x),$$

$$(x^{-1}\,d/dx)^m x^pK_p(x)=(-1)^m x^{p-m}K_{p-m}(x), \quad (8.67)$$

for $m=1$. If we make use of the Wronskian relation[33]

$$K_{p-1}(x)I_p(x)+I_{p-1}(x)K_p(x)=1/x, \quad (8.68)$$

we can obey the initial condition $Y=1$ when $u=0$ or $x=x_0$ by setting $C=x_0^{2(1-p)}$ to get

$$Y(x)=x_0(x/x_0)^p\left[K_{p-1}(x_0)I_p(x)+I_{p-1}(x_0)K_p(x)\right]. \quad (8.69)$$

Using (8.53), (8.65), and (8.67), we obtain

$$4DR(u)=\beta x^2\frac{I_{p-1}(x_0)x^{p-1}K_{p-1}(x)-K_{p-1}(x_0)x^{p-1}I_{p-1}(x)}{I_{p-1}(x_0)x^pK_p(x)+K_{p-1}(x_0)x^pI_p(x)}. \quad (8.70)$$

---

[33] I. M. Ryshik and I. S. Gradstein, *Tables of Series, Products and Integrals* (Plenum Press, New York and VEB Deutscher Verlag der Wissenschaften, Berlin, 1963), p. 329, formula 6; E. Jahnke and F. Emde, *Tables of Functions* (Dover Publications, Inc., New York, 1943), Sec. VIII.7. G. M. Watson, *Bessel Functions* (Cambridge University Press, Cambridge, England, 1948), 2nd ed.

CC-0. In Public Domain. Gurukul Kangri Collection, Haridwar

Digitized by Arya Samaj Foundation Chennai and eGangotri

The exact relations[33]

$$K_p(x) = (\pi/2 \sin p\pi)[I_{-p}(x) - I_p(x)], \quad (8.71)$$

$$\Gamma(p)\Gamma(1-p) = (\pi/\sin p\pi), \quad (8.72)$$

and the behavior[34] as $u\to\infty$ or $x\to 0$:

$$I_p(x) \underset{x\to 0}{\to} [\Gamma(1+p)]^{-1}(x/2)^p[1+(p+1)^{-1}(x/2)^2+\cdots] \quad (8.73)$$

yields the asymptotic behavior

$$Y(x) \underset{x\to 0}{\to} \Gamma(p)(2/x_0)^{p-1} I_{p-1}(x_0) \times \{1+(1-p)^{-1}(x/2)^2 - (1-p)^{-1}\Gamma(2-p)(x/2)^{2p}[\Gamma(1+p)]^{-1} + 2(x/2)^{2p} K_{p-1}(x_0)/[I_{p-1}(x_0)\Gamma(1+p)\Gamma(p)]\}. \quad (8.74)$$

Thus as $u\to\infty$, Y achieves the *stationary value*

$$Y(u=\infty) = \Gamma(p)(2/x_0)^{p-1} I_{p-1}(x_0) \quad (8.75)$$

and $R(u)$ approaches zero rapidly:

$$4DR(u) = Y'(u)/Y(u) = 2\lambda D(\Lambda-\beta)^{-1}\exp(-2\beta u) - 2(\Lambda/\beta)(\Lambda-\beta)^{-1}\Gamma(2-p)(\lambda D/\beta^2)^{\Lambda/\beta}\exp(-2\Lambda u)/\Gamma(1+p) - 4\Lambda K_{p-1}(x_0)(\lambda D/\beta^2)^{\Lambda/\beta}\exp(-2\Lambda u)/[I_{p-1}(x_0)\Gamma(1+p)\Gamma(p)], \quad (8.76)$$

showing that the smoothed O.U. process rapidly forgets a_0, i.e., M_0 becomes truly stationary! This stationary result is what will be observed experimentally, since the duration of the measurement is usually large compared to $1/\beta$ or $1/\Lambda$.

Case 4. $\beta\neq 0$, $\Lambda=0$, *Exponentially Smoothed Weiner Process*

Since we have allowed $\Lambda u\to\infty$ in the asymptotic formula (8.76), this result can not be applied to the $\Lambda=0$ case. We can, however, set $p=\Lambda/\beta=0$ in (8.69) or (8.70), to obtain

$$Y(x) = x_0[K_1(x_0)I_0(x) + I_1(x_0)K_0(x)], \quad (8.77)$$

$$4DR = \beta x[I_1(x_0)K_1(x) - K_1(x_0)I_1(x)]/[I_1(x_0)K_0(x) + K_1(x_0)I_1(x)]. \quad (8.78)$$

The behavior as $x\to 0$

$$xK_1(x)\to 1, \qquad K_0(x) = -\ln(x/2), \quad (8.79)$$

leads to the asymptotic ($u\to\infty$) behavior

$$Y(u) \underset{u\to\infty}{\to} x_0 I_1(x_0)(u+\tau), \quad (8.80)$$

$$4DR(u) \to (u+\tau)^{-1}, \quad (8.81)$$

where

$$\tau = \beta^{-1}\{[K_1(x_0)/I_1(x_0)] - \tfrac{1}{2}\ln(\lambda D/\beta^2)\}. \quad (8.82)$$

Thus Y does not become stationary, and R vanishes very slowly as $u\to\infty$.

Case 5. Arbitrary Positive Smoothing Function $k(s-t)$

Let us summarize our results in the form

$$M_0(t-t_0) = \left\langle \exp\left[-\lambda\int_{t_0}^{t} k(t-s)\,a(s)^2\,ds\right]\right\rangle \quad (8.83)$$

$$= [Y(t-t_0)]^{-\frac{1}{2}}\exp[-a_0^2 R(t-t_0)], \quad (8.84)$$

$$Y(t-t_0) = \exp\left[4D\int_0^{t-t_0} R(u)\,du\right]. \quad (8.85)$$

Stationarity properties of M_0 can then be stated as follows:

M_0 becomes independent of a_0 if $\lim_{u\to\infty} R(u) = 0$ (8.86)

$$Y(t-t_0) \underset{t_0\to -\infty}{\longrightarrow} \text{constant} \quad \text{if} \quad \int_0^\infty R(u)\,du < \infty. \quad (8.87)$$

We see immediately that the second condition can be obeyed ($Y\to$constant) only if the first is obeyed (M_0 independent of a_0); but the converse is not necessarily true, since $R(u)$ may fall off too slowly for the integral to be convergent [as in (8.81)]. A necessary condition for $R(\infty)$ to vanish is $k(\infty)=0$, but this condition is not sufficient, since the equation

$$dR/du = -2\Lambda R - 4DR^2 \quad (8.88)$$

admits two special solutions $R=0$ and $R=-(\Lambda/2D)$. The first of these solutions is stable, but the second can readily be shown to be unstable. If one ever arrived at $R<-(\Lambda/2D)$, one would find a runaway solution $R\to-\infty$. We shall now show that $k(u)>0$ is sufficient to prevent such runaway solutions. Since most smoothing functions obey $k>0$, and we have not found the *necessary* condition on k to prevent

[34] This special case is worked out by Deutsch, Ref. 4 Chap. 7, using forward equation techniques.

CC-0. In Public Domain. Gurukul Kangri Collection, Haridwar

Digitized by Arya Samaj Foundation Chennai and eGangotri

runaway solutions, we shall suppose $k>0$ in all that follows.

Since $k(0)>0$, dR/du is positive at $u=0$, so that R increases from zero and achieves a positive value. Thenceforth, R can never become negative, for if R were to become zero at $u=u_1$, we would have $dR/du_1=\lambda k(u_1)>0$. Moreover, if $k\to 0$ as $u\to\infty$ then R must likewise approach zero, for if R remains larger than (say) $R_1>0$, then for sufficiently large u, dR/du would become negative and lead to a contradiction. The same argument essentially tells us that the condition $k\to 0$ is necessary as well as sufficient for $R(u)$ to vanish as $u\to\infty$, i.e., for M_0 in (8.83) to "forget" a_0^2. A similar argument tells us that if $k\to$constant as $a\to\infty$ then R must also approach a constant, which explains the results in Cases 1 and 2 above.

We must next investigate (8.87), i.e., whether $R(u)$ is integrable. We shall first show that if $\Lambda>0$, R is integrable if and only if k is integrable. Integrate Eq. (8.47) for R from $u=0$ to $u=\infty$ to obtain

$$2\Lambda\int_0^\infty R(u)\,du+4D\int_0^\infty R^2(u)\,du=\lambda\int_0^\infty k(u)\,du-R(\infty). \tag{8.89}$$

Suppose now, that k is integrable, then

$$R(\infty)<\lambda\int_0^\infty k(u)\,du<\infty.$$

Thus the right-hand side of (8.89) is finite, and each of the positive integrals on the left-hand side must converge.

Suppose now that the integral of k diverges. We shall show that the integral of R diverges by proving that

$$Y=\exp\left[4D\int_0^t R\,du\right]$$

cannot approach a constant. Integration of Eq. (8.52) yields

$$dY/dt+2\Lambda Y=2\Lambda+4\lambda D\int_0^t k(u)\,Y(u)\,du. \tag{8.90}$$

If $Y(u)\to$constant as $u\to\infty$, the right-hand side diverges, which forces dY/dt to diverge and contradicts the possibility of Y remaining finite when $\int k\,du$ diverges.

We shall now show that for $\Lambda=0$, R is never integrable. The transformation

$$R=[4Du+T]^{-1} \tag{8.91}$$

yields

$$dT/du=-\lambda k(4Du+T)^2. \tag{8.92}$$

Thus T is a monotonic decreasing function of u. For $u>u_1$, $T(u)<T(u_1)$ and

$$R(u)\geq[4Du+T(u_1)]^{-1}. \tag{8.93}$$

Thus $R(u)$ is not integrable. Our results may be summarized in the

Asymptotic Theorem: *Within the class of positive smoothing functions* $k(t-s)$, *the average*

$$M_0=\left\langle \exp\left[-\lambda\int_{t_0}^t k(t-s)\,a(s)^2\,ds\right]\right\rangle$$

[*where* $a(s)$ *is an Ornstein–Uhlenbeck process subject to* $a(t_0)=a_0$] *becomes independent of* a_0 *as* $t-t_0\to\infty$ *if and only if* $k(u)\to 0$ *as* $u\to\infty$, *and* M_0 *becomes independent of the time in this limit, if and only if* $\Lambda\neq 0$ (the *O.U. process does not reduce to a Weiner process*) *and the integral*

$$\int_0^\infty k(u)\,du<\infty$$

converges.

CC-0. In Public Domain. Gurukul Kangri Collection, Haridwar

Digitized by Arya Samaj Foundation Chennai and eGangotri

Thermal Diffusion in Isotopic Gas Mixtures and Intermolecular Forces

S. C. SAXENA, B. P. MATHUR
Department of Physics, University of Rajasthan, Jaipur, India

Available thermal diffusion data on He, Ne, Ar, Kr, Xe, H_2, N_2, O_2, CO, CH_4, NH_3, HCl of different workers have been discussed. This study has revealed the need and nature of the additional measurements which will be useful and is thus of help in planning new experiments. The problems of temperature assignment and composition dependence of the thermal diffusion factor α_T are examined. The adequacy of the theoretical α_T expression used while interpreting the experimental results is also given proper consideration. Comparison of the experimental data are made with the predictions of the rigorous Chapman–Enskog kinetic theory in conjunction with the three spherically symmetric potentials (Lennard-Jones 12–6, modified Buckingham exp-6, and Morse) for nonpolar gases, while a Stockmayer type 12-6-3 potential for polar gases. Reasonably satisfactory agreement is obtained even for polyatomic gases. The extent to which Chapman-Enskog theory in conjucntion with central force-field models may be expected to hold for polyatomic gases is investigated. The up-to-date knowledge of the kinetic theory which takes into consideration inelastic molecular collisions is reviewed.

I. INTRODUCTION

There have been many attempts in recent years to understand the phenomenon of thermal diffusion both theoretically and experimentally. These efforts primarily arose because of the large sensitivity of the thermal diffusion factor α_T to the nature of intermolecular forces and the importance of its knowledge in the design of thermal diffusion columns for separation purposes. Saxena and Mathur[1] and Saxena and Joshi[2] have recently given the status of our knowledge of the thermal diffusion of binary gas mixtures and the interesting results derived therefrom regarding the force-field between different molecules. This article examines the available α_T data on isotopic mixtures.

The formulation of the rigorous theory of thermal diffusion in gases was given by Chapman,[3] and its adequate description is given in the book of Chapman and Cowling.[4] In this work only the first approximation to α_T, $[\alpha_T]_1$, was discussed but since then Mason[5] and Saxena and Srivastava[6] have extended this work to include second as well as third approximations. These formulas, which are derived according to an approximation procedure described in detail by Chapman and Cowling,[4] will be referred after these authors. Kihara[7] and later Mason[5] developed another procedure for simplifying the infinite determinants which occur in α_T and gave a set of formulas which will be referred after these workers. All these expressions which are essentially for binary gas mixtures are considerably simplified for isotopic mixtures. However, for each isotope one has to choose the right expression for α_T to be able to interpret the experimental results with reliance. This point is discussed here at length when we consider the data on individual isotopes.

For either interpretation or computation of α_T from the rigorous expressions one needs the knowledge of the form of intermolecular potential. We consider in detail the L-J (12–6) and exp-6 potentials but also discuss for a few systems the Morse potential, recently introduced. These potentials can be written explicitly in terms of the potential parameters and the separation between the molecules. If $\phi(r)$ refer to the interaction potential energy between two molecules at a separation distance r then according to the L-J (12–6) potential

$$\phi(r) = 4\epsilon[(\sigma_0/r)^{12} - (\sigma_0/r)^6], \tag{1}$$

for the modified Buckingham exp-6 potential,[5]

$$\phi(r) = [\epsilon\alpha/(\alpha-6)] \times [(6/\alpha)\exp\{\alpha[1-(r/\sigma_m)]\} - (\sigma_m/r)^6], \tag{2}$$

and for the Morse potential,[9]

$$\phi(r) = \epsilon\{\exp\{-2(c/\sigma_0)(r-\sigma_m)\} - 2 \times \exp[-(c/\sigma_0)(r-\sigma_m)]\}. \tag{3}$$

Here ϵ is the depth of the potential energy minimum and is equal to the maximum attractive energy which occurs at $r=\sigma_m$, σ_m, and σ_0 are the finite values of r for which $\phi(r)$ is minimum and zero, respectively, α is a parameter which measures the steepness of the repulsive limb, and c is also a similar parameter which controls the curvature at the minimum also.

[1] S. C. Saxena and B. P. Mathur, Rev. Mod. Phys. **37**, 316 (1965).
[2] S. C. Saxena and R. K. Joshi, J. Sci. Ind. Res. (to be published).
[3] S. Chapman, Phil. Trans. Roy. Soc. (London) **A211**, 433 (1912); **A216**, 279 (1916); **A217**, 115 (1917); Proc. Roy. Soc. (London) **A93**, 1 (1916), **A177**, 38 (1941).
[4] S. Chapman and T. G. Cowling, *The Mathematical Theory of Nonuniform Gases* (Cambridge University Press, New York, 1952), 2nd ed.
[5] E. A. Mason, J. Chem. Phys. **22**, 169 (1954); **27**, 75, 782 (1957).
[6] S. C. Saxena and B. N. Srivastava, J. Chem. Phys. **23**, 1571 (1955); S. C. Saxena, *ibid.* **24**, 1209 (1956).
[7] T. Kihara, *Imperfect Gases* (Asakura Bookstore, Tokyo, Japan, 1949) (English transl.: U.S. Office of Air Research, Wright–Patterson Air Force Base, Ohio); see also Rev. Mod. Phys. **25**, 831 (1953).
[8] J. O. Hirschfelder, C. F. Curtiss, and R. B. Bird, *Molecular Theory of Gases and Liquids* (John Wiley & Sons, Inc., New York, 1964).
[9] S. E. Lovell and J. O. Hirschfelder, University of Wisconsin Theoretical Chemistry Laboratory Report WIS-AF-21 (1952); see also D. D. Konowalow, M. H. Taylor, and J. O. Hirschfelder, Phys. Fluids **4**, 622 (1961).

CC-0. In Public Domain. Gurukul Kangri Collection, Haridwar

Digitized by Arya Samaj Foundation Chennai and eGangotri

We consider the experimental α_T data on the nonpolar gases He, Ne, Ar, Kr, Xe, H_2, N_2, O_2, CO, and CH_4 as a function of temperature and in the case of H_2 isotopes as a function of composition, also. We also review the data on the two polar gases HCl and NH_3. For nonpolar gases we have considered only the spherically symmetric potentials given by Eqs. (1)–(3) while for polar gases a Stockmayer type potential[10] recently worked out in detail by Monchick and Mason[11] is used. According to this potential[11]

$$\phi(r)=4\epsilon[(\sigma_0/r)^{12}-(\sigma_0/r)^6+\delta(\sigma_0/r)^3],$$

$$\delta=\tfrac{1}{4}\mu^{*2}\zeta(\theta_1,\theta_2,\varphi), \qquad \mu^*=\mu/(\epsilon\sigma_0^3)^{\frac{1}{2}},$$

and

$$\zeta(\theta_1,\theta_2,\varphi)=2\cos\theta_1\cos\theta_2-\sin\theta_1\sin\theta_2\cos\varphi, \quad (4)$$

where all the terms have the usual meaning.

Thus, in addition to properly pooling together the data of different workers on a particular system and then interpreting it in terms of an adequate theoretical expression in conjunction with the intermolecular potentials discussed above, the endeavor here is also to throw some light on the composition dependence of α_T and on the problem of assigning a temperature to the measured α_T value. This detailed study automatically brings to light the deficiencies of the existing α_T data and the differences between the values of different experimentalists using different techniques in certain cases. This study is thus intended not only to be just a critical review but also a source of information for planning further α_T measurements. Grew and Ibbs[12] in their excellent monograph discussed the data which were available at that time. Since then many reliable and elaborate measurements have appeared, and also, theoretical expressions which are more accurate have been derived. The calculations of α_T on potentials of Eqs. (2)–(4) have also appeared only after their work. A new method of measuring α_T using a swing separator or Trennschaukel has also since been introduced. Reliable calculations of the composition dependence are possible only now and further some success has also been achieved during these years in assigning the temperature to measured α_T value more unambiguously than before. As contrasted with the earlier work of Grew and Ibbs,[12] this article covers new information from all these view points.

II. THEORETICAL EXPRESSIONS FOR α_T

To list here all the different rigorous and approximate formulas applicable to different isotopes would be a long story which we do not attempt. An extensive critical survey is given by Saxena and Joshi.[2] These formulas are also applicable to isotopes if we incorporate the obvious simplification that molecular interactions are now identical for all the molecular species. This implies to be more specific for a binary mixture that $\epsilon_{12}=\epsilon_{11}=\epsilon_{22}$, $(\sigma_m)_{12}=(\sigma_m)_{11}=(\sigma_m)_{22}$, $(\sigma_0)_{12}=(\sigma_0)_{11}=(\sigma_0)_{22}$, $\alpha_{12}=\alpha_{11}=\alpha_{22}$, and $C_{12}=C_{11}=C_{22}$. Further, the various Chapman–Cowling collision integrals[4] $\Omega_{ij}^{(l,n)*}$ will also have the same simplification, viz. $\Omega_{ij}^{(l,n)*}=\Omega_{ii}^{(l,n)*}=\Omega_{jj}^{(l,n)*}$. For the sake of convenience in reference and interpretation of results, we quote here the pertinent formulas.

Both according to Chapman–Cowling and Kihara–Mason approximation procedures, the first approximation to α_T is given by

$$[\alpha_T]_1=(6C^*-5)(x_1S_1-x_2S_2)(x_1^2Q_1+x_2^2Q_2+x_1x_2Q_{12})^{-1}. \quad (5)$$

The terms are as defined by Saxena and Joshi.[2] The defining relations for Q_i and Q_{12} are different for the two approximation procedures. For heavy isotopes, which are characterised by a small value of the proportionate mass difference $M=(M_1-M_2)/(M_1+M_2)$, M_1 and M_2 being the molecular weights of the two components, Eq. (5) has been expanded in powers of M and on the Kihara approximation scheme to give[13]

$$[\alpha_T']_1=[\alpha_0']_1M\{1-[5-3A^*/2(2A^*-5)]M(x_1-x_2)\}, \quad (6)$$

where

$$[\alpha_0']_1=15(6C^*-5)/16A^*. \quad (7)$$

A^* and C^* are defined in Ref. 13. In Eq. (6) they[13] have neglected terms having powers of M greater than 2. Mason[5] has given the second approximation to α_T on the Kihara–Mason approximation procedure and is

$$[\alpha_T']_2=[\alpha_T]_1[1+K_1']+K_2'. \quad (8)$$

The defining relations for K_1' and K_2' are given by Mason.[5]

III. TEMPERATURE ASSIGNMENT TO THE MEASURED α_T VALUE

Even the most accurate thermal diffusion measurement has to solve the problem of temperature assignment in a unique manner before any adequate interpretation can be based on it. This evidently results from the fact that thermal diffusion measurements are done across a temperature gradient. The early practice has been to calculate the average value of α_T in the temperature range at which the two bulbs are maintained (T_1, T_2) and then calculate the corresponding temperature T_r, by the relation[14]

$$T_r=[(T_1-T_2)/T_1T_2]\ln(T_1/T_2). \quad (9)$$

[10] W. H. Stockmayer, J. Chem. Phys. **9**, 398 (1941).
[11] L. Monchick and E. A. Mason, J. Chem. Phys. **35**, 1676 (1961).
[12] K. E. Grew and T. L. Ibbs, *Thermal Diffusion in Gases* (Cambridge University Press, New York, 1952).
[13] S. C. Saxena and P. A. Pardeshi, Indian J. Phys. **35**, 55 (1961).
[14] H. Brown, Phys. Rev. **58**, 661 (1940).

CC-0. In Public Domain. Gurukul Kangri Collection, Haridwar

Digitized by Arya Samaj Foundation Chennai and eGangotri

Relation (9) implies that α_T varies as

$$\alpha_T = A - (B/T). \tag{10}$$

Srivastava and Madan[15] have used different relations than (10) for temperature assignment, viz.

$$\alpha_T = A - (B/T) + (C/T^2), \quad \text{and} \quad \alpha_T = A + BT. \tag{11}$$

Holleran[16] suggested that

$$\alpha_T = A + B \ln T, \tag{12}$$

so that

$$T_r = (T_1 T_2)^{\frac{1}{2}}. \tag{13}$$

Paul *et al.*[17] also have recently used the latter relation of Eq. (11) while interpreting their recent measurements on Ar; according to this one gets

$$T_r = (T_1 - T_2)/\ln (T_1/T_2). \tag{14}$$

A somewhat better procedure is to make measurements for different values of the temperature of one bulb while keeping the other bulb temperature constant. Such measurements can yield the values of α_T as a function of temperature directly as indicated by Grew,[18] Grew, Johnson, and Neal,[19] Grew and Mundy,[20] Saxena and Mason,[21] and Weissman, Saxena, and Mason.[22]

Corbett and Watson[23] have suggested another way out of this problem of temperature assignment which has also the advantage that it tests the degree of agreement between theory and experiment at the same time. The procedure is based on an earlier suggestion of Srivastava and Madan.[15]

This problem of temperature assignment gets a happy solution in those *trennschaukel* measurements where the difference in the temperatures of the two end-bulbs is small, and as such the different procedures do not lead to any appreciably different values for T_r. Usually the average of T_1 and T_2 is taken as T_r.

In discussing the various measurements where different procedures have been employed for temperature assignment, the uncertainty due to this should be kept in mind. However, for future experiments on the two bulb method the procedure of Grew[18,21] is about the best, and in *trennschaukel* the temperature difference should be kept as small as possible.

IV. COMPOSITION DEPENDENCE OF α_T

To a fairly large extent α_T for isotopic mixtures is independent of the relative proportions of the constituents. This follows directly from theory. If the Eqs. (7) and (8) are expanded in increasing powers of M the coefficient of M is always independent of the composition of the mixture. It is only in the coefficient of M^2 which is always small at least for most of the heavy isotopes, that the dependence on composition appears. Thus, *a priori* we would expect in H_2 and He isotopes only a relatively pronounced composition dependence. This aspect is discussed in detail in the next section. This point is also worth investigating experimentally for it offers one of the crucial tests of theory. Except in the case of hydrogen isotopes, no systematic investigations have ever been undertaken with this view point. It will, however, be worthwhile to plan such experiments specially in view of the results discussed in the next section where the theory predicts appreciable composition dependence in a few other cases also.

V. COMPARISON OF EXPERIMENTAL AND THEORETICAL α_T VALUES

We will now discuss individually the thermal diffusion data of different isotopic mixtures of various workers and assess their relative agreement. These results are also compared with the calculated theoretical values using the appropriate formula and according to different molecular potentials. This comparison will throw some light on the nature of intermolecular forces. This laborious work is not only supported but also receives preference from the well-known fact that thermal diffusion is very sensitive to the nature of molecular interactions.

Helium

The experimental values of α_T for this gas have been reported by McInteer, Aldrich, and Nier,[24] Moran and Watson,[25] Saxena, Kelley, and Watson,[26] Van der Valk and de Varies,[27] and Watson, Howard, Miller, and Schiffrin.[28] All these workers except the first one have used *trennschaukel* for determining α_T. Saxena and Joshi[29] have earlier pointed out that the measured values of Moran and Watson[25] and Saxena *et al.*[26] may be smaller than the actual values due to a fault in the *trennschaukel* design. Very recently Joshi and Saxena[30]

[15] B. N. Srivastava and M. P. Madan, J. Chem. Phys. **21**, 807 (1953).
[16] E. M. Holleran, J. Chem. Phys. **21**, 1901 (1953).
[17] R. Paul, A. J. Howard, and W. W. Watson, J. Chem. Phys. **39**, 3053 (1963).
[18] K. E. Grew, Proc. Roy. Soc. (London) **A189**, 402 (1947).
[19] K. E. Grew, F. A. Johnson, and W. E. J. Neal, Proc. Roy. Soc. (London) **A224**, 513 (1954).
[20] K. E. Grew and J. N. Mundy, Phys. Fluids **4**, 1325 (1961).
[21] S. C. Saxena and E. A. Mason, Mol. Phys. **2**, 379 (1959).
[22] S. Weissman, S. C. Saxena, and E. A. Mason, Phys. Fluids **4**, 643 (1961).
[23] J. W. Corbett and W. W. Watson, J. Chem. Phys. **25**, 385 (1956).
[24] B. B. McInteer, L. T. Aldrich, and A. O. Nier, Phys. Rev. **72**, 510 (1947).
[25] T. I. Moran and W. W. Watson, Phys. Rev. **109**, 1162 (1958).
[26] S. C. Saxena, T. G. Kelley, and W. W. Watson, Phys. Fluids **4**, 1216 (1961).
[27] F. Van der Valk and A. E. de Vries, J. Chem. Phys. **34**, 345 (1961).
[28] W. W. Watson, A. J. Howard, N. E. Miller, and R. M. Schiffrin, Z. Naturforsch. **18a**, 242 (1963).
[29] S. C. Saxena and R. K. Joshi, J. Chem. Phys. **37**, 1170 (1962).
[30] R. K. Joshi and S. C. Saxena, J. Sci. Ind. Res. (India) **24**, **21** (1965).

CC-0. In Public Domain. Gurukul Kangri Collection, Haridwar

Digitized by Arya Samaj Foundation Chennai and eGangotri

Table I. Potential parameters for pure gases.

Potential	L-J (12-6)		exp-6			Morse		
Parameters	ϵ/k	σ	α	ϵ/k	σ_m	C	ϵ/k	σ_m
Gas	(°K)	(°A)		(°K)	(°A)		(°K)	(°A)
He	10.22	2.556[a]	12.4	9.16	3.135[e]	6	8.55	2.687[g]
Ne	35.6	2.749[a]	14.5	38.0	3.147[e]	8	67.1	2.611[h]
Ar	119.8	3.405[a]	14.0	123.2	3.866[e]	5.7	120.0	4.461[i]
H_2	37.0	2.928[a]	14.0	37.3	3.337[e]			
N_2	96.0	3.730[a]	17.0	101.2	4.011[e]			
O_2	128.0	3.398[b]	17.0	132.0	3.726[e]			
CH_4	148.0	4.220[c]	14.0	152.8	4.206[c]			
			15.0	163.7	4.218[f]			
CO	110.0	3.590[d]	17.0	119.1	3.937[e]			

[a] R. J. Lunbeck, thesis, Amsterdam (1951).
[b] C. J. W. Raw and C. P. Elies, J. Chem. Phys. **28**, 1198 (1958).
[c] E. A. Mason and W. E. Rice, J. Chem. Phys. **22**, 525, 843 (1954).
[d] Reference 8.
[e] J. T. Vanderslice, E. A. Mason, and W. G. Maisch, J. Chem. Phys. **31**, 738 (1959).
[f] H. W. Schamp, Jr., E. A. Mason, A. C. B. Richardson, and A. Altman, Phys. Fluids **1**, 329 (1958).
[g] Reference 33.
[h] Reference 34.
[i] A. Saran, Indian J. Phys. **37**, 491 (1963).

worked out the detailed theory of *trennschaukel* operation and gave expressions for the calculation of various correction factors. They have also examined the probable uncertainties in the α_T values of different workers. They conclude that α_T values of Moran and Watson[25] are likely to be very much in error; Saxena *et al.*[26] data may be of relatively better accuracy as the additional corrections discussed in the later paper[30] are almost negligible for this case. Though Van der Valk[27] values are within reasonable accuracy, the values of Watson *et al.*[28] are again associated with some appreciable uncertainty arising from the fact that the connecting capillaries used in construction are somewhat wide, 1.5 mm. A careful knowledge of these facts is essential for a correct assessment of experimental data. We have thus dropped the data of Moran and Watson[25] from Fig. 1 and, also, the value of α_T at 136°K of Watson *et al.*[28] for there may be appreciable quantum corrections around such temperatures.[31] The uncertainties shown in the data of Fig. 1 are just the precision of the measurements claimed by the workers; it is not to be confused with the error which may still be larger. It is not possible to estimate it for the various corrections arising due to nonideal conditions of the *trennschaukel* design and operation have not been applied. Thus, within the scope of rather large uncertainty, it is possible to conclude that the various measurements are consistent with each other. However, the need to evolve a better set of α_T values as a function of temperature is apparent.

In Fig. 1 we also show the computed α_T values for the L-J (12–6), exp-6, and Morse potentials. The potential parameters used are those listed in Table I. Saxena and Pardeshi[13] have computed the theoretical α_T values for a mixture of He^3 and He^4 containing 5% He^3 and according to different formulas on the L-J (12–6) potential. They found the Kihara approximation scheme to yield the best results and that the second approximation formula differs from the first approximation by less than 1%. In view of this it will be quite accurate to use only the first approximation Kihara formula. Sample calculations were also performed by us for the case when the heavier component is in trace, and this revealed that the first approximation formula is accurate within about 2% in the temperature range 400°–800°K. Similar results were found for the exp-6 potential, also. We have, consequently, used the first approximation Kihara formula for our calculations on this system throughout. Calculated curves a, b, and c refer to the isotopic mixtures having 0%, 50%, and 100% of the heavier component, respectively, and refer to the L-J (12–6) potential. It is interesting to note that the theory predicts an appreciable composition dependence for α_T, the value increases as the proportion of the lighter component increases, the maximum vari-

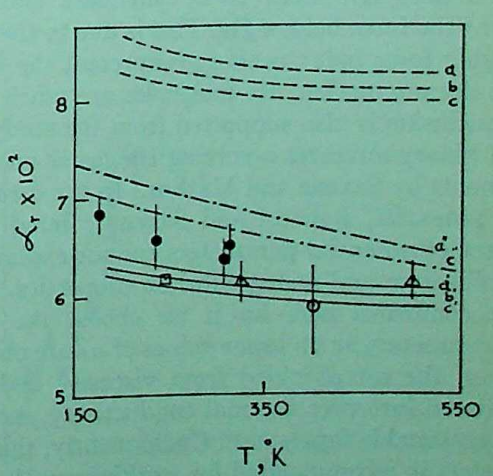

Fig. 1. Temperature dependence of α_T for the He^3–He^4 system. Experimental data: ⊙ McInteer *et al.*; ⊡ Saxena *et al.*; △ Van der Valk *et al.*; ● Watson *et al.* Theoretical curves: – – – L-J (12-6), a(x_1=0), b(x_1=0.5), c(x_1=1); —— exp-6, a′(x_1=0), b′(x_1=0.5), c′(x_1=1); -·-·- Morse potential, a″(x_1=0), c″(x_1=1).

[31] S. C. Saxena, Physica **26**, 730 (1960).

CC-0. In Public Domain. Gurukul Kangri Collection, Haridwar

Digitized by Arya Samaj Foundation Chennai and eGangotri

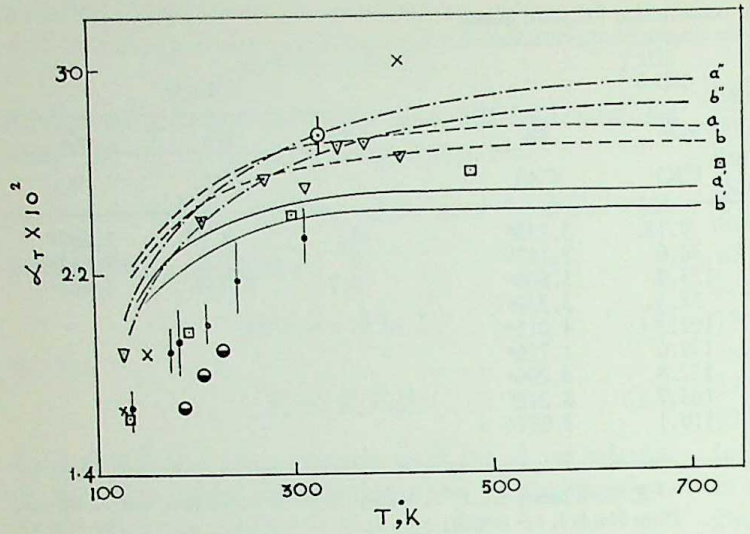

FIG. 2. Temperature dependence of α_T for the system Ne^{20}–Ne^{22}. Experimental points: × Nier; ⊙ Mann; ● Watson *et al.*; ▽ Fischer; ⊡ Grew *et al.*; Saxena *et al.* Calculated curves: – – – L-J (12-6), a(x_1=0), b(x_1=0.5); —— exp-6, a′(x_1=0), b′(x_1=0.5); – · – Morse potential, a″(x_1=0), b″(x_1=0.5).

ation being 3%–4%. Thus, a carefully planned experiment having high precision can check this particular prediction of theory. At the moment even the precision of the available data is relatively more poor than the expected composition dependence. The measurements of Saxena *et al.*,[26] Van der Valk and de Varies,[27] Watson *et al.*,[28] and McInteer *et al.*[24] refer to 5%, 10%, 50%, and trace quantities of He^3, respectively. A somewhat apparent trend of the experimental data with varying composition does fall in line with the prediction of theory.

Only the exp-6 potential leads to a satisfactory agreement between theory and experiment if allowance is made for the fact that at low temperatures quantum corrections may be important. The Lennard-Jones as well as the Morse potentials over-estimate the α_T values. Thus, out of these three intermolecular potentials only the exp-6 potential is capable of correlating the equilibrium and nonequilibrium properties if one recalls the work of Mason and Rice.[32] Lennard-Jones (12–6) potential does not seem to be adequate enough to represent the force field of He. This is due to the choice of a higher force index twelve to represent the overlap part of the interaction; He molecules are much softer. This conclusion is also supported from the study of α_T data of binary mixtures involving He gas as one of the components by Saxena and Mathur.[1] In the case of the Morse potential, Bahethi and Saxena[33] found that a single set of potential parameters cannot explain both the equilibrium and nonequilibrium properties. This is further confirmed here for if we choose the second virial parameters much lower values of α_T are obtained. However, the set obtained from viscosity and found adequate to interpret thermal conductivity and diffusion is reasonable for α_T also. Consequently, this set of parameters is recommended for working on Morse potential while dealing with transport properties. This conclusion is in agreement with the finding of Bahethi, Gambhir, and Saxena,[34] who have studied the various properties of mixtures involving He with the Morse potential.

[32] E. A. Mason and W. E. Rice, J. Chem. Phys. **22**, 525 (1954).
[33] O. P. Bahethi and S. C. Saxena, Phys. Fluids **6**, 1774 (1963).

Neon

Isotopic thermal diffusion factor for Ne has been measured using the conventional two-bulb apparatus by Nier,[35] Stier,[36] Mann,[37] and Grew and Mundy[20]; and using a *trennschaukel* by Moran and Watson,[25] Saxena *et al.*,[26] Fischer,[38] and Watson *et al.*[28] As pointed out earlier by a number of workers,[39,40] and more recently by Grew and Mundy,[20] the data of Stier[36] are probably in error. We also exclude the data of Moran and Watson[25] for reasons already mentioned in connection with the discussion on He. These data are systematically smaller than the values of other workers. Rest of the data are plotted in Fig. 2. The α_T values of Grew and Mundy[20] and Watson *et al.*[23] refer to an approximately equimolar mixture of Ne^{20} and Ne^{22} while in other measurements samples of Ne used were having the natural isotopic abundance. In general, there is a very poor agreement between the data of different workers and unfortunately, even the data obtained using the same technique present serious discrepancies and inconsistencies though the values of a worker as a function of temperature are smooth. It is not possible to pinpoint the source which can lead to simple explanations of the observed discrepancies. The need of a careful and accurate α_T measurement for this system as a function of temperature is still as essential as ever.

Convergence of the theoretical formulas for this system was judged on the basis of the formula applicable to mixtures of heavy isotopes. For L-J (12–6) and

[34] O. P. Bahethi, R. S. Gambhir, and S. C. Saxena, Z. Naturforsch. (to be published).
[35] A. O. Nier, Phys. Rev. **57**, 338 (1940).
[36] L. G. Stier, Phys. Rev. **62**, 548 (1942).
[37] A. K. Mann, Phys. Rev. **73**, 412 (1948).
[38] A. Fischer, Ph.D. thesis, Zurich (1959).
[39] E. A. Mason and W. E. Rice, J. Chem. Phys. **22**, 843 (1954).
[40] S. C. Saxena, Indian J. Phys. **29**, 587 (1955).

CC-0. In Public Domain. Gurukul Kangri Collection, Haridwar

Digitized by Arya Samaj Foundation Chennai and eGangotri

Table II. Calculated values of the $[\alpha_0']_1$ for the Morse potential.

	C						
T^*	3	4	5	5.5	6	8	10
1	−0.354	−0.152	0.0386	0.111	0.160	0.351	0.460
1.4	−0.271	−0.0313	0.101	0.152	0.201	0.370	0.466
2	−0.111	0.0741	0.208	0.264	0.307	0.421	0.514
3	0.0232	0.210	0.319	0.360	0.394	0.505	0.572
4	0.0783	0.266	0.378	0.419	0.452	0.545	0.608
6	0.123	0.309	0.419	0.461	0.496	0.590	0.647
8	0.126	0.320	0.434	0.475	0.509	0.605	0.664
10	0.115	0.320	0.437	0.480	0.515	0.611	0.670
20	0.0323	0.281	0.418	0.466	0.506	0.612	0.675
30	−0.0429	0.244	0.359	0.448	0.490	0.605	0.671
40	−0.107	0.212	0.376	0.432	0.477	0.597	0.668
50	−0.163	0.185	0.360	0.419	0.466	0.591	0.663
60	−0.214	0.162	0.344	0.407	0.457	0.586	0.659
70	−0.261	0.141	0.334	0.407	0.449	0.581	0.656
80	−0.305	0.122	0.322	0.455	0.441	0.577	0.654
90	−0.346	0.104	0.312	0.380	0.435	0.574	0.651
100	−0.386	0.0881	0.303	0.373	0.429	0.570	0.649
200	−0.707	−0.0345	0.237	0.321	0.386	0.548	0.635

exp-6 potentials the tabulations of Saxena,[41] Saxena and Mason,[42] and Srivastava[43] were used. For both the potentials the Kihara approximation formulas seem to be preferable, and the first-approximation expression is accurate within 1%. To investigate the composition dependence, we used Eq. (5) on the Kihara scheme. Calculations in the temperature range 100°–700°K revealed that for both the potentials α_T decreases as the proportion of the heavier component increases though in the range 50%–100%; the change is almost negligible while in the range 0%–50% the change is about 3%. Another interesting conclusion to which these calculations lead is the invalidity of Eq. (7) for this gas and the fact that one should use either Eq. (5) or Eq. (6) for precise estimation of α_T. Similar conclusions also follow for the Morse potential.

Computed values of α_T according to Eq. (5) and on the Kihara approximation scheme are also shown in Fig. 2 for all the three potentials when $X_1=0$ and 0.5. The agreement between theory and experiment is very poor and, due to the large scatter and widely different trends in the data of different workers, it is not possible to comment on the adequacy of any particular potential. The fact that the composition differs is of no help and the discrepancies become still more pronounced if one makes an attempt to reduce the data on the same composition.

Argon

Employing a two-bulb apparatus and a normal sample of Ar (0.307% Ar^{36} and 99.63% Ar^{40}) Stier[36] and Mann[37] have reported the α_T values. Moran and Watson,[25] Saxena *et al.*,[26] and Paul *et al.*[17] on the other hand exploited the *trennschaukel* and obtained the α_T values using isotopic mixture which contained 9.87%, 36.4%, and 50% of Ar^{36}. All the values except those due to Moran and Watson[25] are plotted in Fig. 3 as a function of temperature. The values are in reasonable agreement with each other though it is desirable to have a better set of values with less uncertainty in the individual values. Only such a set will be capable of uniquely answering the appropriateness of a molecular potential.

It was further established that for this case the simpler formulas obtained from the rigorous ones by expanding in powers of the proportionate mass differ-

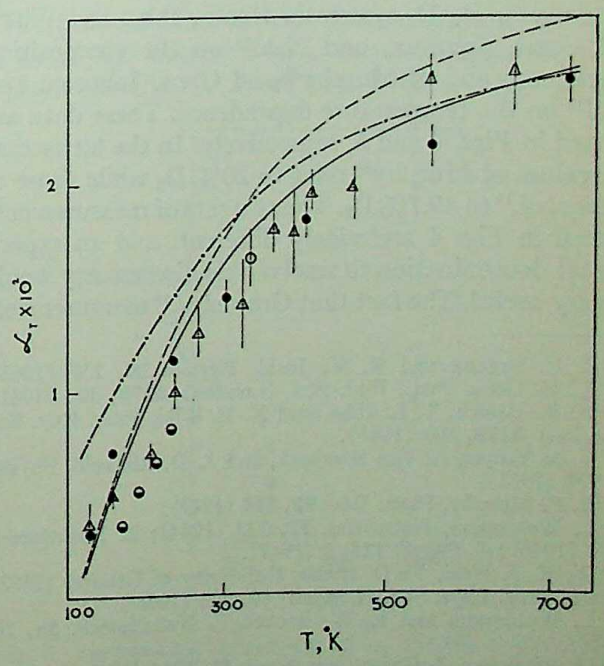

Fig. 3. Temperature dependence of α_T for the Ar^{36}–Ar^{40} system. Experimental points: ● Stier; ⊙ Mann; ◒ Saxena *et al.*; △ Paul *et al.* Theoretical curves; – – – L-J (12-6); —— exp-6; –·–·– Morse potential.

[41] S. C. Saxena, Proc. Phys. Soc. Japan 11, 367 (1956).
[42] S. C. Saxena and E. A. Mason, J. Chem. Phys. 28, 623 (1958).
[43] K. P. Srivastava, Indian J. Phys. 31, 404 (1957).

CC-0. In Public Domain. Gurukul Kangri Collection, Haridwar

Digitized by Arya Samaj Foundation Chennai and eGangotri

ence are quite adequate and that there is no composition dependence. The tabulated values of α_0 of Saxena and Mason[42] were therefore used for L-J and exp-6 potentials. The Morse potential values were obtained from Eq. (7), which was found to be as adequate as Eq. (5) at least in the temperature range of Fig. 3, though it is likely to hold even for still higher temperatures. For future use we tabulate α_0 values according to Eq. (7) on this potential in Table II. The agreement between theory and experiment is best for the exp-6 potential while the other potentials fail either at low temperatures or at high temperatures.

Krypton and Xenon

There are practically no reliable data on Kr and Xe; Corbett and Watson[23] using the two-bulb apparatus were the first to report α_T data for Kr. Later Moran and Watson[25] employed *trennschaukel* to evolve α_T data for Kr and Xe. This latter set for Kr is inconsistent with the earlier values of Corbett and Watson.[23] Further, recently Saxena and Joshi[44] examined the α_T data of Moran and Watson[25] and came to the conclusion that probably these values are systematically low. Thus, unfortunately we have no reliable thermal diffusion data for these two gases and such data will be extremely useful for the proper understanding of the potential-field of these molecules.

Hydrogen

Thermal diffusion factors have been measured by a large number of workers[19,45–55] for the different isotopes of hydrogen both as a function of composition as well as temperature. We will, however, consider here only the data on H_2–D_2 system of Heath, Ibbs, and Wild[46] and Grew, Johnson, and Neal[19] on the composition dependence and of Murphy[48] and Grew, Johnson, and Neal[19] on the temperature dependence. These data are plotted in Figs. 4 and 5, respectively. In the latter case the values of Murphy[48] refer to 20% D_2 while those of Grew *et al.*[19] to 49.7% D_2. The two sets of measurements plotted in Fig. 4 are widely different, and an experimental determination to resolve this discrepancy would be very useful. The fact that Grew *et al.*[19] measurements refer to a slightly smaller temperature cannot explain the large difference in the values of the two groups of workers. Both groups have used the familiar two-bulb apparatus.

Saxena and Pardeshi[56] have made detailed calculations to determine the proper formula to be used for the different combinations of the isotopes of H_2. For H_2–D_2 mixtures, their computations which are according to the exp-6 potential suggest that the Kihara first approximation formula, Eq. (5), is accurate enough. In both Figs. 4 and 5, calculations of α_T are according to this expression and are for L-J (12–6) and exp-6 potentials. Comparison of theory and experiment does not lead to any preference for either of these two potentials as far as Fig. 4 is concerned, but on the basis of Fig. 5, exp-6 potential seems to be a better choice than the (12–6) potential. Not much importance can be attached to the values below 200°K because the magnitude of the quantum corrections is likely to be appreciable.[57] Due to the general failure of the Morse potential[58] in correlating the various properties of H_2 we have excluded it from our consideration.

Nitrogen

Mann[37] and Davenport and Winter[59] have reported the data for N_2 obtained on a two-bulb apparatus. These data are plotted in Fig. 6. Though the data of the two different groups of workers agree with each other still there seem to be large uncertainties in the individual values as the points fail to lie on a smooth curve. Additional measurements are thus apparently needed.

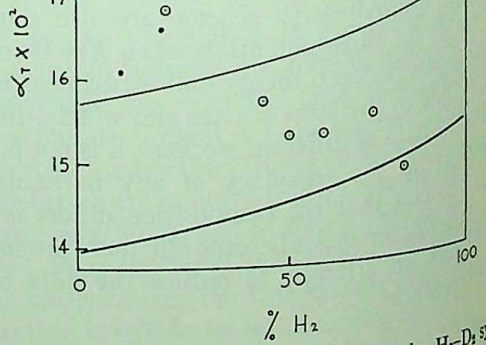

FIG. 4. Composition dependence of α_T for the H_2–D_2 system. Experimental points: ● Heath *et al.* (326°K); ⊙ Grew *et al.* (300°K). Calculated curves: – – – L-J (12-6); —— exp-6; calculated from experimental diffusion and viscosity data.

[42] S. C. Saxena and R. K. Joshi, Physica **29**, 257 (1963).
[45] K. E. Grew, Proc. Roy. Soc. (London) **A178**, 390 (1941).
[46] H. R. Health, T. L. Ibbs, and N. E. Wild, Proc. Roy. Soc. (London) **A178**, 380 (1941).
[47] A. de Troyer, A. Van Itterbeek, and A. D. Rietveld, Physica **17**, 938 (1951).
[48] B. F. Murphy, Phys. Rev. **72**, 834 (1947).
[49] L. Waldmann, Naturwiss. **32**, 223 (1944); Z. Naturforsch. **1**, 59 (1946); Z. Physik **124**, 1 (1947).
[50] W. E. J. Neal, Ph.D. thesis, University of London (1952); see also Proc. Phys. Soc. (London) **82**, 333 (1963).
[51] L. Waldmann and E. W. Becker, Z. Naturforsch. **3a**, 180 (1948).
[52] H. Kitagawa, J. Chem. Soc. Japan **61**, 1243 (1941).
[53] J. Schirdewahn, A. K. Klemm, and L. Waldmann, Z. Naturforsch. **16a**, 133 (1961).
[54] T. Ghozlan, Ph.D. thesis, Amsterdam (1963).
[55] C. J. G. Slieker, Ph.D. thesis, Amsterdam (1964).
[56] S. C. Saxena and P. A. Paradeshi, Indian J. Phys. **36**, (1962).
[57] S. C. Saxena and T. K. S. Narayanan, Can. J. Phys. **4** 527 (1962).
[58] O. P. Bahethi and S. C. Saxena, Indian J. Pure Appl. Phys. **2**, 267 (1964).
[59] A. N. Davenport and E. R. S. Winter, Trans. Faraday Soc. **47**, 1160 (1951).

CC-0. In Public Domain. Gurukul Kangri Collection, Haridwar

Digitized by Arya Samaj Foundation Chennai and eGangotri

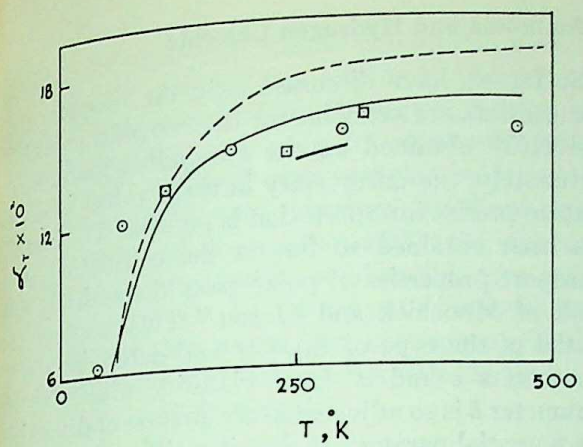

Fig. 5. Temperature dependence of α_T for the H_2–D_2 system. Experimental points: ⊡ Murphy (20% D_2); ⊙ Grew *et al.* (49.7% D_2). Theoretical curves: – – – L-J (12-6) (49.7% D_2); —— exp-6 (49.7% D_2); —— calculated from experimental diffusion and viscosity data.

On the basis of Eq. (5), numerical calculations indicated that there is no composition dependence of α_T and that the formula appropriate for mixtures of heavy isotopes is adequate. Calculated values shown in Fig. 6 are based on the tabulated values of Saxena and Mason[42] for the L-J potential and of Srivastava[43] for the exp-6 potential.

In view of the scatter in the experimental data, both the potentials seem to be equally good, though some preference can be attached to the L-J potential tentatively. Another point against the exp-6 potential lies in the use of the value of the parameter $\alpha=17$, for this choice predicts no reversal in the thermal diffusion factor even at low temperatures which has been observed in a few other cases. For this reason, as pointed out by Madan,[60] the applicability of the exp-6 potential with the parameter α equal to 15 and greater is questionable.

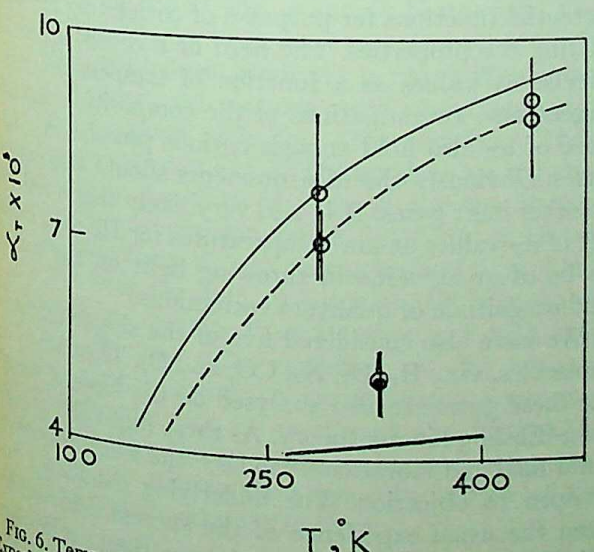

Fig. 6. Temperature dependence of α_T for the N_2^{28}–N_2^{29} system. Experimental data: ● Mann; ⊙ Davenport *et al.* Calculated curves: – – – L-J (12-6); —— exp-6 potential; —— calculated from experimental diffusion and viscosity data.

[60] M. P. Madan, Indian J. Phys. 29, 11 (1955).

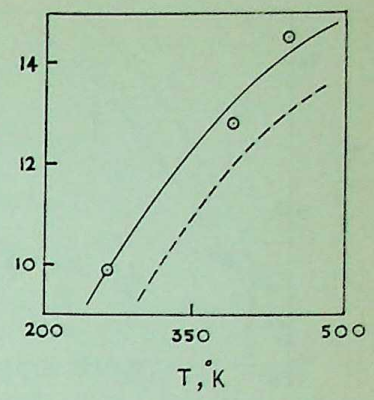

Fig. 7. Temperature dependence of α_T for the O_2^{32}–O_2^{34} system. Experimental points: ⊙ Whalley *et al.* Theoretical curves: – – – – L-J (12-6); —— exp-6 potential.

Oxygen

The only data of Whalley, Winter, and Briscoe[61] on the isotopes of oxygen are indicated in Fig. 7. They used a sample of oxygen 32 and 34 in which the latter was only 0.04% and employed a two-bulb apparatus. α_T values for oxygen are also found to be composition independent by actual calculation like nitrogen. The calculated values shown in Fig. 7 are therefore according to the tabulations of Saxena and Mason[42] for the L-J (12–6) potential and for the exp-6 potential these are according to the first approximation, Eq. (7), tabulated by Srivastava.[43] The existing limited data show preference for the exp-6 potential though in view of what has been said already in the case of N_2 it may be questionable to accept this conclusion. It seems highly desirable to have more extensive measurements of α_T so that more definite information regarding the potential field of this gas may be derived.

Carbon Monoxide

Thermal diffusion data of Davenport and Winter[59] for α_T of CO obtained on a two-bulb apparatus are displayed in Fig. 8. There is a large amount of un-

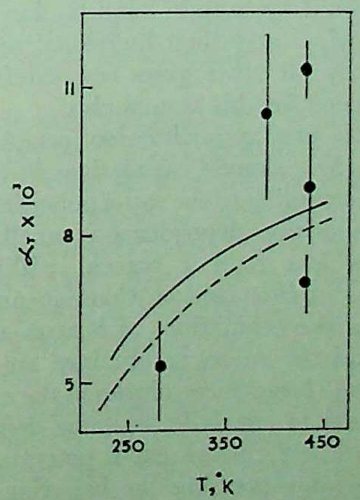

Fig. 8. Temperature dependence of α_T for the $C^{12}O^{16}$–$C^{13}O^{16}$ system. Experimental points: ● Davenport *et al.* Calculated curves: – – – – L-J (12-6); —— exp-6 potential.

[61] E. Whalley, E. R. S. Winter, and H. V. A. Briscoe, Trans. Farday Soc. 45, 1085 (1949).

CC-0. In Public Domain. Gurukul Kangri Collection, Haridwar

Digitized by Arya Samaj Foundation Chennai and eGangotri

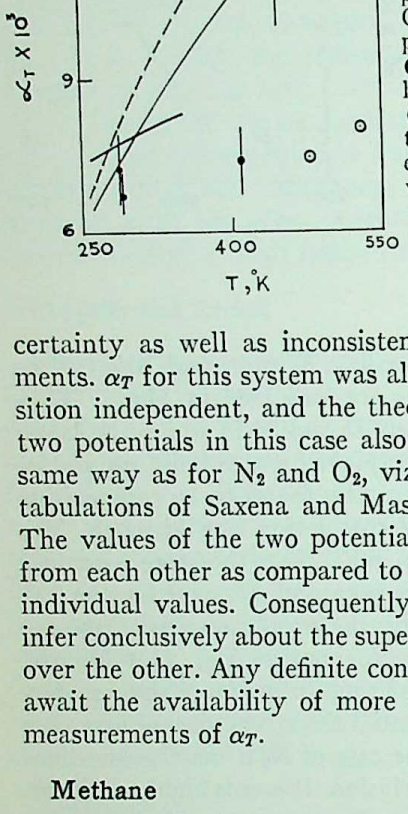

FIG. 9. Temperature dependence of α_T for the $C^{12}H_4$–$C^{13}H_4$ system. Experimental points: ⊙Nier; ● Davenport *et al.* Calculated curves: ---- L-J (12-6); —— exp-6 potential; —— calculated from experimental diffusion and viscosity data.

certainty as well as inconsistency in these measurements. α_T for this system was also found to be composition independent, and the theoretical curves for the two potentials in this case also were obtained in the same way as for N_2 and O_2, viz., on the basis of the tabulations of Saxena and Mason[42] and Srivastava.[43] The values of the two potentials do not differ much from each other as compared to the uncertainty in the individual values. Consequently, it is not possible to infer conclusively about the superiority of one potential over the other. Any definite conclusion must therefore await the availability of more reliable and elaborate measurements of α_T.

Methane

The quasi-spherical molecule methane has very often been found appropriate for interpretation on the basis of spherically symmetric potentials in conjunction with the theory of Chapman–Cowling based on elastic collision of molecules. Nier[62] and Davenport and Winter[59] have reported the α_T data obtained on the two-bulb type apparatus and these are shown in Fig. 9. Unfortunately, the two sets of measurements are not in agreement even if we keep in mind the large scatter of the various points and their individual uncertainties. Like practically all other gases new careful measurements are needed for this system also.

Based on the first approximation formula of Kihara for α_T, [Eq. (5)], sample calculations in this temperature range (according to the exp-6 potential) predicted that the composition dependence is small, and it remains always less than a percent within the two extreme limits of composition. Consequently, for both the potentials the tabulations of Saxena and Mason[42] were used, and the values so obtained are also shown in Fig. 9. Due to large uncertainties in the experimental data, it is hard to conclude anything definite on the adequacy of theory though exp-6 potential may be a better choice for expressing the behavior of this gas bears out from Fig. 9 to some extent. The two sets of available exp-6 potential parameters lead to identical results in the temperature range of Fig. 9.

[62] A. O. Nier, Phys. Rev. 56, 1009 (1939).

Ammonia and Hydrogen Chloride

So far we have discussed only the nonpolar gas... Meager data are available for the two polar gases NH_3 and HCl[64] obtained on the two-bulb apparatus. U... fortunately, the uncertainty in these values is so gr... that no precise interpretation is possible. The best t... has been obtained so far on the calculation of ... transport properties of polar gases theoretically is t... work of Monchick and Mason.[11] They assume a p... tential of the type of Eq. (4) and determine the t... parameters ϵ and σ_0 from viscosity while the t... parameter δ is so adjusted in the process of determi... the potential parameters that it satisfies the relation

$$4\epsilon_0\sigma_0^3\delta_{\max} = 2\mu^2. \quad (17)$$

Within rather large uncertainty in the experimen... data, it is hard to say anything definite and inde... Monchick and Mason[11] found reasonable agreeme... Consequently, at the moment our knowledge of α_T ... polar gases is very poor, and it would be a great ... to obtain reliable measurements of the thermal diffusi... factor.

VI. DISCUSSION OF RESULTS

In the previous section we have discussed in de... the experimental data of three inert gases, viz., He, ... and Ar. These gases, which are composed of monatom... spherically symmetric molecules, are most appropri... for interpretation in terms of the Chapman–Ensk... kinetic theory in conjunction with central force mod... Saxena, Kelley, and Watson[26] have confirmed this e... pectation also by expressing α_T as a function of ... measurable quantities. However, a critical study of ... behavior of these gases tends to suggest that ... probably the exp-6 potential is the best of all the kn... potential functions for purposes of correlating and p... dicting the properties. The need of a consistent se... precise α_T values as a function of temperature is ... urgent one. Investigations of the composition depe... ence of α_T also hold enough curious promise in a f... cases. Obviously the measurements should also ext... to other inert gases. It is also very likely that a reli... set of α_T values at low temperatures for He may p... to be of great value in throwing light on the na... and magnitude of quantum corrections.

We have also considered five of the simple diato... molecules, viz., H_2, D_2, N_2, CO, and O_2. The data of ... for these gases are also analysed on the basis of Ch... man–Enskog kinetic theory. As these molecules pos... rotational and vibrational modes,[65] the whole proce... is open to objection. The underlying confidence ... been the usual experience of the success achieved ... this theory in the description of the various equilibr...

[63] W. W. Watson and D. Woernley, Phys. Rev. 63, 181 ...
[64] A. Z. Kraz and W. W. Watson, Phys. Rev. 91, 1460 ...
[65] S. C. Saxena and J. P. Agrawal, J. Chem. Phys. 35, ... (1961).

CC-0. In Public Domain. Gurukul Kangri Collection, Haridwar

Digitized by Arya Samaj Foundation Chennai and eGangotri

and nonequilibrium properties of polyatomic gases. Incentive to this approach has also been added by the indirect support advanced by Weissman, Saxena, and Mason[22,66] from the study of α_T for mixtures involving polyatomic gases. They[66] expressed the binary α_T expression in favor of such quantities which are experimentally known and showed that within the uncertainties of the experimental data it is possible to correlate the mixture properties of some gas pairs involving polyatomic molecules even on the basis of Chapman–Enskog theory and central interatomic potentials. As shown by Saxena, Kelley, and Watson,[26]

$$A^* = (\tfrac{5}{6})(\rho D/\eta), \tag{16}$$

and

$$(6C^* - 5) = 2[2 - (\partial \ln D/\partial \ln T)_p]. \tag{17}$$

Here ρ, D, η, and p represent the density, diffusion, viscosity, and pressure of the gas, respectively. Let us further assume that Eq. (7) is accurate enough to represent α_0 for these gases. This, as will be seen later, is not a bad approximation in view of the large uncertainty that gets associated with the calculation of α_0 on the basis of Eq. (7) in conjunction with Eqs. (16) and (17). Also Eq. (7) has been shown to be accurate enough for all these gases except the isotopes of H_2. One can therefore compute α_0 easily if the coefficients of diffusion, viscosity, and the slope of $\ln D$ vs $\ln T$ curve at a fixed pressure be known at that temperature. We now report the results so obtained for all these five gases.

For H_2 the diffusion data[67] are available in the temperature range 85°–293°K, and these lead to a linear plot between $\ln D$ and $\ln T$ with a slope of 1.73 over the entire range. This, in conjunction with the viscosity data,[68] leads to α_T values on the basis of Eqs. (5), (16), and (17) as shown in Fig. 5 with a heavy solid line. These values are in reasonable agreement with the direct measured values. Similarly to check the composition dependence calculations were performed again using Eq. (5) along with Eqs. (16) and (17). These α_T values are shown in Fig. 4. These values are in better agreement with the data of Grew *et al.*[19] the discrepancies in the composition range 0%–50% of H_2 are rather serious. Thus, though on the basis of Figs. 4 and 5, it seems that the data of Grew *et al.*[19] is probably relatively more accurate than Heath *et al.*[46] still, even these data are not fully explained on the basis of Chapman–Enskog theory. A careful study suggests a precise redetermination of α_T values, and further the Chapman–Enskog theory is reasonably well competent to correlate the existing data specially in view of the large associated uncertainty in them.

For N_2 the diffusion data have been reported[69] in the temperature range 77°–350°K, and these lead to a constant value of 1.86 for $\partial \ln D/\partial \ln T$. Viscosity data[68] are also available, and when all these are used to compute α_0 according to Eqs. (7), (16), and (17), we get the values shown in Fig. 6 by the heavy solid line. The general large scatter, and the strangeness in the α_T value at 326°K offer some difficulty in interpretation. We can make two general observations. Firstly, the values indirectly obtained from diffusion and viscosity data are smaller than the directly observed values, and secondly, the observed temperature dependence of α_T data is much more pronounced than suggested by the indirect α_T values. Partly, this pronounced disagreement is due to the lack of accurate diffusion data which reflects in our inability to determine $\partial \ln D/\partial \ln T$ with enough precision on which α_T sensitively depends. However, the good agreement of the computed α_T values with the directly measured values is not, in our opinion, fortuitous, and in view of all that has been said above, we may conclude that the assumption of a central force-field is reasonably satisfactory for correlating the properties of this gas at least over the limited temperature range of our investigation. This tentative conclusion may require some modification when α_T data become available at higher temperatures where internal degrees will play a more pronounced role.[65]

An indirect check is further possible regarding the conclusion drawn for N_2 on the basis of CO data. Unfortunately this possibility is seriously handicapped by the lack of diffusion data for CO. Nevertheless, the similarity in the nature and the degree of agreement obtained between theory and experiment for this molecule (Fig. 8) with that for N_2 (Fig. 6) tend to support and substantiate the conclusion drawn in the case of N_2. Diffusion and α_T data at extended temperatures both for N_2 and CO will be of great assistance in further investigating with reliance the possibility of interpreting these simple gases on the basis of central force-field potentials.

O_2 is also an interesting gas for a study of this type. Diffusion data[69] for this gas are available in the temperature range 77°–353°K. The data exhibit enough internal consistency and $\ln D$ vs $\ln T$ was again found to be a linear plot in this temperature range, surprisingly enough, with a slope of two. On the basis of this, α_T value will be zero or at least very small in this temperature range. Direct measurements (Fig. 7) contradict this prediction. Thus, if reliance could be placed on the accuracy of diffusion data, one would doubt about the applicability of Chapman–Enskog theory to this gas. On the other hand, Fig. 7 shows a reasonably good agreement between theory and experiment. Further, since the indirectly generated α_T values are generally smaller than the directly measured values, we may tentatively conclude that the situation as regards this

[66] S. Weissman, S. C. Saxena, and E. A. Mason, Phys. Fluids 3, 510 (1960).
[67] P. Harteck and H. W. Schmidt, Z. Physik. Chem. B21, 447 (1933). References 46 and 49.
[68] H. L. Johnston and K. E. McCloskey, J. Phys. Chem. 44, 1038 (1940).
[69] E. B. Winn, Phys. Rev. 80, 1024 (1950); E. R. S. Winter, Trans. Faraday Soc. 47, 342 (1951).

CC-0. In Public Domain. Gurukul Kangri Collection, Haridwar

Digitized by Arya Samaj Foundation Chennai and eGangotri

gas may be essentially the same as for the other diatomic gases considered here.

We may try a similar procedure for CH_4 because of its quasi-spherical nature. Diffusion data[70] for this gas are available again for the temperature range of 77°–353°K which lead to a constant value of 1.84 for $\partial \ln D/\partial \ln T$. This information in conjunction with the viscosity data[68] and Eqs. (7), (16), and (17) lead to α_T values shown in Fig. 9. The agreement with the directly obtained values can definitely be regarded as satisfactory in view of the large scatter of the thermal diffusion data. Consequently, in this limited temperature range, the correlation of the various properties of this gas on the basis of Chapman–Enskog theory seem to be possible.

On the whole we find that only approximate success is possible in the attempt to interpret the properties of complicated polyatomic molecules on the basis of Chapman–Enskog kinetic theory. Good success has been achieved here for the data considered are limited in temperature range and in most cases are of poor accuracy. The interpretation at high temperatures is likely to suffer more as rotational and vibrational modes will add appreciably to the energy of the molecule. Adequate solution of this difficulty lies in the development of the rigorous kinetic theory of nonspherical molecules. Curtiss and his collaborators[71] have contributed towards this complicated task. They have developed the kinetic theory based on classical mechanics of nonspherical molecules and specialized it for certain shapes of the molecules. Unfortunately, the detailed calculations have not yet been performed to a stage where application to actual systems is possible. A formal quantum-mechanical kinetic theory taking into account the inelastic nature of the molecular collisions has also been developed for pure gases by Wang Chang and Uhlenbeck[72] and de Boer.[73] Taxman[74] also has given the classical theory for such systems as an extension of the Chapman–Enskog kinetic theory. All these approaches[72–74] lead to expressions for the transport coefficients in terms of certain integrals, the solution of which appear almost hopelessly difficult. Recently Mason and Monchick[75] have indicated a practical way of evaluating these integrals and have derived expressions for the transport properties of pure gases. The theory indicated an appreciable correction for the case of thermal conductivity only. Saxena, Saksena, and Gambhir[76] have also developed a theory for the thermal conductivity of polyatomic gases, and the results apparently are similar to those obtained by Mason and Monchick.[75] Recently Monchick, Yun, and Mason have given a formal kinetic theory of polyatomic gas mixtures by extending the Wang Chang and Uhlenbeck theory to mixtures. They have derived expressions for the various properties including α_T but the form is still not appropriate for actual numerical calculations. We hope that they will simplify these expressions as for pure gases,[75] and then the interpretation of data may be possible. The interesting result that they have derived[77] which is relevant for our present discussion is that α_T is likely to be seriously affected by the presence of internal degrees of freedom. No quantitative indication can be made except their calculations for the specialized case of a "dusty gas" which indicates that the values obtained from the Chapman–Enskog theory will be reduced, a trend which is indicated by the indirect calculations of α_T, also. The work on the development of the properties of mixtures of polyatomic gases is rather limited and the only two efforts are in the area of thermal conductivity by Hirschfelder[78] and Saxena, Saksena, Gambhir, and Gandhi.[79]

The prospect of achieving only limited success in explaining α_T data of nonspherical molecules on the basis of Chapman–Enskog theory of spherical molecules has started accumulating in recent years. Becker *et al.*[80] were the first to plan suitable experiments using isotopic–isobaric systems. Work in this direction has also been continued by Schirdewahn *et al.*[53] and Slieker.[55] The former workers[53] have suggested an empirical formula derived on the basis of dimensional analysis which has also received some support from the measurements of Slieker.[55] However, much still remains to be done to make this entirely empirical approach reliable and we hope rigorous theories may provide a lead.

ACKNOWLEDGMENT

This work was supported in part by the Department of Atomic Energy, Bombay, India.

[70] E. B. Winn and E. P. Ney, Phys. Rev. **72**, 77 (1947); **80**, 1024 (1950).

[71] C. F. Curtiss, J. Chem. Phys. **24**, 225 (1956); C. F. Curtiss and C. Muckenfuss, *ibid.* **26**, 1619 (1957); C. Muckenfuss and C. F. Curtiss, *ibid.* **29**, 1257 (1958); P. M. Livingston and C. F. Curtiss, *ibid.* **31**, 1643 (1959); C. F. Curtiss and J. S. Dahler, *ibid.* **38**, 2352 (1963).

[72] C. S. Wang Chang and G. E. Uhlenbeck, "Transport Phenomena in Polyatomic Gases," University of Michigan Engineering Research Rept. No. CM-681 (July 1951); see also Ref. 8, pp. 501–506.

[73] J. de Boer, *Studies in Statistical Mechanics* (North-Holland Publishing Co., Amsterdam, 1964), Vol. II, pp. 241; referred to in Ref. 8, p. 501.

[74] N. Taxman, Phys. Rev. **110**, 1235 (1958).

[75] E. A. Mason and L. Monchick, J. Chem. Phys. **36**, 1622 (1962).

[76] S. C. Saxena, M. P. Saksena, and R. S. Gambhir, Brit. J. Pure Appl. Phys. **15**, 843 (1964); see also J. Chem. Phys. **26**, 282 (1957).

[77] L. Monchick, K. S. Yun and E. A. Mason, J. Chem. Phys. **39**, 654 (1963); see also *ibid.* **38**, 1282 (1963).

[78] J. O. Hirschfelder, *Sixth International Combustion Symposium* (Reinhold Publishing Corporation, New York, 1957), p. 351; see also J. Chem. Phys. **26**, 282 (1957).

[79] S. C. Saxena, M. P. Saksena, R. S. Gambhir, and J. Gandhi, Physica **31**, 333 (1965).

[80] E. W. Becker and E. Dörnenburg, Naturwiss. **37**, 589 (1950); E. W. Becker and W. Beyrich, J. Phys. Chem. **56**, 52 (1952).

CC-0. In Public Domain. Gurukul Kangri Collection, Haridwar

Digitized by Arya Samaj Foundation Chennai and eGangotri

REVIEWS OF

MODERN PHYSICS

VOLUME 38, NUMBER 3 JULY 1966

A Survey of Fast-Neutron Reactions*

N. CINDRO

Institute "Ruđer Bošković," Zagreb, Yugoslavia

A survey of recent experimental and theoretical results (January 1963–July 1965) on fast-neutron-induced reactions is presented. The first part gives an outline of present reaction mechanism theories that may be useful for an experimentalist. A semiclassical and a more exact description of both direct and equilibrium processes is given and a brief discussion of intermediate processes included. The second part gives the experimental results relevant to the understanding of the mechanism of the interaction of neutrons with nuclei: energy spectra, angular distributions, and total cross sections. Finally, a survey is presented of the results and possibilities of utilising fast neutrons for nuclear structure investigations.

CONTENTS

Introduction 391
I. Studies of Reaction Mechanisms and Related Problems 392
A. Reaction Mechanism Theories 392
1. Compound Nucleus Theory: Basic Assumptions 392
2. Statistical Theory: a Semiclassical Treatment .. 393
3. Statistical Theory: General Case 395
4. Direct Reaction Theories: General Predictions .. 397
5. Direct Reaction Theories: the DWBA Method .. 399
6. Intermediate Processes 400
B. Energy Spectra and Angular Distributions 401
1. Very Light Elements ($A<20$) 401
2. Intermediate Elements ($20<A<100$) 403
3. Heavy Elements ($A>100$) 417
C. Total Cross Sections and Excitation Functions 420
1. Total Cross Sections of Neutron-Induced Reactions up to 14 MeV 420
2. Excitation Functions of Neutron-Induced Reactions 423
3. Trends in (n, p), (n, α), and $(n, 2n)$ Cross Sections at 14 MeV 425
4. "Rare" Nuclear Reactions 431
5. Fluctuations in Total Cross Sections 431
D. Isomeric Ratios 433
II. Scattering and Optical Model Studies 433
A. Formulation of the Problem 434
B. Comparison with Experimental Data 436
1. Elastic and Inelastic Scattering 436
2. Polarization and Related Date 438
3. Optical Model Data and Conclusions 439
III. Nuclear Structure and Spectroscopy Studies 440
A. Investigation of Nuclear Levels 440
B. Nuclear Structure Investigations 441

INTRODUCTION

Reactions induced by fast neutrons are probably one of the experimentally hardest fields in nuclear physics, but the information that can be obtained therein is worth the effort and time spent in building special experimental apparatus and performing experiments incomparably longer than the ones where charged-particle beams are used. Moreover, when, in the last decade intense 14-MeV neutron beams became readily available, fast-neutron physics became in many respects the "poor man's physics." It is thus not surprising that in spite of the hardships involved a large number of experimental (and theoretical) papers have been published in recent years.

This survey aims to give an insight in fast-neutron reaction investigations. Of course, we are not able to explore every detail of this work. Our interest is concentrated on the problems concerning the mechanism of the interaction of fast neutrons with nuclei, and, to a somewhat lesser degree, the inferences about the nuclear structure that one can obtain from these interactions. Thus the interesting problems concerning the n–p and n–n scatterings and some of the few-body topics are omitted. It is necessary also to speak of the progress in experimental techniques utilized in the research work with fast neutrons. Considerable progress has, in fact, been achieved in recent years in this field.

The task of reviewing such a vast field of research as fast-neutron reactions poses immediately the problem of systematizing the presentation. In this systematization one might define a partition either by the energy scale or by the reaction products. Another systematic way of presentation would be according to the measured physical quantities, such as total cross sections, energy spectra, and angular distributions. It is our feeling that none of these systematic approaches is completely useful for the space at our disposal. Thus we shall rather divide the information collected in the last few years (January 1963 to approximately July 1965) according to its purpose: reaction mechanism investigations, nuclear structure studies, optical model and related topics.

* Based on a series of lectures held at the Third Winter School of Nuclear Physics, Villars, Switzerland, January 1965.

Copyright © 1966 by The American Physical Society

CC-0. In Public Domain. Gurukul Kangri Collection, Haridwar

Digitized by Arya Samaj Foundation Chennai and eGangotri

This is not always possible because some of the studies interweave structure, mechanism, and other information.

Thus the master plan is as follows: In Sec. I we review studies of reaction mechanism and related parameters obtained by means of energy spectra and angular distributions, total cross sections, and excitation function measurements and isomeric ratio measurements and analysis. Section II contains scattering and optical model studies while, finally, in Sec. III we review data about nuclear structure that can be obtained from fast-neutron reactions.

I. STUDIES OF REACTION MECHANISMS AND RELATED PROBLEMS

The problem of establishing the mechanism of the interaction between nucleons with nuclei is as old as nuclear physics itself, and so far it has not been successfully solved. There exist two different approaches to this basic problem, one that can be called black box or model treatment, the other, more recent, that can be connected with the employment of the many-body methods in nuclear physics.

In the first formulation the dynamics of the nuclear many-body system was dismissed as impossible to handle and the real state of affairs was substituted by a mathematically solvable model. Evaporation, direct reaction theories, and the optical model fall into this category. These models yield expressions for the cross sections, the polarization, and angular distributions without really solving the complete dynamical problem.

The second approach consists essentially in extending to the problem of nuclear reactions the many-body methods used in the study of nuclear structure. It is based on the idea that the unbound continuous states of the collision problem can be treated analogously to the bound levels of nucleons in the atomic nucleus.

The obvious difficulty with this approach is the problem of joining the internal region in which all nucleons interact to the external region in which the system is split into two or more particles. Much effort is being spent on solving this and other problems and it is probably true that a complete theory of nuclear interactions will ultimately follow the lines of the many-body approach. It is also true, however, that so far only a limited class of nuclear phenomena have been quantitatively understood and explained on the basis of many-body calculations. The bulk of our knowledge about the mechanism of interaction still comes from the black box approaches. (*Note added in proof*. From the time this survey was completed, the situation has greatly evolved in favor of the many-body treatment of nuclear problems.) Thus we concentrate on reaction mechanism models and analyse the existing data in terms of direct and compound nucleus theories. In the following pages we outline briefly the main reaction mechanisms. A more detailed description is given in the analysis of experimental data. The reader is also referred to several existing reviews like the one of Ericson[1] for the compound nucleus and of Austern[19] and Glendenning[21] for direct processes.

A. Reaction Mechanism Theories

A commonly employed partition divides the nuclear reactions according to their time duration. Although mathematically we can treat only the extremes—the infinitely short and infinitely long (equilibrium) interactions—it has become customary to consider the reactions which take place within a time comparable to the transit time of energetic nucleons through atomic nuclei (10^{-22} sec) as direct reactions, involving the excitation of only a few of the numerous degrees of freedom available in the nucleus. The reactions lasting one or more orders of magnitude longer are treated as equilibrium processes leading to long lived compound states. The domain inbetween the two extreme cases are the intermediate reactions which made their appearance in nuclear physics only recently.

1. Compound Nucleus Theory: Basic Assumptions

We start by stating the basic ideas and formulating the main equations that govern the extreme case of a slow reaction, the compound nucleus process. When the incident particle interacts with the target nucleus in such a way that its energy and momentum are evenly distributed through the nucleus, a long lived equilibrium system, called the compound nucleus is created. A typical feature of the system in equilibrium is that it is entirely determined by the constants of motion of the system and its size and shape; it is entirely independent of the details of the formation of the system.[1] Thus the mathematical treatment of a compound nuclear system in many ways parallels the treatment of classical thermodynamic systems, such as a liquid drop or radiative emission from a blackbody.

The analogy of an equilibrium system in nuclear reactions and a classical thermodynamic system, as foreseen by Bohr, carries several important implications. As already mentioned, the behavior of a system in equilibrium, in particular its decay, is independent of its mode of creation. The Bohr assumption of a nuclear reaction as a decay of a system in thermodynamic equilibrium (the compound nucleus) leads straightforwardly to the formulation of the expression for the cross section of a nuclear reaction,

$$X(a, b)Y \tag{1.1}$$

in the form[2]

$$\sigma(a, b) = \sigma_c(a) P_c(b),$$

where $\sigma_c(a)$ is the cross section for the formation of the metastable compound system from the incident particle a and the target nucleus X, and $P_c(b)$ the probability that the compound system, once formed

CC-0. In Public Domain. Gurukul Kangri Collection, Haridwar

Digitized by Arya Samaj Foundation Chennai and eGangotri

will decay by emission of particles b. The independence of the modes of creation and decay ("loss of memory" in the compound nucleus) is reflected by the factorization of the cross section.

The compound nucleus as an equilibrium system is created as a result of subsequent scattering of nuclear particles, and the time necessary to attain such equilibrium is of the order of nuclear relaxation times. Hence, considerations based on nuclear recurrence times are important when considering the applicability of the compound nucleus theory to nuclear processes. It is well known that the recurrence time for a wave packet with an energy spread much larger than the level spacing formed of the compound nucleus is of the order of

$$2\pi h/D$$

for nonoverlapping equidistant levels of spacing D. It is thus that the criteria for the applicability of the Bohr assumption are most commonly discussed in terms of the overlap of compound state levels, which can be easily reduced to incident particle energy and target nucleus mass, rather than in terms of a time duration scale.

For incident particles of low energy the levels of the compound nucleus are well separated, and their width Γ is much smaller than their spacing D. The lifetime of such levels

$$\tau=\hbar/\Gamma$$

is much larger than the recurrence time $(2\pi h/D)$ of the system and the Bohr conditions are widely met.[3] Our main interest lies however, in the region of several MeV of incident energy where with increasing excitation of the compound nucleus its lifetime grows shorter as more and more exit channels become available. As the levels become less defined and start overlapping it is not possible any longer to make a general statement about an equilibrium system based on recurrence times. The applicability of the compound nucleus mechanism can, however, be understood in a different way. The energy spread of the incident beam here plays an essential role. For a given energy of excitation several overlapping states will, in general, contribute to the process. These states will interfere: however, there is an averaging effect due to the finite energy spread of the incident beam while an additional averaging is caused by transitions to different final states.

At this point we make use of the statistical hypothesis of the randomness of phases.[4,5] The phases between the different transition amplitudes interfere, and, provided they are randomly distributed, the averaging over the fluctuations inside the energy spread of the incident beam leads to the cancellation of cross-term contributions to the reaction cross section. Thus the statistical hypothesis of random phases of compound nucleus states is equivalent to saying that the contribution of cross terms to the transition amplitude is negligible and most of the transitions come from diagonal terms. Accordingly, the problem can still be treated as a classical one.

The success of the compound nucleus model in explaining intermediate energy nuclear reactions constitutes only an *a posteriori* argument for the validity of the statistical hypothesis.

The mathematical treatment of the compound nucleus theory can be considerably simplified if certain semiclassical concepts and pictures are adopted. Formulas derived in this way are applicable only to reactions leading to continuously populated final states, but in this range their validity is not necessarily less general. The advantage of such a treatment is that it gives a more straightforward insight to the meaning of expressions and parameters that govern a statistical process. For this reason we start with a presentation of the semiclassical treatment of the statistical theory.

2. *Statistical Theory: A Semiclassical Treatment*

The treatment of a nuclear reaction as an equilibrium process implies the knowledge of the two factors, $\sigma_c(a)$ and $P_c(b)$, entering Eq. (1.1). The cross section for compound nucleus formation $\sigma_c(a)$ is most readily calculated from the optical model, as the reaction cross section σ_R (i.e., the total cross section σ_T diminished by the shape elastic cross section σ_{SE})

$$\sigma_R=\sigma_T-\sigma_{SE}.$$

In equating the compound nucleus formation cross section σ_c to the optical model reaction cross section σ_R one tacitly assumes that every nuclear interaction takes place through the formation of a compound nucleus. This is certainly an overestimate of σ_c. The extent of this overestimation is discussed later on; however, the analysis of inelastic scattering data confirms the plausibility of this assumption.[7] The calculation of σ_c is rather complicated and requires the use of fast computers. However, several sets of calculated optical model cross sections are available both for charged particles[8,9] and neutrons.[10] Codes are also available for calculating cross sections using different local and nonlocal optical potentials.

The determination of the second term in (1.1), governing the decay of the compound nucleus, is less straightforward, although considerable progress has been made towards a better understanding of the use of different parameters involved. Derivation of a suitable form of $P_c(b)$ is based on the principle of detailed balance.[1,6] We merely give the final result and add a few comments on its validity. It can be shown that the probability per unit time of the compound nucleus decaying into an open channel leading to the emission of a particle ν with energy in the interval $(\epsilon_\nu, \epsilon_\nu+d\epsilon_\nu)$ is given by

$$P_\nu(\epsilon_\nu)d\epsilon_\nu=g_\nu\cdot(8\pi\mu_\nu\epsilon_\nu/\hbar^2)\sigma_\nu^*(\epsilon_\nu)[\rho_\nu(E_\nu)/\rho_c(E_c)], \tag{1.2}$$

CC-0. In Public Domain. Gurukul Kangri Collection, Haridwar

Digitized by Arya Samaj Foundation Chennai and eGangotri

where g_ν, μ_ν, and ϵ_ν are the spin weight $(2s_\nu+1)$, the reduced mass, and the energy of the emitted particle ν, respectively, and $\sigma_\nu^*(\epsilon_\nu)$ the cross section for the compound nucleus formation by the inverse process (absorption of particle ν with energy ϵ_ν by the residual nucleus). The level density factors $\rho_\nu(E_\nu)$ and $\rho_c(E_c)$ represent the level densities of the residual and compound nuclei at the corresponding excitations.

Equation (1.2) represents the basic equation governing the decay of the compound nucleus. It is based on the principle of detailed balance which in this case (overlapping levels) has a meaning only if applied to the average transition probability for the energy interval $\pm\Gamma$.

Using (1.1) and (1.2) we can readily deduce the cross section for a compound nuclear reaction. The total probability of decay of a compound nucleus is the sum of all particle probabilities over all kinds of particles and all ranges of energies:

$$P=\sum_\nu \int P_\nu(\epsilon_\nu)\, d\epsilon_\nu.$$

Thus the cross section for a specific emission is determined by the competition of different modes of decay, $P_\nu(\epsilon_\nu)/P$, which we can write explicitly by the aid of (1.1) and (1.2)

$$\sigma(a;\epsilon_\nu)\, d\epsilon_\nu=\sigma_c(a)\cdot\frac{g_\nu\mu_\nu\epsilon_\nu\sigma_c^*(\epsilon_\nu)\rho_\nu(\epsilon_\nu)\, d\epsilon_\nu}{\sum_\nu g_\nu\mu_\nu\int_0^{\epsilon\,\mathrm{lim}}\epsilon_\nu\sigma_c^*(\epsilon_\nu)\rho_\nu(\epsilon_\nu)\, d\epsilon_\nu} \tag{1.3}$$

where the symbols have been explained before and the upper limit in the integral is obtained from energy conservation requirements. This is the well-known Weisskopf–Ewing formula for the emission into a particular exit channel in a nuclear reaction.[5]

Expression (1.3) shows that the decay of the compound nucleus, whose probability of formation is given by σ_c, is governed by the available phase space modified by a penetrability factor $\sigma_c^*(\epsilon_\nu)$. So far we have no way of measuring experimentally the cross section for the formation of the compound nucleus by the inverse reaction, which, as a rule will take place with the residual (now target) nucleus in an excited state. So we assume that this cross section is equal to the previously defined simple compound nucleus formation cross section (or, in essence, to σ_R), an assumption borne out by results. Having more or less established the meaning and value of the penetration factor σ_c^*, we discuss the level densities which are a crucial parameter in the determination of spectral shapes and total cross sections.

There are good grounds for the treatment of the nucleus as a system of fermions moving in an average potential. This model, called also the Fermi gas model, accounts for the rapid increase of level densities with excitation energy by the very additivity of energy of states in a system of fermions. In this model the problem of calculating the level densities is a combinatorial one, and can be treated in the usual thermodynamic way.

In the Fermi gas model the number of levels with a given energy E and angular momentum J is given by

$$\Omega(E,J)=[(2J+1)/\pi^{\frac{1}{2}}(2cT)^{\frac{3}{2}}]\times\exp[-(J+\tfrac{1}{2})/2cT]\rho(E), \tag{1.4}$$

where

$$\rho(E)=\text{const.}\ (E+t)^{-\frac{1}{4}}\exp[2(aE)^{\frac{1}{2}}]. \tag{1.4a}$$

We have introduced several new parameters in the formulas (1.4) and (1.4a). The level density parameter a is proportional to the single-particle spacing g_0 near the Fermi energy and related to the Fermi energy itself by

$$a=\tfrac{1}{6}(\pi^2 g_0)=\tfrac{1}{4}[\pi^2(A/\xi_0)]. \tag{1.5}$$

As the Fermi energy of a gas is independent of the number of particles (nucleons) in the gas

$$\xi_0=(3/\pi)^{\frac{2}{3}}(\hbar^2/2Mr_0^2) \tag{1.5a}$$

(M and r_0 are the nucleon mass and radius respectively), the experimentally derived values of the level density parameter a should present a rough proportionality with the mass number A. For appropriate nucleon radii ($r_0=1.1-1.2$ F) the value of the Fermi energy $\xi_0=31$ MeV, which gives for a the value $A/8$. This indeed, is the case.[11] Later on we introduce a more detailed theory that introduces shell effects in the level densities by means of j-dependent a values.

The parameter a is also related to the thermodynamic temperature t by a quadratic dependence

$$E=at^2-t \tag{1.6}$$

which, in essence, is the "equation of state" for a Fermi gas.

It can be shown that the value of $c\hbar^2$ in this model is equal to the rigid body moment of inertia, and the nuclear (to be distinguished from the thermodynamic) temperature T is given by

$$T^{-1}=[d\ln\rho(E)/dE]=(a/E)^{\frac{1}{2}}-\tfrac{5}{2}(2E+t)^{-1}. \tag{1.7}$$

The factor $2cT$ in the exponential of (1.4) is the well-known spin cutoff factor $2\sigma^2$.

The form of the level density energy dependence given in (1.4) is not the one usually employed under the name of Fermi gas model. One should notice, however, that as E becomes large, the preexponential factors

$$(E+t)^{-\frac{1}{4}} \quad \text{and} \quad t^{-1}$$

vary as

$$E^{-\frac{1}{4}} \quad \text{and} \quad E^{-\frac{1}{2}},$$

CC-0. In Public Domain. Gurukul Kangri Collection, Haridwar

Digitized by Arya Samaj Foundation Chennai and eGangotri

respectively, thus giving rise to the high-energy limit form of the level density

$$\rho(E) \propto E^{-2} \exp\left[2(aE)^{\frac{1}{2}}\right] \tag{1.8}$$

which is the commonly employed form. It is questionable, however, how and when this limit is reached in most of the neutron experiments analyzed.

The free fermion gas model is an essential basis of our treatment of nuclei, represented as a system of free, noninteracting nucleons. This picture is in many respects too crude, in the first place because the residual interaction effects are neglected. The importance of these effects is seen in the odd–even differences in nuclear level densities. In order to incorporate at least some of these residual interaction effects (pairing, shell structure etc.) one extends the Fermi gas model by artificially shifting the zero energy levels in odd–A and even–even nuclei by an amount varying up to 2 MeV. Phenomenologically this energy shift can be correlated to the energy necessary to break up a pair of nucleons. Thus the even–even nucleus behaves similarly to the odd–odd nucleus once a pair has been broken and the same number of particles results in each case, however, with an excitation energy decreased by the amount necessary to break up the pair (pairing energy). Thus, if the pairing energy is equal to 2δ, we can write

$$\rho_{\text{odd-odd}}(E) = \rho_{\text{odd}-A}(E-\delta) = \rho_{\text{even-even}}(E-2\delta) \tag{1.9}$$

the odd–A nuclei being somewhat intermediate. Values of δ (negative) obtained from mass formulas are listed in Cameron.[12]

The formulas (1.4)–(1.8) represent the mathematical outcome of the Fermi gas theory. Although other models of nuclear level densities are available, most of the analyses has been performed with this model.

Bohr, Mottelson, and Pines[13] have proposed a model based on the analogy between the spectra of excited nuclei and those of a superconducting metallic state. The essential feature of this model is that above a certain critical energy the nucleus behaves as a common Fermi gas, except that the energy of excitation is measured from a Fermi energy which lies above the even–even mass surface. This model gives, among other things, a different value of the spin cut-off parameter $2\sigma^2$, which is consistently above the free Fermi gas model value.

The salient feature of the nuclear level densities, their fast increase with excitation energy, can be taken into account by the simple expression (constant temperature model)

$$\rho(E) \propto \exp(E/T), \tag{1.10}$$

where T is a parameter often called the nuclear temperature. The expression (1.10) is actually the extreme application of the evaporation concept to atomic nuclei, and although plausible, it is not based on a proper nuclear model. Nevertheless many satisfactory results have been obtained using this expression.

3. *Statistical Theory: General Case*

The formalism developed in the preceding section could be applied to those transitions that lead only to a continuum of final states. There is no reason why compound nucleus reactions should not lead to well separated states with definite spins and parities. In this section we develop a formalism that provides for both cases, in the sense that the case of transitions to many final states can be obtained by appropriate summation of transition probabilities to individual states.[14,15] The account is mostly based on Ref. 16.

The theory is again based on the assumption that all states of the compound nucleus which can be excited on the basis of conservation of energy, angular momentum, and parity do participate in the reaction, but that the formation and decay of the compound nucleus take place in an incoherent way. Thus the cross section for a reaction induced by a particle of energy ϵ_0 and intrinsic spin i on a target with spin I leading to the emission of a particle with energy ϵ and spin i' and a residual nucleus of spin I' is given by[16]

$$\sigma\langle\alpha \mid \alpha'\rangle = \pi\lambda\!\!\!^{-2} \sum_{J,j,l\ j',l'} [(2J+1)/(2i+1)(2I+1)] \times (T^J{}_{\alpha',j',l'} T^J{}_{\alpha,j,l} / \sum_{\alpha'',j'',l''} T^J{}_{\alpha'',j'',l''}), \tag{1.11}$$

where l is the orbital angular momentum of the incoming particle, $j = I+i = J-l$ its channel spin, while l' and $j' = J-l'$ are the corresponding values for the emitted particle. The symbols α and α' mean a set of values characterizing the entrance and the exit channels, respectively, while T stands for penetrabilities.

The sums in (1.11) are submitted to the ordinary laws of angular momentum and parity conservation. The former law requires that only those terms that satisfy

$$|J-l| \leq j \leq J+l$$
$$|J-i| \leq j \leq J+i$$
$$|J-l'| \leq j' \leq J+l'$$
$$|J'-i'| \leq j' \leq J+i'$$

(J stands for the compound nucleus angular momentum) can be included in the first sum in (1.11). Conservation of parity requires that the sum runs over all final states consistent with

$$(-1)^{l'}\pi_q = (-1)^{l}\pi_{\text{initial}}$$
$$(-1)^{l''}\pi_p = (-1)^{l}\pi_{\text{initial}}.$$

Finally the energy conservation restricts the sum in the denominator to levels with energy $E < \epsilon_0$. Similarly, the second (double primed) sum goes over all possible ways through which the compound nucleus can decay when the decay characterized by α', j', l' can occur.

CC-0. In Public Domain. Gurukul Kangri Collection, Haridwar

Digitized by Arya Samaj Foundation Chennai and eGangotri

Equation (1.10) gives the total cross section for the emission of a particle to a specific final state, regardless of the direction of emission. The angular distribution of emitted particles is given by

$$\sigma\langle\alpha \mid \alpha'\Omega\rangle = \tfrac{1}{4}\lambda^2 \sum_{J,l,j,l',j'} \frac{(-1)^{j'-j}}{(2i+1)(2J+1)} \frac{T^J{}_{\alpha jl} T^J{}_{\alpha' j' l'}}{\sum_{\alpha'' j'' l''} T^J{}_{\alpha'' j'' l''}} \times i^{-2L} \sum_L Z(lJlJ; jL) Z(l'Jl'J; j'L) P_L(\cos\theta), \quad (1.12)$$

where L in the last sum should be taken over even values for $L \leq \min(2l, 2l', 2J)$; the rest of the symbols are as in (1.11). The angular momentum factors $Z(abcd; ef)$ are given by Blatt and Biedenharn[17] and can be expressed in terms of Clebsch–Gordan and Racah coefficients.[16] The $Z(a, b, d, d; ef)$ vanish unless $a+c+f$ is even. In our case this means that the only nonvanishing terms in the last summation are those for which

$$2l+L, \quad \text{i.e., } L \text{ is even.}$$

This has the important consequence that in Eq. (1.12), only Legendre polynomials $P_L(\cos\theta)$ of even order are present, i.e., that the angular distribution is symmetric around 90°.

It is interesting to note that the statistical assumption, in which interference terms between different states in the compound nucleus are assumed to average out leads to the fact that l and J, and l' and J' repeat in the Z symbols. Consequently, in the cross section, involving products of wave functions, only terms containing the same l and J values are retained. This same cancelation of interference term means that no polarization of emitted particles can result in compound nuclear reactions. Thus if the incident beam is unpolarized, the cross section depends only on the polar angle θ.

The integration of (1.12) over the solid angle leads to the expression (1.11) for the total cross section for the emission into a separate final state.

The cross section for the compound nuclear transition in the case when final levels are not separated should be obtained from (1.11) by summing (or integrating) over all final states. This should lead to an expression identical to (1.3), obtained in a semiclassical way.

We thus assume that the density of final states is a continuous function of energy and perform explicitly the integration of expression (1.11) over a definite range of energy. For simplicity, competing decay channels α' leading to fission or radiative transitions are neglected, and only particle channels assumed to be important. Furthermore, no parity conservation restrictions are present, since the continuum has equal population of positive and negative parity states.

With these assumptions, the cross section for the reaction induced by a particle a with energy ϵ_0 leading to a particle ν with energy in the interval $\epsilon, \epsilon+d\epsilon$, is given by

$$\sigma_{a,\nu}(\epsilon_0, \epsilon)\, d\epsilon = \pi\lambda^2 \sum_{J,j,l} \frac{2J+1}{(2i+1)(2I+1)} \times \left(T^J{}_{ajl}(\epsilon_0) \cdot \sum_{J'l'I'} T^J{}_{\nu j' l'}(\epsilon) \cdot \rho_\nu(I', E)\, d\epsilon \Big/ \sum_{\nu'' j'' l'' I''} \int_0^{\epsilon_0 - Q_{\nu''}} d\epsilon\, T^J{}_{\nu'' j'' l''}(\epsilon) \rho_{\nu''}(I'', E'')\, dE'' \right). \quad (1.13)$$

The symbols are again as in (1.11) and (1.12) except that the incoming and outgoing channels, α and α' have been replaced by the notation a and ν, respectively. The sum in the denominator runs over all energetically possible emitted particles ν''. $\rho_\nu(I', E)$ is the density of levels of the residual nucleus after the emission of a particle, leaving the residual nucleus with an excitation

$$E = \epsilon_0 - \epsilon - Q, \quad (1.13a)$$

where Q is the Q value of the reaction.

To reduce Eq. (1.13) to a form similar to the Weisskopf–Ewing formula (1.3) two additional assumptions are necessary:

(i) that spin and energy dependence of the level density (I, E) can be factored into

$$\rho(I, E) = (2J+1)\rho(E)$$

(ii) that the penetrabilities T do not depend on j or J but only on l.

With the consequent simplifications in the summations, after the enumeration of the statistical weight factors, Eq. (1.13) reduces to

$$\sigma_{a\nu}(\epsilon_0, \epsilon)\, d\epsilon = \sigma_c(a, \epsilon_0) \left((2i'+1)\epsilon\sigma_{c,\nu}{}^*(\epsilon)\rho_\nu(E)\, d\epsilon \Big/ \sum_{\nu''} (2i''+1) \int_0^{\epsilon_0 - Q_{\nu''}} \epsilon'' \sigma_{c,\nu''}(\epsilon'') \rho_{\nu''}(E'')\, dE'' \right), \quad (1.14)$$

CC-0. In Public Domain. Gurukul Kangri Collection, Haridwar

Digitized by Arya Samaj Foundation Chennai and eGangotri

where the combinations $\sum_l (2l+1)T_l$ have been replaced by the cross sections for compound nucleus formation, $\sigma_{c.n.}$* to which they are proportional.

Equation (1.14) is the well-known Weisskopf–Ewing formula (1.3) derived in the preceding section.

4. Direct Reaction Theories: General Predictions

The other extreme in a time classification of nuclear reactions is given by the extremely fast reactions, with duration times of the order a nucleon takes to cross the nucleus. These reactions are generally known as direct reactions and comprise a number of mechanisms by which a particle can be excited in a direct collision. In a long process during which the nucleon crosses the nucleus several times, many degrees of freedom can be excited. On the contrary, if the nucleon just crosses the nucleus, it excites only a few degrees of freedom. Thus the time scale of nuclear reactions implies a description of direct processes as those involving only a few of the many degrees of freedom of a nucleus. The minimum number of degrees of freedom that must be involved in a nuclear reaction are those required to describe the initial and final channels and direct reaction studies consider just these. Strictly speaking this kind of reasoning contains a sometimes not justifiable mixture of classical (collision time and number of collisions) and quantum concepts (number of degrees of freedom involved). Its only justification is that it provides a simple insight into the energy and angular dependence of the two main mechanisms of interaction.

It is clear that direct interaction processes take only a fraction of the incident wave function. The rest is connected with complicated excitations of many degrees of freedom and result in the gradual formation of a compound nucleus. It is however true that the direct processes, when existing, have a large cross section. The causes for such a large cross section are not yet fully understood, and the answer is probably not unique.

The reason why direct effects are, when existing, large is deeply bound with our knowledge of nuclear structure. Our attitude towards the direct interactions has been—even historically—rather parallel to that towards the shell model. This is clear, since both models rely on the assumption that, to a good approximation, the mean free path of nucleons in nuclear matter is infinite. For reactions involving nucleons, the intrinsic reason of the extraordinary magnitude of direct reactions is found in the same properties which cause the independent particle model to be a good approximation of nuclear behavior. Namely, the attractive part of the two-nucleon force is moderately weak and of long range and thus goes mostly in setting up an average potential responsible for shell model configurations. Now, the low-lying excited states which are in the same shell model configuration as the ground state have a great deal of overlap with the ground state and can be excited strongly in the very initial stages of interaction.

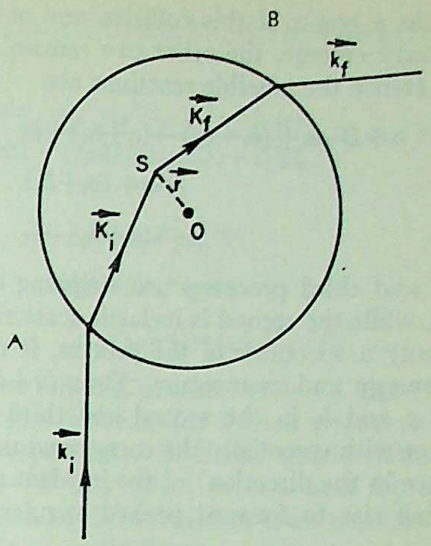

FIG. 1. The semiclassical model of direct reactions (Ref. 19).

Thus strong direct interaction excitations are expected to occur for these states in the cases of (incident) nucleon–(outgoing) nucleon reactions. For composite particles the reasons are more complex, but in general are connected to their low penetrabilities and the excitation of low-lying surface vibrational levels.[16]

The simplest direct interactions involve a three-body rearrangement collision.[19] They are known as *knock-out* scattering (a bombarding particle, which need not be a nucleon, may interact with a particle in the target nucleus, both particles being then lifted to higher states of motion), *stripping* and its inverse *pick-up* (a particle bound in one of a pair of colliding nuclei may make a transition to a bound state in the other), and *collective surface oscillations* (a bombarding particle collides with the surface of a nucleus thereby inducing a collective oscillation, which again results in inelastic scattering). The mathematical expressions governing these processes can be found in several excellent reviews, on which the following presentation is based.[18–21] We briefly review the main ideas and state, when possible, the most widely used formulas.

The treatment of direct reactions is somewhat different for the cases when final levels can or cannot be resolved. In each case a semiclassical treatment (Fig. 1) can be applied, that leads to an asymmetric angular distribution of emitted particles. However, while in the former case the asymmetry can be understood as a consequence of angular momentum conservation, in the latter case it is rather the conservation of linear momentum that causes a general forward peaking.

(*i*) *Sharp levels not resolved.* In this case the theory predicts forward peaked angular distributions and spectra composed predominantly of higher energy particles. The two results can be understood qualitatively in the following way.[19] A direct interaction process can be pictured as involving the collision of a nuclear unit a colliding with a subunit b_1 of a nucleus B, the remaining subunit b_2 of B being only a spectator to this

CC-0. In Public Domain. Gurukul Kangri Collection, Haridwar

Digitized by Arya Samaj Foundation Chennai and eGangotri

collision. As a result of this collision any of the three particles may emerge, the other two remaining bound together. Hence the possible reactions are:

$$a+B\rightarrow a+(b_1+b_2)\rightarrow(a+b_1)+b_2$$
$$\rightarrow a+(b_1+b_2)$$
$$\rightarrow(a+b_2)+b_1.$$

The first and third processes are stripping or pickup processes, while the second is inelastic scattering. Now, as b_2 is only a spectator of the process, it retains its original energy and momentum. Thus $(a+b_1)$ in the first and a and b_1 in the second and third processes will emerge with essentially the energy and momentum (and hence in the direction) of the incident particle a, thus giving rise to forward peaked angular distributions.

A similar argument can explain the hardening of the spectra observed in direct processes. Since the incident particle a and the interacting subunit b_1 are usually of a comparable size, the transfer of momentum will be maximal, favoring the emission of more higher energy particles. A more specific derivation of the shape of the spectra of particles emitted in direct reaction can be obtained by taking into account the fact that in a direct reaction the energy distribution is the result of two competitive processes. For a volume direct interaction the incoming nucleon first interacts with the proton and neutron Fermi sea. For a maximal transfer of energy and momentum, the reaction may take place only on the surface of the Fermi sea. Reactions with less momentum transfer can occur also deeper in the Fermi sea. Thus the maximum in the spectrum comes as a result of the interplay of two factors:

—the Pauli principle making more and more protons available for the interaction and
—the Coulomb barrier, inhibiting their emission.

The expression for the energy spectrum of direct volume reactions is thus given by[22]

$$N(\epsilon)\propto b_1(\epsilon_{\max}-\epsilon)+b_2(\epsilon_{\max}-\epsilon)^2+b_3(\epsilon_{\max}-\epsilon)^3+\cdots, \tag{1.15}$$

where $\epsilon_{\max}$ is the maximum energy transfer. The above expression is valid only for volume interactions. Qualitatively both volume direct and compound nuclear mechanisms lead to similar results for the energy spectrum of emitted particles, since in both cases the distribution is the result of two competitive processes.

(*ii*) *Sharp levels resolved.* In this case it is possible to speak only of angular distributions. The general argument from the preceding section holds again, but the forward peaked asymmetry is modified by angular momentum conservation requirements. In the semiclassical model of Butler[23] the process is pictured as a refraction of the incident ray on the surface of the nucleus followed by the main scattering inside the nucleus and a second refraction when the emitted particle leaves the nucleus. The transfer of momentum to the nucleus is

$$\mathbf{q}=\mathbf{k}_i-\mathbf{k}_f,$$

where $\mathbf{k}_i$ and $\mathbf{k}_f$ are the momenta of the incident and outgoing particles, respectively. In the semiclassical picture we shall assume that the momenta of the particles inside the nucleus are equal to the momenta outside it. Thus the transfer of angular momentum which takes place at S is

$$\Delta\mathbf{L}=\hbar\mathbf{q}\times\mathbf{r}.$$

As the angular momentum is quantized, and restricted to integer values $l\hbar$, the reaction may proceed only at those points $\mathbf{r}$, which satisfy the equation

$$l=|\mathbf{Q}\times\mathbf{r}|.$$

These points lie all on a surface of a cylinder of radius l/Q whose axis passes through the center of the nucleus in the direction $\mathbf{q}$, the so-called *active cylinder*. A further simplification, based on the absorption of particles in nuclear matter, restricts the contributing points to the nuclear surface only ($r\geq R$). Thus the contributing points lie on the intersection between the active cylinder and the nuclear surface, and the total transition amplitude can be obtained by adding coherently all these contributions:

$$T=\int_{ac(r\geq R)}p(r)\exp(i\mathbf{Q}\cdot\mathbf{r})\,d\mathbf{r}. \tag{1.16}$$

$p(r)$ weights the probability that a reaction can take place at a given point and $\exp(i\mathbf{q}\cdot\mathbf{r})$ is a phase factor accounting for the differences in phases between outgoing rays originating from different points in the nucleus.

Performing the integration, (1.16) leads to

$$T=4\pi l\int_R^\infty rdrp(r)\cos(Q^2r^2-l^2)^{\frac{1}{2}}/(Q^2r^2-l^2)^{\frac{1}{2}}. \tag{1.17}$$

The factor $p(r)$ must fall off very rapidly for $r>R$, since it is proportional to the nuclear density. Moreover only as long as $qR<l$, so that the active cylinder does in fact intersect the nuclear surface, will the transition amplitude be different from zero. When $qR<l$ the active cylinder misses the nucleus, and so there are no contributions and the cross section is zero. Combining this with the above assumption on $p(r)$, the angular distribution can be written in the form

$$\sigma(\theta)\propto\cos^2(Q^2r^2-l^2)^{\frac{1}{2}}/(Q^2r^2-l^2) \quad \text{for } qR>l$$
$$\sigma(\theta)\rightarrow 0 \quad \text{for } qR<l. \tag{1.18}$$

Equations (1.17) and (1.18) give all the essential features of a direct reaction angular distribution: the oscillatory behavior, seen as a typical interference effect, and the existence of forbidden regions of emission. Namely, for a reaction in which $l>0$ it may happen

CC-0. In Public Domain. Gurukul Kangri Collection, Haridwar

Digitized by Arya Samaj Foundation Chennai and eGangotri

that for small angles $qR<l$. For this reaction there will be no (in the extreme case) emission in the forward angles.

Despite its shortcomings the simple model gives a better than qualitative insight into the main features of the direct processes. It has, however, been almost abandoned in favor of the more sophisticated approaches, which we briefly review in the next section.

5. *Direct Reaction Theories: The DWBA Method*

The exact matrix for a direct transition between an initial state i and a final state f is given by

$$T_{if}=\langle\phi_f \mid V \mid \psi_i\rangle, \tag{1.19}$$

where ϕ_f and ψ_i are the wave functions of the final and initial states, and V the interaction that causes the transition. The interaction V is usually the nucleon–nucleon interaction, or, in the case of more complex particles, some mathematically solvable prescription. To the present time we are not able to evaluate (1.19) exactly. It can be shown, however,[21] that the exact expression (1.19) can be approximated by .

$$T_{if}\doteq\langle\chi_f^{(-)} \mid V \mid \chi_f^{(+)}\rangle, \tag{1.20}$$

where $\chi_i^{(+)}$ and $\chi_f^{(-)}$ are simple wave functions obtained by factoring the state wave functions into their components:

$$\chi_{i,f}^{(\pm)}=\psi_{i,f}^{(\mathrm{el})}\phi_{i,f}^{(\mathrm{int})}\xi_{i,f}^{(\mathrm{spin})}\Psi(\text{target, residual}), \tag{1.21}$$

where $\psi^{(\mathrm{el})}$, $\phi^{(\mathrm{int})}$, and $\xi^{(\mathrm{spin})}$ stand for the elastic scattering, internal, and spin wavefunctions of the incident (i) viz. outgoing (f) particle, respectively, and $\Psi^{(\mathrm{target})}$ and $\Psi^{(\mathrm{residual})}$ represent the target and the residual nuclei wave functions, respectively.

Up to this point we have not made any physical assumption about the nature of the process. Now we take into account the physical nature of the transition, and appropriately decompose the final state wave function. It is most convenient to consider a (d, p) stripping process, as representative of direct reactions.[21] In this case we decompose the wave function of the residual nucleus on a basis exhibiting the target+stripped neutron,

$$\Psi^{(\mathrm{residual})}(A, \mathbf{r}_n, \mathbf{s}_n)=\sum_{l,j,J_c}\beta_{jl}(J_c, J_f)\Phi(J_c, j, l), \tag{1.22}$$

where Φ is a wave function constructed by vector coupling the extra nucleon in the spin–orbit state $\phi_{l,j}$ to a target wave function with angular momentum J_c. The expansion coefficients β_{jl} represent the degree to which the final state has the configurations indicated by Φ, and are directly related to the reduced widths of the corresponding states.

With the necessary rearrangements,[21] the square of the transition amplitude, i.e., the stripping cross section is given by

$$\frac{d\sigma}{d\Omega}=\frac{m_d^*m_p^*}{(2\pi\hbar^2)^2}\frac{k_p}{k_d}\frac{2J_f+1}{2J_i+1}\sum_{j,l,m}\beta_{jl}^2\mid B_l^m\mid^2, \tag{1.23}$$

where

$$k_p^2=2m^*p\epsilon_p/\hbar^2,$$

$$k_d^2=2m_d^*\epsilon_d/\hbar^2,$$

$$\epsilon_p=\epsilon_\alpha+Q=\epsilon_d+B_n-B_d,$$

m^* are the reduced masses, while ϵ's and B's are kinetic energies in the center of mass system and binding energies respectively. Equation (1.23) holds—*mutatis mutandis*—for any direct process and represents the general form of direct reaction cross sections.

Aside from multiplicative constants, the cross section (1.23) has been decomposed into two factors: the already defined expansion coefficients β_{jl} and the quantities B^m that in essence represent the overlap integrals between the elastic scattering wave functions of the incoming and outgoing particles:

$$B_l^m=i^{-l}(2l+1)^{-\frac{1}{2}}\int\psi_p^*\xi_pV_{np}(r)\psi_d\xi_d\,dr, \tag{1.23a}$$

where ψ_p and ψ_d are elastic scattering proton (outgoing) and deuteron (incoming) wavefunctions and ξ_p and ξ_d are corresponding spin functions. The quantities B_l^m depend sensitively on l, and this is the root of the spectroscopic value of stripping and direct reactions in general.

The effect of antisymmetrization deriving from the fact that the nucleons in the nucleus are indistinguishable modifies the expression (1.23) into

$$\frac{d\sigma}{d\Omega}=\frac{a}{4}\frac{m_f^*m_i^*}{(2\pi\hbar^2)^2}\frac{k_f}{k_i}\frac{2J_f+1}{2J_i+1}C^2\sum_{l,m}S(l)\mid B_l^m\mid^2, \tag{1.24}$$

where

$$S(l)=\sum_j S(l,j)$$

$$S^{\frac{1}{2}}(l,j)=(A+1)^{\frac{1}{2}}\beta_{lj}$$

$$=(A+1)^{\frac{1}{2}}\int\Phi^*(J_c,j,l)\Psi_{J_f}\,d(A+1). \tag{1.24a}$$

a and A are the masses of the incident and target particles in the process, so that the equation (1.24) holds for any transfer reaction

$$A(a, a\mp1)A\pm1.$$

The rest of the symbols used have already been defined.

The importance of Eqs. (1.23) and (1.24) lies as already mentioned in the possibility of factorization. The first factor $S(l)$, called also the *spectroscopic factor*, is connected with the β_{jl}, i.e., with the overlap of the wavefunction Ψ_{J_f} of the residual nucleus and $\Phi_{J_c,j,l}$, the wave function constructed by vector coupling the

CC-0. In Public Domain. Gurukul Kangri Collection, Haridwar

Digitized by Arya Samaj Foundation Chennai and eGangotri

extra particle (nucleon, in general) in the spin orbit state ϕ_{lj}. This factor depends only on the nuclear structure. Vice versa, nuclear structure information can be obtained from knowledge of it. The second factor $|B_l^m|^2$ contains the angular distribution and the incident and outgoing wave functions. The difference between (1.23) and (1.24), introduced by the antisymmetrization does not affect the angular distribution but only the absolute value of the cross section. Hence it is important in obtaining spectroscopic information.

We end this presentation of direct reactions by discussing the elastic scattering wave functions $\psi_{i,f}$ of the incident and outgoing particles. In the plane wave Born approximation (PWBA) we assume that there is no interaction either between the incident particle and the target nucleus or between the outgoing particle and the residual nucleus. Thus the two particles satisfy the field free Schrödinger equation and are represented by plane waves.

Obviously this approximation is too crude. The effect of the optical and the Coulomb potentials of the nucleus distorts the wave functions of the incident and outgoing particles. These wave functions are now solutions of the Schrödinger equation including the nucleon–nucleus interaction. The presence of the distortion affects the B_l^m factors. However, the effect of the distorted wave Born approximation (DWBA) on the angular distribution itself is rather small; it rather changes the absolute value of B_l^m thus influencing the reliability of spectroscopic information obtained.

The potential that distorts the wave functions is the potential determined from the best fit of elastic scattering data. Thus in principle the DWBA method is an exact method which does not allow for any free parameters. In practice there is still considerable ambiguity in the values derived from the DWBA calculations.

6. *Intermediate Processes*

Between the two extremes in nuclear reaction mechanisms—the compound nucleus and the direct interaction—there certainly exists a wide spectrum of intermediate stage processes, characterized by a partial equilibrium resulting from the sharing of the incoming energy among a small number of particles.

Ideas of partial equilibrium were first introduced a long time ago by Bethe as spot heating. Bethe assumed that the nuclear interaction takes place in a rather restricted region of the nucleus, which is excited to a high temperature, and the evaporation takes place only in this region. A new approach to this problem has been given by Izumo.[24] Although Izumo uses the same concept of partial equilibrium, the essentially new idea in this approach is the supposition that the interacting nucleons need not be localized, but can very well be distributed over the whole nuclear volume. In this model the reaction is understood as taking place after a state of partial equilibrium is achieved. In other words, based on the experimental fact of rather broad resonances in the energy dependence of the cross section for a given final state (100–400 keV) Izumo envisages a partial (intermediate) equilibrium taking place after a time τ_μ, several orders of magnitude shorter than the time necessary for a complete equilibrium and yet much longer than the nucleon transit time in the nucleus. The total equilibrium is attained after a time

$$\tau_{CN}=\hbar/\Gamma\doteq 10^{-16}\text{ sec} \qquad (\Gamma=\text{level width})$$

while the nucleon transit time is equal to

$$\tau_{DI}=R/v\sim 10^{-22}\text{ sec}.$$

The intermediate partial equilibrium time should be of the order of

$$\tau_\mu=\hbar/\Gamma_\mu\sim 10^{-20}\text{ sec}.$$

One sees that

$$\tau_{CN}\gg\tau_\mu\gg\tau_{DI}.$$

These considerations lead to the assumption that the reaction proceeds through a certain partial equilibrium in which only a fraction of the nucleons takes part. One divides the nucleons into two groups: the inert core nucleons and the outer nucleons. Izumo's assumption states that only outer nucleons interact strongly with the incident particle, while the inert core remains in its ground state and produces only an average potential for the incident particle.

The essential part of the theory is that the transition amplitude T, although calculated analogously as for the core nucleons, uses a different density of residual states. As these states stem from the interaction of fewer particles, their density is smaller. The result is the same as having the same number of particles in a large potential well (the density of states decreases with R^{-2}). In calculating, therefore, the partial equilibrium transitions we select from all the possible levels of the residual nucleus only those, which one can reach through a partial equilibrium (compound state) process. The density of these states is smaller than for the whole compound nucleus which is accounted for by a smaller value of the parameter a entering in the formula

$$\rho(E)=\text{ const } E^{-2}\exp\left[2(aE)^{\frac{1}{2}}\right].$$

The associated physical picture implies that, as the energy is shared among fewer particles, the temperature is higher, and consequently, a is smaller ($E=aT^2$). Following our argument, this excitation E_0 gives the same level density as an excitation E of a classical compound nucleus given by (1.25)

$$E_0=\left[(A+n)/(N+n)\right]^{\frac{1}{2}}E,$$

where A, N, and n are the masses of the target nucleus, the interacting fragment inside the nucleus, and the incident particle, respectively. The factor $\left[(A+n)/(N+n)\right]^{\frac{1}{2}}$ shows the R^{-2} dependence. The level density $\rho(E)$ for a compound nucleus process is

CC-0. In Public Domain. Gurukul Kangri Collection, Haridwar

Digitized by Arya Samaj Foundation Chennai and eGangotri

then related to the intermediate state level density ρ_μ, as

$$\rho(E)=[(A+n)/(N+n)]^{\frac{1}{2}}\rho_\mu(E_0). \quad (1.26)$$

As the factor in brackets is greater than one, the intermediate state level density is less than the corresponding compound nucleus level density. A good fit for particles of medium energy is obtained with

$$N+n=6,$$

i.e., the interaction is spread over 6 particles.

A different approach has been taken by Feshbach and collaborators,[25] although again the same basic idea of sharing the energy among a smaller number of particles is present. Feshbach considers the different stages of creation of the compound nucleus, that takes part when the degree of complexity of the excitations gradually rises.

(i) The simplest interaction is when the incident particle interacts with what is essentially the real part of the shell model potential of the target nucleus, in elastic scattering, this interaction would correspond to the so-called potential scattering.

(ii) The next step is a two-body interaction between the incident particle and a nucleon from the target nucleus. This interacting particle is raised to higher state and leaves a hole behind. In this way a 3 quasi-particle (two particles–one hole) state has been created that may exhibit some of the features of a resonant state. This state, appropriately called a doorway state consists of two particles (usually two nucleons) the incident one and the excited one, raised to unbound (or bound) states in the nucleus and a hole that is left behind the excited particle.

(iii) This 3 quasi-particle configuration leads either to more complicated 5-, 7-, etc. quasi-particle configurations or dissolves back to a single-particle state in a potential well. In the former case, the gradual rise in complexity of the configurations (ultimately) leads to the creation of a compound nucleus. Hence the name of doorway states.

There is no question that such or similar processes take place. The question is whether this doorway state lives long enough to give rise to resonant structure narrow enough to be observed, or the lifetime of the state is so small that the related structure in the excitation functions is undetectable.

Feshbach has suggested that doorway states having a finite lifetime would give rise to intermediate structure in neutron total cross-section excitation functions. The estimated width of these resonances is 50–100 keV, and they would reveal themselves as a characteristic structure within a single giant (optical model) resonance.

A quantitative estimate of the width of doorway states has been suggested by Le Couteur.[26] The argument of Le Couteur is based on the fact that the total energy of excitation E, present in the process is partitioned between the excitation E_1 of one particle above the Fermi level and the excitation E_2 of the particle above the hole it previously occupied. The corresponding number of states within the range dE of excitation is

$$\tfrac{3}{4}g^2E\cdot dE,$$

where g is the average single-particle spacing,

$$g=(6a/\pi^2)\doteq\tfrac{1}{8}A \text{ MeV}^{-1}.$$

Hence[26] for a nucleus with atomic number A, the average spacing of doorway states is

$$\Delta=\tfrac{4}{3}(6A/8\pi^2)^{-2}E^{-1}=230A^{-2}E^{-1} \text{ MeV}. \quad (1.27)$$

This average distance is modified when considerations of angular momentum are taken into account. For a nucleus with small target spin the spacing is given by

$$\Delta_0=1.7A^{\frac{1}{3}}\Delta. \quad (1.27a)$$

The formula of Le Couteur gives a strong A dependence of the spacing of doorway resonances, contrary to possible experimental evidence.

B. Energy Spectra and Angular Distributions

Although we believe that, globally speaking, at least 80% of interactions of fast neutrons with atomic nuclei proceed via the compound nucleus formation, the investigation of the compound nucleus–direct interaction competition in neutron induced reactions is far from being exhausted. This concerns especially the presence of possible intermediate mechanisms.

There are several means of investigating reaction mechanisms, energy spectra and angular distribution studies being the most popular one. It has, however, been often pointed that none of these methods, taken *per se* provides sufficient information as to ascertain unambiguously the reaction mechanism.[27] Moreover, the determination of parameters connected with different models usually requires more than single-information-type experiments. Several complete experiments have been performed recently or are in progress.

1. Very Light Elements ($A<20$)

A few measurements of neutron reactions on very light elements ($A<20$) have been performed in the last two years. The easy obtainable combination C–N–O, present in nuclear emulsions has been investigated by Sen[28] with 14.3-MeV neutrons. The obtained spectra of alpha particles, although experimentally somewhat uncertain, show typically direct features with unresolved levels. The angular distribution of alpha particles from 14-MeV neutron bombardment of emulsions is shown in Fig. 2. A fit in terms of the three familiar direct interaction mechanisms, namely the pick-up (of He^3), knock-out of (He^4), and heavy-particle stripping has been attempted. For all the three mechanisms, the differential cross sections are given by the spherical

CC-0. In Public Domain. Gurukul Kangri Collection, Haridwar

Digitized by Arya Samaj Foundation Chennai and eGangotri

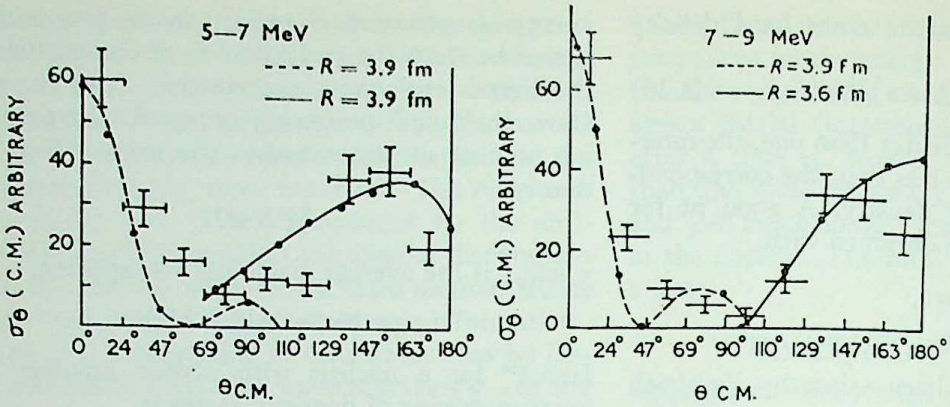

FIG. 2. Angular distribution of alpha particles from 14-MeV neutron bombardment of nuclear emulsion (C-N-O). The dotted line represents a fit with the pick-up mechanism; the full line is heavy-particle stripping (Ref. 28).

Bessel function of order l:

$$\sigma(\theta) \propto f j_l^2(QR), \tag{1.28}$$

where f is the form factor, and the distinction of the three reaction mechanisms comes only in the definition of the momentum transfer $\mathbf{Q}$:

pick-up:

$$\mathbf{Q} = (M_R/M_T)\mathbf{k}_n - \mathbf{k}_\alpha \tag{1.28a}$$

knock-out:

$$\mathbf{Q} = [(M_T - M_\alpha)/M_T]\mathbf{k}_n - [(M_T - M_\alpha)/M_R]\mathbf{k}_\alpha \tag{1.28b}$$

heavy-particle stripping:

$$\mathbf{Q} = \mathbf{k}_n + (M_n/M_R)\mathbf{k}_\alpha. \tag{1.28c}$$

(This is purely a consequence of the different kinematics of the three processes.) A reasonable fit for forward angles with the pick-up process and with heavy-particle stripping for backward angles has been attained. Thus it appears that a better approach to the understanding of the reaction mechanism is to assume a He^3 pick-up than a He^4 knock-out mechanism, in contrast with the results of several other authors. In fact in a later article Chatterjee *et al.*[29] found that the angular distribution of ground-state alphas from C^{12} could be fitted equally well by either [(pick-up, knock-out)+heavy-particle stripping mechanisms]. Furthermore, Al Kitel *et al.*[30] found evidence for clearly knock-out processes in the emission of alpha particles from C^{12} (Figs. 3-5). In their results the strongly forward angular distributions of ground state alphas and alphas from the excited states up to 5 MeV of excitation (it is believed that no alphas are emitted below this energy region, a point that experimentally has yet to be verified) of the residual nucleus are again equally well fitted by the pick-up and knock-out mechanisms. However, an additional argument in favor of the knock-out mechanism—in C^{12} *a priori* more likely—is given by the reduced widths of the ground and first excited states. The ratio of the reduced widths of these states for α emission amounts to 1.5. The knock-out mechanism gives 1.1 while the pure pick-up mechanism yields a ratio of 6.5. Thus our *a priori* guess seems well endorsed by the experimental evidence.

Further data about the $O^{16}(n, \alpha)C^{13}$ reaction are presented by Chatterjee,[31] who measured the angular distribution of alpha particles emitted up to an excitation of 4 MeV of residual nucleus C^{13}. The distribution is peaked in the backward direction and heavy-particle stripping gives an excellent fit. This and the preceding

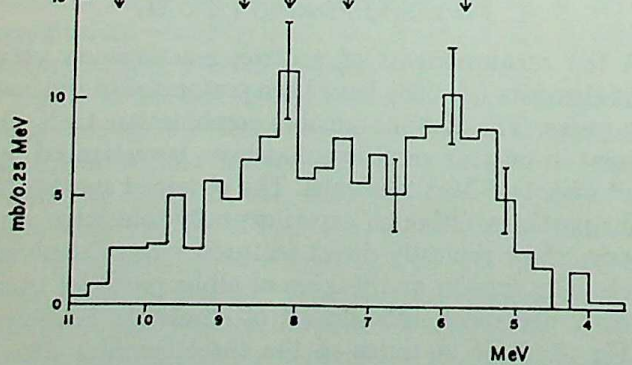

FIG. 3. Energy spectrum of alpha particles emitted from the reaction $C^{12}(n, \alpha)Be^9$; $E_n = 14$ MeV. The ordinate is the total cross section between 0° and 90° in the laboratory system, and the abscissa is $-Q$. Arrows show the known levels of Be^9 labeled with excitation (MeV), spin and parity (Ref. 30).

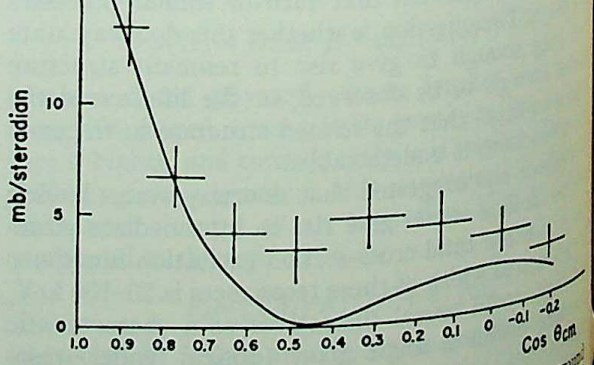

FIG. 4. Angular distribution for the transition to the ground state ($-6.2 < Q < -5.2$) of the reaction $C^{12}(n, \alpha)Be^9$. The solid curve is a theoretical Butler curve with $l=1$ and $R=5$ F. A knock-out mechanism has been assumed (Ref. 30).

CC-0. In Public Domain. Gurukul Kangri Collection, Haridwar

Digitized by Arya Samaj Foundation Chennai and eGangotri

results seem to establish heavy-particle stripping as an exchange process in the (n, α) reactions on light nuclei. This process accounts for most of the backward peaking. The presence of strong heavy-particle stripping contributions in the backward angles for the reaction $O^{16}(n, \alpha)C^{13}$ favor implicitly the presence of knock-out rather than the pick-up process at forward angles (see also Sec. IIIB).

The problem of reaction mechanism on very light nuclei has been also studied by measuring the angular distribution of gamma rays following the inelastic scattering of 14.1-MeV neutrons with C^{12} and Mg^{24}.[32] The angular distributions for both the 4.43-MeV gamma ray in C^{12} and the 1.37-MeV gamma ray of Mg^{24} were symmetrical around 90°, in agreement with the statistical model theory predictions of Satchler,[33] although it is well known that the corresponding inelastic scattering processes are well described by a direct mechanism. Although it is possible that both the direct and statistical theories of gamma emission give similar angular distributions, these results remain open to further speculations.

The interaction of neutrons with very light nuclei has been employed to study a different aspect of reaction mechanisms, more familiar to those working in few nucleon problems, namely the distinction between sequential decay and simultaneous disruption into many bodies. Jeremie[90] has measured the spectra and angular correlations of the two neutrons resulting from the $(n, 2n)$ reaction on Be^9. This reaction can proceed in several ways, the one most in accordance with the experiment being the simultaneous decay into three or four bodies:

$$n+Be^9 \rightarrow (n+n)+Be^8 \rightarrow 2n+2He^4.$$

On the other hand, the results of Batchelor and Towle[34] and Valković[35] on the interaction of fast neutrons with Li isotopes and B^{10} are rather inconclusive as far as the particular direct reaction mechanism is concerned. Only in the case of the $Li^7(n, t)$ reaction Valković[35] reports strong final state interaction of the neutron

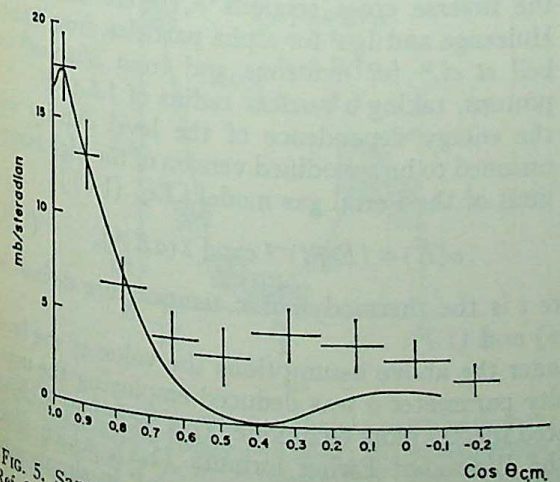

FIG. 5. Same as Fig. 4, with pick-up curve $l=1$, $R=4.45$ F (Ref. 30).

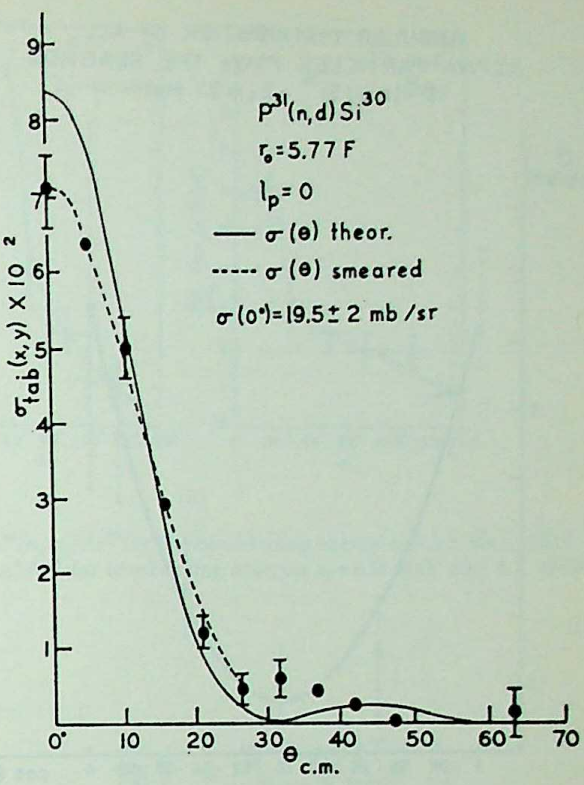

FIG. 6. Angular distribution of deuterons from the reaction $P^{31}(n, d_0)S^{30}$ (ground state). The ordinate values are those from the numerical tables of Lubitz.[37] They are proportional to the square of the Wronskian and contain the whole angular dependence of the cross section. The error flags show statistical counting errors only. Measurements have been extended to 150° lab., but no significant yield has been obtained. The energy of the neutrons was $\epsilon_0=14$ MeV (Ref. 36).

and the alpha particle, giving rise to a strong ground-state peak of tritons, while the continuous part of the triton spectrum is presumably due to sequential decay and not to the simultaneous three-body break-up. We shall again turn to (n, d) and (n, t) reactions when speaking of the cluster structure in light nuclei. A measurement of $N^{14}(n, d)C^{13}$ ground and first excited state distributions shows no appreciable cross section at backward angles.[36] Hence heavy-particle stripping seems to be rather unimportant in (n, d) reactions at 14 MeV. Good fits to these angular distributions have been obtained with plane wave Butler curves, showing that either both Coulomb and nuclear distortions are small or they cancel in a peculiar way (see also Sec. IB2 for results on P^{31} and S^{32}).

2. *Intermediate Elements* $(20<A<100)$

This is a region where, at least in its lower part, the statistical assumptions of the compound nucleus model should not necessarily be fulfilled. In spite of this, the model works surprisingly well in all this region, both for emission of charged particles and neutrons. In fact, direct reactions in this region of nuclei can be traced only for some $(n,$ charged particle$)$ reactions leading to low-lying states in the residual nuclei, e.g., in the case of $P^{31}(n, d)Si^{30}$ ground and first excited states and $S^{32}(n, d)P^{31}$ ground state at 14 MeV[36] (Fig. 6).

CC-0. In Public Domain. Gurukul Kangri Collection, Haridwar

Digitized by Arya Samaj Foundation Chennai and eGangotri

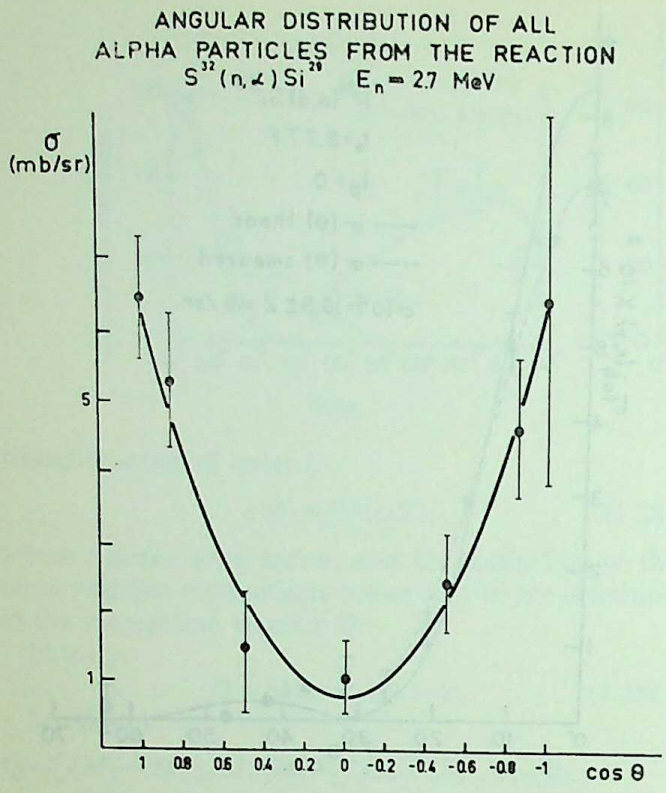

FIG. 7. Angular distribution of ground-state alpha particles from 2.7-MeV neutron bombardment of S^{32} (Ref. 38).

Most of the other results could be interpreted in terms of the compound nucleus mechanism. Even some ground state (n, α) transitions on elements like S^{32} (Ref. 38) for lower energy neutrons show a shape symmetrical around 90° that can be fairly well fitted by a polynomial of the type (Fig. 7).

$$P(A)=a+b\cos^2\theta.$$

Calvi *et al.*[39,40] measured angular distributions from the reaction $Ca^{40}(n, \alpha)A^{37}$ ground state and first excited state measured at neutron energies of 3.6, 4.0, and 4.5 MeV. While the earlier result at 3.6 MeV showed a symmetrical angular distribution for ground state alphas [Fig. 8(a)], the two recent ones at 4.0 and 4.5 MeV showed marked asymmetry both for ground state and first excited state alphas [Fig. 8(b)]. The strong dependence of the angular distributions on neutron energy shows that the results cannot be explained simply, neither in terms of the statistical model nor in terms of the simple direct interaction theory. It is again an example of the inadequacy of judging the reaction mechanism from angular distributions solely.

Actually the direct reaction mechanism could even account for angular distributions practically symmetrical around 90° as, e.g., in the work of Massot *et al.*[41] Using a plane wave approximation and both a zero range and Gaussian potential of interaction these authors obtained differential cross sections for pick-up and knock-out processes in terms of the respective momentum transfers. As shown in Figs. 9(a) and (b), quasi-symmetrical angular distributions could be fitted with a mixture of (pick-up+knock-out) processes. It seems that the range of the assumed interaction does not play an important role [cf. Figs. 9(a) and (b)].

A new field of experimental investigation has been opened by methods employing the targets simultaneously as detectors. This is an illustrative example of how physicists find ingenious devices to circumvent the inherent difficulties of fast neutron work. From the early work of the Milan group[42,43] physicists have discovered that they can use this same technique for a number of other targets: scintillators, gases, and semiconductors. This has proven to be fruitful especially when more subtle techniques, like pulse-shape discrimination and others are added. In this way charged-particle spectra of silicon,[44,45] potassium,[46] and argon[47] have been measured for neutron bombarding energies up to 14 MeV. Figure 10 shows cross sections for (n, α) disintegration of Ar^{40} obtained in this way.[47]

More classical techniques have been used to study spectra and angular distributions of (n, α) reactions on Al^{27} and Co^{59}, (Ref. 48) and P^{31}, S^{32}, and Ca^{40} (Refs. 49, 50), all with 14-MeV neutrons. Both energy spectra and angular distributions (Figs. 11–13) are consistent with an evaporative process provided one does not take into account a slightly excessive emission of higher energy alpha particles.

An extensive study of energy spectra of (n, α) reactions on light and medium weight elements has been performed by Saetta *et al.*[51] They have analyzed a number of spectra in terms of the statistical model using the Weisskopf–Ewing formula (1.3) derived in Sec. IA2. The maximum energy of integration in the denominator of (1.3) was computed from the bombarding energy ϵ_0, the values Q_n and the corresponding pairing energies δ_n for the particular reaction involved. The pairing energies were taken from the calculations of Cameron.[12] The other parameters involved in the analysis were as follows:

—the inverse cross sections σ_c^* were taken from Huizenga and Igo[9] for alpha particles, from Campbell *et al.*[51] for neutrons and from Shapiro[52] for protons, taking a nuclear radius of $1.6A^{\frac{1}{3}}$ F.

—the energy dependence of the level density was assumed to be a modified version of the high energy limit of the Fermi gas model [Eq. (1.8)].

$$\rho(E)\propto(E+t)^{-2}\exp[2(aE)^{\frac{1}{2}}], \tag{1.29}$$

where t is the thermodynamic temperature defined in (1.4a) and (1.7).

Under the above assumptions the value of the level density parameter a was deduced employing the usual reduced spectra plots technique. This technique is based on the Weisskopf–Ewing formula (1.3), which gives the logarithm of the "reduced spectra" in simple pro-

CC-0. In Public Domain. Gurukul Kangri Collection, Haridwar

Digitized by Arya Samaj Foundation Chennai and eGangotri

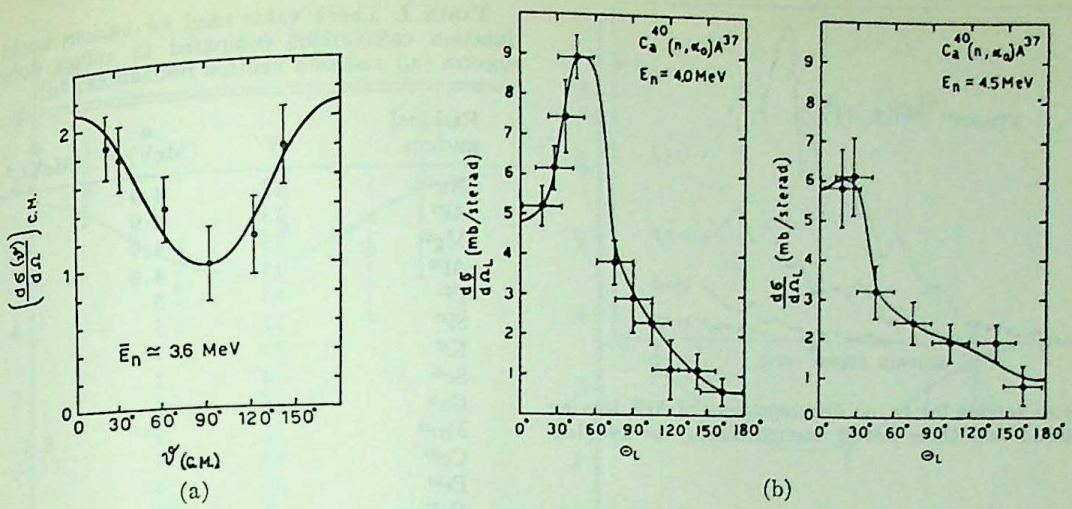

FIG. 8. (a) Angular distribution of alpha particles from the reaction $Ca^{40}(n, \alpha_0)Ar^{37}$ for the bombarding energy $\epsilon_0 = 3.6$ MeV (Ref. 39). (b) Angular distributions of alpha particles from the reaction $Ca^{40}(n, \alpha_0)Ar^{37}$ for bombarding energies $\epsilon_0 = 4.0$ MeV and 4.5 MeV, respectively (Ref. 40).

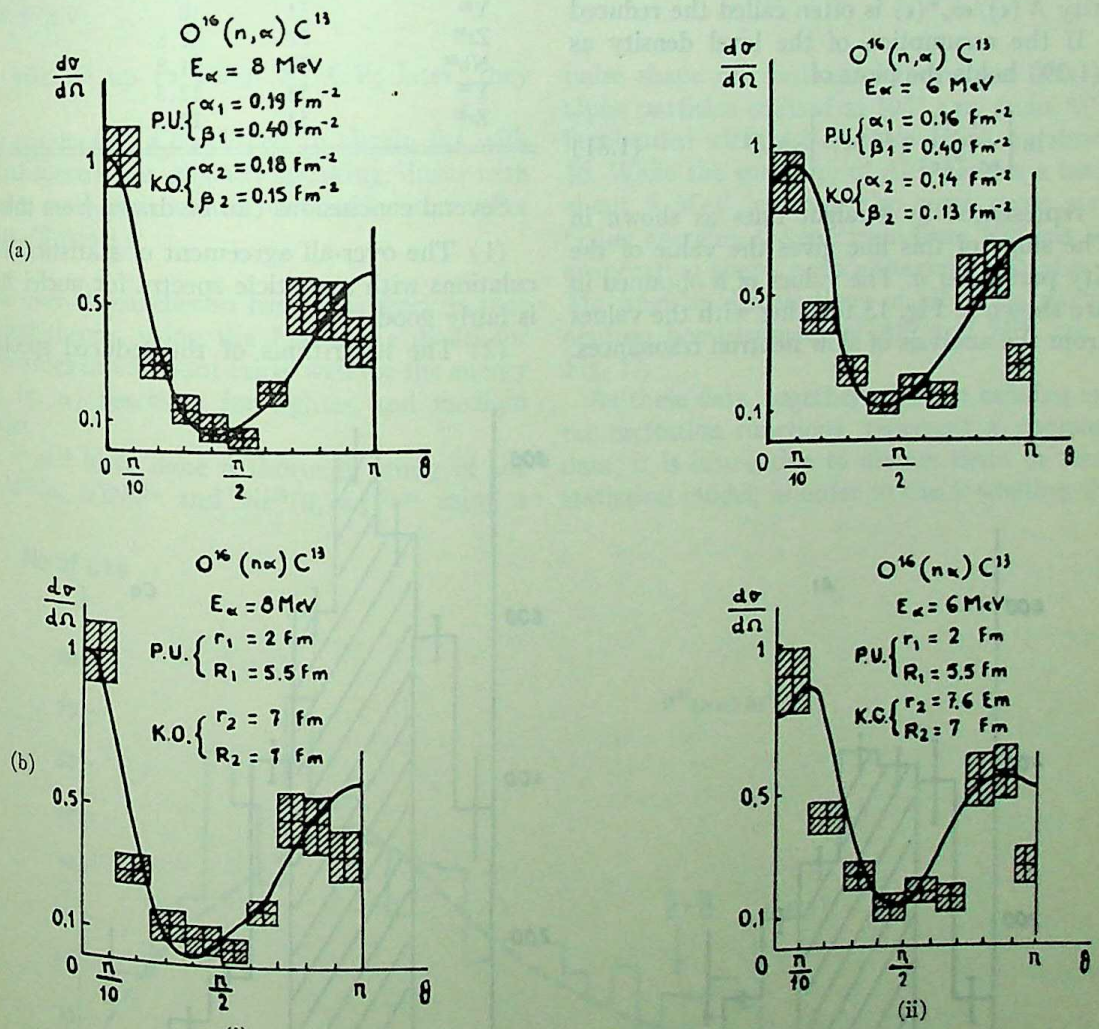

FIG. 9. (a) Angular distribution of alpha particles from the reaction $O^{16}(n, \alpha)C^{13}$ ($\epsilon_0 = 14$ MeV) with a zero range interaction potential for (i) alpha-particle energy $\epsilon = 8$ MeV; (ii) alpha-particle energy $\epsilon = 6$ MeV (Ref. 41). (b) Angular distribution of alpha particles from the reaction $O^{16}(n, \alpha)C^{13}$ ($\epsilon_0 = 14$ MeV) with a Gaussian interaction potential for (i) alpha-particle energy $\epsilon = 8$ MeV, (ii) alpha-particle energy $\epsilon = 6$ MeV (Ref. 41).

CC-0. In Public Domain. Gurukul Kangri Collection, Haridwar

Digitized by Arya Samaj Foundation Chennai and eGangotri

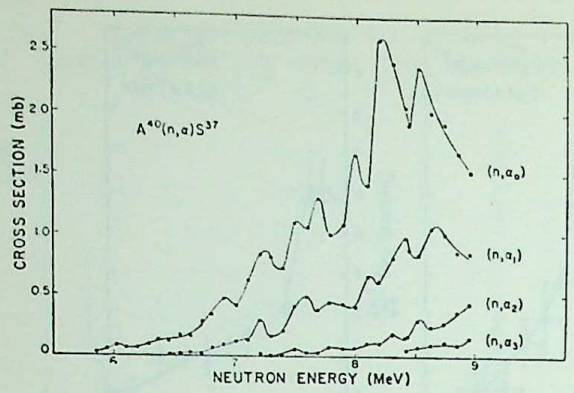

FIG. 10. Cross section for (n, α) disintegrations of Ar^{40}, leaving S^{37} in its ground and three lowest excited states; $\epsilon_0 = 14$ MeV (Ref. 47).

portionality to the level density exponential dependence:

$$N(\epsilon)\, d\epsilon \propto \sigma(\epsilon)\, d\epsilon \propto \sigma_c^*(\epsilon)\rho(E)\, d\epsilon,$$

hence

$$\ln \rho(E) \propto \ln [N(\epsilon)/\epsilon\sigma_c^*(\epsilon)]. \qquad (1.30)$$

The quantity $N(\epsilon)/\epsilon\sigma_c^*(\epsilon)$ is often called the reduced spectrum. If the assumption of the level density as given by (1.29) holds the plots of

$$\ln\left[\frac{N(t)}{\epsilon\sigma_c^*(\epsilon)}\,(E+t)^2\right] \text{ vs } E^{\frac{1}{2}} \qquad (1.31)$$

should be represented by straight lines as shown in Fig. 14. The slope of this line gives the value of the level density parameter a. The values of a obtained in this way are shown in Fig. 15 together with the values obtained from the analysis of slow neutron resonances.

TABLE I. The a value used for various nuclei in excitation function calculations compared to values deduced from the spectra (a_s) and slow neutron resonances (a_D).

Residual nucleus	N	a (MeV)$^{-1}$	a (MeV)$^{-1}$	a (MeV)$^{-1}$
Na^{24}	13	4.9		
Al^{27}	13	4.9		5.5
Mg^{27}	15	4.9		
Al^{28}	15	4.6		
P^{31}	16	5		4.5
Si^{31}	17	5		
K^{42}	23	7		
Sc^{45}	24	7		
Ca^{45}	25	7		
Mn^{56}	31	9	8.3	
Co^{60}	32	9		8.6-10
Fe^{60}	33	9		
Ga^{72}	41	13	12.1	
As^{75}	42	13		13
Ge^{75}	43	13		16.5
As^{76}	43	13	12.8	
Br^{79}	44	12.6		
Se^{79}	45	12.6		
Sr^{89}	51	10.5		
Y^{90}	51	10	9.8	
Zr^{92}	52	11.8		
Nb^{93}	52	11.8		
Y^{92}	53	12.5		
Zr^{93}	53	12.5		

Several conclusions can be drawn from this analysis:

(1) The over-all agreement of statistical model calculations with α-particle spectra for nuclei $20 < A < 80$ is fairly good.

(2) The logarithms of the reduced spectra (1.30)

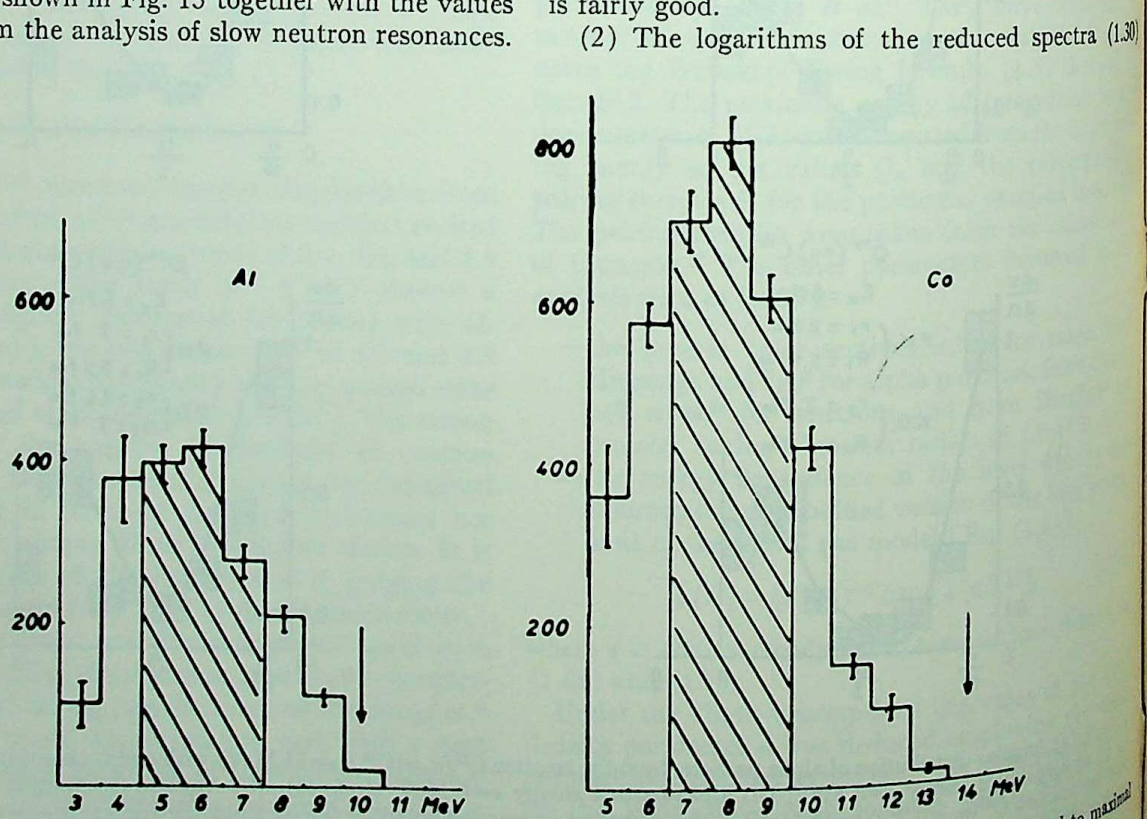

FIG. 11. Energy spectra of alpha particles from 14-MeV neutron bombardment of Al^{27} and Co^{59}. The arrows correspond to maximal energies calculated from Q values (Ref. 48).

CC-0. In Public Domain. Gurukul Kangri Collection, Haridwar

Digitized by Arya Samaj Foundation Chennai and eGangotri

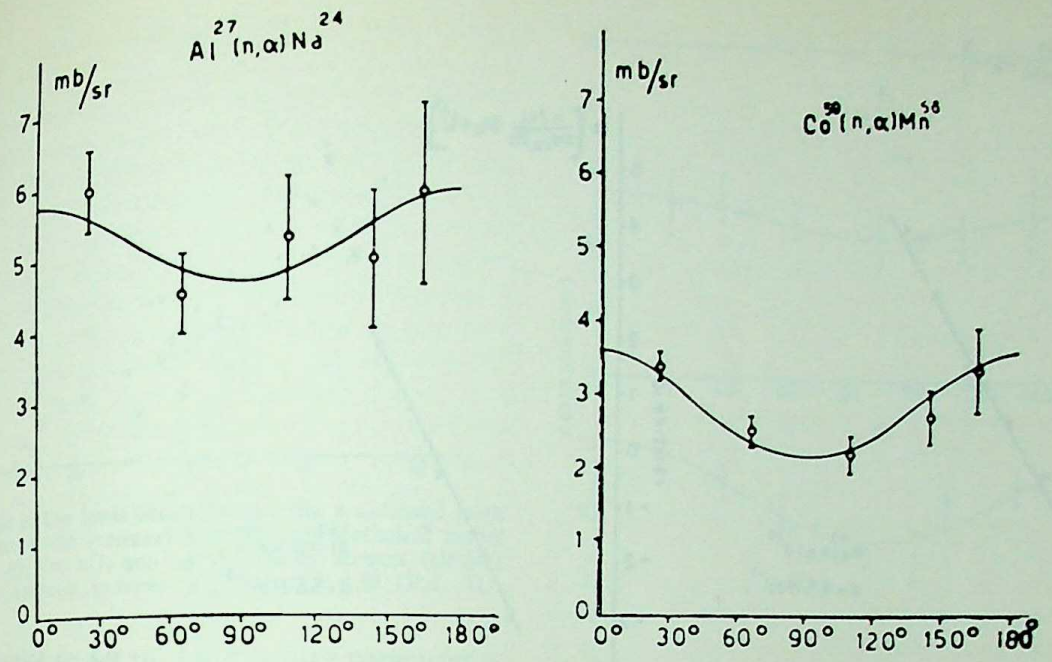

FIG. 12. Angular distribution of alpha particles from 14-MeV bombardment of Al^{27} and Co^{59} (experimental points and theoretical curves) (Ref. 48).

are linear with $E^{\frac{1}{2}}$ up to about 8 MeV; later, they curve up.

(3) The parameters a employed to obtain fits with experimental spectra are, globally speaking, linear with A and agree well with values obtained from other experiments (Table I).

Thus the over-all conclusion from this work is that the statistical theory, using the Fermi gas model for the level densities can account fairly well for the energy spectra of (n, α) reactions for lighter and medium weight nuclei.

Seebeck *et al.*[53] have done a thorough study of the reactions $Al^{27}(n, \alpha)Na^{24}$ and $Ni^{58}(n, \alpha)Fe^{55}$ using a pulse shape discrimination technique. The spectra of alpha particles emitted at 103° c.m. from Al^{27} and Ni^{58} bombarded with 14.1-MeV neutrons are shown in Fig. 16. While the spectrum of Al^{27}, besides a maximum at about 5 MeV, exhibits also some gross structure at higher energies, the spectrum from Ni^{58} has the typical evaporation shape, with a maximum at about 8 MeV. The angular distributions of all alpha particles from neutron bombardment of Al^{27} and Ni^{58} are shown in Fig. 17.

As these data, together with the existing experimental excitation functions, represent a complete set of data, it is instructive to discuss them in terms of the statistical model, in order to check whether this analy-

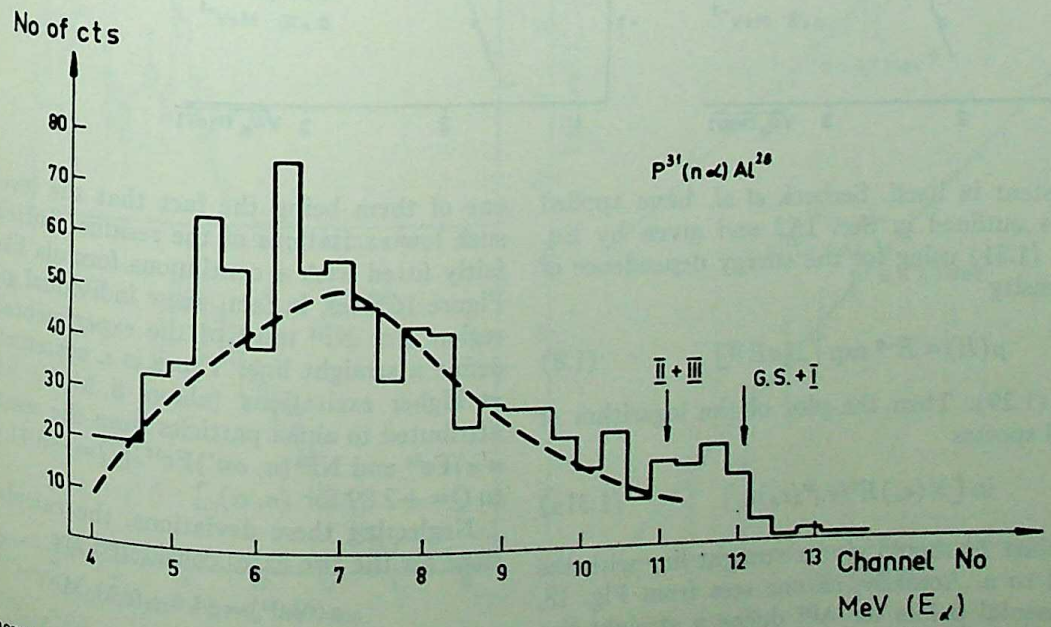

FIG. 13. Energy spectrum of alpha particles from 14.6-MeV neutron bombardment of P^{31} and evaporation calculation (Ref. 50).

CC-0. In Public Domain. Gurukul Kangri Collection, Haridwar

Digitized by Arya Samaj Foundation Chennai and eGangotri

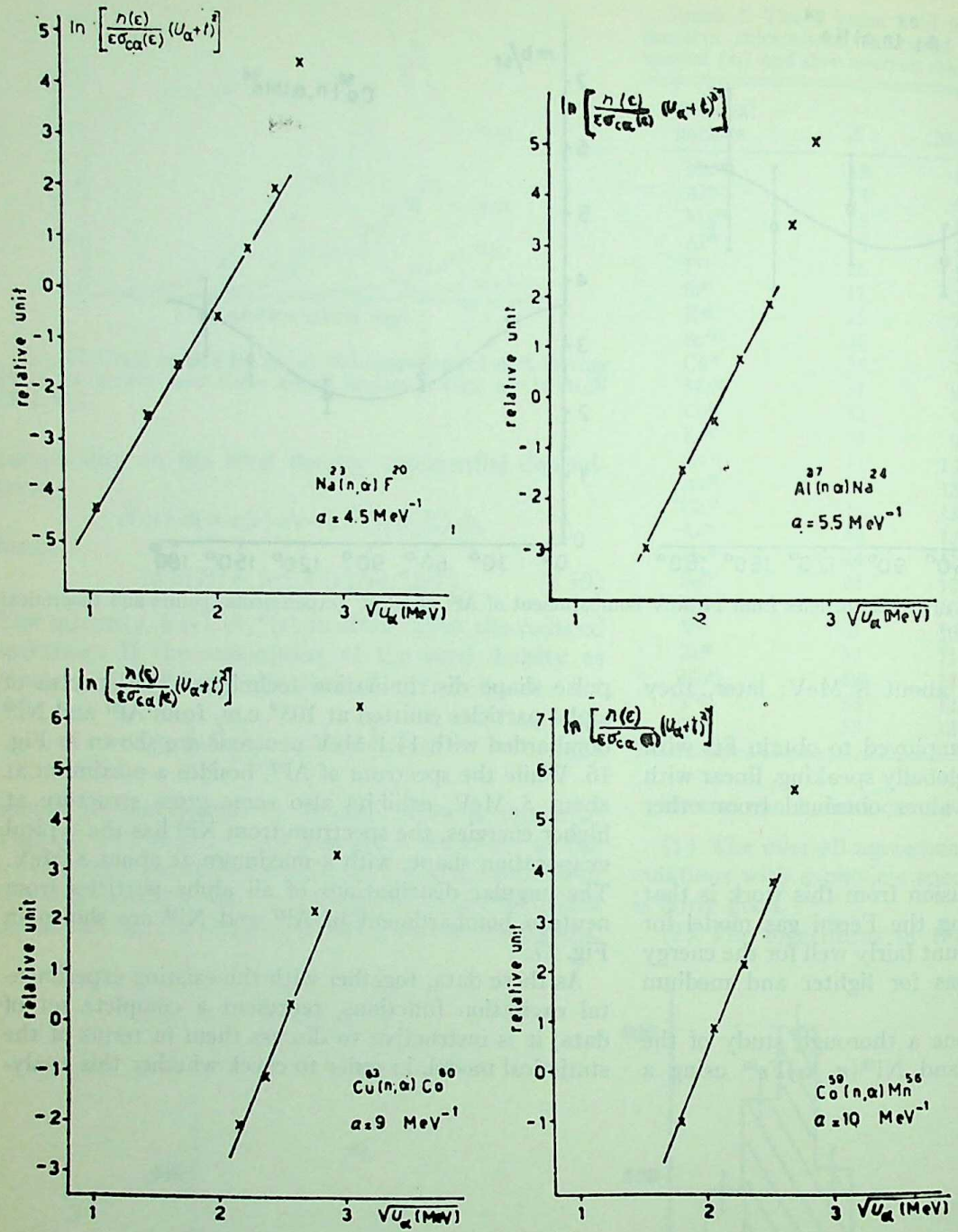

FIG. 14. Values of the parameter a from reduced spectra plots of (n, α) reactions at 14 MeV (Ref. 51).

sis is consistent in itself. Seebeck *et al.* have applied the analysis outlined in Sec. IA2 and given by Eq. (1.30) and (1.31) using for the energy dependence of the level density

$$\rho(E) \propto E^{-2} \exp\left[2(aE)^{\frac{1}{2}}\right] \tag{1.8}$$

instead of (1.29). Then the plot of the logarithm of the reduced spectra

$$\ln\left[N(\epsilon_\alpha)E^2/\sigma_c^*(\epsilon_\alpha)\epsilon_\alpha\right] \tag{1.31a}$$

plotted against $E^{\frac{1}{2}}$ should give a straight line with the slope equal to a. Actually, as one sees from Fig. 18, the experimental points for Al^{27} define a straight line on the average. The deviation from this line for high energy alpha particles can be due to several reasons, one of them being the fact that the level density at such low excitations of the residual nucleus cannot be fairly fitted with a continuous formula like Eq. (1.8). Figure 16 does, in fact, show individual groups in this region. For Ni^{58} most of the experimental points also define a straight line. There is a systematic deviation at higher excitations (above 8 MeV) which can be attributed to alpha particles from the reactions $Ni^{58}(n, n'\alpha)Fe^{54}$ and $Ni^{58}(n, \alpha n')Fe^{54}$. [$Q=-6.41$ as compared to $Q=+2.89$ for (n, α).]

Neglecting these deviations, the calculated average slope for the two cases considered are

$$a(Na^{24}) = (4.8\pm0.3)\ MeV^{-1}$$

$$a(Ni^{55}) = (7.0\pm0.4)\ MeV^{-1}.$$

This compares well to the values of Table I.

CC-0. In Public Domain. Gurukul Kangri Collection, Haridwar

Digitized by Arya Samaj Foundation Chennai and eGangotri

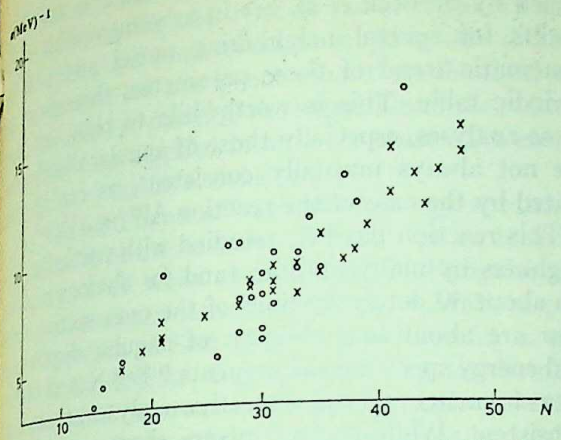

FIG. 15. Value of the level density parameter a obtained from slow neutron resonances (crosses) and from the statistical model analysis of (n, p), (n, n'), and (p, α) energy spectra (circles) plotted vs the neutron number N for $13<N<50$ (Ref. 51).

Using these values for the level density parameter a, one calculates the predicted shape of the energy spectra. The results are shown as dotted lines in Fig. 16 and as expected, appear to be quite satisfactory. Using the excitation energy of the product nucleus corresponding to the maximum of the spectra, and the above level density parameters, one obtains the nuclear temperature T

$$1/T=[d \ln \rho(E)/dE] \mid_{E=E\,(n_{max})}$$

equal to (1.52±0.15) MeV for Na^{24} and (1.39±0.14) MeV for Fe^{55}.

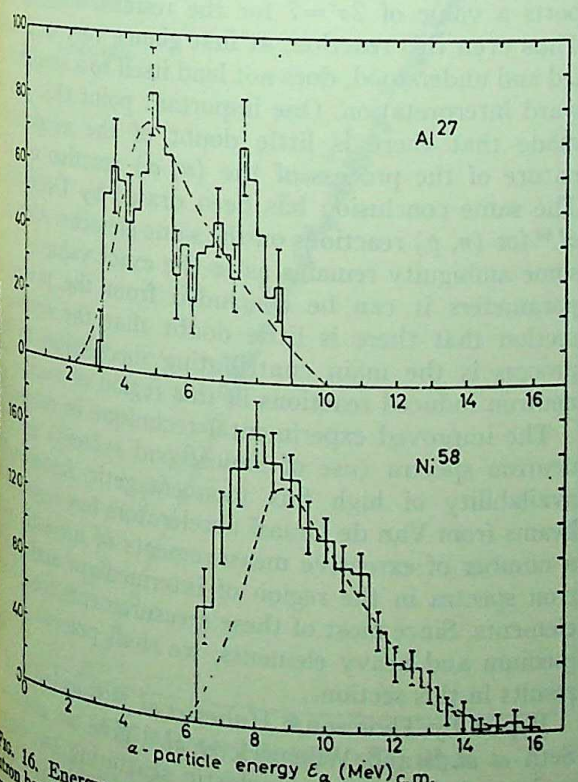

FIG. 16. Energy spectra of alpha particles from 14.1-MeV neutron bombardment of Al^{27} and Ni^{58}. Dotted lines are theoretical curves obtained from statistical model calculations (Ref. 53).

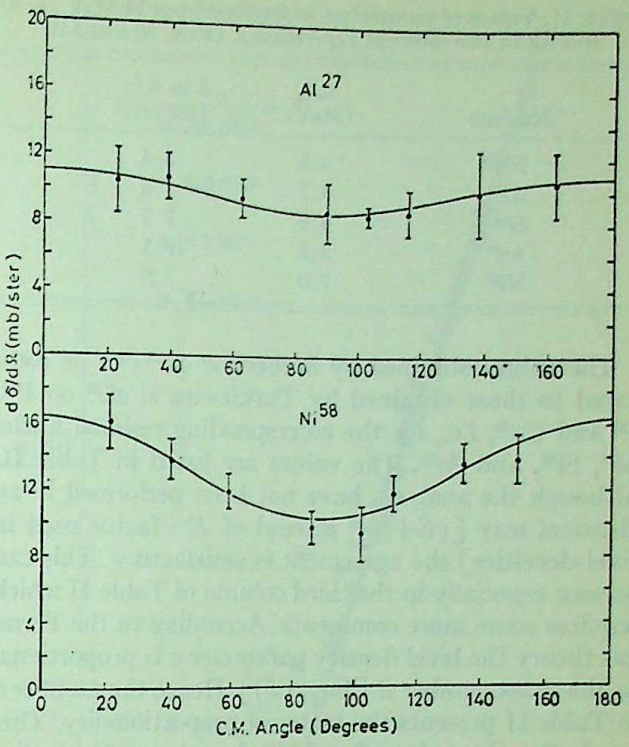

FIG. 17. Angular distribution of all alpha particles from 14.1-MeV neutron bombardment of Al^{27} and Ni^{58}. Dotted lines are theoretical curves obtained from statistical model calculations (Ref. 53).

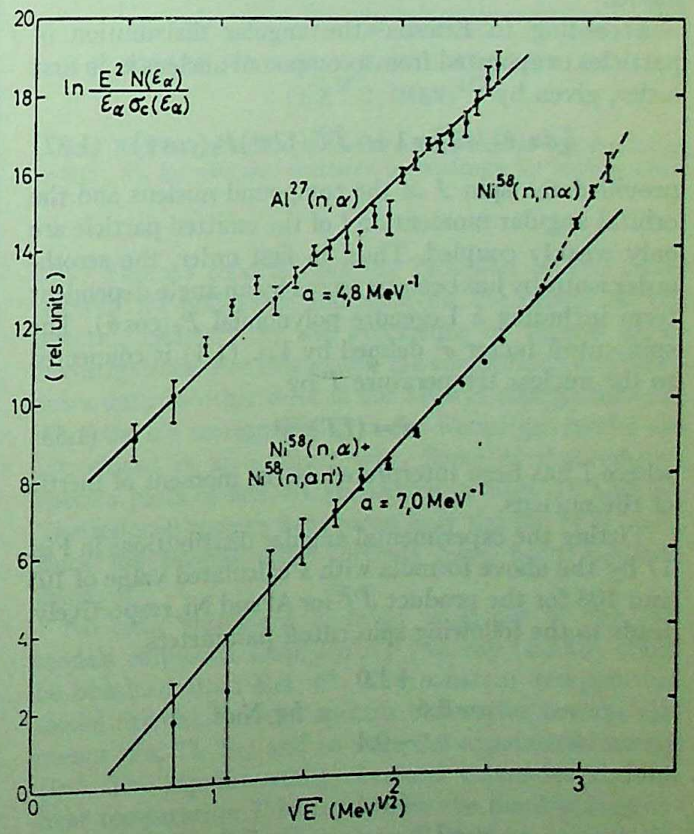

FIG. 18. Reduced spectra plots $\ln N(\epsilon) E^2/\epsilon\sigma_c^*(\epsilon)$ vs $E^{\frac{1}{2}}$ for alpha particles from 14.1-MeV neutron bombardment of Al^{27} and Ni^{58} (Ref. 53).

CC-0. In Public Domain. Gurukul Kangri Collection, Haridwar

Digitized by Arya Samaj Foundation Chennai and eGangotri

TABLE II. Values of parameters a obtained from 14-MeV (n, α) spectra in two different experiments. (Refs. 50 and 53).

Nucleus	a_{exp} $(MeV)^{-1}$	x in A/x (see text)
Na^{24}	4.5	5.4
Al^{28}	3.7	7.6
Si^{29}	4.0	7.2
Ar^{37}	3.5	10.5
Ni^{55}	7.0	7.8

The values obtained by Seebeck *et al.*[53] can be compared to those obtained by Turkiewicz *et al.*[50] on P^{31}, S^{32} and Ca^{40}, i.e., for the corresponding residual nuclei Al^{28}, Si^{29}, and Ar^{37}. The values are listed in Table II. Although the analyses have not been performed in an identical way [$(E+t)^{-2}$ instead of E^{-2} factor used in level densities] the agreement is satisfactory. This can be seen especially in the third column of Table II which requires some more comments. According to the Fermi gas theory the level density parameter a is proportional to the mass number A [Eq. (1.5)]. Hence the number x in Table II presents the factor of proportionality. Theoretically, the value of x depends only on the radius of nucleons. Taking this radius as $r_0=1.15$ one obtains $a=A/7.4$, i.e. $x=7.4$ in agreement with the values in Table II. The relative decrease of a in Ar^{37} ($x=10.5$) can be easily explained by the near magicity of this nucleus (smaller number of levels) while Na^{24} is probably on the lower limit of applicability of the statistical model.

According to Ericson[1] the angular distribution of particles evaporated from a compound nucleus is, in first order, given by

$$[d\sigma(\theta)/d\Omega]=1+(\bar{J}^2\bar{l}^2/12\sigma^4)P_2(\cos\theta) \quad (1.32)$$

provided the spin J of the compound nucleus and the orbital angular momentum l of the emitted particle are only weakly coupled. Thus, in first order, the zeroth-order isotropy has been corrected by an angle-dependent term including a Legendre polynomial $P_2(\cos\theta)$. The spin cutoff factor σ^2 defined by Eq. (1.4) is connected to the nuclear temperature T by

$$\sigma^2=(IT)/\hbar^2 \quad (1.33)$$

where I has been interpreted as the moment of inertia of the nucleus.

Fitting the experimental angular distributions in Fig. 17 by the above formula with a calculated value of 105 and 108 for the product $\bar{J}^2\bar{l}^2$ for Al and Ni, respectively, leads to the following spin cutoff parameters

$$\sigma=2.6^{+1.0}_{-0.4} \quad \text{for } Na^{24}$$

and

$$\sigma=2.2^{+0.4}_{-0.2} \quad \text{for } Fe^{55}.$$

The values of statistical parameters a, σ, and T ob-tained by Seebeck *et al.* are in agreement with sim-results for several neighboring nuclei and with the systematic trend of these parameters throughout the periodic table. This is worthwhile to point out since these analyses, especially those of angular distributions, are not always mutually consistent, as can be illus-trated by the case of the reaction $Al^{27}(n, \alpha)Na^{24}$.

This reaction has been studied with particular thor-oughness by many authors (and for obvious reasons). To about 30 determinations of the cross section added now are about half a dozen of angular distribution and energy spectra measurements.[48,53–58] Not all of these measurements and the respective analyses are mutually consistent. While energy spectra show a more or less consistent shape (see Figs. 11 and 16), the angular distributions vary from nearly isotropic[48,53,54] to strongly curved, with a deep minimum around 90°.[55–57] As we have already seen the angular distribution in the evap-oration model is connected to the so-called spin cutoff factor by the expression (1.32),[1] which can be calcu-lated accordingly. A more isotropic distribution will give rise to a larger value of σ^2 [smaller angular-depend-ent term in (1.32)]. In fact, Patzak *et al.*[46] Cindro *et al.*,[54] Jarwis *et al.*,[57] and Seebeck *et al.*[53] give values of

$$2\sigma^2=13,\ 15,\ 16,\ \text{and}\ 14,$$

respectively, while Irfan *et al.*[56] obtain

$$2\sigma^2=5$$

in accordance with the result of Csikai *et al.*[57] and earlier results of Kumabe[50] of $2\sigma^2<5$. Turkiewicz[50] re-ports a value of $2\sigma^2=7$ for the residual nucleus Al^{28}. Thus even this reaction, at first glance very well stud-ied and understood, does not lend itself to a straightfor-ward interpretation. One important point that can be made that there is little doubt of the evaporation nature of the process of the (n, α) reaction on Al. The same conclusion has been drawn by Debertin *et al.*[60] for (n, p) reactions on the same element. Although some ambiguity remains as to the exact value of some parameters it can be concluded from the preceding section that there is little doubt that the statistical process is the main contributing mechanism to fast neutron induced reactions in this region of nuclei.

The improved experimental technique in measuring neutron spectra (use of nanosecond system) and the availability of high flux monoenergetic fast-neutron beams from Van de Graaff accelerators has resulted in a number of extensive measurements of inelastic neu-tron spectra in the region of intermediate and heavy elements. Since most of these measurements treat both medium and heavy elements, we shall present all the results in this section.

Papers by Thomson,[61] Huber *et al.*,[62] Buccino *et al.*,[63] Seth *et al.*,[64] and Wilenzick *et al.*[65] give an extensive review of the neutron inelastic scattering on several energies and many nuclei. The results have been ana-

CC-0. In Public Domain. Gurukul Kangri Collection, Haridwar

Digitized by Arya Samaj Foundation Chennai and eGangotri

lyzed with the aim of establishing the reaction mechanism and obtaining the related parameters. As most of the results are concordant in singling out the statistical process as the predominant mechanism, the usual procedure of plotting the logarithm of the reduced spectra has been applied in order to obtain the energy dependence of the level density.

The data of Thomson[61] comprise energy spectra of more than 20 elements from Al to Pb at an incident energy of 7 MeV while some spectra and angular distributions have been taken at 4, 5, and 6 MeV, respectively. The data of Seth *et al.*[64] and Wilenzick *et al.*[63] contain measurements of spectra and angular distributions of 6-MeV neutrons in the energy region of 0.5–4 MeV (scattered neutrons). As these results are rather complementary, we discuss them together.

The spectra obtained by Thomson[61] were analyzed in terms of an incomplete Fermi gas model and the exponential (constant temperature) model of level densities:

$$\rho(E) \propto \exp\left[2(a'E)^{\frac{1}{2}}\right] \quad \text{and} \quad \rho(E) \propto \exp\,(E/T).$$

The pre-exponential E-dependent factor ($E^{-\frac{1}{2}}$ or E^{-2}) in the Fermi gas model has not been included. Actually, Thomas reports that the inclusion of the latter showed no noticeable influence on the shape of the spectra, contrary to the experience of several other investigations. For this reason the comparison of Thomson's data to other data is not always straightforward since the a's corresponding to the Fermi gas model are introduced in an indirect way. Some of the reduced spectra plots of Ref. 61 are shown in Figs. 19 and 20. The reduced spectra here mean only the log of $N(\epsilon)/\epsilon$, since the inverse cross sections have been assumed constant.

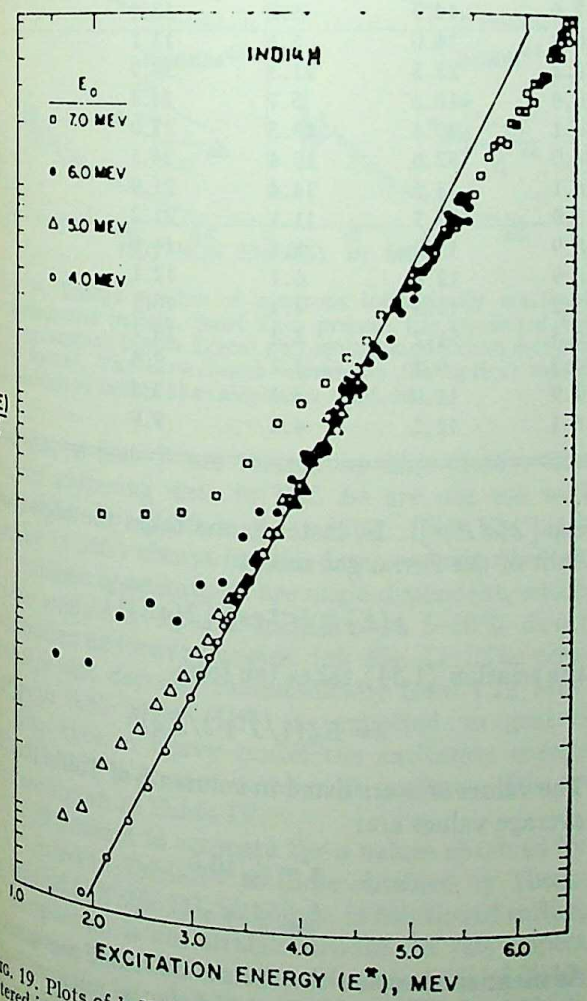

FIG. 19. Plots of $\ln N(\epsilon)/\epsilon$ vs excitation energy E for neutrons scattered inelastically by indium (Ref. 61).

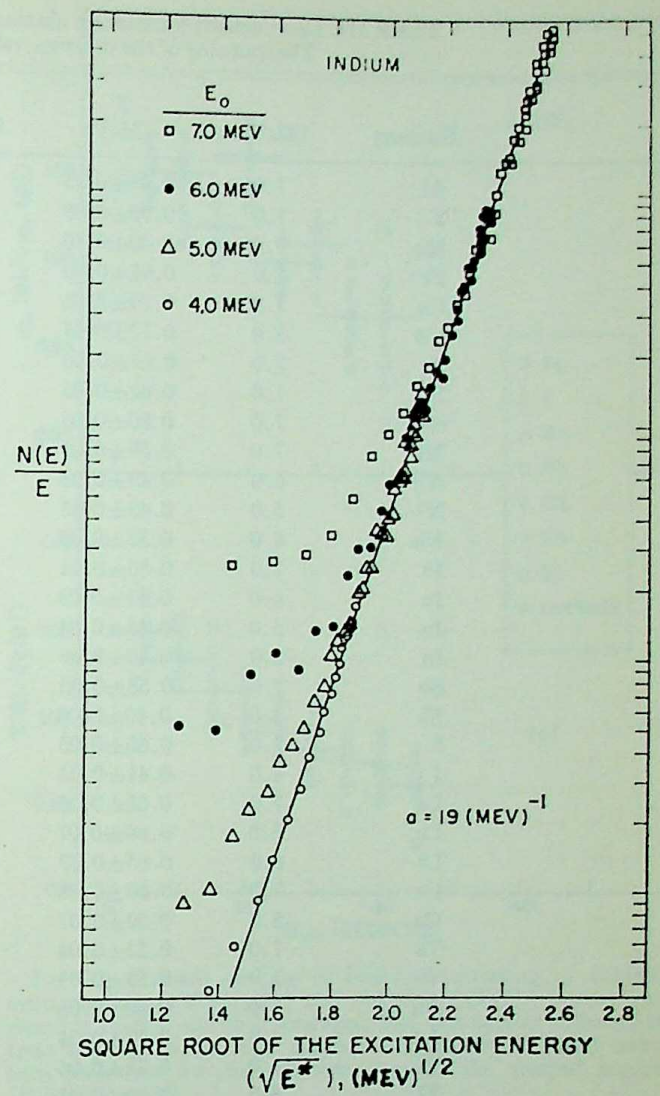

FIG. 20. Plots of $\ln N(\epsilon)/\epsilon$ vs the square root of the excitation energy, $E^{\frac{1}{2}}$, for neutrons scattered inelastically by indium (Ref. 61).

No clear statement in favor of either of the two models employed {$\exp[2(a'E)^{\frac{1}{2}}]$ vs $\exp\,(E/T)$} could be obtained from Ref. 61. The constant temperature model fits the reduced spectra curves for several elements (Fe, Tl, Bi) and so does the exponential model (In). The experimentally obtained values for the nuclear temperature T increase with the bombarding energy, while the reduced spectra plotted vs $E^{\frac{1}{2}}$ give the same value of the parameters a' for all bombarding

CC-0. In Public Domain. Gurukul Kangri Collection, Haridwar

Digitized by Arya Samaj Foundation Chennai and eGangotri

TABLE III. Level density parameters obtained from inelastic neutron scattering (Ref. 61). The meaning of the different values for a is explained in the text.

Element	(MeV)	T (MeV)	a' (MeV^{-1})	a (MeV^{-1})	a_p' (MeV^{-1})	a_p (MeV^{-1})
Al	7.0	0.96±0.15	5.5	10.5	3.2	8.7
V	7.0	0.90±0.09	6.4	11.7	4.6	10.1
Mn	7.0	1.00±0.10	5.0	9.8	3.7	8.8
Fe	7.0	0.95±0.06	5.7	10.7	2.6	8.5
Cu	7.0	0.79±0.06	8.7	14.6	6.4	12.4
Cu	5.0	0.72±0.07	6.9	13.5	4.1	11.5
As	7.0	0.67±0.06	12.6	19.3	9.3	16.3
Se	7.0	0.62±0.05	15.0	22.1	8.0	15.7
Sr	7.0	0.80±0.08	8.4	14.2	4.6	11.0
Nb	7.0	0.59±0.03	16.7	24.2	14.9	22.5
Nb	6.0	0.49±0.05	20.9	29.9	18.3	27.4
Nb	5.0	0.48±0.05	17.5	26.2	14.8	24.3
Nb	4.0	0.33±0.03	30.7	44.0	24.9	38.6
In	7.0	0.56±0.02	18.8	26.2	14.6	22.7
In	6.0	0.52±0.03	18.3	26.8	13.6	22.4
In	5.0	0.48±0.04	17.6	26.9	11.9	21.7
In	4.0	0.40±0.03	20.0	31.3	11.9	24.0
Sb	7.0	0.58±0.05	17.4	24.9	13.5	21.3
Sb	4.0	0.40±0.04	20.0	31.3	12.0	24.1
I	7.0	0.60±0.05	16.1	23.5	12.8	20.3
I	4.0	0.41±0.04	18.9	29.9	11.8	23.6
La	7.0	0.68±0.06	12.2	18.8	11.0	17.7
La	5.0	0.69±0.07	7.6	14.5	6.5	13.6
La	4.0	0.65±0.07	6.4	14.0	5.1	13.1
Ce	7.0	0.60±0.06	16.2	23.5	11.3	18.9
Ce	5.0	0.60±0.07	10.6	18.3	5.7	14.3
Ta	7.0	0.52±0.04	22.1	30.4	18.5	27.0
W	7.0	0.50±0.05	24.0	32.6	15.4	24.5
Au	7.0	0.60±0.06	16.1	23.5	14.4	21.9
Au	4.0	0.47±0.04	13.9	23.7	11.1	21.2
Tl	7.0	0.78±0.06	8.9	15.0	8.1	14.0
Tl	6.0	0.80±0.05	6.9	12.8	6.1	12.1
Tl	5.0	0.81±0.05	5.2	11.3	4.4	10.7
Tl	4.0	0.76±0.05	4.3	11.2	3.4	10.7
Bi	7.0	1.05±0.07	4.5	9.1	3.7	8.5
Bi	5.0	0.68±0.09	7.9	14.9	6.1	13.4
Pb^{206}	7.0	0.92±0.09	6.1	11.2	4.5	9.9

energies. The constant temperature model predicts a faster increase of the level densities with excitation and it has sometimes been interpreted as a sign of a second-order phase transition or "melting" of the nucleus.

The variation of the parameters a and T with the mass number A is shown in Table III. In the column labeled T the value of the nuclear temperature is given. The values a' (fourth column) have been calculated from the relation

$$a'=E_{Av}/T^2, \tag{1.34}$$

where the average excitation has been calculated from the evaporation model as

$$E_{Av}=\epsilon_{inc}-2T. \tag{1.35}$$

The values of a' calculated in this way (1.34) correspond to the incomplete Fermi gas model $\{\rho(E)\propto \exp[2(a'E)^{\frac{1}{2}}]\}$. If, instead, one takes the high-energy limit of the Fermi gas model

$$\rho(E)\propto E^{-2}\exp[2(aE)^{\frac{1}{2}}] \tag{1.8}$$

the relation (1.34) takes the form

$$a=E_{Av}(1/T+2/E_{Av})^2. \tag{1.34a}$$

The values of a are listed in column 5 of Table III. The average values are:

$$a'=A/10.9$$
$$a=A/7.2. \tag{1.36}$$

As mentioned earlier the theoretical value predicted by the Fermi gas model is $A/7.4$ for a nucleon radius $r_0=1.15$ F. A similar result has been obtained also for

CC-0. In Public Domain. Gurukul Kangri Collection, Haridwar

Digitized by Arya Samaj Foundation Chennai and eGangotri

(n, α) spectra, speaking of the reliability of the Fermi gas model.

The reduced spectra analysis of inelastic scattering of 6-MeV neutrons from many nuclei has been performed by Seth *et al.*[64] using, however, optical model values for the inverse cross section σ_c*. After having established that the sets of values σ_c* obtained from the volume local optical potential and the nonlocal optical potential of Perey *et al.*,[66] do not differ appreciably, Seth *et al.* compare the experimental reduced spectra to several forms of level densities:

$$\rho(E) \propto (E+t)^{-n} \exp\left[2(aE)^{\frac{1}{2}}\right] \qquad n=\tfrac{5}{4},\ 2 \qquad (1.36a)$$

$$\rho(E) \propto \exp\left[E/\langle t\rangle\right] \quad \text{or} \quad \exp\left[-\epsilon/T\right], \qquad (1.36b)$$

where T is the nuclear temperature defined by (1.7). Equation (1.36a) derives from the Fermi gas model while (1.36b) is valid under the extreme supposition

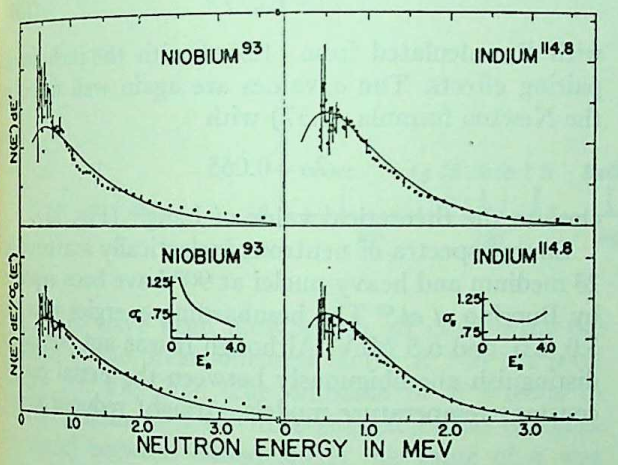

FIG. 21. Energy spectra of neutrons inelastically scattered by niobium and indium. Solid lines present the statistical fits assuming constant (upper figure) and optical model cross sections (lower figure). The little insert represents the optical model cross sections σ_c used in the calculation (Ref. 64).

of $\langle\epsilon\rangle \ll \epsilon_0$. a and T are related by Eq. (1.35). The inelastic scattering data in Ref. 64 are not too well fitted either by (1.36a) or (1.36b). (See Fig. 21.) Actually (1.36b) always fits the data somewhat better. The obtained temperatures are angle-dependent, which can be explained by the inclusion of 5–10% direct contribution at forward angles. (cf. Fig. 22). The temperatures also decrease monotonically from 1.22 MeV (Fe^{56}) to 0.55 MeV (U^{238}) as expected on general grounds, since in heavy nuclei the excitation energy is spread over a greater number of nucleons. The results are shown in Table IV.

It is of interest to compare the a values obtained by Seth,[64] listed in Table IV to those obtained by Thomson,[61] listed in Table III, although, as mentioned earlier, the comparison is not straightforward. In this respect we compare Thomson's a values in column 5 of Table III. The two last columns in Table III have been obtained by including the pairing effects[12] in calculat-

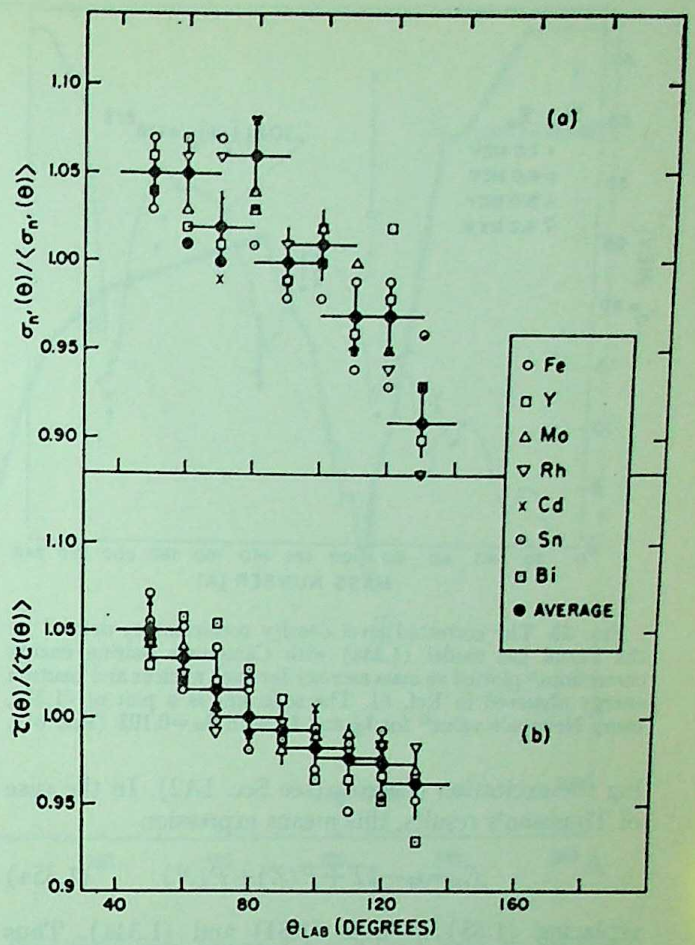

FIG. 22. Forward peaking in inelastic scattering of 6-MeV neutrons: (a) $\sigma_n(\theta)/\langle\sigma_n(\theta)\rangle$ and (b) $T(\theta)/\langle T(\theta)\rangle$ for several elements studied and their averages. The averages of differential cross sections $\langle\sigma_n(\theta)\rangle$ and nuclear temperatures $\langle T(\theta)\rangle$ have been performed for each element over all the studied angles (Refs. 64 and 65).

TABLE IV. Nuclear temperatures and Fermi gas coefficients for $E_n=6$ MeV (Ref. 64).

Element (at. weight)	T (MeV) ±10% using σ_c=const	T (MeV) ±10% using σ_c(opt. model)	a (MeV)$^{-1}$ ±20%, using σ_c(opt. model) $\delta_p=0$
Fe (56)	0.87	1.22	2.4
Y (89)	0.56	0.66	10.9
Nb (93)	0.55	0.65	11.2
Rh (193)	0.54	0.64	11.7
Pd (106.4)	0.51	0.58	14.7
Ag (107.9)	0.54	0.60	13.6
Cd (112.4)	0.52	0.56	15.9
In (114.8)	0.49	0.51	19.2
Sn (118.7)	0.55	0.56	16.0
Te (127.6)	0.61	0.59	14.1
W (183.9)	0.46	0.46	23.8
Pt (195.1)	0.52	0.51	19.0
Au (197)	0.55	0.54	17.1
Hg (200.6)	0.62	0.58	14.7
Pb (207.2)	0.69	0.66	11.0

CC-0. In Public Domain. Gurukul Kangri Collection, Haridwar

Digitized by Arya Samaj Foundation Chennai and eGangotri

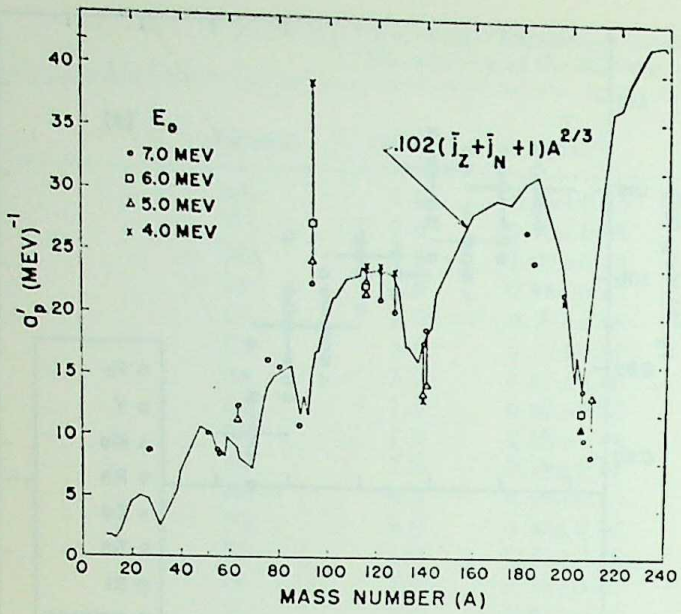

FIG. 23. The corrected level density coefficient a_p defined by the Fermi gas model (1.34a) with Cameron's pairing energy corrections[12] plotted vs mass number for each nucleus and neutron energy observed in Ref. 61. The solid line is a plot of (1.37), using Newton's value[67] for $\bar{\imath}_Z$ and $\bar{\imath}_N$ with $2\alpha=0.102$ (Ref. 61).

ing the excitation energies (see Sec. IA2). In the case of Thomson's results, this means expression

$$E_{Av}=\epsilon_0-2T+P(Z)+P(N) \qquad (1.35a)$$

replacing (1.35) in Eqs. (1.34) and (1.34a). Thus only the values in column 5 of Table III (Ref. 61) and the a values in the Table IV (Ref. 64) are suitable for comparison, since they use an approximately equal form for the energy dependence of the level density and no pairing corrections. Considerable differences can be found in absolute values, but the main trends are similar. The pairing-dependent a values of Thomson[61] (a_p) and Seth *et al.*[64] should be compared to the theoretical values given by Newton[67]

$$a=2\alpha(\bar{j}_Z+\bar{j}_N+1)A^{\frac{1}{3}}, \qquad (1.37)$$

where $\bar{j}_Z$ and $\bar{j}_N$ are defined as the effective values of proton and neutron angular momenta in the outermost shell of the nucleus.[67,68] A good fit for the values of Thomson[61] is achieved with $2\alpha=0.102$, (Fig. 23) while the same excellent agreement for Seth *et al.*[64] is obtained by using $2\alpha=0.075$. (Fig. 24). The difference is obviously due to the incomplete form of the energy dependence employed and to different values for the inverse cross sections. The theoretical value for the parameter 2α given by Lang[69] is

$$2\alpha=0.0784 \qquad (1.37a)$$

almost identical to the experimental value of Seth.[64] Although this identity should not be taken too seriously, alpha particle spectra obtained from 14-MeV neutron bombardment of Nb^{93} yield a value of $2\alpha=0.062$ close to the theoretical value.[70]

Further light on the shell dependence of the level densities in atomic nuclei has been shed by the investigations of Huber *et al.*[62] and Buccino *et al.*[63] Huber *et al.* have investigated the inelastic neutron energy spectra for 15 elements near and at closed shells. The bombarding energy was 14 MeV and the elements ranged from molybdenum to uranium. The analysis of the energy distribution $N(\epsilon)$ was carried out in the range of 0.5–4.5 MeV. The nuclear temperature T was obtained by using the Le Couteur formula,[71] which takes into account that at 14-MeV incident energy nuclei may emit more than one nucleon:

$$N(\epsilon)\propto\epsilon^{5/11}\exp\left[-12\epsilon/11T\right]d\epsilon \qquad (1.38)$$

for the number of neutrons emitted with energy ϵ. From the reduced spectra plots the nuclear temperatures T were obtained, the values of the level density parameters a calculated [using expression (1.34)]

$$a=E_{Av}/T^2 \qquad (1.39)$$

with E_{Av} calculated from (1.35a) with the inclusion of pairing effects. The a values are again well fitted by the Newton formula (1.37) with

$$2\alpha=0.065$$

close to the theoretical value of Lang[69] (Fig. 25).

Energy spectra of neutrons inelastically scattered by 23 medium and heavy nuclei at 90° have been reported by Buccino *et al.*[63] The bombarding energies were 4.0, 5.0, 6.0, and 6.5 MeV. Although it was not possible to distinguish unambiguously between the Fermi gas and constant temperature models, straight reduced spectra

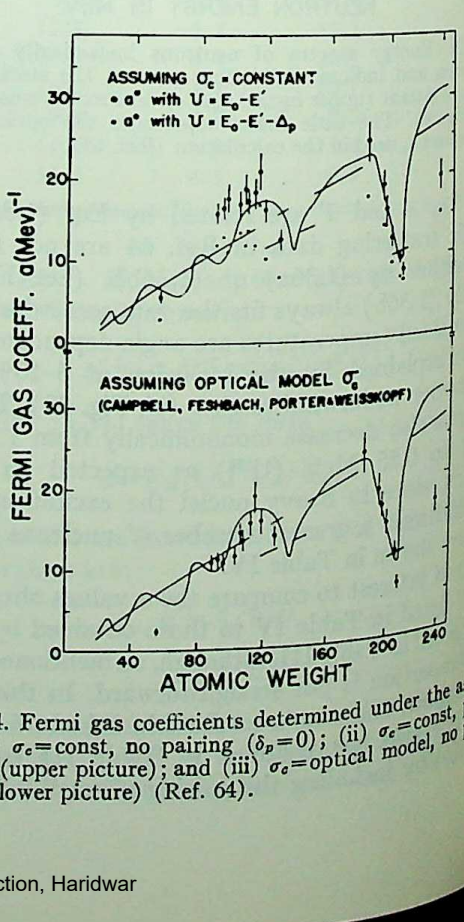

FIG. 24. Fermi gas coefficients determined under the assumptions: (i) σ_c=const, no pairing ($\delta_p=0$); (ii) σ_c=const, pairing included (upper picture); and (iii) σ_c=optical model, no pairing ($\delta_p=0$) (lower picture) (Ref. 64).

CC-0. In Public Domain. Gurukul Kangri Collection, Haridwar

Digitized by Arya Samaj Foundation Chennai and eGangotri

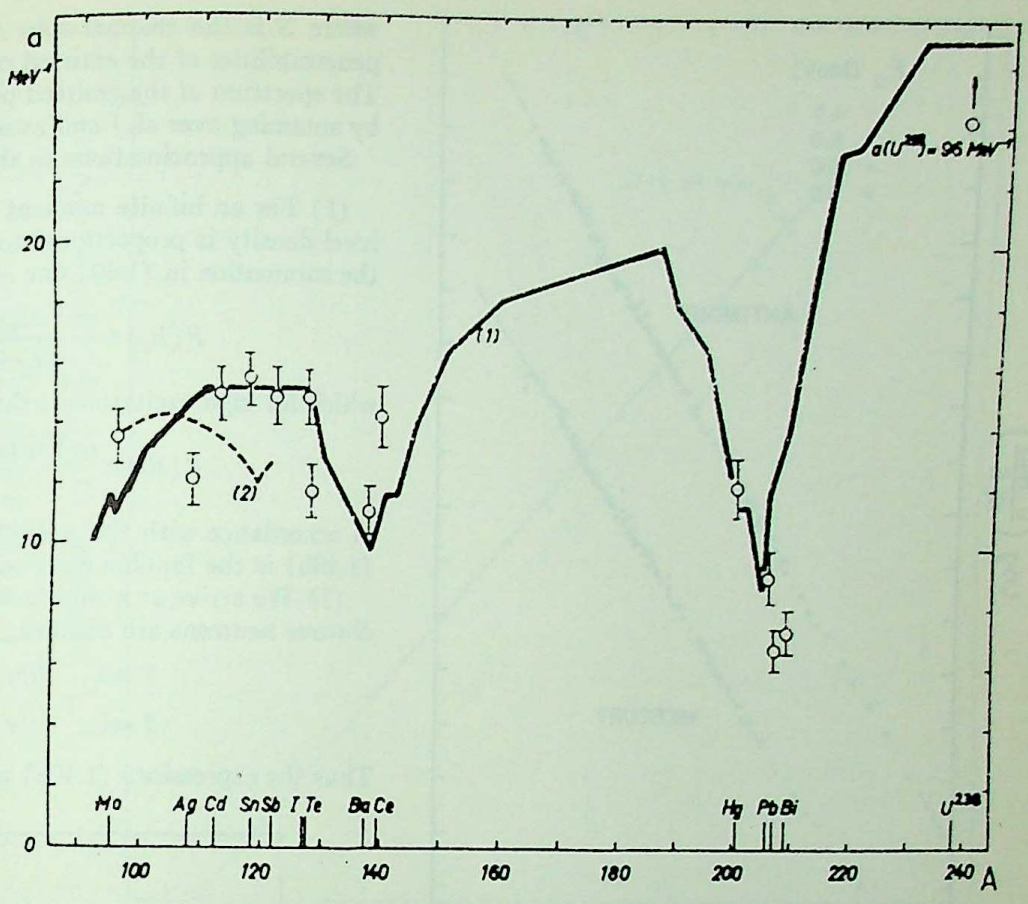

FIG. 25. Values of the level density parameter a derived in Ref. 62 (see text) compared to the Newton formula[67] with $2\alpha=0.065$ (Ref. 62).

plots vs $E^{\frac{1}{2}}$ have been obtained in all cases with the inclusion of the preexponential factor E^{-2} in the level density (cf. Fig. 26). The omission of E^{-2} leads to different values of a for different excitation energies. For nuclei between closed shells the value of a was independent of the bombarding energy, while for nuclei near or at shell closures of $N=82$ and 126 and $Z=82$, the nuclear temperatures were nearly constant over the range of excitations studied. In an overall picture, a general agreement between the experimentally determined values of a and the theoretical values was found, although the average increase of the level density coefficient with mass number A appears to be slower than predicted by a simplified equidistant model.

Results on angular distributions of inelastically scattered neutrons obtained by Thomson[61] (Fig. 27) and Wilenzick *et al.*[65] corroborate the results obtained from the analysis of the spectra. The angular distributions are either symmetric or show an unperceptible but systematic forward peaking, which is more clear if one takes the average of all elements at a given angle. A similar plot of relative nuclear temperatures shows the same behavior. (Fig. 22).

We have purposedly devoted much space to analyzing the neutron inelastic scattering data, since these data for several reasons (absence of Coulomb effects etc.) represent the most reliable source of information about the statistical model parameters, notably the level densities. It appears from the above discussion that the Fermi gas model is a solid base of our treatment of level densities. The use of more accurate expressions for level densities brings the value of the parameter a close to theoretical predictions, and the inclusion of shell and pairing effects accounts for the deviations from the average value. The ever present Fermi gas—constant temperature dilemma appears to be more due to the fact that *both* models satisfy, indicating that the evaporation picture is a better approximation than one would expect at first glance. Anyway as the Fermi gas model for level densities is based on more physical grounds (notably with the success of many-body calculations of nuclear spectra) it is our opinion that it should be used throughout in the analysis of spectra.

In all experiments discussed so far we have tacitly omitted angular momentum effects. At the same time, we have not accounted for the energy variation of the nuclear level density parameters a and T observed in some experiments.[72–74] This variation is a serious problem, since it may imply that the level density expressions chosen are not adequate to describe the actual level density over a wide range of energies. Bodansky[75] has reviewed some of the possible reasons for this variation:

(i) as the incident energy increases, there is an increasing probability of direct processes with a consequent hardening of the spectra;

CC-0. In Public Domain. Gurukul Kangri Collection, Haridwar

Digitized by Arya Samaj Foundation Chennai and eGangotri

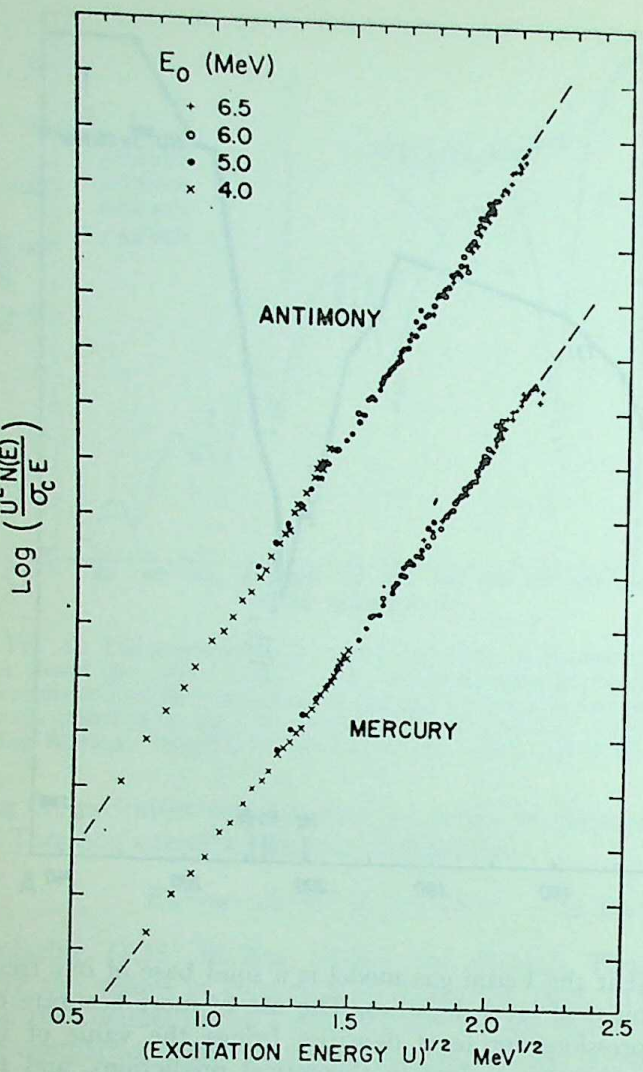

FIG. 26. Plots of $\ln N(\epsilon)E^2/\epsilon\sigma_c^*(\epsilon)$ vs $E^{\frac{1}{2}}$ for antimony and mercury. The dashed lines are drawn along the average slopes (Ref. 63).

(ii) since higher energies produce higher angular momenta in the compound nucleus, there may be an angular momentum effect producing the variation.

Although the first assumption is rather obvious, Thomas[76] has discussed this last possibility in terms of the Fermi gas model, using different degrees of approximation. In terms of the exact Fermi gas model, the number of levels with a given energy E and angular momentum J (level density) is given by Eq. (1.4) which for the high energy limit reduces to (1.8). According to Thomas[76] it is questionable whether this high energy limit is reached in most of the neutron experiments analyzed.

The rate of emission $R\,dE_f$ of a particle with a channel energy ϵ from a compound nucleus with an energy E_c and angular momentum J that leaves a residual nucleus with an energy E_f and angular momentum j is given by

$$R(E_f,j)\,dE_f=h^{-1}[\Omega(E_f,j)/\Omega(E_c,j)] \times \sum_{s=|j-s|}^{j+s}\sum_{l=|J-s|}^{l=J+s} T_l\,dE_f, \quad (1.40)$$

where S is the channel spin $S=s+j$, and T are the penetrabilities of the emitted particle [cf. Eq. (1.13)]. The spectrum of the emitted particles is then obtained by summing over all j and averaging over J.

Several approximations to this formula are possible:

(1) For an infinite moment of inertia ($\mathcal{J}=\infty$) the level density is proportional to $(2J+1)$. Carrying out the summation in (1.40) one obtains:

$$R(E_f)\propto\frac{\epsilon\sigma_c^*\exp[2(aE_f)^{\frac{1}{2}}]}{(E_f+t_f)^{-\frac{1}{2}}T^{\frac{1}{2}}} \quad (1.40a)$$

which for high excitations reduces to

$$R(E_f)\propto\frac{\epsilon\sigma_i^*\exp[2(aE_f)^{\frac{1}{2}}]}{E^2} \quad (1.40b)$$

in accordance with the preceding discussion. Formula (1.40b) is the familiar evaporation formula.

(2) We arrive at a similar result assuming that only S-wave neutrons are emitted, i.e., that

$$T=1 \quad \text{for} \quad l=0$$
$$T=0 \quad \text{for} \quad l\neq 0.$$

Thus the expressions (1.40a) and (1.40b) hold, strictly

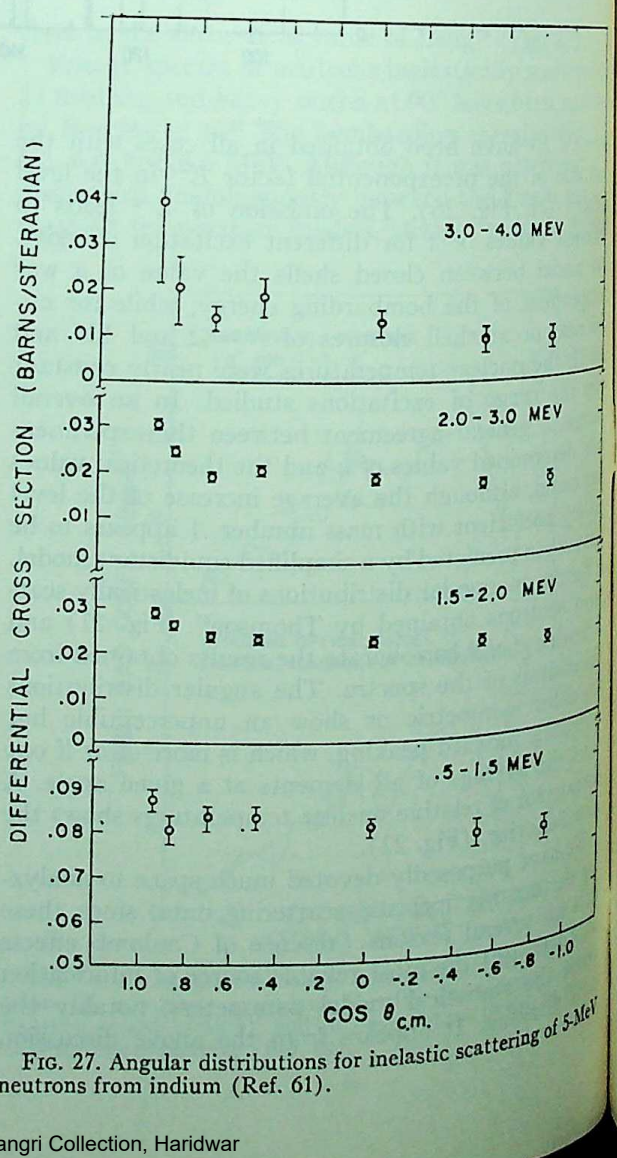

FIG. 27. Angular distributions for inelastic scattering of 5-MeV neutrons from indium (Ref. 61).

CC-0. In Public Domain. Gurukul Kangri Collection, Haridwar

Digitized by Arya Samaj Foundation Chennai and eGangotri

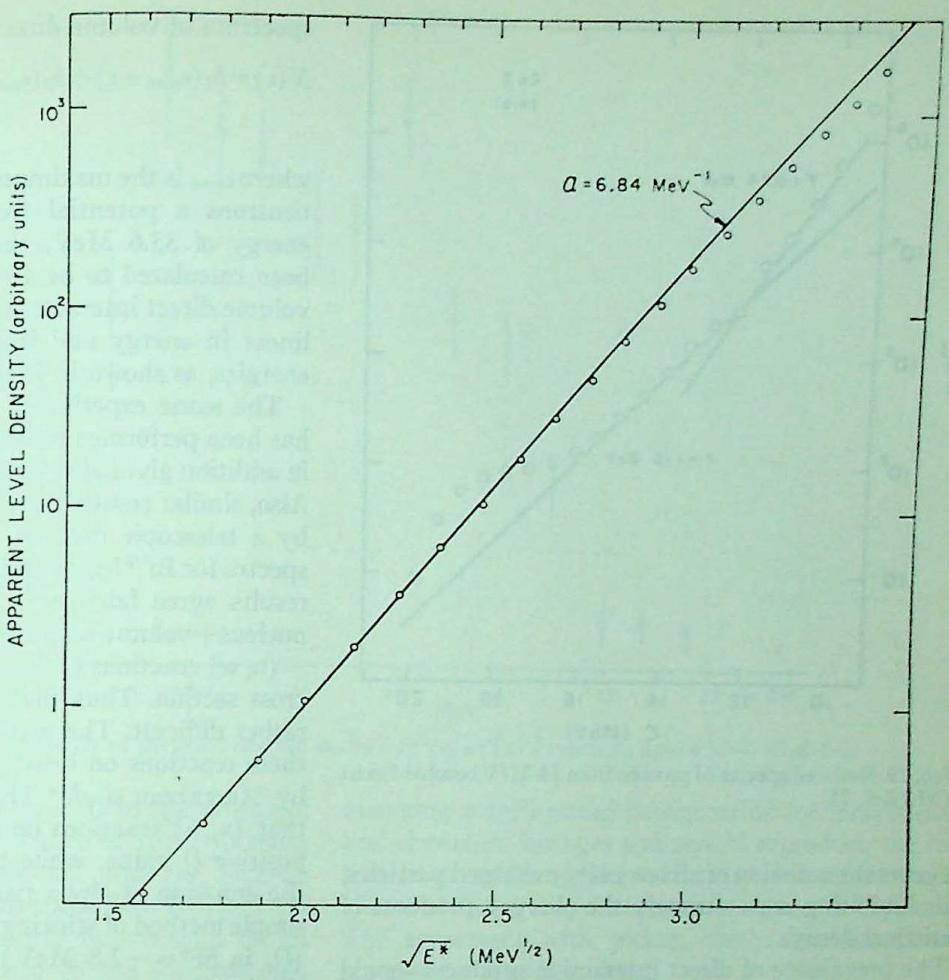

FIG. 28. Apparent level density plot based on the analysis of a calculated evaporating spectrum. The compound nucleus is taken to be Mn^{55} formed by irradiation of V^{51} with 16-MeV alpha particles. For this analysis it has been assumed that the level density is proportional to E^{-2} exp $[2(aE)^{\frac{1}{2}}]$ (Ref. 76).

speaking, only when either (1) the spin cutoff factor $2\sigma^2$ becomes infinite or (2) when only S-wave neutrons are emitted. It is thus possible that the energy variation of the level density parameter a observed when analyzing experimental spectra by the use of (1.40a) or (1.40b) can be connected to angular momentum effects.

To test this assumption Thomas has calculated several theoretical neutron evaporation spectra using the correct formula (1.40) summed over the final angular momenta and averaged over initial angular momenta. The assumed level density was (1.4) and (1.4a). The *same* value of a was used for different bombarding energies.

Afterwards, each calculated spectrum was analyzed, as if it were an experimental one, in terms of the expression (1.40b) to derive an apparent value of a. The result of an analysis of this kind is shown in Fig. 28.

If the supposition on the influence of angular momentum effects on the energy variation of a was correct, one should get the same variation of a with ϵ_{bomb} as in the experimental work. However, *no variation of a with* ϵ_{bomb} has been observed in the range of ϵ_{bomb} 12-20 MeV (for incident alpha particles). However, the a values obtained were about 40% higher than the input a values. Hence, angular momentum effects could not be responsible for the energy variation of a. The value of a obtained from the "experiments" was, however, considerably larger than the one from the Fermi gas model partly for angular momentum effects ($\doteq 50\%$) and partly because of the inadequacy of the expression (1.4) for the actual level density ($\doteq 50\%$).

These results are corroborated also by the analysis of Hurwitz *et al.*[77]

3. *Heavy Elements* ($A > 100$)

Except for neutron inelastic scattering, most of which has been analyzed in the preceding section, results of neutron induced reactions in this region are still scarce and no systematic search has been done so far. It is characteristic of this region of nuclei that the predominant part of the cross section for charged particle production is composed of nonequilibrium (direct) processes, due to the regulating effect of the Coulomb barrier.

The difference between direct and equilibrium processes is that the former are single-stage processes while the latter are multistage ones. Thus the energy and momentum transfer to the reaction product in the case of direct interactions is large, giving rise to particles with energies close to the maximum possible; on the contrary, statistical processes will favor the emission of lower energy particles. The Coulomb barrier, which for nuclei of $A = 100$ is about 10 MeV for protons and deuterons and the double of this value for α particles

CC-0. In Public Domain. Gurukul Kangri Collection, Haridwar

Digitized by Arya Samaj Foundation Chennai and eGangotri

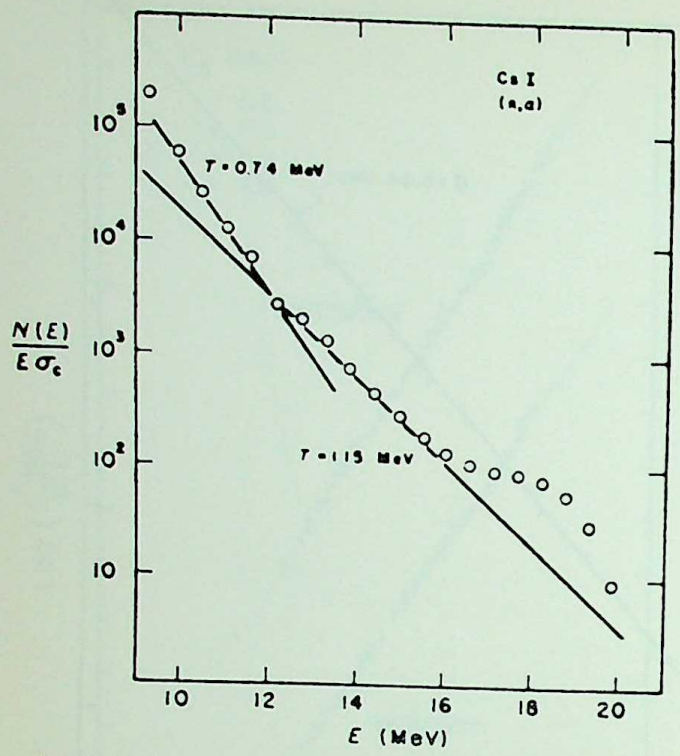

FIG. 29. Reduced spectra of protons from 14-MeV bombardment of CsI (Ref. 78).

prevents the emission of all low energy charged particles, thus inhibiting more strongly the charged products of statistical decay.

The prevalence of direct interaction products should be seen also in the spectra and angular distributions of charged particles emitted from heavy nuclei. Dixon[78] using the pulse-shape discrimination method has measured spectra of protons, deuterons and alpha particles from 14-MeV bombardment of a CsI crystal. It has been noted that Cs^{133} and I^{127} are close in mass number and $Q_{n,\text{charged part}}$ values and that both are odd Z–even N nuclei. Thus it is expected that their spectra are similar and it is meaningful to speak about the spectrum of CsI.

The reduced spectra plot vs the particle energy for protons from 14-MeV bombardment of CsI is shown in Fig. 29. No single straight line could be drawn, and the curve itself can be broken into three sections. The low-energy section, corresponding presumably to admixtures of the reaction (n, np) is characterized by a low nuclear temperature ($T=0.74$ MeV), which corresponds to the low residual excitation of a nucleus after the emission of the fast particle. The medium and higher energy part correspond presumably to prevalently compound and direct processes. The above division gives about $\frac{1}{3}$ statistical and $\frac{2}{3}$ direct emission of protons, as exhibited in Fig. 30, where a possible decomposition of the proton spectrum is shown. As already noted in Sec. IA4 the shape of the spectra for volume direct and statistical processes are rather similar, the main difference being in the shifting of direct spectra toward higher energies. As mentioned, the theory of Brown *et al.*,[22] gives the following expression for the energy spectrum of volume direct reactions:

$$N(\epsilon)=b_1(\epsilon_{\max}-\epsilon)+b_2(\epsilon_{\max}-\epsilon)^2+b_3(\epsilon_{\max}-\epsilon)^3+\ldots, \quad (1.15$$

where $\epsilon_{\max}$ is the maximum energy transfer. For 14-Me neutrons a potential well of 40 MeV and a Fer energy of 33.6 MeV, the ratios b_2/b_1 and b_3/b_1 ha been calculated to be 10^{-2} and 10^{-4}, respectively. T volume direct interaction spectrum should be in essenc linear in energy and its peak should come at highe energies, as shown in Fig. 30.

The same experiment as the one discussed above has been performed independently by Robertson[79] wh in addition gives also total cross sections (see Sec. IC3 Also, similar results have been obtained by Hans *et al.*[8] by a telescopic method. These authors measured th spectra for $In^{115}(n, p)$ and $Au^{197}(n, p)$. The experimenta results agree fairly well with a calculated compou nucleus+volume direct interaction energy distributio

(n, α) reactions on heavy elements have a very sma cross section. Thus their experimental investigation i rather difficult. The first extensive search of spectra o these reactions on heavy elements has been performe by Marcazzan *et al.*[44] They used the experimental fac that (n, α) reactions on heavy elements have a highly positive Q value, while the Coulomb barrier prevents the emission of alpha particles below 12 MeV. Thus a simple method of sticking the targets to a silicon counter (Q_n in $Si^{28}=-2.8$ MeV) has been used to obtain forward and backward spectra. Some of their results are shown in Fig. 31. A clearly direct mechanism for these reactions has been inferred from the rather large forward to backward ratio in the angular distributions.

The same method was used by Cuzsocrea *et al.*[81] to measure alpha-particle spectra from molybdenum isotopes up to several MeV of excitation. (Bombarding energy $\epsilon_n=15$ MeV.) The results obtained suggest also a direct process. Where it was possible, the ground-state transition has been separated and the relative

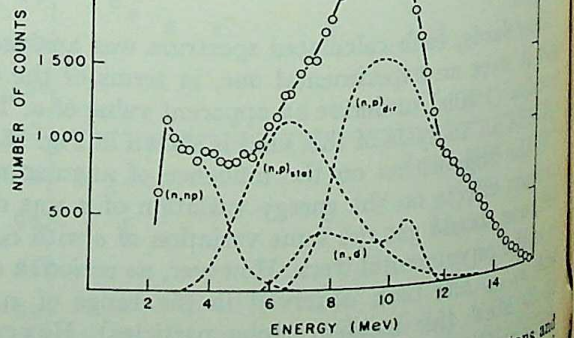

FIG. 30. Full curve: experimental distribution of protons and deuterons from 14-MeV neutron-induced reactions in CsI. Dashed curves: a possible decomposition into four components, as described in the text (Ref. 78).

CC-0. In Public Domain. Gurukul Kangri Collection, Haridwar

Digitized by Arya Samaj Foundation Chennai and eGangotri

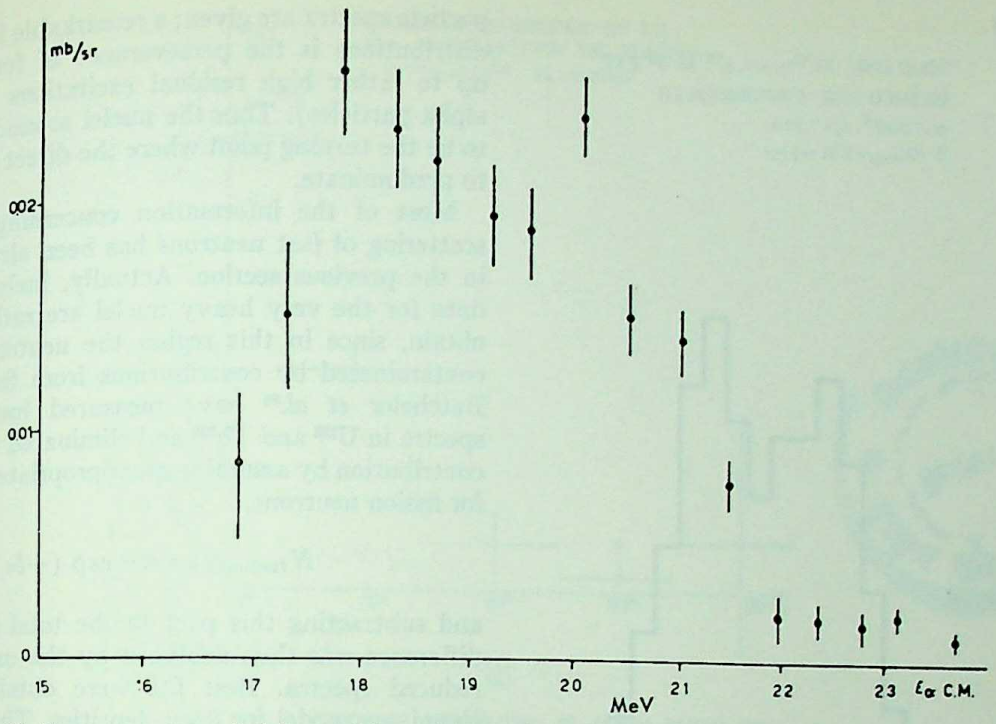

FIG. 31. Energy spectrum of alpha particles emitted in the $Lu^{175}(n, \alpha)Tm^{172}$ reaction; $\epsilon_0 = 14$ MeV (Ref. 44).

intensities of the α_0 groups compared to spectroscopic factors in order to establish which of the two main direct mechanisms—the knock-out and the pick-up processes—is responsible for this transition. In a pick-up process, the transition probability between an initial and a final state is proportional to the spectroscopic factor describing the removal of the various nucleons from the target nucleus. In the case of an (n, α) pick-up process,

$$S = S_n S_{2p}.$$

Considering the ground-state transitions only, the factor S_{2p} should be equal for all the molybdenum isotopes, and hence the transition probability is proportional to S_n. This quantity can be calculated assuming a shell model configuration for molybdenum and zirconium isotopes and should reproduce the relative cross sections. The comparison of calculated S_n values and α_0 group intensities is shown in Table Va. The agreement with pickup mechanism for ground state transitions is striking.

A recent preliminary result of Veselić *et al.* on (n, α) ground-state transitions on zirconium isotopes (Zr^{90}, Zr^{91}, and Zr^{93}) does not seem to confirm the above conclusions. In fact a glance on Table Vb shows that the values of spectroscopic factors S and the relative intensities of the α_0 group do not agree completely. Although the results of Veselić have been taken with a telescopic technique that seems to be more suitable for experiments of this kind, so far they are only preliminary.

Using an elaborate telescopic technique Kulišić *et al.*[70,83] and Lalović *et al.*[84] have measured energy and angular distributions of alpha particles emitted by 14-

TABLE V(a). Comparison of calculated values of the spectroscopic factor S_n and experimental values α_0 of group intensities for molybdenum isotopes. (Ref. 81).

Reaction	Transition	S_n	Group intensity
$Mo^{92}(n, \alpha)Zr^{89}$	$\left(\frac{9}{2}\right)^{10}_{0} \rightarrow \left(\frac{9}{2}\right)^{9}_{9/2}$	10	10±1.0
$Mo^{94}(n, \alpha)Zr^{91}$	$\left(\frac{5}{2}\right)^{2}_{0} \rightarrow \left(\frac{5}{2}\right)^{1}_{5/2}$	2	3±1.0
$Mo^{95}(n, \alpha)Zr^{92}$	$\left(\frac{5}{2}\right)^{3}_{5/2} \rightarrow \left(\frac{5}{2}\right)^{2}_{0}$	0.67	1±0.5
$Mo^{96}(n, \alpha)Zr^{93}$	$\left(\frac{5}{2}\right)^{6}_{0} \rightarrow \left(\frac{5}{2}\right)^{5}_{5/2}$	6	6±0.5
$Mo^{98}(n, \alpha)Zr^{97}$	$\left(\frac{5}{2}\right)^{6}_{0} \rightarrow \left(\frac{5}{2}\right)^{5}_{5/2}$	6	6.3±1.3

TABLE V(b). Comparison of calculated values of the spectroscopic factor S_n and experimental values of α_0 group intensities for zirconium isotopes (Ref. 82).

Reaction	Transition	S_n	α_0 group intensity
$Zr^{90}(n, \alpha)Sr^{87}$	$\left(\frac{9}{2}\right)^{10}_{0} \rightarrow \left(\frac{9}{2}\right)^{9}_{9/2}$	10	2.3
$Zr^{91}(n, \alpha)Sr^{88}$	$\left(\frac{5}{2}\right)^{1}_{5/2} \rightarrow \left(\frac{5}{2}\right)^{10}_{0}$	1	1
$Zr^{92}(n, \alpha)Sr^{89}$	$\left(\frac{5}{2}\right)^{2}_{0} \rightarrow \left(\frac{5}{2}\right)^{1}_{5/2}$	2	1.1

CC-0. In Public Domain. Gurukul Kangri Collection, Haridwar

Digitized by Arya Samaj Foundation Chennai and eGangotri

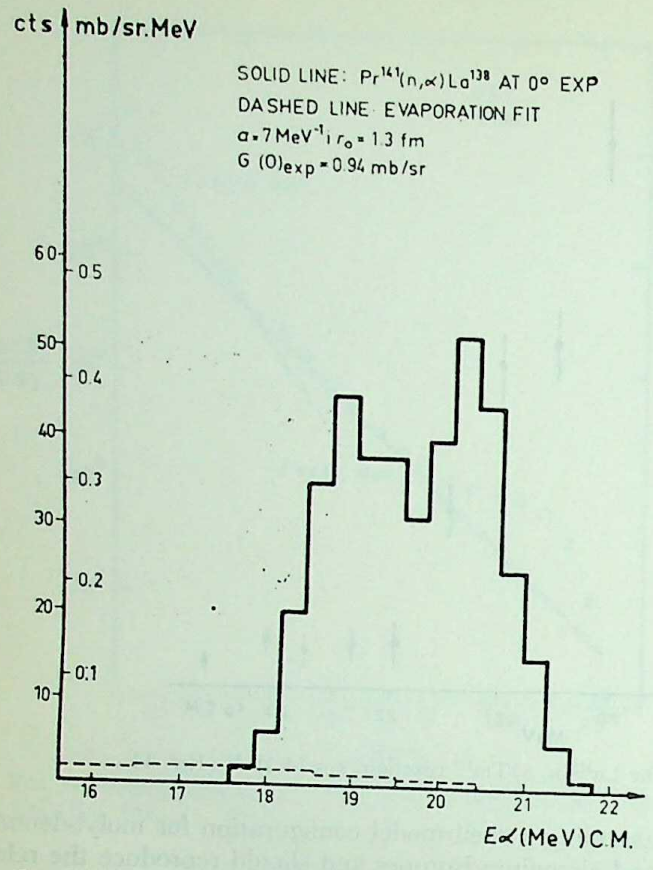

FIG. 32. The energy spectrum of alpha particles from 14-MeV neutron bombardment of Pr^{141}. Dotted lines represent statistical model calculations. (Ref. 70).

MeV neutron bombardment of several heavy nuclei from Nb^{93} to Bi^{209}. Their results, shown in Figs. 32 and 33(a) and (b), have been obtained by a telescopic technique combined with a two-dimensional analysis in dE/dx and E. Except for Nb^{93}, all the spectra and angular distributions are clearly direct. A statistical fit to the spectra could not be obtained even by using unreasonable values of the level density parameter a such as $A/25$. Thus some doubt is cast on the meaning of statistical model fits of (n, α) total cross sections for heavy elements that will be discussed in the next section.[85] The shape of the spectra and angular distributions show a clear surface process, and, contrary to the previously discussed results of Cuzsocrea *et al.*[81] several indications exist that the reactions proceed via a knock-out mechanism. Inferences from this supposition are discussed in Chapter 3.

An outstanding feature of the spectra is the constant position of the peak in the spectrum for the elements studied. The constancy with change in excitation energy is present also in the results of Marcazzan *et al.*[44] Its meaning has not yet been fully understood, although some attempts have been done.[83]

Spectral and angular distributions of alpha particles from 14- and 22-MeV neutron bombardment of silver have been studied by Rössle *et al.* using a gas scintillation telescope described by Mausberg *et al.*[87] (see Chap. 4). Angular distributions of portions of alpha-particle spectra are given; a remarkable feature of these distributions is the perseverance of forward peaking up to rather high residual excitations (lower energy alpha particles). Thus the nuclei around $A=100$ seem to be the turning point where the direct processes start to predominate.

Most of the information concerning the inelastic scattering of fast neutrons has been already discussed in the previous section. Actually, inelastic scattering data for the very heavy nuclei are rather difficult to obtain, since in this region the neutron spectrum is contaminated by contributions from fission neutrons. Batchelor *et al.*[88] have measured inelastic neutron spectra in U^{238} and Th^{232} and eliminated the post-fission contribution by assuming an appropriate spectral shape for fission neutrons,

$$N_{\text{fission}}(\epsilon) = A\epsilon^{\frac{1}{2}} \exp(-b\epsilon), \qquad (1.41)$$

and subtracting this part to the total spectrum. The difference was then analyzed by the usual method of reduced spectra. Best fits were obtained using the Fermi gas model for level densities. The values of the parameter a were independent of incident neutron energy.

Using 14-MeV neutrons, Adam *et al.*[89] have measured the angular correlation of the two neutrons from the reaction $(n, 2n)$ on bismuth in order to check the evaporation assumption of uncorrelated directions of emission. Their results suggest that the pure compound nucleus contribution (uncorrelated events) accounts for at most 70–80% of the $(n, 2n)$ cross section, which is somewhat surprising (see next section), and in contrast to the results of Jeremie,[90] who found no correlation at all between the two outgoing neutrons from the reaction $Bi^{209}(n, 2n)Bi^{208}$.

C. Total Cross Sections and Excitation Functions

In the earlier years, the bulk of information about neutron induced reactions came from total cross section measurements. Only recently, the improvement of detection methods, especially the introduction of telescopic techniques and multiparameter analysis, has shifted the peak of interest to angular and energy distributions. Nevertheless a large amount of data concerning total cross sections has been collected, from which valuable information can still be outlined. Several excellent compilations of total cross sections exist,[91] mostly around 14 MeV and we refer the reader to them, since we will not be able to review all the results.

1. Total Cross Sections of Neutron Induced Reactions up to 14 MeV

Most of the total cross sections have been measured by the activation method. Globally speaking, they corroborate and complement the information obtained from results of spectra and angular distributions dis-

CC-0. In Public Domain. Gurukul Kangri Collection, Haridwar

Digitized by Arya Samaj Foundation Chennai and eGangotri

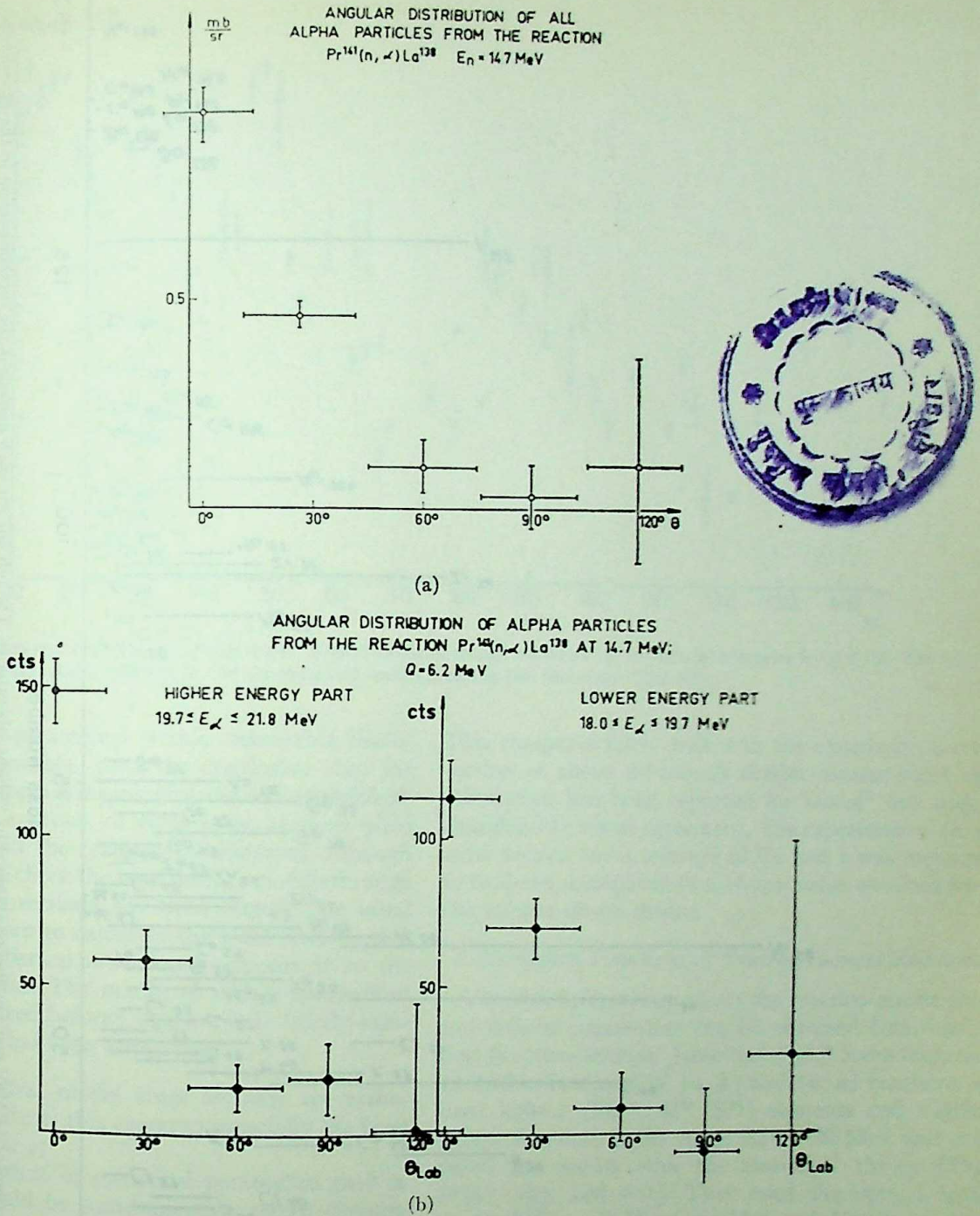

FIG. 33. (a) Angular distribution of all alpha particles from 14-MeV neutron bombardment of Pr^{141} (Ref. 70). (b) Angular distribution of higher and lower energy alpha particles from 14-MeV neutron bombardment of Pr^{141} (Ref. 70).

cussed in the previous sections and add valuable data on statistical and optical model parameters.

In the very low energy range (up to about 1 MeV) only (n, γ) reactions are important in the total cross section.[92] Cross-section measurements at lower energies are reported also by Cuzzocrea *et al.*[93] and Potenza *et al.*[94] However, the bulk of the total cross-section measurements lies, for obvious reasons, around 14 MeV. In these measurements usually the comparison technique was used, with $Al^{27}(n, \alpha)Na^{24}$ taken as a standard with 112–118 mb around 14 MeV. The measurements are reported in the references,[96] and we present here compilation of available data on total cross sections of (n, p) and (n, α) reactions taken from the work of Jeronimo *et al.*[95] (Fig. 34) and Facchini *et al.*[85] (Fig. 35).

It is our opinion that the analysis of total cross sections of neutron induced reactions is meaningful only in the case when a systematic search of many elements in a given region has been done. The underlying philosophy in the analysis should not be to obtain excellent fits for particular cases by an irregular variation of parameters, but to get fair overall fits varying sys-

CC-0. In Public Domain. Gurukul Kangri Collection, Haridwar

Digitized by Arya Samaj Foundation Chennai and eGangotri

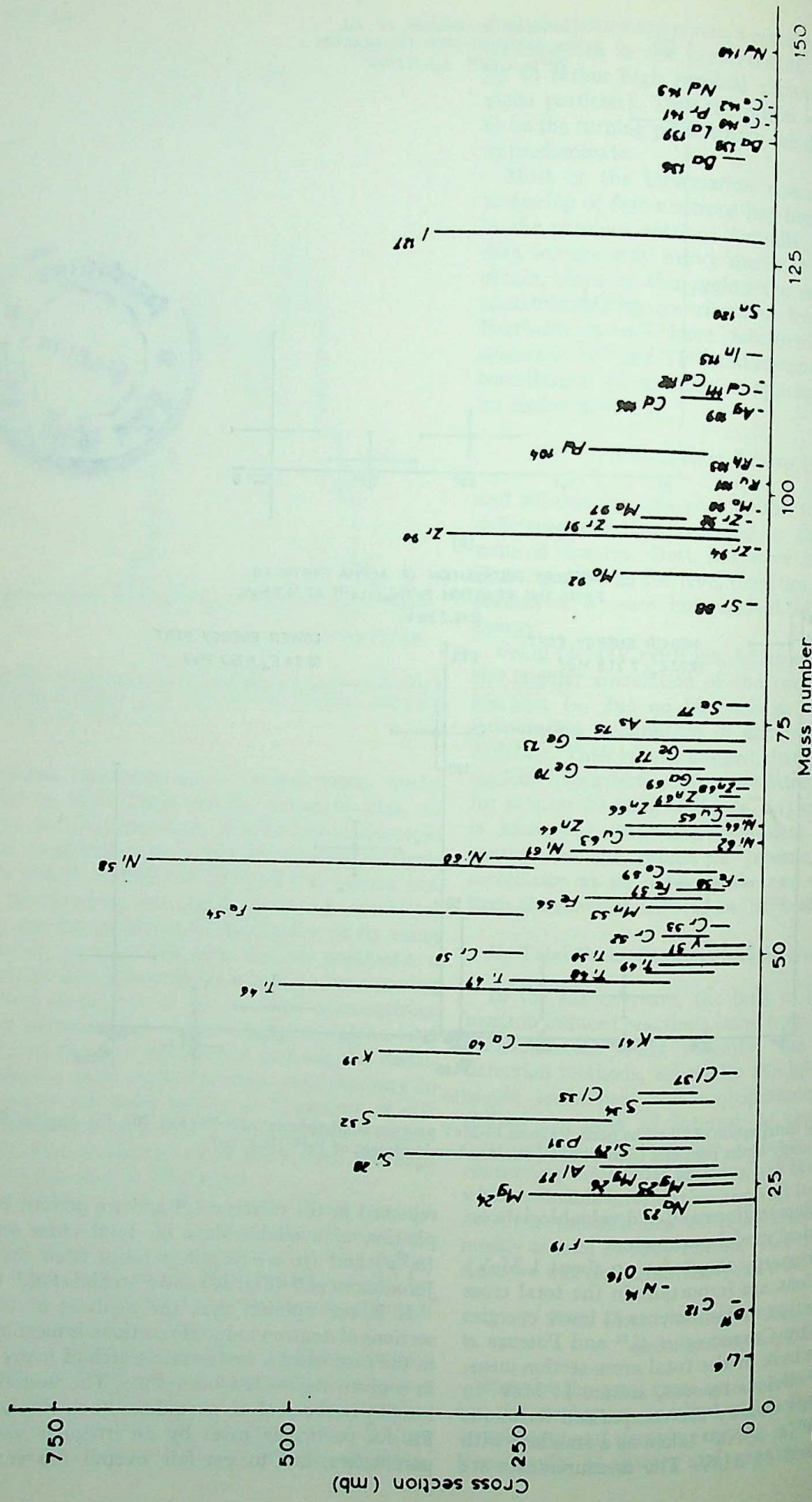

FIG. 34. Total cross sections for (n, p) reactions at 14-MeV neutron energy obtained by various laboratories. The full line for each nucleus is the total dispersion in the experimental values found in literature (Ref. 95).

CC-0. In Public Domain. Gurukul Kangri Collection, Haridwar

Digitized by Arya Samaj Foundation Chennai and eGangotri

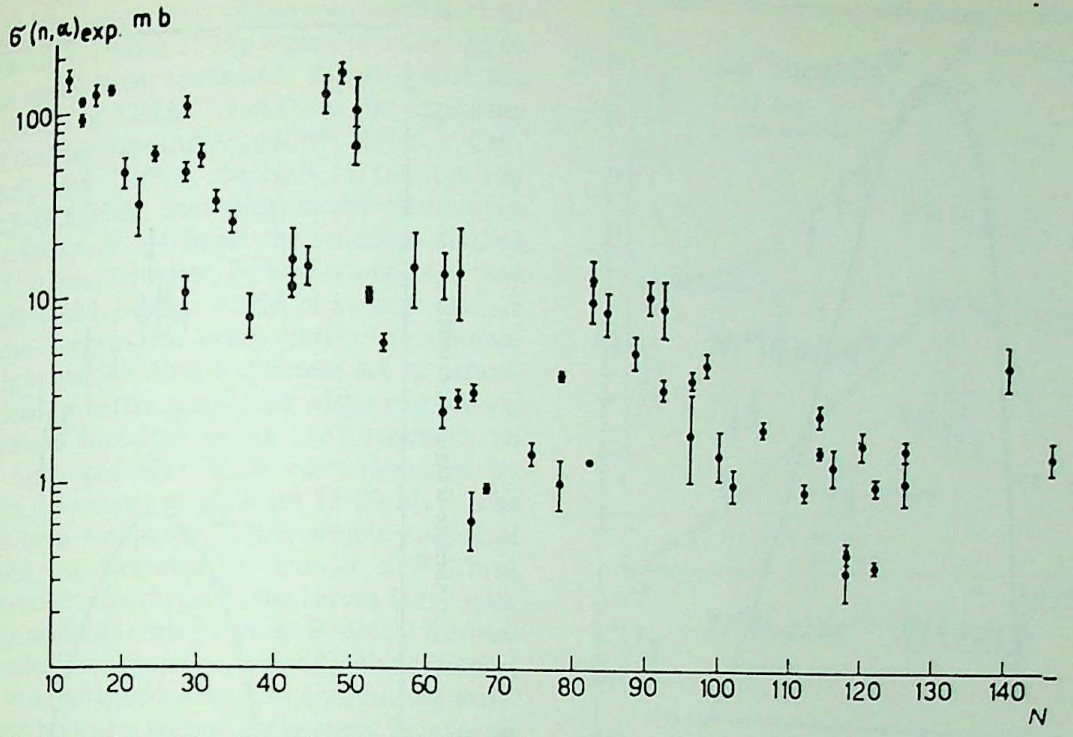

FIG. 35. Total cross sections of (n, α) reactions at 14-MeV neutron energy obtained by various laboratories for $A < 150$. The full line for each nucleus is the total dispersion in the experimental results found in the literature (Ref. 85).

tematically the parameters within reasonable limits. If this is not possible, then the conclusion that the model does not apply is meaningful and well established.

Most of the analyses of total cross sections yield information about the reaction mechanisms, although some attempts to check the level density models through fitting the cross sections has been done.[97] The usual procedure has been to calculate the total cross section through the statistical model and compare it to the experimental value. The merits of such a comparison have been analyzed before[27] and are only briefly summarized here. It has been noted that:

(i) the statistical model cross sections are rather parameter-dependent; this concerns especially the level density parameter a;

(ii) thus a system of statistical parameters used in the analysis should be simultaneously tested through a set of other experiments;

(iii) calculations of total cross sections in terms of direct interaction theories are necessary in order to get a more complete insight into the reaction mechanism of neutron-induced reactions.

Very few calculations of direct interaction total cross sections are available. Robertson[79] has calculated the total cross section of the (n, p) reaction on I^{127}. Using both the volume direct theory of Brown and Muirhead[22] and the statistical theory, Robertson has obtained the total cross section for the reaction $I^{137}(n, p)$ as:

$$\sigma_{\text{direct}} = 16 \text{ mb},$$

$$\sigma_{\text{comp}} = 1 \text{ mb}.$$

This compares fairly well with the experimental cross section of about 12 mb. A similar measurement and calculation has been reported by Dixon[78] but with a considerably worse agreement. The experimental (n, p) cross section for a mixture of Cs and I was measured to be 8 mb, compared to a 16-mb value obtained from the volume direct theory.

2. *Excitation Functions of Neutron-Induced Reactions*

Valuable information about the reaction mechanisms and related parameters can be obtained from excitation function studies. Jeronimo *et al.*[95] have measured excitation functions of (n, p) and (n, α) reactions for some lighter (Mg^{26}, Al^{27}, Si^{28}) elements and medium weight elements in the range $E_n = 6$–20 MeV and compared the results with the statistical theory [Figs. 36(a), (b), and (c)]. They used the optical model penetrabilities of Mani *et al.*[8,10] and Huizenga *et al.*[9] obtained from elastic scattering data and the level densities of Cameron.[12] The meaning of the over-all good fit obtained lies in the fact that it was obtained with *no adjustable* parameters. Thus in this region the compound nucleus model generally reproduces trends in the total cross sections.

Concurring results have been obtained by Bormann *et al.*,[98] the only difference being that these authors allowed a variable energy parameter η which essentially adjusted the excitation energy, replacing the neutron separation energy S_n by an effective value

$$S_n^{\text{eff}} = S_n + \eta.$$

Varying η within a couple of MeV excellent fits have been obtained for a number of excitation functions.

CC-0. In Public Domain. Gurukul Kangri Collection, Haridwar

Digitized by Arya Samaj Foundation Chennai and eGangotri

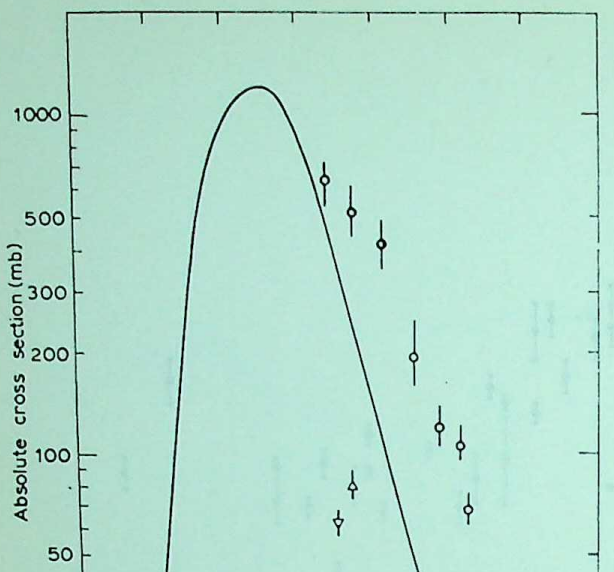

(a)

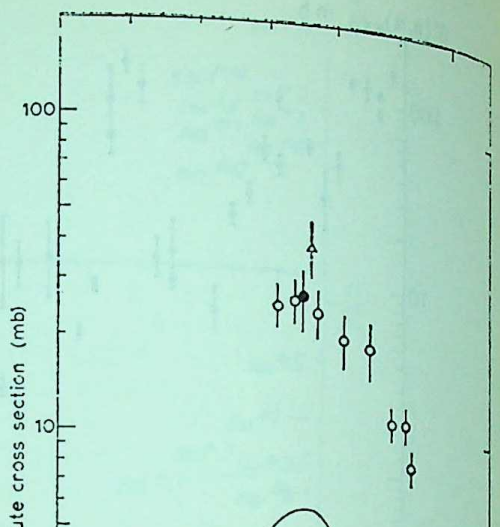

(b)

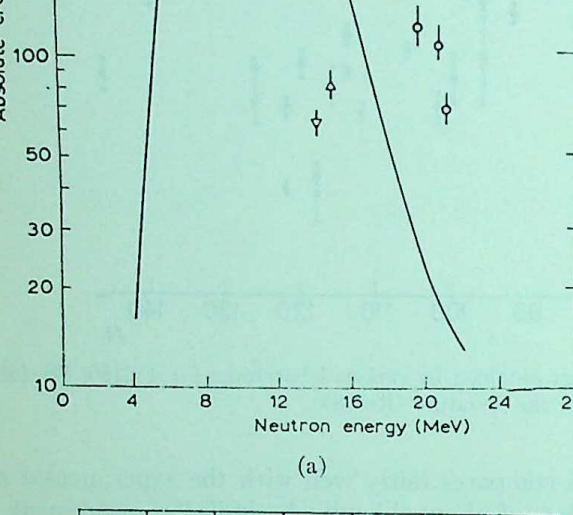

(c)

FIG. 36. (a) Total cross section for the $Co^{59}(n, p)Fe^{59}$ reaction. Experimental points: ○ (Ref. 95), ▽ (Ref. 99), △ (Ref. 100). The full curve is the calculation of Mani *et al.*[101] (Ref. 95). (b) Total cross section for the $Co^{59}(n, \alpha)Mn^{56}$ reaction. Experimental points: ○ (Ref. 95), ● (Ref. 102), △ (Ref. 103). The full curve is the calculation of Mani *et al.*[101] (Ref. 95). (c) Total cross sections for $Ni^{58}(n, np)Co^{57}+N^{58}(n, d)Co^{57}+Ni^{58}(n, pn)Co^{57}$ reactions from Refs. 100 and 104. The curves I, II, III, and IV have been obtained from calculations of Mani *et al.*[101] and represent excitation functions for these reactions and their sum, respectively (Ref. 95).

The underlying argument was that the neutron bombarding energy for which particular (n, p) and (n, α) reactions attain their maxima (in the excitation functions) follow closely, in their Z dependence, the respective Q values.

An extensive analysis of excitation functions of (n, α) reactions in terms of the statistical model has been performed by the Milan group[51] (see Sec. IB). Using the same values of optical penetrabilities as in the analysis of spectra, they obtained a set of values for the level density parameter a in complete agreement with the values obtained from the analysis of the

CC-0. In Public Domain. Gurukul Kangri Collection, Haridwar

Digitized by Arya Samaj Foundation Chennai and eGangotri

spectra. Thus the applicability of the compound nucleus model for (n, α) reactions in the region of nuclei up to $A \lesssim 100$ has again been confirmed. An exception are the recent results of Liskien *et al.*[105] on the excitation functions of the reactions $Cu^{63}(n, \alpha)Co^{60}$, $Ni^{60}(n, p)Co^{60}$, $Ti^{46}(n, p)Sc^{46}$, and $Na^{23}(n, 2n)Na^{22}$ in the neutron range of 12.5–16.5 MeV. Statistical model calculations are off by a factor of 2–4 in all the reactions studied (cf. Fig. 37). It can, however, be hardly expected that the statistical model, being a model of average nuclear properties can account for every particular reaction. Moreover, it is possible that a different set of parameters could lead to better agreement with experiments.

The excitation functions of $(n, 2n)$ reactions on Cu^{63}, Zn^{64}, Ag^{107}, and Sb^{121} have been measured by Rayburn[106] in the energy range from 12–20 MeV. The results have been compared to the simple statistical formulas[6] and the formulas of Barr *et al.*[107] These formulas reproduce the shape of the curves fairly well, but both give too large cross sections. Recently Büttner *et al.*[108] have calculated the cross section for the statistical emission of two particles taking into account the emission of gamma rays as a competing process. It is found that the competition of gamma emission is only important near the threshold of the considered reaction, where the level density formula fails to give a reliable result. Using their formula Büttner *et al.*[108] have obtained satisfactory agreement with $(n, 2n)$ excitation functions for nuclei around $A=60$ over a wide range of energies.

3. *Trends in* (n, p), (n, α), *and* $(n, 2n)$ *Cross Sections at 14 MeV*

For obvious reasons the bulk of total neutron reaction cross sections has been measured around 14 MeV. As mentioned before these results have been compiled,[91] and excellent reviews about the physical inferences from these measurements have appeared in the last few years. Facchini *et al.*[85] and Gardner *et al.*[109] have analyzed the 14-MeV (n, α) cross sections in terms of the statistical model, while in a series of articles Chatterjee *et al.* have analyzed the compound nucleus and shell effects in (n, α)[110] and (n, p)[111] cross sections. The same effects in $(n, 2n)$ reactions have been analyzed by Bormann.[112] Rather than presenting individual measurements we discuss these survey articles in some more detail.

The statistical model analysis of Facchini *et al.*[85] is based on compound nucleus calculations of the (n, α) cross section in terms of the cross section for the emission of inelastic neutrons, based on Eq. (1.3),

$$\frac{\sigma(n,\alpha)}{\sigma(n,n)}=\left(\frac{a_\alpha}{a_n}\right)^{1/2}\left(\frac{A}{A+3}\right)^{-5/2}\frac{g_\alpha m_\alpha}{g_n m_n}\times\frac{\int_{\epsilon_{\min}}^{\epsilon_{\alpha\,\max}}\epsilon_\alpha\sigma_{c\alpha}{}^*(\epsilon_\alpha)\exp\left[2(a_\alpha E_\alpha)^{\frac{1}{2}}\right]/(E_\alpha+t)^2\,d\epsilon}{\int_{\sigma_{\min}}^{\epsilon_{n\,\max}}\epsilon_n\sigma_{cn}(\epsilon_n)\exp\left[2(a_n E_n)^{\frac{1}{2}}\right]/(E_n+t)^2\,d\epsilon},$$

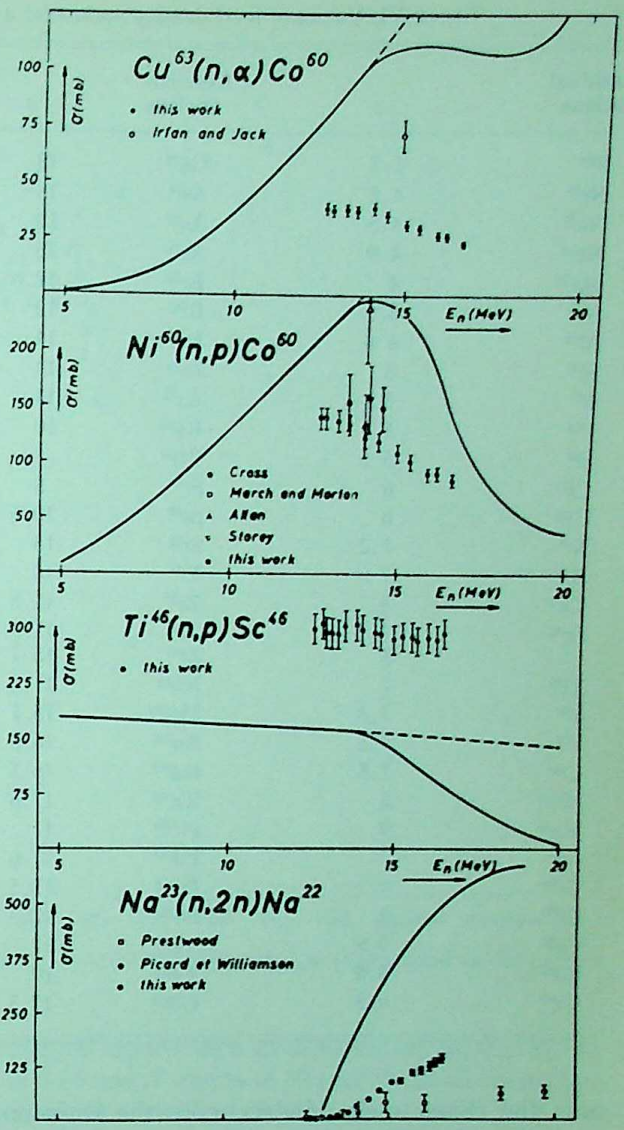

FIG. 37. Statistical model calculations together with the experimental cross sections for various neutron reactions. The dashed line represents theoretical cross sections without regarding second particle emission. Notice that in all the cases statistical model calculations are off by at least a factor of two. (Ref. 105).

where the cross section for inelastic neutron scattering is given by

$$\sigma(n, n)=\sigma_{\text{in}}-\{\sigma(n, p)+\sigma(n, \alpha)\}$$

and σ_{in}, the total inelastic cross section (all outgoing channels), has been computed from experimental data. The lower limit $\epsilon_{\min}$ in the integral in the numerator has been inserted to eliminate possible contributions from the region where $(n, n\alpha)$ and $(n, \alpha n)$ reactions became energetically possible. The other symbols are already familiar to the reader.

The a values used in the computation are shown in Table VI. They yield the same relationship between a and the neutron number N as those of Erba[113] shown in Fig. 38.

The interesting feature of this relationship is the presence of shell effects corresponding to closed neutron shells of $N=50$, 82, and 126 (for the corresponding proton shell effect see below). As the decrease of a

CC-0. In Public Domain. Gurukul Kangri Collection, Haridwar

Digitized by Arya Samaj Foundation Chennai and eGangotri

TABLE VI. Values of level density parameter a used in computing the (n, α) cross sections at 14 MeV.

Residual nucleus	a	Residual nucleus	a	Residual nucleus	a	Residual nucleus	a
F^{20}	4.5	Ga^{72}	13	Cd^{114}	17.5	Dy^{162}	
Ne^{23}	4.5	As^{75}	13	Cd^{115}	18.6	Dy^{164}	23.6
Na^{23}	4.5	As^{76}	13	In^{115}	16	Dy^{165}	22.8
Na^{24}	4.9	As^{78}	13	Sn^{118}	16.4	Dy^{167}	20.2
Mg^{26}	4	Br^{79}	12.6	Sn^{127}	17.5	Er^{168}	23.5
Al^{27}	4.9	Br^{81}	12	Sb^{124}	18	Er^{170}	21.4
Al^{28}	4.6	Br^{82}	14	Te^{130}	17	Yb^{175}	24
Si^{31}	5	Br^{84}	14	I^{127}	18	Hf^{178}	22
P^{31}	5	Kr^{85}	14	I^{130}	17.5	Ta^{181}	23.5
P^{34}	5	Rb^{85}	10	Cs^{133}	17.4	W^{187}	30.6
S^{34}	5.5	Rb^{87}	8	Cs^{136}	15.5	Re^{187}	23.5
Cl^{37}	6	Sr^{88}	8	Ba^{137}	15.5	Re^{188}	27
Cl^{38}	6	Sr^{89}	10.5	Ba^{139}	17	Os^{190}	23.5
K^{41}	7.2	Sr^{91}	13	La^{139}	13.5	Os^{191}	27.7
K^{42}	7	Y^{90}	10	Ce^{139}	13.5	Os^{193}	24
Ca^{47}	8	Zr^{92}	11.8	Ce^{140}	12.5	Ir^{191}	25
Sc^{45}	7	Zr^{94}	13.5	Ce^{142}	15	Ir^{194}	23.7
	8	Zr^{97}	15.7	Ce^{145}	25	Pt^{194}	24
Ti^{50}	7	Nb^{93}	11.8	Nd^{142}	11.5	Pt^{196}	23
V^{51}	7.3	Mo^{100}	15.7	Nd^{148}	21	Pt^{197}	20
V^{52}	8.5	Ru^{105}	16.5	Nd^{149}	24	Au^{197}	20
Cr^{51}	7.5	Ru^{107}	16.5	Nd^{151}	23	Hg^{200}	19
Mn^{55}	8	Rh^{106}	17.6	Sm^{152}	23	Tl^{206}	10.3
Mn^{56}	9	Pd^{108}	17	Sm^{153}	23	Bi^{209}	11.2
Fe^{54}	7	Pd^{109}	17.6	Sm^{154}	24.5	Ra^{227}	24.8
Co^{59}	9	Pd^{110}	17.5	Sm^{157}	22.5	Th^{230}	27.3
Co^{60}	9	Pd^{111}	17.8	Gd^{156}	24.5	Th^{235}	30
Co^{62}	9.5	Ag^{109}	17	Gd^{159}	21.6	U^{238}	29
Cu^{63}	9.5	Ag^{112}	19	Gd^{160}	21.4		
Cu^{65}	9.5	Cd^{112}	17.5	Gd^{161}	18.2		

near the closed shells hinders more the emission of neutrons than the emission of alpha particles (the Coulomb barrier anyway prevents the emission of low-energy alphas corresponding to high excitation of the compound nucleus), the relative cross sections for alpha emission increase near the closed neutron shells.

The comparison between compound nucleus theory and experimental cross sections is shown in Fig. 39. The results can be briefly summarized as follows:

—a fair agreement can be obtained for nuclei up to about the middle of the periodic table ($A \leq 80$);

—nuclei with closed neutron shells ($N=50$ and 82) have a cross section an order of magnitude higher than for neighboring nuclei; there is good agreement between experimental and theoretical values;

—for nuclei with neutron number N in between the two closed shells 50 and 82 the agreement becomes gradually worse, and often the experimental cross section becomes 5–10 times larger than the theoretical (compound nucleus) one. A different choice of parameters may sometimes reduce the disagreement;

—for heavy nuclei ($N>82$) the experimental cross sections are of the order of 1 mb and the disagreement between the experimental and theoretical values becomes at times catastrophic (ratio of 100–1000). No variation of parameters could eliminate this discrepancy. Other reaction mechanisms have to be taken into account (see below).

While very light nuclei have not been included in the survey in Ref. 85, in a recent article Gardner *et al.* have tried to establish trends in (n, α) total cross sections for nuclei with $6 \leq Z \leq 30$. Using a suitable form for the Coulomb barrier, the fractional probability of alpha particle emission F_α has been obtained in a simple form, particularly applicable to ratios of cross sections for neighboring isotopes:

$$\sigma(Z, A+1)/\sigma(Z, A) \doteq [F_\alpha(Z, A+1)/F_\alpha(Z, A)] \doteq \exp 2\{[a(\epsilon_{\max}-\beta_\alpha)]_{A+1}^{\frac{1}{2}}-[a(\epsilon_{\max}-\beta_\alpha)]_A^{\frac{1}{2}}\},$$

where $\epsilon_{\max}$ is the maximum energy of emission for alpha particles and β_α the corresponding Coulomb barrier. However, in this region of nuclei the experimental results are rather scanty, and a meaningful comparison with experiment was not possible.

CC-0. In Public Domain. Gurukul Kangri Collection, Haridwar

Digitized by Arya Samaj Foundation Chennai and eGangotri

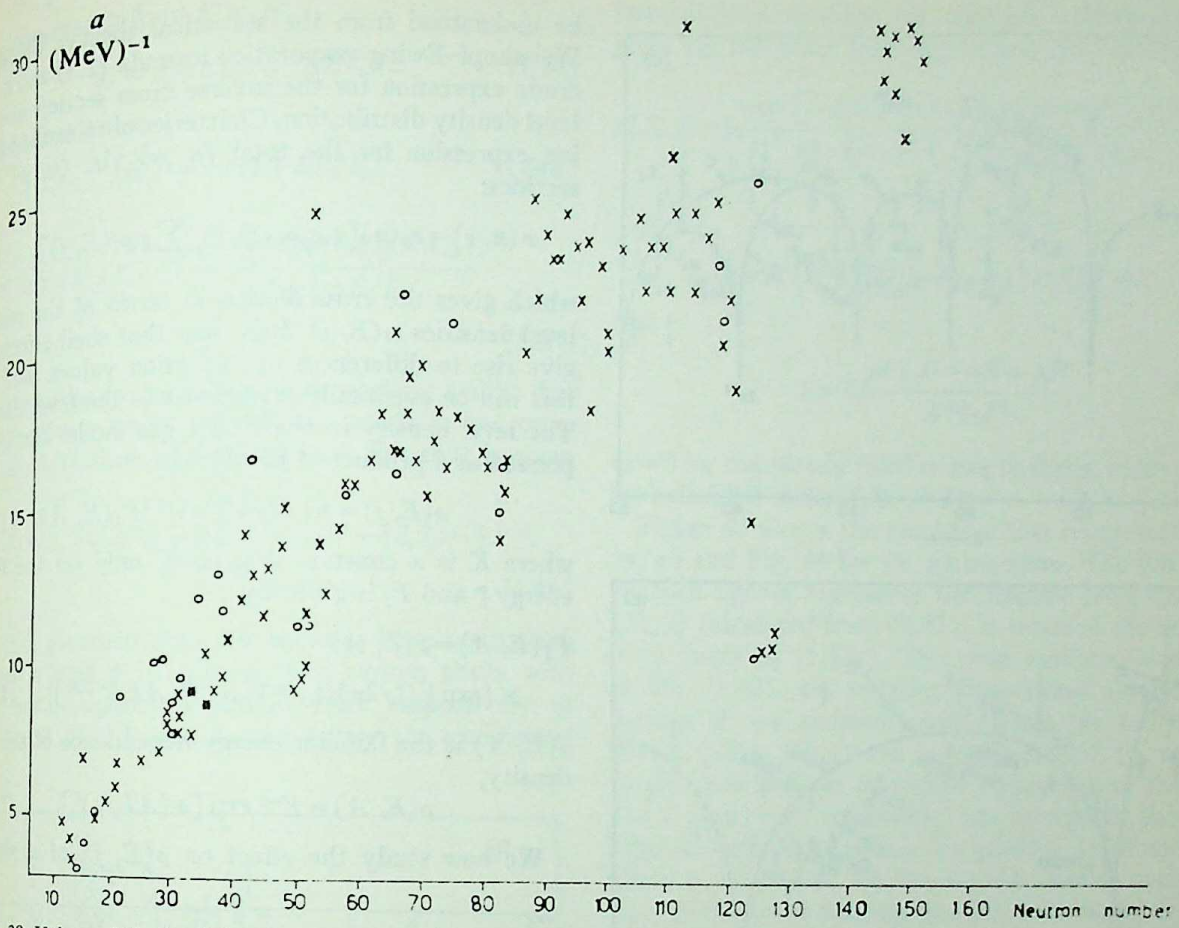

FIG. 38. Values of the level density parameter a from neutron resonances (*) and from energy spectra (○) plotted vs the neutron number N (Refs. 85 and 113).

In a series of articles Chatterjee[110,111] has discussed various aspects of trends in (n, α) and (n, p) reactions, especially shell effects. Shell effects in neutron induced reactions have been observed before[114] and in (n, α) reactions can be observed clearly by plotting the cross sections against the proton number Z and the neutron number N of the target nucleus (Figs. 40 and 41). Chatterjee reports dips at Z values of 10, 22, 30, 40, 52, and 84 and N values of 38 and 78. In all these cases the residual nuclei had closed proton shells. It is true that although in drawing the solid lines in Figs. 40 and 41 especially for large values of Z and N some freedom could have been employed, nevertheless the location of the dips near the closed shell numbers can

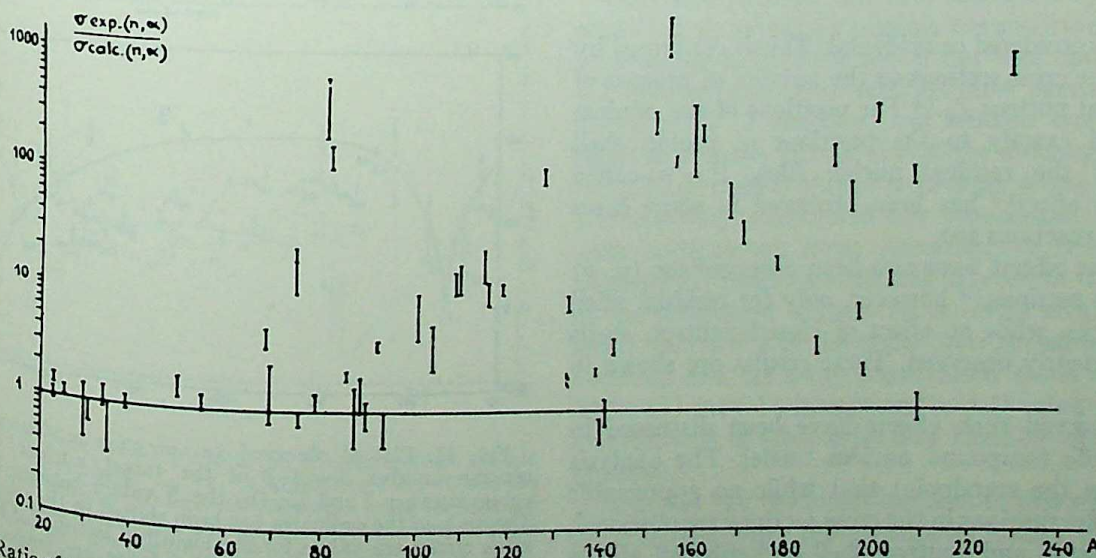

FIG. 39. Ratio of experimental cross sections and theoretical calculations of Facchini *et al.*[85] for (n, α) reactions at 14 MeV (Ref. 41).

CC-0. In Public Domain. Gurukul Kangri Collection, Haridwar

Digitized by Arya Samaj Foundation Chennai and eGangotri

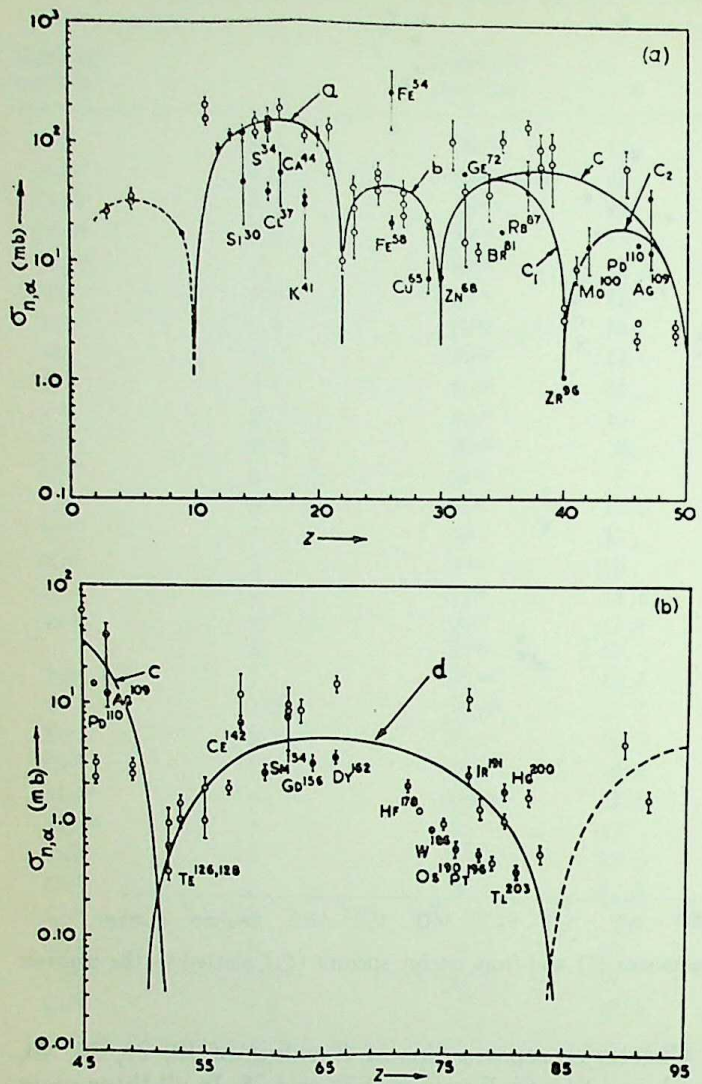

FIG. 40. Plot of the observed (n, α) cross sections against the proton number Z of the target nucleus. (a) the observed values between $Z=0$ and 50; (b) the values between $Z=45$ and 95. The scale of the ordinates has been shifted in the two cases. The isotopes of lesser natural abundance have been marked with black circles and have also been identified in the two plots (Ref. 110).

be hardly considered coincidental. This is confirmed by plotting the cross sections vs the number of protons of the residual nucleus Z_R.[110] The positions of the minima correspond exactly to the positions of proton shell closure of the residual nuclei. Also, the so-called Levkovski effect[115] has been observed in some cases for (n, α) reactions too.

The same effects have also been observed for (n, p) total cross sections,[111] however, only for residual filled proton shells, while no effect of closed neutron shells has been clearly observed. These results are shown in Fig. 42.

The observed shell effects have been discussed in terms of the compound nucleus model. The analysis starts from the standpoint that while no appreciable odd–even fluctuations in the cross sections are observed, distinct proton and neutron shell and subshell effects are present. The question is whether these effects can be understood from the statistical theory. Using the Weisskopf–Ewing evaporation formula (1.3) and a very crude expression for the inverse cross section and the level density distribution, Chatterjee obtains the following expression for the total (n, α) viz. (n, p) cross sections:

$$\sigma(n, \nu)=\sigma_c(n)[g_\nu\mu_\nu\rho_\nu(E, j)/\sum_i g_i\rho_i(E, j)], \quad (1.42)$$

which gives the cross section in terms of the residual level densities $\rho_i(E, j)$. It is clear that shell effects will give rise to differences in excitation values, and thus this will be eventually transposed to the level density. The level density in the Fermi gas model can be expressed as a product of two factors:

$$\rho(E, j)=K[(2j+1)/A^2]P_j(E, A), \quad (1.43)$$

where K is a constant depending only on the Fermi energy ζ and P_j is given by

$$P_j(E, A)=\rho(E, A) \times\{\exp[(1/2\pi)j(j+1)A^{-5/3}(AE/\zeta)^{1/2}]\}. \quad (1.43a)$$

$\rho(E, A)$ is the familiar energy dependence of the level density,

$$\rho(E, A)=E^{-2}\exp[\pi(AE/\zeta)^{\frac{1}{2}}]. \quad (1.43b)$$

We now study the effect on $\rho(E, j)$ of a shift in

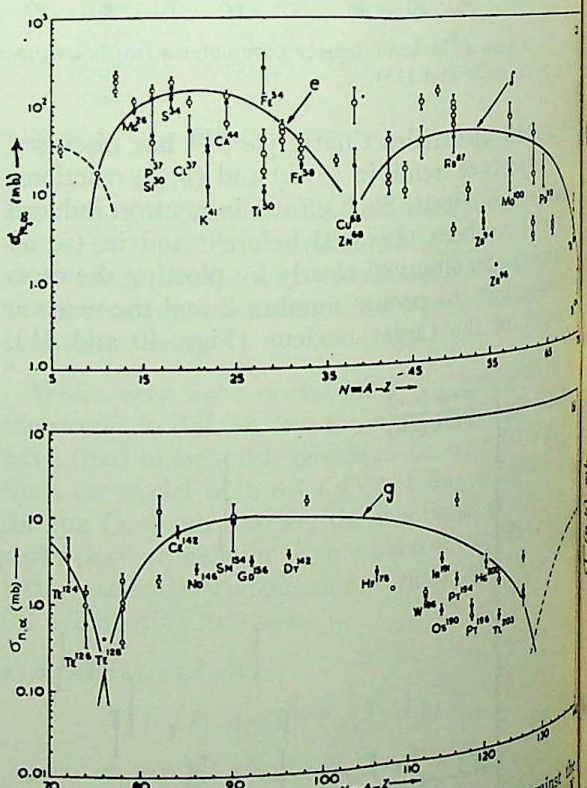

FIG. 41. Plot of observed (n, α) cross sections against the neutron number $N=A-Z$ of the target nucleus. (a) the N values between 5 and 75; (b) the N values between 70 and 130. The scale of the ordinates has been shifted in the two cases. The black circles are values for the identified isotopes of lesser abundance; the isotopes of higher abundance are marked as white circles and unidentified (Ref. 110).

CC-0. In Public Domain. Gurukul Kangri Collection, Haridwar

Digitized by Arya Samaj Foundation Chennai and eGangotri

citation energy from E to E',

$$E'=E+\Delta E, \qquad \Delta E \ll E. \tag{1.44}$$

Thus, to first order,

$$(E')^n=E^n(1+\Delta E/E) \tag{1.44a}$$

and

$$P_j(E', A)=P_j(E, A)\frac{\exp\left[(1/2\pi)(A/\zeta E)^{\frac{1}{2}}\Delta E\right]}{1+2\,\Delta E/E}. \tag{1.45}$$

It is now interesting to explore whether a shift due to shell effects could explain the trends in the cross sections. According to Rosenzweig[117] this shift is given by

$$\Delta E=\tfrac{1}{12}N^2d_n+\tfrac{1}{12}P^2d_p-\tfrac{1}{2}d_n(n-\tfrac{1}{2}N)^2-\tfrac{1}{2}d_p(p-\tfrac{1}{2}P)^2. \tag{1.46}$$

Here it is assumed that the nucleons have occupation number n and p in neutron and proton shells with maximum occupancy N and P, equal, respectively, to $2j_N+1$ and $2j_P+1$, and d_n and d_p are the equidistant fermion-level spacings for neutrons and protons. This gives the following shell-dependent level density:

$$\rho(E_s, j)=\rho_0\frac{\exp\left[-(\pi/36)(\zeta/\Delta E)^{\frac{1}{2}}(N^2+P^2)(1+x)\right]}{1-\left[\zeta(N^2+P^2)/9AE\right](1+x)} \tag{1.47}$$

with

$$\rho_0=K(1/A^2)2(j_N+j_P+1)P_j(E, A) \tag{1.47a}$$

and

$$x=12\frac{n^2+p^2-nN-pP}{N^2+P^2} \tag{1.47b}$$

($x=0$ for completely filled or empty shells, while $x=-3$ for half-filled shells $N/2$, $P/2$).

Figure 43 shows the results of this computation for (n, α) and Fig. 44 for (n, p) reactions. The full curve on both figures represents the relative level densities (E_s, j) calculated from (1.47), in terms of the normalizing factor ρ_0 (1.47a). The cross sections, according to Eq. (1.42), are roughly proportional to the level density of the residual nuclei. Thus the full curves should follow the trends in experimental (n, α) and (n, p) cross sections as, indeed, appears to be the case. For a very crude calculation, the agreement shown in Figs. 43 and 44 is rather remarkable. It should not, however, be pushed too far, since for heavy nuclei the dips in the cross sections are far from being certain. It is nevertheless clear that two important structure effects, the pairing and the shell effects, can be suitably described in terms of the statistical model. In fact, nothing has been said about the contribution of direct reactions to analyze the shell effects. The shell effects are comparable in energy to the pairing effects, but usually are less clearly seen because (i) more attention is usually given to the behavior within a shell than to that across the shells and (ii) no neutron shell effects have been observed.

This last problem has been discussed by Rubbino *et al.*,[118] in an attempt to explain the anomalies in (n, α) cross sections. In particular, it has been observed that (i) experimental cross sections show *maxima* around closed shells of *neutrons*, and *minima* around closed shells of *protons*; (ii) for $A>70$ the disagreement with compound nucleus theory is *stronger* where $\sigma_{\exp}(n, \alpha)$ are relatively *small*, and *less pronounced*, where the cross sections are *large*. According to Rubbino, the anomaly (i) could be explained in terms of the decrease of the compound nucleus (n, α) cross section for the larger values of a in the region near the closed shells of neutrons and far away from closed shells of protons, while (ii) may be interpreted as a Q value effect. The explanations of Chatterjee and Rubbino are not quite consistent.

Analyses like the ones discussed in this section could be criticized from the standpoint[116] that through the uncertainty of the bombarding energy (it is, however,

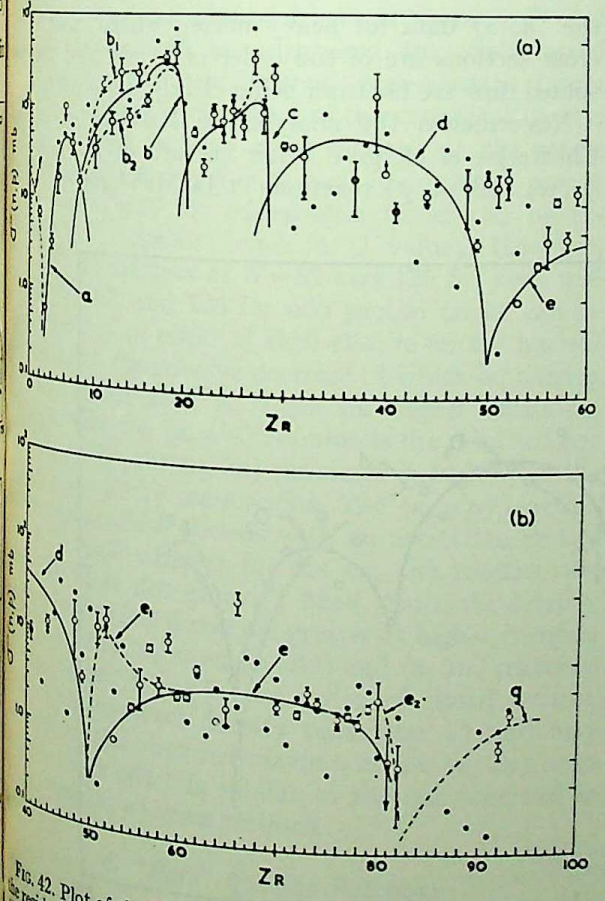

FIG. 42. Plot of the ~14-MeV total (n, p) cross sections against the residual nuclear charge Z_R. (a) values between $Z_R=0$ and 60; (b) values between $Z_R=40$ and 100. Reaction cross sections for only the most abundant target elements have been shown as white circles; the "errors" are the spread in the nominal values. Gardner's predicted values[116] are shown as black dots (Ref. 111).

CC-0. In Public Domain. Gurukul Kangri Collection, Haridwar

Digitized by Arya Samaj Foundation Chennai and eGangotri

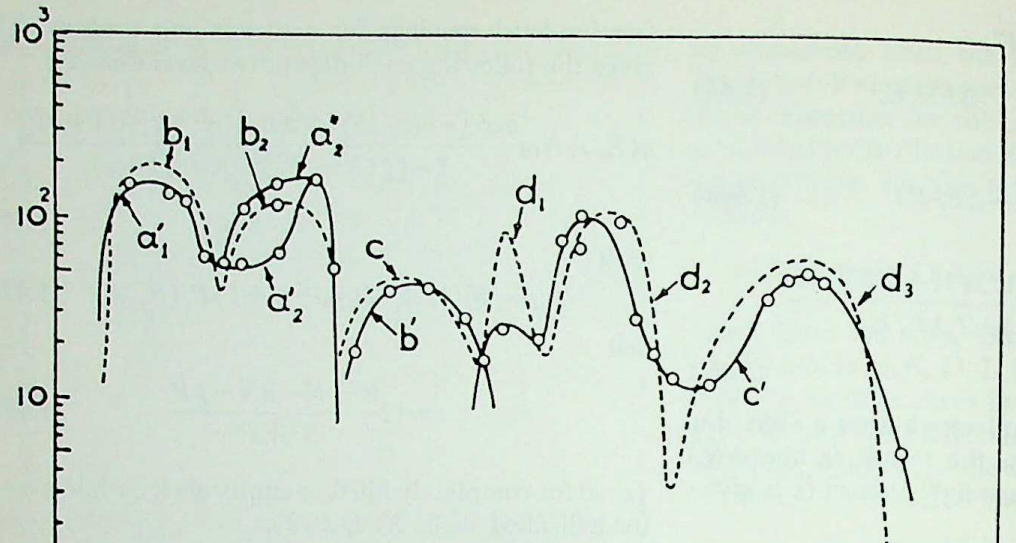

FIG. 43. The computed curves of (n, α) total cross sections (full lines) against Z_R $(9 \leqq Z_R \leqq 55)$ obtained using the shell-dependent level density (1.47). The regions of the three major proton shells a, b, c, use different normalizing factors ρ_0. The ordinate is $\rho(E_{s,i})/\rho_0$. The dotted curves, superimposed for comparison, present trends in experimental (n, α) cross sections (Ref. 110).

true that several measurements[45,119–121] have shown only small variations of $\sigma_{n\alpha}$ with the bombarding energy around 14.5 MeV), the unrealistic error limits, and lack of thorough standardization one can hardly perform a judicious selection of data for such systematic studies. As already mentioned, this concerns especially the (n, α) data for heavy nuclei, where most of the cross sections are of the order of 1 mb, and the presumed dips are far from being clearly discernible.

Nevertheless the analyses of Facchini *et al.* and Chatterjee *et al.* give a fair picture of the trends in (n, α) and (n, p) reactions at 14 MeV and it is hoped

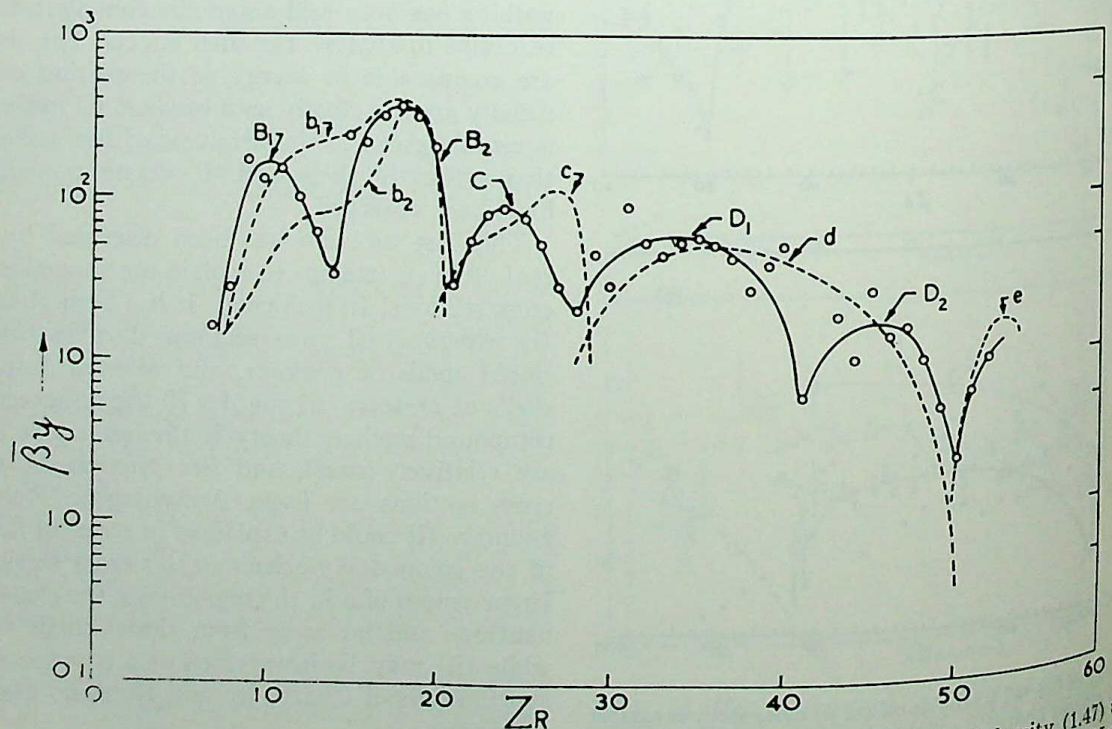

FIG. 44. Plot of the calculated (n, p) total cross sections $(\bar{\beta}_y)$ obtained using the shell-dependent level density (1.47) against residual nuclear charge $Z_R (0 \leqq Z_R \leqq 60)$. The solid curve is drawn through the calculated values shown as white circles. Note the dips between the regions B_2 and C, C and D_1, and D_2 and e, and the subshell dips between B_1 and B_2, and D_1 and D_2. The dotted curves $b_1 - e$ present smooth curves drawn through the experimental points and have been shown here for comparison (Ref. 111).

CC-0. In Public Domain. Gurukul Kangri Collection, Haridwar

Digitized by Arya Samaj Foundation Chennai and eGangotri

to believe that new results can radically alter this picture. The interplay of compound nucleus and direct processes for these reactions can be described as follows:

For elements in the lighter half of the periodic table (up to $A=100$) the main contribution to the reaction mechanism comes from compound nucleus processes and the explanation of the dips in the cross sections as a consequence of the shell effects in the level density is quite plausible. While the direct contribution, stemming mostly from the nuclear surface, remains more or less constant throughout the periodic table, the compound contribution falls down sharply for heavy nuclei due to the effect of the Coulomb barrier. The compound nucleus cross section falls practically to zero for nuclei with $Z=60$–70. Thus the (n, α) cross sections for very heavy nuclei come from purely direct surface effects and is constant up to highest Z values. In fact, Fig. 40 shows a slight increase for $Z=70$ to 90 that could be expected from the increase of the nuclear surface, consistent with the above interpretation.

$(n, 2n)$ reactions have always been considered as evaporative processes *par excellence*. In fact, in this case even the most modest approximations gave satisfactory results. Nevertheless, structure effects in these reactions have been observed several years ago[114] and recently Bormann[122] has discussed the shell model effects in $(n, 2n)$ reactions on even–neutron target nuclei against the background of the statistical theory. Minima in the $(n, 2n)$ cross sections at the magic neutron numbers for $N=28$ and 50 for even–proton nuclei and $N=20$ for odd–proton nuclei can be explained by a similar trend in Q values. However, cross section maxima at $N=82$ and 126 for even and $N=28$, 50, 82, and 126 for odd proton nuclei can be understood as an effect of shell closure on the nuclear level density, the relative decrease of which on passing across a closed shell is larger for higher excitation energies. Now the $(n, n'\alpha)$ reaction is the principal one competing with the $(n, 2n)$ processes at 14 MeV in the medium and heavy mass region. The $(n, n'\alpha)$ reaction leaves the residual nucleus with an excitation energy up to 12 MeV whereas for the $(n, 2n)$ reaction the excitation does not exceed 4 MeV. Since the relative change in the level density is greater at higher energies, the competition between $(n, n'\alpha)$ and $(n, 2n)$ reactions favors the latter one in the region of closed neutron shells (smaller level density parameter a) and may account for the observed maxima in the $(n, 2n)$ cross sections. The effect is similar to the one observed in (n, α) and (n, p) cross sections.

4. "Rare" Nuclear Reactions

The "rare" nuclear reactions, including (n, d), (n, np), (n, pn), (n, t), (n, dn), $(n, 2p)$, (n, He^3), (n, γ), $(n, n\alpha)$, and $(n, \alpha n)$ and $(n, 3n)$, have been measured by the activation technique.[123,124] These reactions are important for the understanding of spectra and angular distributions, since the "rare" reactions often interfere in the region of highly excited residual states. They also give information about the clustering of particles.

In general, the upper limit for most of the above reactions at 14–20-MeV neutron energy is below 1 mb. Exceptions are the (n, pn), (n, np), and (n, d) reactions, whose total sum may exceed several hundreds millibarns (e.g., 520 mb for Ni^{58}) and some $(n, n\alpha)$ reactions. As far as this latter reaction is concerned, a search has been done to establish whether the process

$$n+X \rightarrow Y+\alpha+n$$

proceeds via the direction $(n, \alpha n)$ or $(n,\alpha n)$. This reaction might be supposed to proceed mainly via the n, n' process followed by α emission: the emission of neutrons is easier than that of alphas due to the Coulomb barrier. However, for an alpha particle to compete successfully with the emission of a proton or a second neutron *after* a first neutron has been emitted, the separation energy S must be much less than the corresponding energies S_n and S_p. This, actually, is always the case for S_n, but not for S_p. Thus $(n, n\alpha)$ cannot successfully compete with the (n, np) process and we must turn the $(n, \alpha n)$ reaction as the predominant mechanism for the emission of a neutron and an alpha particle. Indeed, the formula

$$\sigma(n, \alpha n)=\sigma(n, \alpha)P(n) \tag{1.48}$$

with

$$P(n)=\frac{\int_0^{\epsilon_n+Q_{n,\alpha}-S_n} \epsilon_\alpha \sigma_\alpha^*(\epsilon_\alpha)\rho(E)\,d\epsilon_\alpha}{\int_0^{\epsilon_n+Q_{n,\alpha}} \epsilon_\alpha \sigma_\alpha^*(\epsilon_\alpha)\rho(E)\,d\epsilon_\alpha} \tag{1.48a}$$

which is obtained under the supposition that if the residual nucleus has an energy excess of at least S_n, then a neutron is always emitted, gives excellent agreement up to Nb. For higher A values there are no $(n, n\alpha)$ or $(n, \alpha n)$ reactions, since these reactions can hardly arise as a consequence of direct processes.

5. Fluctuations in Total Cross Sections

In this section we review briefly some of the recent experimental information concerning the presence of intermediate structure in reaction excitation functions.

Feshbach[25] has suggested (see Sec. IA6) that structure due to effects of intermediate processes could be expected in excitation functions of neutron total cross sections. Seth[125] has measured average total cross sections for many nuclei from Cu to Tl in the energy range 3–650 keV, with an energy resolution of 8–10 keV. His results can be summarized as follows:

(i) The excitation functions on all elements show a characteristic structure. The structure is not random

CC-0. In Public Domain. Gurukul Kangri Collection, Haridwar

Digitized by Arya Samaj Foundation Chennai and eGangotri

in character, has widths of 75±25 keV over the whole region and amplitudes 10–20 in the $\langle\sigma_t\rangle$ (3–10 times the statistical error);

(ii) the structure is most prominent for monoisotopic elements and small for elements containing many isotopes.

As the known level density for most of the nuclei is of the order of $\langle D\rangle = 10$–100 eV, the average width

$$\langle\Gamma_{\text{exp}}\rangle \gg \langle D\rangle$$

and the observed structure cannot be due to Ericson fluctuations. Seth[125] suggests that they represent evidence of Feshbach's doorway states.

The width of doorway states has been calculated in the region of lead[25] to be of the order of 100 keV. However the mentioned result of Le Couteur[26] (see Sec. IA6) that the width of intermediate states varies as $A^{-5/3}$ [Eqs. (1.27) and (1.27a)] is not confirmed by the experimental evidence in Ref. 125.

Results that could be interpreted along the same lines have been presented by Csikai,[126] and Cabe[127] who have measured $(n, 2n)$ total cross sections in the region around 14 and 17 MeV, respectively. Here the energy resolution of the neutron beam was considerably worse than in the preceding experiments (25–50 keV). Nevertheless, the structure of 50–100-keV width could be seen for all the nuclei studied except the lightest ones.[128] Now for medium weight and heavy nuclei the $(n, 2n)$ cross section accounts for most of the total cross section above 14 MeV, and an interpretation in terms of doorway states is feasible.

The structure in the excitation functions is not confined solely to total cross sections. Characteristic peaks 100–200 keV wide and separated by energy intervals of 300–400 keV have been observed in both the polarization and the differential cross sections of neutrons scattered by F, Na, Al, and P in the energy range 0.2–2.2 MeV.[129] The optical model of Perey *et al.* reproduced the average behavior of the energy dependence of the cross sections and the polarization, but not the fine structure. It is suggested[129] that the resonances are due to doorway states. The supposition is enhanced by the fact that the observed structure is correlated at different scattering angles as a function of energy.

The structure in total cross sections need not, however, be interpreted uniquely in terms of doorway states or intermediate structure in general. Calvi *et al.*[39] have suggested that the resonances found in total cross sections could be interpreted as statistical fluctuations in the level density of the compound nucleus. According to these authors, the mean square relative deviation of the total compound cross section from the average value is inversely proportional to the square root of the level density of the intermediate (compound) nucleus. Manero[130] has measured neutron total cross sections for V, In, I, and Bi in the energy range of 3.2–5.2 MeV, with a neutron energy spread of ±30 keV. The results for vanadium and indium are shown in Fig. 45. Now it is known from earlier work,[11] that the level spacing for bismuth (Bi^{209}) and vanadium (V^{51}) at these excitations is considerably smaller than for indium (In^{115}) and iodine (I^{127}). The use of the level density formula given by Ericson[1] for the equidistant spacing model with the values of the parameter a given by Erba *et al.*,[11] gives the respective level densities for compound nuclei for an average neutron energy ϵ_n= MeV (Table VII). Thus, according to Calvi *et al.*, one should expect large and narrow resonances for vanadium and bismuth, small value of a and smaller but broader resonances of indium and iodine. This indeed seems to be the case (cf. Fig. 45).

Structure in total cross sections for Na, K, and Ca between 4–6-MeV neutron energy has been found also by Stüwer *et al.*[131] Pronounced peaks of 100–150-keV width have been found in each case and their presence attributed to fluctuation in compound nucleus density. Thus although the presence of intermediate resonances in the total cross section seems to be well established

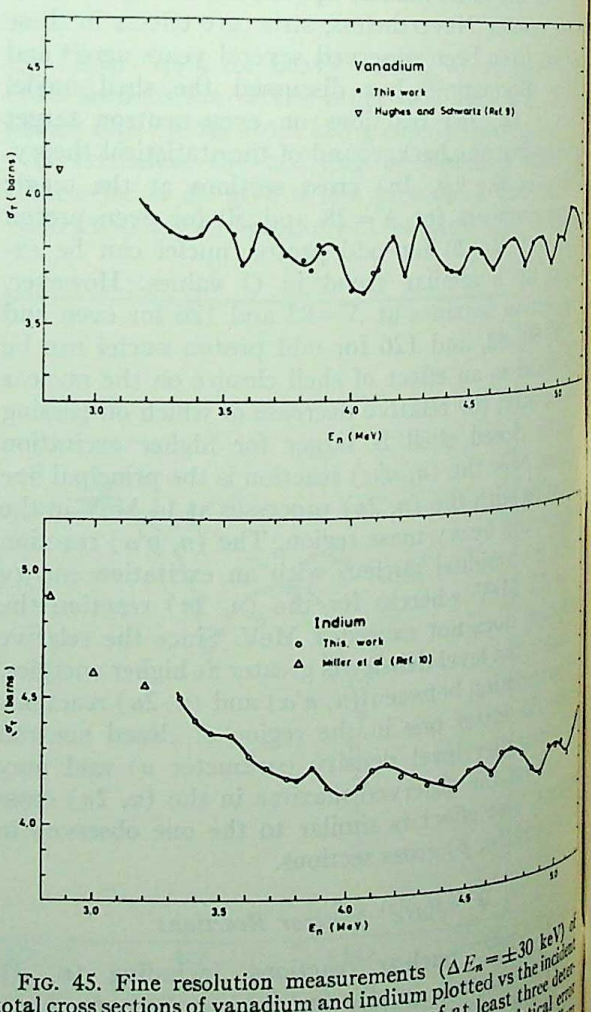

FIG. 45. Fine resolution measurements ($\Delta E_n = \pm 30$ keV) of total cross sections of vanadium and indium plotted vs the incident neutron energy. Each point is the average of at least three determinations of five measurements each. The total statistical error of every point is about 2.5% for vanadium and 2% for indium (Ref. 130).

CC-0. In Public Domain. Gurukul Kangri Collection, Haridwar

Digitized by Arya Samaj Foundation Chennai and eGangotri

the problem of finding an adequate interpretation for these resonances is still open to discussion.

D. Isomeric Ratios

Ratios of cross sections leading to two neighboring isomeric states have been used to complement our knowledge about the reaction mechanisms and especially to obtain information about the distribution of spins in the compound nucleus. The so-called spin cutoff factor $2\sigma^2$, present in the spin distribution of level densities,

$$(2J+1)\exp[-(J+\tfrac{1}{2})^2/2\sigma^2] \qquad (1.49)$$

enters as a crucial parameter in the calculation of isomeric ratios. Thus, if one assumes a compound nucleus mechanism for a specific reaction, the study of experimental isomeric ratios should yield information about this parameter.[132] This method is especially applicable for thermal neutron reactions, where the mechanism is purely a compound nucleus one.[133]

Isomeric ratios of fast neutron induced reactions were measured recently by Meadows *et al.*[134] and Brzosko *et al.*[135] The latter studied the so-called Levkovski effect[115] consisting in the regular decrease of the cross section with the increasing atomic number in (n, p) reactions on different isotopes. They found that a smaller variation in the ratio of Z/A (0.004 for tin and 0.007 for tellurium) than the one reported by Levkovski (0.009) is necessary to reduce the cross section by a factor of two.

Mangal and Gill[136] have measured the isomeric cross section ratios for several $(n, 2n)$ reactions at 14 MeV and compared them to the theory in order to obtain a best fit value of σ in the distribution (1.49). Using the calculations of Huizenga and Vandenbosh[132] and supposing dipole emission only, the value of the parameter σ for several nuclei around $A=100$ was calculated. All the obtained values cluster around 5 (e.g., for Sb^{123} $\sigma=4.5$). A similar analysis was performed by Kolar *et al.* for several neutron induced reactions in order to study the dependence of the isomeric ratios on the respective values of final angular momenta. In the (n, p) and (n, α) reactions studied all the metastates had considerably larger spins than the ground states. However, the measured isomeric ratios were all around unity. Thus the results of Brzosko *et al.*[135] could not be reproduced. Although the statistical model reproduces the experimental results fairly with a cutoff parameter σ corresponding to one-half of the rigid body moment of inertia, these results should be taken with some caution, since they are obtained assuming a very small number of de-excitation gamma rays (in fact $\nu=0$ was used throughout).

In two recent articles Vonach *et al.*[138] and Bishop *et al.*[139] have used the isomeric ratios in order to distinguish between two models of level densities, the Fermi gas and the superconductor model (see Secs. IA2 and IA3). Although the superconductor model predicts only a slight energy dependence of the nuclear temperature at low excitation energies, in agreement with some, but not all experimental results, the single-particle level densities required to reproduce the absolute values of the experimental nuclear temperatures are considerably smaller than expected. The superconductor model predicts a reduction from the rigid body moment of inertia which is consistent with isomeric ratios for nuclei with an odd number of nucleons.

The two models—a Fermi gas model modified to compensate for pairing interactions (the so-called "shifted" Fermi gas model) and the superconductor model have been used to calculate isomeric ratios for the reactions $Au^{127}(n, 2n)$ $Au^{126g,m}$ and $Cd^{116}(n, 2n)$ $Cd^{115g,m}$ for neutron energies from 12–17.5 MeV. For the first reaction excellent fits for σ_m/σ_g have been obtained with the Fermi gas model with $a=19$ MeV^{-1} ($a=15$ and 30 MeV^{-1} gave no agreement). However, in order to obtain any agreement with the superconductor model, the a value should be set below 15 MeV^{-1}, which is incompatible with other experimental results (Fig. 46). The situation is quite opposite for the reaction $Cd^{116}(n, 2n)$ $Cd^{115g,m}$. A reasonable fit is obtained with the superconductor model with $a=25$ MeV^{-1}, which is reasonable for this model,[140] and the Fermi gas requires $a=30$ MeV^{-1}, which is by far too large [Figs. 47(a) and (b)].

Neither of the models is able to explain satisfactorily all the experimental isomeric ratios. All the cases in which the Fermi gas model is satisfactory are odd-odd residual nuclei, while odd mass nuclei either agree well with the superconductor model or lie in between the two.

TABLE VII. Level densities of V^{51}, In^{115}, I^{127}, and Bi^{209} (see text).

Target nucleus	B_n (MeV)	a (MeV^{-1})	(N) (levels/MeV) for $E_n=4.0$ MeV
V^{51}	7.304	8.8	1.9×10^5
In^{115}	6.610	21.0	4.4×10^{11}
I^{127}	6.760	20.6	3.3×10^{11}
Bi^{209}	4.640	10.8	1.4×10^5

II. SCATTERING AND OPTICAL MODEL STUDIES

For the last decade, the elastic neutron scattering has been analyzed in terms of a complex potential.[141] Conversely, information about this potential has been extracted from these data and successfully used to fit neutron inelastic scattering and other nuclear processes. Gradually, the complex potential employed grew in complexity: the square well potential was abandoned in favor of the diffuse edged one[142] and spin orbit interaction has been added to it.[143] In the last few years the energy dependence of the optical model parameters has been, in a sense, circumvented by the use of nonlocal potentials[66] which give a good over-all

CC-0. In Public Domain. Gurukul Kangri Collection, Haridwar

Digitized by Arya Samaj Foundation Chennai and eGangotri

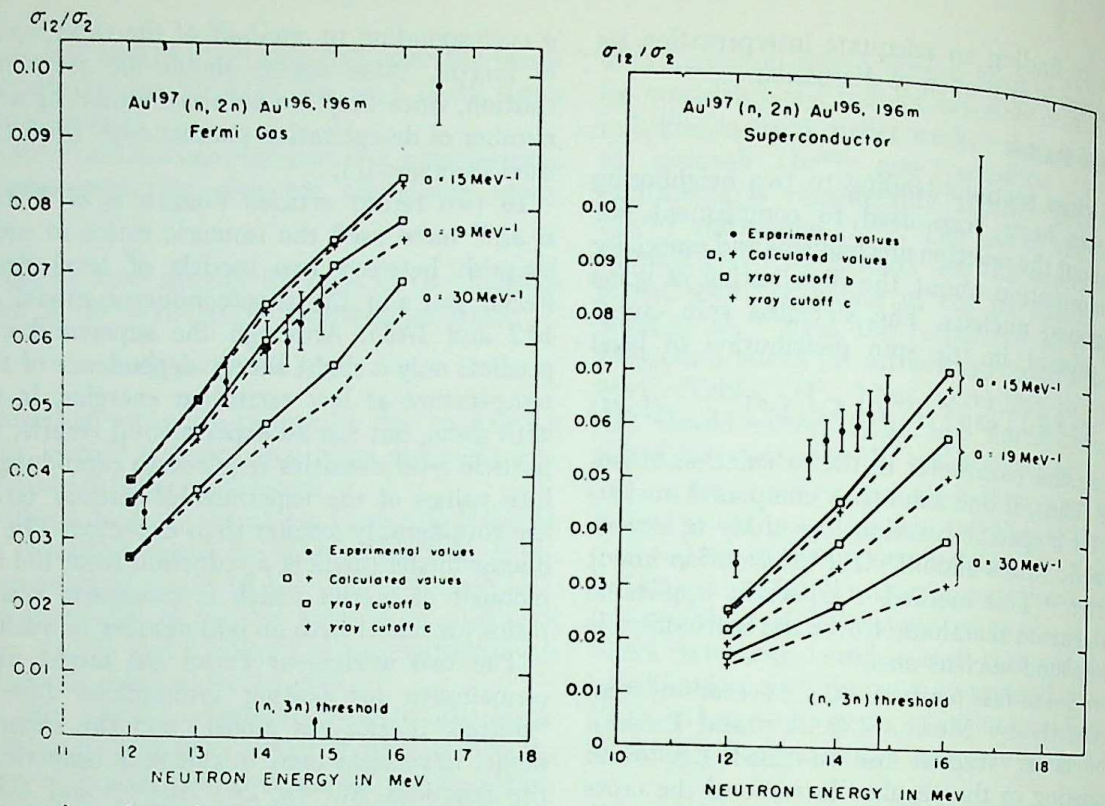

FIG. 46. Comparison of experimental isomeric cross section ratios for the Au^{196} isomers produced by the $Au^{197}(n, 2n)$ reaction with theoretical values calculated with (left) a Fermi gas model for two assumptions about the gamma ray cascade and for several values of the level density parameter a, and (right) a superconductor model for two assumptions about the gamma ray cascade and for two values of the level density parameter a. The effect of the number of gamma rays in a cascade appears to be negligible (Ref. 138).

fit for neutron cross sections over a wide range of energies and elements.

A. Formulation of the Problem

Optical model calculations are nowadays considered as the standard method of analysis of scattering data. They give the expressions necessary to compute the differential elastic cross sections, polarization, and total reaction cross sections. So far the optical model has been applied successfully to particles of spin 0, $\frac{1}{2}$, and 1 incident against 0-spin nuclei. The basic idea of the optical model in its simplest form is to substitute the intricate interaction in the nuclear system by a complex potential well which reproduces the main features of the absorption and the scattering of nuclear particles by atomic nuclei.

The formal statement of the problem[144] starts with the Schrödinger equation

$$[-(\hbar^2/2\mu)\nabla^2+U]\psi=E\psi, \qquad (2.1)$$

where μ and E are the reduced mass and the center of mass energy of incident particle. U is the optical potential that replaces the general particle–nucleus interaction:

$$U=U_{coul}(r)+U_{NR}(r)+iU_{NI}(r) +\{U_{SR}(r)+iU_{SI}(r)\}\hbar^2(\mathbf{s}\cdot\mathbf{L}). \qquad (2.2)$$

The terms in (2.2) that depend only on the distance r between particle and target are the Coulomb, the central real, the central imaginary, the spin–orbit real, and spin–orbit imaginary potential, respectively, while $\mathbf{s}$ and $\mathbf{L}$ represent, respectively, the spin and orbital angular momentum operators of the incident particle. The expression (2.2) can be amplified to include other terms, notably a tensor term for spin-1 particles,[145] but even the form (2.2) is often too complicated to be used. Equation (2.1) could, in general, be solved only numerically, with the aid of fast computers. Several computer programs, differing in the form factor of the assumed potentials are available.[144] The most commonly used form factors are:

—the Woods–Saxon potential[142] for the real central part

$$U_{NR}(r)=V[1+\exp(r-r_R)/a_R]^{-1}, \qquad (2.2a)$$

—a similar volume

$$U_{NI}(r)=W_V[1+\exp(r-r_I)/a_I]^{-1}, \qquad (2.2b)$$

or the surface potential for the imaginary central part

$$U_{NI}(r)=W_S\exp\{-[(r-r_I)/b]^2\}, \qquad (2.2c)$$

—and a Thomas term for the real and imaginary

CC-0. In Public Domain. Gurukul Kangri Collection, Haridwar

Digitized by Arya Samaj Foundation Chennai and eGangotri

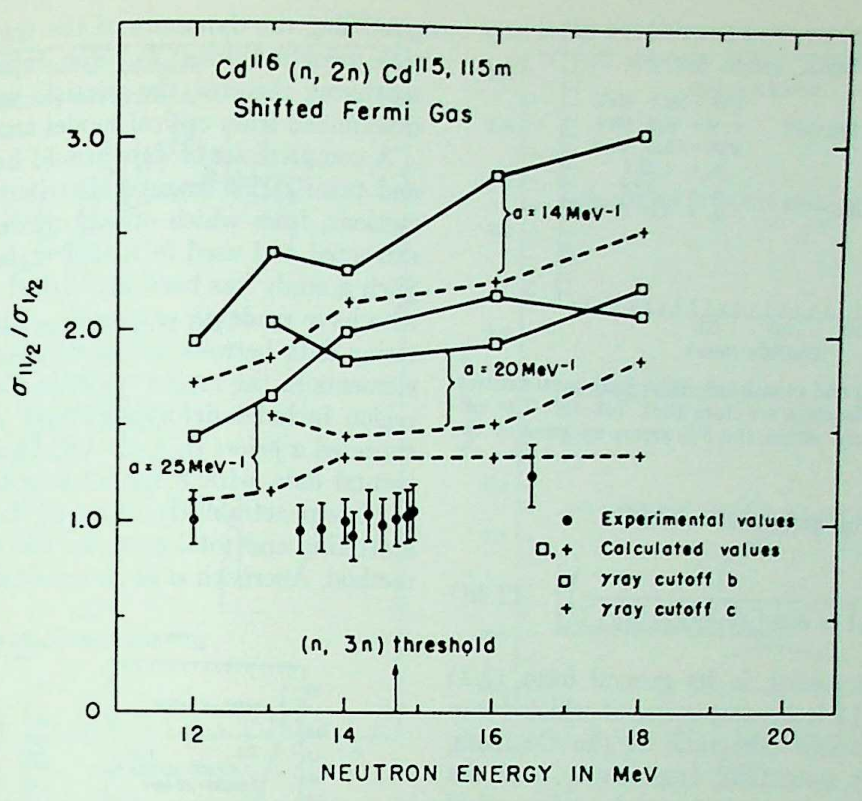

(a)

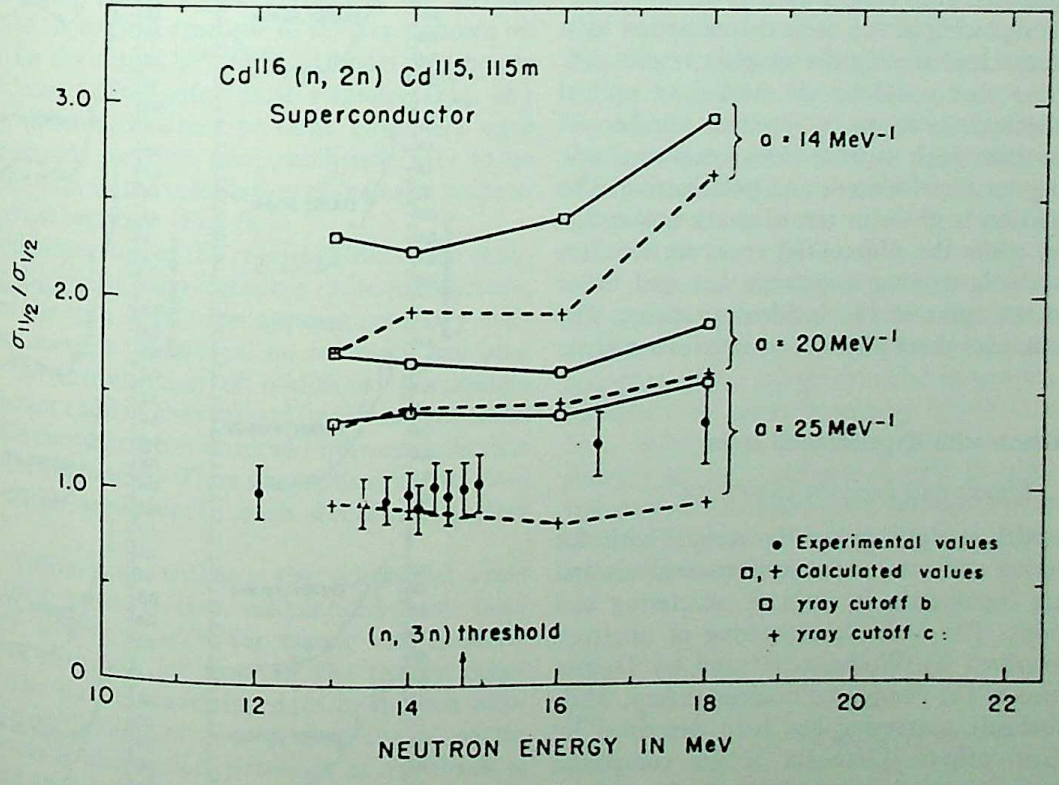

(b)

FIG. 47. (a) Comparison of the experimental isomeric cross section ratios $\sigma_{9/2}/\sigma_{1/2}$ for the Cd^{115} isomers produced by the $Cd^{116}(n, 2n)$ reaction with theoretical values calculated with a shifted Fermi gas model for two assumptions about the gamma ray cascade and for two values of the level density parameter a (Ref. 138). (b) Same as Fig. 47(a), with theoretical values calculated with a superconductor model for two assumptions about the gamma-ray cascade and for two values of the level density parameter a (Ref. 138).

CC-0. In Public Domain. Gurukul Kangri Collection, Haridwar

Digitized by Arya Samaj Foundation Chennai and eGangotri

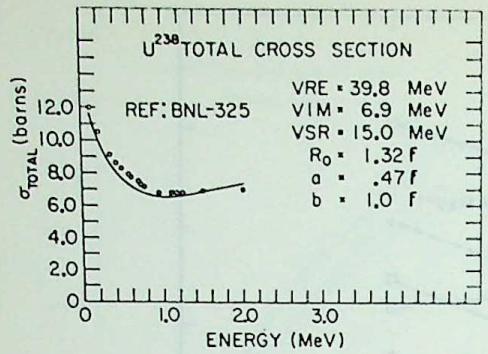

FIG. 48. Experimental and calculated (solid line) total neutron cross sections of U^{238}. The data are from Refs. 148–150. The calculated values are mostly within the 5% errors assigned to the data (Ref. 147).

parts of the spin–orbit potential

$$\left.\begin{matrix} U_{SR} \\ U_{SI} \end{matrix}\right\} = \left.\begin{matrix} V_{SO} \\ W_{SO} \end{matrix}\right\} \frac{2}{\hbar^2 r}\left[\frac{d}{dr}\left(\frac{1}{1+\exp\left[(r-r_{R,I})/a_{R,I}\right]}\right)\right]. \quad (2.2d)$$

Thus the optical potential, in its general form (2.2) allows for at least 11 free parameters, of which 6 can be listed as geometrical (the radii of the Coulomb, real, and imaginary potentials, respectively, and the three shape factors a_R, a_I, and b) and 5 as dynamical (the depths of central and spin–orbit potentials, respectively). Both in practice and in theory some of these parameters are related to each other.

The simple replacing of the nuclear interaction by a complex hole can lead to only the simplest results, i.e., the information that could be obtained from optical model calculations concerns a limited number of physical quantities, such as total cross sections, elastic scattering angular distributions, and polarization. The total cross section is given in terms of the absorption coefficients η_l while the differential cross sections are functions of the scattering amplitude too and differ according to the spins of the incident particles. The explicit formulas for these physical quantities are given in Ref. 144.

B. Comparison with Experimental Data

1. *Elastic and Inelastic Scattering*

Optical model analysis presently serves both for elastic scattering and total cross sections analysis and for producing input data in inelastic scattering and direct reactions. The inelastic scattering of neutrons has been described by Wolfenstein[14] and by Hauser *et al.*[15] in terms of the compound nucleus theory, while the direct inelastic scattering has been described by Banerjee[146] and others. Elements of the compound nucleus theory of inelastic scattering have been given in Sec. IA3, where the cross section for the transition to a particular state in the residual nucleus is given in terms of initial and final state spins and parities, and the transitions amplitudes are summed over all the accessible states in the compound nucleus. The factors governing the dynamics of the transitions are the pa... ticle penetrabilities T_l. The input data in inelastic scattering theories, the particle penetrabilities T_l are determined from optical model analysis.

A complete set of data would hence comprise elastic and polarization angular distributions and total cross sections, from which optical model parameters can be extracted and used in fitting inelastic scattering data. Such a study has been performed by Auerbach *et al.*[15] who have made an extensive analysis of neutron scattering data between 0.1 and 3 MeV for several heavy elements in the region between Ta^{181} and U^{238}. As this region includes deformed nuclei also, it is not to be expected *a priori* that one will be able to fit the experimental data with a spherical optical potential. Using particle penetrabilities obtained from fitting the elastic scattering and total cross section data by the usual χ^2 method, Auerbach *et al.* have obtained good agreement

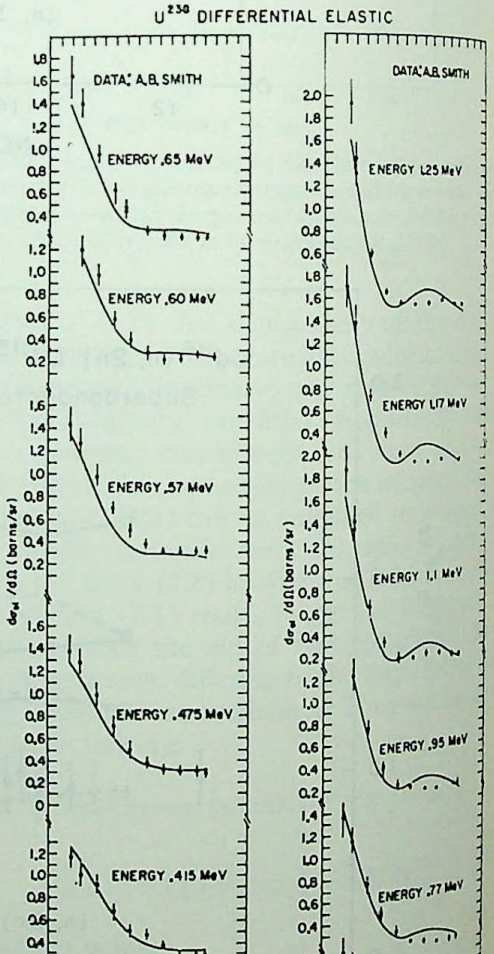

FIG. 49. Experimental and calculated (solid lines) differential elastic cross sections for U for parameters shown in Fig. 48. Calculated values include corrections for compound elastic scattering, using the Hauser–Feshbach theory (Ref. 147).

CC-0. In Public Domain. Gurukul Kangri Collection, Haridwar

Digitized by Arya Samaj Foundation Chennai and eGangotri

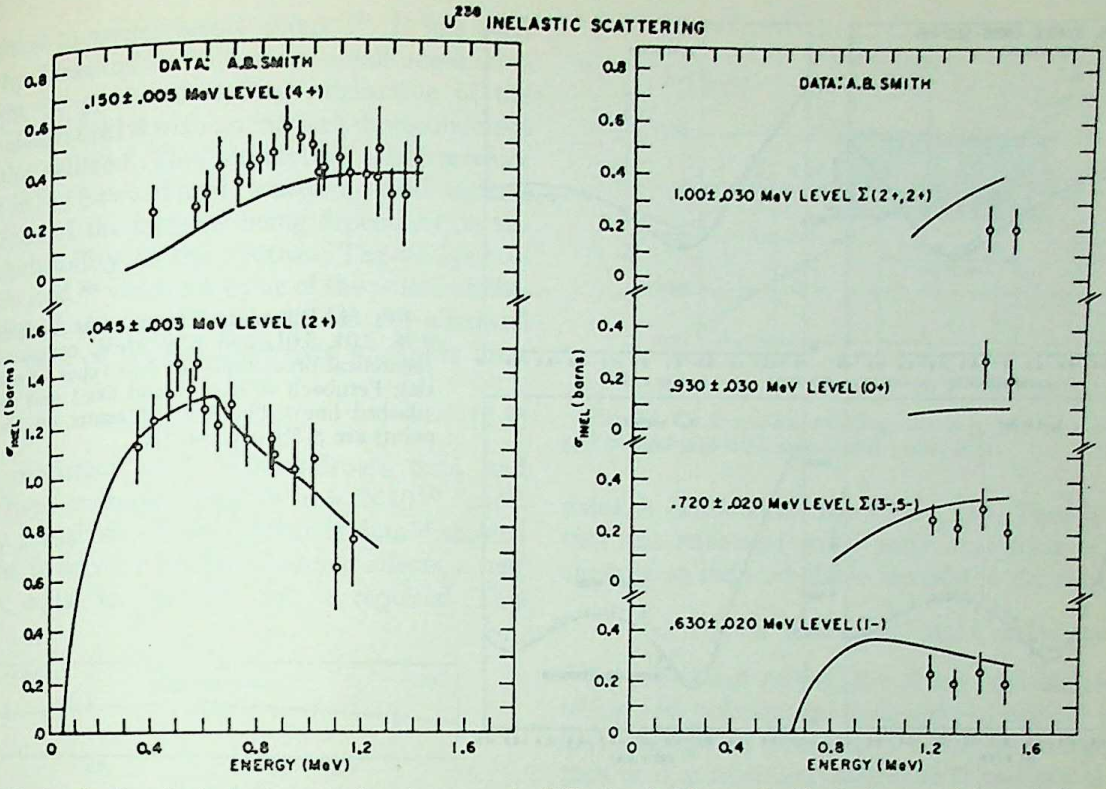

FIG. 50. Calculated values for inelastic scattering of neutrons by U^{238} using the Hauser–Feshbach theory and the optical model parameters determined by fitting the entrance channel data (Ref. 147).

for the inelastic scattering experiments on all the studied nuclei. A typical example of the fits is shown on Figs. 48–50 for the case of U^{238}. Optical model parameters calculated from fitting total cross sections (Fig. 48) and elastic differential cross sections (Fig. 49) were used to determine neutron penetrabilities $T_l(\epsilon)$ to be used as input data in the calculation of inelastic neutron scattering cross sections (Fig. 50).

A detailed inspection of the results of Auerbach *et al.*, shows that the over-all agreement is quite satisfactory. Inclusion of the spin orbit term appears necessary even at such low energies. However, no necessity has been found for the introduction of additional parameters such as different radii of the real and imaginary potential etc. No difference has been observed between spherical and nonspherical nuclei. Thus the optical model does not seem to be sensitive to such details of nuclear structure.[151]

Similar results, but without the additional cross check of total cross section calculations have been obtained by Gilboy *et al.*[152] for elastic and inelastic scattering of neutrons by iron, in the energy range 1–4 MeV. The elastic scattering data have been compared to the predictions of two types of optical potential. The surface absorption potential of Fernbach *et al.*[143] with an absorption depth up to 10 MeV generally yielded a better fit than the non local potential of Perey *et al.*[66] as can be seen from Fig. 51. The latter potential was used in its local energy-dependent approximation. The inelastic scattering angular distributions are all excellently fitted by the Hauser–Feshbach[15] theory using optical model penetrabilities from both the Perey *et al.*[66] and Fernbach *et al.*[143] models (cf. Fig. 52). It appears that the direct interaction contribution to inelastic scattering is negligible. An interesting feature is presented by the excitation function for the 1st excited state in Fe^{56}, which carries the bulk of inelastic scattering at these energies. Penetrabilities calculated from any of the two mentioned potentials did not fit too well this excitation function. Instead, only a strongly energy-dependent ($W_I \propto 1.75\epsilon_0$) imaginary part of the potential yielded acceptable fits.

The available data on absorption, scattering, and polarization by spherical nuclei have been analyzed by Moldauer for neutron energy below 1 MeV. A good fit is obtained with a diffuse surface model, having a sharply peaked absorptive shell at the surface. The comparison has been done through the strength function, Γ_n^0/D, since at very low energy the optical model total cross section approaches

$$\sigma_t = \alpha + \beta/E^{\frac{1}{2}} \tag{2.3}$$

with

$$\alpha = 4\pi R^2 \tag{2.3a}$$

and

$$\beta = 2\pi^2(\epsilon/k^2)(\bar{\Gamma}_n^0/D), \tag{2.3b}$$

where ϵ and k are the incident neutron energy and wave number, respectively, and R the effective radius of interaction. A similar analysis has also been performed by Elwyn *et al.*[154]

Valuable results on elastic and inelastic scattering of fast neutrons have also been obtained by Gilboy *et al.*[155]

CC-0. In Public Domain. Gurukul Kangri Collection, Haridwar

Digitized by Arya Samaj Foundation Chennai and eGangotri

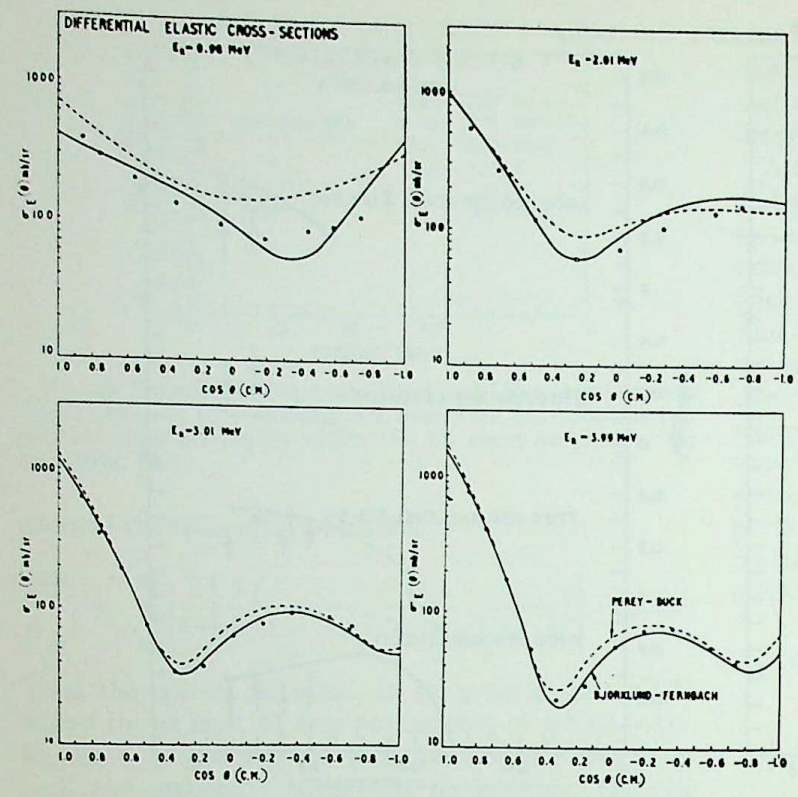

FIG. 51. Differential elastic cross sections for iron at 0.98, 2.01, 3.01, and 3.99 MeV, compared with the theoretical predictions for two types of optical potential: Fernbach *et al.*[143] (solid line) and Perey *et al.* (dashed line). The over-all errors on the measured points are ≦5% (Ref. 152).

in an earlier article ($A=140$–178, $\epsilon_n=1$ MeV) and several other investigators.[156] Total cross sections on Li, U, and Pu isotopes, important in the comparison with neutron cross sections given by the optical model have been measured by MacGregor *et al.*[157]

2. *Polarization and Related Data*

Several references mentioned in the preceding section give also results on polarization of fast neutrons. Scattering of polarized neutrons has been reported by Bucher *et al.*,[158] Kent,[159] Wentzel *et al.*,[160] and Bredin.[161] Optical model analysis has been applied to the scattering of polarized neutrons from the D(d, n) He^3 and T(p, n) He^3 reactions in Refs. 159 and 161, respectively, and satisfactory results have been found in both cases. The angular distribution of elastic polarization of 2-MeV neutrons was found to be strongly element dependent[161] in the region of $A=30$ to 50. Although a surface peaked optical potential yielded excellent fits for all the elements, the sets of optical parameters used differed from element to element. This is hardly unexpected, since it is known that resonances in Al, Si, and Fe do exist. However the same set of parameters gave the best fit for all data (elastic and inelastic scattering and polarization) for each element separately.

Wagner *et al.*[162] have investigated the interaction of polarized and unpolarized 0.35-MeV neutrons with oriented Ho^{165} nuclei in order to search for a possible spin–spin interaction and to study the influence of the deformation of the Ho^{165} nucleus on the interaction. They found that the deformation has some effect on the total cross section of the oriented target. To determine the existence of a possible spin–spin interaction, the total cross section for parallel $\sigma_t^{\uparrow\uparrow}$ and antiparallel $\sigma_t^{\uparrow\downarrow}$ polarizations have been measured. The observed difference

$$\Delta\sigma=\sigma_t^{\uparrow\uparrow}-\sigma_t^{\uparrow\downarrow}$$

has been interpreted as indicating the existence of a spin–spin term to be added to the usual radial+spin-orbit potential.

$$-V_{SS}(\boldsymbol{\sigma}\cdot\mathbf{I})\{1+\exp[(r-r_0A^{\frac{1}{3}})/a]\}^{-1}. \quad (2.4)$$

To account for the observed difference in total cross sections a spin–spin potential depth value V_{SS} of

$$-0.06 \text{ MeV}<V_{SS}<0.13 \text{ MeV}$$

was necessary (Fig. 53). Thus a spin–spin interaction, if present, is practically negligible, since in this case it is less by about two orders of magnitude than the corresponding spin–orbit interaction ($V_{SO}=7.5$ MeV).[97] Other scattering data are discussed in the next chapter.[164,165]

We shall include an interesting application of fast neutron physics to the investigation of the structure of neutrons, which, traditionally is the domain of high-energy physics. This concerns the investigation of the electric polarizability of the neutron by means of small angle elastic scattering, reported by Aleksandrov *et al.*[164] and Walt *et al.*[165] Earlier measurements have shown that the elastic scattering of fast neutrons exhibits an unexpected increase as the angle of scattering is decreased below 15°. Because of its angular dependence this small angle effect could not be attributed either to nuclear or Schwinger scattering effects,[197] the former being a slowly varying function of angle and the latter

CC-0. In Public Domain. Gurukul Kangri Collection, Haridwar

Digitized by Arya Samaj Foundation Chennai and eGangotri

being confined to angles below about 2°. It has been suggested by Aleksandrov[164] that the small angle scattering might be produced by the interaction of the nuclear Coulomb field $\mathcal{E}$ with an induced dipole moment $p=\alpha\mathcal{E}$ of the neutron. This interaction could produce an increase in the forward angle scattering cross section, the magnitude of the increase being dependent on the electric polarizability of the neutron. The analysis of Aleksandrov *et al.*[164] yielded a value of the polarizability $\alpha=8\times10^{-41}$ cm³ that could account for the observed effects. The data of Walt *et al.*[165] fixed an upper limit for α,

$$\alpha\leq2\times10^{-40}\text{ cm}^3, \tag{2.5}$$

seemingly consistent with Aleksandrov's data and estimates from mesonic effects ($\alpha\doteq2\times10^{-41}$ cm³). However, a reanalysis of Aleksandrov's data[164] showed that in order to account for the observed effects, a new value of α, equal to 5×10^{-40} cm³, is required. This value is excluded by the limit (2.5). Thus it appears that the enhanced small angle scattering is not the effect of an induced dipole moment in the neutron.

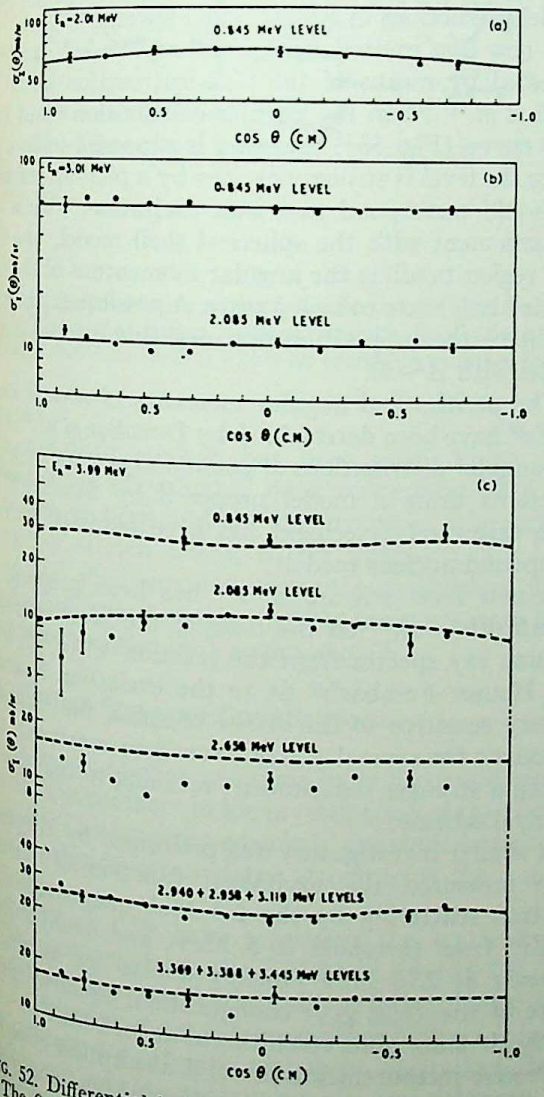

FIG. 52. Differential inelastic scattering cross sections of iron. (a) The 0.845-MeV level at $E_n=2.01$ MeV indicating typical over-all errors. (b) The 0.845- and 2.085-MeV levels at $E_n=3.01$ MeV. (c) Various levels at $E_n=2.99$ MeV. The dashed curves are Hauser-Feshbach[15] predictions (Ref. 152).

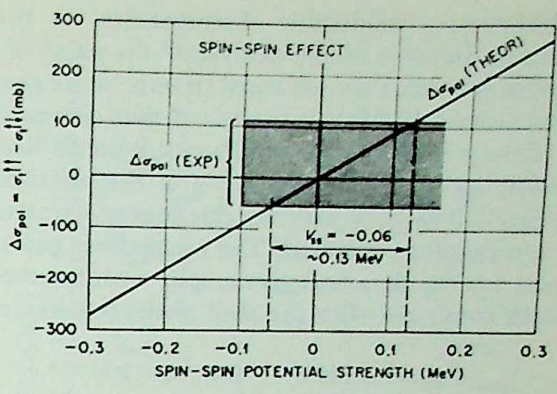

FIG. 53. Cross-section splitting due to a spin–spin interaction, and comparison with experiment (Ref. 162).

3. *Optical Model Data and Conclusions*

As mentioned earlier, the elastic and inelastic scattering and polarization data serve a twofold purpose: first the optical parameters could be extracted and then used as input parameters to fit inelastic scattering and other data. It appears from the preceding discussion that the compound nucleus theory combined with suitable optical model penetrabilities can account for most of the inelastic scattering data. The elastic scattering and polarization data, well fitted by the optical model itself may help to decide between the different forms of optical potentials used, notably the shape of the absorptive part and the depth of the spin–orbit interaction. It seems that consistently better fits are obtained by the use of a surface peaked imaginary potential.[166] No marked difference in favor of nonlocal potentials has been observed so far although an energy dependence of the parameters seems to be necessary.

The existence of shell model effects in the absorptive potential suggested by Lane[167] to account for the very small values of the S-wave strength functions observed in the mass region $A=90$–130 has been substantiated recently by Vonach *et al.*[168] The effect of a closed shell on the imaginary part of the potential can be explained as caused by the reduction of available absorption states near the closed shells. Hence the effects hould be especially large for doubly closed shells. The investigation in Ref. 168 was centered around the doubly closed shell $A=208$. A surface peaked optical potential with $V_{\text{real}}=46$ MeV, $W_{\text{imag}}=14$ MeV and $V_{SO}=7$ MeV was used. This potential gave good over-all fit to neutron scattering data over a wide range of nuclear masses. Good fit was thus obtained for Au^{197} but the agreement rapidly deteriorated when approaching bismuth (Bi^{209}) through mercury and thalium. However, if one allows W_{imag} to decrease from 14 MeV for Au^{197} to 5 MeV for Bi^{209}, the agreement is again restored.

The presence of spin–orbit interaction is generally considered as necessary in optical model analysis. There

CC-0. In Public Domain. Gurukul Kangri Collection, Haridwar

Digitized by Arya Samaj Foundation Chennai and eGangotri

are, however, considerable discrepancies as to its magnitude. In some of the analyses[166] the value of the spin–orbit potential was set equal to zero, but in general a value around 10 MeV is contained that accounts for most of the polarization measurements. Rahman Khan[169] has made an extensive calculation of the polarization of 0.38- and 0.98-MeV neutrons due to elastic scattering over a wide range of nuclei. The calculations generally account for the data and give a spin–orbit interaction strength consistent with the shell model requirements:

$$V_{SO}=7.5 \text{ MeV} \quad \text{for} \quad A<100.$$

$$V_{SO}=15 \text{ MeV} \quad \text{for} \quad A>100.$$

III. NUCLEAR STRUCTURE AND SPECTROSCOPY STUDIES

A. Investigation of Nuclear Levels

The classical method of investigating levels of excited nuclei at neutron binding energies has been the study of the interaction of nuclei with thermal neutrons. A series of interesting measurements has been done in the field of slow neutron capture in several elements[170–173] but we shall not discuss them.

It is well known that fast neutrons as bombarding particles are less suitable for the fine resolution experiments customary in spectroscopic studies. Nevertheless, they have some advantages in comparison to protons and alpha particles. The absence of charge enables the exploration of not too highly excited states and the interpretation of these results, especially for inelastic neutrons scattering is more straightforward than for charged particles. The analysis is performed in terms of either the Hauser–Feshbach[15] or a direct theory of scattering.[20]

Davis *et al.*[174] have investigated the disintegration of C^{12} and O^{16} by fast neutrons in a CO_2 filled ionization chamber. In the energy range below 9 MeV the only reaction leading to charged particles is the (n, α) reaction. While the cross section for the reaction $O^{16}(n, \alpha)\ C^{13}$ g.s. shows a strong resonant structure (21 resonances were observed in O^{17} in the energy range of $E_n=5.0-8.8$ MeV), no such structure has been observed in the $C^{12}(n, \alpha)\ Be^{9}$ g.s. reaction. No plausible explanation of this phenomenon has been advanced.

The resonances in the lithium isotopes were investigated by studying the polarization and differential cross sections for neutrons scattered from Li^6 and Li^7 by Lane *et al.*[175] The scattering and the polarization of neutrons below 1.5 MeV are defined by the resonance at 0.25 MeV determined by $J^\pi=\frac{5}{2}^-$, corresponding to a Li^7 state at 7.47 MeV. For higher energies the experimental data vary smoothly with the incident energy. Similar data have been obtained for Li^7 and interpreted in terms of the nonlocal optical potential of Perey *et al.*[66]

Donoghue *et al.*[176] have used the same method to investigate the parity and angular momenta of levels in O^{19} and N^{16} by measuring the elastic scattering of neutrons in a gas filled recoil counter. CO_2 (O^{18} enriched) and N^{15} were used, respectively. About a hundred angular distributions have been measured in the energy range of 0.4–2.7 MeV (Fig. 54). In the analysis, the cross sections were calculated from the phase shifts, using a formula for the elastic scattering of spin-$\frac{1}{2}$ particles on a spin-0 target derived by Bloch.[177] The phase shifts were calculated from Lane and Thomas.[178] The same phase shifts that fitted the distributions fitted the excitation functions too. The parity of states has been established from the asymmetry $(-)$ or symmetry $(+)$ of the angular distributions around $\pi/2$, while the values of the angular momenta J have been obtained in connection with total cross sections. The results are consistent with the shell model predictions of Elliott and Flowers.[179]

A new first excited state of P^{31} at 451 keV has been detected by means of the pick-up reaction on S^{32} by Colli *et al.*[180] From the angular distribution fitted by a $l=0$ curve (Fig. 55), the state is supposed to be a $\frac{1}{2}^+$. Since the level is strongly excited by a pick-up reaction it should correspond to a hole excitation. This is not in agreement with the spherical shell model, which in this region predicts the angular momentum of the first excited hole state to be a $\frac{5}{2}$ state. A possible explanation might be the supposition of a negative deformation of nuclei with $A\sim30$.

The parities and angular momenta of several states in Fe^{56} have been determined by Donahue *et al.*[181] from the angular distributions of gamma rays from $(n, n'\gamma)$ reactions using a model proposed by Satchler.[182] In each case good agreement has been obtained with the compound nucleus model.

A new level scheme of Y^{89} has been proposed by Schaffroth *et al.*[182] on the basis of the investigation of gamma ray spectra from the reaction $Y^{89}(n, n'\gamma)$. As the Hauser–Feshbach[15] fit to the excitation functions is very sensitive to the choice of spins, the excitation functions for several states have been measured, thus giving a stronger independent meaning to the ascribed spectral scheme.

A similar investigation was performed by Wagner,[183] who measured the excitation function of inelastic neutron scattering by the 2.3 MeV metastable state in Zr^{90} from threshold to 5 MeV, and found a sharp increase at 2.75 MeV possibly due to the missing 1^- state of the $(p_{1/2}, g_{9/2})$ configuration, equal in energy to the 3^- state observed hitherto at 2.75 MeV.

Precise measurements of total absorption cross sections of neutrons have been performed by Cabe *et al.*[184] in the energy range from 0.4–1.2 MeV and 3.6–5.2 MeV with a resolution of 3 keV for a number of elements

CC-0. In Public Domain. Gurukul Kangri Collection, Haridwar

Digitized by Arya Samaj Foundation Chennai and eGangotri

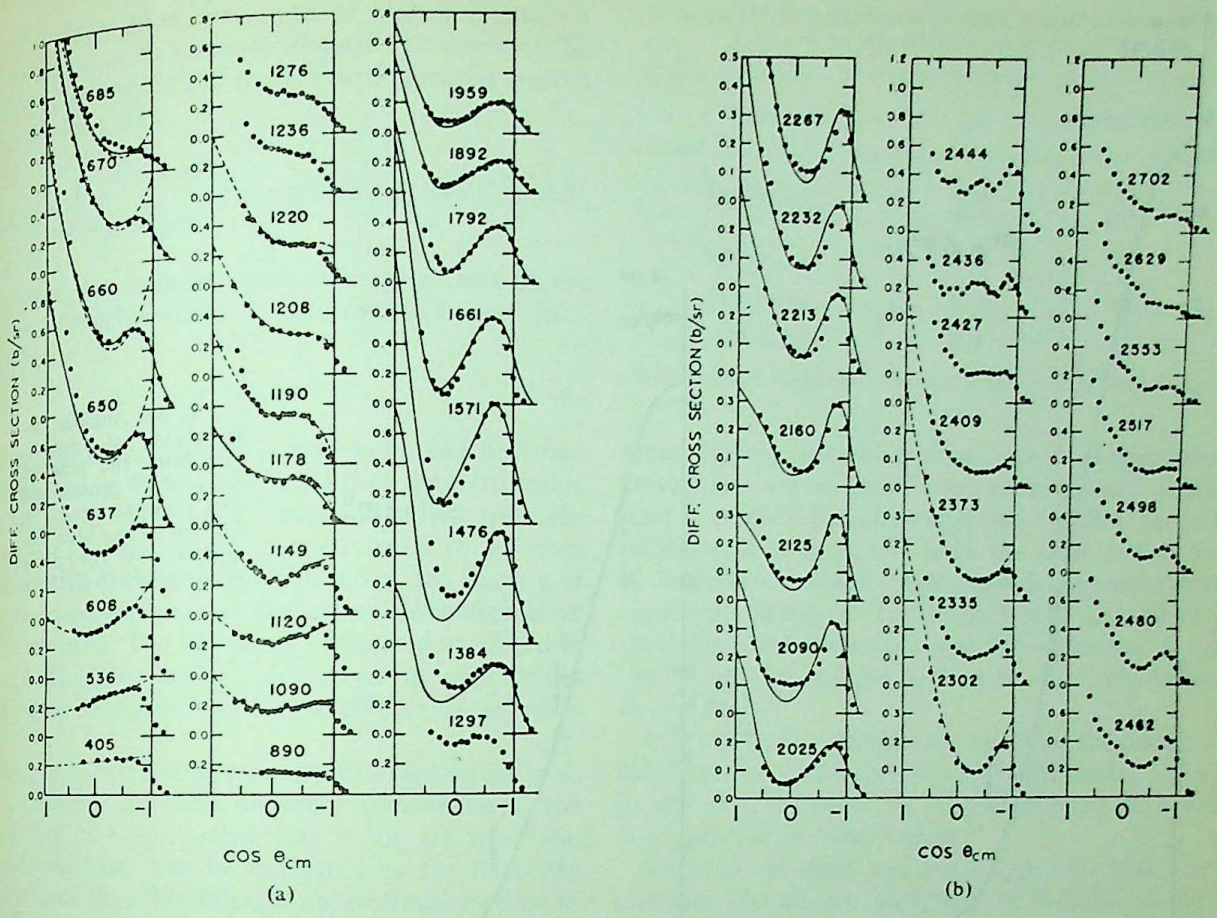

FIG. 54. Representative angular distributions of neutrons elastically scattered from O^{18} for neutron energies (a) below (b) above 2 MeV. The dashed curves represent angular distributions calculated using the phase shifts of Ref. 176. The solid curves represent calculated distributions into which an energy distribution function has been folded (Ref. 176).

A time-of-flight method has been used. These data present a set of valuable data concerning both the total cross sections and the spectroscopic information. A number of new levels, so far unknown, has been found and their angular momenta established using the Breit–Wigner formula. Similar measurements have been presented also by Vaughn *et al.*[185]

B. Nuclear Structure Investigations

Low-energy nuclear reactions have become a tool of increasing importance in the investigation of the nuclear structure. This concerns especially the studies of cluster model configurations and the structure of the nuclear surface.

Bouchez *et al.*[186] have measured the scattering of 14-MeV neutrons from the 7.65-MeV level in C^{12}. The angular distribution exhibits a strong forward maximum and a minimum at $\theta=45°$, suggesting a direct interaction process for $0^+\rightarrow 0^+$ monopole excitation. It is possible to connect this monopole transition to the excitation of an alpha cluster. According to Peele[187] and Wildermuth[188] the angular distribution of inelastically scattered neutrons would in this case take the form

$$\sigma(\theta) \propto j_0^2(kR), \tag{3.1}$$

where j_0 is the zeroth-order spherical Bessel function, k the momentum transfer to the C^{12} nucleus, and R the interaction radius (Fig. 56). The comparison between the experimental curve and the Bessel function is encouraging, although the backward rise should be treated with distorted waves and configuration mixing. The purely backward angular distributions in the reaction O^{16} (n, α) C^{13} (heavy-particle stripping)[29] are a strong additional argument for a four alpha cluster structure of O^{16}.

Some implications about the structure of the nuclear surface can be obtained from the study of (n, α) reactions. Data about nuclear matter at high densities are available from high-energy electron scattering. Far away from the nuclear center the nuclear density decreases. Two alternatives are, however, possible.

(i) as the distance between nucleons increases, the tendency of the nucleons to cluster is not higher than implied by statistics;

CC-0. In Public Domain. Gurukul Kangri Collection, Haridwar

Digitized by Arya Samaj Foundation Chennai and eGangotri

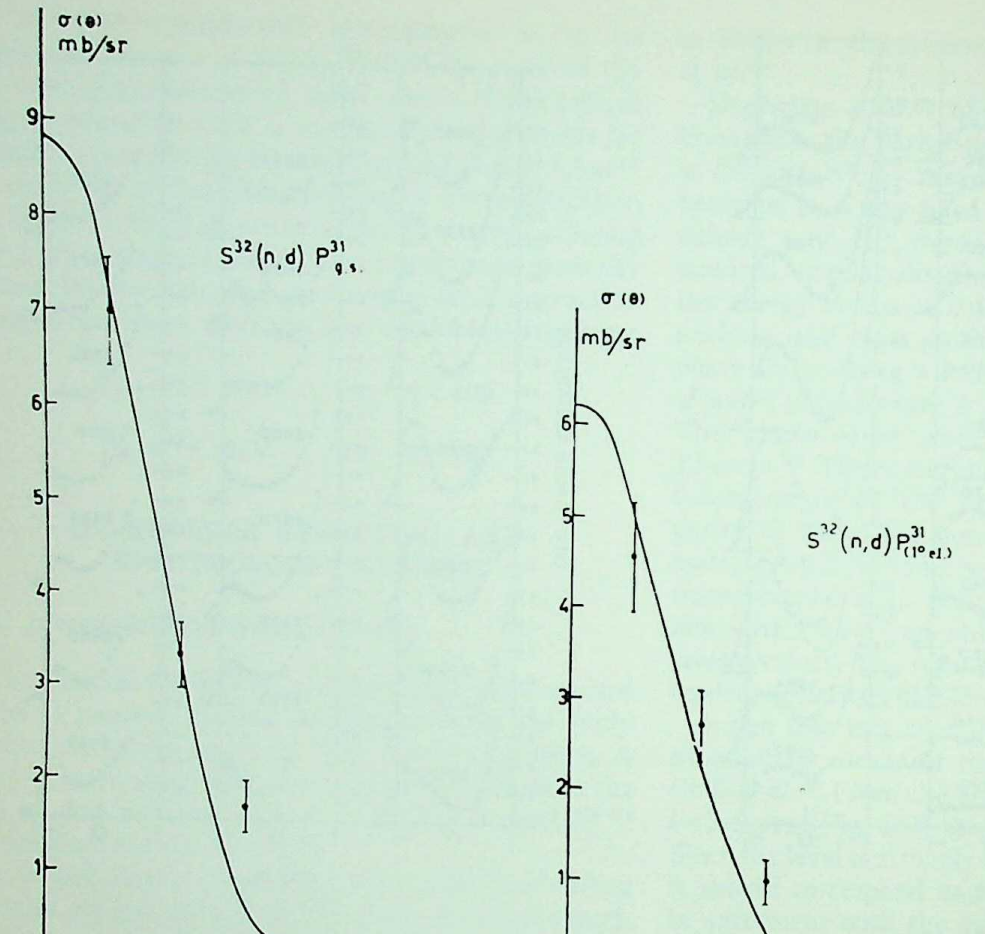

FIG. 55. Angular distribution of deuterons from the reaction $S^{32}(n, d)\,P^{31}$ ground and first excited states. The full curve has been calculated by the plane wave theory (Ref. 180).

(ii) in spite of the decrease of the over-all density, local densities may attain very high values, i.e., the clustering probability increases.

Hodgson[189] and Wilkinson[190] point out that reactions leading to complex nuclei can be used for the investigation of the texture of the nuclear surface. Using the model proposed by Hodgson, Osakiewicz *et al.*[191] and Kulišić *et al.*[83] have investigated (n, α) reactions on heavy nuclei at 14 MeV in order to calculate the probability of alpha clustering on the nuclear surface. This reaction proceeds through a direct process, (Ref. 60 and others) and, due to the small mean free path of alpha particles in nuclear matter, through a surface interaction. Thus the process might be understood as taking place in a thin layer of the nuclear surface, with the incoming neutron knocking off an alpha particle present on the nuclear surface. Assuming a certain distribution of nuclear matter density on the surface, one can calculate the maximum number N_α of alpha particles that can be built up by the nucleons present on the surface,[192] defined arbitrarily as the region with $\rho < \frac{1}{2}\rho_0$. Then the actual number N of alpha particles present at any time on the surface will be

$$N = pN_\alpha,$$

where p is the fraction of its time that a nucleon on the surface spends incorporated in an α-particle cluster. p is in essence the probability of clustering. Assuming that the (n, α) process proceeds in complete analogy to free neutron–alpha scattering and taking into account

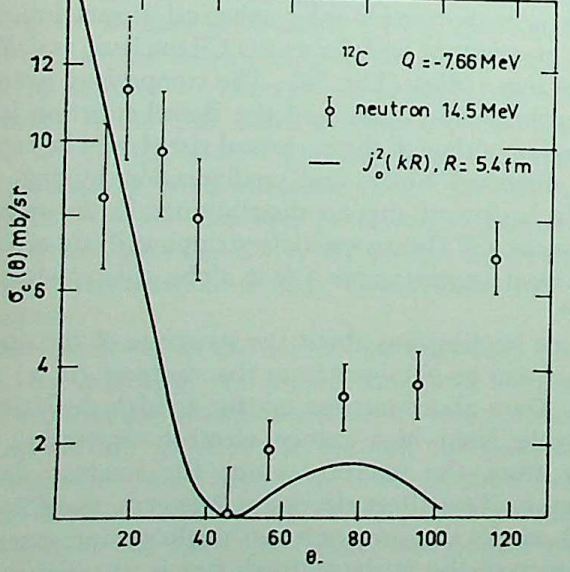

FIG. 56. The experimental angular distribution of 14-MeV neutrons scattered by the 7.65-MeV state in C^{12} and a comparison with a $j_0^2(kR)$ Bessel function (Ref. 186).

CC-0. In Public Domain. Gurukul Kangri Collection, Haridwar

Digitized by Arya Samaj Foundation Chennai and eGangotri

that the short mean free path of alphas in nuclear matter prevents its emission *through* the nucleus, the total cross section for the (n, α) reaction can be written as follows (Fig. 57)

$$\sigma(n, \alpha) = \int_V \int_{\theta_1}^{\theta_2} \int_{\phi_1(\theta)}^{\phi_2(\theta)} \gamma p N_\alpha \sigma(\theta) \sin\theta \, d\phi \, d\theta \, dV, \quad (3.2)$$

where γ is the neutron attenuation coefficient in the nucleus, connected with the neutron mean free path λ by[193]

$$\gamma = \exp x/\lambda \quad (3.2a)$$

and $\sigma(\theta)$ the differential cross section for free neutron–alpha scattering. It was estimated that the latter value was 6.4 mb in the energy region where α's were observed.[194] Thus, knowing the experimental (n, α) cross sections at 14 MeV, the quantity p, i.e., the fraction of time a nucleon spends in an alpha-particle configuration can be deduced. The values of p obtained are listed in Table VIII. They are in fair agreement with values obtained by Hodgson[189] and Gauvin[195] for (p, α) reactions.

This way of calculating p can be criticized on the basis of its crudity, and also on other grounds, e.g., the presence of pick-up mechanisms in (n, α) reactions. The first criticism can be mitigated by the fortunate circumstance that the different approximations used in the calculation (3.2) have opposite effects, thus tending to cancel each other.[83] The assumption of a free (n, α) scattering cross section for the collision cross section in nuclear matter and the neglection of the effects of the Pauli principle (prohibiting certain collisions) will certainly decrease the value of p. On the other hand, equating the experimental total (n, α) cross section to the knock-out one certainly minimizes the latter, since

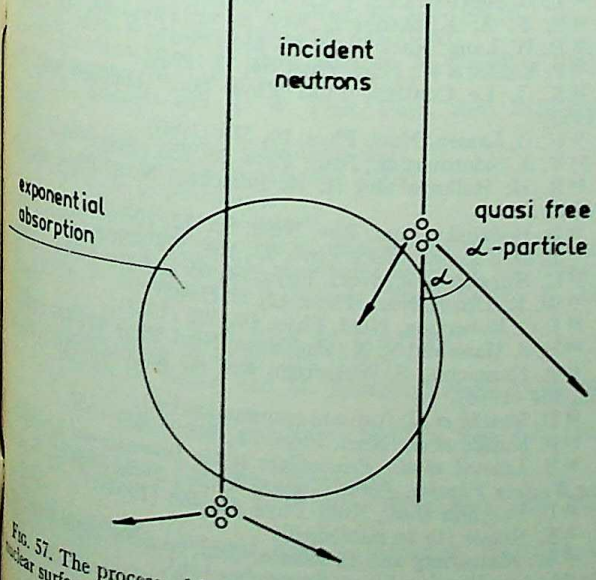

Fig. 57. The process of knocking-out alpha particles from the nuclear surface (Ref. 191).

TABLE VIII. The fraction of its time, p, that a surface nucleon spends incorporated in an alpha cluster.

Reaction	p	Reference
$La^{139}(n, \alpha)$	0.4	83
	0.3	191
$Pr^{141}(n, \alpha)$	0.4	83
$Tb^{159}(n, \alpha)$	0.3	83
$Bi^{209}(n, \alpha)$	0.1	83

some alphas, stemming from other mechanisms of production are counted too; consequently this will tend to increase the value of p (see Fig. 57). Secondary collisions, if present, will have the same effect. As far as the presence of pick-up processes is concerned, several arguments listed by Wilkinson[190] and Lalović *et al.*[84] show that the probability for the formation of a He^3 cluster on the nuclear surface is small compared to that of He^4.

It has to be nevertheless stressed that the calculations based on Eq. (3.2) yield consistently similar values of p, that are, moreover, in good agreement with values of p obtained by other means.[190]

Structure of alpha and other types discussed in the previous section are obviously of dynamical nature. Following an argument of Serebrennikov[196] one could, along the same lines, calculate the lifetime of an alpha cluster on the nuclear surface. This method is based on the shape of the respective alpha spectra.

In the case of dynamical, decaying alpha structures the static spectrum $N_0(\epsilon)$ of the emitted alpha particles is modified by an exponential factor

$$N(\epsilon) = N_0(\epsilon) \exp(-t_{\text{eff}}/\tau_\alpha), \quad (3.3)$$

where t_{eff} is the effective time the alpha particle spends in traveling to the nuclear surface,

$$t_{\text{eff}} = l/v = \{m_\alpha/2(\epsilon+U)\}^{1/2} \quad (3.3a)$$

given in terms of the mass m_α, the outgoing energy ϵ and the shell model potential U of the alpha cluster, and its average shortest distance to the nuclear surface, l. The effect of the exponential factor in expression (3.3) will be to cut off the spectrum of alpha particles at much higher energies than predicted by the Coulomb and optical penetrabilities solely. References 83 and 84 in fact report spectra that are sharply cut off at alpha energies around 17 MeV, while the respective penetrabilities at this energy are around 0.5 (Ref. 9). Assuming reasonable values for the parameters in (3.3a) one obtains lifetimes τ_α of the order of 0.5×10^{-22} seconds. Now, 10^{-22} sec is of the order of transit time of 20-MeV nucleons in nuclei. There is a fair chance that a fast nucleon moving in the nucleus will hit at

CC-0. In Public Domain. Gurukul Kangri Collection, Haridwar

Digitized by Arya Samaj Foundation Chennai and eGangotri

least one alpha cluster and dissolve it. Our result is not contradictory to this interpretation.

Although the model of Serebrennikov[196] succeeds in explaining the absence of alpha particles around Coulomb barrier energies it fails completely when applied to the higher energy part of the spectrum. In fact, instead of the slow rise determined by the square root of the energy, one has a sharp increase of the number of particles[83] unexplainable in terms of this model.

There is no doubt that calculations of this kind do not include a series of effects and cannot be taken very seriously. However, they still give simple straightforward pictures that yield information in rough accordance with that expected on the basis of more refined and sophisticated models.

REFERENCES

[1] T. Ericson, Advan. Phys. **9**, 425 (1960).
[2] N. Bohr, Nature **137**, 344 (1936).
[3] V. F. Weisskopf, Helv. Phys. Acta **23**, 187 (1950).
[4] H. A. Bethe, Rev. Mod. Phys. **9**, 69 (1937); Phys. Rev. **57**, 1125 (1940).
[5] D. H. Ewing and V. F. Weisskopf, Phys. Rev. **57**, 472, 935 (1940).
[6] J. Blatt and W. F. Weisskopf, *Theoretical Nuclear Physics* (John Wiley & Sons, Inc., New York, 1955).
[7] K. K. Seth, R. M. Vilenzick, and T. A. Griffy, Phys. Letters **11**, 308 (1964).
[8] G. S. Mani, M. A. Melkanoff, and I. Iori, Rapport CEA No. 2379 (1963).
[9] J. Huizenga and G. Igo, ANL Report 6373.
[10] G. S. Mani, M. A. Melkanoff, and I. Iori, Rapport CEA, No. 2380 (1963).
[11] E. Erba, U. Facchini, and E. Saetta Mehichella, Nuovo Cimento **22**, 1237 (1961).
[12] A. G. W. Cameron, Can. J. Phys. **36**, 1040 (1958).
[13] A. Bohr, B. R. Mottelson, and R. Pines, Phys. Rev. **110**, 936 (1958); R. Lang, Nucl. Phys. **42**, 353 (1963).
[14] L. Wolfenstein, Phys. Rev. **82**, 690 (1951).
[15] W. Hauser and H. Feshbach, Phys. Rev. **87**, 366 (1952).
[16] H. Goldstein, in *Fast Neutron Physics*, edited by J. B. Marion and J. L. Fowler (Interscience Publishers, Inc., New York, 1963), Vol. II, p. 1525.
[17] J. M. Blatt and L. C. Biedenharn, Rev. Mod. Phys. **24**, 258 (1952); L. C. Biedenharn and A. Simon, "Revised *Z* Tables of Racah Coefficients," ORNL Report 1501 (1952) and ORNL 1501—Suppl. (1954).
[18] J. Blair, "Inelastic Excitation of Collective Levels," in *Lectures on Nuclear Interactions* (Herceg Novi, Yugoslavia, 1962), Vol. II, p. 1.
[19] N. Austern, "Direct Reaction Theories," in *Fast Neutron Physics*, edited by J. B. Marion and J. Fowler (Interscience Publishers, Inc., New York, 1963), Vol. II, p. 113.
[20] S. T. Butler and A. H. Hittmair, *Nuclear Stripping Reactions* (John Wiley & Sons, Inc., New York, 1957).
[21] N. Glendenning, Ann. Rev. Nucl. Sci. **13**, 191 (1963).
[22] G. E. Brown and H. Muirhead, Phil. Mag. **2**, 473 (1957).
[23] S. T. Butler, Proc. Roy. Soc. (London) **208A**, 559 (1951); Phys. Rev. **106**, 272 (1957).
[24] K. Izumo, Progr. Theoret. Phys. (Kyoto) **26**, 807 (1961).
[25] H. Feshbach, Ann. Phys. (N.Y.) **5**, 357 (1958); **19**, 287 (1962); B. Block and H. Feshbach, Ann. Phys. (N.Y.) **23**, 47 (1963); C. M. Shakin, Ann. Phys. (N.Y.) **22**, 373 (1963); A. Karman, Rodberg, and Young, Phys. Rev. Letters **11**, 422 (1963); R. H. Lemmer and C. M. Shakin, Ann. Phys. (N.Y.) **27**, 13 (1964).
[26] K. J. Le Couteur, Phys. Letters **11**, 53 (1964).
[27] N. Cindro, "Total Cross Section Measurement and Analysis," in *Lectures on Nuclear Interactions* (Herceg Novi, Yugoslavia, 1962), Vol. II, p. 290.
[28] B. Sen, Nucl. Phys. **41**, 435 (1963).
[29] M. L. Chatterjee and B. Sen, Nucl. Phys. **51**, 583 (1964).
[30] R. A. Al Kital and R. A. Peck, Jr., Phys. Rev. **130**, 1591 (1963).
[31] M. L. Chatterjee, Nucl. Phys. **65**, 635 (1963).
[32] D. T. Stewart and P. W. Martin, Nucl. Phys. **60**, 349 (1964).
[33] G. R. Satchler, Phys. Rev. **104**, 104 (1956).
[34] R. Batchelor and J. H. Towle, Nucl. Phys. **47**, 385 (1963).
[35] V. Valković, Nucl. Phys. **54**, 465 (1964); **60**, 581 (1964).
[36] M. R. Zatzik and D. R. Moxon, Phys. Rev. **129**, 1728 (1963).
[37] C. R. Lubitz, "Numerical Table of Butler Born Approximation Stripping Cross Sections" (University of Michigan, 1957).
[38] D. Kovač (private communication).
[39] G. Calvi *et al.*, Nucl. Phys. **39**, 621 (1962); **48**, 408 (1963).
[40] G. Calvi, A. S. Figuera, and R. Potenza, *Proceedings International Conference on Nuclear Physics, Paris* (Dunod & Cie., Paris, 1964).
[41] J. N. Massot, E. El Baz, and J. Lafoucriere, Nucl. Phys. **58**, 273 (1964).
[42] U. Facchini *et al.*, Phys. Letters **1**, 6 (1962).
[43] M. G. Marcazzan, F. Merzari, and F. Tonolini, Phys. Letters **1**, 21 (1962).
[44] M. G. Marcazzan, F. Tonolini, and L. Zetta, Nucl. Phys. **46**, 51 (1963).
[45] G. Anderson Lindström, Z. Naturforsch. **17a**, 238 (1962).
[46] R. Bass, U. Fanger, and F. Saleh, Nucl. Phys. **56**, 569 (1964).
[47] E. A. Davis, Nucl. Phys. **55**, 643 (1964).
[48] W. Patzak and H. Vonach, Nucl. Phys. **39**, 263 (1963).
[49] O. N. Koul, Nucl. Phys. **55**, 127 (1964).
[50] I. Turkiewicz *et al.*, Nucl. Phys. **77**, 276 (1966).
[51] E. Saetta Menichella, F. Tonolini, and L. Tonolini-Severgnini, Nucl. Phys. **51**, 449 (1964); E. Campbell *et al.*, MIT Report No. 73 (1960).
[52] M. Shapiro, Phys. Rev. **90**, 171 (1953).
[53] U. Seebeck and M. Bormann, Nucl. Phys. **68**, 387 (1965).
[54] N. Cindro *et al.*, Proc. 2nd Polish–Yugoslav Symposium on Nuclear Physics, Cracow, 1963.
[55] J. Csikai, J. Baczo, and A. Doroczi, Nucl. Phys. **41**, 141 (1963).
[56] M. Irfan and W. Jack, Proc. Phys. Soc. (London) **47**, 225 (1963).
[57] C. J. D. Jarwis, W. R. Dixon, and R. S. Storey, Nucl. Phys. **44**, 680 (1963).
[58] W. R. Dixon and R. S. Storey, Phys. Letters **5**, 208 (1963).
[59] I. Kumabe *et al.*, Phys. Rev. **106**, 155 (1957).
[60] K. Debertin and E. Rossle (unpublished).
[61] D. B. Thomson, Phys. Rev. **129**, 1649 (1963).
[62] P. Huber *et al.*, Phys. Letters **5**, 202 (1963).
[63] S. G. Buccino *et al.*, Nucl. Phys. **60**, 17 (1964).
[64] K. K. Seth, R. M. Wilenzick, and T. A. Griffy, Phys. Letters **11**, 308 (1964).
[65] R. M. Wilenzick *et al.*, Nucl. Phys. **62**, 511 (1965).
[66] F. G. Perey and B. Buck, Nucl. Phys. **32**, 353 (1962).
[67] T. D. Newton, Can. J. Phys. **34**, 804 (1956).
[68] P. F. A. Klinkenberg, Rev. Mod. Phys. **24**, 63 (1952).
[69] D. W. Lang, Nucl. Phys. **26**, 434 (1961).
[70] P. Kulišić *et al.*, Nucl. Phys. **54**, 17 (1964).
[71] K. J. Le Couteur, Proc. Phys. Soc. (London) **465**, 715 (1952).
[72] N. O. Lassen, Nucl. Phys. **19**, 579 (1960).
[73] V. A. Sidorov *et al.*, Nucl. Phys. **35**, 253 (1963).
[74] R. H. Holbrow and H. H. Barschall, Nucl. Phys. **42**, 264 (1963).
[75] D. Bodansky, Ann. Rev. Nucl. Sci. **12**, 107 (1962).
[76] T. D. Thomas, Nucl. Phys. **53**, 558, 577 (1964).
[77] C. Hurwitz *et al.*, Nucl. Phys. **54**, 65 (1964).
[78] W. R. Dixon, Nucl. Phys. **42**, 27 (1963).
[79] J. C. Robertson, Nucl. Phys. **49**, 306 (1963).
[80] H. S. Hans and R. K. Mohindra, Nucl. Phys. **47**, 473 (1963).
[81] P. Cuzzocrea, S. Notarrigo, and A. Rubbino, Nucl. Phys. **55**, 364 (1964).
[82] D. Veselić *et al.* (private communication).
[83] P. Kulišić *et al.*, Nucl. Phys. **73**, 548 (1965).
[84] B. Lalović *et al.*, *Proceedings of the International Conference on Nuclear Physics, Paris* (Dunod & Cie., Paris, 1964).
[85] U. Facchini *et al.*, Nucl. Phys. **51**, 460 (1964).
[86] E. Rössle (to be published).
[87] W. Maussberg and E. Rössle, Conf. on Solid State Detectors in Nuclear Physics, Liege, September 1963.

CC-0. In Public Domain. Gurukul Kangri Collection, Haridwar

Digitized by Arya Samaj Foundation Chennai and eGangotri

[92] R. Batchelor, W. B. Gilboy, and J. H. Towle, Nucl. Phys. 65, 236 (1965).
[93] A. Adam *et al.*, Nucl. Phys. **49**, 489 (1963).
[94] H. Jeremie, Nucl. Phys. **47**, 225 (1963).
[95] H. Neuert and H. Pollehn, *Tables of Neutron Cross Sections*, EUR 122e, 1963; A. Chatterjee (to be published).
[96] M. Cox, Phys. Rev. **133**, 1337B (1964).
[97] P. Cuzzocrea and G. Pappalardo, Nucl. Phys. **48**, 656 (1963).
[98] R. Potenza, R. Ricamo, and A. Rubbino, Nucl. Phys. **41**, 298 (1963).
[99] J. M. F. Jeronimo *et al.*, Nucl. Phys. **47**, 225 (1963).
[100] Other recent total cross-section measurements: G. C. Bonazzola *et al.*, Nucl. Phys. **51**, 337 (1964). J. Csikai, B. Guyarmati, and I. Hunyadi, Nucl. Phys. **46**, 141 (1963). B. Grimeland and P. Opsahl-Andersen, Nucl. Phys. **51**, 302 (1964). B. Grimeland, E. Kjellsby, and J. Vines, Phys. Rev. **137**, B878 (1963). N. K. Majumdar and A. Chatterjee, Nucl. Phys. **41**, 192 (1963). J. Picard and C. F. Williamson, Nucl. Phys. **63**, 673 (1965). S. R. Salisbury, D. B. Fossan, and F. J. Vaughn, Nucl. Phys. 64, 343 (1965). H. Spenke, Nucl. Phys. **51**, 329 (1964).
[101] J. Csikai *et al.*, Phys. Letters **4**, 33 (1963).
[102] M. Bormann *et al.*, Z. Physik **174**, 1 (1963).
[103] D. L. Allen, Nucl. Phys. **24**, 274 (1961).
[104] I. L. Preiss and R. W. Fink, Nucl. Phys. **15**, 326 (1960).
[105] G. S. Mani and M. A. Melkanoff, in *Proceedings of the International Conference on Direct Interactions, Padua, 1962* (Interscience Publishers, Inc., New York, 1962).
[106] R. J. Howerton, UCRL Report 5226 (1958).
[107] E. B. Paul and R. L. Cloake, Can. J. Phys. **31**, 267 (1953).
[108] D. L. Allen, Proc. Phys. Soc. (London) **A70**, 195 (1957).
[109] L. Allen *et al.*, Phys. Rev. **107**, 1363 (1957).
[110] H. Liskien and A. Paulsen, Nucl. Phys. **63**, 393 (1965).
[111] L. A. Rayburn, Phys. Rev. **130**, 731 (1963).
[112] D. W. Ban, I. C. Browne, and J. S. Gillmore, Phys. Rev. 123, 859 (1961).
[113] H. Büttner, A. Lindner, and H. Meldner, Nucl. Phys. **63**, 615 (1965).
[114] D. G. Gardner and Yu-Wen Yu, Nucl. Phys. **60**, 49 (1964).
[115] A. Chatterjee, Nucl. Phys. **47**, 511 (1963); **49**, 686 (1963). A. Chatterjee, Phys. Rev. **134**, B374 (1964).
[116] A. Chatterjee, Nucl. Phys. **60**, 273 (1964).
[117] M. Bormann, Nucl. Phys. **65**, 257 (1965).
[118] E. Erba, U. Facchini, and E. Saetta-Menichella, Nuovo Cimento **22**, 1237 (1961).
[119] P. Strohal, N. Cindro, and B. Eman, Nucl. Phys. **30**, 49 (1962).
[120] V. Levkovski, Zh. Eksperim. i Teor. Fiz. **33**, 1520 (1957) [English transl.: Soviet Phys.—JETP **6**, 1154 (1958)].
[121] D. G. Gardner, Nucl. Phys. **29**, 373 (1962). D. G. Gardner and A. Poularikis, Nucl. Phys. **35**, 303 (1962).
[122] N. Rosenzweig, Phys. Rev. **108**, 817 (1957).
[123] A. Rubbino and D. Zubke, Phys. Letters **11**, 333 (1964).
[124] J. E. Brolley, Jr., *et al.*, Phys. Rev. **99**, 330 (1953).
[125] G. S. Mani *et al.*, Nucl. Phys. **19**, 535 (1960).
[126] M. Bormann *et al.*, J. Phys. Radium **22**, 62, 602 (1961).
[127] M. Bormann, Nucl. Phys. **65**, 257 (1965).
[128] E. T. Bramlitt and R. W. Fink, Phys. Rev. **131**, 2649 (1963).
[129] J. Csikai *et al.* (private communication).
[130] K. K. Seth, Phys. Letters **16**, 306 (1965).
[131] J. Csikai (to be published).
[132] R. Cabe *et al.* (to be published).
[133] For the interpretation of total cross-section fluctuations in light elements see: P. Strohal *et al.*, Phys. Letters **10**, 104 (1964); N. Cindro, P. Kulišić, and P. Strohal, Phys. Letters **6**, 205 (1963).
[134] A. J. Elwyn *et al.*, Nucl. Phys. **59**, 113 (1964).
[135] F. Manero, Nucl. Phys. **65**, 419 (1965).
[136] D. Stüwer, H. Gentz, and M. Bormann, Nucl. Phys. **62**, 165 (1965).
[137] Z. Kolar, P. Strohal, and N. Cindro, J. Inorg. Nucl. Chem. **27**, 2471 (1965).
[138] H. K. Vonach, R. Vandenbosch, and J. R. Huizenga, Nucl. Phys. **60**, 70 (1964).
[139] C. T. Bishop, H. K. Vonach, and J. R. Huizenga, Nucl. Phys. **60**, 241 (1964).
[140] The superconductor model gives, in general, larger values for the level density parameter a than the Fermi gas model.
[141] H. Feshbach, C. E. Porter, and V. F. Weisskopf, Phys. Rev. **97**, 448 (1954).
[142] R. W. Woods and D. S. Saxon, Phys. Rev. **95**, 577(L) (1954).
[143] S. Fernbach, W. Heckrotte, and J. V. Lepore, Phys. Rev. **97**, 1059 (1955); F. Björklund and S. Fernbach, Phys. Rev. **109**, 1295 (1958).
[144] M. A. Melkanoff, J. Roynal, and T. Sawada, in *Methods of Computational Physics*, edited by B. Alder, S. Fernbach, and M. Rotenberg (Academic Press Inc., New York, to be published) Vol. V.
[145] J. Raynal, Phys. Letters **3**, 331 (1963); **7**, 281 (1963).
[146] M. K. Banerjee, "Theory of Stripping and Pickup Reactions," in *Nuclear Spectroscopy*, edited by F. Ajzenberg-Selove (Academic Press Inc., New York, 1960).
[147] E. H. Auerbach and S. O. Moore, Phys. Rev. **135**, B895 (1964).
[148] D. J. Hughes and R. B. Schwartz, *Neutron Cross Sections* (U.S. Government Printing Office, Washington, D.C., 1958), 2nd ed.
[149] H. H. Barshall *et al.*, Los Alamos Report, LA-1060, 1950 (unpublished).
[150] R. L. Henkel *et al.*, Phys. Rev. **94**, 141 (1954).
[151] It is true that the analysis of Auerbach *et al.*[147] does not require, but also does not prejudice the use of additional parameters.
[152] W. B. Gilboy and J. H. Towle, Nucl. Phys. **64**, 130 (1965).
[153] P. A. Moldauer, Nucl. Phys. **47**, 65 (1963).
[154] A. J. Elwin *et al.*, Phys. Rev. **133**, B80 (1964).
[155] W. Gilboy and J. H. Towle, Nucl. Phys. **42**, 86 (1963).
[156] D. Winterhalter, Nucl. Phys. **43**, 339 (1963). D. Reitmann, C. A. Engelbrecht, and A. B. Smith, Nucl. Phys. **48**, 593 (1963). A. H. Armstrong *et al.*, Nucl. Phys. **52**, 505 (1964). D. J. Hooton, Phys. Rev. **138**, B48 (1965).
[157] M. H. Mac Gregor, R. Booth, and W. B. Ball, Phys. Rev. **130**, 1471 (1963).
[158] W. P. Bucher and D. W. Kent, Phys. Rev. **134**, B361 (1963).
[159] D. W. Kent, Phys. Rev. **137**, B401 (1965).
[160] B. E. Wentzel and M. F. Steuer, Phys. Rev. **137**, B80 (1965).
[161] D. J. Bredin, Phys. Rev. **135**, B412 (1964).
[162] R. Wagner *et al.*, Phys. Letters **10**, 316 (1964).
[163] See also Sec. III.
[164] Y. A. Aleksandrov and I. I. Bondarenko, Zh. Eksperim. i Teor. Fiz. **31**, 726 (1956) [English transl.: Soviet Phys.—JETP **4**, 612 (1957)].
[165] M. Walt and D. B. Fossan, Phys. Rev. **137**, B629 (1965).
[166] W. J. MacDonald and J. M. Robson, Nucl. Phys. **59**, 321 (1964). P. W. Martin, D. T. Stewart, and J. Martin, Nucl. Phys. **61**, 524 (1965). M. Conjeaud, B. Fernandez, S. Harar, J. Picard, and G. Souchere, Nucl. Phys. **62**, 225 (1965).
[167] A. M. Lane, Phys. Rev. Letters **2**, 424 (1954).
[168] W. G. Vonach, A. B. Smith, and P. A. Moldauer, Phys. Letters **11**, 331 (1964).
[169] M. Z. Rahman Khan, Nucl. Phys. **59**, 580 (1964).
[170] S. S. Glickstein and R. G. Winter, Phys. Rev. **129**, 1281 (1963).
[171] J. A. Moore, H. Palewsky, and R. E. Clursen, Phys. Rev. **132**, 801 (1963).
[172] R. E. Seegel, R. K. Smither, and R. T. Carpenter, Phys. Rev. **133**, B583 (1964).
[173] L. V. Groshev *et al.*, Nucl. Phys. **58**, 465 (1964).
[174] E. A. Davis *et al.*, Nucl. Phys. **48**, 196 (1963).
[175] R. O. Lane, A. J. Elwyn, and A. Langsdorf, Phys. Rev. **136**, B1710 (1964).
[176] T. R. Donoghue, A. F. Behoff, and S. E. Darden, Nucl. Phys. **54**, 33, 49 (1964).
[177] F. Bloch, Phys. Rev. **58**, 824 (1940).
[178] A. M. Lane and R. G. Thomas, Rev. Mod. Phys. **30**, 257 (1958).

CC-0. In Public Domain. Gurukul Kangri Collection, Haridwar

Digitized by Arya Samaj Foundation Chennai and eGangotri

[179] J. P. Elliott and B. H. Flowers, Proc. Phys. Soc. (London) **242A,** 57 (1957).
[180] L. Colli, P. Forti, and E. Gadioli, Nucl. Phys. **54,** 253 (1964).
[181] D. J. Donahue and R. D. Roberts, Nucl. Phys. **50,** 641 (1964).
[182] G. R. Satchler, Phys. Rev. **104,** 1198 (1956); **411,** 1747 (1958). S. M. Shaffroth, P. N. Trehan, and D. M. Van Patter, Phys. Rev. **129,** 704 (1963).
[183] R. T. Wagner, E. R. Shrunk, and R. B. Day, Phys. Rev. **130,** 1926 (1963).
[184] J. Cabe, M. Laurat, and P. Yvon (to be published).
[185] F. J. Vaughn *et al.*, Nucl. Phys. **64,** 336 (1965).
[186] R. Bouchez, J. Duclos, and P. Perrin, Nucl. Phys. **43,** 628 (1963).
[187] R. W. Peele, Phys. Rev. **105,** 1311 (1957).
[188] K. W. Wildermuth (private communication quoted in Ref. 187).
[189] P. E. Hodgson, Nucl. Phys. **8,** 1 (1958).
[190] D. H. Wilkinson, Proceedings of the International Rutherford Jubellee Conference, Manchester, 1960.
[191] W. Osakiewicz *et al.*, Institute of Nuclear Research, Warsaw, Report No. 505/5, March 1964.
[192] A useful expression for the distribution of density of nuclear matter is the one given by Hahn *et al.* [Phys. Rev. 101, 1131 (1956)]:

$$\rho(r)=\begin{cases}\rho_0 & 0<r<c-z_3\\ \rho_0(c+z_3-r) & c-z_3<r<c+z_3\\ 0 & r>c+z_3,\end{cases}$$

with
$\rho_0=0.18$ nucl/F^3
$c=5.54$ (for La^{138})
$z_3=1.5$ F.
[193] The mean free path of neutrons in nuclear matter is given by

$$\lambda=\hbar/W[(\epsilon_0+V)/2m]^{\frac{1}{2}},$$

where V and W are the real and imaginary part of the optical potential and ϵ_0 and m are the neutron energy and mass, respectively.
[194] M. Arnold *et al.*, Nucl. Phys. **19,** 500 (1960).
[195] H. Gauvin, M. Lefort, and X. Tanago, Nucl. Phys. 36, 447 (1962).
[196] J. I. Serebrennikov, Zh. Eksperim. i Teor. Fiz. 35, 789 (1958) [English transl.: Soviet Phys.—JETP 8, 547 (1959)].
[197] The so-called Schwinger scattering results from the interaction of the neutron magnetic moment with the Coulomb field of the nucleus.

CC-0. In Public Domain. Gurukul Kangri Collection, Haridwar

Digitized by Arya Samaj Foundation Chennai and eGangotri

On the Problem of Hidden Variables in Quantum Mechanics*

JOHN S. BELL†
Stanford Linear Accelerator Center, Stanford University, Stanford, California

The demonstrations of von Neumann and others, that quantum mechanics does not permit a hidden variable interpretation, are reconsidered. It is shown that their essential axioms are unreasonable. It is urged that in further examination of this problem an interesting axiom would be that mutually distant systems are independent of one another.

I. INTRODUCTION

To know the quantum mechanical state of a system implies, in general, only statistical restrictions on the results of measurements. It seems interesting to ask if this statistical element be thought of as arising, as in classical statistical mechanics, because the states in question are averages over better defined states for which individually the results would be quite determined. These hypothetical "dispersion free" states would be specified not only by the quantum mechanical state vector but also by additional "hidden variables"—"hidden" because if states with prescribed values of these variables could actually be prepared, quantum mechanics would be observably inadequate.

Whether this question is indeed interesting has been the subject of debate.[1,2] The present paper does not contribute to that debate. It is addressed to those who do find the question interesting, and more particularly to those among them who believe that[3] "the question concerning the existence of such hidden variables received an early and rather decisive answer in the form of von Neumann's proof on the mathematical impossibility of such variables in quantum theory." An attempt will be made to clarify what von Neumann and his successors actually demonstrated. This will cover, as well as von Neumann's treatment, the recent version of the argument by Jauch and Piron,[3] and the stronger result consequent on the work of Gleason.[4] It will be urged that these analyses leave the real question untouched. In fact it will be seen that these demonstrations require from the hypothetical dispersion free states, not only that appropriate ensembles thereof should have all measurable properties of quantum mechanical states, but certain other properties as well. These additional demands appear reasonable when results of measurement are loosely identified with properties of isolated systems. They are seen to be quite unreasonable when one remembers with Bohr[5] "the impossibility of any sharp distinction between the behavior of atomic objects and the interaction with the measuring instruments which serve to define the conditions under which the phenomena appear."

The realization that von Neumann's proof is of limited relevance has been gaining ground since the 1952 work of Bohm.[6] However, it is far from universal. Moreover, the writer has not found in the literature any adequate analysis of what went wrong.[7] Like all authors of noncommissioned reviews, he thinks that he can restate the position with such clarity and simplicity that all previous discussions will be eclipsed.

II. ASSUMPTIONS, AND A SIMPLE EXAMPLE

The authors of the demonstrations to be reviewed were concerned to assume as little as possible about quantum mechanics. This is valuable for some purposes, but not for ours. We are interested only in the possibility of hidden variables in ordinary quantum me-

* Work supported by U.S. Atomic Energy Commission.
† Permanent address: CERN, Geneva.

[1] The following works contain discussions of and references on the hidden variable problem: L. de Broglie, *Physicien et Penseur* (Albin Michel, Paris, 1953); W. Heisenberg, in *Niels Bohr and the Development of Physics*, W. Pauli, Ed. (McGraw-Hill Book Co., Inc., New York, and Pergamon Press, Ltd., London, 1955); *Observation and Interpretation*, S. Körner, Ed. (Academic Press Inc., New York, and Butterworths Scientific Publ., Ltd., London, 1957); N. R. Hansen, *The Concept of the Positron* (Cambridge University Press, Cambridge, England, 1963). See also the various works by D. Bohm cited later, and Bell and Nauenberg.[8] For the view that the possibility of hidden variables has little interest, see especially the contributions of Rosenfeld to the first and third of these references, of Pauli to the first, the article of Heisenberg, and many passages in Hansen.

[2] A. Einstein, *Philosopher Scientist*, P. A. Schilp, Ed. (Library of Living Philosophers, Evanston, Ill., 1949). Einstein's "Autobiographical Notes" and "Reply to Criticics" suggest that the hidden variable problem has some interest.

[3] J. M. Jauch and C. Piron, Helv. Phys. Acta **36**, 827 (1963).

[4] A. M. Gleason, J. Math. & Mech. **6**, 885 (1957). I am much indebted to Professor Jauch for drawing my attention to this work.

[5] N. Bohr, in Ref. 2.

[6] D. Bohm, Phys. Rev. **85**, 166, 180 (1952).

[7] In particular the analysis of Bohm[6] seems to lack clarity, or else accuracy. He fully emphasizes the role of the experimental arrangement. However, it seems to be implied (Ref. 6, p. 187) that the circumvention of the theorem *requires* the association of *hidden* variables with the apparatus as well as with the system observed. The scheme of Sec. II is a counter example to this. Moreover, it will be seen in Sec. III that if the essential additivity assumption of von Neumann were granted, hidden variables wherever located would not avail. Bohm's further remarks in Ref. 16 (p. 95) and Ref. 17 (p. 358) are also unconvincing. Other critiques of the theorem are cited, and some of them rebutted, by Albertson [J. Albertson, Am. J. Phys. **29**, 478 (1961)].

CC-0. In Public Domain. Gurukul Kangri Collection, Haridwar

Digitized by Arya Samaj Foundation Chennai and eGangotri

chanics and will use freely all the usual notions. Thereby the demonstrations will be substantially shortened.

A quantum mechanical "system" is supposed to have "observables" represented by Hermitian operators in a complex linear vector space. Every "measurement" of an observable yields one of the eigenvalues of the corresponding operator. Observables with commuting operators can be measured simultaneously.[8] A quantum mechanical "state" is represented by a vector in the linear state space. For a state vector ψ the statistical expectation value of an observable with operator O is the normalized inner product $(\psi, O\psi)/(\psi, \psi)$.

The question at issue is whether the quantum mechanical states can be regarded as ensembles of states further specified by additional variables, such that given values of these variables together with the state vector determine precisely the results of individual measurements. These hypothetical well-specified states are said to be "dispersion free."

In the following discussion it will be useful to keep in mind as a simple example a system with a two-dimensional state space. Consider for definiteness a spin $-\frac{1}{2}$ particle without translational motion. A quantum mechanical state is represented by a two-component state vector, or spinor, ψ. The observables are represented by 2×2 Hermitian matrices

$$\alpha + \beta \cdot \sigma, \tag{1}$$

where α is a real number, β a real vector, and σ has for components the Pauli matrices; α is understood to multiply the unit matrix. Measurement of such an observable yields one of the eigenvalues.

$$\alpha \pm | \beta |, \tag{2}$$

with relative probabilities that can be inferred from the expectation value

$$\langle \alpha + \beta \cdot \sigma \rangle = (\psi, [\alpha + \beta \cdot \sigma]\psi).$$

For this system a hidden variable scheme can be supplied as follows: The dispersion free states are specified by a real number λ, in the interval $-\frac{1}{2} \leq \lambda \leq \frac{1}{2}$, as well as the spinor ψ. To describe how λ determines which eigenvalue the measurement gives, we note that by a rotation of coordinates ψ can be brought to the form

$$\psi = \begin{pmatrix} 1 \\ 0 \end{pmatrix}.$$

Let $\beta_x, \beta_y, \beta_z$, be the components of β in the new coordinate system. Then measurement of $\alpha + \beta \cdot \sigma$ on the state specified by ψ and λ results with certainty in the eigenvalue

$$\alpha + | \beta | \text{ sign } (\lambda | \beta | + \tfrac{1}{2} | \beta_z |) \text{ sign } X, \tag{3}$$

where

$$X = \beta_z \quad \text{if } \beta_z \neq 0$$
$$= \beta_x \quad \text{if } \beta_z = 0, \ \beta_x \neq 0$$
$$= \beta_y \quad \text{if } \beta_z = 0, \text{ and } \beta_x = 0$$

and

$$\text{sign } X = +1 \quad \text{if } X \geq 0$$
$$= -1 \quad \text{if } X < 0.$$

The quantum mechanical state specified by ψ is obtained by uniform averaging over λ. This gives the expectation value

$$\langle \alpha + \beta \cdot \sigma \rangle$$
$$= \int_{-\frac{1}{2}}^{\frac{1}{2}} d\lambda \{ \alpha + | \beta | \text{ sign } (\lambda | \beta | + \tfrac{1}{2} | \beta_z |) \text{ sign } X \} = \alpha + \tfrac{1}{2} \beta_z \text{ sign } \beta_z$$

as required.

It should be stressed that no physical significance is attributed here to the parameter λ and that no pretence is made of giving a complete reinterpretation of quantum mechanics. The sole aim is to show that at the level considered by von Neumann such a reinterpretation is not excluded. A complete theory would require for example an account of the behavior of the hidden variables during the measurement process itself. With or without hidden variables the analysis of the measurement process presents peculiar difficulties,[8] and we enter upon it no more than is strictly necessary for our very limited purpose.

III. VON NEUMANN

Consider now the proof of von Neumann[9] that dispersion free states, and so hidden variables, are impossible. His essential assumption[10] is: *Any real linear combination of any two Hermitian operators represents an observable, and the same linear combination of expecta-*

[8] Recent papers on the measurement process in quantum mechanics, with further references, are: E. P. Wigner, Am. J. Phys. **31**, 6 (1963); A. Shimony, *ibid.* **31**, 755 (1963); J. M. Jauch, Helv. Phys. Acta **37**, 293 (1964); B. d'Espagnat, *Conceptions de la physique contemporaine* (Hermann & Cie., Paris, 1965); J. S. Bell and M. Nauenberg, in *Preludes in Theoretical Physics, In Honor of V. Weisskopf* (North-Holland Publishing Company, Amsterdam, 1966).

[9] J. von Neumann, *Mathematische Grundlagen der Quantenmechanik* (Julius Springer-Verlag, Berlin, 1932) [English translation, Princeton University Press, Princeton, N.J., 1955]. All page numbers quoted are those of the English edition. The problem is posed in the preface, and on p. 209. The formal proof occupies essentially pp. 305–324 and is followed by several pages of commentary. A self-contained exposition of the proof has been presented by J. Albertson (see Ref. 7).

[10] This is contained in von Neumann's **B′** (p. 311), **1** (p. 313), and **11** (p. 314).

CC-0. In Public Domain. Gurukul Kangri Collection, Haridwar

Digitized by Arya Samaj Foundation Chennai and eGangotri

tion values is the expectation value of the combination. This is true for quantum mechanical states; it is required by von Neumann of the hypothetical dispersion free states also. In the two-dimensional example of Sec. II, the expectation value must then be a linear function of α and β. But for a dispersion free state (which has no statistical character) the expectation value of an observable must equal one of its eigenvalues. The eigenvalues (2) are certainly not linear in β. Therefore, dispersion free states are impossible. If the state space has more dimensions, we can always consider a two-dimensional subspace; therefore, the demonstration is quite general.

The essential assumption can be criticized as follows. At first sight the required additivity of expectation values seems very reasonable, and it is rather the nonadditivity of allowed values (eigenvalues) which requires explanation. Of course the explanation is well known: A measurement of a sum of noncommuting observables cannot be made by combining trivially the results of separate observations on the two terms—it requires a quite distinct experiment. For example the measurement of σ_x for a magnetic particle might be made with a suitably oriented Stern Gerlach magnet. The measurement of σ_y would require a different orientation, and of $(\sigma_x+\sigma_y)$ a third and different orientation. But this explanation of the nonadditivity of allowed values also establishes the nontriviality of the additivity of expectation values. The latter is a quite peculiar property of quantum mechanical states, not to be expected *a priori*. There is no reason to demand it individually of the hypothetical dispersion free states, whose function it is to reproduce the *measurable* peculiarities of quantum mechanics *when averaged over*.

In the trivial example of Sec. II the dispersion free states (specified λ) have additive expectation values only for commuting operators. Nevertheless, they give logically consistent and precise predictions for the results of all possible measurements, which when averaged over λ are fully equivalent to the quantum mechanical predictions. In fact, for this trivial example, the hidden variable question as posed informally by von Neumann[11] in his book is answered in the affirmative.

Thus the formal proof of von Neumann does not justify his informal conclusion[12]: "It is therefore not, as is often assumed, a question of reinterpretation of quantum mechanics—the present system of quantum mechanics would have to be objectively false in order that another description of the elementary process than the statistical one be possible." It was not the objective measurable predictions of quantum mechanics which ruled out hidden variables. It was the arbitrary assumption of a particular (and impossible) relation between the results of incompatible measurements either of which *might* be made on a given occasion but only one of which can in fact be made.

[11] Reference 9, p. 209.
[12] Reference 9, p. 325.

IV. JAUCH AND PIRON

A new version of the argument has been given by Jauch and Piron.[3] Like von Neumann they are interested in generalized forms of quantum mechanics and do not assume the usual connection of quantum mechanical expectation values with state vectors and operators. We assume the latter and shorten the argument, for we are concerned here only with possible interpretations of ordinary quantum mechanics.

Consider only observables represented by projection operators. The eigenvalues of projection operators are 0 and 1. Their expectation values are equal to the probabilities that 1 rather than 0 is the result of measurement. For any two projection operators, a and b, a third $(a\cap b)$ is defined as the projection on to the intersection of the corresponding subspaces. The essential axioms of Jauch and Piron are the following:

(A) Expectation values of *commuting* projection operators are additive.

(B) If, for some state and two projections a and b,

$$\langle a\rangle=\langle b\rangle=1,$$

then for that state

$$\langle a\cap b\rangle=1.$$

Jauch and Piron are led to this last axiom (4° in their numbering) by an analogy with the calculus of propositions in ordinary logic. The projections are to some extent analogous to logical propositions, with the allowed value 1 corresponding to "truth" and 0 to "falsehood," and the construction $(a\cap b)$ to (a "and" b) In logic we have, of course, if a is true and b is true then (a and b) is true. The axiom has this same structure.

Now we can quickly rule out dispersion free states by considering a 2-dimensional subspace. In that the projection operators are the zero, the unit operator, and those of the form

$$\tfrac{1}{2}+\tfrac{1}{2}\hat{\alpha}\cdot\mathfrak{d},$$

where $\hat{\alpha}$ is a unit vector. In a dispersion free state the expectation value of an operator must be one of its eigenvalues, 0 or 1 for projections. Since from A

$$\langle\tfrac{1}{2}+\tfrac{1}{2}\hat{\alpha}\cdot\mathfrak{d}\rangle+\langle\tfrac{1}{2}-\tfrac{1}{2}\hat{\alpha}\cdot\mathfrak{d}\rangle=1,$$

we have that for a dispersion free state either

$$\langle\tfrac{1}{2}+\tfrac{1}{2}\hat{\alpha}\cdot\mathfrak{d}\rangle=1 \quad \text{or} \quad \langle\tfrac{1}{2}-\tfrac{1}{2}\hat{\alpha}\cdot\mathfrak{d}\rangle=1.$$

Let α and $\hat{\beta}$ be any noncollinear unit vectors and

$$a=\tfrac{1}{2}\pm\tfrac{1}{2}\hat{\alpha}\cdot\mathfrak{d}, \qquad b=\tfrac{1}{2}\pm\tfrac{1}{2}\hat{\beta}\cdot\mathfrak{d},$$

with the signs chosen so that $\langle a\rangle=\langle b\rangle=1$. Then B requires

$$\langle a\cap b\rangle=1.$$

CC-0. In Public Domain. Gurukul Kangri Collection, Haridwar

Digitized by Arya Samaj Foundation Chennai and eGangotri

But with $\hat{\alpha}$ and $\hat{\beta}$ noncollinear, one readily sees that

$$a \cap b = 0,$$

so that

$$\langle a \cap b \rangle = 0.$$

So there can be no dispersion free states.

The objection to this is the same as before. We are not dealing in B with logical propositions, but with measurements involving, for example, differently oriented magnets. The axiom holds for quantum mechanical states.[13] But it is a quite peculiar property of them, in no way a necessity of thought. Only the quantum mechanical averages over the dispersion free states need reproduce this property, as in the example of Sec. II.

V. GLEASON

The remarkable mathematical work of Gleason[4] was not explicitly addressed to the hidden variable problem. It was directed to reducing the axiomatic basis of quantum mechanics. However, as it apparently enables von Neumann's result to be obtained without objectionable assumptions about noncommuting operators, we must clearly consider it. The relevant corollary of Gleason's work is that, if the dimensionality of the state space is greater than two, the additivity requirement for expectation values of *commuting operators* cannot be met by dispersion free states. This will now be proved, and then its significance discussed. It should be stressed that Gleason obtained more than this, by a lengthier argument, but this is all that is essential here.

It suffices to consider projection operators. Let $P(\Phi)$ be the projector on to the Hilbert space vector Φ, i.e., acting on any vector ψ

$$P(\Phi)\psi = (\Phi, \Phi)^{-1}(\Phi, \psi)\Phi.$$

If a set Φ_i are complete and orthogonal,

$$\sum_i P(\Phi_i) = 1.$$

Since the $P(\Phi_i)$ commute, by hypothesis then

$$\sum_i \langle P(\Phi_i) \rangle = 1. \tag{4}$$

Since the expectation value of a projector is nonnegative (each measurement yields one of the allowed values 0 or 1), and since any two orthogonal vectors can be regarded as members of a complete set, we have:

(A) If with some vector Φ, $\langle P(\Phi) \rangle = 1$ for a given state, then for that state $\langle P(\psi) \rangle = 0$ for any ψ orthogonal on Φ.

[13] In the two-dimensional case $\langle a \rangle = \langle b \rangle = 1$ (for some quantum mechanical state) is possible only if the two projectors are identical ($\hat{\alpha} = \hat{\beta}$). Then $a \cap b = a = b$ and $\langle a \cap b \rangle = \langle a \rangle = \langle b \rangle = 1$.

If ψ_1 and ψ_2 are another orthogonal basis for the subspace spanned by some vectors Φ_1 and Φ_2, then from (4)

$$\langle P(\psi_1) \rangle + \langle P(\psi_2) \rangle = 1 - \sum_{i \neq 1, i \neq 2} \langle P(\Phi_i) \rangle$$

or

$$\langle P(\psi_1) \rangle + \langle P(\psi_2) \rangle = \langle P(\Phi_1) \rangle + \langle P(\Phi_2) \rangle.$$

Since ψ_1 may be any combination of Φ_1 and Φ_2, we have

(B) If for a given state

$$\langle P(\Phi_1) \rangle = \langle P(\Phi_2) \rangle = 0$$

for some pair of orthogonal vectors, then

$$\langle P(\alpha\Phi_1 + \beta\Phi_2) \rangle = 0$$

for all α and β.

(A) and (B) will now be used repeatedly to establish the following. Let Φ and ψ be some vectors such that for a given state

$$\langle P(\psi) \rangle = 1, \tag{5}$$

$$\langle P(\Phi) \rangle = 0. \tag{6}$$

Then Φ and ψ cannot be arbitrarily close; in fact

$$|\Phi - \psi| > \tfrac{1}{2}|\psi|. \tag{7}$$

To see this let us normalize ψ and write Φ in the form

$$\Phi = \psi + \epsilon\psi',$$

where ψ' is orthogonal to ψ and normalized and ϵ is a real number. Let ψ'' be a normalized vector orthogonal to both ψ and ψ' (it is here that we need three dimensions at least) and so to Φ. By (A) and (5),

$$\langle P(\psi') \rangle = 0, \qquad \langle P(\psi'') \rangle = 0.$$

Then by (B) and (6),

$$\langle P(\Phi + \gamma^{-1}\epsilon\psi'') \rangle = 0,$$

where γ is any real number, and also by (B),

$$\langle P(-\epsilon\psi' + \gamma\epsilon\psi'') \rangle = 0.$$

The vector arguments in the last two formulas are orthogonal; so we may add them, again using (B):

$$\langle P(\psi + \epsilon(\gamma + \gamma^{-1})\psi'') \rangle = 0.$$

Now if ϵ is less than $\frac{1}{2}$, there are real γ such that

$$\epsilon(\gamma + \gamma^{-1}) = \pm 1.$$

Therefore,

$$\langle P(\psi + \psi'') \rangle = \langle P(\psi - \psi'') \rangle = 0.$$

The vectors $\psi \pm \psi''$ are orthogonal; adding them and again using (B),

$$\langle P(\psi) \rangle = 0.$$

CC-0. In Public Domain. Gurukul Kangri Collection, Haridwar

Digitized by Arya Samaj Foundation Chennai and eGangotri

This contradicts the assumption (5). Therefore,

$$\epsilon > \tfrac{1}{2},$$

as announced in (7).

Consider now the possibility of dispersion free states. For such states each projector has expectation value either 0 or 1. It is clear from (4) that both values must occur, and since there are no other values possible, there must be arbitrarily close pairs ψ, Φ with different expectation values 0 and 1, respectively. But we saw above such pairs could *not* be arbitrarily close. Therefore, there are no dispersion free states.

That so much follows from such apparently innocent assumptions leads us to question their innocence. Are the requirements imposed, which are satisfied by quantum mechanical states, reasonable requirements on the dispersion free states? Indeed they are not. Consider the statement (B). The operator $P(\alpha\Phi_1+\beta\Phi_2)$ commutes with $P(\Phi_1)$ and $P(\Phi_2)$ only if either α or β is zero. Thus in general measurement of $P(\alpha\Phi_1+\beta\Phi_2)$ requires a quite distinct experimental arrangement. We can therefore reject (B) on the grounds already used: it relates in a nontrivial way the results of experiments which cannot be performed simultaneously; the dispersion free states need not have this property, it will suffice if the quantum mechanical averages over them do. How did it come about that (B) was a consequence of assumptions in which only commuting operators were explicitly mentioned? The danger in fact was not in the explicit but in the implicit assumptions. It was tacitly assumed that measurement of an observable must yield the same value independently of what other measurements may be made simultaneously. Thus as well as $P(\Phi_3)$ say, one might measure *either* $P(\Phi_2)$ *or* $P(\psi_2)$, where Φ_2 and ψ_2 are orthogonal to Φ_3 but not to one another. These different possibilities require different experimental arrangements; there is no *a priori* reason to believe that the results for $P(\Phi_3)$ should be the same. The result of an observation may reasonably depend not only on the state of the system (including hidden variables) but also on the complete disposition of the apparatus; see again the quotation from Bohr at the end of Sec. I.

To illustrate these remarks, we construct a very artificial but simple hidden variable decomposition. If we regard all observables as functions of commuting projectors, it will suffice to consider measurements of the latter. Let P_1, P_2, $\cdots$ be the set of projectors measured by a given apparatus, and for a given quantum mechanical state let their expectation values be λ_1, $\lambda_2-\lambda_1$, $\lambda_3-\lambda_2$, $\cdots$. As hidden variable we take a real number $0<\lambda\leq 1$; we specify that measurement on a state with given λ yields the value 1 for P_n if $\lambda_{n-1}<\lambda\leq\lambda_n$, and zero otherwise. The quantum mechanical state is obtained by uniform averaging over λ. There is no contradiction with Gleason's corollary, because the result for a given P_n depends also on the choice of the others. Of course it would be silly to let the result be affected by a mere permutation of the other P's, so we specify that the same order is taken (however defined) when the P's are in fact the same set. Reflection will deepen the initial impression of artificiality here. However, the example suffices to show that the implicit assumption of the impossibility proof was essential to its conclusion. A more serious hidden variable decomposition will be taken up in Sec. VI.[14]

VI. LOCALITY AND SEPARABILITY

Up till now we have been resisting arbitrary demands upon the hypothetical dispersion free states. However, as well as reproducing quantum mechanics on averaging, there *are* features which can reasonably be desired in a hidden variable scheme. The hidden variables should surely have some spacial significance and should evolve in time according to prescribed laws. These are prejudices, but it is just this possibility of interpolating some (preferably causal) space–time picture, between preparation of and measurements on states, that makes the quest for hidden variables interesting to the unsophisticated.[2] The ideas of space, time, and causality are not prominent in the kind of discussion we have been considering above. To the writer's knowledge the most successful attempt in that direction is the 1952 scheme of Bohm for elementary wave mechanics. By way of conclusion, this will be sketched briefly, and a curious feature of it stressed.

Consider for example a system of two spin $-\frac{1}{2}$ particles. The quantum mechanical state is represented by a wave function,

$$\psi_{ij}(\mathbf{r}_1, \mathbf{r}_2),$$

where i and j are spin indices which will be suppressed. This is governed by the Schrödinger equation,

$$\partial\psi/\partial t = -i(-(\partial^2/\partial\mathbf{r}_1^2)-(\partial^2/\partial\mathbf{r}_2^2)+V(\mathbf{r}_1-\mathbf{r}_2) + a\boldsymbol{\sigma}_1\cdot\mathbf{H}(\mathbf{r}_1)+b\boldsymbol{\sigma}_2\cdot\mathbf{H}(\mathbf{r}_2))\psi, \quad (8)$$

where V is the interparticle potential. For simplicity we have taken neutral particles with magnetic moments, and an external magnetic field $\mathbf{H}$ has been allowed to represent spin analyzing magnets. The hidden variables are then two vectors $\mathbf{X}_1$ and $\mathbf{X}_2$, which give directly the results of position measurements. Other measurements are reduced ultimately to position measurements.[15] For example, measurement of a spin component means observing whether the particle emerges with an upward or downward deflection from a Stern–

[14] The simplest example for illustrating the discussion of Sec. V would then be a particle of spin 1, postulating a sufficient variety of spin–external-field interactions to permit arbitrary complete sets of spin states to be spacially separated.

[15] There are clearly enough measurements to be interesting that can be made in this way. We will not consider whether there are others.

CC-0. In Public Domain. Gurukul Kangri Collection, Haridwar

Digitized by Arya Samaj Foundation Chennai and eGangotri

Gerlach magnet. The variables $\mathbf{X}_1$ and $\mathbf{X}_2$ are supposed to be distributed in configuration space with the probability density,

$$\rho(\mathbf{X}_1, \mathbf{X}_2) = \sum_{ij} |\psi_{ij}(\mathbf{X}_1, \mathbf{X}_2)|^2,$$

appropriate to the quantum mechanical state. Consistently, with this $\mathbf{X}_1$ and $\mathbf{X}_2$ are supposed to vary with time according to

$$d\mathbf{X}_1/dt = \rho(\mathbf{X}_1, \mathbf{X}_2)^{-1} \operatorname{Im} \sum_{ij} \psi_{ij}^*(\mathbf{X}_1, \mathbf{X}_2)(\partial/\partial\mathbf{X}_1)\psi_{ij}(\mathbf{X}_1, \mathbf{X}_2),$$

$$d\mathbf{X}_2/dt = \rho(\mathbf{X}_1, \mathbf{X}_2)^{-1} \operatorname{Im} \sum_{ij} \psi_{ij}^*(\mathbf{X}_1, \mathbf{X}_2)(\partial/\partial\mathbf{X}_2)\psi_{ij}(\mathbf{X}_1, \mathbf{X}_2). \tag{9}$$

The curious feature is that the trajectory equations (9) for the hidden variables have in general a grossly nonlocal character. If the wave function is factorable before the analyzing fields become effective (the particles being far apart),

$$\psi_{ij}(\mathbf{X}_1, \mathbf{X}_2) = \Phi_i(\mathbf{X}_1)\chi_j(\mathbf{X}_2),$$

this factorability will be preserved. Equations (8) then reduce to

$$d\mathbf{X}_1/dt = [\sum_i \Phi_i^*(\mathbf{X}_1)\Phi_i(X_1)]^{-1} \times \operatorname{Im} \sum_i \Phi_i^*(\mathbf{X}_1)(\partial/\partial\mathbf{X}_1)\Phi_i(X_1),$$

$$d\mathbf{X}_2/dt = [\sum_j \chi_j^*(\mathbf{X}_2)\chi_j(X_2)]^{-1} \times \operatorname{Im} \sum_j \chi_j^*(\mathbf{X}_2)(\partial/\partial\mathbf{X}_2)\chi(X_2).$$

The Schrödinger equation (8) also separates, and the trajectories of $\mathbf{X}_1$ and $\mathbf{X}_2$ are determined separately by equations involving $\mathbf{H}(\mathbf{X}_1)$ and $\mathbf{H}(\mathbf{X}_2)$, respectively. However, in general, the wave function is not factorable. The trajectory of 1 then depends in a complicated way on the trajectory and wave function of 2, and so on the analyzing fields acting on 2—however remote the may be from particle 1. So in this theory an explic causal mechanism exists whereby the disposition of one piece of apparatus affects the results obtained with a distant piece. In fact the Einstein-Podolsky-Rosen paradox is resolved in the way which Einstein would have liked least (Ref. 2, p. 85).

More generally, the hidden variable account of a given system becomes entirely different when we remember that it has undoubtedly interacted with numerous other systems in the past and that the total wave function will certainly not be factorable. This same effect complicates the hidden variable account of the theory of measurement, when it is desired to include part of the "apparatus" in the system.

Bohm of course was well aware[6,16–18] of these features of his scheme, and has given them much attention. However, it must be stressed that, to the present writer's knowledge, there is no *proof* that *any* hidden variable account of quantum mechanics *must* have this extraordinary character.[19] It would therefore be interesting, perhaps,[1] to pursue some further "impossibility proofs," replacing the arbitrary axioms objected to above by some condition of locality, or of separability of distant systems.

ACKNOWLEDGMENTS

The first ideas of this paper were conceived in 1952. I warmly thank Dr. F. Mandl for intensive discussion at that time. I am indebted to many others since then and latterly, and very especially, to Professor J. M. Jauch.

---

[16] D. Bohm, *Causality and Chance in Modern Physics* (D. Van Nostrand Co., Inc., Princeton, N.J., 1957).

[17] D. Bohm, in *Quantum Theory*, D. R. Bates, Ed. (Academic Press Inc., New York, 1962).

[18] D. Bohm and Y. Aharonov, Phys. Rev. **108**, 1070 (1957).

[19] Since the completion of this paper such a proof has been found [J. S. Bell, Physics **1**, 195 (1965)].

CC-0. In Public Domain. Gurukul Kangri Collection, Haridwar

Digitized by Arya Samaj Foundation Chennai and eGangotri

A Proposed Solution of the Measurement Problem in Quantum Mechanics by a Hidden Variable Theory

D. BOHM, J. BUB

Birkbeck College, University of London, London, England

The measurement problem in quantum mechanics is re-examined and it is shown that it cannot really be solved in a satisfactory way, within the framework of the usual interpretation of the theory. We then discuss von Neumann's attempts to prove that quantum mechanics is incompatible with the introduction of hidden variables, and develop a more detailed form of Bell's argument, showing that von Neumann's analysis is invalid. Using certain ideas that are implicit in the "differential-space" theory of Wiener and Siegel, we go on to propose a new deterministic equation of motion, describing a kind of coupling of the measuring instrument to the observed system that explains in detail how the wave packet is "reduced" during a measurement in a continuous and causally determined way. By averaging over the hidden parameters, we then recover the usual statistical results of quantum mechanics as a special case. However, a more detailed analysis of the theory shows that new experimental and theoretical questions can now be raised, which go outside the framework of the quantum theory as it is now formulated. These questions are examined briefly.

1. INTRODUCTORY REMARKS

In recent years a number of articles have been published indicating a revival of interest in the problem of the physical interpretation of quantum mechanics. In these articles it becomes evident that the whole question is far from being settled in a clear and simple way. It therefore seems worthwhile to go into this subject as carefully as possible. We shall attempt to clarify the nature of these questions and problems, as well as to suggest some tentative steps towards answers and solutions.

Now, in one of the most widely accepted interpretations of the quantum theory, i.e., that of the Copenhagen school,[1,2] the physical state of a system is assumed to be completely specified by its wave function which, however, defines only the probabilities of results that can be obtained in a statistical ensemble of similar measurements. The possibility that there exist further dynamical variables determining the actual behavior of each individual system at the quantum level is rejected. In support of this orthodox doctrine there is the well-known proof of von Neumann[3] that the assumption of such "hidden variables" is incompatible with the established results of quantum mechanics.

On the other hand, there are theoretical as well as practical reasons for regarding the present form of the quantum theory as unsatisfactory. The now classic Einstein–Podolsky–Rosen paradox[4] suggests that the theory is incomplete (in spite of refutations by Bohr and others). The results of experiments involving very high energies (of the order of 10^9 eV or more) or very short distances (of the order of 10^{-13} cm or less) are becoming increasingly more difficult to explain without ad hoc extensions to the theory. In addition, many authors have suggested that the reasoning involved in von Neumann's proof is circular and that the conclusion is tacitly assumed in the premises on which the argument is based. Other authors (the most recent of whom are Jauch and Piron[5]) deny that the conclusion depends on a circular argument. Still others[6,7] fully accept neither the Copenhagen interpretation nor von Neumann's point of view and yet, at least by implication, agree that the usual interpretation is in essence the only possible one. Finally, it has recently been pointed out by Bell[8] that von Neumann's proof is based on certain unnecessarily restrictive assumptions and that when these are not made the proof breaks down.

It seems, then, that the question of the possibility of hidden variables underlying the quantum theory is still problematic. Besides, as we shall make clear, if the claims based on von Neumann's theorem are accepted as valid then it would follow, from the facts confirming the current quantum theory, that a different general structure of concepts is impossible. Thus, it is made to appear that the linguistic structure of quantum mechanics prevents even the assertion of the *possibility* that the basic postulates underlying the theory may be false. In effect, this would mean that certain features of the basic postulates of the current theory are absolute truths that can never be falsified, or shown to be valid only as approximations or limiting cases. This

[1] N. Bohr, article in *Albert Einstein: Philosopher-Scientist*, P. A. Schilpp, Ed. (Library of Living Philosophers, Inc., Evanston, Ill., 1949).
[2] W. Heisenberg, article in *Niels Bohr and the Development of Physics*, W. Pauli, Ed. (Pergamon Press, Ltd., London, 1955).
[3] J. von Neumann, *The Mathematical Foundations of Quantum Mechanics* (Princeton University Press, Princeton, N.J., 1955).
[4] A. Einstein, B. Podolsky, and N. Rosen, Phys. Rev. **47**, 777 (1935).
[5] J. M. Jauch and C. Piron, Helv. Phys. Acta **36**, 827 (1963).
[6] H. Margenau, Ann. Phys. (N.Y.) **23**, 469 (1963).
[7] H. Margenau, Phil. Sci. **30**, 1, 138 (1963).
[8] J. S. Bell, Rev. Mod. Phys. **38**, 447 (1966).

CC-0. In Public Domain. Gurukul Kangri Collection, Haridwar

Digitized by Arya Samaj Foundation Chennai and eGangotri

kind of unfalsifiability would be almost as dangerous in any theory as is the claim to unfalsifiability on *a priori* grounds.

There have been many attempts to develop other interpretations of quantum mechanics and a number of hidden variable theories have been proposed,[2,9–11] which supply explicit refutations of von Neumann's proof. Nevertheless, these theories have all suffered from various inadequacies and, for this reason, are largely ignored in current research. From the outset, however, this whole controversy has been plagued by tacit assumptions, very often of a philosophical rather than a physical character, leading to the kind of difficulties referred to above concerning the relationship of hidden variable theories to the experimental content of quantum mechanics and the relevance of von Neumann's proof. In addition, the theory of the process of measurement involves a great many unclear features and unresolved problems, arising mainly because the role of the measuring instrument in the phenomenon of the "collapse" of the wave packet in a quantum mechanical measurement process is obscure. This has been referred to as the *measurement problem* in quantum mechanics.

In this article, as has been indicated, it is hoped to present the controversy in a more coherent and unified manner and to investigate and propose a solution to the measurement problem. After a review of the basic principles of quantum mechanics with the aim of clarifying the problem, we shall consider the Copenhagen interpretation, along with one of its modern variants,[12] which latter aims to give a more detailed mathematical treatment of the role of the observing apparatus than Bohr does. These attempts to treat the "collapse" within the framework of quantum mechanics will be seen to avoid the real problem, because they do not, in fact, propose a scheme which adequately incorporates the role of the measuring instrument into the dynamics of a theory that includes the measurement process. The idea that the quantum mechanical description of phenomena is incomplete, and that there are additional variables (at present "hidden") which must be taken into account, seems therefore to provide a very natural basis for a proper understanding of the situation. Before proceeding with the development of such a theory, however, it is of course necessary to consider the claim that a hidden variable theory underlying quantum mechanics is impossible. In this connection, we shall discuss the assumptions underlying von Neumann's proof[3] and expose their inadequacy. (Besides this proof, there has been a more recent attempt by Jauch and Piron[5] to establish the impossibility of a hidden variable quantum mechanics. This will be discussed in a subsequent paper.)

We present a hidden variable theory which is an extension of the "differential space" theory of Wiener and Siegel[11,13,14] and develop certain ideas which are only tacitly implied in their work. A deterministic equation of motion is introduced which couples the measuring instrument to the observed system and explicitly incorporates the role of the measuring instrument into the dynamics of the theory. Since the apparatus may be regarded, from a physical point of view, as merely a particular case of the large-scale environment of the system, this suggests a multi-level theory in which the general movement of a system is determined by an equation of motion coupling the large scale to the small scale. A measurement process is then interpreted as a special case of this movement to which each system is always subject.

An important feature of any such hidden variable theory is its potential contradiction with quantum mechanics. The latter is, of course, recovered in a certain special case. This theory therefore opens up new experimental possibilities, which are briefly examined.

It is definitely not proposed that the theory developed here is likely to be a "right" one. Rather, the main aim of this theory is to provide a language and a set of concepts in which it is possible to show clearly the meaning behind the different interpretations of quantum mechanics and to indicate what it means to assert or deny the existence of hidden variables. However, the discussion of the questions outlined above would almost certainly be relevant in any new hidden variable theory which might be developed, even if the form of the latter were very different from the theory proposed here. Thus, while this theory serves mainly as an example for making the discussion more concrete, at the same time it also suggests certain new kinds of experimental and theoretical questions whose relevance transcends the particular example of the theory in which they are raised.

2. REVIEW OF THE BASIC PRINCIPLES OF QUANTUM MECHANICS

The basic principles of quantum mechanics have been expressed in many different ways in various publications. It is, however, necessary to discuss briefly here certain essential features of the quantum description, with the aim of clarifying what the assumptions behind the usual interpretation of quantum mechanics actually are and how these may be changed in the development of a theory of hidden variables. In addition, we shall attempt to distinguish clearly between those assumptions confirmed in experiment and those based on largely tacit notions which are essentially philosophical

[9] D. Bohm, Phys. Rev. **85**, 166, 180 (1952).
[10] L. de Broglie, *The Current Interpretation of Wave Mechanics* (Elsevier Publ. Co., Inc., Paris, 1964).
[11] N. Wiener and A. Siegel, Nuovo Cimento Suppl. **2**, Ser. X, 304 (1955).
[12] A. Daneri, A. Loinger, and G. M. Prosperi, Nucl. Phys. **33**, 297 (1962).
[13] A. Siegel and N. Wiener, Phys. Rev. **101**, 429 (1956).
[14] N. Wiener and S. Siegel, Phys. Rev. **91**, 1551 (1953).

CC-0. In Public Domain. Gurukul Kangri Collection, Haridwar

Digitized by Arya Samaj Foundation Chennai and eGangotri

rather than physical. It will become evident in this discussion that some of these philosophical assumptions underlying the usual interpretation are misleadingly vague and unclear, especially on the question of the relation between the properties of individual systems and those of statistical ensembles.

Two of the basic postulates of quantum mechanics are the following:

(1) The state of a quantum mechanical system is defined by a continuous, single-valued wave function, $\Psi(\mathbf{x}, t)$, which obeys a deterministic equation of motion, Schrödinger's equation:

$$i\hbar(\partial\Psi/\partial t) = H\Psi. \tag{2.1}$$

(2) The wave function determines the probabilities of the possible results of any measurement on the system. Equivalently, the average or expectation value for an ensemble of measurements of any observable R is derived from Ψ through the algorithm:

$$\bar{R} = (\Psi, \mathrm{R}\Psi) = \int \Psi^*(\mathbf{x}) R(\mathbf{x}, -i\hbar\nabla)\Psi(\mathbf{x})\, d\mathbf{x}, \tag{2.2}$$

where R is the operator corresponding to the observable R.

These two postulates, which are fundamental in any conventional formulation of quantum mechanics, incorporate the notion of probability into the theory in an inherent way. Yet it is not immediately clear how the ensembles, to which these probabilities refer, are formed and what their individual elements are. For the very terminology of quantum mechanics contains an unusual and significant feature, in that what is called the *physical state* of an *individual* quantum mechanical system is assumed to manifest itself only in an *ensemble of systems*.

Because it is indeed mysterious for an individual system thus to manifest itself only in a statistical ensemble, there is a tendency among physicists tacitly to avoid this problem by interpreting the wave function as referring directly to an ensemble rather than to an individual system. In other words, it is quite often supposed that a wave function is not to be associated with an individual system, but *only* with an ensemble of similar systems. This interpretation is in fact untenable, as can be seen by the analysis of a simple hypothetical experiment.

Consider a two-slit diffraction experiment with electrons, which is set up with a movie camera replacing the single photographic plate in the usual arrangement. If the film moves at the rate of one frame per second and the electrons arrive at the slit system one at a time at intervals of one second, then each frame will record a different individual track. If each electron is similarly prepared, then their wave packets are similar in shape and will each be represented by the same function Ψ. For example, suppose that the electron passes through a slit system and a time gate which localizes it to within a region of size Δr. According to Schrödinger's equation, there will be a slowly expanding wave packet, initially of this width, which moves through the slit system to the plate. From this wave packet, something is known about the individual system; viz., *that the electron is somewhere in the region where the wave function is appreciable.* Likewise, the momentum of the electron is somewhere in the region in which the Fourier coefficient of the wave function is appreciable. Indeed, this is just how quantum mechanics approaches the definiteness of the classical concepts of momentum and position of an individual electron, which are, however, limited in their degree of simultaneous definition by the uncertainty principle. Therefore, if one considers the movement of the packet representing an individual electron as it passes through the slit system and develops a set of fringes, according to Schrödinger's equation, one can predict that it will strike a certain region of one frame of the film in which the transformed wave function Ψ is appreciable. After the experiment, a superposition of all the frames will yield the diffraction pattern determined by $|\Psi|^2$, where Ψ is a *typical* wave function. Although they are all represented formally by the same function of $\mathbf{x}$, each electron has a wave function that depends on the time t in its own way (such that only one electron is in the system at the time). The packets are similar in shape, but different in their times of going through the slit system.

Therefore, the wave function refers primarily to an individual electron and the statistical ensembles refers to a set of electrons having different wave functions of similar shapes. Nevertheless, because the probability interpretation is the only physical meaning given for the precise shape of the wave function (as opposed to its general extension in $\mathbf{x}$ or $\mathbf{p}$ space), it cannot give a model of how the electron moves in the slit system, which is more detailed than the limits of applicability of classical concepts to individual particles, as determined by the uncertainty principle. To bring out in more detail what this means, we note that the wave function of the electron at a point $\mathbf{x}$ to the right of the slits is

$$\Psi(\mathbf{x}) = \Psi_A(\mathbf{x}) + \Psi_B(\mathbf{x}), \tag{2.3}$$

where $\Psi_A(\mathbf{x})$ represents that part of the wave reaching the point $\mathbf{x}$ that has come from slit A and $\Psi_B(\mathbf{x})$ represents that part which has come from slit B. If only slit A were open, then the probability of an electron reaching the point $\mathbf{x}$ would be equal to $P_A(\mathbf{x}) = |\Psi_A(\mathbf{x})|^2$, while if only slit B were open this probability would be $P_B(\mathbf{x}) = |\Psi_B(\mathbf{x})|^2$. When both slits are open, however, the probability is

$$\begin{aligned} P(\mathbf{x}) &= |\Psi_A(\mathbf{x}) + \Psi_B(\mathbf{x})|^2 \\ &= P_A(\mathbf{x}) + P_B(\mathbf{x}) + \Psi_A^*(\mathbf{x})\Psi_B(\mathbf{x}) + \Psi_B^*(\mathbf{x})\Psi_A(\mathbf{x}). \end{aligned} \tag{2.4}$$

CC-0. In Public Domain. Gurukul Kangri Collection, Haridwar

Digitized by Arya Samaj Foundation Chennai and eGangotri

In addition to the "classical" probability terms P_A+P_B, P contains the interference terms, $\Psi_A^*\Psi_B+\Psi_B^*\Psi_A$, which would not be present if the experiment involved a probability distribution of classical particles, coming either through slit A or slit B. (These terms may, for example, cause Ψ to vanish at certain points where there would have been a nonvanishing probability with only one slit open.) Therefore the particle model fails as a description of the details of the motion of an individual electron within the slit system. On the other hand, since the electron acts like an individual particle in producing a track on one frame of the film, the wave model also fails to describe the order and structure of this motion adequately.

At the risk of laboring an obvious point, we repeat: Each individual quantum system is associated with a certain wave function. All information about the system is assumed to be contained in the wave function through the probabilities that can be deduced from it. But this function provides no representation of the detailed movement of an individual electron. To call Ψ the *state function* of such an individual electron therefore leads to confusion, because the significance of this function is in general manifested physically only in an ensemble of systems having wave functions of a similar form. On the other hand, because these functions actually all refer in a certain way to different systems, it is also wrong to say that the wave function belongs *only* to an ensemble.

It seems therefore that there is no clear *physical* concept of the detailed state of movement of the individual electron. At best, then, the quantum theory can be regarded as an elaborate system of algorithms for computing the probabilities of experimental results. Nevertheless, most of those physicists who follow the usual probabilistic interpretation of the theory are not content to do this, so that they are ultimately faced with the inability to provide a satisfactory resolution of the question of how the individual and the ensemble are related, as they try to interpret the algorithms with the aid of physical concepts. It will be our intention to show that this difficulty can be removed by extending the concepts of the theory, in a manner equivalent to the introduction of *some* kind of hidden variables.

Before continuing with a third, and yet more problematic, postulate of the usual theory, we shall digress here briefly in order to clarify the distinction between pure and mixed ensembles in quantum mechanics.

A *pure* (or homogeneous) ensemble consists of individuals (e.g., electrons) which all have similar wave functions, although they are generally ordered in different places or times. In a pure ensemble, therefore, the typical wave function Ψ defines the probability distribution for the ensemble, so that the expectation value of an observable R is given by the relation:

$$\bar{R}=\int \Psi^*(\mathbf{x})R(\mathbf{x}, -i\hbar\nabla)\Psi(\mathbf{x})\,d\mathbf{x}. \qquad (2.5)$$

A *mixed* ensemble is composed of individuals wh wave packets are not all similar; e.g., electrons wh boil out of a filament have a distribution of energ hence a distribution of wave functions. If, in a gi representation, the coefficients of the expansion of wave function Ψ into an orthonormal (discrete, simplicity) set of basis functions $S_i(\mathbf{x})$ are ψ_i, then t expectation value determined by this wave functi for an observable R may be expressed as:

$$\bar{R}=\sum_{ij}\psi_i^*R_{ij}\psi_j, \qquad (2.6)$$

where R_{ij} is the matrix $(S_i, \mathbf{R}S_j)$. For a mixed ensemble the expectation value is determined by averaging ov all the wave functions present, i.e.,

$$\langle\bar{R}\rangle_{\text{Av}}=\sum_{ij}\langle\psi_i^*\psi_j\rangle_{\text{Av}}R_{ij}$$
$$=\sum_{ij}\rho_{ji}R_{ij}, \qquad (2.7)$$

where $\rho_{ji}=\langle\psi_i^*\psi_j\rangle_{\text{Av}}$ is the statistical matrix (or densi matrix), so that:

$$\langle R\rangle_{\text{Av}}=\text{Tr}\,(f\cdot\mathbf{R}). \qquad (2.8)$$

From the above assumptions, it follows that f Hermitian and $\langle\bar{R}\rangle_{\text{Av}}$ is real.

We come now to postulate (3):

(3) After a precise measurement of the observabl represented by the operator $\mathbf{R}$ yielding the eigenvalu R_i, the wave function $\Psi(\mathbf{x})=\sum_i\psi_iR_i(\mathbf{x})$ becom $R_i(\mathbf{x})$.

This phenomenon is known as the "collapse" o "reduction" of the wave packet and the postulate i question is sometimes referred to as the "projectio postulate", because the vector in Hilbert space repr senting Ψ is projected after the measurement onto on of the basis vectors of the representation in which th matrix of the operator representing the observable measured is diagonal. The postulate is necessary to en sure the *reproducibility* of measurement results: after measuring R and finding the result R_i, an immediate subsequent measurement should yield the same value R_i, or the theory would clearly be inadequate. It is however, incompatible with Schrödinger's equation, since an ensemble of measurements on systems similarly prepared with wave functions Ψ, i.e., a *pure* ensemble will yield a *mixed* ensemble represented by a prob ability distribution of eigenfunctions, $R_i(\mathbf{x})$, each with weight $p_i=|\psi_i|^2$. This represents an irreversible change involving a nonunitary transformation of Ψ. In con trast to the classical situation, where every dynamica process is, in principle, covered by Hamilton's equa tions, the measurement process in quantum mechanics is placed in a category on its own.

It may perhaps clarify the situation to point out here that, according to the usual interpretation of quantum mechanics, the process of collapse is equiva lent to assuming that a given wave function is replaced

CC-0. In Public Domain. Gurukul Kangri Collection, Haridwar

Digitized by Arya Samaj Foundation Chennai and eGangotri

by a second wave function after measurement, but for no assignable reason: the second wave function cannot be derived as a solution of the Schrödinger equation of motion for the system initially described by the first wave function. If we consider a pure ensemble of similar first wave functions, as in the cine camera experiment, then this ensemble is associated with an ensemble of second wave functions which will not in general be pure, i.e., the individual members will have different wave functions. The relative frequencies of these different second wave functions are given by the usual rules of the quantum theory.

It is not easy to avoid the feeling that such a sudden break in the theory (i.e., the replacement, unaccounted for in the theory, of one wave function by another when an individual system undergoes a measurement) is rather arbitrary. Of course, this means the renunciation of a deterministic treatment of physical processes, so that the statistics of quantum mechanics becomes *irreducible* (whereas in classical statistical mechanics it is a simplification—in principle more detailed predictions are possible with more information). More significant still, a precise conceptual description of the process of measurement in quantum mechanics becomes in principle impossible, so that one also gives up all hope of ever being able to obtain a clear conception of the *nature* of the individual electron or of how it moves. The physicist may have a rough picture of a wave packet, which supplies a limited kind of physical intuition, but this does not in any sense complete the picture of what the electron is and of what it does.

The deeper significance of the lack of such a clear concept of the electron and its motion can be brought out more clearly by considering the fact that, in an ensemble of electrons with similar first wave functions, the differences among the second wave functions cannot be referred to differences that exist in the individual members of the first "pure" ensemble. Does it not seem natural, however, to suppose that differences in the later states of an ensemble of systems should be related to corresponding differences in the earlier states of the systems? The assumption that differences appear in time which are totally unrelated to *any* differences whatsoever in the earlier states of the systems implies a kind of breakdown of physical law that should not be accepted lightly without some clear proof that an assumption of this nature is unavoidable. For, once it is accepted, we shall tend very strongly to cease to be interested in looking for such relationships, so that even if they should exist, we are unlikely to find them.

At this point, the idea seems quite naturally to suggest itself that the differences in the second wave functions (after a measurement) could be referred to differences, before the measurement, in the values of some new kinds of variables, at present "hidden" (but in principle ultimately observable with the aid of suitable new methods of observation may later be suggested by thinking in terms of such variables). Since the behavior of each system would depend on these hidden variables, as well as on the wave function, we can understand how electrons with initially similar wave functions can display different properties when they are observed, through the differences of the hidden variables before measurement. The quantum mechanical distributions of observed results could then be recovered by averaging over a suitable ensemble of hidden variables in the first (pure) ensemble.

Such a theory would, in certain ways, be rather similar to classical statistical mechanics, in which the large-scale thermodynamic properties, relationships of P, V, T, etc., are explained in terms of statistical distributions of atomic variables. Relative to the large-scale level, these variables are at first "hidden," but (as has been suggested with regard to hidden variables of quantum mechanics) they are ultimately observable with new kinds of instruments—Geiger counters or cloud chambers instead of thermometers and pressure gauges—which have in fact been developed as a result of the new ideas suggested by thinking in terms of atomic concepts.

3. INADEQUACY OF THE COPENHAGEN INTERPRETATION AND OTHER RELATED THEORIES OF MEASUREMENT

There are various reasons for developing such a hidden variable theory. As we have indicated, the Copenhagen interpretation of quantum mechanics, in which the collapse of the wave packet is accepted as a fundamental and irreducible phenomenon (an ultimate fact of nature which is incapable of any further analysis), entails the renunication of any conception of the order and structure of movement of a microsystem in favor of a set of rules for the prediction of the results of specific experiments. Of course, a system of calculation of experimental probabilities is useful. Nevertheless, science is surely more than *merely* a set of algorithms for an engineer's handbook. Science also aims at an *understanding* of the over-all structure and order of movement of matter from the atom to the galaxies. While science also has the aim of prediction and useful application, these in themselves cannot correctly be identified with the whole of the act of understanding, in which one grasps the order the structure of a complex process in a unified coherent set of concepts. From these latter, one can abstract relationships of the parts, which make predictions possible. However, the difference between understanding and *mere* prediction can be illustrated by the example of trying to find one's way through a city that one does not know. One may be given directions, which in effect constitute predictions of the order of streets and buildings that one will discover if one walks in certain ways. But a map of the city gives a unified coherent understanding of its over-all order and structure, from which useful predictions can be taken by reading it. Quantum

CC-0. In Public Domain. Gurukul Kangri Collection, Haridwar

Digitized by Arya Samaj Foundation Chennai and eGangotri

mechanics at present yields a coherent structure of *mathematics*. However, its *physical concepts* resemble the giving of directions to find one's way through a city. Thus, if electrons enter a slit system, quantum mechanics predicts the distribution with which they will leave. But this is not deduced from a concept of the over-all order and structure of movement of the electrons. Rather, as has been indicated, it has the character of a mathematical algorithm, equivalent to a set of "directions." This algorithm is surely a reflection of the whole of natural law. But to assume that *all* theories must henceforth take the form of such algorithms will evidently limit understanding and channel research into a study of the statistical properties of observation processes involving such "collapses."

This point can perhaps be further clarified by considering the fact that there is a very important methodological justification for the consideration of hidden variable theories, even those which are not necessarily seriously regarded as "right" ones. For the language of quantum mechanics in the usual interpretation of the formalism makes it virtually impossible even to assert linguistically what is to be meant by the detailed order and structure of this process of collapse, because the denial that this process has any meaning is incorporated into the very structure of the language. In this way the theory seems to provide a justification for an inherently statistical concept of an individual system.

This, by itself, is a very serious fault in the present formulation of quantum mechanics. As Popper[15,16] has indicated, it is a basic requirement of any scientific theory that it should be expressed in terms that make it *falsifiable*. But current quantum mechanics has been given a linguistic form that prevents even the hypothetical assertion of the contrary to any of the basic postulates, because this would apparently entail a change in the experimental facts on which the theory is based. (As will be shown later, it was the aim of von Neumann's theorem to prove this.) Since to deny the experimental content of the theory is evidently absurd, and since we can neither say nor think anything contrary to the basic principles of quantum mechanics, it seems that the latter are inescapable and absolute truths, proved by a tremendous number of experiments.

It is not generally realized that in the present language we can only ask questions and consider experiments that do not go outside the structure of this language. As long as we use this language, no experiment is *ever* likely to be devised that could conceivably refute the basic postulates of quantum mechanics and thus in principle provide a test of these postulates. We shall always search for energy levels, scattering probabilities, magnetic moments, etc., and if they are not as predicted we can always suppose that a change of the forces between atoms, the introduction of particles with new properties, new groups such as SU_3, SU_4, U_3 and other such orders, etc., will eventually bring experiments back into agreement with the theory, without changing the *basic* postulates given above, except in the way of enriching and adding to them: we need never take a step that contradicts them. Of course, in a way, every theory can be adapted by means of enough assumptions to accommodate any kind of data whatsoever. But the current linguistic form of quantum mechanics has the further special feature that it asserts the logical impossibility of any other scheme that would fit the facts as they are known today. It is, therefore, necessary to *challenge* such a point of view, for otherwise it might lead to our being trapped in a given set of concepts, without our even realizing that we are thus trapped. As we have already indicated, we shall do this by changing the language of quantum mechanics, so that questions may be asked which would show what it could mean if the basic postulates of the current theory were false. Even if the theory in terms of which the new language is embodied should not be correct in detail, such a questioning on a theoretical basis can be useful, because it may ultimately lead to the proposal of experiments that test these postulates.

A number of authors, notably Ludwig,[17] Green,[18] and the group Daneri, Loinger, and Prosperi[19] have proposed theories of measurement which take into account the macroscopic nature of the measuring instrument. This point of view differs from that of Bohr and the Copenhagen school, since the macroscopic measuring instrument is in fact treated as a quantum mechanical system, with certain added conditions which enable "macroscopically distinguishable states" of the system to be defined in some way. These macrostates are, of course, related to probability distributions over microstates of the system, so that the measurement process is treated as a problem of quantum statistical mechanics. Before the measurement interaction, the apparatus is assumed to be in a thermodynamically metastable state, such that a very small perturbation makes it evolve (irreversibly) towards a thermodynamically stable state, dependent on the state of the microsystem.

The most sophisticated and general analysis along these lines has been given by Daneri, Loinger, and Prosperi and many prominent physicists, including Rosenfeld,[19] have favored this apparent solution to the problem. The argument is essentially that the collapse of the wave packet in a measurement process is not really a problem, because interference is destroyed in

[15] K. R. Popper, *The Logic of Scientific Discovery* (Hutchinson, London, 1959).
[16] K. R. Popper, *Conjectures and Refutations* (Routledge and Kegan Paul, London, 1962).
[17] G. Ludwig, article in *Werner Heisenberg und die Physik Unserer Zeit* (Friedrich Vieweg und Sohn, Braunschweig, 1961).
[18] H. S. Green, Nuovo Cimento 9, 880 (1958).
[19] L. Rosenfeld, "The Measuring Process in Quantum Mechanics," preprint (May 1965).

CC-0. In Public Domain. Gurukul Kangri Collection, Haridwar

Digitized by Arya Samaj Foundation Chennai and eGangotri

the process of *amplification* involved in the detection of a microsystem by a macroinstrument, so that probability amplitudes become ordinary probabilities in the irreversible transition of the amplifying apparatus to a condition of stable equilibrium. Hence what "collapses" is only our *knowledge* of the system and not some property of the system itself. However, in the cine camera experiment, we have seen that, according to the basic principles of quantum mechanics, the wave function always refers to an individual system. The fact that interference between different parts of the wave function, corresponding to different values for the observable measured, is effectively destroyed in the amplification process does not explain why the wave function of the *individual total* system "condenses" onto one and only one of the component noninterfering wave packets that are produced in the interaction with the measuring apparatus. Thus, the question of the behavior of an individual total system is avoided.

In order to clarify this criticism, we can also refer to the example of the measurement of the z component of the angular momentum of an atom with angular momentum $\hbar/2$ by means of a Stern–Gerlach experiment (Ref. 20, p. 593). In this experiment, an atom is passed through an inhomogeneous magnetic field which gives it a momentum that is directed up or down, according to whether the spin is up or down. The resulting s motion of the atom after it leaves the field carries it to a height that depends on the spin and, in this way, a rather rough observation of the position determines whether the spin was up or down.

It can be shown that, after the measurement interaction, the wave function of the total system of atom plus measuring instrument takes the form of two localized wave packets which no longer interfere significantly. But this does not alter the fact that only *one* of these packets can be "actual" if the total system is to be in a certain definite state after the measurement. In terms of the cine camera experiment, if an individual electron is sent through this apparatus, until it arrives at the photographic film it is represented by a wave packet spread over a large region of space. When this packet arrives at the film it begins to interact with the wave functions of the atoms of the film. In the interaction it is "broken up" into many very small packets, which cease to interfere coherently. What is still unexplained, however, is that only one of these packets contains the electron: there is no possibility within the theory of understanding how and why the individual electron suddenly "condenses" into one of the packets. In other words, there is no *logical connection* between the first wave function, which may be regarded as "broken up" into noninterfering localized packets, and the second wave function, which represents a definite result.

To be sure, if we now average over the resulting wave functions in an ensemble of measurements on similarly prepared systems, then the pure ensemble of similar first wave functions is connected statistically to the ensemble of second wave functions, i.e., the probability distribution of second wave functions is determined by the algorithm of quantum mechanics. But this averaging process can only be understood as an *empirical* average over the wave functions which are actually present after an ensemble of measurements: there is no corresponding distribution of any parameter over the ensemble of first wave functions which can be averaged over to produce the resulting distribution of second wave functions. This amounts to a confusion between the individual and the statistical interpretation of the meaning of the wave function. For, the attempt to regard the different components of the "broken up" first wave function as nothing more than probabilities would make sense if the wave function were given *only* a statistical interpretation. The purely statistical aspects of the treatment are in themselves therefore perfectly clear, and would be still clearer, if it made no claims at all (beyond limits determined by the uncertainty principle) to discuss the details of the movement of individual electrons. But then, it would also be very obvious that no explanation has been given for how an individual electron arrives in *one* of the packets. The assertion that the individual has in fact been adequately treated is just what leads to the confusion, in which the one word "electron" is required at the same time to refer to individual and statistical ensemble. And this assertion is based on the tacit assumption that the current interpretation of quantum mechanics is complete.

Thus, although the analyses of Daneri, Loinger, and Prosperi, and other such treatments do help to clarify the measurement process to a certain extent by emphasizing the existence of an amplifying stage in the process, the basic problem is still unresolved. A thermodynamic averaging operation is performed over an ensemble and reasonable probability functions are obtained, but it remains unclear exactly what the statistical mechanical parameters are. The question of the behavior of an individual system, for example the process of movement of an individual electron through the apparatus of the movie camera experiment, is not answered. The analysis of Daneri, Loinger, and Prosperi does not alter the fact that the extended wave model is needed to describe the movement of the electron through the slits, while after the packet reaches the film and interacts with it there is a set of noninterfering localized packets, only one of which contains the electron.

We conclude that the attempts to develop a theory of measurement within the quantum theory do not succeed in solving the real problem, and that the order and structure of the process by which a microsystem

[20] D. Bohm, *Quantum Theory* (Prentice-Hall, Inc., Englewood Cliffs, N.J., 1951).

CC-0. In Public Domain. Gurukul Kangri Collection, Haridwar

Digitized by Arya Samaj Foundation Chennai and eGangotri

such as an electron is measured cannot be conceived within the formalism of quantum mechanics alone. Before proceeding with the development of a hidden variable theory, however, we must first dispose of von Neumann's proof that any attempt to explain the probability distributions of quantum mechanics in this way would be impossible, because it would contradict the experimental facts on which the theory is based.

4. VON NEUMANN'S PROOF

Von Neumann's proof[21] that hidden variables can be excluded in quantum mechanics, contained in Chap. IV of the "Mathematical Foundations of Quantum Mechanics," is based on the following assumptions:

(i) There corresponds to each observable of a quantum mechanical system a unique hypermaximal Hermitian operator in Hilbert space. This correspondence is assumed to be one-one, i.e., each such operator corresponds to an observable. (Page 313.) (In place of the term "observable", von Neumann uses the neutral phrase "physical quantity," but with the same connotation.)

(ii) If the observable R has the operator $\mathbf{R}$, then the observable $f(R)$ has the operator $f(\mathbf{R})$. (I, page 313.)

(iii) If the observables $R, S, \cdots$ have the operators $\mathbf{R}, \mathbf{S}, \cdots$, then the observable $R+S+\cdots$ has the operator $\mathbf{R}+\mathbf{S}+\cdots$. (The simultaneous measurability of $R, S, \cdots$ is not assumed.) (II, page 314.)

(iv) If the observable R is by nature a nonnegative quantity, for example, if it is the square of another quantity S, then $\bar{R}\geq 0$, where $\bar{R}$ is the expectation value of R for an ensemble of measurements. (A′, page 311.)

(v) If $R, S, \cdots$ are arbitrary observables and $a, b, \cdots$ real numbers, then $\langle aR+bS+\cdots\rangle_{\mathrm{Av}}=a\bar{R}+b\bar{S}+\cdots$. (B′, page 311.)

Two definitions are also relevant:

(a) An ensemble is *dispersion-free* if $(\bar{R})^2=\langle R^2\rangle_{\mathrm{Av}}$ for every observable R. (α', page 312.)

(b) An ensemble is *homogeneous* or *pure* if it cannot be split into subensembles with different statistical properties. In other words, if the ensemble is split into any two subensembles, so that $\bar{R}=\bar{R}'+\bar{R}''$ for every observable R, then $\bar{R}'=c'\bar{R}$, $\bar{R}''=c''\bar{R}$ (where c', c'' are constants $c'+c''=1$; $c', c''>0$).

On the basis of these assumptions, von Neumann demonstrated that there exists a linear, semidefinite, Hermitian matrix U_{mn}, such that for any observable R:

$$\bar{R}=\sum_{mn} U_{nm}R_{mn}=\mathrm{Tr}\,(\mathbf{UR}). \qquad (4.1)$$

Thus, every ensemble in quantum mechanics is characterized by a certain (density) matrix (or statistical operator), from which the average of any observable can be deduced according to a certain algorithm.

Since there is no physically meaningful density matrix which gives zero dispersion for all observables R, von Neumann's first conclusion was that there are no dispersion free ensembles. In addition, there are density matrices which represent homogeneous ensembles, which means that it is not always possible to split an ensemble into subensembles with different statistical properties. The interpretation of this result for the question of hidden variables is that the statistics of the homogeneous ensemble cannot result from averaging over the hidden variables because, firstly, the homogeneous ensemble could then be represented as a mixture of two different ensembles and, secondly, because the dispersion free subensembles consisting of one or more individual systems in the same precisely defined state do not exist.

The argument here follows the analogy with classical statistical mechanics. A classical observable is defined as a function of the coordinates and momenta (hidden variables) which determine the microstates of the system:

$$R=R(q_1, q_2, \cdots; p_1, p_2, \cdots), \qquad (4.2)$$

which is abbreviated symbolically to $R(q,p)$. If the "state" of the system is only defined by certain thermodynamic (i.e., large-scale) variables, then the expectation value of R for such a system is computed as the average over a suitably defined ensemble of systems:

$$\bar{R}=\int \rho(T, q, p)R(q, p)\,dq\,dp=\bar{R}(T), \qquad (4.3)$$

where the symbol T is used to represent the thermodynamic variables which define the "state" of the system macroscopically and ρ is a probability density. In the equilibrium case the statistical or thermodynamic properties of the system may be derived from the "normal" Boltzmann distribution function $C\exp(-E/kT)$:

$$\bar{R}=\int C\exp\left(-E(q, p)/kT\right)R(q, p)\,dq\,dp, \qquad (4.4)$$

where T is the temperature. In general we may consider any distribution function $\rho(T, q, p)$, in particular the extreme case of a δ-function, representing a dispersion free ensemble in which the values q, p are precisely defined and determine a value for every observable $R(q, p)$ without dispersion.

Similarly, in a statistical explanation of quantum mechanics by hidden variables, there should be "nonnormal" distributions of these parameters possible as well as a "normal" distribution which would reproduce the results of quantum mechanics. The extreme case of such a "nonnormal" distribution would be the dispersion free ensemble, in which the values of all hidden parameters are precisely defined and hence determine

[21] Reference 19, Chap. IV, Parts 1 and 2 (pages 295–328).

CC-0. In Public Domain. Gurukul Kangri Collection, Haridwar

Digitized by Arya Samaj Foundation Chennai and eGangotri

a particular value for every observable. Von Neumann demonstrated that the existence of such "nonnormal" ensembles, with statistical properties violating those of quantum mechanics (which is certainly implicit in any hidden variable theory), is impossible. He concluded this proof with the remark that:

"...we need not go any further into the mechanism of the 'hidden parameters' since we now know that the established results of quantum mechanics can never be re-derived with their help"[22]

and he even stressed that:

"...it is therefore not, as is often assumed, a question of a re-interpretation of quantum mechanics,—the present system of quantum mechanics would have to be objectively false, in order that another description of the elementary processes than the statistical one be possible."[22]

Thus, since the concept of hidden variables is incompatible with von Neumann's assumptions, and since the denial of these assumptions would seem to entail the denial of the postulates of quantum mechanics as a special case, it appears that any hidden variable theory would contradict the experimental results confirming quantum mechanics.

If von Neumann's assumptions are accepted, then his conclusion is indeed inescapable. However, these assumptions, in spite of their apparent innocence, are unnecessarily restrictive. If the dispersion in the measured values of an observable R is assumed to be due to a distribution in the values of certain hidden parameters over the ensemble of systems measured, then the expectation value of R, $\bar{R}$, is clearly to be regarded as an average over this distribution of hidden variables. Hence, the relation

$$\bar{R}=\sum_{mn} U_{nm}R_{mn}$$

should be expressed as:

$$\bar{R}=\sum_{mn} \bar{U}_{nm}R_{mn}, \tag{4.5}$$

where $\bar{U}_{mn}$, the matrix defining the statistics of a quantum mechanical ensemble, is computed as an average over the distribution of hidden variables in the ensemble. Explicitly:

$$\bar{U}_{mn}=\int U_{mn}(\Psi,\lambda)\rho(\lambda)\,d\lambda, \tag{4.6}$$

so that:

$$\bar{R}=\sum_{mn}\int U_{nm}(\Psi,\lambda)R_{mn}\rho(\lambda)\,d\lambda, \tag{4.7}$$

where the symbol λ is used generically to denote the set of hidden variables $\lambda_1, \lambda_2, \cdots$ and $\rho(\lambda)=\rho(\lambda_1, \lambda_2, \cdots)$ is a probability distribution function defined over the hidden variables. [The above expression is, of course, only true for a pure ensemble. In the case of a mixed ensemble, there is a certain probability, $P(\Psi)$, of any particular quantum state. Hence R must be averaged over the distribution of quantum states as well as the distribution of hidden variables:

$$\langle\bar{R}\rangle_{Av}=\sum_{mn}\int \bar{U}_{nm}R_{mn}\rho(\lambda)\,d\lambda, \tag{4.8}$$

where $\bar{U}_{mn}$ is averaged over the distribution of wave functions, not over λ.]

This relation for $\bar{R}$ implies that, for particular values of Ψ and λ (i.e., the dispersion free case), the value of R is determined by a relation of the form:

$$R'=\sum_{mn} U_{nm}(\Psi',\lambda')R_{mn}, \tag{4.9}$$

where the $'$ is used to denote a particular value of the relevant parameter. This is a linear relation between the value of the observable R and its associated matrix R_{mn}. Now, *a priori*, there is no reason why the value of R should not be determined by some *nonlinear* function of Ψ, the hidden variables and the matrix R_{mn}:

$$R=F(\Psi,\lambda,R_{mn}). \tag{4.10}$$

In an ensemble:

$$\bar{R}=\int F(\Psi,\lambda,R_{mn})\rho(\lambda)\,d\lambda \tag{4.11}$$

and we would expect to obtain the statistical results of quantum mechanics from a "normal" ensemble specified by some $\rho_N(\lambda)$.

Von Neumann's implicit choice of a particular linear form for F as a function of the R_{mn}, i.e.,

$$F=\sum_{mn} U_{nm}(\Psi,\lambda)R_{mn}, \tag{4.12}$$

depended essentially on the linearity assumption (v), i.e., for any set of observables $R, S, \cdots$, whether simultaneously measurable or not, $\langle aR+bS+\cdots\rangle_{Av}=a\bar{R}+b\bar{S}+\cdots$. Clearly (v) follows immediately from the assumption of linearity for the function F:

$$\langle R+S\rangle_{Av}=\sum_{mn}\int U_{nm}(\Psi,\lambda)(R+S)_{mn}\rho(\lambda)\,d\lambda$$

$$=\sum_{mn}\int U_{nm}(\Psi,\lambda)(R_{mn}+S_{mn})\rho(\lambda)\,d\lambda$$

$$=\sum_{mn}\int U_{nm}(\Psi,\lambda)R_{mn}\rho(\lambda)\,d\lambda$$

$$+\sum_{mn}\int U_{nm}(\Psi,\lambda)S_{mn}\rho(\lambda)\,d\lambda=\bar{R}+\bar{S}.$$

[22] Reference 19, pages 324, 325.

CC-0. In Public Domain. Gurukul Kangri Collection, Haridwar

Digitized by Arya Samaj Foundation Chennai and eGangotri

Von Neumann justified the assumption (v) by the remark that it is always true in quantum mechanics, i.e., for any quantum state Ψ:

$$(\Psi, (R+S)\Psi) = (\Psi, R\Psi) + (\Psi, S\Psi).$$

Hence (v) is true for every pure or mixed ensemble. But this relationship could conceivably be reproduced for *normal* ensembles, specified by some $\rho_N(\lambda)$ without rejecting the possibility of a nonlinear function F. This would imply that the assumption (v) is in general false and is valid only in a certain special case which includes the ensembles of quantum mechanics. (This has been pointed out by Bell.[8])

Without the assumption of linearity

$$\bar{R} = \sum_{mn} \int U_{nm}(\Psi, \lambda) R_{mn} \rho(\lambda)\, d\lambda$$

tacitly contained in von Neumann's assumption (v), the proof fails, because it is based on an analysis of the statistical properties of the density matrix

$$\bar{U}_{mn} = \int U_{mn}(\Psi, \lambda) \rho(\lambda)\, d\lambda,$$

which is now no longer characteristic of all conceivable ensembles.

This proof discouraged further work on hidden variable theories for some time. In the light of the above analysis it seems that the proof rejects only those hidden variable theories which depend on a linear law of the form (4.7). We shall therefore turn our attention to theories which contain the more general assumption (4.11):

$$\bar{R} = \int F(\Psi, \lambda, R_{mn}) \rho(\lambda)\, d\lambda.$$

As we have demonstrated, the assumption (v) is now no longer valid and von Neumann's proof breaks down. A more recent impossibility proof has been proposed by Jauch and Piron, in which they come to the same conclusion as von Neumann without using the linearity assumption (4.7) or (v). We shall demonstrate the inadequacy of this proof in a subsequent article.

A theory which embodied the possibility of such a nonlinear assumption for R was first proposed by one of us in 1951.[9] However, that theory was suggested merely in order to demonstrate, by a counter-example to von Neumann's proof, the possibility of a hidden variable theory. It was not seriously envisaged as an ideal theory and suffered from a lack of simplicity and elegance of structure. We now wish to propose a hidden variable theory, an extension of certain ideas of Wiener and Siegel, which we consider is at least a step toward what could seriously be considered as a tentative theory, insofar as it suggests certain questions which we feel to be relevant.

5. THE THEORY

We propose, firstly, that one of the basic variables of the theory is the wave function Ψ. In fact, as indicated in Sec. 2 ("Review of the Basic Principles of Quantum Mechanics") we regard the Ψ as playing a role somewhat analogous to the thermodynamic variables P, V, T, etc. in classical statistical mechanics. As P, V, T, can be known from measurements on a classical thermodynamic system done with the aid of suitable instruments, so the measurement of a "complete set of observables" enables us to know the wave function of a quantum mechanical system (by finding the eigenfunctions of the corresponding operators). Thus, after a measurement, the wave function can be known. At this stage, this is a basic postulate of the usual theory, but we shall later derive it from deeper assumptions concerning the hidden variables.

In order to simplify the presentation in the following we shall consider the problem of a system whose wave function can be represented as a vector in a two-dimensional Hilbert space, for example a spin-$\frac{1}{2}$ particle without translational motion. Using the Dirac notation to represent vectors in Hilbert space, the vector $|\Psi\rangle$ may be expressed in the form:

$$|\Psi\rangle = \psi_1 |S_1\rangle + \psi_2 |S_2\rangle, \tag{5.1}$$

where $|S_1\rangle$, $|S_2\rangle$ is the basis in which the operator of the spin observable S is diagonal. We assume that $|\Psi\rangle$ is normalized ($|\psi_1|^2 + |\psi_2|^2 = 1$).

We postulate a *dual* Hilbert space, a typical vector of which is represented with respect to the same basis by:

$$\langle\xi| = \xi_1 \langle S_1| + \xi_2 \langle S_2|. \tag{5.2}$$

This dual vector space is *different* to the original space and, whereas the vector $|\Psi\rangle$ satisfies Schrödinger's equation, the dual vector $\langle\xi|$ obeys an entirely different equation of motion, which we shall discuss presently. We shall use the components of the vector $\langle\xi|$ to represent the hidden variables corresponding to the λ in Eqs. (4.10), (4.11).

We propose also that for the "normal" quantum mechanical ensemble these hidden variables are randomly distributed on the hypersphere of unit radius in Hilbert space defined by $\sum_i |\xi_i|^2 = 1$. With the aid of certain further assumptions, which in effect define the function F of Eqs. (4.10), (4.11), we shall demonstrate that this distribution reproduces the usual quantum mechanical averages for all observables. Nevertheless, the theory also allows subensembles which have less dispersion than the "normal" ones and even, in the limiting case, dispersion free ensembles, in which the ξ_i are all precisely defined.

We define the two ratios:

$$R_1 = |\psi_1|^2 / |\xi_1|^2 = J_1 / |\xi_1|^2 \tag{5.3}$$
$$R_2 = |\psi_2|^2 / |\xi_2|^2 = J_2 / |\xi_2|^2$$

CC-0. In Public Domain. Gurukul Kangri Collection, Haridwar

Digitized by Arya Samaj Foundation Chennai and eGangotri

and postulate that, in addition to the change in $|\Psi\rangle$ defined by the Schrödinger equation, the following deterministic equations operate during a measurement process of the observable S:

$$d\psi_1/dt=\gamma(R_1-R_2)\psi_1 J_2$$
$$d\psi_2/dt=\gamma(R_2-R_1)\psi_2 J_1, \qquad (5.4)$$

where γ is a suitable quantity that remains nearly constant during a measurement and negligible before and after. (We assume that γ is always positive.)

(For simplicity, we are considering an *impulsive* measurement, where the interaction with the apparatus is so great that the effects of the Hamiltonian of the undisturbed system can be neglected during the interaction. The generalization to include arbitrary measurements is straightforward and does not essentially alter the argument.)

From these equations it follows that:

$$dJ_1/dt=2\gamma(R_1-R_2)J_1J_2$$
$$dJ_2/dt=2\gamma(R_2-R_1)J_2J_1. \qquad (5.5)$$

Hence $d(J_1+J_2)\,dt=0$, so that $|\Psi\rangle$ remains normalized during the measurement process.

Also:

$$d(\log J_1)\,dt=2\gamma(R_1-R_2)J_2$$
$$d(\log J_2)\,dt=2\gamma(R_2-R_1)J_1. \qquad (5.6)$$

(We assume for the present that the ξ_i are constants, at least during a measurement process. They may be changing, but so slowly that this change can be neglected during the measurement interaction. Later, in fact, we shall discuss such relatively slow changes in the ξ_i.)

If $R_1>R_2$ and $J_2\neq 0$, then J_1 must always increase and J_2 must always decrease. Since $J_1+J_2=1$, this process will continue until $J_1=1$ and $J_2=0$; so $|\Psi\rangle\rightarrow \exp(i\phi_1)\,|S_1\rangle$. Similarly, if $R_2>R_1$ initially and $J_1\neq 0$, then $|\Psi\rangle\rightarrow \exp(i\phi_2)\,|S_2\rangle$. ($\phi_1$ and ϕ_2 are phase factors.)

Thus, the motion described by these equations produces the eigenstate $|S_1\rangle$ or $|S_2\rangle$ after a measurement of S, representing a spin value of $+\hbar/2$ or $-\hbar/2$, respectively. In an ensemble of measurements, this results in the mixture represented by the statistical operator $f=|\psi_1|^2\,|S_1\rangle\langle S_1|+|\psi_2|^2\,|S_2\rangle\langle S_2|$. We see that the result of a measurement of the spin is determined both by the Hilbert space vector of the system $|\Psi\rangle$ and by the dual vector $\langle\xi|$, in wuch a way that if $R_1>R_2$, or $|\psi_1|^2/|\xi_1|^2>1$, then the result is $+\hbar/2$, while if $R_2>R_1$, or $|\psi_2|^2/|\xi_2|^2>1$, then the result is $-\hbar/2$.

These two possibilities are mutually exclusive and between them they cover every possible set of values of the components of the dual vector ξ_1, ξ_2 whenever the quantum state, i.e., ψ_1, ψ_2, is determined. For, if $R_1>R_2$, $|\psi_1|^2>|\xi_1|^2$ (and $|\psi_2|^2<|\xi_2|^2$), while if $R_2>R_1$, $|\psi_2|^2>|\xi_2|^2$ (and $|\psi_1|^2<|\xi_1|^2$). This leaves only the case: $|\psi_1|^2=|\xi_1|^2$ and $|\psi_2|^2=|\xi_2|^2$, a set of measure zero which has no effect on the statistics: whatever we assume for this case it will have no significance for physical measurements, which are never *perfectly* precise.

Now, in general, the hidden parameters ξ_1, ξ_2 could have any conceivable statistical distribution. As indicated earlier, we demonstrate that a certain "normal" distribution, with probability function ρ_N, determines the usual results of quantum mechanics.

We write:

$$\xi_1=\rho_1\exp(i\theta_1)=a_1+ib_1$$
$$\xi_2=\rho_2\exp(i\theta_2)=a_2+ib_2. \qquad (5.7)$$

Substituting:

$$\rho_1=\rho\cos\phi$$
$$\rho_2=\rho\sin\phi \qquad (5.8)$$

we transform to spherical coordinates. The element of volume in the space of hidden parameters is

$$d\Omega=da_1\,db_1\,da_2\,db_2=\rho_1\rho_2\,d\rho_1\,d\rho_2\,d\theta_1\,d\theta_2$$
$$=\rho^3\cos\phi\sin\phi\,d\rho\,d\phi\,d\theta_1\,d\theta_2$$
$$=\tfrac{1}{2}\rho^3\,d(\sin^2\phi)\,d\rho\,d\theta_1\,d\theta_2. \qquad (5.9)$$

We assume now that the dual vector is also normalized, i.e., $\rho=1$, so that the dual point is on the surface of the three-dimensional hypersphere of unit radius in the four-dimensional space—i.e., the complex two-dimensional space. Hence we ignore $d\rho$ hereafter; the element of volume of interest (with $\rho=1$) is

$$d\Omega=\tfrac{1}{2}\,d(\sin^2\phi)\,d\theta_1\,d\theta_2. \qquad (5.10)$$

Our basic assumption is that $\rho_N=$ constant over this hyperspherical "shell," i.e., a random distribution for ξ_1, ξ_2.

The integral over all points in the dual space for which the following conditions are satisfied:

(a) $|\psi_1|^2/|\xi_1|^2>|\psi_2|^2/|\xi_2|^2$, i.e., $|\psi_1|^2/\rho_1^2>|\psi_2|^2/\rho_2^2$

(b) $|\psi_1|^2+|\psi_2|^2=1$

(c) $|\xi_1|^2+|\xi_2|^2=1$, i.e., $\rho_1^2+\rho_2^2=1$ or $\rho^2=1$

will give the probability of the result corresponding to the state $|S_1\rangle$.

We have:

$$|\psi_1|^2\,\rho_2^2>|\psi_2|^2\,\rho_1^2$$
$$|\psi_1|^2\,\rho_2^2>|\psi_2|^2(1-\rho_1^2)$$
$$\rho_2^2>|\psi_2|^2$$
$$\sin^2\phi>|\psi_2|^2. \qquad (5.11)$$

CC-0. In Public Domain. Gurukul Kangri Collection, Haridwar

Digitized by Arya Samaj Foundation Chennai and eGangotri

Integration over the range of $\sin^2\phi$ gives (with the correct normalization for the surface area of the hypersphere):

$$\frac{2}{(2\pi)^2}\int_{|\psi_2|^2}^{1}\tfrac{1}{2}\,d(\sin^2\phi)=\frac{1}{(2\pi)^2}\,(1-|\psi_2|^2)=\frac{1}{(2\pi)^2}\,|\psi_1|^2. \tag{5.12}$$

Integration over θ_1, θ_2 (from 0 to 2π) then gives the measure or probability of the set of points (on the unit "shell") for which $R_1>R_2$ as:

$$P_1=|\psi_1|^2. \tag{5.13}$$

For $R_2>R_1$, a similar calculation gives the result $|\psi_2|^2$.

The form of the deterministic equations guarantees that the Hilbert space vector representing the wave function of the system after a measurement of the spin S is $|S_1\rangle$ if $R_1>R_2$ and $|S_2\rangle$ if $R_2>R_1$. The inequality $R_1>R_2$ or $R_2>R_1$ is maintained after a measurement, since either $J_1=|\psi_1|^2$ or $J_2=|\psi_2|^2$ becomes and remains unity in this representation while the other becomes and remains zero. So, if $R_1>R_2$ *before* the measurement then, since $R_1=J_1/|\xi_1|^2$ increases (or remains the same) during the measurement, while $R_2=J_2/|\xi_2|^2$ decreases to zero (or remains the same), this inequality is satisfied *after* the measurement as well. Hence the result of a measurement will be reproduced if the same observable is measured immediately afterwards on the same system. This conclusion is not altered if the ξ_i should undergo a change after completion of the measurement, because if, for example, $J_1=1$, $J_2=0$ we always have $R_1=|\psi_1|^2/|\xi_1|^2=1/|\xi_1|^2>1$ (and $R_2=|\psi_2|^2/|\xi_2|^2=0$) for any values of ξ_1, ξ_2 (except $|\xi_1|^2=1$ and $|\xi_2|^2=0$, a set of measure zero which can be neglected.)

It is clear that we have developed here a theory of hidden variables that reproduces the usual probabilities of quantum mechanics as well as the feature of the "collapse" of the wave packet. However, the probabilities are now the result of a random distribution of "hidden" variables (and not "irreducible") and the "collapse" is due to a deterministic process that satisfies a law that could in principle be studied with regard to its order and structure of movement. Of course, the theory is similar to the usual quantum theory in that it also makes statistical assumptions of a certain kind. But it is different in the crucial respect that these assumptions permit a more general kind of statistics, containing the usual quantum statistics as one possible limit, and a "delta function" distribution of the hidden variables as another limit (in which the behavior is in fact completely specified and determined). In addition, the theory opens up the possibility of a further study, aimed at demonstrating that our statistical assumptions might be justified (as is done in classical statistical mechanics) by showing that the equations of motion of complex systems imply a quasi-ergodic character to the solutions. Evidently, such questions would have no meaning in terms of the usual linguistic structure of quantum mechanics.

Before investigating these consequences of the theory further, we shall outline briefly the generalization to a Hilbert space of N dimensions (where, in principle, $N\to\infty$).

The generalized deterministic equations describing the change in $|\Psi\rangle$ during a measurement process are:

$$d\psi_i/dt=\gamma\psi_i\sum_j J_j(R_i-R_j)\qquad(i=1,2,\cdots,N). \tag{5.14}$$

If $\sum_i|\psi_i|^2=\sum_i J_i=1$ initially, a simple calculation shows that $d(\sum_i J_i)/dt=0$ and the normalization of $|\Psi\rangle$ is therefore unaltered. Further, it is easily demonstrated that if R_s is a maximum then J_s will increase faster than any other J_i, so that eventually $J_s\to1$ and all the other $J_i\to0$. Thus, $|\Psi\rangle$ is projected onto the vector corresponding to the result s. If we assume that the dual vector $\langle\xi|$ is randomly distributed over the hyperspherical surface $\sum_i|\xi_i|^2=1$, then a similar calculation gives for the probability of the result s: $P_s=|\psi_s|^2$, in agreement with quantum mechanics. A remeasurement of the same observable will always yield the same result.

6. SOME CONSEQUENCES OF THE THEORY

It may now be of interest to re-examine von Neumann's proof in the light of this theory. As already indicated, the theory goes beyond the assumption of linearity in the proof: $\langle aR+bS+\cdots\rangle_{Av}=a\bar{R}+b\bar{S}+\cdots$. For example, in the spin case, let:

$$\mathrm{R}=\mathfrak{d}_x,\qquad \mathrm{S}=\mathfrak{d}_y,\qquad \mathrm{T}=\mathfrak{d}_z$$
$$a\mathrm{R}+b\mathrm{S}+c\mathrm{T}=\mathfrak{d}=\cos\alpha\mathfrak{d}_x+\cos\beta\mathfrak{d}_y+\cos\gamma\mathfrak{d}_y. \tag{6.1}$$

$\mathfrak{d}_x$, $\mathfrak{d}_y$, and $\mathfrak{d}_z$ are operators representing the components of the spin in three orthogonal directions. The operator $\mathfrak{d}$ represents the component of the spin in some arbitrary direction inclined to these axes. Consider the special case of a dispersion free ensemble, in which the hidden variables ξ_1, ξ_2, the components of the vector $\langle\xi|$ in the dual space, are precisely defined. These parameters determine the result of every possible measurement. Now, every measurement gives either $+1$ or -1 for σ_x, σ_y, σ_z, and σ. Hence, since the distribution is now a delta function of the hidden variables, we have

$$\bar{\sigma}=\sigma=\cos\alpha\sigma_x+\cos\alpha\sigma_y+\cos\alpha\sigma_z$$
$$=\cos\alpha(\pm1)+\cos\beta(\pm1)+\cos\gamma(\pm1). \tag{6.2}$$

On the other hand, we also have:

$$\sigma=\pm1.$$

Therefore, in general, it is not true that $\bar{\sigma}=\cos\alpha\bar{\sigma}_x+\cos\beta\bar{\sigma}_y+\cos\gamma\bar{\sigma}_z$. So the linearity assumption is not

CC-0. In Public Domain. Gurukul Kangri Collection, Haridwar

Digitized by Arya Samaj Foundation Chennai and eGangotri

satisfied by this model and von Neumann's proof has no relevance here.

The deterministic equations which we have postulated in addition to the movement defined by Schrödinger's equation have a form dependent on the representation in which the matrix of the operator representing the observable measured is diagonal:

$$\dot{\psi}_i=\gamma\psi_i\sum_j J_j(R_i-R_j).$$

Physically, we postulate that the representation chosen depends on the effect of the measuring apparatus. Thus, an apparatus that measures σ_x creates a different motion in the Hilbert space of the wave function than an apparatus that measures σ_y. These two motions are incompatible: a movement projecting the vector representative of Ψ onto one or another of a particular set of axes in Hilbert space cannot be carried out at the same time as a movement onto another set of axes. This provides a simple explanation of the impossibility of measuring simultaneously two "observables" whose operators do not commute. The two "observables" are associated with two different measuring instruments, represented in the theory by two different orthonormal bases in Hilbert space. From the point of view of the system alone, these "observables" represent certain "potentialities" only, i.e., the wave function of the system, represented as a vector in Hilbert space, determines only a set of potential results for each "observable". By defining a particular set of axes in the space, the formal effect of each apparatus is to choose a particular set of potentialities and the hidden variables, represented by the dual vector, then determine which result in this set is actually realized.

For this reason the term "observable" as used in ordinary quantum mechanics seems to be highly inappropriate. In our theory, the state of a system is determined by the wave function as well as the values of a certain set of hidden variables, i.e., these parameters are sufficient to determine the dynamical behavior of the system. These additional variables are regarded as being in principle observable or measurable, as in the statistical explanation of the macroscopic properties of matter we assume that the atomic variables are measurable. On the other hand, the quantum "observable" is no longer identified with any physical quantity or measurable property of the system in the usual (classical) sense of these terms and is not a dynamical variable of the system *alone*. Instead, each quantum observable is to be associated with a specific process of interaction between the system and a certain "apparatus", i.e., another system with certain well-defined characteristics which differentiate it both from the original system and from other apparatus systems. The hidden variables which define the state of the system in the sub-quantum level determine the outcome of this process and it is this result which is labelled with a specific value of the quantum observable. The process of interaction is said to constitute a "measurement" of the "observable."

Physically, the measuring apparatus is merely part of the large-scale environment of the system and it would be completely artificial to postulate a particular process for "measurement interactions" which would not also be characteristic of all interactions between a quantum system and its large-scale environment. Instead of Schrödinger's equation, therefore, we suggest that the equation of motion of the system is in general of the form:

$$\dot{\psi}_i=\gamma\psi_i\sum_j J_j(R_i-R_j)-(i/\hbar)\sum_j H_{ij}\psi_j \quad (i=1, 2,\cdots, n) \tag{6.3}$$

where the additional nonunitary term represents the effect of the large-scale environment on the system.

We may consider the possibility that the motion of the wave function depends to some extent on all levels of its environment, out to the cosmological scale. There may, for example, be a "natural" set of variables on the large-scale, say space and time, determined in some as yet unknown way by the relationship of the atomic to the cosmological level. Einstein's notion in the general theory of relativity, that the metric depends on the large-scale distribution of matter in the universe, does suggest a deep relation between the large-scale and small-scale levels. It is interesting to consider such an extension of his idea to include the "natural" observables.

Since our theory explicitly couples the large-scale and the small-scale levels together, all macro-quantities can not be calculated completely from the micro-laws. In fact, according to the Copenhagen interpretation, this was always implicit in quantum mechanics, but with the unacceptable qualification that such a multi-level theory dealing with the totality, in which quantum and subquantum movements depend on the large-scale movement and vice versa, is in principle incapable of being developed.

Lastly, it is clear that the idea of a measurement *disturbing* a system is completely inappropriate in this model. We have proposed that the wave function and Schrödinger equation do not provide adequate terms of description of the whole physical process, and we have extended these terms to include the dual space, the effects of the large-scale level (which includes the measuring instrument as a special case) and the equation coupling the wave function, the dual vector and the large-scale level. The motion described by Eq. (6.3) is in fact the usual motion of the system and a measurement process is only a special and simple case of this motion which leads to results that are easy to interpret. In practice, it is realized by an arrangement of matter for which γ is appreciable for long enough to carry

CC-0. In Public Domain. Gurukul Kangri Collection, Haridwar

Digitized by Arya Samaj Foundation Chennai and eGangotri

Ψ over to one of the eigenfunctions of the representation. If γ were not great enough during the time of the interaction, no *measurement* would be possible, but there would still be a complex change in Ψ that would be difficult to interpret. Thus, when a measurement takes place, the motion of the wave function is only *quantitively* different from otherwise, not *qualitatively*.

7. THE POSSIBILITY OF AN EXPERIMENTAL TEST OF THE THEORY

The theory has certain interesting consequences which suggest situations in which it might be possible to test these against the predictions of quantum mechanics.

In the two-dimensional example, which we have analyzed in detail, suppose a measurement of the spin is made in a certain direction. Now, in order to reproduce the usual quantum mechanical probabilities it was necessary to assume that the dual vector $\langle\xi|$ was randomly distributed on the surface of the unit hypersphere. However, after the measurement, this vector will no longer be completely random, since from the result of the measurement it is possible to deduce that the components of $\langle\xi|$ satisfy one or other of the relations:

$$|\psi_1|^2/|\xi_1|^2>1 \qquad (\text{and } |\psi_2|^2/|\xi_2|^2<1) \qquad (7.1)$$

or

$$|\psi_1|^2/|\xi_1|^2<1 \qquad (\text{and } |\psi_2|^2/|\xi_2|^2>1). \qquad (7.2)$$

Therefore, the quantum mechanical probabilities will not in general be reproduced for a subsequent measurement of the spin component in some other direction, unless there are further equations of motion which define a quasi-ergodic movement of the ξ_i, leading to an eventual random distribution of these variables over the unit "shell." These equations may, for example, be due to a coupling of the ξ_i with the ψ_i which is negligible during a measurement. As we have shown, such a movement in the ξ_i after measurement will not affect the inequalities $R_1>R_2$ or $R_2>R_1$, and so will not alter the requirement of reproducibility of the measurement result. However, in a long enough time after a measurement the ξ_i may be completely randomized so that the theory will imply the usual quantum mechanical probabilities for the results of a subsequent measurement.

This raises the interesting question of the amount of time needed to randomize the dual vector. This is, of course, unknown, but some plausible suggestions can be made at this stage.

(i) Since most systems are either in thermal equilibrium or have emerged from a source in equilibrium, it seems plausible to assume a random process resulting from this. The characteristic unit of time of thermal processes in relation to quantum mechanics is: $\tau=\hbar/kT\simeq10^{-13}$ sec, for room temperatures. Typical measurements generally involve longer times, so that the usual results of quantum mechanics are to be expected.

(ii) The time for randomization might be related to the lifetime τ_0 of the quantum state in the conventional sense of the word. This would require that the equations of motion for the dual vector couple it to the wave function in additional ways that would make the randomization process depend on what is at present called the "quantum state."

The double Stern–Gerlach experiment, in which two consecutive measurements are made of the spin components in different directions, might provide a possible test of the theory. Such experiments have not so far been done for short enough times with the required accuracy in statistics (about 1%).

Otherwise, phenomena of superconductivity, superfluidity, or low-temperature measurements seem to offer the best possibilities of tests.

Besides investigating the dependence of the statistics of successive measurements on the time between them, one could investigate the time needed to "complete" a measurement, i.e., to bring ψ_s to exp $(i\phi_s)$ and all the other ψ_i to 0 (the "collapse" of the wave packet).

A discrepancy with the usual predictions of quantum mechanics would overthrow the whole conceptual structure and logical foundation of orthodox quantum mechanics and open up the possibility of investigating the order and structure in the process of measurement.

8. MEASUREMENT OF THE "HIDDEN VARIABLES"

As indicated, the ψ_i are "observable." At present, the ξ_i are *unobserved*, since no experiments have so far been designed to test for their effects. This is, of course, understandable since the very existence of such variables has generally been tacitly and explicitly assumed to be in conflict with the experimental facts of quantum mechanics. However, they are not intrinsically unobservable. Thus, in the spin example, after the measurement of the spin component in a certain direction, if there has been no time for randomization, $|\Psi\rangle$ is either $|S_1\rangle$ or $|S_2\rangle$ and hence the variables ξ_1, ξ_2 must be such as to satisfy either the inequality $R_1>1$, or $R_2>1$. This is a *rough* observation of the ξ_i. A subsequent measurement of the spin component in a different direction would restrict the possible range of values for the ξ_i still further. This process can be continued until a fairly accurate measurement has been made. It is clear that the "hidden" variables are in principle as observable as the ψ_i, but they must be observed with the aid of techniques based on new relationships arising in a time sequence of successive measurements relationships that cannot even be stated or thought about in terms of the linguistic structure of the usual interpretation of the mathematical formalism of quantum mechanics.

CC-0. In Public Domain. Gurukul Kangri Collection, Haridwar

Digitized by Arya Samaj Foundation Chennai and eGangotri

9. GENERALIZATION TO A RELATIVISTIC THEORY

It may be as well to mention here that the equation of motion:

$$\dot{\psi}_i=\gamma\psi_i\sum_j J_j(R_i-R_j)-(i/\hbar)\sum_j H_{ij}\psi_j \quad (i=1,2,\cdots,n) \tag{6.3}$$

is both nonlocal and nonlinear. The change in the component ψ_i of the state vector depends in a complicated way on the values of all the other components. The analogous equation for the continuous case:

$$\psi_x=\gamma\psi_x\int J_y(R_x-R_y)\,dy-(i/\hbar)H\psi_x \tag{9.1}$$

would therefore imply that the change in the wave function at a particular point in space depends on the values of the wave function at every other point in space. Clearly there is no possibility of generalizing this theory to include relativistic phenomena if the equation of motion is retained in its present form, which incorporates an explicit causal mechanism whereby any effect in one part of space is instantaneously transmitted to another part. The theory is therefore limited to nonrelativistic phenomena.

Another limitation of the theory, connected with this nonlocal character of the equation of motion, is that only *complete* measurements are now feasible. For example, in the case of a composite system consisting of two interacting particles, the theory only deals with a process of measurement in which the state vector of the composite system "collapses" onto an eigenvector of an observable of the composite system. The possibility of carrying out a measurement on one particle alone does not exist: this can be interpreted now only in the sense that a complete measurement has been made and certain information ignored. Consequently, the paradox of Einstein, Podolski, and Rosen does not arise in this theory, because a composite system must always be regarded as an indivisible totality which in principle cannot be subdivided into independently existing units. (This is really the essence of Bohr's refutation of the paradox.) Of course, this is a fault and not an advantage of the theory, which has been formulated in terms which exclude the framing of the paradox. If the paradox is accepted as a real inadequacy in our present theoretical description of certain phenomena, then the problem of finding a theory which satisfactorily resolves the paradox remains.

As we have repeatedly emphasized, we regard the present nonrelativistic theory merely as a step towards a more elaborate theory, which should include relativistic phenomena. The Einstein–Podolski–Rosen paradox seems relevant in this connection and suggests a possible line of research, i.e., we require a theory which resolves the paradox in the terms in which it is presented. Nevertheless, in spite of its shortcomings, the nonrelativistic theory does provide a theoretical structure which makes it possible to discuss relationships which go beyond those of formal quantum mechanics, relationships which we believe are relevant to the understanding of the measurement problem.

10. IRREVERSIBILITY OF THE FUNDAMENTAL EQUATIONS OF MOTION

It is a well-known fact that the equations of motion of both classical and quantum mechanics are time-reversible, in the sense that to every solution of the equations representing a forward motion there is a corresponding solution representing a reversed motion. The irreversible behavior of macro-systems is explained in a statistical sense as the average or probable movement of a system from one imprecisely defined state to another. Boltzmann's H theorem is applicable to such systems and the irreversible transition to a condition of macroscopic or thermodynamic equilibrium is characterized as a transition to a condition corresponding to a minimum value of H, i.e., a maximum value of the entropy, $-H$. In formal quantum mechanics, an entropy can be defined which is zero for pure ensembles and positive for mixed ensembles so that the collapse of the wave packet leads to an increase in entropy, i.e., the process of measurement itself introduces an irreversible change in the state of the system measured. However, as we have seen, the measurement process in quantum mechanics is rather obscure and even an analysis which treats the measuring instrument as a macroscopic system cannot avoid certain inherent problems. Nevertheless, it does seem that the irreversibility associated with a measurement process, in the sense of an interaction between a micro-system and a macro-system, may be very significant for the whole question of irreversibility and the "arrow of time" in general which, in view of certain recent experiments indicating a breakdown of the CPT theorem, is still a controversial subject.

In the theory developed here, the fundamental equations of motion are clearly irreversible. The terms $\gamma\psi_i\sum_j J_j(R_i-R_j)$ in the equations (6.3):

$$\dot{\psi}_i=\gamma\psi_i\sum_j J_j(R_i-R_j)-(i/\hbar)\sum_j H_{ij}\psi_j \quad (i=1,2,\cdots,n)$$

describe an exponential-type decay of $(n-1)$ components ψ_j of the wave function in a particular representation and a simultaneous exponential-type growth of one component ψ_s to a limiting absolute value of 1. This process is intrinsically different in character from the reverse process [an exponential-type growth of $(n-1)$ components of the wave function and a simultaneous exponential-type decay of one component], which could not, therefore, be described by equations

CC-0. In Public Domain. Gurukul Kangri Collection, Haridwar

Digitized by Arya Samaj Foundation Chennai and eGangotri

of the same form. Hence there is no reverse motion of the system which would develop the initial past wave function from the final eigenfunction produced by the movement described by these equations.

As well as being reversible, the equations of motion of classical mechanics are time-symmetrical with repect to the *prediction* of the results of future measurements from a given initial state and the *retrodiction* of the results of past measurements from a given final state. Thus, Hamilton's equations can be used to retrodict the past, by following the solution of the equations backwards in time, in the same way that they can be used to predict the future, by following the solution forwards in time. On the other hand, in quantum mechanics, whereas the equation of motion for the wave function is formally time-reversible, the probabilistic interpretation introduces an asymmetry with respect to prediction and retrodiction. For example, an initial pure ensemble of systems, each in the same quantum state, will yield a mixed ensemble after measurement. From a knowledge of the initial quantum state, it is possible to predict the relative frequencies with which the different states will actually be found in the measurement. However, if one uses Schrödinger's equation to calculate what the wave function must have been before the measurement, this will not in general give a correct statistical retrodiction of the earlier states, from which the system came (assuming, for example, that someone else had already made such a set of measurements and that the data were available).

It seems to be characteristic of all statistical theories, and not necessarily a feature of quantum mechanics alone, that the predictive and retrodictive situations are symmetrical only under certain special circumstances. Watanabe[23] has argued that phenomenological one-way-ness has its origin in the very notion of probability, i.e., the temporal asymmetry is related to irretrodictability and has nothing to do with the structure of the dynamical laws. He formulates general criteria for retrodictability and predictability and shows that quantum mechanics is irretrodictable, microscopically as well as macroscopically, whether or not it is invariant with respect to time-reversal in the usual sense.

Aharanov, Bergmann, and Lebowitz[24] have also investigated time-symmetrical situations in quantum mechanics. They demonstrate that if both the initial and final states are fixed, then the predictive and retrodictive formulae, from the initial and final state, respectively, to an intermediate state (later in time than the initial state, but earlier in time than the final state) are symmetrical. If only one state is fixed, i.e., the initial or final state, the predictive and retrodictive formulae are asymmetrical. The explanation suggested for this asymmetry is that, while the future behavior of a micro-system depends on the present (macroscopic) boundary conditions, which define its quantum state, we do not believe that the past behavior of the system can be affected by the boundary conditions which we choose to establish now.

In our theory, the equations of motion (6.3) can be used to predict, for a certain future time, the result of the measurement of the "observable" defining the representation, if the hidden variables are known, or the probabilities of different results if the hidden variables are not known. They make no sense retrodictively. Thus, the asymmetry of prediction and retrodiction is associated with the time irreversibility of the fundamental equations.

In order to solve the problem of measurement in quantum mechanics, we have proposed a hidden variable theory which incorporates a basic irreversibility into the dynamics of an interaction coupling micro- and macro-levels. This is a new concept; it provides a fresh insight into the asymmetry of prediction and retrodiction in quantum mechanics and its development in a more sophisticated theory might conceivably clarify the relationship between macro- and micro-physics and the nature and origin of irreversibility in general.

11. CONCLUSION

We have demonstrated the falsity of von Neumann's proof, which rejects the possibility of hidden variables underlying the statistics of quantum mechanics, both by exposing the inadequacy of the assumptions upon which the proof is based and by explicitly developing a hidden variable theory.

The current formulation of quantum mechanics must be regarded merely as a statistical algorithm, which provides no conceptual structure in terms of which the movement of individual systems can be understood. In order to be able to raise questions about the behavior of individual systems, it seems to be necessary to extend the linguistic structure of the theory by the concept of hidden variables. The problem of measurement is at present a problem only because of an inadequate set of concepts and the confusion which arises with the attempt to interpret this set as complete. There is, therefore, no solution to the measurement problem within the framework of quantum mechanics.

A careful analysis of the reasons for the inadequacy of the von Neumann proof suggests that, in order to succeed, a hidden variable theory should incorporate a nonlinear relation between the value of a quantum mechanical observable and the precise state of the system. In the theory proposed here, a completely specified physical state is defined by two vectors: the Hilbert space vector of the system and the dual vector.

[23] S. Watanabe, Suppl. Progr. Theoret Phys. (Kyoto) Extra Number (Commemorative Issue for the 30th Anniversary of the Meson Theory by Dr. H. Yukawa), p. 135 (1965).

[24] Y. Aharanov, P. G. Bergmann, and J. L. Lebowitz, Phys. Rev. 134, B1410 (1964).

CC-0. In Public Domain. Gurukul Kangri Collection, Haridwar

Digitized by Arya Samaj Foundation Chennai and eGangotri

From this point of view, the quantum mechanical specification of the state of a system by a wave function only, represented by a vector in Hilbert space, is incomplete and we recover the statistical results of quantum mechanics from an ensemble of systems with the same $|\Psi\rangle$ vector but with a random distribution for the dual vector $\langle\xi|$ representing the hidden variables. The "collapse" of the wave packet in a measurement process is described, by a nonlinear deterministic equation of motion, as a real dynamical process which takes a certain amount of time to complete. The measuring apparatus is regarded as a part of the large-scale environment of the system and its influence is reflected in the above equation of motion by the representation chosen. This suggests a general modification to Schrödinger's equation and an interpretation of a physical process as a coupling of the large-scale and small-scale levels. The measurement process is then merely a particular case of this process. This theory has some interesting consequences, which may be used to provide an experimental comparison with the predictions of quantum mechanics. In particular, the equation of motion introduces an inherent irreversibility into all physical processes, which becomes especially significant in the case of a measurement process.

The theory, in its present form, suffers from a number of inadequacies, but it does provide a new conceptual structure in which certain questions can be considered, which cannot even be formulated within the framework of quantum mechanics. Thus, to describe the same facts in a new linguistic structure may be significant. The rather prevalent idea that differences of language for saying the same thing are *always* unimportant is false. In some cases a different language opens up a different structure of thinking and thus leads to new kinds of actions in relationship to nature. What is needed now is a hypothetical tentative approach, to attempt both by theory and by experiment to inquire into the conditions in which quantum mechanics might break down, to reveal a new structure of physical law and a new order in physical movement. Experiments devised in order to study questions raised in such an inquiry could, in principle, falsify the basic principles of quantum mechanics and show the need for new ones.

CC-0. In Public Domain. Gurukul Kangri Collection, Haridwar

Digitized by Arya Samaj Foundation Chennai and eGangotri

A Refutation of the Proof by Jauch and Piron that Hidden Variables Can Be Excluded in Quantum Mechanics

D. BOHM, J. BUB

Birkbeck College, London University, London, England

In this paper, we examine an argument of Jauch and Piron, which aims to prove the impossibility of hidden variables underlying the quantum theory, on the basis of certain assumptions that are weaker than those used by von Neumann for the same purpose. We show that, while the assumptions of Jauch and Piron are in fact weaker than those of von Neumann, the net result is that they actually prove nothing new at all. The conclusions of Jauch and Piron concerning the nonexistence of hidden variables are indeed seen to follow from a false assumption; i.e., that the impossibility of propositions that describe simultaneously the results of measurements of two noncommuting observables is an "empirical fact." Actually, it is shown that this assumption follows if and only if one first assumes what the authors set out to prove, i.e., that the current linguistic structure of quantum mechanics is the only one that can be used correctly to describe the empirical facts underlying the theory.

INTRODUCTION

In a previous paper[1] we analyzed the classic von Neumann proof of the impossibility of a "hidden variable" theory underlying quantum mechanics and found that the argument excluded only a certain very restricted class of hidden variable theories. A more general theory, which went beyond the assumptions of von Neumann, was developed, and it was shown that the usual results of quantum mechanics could be recovered in certain limiting cases. In particular, we showed that one need not make the linearity assumption of von Neumann, i.e., that for any real linear combination of observables, whether simultaneously measurable or not, the expectation value of the sum in an ensemble of measurements is equal to the sum of the expectation values. This property follows as a theorem in quantum mechanics, but it is quite possible to construct theories in which this relation does not hold in general but is true only in the case of specially constructed ensembles.

A more recent impossibility proof has been proposed by Jauch and Piron,[2] in which they come to the same conclusion as von Neumann without using this assumption. We examine their proof here.

SUMMARY OF THE ARGUMENT

The argument by which Jauch and Piron attempt to prove that the structure of the quantum theory is incompatible with the assumption of hidden variables is based on an analysis of the type of experimental question that can be asked in the theory. Thus, they consider those observables of a physical system which are associated with only two alternatives or possibilities, which may be designated by 1 or 0, yes or no, true or false, and are represented in quantum mechanics by the projection operators. The results of such yes-no experiments, for example, that a certain observable P has the value P', or that the value of P is positive, etc., are referred to as the *propositions* of the system, and these are classified as *compatible* or *incompatible*, depending on whether or not the corresponding measurements can be performed simultaneously. Jauch and Piron refer to a paper by Birkhoff and von Neumann[3] on "The Logic of Quantum Mechanics," in which these authors formally develop a logical calculus of propositions for quantum mechanics, based on the relation between the propositions of a quantum mechanical system and the associated projection operators. In contrast to the usual propositional calculus of ordinary logic, applicable to classical mechanics, this system is extended by the concept of "incompatibility" characteristic of quantum mechanics. The contribution of Jauch and Piron is to prove as a theorem in this calculus that if a propositional system admits hidden variables then all propositions are compatible. This is the conclusion of Theorem I and Theorem II (proved under slightly weaker assumptions) in their paper. Since the propositions of a quantum mechanical system are not all compatible, because there are certain measurements which cannot be carried out on the system simultaneously, the possibility of hidden variables underlying the quantum theory is rejected. This rejection does not make use of von Neumann's linearity assumption (see Ref. 1, Sec. 4), which has been shown by various authors to be unnecessarily restrictive.

Now, at first sight, it is not at all clear why the authors should wish to use the terminology of logic to describe the experimental questions of a physical theory, unless they intend to propose a deep connection between all human reasoning and the theory. If this is the case,

[1] D. Bohm and J. Bub, Rev. Mod. Phys. **38**, 453 (1966).
[2] J. M. Jauch and C. Piron, Helv. Phys. Acta **36**, 827 (1963).
[3] G. Birkhoff and J. von Neumann, Ann. Math. **37**, 823 (1936).

CC-0. In Public Domain. Gurukul Kangri Collection, Haridwar

Digitized by Arya Samaj Foundation Chennai and eGangotri

then the impossibility of developing a hidden variable theory for microsystems could be traced to a limitation in our thought processes. Unfortunately, the treatment of this question is rather vague, especially with regard to the significance of "incompatible propositions" in the general sense, and a careful analysis of the argument will be necessary in order to clarify what is in fact implied.

As we see, however, such an analysis indicates that Jauch and Piron are really only making assumptions about physics and that the suggested relationship with logic is both artificial and misleading. If this is so, then it is important to discover what these physical assumptions are and to consider whether they are well founded. In this connection, a key point for consideration is the claim that the existence of incompatible propositions is an "empirical fact." Such incompatible propositions could be taken as necessary inferences from experiment, however, only if it could be established that no other propositions besides those of quantum mechanics are applicable to a microsystem, from which it would follow that the only relevant experimental questions are those of quantum mechanics. But this is in essence just what Jauch and Piron have set out to prove in their efforts to exclude hidden variables from the quantum theory. For if there are such hidden variables, then (as we see in more detail in the present paper) they do make possible a language in terms of which relevant experimental questions do not involve any *incompatible propositions*, but only incompatible processes of measurement, in which the actions needed in making one kind of measurement may interfere physically with those needed for making another kind of measurement. In this way, it becomes clear that the basic assumption of Jauch and Piron is that the conceptual structure of all the laws of physics is the same as that of the laws of current quantum mechanics and nothing else. But it has long been fairly clear that without extending or otherwise altering the basic conceptual structure of the laws of quantum theory, no hidden variables can be introduced into the theory. So in fact, Jauch and Piron have actually proved essentially nothing new at all. This fact may, however, be obscured by the use of a logical terminology for the description of the properties of physical systems, which might perhaps at first sight cause the old conceptual structure to appear as if it had a new meaning.

We now proceed to a more detailed examination of the argument.

THE LOGIC OF QUANTUM MECHANICS

As we have indicated, Jauch and Piron propose that the propositions of a quantum mechanical system are represented in the formalism by projection operators. Each projection operator $\mathbf{P}_a$ defines a certain closed subspace V_a of the Hilbert space $\mathcal{H}$, spanned by the eigenvectors of V_a with eigenvalue 1. The (normalized) vectors of V_a all represent states of the system for which the proposition a is true with certainty, whereas for those states represented by the vectors orthogonal to the members of V_a the proposition a is certainly false. If $\mathbf{P}_a$, V_a belong to the proposition a, then it follows that $\mathbf{1}-\mathbf{P}_a$, $\mathcal{H}-V_a$ belong to the denial of a, the proposition "not a," denoted by a'. If the proposition a is always true, then $\mathbf{P}_a=\mathbf{1}$, $V_a=\mathcal{H}$. If the proposition a is never true, i.e., impossible, then $\mathbf{P}_a=\mathbf{0}$, $V_a=0$. The trivially true proposition is denoted by I and the absurd or trivially false proposition by ϕ.

If the projection operators $\mathbf{P}_a\cdot\mathbf{P}_b$ of the propositions a, b commute, then the additional propositions "a and b" and "a or b" can be formed. The proposition "a and b," denoted by $a\cap b$, is true if the propositions a and b are both true, and it is false if one of them is false. The corresponding projection operator is $\mathbf{P}_a\cdot\mathbf{P}_b$, and the closed subspace is the set of vectors common to both V_a and V_b. "a or b," denoted by $a\cup b$, can be expressed as "not [(not a) and (not b)]," or $(a'\cap b')'$, and its operator is therefore, $\mathbf{1}-(\mathbf{1}-\mathbf{P}_a)(\mathbf{1}-\mathbf{P}_b)=\mathbf{P}_a+\mathbf{P}_b-\mathbf{P}_a\cdot\mathbf{P}_b$, which is also a projection operator. The associated closed subspace is defined by the set of all vectors which are linear combinations of a vector from V_a and a vector from V_b.

As long as all operators commute, then the use of projection operators to represent the answers to yes–no questions that can be "asked" in an experiment is merely a formal representation of Boolean algebra of ordinary logic in terms of quantum mechanical operator theory. However, if the field of operators is extended to include noncommuting projection operators, then new features are introduced. In terms of the usual quantum mechanical language, one says that when two operators do not commute, then the corresponding measurements cannot both give rise to precise and unambiguous results simultaneously. Jauch and Piron transcribe this notion into their own language by asserting that the *propositions* corresponding to the operators in question are *incompatible*.

Here it is necessary to consider carefully whether this change in the language in fact implies a change in the physical assumptions underlying the theory, or whether what has been introduced is merely a new terminology for the treatment of the same assumptions. If what is involved is merely a change in terminology, then, of course, the authors cannot really have gone beyond the result of von Neumann, the inadequacy of which has been demonstrated in our previous article. On the other hand, if Jausch and Piron have actually introduced new physical assumptions going beyond those of the usual (probabilistic) interpretation of the quantum theory, incorporated in the formulation of von Neumann, then the question arises as to whether or not these assumptions are justified in the context of the proof.

CC-0. In Public Domain. Gurukul Kangri Collection, Haridwar

Digitized by Arya Samaj Foundation Chennai and eGangotri

In explaining the meaning of their terminology, Jauch and Piron define the concept of compatibility, characterizing the propositions corresponding to commuting projection operators, as a certain formal relationship between pairs of propositions. Two propositions a and b are said to be compatible if they satisfy the relation,

$$(a\cap b')\cup b=(b\cap a')\cup a, \tag{1}$$

which is equivalent to the property that the projection operators $\mathbf{P}_a$, $\mathbf{P}_b$ commute. It is clear that in the case of incompatible propositions, corresponding to noncommuting projection operators, the intersection $a\cap b$ and union $a\cup b$ of propositions will lead almost always to the absurd proposition ϕ and the trivially true proposition I, respectively. If $\mathbf{P}_a$ and $\mathbf{P}_b$ do not commute, then, although there may exist simultaneous eigenvectors of both projection operators, such vectors can not form a complete set. In general, the subspace $V_{a\cap b}$ will be empty and $V_{a\cup b}$ will be the whole space, so that,

$$a\cap b=a'\cap b=a\cap b'=a'\cap b'=\phi$$

and

$$a\cup b=I. \tag{2}$$

Now, it is demonstrated in the paper by Birkhoff and von Neumann that the propositions of a physical system form an ortho-complemented lattice—i.e., essentially a set with a partial ordering relation, a greatest lower bound (and least upper bound) for every nonempty set of propositions and an operation with the formal properties of the negation in the propositional calculus of ordinary logic. The partial ordering relation is defined as the relation of implication,

$$a\subseteq b \qquad \text{if, whenever } a \text{ is true, } b \text{ is also true.} \tag{3}$$

However, although the propositions of classical systems (represented by functions on the phase space with the two values 1 and 0) obey the distributive law:

$$a\cap(b\cup c)=(a\cap b)\cup(a\cap c)$$

and

$$a\cup(b\cap c)=(a\cup b)\cap(a\cup c), \tag{4}$$

the lattice of quantum propositions is nondistributive. Birkhoff and von Neumann quote the following example to demonstrate this point:

If a denotes the experimental observation of a wave packet ψ on one side of a plane in ordinary space, a' correspondingly the observation of ψ on the other side and b the observation of ψ in a state symmetric about the plane, then

$$b\cap(a'\cup a)=b\cap I=b\supset\phi=(b\cap a)=(b\cap a')$$
$$=(b\cap a)\cup(b\cap a') \tag{5}$$

(where the notation $b\supset\phi$ means $b\supseteq\phi$ but not $b=\phi$). The fact that the lattice of quantum propositions is nondistributive (which is evidently a direct consequence of the existence of propositions which are "incompatible") means that, whereas the propositional calculus of classical mechanics forms a Boolean algebra, the propositional calculus of quantum mechanics does not.

At this point, one must be careful to avoid a kind of confusion that tends to result from the replacement of the usual term "experimental questions" by the term "proposition." The fact that different experimental questions cannot all be answered simultaneously is, of course, characteristic of the quantum theory (whereas in the classical theory the corresponding questions can all be answered together). But by using the term "proposition" instead of "question" and by asserting that propositions corresponding to noncommuting operators are "incompatible," the authors would seem, at least at first sight, to be suggesting that their basic assumptions refer, not to particular physical theories such as classical or quantum mechanics, but rather to the structure of the *logic* that applies in the whole field of human reasoning. If there is in fact such a perfect correspondence between the possible structures of all logical reasoning and the structures of these two particular physical theories, then to establish this as true would indeed be a very revolutionary discovery, in all probability far transcending both classical and quantum mechanics in its ultimate significance. Unfortunately, the authors do not make it very clear what their intentions are with regard to this point. Are they proposing, for example, that in ordinary reasoning one could extend the operations of intersection and union to "incompatible" propositions, similar to those represented by noncommuting operators? As we have remarked, this would lead almost always to the absurd or trivially true proposition; such a proposal does not, therefore, appear to be particularly meaningful. It is surely significant here that Jauch and Piron and Birkhoff and von Neumann continue to employ the conventional "classical" logic in their own reasoning and make no attempt to persuade the reader by a non-Boolean argument. From this fact, it seems fairly safe to infer that the authors do not actually wish to suggest that their assumptions about "propositions" should apply generally in the whole field of human logic, but rather, they would seem to be tacitly restricting such assumptions to particular physical theories.

If this is so, then the replacement of the term "experimental question" by the term "proposition" can in itself add nothing new to the structure of the theory and has the disadvantage of tending to lead the reader into a kind of confusion between physical assumptions and the structure of all logic.

THE ASSUMPTIONS OF JAUCH AND PIRON

Accepting that Jauch and Piron do not wish to make new assumptions about the whole field of human reasoning, we come then to the question of what new assumptions, if any, are actually involved in their proof. In this connection, we find a possible clue by noting that they interpret the example of Birkhoff

CC-0. In Public Domain. Gurukul Kangri Collection, Haridwar

Digitized by Arya Samaj Foundation Chennai and eGangotri

and von Neumann "empirically." In other words, they regard the nondistributivity of what they call "quantum propositions" (but what we would prefer to call "experimental questions that can be raised in the quantum theory") as a fundamental and factually established property of the structure of the objectively existing systems themselves, and not merely as a feature of the *theory* used to describe these systems. Thus, Jauch and Piron prove as a theorem that a lattice is distributive if and only if any two propositions are compatible, in the sense defined, and conclude that, since the distributivity law is "empirically false" for quantum systems, it is "empirically established" that for such systems there always exist propositions which are not compatible. As they remark: "This important point will be essential in the argument to be presented establishing the impossibility of hidden variables." (Ref. 2, p. 831.)

In the thesis of Piron, to which the authors also refer, it is shown that the compatibility relation is equivalent to the relation,

$$(a\cap b)\cup(a'\cap b)\cup(a\cap b')\cup(a'\cap b')=I. \qquad (6)$$

Using this relation, Piron constructs another example by which he attempts to prove that: "The existence of systems of propositions not all compatible amongst themselves, that is to say of non-distributive systems of propositions, is a fact of experience." (Ref. 4, p. 467, note 9.) He considers a beam of light crossing a crystal of tourmaline. If the incident beam contains only a single photon, the emergent beam will contain either a whole photon of energy equal to the original photon or no photon at all. Thus the crystal constitutes a measuring apparatus and the corresponding proposition may be denoted by a_0. The proposition corresponding to the same crystal turned through an angle α is denoted by a_α. The ortho-complementary proposition to a_0, defined by the interchange of the yes and the no, corresponds to the crystal turned through $\frac{1}{2}\pi$. Piron demonstrates that a_0 and a_α constitute a pair of incompatible propositions if $\alpha\neq\frac{1}{2}n\pi$ (where n is an integer).

"It suffices to verify:

$$x=(a_0\cap a_\alpha)\cup(a_{\pi/2}\cap a_\alpha)\cup(a_0\cap a_{\alpha+\pi/2})\cup(a_{\pi/2}\cap a_{\alpha+\pi/2})\neq I.$$

Now $a_\alpha\cap a_\beta=\phi$ for $\alpha-\beta\neq n\pi$, for by definition $a_\alpha\cap a_\beta$ is true if and only if a_α and a_β are both true. Now there exists no photon which can with certainty traverse each of the two crystals if their optic axes form an angle different from zero. Thus $x=\phi$." (Ref. 4, p. 467, note 9.)

It seems clear then that Jauch and Piron regard the necessity for describing quantum mechanical experiments in terms of "incompatible propositions" as a physically demonstrated fact. But actually, it is only when one is restricted to the language of quantum theory that the experiment described above necessarily leads to "incompatible propositions" (i.e., when the state of the photon is assumed to be completely defined by a vector in Hilbert space). Indeed, as has been shown in our previous article, an entirely different structure of theoretical ideas can be proposed for describing this experiment, in terms of a set of hidden variables which do in fact determine the future behavior of the photon completely (so that, for example, there do exist photons which can *with certainty* traverse both crystals). Therefore, the need to describe this experiment in terms of incompatible propositions would be a "fact" only if it could be proved that the language of quantum mechanics is necessarily universally applicable to all possible physical phenomena and is the only one that is of this nature. To *begin* with such an assumption, without experimental or theoretical justification, would however evidently amount to circular reasoning, because this is just what the argument of Jauch and Piron aims to prove. Since no justification for an assumption of the kind described above is in fact offered, it seems clear that the proof of Jauch and Piron breaks down.

THE PROOF OF THE THEOREM

To see in more detail how this happens, we note that their object is to establish that, if a propositional system admits hidden variables, then all propositions are compatible. This is proved in Theorem II of their paper. (The conclusion of Theorem I is the same, but the proof depends on slightly stronger assumptions.)

"This theorem permits the reduction of the question concerning hidden variables to an empirical one, viz., whether there exist propositions which are not compatible. Since the lattice operations have a physical interpretation which is accessible to an empirical verification, we can decide the question by examining the actual behavior of specific propositions under observation. To rule out hidden variables, it suffices to exhibit two propositions of a physical system which are not compatible. It turns out that this is quite easy. In fact, the occurrence of incompatible propositions leads to gross macroscopic effects which can easily be verified. With this result the possible existence of hidden variables is decided in the negative." (Ref. 2, pp. 836, 837.)

In spite of the unfortunate wording—it is difficult to see how propositions, "incompatible" or otherwise, could lead to gross macroscopic effects—the error in the above reasoning is clear. The authors refer to the thesis of Piron and the article of Birkhoff and von Neumann for examples, and we have already indicated that these examples are not really "empirical" because they are based on tacitly assuming just what the authors wish to prove, i.e., that the language of propositions corresponding to projection operators in Hilbert space is the only one that can be used to describe the actual experimental facts about the examples in question.

Of course, if quantum mechanics is assumed from the outset as the theory to which all experimental

[4] C. Piron, Helv. Phys. Acta **37**, 439 (1964).

CC-0. In Public Domain. Gurukul Kangri Collection, Haridwar

Digitized by Arya Samaj Foundation Chennai and eGangotri

propositions must necessarily refer, then it is possible to introduce the concept of compatibility of propositions as a formal reflection of the commutativity of projection operators. But then the term *experimental proposition* is little more than another name for *projection operator*, and the *incompatibility of propositions* means nothing more than the *noncommutativity of projection operators*.

Jauch and Piron define the "state" of a physical system by a probability function $\omega(a)$ on the set of all propositions $a \in \mathfrak{L}$, where $\mathfrak{L}$ is the lattice in question, i.e., the state of a system is determined if for each proposition of the system we know the probability of obtaining the answer yes during a measurement. Two states are different if there exists a proposition a such that $\omega_1(a) \neq \omega_2(a)$. If ω_1 and ω_2 are two different states, then

$$\omega(a) = \lambda_1\omega_1(a) + \lambda_2\omega_2(a),$$

with

$$\lambda_1 > 0, \qquad \lambda_2 > 0, \qquad \lambda_1 + \lambda_2 = 1, \tag{7}$$

defines a new state which is different from either one. Such a state, which can be represented with two different states, is called a *mixture* and distinguished from the *pure* or *homogeneous* state. A system of propositions $\mathfrak{L}$ which admits hidden variables is defined as a lattice on which every state is a mixture of dispersion-free states, so that every state can be expressed in the form:

$$\omega(a) = \sum_i \lambda_i \omega_i(a)$$

with

$$\lambda_i > 0, \qquad \sum_i \lambda_i = 1, \tag{8}$$

where $\omega_i(a)$ is dispersion-free.

Whether or not one agrees with the manner in which the term "state" is introduced, quite obviously, if quantum mechanics is assumed, there are no "dispersion-free states," i.e., states which give zero dispersion for all the observables or propositions represented by all projection operators in Hilbert space. The conclusion of Jauch and Piron is therefore completely trivial.

This becomes immediately obvious with a closer examination of the definition of the function $\omega(a)$. $\omega(a)$ is defined as a function with the following properties:

(1) $0 \leq \omega(a) \leq 1$;

(2) $\omega(\phi) = 0, \qquad \omega(I) = 1$;

(3) if a is compatible with b, then $\omega(a) + \omega(b) = \omega(a \cap b) + \omega(a \cup b)$;

(4) if $\omega(a_i) = 1$, then

$$\omega(\bigcap_i a_i) = 1;$$

(5) if $a = \phi$, then there exists a state ω such that $\omega(a) \neq 0$.

In the proof of Theorem II, (4) is replaced by the weaker assumption (4°)

$$\omega(a) = \omega(b) = 1 \quad \text{implies} \quad \omega(a \cap b) = 1.$$

Now if a and b are incompatible, i.e., if the corresponding projection operators do not commute and have no common eigenvectors, then, as we have already pointed out, $a \cap b = a' \cap b = a \cap b' = a' \cap b' = \phi$. Since $\omega(\phi) = 0$, by the requirement (2), $\omega(a)$ and $\omega(b)$ cannot both be equal to 1. Thus, their definition of an acceptable state ω rules out states in which the result of the measurement of a and b can be predicted with certainty if the projection operators corresponding to a and b do not commute. On the other hand, the very essence of a hidden variable theory is that, for a completely specified state of the system, in which the values of the hidden variables are all determined, the result of a measurement of any observable can be predicted with certainty. This has been pointed out by Bell.

"QUANTUM PROPOSITIONS" IN TERMS OF A HIDDEN VARIABLE THEORY

As we have shown in our previous article, by explicitly developing a hidden variable theory, it is possible to go beyond the assumptions of quantum mechanics and, with the aid of dynamical variables (at present "hidden") which are not represented by projection operators in Hilbert space, to define a "dispersion-free state" in the sense that all results of all possible measurements on the system are determined. In this theory, the measurement process of an observable P, represented by the Hermitian operator $\mathbf{P}$ with eigenvalues P_i and eigenvectors $|P_i\rangle$, is described by a set of equations of the form:

$$d\psi_i/dt = \gamma\psi_i \sum_j |\psi_j|^2 (R_i - R_j) \qquad (i = 1, 2, \cdots, n). \tag{9}$$

The ψ_i are the components of the Hilbert space vector of the system—the "state" vector in quantum mechanics—in the representation in which the matrix of $\mathbf{P}$ is diagonal:

$$|\Psi\rangle = \sum_i \psi_i |P_i\rangle. \tag{10}$$

The hidden variables are represented by the components of a normalized vector in the dual space:

$$\langle\xi| = \sum_j \xi_j \langle P_j| \tag{11}$$

and appear in the terms R_i, R_j, which are defined as

$$R_i = |\xi_i|^2/|\psi_i|^2, \qquad R_j = |\xi_j|^2/|\psi_j|^2. \tag{12}$$

γ is a constant representing the strength of the interaction between the apparatus and the system measured. If R_s is the greatest such term, then these equations describe a dynamical process in which ψ_s increases to 1 and all the other ψ_i decrease to 0, assuming the vector

CC-0. In Public Domain. Gurukul Kangri Collection, Haridwar

Digitized by Arya Samaj Foundation Chennai and eGangotri

$|\Psi\rangle$ is normalized, so that the result of the measurement is the eigenvalue P_s and the system is left in the "quantum state" $|P_s\rangle$. The result of the measurement is therefore determined by the vector $|\Psi\rangle$, the hidden variables and the apparatus, which we characterize as a macroscopic system defining the representation.

Thus, a completely specified physical state is defined in this theory by two vectors: the Hilbert space vector of the system and the dual vector. From our point of view, the quantum mechanical specification of the state of a system by a wave function only, represented by a vector in Hilbert space, is incomplete, and we recover the statistical results of quantum mechanics from an ensemble of systems with the same $|\Psi\rangle$ vector but with a random distribution for the dual vector $\langle\xi|$. The propositions of this theory are statements about the Hilbert space vector of the system, the hidden variables represented in the dual space, which are also in principle measurable, and the measuring apparatus. There does not seem to be any sense in which two such statements can be considered to be "incompatible." However, each quantum mechanical observable is associated with a specific process of interaction between the system and a suitable measuring apparatus, and if we consider two different processes for the measurement of two observables P, Q whose operators do not commute, then these *processes* are incompatible in the obvious sense that their actions interfere. If

$$|\Psi\rangle=\sum_i \psi_i |P_i\rangle=\sum_j \varphi_j |Q_j\rangle, \tag{13}$$

then the process tending to develop ψ_s to 1 and ψ_i $(i\neq s)$ to 0 in the measurement of P conflicts with the process developing φ_t to 1 and φ_j $(j\neq t)$ to 0 in the measurement of Q. In this theory, two quantum propositions a and b, represented by noncommuting projection operators, can both be "true" with certainty in the sense that they would each be verified as true by the corresponding processes, whereas there is clearly no process for the proposition $a\cap b$. For example, if two systems are prepared in the same completely specified physical state, i.e., with the same $|\Psi\rangle$ vectors and the same $\langle\xi|$ vector, then the one system could be used to verify the proposition a and the other to verify the proposition b. If the state is defined in such a way that the results of both measurements can be predicted as positive with certainty, then for this state we would have

$$\omega(a)=\omega(b)=1 \quad \text{but} \quad \omega(a\cap b)=0, \tag{14}$$

since the proposition $a\cap b$ is certainly false. As to the example of Piron, it is clear that if the state of the photon is completely defined, by specifying the hidden variables as well as the "quantum state," then it is possible to predict with certainty whether or not the photon will pass through both crystals from the equations of measurement.

In our theory, every (quantum) proposition is either true or false with certainty, if the values of the hidden variables are known. However, these propositions refer to the results of experiments on the system, i.e., physical processes involving the system in interaction with a measuring apparatus, and to *realize* the truth or falsity of experimental propositions representing projection operators which do not commute involves *incompatible processes*. All quantum propositions are compatible as potentialities referring to the outcomes of various dynamical processes for the system. Although the concept of incompatibility of propositions seems to be meaningless, except in the sense of a rather inappropriate synonym for the noncommutativity of projection operators, the concept of incompatibility of processes is quite clear: two processes are incompatible if their actions interfere in the sense that the one process implies an order of movement which conflicts with that needed for the other to take place.

To sum up, the argument of Jauch and Piron is circular since they are really assuming quantum mechanics, whereas von Neumann's proof does rule out a certain restricted class of hidden variable theories. They are led to the idea of incompatible propositions only because they tacitly suppose that all experiments must be analyzed in terms of the usual terminology of quantum mechanics, which we have suggested provides an inadequate set of propositions for the problem.

CC-0. In Public Domain. Gurukul Kangri Collection, Haridwar

Digitized by Arya Samaj Foundation Chennai and eGangotri

REVIEWS OF MODERN PHYSICS VOLUME 38, NUMBER 3 JULY 1966

Present Phenomenological Status of the Regge Pole Theory

E. LEADER*

Lawrence Radiation Laboratory, University of California, Berkeley, California

Few theories have generated so much emotion amongst physicists as the Regge Pole theory has ··· and still does. With the gradual accumulation of a vast amount of precise experimental data, it has become possible to attempt to give an objective survey of the present status of the theory in relation to experiment. The analysis herein is restricted to elastic and charge-exchange scattering processes in the region of high energies and small momentum transfers. A strong distinction is made between strictly forward ($t=0$) and nonforward ($t\lesssim 0$) processes. In discussing the latter, an attempt is made to examine the phenomenological validity of the so called "factorisation theorem," the proof of which depends critically upon the assumption of the Regge poles being simple poles.

I. INTRODUCTION

Perhaps the most unified of all theories of elementary particles ever proposed was the "Regge pole theory" of Chew and Frautschi.[1] Following on the brilliant analysis of potential scattering by Regge,[2] in which the whole concept of complex angular momentum was introduced, Chew and Frautschi suggested that all the known particles and resonances could be grouped into families, each family being associated with a given Regge trajectory, and consisting of several members differing only in their spin quantum number. A spin-J member of a family would appear as a manifestation of the passage of the Regge trajectory $\alpha(t)$ through an integral or half-integral value of J. Actually, only *alternate* integer or half-integer values of J along a given trajectory would appear as particles or resonances, owing to the concept of "J parity." The square of the mass of the particle of spin J would be the value of t for which $\mathrm{Re}\,\alpha(t)=J$.

Moreover, a knowledge of $\alpha(t)$ for $t\lesssim 0$ plus the assumption that the residue functions $r(t)$ were slowly varying would suffice to specify the behavior of the scattering amplitude at high energies in the cross channel.

More detailed considerations led to startling predictions, e.g., at asymptotically high energies the total cross sections for $\pi\pi$, πN, and NN scattering would satisfy the relation

$$\sigma^2_{\pi N}=\sigma_{\pi\pi}\sigma_{NN}.$$

A further unification of the theory was afforded by the suggestion that the trajectory families themselves could be grouped together into multiplets according to some set of internal quantum numbers, e.g., into $SU(3)$ multiplets.

The experimental successes of the Regge pole theory in its earliest period were very impressive. Since then a vast amount of precise experimental data has been accumulated, and the whole status of the Regge pole theory is much less secure. In the following, we attempt to give an objective and coherent survey of the present phenomenological status of the theory. We also point out possibilities for testing some of the fundamental properties of the theory.

It is our aim to discuss in detail only those aspects of the situation which allow reasonable quantitiative tests of the validity of the theory. Thus we concentrate primarily upon the field of small angle, high energy scattering, i.e., the region $t\lesssim 0$, and we do not attempt to analyze the situation for $t>0$. The latter region, in which one tries to find sets of particles and resonances which lie on the same trajectory, and multiplets of trajectories which fit into group theoretical symmetry schemes, abounds with interesting and exciting possibilities, but these are of a much more speculative nature and do not easily provide genuinely critical tests of the theory.

In Sec. II we briefly review the basic tools of the Regge pole theory and their origin in potential scattering.

In Sec. III we summarize the results of the original one-pole approach and then discuss the rules for generalizing to the case of several Regge poles.

Section IV, which is the main section of this survey, contains a detailed analysis of the present experimental situation and its relationship to the theory.

In Sec. V we attempt to summarize the over-all situation.

II. BASIC TOOLS OF THE THEORY

Consider a scattering process

$$A+B\to A'+B',$$

described by a scattering amplitude $f(s,\theta_s)$, where

$$\left.\begin{aligned} s&=(\text{center-of-mass energy})^2\\ \theta_s&=\text{scattering angle in c.m.}\end{aligned}\right\}\ \text{for MAIN PROCESS.}\quad (2.1)$$

* Present address: Physics Department, Cavendish Laboratory, University of Cambridge, Cambridge, England.

[1] G. F. Chew and S. Frautschi, Phys. Rev. Letters **7**, 394 (1961); **8**, 41 (1962).

[2] See, A. Bottino, A. M. Longoni, and T. Regge, Nuovo Cimento **23**, 954 (1962).

CC-0. In Public Domain. Gurukul Kangri Collection, Haridwar

Digitized by Arya Samaj Foundation Chennai and eGangotri

We refer to this as the MAIN PROCESS. It is represented schematically in Fig. 1. Related to the main process, we may also consider the CROSSED PROCESS,

$$A+\bar{A}'\rightarrow\bar{B}+B',$$

described by a scattering amplitude $f(t,\theta_t)$, where

$$\left.\begin{aligned} t&=(\text{center-of-mass energy})^2\\ \theta_t&=\text{scattering angle in c.m.}\end{aligned}\right\}\ \text{for CROSSED PROCESS.} \tag{2.2}$$

Let us digress for a moment and imagine that the process $A+\bar{A}'\rightarrow\bar{B}+B'$ was governed by a nonrelativistic potential. Then the results of Regge on potential scattering would apply and would tell us that if we take the limit (of course it is a formal, unphysical one) of letting $\cos\theta_t\rightarrow\infty$, then $f(t,\theta_t)$ has the simple form

$$f(t,\theta_t)\xrightarrow[\cos\theta_t\rightarrow\infty]{}[\beta(t)/\sin\pi\alpha(t)](\cos\theta_t)^{\alpha(t)}, \tag{2.3}$$

where $\alpha(t)$ is the "trajectory function" associated with the Regge pole which lies farthest to the right in the complex J plane for the given t value and $\beta(t)$ is the "residue function" associated with it.

The relativistic generalization of Regge's results cannot be proved rigorously. However, one can show that a reasonable heuristic attempt is to replace the formula (2.3) by

$$f(t,\theta_t)\xrightarrow[\cos\theta_t\rightarrow\infty]{}\xi(t)\beta(t)(\cos\theta_t)^{\alpha(t)} \tag{2.4}$$

where $\xi(t)$, the "signature factor," is given by

$$\xi(t)=\{1+\tau\exp[-i\pi\alpha(t)]\}/\sin\pi\alpha(t), \tag{2.5}$$

and $\tau=\pm1$ is the "J parity" associated with the Regge pole. The complication introduced in (2.4) is simply due to the fact that in the relativistic case both *direct* and *exchange* forces play a role.

It will be useful to write (2.5) in a simpler form. We have

$$\begin{aligned}\xi(t)&=\tfrac{1}{2}[\cot\tfrac{1}{2}\pi\alpha(t)-i], &&\text{Im }\xi=-\tfrac{1}{2}\quad\text{for }\tau=+1,\\ \xi(t)&=\tfrac{1}{2}[\tan\tfrac{1}{2}\pi\alpha(t)+i], &&\text{Im }\xi=+\tfrac{1}{2}\quad\text{for }\tau=-1.\end{aligned} \tag{2.6}$$

Let us now return to our main problem. The so-called *crossing theorem* allows us to relate our main process to the crossed process. In fact, if all the particles were spinless, it would just tell us that

$$f(s,\theta_s)=f(t,\theta_t), \tag{2.7}$$

i.e., that one single function describes both the main and crossed processes. In the general case we still have some simple relationship which we denote very schematically as

$$f(s,\theta_s)\approx f(t,\theta_t). \tag{2.8}$$

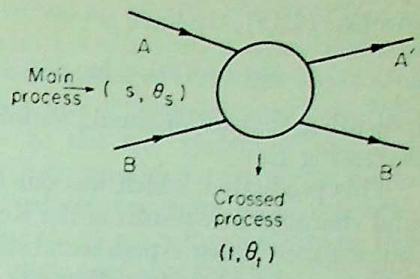

FIG. 1. Main and crossed processes.

If we now note that

$$\cos\theta_t=-1+[2s/(4m^2-t)], \tag{2.9}$$

and that $t=-$(momentum transfer)^2 for the main process, we see that the region of high energies ($s\gg2m^2$) and small momentum transfers ($|t|<4m^2$) for the main process just corresponds to having $\cos\theta_t\gg1$. Thus we can use the Regge asymptotic form (2.4), the crossing relation (2.8), and Eq. (2.9) to get

$$f(s,\theta_s)\approx\xi(t)\beta(t)(s/2m^2)^{\alpha(t)}, \tag{2.10}$$

which is valid for $s\gg2m^2$ and $|t|<4m^2$.

To simplify the following, let us choose units in which $m=1$, and use the fact that $s/2m^2\approx E=lab$ kinetic energy. We also use θ for θ_s from now on. Thus our fundamental formula (2.10) becomes

$$f(E,\theta)\approx\xi(t)\beta(t)E^{\alpha(t)}. \tag{2.11}$$

Finally, to make contact with experiment, we note that by the optical theorem,

$$\sigma_{\text{tot}}(E)\approx E^{-1}\,\text{Im}\,f(E,\theta=0). \tag{2.12}$$

Also, we have

$$(d\sigma/dt)(E,t)\approx E^{-2}|\beta(t)\xi(t)E^{\alpha(t)}|^2. \tag{2.13}$$

III. THE ESSENTIALS OF REGGE POLOLOGY

A. The One-Pole Approach

It was originally assumed that the above formulas (2.11)–(2.13) might be valid with $\alpha(t)$ referring simply to the dominant Regge pole P (the Pomeranchuk pole). Then very powerful predictions could be made.

(i) The approximate constancy of total cross sections at high energies implied $\alpha_P(0)\approx1$. This, coupled with the Froissart result that $\alpha(0)\leq1$, led to the appealing suggestion that "forces were as strong as possible," i.e., $\alpha_P(0)=1$.

(ii) Chew and Frautschi, making the simplest possible assumption, drew straight lines representing $\alpha(t)$, joining particles with the same internal quantum numbers, but differing by two units of spin, and deduced the slope $\alpha'(t)\approx1/(\text{BeV}/c)^2$.

(iii) Assuming this holds also for small negative t, and putting

$$\alpha(t)=\alpha(0)+t\alpha'(0)\approx1+t$$

CC-0. In Public Domain. Gurukul Kangri Collection, Haridwar

Digitized by Arya Samaj Foundation Chennai and eGangotri

into Eq. (2.13), we have

$$\log (d\sigma/dt) \approx \log \beta(t) + t \log E, \tag{3.1}$$

indicating that $d\sigma/dt$ should shrink quite rapidly with increasing E.

This prediction, which was one of the most startling and characteristic results of the Regge pole theory, was immediately given experimental support from measurements on the pp system. However, it was soon realized that not all processes were exhibiting shrinkage, and in order to cope with this situation, it was necessary to include the effect of several secondary Regge poles.

B. The Many-Pole Approach

We must now learn the rules needed for handling several Regge poles.

(i) If there are several different Regge poles that can contribute to a process, we simply replace formula (2.11) by a sum of terms, each one referring to one definite Regge pole.

(ii) Since *all* total cross sections look as though they will ultimately become constant, the leading Regge pole, P, should have the quantum numbers of the vacuum: $C=P=G=+1$, $\tau=+1$, $I=0$.

(iii) An analysis by Igi,[3] in which the πN scattering length was calculated using a forward dispersion relation which had built into it a Regge type asymptotic behavior, indicated that there is a second pole, P', of the same type as P, with $\alpha_{P'}(0)\approx\frac{1}{2}$. A recent, more accurate calculation by Scanio[4] indicates $\alpha_{P'}(0)\approx 0.65$.

(iv) A given Regge pole can be exchanged in any process provided that the t channel (the crossed channel) is able to communicate with systems which have the quantum numbers of the pole.

(v) The *relative sign* of the contribution of a given Regge pole to any process can be determined from its internal quantum numbers, as is indicated below.

For brevity we represent the *amplitude* arising from a given pole by the symbol for the particle (if it exists) with the quantum numbers of the pole. The relevant poles are listed below, and they seem to be more or less a minimal set.

Symbol	Quantum Numbers of Regge Poles				
	P	C	G	I	τ
P, P'	+	+	+	0	+
ρ	−	−	+	1	−
ω	−	−	−	0	−
R	+	+	−	1	+

Let us illustrate the rules[5] by considering the systems pp, pn, and $\bar{p}p$.

Remembering (2.12) and (2.6), let us write, for the $\bar{p}p$ total cross section (the signs are arbitrary at this point),

$$\sigma_T(\bar{p}p) \approx -E^{-1} \operatorname{Im} (P+P'-\rho-\omega+R). \tag{3.2}$$

To change $\bar{p}\to p$, reverse the signs of ρ and ω;

$$\sigma_T(pp) \approx -E^{-1} \operatorname{Im} (P+P'+\rho+\omega+R). \tag{3.3}$$

To change $p\to n$, reverse the signs of ρ and R;

$$\sigma_T(pn) \approx -E^{-1} \operatorname{Im} (P+P'-\rho+\omega-R). \tag{3.4}$$

The same rules will apply to πN and KN systems. They will also apply in Eq. (2.13) for $d\sigma/dt$. Thus the term $\beta(t)\zeta(t)E^{\alpha(t)}$ is replaced by

$$\sum_{\substack{\text{poles}\\ n}} \beta_n(t)\zeta_n(t)E^{\alpha_n(t)}. \tag{3.5}$$

We can now turn to a study of the present experimental situation and its implications for the Regge pole theory.

IV. THE PRESENT EXPERIMENTAL SITUATION

We separate our analysis into two main categories: (i) $t=0$ and (ii) $t<0$. In (ii) we further subdivide into predictions which do or do not depend on "factorization" (to be discussed below). As mentioned in the Introduction, we do not attempt to analyze the more speculative region in which $t>0$.

A. Processes for which t = 0

Consider first the difference of the π^-p and π^+p total cross sections. Since

$$\sigma_T(\pi^-p) \approx -E^{-1} \operatorname{Im} (P+P'+\rho)$$

and

$$\sigma_T(\pi^+p) \approx -E^{-1} \operatorname{Im} (P+P'-\rho), \tag{4.1}$$

the difference $\Delta(\pi p)=\sigma_T(\pi^-p)-\sigma_T(\pi^+p)$ depends only on ρ. Its energy dependence[6] is $E^{-\frac{1}{2}}$ and determines

$$\alpha_\rho(0)\approx 0.5. \tag{4.2}$$

The small value of $\Delta(\pi p)$ indicates that ρ couples weakly to $N\bar{N}$ and $\pi\pi$. Also, from (2.6),

$$\zeta_\rho(0)=\tfrac{1}{2}(1+i), \tag{4.3}$$

i.e., *the real part of the ρ amplitude relative to the imaginary part is completely determined.*

Consider now the value and energy dependence of $d\sigma/dt\,|_{t=0}$ for the charge-exchange process[7] $\pi^-p\to\pi^0n$. We have

$$(d\sigma/dt)(\pi^-p\to\pi^0n)\,|_{t=0} \approx |\rho|^2 \approx |1+i|^2 E^{-1}. \tag{4.4}$$

That the *imaginary part* of the amplitude must have the above energy dependence follows from the optical

[3] K. Igi, Phys. Rev. **130**, 820 (1963).
[4] J. J. G. Scanio (unpublished).
[5] A. Ahmadzadeh and E. Leader, Phys. Rev. **134**, B1058 (1964).
[6] W. Galbraith, E. W. Jenkins, T. F. Kycia, B. A. Leontic, R. H. Phillips, A. L. Reed, and R. Rubinstein, Report presented to Dubna Conference (1964).
[7] A. V. Stirling, P. Sonderegger, J. Kirz, P. Falk-Vairant, O. Guisan, C. Bruneton, P. Borgeand, M. Yvert, J. P. Guillaud, C. Caverzasio, and B. Amblard, Phys. Rev. Letters **14**, 763 (1965).

CC-0. In Public Domain. Gurukul Kangri Collection, Haridwar

Digitized by Arya Samaj Foundation Chennai and eGangotri

theorem. There are *two* predictions in (4.4): (a) that the real part has the *same energy dependence* as the imaginary part; (b) that the real part is *as large as* the imaginary part, so that $d\sigma/dt\,|_{t=0}$ should be about *twice* the optical theorem value. Both these predictions are strikingly confirmed.

Using $\alpha_P(0)=1$ and our values of $\alpha_\rho(0)$, we can study the energy variation of $\sigma_T(\pi^- p)$, and we find that a good fit is obtained with

$$\alpha_{P'}(0)\approx 0.5. \tag{4.5}$$

From (2.6) follows

$$\zeta_{P'}(0)=\tfrac{1}{2}(1-i), \tag{4.6}$$

in contrast to (4.3) for the ρ.

Let us now turn to the NN system. From (3.3) and (2.6) we have

$$\Delta=\sigma_T(pn)-\sigma_T(pp)\approx E^{-1}\,\mathrm{Im}\,(\rho+R). \tag{4.7}$$

Experimentally Δ changes sign (becomes positive) at $E\gtrsim 6$ BeV. This sign change would be impossible with just ρ. Thus, although an R particle has not yet been identified (it may be the 2^+A_2), it is concluded that the R pole exists. This argument is somewhat dangerous, since one is talking about rather low energies. We see later that there are other tests for the existence of R.

The energy variation of Δ in (4.7) can be used to give

$$\alpha_R(0)\approx 0.3, \tag{4.8}$$

and by Eq. (2.6) follows

$$\zeta_R(0)\approx\tfrac{1}{2}(1.7-i). \tag{4.9}$$

Consider now the charge-exchange process $np\to pn$, for which

$$d\sigma/dt\,|_{t=0}\approx E^{-1}\,|\,\rho+R\,|^2. \tag{4.10}$$

From (4.9) and (4.3) we see that the *real parts tend to add* in (4.10), whereas the *imaginary parts tend to cancel*. Thus the theory predicts that the $np\to pn$ forward cross section should be much larger than the optical value, as is indeed found experimentally.[8] Also, the energy variation is correctly predicted.

A similar argument would predict that the process $\bar{p}p\to n\bar{n}$ should be about equal to the optical value, but as yet there are no experimental results.

Consider now the difference[6]

$$\bar{\Delta}=\sigma_T(\bar{p}p)-\sigma_T(pp)\approx E^{-1}\,\mathrm{Im}\,(\rho+\omega). \tag{4.11}$$

The energy variation indicates

$$\alpha_\omega(0)\approx 0.5, \tag{4.12}$$

so, that from (2.6),

$$\zeta_\omega(0)=\tfrac{1}{2}(1+i). \tag{4.13}$$

The size of the difference indicates that the ω coupling to NN is much greater than the ρ coupling.

[8] See, A. Ahmadzadeh, Phys. Rev. **134**, B633 (1964).

Since we now have values of $\alpha(0)$ for P, P', ρ, ω, and R, the energy variation of $\sigma_T(pp)$ can be computed and *the result is in good agreement with experiment.* One learns also that both P and P' couple strongly to NN.

Let us turn now to the KN system. A detailed analysis has recently been carried out by Phillips and Rarita.[9] Using $\alpha(0)$ values very close to above-mentioned ones, they are able to get very good fits to the highly precise data[6] now available for the $K^\pm p$ and $K^\pm n$ total cross sections.

The forward charge-exchange processes $K^+n\to K^0p$ and $K^-p\to\bar{K}^0n$ are strictly analogous to $np\to pn$ and $\bar{p}p\to\bar{n}n$, respectively. Hence, the above discussion would predict

$$(d\sigma/dt)\,(K^+n\to K^0p)\,|_{t=0}\gg\text{optical value} \tag{4.14}$$

and

$$(d\sigma/dt)\,(K^-p-\bar{K}^0n)\,|_{t=0}\approx\text{optical value}. \tag{4.15}$$

There are as yet no data on (4.14).[9a] There are data on (4.15) at one energy only, 9.5 BeV, and the prediction of (4.15) is well fulfilled. The experimental uncertainty is not small, but if there were no R pole one would have $d\sigma/dt\approx$twice the optical value. *Thus the KN system gives added evidence for the existence of R.*

Let us now attempt to summarize the situation at $t=0$. The Regge pole theory, using a small number of parameters, is eminently successful in correlating a large amount of precise data. But what of other theories? The only other general possibility at present is to use forward dispersion relations.[10] Assuming that the imaginary part is given at high energies by a simple combination of fractional powers of E, and using the experimental data at lower energies, one uses the dispersion relation to compute the real part.

Now it is clear that the Regge pole amplitude satisfies (more or less) a Mandelstam representation and in particular, therefore, a fixed momentum-transfer dispersion relation. Thus the real part of a Regge amplitude will *emerge* from a dispersion-relation calculation if the imaginary part is given the Regge behavior, which it must be in order to agree with the total cross-section data. Thus, for a given process there will be nothing to distinguish the two types of theory.

However, suppose that we now use the dispersion method for a series of interrelated processes. By taking various linear combinations of these processes, we discover that what we have been doing is *equivalent* to asserting that the exchange of a *given set of internal quantum numbers* always contributes a certain *characteristic power behavior* to the imaginary part, which is precisely what the Regge pole theory tells us. Thus the Regge theory provides a simple and aesthetic underlying

[9] R. J. N. Phillips and W. Rarita, Phys. Rev. **139**, B1336 (1965).

[9a] *Note added in proof.* The new results of I. Butterworth *et al.*, Phys. Rev. Letters **15**, 734 (1965) support the predictions of Eq. (4.14).

[10] See, for example, P. Soding, Phys. Letters **8**, 285 (1964).

CC-0. In Public Domain. Gurukul Kangri Collection, Haridwar

Digitized by Arya Samaj Foundation Chennai and eGangotri

picture for the power law behavior used in the dispersion-relation methods.

B. Processes for which $t \neq 0$

1. Processes that do not Involve the Factorization Theorem

The most beautiful result of the original Regge pole theory was its prediction about the energy and momentum-transfer dependence of $d\sigma/dt$. With the simplest assumptions, namely, $\alpha(t)$ linear and $\beta(t)$ approximately constant, one had the prediction of the shrinkage phenomenon and at *the same time* an explanation of the exponential dropoff of $d\sigma/dt$ with increasing $|t|$ [see Eq. (3.1)].

The more precise experimental evidence that shows that only the pp (and perhaps K^+p) differential cross sections are shrinking, and that the rate of shrinkage is so much smaller than originally supposed, has destroyed the essential beauty and simplicity of the Regge Pole theory. This does not mean that the Regge Pole theory fails to account for the new data. Rather, it means that the situation is much less simple and far more a contrived one. Thus by using several poles and very flat trajectories $\alpha(t)$, Phillips and Rarita[9] are able to get excellent agreement with experiment for all the processes thus far measured. But the very use of flat trajectories means that one has lost the automatic mechanism for producing the sharp exponential dropoff of $d\sigma/dt$. Instead, one has to put the entire burden for this into the residue functions $\beta(t)$, introducing several *ad hoc* parameters to describe their behavior.

There does exist, however, one class of experiment that might prove crucial in deciding the merits of the Regge pole theory. These are the situations in which one believes that just *one* Regge pole plays a role. The prime example is the charge-exchange process $\pi^-p\to\pi^0n$, which, as discussed earlier [see Eq. (4.4)], depends solely on the ρ pole. We have thus

$$(d\sigma/dt)(\pi^-p\to\pi^0n)$$
$$\approx(1/E^2)\beta_\rho(t)^2\,|\tan(\pi/2)\alpha_\rho(t)+i\,|^2E^{2\alpha_\rho(t)}. \quad (4.16)$$

Assuming a linear behavior of $\alpha_\rho(t)$ for small t, one has

$$\alpha_\rho(t)\approx 0.5+t\alpha_\rho'(0); \quad (4.17)$$

we get from (4.16)

$$(d\sigma/dt)(\pi^-p\to\pi^0n)\approx E^{-1}\beta_\rho^2(t)\,|\,1+\pi t\alpha_\rho'(0)\,|\,E^{2t\alpha_\rho'(0)}, \quad (4.18)$$

and the process *will certainly exhibit shrinkage unless* $\alpha'(0)$ is exceeding small. However, the detailed analysis of Phillips and Rarita indicated a value

$$\alpha_\rho'(0)\approx 0.7, \quad (4.19)$$

so that a definite measurable shrinkage is predicted.

The latest experimental data[7] indicate that there may be some shrinkage, but the measurements are not yet sufficiently accurate to make a more definitive statement.

Let us speculate a little and ask ourselves to what extent a more definitive result will influence our belief in the theory. If there is no shrinkage, then I believe that one has a clear-cut case against the theory. However, a true diehard will always be able to wiggle out of this difficulty by postulating the existence of a second Regge pole with the same quantum numbers at the ρ and in this way explain away the nonshrinkage. If, on the other hand, there is shrinkage, one has a strong case in favor of the theory.

There is one further general prediction which might eventually be used as a quantitative criterion for the validity of the Regge pole theory. It is generally felt by theoretical physicists that in "conventional" models of diffractive scattering the probability of a spin flip scattering in a given collision will drop off with increasing energy much more rapidly than will the nonspin flip probability. Neither the author nor any of the many colleagues whose opinion he has canvassed have been able to offer a *proof* of this assertion. Yet without exception the assertion seems to be accepted as fact. If it is indeed fact, then the Regge pole theory is highly unconventional in that it predicts *spin flip amplitudes* which *remain as large as the nonspin flip ones*; i.e., spin flip and nonspin flip amplitudes have the same energy dependence. Thus it will be possible to find certain spin-dependent parameters, e.g., spin correlation coefficients in NN scattering, which tend to constant, nonzero values as $E\to\infty$.[11] Note that this will not be true for the polarization. This is because the polarization always depends on the *imaginary part* of the product of a spin flip and a nonspin flip amplitude. It is therefore nonzero only if there is a phase difference between the spin flip and nonspin flip amplitudes. In the Regge model the *leading terms* in these amplitudes turn out to have the same phase and, therefore, fail to contribute to the polarization.

Some interesting evidence that this kind of behavior occurs in practice is afforded by the charge exchange process $\pi^-p\to\pi^0n$. Experimentally, the differential cross section $d\sigma/dt$ first *rises* as we move away from $t=0$, reaches a maximum at $t\approx-0.05$ and then decreases. This is very simply explained if there is a strong spin flip amplitude, which of course has to be identically zero at $t=0$ to conserve angular momentum, and which then increases rapidly to a magnitude comparable with the nonspin flip amplitude. This is by no means a unique explanation of the peak in $d\sigma/dt$, but if it is correct then the energy variation of this peak gives some indication that both nonspin flip and spin flip amplitudes have the same energy dependence.

[11] R. J. N. Phillips and W. Rarita, UCRL-16185 (1965); E. Leader and R. Slansky, UCRL-16597 (1965).

CC-0. In Public Domain. Gurukul Kangri Collection, Haridwar

Digitized by Arya Samaj Foundation Chennai and eGangotri

2. Processes that Involve the Factorization Theorem

In all the above, our decisions (with the possible exception of $\pi^- p \to \pi^0 n$ and the spin flip behavior) *pro or contra* the Regge pole theory were unfortunately of an aesthetic nature only. We wish now to examine a class of phenomena which we believe offer the possibility of a more fundamental decision.

Consider first the derivation of the factorization theorem. Suppose we have a system which for a given J can exist in two states $|1\rangle$ and $|2\rangle$ (a concrete example to keep in mind would be the two $N\bar{N}$ triplet states with $l=J\pm1$), and suppose that $|1\rangle$ and $|2\rangle$ can communicate with each other and with the two-pion state $|\pi\pi\rangle$ via the unitarity condition. Then if f_{ij} is the transition amplitude for $|i\rangle \to |j\rangle$, one can show that the partial-wave amplitude $f_{ij}(t, J)$ is given by

$$f_{ij}(t, J) \approx r_{ij}(t)/[J-\alpha(t)], \tag{4.20}$$

for J close to $\alpha(t)$ for a given fixed t value.

The factorization theorem now asserts that

$$r^2_{ij} = r_{ii} r_{jj}, \tag{4.21}$$

e.g., that $r_{11}(t) r_{22}(t) = [r_{12}(t)]^2$.

It is this fundamental property which leads, for example, to the relationship

$$\sigma^2_{\pi N} = \sigma_{\pi\pi}\sigma_{NN}. \tag{4.22}$$

It will be some time before we can test relationships like (4.22), so we must look elsewhere to test (4.21). A good place is in NN scattering, where, however, the argument depends on a detailed consideration of the spin complications. We give an outline of the argument, suppressing as many inessential considerations as possible.

There are five independent helicity amplitudes ϕ_i, $i=1$–5 needed to describe $NN \to NN$ scattering in the main s channel. By means of very general crossing properties, one can relate the ϕ_i to the five amplitudes f_j needed to describe the t-channel process $N\bar{N} \to N\bar{N}$.[12] Schematically,

$$\phi_i = M_{ij} f_j. \tag{4.23}$$

These f_j are the $N\bar{N} \to N\bar{N}$ transition amplitudes in a singlet-triplet spin representation.[5]

The $NN \to NN$ differential cross section is simply

$$d\sigma/dt \approx (1/E^2) \sum_i |\phi_i|^2. \tag{4.24}$$

If each f_j is now replaced by its Regge asymptotic form, using just the poles discussed above, one gets

$$\begin{aligned} f_1 &= 0, \\ f_2 &= \sum_n \zeta_n r_{11}^{(n)} E^{\alpha_n(t)}, \\ f_3 &= -t \sum_n \zeta_n \alpha_n (\alpha_n - 1) r_{22}^{(n)} E^{\alpha_n(t)-2}, \\ f_4 &= t \sum_n \zeta_n \alpha_n^2 r_{22}^{(n)} E^{\alpha_n(t)-1}, \\ f_5 &= \sum_n \zeta_n \alpha_n r_{12}^{(n)} E^{\alpha_n(t)-1}, \end{aligned} \tag{4.25}$$

where n runs over P, P', ρ, ω, R.

If we utilize the factorization theorem, Eq. (4.21), by putting

$$r_{11}(t) = b_1^2(t), \qquad r_{12}(t) = b_1(t) b_2(t),$$

and

$$r_{22}(t) = b_2^2(t), \tag{4.26}$$

then, as first shown by Wagner,[13] Eq. (4.24) takes on the simple form

$$d\sigma/dt \approx \sum_{l,n} \zeta_l^* \zeta_n (b_1^{(l)} b_1^{(n)} - \alpha_l \alpha_n b_2^{(l)} b_2^{(n)} t)^2 E^{\alpha^l + \alpha^n - 2}. \tag{4.27}$$

Remembering our rule [see Eqs. (3.2) and (3.3)] for going from the $p\bar{p}$ to the pp system, we see that

$$\begin{aligned} (d\sigma/dt)(p\bar{p} \to p\bar{p}) - (d\sigma/dt)(pp \to pp) \approx \sum_{l \neq \rho, \omega} \mathrm{Re}\,(\zeta_l^* \zeta_\omega) \\ \times (b_1^{(l)} b_1^{(\omega)} - \alpha_l \alpha_\omega b_2^{(l)} b_2^{(\omega)} t)^2 E^{\alpha_l + \alpha_\omega - 2} + (\text{term with } \omega \to \rho). \end{aligned} \tag{4.28}$$

Now, since l in (4.28) refers only to poles of even signature, we get, from (2.6),

$$\mathrm{Re}\,(\zeta_l^* \zeta_\omega) = \tfrac{1}{4}[1 - \cot \tfrac{1}{2}\pi\alpha_l(t) \tan \tfrac{1}{2}\pi\alpha_\omega(t)], \tag{4.29}$$

and similarly for ρ. Thus the only factor in (4.28) that can possibly change sign are $\mathrm{Re}\,(\zeta_l^* \zeta_\omega)$ and $\mathrm{Re}\,(\zeta_l^* \zeta_\rho)$. *But experimentally the difference in* (4.28) *changes sign at* $t \approx -0.15$. To produce such a sign change would require enormous slopes for $\alpha(t)$, slopes many times as great as allowed by the fits to experiment discussed in Sec. IVB1.

We have undertaken a detailed analysis to try to understand to what extent one can escape the above conclusion. We find that even with the inclusion of correction terms, beyond the assymptotic form, or the introduction of additional hitherto unused Regge poles, the above conclusion is inevitable. There is, however, one weak point in this conclusion. Namely, it is not really possible to show rigorously that the functions

[12] M. L. Goldberger, M. T. Grisaru, S. W. MacDowell, and D. Y. Wong, Phys. Rev. **120**, 2250 (1960).

[13] W. G. Wagner, Phys. Rev. Letters **10**, 202 (1963).

CC-0. In Public Domain. Gurukul Kangri Collection, Haridwar

Digitized by Arya Samaj Foundation Chennai and eGangotri

$b_1(t)$, $b_2(t)$ introduced in (4.26) are necessarily *real functions*. Thus, if they suddenly become *purely imaginary* at $t=-0.15$, then a term like $b_1^2(t)$ could become negative. However, this is a rather unpalatable situation, and it seems very difficult to imagine a dynamical model in which this could happen.

It is thus of great importance to find a test for the factorization theorem which really has no loopholes. One such possibility is to measure the energy dependence of the spin-correlation parameter C_{NN} in nucleon-nucleon scattering. It turns out that the expression for C_{NN} contains terms like

$$\sum_{n,l} | r_{11}^{(n)} r_{22}^{(l)} - r_{12}^{(n)} r_{12}^{(l)} |^2 E^{\alpha_n+\alpha_l-2}. \quad (4.30)$$

Thus the highest power in E would come from the Pomeranchuk pole, i.e., from the term with $n=l=$ Pomeranchuk. Since $\alpha_P=1$ for $t=0$ we would have as leading term

$$C_{NN} \approx \text{const} \, | \, r_{11}^{(P)} r_{22}^{(P)} - [r_{12}^{(P)}]^2 \, |^2. \quad (4.31)$$

But by the *factorization theorem this is identically zero.* Thus in fact, if the factorization theorem holds, we will have as leading term something like

$$C_{NN} \approx | \, r_{11}^{(P)} r_{22}^{(\omega)} - r_{12}^{(P)} r_{12}^{(\omega)} \, |^2 E^{\alpha_P+\alpha_\omega-2}$$

$$\approx \text{const} \, E^{-\frac{1}{2}} \qquad \text{at } t=0. \quad (4.32)$$

If, on the other hand, the factorization theorem does not hold, then presumably we would find,

$$C_{NN} \underset{E\to\infty}{\longrightarrow} \text{const} \qquad \text{at } t=0$$

except for possible logarthmic factors.

Thus we might expect that roughly

$$\frac{C_{NN}(E) \text{ with fact. theorem}}{C_{NN}(E) \text{ without fact. theorem}} \approx E^{-\frac{1}{2}}. \quad (4.33)$$

A merasurement of C_{NN} would thus decide whether or not the factorization theorem is satisfied.[14]

V. CONCLUSION

We attempt herein to summarize the rather complex situation.

One the one hand, the Regge pole theory provides a simple and elegant explanation of the properties of cross sections, both direct and charge-exchange, in the forward direction. It also provides a neat, and probably correct, description of the relationship between the real and imaginary parts of the forward scattering amplitude. For nonforward processes it provides an acceptable but aesthetically much less pleasing description.

On the other hand, the fundamental and intrinsic property of residue factorizability appears to be at variance with the empirical data, and this matter deserves urgent experimental attention.

We thus conclude that what we are observing in these high-energy experiments is almost certainly the leading singularities in the complex J plane, but that the assumption that these singularities are purely poles is too naive. Of course the idea that there are branch cuts as well as poles in the complex J plane is an old one, and there is an extensive literature concerning their dynamical origin. However, none of these theoretical treatments would claim to be conclusive. Thus we feel that the direct breakdown of the factorization theorem is excellent phenomenological evidence for the relative complexity of the complex J plane.

ACKNOWLEDGMENTS

The author is grateful to Dr. David Judd for suggesting that this survey talk should be circulated to a wider audience. He is also grateful to the U.S. Atomic Energy Commission for support.

[14] This conclusion was reached independently by R. J. N. Phillips at Lawrence Radiation Laboratory (private communication).

CC-0. In Public Domain. Gurukul Kangri Collection, Haridwar

Digitized by Arya Samaj Foundation Chennai and eGangotri

Hamiltonian Path-Integral Methods

CLAUDE GARROD
University of California, Davis, California

A path-integral formulation of quantum mechanics is investigated which is closely related to that of Feynman. It differs from Feynman's formulation in that it involves the Hamiltonian function of the canonically conjugate coordinates and momenta. The classical limit yields the variational principle: $\delta\int(p\dot{\mathbf{q}}-N)dt=0$. A path-integral formula is also obtained for the energy eigenstate projection operator associated with the time-independent Schrödinger equation. The classical limit of the projection operator formula yields a modified form of the well-known variational principle for the phase–space orbit of given energy. Relativistically covariant Hamiltonian variational principles are analyzed and lead naturally to a relativistic scalar wave equation which involves a proper time variable which is canonically conjugate to the mass in the same manner as the ordinary time variable is conjugate to the energy in nonrelativistic quantum theory.

I. INTRODUCTION

In 1948 the now well-known paper by R. Feynman[1] appeared, which presented a new formulation of nonrelativistic quantum mechanics. This formulation had three distinctive features.

(i) It concentrated attention on the propagator of the Schrödinger wave function rather than on the wave function itself, expressing this propagator (in a way to be described later) as an integral over all possible paths from one given point to another.

(ii) It introduced a new mathematical concept into quantum theory, namely the function space integral or "sum over paths."

(iii) It was directly related to Lagrangian rather than Hamiltonian classical dynamics. Thus the system to be quantized was not first described in terms of N coordinates and their canonical momenta.

The formulation presented in this paper is patterned after that of Feynman in that it retains the first two features mentioned above. It differs from Feynman's work in that it requires the description of the classical system in terms of canonical variables and in the classical limit reduces to a Hamiltonian variational principle. An advantage of the Hamiltonian formulation is that if the path integral is defined in the simplest and most obvious way there is no need to introduce special normalization constants to maintain the unitarity of the propagator. In the conversion from the Hamiltonian formulation to Feynman's formulation the correct normalization constants automatically appear. Besides the Hamiltonian path integral formulation for the time-dependent Schrödinger equation a path integral formula is also derived for the time-independent energy eigenvalue equation. The last section is devoted to the relativistic extension of the formulation; particularly to the derivation and interpretation of an equation for scalar particles which involves a proper time variable.

II. THE FEYNMAN METHOD

Since we are concerned with phase–space integrals throughout this paper it is convenient to choose units such that h (not $\hbar$), the natural unit of phase–space volume, is unity. The Schrödinger equation is then

$$-(8\pi^2m)^{-1}\nabla^2\psi+V(\mathbf{x})\psi=(i/2\pi)\,\partial_t\psi. \qquad (2.1)$$

We define a propagator, $K(\mathbf{x}'',\mathbf{x}',t''-t')$ for the equation by stating that if $\psi(\mathbf{x},t)$ is any solution (for all values of t) then

$$\psi(\mathbf{x}'',t'')=\int K(\mathbf{x}'',\mathbf{x}',t''-t')\psi(\mathbf{x}',t')\,d^3x' \qquad (2.2)$$

for all t'' and t'. This is different from the more common practice of defining the propagator to be zero for negative values of $t''-t'$ but it proves more useful when discussing the time-independent Schrödinger equation. $K(\mathbf{x}'',\mathbf{x}',t)$ may be expressed in terms of the energy eigenfunctions by the equation

$$K(\mathbf{x}'',\mathbf{x}',t)=\sum_n\phi_n(x'')\phi_n^*(x')\exp(-2\pi iE_nt) \qquad (2.3)$$

where the sum, which may actually include an integral if the spectrum is partly continuous, is over the complete set of normalized eigenstates. Using this formula we can see that

$$P(\mathbf{x}'',\mathbf{x}',E)=\int_{-\infty}^{\infty}K(\mathbf{x}'',\mathbf{x}',t)\exp(2\pi iEt)\,dt \qquad (2.4)$$

$$=\sum_n\delta(E-E_n)\phi_n(\mathbf{x}'')\phi_n^*(\mathbf{x}')$$

is a projection operator for the time-independent states of energy E.

In his paper on nonrelativistic quantum mechanics, Feynman presented the following recipe for calculating $K(\mathbf{x}'',\mathbf{x}',t)$:

Let us denote by Ω the set of all continuous, piecewise differentiable functions $\mathbf{x}(t)$ which satisfy the conditions that $\mathbf{x}(t')=\mathbf{x}'$ and $\mathbf{x}(t'')=\mathbf{x}''$. For each function in Ω (which can obviously represent the trajectory of a particle moving from $\mathbf{x}'$ to $\mathbf{x}''$ in time interval t' to t'') we calculate the action integral

$$A[\mathbf{x}(t)]=\int_{t'}^{t''}L\,dt=\int_{t'}^{t''}\{\tfrac{1}{2}m\dot{\mathbf{x}}^2(t)-V(\mathbf{x}(t))\}\,dt. \qquad (2.5)$$

[1] R. Feynman, Rev. Mod. Phys. **20**, 367 (1948).

CC-0. In Public Domain. Gurukul Kangri Collection, Haridwar

Digitized by Arya Samaj Foundation Chennai and eGangotri

We define a method of integrating a functional over the set of functions Ω which allows us to write the propagator as

$$K(\mathbf{x}'', \mathbf{x}', t''-t') = \int_{\Omega} \exp\{2\pi i A[\mathbf{x}(t)]\}\, d[\mathbf{x}(t)]. \quad (2.6)$$

To define the function space integral let us consider a sequence of partitions of the interval $t' \leq t \leq t''$ such as used in defining the Riemann Integral. The Nth partition is given by choosing the $N+1$ points: $t_0 \equiv t' < t_1 < t_2 < \cdots < t_{N-1} < t_N \equiv t''$. For the Nth partition consider the piecewise linear function which has the values $\mathbf{x}_j$ at t_j. That is,

$$\mathbf{x}(t) = \mathbf{x}_{j-1}\left(\frac{t_j - t}{t_j - t_{j-1}}\right) + \mathbf{x}_j\left(\frac{t - t_{j-1}}{t_j - t_{j-1}}\right) \quad \text{for} \quad t_{j-1} \leq t \leq t_j, \quad (2.7)$$

where $\mathbf{x}_0 \equiv \mathbf{x}'$ and $\mathbf{x}_N \equiv \mathbf{x}''$.

In the Nth approximation to the functional integral we integrate over all such functions with a normalization constant which is chosen so that K_N approaches a unitary kernal. Such a normalization constant is

$$C_N = \prod_{j=1}^{N}\left(\frac{-im}{t_j - t_{j-1}}\right)^{\frac{3}{2}}.$$

Thus

$$K(\mathbf{x}'', \mathbf{x}', t''-t') = \lim_{N\to\infty}\left\{\prod_{j=1}^{N}\left(\frac{-im}{t_j - t_{j-1}}\right)^{\frac{3}{2}} \int d^3x_1 \cdots d^3x_{N-1} \exp\{2\pi i A[\mathbf{x}]\}\right\}. \quad (2.8)$$

In the classical limit, in which the potential changes only slightly over a DeBroglie wavelength of the particle, the only paths which contribute appreciably to the functional integral are those which are close to the classical path from $\mathbf{x}'$ to $\mathbf{x}''$ in time $t''-t'$. This is due to the fact that in this limit one may evaluate the integral by stationary phase and the trajectory which makes the phase stationary is the one for which $A[\mathbf{x}(t)]$ is stationary, but by Hamilton's Principle, this is just the classical path.

III. NONRELATIVISTIC HAMILTONIAN FORMULATION

The quantum mechanical path-integral formulas which we use are related to the following phase-space variational principles:

We consider a system described by N coordinates $q_1, \cdots, q_N$ and their canonical momenta $p_1, \cdots, p_N$. The system has a Hamiltonian $H(q, p)$. The first variational principle is an answer to the problem: Given that the total energy of the system is E and that at some unspecified times during its motion the coordinates of the system had the values $q_1', \cdots, q_N'$ and $q_1'', \cdots, q_N''$, what must have been the corresponding values of the canonical momenta, $p_1', \cdots, p_N'$ and $p_1'', \cdots, p_N''$ and what path through the system phase-space must have been taken in going from the point q', p' to q'', p''? At what rate the system point moved along the curve is not asked and is not obtained from the variational principle. The equation $H(q, p) = E$ defines a $(2N-1)$-dimensional energy surface. Consider the set of all curves on this energy surface which begin with coordinates q' and end with coordinates q''. For each such curve we calculate the integral:

$$I_0 = \int_{q'}^{q''} \sum p_j\, dq_j. \quad (3.1)$$

Any curve for which I_0 is an extremum is a solution to the problem posed.

The second variational principle is obviously related to the above but yields the explicit time dependence of the coordinates and momenta. Given that the coordinates of the system at times t' and t'' are, respectively, $q_1', \cdots, q_N'$ and $q_1'', \cdots, q_N''$ we consider the set of all phase-space trajectories $q(t)$, $p(t)$ which satisfy the given initial and final conditions with no restrictions on the energy or the initial and final values of the momenta. Among this set the path (or paths) which makes

$$I = \int_{t'}^{t''} \{\sum_j p_j \dot{q}_j - H(q(t), p(t))\}\, dt \quad (3.2)$$

an extremum is a solution of Hamilton's equations of motion with the specified initial and final conditions. We consider now the corresponding quantum mechanical principle.

We consider a system described by n coordinates $q_1, \cdots, q_n$ (denoted collectively as Q) and their canonical momenta $p_1, \cdots, p_n$ (denoted P). The probability that, at time t, the system has coordinates in the range d^nQ about Q is given by the absolute square of a complex valued amplitude $\psi(Q, t)$. $\psi(Q, t)$ satisfies an equation of the form:

$$\psi(Q', t') = \int K(Q', Q, t'-t)\psi(Q, t)\, d^nQ. \quad (3.3)$$

There may or may not exist a differential (or local) equation for ψ depending upon the form of the Hamiltonian function $H(Q, P)$. [The procedure of replacing p_j by $-i\hbar(\partial/\partial q_j)$ is reliable only in rectangular coordinates.] The essential element in the Hamiltonian formulation is the following prescription for calculating $K(Q', Q, t'-t)$.

We want to define an integral over the set of paths mentioned in the second Hamiltonian variational principle. In order to do this we consider a sequence of better and better approximations to any given path in terms of an ever increasing number of parameters. The Nth approximation is constructed by partitioning the time interval $t' \leq t \leq t''$ into N parts. The function $Q(t)$ is then approximated by a piecewise linear function

CC-0. In Public Domain. Gurukul Kangri Collection, Haridwar

Digitized by Arya Samaj Foundation Chennai and eGangotri

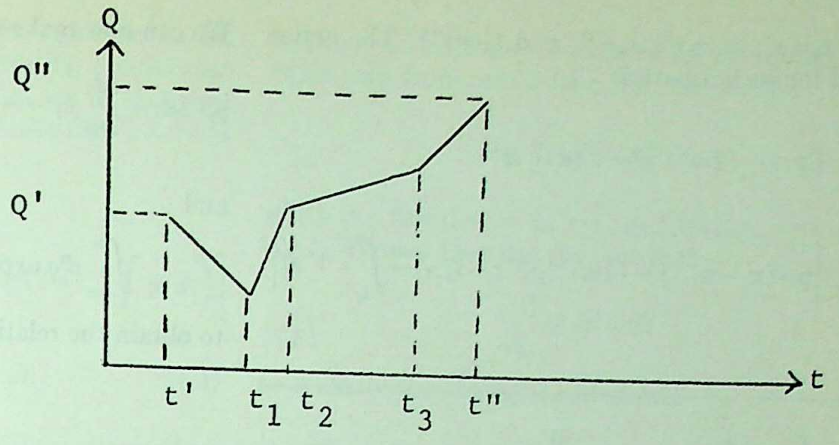

FIG. 1. Phase–space path, $Q(t)$, $P(t)$.

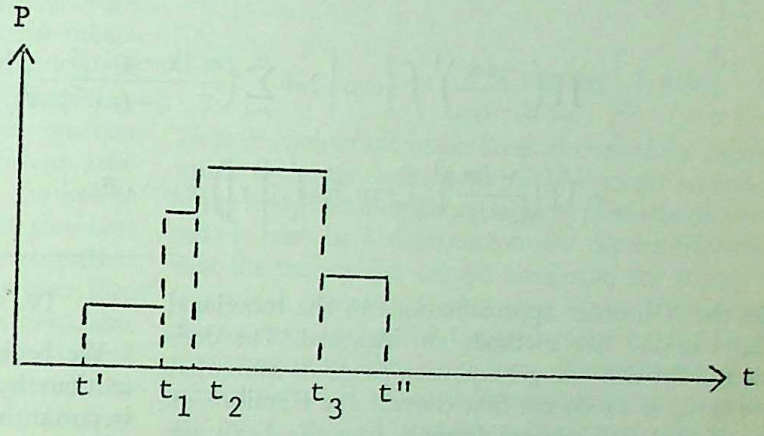

going from Q_{j-1} to Q_j in the interval t_{j-1} to t_j. (See Fig. 1.)

The function $P(t)$ is, in the same interval, approximated by a constant P_j. The piecewise constant but discontinuous approximation for the momentum is consistent with the fact that the velocity associated with our Nth approximation to $Q(t)$ is piecewise constant but discontinuous. For any functional $F[Q(t), P(t)]$ of the phase–space trajectory the integral over paths is defined as:

$$\int F[Q, P]\,d[Q(t)]\,d[P(t)]$$

$$\equiv \lim_{N\to\infty} \int F[Q, P]\, dQ_1 \cdots dQ_{N-1}\, dP_1 \cdots dP_N. \quad (3.4)$$

It will not be necessary to include any N-dependent normalization constant. With this definition the propagator $K(Q'', Q', t''-t')$ is given by

$$K(Q'', Q', t''-t') = \int \left\{\exp 2\pi i \left(\int_{Q'}^{Q''} P\,dQ - \int_{t'}^{t''} H\,dt\right)\right\} \times d[Q(t)]\,d[P(t)], \quad (3.5)$$

where

$$\int_{Q'}^{Q''} P\,dQ \equiv \int_{t'}^{t''} \left(\sum_{j=1}^{n} p_j \dot{q}_j\right) dt.$$

If Q is a rectangular coordinate and the Hamiltonian has the form.

$$H = (p^2/2m) + V(\mathbf{x}) \quad (3.6)$$

the above prescription may be readily converted into the Feynman formula. To do this we look at the Nth-order approximation for the integral over paths. The paths included are then as shown in Fig. 2 for $N=4$.

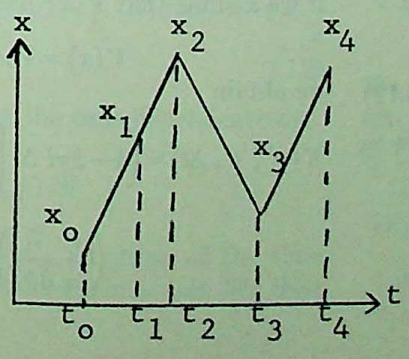

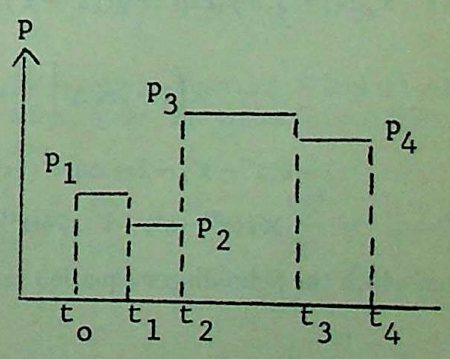

FIG. 2. Phase–space path, $x(t)$, $p(t)$.

CC-0. In Public Domain. Gurukul Kangri Collection, Haridwar

Digitized by Arya Samaj Foundation Chennai and eGangotri

Note: ($x_0=x'$, $x_N=x''$, $t_0=t'$, and $t_N=t''$). The action integral for such a path is

$$I=\int_{t'}^{t''}[\mathbf{p}\cdot\dot{\mathbf{x}}-(2m)^{-1}p^2-V(\mathbf{x})]\,dt$$

$$=\sum_{j=1}^{N}\left\{\mathbf{p}_j\cdot(\mathbf{x}_j-\mathbf{x}_{j-1})-(2m)^{-1}p_j^2(t_j-t_{j-1})-\int_{t_{j-1}}^{t_j}V\,dt\right\}. \tag{3.7}$$

We can now make use of the formulas:

$$\mathbf{p}_j\cdot\Delta\mathbf{x}_j-\frac{\Delta t_j}{2m}p_j^2=-\frac{\Delta t_j}{2m}\left(\mathbf{p}_j-\frac{m}{\Delta t_j}\Delta\mathbf{x}_j\right)^2+\tfrac{1}{2}m\frac{(\Delta\mathbf{x}_j)^2}{\Delta t_j} \tag{3.8}$$

and

$$\int_{-\infty}^{\infty}d^3q\exp\left[2\pi i\left(-\frac{\Delta t_j}{2m}q^2\right)\right]=\left(\frac{-im}{\Delta t_j}\right)^{\frac{3}{2}} \tag{3.9}$$

to obtain the relation

$$\int\left\{\exp\left[2\pi i\int(p\cdot\dot{x}-H)\,dt\right]\right\}d^3p_1\cdots d^3p_N\,d^3x_1\cdots d^3x_{N-1}$$

$$=\prod_{j=1}^{N}\left(\frac{-im}{t_j-t_{j-1}}\right)^{\frac{3}{2}}\int\left\{\exp\left[2\pi i\sum_{j=1}^{N}\left(\frac{m}{2}\frac{(\mathbf{x}_j-\mathbf{x}_{j-1})^2}{t_j-t_{j-1}}-\int_{t_{j-1}}^{t_j}V\,dt\right)\right]\right\}dx_1\cdots dx_{N-1}$$

$$=\prod_{j=1}^{N}\left(\frac{-im}{t_j-t_{j-1}}\right)^{\frac{3}{2}}\int\exp 2\pi i\left(A\left[x\right]\right)d^3x_1\cdots d^3x_{N-1}. \tag{3.10}$$

Thus the Nth order approximations to the functional integral in the two methods are identical. The derivation of the Schrödinger equation proceeds somewhat more easily if we do not first convert the Hamiltonian form of the path-integral formula into the Feynman formula since the latter contains terms involving negative powers of the time differences. In order to derive the equation we assume that when $\Delta t=t''-t'$ is sufficiently small we may approximate the functional integral by its first-order approximation. It is clear that such an assumption must be valid if the functional integrals are to converge at all as $N\to\infty$, which has been shown to be the case for a wide class of potentials. We can then write:

$$K(\mathbf{x}'',\mathbf{x}',\Delta t)=\int d^3p\exp 2\pi i(\mathbf{p}\cdot(\mathbf{x}''-\mathbf{x}')-(1/2m)p^2\,\Delta t-\bar{V}\,\Delta t), \tag{3.11}$$

where $\bar{V}$ is the average of $V(\mathbf{x})$ over the straight line connecting $\mathbf{x}'$ and $\mathbf{x}''$. Expanding the exponential to first order in Δt we obtain

$$K(\mathbf{x}'',\mathbf{x}',\Delta t)=\int d^3p(\exp 2\pi i\mathbf{p}\cdot(\mathbf{x}''-\mathbf{x}'))\times\left(1-2\pi i\,\Delta t\left[\frac{p^2}{2m}+\bar{V}\right]\right) \tag{3.12}$$

$$=\delta(\mathbf{x}''-\mathbf{x}')-2\pi i\,\Delta t[-(8\pi^2m)^{-1}\nabla^2\times\delta(\mathbf{x}''-\mathbf{x}')+V(\mathbf{x})\,\delta(\mathbf{x}''-\mathbf{x}')]$$

from which the Schrödinger equation easily follows.

IV. CANONICAL TRANSFORMATION

We begin our consideration of canonical transformations by looking at one of the simplest but most important examples, namely the transformation:

$$x\longrightarrow p\qquad p\longrightarrow -x.$$

With this transformation our equation for the propagator becomes

$$K(p'',p',t''-t')=\lim_{N\to\infty}\int dx_1\cdots dx_N\,dp_1\cdots dp_{N-1}\times\exp 2\pi i\left(-\int x\,dp-\int H\,dt\right). \tag{4.1}$$

If $H=(1/2m)p^2+V(x)$ and $\Delta t=t''-t'$ is small, then

$$K(p'',p',\Delta t)=\int dx\exp\left(-2\pi i\left[x(p''-p')+(2m)^{-1}\int p^2\,dt+\Delta tV(x)\right]\right). \tag{4.2}$$

If we assume that $V(x)$ has a power series expansion:

$$V(x)=V_0+V_1x+\cdots$$

we obtain

$$K(p'',p',\Delta t)=\left(1-2\pi i\,\Delta t\left[\frac{p^2}{2m}+V_0+V_1\left(\frac{i}{2\pi}\frac{\partial}{\partial p''}\right)+V_2\left(\frac{i}{2\pi}\frac{\partial}{\partial p''}\right)^2+\cdots\right]\right)\delta(p''-p') \tag{4.3}$$

CC-0. In Public Domain. Gurukul Kangri Collection, Haridwar

Digitized by Arya Samaj Foundation Chennai and eGangotri

which again yields the Schrödinger equation in its momentum representation. An interesting special case is that of a constant force, $V=-F_0x$, for in that case the first approximation is exact for finite time intervals yielding:

$$K(p'',p',t)$$
$$=\int dx \exp\left(-2\pi i\left[x(p''-p'-F_0t)+(2m)^{-1}\int p^2\,dt\right)\right]$$
$$=\delta(p''-p'-F_0t)\exp(-2\pi i)\int_0^t \frac{p^2}{2m}\,dt. \tag{4.4}$$

Before discussing nonlinear canonical transformations we should take note of the fact that, in contrast to the usual quantization techniques which involve the substitution of operators for classical scalar variables, the Hamiltonian path-integral formulation is completely unambiguous. The question therefore arises whether this procedure of quantization commutes with an arbitrary canonical transformation. That is, is one free to transform canonically the Hamiltonian into the most convenient form before calculating the sum over paths? If one is free to do so then we may take over into quantum theory the complete paraphernalia of canonical transformations including action-angle variables and the like. The question is at present unanswered. An example of the use of nonlinear canonical transformations is given in Appendix A where the harmonic oscillator is transformed to action-angle variables before quantization.

V. TIME-INDEPENDENT EQUATION

Using the relation between the propagator and the projection operator for the time-independent energy eigenstates it is rather easy to derive a path integral formula for the latter. We recall from Sec. II that

$$P(x'',x',E)=\int_{-\infty}^{\infty} K(x'',x',t)\exp(2\pi iEt)\,dt. \tag{5.1}$$

We may thus write an Nth-order approximation for P as:

$$P_N(x'',x',E)=\int dt\int dp_1\cdots dp_N\,dx_1\cdots dx_{N-1}$$
$$\times\exp 2\pi i\left[\sum p_j(x_j-x_{j-1})-\int_0^t H(x,p)\,dt'+Et\right]. \tag{5.2}$$

In order to extract explicitly the time dependence of

$$\int_0^t H(x,p)\,dt$$

let us choose for our Nth-order partition of the time interval a partition into N equal subintervals. We then describe the trajectory in terms of a parameter $\alpha\equiv t'/t$ which runs from zero to one. We also define:

$$\bar{H}\equiv\int_0^1 H(x,p)\,d\alpha \tag{5.3}$$

which is a function of $x_1,\cdots,x_{N-1}$ and $p_1,\cdots,p_N$ but not t. We may then use the fact that

$$\int_0^t H\,dt'=t\bar{H} \tag{5.4}$$

to evaluate the t integral and obtain

$$P_N(x'',x',E)=\int dp\cdots dp_N\,dx_1\cdots dx_{N-1}\,\delta(\bar{H}-E)$$
$$\times\exp 2\pi i\left[\int p\,dx\right]. \tag{5.5}$$

Thus P is obtained as an integral over those paths for which the average energy is E. This seems reminiscent of the first Hamiltonian variational principle of Sec. III but yet has a basic difference in that there we demanded that the trajectories remain always on the energy surface which is more stringent than the requirement that the average energy on the trajectory be E. We may now show that the usual form of the classical variational principle in which one considers only paths on the energy surface is unnecessarily restrictive and can be generalized so as to match our formula for the projection operator exactly.

We consider a set of phase–space paths described in terms of a parameter α running from zero to one. We demand that

$$x(0)=x',\quad x(1)=x'',$$

and

$$\int_0^1 H(x(\alpha),p(\alpha))\,d\alpha=E. \tag{5.6}$$

We then want to find the path for which the functional

$$A=\int p\,dx \tag{5.7}$$

is stationary with respect to variations within this set of paths. We do this by means of a Lagrange parameter, considering, instead of A, the functional

$$F_\lambda=\int_0^1 p(\alpha)\frac{dx}{d\alpha}\,d\alpha-\lambda\int_0^1 H(x(\alpha),p(\alpha))\,d\alpha. \tag{5.8}$$

We now drop the restriction involving E and set arbitrary variations (except for the end-point conditions) of F_λ equal to zero.

$$\delta F_\lambda=\int_0^1\left\{\delta p\frac{dx}{d\alpha}-\delta x\frac{dp}{d\alpha}-\lambda\frac{\partial H}{\partial x}\delta x-\lambda\frac{\partial H}{\partial p}\delta p\right\}d\alpha=0. \tag{5.9}$$

CC-0. In Public Domain. Gurukul Kangri Collection, Haridwar

Digitized by Arya Samaj Foundation Chennai and eGangotri

This yields

$$dx/d\alpha=\lambda(\partial H/\partial p)$$

and

$$dp/d\alpha=-\lambda(\partial H/\partial x) \tag{5.10}$$

as conditions for a stationary point. But we then see that, regardless of the value of λ, the rate of change of H along the path, namely,

$$\frac{dH}{d\alpha}=\frac{\partial H}{\partial x}\frac{dx}{d\alpha}+\frac{\partial H}{\partial p}\frac{dp}{d\alpha}=0. \tag{5.11}$$

Hence the variational principle for the classical phase-space orbit may be put into a form in which it bears the same relation to the quantum mechanical projection operator for the states of energy E as the classical variational principle for the time dependence of the phase point bears to the time-dependent quantum mechanical propagator.

As an example of the above formula (and the only simple example) we consider a one-dimensional free particle. The Nth-order approximation is then

$$P_N(x'', x', E)=\int dp_1\cdots dp_N\, dx_1\cdots dx_{N-1}\,\delta(E-\bar{H}_N)$$
$$\times\exp 2\pi i\Big(\sum p_j(x_j-x_{j-1})\Big), \tag{5.12}$$

where

$$\bar{H}_N=N^{-1}\sum(p_j^2/2m).$$

By using the fact that

$$\sum p_j(x_j-x_{j-1})=p_Nx''-p_1x'+(p_1-p_2)x_1$$
$$+\cdots+(p_{N-1}-p_N)x_{N-1} \tag{5.13}$$

and doing the x_j integrations we obtain

$$P_N(x'', x', E)=\int dp\;\delta\left(E-\frac{p^2}{2m}\right)\exp 2\pi ip(x''-x')$$
$$=[(2m)^{\frac{1}{2}}/E]\cos[2\pi(2mE)^{\frac{1}{2}}(x''-x')]$$
$$=\phi_p(x'')\phi_p{}^*(x')+\phi_{-p}(x'')\phi_{-p}{}^*(x'), \tag{5.14}$$

where $\phi_p(x)$ is the properly normalized state of momentum $(2mE)^{\frac{1}{2}}$.

VI. RELATIVISTIC VARIATIONAL PRINCIPLES

Before we discuss the relativistic form of the Hamiltonian path integral formulation of quantum theory it would be useful to describe carefully the associated classical variational principles. In going from a nonrelativistic to a relativistic form of either the first or second Hamiltonian variational principles the most obvious thing to do is simply to modify the function $H(\mathbf{p}, \mathbf{x})$ so as to obtain the correct relativistic form of the equations of motion. For a particle of charge e in an electromagnetic field derived from the scalar and vector potentials A_0 and $\mathbf{A}$ a form of H which accomplishes the desired end is

$$H=[m^2+(\mathbf{p}-e\mathbf{A})^2]^{\frac{1}{2}}+eA_0. \tag{6.1}$$

Details of the calculation can be found in any text on relativistic mechanics. It has often been noted that when this Hamiltonian is employed in the variational principle:

$$\delta\int(\mathbf{p}\cdot d\mathbf{x}-H\,dt)=0. \tag{6.2}$$

The resulting theory is not explicitly covariant. It is possible to formulate this variational principle in a way which resembles the first Hamiltonian variational principle and which does have the property of being obviously covariant. In order to do this we first replace H by the symbol p_0 and solve Eq. (6.1) for the mass.

$$m=[(p_0-eA_0)^2-(\mathbf{p}-e\mathbf{A})^2]^{\frac{1}{2}}\equiv[(p-eA)^2]^{\frac{1}{2}}\equiv M(p,x). \tag{6.3}$$

The equation: $M(p, x)=m$ defines a surface in the eight-dimensional phase space of points (p, x). If we consider the set of phase-space trajectories which lie in that surface and also have the space-time points x' and x'' as end points then within this set the "invariant action integral"

$$A=\int_{x'}^{x''}(p\,dx) \tag{6.4}$$

is an extremum for the actual trajectory of a particle of mass m. Thus we see that the variational principle has the same form as the nonrelativistic one but has taken one step up in dimensionality while the three-dimensional scalar $H(\mathbf{p}, \mathbf{x})$ has been replaced by the four-dimensional scalar $M(p, x)$. We must notice however that it was the second Hamiltonian variational principle in three dimensions which was transformed into the first Hamiltonian variational principle in four dimensions. We presently discuss the hierarchy of first and second variational principles but first state and prove the four-dimensional form of the second Hamiltonian variational principle. We consider the set of phase-space trajectories described by a parameter τ which satisfy the endpoint conditions:

$x(\tau'')=x'$ and $x(\tau'')=x''$ where we assume x'' is in the future light cone of x'. For each such trajectory we calculate:

$$I=\int_{\tau'}^{\tau''}\left\{p(\tau)\frac{dx}{d\tau}-M(p(\tau), x(\tau))\right\}d\tau. \tag{6.5}$$

Unless $\tau''-\tau'>x_0''-x_0'$ there usually exists a trajectory for which I is an extremum. That trajectory satisfies the relativistic equations of motion for a particle of mass m where the value of m depends on the end-point

CC-0. In Public Domain. Gurukul Kangri Collection, Haridwar

Digitized by Arya Samaj Foundation Chennai and eGangotri

conditions imposed. Furthermore the path is such that the parameter τ is equal to the proper time along the path. To prove these assertions we set the variation of I equal to zero, obtaining:

$$\int_{\tau'}^{\tau''}\left\{\delta p_0\dot{x}_0-\delta p_j\dot{x}_j-\delta x_0\dot{p}_0+\delta x_j\dot{p}_j-\frac{\partial M}{\partial p_0}\,\delta p_0\right.$$

$$\left.-\frac{\partial M}{\partial p_j}\,\delta p_j-\frac{\partial M}{\partial x_0}\,\delta x_0-\frac{\partial M}{\partial x_j}\,\delta x,\,d\tau=0,\right. \quad (6.6)$$

from which we get the following equations of motion:

$$\dot{x}_0=\partial M/\partial p_0 \qquad \dot{x}_j=-(\partial M/\partial p_j)$$

$$\dot{p}_0=-(\partial M/\partial x_0) \qquad \dot{p}_j=\partial M/\partial x_j \quad (6.7)$$

which immediately imply that

$$dM/d\tau=0. \quad (6.8)$$

Thus M is a constant of the motion which we denote as m. For the specific form of M in the electromagnetic case; namely,

$$M=[(p-eA(x))^2]^{\frac{1}{2}} \quad (6.9)$$

the detailed equations of motion are

$$m\dot{x}_0=p_0-eA_0, \quad (6.10a)$$

$$m\dot{x}_j=p_j-eA_j, \quad (6.10b)$$

$$\dot{p}_0=\frac{e}{m}\left[(p_0-eA_0)\,\frac{\partial A_0}{\partial x_0}-(p_j-eA_j)\,\frac{\partial A_j}{\partial x_0}\right], \quad (6.10c)$$

$$=e\dot{x}(\partial A/\partial x_0),$$

and

$$\dot{p}_j=e\dot{x}(\partial A/\partial x_j). \quad (6.10d)$$

These are the well-known equations of motion of a point charge of mass m which can easily be shown to imply that

$$d\tau=[(dx)^2]^{\frac{1}{2}}. \quad (6.11)$$

Let us return now to an analysis of the connections among this array of variational principles. In deriving the fact that M is a constant on the trajectory we made use of an assumption that the function M has no explicit dependence on the parameter τ. This assumption is all that is needed to derive the fact that M is a constant. Suppose, for given end-point conditions, we had deduced the value of the constant m. We would then be free to restrict our variational trajectories to those which lie totally within the surface $M=m$ secure in the knowledge that we were including the desired solution in our restricted set. This alone would not reduce our variational principle to one of the first kind because we would still have to maintain the end-point conditions. Now let us notice that within this restricted set, the functional we are minimizing can be written:

$$I=\int p\,dx-m(\tau''-\tau'). \quad (6.12)$$

The second term, due to the fixed range of τ, is simply a constant, independent of the trajectory while the first term which must therefore be separately stationary is independent of the parameterization. We may therefore ignore the restrictions on the parameterization, drop the second term and demand that the first term be stationary within our restricted set. We thus obtain the four-dimensional form of the Hamiltonian variational principle of the first kind. Now it is easy to show that the four-dimensional form of the first Hamiltonian variational principle is identical with the three-dimensional form of the second Hamiltonian principle. One simply solves the equation $M=m$ for p_0 as a function of $\mathbf{p}, \mathbf{x}$, and x_0, containing m as a parameter. If one assumes that $M(p, x)$ and therefore $H(p, \mathbf{x}, \mathbf{x}_0)$ is independent of x_0 it is possible to carry the reduction in dimensionality one step further and in fact the process may be continued as long as cyclic coordinates can be found. The sequence of variational principles thus forms an overlapping hierarchy, the lower dimensional ones utilizing more and more constants of the motion and thus having smaller and smaller ranges of variation. We have gone into this long discussion of variational principles, not as an exercise in classical physics, but because we shall see that the quantum mechanical theory we obtain depends in an essential way upon the stage in this hierarchy at which we impose quantization. To be more explicit; if we extend the variational principle:

$$\delta\int(p\,dx-M\,d\tau)=0 \quad (6.13)$$

to a formula for a quantum mechanical propagator, which as we shall see will describe particles of arbitrary mass, and then look at the mass eigenvalues of the theory we obtain an equation of motion different from that which we obtain if we directly quantize the fixed mass classical variational principle; namely,

$$\delta\int(\mathbf{p}\cdot d\mathbf{x}-H\,dt)=0. \quad (6.14)$$

Before we attempt the quantization of these classical variational principles a few words are in order regarding the physical interpretation of quantum theories involving the proper time. Such theories have been discussed previously[2,3] but the introduction of τ into the theory has usually had a more formal character than it will here. We shall see that the variable τ is canonical to the mass which will be a dynamical variable rather than a scalar parameter in the theory. The relation between the proper time and the mass will be an almost exact analogy to the relation between the time and the energy in the nonrelativistic theory. To see how the proper time may be incorporated into the theory let

[2] R. Feynman, Phys. Rev. **80**, 440 (1950).
[3] Y. Nambu, Prog. Theoret. Phys. (Kyoto) **5**, 82 (1950).

CC-0. In Public Domain. Gurukul Kangri Collection, Haridwar

Digitized by Arya Samaj Foundation Chennai and eGangotri

us consider the following classical problem which is the daily concern of cosmic-ray physicists. Suppose we know that within a certain region of space–time a particle is created with a certain probability distribution in velocities. Assuming we know the electromagnetic fields present and assuming the particle is an unstable particle whose decay pattern we know we may ask what is the probability that the particle will decay in some other given region of space–time. In order to answer this question we construct an ensemble of particles which at $\tau=0$ has the given initial velocity distribution and follow this ensemble density $\rho(x,\tau)$ as τ progresses. The probability that the particle will decay in any given region of space–time is then proportional to the product of the amount of proper time it spends in that region and the probability that it reaches the region in question. The second factor depends upon the complete path which the particle takes in going from one region to the other but that fact introduces no difficulty into the classical analysis since the path (or paths) from one region to another are determined in detail. To determine the proper time of the particle if and when it reaches the region in question one simply integrates along the classical path from the initial region. There is no reason why one might not consider the same problem from a quantum mechanical viewpoint. (This is not to be confused with the field-theoretic calculations of decay processes where one calculates the decay pattern which is here assumed empirically known.) We assume a particle is created within some limited space–time region in a state $\psi(x)$ which within that region satisfies the Schrödinger equation. We may then use the Schrödinger equation to continue the wave function outside the region. We may therefore determine the probability that, if the particle were stable, it would be found at the space–time point x. (simply $|\psi(x)|^2$). But there is no satisfactory way from the Schrödinger equation point of view to assign a proper time value to the particle at x and this is essential for determining the decay probability. All knowledge of how the particle got from one point to the other has been lost. It seems to the author that one must approach this problem via a path-integral formulation. We now have the option of using a path integral formulation based on a variational principle which is not explicitly covariant and, for each path, calculating the proper time or using a path integral method which is related to the explicitly covariant variational principle which involves the proper time. That the two methods will not agree may be seen from the following considerations.

Up until now we have not carefully stated what our physical definition is of what we have been calling proper time. Although we specify the space–time location of a particle by a single point we shall always picture the particle as a dynamical system for which there is a variable which measures the internal evolution of the system. We shall call this variable the "particle time." If our particle were a miniature alarm clock this would be simply the reading on the face of the clock. Given a particular trajectory in space–time we may also define a "proper time" by taking the integral of $[(dx)^2]^{\frac{1}{2}}$ along the path. It is a principle of relativity that, at least for classical physics, these two definitions will coincide. We must realize, however, that in the path integral formula which is related to our variational principle there are finite contributions from nonclassical paths including those along which the parameter τ does not coincide with the integral of the proper time along the path. Thus, if we are to give any consistent physical interpretation to the parameter it seems most natural to interpret it as the dynamically defined particle time rather than the geometrically defined proper time. This would certainly agree with our use of the parameter in the unstable particle problem mentioned before.

We thus shall describe a particle by a wave function $\psi(x,\tau)$ which we interpret by stating that $|\psi(x,\tau)|^2$ is the probability that the particle will occupy space–time point x when the particle time is τ. We see that ψ satisfies an equation

$$(1/2\pi i)\,(\partial\psi/\partial\tau)=\hat{M}\psi, \tag{6.15}$$

where $\hat{M}$ is an integral operator which will shortly be derived from the path integral theory.

The extension of our classical variational principle to a quantum mechanical principle yields the propagator equation:

$$K(x'',x',\tau''-\tau')=\int\left\{\exp 2\pi i\left[-\int p\,dx+\int M\,d\tau\right]\right\}d[x(\tau)]\,d[p(\tau)]. \tag{6.16}$$

(The sign in the exponential has been changed in order to ensure that the formula reduces to the nonrelativistic one in the appropriate limit.)

We consider this equation in some detail for the case of a free particle for which

$$M=[p_0^2-\mathbf{p}^2]^{\frac{1}{2}}.$$

Since we are integrating over all values of p we must carefully define the double-valued square root function. We do this by temporarily extending p_0 to a complex variable and then imposing the condition that, whenever the mass is real, it is positive. The p_0 integrations then take place over the contour shown in Fig. 3, where $p_0=u+iv$:

With this definition $M=i[\mathbf{p}^2-p_0^2]^{\frac{1}{2}}$ when $p_0^2<p^2$. If in the Nth-order approximation to K we first do the integrals over $d^4x_1\cdots d^4x_{N-1}$ we find that due to the fact that M is not a function of x the Nth-order prop-

CC-0. In Public Domain. Gurukul Kangri Collection, Haridwar

Digitized by Arya Samaj Foundation Chennai and eGangotri

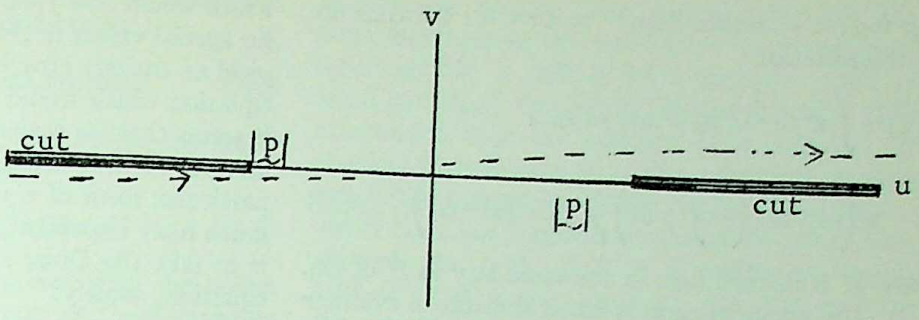

FIG. 3. Path of integration: $\tau=u+iv$.

agator reduces to the first-order propagator. Thus:

$$K(x'',x',\tau''-\tau')=\int d^4p$$

$$\times \exp 2\pi i[-p(x''-x')+(\tau''-\tau')(p^2)^{\frac{1}{2}}]. \quad (6.17)$$

In contrast to the nonrelativistic case we are forced to consider only that propagator which is defined to be zero for negative $\tau''-\tau'$ since the space-like part of the momentum integration would strongly diverge for $\tau''-\tau'<0$. Let us now consider the plane wave solutions of the equation of motion:

$$\psi(x'',\tau'')=\int K(x'',x',\tau''-\tau')\psi(x',\tau')\,d^4x'. \quad (6.18)$$

If we assume ψ is of the form

$$\psi(x,\tau)=c\exp 2\pi i(-kx+m\tau) \quad (6.19)$$

we find that the equation is satisfied only if

$$m=(k^2)^{\frac{1}{2}}. \quad (6.20)$$

Consider now the behavior of a localized wave packet containing a small range of momentum components centered about the momentum k in the following three cases.

(i) $k_0>|\mathbf{k}|$. (Forward light cone) as τ increases the wave packet moves with a velocity $dx/d\tau=k/m$ where $m=(k^2)^{\frac{1}{2}}$.

(ii) $-k_0>|\mathbf{k}|$ (Backward light cone) as τ increases the wave packet moves with a velocity $dx/d\tau=k/m$ as before however since k_0 is negative we see that the time and the particle time increase in opposite directions along the trajectory. The physical interpretation of this phenomenon has been discussed in detail by Stückelberg[4] and R. Feynman.[2,5,6]

(iii) $|k_0|<|\mathbf{k}|$ (Space-like momentum) as τ increases the position in space–time of the wave packet does not change but its amplitude diminishes with decay constant $(k^2-k_0^2)^{\frac{1}{2}}$. Thus there do not exist propagating solutions of imaginary mass. By decomposing any solution of Eq. (6.15) into its plane wave components it can easily be seen that the integral operator $\hat{M}$ mentioned above has the kernal:

$$M(x,y)=\int d^4k\{[k^2]^{\frac{1}{2}}\exp 2\pi i(-k(x-y))\}. \quad (6.21)$$

The propagator $K(x,\tau)$ (where x is now written for $x''-x'$ and τ for $\tau''-\tau'$) satisfies an equation:

$$[(2\pi i)^{-1}(\partial/\partial\tau)-\hat{M}]K(x,\tau)=(2\pi i)^{-1}\,\delta(\tau)\,\delta(x), \quad (6.22)$$

where the $\delta(\tau)$ arises from the fact that K is defined to be zero for negative τ and the $\delta(x)$ is simply the limit of $K(x,\tau)$ as $\tau\to 0$.

In order to study the fixed mass theory we use the same method as was used to derive the time-independent theory from the time-dependent theory in the nonrelativistic case. Thus we define a function $G(x,m)$, where hereafter the dependence on m will not be explicitly indicated, by

$$G(x)=\int_0^\infty d\tau\exp[-2\pi i(m-i\epsilon)\tau]K(x,\tau) \qquad (\epsilon\to 0). \quad (6.23)$$

A small imaginary part has been added to the mass in order to make any purely oscillatory parts converge. As indicated the limit as $\epsilon\to 0$ is to be taken. Using this definition and the equation satisfied by K an equation for $G(x)$ may be derived in a straightforward manner. The equation is

$$MG-mG=-(1/2\pi i)\,\delta(x). \quad (6.24)$$

Thus we see that $G(x)$ is the propagator (or Green's function) for the mass eigenvalue equation. It is shown in Appendix B that, as might be expected, it is a propagator of the Feynman type. That is, for $x_0<0$ it has only negative energy components while for $x_0>0$ it has only positive energy components. We may develop a path-integral formula for $G(x)$ by a method identical to that used in the nonrelativistic case. The only significant difference is that here we integrate over the

[4] E. C. C. Stückelberg, Helv. Phys. Acta **15**, 23 (1942).
[5] R. Feynman, Phys. Rev. **76**, 749 (1949).
[6] R. Feynman, Phys. Rev. **76**, 769 (1949).

CC-0. In Public Domain. Gurukul Kangri Collection, Haridwar

Digitized by Arya Samaj Foundation Chennai and eGangotri

range $0<\tau<\infty$ rather than $-\infty<\tau<\infty$. We thus obtain the formula:

$$G_N(x)=\int d^4p_1\cdots d^4p_N\, d^4x_1\cdots d^4x_{N-1}$$

$$\times\left(\exp 2\pi i\left(-\int p\,dx\right)\Big/\bar{M}-(m-i\epsilon)\right), \quad (6.25)$$

where $\bar{M}$ is defined here in the same way as $\bar{H}$ of Eq. (5.3). The above integral is rather difficult to evaluate even in the free-particle case.

The eigenvalue equation:

$$(\hat{M}-m)\psi=0 \quad (6.26)$$

associated with the above Green's function is the eigenvalue equation for the operator M which is a sort of operator square root of the D'Alembertian operator. Thus the above equation is a square root of the Klein–Gordon equation:

$$\Box\psi=m^2\psi. \quad (6.27)$$

Square roots of this equation have been considered before but they have been attempts to eliminate the negative energies by first writing the equation in the form:

$$-\partial_0{}^2\psi=(-\nabla^2+m^2)\psi \quad (6.28)$$

and then taking the square root of the operators on both sides, obtaining

$$i\partial_0\psi=+(-\nabla^2+m^2)^{\frac{1}{2}}\psi. \quad (6.29)$$

Here we have, using the ideas of Stückelberg and Feynman, interpreted the negative energy states as antiparticles but have eliminated the negative masses. One might remark here that we could have avoided these square root operators by using a different form for the covariant Hamiltonian variational principle. One such form, found in the literature, is

$$\delta\int(-p\,dx+\mathcal{H}\,d\tau)=0, \quad (6.30)$$

where

$$\mathcal{H}=(p-eA)^2/2m.$$

However, the above variational principle is in direct conflict with an essential property of the covariant Hamiltonian principle which is that the mass is treated as an initial condition which is conserved only due to the fact that $M(p,x)$ is not explicit function of τ. The above variational principle would only yield a correct classical equation for special values of the end-point conditions and to use it as a starting point for path-integral quantization, where propagation along paths not on the mass shell is important, would be equivalent to using in the nonrelativistic theory the variational principle:

$$\delta\int(\mathbf{p}\cdot d\mathbf{x}-[H^2(\mathbf{p},\mathbf{x})/2E]\,dt)=0 \quad (6.31)$$

which would also yield the correct equations of motion for special values of the end-point conditions but would yield an entirely erroneous time-dependent Schrödinger equation which would contain the parameter E. Thus it seems that for scalar particles the Hamiltonian path-integral method strongly suggests the validity of the particular form of square root equation used here. A much more important variation on what was done here is to take the Dirac square root of the Klein-Gordon equation; namely:

$$i\gamma^\nu\partial_\nu\psi=m\psi, \quad (6.32)$$

where

$$\gamma^\nu\gamma^\mu+\gamma^\mu\gamma^\nu=2g^{\nu\mu}.$$

This equation could be derived formally from a "classical" mass function:

$$M(p)=\gamma^\nu p_\nu \quad (6.33)$$

but the question of convergence of the path integral seems much more complicated than it was for the scalar equation due to the fact that γ^1, γ^2, and γ^3 are anti-Hermitian matrices. We shall not consider the Dirac equation here.

VII. ACKNOWLEDGMENTS AND FURTHER REFERENCES

The author gratefully acknowledges the support of the Crocker Nuclear Laboratory and the Atomic Energy Commission while this work was in progress. He also gladly thanks Professor J. Hurley for many suggestions, criticisms, and hours of invaluable conversation on the subjects of this paper.

After this work was completed the author came across a summary[7] of work done by R. Abe[8] on the calculation of the quantum mechanical partition function which is closely related to work presented here. The paper is especially valuable in that, after the transformation from temperature to time variable is made, it completely elucidates the connection between the concepts of the Hamiltonian path integral as the propagator for finite time and the Hamiltonian operator as the propagator for infinitesimal time. The non-relativistic variational principles used here may be found presented clearly and in great detail by J. A. Wheeler.[9] A complete bibliography through 1960 can be found in the review article by S. G. Brush.[7]

APPENDIX A

We consider the special case of a harmonic oscillator with Hamiltonian

$$H=\tfrac{1}{2}(p^2+x^2). \quad (A1)$$

[7] S. G. Brush, Rev. Mod. Phys. **33**, 79 (1961).
[8] R. Abé, Busseiron Kenkyu **79**, 101 (1954).
[9] J. A. Wheeler, "Geometrodynamics and the Issue of the Final State," in *Relativity, Groups, and Topology*, edited by C. DeWitt (Gordon and Breach Science Publishers, Inc., New York, 1963).

CC-0. In Public Domain. Gurukul Kangri Collection, Haridwar

Digitized by Arya Samaj Foundation Chennai and eGangotri

The phase space for the system is the Euclidean x-p plane. Using the canonical transformation:

$$x=(2\rho)^{\frac{1}{2}}\cos\theta \qquad p=(2\rho)^{\frac{1}{2}}\sin\theta \tag{A2}$$

we may map all points in the plane except the origin onto the doubly connected region:

$$0<\rho<\infty \qquad 0\leq\theta\leq 2\pi \tag{A3}$$

where the points $(\rho, 0)$ are identified with the points $(\rho, 2\pi)$. The Hamiltonian in terms of these variables takes the trivial form

$$H=\rho. \tag{A4}$$

We want to derive an equation of motion for the wave function $\psi(\theta, t)$. In calculating the propagator for ψ we shall use the first-order approximation to the path integral since we are interested only in infinitesimal times. (Actually the result is good for all time.) In this approximation we are to take a straight-line path from θ' to θ'' but due to the double-connectedness there are an infinity of such straight-line paths. They must all be included in the first-order contribution. That this is necessary even for infinitesimal time can be seen from the fact that these paths would all make finite contributions to a stationary phase evaluation of the functional integral. Thus, if we denote by K_1 the first-order propagator, we have

$$K_1(\theta'', \theta', t)=\int_{\rho>0} d\rho \sum_{n=-\infty}^{\infty} \exp 2\pi i[\rho(\theta''-\theta'+2\pi n)-\rho t]. \tag{A5}$$

Using the relation:

$$\sum_{n=-\infty}^{\infty} \exp(2\pi i\alpha n)=\sum_{K=-\infty}^{\infty} \delta(\alpha-K) \tag{A6}$$

we obtain

$$K_1(\theta'', \theta', t)=(2\pi)^{-1}\sum_{K=1}^{\infty} \exp iK(\theta''-\theta'-t). \tag{A7}$$

This equation indicates that the values of $\psi(\theta, t)$ considered as mapped on a unit circle rotate with constant angular velocity in complete analogy with the classical phase–space density. The energy spectrum has the same structure as the well-known harmonic oscillator spectrum but is shifted by a constant. ($\frac{1}{2}\hbar\omega$ in the usual notation.) One could dismiss this shift with the observation that the addition of a constant to the classical Hamiltonian is itself a canonical transformation but it does seem to lessen the likelihood that a free use of canonical transformations before quantization is allowed. As $t\to 0$, $K(\theta'', \theta', t)$ does not approach $\delta(\theta''-\theta')$ but it does approach the unit operator on the subspace of positive energy states. That the first-order propagator in this case is exact for finite time can easily be seen from the fact that it satisfies the equation:

$$K_1(\theta'', \theta', t)=\int_0^{2\pi} d\theta K_1(\theta'', \theta, t-\tau)K_1(\theta, \theta', \tau).$$

APPENDIX B

Given the τ-dependent propagator:

$$K(x, \tau)=\int d^4p \exp 2\pi i[-px+\tau(p^2)^{\frac{1}{2}}].$$

We want to investigate the properties of the Green's function (of the mass eigenvalue equation) defined by

$$G(x, m)\equiv\int_0^{\infty} d\tau K(x, \tau) \exp[-2\pi i(m-i\epsilon)\tau].$$

Carrying out the τ integration and defining a variable $q\equiv|\mathbf{p}|$ we obtain:

$$G=\frac{i}{2\pi}\int d^3p \exp(2\pi i\mathbf{p}\cdot\mathbf{x})I(q)$$

where

$$I(q)=\int_C dp_0 \exp(-2\pi i x_0 p_0)/(p_0^2-q^2)^{\frac{1}{2}}-(m-i\epsilon)$$

and the contour C is shown in Fig. 4.

The denominator vanishes at two points infinitesimally inside the second sheet at which: $u=\pm(m^2+q^2)^{\frac{1}{2}}$.

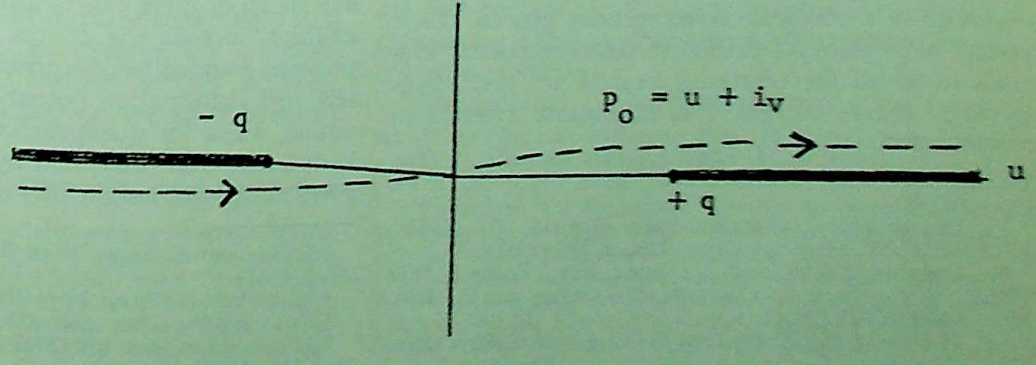

FIG. 4. Path of integration.

CC-0. In Public Domain. Gurukul Kangri Collection, Haridwar

Digitized by Arya Samaj Foundation Chennai and eGangotri

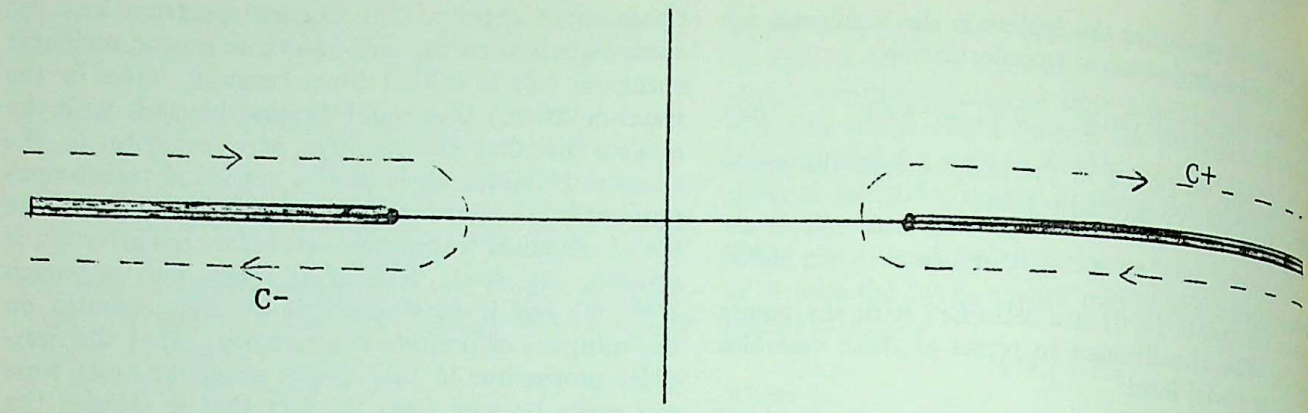

FIG. 5. Deformed paths of integration.

If $x_0>0$ the contour C may be deformed into the contour $C+$ shown in Fig. 5, while if $x_0<0$ the contour C may be deformed into the contour $C-$.

Thus, for $x_0>0$, the integral may be converted into one involving only positive frequencies, while for $x_0<0$ it may be converted into an integral over negative frequencies. The author has not succeeded in obtaining an explicit evaluation of the integrals.

Note added in proof. Since this article was submitted for publication, the author has become aware of some earlier work done on the subject. The earliest derivation of the Hamiltonian path-integral method can be found in Appendix B of R. Feynman, Phys. Rev. 84, 108 (1951). See also: W. Tobocman, Nuovo Cimento 3, 1213 (1956); and H. Davies, Proc. Cambridge Phil. Soc. **59**, 147 (1963).

REVIEWS OF MODERN PHYSICS VOLUME 38, NUMBER 3 JULY 1966

High-Frequency Conductivity of a Solid-State Plasma with Dynamically Screened Interactions. I. Thermal Equilibrium

D. E. McCUMBER
Bell Telephone Laboratories, Murray Hill, New Jersey

Dawson–Oberman high-frequency long-wavelength conductivities of solid-state plasmas in thermal equilibrium are derived using a variational formalism. These derivations are different from those of other authors and give additional insight into the nature of the approximations implicit in their results. The final expressions reflect screened carrier–carrier and carrier–phonon interactions. They extend published conductivity formulas principally in their inclusion of deformation-potential phonon–carrier coupling.

1. INTRODUCTION

It has been demonstrated by Perel' and Eliashberg[1] and by Dawson and Oberman[2] how dynamic electron screening of static ions affects the high-frequency conductivity of a classical one-component plasma. Their results have been generalized to multicomponent systems in which the scattering centers are themselves dynamic charge carriers,[3,4] to degenerate systems in which the carriers are described by quantum statistics,[5,6] and to solid systems in which the carriers are scattered by polar lattice vibrations (polar phonons).[7,8] In this paper we derive general conductivity expressions which include all of these effects simultaneously and which in addition include the effects of carrier scattering by phonons coupled to the carriers through a dynamically screened deformation potential. Our method of derivation, valid for quantum and for classical statistics, is different from that used by previous authors[1–8] and gives additional insight into the nature of the approxi-

[1] V. I. Perel' and G. M. Éliashberg, Zh. Eksperim. i Teor. Fiz. **41**, 886 (1961) [English transl.: Soviet Phys.—JETP **14**, 633 (1962)].
[2] J. Dawson and C. Oberman, Phys. Fluids **5**, 517 (1962); J. Dawson and C. Oberman, Phys. Fluids **6**, 394 (1963).
[3] C. Oberman, A. Ron, and J. Dawson, Phys. Fluids **5**, 1514 (1962); R. Guernsey, C. Oberman, J. Dawson, and A. Ron, Phys. Fluids **7**, 921 (1964).
[4] D. F. Dubois, V. Gilinsky, and M. G. Kivelson, Phys. Rev. **129**, 2376 (1963).
[5] A. Ron and N. Tzoar, Phys. Rev. **131**, 12 (1963); [E] **132**, 2800 (1963).
[6] A. Ron and N. Tzoar, Phys. Rev. **131**, 1943 (1963).
[7] N. Tzoar, Phys. Rev. **132**, 202 (1963).
[8] A. Ron, Phys. Rev. **131**, 2041 (1963); A. Ron and N. Tzoar, *ibid.* **133**, A1378 (1964).

CC-0. In Public Domain. Gurukul Kangri Collection, Haridwar

Digitized by Arya Samaj Foundation Chennai and eGangotri

mations implicit in their results. To simplify the analysis, we only consider homogeneous isotropic materials for which the carrier kinetic energy is described by a scalar effective mass. We assume in this paper that the carrier-phonon system is in thermal equilibrium; in a second paper we consider steady-state systems with drifting carriers.

Our derivations emphasize the dynamic self-consistent fields interacting with the carriers. Because charged particles and polar phonons interact with carriers through a common electric field and because this field is different from the field relevant to the interaction of carriers with deformation-potential phonons, we can anticipate that deformation-potential phonons affect the Dawson–Oberman conductivity in a fundamentally different way from the polar phonons, as indeed is found in Sec. 5. Deformation-potential coupling can be important even in some polar materials. For example, as we shall discuss in detail in a later paper, in room-temperature GaAs it significantly damps the single-stream instability of McCumber and Chynoweth,[9] whereas polar optical-phonon and piezoelectric-phonon effects are negligible.

The general conditions under which the Dawson–Oberman approach obtains have been discussed by other authors.[4–8] The three basic requirements are (i) that the number of particles in the Debye sphere be large,[10] (ii) that the driving frequency ω be large relative to the cumulative 90° collision frequency ν_c of the particles, and (iii) that the Born approximation describe carrier scattering by the dynamically screened potentials. These conditions insure that the principal collective modes of the plasma are described by a Vlasov, random-phase, or effective-field approximation[11] and that, once screening has been properly taken into account, scattering collisions may be treated perturbatively. Provided only that $\omega > \nu_c$, there is no restriction on the frequency ω and, in particular, it may range over plasma resonance frequencies. Consistent with previous authors, we restrict our treatment to the long-wavelength limit ($k = 2\pi/\lambda \to 0$). This is the case of primary interest because it is in this limit that Landau damping is ineffective. Because Landau damping is of lower order in the interaction parameters than the scattering mechanisms we consider, it is expected to dominate at short wavelengths.

To introduce notation and to place subsequent generalizations in their proper perspective, let us briefly review previous results. Consider initially a single species (effective mass m, charge e, average density n) of charge carriers which interact with statistically distributed static impurity ions of charge Ze and average density $n_I = N_I/V$.[12] To lowest order in the collision frequency, the complex high-frequency long-wavelength ($k \to 0$) conductivity for such a system is[1,2,6,13]

$$\tilde{\sigma}(\omega+i\epsilon) = \lim_{k\to 0} \tilde{\sigma}(\omega)^0 \left\{1 - \frac{Z^2e^2n_I}{m\omega^2} \int \frac{(dk'')}{(2\pi)^3} \left(\frac{\mathbf{e}\cdot\mathbf{k}''}{k''}\right)^2 + \left[\frac{1}{\epsilon(\mathbf{k}''; \omega+i\epsilon)^0} - \frac{1}{\epsilon(\mathbf{k}; 0)^0}\right] C_I(\mathbf{k}'')\right\}, \quad (1.1)$$

where $\mathbf{e}$ is a unit vector in the direction of the electric field, where

$$\tilde{\sigma}(\omega)^0 = ie^2n/\omega m \quad (1.2)$$

is the free-particle conductivity, and where

$$C_I(\mathbf{k}'') = \langle N_I^{-1} \sum_{ij} \exp\left[i\mathbf{k}''\cdot(\mathbf{R}_i - \mathbf{R}_j)\right]\rangle \quad (1.3)$$

characterizes ion spatial correlations. The ensemble average in (1.3) is over all admissible ion configurations; for randomly distributed ions $C_I(\mathbf{k}'') = 1$.

The function $\epsilon(\mathbf{k}; \omega+i\epsilon)^0$ in Eq. (1.1) is the finite-wavelength collisionless dielectric function appropriate to no impurity scattering. It is a Vlasov or self-consistent-field approximation to the dielectric function $\epsilon(\mathbf{k}; \omega+i\epsilon)$, where this latter function describes the retarded electric displacement produced by a longitudinal electric field of wave vector $\mathbf{k}$ and frequency ω. [For a longitudinal field the unit vector $\mathbf{e}$ in (1.1) is parallel to $\mathbf{k}$.] If ϵ_∞ is the high-frequency dielectric constant of the host material and if

$$\hbar v(k) = 4\pi e^2/k^2V \quad (1.4)$$

is the Fourier transform of the Coulomb interaction between carriers, then

$$\epsilon(\mathbf{k}; z)^0 = \epsilon_\infty - v(k)\, R'(\mathbf{k}; z)^0, \quad (1.5)$$

where

$$R'(\mathbf{k}; z)^0 = \sum_{\mathbf{k}_1} R'(\mathbf{k}; \mathbf{k}_1; z)^0, \quad (1.6a)$$

$$R'(\mathbf{k}; \mathbf{k}_1; z)^0 = \left[N(\mathbf{k}_1 - \tfrac{1}{2}\mathbf{k}) - N(\mathbf{k}_1 + \tfrac{1}{2}\mathbf{k})\right]/(z - \hbar\mathbf{k}\cdot\mathbf{k}_1/m) \quad (1.6b)$$

are free-particle density propagators. The extensive parameters $N(\mathbf{k}_1)$ describe the average momentum distribution of carriers.

The functions (1.6) are analytic functions of z everywhere except on the real axis. In evaluating the $\mathbf{k}_1$

---

[9] D. E. McCumber and A. G. Chynoweth, Phys. Rev. Letters 13, 651 (1964).

[10] If n is the density of carriers of charge e and mass m, condition (i) requires $4\pi n\, r_0^3/3 \gg 1$, where for a degenerate Fermi–Dirac distribution $r_0 = 1/k_{FT} = (\hbar/2e)m^{\frac{1}{2}} \times (\pi/3n)^{1/6}$ and for a temperature-T Maxwell–Boltzmann distribution $r_0 = 1/k_D = (kT/4\pi ne^2)^{\frac{1}{2}}$. Physically this condition ensures that the mean potential energy between carriers is small relative to their mean kinetic energy.

[11] P. A. Wolff, Phys. Rev. **126**, 405 (1962).

[12] We assume that the impurity ions are uniformly distributed on the average and than any excess charge is compensated by a suitable uniform background distribution.

[13] Throughout this paper we assume $\omega \gg \nu_c > 0$ real and $\epsilon = 0^+$. We represent general complex frequencies by z, a special case of which is $z = \omega + i\epsilon$. Fourier transforms $F(\mathbf{k}, \omega) = \int (dr)\, dt f(\mathbf{r}, t) \times \exp(i\omega t - i\mathbf{k}\cdot\mathbf{r})$ and $f(\mathbf{r}, t) = (1/V)\sum_{\mathbf{k}} \int (d\omega/2\pi) F(\mathbf{k}, \omega) \times \exp(-i\omega t + i\mathbf{k}\cdot\mathbf{r})$.

CC-0. In Public Domain. Gurukul Kangri Collection, Haridwar

Digitized by Arya Samaj Foundation Chennai and eGangotri

summation of (1.6a), we freely make the large-volume replacement

$$\sum_{\mathbf{k}_1} \leftrightarrow V \int (dk_1)/(2\pi)^3 \tag{1.7}$$

already used in the derivation of Eq. (1.1). We use the convention that principal-value integrals are understood whenever the argument z is purely real, as it is, for example, in $\epsilon(\mathbf{k}''; 0)^0$ of Eq. (1.1). For complex z the integrals are unambiguous.

The dielectric function and the electrical conductivity are related. For a homogeneous isotropic medium such as we consider here the long-wavelength conductivity, excluding ϵ_∞ displacement-current contributions, is

$$\tilde{\sigma}(z) = \lim_{k\to 0} [\epsilon(\mathbf{k}; z) - \epsilon_\infty] z/4\pi i. \tag{1.8}$$

Approximating $\epsilon(\mathbf{k}; z)$ in (1.8) by the collisionless function (1.5), we correctly obtain the free-particle conductivity (1.2). Representative dielectric functions appropriate to Dawson–Oberman conductivities like that of Eq. (1.1) are computed in subsequent sections.

The real part of the conductivity (1.1), that part associated with energy dissipation and Joule heating, is[13]

$$\sigma(\omega) \equiv \mathrm{Re}\,\tilde{\sigma}(\omega + i\epsilon) = \frac{e^4 Z^2 n n_I}{\omega^3 m^2} \int \frac{(dk'')}{(2\pi)^3} \left(\frac{\mathbf{e}\cdot\mathbf{k}''}{k''}\right)^2 \frac{\mathrm{Im}\,\epsilon(\mathbf{k}''; \omega - i\epsilon)^0}{|\,\epsilon(\mathbf{k}''; \omega - i\epsilon)^0\,|^2}. \tag{1.9}$$

If Eqs. (1.5) and (1.6) are used to express $\mathrm{Im}\,\epsilon(\mathbf{k}''; \omega - i\epsilon)^0$ in terms of the momentum distribution parameters $N(\mathbf{k}_1)$, Eq. (1.9) can be interpreted in terms of the elementary processes indicated in Fig. 1(b). A charge carrier, in scattering from an ionized impurity, emits or absorbs an electric-field quantum of wave vector $\mathbf{k}$ and frequency ω. The interaction strength at the scattering vertex is proportional to

$$Zv(k)/|\,\epsilon(\mathbf{k}; \omega - i\epsilon)^0\,|,$$

the Coulomb potential $Zv(k)$ dynamically screened by the dielectric function $\epsilon(\mathbf{k}; \omega - i\epsilon)^0$.

The diagrams of Fig. 1(b) should be contrasted with those of Fig. 1(a), which relate to free-carrier conduction. In the free-carrier processes of Fig. 1(a) both energy and momentum are conserved, whereas in the impurity-moderated processes of Fig. 1(b) the carriers transfer momentum to the ionized impurities. The restrictions of energy and momentum conservation in the processes of Fig. 1(a) prevent the emission or absorption of long-wavelength finite-frequency field quanta. A consequence is that the free-particle conductivity (1.2) is purely reactive (imaginary). Real absorption and emission processes can occur if the wavelength of the field quanta is sufficiently short [$k/\omega \gtrsim k_f$ for a degenerate Fermi–Dirac distribution or $k/\omega \gtrsim (2m\kappa T/\hbar^2)^{\frac{1}{2}}$ for a temperature-T Maxwell–Boltzmann distribution]. These are associated with familiar Landau damping.

Equations (1.1) and (1.9) pertain to carrier scattering by fixed ions. The corresponding expressions[4] appropriate to mobile ions of finite mass are somewhat more complicated, because the moving ions contribute to the electric current and because in their recoil after collisions the ions can absorb energy as well as momentum. Consider a system composed of several different species s of mobile charge carriers, each species characterized by its charge $Z_s e$, effective mass m_s, and average momentum distribution $N(\mathbf{k}_1)_s$. For each species we define auxiliary functions analogous to the functions (1.6). In terms of these functions the collisionless dielectric function of the Vlasov or self-consistent-field approximation is [compare Eq. (1.5)]

$$\epsilon(\mathbf{k}; z)^0 = \epsilon_\infty - v(k) \sum_s Z_s^2 R'(\mathbf{k}; z)_s{}^0. \tag{1.10}$$

Dawson–Oberman collision corrections to this dielectric function are computed in Sec. 3. Using that corrected dielectric function in Eq. (1.8), we are led to generalizations of Eqs. (1.1) and (1.9) which are equivalent (cf. Appendix B) to those found by Ron and Tzoar[14]:

$$\tilde{\sigma}(\omega + i\epsilon) = \tilde{\sigma}(\omega)^0 + i\tfrac{1}{2} \sum_{\mathbf{k}''} \frac{e^2}{\hbar\omega^3 V} [\hbar v(k'')\mathbf{e}\cdot\mathbf{k}'']^2 \sum_{ss'} Z_s^2 Z_{s'}^2 \left(\frac{Z_s^2}{m_s^2} - \frac{Z_s Z_{s'}}{m_s m_{s'}}\right) \left(\int_{-\infty}^{\infty} \frac{d\omega_1 d\omega_2}{\pi^2} \frac{\coth(\beta\omega_1/2)}{\omega + i\epsilon - (\omega_1 - \omega_2)} \times \mathfrak{F}\{[R'(\mathbf{k}''; \omega_1)_s{}^0 - R'(\mathbf{k}''; \omega_2)_s{}^0][R'(\mathbf{k}''; \omega_1)_{s'}{}^0 - R'(\mathbf{k}''; \omega_2)_{s'}{}^0]/\epsilon(\mathbf{k}''; \omega_1)^0 \epsilon(\mathbf{k}''; \omega_2)^0\} - \int_{-\infty}^{\infty} \frac{d\bar{\omega}}{\pi} \coth(\beta\bar{\omega}/2) \mathfrak{F}\left\{\frac{R'(\mathbf{k}''; \bar{\omega})_s{}^0 R'(\mathbf{k}''; \bar{\omega})_{s'}{}^0}{\epsilon_\infty \epsilon(\mathbf{k}''; \bar{\omega})^0}\right\}\right), \tag{1.11a}$$

$$\sigma(\omega) \equiv \mathrm{Re}\,\tilde{\sigma}(\omega + i\epsilon) = \underset{\omega\neq 0}{\tfrac{1}{2}} \sum_{\mathbf{k}''} \frac{e^2}{\hbar\omega^3 V} [\hbar v(k'')\mathbf{e}\cdot\mathbf{k}'']^2 \sum_{ss'} Z_s^2 Z_{s'}^2 \left(\frac{Z_s^2}{m_s^2} - \frac{Z_s Z_{s'}}{m_s m_{s'}}\right) \int_{-\infty}^{\infty} \frac{d\omega_1}{\pi} \coth(\beta\omega_1/2) \times \mathfrak{F}\{[R'(\mathbf{k}''; \omega_1)_s{}^0 - R'(\mathbf{k}''; \omega_2)_s{}^0][R'(\mathbf{k}''; \omega_1)_{s'}{}^0 - R'(\mathbf{k}''; \omega_2)_{s'}{}^0]/\epsilon(\mathbf{k}''; \omega_1)^0 \epsilon(\mathbf{k}''; \omega_2)^0\}_{\omega_2 = \omega_1 - \omega}. \tag{1.11b}$$

[14] Equation (33), Ref. 5, is equivalent (cf. Appendix B) to our Eq. (1.11a). Our $R'(\mathbf{k}; z)_s{}^0$ and $\epsilon(\mathbf{k}; z)^0$ correspond to Wilkie's simple factors to their $Q_a(z, s)$ and $1/U_a(z)$, respectively.

CC-0. In Public Domain. Gurukul Kangri Collection, Haridwar

Digitized by Arya Samaj Foundation Chennai and eGangotri

In Eq. (1.11a)

$$\tilde{\sigma}(\omega)^0 = \sum_s i(Z_s e)^2 n_s/m_s\omega \qquad (1.12)$$

is the free-carrier conductivity obtained by using (1.10) in Eq. (1.8). The real functionals $\mathfrak{F}\{\cdots\}$ are defined as follows.

If $g(\omega_1)$ and $f(\omega_1, \omega_2)$ are real functions of the real frequencies ω_1 and ω_2, we define

$$\mathfrak{F}\{g(\omega_1)\} \equiv (i/2)\{g(\omega_1+i\epsilon) - g(\omega_1-i\epsilon)\}, \qquad (1.13a)$$

$$\mathfrak{F}\{f(\omega_1,\omega_2)\} \equiv (i/2)^2\{f(\omega_1+i\epsilon, \omega_2+i\epsilon) - f(\omega_1-i\epsilon, \omega_2+i\epsilon) - f(\omega_1+i\epsilon, \omega_2-i\epsilon) + f(\omega_1-i\epsilon, \omega_2-i\epsilon)\}, \qquad (1.13b)$$

where $\epsilon = 0^+$. If the function $f(\omega_1, \omega_2)$ is separable in the sense that

$$f(\omega_1,\omega_2) = \sum_{m=1}^{M} g_{m1}(\omega_1)\, g_{m2}(\omega_2), \qquad M < \infty, \qquad (1.14a)$$

it follows easily from the definitions (1.13) that

$$\mathfrak{F}\{f(\omega_1,\omega_2)\} = \sum_{m=1}^{M} \mathfrak{F}\{g_{m1}(\omega_1)\}\mathfrak{F}\{g_{m2}(\omega_2)\}. \qquad (1.14b)$$

The functionals (1.13) enter our formulas as *spectral functions* characterizing the intrinsic frequency or energy spectra of their arguments. For example, using

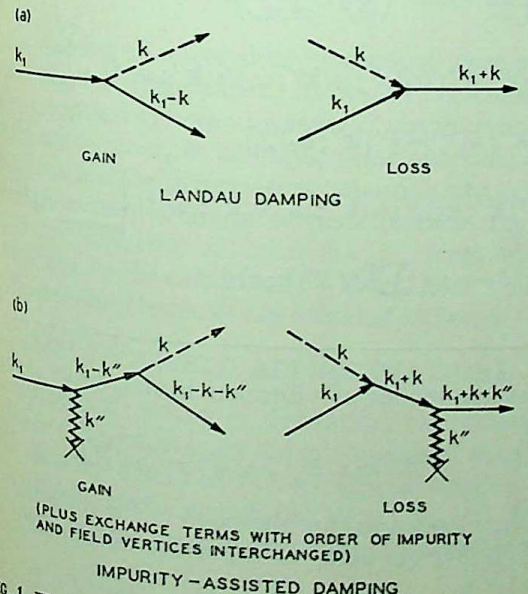

FIG. 1. Elementary processes contributing to the conductivity of a system of charged carriers. Diagrams (a) show processes relevant to Landau damping in which the carrier (solid line) emits (GAIN) or absorbs (LOSS) a quantum of the perturbing electric field (dashed line). Diagrams (b) show processes in which the carrier is scattered through interaction (folded line) with a fixed impurity.

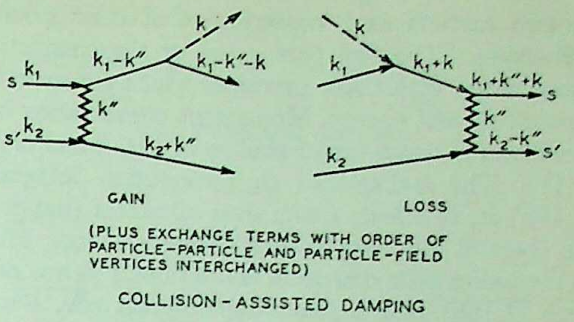

FIG. 2. Elementary two-carrier-collision processes contributing to the conductivity of a multicomponent plasma. A quantum of the perturbing electric field (dashed line) is emitted (GAIN) or absorbed (LOSS) by a charge carrier (solid line) of species s which collides or interacts (folded line) with a carrier of species s'.

(1.6b) with (1.13a), we find that[15]

$$\mathfrak{F}\{R'(\mathbf{k};\mathbf{k}_1;\omega)^0\} = \pi[N(\mathbf{k}_1-\tfrac{1}{2}\mathbf{k}) - N(\mathbf{k}_1+\tfrac{1}{2}\mathbf{k})]\delta(\omega-\hbar\mathbf{k}\cdot\mathbf{k}_1/m) \qquad (1.15a)$$

$$= \pi\{[1\pm N(\mathbf{k}_1+\tfrac{1}{2}\mathbf{k})]N(\mathbf{k}_1-\tfrac{1}{2}\mathbf{k}) - [1\pm N(\mathbf{k}_1-\tfrac{1}{2}\mathbf{k})]N(\mathbf{k}_1+\tfrac{1}{2}\mathbf{k})\} \times \delta[\omega-\hbar(\mathbf{k}_1+\tfrac{1}{2}\mathbf{k})^2/2m+\hbar(\mathbf{k}_1-\tfrac{1}{2}\mathbf{k})^2/2m]. \qquad (1.15b)$$

This can be recognized as the free-carrier excitation spectrum of the effective-mass approximation.

In a plasma in which carrier interactions are taken into account through a Vlasov or self-consistent-field approximation the excitation spectrum of "dressed" carriers is more appropriately described by

$$\mathfrak{F}\{R'(\mathbf{k};\mathbf{k}_1;\omega)^0/\epsilon(\mathbf{k};\omega)^0\}$$

than it is by the spectrum (1.15). Returning to Eq. (1.11b), we see that the spectral function of the last integral is of the form (1.14) with two distinct types of terms in its decomposition (1.14b): those of the type

$$\mathfrak{F}\{R'(\mathbf{k}'';\omega_1)_s{}^0/\epsilon(\mathbf{k}'';\omega_1)^0\}\mathfrak{F}\{R'(\mathbf{k}'';\omega_2)_{s'}{}^0/\epsilon(\mathbf{k}'';\omega_2)^0\} \qquad (1.16a)$$

and those of the type

$$\mathfrak{F}\{R'(\mathbf{k}'';\omega_1)_s{}^0 R'(\mathbf{k}'';\omega_1)_{s'}{}^0/\epsilon(\mathbf{k}'';\omega_1)^0\}\mathfrak{F}\{\epsilon^{-1}(\mathbf{k}'';\omega_2)^0\}. \qquad (1.16b)$$

Noting that (1.16a) is the product of two dressed-carrier spectral functions, we can interpret their contribution to (1.11b) physically in terms of the elementary processes of Fig. 2 in which an electric-field quantum of wave vector $\mathbf{k}$ and frequency ω is emitted or absorbed by one of a pair of interacting dressed charge carriers.[16] The field momentum and energy is partitioned between

[15] The upper signs in Eq. (1.15b) apply to carriers which are bosons, the lower to fermions.

[16] Figures 1–3 have been introduced to distinguish the different physical contributions to the conductivity. They are not meant to illustrate the totality of Feynman-like "diagrams" which, in the context of one of several specific calculational formalisms, have been included in our results. Interested readers will find the latter diagrams illustrated in Refs. 5 and 7 and in the second of Ref. 8.

CC-0. In Public Domain. Gurukul Kangri Collection, Haridwar

Digitized by Arya Samaj Foundation Chennai and eGangotri

the two carriers as a consequence of their Coulomb interaction. [The real part $\sigma_k(\omega)$ of the conductivity is associated with those processes which conserve both momentum and energy. Momentum conservation is ensured by the wave-vector choices of Fig. 2 and of Eqs. (1.11). The ω-displaced ω_1 convolution integral in (1.11b) is, in effect, a sum over all states (implicit in the spectral functions) which conserve energy, subject to the indicated momentum restrictions.] Terms of the type (1.16b) play a somewhat different role. Because the two particles of Fig. 2 both propagate through the same medium, because both particles thereby see the same effective field as it is reflected in the dielectric function $\epsilon(\mathbf{k}'';z)^0$ of Eq. (1.10), and because both particles contribute to that dielectric function, the dynamics of the two particles are not independent but are correlated through the dielectric response. The terms (1.16b) are "correlation corrections" compensating for this fact.

The preceding results pertain to systems of interacting charged particles. This model is generalized in Sec. 4 to include polar lattice vibrations.[7,8] Using the dielectric function derived there, we find from Eq. (1.8) that[17]

$$\tilde{\sigma}(\omega+i\epsilon)=\tilde{\sigma}(\omega)^0+i\tfrac{1}{2}\sum_{\mathbf{k}''}\frac{e^2}{\hbar\omega^3 V}[\hbar v(k'')\mathbf{e}\cdot\mathbf{k}'']^2\Bigg[\sum_{ss'}Z_s^2Z_{s'}^2\left(\frac{Z_s^2}{m_s^2}-\frac{Z_sZ_{s'}}{m_sm_{s'}}\right)\Bigg(\int_{-\infty}^{\infty}\frac{d\omega_1\,d\omega_2}{\pi^2}\frac{\coth(\beta\omega_1/2)}{\omega+i\epsilon-(\omega_1-\omega_2)}$$
$$\times\mathfrak{F}\{[R'(\mathbf{k}'';\omega_1)_s{}^0-R'(\mathbf{k}'';\omega_2)_s{}^0][R'(\mathbf{k}'';\omega_1)_{s'}{}^0-R'(\mathbf{k}'';\omega_2)_{s'}{}^0]/\epsilon(\mathbf{k}'';\omega_1)^0\epsilon(\mathbf{k}'';\omega_2)^0\}$$
$$-\int_{-\infty}^{\infty}\frac{d\bar{\omega}}{\pi}\coth(\beta\bar{\omega}/2)\mathfrak{F}\left\{\frac{R'(\mathbf{k}'';\bar{\omega})_s{}^0R'(\mathbf{k}'';\bar{\omega})_{s'}{}^0}{\epsilon_\infty\epsilon(\mathbf{k}'';\bar{\omega})^0}\right\}\Bigg)+\sum_s\sum_r(Z_s^4/m_s^2)|\,p_r(\mathbf{k}'')|^2$$
$$\times\Bigg(\int_{-\infty}^{\infty}\frac{d\omega_1\,d\omega_2}{\pi^2}\frac{\coth(\beta\omega_1/2)}{\omega+i\epsilon-(\omega_1-\omega_2)}\mathfrak{F}\{[R'(\mathbf{k}'';\omega_1)_s{}^0-R'(\mathbf{k}'';\omega_2)_s{}^0]$$
$$\times[A'(\mathbf{k}'';\omega_1)_r{}^0-A'(\mathbf{k}'';\omega_2)_r{}^0]/\epsilon(\mathbf{k}'';\omega_1)^0\epsilon(\mathbf{k}'';\omega_2)^0\}-\int_{-\infty}^{\infty}\frac{d\bar{\omega}}{\pi}\coth(\beta\bar{\omega}/2)\mathfrak{F}\left\{\frac{R'(\mathbf{k}'';\bar{\omega})_s{}^0A'(\mathbf{k}'';\bar{\omega})_r{}^0}{\epsilon_\infty\epsilon(\mathbf{k}'';\bar{\omega})^0}\right\}\Bigg)\Bigg] \quad (1.17a)$$

and that

$$\sigma(\omega)\equiv\operatorname{Re}\tilde{\sigma}(\omega+i\epsilon)$$
$$=\underset{\omega\neq0}{\sigma(\omega)^0}+\tfrac{1}{2}\sum_{\mathbf{k}''}\frac{e^2}{\hbar\omega^3V}[\hbar v(k'')\mathbf{e}\cdot\mathbf{k}'']^2\int_{-\infty}^{\infty}\frac{d\omega_1}{\pi}\coth(\beta\omega_1/2)\Bigg[\sum_{ss'}Z_s^2Z_{s'}^2\left(\frac{Z_s^2}{m_s^2}-\frac{Z_sZ_{s'}}{m_sm_{s'}}\right)$$
$$\times\mathfrak{F}\{[R'(\mathbf{k}'';\omega_1)_s{}^0-R'(\mathbf{k}'';\omega_2)_s{}^0][R'(\mathbf{k}'';\omega_1)_{s'}{}^0-R'(\mathbf{k}'';\omega_2)_{s'}{}^0]/\epsilon(\mathbf{k}'';\omega_1)^0\epsilon(\mathbf{k}'';\omega_2)^0\}$$
$$+\sum_s\sum_r(Z_s^4/m_s^2)|\,p_r(\mathbf{k}'')|^2\mathfrak{F}\{[R'(\mathbf{k}'';\omega_1)_s{}^0-R'(\mathbf{k}'';\omega_2)_s{}^0]$$
$$\times[A'(\mathbf{k}'';\omega_1)_r{}^0-A'(\mathbf{k}'';\omega_2)_r{}^0]/\epsilon(\mathbf{k}'';\omega_1)^0\epsilon(\mathbf{k}'';\omega_2)^0\}\Bigg]_{\omega_2=\omega_1-\omega}, \quad (1.17b)$$

where

$$\epsilon(\mathbf{k};z)^0=\epsilon_\infty-v(k)\sum_r|\,p_r(\mathbf{k})|^2A'(\mathbf{k};z)_r{}^0-v(k)\sum_s{}'Z_s^2R'(\mathbf{k};z)_s{}^0 \quad (1.18)$$

is the dielectric function of the collisionless system, where $\tilde{\sigma}(\omega)^0$ is the conductivity obtained by using (1.18) in (1.8), and where $A'(\mathbf{k};z)_r{}^0$ is the free-phonon propagator analogous to the particle propagators $R'(\mathbf{k};z)_s{}^0$. If in a harmonic lattice of cubic symmetry $\omega_{\mathbf{k}}{}^r=\omega_{-\mathbf{k}}{}^r$ are the frequencies in phonon branch r of the transverse modes of vibration having wave vector $\mathbf{k}$, then[18]

$$A'(\mathbf{k};z)_r{}^0=2\omega_{\mathbf{k}}{}^r/[z^2-(\omega_{\mathbf{k}}{}^r)^2]. \quad (1.19)$$

The frequencies $\omega_{\mathbf{k}}{}^r$ are the poles of the dielectric function (1.18); the zeros of the dielectric function relate

[17] Although parts of Eq. (1.17) are similar in form to Eq. (1.11), the collisionless dielectric function $\epsilon(\mathbf{k}'';z)^0$ used in the two equations is different.

[18] The function $A'(\mathbf{k};z)_r{}^0$ differs from the similar function $D_k(z)$ of Ron and Tzoar, Refs. 7 and 8, in that the frequencies of the latter function are renormalized to absorb the phonon–phonon components of the polar interaction Hamiltonian (4.3) below. For this same reason the dielectric function (20), Ref. 7, has a different form from our (1.18), although the two expressions are equivalent. [Phonon renormalization arises again in Eq. (4.14)ff below.] When it is specialized to a single species of carrier and to a single species of polar phonon, Eq. (1.17a) can be shown (cf. Appendix B) to be equivalent to Eq. (27), Ref. 7.

CC-0. In Public Domain. Gurukul Kangri Collection, Haridwar

Digitized by Arya Samaj Foundation Chennai and eGangotri

to the longitudinal lattice vibrations.[19,20] The phonon–particle coupling parameters $p_r(\mathbf{k})$ in Eqs. (1.17) and (1.18) are a measure of the polar character of the $(\mathbf{k}, r)$ vibration.[21]

The interpretation of Eqs. (1.17) parallels that of Eqs. (1.11). In addition to the single-carrier and single-phonon resonant "Landau" processes of the collisionless approximation [Figs. 1(a) and 3(a)] and to the two-carrier processes of Fig. 2, the conductivity (1.17) includes phonon–carrier processes of the type indicated in Fig. 3(b), in which field momentum and energy is partitioned between a carrier and a polar phonon.[16] The excitation spectrum of the "dressed" phonons is contained in $\mathfrak{F}\{A'(\mathbf{k};\omega)_r{}^0/\epsilon(\mathbf{k};\omega)^0\}$. Because this spectrum also contains collective particle effects,[20] the integrands of Eqs. (1.17) contain correlation corrections analogous to those previously noted in Eqs. (1.11).

Equations (1.17) pertain to carriers plus polar phonons. The simplifying feature of this system is that the charged particles and the lattice vibrations couple through the same electrostatic field. More general carrier-phonon interactions—for example, those relevant to deformation-potential coupling—are considered in Sec. 5 where we develop the necessary notation for their discussion.

The results of the present paper apply to systems which, in the absence of the high-frequency perturbing field, are in thermal equilibrium. The basic variational technique underlying our method of derivation is outlined in Sec. 2. A related but slightly more complicated technique applies when thermal equilibrium does not obtain.[22] We shall use this technique in a second paper concerned with the high-frequency Dawson–Oberman conductivity of steady-state systems having drifting carriers.

Three systems of successively increasing generality are considered in this paper. In Sec. 3 we consider systems composed of several species of charge carriers; in Sec. 4 we consider, in addition, polar phonons; and in Sec. 5 we include deformation-potential interaction between phonons and charge carriers. In each case we compute the dielectric function $\epsilon(\mathbf{k};z)$, from which conductivities can be calculated by Eq. (1.8).

Brief concluding remarks are included in Sec. 6.

2. EFFECTIVE-FIELD APPROXIMATIONS

To outline our method of derivation, we focus out attention in this section upon a single species of charge-e mass-m particles described in second quantization by annihilation and creation operators $\psi_{\mathbf{k}_1}(t)$, $\psi_{\mathbf{k}_1}{}^\dagger(t)$. Particle density is governed in momentum space by the operator

$$\rho_{\mathbf{k}_1}{}^{\mathbf{k}}(t)=\psi_{\mathbf{k}_1-\frac{1}{2}\mathbf{k}}{}^\dagger(t)\psi_{\mathbf{k}_1+\frac{1}{2}\mathbf{k}}(t)\,; \qquad (2.1)$$

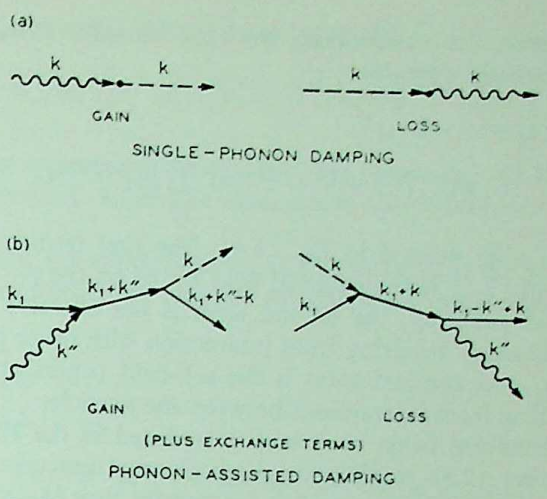

FIG. 3. Elementary phonon processes contributing to the conductivity of a solid-state plasma. Diagrams (a) show simple processes analogous to the Landau processes of Fig. 1(a) in which a quantum of the perturbing electric field (dashed line) is emitted (GAIN) or absorbed (LOSS) with the consequent destruction or excitation of a polar lattice phonon (wavy line). Diagram (b) show processes in which charged particles and phonons share the energy and momentum of the field quantum. For simplicity we have only shown processes in which field-quantum generation is accompanied by phonon annihilation; all combinations are actually included in Eqs. (1.17).

the more familiar spatial-density operator is the Fourier transform

$$\rho(\mathbf{r},t)=V^{-1}\sum_{\mathbf{k}}\exp(i\mathbf{k}\cdot\mathbf{r})\sum_{\mathbf{k}_1}\rho_{\mathbf{k}_1}{}^{\mathbf{k}}(t). \qquad (2.2)$$

We assume that particle dynamics is described by the Hermitian Hamiltonian

$$\begin{aligned}H_e(t)=&\sum_{\mathbf{k}_1}(\hbar^2k_1^2/2m)\rho_{\mathbf{k}_1}{}^0(t)\\&+(\hbar/\epsilon_\infty)\sum_{\mathbf{k}}\{[\phi(\mathbf{k};t)+u(\mathbf{k};t)]\sum_{\mathbf{k}_1}\rho_{\mathbf{k}_1}{}^{-\mathbf{k}}(t)\\&+\tfrac{1}{2}v(k)\sum_{\mathbf{k}_1\mathbf{k}_2}\psi_{\mathbf{k}_1-\frac{1}{2}\mathbf{k}}{}^\dagger(t)\psi_{\mathbf{k}_2+\frac{1}{2}\mathbf{k}}{}^\dagger(t)\psi_{\mathbf{k}_2-\frac{1}{2}\mathbf{k}}(t)\psi_{\mathbf{k}_1+\frac{1}{2}\mathbf{k}}(t)\\&+\xi(\mathbf{k};t)u(-\mathbf{k};t)\}+H_e'(t), \qquad (2.3)\end{aligned}$$

which depends explicitly upon time through external (numerical, not operator) fields such as $\phi(\mathbf{k};t)=\phi(-\mathbf{k};t)^*$ and $\xi(\mathbf{k};t)=\xi(-\mathbf{k};t)^*$. In this Hamiltonian $u(\mathbf{k};t)=u(-\mathbf{k};t)^\dagger$ and $H_e'(t)=H_e'(t)^\dagger$ are operators independent of the fields $\phi(\mathbf{k};t)$, $\xi(\mathbf{k};t)$ and of the particle operators $\psi_{\mathbf{k}_1}(t)$ and $\psi_{\mathbf{k}_1}{}^\dagger(t)$—that is, they depend upon particle species and external fields different from those under scrutiny.

The Hamiltonian (2.3) implies the equations of motion

$$\begin{aligned}i(\partial/\partial t)\psi_{\mathbf{k}_1}(t)=&(\hbar k_1^2/2m)\psi_{\mathbf{k}_1}(t)\\&+\sum_{\mathbf{k}''}w(\mathbf{k}'';t)\psi_{\mathbf{k}_1-\mathbf{k}''}(t), \qquad (2.4a)\\-i(\partial/\partial t)\psi_{\mathbf{k}_1}{}^\dagger(t)=&(\hbar k_1^2/2m)\psi_{\mathbf{k}_1}{}^\dagger(t)\\&+\sum\psi_{\mathbf{k}_1+\mathbf{k}''}{}^\dagger(t)w(\mathbf{k}'';t) \qquad (2.4b)\end{aligned}$$

[19] M. Born and K. Huang, *Dynamical Theory of Crystal Lattices* (Clarendon Press, Oxford, England, 1954), pp. 82–100.
[20] B. B. Varga, Phys. Rev. **137**, A1896 (1965).
[21] Cf. Sec. 4 below.
[22] J. Schwinger, J. Math. Phys. **2**, 407 (1961).

CC-0. In Public Domain. Gurukul Kangri Collection, Haridwar

Digitized by Arya Samaj Foundation Chennai and eGangotri

in which, for conciseness, we have introduced the effective-field *operator*

$$w(\mathbf{k};t)=w(-\mathbf{k};t)^{\dagger}$$
$$=[\phi(\mathbf{k};t)+u(\mathbf{k};t)+v(k)\sum_{\mathbf{k}_1}\rho_{\mathbf{k}_1}{}^{\mathbf{k}}(t)]/\epsilon_\infty \quad (2.5)$$

with $v(k)$ defined in Eq. (1.4). The first term on the rhs of (2.5) is the external field acting on the particles under scrutiny, the second term is the effective field (operator) resulting from interaction with other particles, and the last term is the self-field (operator) resulting from interactions between the particles.

External fields have been introduced in the Hamiltonian (2.3) to simulate weak external perturbations (such as those responsible for current flow in conductivity measurements) and to facilitate the derivation of tractable approximations.[23] Once these external fields have served their formal purposes, we set all external fields identically equal to zero and compute operator expectation values appropriate to the thermal-equilibrium ensemble derived from the stationary Hamiltonian $H=H_e(t)$ with $\phi(\mathbf{k};t)$, etc.$=0$. Formalisms to expedite calculations of this type have been extensively discussed in the literature.[24,25]

Basic to those formalisms are expectation values like

$$\bar{\rho}(\mathbf{k};\mathbf{k}_1;t)_e=\langle\rho_{\mathbf{k}_1}{}^{\mathbf{k}}(t)\rangle_e \quad \text{and} \quad \bar{w}(\mathbf{k};t)_e=\langle w(\mathbf{k};t)\rangle_e \quad (2.6)$$

which are implicitly analytic functions of a complex variable β. In a thermal ensemble of temperature T, $\beta=\hbar/\kappa T$. The subscript "e" in (2.6) will be omitted when the auxiliary external fields in $H_e(t)$ are set equal to zero. The thermal-equilibrium ensemble appropriate to that case is space–time independent, in which case it is convenient to supplement Eqs. (2.6) by the definitions

$$\bar{\rho}(\mathbf{k};\mathbf{k}_1;t)=N(\mathbf{k}_1)\,\delta(\mathbf{k},0), \quad (2.7a)$$
$$[\delta/\delta\eta(\mathbf{k}',t')]\bar{\rho}(\mathbf{k};\mathbf{k}_1;t)_e\,|_{\phi,\text{etc.}=0}$$
$$=\delta(\mathbf{k},\mathbf{k}')\bar{\rho}_\eta'(\mathbf{k};\mathbf{k}_1;t-t'), \quad (2.7b)$$
$$[\delta^2/\delta\eta(\mathbf{k}',t')\,\delta\eta'(\mathbf{k}'',t'')]\bar{\rho}(\mathbf{k};\mathbf{k}_1;t)_e\,|_{\phi,\text{etc.}=0}$$
$$=\delta(\mathbf{k},\mathbf{k}'+\mathbf{k}'')\bar{\rho}_{\eta\eta'}''(\mathbf{k},\mathbf{k}',\mathbf{k}'';\mathbf{k}_1;t,t',t''), \quad (2.7c)$$

etc., where $\eta(\mathbf{k},t)$ and $\eta'(\mathbf{k},t)$ represent any of the several external fields in $H_e(t)$. Boundary conditions appropriate to the calculational formalisms imply typically that

$$\bar{\rho}_\eta'(\mathbf{k};\mathbf{k}_1;t-t')=(i/\beta)\sum_{n=-\infty}^{\infty}R_\eta'(\mathbf{k};\mathbf{k}_1;z_n)\times\exp[-iz_n(t-t')] \quad (2.8a)$$

$$\bar{\rho}_{\eta\eta'}''(\mathbf{k},\mathbf{k}',\mathbf{k}'';\mathbf{k}_1;t,t',t'')=(i/\beta)^2\sum_{n,l=-\infty}^{\infty}R_{\eta\eta'}''(\mathbf{k},\mathbf{k}',\mathbf{k}'';\mathbf{k}_1;z_n,z_l)\times\exp[-iz_n(t-t')]\exp[-iz_l(t-t'')], \quad (2.8b)$$

where $z_n=i2\pi n/\beta$.[26] As in Eq. (1.6a), we also use the abbreviation

$$R_\eta'(\mathbf{k};z)=\sum_{\mathbf{k}_1}R_\eta'(\mathbf{k};\mathbf{k}_1;z) \quad (2.9)$$

where it is convenient. Fourier coefficients W_η' and $W_{\eta\eta'}''$ similar to those defined in Eqs. (2.8) but appropriate to the functions $\bar{w}(\mathbf{k};t)_e$ will be introduced as required. As the notation is meant to suggest, it is useful to view the Fourier coefficients in Eqs. (2.8) as the values taken by analytic functions $R_\eta'(\mathbf{k};\mathbf{k}_1;z)$, etc., at discrete values z_n of their argument z.[27] These functions are intimately related to Fourier–Laplace transforms of system impulse-response functions.

Using the equations of motion (2.4) with the functions $\bar{\rho}(\mathbf{k};\mathbf{k}_1;t)_e$ of Eq. (2.6), we obtain

$$\left(i\frac{\partial}{\partial t}-\frac{\hbar\mathbf{k}\cdot\mathbf{k}_1}{m}\right)\bar{\rho}(\mathbf{k};\mathbf{k}_1;t)_e$$
$$=\sum_{\mathbf{k}''}[\langle\psi_{\mathbf{k}_1-\frac{1}{2}\mathbf{k}}{}^{\dagger}(t)w(\mathbf{k}'';t)\psi_{\mathbf{k}_1-\mathbf{k}''+\frac{1}{2}\mathbf{k}}(t)\rangle-\langle\psi_{\mathbf{k}_1+\mathbf{k}''-\frac{1}{2}\mathbf{k}}{}^{\dagger}(t)w(\mathbf{k}'';t)\psi_{\mathbf{k}_1+\frac{1}{2}\mathbf{k}}(t)\rangle] \quad (2.10a)$$
$$=\sum_{\mathbf{k}''}\{\bar{w}(\mathbf{k}'';t)_e+iv(k'')[\delta/\delta\phi(-\mathbf{k}'';t)]+i[\delta/\delta\xi(-\mathbf{k}'';t)]\}\times[\bar{\rho}(\mathbf{k}-\mathbf{k}'';\mathbf{k}_1-\tfrac{1}{2}\mathbf{k}'';t)_e-\bar{\rho}(\mathbf{k}-\mathbf{k}'';\mathbf{k}_1+\tfrac{1}{2}\mathbf{k}'';t)_e]. \quad (2.10b)$$

These equations are exact. Their proof follows directly from properties of the β ensemble used in the expectation values (2.6).[22–24] The Dawson–Oberman collision corrections are contained in the ϕ and ξ derivatives of Eq.

[23] J. Schwinger, Proc. Natl. Acad. Sci. U.S. **37**, 542 (1951).
[24] P. C. Martin and J. Schwinger, Phys. Rev. **115**, 1342 (1959), Sec. 6.
[25] L. P. Kadanoff and G. Baym, *Quantum Statistical Mechanics* (W. A. Benjamin, Inc., New York, 1964), Chap. 5ff.
[26] All of the operators here considered satisfy the Bose–Einstein statistics implicit in Eqs. (2.8). For Fermi–Dirac statistics $z_n=2\pi i(n+\frac{1}{2})/\beta$.
[27] G. Baym and N. D. Mermin, J. Math. Phys. **2**, 232 (1961). When the time-dependent functions contain a constant time-independent component in addition to time-dependent parts having the periodicity required by the thermal-equilibrium formalism, it may be necessary to include a supplemental constant in the z_0 Fourier coefficient over and above the $z=z_0$ value of an analytic coefficient function.

CC-0. In Public Domain. Gurukul Kangri Collection, Haridwar

Digitized by Arya Samaj Foundation Chennai and eGangotri

(2.10b). If we neglect such derivatives, Eq. (2.10b) reduces to the collisionless Vlasov equation

$$[i(\partial/\partial t)-(\hbar\mathbf{k}\cdot\mathbf{k}_1/m)]\bar{\rho}(\mathbf{k};\mathbf{k}_1;t)_e=\sum_{\mathbf{k}''}\bar{w}(\mathbf{k}'';t)_e[\bar{\rho}(\mathbf{k}-\mathbf{k}'';\mathbf{k}_1-\tfrac{1}{2}\mathbf{k}'';t)_e-\bar{\rho}(\mathbf{k}-\mathbf{k}'';\mathbf{k}_1+\tfrac{1}{2}\mathbf{k}'';t)_e], \quad (2.11)$$

an equation which would be exact if $\bar{w}(\mathbf{k};t)_e$ were an externally imposed force field. For this reason Eq. (2.11) is sometimes called an effective-field approximation; alternatively it is called a random-phase approximation or a time-dependent Hartree approximation.

To derive the results outlined in Section 1, we proceed beyond the approximation (2.11) to include the ϕ and ξ derivatives in (2.10b) to lowest order. Using the Fourier representations (2.8) in external-field derivatives of Eq. (2.10b), we find after straightforward manipulations that

$$R_\eta'(\mathbf{k};\mathbf{k}_1;z_n)=R'(\mathbf{k};\mathbf{k}_1;z_n)^0W_\eta'(\mathbf{k};z_n)-(z_n-\hbar\mathbf{k}\cdot\mathbf{k}_1/m)^{-1}\beta^{-1}\sum_{l=-\infty}^{\infty}$$

$$\times\sum_{\mathbf{k}''}\{v(k'')[R_{\phi\eta}''(\mathbf{k}-\mathbf{k}'',-\mathbf{k}'',\mathbf{k};\mathbf{k}_1-\tfrac{1}{2}\mathbf{k}'';z_l,z_n)-R_{\phi\eta}''(\mathbf{k}-\mathbf{k}'',-\mathbf{k}'',\mathbf{k};\mathbf{k}_1+\tfrac{1}{2}\mathbf{k}'';z_l,z_n)]$$

$$+[R_{\xi\eta}''(\mathbf{k}-\mathbf{k}'',-\mathbf{k}'',\mathbf{k};\mathbf{k}_1-\tfrac{1}{2}\mathbf{k}'';z_l,z_n)-R_{\xi\eta}''(\mathbf{k}-\mathbf{k}'',-\mathbf{k}'',\mathbf{k};\mathbf{k}_1+\tfrac{1}{2}\mathbf{k}'';z_l,z_n)]\}, \quad (2.12)$$

where $R'(\mathbf{k};\mathbf{k}_1;z)^0$ is defined in Eq. (1.6b). Similarly, from Eq. (2.11) we obtain

$$R_{\eta'\eta}''(\mathbf{k}-\mathbf{k}'',-\mathbf{k}'',\mathbf{k};\mathbf{k}_1;z_l,z_n)$$

$$=W_{\eta'\eta}''(\mathbf{k}-\mathbf{k}'',-\mathbf{k}'',\mathbf{k};z_l,z_n)R'(\mathbf{k}-\mathbf{k}'';\mathbf{k}_1;z_l+z_n)^0+[z_l+z_n-\hbar(\mathbf{k}-\mathbf{k}'')\cdot\mathbf{k}_1/m]^{-1}$$

$$\times\{W_{\eta'}'(-\mathbf{k}'';z_l)[R_\eta'(\mathbf{k};\mathbf{k}_1+\tfrac{1}{2}\mathbf{k}'';z_n)-R_\eta'(\mathbf{k};\mathbf{k}_1-\tfrac{1}{2}\mathbf{k}'';z_n)]$$

$$+W_\eta'(\mathbf{k};z_n)[R_{\eta'}'(-\mathbf{k}'';\mathbf{k}_1-\tfrac{1}{2}\mathbf{k};z_l)-R_{\eta'}'(-\mathbf{k}'';\mathbf{k}_1+\tfrac{1}{2}\mathbf{k};z_l)]\} \quad (2.13a)$$

$$\approx W_{\eta'\eta}''(\mathbf{k}-\mathbf{k}'',-\mathbf{k}'',\mathbf{k};z_l,z_n)R'(\mathbf{k}-\mathbf{k}'';\mathbf{k}_1;z_l+z_n)^0+\frac{W_{\eta'}'(-\mathbf{k}'';z_l)W_\eta'(\mathbf{k};z_n)}{z_l+z_n-\hbar(\mathbf{k}-\mathbf{k}'')\cdot\mathbf{k}_1/m}$$

$$\times\{[R'(\mathbf{k};\mathbf{k}_1+\tfrac{1}{2}\mathbf{k}'';z_n)^0-R'(\mathbf{k};\mathbf{k}_1-\tfrac{1}{2}\mathbf{k}'';z_n)^0]$$

$$+[R'(-\mathbf{k}'';\mathbf{k}_1-\tfrac{1}{2}\mathbf{k};z_l)^0-R'(-\mathbf{k}'';\mathbf{k}_1+\tfrac{1}{2}\mathbf{k};z_l)^0]\}. \quad (2.13b)$$

where in (2.13b) we have replaced the R_η' in (2.13a) by the first term of Eq. (2.12), an approximation consistent with the derivation of (2.13a) from (2.11). In this same spirit we shall linearize Eq. (2.13b) by setting $W_{\eta'}'(-\mathbf{k}'';z)=W_{\eta'}'(-\mathbf{k}'';z)^0$, an approximation to $W_{\eta'}'$ derived from equations based upon Eq. (2.11). With this approximation we assume, in effect, that Landau damping dominates most of the $\mathbf{k}''$ region relevant to the use of Eq. (2.13) in (2.12). A similar approximation to $W_\eta'(\mathbf{k};z_n)$ in (2.13) is inadmissible because in the long-wavelength $k\to0$ limit the Dawson–Oberman corrections exceed the Landau damping. Keeping $W_\eta'(\mathbf{k};z_n)$ intact in (2.13) is equivalent to summing the "most divergent 'bubble' diagrams" of a perturbation expansion. Physically, it insures that external force fields are properly screened.[28]

Making this final linearizing approximation in Eq. (2.13b) and passing to the long-wavelength $k\to0$ limit, we find after some manipulation that these approximations give

$$\sum_{\mathbf{k}_1}R_{\eta'\eta}''(\mathbf{k}-\mathbf{k}'',-\mathbf{k}'',\mathbf{k};\mathbf{k}_1;z_l,z_n)$$

$$\underset{k\to0}{\approx}R'(-\mathbf{k}'';z_l+z_n)^0W_{\eta'\eta}''(\mathbf{k}-\mathbf{k}'',-\mathbf{k}'',\mathbf{k};z_l+z_n)$$

$$+W_\eta'(\mathbf{k};z_n)W_{\eta'}'(-\mathbf{k}'';z_l)^0(\hbar\mathbf{k}\cdot\mathbf{k}''/mz_n^2)$$

$$\times[R'(-\mathbf{k}'';z_l+z_n)^0-R(-\mathbf{k}'';z_l)^0]. \quad (2.14)$$

This equation, which is to be used with the exact Eq. (2.12), reflects the basic approximations of the Dawson–Oberman theory. The corresponding collisionless Vlasov theory would be based solely upon Eq. (2.12) in which the second field derivatives $R_{\eta'\eta}''=0$. Because in improving this collisionless theory we have included derivative corrections only to lowest order—that is, in Eq. (2.12) but not in Eq. (2.13) or (2.14)—collisions have been treated in the Born approximation. However, the collision potentials are dynamically screened.

In the following sections we apply these improved effective-field approximations to specific systems. Details of notation and procedure will change to accom-

[28] D. Pines, *Elementary Excitations in Solids* (W. A. Benjamin, Inc., New York, 1963), pp. 138–141.

CC-0. In Public Domain. Gurukul Kangri Collection, Haridwar

Digitized by Arya Samaj Foundation Chennai and eGangotri

modate the different physical situations, but the basic approximations will remain as outlined above.

3. SEVERAL SPECIES OF CHARGED PARTICLES

To verify that the preceding prescription reproduces Dawson–Oberman results, consider a system in which several species of charged particles interact through the Coulomb potential.[5] Because all particles here see the same electrostatic field, it is sufficient to introduce a single external potential field $\phi(\mathbf{k};t)$ seen by all particles. If $Z_s e$ is the charge and m_s the effective mass of particles of species s, then the Hamiltonian (2.3) appropriate to this system is

$$H_e(t)=\sum_s\sum_{\mathbf{k}_1}(\hbar^2k_1^2/2m_s)\rho_{\mathbf{k}_1}{}^0(t)_s+(\hbar/\epsilon_\infty)\sum_{\mathbf{k}}\{\phi(\mathbf{k},t)\sum_s Z_s\sum_{\mathbf{k}_1}\rho_{\mathbf{k}_1}{}^{-\mathbf{k}}(t)_s$$
$$+\tfrac{1}{2}v(k)\sum_{ss'}Z_sZ_{s'}\sum_{\mathbf{k}_1\mathbf{k}_2}\psi_{\mathbf{k}_1-\frac{1}{2}\mathbf{k}}{}^\dagger(t)_s\psi_{\mathbf{k}_2+\frac{1}{2}\mathbf{k}}(t)_{s'}\psi_{\mathbf{k}_2-\frac{1}{2}\mathbf{k}}(t)_{s'}\psi_{\mathbf{k}_1+\frac{1}{2}\mathbf{k}}(t)_s\}. \quad (3.1)$$

For species s the appropriate form of the equation of motion (2.10b) is

$$[i(\partial/\partial t)-(\hbar\mathbf{k}\cdot\mathbf{k}_1/m_s)]\bar{\rho}_s(\mathbf{k};\mathbf{k}_1;t)_e=Z_s\sum_{\mathbf{k}''}\{\bar{w}(\mathbf{k}'';t)_e+iv(k'')[\delta/\delta\phi(-\mathbf{k}'';t)]\}$$
$$\times[\bar{\rho}_s(\mathbf{k}-\mathbf{k}'';\mathbf{k}_1-\tfrac{1}{2}\mathbf{k}'';t)_e-\bar{\rho}_s(\mathbf{k}-\mathbf{k}'';\mathbf{k}_1+\tfrac{1}{2}\mathbf{k}'';t)_e], \quad (3.2)$$

where the average effective field

$$\bar{w}(k;t)_e=[\phi(\mathbf{k},t)+v(k)\sum_s Z_s\sum_{\mathbf{k}_1}\bar{\rho}_s(\mathbf{k};\mathbf{k}_1;t)_e]/\epsilon_\infty. \quad (3.3)$$

From Eq. (3.2) the following form of Eq. (2.12) obtains:

$$R_\phi'(\mathbf{k};\mathbf{k}_1;z_n)_s=Z_sR_\phi'(\mathbf{k};\mathbf{k}_1;z_n)_s{}^0W'(\mathbf{k};z_n)-\frac{Z_s}{z_n-\hbar\mathbf{k}\cdot\mathbf{k}_1/m_s}\beta^{-1}\sum_{l=-\infty}^{\infty}\sum_{\mathbf{k}''}v(k'')$$
$$\times[R_{\phi\phi}''(\mathbf{k}-\mathbf{k}'',-\mathbf{k}'',\mathbf{k};\mathbf{k}_1-\tfrac{1}{2}\mathbf{k}'';z_l,z_n)_s-R_{\phi\phi}''(\mathbf{k}-\mathbf{k}'',-\mathbf{k}'',\mathbf{k};\mathbf{k}_1+\tfrac{1}{2}\mathbf{k}'';z_l,z_n)_s], \quad (3.4)$$

where the definitions (1.6) obtain as before except that $m\to m_s$ and $N(k_1)\to N(k_1)_s$. Summing this over $\mathbf{k}_1$ and passing to the $k\to0$ limit, we find

$$R_\phi'(\mathbf{k};z_n)_s=\sum_{\mathbf{k}_1}R_\phi'(\mathbf{k};\mathbf{k}_1;z_n)_s$$
$$=Z_sR'(\mathbf{k};z_n)_s{}^0W_\phi'(\mathbf{k};z_n)-Z_s\sum_{\mathbf{k}''\mathbf{k}_1}\frac{(\hbar\mathbf{k}\cdot\mathbf{k}''/m_s)}{(z_n-\hbar\mathbf{k}\cdot\mathbf{k}_1/m_s)^2-(\hbar\mathbf{k}\cdot\mathbf{k}''/2m_s)^2}$$
$$\times v(k'')\beta^{-1}\sum_{l=-\infty}^{\infty}R_{\phi\phi}''(\mathbf{k}-\mathbf{k}'',-\mathbf{k}'',\mathbf{k};\mathbf{k}_1;z_l,z_n)_s \quad (3.5a)$$
$$\underset{k\to0}{\to}Z_sR'(\mathbf{k};z_n)_s{}^0W_\phi'(\mathbf{k};z_n)-Z_s\sum_{\mathbf{k}''}(\hbar\mathbf{k}\cdot\mathbf{k}''/m_sz_n^2)v(k'')$$
$$\times\sum_{\mathbf{k}_1}\beta^{-1}\sum_{l=-\infty}^{\infty}R_{\phi\phi}''(\mathbf{k}-\mathbf{k}'',-\mathbf{k}'',\mathbf{k};\mathbf{k}_1;z_l,z_n)_s. \quad (3.5b)$$

The corresponding form of Eq. (2.14) is

$$\sum_{\mathbf{k}_1}R_{\phi\phi}''(\mathbf{k}-\mathbf{k}'',-\mathbf{k}'',\mathbf{k};\mathbf{k}_1;z_l,z_n)_s\underset{k\to0}{\approx}Z_sR'(-\mathbf{k}'';z_l+z_n)_s{}^0W_{\phi\phi}''(\mathbf{k}-\mathbf{k}'',-\mathbf{k}'',\mathbf{k};z_l,z_n)$$
$$+Z_s^2W_\phi'(\mathbf{k};z_n)W_\phi'(-\mathbf{k}'';z_l)^0(\hbar\mathbf{k}\cdot\mathbf{k}''/m_sz_n^2)[R'(-\mathbf{k}'';z_l+z_n)_s{}^0-R'(-\mathbf{k}'';z_l)_s{}^0]. \quad (3.6)$$

These equations must be solved in conjunction with the following equations derived easily from Eq. (3.3):

$$\epsilon_\infty W_\phi'(\mathbf{k};z_n)=1+v(k)\sum_s Z_sR_\phi'(\mathbf{k};z_n)_s; \quad (3.7a)$$

$$\epsilon_\infty W_{\phi\phi}''(\mathbf{k}-\mathbf{k}'',-\mathbf{k}'',\mathbf{k};z_l,z_n)=v(\mathbf{k}-\mathbf{k}'')\sum_s Z_s\sum_{\mathbf{k}_1}R_{\phi\phi}''(\mathbf{k}-\mathbf{k}'',-\mathbf{k}'',\mathbf{k};\mathbf{k}_1;z_l,z_n)_s. \quad (3.7b)$$

CC-0. In Public Domain. Gurukul Kangri Collection, Haridwar

Digitized by Arya Samaj Foundation Chennai and eGangotri

Consider first the function $W_\phi'(-k''; z_l)^0$. Following the prescription outlined at the end of Sec. 2, we compute this function by neglecting the $R_{\phi\phi}''$ terms of (3.5a) and by using the resulting simplified equation with (3.7a). Thus,

$$W_\phi'(-\mathbf{k}''; z_l)^0 = \epsilon_\infty^{-1}\{1+v(-k'')\sum_s Z_s^2 R'(-\mathbf{k}''; z_l)_s{}^0 W_\phi'(-\mathbf{k}''; z_l)^0\}$$

$$= \{\epsilon_\infty - v(-k'')\sum_s Z_s R'(-\mathbf{k}''; z_l)_s{}^0\}^{-1} \tag{3.8a}$$

$$= 1/\epsilon(-\mathbf{k}''; z_l)^0, \tag{3.8b}$$

where $\epsilon(\mathbf{k}; z)^0$ is the collisionless dielectric function introduced in Eq. (1.10). That $W_\phi'(\mathbf{k}; z)^0$ and, more generally, $W_\phi'(\mathbf{k}; z)$ should be related to system dielectric functions follows physically from the fact that W_ϕ' describes the (dielectrically screened or self-consistent) internal field induced by a small perturbing external field.[24,25]

Using the result (3.8) in (3.6), we similarly solve Eqs. (3.6) and (3.7) to find

$$\sum_{\mathbf{k}_1} R_{\phi\phi}''(\mathbf{k}-\mathbf{k}'', -\mathbf{k}'', \mathbf{k}; \mathbf{k}_1; z_l, z_n)_s$$

$$\underset{k\to 0}{=} \frac{Z_s W_\phi'(\mathbf{k}; z_n)}{\epsilon(-k''; z_l)^0}\left\{\frac{v(k'')R'(-\mathbf{k}''; z_l+z_n)_s{}^0}{\epsilon(-\mathbf{k}''; z_l+z_n)^0}\sum_{s'} Z_{s'}{}^3\left(\frac{\hbar\mathbf{k}\cdot\mathbf{k}''}{m_{s'}z_n{}^2}\right)[R'(-\mathbf{k}''; z_l+z_n)_{s'}{}^0 - R'(-\mathbf{k}''; z_l)_{s'}{}^0]\right.$$

$$\left. + Z_s(\hbar\mathbf{k}\cdot\mathbf{k}''/m_s z_n{}^2)[R'(-\mathbf{k}''; z_l+z_n)_s{}^0 - R'(-\mathbf{k}''; z_l)_s{}^0]\right\}. \tag{3.9}$$

Substituting this expression into (3.5b) and using Eq. (3.7b), we solve for $W_\phi'(k; z_n)$ to find after considerable manipulation

$$\epsilon(\mathbf{k}; z_n) = [W'(\mathbf{k}; z_n)]^{-1}$$

$$= \epsilon(\mathbf{k}; z_n)^0 + (2\beta)^{-1}\sum_{l=-\infty}^{\infty}\sum_{\mathbf{k}''} v(k)\left(\frac{\hbar\mathbf{k}\cdot\mathbf{k}''}{z_n{}^2}\right)^2 \frac{|v(k'')|^2}{\epsilon(\mathbf{k}''; z_n+z_l)^0\epsilon(\mathbf{k}''; z_l)^0}$$

$$\times\left\{\left(\sum_s \frac{Z_s{}^3}{m_s}[R'(\mathbf{k}''; z_n+z_l)_s{}^0 - R'(\mathbf{k}''; z_l)_s{}^0]\right)^2 + \frac{\epsilon(\mathbf{k}''; z_n+z_l)-\epsilon(\mathbf{k}''; z_l)}{v(k'')}\right.$$

$$\left.\times\sum_s \frac{Z_s{}^4}{m_s{}^2}[R'(\mathbf{k}''; z_n+z_l)_s{}^0 - R'(\mathbf{k}''; z_l)_s{}^0]\right\} \tag{3.10a}$$

$$= \epsilon(\mathbf{k}; z_n)^0 + (2\beta)^{-1}\sum_{l=-\infty}^{\infty}\sum_{\mathbf{k}''} v(k)\left(\frac{\hbar\mathbf{k}\cdot\mathbf{k}''}{z_n{}^2}\right)^2 \frac{|v(k'')|^2}{\epsilon(\mathbf{k}''; z_n+z_l)^0\epsilon(\mathbf{k}''; z_l)^0}$$

$$\times\sum_{ss'} Z_s{}^2 Z_{s'}{}^2\left(\frac{Z_s Z_{s'}}{m_s m_{s'}} - \frac{Z_s{}^2}{m_s{}^2}\right)[R'(\mathbf{k}''; z_n+z_l)_s{}^0 - R'(\mathbf{k}''; z_l)_s{}^0][R'(\mathbf{k}''; z_n+z_l)_{s'}{}^0 - R'(\mathbf{k}''; z_l)_{s'}{}^0]. \tag{3.10b}$$

In order to obtain this result, we used the fact that

$$\epsilon(\mathbf{k}; z_n) = \epsilon(-\mathbf{k}; -z_n), \tag{3.11}$$

the fact that z_n has one of the discrete values $z_n = i2\pi n/\beta$ appropriate to the expansion (2.8), and the fact that, because the l summation in (3.4) extends over all integral l, it is invariant with respect to the displacement $l \to l \pm n$.

Equation (3.10b) is equivalent to Eqs. (29) and (30) of Ron and Tzoar.[5] This justifies our assertion that the prescription of Sec. 2 reproduces the Dawson–Oberman approximation.

To proceed, we rearrange the terms of (3.10b) and

CC-0. In Public Domain. Gurukul Kangri Collection, Haridwar

Digitized by Arya Samaj Foundation Chennai and eGangotri

introduce dispersion relations to represent the functions of z_l in terms of their spectral functions. (Typical dispersion relations and the basic elements in their proof are indicated in Appendix A.)

$$\epsilon(\mathbf{k};z_n)=\epsilon(\mathbf{k};z_n)^0-\tfrac{1}{2}\sum_{\mathbf{k}''}v(k)\,(\hbar\mathbf{k}\cdot\mathbf{k}''v(k'')/z_n^2)^2\sum_{ss'}Z_s^2Z_{s'}^2\left(\frac{Z_s^2}{m_s^2}-\frac{Z_sZ_{s'}}{m_sm_{s'}}\right)$$

$$\times\beta^{-1}\sum_{l=-\infty}^{\infty}\left(\left\{\frac{R'(\mathbf{k}'';z_l+z_n)_s{}^0R'(\mathbf{k}'';z_l+z_n)_{s'}{}^0}{\epsilon(\mathbf{k}'';z_l+z_n)^0}[[\epsilon(\mathbf{k}'';z_l)^0]^{-1}-\epsilon_\infty{}^{-1}]+\frac{R'(k'';z_l)_s{}^0R'(k'';z_l)_{s'}{}^0}{\epsilon(\mathbf{k}'';z_l)^0}\right.\right.$$

$$\times[[\epsilon(\mathbf{k}'';z_l+z_n)^0]^{-1}-\epsilon_\infty{}^{-1}]-[R'(\mathbf{k}'';z_l+z_n)_s{}^0R'(\mathbf{k}'';z_l)_{s'}{}^0$$

$$\left.+R'(\mathbf{k}'';z_l)_s{}^0R'(\mathbf{k}'';z_l+z_n)_{s'}{}^0]/\epsilon(\mathbf{k}'';z_l+z_n)^0\epsilon(\mathbf{k}'';z_l)^0\right\}$$

$$\left.+\left\{\frac{R'(\mathbf{k}'';z_l+z_n)_s{}^0R'(\mathbf{k}'';z_l+z_n)_{s'}{}^0}{\epsilon_\infty\epsilon(\mathbf{k}'';z_l+z_n)^0}+\frac{R'(\mathbf{k}'';z_l)_s{}^0R'(\mathbf{k}'';z_l)_{s'}{}^0}{\epsilon_\infty\epsilon(\mathbf{k}'';z_l)^0}\right\}\right)\quad(3.12a)$$

$$=\epsilon(\mathbf{k};z_n)^0-\tfrac{1}{2}\sum_{\mathbf{k}''}v(k)\,(\hbar\mathbf{k}\cdot\mathbf{k}''v(k'')/z_n^2)^2\sum_{ss'}Z_s^2Z_{s'}^2\left(\frac{Z_s^2}{m_s^2}-\frac{Z_sZ_{s'}}{m_sm_{s'}}\right)\beta^{-1}\sum_{l=-\infty}^{\infty}\left(\int_{-\infty}^{\infty}\frac{d\omega_1\,d\omega_2}{\pi^2}\right.$$

$$\times[(z_l+z_n-\omega_1)(z_l-\omega_2)]^{-1}\mathfrak{F}\{[R'(\mathbf{k}'';\omega_1)_s{}^0-R'(\mathbf{k}'';\omega_2)_s{}^0]$$

$$\times[R'(\mathbf{k}'';\omega_1)_{s'}{}^0-R'(\mathbf{k}'';\omega_2)_{s'}{}^0]/\epsilon(\mathbf{k}'';\omega_1)^0\epsilon(\mathbf{k}'';\omega_2)^0\}$$

$$\left.+2\int_{-\infty}^{\infty}\frac{d\bar\omega}{\pi}\frac{1}{z_l-\bar\omega}\mathfrak{F}\left\{\frac{R'(\mathbf{k}'';\bar\omega)_s{}^0R'(\mathbf{k}'';\bar\omega)_{s'}{}^0}{\epsilon_\infty\epsilon(\mathbf{k}'';\bar\omega)^0}\right\}\right).\quad(3.12b)$$

The real functionals $\mathfrak{F}\{\cdots\}$ are defined in Eqs. (1.13). The separation of terms in (3.12a) ensures that the first bracket $\{\cdots\}$ in (3.12a) vanishes when either z_l or $z_n\to\infty$, a prerequisite to the dispersion relations used in Eq. (3.12b).

Interchanging the order of the l-series summation and the double (ω_1,ω_2) integral, permissible because the series converges uniformly in the variables ω_1 and ω_2, we are led to consider the sum[29]

$$\beta^{-1}\sum_{l=-\infty}^{\infty}(z_l+z_n-\omega_1)^{-1}(z_l-\omega_2)^{-1}$$

$$=-[z_n-(\omega_1-\omega_2)]^{-1}\left\{[(\beta\omega_2)^{-1}-(\beta\omega_1)^{-1}]+\sum_{l=1}^{\infty}\left[\frac{2\beta\omega_2}{(\beta\omega_2)^2-(2\pi il)^2}-\frac{2\beta\omega_1}{(\beta\omega_1)^2-(2\pi il)^2}\right]\right\}$$

$$=\frac{1}{2}\frac{\coth(\beta\omega_1/2)-\coth(\beta\omega_2/2)}{z_n-(\omega_1-\omega_2)}.\quad(3.13a)$$

The single-integral term of (3.12b) can be similarly treated if we introduce the convergence factor $\exp(-\epsilon|z_l|)$, $\epsilon=0^+$, which does not change the value of that term but which does permit interchange of the order of series summation and $\bar\omega$ integration. After this interchange we are left with[29]

$$\beta^{-1}\sum_{l=-\infty}^{\infty}\frac{\exp(-\epsilon|z_l|)}{z_l-\bar\omega}=-\left[(\beta\bar\omega)^{-1}+\sum_{l=1}^{\infty}\frac{2\beta\bar\omega\exp(-\epsilon z_l)}{(\beta\bar\omega)^2-(2\pi il)^2}\right]$$

$$=-\left[(\beta\bar\omega)^{-1}+\sum_{l=1}^{\infty}\frac{2\beta\bar\omega}{(\beta\bar\omega)^2+(2\pi l)^2}\right]\quad(3.13b)$$

$$=-\tfrac{1}{2}\coth(\beta\bar\omega/2).$$

[29] K. Knopp, *Theory and Application of Infinite Series* (Hafner, New York, 1951), 2nd ed., pp. 204–208.

CC-0. In Public Domain. Gurukul Kangri Collection, Haridwar

Digitized by Arya Samaj Foundation Chennai and eGangotri

Using these results in Eq. (3.12b), we finally obtain

$$\epsilon(\mathbf{k};z_n)=\epsilon(\mathbf{k};z_n)^0-\tfrac{1}{2}\sum_{\mathbf{k}''}v(k)\,(\hbar\mathbf{k}\cdot\mathbf{k}''v(k)/Z_n^2)^2\sum_{ss'}Z_s^2Z_{s'}^2\left(\frac{Z_s^2}{m_s^2}-\frac{Z_sZ_{s'}}{m_sm_{s'}}\right)$$

$$\times\left(\int_{-\infty}^{\infty}\frac{d\omega_1\,d\omega_2}{\pi^2}\,\frac{1}{2}\,\frac{\coth(\beta\omega_1/2)-\coth(\beta\omega_2/\beta)}{z_n-(\omega_1-\omega_2)}\,\mathfrak{F}\{[R'(\mathbf{k}'';\omega_1)_s{}^0-R'(\mathbf{k}'';\omega_2)_s{}^0]\right.$$

$$\times[R'(\mathbf{k}'';\omega_1)_{s'}{}^0-R^1(\mathbf{k}'';\omega_2)_{s'}{}^0]/\epsilon(\mathbf{k}'';\omega_1)^0\epsilon(\mathbf{k}'';\omega_2)^0\}$$

$$\left.-\int_{-\infty}^{\infty}\frac{d\bar{\omega}}{\pi}\coth(\beta\bar{\omega}/2)\mathfrak{F}\left\{\frac{R'(\mathbf{k}'';\bar{\omega})_s{}^0R'(\mathbf{k}'';\bar{\omega})_{s'}{}^0}{\epsilon_\infty\epsilon(\mathbf{k}'';\bar{\omega})^0}\right\}\right) \quad (3.14a)$$

$$=\epsilon(\mathbf{k};z_n)^0-\tfrac{1}{2}\sum_{\mathbf{k}''}v(k)\,(\hbar\mathbf{k}\cdot\mathbf{k}''v(k)/Z_n^2)^2\sum_{ss'}Z_s^2Z_{s'}^2\left(\frac{Z_s^2}{m_s^2}-\frac{Z_sZ_{s'}}{m_sm_{s'}}\right)\left(\int_{-\infty}^{\infty}\frac{d\omega_1\,d\omega_2}{\pi^2}\,\frac{\coth(\beta\omega_1/2)}{z_n-(\omega_1-\omega_2)}\right.$$

$$\times\mathfrak{F}\{[R'(\mathbf{k}'';\omega_1)_s{}^0-R'(\mathbf{k}'';\omega_2)_s{}^0][R'(\mathbf{k}'';\omega_1)_{s'}{}^0-R'(\mathbf{k}'';\omega_2)_{s'}{}^0]/\epsilon(\mathbf{k}'';\omega_1)^0\epsilon(\mathbf{k}'';\omega_2)^0\}$$

$$\left.-\int_{-\infty}^{\infty}\frac{d\bar{\omega}}{\pi}\coth(\beta\bar{\omega}/2)\mathfrak{F}\left\{\frac{R'(\mathbf{k}'';\bar{\omega})_s{}^0R'(\mathbf{k}'';\bar{\omega})_{s'}{}^0}{\epsilon_\infty\epsilon(k'';\bar{\omega})^0}\right\}\right), \quad (3.14b)$$

where in going to (3.14b) we made the change of variable $(\omega_1,\omega_2)\rightarrow(-\omega_2,-\omega_1)$ and used (3.11) in the $\coth(\beta\omega_2/2)$ part of the double integral.

When the result (3.14b) is analytically continued[27] from discrete z_n to arbitrary complex z and when the result is used in Eq. (1.8), the conductivities (1.11) follow immediately.

4. CHARGED PARTICLES AND POLAR PHONONS

It is not difficult to extend the results of Sec. 3 to include the contributions from polar phonons. Because charged carriers and polar phonons interact through the same electric potential responsible for particle–particle interactions, a single effective field still pertains. Modifying the effective field (3.3) so as to include lattice polarization, we obtain the new average effective field

$$\bar{\phi}(\mathbf{k};t)_e=[\phi(\mathbf{k};t)+v(k)\sum_s Z_s\sum_{\mathbf{k}_1}\bar{\rho}_s(\mathbf{k};\mathbf{k}_1;t)_e$$

$$+v(k)\sum_r p_r(\mathbf{k})\bar{\alpha}_r(\mathbf{k};t)_e]/\epsilon_\infty, \quad (4.1)$$

where $\bar{\alpha}_r(\mathbf{k};t)_e$ is the expectation value (2.6) of the phonon operator $\alpha_r(\mathbf{k};t)$ which measures the wave-vector-$\mathbf{k}$ branch-r component of lattice displacement and where the parameters $p_r(\mathbf{k})=p_r(-\mathbf{k})^*$ measure the polar character of that displacement.

Considering for definiteness the harmonic lattice of cubic symmetry for which Eq. (1.17) obtains, we define

$$\alpha_r(\mathbf{k};t)=a_r(\mathbf{k};t)+a_r{}^\dagger(-\mathbf{k};t), \quad (4.2)$$

where $a_r(\mathbf{k})$, $a_r{}^\dagger(\mathbf{k})$ are phonon annihilation, creation operators satisfying the usual commutation rules of Bose–Einstein statistics: $[a_r(\mathbf{k}),a_{r'}{}^\dagger(\mathbf{k}')]=\delta_{rr'}\delta_{\mathbf{k}\mathbf{k}'}$. Consistent with (4.1), the phonon components of the system Hamiltonian are

$$H_e(t)\,|_{\text{phonon}}=\hbar\sum_r\sum_{\mathbf{k}}\omega_{\mathbf{k}}{}^r a_r{}^\dagger(\mathbf{k};t)a_r(\mathbf{k};t)$$

$$+(\hbar/\epsilon_\infty)\sum_r\sum_{\mathbf{k}}\{[\phi(\mathbf{k};t)+\sum_s Z_sv(k)\sum_{\mathbf{k}_1}\rho_{\mathbf{k}_1}{}^{\mathbf{k}}(t)_s]$$

$$\times p_r(-\mathbf{k})\alpha_r(-\mathbf{k};t)+\tfrac{1}{2}v(k)\,|\,p_r(\mathbf{k})\,|^2\alpha_r(\mathbf{k};t)\alpha_r(-\mathbf{k};t)\}. \quad (4.3)$$

The total Hamiltonian equals this plus the particle Hamiltonian (3.1). From (4.3) we obtain the equation of motion

$$\{[i(\partial/\partial t)]^2-(\omega_{\mathbf{k}}{}^r)^2\}\bar{\alpha}_r(\mathbf{k};t)_e=2\omega_{\mathbf{k}}{}^r p_r(-\mathbf{k})\bar{w}(\mathbf{k};t)_e. \quad (4.4)$$

If $A_\phi{}'(\mathbf{k};z_n)_r$, etc., are coefficients in Fourier-series representations of the type (2.8) and if $A'(\mathbf{k};z)_r{}^0$ is defined as in Eq. (1.17), it follows easily from Eq. (4.4) that

$$A_\phi{}'(\mathbf{k};z_n)_r=A'(\mathbf{k};z_n)_r{}^0p_r(-\mathbf{k})W_\phi{}'(\mathbf{k};z_n), \quad (4.5a)$$

$$A_{\phi\phi}{}''(\mathbf{k}-\mathbf{k}'',-\mathbf{k}'',\mathbf{k};z_l,z_n)_r$$

$$=A'(\mathbf{k}-\mathbf{k}'';z_l+z_n)_r{}^0p_r(\mathbf{k}''-\mathbf{k})$$

$$\times W_{\phi\phi}{}''(\mathbf{k}-\mathbf{k}'',-\mathbf{k}'',\mathbf{k};z_l,z_n). \quad (4.5b)$$

For the particle Fourier coefficients Eqs. (3.4)–(3.6) obtain as before. Equations (3.7) must be slightly

CC-0. In Public Domain. Gurukul Kangri Collection, Haridwar

Digitized by Arya Samaj Foundation Chennai and eGangotri

modified to include phonon contributions:

$$\epsilon_\infty W_\phi'(\mathbf{k};z_n) = 1+v(k)\{\sum_s Z_s R_\phi'(\mathbf{k};z_n)_s+\sum_r p_r(\mathbf{k})A_\phi'(\mathbf{k};z_n)_r\}, \tag{4.6a}$$

$$\epsilon_\infty W_{\phi\phi}''(\mathbf{k}-\mathbf{k}'',-\mathbf{k}'',\mathbf{k};z_l,z_n) = v(\mathbf{k}-\mathbf{k}'')\{\sum_s Z_s\sum_{\mathbf{k}_1} R_{\phi\phi}''(\mathbf{k}-\mathbf{k}'',-\mathbf{k}'',\mathbf{k};\mathbf{k}_1;z_l,z_n)_s + \sum_r p_r(\mathbf{k}-\mathbf{k}'')A_{\phi\phi}''(\mathbf{k}-\mathbf{k}'',-\mathbf{k}'',\mathbf{k};z_l,z_n)_r\}. \tag{4.6b}$$

With these equations we proceed as in Sec. 3 to compute first the function $W_\phi'(-\mathbf{k}'';z)^0$, neglecting the $R_{\phi\phi}''$ terms of (3.5a) as outlined in Sec. 2. We find thereby the collisionless dielectric function of Eq. (1.16):

$$W_\phi'(-\mathbf{k}'';z_l)^0 = 1/\epsilon(-\mathbf{k}'';z_l)^0 \tag{4.7a}$$

$$= \{\epsilon_\infty - v(k'')[\sum_r |p_r(\mathbf{k}'')|^2 A'(-\mathbf{k}'';z_l)_r + \sum_s Z_s^2 R'(-\mathbf{k}'';z_l)_s{}^0]\}^{-1}. \tag{4.7b}$$

Substituting this expression into Eq. (3.6), we solve that equation with Eqs. (4.5b) and (4.6b) to obtain a result identical in *form* to Eq. (3.9). The essential difference is that the dielectric function (4.7) must be used in place of the function (3.8) used previously. Using Eq. (3.9) in Eq. (3.5b), we find with Eqs. (4.5a) and (4.6a) that

$$\epsilon(\mathbf{k};z_n) = [W_\phi'(\mathbf{k};z_n)]^{-1}$$

$$= \epsilon(\mathbf{k};z_n)^0+(2\beta)^{-1}\sum_{l=-\infty}^{\infty}\sum_{\mathbf{k}''} v(k)\left(\frac{\hbar\mathbf{k}\cdot\mathbf{k}''}{z_n{}^2}\right)^2 \frac{|v(k'')|^2}{\epsilon(\mathbf{k}'';z_n+z_l)^0\epsilon(\mathbf{k}'';z_l)^0} \times\left\{\left(\sum_s \frac{Z_s{}^3}{m_s}[R'(\mathbf{k}'';z_n+z_l)_s{}^0-R'(\mathbf{k}'';z_l)_s{}^0]\right)^2+\frac{\epsilon(\mathbf{k}'';z_n+z_l)^0-\epsilon(\mathbf{k}'';z_l)^0}{v(k'')} \times\sum_s \frac{Z_s{}^4}{m_s{}^2}[R'(\mathbf{k}'';z_n+z_l)_s{}^0-R'(\mathbf{k}'';z_l)_s{}^0]\right\} \tag{4.8a}$$

$$= \epsilon(\mathbf{k};z_n)^0+(2\beta)^{-1}\sum_{l=-\infty}^{\infty}\sum_{\mathbf{k}''} v(k)\left(\frac{\hbar\mathbf{k}\cdot\mathbf{k}''}{z_n{}^2}\right)^2 \frac{|v(k'')|^2}{\epsilon(k'';z_n+z_l)^0\epsilon(k'';z_l)^0} \times\left\{\sum_{ss'} Z_s{}^2Z_{s'}{}^2\left(\frac{Z_sZ_{s'}}{m_sm_{s'}}-\frac{Z_s{}^2}{m_s{}^2}\right)[R'(\mathbf{k}'';z_n+z_l)_s{}^0-R'(\mathbf{k}'';z_l)_s{}^0][R'(\mathbf{k}'';z_n+z_l)_{s'}{}^0-R'(\mathbf{k}'';z_l)_{s'}{}^0] - \sum_s\sum_r (Z_s{}^4/m_s{}^2)|p_r(\mathbf{k}'')|^2[R'(\mathbf{k}'';z_n+z_l)_s{}^0-R'(\mathbf{k}'';z_l)_s{}^0][A'(\mathbf{k}'';z_n+z_l)_r{}^0-A'(\mathbf{k}'';z_l)_r{}^0]\right\}. \tag{4.8b}$$

As in the derivation of Eq. (3.10), we used Eq. (3.11) and the fact that z_n and z_l have discrete values. Equation (4.8a) is identical in form to Eq. (3.10a); this correspondence parallels that noted earlier of the $R_{\phi\phi}''$ expressions.

If we proceed as in Eqs. (3.12)–(3.14), using dispersion relations of the type illustrated in Appendix A, we find from Eq. (4.8b) that

$$\epsilon(\mathbf{k};z_n) = \epsilon(\mathbf{k};z_n)^0-\tfrac{1}{2}\sum_{\mathbf{k}''} v(k)\left(\frac{\hbar\mathbf{k}\cdot\mathbf{k}''v(k'')}{z_n{}^2}\right)^2\left[\sum_{ss'} Z_s{}^2Z_{s'}{}^2\left(\frac{Z_s{}^2}{m_s{}^2}-\frac{Z_sZ_{s'}}{m_sm_{s'}}\right)\left(\int_{-\infty}^{\infty}\frac{d\omega_1\,d\omega_2}{\pi^2}\frac{\coth(\beta\omega_1/2)}{z_n-(\omega_1-\omega_2)} \times\mathfrak{F}\{[R'(\mathbf{k}'';\omega_1)_s{}^0-R'(\mathbf{k}'';\omega_2)_s{}^0][R'(\mathbf{k}'';\omega_1)_{s'}{}^0-R'(\mathbf{k}'';\omega_2)_{s'}{}^0]/\epsilon(\mathbf{k}'';\omega_1)^0\epsilon(\mathbf{k}'';\omega_2)^0\} -\int_{-\infty}^{\infty}\frac{d\bar\omega}{\pi}\coth(\beta\bar\omega/2)\mathfrak{F}\left\{\frac{R'(\mathbf{k}'';\bar\omega)_s{}^0R'(\mathbf{k}'';\bar\omega)_{s'}{}^0}{\epsilon_\infty\epsilon(\mathbf{k}'';\bar\omega)^0}\right\}\right)+\sum_s\sum_r (Z_s{}^4/m_s{}^2)|p_r(k'')|^2\left(\int_{-\infty}^{\infty}\frac{d\omega_1\,d\omega_2}{\pi^2}\frac{\coth(\beta\omega_1/2)}{z_n-(\omega_1-\omega_2)} \times\mathfrak{F}\{[R'(\mathbf{k}'';\omega_1)_s{}^0-R'(\mathbf{k}'';\omega_2)_s{}^0][A'(\mathbf{k}'';\omega_1)_r{}^0-A'(\mathbf{k}'';\omega_2)_r{}^0]/\epsilon(\mathbf{k}'';\omega_1)^0\epsilon(\mathbf{k}'';\omega_2)^0\} -\int_{-\infty}^{\infty}\frac{d\bar\omega}{\pi}\coth(\beta\bar\omega/2)\mathfrak{F}\left\{\frac{R'(\mathbf{k}'';\bar\omega)_s{}^0A'(\mathbf{k}'';\bar\omega)_r{}^0}{\epsilon_\infty\epsilon(\mathbf{k}'';\bar\omega)^0}\right\}\right)\Bigg]. \tag{4.9}$$

CC-0. In Public Domain. Gurukul Kangri Collection, Haridwar

Digitized by Arya Samaj Foundation Chennai and eGangotri

When analytically continued from discrete to arbitrary z, this expression and Eq. (1.8) give the conductivities (1.17).

Before we consider a further generalization of the Dawson–Oberman expressions, it is useful to digress briefly to identify the parameters $p_r(k)$ more phenomenologically. Consider with Fröhlich[30] a crystal of cubic symmetry having a single set of infrared-active optical-phonon branches (two transverse, one longitudinal). In the absence of carriers the dielectric function (1.16) equals

$$\epsilon(\mathbf{k};z)_p{}^0=\epsilon_\infty-v(k)\sum_r|p_r(\mathbf{k})|^2A'(\mathbf{k};z)_r{}^0, \quad (4.10)$$

where $p_r(\mathbf{k})$ is different from zero only for the optically active branches. If the two transverse optical branches are characterized by a single $\mathbf{k}$-independent frequency ω_t, then the phonon function (1.17) for all three active branches ($r=TO_a$, TO_a, and LO_a) is

$$A'(\mathbf{k};z)_{O_a}{}^0=2\omega_t/(z^2-\omega_t^2), \quad (4.11)$$

independent of $\mathbf{k}$. The characteristic frequency ω_l of the longitudinal branch corresponds to a zero, not a pole, of the dielectric function; it is related to the transverse frequency ω_t by a Lyddane–Sachs–Teller relation, which, when Eqs. (4.10) and (4.11) obtain, is

$$\omega_l^2=\omega_t^2\epsilon(0;0)_p{}^0/\epsilon_\infty. \quad (4.12)$$

This expression contains the ratio of the low-frequency and high-frequency (relative to lattice frequencies) dielectric function. More generally, we see from Eqs. (4.10) and (4.11) that

$$v(k)\sum_r|p_r(\mathbf{k})|^2=\omega_t[\epsilon(\mathbf{k};0)_p{}^0-\epsilon_\infty]/2, \quad (4.13)$$

where the r summation extends over the infrared-active optical branches. If the longitudinal branch dominates the summation, as is generally the case,[19] we can use (4.13) to evaluate the only important coefficient $p_{LO_a}(\mathbf{k})$. Using this coefficient in the Hamiltonian (4.3), we find that the phonon-generated electric potential seen by carriers of unit charge is

$$\phi(\mathbf{r},t)|_{LO_a}=\left[\frac{\epsilon(\mathbf{k};0)_p{}^0}{\epsilon_\infty}\right]^{\frac{1}{2}}4\pi\left[\frac{e^2\hbar\omega_l}{8\pi V}\left(\frac{1}{\epsilon_\infty}-\frac{1}{\epsilon(\mathbf{k};0)_p{}^0}\right)\right]^{\frac{1}{2}}\times\sum_{\mathbf{k}}\frac{\exp(i\mathbf{k}\cdot\mathbf{r})}{k}\alpha_{LO_a}(k;t). \quad (4.14)$$

This is equivalent to the potential derived by Fröhlich,[30] although Fröhlich uses slightly different phonon coordinates. He has chosen coordinates which diagonalize the first *and last* terms of (4.3), all of the purely phonon parts of the Hamiltonian. In these coordinates the operators (4.2) absorb the first factor of (4.14):

$$\alpha_{LO_a}(\mathbf{k};t)|_{\text{Fröhlich}}=[\epsilon(\mathbf{k};0)_p{}^0/\epsilon_\infty]^{\frac{1}{2}}\alpha_{LO_a}(\mathbf{k};t). \quad (4.15)$$

[30] H. Fröhlich, Advan. Phys. **3**, 325 (1954).

In piezoelectric crystals the phonon coupling parameters $p_r(\mathbf{k})$ will be different from zero in acoustic branches. A detailed treatment is generally complicated by crystal assymmetry, a feature we have chosen to ignore. Briefly however, if $\epsilon_{mn}{}^S$ is the dielectric tensor at constant lattice strain S_{mn}, then we define a piezoelectric tensor $e_{l,mn}$ through the relation[31]

$$D_l=4\pi\sum_{mn}e_{l,mn}S_{mn}+\sum_m\epsilon_{lm}{}^SE_m \quad (4.16)$$

connecting the electric displacement to the lattice-strain and electric fields. In terms of this tensor the piezoelectric potential seen by a carrier of unit charge is [compare Eq. (4.14)]

$$\phi(\mathbf{r},t)|_{\text{piezoelectric}}=(4\pi/\epsilon_\infty)\sum_{\mathbf{k}}\exp(i\mathbf{k}\cdot\mathbf{r})\sum_{lmn=1}^{3}(k_le_{l,mn}/k^2)\times\sum_r s_{mn}(\mathbf{k})_r\alpha_r(\mathbf{k};t), \quad (4.17)$$

where $s_{mn}(\mathbf{k})_r$ describes that fraction of the lattice strain associated with the lattice displacement operator $\alpha_r(\mathbf{k};t)$ and where the r summation extends over all piezoelectrically active acoustic-phonon branches. In order-of-magnitude calculations one can approximate $s_{mn}(\mathbf{k})_r$ in the active modes by

$$s(\mathbf{k})=[\hbar k/2\rho_m\bar{v}]^{\frac{1}{2}}, \quad (4.18)$$

a form appropriate to lattice dilation in a simple Debye model for a crystal of mass density ρ_m and average sound velocity $\bar{v}$. Comparing the potential (4.17) with that used in the Hamiltonian (4.3), we see that for piezoelectric coupling the acoustic-branch coupling parameters are

$$p_r(\mathbf{k})=[4\pi e/\hbar v(k)]\sum_{lmn}(k_le_{l,mn}/k^2)s_{mn}(\mathbf{k})_r. \quad (4.19)$$

5. GENERAL PHONON COUPLINGS

From the examples of the preceding two sections it is clear how to incorporate additional dynamic components which couple through the effective electric field $\bar{w}(k;t)_e$. It is only slightly more difficult in principle to incorporate components which couple in more general ways—for example, phonons which couple to carriers through deformation potentials. In this section we generalize the results of Sec. 4 to include such phonon couplings. To simplify our derivation and to eliminate phase complications in the carrier–phonon interactions, we assume that phonon branches which couple to carriers through deformation potentials are not polar. Because for each branch one type of coupling usually dominates, this is a reasonable approximation for many applications.

[31] W. P. Mason, *Piezoelectric Crystals and Their Application to Ultrasonics* (D. Van Nostrand Company, Inc., Princeton, New Jersey, 1950), Chap. 5, esp. Eq. (3.60).

CC-0. In Public Domain. Gurukul Kangri Collection, Haridwar

Digitized by Arya Samaj Foundation Chennai and eGangotri

To distinguish the new phonons from the polar phonons of the preceding section, we introduce new phonon annihilation, creation operators $b_r(\mathbf{k})$, $b_r^\dagger(\mathbf{k})$ analogous to the operators $a_r(\mathbf{k})$, $a_r^\dagger(\mathbf{k})$ of Eq. (4.2) ff. We assume that these phonons couple to the carrier density through the operator

$$\beta_r(\mathbf{k};t)=b_r(\mathbf{k};t)+b_r^\dagger(-\mathbf{k};t). \tag{5.1}$$

Using this operator, we describe the dynamics of the nonpolar phonons and their coupling to the carriers by the Hamiltonian

$$H_e(t)|_{\text{nonpolar phonons}}=\hbar\sum_r\sum_{\mathbf{k}}\omega_{\mathbf{k}}{}^r b_r^\dagger(\mathbf{k};t)b_r(\mathbf{k};t)$$
$$+\hbar\sum_r\sum_{\mathbf{k}}[\xi(\mathbf{k};t)+\sum_s E_s\sum_{\mathbf{k}_1}\rho_{\mathbf{k}_1}{}^{\mathbf{k}}(t)_s]$$
$$\times d_r(-\mathbf{k})\beta_r(-\mathbf{k};t). \tag{5.2}$$

The total Hamiltonian equals this plus the compone... Hamiltonians (3.1) and (4.3). The parameters $d_r(\mathbf{k})=$ $d_r(-\mathbf{k})^*$ in (5.2) describe the nonpolar coupling of the wave-vector–$\mathbf{k}$ branch–r phonons; the real parameter E_s measures the over-all strength of that coupling for carrier species s.

The Hamiltonian (5.2) leads to a new effective field

$$\bar{y}(\mathbf{k};t)_e=\xi(\mathbf{k};t)+\sum_s E_s\sum_{\mathbf{k}_1}\bar{\rho}_s(\mathbf{k};\mathbf{k}_1;t)_e \tag{5.3}$$

which supplements the effective field $\bar{w}(\mathbf{k};t)_e$ of Eq. (4.1). These two average effective fields together with their associated external fields $\xi(\mathbf{k};t)$ and $\phi(\mathbf{k};t)$ are sufficient for the analysis of the present simple system. More complicated systems might require additional fields.

Using the Hamiltonians (3.1), (4.3), and (5.2) to compute equations of motion, we find [compare Eqs. (3.2) and (4.4)]

$$\left(i\frac{\partial}{\partial t}-\frac{\hbar\mathbf{k}\cdot\mathbf{k}_1}{m_s}\right)\bar{\rho}_s(\mathbf{k};\mathbf{k}_1;t)_e$$
$$=\sum_{\mathbf{k}''}\left\{Z_s\left[\bar{w}(\mathbf{k}'';t)_e+iv(k'')\frac{\delta}{\delta\phi(-\mathbf{k}'';t)}\right]+E_s\left[\sum_r d_r(\mathbf{k}'')\bar{\beta}_r(\mathbf{k}'';t)_e+i\frac{\delta}{\delta\xi(-\mathbf{k}'';t)}\right]\right\}$$
$$\times[\bar{\rho}_s(\mathbf{k}-\mathbf{k}'';\mathbf{k}_1-\tfrac{1}{2}\mathbf{k}'';t)_e-\bar{\rho}_s(\mathbf{k}-\mathbf{k}'';\mathbf{k}_1+\tfrac{1}{2}\mathbf{k}'';t)_e], \tag{5.4a}$$
$$\{[i(\partial/\partial t)]^2-(\omega_{\mathbf{k}}{}^r)^2\}\bar{\alpha}_r(\mathbf{k};t)_e=2\omega_{\mathbf{k}}{}^r p_r(-\mathbf{k})\bar{w}(k;t)_e, \tag{5.4b}$$
$$\{[i(\partial/\partial t)^2-(\omega_{\mathbf{k}}{}^r)^2\}\bar{\beta}_r(\mathbf{k};t)_e=2\omega_{\mathbf{k}}{}^r d_r(-\mathbf{k})\bar{y}(\mathbf{k};t)_e. \tag{5.4c}$$

Introducing Fourier-series representations of the type (2.8), we use Eqs. (5.4) and the methods outlines in Sec. ... to evaluate the series coefficients.

From Eq. (5.4a) we find [compare Eqs. (2.12), (3.4), and (3.5)]

$$R_\eta'(\mathbf{k};z_n)=[Z_sW_\eta'(\mathbf{k};z_n)+E_s\sum_r d_r(\mathbf{k})B_\eta'(\mathbf{k};z_n)_r]R'(\mathbf{k};z_n)_s{}^0$$
$$-\sum_{\mathbf{k}''\mathbf{k}_1}\frac{(\hbar\mathbf{k}\cdot\mathbf{k}''/m_s)}{(z_n-\hbar\mathbf{k}\cdot\mathbf{k}_1/m_s)^2-(\hbar\mathbf{k}\cdot\mathbf{k}''/2m_s)^2}\beta^{-1}\sum_{l=-0}^{\infty}[Z_sv(k'')R_{\phi\eta}''(\mathbf{k}-\mathbf{k}'',-\mathbf{k}'',\mathbf{k};\mathbf{k}_1;z_l,z_n)_s$$
$$+E_sR_{\xi\eta}''(\mathbf{k}-\mathbf{k}'',-\mathbf{k}'',\mathbf{k};\mathbf{k}_1;z_l,z_n)_s] \tag{5.5a}$$
$$\underset{k\to 0}{\to}[Z_sW_\eta'(\mathbf{k};z_n)+E_s\sum_r d_r(\mathbf{k})B_\eta'(\mathbf{k};z_n)_r]R'(\mathbf{k};z_n)_s{}^0$$
$$-\sum_{\mathbf{k}''}(\hbar\mathbf{k}\cdot\mathbf{k}''/m_sz_n{}^2)\sum_{\mathbf{k}_1}\beta^{-1}\sum_{l=-\infty}^{\infty}[Z_sv(k'')R_{\phi\eta}''(\mathbf{k}-\mathbf{k}'',-\mathbf{k}'',\mathbf{k};\mathbf{k}_1;z_l,z_n)_s$$
$$+E_sR_{\xi\eta}''(\mathbf{k}-\mathbf{k}'',-\mathbf{k}'',\mathbf{k};\mathbf{k}_1;z_l,z_n)_s], \tag{5.5b}$$

where $\eta=\phi$ or ξ. Likewise [compare Eqs. (2.14) and (3.6)]

$$\sum_{\mathbf{k}_1}R_{\eta'\eta}''(\mathbf{k}-\mathbf{k}'',-\mathbf{k}'',\mathbf{k};\mathbf{k}_1;z_l,z_n)_s$$
$$\underset{k\to 0}{\approx}[Z_sW_{\eta'\eta}''(\mathbf{k}-\mathbf{k}'',-\mathbf{k}'',\mathbf{k};z_l,z_k)+E_s\sum_r d_r(\mathbf{k}-\mathbf{k}'')B_{\eta'\eta}''(\mathbf{k}-\mathbf{k}'',-\mathbf{k}'',\mathbf{k};z_l,z_n)_r]$$
$$\times R'(-\mathbf{k}'';z_l+z_n)_s{}^0+[Z_sW_\eta'(\mathbf{k};z_n)+E_s\sum_r d_r(\mathbf{k})B_\eta'(\mathbf{k};z_n)_r]$$
$$\times[Z_sW_{\eta'}'(-\mathbf{k}'';z_l)^0+E_s\sum_r d_r(-\mathbf{k}'')B_{\eta'}'(-\mathbf{k}'';z_l)_r{}^0]$$
$$\times(\hbar\mathbf{k}\cdot\mathbf{k}''/m_sz_n{}^2)[R'(-\mathbf{k}'';z_l+z_n)_s{}^0-R'(-\mathbf{k}'';z_l)_s{}^0]. \tag{5.6}$$

CC-0. In Public Domain. Gurukul Kangri Collection, Haridwar

Digitized by Arya Samaj Foundation Chennai and eGangotri

Here, as explained in previous sections, $W_{\eta'}'(-\mathbf{k}''; z_l)^0$ and $B_{\eta'}'(-\mathbf{k}''; z_l)_r{}^0$ are approximate expressions obtained by neglecting the $R_{\eta'\eta}''$ terms of Eqs. (5.5).

The function $B_\eta'(-\mathbf{k}''; z_l)_r{}^0$, an approximate form of the function $B_{\eta'}'(-\mathbf{k}''; z_l)_r$, is not to be confused with the useful auxiliary function

$$B'(\mathbf{k}; z)_r{}^0 = 2\omega_{\mathbf{k}}{}^r/[z^2 - (\omega_{\mathbf{k}}{}^r)^2] \tag{5.7}$$

which is the direct analog for the nonpolar phonons of the function $A'(\mathbf{k}; z)_r{}^0$ of Eq. (1.17). Using the definition (5.7) with Eqs. (5.3) and (5.4c), we find that, if $\eta = \phi$ or ξ,

$$B_\eta'(\mathbf{k}; z_n)_r = B'(\mathbf{k}; z)_r{}^0\, d_r(-\mathbf{k})\, Y_\eta'(\mathbf{k}; z_n), \tag{5.8a}$$

$$B_{\eta'\eta}''(\mathbf{k}-\mathbf{k}'', -\mathbf{k}'', \mathbf{k}; z_l, z_n)_r = B'(\mathbf{k}-\mathbf{k}''; z_l+z_n)_r{}^0\, d_r(\mathbf{k}''-\mathbf{k})\, Y_{\eta'\eta}''(\mathbf{k}-\mathbf{k}'', -\mathbf{k}'', \mathbf{k}; z_l, z_n). \tag{5.8b}$$

The corresponding Eqs. (4.5) for the polar phonons obtain essentially as before because the equation of motion (5.4b) is identical to (4.4).

The preceding equations must be supplemented by equations defining the variational derivatives of the average effective fields $\bar{w}(\mathbf{k}; t)_e$ and $\bar{y}(\mathbf{k}; t)_e$. The $\bar{w}$-field Eqs. (4.6) obtain essentially as before:

$$\epsilon_\infty W_\phi'(\mathbf{k}; z_n) = 1 + v(k)\Big[\sum_s Z_s R_\phi'(\mathbf{k}; z_n)_s + \sum_r p_r(\mathbf{k})\, A_\phi'(\mathbf{k}; z_n)_r\Big], \tag{5.9a}$$

$$\epsilon_\infty W_\xi'(\mathbf{k}; z_n) = v(k)\Big[\sum_s Z_s R_\xi'(\mathbf{k}; z_n)_s + \sum_r p_r(\mathbf{k})\, A_\xi'(\mathbf{k}; z_n)_r\Big], \tag{5.9b}$$

and, if $\eta, \eta' = \phi$ or ξ,

$$\epsilon_\infty W_{\eta'\eta}''(\mathbf{k}-\mathbf{k}'', -\mathbf{k}'', \mathbf{k}; z_l+z_n) = v(\mathbf{k}-\mathbf{k}'')\Big[\sum_s Z_s \sum_{\mathbf{k}_1} R_{\eta'\eta}''(\mathbf{k}-\mathbf{k}'', -\mathbf{k}'', \mathbf{k}; \mathbf{k}_1; z_l, z_n)_s + \sum_r p_r(\mathbf{k}-\mathbf{k}'')\, A_{\eta'\eta}''(\mathbf{k}-\mathbf{k}'', -\mathbf{k}'', \mathbf{k}; z_l, z_n)_r\Big]. \tag{5.9c}$$

The corresponding $\bar{y}$ equations are

$$Y_\phi'(\mathbf{k}; z_n) = \sum_s E_s R_\phi'(\mathbf{k}; z_n)_s, \tag{5.10a}$$

$$Y_\xi'(\mathbf{k}; z_n) = 1 + \sum_s E_s R_\xi'(\mathbf{k}; z_n)_s, \tag{5.10b}$$

$$Y_{\eta'\eta}''(\mathbf{k}-\mathbf{k}'', -\mathbf{k}'', \mathbf{k}; z_l, z_n) = \sum_s E_s \sum_{\mathbf{k}_1} R_{\eta'\eta}''(\mathbf{k}-\mathbf{k}'', -\mathbf{k}'', \mathbf{k}; \mathbf{k}_1; z_l, z_n)_s. \tag{5.10c}$$

With these equations we proceed as in prior sections to compute first the results appropriate to the collisionless approximation in which the $R_{\eta'\eta}''$ terms of (5.5) are neglected. We find thereby the collisionless dielectric function

$$\epsilon(\mathbf{k}; z)^0 = [W_\phi'(\mathbf{k}; z)^0]^{-1}$$

$$= \epsilon_\infty - v(k)\left(\sum_r |p_r(\mathbf{k})|^2 A'(\mathbf{k}; z)_r{}^0 + \sum_s Z_s{}^2 R'(\mathbf{k}; z)_s{}^0 + \frac{[\sum_s E_s Z_s R'(\mathbf{k}; z)_s{}^0]^2 \sum_r |d_r(\mathbf{k})|^2 B'(\mathbf{k}; z)_r{}^0}{1 - \sum_s E_s{}^2 R'(\mathbf{k}; z)_s{}^0 \sum_r |d_r(\mathbf{k})|^2 B'(\mathbf{k}; z)_r{}^0}\right), \tag{5.11}$$

which correctly reduces to the expression (1.16) when the nonpolar corrections of the last term are omitted. Note that the nonpolar phonons, in contrast to the polar phonons, contribute only indirectly to the dielectric function through their interaction with the carriers. In addition to the result (5.11) we also find with the $R_{\eta'\eta}''$ terms of (5.5) neglected that

$$W_\xi'(\mathbf{k}; z)^0 = \frac{v(k)\sum_s E_s Z_s R'(\mathbf{k}; z)_s{}^0 \sum_r |d_r(\mathbf{k})|^2 B'(\mathbf{k}; z)_r{}^0}{\epsilon(k; z)^0[1 - \sum_s E_s{}^2 R'(\mathbf{k}; z)_s{}^0 \sum_r |d_r(\mathbf{k})|^2 B'(\mathbf{k}; z)_r{}^0]}, \tag{5.12a}$$

$$\sum_r d_r(\mathbf{k})\, B_\phi'(\mathbf{k}; z)_r{}^0 = \frac{\sum E_s Z_s R'(\mathbf{k}; z)_s{}^0 [\sum_r |d_r(\mathbf{k})|^2 B'(\mathbf{k}; z)_r{}^0]}{\epsilon(\mathbf{k}; z)^0[1 - \cdots]}, \tag{5.12b}$$

$$\sum_r d_r(\mathbf{k})\, B_\xi'(\mathbf{k}; z)_r{}^0 = \frac{\{\epsilon_\infty - v(k)[\sum_s Z_s{}^2 R'(\mathbf{k}; z)_s{}^0 + \sum_r |p_r(\mathbf{k})|^2 A'(\mathbf{k}; z)_r{}^0]\} \sum_r |d_r(\mathbf{k})|^2 B'(\mathbf{k}; z)_r{}^0}{\epsilon(\mathbf{k}; z)^0[1 - \cdots]}. \tag{5.12c}$$

CC-0. In Public Domain. Gurukul Kangri Collection, Haridwar

Digitized by Arya Samaj Foundation Chennai and eGangotri

Substituting these expressions into Eq. (5.6) and using that equation with Eqs. (4.5), (5.5), and (5.7)–(5.10), we find after considerable algebraic manipulation that the Dawson–Oberman dielectric function is

$$\epsilon(\mathbf{k};z_n)=[W_\phi'(\mathbf{k};z_n)]^{-1}=\epsilon_\infty-v(k)\left(\sum_r|p_r(\mathbf{k})|^2A'(\mathbf{k};z_n)_r{}^0+\sum_{ss'}Z_sZ_{s'}M(\mathbf{k};z_n)_{ss'}\right.$$
$$\left.+\frac{\sum_r|d_r(\mathbf{k})|^2B'(\mathbf{k};z_n)_r{}^0[\sum_{ss'}Z_sE_{s'}M(\mathbf{k};z_n)_{ss'}]^2}{1-\sum_r|d_r(\mathbf{k})|^2B'(\mathbf{k};z_n)_r{}^0\sum_{ss'}E_sE_{s'}M(\mathbf{k};z_n)_{ss'}}\right), \quad (5.13)$$

where the auxiliary function

$$M(\mathbf{k};z_n)_{ss'}=\delta_{ss'}R'(\mathbf{k};z_n)_s{}^0+\sum_{\mathbf{k}''}\frac{(\hbar\mathbf{k}\cdot\mathbf{k}''/z_n{}^2)^2}{m_sm_s'}(2\beta)^{-1}\sum_{l=-\infty}^{\infty}\{\delta_{ss'}[v_{\rm eff}(\mathbf{k}'';z_l+z_n)_{ss'}-v_{\rm eff}(\mathbf{k}'';z_l)_{ss'}]$$
$$\times[R'(\mathbf{k}'';z_l+z_n)_s{}^0-R'(\mathbf{k}'';z_l)_s]-v_{\rm eff}(\mathbf{k}'',z_l)_{ss'}v_{\rm eff}(\mathbf{k}'';z_l+z_n)_{ss'}[R'(\mathbf{k}'';z_l+z_n)_s{}^0-R'(\mathbf{k}'';z_l)_s{}^0]$$
$$\times[R'(\mathbf{k}'';z_l+z_n)_{s'}{}^0-R'(\mathbf{k}'';z_l)_{s'}{}^0]\}. \quad (5.14)$$

In this last expression $\delta_{ss'}$ is the Kronecker delta symbol and $v_{\rm eff}(\mathbf{k};z_n)_{ss'}$ is the effective particle–particle interaction

$$v_{\rm eff}(\mathbf{k};z_n)_{ss'}=v_{\rm eff}(\mathbf{k};z_n)_{s's}=\{Z_sZ_{s'}v(k)+([Z_sE_{s'}+E_sZ_{s'}]v(k)\sum_{s''}Z_{s''}E_{s''}R'(\mathbf{k},z_n)_{s''}{}^0$$
$$+E_sE_{s'}[\epsilon_\infty-v(k)\sum_r|p_r(\mathbf{k})|^2A'(\mathbf{k};z_n)_r{}^0-v(k)\sum_{s''}Z_{s''}{}^2R'(\mathbf{k},z_n)^0{}_{s''}])$$
$$\times\sum_r|d_r(\mathbf{k})|^2B'(\mathbf{k};z_n)_r{}^0/[1-\sum_{s''}E_{s''}{}^2R'(\mathbf{k};z_n)_{s''}{}^0\sum_r|d_r(\mathbf{k})|^2B'(\mathbf{k},z_n)_r{}^0]\}/\epsilon(\mathbf{k};z)^0. \quad (5.15)$$

When the nonpolar interaction vanishes [$E_s=0$ for all s] the result (5.13) correctly reduces to the expression (4.8).

Introducing dispersion relations and proceeding as in previous sections, we can rewrite the auxiliary function (5.14) in a form convenient for analytically continuing the result (5.13) from discrete z_n to arbitrary complex z:

$$M(\mathbf{k};z)_{ss'}=\delta_{ss'}R'(\mathbf{k};z)_s{}^0-\tfrac{1}{2}\sum_{\mathbf{k}''}\frac{(\hbar\mathbf{k}\cdot\mathbf{k}''/z^2)^2}{m_sm_{s'}}\left[\delta_{ss'}\left(\int_{-\infty}^{\infty}\frac{d\omega_1\,d\omega_2}{\pi^2}\frac{\coth(\beta\omega_1/2)}{z-(\omega_1-\omega_2)}\mathfrak{F}\{v_{\rm eff}(\mathbf{k}'';\omega_1)_{ss}R'(\mathbf{k}'';\omega_2)_s{}^0\right.\right.$$
$$\left.+v_{\rm eff}(\mathbf{k}'';\omega_2)_{ss}R'(\mathbf{k}'';\omega_1)_s{}^0\}+\int_{-\infty}^{\infty}\frac{d\bar\omega}{\pi}\coth(\beta\bar\omega/2)\mathfrak{F}\{v_{\rm eff}(\mathbf{k}'';\bar\omega)_{ss}R'(\mathbf{k}'';\bar\omega)_s{}^0\}\right)+\left(\int_{-\infty}^{\infty}\frac{d\omega_1\,d\omega_2}{\pi^2}\frac{\coth(\beta\omega_1/2)}{z-(\omega_1-\omega_2)}\right.$$
$$\times\mathfrak{F}\{v_{\rm eff}(\mathbf{k}'';\omega_1)_{ss'}v_{\rm eff}(\mathbf{k}'';\omega_2)_{ss'}[R'(\mathbf{k}'';\omega_1)_s{}^0-R'(\mathbf{k}'';\omega_2)_s{}^0][R'(\mathbf{k}'';\omega_1)_{s'}{}^0-R'(\mathbf{k}'';\omega_2)_{s'}{}^0]\}$$
$$\left.\left.-\int_{-\infty}^{\infty}\frac{d\bar\omega}{\pi}\coth(\beta\bar\omega/2)\mathfrak{F}\{[Z_sZ_{s'}v(k'')/\epsilon_\infty]v_{\rm eff}(\mathbf{k}'';\bar\omega)_{ss'}R'(\mathbf{k}'';\bar\omega)_s{}^0R'(\mathbf{k}'';\bar\omega)_{s'}{}^0\}\right)\right]. \quad (5.16)$$

Using the continued dielectric function (5.13) in Eq. (1.8), one can compute the conductivity $\tilde\sigma(\omega+i\epsilon)$.

It may be useful in concluding this section to indicate briefly the specific form of the parameters $d_r(\mathbf{k})$ for deformation-potential coupling. If $s(\mathbf{k})_r$ describes the strain dilation associated with the lattice displacement operator $\beta_r(\mathbf{k};t)$ of (5.1), then the deformation potential seen by carriers of type s is [compare Eqs. (4.14) and (4.17)]

$$\phi(\mathbf{r},t)|_{\text{deformation potential}}=\hbar E_s\sum_{\mathbf{k}}\exp(i\mathbf{k}\cdot\mathbf{r})\sum_r s(\mathbf{k})_r\beta_r(\mathbf{k};t), \quad (5.17)$$

where $\hbar E_s$ is the deformation-potential energy constant for those carriers and where the r summation is over all acoustic modes. Comparing the potential (5.17) with that used in the Hamiltonian (5.2), we see that

$$d_r(\mathbf{k})=s(\mathbf{k})_r, \quad (5.18)$$

the strain dilation coefficient. In a Debye model of acoustic phonons $s(\mathbf{k})_r$ has the form (4.18), while for optical phonons the corresponding expression is

$$s(\mathbf{k})_r=(\hbar K^2/2\rho_mV\omega_{\mathbf{k}}{}^r)^{\frac{1}{2}}, \quad (5.19)$$

where $\mathbf{K}$ is a vector of the reciprocal lattice.

CC-0. In Public Domain. Gurukul Kangri Collection, Haridwar

Digitized by Arya Samaj Foundation Chennai and eGangotri

6. CONCLUDING REMARKS, DRIFTING CARRIERS

In the preceding sections we have indicated how Dawson–Oberman high-frequency long-wavelength conductivities can be systematically derived for systems in thermal equilibrium by a variational formalism, and we have used that formalism to take into account carrier–phonon as well as carrier–carrier interactions. In a later publication we shall use our formulas to analyze single-stream instabilities. For this purpose we shall require expressions appropriate to drifting carriers. The preceding derivations are based upon thermal-equilibrium ensembles in which there is, on the average, no net energy or momentum transfer between different carrier or phonon components. In normal solids of finite conductivity a uniform applied field results in a stationary or stead-state configuration which is not a thermal-equilibrium configuration. The drifting carriers gain energy and momentum from the applied field; this they transfer to the lattice through phonon and impurity interactions.

The thermal-equilibrium assumption, upon which the Fourier-series expansion (2.8) is based, leads through identities of the type (3.13) to the coth $(\beta\omega/2)$ factors which appear in our final results and which involve the ensemble temperature explicitly in the parameter $\beta=\hbar/kT$. These factors describe the thermal excitation of collective plasmon–phonon resonances as well as the thermal distribution of carriers. For this reason they cannot be easily modified to describe steady-state systems which are not in thermal equilibrium. Useful variational equations similar to Eq. (2.10) have been derived for nonequilibrium ensembles.[22] In a second paper we shall use such equations to extend the thermal-equilibrium results to more general stationary ensembles.

ACKNOWLEDGMENTS

I wish to acknowledge fruitful conversations in the course of preparing this paper with N. Tzoar, P. M. Platzman, and P. A. Wolff.

APPENDIX A

Dispersion Relations

In going from Eq. (3.12a) to (3.12b), we have used dispersion relations of the following typical types:

$$\frac{R'(\mathbf{k};z)^0}{\epsilon(\mathbf{k};z)^0}=\int_{-\infty}^{\infty}\frac{d\omega}{\pi}(z-\omega)^{-1}\mathfrak{F}\left\{\frac{R'(\mathbf{k};\omega)^0}{\epsilon(\mathbf{k};\omega)^0}\right\}, \quad \text{(A1a)}$$

$$[\epsilon(k;z)^0]^{-1}=\epsilon_\infty^{-1}+\int_{-\infty}^{\infty}\frac{d\omega}{\pi}(z-\omega)^{-1}\mathfrak{F}\{\epsilon(k;\omega)^0\}^{-1}. \quad \text{(A1b)}$$

The principal steps in the derivation of these expressions are as follows. (Similar derivations apply to all of the dispersion relations which we require.) Starting from Eqs. (1.5) and (1.6) with $\mathbf{k}$ finite and using the discrete-$\mathbf{k}_1$ summation of (1.6a), we infer from the Mittag-Leffler partial-fractions theorem[22] that the functions $R'(\mathbf{k};z)^0/\epsilon(\mathbf{k};z)^0$ and $1/\epsilon(\mathbf{k};z)^0$ can both be written in the form

$$f(z)=f_\infty+\sum_s f_s/(z-z_s), \quad \text{(A2)}$$

where $f_\infty=\lim f(z)$ as $z\to\infty$. Noting from Eqs. (1.6) that $R'(\mathbf{k};z)^0$ already has this form with *real* parameters $\{z_s, f_s, f_\infty\}$, we can easily establish by studying the parameters of (A2) as a function of the strength of the coefficient $v(k)$ in Eq. (1.5) that $\{z_s, f_s, f_\infty\}$ in (A2) are also real. Hence, if ω is real and $\epsilon=0^+$, then, using the definition (1.13a), we note that

$$\mathfrak{F}\{f(\omega)\}=\tfrac{1}{2}i\sum_s\left[\frac{f_s}{\omega-z_s+i\epsilon}-\frac{f_s}{\omega-z_s-i\epsilon}\right]$$

$$=\pi\sum_s f_s\delta(\omega-z_s), \quad \text{(A3)}$$

where $\delta(\omega-z_s)$ is the Dirac δ function. Equations (A1) and the identification of $\mathfrak{F}\{f(\omega)-f_\infty\}=\mathfrak{F}\{f(\omega)\}$ with an energy spectrum follow immediately from this result.

APPENDIX B

Alternative Forms for Eqs. (1.11a) and (1.17a)

To establish the equivalence of Eqs. (1.11a) and (1.17a) with results previously derived by Ron and Tzoar[5,14] and by Tzoar,[7,15] we establish in this appendix an alternative form for the expression

$$\int_{-\infty}^{\infty}\frac{d\omega_1 d\omega_2}{\pi^2}\frac{\coth(\beta\omega_1/2)}{\omega+i\epsilon-(\omega_1-\omega_2)}$$

$$\times\mathfrak{F}\{[R(\omega_1)-R(\omega_2)][A(\omega_1)-A(\omega_2)]/\epsilon(\omega_1)^0\epsilon(\omega_2)^0\}$$

$$-\int_{-\infty}^{\infty}\frac{d\omega_1}{\pi}\coth(\beta\omega_1/2)\mathfrak{F}\{R(\omega_1)A(\omega_1)/\epsilon(\omega_1)^0\epsilon_\infty\}, \quad \text{(B1)}$$

in which we have abbreviated

$$R(\omega)=R'(\mathbf{k}'';\omega)_s^0, \qquad \epsilon(\omega)^0=\epsilon(\mathbf{k}'';\omega)^0, \quad \text{(B2a)}$$

and

$$A(\omega)=R'(\mathbf{k}'';\omega)_s^0 \text{ or } A'(\mathbf{k}'';\omega)_s^0. \quad \text{(B2b)}$$

The first of Eqs. (B2b) pertains to Eq. (1.11a) and to Sec. 3, the second to Eq. (1.17a) and to Sec. 4.

[22] K. Knopp, *Theory of Functions* (Dover Publishers, Inc., New York, 1947), Vol. 2, Chap. 2.

CC-0. In Public Domain. Gurukul Kangri Collection, Haridwar

Digitized by Arya Samaj Foundation Chennai and eGangotri

Removing the ω_1 integration and the factor $\coth(\beta\omega_1/2)$ from (B1), we initially consider the integrand

$$I(\omega,\omega_1)=\int_{-\infty}^{\infty}\frac{d\omega_2}{\pi}(\omega+i\epsilon-\omega_1+\omega_2)^{-1}\mathfrak{F}\{[R(\omega_1)-R(\omega_2)][A(\omega_1)-A(\omega_2)]/\epsilon(\omega_1)^0\epsilon(\omega_2)^0\}-\mathfrak{F}\{R(\omega_1)A(\omega_1)/\epsilon(\omega_1)^0\epsilon_\infty\}$$

$$=-\int_{-\infty}^{\infty}\frac{d\omega_2}{\pi}(\omega_1-\omega-\omega_2-i\epsilon)^{-1}[\mathfrak{F}\{1/\epsilon(\omega_2)^0\}\mathfrak{F}\{R(\omega_1)A(\omega_1)/\epsilon(\omega_1)^0\}+\mathfrak{F}\{1/\epsilon(\omega_1)^0\}\mathfrak{F}\{R(\omega_2)A(\omega_2)/\epsilon(\omega_2)^0\}$$
$$-\mathfrak{F}\{R(\omega_2)/\epsilon(\omega_2)^0\}\mathfrak{F}\{A(\omega_1)/\epsilon(\omega_1)^0\}-\mathfrak{F}\{A(\omega_2)/\epsilon(\omega_2)^0\}\mathfrak{F}\{R(\omega_1)/\epsilon(\omega_1)^0\}]$$
$$-\mathfrak{F}\{R(\omega_1)A(\omega_1)/\epsilon(\omega_1)^0\epsilon_\infty\} \quad \text{(B3b)}$$

$$=-[[\epsilon^-(\omega_1-\omega)^0]^{-1}-\epsilon_\infty^{-1}]\mathfrak{F}\{R(\omega_1)A(\omega_1)/\epsilon(\omega_1)^0\}-[R^-(\omega_1-\omega)A^-(\omega_1-\omega)/\epsilon^-(\omega_1-\omega)^0]$$
$$\times\mathfrak{F}\{1/\epsilon(\omega_1)^0\}+[R^-(\omega_1-\omega)/\epsilon^-(\omega_1-\omega)^0]\mathfrak{F}\{A(\omega_1)/\epsilon(\omega_1)^0\}+[A^-(\omega_1-\omega)/\epsilon^-(\omega_1-\omega)^0]$$
$$\times\mathfrak{F}\{R(\omega_1)/\epsilon(\omega_1)^0\}-\epsilon_\infty^{-1}\mathfrak{F}\{R(\omega_1)A(\omega_1)/\epsilon(\omega_1)^0\}. \quad \text{(B3c)}$$

In Eq. (B3b) we have used the property (1.14). In Eq. (B3c) we have used dispersion relations of the type illustrated in Appendix A, and we have used the abbreviated notation of Ron and Tzoar in which $R^\pm(\omega)=R(\omega\pm i\epsilon)$, etc. Using (B3c) in (B1), we find with equations like (3.11) that

$$\int_{-\infty}^{\infty}\frac{d\omega_1}{\pi}\coth(\beta\omega_1/2)I(\omega,\omega_1)=-\int_{-\infty}^{\infty}\frac{d\omega_1}{\pi}\coth(\beta\omega_1/2)I(\omega,-\omega_1)$$

$$=\int_{-\infty}^{\infty}\frac{d\omega_1}{\pi}\frac{\coth(\beta\omega_1/2)}{\epsilon^+(\omega_1+\omega)^0}[\mathfrak{F}\{R(\omega_1)A(\omega_1)/\epsilon(\omega_1)^0\}$$
$$+R^+(\omega_1+\omega)A^+(\omega_1+\omega)\mathfrak{F}\{1/\epsilon(\omega_1)^0\}-R^+(\omega_1+\omega)\mathfrak{F}\{A(\omega_1)/\epsilon(\omega_1)^0\}$$
$$-A^+(\omega_1+\omega)\mathfrak{F}\{R(\omega_1)/\epsilon(\omega_1)^0\}]$$
$$=\int_{-\infty}^{\infty}\frac{d\omega_1}{\pi}\coth(\beta\omega_1/2)\{[R^+(\omega_1)-R^+(\omega_1+\omega)]$$
$$\times[A^+(\omega_1)-A^+(\omega_1+\omega)]/\epsilon^+(\omega_1)^0\epsilon^+(\omega_1+\omega)^0-[R^-(\omega_1)$$
$$-R^+(\omega_1+\omega)][A^-(\omega_1)-A^+(\omega_1+\omega)]/\epsilon^-(\omega_1)^0\epsilon^+(\omega_1+\omega)^0\}. \quad \text{(B4)}$$

This last result follows by simple algebra from the definitions (1.13a) of the spectral functions $\mathfrak{F}\{\cdots\}$.

Using (B4) with the definitions (B2), we can easily demonstrate that in the appropriate limits our results are equivalent to those of Ron and Tzoar.

CC-0. In Public Domain. Gurukul Kangri Collection, Haridwar

Digitized by Arya Samaj Foundation Chennai and eGangotri

REVIEWS OF MODERN PHYSICS VOLUME 38, NUMBER 3 JULY 1966

Atomic Fluorescence Yields

R. W. FINK
School of Chemistry, Georgia Institute of Technology, Atlanta, Georgia

R. C. JOPSON, HANS MARK, C. D. SWIFT
Lawrence Radiation Laboratory, University of California, Livermore, California

The mechanisms of the reorganization of atoms with inner shell vacancies are reviewed. All available experimental values of K-, L-, and M-shell fluorescence yields, together with L-shell Coster–Kronig yields are summarized and compared with available theoretical calculations. Rather good agreement exists in general between theory and experiment for the K shell, but experimental values of the L_2 and L_3 subshell fluorescence yields disagree substantially with the semitheoretical results of Listengarten. Related phenomena in μ-mesic atoms are included. Experimental methods of measurement are summarized and discussed, together with suggestions for future studies with high resolution techniques. Results from the literature have been included up to 10 May 1966.

1. Introduction and Definitions 513
1.1. Fluorescence and Auger Yields 513
1.2. Subshell Yields and Coster–Kronig Transitions 514
1.3. Quantitative Relationships and Notation 514
2. Creation of Primary Vacancies 516
2.1. Photoelectric Absorption 516
2.2. Ionization by Impact of Electrons and Heavy Charged Particles 517
2.3. Ionization of Higher Shells by Transitions to K-Shell Vacancies 518
2.4. Ionization by Electron Capture or Internal Conversion 518
2.5. Critical Excitation of Specific Subshell Vacancies 518
3. Rearrangement of Vacancies 519
3.1. Shifting of Vacancies between Major Shells 519
3.2. Shifting of Vacancies among Subshells: Coster–Kronig Transitions 520
4. Filling of Vacancies and Measurement of Auger Electron and X-Ray Intensities 521
4.1. Auger Electron Measurements 521
4.2. X-Ray Intensity Measurements 521
4.2.1. Photographic Detection of X Rays 521
4.2.2. Ionization Chambers and Geiger Counters 522
4.2.3. Proportional Counters 522
4.2.4. Scintillation Counters 523
4.2.5. Coincidence Methods 523
4.2.6. High-Resolution Techniques 525
5. Experimental Results and Comparison with Theory 526
5.1. K-Shell Fluorescence Yields 526
5.2. L-Shell Fluorescence and Coster–Kronig Yields 531
5.3. M-Shell Fluorescence Yields 534
5.4. Mesic X-Ray Fluorescence Yields 537
6. List of References 538

1. INTRODUCTION AND DEFINITIONS

1.1. Fluorescence and Auger Yields

The creation of a vacancy in an atomic shell initiates a series of rearrangement processes which may become quite complicated. A single vacancy created, for example, in the K shell is filled in a time of the order of 10^{-17}–10^{-14} sec by an electron coming from some higher shell (e.g., the L_2 subshell), thus shifting the vacancy to the higher shell. The difference in binding energy between the two shells (e.g., the $K-L_2$ energy difference) either is released as a K x-ray photon or is transferred to another bound electron (e.g., an L_3 electron) which is ejected (e.g., a $K-L_2L_3$ Auger transition). This results in an atom with two vacancies. Continuation of these processes gives rise to the emission of L, M, N, etc. x rays and Auger electrons, resulting in an atom with multiple vacancies in its outermost shells; i.e., a highly charged ion. In principle, both the radiative and the Auger process are well understood. The radiative transitions can be adequately explained in terms of multipole theory which predicts that by far the most important mode is the electric dipole, although other multipoles also may cause observable effects. The nonradiative, or Auger, transitions occur because of the Coulomb interaction existing among the different electrons in the atom (Be-64). Detailed theories exist which can accurately predict nonradiative transition rates (As-59, As-65, Li-60, Li-62, Di-63, Ca-63b, a).

High resolution spectrometry has made it possible to determine the binding energies of a vast number of atomic levels (2-Ha-64), but the transition rates between levels and the branching ratios between different decay modes are not nearly as well known. The present review summarizes the situation existing today in a restricted class of these branching ratios—the atomic fluorescence yields and Coster–Kronig yields.

Historically, the fluorescence yield of an element was defined in terms of the intensity of fluorescent radiation produced when a sample of the material was exposed to a beam of energetic x rays. More recently, it has been defined in terms of the probability that a vacancy in a given shell results in a radiative transition. The fluorescence yield of the ith subshell of an atom, ω_i, is the probability that a vacancy in that subshell is filled by a radiative transition. The Auger yield of the same shell, a_i, is defined as the probability that an electron is emitted when the vacancy is filled from a higher shell. Great care must be taken in applying these definitions in practical situations because several complicated rearrangements may occur before the vacancy is filled. These definitions can be applied in a straightforward manner to the K shell, which consists of two $s_{\frac{1}{2}}$ electrons. The fluorescence yield of the K shell, ω_K, can thus be obtained by measuring the number of characteristic K x rays emitted per K-shell vacancy. Since the K shell has only one subshell, the

CC-0. In Public Domain. Gurukul Kangri Collection, Haridwar

Digitized by Arya Samaj Foundation Chennai and eGangotri

experiment results in a quantity directly related to the fluorescence yield as defined above.

1.2. Subshell Yields and Coster–Kronig Transitions

The situation is more complicated in the case of higher atomic shells. In the L shell, for instance, there are eight electrons grouped into three subshells (L_1, L_2, and L_3) each of which corresponds to a different quantum state. The fluorescence yield of each of these subshells can be defined as before; however, two circumstances make it difficult to apply the definition in practical situations:

(1) In most experiments it is very difficult to ionize only one of the three L subshells. Usually, all three subshells are ionized in some specific ratio, so that the L shell fluorescence yield measured in a typical experiment is an average fluorescence yield ($\bar{\omega}_L$). Since the fluorescence yields of the three subshells (ω_1, ω_2, and ω_3) generally are not equal, the mean fluorescence yield, $\bar{\omega}_L$, will depend on the ratio of the number of primary vacancies produced in the three subshells and thus on the way in which the L shell is ionized.

(2) A second complicating factor is that in certain regions of the periodic table, radiationless transitions occur that move a vacancy in one L subshell to another ($L_1 \rightarrow L_3$, $L_1 \rightarrow L_2$, or $L_2 \rightarrow L_3$). Therefore, a primary vacancy which originally is created in the L_1 shell may move to the L_2 or L_3 shell before it is filled by an electron from a higher (M, N, etc.) shell. These transitions are called Coster–Kronig transitions (Co-35), and they complicate the situation by changing the distribution of primary vacancies among the three subshells. Great care must be taken to insure that this effect is properly included in the calculation of the subshell yields ω_1, ω_2, and ω_3 from measured average fluorescence yield, $\bar{\omega}_L$.

In the case of fluorescence yields for shells higher than the L shell, the situation is even more complex. The M shell, for example, has five subshells which may be ionized each with different probabilities by the primary excitation process. After the initial ionization, Coster–Kronig transitions may redistribute the primary vacancies before these are filled by electrons from higher shells. If all of the M subshells are ionized, there may be eight or ten different processes before the event is over. To trace all of these in detail is quite complicated (Di-63). Since very little experimental data on M- or higher-shell fluorescence yields are available, not much attention can be given to these complications other than to mention that they exist.

1.3. Quantitative Relationships and Notation

To make certain that various experiments are properly interpreted, it is important that a uniform notation system be employed. There is a fairly large literature on L-shell fluorescence yields for which the notation system is rather well standardized. The relationships between the various important quantities will be developed here for the L shell to account for the two complications discussed in the preceding section. These are the existence of subshells (in shells above the K shell) and the possibility that radiationless transitions between the subshells change the initial distribution of primary vacancies.

In an L-shell fluorescence yield experiment in which vacancies are created in all three subshells and no Coster–Kronig transitions occur, an average L-fluorescence yield is measured. This average fluorescence yield may be expressed in terms of the individual subshell fluorescence yields as

$$\bar{\omega}_L = N_1\omega_1 + N_2\omega_2 + N_3\omega_3, \tag{1}$$

where N_1, N_2, and N_3 are the relative numbers of primary vacancies in the three subshells, respectively. It follows that

$$N_1 + N_2 + N_3 = 1 \tag{2}$$

and it is easy to see that Eq. (1) is consistent with the general definition of the fluorescence yield given in Sec. 1.1. Since the quantities of theoretical interest are the subshell fluorescence yields ω_1, ω_2, and ω_3, it is clear that no information about these can be obtained from Eq. (1) unless further measurements are made. In general, it is necessary to perform two other measurements of mean L-fluorescence yields, $\bar{\omega}_L'$ and $\bar{\omega}_L''$ for *different* ratios of primary vacancies $N_1':N_2':N_3'$ and $N_1'':N_2'':N_3''$. If all of the primary vacancy distributions are known, then the subshell fluorescence yields ω_1, ω_2, and ω_3 can be calculated from the set of equations

$$\begin{aligned} \bar{\omega}_L &= N_1\omega_1 + N_2\omega_2 + N_3\omega_3 \\ \bar{\omega}_L' &= N_1'\omega_1 + N_2'\omega_2 + N_3'\omega_3 \\ \bar{\omega}_L'' &= N_1''\omega_1 + N_2''\omega_2 + N_3''\omega_3. \end{aligned} \tag{3}$$

It is clear that in any L-shell fluorescence yield experiment, the determination of the subshell vacancy distribution is as important as the measurement of the mean L-fluorescence yield itself.

Equations (1), (2), and (3) are applicable only if the primary vacancy distribution remains unaltered before the vacancies are filled by transitions from higher shells. If Coster–Kronig transitions (Co-35) occur within the subshell, then the situation is more complicated. Under such circumstances, two views are possible: One is to regard the measured mean L-fluorescence yield, $\bar{\omega}_L$, as a linear combination of the subshell fluorescence yields ω_1, ω_2, and ω_3, with a vacancy distribution altered by Coster–Kronig transitions. This is the view taken by Listengarten (Li-60). The other view is to let the mean L-fluorescence yield, $\bar{\omega}_L$, be a linear combination of the *primary* vacancy distribution N_1, N_2, and N_3 and to redefine the fluorescence yields of the subshells to account for the Coster–Kronig transitions, as was done by Wapstra, Nijgh, and van Lieshout (Wa-59). The latter system is some-

CC-0. In Public Domain. Gurukul Kangri Collection, Haridwar

Digitized by Arya Samaj Foundation Chennai and eGangotri

what more convenient from the experimental viewpoint, since the equations are written in terms of the primary vacancy distribution $N_1:N_2:N_3$, which is usually known in a given experiment. It is important to recognize that the two notation systems are completely equivalent. The appropriate transformation equations between them will now be developed.

If the mean L-fluorescence yield is regarded as a linear combination of the three subshell yields, ω_1, ω_2, and ω_3, then it may be expressed as:

$$\bar{\omega}_L = V_1\omega_1 + V_2\omega_2 + V_3\omega_3. \tag{4}$$

The coefficients V_1, V_2, and V_3 represent a modified vacancy distribution in which Coster–Kronig processes are taken into account. It should be noted that

$$V_1 + V_2 + V_3 \geq 1. \tag{5}$$

The N's are relative primary vacancy distributions and thus, by definition, obey Eq. (2). Because of the way the fluorescence yields are defined, the condition (5) applies to the V's, because some of the vacancies created in the L_1 and L_2 subshells must be counted twice since they may be shifted to higher shells. The final vacancy distribution $V_1:V_2:V_3$ can be rewritten in terms of the primary vacancy distribution $N_1:N_2:N_3$ using the appropriate Coster–Kronig yields,

$$\begin{aligned} V_1 &= N_1 \\ V_2 &= N_2 + f_{12}N_1 \\ V_3 &= N_3 + f_{23}N_2 + (f_{13} + f_{12}f_{23})N_1, \end{aligned} \tag{6}$$

where f_{12}, f_{13}, and f_{23} are the respective probabilities for the occurrence of the Coster–Kronig transitions $L_1 \rightarrow L_2$, $L_1 \rightarrow L_3$, and $L_2 \rightarrow L_3$. Listengarten (Li-60) also defines three other quantities which are often useful,

$$\begin{aligned} X_1 &= V_1\omega_1, \\ X_2 &= V_2\omega_2, \\ X_3 &= V_3\omega_3. \end{aligned} \tag{7}$$

The quantities X_1, X_2, and X_3 are the respective fractions of x-ray quanta emitted per *total* L-shell vacancy with energies corresponding to transitions *to* each of the L subshells.

If the mean L-fluorescence yield is expressed in terms of the primary vacancy distribution, the following equation results:

$$\bar{\omega}_L = N_1\nu_1 + N_2\nu_2 + N_3\nu_3. \tag{8}$$

The coefficients ν_1, ν_2, and ν_3, denoted as ν_{L_1}, $\nu_{L_{11}}$, and $\nu_{L_{111}}$ by Wapstra, Nijgh, and van Lieshout (Wa-59), are specially defined "fluorescence yields." The quantity ν_1 is the fraction of *all* L x rays observed per vacancy in the L_1 subshell. Note that this is quite different from the definition of the actual fluorescence yield for that subshell ω_1, when it is required that the L x-ray transitions go *only* to the L_1 subshell. It is instructive at this point to emphasize that the products $V_i\omega_i$, called X_i by Listengarten (Li-60), and $N_i\nu_i$ are *not* equal. Only the sums of the products for all three subshells are equal to the mean fluorescence yield $\bar{\omega}_L$, [see Eqs. (4) and (8)]. This is obvious from the respective physical definitions: The product $V_i\omega_i$ (or X_i) represents the number of L x rays filling vacancies in the ith subshell per vacancy in the entire L shell. The product $N_i\nu_i$, on the other hand, represents the number of L x rays observed per vacancy created in the ith subshell. It is readily seen from Eqs. (8), (6), and (4) that the relations between the quantities ν_1, ν_2, and ν_3 and ω_1, ω_2, and ω_3 are

$$\begin{aligned} \nu_1 &= \omega_1 + f_{12}\omega_2 + (f_{13} + f_{12}f_{23})\omega_3, \\ \nu_2 &= \omega_2 + f_{23}\omega_3, \\ \nu_3 &= \omega_3. \end{aligned} \tag{9}$$

In some of the early papers in this field (Kü-35), before the mechanism of Coster–Kronig transitions was discovered (Co-35), no distinction was made between the ν's and the ω's. This has led to some confusion, since some of the values quoted as "subshell fluorescence yields" in certain tables (Bu-52) are in fact ν's and not ω's.

It is obvious from the foregoing discussion that a determination of the three subshell yields ω_1, ω_2, and ω_3 may be a fairly complex procedure. If Coster–Kronig yields are included, a set of simultaneous equations such as the set (3) is obtained, except that instead of the primary vacancy distributions N_1, N_2, N_3, the more complicated expressions given in Eq. (6) must be employed. In general, three different mean L-fluorescence yields measured for three different primary vacancy distributions *and* the appropriate Coster–Kronig yields must be known to deduce values of ω_1, ω_2, and ω_3. Fortunately, the conditions can often be adjusted to reduce the complexity. It is generally possible to measure ω_3 alone using the critical excitation method (Sec. 2.5). Furthermore, there are certain regions of the periodic table for which some of the Coster–Kronig yields are small so that the equations can be greatly simplified (see Sec. 3.2).

As yet, no mention has been made of the Auger yields, which are the complementary quantities to the fluorescence yields. The fluorescence yield ω_i has been defined as the probability that a vacancy in the ith subshell is filled by an electron making a radiative transition. The Auger yield a_i is the probability that a vacancy in the ith shell is filled with an electron making a nonradiative transition *from a higher shell* (see Sec. 3.1). The underlined phrase in the definition is important, since the Coster–Kronig transitions are *excluded* from the definition of the Auger yields. The Coster–Kronig yield is the probability that a vacancy is filled with an electron making a nonradiative transition from a *higher subshell* in the *same* major shell (see Sec. 3.2). From these definitions, it is obvious that

CC-0. In Public Domain. Gurukul Kangri Collection, Haridwar

Digitized by Arya Samaj Foundation Chennai and eGangotri

the following relations must hold between the fluorescence yields, the Auger yields, and the Coster–Kronig yields for the L shell:

$$\omega_3+a_3=1,$$
$$\omega_2+a_2+f_{23}=1,$$
$$\omega_1+a_1+f_{12}+f_{13}=1. \quad (10)$$

The expressions for mean L-shell Auger yields can be developed in precisely the same way as for the fluorescence yields. In the Listengarten notation (Li-60),

$$\bar{a}_L=a_1V_1+a_2V_2+a_3V_3=A_1+A_2+A_3. \quad (11)$$

It can be shown from Eqs. (10), (6), and (4) that the sum of the mean fluorescence yield and the mean Auger yield for the *same* initial vacancy distribution is

$$\bar{a}_L+\bar{\omega}_L=1. \quad (12)$$

Another important fact should be mentioned at this point. The total "width" of an energy level (i.e., an inner shell vacancy in an atom) is the sum of the partial widths of all of the processes by which the level can decay (i.e., processes by which the vacancy can be filled). Thus,

$$\Gamma_{T_i}=\Gamma_{X_i}+\Gamma_{a_i}+\sum_{k>i}\Gamma_{ik}, \quad (13)$$

where Γ_{T_i} is the total width, Γ_{X_i} the radiation width, and Γ_{a_i} is the Auger width for the ith subshell. The quantities Γ_{ik} are the widths for the Coster–Kronig transitions $k\rightarrow i$. From the definitions of ω_i, a_i, and f_{ik}, it can be seen that (Ki-48a)

$$\omega_i=\Gamma_{X_i}/\Gamma_{T_i},$$
$$a_i=\Gamma_{a_i}/\Gamma_{T_i},$$
$$f_{ik}=\Gamma_{ik}/\Gamma_{T_i}. \quad (14)$$

The method of using radiation width measurements has been employed to determine fluorescence and Auger yields at high Z (see Sec. 5.1).

In addition to the system developed above for the fundamental quantities dealt with in this review, there are several other derived quantities which are important enough to deserve special attention. A partial L-shell fluorescence yield which is often used is the fluorescence yield of the L shell following K x-ray emission, ω_{KL}. The quantity ω_{KL} may be defined as

$$\omega_{KL}=N_2\nu_2+N_3\nu_3, \quad (15)$$

where $N_2=(K_{\alpha_2}/K_\alpha)$ and $N_3=(K_{\alpha_1}/K_\alpha)$, the ratio of K_{α_2} and K_{α_1} x rays to the total K_α x-ray emission, respectively.

Another quantity often determined experimentally is the partial L-shell fluorescence yield following L-electron capture, ω_{LL}. The quantity ω_{LL} depends on ω_1, ω_2, ω_3, and the Coster–Kronig yields f_{12}, f_{13}, and f_{23}. Since for allowed and first-forbidden L capture, $N_1\approx 1$ and N_2, $N_3\ll 1$ (RF-55, RF-60), we define ω_{LL} as

$$\omega_{LL}\approx\nu_1=\omega_1+f_{12}\omega_2+(f_{13}+f_{12}f_{23})\omega_3. \quad (16)$$

In general, one may think of ω_{KL} as a special case of the mean L-fluorescence yield $\bar{\omega}_L$ for which $N_1\approx 0$, and of ω_{LL} as a special case of $\bar{\omega}_L$ for which $N_1\approx 1$. The quantity ω_{LL} is particularly important in most electron capture and in certain internal conversion experiments because these processes create vacancies predominantly in the L_1 subshell.

2. CREATION OF PRIMARY VACANCIES

2.1. Photoelectric Absorption

The primary vacancies in most fluorescence yield measurements are usually produced by bombarding the atom with photons, electrons, or with heavy charged particles of sufficient energy to cause ionization. The vacancies also can be produced by such radioactive decay processes as electron capture and internal conversion. If the shell to be ionized consists of more than one subshell, then each of these processes results in a different distribution of primary vacancies. Furthermore, the distribution may also depend on the energy of the incident radiation or particles.

Most of the early work on fluorescence yields was performed using photoelectric ionization to create the primary vacancies. (Indeed, the name "fluorescence yield" came from the fact that the measurement involves the observation of fluorescent x rays during the irradiation of a sample.) The measurements of K-shell fluorescence yields were performed using the schematic geometry shown in Fig. 1. The detector A observes the fluorescent x rays, and the detector B measures the transmitted beam. When the sample is removed, detector B measures the incident beam intensity. The difference in the observed intensities is a measure of the attenuation in the target and thus depends on the rate

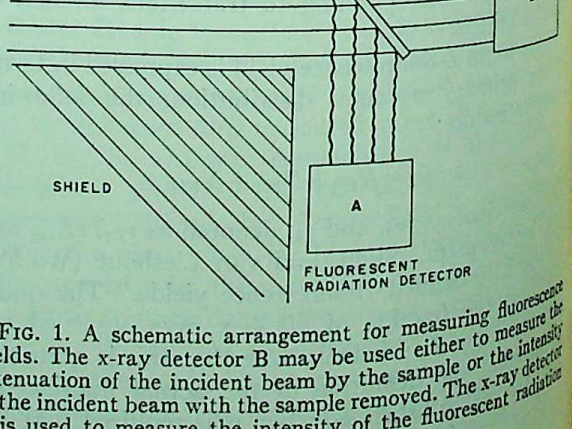

FIG. 1. A schematic arrangement for measuring fluorescence yields. The x-ray detector B may be used either to measure the attenuation of the incident beam by the sample or the intensity of the incident beam with the sample removed. The x-ray detector A is used to measure the intensity of the fluorescent radiation from the sample.

CC-0. In Public Domain. Gurukul Kangri Collection, Haridwar

Digitized by Arya Samaj Foundation Chennai and eGangotri

at which vacancies are created by the incident beam. When this is compared with the counting rate observed in detector A, the fluorescence yield can be calculated according to the definition given in Sec. 1.1. In practice, it is not enough simply to measure the attenuation, since too many other mechanisms can lead to absorption of x rays from the incident beam. Even the very early workers in the field (La-34) used theoretical estimates to calculate the fraction of the incident x rays which cause vacancies in the appropriate atomic shells. Fortunately, theoretical values of the ionization cross sections (or partial absorption coefficients) for the K shell are well known over a wide energy region, so that the necessary calculations can easily be performed if the spectrum of the incident radiation is known. For a complete discussion, see C. M. Davisson (Da-64). The reliance upon theoretical values for the computation of the creation of primary vacancies is justified for the K shell.

In the case of higher atomic shells, however, it is necessary to know not only the total absorption coefficient, but also how the vacancies created are distributed among the subshells. In the case of the L shell, for instance, this is necessary if some information about the actual subshell yields ω_1, ω_2, and ω_3 is desired. The best discussion of vacancy creation by photoionization of the L shell is given by Ross, Cochran, Hughes, and Feather (Ro-55). If relatively soft x rays are used to ionize the L shell (i.e., x rays with quantum energies between two and five times the mean binding energy of the L-shell electrons), the ratio of primary vacancies is approximately $N_1:N_2:N_3=1:2:3$. This ratio was obtained from several experimental measurements quoted in Ro-55, and it should not be considered as being very reliable. Indeed, the photoelectric method of creating vacancies in higher shells has not been extensively employed precisely because the subshell vacancy ratio is difficult to determine. Recently, a number of more effective methods (see Secs. 2.2, 2.3, and 2.4) of creating vacancies in higher shells have been developed, where it is possible to determine the vacancy ratio with greater accuracy. Consequently, photoelectric excitation of L- and higher-shell vacancies is no longer used extensively for precise measurements of subshell fluorescence yields.

2.2. Ionization by Impact of Electrons and Heavy Charged Particles

Electron beams have been employed to produce primary vacancies for fluorescence yield measurements. This method has the drawback that it is generally not possible to measure the rate of vacancy creation directly, but that it must be calculated using the theory of ionizing collisions. Fortunately, such calculations can be performed quite accurately for a variety of incident electron energies (Be-30, Be-33).

The electron beam current must be determined accurately if the appropriate fluorescence yield is to be calculated. This is accomplished by placing the target in a biased Faraday cup to eliminate the effect of secondary electrons on the current observed. In such experiments, the fluorescence yield is determined by comparing the observed x-ray intensity with the yield calculated on the assumption that all vacancies are filled by radiative transitions.

For measurements in higher atomic shells, the primary vacancy distribution among the subshells also must be determined. For electron energies far above the ionization potential, the ratio of vacancies is proportional simply to the electron population in each subshell. Thus, for the L subshells, the vacancy ratio is approximately $N_1:N_2:N_3=1:1:2$. For lower energies, a more precise calculation of the vacancy ratio is necessary. Bethe (Be-30, Be-33) has developed a theoretical expression from which the relative ionization in the various L subshells due to electron bombardment can be calculated. For electrons having kinetic energies greater than 40 keV,

$$N_1:N_2:N_3=(1/E_1):(1/E_2):(2/E_3), \qquad (17)$$

where E_1, E_2, and E_3 are the respective binding energies of the L_1, L_2, and L_3 subshells. This formula has been verified experimentally to within 15% in bombardments with electrons having energies greater than 40 keV (Vi-61).

Heavy charged particles can also be employed for primary vacancy creation. Cross sections for x-ray production for many elements using protons and alpha-particles with energies between 0.1 and 4.3 MeV have been measured (Ge-37, Jo-62, Le-53). However, no measurements of fluorescence yields have been attempted. The reason for this situation is that the calculation of the vacancy creation rate using available theoretical models for heavy charged particles is not reliable for incident particle energies below some 10 to 20 times the ionization energy (Jo-62). Thus, while it is relatively easy to observe characteristic x rays emitted by targets bombarded with heavy charged particles, there is no precise way of computing the fluorescence yield from these data. If more accurate theoretical calculations of ionization cross sections were available, then the heavy charged particle excitation could become a very useful method for obtaining fluorescence yields from measurements of x-ray intensities during bombardment. One advantage is that the characteristic x rays produced are free of the usual bremsstrahlung background present when electron bombardment is used. The very high intensity, low-energy ion accelerators now being built (Ma-64) could be employed to great advantage. The x rays produced by such machines are of sufficient intensity that high resolution diffraction spectrometers could be employed to separate x-ray transitions leading to vacancies in different subshells. This point will be amplified in greater detail in Sec. 4.

CC-0. In Public Domain. Gurukul Kangri Collection, Haridwar

Digitized by Arya Samaj Foundation Chennai and eGangotri

2.3. Ionization of Higher Shells by Transitions to K-Shell Vacancies

A method which has been developed recently to to determine L- and M-shell fluorescence yields is to use the L- and M-shell vacancies produced by transitions to vacancies in the K shell, which usually are produced by photoelectric absorption (Jo-63, Jo-64, a, b), but also may be created by other means (Ho-63, Ho-64). The radiative transitions to the K-shell vacancies are employed as a signal to indicate the presence of a vacancy in one of the higher shells. This method has several advantages over those employed previously for determining L-shell fluorescence yields. The primary vacancy distribution in the L subshells is determined precisely by the relative intensities of the K_α x rays ($N_1:N_2:N_3 \approx 0:1:2$), so that no theoretical estimates are required to determine the proper primary vacancy distribution. Precise values of the vacancy ratios are given in Wapstra, Nijgh, and van Lieshout (Wa-59). Furthermore, since each L-shell vacancy is preceded by a K_α x ray, coincidence measurements can be used to measure the fluorescence yield of the L shell. The mean L-fluorescence yield ω_{KL} will be determined by the coincidence rate observed between the L and the K x rays. Therefore, no theoretical calculation is necessary to determine the number of primary vacancies—the K_α x ray serves as a marker that the vacancy is in place. This method of creating primary vacancies also has been employed to determine certain M-shell mean fluorescence yields (Jo-65). In these experiments, the L shell was ionized by photon bombardment, and the coincidence rate between the L and the M x rays emitted by the foil was determined. The results of these measurements are discussed in Sec. 5.3.

2.4. Ionization by Electron Capture or Internal Conversion

Electron capture and internal conversion also produce primary vacancies in atomic shells. Electron capture processes particularly are useful, because the primary vacancy distribution usually is known from the nature of the transition (RF-55, RF-60). Moreover, each transition usually is accompanied by an x ray or a gamma ray which can be employed to mark the existence of a vacancy in much the same way that the K x rays were employed in the method described in Sec. 2.3. A good example is the isotope W^{181} (Jo-61). This isotope decays by electron capture to the ground state predominantly, but also to excited levels at 152 and 137 keV. The fact that about one-third of W^{181} decays lead to the first excited state of Ta^{181} at 6.3 keV does not alter the conclusion that the L-shell vacancies created in this decay are predominantly in the L_1 subshell. The 6.3-keV transition is not converted in the L shell and the electron capture transition from W^{181} to the 6.3-keV level, as well as to the ground state, is allowed. The ground state transition can proceed by K electron capture, giving a Ta^{181} atom ionized in the K shell. The coincidence rate between K and L x rays can be used to determine the same fluorescence yield (ω_{KL}) of the L shell as before, since it does not matter how the K shell is ionized.

The decay to the excited nuclear levels can be employed (Ra-65b) to measure a slightly different partial fluorescence yield. If the decay energy is not large enough to permit transitions to the excited levels by K-electron capture, then all of these transitions must cause vacancies in the L or higher atomic shells. In the case of allowed and first-forbidden transitions, almost all of the primary vacancies are created in the L_1 subshell. The coincidence rate between the gammas emitted in the nuclear decay process and the L x rays thus determines a different partial L-shell fluorescence yield (ω_{LL}), defined in Sec. 1.3, than that measured using the K capture to the ground state. This illustrates the necessity of knowing the primary vacancy distribution to determine the precise partial fluorescence yield in measurements of shells above the K shell. It also demonstrates how a knowledge of nuclear decay schemes may be used to determine primary vacancy distributions.

Internal conversion processes also ionize various atomic shells. A nuclear state decaying by K conversion may be used to determine ω_{KL} in a manner similar to K capture. The L conversion also may be employed to determine M-shell fluorescence yields by measuring L and M x-ray coincidence rates. The coincidence method between gammas and L x rays cannot be employed since, in general, no unique gamma ray accompanies an L conversion event. As is the case for electron capture processes in higher shells, the primary vacancy distribution in the L shell (and higher shells) produced by internal conversion is determined by the properties of the nuclear decay. An electric quadrupole (E2) transition, for example, will not lead to the same distribution of L-shell vacancies as a transition having a different multipole order. There is also a difference between electric and magnetic multipole orders. Owing to these complications, electron capture transitions are generally more useful than internal conversion for fluorescence yield determinations.

If a particular decay scheme is really well known, or if theory can be applied with great confidence, then it is unnecessary to use the coincidence methods described here. For such cases, the number of primary vacancies can be determined by measuring the decay rate of the source using one of the other radiations emitted (α, β, or γ) and then using the known decay scheme to calculate the number of primary vacancies produced per decay. For example, $[(\alpha)(L \text{ x ray})]$ coincidences were used for plutonium (Sa-61), together with $L_2:L_3$ x-ray intensities.

2.5. Critical Excitation of Specific Subshell Vacancies

It has been shown that for higher atomic shells the vacancy distribution usually depends on the method of

CC-0. In Public Domain. Gurukul Kangri Collection, Haridwar

Digitized by Arya Samaj Foundation Chennai and eGangotri

excitation. In some of the very early experiments, attempts to control the vacancy distribution more precisely were made (Kü-35, St-37). For example, it is relatively easy to determine ω_3, the fluorescence yield of the L_3 subshell. This subshell is the least tightly bound L subshell. By adjusting the energy of the incident radiation or particles appropriately, it is possible to excite vacancies only in the L_3 subshell and thus to determine ω_3. In the experiments quoted in Kü-35 and St-37, this was done by fixing the energy of the incident bremsstrahlung beam so that the endpoint of the spectrum fell between the L_2- and L_3-subshell binding energies. In principle, the method of critical excitation described here can be extended to measure ω_2 and ω_1. If the endpoint energy of the incident bremsstrahlung spectrum is made to lie between the L_2 and the L_1 subshells, then vacancies in the L_2 and L_3 subshells only will be produced. The mean L-fluorescence yield measured in this way will be a linear combination of ω_2 and ω_3. Since ω_3 will be known from the previous measurement, ω_2 can be computed if the vacancy distribution and the Coster–Kronig yield f_{23} are known. In principle, the method can be extended to determine ω_1 if the vacancy distribution and the appropriate Coster–Kronig yields are known (Ro-54). In practice, the critical excitation method is useful primarily for the determination of ω_3, since uncertainties in the primary vacancy distribution make measurements of ω_2 and ω_1 unreliable.

An interesting variation of the critical excitation method has been employed with the K and L x-ray coincidence technique described in Sec. 2.3. The L shell vacancy distribution following K_α x-ray emission is $N_1:N_2:N_3=0:1:2$. The average fluorescence yield, ω_{KL}, determined by this method is the appropriate linear combination of the L_2 and L_3 subshell fluorescence yields defined in Eq. (15) with $N_2:N_3=1:2$,

$$\omega_{KL}\approx 1/3\omega_2+2/3\omega_3. \tag{18}$$

This average yield is measured because the K x-ray detector cannot resolve the K_{α_1} and the K_{α_2} x rays. (The K_{α_1} line is the transition $L_3\rightarrow K$, and the K_{α_2} line is the transition $L_2\rightarrow K$.) The coincidence method also can be employed to measure ω_3 separately. Instead of observing the K x rays directly, the K x-ray detector now is shielded from the direct radiations from the sample. A radiator foil is placed in the direct sample beam and the K x-ray counter is set to observe the radiator. For certain materials, it is possible to choose the radiator in such a way that the K shell of the radiator atoms can be ionized only by the K_{α_1} and not by the K_{α_2} x rays emitted by the sample. A signal observed in the K x-ray counter therefore indicates a vacancy in the L_3 shell, and hence the coincidence rate observed will be proportional to ω_3. If ω_{KL} is also known, then ω_2 can be calculated using Eq. (18). This method of determining ω_2 and ω_3 has been applied successfully to several elements in the region between $Z=67$ and $Z=83$ (Jo-64a). (The possibility of using high-resolution detection to resolve the K_{α_1} and K_{α_2} x rays will be discussed in Sec. 4.)

3. REARRANGEMENT OF VACANCIES

3.1. Shifting of Vacancies between Major Shells

In the filling of a K-shell vacancy by an electron of a higher shell, the vacancy of course reappears in the higher shell. The number of L-shell vacancies produced in the filling of a K-shell vacancy is n_{KL} (RF-55, RF-60) and is given by

$$n_{KL}=k\omega_K+a_K\left\{\left[\frac{2(K-LL)+(K-LX)}{\sum \text{Auger electrons}}\right]\right\} \tag{19}$$

where k is K_α/K, the ratio of K_α x-ray intensity to the total K series x-ray intensity, a_K is the K shell Auger yield $(1-\omega_K)$, and $(K-LX)$ is a partial Auger yield where X denotes $M-$, $N-$, etc. shell electrons. For example, $K-LX$ is the probability that a K-shell vacancy is filled by an L-shell electron with the binding energy difference transferred to an electron in the X shell which is ejected. Values of n_{KL} have been computed by Robinson and Fink (RF-55, RF-60) and by Listengarten (Li-60). A similar quantity f_{KL_i} given by Wapstra, Nijgh, and van Lieshout (Wa-59) is related to n_{KL} by the relation

$$n_{KL}=\sum f_{KL_i}. \tag{20}$$

Similarly, the fraction of K vacancies shifted to the M shell is n_{KM}, and the fraction of L-shell vacancies shifted to the M shell is n_{LM}. Owing to the paucity of data on partial L-shell Auger electron yields, accurate values of n_{LM} are not yet available.

The appearance in higher shells of vacancies shifted up in the course of filling lower shells is important in experiments where a fluorescence yield is measured by determining the relative intensities of emitted x rays or Auger electrons, as for example in electron capture excitation (Sec. 2.4). The relative intensities of L and K x rays, I_L/I_K, have been measured for several electron capturers, for which the orbital electron capture ratio, P_L/P_K, is known either from direct measurement or from computation from the electron capture decay energy (Q_{EC}). A mean L-fluorescence yield is then obtained by means of the relation (Fi-55)

$$\bar{\omega}_L=\frac{(I_L/I_K)\omega_K}{(P_L/P_K+n_{KL})}. \tag{21}$$

In principle, mean M-shell fluorescence yields can be obtained in a similar manner from measurements of M, L, and K x-ray intensities, with account being taken of P_M/P_L, the ratio of probabilities for $M-$ and $L-$ capture, P_L/P_K, n_{KL}, n_{KM}, and n_{LM}. No measurements of M-shell fluorescence yields by this method have been reported to date.

CC-0. In Public Domain. Gurukul Kangri Collection, Haridwar

Digitized by Arya Samaj Foundation Chennai and eGangotri

3.2. Shifting of Vacancies among Subshells: Coster–Kronig Transitions

Radiationless transitions occurring within a subshell are of great importance in the measurements of fluorescence yields other than ω_K. These transitions alter the initial distribution of primary vacancies, and they must be taken into account in the computation of individual subshell yields from measured average fluorescence yields for the entire shell. The formal way in which this effect is included in the equations has been discussed (for the L shell) in Sec. 1.3, and the Coster–Kronig transition probabilities f_{13}, f_{12}, and f_{23} have been defined (again for the L shell).

There are two important points regarding the magnitude and the behavior of the Coster–Kronig yields which must be understood. One is that the radiationless transition probabilities for the shifting of vacancies between subshells are of the same order of magnitude as the radiative transition probabilities for filling the vacancies from *higher* shells. If this were not the case, then the initial vacancy distribution produced in a given experiment would not be altered *before* the vacancies were filled by radiative processes. There is abundant evidence that rearrangements within the shell do, in fact, occur before the atom radiates (Bu-52).

The second point is that the actual magnitudes of the Coster–Kronig transition rates tend to vary strongly with atomic number. If a vacancy is shifted from a lower subshell to a higher one, then an energy equal to the difference between these levels must be released. This energy is transferred to an electron in a higher shell by the Coulomb interaction.

Thus, Coster–Kronig transitions are Auger transitions in which the vacancy shifts from one subshell to another within a given shell (Co-35). In the general Auger case, the radiative and nonradiative transition rates are comparable, but in the Coster–Kronig case, the radiative transition rates among the subshells are negligible compared to nonradiative ones. Thus, no x rays corresponding to transitions of the type $L_1 \rightarrow L_2$, etc., are observed (Bu-52), but the effects of nonradiative transitions cannot be ignored. Recently, direct observation of low-energy electrons (<1 keV) from L-shell Coster–Kronig transitions has been reported (Al-61, Va-62) as well as from the M shell (Me-65) A Coster–Kronig process is characterized by the two subshells between which the vacancy shift occurs and the electron in the higher shell which removes the energy. The process is usually denoted in the manner, for example, $L_1-L_3M_4$, which means that a vacancy has shifted from the L_1 to the L_3 subshell, and that the binding energy difference released has been removed by an M_4 electron which is ejected from the atom, leaving a vacancy in the M_4 shell. Whether or not such a process can occur with a large probability depends upon whether an electron is energetically available in the next higher shell to absorb the energy. If all of the M electrons, for instance, have binding energies larger than the energy differences between the L subshells, then Coster–Kronig yields are generally very small, since it is more difficult to transfer the transition energy to an electron in the N or even a higher shell. The situation outlined here explains why Coster–Kronig yields tend to vary strongly as a function of atomic number. In certain regions of the periodic table all M electrons have higher binding energies than the energy differences between the L subshells. In these regions, the Coster–Kronig yields will be small (less than 0.1). In other regions, M electrons may be ejected in Coster–Kronig processes, and thus the yields may be quite large (≈ 0.7). This "threshold" effect thus accounts for the observed variation of the Coster–Kronig yields. See Table XIII in Burhop (Bu-52).

Several theoretical calculations and experimental measurements of Coster–Kronig yields have been performed which are of use in computing subshell fluorescence yields from measured average fluorescence yields. The method employed in the calculation is identical to that introduced by Wentzel (We-27) for the calculation of Auger electron emission rates. The most recent calculations are those by Callan (Ca-63a) and Asaad (As-65), who computed the Coster-Kronig yields for the transitions $L_1L_{2,3}-M_{4,5}$. (It should be noted that these are not quite the same as the total Coster–Kronig yields f_{12} and f_{13}, because only those transitions in which the electron ejected is in the M_4 or M_5 levels are considered.) The results exhibit the characteristic behavior of Coster–Kronig yields in that the values have a strong dependence on atomic number. It was shown also that the magnitudes of the calculated Coster–Kronig yields depend quite critically on the electronic wave functions used to compute the matrix elements. Unfortunately, the calculations of Callan are available only between $Z=21$ and $Z=50$. Many of the measurements for which a precise knowledge of the Coster–Kronig yields are needed are for values of $Z \geq 50$, so that these calculations cannot be employed.

For heavier atoms, there are a number of experimental values of Coster–Kronig yields which are available. Ferreira, Costa, Concalves, and Salguero (Fe-65) have determined the f_{13} Coster–Kronig yields for six elements between $Z=73$ and $Z=92$ by comparing the intensities of L x-ray lines with L_α and L_{β_2} satellite lines. Dionisio (Di-63) has measured soft Auger electron spectra emitted in the decays of Em^{220} (thoron) and Em^{222} (radon). The Coster–Kronig yields, f_{12} and f_{13}, for Po, Bi, Pb, and Tl have been calculated from these data. Very recently, Melhorn (Me-65) has reported the first measurement of an M-shell Coster–Kronig yield ($M_2-M_{3,4}N_5$) in krypton. This yield was deduced from the measured Auger electron spectrum resulting from irradiating krypton with monoenergetic electrons at two different energies, 2000-eV and 20[illegible] eV incident energy. The experimental result agrees

CC-0. In Public Domain. Gurukul Kangri Collection, Haridwar

Digitized by Arya Samaj Foundation Chennai and eGangotri

qualitatively with theoretical predictions that the probability for a Coster–Kronig transition is much greater than for an Auger transition, if the former is energetically possible.

A summary of all available Coster–Kronig yields is given in Table IV in Sec. 5.2. More extensive measurements and calculations of Coster–Kronig yields for a broader range of elements are urgently needed.

4. FILLING OF VACANCIES AND MEASUREMENT OF AUGER ELECTRON AND X-RAY INTENSITIES

4.1. Auger Electron Measurements

Precision beta-spectrometers have been used for many years to measure the energies and intensities of Auger electrons. The latest review of this work is that of Bergström (Be-64), as mentioned in Sec. 1.1. Electron intensity measurements have been most useful in determining K-shell fluorescence yields by comparing the intensities of the electron transitions to the total linewidth. Auger electron measurements have not been used extensively for the determination of fluorescence yields of higher atomic shells because the electron energies resulting from the filling of higher shell vacancies generally are too low. Since excellent discussions of electron spectroscopy are available (Si-64), no detailed description of the experiments for the measurement of K-shell fluorescence yields will be given. Some of the features of the ω_K experiments will be discussed in Sec. 5.1 to compare the measurements with theory.

Many of the L-shell measurements using electron spectrometry have been performed by Haynes and his collaborators (Na-60, Bu-58, 2-Ha-55, Le-58). A good example of an L-Auger electron spectrum obtained with a medium resolution lens spectrometer is shown in Fig. 7 of Ref. Na-60. Measurements of $\bar{a}_L$ and $\bar{\omega}_L$ for Hg are described in this paper (Na-60).

A novel variation of the electron technique was used by Päschke (Pä-63) to measure $\bar{a}_L$, ω_1, ω_2, and ω_3 for Au. A 50-Å foil was suspended in a beam of 55-keV electrons. This foil was located between the poles of a magnetic spectrometer. Electrons from the primary beam were collected in a Faraday cup and the Auger electrons were bent through collimating slits between the poles and detected 180° from the foil in a Geiger counter. Simultaneously, the L x rays from the foil were detected by a NaI(Tl) crystal spectrometer looking between the poles. A drawing of the experimental arrangement is shown in Fig. 2. The Auger spectrum and the L x-ray spectrum provide enough information, along with the measured efficiency of the equipment, to determine the Auger and the fluorescence yields.

4.2. X-Ray Intensity Measurements

A great many methods for measuring the x-ray intensities in fluorescence yield experiments have been developed. These fall into two large categories, those involving the use of high-resolution spectrometers, and the large majority of measurements in which low-resolution devices are employed. The advantage of using high-resolution equipment is of course that it is then possible to investigate the shape and intensity of each individual transition in a spectrum of characteristic x rays. Unfortunately, diffraction spectrometers have very low efficiencies and it is necessary, therefore, to use very intense sources, or else data must be taken for long periods of time. In addition, this low efficiency usually rules out the possibility of using the diffraction spectrometer as one of the two detectors in a coincidence-type experiment.

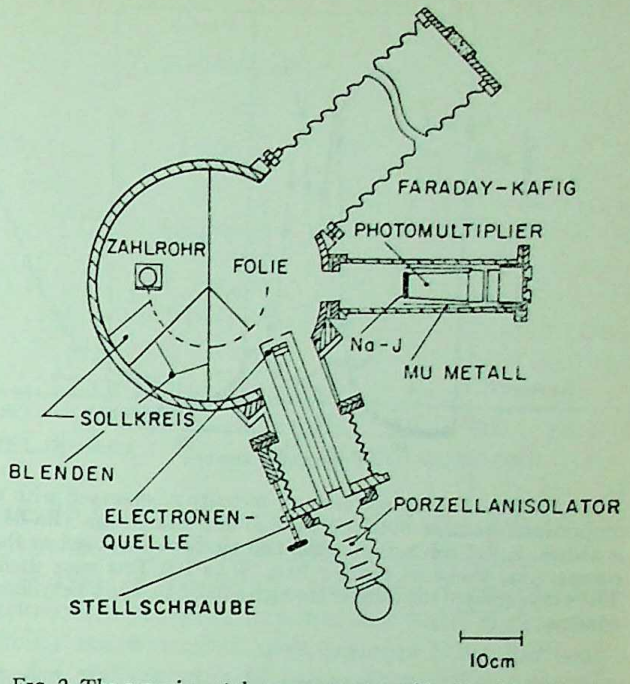

FIG. 2. The experimental arrangement used by Päschke (Pä-63) for the measurement of fluorescence and Auger yields in gold. The magnetic field is perpendicular to the plane of the paper. The Auger electrons emitted by the sample foil mounted in the chamber are counted with the proportional counter inside the vacuum chamber, and the L x rays are detected by the scintillation counter mounted on the right side of the chamber.

Low-resolution devices have in common the advantage of high efficiency and convenience of use. These detectors can in practice be designed to have efficiencies of 100% in a 4π geometry. The low resolution of these detectors makes it impossible to separate and investigate individual transitions, except in a few isolated cases where critical absorption techniques are usable, or where peculiar vacancy populations occur. In the remainder of this section, a number of examples illustrating how the various x-ray detectors are employed will be discussed. In addition, an attempt will be made to evaluate the potentialities of some of the newer developments in the field of radiation detection.

4.2.1. Photographic Detection of X Rays

Although this technique is no longer employed, it is of some historical interest, since some of the first

CC-0. In Public Domain. Gurukul Kangri Collection, Haridwar

Digitized by Arya Samaj Foundation Chennai and eGangotri

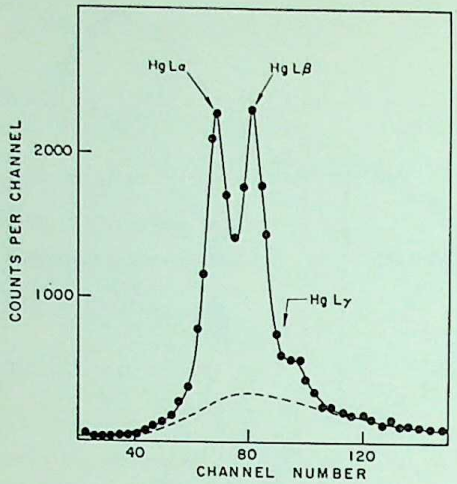

FIG. 3. The L x-ray spectrum of mercury as observed with a proportional counter obtained by Rao and Crasemann (Ra-64) is shown. A 9:1 mixture of argon and methane was used as the counter gas. Pressures ranging from 30 to 160 Torr were used. The x rays entered the counter through a 0.005-in.-thick beryllium window.

comprehensive measurements of both K- and L-shell fluorescence yields were performed using photographic plates to measure x-ray intensities. H. Lay in 1934 (La-34) used photographic plates to determine both the intensity of the incident beam and fluorescent radiation by measuring the time ratio necessary to obtain roughly equal darkening of the film and then making the appropriate corrections for the difference in film efficiency for the incident and fluorescent radiation. In view of the uncertainties involved in the photographic method, it is remarkable how well Lay's results have stood the test of time; 32 years later, Lay's values of ω_K and $\bar{\omega}_L$ are still considered to be among the better measurements of these quantities.

4.2.2. *Ionization Chambers and Geiger Counters*

Another series of early measurements were those made using ionization chambers to detect the primary and the fluorescent radiation. Küstner and Arends (Kü-35) and Stephenson (St-37) used variations of the ionization chamber technique to measure the ratio of fluorescent radiation to the primary beam intensity. In each case, the vacancy production rate was computed from the measured primary beam intensity. Calibrated Geiger–Müller counters with known spectral responses were used by Kinsey (Ki-48b) to detect L x rays from Pb^{212} (ThB) to measure an L-fluorescence yield.

4.2.3. *Proportional Counters*

The development of proportional counters has made it possible to resolve x-ray lines caused by the filling of vacancies in specific shells. At 10 keV, a good proportional counter may have a resolution of 10 to 15% of the incident quantum energy. It is possible therefore to resolve partially the L_α, L_β, and L_γ x-ray groups at high Z (see Fig. 3). The most common use of the proportional counter, however, is to separate the L x rays from the K x rays emitted by a given atom. The L-shell fluorescence yields thus have been measured by using proportional counters to determine the x-ray intensity, and by making a separate measurement or calculation of the number of vacancies (Ro-55, Fi-57). A recent example of this is the experiment of Zimmerman and Flammersfeld (Zi-63) to determine the L-fluorescence yield of Dy. The experiment consisted of measuring the conversion electrons from the decay of Dy^{165m} (1.26 min). These electrons were counted in an anthracene crystal spectrometer. Assuming the conversion coefficients are known, the intensity of the conversion electrons gives the number of vacancies in the L shell. By then counting the L x rays detected in the proportional counter, the L-shell fluorescence yield is determined.

In another example of this method, Winkenbach (Wi-58) measured mean L-fluorescence yields of thallium ($Z=81$) and bismuth ($Z=83$) from the decay of Pb^{212}–Bi^{212}–Tl^{208} series (Th–B–C–C′). Here the ionization in the L shell is known accurately from the conversion in bismuth of the 238-keV gamma in Pb^{212} decay, and in thallium from conversion of the 40-keV gamma following Bi^{212} α-decay. Thus, a proportional counter determination of the total intensity of the L x rays emitted from Pb^{212} (ThB) and Bi^{212} (ThC) sources measures the mean L-fluorescence yields of bismuth and thallium, respectively. Furthermore, by partially resolving the L_α, L_β, and L_γ x rays in Bi^{212} decay, the fluorescence yield for the L_3 shell of thallium was found, $\omega_3=0.33\pm0.02$ (Wi-58).

An interesting variation of the proportional counter method is to employ internally mounted sources of radiation. These can be either radioisotopes or atoms in the counter gas (or wall) used as fluorescent radiators. The internal source method was employed by Konstantinov *et al.* (Ko-60, Ko-61, Ko-64, Ko-65) to measure fluorescence yields in Ga, Cu, V, and Mn for the L shell, and in V, Mn, Cu, Ga, Mg, and Al for the K shell. Similar measurements with a double proportional counter were made by Kramer (Kr-61, Kr-62). If the proper gas, pressure, and counter dimensions are chosen, the counter will detect the L and K x rays from the source with known efficiency, close to 100%. Observation of a K x ray then indicates the presence of a certain number of L-shell vacancies. Using a calculation similar to that outlined in Sec. 3.1, it can be shown that about 1.3 L-shell vacancies are produced for each K-shell vacancy. The observed L to K x-ray intensity ratio, corrected for this factor, thus is a direct measure of the L-shell fluorescence yield ω_{KL}.

A novel method of employing the proportional counter gas as an internal source was used by Curran *et al.* (Cu-49) and Godeau (Go-61) to measure ω_K of argon. Radiation of energy above the K edge of argon is directed into the counter (Godeau used 6-keV x rays from Fe^{55} source). This radiation is absorbed in the

CC-0. In Public Domain. Gurukul Kangri Collection, Haridwar

Digitized by Arya Samaj Foundation Chennai and eGangotri

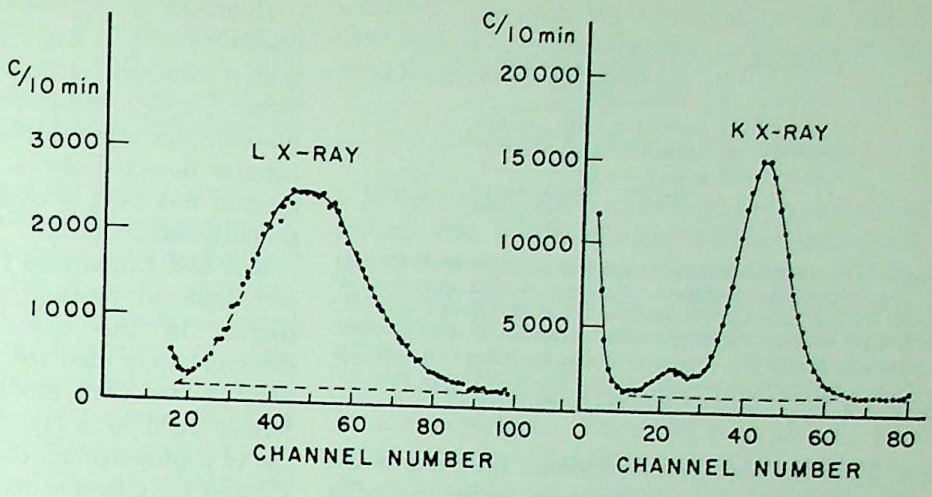

FIG. 4. The x-ray spectra of Pb^{203}, measured with a $1\frac{1}{2}$- $\times\frac{1}{4}$-in. NaI(Tl) scintillation detector are shown. The crystal was covered with a 0.001 - in. aluminum foil. These spectra were obtained by Persson and Sujkowski (Pe-61).

gas, and a large fraction of it photoionizes the argon K shell. With low enough pressure and small enough counter size, most of the argon K x rays emitted will escape from the counter, and only the escape peak will be observed (i.e., a peak corresponding to the energy of the incident radiation less the energy carried away by the escaping argon K x ray). However, if the vacancy in the argon K shell is filled by an Auger transition, there will be no K x ray emitted and the K-Auger electron will not escape. Therefore, a peak corresponding to the full energy of the incident radiation will be observed. Hence, the ratio of the counts in the escape peak to the counts in the full-energy photopeak, with small corrections for nonescaping K x rays, is a direct measure of ω_K for argon.

In the decay of pure electron capturing Cs^{131}, the mean L-fluorescence yield $\bar{\omega}_L$ of xenon has been measured from a determination of the relative L/K x-ray intensity ratio I_L/I_K with thin NaI(Tl) detectors (Ho-64) or proportional counters (Fi-55). Similar measurements have been made in the decay of Tl^{204} (Sc-57) and (Ra-65a). In these studies, the experimental or theoretical value of P_L/P_K, the ratio of probabilities for L and K capture, is required (RF-55, RF-60, Mo-63) together with the value of n_{KL}, the number of L vacancies produced in the filling of a K vacancy. The value of n_{KL} is found from the K Auger electron spectrum and total Auger electron intensity and has been given by RF-60, RF-55, and Li-60 (see Sec. 3.1). The mean L-fluorescence yield then is given by Eq. (21), with appropriate corrections for counting efficiencies of the L and K x rays.

A typical x-ray spectra observed using a proportional counter is shown in Fig. 3.

4.2.4. *Scintillation Counters*

Inorganic and organic scintillation detectors also have been widely employed in fluorescence yield measurements. Scintillation counters have some of the same advantages as the proportional counters. The NaI(Tl) crystals can be used to detect K x rays from elements with $Z \geq 20$ and L x rays emitted by elements with $Z \geq 50$. They also are very efficient in that all the x rays incident on the scintillator are counted.

In 1957, Roos (Ro-57) measured various K-shell fluorescence yields using a movable NaI(Tl) detector. Similar measurements were performed by Patronis, Braden, and Wyly (Pa-57) (using a proportional counter with variable solid angle). In this type of experiment, foils of the element under investigation were placed in a highly collimated flux of gamma radiation. The detector is placed such that the collimated radiation passing through the foil is incident on the detector. By moving the detector away from and toward the foil, the solid angle subtended by the detector can be varied. Since the fluorescent radiation from the foil is isotropic, the intensity of collimated radiation can be measured in the far position, and the sum of collimated radiation and the fluorescent radiation can be measured in the near position. Knowing the absorption of the primary radiation in the K shell gives the number of vacancies, and measuring the fluorescent radiation then gives the K-shell fluorescence yield.

In addition to their employment as simple x-ray detectors, scintillation counters also have found important applications in some of the more specialized experiments to be discussed in the following section.

Some typical x-ray spectra observed with NaI(Tl) scintillation detectors are shown in Fig. 4.

4.2.5. *Coincidence Methods*

The coincidence method has proved to be one of the more fruitful methods for investigation of atomic fluorescence yields. The principle has already been outlined in Sec. 2.3. The creation of a vacancy in an atomic shell may be accompanied by the emission of either a nuclear radiation or an x ray. If these accompanying radiations can be detected, they can be used to signal the creation of a vacancy in that shell. The coincidence counting rate between the accompanying radiation and the x rays produced in the filling of the vacancy is proportional to the fluorescence yield. Thus,

$$N_c = KN_{p_i}\omega_i, \tag{22}$$

CC-0. In Public Domain. Gurukul Kangri Collection, Haridwar

Digitized by Arya Samaj Foundation Chennai and eGangotri

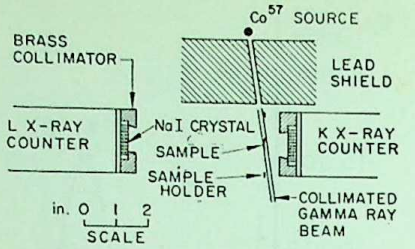

FIG. 5. The experimental arrangement used to measure ω_{KL} using the coincidence technique is shown. A thin sample is irradiated with a carefully collimated beam of 125-keV gammas from a Co^{57} source. These produce vacancies in the K shell. The resulting K and L x rays are counted by using two NaI(Tl) scintillation detectors connected so that the coincidence rate and the K and L x-ray counting rates can be determined.

where N_c is the observed coincidence rate, N_{p_i} is the number of radiations observed accompanying vacancies in the ith shell, and ω_i is the fluorescence yield of the ith shell. The constant K depends on the geometrical arrangement, the efficiency of the detector observing the ith shell radiations, and on the nature of the transition producing the vacancy in the ith shell.

Hagedoorn and Wapstra (Ha-60) first used this method to measure ω_K in Ti, Co, Cr, Zn, and Zr. Radioisotopes of these elements were used in this experiment, and a NaI(Tl) scintillation counter was used to detect the nuclear radiations which signaled the creation of a K-shell vacancy. A proportional counter was then used to observe the K x rays emitted in coincidence with the nuclear radiation.

Jopson *et al.* (Jo-61, Jo-63, Jo-64a, b, Jo-65) extended this method to measure L- and M-shell fluorescence yields. In Jo-61, radioisotopes were used to produce K-shell vacancies by electron capture processes, while in subsequent experiments, the K-shell vacancies were produced by photoionizing the K shell with an incident beam. In both cases, the coincidence rate between the K and L x rays was used to determine the mean L-fluorescence yield ω_{KL}. The K x rays were observed with thin NaI(Tl) scintillation detectors. Either scintillation or proportional counters were used to observe the L x rays, depending on the quantum energy of the x rays. The arrangement for these experiments is shown in Fig. 5. In Sec. 2.3, the method of measuring ω_3 separately was mentioned briefly. The experimental geometry for this experiment is shown in Fig. 6. Here, the K x-ray detector is shielded from the direct radiations of the target foil, and is surrounded by an annular radiator which views the target foil. This radiator is made of an element with the K edge between the energies of the $K_{\alpha 1}$ and $K_{\alpha 2}$ x rays coming from the target foil. Therefore, when $K_{\alpha 1}$ or K_β x rays strike the radiator, it reradiates its characteristic x rays into the x-ray detector. In this way, the K detector is triggered only by $K_{\alpha 1}$ or K_β x rays from the target and thus signals only vacancies in the L_3 or M, N, etc., shells. The coincidence rate between these events and the L x rays observed in the other counter thus depends only on ω_3.

Hohmuth *et al.* (Ho-63, Ho-64) measured L-fluorescence yields in Ru, Nb, Ag, Te, La, Ho, and Hg by taking coincidences between L and K x rays and between L x rays and gammas from radioisotope sources placed inside a proportional counter. The proportional counter detected the L x rays, while a scintillation counter was used to observe the K x rays outside the proportional counter.

Rao and Crasemann (Ra-65a) used the coincidence technique to measure ω_2 using a radioactive Tl^{201} source. In this experiment, NaI(Tl) scintillation detectors were used for the L and K x rays. The apparatus was then modified to measure the Coster-Kronig yield f_{23} in Hg. This modification involved the use of a proportional counter capable of resolving the $L_{\alpha 1}$ and $L_{\alpha 2}$ x rays of mercury from a thin Tl^{201} source (Ra-65b). In addition, the K x-ray detection system was modified with critical absorbers. Tungsten has its K edge between the $K_{\alpha 1}$ and $K_{\alpha 2}$ energies of mercury. By thus using a combination of tungsten, erbium, and tin, the $K_{\alpha 1}$ component of the Hg spectrum was substantially reduced in intensity, while the $K_{\alpha 2}$ component was retained. Coincidences were then taken between the $K_{\alpha 2}$ x rays and the $L_{\alpha 1}$ x rays. Since the $K_{\alpha 2}$ radiation indicates the occurrence of a $K-L_2$ transition and the $L_{\alpha 1}$ radiation indicates the filling of a vacancy in the L_3 subshell, the coincidence rate between $K_{\alpha 2}$ x rays and $L_{\alpha 1}$ x rays depend on the Coster–Kronig transition rate, f_{23}, for transfer of vacancies from the L_2 to the L_3 subshell. The quantitative relationships are

$$I_{L_3}/I_{L_2}=f_{23}(\omega_3/\omega_2) \tag{23}$$

$$\omega_2+f_{23}\omega_3=\nu_2=N_c/kN(K_{\alpha 2}) \tag{24}$$

$$\omega_{KL}=N_2\nu_2+N_3\omega_3=N_2(N_c/kN_{K\alpha 2})+N_3\omega_3, \tag{25}$$

where $k=\epsilon_L a_L \Omega_L$, the L x-ray detection efficiency, absorption factor, and geometry, respectively. These three equations (Ra-65b) can be solved to find f_{23}, ω_2, and ω_3, once the values of ν_2, I_{L_3}/I_{L_2} (the ratio of

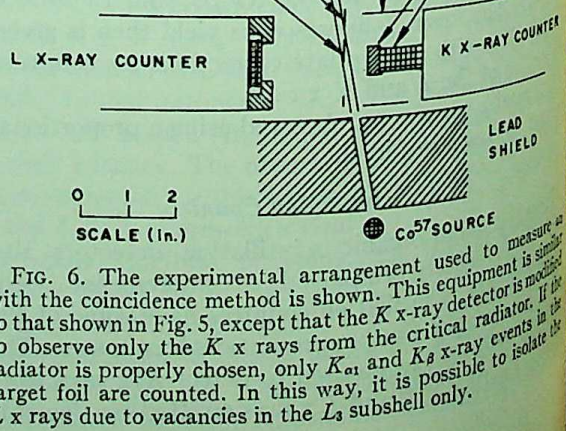

FIG. 6. The experimental arrangement used to measure ω_{KL} with the coincidence method is shown. This equipment is similar to that shown in Fig. 5, except that the K x-ray detector is modified to observe only the K x rays from the critical radiator. If the radiator is properly chosen, only $K_{\alpha 1}$ and K_β x-ray events in the target foil are counted. In this way, it is possible to isolate the L x rays due to vacancies in the L_3 subshell only.

CC-0. In Public Domain. Gurukul Kangri Collection, Haridwar

Digitized by Arya Samaj Foundation Chennai and eGangotri

L_3 to L_2 x rays emitted), and ω_{KL} have determined experimentally. In these equations, N_c = the number of coincidences counted between L_{α_1} and K_{α_2} x rays; $N(K_{\alpha_2})$ is the number of K_{α_2} x rays counted; and k is the detection efficiency for L x rays as defined above for the L x-ray counter.

It should be pointed out that the results of this experiment depend quite critically on knowing precisely the properties of the critical absorber used to eliminate the K_{α_1} component of the Hg K x-ray spectrum.

Halley and Engelkemeir (1-Ha-64) have measured high Z (Ra, Th, U, Pu, and Cm) L-fluorescence yields. Three methods were used. One involved counting the number of alphas emitted by a thin source and then calculating the fraction of these alphas, giving rise to L-shell vacancies. The L x rays were then counted and the fluorescence yield determined. This method also was used by Fink (Fi-57) to measure the mean L-fluorescence yield of bismuth $\bar{\omega}_L$ from Pb^{210} (RaD) decay (Ro-55). In this case, the L x rays from a carrier-free source of Pb^{210} were counted in a proportional counter, the number of L-shell vacancies being obtained from the counting of alphas from the Po^{210} daughter, in equilibrium with Pb^{210} parent through 4-day Bi^{210} (RaE). The alphas were counted with a very thin ZnS layer deposited on a photomultiplier tube. Very old (some years) sources of RaDEF had to be used to insure that the three isobars were in true radioactive equilibrium. Carrier-free sources were used to avoid spurious effects arising from fluorescent excitation from alpha and beta particles acting on solid sources (Fi-57). A second method (1-Ha-64) involved the coincidence method in which coincidences between L x rays and gammas were measured using NaI(Tl) detectors. In a third experiment (1-Ha-64), coincidences between L x rays detected in NaI(Tl) scintillation counters and alpha particles counted with solid-state detectors were determined.

Akalaev, Vartanov, and Samoilov (Ak-64) have measured $\bar{\omega}_L$ for Pu from a mixed source of $Cm^{242,244}$ and Eu^{154}, using the experimental relationship:

$$\bar{\omega}_L = (I_K/I_\gamma)\,(N_K/N_L)\,(1/\alpha_K),$$

where (I_K/I_γ) = ratio of Pu L x rays to 123-keV gamma of Eu^{154} decay. (N_K/N_L) = ratio of K x rays from Eu^{154} decay to the total L Auger electron intensity of Pu; and α_K = conversion coefficient of the 123-keV E2 gamma in Eu^{154} decay. The same authors (Ak-64) measured $\bar{\omega}_L = 0.66 \pm 0.08$ for Np from an Am^{241} source by measuring the L Auger electron spectra and its total intensity in a magnetic spectrometer, together with the intensity of the 60-keV E2 gamma from Am^{241} decay with NaI(Tl). From the L Auger electron spectrum, subshell Auger yields, $a_1 = 0.16 \pm 0.03$, $a_2 = 0.20 \pm 0.06$, and $a_3 = 0.43 \pm 0.09$ were found for Np ($Z = 93$), and assuming from Li-60 that $f_{12} = 0.10 \pm 0.04$, the Coster–Kronig yields f_{13} and f_{23} were evaluated. (See Table IV.) From the measured value of $\bar{\omega}_L$ and the Coster–Kronig and Auger subshell yields, the L-subshell fluorescence yields ω_1, ω_2, and ω_3 for $Z = 93$ also were found. (See Table III.)

4.2.6. *High-Resolution Techniques*

It has already been mentioned that the use of detectors with high resolution would substantially increase the scope of the experimental work in this field. In certain isolated cases, high-resolution detection methods have already been applied to good advantage. An interesting example of this is the determination of ω_2, f_{23}, and a_2 for plutonium by Salguero *et al.* (Sa-60). In this experiment, calculations of the L_2 subshell yields were computed from two sets of measurements, the coincidence rate between the L x rays and the alpha particles emitted by a Cm^{242} source, and the relative intensities of the L x-ray spectrum lines observed with a bent crystal spectrometer. The measured line intensities and available estimates of the Coster–Kronig yields f_{12} and f_{13} make it possible to compute the rate of vacancy creation per alpha decay in the L_2 subshell, and hence to evaluate the quantities ω_2, a_2, and f_{23} for that shell. This experiment can only be performed if strong radioactive sources (millicuries) are available, since the high-resolution bent crystal spectrometer has an efficiency much less than one percent. Correction for the variation in reflectivity with x-ray wavelength of the bent crystal must be made in this work. Careful measurements of the reflectivity variation have been reported by Cochran and Ross (Co-58) and Knowles (Kn-64).

A recent development of great promise is that of lithium-drifted silicon and germanium detectors suitable for low-energy x-ray spectrometry. Such detectors can be fabricated essentially windowless (i.e., with no dead layer) and used to observe x rays of energies down to a few keV with excellent resolution. For example, a Si(Li) detector operated at liquid-nitrogen temperature (77°K) in combination with a low-noise FET preamplifier whose input field-effect transistor is mounted next to the detector and cooled to 77°K can be optimized to achieve a resolution for the K_α x-ray group of better than 740-eV FWHM. This is adequate to resolve the K_β x-ray group from the K_α group for all elements of atomic number greater than $Z = 32$ (germanium). This can be seen in Fig. 7, which displays the characteristic K x rays of iron, germanium, and zirconium taken with such a cooled Si(Li) detector system having an active area of 110 mm² and a 3-mm sensitive depth. The spectra were taken through a 0.010-in. beryllium window. Similar spectra also have been obtained with windowless lithium-drifted germanium detectors. One interesting application of Si(Li) and Ge(Li) x-ray detectors would be to measure the fluorescence yields of the M shell in several elements by taking the coincidence rate between the K_β-series x rays, which mark vacancies in the M shell, and M x rays.

CC-0. In Public Domain. Gurukul Kangri Collection, Haridwar

Digitized by Arya Samaj Foundation Chennai and eGangotri

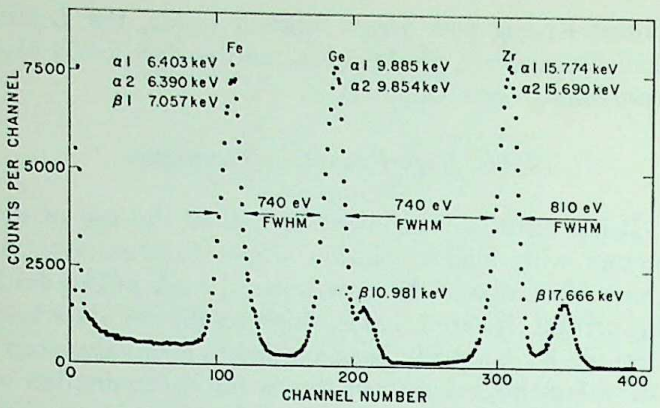

FIG. 7. Characteristic K x-ray spectra of iron, germanium, and zirconium taken with a 110 mm²×3 mm lithium-drifted silicon detector cooled to 77°K connected to a FET preamplifier whose input field-effect transistor also was cooled to 77°K. Typical resolution for the K_α x-ray group is about 740-eV FWHM. The K_β x-ray group is clearly separated for elements with atomic number above germanium ($Z=32$). This spectrum was furnished by D. Grunau of Technical Measurements Corporation. Similar spectra have also been obtained with windowless lithium-drifted germanium detectors.

Another potentially important new device which could be employed for fluorescence yield measurements is the high-current (≈10 mA), low-energy (≈500 keV) ion accelerator, already mentioned in Sec. 2.2. Using intense proton or alpha-particle beams to excite primary vacancies, it is possible that high-resolution detectors and coincidence methods could be employed to great advantage in determining more precisely the fluorescence yields of higher atomic shells. For this work, it would be highly desirable to have available more precise calculations of the atomic ionization cross sections of heavy charged particles.

5. EXPERIMENTAL RESULTS AND COMPARISON WITH THEORY

5.1. *K*-Shell Fluorescence Yields

The earliest theoretical calculations of the Auger fluorescence yield ω_K are due to Wentzel (We-27), who took into account only the L-shell participation in the Auger process:

$$\omega_K=(1+a/Z^4)^{-1}, \quad \text{where} \quad a=\approx 10^6. \tag{26}$$

More detailed calculations were made by Burhop (Bu-35) and by Pincherle (Pi-35) using nonrelativistic theory, and by Massey and Burhop (Ma-36) using a relativistic theory. Hydrogen-like single-electron wave functions with Slater screening were used. Account is taken of transitions involving M and N shells in the Auger process if the following values of the parameter a are used: (Bu-52) $a=9\times10^5$ for $Z<10$; $a=1.19\times10^6$ for $10\leq Z\leq 18$; and $a=1.27\times10^6$ for $Z>18$. These theoretical calculations corroborated Eq. (26), according to which the values of ω_K should be independent of the frequency of the exciting radiation, or of the manner in which K-shell vacancies are created. Comparison with experiment has fully substantiated this expectation (Bu-52), based on our present understanding of the Auger processes.

Rubinstein and Snyder (Ru-55) used the Hartree self-consistent field method of computing the initial wave functions for argon, krypton, and silver. Higher values of ω_K were obtained, in better agreement with experiment, particularly in the case of argon, for which their calculation gives $\omega_K=0.13$, rather than 0.08 according to Burhop (Bu-52). The approximations used, however, in particular the central field polynomial, are likely to lead to larger errors for low Z elements, so that the disagreement with the earlier calculations at low Z may not be significant.

Attempts have been made to fit a semiempirical formula of the type

$$\omega_K=[1+a(Z-b-cZ^3)^{-4}]^{-1}, \tag{27}$$

which can be written in the more usual alternate form

$$[\omega_K/(1-\omega_K)]^{-4}=-A+BZ+CZ^3, \tag{28}$$

to the experimental results (Bu-55, La-56a, Li-60). The term involving the constant A essentially is a correction for screening, while the term involving CZ^3 carries the relativistic correction. The latter is negligible at low Z; on the other hand, the screening factor is very important at low Z, but it is difficult to determine it accurately, since its effect is small for medium- and high Z, where the experimental measurements are more accurate. Thus, Eqs. (27) and (28) introduce a considerable error when extrapolated to low Z ($Z<18$). These early theories assumed, moreover, that all of the electrons involved lie in discrete energy states, as in a gaseous atom, but this in fact is not true for low Z elements, in which the L electrons lie in the valance band and have wave functions which depend on the structure of the solid.

Furthermore, no allowance is made for the fact that the L- and M shells below $Z=18$ are incomplete. For ω_K values below $Z=18$, Achard (Ac-60) has shown that the theory of K-shell ionization by electron impact predicts the correct variation of K x-ray yields down to boron ($Z=5$), provided that Eq. (26) (Bu-52), rather than Eq. (27) or (28), is used for ω_K. The only serious disagreement between theory and experiment then remaining at very low Z is for beryllium ($Z=4$), where the observed K x-ray yield is only about half that predicted (Cam-63). Although considerable systematic error could be present in the beryllium experiments, the likely explanation of the disagreement is a breakdown of the formula for ω_K.

The constants A, B, and C in Eq. (28) are obtained from experiment by least-squares analysis. Curves of Eq. (27) or (28), together with available experimental points, have been published by many authors (Wa-58, Gr-56, Be-55, La-56a, Br-53, Bu-55, Bu-52, and Ro-57). Listengarten (Li-60) has compared available ω_K values

CC-0. In Public Domain. Gurukul Kangri Collection, Haridwar

Digitized by Arya Samaj Foundation Chennai and eGangotri

with Eq. (28) using values of constants A, B, and C from the literature, as shown in Table I. As Listengarten (Li-60) has observed, the curves of Li-56a and Wa-59 are rather similar, in agreement with available experimental data. In the region $23 \leq Z \leq 57$, the two curves are rather close, within 10% at the edges of the region, and giving the same value of ω_K for $Z \approx 40-45$.

Taylor and Merritt (Ta-63) have recently reported a new set of precision ω_K measurements for V, Cr, and Cu, using radioactive electron-capture sources of Cr^{51}, Mn^{54}, and Zn^{65}, respectively. Account was taken of the ratios of K/total capture and of capture from higher shells. Corrections for electron exchange effects were applied as given by Bahcall (Ba-63), which resolve the discrepancy previously noted between measured allowed L/K-capture ratios and their theoretical values (RF-55, RF-60, Mo-63). Since the ω_K values of Ta-63 are based on absolute measurements of disintegration rates and K x-ray emission rates, they are not subject to errors arising from self-absorption-scattering of low-energy Auger electrons in the solid sources or from quantitative measurement of Auger electron intensities. Likewise, the difficulties of resolving electron or K x-ray peaks or of determining detector efficiencies as a function of energy are avoided. The largest corrections are for capture from higher shells and for K x rays stopped in the Auger electron absorbers. The latter correction was directly measured and was kept small ($\sim 3\%$). Reproducibility of the results was 0.2% or better. The quoted errors of $\pm 2\%$ (Table II) include allowances for possible systematic errors, corrections, and capture ratios. The ω_K values of Ta-63 are significantly larger than previously accepted experimental values (Table II) in the region $24 \leq Z \leq 29$, as well as larger than Callan's theoretical values (Ca-63b) in this region, but not as large as the earlier theoretical estimates of Rubenstein and Snyder (Ru-55).

Listengarten (Li-62) has carried out new calculations of the probability of the Auger effect for elements with $Z=65$, 81, and 92. Previous nonrelativistic calculations of the relative intensities of the K-LL series of Auger lines (from which values of ω_K are computed) disagreed with experiment by some 30–40% for medium Z and by some 400% for $Z>81$. The relativistic calculations of Massey and Burhop (Ma-36) did not remove the disagreement in the K-LL Auger intensities. Recently, Asaad (As-59, As-65) gave results for relativistic calculations for $Z=80$, the screening being taken into account by means of nonrelativistic self-consistent Hartree field.

In Listengarten's calculations (Li-62), more accurate relativistic expressions (in jj coupling) for the probability of the various K-LL Auger transitions were obtained from general electrodynamic quantum theory. Screening was taken into account through the use of the Thomas–Fermi–Dirac statistical model. These results show that the total probability for K-LL Auger transitions is more than twice as large as the corresponding nonrelativistic value, the greatest increase being in the probabilities for K-L_1L_1 and K-L_1L_2 Auger transitions. The probability of an Auger transition involving only the p-electrons is essentially unchanged, but the relative contribution from the K-L_2L_2, K-L_2L_3, and K-L_3L_3 transitions is significantly reduced, which is in good agreement with experiment.

TABLE I. Values of empirical constants in Eq. (2a) from various authors (Cf. Li-60).

Constants	Bu-52	La-56a	Wa-59
$A\times 10^2$	4.4	2.17	6.4
$B\times 10^2$	3.46	3.318	3.4
$C\times 10^6$	1.35	1.14	1.03

To evaluate the K-fluorescence yield ω_K a knowledge of the total width of the K level is required, together with the value of the radiation width of the K level, since $\omega_K=\Gamma_{X_K}/\Gamma_{T_K}$. Using the ratio of Auger electron intensities

$$[(K-LX)+(K-XY)]/(K-LL),$$

where the numerator is obtained from experiment (Cf. Li-60) and the denominator from the theoretical total K-LL Auger probability (Li-62), the total width of the K level can be found; as given by Listengarten, $\Gamma_{T_K}=2.07$ eV for $Z=65$; 2.52 eV for $Z=81$; and 4.16 eV for $Z=92$.

The radiation width of the K level for emission of K_α x rays can be obtained from the K-$L_{2,3}$ Auger transition probability for $Z=80$ calculated by Asaad (As-59, Aa-65), $\Gamma_{X_K}=49.6$ eV at $Z=80$. Evaluation of Γ_{X_K} for other values of Z between 51 and 92 is done by means of the calculations of Massey and Burhop (Ma-36), which give a Z^4 dependence of the K-$L_{2,3}$ (the K_α transition) probability. The ratio of $K_\alpha/K_{\text{total}}$ x-ray quanta in these calculations was obtained from Wa-59. Although the absolute values from Massey and Burhop (Ma-36) are too low, owing to their use of Slater screening constants, the relative Z^4 dependence can be accepted as approximately correct. From this method, Listengarten (Li-62) has computed theoretical values of $\Gamma_{X_K}=20$ eV at $Z=65$; 49 eV at $Z=81$; and 81.5 eV at $Z=92$. Extrapolating for other values of Z in the region $Z=65$ to 93, Listengarten has evaluated values of the K-fluorescence yield from $\omega_K=\Gamma_{X_K}/\Gamma_{T_K}$, and these are given in Table II, and are used in Fig. 8 to construct the theoretical curve in this region of atomic number.

Comparison of these results with experiment (Table II and Fig. 8) shows that the agreement with experimental data is better at high Z for Listengarten's relativistic calculations than for the older nonrelativistic results, the best agreement coming in the heavy element region $Z=92$–94, for which no previous relativistic calculations exist.

CC-0. In Public Domain. Gurukul Kangri Collection, Haridwar

Digitized by Arya Samaj Foundation Chennai and eGangotri

TABLE II. Summary of K-fluorescence yields and comparison with theory.[a]

Z	Element	ω_K(experimental)	Ref.	ω_K(theory)	Ref.
6	C	0.0009	Br-53		
7	N	0.0015	Br-53		
8	O	0.0022	Br-53		
10	Ne	0.0081	Br-53		
12	Mg	0.043±0.004	Fr-58		
		0.0280±0.011	Ko-64		
		0.013	Br-53		
		0.008±0.003	Ri-59		
13	Al	0.008±0.003	Fr-58		
		0.0381±0.015	Ko-64		
		0.045±0.002	Be-59		
14	Si	0.038	Br-53		
16	S	0.083	Br-53	0.098	Ca-63b
17	Cl	0.093±0.003	Be-59	0.117	Ca-63b
		0.108	Br-53		
18	Ar	0.081±0.006	1-Ha-55	0.138	Ca-63b
		0.087±0.007	Go-61	0.13	Ru-55
		0.123	Br-53		
		0.129±0.011	He-55		
		0.140±0.0014	Wa-62		
19	K			0.155	Ca-63b
20	Ca	0.15	Br-53	0.165	Ca-63b
		0.207	La-34		
22	Ti	0.180±0.010	Ha-57	0.213	Ca-63b
			Ha-60		
		0.22	Ru-62		
23	V	0.24	Ru-62		
		0.253±0.005	Ta-63		
		0.305±0.027	Fr-58	0.242	Ca-63b
		0.23±0.02	Ko-61		
24	Cr	0.26	Ru-62		
		0.222±0.003	Kr-62	0.272	Ca-63b
			Kr-61		
		0.277±0.042	Ba-65		
			Le-65		
		0.264 (av)	Br-53		
		0.219±0.012	Ha-60		
		0.20±0.03	2-Mo-61		
		0.285±0.006	Ta-63		
25	Mn	0.273±0.003	Kr-62	0.291	Ca-63b
			Kr-61		
		0.28	Ru-62		
		0.308±0.015	Fr-58		
		0.27±0.02	Ko-61		
		0.33±0.03	2-Mo-61		
26	Fe	0.308±0.015	Ro-57	0.319	Ca-63b
		0.375	Br-53		
		0.314	Br-53		
		0.32	Br-53		
		0.343	La-34		
27	Co	0.310±0.010	Ko-58a	0.346	Ca-63b
			Ko-58b		
			Ha-60		
			Ha-57		
28	Ni	0.366±0.011	Ro-57	0.378	Ca-63b
		0.38±0.01	Be-59		
		0.33±0.02	Pa-57		
		0.385	Br-53		
		0.374	Br-53		
		0.436	La-34		
29	Cu	0.400±0.004	Kr-61	0.407	Ca-63b
			Kr-62		
		0.42±0.02	Ko-61		
		0.410±0.012	Ro-57		
		0.454±0.009	Ta-63		
		0.390±0.020	1-Ha-55		
			Pa-57		
		0.419	Br-53		
30	Zn	0.446±0.012	Ro-57	0.438	Ca-63b
		0.440±0.020	Pa-57		
		0.430±0.020	Ha-60		
		0.440	Br-53		
		0.476	La-34		

CC-0. In Public Domain. Gurukul Kangri Collection, Haridwar

Digitized by Arya Samaj Foundation Chennai and eGangotri

TABLE II (*Continued*)

Z	Element	ω_K(experimental)	Ref.	ω_K(theory)	Ref.
31	Ga	0.427±0.004	Kr-61	0.469	Ca-63b
			Kr-62		
		0.47±0.02	Ko-61		
		0.53±0.03	Dr-57		
32	Ge			0.510	Ca-63b
33	As	0.53	Br-53	0.548	Ca-63b
34	Se	0.575	St-37	0.585	Ca-63b
		0.578	Br-53		
		0.547	Br-53		
		0.585	La-34		
35	Br	0.565	Br-53	0.628	Ca-63b
		0.623 (av)	Br-53		
36	Kr	0.620±0.030	We-55	0.660	Ca-63b
		0.660±0.020	He-55	0.67	Ru-55
		0.67	Br-53		
37	Rb			0.680	Ca-63b
38	Sr	0.640±0.030	Ha-60	0.702	Ca-63b
		0.644	Br-53		
39	Y			0.719	Ca-63b
40	Zr	0.700±0.020	Ro-57	0.737	Ca-63b
		0.69	St-37		
		0.645	Gr-56		
41	Nb	0.730±0.020	Ro-57	0.754	Ca-63b
		0.713	Gr-56		
42	Mo	0.730±0.020	Ro-57	0.770	Ca-63b
		0.714	Gr-56		
		0.785	Br-53		
		0.735	St-37		
		0.765 (av)	Br-53		
43	Tc	0.697(+0.060, −0.046)	Ra-61	0.785	Ca-63b
		0.700±0.030	La-56a, b		
44	Ru			0.799	Ca-63b
45	Rh	0.786±0.015	Ro-57	0.812	Ca-63b
		0.801	Br-53		
		0.779	Gr-56		
		0.77	St-37		
46	Pd	0.790±0.015	Ro-57	0.822	Ca-63b
		0.835	Br-53		
		0.781	Gr-56		
47	Ag	0.821±0.019	Ro-57	0.833	Ca-63b
		0.840 (av)	Br-53	0.85	Ru-55
		0.81	St-37		
		0.813	Gr-56		
48	Cd	0.827±0.015	Ro-57	0.843	Ca-63b
		0.846	Br-53		
		0.819	Gr-56		
		0.773 (av)	Br-53		
49	In	0.820±0.020	1-Ha-55		
		0.87±0.03	La-56a, b		
50	Sn	0.846±0.012	Ro-57		
		0.836±0.013	Fa-57		
		0.840	Gr-56		
		0.855	Br-53		
		0.81	St-37		
51	Sb	0.862	Br-53		
52	Te	0.872	Br-53		
53	I	0.91±0.03	Fo-59		
		0.88	Br-53		
54	Xe	0.880±0.030	He-55	0.872	Ca-63b
		0.81	Br-53		
55	Cs	0.873±0.015	Er-61		
		0.898±0.002	Gr-61b		
		0.890	Br-53		
56	Ba	0.870±0.007	Br-53		
		0.85	Gr-56		
57	La	0.88±0.01	Ke-56		
		0.94	Gr-56		
58	Ce	0.90	Gr-56		
59	Pr				
59	Pr	0.88	Br-53		
63	Eu	0.908±0.007	Su-62		

CC-0. In Public Domain. Gurukul Kangri Collection, Haridwar

Digitized by Arya Samaj Foundation Chennai and eGangotri

TABLE II (*Continued*)

Z	Element	ω_K (experimental)	Ref.	ω_K (theory)	Ref.
64	Gd	0.925±0.005	1-Mo-61		
65	Tb			0.924	Li-62
66	Dy	0.943±0.007	Gr-61a		
67	Ho			0.930	Li-62
68	Er	0.955±0.022	Br-59		
69	Tm			0.936	Li-62
70	Yb	0.936±0.010	Gr-56		
71	Lu			0.941	Li-62
73	Ta			0.946	Li-62
74	W			0.945	Ca-63b
75	Re			0.951	Li-62
77	Ir			0.956	Li-62
78	Pt	0.942	Br-53		
79	Au			0.960	Li-62
80	Hg	0.952±0.003	Na-60	0.953	Ca-63b
		0.946±0.008	Br-53	0.961	Li-62
81	Tl			0.955	Ca-63b
82	Pb	0.96	Gr-56	0.962	Li-62
83	Bi	0.96	Gr-56	0.963	Li-62
		0.934	Br-53	0.963	Li-62
		0.976	Br-53	0.958	Ca-63b
84	Po	0.944±0.008	Gr-56	0.963	Li-62
		0.894	Br-53		
90	Th			0.963	Li-62
91	Pa			0.963	Li-62
92	U	0.967±0.010	Gr-56	0.963	Li-62
93	Np	0.938±0.010	Ho-58	0.963	Li-62

[a] Most values before review of Gr-56 and Br-53 are referred to in those summaries, respectively. This accounts for different values with same reference number. (Cloud chamber and approximate results have not been included.)

Callan (Ca-63b) has computed radiation and Auger level widths for K levels in the region of $16 \leq Z \leq 83$. The former were computed empirically from the quasi-hydrogenic approximation

$$\Gamma_{X_K} = \sum_n A_n Z^4, \tag{29}$$

where the empirical coefficients A_n are averaged values of the $1s$-np dipole transition probabilities. The approximation was used of multiplying the A_n coefficient for a full shell by the fraction of electrons in the shell, which accounts adequately for the fraction of the widths due to an unfilled shell. The Auger widths, Γ_{a_K} (from which the total width $\Gamma_{T_K} = \Gamma_{X_K} + \Gamma_{a_K}$) were computed from K-LL widths corrected both for $(K$-$XY)/(K$-$LL)$ ratios from Geffrion and Nadeau (Ge-59) and for relativistic effects for heavy elements.

The results for Γ_{X_K} and $\Gamma_{T_K} = \Gamma_{X_K} + \Gamma_{a_K}$ agree within 5% for all but the lightest elements with those given by Parratt (Pa-59); for the lightest elements, the differences in Γ_{T_K} are less than 0.15 eV.

The K-shell fluorescence yields from

$$\omega_K = \Gamma_{X_K}/(\Gamma_{X_K} + \Gamma_{a_K})$$

thus were computed by Callan in the region $Z = 16-83$. They agree well with the theoretical results of Listengarten (Li-62), as seen in Table II and Fig. 8, for the high-Z region. When compared to curves based on Eq. (28), Callan's results lie slightly higher than those of Wa-59 and Bu-55 in the middle-Z region. From $Z = 40$ to 50, Callan's results also tend to be higher than the values of Roos (Ro-57), which may be the result of neglect of the relativistic increase in the Auger yield in this region. However, the maximum deviation does not exceed about 0.04 from the experimental values in the middle-Z region, and one concludes that the use of screened hydrogenic-type approximations is reasonably well justified for both Γ_{X_K} and Γ_{a_K} widths for the K shell. Callan's values are shown in Table II, and they are used to construct the theoretical curve in the middle-Z region shown in Fig. 8.

The K-fluorescence yield can be measured experimentally if the fraction of the total number of orbital electron capture events by a radioactive nuclide which produce a K-shell vacancy is known, since one can determine the ratio of the rate of K x-ray emission to the total electron capture rate (see Ta-63). However, to calculate theoretically the fraction of the total electron capture events producing a K-shell vacancy, one must correct for the effect of electron exchange and imperfect atomic overlap according to Bahcall (Ba-63)

$$\lambda_K/\lambda_{\text{total}} = (\lambda_K/\lambda_{\text{total}})^0 B_K, \tag{30}$$

where $(\lambda_K/\lambda_{\text{total}})^0$ is the usual theoretical ratio of the probability of K capture to the total electron capture probability (Br-58), and B_K is the exchange correction factor defined by Bahcall as

$$B_K = |f(1s')/\psi(1s)(0)|^2, \tag{31}$$

where $f_{(1s')}$ is the amplitude for the production of a vacancy in the K shell of the *daughter* atom, and $\psi(1s)(0)$ is the one-electron K-shell wave function.

CC-0. In Public Domain. Gurukul Kangri Collection, Haridwar

Digitized by Arya Samaj Foundation Chennai and eGangotri

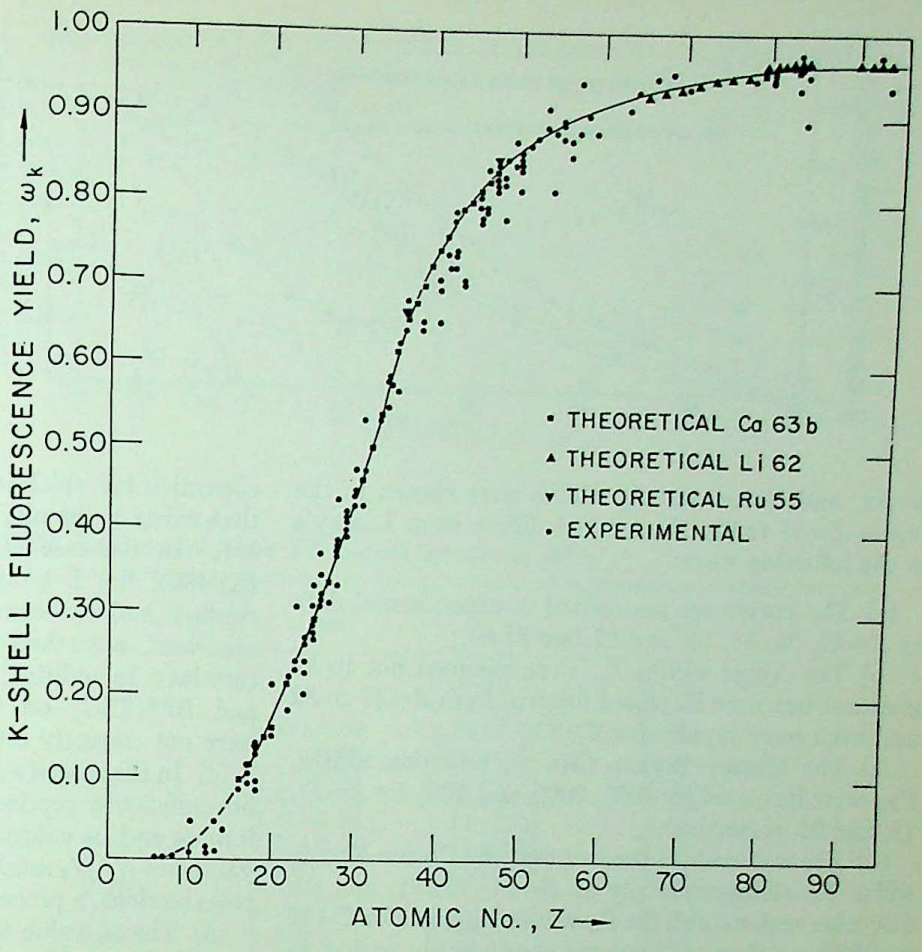

FIG. 8. The K-shell fluorescence yields are shown as a function of atomic number. The closed circles represent experimental values. The theoretical values from three different calculations are shown. The solid curve is the "best fit" theoretical curve.

evaluated at the nucleus, of electrons in the *initial* atom. Numerical values of B_K have been computed by Bahcall (Ba-63) using the analytic Hartree–Fock wave functions of Watson and Freeman (Wa-61) in the region limited to $14 \leq Z \leq 37$. These values of B_K are given by the formula

$$B_K = 1 - 0.929/Z + 20.98/Z^2 - 316.5/Z^3,$$

for

$$14 \leq Z \leq 37. \tag{32}$$

The exchange correction is accurate to within about 2%.

All available theoretical and experimental values of ω_K are gathered in Table II and exhibited in Fig. 8. Experimental ω_K values before the summary of Broyles, Thomas, and Haynes (Br-53) are taken or averaged from these authors for elements for which no other data exists, except that no result based on the unreliable cloud chamber method has been included. Similarly, the summary of ω_K values of Gray (Gr-56) was used to obtain more recent experimental values appearing since Br-53. All other experimental data were collected from the literature through 10 May 1966.

Those values of ω_K which were measured by means of the more accurate experimental techniques discussed above appear to agree best with the theoretical curve, Fig. 8, which has been drawn from the theoretical results of Callan (Ca-63b) and Listengarten (Li-62).

When one requires a value of the K-fluorescence yield for other purposes, a suitable procedure would be to take the value from the curve, Fig. 8, especially in cases where a variety of experimental points is offered.

5.2. *L*-Shell Fluorescence and Coster–Kronig Yields

An early attempt to compute theoretical values of mean L-shell fluorescence yields was made by Pincherle (Pi-35). He employed nonrelativistic, hydrogen-like wave functions with Slater screening. These results do not agree satisfactorily with experimental results (Bu-52). A recent theoretical calculation of the Auger effect in the L shell (As-65) has been performed. The only other theoretical work which bears on L-shell fluorescence yields is that of Massey and Burhop (Ma-36) who have given theoretical values of Γ_{X_i} for the L subshells; see Eqs. (13) and (14). As stated in Ref. Li-60, these values are too small. The probable reason for this circumstance is that Slater screening was used rather than more accurate atomic wave functions. Listengarten (Li-60) has generated semitheoretical curves for the fluorescence and Coster–Kronig yields of the L subshells. These are shown as curves in Figs. 9, 10, and 11 on which experimental points are also shown for comparison.

The Listengarten curves were constructed in a manner similar to that of Kinsey (Ki-48a). Radiation,

CC-0. In Public Domain. Gurukul Kangri Collection, Haridwar

Digitized by Arya Samaj Foundation Chennai and eGangotri

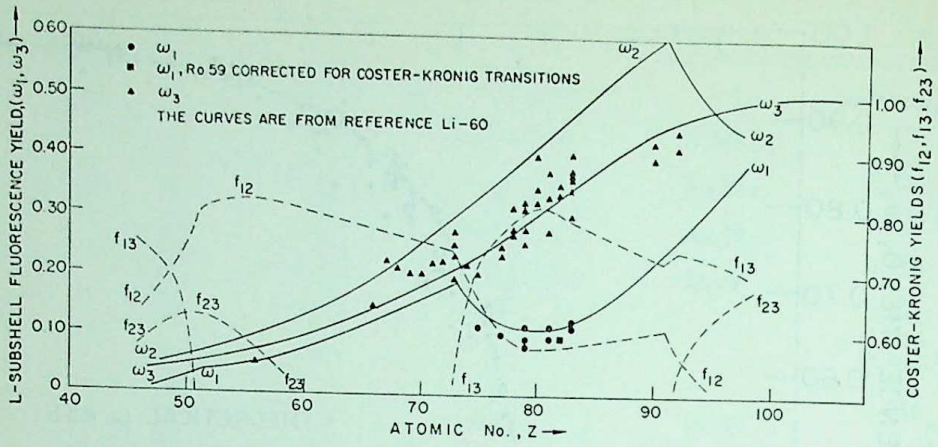

FIG. 9. The values of ω_1 and ω_3 are shown, together with the semi-theoretical estimates of Listengarten (Li-60) in the form of the curves.

Auger, and Coster–Kronig widths were chosen in the region $Z=47$ to 98. The method differs from Kinsey's in the following ways:

(a) The curves are normalized to experimental data at $Z=47$, 54, 55, 56, and 82 (see Li-60);

(b) The Auger widths Γ_{a_i} were assumed not to be constant but were increased linearly from $Z=47$ to 82 and even more rapidly for $Z\geq 82$;

(c) The Massey–Burhop (Ma-36) radiation widths, Γ_{x_i}, were increased by 40%, 20%, and 10% for $Z=51$, 79, and 92, respectively;

(d) Use was made of the fact that the Coster–Kronig width Γ_{ik} changes sharply at $Z=51$, 73, 91, and 92. For other regions of Z, the Γ_{ik} values obtained for $Z=55$ and 82 were then extrapolated continuously with Z in accordance with Coster–Kronig electron energies. It was further assumed that $L_2\rightarrow L_3M_{4,5}$ transitions cause Γ_{23} to increase for $Z\geq 91$ in the same way as Γ_{13} increases for $Z\geq 73$.

In Fig. 9, which shows Listengarten's curves, experimental values for ω_1 and ω_3 have been entered. Figure 10 shows the Listengarten curves and the experimental points for ω_2. In these figures, the experimental values for ω_1 and ω_2 reported by Küstner and Arends (Kü-35) and Roos (Ro-59) shown in Table III are not entered because:

(a) In the case of ω_1, the results do not take into account Coster–Kronig transitions ($L_1\rightarrow L_{2,3}$), the correction for which introduces even more uncertainty than exists in the original data;

(b) In the case of ω_1 values obtained by Kinsey (Ki-48b), the L x-ray transitions ascribed to the L_1 subshell had to be measured with the aid of critical absorbers, a method which involves considerable uncertainty. In addition, the decay schemes of Pb^{210}(RaD) and Bi^{212}(ThC) on which assumptions were based were not correctly established at the time;

(c) In the case of ω_2, the critical absorption method is not sufficiently precise to permit an accurate separation into ω_2 and ω_3 values. Moreover, the ratio of subshell vacancies $N_2:N_3$ must be calculated from photoelectric cross sections, a procedure involving some inaccuracies;

(d) The ω_2 value for $Z=79$ of Päschke (Pä-63) depends on assuming a value for f_{23} and is therefore not entered. Similarly, the ω_3 value which depends on assumed values for f_{12}, f_{13}, and f_{23} is omitted. On the other hand, Päschke's value for ω_1, determined by analyzing the Auger electrons and the L x rays, depends on a calculated subshell vacancy ratio of $N_1:N_2:N_3=1:1:2$ for excitation by electron bombardment, but not on the assumption of values of Coster-Kronig yields, and so it is retained on the plot.

The ω_1 points retained in Fig. 9 were measured by various methods based on Auger electron intensity measurements with high resolution beta spectrometry (Pä-63, Su-61a), or by the measurement of radiation widths according to Kinsey (Ki-48b).

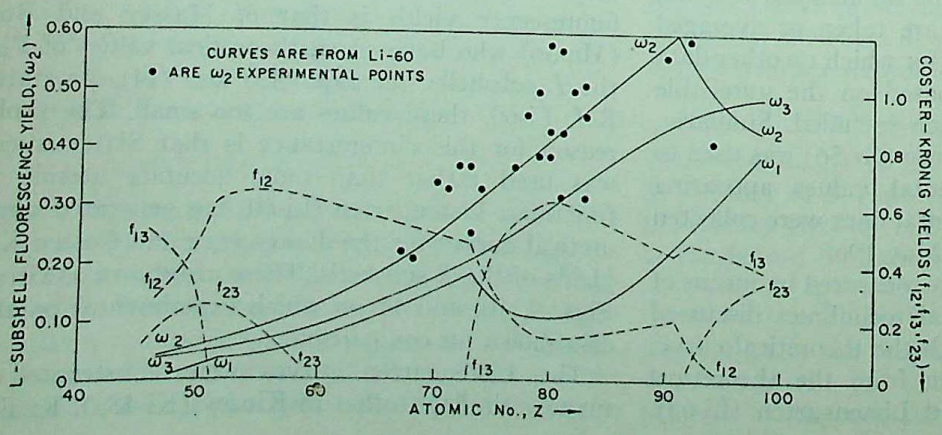

FIG. 10. The values of ω_2 are shown, together with the semi-theoretical estimates of Listengarten (Li-60) in the form of the curves.

CC-0. In Public Domain. Gurukul Kangri Collection, Haridwar

Digitized by Arya Samaj Foundation Chennai and eGangotri

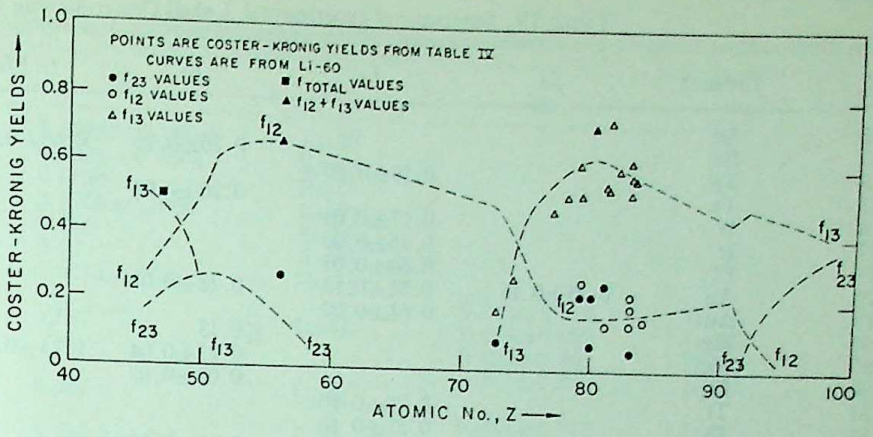

FIG. 11. This figure shows the available values of L shell Coster–Kronig yields compared with the semi-theoretical estimates of Listengarten (Li-60) in the form of the curves.

TABLE III. Experimental values of L-subshell fluorescence yields.

Z	Element	ω_1	ω_2	ω_3	Ref.
56	Ba			0.05±0.01	Bu-58
66	Dy			0.145±0.055	Zi-63
67	Ho		0.22±0.04	0.22±0.03	Jo-64a
68	Er		0.21±0.04	0.21±0.03	Jo-64a
70	Yb		0.34±0.05	0.20±0.02	Jo-64a
71	Lu		0.33±0.06	0.22±0.03	Jo-64a
72	Hf		0.37±0.06	0.22±0.03	Jo-64a
73	Ta	0.28±0.07	0.23±0.04	0.23±0.02	Ro-59
			0.25±0.02	0.27±0.01	Ra-65
	Ta	0.284[a]	0.326[a]	0.191[a]	Kü-35[a]
	Ta		0.37±0.06	0.25±0.03	Jo-64a
74	W	0.305[a]	0.311[a]	0.207[a]	Kü-35
	W		0.33		Ki-48
75	Re	0.11		0.20	Ki-48
77	Ir	0.370[a]	0.281[a]	0.244[a]	Kü-35[a]
	Ir	0.10	0.37	0.23	Ki-48
78	Pt	0.35±0.08	0.31±0.04	0.275±0.03	Ro-59
	Pt	0.392[a]	0.274[a]	0.262[a]	Kü-35[a]
	Pt		0.46±0.07	0.31±0.04	Jo-64a
79	Au	0.08±0.01	0.26±0.03	0.24±0.02	Pä-63
	Au	0.410[a]	0.272[a]	0.276[a]	Kü-35[a]
	Au	0.09	0.39	0.25	Ki-48
			0.343±0.007		La-65
	Au	0.36±0.09	0.27±0.04	0.32±0.03	Ro-59
	Au		0.50±0.08	0.31±0.04	Jo-64a
80	Hg		0.433±0.090	0.342±0.010	2-Ha-55
			0.39±0.03	0.40±0.02	Ra-65a
	Hg		0.58±0.10	0.32±0.05	Jo-64a
81	Tl	0.09	0.43	0.27	Ki-48
	Tl			0.33±0.02	Wi-58
	Tl	0.11±0.025	0.32±0.05		Su-61a
	Tl		0.57±0.10	0.37±0.06	Jo-64a
82	Pb	0.475[a]	0.264[a]	0.337[a]	Kü-35[a]
	Pb	0.37±0.04	0.24±0.04	0.35±0.04	Ro-59
	Pb		0.50±0.08	0.35±0.05	Jo-64a
83	Bi	0.11[b]	0.32[b]	0.34[b]	To-58[b]
	Bi	0.487[a]	0.255[a]	0.367[a]	Kü-35
	Bi		0.46	0.30	Ki-48
	Bi			0.36	Ri-60
	Bi		0.51±0.08	0.37±0.05	Jo-64a
	Bi	0.12±0.01	0.32±0.04	0.40±0.05	Ro-55
90	Th		0.56	0.39	Ki-48
	Th			0.42	2-Ha-55
92	U		0.59	0.41	Ki-48
	U			0.44	St-37
93	Np	0.19±0.04[c]	0.78±0.19[c]	0.57±0.12[c]	Ak-64
94	Pu		0.413±0.02		Sa-61

[a] Uncorrected for Coster–Kronig transitions.
[b] Assuming $f_{12}=0$. This assumption is also made for all ω_2 values given in Jo-64a.
[c] Assuming from Li-60 that $f_{12}=0.10\pm0.04$.

CC-0. In Public Domain. Gurukul Kangri Collection, Haridwar

Digitized by Arya Samaj Foundation Chennai and eGangotri

TABLE IV. Summary of experimental L-shell Coster–Kronig yields.

Z	Element	f_{12}	f_{13}	f_{23}	$f_{12}+f_{13}$	f_{total}	Reference
47	Ag			0.26±0.26	0.66±0.07	≈0.5	Bu-52
56	Ba		0.19±0.20				Bu-58
73	Ta			0.20±0.04			Fe-65
73	Ta		0.27±0.03				Ra-65a
74	W		0.46±0.06				Fe-65
77	Ir		0.50±0.05				Fe-65
78	Pt	0.25±0.13	0.51±0.13	0.22±0.07[a]			Fe-65
79	Au		0.61±0.07				Pä-63
79	Au			≤0.13			Fe-65
80	Hg			0.22±0.04	0.74±0.04		Ra-64
80	Hg			0.08±0.02			Na-60
80	Hg		0.76±0.10				Ra-65a
81	Tl		0.57±0.10				Fe-65
81	Tl	0.17±0.05	0.56±0.07	0.25±0.13		0.73[a]	Pe-61
81	Tl	0.24	0.52	0[a]			Su-61a
81–83		0.16	0.60	0[a]	(calculated from Ki-48b)		Bu-56
82	Pb	0.16	0.62	0[a]			Li-60
83	Bi	0.19±0.05	0.58±0.05	0.06(+0.14, −0.06)			To-58
83	Bi	0.19	0.58	0([a])			Ro-55
83	Bi	0.10±0.04[a]	0.55±0.09	0.02±0.05			Ri-58
93	Np						Ak-64

[a] Assumed in order to obtain the other values.

Table IV shows a summary of experimental L-shell Coster–Kronig yields. These are plotted in Fig. 11, together with the semitheoretical curves of Listengarten (Li-60).

Table V lists experimental values of ω_{KL} and some mean L-fluorescence yields, $\bar{\omega}_L$, measured by various methods. Figure 12 shows ω_{KL} as a function of Z, and Fig. 13 shows $\bar{\omega}_L$ vs Z. In Figs. 12 and 13, measurements based on photoexcitation are shown as solid points and those from radioactive excitation by open circles. In Fig. 13, the solid line for the mean L-fluorescence yields represents Lay's data (La-34). The sharp break at $Z\approx 70$ in Fig. 13 represents the onset of the Coster–Kronig yield ($L_1 \rightarrow L_{2,3}M_{4,5}$) which is energetically forbidden for $50 \leq Z \leq 73$ (see Fig. 11). The existence of this sharp break has not been established experimentally. A break of this type does not appear in Fig. 12, where only the L_2 and L_3 subshells are ionized in the primary process. In Fig. 13, where excitation of the L_1 subshell makes a substantial contribution to the mean L-fluorescence yield, $\bar{\omega}_L$, such a break and increase in the fluorescence yield is expected.

Table VI summarizes experimental L-shell fluorescence yields following L-capture ω_{LL} (discussed in Sec. 1.3).

5.3. M-Shell Fluorescence Yields

Very little information is available about fluorescence yields in shells higher than the L shell. Six

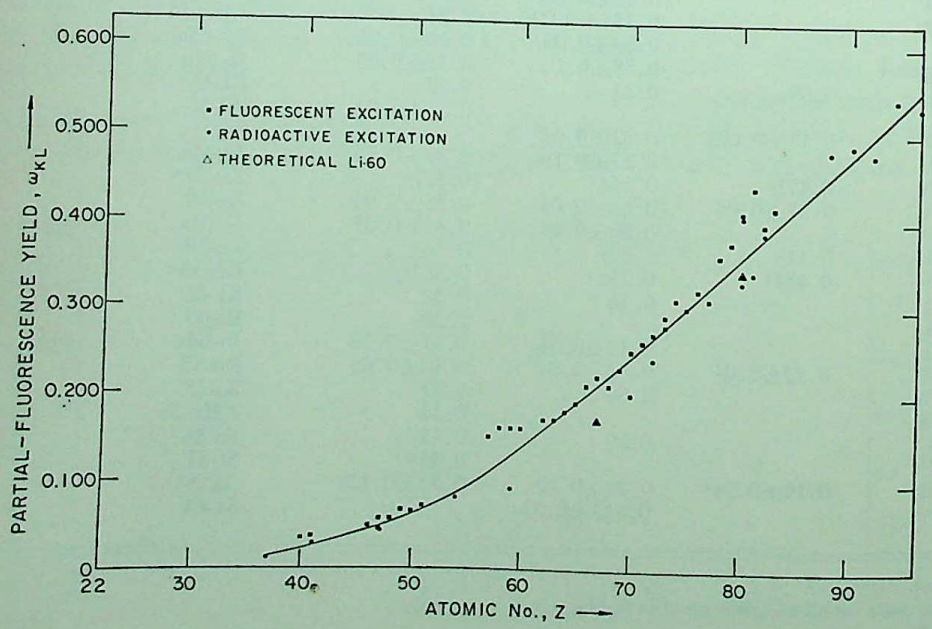

FIG. 12. The values of ω_{KL} as a function of atomic number are shown. The solid squares are measurements using photoexcitation of the K shell and the closed circles represent experiments in which the K shell was ionized by electron capture or internal conversion in radioactive decay.

CC-0. In Public Domain. Gurukul Kangri Collection, Haridwar

Digitized by Arya Samaj Foundation Chennai and eGangotri

TABLE V. Experimental mean L-shell fluorescence yields.

Z	Element	$\bar{\omega}_L$	Ref.	ω_{KL}	Ref.
23	V	0.00235±0.00025	Ko-60		
25	Mn	0.0029_5±0.0004	Ko-65		
29	Cu	0.0056	Ko-61		
31	Ga	0.0064±0.0004	Ko-60		
36	Kr	0.075	Bo-36		
	Kr	0.13	Au-25		
37	Rb	0.011±0.001	Ho-63		
	Rb			0.013±0.002	Ho-63
40	Zr	0.057	La-34	0.034±0.012	Jo-64b
41	Nb			0.022±0.002	Ho-63
	Nb			0.036±0.012	Jo-64b
42	Mo	0.067	La-34		
46	Pd			0.047±0.012	Jo-64b
47	Ag	0.047 (theory)	Li-60	0.045±0.003	Ho-63
	Ag			0.054±0.014	Jo-64b
	Ag			0.044±0.0003	Ho-64
	Ag	0.047±0.002	Be-59		
	Ag	0.029±0.003	Be-54		
	Ag	0.100	La-34		
48	Cd				
49	In			0.055±0.014	Jo-64b
50	Sn			0.065±0.014	Jo-64b
51	Sb			0.064±0.014	Jo-64b
	Sb	0.119	La-34	0.070±0.015	Jo-64b
52	Te	0.073±0.007	Ho-63		
		0.071 (theory)	Li-60		
	Te	0.122	La-34		
54	Xe	0.103±0.010	Fi-55		
	Xe	0.11±0.01	Ho-64		
	Xe	0.21	Bo-36		
	Xe			0.08±0.01	Ho-64
	Xe	0.25	Au-25		
56	Ba	0.148	La-34		
57	La	0.099 (theory)	Li-60	0.15±0.02	Jo-63
	La	0.092±0.007	Ho-63		
	La	0.158	La-34		
58	Ce			0.16±0.02	Jo-63
	Ce	0.163	La-34		
59	Pr			0.16±0.02	Jo-63
	Pr	0.167	La-34		
	Pr			0.09±0.01	Ho-64
60	Nd			0.16±0.02	Jo-63
	Nd	0.170	La-34		
62	Sm			0.17±0.01	Jo-63
	Sm	0.188	La-34		
63	Eu			0.17±0.01	Jo-63
	Eu	0.17	Bi-56		
64	Gd			0.18±0.02	Jo-63
	Gd	0.198	La-34		
65	Tb			0.19±0.01	Jo-63
	Tb			0.19	2-La-58
66	Dy	0.14±0.02	Zi-63		
	Dy			0.21±0.01	Jo-63
67	Ho			0.17±0.01	Ho-63
				0.17 (theory)	Li-60
	Ho			0.22±0.01	Jo-63
68	Er			0.21±0.03	Jo-63
	Er	0.228	La-34		
69	Tm			0.23±0.03	Jo-63
70	Yb			0.25±0.02	Jo-63
				0.20±0.02	Co-65
	Yb			0.20	2-La-58
71	Lu			0.26±0.03	Jo-63
72	Hf	0.260	La-34		
	Hf	0.17	2-Bi-56		
	Hf			0.24	2-La-58
	Hf			0.27±0.02	Jo-63
73	Ta			0.28±0.01	Ra-65a
				0.29±0.02	Jo-63
74	W	0.298	La-34		
75	W			0.31±0.04	Jo-63
76	Re			0.30±0.04	Jo-63
	Os	0.348	La-34		
	Os			0.32±0.04	Jo-63

CC-0. In Public Domain. Gurukul Kangri Collection, Haridwar

Digitized by Arya Samaj Foundation Chennai and eGangotri

TABLE V (*Continued*)

Z	Element	ω_L	Ref.	ω_{KL}	Ref.
77	Ir			0.31±0.04	Jo-63
78	Pt	0.348	La-34		
	Pt	0.32±0.02	Jo-62[a]		
	Pt			0.36±0.02	Jo-63
79	Au	0.365	La-34		
	Au			0.374±0.018	Jo-63
79	Au	0.430±0.012	La-65	0.287±0.04	La-65
80	Hg	0.410±0.040	Na-60		
	Hg	0.34±0.04	Sc-57		
	Hg	0.41±0.04	Le-62		
	Hg			0.34	2-La-58
	Hg	0.40±0.04	Ra-64		
	Hg	0.371±0.035	2-Ha-55	0.34 (theory)	Li-60
	Hg	0.24±0.05	Ja-54		
	Hg			0.33±0.02	Ho-63
	Hg			0.41±0.05	Jo-63
	Hg	0.39±0.06	Ra-64[a]		
	Hg			0.405±0.020	Ra-64
81	Tl	0.32±0.02	Wi-58		
	Tl	0.50±0.02	Bu-56		
	Tl	0.41±0.04	Ra-62		
	Tl	0.48±0.03	Ri-58		
	Tl			0.34	2-La-58
	Tl			0.44±0.05	Jo-63
82	Pb	0.39±0.02	Pa-57		
	Pb	0.398	La-34		
	Pb			0.385	2-La-58
	Pb			0.395±0.020	Jo-63
	Pb	0.36±0.02	Jo-62[a]		
83	Bi	0.38±0.02	Fi-57		
	Bi	0.38±0.04	Le-58		
	Bi	0.40±0.02	Wi-58		
	Bi	0.402	La-34		
	Bi	0.51±0.03	Bu-56		
	Bi			0.414±0.021	Jo-63
88	Ra			0.480±0.012	1-Ha-64
88	Ra	0.40±0.03	Gi-66		
	Ra	0.52±0.05	Bo-56		
90	Th			0.488±0.008	1-Ha-64
91	Pa	0.52±0.03	Ad-62[a]		
92	U			0.478±0.009	1-Ha-64
92	U	0.603±0.04	La-65	0.409±0.04	La-65
	U	0.45	La-34		
93	Np	0.66±0.08	Ak-64		
94	Pu			0.540±0.009	1-Ha-64
	Pu	0.486±0.01	Sa-61		
96	Cm			0.531±0.010	1-Ha-64

[a] ω_{LL} with $n_1, n_2, n_3 \approx 1, 0, 0$.

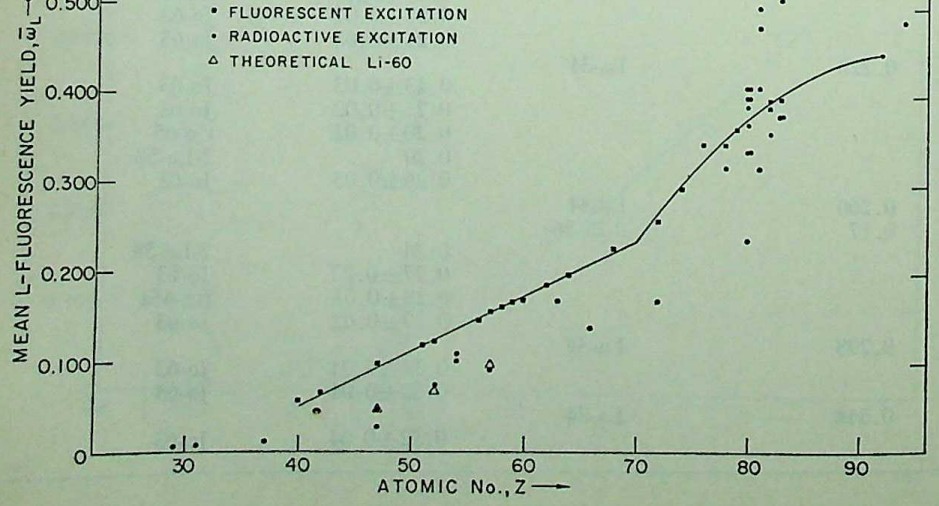

FIG. 13. The measured values of selected mean L-fluorescence yields, $\bar{\omega}_L$, are shown in this plot. The solid curve is drawn through the experimental points obtained by Lay (La-34).

CC-0. In Public Domain. Gurukul Kangri Collection, Haridwar

Digitized by Arya Samaj Foundation Chennai and eGangotri

measurements of mean M-fluorescence yields have been reported in the literature for elements between $Z=76$ and $Z=92$. The earliest measurement is that of Lay (La-34), who determined a mean M-fluorescence yield of uranium using photoionization of the M shell and photographic plates to measure the x-ray intensity (Sec. 4.2.1). Jaffe (Ja-54) has measured a mean M-shell fluorescence yield of bismuth by using the known M-shell conversion coefficient of the 46.5-keV transition following Pb^{210}(RaD) decay to compute the M-shell vacancies and then observed the M x rays with a proportional counter.

Finally, mean M-fluorescence yields of Os, Au, Pb, and Bi have been measured using the coincidence method with proportional counters, as described in Sec. 4.2.5. The mean M-shell yield measured in this way is designated ω_{LM} (in analogy with the similar quantity ω_{KL} defined for the L shell). It can be shown that ω_{LM} is approximately equal to a linear combination of the subshell fluorescence yields of the M_4 and M_5 subshells,

$$\omega_{LM}=0.4\omega_{M_4}+0.6\omega_{M_5}. \tag{33}$$

For a complete discussion of the procedure used to find Eq. (33), see Jo-65. Fluorescence yields for the M shell are summarized in Table VII.

The calculations of Ramberg and Richtmeyer (Ra-37) give the following values for M subshell fluorescence yields of gold ($Z=79$): $M_1=0.0050$, $M_2=0.0084$, $M_3=0.0045$, $M_4=0.017$, and $M_5=0.019$. These values when substituted into Eq. (33) for ω_{LM} give a somewhat lower value than that observed experimentally (Table VII).

5.4. Mesic X-Ray Fluorescence Yields

When fast negative mesons such as μ^-, π^-, or K^- have been slowed down to energies of a few eV, they can be captured into bound atomic orbits to form mesic atoms characterized by large values of the principal and orbital quantum numbers (n, 1∼16). The wave functions of these states with high quantum numbers have little overlap with the nucleus. Before the meson can be captured by a nuclear proton, it must cascade down into a state of low atomic excitation having considerable overlap with the nucleus. In this cascade both radiative and Auger transitions occur. The theory of Fermi and Teller (Fe-47) indicates that the principal quantum numbers below which radiative transitions dominate over the Auger transitions, for example in nuclear emulsions, are $n\approx4.8$ for bromine and $n\approx5.6$ for silver. Wheeler (Wh-49) has calculated the Auger and mesic x-ray transition probabilities per unit time for the $2s\rightarrow2p$, $2s\rightarrow1s$, and $2p\rightarrow1s$ transitions in μ^- and π^- -mesic atoms, assuming a point-charge nucleus. The results of Wheeler's calculation show that for low Z, Auger electron emission is predominant for transitions depopulating the $2s$ level.

TABLE VI. L-shell fluorescence yields following L capture, ω_{LL}.

Z	Element	Value of ω_{LL} (experimental)	Ref.
73			
78	Ta	0.23±0.01	Ra-65b
80	Pt	0.32±0.02	Jo-62
82	Hg	0.39±0.06	Ra-64
91	Pb	0.36±0.02	Jo-62
	Pa	0.52±0.03	Ad-62

TABLE VII. Summary of mean M-shell fluorescence yields.

Z	Element	Experimental ω_{LM}	$\bar{\omega}_M$	Ref.
76	Os	0.016±0.003		Jo-65
79	Au	0.030±0.006		Jo-65
82	Pb	0.032±0.006		Jo-65
83	Bi	0.037±0.007		Jo-65
83	Bi		0.037±0.007	Ja-54
92	U		0.06	La-34

In addition to the theoretical studies, there also has been considerable experimental work reported for radiative transitions in μ^--mesic atoms in cosmic rays (Ch-54, Hi-51, Fa-52, Ha-53, 1-Bu-53) and with machine-produced muons (Fi-53, St-54, Ko-54, Co-64). Auger transitions in μ^--mesic atoms have been found in cosmic ray investigations (Co-49, 1-Fr-50, 2-Fr-50, Bo-51, Gr-51) and with machine-produced muons (Mo-53, Fr-53). Experimental evidence for radiative transitions (Ca-55, Sc-53, St-54, Mc-54) and for Auger electron emission (Me-50, Sa-62, Cu-62) in π^--mesic atoms has been obtained with machine-produced pions. In one investigation, the π^--mesic Auger yields were compared with those from K^--mesic atoms with the finding that the latter yields are about 75% larger than those from π^--mesic atoms in emulsions (Ch-58).

The experimental evidence shows that the Auger electrons from mesic atoms are emitted with quite low energies. In nuclear emulsion studies, the lower limit of detectability for electrons is about 14 keV. These low-energy electrons must arise from Auger transitions in silver and bromine associated with principal quantum numbers in the range of $n=4$ to 8, consistent with the theory of Fermi and Teller (Fe-47). Some of the higher energy (75–125 keV) Auger electrons observed may be due to $2s\rightarrow1s$ transitions in light elements such as carbon, nitrogen, and oxygen in the emulsions, assuming that the probability of cascade through the $2s$ state is not negligible. In low-Z elements (Be, B, C, N, O) the emission of Auger electrons predominates for transitions between states above $n=3$, below which the radiative transitions become important.

Once the meson has cascaded down to quantum states of low principal quantum number, capture by the nucleus competes strongly with radiative transitions in depleting these states. Finally, when the meson reaches the $1s$ state, it lives a relatively long time (of the order of 10^{-6} sec) before it is captured by the nucleus, as

CC-0. In Public Domain. Gurukul Kangri Collection, Haridwar

Digitized by Arya Samaj Foundation Chennai and eGangotri

compared to the time required for it to cascade down to the $1s$ state (generally less than 10^{-12} sec). Extensive calculations of the cascade time have been made (2-Bu-53, De-54, Jo-52). The fact of the long lifetime in the $1s$ state is convincing evidence that the interaction between muons and nucleons is weak (Wh-49).

Since the radii of mesic orbits are some 200 times smaller than the electron orbits for the same principal quantum number, mesic orbits below about $n=3$ in low Z elements and about $n=5$ for middle Z elements lie wholly within the radius of the K-electron orbit where the mean electron density is so small that Auger transitions become negligible. For this reason the mesic x-ray fluorescence yields for transitions between quantum states of low principal quantum number are close to unity, with the exception of the $2s \rightarrow 1s$ transition, for which the radiative transition is absolutely forbidden. Good evidence, both experimental and theoretical, exists that low-Z elements such as Be, B, C, N, O, Mg, Al, give one K-mesic x ray for each stopping muon or pion.

It may be noted that in addition to radiative transitions and direct capture of the meson by the nucleus, the two principal processes depopulating states of low quantum number, other effects also occur. One such effect is a process by which the muon, bound in a $3d$ orbit in a very heavy element (Th, U), makes a nonradiative transition to the $1s$ state accompanied by an $E2$ Coulomb excitation of a nuclear energy state. This process may have a transition probability large enough to cause a significant decrease in the yield of $3d \rightarrow 2p$ and $2p \rightarrow 1s$ mesic x rays (2-Ru-62, Ki-62, Fo-60). It has been found that the K mesic x-ray yields per stopped muon from Th^{232}, U^{235}, and U^{238} are, respectively, 15, 29, and 23% lower than that from lead (Mu-60). Thus the $3d \rightarrow 1s$ nonradiative transition of the muon, with the energy going to excite an $E2$ transition in the nucleus, may compete significantly in heavy elements with the radiative $3d \rightarrow 2p$ and $2p \rightarrow 1s$ cascade.

As newer accelerators, capable of producing very high fluxes of mesons ("meson factories") come into operation, further studies of the details of the deexcitation of the atomic states of mesic atoms will become feasible. As the mesic x rays have much higher energies than the corresponding x rays from electronically excited atoms, the study of the fluorescence yields and of Auger transitions might be extended to the M, N, etc. shells with detailed measurements of the yields from these higher shells in mesic atoms.

ACKNOWLEDGMENTS

The authors are grateful to their colleagues in this field for supplying some of their data before publication. We would also like to express our thanks to Dr. T. C. Merkle for his continued support and encouragement. This work was supported by the U.S. Atomic Energy Commission.

6. LIST OF REFERENCES

This is a complete list of references for all relevant material up to 10 May 1966.

Ac-60 G. D. Achard, *Proceedings of the Second Symposium on X-Ray Microscopy and Microanalysis* (Elsevier Publishing Co., Ltd., Amsterdam, 1960), pp. 39[illegible].

Ad-62 A. M. Adamson, M. Duquesne, and R. Foucher, J. Phys. Radium **23**, 580 (1962).

Ak-64 G. G. Akalaev, N. A. Vartanov, and P. S. Samoilov, Izv. Akad. Nauk SSSR, Ser. Fiz. **28**, 1158, 1255 (1964) [Bull. Acad. Sci. USSR, Phys. Columbia Tech. Transl. **28**, 1260 (1964)].

Al-61 R. G. Albridge and J. M. Hollander, Nucl. Phys. **27**, 554 (1961).

Ar-35 E. Arends, Ann. Physik **22**, 281 (1935).

As-59 W. N. Asaad, Proc. Roy. Soc. (London) A249, 555 (1959).

As-65 Nucl. Phys. **66**, 494 (1965); 63, 337 (1965).

Au-25 P. Auger, J. Phys. Radium **6**, 205 (1925).

Ba-63 J. N. Bahcall, Phys. Rev. **132**, 362 (1963).

Ba-65 W. Bambynek, E. De Roost, A. Spernol, W. Van Der Eijk, and P. Vaninbrouk, Euratom Rept. EUR-2524.e (1965) (unpublished).

Be-30 H. Bethe, Ann. Physik **5**, 325 (1930).

Be-33 H. Bethe, in *Handbuch der Physik* (Julius Springer-Verlag, Berlin, 1933), Vol. 24, p. 273ff.

Be-54 G. Bertolini, A. Bisi, Lazarrini, and L. Zappa, Nuovo Cimento **11**, 539 (1954).

Be-55 I. Bergström, in *Beta- and Gamma-Spectroscopy*,

Be-64 edited by I. Bergström, (1955); and I. Bergström and C. Nordling, in *Alpha-, Beta-, and Gamma-Spectroscopy*, edited by K. Siegbahn (North-Holland Publishing Co., Amsterdam, 1964), p. 1523ff.

Be-59 F. Bertrand, G. Charpak, and F. Suzor, J. Phys. Radium **20**, 956 (1959); **20**, 462 (1959).

1-Bi-56 A. Bisi, E. Germagnoli, and L. Zappa, Nucl. Phys. **1**, 593 (1956).

2-Bi-56 A. Bisi, L. Zappa, and E. Zimmer, Nuovo Cimento **4**, 307 (1956).

Bo-36 J. C. Bower, Proc. Roy. Soc. (London) A157, 662 (1936).

Bo-51 A. Bonetti and G. Tomasini, Nuovo Cimento **8**, 693 (1951).

Bo-56 E. Booth, L. Madansky, and F. Rasetti, Phys. Rev. **102**, 800 (1956).

Br-53 C. Broyles, D. Thomas, and S. Haynes, Phys. Rev. **89**, 715 (1953).

Br-58 H. Brysk and M. E. Rose, Rev. Mod. Phys. **30**, 1169 (1958); and ORNL-1830 (1955).

Br-59 V. Brabets, K. Gromov, B. Dzhelepov, and V. Morozov, Bull. Acad. Sci. USSR, Columbia Tech. Transl. **23**, 805 (1959).

Bu-35 E. H. S. Burhop, Proc. Roy. Soc. (London) A148, 272 (1935).

Bu-52 E. H. S. Burhop, *The Auger Effect and Other Radiationless Transitions* (Cambridge University Press, Cambridge, England, 1952).

1-Bu-53 F. D. S. Butement, Phil. Mag. **44**, 208 (1953).

2-Bu-53 G. R. Burbridge and A. H. DeBorde, Phys. Rev. **89**, 189 (1953).

Bu-55 E. H. S. Burhop, J. Phys. Radium **16**, 625 (1955).

Bu-56 J. Burde and S. G. Cohen, Phys. Rev. **104**, 1085 (1956).

Bu-58 A. O. Burford and S. K. Haynes, Bull. Am. Phys. Soc. **3**, No. 3, 208 (1958).

Ca-55 M. Camac, A. D. McGuire, J. B. Platt, and H. J. Schulte, Phys. Rev. **99**, 897 (1955); **88**, 134 (1952).

Ca-61 E. J. Callan, Phys. Rev. **124**, 793 (1961).

Ca 63a E. J. Callan, Rev. Mod. Phys. **35**, 524 (1963).

Ca-63b E. J. Callan, preprint (1963) (unpublished); Bull. Am. Phys. Soc. **7**, N416 (1962).

Cam-63 A. J. Campbell, Proc. Roy. Soc. (London) A274, 319 (1963).

Ch-54 W. Y. Chang, Rev. Mod. Phys. **21**, 133 (1949); Phys. Rev. **95**, 1288 (1954).

Ch-58 E. B. Chesick and J. Schnepps, Phys. Rev. **112**, 1810 (1958).

CC-0. In Public Domain. Gurukul Kangri Collection, Haridwar

Digitized by Arya Samaj Foundation Chennai and eGangotri

Co-35 D. Coster and R. Kronig, Physica **2**, 13 (1935).

Co-49 M. G. E. Cosyns, C. C. Dilworth, G. P. S. Occhialini, M. Schoenberg, and N. Page, Proc. Phys. Soc. (London) **A62**, 801 (1949).

Co-58 A. J. Cochran and M. A. S. Ross, Proc. Phys. Soc. (London) **A71**, 1011 (1958).

Co-64 R. C. Cohen, S. Devons, and A. D. Kanaris, Nucl. Phys. **57**, 255 (1964).

Co-65 G. D. Cole and A. Mukerji, Bull. Am. Phys. Soc. **10**, No. 2, 262 (1965).

Cu-49 S. C. Curran, J. Angus, and A. L. Cockcroft, Phil. Mag. **40**, 36, 929 (1949).

Cu-62 J. E. Cuevas, M.S. thesis, Marquette University, Milwaukee, Wisconsin (1962).

Da-64 C. M. Davisson, in *Alpha-, Beta-, and Gamma-Spectroscopy*, edited by K. Siegbahn (North-Holland Publishing Co., Amsterdam, 1964), p. 37ff.

De-54 A. H. deBorde, Proc. Phys. Soc. (London) **A67**, 57 (1954).

Di-63 J. S. Dionisio, Ann. Phys. (Paris) **8**, 747 (1963); and thesis (Paris) (1963).

Dr-57 R. W. P. Drever and A. Moljk, Phil. Mag. **2**, 427 (1957).

Dy-62 B. B. D'yakov and I. M. Rogachev, Izv. Akad. Nauk SSSR, Ser. Fiz. **26**, 191 (1962) [Bull. Acad. Sci. USSR Columbia Tech. Transl. Phys. **26**, 191 (1962)].

Er-61 P. Erman and Z. Sujkowski, Arkiv Fys. **20**, 209 (1961).

Fa-52 A. Farfarman and M. H. Schamos, Phys. Rev. **87**, 219 (1952).

Fa-57 J. A. V. Fairbrother, D. G. Parkyn, and B. M. O'Connor, Proc. Phys. Soc. (London) **A70**, 262 (1957).

Fe-47 E. Fermi and E. Teller, Phys. Rev. **72**, 399 (1947); cf. also B. Feretti, Nuovo Cimento **5**, 325 (1948).

Fe-65 J. G. Ferreira, M. O. Costa, M. I. Goncalves, and L. Salgueiro, J. Phys. (Paris) **26**, 5 (1965).

Fi-53 V. Fitch and J. Rainwater, Phys. Rev. **92**, 789 (1953).

Fi-55 R. W. Fink and B. L. Robinson, Phys. Rev. **98**, 1293 (1955).

Fi-57 R. W. Fink, Phys. Rev. **106**, 266 (1957).

Fo-59 R. N. Forest and H. T. Easterday, Phys. Rev. **112**, 950 (1959).

Fo 60 B. Forkman and S. A. E. Johansson, Nucl. Phys. **20**, 136 (1960).

1-Fr-50 C. Franzinetti, Phil. Mag. **41**, 86 (1950).

2-Fr-50 W. F. Fry, Phys. Rev. **79**, 893 (1950).

Fr-53 W. F. Fry, Nuovo Cimento **10**, 490 (1953).

Fr-58 W. F. Frey, R. E. Johnston, and J. I. Hopkins, Phys. Rev. **113**, 1057 (1958); Bull. Am. Phys. Soc. **3**, No. 4, 299 (1958); TID-14854 (1958).

Ge-37 F. Genevese, M. S. Livingston, and E. J. Konopinski, Phys. Rev. **51**, 835 (1937).

Ge-59 C. Greffrion and G. Nadeau, Air Force Office of Scientific Res. Report TR-59-145 (1959) (unpublished).

Gi-66 F. B. Gil, C. F. Miranda, J. S. Lobo, and J. G. Ferreira, Port. Phys. **4**, 17 (1965) (in Portuguese); Nuclear Sci. Abstr. **20**, 10075 (1966).

Go-61 C. Godeau, Natl. Bur. Std. Tech Note No. 91 (1961) (unpublished).

Gr-51 G. Groetzinger, L. B. Leder, and F. L. Ribe, Phys. Rev. **81**, 626 (1951).

Gr-56 P. R. Gray, Phys. Rev. **101**, 1306 (1956); and AEC Report UCRL-3104 (1955).

Gr-61a R. L. Graham and J. S. Merritt, Can. J. Phys. **39**, 1058 (1961).

Gr-61b R. L. Graham, F. Brown, G. T. Ewan, and J. Uhler, Can. J. Phys. **39**, 1086 (1961).

Ha-53 G. G. Harris and T. J. B. Shanley, Phys. Rev. **89**, 983 (1953).

1-Ha-55 G. R. Harrison, R. C. Crawford, and J. I. Hopkins, Phys. Rev. **99**, 1629A (1955); Phys. Rev. **100**, 841 (1955).

2-Ha-55 S. K. Haynes and W. T. Achor, J. Phys. Radium **16**, 635 (1955).

Ha-57 H. L. Hagedoorn and J. Konijn, Physica **23**, 1069 (1957).

Ha-60 H. L. Hagedoorn and A. H. Wapstra, Nucl. Phys. **15**, 146 (1960).

1-Ha-64 J. W. Halley and D. Engelkemeir, Phys. Rev. **134**, A24 (1964).

2-Ha-64 S. Hagström, C. Nordling, and K. Siegbahn, in *Alpha-, Beta-, and Gamma-Spectroscopy*, edited by K. Siegbahn (North-Holland Publishing Co., Amsterdam, 1964), Appendix 2.

He-55 J. Heintze, Z. Physik **143**, 153 (1955); Z. Naturforsch. **9a**, 469 (1954).

Hi-51 E. P. Hincks, Phys. Rev. **81**, 313 (1951).

Ho-58 D. Hoffman and B. Dropesky, Phys. Rev. **109**, 1211 (1958).

Ho 63 K. Hohmuth, G. Müller, and J. Schintlmeister, Nucl. Phys. **48**, 209 (1963).

Ho 64 K. Hohmuth and G. Winter, Phys. Letters **10**, 58 (1964) and private communication (1964).

Ja-54 A. A. Jaffe, Bull. Res. Council (Israel) **3**, No. 4, 316 (March 1954); [see Phys. Abstr. **58**, 360, No. 2782 (1955)].

Jo-52 B. L. Jaffe and I. Ya. Pomeranchuk, Zh. Eksperim. i Teor. Fiz. **23**, 123 (1952).

Jo-60 B. R. Joshi, Proc. Phys. Soc. (London) **A77**, 1205 (1960).

Jo-61 R. C. Jopson, H. Mark, C. D. Swift, and J. H. Zenger, Phys. Rev. **124**, 157 (1961).

Jo-62 R. C. Jopson, H. Mark, and C. D. Swift, Phys. Rev. **127**, 1612 (1962).

Jo-63 R. C. Jopson, H. Mark, C. D. Swift, and M. A. Williamson, Phys. Rev. **131**, 1165 (1963); Bull. Am. Phys. Soc. **8**, No. 1, 49 (1963); **7**, 491 (1962).

Jo-64a R. C. Jopson, J. M. Khan, H. Mark, C. D. Swift, and M. A. Williamson, Phys. Rev. **133**, A381 (1964); Bull. Am. Phys. Soc. **9**, No. 1, 51 (1964).

Jo-64b R. C. Jopson, H. Mark, C. D. Swift, and M. A. Williamson, Phys. Rev. **136**, A69 (1964).

Jo-65 R. C. Jopson, H. Mark, C. D. Swift, and M. A. Williamson, Phys. Rev. **137**, A1353 (1965).

Ke-56 B. Kettele, H. Thomas, and A. Brosi, Phys. Rev. **103**, 190 (1956).

Ki-48a B. B. Kinsey, Can. J. Res. **A26**, 404 (1948).

Ki-48b B. B. Kinsey, Can. J. Res. **A26**, 421 (1948).

Ki-62 Y. N. Kim, Phys. Letters **3**, 33 (1962).

Kn 65 J. W. Knowles, in *Alpha-, Beta-, and Gamma-Spectroscopy*, edited K. Siegbahn (North-Holland Publishing Co., Amsterdam, 1964), p. 203ff.

Ko-54 S. Koslov, V. Fitch, and J. Rainwater, Phys. Rev. **95**, 291, 625 (1954).

Ko-58a J. Konijn, H. L. Hagedoorn, and B. van Nooyen, Physica **24**, 129 (1958).

Ko-58b J. Konijn, B. van Nooyen, and H. L. Hagedoorn, Physica **24**, 377 (1958).

Ko-60 A. A. Konstantinov, T. E. Sazonova, and V. V. Perepelkin, Izv. Akad. Nauk SSSR, Ser. Fiz. **24**, 1480 (1960) [Bull. Acad. Sci. USSR, Phys., Columbia Tech. Transl. **24**, 1472 (1960)].

Ko-61 A. A. Konstantinov, I. A. Sokolova, and T. E. Sazonova, Izv. Akad. Nauk SSSR, Ser. Fiz. **25**, 228 (1961) [Bull. Acad. Sci. USSR, Phys., Columbia Tech. Transl. **25**, 219 (1961)].

Ko-64 A. A. Konstantinov, V. V. Perepelkin, and T. E. Sazonova, Izv. Akad. Nauk SSSR, Ser. Fiz. **28**, 107 (1964) [Bull. Acad. Sci. USSR, Phys., Columbia Tech. Transl. **28**, 103 (1964)].

Ko-65 A. A. Konstantinov and T. E. Sazonova, Izv. Akad. Nauk SSSR, Ser. Fiz. **29**, 302 (1965) [Bull. Acad. Sci. USSR, Phys. Columbia Tech. Transl. **29**, 305 (1965)].

Kr-61 P. Kramer, thesis, Amsterdam (1961).

Kr-62 P. Kramer, A. De Beer, E. C. Bos, and J. Blok, Physica **28**, 582 (1962).

Kü-35 H. Küstner and E. Arends, Ann. Physik **22**, 443 (1935).

La-34 H. Lay, Z. Physik **91**, 533 (1934).

La-56a J. Laberrigue and P. Radvanyi, J. Phys. Radium **17**, 944 (1956); Compt. Rend. **242**, 901 (1956).

CC-0. In Public Domain. Gurukul Kangri Collection, Haridwar

Digitized by Arya Samaj Foundation Chennai and eGangotri

La-56b J. Laberrigue-Frolow, P. Radvanyi, and M. Langevin, J. Phys. Radium **17**, 530 (1956).

1-La-58 W. Laskar, Ann. Physique **3**, 258 (1958).

2-La-58 N. H. Lazar and W. S. Lyon, Bull. Am. Phys. Soc. **3**, No. 1, 29 (1958); and private communication (1958).

La-65 M. A. D. Lazzaro and G. Missoni, Istituto di Superiore di Sanita; Laboratori di Fisica Report (in English) ISS-65/11, Rome, Italy (1965) (unpublished).

Le-53 H. W. Lewis, B. E. Simmons, and E. Merzbacher, Phys. Rev. **91**, 943 (1953); **95**, 83 (1954).

Le-58 N. K. Lee, thesis, Vanderbilt Univ., Report TID-14963 (1958) (unpublished).

Le-62 H. Leutz and K. Ziegler, Z. Physik **166**, 582 (1962).

Le-65 M. Leistner and K. Friedrich, Atomkernenergie **8**, 311 (1965).

Li-60 M. A. Listengarten, Izv. Akad. Nauk SSSR, Ser. Fiz. **24**, 1041 (1960) [Bull. Acad. Sci. USSR, Phys. **24**, 1050 (1960)].

Li-62 M. A. Listengarten, Izv. Akad. Nauk SSSR, Ser. Fiz. **26**, 182 (1962) [Bull. Acad. Sci. USSR, Phys., Columbia Tech. Transl. **26**, 182 (1962)]; Izv. Akad. Nauk SSSR, Ser. Fiz. **25**, 792 (1961) [Bull. Acad. Sci. USSR, Phys., Columbia Tech. Transl. **25**, 803 (1961)].

Ma 36 H. S. W. Massey and E. H. S. Burhop, Proc. Roy. Soc. (London) **A153**, 661 (1936).

Ma 64 Hans Mark, Nucl. Instr. Methods **28**, 131 (1964).

Mc 54 A. D. McGuire, M. Camac, M. L. Halbert, and J. B. Platt, Phys. Rev. **95**, 625 (1954).

Me 50 M. G. K. Menon, H. Muirhead, and O. Rochat, Phil. Mag. **41**, 583 (1950).

Me-65 W. Mehlhorn, Phys. Letters **15**, 46 (1965); Z. Physik **187**, 21 (1965).

Mo-53 H. Morinaga and W. F. Fry, Nuovo Cimento **10**, 308 (1953).

1-Mo-61 E. Morrand and A. Moussa, Nucl. Phys. **25**, 292 (1961).

2-Mo-61 R. B. Moler and R. W. Fink, Bull. Am. Phys. Soc. **6**, No. 5, 428 (1961).

Mo-63 R. B. Moler and R. W. Fink, Phys. Rev. **131**, 821 (1963).

Mu-60 A. I. Muhkin, M. J. Balatz, L. N. Kondratiev, L. G. Landsburg, P. I. Lebedev, Yu. V. Obukliov, and B. Pontecorvo, *Proceedings of the High Energy Physics Conference, Rochester, 1960* (Interscience Publishers, Inc., New York, 1960), p. 550.

Na-60 J. C. Nall, Q. L. Baird, and S. K. Haynes, Phys. Rev. **118**, 1278 (1960).

Pa-57 E. T. Patronis, Jr., C. H. Braden, and L. D. Wyly, Phys. Rev. **105**, 681 (1957).

Pa-59 L. G. Parratt, Rev. Mod. Phys. **31**, 616 (1959).

Pä-63 R. Päschke, Z. Physik **176**, 143 (1963).

Pe-61 L. Persson and Z. Sujkowski, Arkiv Fys. **19**, 309 (1961).

Pi-35 L. Pincherle, Nuovo Cimento **12**, 81 (1935).

Ra-37 E. G. Ramberg and F. K. Richtmeyer, Phys. Rev. **51**, 913 (1937).

Ra-61 J. Ravier, P. Marguin, and A. Moussa, J. Phys. Radium **22**, 249 (1961).

Ra-62 M. K. RamaSwamy, Nucl. Phys. **33**, 320 (1962); Bull. Am. Phys. Soc. **7**, No. 4, 342 (1962).

Ra-64 P. V. Rao and B. Crasemann, Bull. Am. Phys. Soc. **9**, No. 7, 720 (1964).

Ra 65a P. V. Rao and B. Crasemann, Phys. Rev. **137**, B64 (1965); Bull. Am. Phys. Soc. **9**, No. 4, 396 (1964).

Ra-65b P. V. Rao and B. Crasemann, Phys. Rev. **142**, [illegible] (1966); Bull. Am. Phys. Soc. **10**, No. 5, [illegible] (1965); and private communication (1965).

RF-55 B. L. Robinson and R. W. Fink, Rev. Mod. Phys. **27**, 424 (1955).

RF-60 B. L. Robinson and R. W. Fink, Rev. Mod. Phys. **32**, 117 (1960).

Ri-58 K. Risch, Z. Physik **150**, 87 (1958).

Ri-59 R. A. Rightmire, J. R. Simanton, and T. P. Kohman, Phys. Rev. **113**, 1069 (1957); R. A. Rightmire, thesis, Carnegie Tech., Report NYO-6633 (1957).

Ri-60 K. Risch, Z. Physik **159**, 89 (1960).

Ro-55 M. A. S. Ross, A. J. Cochran, J. Hughes, and N. Feather, Proc. Phys. Soc. (London) **A68**, [illegible] (1955).

Ro 57 C. E. Roos, Phys. Rev. **105**, 931 (1957); **100**, [illegible] (1955); **93**, 401 (1954); Bull. Am. Phys. Soc. **30**, No. 7, 40 (1955).

Ro-59 C. E. Roos, private communication to B. L. Robinson, quoted in RF-60 (1959).

Ru-55 R. A. Rubenstein and J. N. Snyder, Phys. Rev. **97**, 1653 (1955).

1-Ru-62 M. A. Rumsh and V. N. Shchemelev, Zh. Eksperim. i Teor. Fiz. **42**, 727 (1962) [English transl. Soviet Phys.—JETP **15**, 507 (1962)].

2-Ru-62 J. E. Russell, Phys. Rev. **127**, 245 (1962).

Sa-61 L. Salgueiro, J. G. Ferreira, J. J. H. Park, and M. A. S. Ross, Proc. Phys. Soc. (London) **77**, 657 (1961).

Sa-62 J. Sacton, thesis, quoted in Cu-62.

Sc-53 H. J. Schulte, J. B. Platt, and M. Camac, Phys. Rev. **89**, 905 (1953).

Sc-57 H. Schmied and R. W. Fink, Phys. Rev. **107**, [illegible] (1958).

Si-64 K. Siegbahn, *Alpha-, Beta-, Gamma-Spectroscopy* (North-Holland Publishing Co., Amsterdam, 1964), p. 79ff.

St-37 R. J. Stephenson, Phys. Rev. **51**, 637 (1937).

St-54 M. B. Sterns, S. DeBenedetti, M. Sterns, and L. Leipuner, Phys. Rev. **93**, 1123 (1954); **95**, 625, 1353; **96**, 804 (1954); **97**, 240 (1955).

Su-61a Z. Sujkowski and O. Melin, Arkiv Fys. **20**, 193 (1961).

Su-61b Z. Sujkowski, Arkiv Fys. **20**, 243 (1961).

Su-62 T. Suter and P. Reyes-Suter, Arkiv Fys. **20**, 387 (1962).

Ta-63 J. G. V. Taylor and J. S. Merritt, Proc. Conf. *Atomic Electrons in Nuclear Transformations*, Warsaw, Poland, Vol. III, 465 (1963).

To-58 J. Tousset and A. Moussa, J. Phys. Radium **19**, 39 (1958).

Va-62 J. Valentin, Compt. Rend. **254**, 858 (1962).

Vi-61 C. Victor, Ann. Phys. (Paris) **6**, 183 (1961).

Wa-59 A. Wapstra, G. Nijgh, and R. van Lieshout, *Nuclear Spectroscopy Tables* (North-Holland Publishing Co., Amsterdam, 1959).

Wa-61 R. E. Watson and A. J. Freeman, Phys. Rev. **123**, 521 (1961); **124**, 1117 (1961); **118**, 1036 (1960); and MIT Tech. Rept. No. 12 (1959).

Wa-62 T. Wanabe, H. W. Schnopper, and F. N. Gillis, Phys. Rev. **127**, 2055 (1962) and Air Force Report AFOSR-1932 (1961).

We-27 G. Wentzel, Z. Physik **43**, 524 (1927).

We-55 J. P. Welker and M. L. Perlman, Phys. Rev. **100**, 74 (1955).

Wh-49 J. A. Wheeler, Rev. Mod. Phys. **21**, 133 (1949).

Wi-58 H. Winkenbach, Z. Physik **152**, 387 (1958).

Zi-63 T. Zimmerli and A. Flammersfeld, Z. Physik **176**, 323 (1963).

CC-0. In Public Domain. Gurukul Kangri Collection, Haridwar

Digitized by Arya Samaj Foundation Chennai and eGangotri

REVIEWS OF MODERN PHYSICS VOLUME 38, NUMBER 3 JULY 1966

Classical Noise IV: Langevin Methods

MELVIN LAX
Bell Telephone Laboratories, Murray Hill, New Jersey

A Langevin theory for linear and nonlinear, stationary and nonstationary, processes is developed and compared with Markoff methods. For short correlation times τ_c, we find the Markoff process that is a good approximation to the Langevin process for $\Delta t > \tau_c$. Conversely, given the diffusion coefficients D_n of a Markoff process, we find the moments (to all orders) of the Langevin forces that lead to the same process—exactly for homogeneous noise, approximately for the general nonlinear case. The techniques are illustrated by applications to Fokker–Planck processes, homogeneous noise with linear damping, the one-dimensional impurity band, spin diffusion, and population fluctuations.

CONTENTS

1. Introduction 541
2. Langevin Treatment of Linear Markoff Processes 543
3. Langevin Treatment of the Fokker–Planck Process 546
4. One-Dimensional Impurity Band 548
5. Markoffian Representation of Processes with Short Correlation Times 550
6. Distribution Function Treatment of Short Correlation Time Problem 554
7. Spin Diffusion 556
8. The (Approximate) Langevin Forces Appropriate to a Markoff Problem 558
9. Population Fluctuations 560
10. Summary 565

1. INTRODUCTION

Our quasilinear approach to stationary, Markoffian random processes[1,2] has recently been generalized[3] to include nonstationary,[4] nonlinear processes treated from a Markoffian point of view, i.e., using generalized forward and backward Eqs. III (5.13), (5.19) [or corresponding equations for the characteristic functions Eq. III (6.18)]. The purpose of the present paper is to review the same problem from a Langevin (noise-source) viewpoint.[2]

While many random problems are actually solved using the Markoff techniques described in III we present the Langevin approach because of its greater flexibility:

(1) If two systems, each of which is subject to dissipative processes and fluctuations, are coupled together in a deterministic way (e.g., by adding a coupling term to the Hamiltonian) then the Langevin noise sources are unchanged by the coupling—although the response to these sources may be completely different than in the absence of the coupling. We have used this technique to discuss noise in masers[5] with the atoms constituting one system, and the radiation field constituting the other.

(2) Langevin noise sources can at no extra cost be given the finite correlation times needed in non-Markoffian processes. Gaussian noise sources with a nonwhite spectrum are in fact a well-known way[6] to deal with linear non-Markoffian processes. For nonlinear processes, the Gaussian approximation is inadequate. If the correlation time of the noise sources is long, the sources can be treated quasistatically,[7] i.e., the random variables $\mathbf{a}$ are solved ("adiabatically") in terms of static forces $\mathbf{F}$. The result is then averaged over the distribution of F's at one time. We shall not review such quasistatic or "statistical"[8] methods here. If the correlation time τ_c of the sources is short (compared to typical relaxation times) then the system will behave in a Markoffian manner over time intervals greater than τ_c. The Markoffian representation of short correlation time processes[9,10] is discussed in Secs. 5 and 6.

(3) It is easier to transform from one set of variables $\mathbf{a}$ to another $\mathbf{a}'$ in the Langevin formulation than the Markoff formulation. (See Sec. 3.)

(4) If one has a set of N variables $\mathbf{a}=a_1, a_2, \cdots, a_N$, then moment techniques, even in the quasilinear case,

[1] M. Lax, Rev. Mod. Phys. **32**, 25 (1960). This paper will be referred to as I.
[2] M. Lax, Phys. Chem. Solids **14**, 248 (1960). This paper will be referred to as II.
[3] M. Lax, Rev. Mod. Phys. **38**, 359 (1966). This is "Classical Noise III." The references given in I and III provide a review of the literature, and will not be duplicated here. The notation in this paper, if not explained, follows that of III.
[4] The appropriate definition of the noise spectrum for nonstationary systems when the noise is a function of both time and frequency is given in paper QII: M. Lax, Phys. Rev. **129**, 2342 (1963) where quantum fluctuations in nonequilibrium states are discussed. Paper QI, *ibid.* **109**, 1921 (1958) includes a discussion of quantum noise in equilibrium states.
[5] See the papers in our series on quantum noise QIV, Phys. Rev. **145**, 110 (1966); QV in *Physics of Quantum Electronics*, P. L. Kelley, B. Lax, and P. E. Tannenwald, Eds. (McGraw-Hill Book Co., Inc., New York, 1966), p. 735; QVII and QIX in J. Quantum Electron. (to be published).
[6] See, for example, S. O. Rice, Bell Syst. Tech. J. **23**, 282 (1944); **24**, 46 (1945).
[7] See for example R. L. Stratanovich, *Topics in the Theory of Random Noise* (Gordon and Breach, Inc., New York, 1963), Vol. I.
[8] See for example H. Margenau and W. W. Watson, Rev. Mod. Phys. **8**, 22 (1936); J. H. Van Vleck and V. F. Weisskopf, *ibid.* **17**, 227 (1945), for a summary of the statistical treatment of collision broadened spectral lines, and M. Lax, J. Chem. Phys. **20**, 1752 (1952) for a discussion of the Franck–Condon principle as an adiabatic treatment of vibrational broadening of spectral lines.
[9] R. Kubo in *Fluctuation, Dissipation and Resonance in Magnetic Systems*, edited by D. ter Haar (Plenum Press, Inc., New York, 1962).
[10] M. Lax, J. Phys. Chem. Solids **25**, 487 (1964). This is paper QIII in our series on relaxation and noise in quantum systems. The dissipative and fluctuating effects of a reservoir on a system are displayed in the equation for the density matrix of the system obtained by integrating out the reservoir coordinates.

CC-0. In Public Domain. Gurukul Kangri Collection, Haridwar

Digitized by Arya Samaj Foundation Chennai and eGangotri

generally require the solution of N^2 equations whereas Langevin techniques require only the solution of N equations.

To see why this is so, we remind the reader, that the essential content of I is that[11]

$$\langle \boldsymbol{\alpha}(t)\,\boldsymbol{\alpha}^*(0)\rangle = \exp(-\boldsymbol{\Lambda}t)\,\langle \boldsymbol{\alpha}(0)\,\boldsymbol{\alpha}^*(0)\rangle, \quad (1.1)$$

where $\boldsymbol{\alpha}=\mathbf{a}-\mathbf{a}_0$ is the deviation from the operating point $\mathbf{a}_0$ and $\boldsymbol{\Lambda}$ is the decay matrix describing the mean equations of motion

$$d\langle \boldsymbol{\alpha}(t)\rangle/dt = -\boldsymbol{\Lambda}\langle \boldsymbol{\alpha}(t)\rangle. \quad (1.2)$$

[This result is true even for quantum systems as shown in QII.[4]] Thus the noise matrix $\mathbf{G}$ defined by

$$\tfrac{1}{2}\mathbf{G}(\boldsymbol{\alpha}) = \int_{-\infty}^{\infty} \exp(-i\omega t)\,\langle \boldsymbol{\alpha}(t)\,\boldsymbol{\alpha}^*(0)\rangle\,dt \equiv \boldsymbol{\alpha}_\omega \boldsymbol{\alpha}_\omega^* \quad (1.3a)$$

$$= (i\omega+\boldsymbol{\Lambda})^{-1}\langle \boldsymbol{\alpha}\boldsymbol{\alpha}^*\rangle + \langle \boldsymbol{\alpha}\boldsymbol{\alpha}^*\rangle(-i\omega+\boldsymbol{\Lambda}^\dagger)^{-1} \quad (1.3b)$$

(where ω is written briefly for ω times the unit matrix) has a spectrum determined by the relaxation times associated with the mean motion (1.2), but a magnitude determined by the fluctuations at one time

$$\langle \boldsymbol{\alpha}(0)\,\boldsymbol{\alpha}(0)^*\rangle = \langle \boldsymbol{\alpha}\boldsymbol{\alpha}^*\rangle.$$

The latter, unfortunately must be obtained by solving the N^2 equations contained in the generalized Einstein Eq. I (5.18):

$$2\mathbf{D} = \boldsymbol{\Lambda}\langle \boldsymbol{\alpha}\boldsymbol{\alpha}^*\rangle + \langle \boldsymbol{\alpha}\boldsymbol{\alpha}^*\rangle\boldsymbol{\Lambda}^\dagger, \quad (1.4)$$

where

$$2\mathbf{D} = \lim_{\Delta t\to 0} (\Delta t)^{-1}\langle [\boldsymbol{\alpha}(t+\Delta t)-\boldsymbol{\alpha}(t)][\boldsymbol{\alpha}(t+\Delta t)-\boldsymbol{\alpha}(t)]^*\rangle \quad (1.5)$$

is a Hermitian matrix. When time reversal is obeyed (I Sec. 6) the two terms in (1.4) are equal, and

$$\langle \boldsymbol{\alpha}\boldsymbol{\alpha}^*\rangle = \boldsymbol{\Lambda}^{-1}\mathbf{D} \quad (1.6)$$

can be obtained by inverting an $N\times N$ matrix. If $\boldsymbol{\Lambda}^{-1}\mathbf{D}$ is a Hermitian matrix, then time reversal is indeed obeyed and (1.6) is already the correct answer.[12] In the absence of time reversal, one is faced either with the use of the unpleasant formula I (5.19)

$$\langle \boldsymbol{\alpha}\boldsymbol{\alpha}^*\rangle = 2\int_0^\infty \exp(-\boldsymbol{\Lambda}t)\mathbf{D}\exp(-\boldsymbol{\Lambda}^\dagger t)\,dt, \quad (1.7)$$

or with direct solution of the N^2 equations (1.4) which is usually simpler for small N.

The Langevin equation

$$d\boldsymbol{\alpha}/dt + \boldsymbol{\Lambda}\boldsymbol{\alpha} = \mathbf{F} \quad (1.8)$$

suggests a more efficient procedure[13]:

$$\boldsymbol{\alpha}_\omega = (i\omega+\Lambda)^{-1}\mathbf{F}_\omega; \quad \boldsymbol{\alpha}_\omega^* = \mathbf{F}_\omega^*(-i\omega+\boldsymbol{\Lambda}^\dagger)^{-1}, \quad (1.9)$$

$$\langle \boldsymbol{\alpha}_\omega \boldsymbol{\alpha}_\omega^*\rangle = (i\omega+\boldsymbol{\Lambda})^{-1}\langle \mathbf{F}_\omega \mathbf{F}_\omega^*\rangle(-i\omega+\Lambda^\dagger)^{-1}, \quad (1.10)$$

where

$$\langle \mathbf{F}_\omega \mathbf{F}_\omega^*\rangle \equiv \tfrac{1}{2}\mathbf{G}(\mathbf{F}) = \int_{-\infty}^{\infty} \exp(-i\omega t)\,dt\,\langle \mathbf{F}(t)\mathbf{F}(0)^*\rangle \quad (1.11)$$

in accord with (1.3a). But the Langevin forces possess the autocorrelation

$$\langle \mathbf{F}(t)\mathbf{F}(u)^*\rangle = 2\mathbf{D}\delta(t-u). \quad (1.12)$$

Combining (1.9)–(1.12) *we obtain the desired noise spectrum*

$$\tfrac{1}{2}\mathbf{G}(\boldsymbol{\alpha}) \equiv \langle \boldsymbol{\alpha}_\omega \boldsymbol{\alpha}_\omega^*\rangle = (i\omega+\boldsymbol{\Lambda})^{-1}2\mathbf{D}(-i\omega+\boldsymbol{\Lambda}^\dagger)^{-1} \quad (1.13)$$

in a way that completely avoids the need to determine $\langle \boldsymbol{\alpha}\boldsymbol{\alpha}^*\rangle$.

It is, of course, easy to verify that (1.13) and (1.3b) are algebraically equivalent with the help of the Einstein relation (1.4). However, we would not have discovered (1.13) without the Langevin procedure. Although Langevin procedures have been used for many years, the general formula (1.13) for the final noise-spectrum, and its simplicity compared to (1.3b) may not have been emphasized previously.

The autocorrelation can now be obtained by inverting (1.3a)!

$$\langle \boldsymbol{\alpha}(t)\,\boldsymbol{\alpha}^*(0)\rangle = \frac{1}{2\pi}\int_{-\infty}^{\infty} \exp(i\omega t)\,d\omega(i\omega+\boldsymbol{\Lambda})^{-1}(2\mathbf{D})(-i\omega+\boldsymbol{\Lambda}^\dagger)^{-1}, \quad (1.14)$$

and the simplest expression for $\langle \boldsymbol{\alpha}\boldsymbol{\alpha}^*\rangle$ when N is large is then

$$\langle \boldsymbol{\alpha}\boldsymbol{\alpha}^*\rangle = \frac{1}{2\pi}\int_{-\infty}^{\infty} d\omega(i\omega+\boldsymbol{\Lambda})^{-1}2\mathbf{D}(-i\omega+\boldsymbol{\Lambda}^\dagger)^{-1} \quad (1.15)$$

which can always be done by residue techniques.

---

[11] These results are summarized in Sec. 15 of I. The equations that follow constitute a slight generalization of I to the case in which the variables $\boldsymbol{\alpha}$ are permitted to be complex, but the two sets $\boldsymbol{\alpha}$ and $\boldsymbol{\alpha}^*$ are not coupled by $\boldsymbol{\Lambda}$. (If they are coupled, one may as well introduce real variables and use the equations of I.) The conjugate variables then obey

$$d\langle \boldsymbol{\alpha}^*(t)\rangle/dt = -\boldsymbol{\Lambda}^*\langle \boldsymbol{\alpha}^*(t)\rangle = -\langle \boldsymbol{\alpha}^*(t)\rangle\boldsymbol{\Lambda}\dagger,$$

where $\boldsymbol{\Lambda}\dagger$ is the Hermitian adjoint of $\boldsymbol{\Lambda}$, as remarked at I (3.11).

[12] See II, Appendix A, last paragraph, where the equivalence of time reversal and the symmetry of $\boldsymbol{\Lambda}^{-1}\mathbf{D}$ (for real $\boldsymbol{\alpha}$) is established. See also III (7B6).

[13] Strictly speaking, only $\boldsymbol{\alpha}_\omega\boldsymbol{\alpha}_\omega^*$ is defined by (1.3a), not $\boldsymbol{\alpha}_\omega$ separately. If we define

$$\boldsymbol{\alpha}(\omega) = \int_{-\infty}^{\infty} \exp(-i\omega t)\,\boldsymbol{\alpha}(t)\,dt,$$

then $\langle \boldsymbol{\alpha}(\omega)\,\boldsymbol{\alpha}(\omega')^*\rangle$ is expressible in terms of $\langle \boldsymbol{\alpha}(t)\,\boldsymbol{\alpha}(u)\rangle$ and hence by (1.3a) in terms of $\boldsymbol{\alpha}_\omega\boldsymbol{\alpha}_\omega^*$ with the result

$$\langle \boldsymbol{\alpha}(\omega)\,\boldsymbol{\alpha}(\omega')^*\rangle = 2\pi\langle \boldsymbol{\alpha}_\omega\boldsymbol{\alpha}_\omega^*\rangle\delta(\omega-\omega').$$

Thus, when we manipulate with $\boldsymbol{\alpha}_\omega$ separately from $\boldsymbol{\alpha}_\omega^*$ we are really using $\boldsymbol{\alpha}(\omega)$. In the end, however, we deal with bilinear quantities and the factor $2\pi\delta(\omega-\omega')$ cancels from both sides of the equation.

CC-0. In Public Domain. Gurukul Kangri Collection, Haridwar

Digitized by Arya Samaj Foundation Chennai and eGangotri

(5) *A fifth advantage of Langevin methods over moment methods is that they are usable even in unstable situations.*[14] Gurevich[15] has recently studied unstable systems by Langevin methods and we have studied self-sustained oscillators.[16] To deal with masers we have developed a set of noncommuting operator noise sources[17] to add to equations for $d(a_i^\dagger a_j)/dt$ where $a_i^\dagger a_j$ destroys a particle in state j and creates one in state i.

Let us note that in an unstable situation at least one of the moments $\langle \boldsymbol{\alpha}(t)\, \boldsymbol{\alpha}(t)^* \rangle$ will grow with time even if the underlying transition probabilities are stationary. Thus (1.13) can yield the correct noise spectrum when (1.3b) is meaningless because $\langle \boldsymbol{\alpha}\boldsymbol{\alpha}^* \rangle$ does not exist. For example, a one-dimensional system moving under simple Brownian motion has $\Lambda = 0$,

$$\langle \boldsymbol{\alpha}_\omega \boldsymbol{\alpha}_\omega^* \rangle = 2D/\omega^2 \tag{1.16}$$

and the integral (1.15) does not converge.

2. LANGEVIN TREATMENT OF LINEAR MARKOFF PROCESSES

In this section, we shall present the Langevin formulation for all Markoff examples discussed in III Sec. 7, but the Fokker–Planck process. Since all these processes (but the Fokker–Planck process) are special cases of example[18] F, homogeneous noise plus linear damping, we shall present this general case first and then indicate briefly how the results simplify in each of the special cases.

Homogeneous Noise with Linear Damping (F)

Let us define our Langevin process F by the equations

$$d\mathbf{a}/dt + \boldsymbol{\Lambda}(t)\cdot\mathbf{a} = \mathbf{F}(t), \tag{2.1}$$

where the randomness in $\mathbf{a}$ is induced by the random noise sources $\mathbf{F}$. The statistics of the noise sources will be defined by

$$\langle \mathbf{F}(t) \rangle = 0 \tag{2.2}$$

$$\langle \mathbf{F}(t_1)\mathbf{F}(t_2) \rangle = 2\mathbf{D}(t_1)\,\delta(t_1 - t_2) \tag{2.3}$$

$$\langle \mathbf{F}(t_1)\cdots\mathbf{F}(t_n) \rangle^L = n!\mathbf{D}_n(t_1)\prod_{i=1}^{n-1}\delta(t_i - t_{i+1}), \tag{2.4}$$

where the $\mathbf{D}_n$'s may be functions of the time, but not of $\mathbf{a}$. The linked averages are defined by Eq. III (6.8), i.e.,

$$\left\langle \exp i\int \mathbf{y}(s)\cdot\mathbf{F}(s)\,ds \right\rangle = \exp\left\{ \left\langle \exp\left[i\int \mathbf{y}(s)\cdot\mathbf{F}(s)\,ds \right] - 1 \right\rangle^L \right\}, \tag{2.5}$$

where $\mathbf{y}(s)$ is an arbitrary (vector) function of s. The choice (2.4) permits us to simplify the right-hand side into the form

$$\left\langle \exp i\int \mathbf{y}(s)\cdot\mathbf{F}(s)\,ds \right\rangle = \exp\sum_{n=1}^{\infty} i^n \int ds [\mathbf{y}(s)]^n : \mathbf{D}_n(s) \tag{2.6}$$

$$= \exp\left[-\int ds K(\mathbf{y}(s), s) \right]. \tag{2.7}$$

Equation (2.7) defines $K(\mathbf{y}, s)$. Compare with III (7F.2).

If $\boldsymbol{\lambda}(s)$ and $\boldsymbol{\mu}(s)$ are not both nonzero simultaneously, i.e.,

$$\lambda_i(s)\mu_j(s) = 0$$

except at a set of points of measure zero, then almost everywhere

$$[\boldsymbol{\lambda}(s) + \boldsymbol{\mu}(s)]^n = [\boldsymbol{\lambda}(s)]^n + [\boldsymbol{\mu}(s)]^n,$$

$$\left\langle \exp i\int [\boldsymbol{\lambda}(s) + \boldsymbol{\mu}(s)]\cdot\mathbf{F}(s)\,ds \right\rangle = \left\langle \exp i\int \boldsymbol{\lambda}(s)\cdot\mathbf{F}(s)\,ds \right\rangle \left\langle \exp i\int \boldsymbol{\mu}(s)\cdot\mathbf{F}(s)\,ds \right\rangle. \tag{2.8}$$

Thus $\int \boldsymbol{\lambda}(s)\cdot\mathbf{F}(s)\,ds$ and $\int \boldsymbol{\mu}(s)\cdot\mathbf{F}(s)\,ds$ are independent random variables. In particular

$$\int_t^{t'} \mathbf{y}(s)\cdot\mathbf{F}(s)\,ds \quad \text{and} \quad \int_{t'}^{t''} \mathbf{y}(s)\cdot\mathbf{F}(s)\,ds \tag{2.9}$$

are *independent random variables* for *any* $\mathbf{y}(s)$ since the intervals (t, t') and (t', t'') overlap in only one point.

If $\mathbf{n}(t)$ is defined as the solution of

$$d\mathbf{n}(t)/dt = -\boldsymbol{\Lambda}(t)\cdot\mathbf{n}(t) \tag{2.10}$$

subject to $\mathbf{n}(0) = 1$, and

$$\mathbf{n}(t, s) = \mathbf{n}(t)[\mathbf{n}(s)]^{-1} \tag{2.11}$$

as the solution subject to $\mathbf{n}(s, s) = 1$, then

$$\mathbf{a}(u) = \int_0^u \mathbf{n}(u, s)\cdot\mathbf{F}(s)\,ds + \mathbf{n}(u)\cdot\mathbf{a}(0) \tag{2.12}$$

$$\mathbf{a}(t) = \int_u^t \mathbf{n}(t, s)\cdot\mathbf{F}(s)\,ds + \mathbf{n}(t, u)\cdot\mathbf{a}(u). \tag{2.13}$$

[14] Of course, if the system is unstable the procedure that leads to (1.13) is valid only as long as the motion stays within the domain of validity of quasilinearity. Otherwise, the more elaborate procedures developed in this paper must be used.

[15] V. L. Gurevich, Zh. Eksperim. i Teor. Fiz. **46**, 354 (1963) [English transl.: Soviet Phys.—JETP **19**, 242 (1964)].

[16] Reference 5 and "Classical Noise V" (to be published).

[17] The moments of the noise sources are shown in QIV to be determined by the diffusion coefficients. Vanishings in these coefficients caused by the averaging process (5.37) are shown in QIV to be important in quantum systems.

[18] The examples A to F refer to Sec. 7 of III, Ref. 3.

CC-0. In Public Domain. Gurukul Kangri Collection, Haridwar

Digitized by Arya Samaj Foundation Chennai and eGangotri

Thus for $0<u<t$, we can compute $\mathbf{a}(t)$ in terms of $\mathbf{a}(u)$ and the statistics of $\mathbf{F}(s)$ in the interval (u, t). Moreover, the specification of $\mathbf{a}(u)$ which selects those $\mathbf{F}$'s with a particular value of

$$\int_0^u \mathbf{n}(u,s)\mathbf{F}(s)\,ds$$

does not influence the statistics of F in the interval (u, t) because of the independence established in (2.9) of the F's in two different time intervals. Thus $\mathbf{a}(t)$ depends on $\mathbf{a}(u)$ but not in any way on the previous history. This establishes that our process is Markoffian. The delta-function correlations of (2.4) are essential to this argument. One can consider processes (2.1) with random forces possessing a finite correlation time, but the resulting processes exhibit non-Markoffian memory effects.

By using (2.12) and interchanging the order of the u and s integrations we obtain

$$\left\langle \exp i\int_0^t \mathbf{q}(u)\cdot\mathbf{a}(u)\,du \right\rangle$$

$$= \exp i\int_0^t \mathbf{q}(u)\cdot\mathbf{n}(u)\cdot\mathbf{a}(0)\,du$$

$$\times\left\langle \exp\left[i\int_0^t ds\mathbf{h}(s,t)\cdot\mathbf{F}(s)\right]\right\rangle, \quad (2.14)$$

where

$$\mathbf{h}(s,t)=\int_s^t du\mathbf{q}(u)\cdot\mathbf{n}(u,s). \quad (2.15)$$

Making use of (2.7) we obtain

$$\left\langle \exp i\int_0^t \mathbf{q}(u)\cdot\mathbf{a}(u)\,du\right\rangle = \exp\left[i\int_0^t \mathbf{q}(s)\cdot\langle\mathbf{a}(s)\rangle\,ds\right]$$

$$\times\exp\left[-\int_0^t dsK\left(\int_s^t du\mathbf{q}(u)\cdot\mathbf{n}(u,s),s\right)\right], \quad (2.16)$$

where $\langle\mathbf{a}(s)\rangle=\mathbf{n}(s)\cdot\mathbf{a}(0)$. This result is in agreement with III (7F.21) when we make use of

$$\mathbf{m}(u)^{-1}=\mathbf{n}(u),$$

$$\mathbf{m}(u,s)\equiv\mathbf{m}(u)^{-1}\mathbf{m}(s)=\mathbf{n}(u)\cdot\mathbf{n}(s)^{-1}\equiv\mathbf{n}(u,s). \quad (2.17)$$

Indeed, the procedure given here, is the one by which we first solved the problem. In summary, our agreement between (2.16) and III (7F.21) demonstrates the equivalence between our assignment (2.4) of Langevin forces, and the Markoff definition III (5.4) of the nth-order diffusion coefficients D_n.

Ornstein–Uhlenbeck Process

We can specialize to the Ornstein–Uhlenbeck process,[18] C, by setting

$$K(\mathbf{y},s)=\mathbf{y}\cdot\mathbf{D}\cdot\mathbf{y} \quad (2.18)$$

with all $D_n=0$ for $n>2$, and $\mathbf{D}$ and $\mathbf{\Lambda}$ independent of t, so that $\mathbf{n}(t)=\exp(-\mathbf{\Lambda}t)$. The multidimensional Weiner process,[18] A, is obtained by the further specialization $\mathbf{\Lambda}=0$.

The Homogeneous Process E

The homogeneous process,[18] E, with no damping, retains all $\mathbf{D}_n$, but replaces

$$\mathbf{D}_1(a)=\mathbf{A}(a)=\mathbf{A} \quad (2.19)$$

by a constant rather than $-\mathbf{\Lambda}\mathbf{a}$. The equation

$$d\mathbf{a}/dt=\mathbf{A}+\mathbf{F}(t)=\mathbf{G}(t) \quad (2.20)$$

can be handled as before. Equation (2.16) remains correct providing we make the replacements

$$\langle\mathbf{a}(s)\rangle=\mathbf{a}(0)+\mathbf{A}s; \qquad \mathbf{n}(u,s)=1. \quad (2.21)$$

Comparison with Eq. III (7E.9) shows that A plays the role of the unperturbed frequency ω_{if} and $F(s)$ corresponds to the random frequency $\omega(s)-\omega_{if}$.

In this homogeneous case, we note that the linked averages of $\mathbf{G}$ are identical to those of $\mathbf{F}$ for $n\geq 2$ since $\mathbf{A}$ cancels out of such linked averages.

The Poisson Process (Shot Noise)

The Poisson process,[18] D, in view of III (7D.8) and (2.4) has the simple correlations

$$\langle G(t)\rangle=\nu,$$

$$\langle G(t_1)G(t_2)\rangle^L=\nu\delta(t_1-t_2),$$

$$\langle G(t_1)\cdots G(t_n)\rangle^L=\nu\delta(t_1-t_2)\cdots\delta(t_{n-1}-t_n), \quad (2.22)$$

where

$$da/dt=G(t). \quad (2.23)$$

These results are succintly summarized by

$$\left\langle \exp i\int y(s)G(s)\,ds\right\rangle$$

$$= \exp\left(\nu\int ds\{\exp[iy(s)]-1\}\right). \quad (2.24)$$

The Poisson process can also be described in terms of "shot noise," i.e., a series of impulses distributed randomly in time, by setting

$$G(s)=\sum_k\delta(s-t_k). \quad (2.25)$$

To prove the equivalence of these two viewpoints, let us suppose that N impulses are distributed over the time interval T, at the rate $N/T=\nu$. Since the t_k are independent, we can factor the average:

$$\left\langle \exp i\int_0^T y(s)G(s)\,ds\right\rangle=\prod_{k=1}^N\langle\exp iy(t_k)\rangle. \quad (2.26)$$

Each t_k is uniformly distributed on T, i.e., we multiply by dt_k/T and integrate to take the average over t_k

CC-0. In Public Domain. Gurukul Kangri Collection, Haridwar

Digitized by Arya Samaj Foundation Chennai and eGangotri

Moreover, all such averages are identical. Thus

$$\prod_{k=1}^{N}\langle\exp[iy(t_k)]\rangle=\left[\int_0^T \exp[iy(t_k)]\,dt_k/T\right]^N$$

$$=\left[1+T^{-1}\int_0^T\{\exp[iy(\tau)]-1\}\,d\tau\right]^N. \tag{2.27}$$

If $y(\tau)$ is some function that is large near $\tau=t$ and falls off sufficiently rapidly as τ moves away from t for the integral over τ to converge, we obtain using

$$[1+(x/T)]^N\approx\exp[(N/T)x]=\exp\nu x:$$

$$\lim_{T\to\infty}\left\langle\exp i\int_0^T y(s)G(s)\,ds\right\rangle$$

$$=\exp\nu\int_{-\infty}^{\infty}d\tau\{\exp[iy(\tau)]-1\} \tag{2.28}$$

in agreement with III (7D.11) when $y(s)=y$ for $0\le s\le t$. The usual shot noise calculation is based on a choice of the form

$$y(s)=\lambda f(t-s) \tag{2.29}$$

and Eq. (2.28) then states that

$$\langle\exp[i\lambda\sum_k f(t-t_k)]\rangle$$

$$=\exp\left\{\nu\int_{-\infty}^{\infty}ds\{\exp[i\lambda f(t-s)]-1\}\right\}$$

$$=\exp\left\{\nu\int_{-\infty}^{\infty}dt\{\exp[i\lambda f(t)]-1\}\right\} \tag{2.30}$$

in agreement with the usual shot noise calculations.[6]

The Homogeneous Process E

The "shot noise" representation (2.25) of the Poisson process can be extended to a general homogeneous process[18] by writing

$$da/dt=G(t)=\sum\eta_k\delta(t-t_k), \tag{2.31}$$

where the jumps η_k occur at a rate ν, and with the normalized distribution $g(\eta)$ as in III Sec. 7E. The moments D_n can be determined as in (2.26)–(2.30) by computing

$$\left\langle\exp i\int_0^T y(s)G(s)\,ds\right\rangle$$

$$=\prod_{k=1}^{N}\langle\exp i\eta_k y(t_k)\rangle$$

$$=\prod_{k=1}^{N}\int g(\eta_k)\,d\eta_k\left[1+T^{-1}\int_0^T\{\exp[i\eta_k y(t_k)]-1\}\,dt_k\right]$$

$$=\left[1+T^{-1}\int g(\eta)\,d\eta\int_0^T\{\exp[i\eta y(\tau)]-1\}\,d\tau\right]^N$$

$$=\exp\left[\nu\int g(\eta)\,d\eta\int_0^T\{\exp[i\eta y(\tau)]-1\}\,d\tau\right]. \tag{2.32}$$

Expanding the exponent in powers of y and comparing with (2.6) we obtain III (7E.3),

$$n!D_n=\nu\int g(\eta)\,d\eta\eta^n\equiv\nu\langle\eta^n\rangle, \tag{2.33}$$

so that the linked moments of G are [c.f. (2.4)]

$$\langle G(t_1)\cdots G(t_n)\rangle^L=\nu\langle\eta^n\rangle\prod_{i=1}^{n-1}\delta(t_i-t_{i+1}) \tag{2.34}$$

for all $n\ge1$.

Equation (2.32) with $y(s)=f(t-s)$ permits us to generalize (2.30) to[6]

$$\langle\exp[i\sum_k\eta_k f(t-t_k)]\rangle$$

$$=\exp\left\{\nu\int g(\eta)\,d\eta\int_{-\infty}^{\infty}ds\{\exp[i\eta f(t-s)]-1\}\right\}. \tag{2.35}$$

By specializing (2.16) to a one-dimensional case with $\Lambda=0$, we determine the characteristic functional:

$$\left\langle\exp i\int_0^t q(u)a(u)\,du\right\rangle=\exp\left[i\nu\langle\eta\rangle\int_0^t q(s)s\,ds\right]$$

$$\times\exp\left\{-\nu\int_0^t ds\left[\phi\left(\int_s^t q(u)\,du\right)-1-i\langle\eta\rangle\int_s^t q(u)\,du\right]\right., \tag{2.36}$$

where

$$\phi(\lambda)=\langle\exp(i\lambda\eta)\rangle=\int g(\eta)\,d\eta\exp(i\lambda\eta) \tag{2.37}$$

is the characteristic function of the jump distribution $g(\eta)$.

An interesting special case of the homogeneous process is that in which the jumps η_k can only take the values ±1:

$$g(\eta)=p_{\text{in}}\delta(\eta-1)+p_{\text{out}}\delta(\eta+1);\quad p_{\text{in}}+p_{\text{out}}=1. \tag{2.38}$$

In this case, the random variable a can be interpreted as the (integral) occupancy of some state, with jumps into the state, and out of the state occurring randomly at the rates

$$\nu_{\text{in}}=\nu p_{\text{in}};\qquad \nu_{\text{out}}=\nu p_{\text{out}};\qquad \nu_{\text{in}}+\nu_{\text{out}}=\nu. \tag{2.39}$$

The moments are then given by

$$n!D_n=\nu_{\text{in}}+(-1)^n\nu_{\text{out}}. \tag{2.40}$$

Nonlinear Decay Plus Homogeneous Noise

A Markoff process with $\mathbf{D}_1=\mathbf{A}(\mathbf{a},t)$ but all $\mathbf{D}_n=\mathbf{D}_n(t)$, $n\ge2$, is a process with homogeneous noise plus nonlinear decay. Such a process is adequately described by

$$d\mathbf{a}/dt=\mathbf{A}(\mathbf{a},t)+\mathbf{F}(t), \tag{2.41}$$

where $\mathbf{F}$ *has the linked moments given by* (2.2)–(2.4). The statistics of $\mathbf{a}(t)$ are not readily obtainable, but those of the Langevin form $\mathbf{F}$ are not affected by the

CC-0. In Public Domain. Gurukul Kangri Collection, Haridwar

Digitized by Arya Samaj Foundation Chennai and eGangotri

nonlinearity of the decay. Thus **F** can represent Gaussian noise, or shot noise, or a general homogeneous noise just as in the linear case.

3. LANGEVIN TREATMENT OF THE FOKKER-PLANCK PROCESS

Let us consider the nonlinear Langevin process defined by

$$da/dt=B(a)+\sigma(a)f(t), \tag{3.1}$$

where $f(t)$ is a Gaussian random variable with

$$\langle f(t)\rangle=0, \qquad \langle f(t)f(u)\rangle=2\delta(t-u), \tag{3.2}$$

and the Gaussian properties insure that all higher linked moments vanish

$$\langle f(t_1)f(t_2)\cdots f(t_n)\rangle^L=0, \qquad n>2. \tag{3.3}$$

The coefficients B and σ may depend explicitly on the time, but we will not display this dependence in our equations.

The process (3.1) is a Markoff process because $a(t+\Delta t)$ can be calculated in terms of $a(t)$, and the result is uninfluenced by information concerning $a(u)$ for $u<t$ because of the independence of f at different times demonstrated explicitly in (2.9).

As a Markoff process, (3.1) is characterized by the moments III (6.10):

$$D_n(a,t)=(n!)^{-1}\lim_{\Delta t\to 0}\langle[a(t+\Delta t)-a(t)]^n\rangle^L/\Delta t. \tag{3.4}$$

Thus we need evaluate $\Delta a=a(t+\Delta t)-a(t)$ and its powers, only to first order in Δt. In view of (3.3), this means that we need not retain powers of f greater than 2. We therefore rewrite (3.1) as an integral equation

$$a(t+\Delta t)-a(t)=\int_t^{t+\Delta t}B(a(s))\,ds + \int_t^{t+\Delta t}\sigma(a(s))f(s)\,ds \tag{3.5}$$

and iterate by inserting $a(s)=a(t)$ as zeroth approximation on the right-hand side. Our first approximation is then

$$(\Delta a)_1=B(a(t))\Delta t+\sigma(a(t))\int_t^{t+\Delta t}f(s)\,ds. \tag{3.6}$$

The first term is already of order Δt and need not be calculated more accurately. In the second term of (3.5) we insert the first approximation

$$a(s)=a(t)+B(a(t))(s-t)+\sigma(a(t))\int_t^s f(u)\,du. \tag{3.7}$$

Retaining only terms of order Δt, or f^2 but not Δtf, or higher, we arrive at our second and final approximation

$$(\Delta a)_2=B(a(t))\Delta t+\sigma(a(t))\int_t^{t+\Delta t}f(s)\,ds + \sigma(a(t))\partial\sigma/\partial a(t)\int_t^{t+\Delta t}ds\int_t^s du f(s)f(u). \tag{3.8}$$

For $n>2$, the minimum powers that appear in $(\Delta a)^n$ are f^n or $f^{n-1}\Delta t$, etc., so that to order Δt,

$$\langle(\Delta a)^n\rangle^L=0 \quad \text{for} \quad n>2.$$

Thus all $D_n=0$ for $n>2$ and we have a Fokker-Planck process. For $n=2$, it is adequate to use $(\Delta a)_1$ and we obtain

$$\langle(\Delta a)^2\rangle^L=\sigma^2\int_t^{t+\Delta t}\int_t^{t+\Delta t}ds\,du\langle f(s)f(u)\rangle = 2\sigma^2\Delta t=2!D_2\Delta t. \tag{3.9}$$

For $n=1$, it is necessary (and adequate) to use $(\Delta a)_2$ to obtain

$$\langle\Delta a\rangle=B(a(t))\Delta t+\sigma(a)\partial\sigma/\partial a\int_t^{t+\Delta t}\int_t^s ds\,du 2\delta(s-u) = B(a)\Delta t+\sigma\partial\sigma/\partial a\Delta t \tag{3.10}$$

since only half the area of the delta function contributes at the boundary point s. This is easy to see if $\langle f(s)f(u)\rangle$ is first given a finite correlation time, and the delta functions limit is taken after the integrals are done. In summary, we have a Fokker–Planck process with

$$D(a)=[\sigma(a)]^2, \tag{3.11}$$

$$A(a)=B(a)+\sigma\partial\sigma/\partial a=B(a)+\tfrac{1}{2}\partial D/\partial a. \tag{3.12}$$

Equation (3.1) suggests that when σ does not depend explicitly on t and

$$B=A-\tfrac{1}{2}\partial D/\partial a=0, \tag{3.13}$$

an exact solution can be found for the Fokker-Planck equation by the transformation

$$dx=da/\sigma(a)=f(t)\,dt. \tag{3.14}$$

Thus,

$$\langle x(t)\rangle=0,$$

$$\langle[x(t)-x(0)]^2\rangle=\int_0^t\int_0^t ds\,du\langle f(s)f(u)\rangle=2t,$$

i.e., $x(t)$ is a Weiner process with unit diffusion constant. The distribution in x is thus given by III (7A.3):

$$P(x,t\mid x_0,0)\,dx=(4\pi t)^{-\frac{1}{2}}\exp[-(x-x_0)^2/4t]\,dx \tag{3.15}$$

or inserting $dx/da=1/\sigma(a)$, and transforming back to a as variable:

$$P(a,t\mid a_0,0)\,da=[4\pi D(a)t]^{-\frac{1}{2}} \times\exp\left\{-(4t)^{-1}\left[\int_{a_0}^a da'/\sigma(a')\right]^2\right\}da. \tag{3.16}$$

This result could also have been obtained by rewriting the Fokker–Planck equation in the form

$$\frac{\partial P}{\partial t}=-\frac{\partial}{\partial a}[BP]+\frac{\partial}{\partial a}\left[\sigma\frac{\partial}{\partial a}(\sigma P)\right] \tag{3.17}$$

CC-0. In Public Domain. Gurukul Kangri Collection, Haridwar

Digitized by Arya Samaj Foundation Chennai and eGangotri

or with $B=0$, and $\sigma\partial/\partial a=\partial/\partial x$

$$\frac{\partial}{\partial t}(\sigma P)=\sigma\frac{\partial}{\partial a}\sigma\frac{\partial}{\partial a}(\sigma P)=\frac{\partial^2}{\partial x^2}(\sigma P)$$

so that σP obeys the usual diffusion equation with diffusion constant unity in the variable x.

Note that if $f(t)$ has a finite correlation time, the process is not Markoffian, nor does it lead to a Fokker–Planck equation. But if $f(t)$ is Gaussian, our Langevin analysis remains valid, we must simply use the original value

$$\langle[x(t)-x(0)]^2\rangle=\int_0^t\int_0^t ds\,du\langle f(s)f(u)\rangle \tag{3.18}$$

in place of $2t$ wherever t appears in (3.15). Even more generally, if $f(t)$ is not Gaussian, but

$$b=x(t)-x(0)=\int_0^t f(t)\,dt$$

is described by a distribution $W(b)\,db$ then

$$P(at\mid a_0 0)\,da=\frac{1}{\sigma(a)}W\left(\int_{a_0}^{a}\frac{da'}{\sigma(a')}\right)da. \tag{3.19}$$

The results of this section can be immediately generalized to the multidimensional case by setting

$$da_i/dt=B_i+\sigma_{im}f_m(t), \tag{3.20}$$

where $f_m(t)$ are a set of Gaussian variables with

$$\langle f_m(t)f_n(u)\rangle=2\delta_{mn}\delta(t-u). \tag{3.21}$$

Repeated indices, such as m in (3.20) are understood to be summed over. A repeat of the one-dimensional procedure leads to a Fokker–Planck equation with

$$A_i=B_i+\sum_{mk}(\partial\sigma_{im}/\partial a_k)\sigma_{km}, \tag{3.22}$$

$$D_{ij}=\sum_m\sigma_{im}\sigma_{jm}. \tag{3.23}$$

Conversely, if a Fokker–Planck process is given, we can construct the corresponding Langevin process, as noted by Stratanovitch,[7] since D_{ij} is a symmetric matrix, and necessarily possesses a symmetric square root. Thus σ is the symmetric square root of D, and B_i can then be constructed from A_i.

Behavior of the Diffusion Coefficients under Transformations

If we make a change of variables from a_i to

then $$a_i'=a_i'(\mathbf{a},t),$$

$$da_i'/dt=\partial a_i'/\partial t+(\partial a_i'/\partial a_k)(da_k/dt)$$

$$=B_i'+\sigma_{ij}'f_j. \tag{3.24}$$

$$B_i'=\partial a_i'/\partial t+(\partial a_i'/\partial a_k)B_k, \tag{3.25}$$

$$\sigma_{ij}'=(\partial a_i'/\partial a_k)\sigma_{kj}. \tag{3.26}$$

Making use now of Eqs. (3.22) and (3.23) we find that

$$D_{ij}'=(\partial a_i'/\partial a_k)(\partial a_j'/\partial a_l)D_{kl}, \tag{3.27}$$

$$A_i'=\partial a_i'/\partial t+(\partial a_i'/\partial a_k)A_k+(\partial^2 a_i'/\partial a_m\partial a_n)D_{mn}. \tag{3.28}$$

Preservation of normalization requires that

$$P'(\mathbf{a}',t)\equiv JP(\mathbf{a},t), \tag{3.29}$$

where

$$J=\det(\partial a_i/\partial a_j') \tag{3.30}$$

is the Jacobian of the transformation. A direct proof that

$$\frac{\partial P'}{\partial t}=\left[-\frac{\partial}{\partial a_i'}A_i'+\frac{\partial}{\partial a_i'}\frac{\partial}{\partial a_j'}D_{ij}'\right]P' \tag{3.31}$$

reduces to

$$\frac{\partial P}{\partial t}=\left[-\frac{\partial}{\partial a_m}A_m+\frac{\partial}{\partial a_m}\frac{\partial}{\partial a_n}D_{mn}\right]P \tag{3.32}$$

we leave as a nontrivial exercise for the reader. Hint:

$$J^{-1}\partial J/\partial a_i'=\sum_{qp}\frac{\partial a_q'}{\partial a_p}\frac{\partial}{\partial a_i'}\left(\frac{\partial a_p}{\partial a_q'}\right)=\sum_p\frac{\partial}{\partial a_p}\left(\frac{\partial a_p}{\partial a_i'}\right). \tag{3.33}$$

Our transformation properties (3.27), (3.28) can be shown to be valid independent of the Langevin procedure which led us to them by noting that with $\Delta a_i'=a_i'(t+\Delta t)-a_i'(t)$

$$\Delta a_i'=\partial a_i'/\partial t\Delta t+\partial a_i'/\partial a_k\Delta a_k+(\partial^2 a_i'/\partial a_m\partial a_n)\tfrac{1}{2}\Delta a_m\Delta a_n. \tag{3.34}$$

The mean of this equation leads immediately to (3.28) and the mean of $\frac{1}{2}\langle\Delta a_i'\Delta a_j'\rangle$ leads immediately to (3.27).

Doobian Integrals and the Fokker–Planck Process

There is an apparent contradiction between our result (3.12) that the drift vector A is modified by the presence of a nonlinear diffusion coefficient and Doob's result[19] that there is no such modification. This contradiction arises because Doob regards our differential Eq. (3.1) as equivalent to an integral equation

$$a(t)=a(t_0)+\int_{t_0}^{t}[B(a(s),s)+\sigma(a(s),s)f(s)]\,ds \tag{3.35}$$

and then introduces a special rule for stochastic integrals of the form[20]

$$\int_{t_0}^{t}\sigma(a(s),s)f(s)\,ds=\sum\sigma(a(t_j),t_j)[y(t_{j+1})-y(t_j)], \tag{3.36}$$

[19] J. L. Doob, *Stochastic Processes* (John Wiley & Sons, Inc., New York, 1953), Chap. VI, Sec. 3. Compare Doob's equations (3.1) and (3.4). See also K. Ito, Mem. Am. Math. Soc. **4**, 1 (1951).

[20] When this Doob rule of integration (3.36) is used, the meaning of the differential equation (3.1) has been modified, and it is referred to as a *stochastic differential equation*. E. Wong and M. Zakai (to be published), have shown that if one replaces $y(t)$ of (3.37) by a convergent sequence $y^{(n)}(t)$ of continuous, piecewise linear functions, the corresponding solutions $a^{(n)}(t)$ converge to a solution of the random problem described by (3.12) containing the "dynamic friction" contribution to $A(a)$.

CC-0. In Public Domain. Gurukul Kangri Collection, Haridwar

Digitized by Arya Samaj Foundation Chennai and eGangotri

where

$$y(t)=\int^t f(s)\,ds. \tag{3.37}$$

This special rule, which we shall refer to as the Doobian integral, seemed necessary because the usual rule for Stieltjes integration requires that $y(t)$ be of bounded variation. But $y(t)$ is a simple Brownian motion process, which is not of bounded variation. Thus if σ were evaluated at t_{j+1} instead of t_j, a *different* integration rule results.

We have chosen *not* to modify the rules of integration. Then we cannot evaluate $a(s)$ as $a(t_j)$, instead we write it as $a(t_j)+[a(s)-a(t_j)]$ and obtain the second term by iteration.[20]

Our procedure can be justified by the following argument: A Brownian motion process is over-idealized because it describes a noise spectrum that is flat to infinite frequency. For a physicist, this is an adequate approximation for most purposes, to a realistic spectrum that is flat over a wide range but whose integrated power converges at infinity. Such a realistic spectrum can be assumed to converge rapidly enough at infinity for $y(t)$ to have bounded variation. Stated differently $\langle f(s)f(s')\rangle$ is not $\delta(s-s')$ but a rapidly decreasing function of $s-s'$ for $s-s'>$ some correlation time τ_c. The Stieltjes integral will then converge if $\Delta t_j=t_{j+1}-t_j$ is chosen small compared to τ_c. Our stochastic integration procedure is equivalent to evaluating the integral for finite τ_c and *then* taking the limit $\tau_c\to 0$.

The use of Doobian integrals for defining Brownian motion processes, and Stieltjes integrals for finite correlation time processes would lead to an apparent discontinuity in comparing such processes, whereas our discussion of short correlation time processes in Secs. 5 and 6 lead to corrections to the drift vector A that approach our result (3.12) in the limit as the correlation time is made to go to zero.

There are some related peculiarities of Brownian motion processes that have been emphasized recently.[21] For example, one can not write

$$df(a)/dt=\partial f/\partial a\; da/dt \tag{3.38}$$

since Δa for a Brownian motion process contains terms of order $(\Delta t)^{\frac{1}{2}}$ so that there are correction terms of the form:

$$\langle df(a)/dt\rangle_a=\partial f/\partial a\langle\Delta a/\Delta t\rangle+\tfrac{1}{2}\partial^2 f/\partial a^2\langle(\Delta a)^2\rangle/\Delta t$$
$$=(\partial f/\partial a)A(a)+\partial^2 f/\partial a^2 D(a). \tag{3.39}$$

Then results are special cases of our general formula III (5.6)

$$(\partial/\partial t)\langle f(\mathbf{a})\rangle=\langle A_j\partial f/\partial a_j\rangle+\sum_{ij}\langle D_{ij}\partial^2 f/\partial a_i\partial a_j\rangle$$
$$+\sum_{ijk}\langle D_{ijk}\partial^3 f/\partial a_i\partial a_j\partial a_k\rangle+\cdots. \tag{3.40}$$

These results seem to cause difficulty in a comparison between a finite correlation-time process for which (3.38) is valid, and a zero correlation-time (Markoffian) process for which (3.40) is valid. We should remember, however, that (3.38) is valid only for $\Delta t\ll\tau_c$ whereas a Markoffian process should be regarded as a short correlation-time process evaluated for $\Delta t\gg\tau_c$. When one examines short correlation-time processes for $\Delta t\gg\tau_c$ they behave in an approximately Markoffian manner, and the correction terms in (3.40) appear, and can be evaluated to estimate the D_n's.

4. ONE-DIMENSIONAL IMPURITY BAND

The one-dimensional impurity band with delta function potentials[22–24] described by the Schrödinger equation

$$\left[-\frac{\hbar^2}{2m}\frac{d^2}{dx^2}-|V_0|\sum_j\delta(x-x_j)\right]\psi(x)=E\psi(x) \tag{4.1}$$

provides an excellent example of a Markoff process described in terms of a Langevin noise source. To maintain the analogy, we must think of x as the time, and $\psi(x)$, $\psi'(x)$ as a two-dimensional Markoff process whose "future" is computable in terms of $\psi'(x)$ and $\psi''(x)$ which are given. In terms of the reciprocal lengths κ_0 and κ defined by

$$\kappa_0=m|V_0|/\hbar^2,\qquad \kappa^2=-2mE/\hbar^2=-\lambda, \tag{4.2}$$

Eq. (4.1) simplifies to

$$\psi''(x)+2\kappa_0\sum_j\delta(x-x_j)\psi(x)=\kappa^2\psi(x)=-\lambda\psi(x). \tag{4.3}$$

The transformation to Riccati form

$$z=\psi'(x)/\psi(x)$$
$$dz/dx=-(z^2+\lambda)-2\kappa_0\sum_j\delta(x-x_j)=A(z)+G(x) \tag{4.4}$$

shows that z, alone, is a Markoffian variable subject to a nonrandom drift $A(z)=-(z^2+\lambda)$ and a Poisson random force $G(x)$ that induces jumps in z of $-2\kappa_0$:

$$z(x_j+0)-z(x_j-0)=\int_{x_j-}^{x_j+}dz/dx=-2\kappa_0. \tag{4.5}$$

[21] See, for example, K. Ito, Nagoya Math. J. **3**, 55 (1951); G. Maruyama, Rend. Circ. Mat. Palermo, Ser. 2, **4**, 48 (1955); E. Nelson in *Analysis in Function Space*, edited by W. T. Martin and I. Segal (Technology Press, Cambridge, Massachusetts, 1964); and E. Wong and M. Zakai, Ref. 20.

[22] M. Lax and J. C. Phillips, Phys. Rev. **110**, 41 (1958).
[23] A review of impurity band calculations is given by I. M. Lifschitz, Zh. Eksperim. i Teor. Fiz. **44**, 1723 (1963) [English transl.: Soviet Phys.—JETP **17**, 1159 (1963)].
[24] H. L. Frisch and S. P. Lloyd, Phys. Rev. **120**, 1175 (1960).

CC-0. In Public Domain. Gurukul Kangri Collection, Haridwar

Digitized by Arya Samaj Foundation Chennai and eGangotri

rather than the unit jumps induced by the normalized Poisson force (2.25). The probability density $P(z, x)$ at "time" x then obeys:

$$\partial P/\partial x=(\partial/\partial z)[(z^2+\lambda)P(z)]+n[P(z+2\kappa_0)-P(z)], \tag{4.6}$$

where n is the average number of delta potentials per unit length. The first term arises from the smooth drift term $A(z)$ in the usual way, and the second term $G(x)$ is the usual Poisson term of Eq. III (7E.2) with $\eta=-2\kappa_0$. Equation (4.6) was first written down by Frisch and Lloyd[24] using an argument based on conservation of points in phase space.

Equation (4.5) can also be written in the form of a conservation law as

$$\partial P/\partial x=-\partial J(z, x)/\partial z, \tag{4.7}$$

where

$$J(z, x)=-(z^2+\lambda)P(z, x)-n\int_z^{z+2\kappa_0} P(\zeta, x)\,d\zeta \tag{4.8}$$

is the flux or number of times per unit ("time") x that the random variable z crosses the numerical value z. For stationary solutions, we obtain

$$J(z)=-(z^2+\lambda)P(z)-n\int_z^{z+2\kappa_0} P(\zeta)\,d\zeta$$
$$=J=\text{ constant}, \tag{4.9}$$

just as in III (7B.7) for the Fokker–Planck case.

The original impurity band problem[22–24] required the calculation of the density of states in the impurity band. For this purpose, the Sturm–Liouville theorem can be used[25]: the number of states of the system with energy less than E [the cumulative density of state $\mathfrak{N}(E)$] is given by the number of zeros of $\psi(x, E)$ over the length of the "crystal." Lax and Phillips[22] computed

$$N(E)=\mathfrak{N}(E)/N, \tag{4.10}$$

the number of zeros per impurity atom by a direct zero-counting, Monte Carlo solution of (4.3).

Note that when $\psi=0$, $z=\infty$, and that by Eq. (4.4) z always moves toward $-\infty$ (reappearing afterward at $+\infty$). Thus the flux toward $-\infty$, $-J(-\infty)=-J$ is the number of zeros per unit x and

$$\mathfrak{N}(E)=-J\times(\text{length of crystal}),$$
$$N(E)=\mathfrak{N}(E)/N=-J/n, \tag{4.11}$$

where n is the number of impurity atoms per unit length. But $J(z)=J$ can be evaluated at any z. Letting $z\to\pm\infty$, in (4.9) we obtain

$$N(E)=(1/n)\lim_{z\to\pm\infty} z^2P(z) \tag{4.12}$$

$$=(1/n)\lim_{z\to\pm\infty} z^2P(z)\Big/\int_{-\infty}^{\infty}P(z)\,dz, \tag{4.13}$$

where the second form is independent of the normalization of P.

If we multiply Eq. (4.9) by $\exp(isz)$ and integrate from $-\infty$ to ∞ over z, we find that the characteristic function

$$\phi(s)=\int_{-\infty}^{\infty}\exp(isz)P(z)\,dz \tag{4.14}$$

obeys

$$[(d^2/ds^2)-\lambda]\phi(s)+(n/is)[\exp(-2is\kappa_0)-1]\phi(s)$$
$$=-2\pi nN(E)\delta(s), \tag{4.15}$$

where J has been replaced by $-nN(E)$ on the right-hand side and an integration by parts was performed to obtain the second term on the left. The delta function on the right tells us that

$$\phi'(0+)-\phi'(0-)=-2\pi nN(E). \tag{4.16}$$

To understand this discontinuity, we note that

$$P(z)=\frac{nN(E)}{z^2+\lambda}-\frac{n}{z^2+\lambda}\int_z^{z+2\kappa_0}P(\zeta)\,d\zeta\equiv P_1-P_2. \tag{4.17}$$

The characteristic function $\phi(s)$ can then be written

$$\phi(s)=\phi_1(s)-\phi_2(s),$$
$$\phi_1(s)=\int_{-\infty}^{\infty}\exp(isz)\,dznN(E)/(z+\lambda^2)$$
$$=nN(E)\pi\lambda^{-\frac{1}{2}}\exp(-|s|\lambda^{\frac{1}{2}}), \tag{4.18}$$
$$\phi_1'(0^+)=-\pi nN(E),$$
$$\phi_1'(0^-)=\pi nN(E), \tag{4.19}$$
$$\phi_2(s)=\int_{-\infty}^{\infty}\exp(isz)\,dzP_2(z),$$
$$\phi_2'(0)=i\int_{-\infty}^{\infty}dzzP_2(z).$$

Since the last integral converges, $\phi_2'(0)$ exists and is pure imaginary[26] and $\phi_1(s)$ contains the discontinuity in Re $\phi'(s)$ at $s=0$. Thus $\phi(0)=1$, Re $\phi'(0)=-\pi nN(E)$ or

$$N(E)=-(\pi n)^{-1}\,\text{Re}\,[\phi'(0)/\phi(0)], \tag{4.20}$$

where $\phi(s)$ is any solution of the homogeneous part of (4.15) such that $\phi(s)\to 0$ as $s\to+\infty$.

[25] Application of the Sturm–Liouville theorem to impurity bands was first made by H. M. James and A. S. Ginzbarg, J. Phys. Chem. **57**, 840 (1953).

[26] This justifies a step omitted in the Frisch–Lloyd proof of (4.21).

CC-0. In Public Domain. Gurukul Kangri Collection, Haridwar

Digitized by Arya Samaj Foundation Chennai and eGangotri

Unfortunately neither Eq. (4.6) for $P(z)$, nor (4.15) for $\phi(s)$ can be integrated exactly. Frisch and Lloyd[24] therefore integrated (4.15) numerically from a known asymptotic behavior as $s\to\infty$ into the point $s=0$.

The High-Density Limit

At high densities,[27] as is well known, Poisson statistics can be replaced by Gaussian statistics. This can be accomplished by using (4.4) with

$$\langle G(x)\rangle = -2n\kappa_0, \qquad \langle G(x)G(x')\rangle^L = (2\kappa_0)^2 n\delta(x-x') \tag{4.21}$$

and all higher linked averages equal to zero. [All reference to the $\delta(x-x_j)$ is now lost. The potential $V(x)$ is a Gaussian white noise source of arbitrary origin.] Our Langevin process then reduces to the form (3.1) which leads to a Fokker–Planck equation. The resulting equation can be obtained directly from (4.6) by expanding $P(z+2\kappa_0)$ as a Taylor expansion around z and retaining two terms. Keeping one *extra term* we obtain

$$\frac{\partial P}{\partial x} = \frac{\partial}{\partial z}\left[(z^2+\lambda+2n\kappa_0)P(z)\right] + 2n\kappa_0{}^2\frac{d^2P}{dz^2} + \tfrac{4}{3}n\kappa_0{}^3\frac{d^3P}{dz^3} + \cdots. \tag{4.22}$$

We pass to dimensionless variables by setting

$$x = Ly, \qquad z = w/L, \tag{4.23}$$

where L is a length chosen to be

$$L = (2n\kappa_0{}^2)^{-\frac{1}{3}}. \tag{4.24}$$

so that in the new units, the diffusion coefficient is unity:

$$\frac{\partial P}{\partial y} = \frac{\partial}{\partial w}\left[(w^2+\Lambda)P(w)\right] + \frac{\partial^2 P}{\partial w^2} + \frac{2^{5/3}}{3\epsilon^{1/3}}\frac{\partial^3 P}{\partial w^3} + \cdots, \tag{4.25}$$

where

$$\epsilon = n/\kappa_0, \qquad \Lambda = (2\epsilon)^{-\frac{2}{3}}\left[(\lambda/\kappa_0{}^2)+2\epsilon\right]. \tag{4.26}$$

As remarked by Lax and Phillips,[22] the density of states is a function of the energy in the units $\kappa^2/\kappa_0{}^2 = -\lambda/\kappa_0{}^2$ and the single dimensionless density $\epsilon = n/\kappa_0$. At high densities, $\epsilon\gg 1$, the derivatives higher than the second in (4.25) can be omitted. This justifies the Fokker–Planck equation and the Gaussian approximation (4.21) which leads to it. Moreover $N(E)$ is a function $N(\Lambda)$ of a single dimensionless parameter Λ, permitting a universal curve to be plotted for all ϵ (valid, of course, for all $\epsilon\gg 1$).

The equation for the characteristic function $\phi(s)$ of (4.15) in the Fokker–Planck approximation is obtained by expanding the exponential in (4.15) in powers of κ_0 and retaining terms of order $\kappa_0{}^2$:

$$\left[(d^2/ds^2) - (\lambda+2n\kappa_0) + i2n\kappa_0{}^2 s\right]\phi(s) = 0. \tag{4.27}$$

Transforming to dimensionless variables

$$s = Lt, \qquad \phi(Lt) = \psi(t),$$

$$\left[(d^2/dt^2) - \Lambda + it\right]\psi = 0, \tag{4.28}$$

$$N(E) = -(\pi nL)^{-1}\,\mathrm{Re}\left[\psi'(0)/\psi(0)\right].$$

We now follow a procedure of Halperin[27] to obtain the density of states and set

$$u = it - \Lambda, \qquad (d/dt)^2 = -(d/du)^2, \qquad \psi(t) = G(u),$$

$$d^2G/du^2 = uG(u), \tag{4.29}$$

$$N(E) = (\pi nL)^{-1}\,\mathrm{Im}\left[G'(-\Lambda)/G(-\Lambda)\right]. \tag{4.30}$$

The solution of the differential Eq. (4.29) are the Airy functions[28] $Ai(u)$ and $Bi(u)$. The linear combination which vanishes as $t\to\infty$, i.e., $u\to i\infty$ is $Ai(u)+iBi(u)$. Making use of the Wronskian,

$$Bi'(u)\,Ai(u) - Ai'(u)\,Bi(u) = 1/\pi, \tag{4.31}$$

we obtain Halperin's result[27]

$$N(E) = (\pi^2 nL)^{-1}\{\left[Ai(-\Lambda)\right]^2 + \left[Bi(-\Lambda)\right]^2\}^{-1}. \tag{4.32}$$

For large positive energies $\Lambda\gg 0$, the density of states reduces to the usual "virtual crystal" approximation[29]

$$N(E) \approx (\pi nL)^{-1}\Lambda^{\frac{1}{2}} = (\pi n)^{-1}(\lambda+2n\kappa_0)^{\frac{1}{2}}. \tag{4.33}$$

For large negative energies, i.e., deep in the band tail, the asymptotic form of the Airy functions[30] leads to

$$N(E) \approx (\pi nL)^{-1}\,|\,\Lambda\,|^{\frac{1}{2}}\exp\left[-\tfrac{4}{3}\,|\,\Lambda\,|^{\frac{3}{2}}\right]. \tag{4.34}$$

An approximation technique that yields this form of asymptotic behavior, but which can be applied to two- and three-dimensional impurity bands (whose behavior is non-Markoffian) has been developed by Halperin and Lax.[31]

5. MARKOFFIAN REPRESENTATION OF PROCESSES WITH SHORT CORRELATION TIMES

In the last three sections, we have seen that delta-correlated Langevin forces lead to Markoffian processes. The delta-function correlations are, of course, necessary to permit the immediate forgetting of the past, characteristic of a Markoffian process. Often,

[27] B. Halperin, Phys. Rev. **139**, A104 (1965).

[28] J. C. P. Miller, "The Airy Integral," *British Association for The Advancement of Science Tables* (Cambridge University Press, Cambridge, England, 1946), Part V, Vol. B.

[29] This approximation is incorrectly called the optical model by Lax and Phillips (Ref. 22). The optical-model approximation should be reserved for a procedure that replaces potentials by scattering matrices as in J. R. Klauder, Ann. Phys. (N.Y.) **14**, 43 (1961).

[30] H. and B. S. Jeffreys, *Methods of Mathematical Physics* (Cambridge University Press, Cambridge, England, 1950).

[31] B. Halperin and M. Lax (to be published); and Bull. Am. Phys. Soc. **10**, 302 (1965).

CC-0. In Public Domain. Gurukul Kangri Collection, Haridwar

Digitized by Arya Samaj Foundation Chennai and eGangotri

the Langevin forces possess correlation times τ_c short compared to typical relaxation times $1/\Lambda$. It is then possible to choose time intervals Δt long enough ($\Delta t \gg \tau_c$) for "forgetting" to take place, yet short enough ($\Delta t \ll 1/\Lambda$) for changes in the system to be created on an "infinitesimal" basis. With $\partial P/\partial t$ understood to mean $\Delta P/\Delta t$, we should be able to obtain a generalized Fokker–Planck, or Markoffian description of the motion on the scale Δt.

Let us illustrate this idea by considering the simple example

$$d\mathbf{a}/dt = \xi(t), \tag{5.1}$$

where $\xi(t)$ is a Langevin force that is *not* delta-correlated as $\mathbf{f}(t)$ was. Then

$$\phi(\mathbf{y}, t) = \langle \exp[i\mathbf{y}\cdot\mathbf{a}(t)] \rangle = \exp[i\mathbf{y}\cdot\mathbf{a}(0)]M, \tag{5.2}$$

$$M = \left\langle \exp i\mathbf{y}\cdot\int_0^t \xi(s)\, ds \right\rangle$$

$$= \exp\left[\left\langle \exp i\mathbf{y}\cdot\int_0^t \xi(s)\, ds \right\rangle^L - 1 \right]$$

$$= \exp\left[\sum_{n=1}^{\infty} (i\mathbf{y})^n : \int_0^t ds_1 \cdots \int_0^t ds_n\, \mathbf{d}_n(s_1, \cdots, s_n) \right], \tag{5.3}$$

where

$$n!\,\mathbf{d}_n(s_1, \cdots, s_n) = \langle \xi(s_1)\xi(s_2)\cdots\xi(s_n) \rangle^L \tag{5.4}$$

is a linked correlation that is large only if all $|s_i - s_j|$ are of the order τ_c or smaller. Thus,

$$\mathbf{e}_n(s, t) = \int_0^t ds_2 \cdots \int_0^t ds_n\, \mathbf{d}_n(s, s_2, \cdots, s_n) \tag{5.5}$$

for any s in the interior of the region $0 < s < t$ is nearly independent of s and t with the numerical value

$$\mathbf{e}_n(s, t) \approx \mathbf{D}_n \equiv \int_{-\infty}^{\infty} ds_2 \cdots \int_{-\infty}^{\infty} ds_n\, \mathbf{d}_n(s, s_2, \cdots, s_n), \tag{5.6}$$

and

$$\mathbf{M}_n(t) = \int_0^t ds_1 \cdots \int_0^t ds_n\, \mathbf{d}_n(s_1, \cdots, s_n) = \int_0^t \mathbf{e}_n(s, t)\, ds \tag{5.7}$$

is, for $t \gg \tau_c$, linear in t with the value $\mathbf{D}_n t$. Thus our non-Markoffian process is approximately equivalent to a stationary Markoffian process with parameters $\mathbf{D}_n$. A comparison with Eq. (2.6):

$$\exp \sum (i\mathbf{y})^n : \mathbf{M}_n(t) \to \exp\left[\sum (i\mathbf{y})^n : \int_0^t \mathbf{D}_n(s)\, ds \right] \tag{5.8}$$

shows a *precise* equivalence [for the purpose of computing $\phi(\mathbf{y}, t)$, or $P(\mathbf{a}t \mid \mathbf{a}_0 t_0)$] between our non-Markoffian process, and a nonstationary Markoffian process with

$$\mathbf{D}_n(s) = \partial \mathbf{M}_n(s)/\partial s. \tag{5.9}$$

This precise equivalence will not hold if we ask questions about more than two times, or if we use a system with a finite relaxation matrix $\mathbf{\Lambda}$. Thus for

$$d\mathbf{a}/dt + \mathbf{\Lambda}\cdot\mathbf{a} = \xi(t) \tag{5.10}$$

we have using Eq. (2.14):

$$\left\langle \exp i\int_0^t \mathbf{q}(u)\cdot\mathbf{a}(u)\, du \right\rangle$$

$$= \left[\exp i\int_0^t \mathbf{q}(u)\cdot\mathbf{n}(u)\cdot\mathbf{a}(0)\, du \right] M$$

$$M = \left\langle \exp\left[i\int_0^t ds\mathbf{h}(s, t)\cdot\xi(s) \right] \right\rangle. \tag{5.11}$$

$$M = \exp \sum_1^{\infty} (i)^n \int_0^t ds_1 \cdots \int_0^t ds_n h(s_1, t)\cdots h(s_n, t) \times d_n(s_1, \cdots, s_n), \tag{5.12}$$

where

$$h(s, t) = \int_s^t du\mathbf{q}(u)\cdot\mathbf{n}(u, s) = \int_s^t du\mathbf{q}(u) \times \exp[\mathbf{\Lambda}(s-u)]. \tag{5.13}$$

Thus $h(s, t)$ is a function that has been smoothed over a time interval $1/\Lambda$. If $\tau_c \ll 1/\Lambda$, the d_n can be regarded as nearly a delta function as far as the h functions are concerned, and

$$M \approx \exp \sum (i)^n \int_0^t ds[h(s, t)]^n e_n(s, t)$$

$$\approx \exp \sum (i)^n D_n \int_0^t ds[h(s, t)]^n \tag{5.14}$$

which is the Markoffian result with parameters D_n given by (5.6). This result is clearly valid only if $\tau_c \ll 1/\Lambda$, and no precise equivalence is possible even if we set $\mathbf{q}(u) = \mathbf{q} =$ constant to ask a two-time question.

When the random force $\xi(t)$ appears in a nonlinear function $G(\mathbf{a}, \xi)$:

$$d\mathbf{a}/dt = G(\mathbf{a}(t), \xi(t)). \tag{5.15}$$

The analysis is appreciably more complicated, but for time intervals $\Delta t > \tau_c$ we again expect a Markoffian description to be valid. Just as in our discussion of the delta-correlated case, the Eq. (5.15) must then be solved by iteration. The iteration can, in principle, be carried to any order, but unless $G(\mathbf{a}, \xi)$ is an especially simple function, the higher order contributions will look rather complicated. If one needs to go beyond the second order, one will have to go to infinite order to get sensible results.[32] This may be possible for special

[32] R. F. Pawula, thesis, California Institute of Technology, 1965 (unpublished) has used the Cauchy–Schwarz inequality $\langle (\Delta a)^{m+n} \rangle^2 \leq \langle (\Delta a)^{2m} \rangle \langle (\Delta a)^{2n} \rangle$ to derive the inequality $A_{2m} \geq A_{m+n}^2 / A_{2n}$, where $A_n = n! D_n$. From this we can deduce that if $A_n \neq 0$ for any $n > 2$, an infinite sequence of A_n's must be non-vanishing.

CC-0. In Public Domain. Gurukul Kangri Collection, Haridwar

Digitized by Arya Samaj Foundation Chennai and eGangotri

functions $G(\mathbf{a}, \xi)$, but not in general. We shall therefore iterate once, leading to results accurate to the second order, and to a Fokker–Planck equation.

Let us define the averages

$$\langle G_i(\mathbf{a}, \xi(t), t)\rangle = B_i(\mathbf{a}, t), \tag{5.16}$$

$$\langle G_i(\mathbf{a}, \xi(t), t) G_j(\mathbf{a}', \xi(t'), t')\rangle_L = 2!\, d_{ij}(\mathbf{a}t; \mathbf{a}'t'). \tag{5.17}$$

We have displayed $\mathbf{a}$ without a time dependence $\mathbf{a}(t)$ to indicate that in this average, $\mathbf{a}$ is held fixed, and only ξ is averaged. Thus we can write

$$da_i/dt = B_i(\mathbf{a}(t), t) + F_i(\mathbf{a}(t), \xi(t), t), \tag{5.18}$$

where $\langle F_i(\mathbf{a}, t)\rangle = 0$ at fixed $\mathbf{a}$. We shall now suppose that any *dissipative* time constants in B_i are long compared to the correlation times of the F_i forces. Thus the response of the a_i involves an average of the F_i over times long compared to their correlation time. A good approximation for the a_i can then be obtained by neglecting the F_i, i.e., $a_i \approx \bar{a}_i(t)$, where $\bar{a}_i(t) \equiv \bar{a}_i(t, t_0, b)$ is a solution of the "noise-free" equation of motion

$$d\bar{a}_i/dt = B_i(\bar{\mathbf{a}}(t, t_0, \mathbf{b}), t) \tag{5.19}$$

with

$$\bar{\mathbf{a}}(t_0, t_0, \mathbf{b}) = \mathbf{b} \tag{5.20}$$

as initial condition. Let us now make a transformation

$$\mathbf{a}(s) = \bar{\mathbf{a}}(s, t_0, \mathbf{b}(s)) \tag{5.21}$$

to new variables $\mathbf{b}(s)$ that in the absence of noise would be the initial conditions, and hence would not change in time. Thus

$$db_m/ds = \partial b_m/\partial s + (\partial b_m/\partial a_i) B_i + (\partial b_m/\partial a_i) F_i$$

$$db_m/ds = (\partial b_m/\partial a_i) F_i(\bar{\mathbf{a}}(s, t_0, \mathbf{b}(s)), \xi(s)) \tag{5.22}$$

since we know that $db_m/ds = 0$ when all $F_i = 0$. In this way, any rapid *nondissipative* motion of the a_i has been eliminated.

With the abbreviation $\Delta a_i = a_i(t+\Delta t) - a_i(t)$, we have

$$\Delta a_i = \bar{a}_i(t+\Delta t, t_0, \mathbf{b}(t+\Delta t)) - \bar{a}_i(t, t_0, \mathbf{b}(t))$$
$$= \frac{\partial \bar{a}_i}{\partial t}\Delta t + \frac{\partial \bar{a}_i(t)}{\partial b_m(t)}\Delta b_m + \frac{1}{2}\frac{\partial^2 \bar{a}_i(t)}{\partial b_m(t)\partial b_n(t)}\Delta b_m \Delta b_n + \cdots. \tag{5.23}$$

To second-order accuracy, the diffusion and drift coefficients are

$$D_{ij} = \tfrac{1}{2}\langle \Delta a_i \Delta a_j\rangle/\Delta t = [\partial \bar{a}_i(t)/\partial b_m(t)][\partial \bar{a}_j(t)/\partial b_n(t)] \times \tfrac{1}{2}\langle \Delta b_m \partial b_n\rangle/\Delta t, \tag{5.24}$$

$$A_i = \frac{\partial \bar{a}_i}{\partial t} + \frac{\partial \bar{a}_i(t)}{\partial b_m(t)}\frac{\langle \Delta b_m\rangle}{\Delta t} + \frac{\partial^2 \bar{a}_i}{\partial b_m(t)\partial b_n(t)}\frac{1}{2}\frac{\langle \Delta b_m \Delta b_n\rangle}{\Delta t}. \tag{5.25}$$

The use of Eqs. (5.24), (5.25) is equivalent to calculating the A and D coefficients for the $\mathbf{b}$ process, followed by the transformation (3.27), (3.28) that carries the $\mathbf{b}$ variables into the $\mathbf{a}$ variables.

Using Eq. (5.22) we calculate Δb_m to second order by a procedure analogous to that used in (3.8):

$$\Delta b_m = b_m(t+\Delta t) - b_m(t)$$
$$\equiv \int_t^{t+\Delta t} ds' \frac{\partial b_m(s')}{\partial a_j(s')} F_j(\mathbf{a}(s', t_0, \mathbf{b}(s')), \xi(s')) \tag{5.26}$$
$$\approx \int_t^{t+\Delta t} ds' F_j(s') \frac{\partial b_m(s')}{\partial a_j(s')}$$
$$+ \int_t^{t+\Delta t} ds' \frac{\partial}{\partial b_n(s')}\left[\frac{\partial b_m(s')}{\partial a_j(s')} F_j(s')\right] \times \int_t^{s'} ds \frac{\partial b_n(s)}{\partial a_k(s)} F_k(s). \tag{5.27}$$

Since the first term in (5.27) is squared before use in calculating the diffusion constant, and the second term is already of second order in the Langevin forces, we shall approximate all random variables in (5.27) other than $\xi(t)$ by their values in the absence of noise. Thus we shall set

$$b_n(s) \approx b_n(t) = b_n,$$

$$a_l(s) = \bar{a}_l(s, t_0, \mathbf{b}(s)) \approx \bar{a}_l(s, t_0, \mathbf{b}), \tag{5.28}$$

where the constants $\mathbf{b}$ are determined by the conditions at time t:

$$a_j(t) \equiv a_j = \bar{a}_j(t, t_0, \mathbf{b}), \tag{5.29}$$

so that

$$a_l(s) \approx \bar{a}_l(s, t_0, \mathbf{b}) = \bar{a}_l(s, t, \mathbf{a}) \equiv \bar{a}_l(s) \tag{5.30}$$

$$F_j(s') \approx F_j(\bar{\mathbf{a}}(s', t, \mathbf{a}), \xi(s')). \tag{5.31}$$

To our desired accuracy, therefore,

$$\Delta b_m \approx \int_t^{t+\Delta t} ds' F_j(\bar{\mathbf{a}}(s'), \xi(s')) \frac{\partial b_m}{\partial \bar{a}_j(s')}$$
$$+ \int_t^{t+\Delta t} ds' \frac{\partial}{\partial b_n}\left[\frac{\partial b_m}{\partial \bar{a}_j(s')} F_j(\bar{\mathbf{a}}(s'), \xi(s'))\right] \times \int_t^{s'} ds \frac{\partial b_n}{\partial \bar{a}_k(s)} F_k(\bar{\mathbf{a}}(s), \xi(s)). \tag{5.32}$$

Inserting the first term of (5.32) into (5.24) [and noting that $\bar{a}_i(t) \equiv a_i$] we obtain the diffusion constant

$$D_{ij}(t) = \frac{1}{2\Delta t}\int_t^{t+\Delta t}\int_t^{t+\Delta t} ds'\, ds \frac{\partial a_i}{\partial \bar{a}_k(s', t, \mathbf{a})}\frac{\partial a_j}{\partial \bar{a}_l(s, t, \mathbf{a})} \times \langle F_k(s') F_l(s)\rangle, \tag{5.33}$$

where

$$\langle F_k(s') F_l(s)\rangle \equiv \langle F_k(\bar{\mathbf{a}}(s', t, \mathbf{a}), \xi(s')) F_l(\bar{\mathbf{a}}(s, t, \mathbf{a}), \xi(s))\rangle, \tag{5.34}$$

CC-0. In Public Domain. Gurukul Kangri Collection, Haridwar

Digitized by Arya Samaj Foundation Chennai and eGangotri

result (5.33) that is manifestly independent of t_0. Interchange of the dummy indices k, l and s', s shows that

$$D_{ij}(t)=D_{ji}(t). \tag{5.35}$$

In (5.33) we set $s=s'+u$, and for $\Delta t \gg$ the correlation time τ_c, we have

$$\int_{-(s'-t)}^{t+\Delta t-s'} du \to \int_{-\infty}^{\infty} du, \tag{5.36}$$

$$D_{ij}(t)=(\Delta t)^{-1}\int_t^{t+\Delta t} ds' D_{ij}(s',t), \tag{5.37}$$

where

$$D_{ij}(s',t)\equiv\frac{1}{2}\int_{-\infty}^{\infty} du \frac{\partial a_i}{\partial \bar{a}_k(s',t,\mathbf{a})}\frac{\partial a_j}{\partial \bar{a}_l(s'+u,t,\mathbf{a})} \times\langle F_k(s')F_l(s'+u)\rangle. \tag{5.38}$$

If the noise-free motion has a rapid oscillatory component, the average over s' in (5.37) is necessary, and may even cause some D_{ij} to vanish.[17] If *both* the non-dissipative and dissipative motion induced by $\mathbf{B}(\mathbf{a})$ is small during a correlation time τ_c, then we can omit the average over s':

$$D_{ij}(t)\approx D_{ij}(t,t) \tag{5.39}$$

$$=\frac{1}{2}\int_{-\infty}^{\infty} ds \frac{\partial a_j}{\partial \bar{a}_l(s,t,\mathbf{a})} \times\langle F_i(\mathbf{a},\xi(t))F_l(\bar{\mathbf{a}}(s,t,\mathbf{a}),\xi(s))\rangle \tag{5.40}$$

$$=\frac{1}{2}\int_{-\infty}^{\infty} ds' \langle F_k(\bar{\mathbf{a}}(s',t,\mathbf{a}),\xi(s'))F_j(\mathbf{a},\xi(t))\rangle \times\frac{\partial a_i}{\partial \bar{a}_k(s',t,\mathbf{a})}, \tag{5.41}$$

where the second form results from (5.33) if one integrates first over s' instead of s, or if one interchanges j and i in (5.40).

A symmetric formula can be obtained directly by defining[33]

$$D_{ij}(t)=\tfrac{1}{2}(d/dt)\langle[a_i(t)-a_i(t-\Delta t)] \times[a_j(t)-a_j(t-\Delta t)]\rangle, \tag{5.42}$$

which is suggested by (5.9). After differentiation, one lets $\Delta t\to\infty$ to obtain

$$D_{ij}=\frac{1}{2}\int_{-\infty}^{t} ds' \langle F_k(\bar{\mathbf{a}}(s',t,\mathbf{a}),\xi(s'))F_j(\mathbf{a},\xi(t))\rangle \times\frac{\partial a_i}{\partial \bar{a}_k(s',t,\mathbf{a})} +\frac{1}{2}\int_{-\infty}^{t} ds \langle F_i(\mathbf{a},\xi(t))F_l(\bar{\mathbf{a}}(s,t,\mathbf{a}),\xi(s))\rangle \times\frac{\partial a_j}{\partial \bar{a}_l(s,t,\mathbf{a})}. \tag{5.43}$$

This result (5.43) is equivalent to the unsmoothed "instantaneous" $D_{ij}(t,t)$ of (5.40), (5.41) rather than the smoothed diffusion coefficient (5.37).

To obtain A_i, we evaluate the second term of (5.25) with the help of (5.32):

$$\frac{\partial a_i}{\partial b_m}\frac{\langle\Delta b_m\rangle}{\Delta t}=\int_t^{t+\Delta t} ds'\int_t^{s'} ds C(s',s), \tag{5.44}$$

$$C(s',s)=\frac{\partial a_i}{\partial b_m}\left\langle\frac{\partial}{\partial b_n}\left[\frac{\partial b_m}{\partial \bar{a}_j(s')}F_j(s')\right]F_k(s)\frac{\partial b_n}{\partial \bar{a}_k(s)}\right\rangle =I+II, \tag{5.45}$$

where I is obtained by moving $\partial a_i/\partial b_m$ underneath the derivative

$$I=\left\langle\frac{\partial b_n}{\partial \bar{a}_k(s)}\frac{\partial}{\partial b_n}\left[\frac{\partial a_i}{\partial b_m}\frac{\partial b_m}{\partial \bar{a}_j(s')}F_j(s')\right]F_k(s)\right\rangle =\left\langle\frac{\partial}{\partial \bar{a}_k(s)}\left[\frac{\partial a_i}{\partial \bar{a}_j(s')}F_j(s')\right]F_k(s)\right\rangle \tag{5.46}$$

and II is obtained by subtracting the explicit derivative of $\partial a_i/\partial b_m$ by $\partial/\partial b_n$ to correct for the error in I:

$$II=-\frac{\partial^2 a_i}{\partial b_n\partial b_m}\frac{\partial b_m}{\partial \bar{a}_j(s')}\frac{\partial b_n}{\partial \bar{a}_k(s)}\langle F_j(s')F_k(s)\rangle. \tag{5.47}$$

The last term in (5.25) can be written

$$\frac{\partial^2 a_i}{\partial b_m\partial b_n}\frac{1}{2}\frac{\langle\Delta b_m\Delta b_n\rangle}{\Delta t}=\int_t^{t+\Delta t}\int_t^{t+\Delta t} ds'\, ds III(s',s),$$

$$III(s',s)=\frac{1}{2}\frac{\partial^2 a_i}{\partial b_m\partial b_n}\frac{\partial b_m}{\partial \bar{a}_j(s')}\frac{\partial b_n}{\partial \bar{a}_k(s)}\langle F_j(s')F_k(s)\rangle. \tag{5.48}$$

The terms II and III depend explicitly on t_0 and $\mathbf{b}$. Fortunately, we can use the symmetry of II in s and s' to write

$$\int_t^{t+\Delta t} ds'\int_t^{s'} ds II(s',s)=\frac{1}{2}\int_t^{t+\Delta t} ds'\int_t^{t+\Delta t} ds II(s',s) \tag{5.49}$$

so that II and III cancel exactly.

[33] R. F. Pawula, Ref. 32, discusses the relation between forward and backward moments. He also proves that non-Markoffian processes obey a generalized Fokker–Planck equation [as in Eq. (5.9), but the coefficients are expectations of $(\Delta a)^n$ conditional on information at *two* previous times and t and t_0. For non-Markoffian processes, there is no general method of evaluating these coefficients without detailed knowledge of the yet unknown conditional probabilities. For similar results see I. Oppenheim and K. E. Shuler, Phys. Rev. **138**, B1007 (1965).

CC-0. In Public Domain. Gurukul Kangri Collection, Haridwar

Digitized by Arya Samaj Foundation Chennai and eGangotri

If we set $s=s'+u$, the integration over u can be extended to $-\infty$ since Δt is large compared to the correlation time [cf. (5.36)]. Thus we obtain from (5.25):

$$A_i(\mathbf{a},t)=\frac{1}{\Delta t}\int_t^{t+\Delta t} ds' A_i(\mathbf{a},s',t), \tag{5.50}$$

$$A_i(\mathbf{a},s',t)\equiv B_i(\mathbf{a},t)+\int_{-\infty}^{s'} ds \times\left\langle \frac{\partial}{\partial \bar{a}_k(s)}\left[\frac{\partial a_i}{\partial \bar{a}_j(s')}F_j(\bar{\mathbf{a}}(s'),\xi(s'))\right]F_k(\bar{\mathbf{a}}(s),\xi(s))\right\rangle. \tag{5.51}$$

For the case in which the noise free motion is small during a correlation time, the average over s' is unimportant and we can set $s'=t$:

$$A_i(\mathbf{a},t)\approx B_i(\mathbf{a},t) +\int_{-\infty}^{t} ds\left\langle \frac{\partial}{\partial \bar{a}_k(s)}[F_i(\mathbf{a},\xi(t))][F_k(\bar{\mathbf{a}}(s),\xi(s))]\right\rangle \tag{5.52}$$

since $\partial a_i/\partial \bar{a}_j(t)=\partial a_i/\partial a_j=\delta_{ij}$.

It is gratifying that we have succeeded in making the final expressions (5.51), (5.52) for A_i independent of t_0 and b.

6. DISTRIBUTION FUNCTION TREATMENT OF SHORT CORRELATION TIME PROBLEM

The problem of treating short but nonzero correlation times is sufficiently important that we shall provide another treatment, based on distribution functions, that is analogous to our previous treatment of quantum relaxation.[10] For this purpose, we need

THEOREM 6.1: Let $\mu(\mathbf{a},t)$ be the density of systems at $\mathbf{a}$ and time t that obey the equations of motion

$$da_i/dt=G_i(\mathbf{a}(t),\xi(t)). \tag{6.1}$$

Then

$$(\partial\mu/\partial t)+(\partial/\partial a_i)[G_i(\mathbf{a},\xi(t))\mu]=0, \tag{6.2}$$

where summation on repeated indices is understood.

Proof: Consider first a single system. Let $b_i(t)$ be a solution of Eq. (6.1) subject to some specified initial condition, e.g., $b_i(t)=a_i(t)$; $b_i(t_0)=a_i^0$. Then

$$\mu(\mathbf{a},t)=\delta(\mathbf{a}-\mathbf{b}(t)) \tag{6.3}$$

is the density that describes the trajectory $\mathbf{a}=\mathbf{b}(t)$ in our space. Let $g(\mathbf{a})$ be an arbitrary function of $\mathbf{a}$. Then $g(\mathbf{b}(t))$ obeys

$$\frac{dg(\mathbf{b}(t))}{dt}=\frac{\partial g}{\partial b_i}\frac{db_i}{dt}=\frac{\partial g}{\partial b_i}G_i(\mathbf{b}(t),\xi(t)). \tag{6.4}$$

However, we can also write

$$g(\mathbf{b}(t))=\int \mu(\mathbf{a},t)g(\mathbf{a})\,d\mathbf{a} \tag{6.5}$$

$$\frac{\partial g}{\partial b_i}G_i(\mathbf{b}(t),\xi(t))=\int \mu(\mathbf{a},t)\frac{\partial g}{\partial a_i}G_i(\mathbf{a},\xi(t))\,d\mathbf{a} =-\int g(\mathbf{a})\frac{\partial}{\partial a_i}[G_i(\mathbf{a},\xi(t))\mu]\,d\mathbf{a}, \tag{6.6}$$

$$\frac{dg(b(t))}{dt}-\frac{\partial g}{\partial b_i}G_i=\int g(a)\left\{\frac{\partial\mu}{\partial t}+\frac{\partial}{\partial a_i}[G_i(\mathbf{a},\xi(t))\mu]\right\}d\mathbf{a} =0. \tag{6.7}$$

Since $g(\mathbf{a})$ is arbitrary, the factor in braces must vanish, and we have derived (6.2) for a single system. For an ensemble of systems, however, μ is a superposition of results for single systems and necessarily obeys the same equations.

Only if the flow is "incompressible,"

$$\partial G_i/\partial a_i=0, \tag{6.8}$$

does our equation reduce to the usual "Liouville" form

$$\partial\mu/\partial t+G_i(\mathbf{a},\xi(t))(\partial\mu/\partial a_i)=0. \tag{6.9}$$

Our original form (6.2) is then more general, and indeed it is the usual Fokker–Planck equation without the diffusion terms. The diffusion terms are not present because μ has been computed for a particular $\xi(t)$, i.e., in the presence of a known force.

With $\xi(t)$ now regarded as a random variable, the distribution we are interested in is

$$P(\mathbf{a},t)=\langle\mu(\mathbf{a},t)\rangle. \tag{6.10}$$

Note that $\mathbf{a}$ and $P(\mathbf{a},t)$ are not random, but μ in its dependence on ξ is. In this section, all averages are therefore taken over ξ with $\mathbf{a}$ held fixed.

Let us now decompose the motion of μ into an unperturbed (nonrandom) part and a random perturbation:

$$\partial\mu/\partial t=(\Omega_0+\Omega_1)\mu, \tag{6.11}$$

$$\Omega_0=-(\partial/\partial a_i)B_i(\mathbf{a},t)=-(\partial/\partial a_i)\langle G_i(\mathbf{a},\xi(t))\rangle, \tag{6.12}$$

$$\Omega_1=-(\partial/\partial a_i)F_i(\mathbf{a},\xi(t)), \tag{6.13}$$

where

$$F_i(\mathbf{a},\xi(t))=G_i(\mathbf{a},\xi(t))-B_i(\mathbf{a},t)$$

and the derivatives $\partial/\partial a_i$ in Ω_0 and Ω_1 are operators that are understood to act on everything to the right, including μ.

By averaging Eq. (6.11) we can write (compare with QIII, Ref. 10):

$$\partial P/\partial t=\Omega_0 P+\langle\Omega_1\mu\rangle=\Omega_0 P+\langle\Omega_1\Delta\mu\rangle, \tag{6.14}$$

CC-0. In Public Domain. Gurukul Kangri Collection, Haridwar

Digitized by Arya Samaj Foundation Chennai and eGangotri

where $\mu = P + \Delta\mu$. Subtracting (6.14) from (6.11) we obtain an equation for $\Delta\mu$:

$$\partial\Delta\mu/\partial t = \Omega_0\Delta\mu + \Omega_1\mu - \langle\Omega_1\mu\rangle,$$

$$\partial\Delta\mu/\partial t = \Omega_0\Delta\mu + \Omega_1 P + [\Omega_1\Delta\mu - \langle\Omega_1\Delta\mu\rangle]. \quad (6.15)$$

Since $\Delta\mu$ is first order in the fluctuation, $\Omega_1\Delta\mu$ is second order. Thus the term in brackets is of second order *and* has mean zero. One can therefore start an iteration procedure by neglecting this term.[10] To first order, then we can solve (6.15) for $\Delta\mu$:

$$\Delta\mu(t) \approx \int_{t_0}^{t} ds U^{-1}(s,t)\Omega_1(s)U(s,t)U(t,s)P(s), \quad (6.16)$$

where we have assumed that $\mu(t_0)$ is nonrandom so that $\Delta\mu(t_0) = \mu(t_0) - P(t_0) = 0$, and U is defined by

$$\partial U(t,t_0)/\partial t = \Omega_0 U(t,t_0), \qquad U(t_0,t_0) = 1,$$

$$U(t,t_0) = T_{\leftarrow} \exp \int_{t_0}^{t} \Omega_0(s)\, ds,$$

$$U(t,t_0) = \exp[\Omega_0(t-t_0)], \quad (6.17)$$

where the last form is valid when Ω_0 does not depend explicitly on the time and $T_{\leftarrow}$ orders the Ω's from right to left in order of increasing time, c.f. Eq. III (7F.11). If we define $\bar{\mathbf{a}}(t,t_0)$ by

$$\bar{\mathbf{a}}(t,t_0) = U(t,t_0)^{-1}\mathbf{a}U(t,t_0), \quad (6.18)$$

or using (6.17), (6.12),

$$d\bar{a}_i(t,t_0)/dt = U^{-1}B_i(\mathbf{a},t)U$$

$$= B_i(U^{-1}\mathbf{a}U, t) = B_i(\bar{\mathbf{a}}(t,t_0), t), \quad (6.19)$$

then $\bar{\mathbf{a}}(t,t_0)$ has the same meaning as in the previous section. It is the solution of the unperturbed (nonrandom) equation of motion (6.19) subject to the initial condition $\bar{\mathbf{a}}(t_0,t_0) = \mathbf{a}$.

If we now insert (6.16) into (6.14), we find that P obeys

$$\partial P/\partial t = \Omega_0 P + \int_{t_0}^{t} \langle\Omega_1(\mathbf{a},t)\Omega_1(\bar{\mathbf{a}}(s,t),s)\rangle\, ds U(t,s)P(s), \quad (6.20)$$

an equation that exhibits memory effects. But $U(t,s)P(s)$ is the density function $P(t)$ that one would obtain at time t, with $P(s)$ as initial condition, if the evolution from s to t takes place ignoring Ω_1, i.e., ignoring the dissipation. Since the correlation time is short, the dissipation over the relevant time interval $t - s \sim \tau_c$ is negligible, and we can write $U(t,s)P(s) \approx P(t)$. Thus we obtain the Markoffian equation

$$\partial P/\partial t = \Omega_0 P + \int_{t_0}^{t} \langle\Omega_1(\mathbf{a},t)\Omega_1(\bar{\mathbf{a}}(s,t),s)\rangle\, ds P(t). \quad (6.21)$$

This equation has also been derived by Kubo[9] using the linked (or cumulant) moment expansion[34] that he has popularized recently. With the notation already set up, we can present a brief simplification of his proof. Let

$$\mu(\mathbf{a},t) = U(t,t_0)VP(t_0). \quad (6.22)$$

Then the equation for μ implies that

$$dV/dt = U(t,t_0)^{-1}\Omega_1(\mathbf{a},t)U(t,t_0)V$$

$$= \Omega_1(\bar{\mathbf{a}}(t,t_0),t)V, \quad (6.23)$$

$$V = T_{\leftarrow} \exp \int_{t_0}^{t} \Omega_1(\bar{\mathbf{a}}(s,t_0),s)ds. \quad (6.24)$$

The average of Eq. (6.22) now yields

$$P(t) = U(t,t_0)\langle V\rangle P(t_0). \quad (6.25)$$

Let

$$d\langle V\rangle/dt = G\langle V\rangle \quad (6.26)$$

define the operator G. Then

$$dP/dt = [dU/dt\langle V\rangle + UG\langle V\rangle]P(t_0)$$

$$= [\Omega_0 + U(t,t_0)GU(t,t_0)^{-1}]P(t) \quad (6.27)$$

constitutes our exact equation of motion. As in (5.9) a *stationary non-Markoffian process has been replaced rigorously by a nonstationary Markoffian process* for the purpose of computing $P(\mathbf{a}t \mid \mathbf{a}_0t_0)$.

To obtain G, we compare $\langle V\rangle$ evaluated from (6.24) with $\langle V\rangle$ evaluated from (6.26):

$$\langle V\rangle = T_{\leftarrow} \exp \int_{t_0}^{t} G(s)\, ds$$

$$= 1 + \int_{t_0}^{t} G(s)\, ds + \int_{t_0}^{t} G(s)\, ds \int_{t_0}^{s} G(s')\, ds' + \cdots$$

$$= 1 + \int_{t_0}^{t} ds \int_{t_0}^{s} ds' \langle\Omega(s)\Omega(s')\rangle$$

$$+ \int_{t_0}^{t} ds_1 \int_{t_0}^{s_1} ds_2 \int_{t_0}^{s_2} ds_3 \int_{t_0}^{s_3} ds_4$$

$$\times \langle\Omega(s_1)\Omega(s_2)\Omega(s_3)\Omega(s_4)\rangle + \cdots, \quad (6.28)$$

where

$$\Omega(s) \equiv \Omega_1(\bar{\mathbf{a}}(s,t_0),s) \quad (6.29)$$

and we have made use of $\langle\Omega_1\rangle = 0$ to kill all terms of odd order. We find that

$$G(s) = \int_{t_0}^{s} ds' \langle\Omega(s)\Omega(s')\rangle + \int_{t_0}^{s} ds_2 \int_{t_0}^{s_2} ds_3 \int_{t_0}^{s_3} ds_4$$

$$\times \langle\Omega(s)\Omega(s_2)\Omega(s_3)\Omega(s_4)\rangle - \int_{t_0}^{s} \langle\Omega(s)\Omega(s_1)\rangle\, ds_1$$

$$\times \int_{t_0}^{s} ds' \int_{t_0}^{s'} ds_1' \langle\Omega(s')\Omega(s_1')\rangle + \cdots. \quad (6.30)$$

If $\Omega(s)$ were a Gaussian variable, and commuted with itself at different times, the two fourth-order terms in

[9] R. Kubo, J. Phys. Soc. Japan **17**, 1100 (1962).

CC-0. In Public Domain. Gurukul Kangri Collection, Haridwar

Digitized by Arya Samaj Foundation Chennai and eGangotri

(6.30) (and all higher-order terms) would cancel. To second-order accuracy, we have

$$U(t,t_0)G(t)U(t,t_0)^{-1}\approx\int_{t_0}^{t}dsU(t,t_0)\times\langle\Omega_1(\bar{\mathbf{a}}(t,t_0),t)\Omega_1(\bar{\mathbf{a}}(s,t_0),s)\rangle U(t,t_0)^{-1}=\int_{t_0}^{t}ds\langle\Omega_1(\mathbf{a},t)\Omega_1(\bar{\mathbf{a}}(s,t),s)\rangle \tag{6.31}$$

in agreement with (6.21).

Inserting the expressions (6.12), (6.13) for Ω_0 and Ω_1 into (6.21) we obtain

$$\partial P/\partial t=-(\partial/\partial a_i)[B_i(\mathbf{a},t)P]+\int_{t_0}^{t}ds\langle(\partial/\partial a_i)\{F_i(\mathbf{a},\xi(t))[\partial/\partial\bar{a}_k(s,t)]\times[F_k(\bar{\mathbf{a}}(s,t),\xi(s))\rangle P]\}. \tag{6.32}$$

But

$$\frac{\partial}{\partial a_i}F_i\frac{\partial}{\partial\bar{a}_k}F_k=\frac{\partial}{\partial a_i}F_i\frac{\partial a_j}{\partial\bar{a}_k}\frac{\partial}{\partial a_j}F_k=\frac{\partial}{\partial a_i}\frac{\partial}{\partial a_j}F_iF_k\frac{\partial a_j}{\partial\bar{a}_k}-\frac{\partial}{\partial a_i}\frac{\partial}{\partial a_j}\left[F_i\frac{\partial a_j}{\partial\bar{a}_k}\right]F_k, \tag{6.33}$$

so that

$$D_{ij}=\int_{t_0}^{t}ds\langle F_i(\mathbf{a},\xi(t))F_k(\bar{\mathbf{a}}(s,t),\xi(s))\rangle\frac{\partial a_j}{\partial\bar{a}_k(s,t)}, \tag{6.34}$$

$$A_i=B_i+\int_{t_0}^{t}ds\left[\left\langle\frac{\partial a_j}{\partial\bar{a}_k}\frac{\partial F_i}{\partial a_j}F_k+F_iF_k\frac{\partial}{\partial a_j}\left(\frac{\partial a_j}{\partial\bar{a}_k}\right)\right\rangle\right]$$

$$=B_i+\int_{t_0}^{t}ds\left\langle\frac{\partial F_i(\mathbf{a},\xi(t))}{\partial\bar{a}_k(s,t)}F_k(\bar{\mathbf{a}}(s,t),\xi(0))\right\rangle+\int_{t_0}^{t}ds\langle F_i(\mathbf{a},\xi(t))F_k(\bar{\mathbf{a}}(s,t),\xi(s))\rangle\times\frac{\partial}{\partial a_j}\left[\frac{\partial a_j}{\partial\bar{a}_k(s,t)}\right]. \tag{6.35}$$

Thus D_{ij} [after replacement by $\frac{1}{2}(D_{ij}+D_{ji})$] and the first two terms of A_i agree with our previous results using the "particle equations of motion," Eqs. (5.41) and (5.52). The last term of (6.35) is a strange one, however, because it does not appear to transform under the change of coordinates $a_i\to a_i'$ according to the rule (3.28) whereas under such a transformation

$$B_i'=\partial a_i'(\mathbf{a},t)/\partial t+(\partial a_i'/\partial a_k)B_k,$$

$$I_i'=\int_{-\infty}^{t}ds\left\langle\frac{\partial F_i'}{\partial\bar{a}_k'(s,t)}F_k'(s)\right\rangle=\int_{-\infty}^{t}ds\left\langle\frac{\partial}{\partial a_k'(s)}\left[\frac{\partial a_i'}{\partial a_m}F_m\right]\frac{\partial a_k'(s)}{\partial a_n(s)}F_n\right\rangle=\int_{-\infty}^{t}ds\left\langle\frac{\partial}{\partial a_n(s)}\left[\frac{\partial a_i'}{\partial a_m}F_m\right]F_n\right\rangle$$

$$=\frac{\partial a_i'}{\partial a_m}\int_{-\infty}^{t}ds\left\langle\frac{\partial F_m}{\partial a_n(s)}F_n\right\rangle+\int_{-\infty}^{t}\frac{\partial}{\partial a_n(s)}\left[\frac{\partial a_i'}{\partial a_m}\right]\langle F_mF_n\rangle ds \tag{6.37}$$

$$=\frac{\partial a_i'}{\partial a_m}I_m+\frac{\partial^2a_i'}{\partial a_j\partial a_m}\int_{-\infty}^{t}\frac{\partial a_j}{\partial a_n(s)}\langle F_mF_n\rangle ds$$

$$=\frac{\partial a_i'}{\partial a_m}I_m+\frac{\partial^2a_i'}{\partial a_j\partial a_m}D_{mj}. \tag{6.38}$$

Thus $B+I$ has the correct transformation properties, (3.27)–(3.28), and the last term (IV) of (6.35) to be consistent should obey

$$IV_i'=(\partial a_i'/\partial a_m)IV_m, \tag{6.39}$$

but Eq. (6.35) seems to prevent such a simple transformation property.

We interpret the noncovariant nature of this extra contribution to stem from the fact that the truncation of a cumulant expansion by a Gaussian approximation depends on the choice of reference frame. It is more likely to be valid, for example, in a reference frame in which the (noise-free) equations of motion are linear. In such a frame, the noncovariant term in (6.35) vanishes.

7. SPIN DIFFUSION

In this section we apply the methods of the two preceding sections to the diffusion of a classical spin in a random external field[9] $\mathbf{h}(t)$:

$$d\mathbf{M}/dt=(\mathbf{H}\times\mathbf{M})+[\mathbf{h}(t)\times\mathbf{M}] \tag{7.1}$$

as well as a constant field $\mathbf{H}$ whose direction we take to be the z direction of our coordinate system. [In (7.1), to save writing, we have absorbed the gyromagnetic ratio into the fields, so that they have the dimensions of frequency.] With the notation

$$h_\pm=h_x\pm ih_y,\qquad M_\pm=M_x\pm iM_y \tag{7.2}$$

CC-0. In Public Domain. Gurukul Kangri Collection, Haridwar

Digitized by Arya Samaj Foundation Chennai and eGangotri

we can rewrite (7.1) in the form

$$dM_z/dt=(\mathbf{h}\times\mathbf{M})_z=\tfrac{1}{2}i[h_+M_--h_-M_+],$$
$$dM_+/dt=iHM_++(\mathbf{h}\times\mathbf{M})_+=iHM_++i(h_zM_+-h_+M_z),$$
$$dM_-/dt=-iHM_-+(h\times M)_-$$
$$=-iHM_--i(h_zM_--h_-M_z). \tag{7.3}$$

The statistics of our random fields will be assumed to have cylindrical symmetry:

$$\langle h_z(t)h_z(s)\rangle=\phi_{11}(t-s),$$
$$\langle h_x(t)h_x(s)\rangle=\langle h_y(t)h_y(s)\rangle=\phi_\perp(t-s), \tag{7.4}$$
$$\langle h_x(t)h_y(s)\rangle=0. \tag{7.5}$$

Thus our circular components obey

$$\langle h_-(t)h_+(s)\rangle=\langle h_+(t)h_-(s)\rangle=2\phi_\perp(t-s)=\text{real}. \tag{7.6}$$

We have chosen the circularly polarized components $M_\pm$ rather than the Cartesian components M_x, M_y, because of the great simplicity of their noise-free motion:

$$\bar{M}_+(s)\equiv\bar{M}_+(s,t)=\exp[iH(s-t)]M_+,$$
$$\bar{M}_-(s)=\exp[-iH(s-t)]M_-,$$
$$\bar{M}_z(s)\equiv\bar{M}_z(s,t)=M_z. \tag{7.7}$$

Application of Eq. (5.51) for the drift to the present problem yields

$$A_i(s',t)=B_i+\frac{\partial M_i}{\partial\bar{M}_i(s')}\int_{-\infty}^{s'}ds$$
$$\times\left\langle[\mathbf{h}(s)\times\overline{\mathbf{M}}(s)]_k\frac{\partial}{\partial\bar{M}_k(s)}\cdot[\mathbf{h}(s')\times\overline{\mathbf{M}}(s')]_i\right\rangle \tag{7.8}$$

since

$$\partial M_i/\partial\bar{M}_j(s')=\delta_{ij}\times[\exp(\mp iH(s'-t))\ \text{ or }\ 1] \tag{7.9}$$

when the indices i, j, k take on the values $+$, $-$ or z. Thus

$$A_z(s',t)=\int_{-\infty}^{s'}ds\left\langle[\mathbf{h}(s)\times\overline{\mathbf{M}}(s)]_+\frac{\partial}{\partial\bar{M}_+(s)}\right.$$
$$\left.\times[\mathbf{h}(s')\times\overline{\mathbf{M}}(s')]_z+\text{c.c.}\right\rangle \tag{7.10}$$
$$=\int_{-\infty}^{s'}ds\,\langle i[h_z(s)\bar{M}_+(s)-h_+(s)\bar{M}_z(s)]$$
$$\times[\partial/\partial\bar{M}_+(s)]\tfrac{1}{2}i[h_+(s')\bar{M}_-(s')$$
$$-h_-(s')\bar{M}_+(s')]+\text{c.c.}\rangle$$
$$=-\frac{1}{2}\int_{-\infty}^{s'}ds\,\langle h_+(s)h_-(s')\rangle$$
$$\times\exp[iH(s'-s)]+\text{c.c.}$$
$$=-\int_0^\infty du\phi_+(u)\exp(iHu)+\text{c.c.}$$
$$=-(a+a^*). \tag{7.11}$$

We note that $A_z(s',t)$ is independent of s' (as well as t) so that the average over s' in (5.50) can be omitted. In other words, the simpler (unsmoothed) formulas (5.52), (5.40) for A and D can be used from the start. In this way, we obtain the three "Bloch" equations:

$$d\langle M_z\rangle/dt=-\langle M_z\rangle/T_1,$$
$$d\langle M_\pm\rangle/dt=\pm iH'\langle M_\pm\rangle-\langle M_\pm\rangle/T_2, \tag{7.12}$$

where

$$1/T_1=a+a^*,\qquad a=\int_0^\infty du\phi_\perp(u)\exp(iHu)$$
$$=a'+ia'', \tag{7.13}$$
$$1/T_2=b+a',\qquad b=\int_0^\infty du\phi_{11}(u), \tag{7.14}$$
$$H'=H+a'', \tag{7.15}$$

and $a''=\operatorname{Im}a$ yields a frequency shift. Here T_1 and T_2 are referred to as the longitudinal and transverse relaxation times. Since a change in M_z produces a change in the Zeeman energy of the system, longitudinal relaxation requires a lattice to dispose of the energy, and T_1 is also referred to as the spin–lattice relaxation time, whereas T_2 is called the spin–spin relaxation time.

The diffusion constant formula (5.38) can be simplified to

$$D_{ij}(s',t)=\frac{1}{2}\frac{\partial M_i}{\partial\bar{M}_i(s')}\int_{-\infty}^{\infty}ds\frac{\partial M_j}{\partial\bar{M}_j(s)}$$
$$\times\langle[\mathbf{h}(s')\times\overline{\mathbf{M}}(s')]_i[\mathbf{h}(s)\times\mathbf{M}(s)]_j\rangle. \tag{7.16}$$

We illustrate this formula by calculating D_{-+}:

$$D_{-+}(s',t)=\frac{1}{2}\int_{-\infty}^{\infty}ds\exp[iH(s'-s)]$$
$$\times\langle[\mathbf{h}(s')\times\overline{\mathbf{M}}(s')]_-[\mathbf{h}(s)\times\overline{\mathbf{M}}(s)]_+\rangle \tag{7.17}$$

where the ensemble average can be simplified to

$$\langle-i[h_z(s')\bar{M}_-(s')-h_-(s')\bar{M}_z(s')]$$
$$\times i[h_z(s)\bar{M}_+(s)-h_+(s)\bar{M}_z(s)]\rangle$$
$$=\exp[iH(s-s')]M_-M_+\langle h_z(s')h_z(s)\rangle$$
$$+M_z^2\langle h_-(s')h_+(s)\rangle$$

or

$$D_{-+}=bM_-M_++2a'M_z^2. \tag{7.18}$$

Our results for the diffusion coefficients are

$$D_{zz}=a'(M_x^2+M_y^2),$$
$$D_{z+}=-aM_zM_+,\qquad D_{z-}=-a^*M_zM_-,$$
$$D_{++}=-bM_+^2,\qquad D_{--}=-bM_-^2,$$
$$D_{-+}=D_{+-}=b(M_x^2+M_y^2)+2a'M_z^2. \tag{7.19}$$

CC-0. In Public Domain. Gurukul Kangri Collection, Haridwar

Digitized by Arya Samaj Foundation Chennai and eGangotri

We now construct the operator $L^\dagger$ of III (5.9):

$$-L^\dagger=\sum \mathbf{D}_n(a):\left(\frac{\partial}{\partial \mathbf{a}}\right)^n$$

$$=A_z\frac{\partial}{\partial M_z}+A_+\frac{\partial}{\partial M_+}+A_-\frac{\partial}{\partial M_-}+D_{zz}\left(\frac{\partial}{\partial M_z}\right)^2$$

$$+2D_{z+}\frac{\partial}{\partial M_z}\frac{\partial}{\partial M_+}+2D_{z-}\frac{\partial}{\partial M_z}\frac{\partial}{\partial M_-}+D_{++}\left(\frac{\partial}{\partial M_+}\right)^2$$

$$+D_{--}\left(\frac{\partial}{\partial M_-}\right)^2+2D_{+-}\frac{\partial}{\partial M_+}\frac{\partial}{\partial M_-}. \quad (7.20)$$

Inserting the A's and D's from (7.12), (7.19), and transforming to Cartesian coordinates with the help of

$$\frac{\partial}{\partial M_+}=\frac{1}{2}\left(\frac{\partial}{\partial M_x}-i\frac{\partial}{\partial M_y}\right), \quad (7.21)$$

our results can be rearranged in the convenient operator notation

$$-L^\dagger=a'(\mathbf{M}\times\nabla_M)^2+(b-a')(\mathbf{M}\times\nabla_M)_z^2$$

$$+H'(\mathbf{M}\times\nabla_M)_z$$

$$=-a'\mathbf{L}^2+(a'-b)L_z^2+iH'L_z, \quad (7.22)$$

where

$$\mathbf{L}=\mathbf{M}\times(1/i)\nabla_M, \quad (7.23)$$

$$L_z=\left(\frac{1}{i}\right)\left(M_x\frac{\partial}{\partial M_y}-M_y\frac{\partial}{\partial M_x}\right), \quad (7.24)$$

are like the angular momentum operators of quantum mechanics $\mathbf{r}\times\mathbf{p}\sim\mathbf{r}\times(1/i)\nabla_r$, and $H'=H+a''$ is the shifted frequency of (7.15). The operator L of III (5.16) is the adjoint of $L^\dagger$ and may be obtained by reversing the sign of ∇_M:

$$-L=-[a'\mathbf{L}^2+(b-a')L_z^2+iH'L_z], \quad (7.25)$$

and according to III (5.13)

$$\partial P(\mathbf{M},t)$$

$$=-[a'\mathbf{L}^2+(b-a')L_z^2+i(H+a'')L_z]P(\mathbf{M},t). \quad (7.26)$$

We note that with $M_z=M\cos\theta$, $M_\pm=M\sin\theta\times\exp(\pm i\phi)$

$$\mathbf{L}^2=(\sin\theta)^{-1}(\partial/\partial\theta)[\sin\theta(\partial/\partial\theta)]+(\sin^2\theta)^{-1}(\partial^2/\partial\phi^2),$$

$$iL_z=\partial/\partial\phi, \quad (7.27)$$

so that $\mathbf{L}$ is a purely angular operator. Thus any $W(M)$, $M=|\mathbf{M}|$, is a steady-state solution: rotational diffusion will not disturb an isotropic distribution. This remark is true even though we have not assumed that our random forces are isotropic which would require

$$\phi_{||}(u)=\phi_\perp(u). \quad (7.28)$$

If, in addition, one sets $H=\Omega$ to eliminate z as a preferred direction, one obtains $a''=0$, $b=a'=a=$ real, and

$$\partial P(\mathbf{M},t)/\partial t=-a\mathbf{L}^2P \quad (7.29)$$

as the description of purely isotropic diffusion.

For the spin-diffusion problem, the equations of motion are linear. Thus the spurious last term of (6.35) vanishes, and our equation (7.26) for the distribution function can also be derived directly from (6.21): From (6.2) we can write

$$\partial\mu/\partial t=-d/d\mathbf{M}\{[(\mathbf{H}+\mathbf{h})\times\mathbf{M}]_\mu\}$$

$$=-i(\mathbf{H}+\mathbf{h})\times\mathbf{M}\cdot(1/i)(d/d\mathbf{M})_\mu$$

$$=-i(\mathbf{H}+\mathbf{h})\cdot\mathbf{L}_\mu \quad (7.30)$$

$$\Omega_0=-i\mathbf{H}\cdot\mathbf{L}, \qquad \Omega_1=-i\mathbf{h}\cdot\mathbf{L}. \quad (7.31)$$

Equation (6.21) then yields

$$\partial P/\partial t=-i\mathbf{H}\cdot\mathbf{L}P$$

$$-\int_{t_0}^{t}\langle[\mathbf{h}(t)\cdot\mathbf{L}][\mathbf{h}(s)\cdot\mathbf{L}(s,t)]\rangle\,ds P(t), \quad (7.32)$$

where

$$\mathbf{L}(s,t)=\exp[-(s-t)\Omega_0]\mathbf{L}\exp[(s-t)\Omega_0]$$

$$=\exp[i(s-t)\mathbf{H}\cdot\mathbf{L}]\mathbf{L}\exp[-i(s-t)\mathbf{H}\cdot\mathbf{L}] \quad (7.33)$$

using (6.17), (6.18). With $\mathbf{H}$ in the z direction,

$$L_z(s,t)=L_z, \qquad L_+(s,t)=\exp[iH(s-t)]L_+,$$

$$L_-(s,t)=\exp[-iH(s-t)]L_-, \quad (7.34)$$

$$\langle\mathbf{h}(t)\cdot\mathbf{L}[\mathbf{h}(s)\cdot\mathbf{L}(s,t)]\rangle=\langle h_z(t)h_z(s)\rangle L_z^2$$

$$+\tfrac{1}{4}\langle h_-(t)h_+(s)\rangle L_+L_-\exp[-iH(s-t)]$$

$$+\tfrac{1}{4}\langle h_+(t)h_-(s)\rangle L_-L_+\exp[iH(s-t)], \quad (7.35)$$

$$\partial P/\partial t=-[iHL_zP+bL_z^2+\tfrac{1}{2}aL_+L_-+\tfrac{1}{2}a^*L_-L_+]P, \quad (7.36)$$

which reduces to (7.26) on using

$$\tfrac{1}{2}(L_+L_-+L_-L_+)=L_x^2+L_y^2,$$

$$\tfrac{1}{2}(L_+L_--L_-L_+)=L_z. \quad (7.37)$$

8. THE (APPROXIMATE) LANGEVIN FORCES APPROPRIATE TO A MARKOFF PROCESS

In Sec. 3 we showed how to start with a given set of delta-correlated Langevin forces and derive a corresponding Markoff process. We now ask the inverse question: given a transition probability $P(a't+\Delta t|a)$ or a set of diffusion coefficients $\mathbf{D}_n(\mathbf{a},t)$, what properties can we assign to the Langevin forces $\mathbf{F}(\mathbf{a},t)$ in

$$da/dt=\mathbf{A}(\mathbf{a},t)+\mathbf{F}(\mathbf{a},t) \quad (8.1)$$

so as to reproduce the original Markoff process. There may be no unique answer to the construction of $\mathbf{F}$, since $\mathbf{F}=\mathbf{F}(\mathbf{a},\mathbf{f}(t),t)$ depends both on a random force $\mathbf{f}(t)$ and on an arbitrary function of $\mathbf{a}$. However, the moments taken with $\mathbf{a}(t_0)=\mathbf{a}_0$ fixed, but $\mathbf{a}(t)$ varying

CC-0. In Public Domain. Gurukul Kangri Collection, Haridwar

Digitized by Arya Samaj Foundation Chennai and eGangotri

accord with the solution of (8.1), are undoubtedly unique. As an *approximate* set of moments, we propose

$$\langle \mathbf{F}(t) \rangle_0 = 0, \tag{8.2}$$

$$\langle \mathbf{F}(t_1)\mathbf{F}(t_2) \rangle_0 = 2!\langle \mathbf{D}_2(\mathbf{a}, t_1) \rangle_0 \delta(t_1 - t_2), \tag{8.3}$$

$$\langle \mathbf{F}(t_1)\mathbf{F}(t_2)\cdots\mathbf{F}(t_n) \rangle_0{}^L = n!\langle \mathbf{D}_n(\mathbf{a}, t_1) \rangle_0 \prod_{i=1}^{n-1} \delta(t_i - t_{i+1}). \tag{8.4}$$

All of these averages are understood to be taken with $\mathbf{a}(0)$ fixed, i.e., $\langle \mathbf{F}(t) \rangle_0 = \langle \mathbf{F}(t) \rangle_{\mathbf{a}_0}$ and

$$\langle \mathbf{D}_n(\mathbf{a}, t_1) \rangle_0 \equiv \int \mathbf{D}_n(\mathbf{a}, t_1) P(\mathbf{a}, t_1 \mid \mathbf{a}_0, t_0)\, d\mathbf{a}. \tag{8.5}$$

Of course, if these averages are correct for fixed $\mathbf{a}_0$ they are *a fortiori* correct after a subsequent average over $\mathbf{a}_0$.

A term with the $(n-1)$-fold delta-function character of (8.4) is necessary in order that $\langle [\mathbf{a}(t_0+\Delta t) - \mathbf{a}(t_0)]^n \rangle$ contain a term linear in Δt for small Δt. Moreover, the coefficient has been chosen to yield the correct result $\mathbf{D}_n(\mathbf{a}_0, t_0)\Delta t$ for the coefficient of Δt. The most likely error in (8.4) is the omission of terms that involve a smaller number of delta functions (or none).

Equation (8.2) is, of course, exact since it is equivalent to the requirement

$$d\langle \mathbf{a} \rangle_0 / dt = \langle \mathbf{A}(\mathbf{a}, t) \rangle_0, \qquad t > t_0, \tag{8.6}$$

which is simply the correct first-moment equation III (5.10), I (5.9), subject to $\mathbf{a}(t_0) = \mathbf{a}_0$ as an initial condition, so that $\langle \mathbf{F} \rangle_0 \equiv \langle \mathbf{F} \rangle_{\mathbf{a}_0} = 0$. These statements must be interpreted carefully. For example, the Langevin process

$$da/dt = B(a) + \sigma(a) f(t) \tag{8.7}$$

of (3.1) leads to a result (3.10) that must be interpreted to mean

$$\langle \sigma(a) f(t) \rangle = \sigma \partial\sigma/\partial a, \tag{8.8}$$

so that for this example, we must write

$$da/dt = [B(a) + \sigma\partial\sigma/\partial a] + F; \qquad F = \sigma f(t) - \sigma\partial\sigma/\partial a \tag{8.9}$$

for (8.2) to be true. We have omitted the $\mathbf{a}$'s *inside* the $\mathbf{F}$'s in (8.2)–(8.4) to remind us that they are not held fixed during the average process, so that correction terms of the form (8.8) are *included* in the results.

That Eq. (8.3) is also exact can be established by showing that the second moment vanishes for $t_1 \neq t_2$ so that no non-delta-function term can occur. Since the expression is symmetric in t_1 and t_2, we shall confine ourselves to the case $t_1 > t_2$ and write

$$\langle (d\mathbf{a}/dt_1 - \mathbf{A}_1)\mathbf{A}_2 \rangle = \langle \langle d\mathbf{a}/dt_1 - \mathbf{A}_1 \rangle_2 \mathbf{A}_2 \rangle = 0. \tag{8.10}$$

The right-hand side indicates that an average over $\mathbf{a}_1$ can be performed first, conditional upon $\mathbf{a}_2$, followed by an average over $\mathbf{a}_2$. But the conditional average vanishes because of (8.6) with $t \to t_1$ and $t_0 \to t_2$.

Similarly

$$\left\langle \left(\frac{d\mathbf{a}}{dt_1} - \mathbf{A}_1\right)\frac{d\mathbf{a}}{dt_2} \right\rangle = \frac{d}{dt_2}\left\langle \left\langle \frac{d\mathbf{a}}{dt_1} - \mathbf{A}_1 \right\rangle_2 \mathbf{a}(t_2) \right\rangle = 0. \tag{8.11}$$

These last two results can be combined into

$$\left\langle \left(\frac{d\mathbf{a}}{dt_1} - \mathbf{A}_1\right)\left(\frac{d\mathbf{a}}{dt_2} - \mathbf{A}_2\right) \right\rangle = 0 \quad \text{if} \quad t_1 \neq t_2. \tag{8.12}$$

a result that confirms the delta-function character of (8.3). This result establishes that

$$\int_a^b \mathbf{F}(t)\, dt \quad \text{and} \quad \int_c^d \mathbf{F}(t)\, dt \tag{8.13}$$

are *uncorrelated* random variables as long as the intervals (a, b) and (c, d) overlap in a set of measure zero. *If* we could assume that

$$\langle \mathbf{F}(t_1)\mathbf{F}(t_2)\cdots\mathbf{F}(t_n) \rangle^L = 0 \tag{8.14}$$

when any two times are unequal, then we could conclude that the two integrals in (8.13) are not merely uncorrelated, but *independent*. While this is not precisely true for problems in which $\mathbf{D}_n$ depends on $\mathbf{a}$, let us examine the consequences of this independence assumption, by writing

$$\left\langle \exp\left[i\int_{t_0}^t \mathbf{q}(s)\cdot\mathbf{F}(s)\, ds \right] \right\rangle \approx \prod_j \left\langle \exp\left[i\mathbf{q}(t_j)\cdot\int_{t_j}^{t_{j+1}} \mathbf{F}(s)\, ds \right] \right\rangle = \prod_j \exp \sum_{n=1}^{\infty} (n!)^{-1}[i\mathbf{q}(t_j)^n] : \langle (\Delta\mathbf{b}_j)^n \rangle^L, \tag{8.15}$$

where

$$\Delta\mathbf{b}_j = \int_{t_j}^{t_{j+1}} \mathbf{F}(s)\, ds = \int_{t_j}^{t_{j+1}} [d\mathbf{a}/ds - \mathbf{A}]\, ds \approx \mathbf{a}(t_{j+1}) - \mathbf{a}(t_j) - \mathbf{A}(\mathbf{a}(t_j))\Delta t_j. \tag{8.16}$$

Taking all $\Delta t_j = t_{j+1} - t_j$ to be small enough so that it is adequate to retain only linear terms in Δt_j we have

$$\langle \Delta\mathbf{b}_j \rangle = 0, \tag{8.17}$$

$$\langle (\Delta\mathbf{b}_j)^n \rangle^L \approx \langle [\mathbf{a}(t_{j+1}) - \mathbf{a}(t_j)]^n \rangle^L = n!\Delta t_j \int D_n(\mathbf{a}_j, t_j)\, d\mathbf{a}_j P(\mathbf{a}_j t_j \mid \mathbf{a}_0 t_0) = n!\Delta t_j \langle D_n(\mathbf{a}, t_j) \rangle_0, \tag{8.18}$$

$$\left\langle \exp\left[\int_{t_0}^t \mathbf{q}(s)\cdot\mathbf{F}(s)\, ds \right] \right\rangle \approx \exp \sum_{n=2}^{\infty} \sum_j [i\mathbf{q}(t_j)]^n : \langle D_n(\mathbf{a}, t_j) \rangle_0 \Delta t_j \approx \exp \sum_{n=2}^{\infty} \int ds [i\mathbf{q}(s)]^n : \langle D_n(\mathbf{a}, s) \rangle_0 \approx \exp\left[-\int_{t_0}^t ds \langle \overset{\circ}{K}(\mathbf{q}(s), \mathbf{a}, s) \rangle_0 \right], \tag{8.19}$$

CC-0. In Public Domain. Gurukul Kangri Collection, Haridwar

Digitized by Arya Samaj Foundation Chennai and eGangotri

where K of III (7F.2) is the part of $L(\mathbf{y}, \mathbf{a}, t)$ that omits the drift term, and

$$\langle K(\mathbf{q}(s), \mathbf{a}, s)\rangle_0 = \int K(\mathbf{q}(s), \mathbf{a}, s) P(\mathbf{a}s \mid \mathbf{a}_0 t_0)\, d\mathbf{a}. \tag{8.20}$$

The left-hand side of (8.19) can be rewritten using our linked average result III (6.8) as

$$\left\langle \exp\left[i\int_{t_0}^{t} \mathbf{q}(s)\cdot\mathbf{F}(s)\, ds\right]\right\rangle_0 = \exp\sum \frac{(i)^n}{n!}\int_{t_0}^{t} ds_1 \cdots \int_{t_0}^{t} ds_n A_n,$$

$$A_n = [\mathbf{q}(s_1)\cdots\mathbf{q}(s_n)]:\ \langle \mathbf{F}(s_1)\cdots\mathbf{F}(s_n)\rangle_0^L. \tag{8.21}$$

Comparison with the right-hand side of (8.19) for arbitrary $\mathbf{q}(s)$ establishes the result (8.4)—not only its delta-function character, but the coefficient in front. Thus the linked-moment assumption (8.4) is equivalent to the assumption of independence of the integrals of (8.13). Either can be derived from the other. For the case when all $\mathbf{D}_n$ ($n \geq 2$) are independent of $\mathbf{a}$, these results are exact. We hope to discuss the corrections to (8.21) for inhomogeneous noise at another time. (See also Sec. 9.)

For the case in which the decay is linear,

$$d\mathbf{a}/dt + \mathbf{\Lambda}(t)\cdot\mathbf{a} = \mathbf{F}(t), \tag{8.22}$$

we can as in (2.14) rewrite

$$\left\langle \exp i\int_{t_0}^{t} \mathbf{q}(u)\cdot\mathbf{a}(u)du\right\rangle = \exp i\int \mathbf{q}(u)\cdot\mathbf{n}(u)\cdot\mathbf{a}(0)\, du \times \left\langle \exp\left[i\int_{t_0}^{t} ds\mathbf{h}(s,t)\cdot\mathbf{F}(s)\right]\right\rangle, \tag{8.23}$$

where

$$\mathbf{h}(s,t) = \int_s^t du\mathbf{q}(u)\cdot\mathbf{n}(u,s), \tag{8.24}$$

$$\mathbf{n}(u) \doteq \exp(-\mathbf{\Lambda}u),$$

$$\mathbf{n}(u,s) = \mathbf{n}(u)[\mathbf{n}(s)]^{-1} \doteq \exp[-\mathbf{\Lambda}(u-s)], \tag{8.25}$$

where $\doteq$ means equal when $\mathbf{\Lambda}(t) = \mathbf{\Lambda}$ is not explicitly dependent on the time, the more general case being covered by (2.10). The point of the transformation (8.23) is that our result is reduced to an integral over F for which an approximate average is given by (8.19). Thus we obtain the *approximate* result

$$\left\langle \exp\left[i\int_{t_0}^{t} \mathbf{q}(u)\cdot\mathbf{a}(u)\, du\right]\right\rangle \approx \exp\left[i\int_{t_0}^{t} \mathbf{q}(u)\cdot\langle\mathbf{a}(u)\rangle\, du\right] \times \exp\left[-\int_{t_0}^{t} ds\langle K(\mathbf{h}(s,t), \mathbf{a}, s)\rangle\right], \tag{8.26}$$

which reduces immediately to the *exact* result (2.16) in the case of homogeneous noise when K is independent of $\mathbf{a}$.

If we set $\mathbf{q}(u) = \mathbf{y}\delta(u-t)$ we obtain an approximate expression for the characteristic function

$$\langle \exp[i\mathbf{y}\cdot\mathbf{a}(t)]\rangle = \exp[i\mathbf{y}\cdot\langle\mathbf{a}(t)\rangle - N(\mathbf{y}, t)],$$

$$N(\mathbf{y}, t) = \int_{t_0}^{t} ds\int K(\mathbf{y}\cdot\mathbf{n}(t,s), \mathbf{a}, s) d\mathbf{a} P(\mathbf{a}, s \mid \mathbf{a}_0, t_0). \tag{8.27}$$

9. POPULATION FLUCTUATIONS

Generation Recombination Model

Let us start, for simplicity, with a one-dimensional case in which our variable $a = n =$ the occupancy of some state. Let us assume that "particles" are generated at the rate $G(n)$ and disappear at the rate $R(n)$ ("recombination"), so that our mean equation of motion is

$$\partial\langle n\rangle/\partial t = \langle G(n)\rangle - \langle R(n)\rangle. \tag{9.1}$$

This is a generalization of our previous discussion of shot noise in III (7D) and Eq. (2.22) ff. from a case in which $R = 0$ and $G(n) = \nu =$ a constant independent of n to a case in which recombination and generation are both present, and are arbitrary nonlinear functions of n. Since the occupancy of state n is enhanced by generation from state $n-1$, and reduced by generation out of n, the possibility distribution $P(n, t)$ obeys

$$\partial P(n,t)/\partial t = G(n-1)P(n-1,t) - G(n)P(n,t) + R(n+1)P(n+1,t) - R(n)P(n,t), \tag{9.2}$$

where the last two terms reflect recombination from $n+1$ entering n, and recombination from n leaving n. To obtain the moments of the Langevin forces as in (2.4), we need the rth-order diffusion coefficient D_r. We can obtain these by writing

$$\partial P/\partial t = [\exp(-\partial/\partial n) - 1]G(n)P(n) + [\exp(\partial/\partial n) - 1]R(n)P(n) = \sum_{r=1}^{\infty} (r!)^{-1}(-\partial/\partial n)^r\{[G(n) + (-1)^r R(n)]P(n)\}. \tag{9.3}$$

Comparison with III (5.13) yields

$$r!D_r = G(n) + (-1)^r R(n). \tag{9.4}$$

The first moment $D_1 = A$ simply yields our starting Eq. (9.1). The second moment, which is the most important for problems that can be treated in the quasilinear approximation, yields the result

$$2D_2 = G + R = \text{rate in} + \text{rate out}. \tag{9.5}$$

This result was obtained for a multidimensional case in I (12.25). We see in (9.4) that the rates in and

CC-0. In Public Domain. Gurukul Kangri Collection, Haridwar

Digitized by Arya Samaj Foundation Chennai and eGangotri

cates out add in all even moments, subtract in all odd moments. This feature will persist in our treatment below of the multidimensional case.

A comparison with (2.22) suggests that we write a Langevin equation in the form

$$dn/dt=G(t)-R(t). \tag{9.6}$$

According to (8.4) the most singular parts of the moments of G and R are given by:

$$\langle G(t_1)\cdots G(t_r)\rangle^L=G(n)\,\delta(t_1-t_2)\cdots\delta(t_{r-1}-t_r),$$
$$\langle R(t_1)\cdots R(t_r)\rangle^L=R(n)\,\delta(t_1-t_2)\cdots\delta(t_{r-1}-t_r), \tag{9.7}$$
$$\langle[G(t_1)-R(t_1)]\cdots[G(t_r)-R(t_r)]\rangle$$
$$=[G(n)+(-1)^rR(n)]\delta(t_1-t_2)\cdots\delta(t_{r-1}-t_r). \tag{9.8}$$

If the averages on the left are taken relative to an initial condition $n(t_0)=n_0$, then on the right-hand side, G and R are to be replaced by the conditional averages $\langle G\rangle_0$ and $\langle R\rangle_0$ as in (8.5).

In order to test the accuracy of the moments (9.8), let us consider the evaluation of III (6.21):

$$M_0=\left\langle\exp\left[-\int_{t_0}^{t}q(s)n(s)\,ds\right]\right\rangle=\hat\phi(0,t), \tag{9.9}$$

where

$$\hat\phi(y,t)=\sum_n\exp(iyn)\hat P(nt\mid n_0t_0) \tag{9.10}$$

and $\hat P$ according to III (5.13) obeys

$$\partial\hat P/\partial t=-[q(t)n+L(y_{\rm op},n)]\hat P(nt\mid n_0t_0), \tag{9.11}$$

where a comparison with (9.3) yields

$$-L(y,n)=(e^{iy}-1)G(n)+(e^{-iy}-1)R(n), \tag{9.12}$$

$$y_{\rm op}=i\partial/\partial n,\qquad n_{\rm op}=-i\partial/\partial y. \tag{9.13}$$

Then by III (6.18), $\hat\phi(y,t)$ obeys

$$\partial\hat\phi/(y,t)=-[q(t)n_{\rm op}+L(y,n_{\rm op})]\hat\phi(y,t). \tag{9.14}$$

If $G(n)$ and $R(n)$ are linear functions of n, $\hat\phi$ will obey a first-order differential equation that is solvable by the method of characteristics. Let us consider the interesting special case

$$G(n)=G=\text{constant},\qquad R(n)=rn. \tag{9.15}$$

In this case, the transformation

$$z=e^{iy},\qquad \hat\phi(y,t)=\hat\psi(z,t)=\sum_n z^nP(nt\mid n_0t_0) \tag{9.16}$$

simplifies the equation to

$$\partial\hat\psi/\partial t+[(z-1)r+zq(t)]\partial\hat\psi/\partial z=G(z-1)\hat\psi \tag{9.17}$$

$$\hat\psi(z,0)=z^{n_0}. \tag{9.18}$$

Because of the definition (9.16) we can refer to $\hat\psi$ as the generating function.

Let $\bar z(s\mid z_1t_1)$ be the solution at s of the characteristic equation

$$dz/ds=[r+q(s)]z-r \tag{9.19}$$

subject to $z=z_1$ at $t=t_1$. Then the solution of (9.17) subject to the initial condition (9.18) is

$$\hat\psi(z,t)=[z_0(z,t)]^{n_0}\exp\left\{G\int_{t_0}^{t}ds[\bar z(s\mid zt)-1]\right\}, \tag{9.20}$$

where

$$z_0(z,t)=\bar z(t_0\mid zt)$$

is the inverse of the usual solution $\bar z(t\mid z_0t_0)$. It is convenient to write the solution (9.20) in the form

$$\hat\phi=[1+x_0(x,t)]^{n_0}\exp\left[G\int_{t_0}^{t}ds\bar x(s\mid xt)\right], \tag{9.21}$$

where

$$x=z-1=e^{iy}-1 \tag{9.22}$$

and $x_0(x,t)=\bar x(t_0\mid xt)$.

To obtain the characteristic function ϕ itself, we must specialize to $q=0$, in which case $dx/ds=rx$,

$$x(s)=x(t)\,\exp[r(s-t)],$$
$$\int_{t_0}^{t}ds\bar x(s\mid xt)=\int_0^t dsx\exp[r(s-t)]$$
$$=(1/r)[1-\exp(-rt)], \tag{9.23}$$

where we have set $t_0=0$ to save writing. Thus

$$\phi(y,t)=[1+xe^{-rt}]^{n_0}\exp[(G/r)(1-e^{-rt})x] \tag{9.24}$$

with $x=e^{iy}-1$, is a product of two characteristic functions. The first

$$\psi_1=[1+xe^{-rt}]^{n_0}=[1-e^{-rt}+ze^{-rt}]^{n_0}=[1+(e^{iy}-1)p]^{n_0} \tag{9.25}$$

is a binomial distribution with n_0 particles being deposited with probability $p=e^{-rt}$ into the state and probability $1-e^{-rt}$ out of the state. The second

$$\psi_2=\phi_2=\exp[n_2(e^{iy}-1)]$$
$$n_2=(G/r)(1-e^{-rt}) \tag{9.26}$$

is a pure shot-noise result [cf. III (7D11)] with the mean number $(G/r)(1-e^{-rt})=n_2$.

The product nature of the characteristic function implies that the result n is simply the sum of these two independent random processes. A simple consequence is that the linked moments of the two contributions are additive. The relation III (6.8),

$$\exp\langle\exp[iy\cdot n(t)]-1\rangle_0^L=\exp[n_2(e^{iy}-1)]$$
$$\times\exp\{n_0\ln[1+(e^{iy}-1)p]\}, \tag{9.27}$$

leads to the moments

$$\langle n(t)\rangle=n_2+pn_0,$$
$$\langle n(t)^2\rangle_0^L=n_2+p(1-p)n_0,$$
$$\langle n(t)^3\rangle_0^L=n_2+p(1-p)(1-2p)n_0,$$
$$\langle n(t)^4\rangle_0^L=n_2+p(1-p)[1-6p(1-p)]n_0,$$
$$\langle n(t)^s\rangle_0^L=n_2+n_0\sum_{r=1}^{s}(p^r/r)\sum_{l=1}^{r}(-1)^{l+1}{}_rC_l\,l^s, \tag{9.28}$$

CC-0. In Public Domain. Gurukul Kangri Collection, Haridwar

Digitized by Arya Samaj Foundation Chennai and eGangotri

where

$$n_2=(G/r)(1-e^{-rt}), \qquad p=e^{-rt}, \qquad {}_rC_l=r!/[l!(r-l)!].$$

We now return to the more general question of the evaluation of M_0, Eq. (9.9). This requires the solution of

$$dx/ds=[q(s)+r]x+q(s) \tag{9.29}$$

or

$$x(s)=x(t)\exp[r(s-t)]\exp\left[\int_t^s q(u)\,du\right]$$

$$+\int_t^s duq(u)\exp[r(s-u)]\exp\left[\int_u^s q(u')\,du'\right]. \tag{9.30}$$

The right-hand side is $\bar{x}(s\,|\,xt)$, and this result with $s=s$ and with $s=t_0=0$ can be substituted directly into (9.21). Since we are interested in $\hat{\phi}(0,\,t)$, we can set $x(t)=e^{iv}-1=0$. Our result again takes the product form

$$M_0=\exp\left[-G\int_0^t ds\int_s^t duq(u)\exp\left(\int_u^s[q(u')+r]\,du'\right)\right]$$

$$\times\left[1-\int_0^t du\exp\left(-\int_0^u[q(u')+r]\,du'\right)q(u)\right]^{n_0}. \tag{9.31}$$

As we check on our accuracy, we note that when $r=0$, we are dealing with a pure shot noise process, and M_0 reduces to the result

$$M_0(r=0)=\exp\left[-n_0\int_0^t q(s)\,ds\right]$$

$$\times\exp G\int_0^t ds\left[\exp\left(-\int_s^t q(u)\,du\right)-1\right] \tag{9.32}$$

expected from (8.26) or III (7F.21) for the shot-noise case.

A comparison between (9.31) and

$$M_0=\left\langle\exp\left[-\int_0^t q(s)n(s)\,ds\right]\right\rangle_0$$

$$=\exp\left[\sum_{r=1}^{\infty}\frac{(-1)^r}{r!}\int_0^t ds_1\cdots\int_0^t ds_r q(s_1)\cdots q(s_r)\right.$$

$$\left.\times\langle n(s_1)\cdots n(s_r)\rangle_0{}^L\right] \tag{9.33}$$

permits us to determine the linked moments:

$$\langle n(u)\rangle_0{}^L=(G/r)(1-e^{-ru})+n_0e^{-ru}, \tag{9.34}$$

$$\langle n(u_1)n(u_2)\rangle_0{}^L=(G/r)\{\exp[-r\,|\,u_1-u_2\,|\,)$$

$$-\exp[-r(u_1+u_2)]\},$$

$$+[n_0-(G/r)]\{\exp(-u_>)\rangle-\exp[-r(u_1+u_2)]\}, \tag{9.35}$$

$$\langle n(u_1)n(u_2)n(u_3)\rangle_0{}^L=(G/r)\{\exp[-r(u_l-u_s)]$$

$$-\exp(-ru_l)\}$$

$$+n_0\{\exp(-ru_l)-\exp[-r(u_1+u_3)]$$

$$-\exp[-r(u_1+u_2)]-\exp[-r(u_2+u_3)]$$

$$+2\exp[-r(u_1+u_2+u_3)]\}, \tag{9.36}$$

where $u_>$ is the larger of u_1, u_2; u_l is the largest of u_1, u_2, u_3 and u_s is the smallest of u_1, u_2, u_3. These results (9.35), (9.36) can be checked against (9.28) by setting $u_1=u_2=u_3=t$.

The quasilinear approximation exploited in I [in which the $D_s(n)$ are replaced by $D_s(G/r)$ for $s\geq 2$] yields the first term in (9.35), using I (8.18), but not the second term. Of course, if we average over n_0, the second term disappears. In other words, the quasilinear method gives second moments correctly, which justifies its use in I, but *not* conditional second moments that really contain third-moment information.

The approximation formula (8.26), yields the correct conditional second moment (9.35), but fails to yield the correct conditional third moment (9.36). This verifies our claim that the Langevin forces have the first and second moments (8.2), (8.3), but that higher moment (8.4) omits terms possessing a smaller number of delta functions.

Multidimensional Population Fluctuations

The procedures we have used to discuss one-dimensional population fluctuations can be immediately generalized to the multidimensional case. Equation (9.1 for the mean motion is to be replaced by

$$d\langle n(a)\rangle/dt=\sum_b\langle R_{ab}(\mathbf{n})\rangle$$

$$=\langle R_{aa}(\mathbf{n})\rangle+\sum_{b\neq a}\langle R_{ab}(\mathbf{n})\rangle, \tag{9.37}$$

where $\mathbf{n}$ stands for the whole set of occupancies $n(a)$ and R_{ab}, the rate of transitions from state b to state a, is an arbitrary function of the initial occupation numbers.

The probability $P[\mathbf{n},\,t]$ of a given set of occupation numbers $\mathbf{n}$ obeys a master equation

$$\partial P[\mathbf{n},\,t]/\partial t=\sum_{\mathbf{n}'}W(\mathbf{n},\mathbf{n}')P(\mathbf{n}',t)$$

$$-[\sum_{\mathbf{n}'}W(\mathbf{n}',\mathbf{n})]P(\mathbf{n},t) \tag{9.38}$$

where the transition probability from state $\mathbf{n}'$ to $\mathbf{n}$ is given by

$$W(\mathbf{n},\mathbf{n}')=\sum_{a,b}R_{ab}[\mathbf{n}']\delta[n(a),n'(a)+1]$$

$$\times\delta[n(b),n'(b)-1]\prod, \tag{9.39}$$

$$\prod\equiv\prod_{c\neq a,b}\delta[n(c),n'(c)],$$

includes the contributions of transitions from all states b to all states a (compare with I Sec. 12). Interchanging indices n and n',

$$W(\mathbf{n}',\mathbf{n})=\sum_{ab}R_{ab}[\mathbf{n}]\delta[n'(a),n(a)+1]$$

$$\times\delta[n'(b),n(b)-1]\prod, \tag{9.40}$$

$$\sum_{\mathbf{n}'}W(\mathbf{n}',\mathbf{n})=\sum_{ab}R_{ab}[\mathbf{n}].$$

Inserting these results into (9.38), the master equation

CC-0. In Public Domain. Gurukul Kangri Collection, Haridwar

Digitized by Arya Samaj Foundation Chennai and eGangotri

mplifies to

$$\frac{\partial P[\mathbf{n}, t]}{\partial t} = \sum_{a,b}\left\{\exp\left[\frac{\partial}{\partial n(b)}\right] \times \exp\left[-\frac{\partial}{\partial n(a)}\right] - 1\right\} R_{ab}(\mathbf{n})\, P[\mathbf{n}, t]. \quad (9.41)$$

The terms with $b=a$ cancel out of (9.41). In what ollows, therefore, we can take $R_{aa}=0$. The correspond- ng equation for the characteristic function obeys

$$\frac{\partial \phi(\mathbf{y}, t)}{\partial t} = \sum_{ab}[\exp(-iy_b)\exp(iy_a) - 1] R_{ab}\left(-\frac{\partial}{\partial \mathbf{y}}\right)\phi(\mathbf{y}, t). \quad (9.42)$$

The cases of Bose, Fermi, and Boltzmann collisions with a reservoir are described by

$$R_{ab} = [1+\epsilon n(a)]\, w_{ab} n(b) \quad (9.43)$$

or $\epsilon=1$, -1, and 0, respectively, as discussed in I Sec. 12 using the notation $x(a', a)$ for $R_{a'a}$. More general cases involving two-body collisions are discussed by Mathews, Shapiro and Falkoff.[35] The case (9.43) has the special simplicity of leading to a second-order partial differential equation. The Boltzmann case leads to a first-order differential equation solvable by the method of characteristics. In terms of the generating function[36]

$$\psi(\mathbf{z}, t) = \sum_{\mathbf{n}}\prod_{a} z_a{}^{n(a)} P(\mathbf{n}t \mid \mathbf{n}_0 t_0) \equiv \phi(\mathbf{y}, t), \quad (9.44)$$

where $\mathbf{z} = \exp(i\mathbf{y})$, the Boltzmann case simplifies to[35]

$$\partial\psi/\partial t = \sum_{ab} w_{ab}(z_a - z_b)\,\partial\psi/\partial z_b,$$

$$\psi(z, 0) = \prod_{c} z_c{}^{n(c,0)}, \quad (9.45)$$

If the system starts with occupancies $n(c, 0)$ at time 0. The characteristic equations are

$$d\mathbf{z}/dt = \mathbf{z}\cdot\mathbf{\Lambda}, \quad (9.46)$$

$$\Lambda_{bc} = -w_{bc}, \qquad \Lambda_{bb} = \sum_{c} w_{cb}, \quad (9.47)$$

so that the complete formal solution is

$$\psi(\mathbf{z}, t) = \prod_{c}[(\mathbf{z}\cdot\mathbf{U})_c]^{n(c,0)} = \prod_{c}[\sum_{a} z_a U_{ac}]^{n(c,0)}, \quad (9.48)$$

where

$$\mathbf{U} = \exp(-\mathbf{\Lambda}t), \qquad U_{ac} = [\exp(-\mathbf{\Lambda}t)]_{ac}. \quad (9.49)$$

The product implies that the total occupancy of state a is a sum of independent contributions from each of the $n(c, 0)$. For one of these contributions, with $p_a = U_{ac}$

$$[\sum z_a p_a]^{n(c,0)} = \sum\prod_{b} z_b{}^{n_b} p_b{}^{n_b}\frac{n(c,0)!}{n_b!}. \quad (9.50)$$

The coefficients of a given monomial $\prod_b z_b{}^{n_b}$, is the probability associated with that state [see (9.44)]. This coefficient

$$p_1{}^{n_1} p_2{}^{n_2}\cdots p_r{}^{n_r}\frac{n(c,0)!}{n_1!n_2!\cdots n_r!} \quad (9.51)$$

is simply the multinomial distribution that says that the $n(c, 0)$ particles are tossed randomly into the states with probability p_a of occupying state a. The complete probability distribution is a convolution of the separate distributions (for each c), and is not, in general, a multinomial distribution.[37] However, the linked moments for independent contributions are additive. Thus we can compute such *linked* moments *for each multinomial distribution and then add the results.* For any one factor $\psi_c(z, t)$, the *unlinked moments* are computed most easily by differentiation

$$\langle n(a, t)^{s_1} n(b, t)^{s_2} n(c, t)^{s_3}\cdots\rangle = \left(z_a\frac{\partial}{\partial z_a}\right)^{s_1}\left(z_b\frac{\partial}{\partial z_b}\right)^{s_2}\left(z_c\frac{\partial}{\partial z_c}\right)^{s_3}\cdots\psi_c(z, t). \quad (9.52)$$

Thus, for example,

$$\langle n(a, t)\rangle_0 = U_{ac} n(c, 0) \equiv \langle n(a, t)\rangle_0{}^L, \quad (9.53)$$

which is simply a solution of the first-moment equation

$$d\langle n(a, t)\rangle/dt = -\sum_{c}\Lambda_{ac}\langle n(c, t)\rangle,$$

subject to $\langle n(a, 0)\rangle = n(c, 0)\,\delta_{ac}$.

The use of $z_a\partial/\partial z_a\; z_b\partial/\partial z_b$ yields a contribution from $n(c, 0)$ of

$$\langle n(a, t) n(b, t)\rangle_0 = \delta_{ab} U_{bc} n(c, 0) + n(c, 0)[n(c, 0) - 1] U_{ac} U_{bc}, \quad (9.54)$$

$$\langle n(a, t)\rangle_0\langle n(b, t)\rangle_0 = [n(c, 0)]^2 U_{ac} U_{bc}. \quad (9.55)$$

Such *unlinked* moments are, strictly speaking, correct only if $n(d, 0) = 0$ for all $d \neq c$, and are not to be summed over c. The difference between (9.54) and (9.55) is a linked moment, however, and it is additive over c:

$$\langle n(a, t) n(b, t)\rangle_0{}^L = \sum_{c}[\delta_{ab} U_{bc} - U_{ac} U_{bc}] n(c, 0).$$

As $t\to\infty$, if $\mathbf{\Lambda}$ is well behaved,[38] the system approaches a *unique* steady state:

$$U_{ac} = [\exp(-\mathbf{\Lambda}t)]_{ac} \to p_a \qquad n(a, t) \to \bar{n}(a) = N p_a,$$

[35] P. M. Mathews, I. I. Shapiro, and D. L. Falkoff, Phys. Rev. 120, 1 (1960).

[36] W. Feller, *An Introduction to Probability Theory and Its Applications* (John Wiley & Sons, Inc., New York, 1950), Vol. I.

[37] If the initial condition is a multinomial distribution:

$$\psi(z, 0) = [\Sigma z_c p_c]^N$$

then

$$\psi(z, t) = [\Sigma z_a U_{ac} p_c]^N$$

remains a multinomial distribution [with probability $p_a(t) = \Sigma\, U_{ac}(t) p$] for all time (Ref. 35).

[38] Conditions on Λ that lead to a unique steady solution are discussed by S. Karlin and J. McGregor, Proc. Natl. Acad. Sci. 41, 387 (1955); and by W. Feller, Ann. Math. 65, 527 (1957).

CC-0. In Public Domain. Gurukul Kangri Collection, Haridwar

Digitized by Arya Samaj Foundation Chennai and eGangotri

where $N=\sum_c n(c,0)$ is the total number of particles. In the steady state:

$$\langle n(a)\rangle=\bar{n}(a),$$

$$\langle n(a)n(b)\rangle^L=\delta_{ab}\bar{n}(a)-(\bar{n}(a)\bar{n}(b)/N). \quad (9.56)$$

These results have previously been obtained in the quasilinear approximation I (12.36).

We now consider the characteristic functional

$$M_0=\left\langle \exp\left[-\int_0^t \mathbf{q}(s)\cdot\mathbf{n}(s)\,ds\right]\right\rangle_0=\hat{\phi}(0,t), \quad (9.57)$$

where $\hat{\phi}(\mathbf{y},t)$ and $\hat{P}(\mathbf{n},t)$ obey equations identical to (9.41), (9.42) except for an additive term $-\mathbf{q}(t)\cdot\mathbf{n}_{0p}$ as in (9.14). With $\hat{\phi}(\mathbf{y},t)\equiv\hat{\psi}(\mathbf{z},t)$, $\mathbf{z}=\exp(i\mathbf{y})$, Eq. (9.45) is modified to take the form

$$\partial\hat{\psi}/\partial t=\sum_{a,b}[z_a w_{ab}-(w_{ab}+q_b\delta_{ab})z_b]\partial\psi/\partial z_b$$

$$=-d\mathbf{z}/dt\cdot\partial\psi/\partial\mathbf{z} \quad (9.58)$$

with

$$d\mathbf{z}/dt=\mathbf{z}\cdot(\mathbf{\Lambda}+\mathbf{Q}), \quad (9.59)$$

where $\mathbf{\Lambda}$ is given by (9.47), as before, and

$$\mathbf{Q}_{ab}=q_b(t)\,\delta_{ab} \quad (9.60)$$

is a diagonal matrix.

Our general solution (9.48) *remains valid*, therefore, providing we interpret $\mathbf{U}$ now to be the solution of

$$d\mathbf{U}/dt=-(\mathbf{\Lambda}+\mathbf{Q})\cdot\mathbf{U}. \quad (9.61)$$

Setting $\mathbf{y}=0$, or $z_a=1$ in (9.48) we obtain

$$M_0=\left\langle \exp\left[-\int_0^t \mathbf{q}(s)\cdot\mathbf{n}(s)\,ds\right]\right\rangle_0$$

$$=\prod_c[\sum_a U_{ac}(t)]^{n(c,0)}. \quad (9.62)$$

In preparation for an expansion in powers of $\mathbf{Q}$ we set

$$\mathbf{U}=[\exp(-\mathbf{\Lambda}t)]\mathbf{W}, \quad (9.63)$$

$$d\mathbf{W}/dt=[\exp(\mathbf{\Lambda}t)\mathbf{Q}\exp(-\mathbf{\Lambda}t)]\mathbf{W}=\mathbf{V}(t)\mathbf{W}, \quad (9.64)$$

and make use of conservation of probability (9.47) to write

$$\sum_a \Lambda_{ab}=0, \qquad \sum_a[\exp(-\mathbf{\Lambda}t)]_{ab}=1,$$

$$\sum_a U_{ac}=\sum_a[\exp(-\Lambda t)]_{ab}W_{bc}=\sum_b W_{bc}. \quad (9.65)$$

The solution of (9.64) yields

$$\mathbf{W}=1+\int_0^t \mathbf{V}(s)\,ds+\int_0^t ds_1\int_0^{s_1}\mathbf{V}(s_1)\mathbf{V}(s_2)\,ds_2+\cdots, \quad (9.66)$$

$$\sum_a W_{ac}=1+\sum_b\int_0^t q_b(s)[\exp(-\mathbf{\Lambda}s)]_{bc}ds$$

$$+\int_0^t ds_1\int_0^{s_1}ds_2\sum_{b,d}q_b(s_1)\{\exp[-\mathbf{\Lambda}(s_1-s_2)]\}_{bd}$$

$$\times[\exp(-\mathbf{\Lambda}s_2)]_{dc}+\cdots. \quad (9.67)$$

Comparison with a linked moment expansion [see Eq. (8.21)] of the left-hand side of (9.62) yields the various conditional linked moments

$$\langle n(b,s)\rangle_0=[\exp(-\mathbf{\Lambda}s)]_{bc}n(c,0),$$

$$\langle n(a,t)n(b,u)\rangle_0^L$$

$$=\sum_c\{[\exp(-\mathbf{\Lambda}(t-u))]_{ab}[\exp(-\mathbf{\Lambda}u)]_{bc}$$

$$-[\exp(-\mathbf{\Lambda}t)]_{ac}[\exp(-\mathbf{\Lambda}u)]_{bc}\}n(c,0). \quad (9.68)$$

These results can be immediately specialized to a two level system

$$dn_2/dt=w_{21}n_1-w_{12}n_2=g(N-n_2)-rn_2$$

$$=w_{12}n_2-w_{21}n_1=-dn_2/dt. \quad (9.69)$$

We leave it as an exercise for the reader to discuss the statistics of such a two-level system, and to show that in the limit

$$N\to\infty, \qquad g\to 0, \qquad gN\to G, \quad (9.70)$$

these results reduce to those found in the generation-recombination model discussed earlier in this section.

General-Order Diffusion Coefficients

For use with Langevin techniques, it is convenient to have the general-order diffusion coefficients. These may be obtained by expanding (9.41):

$$\frac{\partial P[\mathbf{n},t]}{\partial t}=\sum_{a,b}\sum_{r,s}{}'\left[\frac{\partial}{\partial n(b)}\right]^r\left[\frac{\partial}{\partial n(a)}\right]^s\frac{(-1)^s}{r!s!}$$

$$\times[R_{ab}(\mathbf{n})P(\mathbf{n})], \quad (9.71)$$

where the primed sum omits the $r=0$, $s=0$ term and we take $R_{aa}=0$. Comparison of (9.71) with the generalized Fokker–Planck equation III (5.13) yields

$$r!s!D_{b^r a^s}=(-1)^r R_{ab}(\mathbf{n}), \quad (9.72)$$

where $D_{b^r a^s}$ is an abbreviation for a subscript containing $n(b)$ r times and $n(a)$ s times. If we set $b=c$, $r=1$, $s=0$ and $a=c$, $s=t$, $r=0$, we obtain all terms containing $[\partial/\partial n(c)]^t$. Thus

$$t!D_{(c)^t}=\sum_b R_{cb}+(-1)^t\sum_a R_{ac}$$

$$=\text{rate in}+(-1)^t(\text{rate out}). \quad (9.73)$$

just as in (9.4). For the special case $r=s$, it is convenient to symmetrize (9.72):

$$(r!)^2D_{b^r a^r}=(-1)^r\tfrac{1}{2}[R_{ab}+R_{ba}]. \quad (9.74)$$

The second moments (9.73) for $t=2$ and (9.74) for $r=1$ were obtained previously in I (12.25), I (12.24). They lead to the appropriate "shot-noise" Langevin forces:

$$\langle F_c(t)F_c(u)\rangle=\delta(t-u)[\sum_b R_{cb}+\sum_a R_{ac}], \quad (9.75)$$

$$\langle F_a(t)F_b(u)\rangle=-\delta(t-u)[R_{ab}+R_{ba}].$$

CC-0. In Public Domain. Gurukul Kangri Collection, Haridwar

Digitized by Arya Samaj Foundation Chennai and eGangotri

10. SUMMARY OF RESULTS

For a (nonstationary) Markoff process with linear decay: $\mathbf{A}\equiv\mathbf{D}_1=-\mathbf{\Lambda}(t)\cdot\mathbf{a}$ and homogeneous noise, i.e., whose nth order diffusion coefficients obey $\mathbf{D}_n(\mathbf{a},t)=D_n(t)$ for $n\geq 2$, we have shown that the corresponding Langevin description is given by[39]

$$d\mathbf{a}/dt+\mathbf{\Lambda}(t)\cdot\mathbf{a}=\mathbf{F}(t), \qquad (10.1), (2.1)$$

where $\langle\mathbf{F}(t)\rangle=0$, and the set of Langevin forces $\mathbf{F}$ possess the higher moments

$$\langle\mathbf{F}(t_1)\cdots\mathbf{F}(t_n)\rangle^L=n!D_n(t_1)\prod_{i=1}^{n-1}\delta(t_i-t_{i+1}), \quad (10.2), (2.4)$$

where the linked averages $\langle\ \rangle^L$ are defined in III (6.8) or in (2.5). Moreover, we have in (2.16) evaluated

$$\left\langle \exp i\int_0^t \mathbf{q}(u)\cdot\mathbf{a}(u)\,du\right\rangle,$$

where $\mathbf{q}(u)$ is an arbitrary (vector) function of the time.

For a process in which a single variable a is subject to jumps η at a rate ν with normalized distribution $g(\eta)$, we show that the moments D_n that determine either the generalized forward equation III (5.13) or the Langevin moments (2.34) are given by

$$n!D_n=\nu\langle\eta^n\rangle=\nu\int g(\eta)\,d\eta\eta^n. \quad (10.3), (2.33)$$

For the special case in which a is a population and particles enter or leave (at a total rate ν) with probabilities p_{in} and p_{out}, this reduces to

$$n!D_n=\nu[p_{\text{in}}+(-1)^n p_{\text{out}}]=\nu_{\text{in}}+(-1)^n\nu_{\text{out}}. \qquad (10.4), (2.40)$$

In Sec. 3, we have shown that the nonlinear Langevin process

$$da_i/dt=B_i(\mathbf{a},t)+\sum\sigma_{im}(\mathbf{a},t)f_m(t), \qquad (10.5), (3.20)$$

where the $f_m(t)$ are Gaussian variables with

$$\langle f_m(t)f_n(u)\rangle=2\delta_{mn}\delta(t-u), \quad (10.6), (3.21)$$

is precisely equivalent to a Fokker–Planck problem with drift vector $\mathbf{D}_1=\mathbf{A}$ and diffusion coefficient $\mathbf{D}_2$ given by

$$A_i=B_i+\sum_{mk}(\partial\sigma_{im}/\partial a_k)\sigma_{km}, \quad (10.7), (3.22)$$

$$D_{ij}=\sum_m\sigma_{im}\sigma_{jm}. \qquad (10.8), (3.23)$$

Under the transformation to new variables $a_i'=a_i'(\mathbf{a},t)$ we find

$$D_{ij}'=(\partial a_i'/\partial a_k)(\partial a_j'/\partial a_l)D_{kl}, \qquad (10.9), (3.27)$$

$$A_i'=\partial a_i'/\partial t+(\partial a_i'/\partial a_k)A_k+(\partial^2 a_i'/\partial a_m\partial a_n)D_{mn}, \qquad (10.10), (3.28)$$

so that A_i does *not* transform as a vector.

In Sec. 4 we show that the one-dimensional impurity band is a nonlinear Langevin problem with a "shot noise" random source. We derive the forward equation and the solution in the high density (Gaussian white noise) limit.

In Sec. 5, we consider the nonlinear, nonstationary random process

$$da_i/dt=B_i(\mathbf{a},t)+F_i(\mathbf{a},t,\xi(t)), \quad (10.11), (5.18)$$

where $\langle\mathbf{F}_i\rangle=0$ if the average is taken with $\mathbf{a}$ fixed, and $\xi(t)$ is a random variable with a finite correlation time short compared to the relaxation times contained in B_i but not necessarily short compared to all the natural frequencies of the system. We show that the drift vector A_i, and diffusion coefficient D_{ij} are given approximately by

$$A_i(\mathbf{a},t)=\frac{1}{\Delta t}\int_t^{t+\Delta t}ds'A_i(\mathbf{a},s',t), \quad (10.12), (5.50)$$

$$A_i(\mathbf{a},s',t)=B_i(\mathbf{a},t)+\int_{-\infty}^{s'}ds\left\langle\frac{\partial}{\partial\bar a_k(s)}\left[\frac{\partial a_i}{\partial\bar a_j(s')}F_j(s')\right]F_k(s)\right\rangle, \qquad (10.13), (5.51)$$

$$D_{ij}(t)=\frac{1}{\Delta t}\int_t^{t+\Delta t}ds'D_{ij}(s',t), \quad (10.14), (5.37)$$

$$D_{ij}(s',t)=\frac{1}{2}\int_{-\infty}^{\infty}ds\frac{\partial a_i}{\partial\bar a_k(s')}\frac{\partial a_j}{\partial\bar a_l(s)}\langle F_k(s')F_l(s)\rangle, \qquad (10.15), (5.38)$$

where $\bar a_i(s)$ is the solution at s to

$$da_i/ds=B_i(\mathbf{a}(s),s) \quad (10.16), (5.19)$$

subject to the initial conditions $\bar a_k(t)=a_k$, and $F_i(s)$ is an abbreviation

$$F_i(s)\equiv F_i(\bar{\mathbf{a}}(s),s,\xi(s)). \quad (10.17), (5.34)$$

The average over s' is to be taken over a time Δt large compared to the (fast natural frequencies)$^{-1}$ of the noise free motion, but small compared to the relaxation times. If the correlation time is short compared to all (frequencies)$^{-1}$ in the problem, the average over s' can be omitted, and s' simply replaced by t. In the spin-diffusion problem, Sec. 7, this condition was not met, yet the average over s' was found to be unnecessary. We found the average necessary in our discussion of quantum noise sources.[17]

[39] The second equation number gives the number in the main text where this equation appears.

CC-0. In Public Domain. Gurukul Kangri Collection, Haridwar

Digitized by Arya Samaj Foundation Chennai and eGangotri

In Sec. 6, a distribution function approach led to results that (a) were not averaged over s' (b) yielded an A_i in (6.35) that did not transform by the proper rule (3.28).

In Sec. 8, we attempt to find the Langevin process that corresponds to an arbitrary Markoff process with the moments $\mathbf{D}_1=\mathbf{A}(\mathbf{a}, t)$, $\mathbf{D}_2(\mathbf{a}, t)\cdots\mathbf{D}_n(\mathbf{a}, t)\cdots$. We find that

$$d\mathbf{a}/dt=\mathbf{A}(\mathbf{a}, t)+\mathbf{F}(\mathbf{a}, t), \quad (10.18), (8.1)$$

where

$$\langle\mathbf{F}(t)\rangle_0=0, \quad (10.19), (8.2)$$

$$\langle\mathbf{F}(t_1)\mathbf{F}(t_2)\rangle_0=2!\langle\mathbf{D}_2(\mathbf{a}, t_1)\rangle\delta(t_1-t_2), \quad (10.20), (8.3)$$

but that the higher linked moments, in addition to

$$\langle\mathbf{F}(t_1)\cdots\mathbf{F}(t_n)\rangle_0^L\approx n!\langle\mathbf{D}_n(\mathbf{a}, t_1)\rangle_0\prod_{i=1}^{n-1}\delta(t_i-t_{i+1}), \quad (10.21), (8.4)$$

also contain terms with fewer than $n-1$ delta functions. [The subscript 0 means averages holding $\mathbf{a}(t_0)$ fixed.]

In Sec. 9, we consider the problem of population fluctuations

$$dn(a)/dt=\sum_b R_{ab}(\mathbf{n})-\sum_b R_{ba}(\mathbf{n})+F_a(t), \quad (10.22), (9.37)$$

where R_{ab}, the rate of collisions that take a particle from state b to state a, can be an arbitrary function of $\mathbf{n}$. We show that the Langevin forces obey $\langle\mathbf{F}\rangle=0$ and

$$\langle\mathbf{F}_a(t)F_a(u)\rangle=\delta(t-u)[\sum_b R_{ab}(\mathbf{n})+\sum_b R_{ba}(\mathbf{n})],$$

$$\langle F_a(t)F_b(u)\rangle=-\delta(t-u)[R_{ab}+R_{ba}]. \quad (10.23), (9.3)$$

These are typical "shot-noise" results: The first bracket is the total rate in, plus the total rate out, of $\mathbf{a}$; the second is the sum of the rates from $\mathbf{a}$ to $\mathbf{b}$ and $\mathbf{b}$ to $\mathbf{a}$. The higher moments D_n are also obtained, in terms of the $R_{ab}(\mathbf{n})$.

In the usual Boltzmann case $R_{ab}(\mathbf{n})=w_{ab}n(b)$ is a linear function of $\mathbf{n}$, so that moments $\mathbf{D}_n$ are $\mathbf{n}$ dependent. Nevertheless, we find an exact solution (9.62) for the characteristic functional:

$$M_0=\left\langle\exp\left[-\int_0^t\mathbf{q}(s)\cdot\mathbf{n}(s)\,ds\right]\right\rangle_0.$$

We also discuss in detail the exact solution for the generation recombination problem $d\langle n\rangle/dt=g-r\langle n\rangle$ whose D_n's are linear in n. We show in this example that the conditional second moments of the Langevin forces are given correctly by (10.20) but that higher moments must have, in addition to (10.21) some less singular contributions.

ACKNOWLEDGMENTS

The author wishes to thank J. R. Klauder and D. R. Fredkin for numerous discussions during the development of this paper.

CC-0. In Public Domain. Gurukul Kangri Collection, Haridwar

Digitized by Arya Samaj Foundation Chennai and eGangotri

REVIEWS OF
MODERN PHYSICS

VOLUME 38, NUMBER 4 OCTOBER 1966

Quantization of Macroscopic Motions and Hydrodynamics of Rotating Helium II

E. L. ANDRONIKASHVILI, YU. G. MAMALADZE
Institute of Physics, Academy of Sciences of the Georgian SSR, Tbilissi, U.S.S.R.

This paper is a review of experimental data and theoretical studies devoted to the rotating helium II problem. The problem arose when helium II appeared to be rotating as a whole in a uniformly rotated container, while dragging of its superfluid component into rotation of a cylindrical vessel seemed impossible due to the absence of viscosity and Landau's requirement curl $\mathbf{v}_s=0$. Later it was found that imitation of a solid body rotation by helium II is realized by means of Onsager–Feynman's vortex lines which possess quantized circulation. In a uniformly rotating vessel they are distributed approximately uniformly along its cross section, aligned parallel to the axis of rotation, and cause a complicated velocity distribution at which curl $\mathbf{v}_s=(2\pi\hbar/m)\Sigma_v\delta(\mathbf{r}-\mathbf{r}_v)$, that is, Landau's requirement is valid everywhere excluding singular lines where the curl is equal to infinity ($\mathbf{r}_v$ is a two-dimensional radius vector of a vortex line in an arbitrary plane perpendicular to the axis of rotation).

In the review the experiments are described in which both an averaged picture of the joint rotation of the superfluid and the normal components is displayed and the studies in which the existence of vortex peculiarities is manifested in a clear manner. The measurements of the meniscus of rotating helium II and its angular momentum belong to the first group of these experiments ("integral" ones). Propagation of second sound, oscillations of solid bodies immersed into helium II, passage of negative ions, and different relaxation processes (acceleration and deceleration of the vessel, changes of temperature, etc.) form the second group ("local" experiments). The experiments in which the superfluid performs potential rotation, which can be persistent in the vessel at rest are also described. Vortex lines are absent there and the circulation of velocity can reach the value equal to a lot of elementary circulations.

Special attention is devoted to the problem of the nature of the phase transition helium I–helium II (and back) in the state of rotation.

The properties of rotating helium II illustrate brightly the main peculiarity of a quantum liquid, i.e., its complete inability to perform nonpotential motions. They show that Landau's requirement curl $\mathbf{v}_s=0$ remains valid even when the thermodynamical condition of the free-energy ($E-L\omega_0$) minimization gives preferrence to the velocity distribution of the type $v=\omega_0 r$.

CONTENTS

1. The Origin of the Rotating Helium II Problem..... 568
1.1. How the Problem of Rotating Helium II Has Arisen. 568
1.2. The First Observations of Rotating Helium II..... 569
1.3. Is Rotating Helium II a Superfluid?..... 569
1.4. Summary of the Aspects of the Rotating Helium II Problem by 1955..... 569
1.5. Purpose and the Plan of this Review..... 570
2. Principles of Onsager–Feynman Theory..... 570
2.1. Vortex Lines in the Superfluid Component of Helium II..... 570
2.2. Quantization of the Circulation..... 571
2.3. Energy and Tension of Vortex Lines..... 572
2.4. Rotation of a Superfluid Liquid..... 572
2.5. Density of Vortex Lines..... 572
2.6. The Critical Velocity of Vortex Formation..... 573
3. Vortex Lines in Uniformly Rotating Helium II. Imitation of the Solid Body Rotation by a Liquid..... 573
3.1. Meniscus of Rotating Helium II..... 573
3.2. The Angular Momentum of Rotating Helium II.... 574
3.3. Capture of Negative Ions by Rotating Helium II... 574
3.4. Does Helium II Rotate as a Whole?..... 576
3.5. Distribution of Vortex Lines over the Cross Section of a Rotating Vessel. Irrotational Regions..... 577
3.6. Distribution of Vortex Lines when There Is a Free Surface..... 579
3.7. Direct Observations of Vortex Lines in a Uniformly Rotating Helium II..... 579
4. Hydrodynamics of Rotating Helium II..... 580
4.1. Averaged Hydrodynamics of Rotating Helium II... 580
4.2. The Equations of Hydrodynamics of Rotating Helium II..... 581
4.3. Additional Boundary Conditions..... 581
5. Oscillations of Solid Bodies with Axial Symmetry in Rotating Helium II and Anisotropy of its Elastic–Viscous Properties..... 582
5.1. Anisotropy of Elastic–Viscous Properties of Rotating Helium II..... 582
5.2. Hydrodynamics of Small Oscillations of Bodies with Axial Symmetry in Rotating Helium II..... 585
5.3. Transverse Waves..... 586
5.4. The Mechanism of Interaction of an Oscillating Disk with a Rotating Viscous Liquid..... 587
5.5. The Mechanism of Interaction of an Oscillating Disk with a Rotating Superfluid Liquid..... 587
5.6. Resonance Phenomena..... 589
6. Oscillations of Solid Bodies with Axial Symmetry in Rotating Helium II (continuation). Sliding of Vortex Lines and Collectivization of Vortex Oscillations..... 591
6.1. Sliding of Vortex Lines..... 591
6.2. The Role of Sliding in an Interaction of an Oscillating Disk with Rotating Helium II..... 592
6.3. Collectivization of Vortex Line Oscillations..... 592

Copyright © 1966 by The American Physical Society
CC-0. In Public Domain. Gurukul Kangri Collection, Haridwar

Digitized by Arya Samaj Foundation Chennai and eGangotri

7. Mutual Friction between the Superfluid and Normal Components 594
7.1. The Concept of Mutual Friction in Rotating Helium II 594
7.2. The First Experimental Confirmation of Feynman's Theory 595
7.3. Further Investigations 595
8. Persistent Currents of the Superfluid Liquid 597
8.1. Observations of Persistent Currents 597
8.2. Persistent Current with an Elementary Circulation 597
8.3. An Irrotational Region and a Persistent Current ... 598
8.4. Dependence of a Persistent Current on Temperature 598
8.5. A Superfluid Gyroscope 599
8.6. The Critical Velocity 600
9. Stability of Helium II Motion between Two Cylinders Rotating with Different Angular Velocities 601
9.1. The First Experiments 601
9.2. Distribution of Velocities in a Liquid Rotating between Two Cylinders 601
9.3. Stability of Rotation of an Ideal Liquid 602
9.4. Stability of a Viscous Liquid Rotation 602
9.5. Stability of Helium II Rotation 602
10. Formation and Decay of Vortex Lines in Helium II 604
10.1. Dragging of Helium II into Rotation by a Moving Wall of a Container 604
10.2. Decay of Vortex Lines at the Stop of Rotation ... 607
10.3. Formation of Vortex Lines in Rotating Helium II at the Passage through the Point of the Phase Transition 608
10.4. Change of Vortex Damping at the Variation of Temperature 609
11. The Phase Transition in Rotating Helium II 611
11.1. A Central Macroscopic Vortex 611
11.2. Peculiarities of the Phase Transition of Helium II into Helium I in the State of Rotation 611
11.3. Does the Point of the Phase Transition Shift in Rotating Helium II? 613
11.4. The Order of the Phase Transition in Rotating Liquid Helium 614
12. Phenomenological and Microscopic Theory of Quantum Liquid Rotation 615
12.1. Phenomenological Quantum Theory of Helium II ... 615
12.2. Rotating Helium II in the Phenomenological Theory 615
12.3. Free Energy of Rotating Helium II 617
12.4. Critical Velocities and the λ-Point Shift 617
12.5. Why are Vortex Lines Formed in Rotating Helium II? 618
12.6. The Character of the Phase Transition at a Change of Temperature of Rotating Helium II 620
12.7. Rotation of Bose Gas 621
12.8. Vortex Lines in the Gas of Weakly Interacting Bose Particles and Rotation of Non-Ideal Bose Gas .. 622
12.9. The Rotating Helium II Problem and the Microscopic Theory of Superfluidity 623
Summary 623

1. THE ORIGIN OF THE ROTATING HELIUM II PROBLEM

1.1. How the Problem of Rotating Helium II Has Arisen

While explaining the experiments of Kapitza (1938a, b, 1941a, b), who discovered and studied the phenomenon of superfluidity, Landau (1941) suggested the two-fluid theory of a quantum liquid (see, also, Landau, 1944, 1947; Lifshitz and Andronikashvili, 1959). Using not quite rigorous, but very convenient, and therefore widely spread, terminology for the physical interpretation of the experimental facts, we can describe the main principles of this theory in the following way. Helium II consists of two fluids, one of them is a normal (n) component, which is an ordinary viscous liquid. The properties of this liquid depend on the existence of thermal excitations in helium, which are called rotons and phonons (in accordance with the different types of energy dependence on the momentum in different parts of the dispersion curve). The other one is a superfluid (s) component with zero viscosity and zero entropy. In addition, it cannot perform rotational potential motions. The character of motion of each of the components can be quite different. In other words, one can axcribe two celocities $\mathbf{v}_n$ and $\mathbf{v}_s$ and two densities ρ_n and ρ_s to each point of space, so that $\rho_n+\rho_s=\rho$. Here ρ is an ordinary density of the liquid, while ρ_n and ρ_s are the effective densities of motions performed with the velocities $\mathbf{v}_n$ and $\mathbf{v}_s$, respectively. With a rise in temperature, elementary excitations (phonons and rotons) involve larger and larger parts of the liquid in thermal motion, and thus the normal component density is increased, while that of the superfluid one is decreased: $\rho_n/\rho=0$, when $T=0°\mathrm{K}$ and $\rho_n/\rho=1$, when $T=T_\lambda=2.17°\mathrm{K}$. The latter temperature corresponds to the point of the phase transition.

Simultaneous with the creation of his theory, Landau suggested some experiments to test its validity. One was an experiment in which the properties of helium II in a rotating vessel would be studied. It was assumed that, because of the absence of viscosity and the necessity of maintaining the condition curl $\mathbf{v}_s=0$, the superfluid component would not take part in the rotation of the vessel and only the normal component would be rotated.

Such an experiment, the aim of which was to show directly the possibility of the simultaneous existence of two independent fields of velocities $\mathbf{v}_s$ and $\mathbf{v}_n$, was really performed by Andronikashvili (1946, 1948a), but in quite a modified form. Axial oscillations of a vessel with a pile of closely spaced parallel thin disks, suspended in helium II by means of an elastic thread, were realized instead of rotation. The normal component was dragged into the motion of the disks completely, while the superfluid one did not take any part in it. One could detect this phenomenon by measurements of the period of oscillations of the suspended system, determined by its moment of inertia. This moment of inertia consisted of the moment of inertia of the vessel and that of the normal component. The investigations performed allowed confirmation of the existence of the two components in helium II and the possibility of the simultaneous realization of two different motions in this liquid, as well as establishing the temperature dependence of ρ_n.

At that time, the difference between rotation and axial oscillations seemed quite unessential. But soon, when Andronikashvili (1948b, published in the paper of Andronikashvili and Kaverkin, 1955) performed an experiment with really rotating helium, the result was

CC-0. In Public Domain. Gurukul Kangri Collection, Haridwar

Digitized by Arya Samaj Foundation Chennai and eGangotri

quite different. Helium II seemed to rotate like a solid body.

1.2. The First Observations of Rotating Helium II

The idea of the experiment mentioned above, as well as that of the similar Osborne's experiment (1950), was the following. As is well known, a rotating viscous liquid eventually forms a parabolic meniscus, the shape of which depends on the force of gravitation and on centripetal force. Because of that, in particular, the depth of the meniscus h is equal to

$$h=\omega_0^2R^2/2g, \qquad (1.2.1)$$

where ω_0 is the angular velocity of rotation, R is the radius of the vessel, and g is the acceleration of gravity. It would seem that in the case of helium II the whole thing would be quite different. In this case the force of gravity acts on the whole bulk of the liquid, while the centripetal force would have to act only on its normal component, since it is assumed that the superfluid component does not rotate. Therefore, one should expect that the shape of the meniscus would depend on the amount of the superfluid component, i.e., on temperature, and its depth would be determined by the formula

$$h=(\rho_n/\rho)(\omega_0^2R^2/2g). \qquad (1.2.2)$$

In both experiments described, vessels with a radius of the order of centimeters were used and the velocity of rotation was about some tens of radians per second. There was no difference in the depths of the meniscus of helium I and helium II at any temperature and velocity of rotation. Formula (1.2.1) was always rigorously maintained, which gave an impression that helium rotated like a solid body.

Thus, in these experiments helium II behaved as if it were rotating as a classical liquid. The only small difference which could be noticed at maximum velocities of rotation was that a small conic pit appeared at maximum velocities of rotation on the lower part of the parabolic meniscus (Andronikashvili and Kaverkin, 1955).

Participation of the superfluid component in rotation of the vessel was also found in the experiments of Hall (1955; see, also, Hall and Vinen, 1955), who used a vessel filled with closely spaced disks for this purpose, which dragged the normal component into motion completely. The angular momentum of helium II was measured by determination of the torsion effect, which was required to accelerate and slow down the liquid.

In addition, Hall and Vinen (1955) have shown that rotating helium II renders an additional resistance to propagation of thermal waves called second sound. Attenuation of these waves in their propagation perpendicularly to the axis of rotation depended on velocity, increasing linearly with an increase of ω_0. For propagation of second sound along the rotation axis, its attenuation was the same as in helium II at rest.

1.3. Is Rotating Helium II a Superfluid?

At the time when nothing was known about the physical nature of critical phenomena in helium II, any interaction of the superfluid component with the walls of the vessel or with the normal component caused an idea of the breakdown of superfluidity. Such a possibility was foreseen by Landau's theory, according to which a body moving in helium II with the velocity of about 60 m/sec could generate thermal excitations (rotons) there. In this way, the liquid lost the ability to flow without friction. The idea of the breakdown of superfluidity also appeared in the association of the establishment of a solid-body rotation of helium. But it was found (Andronikashvili and Kaverkin, 1955) that the fountain effect[1] continued to exist in rotating helium II and had the same value as in helium II at rest. This fact was an obvious demonstration of the existence of the superfluid, which, being a liquid with zero entropy, flows towards a source of heat to get entropy and become normal. Moreover, it was also established that the relative content of the superfluid and normal components did not depend on the velocity of rotation.

We have already mentioned the experiments performed by Hall and Vinen (1955). In them the existence of the superfluid component in rotating helium II and the independence of its amount on the velocity of rotation were displayed in the absence of any dependence of the velocity of second-sound propagation u on ω_0 (u is, as is known, a function of the ratio ρ_s/ρ_n).

1.4. Summary of the Aspects of the Rotating Helium II Problem by 1955

Thus the rotating helium II problem arose in Andronikashvili's and Osborne's experiments as early as the end of the forties, when oscillating disk experiments were already finished, and not in 1941, when Landau proposed an experiment with rotating helium II. We can hardly be sorry about this delay. On the contrary, though it may sound paradoxical, one might fear that the discovery of the superfluid participation in the rotation of the container could have slowed down the development of the theory of superfluidity for several years. Fortunately, this fact was established only after the first confirmations of Landau's theory had been obtained in the experiments with a pile of oscillating

[1] The fountain effect is a phenomenon in which the superfluid component has a tendency to move through narrow pores or slits towards a source of heat. Since the normal component under such conditions cannot move towards the superfluid, a pressure difference arises on the porous partition. It is one of the particular manifestations of the thermomechanical effect which causes the superfluid component motion in the direction of the temperature gradient, while the normal component flows in the opposite direction [see Eqs. (4.2.1) and (4.2.2)].

CC-0. In Public Domain. Gurukul Kangri Collection, Haridwar

Digitized by Arya Samaj Foundation Chennai and eGangotri

disks and in experiments with second sound. A number of successes of the theory followed, and an unexpected result of one experiment could not have shaken the confidence in the validity of the principal ideas of the two-fluid hydrodynamics of helium II. In addition, the qualitative characteristics of many phenomena, which were specific for superfluid helium, were well studied by that time. Some of them, in particular the fountain effect and second sound, had been observed in rotating helium. This was a very essential thing, which showed that the existence of the superfluid component rotation did not mean the breakdown of superfluidity. In this respect, the experiment did not contradict Landau's theory, according to which the corresponding critical velocity was about 60 m/sec, while in the experiments of Osborne, Andronikashvili, and Kaverkin, and Hall and Vinen the maximum velocity on the periphery of the container was several orders smaller. Only the existence of the superfluid component in these experiments showed that the nature of the critical phenomena is not connected with the breakdown of superfluidity spoken about in Landau's theory.

Nevertheless, the mechanism of dragging of the superfluid component into rotation and the very character of this rotation remained quite obscure. In particular, the question of the maintenance of the Landau condition, curl $\mathbf{v}_s=0$, remained open. It seemed that most probably this condition was broken, and the theory required an essential revision of its principles.

1.5. The Purpose and the Plan of this Review

While writing this review, the authors aimed at showing how the problems summarized in the previous paragraph were explained and at describing the further development of theoretical and experimental studies of rotating helium II. Section 2 is devoted to ideas of Onsager and Feynman, who developed Landau's theory for supercritical phenomena. The Landau–Onsager–Feynman conception is the basis of all further considerations. Then, beginning with Sec. 3, without any chronological order, the authors systematically describe the main results of practically all experimental and theoretical investigations devoted to the rotating helium problem.

However, attention is mainly devoted to those experiments, the precision and clarity of purposes of which provided the possibility of a quantitative treatment of the data obtained, or at least extraction of important qualitative conclusions from them. A similar principle has been used for the description of the results of theoretical investigations when we tried, in the main, to show clearly the physical picture of the phenomena considered. Wishing to describe all the observed phenomena from one general point of view, the authors have deliberately avoided Lin's hydrodynamics (1959, 1963), in spite of the fact that without doubt it is interesting and deserves great attention. The authors think that at present there are not sufficient data to oppose this theory to the Landau–Onsager–Feynman conception or to give a parallel interpretation of phenomena using Lin's conception. On the one hand, there are no results of some decisive experiment, which could not have been explained by the Landau–Onsager–Feynman theory. On the other hand, there are no solutions of sufficient number of concrete problems within the framework of Lin's theory, without which it is impossible to describe all or at least the most available data from the point of view of this theory.

2. PRINCIPLES OF ONSAGER–FEYNMAN THEORY

2.1. Vortex Lines in the Superfluid Component of Helium II

It has already been noted that the critical phenomena connected with the appearance of an interaction of the superfluid component and solid bodies have nothing to do with the breakdown of superfluidity. In accordance with Onsager's assumption (1949), they are connected with the appearance of vortex lines in the superfluid component of helium II. The circulation of such vortex lines is quantized in units of $\Gamma_0=h/m$ (where h is Planck's constant and m is the mass of the helium atom). In the precritical regime, the superfluid does not interact with solids (Dalamber's paradox). But in the postcritical regime, when vortex lines are present, it can have such an interaction without losing its superfluid properties. Let us recollect that a classical ideal liquid, when it has vortex lines, also breaks Dalamber's paradox (vortex resistance).

As for the circulation quantization, it explains the very fact of the critical velocity's existence. Indeed, if a vortex line cannot exist in a state with an arbitrary small intensity (circulation), then vortex formation can take place only if some minimum energy is available in the stream of fluid or in a body immersed into the liquid.

However, it is well known that the classical theorems of Helmholtz–Thomson–Lagrange forbid general vortex formation in an absolutely ideal liquid performing potential motion. Even now it is not quite clear what properties of a quantum liquid allow breaking the requirements of those theorems. Nevertheless, Feynman used quantum-mechanical ideas to explain the possibility of vortex formation and showed that a vortex hypothesis can explain the established fact of the superfluid rotation (1955, 1957).

The argument in favor of the possibility of vortex existence in a superfluid is associated with consideration of the following situation. Let helium II at the temperature absolute zero ($\rho_n=0$) be at rest in a semispace $z<0$ and in the state of uniform motion along the x axis in the semispace $z>0$. Then if the wave function of the liquid at rest is Φ_0, the wave function in the upper semispace will be $\Phi_0 \exp(ikx)$, where k is the wave number, related in the usual way to the velocity of motion. We shall question what will happen further.

CC-0. In Public Domain. Gurukul Kangri Collection, Haridwar

Digitized by Arya Samaj Foundation Chennai and eGangotri

whether such a state of the liquid will remain or whether an interaction between the semispaces will take place, bringing into motion the liquid in the lower semispace as well. The absence of viscosity excludes the presence of tangent forces on the interface $z=0$, and one can think that volumes of helium in the state of motion and of helium at rest are really isolated from each other and that the surface energy of the interface $z=0$ is higher, the higher is the relative velocity [Fig. 2.1(a)]. But we pay attention to the fact that the function $\Phi_0 \exp(ikx)$ turns periodically into Φ_0 with the period $\Delta x = 2\pi/k$. On the corresponding lines (parallel to the y axis), the conception of the surface energy of the interface becomes senseless and nothing can prevent moving helium from flowing into the region of helium at rest and make it move to the other side of the interface. But the interface cannot exist in the form of flat strips; their cross sections are shown in Fig. 2.1(b). The surface tension should draw them up into lines (points in the section), and they would quite disappear if there were no centrifugal forces created by rotation of the liquid [Fig. 2.1(c)]. Estimation of the radius of cylinders formed in such a way, according to the equilibrium of the surface tension forces and centrifugal one, gives a meaningless value of the order of some tenths of an angstrom. It is clear that in such a case either the radius of the order of interatomic distances in helium II (Feynman used the magnitude $a_0 = 4$ Å) would be ascribed to this cylinder (to the vortex core) or the use of such macroscopic conceptions as surface tension or size of a hollow core in general should be renounced in favor of a more detailed description. For such a more detailed quantum description, a vortex line should be considered as a node line of the wave function, i.e., the line on which the wave function is equal to zero.[2] Then the parameter a_0 acquires the meaning of a characteristic distance from this line, within which the density of the liquid is appreciably different from its value in bulk. We return to such a description in Sec. 12.

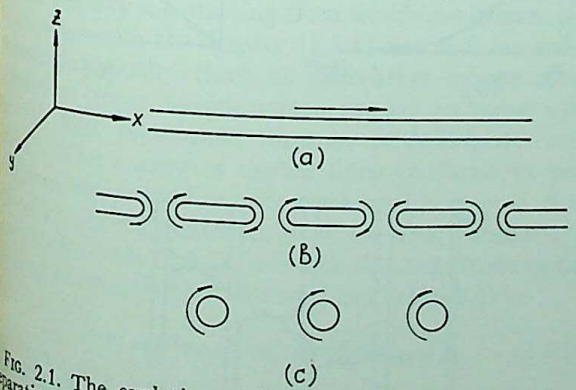

FIG. 2.1. The evolution of ideas on the nature of interface separating semispaces with helium II at rest and in the state of motion: (a) solid surface; (b) the surface torn along the lines on which wave functions of helium at rest and in motion coincide; (c) surface tension and centrifugal force make the "strips" of the interface cylindrical.

[2] It should be noted, as Feynman pointed out, that the appearance of node lines in an excited state is characteristic of the general behavior of quantum systems. Let us recollect, for instance, a harmonic oscillator. Its wave function in an unexcited state has no nodes, and each next stage of excitation increases the number of its nodes.

Though the present consideration represents a speculative experiment rather than a study of some real process, we think it has a deeper sense. Evidently it shows instability of tangent discontinuity of velocity well known in the case of a classical liquid (Landau and Lifshitz, 1953). Figure 2.1 then represents to some extent the real course of the events after a jet of superfluid flows from a hole into a large volume. Apparently the process of a vortex street formation following the motion of a body in a superfluid liquid is developed in a similar way (von Karman's chains).

2.2. Quantization of the Circulation

Having generalized the wave function of uniformly moving helium II $\Phi_0 \exp[(m/\hbar)\sum_a \mathbf{v}\cdot\mathbf{R}_a]$ (the sum is taken over all the atoms of the system), Feynman suggested writing the wave function arbitrarily moving helium II ($T=0°$K) in the form $\Phi_0 \exp(i\phi)$. The velocity of the liquid flow is related with the phase of the wave function by the expression $\mathbf{v}_s = \hbar\nabla\phi/m$. The existence of a vortex line requires a change of the wave function phase on going once round a singular point (line). However, because of the unambiguity of the wave function, the change of its phase cannot be arbitrary at one complete revolution, but should be a multiple of 2π. Considering rotation of a liquid particle round a vortex line, the phase change per revolution along the circumference with a vortex line as its center will be equal to

$$\oint \nabla\phi = d\mathbf{r}\frac{2\pi r m v_s}{\hbar};$$

hence, the condition of circulation quantization will be (n is an integer):

$$2\pi r v_s = n(2\pi\hbar/m), \qquad (2.2.1)$$

or in a more general form (for an arbitrary contour),

$$\Gamma \equiv \oint \mathbf{v}_s \cdot d\mathbf{r} = n(2\pi\hbar/m) \equiv n\Gamma_0. \qquad (2.2.2)$$

Since the circulation along any contour is equal to a sum of circulations along the contours it contains, condition (2.2.2) is valid for integration over a closed curve including a number of vortex lines. The number n in this case is a sum of integers, characterizing intensities of different vortex lines. In particular, if all the vortex lines are unit ones (with the circulation Γ_0), this number is simply equal to the number of vortex lines in the contour.

Thus the formation of superfluid vortex lines was the first phenomenon that required application of the quantization principle, similar to Bohr's postulate, to the motion the scale of which can be measured even

CC-0. In Public Domain. Gurukul Kangri Collection, Haridwar

Digitized by Arya Samaj Foundation Chennai and eGangotri

by centimeters. It is essential that according to (2.2.1) the distribution of the superfluid velocity round the vortex line is given by the law

$$v_s = n\hbar/mr. \qquad (2.2.3)$$

It means that one of the main requirements of Landau's theory, namely, curl $\mathbf{v}_s = 0$, which remains valid over all the bulk of the liquid (because of the determination of the velocity by means of the gradient of the phase), is broken only on vortex lines themselves, where the curl is infinite but the density is equal to zero.

2.3. Energy and Tension of Vortex Lines

Now let us calculate the energy of a liquid rotating according to law (2.2.3). For unit length of a vortex line, it is

$$\epsilon = \int \frac{\rho_s v_s^2}{2} 2\pi r\, dr = \pi\rho_s \frac{\hbar^2}{m^2} \ln\frac{b}{a_0}, \qquad (2.3.1)$$

where b is the effective radius of a vortex line determined by the dimensions of the vessel (if there is one vortex line) or by the vortex separation (if there are many vortex lines).

According to Bernoulli's equation, pressure in a liquid is equal to $P = P_0 - \rho_s v_s^2/2$, where, in the case of rotation according to (2.2.3), P_0 is the maximum pressure at an infinite distance from a vortex line. Nearer the core of a vortex line, the pressure decreases, creating the force with which a vortex line is attached to the surface on which it ends (Hall, 1957a). As a result, a vortex line is in a strained state and its tension force is $\int (P_0 - P) 2\pi r\, dr$, and according to (2.3.1) it coincides numerically with the energy ϵ of its unit length [this is clear, since its tension is equal to $\partial(\epsilon s)/\partial s$, where s is the vortex line length]. Elastic properties of vortex lines are determined by these phenomena.

2.4. Rotation of a Superfluid Liquid

The physical nature of critical phenomena in helium II is connected with the fact that a superfluid liquid, remaining superfluid, interacts, because of the existence of vortex lines, with solids or with the normal component.

Feynman has shown that the critical velocities of vortex formation are much lower than that of the breakdown of superfluidity caused by roton formation (according to Landau this velocity is 60 m/sec). It should be emphasized once more that critical phenomena at low velocities have nothing in common with the breakdown of superfluidity and, therefore, do not contradict Landau's theory.

Potential rotation, described by formula (2.2.3), is unfavorable thermodynamically. Rotation performed according to the law

$$v = \omega_0 r, \qquad (2.4.1)$$

characteristic of a viscous liquid, provides a smaller value of the energy E at a given momentum $\mathbf{L}$ or, that is the same a smaller value of the free energy $F = E - \mathbf{L}\cdot\boldsymbol{\omega}_0$. But Feynman has noticed that in the presence of a great number of vortex lines, which (interacting with each other and being also attached to the bottom and top or to a free surface) rotate together with the vessel, the summary distribution of velocities in a superfluid liquid approaches closely law (2.4.1). This situation is illustrated by Fig. 2.2, which shows schematically that the mean velocity of the superfluid is also determined by the formula $\bar{v}_s = \omega_0 r$ at the motion of vortex lines according to the law $v_L = \omega_0 r$. The difference between the true value of the velocity in a given point and the mean velocity is essential only in the vicinity of the considered vortex line. The existence of a number of vortex lines with unit circulation provides greater proximity of $\bar{v}_s$ to $\omega_0 r$ than the existence of a smaller number of vortex lines with great circulations. Therefore it is natural to consider that all the vortex lines have the circulation Γ_0 in uniformly rotating helium II.

2.5. Density of Vortex Lines

Let us consider some circumference with the center on the axis of rotation. The circulation of the mean velocity on it will be $2\pi r \cdot \omega_0 r$; on the other hand, as it has been already mentioned, it is equal to the number of vortex lines multiplied by Γ_0. Therefore the number

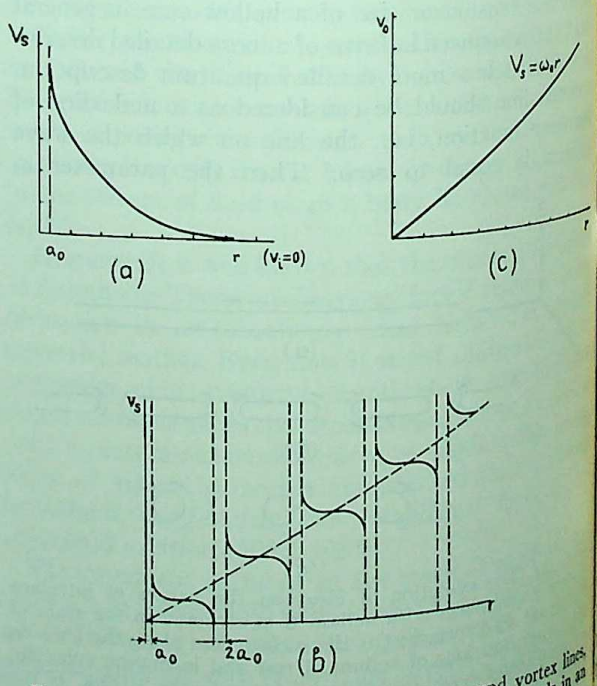

FIG. 2.2. Curl-free rotation of the liquid around vortex lines which in their turn rotate around the common axis, leads in an average to solid-body rotation of the liquid around this axis. The figure shows: (a) the distribution of velocity around unit stationary vortex line, a_0 is the radius of the vortex core; (b) the distribution of velocities around some vortices the cores of which rotate according to the law $v_L = \omega_0 r$; (c) the distribution of velocities averaged over the volume containing several vortices.

CC-0. In Public Domain. Gurukul Kangri Collection, Haridwar

Digitized by Arya Samaj Foundation Chennai and eGangotri

of vortex lines piercing the unit cross section of the liquid is

$$N = 2\omega_0/\Gamma_0 = m\omega_0/\pi\hbar. \qquad (2.5.1)$$

When $\omega_0 = 1$ sec^{-1}, this formula gives $N \approx 2\times 10^3$ vortex lines per square centimeter.

2.6. The Critical Velocity of Vortex Formation

The angular velocity of rotation at which the first vortex line appears on the axis of a cylindrical vessel with the radius R was calculated by Arkhipov (1957) and Vinen (1958a):

$$\omega_{c1} = [\hbar/m(R^2 - a_0^2)] \ln (R/a_0). \qquad (2.6.1)$$

When $\omega_0 > \omega_{c1}$,[3] the contribution of a vortex line into the magnitude $E - L\omega_0$ becomes negative as the value of E for unit lengths is determined by formula (2.3.1) and $l = L/s = \pi\rho_s\hbar(R^2 - a_0^2)/m$. It is easy to see by means of the direct calculation of the integral $l = \int \rho_s v_s \cdot 2\pi r\, dr$, where v_s is determined by formula (2.2.3). Therefore, starting from this velocity, the vortex formation is favorable thermodynamically. The critical velocity ω_{c1} is very small. When $R \sim 10$ cm, it is $\omega_{c1} \sim 10^{-5}$ sec^{-1}, when $R \sim 1$ cm, it is $\omega_{c1} \sim 10^{-3}$ sec^{-1}. Hence, almost at any real velocities of the vessel, rotating helium is in the supercritical regime and contains a lot of vortex lines. The only exception arises for devices with extremely small characteristic dimensions.

When $\omega_0 \gtrsim \omega_{c1}$, the number of vortex lines is not yet determined by Feynman's formula (2.5.1). Formula (2.5.1), when $\omega_0 = \omega_{s1}$, gives the expression $N \cdot \pi R^2 = \ln (R/a_0)$ for the total number of vortex lines in the cylinder instead of unity. This magnitude is always bigger than unity. In this connection, Kiknadze, Mamaladze, and Cheishvili have also estimated the critical velocity ω_{s1}' starting from which the presence of vortex lines with the density (2.5.1) becomes favorable thermodynamically. Such an estimation can be made proceeding from considerations similar to those used for the just mentioned formula of Arkhipov–Vinen (2.6.1). The energy of vortex lines (reduced to unit height of the vessel) is estimated in this case as $E_1 = E_{sb} + E_v$; $E_{sb} = 0.25\omega_0^2 R^4 \pi\rho_s' E_v = N \cdot \pi R^2 \cdot \epsilon$, where ϵ is given by formula (2.3.1), in which the magnitude of the order of $(\hbar/m\omega_0)^{\frac{1}{2}}$ should be used as $b(\pi b^2 \sim 1/N)$:

$$E_v = \omega_0 R^2 \pi\rho_s (\hbar/m) \ln (\hbar/m\omega_0 a_0^2)^{\frac{1}{2}}. \qquad (2.6.2)$$

The angular momentum of the superfluid component caused by vortex lines L_1 (also reduced to unit height), when there is a lot of vortex lines, coincides with its value at rotation of the liquid as a whole. As the contribution of each vortex line is $\pi\rho_s(\hbar/m)(R^2 - r^2)$, where r is the distance from the vortex line to the cylinder axis, we have the following:

$$L_1 \approx \int_0^R \pi\rho_s \frac{\hbar}{m}(R^2 - r^2)\frac{m\omega_0}{\pi\hbar} 2\pi r\, dr = \tfrac{1}{2}\omega_0 R^4 \pi\rho_s. \qquad (2.6.3)$$

Hence, the contribution made by vortex lines to the magnitude $E - L\omega_0$ becomes negative when $\omega_0 = \omega_{c1}'$, where $\omega_{c1}' = E_1/L_1$:

$$\omega_{c1}' = (4\hbar/mR^2) \ln (\hbar/m\omega_{c1}' a_0^2)^{\frac{1}{2}} \sim 4\omega_{c1}. \qquad (2.6.4)$$

As the value of the magnitude ω_{c1} is small, one can conclude from formula (2.6.4) that the formation of vortex lines and the increase of their density until equal to the values corresponding to formula (2.5.1) takes place in a very narrow interval of angular velocities in rotating vessels, the dimensions of which are not extremely small. At the beginning of this interval, the number of vortex lines could be equal to $\ln R/a_0$, according to (2.5.1), but the presence of only one vortex line is favorable thermodynamically. At the end of this interval, the favorable number of vortex lines is equal to $2 \ln (\hbar/m\omega_{c1}' a_0^2)^{\frac{1}{2}}$; that is in complete agreement with formula (2.5.1).

3. VORTEX LINES IN UNIFORMLY ROTATING HELIUM II. IMITATION OF THE SOLID BODY ROTATION OF A LIQUID

3.1. Meniscus of Rotating Helium II

It was said in the previous sections that, in the experiments of Osborne (1950) and Andronikashvili and Kaverkin (1955), the meniscus of rotating helium II was such as if the liquid rotated like a solid body.

Turkington, Brown, and Osborne (1963) reduced the minimum value of the angular velocity to $\omega_0 = 1.58$ sec^{-1} and used an oblique light beam, reflected from the meniscus, to measure the curvature of the free surface of the liquid. The results are shown in Fig. 3.1.

The curvature of the free surface of a thin layer of helium II at the bottom of a rotating cylindrical container was measured by a very sensitive method by Meservey (1964). The depth of the liquid layer was only 5×10^{-3} cm. The meniscus of rotating helium II, at rotation with the velocity to 0.29 sec^{-1}, at 1.1°K, was indistinguishable from the meniscus of a classical liquid. The results of Meservey are given in Fig. 3.2.

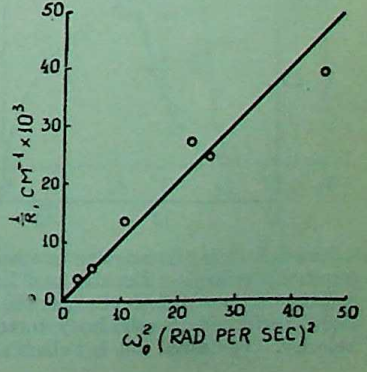

FIG. 3.1. Dependence of the meniscus curvature on the rotation velocity according to the data of Turkington, Brown, and Osborne (1963).

[3] The symbol ω_{c1} is introduced in an analogy with the first critical field H_{c1}, beginning from which Abrikosov's vortex lines are created in superconductors of the second kind.

CC-0. In Public Domain. Gurukul Kangri Collection, Haridwar

Digitized by Arya Samaj Foundation Chennai and eGangotri

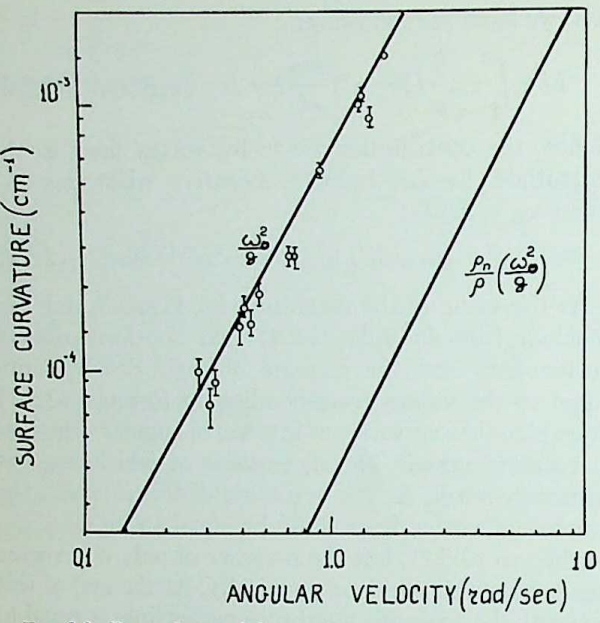

FIG. 3.2. Dependence of the meniscus curvature on the rotation velocity according to the data of Meservey (1964).

3.2. The Angular Momentum of Rotating Helium II

The experiment of Hall mentioned previously (Hall 1955, Hall and Vinen, 1955), developed in his next paper (1957), was a direct realization of Landau's suggestion on the measurement of the moment of inertia of rotating helium II. The angular momentum and, hence, the moment of inertia were found to correspond to the rigid body rotation of the liquid (see, however, Secs. 8.1, 8.6).

Reppy, Depatie, and Lane (1960) observed rotation of a transparent cylindrical vessel, filled with helium II around a vertical axis. The vessel suspended by means of a Beams type magnetic bearing, obtained suddenly an angular momentum during 0.5 sec. After that observations were made of the time dependence of the rotation velocity. It is found that the angular momentum of the liquid in these experiments is always a classical one, in other words, the liquid under all conditions performs a solid body rotation together with the vessel. In Fig. 3.3 the temperature dependence is given

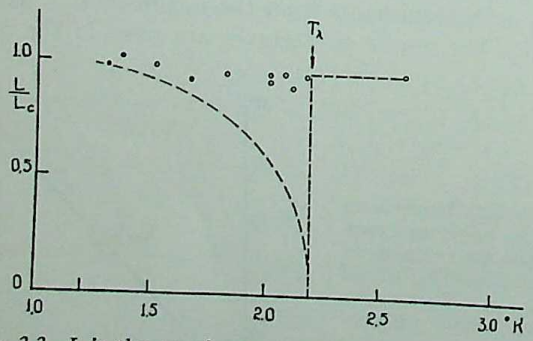

FIG. 3.3. L is the angular momentum of rotating helium II, measured by Reppy, Depatie, and Lane (1960). The velocity of rotation is about 0.2 sec^{-1}. L_c is the classical momentum of the liquid performing a solid-body rotation with the same angular velocity. The dashed line is Pellam's curve (compare Fig. 3.10).

of the ratio L/L_c, where L is the measured angular momentum and L_c is its classical value, corresponding to the solid body rotation. This ratio is equal to unity over all the range of measured temperatures.

3.3. Capture of Negative Ions by Rotating Helium II

A number of papers is devoted to ion motion in liquid helium [see, for instance, reviews of Careri (1961, 1963) and Atkins (1963)]. In particular, having studied vortex rings formed by fast moving ions in helium II, Rayfield and Reif (1963, 1965) proved quantization of their circulation and measured the radius of their core, obtaining the value $a_0 \sim 1$ Å.

The results of study of ion motion in rotating helium II were some of the serious confirmations of the existence of vortex lines in it.

Careri, McCormick, and Scaramuzzi (1962) found an appreciable decrease of the current intensity of negative

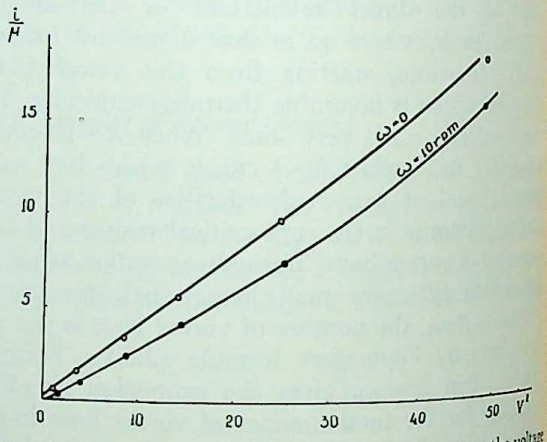

FIG. 3.4. Dependence of the negative-ion current on the voltage (in volts) in helium II at rest ($\omega_0=0$) and in rotating helium ($\omega_0 \approx 1$ sec^{-1}) according to the data of Careri, McCormick, and Scaramuzzi (1962). i is the current intensity, μ is the mobility of ions.

ions formed by a radioactive source Po^{210} in rotating helium II at their radial motion. If the current was directed along the axis of rotation, then it did not depend at all on the angular velocity. A decrease of the current intensity of ions moving perpendicularly to the axis of rotation was found to be dependent on the angular velocity and on the temperature till the λ-point. In Fig. 3.4 the plot is given of the current intensity divided by the mobility versus the square of the applied voltage, when $\omega_0=0$ and $\omega_0 \approx 1$ sec^{-1}. Nonlinearity of the latter graph allowed the authors to make a conclusion that the effect of the current decrease cannot be explained only by a decrease of the mobility of ions, which should be connected with the appearance of new centers of scattering (vortex lines). The data obtained show the capture of a definite number of ions in the gap between the electrodes (see Fig. 3.5), i.e., formation of a space charge, caused by the capture of negative ions by vortex lines of rotating helium II. According to a widely held model of a negative ion, it is an electron

CC-0. In Public Domain. Gurukul Kangri Collection, Haridwar

Digitized by Arya Samaj Foundation Chennai and eGangotri

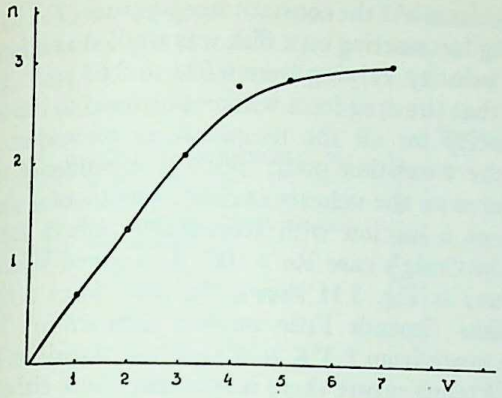

FIG. 3.5. The number of ions (in 10^6 cm^{-3}), trapped by vortex lines of rotating helium II calculated by Careri, McCormick, and Scaramuzzi (1962) according to the data represented in Fig. 3.4.

in a cavity with the diameter of several interatomic distances. Therefore, the capture of such a formation by a vortex line, which represents a node line of the wave function, i.e., the region with reduced density, is very probable. Careri *et al.* refer to a private communication of Onsager to support such a point of view.

The observations of capture of negative and positive ions in rotating helium II as well as some measurements of their mean time of capture and their mobility parallel to the axis of rotation at the temperature between 1.20° and 1.72°K were also realized by Douglass (1964). He did not find any evidence of positive ion capture. It was found that the probability of negative ion capture is proportional to the angular velocity till 45 min^{-1} and that the mean time of capture strongly depends on temperature (see Fig. 3.6). Douglass' data are described well by the relation $\tau \sim \exp(E_0/kT)$, $E_0 = 0.012$ eV, where E_0 is assumed to be associated with the depth of the potential well into which negative ions are trapped.

Tanner, Springett, and Donnelly (1965) have shown that the proportionality between the relative change of the negative ion current and the angular velocity of rotation is maintained at different directions of the

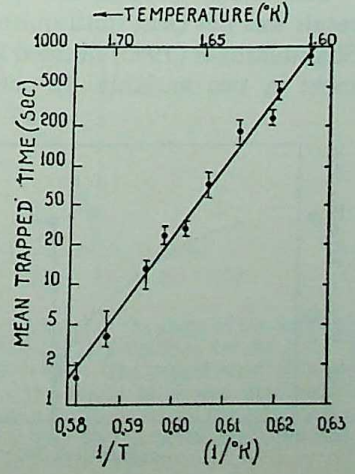

FIG. 3.6. Dependence of the trap time of negative ions on temperature according to the data of Douglass (1964).

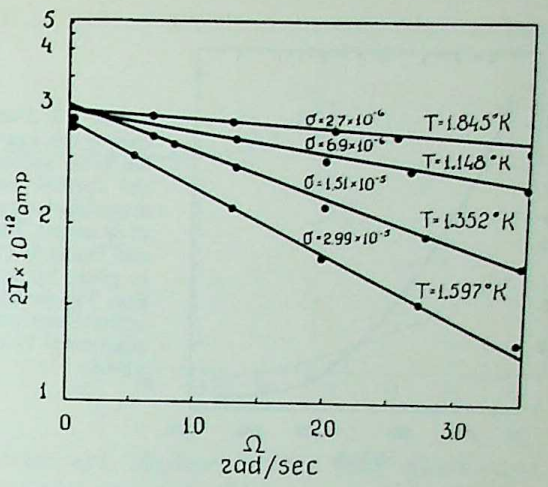

FIG. 3.7. The dependence of the negative-ion current I on the angular velocity of helium II rotation according to Springett, Tanner, and Donnelly (1965). σ is the capture cross section in cm.

current with respect to the axis of rotation. The effect disappears suddenly at an increase of temperature to $T \approx 1.6$°K. Further results of the same authors (Springett, Tanner, and Donnelly, 1965) are given in Fig. 3.7. They determined the cross section of capture σ calculated from a simple formula

$$I = I_0 \exp[-(m\omega_0/\pi\hbar)\sigma y],$$

where I is the current intensity, $m\omega_0/\pi\hbar$ is the density of vortex lines, and y is the distance passed by an ion along the applied field. σ shows a complex dependence on temperature (Fig. 3.8, a solid line). The experimentally found dependence of σ on the applied field is shown in Fig. 3.9 (also a solid line). The dashed lines are the results of the theoretical calculation made by Donnelly (1965), at the effective mass of a negative ion equal to 100 m, while its radius was 12.1 Å. The discrepancy between the theoretical and experimental results, rather considerable in Figs. 3.8, 3.9, the author explains by the presence of a space charge making the

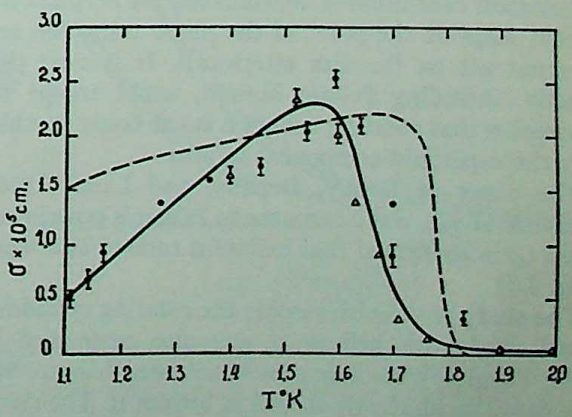

FIG. 3.8. Temperature dependence of the capture cross section of negative ions by vortex lines in rotating helium II according to the data of Springett, Tanner, and Donnelly (1965) is given by a solid line. The dashed line represents the theoretical calculations of Donnelly (1965).

CC-0. In Public Domain. Gurukul Kangri Collection, Haridwar

Digitized by Arya Samaj Foundation Chennai and eGangotri

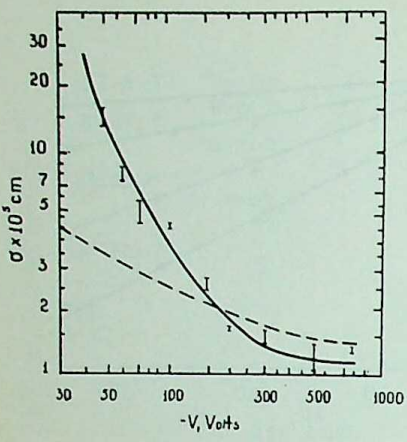

FIG. 3.9. Dependence of the negative-ion cross section on the applied voltage according to the data of Springett, Tanner, and Donnelly (1965) is given by a solid line. The dashed line is the theoretical calculation of Donnelly (1965).

electrostatic field nonuniform. The cross section of the capture for positive charges at the same mass of 100 m is somewhat smaller. However, the difference of probabilities of escaping the trap is so great for positive and negative ions that a weakening of the current of positive ions at temperatures higher than 1°K is impossible to observe. There is some probability to observe this phenomenon only when $T<1$°K.

3.4. Does Helium II Rotate as a Whole?

Perhaps the only paper stating that helium II does not rotate as a whole was that by Pellam (1960), who observed a deviation of the Rayleigh disk, suspended at an angle 45° to current lines of helium II, rotating in a cylindrical vessel. A light beam fell on the Rayleigh disk, the suspension point of which was stationary in the laboratory system of coordinates. The reflection angle of the beam served as a criterion of the moment of forces acting on the disk. It is seen in Fig. 3.10 that the effective density of a rotating liquid acting on the Rayleigh disk is equal to the total density of helium I. At the point of the phase transition, it becomes equal to zero and in helium II again increases as ρ_s at the further decrease of temperature. Thus a paradoxical conclusion is unavoidable, the normal component stops at the point of the phase transition and does not act on the disk afterwards. It is clear that nobody, including Pellam himself, could accept the conception that rotating helium II is the liquid in which only the superfluid component rotates.

The paper of Reppy, Depatie, and Lane (1960), described above, was a response to Pellam's experiment. They again confirmed that helium II rotated as a whole (Fig. 3.3).

The study of velocities inside the rotating cylindrical vessel filled with helium II was also performed by Craig (1961). With this aim a torsional balance was suspended on an elastic thread in helium II. The center of the balance suspension was stationary in the laboratory system of coordinates. The balance had a pair of disks fastened to the ends of its beam. The disks were placed so that the flow of liquid was perpendicular to their surfaces. At the constant temperature ($T<2.17$°K) the drag force acting on a disk was studied as a function of the velocity varying from 0.022 to 0.63 sec^{-1}. It was found that the drag force was proportional to the square of velocity for all the temperatures somewhat lower than the transition point. Such a dependence of the drag force on the velocity is characteristic of a classical liquid at a motion with Reynolds numbers $\mathrm{Re}>50$, while in Craig's case $\mathrm{Re}>100$. At a given velocity of rotation, as Fig. 3.11 shows, the drag force acting on the disks depends little on the temperature in the whole range from 1.3°K to almost the transition point. At this temperature there is no break there either.

In another paper of Craig (1964), the question was put whether Helmholtz flow could be realized under conditions of Pellam's experiment (a large angle of attack) instead of a potential flow round the disk. This hypothesis was verified and confirmed in the paper of Kitchens, Steyert, Taylor, and Craig (1965), who observed trajectories of hard particles of hydrogen-deuterium mixture suspended in liquid helium II by means of a cinema film. Helium II rotated in a cylindrical vessel, and a wing (a flat plate) was immersed in it. Under such conditions, very similar to those of Pellam's experiment, tearing away of jets behind the wing was clearly observed as well as formation of eddies. These effects were increased at an increase of the attack angle from 27° to 45° and then to 90°. Evidently, the observed phenomena were connected with the normal component motion, as the superfluid component of helium II in the similar conditions (the velocity of the flow did not exceed several centimeters per second) flows around the Rayleigh disk in a potential way (Craig and Pellam, 1957, Köeller and Pellam, 1962). In spite of the certain interest caused by the data obtained in this paper, independence of the effect on temperature made Craig *et al.* give up the hope of explaining the strange behavior of the Rayleigh disk in Pellam's experiment.

Pellam (1965) has repeated a detailed study of the Rayleigh disk behavior in rotating helium II, but he only confirmed his previous results.

The cause of Pellam's paradoxical experimental result was not clear until quite recently; Tsakadze and Shanshiashvili (1965) decided to repeat Pellam's experiment in two variants. In one case a light beam was

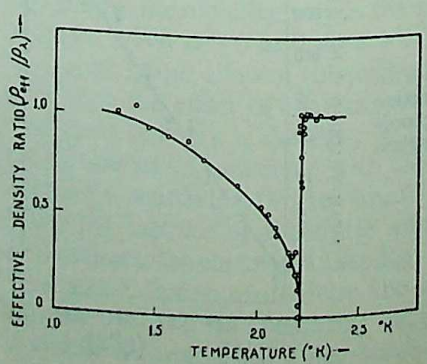

FIG. 3.10. Temperature dependence of the effective density determined by Pellam (1960) by a deflection of the Rayleigh disk, immersed into rotating helium II. ρ_λ is the density of liquid helium at the λ-point.

CC-0. In Public Domain. Gurukul Kangri Collection, Haridwar

Digitized by Arya Samaj Foundation Chennai and eGangotri

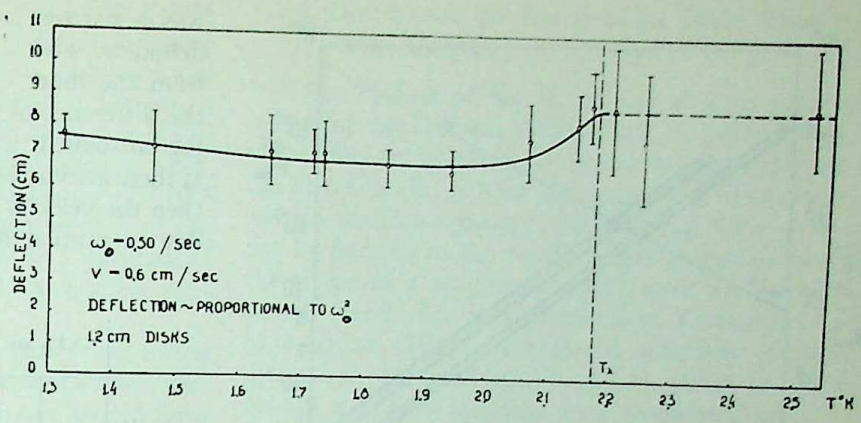

FIG. 3.11. Temperature dependence of the deflection of the disks fixed perpendicularly to the current lines of rotating helium II to the ends of the torsional balance beam (Craig, 1961).

reflected directly from the Rayleigh disk (as in Pellam's device); in the other case a mirror was placed above the rotating vessel and the light beam did not fall on the body immersed into liquid helium. In the first variant, the authors obtained a curve very similar to that of Pellam. In the second variant, the deflection of the Rayleigh disk was equal at all temperatures to that in helium I (Fig. 3.12).

Thus, at present we can definitely state that the results of Pellam's experiment were caused completely by the action of light.

3.5. Distribution of Vortex Lines over the Cross Section of a Rotating Vessel, Irrotational Regions

Usually it was thought that the distribution of vortex lines in a uniformly rotating helium II was uniform. However, Hall (1960), minimizing the free energy of the liquid, has shown that there should exist some region near the side surface of a cylinder in which there are no vortex lines and the motion is determined by the law $v_s = \Gamma/2\pi r$. Here Γ is the sum of circulations of all the vortex lines existing in the vessel. It is natural to call such a region "irrotational," as then not only the curl of the local velocity, but also that of the mean velocity is equal to zero.

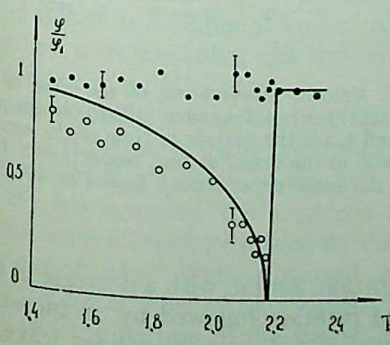

FIG. 3.12. Temperature dependence of the angle of the Rayleigh disk deflection in rotating helium II according to the data of Tsiklauri, Tsiadakze and Shanshiashvili (1965). The points were obtained when a mirror placed above the liquid level was illuminated; the circles when the Rayleigh disk was illuminated; the solid line is Pellam's curve (1960) shown in Fig. 3.10. φ_1 is the angle of deflection in helium I. ($\varphi/\varphi_1 = \rho_{eff}/\rho_\lambda$.)

Bendt and Oliphant (1961) have shown that an irrotational region should be created round the inner cylinder at rotation of helium II in an annulus between two coaxial cylinders moving with the common angular velocity. Proceeding from the minimization of the free energy $E - L\omega_0$, they have calculated the velocity dependence of the irrotational region radius and the value of the circulation in this region (Figs. 3.13, 3.14). It was found that the velocity circulation Γ round the inner cylinder can reach hundreds of thousands of quanta h/m. It is more favorable thermodynamically to allow the possibility of the existence of such values of Γ which are incompatible with the continuity of the mean velocity on the boundary between the region occupied by vortex lines and the irrotational region (sliding).

Formation of an irrotational region round the inner

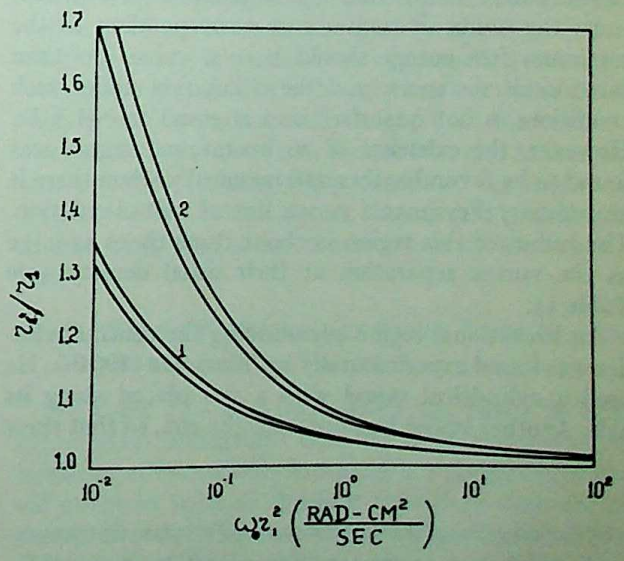

FIG. 3.13. The results of Bendt and Oliphant's calculations (1961). r_i is the radius of the irrotational region, r_1 is the radius of the inside cylinder. Band 1 corresponds to the calculation made on the assumption of continuity of the averaged velocity on the boundary between the irrotational region and the region occupied by vortex lines; band 2 corresponds to the calculation made without this limitation. Band use instead of curves is connected with a weak dependence of $\ln(b/a_0)$ on ω_0; b is the effective radius of a vortex line (outside the irrotational region).

CC-0. In Public Domain. Gurukul Kangri Collection, Haridwar

Digitized by Arya Samaj Foundation Chennai and eGangotri

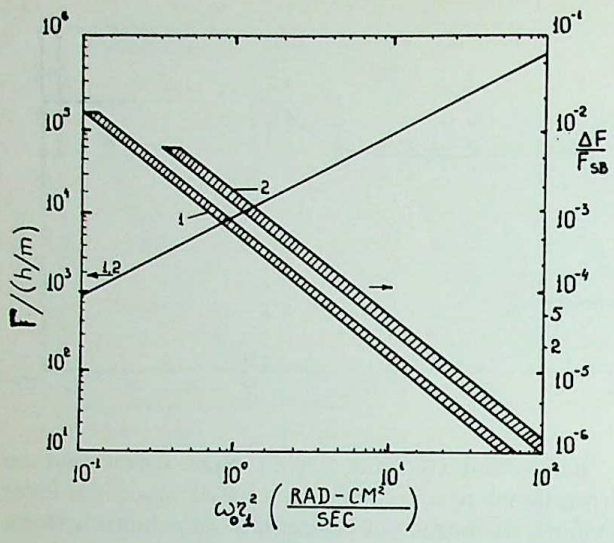

FIG. 3.14. The results of calculations of Bendt and Oliphant (1961). Γ is the velocity circulation around the inside cylinder (in the irrotational region). F is the free energy of rotating helium in the presence of the irrotational region; F_{sb} is the free energy of the solid-body rotation simulated by the presence of uniformly distributed vortex lines, $\Delta F = F - F_{sb}$ ($\Delta F < 0$, $F_{sb} < 0$). The sense of the notations 1 and 2 and the reason for the use of bands instead of lines are explained in the caption to Fig. 3.13.

cylinder was discussed in the paper of Kemoklidze and Khalatnikov as well (1964).

If the existence of an inside irrotational region is favorable thermodynamically, then it is natural to ask whether its creation is possible when there is no inner cylinder, in which case the liquid could have formed a hollow cylindrical core. Kemoklidze and Mamaladze (1964a) have shown that it is impossible for two reasons: the radius of such a core corresponding to the minimum free energy should have a value less than interatomic distances, and the circulation under such conditions is not quantized and is equal to $\sim 1.5\ \Gamma_0$. However, the existence of an irrotational region was found to be favorable thermodynamically when there is an ordinary Feynman's vortex line of unit circulation. The radius of this region is about three times as large as the vortex separation at their usual density (see Table I).

An irrotational region surrounding the central cylinder was found experimentally by Tsakadze (1964b). He used a cylindrical vessel with a rod placed along its axis. Another vessel was put onto the rod, so that there was a narrow gap between the bottoms of the two cylinders. The superfluid had to leak through a slit from the inner cylinder not glued to the rod due to the difference of levels. Flowing into the gap between the bottoms, it was moving in the horizontal direction. If there are vortex lines in the gap between the bottoms then the velocity of the liquid flow out should depend, due to mutual friction (see Sec. 7), on the angular velocity of rotation. And if, with a decrease of the angular velocity of rotation followed by an increase of the irrotational region radius, vortex lines leave the gap between the bottoms, the rate of the leakage becomes constant. Tsakadze sucked the liquid into the inside vessel by means of the thermomechanical effect and then measured the time of its leakage as a function of the angular velocity of rotation (Fig. 3.15).

TABLE I.

ω_0 sec^{-1}	$10^2 r_i$ cm	$r_i/b[b=(\hbar/m\omega_0)^{\frac{1}{2}}]$
0.01	82	6.6
0.1	25	6.4
1	7.8	6.2
5	3.4	6.0
10	2.4	6.0
20	1.7	5.9
30	1.4	5.9

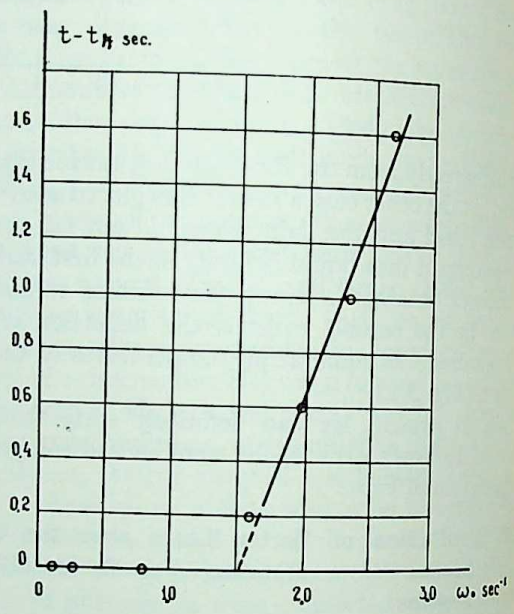

(a)

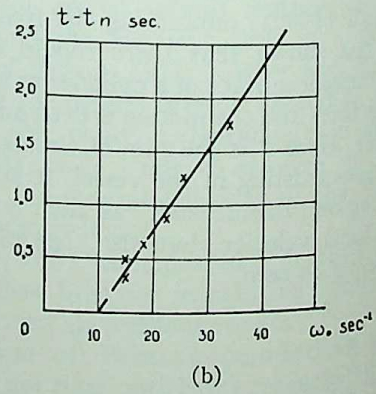

(b)

FIG. 3.15. (a) Velocity dependence of the time of helium II outflow in the experiment of Tsakadze (1964b) in the presence of an axial rod. t and t_n are the periods of time of the outflow in the rotating vessel and in the vessel at rest, respectively. $T = 1.75$°K. (b) Results of the same experiment (Tsakadze, 1964b) at $T = 1.46$°K.

CC-0. In Public Domain. Gurukul Kangri Collection, Haridwar

Digitized by Arya Samaj Foundation Chennai and eGangotri

A break on the curve observed in such a way means that, when $\omega_0=1.5$ sec^{-1}, the radius of the irrotational region r_i becomes equal to the outside radius of the inside vessel, equal to 0.8 cm. The radius of the rod is $r_1=0.5$ cm. Under such conditions the ratio $r_i/r_1=1.6$. Meanwhile, according to Bendt and Oliphant (Fig. 3.13), such a value should be obtained when $\omega_0\sim 2\times10^{-2}$ sec^{-1} in an obvious contradiction with the data of the experiment. The discrepancy increases at a decrease of temperature, though the theoretical calculation concerns the case $T=0$°K.

A similar, but rather smaller discrepancy was found between the observations and calculations of Kemoklidze and Khalatnikov, according to which one should have $r_i-r_1=0.055$ cm, when $\omega_0=1.5$ sec^{-1} and $r_i-r_1=0.022$ cm, when $\omega_0=10$ sec^{-1}. This disagreement of theoretical calculations with the experimentally found values $r_i-r_1=0.3$ cm could be explained, at least partially,

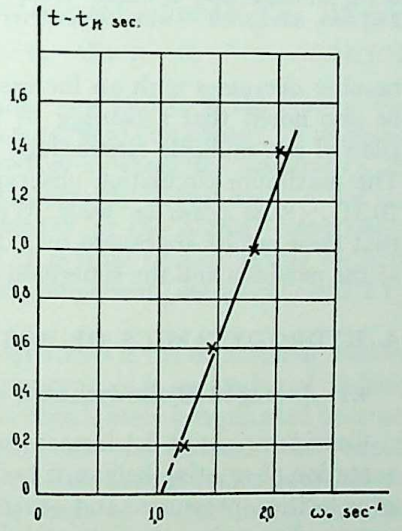

FIG. 3.16. Dependence of the time of helium II outflow through a capillary in the absence of an axial rod. $T=1.38$°K. (Tsakadze, 1964b.)

by the conditions under which the experiment was performed. In Tsakadze's device the narrow gap between the bottoms was transformed into a volume limited from the top by the free surface at a higher level than the bottom of the inside vessel. Meanwhile, the calculations of Bendt and Oliphant and of Kemoklidze and Khalatnikov were made for the case when the liquid flew between two parallel planes.

A similar technique was used by Tsakadze to find an irrotational region without the inside cylinder. With this aim he chose a version of the just now described device. He has removed the axial rod and made the liquid leak from a capillary placed on the rotation axis. Flowing out of the capillary, it passed through the gap between the lower edge of the capillary (it had a flat section) and the bottom of the vessel. The results are shown in Fig. 3.16. The radius of the irrotational region was equal to $r_i=0.1$ cm, when $\omega_0=1$ sec^{-1}. Calculations of Kemoklidze and Mamaladze gave under such conditions $r_i=0.08$ cm (the experiment was made at $T=1.38$°K).

3.6. Distribution of Vortex Lines when There Is a Free Surface

A free surface of the liquid can also be a peculiar reason of nonuniform distribution of vortex lines. A vortex line in equilibrium should be perpendicular to the free surface, so that the tangential component of tension would not make it drift. But in this case it will not be parallel to the rotation axis as the surface has the shape of a nonflat meniscus near which vortices should bend. In this connection Kemoklidze and Mamaladze (1946b) considered solutions of hydrodynamical equations (4.2.1), (4.2.2), (4.2.3) of rotating helium II. These solutions were considered under the usual boundary conditions on solid surfaces and under the condition on the free surface (using the tensor of momentum flux, see, for instance, Landau and Lifshitz, 1953), which should be self-consistent with the solution of the equations mentioned above.

The authors did not manage to solve this problem completely because of great difficulties of calculations. But they have shown that the solution $v_s=\omega_0 r$ and $|\operatorname{curl}\mathbf{v}_s|=\omega_z=2\omega_0=$ const (the constancy of the density of vortex lines) is not compatible with the parabolic meniscus. Small deviations from this solution show the tendency to an increase of curl $\mathbf{v}_s$ (increase of vortex line density) at the approach to the rotation axis and to the deepening of the meniscus near this axis, in the immediate vicinity of which deviations become large. Evidently, a conic pit on the meniscus observed by Andronikashvili (Andronikashvili and Kaverkin, 1955) is the result of these circumstances. One would rather assume that, in the vicinity of the rotation axis, the region of closely spaced vortex lines is replaced by an irrotational region [where Eqs. (4.2.1), (4.2.2), (4.2.3) are already not applicable] and a unit vortex line is situated on the very axis. As the confirmation of such an assumption can be used the results of the mentioned above (3.5) Kemoklidze and Mamaladze paper (1964a). Though they concerned the case of the liquid confined by flat planes, they should remain valid at distances deep under the meniscus of the liquid as well.

3.7. Direct Observations of Vortex Lines in a Uniformly Rotating Helium II

We begin this paragraph from the paper in which rather clear indications were obtained concerning the existence of vortex lines arranged in a definite geometrical order, in spite of the fact that they were not observed directly. That was Chase's experiment (1960a). He rotated round the vertical axis a horizontally placed tube with the diameter 2.62 mm packed with 70 thin wires with the diameter 0.25 mm. These wires produced a large number of narrow parallel channels of irregular cross section. A heat current was switched on along these channels filled with helium II. The critical value of this current w_c should depend according to Vinen

CC-0. In Public Domain. Gurukul Kangri Collection, Haridwar

Digitized by Arya Samaj Foundation Chennai and eGangotri

(1957a, b, c, 1958b) on the presence of vortex lines. Measuring w_c as a function of the square root of the angular velocity of rotation, Chase has obtained that this dependence has a step shape, and the first step is characterized by an appreciable hysteresis which is absent at high angular velocities (see Fig. 3.17). The points were taken under the conditions of an accelerated rotation (open circles) and its slowing down as well (solid circles). There are no vortex lines at the first step. Their sudden appearance corresponds to creation of the stable configuration of vortex lines with the separation $(\pi\hbar/m\omega_0)^{\frac{1}{2}}$ equal to 0.34 mm. This value is compatible with the wire size. Separation of vortex lines equal to 0.17 and 0.11 mm corresponds to transitions to the next steps, i.e., the separation of vortex lines for different steps gives the ratio $1:\frac{1}{2}:\frac{1}{3}$. Such a situation could take place only if there exists some discrete succession of stable configurations of vortex arrays.

Unfortunately, Chase has not obtained such clear results for channels of another shape and larger size (Fig. 3.18, Chase, 1960b). Maybe the vortex lines formed in such channels are "blown away" by a heat current or the conditions of their fastening are sharply different from those existing between the thin wires of the first of capillaries used by him.

A direct observation of vortex lines in rotating helium II was realized by Steyert, Taylor, and Kitchens (1965). For this purpose they observed (and took photos as well) the motion of tiny particles of solidified hydrogen–deuterium mixture. Most of such particles moved in rotating helium II along smooth circular trajectories with the center on the rotation axis. But a part of them made small closed loops from time to time. That meant undoubtedly that a particle was in the vicinity of a vortex line. It was easy to calculate the vortex line circulation if to know the loop diameter and the period of revolution. The results of the similar calculations given in the mentioned paper show that together with vortex lines with the circulation close to unit one (Γ_0), there are vortex lines with $\Gamma=2\Gamma_0$, $3\Gamma_0$, etc. Their

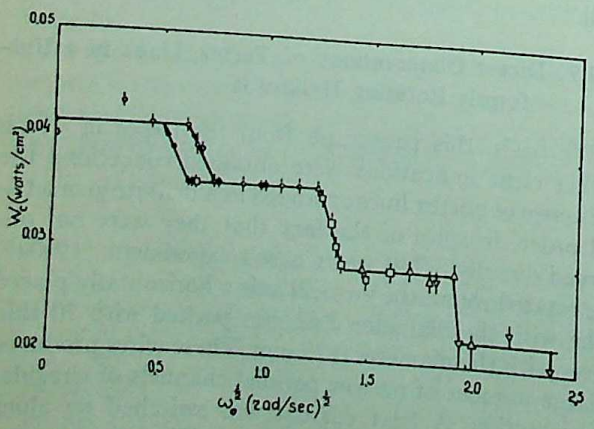

FIG. 3.17. Dependence of the critical thermal flux W_c on the velocity of rotation in the experiment of Chase (1960a).

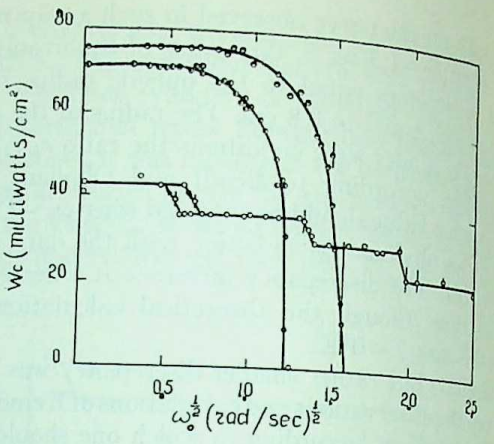

FIG. 3.18. Dependence of the critical thermal flux W_c on the velocity of rotation in the experiment of Chase (1960b). The upper curve is obtained with 9 rectangular canals 0.102×0.051 cm (the long axis is in the plane of rotation). The middle curve is obtained with the same canals, but with the long axis perpendicular to the plane of rotation. The lower curve reproduces the result of the previous paper of Chase (1960a) with a tube of diameter 2.62 mm, filled with 70 wires of diameter 0.252 mm.

number decreases with an increase of Γ/Γ_0. It should be also noted that according to their data there are allowed not multiple circulations $\Gamma=0.8\Gamma_0$, $1.5\Gamma_0$, etc. The maximum circulation observed in this study was $10.5\Gamma_0$. (*Note added in proof.* We think it is possible that these results are caused by a difference in velocities of the particles and the superfluid component.)

4. HYDRODYNAMICS OF ROTATING HELIUM II

4.1. Averaged Hydrodynamics of Rotating Helium II

Considerations of 2.4 formed the basis for the representation of rotating helium II hydrodynamics in terms of velocities, pressures, and other physical magnitudes averaged over the volume containing many vortex lines. Such an averaging is desirable, because at solution of hydrodynamical problems, associated with the existence of many vortex lines, it would be necessary to give boundary conditions on each of them, which would take into account such "local" forces as tension, Magnus force,[4] and forces caused by interaction of vortices with thermal excitations. The offered averaging does not only simplify the complex picture of velocity distribution (Fig. 2.2), but ascribes to local forces a character of space ones. Thus the necessity of taking into account numerous boundary conditions is excluded. But the new space forces which have appeared in such a manner should be included into hydrodynamical equations. Due to this fact the latter become more complicated than usual Landau equations of two component hydrodynamics.

[4] If the velocity $\mathbf{v}_s$ of the superfluid component in the points through which the vortex line passes is different from the velocity $\mathbf{v}_L$ of the vortex line itself, then the following force (reduced to unit length) acts on a vortex line with the circulation Γ:

$$\mathbf{f}=\rho_s[\mathbf{v}_s-\mathbf{v}_L,\ \boldsymbol{\Gamma}].$$

CC-0. In Public Domain. Gurukul Kangri Collection, Haridwar

Digitized by Arya Samaj Foundation Chennai and eGangotri

4.2. The Equations of Hydrodynamics of Rotating Helium II

The averaged hydrodynamics of rotating helium II was formulated in succession at first in Hall's papers (1957a, 1960), then by Mamaladze and Matinyan (1960a) (see, also Andronikashvili, Mamaladze, Matinyan, and Tsakadze, 1961) and at last by Bekarevich and Khalatnikov (1961). If to take only the case of low (in comparison with the velocity of second sound) relative velocities of the superfluid and the normal components and small temperature gradients, then the complete set of equations of hydrodynamics of helium II will be

$$(\partial \mathbf{v}_s/\partial t)+(\mathbf{v}_s, \nabla)\mathbf{v}_s+\nu_s[\boldsymbol{\omega}, \operatorname{curl}(\boldsymbol{\omega}/\omega)]$$
$$=-\rho^{-1}\nabla(\rho+\eta_s\omega)+s\nabla T+\mathbf{F}_{sn}, \quad (4.2.1)$$

$$(\partial \mathbf{v}_n/\partial t)+(\mathbf{v}_n, \nabla)\mathbf{v}_n-\nu_n\Delta\mathbf{v}_n$$
$$=-\rho^{-1}\nabla(P+\eta_s\omega)-(\rho_s/\rho_n)s\nabla T-(\rho_s/\rho_n)\mathbf{F}_{sn}, \quad (4.2.2)$$

$$\operatorname{div}\mathbf{v}_s=\operatorname{div}\mathbf{v}_n=0, \quad (4.2.3)$$

where $\nu_s=\epsilon/\rho_s\Gamma_0=\eta_s/\rho_s$, $\boldsymbol{\omega}=\operatorname{curl}\mathbf{v}_s$ is the curl of the mean velocity of the superfluid component (symbols of averaging are omitted everywhere for simplicity), P is the pressure, s is the entropy of unit mass, $\nu_n=\eta_n/\rho_n$ is the kinematic viscosity of the normal component, and $\mathbf{F}_{sn}$ is the force of mutual friction acting on unit mass of the superfluid component [see formulas (7.2.1) and (7.3.4)].

The first of these equations is the equation of motion of the superfluid component; it is an analog of Euler's equation for the ideal liquid, more complicated because of taking into account the thermomechanical effect (the term $s\nabla T$) and the existence of vortex lines (terms containing ω and the force of mutual friction). The second equation is the equation of motion of the normal component, similar to the Navier–Stokes equation for a viscous liquid and also containing some additional terms taking into account the same effects. In the equations of continuity (4.2.3), both components appear as incompressible liquids, and it is natural, in the cases when motions with high velocities or nonstationary processes of mutual transformations of the components are not considered. In the latter cases the equation,

$$(\partial\rho/\partial t)+\operatorname{div}(\rho_s\mathbf{v}_s+\rho_n\mathbf{v}_n)=0, \quad (4.2.3a)$$

should be used instead of (4.2.3).

The terms, containing ω and the magnitude $\mathbf{F}_{sn}$ provide taking into account vortex singularities to such an extent as is necessary after averaging as well. In particular, the term $\eta_s\omega$ added to the pressure P is associated with the additional pressure caused by the tension of vortex lines ($m\omega_0\epsilon/\pi\hbar=\eta_s\omega$). Further a special role of the term $\nu_s[\boldsymbol{\omega}, \operatorname{curl}(\boldsymbol{\omega}/\omega)]$ should be emphasized more than once. Therefore, it is necessary to explain its origin. It describes elastic properties of vortex lines, due to which straightening forces are created preventing distortion of vortex lines (Fig. 4.1). The straightening force (reduced to unit length) for one vortex line, the tension of which is $\boldsymbol{\varepsilon}=\epsilon\boldsymbol{\omega}/\omega$, is equal to $\epsilon/R_c=\epsilon(\boldsymbol{\omega}/\omega, \nabla)\boldsymbol{\omega}/\omega$, where R_c is the radius of curvature. Let us recollect now that the density of vortex lines is ω/Γ_0 and $\nu_s=\epsilon/\rho_s\Gamma_0$; then calculate the mean straightening force reduced to unit mass of the superfluid component:

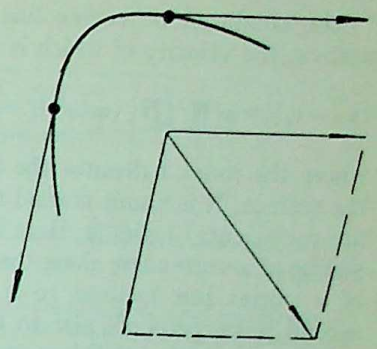

FIG. 4.1. The sum of tension forces, acting on an element of a distorted vortex line, constitutes a straightening effort.

$$\left(\frac{1}{\rho_s}\right)\left\{\epsilon\left(\frac{\boldsymbol{\omega}}{\omega}, \nabla\right)\frac{\boldsymbol{\omega}}{\omega}\right\}\left(\frac{\omega}{\Gamma_0}\right)=\nu_s(\boldsymbol{\omega}, \nabla)\frac{\boldsymbol{\omega}}{\omega}=-\nu_s\left[\boldsymbol{\omega}, \operatorname{curl}\frac{\boldsymbol{\omega}}{\omega}\right].$$

The existence of the second derivatives of velocity over the coordinates in this expression makes two equations similar by their mathematical structure: the equation of the superfluid liquid and that of the normal liquid containing the viscous term $\nu_n\Delta\mathbf{v}_n$. It is shown in Sec. (5.5) that the presence of terms with second derivatives of velocities causes peculiar processes of energy dissipation (though, as it has just been shown, the term $\nu_s[\boldsymbol{\omega}, \operatorname{curl}\boldsymbol{\omega}/\omega]$ is a purely elastic one by its physical meaning) and that the constant ν_s acts as a peculiar "kinematic viscosity of the superfluid component." One can emphasize that its dimension coincides with the dimension of ν_n. The numerical values of ν_n ν_s are of the same order of magnitude, rather close to each other, at least in the range of temperatures in which the experiments discussed in this review were made.

4.3. Additional Boundary Conditions

The necessity of additional boundary conditions is also a consequence of the existence of the velocity second derivatives. In addition to the evident condition for the velocity component of the superfluid liquid perpendicular to the wall (the liquid does not flow into the wall and does not flow out of it at the constant temperature), we have to look for conditions for the tangential component as well. Such conditions are given indirectly. At first the conditions of vortex fastening to the surface crossing them are written down, and then the relation between the velocity of vortex lines $\mathbf{v}_L$ and the velocity of the superfluid component $\mathbf{v}_s$ is used to transform the boundary conditions for $\mathbf{v}_L$ into the boundary conditions for $\mathbf{v}_s$. This program is realized by the following equations.

CC-0. In Public Domain. Gurukul Kangri Collection, Haridwar

Digitized by Arya Samaj Foundation Chennai and eGangotri

The condition of vortex line fastening to a solid surface, the velocity of which is $\mathbf{v}_\sigma$ has the form

$$(\mathbf{v}_L-\mathbf{v}_\sigma)_t=a\{\mathbf{N},[\mathbf{N},(\boldsymbol{\omega}/\omega)]\}-a'[\mathbf{N},(\boldsymbol{\omega}/\omega)], \quad (4.3.1)$$

where the index t denotes the tangent component to the surface; $\mathbf{N}$ is a unit normal to the surface. a and a' are coefficients of sliding. Here the first term describes sliding of a vortex line along the surface due to tension of a vortex line inclined to it ($\mathbf{v}_L-\mathbf{v}_\sigma\sim\epsilon\boldsymbol{\omega}/\omega$). The second term, perpendicular to the first one, is caused by Magnus effect "drifting away" the sliding vortex line. Let us note that two terms of formula (4.3.1) correspond to two terms of expression (7.2.1) for the force $\mathbf{F}_{sn}$. Really the first term describes the direct action of some force, and the other one describes a secondary effect directed perpendicularly to the "drag" force. Therefore, it is natural that Bekarevich and Khalatnikov (1961) predicted the following proportionality of the coefficients a and a' on the one hand and B, B' on the other hand (we remind that $B'<0$):

$$a/a'=-B/B'. \quad (4.3.2)$$

In the absence of sliding, $a=a'=0$. When there is a complete sliding, $a=a'=\infty$. Roughness of a solid surface, made, for instance, of grains of sand attached to it, prevents sliding of vortex lines, as stretched vortices tending to have the minimum length are fastened to the grains. Accordingly, Bekarevich and Khalatnikov (1961) obtained the following estimate:

$$a\sim(\hbar/m\delta)B(\rho_n/\rho), \quad (4.3.3)$$

where δ is the height of a grain.

If vortex lines are parallel to the rotation axis, then curl $\boldsymbol{\omega}/\omega=0$; there is no term with ν_s in Eq. (4.2.1), and the necessity in additional boundary conditions disappears.

The relationship between $\mathbf{v}_L$ and $\mathbf{v}_s$ is realized by means of formula

$$[\boldsymbol{\omega},\mathbf{v}_s-\mathbf{v}_L]+\nu_s[\boldsymbol{\omega},\text{curl }\boldsymbol{\omega}/\omega]+\mathbf{F}_{sn}=0 \quad (4.3.4)$$

or formula

$$(\partial\mathbf{v}_s/\partial t)-[\mathbf{v}_L,\boldsymbol{\omega}]=-\rho^{-1}\nabla(P+\eta_s\omega)+s\nabla T-\tfrac{1}{2}\nabla v_s^2. \quad (4.3.5)$$

Equation (4.3.4) is the condition of equilibrium of Magnus force, straightening force, and force of mutual friction which act on vortex lines. When such a condition is maintained (and not when one of these forces is equal to zero), vortex lines are free.

We note, in the association with Eq. (4.3.5), that an equality of the type $(\partial\mathbf{v}_s/\partial t)-[\mathbf{v}_L,\boldsymbol{\omega}]=\nabla G$, where G is an arbitrary function, gives $(\partial\boldsymbol{\omega}/\partial t)-\text{curl}\,[\mathbf{v}_L,\boldsymbol{\omega}]=0$ and describes the transport of the magnitude $\boldsymbol{\omega}$ with the velocity $\mathbf{v}_L$.

5. OSCILLATIONS OF SOLID BODIES WITH AXIAL SYMMETRY IN ROTATING HELIUM II AND ANISOTROPY OF ITS ELASTIC-VISCOUS PROPERTIES

5.1. Anisotropy of Elastic-Viscous Properties of Rotating Helium II

Experiments, in which small oscillations of solids immersed in rotating helium II were studied, have given abundant information on properties of vortex lines. In these experiments, solid bodies of axial symmetrical shape performed rotation together with helium II and small oscillations superimposed on their rotational motion.

Though chronologically we should begin from the experiments in which dampling of an oscillating disk was determined (Andronikashvili and Tsakadze, 1959b), let us start the description of such investigations from the simplest one made by Tsakadze (1962a). Tsakadze measured the logarithmic decrement of damping of an upside-down hollow cylinder, performing two motions simultaneously: rotation together with helium II and oscillation upwards and downwards, so that the side of the cylinder moved along vortex lines. As a result of the measurements, it was found that damping in rotating helium II is indistinguishable from that taking place in helium II at rest. It does not depend on the angular velocity of rotation ω_0, i.e., it does not depend on the number of vortex lines. In such an experiment, helium II behaves as a classical liquid.

In another experiment (Tsakadze and Chkheidze, 1960), a cylinder, turned upside down and suspended on an elastic thread, performed in addition to rotation with helium II axial oscillations around the rotation axis. In the case of a classical liquid, damping of such oscillations does not depend on the velocity of rotation. But, in rotating helium II, a layer of the normal component, adjacent to the wall of the cylinder at the distance of the order of the penetration depth, dragged, due to mutual friction (Sec. 7), all those vortex lines which pierced this layer into its motion. Therefore the damping of the cylinder was different from that in a liquid at rest and increased proportionally to the angular velocity in accordance with the increase of the density of vortex lines according to formula (2.5.1). The data of the experiment made by Tsakadze and Chkheidze are shown in Fig. 5.1, where solid lines show the results of calculations made according to the formula obtained by Mamaladze and Matinyan (1960b).

The common feature for these two experiments is that both the shape of the oscillating surface and the direction of its motion do not cause immediate contact of vortex lines with the moving body.

This situation is changed when axial oscillations of the surfaces of a disk or a pile of disks suspended on an elastic thread crossing the array of Onsager–Feynman vortex lines are considered. Vortex lines fastened to these oscillating surfaces are distorted during the disk motion,

CC-0. In Public Domain. Gurukul Kangri Collection, Haridwar

Digitized by Arya Samaj Foundation Chennai and eGangotri

and waves propagate along them. Thus the changes of the character of oscillations of a solid body carry information on elastic properties of vortex lines. Propagation of elastic waves is a common phenomenon for all the experiments of such a type, because, due to mutual friction between the components, the waves on vortex lines are excited even in the complete absence of direct contact between them and the solid surface (sliding).

First of all, one should expect some manifestation of vortex elasticity with an increase in frequency of the disk oscillations, the fact observed in the experiment made by Andronikashvili and Tsakadze (1962). The data of these measurements with a sufficiently light disk, "feeling" the elasticity of vortex lines, are given in Fig. 5.2. At small angular velocities, the frequency

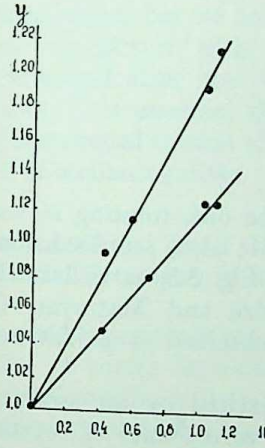

FIG. 5.1. Dependence of damping of the cylinder axial oscillations on the velocity of rotation. $y=A(\delta_2-\delta_1)/(l_2-l_1)$, where δ_2 and δ_1 are the logarithmic decrements of damping of the cylinder oscillations at its immersion to the depths l_2 and l_1, respectively; $A=(I/2\pi^2R^3)(\Omega/2\eta_n\rho_n)^{\frac{1}{2}}$; I is the moment of inertia of the oscillating system; R is the radius of the cylinder; Ω is the frequency of oscillations; η_n and ρ_n are the viscosity and the density of the normal component, respectively. The points are the experimental data of Tsakadze and Chkheidze (1960). The straight lines are plotted according to formula (7.3.1) (Mamaladze and Matinyan, 1960b). The upper straight line represents the case when $T=1.48$°K, the lower one when $T=1.75$°K.

of oscillations increases in accordance with the increase of the number of vortex lines. But when $2\omega_0/\Omega\sim0.2$, where Ω is the frequency of oscillations, the rate of frequency increase slows down sharply and the experimental curve begins to show the tendency to saturation. This phenomenon is caused by collectivization of vortex oscillations, which takes place at such a ratio of frequencies. The collectivization of vortices is discussed in more detail in Sec. 6.3. The experiment of Andronikashvili and Tsakadze clearly establishes the fact of existence of the modulus of rigidity in rotating helium II, manifested in elastic counteraction to the torsion deformation of this liquid with respect to the axis of its rotation.

As noted in 4.2 {at the consideration of the physical sense of the term $\nu_s[\omega, \text{curl}\,(\omega/\omega)]$ in the equation of motion of the superfluid component}, the elastic prop-

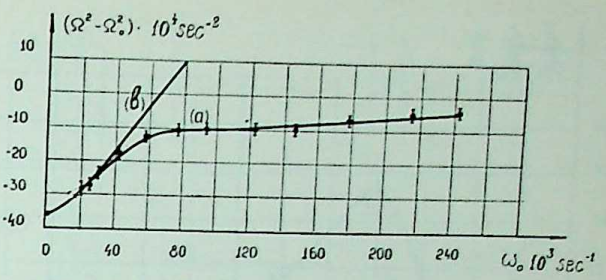

FIG. 5.2. Dependence of the frequency of axial oscillations of a "light" disk on the velocity of rotation. Curve (a) shows the experimental data of Andronikashvili and Tsakadze (1962); curve (b) is plotted according to formula (5.2.1) (when the edge corrections are taken into account).

erties of vortex lines can be also seen in a very "inelastic manner," being the cause of dissipative processes. The first indication of such a possibility was the experiment of Andronikashvili and Tsakadze (1959b) in which the damping of a disk suspended on an elastic thread, rotating with helium II, and performing simultaneous axial oscillations around the axis of rotation was measured. First of all, a disk with a rough surface, with grains of sand ($\sim$50 μ) glued to it, and a smooth disk show different dependencies of damping on the angular velocity of rotation (Figs. 5.3, 5.4). It is connected with conditions (4.3.1) of fastening vortex lines to the surface (Andronikashvili, Tsakadze, and Mesoed, 1961). Indeed, as mentioned in 4.3, a grain of sand on the disk fastens a vortex line. Actually, a vortex line having slid off the grain has to become longer, i.e., to increase its energy. Therefore, the tension of a vortex line sliding from the grain tends to return it.

Increasing the period of the disk oscillations, we apparently improve the conditions of vortex line fastening to its surface. That is why a smooth disk begins to behave quite similarly to a rough one (Fig. 5.4). But in any case and at any temperature, the dependence of damping on the angular velocity had a maximum at

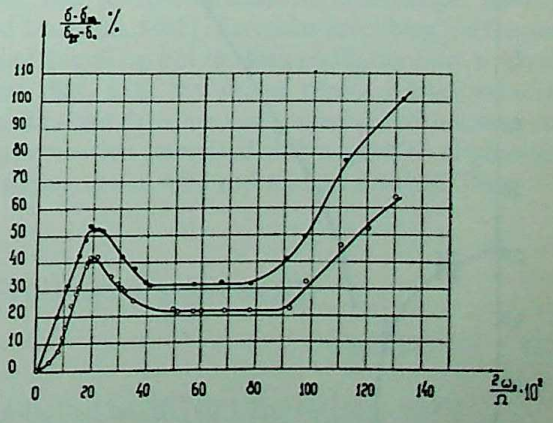

FIG. 5.3. Dependence of the damping of axial oscillations of a rough disk on the velocity of rotation according to the data of Andronikashvili and Tsakadze (1959b). The upper curve is obtained at the frequency of oscillations $\Omega=0.361$ sec^{-1}, the lower one at $\Omega=0.581$ sec^{-1}, δ_n is the logarithmic decrement of damping of the disk in the liquid at rest. δ_0 is that in the vacuum. The disks are "heavy" ($\Omega\approx\Omega_0$). $T=1.78$°K.

CC-0. In Public Domain. Gurukul Kangri Collection, Haridwar

Digitized by Arya Samaj Foundation Chennai and eGangotri

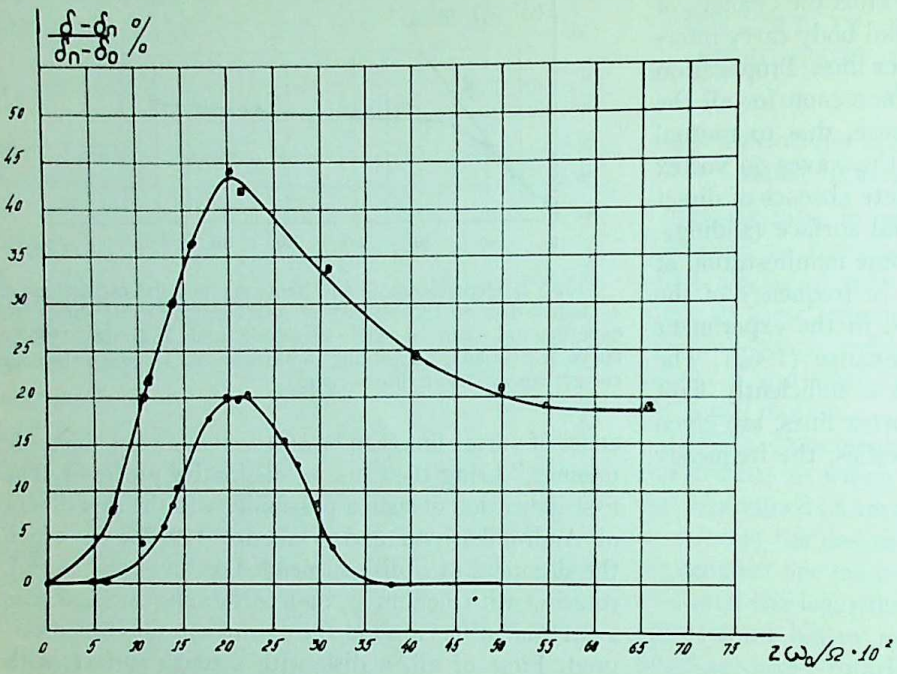

FIG. 5.4. Dependence of the oscillation damping of a smooth disk on the velocity of rotation (Andronikashvili, Tsakadze, and Mesoed, 1961). The symbols are explained in the caption to Fig. 5.3. The upper curve is for $\Omega=0.368$ sec^{-1}, the lower one for $\Omega=0.551$ sec^{-1}. The disks are "heavy" ($\Omega\approx\Omega_0$). $T=1.78$°K.

$2\omega_0/\Omega\sim0.2$, i.e., at the value at which the increase of the frequency of a light disk shows the tendency to saturation.

The dependence obtained for rotating helium II does not resemble the dependence obtained for a classical liquid, which shows a deep minimum of the logarithmic decrement of damping when $2\omega_0/\Omega\sim1$. The results of measurements of the velocity dependence for damping of oscillations of the disk rotating in water (Mesoed and Tsakadze, 1961; also, see Tsakadze and Shultz 1960) are given in Fig. 5.5, as well as the theoretical curve of Mamaladze and Matinyan (1960c). The similar results are obtained at oscillations of a disk in helium I.

Elastic waves, excited by an oscillating disk and propagating along vortex lines of rotating helium II,

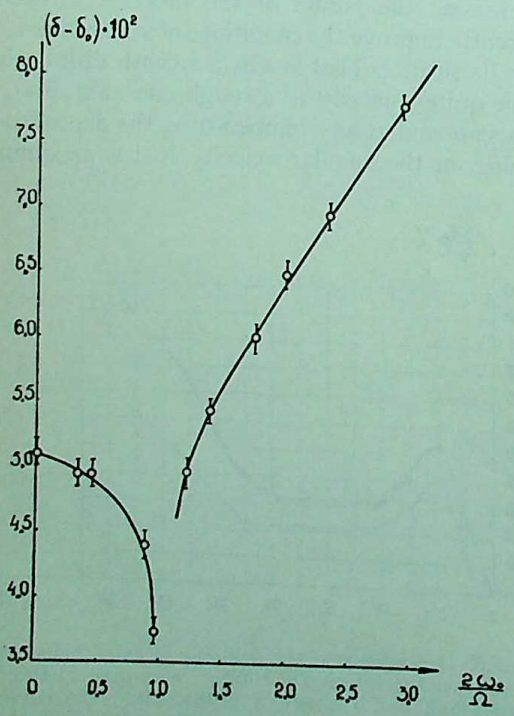

FIG. 5.5. Dependence of the damping of the disk oscillations on the velocity of rotation in the case of the classical liquid. The experimental data were obtained by Mesoed and Tsakadze (1961) in rotating water. The solid curves represent the theoretical results (Mamaladze and Matinyan, 1960c).

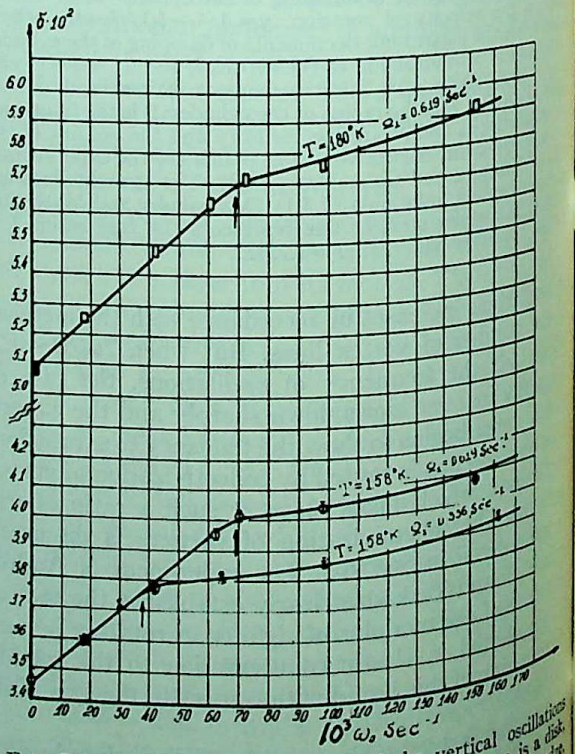

FIG. 5.6. Dependence of damping of the vertical oscillations of the cylinder on the velocity of rotation when there is a disk below the cylinder, oscillating with the frequency $\omega_0=0.11\Omega_1$ (Tsakadze, 1963d). Arrows show the angular velocities from which the collectivization of vortex oscillations starts.

CC-0. In Public Domain. Gurukul Kangri Collection, Haridwar

Digitized by Arya Samaj Foundation Chennai and eGangotri

change the character of its interaction with a vertically oscillating cylinder as well. Placing an oscillating disk under this cylinder (Tsakadze, 1962b, 1963a,d), damping of the cylinder shows the linear dependence on the velocity of rotation (i.e., on the number of vortex lines). As is shown in Fig. 5.6, the velocity of rotation at which $2\omega_0/\Omega_1 \sim 0.2$ (Ω_1 is the frequency of disk oscillations and not that of the cylinder) is connected in this case as well with the existence of a certain peculiarity leading to a break on the experimental curves.

Figure 5.7 gives a summary of the results described in this paragraph concerning the velocity dependence of damping in rotating helium II for bodies of different shape. It gives a clear picture of anisotropy of elastic–viscous properties of rotating helium II. Detailed analysis of the peculiarities of the observed curves is given in the next paragraphs, but we note here the complete agreement of this picture with the conceptions on vortex lines arranged along the rotation axis. In the two latter cases, it is essential that vortex lines are deformed by transversal motion of their ends fastened to the surface of oscillating disks.

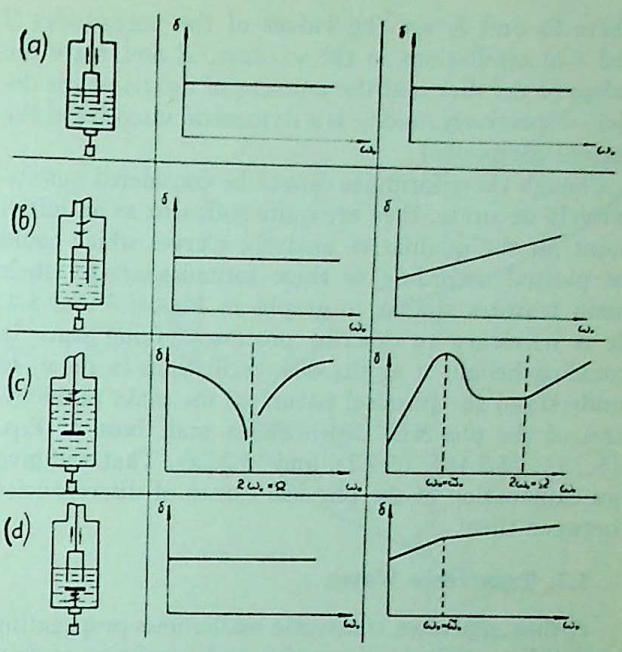

FIG. 5.7. Summary of the data on the dependence of oscillation damping upon the velocity of rotation. The schematic representation of the oscillating body and the direction of its oscillations are given in the first column; the velocity dependencies of damping of the corresponding bodies in the classical liquid are given in the second column (in arbitrary units); the same dependencies in helium II are given in column three.

5.2. Hydrodynamics of Small Oscillations of Bodies with Axial Symmetry in Rotating Helium II

All the described experiments are united by a common idea: properties of vortex lines and properties of the stationary state of rotating helium II are studied by the method of superimposing small perturbations on this state. Quasi-stationarity of these perturbations, which have the character of harmonic oscillations and smallness of their amplitude, simplifies the hydrodynamical analysis of the corresponding problems, as Eqs. (4.2.1) and (4.2.2) as well as condition (4.3.1) and equalities (4.3.4) and (4.3.5) are linearized in such a situation and exponential factors containing time (and the amplitude) cancel. But even linearized equations do not have simple solutions at all boundary conditions.

Problems of motion of cylinders oscillating in a vertical direction (Mamaladze, 1960a) or in an axial one (Mamaladze and Matinyan, 1960b) are solved rather easily. Solutions of the set (4.2.1), (4.2.2), (4.3.3) in such cases are radially propagating transverse waves of the normal component. They drag or do not drag the superfluid component as well, depending on the orientation of vortex lines and on the direction of oscillations in these viscous waves coinciding with the direction of oscillations of the cylinder. The study of such phenomena gives the information on orientation and density of vortex lines, we mentioned in the previous paragraph, and on the character of interaction of vortex lines with the normal component.

In the case of disk oscillations, the solution of the set of equations of rotating helium II hydrodynamics is much more complicated (Mamaladze and Matinyan, 1961; also, see Andronikashvili, Mamaladze, Matinyan, and Tsakadze, 1961). Formulas describing the frequency Ω and dampling δ of the disk oscillations are so cumbersome that, with the aim of physical interpretation of the obtained data, we limit ourselves with a very rough approximation associated with neglection of phenomena of sliding ($a=a'=0$) and mutual friction. Then

$$\Omega^2-\Omega_0^2=(\pi R^4\Omega/2I)\left[-(\eta_n\rho_n/2)^{\frac{1}{2}}\left[(\Omega+2\omega_0)^{\frac{1}{2}}+(\Omega-2\omega_0)^{\frac{1}{2}}\right]+(\nu_s)^{\frac{1}{2}}\rho_s(2\omega_0/\Omega)(\Omega+2\omega_0)^{\frac{1}{2}}\right],$$

when $2\omega_0<\Omega$; (5.2.1)

$$\Omega^2-\Omega_0^2=(\pi R^4\Omega/2I)\left\{-(\eta_n\rho_n/2)^{\frac{1}{2}}\left[(\Omega+2\omega_0)^{\frac{1}{2}}-(2\omega_0-\Omega)^{\frac{1}{2}}\right]+(\nu_s)^{\frac{1}{2}}\rho_s(2\omega_0/\Omega)\left[(\Omega+2\omega_0)^{\frac{1}{2}}+(2\omega_0-\Omega)^{\frac{1}{2}}\right]\right\},$$

when $2\omega_0>\Omega$; (5.2.1a)

$$-(\Omega_0/\Omega)\,\delta_0=(2\pi^2R^4/I\Omega)\left\{(\eta_n\rho_n/2)^{\frac{1}{2}}\left[(\Omega+2\omega_0)^{\frac{1}{2}}+(\Omega-2\omega_0)^{\frac{1}{2}}\right]+(\nu_s)^{\frac{1}{2}}\rho_s(2\omega_0/\Omega)(\Omega-2\omega_0)^{\frac{1}{2}}\right\},$$

when $2\omega_0<\Omega$; (5.2.2)

$$-(\Omega_0/\Omega)\,\delta_0=(2\pi^2R^4/I\Omega)(\eta_n\rho_n/2)^{\frac{1}{2}}\left[(2\omega_0+\Omega)^{\frac{1}{2}}+(2\omega_0-\Omega)^{\frac{1}{2}}\right],$$

when $2\omega_0>\Omega$; (5.2.2a)

CC-0. In Public Domain. Gurukul Kangri Collection, Haridwar

Digitized by Arya Samaj Foundation Chennai and eGangotri

where Ω_0 and δ_0 are the values of the magnitudes Ω and δ at oscillations in the vacuum, R and I are the radius of the disk and the moment of inertia of the device, respectively, and η_n is a dynamical viscosity of the normal component.

Though these formulas cannot be considered quantitatively accurate, they are quite sufficient as an initial point for the qualitative analysis. Curves which could be plotted according to these formulas are by their main features similar to graphs in Figs. 5.3 and 5.4. It is necessary to describe processes taking place in rotating helium II at the disk oscillations in detail to understand the physical nature of the main peculiarities of the observed dependencies and those of Eqs. (5.2.1), (5.2.1a), (5.2.2), and (5.2.2a). That will give an explanation of the physical causes of discrepancies between them.

5.3. Transverse Waves

A disk generates transverse oscillations propagating parallel to the axis of rotation and consisting of four waves. The relative amplitudes of these waves are different in the superfluid and normal components; therefore, they can be called s^+, s^-, n^+, and n^-, because if there had been no mutual friction, the waves $s^\pm$ would have propagated only in the superfluid component and $n^\pm$ only in the normal one. The sign "+" is used for the wave numbers of these waves described by the term $\Omega+2\omega_0$, and the sign "−" for those described by the term $\Omega-2\omega_0$ [see formulas (5.3.1) and 5.3.2)]. "Plus" and "minus" waves have opposite circular polarization.

In the approximation $\mathbf{F}_{sn}=0$[5] the waves called $S^\pm$ are elastic waves, their complex wave numbers[6] are determined in the following way:

$$k_{s0}^{(\pm)2}=\mp\,(\Omega\pm2\omega_0)/\nu_s, \qquad \mathrm{Im}\,k_{s0}^{(\pm)}>0 \quad (5.3.1)$$

(the index 0 means a zero approximation over the mutual friction).

In the same approximation the waves called $n^\pm$ are viscous waves with the wave numbers

$$k_{n0}^{(\pm)2}=-i\,(\Omega\pm2\omega_0)/\nu_n, \qquad \mathrm{Im}\,k_{n0}^{(\pm)}>0. \quad (5.3.2)$$

Let us note once more the similarity of formulas (5.3.1) and (5.3.2) that recalls the analogous role of the elastic constant ν_s and viscous constant ν_n, but let us still emphasize a very different character of the waves, described by them.

The wave $k_{n0}^{(+)}$ has a usual character of a viscous wave. The same may be said about the wave $k_{n0}^{(-)}$ if Ω is not very close to $2\omega_0$.[7] Their penetration depth is rather small in comparison with the wavelength and the conception "wave" is somewhat conventional (Fig. 5.8). It would be better to speak about oscillations of a layer with the effective thickness $\frac{1}{2}\lambda$ adjacent to the disk (Landau and Lifshitz, 1953). The reason for these circumstances is the equality of the real and imaginary parts of $k_{n0}^{(\pm)}$ (see footnote 6) and in this connection the following relationship is obtained:

$$L_{n0}^{(\pm)}=2\pi\lambda_{n0}^{(\pm)}$$

$$\lambda_{n0}^{(\pm)}=(1/2\pi)\,L_{n0}^{(\pm)}=(2\nu_n/|\,\Omega\pm2\omega_0\,|)^{\frac{1}{2}}. \quad (5.3.3)$$

Under the conditions of the experiments of Andronikashvili, Tsakadze, and Chkheidze (the usual conditions of such experiments), the values of $\lambda_n^{(\pm)}$ are usually of the order of fractions of a millimeter and do not exceed a few millimeters. If there are solid

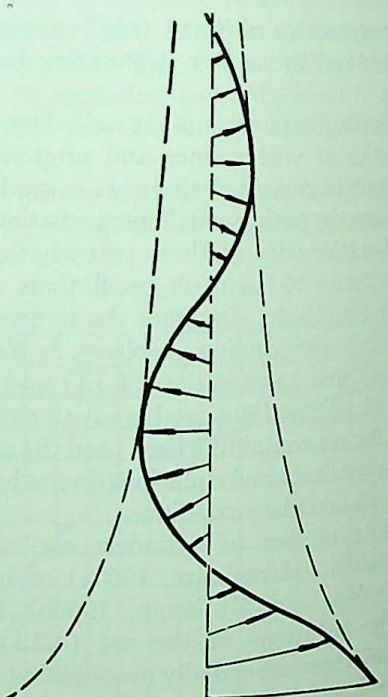

FIG. 5.8. Hodograph of velocities of the liquid motion in the viscous waves with circular polarization. To make the drawing simpler the scale is distorted. In reality, at the distance from the disk surface equal to one-half wavelength the velocity is exp $(-\pi)\approx0.043$ times less than that on this surface, and at the distance equal to the wavelength exp $(-2\pi)=0.0019$ times. Only the first half turn of the hodograph, shown in this figure, exists effectively.

[5] Having solved the equation of motion of the superfluid liquid (4.2.1) in this approximation Hall (1958) has found expressions of the wave numbers $k_{s0}^{(\pm)}$ (5.3.1) and used them to determine ν_s. The following expressions (5.3.2) for $k_{n0}^{(\pm)}$ are characteristic of the classical viscous liquid (Mamaladze and Matinyan, 1960c). The complete expressions of the wave numbers $k_s^{(\pm)}$, $k_n^{(\pm)}$ taking into account the mutual friction between the components are found by Mamaladze and Matinyan (1960a, more accurate formulae are published in the paper of Mamaladze and Matinyan 1961 and in the paper of Andronikashvili, Mamaladze, Matinyan, and Tsakadze, 1961).

[6] A complex wave number $k\equiv\sigma+i\tau$ determines the wavelength L and the depth of the wave penetration λ: $L=2\pi/|\,\sigma\,|$, $\lambda=1/\tau$ (it is implied that $\tau>0$).

[7] We imply everywhere that the case $\Omega-2\omega_0\gg\gamma$ is considered, where γ is the coefficient of damping ($\gamma=\Omega\delta/2\pi$), δ is the logarithmic decrement of damping). That excludes some interval of angular velocities of rotation from consideration. Phenomena taking part in this interval are not sufficiently studied and are not described in this paper. Deep penetrating viscous waves are observed in a classical liquid in this interval (Mamaladze, Mesoed and Tsakadze, 1964, Mamaladze, 1964).

CC-0. In Public Domain. Gurukul Kangri Collection, Haridwar

Digitized by Arya Samaj Foundation Chennai and eGangotri

surfaces at intervals of the order of a few centimeters from the disk, we can consider that the disk is immersed in an infinite liquid.

The wave number $k_{s0}^{(+)}$ is always obtained as a purely imaginary one. The same is true for the number $k_{s0}^{(-)}$, when $2\omega_0>\Omega$. Hence, the corresponding wavelengths are infinite and the penetration depths are equal to

$$\lambda_{s0}^{(+)}=(\nu_s/\Omega+2\omega_0)^{\frac{1}{2}} \qquad (5.3.4)$$

$$\lambda_{s0}^{(-)}=(\nu_s/2\omega_0-\Omega)^{\frac{1}{2}}, \quad \text{when} \quad 2\omega_0/\Omega>1. \qquad (5.3.5)$$

They are of small magnitudes of the same order as $\lambda_{n0}^{(\pm)}$. There are even fewer reasons here to use the conception "wave." In addition to the fact that the hodograph of velocities again has the shape shown in Fig. 5.8, the oscillations of the liquid in this case occur everywhere in the same phase (Fig. 5.9), i.e., there is no wave in general. Nevertheless we shall use the term s^- "waves", when $2\omega_0>\Omega$ and s^+ "waves," meaning that under real conditions the mutual friction makes these wavelengths finite and thus makes them like $n^\pm$ waves.

Only the wave s^-, when $2\omega_0<\Omega$ has the character completely corresponding to the ideas associated with the conception of an "elastic wave." The wave number $k_{n0}^{(-)}$, when $2\omega_0<\Omega$ is purely real. The penetration depth $\lambda_{s0}^{(-)}$ in this case is infinite. The velocity amplitude does not depend on the distance from the oscillating disk and an instantaneous profile of velocities as well as an instantaneous photo of a vortex line have the shape shown in Fig. 5.10. The wavelength is expressed by the formula

$$L_{s0}^{(-)}=(\nu_s/\Omega-2\omega_0)^{\frac{1}{2}}, \quad \text{when} \quad 2\omega_0<\Omega. \qquad (5.3.6)$$

It is natural that the mutual friction does not leave the penetration depth of this wave equal to infinity. However, even when the dissipation of energy due to mutual friction is taken into account, the penetration depth $\lambda_s^{(-)}$, when $2\omega_0<\Omega$ is (under usual conditions) larger than the other three ($\lambda_s^{(+)}$, $\lambda_n^{(\pm)}$) and larger than the wavelength $L_s^{(-)}$. But $\lambda_s^{(-)}$ is smaller than

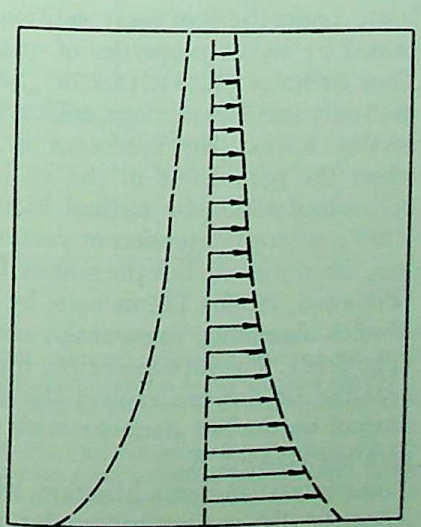

Fig. 5.9. Hodograph of velocities in the s^+ wave in the absence of mutual friction ($L_{s0}^{(+)}=\infty$). The value of the velocity decreases at the removal from the disk along the z axis, according to the exponential law $\exp(-z/\lambda_{s0}^{(+)})$. A similar situation exists for the s^- wave when $2\omega_0>\Omega$.

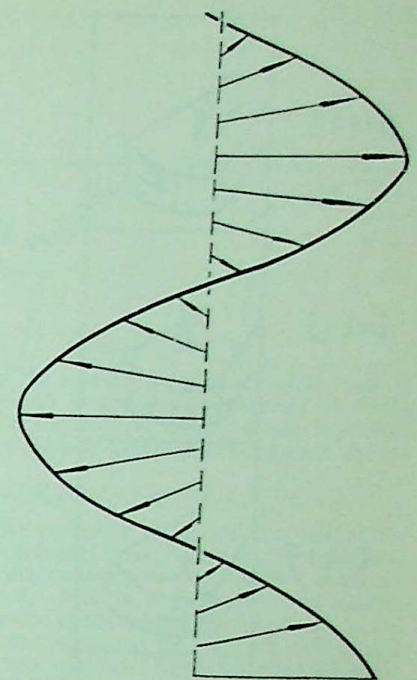

Fig. 5.10. Hodograph of velocities in the s^- wave when $2\omega_0<\Omega$ in the absence of mutual friction ($\lambda_{s0}^{(-)}=\infty$).

the distances of the order of ten centimeters or in some cases even smaller than one centimeter [formula (7.3.3)]. Therefore it is not difficult to create such conditions when the disk is oscillating in an "infinite" liquid.

5.4. The Mechanism of Interaction of an Oscillating Disk with a Rotating Viscous Liquid

Now we can return to the interpretation of formulas (5.2.1), (5.2.1a), (5.2.2), and (5.2.2a). They describe the summarized effects of action of the normal and the superfluid components on the disk. The normal component interacts with the disk by means of viscous forces, which are proportional to the coefficient of viscosity η_n and to the gradient of velocity, i.e., inversely proportional to the penetration depth λ (see Fig. 5.8). Therefore the contribution of $n^\pm$ waves into the change of frequency and damping of oscillations, described by formulas (5.2.1), (5.2.1a), (5.2.2), (5.2.2a) contain terms proportional [according to (5.3.3)] to $(\eta_n\rho_n)^{\frac{1}{2}}\times(|\Omega\pm2\omega_0|)^{\frac{1}{2}}$. The same expressions describe the frequency and damping of the axial disk oscillations in a rotating classical liquid (Mamaladze and Matinyan, 1960c). When $2\omega_0<\Omega$ they give a decrease of oscillation damping at an increase of the velocity of rotation (negligible, when $2\omega_0/\Omega\lesssim0.5$). When $2\omega_0>\Omega$, this decrease is replaced by an increase of damping. This fact is associated with the change of the sequence of terms in the difference $|\Omega-2\omega_0|$. Thus expressions (5.3.3) for the penetration depths of viscous waves explain the existence of the minimum in Fig. 5.5.

5.5. The Mechanism of Interaction of an Oscillating Disk with a Rotating Superfluid Liquid

In contrast to the normal component, the superfluid component of rotating helium II interacts with the disk

CC-0. In Public Domain. Gurukul Kangri Collection, Haridwar

Digitized by Arya Samaj Foundation Chennai and eGangotri

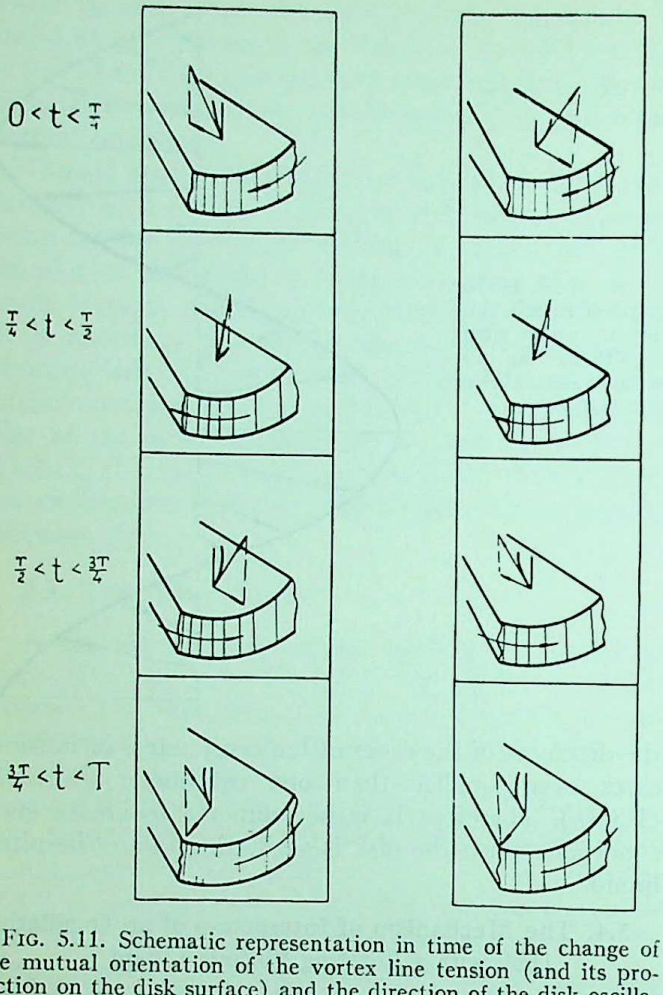

FIG. 5.11. Schematic representation in time of the change of the mutual orientation of the vortex line tension (and its projection on the disk surface) and the direction of the disk oscillations. The action of the s^+ wave is shown in the first column. Similarly the s^- wave acts when $2\omega_0>\Omega$; only the direction of the circular polarization changes. The action of the s^- wave when $2\omega_0<\Omega$ is shown in the second column.

by means of tension in vortex lines curved by the waves. The corresponding tangent forces are proportional to the density of vortex lines and to their tension and inversely proportional to the wavelength of s^-, when $2\omega_0<\Omega$ (Fig. 5.10). When $2\omega_0>\Omega$, then the tangent forces are inversely proportional to the penetration depth of the same s^- wave, and in all the cases to the penetration depth of the wave s^+ (Fig. 5.9). Therefore the contributions of these waves are proportional to $(\omega_0/\Gamma)\epsilon/L_{s0}^{(-)}$ or $(\omega_0/\Gamma)\epsilon/\lambda_{s0}^{(\pm)}$, respectively, i.e., to $\omega_0(\nu_s)^{\frac{1}{2}}\rho_s(|\Omega\pm 2\omega_0|)^{\frac{1}{2}}$.

Considering formulas (5.2.1), (5.2.1a), (5.2.2), and (5.2.2a) from this point of view, we should pay attention to the fact that when $2\omega_0<\Omega$, the s^+ wave contributes only to the change of oscillation frequency and the s^- wave only to damping. When $2\omega_0>\Omega$ both $s^\pm$ waves contribute only to the frequency. Damping in this case is completely determined by $n^\pm$ waves.

The cause of such a separation of functions between the components of a complex wave could be explained if you make a more detailed analysis of solutions of hydrodynamical equations (Mamaladze, 1960b). Its results are schematically shown in Fig. 5.11. It is seen that the s^+ wave distorts a vortex line so that every quarter of the period it sometimes accelerates an approach of the disk to the position of the equilibrium, sometimes slows down its removal from this position. It is clear that such an interaction can change only the oscillation frequency, but does not cause their damping. When $2\omega_0>\Omega$, the s^- wave has the opposite direction of the circular polarization, nevertheless it acts on the disk in the same way as the s^+ wave. But when $2\omega_0<\Omega$, the difference between the s^- and s^+ waves is connected not only with the different signs of polarization, but with the existence of a difference of the initial phases as well. As a result of this the s^- wave distorts a vortex line so that it continuously slows down the disk motion. This fact causes damping of oscillations.

So the nature of the disk vortex damping is similar to the physical nature of radiation damping of electric charge oscillations. The dissipation of the energy of the disk oscillating axially in rotating helium II is caused (in addition to the action of viscous forces) by leakage of energy along oscillating vortex lines in the form of the energy flux of s^- waves.

An idealized picture drawn here, neglecting vortex line sliding and the mutual friction, in reality could have led to disk oscillation damping only in a truly infinite liquid. In the opposite case the energy transferred to vortex lines would return to the disk by waves reflected from the boundaries of the liquid. Under real conditions sliding of vortex lines should be taken into account. It decreases the intensity of the waves running from a given surface, both from a generating surface and a reflecting one. The mutual friction also should be taken into account, as it has been already mentioned, it gives a finite value $\lambda_s^{(-)}$ (instead of $\lambda_{s0}^{(-)}=\infty$) to the penetration depth of an s^- wave. If the distance between the disk and the reflecting surface is sufficiently large in comparison with $\lambda_s^{(-)}$ (not necessarily much larger than $\lambda_s^{(-)}$) then the reflected waves are really absent. Then the dissipation of the disk energy carried away by means of waves along vortex lines, is realized by mutual friction. But the mechanism of energy transfer is still, under the most real conditions of the experiment, caused by elastic properties of quantized vortex lines. Thus formulas (5.2.1), (5.2.1a), (5.2.2), and (5.2.2a) need only small corrections, taking into account mutual friction forces. The exception is the region $2\omega_0\approx\Omega$ where the parameters of the s^- (and n^-) wave are determined rather by mutual friction, and the region $T\approx T_\lambda$, where the tension of vortex lines, proportional to ρ_s, is very small, but the mutual friction is significant (Pitaevski, 1958b). Let us note, by the way, that below $T\sim 2°K$ dampling, apparently, changes roughly as ρ_s (Fig. 5.12). The increase of the role of mutual friction near the λ-point can explain the slowing down of the drop of vortex line damping with an increase of temperature above 2°K.

In contrast to mutual friction, sliding of vortex lines along the disk surface has, under all real conditions, a

CC-0. In Public Domain. Gurukul Kangri Collection, Haridwar

Digitized by Arya Samaj Foundation Chennai and eGangotri

very important role in the determination of the character of vortex oscillation influence on the disk motion (though sliding does not influence the expressions for the wave numbers of the $s^{\pm}$, $n^{\pm}$ waves). Let us nevertheless note that even without taking sliding into account, formula (5.2.2) gives the possibility to understand the main peculiarity of the graphs in Figs. 5.3 and 5.4 distinguishing them from the graph in Fig. 5.5, i.e., instead of a minimum at oscillations in classical liquids including helium I, there is a maximum of damping at oscillations in helium II.

Damping in the rotating normal component (similarly to that in a classical liquid) decreases with an increase of the velocity of rotation almost till $2\omega_0 \sim \Omega$ and damping in helium II is always greater than in a liquid at rest. This means that the main term in formula (5.2.2) is the vortex term (containing $\rho_s \nu_s^{1/2}$). But there is a product $\omega_0(\Omega-2\omega_0)^{1/2}$ in this term that gives a maximum, when $2\omega_0/\Omega=\frac{2}{3}$. The origin of this maximum is easy to understand if you recall that the factor ω_0 characterizes the density of vortex lines and $(\Omega-2\omega_0)^{1/2}$ determines the value of the projection of the vortex line tension on the disk surface. The number of vortex lines increases with an increase of ω_0, but the action of each of them on the disk oscillations is weakened, because of a decrease of the inclination of a vortex line to the disk surface, caused by an increase of the wavelength $L_{s0}^{(-)}$. The struggle of such opposite tendencies leads just to the maximum of δ when $2\omega_0/\Omega=\frac{2}{3}$. But this magnitude is about three times as large as the experimental one. The cause of this discrepancy cannot be understood without consideration of vortex sliding, which is considered in the next section.

5.6. Resonance Phenomena

The waves $n^{\pm}$, $s^{\pm}$, being generated by an oscillating disk and reflected from the top or the bottom of the vessel, from the free surface of the liquid, or from the surface of another oscillating disk, could interfere in a different way in dependence on the passed distance. The maximum and the minimum intensities would then be achieved at different distances between the surfaces, multiple to the half-wavelength or a quarter wavelength, in dependence on the character of the surface and its motion. The surface may be free or solid. In the latter case it may be at rest or oscillate.

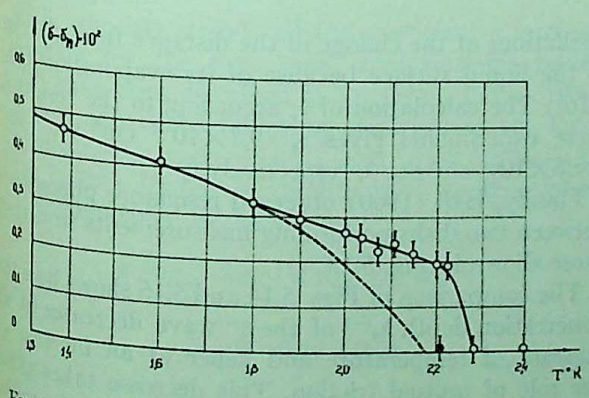

Fig. 5.12. Temperature dependence of the disk axial oscillation damping at $2\omega_0/\Omega=0.21$ (corresponding to the maximum in Fig. 5.3). The dashed line shows the law $\delta-\delta_n \sim \rho_s$; δ_n is the decrement of damping in helium II at rest. The experimental data shown by open circles (Andronikashvili, Mesoed, and Tsakadze, 1964) are stable when $T<T_\lambda$, but when $T>T_\lambda$ they are obtained only at the transition from helium II into helium I in the state of rotation (11.2). The stable value obtained by rotation at $T>T_\lambda$ is given by a circle with a cross.

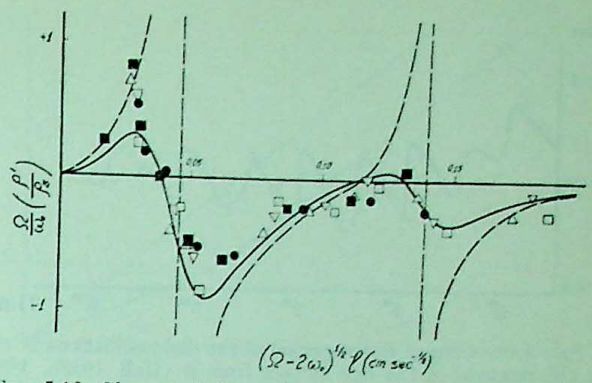

Fig. 5.13. Change of the oscillation frequency of the pile of disks at the change of disk separation $2l$, according to Hall's data (1958a, 1960). ρ' is the effective density of the superfluid component dragged into the pile oscillations, determined by the formula

$$\rho'/\rho_s=[(T_\omega^2-T_0^2)/(T_2^2-T_1^2)][(I_2-I_1)/I_s],$$

where $T\omega$ and T_0 are the periods of oscillation of a disk in the rotating helium II and in helium II at rest. T_2 and T_1 are the periods of oscillation at room temperature; the corresponding moments of inertia are I_2 and I_1; I_2-I_1 is the known moment of inertia; I_s is the moment of inertia of the superfluid component in the pile. The dashed line was calculated by Hall not taking into account vortex sliding. The solid line is obtained when sliding is taken into account (6.1). Different symbols for the experimental points correspond to different conditions of the experiment. In all cases, $2\omega_0<\Omega$.

Therefore it is clear that waves, the penetration depths of which are small in comparison with the wavelengths ($n^{\pm}$, s^{+}, and s^{-} when $2\omega_0>\Omega$) could not manifest themselves appreciably in resonance phenomena. Only a s^{-} wave has such an ability, when $2\omega_0<\Omega$.

In actuality, having studied the velocity dependence of the oscillation frequency of a pile of disks in rotating helium II, Hall (1958a) found resonance phenomena disappearing when $2\omega_0>\Omega$. It was found that, when $2\omega_0<\Omega$, the frequency of oscillations Ω sometimes decreases, sometimes increases with an increase of the velocity of rotation in such a way that some function of Ω (see Fig. 5.13) depends almost sinusoidally on the combination $(2\omega_0-\Omega)^{1/2}l$ (where l is the half of the disk separation). Let us recall that Hall's pile of disks had variable separation between the disks. The magnitude $(2\omega_0-\Omega)^{1/2}l$ is proportional to the ratio of $2l$ to the length of the S^{-} wave. Hall has determined the parameter ν_s entering formula (5.3.6) for $L_{s0}^{(-)}$ for the known distance between two nearest maxima (minima) on the curve in Fig. 5.13. He has obtained for ν_s the value $\nu_s=(8.5\pm1.5)10^{-4}$ cm^2 sec^{-1}. In addition he made an estimation of the radius of the core of a vortex line

CC-0. In Public Domain. Gurukul Kangri Collection, Haridwar

Digitized by Arya Samaj Foundation Chennai and eGangotri

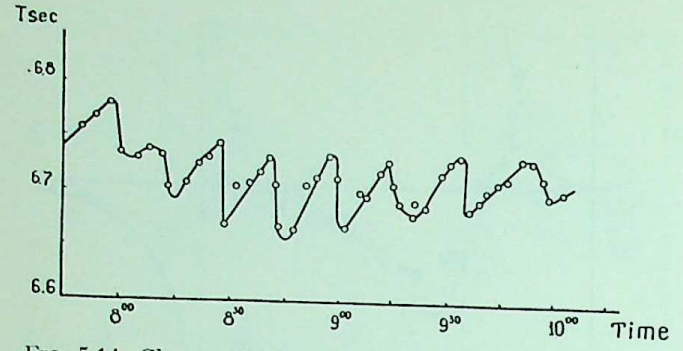

FIG. 5.14. Change of the period of the disk oscillations in time at the removal of the free surface from it (Hall, 1958b, 1960). $T=1.3°K$, $2\omega_0<\Omega$.

(entering the expression for ν_s). According to his estimation $a_0\approx 7$ Å, but Gopal (1964), having recalculated data of Hall's experiment, has shown that they correspond to the value $a_0\approx 4$ Å.

The described investigation made by Hall and the similar results published by Andronikashvili and Tsakadze (1958),[8] in which oscillations of a pile of disks were studied, were the first ones in the series of the following studies of solid body motion in rotating helium II. Many of these studies have already been described in the previous paragraphs. Just the experiment with a pile of disks was the basis of the statement of Andronikashvili and Tsakadze on the existence of the modulus of rigidity in rotating helium II with respect to the rotation axis. However, Hall who was the first to determine the parameters of elastic waves $s^{\pm}$, nevertheless has interpreted the results of his experiments in terms of "effective density of the superfluid component dragged into oscillations of the pile of disks." In particular, he considered the observed increase of the frequency as an indication of the effective decrease of the moment of inertia. Therefore he explained it by the superfluid motion in the antiphase to the motion of disks of the pile. However, it would be more natural to consider the observed phenomena as a result of the torque increase as it was made by Andronikashvili and Tsakadze.[9] In this connection we should mention the

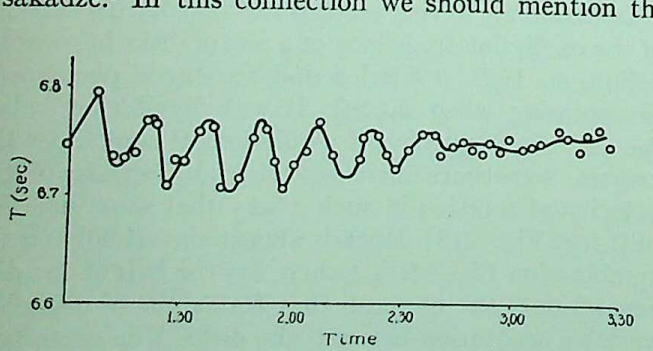

FIG. 5.15. Same as in Fig. 5.14, but at the temperature $T=1.6°K$ (Hall, 1958b, 1960). Comparison of Figs. 5.14 and 5.15 shows how the penetration depth of the s^- wave decreases at an increase of mutual friction, when the wavelength practically does not change [compare formulae (5.3.6), (7.3.3), and (7.3.5)].

[8] The results of both experiments were reported simultaneously by both groups of authors at the Fourth All-Union Conference on Low Temperature Physics, Moscow, 1957.

results of a detailed analysis of hydrodynamical equations. This analysis shows that when vortex lines are completely fastened onto the surface of the disk, the superfluid component oscillates in the radial direction, i.e., not in the phase or antiphase with the disks, but perpendicular to the direction of their oscillations. Certainly, this phenomenon is connected with the Magnus effect. In general, one should always remember that the superfluid component does not interact directly with a solid body, just vortex lines existing in it do that.

Resonance phenomena were also observed at oscillations of a single disk under the free surface of rotating helium II. Hall (1958b, 1960) has measured the period of the disk oscillations as a function of the distance from it to the free surface changed as a result of helium inflow along the film (Figs. 5.14 and 5.15). Andronikashvili and Tsakadze (1959a) have measured the damping of

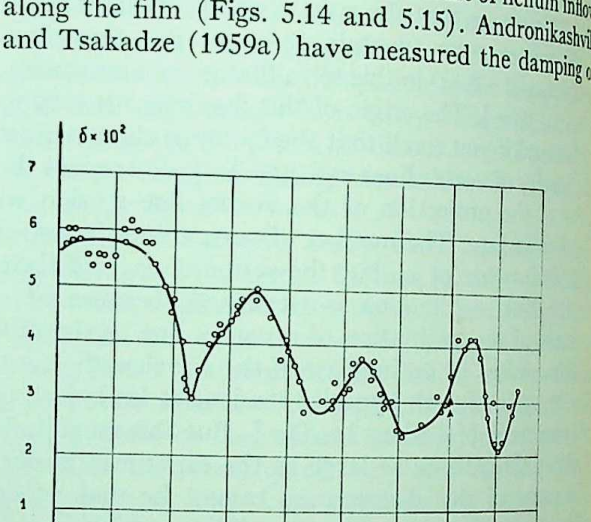

FIG. 5.16. Change of the disk oscillation damping in time at an approach of the free surface to the disk (Andronikashvili and Tsakadze, 1959a). Here n is the number of half-periods of oscillations. $2\omega_0<\Omega$.

oscillations at the change of the distance from the disk to the liquid surface because of its evaporation (Fig. 5.16). The calculation of ν_s according to the results of these experiments gives $\nu_s=9.7\times10^{-4}$ cm^2 sec^{-1} and $\nu_s\approx 8\times10^{-4}$ cm^2 sec^{-1}, respectively.

Finally, Hall (1960) observed resonance phenomena between two disks performing measurements similar to those shown in Fig. 5.13.

The comparison of Figs. 5.14 and 5.15 shows how the penetration depth $\lambda_s^{(-)}$ of the s^- wave decreases at an increase of temperature and hence at an increase of the role of mutual friction. This decrease takes place practically at its constant length $L_s^{(-)}$ and at the maintenance of the unequality $\lambda_s^{(-)}\gg L_s^{(-)}\approx L_{s0}^{(-)}$. The weakness of the dependence of $L_s^{(-)}$ on temperature

[9] More detail is given on the difference between Hall's conception and that of the Tbilissi group as well as on the more accurate interpretation of Hall's experiments in the paper of Andronikashvili, Mamaladze, Matinyan, and Tsakadze (1961).

CC-0. In Public Domain. Gurukul Kangri Collection, Haridwar

Digitized by Arya Samaj Foundation Chennai and eGangotri

was also found as a result of Hall's experiment with the disks.

6. OSCILLATIONS OF SOLID BODIES WITH AXIAL SYMMETRY IN ROTATING HELIUM II (CONTINUATION). SLIDING OF VORTEX LINES AND COLLECTIVIZATION OF VORTEX OSCILLATIONS

6.1. Sliding of Vortex Lines

The coefficients a and a' first mentioned in Sec. 4.3, in the boundary conditions of Bekarevich, Khalatnikov (4.3.1) being practically always not equal to zero, describe sliding of vortex lines along the disk surface. Their values depend on many conditions. According to formulas (4.3.2), (4.3.3) the coefficient a depends on the scale of roughness of the considered surface and the coefficient a' can be very small in comparison with the coefficient a. In the temperature interval $T>1°K$, it does not exceed $\sim 0.3a$. [*Note added in proof*. According to a new estimation of the coefficient B', made by Iordanski (Sec. 12.8), even the ratio $a'/a\sim 0.3$ should be considered as too large.] Thus we can take into account only the coefficient a in the interpretation of many experimental data.

In addition to the size of protuberances the following factors may influence the values of the coefficients of sliding: the number of protuberances on the surface and the velocity of rotation determining the ratio between the number of protuberances and the number of vortex lines; the frequency of oscillations of the surface, determining together with the velocity of rotation the values of forces dragging the vortex line along the surface; the amplitude of oscillation determining the change of vortex energy as a result of which it either becomes longer at the removal from the position of equilibrium or it slides off the proturberance of a given size, and finally it is also reduced to the value of the drag force, etc.

Hall, who has introduced the coefficient a into consideration for the first time, analyzing his results, which have been described in 5.6 (Hall, 1958a, 1960), has determined the following empirical values for a: $a=0.5\Omega/k_{s0}^{(-)}$, when $2\omega_0<\Omega$ and $a=0.5\Omega(2\omega_0/\nu_s)^{-\frac{1}{2}}$, when $2\omega_0\gg\Omega$. Under the conditions of the experiments that corresponded to the values

$$a\sim(1.5\div 2.3)\times 10^{-2}\ \text{cm sec}^{-1}$$

when

$$2\omega_0/\Omega\sim 0.13\div 0.26$$

and

$$a\sim(2.3\div 3)\times 10^{-1}\ \text{cm sec}^{-1}$$

when

$$2\omega_0/\Omega\sim 6\div 8.$$

The necessity to obtain at least an approximate estimation of the coefficient of sliding was connected with the fact that the magnitude plotted along the ordinate in Fig. 5.13, has, in the theory neglecting sliding, infinite jumps between its experimental maxima and minima (i.e., near the second, fourth, and the following even zeros).

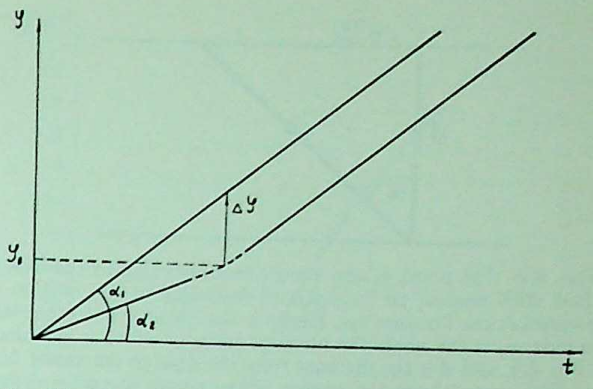

FIG. 6.1. Change in time of the deflection angle of the suspension head with respect to the rotating vessel takes place according to the law $\varphi=\omega_0' t(\omega_0'=tg\alpha_1)$. The deflection angle of the disk changes in time by the law

$$\varphi=\begin{cases} t\cdot tg\alpha_2 & \text{at } \varphi<\varphi_0 \\ \omega_0' t-\Delta\varphi & \text{at } \varphi>\varphi_0 \end{cases}$$

(Gamtsemlidze, Japaridze, Salukvadze, and Turkadze, 1966). The constancy in time of the disk delay from the suspension head, taking place at $\varphi=\varphi_0$, means that vortex sliding prevents their further distortion.

The direct measurement of a was made by Gamtsemlidze, Japaridze, Salukvadze, and Turkadze (1966) in an experiment, the idea of which arose from the following circumstances. Osborne (1961) made an attempt to measure the force with which vortex lines are fastened to a solid surface. For this purpose he deflected for some angle a disk suspended on an elastic thread near the bottom of the rotating vessel and taking part in the rotation. The experiment failed, because vortex lines, sliding along the surface of the disk or the bottom, became parallel again to the rotation axis. After that they could not already create the torque acting on the disk. Therefore Gamtsemlidze *et al.* decided to use a disk performing continuous motion with respect to the vessel bottom. They constructed a device in which the vessel with helium II and the disk rotated together. An additional rotation of the disk suspension head was superimposed on this rotation. Depending on the forces acting on it, the disk could either rotate with the same velocity as its suspension head, or rotate with some delay with respect to it. At the start of an extra rotation the disk was at first behind the suspension head, being slowed down due to inclined vortex lines (Fig. 6.1). But with an increase of delay the torque of the suspension head increased gradually, while an increase of slowing down action of the inclined vortex lines was limited by their sliding. If we neglect the coefficient a' then the boundary condition (4.3.1) gives in this case $\omega_0' r\approx a\sin\alpha\approx ar\phi_0/d$ (Fig. 6.2) or $a=\omega_0' d/\phi_0$, where ϕ_0 is the angle of torsion at which the disk delay reaches some constant value,

CC-0. In Public Domain. Gurukul Kangri Collection, Haridwar

Digitized by Arya Samaj Foundation Chennai and eGangotri

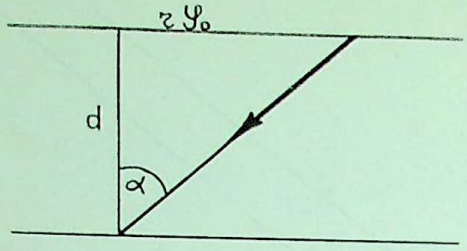

FIG. 6.2. The point of the vortex line fastening to the disk is shifted with respect to its point of fastening to the bottom of the vessel at the distance $r\varphi_0$. Here r is the distance from the rotation axis, φ_0 is the angle the physical sense of which is explained by Fig. 6.1, and d is the distance from the disk to the vessel bottom. The arrow shows the tension of the vortex line after deflection.

d is the distance from the disk to the bottom, and ω_0' is the angular velocity of the additional rotation.[10]

The estimation obtained in such a way gave $a=0.1$ cm sec^{-1}, when $\omega_0=0.038$ sec^{-1} (and $\omega_0'=0.0035$ sec^{-1}). Within an order of magnitude it agrees rather well both with Hall's data (1960) and with the estimation (4.3.3) as the size of sand grains glued to the disk was $\delta\sim 50\,\mu$.

6.2. The Role of Sliding in an Interaction of an Oscillating Disk with Rotating Helium II

Let us return now to the problem of axial oscillations of a disk in helium II. If sliding is taken into account formulas (5.2.1), (5.2.1a), (5.2.2), and (5.2.2a) became much more complex. We shall not write the corresponding cumbersome expressions, but we shall note (Mamaladze, 1965) that sliding changes the relation of phases of the s^+ and s^- waves and each of them begins to contribute both to damping and to oscillation frequency. In addition, as it was already noted, sliding influences the value of the tangent component of the vortex line tension. Let us take into account all these factors, without taking the mutual friction into account explicitly, though it enters all these phenomena not explicitly, since it is possible to neglect the reflected waves. Then the calculation of vortex damping at different coefficients of sliding leads to the results given in Fig. 6.3. An increase of the coefficient a leads at first to an increase of damping and then to its drop. The coefficient a' has a comparatively insignificant role.

The curves in Fig. 6.3 are very much like the experimental curves in Figs. 5.3 and 5.4. The only essential difference between them is the position of the maximum, which, as it was before sliding was taken into account, is on the calculated curves at the value of $2\omega_0/\Omega$ much greater than in reality.

Comparing Fig. 6.3 with Figs. 5.3 and 5.4, we can note that experimental curves hardly correspond to some constant values of the coefficients of sliding. That should not be expected, if we take into account their probable dependence on the velocity of rotation. The first portions of the experimental curves (especially in the case of a smooth disk) have a small slope indicating that the sliding coefficient a has large values. Relatively high maxima, on the contrary, show that a is rather small. It becomes clear that the experimental maximum is associated with the minimum of sliding and the shapes of the experimental curves are due to its smooth change.

Numerical calculations made by a computer have shown (Fig. 6.4) that the experimental data agree completely with the theory, when both sliding and mutual friction are taken into account. Here it was suggested that the coefficient of sliding is a function of the velocity of rotation as it is shown in Fig. 6.5 (Andronikashvili, Mamaladze, Matinyan, and Tsakadze, 1961). The order of magnitude of a according to these data also agrees with the data of other authors.

6.3. Collectivization of Vortex Line Oscillations

The maximum on the curves of the disk damping dependence on the velocity of rotation is always found at $2\omega_0/\Omega\approx 0.2$ and its position does not depend either on temperature or on the extent of roughness of the disk surface. The minimum of the sliding coefficient is always located at this point and the reason for this fact does not depend directly on the peculiarities of the phenomenon of sliding itself. Here the properties of vortex lines and of waves running along them are displayed and lead, when $2\omega_0/\Omega\approx 0.2$, to the phenomenon of collectivization of vortex oscillations [Mamaladze, see, for instance, Andronikashvili and Tsakadze (1959b) and Andronikashvili, Mamaladze, Matinyan,

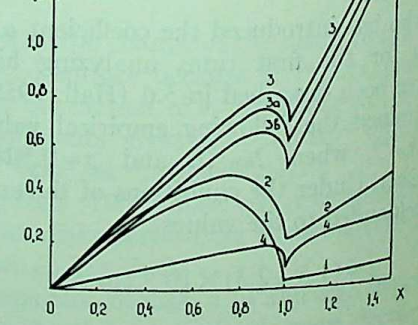

FIG. 6.3. Dependence of axial oscillation damping of the disk on the velocity of rotation of the superfluid at different values of coefficients of sliding according to calculations of Mamaladze (1965). The symbols are $x=2\omega_0/\Omega$,

$$f_4(x)=\frac{2I\Omega^{\frac{1}{2}}(\delta-\Omega_0\delta_0/\Omega)}{\pi^2R^4\rho_s(\nu_s)^{\frac{1}{2}}}.$$

The coefficient b equal to $b=a/(\Omega\nu_s)^{\frac{1}{2}}$ takes the following values on the curves 1, 2, 3, and 4, where the coefficient $a'=0$: (1) $b=10^{-2}$; (2) $b=10^{-1}$; (3) $b=1$; (4) $b=10$. On curves 3a and 3b as well as on curve 3, $b=1$, and the coefficient b' equal to $b'=a'/(\Omega\nu_s)^{\frac{1}{2}}$ takes the values: (3a) $b'=10^{-1}$; (3b) $b'=3\times 10^{-1}$.

[10] Apparently, the absolute sense should not be attributed to Fig. 6.2. In reality vortex lines slide off the grains and try to straighten, but fasten themselves to new grains and become inclined again, etc. Figure 6.2 can be considered as a result of the averaging of this process in time.

CC-0. In Public Domain. Gurukul Kangri Collection, Haridwar

Digitized by Arya Samaj Foundation Chennai and eGangotri

and Tsakadze (1961)]. Let us begin the description of this phenomenon.

When a wave runs along a vortex line, the superfluid liquid both rotates around the vortex line and oscillates with it as well. The distances from a vortex line at which the liquid takes an effective part in rotation around one of the vortex lines can differ significantly from distances at which it participates in vortex oscillations. The participation of the superfluid component in vortex oscillations is characterized by the additional energy ϵ' (Pitaevski, 1958b).

$$\epsilon' = \pi\rho_s(\hbar^2/m^2)\tfrac{1}{2}(q^2\sigma^2)\ \ln\,(\sigma a)^{-1}, \qquad (6.3.1)$$

where q is the amplitude of oscillations and σ is the real wave number. Comparing this expression with formula (2.3.1) for the energy of the liquid rotation in a vortex, we obtain the following estimation for the effective radius b_1 of the region where the liquid oscillates together with a vortex line

$$b_1 \approx 1/\sigma. \qquad (6.3.2)$$

This estimate agrees with the Kelvin formula (1880) according to which $b_1 = 1.046/\sigma$.

As noted in Sec. 5.3, when $2\omega_0 < \Omega$, the s^- waves are the main ones running along vortex lines. To estimate the value of b_1 for these waves, the wave number $k_{s0}^{(-)}$ should be substituted into formula (6.3.2). Neglecting the mutual friction, we obtain

$$b_1 = [\nu_s/(\Omega - 2\omega_0)]^{\frac{1}{2}}. \qquad (6.3.3)$$

At sufficiently small velocities of rotation, the vortex line separation $(\pi\hbar/m\omega_0)^{\frac{1}{2}}$ is large and exceeds the effective radius of oscillations b_1. Under such conditions,

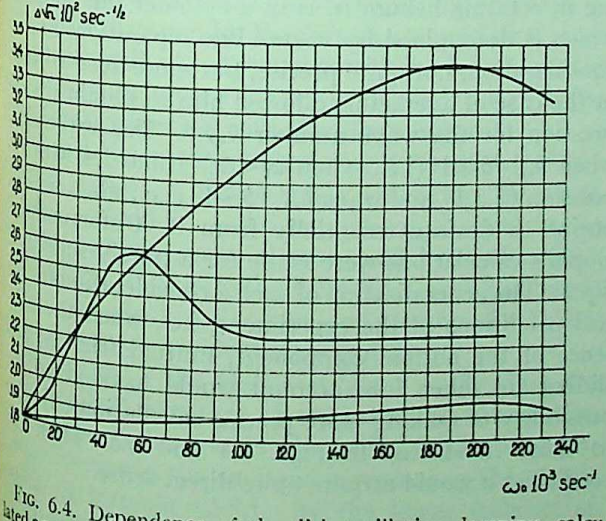

Fig. 6.4. Dependence of the disk oscillation damping, calculated according to the formula which takes into account completely both sliding and mutual friction (Andronikashvili, Mamaladze, Matinyan, and Tsakadze, 1961). The parameters of the device and the temperature correspond to the conditions of the experiment described by the lower curve in Fig. 5.3. Δ denotes $\delta - \Omega_0\delta_0/\Omega$. The upper curve is calculated when $a=0$, the lower one when $a=\infty$. The middle curve reproduces the experimental data and is obtained using a variable a, the velocity dependence of which is shown in Fig. 6.5.

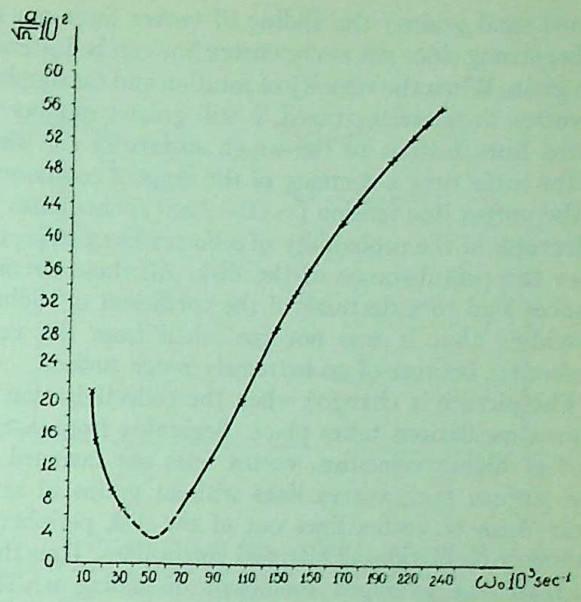

Fig. 6.5. Empirically established dependence of the coefficient of sliding a on the angular velocity of rotation under the conditions of the experiment described by the lower curve in Fig. 5.3. (Andronikashvili, Mamaladze, Matinyan, and Tsakadze, 1961).

the whole superfluid liquid moved by vortex lines does not participate in oscillations, but only some part of it, directly adjacent to them. Oscillations of separate vortex lines are independent. But when the velocity of rotation is increased, the distance between vortex lines decreases while the effective radius of oscillations b_1 increases. At the velocity, which we shall denote as $\tilde{\omega}_0$, the effective radius b_1 becomes equal to half of the vortex separation

$$[\nu_s/(\Omega - 2\tilde{\omega}_0)]^{\frac{1}{2}} = \tfrac{1}{2}(\pi\hbar/m\tilde{\omega}_0)^{\frac{1}{2}},$$

hence,

$$2\tilde{\omega}_0/\Omega = (2m\nu_s/\pi\hbar + 1)^{-1}. \qquad (6.3.4)$$

Beginning from the velocity $\tilde{\omega}_0$ and when $\omega_0 > \tilde{\omega}_0$ the effective radii of vortex oscillations overlap and their mutual interaction occurs. Under such conditions, oscillations of a vortex line are transferred to its neighbors and, on the contrary, the existence of nonoscillating neighbors prevents vortex line oscillations.

If we substitute numerical values for the parameters which are in the right-hand side of formula (6.3.4), then $2\tilde{\omega}_0/\Omega$ is of the order of 0.2. This value coincides with the point of maximum on the experimental curves of damping dependence on the velocity of rotation (Figs. 5.3, 5.4) and with the point of the minimum on the curve of the sliding coefficient a dependence on the velocity of rotation (Fig. 6.5). Proceeding from the idea of collectivization of vortex oscillations the character of the latter curve can be understood in the following way.

At small velocities of rotation when there are few vortex lines, the coefficient of sliding depends mainly on the roughness of the surface. We should take into account that even in the presence of artificial roughness

CC-0. In Public Domain. Gurukul Kangri Collection, Haridwar

Digitized by Arya Samaj Foundation Chennai and eGangotri

(glued sand grains) the sliding of vortex lines can be rather strong since not every vortex line can be fastened to a grain. When the velocity of rotation and the number of vortex lines are increased, a still greater number of vortex lines fastens to the rough surface of the disk. At the same time a decrease of the tangent component of the vortex line tension $[\sim(\Omega-2\omega_0)^{\frac{1}{2}}]$ contributes to a decrease of the probability of a vortex line tearing off from the protuberance of the disk. All these circumstances lead to a decrease of the coefficient of sliding, providing that it was not too small from the very beginning, because of an extremely rough surface.

The picture is changed when the collectivization of vortex oscillations takes place. Beginning from $\omega_0\approx\tilde{\omega}_0$ and at higher velocities, vortex lines not fastened to the surface (i.e., vortex lines without grains of sand near them or vortex lines out of the disk periphery) influence oscillations of fastened vortex lines. Thus they increase the averaged coefficient of sliding a. This increase of sliding leads just to the maximum of damping (Figs. 5.3, 5.4). As noted before (Fig. 6.3) even stronger damping of disk oscillations corresponds to smaller coefficients of sliding than in the case $a=0$. Such a phenomenon is connected with the fact that when there is sliding, the s^+ wave, in addition to the change of frequency of disk oscillations (5.5), begins to participate in the increase of damping. In its turn large coefficients a correspond to weak damping, as the projection of vortex tension does not sufficiently slow down the disk oscillations.

Now it is possible to understand another phenomenon in which the special role of the point $2\tilde{\omega}_0/\Omega\approx0.2$ is seen. It is a sharp slowing down of the frequency increase

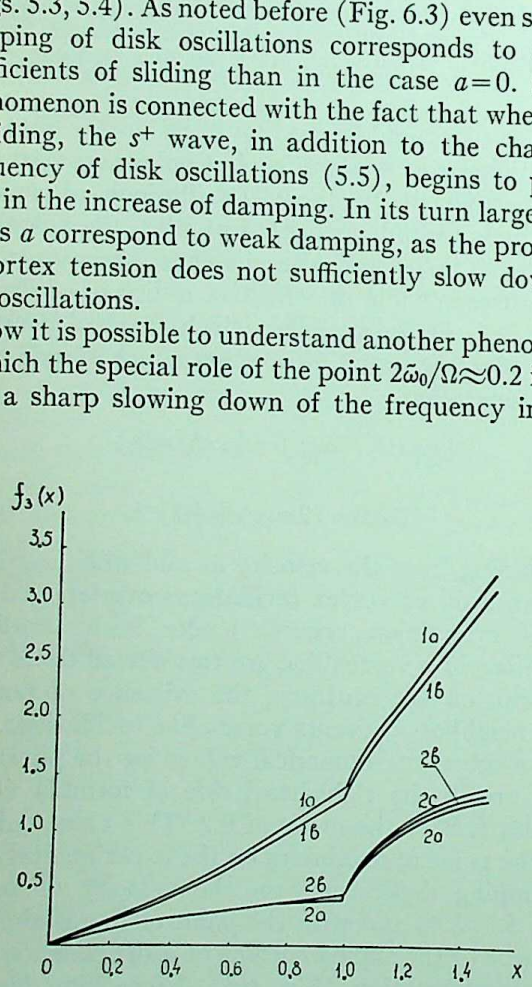

FIG. 6.6. The influence of sliding on the velocity dependence of the disk oscillation frequency in the rotating superfluid. It was calculated when mutual friction was not taken into account (Mamaladze 1965). The symbols used are: $x=2\omega_0/\Omega$,

$$f_3(x)=2I(\Omega^2-\Omega_0^2)/\pi R^4\rho_s(\nu_s\Omega)^{\frac{1}{2}}.$$

The symbols b and b' are the same as in Fig. 6.3. Their values on different curves: (1a) $b=10^{-1}$, $b'=0$; (1b) $b=10^{-1}$, $b'=3\times10^{-2}$; (2a) $b=1$, $b'=0$; (2b) $b=1$, $b'=10^{-1}$; (2c) $b=1$, $b'=3\times10^{-1}$.

of light disk oscillations, depending on the velocity of rotation. In the beginning of the curve in Fig. 5.2, the experimental data agree rather well with formula (5.2.1), which does not take sliding into account. But when $2\omega_0/\Omega>0.2$ an increase of sliding leads to a decrease of vortex line contribution to the torsion momentum acting on the disk. Then the increase of frequency is slowed down (Fig. 6.6).

The third fact confirming the validity of the considerations on the role of collectivization is the break of the curves in Fig. 5.6. When $2\omega_0/\Omega_1>0.2$ vortex lines begin to slide along the disk surface, which is a generator of waves. The intensity of s^- waves, running along them, decreases as well as the damping of the cylinder performing vertical oscillations.

The hydrodynamics of rotating helium II by its very nature cannot take into account completely the phenomenon of collectivization of vortex line oscillations. It deals with magnitudes averaged over the volume containing many vortex lines and therefore the parameters b_1 or $\tilde{\omega}_0$ do not appear naturally in the equations of hydrodynamics or in their solutions. The considerations used to determine these parameters were beyond the frames of an averaged hydrodynamical treatment and the phenomena associated with the collectivization of oscillations were described, in the language of hydrodynamics of rotating helium II, as changes of the averaged coefficient a. Thus it is an arbitrary parameter, selected to achieve an agreement between the theory and experiment (Figs. 6.4 and 6.5).

Gopal (1964a,b) approached this problem in another way, without averaging, while solving the problem of single vortex line oscillations in a cylindrical vessel (1963). Then he imagined that each vortex line, appearing in rotating helium II, is in a cylinder the radius of which is determined by vortex line separation. Such a consideration, not quite precise, but more detailed than in the case of averaging, allowed him to obtain the expression for the wave number $k_{s0}^{(-)}$. This expression, when $k_{s0}^{(-)}b\ll1$ (i.e., when $\omega_0<\tilde{\omega}_0$) coincides with expression (5.3.1) and when $k_{s0}^{(-)}b\sim1$, (i.e., when $\omega_0\sim\tilde{\omega}_0$) begins to deviate essentially from it. Unfortunately, Gopal's calculations were made for a purely superfluid liquid. The generalization of such a consideration for the real conditions of the experiment, i.e., when the existence of the normal component, mutual friction, and sliding are taken into account would have given the possibility of making more precise calculations, similar to those illustrated in Figs. 6.4 and 6.5. Then the coefficient a would acquire more direct sense.

7. MUTUAL FRICTION BETWEEN THE SUPERFLUID AND NORMAL COMPONENTS

7.1. The Conception of Mutual Friction in Rotating Helium II

Preliminary data on mutual friction between the superfluid and normal components of rotating helium II

CC-0. In Public Domain. Gurukul Kangri Collection, Haridwar

Digitized by Arya Samaj Foundation Chennai and eGangotri

were given in the paper of Hall and Vinen (1955). The anisotropic character of such an interaction was also emphasized there. Feynman's point of view on the nature of critical phenomena in helium II explains completely both the causes of the creation of mutual friction and its anisotropic character. The mutual friction is due to scattering of thermal excitations on singularities, which are vortex lines. In rotating helium II where vortex lines are aligned along the rotation axis, the transfer of the thermal excitation momentum to a vortex line (i.e., of the normal component momentum to the superfluid liquid) should be essentially different in radial and axial directions.

7.2. The First Experimental Confirmation of Feynman's Theory

In the investigations which gave the first experimental confirmation of Feynman's theory, the force of mutual friction reduced to unit mass of the superfluid component was expressed by Hall and Vinen (1955, 1956a, b) in the following way:

$$\mathbf{F}_{sn}=-\tfrac{1}{2}(\rho_n/\rho)B[(\boldsymbol{\omega}/\omega),[\boldsymbol{\omega},\mathbf{v}_n-\mathbf{v}_s]]$$
$$-\tfrac{1}{2}(\rho_n/\rho)B'[\boldsymbol{\omega},\mathbf{v}_n-\mathbf{v}_s]. \quad (7.2.1)$$

In this formula the both terms are proportional to the values of two vectors, to the relative velocity $\mathbf{v}_n-\mathbf{v}_s$ and to $\boldsymbol{\omega}=$ curl $\mathbf{v}_s$ (because of the linear dependence of the number of vortex lines on the velocity of rotation). The first term with the coefficient B has the direction of the relative velocity projection $\mathbf{v}_n-\mathbf{v}_s$ on the plane perpendicular to the rotation axis. It is just the direction which one could imagine at an elementary consideration of the action of the normal component flow on vortex lines existing in the superfluid component. But in the expression for $\mathbf{F}_{sn}$ there is a second term, with the coefficient B' also directed perpendicularly to vortex lines and at the same time perpendicular to $\mathbf{v}_n-\mathbf{v}_s$. Its existence is connected with the Magnus effect.

Hall and Vinen used second-sound resonators of two different types: a radial mode resonator, in which emission, reflection, and reception of thermal waves were realized by means of two coaxial cylinders with side surfaces facing each other and an axial mode resonator in which the bottom and the top of a hollow cylinder were used with the same aim.

The results of the Hall and Vinen study were the following: (a) detection of second-sound attenuation due to mutual friction in the radial mode resonator and its absence in the axial mode resonator, (b) confirmation of formula (2.5.1) by the linear increase of mutual friction with an increase of velocity of rotation, (c) a theoretical analysis of scattering of thermal excitations on vortex lines and comparison of the calculated values of the mutual friction coefficients B with its experimental dependence on temperature, (d) confirmation of circulation quantization (Fig. 7.1). Hall and Vinen did not manage to measure the coefficient B'.

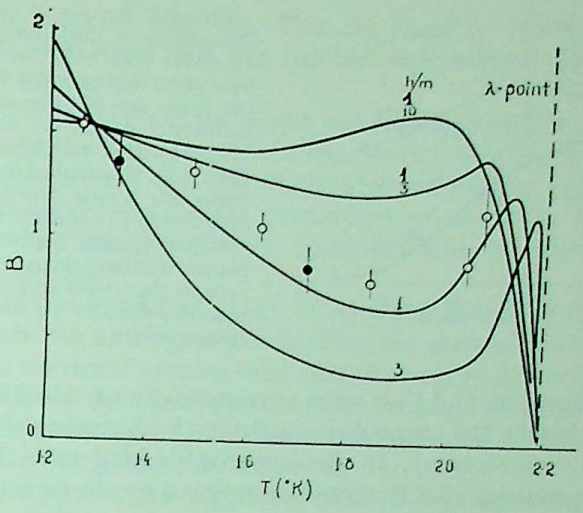

Fig. 7.1. Dependence of the coefficient of mutual friction B on temperature studied experimentally by Hall and Vinen, and calculated by them at different values of the vortex circulation, which are given (in units of h/m) above each curve (Hall and Vinen, 1956a, b).

7.3. Further Investigations

Lifshitz and Pitaevski (1957) have critically considered the calculations of Hall and Vinen and showed the necessity of replacing Born's approximation, used by them at the consideration of scattering of thermal excitations on vortex lines, by a quasi-classical one. That did not lead to sufficient results. To achieve agreement of the theory with the experiments of Hall and Vinen on measurements of B, it was necessary to introduce such a mechanism of roton scattering, at which a roton passes an intermediate stage of its capture to a stationary orbit by a vortex line. Having selected the effective radius of this capture ~10 Å, Lifshitz and Pitaevski have brought their calculations to agreement with the experimental values of B and obtained the theoretical dependence of B' on temperature shown in Fig. 7.2.

Dependence of B and B' on temperature in the vicinity of the λ-point is studied in comparatively less detail. Pitaevski (1958b) has shown that here one should not expect a gradual approach of B and B' to zero and large values of both coefficients are possible.

The data of Tsakadze and Chkheidze (1960, see Fig. 5.1) also give a possibility to measure B. According to Mamaladze and Matinyan (1960b), the results of their experiments should be described by the formula

$$\frac{\delta_2-\delta_1}{l_2-l_1}=\frac{2\pi^2R^3}{I}\left(\frac{2\eta_n\rho_n}{\Omega}\right)^{\frac{1}{2}}\left(1+\frac{\omega_0}{\Omega}\frac{\rho_s}{2\rho}B\right). \quad (7.3.1)$$

(Symbols used are the same as in caption to Fig. 5.1.) The agreement of the theory and the experiment shown in Fig. 5.1 confirms the calculations made by Lifshitz and Pitaevski (1957), as the values obtained by them for B were used while plotting the theoretical straight lines.

CC-0. In Public Domain. Gurukul Kangri Collection, Haridwar

Digitized by Arya Samaj Foundation Chennai and eGangotri

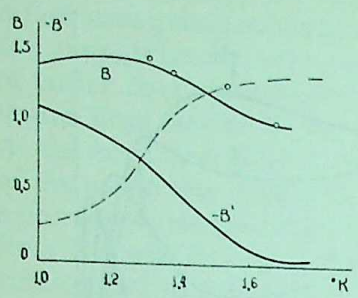

FIG. 7.2. Results of the calculations of Lifshitz and Pitaevski (1957). The solid lines give: the upper one B, the lower one B'. The experimental points are obtained by Hall and Vinen (Fig. 7.1). The dashed line shows the wrong dependence $B=B(T)$ obtained at the quasiclassical approximation without taking into account the temporary capture of rotons to the stationary orbits.

Formula (7.3.1) is valid at relatively small velocities satisfying the unequality $\omega_0\rho_s B/\rho\Omega\ll 1$ (depending also on temperature). In the opposite limiting case the dependence (7.3.1) should be replaced by the formula of Mamaladze:

$$\frac{\delta_2-\delta_1}{l_2-l_1}=\frac{2\pi^2R^3}{I}\left(\frac{2\eta_n\rho}{\Omega}\right)^{\frac{1}{2}}. \qquad (7.3.2)$$

Equation (7.3.2) does not give the dependence of damping on the velocity of rotation. It is especially interesting that it contains the total density ρ instead of ρ_n. Thus the formula has such a form as if oscillations take place in a liquid at rest with the density ρ, but viscosity η_n.

In the method of an oscillating cylinder edge effects are excluded by subtraction of damping measured at different depth of immersion. Because of this the described method is very convenient for measurements of viscosity of different liquids (Tsakadze and Mesoed, 1962). Formula (7.3.2) should be used for classical liquids (η_n is replaced by η).

The coefficient B' is not sufficiently well studied experimentally so far. It was not determined in the experiments of Hall and Vinen (1956a, b), because of a lack of accuracy in the measurements. The accuracy of measurements of this magnitude was also insufficient in Hall's experiment with two disks. In that experiment, as mentioned earlier, the length $L_s^{(-)}$ of an s^- wave was determined. After making a correction in formula (5.3.6) for mutual friction, $L_s^{(-)}$ can be expressed in the following way (when $2\omega_0\ll\Omega$, $\rho_n B'/4\rho\ll 1$):

$$L_s^{(-)}=2\pi\left(\frac{\nu_s}{\Omega-2\omega_0}\right)^{\frac{1}{2}}\left(1-\frac{\rho_n}{4\rho}\frac{\Omega}{\Omega-2\omega_0}B'\right). \qquad (7.3.3)$$

According to Sneider's preliminary data (1963) (he used a cubic mode resonator of second sound), $B'\ll 1$ at $T<2$°K. The coefficient B' increases at a temperature rise. Lifshitz and Pitaevski (1957) predicted its increase at temperatures below 1.4°K as well. However such a phenomenon was not found in Sneider's experiment.[11] The data on the final results of this study are not known to us.

[11] These results are in complete agreement with the theoretical calculation of Iordanski (1965b), whose paper we read when this chapter was already written (see 12.8).

At the consideration of the phenomena, in which vortex lines are parallel to the rotation axis, it is quite sufficient to use the expression for the force of mutual friction. But when transverse waves run along vortex lines, a more complete formula should be used (Bekarevich and Khalatnikov, 1961; also, see, Hall, 1960):

$$\mathbf{F}_{sn}=\frac{\rho_n}{2\rho}B\left[\frac{\boldsymbol{\omega}}{\omega},\left[\mathbf{v}_n-\mathbf{v}_s-\nu_s\,\mathrm{curl}\,\frac{\boldsymbol{\omega}}{\omega},\boldsymbol{\omega}\right]\right]$$
$$+\frac{\rho_n}{2\rho}B'\left[\mathbf{v}_n-\mathbf{v}_s-\nu_s\,\mathrm{curl}\,\frac{\boldsymbol{\omega}}{\omega},\boldsymbol{\omega}\right]$$
$$+\frac{\rho_n}{2\rho}B''\left(\frac{\boldsymbol{\omega}}{\omega},\mathbf{v}_n-\mathbf{v}_s-\nu_s\,\mathrm{curl}\,\frac{\boldsymbol{\omega}}{\omega}\right). \qquad (7.3.4)$$

This formula is a result of decomposition of the force $\mathbf{F}_{sn}$ into three vectors with mutually perpendicular directions. Each of these three components of the force of mutual friction is proportional to the density of vortex lines, represented by the curl of the mean velocity of the superfluid component, and to the velocity of the normal component with respect to a vortex line. This velocity is represented by the vector

$$\mathbf{v}_n-\mathbf{v}_s-\nu_s\,\mathrm{curl}\,(\boldsymbol{\omega}/\omega).$$

In calculations the results of which are given in Figs. 6.4 and 6.5 just this formula was used in which B'' is put equal to zero and the values of B and B' correspond to those of Lifshitz and Pitaevski (1957). Earlier calculations made by Mamaladze and Matinyan (1960a) were performed using formula (7.2.1); i.e., without taking into account the term with ν_s curl (ω/ω). The comparison of the results shows that this term has no special role in the calculation of the disk oscillation damping. But it influences the expression of the penetration depth of the s^- wave essentially. This penetration depth, when $2\omega_0\ll\Omega$, at the first approximation over the mutual friction is determined by formula

$$\lambda_s^{(-)}\approx 4\rho[(\Omega-2\omega_0)\nu_s]^{\frac{1}{2}}/\rho_n\Omega B. \qquad (7.3.5)$$

The assumption $B''=0$ encountered in papers of many authors is associated both with experimental facts and the theoretical considerations on the impossibility of mutual friction existence along vortex lines. Hall and Vinen (1956a, b) have not found any additional damping in an axial mode resonator. Mamaladze (1960a) suggested to use, with the aim of verification of equation $B''=0$ (or for measurements of B'' if it is different from zero), vertical oscillations of a cylinder, for which, similarly to (7.3.1), we obtain

$$\frac{\delta_2-\delta_1}{l_2-l_1}\sim 1+\frac{\omega_0}{\Omega}\frac{\rho_s}{2\rho}B''. \qquad (7.3.6)$$

The results of Tsakadze's experiment (1962a), in which the independence of δ on ω_0 was shown (see Sec. 5.1), mean that $B''=0$. If we take into account the

CC-0. In Public Domain. Gurukul Kangri Collection, Haridwar

Digitized by Arya Samaj Foundation Chennai and eGangotri

errors of the experiment we must write down more precisely that $B''=0\pm0.025$ (when $B\sim1$ at $T=1.86°K$).

In the paper of Sneider (1963) already mentioned, the author did not manage to obtain reproducible values of B''. In 30% of events $B''=0$. In the other cases B'' was always much less than B in a wide range of temperatures from 1.34° to 2.17°K, while the ratio B''/B varied between 0.25 and 0.01. At the highest temperatures it even reached 0.002. Unfortunately, the errors of these data are not given. It is also difficult to say whether the values of B'' different from zero correspond to the equilibrium configurations of vortex lines.

The results of another experiment by Tsakadze (1962b, 1963a) with vertical oscillations of a cylinder above an axially oscillating disk (5.1) show that vortex line oscillations lead to the creation of mutual friction along the rotation axis (as this axis is not parallel to vortex lines). But it means that a rather small effective value of B'' can arise even without artificial generation of vortex oscillation as well, because vortex lines always experience zero and thermal oscillations.

The difference between the coefficients B, B', and B'' determining the intensity of mutual friction in three mutually perpendicular directions once more speaks in favor of anisotropy of elastic–viscous properties of rotating helium II.

8. PERSISTENT CURRENTS OF THE SUPERFLUID LIQUID

8.1. Observations of Persistent Currents

The best illustration of the complete absence of viscosity of the superfluid component is the existence of circular currents which, once formed, exist for an arbitrary long time.

The first attempt to find such currents of the superfluid component was made by Andronikashvili (1952). For this purpose, he used a pile of strictly parallel light disks spaced 0.2 mm apart and surrounded by a thin walled aluminium shell. The pile suspended on an elastic thread was carefully protected from light, which could cause some mechanical effects due to its thermal action. The pile was brought into a uniform rotation at temperatures close to that of the transition point. Then under the conditions of a continuous rotation of the pile, the helium bath was cooled to 1.5°K and after that the suspended system was smoothly (aperiodically) slowed down. This process was realized by electromagnetic forces acting on a special metal ring placed much higher than the pile. After a certain period of time, the pile was heated during $\frac{1}{4}$ of the period of the suspended system oscillation to a temperature of 1.65°K. That led to the transition of $\sim$10% of the superfluid component into the normal state. Heating was realized by eddy currents, which were induced in the cylindrical case of the pile by a high-frequency generator with a frequency of 2000 cps. Thus an absolute symmetry of the thermal flow was reached with respect to the rotation axis.

No deviation of the device was found, though it had to appear if the superfluid component, continuing to rotate around the axis of the stopped device, would have given its angular momentum to the walls and disks of the pile after its transition into the normal component.

In the published paper of Andronikashvili (1952) there was an error in calculations, but even without it the statement remains valid that the measured random angles of the pile deviation at the moment of heating were much less than the calculated one, which highly exceeded the experimental errors.

At present the negative results of this experiment should be ascribed to critical velocities, but in 1952 nothing was known about their values for rotating systems.

The first indication of the existence of the persistent current was presented in Hall's investigation (1957). It was shown that a rather slowly rotating vessel with a pile of disks [similar to Andronikashvili's device (1952)] does not give away, at its slowing down, the whole angular momentum obtained at its acceleration. It was found that there is conserved some angular momentum in the stopped vessel at least for about 25 min.

8.2. Persistent Current with an Elementary Circulation

Vinen (1958a, 1961a, b) has observed the existence of circulation (not exceeding two quanta of this magnitude) during a long time in the stopped device. The aim of his experiment was not the study of the persistent current, but the direct observation of a unit quantum circulation. It was found that it is more convenient to make such measurements after the stop of the vessel's rotation. That is why we discuss Vinen's experiments in this chapter. The idea of the experiment was the following. Oscillations of a stretched string are doubly degenerate, as they can be decomposed into two mutually perpendicular linearly polarized oscillations. Each of these oscillations will be quite equivalent to the second one. The same statement is valid at the decomposition into two oscillations with mutually opposite circular polarization. The situation changes when the string is run around by the circulation motion of the liquid. Then degeneration disappears and the oscillations with the circular polarization (the direction of rotation of one of which coincides with the imposed circulation, while the other one is opposite to it) acquire different frequencies. Indeed, depending on the mutual direction of the rotation of some elementary portion of the wire and the rotation of the fluid around it, the Magnus force is either added to the elastic straightening force or is subtracted from it. The vector sum of these two forces determines the value of the centrifugal

CC-0. In Public Domain. Gurukul Kangri Collection, Haridwar

Digitized by Arya Samaj Foundation Chennai and eGangotri

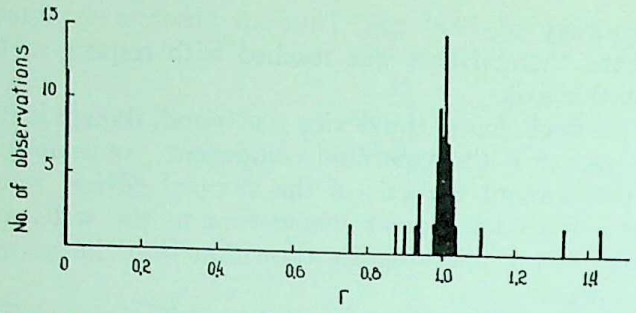

FIG. 8.1. The histogram confirming quantization of circulation (Vinen, 1961a, b).

force and hence the frequency of the wire's rotation. In Vinen's experiment a thin wire with a diameter of 2.5×10 cm^{-3} was stretched along the rotation axis of a narrow cylinder with a diameter of 0.5 cm, filled with helium II. The wire was placed in an external magnetic field and its oscillations excited by a short current pulse as a result of a capacity discharge. The registration of oscillations was made by observation of the current induced by a magnetic field in this wire. The difference of frequencies of the main modes of oscillations led to the generation of beats and that allowed the rather accurate measurement of the circulation of the liquid velocity determining the difference between frequences of oscillations with the opposite circular polarization.

At the above-mentioned value of the diameter of the rotating vessel there could arise from one to three vortex lines in the range of velocities used by Vinen $\omega_0\simeq2\times10^{-3}\div2\times10^{-2}$ sec^{-1}. Directly measured values of circulations were not always integers in units of h/m. The fact is that vortex lines could only partially cover the wire, fastening by one of the ends or by both of them to any point of the device. Shaking of the device had to give a more stable configuration to a vortex line and really, because of shaking the value of the measured circulation changed. The results are shown in Fig. 8.1 and leave no doubts as to the existence of vortex lines with unit circulation. They are obtained as a result of starting the device rotation above the λ-point, its cooling lower than this temperature and shaking more than once to obtain the stable circulation.

Vinen's conclusion that the data of his experiment correspond to the value of the vortex core $a_0\sim10^{-4}$ cm agrees poorly with the theory of Onsager and Feynman. However, Griffiths (1964) doubted the validity of Vinen's analysis (1961a, b), which had led to a such conclusions. According to Griffiths' estimation the core of Vinen's vortex lines had a radius not larger than 3×10^{-6} cm and probably much smaller.

Recently, Whitmore and Zimmermann (1965) have repeated Vinen's experiment. They have noticed an increase of stable circulation around the wire while increasing the diameter of the wire and the velocity of rotation. Their data, obviously, have something in common with the calculations of Bendt and Oliphant (1961), according to which (see Sec. 3.5) an increase of $\omega_0 r_1^2$ causes an increase of Γ.

8.3. An Irrotational Region and a Persistent Current

It was assumed by Bendt and Oliphant (1961) that an irrotational motion of the superfluid in an annulus can be conserved as a metastable state after the stop of the device as well.

The corresponding measurements were made by Bendt (1961, 1962) to find the persistent current in the annulus formed by two cylindrical surfaces rotating together until the stop; he immersed in helium II wings suspended on an elastic thread or a foil strip used as a peculiar Rayleigh disk. The most interesting results were obtained with the second version of the device. At an immersion of the strip to a definite depth (0.3 cm), the existence of a persistent current was registered. But at the repeated immersion of the foil the persistent current was not found. The disappearance of the current indicated firstly that the state with the persistent current in the stopped device is metastable and secondly the coherence of such a kind of flow, since at the repeated immersion of the foil the absence of the current was established until the depth of 1.3 cm (0.3 cm is about $\frac{1}{5}$ of the annulus depth).

8.4. Dependence of a Persistent Current on Temperature

Depatie, Reppy, and Lane (1962) have observed persistent currents in a device similar to that of Andronikashvili (1952) with the only difference that heating of the liquid, needed for the transition of the superfluid component into the normal one, was realized by a light beam. In addition, the vessel with a pile of disks was suspended not on an elastic thread, but by means of a magnetic suspension. This allowed the vessel to rotate practically without friction. When the initially uniformly rotated vessel was slowed down, then freed and heated, the velocity of its rotation increased and this indicated the existence of a persistent current in the slowed down vessel (Fig. 8.2). This effect occurred in the liquid which could be placed both in

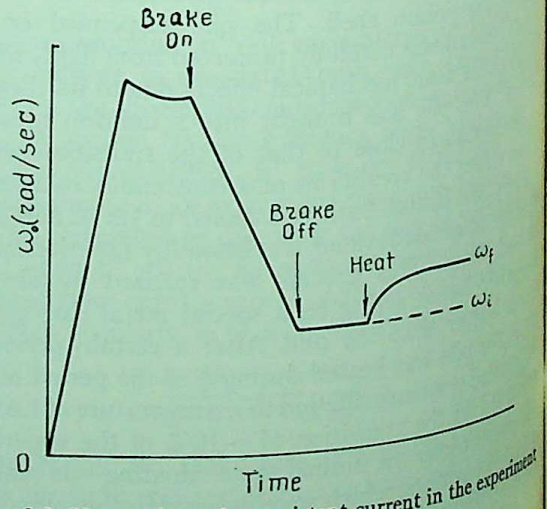

FIG. 8.2. Observations of a persistent current in the experiment of Depatie, Reppy, and Lane (1962).

CC-0. In Public Domain. Gurukul Kangri Collection, Haridwar

Digitized by Arya Samaj Foundation Chennai and eGangotri

the devices with doubly connected and with simply connected regions. In the first case the disk spacers were placed in the center of the vessel and in the second one they were at the periphery.

Reppy and Depatie (1964) used this technique to study the temperature dependence of the persistent current angular momentum. It was found that it is proportional to ρ_s, but not the value of ρ_s at the start or slowing down of the rotation, which leads to the formation of a persistent current. On the contrary the angular momentum is proportional to the value of ρ_s at the temperature from which the freed vessel is heated with the aim to show the conserved angular momentum (Fig. 8.3). Thus in a slowed down vessel the angular momentum changes as ρ_s during variation of temperature. That is explained by *conservation of the*

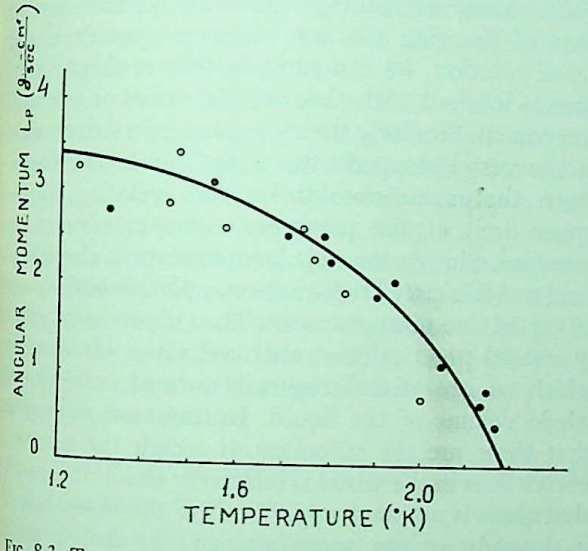

Fig. 8.3. Temperature dependence of the angular momentum of a persistent current according to the data of Reppy and Depatie (1964). The solid line corresponds to the law $L_P \sim \rho_s$; solid circles represent the data obtained at constant temperature; open circles show data obtained by lowering the temperature after a persistent current was formed until it was found.

velocity circulation, i.e., of an integral over the contour of $\mathbf{v}_s$, which represents a part of the integral of $\rho_s[\mathbf{r}, \mathbf{v}_s]$ over the volume which is equal to the angular momentum.

8.5. A Superfluid Gyroscope

Later Reppy (1965), having used the gyroscopic method of observation of a persistent current, developed by Clow, Depatie, Weaver, and Reppy (1965), had investigated the dependence of the angular momentum of a persistent current on temperature. The temperature range studied earlier was extended to the λ-point, to 10^{-5} °K. The superfluid current was formed in an annular container filled with fibrous foam to increase the critical velocity. This system constituted a superfluid gyroscope the angular momentum of which L_P was directed in the horizontal plane. One could judge the

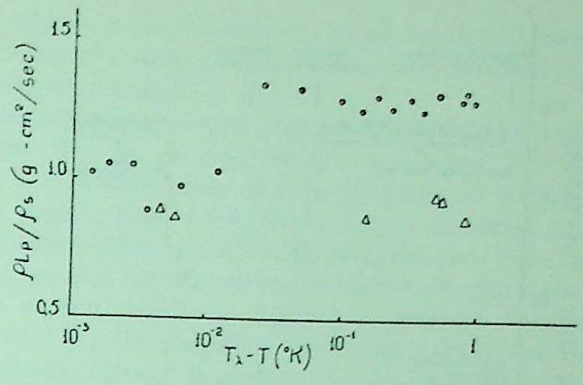

Fig. 8.4. The transition of a persistent current into a more stable state by liquid heating (Reppy, 1965). Circles give the data when the current was formed at $T_\lambda - T > 2\times10^{-2}$°K. Triangles show the data when the current was formed at $T_\lambda - T < 2\times10^{-2}$°K.

existence of a superfluid current, perpendicular to the L_P horizontal torque, required for excitation of gyroscope rotation around the vertical axis. The magnitude of $\rho(L_P/\rho_s)$ was determined, that excluded the dependence of L_w on temperature associated with the conservation of the circulation. Figure 8.4 shows that, when $T_\lambda - T \sim 2\times10^{-2}$ °K, persistent currents formed at lower temperatures display a tendency to transfer to a more stable state. This state, in the case when the current is formed near the λ-point and a smooth cooling followed, was not changed in time. In the vicinity of the λ-point the magnitude $\rho(L_P/\rho_s)$ characterizing in reality the flow rate, changes suddenly from the value larger than zero in helium II to zero in helium I. as shown in Fig. 8.5. This phenomenon takes place in the temperature range, which differs from T_λ by $\pm10^{-5}$ °K. The magnitude $\rho(L_P/\rho_s)$ has a tendency to a decrease at $\Delta T = T_\lambda - T \to 0$. This tendency is displayed when $T_\lambda - T$ drops from 4×10^{-5} °K to 0.5×10^{-5} °K. But this decrease of $\rho(L_P/\rho_s)$ does not exceed explicitly the errors of measurements.

Gyroscopic observations of a persistent current were also made by Mehl and Zimmerman (1965). They used a spherical vessel, filled with a porous substance,

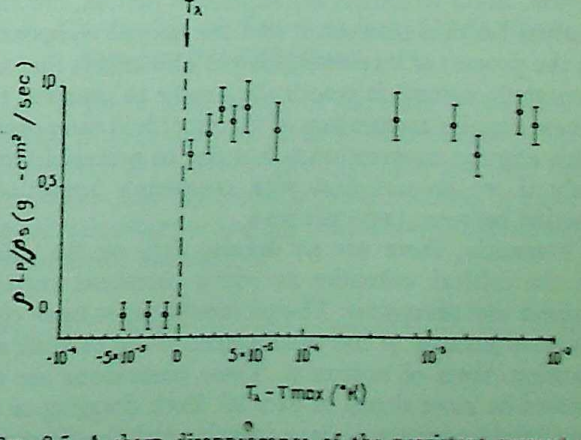

Fig. 8.5. A sharp disappearance of the persistent current at $T = T_\lambda$ (Reppy, 1965).

CC-0. In Public Domain. Gurukul Kangri Collection, Haridwar

Digitized by Arya Samaj Foundation Chennai and eGangotri

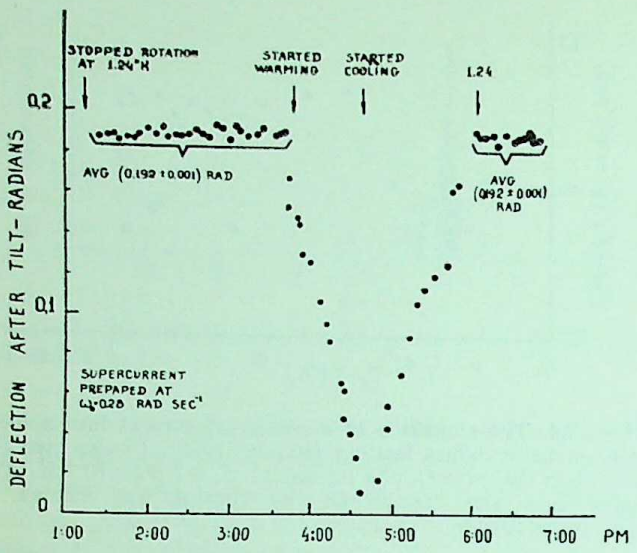

FIG. 8.6. Reversible change of the angular momentum of a persistent current on heating from 1.24°K to $T \lesssim T_\lambda$ and cooling till 1.24°K (Mehl and Zimmerman, 1965).

hanging freely on an elastic thread. During the measurements, after the rotation was stopped, this vessel was turned by a magnetic field for ~90°. As a result the persistent current angular momentum, which was directed vertically, changed its orientation into a horizontal one. The change was compensated by a deflection of the suspended system with respect to the vertical axis, permitting one to judge the existence of a persistent current, and the value of its angular momentum. Heating and cooling of the system have confirmed the conservation of circulation and the dependence $L_P \sim \rho_s$ in this case as well, as shown in Figs. 8.6 and 8.7.

8.6. The Critical Velocities

The uniform rotation of the superfluid component, taking place with an averaged velocity $v_s = \omega_0 r$ and accompanying the uniform rotation of the normal component, is realized by means of an array of Onsager–Feynman vortex lines. However, after the stop of the vessel, vortex lines existing outside the irrotational region, begin to inhibit the superfluid motion, creating mutual friction between it and the normal component in the process of its slowing down. This means that the persistent current is practically unable to conserve the whole angular momentum of the superfluid component. This angular momentum is lost due to mutual friction only if we do not deal with completely irrotational motion between two cylinders.

Presently, there are no definite data on the values of the critical velocities at which persistent currents appear and disappear. The picture becomes more complicated because of the peculiarities of the twisting and slowing down of helium II. These phenomena are discussed in more detail in Sec. 10. Both dragging of the superfluid component into rotation and the disappearance of vortex lines after the vessel is stopped take rather a long time. At low velocities of vessel rotation ($\omega_0 \sim 0.1$ sec^{-1}), the superfluid liquid can even remain stopped for a rather long time ($\tau \sim 10^3$ sec) before an interaction with the rotating container will take place. This phenomenon is especially clearly pronounced if before rotation helium was at rest for a long time, being in the state of helium I. At high velocities of rotation ($\omega_0 \gtrsim 0.2$ sec^{-1}), the interaction of the vessel with the superfluid begins practically at once and is over after a time of the order of $10^3 \div 10^2$ sec. After the rotated vessel is stopped, the vortex lines decay according to the exponential law with the period of half-decay of the order of 30 sec.

Let us assume that a slowly rotating vessel was stopped and we have not found any persistent current. Does that mean that at such angular velocities this annular current cannot be realized in general? Taking into account everything mentioned above about the time of dragging the superfluid component into the vessel rotation, we can suppose that it simply had no time to interact with the rotating vessel or the normal component. Similarly the absence of a persistent current in the vessel stopped after a rapid rotation does not mean that some absolute critical velocity, i.e., the upper limit of the persistent current existence, was exceeded. Simply the angular momentum of the superfluid was dissipated before the completion of the process of vortex line disappearance. Thus a persistent current is created practically at such velocities of rotation at which an irrotational region is formed occupying the whole volume of the liquid. In any case one can say that these are the velocities at which the number of vortex lines in the vessel is relatively small. It is possible that there is no exact upper limit of the vessel velocity, it depends on the sensitivity of the device, on the possibility of finding a much weakened persistent current.

Considerations just described explain the failure of Andronikashvili's experiment (1952) in which $\omega_0 \gtrsim 1$ sec^{-1}. The same consideration concerns Hall's experiment (1957), in which he had not observed any retention of the angular momentum by the superfluid component at slowing down of the container which rotated

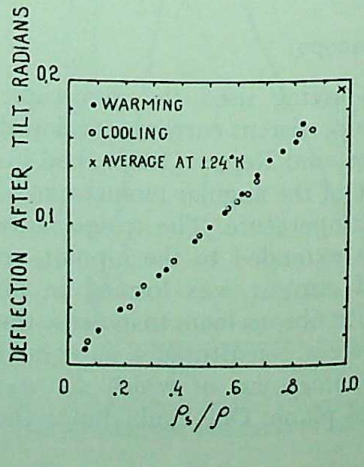

FIG. 8.7. The data of Fig. 8.6 confirm the law $L_P \sim \rho_s$ (Mehl and Zimmerman, 1965).

CC-0. In Public Domain. Gurukul Kangri Collection, Haridwar

Digitized by Arya Samaj Foundation Chennai and eGangotri

with high velocity. Only at small velocities was the momentum lost by slowing down helium II smaller than the momentum L_c obtained by the liquid at twisting. Similarly in the Walmsley and Lane experiments (1958) the angular momentum obtained from slowing down helium II was smaller than L_c, but it tended to this value at an increase of the velocity of rotation and of temperature rise.

According to Bendt (1962), who made experiments with the annular channel between cylindrical surfaces with the radii $R_1=8.72$ cm and $R_2=8.94$ cm and the height 0.18 cm, the critical velocity had the value varying in the interval $1.75\div1.19$ rpm depending on the initial state of the liquid, which could be either rotated before the experiment or be at rest. Bendt determined critical velocities of rotation below which the appearance of a persistent current was not observed. He noticed quite reasonably that there were no grounds to think that a persistent current rotates with the same velocity as the vessel before its stop.

In the case when the device was filled with a porous substance the vortex formation became more difficult and the critical velocity increased. At sufficiently small dimensions of the pores of the used substance, such conditions could be created when the critical velocity limiting the value of the persistent current is the velocity of the breakdown of superfluidity (in Landau's sense) and not the velocity of vortex formation. Using the results of the paper of Mamaladze and Cheishvili (1965)[12] for rough estimation of this velocity, it is described by the equation

$$v_c=(\hbar/\sqrt{3}ma_0)\left[1-(\delta_c^2a_0^2/\delta^2)\right]^{\frac{1}{2}}, \qquad (8.6.1)$$

where $a_0=4.3\times10^{-8}(T_\lambda-T)^{-\frac{1}{2}}$ cm is a characteristic dimension of the phenomenological quantum theory of superfluidity near the λ-point (see Sec. 12.1), δ is the size of pores, $\delta_c\sim3\div5$ (dimensionless critical size of pores). When $\delta\gg a_0$ and $T\approx T_\lambda$ this formula gives a very large value (~30 m/sec) close by the order of the magnitude of Landau's critical velocity of the breakdown of superfluidity. However, according to (8.6.1), when T approaches T_λ, $v_c\to0$. It is interesting in this connection to discuss Reppy's results described in the previous paragraph (Fig. 8.5). Reppy did not find that v_c tends to zero, when $T\to T_\lambda$, and concluded that the critical velocity experiences a jump at $T=T_\lambda$. That would distinguish the superfluid persistent current from a superconducting persistent current. The critical velocity of the latter tends smoothly to zero as the temperature of the point of the phase transition is approached.

Meanwhile there is no principal difference here. An essential difference, but not a principal one is only that the parameter in the phenomenological theory of superfluidity a_0 is much smaller than the similar parameter in the theory of superconductivity, i.e., than the length of coherence. An increase of a_0 and the corresponding decrease of v_c take place in a very narrow interval of temperatures near T_λ.

In Reppy's experiment, apparently, δ is always much larger than a_0, as $a_0\leq1.9\times10^{-5}$ cm, when $T_\lambda-T\geq5\times10^{-6}$ °K (the value of δ in the paper of Reppy is not given). Then $v_c\approx\hbar/\sqrt{3}ma_0$, i.e., v_c decreases from the value -30 m/sec at low temperatures to ~5 cm/sec. Such a value corresponds to the maximum approach to the λ-point which in Reppy's experiment reached 5×10^{-6} °K. On the other hand, the velocity of the persistent current in Reppy's device was about 0.2 cm/sec. Hence when the λ-point is approached down to 5×10^{-6} °K, that decreases the value of the critical velocity to 5 cm/sec, it is not sufficient to find a smooth drop of the critical velocity to zero. The persistent current all the time has a velocity much less than the critical one.

9. STABILITY OF HELIUM II MOTION BETWEEN TWO CYLINDERS ROTATING WITH DIFFERENT ANGULAR VELOCITIES

9.1. The First Experiments

As early as 1941 Kapitza noticed that rotation of a thin rod set into a capillary with helium II sharply changes the character of heat transfer along the circular slit formed by them (Kapitza, 1941). Then Wheeler, Blackwood, and Lane (1955) measured damping of second sound in rotating helium II. In contrast to the experiments made by Hall and Vinen (1955, 1056a, b) about the same time, they found a considerable increase of scattering of thermal waves as a result of rotation, though the direction of propagation of these waves was parallel to the axis of rotation. In the device constructed by Wheeler, Blackwood, and Lane, helium II was between the two cylinders, the inside cylinder was rotating and the outside one was at rest. Therefore their results should be considered as an indication of an instability of such a kind of motion under the conditions of these experiments. The same can be said about Kapitza's experiments.

9.2. Distribution of Velocities in a Liquid Rotating Between Two Cylinders

Let us give a brief survey of the state of theories of stability of such motions. Both in viscous and in ideal fluids, which are between two cylinders with the radii R_1 (inside) and R_2 (outside) and rotating with the angular velocities ω_{01} and ω_{02} the following distribution of velocities is established:

$$v_r=v_z=0, \qquad v_\phi=\frac{\omega_{02}R_2^2-\omega_{01}R_1^2}{R_2^2-R_1^2}r+\frac{(\omega_{01}-\omega_{02})R_1^2R_2^2}{R_2^2-R_1^2}\frac{1}{r}. \qquad (9.2.1)$$

Equations (9.2.1) represent the only solution of the Navier–Stokes equation, corresponding to the con-

[12] Mamaladze and Cheishvili (1965) have considered strictly speaking not a rotational, but a translational motion.

CC-0. In Public Domain. Gurukul Kangri Collection, Haridwar

Digitized by Arya Samaj Foundation Chennai and eGangotri

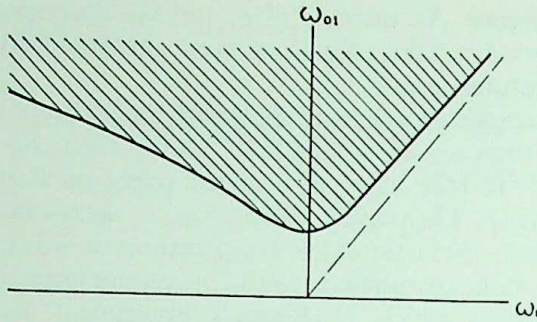

FIG. 9.1. The dashed line corresponds to the equation $\omega_{02}{}^2R_2{}^2=\omega_{01}R_1{}^2$. The region of stability of a classical ideal liquid is situated between this dashed line and the line $\omega_{01}=0$. The region of stability of a real (viscous) classical liquid is wider and extends to the hatched region. (The figure is taken from the book of Landau and Lifshitz, 1953.)

sidered boundary conditions. They do not contain viscosity and therefore are valid for an ideal liquid as well. However, the Euler equations allow other solutions. As to the equations of hydrodynamics of rotating helium II, the distribution (9.2.1) is also the only possible solution for them. It is required by the normal component, and the mean velocities of both components under the stationary conditions reach the same values due to mutual friction.

9.3. Stability of Rotation of an Ideal Liquid

The problem of stability for a laminar motion (9.2.1) for an ideal liquid was studied by Rayleigh (1916). He showed that at rotation of cylinders in the opposite directions the motion is unstable, while at the same direction of rotation the condition of stability has the form

$$\omega_{02}R_2{}^2-\omega_{01}R_1{}^2>0. \qquad (9.3.1)$$

In particular, this means instability in case of the rotation of the inside cylinder, when the outside one is at rest ($\omega_{02}=0$).

For the further representation of the material it is essential to note that the sense of the Rayleigh condition is connected with the following considerations. Let an element of the liquid M occasionally leave the orbit of its rotation, i.e., a circumference with the radius $_p$, and let it be displaced for some distance. Before this fluctuation occurred the centrifugal force $Mv_\phi{}^2/r=L^2/Mr^3$ (here L is the angular momentum) P and the force caused by the gradient of pressure $(M/\rho)\partial P/\partial r$ balance each other ($\partial P/\partial r=\rho v_\phi{}^2/r$). As a result of fluctuation the element considered is in the region with another value of the pressure gradient. But the magnitude L is conserved and the stability or instability of the motion depends on the ratio of two forces having opposite directions: which of them will be larger? Will the element be returned to its orbit? As shown in the book of Landau and Lifshitz (1953) the solution of this problem leads to the Rayleigh condition (9.3.1).

9.4. Stability of a Viscous Liquid Rotation

In Fig. 9.1 is shown how the Rayleigh condition is modified if, according to Taylor (1923), the role of viscosity is taken into account. For this one studies the Navier–Stokes equation (instead of the Euler equation) to determine the stability of its solution (9.2.1) with respect to relatively small perturbations.

9.5. Stability of Helium II Rotation

A similar thing for helium II was studied by Chandrasekhar and Donnelly (1957). They concluded that there are two conditions of stability for this liquid. One of them, when there is no mutual friction, leads to condition (9.3.1), the other one to that shown in Fig. 9.1. That means, for instance, that if there is an outside cylinder at rest and the angular velocity of the inside cylinder is increased (that was done in Donnelly's experiment (1959)], then one will find the existence of two critical points: one of them corresponds to the appearance of the Rayleigh's instability of the superfluid component rotation, the other to Taylor's instability of the normal component rotation.

Donnelly's device was a viscometer, the inside cylinder of which was rotating causing deflection of the outside cylinder suspended on an elastic thread. At small velocities (large periods θ) the deflection of the outside cylinder did not depend on θ, but with the decrease of this magnitude two critical points were observed (Fig. 9.2), θ_s and θ_n, marking the appearance

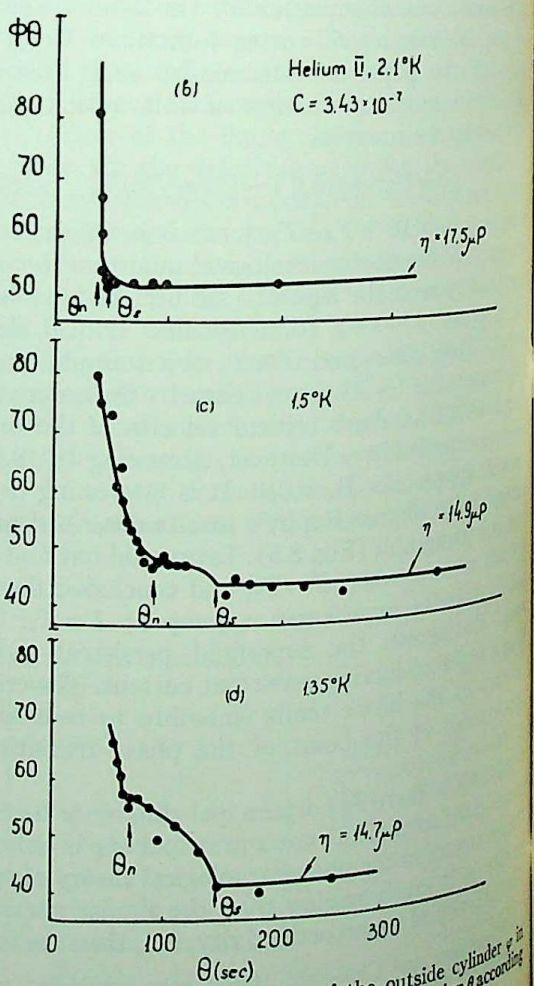

FIG. 9.2. The angle of deflection of the outside cylinder φ as dependence on the period of the inside cylinder rotation θ according to the data of Donnelly (1959).

CC-0. In Public Domain. Gurukul Kangri Collection, Haridwar

Digitized by Arya Samaj Foundation Chennai and eGangotri

of instability of motion of the corresponding components predicted by the theory of Chandrasekhar and Donnelly. However, quantitative data of this experiment did not agree with the theory.

The reason for this discrepancy was explained by Mamaladze and Matinyan (1963), who paid attention to the fact that the existence of vortex lines in rotating helium II is not completely taken into account in the equations used by Chandrasekhar and Donnelly. The mutual friction is included, but the term $\nu_s[\omega, \text{curl } \omega/\omega]$ is absent and this term, as we know, describes the elastic properties of vortex lines. As shown in Fig. 9.3, the role of elastic effects can be very essential for the solution of the problem of stability. To verify this assumption Mamaladze and Matinyan studied Eq. (4.2.1) with $F_{sn}=0$ and div $v_s=0$ for the stability of solution (9.2.1) with respect to small perturbations. As one should expect in the condition of equilibrium obtained in such a way

$$\omega_2^2 R_2^2 - \omega_{01}^2 R_1^2 > -\tfrac{1}{2}\pi^2 \nu_s [(R_2+R_1)/(R_2-R_1)], \quad (9.5.1)$$

the stabilizing action of vortex lines is clearly expressed indeed. It shifts the boundary of stability in comparison with condition (9.3.1). Though condition (9.5.1) is valid strictly speaking only when $T=0$°K, nevertheless it can be compared with the data of Donnelly, as they are reduced to the temperature 1.35°K and at such a temperature the relative density of the normal component is only about 7%. Therefore one can consider that, when $T=1.35$°K the role of the mutual friction is not very essential and the critical point $\theta_s \sim 140$ sec in Fig. 9.2 should agree with condition (9.5.1). And indeed, using the values of ν_s obtained in different experiments (see Sec. 5.6), we get, according to (9.5.1), $\theta_s = 120 \div 150$ sec.

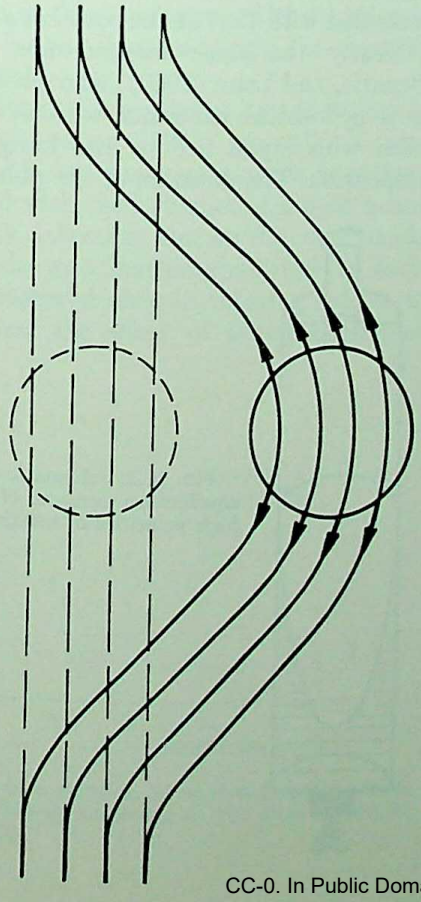

Fig. 9.3. Tension of the distorted vortex lines (solid lines) promotes the return of an occasionally shifted element of the liquid (a circle) to its initial position (dashed lines).

Hollis–Hallett (1953) in contrast to Donnelly (1959) has used a viscosimeter with rotating outside cylinder, while the inside cylinder, suspended by means of an elastic thread was at rest. According to (9.5.1) in this case ($\omega_{01}=0$) the motion of the superfluid component should be stable. However, such an assumption cannot be considered sufficiently rigorous. Indeed, condition (9.5.1) does not take into account actions both of viscous forces and mutual friction force. Besides, condition (9.5.1) determines instability with respect to infinitesimal perturbations, but there can exist instability with respect to finite perturbations, realized in a classical liquid even in the unhatched region in Fig. 9.1. That suggests an idea that instability of motion should appear in the case of helium II as well, even when $\omega_{01}=0$. The results of the calculations of Chandrasekhar and Donnelly (1957) as well as those of Donnelly's experiment (Fig. 9.2) allow one to expect that when the Hollis-Hallett viscosimeter is used there should be manifested two critical velocities v_{cn} and v_{cs}.

Meanwhile, Heikkila and Hollis–Hallett (1955), while measuring the viscosity of the normal component of helium II, decreased the velocity of rotation of Hollis–Hallett's viscosimeter only a little lower than the critical velocity v_c found by them. (They measured the effective viscosity defined by the formula of the classical hydrodynamics. The dependence of this effective viscosity on the velocity of rotation disappears just at this velocity v_c, when $v \leq v_c$.) Woods and Hollis–Hallett (1958) have shown that the velocity v_c has a classical nature, as it is manifested in the experiments with classical liquids as well. They have shown that between this experiment and the helium experiment there is maintained similarity according to Reynolds number, calculated in the latter case with the use of the viscosity of the normal component. Thus the velocity v_c is a critical velocity v_{cn} and there are all the grounds to assume that at lower velocities the second critical point v_{cs} may appear (compare Fig. 9.2, where $\theta_s > \theta_n$).

The viscosity of helium II measured by a rotating viscosimeter is somewhat different from the viscosity measured by means of an oscillating disk (Andronikashvili, 1948c). (The results of many other authors who used this method later confirm the data of his paper.) Such a difference between "rotating" and "oscillating" viscosities of helium II is undoubtedly connected with insufficient analysis of one of the procedures of measurement (or even of both of them). We think that the attempt to find the second critical point v_{cs} in the experiments with the rotating viscosimeter could elucidate this problem as the viscosity measured when $v < v_{cs}$ could coincide with the "oscillating" one.

Another possible source of misunderstanding in the

CC-0. In Public Domain. Gurukul Kangri Collection, Haridwar

Digitized by Arya Samaj Foundation Chennai and eGangotri

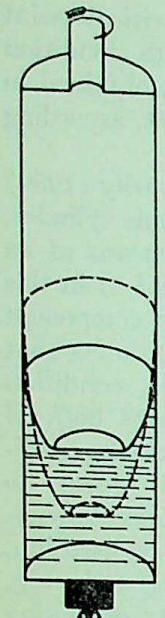

FIG. 10.1. Schematic representation of the gradual development of the meniscus at the dragging of helium II into rotation.

analysis of the results obtained with the rotating viscosimeter can be insufficient clarity of the picture of vortex line arrangement in such a device. At present we do not even know if there are vortex lines in it when $v<v_c$. Indeed, nobody has made calculations similar to those made by Bendt and Oliphant (1961) for cylinders rotating with different velocities. If the superfluid in a rotation viscosimeter does not move at all when $v<v_c$, then there are no grounds for appearance of the critical velocity v_{is} smaller than v_c. If it moves then, in addition to the possibility of v_{cs} appearance, there is another possibility of the existence of complications which were not taken into account so far. It is not excluded that at low temperatures vortex separation or the distance between vortices and the wall can be comparable with the free path length of thermal excitations and thus the law of the momentum transfer from the moving cylinder to the cylinder at rest can be changed.

We think that the question about the difference of viscosities measured by the two methods deserves great attention and its solution can form a source of interesting information on properties of helium II.

10. FORMATION AND DECAY OF VORTEX LINES IN HELIUM II

10.1. Dragging of Helium II into Rotation by a Moving Wall of a Container

The first data on kinetics of helium II dragged into rotation were published by Andronikashvili and Kaverkin (1955). The experiment was made with a transparent cylindrical container, which was rapidly brought from the state of rest into the state of uniform rotation.

Every normal liquid under such conditions would rather soon form a parabolic meniscus, the depth of which would gradually increase in time. Such behavior, for instance, is established for water and helium I. But the behavior of helium II is quite different as compared with that of usual liquids. In particular, at first only its peripheral layers are dragged into rotation, while the central part of the meniscus remains flat.

Gradually the radius of the flat part of the meniscus becomes narrower (see Fig. 10.1) and at last a parabola is formed the usual shape of which is indistinguishable at low and moderate velocities of rotation from the parabolic meniscus of viscous liquids. But already at an angular velocity about 30 sec^{-1} a characteristic conic pit appears on the lower part of the parabola. This fact was mentioned at the beginning of this paper (Fig. 10.2).

At angular velocities of the order of 30 sec^{-1} the equilibrium shape of the meniscus is formed during 120 sec, that corresponds to the velocity of the vortex front propagation of the order of 0.1 mm/sec.

The process of helium II dragging into rotation was studied by Eselson, Lazarev, Sinelnikov, and Shvetz (1956), who brought into rotation, during the period of the order of some seconds a pile of narrow disks with the separation equal to 0.15 mm and surrounded by a thin metal case. The device was hung by means of a magnetic suspension and rotated with velocities of several revolutions per second. The authors reported that the bulk of helium was dragged into the device rotation during not more than 2 sec. The vortex front traveled in this case with the velocity more than 0.04 mm/sec, if the direction of the front propagation coincided with that of the rotation axis.

Nearly the same method was used by Reppy, Depatie, and Lane (1960), who gave a rotational pulse to a cylindrical container without the pile of disks, filled with liquid helium and hung on the magnetic suspension. The duration of the pulse was 0.5 sec. The

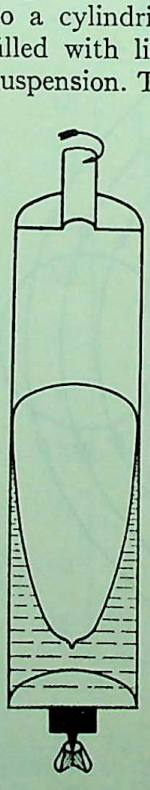

FIG. 10.2. Schematic representation of the equilibrium meniscus of rotating helium II at high velocities of rotation.

CC-0. In Public Domain. Gurukul Kangri Collection, Haridwar

Digitized by Arya Samaj Foundation Chennai and eGangotri

authors reached the velocity of rotation of ~ 0.2 sec^{-1}. Under such conditions, in contrast to the results of Eselson *et al.*, they observed the subsequent slowing down of the container due to redistribution of the angular momentum between it and the liquid. Reppy *et al.* found that the laws of helium II dragging into rotation and those of helium I are quite different (see Fig. 10.3).

Reppy and Depatie (1961) used a similar technique, but at still lower velocities of vessel rotation and found some additional details of the process of the superfluid liquid twisting, as mentioned in Sec. 8.6. It was found that rather slow twisting of helium II observed at the initial portions of curves similar to that shown in Fig. 10.3, when $\omega_0 \sim 0.2$ sec^{-1}, was replaced by a long delay of the beginning of twisting at smaller values of ω_0. When $\omega_0 \approx 0.1$ sec^{-1} and $T = 1.2$°K ($\rho_n/\rho = 3\%$), the superfluid can remain at rest during some thousands of seconds even when the vessel gets additional pulses of rotation acceleration. However, it concerns only the cases when helium II was at rest during a sufficiently long time, and, if it rotated previously not for a long time, then during the start of its repeated twisting there was not any appreciable relaxation. When $\omega_0 \approx 0.065$ sec^{-1}, the twisting of the superfluid component was not observed till the end of the experiment (during 10^4 sec). In their recent paper Reppy and Lane (1965) have shown that these delays disappear completely if there is an artificial protuberance on the inner side surface. Dragging of the liquid into rotation begins without any delay even at the minimum velocity $\omega_0 = 0.05$ sec^{-1}, used in this experiment. The dragging is always completed by the liquid aquiring the classical angular momentum L_c.

There is some information on the process of helium II twisting in Pellam's paper (1960) as well. It was mentioned in Sec. 3.5 that the results of his investigation were connected with the influence of a light beam on the Rayleigh disk deflection. But on the other hand, according to Tsakadze and Shanshiashvili (1965), such an influence was observed only in rotating helium II (in the liquid at rest the effect of illumination was

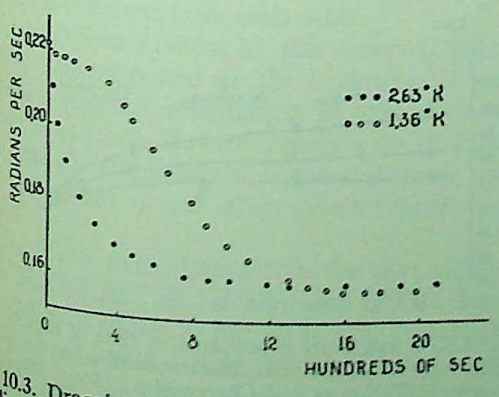

Fig. 10.3. Dragging into rotation of helium I (solid circles) and helium II (open circles) according to the data of Reppy, Depatie, and Lane (1960).

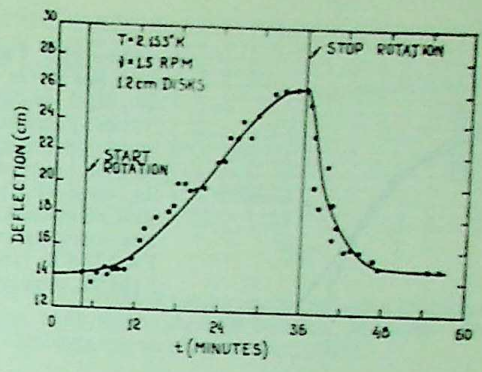

Fig. 10.4. Change of the angle of the torsional balance deflection in time in the experiment of Craig (1961).

much smaller). Therefore Pellam's data on some increase of the delay of the Rayleigh disk at its removal from the wall of the rotating vessel indicate the propagation of the rotation front from the periphery to the axis of the container. At the rotation velocity 2 rpm and $T = 2$°K the velocity of the front was of the order of 2 mm/min.

A similar method was used by Craig (1961) for the study of helium II dragging into rotation. He suspended a beam of a torsional balance with two wings immersed into liquid helium above the cylindrical vessel and studied the moment of forces acting on the device. The angle of torsion of an elastic suspension to which the beam of the balance was fastened (the balance was at rest in the laboratory system of coordinates) was the measure of dragging the liquid into rotation. Craig's results are given in Fig. 10.4, where it is seen that he has also observed a delay at the beginning of twisting, and that at the angular velocity 1.5 rpm the complete dragging of helium II into rotation takes about 30 min.

It is seen that the mechanism of dragging of helium II into rotation is quite different from that valid for classical liquids. The process of dragging of classical and quantum liquids into rotation of a container was studied in particular detail by Tsakadze (1964c) and by Tsakadze and Cheremisina (1966).

First of all it was shown by precise measurements of the meniscus depth z on stills of a film taken by a cinematographic camera, which was switched on every 3 sec by an electronic circuit, that the character of the meniscus deepening is quite different for helium I and helium II. Figure 10.5 shows that $\log \Delta z$(He I) is a straight line breaking after some time, which depends linearly on the angular velocity of rotation.

At the point of the phase transition the character of the meniscus development is changed in a jump and $\log \Delta z$ in He II gives a curve without any breaks, immediately after the temperature is reduced below $T = 2.17$°K.

The time of helium I twisting was less than that of helium II in the studied cases. An increase of the container radius caused the linear increment of the velocity of the meniscus deepening for helium I, while for helium

CC-0. In Public Domain. Gurukul Kangri Collection, Haridwar

Digitized by Arya Samaj Foundation Chennai and eGangotri

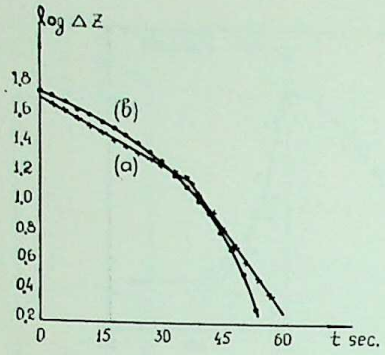

FIG. 10.5. Time dependence of the meniscus depth of helium I (curve a) and helium II (curve b) brought into rotation, according to the data of Tsakadze and Cheremisina (1966). The temperatures are $T=2.186°K$ and $T=2.164°K$, respectively.

II it dropped in the initial portion of the curve according to the law close to a hyperbola. The dependence of the time of helium II dragging into rotation on the angular velocity ω_0 was the same in character. The dependence of the time of acceleration on ω_0 for helium I is a straight line with a negative slope. The same time for helium II decreases slowly with an increase of temperature and only in the interval 2.0–2.17°K this dependence becomes sharper (Figs. 10.6, 10.7, 10.8, 10.9).

At the beginning of the analysis of the results of this paper, all the experiments were made at high Reynolds numbers ($Re\sim5\times10^5\div2\times10^7$). That excluded the possibility of laminar regimes of helium I dragging into rotation or that of the normal component of helium II. Therefore the observed durations of the liquid acceleration obtained were much shorter than those expected for a laminar regime, i.e., $R^2/\nu\sim10^6$ sec.

The turbulent character of the motion makes the treatment of the results, obtained in this case, more difficult for the classical liquid. But it simplifies, and that sounds paradoxical, the understanding of the processes of helium II dragging into rotation.

First of all as seen from the shape of the meniscus of helium II in the process of its acceleration and from the figures given in this paragraph, the quantum turbulence in a certain sense depresses the classical one as soon as in all the cases dragging into motion of the normal component of helium II takes place slower than that of helium I.

The authors of the paper give reliable considerations that help us to understand the character of the experimental data obtained by them, proceeding from an assumption that quantized vortex lines are generated

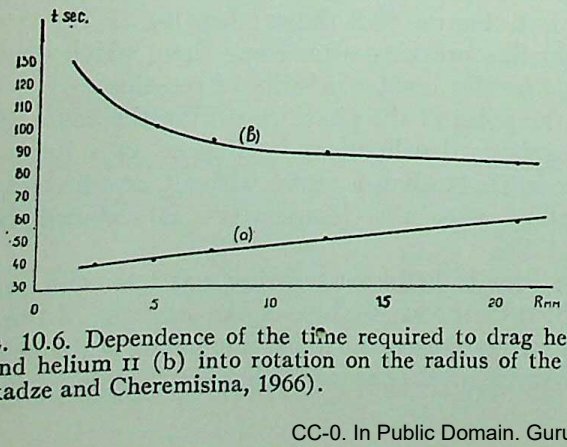

FIG. 10.6. Dependence of the time required to drag helium I (a) and helium II (b) into rotation on the radius of the vessel (Tsakadze and Cheremisina, 1966).

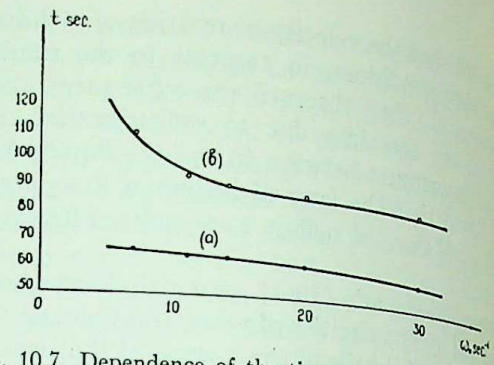

FIG. 10.7. Dependence of the time required to drag helium I (a) and helium II (b) into rotation on the angular velocity of rotation (Tsakadze and Cheremisina, 1966).

at the periphery and propagate to the rotation axis. According to (2.5.1) the total number of vortex lines formed by the end of the process of acceleration is proportional to the cross section of the vessel and to the angular velocity: $N_0\sim R^2\omega_0$. In addition, let the number of vortex lines n generated in unit time per unit of the vessel periphery depend on the difference of mean velocities of the normal and the superfluid liquids v according to the law $n\sim v^\alpha$. This magnitude varies from the value $\omega_0 R$ at the beginning of the process till zero by its end. It is natural to assume that a stationary regime of rotation will be established at formation of an equilibrium number of quantized vortex lines in the container. Then

$$t\sim(N_0/Rn)\sim(\omega_0 R)^{1-\alpha}.$$

Hence at any law of the form $n\sim v^\alpha$ there appears an universal dependence of the time of dragging into rotation t on the velocity. Just such a conclusion is given by the experiment (Fig. 10.8).

The observed decrease of t with an increase of ω_0 and v requires $\alpha>1$. The numerical estimation shows that the experimental curve shown in Fig. 10.6 corresponds to an averaged value $\alpha\approx1.3$. Let us note for comparison that in Vinen's paper (1957c), devoted to the study of the quantized turbulence in the thermal flux, the dependence of the type $n\sim v^2$ is obtained, i.e., $\alpha=2$.

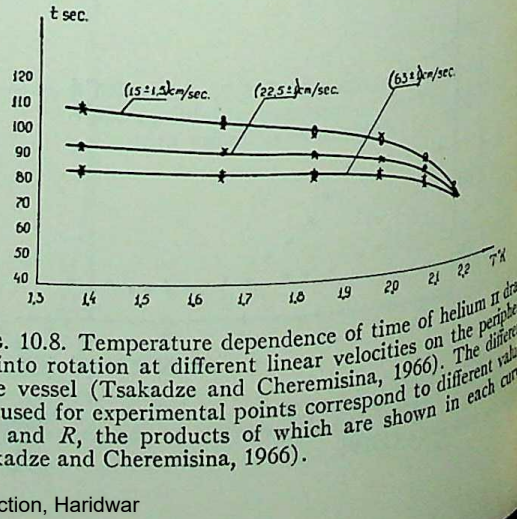

FIG. 10.8. Temperature dependence of time of helium II dragging into rotation at different linear velocities on the periphery of the vessel (Tsakadze and Cheremisina, 1966). The different signs used for experimental points correspond to different values of ω_0 and R, the products of which are shown in each curve (Tsakadze and Cheremisina, 1966).

CC-0. In Public Domain. Gurukul Kangri Collection, Haridwar

Digitized by Arya Samaj Foundation Chennai and eGangotri

10.2. Decay of Vortex Lines at the Stop of Rotation

The first information on rotating helium II slowing down was given in the paper of Andronikashvili and Kaverkin (1955). In a suddenly stopped cylindrical container an initially parabolic meniscus begins to straighten at the walls and only a conic crater is left in the center, disappearing in 30 sec. Thus the time of slowing down is one fourth as long as the time of dragging into rotation.

Pellam (1960) has also noted that slowing down proceeds much quicker than acceleration and that the beginning of slowing down of the liquid in the vessel takes place immediately after its stop.

Craig (1961) described the action of forces applied to the torsional balance wings immersed into helium II. Confirming Andronikashvili's observations (Andronikashvili and Kaverkin, 1955), he has noticed that a sharp decrease of the drag force at slowing down occurs

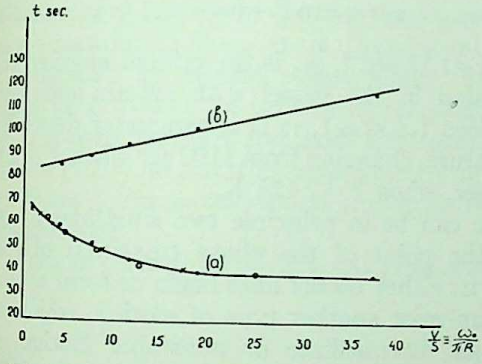

Fig. 10.9. The time of helium I dragging into rotation at different ω_0 and R is an universal function of ω_0/R (compare Fig. 10.8). This situation is illustrated by curve (a) on which points for different ω_0 and R are denoted in a different way. The time of helium II dragging into rotation is shown by curve (b). Here the dependence of t on ω_0/R is linear, but not universal (Tsakadze and Cheremisina, 1966).

three or four times as fast as its increase at acceleration. An essential difference in the absolute values of time measured in Andronikashvili's experiment on the one hand and that of Craig on the other hand is explained by the fact that angular velocities of rotation were many times different from each other.

Hall and Vinen (1956a, b) also observed relaxation effects at the stop and at the beginning of motion, when they studied attenuation of second sound in rotating resonators. However, such a great difference in the time of establishment of the stationary rotation regime of helium II and of its slowing down was not observed.

Similar data were obtained in the investigation of Careri, McCormick, and Scaramuzzi (1962) described in Sec. 3.3. It is shown in Fig. 10.10 that an equilibrium value of the current (after switching on of rotation) is reached in ~2 min (when $T=1.27$°K). Approximately the same time is required for the current to reach almost its initial value after the stop of rotation.

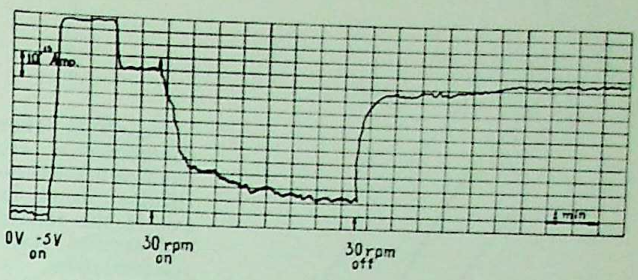

Fig. 10.10. Changes of the currents of negative ions in helium II: at voltage application, start of rotation and stop of rotation (Careri, McCormick, and Scaramuzzi, 1962).

However, a complete recovery of the current takes much longer time. At $T=0.9$°K it is about an hour and near the λ-point it is several minutes.

Further, the same authors (1963) reported that the period of half-decay of vortex lines τ after the stop of rotation was inversely proportional to the total number of thermal excitations, determined in the paper of Bendt, Cohwan, and Yarnell (1959). This conclusion is confirmed by Table II. There are the data obtained at a velocity of 10 rpm and at a voltage of 4 V. Careri *et al.* think that this result shows the participation of all the thermal excitations in the process of vortex line decay.

Interesting experiments for the study of the process of decay of vortex lines were made by Gamtsemlidze, Japaridze, and Turkadze (1965), who observed attenuation of the torsional pendulum (a flat disk) suspended inside of a uniformly rotating cylindrical container. The idea of the experiment was the following: The existence of vortex lines causes an additional attenuation of a torsional pendulum (5.1, 6.5). By watching the decrease of this additional attenuation after the stop of the container, it is possible to determine the time dependence of the number of vortex lines. An extra attenuation α was determined as the difference of two attenuations $\alpha=\delta_t-\delta_\infty$, where δ_∞ is the attenuation of the disk in helium II at rest and δ_t is the attenuation at some moment of time after the container stops.

As seen from the curves of Fig. 10.11, the extra attenuation can be described by an exponential law

$$\alpha=\alpha_0 \exp\left[-(\ln 2\tau/)t\right], \qquad (10.2.1)$$

where $\ln 2/\tau$ is the angle of the slope of the curves $\ln 2$ (t), τ is the period of half-decay. Curve A corre-

Table II.

T°K	τ sec	$10^{-19}N$ cm^{-3}	$10^{-22}\tau N$ cm^{-3} sec
0.87	510	1.56	0.8
1.12	192	5.43	1.0
1.27	105	11.4	1.2
1.40	96	20.4	2.0
1.54	48	37.0	1.8
1.93	12	154	1.8
2.05	6	233	1.4
2.12	3	313	0.9

CC-0. In Public Domain. Gurukul Kangri Collection, Haridwar

Digitized by Arya Samaj Foundation Chennai and eGangotri

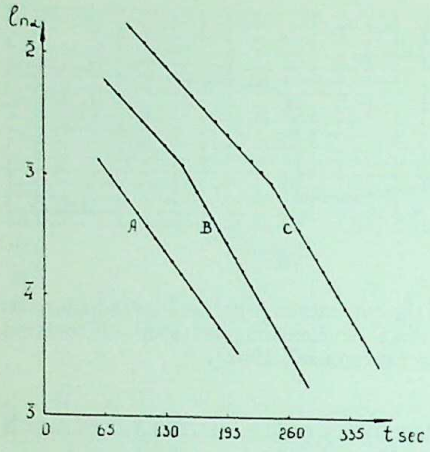

FIG. 10.11. Time dependence of the damping of a disk oscillating round its axis in the rotated and stopped vessel (Gamtsemlidze, Japaridze, and Turkadze, 1966).

sponded to a decay at the velocity of rotation $\omega_0 = (0.10 \pm 0.02)$ sec^{-1}, measured before the stop of the device. This velocity was closer to that $\tilde{\omega}_0$ at which collectivization of vortex lines takes places (6.3). Under the conditions of this experiment $\tilde{\omega}_0 = 0.11$ sec^{-1}.

But at the velocities $\omega_0 > \tilde{\omega}_0$ there is a sharp break on Curves B ($\omega_0 = 0.24$ sec^{-1}) and C ($\omega_0 = 0.48$ sec^{-1}). At small velocities the period of half-decay of vortex lines τ is equal to (55 ± 5) sec and at higher velocities the decay takes place with another half-period τ_1, for instance, for curve B $-\tau_1 = (70 \pm 5)$ sec. It is rather evident that an increase of the period of half-decay is caused by the process of collectivization. Actually, the estimation according to the formula $\omega_1 = \omega_0 \exp(-t_1 \ln 2/\tau_1)$, (where t_1 is the time from the moment of the rotation stop until the moment of the break of curves in Fig. 10.11) leads in each case to the value $\omega_1 \approx \tilde{\omega}_0$.

The decay of vortex lines was studied by the method of second sound by Bablidze (1965). He has established that the slowing down of rotating helium II is characterized by the period of half-decay $\tau = 30$ sec.

The conditions of this experiment differ essentially from those of Gamtzemlidze *et al.* (1966). Therefore it is, so far, difficult to indicate definitely the cause of some difference in their results ($\tau = 30$ sec should be compared with $\tau = 55$ sec).

10.3. Formation of Vortex Lines in Rotating Helium II at the Passage through the Point of the Phase Transition

The study of formation of Onsager–Feynman's vortex lines at cooling of uniformly rotating helium I lower than the temperature of the phase transition was undertaken in detail by Andronikashvili, Bablidze, and Tsakadze (Andronikashvili, Bablidze, Gujabidze, and Tsakadze, 1964a,b; Andronikashvili, Bablidze, and Tsakadze, 1965, 1966; Bablidze, 1965).

With this aim a radial mode resonator was constructed in which the waves of second sound generated on the surface of the inside cylinder were reflected on the inner surface of the outside cylinder and then received by a detector, wound on the inside cylinder.

The resonator was tuned to some temperature, then liquid helium was heated till $T = 2.21$°K at which it rotated about 30 min. After that, without a stop of the container rotation, it was cooled to the temperature at which second sound was tuned for resonance.

By means of this device it was established by attenuation of second-sound waves that vortex lines in rotating helium II appear at the passage through the point of the phase transition with a considerable delay. At the velocity of the liquid rotation $\omega_0 = 1.76$ sec^{-1} the resonance amplitude reaches its equilibrium value ($T = 2.168$°K) only after 300 sec (see Fig. 10.12).

Depending on the rate of cooling the relaxation phenomena accompany the process of rotation till 2.12°K. Below this temperature nonequilibrium phenomena were not observed at any velocity of rotation. The time of relaxation was dependent on the angular velocity ω_0 and on the value of overcooling $(T_\lambda - T)$. An empirical formula was obtained in the following form (see Fig. 10.13):

$$\tau = \tau_0 \exp\left[-(\omega_0 - \omega_{0c})/\alpha\right], \qquad (10.3.1)$$

where $\alpha = 1.18$ sec^{-1}, ω_{0c} is the critical angular velocity of rotation in the vessel with certain characteristic dimensions ($\omega_{0c} \ll \omega_0$), τ_0 is a parameter dependent on temperature, changing from 1100 sec when $T = 2.165$°K to 500 sec, when $T = 2.125$°K.

There can be in principle two situations at cooling below the point of the phase transition of rotating helium II: either vortex lines begin to form at once, or there can exist another type of motion, which can be called an intermediate or nonstable motion, which transforms into a stable form realized by an array of

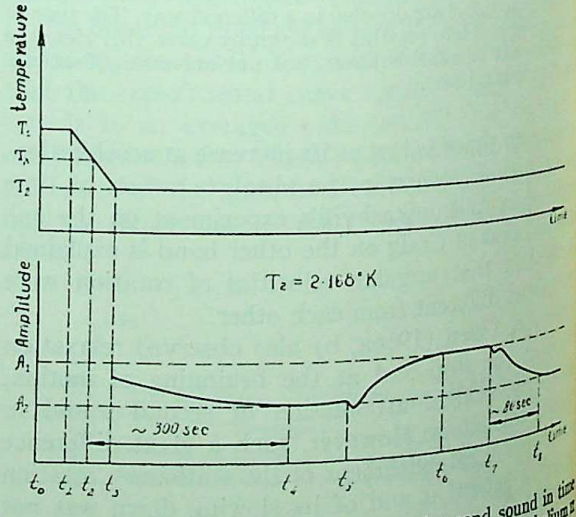

FIG. 10.12. Change of the amplitude of second sound in time in the radial mode resonator after the transition helium I–helium II, taking place during rotation (Andronikashvili, Bablidze, and Tsakadze, 1965). The time notations: t_1 is the beginning of cooling; t_2 is the transition through the λ-point; t_3, the cooling has been finished; t_4, the amplitude of second sound has reached its equilibrium value ($t_4 - t_2 = \tau$); t_6, the termination of rotation; t_7, the repeated beginning of rotation; t_8, again the equilibrium amplitude of second sound has reached its resonance value (under the conditions of rotation) value of the amplitude has been reached. $\omega_0 = 1.76$ sec^{-1}.

CC-0. In Public Domain. Gurukul Kangri Collection, Haridwar

Digitized by Arya Samaj Foundation Chennai and eGangotri

vortex cores aligned parallel to the rotation axis. This transformation takes place both at a lowering of the temperature and in time.

A slow decrease of the second-sound amplitude with time, shown in Fig. 10.12, cannot solve this problem in favor of either assumption. It was necessary to construct another axial mode resonator to answer this question. In such a resonator the second-sound generator was fixed on the cover of the device and the receiver on its bottom.

From the papers of Hall and Vinen (1956a, b), it was known that propagation of second sound along vortex lines does not lead to an additional attenuation of its amplitude. Therefore if vortex lines, oriented along the rotation axis, were the only cause of an additional second-sound scattering (in a radial mode resonator), then rotating helium II in their presence would seem transparent for thermal waves propagating in an axial mode resonator.

The experiments made by Andronikashvili, Bablidze, and Tsakadze have shown that in the vicinity of the λ-point, rotating helium II is "opalescent" at its "translucence" by second sound along the axis of rotation (Fig. 10.14). In time or at removal from the λ-point, it becomes more and more translucent. And at last after ~200 sec, at the same velocity of rotation ω_0=1.76 sec^{-1}, the second-sound amplitude reaches its resonance value.

The use of resonators of different geometrical shape

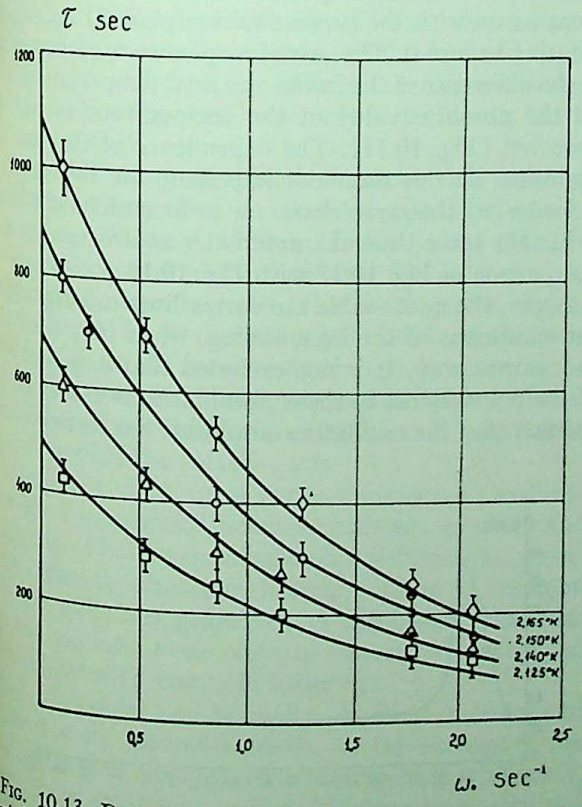

Fig. 10.13. Dependence of the relaxation time τ (equal to t_4-t_2 in Fig. 10.12) on the velocity of rotation at different temperatures (Andronikashvili, Bablidze, and Tsakadze, 1965).

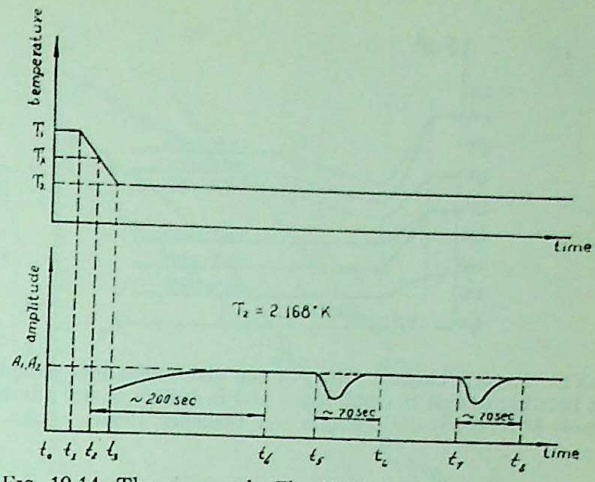

Fig. 10.14. The same as in Fig. 10.12, but with the use of an axial mode resonator (Andronikashvili, Bablidze, and Tsakadze, 1965).

shows that the change of an inner surface of a rotating vessel does not influence the formation of vortex lines.

Thus there can exist another intermediate type of motion than vortex lines, which makes rotating helium II isotropic with respect to second-sound propagation.

Evidently at such a stage vortex nuclei are generated in rotating helium II and vortex lines are formed gradually from them.

According to (10.3.1), the smaller the angular velocity is, i.e., the smaller the number of vortices, the longer the time is during which vortex nuclei can form a vortex line. This is clear, since the mean diffusion path of a nucleus, until it encounters a vortex core, is bigger for each nucleus when there are few vortex lines to be formed.

The time needed for a vortex line formation at the passage through the point of the phase transition (~300 sec) is comparable, by the order of the magnitude at the same ω_0, with the decay time and the time of vortex formation taking place at sudden switching on and off of the cylindrical container rotation (~70 sec).

This made us think that in this case as well vortex lines are formed from vortex line nuclei (or they decay on them). But the turbulent regime of the normal component leads in this case to reduction (3–4 time shorter) of the duration of the relaxation.

The idea of formation of vortex nuclei found its theoretical treatment in Iordanski's paper (1965a). It is shown there that in the presence of sufficiently high relative velocity of motion of the normal and the superfluid components, vortex formation begins in the latter, passing the initial stage of nucleus formation (the author considers the process of formation of ring vortices). The intensity of this process is calculated.

10.4. Change of Vortex Damping at the Variation of Temperature

We already know that at the change of temperature the number of vortex lines per unit of rotating liquid

CC-0. In Public Domain. Gurukul Kangri Collection, Haridwar

Digitized by Arya Samaj Foundation Chennai and eGangotri

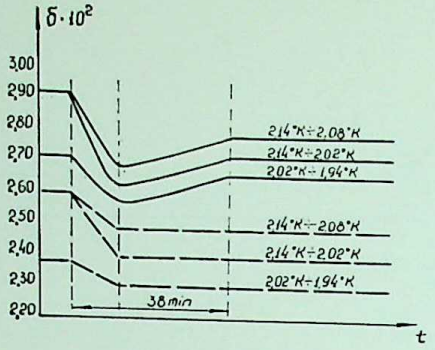

FIG. 10.15. Change in time of the disk oscillations damping in rotating helium II (solid lines) and in helium at rest (dashed lines) at its cooling (Gujabidze and Tsakadze, 1966).

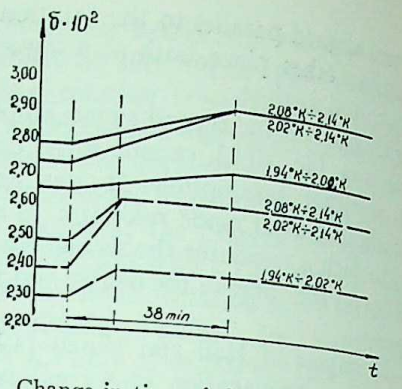

FIG. 10.17. Change in time of the disk oscillation damping in rotating helium II (solid lines) and helium II at rest (dashed lines) at its heating (Gujabidze and Tsakadze, 1966).

cross section does not change, but the amount of the superfluid component taking part in vortex motion does.

The study of relaxation processes at the change of temperature was made by Gujabidze and Tsakadze (1966). It was found that by lowering the temperature the normal component, having passed into the superfluid one, is dragged into the motion of already existing vortex lines during a very long time, in some cases reaching 40 min.

This process of enrichment of vortex lines by the superfluid component was studied by the time dependence of an additional damping of a disk oscillating in helium II and performing together with it a uniform rotation. As the tension of the vortex line according to formula (2.3.1) is porportional to ρ_s, then the projection of the tension on the plane of the disk causing an additional damping also depends on the amount of the superfluid component already dragged into a vortex motion. Figure 10.15 shows that there are two portions of the curve $\delta=f(t)$. One of them is associated directly with the process of temperature lowering, in particular, with the change in viscosity of the normal component. This process takes about 5 min. The other portion is associated only with the process of vortex line enrichment and it takes about 30–35 min.

The time necessary for a vortex line to drag the superfluid component into motion depends little on the value of the difference of the initial and finite temperatures, the same as on the absolute value of temperature. But it depends essentially on the angular velocity.

Figure 10.16 shows that the time of vortex enrichment is increased with an increase of the number of vortex lines and reaches the maximum when $2\omega_0/\Omega \approx 0.2$, i.e., when collectivization of vortex lines takes place. After that it begins to decrease. Beginning from the velocities $\omega_0 \approx 0.25\,\Omega$, the time of vortex enrichment does not already depend on the angular velocity, remaining strictly constant. Thus a vortex line has the most stable configuration, with respect to dragging of new amounts of the superfluid component into motion, under the conditions of its strongest fastening.

The phenomenon of exclusion of the normal component from vortex motion at an increase of temperature was studied by the same authors. This process, connected with heating, proceeds more smoothly in comparison with the process taking place at cooling of rotating helium II. The same independence on the value of the difference of the initial and final temperatures and on the absolute value of the temperature as well is observed (Fig. 10.17). The dependence of the time of exclusion of the normal component on the angular velocity has the same character as at enrichment. And it has the same time characteristics as it is seen at the comparison of Fig. 10.18 with Fig. 10.16.

Again, the most stable are vortex lines existing under the conditions of the least sliding, when they decay in the slowest way. It is not excluded that a special role of the point $\omega_0=\tilde{\omega}_0$ in these phenomena is explained by the fact that the oscillation amplitude has its maximum

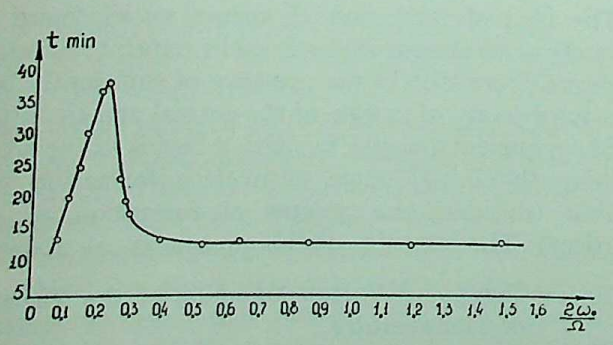

FIG. 10.16. Dependence of the duration of the process of vortex enrichment by the superfluid component (Fig. 10.15) on the velocity of rotation at a given rate of cooling (Gujabidze and Tsakadze, 1966).

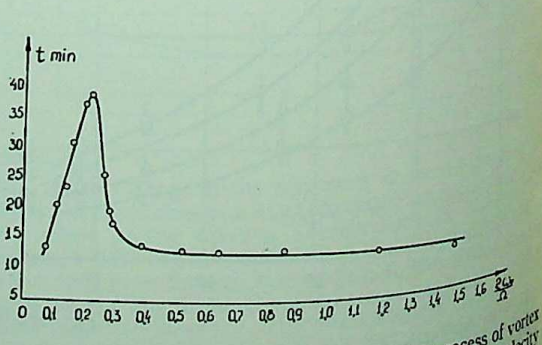

FIG. 10.18. Dependence of the duration of the process of vortex losing the superfluid component (Fig. 10.17) on the velocity of rotation (Gujabidze and Tsakadze, 1966), at a given rate of heating.

CC-0. In Public Domain. Gurukul Kangri Collection, Haridwar

Digitized by Arya Samaj Foundation Chennai and eGangotri

value at the best fastening of a vortex line. Being involved into such a vortex or "turned off" out of it the liquid should reconstruct most radically the character of its motion and that explains the maximum of relaxation time in Figs. 10.16 and 10.18.

The problem of the vortex decay at heating of rotating helium II was considered by Andreev (1964). He has shown that at heating two vortices (a superfluid and a normal one) with compatible cores are formed instead of one superfluid vortex. The newly formed normal vortex becomes more spread in time due to viscous forces. The duration of this process, estimated by Andreev on the basis of the analysis of dimensions is 10 min in the order of magnitude.

11. THE PHASE TRANSITION IN ROTATING HELIUM II

11.1. A Central Macroscopic Vortex

In Sec. 10.3 the phenomenon of delay at the vorticity formation was described at the phase transition helium I-helium II, under the conditions of rotation. A similar phenomenon of "overcooling" of the motion type is observed in the study of a central macroscopic vortex.

As early as 1948 Andronikashvili, studying rotation of liquid helium, found that under certain conditions in rapidly cooled rotating helium, there is observed a central macroscopic vortex piercing the whole liquid until the very bottom and forming something like a hollow rotation axis in helium II (Andronikashvili and Kaverkin, 1955). Andronikashvili's observations were confirmed by Donnelly, Chester, Walmsley, and Lane, (1956), who observed the central macroscopic vortex formation (see Fig. 11.1) not only in helium II, but in helium I as well.

A detailed study of this phenomenon was made by Tsakadze, who called it "Andronikashvili's vortex" (Tsakadze, 1963b,c,e, 1964a). He has found that this vortex is always formed in helium I. He has shown, by model experiments in water, that boiling of a rapidly rotating liquid leads to motion of vapor bubbles not in the direction to the surface, but in the direction to the axis of rotation. If boiling proceeds sufficiently intensively, then these bubbles are fused into a hollow axis, coinciding with the rotation axis.

In helium I, the central vortex forms a cord with the diameter 2 mm, which behaves restlessly, twisting and oscillating. Thus Andronikashvili's vortex is an essentially classical formation, having nothing in common with the quantum properties of the liquid. Tsakadze did not manage even once to observe formation of Andronikashvili's vortex in helium II.

But this vortex can be really observed in helium II, as reported by Andronikashvili. At the passage of the phase transition point this vortex, created in helium I, continues to exist for a sufficiently long time until the temperature 2.09°K. As soon as the temperature 2.17°K is passed, it stretches like a string and the meniscus of rotating helium II obtains the shape shown in Fig.

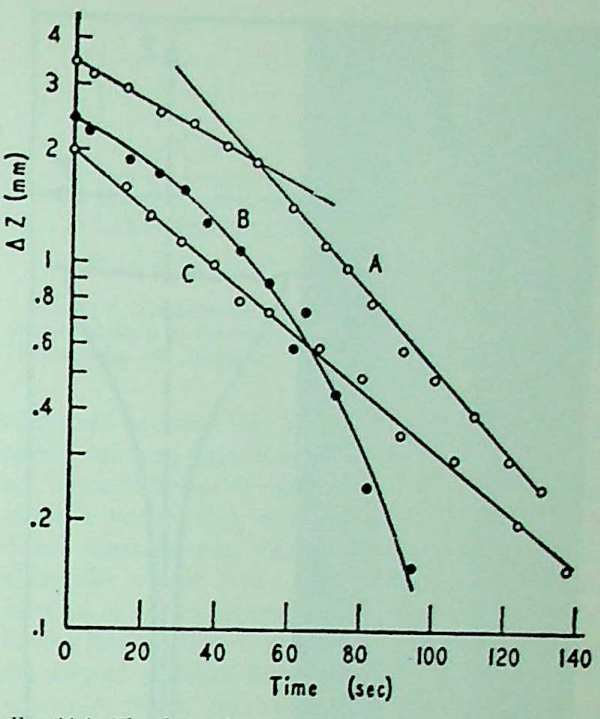

FIG. 11.1. The change in time of the meniscus depth of helium II brought into rotation (in the logarithmic scale), according to the data of Donnelly, Chester, Walmsley, and Lane (1956). Curve C shows the most frequently encountered case in these experiments. Sometimes the events develop as shown by curve B. Then the meniscus has a conic pit. In other cases the development of the pit is delayed. Then curve A is obtained. All these processes as well as the instability of the pit and formation of a central macroscopic vortex were observed both in helium I and in helium II. While according to Tsakadze (1964a) the curve of type A is possible only in helium I and B in helium II.

11.2. In time or at sufficiently low temperature, the central vortex tears off from the bottom of the container and begins to shorten gradually forming a conic deepening on the lower part of the parabolic meniscus.

It is a characteristic fact that this deepening, typical of a quantum liquid (see Sec. 3.6) remains in helium I for a long time. It can be observed there at a rapid heating from $T<T_\lambda$ until the temperature 3°K.

We dwell on these phenomena because they allow us to notice once more (compare Sec. 10.4) that at a transition from a classical liquid into a quantum one an overcooling is possible (though a temporary one) of classical kinds of motion, nonequilibrium for quantum systems. The similar phenomena—an overheating of quantum types of motion, nonequilibrium for classical liquids, can be observed at a reverse transition.

11.2. Peculiarities of the Phase Transition of Helium II into Helium I in the State of Rotation

It seemed evident that in the point of the phase transition, in which ρ_s becomes zero, the vortex damping described in detail in Secs. 5.1, 5.5, 6.2 should disappear.

Meanwhile the experiments of Andronikashvili, Mesoed, and Tsakadze (1964) have shown that the damping of an oscillating disk, rotating together with helium II and performing, in addition, axial oscillations remains constant by its character even above $T=$

CC-0. In Public Domain. Gurukul Kangri Collection, Haridwar

Digitized by Arya Samaj Foundation Chennai and eGangotri

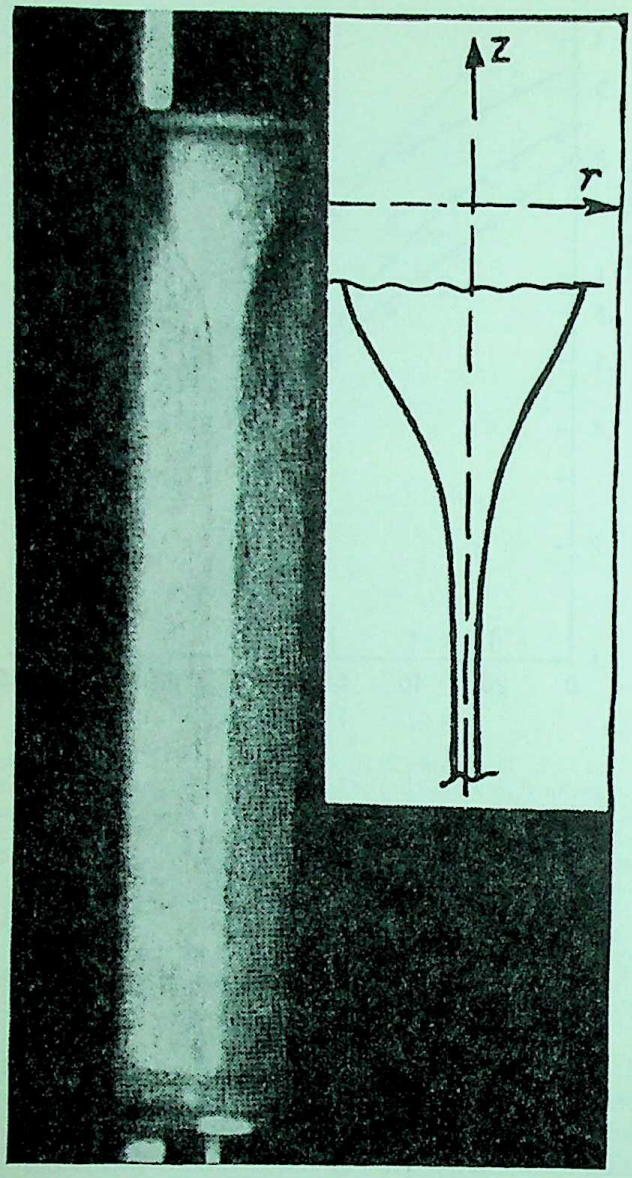

FIG. 11.2. The central macroscopic vortex in helium II: the photograph of the vortex and the result of the calculation according to the formula

$$z=-g^{-1}\left[\frac{1}{2}\left(\omega_0-\frac{\Gamma}{2\pi R^2}\right)^2(R^2-r^2)+\frac{\Gamma^2}{2\pi^2}\left(\frac{1}{r^2}-\frac{1}{R^2}\right)+\frac{\Gamma}{\pi}\left(\omega_0-\frac{\Gamma}{2\pi R^2}\right)\ln\frac{R}{r}\right],$$

when $\Gamma=10^2$ cm^2 sec^{-1} (Tsakadze, 1964a).

2.17°K, if only the phase transition of helium I into helium II takes place in the state of rotation (Fig. 5.12).

All attempts to find vortex damping in liquid helium brought into rotation above the λ-point and not cooled afterwards till temperatures corresponding to helium II, failed.

Thus it remained to assume that the existence of vortex lines in helium II is associated with extremely long relaxation time. The further experiments have confirmed these assumptions (Andronikashvili, Bablidze, Gujabidze, and Tsakadze, 1964a, b; Andronikashvili, Gujabidze, and Tsakadze, 1965, 1966).

It was natural to suppose that at the transition through 2.17°K, the whole superfluid component participating in the vortex motion, having passed into the normal state, begins to slow down sufficiently rapidly. This had to influence the energy of the vortex line, determining its tension. Thus if even the number of vortex lines would exist for some time at $T>2.17$°K and their number would be conserved constant, then due to a decrease of tension the vortex damping had to reduce.

But the obtained experimental data represent the time dependence of the logarithmic decrement of damping at the transition from rotating helium II into rotating helium I in the form shown in Fig. 11.3.

In a particular case when $\omega_0=\tilde{\omega}_0$, vortex lines, having passed through the λ-point, are conserved completely within the errors of the experiment during 18 min. Their existence causes the conservation of the corresponding maximum value of the decrement, characteristic of rotating helium II. This value of the decrement is associated, as we know, with the fact that the energy of the disk oscillations is carried away along the vortex lines. After 18 min a sudden vortex tearing off from the disk takes place during about one minute. This leads to a sharp decrease of the decrement and it decreases even lower than the value which should be expected for helium I, rotating as a solid body.

The latter circumstance can be understood by recalling that the logarithmic decrement of oscillation damping in helium II is expressed by formula (5.2.2), the main terms of which have the form:

$$\delta-(\Omega_0/\Omega)\,\delta_0\sim(\tfrac{1}{2}\eta_n\rho_n)^{\frac{1}{2}}[(\Omega+2\omega_0)^{\frac{1}{2}}+(\Omega-2\omega_0)^{\frac{1}{2}}]+(\eta_s\rho_s)^{\frac{1}{2}}(\Omega-2\omega_0)^{\frac{1}{2}} \quad (11.2.1)$$

and in helium I it should be:

$$\delta-(\Omega_0/\Omega)\,\delta_0\sim(\tfrac{1}{2}\eta\rho)^{\frac{1}{2}}[(\Omega+2\omega_0)^{\frac{1}{2}}+(\Omega-2\omega_0)^{\frac{1}{2}}]. \quad (11.2.2)$$

The first term of formula (11.2.1) is associated with the usual for a viscous liquid character of its interaction with an oscillating surface, which is realized between the disk and the normal component. The same process is described by formula (11.2.2) as well. As to the second term of formula (11.2.1), it is associated with the already mentioned mechanism of the disk energy loss by means of the waves, running along vortex lines.

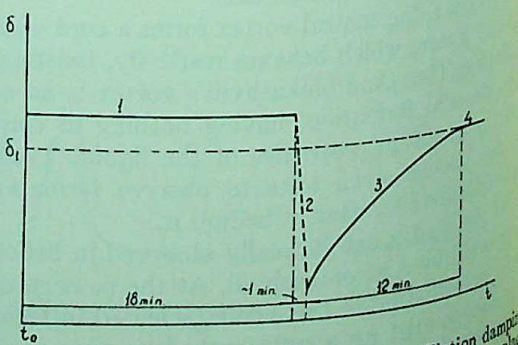

FIG. 11.3. The change in time of the disk oscillation damping in rotating helium I, after the phase transition has taken place at the moment t_0 in the state of rotation (Andronikashvili, Gujabidze, and Tsakadze, 1965).

CC-0. In Public Domain. Gurukul Kangri Collection, Haridwar

Digitized by Arya Samaj Foundation Chennai and eGangotri

In a metastable regime of rotation of helium I, when the system of vortex lines still continues to be connected with the disk, formula (11.2.1) has its initial meaning which is reflected by means of the first straight line portion of the given graph. At the moment of vortex tearing off, the second term of formula (11.2.1) decreases rapidly to zero. However, the amount of the liquid which participated in vortex motion is not dragged into the regime of the solid body rotation immediately. Therefore, beginning from the moment of vortex line tearing off, the decrement is expressed by formula (11.2.2) with the only difference that instead of the total density of the liquid ρ there is some effective density ρ' in it.

An increase of ρ' from the values near the value ρ_n, corresponding to the beginning of helium heating, until the total density ρ characteristic of the end of the experiment, represents the physical sense of the third portion of the graph in Fig. 11.3. The duration of this process is of the order of 12 min.

It was mentioned in Sec. 10.4 that superfluid vortex lines in helium II have the highest stability (in a sense of enrichment or losing the superfluid component) under the conditions of minimum sliding. The same is true in helium I as well: metastable vortex lines have the highest stability, i.e., the longest time until tearing off from the disk, when $\omega_0=\tilde{\omega}_0$. At the velocities larger or smaller than $\tilde{\omega}_0$, the time of vortex array tearing off from the disk surface becomes much shorter. It also becomes shorter at the temperature rise of helium I, at which the experiment takes place. Figure 11.4 illustrates this fact. At temperatures above 2.27°K one did not manage to observe the metastable vortex line array.

A question arises as to what reasons caused the sudden vortex array tearing off from the disk surface. The experiment shows that vortex lines of helium I,

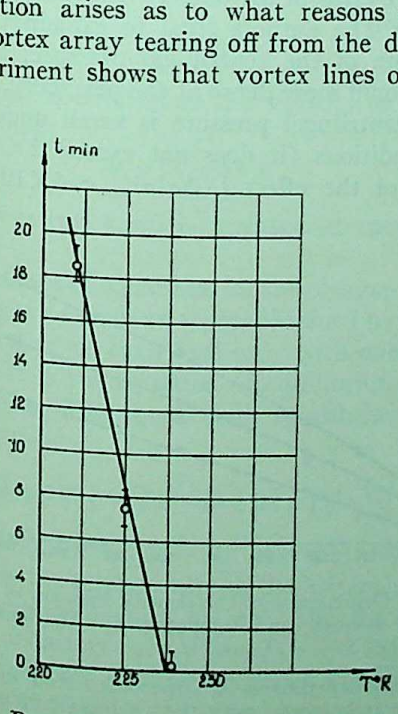

Fig. 11.4. Dependence of the duration of the first portion of Fig. 11.3 on the temperature (Andronikashvili, Gujabidze, and Tsakadze, 1965).

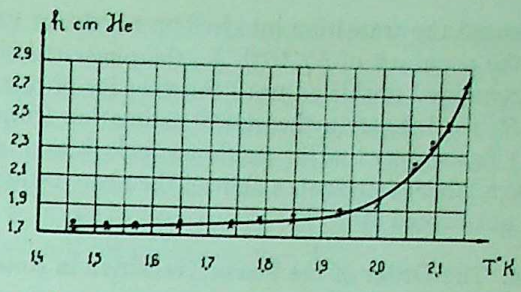

Fig. 11.5. Temperature dependence of the fountain effect in rotating helium II (crosses) and in helium II at rest (points) (Zamtaradze and Tsakadze, 1964).

stretched between two surfaces, are very stable and slowly damping formations until the moment of tearing off. Some decreases of the velocity of the liquid motion inside a vortex line, sufficiently small to escape the direct measurement, causes an increase of pressure along the vortex core. As a result of this pressure increase, a vortex separates from the solid surface and having become free decays. This explains the fact why the largest stability is observed in those vortex line arrays for which the coefficient of sliding is minimum.

This statement is confirmed by the fact that the relaxation time for vortex lines fixed to a smooth surface is four times as small as that for vortex lines fixed to a rough surface (when $\omega_0=\tilde{\omega}_0$).

11.3. Does the Point of the Phase Transition Shift in Rotating Helium II?

Some features of the phase transition in rotating helium described in two previous paragraphs, are very peculiar and extend to rather large temperature intervals.

The conservation of vortex damping in helium I, the delay of the vortex structure formation at the transition from rotating helium I into rotating helium II (9.3), and some other facts made it necessary to perform special investigations of the position of the phase transition point as a function of the angular velocity. With this aim Zamtaradze and Tsakadze (1964) studied the thermomechanical effect in rotating helium II and in helium II at rest near the phase transition point.

At first the experiment was made with a capillary filled with pressed rouge and equipped with an electrical heater, mounted along the rotation axis. The authors made another experiment as well, in which the thermomechanical effect was observed in a narrow annular gap near the cylindrical wall of the rotating container. As Fig. 11.5 shows, the curve of the thermomechanical effect in rotating helium II does not differ from that for helium II at rest.

Bablidze, Tsakadze, and Chanishvili (1964) made another attempt to find the phase transition point shift. With this aim they observed the break on the curve of cooling or heating of a phosphor-bronze thermometer placed in rotating helium and then in liquid helium at rest. This break was connected with a jump of thermal resistivity taking place while helium II

CC-0. In Public Domain. Gurukul Kangri Collection, Haridwar

Digitized by Arya Samaj Foundation Chennai and eGangotri

experienced the transition into helium I and vice versa. With the accuracy of 5×10^{-4} °K, the phase transition point remained unshifted until the velocity of rotation $\omega_0=0.56$ sec^{-1}. Later a theoretical estimation (formula 12.4.1) has shown that at maximum velocities of rotation, available at present, a shift of the phase transition could not exceed 10^{-9} °K.

11.4. The Order of the Phase Transition in Rotating Liquid Helium

Phenomena of "overcooling" and "overheating" of motion, characteristic of two states of liquid helium and observed at the phase transition in this liquid, suggested the idea that we are dealing with a first-order transition and not with a second-order one. However, to solve this problem, it was necessary to perform experiments of a thermodynamical and not hydrodynamical character.

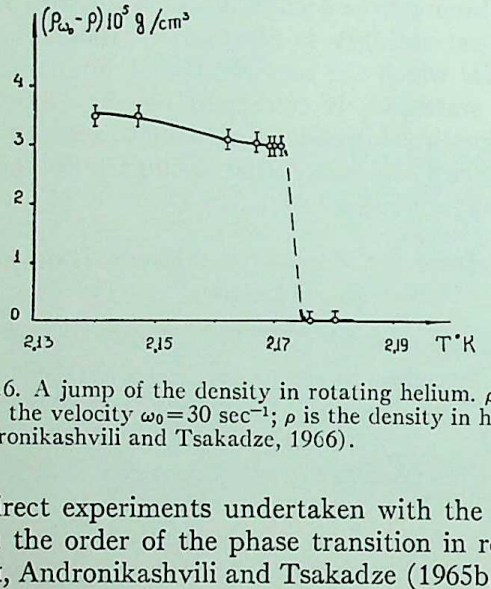

FIG. 11.6. A jump of the density in rotating helium. ρ_{ω_0} is the density at the velocity $\omega_0=30$ sec^{-1}; ρ is the density in helium at rest (Andronikashvili and Tsakadze, 1966).

For direct experiments undertaken with the aim to establish the order of the phase transition in rotating helium II, Andronikashvili and Tsakadze (1965b, 1966) have used the method of a rotating pyknometer. This device was sufficiently sensitive for registration of the slightest changes of the helium density taking place at the change of the temperature or angular velocity of rotation.

The character of the behavior of this magnitude which is the first derivative of the thermodynamical potential, determines the order of the phase transition unambigously.

A pyknometer with a volume of 37.093 cm³, representing a copper cylindrical reservoir, had a glass capillary with an inner diameter of 0.160 cm. In its upper part the capillary was blown into a small sphere and joined to a valve by means of which one could change the level of helium in the capillary. The observations were made by means of a cathetometer. At the rotation of the pyknometer with a velocity of $\omega_0=30$ sec^{-1}, in the temperature interval 2.18°—2.172°K, $\rho_{\omega 0}-\rho$ remains constant, at the further cooling a discontinuity appears, shown in Fig. 11.6. The comparison with the curve of the temperature dependence of density

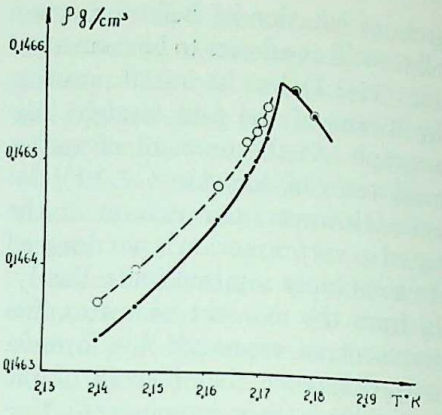

FIG. 11.7. Temperature dependence of densities of rotating helium and helium at rest (Andronikashvili and Tsakadze, 1966). The solid line is Kerr's curve (1957).

obtained by Kerr (1957) (Fig. 11.7) allows us to make the conclusion that the density of liquid helium changes at the phase transition point by a jump of about 0.02%.

That shows that in the state of rotation the order of the phase transition changes: liquid helium under such conditions experiences a phase transition of the first order superimposed on the transition of the second order (see Sec. 12.6).

Pyknometric studies (Andronikashvili and Tsakadze, 1965a,b, 1966) show that helium II brought into rotation increases its density appreciably. This fact contradicts the opinion of many physicists, who thought the vortex structure should reduce helium II density. As seen in Figs. 11.6, 11.7, 11.8 the density change is the higher, the lower in the temperature. An increase of the angular velocity also leads to an increase of helium II density. Naturally such effects are not observed in helium I.

Such experiments were made with a great accuracy (the relative error in the density determination is only 0.0009%).[13] The authors tried to explain the results by an action of the centrifugal pressure, tending to make the liquid more dense at the periphery. However, since the centrifugal pressure is small under the described conditions (it does not exceed 2×10^{-4} atm) the value of the effect $[(\Delta\rho/\rho)_{max}\sim4\times10^{-4}]$ would

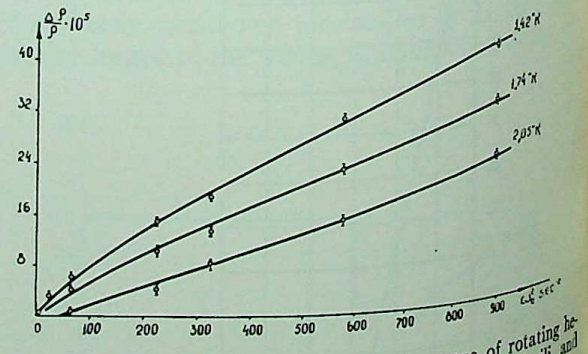

FIG. 11.8. Dependence of the density increase of rotating helium II on velocity and temperature (Andronikashvili and Tsakadze, 1966).

[13] In several experiments of Andronikashivli and Tsakadze (1965a, b) a pyknometer with the volume 52.57 cm³ and with the diameter of the capillary equal to 0.175 cm was used. The change of the level in the capillary was determined within the error ±0.02 cm.

CC-0. Mumukshu Bhawan Varanasi Collection. Digitized by eGangotri
CC-0. In Public Domain. Gurukul Kangri Collection, Haridwar

Digitized by Arya Samaj Foundation Chennai and eGangotri

require the value of the coefficient of compressibility exceeding the real value of this magnitude ($\sim 10^{-2}$ atm^{-1}) by two orders. (*Note added in proof.* Bablidze and Gavrilidi have measured the first sound velocity in rotating helium II and showed that its compressibility did not depend on the velocity of rotation.)

Besides, due to the known properties of the coefficient of compressibility, the effect of compression by centrifugal pressure should be increased with an increase of temperature, and the derivative $\partial\rho/\partial\omega_0^2$ should be decreased with an increase of the angular velocity. In reality only a decrease of $\partial\rho/\partial\omega_0^2$ at an increase of ω_0 is observed. But an increase of temperature decreases the observed packing.

12. PHENOMENOLOGICAL AND MICROSCOPIC THEORY OF QUANTUM LIQUID ROTATION

12.1. Phenomenological Quantum Theory of Helium II

The wave function, we mentioned in Sec. 2, while speaking on Feynman's ideas, is a function of coordinates of all the atoms of liquid helium. But a quantum liquid can be described phenomenologically by a simpler wave function depending only on three spatial coordinates (and may be on time). Ginzburg and Pitaevski (1958), proceeding from an analogy with the phenomenological theory of superconductivity of Ginzburg and Landau, suggested using a complex wave function for description of the superfluid component of helium II

$$\psi = f \exp(i\phi). \tag{12.1.1}$$

Its modulus f determines the density of the superfluid component

$$\rho_s = mf^2 \tag{12.1.2}$$

and the phase ϕ determines the velocity of the superfluid component

$$\mathbf{v}_s = (\hbar/m)\nabla\phi. \tag{12.1.3}$$

The condition curl $\mathbf{v}_s = 0$ is maintained automatically here.

A complete set of equations for the phenomenological quantum theory of helium II was obtained by Pitaevski (1958). Further we shall deal only with one equation of this set. It is the equation of equilibrium, valid in the static case. The equation of equilibrium has the following form:

$$\tfrac{1}{2}m[i(\hbar/m)\nabla + \mathbf{v}_n]^2\psi - \alpha\psi + \beta|\psi|^2\psi = 0, \tag{12.1.4}$$

where $\alpha \approx 4.5\times10^{-17}$ $(T_\lambda - T)$ erg and $\beta \approx 4\times10^{-40}$ erg cm^3, T_λ is the temperature of the λ-transition in an infinite volume of helium at rest. The theory has a sufficient foundation only when $T_\lambda - T \ll T_\lambda$, but one may hope that its qualitative conclusions are valid when $T \ll T_\lambda$ as well.

It should be emphasized that the main peculiarity of this equation is the direct association between the motion of the normal component and the velocity and the density distributions of the superfluid component. This fact distinguishes the phenomenological quantum theory from hydrodynamics formulated in Sec. 4.2, which provides the association between motions of the components only when there are vortex lines (terms with $\mathbf{F}_{sn}$), while the density ρ_s is considered as the constant not dependent on $\mathbf{v}_n - \mathbf{v}_s$.[14]

12.2. Rotating Helium II in the Phenomenological Theory

Kiknadze, Mamaladze, and Cheishvili (1965) used Eq. (12.1.4) to consider uniform rotation of helium II. In this case the motion of the normal component is determined $\mathbf{v}_n = [\boldsymbol{\omega}_0, \mathbf{r}]$ and Eq. (12.1.4) has the form

$$\tfrac{1}{2}m\{i(\hbar/m)\nabla + [\boldsymbol{\omega}_0, \mathbf{r}]\}^2\psi - \alpha\psi + \beta|\psi|^2\psi = 0. \tag{12.2.1}$$

The other equations of the complete set of Pitaevski are reduced to the absence of the temperature gradient and to the requirement of a stationary distribution of all the physical magnitudes in the rotating frame of reference.

It was shown earlier (Ginzburg and Pitaevski, 1958) that Eq. (12.1.4) when $\mathbf{v}_n = 0$ has solutions describing a unit vortex line in an infinite liquid. Then in accordance with formula (2.2.3) the gradient of the wave function phase has the value $|\nabla\phi| = 1/r$ and it is directed along the tangent to the circumference $r = $ const. The same circumferences are the lines of the constant density ρ_s: the modulus of the wave function $f(\mathbf{r}) = f(r)$ is equal to zero on the vortex axis $r = 0$, $f(r) \approx 0.6(\alpha/\beta)^{\frac{1}{2}} r/a_0$, where $r \ll a_0 = \hbar/(2m\alpha)^{\frac{1}{2}}$ and $f(r) \approx (\alpha/\beta)^{\frac{1}{2}}(1 - a_0^2/2r^2)$, when $r \gg a_0$. The parameter a_0 is a characteristic dimension of the theory. It is equal to $a_0 \approx 4.3\times10^{-8}(T_\lambda - T)^{-\frac{1}{2}}$ and appreciably exceeds interatomic distances in liquid helium only at temperatures very close to T_λ. This parameter represents simultaneously the radius of the vortex core; that is the reason why the symbol a_0 is used.

Kiknadze, Mamaladze, and Cheishvili (1965) have shown that Eq. (12.2.1) also has solutions similar to the just described one, with the only difference that the vortex axis, i.e., the line on which $f = 0$, moves together with the normal component (i.e., it takes part in the rotation of the vessel). Furthermore, it was found that Eq. (12.2.1) has solutions describing the existence of two-dimensional regular lattices of vortex lines in a rotating liquid, similar to vortex lattices of Abrikosov (1957). Such lattices can rotate together with the normal component without distortion of their motion. The distribution of the superfluid component density at the square or triangular symmetry of vortex arrangement coincides exactly with the distribution of superconducting electron density in the corresponding square

[14] The latter circumstance is associated with the fact that only the case of small $|\mathbf{v}_n - \mathbf{v}_s|$ was considered in Sec. 4.2. In the general case Landau's two fluid hydrodynamics and hydrodynamics of rotating helium II as well, take into account the dependence of ρ_n and ρ_s on $\mathbf{v}_n - \mathbf{v}_s$.

CC-0. In Public Domain. Gurukul Kangri Collection, Haridwar

Digitized by Arya Samaj Foundation Chennai and eGangotri

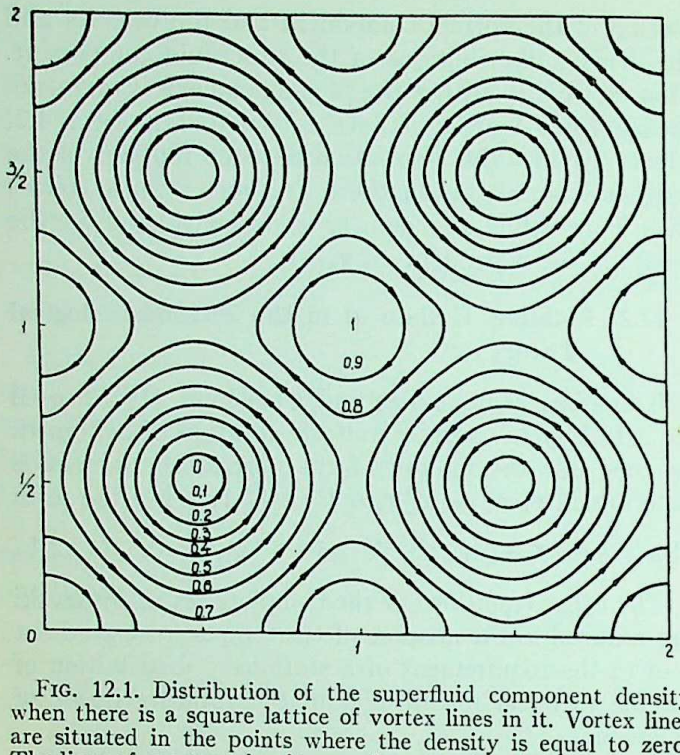

FIG. 12.1. Distribution of the superfluid component density when there is a square lattice of vortex lines in it. Vortex lines are situated in the points where the density is equal to zero. The lines of constant density are shown; values in units of maximum density ρ_s are shown on them. The same lines are the lines of the superfluid component curernt in the reference system rotating together with vortex lines, the normal component, and the vessel. Arrows show the direction of motion. The figure is plotted for the case when $\omega_0 \approx \alpha/\hbar \approx 4.3\times10^{10}\ (T_\lambda - T)\,\mathrm{sec}^{-1}$ and is taken from Abrikosov's paper (1957).

(Abrikosov, 1957, Fig. 12.1) or triangular (Cleiner, Roth, and Autler, 1964, Fig. 12.2) lattices.[15]

The imaginary part of Eq. (12.2.1) has the form

$$(\nabla f,\ (\hbar/m)\nabla\phi - [\boldsymbol{\omega}_0,\ \mathbf{r}]) = 0, \qquad (12.2.2)$$

and that means the lines of the constant density shown in Figs. 12.1, 12.2 are at the same time lines of a superfluid current in the rotating system of reference. On looking at Figs. 12.1 and 12.2 from this point of view, we cannot help but notice that near the points where f is maximum (we denote them $\mathbf{r}_m$), the superfluid component rotates in the opposite direction with respect to the direction of its rotation around vortex points (where $f=0$). A more detailed consideration shows that in the vicinity of $\mathbf{r}_m$ this rotation is performed according to the law $\mathbf{v}_s \approx -[\boldsymbol{\omega}_0,\ \mathbf{r}-\mathbf{r}_m]$ (the next term of the expansion $\mathbf{v}_s$ over the powers of $\mathbf{r}-\mathbf{r}_m$ is equal to zero). At the transformation to the laboratory system of coordinates, we get $\mathbf{v}_s = [\boldsymbol{\omega}_0,\ \mathbf{r}] - [\boldsymbol{\omega}_0,\ \mathbf{r}-\mathbf{r}_m] = [\boldsymbol{\omega}_0,\ \mathbf{r}_m]$, i.e., the vicinity of any point of $\mathbf{r}_m$ is a domain in which the linear velocity of rotation is constant. But the angular velocity is different for different domains (compare Fig. 12.3). Let us note that Pellam (1962) suggested a model of domains instead of the vortex model of rotating helium II.

The centers of these domains rotate together with the vessel and rotation of the superfluid liquid in the opposite direction takes place inside of them, that provides the constant linear velocity and the equality $\operatorname{curl} \mathbf{v}_s = 0$. It is interesting that Pellam's intuition was justified to some extent, but the existence of such domains in intervortex regions was a direct consequence of the vortex existence and there is no necessity to oppose it to the vortex model.

Thus the phenomenological quantum theory has confirmed and made somewhat more precise the quasi-classical considerations taken as the basis of rotating helium II hydrodynamics: the existence of vortex lines, their rotation together with the vessel, the validity of the equation $\operatorname{curl} \mathbf{v}_s = 0$ throughout the liquid at the mean velocity characterized by the curl equal to $2\boldsymbol{\omega}_0$. Figure 2.2 given in Sec. 2.4, plotted on the basis of purely qualitative considerations have now obtained a deeper substantiation. In particular, it became known that the curve of the superfluid velocity crosses the line $v_s = \omega_0 r$ in each intervortex space (in the points $\mathbf{r}_m$) being parallel to the abscissa. This makes the velocity distribution closer to the law $v = \omega_0 r$, most favorable thermodynamically.

However, the statement on the advantages of liquid rotation as a solid body now requires a verification. Indeed, for the complex motion of the liquid consisting of two components, the densities of which depend on the character of motion, the variation problem on the minimum of the free energy should be formulated and solved anew.

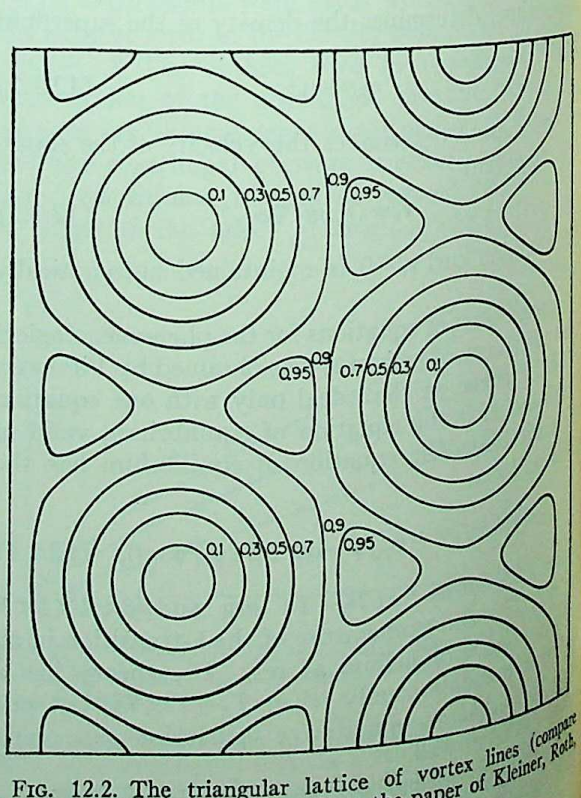

FIG. 12.2. The triangular lattice of vortex lines (compare Fig. 12.1). The figure is taken from the paper of Kleiner, Roth, and Autler (1964).

[15] The existence of Eq. (12.2.1) solutions describing regular systems of vortex lines, does not mean that all such systems are realized (compare Sec. 12.3). Some authors even state that only random, uniform in average, distribution of vortex lines is possible, in difference from superconductors of the second kind. But, we think that this problem is so far open. Ikachenko has shown that a two-dimension vortex lattice with a triangle symmetry is stable.

CC-0. In Public Domain. Gurukul Kangri Collection, Haridwar

Digitized by Arya Samaj Foundation Chennai and eGangotri

12.3. Free Energy of Rotating Helium II

The energy e and the angular momentum $\mathbf{l}$ of unit volume of liquid helium II are composed by means of equations

$$e=e_{s0}+\tfrac{1}{2}\rho_s v_s^2+\tfrac{1}{2}\rho_n v_n^2+(\hbar^2/8m^2)[(\nabla\rho_s)^2/\rho_s], \quad (12.3.1)$$

$$\mathbf{l}=[\mathbf{r},\ \rho_s\mathbf{v}_s+\rho_n\mathbf{v}_n], \quad (12.3.2)$$

where e_{s0} is the internal energy and the last term of formula (12.3.1) describes a purely quantum effect, connected with the contribution of any inhomogeneity into energy, due to the relation of uncertainties. The matter is that the statement on the existence of the density gradient is associated with the statement on the concentration of some additional number of particles in some volume, and an uncertainty of momentum, contributing into the kinetic energy, is associated with any restrictions of coordinates of particles.

Expressing ρ_s, $\mathbf{v}_s$, and $\rho_n=\rho-\rho_s$ by a phenomenological wave function ψ, and taking $\mathbf{v}_n=[\boldsymbol{\omega}_0, \mathbf{r}]$, and expanding e_{s0} in powers of ρ_s (Ginzburg and Pitaevski, 1958)

$$e_{s0}=e_{n0}-\alpha f^2+\tfrac{1}{2}\beta f^4 \quad (12.3.3)$$

then the free energy density will have the form

$$e-\mathbf{l}\cdot\boldsymbol{\omega}_0=e_{s0}+(\alpha^2/2\beta)\ -\alpha\,|\,\psi\,|^2+\tfrac{1}{2}\beta\,|\,\psi\,|^4$$
$$+(\hbar^2/2m)\ |\,\nabla\psi\,|^2-(\hbar/2i)\,(\psi^*\nabla\psi-\psi\nabla\psi^*,\,[\boldsymbol{\omega}_0,\,\mathbf{r}])$$
$$+\tfrac{1}{2}m\,|\,\psi\,|^2\omega_0^2r^2-\tfrac{1}{2}\rho\omega_0^2r^2. \quad (12.3.4)$$

Equation (12.2.1), which we had in Sec. 12.2 is just the solution of the variation problem on the minimum of the integral over the volume of expression (12.3.4). Substituting in its turn this equation into the minimized integral, we obtain the condition

$$\int(e-\mathbf{l}\cdot\boldsymbol{\omega}_0-e_{s0}+\tfrac{1}{2}\rho\omega_0^2r^2)\ dV=\frac{\alpha^2}{2\beta}\int\left(1-\frac{\beta^2}{\alpha^2}f^4\right)dV=\min, \quad (12.3.5)$$

which should be used with the purpose of choosing the most thermodynamically favorable solution of Eq. (12.2.1), when at given boundary conditions it has several solutions.

Let us note that the left-hand side of expression (12.3.5) is the difference of the "kinetic" free energy of rotating helium II and the free energy of rotation as a whole. In other words this condition describes the tendency of helium II to its inaccessible ideal, i.e., to solid body rotation. And the closeness of f to its maximum possible value $f=(\alpha/\beta)^{\frac{1}{2}}$ promotes the approach to such an "ideal."

The direct consequence of condition (12.3.5), which is reduced to the requirement $\int f^4\,dV=\max$, is the advantage of the superfluid component existence in the whole considered volume. The equality $f\equiv 0$ is very undesirable from the point of view of this consideration. Therefore the transition of the whole liquid into the normal state can be realized only because of the absence of nonzero solutions of Eq. (12.2.1) at given boundary conditions (or if there are no solutions with real positive f, which cannot be negative or complex by its definition). When $T=T_\lambda$ the coefficient $\alpha=4.5\times10^{-17}(T_\lambda-T)$ erg becomes zero and the density of the superfluid component vanishes as well, since this density in the stationary infinite liquid is equal to $m\alpha/\beta$ and is proportional to this magnitude in any other case. [The previous statement is connected with the circumstance that Eq. (12.2.1) can be rewritten in a dimensionless form with $|\,\psi\,|$ measured in the units $(\alpha/\beta)^{\frac{1}{2}}$.] In the moving liquid or in the presence of boundary surfaces reduction of ρ_s to zero takes place at $T\leq T_\lambda$ as well (a shift of the λ-point).

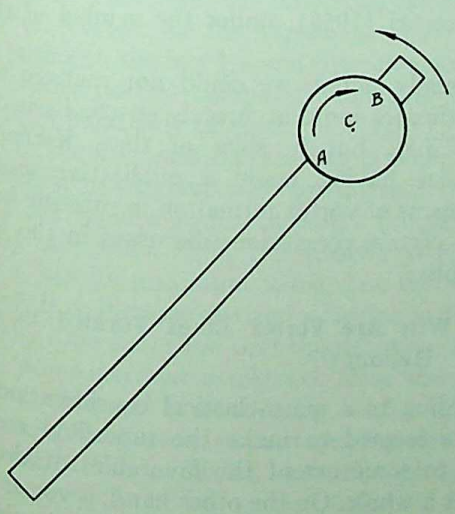

Fig. 12.3. A circle is placed on the rod rotating counter clockwise around the axis passing through one of its ends; the circle itself rotates clockwise. If the velocity at point C is equal to $\omega_0 R_C$, then the velocity at point A is equal to $\omega_0 R_A+\omega_0(R_C-R_A)=\omega_0 R_C$ and the velocity at point B is equal to $\omega_0 R_B-\omega_0(R_B-R_C)=\omega_0 R_C$. Similarly, one can be convinced that all the points of the circle have the same linear velocity $[\omega_0, R_C]$.

12.4. Critical Velocities and the λ-Point Shift

The possibility of reduction of ρ_s to zero [meaning the absence of solutions of Eq. (12.2.1)] is realized in the case of an infinite liquid, rotating with the angular velocity ω_0 which we shall denote as ω_{c2} [16]; $\omega_{c2}=(\alpha/\hbar)\approx 4.3\times10^{10}\,(T_\lambda-T)$ sec^{-1}. When ω_0 tends to ω_{c2}, the wave function of helium II, rotating in an infinite volume, tends to zero smoothly and disappears gradually (the phase transition of the second order). Thus rotation causes a shift of the point of the phase transition

$$\delta T_\lambda\approx-2.3\times10^{-11}\omega_0\ ^\circ\mathrm{K}, \quad (12.4.1)$$

where ω_0 is measured in sec^{-1}.

Calculations of Kiknadze, Mamaladze, and Cheishvili (1965) leading to the determination of the superfluid velocity near the points $\mathbf{r}_m$ which are the centers of the regions of rotation in the opposite direction were made

[16] The symbol ω_{c2} is introduced as an analogy with the second critical field H_{c2}, at which a superconductor of the second kind becomes normal.

CC-0. In Public Domain. Gurukul Kangri Collection, Haridwar

Digitized by Arya Samaj Foundation Chennai and eGangotri

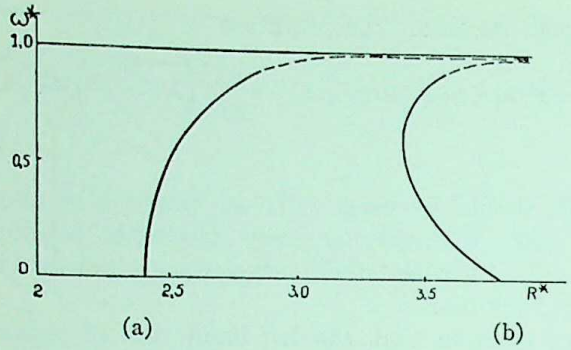

FIG. 12.4. The state diagram of rotating helium II. The symbols: $\omega^*=\hbar\omega_0/\alpha$ is the angular velocity in units $4.3\times10^{10}\,(T_\lambda-T)\,\mathrm{sec}^{-1}$, $R^*=R/a_0$ is the radius of the cylinder in units $4.3\times10^{-8}\,(T_\lambda-T)^{-\frac{1}{2}}$ cm. To the left and above line (a) there is a region of the normal state. To the right and below line (a) there is a region of the superfluid state. The density of the superfluid component is equal to zero on line (a). The existence of vortex lines between lines (a) and (b) is impossible. The existence of a vortex line is allowed to the right and below line (b). The density of the superfluid component on line (b) is equal to zero when there is one vortex line on the axis of the cylinder.

at $\omega_0 \lesssim \omega_{c2}$. The statement of these authors on the possibility of the description of the superfluid rotation picture by Figs. 12.1 and 12.2, also concerns the mentioned range of velocities. Condition (12.3.5) makes us prefer a two-dimensional lattice of vortex lines with the triangular symmetry in comparison with the square one.

Kiknadze and Mamaladze have also determined the critical velocities of rotating helium II at which the superfluid density becomes zero in vessels of finite size. These critical velocities at which helium II passes into the normal state depend on the dimensions of the vessel with a finite radius R (see Fig. 12.4). This figure determines in fact the region of the superfluid state existence on the diagram (ω_0, T), since the dimensionless radius R^* and the dimensionless angular velocity ω^*, used at its plotting are functions of temperature.

The family of curves on the diagram (ω_0, T) corresponds to one curve in Fig. 12.4, each of them is characterized by a definite value of the radius. The change of temperature at the constant radius corresponds to a shift from the right to the left in Fig. (12.4) along the line asymptotically tending to parallelity with the abscissa, when $T\to0$ and to the coincidence with the ordinate, when $T\to T_\lambda$ (see Fig. 12.7). Here since the wave function in the point of intersection of such a line with the curve (a) (taken from Fig. 12.4) becomes smoothly zero, then a shift of the λ-point should occur. As seen in Fig. 12.4 ,at relatively small velocities the phase transition takes place when $R^*\approx2.4$ (more accurately, when $R^*=j_{01}$, where j_{01} is the first root of the Bessel function J_0). Returning to usual units (cm, degree) we obtain

$$\delta T_\lambda \approx -(1.1\times10^{-14})/R^2\ ^\circ\mathrm{K}, \qquad (12.4.2)$$

where R is measured in centimeters. Independence of δT_λ from ω_0 takes place throughout the whole almost vertical portion of curve (a).

Because of a large value of the unit used in Fig. 12.4 of ω_0 measuring, the almost vertical portion of curve (a) overlaps practically the whole interval of the attainable velocities of rotation. At such velocities, an appreciable shift of the λ-point can be observed only in very narrow capillaries [formula (12.4.2)]. At a further increase of ω_0 the shift δT_λ depends both on R and on ω_0, and at last at extremely large ω_0, it hardly depends on R. The transition takes place at $\omega_0=\omega_{c2}$ in the vessel with an arbitrary large radius and δT_λ is determined by formula (12.4.1). As the magnitude a_0, used as a unit of the radius, is very small (if only T is not too close to T_λ), then ω_{c2} is the critical velocity of transition into the normal state for a vessel of any, but not extremely small size.

Using condition (12.3.5), it would be possible in principle to solve the problem of the lower critical velocity ω_{c1}, at which the first vortex line is formed. But in the process of such a calculation great difficulties arise.

An exception is the case of large radii R^*, which involves all practically interesting values of R, if only T is not too close to T_λ. When $R\gg a_0$, the structure of the vortex core has no special role. Therefore, to determine the critical velocity of vortex formation, the considerations which led to the Arkhipov-Vinen formula (2.6.1), for creation of the first vortex line

$$\omega_{c1}\approx(\hbar/mR^2)\ln(R/a_0) \qquad (12.4.3)$$

and to formula (2.6.4) for the velocity

$$\omega_{c1}'\approx(4\hbar/mR^2)\ln(\hbar/m\omega_{c1}'a_0^2)^{\frac{1}{2}} \qquad (12.4.4)$$

are sufficient. Here ω_{c1}' is the velocity starting from which the density of vortex lines corresponds to Feynman's formula (2.5.1). Keeping in mind the estimating character of given formulae, we neglect a_0^2 in comparison with R^2 in formula (2.6.1) and do not introduce the numerical factor, determined by Ginzburg and Pitaevski (1958), under the symbol of the logarithm.

As already noted, we could not manage to make these estimates more accurately on the basis of condition (12.3.5), but in spite of that, Kiknadze and Mamaladze having made a qualitative analysis of the problems of vortex formation in rotating helium II, came to certain conclusions discussed in the following paragraphs.

12.5. Why Are Vortex Lines Formed in Rotating Helium II?

According to a quasi-classical consideration, vortex lines are formed to make the superfluid component imitate to some extent the favorable rotation of the liquid as a whole. On the other hand, a vortex line is a node line of the wave function and the density of the superfluid is small in its core. It would seem to create an unfavorable situation from the point of view of condition (12.3.5). But now it will be shown that in reality, strange as it may seem, the existence of vortex lines increases the density of the superfluid component in a

CC-0. In Public Domain. Gurukul Kangri Collection, Haridwar

Digitized by Arya Samaj Foundation Chennai and eGangotri

rotating vessel. It should drop catastrophically if vortex lines were not formed or if they were not formed in sufficient number.

This statement is based on the analysis of solutions of two equations, which are the real parts of Eq. (12.2.1)[17] in two different cases: when there is no motion of the superfluid component ($\nabla\phi=0$) and when its motion is caused by the existence of one vortex line on the axis of rotation of the normal component ($|\nabla\phi|=1/r$). When there are no vortex lines, Eq. (12.2.1) has the form

$$(\hbar^2/2m)\Delta f+\alpha f-\beta f^3=\tfrac{1}{2}m\omega_0^2r^2f. \qquad (12.5.1)$$

Rotation, when there is one vortex line in the superfluid component, reduces Eq. (12.5.1) to the form

$$(\hbar^2/2m)\Delta f+\alpha f-\beta f^3=\tfrac{1}{2}m[\omega_0r-(\hbar/mr)]^2f. \qquad (12.5.2)$$

The analytical form of solutions of these equations is determined by the authors only for some particular cases. However, for the purposes of this section, the results of the qualitative analysis are sufficient. It is valid in the general case and it takes into account that an increase of $|\mathbf{v}_n-\mathbf{v}_s|$ leads to a decrease of ρ_s (see Fig. 12.5).

The density of the superfluid component is equal to zero on a solid surface, but at the distance of the order of a_0 from the wall the density of the superfluid component already reaches a value of the order of $m\alpha/\beta$, which is an equilibrium value for an infinite medium (curve 1 in Fig. 12.5; it is implied that $R\gg a_0$). As already noted in Sec. 12.2, $\rho_s=0$ on the vortex line and also reaches the order of $m\alpha/\beta$ at a distance of the order of a_0 from the vortex line axis (curve 3). Rotation of the normal component creates an action similar to that of a vortex line: the density of the superfluid component is smaller in regions where the velocity of rotation is higher. Therefore the difference between the character of rotation of the superfluid liquid taking place according to the law $1/r$ and the character of the rotation of the normal component, obeying the law ω_0r [the right-hand side of equation (12.5.1)] is very essential. In the first case the velocity is infinite when $r=0$ and there $\rho_s=0$, but with an increase of r the velocity drops rapidly and ρ_s increases (curve 3). In the second case when $r=0$, the velocity is equal to zero and ρ_s has its maximum value, but the velocity increases with an increase of r and ρ_s begins to decrease more rapidly. One may show that this decrease becomes especially pronounced at a distance from the axis of the order of $(\hbar/m\omega_0)^{\frac{1}{2}}$ [curve 2, Fig. 12.5 is given in arbitrary units for illustrative purposes, but one should keep in mind that at usual velocities of rotation $(\hbar/m\omega_0)^{\frac{1}{2}}\gg a_0$].

So if in a vessel, the radius R of which exceeds $(\hbar/m\omega_0)^{\frac{1}{2}}$, only the normal component would rotate, the density of the superfluid component in this vessel would be strongly reduced in the whole peripheral region $R>r>(\hbar/m\omega_0)^{\frac{1}{2}}$. In other words, at small velocities of the vessel rotation, the effect of the superfluidity depression by the rotation of the normal component is rarely seen. But when the angular velocity, equal by the order of the magnitude to $\omega_0\sim\hbar/mR^2$ is exceeded, this effect is stronger pronounced.

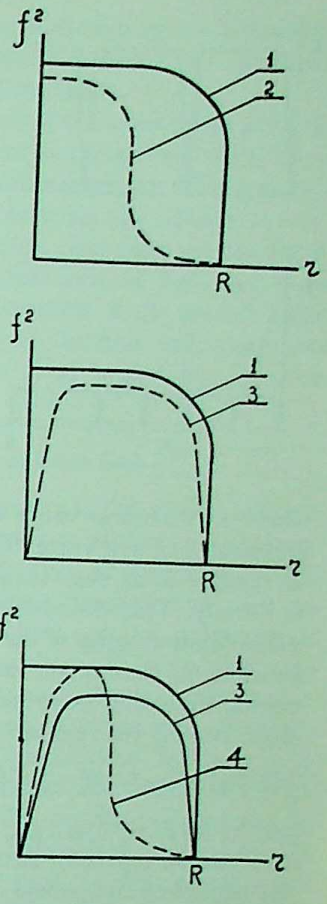

FIG. 12.5. Distribution of the superfluid component density ($\rho_s=mf^2$): (1) in the stationary cylindrical vessel; (2) with rotation of only the normal component ($v_n=\omega_0r$, $v_s=0$); (3) with rotation of the superfluid component caused by the presence of only one vortex line ($v_n=0$, $v_s=\hbar/mr$); (4) when the both components rotate ($v_n=\omega_0r$, $v_s=\hbar/mr$). The drawing is plotted in arbitrary units.

It would seem that the existence of a vortex line also decreasing ρ_s can only make this unfavorable situation still worse. But Eq. (12.5.2) (in the right-hand side of which we have *the difference* of ω_0r and $\hbar/mr$) shows that the effect of rotation of each of the components depressing superfluidity takes place only in the regions $r\ll(\hbar^2/m\omega_0)^{\frac{1}{3}}$ where a vortex line dominates or $r\gg(\hbar/m\omega_0)^{\frac{1}{2}}$, where the normal component dominates. In the region $r\approx(\hbar/m\omega_0)^{\frac{1}{2}}$ the mutual compensation of these influences takes place and the density of the superfluid component reaches the value characteristic of the liquid at rest (curve 4).

Hence two conclusions follow. Firstly, starting from the velocities of the order $\hbar/mR^2$ the formation of vortex lines on the rotation axis can be favorable (compare formula 12.4.3). Really, by decreasing the density ρ_s at the distance of the order of a_0 the vortex promotes its increase in a wider region. Thus it prevents the decrease of ρ_s at a distance from the axis of the order of $(\hbar/m\omega_0)^{\frac{1}{2}}$. Secondly, if the size of the vessel or the velocity of rotation is sufficiently large, then in the presence of a vortex line ρ_s will still decrease some-

[17] The real part of Eq. (12.1.4) has the form

$$(\hbar^2/2m)\Delta f+\alpha f-\beta f^3=\tfrac{1}{2}m(\mathbf{v}_n-\mathbf{v}_s)^2f.$$

CC-0. In Public Domain. Gurukul Kangri Collection, Haridwar

Digitized by Arya Samaj Foundation Chennai and eGangotri

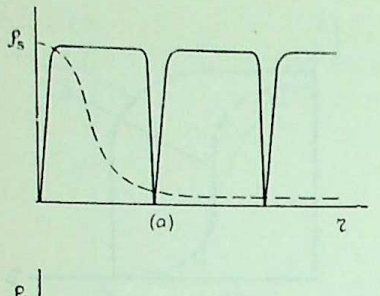

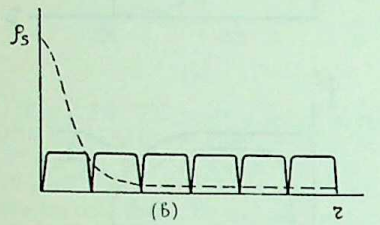

FIG. 12.6. Distribution of the density of the superfluid component in rotating helium II, containing an equilibrium number of vortex lines: (a) at relatively small velocity and (b) at relatively large velocity. The graph is plotted in arbitrary units. The dashed line shows the distribution that would be realized in the absence of vortex lines.

where at distances more than $r \approx (\hbar/m\omega_0)^{\frac{1}{2}}$. Only the appearance of new vortex lines can present this decrease of density ρ_s as they must be distributed apparently uniformly. This distribution should be such that the value of the velocity of the superfluid component would be close to that of the normal component in all the points, excluding those located in the vicinity of vortices. Indeed, the real part of Eq. (12.2.1) has the form

$$(\hbar^2/2m)\Delta f + \alpha f - \beta f^3 = \tfrac{1}{2}m\{[\omega_0, \mathbf{r}] - (\hbar/m)\nabla\phi\}^2 \quad (12.5.3)$$

and if $\hbar\nabla\phi/m \approx [\omega_0, \mathbf{r}]$, considerations, treated just now can be repeated. According to them the value of the superfluid component density is close to its value in the liquid at rest. Let us consider an arbitrary point, not too near a vortex line. Such a point can be located at approximately equal distances from nearest vortices. Then their contribution to the magnitude $\nabla\phi$ in the point under consideration is mutually compensated. Or the condition, according to which, $\hbar/mr'$ is not too large in comparison with $\omega_0 r$ should be satisfied. Here r and r' are the distances from the mentioned point to the rotation axis and to the nearest vortex line, respectively. $\hbar\nabla\phi/m$ in such a point differs little from the mean velocity on a circumference with the radius r. That mean velocity is determined by the number of vortex lines N_r in this circumference in accordance with condition (2.2.2). Thus

$$\hbar/m \mid \nabla\phi \mid \approx N_r\Gamma_0/2\pi r, \qquad (12.5.4)$$

where $N_r = \pi r^2 N$, N is the density of vortex lines. If it is required that equality $\hbar\nabla\phi/m \approx \omega_0 r$ should be valid, then it follows from (12.5.4) that $N \approx 2\omega_0/\Gamma_0$.

That corresponds exactly to Feynman's formula (2.5.1), according to which an area $\pi\hbar/m\omega_0$ corresponds to each vortex line. This area if it were a circumference would have the radius $(\hbar/m\omega_0)^{\frac{1}{2}}$. At a square structure of a vortex lattice the vortex separation is then $(\pi\hbar/m\omega_0)^{\frac{1}{2}}$, at a triangular one it is $(8\pi\hbar/3\sqrt{3}m\omega_0)^{\frac{1}{2}}$. The distribution of ρ_s at such a vortex density is shown schematically in Fig. 12.6. More accurately "the topology" of this distribution was shown in Figs. 12.1 and 12.2 concerning the case when $\omega_0 \leq \omega_{c2}$. In the latter case $(\hbar/m\omega_0)^{\frac{1}{2}}$ is comparable with a_0 and maximum values of ρ_s are small (as it was noted $\rho_s \to 0$ when $\omega_0 \to \omega_{c2}$). But when $(\hbar/m\omega_0)^{\frac{1}{2}} \gg a_0$, that is valid at any practically achieved velocities ω_0, ρ_s has almost everywhere the value very close to the superfluid component density in an infinite liquid at rest.

Thus vortex lines formed in rotating helium II were found to be the means preventing the breakdown of the superfluidity by rotation of the normal liquid.

12.6. The Character of the Phase Transition in Rotating Helium II

It has already been noted in Sec. 12.4 that a change of temperature of rotating helium II on the diagram (ω^*, R^*) may be represented by a line tending to parallelity with the abscissa when $T \to 0$ and to a coincidence with the ordinate when $T \to T_\lambda$. In Fig. 12.7 there are shown, in addition to the mentioned line, the boundaries of the existence for vortexless and single-vortex solutions of Eq. (12.2.1). They are given by curves (a) and (b), which were earlier shown in Fig. 12.4. (Figure 12.7, in contrast to Fig. 12.4, is plotted in an arbitrary scale to the more illustrative.) Curve (c) is also given there, it is a boundary of thermodynamical advantages of the vortex existence. It has been already noted that the curve is computed only in the region $R^* \gg 1$ and $\omega^* \ll 1$, where it is given by formula (12.4.3). The other portion of the curve is plotted (in arbitrary units) on the basis of the following simple considerations. In the immediate vicinity of curve (b), below it, in spite of the fact that here the solution of Eq. (12.5.2) exists, the presence of a vortex line cannot be thermodynamically favorable, because the function f of a single vortex is small. Condition (12.3.5) gives preference to a vortexless situation here. Therefore curve (c) should turn back and repeat in its upper part the outline of curve (b). A similar shape should have the curves confining the regions of thermodynamical advantages of existence of two vortex lines, etc. When $R^* \to \infty$ their upper branches tend to a straight line

$$\omega^* = 1 \qquad (\omega_0 = \omega_{c2}).$$

Let us now move from the left to the right along the line of helium cooling. Superfluidity will appear in the

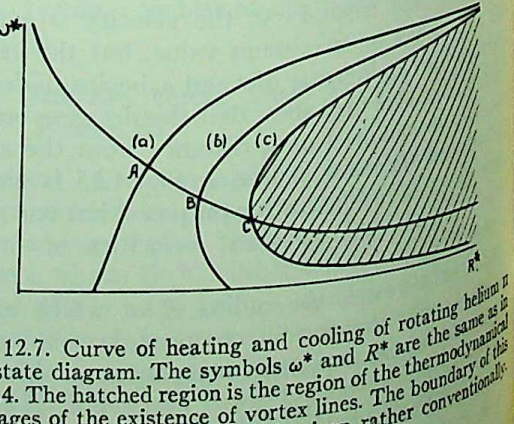

FIG. 12.7. Curve of heating and cooling of rotating helium II on its state diagram. The symbols ω^* and R^* are the same as in Fig. 12.4. The hatched region is the region of the thermodynamical advantages of the existence of vortex lines. The boundary of this region represented by curve (c) is given rather conventionally. The figure is plotted in arbitrary units.

CC-0. In Public Domain. Gurukul Kangri Collection, Haridwar

Digitized by Arya Samaj Foundation Chennai and eGangotri

point of intersection with curve (a), and the function f which is the solution of Eq. (12.5.1) increases, beginning from the zero value, i.e., it is continuous in this point. It is the phase transition of the second order, taking place with the shift of the λ-point, that was mentioned in Sec. 12.4. In contrast to the intersection with curve (a), the intersection with curve (b) does not cause any essential consequences. The superfluid liquid remains at rest. Its state changes only at the intersection with the curve (c), when a vortex appears and a new state of the superfluid component is described by the solution of Eq. (12.5.2). This change of the function f takes place by a jump, as only the integrals taken of the fourth power of the modulus of vortexless and single vortex functions ψ are equal to each other on curve (c) [because of condition (12.3.5)], but the functions themselves are different. It is already the phase transition of the first order.

Let us consider this problem in more detail. $\int f_0^4\,dV$ and $\int f_1^4\,dV$ will denote contributions into the free energy of rotating helium II, which are generally speaking different for a vortexless and single vortex states. When point C is approached from the left, the first of these integrals decreases [vortexless state becomes less favorable (12.7)], the second integral increases. In point C itself, the integral $\int f^4\,dV$ is continuous, as $\int f_0^4\,dV = \int f_1^4\,dV$. But here the transition from a decrease of the integral $\int f^4\,dV$ to its increase takes place and hence the derivative of the integral $\int f^4\,dV$ along the curve of cooling experiences a discontinuity. If we calculate the first derivative of the free energy with respect to temperature, there appears a term

$$\frac{\partial}{\partial T}\int f^4\,dV = \frac{\partial R^*}{\partial T}\frac{\partial}{\partial R^*}\int f^4\,dV + \frac{\partial \omega^*}{\partial T}\frac{\partial}{\partial \omega^*}\int f^4\,dV,$$

i.e., this derivative experiences a discontinuity, and that characterizes the phase transition of the first order. The consideration of the processes of formation of the following vortex lines will lead, apparently, to similar results.

But one should keep in mind, firstly, that the considerations just mentioned are purely qualitative ones, as they are not based on the treatment of the computed portion of the phase diagram. Secondly, only the principal importance should be ascribed to the statement on the character of the phase transition. It means, for instance, that relaxation phenomena connected with vortex formation are possible. But thermodynamical effects of the type of the latent heat can be too insignificant for direct measurement (see, however, Sec. 11.4).

Relaxation effects can significantly influence the character of the considered phenomena. Even at not very rapid cooling, the state of liquid can be vortexless until the values R^* corresponding to a rather large equilibrium number of vortex lines at a given ω^*.

At heating of the liquid, processes proceed in the reverse succession. Here also relaxation phenomena connected with the vortex disappearance are unavoidable. But at an intersection with curve (a) the superfluidity disappears instantaneously.

Under the real conditions of the experiment with the passage through the λ-point, intersections with curves (a) (the point A) and with curve (c) (the point C) and also with the curves confining the regions of two-, three- and many-vortex states, take place almost simultaneously. Thus, some transitions of the first order coincide with the phase transition of the second order. However these transitions of the first order may not take place because of the great probability of overcooling or overheating.

12.7. Rotation of the Ideal Bose Gas

Since at present the microscopic theory of helium II cannot give a complete answer to all the problems encountered by it, the consideration of simplified models becomes especially interesting. Such models are an ideal Bose gas, a rarefied Bose gas, or a system of weakly interacting Bose particles. In particular only in the theory of these systems is there a microscopic consideration of such problems as vortex core structure, the spectrum of vortex line oscillations, interaction of vortex lines with thermal excitations, determination of the moment of inertia (or the angular momentum) of the rotating substance, etc. A short review of the results of such a type directly concerning the topic of our paper is given in this and the following section.

The problem of rotation of the ideal Bose gas was considered by Blatt and Butler (1955), who have shown that at low velocities of the vessel rotation, the particles, having experienced Bose–Einstein condensation in the state with the zero momentum, do not take part in the rotation and the angular momentum is expressed by the formula

$$L = (T/T_{cr})^{\frac{3}{2}} L_c, \qquad (12.7.1)$$

where T_{cr} is the temperature at which condensation begins, L_c is the classical angular momentum of the liquid rotation as a whole. When $T < T_{cr}$, $L < L_c$ (superfluidity). Beginning from $T = T_{cr}$, $L = L_c$ always (a classical behavior).

When the angular velocity is increased, there arises such a situation, when particles of condensate are involved into rotation. Here the angular momentum experiences a jump with the value $N_0\hbar$, where N_0 is the number of particles in the condensate. The internal energy changes by a jump as well. That takes place at the angular velocity of rotation

$$\omega_1 = 4.45\hbar/mR^2. \qquad (12.7.2)$$

The further increase of the angular velocity causes, again and again such jumps, which are the phase transitions of the first order. As the states of the condensate are described by Bessel functions $J_n(j_{1n}r/R)$ the expression for critical velocity ω_n of each nth transition is connected with the first roots of these functions j_{1n} (compare Sec. 12.4, Fig. 12.4). Having used the

CC-0. In Public Domain. Gurukul Kangri Collection, Haridwar

Digitized by Arya Samaj Foundation Chennai and eGangotri

asymptotic expression for j_{1n}, Blatt and Butler have received the following formula for the velocity ω_n, at which the transition into the state with the angular momentum of the condensate $N_0 n\hbar$ takes place:

$$\omega_n \approx [n+2.47n^{\frac{1}{2}}-0.5+O(m^{-\frac{1}{2}})]\hbar/mR^2. \quad (12.7.3)$$

All these phase transitions are very close to each other and *coincide* in fact. At very large n we have $\omega_n \approx n\hbar/mR^2$ and

$$L_n = N_0 n\hbar + \tfrac{1}{2}m(N-N_0)R^2\omega_n \approx \tfrac{1}{2}m(N+N_0)R^2\omega_n$$
$$= [1+(N_0/N)]L_c = [2-(T/T_{cr})^4]L_c. \quad (12.7.4)$$

The analogy with the behavior of helium II finishes here. At large velocities of rotation the ideal Bose gas has a smoothed angular momentum, even larger than at rotation as a whole. In this association Blatt and Butler spoke of the gas "infrafluidity." The physical reason for such a behavior of the system is the following: because of the properties of the function $J_n(j_{n1}r/R)$, the particles of the condensate are concentrated near the walls of the cylinder and then contributions of each of them into the moment of inertia are close to mR^2. That distinguishes the rotating condensate from the rotating substance with the uniform distribution of particles, in which the mean contribution of a particle into the moment of inertia is $0.5mR^2$.

12.8. Vortex Lines in the Gas of Weakly Interacting Bose Particles and Rotation of Nonideal Bose Gas

The fundamental work of Bogolubov (1947) formed the basis of the microscopic theory of a nonideal Bose gas. It influenced decisively all the following development of the theory. Unfortunately we cannot dwell on those aspects of that theory which do not directly concern the topic of our review. As to its connection with the problem of rotating helium II, it is sufficient to note that the wave function of the condensate in the theory of nonideal Bose gas satisfies, under the conditions of equilibrium, the equation quite similar to Eq. (12.1.4) when $v_n=0$ (Pitaevski, 1961; Gross, 1961).[18]

$$(\hbar^2/2m)\Delta\psi + n_0V_0\psi - V_0|\psi|^2\psi = 0. \quad (12.8.1)$$

Here the modulus and the phase of ψ determine the density and the velocity of the condensate flow similarly as in formulas (12.1.2), (12.1.3), n_0 is the density of the condensate particles in an infinite and stationary liquid. The characteristic dimension in this case is expressed as $a_0=\hbar(2mn_0V_0)^{-\frac{1}{2}}$ and the region of application of the theory is restricted by the requirement of smallness of the product n_0V_0 sufficient that the parameter a_0 would be much larger than interatomic distances.

In the connection of the similarity of Eqs. (12.2.1) and (12.8.1), it is quite clear that the latter of them as well as the former one has solutions describing a single vortex line.

Fetter (1965) has described the array of vortex lines formed in a rotating vessel by an approximate function

$$\psi(\mathbf{r}) = n_0^{\frac{1}{2}} \prod_k \frac{|\mathbf{r}-\mathbf{r}_k|}{[(\mathbf{r}-\mathbf{r}_k)^2+a_0^2]^{\frac{1}{2}}} \exp(i\theta_k), \quad (12.8.2)$$

where $\mathbf{r}_k$ is the coordinate of the kth vortex line, $\theta_k = \arctan[(y-y_k)/(x-x_k)]$. In this approximation he made the minimization of the magnitude $E-L\omega_0$ and became convinced that vortex lines should be distributed with the density corresponding to Feynman's formula (2.5.1) and $L=L_c$ [compare formula (2.6.3)]. The angular momentum value per each particle is equal to $0.5N_R\hbar$, where N_R is the total number of vortex lines in the cylinder with the radius R.

The difference between the results of Blatt and Butler (12.7.4) and those of Fetter ($L=L_c$) is due not only to the circumstance that the former ones considered in fact one vortex line with a large circulation and the latter a lot of vortex lines. The nonlinearity of Eq. (12.8.1) is also very essential. It takes into account the interaction of the particles, due to which the modulus of the wave function is maintained at the constant level equal to $n_0^{\frac{1}{2}}$ everywhere besides the immediate vicinity of vortex lines and that of solid boundaries. Therefore even at consideration of an intensive ($\Gamma=n\Gamma_0$) single vortex line on the axis of the vessel with sufficiently large radius ($R \gg na_0$), the double contribution of condensate particles to the moment of inertia because of their "centrifuging" is not obtained. The expression of the type $J_n(j_{n1}r/R)$ does not already describe the distribution of the condensate particles. $\psi \to 0$ only near the vortex line, but almost throughout the whole vessel $|\psi| \approx n_0^{\frac{1}{2}}$ (see curves 1 and 3 in Fig. 12.5).

Scattering of thermal excitations on vortex lines in a rotating nonideal Bose gas was considered by Iordanski (1964) as well as the force of mutual friction caused by this scattering. Having made more accurate calculations Tordanski (1965b) has shown that the force of mutual friction is not expressed directly by the transport cross section of scattering of thermal excitations on vortex lines as it was assumed in papers of Hall and Vinen (1965b), Lifshitz and Pitaevski (1957), and Pitaevski (1958c). It was found that a model of a weak ideal Bose gas indicates the existence of the Magnus force (see footnote 4), which was not taken into account before the expression for which contains ρ_n and $\mathbf{v}_n$ instead of ρ_s and $\mathbf{v}_s$. As the final results contain only the density ρ_n and the relative velocity $\mathbf{v}_L-\mathbf{v}_n$, they depend little on the model of the substance, Iordanski has calculated the coefficients B and B' for helium II. He has obtained the temperature dependence of B (Iordanski 1965b) similar to that shown in Fig. 7.2 at the symmetric cross section of absorption of exitation

[18] Equation (12.8.1) is put down in the form corresponding to a short-range, repulsive interaction, with the potential

$$U_{12}(\mathbf{r}_1-\mathbf{r}_2) = V_0\delta(\mathbf{r}_1-\mathbf{r}_2).$$

CC-0. In Public Domain. Gurukul Kangri Collection, Haridwar

Digitized by Arya Samaj Foundation Chennai and eGangotri

momentum equal to 8.5 Å. The temperature dependence of B' was then greatly different from that shown in Fig. 7.2. The value of $(-B')$ increases monotonously practically from zero at $T=1.1°K$ to about 0.05 at $T=1.7°K$.

12.9. The Rotating Helium II Problem and the Microscopic Theory of Superfluidity

The phenomenological theory of helium II, used in Secs. 12.1–12.6, as has been noted, has a restricted region of application. The quantitative results of this theory are valid only in the region $T_\lambda - T \ll T_\lambda$, when the characteristic dimension a_0 is much larger than interatomic distances. The assumption on, at least, qualitative validity of the conclusions of the phenomenological theory in the whole range of temperatures $0<T<T_\lambda$, though it seems rather plausible, still awaits its substantiation by the microscopic theory.[19] The microscopic theory of an ideal and even nonideal Bose gas is not sufficient for a complete solution of this problem.

The description of the situation existing nowadays in the microscopic theory of helium II is beyond the scope of this review. Therefore we shall limit ourselves with a short statement on some facts. (See for more detail Chester, 1963.) Papers of Onsager and Penrose (Penrose 1951, Penrose and Onsager 1956, Penrose 1957) allow us to consider superfluidity of helium II as a result of Bose–Einstein condensation of some macroscopic part of atoms in this liquid into the state with zero momentum. The velocity of the superfluid liquid can be considered as the gradient of the wave function phase of the condensate. So far the question of the physical interpretation of the density of the superfluid component is not clear. This density, apparently, does not coincide with the relative density of the condensate. In this connection one cannot consider that the question on the sense of the wave function describing the superfluid component is solved completely. Strictly speaking even the possibility of introduction of such a function at any temperatures is not clear.

The latter question has a direct relation to the conception of Landau–Onsager–Feynman, according to which the superfluid component is an ideal liquid, which can perform only potential (curl $\nabla\phi \equiv 0$) motions. If the conclusions just mentioned here from the Onsager and Penrose papers obtain sufficiently general basis, then possible doubts in the validity of the conception of Landau–Onsager–Feynman will have no grounds at all and the equations of Landau's two-liquid hydrodynamics will not be considered as only one of the possibilities allowed by a more general consideration (Lin, 1963).

[19] The phenomenological theory of superconductivity, as is known, has received such a substantiation in Gorkov's investigations. The wave function of superconducting electrons was found to be directly connected with the width of the gap in the energy spectrum of a superconductor.

SUMMARY

A rapid and successful development of ideas on the nature of rotating helium II has allowed us, during less than a decade, to obtain a more or less clear understanding of the mechanisms of the phenomena taking place in this liquid, instead of accumulation of paradoxical facts.

A vast experimental material has been collected and a lot of theoretical studies were made, confirming the ideas of curl-free rotation of the superfluid component accompanied by quantization of circulation. Thus a new confirmation was obtained for the assumption of Landau's theory (curl $\mathbf{v}_s=0$), the violation of which was the first impression obtained from the experiments on rotation of helium II.

At present much is known on properties of Onsager–Feynman vortex lines which are formed in rotating helium II. Studies of irrotational motion of the superfluid liquid, leading to the creation of gyroscopes, are developed successfully.

Apparently, in the near future one should expect further great successes both in the study of quantized vortex lines and in the study of persistent currents. We think that the main directions, in which such advances are possible and especially desirable, are connected with the problems of the mechanism of vortex formation, stability of vortex arrays, quantum coherence, and the microscopic basis of the theory.

It should be believed that solution of these problems will lead not only to the necessary basis and confirmation of the complete validity of the conception of Landau–Onsager–Feynman, but to the further development of the ideas on the nature of superfluidity as well.

ACKNOWLEDGMENT

The authors wish to acknowledge their gratitude to Mrs. A. R. Azo for her valuable assistance in the preparation of the manuscript of this review, the last chapter of which was written without the participation of E. L. Andronikashvili.

REFERENCES

Abrikosov, A. A., 1957, Zh. Eksperim. i Teor. Fiz. **32**, 1442 [English transl.: Soviet Phys.—JETP **5**, 1174 (1957)].

Andreev, A. F., 1964, Zh. Eksperim. i Teor. Fiz. **46**, 1456 [English transl.: Soviet Phys.—JETP **19**, 983 (1964)].

Andronikashvili, E. L., 1946, J. Phys. USSR **10**, 201.

——, 1948a, Zh. Eksperim. i Teor. Fiz. **18**, 424.

——, 1948b, dissertation, Inst. Fiz. Problem Akad. Nauk SSSR (unpublished).

——, 1948c, Zh. Eksperim. i Teor. Fiz. **18**, 429.

——, 1952, Zh. Eksperim. i Teor. Fiz. **22**, 62.

——, R. A. Bablidze, G. V. Gujabidze, and J. S. Tsakadze, 1964a, Second All Union Congress on Theoretical and Applied Mechanics (Summaries of papers), Moscow, edited by Acad. Sci. USSR, p. 16.

——, R. A. Bablidze, G. V. Gujabidze, and J. S. Tsakadze, 1964b, preprint, Institute of Physics, Akad. Nauk GSSR (unpublished).

——, J. S. Tsakadze, and R. A. Bablidze, 1962, Zh. Eksperim. i Teor. Fiz. **43**, 1562 [English transl.: Soviet Phys.—JETP **16**, 1103 (1963)].

CC-0. In Public Domain. Gurukul Kangri Collection, Haridwar

Digitized by Arya Samaj Foundation Chennai and eGangotri

——, R. A. Bablidze, and J. S. Tsakadze, 1965, *Proceedings of the Ninth International Conference on Low Temperature Physics*, J. G. Daunt, D. V. Edwards, F. J. Milford, and M. Yaqub, Eds. (Plenum Press, Inc., New York), p. 155.
——, R. A. Bablidze, and J. S. Tsakadze, 1966, Zh. Eksperim. i Teor. Fiz. **50**, 46 [English transl.: Soviet Phys.—JETP **23**, 31 (1966)].
——, G. V. Gujabidze, and J. S. Tsakadze, 1965, *Proceedings of the Ninth International Conference on Low Temperature Physics*, J. G. Daunt, D. V. Edwards, F. J. Milford, and M. Yaqub, Eds. (Plenum Press, Inc., New York), p. 159.
——, G. V. Gujabidze, and J. S. Tsakadze, 1966, Zh. Eksperim. i Teor. Fiz. **50**, 51 [English transl.: Soviet Phys.—JETP **23**, 34 (1966)].
——, and I. P. Kaverkin, 1955, Zh. Eksperim. i Teor. Fiz. **28**, 126 [English transl.: Soviet Phys.—JETP **1**, 174 (1955)].
——, Yu. G. Mamaladze, S. G. Matinyan, and J. S. Tsakadze, 1961, Usp. Fiz. Nauk **73**, 3 [English transl.: Soviet Phys.—Usp. **4**, 1 (1961)].
——, K. B. Mesoed, and J. S. Tsakadze, 1964, Zh. Eksperim. i Teor. Fiz. **46**, 157 [English transl.: Soviet Phys.—JETP **19**, 113 (1964)].
——, and J. S. Tsakadze, 1958, Bull. Acad. Sci. GSSR **20**, 667.
——, and J. S. Tsakadze, 1959a, Zh. Eksperim. i Teor. Fiz. **37**, 322 [English transl.: Soviet Phys.—JETP **10**, 227 (1960)].
——, and J. S. Tsakadze, 1959b, Zh. Eksperim. i Teor. Fiz. **37**, 562 [English transl.: Soviet Phys.—JETP **10**, 397 (1960)].
——, and J. S. Tsakadze, 1962, Tr. Inst. Fiz. Akad. Nauk Gruz. SSR **8**, 209.
——, and J. S. Tsakadze, 1965a, Phys. Letters **18**, 26.
——, and J. S. Tsakadze, 1965b, ZhETF Pis' ma **2**, 278 [English transl.: JETP Letters **2**, 177 (1965)].
——, and J. S. Tsakadze, 1966, Phys. Letters **20**, 446.
——, J. S. Tsakadze, and K. B. Mesoed, 1961, *Proceedings of the Seventh International Conference on Low Temperature Physics* (University of Toronto Press, Toronto), p. 454.
Arkhipov, R. G., 1957, Zh. Eksperim. i Teor. Fiz. **33**, 116 [English transl.: Soviet Phys.—JETP **6**, 90 (1958)].
Atkins, K. R., 1963, *Proceedings of the International School of Physics, "Enrico Fermi"* (Academic Press Inc., New York), p. 403.
Bablidze, R. A., 1965, dissertation, Tbilissi State University.
——, J. S. Tsakadze, and G. V. Chanishvili, 1964, Zh. Eksperim. i Teor. Fiz. **46**, 843 [English transl.: Soviet Phys.—JETP **19**, 577 (1964)].
Bekarevich, I. L., and I. M. Khalatnikov, 1961, Zh. Eksperim. i Teor. Fiz. **40**, 920 [English transl.: Soviet Phys.—JETP **13**, 643 (1961)].
Bendt, P. J., 1961, *Proceedings of the Seventh International Conference on Low Temperature Physics* (University of Toronto Press, Toronto), p. 576.
——, 1962, Phys. Rev. **127**, 1441.
——, R. D. Cowan and J. L. Yarnell, 1959, Phys. Rev. **113**, 1386.
——, and J. A. Oliphant, 1961, Phys. Rev. Letters **6**, 213.
Blatt, J. M., and S. T. Butler, 1955, Phys. Rev. **100**, 476.
Careri, G., 1961, *Progress in Low Temperature Physics* (North-Holland Publ. Co., Amsterdam), Vol. III, Chap. II.
——, 1963, *Proceedings of the International School of Physics. "Enrico Fermi"* (Academic Press Inc., N.Y.), p. 423.
——, W. D. McCormick and F. Scaramuzzi, 1961, *Proceedings of the Seventh International Conference on Low Temperature Physics* (University of Toronto Press, Toronto), p. 502.
——, W. D. McCormick and F. Scaramuzzi, 1962, Phys. Letters **1**, 61.
——, W. D. McCormick and F. Scaramuzzi, 1963, *Proceedings of the Eighth International Conference on Low Temperature Physics* R. O. Davies, Ed. (Butterworths Scientific Publications Ltd., London), p. 88.
Chandrasekhar, S., and R. J. Donnelly, 1957, Proc. Roy. Soc. (London) **A241**, 9.
Chase, C. E., 1960a, Phys. Rev. Letters **4**, 220.
——, 1960b, *Proceedings of the Seventh International Conference on Low Temperature Physics* (University of Toronto Press, Toronto), p. 438.
Cheishvili, O. D., and Yu. G. Mamaladze, 1965, Phys. Letters **18**, 278.
Chester, G. V., 1963, *Proceedings of the International School of Physics. "Enrico Fermi"* (Academic Press Inc., New York), p. 51.
Clow, J. R., D. A. Depatie, J. C. Weaver, and J. D. Reppy, 1965, *Proceedings of the Ninth International Conference on Low Temperature Physics*, J. G. Daunt, D. V. Edwards, F. J. Milford, and M. Yaqub, Eds. (Plenum Press, Inc., New York), p. 325.
Craig, P. P., 1961, Phys. Rev. Letters **7**, 331.
——, 1964, Phys. Rev. Letters **13**, 708.
——, and J. R. Pellam, 1957, Phys. Rev. **108**, 1109.
Depatie, D., J. D. Reppy, and C. T. Lane, 1963, *Proceedings of the Eighth International Conference on Low Temperature Physics*, R. O. Davies, Ed. (Butterworths Scientific Publications Ltd., London), p. 75.
Donnelly, R. J., 1959, Phys. Rev. Letters **3**, 507.
——, 1965, Phys. Rev. Letters **14**, 39.
——, G. V. Chester, R. H. Walmsley, and C. T. Lane, 1956, Phys. Rev. **102**, 3.
Douglass, R. L., 1964, Phys. Rev. Letters **13**, 79.
Eselson, B. N., B. G. Lazarev, K. D. Sinelnikov, and A. D. Shvets, 1956, Zh. Eksperim. i Teor. Fiz. **31**, 912 [English transl.: Soviet Phys.—JETP **4**, 774 (1957)].
Feynman, R. P., 1955, *Progress in Low Temperature Physics* (North-Holland Publ. Co., Amsterdam), Vol. 1, Chap. 2.
——, 1957, Rev. Mod. Phys. **29**, 205.
Gamtsemlidze, G. A., Sh. A. Japaridze, Ts. M. Salukvadze, and K. A. Turkadze, 1966, Zh. Eksperim. i Teor. Fiz. **50**, 323 [English transl.: Soviet Phys.—JETP **23**, 214 (1966)].
——, Sh. A. Japaridze and K. A. Turkadze, 1966, Zh. Eksperim. i Teor. Fiz. **50**, 327 [English transl.: Soviet Phys.—JETP **23**, 217 (1966)].
Ginzburg, V. L., and L. P. Pitaevski, 1958, Zh. Eksperim. i Teor. Fiz. **34**, 1240 [English transl.: Soviet Phys.—JETP **7**, 858 (1958)].
Gopal, E. S. Raja, 1963, Ann. Phys. (N.Y.) **25**, 196.
——, 1964a, Phys. Letters **9**, 230.
——, 1964b, Ann. Phys. (N.Y.) **29**, 350.
Griffiths, D. J., 1964, Proc. Roy. Soc. (London) **A277**, 214.
Gujabidze, G. V., and J. S. Tsakadze, 1966, Zh. Eksperim. i Teor. Fiz. **50**, 55 [English transl.: Soviet Phys.—JETP **23**, 37 (1966)].
Hall, H. E., 1955, Conference de Phusique des Basses Temperature (Paris), p. 63.
——, 1957, Phil. Trans. Roy. Soc. London **A250**, 359.
——, 1958a, Proc. Roy. Soc. (London) **A245**, 546.
——, 1958b, *Proceedings of the Kamerlingh-Onnes Conference on Low Temperature Physics* (Suppl. to Physica **24**, 141).
——, 1960, Phil. Mag. Suppl. **9**, 89.
——, and W. F. Vinen, 1955, Phil. Mag. **46**, 546.
——, and W. F. Vinen, 1956a, Proc. Roy. Soc. (London) **A238**, 204.
——, and W. F. Vinen, 1956b, Proc. Roy. Soc. (London) **238**, 215.
Heikkila, W. J., and A. C. Hollis-Hallett, 1955, Can. J. Phys. **33**, 420.
Hollis-Hallett, A. C., 1953, Proc. Cambridge Phil. Soc. **49**, 717.
Iordanski, S. V., 1964, Ann. Phys. (N.Y.) **29**, 335.
——, 1965a, Zh. Eksperim. i Teor. Fiz. **48**, 708 [English transl.: Soviet Phys.—JETP **21**, 467 (1965)].
——, 1965b, Zh. Eksperim. i Teor. Fiz. **49**, 225 [English transl.: Soviet Phys.—JETP **22**, 160 (1966)].
Kapitza, P. L., 1938a, Dokl. Akad. Nauk SSSR **18**, 21.
——, 1938b, Nature **141**, 74.
——, 1941a, J. Phys. USSR **4**, 181.
——, 1941b, J. Phys. USSR **5**, 59.
Kelvin, W., 1880, Phil. Mag. **10**, 155.
Kemoklidze, M. P., and Yu. G. Mamaladze, 1964a, Zh. Eksperim. i Teor. Fiz. **46**, 165 [English transl.: Soviet Phys.—JETP **19**, 118 (1964)].
——, and Yu. G. Mamaladze, 1964b, Zh. Eksperim. i Teor. Fiz. **46**, 804 [English transl.: Soviet Phys.—JETP **19**, 547 (1964)].
——, and I. M. Khalatvikov, 1964, Zh. Eksperim. i Teor. Fiz. **46**, 1677 [English transl.: Soviet Phys.—JETP **19**, 1134 (1964)].
Kerr, E. C., 1957, J. Chem. Phys. **26**, 511.
Kiknadze, L. V., Yu. G. Mamaladze, and O. D. Cheishvili, 1965, Zh. Eksperim. i Teor. Fiz. **48**, 1520 [English transl.: Soviet Phys.—JETP **21**, 1018 (1965)].
Kleiner, W. H., Z. M. Roth, and S. H. Autler, 1964, Phys. Rev. **133**, A1226.
Kitchens, T. A., W. A. Steyert, R. D. Taylor, and P. P. Craig, 1965, Phys. Rev. Letters **14**, 942.

CC-0. In Public Domain. Gurukul Kangri Collection, Haridwar

Digitized by Arya Samaj Foundation Chennai and eGangotri

Koehler, T. R., and J. R. Pellam, 1962, Phys. Rev. **125**, 791.
Landau, L. D., 1941, J. Phys. USSR **5**, 71.
—, 1944, J. Phys. USSR **8**, 1.
—, 1947, J. Phys. USSR **11**, 91.
—, and E. M. Lifshitz, 1953, *Mechanics of Continuum Media* (Gostekhizdat, Moscow).
Lifshitz, E. M., and E. L. Andronikashvili, 1959, *A Supplement to "Helium"* (Consultants Bureau Enterprises, Inc., N.Y.; Chapman and Hall, Ltd., London).
—, and L. P. Pitaevski, 1957, Zh. Eksperim. i Teor. Fiz. **33**, 535 [English transl.: Soviet Phys.—JETP **6**, 418 (1958)].
Lin, C. C., 1959, Phys. Rev. Letters **2**, 245.
—, 1963, *Proceedings of the International School of Physics. "Enrico Fermi"* (Academic Press Inc., New York), p. 93.
Mamaladze, Yu. G., 1960a, Zh. Eksperim. i Teor. Fiz. **39**, 859 [English transl.: Soviet Phys.—JETP **12**, 595 (1961)].
—, 1960b, Seventh All Union Congress on Low Temperature Physics, theses of papers, Kharkov, edited by Acad. Sci. Ukr.SSR, p. 7.
—, 1964, Prikl. Mat. Mekhan. USSR **28**, 952.
—, 1965, Collected papers on Low Temperature Physics, Publishing House "Metsniereba".
—, and S. G. Matinyan, 1960a, Zh. Eksperim. i Teor. Fiz. **38**, 184 [English transl.: Soviet Phys.—JETP **11**, 134 (1960)].
—, and S. G. Matinyan, 1960b, Zh. Eksperim. i Teor. Fiz. **38**, 656 [English transl.: Soviet Phys.—JETP **11**, 471 (1960)].
—, and S. G. Matinyan, 1960c, Prikl. Mat. Mekhan. USSR **24**, 473.
—, and S. G. Matinyan, 1961, *Proceedings of the Seventh International Conference on Low Temperature Physics* (University of Toronto Press, Toronto).
—, and S. G. Matinyan, 1963, Zh. Eksperim. i Teor. Fiz. **44**, 2118 [English transl.: Soviet Phys.—JETP **17**, 1424 (1963)].
—, K. B. Mesoed and J. S. Tsakadze, 1964, Second All Union Congress on Theoretical and Applied Mechanics, summaries of the papers, Moscow, edited by Acad. Sci. USSR, p. 144.
Mehl, J. B., and W. Zimmerman, Jr., 1965, Phys. Rev. Letters **14**, 815.
Meservey, R., 1964, Phys. Rev. **133**, 1471.
Mesoed, K. B., and J. S. Tsakadze, 1961, Bull. Acad. Sci. GSSR **26**, 145.
—, and J. S. Tsakadze, 1963, Tr. Inst. Fiz. Akad. Nauk Gruz. SSR **9**, 147.
Onsager, L., 1949, Nuovo Cimento, Suppl. 2, 249.
Osborne, D. V., 1950, Proc. Phys. Soc. (London) **A63**, 909.
—, 1961, *Proceedings of the Seventh International Conference on Low Temperature Physics* (University of Toronto Press, Toronto), p. 449.
Pellam, J. R., 1960, Phys. Rev. Letters **5**, 189.
—, 1962, Phys. Rev. Letters **9**, 281.
—, 1965, *Proceedings of the Ninth International Conference on Low Temperature Physics*, J. G. Daunt, D. V. Edwards, F. J. Milford, and M. Yaqub, Eds. (Plenum Press, Inc., New York), p. 191.
Penrose, O., 1951, Phil. Mag. **42**, 1373.
—, and L. Onsager, 1956, Phys. Rev. **104**, 576.
Pitaevski, L. P., 1958a, Zh. Eksperim. i Teor. Fiz. **35**, 408 [English transl.: Soviet Phys.—JETP **8**, 282 (1959)].
—, 1958b, dissertation, Institut Fiz. Problem Akad. Nauk SSSR (unpublished).
—, 1958c, Zh. Eksperim. i Teor. Fiz. **35**, 1271 [English transl.: Soviet Phys.—JETP **8**, 888 (1959)].
Rayfield, G. W., and F. Reif, 1963, Phys. Rev. Letters **11**, 305.
—, and F. Reif, 1965, Phys. Rev. **136**, 1194.
Reppy, J. D., 1965, Phys. Rev. Letters **14**, 733.
—, and D. Depatie, 1961, *Proceedings of the Seventh International Conference on Low Temperature Physics* (University of Toronto Press, Toronto), p. 442.
—, and D. Depatie, 1964, Phys. Rev. Letters **12**, 187.
—, D. Depatie and C. T. Lane, 1960, Phys. Rev. Letters **5**, 541.
—, and C. T. Lane, 1961, *Proceedings of the Seventh International Conference on Low Temperature Physics* (University of Toronto Press, Toronto), p. 443.
—, and C. T. Lane, 1965, Phys. Rev. **140**, A106.
Rayleigh, Lord, 1916, *Scientific Papers* (Cambridge University Press, New York), Vol. 6, p. 447.
Snyder, H. A., 1963, Phys. Fluids **6**, 755.
Springett, B. E., D. J. Tanner, and R. J. Donnelly, 1965, Phys. Rev. Letters **14**, 585.
Steyert, W. A., R. D. Taylor, and T. A. Kitchens, 1965, Phys. Rev. Letters **15**, 546.
Tanner, D. J., B. E. Springett, and R. J. Donnelly, 1965, *Proceedings of the Ninth International Conference on Low Temperature Physics*, J. G. Daunt, D. V. Edwards, F. J. Milford, and M. Yaqub, Eds. (Plenum Press, Inc., N.Y.), p. 346.
Taylor, G. I., 1923, Phil. Trans. Roy. Soc. London **A223**, 289.
Tsakadze, J. S., 1962a, Zh. Eksperim. i Teor. Fiz. **42**, 985 [English transl.: Soviet Phys.—JETP **15**, 681 (1962)].
——, 1962b, *Eighth International Conference on Low Temperature Physics*, Preprints of Papers, London, p. 388.
——, 1963a, Zh. Eksperim. i Teor. Fiz. **44**, 103 [English transl.: Soviet Phys.—JETP **17**, 70 (1963)].
——, 1963b, Zh. Eksperim. i Teor. Fiz. **44**, 105 [English transl.: Soviet Phys.—JETP **17**, 72 (1963)].
——, 1963c, Tr. Inst. Fiz. Akad. Nauk Gruz. SSR **9**, 151.
——, 1963d, *Proceedings of the Eighth International Conference on Low Temperature Physics*, R. O. Davies, Ed. (Butterworths Scientific Publications Ltd., London), p. 104.
——, 1963e, Bull. Acad. Sci. GSSR **30**, 25.
——, 1964a, Zh. Eksperim. i Teor. Fiz. **46**, 153 [English transl.: Soviet Phys.—JETP **19**, 110 (1964)].
——, 1964b, Zh. Eksperim. i Teor. Fiz. **46**, 1553 [English transl.: Soviet Phys.—JETP **19**, 1050 (1964)].
——, 1964c, Zh. Eksperim. i Teor. Fiz. **46**, 505 [English transl.: Soviet Phys.—JETP **19**, 343 (1964)].
——, and L. V. Cheremisina, 1966, Zh. Eksperim. i Teor. Fiz. **50**, 58 [English transl.: Soviet Phys.—JETP **23**, 39 (1966)].
——, and I. M. Chkheidze, 1960, Zh. Eksperim. i Teor. Fiz. **38**, 637 [English transl.: Soviet Phys.—JETP **11**, 457 (1960)].
——, and K. B. Mesoed, 1962, Tr. Inst. Fiz. Akad. Nauk Gruz. SSR **8**, 213.
——, and L. Shanshiashvili, 1965, ZhETF Pis' ma **2**, 305 [English transl.: JETP Letters **2**, 194 (1965)].
——, and T. M. Shults, 1960, Tr. Tbil. Gos. Univ. **86**, 51.
Turkington, R. E., J. B. Brown, and D. V. Osborne, 1963, Can. J. Phys. **41**, 820.
Vinen, W. F., 1957a, Proc. Roy. Soc. (London) **A240**, 114.
——, 1957b, Proc. Roy. Soc. (London) **A240**, 128.
——, 1957c, Proc. Roy. Soc. (London) **A242**, 493.
——, 1958a, Nature **181**, 1524.
——, 1958b, Proc. Roy. Soc. (London) **A243**, 400.
——, 1961a, *Progress in Low Temperature Physics* (North-Holland Publ. Co., Amsterdam), Vol. 3, Chap. 1.
——, 1961b, Proc. Roy. Soc. (London) **A260**, 218.
Walmsley, R. H. and C. T. Lane, 1958, Phys. Rev. **112**, 1041.
Wheeler, R. C., C. U. Blakewood, and C. T. Lane, 1955, Phys. Rev. **99**, 1667.
Whitmore, S. C. and W. Zimmerman, 1965, Phys. Rev. Letters **15**, 389.
Woods, A. D. B. and A. C. Hollis-Hallett, 1958, *Low-Temperature Physics and Chemistry*, J. R. Dillinger, Ed. (University of Wisconsin Press, Madison, Wisc.), p. 16.
Zamtaradze, L. A. and J. S. Tsakadze, 1964, Zh. Eksperim. i Teor. Fiz. **46**, 162 [English transl.: Soviet Phys.—JETP **19**, 116 (1964)].

CC-0. In Public Domain. Gurukul Kangri Collection, Haridwar

Digitized by Arya Samaj Foundation Chennai and eGangotri
REVIEWS OF MODERN PHYSICS VOLUME 38, NUMBER 4 OCTOBER 1966

High-Energy Electromagnetic Conversion Processes in Intense Magnetic Fields

THOMAS ERBER

Department of Physics, Illinois Institute of Technology, Chicago, Illinois

General characteristics of magnetic bremsstrahlung (synchrotron radiation) are derived on the basis of calculations utilizing exact relativistic matrix elements. The spectral and total energy losses may be described by compact expressions incorporating radiative and quantum corrections. Comparisons of the relative efficacy of matter and magnetic fields as bremsstrahlung radiators indicate that even under relatively conservative conditions the natural conversion rates associated with the magnetic process (i.e., 9.6×10^3 BeV/mm) tends to favor this type of conversion over ordinary bremsstrahlung.

Discussions of a similar scope—including detailed calculations, and comparisons with the corresponding processes in material media—are also carried out for magnetic pair production, direct and indirect trident cascades, and magnetic photon splitting.

Circumstances peculiar to a class of external field radiative processes involving cooperative vacuum polarization corrections are illustrated by a discussion of magnetic Čerenkov radiation.

1. INTRODUCTION

Electromagnetic conversion processes such as bremsstrahlung, pair production, and photon splitting may be catalyzed by the presence of external magnetic fields in essentially the same way as they may be catalyzed by the presence of external electric fields. In fact, from a theoretical point of view, the only significant distinction between these two kinds of processes arises from the circumstance that the symmetry between electric and magnetic vacuum polarization corrections is disturbed by the apparent absence of magnetic monopoles. A simple consequence of this asymmetry is the stability of arbitrarily strong uniform magnetic fields against spontaneous pair conversion as contrasted with the "Klein catastrophe" which is manifested in the corresponding electric case [B1]. Practically speaking however electromagnetic conversion processes occurring in external electric fields are far more familiar since the intense Coulomb fields surrounding atomic nuclei provide a readily accessible means for experimentally studying these transformations—notably bremsstrahlung and pair production. In contrast the only magnetic conversion process which has received any detailed attention to date is synchrotron radiation—or more precisely, magnetic bremsstrahlung—which may be observed at relatively low field intensities, and which is of some technical importance in connection with the design of accelerators.

Just as in the corresponding Coulomb case, magnetically induced conversion processes generally require both high-field strengths and high energies. This is essentially due to the fact that the transition probabilities are principally governed by a single parameter Υ defined by

$$\Upsilon\equiv(E/mc^2)(H/H_{\rm cr}), \tag{1.1}$$

where E is an energy characteristic of the process, e.g., the bombarding energy, H is the ambient magnetic field strength, mc^2 is the electron rest mass, and the quantity

$$H_{\rm cr}\equiv m^2c^3/e\hbar=4.414\times10^{13}\ \text{G}, \tag{1.1a}$$

denotes the natural quantum mechanical measure of magnetic field strength. The transition probabilities are generally increasing functions of Υ (in the range $\Upsilon\lesssim1$) and therefore significant conversion rates require both high energies and very intense magnetic fields.[1] In order to fix the relevant orders of magnitude it is instructive to refer to the early calculations of magnetic bremsstrahlung carried out in connection with betatron and synchrotron design [e.g., I1, B2]: These estimates were based on energy requirements principally in the 0.1- to 1.0-BeV range, and presumed magnetic steering field capabilities of the order of 5 to 15 kG. In keeping with these constraints, the calculations were based on Υ factors of the order of 10^{-7}; and, in view of the Υ^2 dependence of the bremsstrahlung matrix elements, led to the prediction of relatively feeble radiation rates. However it was already appreciated at this early stage that much greater bremsstrahlung rates, as well as a variety of other electromagnetic conversion processes, e.g., pair production and photon splitting, would become accessible if larger values of Υ could be achieved.

In this respect the experimental situation has altered appreciably: Various technical developments in the intervening years have resulted in drastic upward shifts of the attainable ranges of Υ. In particular, high-energy particle accelerators either committed, de-

[1] This relationship has some similarities to the link between high magnetic fields and cryogenics: The appropriate factor in this case is the Langevin parameter $\mathcal{L}=\mu H/kT$. In cases where μ may be identified with the Bohr magneton, this can be rewritten as the product of two dimensionless factors, viz., $\mathcal{L}=(mc^2/kT)(H/H_{\rm cr})$. As is well known, appreciable cooperative effects require values of $\mathcal{L}$ approaching unity, and this clearly indicates the advantage of combining low temperatures and high fields. The analogy with the Υ parameter defined by Eq. (1.1) is evident.

CC-0. In Public Domain. Gurukul Kangri Collection, Haridwar

Digitized by Arya Samaj Foundation Chennai and eGangotri

signed, or planned have made it plausible to consider characteristic conversion energies of the order of 20 to 800 BeV; and the introduction of explosive flux compression techniques ("pulse-imploders") has boosted realizable magnetic field strengths to the 5- to 25-MG range.[2] Taken together, these figures imply Υ values in excess of 10^{-2}, or a total increase of five orders of magnitude over the older working estimates. Under these conditions it becomes possible to consider the extension of measurements of familiar effects such as magnetic bremsstrahlung to previously inaccessible ranges. It also becomes feasible to enhance external field radiative and quantum corrections to the point where they may be detectable as perturbations of familiar effects. And finally, the prospect of observing qualitatively new effects such as electrodynamic strong coupling modifications and vacuum polarization Čerenkov radiation moves closer to realization.[3]

In view of these developments it seems appropriate to review in some detail a number of the principal features of high-energy–high-field electromagnetic conversion processes, and to provide some tentative estimates of the technical requirements which will play a role in eventual experimental programs. The specific processes considered in the present review include: (a) magnetic bremsstrahlung [Sec. 2]; (b) magnetic pair production [Sec. 3]; (c) direct and indirect trident cascades [Sec. 4]; (d) photon splitting and magnetic Čerenkov radiation [Sec. 5]. As indicated previously, a number of related high-field–low-energy processes have already been considered elsewhere [E1, E2]. Most of the key points of the present survey are summarized in the following paragraphs:

(*a*) *Magnetic bremsstrahlung.* This process, under its more familiar name, "synchrotron radiation," is usually associated with direct microwave and optical emission from the circulating particle beams in high-energy accelerators.[4] In this context, magnetic bremsstrahlung is generally considered to be a low-energy phenomenon. Nevertheless, the intrinsic conversion rates (R_0) available with this process are of the order of 9.6×10^3 BeV/mm. The essential point is that under customary circumstances the value of Υ^2 is about 10^{-14}, and therefore the total emission rate—which is proportional to $R_0\Upsilon^2$—corresponds to comparatively insignificant radiative losses. For larger values of Υ however magnetic bremsstrahlung becomes more appreciable, and in fact under the conditions

$$(E/mc^2)\,(H/H_{cr})^2\sim10^{-9}, \qquad (1.2)$$

the total radiation rate begins to compete favorably with the ordinary (Coulomb) bremsstrahlung conversion efficiency of solid copper. The magnetic bremsstrahlung spectrum has a peak in the vicinity of $E[3\Upsilon/(2+3\Upsilon)]$, and this provides some fiducial characteristics for energy calibration, as well as additional flexibility in the selective enhancement of radiation.

The bremsstrahlung calculations discussed in Sec. 2 are based on exact matrix elements utilizing the relativistic Dirac wave functions for uniform magnetic fields. It is therefore possible to treat relativistic and quantum effects with some confidence. One consequence is that previous conjectures [S1, N1] regarding the special significance of relativistic effects in enhancing quantum corrections have been confirmed in numerical detail. Experimentally, these effects are manifested in a reduction of the photon emission into portions of the spectrum above the normal bremsstrahlung peak. Values of Υ of the order of 10^{-2} are sufficient to demonstrate the onset of these quantum corrections [E7].

A practically unique feature of high-energy magnetic bremsstrahlung is the possibility of investigating electrodynamic strong coupling modifications. These effects become important when the forces of radiation reaction ($\mathbf{F}_R$) become comparable in magnitude to the Lorentz forces ($\mathbf{F}_L$) which ordinarily control the particle motion [E4]. Quantitatively this condition may be expressed in the form

$$|\,\mathbf{F}_R\,|/|\,\mathbf{F}_L\,| = \tfrac{1}{2\,0\,0}(H/H_{cr})\,(E/mc^2)^2\rightarrow1; \qquad (1.3)$$

which implies experimental arrangements roughly on par with those required for the observation of quantum effects, i.e., $\Upsilon\sim10^{-2}$. By means of suitable variations of the experimental conditions it is in fact possible to study strong radiative corrections for magnetic bremsstrahlung with minimal interference from quantum mechanical effects. In this sense a nontrivial separation of these effects is feasible. The strong coupling features appear when one attempts to include these large radiative corrections in the usual quantum mechanical description: Simple perturbation theory then is no longer adequate, and the exact propagators must incorporate radiative modifications in addition to those already accounted for in the relativistic bound state Green's functions [e.g., K1, K2]. In contrast to other types of high-energy scattering experiments, non-electromagnetic strong interaction effects in this case remain isolated in higher-order vacuum polarization loops.

(*b*) *Magnetic pair production.* This process has not yet been observed experimentally. Although the minimum energy requirements are rather modest, i.e.,

[2] The technical basis for explosive flux compression [F1, F2, C1, E11, S10] is a conversion of chemical energy to magnetic field energy. The energy density of high explosives (circa 10^3 g-cal/cm^3) is roughly comparable to the energy densities of megagauss fields. Ultimately, higher field intensities may be achieved with pulse-imploders driven by nonconventional explosives.

[3] There are also a number of high-field low-energy effects of related interest. These depend on dispersive properties of magnetic vacuum polarization and generally involve experimental conditions of a completely different kind. These effects have been discussed in some detail in references [E1, E2, E3].

[4] These may be galaxies.

CC-0. In Public Domain. Gurukul Kangri Collection, Haridwar

Digitized by Arya Samaj Foundation Chennai and eGangotri

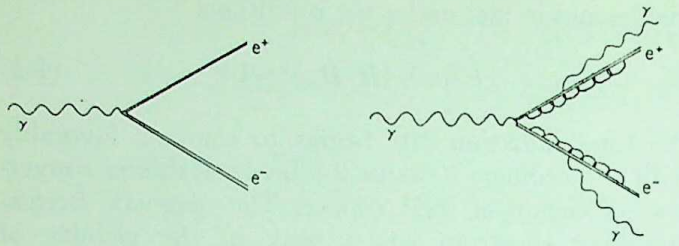

FIG. 1. (a) Pair production in a moderately strong field. The double lines denote the binding effects. (b) Pair production in a strong field. The bound propagators are modified by virtual photon (radiation reaction) loops.

$E/mc^2 \sim 2$, practical considerations place the actual threshold at

$$\Upsilon \gtrsim 10^{-1}, \tag{1.4}$$

which is technically a much more severe demand. Inasmuch as magnetic pair production is so closely linked to electric pair production there would seem to be little theoretical interest in studying its properties. Nevertheless there are certain questions of principle that may be more suitably explored with quasi-uniform magnetic fields than with spatially limited nuclear Coulomb fields. The basic concern is again with the influence of large external-field radiative corrections on the transition amplitudes for electromagnetic conversion processes (compare Fig. 1): Suppose for instance that magnetic pair production occurred at sufficiently high energies and in fields intense enough so that the effective threshold inequality (1.4) were satisfied. Then in almost all foreseeable circumstances at least one of the emerging particles would receive sufficient energy to place it well up near the strong radiation reaction limit given in (1.3). Experimentally this implies that the particle would itself become the source of intense secondary bremsstrahlung. Due to the strong radiation reaction the corresponding particle propagator would then have to include modifications over and above those already accounted for in relativistic and binding effects [T1, D1]. In this respect the situation parallels that already discussed in connection with magnetic bremsstrahlung. The new feature that makes an appearance in magnetic pair conversion is that the production vertex itself should in principle be calculated with this modified propagator. It is entirely possible that a self-consistent calculation utilizing nonperturbative techniques would yield results differing significantly from those implied by the estimates leading to (1.4). These types of strong coupling problems arising in connection with high-energy–high-field pair conversion calculations are very similar to those encountered in estimates of magnetic monopole production [M1, A1].

Some estimates for magnetic pair production are given in Sec. 3. In the absence of tractable nonperturbative techniques, the calculations have been optimized by employing the most accurate relativistic bound state propagators presently available. The final results should at least be adequate for preliminary experimental orientation.

Under conditions approximating (1.4), magnetic pair production becomes competitive with ordinary pair production in matter. For slightly larger values of Υ magnetic pair production in fact tends to become the dominant process. Basically the advantage lies with the magnetic fields because both the electric and magnetic conversion amplitudes approach an upper limit, i.e., saturate, as Υ increases past unity.[5] At very high energies the over-all transition rates are then limited by the total field volumes available for the conversions. In material media, the presence of bound electrons in the vicinity of nuclei places an effective upper limit on the Coulomb field volumes, and this leads to the well known screening limits on pair production. These equivalent Coulomb volumes are roughly of the order of (Avogadro's number)$\times$(Compton wavelength)^3, or approximately 10^{-8} cm^3. As a consequence even very modest magnetic field volumes (of suitable intensity) can become competitive pair converters. This line of argument is of course not limited to pair production: in general under extreme conditions the combined influence of amplitude saturation and (Coulomb) volume limitations tends to favor magnetically induced conversion processes over the corresponding electric conversion processes.

The progressive saturation of Coulomb pair production, and related processes, at very high energies also has the practical consequence that the cross sections gradually become more insensitive to energy variations. This leads to difficulties in establishing reliable energy scales—particularly in the range above 10^{12} eV where cascade shower estimates are currently almost the only means for gauging the orders of magnitude of pertinent energies. These problems can in principle be overcome by taking advantage of the "tunability" available in adjusting the value of Υ for various magnetic conversion processes. As a specific illustration let us consider magnetic pair production where good energy calibrations can be achieved by choosing Υ to be in the range $\Upsilon \gtrsim \frac{1}{3}$. The total transition rates in this case depend principally on the rapidly varying factor

$$\exp\{-\tfrac{8}{3}[(E/mc^2)(H/H_{cr})]^{-1}\},$$

and it is evident that H may be chosen appropriately so as to bring the desired energy variations into this most sensitive range.

---

[5] More precisely, in the case of the magnetic scattering amplitudes, there is a leveling off and a subsequent decrease as Υ increases past unity. In the electric case the situation is completely analogous if one makes the replacement $\Upsilon \to \Upsilon\mathcal{E}/\mathcal{E}_{cr}$ in the corresponding scattering amplitudes. In this case $\mathcal{E}$ denotes ambient electric field strength, and $\mathcal{E}_{cr} = (E/mc^2)(\mathcal{E}/\mathcal{E}_{cr})$ $m^2c^3/e\hbar = 1.323\times10^{16}$ V/cm. The relationship between the saturation of the scattering amplitudes and vacuum polarization effects has been discussed in detail in reference [E5].

CC-0. In Public Domain. Gurukul Kangri Collection, Haridwar

Digitized by Arya Samaj Foundation Chennai and eGangotri

(*c*) *Trident cascades.* The characteristic lengths associated with electromagnetic conversion processes are all of the order of a Compton wavelength ($\approx 3.85\times10^{-11}$ cm). Accordingly, magnetic fields spanning volumes even as small as a cubic millimeter appear to be of practically infinite extent in comparison with the individual conversion vertices. If conditions are adjusted so that the transition probabilities are not vanishingly small, one would then expect that the individual conversion events would rapidly multiply into cascade showers.[6] A crucial step in the initial growth and development of these showers is the occurrence of trident conversions, i.e., the processes

$$e^{\pm}+H\rightarrow e^{\pm}+\gamma+H\rightarrow e^{\pm}+e^{+}+e^{-}+H, \qquad (1.5)$$

where H represents the external magnetic field, and the intermediate photons may be either real or virtual. Estimates of the relevant transition amplitudes (Sec. 4) bear out the expectation that under extreme conditions, i.e., $\Upsilon \gtrsim \frac{1}{10}$, these trident cascades do in fact become an important component of the total magnetic attenuation.

(*d-1*) *Photon splitting.* A number of the usual selection rules of quantum electrodynamics are subject to modifications when external fields are present. One illustration of this is provided by photon splitting, or photon coalescence, which is ordinarily forbidden by Furry's theorem [F3; see also Fig. 2]. This process has not yet been observed experimentally, although in the particular case of Coulomb fields the cross sections are not impractically minute. Significant conversion rates for the corresponding magnetic process of course require extreme conditions, i.e., Υ values of the order of 0.02; but experimentally one has the advantage that competing processes such as double Compton scattering from atomic electrons may in principle be eliminated. Estimates and comparisons of magnetic and Coulomb photon splitting rates are summarized in Sec. 5.

(*d-2*) *Magnetic Čerenkov radiation.* Beyond the strong coupling modifications associated with extreme radiation reaction conditions [cf. (1.3)], there lies the possibility of cooperative radiative corrections arising from collective excitations of (external field) vacuum polarization loops. One effect of this type which has already been discussed on a number of previous occasions [e.g., E2, E3] is vacuum polarization Čerenkov radiation. Phenomenologically this effect is completely analogous to ordinary Čerenkov emission: Electromagnetic radiation propagating across a magnetic field in a direction perpendicular to the lines of flux will travel with a phase velocity less than the phase velocity of light in vacuum [T1, K1, K2]. Consequently charged particles with sufficiently high energies can traverse

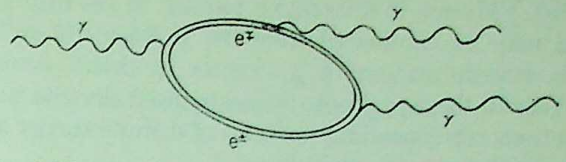

FIG. 2. Photon splitting in a strong field. One of the intermediate particles in a vacuum polarization loop emits a photon.

these fields with velocities exceeding the ambient light velocity, and may be expected to dissipate some of their energy through Čerenkov emission. Estimates based on phenomenological quantum electrodynamics [J1] yield a threshold for this effect of the order of $\Upsilon \gtrsim 60$. Since radiation reaction corrections are very important under these conditions these results are however liable to considerable modification. Semi-quantitative estimates of the expected orders of magnitude—taking into account interference from magnetic bremsstrahlung—are discussed in Sec. 5.

2. MAGNETIC BREMSSTRAHLUNG

A. Spectral Distribution and Total Energy Dissipation

Quantum mechanical calculations of magnetic bremsstrahlung are usually carried out within the framework of a bound state formalism, i.e., the Furry representation [F4]. The transition probabilities in this case lead to radiation rates rather than to cross sections. It is convenient to idealize the calculation by assuming that the entire process takes place in a uniform magnetic field (H) which is of infinite extent. The initial and final electron states (ψ_{e^-}) may then be represented as superpositions of bound state eigenfunctions derived from the Dirac Hamiltonian for a uniform magnetic field. ([J2], and further references cited therein.) These eigenfunctions can be conveniently classified according to their energy (E) and spin along the magnetic field direction (σ_H) in a suitable diagonal representation indexed with the corresponding quantum numbers n and s. The eigenvalue equation relating these quantities is given by

$$E=\pm mc^2[1+(H/H_{cr})(2n+s+1)]^{1/2};$$
$$n=0, 1, \cdots; \; s=\pm 1. \qquad (2.1a)$$

There is an additional degree of freedom which represents the arbitrariness of spatial position in a plane perpendicular to the field direction. This indeterminacy gives rise to an infinite (energy) degeneracy with respect to the location of the orbit centers (r_0). The corresponding quantum number (l) may then be obtained from the eigenvalue condition

$$r_0^2\psi_{e^-}=\{(2l+1)(H_{cr}/H)\lambda\!\!\!^{-}_{c}{}^2\}\psi_{e^-}. \qquad l=1, 2, \cdots; \qquad (2.1b)$$

which exhibits the imprecision in the values of r_0^2. [As usual, $\lambda\!\!\!^{-}_{c}=\hbar/mc$; and the critical field is given by

[6] In view of the tremendous energy degradation of the individual shower components, this may be considered a "gedanken" device for shielding against ultrahigh-energy particles.

CC-0. In Public Domain. Gurukul Kangri Collection, Haridwar

Digitized by Arya Samaj Foundation Chennai and eGangotri

(1.1a).] Motion in a direction parallel to the magnetic field may be eliminated from the problem through a tacit transformation to a "center of drift" system.

With all these provisos, the normalized electron wave functions corresponding to states of definite energy and polarization may be written as

$$\psi_{e^-} = \sum_l | n, s, l \rangle; \tag{2.2}$$

where the explicit analytical forms are given in [J2]. The transition probability for magnetic bremsstrahlung, in simplest approximation, then may be computed by methods of ordinary first-order perturbation theory, viz.

$$W = 2\pi(\alpha/\nu) \times \sum_{ss'll'n'\epsilon} | \langle n', s', l' | \alpha \cdot \epsilon \exp(-ik \cdot r) | n, s, l \rangle |^2, \tag{2.3}$$

where $\nu = c\,|\,\mathbf{k}\,|/2\pi$ denotes the frequency of the emitted photon, and all the other symbols have their customary meaning (e.g., [K3]).

Of the nine operations indicated in (2.3), seven may be carried out by relatively straightforward methods: The summations and averages over the polarization ϵ and the spin indices s,s' are easily performed with the help of standard reductions from Dirac algebra. The n' summation is also immediate since this merely involves a projection of all the final-state components consistent with energy conservation. The spatial integrations—which include Laguerre functions arising from (2.2)—lead to standard hypergeometric functions. The technical difficulties enter at the next stage when one attempts to carry out the l, l' summations. These indices now appear as parameters in hypergeometric functions and at present there are no known closed forms for the requisite sums. This situation has some resemblance to the "azimuthal" quantum number summation problem in the corresponding Coulomb case (e.g., [E6]), and can be dealt with by analogous methods. The essential device that is required is an appropriate asymptotic simplification of the hypergeometric functions. In the present instance this is tantamount to specializing all the electromagnetic conversion processes to the extreme relativistic range. Specifically, *here and in all the succeeding calculations*, it is assumed that the experimental conditions are consistent with the inequalities

$$E/mc^2 \gg 1, \quad \text{and} \quad (E-h\nu)/mc^2 \gg 1, \tag{2.4}$$

where E now represents the *initial* electron energy, and $h\nu$ is the energy of the emitted photon.[7]

[7] The asymptotic expansion of the hypergeometric functions with respect to the parameters also requires the auxiliary condition $(h\nu/mc^2)^2 \gg H/H_{cr}$, which ostensibly eliminates very soft photon conversion processes. In the bremsstrahlung case one can however *a posteriori* extend the final results [compare the Eqs. (2.10) and (2.11) of the text] down to the lower limit of the corresponding classical treatment [S2], viz., $h\nu/mc^2 \gg (mc^2/E)(H/H_{cr})$. The assumption $H \leqq H_{cr}$ is also implicit in most of the computations (compare [T1]).

This part of the magnetic bremsstrahlung calculation was first explicitly carried through by N. P. Klepikov [K4]. His final result for the spectral distribution of the radiation emitted per unit distance may be written in the form:

$$I(E, h\nu, H) = \frac{3\alpha}{\pi^2}\frac{mc^2}{\lambda\!\!\!^{-}_c}\frac{\Upsilon}{(2+3\Upsilon)^2}\frac{y^2}{E}\mathfrak{M}(y, \Upsilon), \tag{2.5a}$$

where

$$\mathfrak{M}(y, \Upsilon) = \sum_{i=1}^{3}\mathfrak{M}_i(h\nu/E)\mathcal{J}_i(y, \Upsilon), \tag{2.5b}$$

and

$$\mathfrak{M}_1(h\nu/E) = 1+(1-h\nu/E)^{-2},$$
$$\mathfrak{M}_2(h\nu/E) = 2/(1-h\nu/E), \tag{2.5c}$$
$$\mathfrak{M}_3(h\nu/E) = \left[\frac{h\nu/E}{1-h\nu/E}\right]^2;$$

furthermore

$$\mathcal{J}_1(y, \Upsilon) = \int_0^\infty dx \cosh^5 x\, K^2_{2/3}\left[\frac{y}{2+3\Upsilon(1-y)}\cosh^3 x\right],$$

$$\mathcal{J}_2(y, \Upsilon) = \int_0^\infty dx \cosh^3 x \sinh^2 x \times K^2_{1/3}\left[\frac{y}{2+3\Upsilon(1-y)}\cosh^3 x\right], \tag{2.5d}$$

$$\mathcal{J}_3(y, \Upsilon) = \int_0^\infty dx \cosh^5 x\, K^2_{1/3}\left[\frac{y}{2+3\Upsilon(1-y)}\cosh^3 x\right].$$

As in the preceding [compare (1.1)], the parameter Υ is defined by

$$\Upsilon = (E/mc^2)(H/H_{cr}). \tag{2.5e}$$

The K's appearing in the integrands of (2.5d) are modified Bessel functions conforming to Watson's conventions [W1]. The new notation

$$y = h\nu/h\nu_{cr}, \qquad h\nu_{cr} = E[3\Upsilon/(2+3\Upsilon)], \tag{2.5f}$$

has been introduced for convenience in characterizing the spectral distribution. (*Note*: $0 \leq h\nu \leq E$ corresponds to $0 \leq y \leq 1+2/3\Upsilon$.) As usual we write $\alpha = e^2/\hbar c$ for the fine structure constant.

The general behavior of the spectral function $I(E, h\nu, H)$ with respect to variations of the individual parameters of physical interest is rather complex. The situation can however be simplified considerably by taking advantage of the convenient circumstance that with the single additional restriction

$$h\nu \ll E, \tag{2.6}$$

the entire complex of analytical expressions (2.5a–d) may be reduced to a concise form which turns out to

CC-0. In Public Domain. Gurukul Kangri Collection, Haridwar

Digitized by Arya Samaj Foundation Chennai and eGangotri

be substantially identical to that derived from the corresponding classical problem.

We begin by expanding the $\mathfrak{M}_i$'s to first order in $h\nu/E$:

$$\mathfrak{M}_1(h\nu/E)\cong 2[1+(h\nu/E)],$$
$$\mathfrak{M}_2(h\nu/E)\cong 2[1+(h\nu/E)], \qquad (2.7)$$
$$\mathfrak{M}_3(h\nu/E)\cong \mathcal{O}(h\nu/E)^2\to 0.$$

As a consequence of the elementary inequality

$$\partial K_\nu(z)/\partial\nu>0, \qquad \text{for } \nu>0,\ z>0; \qquad (2.8a)$$

one may also show that

$$\mathcal{J}_1(y,\Upsilon)\geq\mathcal{J}_3(y,\Upsilon); \qquad (2.8b)$$

and this leads to the rigorous upper bound

$$\frac{\mathfrak{M}_3(h\nu/E)\,\mathcal{J}_3(y,\Upsilon)}{\mathfrak{M}_1(h\nu/E)\,\mathcal{J}_1(y,\Upsilon)}\leq(h\nu/E)^2. \qquad (2.8c)$$

To first order in $h\nu/E$, the $\mathfrak{M}$-representation (2.5b) may then be contracted to the single term

$$\mathfrak{M}(y,\Upsilon)\cong 2(1+h\nu/E)$$
$$\times\int_0^\infty dx\,\left\{\cosh^5 x\,K^2_{2/3}\left[\frac{y}{2+3\Upsilon(1-y)}\cosh^3 x\right]\right.$$
$$\left.+\cosh^3 x\sinh^2 x\,K^2_{1/3}\left[\frac{y}{2+3\Upsilon(1-y)}\cosh^3 x\right]\right\}. \qquad (2.8d)$$

The essential step of the entire reduction now follows from the identity

$$\int_0^\infty dx\{\cosh^5 x\,K^2_{2/3}(\zeta\cosh^3 x)$$
$$+\cosh^3 x\sinh^2 x\,K^2_{1/3}(\zeta\cosh^3 x)\}$$
$$=\frac{\pi}{2\sqrt{3}}\zeta^{-1}\int_{2\zeta}^\infty dx\,K_{5/3}(x), \qquad \zeta>0, \qquad (2.8e)$$

which is proved in Appendix 1. This permits the further simplification of (2.8d) to

$$\mathfrak{M}(y,\Upsilon)=\frac{\pi}{\sqrt{3}}(1+h\nu/E)\zeta^{-1}\int_{2\zeta}^\infty dx\,K_{5/3}(x), \qquad (2.8f)$$

where

$$\zeta\equiv\frac{y}{2+3\Upsilon(1-y)}=\frac{y}{(2+3\Upsilon)(1-h\nu/E)}$$
$$\cong(3\Upsilon)^{-1}\frac{h\nu}{E}\left(1+\frac{h\nu}{E}\right); \qquad (2.8g)$$

the last approximation following from (2.6).

It is now convenient to introduce the auxiliary (bremsstrahlung) function

$$\kappa(z)\equiv z\int_z^\infty dx\,K_{5/3}(x), \qquad (2.9)$$

corresponding to the incomplete Bessel function integrals appearing in (2.8e, f). This leads to a very compact final expression for the bremsstrahlung spectral distribution:

$$I(E,h\nu,H)=(\sqrt{3}\alpha/2\pi)(mc^2/\lambda\!\!\!^{-}_c)(\Upsilon/E)(1-h\nu/E)\kappa(2\zeta), \qquad (2.10)$$

where all the notations and hypotheses are as specified in the equations (2.1b) to (2.9) of the preceding. The corresponding classical relativistic result [S2, S3, A2] may be put into the form[8]

$$I(E,h\nu,H)=\frac{\sqrt{3}\alpha}{2\pi}\frac{mc^2}{\lambda\!\!\!^{-}_c}\frac{\Upsilon}{E}\kappa\left(\frac{2}{3\Upsilon}\frac{h\nu}{E}\right). \qquad (2.11)$$

It is clear that the classical and quantum mechanical expressions are almost identical. The most important distinctions arise from the fact that Υ is *not* necessarily restricted by the condition $\Upsilon\gg 1$ in (2.10); and also that the argument of κ in the quantum mechanical form is modified by the factor $(1+h\nu/E)$. These points are discussed in some detail in Sec. 2B.

Various properties of the bremsstrahlung function $\kappa(z)$ are derived in Appendix 2. For reference we note the limiting forms

$$\kappa(z)\nearrow 2.149z^{1/3}, \qquad z\ll 1$$
$$\kappa(z)\searrow 1.253z^{1/2}e^{-z}, \qquad z\gg 1. \qquad (2.12)$$

The function is displayed graphically in Fig. 3; numerical values are given in Table I.

These formulas may be simplified still further in circumstances where the additional restriction

$$(h\nu/E)(1+h\nu/E)\ll\Upsilon, \qquad (2.13)$$

is applicable. In view of (2.6) this is in fact satisfied identically in the quantum mechanical regime $\Upsilon\gtrsim 1$. From (2.10) and (2.12) we then find

$$I(E,h\nu,H)=0.517\alpha\frac{mc^2}{\lambda\!\!\!^{-}_c}\frac{\Upsilon^{2/3}}{E}\left(\frac{h\nu}{E}\right)^{1/3}\left(1-\frac{2}{3}\frac{h\nu}{E}\right), \qquad (2.14)$$

[8] The usual forms of this equation are easily recovered by shifting from an energy to a frequency scale ($I\to\hbar I$); and converting the quantum mechanical critical field to the corresponding classical expression [L1], e.g., $\alpha^{-1}H_{cr}=m^2c^4/e^3=H_{cr}$(classical).

CC-0. In Public Domain. Gurukul Kangri Collection, Haridwar

Digitized by Arya Samaj Foundation Chennai and eGangotri

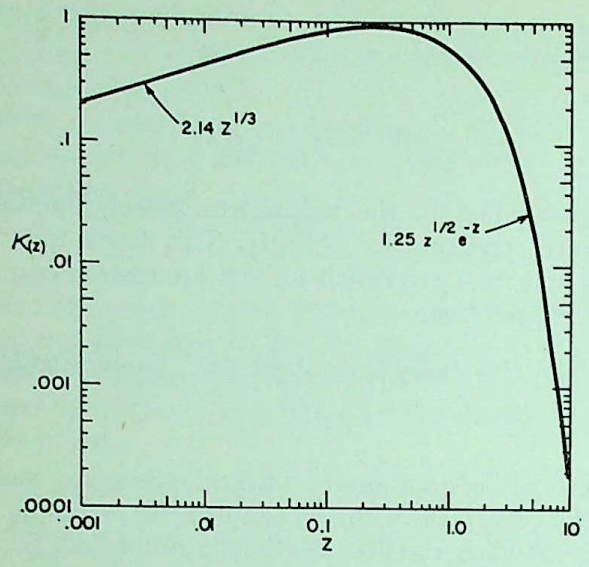

FIG. 3. Graph of the bremsstrahlung function;

$$\kappa(z)=z\int_z^\infty dx K_{5/3}(x).$$

where

$$\alpha(mc^2/\lambda\!\!\!^{-}_c)=9.657\times10^3\ \text{BeV/mm} \qquad (2.14a)$$

is the intrinsic rate of magnetic bremsstrahlung.

It is also useful to have an explicit formula for the total radiation per unit distance into the spectral region between $h\nu_1$ and $h\nu_2$. This follows immediately from (2.14);

$$\frac{\mathcal{E}(h\nu_1,\,h\nu_2)}{\Delta x}=4.99\times10^3\,\Upsilon^{2/3}\int_{h\nu_1/E}^{h\nu_2/E}dx\,x^{1/3}\,(1-\tfrac{2}{3}x)\ \text{BeV/mm}. \qquad (2.15)$$

In particular, for the integral spectrum we obtain

$$\mathcal{E}(0,\,h\nu)/\Delta x\cong 3.75\times10^3\,\Upsilon^{2/3}\,(h\nu/E)^{4/3}\ \text{BeV/mm}. \qquad (2.16)$$

A rough measure of the value of Υ in a given experimental situation may be derived from the position of the maximum intensity of the bremsstrahlung spectrum. This is a consequence of inverting (2.5f) to give

$$\Upsilon=\frac{2}{3}\frac{h\nu_{cr}/E}{1-h\nu_{cr}/E}, \qquad (2.17)$$

and identifying $h\nu_{cr}$ with the bremsstrahlung peak [compare (2.8g)]. In general this maximum increases with increasing values of Υ; and ultimately for $\Upsilon>\frac{2}{3}$, the magnitude of $h\nu_{cr}$ tends towards the top end of the spectrum, i.e., $h\nu_{cr}\to E$. Further information on E and H may in principle be obtained by combining measurements of the differential spectrum, such as (2.15), with determinations of the bremsstrahlung peak.

The total energy dissipation per unit distance may be obtained from the basic expression (2.5a) by an integration over all frequencies. The exact analytical form of this result has been given by Klepikov [K4]. It is convenient to write this as

$$\Delta\mathcal{E}(\Upsilon)/\Delta x=\tfrac{2}{3}\alpha(mc^2/\lambda\!\!\!^{-}_c)\,g(\Upsilon), \qquad (2.18)$$

where

$$g(\Upsilon)=\begin{cases}\Upsilon^2(1-5.953\Upsilon), & \Upsilon\ll1; \quad (2.18a)\\ 0.5563\Upsilon^{2/3}, & \Upsilon\gg1. \quad (2.18b)\end{cases}$$

A graph of the exact function is given in Fig. 4.

Both limiting cases corresponding to $\Upsilon\gtrless1$ may be obtained directly from (2.10). In particular it is easy to check that the expression (2.16), with the ratio $h\nu/E\to1$, lies within 5% of the exact quantum mechanical limit (2.18b). The leading term of the small Υ-expansion (2.18a) of course coincides with the classical result.

B. Quantum Corrections and Radiation Reaction

Under conditions of high momentum transfer it is expected that quantum effects will appreciably influence the characteristics of magnetic bremsstrahlung. The classical theory may therefore be considered reliable only under circumstances where the ratio of the photon to the particle momentum is essentially neg-

TABLE I. Numerical values for the function $\kappa(z)$.

z	$\kappa(z)$	z	$\kappa(z)$
0.001	0.213	1.0	0.651
0.01	0.445		
0.02	0.547	2	0.300
0.03	0.614		
0.04	0.663	4	0.053(+0, −0.002)
0.05	0.701		
0.06	0.733	5	0.0214(+0, −0.0008)
0.07	0.760		
0.08	0.782	6	0.00845(+0, −0.00008)
0.09	0.801		
0.1	0.818	7	0.00338
0.2	0.903		
0.3	0.924	8	0.00129
0.4	0.905		
0.5	0.871	9	0.00049
0.6	0.831	10	0.00019
0.7	0.788		
0.8	0.742		
0.9	0.696		

CC-0. In Public Domain. Gurukul Kangri Collection, Haridwar

Digitized by Arya Samaj Foundation Chennai and eGangotri

ligible. A rough criterion for this is

$$\frac{h\nu_{cr}/c}{E/c}\sim\Upsilon\ll 1. \tag{2.19}$$

At extremely high energies however relativistic effects may enhance the influence of quantum corrections: Various features of high-energy bremsstrahlung depend sensitively on the velocity increment $c-v\sim(c/2)(mc^2/E)^2$, and in the ultrarelativistic region this is diminished to magnitudes comparable with the quantum fluctuations. More refined wave packet arguments [S1] have in fact indicated that the inequality (2.19) ought to be replaced by the stricter condition

$$\Upsilon^{1/2}\ll 1; \tag{2.19a}$$

and it has been conjectured [N1] that quantum modifications may actually be manifested under even more conservative conditions. The observation of these effects is of course favored by circumstances sensitive to the relativistic enhancement. It will appear that the shape of the upper portion of the bremsstrahlung spectrum exhibits significant quantum corrections even for Υ values as low as 10^{-2}.

These points may be checked in quantitative detail with the aid of the classical and quantum mechanical expressions (2.11) and (2.10). The total radiated energy emitted (per unit distance) into portions of the bremsstrahlung spectrum between $h\nu_1$ and $h\nu_2$ is given by

$$\frac{\Delta\mathcal{E}(h\nu_1, h\nu_2)}{\Delta x}=\int_{h\nu_1}^{h\nu_2} d(h\nu)\,I(E, h\nu, H). \tag{2.20}$$

In the classical case the explicit form of this result is

$$\frac{\Delta\mathcal{E}^{cl}(h\nu_1, h\nu_2)}{\Delta x}=\frac{3^{3/2}\alpha}{4\pi}\frac{mc^2}{\lambda\!\!\!^{-}_c}\Upsilon^2\int_{y_1}^{y_2} dy\,\kappa(y), \tag{2.20a}$$

where[9] $y=(2/3\Upsilon)(h\nu/E)$. The corresponding quantum mechanical expression is

$$\frac{\Delta\mathcal{E}^{QM}(h\nu_1, h\nu_2)}{\Delta x}$$

$$=\frac{3^{3/2}\alpha}{4\pi}\frac{mc^2}{\lambda\!\!\!^{-}_c}\Upsilon^2\int_{y_1}^{y_2} dy\left(1-\frac{3\Upsilon}{2}y\right)\kappa\left(y+\frac{3\Upsilon}{2}y^2\right). \tag{2.20b}$$

Although y itself is not necessarily a small quantity, we shall assume that $\Upsilon y^2\ll 1$, and then introduce the series

[9] This is consistent with the previous notation (2.5f) in cases where $\Upsilon\ll 1$.

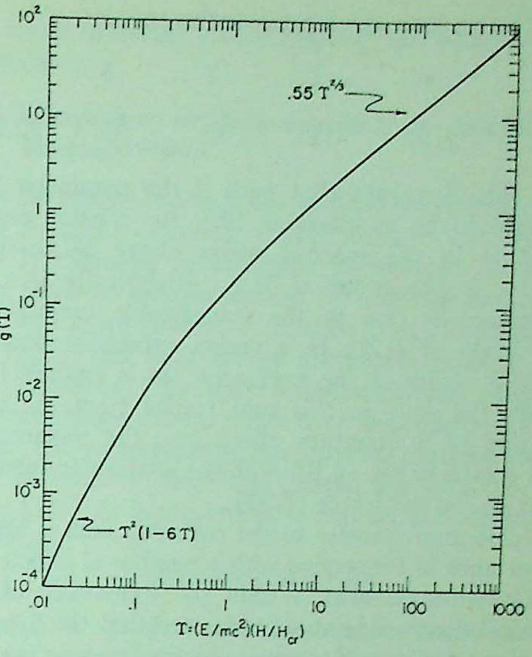

FIG. 4. Graph of the auxiliary function $g(T)$ [cf. (2.18)].

expansion

$$\kappa[y+(3\Upsilon/2)y^2]\approx\kappa(y)+(3\Upsilon/2)y^2\,\kappa'(y)+\mathcal{O}(\Upsilon^2y^4). \tag{2.21}$$

Then

$$\int_{y_1}^{y_2} dy[1-(3\Upsilon/2)y)\,\kappa(y+(3\Upsilon/2)y^2]\approx\int_{y_1}^{y_2} dy\,\kappa(y)$$

$$+\tfrac{3}{2}\Upsilon\left\{y_2^2\,\kappa(y_2)-y_1^2\,\kappa(y_1)-3\int_{y_1}^{y_2} dy\,y\,\kappa(y)\right\}. \tag{2.22}$$

Evidently the region $0.3<y_1,\ 5\lesssim y_2$ is of greatest interest. However since the function $\kappa(y)$ is already very small in the range $y>5$, the y_2 dependence will in fact not be too crucial. [For the same reason even the limit $y_2\to\infty$ does not clash with the initial assumption (2.21).] The quantum corrections to the upper portion of the bremsstrahlung spectrum then may be written in the compact form

$$\frac{\Delta\mathcal{E}^{cl}(h\nu,\infty)-\Delta\mathcal{E}^{QM}(h\nu,\infty)}{\Delta\mathcal{E}^{cl}(h\nu,\infty)}=\Upsilon\,f\left(\frac{2}{3\Upsilon}\frac{h\nu}{E}\right), \tag{2.23a}$$

where

$$f(y)=\frac{3}{2}\left(\left[y^2\,\kappa(y)+3\int_y^\infty dz\,z\,\kappa(z)\right]\Big/\int_y^\infty dz\,\kappa(z)\right). \tag{2.23b}$$

CC-0. In Public Domain. Gurukul Kangri Collection, Haridwar

Digitized by Arya Samaj Foundation Chennai and eGangotri

For $f(y)$ we have the representative values:

y	1	2	3	(2.23c)
$f(y)$	11	20	35.	

It is then apparent that even if the parameter Υ is assumed to be as small as 10^{-2}, the relative energy depletion in the spectral region above $h\nu/E\sim 0.004$ will be of the order of 35%. Analytically this enhancement is due to the considerable variation in magnitude of $\kappa(2\zeta)$ in a region expecially sensitive to small shifts of the argument. As is evident from (2.8g) the shift in this case results from the combination of a quantum effect, i.e., the replacement $1\rightarrow 1+h\nu/E$ in Eq. (2.10) with the relativistic enhancement due to the factor $(2/3\Upsilon)$.

Momentum transfer to the radiation field is also of importance in connection with a number of effects due to radiation reaction. Within the framework of the classical theory it is usually assumed that the dynamical characteristics of magnetic bremsstrahlung may be derived from the equation [E4]

$$\mathbf{F}_L+\mathbf{F}_R=\mathbf{P}, \tag{2.24}$$

where $\mathbf{F}_L$ is the Lorentz force exerted by the magnetic field and $\mathbf{F}_R$ represents the force of radiation reaction. It is well known that there are a number of unresolved theoretical difficulties associated with the derivation and application of this equation. In most cases of practical interest however these problems are of no concern since the experimental conditions imply the inequality

$$|\,\mathbf{F}_R\,|\ll|\,\mathbf{F}_L\,|, \tag{2.25}$$

and this permits the calculation of all necessary radiative corrections from (2.24) by simple perturbation methods. These approximations lead to analytically well defined results a d have the virtue of automatically avoiding the "runaway solutions" and other unpleasant features inherent in the exact form of (2.24). In the special case of magnetic bremsstrahlung it is however feasible to create experimental conditions for which the inequality (2.25) is no longer valid. The rigorous consequence of the "exact" radiation reaction theory may then be checked in a nontrivial way.

We again consider intense magnetic fields and bremsstrahlung in the ultrarelativistic limit: The Lorentz force in this case is given by

$$\mathbf{F}_L\sim e\hat{v}\times\mathbf{H}, \tag{2.26a}$$

where $\hat{v}$ is the unit velocity vector associated with the particle motion. The corresponding reaction force may then be estimated in an essentially model-independent way from the momentum transfer to the radiation field. Since most of the bremsstrahlung is emitted into a forward cone of half-angle $\sim mc^2/E(\ll 1)$, the transverse momentum components may be neglected and $\mathbf{F}_R$ obtained directly from (2.18), i.e.,

$$\mathbf{F}_R\sim-\frac{d(E/c)}{dt}\,\hat{v}=-\frac{2}{3}\,\alpha\,\frac{mc^2}{\lambda\!\!\!^{-}_c}\,g(\Upsilon)\hat{v}. \tag{2.26b}$$

From an experimental point of view the most favored situations involve the condition $\Upsilon\ll 1$; and this implies the further simplification $g(\Upsilon)\rightarrow\Upsilon^2$ [compare (2.18a)]. In these cases the momentum transfer ratio is explicitly given by

$$|\,\mathbf{F}_R\,|/|\,\mathbf{F}_L\,|\sim\tfrac{2}{3}\alpha(H/H_{\rm cr})(E/mc^2)^2. \tag{2.27a}$$

From this expression it is obvious that the equality

$$|\,\mathbf{F}_R\,|\sim|\,\mathbf{F}_L\,|, \tag{2.27b}$$

can indeed be satisfied with a variety of plausible experimental arrangements. Some representative choices for E and H are:

E (BeV)	20	40	200	300	1000
H (gauss)	6.0×10^6	1.5×10^6	6.0×10^4	2.6×10^4	2.4×10^3
Υ	5.4×10^{-3}	2.7×10^{-3}	5.4×10^{-4}	3.5×10^{-4}	1.1×10^{-5}

(2.28)

(See also Table IV.) Under these conditions one would expect appreciable changes in the dynamics and the radiation characteristics of magnetic bremsstrahlung.

It is important to recognize that the equality (2.27b) does not necessarily imply a breakdown of classical electrodynamics. This is presumably a Lorentz-covariant theory and the criteria limiting its domain of validity ought to have a Lorentz-invariant significance. This obviously is not the case for (2.27a) which is merely the ratio of the magnitudes of 3-vectors. For this reason a number of authors have proposed that the value assumed by (2.27a) in the particle rest system—evidently an invariant—be identified as the actual limit for the internal consistency of the theory

CC-0. In Public Domain. Gurukul Kangri Collection, Haridwar

Digitized by Arya Samaj Foundation Chennai and eGangotri

[P1, L1, E4]. Elementary transformations of this ratio yield

$$(|F_R|/|F_L|)_{\text{rest}} \sim \tfrac{2}{3}\alpha(E/mc^2)(H/H_{\text{cr}}), \qquad (2.29)$$

where E and H retain their meaning as energy and field strength measured with respect to the laboratory system. It is apparent that the invariant criterion $(|F_R| \ll |F_L|)_{\text{rest}}$ is far more conservative than (2.25).

This line of argument, apart from its theoretical significance, has the practical merit of suggesting a reasonable approach to the computation of radiation reaction effects even under conditions violating the inequality (2.25): A comparison of the two ratios (2.29) and (2.27a) indicates that Lorentz transformations to the rest system generally tend to diminish the importance of radiation reaction. This implies that perturbation methods may be legitimately applied in the rest system under circumstances where this is not directly feasible in the laboratory system. Specifically in cases where the equality (2.27b) applies but the ratio (2.29) still remains small, radiation reaction effects may be evaluated by perturbation theory in the rest frame, and the results then transformed back to the laboratory system. These perturbed solutions may of course differ considerably from the initial solutions. The net result of the radiation reaction feedback will be to alter the normal spectral distribution [i.e., (2.11)] of the bremsstrahlung.

A special feature of high-energy magnetic bremsstrahlung is that the spectral perturbations due to quantum mechanical effects and radiation reaction corrections can in principle be distinguished from each other. This possibility is a consequence of the differences in the respective threshold criteria, i.e. (2.23a, b) and (2.27a, b). Theoretically this is an extremely interesting situation since in all other known cases (see [E4]) quantum effects intervene well before conditions reach the point where radiative corrections become important. This is reflected in the usual theoretical sequence in which quantum mechanical descriptions are first substituted for the classical formulations; and only afterwards—if necessary—supplemented by quantum mechanical perturbations which correct for the radiative effects. The Lamb shift and the Schwinger correction [S4] are well-known illustrations of the success of this approach both for low- and high-energy radiation reaction effects. In the magnetic bremsstrahlung case however it is evident that experimental conditions can be adjusted so that at the point where quantum corrections become important strong radiation reaction effects already prevail. This corresponds to an inadequacy of the relativistic electron propagators [K2, T1] even in lowest approximation. A proper description would obviously have to incorporate radiative corrections *ab initio*. In this sense high-energy bremsstrahlung becomes a problem in quantum electrodynamics involving *strong coupling but without strong interactions*.

C. Comparison of Bremsstrahlung in Matter and Magnetic Fields

In the energy region above 10 BeV, and for magnetic field strengths exceeding 1 MG, electron bremsstrahlung in magnetic fields begins to compete favorably with electron bremsstrahlung in material media. In this section we present a detailed comparison of the differential and total energy dissipation rates for the two processes. The basic expressions for magnetic bremsstrahlung can be taken over from the preceding work. The corresponding formulas for material media may be obtained from the compilation of Koch and Motz [K6]. It is convenient to restrict the energies to the range

$$1600/Z \ll E/mc^2 \lesssim 10^6, \qquad (2.30)$$

where Z is atomic number. Ionization losses at low energies may then be ignored, and theoretical complications peculiar to super-high energies (cf. Sec. 2D) will not vitiate the comparisons.

The best estimates currently available for the spectral intensity of very-high-energy electron bremsstrahlung in materials characterized by density ρ, atomic weight A, and atomic number Z lead to the expression

$$I(h\nu, Z) = \tfrac{8}{3}\alpha N_0 \lambda\!\!\!^{-}_c{}^2 h(Z), \qquad (2.31a)$$

where N_0 is Avogadro's number, $\lambda\!\!\!^{-}_c$ is the Compton wavelength, and $\alpha =$ "1/137". Screening effects and Coulomb corrections are included in the auxiliary function $h(Z)$ which is given by

$$h(Z) = 6(\rho/A)(\alpha Z)^2 [\ln(183/Z^{1/3}) + 0.083 - 1.20(\alpha Z)^2 \{1 - 0.86(\alpha Z)^2\}]. \qquad (2.31b)$$

This form of $I(h\nu, Z)$ is a good first approximation for the spectral bremsstrahlung per unit distance appropriate in the extreme relativistic region. It omits a weak dependence on photon energy and cannot be relied upon at all near the bremsstrahlung tip, $h\nu \sim E$. (Both Coulomb and magnetic bremsstrahlung cross-section estimates in this region are still rather uncertain.) For purposes of comparison we shall use (2.31a) to represent the effects of bremsstrahlung in material media, and the expression (2.10) for the corresponding magnetic spectrum, viz.

$$I(E, h\nu, H) = \frac{\sqrt{3}\alpha}{2\pi}\frac{mc^2}{\lambda\!\!\!^{-}_c}\frac{\Upsilon}{E}\left(1 - \frac{h\nu}{E}\right)\kappa(2\zeta). \qquad (2.32)$$

The total bremsstrahlung energy dissipation per unit distance in material media is given by

$$\frac{\Delta\mathcal{E}(Z)}{\Delta x} = \int^{E} d(h\nu)\, I(h\nu, Z); \qquad (2.33)$$

CC-0. In Public Domain. Gurukul Kangri Collection, Haridwar

Digitized by Arya Samaj Foundation Chennai and eGangotri

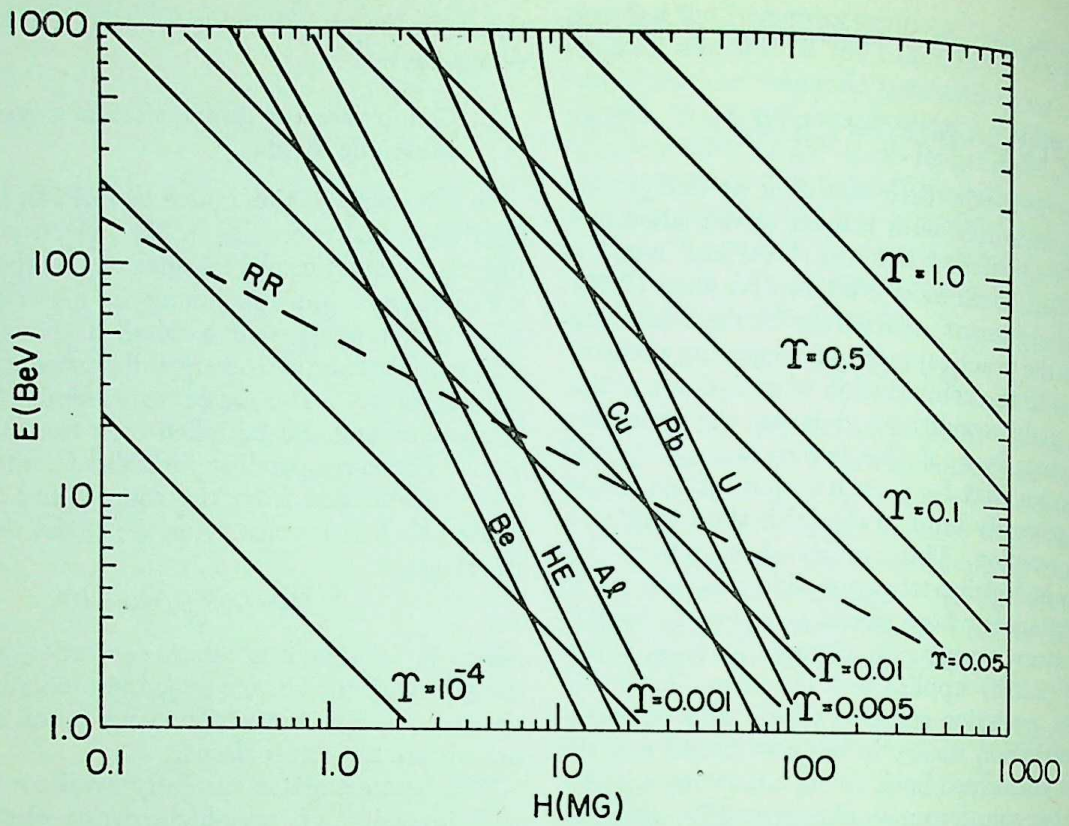

FIG. 5. Summary of the total bremsstrahlung break-even conditions (2.38) for various materials. The regions to the right of the curves labeled Be, HE, Al, etc. correspond to experimental conditions favoring magnetic bremsstrahlung. As an illustration we note that at 300 BeV the minimum magnetic field required to enhance magnetic bremsstrahlung over ordinary bremsstrahlung in high explosives is 1 MG (≡megagauss).

The curves below $\Upsilon=0.01$ represent the equations

$$E_{\mathrm{BeV}}H^2_{\mathrm{MG}}=3.44\times10^4\,h(z); \quad \text{[cf. (2.39)]}.$$

The remaining portions correspond to solutions of the implicit conditions

$$g(\Upsilon)=6.77\times10^{-5}E_{\mathrm{BeV}}\,h(z); \quad \text{[cf. Fig. 4]}.$$

The line "RR" marks the onset of the strong radiation reaction regime (2.27a, b).

and the best current estimate for this quantity is

$$\Delta\mathcal{E}(Z)/\Delta x=\tfrac{2}{3}\alpha N_0\lambda\!\!\!^{-}_c{}^2\,E\,h(Z). \qquad (2.34)$$

The corresponding magnetic expression [compare (2.18)] is

$$\Delta\mathcal{E}(\Upsilon)/\Delta x=\tfrac{2}{3}\alpha(mc^2/\lambda\!\!\!^{-}_c)g(\Upsilon). \qquad (2.35)$$

Since we are principally interested in assessing the comparative magnitudes of these quantities it is convenient to introduce two ratios: the total energy dissipation ratio

$$R_B=\frac{\Delta\mathcal{E}(\Upsilon)/\Delta x}{\Delta\mathcal{E}(Z)/\Delta x}=2.89\times10^7\frac{mc^2}{E}\frac{g(\Upsilon)}{h(Z)}; \qquad (2.36)$$

and the spectral intensity ratio

$$R_B(h\nu)=\frac{I(E,h\nu,H)}{I(h\nu,Z)}=0.89\times10^7\left(1-\frac{h\nu}{E}\right)\frac{H}{H_{\mathrm{cr}}}\frac{\kappa(2\zeta)}{h(Z)}. \qquad (2.37)$$

The large numerical factor ($\sim10^7$) which appears in both of these expressions represents the total "Compton volume" $N_0\lambda\!\!\!^{-}_c{}^3(=3.465\times10^{-10})$ which provides the natural scale for Coulomb-induced conversion processes in bulk matter under fully screened conditions. The small value of this quantity is one of the factors favoring the magnetically catalyzed conversions.

A fairly quick way of becoming familiar with the various experimental possibilities covered by R_B and $R_B(h\nu)$ is to consider first the break-even point for the total radiation rates. The corresponding experimental conditions are then implicitly determined by the equation (2.38)

$$R_B=1.$$

In cases where $\Upsilon\ll\frac{1}{6}$, this is equivalent to the simple relation (2.39)

$$(E/mc^2)(H/H_{\mathrm{cr}})^2=3.46\times10^{-8}\,h(Z).$$

Under more extreme conditions the exact form of (2.36) must be used. Representative values for $h(Z)$ are given in Table II. The experimental conditions required to reach break-even for a number of materials are summarized graphically on Fig. 5. For convenience,

CC-0. In Public Domain. Gurukul Kangri Collection, Haridwar

Digitized by Arya Samaj Foundation Chennai and eGangotri

TABLE II. Representative values for $h(Z)$.

	Beryllium	Air	High explosive	Aluminum	Copper	Lead	Uranium
Z	4	~7	~8	13	29	82	92
A	9	~14	~16	27	63	204	238
ρ	1.84	1.25×10^{-3}	1.7	2.70	8.89	11.00	18.7
$h(Z)$	5.00×10^{-3}	6.44×10^{-6}	9.89×10^{-3}	0.024	0.156	0.409	0.734

curves of constant Υ are also indicated on the figure (compare Table III).

Figure 5 shows that for magnetic fields in the 1–10 MG range and energies above 10-BeV magnetic bremsstrahlung does indeed begin to compete favorably with bremsstrahlung in material media. In the range 100–1000 BeV—which is of interest in connection with projected high energy accelerators—even fields as modest as 1 MG (i.e., pulsed coil configurations or magnetically driven Cnare imploders) can be considered as practical bremsstrahlung converters. These trends become increasingly pronounced at still higher magnetic field strengths. Some of the estimates shown on Fig. 5 must be regarded with caution since the comparisons involving curves above the RR-line are subject to considerable radiation reaction corrections.[10]

A comparison of the spectral intensities of Coulomb and magnetic bremsstrahlung is given in Fig. 6. The curves illustrate the special case of a 20-BeV electron accelerator with a magnetic target adjusted to a field strength of 3 MG. This normalizes the total magnetic bremsstrahlung to the same level as the total ordinary (Coulomb) bremsstrahlung in beryllium, cf. the break-even criteria (2.38), (2.39). It is clear from the figure that under these conditions the low energy end of the spectrum will be completely dominated by magnetic bremsstrahlung. The energy $h\nu_1$ indicated on this graph is defined by the relation

$$h\nu_1 = 1.5E\Upsilon; \qquad (2.40)$$

and serves as a convenient marker of the upper end of the most intense part of the magnetic bremsstrahlung spectrum. The quantity $h\nu_2(\equiv 5h\nu_1)$ which also appears on the figure corresponds roughly to the upper energy limit of the useful portion of the spectrum; beyond this point the intensity dwindles very rapidly. Entries listing values of $h\nu_1$ and $h\nu_2$ corresponding to various experimental conditions are given in Table IV.

Figure 6 also exhibits the situation for a 1000-BeV device: In this case the beryllium target bremsstrahlung extends up towards 1000 BeV, but in virtue of the saturation of the transition amplitudes the absolute magnitude of the intensity does not increase beyond the level reached at 20 BeV. The peak of the corresponding magnetic spectrum ($H=3$ MG) is shifted to approximately 70 BeV, with a useful intensity excess extending up to about 700 BeV. Beyond this point present bremsstrahlung estimates become too uncertain to warrant detailed comparisons. The R_B ratio (2.36) appropriate to this case is of the order of 40.

Table IV contains a summary of the results of similar analyses for a variety of energies, field strengths, and target materials. The general trend of these comparisons supports the view that higher energies favor the magnetic interactions.

D. Bremsstrahlung Comparisons (continued)

There are a number of ultrahigh-energy effects which lead to modifications of the simple bremsstrahlung com-

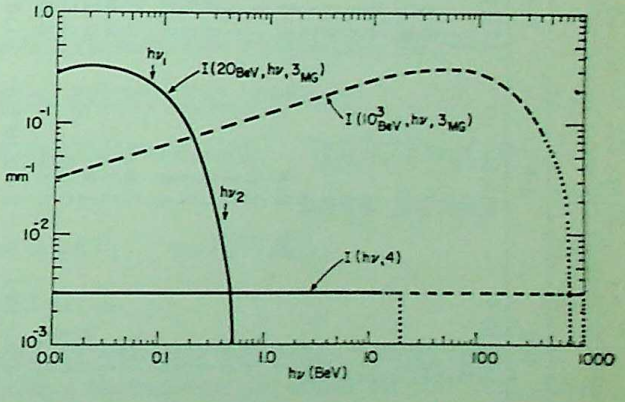

FIG. 6. Comparison of electron bremsstrahlung in beryllium and magnetic fields. In practical units

$$I(E, h\nu, H) \quad 0.12H_{MG}\,K\left(\frac{2}{3\Upsilon}\frac{h\nu}{E}\right)\text{mm}^{-1}, \qquad [\text{cf. (2.32)}];$$

and

$$I(h\nu, Z) \simeq 0.58h(Z)\,\text{mm}^{-1}, \qquad [\text{cf. (2.31a)}].$$

The actual radiation rates, in units of energy/mm, are given by $I(h\nu, Z)\Delta(h\nu)$ and $I(E, h\nu, H)\Delta(h\nu)$. The solid curves indicate the intensities for the conditions $E=20$ BeV and $H=3$ MG which have been adjusted to correspond to break-even, i.e., $R_B=1$ as in (2.38). The dashed curves represent the situation at $E=1000$ BeV with H remaining at 3 MG. The curve segments set off by ··· correspond to regions of theoretical uncertainty near the bremsstrahlung tip. For the definitions of $h\nu_1$ and $h\nu_2$, see (2.40) of the text.

[10] Present bremsstrahlung target materials are limited to total beam power loads of the order of 30 kW/cm² [M2]. It remains to be seen whether this limitation will favor magnetic targets in high-energy high-current devices.

CC-0. In Public Domain. Gurukul Kangri Collection, Haridwar

TABLE III. Values of $\Upsilon = 4.43 \times 10^{-5} E(\text{BeV}) H(\text{MG})$.

E_{BeV}	H_{MG}									
	0.1	0.5	1.0	2.0	3.0	4.0	5.0	6.0	7.0	8.0
1000	4.4×10^{-3}	22×10^{-3}	44×10^{-3}	89×10^{-3}	13×10^{-2}	18×10^{-2}	22×10^{-2}	27×10^{-2}	31×10^{-2}	36×10^{-2}
900	4.0	20	40	80	12	16	20	24	28	32
800	3.6	18	36	71	11	14	18	21	25	28
700	3.1	16	31	62	9.3	12	16	19	22	25
600	2.7	13	27	53	8.0	11	13	16	19	21
500	2.2	11	22	44	6.7	8.9	11	13	16	18
400	1.8	8.9	18	36	5.3	7.1	8.9	11	12	14
300	1.3	6.7	13	27	4.0	5.3	6.7	8.0	9.3	11
200	0.89	4.4	8.9	18	2.7	3.6	4.4	5.3	6.2	7.1
100	0.44	2.2	4.4	8.8	1.3	1.8	2.2	2.7	3.1	3.6
90	0.40	2.0	4.0	8.0	1.2	1.6	2.0	2.4	2.8	3.2
80	0.36	1.8	3.6	7.1	1.1	1.4	1.8	2.1	2.5	2.8
70	0.31	1.6	3.1	6.2	0.93	1.2	1.6	1.9	2.2	2.5
60	0.27	1.3	2.7	5.3	0.80	1.1	1.3	1.6	1.9	2.1
50	0.22	1.1	2.2	4.4	0.67	0.89	1.1	1.3	1.6	1.8
40	0.18	0.89	1.8	3.6	0.53	0.71	0.89	1.1	1.2	1.4
30	0.13	0.67	1.3	2.7	0.40	0.53	0.67	0.80	0.93	1.1
20	8.9×10^{-5}	0.44	0.89	1.8	0.27	0.36	0.44	0.53	0.62	0.71
10	4.4	0.22	0.44	0.88	0.13	0.18	0.22	0.27	0.31	0.36
6	2.7	0.13	0.27	0.53	8.0×10^{-4}	0.11	0.13	0.16	0.19	0.21
1	4.4×10^{-6}	2.2×10^{-5}	4.4×10^{-5}	8.9×10^{-5}	1.3	1.8×10^{-4}	2.2×10^{-4}	2.7×10^{-4}	3.1×10^{-4}	3.6×10^{-4}

E_{BeV}	H_{MG}										
	9.0	10	20	30	40	50	60	70	80	90	100
1000	40×10^{-2}	44×10^{-2}	88×10^{-2}	1.3	1.8	2.2	2.7	3.1	3.6	4.0	4.4
900	36	40	80	1.2	1.6	2.0	2.4	2.8	3.2	3.6	4.0
800	32	36	71	1.1	1.4	1.8	2.1	2.5	2.8	3.2	3.6
				($\Upsilon=1$, $E=752$)							
700	28	31	62	0.93	1.2	1.6	1.9	2.2	2.5	2.8	3.1
600	24	27	53	0.80	1.1	1.3	1.6	1.9	2.1	2.4	2.7
500	20	22	44	0.67	0.89	1.1	1.3	1.6	1.8	2.0	2.2
400	16	18	36	0.53	0.71	0.89	1.1	1.2	1.4	1.6	1.8
300	12	13	27	0.40	0.53	0.67	0.80	0.93	1.1	1.2	1.3
											($\Upsilon=1$, $E=225$)
200	8.0	8.9	18	0.27	0.36	0.44	0.53	0.62	0.71	0.80	0.89
100	4.0	4.4	8.8	0.13	0.18	0.22	0.27	0.31	0.36	0.40	0.44
90	3.6	4.0	8.0	0.12	0.16	0.20	0.24	0.28	0.32	0.36	0.40
80	3.2	3.6	7.1	0.11	0.14	0.18	0.21	0.25	0.28	0.32	0.36
70	2.8	3.1	6.2	9.3×10^{-2}	0.12	0.16	0.19	0.22	0.25	0.28	0.31
60	2.4	2.7	5.3	8.0	0.11	0.13	0.16	0.19	0.21	0.24	0.27
50	2.0	2.2	4.4	6.7	8.9×10^{-2}	0.11	0.13	0.16	0.18	0.20	0.22
40	1.6	1.8	3.6	5.3	7.1	8.9×10^{-2}	0.11	0.12	0.14	0.16	0.18
30	1.2	1.3	2.7	4.0	5.3	6.7	8.0×10^{-2}	9.3×10^{-2}	0.11	0.12	0.13
20	0.80	0.89	1.8	2.7	3.6	4.4	5.3	6.2	7.1×10^{-2}	8.0×10^{-2}	8.9×10^{-2}
10	0.40	0.44	0.88	1.3	1.8	2.2	2.7	3.1	3.6	4.0	4.4
6	0.24	0.27	0.53	0.80	1.1	1.3	1.6	1.9	2.1	2.4	2.7
1	4.0×10^{-4}	4.4×10^{-4}	8.8×10^{-4}	0.13	0.18	0.22	0.27	0.31	0.36	0.40	0.44

CC-0. In Public Domain. Gurukul Kangri Collection, Haridwar

Digitized by Arya Samaj Foundation Chennai and eGangotri

Digitized by Arya Samaj Foundation Chennai and eGangotri

TABLE IV. Summary of magnetic bremsstrahlung characteristics.

Accelerator energy	Material	Magnetic "break-even" field	Υ	Total energy dissipation	$h\nu_1$[d]	$R_B(h\nu_1)$	$h\nu_2$[d]	$R_B(h\nu_2)$
20 BeV	RR[a]	6.0 MG	5.3×10^{-3}	180 MeV/mm	160 MeV	...	...	...
	Be	3.0	2.7	45	79	79	400 MeV	2.5
	HE[b]	4.2	3.7	90	110	56	560	1.8
	Al	6.4	5.7	210	170	35	850	1.1
40 BeV	RR	1.5	2.7×10^{-3}	45	160	...	...	...
	Be	2.1	3.7	89	220	55	1.1 BeV	1.8
	HE	3.0	5.3	180	320	40	1.6	1.3
	Al	4.5	8.0	410	480	25	2.4	0.80
	Cu	10	18	2100	1100	8.6	5.4	0.27
500 BeV	RR	2.6×10^4 G	3.5×10^{-4}	0.77 MeV/mm	160 MeV	...	...	...
	Be	0.75 MG	1.0×10^{-2}	0.64 BeV/mm	4.5 BeV	20	23 BeV	0.63
	HE	0.98	1.3	1.1	5.9	13	29	0.42
	Al	1.5	2.0	2.6	9.0	8.2	45	0.26
	Cu	4.5	6.0	23	27	3.7	...[c]	...
	Pb	7.2	9.6	55	43	2.3	...	...
	U	11	14	96	60	1.9	...	...
1000 BeV	RR	2.4×10^3 G	1.1×10^{-4}	72 keV/mm	160 MeV	...	...	...
	Be	0.38 MG	0.017	2.2 BeV/mm	26 BeV	10.0	130 BeV	...
	HE	0.52	0.023	4.3	35	6.7	170	...
	Al	0.84	0.037	10	56	4.6	280	...
	Cu	2.5	0.11	68	170	2.1	...	...
	Pb	5.0	0.22	180	330	1.6	...	...
	U	7.9	0.35	320	525	...[c]	...	...

[a] RR refers to the radiation reaction condition (2.27a, b); compare Fig. 5.
[b] HE=high explosives (PBX or Composition "B").
[c] Entries omitted because the condition $h\nu \ll E$ is violated.
[d] For definitions of these energies see Eq. (2.40) and the subsequent remarks.

parisons considered in the previous section. In particular it has already been emphasized that magnetic bremsstrahlung under strong radiation reaction conditions, i.e., in the region above "RR" on Fig. 5, will exhibit deviations from the quantum mechanical results (2.32) and (2.35). There are similar corrections for ordinary bremsstrahlung which arise from coherent effects in condensed material media. Generally these effects introduce nontrivial frequency variations in the flat Bethe–Heitler spectrum (2.31a) and are responsible for reductions in the over-all radiative losses. In the energy region of interest, i.e., 10–10^3 BeV, the most important of these coherent effects is the multiple scattering inhibition originally discussed by Landau and Pomeranchuk [L3, M3, M4, D2]. This originates in the relativistic amplification of the intrinsic coherence length associated with the bremsstrahlung scattering amplitude [S5]. At incident electron energies exceeding 10^8 eV this coherence length becomes comparable to interatomic distances and the bremsstrahlung conversion can no longer be idealized as occurring in the vicinity of a single nucleus.[11] In order to discuss this process quantitatively it is convenient to introduce several characteristic energies [G1, G2]:

$$E_l \simeq [200/h(Z)][\rho Z/A]^{1/2}\, mc^2; \tag{2.41}$$

$$E_0 \simeq 3.5\times10^6\, mc^2/h(Z); \qquad [\text{for } h(Z) \text{ see (2.31b)}] \tag{2.42}$$

$$h\nu_l \simeq \gamma E^{2/3}, \qquad \gamma = E_l^{4/3}/E_0; \tag{2.43}$$

$$h\nu_u \simeq E^2/E_0. \tag{2.44}$$

Multiple scattering corrections become important for incident electron energies above the threshold $E > E_l$. The bremsstrahlung region most strongly affected lies between the limits

$$\nu_l \lesssim \nu \lesssim \nu_u. \tag{2.45}$$

In this interval the Bethe–Heitler spectrum is modified by the inhibiting factor q as follows:

$$I(h\nu, Z) \to q(E, h\nu, Z)\, I(h\nu, Z),$$

where

$$q(E, h\nu, Z) \simeq [(2\times10^3)/E][h\nu\, mc^2/h(Z)]^{1/2}. \tag{2.46}$$

For example, $q(10^3 \text{ BeV}, 0.1 \text{ BeV}, 4) \sim \frac{1}{5}$, which confirms that under certain conditions the reduction of the

[11] This coherence phenomenon is a direct relativistic counterpart to coherent multiple photon scattering [B3, B4].

CC-0. In Public Domain. Gurukul Kangri Collection, Haridwar

Digitized by Arya Samaj Foundation Chennai and eGangotri

TABLE V. Critical energies (eV).

	Beryllium	Air	High explosive	Aluminum	Copper	Lead	Uranium
E_l	1.8×10^{10}	3.9×10^{11}	9.2×10^{9}	4.7×10^{9}	1.3×10^{9}	5.1×10^{8}	3.6×10^{8}
E_0	3.5×10^{14}	2.7×10^{17}	1.8×10^{14}	7.3×10^{13}	1.1×10^{13}	4.3×10^{12}	2.4×10^{12}
γ	0.13	0.011	0.13	0.13	0.12	0.11	0.11

ordinary bremsstrahlung intensity may indeed be considerable. In the special case $E\to E_l$, and $\nu\to\nu_l$, it is easy to check that $q\to1$, so that the inhibition vanishes. In the opposite limit $\nu\to\nu_u$ (but $E>E_l$), the factor q on the left-hand side of (2.46) must be replaced by $q(1-q)^{-1/2}$, and one again finds $q\to1$. Under conditions corresponding to $E>E_l$, but $\nu<\nu_l$ (i.e., $h\nu\lesssim10^8$ eV), the expression (2.46) no longer applies and the Landau–Pomeranchuk spectrum goes into the Ter-Mikaeljan spectrum.[12] A number of related possibilities are discussed in reference [G1].

Values of the critical energies for a number of materials are summarized in Table V. This information is also given graphically on Fig. 7. For illustration the spectral regions exhibiting the multiple scattering reduction corresponding to the specific incident energy 10^3 BeV are indicated on the figure.

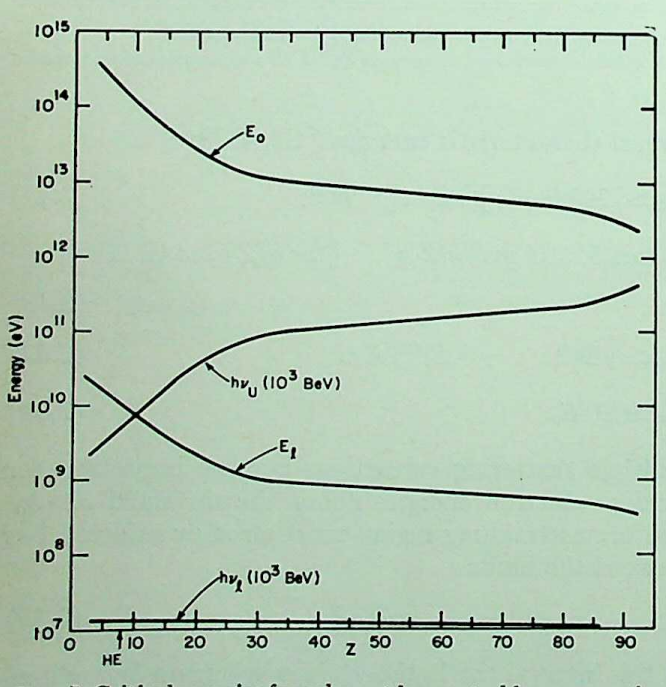

FIG. 7. Critical energies for coherent bremsstrahlung corrections. The curves $h\nu_l$ and $h\nu_u$ [compare (2.43) and (2.44)] mark the boundaries of the spectral regions which are damped by the Landau–Pomeranchuk effect corresponding to the special choice $E\sim10^3$ BeV.

[12] This refers to an additional reduction of low-energy bremsstrahlung emission due to the effects of the polarization of the medium [T2]. Several other effects of this type have been considered by Toptygin [T3] and Feinberg and Pomeranchuk [F5].

At this stage one could in principle return to Sec. 2C and undertake a revision of all the previously computed high-energy (i.e., $E>E_l$) bremsstrahlung comparisons to allow for the Landau–Pomeranchuk effect. However in view of the likely prospect of still further revisions which may eventually be required for radiation reaction and other coherent effects this does not seem advisable at present. It will be sufficient to illustrate the kinds of modifications that can be expected by considering one specific case: If we refer back to Fig. 6 we may easily obtain the values of the differential magnetic Coulomb bremsstrahlung comparison factor $R_B(h\nu)$ appropriate to beryllium. Comparing with Fig. 7, it is evident that for incident energies $E\sim10^3$ BeV, the Landau–Pomeranchuk spectrum includes the special value $h\nu\sim0.1$ BeV. According to the preceding discussion the corresponding q-reduction for these specific conditions is $\sim\frac{1}{5}$. In this instance therefore the multiple scattering inhibition enhances the relative importance of magnetic bremsstrahlung by boosting the spectral ratio $R_B(0.1\text{ BeV})$ from 20 to 100.

Similar trends in the relative enhancement of magnetic bremsstrahlung can be discerned in connection with a number of other coherent effects.[13] For example the coherence length associated with the Landau-Pomeranchuk inhibition is approximately given by

$$l\simeq2\times10^3\,\lambda\!\!\!^{-}_c E\,[h\nu\times mc^2\times h(Z)]^{-1/2}. \tag{2.47}$$

At very high energies this length can become comparable to the macroscopic target dimensions and the corresponding bremsstrahlung matrix elements will contain terms dependent on the surface configuration. In cases where these targets are "thin" relative to l, the bremsstrahlung dissipation may be expected to exhibit a saturation. For energies of the order of 10^5E_0 self-absorption due to pair production begins to play a role and bremsstrahlung emission is damped still further.[14]

[13] Probable exceptions in this respect are corrections of the Frisch–Überall type [F6, U1].

[14] More precisely, we expect that the total bremsstrahlung losses will exhibit an energy dependence $\Delta\mathcal{E}/\Delta x\sim\mathcal{O}(E^{\frac{1}{2}})$, for $E_l\lesssim E\lesssim1.4\times10^5E_l$; and furthermore that $\Delta\mathcal{E}/\Delta x\sim\mathcal{O}(E^{-1})$, for $E\gtrsim1.4\times10^5E_l$ [G2]. In the absence of corresponding modifications for $g(\Upsilon)$, this implies that $R_B\to\infty$ for $E\to\infty$ [compare (2.36)].

CC-0. In Public Domain. Gurukul Kangri Collection, Haridwar

Digitized by Arya Samaj Foundation Chennai and eGangotri

There are some special circumstances in which the observation of the recoil electrons associated with (quasi-elastic) bremsstrahlung can be of practical interest. A particular example is the detection and calibration of transient magnetic fields trapped in the interior of explosive flux compressors [F1]. This type of experiment is based on the fact that explosive materials are relatively transparent to incident electrons with sufficiently high energy [compare Fig. 5]. In particular under conditions where $E>E_l$, electrons traverse high explosives with a mean deflection angle [per coherence length (2.47)] given approximately by

$$\theta_{\mathrm{HE}}\simeq\bar{q}^{-1/2}\,mc^2/E, \tag{2.48a}$$

where the factor $\bar{q}$, corresponding to the Landau–Pomeranchuk region, may be derived from (2.46).

On the other hand, a transverse magnetic field $H_\perp$ localized in a region of diameter d scatters such electrons through an angle

$$\theta_{H\perp}\simeq\frac{d}{\lambda\!\!\!^{-}_c}\frac{H_\perp}{H_{\mathrm{cr}}}\frac{mc^2}{E}. \tag{2.48b}$$

Experimental conditions can in fact be adjusted so that $\theta_{H\perp}\gg\theta_{\mathrm{HE}}$, and these large-angle deflections advantageously exploited for high-field studies.

3. PAIR PRODUCTION

A. General Remarks on Magnetic Field–Photon Interactions

Among the many different kinds of mechanism available for mediating magnetic field-photon interactions there are two particular processes which are closely linked through crossing symmetry and time reversal to the bremsstrahlung matrix elements discussed in the previous section.

One of these processes is inverse-bremsstrahlung [Fig. 8(a)], which for strongly bound initial states may be regarded as a direct analog of the atomic photoeffect. In the present context this type of conversion is relevant for experimental arrangements concerned with the generation of intense magnetic fields containing a plasma: This kind of system is essentially the equivalent of an n-electron "super-atom" capable of sustaining large momentum transfers during internal transitions. If such a magnetically stiffened plasma matrix (or plasma counter) is bombarded with high-energy photons it should in principle exhibit an enormous opacity in virtue of inverse-bremsstrahlung since the basic energy transfer rates are scaled by the same factors that appear in the direct process, i.e., $\alpha mc^2/\lambda\!\!\!^{-}_c\sim10^4$ BeV/mm (2.14a). Some qualitative features of this type of conversion may be inferred from the magnetic Compton scattering calculations of Robl [R1]. More refined estimates are unfortunately not available at present.

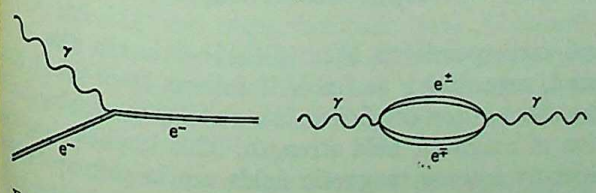

FIG. 8. (a) Feynman diagram for inverse-bremsstrahlung in a magnetic field. (b) Feynman diagram for a simple vacuum polarization loop.

The other photon interaction related to bremsstrahlung is pair production [Fig. 1(a)]. This process differs from bremsstrahlung in the important respect that although conservation laws do not forbid the interaction for photon energies above the threshold $h\nu\gtrsim2mc^2$, the conversion rate is impractically small unless the condition $\frac{1}{2}(h\nu/mc^2)\,(H/H_{\mathrm{cr}})\equiv\chi\rightarrow0.1$ is satisfied. This is a very severe requirement, and in fact magnetic pair production has not yet been observed experimentally. However once the parameter χ reaches the range $\chi\gtrsim0.1$, the photon attenuation coefficient increases rapidly and magnetic pair production begins to dominate the corresponding process in matter. In principle strong magnetic fields are capable of degrading photons of arbitrarily high initial energy through direct pair production, as well as by means of other higher-order processes such as trident production, and electromagnetic shower development [e.g. Fig. 1(b)]. These points are discussed in quantitative detail in the following sections.

For purposes of computation it is convenient to order the magnetic field–photon conversion processes according to the powers of the coupling constant (α) which appear in the matrix elements. However just as in the case of the corresponding sequence of interactions associated with the Coulomb field, i.e., the photoeffect, Compton scattering, pair production, etc. a simple ordering according to powers of the coupling constant does not necessarily reflect the actual experimental importance of each process. A simple illustration of this is provided by magnetic vacuum polarization [Fig. 8(b)], which is a significant component in a number of physical effects including the reduction of the velocity of light in transverse magnetic fields, despite the fact that it is of second order in α and involves virtual pairs in the intermediate states. These types of vacuum polarization effects are essentially high-field–low-energy phenomena and can be observed under circumstances where lower-order processes such as pair production do not exist [E1, E2].

Returning to high-energy–high-field phenomena, we note that further examples of magnetic field–photon interactions include photon splitting [S6, E8] and photon coalescence [K7]. These are represented by the third-order bubble diagrams shown on Fig. 2. Under appropriate conditions magnetic photon splitting can actually dominate magnetic pair production. These problems are discussed in some detail in Sec. 5B.

CC-0. In Public Domain. Gurukul Kangri Collection, Haridwar

Digitized by Arya Samaj Foundation Chennai and eGangotri

B. Magnetic Pair Production

It is convenient to idealize the physical situation corresponding to magnetic pair production by considering the propagation of light across a uniform unbounded magnetic field in a direction perpendicular to the lines of flux. Since the magnetic field may absorb momentum, there is a nonvanishing probability that photons with sufficient energies ($h\nu \gtrsim 2mc^2$) will convert into electron–positron pairs. For a bound-state problem of this kind it is appropriate to express the conversion probability in terms of a photon attenuation coefficient $\alpha(\chi)$, which determines the actual number of pairs (n_{pairs}) created for a photon path length (d) in the magnetic field (H),

$$n_{\text{pairs}} = n_{\text{photons}} \{1 - \exp[-\alpha(\chi)\, d]\} \simeq n_{\text{photons}}\, \alpha(\chi)\, d. \tag{3.1}$$

The parameter $\chi \equiv \frac{1}{2}(h\nu/mc^2)(H/H_{\text{cr}})$ appearing in this expression is the essential factor governing the rate of pair conversion. It plays a role analogous to the parameter Υ in bremsstrahlung. The matrix element for this process, corresponding to the diagram of Fig. 1(a), leads to the expression

$$\alpha(\chi) = 2\pi(\alpha/\nu) \times \sum_{ss'll'nn'\epsilon} |\langle n', s', l' \,|\, \boldsymbol{\alpha}\cdot\boldsymbol{\varepsilon} \exp(-i\mathbf{k}\cdot\mathbf{r}) \,|\, n, s, l\rangle|^2, \tag{3.2}$$

which is analogous to the bremsstrahlung form (2.3) except that now the "initial" spinor represents an outgoing positron. The explicit evaluation of this attenuation coefficient in the ultrarelativistic limit, neglecting all but the leading terms in $E(e^{\pm})/mc^2$, assuming $H \ll H_{\text{cr}}$, and disregarding various kinds of magnetic and electron–positron bound-state resonances [E2, G3, A3], has been described in detail on a number of previous occasions [R2, T1, K4]. The final results may be expressed in the form

$$\alpha(\chi) = \tfrac{1}{2}(\alpha/\lambda\!\!\!^{-}_c)(H/H_{\text{cr}})\, T(\chi), \tag{3.3a}$$

where the dimensionless auxiliary function $T(\chi)$ is given by

$$T(\chi) = \frac{4}{3\pi^2\chi^2}\int_0^\infty\!\!\int_0^\infty du\, dw \times \Big\{[2\cosh^2 w \cosh^5 u - \sinh^2 u \cosh^3 u] \times K^2{}_{1/3}\Big(\frac{2}{3\chi}\cosh^2 w \cosh^3 u\Big) + [2\cosh^2 w - 1] \cdot \times \cosh^5 u\, K^2{}_{2/3}\Big(\frac{2}{3\chi}\cosh^2 w \cosh^3 u\Big)\Big\}. \tag{3.3b}$$

The asymptotic properties of the modified Bessel functions appearing in this integral representation may be used to establish the limiting cases:

$$T(\chi) = \begin{cases} 0.46 \exp\{-4/(3\chi)\}, & \chi \ll 1; \\ 0.60\, \chi^{-1/3}, & \chi \gg 1. \end{cases} \tag{3.3c}$$

An excellent analytic approximation for $T(\chi)$ is given by the expression

$$T(\chi) \cong 0.16 \chi^{-1} K^2{}_{1/3}(2/3\chi). \tag{3.3d}$$

This function is graphed in Fig. 9; some representative values are listed in Table VI.

Equations (3.3a) and (3.3d) may be combined to give a concise expression for the photon attenuation coefficient,

$$\alpha\Big(\frac{1}{2}\frac{h\nu}{mc_2}\frac{H}{H_{\text{cr}}}\Big) = 0.16\,\frac{\alpha}{\lambda\!\!\!^{-}_c}\frac{mc^2}{h\nu} K^2{}_{1/3}\Big(\frac{4}{3}\frac{mc^2}{h\nu}\frac{H_{\text{cr}}}{H}\Big). \tag{3.4}$$

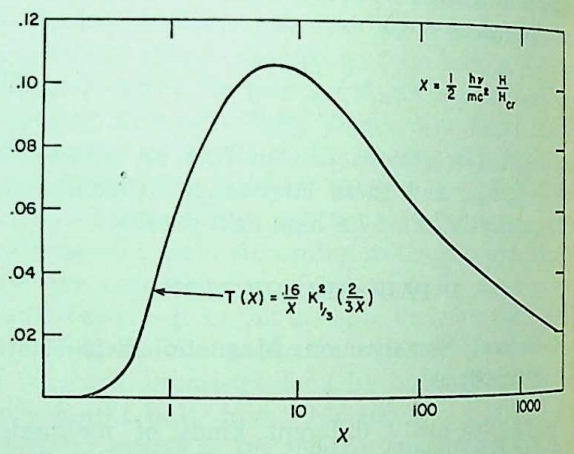

FIG. 9. The magnetic pair production function $T(\chi)$; compare (3.4a-d).

This indicates clearly that the attenuation coefficient is not a symmetric function of the magnetic field strength and photon energy. In particular, considering H to be fixed, it is easy to verify that $\alpha(\chi)$ has a unique maximum with respect to variations of the photon energy which occurs at the point

$$h\nu_{\text{max}}/mc^2 \simeq 12(H_{\text{cr}}/H); \tag{3.5}$$

and corresponds to $\text{Max}\{T(6)\} \sim 0.1$. On the other hand, regarding ν as fixed, it follows from (3.4) that the attenuation coefficient is a strictly increasing function of magnetic field strength. This implies that sufficiently intense magnetic fields are in principle completely efficient pair converters for photons of arbitrarily high energy. Comparing with (3.1) we see that this is equivalent to the condition $\alpha(\chi)\, d' \to 1$, or the

CC-0. In Public Domain. Gurukul Kangri Collection, Haridwar

Digitized by Arya Samaj Foundation Chennai and eGangotri

explicit criterion

$$H(\mathrm{MG})\, d'(\mathrm{mm}) \rightarrow 46. \tag{3.6a}$$

The associated photon energies are approximately bounded from below by

$$h\nu/mc^2 \gtrsim 6\times 10^6\, d'(\mathrm{mm}). \tag{3.6b}$$

This characteristic shielding distance (d') is still very much smaller than the radius of curvature (R) of the emergent photopairs. This follows immediately from the relation

$$R/d' \sim 10^3\, d'(\mathrm{mm}). \tag{3.6c}$$

C. Pair Production Comparisons

We now evaluate the relative efficacy of magnetic fields and material targets as pair converters. It is convenient to carry out these comparisons in terms of the respective attenuation coefficients. The pertinent result for magnetic fields is given by (3.3a). The best current estimate for the corresponding attenuation coefficient in material media, including both relativistic and Coulomb corrections, is given by the expression [D3]

TABLE VI. The magnetic pair production function $T(\chi)$.

χ	$T(\chi)$
0.2	2×10^{-4}
0.3	2.2×10^{-3}
0.4	6.6×10^{-3}
0.7	0.026
1.2	0.055
3.0	0.094
5.0	0.10
6.0	0.10
7.0	0.10
9.0	0.10
15	0.099
30	0.085

where

$$\beta(Z) = \tfrac{14}{27}\,\alpha N_0 \lambda_c^2 \hat{h}(Z), \tag{3.7}$$

$$\hat{h}(Z) = h(Z) - 0.640(\rho/A)(\alpha Z)^2, \tag{3.7a}$$

and $h(Z)$ is the function defined in (2.31b). Since we are considering the ultrarelativistic case ($h\nu \gg mc^2$), the matrix elements leading to (3.7) have been evaluated in the fully screened limit and this results in an attenuation coefficient which is independent of the energy.

The condition for competition of pair production in matter and magnetic fields then is equivalent to

$$\alpha(\chi) \simeq \beta(Z);$$

and inserting (3.3a) and (3.7), this leads to the requirement

$$(H/H_{cr})\, T(\chi) \simeq 3.59\times 10^{-3}\, \hat{h}(Z). \tag{3.8}$$

TABLE VII. Break-even points for pair production in material media and magnetic fields.[a]

Substance	Attenuation coefficient (mm^{-1})	Energy (BeV) 20	40	300	1000	10 000
Air	4×10^{-6}	200	100	15	5	...
Be	3×10^{-3}	300	160	30	10	2
Cu	0.1	...	300	50	20	5
Pb	0.3	...	320	70	30	8

[a] Table entries in megagauss (MG).

Due to the high-energy saturation of pair production in material media it is clear that magnetic pair production will eventually dominate under sufficiently extreme conditions. The precise values of the photon energies and magnetic field strengths corresponding to the break-even point may be obtained by inverting the equality (3.8). Results for a number of representative cases are listed in Table VII and given graphically on Fig. 10.

The general trend of these figures indicates that magnetic pair production becomes a significant competitor for pair conversion in material media only in

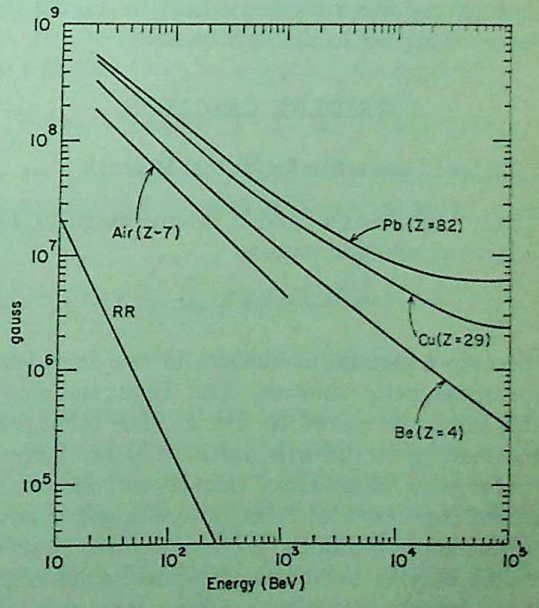

FIG. 10. Break-even curves for pair production in magnetic fields and various material media. The position of the "RR" line (2.27a, b) indicates that *all* of these curves lie in the strong radiation reaction region.

CC-0. In Public Domain. Gurukul Kangri Collection, Haridwar

Digitized by Arya Samaj Foundation Chennai and eGangotri

TABLE VIII. Minimum magnetic fields for break-even in pair production.

Element	Field (MG)	Energy (BeV)	Υ
Be	0.08	4×10^6	~14
Cu	2.4	1.3×10^5	~14
Pb	6.3	5×10^4	~14

the region $H\gtrsim 10$ MG, $h\nu\simeq 100$ BeV. The associated photon attenuation rates vary from moderate, i.e., 0.003 mm^{-1} corresponding to break-even for beryllium, to severe, i.e., 0.3 mm^{-1} corresponding to break-even for lead. In view of the comparisons with air it is however clear that the *existence* of magnetic pair production could in principle be demonstrated under experimentally less demanding conditions.

The absorption maximum discussed previously in connection with the attenuation coefficient (3.4) may also be utilized to find the *minimum* magnetic field strength compatible with the break-even condition (3.8). The corresponding photon energy may then be determined from equation (3.5). Some of these results are given in Table VIII. Evidently the energies associated with break-even for minimum magnetic fields are quite large. In view of the fact that the corresponding Υ values are greater than unity, these results should however be considered only as semiquantitative indications. As emphasized previously, magnetic pair production under these conditions can be expected to exhibit considerable modifications due to radiation reaction effects, and reliable methods for taking these into account are not available at present.

4. TRIDENT CASCADES

A. Trident Production by Virtual Photons

At very high energies and in intense magnetic fields the trident production process

$$e^{\pm}\rightarrow e^{\pm}+e^{+}+e^{-} \tag{4.1}$$

can become a significant element in the development of electromagnetic showers. The Feynman diagram for this process is shown on Fig. 11. The intermediate photon leading to the pair vertex may be either real or virtual; and in an exact calculation coherent contributions from both of these processes will appear in the transition amplitudes. We are however at present interested only in a preliminary quantitative orientation and interference effects arising from this source will be neglected. In the present section we estimate the virtual photon contribution to trident production on the basis of the Fermi–Weizsäcker–Williams (FWW) approximation. In the next section we evaluate the real photon contribution as a two step process involving bremsstrahlung and subsequent pair production. In the last section the relative conversion rates of these two processes are consolidated and compared with the corresponding rates of trident production in material media.

It is convenient to express the results of the trident production calculations directly in terms of the expected number of events per unit path length. Specifically for the virtual photon trident process we introduce the function $N_V^{(T)}(E,H)$ to represent the average number of events occurring during the passage of n electrons of energy E through a path length d in a transverse magnetic field H. This is given by

$$N_V^{(T)}(E,H)=nd\sum_{\nu}\mathfrak{N}(\nu)\alpha(\nu); \tag{4.2}$$

where $\mathfrak{N}(\nu)$ is the number of equivalent photons of frequency ν carried along by an electron, and $\alpha(\nu)$ is the absorption coefficient for pair production (3.3a). The Fourier resolution of the electron field then leads to the expression[15] [F7, W3, W4]

$$\mathfrak{N}(\nu)=(2/\pi)(\alpha/h\nu)W(h\nu/E)\,d(h\nu), \tag{4.3a}$$

where

$$W(\chi)=\chi K_0(\chi)K_1(\chi)-(\chi^2/2)[K_1^2(\chi)-K_0^2(\chi)]. \tag{4.3b}$$

Appropriate expansions of the modified Bessel functions in this expression yield the limiting cases

$$W(\chi)=\begin{cases}-\ln\chi, & \chi\ll 1;\\ (\pi/4)\,e^{-2\chi}, & \chi\gg 1.\end{cases} \tag{4.3c}$$

Since the pair production coefficient has a maximum in the vicinity of $h\nu\sim 12(H/H_{cr})mc^2$, it is clear from (4.3c) that trident conversion may be expected to increase logarithmically with energy. This is indeed confirmed by the details of the calculation. In order to obtain an explicit expression for the virtual photon trident conversion rate we substitute (4.3a) and (3.3a)

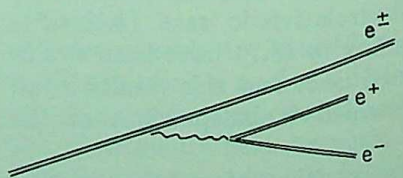

FIG. 11. Diagram for trident production in an external field.

[15] These estimates could in principle be improved with a covariant form of the Fermi–Weizsäcker–Williams approximation [B5].

CC-0. In Public Domain. Gurukul Kangri Collection, Haridwar

Digitized by Arya Samaj Foundation Chennai and eGangotri

into (4.2). After some rearrangement this can be written in the form

$$N_V^{(T)}(E,H) = nd(0.32/\pi)(\alpha^2/\lambda\!\!\!^{-}_c)(H/H_{cr})\hat{\Omega}(\Upsilon), \quad (4.4)$$

where

$$\hat{\Omega}(\Upsilon) = \int_0^\infty du\, u^{-2}\, W(u/\Upsilon) K^2_{1/3}(4/3u). \quad (4.4a)$$

An important feature of this representation is that it exhibits the fact that trident conversion depends principally on the parameter

$$\Upsilon = (E/mc^2)(H/H_{cr}),$$

where E, as noted above, is the energy of the initial electron.

The exact analytical form of $\hat{\Omega}(\Upsilon)$ is too cumbersome to provide any useful insight. As shown in Appendix 3, it has the asymptotic limits

$$\hat{\Omega}(\Upsilon) = \begin{cases} (\pi^{5/2}/16)(3\Upsilon)^{1/4} \exp\{-8(3\Upsilon)^{-1/2}\}, & \Upsilon \ll 1; \\ (\pi^2/2) \ln \Upsilon, & \Upsilon \gg 1. \end{cases} \quad (4.4b)$$

Numerical values may be obtained from the graph given in Fig. 12. We see that the high-energy limit—or more precisely, the large Υ limit—of $\hat{\Omega}(\Upsilon)$ does in fact exhibit the expected logarithmic behavior. The other asymptotic limit has a slightly more complicated functional dependence. This is consistent with the general trend that one would anticipate for conversion processes of increasingly higher order. Comparing with the corresponding limit of ordinary pair production, e.g. (3.3a–c), we see that trident conversion is diminished by a factor of α (second-order process!) but decreases far less rapidly with energy, i.e., $\exp(-\Upsilon^{-1/2})$ as compared with $\exp(-\Upsilon^{-1})$. A detailed discussion of (4.4) and an evaluation of its significance relative to other trident production processes is given in Sec. 4C.

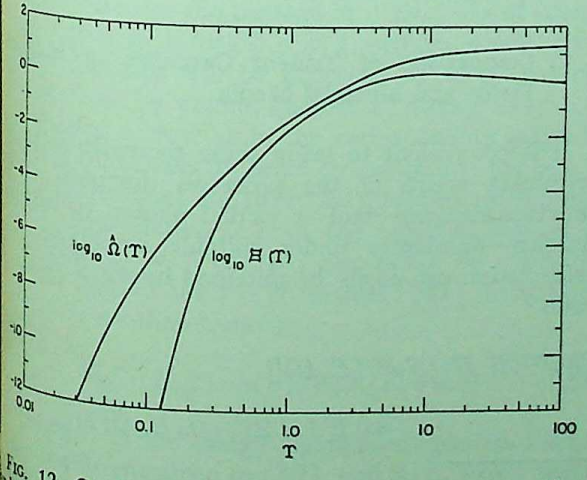

FIG. 12. Graphs of the trident production functions: $\hat{\Omega}(\Upsilon)$ and $\Xi(\Upsilon)$ correspond to virtual and real intermediate photon states, respectively. Compare Eqs. (4.4a) and (4.6b).

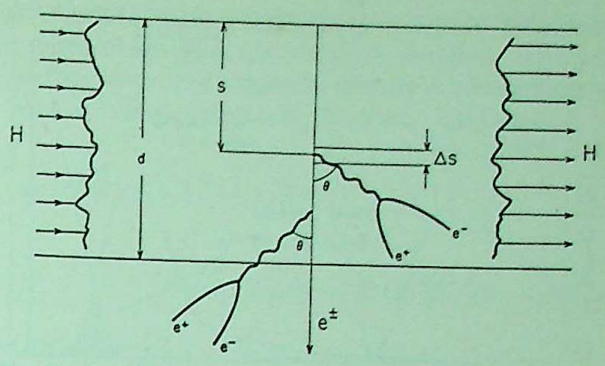

FIG. 13. Trident cascades resulting from magnetic bremsstrahlung and subsequent pair conversion. Essentially the same diagram describes the analogous processes occurring in material media. In the ultrarelativistic limit $\theta \sim 0\,(mc^2/E) \to 0$.

B. Trident Production by Real Photons

The conversion rate governing this process can be estimated by considering the two-step sequence "magnetic bremsstrahlung→magnetic pair production" which is schematically indicated on Fig. 13. The number of bremsstrahlung photons radiated into the energy interval $\Delta(h\nu)$ over a distance ΔS is given by

$$nI(E,H,h\nu)(\Delta S/c)[\Delta(h\nu)/h\nu];$$

where $nI(E,H,h\nu)$ is the spectral function corresponding to bremsstrahlung emission by n electrons with energy E traversing a perpendicular magnetic field H [compare (2.5a)]. These photons partially convert into pairs, and according to Fig. 13 and the photon attenuation equation (3.1), at a depth d one expects

$$n\alpha(\nu)I(E,H,h\nu)(d-S)(\Delta S/c)[\Delta(h\nu)/h\nu]$$

pairs to have been produced. The total number of tridents arising from real photon conversion then is given by

$$N_R^{(T)}(E,H) = n \sum_{\nu} \sum_{s} \alpha(\nu) I(E,H,h\nu)(d-S) \times (\Delta S/c)[\Delta(h\nu)/h\nu]. \quad (4.4c)$$

This representation is analogous to Eq. (4.2) which determines the rate for virtual photon trident production. The detailed numerical evaluation of this expression of course requires explicit forms for the photon attenuation coefficient and the bremsstrahlung spectral function. It is convenient to introduce the auxiliary variables

$$\sigma = (h\nu/mc^2)(H/H_{cr}), \quad \text{and} \quad \Upsilon = (E/mc^2)(H/H_{cr}). \quad (4.5)$$

CC-0. In Public Domain. Gurukul Kangri Collection, Haridwar

Digitized by Arya Samaj Foundation Chennai and eGangotri

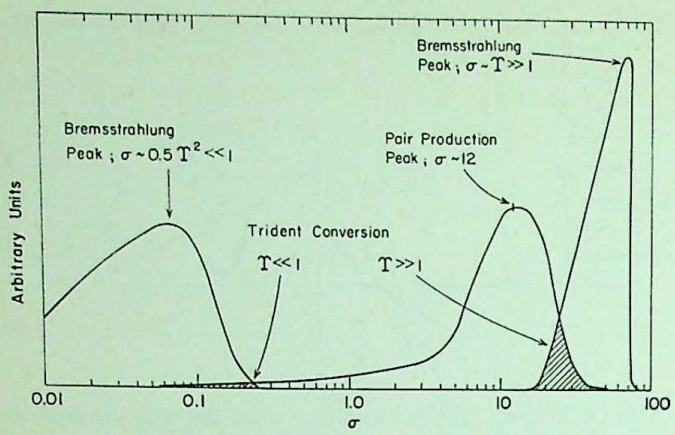

FIG. 14. Sketch of the bremsstrahlung and pair production curves for real photon trident cascades. The principal contributions to $N_R^{(T)}(E, H)$ [compare (4.4c)] arise from the cross-hatched overlap regions.

Energy conservation implies the constraint $\sigma \leq \Upsilon$. In terms of these variables we then have [compare (3.3a)]

$$\alpha(\nu) = 0.16(\alpha/\lambda\!\!\!^{-}_c)(H/H_{cr})\sigma^{-1} K^2_{1/3}(4/3\sigma), \quad (4.5a)$$

and [compare (2.5a)]

$$c^{-1} I(E, H, h\nu) = \frac{1}{3\pi^2}\frac{\alpha}{\lambda\!\!\!^{-}_c}\left(\frac{\sigma}{\Upsilon^2}\right)^2 \frac{H}{H_{cr}} \mathfrak{M}(\sigma, \Upsilon), \quad (4.5b)$$

where $\mathfrak{M}(\sigma, \Upsilon) = \mathfrak{M}(y, \Upsilon)$, represents the auxiliary function defined in Eq. (2.5b). Inserting these expressions into (4.4c), and carrying out the spatial integration, we obtain

$$N_R^{(T)}(E, H) = \frac{\sqrt{3}}{25\pi} n \left(\alpha \frac{d}{\lambda\!\!\!^{-}_c}\frac{H}{H_{cr}}\right)^2 \Xi(\Upsilon), \quad (4.6a)$$

where

$$\Xi(\Upsilon) = \frac{2\sqrt{3}}{9\pi}\Upsilon^{-4}\int_0^\Upsilon d\sigma\, \mathfrak{M}(\sigma, \Upsilon) K^2_{1/3}(4/3\sigma). \quad (4.6b)$$

This representation shows clearly that real photon trident cascades tend to increase quadratically with distance and field strength—as would be expected for a second-order process. The importance of the parameter Υ is also once again exhibited.

The general behavior of $\Xi(\Upsilon)$ may be inferred from the curves sketched in Fig. 14. For values of Υ less than unity, the bremsstrahlung spectrum will consist principally of low-energy photons and the probability for pair conversion will be negligibly small. In fact in the limit $\Upsilon \ll 1$ one would expect that real photon trident conversion would decrease even more rapidly than pair production. In the opposite limit ($\Upsilon \gg 1$) one would also anticipate a decrease in the conversion rate. This is essentially due to the fact that in this case most of the bremsstrahlung emission is concentrated near the high-energy end of the spectrum. Since pair production decreases in the range $\sigma < 12$, it is evident that the overlap between bremsstrahlung and photon attenuation will progressively diminish as Υ increases in magnitude. An immediate consequence of these considerations is that trident cascades mediated by virtual photons will tend to dominate in both of the ranges $\Upsilon \ll 1$ and $\Upsilon \gg 1$.

The situation sketched in Fig. 14 also suggests some analytical simplifications for expediting the evaluation of $\Xi(\Upsilon)$. First we remark that in cases where $\Upsilon \gg 1$, it is evident that only values of $\mathfrak{M}(\sigma, \Upsilon)$, corresponding to the range $\sigma \ll \Upsilon$, will contribute significantly to trident conversion. Under these circumstances we have the approximate reduction

$$\mathfrak{M}(\sigma, \Upsilon) \simeq (9\pi/2\sqrt{3})(\Upsilon^2/\sigma)^2 \kappa(2\sigma/3\Upsilon^2), \quad (4.7)$$

which was derived and discussed in Sec. 2A. A particularly useful feature of this representation is that it continues to be valid in the range $\Upsilon \ll 1$, *without* the necessity for any special restrictions[16] on the values of σ. This implies that in both of the extreme cases $\Upsilon \gtrless 1$, the value of $\Xi(\Upsilon)$ may be estimated from the representation

$$\Xi(\Upsilon) \simeq \int_0^\Upsilon d\sigma\, \sigma^{-2} \kappa(2\sigma/3\Upsilon^2) K^2_{1/3}(4/3\sigma), \quad (4.8)$$

where $\kappa(z)$ is the bremsstrahlung function previously defined in equation (2.9). In Appendix 4 it is shown that in the appropriate ranges $\Xi(\Upsilon)$ is given by

$$\Xi(\Upsilon) \simeq \begin{cases} 0.4\Upsilon^{1/2} \exp(-10/3\Upsilon), & \Upsilon \ll 1; \\ 4.4\Upsilon^{-2/3} \ln \Upsilon, & \Upsilon \gg 1. \end{cases} \quad (4.9)$$

For intermediate values of $\Upsilon (\sim 1)$, Ξ must be calculated directly from (4.6b) by numerical integration. A graph of $\Xi(\Upsilon)$ is given in Fig. 12.

C. Comparison of Trident Cascades in Magnetic Fields and Material Media

It is convenient to begin these comparisons by determining which of the processes discussed in the previous sections—real or virtual photon trident production—dominates under suitable conditions. This information can easily be obtained by considering the ratio

$$[N_R^{(T)}(E, H)/N_V^{(T)}(E, H)] = 0.2[d\, H\, \Xi(\Upsilon)/\lambda\!\!\!^{-}_c H_{cr} \hat{\Omega}(\Upsilon)], \quad (4.10)$$

[16] The immediate vicinity of the bremsstrahlung tip ($\sigma \sim \Upsilon$) is excluded. In cases where $\Upsilon \ll 1$, the omission of this region is of negligible significance.

CC-0. In Public Domain. Gurukul Kangri Collection, Haridwar

Digitized by Arya Samaj Foundation Chennai and eGangotri

for various values of the parameters. The numerical work can be simplified by measuring distances in millimeters and magnetic field strength in units of 10 MG, i.e., $H \equiv \mathrm{H} \times 10^7$. If we also introduce logarithms (base 10), then the ratio (4.10) can be rewritten in the form

$$\log [N_R^{(T)}(E, H)/N_V^{(T)}(E, H)] = 2.1 + \log (d\mathrm{H}) + \log \Xi(\Upsilon) - \log \hat{\Omega}(\Upsilon). \quad (4.10a)$$

With the aid of the curves given in Fig. 12 it is then a straightforward matter to determine the conditions under which one or the other process is dominant.

Generally speaking, for values of $\Upsilon < 0.2$, the virtual photon trident rate tends to be greater. From an experimental point of view however this is of almost no significance since one can easily check that in this region the total trident production rate is vanishingly small. Conditions are much more favorable in the range $\Upsilon > 0.2$. Assuming that the fields and distances satisfy the requirement $d\mathrm{H} > 1$, one may verify from (4.10a) that the real photon (cascade) process dominates in this region. The magnetic trident production rate increases to the point where it can compete favorably with the corresponding process in material media. Under still more extreme conditions, i.e., values of $\Upsilon \gg 100$—which are of course experimentally very implausible—the virtual photon trident process again tends to dominate. However this is not to be taken seriously even as a theoretical indication, since damping corrections [H1] begin to alter the ratio (4.10a) for much smaller values of Υ, i.e., $1 \lesssim \Upsilon \lesssim 10$.

Trident conversion with either real or virtual photon intermediate states can of course also occur in material media. It is in fact an important component of high-energy cosmic-ray showers and has been studied with a variety of experimental techniques [A4, C3, K8]. In order to obtain estimates of these conversion rates let us again consider the passage of n electrons of energy E through a path length d in a medium which in the present instance will be supposed to be a material characterized by atomic number Z, atomic weight A, and density ρ. Just as in the corresponding magnetic case it is convenient to begin by computing the rate of trident conversions due to virtual intermediate photons. In the ultra-relativistic limit the expected number of such tridents, $\bar{N}_V^{(T)}(E, Z)$, can easily be estimated with the help of the FWW method [M5]. In analogy with (4.2) we then have

$$\bar{N}_V^{(T)}(E, Z) = n\, d\, \beta(Z) \mathfrak{N}(E, \eta\, mc^2), \quad (4.11)$$

where $\beta(Z)$ is the energy-independent photon attenuation coefficient given in (3.7), and $\mathfrak{N}(E, \eta\, mc^2)$ represents the total number of virtual photons with energies $E \geq h\nu \geq \eta\, mc^2$, present in the Fourier resolution of the field associated with an electron of energy E. Since only the high-energy limit of (4.11) is required, we have $E/mc^2 \gg \eta \gg 1$, which implicitly defines the parameter η.

Now it follows from (4.3a, b) that

$$\int^{\zeta} dx\, x^{-1} W(x) = \tfrac{1}{2}(\zeta^2 - 1) K_0^2(\zeta) + \frac{\zeta}{2} [K_0(\zeta) - \zeta K_1(\zeta)] K_1(\zeta); \quad (4.12)$$

and therefore

$$\mathfrak{N}(E, \eta\, mc^2) = \frac{2\alpha}{\pi} \int_{\eta(mc^2/E)}^{1} dx\, x^{-1} W(x); \quad (4.12a)$$

$$\simeq (\alpha/\pi) \ln^2 (E/mc^2), \quad \text{for } E/mc^2 \gg \eta \gg 1. \quad (4.12b)$$

This finally leads to the estimate [B6]

$$\bar{N}_V^{(T)}(E, Z) = nd(\alpha^2/\pi) N_0 \lambda\!\!\!^{-}_c{}^2\, h(Z) \ln^2 (E/mc^2), \quad (4.13)$$

where $\hat{h}(Z)$ is the function defined in (3.7a), and N_0 and $\lambda\!\!\!^{-}_c$ as usual denote Avogadro's number and the Compton wavelength.

Real photon trident cascades in material media may be visualized as shown in the sketch in Fig. 13. In the ultra-relativistic limit all the reaction products essentially go in the forward direction, and so the corresponding conversion rate, which we shall denote by $\bar{N}_R^{(T)}(E, Z)$, can be written down in direct analogy with (4.4c), i.e.,

$$\bar{N}_R^{(T)}(E, Z) = n\beta(Z) \sum_{\nu} \sum_{s} I(h\nu, Z)(d - S)\, \Delta S[\Delta(h\nu)/h\nu]; \quad (4.14)$$

where the photon attenuation coefficient, $\beta(Z)$, is now given by (3.7), and $I(h\nu, Z)$ represents the rate of bremsstrahlung in material media (2.31a). The integrations in the present instance are trivial, and we find the explicit form [B7]

$$\bar{N}_R^{(T)}(E, Z) = [(7 \times 2^3)/3^5]\, n\, [d\alpha N_0 \lambda\!\!\!^{-}_c{}^2]^2\, h(Z) \hat{h}(Z) \ln (E/mc^2), \quad (4.15)$$

where $h(Z)$ and $\hat{h}(Z)$ are given by (2.31b) and (3.7a), respectively. As expected, the cascade rate increases quadratically with the distance.

The relative importance of real and virtual photon trident production in material media may now be

CC-0. In Public Domain. Gurukul Kangri Collection, Haridwar

Digitized by Arya Samaj Foundation Chennai and eGangotri

gauged by considering the ratio

$$\frac{\bar{N}_V^{(T)}(E,Z)}{\bar{N}_R^{(T)}(E,Z)}=2.1\times10^7\frac{\lambda\!\!\!^{-}_c}{d}\frac{\ln(E/mc^2)}{h(Z)}. \quad (4.16)$$

In the present discussion the ranges of interest for the parameters are $d\sim1$ mm, and $E/mc^2\gg1$. It is then a simple matter to verify that for $Z\lesssim13$,

$$\bar{N}_V^{(T)}(E,Z)>\bar{N}_R^{(T)}(E,Z); \quad (4.16a)$$

so that in these cases the virtual photon processes dominate.

On the other hand if we consider $Z\gtrsim29$, but restrict $E\lesssim10^3$ BeV, then

$$\bar{N}_V^{(T)}(E,Z)<\bar{N}_R^{(T)}(E,Z); \quad (4.16b)$$

so that in this range the real photon cascades dominate. In principle the two types of trident conversion can of course also be distinguished through measurements of the energy and angular distributions of the emergent particles, but this requires more refined experimental techniques and involves problems beyond the scope of the present discussion.

It is now possible to proceed with the intercomparisons of trident production rates in magnetic fields and material media. Let us consider first the ratio

$$\frac{N_R^{(T)}(E,H)}{\bar{N}_V^{(T)}(E,Z)}=3.8\times10^6\frac{d}{\lambda\!\!\!^{-}_c}\left(\frac{H}{H_{cr}}\right)^2\frac{\Xi(\Upsilon)}{\hat{h}(Z)\ln^2(E/mc^2)}; \quad (4.17)$$

which is appropriate for gauging the relative rates in the range $Z\lesssim13$. For computational purposes it is again convenient to take the logarithm of the ratio (4.17), and to measure distances in millimeters, and field intensity in units of 10 MG, i.e., $H=\mathrm{H}\times10^7$. Then since

$$0.7\lesssim\log\log(E/mc^2)\lesssim0.8 \quad \text{for } 50\text{ BeV}\lesssim E\lesssim1000\text{ BeV},$$

the energy dependence in the iterated logarithm may be ignored, and the break-even condition, $N_R^{(T)}(E,H)\sim\bar{N}_V^{(T)}(E,Z)$, expressed in the form

$$\log d\mathrm{H}^2+\log\Xi(\Upsilon)=\log\hat{h}(Z)-0.6. \quad (4.17a)$$

This is an implicit equation connecting E, H, Z, and d, which with the help of the curve given in Fig. 12, may easily be solved for various values of the parameters. In particular the beryllium ($Z=4$) and high explosives ($Z\simeq8$) break-even curves shown in Fig. 15 correspond to solutions of (4.17a) with the special choice $d=2$ mm. Comparing with the pair-production break-even curves given in Fig. 10, we see that the conditions for competitive conversion generally tend to require slightly higher energies and field strengths. The sensitivity with respect to variations of Υ, already noted in connection with other magnetic conversion processes, is again exhibited in the trident production rates. If for example we refer to Fig. 15 and consider the Be and HE break-even curves corresponding to $H\sim60$ MG, then an upward shift in energy of approximately 10%, i.e., 140 BeV to 155 BeV, changes the conversion rates from about 4×10^{-3} to 8×10^{-3}, or roughly a factor of two!

In circumstance where it is of interest to compare the relative rates of trident conversion in magnetic fields and material media with $Z\gtrsim29$, the appropriate ratio to consider is

$$\frac{N_R^{(T)}(E,H)}{\bar{N}_R^{(T)}(E,Z)}=0.8\times10^{14}\left(\frac{H}{H_{cr}}\right)^2\frac{\Xi(\Upsilon)}{h(Z)\hat{h}(Z)\ln(E/mc^2)}. \quad (4.18)$$

Since both processes involve only real intermediate photons, the distance, d, cancels in the ratio. Proceeding as before, one may readily derive an explicit equation for the break-even condition, viz.,

$$2\log\mathrm{H}+\log\Xi(\Upsilon)=\log\{h(Z)\hat{h}(Z)\}+0.5. \quad (4.18a)$$

The copper ($Z=29$) and lead ($Z=82$) curves given in Fig. 15 have been constructed from this equation. The position of these curves relative to the "complete conversion" line indicated in this figure again emphasizes the fact that extremely intense magnetic fields are excellent energy degraders for ultrahigh-energy electromagnetic showers.[17]

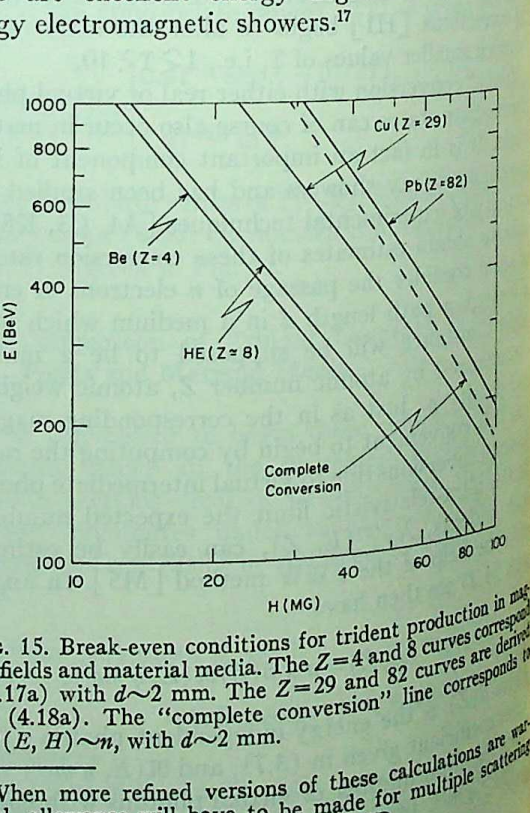

FIG. 15. Break-even conditions for trident production in magnetic fields and material media. The $Z=4$ and 8 curves correspond to (4.17a) with $d\sim2$ mm. The $Z=29$ and 82 curves are derived from (4.18a). The "complete conversion" line corresponds to $N_R^{(T)}(E,H)\sim n$, with $d\sim2$ mm.

[17] When more refined versions of these calculations are warranted, allowance will have to be made for multiple scattering corrections of the type discussed in Sec. 2D.

CC-0. In Public Domain. Gurukul Kangri Collection, Haridwar

Digitized by Arya Samaj Foundation Chennai and eGangotri

5. ČERENKOV RADIATION AND PHOTON SPLITTING

A. Vacuum Polarization Čerenkov Radiation

A particularly interesting aspect of quantum electrodynamic processes occurring in extremely intense electromagnetic fields is the existence of a special class of radiative modifications which are due to coherent vacuum polarization effects. Qualitatively speaking, it is not too difficult to see how such collective radiative effects could arise: The essential point is that in an approximation where vacuum polarization corrections can be described in terms of a Lagrangian of the Born–Infeld type [H2, E9], the corresponding equations governing the behavior of the electromagnetic fields include a number of nonlinear terms. These are not only responsible for light–light and light–field [Delbrück] scattering, but also permit complex propagating modes which are inherently suppressed in the linear theory. A typical example of this kind of nonlinear disturbance is the formation of electromagnetic "shock" waves; a phenomenon which has already been discussed in detail by Lutzky and Toll [L4]. If one now considers the added complication of a charged particle propagating through such vacuum polarization "plasmas," it is clear that a variety of still more complex interactions can be expected to occur. All effects of this type which are inherently nonlinear in the sense that they *cannot* be described in terms of simple perturbations of the linear theory represent collective modifications of the vacuum polarization.[18]

Under conditions where vacuum polarization may be described by a phenomenological quantum electrodynamics [J1], it can be shown that collective radiative effects will give rise to Čerenkov emission by high-energy charged particles in intense external fields. In the present section we briefly review some of the pertinent results and supplement our earlier discussions [E2, E3] with detailed comparisons of magnetic bremsstrahlung and vacuum polarization Čerenkov radiation.

Let us consider first the propagation of light through a strong external magnetic field in a direction normal to the lines of flux. Under these circumstances there will be photon–field interactions of the type shown in Fig. 8(b), and the phase velocity of light is reduced below its free space value [T1, S7]. This situation may be conveniently described by assigning an index of refraction $n(\nu)$ to the magnetic field. Quantitatively this may be derived from the forward coherent part of the scattering amplitude associated with the diagram of Fig. 8(b). This in turn may be computed from the pair–production interaction, Fig. 1(a), by means of a dispersion relation. Specifically, for the index of refraction we write

$$n(\nu)=1+\Delta n(\nu). \tag{5.1}$$

Then $\Delta n(\nu)$ can be directly obtained from the dispersion integral

$$\Delta n(\nu)=\frac{c}{2\pi^2}\int_0^\infty d\bar{\nu}\,\frac{\alpha(\bar{\nu})}{\bar{\nu}^2-\nu^2}, \tag{5.2}$$

where $\alpha(\bar{\nu})$ represents the magnetic pair-production function given in (3.3a). The explicit form of $\Delta n(\nu)$ is

$$\Delta n(\nu)=(\alpha/4\pi)\,(H/H_{cr})^2\,\mathcal{J}(\chi), \tag{5.3a}$$

where

$$\mathcal{J}(\chi)=-0.027\pi^2\chi^{-2}\{K_{1/3}(\bar{\chi})[I_{1/3}(\bar{\chi})+I_{-1/3}(\bar{\chi})] +2[I_{-1/3}(\bar{\chi})\tilde{I}_{1/3}(\bar{\chi})+I_{1/3}(\bar{\chi})\tilde{I}_{-1/3}(\bar{\chi})]\} \tag{5.3b}$$

and $\bar{\chi}=\frac{2}{3}\chi=\frac{1}{3}(h\nu/mc^2)\,(H/H_{cr})$ [compare (3.1)]. The "tilde" functions are derivatives of modified Bessel functions with respect to the index, i.e., $\tilde{I}_\nu\equiv(\partial/\partial\nu)I_\nu$ [E10].

The asymptotic limits of $\mathcal{J}(\chi)$ are

$$\mathcal{J}(\chi)=\begin{cases}0.22+0.30\chi^2, & \chi\ll 1;\\ -0.56\chi^{-4/3}, & \chi\gg 1.\end{cases} \tag{5.4}$$

Some numerical values of $\mathcal{J}(\chi)$ are listed in Table IX. A graph of this function is given in Fig. 16.

TABLE IX. Numerical values of $\mathcal{J}(\chi)$.

χ	$\mathcal{J}(\chi)$
0	0.22
0.17	0.23
0.22	0.24
0.40	0.25
1.00	0.17
2.22	0.059
3.33	0.027
6.66	+0.003
9.52	−0.0009

We now consider an electron with energy E traversing a magnetic field H in a direction normal to the lines of flux. At sufficiently high energies its velocity matches—and eventually exceeds—the ambient phase velocity of light. The corresponding Čerenkov threshold is then given by

$$E/mc^2\geq[2\Delta n(\nu_m)]^{-1/2}, \tag{5.5}$$

where ν_m, the frequency which *first* appears in the Čerenkov spectrum, is determined by $\mathrm{Max}\{\Delta n(\nu)\}$. In the present instance we have $\mathrm{Max}\{\mathcal{J}(\chi)\}\simeq 0.25$ for

[18] Nonperturbative binding corrections for the particle propagators are also assumed.

CC-0. In Public Domain. Gurukul Kangri Collection, Haridwar

Digitized by Arya Samaj Foundation Chennai and eGangotri

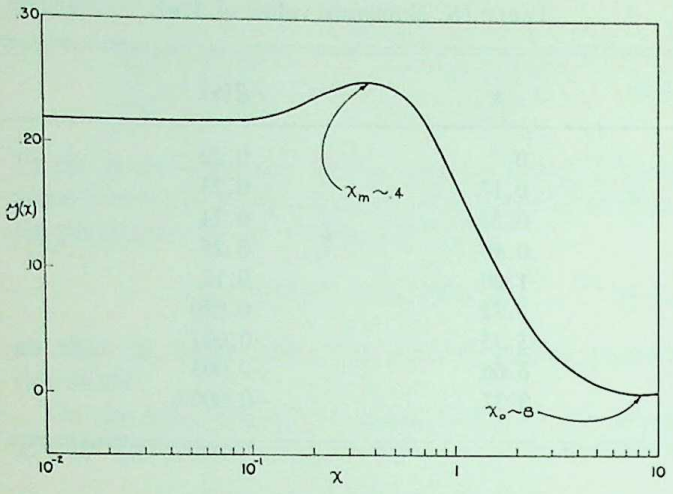

FIG. 16. Index of refraction of a magnetic field:

$$n=1+(\alpha/4\pi)\,(H/H_{cr})^2\mathcal{G}(\chi), \qquad \chi=\tfrac{1}{2}(h\nu/mc^2)\,(H/H_{cr}).$$

$\mathcal{G}(\chi)$ has a maximum at $\chi\simeq 0.4$, and crosses the abscissa at $\chi\simeq 8$.

$\chi\equiv\chi_m\simeq 0.4$; and therefore the threshold energy $E_m(\nu_m)$, associated with ν_m, is given by

$$\frac{E_m(\nu_m)}{mc^2}\,\frac{H}{H_{cr}}=\left[\frac{2\pi}{\alpha\mathcal{G}(\chi_m)}\right]^{1/2}\cong 58.5; \qquad (5.6a)$$

furthermore (see Fig. 16)

$$(h\nu_m/mc^2)\,(H/H_{cr})\cong 0.8. \qquad (5.6b)$$

At energies exceeding the threshold value additional frequencies will appear in the Čerenkov spectrum. Corresponding to each frequency there is a unique minimum energy $E_m(\nu)$ which marks its first appearance in the spectrum. We now introduce the notation $q(\nu)=E/E_m(\nu)$. The spectral intensity of the Čerenkov radiation then may be written in the form

$$\hat{I}(E, h\nu, H)=(2/\pi)\alpha^2(mc^2/\lambda\!\!\!^{-}_c)\chi\mathcal{G}(\chi)[1-q^{-2}(\nu)]. \qquad (5.7)$$

Since Max $\{\chi\mathcal{G}(\chi)\}\simeq 0.18$ for $\chi\simeq 1.4$, one may easily check that the Čerenkov radiation rates are of the order of 12 BeV/mm. These rates are however considerably smaller than the corresponding magnetic bremsstrahlung losses. A detailed comparison can be conveniently made if we recall that the preceding relations imply the estimate

$$\frac{h\nu}{E}=\frac{2\chi}{q(\nu)}\left[\frac{2\pi}{\alpha\mathcal{G}(\chi)}\right]^{-1/2}\ll 1. \qquad (5.8)$$

In this case the magnetic bremsstrahlung intensity $I(E, h\nu, H)$ is accurately represented by the expression (2.14); and the ratio of the intensities may be reduced to the compact form

$$\hat{I}(E, h\nu, H)/I(E, h\nu, H)=[0.86\alpha\chi\mathcal{G}(\chi)q(\nu)]^{2/3}[1-q^{-2}(\nu)]. \qquad (5.9)$$

Just above the threshold, i.e., $q(\nu)\lesssim 1$, this gives $\hat{I}\sim 10^{-2}I$; and therefore Čerenkov emission is negligible in these cases. There is however a strong analogy to the relation between ordinary bremsstrahlung and Čerenkov radiation in material media: The essential feature of this situation—which of course underlies the operation of all conventional Čerenkov counters—is that the low end of the observed spectrum is completely dominated by Čerenkov emission under circumstances where the radiating particle has an energy far above threshold. An analogous relation for the magnetic processes is implied by (5.9). Far above threshold we have

$$\hat{I}(E, h\nu, H)/I(E, h\nu, H)\sim 10^{-2}\,q^{2/3}(\nu), \qquad (5.9_2)$$

and at super-high energies Čerenkov radiation becomes dominant.[19]

In this connection it should be noted that there is an option in the spatial discrimination of bremsstrahlung and Čerenkov emission. The opening angle of the vacuum polarization Čerenkov cone is given by [E3]

$$\theta_C=(H/H_{cr})[(\alpha/2\pi)\,\mathcal{G}(\chi)\{1-q^{-2}(\nu)\}]^{1/2}. \qquad (5.10)$$

The preferred angle for bremsstrahlung emission is $\theta_B\sim mc^2/E$; and the differential cross section in first approximation is proportional to $\sim\{1+[(E/mc^2)\theta]^2\}^{-2}$. It is then easy to show that $\theta_C\sim q(\nu)\theta_B\geq\theta_B$; and if we compare the respective radiation rates at the *larger* angle, i.e., θ_C, the ratio (5.9a) is replaced by the more conservative estimate

$$[\hat{I}(E, h\nu, H)/I(E, h\nu, H)]\,|_{\theta_C}\sim 10^{-2}\,q^{8/3}(\nu). \qquad (5.11)$$

B. Photon Splitting

To lowest order photon splitting is described by the diagram shown in Fig. 2. The external fields responsible for the binding of the intermediate state pairs may of course be either electric or magnetic. At low energies, i.e., for $h\nu\ll mc^2$, and in the weak-field limit,

$$H\ll m^2c^3/e\hbar\gg\mathcal{E},$$

photon splitting can be reliably estimated from the equivalent vacuum polarization Lagrangian of the Born–Infeld theory [H2, S8]. At higher energies it is advisable to derive the results directly from quantum

[19] In particular, for $E\sim 10^{19}$ eV, $H\sim 0.1$ MG, Čerenkov radiation will dominate in the spectral region $h\nu\gtrsim 10^{14}$ eV. These estimates are of course contingent on the semiquantitative reliability of (2.14) even under conditions of strong radiative corrections.

CC-0. In Public Domain. Gurukul Kangri Collection, Haridwar

Digitized by Arya Samaj Foundation Chennai and eGangotri

electrodynamics. However even for the single loop diagram (Fig. 2) this calculation is extremely tedious, and the best results available correspond to Born expansions in the binding of the intermediate states. Photon splitting due to vacuum polarization has not yet been observed experimentally.

Suppose we consider a photon propagating through a uniform magnetic field in a direction normal to the lines of flux. Then according to Skobov [S9] the attenuation coefficient for photon splitting $\mathcal{S}(h\nu, H)$ is given by the expression

$$\mathcal{S}(h\nu, H) = \frac{5}{3(144\pi)^2} \frac{\alpha^3}{\lambda\!\!\!^{-}_c} \frac{h\nu}{mc^2} \left(\frac{H}{H_{cr}}\right)^2; \qquad (5.12)$$

where the principal approximation in the derivation is $H \ll H_{cr}$. It is characteristic for external field photon transformations of this type that the conversion rates are smoothly varying functions of the field strengths and photon energies. This is in sharp contrast to processes such as pair conversion where the attenuation rates diminish very rapidly for conditions such that $(h\nu/mc^2)(H/H_{cr}) \lesssim \frac{1}{3}$ [compare (3.3a–c)]. In principle therefore photon splitting may be observable under circumstances where the characteristic energies are low but very intense illumination is available. Unfortunately most schemes involving lasers or pulsed x-ray devices lead to marginal photon splitting rates and depend on optimistic estimates of the tolerable signal-to-noise ratios. If one considers high fields set up in the vicinity of material media—for example pulse-implosion generators of megagauss fields—then photon splitting at low energies ($h\nu \lesssim mc^2$) will tend to be masked by double Compton scattering in the surrounding explosives and liners.

These difficulties persist at higher energies. The principal competing processes in material media then are photon splitting in the nuclear Coulomb fields and double Compton scattering. In particular the photon splitting coefficient, analogous to (5.12), for a medium of density ρ, atomic number Z and weight A, is approximately given by [T4, B7, S6]

$$\mathcal{S}(h\nu, Z) \simeq 3.5 \times 10^{-8}\, \alpha^3 (\alpha Z)^2 (\rho/A) \ln (h\nu/mc^2), \qquad (5.13)$$

where it is assumed that $h\nu \gg mc^2$, and shielding corrections have been ignored. Under these conditions double Compton scattering becomes less important since the cross section is bounded from above by $\alpha^2 \lambda\!\!\!^{-}_c{}^2 (mc^2/h\nu) \ln (h\nu/mc^2)$. It is in fact easy to check that for energies satisfying the inequality

$$\alpha(\alpha Z) h\nu/mc^2 > 1, \qquad (5.14)$$

Coulomb field photon splitting will be the dominant process.

Comparing (5.12) and (5.13) it is then evident that in principle at least there are circumstances where magnetic photon splitting can compete favorably with photon splitting in material media. The order of magnitude of the break-even point is given by

$$\left(\frac{H}{H_{cr}}\right)^2 \sim 4 \times 10^{-3} (\alpha Z)^2 \frac{\rho}{A} \frac{mc^2}{h\nu} \ln \left(\frac{h\nu}{mc^2}\right); \qquad (5.15)$$

but this requires rather exotic conditions. For example, if we consider incident photon energies of the order of 300 BeV, and high explosives, i.e., $Z \simeq 8$, then magnetic photon splitting will predominate for fields in the range $\gtrsim 2 \times 10^8$ G. Experimentally however this is of no significance since in this case the principal photon conversion process would actually be magnetic pair production. Under more realistic circumstances, e.g., $(h\nu/mc^2)(H/H_{cr}) \sim 10^{-2}$, photon splitting should indeed be observable but this depends on the development of techniques for maintaining intense fields—either $H \sim 10^7$ G or $\mathcal{E} \sim 10^9$ V/cm—momentarily in evacuated regions.

ACKNOWLEDGMENTS

Part of this work was carried out at the Université Libre de Bruxelles. It is a pleasure to thank Professor I. Prigogine for his kind hospitality. Numerous auxiliary calculations for this paper were carried out by Dr. S. M. Prastein, H. C. Shih, and J. Schweigert. The support of the U. S. Army Research Office, Durham, is gratefully acknowledged.

APPENDIX I: INTEGRAL IDENTITIES FOR MODIFIED BESSEL FUNCTIONS

We wish to establish the modified Bessel function identity [K5]

$$y \int_y^\infty dx\, K_{5/3}(x) = \frac{\sqrt{3}}{\pi} y^2 \int_0^\infty dx \{\cosh^5 x\, K^2_{2/3}(\tfrac{1}{2} y \cosh^3 x) + \cosh^3 x \sinh^2 x\, K^2_{1/3}(\tfrac{1}{2} y \cosh^3 x)\}, \qquad y > 0, \quad (A1)$$

which is substantially equivalent to that required for the transition from Eq. (2.8d) to Eq. (2.8f) of the text. The proof given here is based on a slight extension of several ideas originally due to Lerch and Hardy (p. 382 of [W1], [L2]).

Let us suppose that we are faced with the problem of verifying the equality of two functions, $f_1(y)$ and $f_2(y)$, which are specified in terms of representations (these may be integral representations) that are sufficiently complicated so that a direct comparison is rendered impractical. This problem can often be dealt with by introducing a parametric transformation of the functions to a more tractable form. Specifically, let us consider a mapping operation $\mathcal{O}(p \mid y)$ which transforms the f's according to the rule

$$\mathcal{O}(p \mid y) f(y) \to \hat{f}(p). \qquad (A2)$$

CC-0. In Public Domain. Gurukul Kangri Collection, Haridwar

Digitized by Arya Samaj Foundation Chennai and eGangotri

With an appropriate choice of $\mathcal{O}(p \mid y)$ it may then be possible to simplify the explicit form of the $\hat{f}$'s to the point where the identity $\hat{f}_1 = \hat{f}_2$ can in fact be established directly. Schematically this entire process may be represented by the diagram:

$$\begin{array}{ccc} f_1(y) & \overset{?}{=} & f_2(y) \\ \Updownarrow & & \Updownarrow \\ \mathcal{O}(p \mid y)\, f_1(y) \equiv \hat{f}_1(p) = \hat{f}_2(p) \equiv \mathcal{O}(p \mid y)\, f_2(y). & & \end{array} \tag{A3}$$

The essential links in this sequence are the proof of the invertibility of the mapping (A2), and the explicit verification of the identity $\hat{f}_1 = \hat{f}_2$. In the present instance a convenient choice for the operator $\mathcal{O}(p \mid y)$ is the Mellin transform, i.e.,

$$\mathcal{O}(p \mid y)\, f(y) \rightarrow \int_0^\infty dy\, y^p f(y) = \hat{f}(p); \tag{A4}$$

since this permits an elementary computation of the $\hat{f}$'s, and leads to a unified treatment of the comparison question ($\hat{f}_1 = \hat{f}_2$), within the general framework of the Stieltjes' moment problem [W2].

We begin with the obvious identifications

$$f_1(y) \equiv y \int_y^\infty dx\, K_{5/3}(x), \tag{A5a}$$

and

$$f_2(y) \equiv \frac{\sqrt{3}}{\pi} y^2 \int_0^\infty dx \{\cosh^5 x\, K^2_{2/3}(\tfrac{1}{2} y \cosh^3 x) + \cosh^3 x \sinh^2 x\, K^2_{1/3}(\tfrac{1}{2} y \cosh^3 x)\}. \tag{A5b}$$

It is also convenient to restrict the $\hat{f}(p)$'s of (A4) to integer values of the argument so that they reduce to simple moments. For these we introduce the notation

$$C_n^{(1)} = \int_0^\infty dy\, y^n f_1(y), \qquad n = 0, 1, \cdots; \tag{A6a}$$

and

$$C_n^{(2)} = \int_0^\infty dy\, y^n f_2(y), \qquad n = 0, 1, \cdots. \tag{A6b}$$

At this point we invoke the *sufficient* conditions for the uniqueness of the Stieltjes' moment problem. These may be concisely stated in terms of

Carleman's Theorem [C2]: Suppose that we have two nonnegative functions

$$f_1(y) \geq 0, \quad \text{and} \quad f_2(y) \geq 0; \tag{A7a}$$

for which an infinite sequence of moments is equal,

$$C_n^{(1)} = C_n^{(2)}, \qquad n = 0, 1, 2, \cdots. \tag{A7b}$$

If these moments satisfy the divergence criterion

$$\sum_n^\infty (1/C_n)^{1/2n} \rightarrow \infty; \tag{A7c}$$

then the conclusion is that the moment problem does have a unique solution, i.e.,

$$f_1(y) \equiv f_2(y). \tag{A7d}$$

Carleman's theorem therefore insures that with appropriate conditions the mapping (A2) is indeed invertible. The explicit proof of the basic identity (A1) is now reduced to checking that all the analytical details involved in the sequence (A3) are in fact consistent with the hypotheses (A7a) through (A7c).

The first condition (A7a) may easily be satisfied by requiring that $y > 0$ in (A5a) and (A5b). The next step consists of verifying that all the moments are indeed equal. This requires the explicit calculation of (A6a) and (A6b). A number of auxiliary integrals are useful in this connection:

$$\int_0^\infty du (\cosh u)^{-\tau} = 2^{\tau-2}[\Gamma(\tau/2)]^2/\Gamma(\tau), \qquad \tau > 0$$

$$\int_0^\infty du\, u^\sigma K_\nu(u) = 2^{\sigma-1}\, \Gamma[\tfrac{1}{2}(\sigma+1-\nu)]\Gamma[\tfrac{1}{2}(\sigma+1+\nu)], \qquad \mathrm{Re}\{\sigma+1\} > |\mathrm{Re}\{\nu\}|,$$

$$\int_0^\infty du\, u^\sigma K_\nu^2(u) = 2^{\sigma-2}\, \Gamma[\tfrac{1}{2}(\sigma+1)+\nu]\Gamma[\tfrac{1}{2}(\sigma+1)-\nu] \times (\Gamma[\tfrac{1}{2}(\sigma+1)])^2/\Gamma(\sigma+1), \qquad \mathrm{Re}\{\sigma+1\} > 2|\mathrm{Re}\{\nu\}|. \tag{A8}$$

Then

$$C_n^{(1)} = \int_0^\infty dy\, y^{n+1} \int_y^\infty dx\, K_{5/3}(x) = (n+2)^{-1} \int_0^\infty dy\, y^{n+2} K_{5/3}(y), \tag{A9a}$$

or

$$C_n^{(1)} = \frac{2^{n+1}}{n+2}\, \Gamma[\tfrac{1}{2}(n+3)+\tfrac{5}{6}]\Gamma[\tfrac{1}{2}(n+3)-\tfrac{5}{6}]. \tag{A9b}$$

For the other moments we make the decomposition

$$C_n^{(2)} = (\sqrt{3}/\pi)(\mathcal{J}_1 + \mathcal{J}_2), \tag{A10a}$$

where

$$\mathcal{J}_1 = \int_0^\infty dy \int_0^\infty dx\, y^{n+2} K^2_{1/3}(\tfrac{1}{2} y \cosh^3 x) \cosh^3 x \sinh^2 x, \tag{A10b}$$

CC-0. In Public Domain. Gurukul Kangri Collection, Haridwar

Digitized by Arya Samaj Foundation Chennai and eGangotri

and

$$\mathcal{J}_2=\int_0^\infty dy \int_0^\infty dx\, y^{n+2}\, K^2_{2/3}(\tfrac{1}{2}y\cosh^3 x)\cosh^5 x. \tag{A10c}$$

Introducing the new variable $u=\frac{1}{2}y\cosh^3 x$ in both integrals,[20] we find

$$\mathcal{J}_1=\int_0^\infty dx \left(\frac{2}{\cosh^3 x}\right)^{n+3} \cosh^3 x \sinh^2 x \times \int_0^\infty du\, u^{n+2}\, K^2_{1/3}(u), \tag{A10d}$$

and

$$\mathcal{J}_2=\int_0^\infty dx \left(\frac{2}{\cosh^3 x}\right)^{n+3} \cosh^5 x \int_0^\infty du\, u^{n+2}\, K^2_{2/3}(u). \tag{A10e}$$

With the help of the auxiliary integrals (A8), these quadratures may be carried out explicitly,

$$\mathcal{J}_1=\frac{2^{5(n+1)}}{3n+5}\,\Gamma[\tfrac{1}{2}(n+3)+\tfrac{1}{3}]\Gamma[\tfrac{1}{2}(n+3)-\tfrac{1}{3}] \times(\Gamma[\tfrac{1}{2}(n+3)]\Gamma(\tfrac{3}{2}n+2))^2/(\Gamma(3n+4)\Gamma(n+3)), \tag{A10f}$$

and

$$\mathcal{J}_2=2^{5(n+1)}\,\Gamma[\tfrac{1}{2}(n+3)+\tfrac{2}{3}]\Gamma[\tfrac{1}{2}(n+3)-\tfrac{2}{3}] \times(\Gamma[\tfrac{1}{2}(n+3)]\Gamma(\tfrac{3}{2}n+2))^2/(\Gamma(3n+4)\Gamma(n+3)). \tag{A10g}$$

Finally, (A10a), (A10f), and (A10g) may be combined to give

$$C_n^{(2)}=\sqrt{3}\,2^n\,\frac{\Gamma(\frac{3}{2}n+2)\,\Gamma[\frac{1}{2}(n+3)]}{\Gamma(\frac{3}{2}n+2+\frac{1}{2})\,\Gamma(\frac{1}{2}n+2)} \times\{\Gamma[\tfrac{1}{2}(n+3)+\tfrac{2}{3}]\Gamma[\tfrac{1}{2}(n+3)-\tfrac{2}{3}] +(3n+5)^{-1}\,\Gamma[\tfrac{1}{2}(n+3)+\tfrac{1}{3}]\Gamma[\tfrac{1}{2}(n+3)-\tfrac{1}{3}]\}. \tag{A11}$$

Elementary computations now yield the special values:

$$C_0^{(1)}=C_0^{(2)}=(8/3^{5/2})\pi,$$
$$C_1^{(1)}=C_1^{(2)}=(5\times 11/3^4)\pi, \tag{A12}$$
$$C_2^{(1)}=C_2^{(2)}=(7\times 32/3^{9/2})\pi,$$

[20] These interchanges can be justified on the basis of absolute convergence.

These provide the basis for an inductive proof of the identity of $C_n^{(1)}$ and $C_n^{(2)}$. It is convenient to carry the induction from n to $n+2$. The key step is the verification of the equality $C^{(1)}{}_{n+2}=C^{(2)}{}_{n+2}$, expressed in terms of (A9b) and (A11). This can be reduced to establishing the identity

$$[2/(n+4)]\Gamma[\tfrac{1}{2}(n+5+\tfrac{5}{3})]\Gamma[\tfrac{1}{2}(n+5-\tfrac{5}{3})] =3^{-1/2}\,\frac{\Gamma(\frac{3}{2}n+5)\Gamma[\frac{1}{2}(n+3)+1]}{\Gamma[\frac{1}{2}(3n+1)+5]\Gamma(\frac{1}{2}n+3)} \times\{\Gamma[\tfrac{1}{2}(n+3)+1+\tfrac{2}{3}]\Gamma[\tfrac{1}{2}(n+3)+1-\tfrac{2}{3}] +(3n+11)^{-1}\,\Gamma[\tfrac{1}{2}(n+3)+1+\tfrac{1}{3}] \times\Gamma[\tfrac{1}{2}(n+3)+1-\tfrac{1}{3}]\},\qquad n=0,1,\cdots. \tag{A13}$$

Elementary algebraic reductions show that this identity hinges on the validity of the equation

$$\frac{3j+5}{3j+7}=\frac{\Gamma[\frac{1}{2}(j+3)+\frac{1}{3}]\Gamma[\frac{1}{2}(j+3)-\frac{1}{3}]}{\Gamma[\frac{1}{2}(j+3)+\frac{2}{3}]\Gamma[\frac{1}{2}(j+3)-\frac{2}{3}]},\qquad j=0,1,\cdots; \tag{A14}$$

and this in turn depends on the auxiliary lemmas

$$\frac{3j+4}{3j+5}=\frac{1}{2}\prod_{m=1}^{j+1}\frac{1-(1/3m)^2}{1-(2/3m)^2},\qquad j=0,1,\cdots; \tag{A15a}$$

and

$$\frac{6j+5}{6j+7}=-\prod_{m=1}^{j+1}\frac{1-(2/[3(2m-1)])^2}{1-(4/[3(2m-1)])^2},\qquad j=0,1,\cdots. \tag{A15b}$$

It can easily be verified that this entire sequence of implications may be reversed: (A15b) and (A15a) together yield (A14); this in turn implies (A13); and in view of (A12) an appeal to induction finally establishes the equality of the moments, $C_n^{(1)}=C_n^{(2)}$. The remaining divergence criterion (A7c) now follows as an elementary consequence of Stirling's approximation applied to the C_n's. We find

$$C_n^{(1)}=C_n^{(2)}\approx\pi\, n^{n+1}\, e^{-n}\qquad \text{for } n\gg 1; \tag{A16}$$

and this implies

$$\sum_n^\infty (1/C_n)^{1/2n}\to\sum_n^\infty n^{-1/2}\to\infty. \tag{A17}$$

All the hypotheses of Carleman's theorem are thereby satisfied and in virtue of (A3) and (A7d) the equality of both sides of (A1) is proved.

CC-0. In Public Domain. Gurukul Kangri Collection, Haridwar

Digitized by Arya Samaj Foundation Chennai and eGangotri

A related expression is the index-shifting representation

$$K_\nu(z)=\left(\frac{2z}{\pi}\right)^{1/2}\int_0^\infty d\tau(\cosh\tau)^{\nu+1/2}K_{\nu-1/2}(z\cosh\tau),$$
$$z>0,\ \mathrm{Im}\{\nu\}=0, \quad \text{(A18)}$$

which arises in connection with calculations of trident cascades (Sec. 4). This identity may be verified by methods similar to those of the above. Here

$$f_1(y)=K_\nu(y), \quad \text{(A19a)}$$

and

$$f_2(y)=\left(\frac{2y}{\pi}\right)^{1/2}\int_0^\infty d\tau(\cosh\tau)^{\nu+1/2}K_{\nu-1/2}(y\cosh\tau). \quad \text{(A19b)}$$

Then

$$C_n^{(1)}=\int_0^\infty dy\,y^n K_\nu(y)$$
$$=2^{n-1}\Gamma[\tfrac{1}{2}(n+1-\nu)]\Gamma[\tfrac{1}{2}(n+1+\nu)], \quad \text{(A20a)}$$

and

$$C_n^{(2)}=\left(\frac{2}{\pi}\right)^{1/2}\int_0^\infty dy\int_0^\infty d\tau\,y^{n+1/2}$$
$$\times(\cosh\tau)^{\nu+1/2}K_{\nu-1/2}(y\cosh\tau). \quad \text{(A20b)}$$

Introducing the new variable $\chi=y\cosh\tau$, and presuming sufficiently large values for the moment index[21] n, i.e., $n>\nu-2$, (A20b) may be transformed to

$$C_n^{(2)}=\left(\frac{2}{\pi}\right)^{1/2}\int_0^\infty d\tau(\cosh\tau)^{\nu-n-1}\int_0^\infty d\chi\,\chi^{n+1/2}K_{\nu-1/2}(\chi),$$
$$=\frac{2^{2n-\nu-1}}{\pi^{1/2}}\Gamma[\tfrac{1}{2}(n+1+\nu)]\Gamma[\tfrac{1}{2}(n+2-\nu)]$$
$$\times(\Gamma[\tfrac{1}{2}(n+1-\nu)])^2/\Gamma(n+1-\nu). \quad \text{(A20c)}$$

These expressions for the moments are sufficiently simple so that their equivalence can be established without recourse to an inductive proof: A few elementary cancellations show that the conditions $C_n^{(1)}=C_n^{(2)}$, in this instance, reduce to

$$\Gamma(n+1-\nu)=(2^{n-\nu}/\pi^{1/2})\Gamma[\tfrac{1}{2}(n+1-\nu)]\Gamma[\tfrac{1}{2}(n+2-\nu)], \quad \text{(A20d)}$$

and this of course is immediately recognizable as an identity equivalent Legendre's duplication formula.

[21] Strictly speaking (A7b) must hold only for an infinite set of moments $n\geq N>0$; the particular value of n corresponding to the "first" moment is actually irrelevant. The requirement $n>\nu-2$ can therefore always be met.

Finally, we note the asymptotic estimates

$$C_n^{(1)}=C_n^{(2)}\approx\pi\exp[-(n+1)]n^n, \quad n\gg1. \quad \text{(A21a)}$$

These lead to

$$\sum_n^\infty(1/C_n)^{1/2n}\to\sum_n^\infty n^{-1/2}\to\infty, \quad \text{(A21b)}$$

and evidently Carleman's divergence criterion is once more satisfied. (A21b) and (A20d) together then insure the invertibility of the mapping (A2), and this completes the proof of the validity of (A18).[22]

APPENDIX 2: PROPERTIES OF THE BREMSSTRAHLUNG FUNCTION $\kappa(z)$

The function $\kappa(z)$ is defined by the integral representation

$$\kappa(z)=z\int_z^\infty dx\,K_{5/3}(x), \quad \text{(A22)}$$

where $K_{5/3}(x)$ is a modified Bessel function. Evidently for $z\geq0$, the function $\kappa(z)$ is nonnegative. We have the special values $\kappa(0)=\kappa(\infty)=0$; and note that $\kappa(z)$ has a broad maximum in the vicinity of $z\sim3$. More precisely, $\mathrm{Max}\{\kappa(z)\}=\kappa(.28)=0.925$, and this value of z of course also coincides with a zero of the derivative, viz.

$$\kappa'(z)=z^{-1}\kappa(z)-\{\tfrac{4}{3}K_{2/3}(z)+zK_{1/3}(z)\}. \quad \text{(A23)}$$

The general behavior of $\kappa(z)$ is indicated graphically in Fig. 3; numerical values are given in Table I.

Another representation for $\kappa(z)$, especially suited for computations in the range $0\leq z\leq2$, may be obtained from (A22) with the help of the Bessel function transformation

$$K_{5/3}(x)=-\{K_{1/3}(x)+2K'_{2/3}(x)\}.$$

This leads to the expression

$$\kappa(z)=z\left\{-\frac{\pi}{\sqrt{3}}+2K_{2/3}(z)+\int_0^z dx\,K_{1/3}(x)\right\}, \quad \text{(A24)}$$

in which the $z\to0$ limit is no longer troublesome in the limits of integration. We now insert the series expansion

$$K_\nu(x)=\frac{\pi/2}{\sin(\nu\pi)}\left\{(x/2)^{-\nu}\sum_{n=0}^\infty\frac{(x/2)^{2n}}{n!\Gamma(n-\nu+1)}\right.$$
$$\left.-(x/2)^\nu\sum_{n=0}^\infty\frac{(x/2)^{2n}}{n!\Gamma(n+\nu+1)}\right\}; \quad \text{(A25)}$$

[22] The method of moments does not of course yield the most general conditions for the validity of (A1) and (A18). The hypotheses may be considerably relaxed by an appeal to analytic continuation in both the "argument" and "index" variables.

CC-0. In Public Domain. Gurukul Kangri Collection, Haridwar

Digitized by Arya Samaj Foundation Chennai and eGangotri

and carry out the integration:

$$\int_0^z dx\, K_{1/3}(x) \equiv \hat{K}(z) = 2.53143825 z^{2/3}[1+0.09375000 z^2+0.00401786 z^4+0.00008789 z^6+\mathcal{O}(z^8)]$$
$$-1.20910963 z^{4/3}[1+0.07500000 z^2+0.00251116 z^4+0.00004566 z^6+\mathcal{O}(z^8)] \quad \text{(A26)}$$

Since $K_{2/3}(z)$ is a widely tabulated function, (A26) and (A24) are a convenient means for obtaining numerical values of $\kappa(z)$ for $0 \leq z \leq 2$ to better than $\frac{1}{2}\%$ accuracy (see Table X). The leading terms for very small z are

$$\kappa(z) \cong 2.1495\, z^{1/3} - 1.8138\, z + \mathcal{O}(z)^{7/3}, \qquad z \ll 1. \quad \text{(A27)}$$

The computation of $\kappa(z)$ for values of $z \geq 4$ may be based on the exact transformation

$$\int_z^\infty dx \left[1+\frac{7}{2}\left(\frac{4}{3x}\right)^4\right] K_{5/3}(x) = \frac{2}{3z} K_{1/3}(z) \left[1+2\left(\frac{4}{3z}\right)^2\right]$$
$$+ K_{2/3}(z) \left[1-\frac{1}{2}\left(\frac{4}{3z}\right)^2+\left(\frac{4}{3z}\right)^4\right]. \quad \text{(A28)}$$

In case $z>0$, the integral may be simplified with the mean value theorem, i.e.,

$$\int_z^\infty dx \left[1+\frac{7}{2}\left(\frac{4}{3x}\right)^4\right] K_{5/3}(x)$$
$$= \left[1+\frac{7}{2}\left(\frac{4}{3x_0}\right)^4\right] \int_z^\infty dx\, K_{5/3}(x); \qquad x_0 \geq z. \quad \text{(A28a)}$$

For values of $z \gtrsim 4$, the terms of order z^{-4} may be dropped, and we find the expression

$$\kappa(z) \cong \tfrac{2}{3} K_{1/3}(z)[1+2(4/3z)^2] + z K_{2/3}(z)[1-\tfrac{1}{2}(4/3z)^2]. \quad \text{(A29)}$$

The accuracy of this approximation is better than 4% for $z \sim 4$; and better than 1% for $z \gtrsim 5.7$.

Finally, for $z \gg 1$, we have the asymptotic estimate

$$\kappa(z) \to 1.2533\, z^{1/2} e^{-z}; \quad \text{(A30)}$$

but this is not well suited for numerical work.

APPENDIX 3: EVALUATION OF THE AUXILIARY FUNCTION $\hat{\Omega}(\Upsilon)$

In connection with estimates of trident production by virtual photons it is necessary to compute the function

$$\hat{\Omega}(\Upsilon) = \int_0^\infty du\, u^{-2}\, W(u/\Upsilon) K^2_{1/3}(4/3u), \quad \text{(A31)}$$

where W represents the Weizsäcker–Williams spectral distribution given in (4.3b), and K_ν, $\nu=\frac{1}{3}$, etc., denotes a modified Bessel function. It is convenient to introduce the integral representation

$$W(x) = \int_x^\infty d\sigma\, \sigma\, K_1^2(\sigma); \quad \text{(A32)}$$

and carry through the calculations with the auxiliary variable $\beta \equiv \frac{4}{3}\Upsilon^{-1}$. The quantity to be evaluated then is

$$\hat{\Omega}(\Upsilon) \equiv \Omega(\beta) = \int_0^\infty du \int_{4u\beta/3}^\infty d\sigma\, u^{-2}\sigma K_1^2(\sigma) K^2_{1/3}(4/3u). \quad \text{(A33)}$$

This form suggests that it is advantageous to consider the derivative $\Omega'(\beta)$. Absorbing the 4/3-factor into the u-integration, we have

$$\Omega'(\beta) = -\beta \int_0^\infty du\, K_1^2(\beta u) K^2_{1/3}(u^{-1}). \quad \text{(A34)}$$

Since convergence is not a problem here, we can intro-

TABLE X. Values of the auxiliary function $\hat{K}(z)$.

z	$\hat{K}(z)$	z	$\hat{K}(z)$
0.01	0.1148	0.2	0.7271
0.02	0.1799	0.3	0.8995
0.03	0.2331	0.4	1.034
0.04	0.2795	0.5	1.143
0.05	0.3213	0.6	1.234
0.06	0.3596	0.7	1.310
0.07	0.3952	0.8	1.374
0.08	0.4285	0.9	1.429
0.09	0.4599	1.0	1.476
0.1	0.4897	2.0	1.71

CC-0. In Public Domain. Gurukul Kangri Collection, Haridwar

Digitized by Arya Samaj Foundation Chennai and eGangotri

duce the integral reduction

$$K_\nu^2(z)=2\int_0^\infty d\tau\, K_0(2z\cosh\tau)\cosh(2\nu\tau),$$
$$|\arg(z)|<\pi/2 \quad \text{(A34a)}$$

for both of the Bessel functions in (A34), and so obtain

$$\Omega'(\beta)=-4\beta\int_0^\infty du\int_0^\infty d\tau\int_0^\infty d\rho\cosh(2\tau)\cosh(\tfrac{2}{3}\rho)$$
$$\times K_0([2\beta\cosh\tau]u)K_0([2\cosh\rho]u^{-1}). \quad \text{(A35)}$$

Interchanging the orders of integration, and recalling the identity

$$\int_0^\infty du\, K_\nu(\alpha u)K_\nu(\beta u^{-1})=(\pi/\alpha)K_{2\nu}(2[\alpha\beta]^{1/2});$$
$$\text{Re}(\alpha)>0,\ \text{Re}(\beta)>0; \quad \text{(A35a)}$$

we find

$$\Omega'(\beta)=-2\pi\int_0^\infty d\tau\int_0^\infty d\rho\cosh(2\tau)\cosh(\tfrac{2}{3}\rho)$$
$$\times[\cosh\tau]^{-1}K_0(4[\beta\cosh\tau\cosh\rho]^{1/2}). \quad \text{(A36)}$$

It is convenient to reduce this further by inserting the representation

$$K_0(2[\alpha\beta]^{1/2})=\frac{1}{2}\int_0^\infty d\hat{u}\,\hat{u}^{-1}\exp\{-(\alpha\hat{u}+\beta\hat{u}^{-1})\};$$
$$\alpha>0,\ \beta>0. \quad \text{(A37)}$$

This leads to

$$\Omega'(\beta)=-\pi\int_0^\infty d\tau\int_0^\infty d\rho\int_0^\infty d\hat{u}\cosh(2\tau)\cosh(\tfrac{2}{3}\rho)$$
$$\times[\hat{u}\cosh\tau]^{-1}\exp\{-(\hat{u}\cosh\rho+4\beta\hat{u}^{-1}\cosh\tau)\}. \quad \text{(A38)}$$

Again there are no convergence problems, and we may differentiate with respect to β. The τ and ρ integrals are then expressible in terms of Bessel functions. It is also convenient to change variables $\hat{u}\to u^{-1}$; the final result of these operations is

$$\Omega''(\beta)=4\pi\int_0^\infty du\, K_2(4\beta u)K_{2/3}(u^{-1}). \quad \text{(A39)}$$

Comparing with (A34) we see that the net gain has been the elimination of the squares of the Bessel functions in the integral representation. In fact using known generalizations of the identity (A35a) for unequal indices of the Bessel functions, it is straightforward to obtain closed forms for $\Omega(\beta)$ from (A39) in terms of generalized hypergeometric functions. This is however superfluous for our present purposes, and it will be sufficient to derive asymptotic expansions from (A39).

We begin by remarking that $K_\nu(z)$ is an increasing function of ν for positive values of z and ν. This leads to the double inequality

$$\int_0^\infty du\, K_{2/3}(4\beta u)K_{2/3}(u^{-1})<\int_0^\infty du\, K_2(4\beta u)K_{2/3}(u^{-1})<\int_0^\infty du\, K_2(4\beta u)K_2(u^{-1}). \quad \text{(A40)}$$

Applying the identity (A35a), we obtain the bounds

$$K_{4/3}(4\beta^{1/2})<(\beta/\pi^2)\Omega''(\beta)<K_4(4\beta^{1/2}). \quad \text{(A41)}$$

Suppose now that $\beta\gg1$; then both sides of the inequality approach each other since the leading terms of the asymptotic expansion of the Bessel functions are independent of the index. This yields the estimate

$$\Omega''(\beta)\to2^{-3/2}(\pi^2/\beta)^{5/4}\exp\{-4\beta^{1/2}\},\qquad \beta\gg1. \quad \text{(A42)}$$

In the present instance integration of this asymptotic estimate is legitimate. Recalling $\Omega'(\infty)=\Omega(\infty)=0$, and reconverting to $\hat{\Omega}(\Upsilon)$, we find

$$\hat{\Omega}(\Upsilon)\to(\pi^{5/2}/16)(3\Upsilon)^{1/4}\exp\{-8(3\Upsilon)^{-1/2}\},\qquad \Upsilon\ll1. \quad \text{(A43)}$$

This is one of the limiting forms given in Eq. (4.4b) of the text.

The asymptotic expansion of $\Omega(\beta)$ for $\beta\to0$, can also be conveniently derived from (A39). We insert the representation

$$K_\nu(\alpha z)=\frac{(2z)^\nu\Gamma(\nu+\frac{1}{2})}{\alpha^\nu\Gamma(\frac{1}{2})}\int_0^\infty dv\,\frac{\cos(\alpha v)}{(v^2+z^2)^{\nu+1/2}},$$
$$\text{Re}\{\nu+\tfrac{1}{2}\}\geq0,\ |\arg z|<\pi/2,\ \alpha>0, \quad \text{(A44)}$$

for $K_2(4\beta u)$ in (A39). The result may be written as

$$\Omega''(\beta)=\tfrac{3}{4}\pi\beta^{-2}\mathfrak{M}(\beta), \quad \text{(A45a)}$$

where

$$\mathfrak{M}(\beta)=\int_0^\infty du\int_0^\infty dv\,\frac{u^2\cos(4\beta v)}{(u^2+v^2)^{5/2}}K_{2/3}(u^{-1}). \quad \text{(A45b)}$$

It can easily be verified that $\mathfrak{M}(\beta)$ has a series expansion about the origin; and in particular that $\mathfrak{M}(0)=\frac{3}{2}\pi$.

CC-0. In Public Domain. Gurukul Kangri Collection, Haridwar

Digitized by Arya Samaj Foundation Chennai and eGangotri

Combining this with (A45a), and keeping only the dominant terms, we find the asymptotic estimate

$$\Omega(\beta)\rightarrow-(\pi^2/2)\ln\beta, \qquad \beta\ll 1. \tag{A46}$$

Since $\Omega(\beta)=\hat{\Omega}(\Upsilon)$, this leads to the expression corresponding to $\Upsilon\gg 1$ given in (4.4b).

APPENDIX 4: EVALUATION OF THE AUXILIARY FUNCTION $\Xi(\Upsilon)$

This function is defined in terms of the integral representation

$$\Xi(\Upsilon)=\int_0^{\Upsilon} d\sigma\,\sigma^{-2}\,\kappa\left(\frac{2\sigma}{3\Upsilon^2}\right)K^2_{1/3}\left(\frac{4}{3\sigma}\right), \tag{A47}$$

where

$$\kappa(z)=z\int_z^{\infty} dx\,K_{5/3}(x).$$

As shown in the discussion of Sec. 4B the evaluation of the rate of trident production for real photon intermediate states requires estimates of $\Xi(\Upsilon)$ corresponding to both of the ranges $\Upsilon\gg 1$ and $\Upsilon\ll 1$.

It is convenient to begin by considering the case $\Upsilon\gg 1$. The argument of the bremsstrahlung function $\kappa(z)$ in this instance is always very much less than unity and it is possible to use the simplifying approximation [compare (2.12)]

$$\kappa(z)\simeq 2.15\,z^{1/3}.$$

The basic integral representation (A47) can then be rewritten in the form

$$\Xi(\Upsilon)\simeq 1.55\,\Upsilon^{-2/3}\,\xi(\tau_0,\Upsilon), \qquad \Upsilon\gg 1; \tag{A48a}$$

where

$$\xi(\tau_0,\Upsilon)=\int_{4/3\tau_0}^{\infty} d\tau\,\tau^{-1/3}\,K^2_{1/3}(\tau). \tag{A48b}$$

Since the bremsstrahlung spectrum is not well represented by $\kappa(2\sigma/3\Upsilon^2)$ in the region of the tip, i.e., the range $\sigma\rightarrow\Upsilon$, it is advisable to cut off the integration at a lower energy. This is the significance of the auxiliary constant τ_0, where $1\ll\tau_0<\Upsilon$, which has been introduced in (A48b). In order to obtain the leading term of $\Xi(\Upsilon)$ for $\Upsilon\gg 1$, we now perform a parts integration, viz.

$$\xi(\tau_0,\Upsilon)=-\left(\frac{4}{3\tau_0}\right)^{2/3}\ln\left(\frac{4}{3\tau_0}\right)K^2_{1/3}\left(\frac{4}{3\tau_0}\right)$$
$$-\int_{4/3\tau_0}^{\infty} d\tau\,\ln\tau\,\frac{d}{d\tau}\left[\tau^{2/3}\,K^2_{1/3}(\tau)\right]. \tag{A49a}$$

It is easy to check that this reduces to the expression

$$\xi(\tau_0,\Upsilon)\simeq\left[2^{-2/3}\,\Gamma\left(\tfrac{1}{3}\right)\right]^2\ln(3\tau_0/4)$$
$$+O(\tau_0^{-2/3}\ln\tau_0), \qquad \text{for } \tau_0\gg 1. \tag{A49b}$$

The uncertainty regarding the contribution of the bremsstrahlung tip now enters only through the slowly varying factor $\ln\tau_0$. For our present purposes it is sufficient to single out the limit $\xi(\Upsilon,\Upsilon)$ which, in conjunction with the previous results, then leads to the compact estimate

$$\Xi(\Upsilon)\simeq 4.4\,\Upsilon^{-2/3}\ln\Upsilon, \qquad \Upsilon\gg 1. \tag{A50}$$

Similar methods can be used to obtain approximations for $\Xi(\Upsilon)$ which are valid in the range $\Upsilon\ll 1$. In this case it is possible to take advantage of the asymptotic expansion

$$K^2_{1/3}(4/3\sigma)\simeq(3\pi/8)\sigma\exp(-8/3\sigma), \qquad \sigma\ll 1;$$

to simplify the integrand of (A47). It is convenient to introduce the abbreviation $p\equiv 8/9\Upsilon^2$, and rearrange the variables of integration. $\Xi(\Upsilon)$ can then be represented in the form

$$\Xi(\Upsilon)\simeq(3\pi/8)\,p\,\xi(\Upsilon), \qquad \Upsilon\gg 1, \tag{A51a}$$

where

$$\xi(\Upsilon)=\int_0^{3\Upsilon/4} d\tau\,e^{-2/\tau}\int_{p\tau}^{\infty} dx\,K_{5/3}(x). \tag{A51b}$$

This expression can be simplified still further with the help of the identity

$$\xi(\Upsilon)+\xi_1(\Upsilon)-\tfrac{1}{2}\xi_2(\Upsilon)=\tfrac{3}{8}(\Upsilon/p)\exp(-8/3\Upsilon)\,\kappa(\tfrac{3}{4}p\Upsilon); \tag{A52a}$$

where

$$\xi_1(\Upsilon)=\int_0^{3\Upsilon/4} d\tau\,\tau\,e^{-2/\tau}\int_{p\tau}^{\infty} dx\,K_{5/3}(x), \tag{A52b}$$

and

$$\xi_2(\Upsilon)=p\int_0^{3\Upsilon/4} d\tau\,\tau^2\,e^{-2/\tau}\,K_{5/3}(p\tau). \tag{A52c}$$

Now in virtue of the mean value theorem we have

$$\xi_1(\Upsilon)=\bar{\tau}\,\xi(\Upsilon), \qquad \text{where } 0\leq\bar{\tau}\leq\tfrac{3}{4}\Upsilon. \tag{A53}$$

Since Υ itself is bounded from above by $\Upsilon\ll 1$, we may obviously neglect ξ_1 relative to ξ in Eq. (A52a).

The auxiliary function $\xi_2(\Upsilon)$ can be dealt with by analogous methods. For this purpose it is useful to note the

Lemma:

$$y(1+y)^{-1}\,K_{5/3}(y)\leq\frac{5}{3}\int_y^{\infty} dx\,K_{5/3}(x), \qquad y>0. \tag{A54}$$

CC-0. In Public Domain. Gurukul Kangri Collection, Haridwar

Digitized by Arya Samaj Foundation Chennai and eGangotri

This inequality may be verified by considering the function

$$Q(y)\equiv y(1+y)^{-1}K_{5/3}(y)\Big/\int_y^\infty dx\,K_{5/3}(x), \qquad y>0. \tag{A55}$$

From the mean value theorem it follows that

$$Q(y)=\left.\frac{\frac{d}{dy}\{y(1+y)^{-1}K_{5/3}(y)\}}{\frac{d}{dy}\left\{\int_y^\infty dx\,K_{5/3}(x)\right\}}\right|_{y=y_0},$$

for some $y_0\geq y$. (A56a)

Carrying out the differentiations, we obtain

$$Q(y)=(1+y_0)^{-1}\{\tfrac{5}{3}-(1+y_0)^{-1}+y_0[K_{2/3}(y_0)/K_{5/3}(y_0)]\}. \tag{A56b}$$

Since $K_{2/3}(y_0)<K_{5/3}(y_0)$, it is easy to show that

$$0\leq Q(y)\leq\tfrac{5}{3}, \tag{A56c}$$

and this establishes the lemma.

Now inserting (A54) into (A52c), and again applying the mean value theorem, we find

$$\xi_2(\Upsilon)\leq\tfrac{5}{3}\bar{\tau}(1+p\bar{\tau})\xi(\Upsilon),$$

where

$$0\leq\bar{\tau}\leq\tfrac{3}{4}\Upsilon. \tag{A57}$$

This estimate, together with the previous results, implies that (A52a) may be rewritten in the form

$$\xi(\Upsilon)\simeq\tfrac{3}{8}(\Upsilon/p)[1-\Theta(\Upsilon)]^{-1}\times\exp(-8/3\Upsilon)\kappa(\tfrac{3}{4}p\Upsilon), \qquad \Upsilon\ll1; \tag{A58}$$

where the quantity $\Theta(\Upsilon)$ derives from the $\mathcal{O}(\bar{\tau}^2)$ term in (A57). It can easily be verified that $0\leq\Theta(\Upsilon)\leq5/12$; and in the present order of approximation this may be neglected. The bremsstrahlung function appearing in (A58) may be simplified since $\frac{3}{4}p\Upsilon\gg1$, and one of the asymptotic expansions of (2.12) can be used. The corresponding estimate for $\Xi(\Upsilon)$ can then be written as

$$\Xi(\Upsilon)\simeq0.4\Upsilon^{1/2}\exp(-10/3\Upsilon), \qquad \Upsilon\ll1. \tag{A59}$$

REFERENCES

A1 Amaldi, E., *et al.* CERN Rept. 63-13, p. 5.
A2 Arzimovich, L., and I. Pomeranchuk, J. Phys. USSR **9**, 267 (1945).
A3 Alekseev, A. I., Zh. Eksperim. i Teor. Fiz. **31**, 909 (1956) [English transl.: Soviet Phys.—JETP **4**, 771 (1957)].
A4 Aditya, P. K., Nuovo Cimento **11**, 546 (1959).
B1 Beck, F., H. Steinwedel, and G. Sussman, Z. Physik **171**, 189 (1963).
B2 Blewett, J. P., Phys. Rev. **69**, 87 (1946).
B3 Barrat, J. P., Ph.D. dissertation, Université de Paris (1959).
B4 Barrat, J. P., J. Physique **20**, 541 (1959).
B5 Badalyan, A. M., and Ya. A. Smorodinskii, Zh. Eksperim. i Teor. Fiz. **40**, 1231 (1961) [English transl.: Soviet Phys.—JETP **13**, 865 (1961)].
B6 Bhabha, H. J., Proc. Roy. Soc. (London) **A152**, 559 (1935).
B7 Block, M. M., and D. T. King, Phys. Rev. **95**, 171 (1954).
B8 Bolsterli, M., Phys. Rev. **94**, 367 (1954).
C1 Caird, R. S., W. B. Garn, D. B. Thomson, and C. M. Fowler, J. Appl. Phys. **35**, 781 (1964).
C2 Carleman, T., *Les fonctions quasi-analytiques* (Herman et Cie., Paris, 1926).
C3 Criegee, L., Z. Physik **158**, 433 (1960).
D1 Demeur, M., Acad. Roy. Belg. Cl. Sci. Mem. Coll. **28**, No. 5 (1953).
D2 Dovzhenko, O. I., and A. A. Pomanskii, Zh. Eksperim. i Teor. Fiz. **45**, 268 (1963) [English transl.: Soviet Phys.—JETP **18**, 187 (1964)].
D3 Davies, H., H. A. Bethe, and L. C. Maximon, Phys. Rev. **93**, 788 (1954).
E1 Erber, T., Nature **190**, 25 (1961).
E2 Erber, T., in *High Magnetic Fields*, edited by H. Kolm *et al.* (Technology Press, Cambridge, Mass., 1962), p. 706.
E3 Erber, T., and H. C. Shih, Acta Phys. Austriaca **19**, 17 (1964).
E4 Erber, T., Fortschr. Phys. **9**, 343 (1961).
E5 Erber, T., and H. C. Shih, in *Proceedings of the Conference on the Role of Atomic Electrons in Nuclear Transformations* (Polish Academy of Sciences, Warsaw, 1965), Vol. 3, p. 520.
E6 Erber, T., Ann. Phys. (N.Y.) **8**, 435 (1959).
E7 Erber, T., Bull. Am. Phys. Soc. **10**, 536 (1965).
E8 Ehlotzky, F., Acta Phys. Austriaca **18**, 266 (1964).
E9 Euler, H., Ann. Physik **26**, 398 (1936).
E10 Erber, T., and A. Gordon, Math. Computation **17**, 162 (1963).
E11 Erber, T., and H. G. Latal, Bull. Am. Phys. Soc. **10**, 1103 (1965).
F1 Fowler, C. M., W. B. Garn, and R. S. Caird, J. Appl. Phys. **31**, 588 (1960).
F2 Fowler, C. M., R. S. Caird, W. B. Garn, and D. B. Thomson in *High Magnetic Fields*, edited by H. Kolm *et al.* (Technology Press, Cambridge, Mass., 1962), p. 269.
F3 Furry, W. H., Phys. Rev. **51**, 125 (1937).
F4 Furry, W. H., Phys. Rev. **81**, 115 (1951).
F5 Feinberg, E. L., and I. Pomeranchuk, Suppl. Nuovo Cimento **3**, 652 (1956).
F6 Frisch, O. R., Acta Phys. Austriaca **12**, 331 (1959).
F7 Fermi, E., Z. Physik **29**, 315 (1924).
G1 Galitsky, V. M., and I. I. Gurevitch, Nuovo Cimento **32**, 396 (1964).
G2 Galitsky, V. M., and V. V. Yakimets, Zh. Eksperim. i Teor. Fiz. **46**, 1066 (1964) [English transl.: Soviet Phys.—JETP **19**, 723 (1964)].
G3 Guzenko, S. Ya., and P. I. Fomin, Zh. Eksperim. i Teor. Fiz. **47**, 2276 (1964) [English transl.: Soviet Phys.—JETP **20**, 1523 (1965)].
H1 Heitler, W., *Quantum Theory of Radiation* (Clarendon Press, Oxford, England, 1954), 3rd ed., p. 337.
H2 Heisenberg, W., and H. Euler, Z. Physik **98**, 714 (1935).
I1 Iwanenko, D., and I. Pomeranchuk, Phys. Rev. **65**, 343 (1944).
J1 Jauch, J. M., and K. M. Watson, Phys. Rev. **74**, 950 (1948); **74**, 1485 (1948).
J2 Johnson, M. H., and B. A. Lippmann, Phys. Rev. **76**, 828 (1949).
K1 Kaitna, R., Ph.D. dissertation, Universität Graz (1963).
K2 Kaitna, R., and P. Urban, Nucl. Phys. **56**, 518 (1964).
K3 Källén, A. O. G., *Handbuch der Physik*, S. Flügge, Ed. (Springer-Verlag, Berlin, 1958), Vol. 5, Part 1.
K4 Klepikov, N. P., Zh. Eksperim. i Teor. Fiz. **26**, 19 (1954).
K5 Klepikov, N. P., Ph.D. thesis, University of Moscow (1952).

CC-0. In Public Domain. Gurukul Kangri Collection, Haridwar

Digitized by Arya Samaj Foundation Chennai and eGangotri

K6 Koch, H. W., and J. W. Motz, Rev. Mod. Phys. **31**, 920 (1959).

K7 Kuraev, E. A., and S. S. Sannikov, Zh. Eksperim. i Teor. Fiz. **44**, 1015 (1963) [English transl.: Soviet Phys.—JETP **17**, 688 (1963)].

K8 Katz, L., and K. H. Lokan, Nucl. Instr. Methods **11**, 7 (1961).

L1 Landau, L. D., and E. M. Lifshitz, *The Classical Theory Fields* (Pergamon Press, Oxford, England, 1962), revised second edition, p. 235.

L2 Lerch, M., Acta Math. **27**, 339 (1903).

L3 Landau, L., and I. Pomeranchuk, Doklady Akad. Nauk SSSR **92**, 535, 735 (1953).

L4 Lutzky, M., and J. S. Toll, Phys. Rev. **113**, 1649 (1959).

M1 Malkus, W. V. R., Phys. Rev. **83**, 899 (1951).

M2 Mark, H., Nucl. Instr. Methods **28**, 131 (1964).

M3 Migdal, A. B., Phys. Rev. **103**, 1811 (1956).

M4 Migdal, A. B., Zh. Eksperim. i Teor. Fiz. **32**, 633 (1957).

M5 Murota, T., A. Ueda, and H. Tanaka, Progr. Theoret. Phys. **16**, 482 (1956).

N1 Neuman, M., Phys. Rev. **90**, 682 (1953).

P1 Pomeranchuk, I., J. Phys. (USSR) **2**, 65 (1940).

R1 Robl, H., Acta Phys. Austriaca **6**, 45 (1952).

R2 Robl, H., Acta Phys. Austriaca **6**, 105 (1952).

S1 Schiff, L. I., Am. J. Phys. **20**, 474 (1952).

S2 Schwinger, J., Phys. Rev. **75**, 1912 (1949).

S3 Schott, G. A., *Electromagnetic Radiation* (Cambridge University Press, Cambridge, England, 1912).

S4 Schwinger, J., Phys. Rev. **75**, 898 (1949).

S5 Smith, F. T., Phys. Rev. **118**, 349 (1960).

S6 Sannikov, S. S., Zh. Eksperim. i Teor. Fiz. **42**, 282 (1962) [English transl.: Soviet Phys.—JETP **15**, 196 (1962)].

S7 Synge, J. L., *Principal Null Directions Defined in Space Time by an Electromagnetic Field* (University of Toronto Press, Toronto, 1935), Appl. Math. Ser. No. 1.

S8 Schrödinger, E., Proc. Roy. Irish Acad. **A47**, 77 (1942).

S9 Skobov, V. G., Zh. Eksperim. i Teor. Fiz. **35**, 1315 (1958) [English transl.: Soviet Phys.—JETP **8**, 919 (1959)].

S10 Sakharov, A. D., *et al.*, Dokl. Akad. Nauk SSSR **165**, 65 (1965) [English transl.: Soviet Phys.—Doklady **10**, 1045 (1966)].

T1 Toll, J., Ph.D. dissertation, Princeton University (1952).

T2 Ter-Mikaeljan, M. L., Doklady Akad. Nauk SSSR **94**, 1033 (1954).

T3 Toptygin, I. N., Zh. Eksperim. i Teor. Fiz. **46**, 851 (1964) [English transl.: Soviet Phys.—JETP **19**, 583 (1964)].

T4 Tomonaga, S., and M. Kobayasi, Sci. Papers Inst. Phys. Chem. Res. (Tokyo) **34**, 1643 (1938).

U1 Überall, H., Phys. Rev. **103**, 1055 (1956).

W1 Watson, G. N., *Bessel Functions* (Cambridge University Press, Cambridge, England, 1952).

W2 Wall, H. S., *Analytic Theory of Continued Fractions* (D. Van Nostrand Co., Inc., New York, 1948), pp. 327–330.

W3 Weizsäcker, C. F., Z. Physik **88**, 612 (1934).

W4 Williams, E. J., Kgl. Danske Videnskab. Selskab, Mat.-Fyz. Medd. **13**, No. 4 (1935).

CC-0. In Public Domain. Gurukul Kangri Collection, Haridwar

Digitized by Arya Samaj Foundation Chennai and eGangotri

Accelerator Calibration Energies*

JERRY B. MARION†
California Institute of Technology, Pasadena, California

The absolute measurements of nuclear reaction energies appropriate for calibration purposes are critically reviewed and recommended values are given. A sufficent number of points are now known with precision to permit the calibration of proton beams up to 60 MeV.

I. INTRODUCTION

Because only a few accelerators are, at the present time, equipped with absolute instruments for measuring the beam energy, most nuclear reaction experiments are performed with energy analyzers that require calibration. As techniques become more sophisticated, it is increasingly necessary that calibration points of high precision be available. The status of accurately known resonance and threshold energies that are suitable for calibration purposes was reviewed in 1961 (Ma 61) and again in 1963 (Ma 64). Since the last report, the situation has improved sufficiently to warrant a new survey and to list a new set of recommended calibration energies. A more critical evaluation of the data is attempted in this report than was felt appropriate in the past.

Measurements of 16 different reaction energies have been considered and weighted averages are given (see the tables below). These energies cover the range up to $E \cong 10$ MeV with reasonable uniformity. In addition, calculated energies (based on the most recent adjustment of atomic masses) are given for several nuclear reactions which will permit the calibration of magnetic beam analyzers for proton energies up to 60 MeV.

II. SELECTION OF DATA

In recent years, experimenters have become increasingly aware of the subtleties involved in performing precision measurements of nuclear reaction energies. Indeed, most of the work reported in the past few years is characterized by careful attention to minute details of procedure. These recent measurements with improved, modern equipment have yielded several results with a precision approaching (and even exceeding) 1 part in 10^4. The older measurements are generally of lower precision and in some cases were made without proper regard for effects that are now known to be important. The correction of these older measurements to conform to currently accepted practice is at best difficult (and often impossible) to perform with reliability. In view of these facts, it was decided to include only recent measurements (post-1958) in determining recommended values of reaction energies. (1958, the date of the first publication of the initial measurements with the 2-m electrostatic analyzer at the U. S. Naval Research Laboratory, marks the beginning of the current generation of precision energy measurements.) Some discussion of the omitted measurements is given in the appropriate sections below.

In addition to the omission of pre-1958 results, the energy measurements made in 1959–60 with the electrostatic analyzer at Associated Electrical Industries, Aldermaston, England, have also been deleted from the analysis. The reason is an apparent systematic error in the AEI results. Whereas the weighted mean value of all other results for the $Al^{27}(p, \gamma)Si^{28}$ resonance energy is 991.90±0.04 keV, the AEI value is 994.0±1.0 keV; similarly, for the $F^{19}(p, \alpha\gamma)O^{16}$ resonance, the weighted mean is 872.11±0.20 keV compared to 873.9±0.8 keV measured at AEI (Hu 60). The deviation in each case is about 0.2%, twice the stated uncertainty and about ten times the standard deviation in the weighted mean of all the other measurements. At the lower energy $F^{19}(p, \alpha\gamma)O^{16}$ resonance, the AEI value is also high (340.9±0.3 keV compared to 340.46 keV for the mean), but only by 0.13%. Thus, the AEI results appear to be systematically high by about 0.2%, an intolerably large discrepancy in view of the precision of (and close agreement among) the other measurements.

Having eliminated the pre-1958 and the AEI measurements, we further restrict the set of input data by choosing only *absolute* measurements (electrostatic, magnetic, or velocity). We relax this requirement slightly to allow also the inclusion of results obtained by the direct comparison of beam energy with the energy (measured absolutely) of α particles from such sources as Po^{210}, ThC, and ThC′, since these energies are now known with considerable precision (Wa 64). By considering only absolute measurements, a large number of *relative* energy measurements are excluded. Such measurements, which frequently are based on more than one calibration point, are difficult to adjust for changes in calibration energies. Furthermore, if the measured energy is far removed from the calibration energy [for example, basing an energy for the $N^{14}(p, n)O^{14}$ threshold at 6.36 MeV on the $C^{13}(p, n)N^{13}$ threshold energy at 3.236 MeV], the result depends heavily on the linearity of the beam energy analyzer

* Work supported in part by the U.S. Office of Naval Research Contract [Nonr-220(47)].

† John Simon Guggenheim Fellow, on leave from the University of Maryland, College Park, Maryland, 1965–66.

CC-0. In Public Domain. Gurukul Kangri Collection, Haridwar

Digitized by Arya Samaj Foundation Chennai and eGangotri

(which usually is not—or cannot be—demonstrated). However, in the list of nuclear reactions chosen for this survey, the number of relative energy measurements that could otherwise have been included is rather small. [Only in the cases of the $F^{19}(p, n)Ne^{19}$ and $Al^{27}(p, n)Si^{27}$ reactions have a significant number of relative measurements been excluded.] Fortunately, a sufficiently large number of absolute experiments has been performed that it is no longer necessary to rely on the less precise relative measurements.

III. CORRECTION OF DATA

Alterations of some published energy values used in this survey have been made for two reasons: (1) errors in computation or in analysis technique, and (2) adjustments necessitated by changes in the recommended values of the fundamental constants that enter the calculation. The latter are easily made by substituting the latest values (Co 65) for the ones used in the original calculations. Into this category fall the following:

(a) Gasten's measurements (Ga 63) of the $Li^7(p, n)Be^7$ threshold energy and the $Al^{27}(p, \gamma)Si^{28}$ resonance energy have been increased by 39 parts per million (ppm) because of the change in the proton mass from 938.219 MeV to 938.256 MeV. This correction amounts to +0.07 keV and +0.04 keV in the two energies.

(b) The $F^{19}(p, \alpha\gamma)O^{16}$ resonance energy of Seagrave *et al.* (Se 64) has also been corrected (by +26 ppm) for a change in m_pc^2.

(c) The Rice measurements (Be 61, Bo 66) have been corrected for a decrease of 41 ppm in the value of the gyromagnetic ratio of the proton and for a decrease of 48 ppm in the value of e/m for the proton. These quantities enter as $(e/m)/\gamma_p^2$, so the net effect is to increase the stated energies by 34 ppm.

Changes in the least-squares-adjusted values of the fundamental constants since the time of publication cause changes in all of the other energy values that are negligibly small (a few eV at most).

Only one case of a correction of type (1) has been made:

(a) In Gasten's report (Ga 63) of his velocity measurements, the various contributions to the uncertainties in the results are tabulated. For the $Al^{27}(p, \gamma)Si^{28}$ resonance energy and the $Li^7(p, n)Be^7$ threshold energy, the rms errors are 20 and 32, respectively, in units of $\%E\times10^{-3}$. These are *relative* errors, but they have apparently been applied as *absolute* errors; this results in no change for the uncertainty in the $Al^{27}(p, \gamma)Si^{28}$ value (±0.2 keV), but the listed error for the $Li^7(p, n)Be^7$ threshold energy (±0.3 keV) should properly be ±0.6 keV. The latter error is shown in Table II and has been used in the calculation of the weighted mean threshold energy.

IV. TREATMENT OF DATA

In order to compute a weighted mean value for each of the energy points selected, it is necessary to decide whether the rules of standard statistical analysis apply. For a statistical sample, the weighting factor for the ith measurement is

$$\text{weighting factor} = w_i = (\Delta E_i)^{-2}, \tag{1}$$

where ΔE_i is the stated uncertainty in the ith value. This procedure is valid: (a) if all of the uncertainties have been assigned in a uniform manner (e.g., standard deviations), and (b) if a sufficient number of measurements has been made to constitute a "statistical sample." In the previous surveys (Ma 61, Ma 63), it was argued that neither of these criteria is met and therefore that an arbitrary weighting procedure is perhaps more reasonable than that dictated for truly statistical cases; it was decided to assign weights according to $w_i = (\Delta E_i)^{-1}$ as a compromise between *no* weighting and the severe *statistical* weighting.

Although several new measurements have been made since the last survey, the older measurements have now been excluded so that there is actually no significant increase in the number of input data; that is, we are no nearer to a "statistical sample" now than before. However, the recent measurements all appear to have been analyzed rather uniformly (see some specific comments below) so that the first objection to statistical weighting has now been met to an acceptable degree. This latter fact seems crucial and for the purposes of this survey outweighs the paucity of data. Therefore, standard statistical methods have been used in this analysis. That is, the weighting factors have been computed according to Eq. (1) and the *internal* and *external* errors are given by

$$e_{\text{int}}^2 = \Sigma w_i^2(\Delta E_i)^2/(\Sigma w_i)^2 = (\Sigma w_i)^{-1} \tag{2}$$

and

$$e_{\text{ext}}^2 = (N-1)^{-1}(\Sigma w_i\delta_i^2)(\Sigma w_i)^{-1}, \tag{3}$$

where $\delta_i = E_i - \bar{E}$ is the deviation of the ith value from the weighted mean. (*Standard deviations* rather than *probable errors* have been used throughout.)

The recommended value in each case is assigned an uncertainty equal to the *larger* of e_{int} or e_{ext}.

Fortunately, all of the experimenters who, in the recent past, have been engaged in precision energy measurements have followed the practice of listing all known contributions to uncertainties in their results and of calculating the rms error (in all cases, presumably the standard deviation). In the Rice experi-

CC-0. In Public Domain. Gurukul Kangri Collection, Haridwar

Digitized by Arya Samaj Foundation Chennai and eGangotri

ments (Be 61, Bo 66), the rms error was given but a somewhat larger uncertainty was arbitrarily assigned to each result. This practice is not to be encouraged. After the most careful possible assessment of the experimental conditions and the estimation of the contributing uncertainties, the rms error is the most meaningful representation of the reliability of the data; to assign an additional "safety factor" unnecessarily distorts the results when viewed in the total context of all similar measurements. [For an amplification of this point, see Cohen and DuMond (Co 65, Sec. 1.4).] Therefore, in calculating the weighted mean values, the results of Beckner *et al.* (Be 61), and Bonner *et al.* (Bo 66) have been given weights inversely proportional to the squares of the rms errors, before the introduction of the "safety factor."

The results for resonance widths Γ have been treated in the same manner as the energy values.

V. ENERGY STANDARDS VERSUS THE "TRUTH"

This analysis of precision energy measurements aims to provide a recommended set of energy values that can be used for calibration purposes under normal laboratory conditions. Thus, if a well-defined procedure leads to a convenient method for the reproducible extraction of a number which we call, for example, the "neutron threshold" for a reaction, this is (by definition) a *calibration point;* it matters not at all whether the number so defined is the "true" neutron threshold in the sense that the Q value for the reaction can be accurately obtained therefrom.

For several years it has been recognized that the discrete nature of the energy loss process for ions traversing matter can influence the shape and the position of resonance and threshold yield curves. This Lewis effect (Le 62) has been incorporated into the analysis of the yield curves for (p, γ) resonances (see, e.g., Wa 62 and Bo 63) and for (p, n) thresholds (Be 64, Pa 66). These experiments and calculations have shown that the difference between the apparent resonance or threshold position and the "true" position can amount to 100–200 eV. Since we are not concerned here with precision measurements of Q values or energy level positions, these differences are not important—*if* it is possible to establish a standard procedure for defining the "calibration energy."

The procedure for determining a neutron threshold energy is dictated by the fact that the yield of s-wave neutrons from a thick target varies as the $\frac{3}{2}$ power of the neutron energy, i.e., approximately as $(\Delta E)^{\frac{3}{2}}$, where ΔE is the difference between the bombarding energy and the threshold energy. [This is not strictly true for the $Li^7(p, n)Be^7$ reaction in which a strong resonance occurs near threshold. However, the modification of the $(\Delta E)^{\frac{3}{2}}$ yield expression is not great.] Thus, a plot of $(\text{yield})^{\frac{2}{3}}$ versus bombarding energy can be extrapolated linearly to zero yield to determine the threshold energy. The effects on the extrapolated intercepts due to finite beam energy resolution and to discrete energy loss have been extensively investigated by Bondelid and Whiting (Bo 64) and by Palmer *et al.* (Pa 66). The mutual conclusion of these groups is that the extrapolated $(\text{yield})^{\frac{2}{3}}$ intercept lies 100–200 eV *below* the true threshold, the exact value depending on the beam energy resolution. However, for high resolution beams as are generally employed in present-day experiments (i.e., $E/\Delta E \approx 0.01-0.03\%$). The extrapolation of $(\text{yield})^{\frac{2}{3}}$ gives an intercept that is defined and reproducible to within about 100 eV. Therefore, since all of the results used here were obtained from measurements with high resolution beams, the intercept of the linear extrapolation of $(\text{yield})^{\frac{2}{3}}$ serves adequately to define the neutron threshold calibration points. It would be preferable to have a collection of absolute measurements with beams of known resolution and with the analysis performed in the manner of Bondelid and Whiting (Bo 64) or Palmer *et al.* (Pa 66); all presently known effects would then be taken into account. Tables are even available to expedite this procedure for the $Li^7(p, n)Be^7$ threshold (Pa 66). At present, the only absolute measurements that have been so analyzed are those of Bondelid and Whiting (Bo 64). Furthermore, such a procedure is usually more time-consuming than is warranted for most calibration purposes. Therefore, the $(\text{yield})^{\frac{2}{3}}$ extrapolation procedure seems sufficiently accurate for all but the most demanding present-day situations.

Similar comments apply for reasonance reactions. The familiar arctangent thick-target yield curve is modified by the discrete energy loss effect and an overshoot occurs at the peak of the curve (the Lewis effect). If the energy loss process were continuous rather than discrete, the midpoint of the arctangent curve would be the resonance position. The point at which the yield has risen to one-half of the constant yield at bombarding energies above the Lewis effect hump corresponds closely to the resonance energy. The displacement amounts to about 100 eV for the $Al^{27}(p, \gamma)Si^{28}$ resonance when a pure aluminum target is used. If the surface is partially oxidized, the displacement and the height of the Lewis effect hump are greatly reduced. Indeed, with partially oxidized targets as are commonly used for calibration purposes, there may actually be no displacement at all (Bo 63). In any event, if high resolution beams are employed, the half-maximum-yield point is defined and reproducible to within about 100 eV. Again, the procedure that neglects the Lewis effect is quite adequate for calibration purposes.

VI. LOW-ENERGY CALIBRATION POINTS

The vast majority of precision measurements of nuclear reaction energies have been made for bom-

CC-0. In Public Domain. Gurukul Kangri Collection, Haridwar

Digitized by Arya Samaj Foundation Chennai and eGangotri

barding energies below 3.5 MeV. Traditionally, the $Al^{27}(p, \gamma)Si^{28}$ resonance near 992 keV and the $Li^7(p, n)Be^7$ threshold near 1881 keV have served as the main calibration points for low-energy electrostatic accelerators. Since the deterioration of carbon targets is less severe than for aluminum or lithium targets, it has been suggested (Ph 64) that the $C^{13}(p, \gamma)N^{14}$ resonance near 1747 keV and the $C^{13}(p, n)N^{13}$ threshold near 3236 keV be adopted as the primary calibration points. Although there is much merit in this proposal, there is not a sufficient number of absolute measurements of these energies available at present to offer a precision comparable with the aluminum and lithium points. These latter points will probably be the best established markers on the nuclear energy scale for some time to come.

A. $Al^{27}(p, \gamma)Si^{28}$

The five values of the $Al^{27}(p, \gamma)Si^{28}$ resonance energy that have been reported in the post-1958 period are shown in Table I. Several of the values have been corrected as explained in the preceding sections. All of the energies (except the one from Bo 63) were determined by taking the midpoint of the thick-target yield curve. The value listed for the Bondelid and Butler experiment (Bo 63) requires some comment. The first publication of a result for the $Al^{27}(p, \gamma)Si^{28}$ resonance energy by the NRL group was in 1959 when 992.4±0.5 keV was obtained (Bo 59). The experiment was repeated the following year with the result E_R= 992.0 keV (Bo 60a), which value, as pointed out in Bo 63, was rounded up from 991.95 keV. The data of Bo 60a were re-analyzed in Bo 63 and the same result, 991.95 keV, was obtained because the effects of surface

TABLE I. $Al^{27}(p, \gamma)Si^{28}$ resonance energies.

E_R(keV)	Γ(keV)	Method	Reference
	0.1 ±0.05		Bo 59
992.23 ±0.27[a]			
991.83 ±0.10[b]	0.10±0.02[b]	Absolute magnetic	Be 61
991.91 ±0.30[b]		Absolute magnetic	Ry 62
991.64 ±0.2[c]		Absolute electrostatic	Bo 63
991.912±0.043		Absolute velocity	Ga 63
		Absolute velocity	Ro 66
	0.090±0.035		Fe 66

Weighted mean: E_R=991.90 keV

e_{int}=0.04 keV

e_{ext}=0.04 keV

Recommended: E_R=991.90±0.04 keV; Γ=0.10±0.02 keV

[a] Corrected (from 992.2±0.5) as explained in the text.
[b] Supercedes an earlier published value.
[c] Corrected (from 991.6±0.2) as explained in the text.

TABLE II. $Li^7(p, n)Be^7$ threshold energies.

E_{th}(keV)	Method	Reference
1880.56 ±0.55[a]	Absolute magnetic	Be 61
1880.48 ±0.25[b]	Absolute magnetic	Ry 61a
1879.87 ±0.6[c]	Absolute velocity	Ga 63
1881.11 ±0.94[b]	Absolute electrostatic	Bo 64
1880.8 ±0.7[b]	Magnetic; comparison of E_{th} with Po α energy	Br 64 Wa 65
1880.617±0.078	Absolute velocity	Ro 66

Weighted mean: E_{th}=1880.60 keV

e_{int}=0.07 keV

e_{ext}=0.05 keV

Recommended: E_{th}=1880.60±0.07 keV

[a] Corrected (from 1880.5±0.8) as explained in the text.
[b] Supercedes an earlier published value.
[c] Corrected (from 1879.8±0.3) as explained in the text.

impurity happened to exactly cancel the slight decrease of the resonance energy brought about by the discrete energy loss effect. This value was then averaged with six other results from similar analyses of new measurements with different targets; the unweighted mean was 991.91±0.30 keV. Although this number refers to the *true* resonance energy rather than the midpoint of the rise, the discussion above clearly indicates that this difference can be at most a few tens of eV. Therefore, there seemed no point in attempting to adjust this value, especially in view of the fact that this result contributes only 4% to the weighted mean.

In addition to the AEI result, one older measurement has been omitted from the list, viz., 993.3±1.0 keV by Herb *et al.* (He 49). Although this experiment provided a valuable service in that an absolute nuclear energy scale was established for the first time, it probably suffered from excessive surface contamination of the target (high vacuum practice was not nearly the advanced art that it is today) which caused the resonance energy to be considerably higher than the value now accepted.

B. $Li^7(p, n)Be^7$

The six recent determinations of the threshold energy for the $Li^7(p, n)Be^7$ reaction are shown in Table II. Generally, the values are derived from the extrapolation of $(\text{yield})^{\frac{1}{2}}$, as discussed in Sec. V; the exceptions are as follows: The figure in the report by Beckner *et al.* (Be 61) which shows a typical yield curve for the $Li^7(p, n)Be^7$ reaction is *linear* in the yield. However, these authors state that $(\text{yield})^{\frac{1}{2}}$ extrapolations were also made and that no difference in the values was found. This result is probably due to the fact that the

CC-0. In Public Domain. Gurukul Kangri Collection, Haridwar

Digitized by Arya Samaj Foundation Chennai and eGangotri

TABLE III. $F^{19}(p, \alpha\gamma)O^{16}$ resonance energies.

E_R(keV)	Γ(keV)	Method	Reference
340.5 ±0.3	2.4±0.2	Absolute electrostatic	Bo 59
340.6 ±0.5[a]		Absolute magnetic	St 60
340.46±0.04[b]	2.4	Absolute velocity	Se 64

Weighted mean: E_R=340.45 keV

ϵ_{int}=0.04 keV

ϵ_{ext}=0.01 keV

Recommended: E_R=340.46±0.04 keV; Γ=2.4±0.2 keV

[a] Supercedes an earlier published value.
[b] Corrected (from 340.45±0.04) as explained in the text.

beam energy resolution used in this experiment ($R\approx$ 0.05%) was not particularly high by present-day standards. At high resolutions ($R\approx$0.02%), a (yield)$^{\frac{1}{2}}$ plot is distinctly more linear than a (yield)^{1} plot.

Browne *et al.* (Br 60, Br 64) have made an extensive series of measurements to compare the $Li^7(p, n)Be^7$ threshold energy with the energy of Po^{210} α particles. Their latest results (Br 64) are expressed as follows: assuming a threshold energy of 1880.7 keV, the energy of Po^{210} α particles is 5304.2±2.0 keV. The best value for the Po^{210} α-particle energy is now 5304.51±0.47 keV (Wa 64), so that the threshold energy becomes 1880.8±0.7 keV. In obtaining this energy ratio result, Browne *et al.* used both H^+ and H_2^+ beams. Because it has been recognized (Da 60, Wa 62, Bo 63a) that resonance and threshold shapes measured with H_2^+ ions can be quite different from those obtained with protons (H^+), it was necessary to fit the H_2^+ neutron yield curve with a theoretical formula in order to obtain the proper intercept. In spite of this difference in procedure, it still seems reasonable to include Browne's value along with the other results using (yield)$^{\frac{1}{2}}$ extrapolations.

Four pre-1958 measurements have been excluded from the threshold energy list. The electrostatic measurement of Herb *et al.* (He 49) which gave 1882.2±1.9 keV and the velocity measurement of Shoupp *et al.* (Sh 49) which gave 1881.2±1.9 keV suffer from inadequate beam energy resolution and probably also from target contamination problems. Sturm and Johnson (St 51) compared the threshold energy with the energy of α particles from RaC′. The sources used had not been freshly prepared and it is now known that fresh sources are a necessity for precise experiments. Jones *et al.* (Jo 54), using inelastic scattering techniques, compared the threshold energy with the energy of the first excited state of Mg^{24}. It is possible to obtain a corrected threshold energy by combining the energy ratio with the recent precision measurement of the energy of Mg^{24*} made by Murray *et al.* (Mu 65); the result is 1879.6±1.0 keV. Apart from the fact that this experiment falls into the "old" group, the exclusion of this result from the weighted mean can also be made on the following grounds: (a) The intercalibration of the two electrostatic analyzers used in the experiment was made with H_2^+ beams but no analysis of the type now known to be necessary (Da 60, Wa 62, Bo 63a, Br 64) was made. (b) Linear extrapolation of the yield was made. (c) The results also depend on a line-shape analysis since the inelastic scattering was performed on a narrow resonance. All of these factors contribute sufficient uncertainty in the reliability of the result to warrant its exclusion.

It must be emphasized that although the threshold energy 1880.60±0.07 keV is recommended for calibration purposes [i.e., the intercept of a (yield)$^{\frac{1}{2}}$ extrapolation], this value is not appropriate for a Q-value calculation; the *true* threshold probably is about 150 eV higher.

C. $F^{19}(p, \alpha\gamma)O^{16}$

The results for the $F^{19}(p, \alpha\gamma)O^{16}$ resonances at 340.46 and 872.11 keV are shown in Tables III and IV. These resonances tend to be less suitable for calibration purposes because of their appreciable widths. It is unfortunate that more measurements of the widths are not available; a few additional measurements would increase the usefulness of these resonances considerably.

The weighted mean of the 340-keV resonance is completely dominated by the result of Seagrave *et al.* (Se 64) which has an assigned uncertainty that is an order of magnitude smaller than the other errors. The instrument with which this experiment was performed is certainly capable of a precision of 0.01%, as was demonstrated by other measurements with the same apparatus (Ro 66). However, it appears overly optimistic to expect that the position of a resonance peak can be identified with an uncertainty of only 40 eV when the width of the resonance is 2.4 keV. This seems especially true in view of the fact that no uncertainty is quoted for the width measurement. Therefore, even though E_R=340.46 keV is retained as the recom-

TABLE IV. $F^{19}(p, \alpha\gamma)O^{16}$ resonance energies.

E_R(keV)	Γ(keV)	Method	Reference
872.4 ±0.4	4.5±0.3	Absolute electrostatic	Bo 59
872.33±0.27[a]		Absolute magnetic	Be 61
871.80±0.25[b]	4.8±0.2	Absolute magnetic	Ry 62

Weighted mean: E_R=872.11 keV

ϵ_{int}=0.17 keV

ϵ_{ext}=0.20 keV

Recommended: E_R=872.11±0.20 keV; Γ=4.7±0.2 keV

[a] Corrected (from 872.3±0.5) as explained in the text.
[b] Supercedes an earlier published value.

CC-0. In Public Domain. Gurukul Kangri Collection, Haridwar

Digitized by Arya Samaj Foundation Chennai and eGangotri

...ended energy, the standard deviation, ±0.04 keV, ...s artificially small.

D. $C^{13}+p$

The $C^{13}(p, \gamma)N^{14}$ resonance at 1747.6 keV and the $C^{13}(p, n)N^{13}$ threshold at 3235.7 keV have received too ...ttle attention in view of their importance as energy ...standards. A single absolute measurement of the reso...nance energy is available and only two laboratories ...ave produced absolute values for the threshold energy. ...These results are shown in Table V. It is to be hoped ...hat additional measurements will be made in the near ...uture.

The data of Bondelid and Kennedy (Bo 59) for the ...$C^{13}(p, \gamma)N^{14}$ resonance gave a midpoint energy of ...1747.6±0.9 keV. The same data were later re-analyzed ...(Bo 63) by taking into account the discrete energy ...loss effect and a *true* resonance energy of 1747.06±0.53 ...keV was obtained. In Table V, the midpoint value is ...listed as the one appropriate for calibrations in accord...ance with the discussion in Sec. V. Similarly, the ...(yield)$^{\frac{1}{3}}$ extrapolated value of 3236.9±1.6 keV is given ...for the threshold energy (Bo 64); the same data gave ...3237.2±1.6 keV when linearly extrapolated (Bo 59) ...and 3237.1±1.6 keV when analyzed with the discrete ...energy loss theory (Bo 64). Bondelid and Whiting ...(Bo 64) point out that the (yield)$^{\frac{3}{2}}$ extrapolated value ...is correct for their beam energy resolution (0.03%) ...and will be slightly different for other conditions. The ...three measurements (Be 61, Bo 66) were made with similar resolutions, so the three results can properly be averaged.

TABLE V. $C^{13}+p$ calibration energies.

$C^{13}(p, \gamma)N^{14}$			
E_r(keV)	Γ(keV)	Method	Reference
	0.077±0.012	Resonance absorption	Ha 59
1747.6±0.9	0.075±0.050	Absolute electrostatic	Bo 59
$C^{13}(p, n)N^{13}$			
E_{th}(keV)	Method		Reference
3235.41±1.1[b]	Absolute magnetic		Be 61
3236.9 ±1.6[a]	Absolute electrostatic		Bo 64
3235.51±1.1[c]	Absolute magnetic		Bo 66
Weighted mean: E_{th}=3235.7 keV			
e_{int}=0.7 keV			
e_{ext}=0.4 keV			
Recommended: E_{th}=3235.7±0.7 keV			

[a] Supercedes an earlier published value.
[b] Corrected (from 3235.3±1.5) as explained in the text.
[c] Corrected (from 3235.4±2.4) as explained in the text.

VII. CALIBRATION POINTS FOR HIGHER ENERGY PROTONS

Table VI lists the results of all the absolute measurements of (p, n) thresholds for bombarding energies between 4.2 and 9.5 MeV. These values are from three sources—the absolute magnetic measurements made at Rice (Be 61, Bo 66) and at Zürich (Ry 61) and the comparison of threshold energies with α-particle energies made at Harwell (Fr 65). The agreement among the results is satisfactory although it is not as good as at lower energies.

At these high bombarding energies, the normal neutron background tends to be large and to obscure the relatively weak neutron yield at threshold. Therefore, extraordinary precautions must usually be taken, such as using thin targets and stopping the proton beam only after it is some distance away from the detector area (Ph 64); alternatively, the beam can be chopped and the target radioactivity (annihilation radiation from β^+ decay) can be detected (Fr 65).

Recently, several narrow levels have been discovered at high excitation energies in light nuclei. The small widths of these levels result from the fact that they are forbidden (at least in first order) by isobaric spin conservation to decay by particle emission. One such level that is of interest from the calibration standpoint is the first $T=\frac{3}{2}$ level of N^{13}. This state has been observed in the $B^{11}(He^3, n)N^{13}$ reaction (which is not isobaric-spin forbidden) by Adelberger and Barnes (Ad 65) who determined that the excitation energy is 15.068± 0.008 MeV and that the width is less than 20 keV. This level has also been observed (Br 66) in the scattering of protons by C^{12} (an isobaric-spin forbidden reaction which proceeds only by virtue of a small $T=\frac{1}{2}$ impurity in the state); the width was found to be less than 1 keV. Since the scattering anomaly is quite pronounced (Br 66), this resonance provides a convenient calibration point at a proton bombarding energy of 14.233±0.008 MeV (see Table VII).

Other narrow, T-forbidden resonances should also be suitable for calibration purposes. Two candidates are to be found, for example, in the scattering (and, presumably, also in the capture) of protons by O^{16}. Narrow levels (Γ<5 keV) have been found at bombarding energies of 12.671 and 13.215 MeV (Ha 63). These states appear to be the analogs of N^{17} excited states. The analogue of the ground state was not observed; it may be sufficiently narrow to have escaped detection. Recent measurements (Wi 66) have shown that the previous results for the lower $O^{16}+p$ resonance are somewhat inaccurate. The resonance energy is 12.728±0.010 MeV and the width is Γ<2 keV (Wi 66). The scattering anomaly is well defined so that this resonance energy should be a most useful high-energy

CC-0. In Public Domain. Gurukul Kangri Collection, Haridwar

Digitized by Arya Samaj Foundation Chennai and eGangotri

TABLE VI. Higher energy (p, n) threshold energies.

Reaction	E_{th}(keV)	Method	Reference	Recommended value
$F^{19}(p, n)Ne^{19}$	4233.34±1.5[a] 4234.7 ±1.0	Absolute magnetic Absolute magnetic	Be 61 Ry 61	4234.3±0.8 keV
$Al^{27}(p, n)Si^{27}$	5794.5 ±2.4[b] 5802.9 ±3.8	Absolute magnetic ThC α (6089.7 keV)	Bo 66 Fr 65	5796.9±3.8 keV
$S^{34}(p, n)Cl^{34}$	6451.1 ±4.5	ThC α (6089.7 keV)	Fr 65	
$Ni^{60}(p, n)Cu^{60}$	7023.84±3.9[c]	Absolute magnetic	Bo 66	
$Fe^{54}(p, n)Co^{54}$	9202.7 ±4.8	ThC′ α (8786.4 keV)	Fr 65	
$Ni^{58}(p, n)Cu^{58}$	9516.32±3.5[d] 9512.9 ±5.0	Absolute magnetic ThC′ α (8786.4 keV)	Bo 66 Fr 65	9515.2±2.9 keV

[a] Corrected (from 4233.2±2.0) as explained in the text.
[b] Corrected (from 5794.3±4.7) as explained in the text.
[c] Corrected (from 7023.6±7.1) as explained in the text.
[d] Corrected (from 9516.0±7.8) as explained in the text.

calibration point. An improvement in the precision of the above result should be forthcoming (Wi 66).

Another calibration point that is available in the $C^{12}+p$ system is the as yet unobserved (p, n) threshold. The Q value for the $C^{12}(p, n)N^{12}$ reaction can be obtained from the 1964 least-squares adjustment of atomic masses (Ma 65) and the threshold is readily calculated to be 19.684±0.008 MeV (see Table VII). Although detection of the threshold neutrons at such a high bombarding energy will be difficult, the short half-life of N^{12} means that the detection of the induced radioactivity should be relatively easy.

VIII. $O^{16}+d$ THRESHOLD ENERGIES

The threshold energy for the $O^{16}(d, n)F^{17}$ reaction has been measured by Bondelid *et al.* (Bo 60) who found $E_{th}=1829.2\pm0.6$ keV. For the purposes of calibrating high-energy electrostatic accelerators, this reaction may be used by reversing the roles of the target and projectile so that the reaction becomes $H^2(O^{16}, n)F^{17}$ (Go 58). By accelerating oxygen ions in various charge states and determining the threshold positions, a magnetic beam analyzer can be calibrated at equivalent proton energies of 6.45, 9.29, 14.52, and 25.63 MeV with considerable precision (see Table VIII).

TABLE VII. $C^{12}+p$ calibration energies.

Resonance excitation of first $T=\frac{3}{2}$ state of N^{13}				
Reaction	E_x(MeV)	E_R(MeV)	Γ(keV)	Reference
$C^{12}(p, p)C^{12}$	15.068±0.008	14.233±0.008	<20	Ad 65[a]
			<1	Br 66

Neutron threshold (calculated from 1964 masses)			
Reaction	Q(MeV)	E_{th}(MeV)	Reference
$C^{12}(p,n)N^{12}$	−18.14645±0.007	19.684±0.008	Ma 65

[a] Used the $B^{11}(He^3, n)N^{13}$ reaction.

IX. HELIUM ION ENERGIES

Only three absolute measurements have been made of helium-ion-induced neutron thresholds. These are listed in Table IX—two for the $C^{12}(He^3, n)O^{14}$ reaction and one for the $Li^6(He^3, n)B^8$ reaction. The threshold energies for several other reactions can be calculated from the atomic masses given by Mattauch *et al.* (Ma 65); these are also shown in Table IX. By using singly and doubly charged helium ions, these thresholds will provide calibration points for magnetic analyzers up to an equivalent proton energy of 60.4 MeV. Although none of the higher energy (α, n) thresholds have been observed, these reactions are probably the best prospects for precision calibrations of magnets at high field strengths.

Some (α,γ) resonances are also useful as calibration points. Of particular interest in the resonance at $E_\alpha=$

TABLE VIII. $O^{16}+d$ threshold energies.

$O^{16}(d,n)F^{17}$		
E_{th}(keV)	Method	Reference
1829.2±0.6	Absolute electrostatic	Bo 60

$H^2(O^{16}, n)F^{17}$		
Charge state	O^{16} energy (MeV±keV)	Equivalent proton energy[a] (MeV±keV)
+3	14.5255±5	25.627±9
+4	14.5250±5	14.519±5
+5	14.5245±5	9.292±3
+6	14.5240±5	6.452±2

[a] Proton energy in the same magnetic field as required for the oxygen ion at threshold.

CC-0. In Public Domain. Gurukul Kangri Collection, Haridwar

Digitized by Arya Samaj Foundation Chennai and eGangotri

TABLE IX. Helium ion threshold energies.

Reaction	E_{th} (keV)	Method	Reference
Experimentally determined values			
$C^{12}(He^3, n)O^{14}$	1436.2±0.9	Absolute electrostatic	Bu 61
	1436.9±0.6	Absolute velocity	Ro 66
Weighted mean: $E_{th}=1436.7\pm0.5$ keV			
$Li^6(He^3, n)$	2966.1±1.7	Absolute electrostatic	Du 58

Reaction	E_{th} (MeV±keV)	Equivalent proton energy[a] (MeV±keV)	
		For He^+	For He^{++}
Calculated from 1964 masses (Ma 65)			
$Li^6(He^3, n)B^8$	2.9650±1.5	8.8826±4.5	2.2198±1.1
$Li^6(\alpha, n)B^9$	6.6239±2.6	26.345 ±11	6.5844±2.6
$Li^7(\alpha, n)B^{10}$	4.3843±1.9	17.4321±7.4	4.3568±1.9
$C^{12}(He^3, n)O^{14}$	1.4366±0.5	4.3026±1.5	1.0753±0.4
$C^{12}(\alpha, n)O^{15}$	11.3463±1.7	45.1553±6.8	11.2857±1.7
$N^{14}(\alpha, n)F^{17}$	6.0888±0.8	24.2148±3.1	6.0520±0.8
$N^{15}(\alpha, n)F^{18}$	8.1324±1.5	32.3509±6.1	8.0855±1.5
$O^{16}(He^3, n)Ne^{18}$	3.7987±5.7	11.382 ±17	2.8444±3.6
$O^{16}(\alpha, n)Ne^{19}$	15.1761±2.0	60.4279±8.0	15.1028±2.0

[a] Proton energy in the same magnetic field as required for the helium ion at threshold.

9.8±1.0 keV in the Mg^{24} $(\alpha,\gamma)Si^{28}$ reaction (Ry63). he width of this resonance is 1.8±0.3 keV and the crease of yield from a semi-thick target is quite nounced, thereby rendering the resonance suitable r calibration purposes.

TABLE X. Summary of proton calibration energies.

Reaction	E_R or E_{th} (keV)	Γ (keV)
$(p, \alpha\gamma)O^{16}$	340.46±0.04	2.4 ±0.2
$(p, \alpha\gamma)O^{16}$	872.11±0.02	4.7 ±0.2
$(p, \gamma)Si^{28}$	991.90±0.04	0.10 ±0.02
$(p, \gamma)N^{14}$	1747.6 ±0.9	0.077±0.012
$(p, n)Be^7$	1880.60±0.07	
$(p, n)N^{13}$	3235.7 ±0.7	
$(p, n)Ne^{19}$	4234.3 ±0.8	
$(p, n)Si^{27}$	5796.9 ±3.8	
$(p, n)Cl^{34}$	6451.1 ±4.5	
$(p, n)Cu^{60}$	7023.6 ±3.9	
$(p, n)Co^{54}$	9202.7 ±4.8	
$(p, n)Cu^{58}$	9515.2 ±2.9	
$(p, p)O^{16}$	12 728 ±10	<2
$(p, p)C^{12}$	14 233 ±8	<1
$(p, n)N^{12}$	19 684 ±8	

X. SUMMARY

The precision of absolute energy measurements is now sufficiently high that there seems to be little likelihood that the recommended values for the primary, low-energy calibration points will change by significant amounts due to subsequent experiments. Unless future absolute measurements are analyzed by taking into account the known effects of surface contaminants and the discrete energy loss of the incident particles, there also seems to be little prospect that the precision can be improved. All users who would take advantage of the increased precision also would be forced to make detailed analyses of the yield curves rather than merely take the midpoint of thick-target resonance curves or the intercept of a $(\text{yield})^{\frac{3}{2}}$ extrapolation. We have essentially reached the limit of these quick but crude methods and the next advance in precision will require much more sophisticated data analysis techniques.

At the higher energies ($E_p \gtrsim 3$ MeV), there is still considerable room for improvement. Instruments in use at the present time can be used to provide a greater amount of data for neutron thresholds and isobaric-spin forbidden resonances up to proton bombarding energies of 10 or 15 MeV, but until some significant improvements are made, direct absolute measurements at higher energies will probably not be possible. The use of inverse reactions and calculated threshold energies must serve until these improvements are made.

Table X summarizes the proton calibration points;

CC-0. In Public Domain. Gurukul Kangri Collection, Haridwar

Digitized by Arya Samaj Foundation Chennai and eGangotri

Tables VIII and IX contain the deuteron and helium ion data, respectively.

REFERENCES

Ad 65. E. Adelberger and C. A. Barnes, Bull. Am. Phys. Soc. **10**, 1195 (1965).

Be 61. E. H. Beckner, R. L. Bramblett, G. C. Phillips, and T. A. Eastwood, Phys. Rev. **123**, 2100 (1961).

Bo 59. R. O. Bondelid and C. A. Kennedy, Phys. Rev. **115**, 1601 (1959).

Bo 60. R. O. Bondelid, J. W. Butler, and C. A. Kennedy, Phys. Rev. **120**, 889 (1960).

Bo 60a. R. O. Bondelid, J. W. Butler, C. A. Kennedy, and A. del Callar, Phys. Rev. **120**, 887 (1960).

Bo 63. R. O. Bondelid and J. W. Butler, Phys. Rev. **130**, 1078 (1963).

Bo 63a. R. O. Bondelid and J. W. Butler, Phys. Rev. **132**, 1710 (1963).

Bo 64. R. O. Bondelid and E. E. D. Whiting, Phys. Rev. **134**, B591 (1964).

Bo 66. B. E. Bonner, G. Rickards, D. L. Bernard, and G. C. Phillips, Nucl. Phys. (to be published); see also Ph 64.

Br 60. C. P. Browne, J. A. Galey, J. R. Erskine, and K. L. Warsh, Phys. Rev. **120**, 905 (1960).

Br 64. C. P. Browne, in *Proceedings of the Second International Conference on Nuclidic Masses*, 1963, W. H. Johnson, Jr., Ed. (Springer-Verlag, Vienna, 1964), p. 229.

Br 66. D. J. Bredin, O. Hansen, G. M. Temmer, and R. Van Bree, Bull. Am. Phys. Soc. **11**, 625 (1966); and private communications.

Bu 61. J. W. Butler and R. O. Bondelik, Phys. Rev. **121**, 1770 (1961).

Co 65. E. R. Cohen and J. W. M. DuMond, Rev. Mod. Phys. **37**, 537 (1965).

Da 60. P. F. Dahl, D. G. Costello, and W. L. Walters, Nucl. Phys. **21**, 106 (1960).

Du 58. K. L. Dunning, J. W. Butler, and R. O. Bondelid, Phys. Rev. **110**, 1076 (1958).

Fe 66. J. A. Ferry, G. Wendt, D. W. Palmer, and J. M. Donhowe, Phys. Rev. **143**, 825 (1966).

Fr 65. J. M. Freeman, J. H. Montague, G. Murray, R. E. White, and W. E. Burcham, Nucl. Phys. **65**, 113 (1965).

Ga 63. B. R. Gasten, Phys. Rev. **131**, 1759 (1963).

Go 58. H. E. Gove, J. A. Kuehner, A. E. Litherland, E. Almqvist, D. A. Bromley, A. J. Ferguson, P. H. Rose, R. P. Bastide, N. Brooks, and R. J. Conner, Phys. Rev. Letters **1**, 251 (1958).

Ha 59. S. S. Hanna and L. Meyer-Schützmeister, Phys. Rev. **115**, 986 (1959).

Ha 63. G. Hardie, R. L. Dangle, and L. D. Oppliger, Phys. Rev. **129**, 353 (1963).

He 49. R. G. Herb, S. C. Snowden, and O. Sala, Phys. Rev. **75**, 246 (1949).

Hu 55. S. E. Hunt and K. Firth, Phys. Rev. **99**, 786 (1955).

Hu 60. S. E. Hunt, R. A. Pope, D. V. Freck, and W. W. Evans, Phys. Rev. **120**, 1740 (1960).

Jo 54. K. W. Jones, R. A. Douglas, M. T. McEllistrem, and H. T. Richards, Phys. Rev. **94**, 947 (1954).

Le 62. H. W. Lewis, Phys. Rev. **125**, 937 (1962).

Ma 61. J. B. Marion, Rev. Mod. Phys. **33**, 139 (1961).

Ma 64. J. B. Marion, in *Proceedings of the Second International Conference on Nuclidic Masses*, 1963, W. H. Johnson, Jr., Ed. (Springer-Verlag, Vienna, 1964), p. 279.

Ma 65. J. H. E. Mattauch, W. Thiele, and A. H. Wapstra, Nucl Phys. **67**, 73 (1965).

Mu 65. G. Murray, R. L. Graham, and J. S. Geiger, Nucl. Phys. **63**, 353 (1965).

Pa 66. D. W. Palmer, W. G. Mourad, J. M. Donhowe, K. E. Nielsen, and R. J. Nickles, Nucl. Phys. **75**, 515 (1966).

Ph 64. G. C. Phillips, in *Proceedings of the Second International Conference on Nuclidic Masses*, 1963, W. H. Johnson, Jr., Ed. (Springer-Verlag, Vienna, 1964), p. 261.

Ro 66. M. L. Roush, L. West, J. V. Mullendore, H. L. Fann, and J. B. Marion, Phys. Letters (to be published).

Ry 61. A. Rytz, H. Winkler, F. Zamboni, and W. Zych, Helv. Phys. Acta **34**, 819 (1961).

Ry 61a. A. Rytz, H. H. Staub, and H. Winkler, Helv. Phys. Acta **34**, 960 (1961).

Ry 62. A. Rytz, H. H. Staub, H. Winkler, and W. Zych, Helv. Phys. Acta **35**, 341 (1962).

Ry 63. A. Rytz, H. H. Staub, H. Winkler, and F. Zamboni, Nucl. Phys. **43**, 229 (1963).

Se 64. J. D. Seagrave, J. E. Brolley, Jr., and J. G. Beery, Rev. Sci. Instr. **35**, 1290 (1964).

Sh 49. W. E. Shoupp, B. Jennings, and W. Jones, Phys. Rev. **76**, 502 (1948).

St 51. W. J. Sturm and V. Johnson, Phys. Rev. **83**, 543 (1951).

St 60. H. H. Staub and H. Winkler, Nucl. Phys. **17**, 271 (1960).

Wa 62. W. L. Walters, D. G. Costello, J. G. Skofronick, D. W. Palmer, W. E. Kane, and R. G. Herb, Phys. Rev. **125**, 2012 (1962).

Wa 64. A. H. Wapstra, Nucl. Phys. **57**, 48 (1964).

Wi 66. H. Winkler and C. Zaidins (private communication).

CC-0. In Public Domain. Gurukul Kangri Collection, Haridwar

Digitized by Arya Samaj Foundation Chennai and eGangotri

REVIEWS OF MODERN PHYSICS VOLUME 38, NUMBER 4 OCTOBER 1966

Some Simple Isothermal Equations of State

J. ROSS MACDONALD
Texas Instruments Incorporated, Dallas, Texas 75222

Previous work on the Tait equation of state, usually applied to liquids, is discussed together with a review of work on a closely related simple equation arising both from the theory of finite strain and from microscopic considerations. The latter equation has been primarily used for fitting hydrostatic compression pressure–volume data for solids. A detailed discussion of methods for assessing goodness-of-fit of data to equations of state is presented along with an analysis of ways to help decide which of two similar equations is the more applicable for given data. Nonlinear least squares fitting of the above two-parameter equations of state is carried out for the first time using published P–V–T data for water, a very compressible hydrocarbon liquid, zinc, lithium, sodium, potassium, and rubidium and the results compared with those of previous analyses of these data. Careful fitting of the present type can lead to new conclusions and insights not so apparent from less careful fitting of the present equations or from fitting with other equations. For most of the materials and data considered here the finite-strain equation was found to be superior to the Tait equation. Reasons are advanced, however, why both equations should be primarily considered only as empirical, with theoretical justifications for them applicable only over limited pressure–volume ranges.

INTRODUCTION

In recent years there seems to be renewed interest in the semi-empirical Tait equation (abbreviated TE) relating volume of a material under hydrostatic compression to the applied pressure. Although the TE was originally proposed for water and has been applied to a wide variety of other liquids, it is now being put forward as an appropriate equation for fitting pressure–volume results for such compressible solids as the alkali metals. This paper discusses some useful but infrequently applied methods of comparing the applicability of different equations of state and employs them in comparing, for several materials, the TE with a closely related but frequently superior equation (the modified equation, abbreviated ME).

It is important to point out that the conclusion that the TE is *the* equation of state of a given material, frequently drawn in an uncritical manner on the basis of a "reasonable" fit to the data, should only be made after a careful comparison with other equations and examination of several goodness-of-fit criteria. Although the ME has been used for a number of years, its existence, close relation to the TE, and wide applicability to both solids and liquids seems unknown to those who have employed the TE. The present paper draws together the work of the several investigators who have used the TE with those who have employed the ME (and without consideration of the TE), discusses their work in some detail, and presents and discusses improved analyses of some published pressure–volume data.

The TE (see Appendix) suffers from the defect that it leads to negative volumes at sufficiently high pressures. In the Appendix, it is shown how simple modifications of the TE lead to the modified equation

$$V/V_0=(1+n\beta_0 p)^{-1/n}. \tag{1}$$

Here β_0 and V_0 are the isothermal compressibility and volume, respectively, at $P=P_0$, a reference pressure conveniently taken as one atmosphere. The reduced pressure $p\equiv P-P_0$, and n is a pressure-independent parameter usually greater than unity which is also nearly temperature-independent. Of course, n and β_0 are pressure-independent only in the absence of polymorphic transformations, a condition assumed throughout this paper. As shown in the Appendix, the ME may be made to agree identically with the TE to second order in $\beta_0 p$ and very nearly to third order. The ME only leads to zero volume in the limit $p\to\infty$, however, and hence may be expected to be superior to the TE at least at such high pressures that $V/V_0<0.2$ or so. It should be applicable to both solids and liquids.

DISCUSSION OF PREVIOUS WORK

Although Eq. (1) was derived independently by Macdonald and Barlow[1] as in the Appendix in order to obtain an improvement to the TE, and although the ME was stated by the author[2] to fit almost all of Bridgman's data on compression of solids and liquids very well, it was later discovered to be by no means a new equation. As Gilvarry[3] has mentioned, it is identical to Murnaghan's[4] equation derived from his "integrated linear theory of finite strain." The derivation of (1) from this macroscopic theory gives it a theoretical justification which Gilvarry feels is superior to that of equations obtained thus far from quantum mechanics or a lattice model.

Equation (1) is also a simplified version of a very general equation of state given by Gilvarry.[5] He has shown[6] that for solids n in (1) may be identified as $2\gamma_{Av}+\frac{1}{3}$, where γ_{Av} is the average value of the Grüneisen parameter over the pressure range of interest. The ME has been used independently by Ryabinin[7] who, ap-

[1] J. R. Macdonald and C. A. Barlow, Jr., J. Chem. Phys. **36**, 3062 (1962).
[2] J. R. Macdonald, J. Chem. Phys. **40**, 1792 (1964).
[3] J. J. Gilvarry, J. Appl. Phys. **28**, 1253 (1957).
[4] F. D. Murnaghan, *Finite Deformation of an Elastic Solid* (John Wiley & Sons, Inc., New York, 1951), Chap. 4; Proc. Natl. Acad. Sci. **30**, 244 (1944).
[5] J. J. Gilvarry, Phys. Rev. **102**, 331 (1956).
[6] J. J. Gilvarry, Phys. Rev. **102**, 325 (1956).
[7] Yu. N. Ryabinin, Z. Tekh. Fiz. **30**, 739 (1960) [English transl.: Soviet Phys.—Tech. Phys. **5**, 693 (1960)].

CC-0. In Public Domain. Gurukul Kangri Collection, Haridwar

Digitized by Arya Samaj Foundation Chennai and eGangotri

parently unaware of Gilvarry's work, derived (1) from theoretical results of Debye and Grüneisen and obtained $n=2\gamma+\frac{1}{3}$. In addition, Cook and Rogers[8] have independently derived the ME (wrongly identified as the TE yet shown to be the same in form as Murnaghan's equation) from the virial theorem and the Thomas–Fermi atomic model. They obtained $n=\gamma+1$, in disagreement with the above results. The value $n=2\gamma+\frac{1}{3}$ follows immediately from (1), the Debye–Slater[9] expression for γ, and the present assumption of a pressure-independent n. The Debye–Slater relation was derived for an isotropic material with volume-independent Poisson ratio. Finally, Gombas,[10] in a treatment of alkali metals, has given an expression for $\beta\equiv-V^{-1}(\partial V/\partial P)_T$ consistent with (1) provided $n=10/3$. This value of n is discussed later for several alkali metals.

In unpublished work, the author has found that nonlinear least-squares fitting of Bridgman's data (in regions of no polymorphic transition) on the compression of many solids and liquids yields excellent values of the initial compressibility, β_0, and plausible results for n. This work was not published because it was found that Murnaghan,[4] Riabinin,[11] and Cook and Rogers[8] had, to some extent, done it earlier. However, more precise and meaningful comparisons between theory and experiment may be made than any carried out by these authors.[11a]

Recently, in a paper marked I, Ginell and Quigley[12] have applied the TE to Bridgman's data for alkali metals. These authors seem unaware of the ME and although they consider that their results show the TE to be applicable, several of their derived constants have implausible values. A better comparison of both the ME and TE with these data is presented below.

Gilvarry[3] has shown how Eq. (1) (or his generalization of it) may be modified to take temperature dependence into account. He assumes n to be temperature-independent, however. The only temperature dependence then remaining on the right-hand side is that of β_0. Its dependence is frequently known or can be readily measured independently. However, sometimes n does apparently vary somewhat with temperature as well.

There have been several independent derivations of the TE. Some of these might also be applicable for deriving the ME. In 1956, Simha and Hadden[13] showed from cell theory that r (a parameter in the TE corresponding to n in the ME) should be approximately independent of pressure and temperature and that B (see Appendix), the second parameter in the TE, is related to the cohesive energy density of the liquid. It is more meaningful to relate B to the initial compressibility, as in the present work. Recently, Nanda and Simha[14] found (using cell theory and the principle of corresponding states) that for oligomer and polymer liquids r varied theoretically with reduced volume or temperature only from 9.4 to 11.1 over a wider than experimental temperature range. Application of the TE to experimental results for many hydrocarbons with the constant value $r\cong11.2$ yielded[15] good agreement between experimental values of V/V_0 and those predicted by the TE. Although the same value of r could be used for different materials and different temperatures, somewhat greater fitting accuracy could have been obtained had r been allowed to vary (see later discussion). The ordinary least-squares method used to obtain values of the Tait constant B is also subject to some criticism as discussed in the following section. Thus, the utility of the constant value of r found in the study is not a conclusive proof of its actual constancy. This same value of r has been used,[16] in apparently the same way, in a TE fitting to results for polymer liquids and glasses up to pressures of about 2000 atm.

Ginell[17] has also derived the TE equation without reference to the work of Simha and Hadden.[13] For this derivation, the virial equation of state in closed form was used. The derivation had a geometric basis and used association or cluster theory. The meaning of the TE parameters (see Appendix) $J\equiv V_0/r$ and B (designated L by Ginell) was also examined by Ginell on the basis of association theory.[18] Further, Ginell and Quigley[12] have given a qualitative discussion of why the TE might be applicable to polycrystalline solids.

In concluding this section on previous work, which must certainly still be incomplete, it is pertinent to mention that a compilation of 56 equations of state appears in Ref. 19. In addition, a lengthy, yet still quite incomplete annotated bibliography of high-pres-

[8] M. A. Cook and L. A. Rogers, J. Appl. Phys. **34**, 2330 (1963).
[9] J. C. Slater, *Introduction to Chemical Physics* (McGraw-Hill Book Company, Inc., New York, 1939), p. 239, Eqs. (4.3), (4.5).
[10] P. Gombas, Ann. Phys. (Leipzig) **9**, 70 (1951).
[11] Yu. N. Ryabinin, Fiz. Metal. i Metalloved. **9**, 312 (1960).
[11a] *Note added in proof.* Since this work was completed, a valuable approach to the ME quite different from that herein has come to my attention [O. L. Anderson, J. Phys. Chem. Solids **27**, 547 (1966)]. Anderson assumes that the bulk modulus (β^{-1}) is linear with pressure [see Eq. (A12) of the Appendix] and determines adiabatic values of β_0^{-1} and n by precision sound velocity measurements at low pressures. These results are then converted to corresponding isothermal values. Anderson finds good agreement between the ME, with such parameters derived from low-pressure measurements, and compression results for many solids up to very high pressures. In some instances, this "extrapolation from the origin" method of determining ME parameters will be preferable to the statistical approach examined herein. The latter has the advantage of obtaining the parameters directly from many data points, averaging out random errors to some degree. Careful error analysis and comparison of the ME parameters obtained for the same material by the two approaches should help in deciding which method is most appropriate in any given instance.
[12] R. Ginell and T. J. Quigley, J. Phys. Chem. Solids **26**, 1157 (1965).
[13] R. Simha and S. T. Hadden, J. Chem. Phys. **25**, 702 (1956).
[14] V. S. Nanda and R. Simha, J. Chem. Phys. **41**, 1884 (1964).
[15] W. G. Cutler, R. H. McMickle, W. Webb, and R. W. Schiessler, J. Chem. Phys. **29**, 727 (1958).
[16] V. S. Nanda and R. Simha, J. Chem. Phys. **41**, 3870 (1964).
[17] R. Ginell, J. Chem. Phys. **34**, 1249, 2174 (1961).
[18] R. Ginell, J. Chem. Phys. **35**, 1776 (1961).
[19] *Handbuch der Experimentalphysik*, W. Wien and F. Harms, Eds. (Academische Verlagsgesellschaft M. B. H., Leipzig, 1926–1937), Vol. 8, part 2, pp. 224–228.

CC-0. In Public Domain. Gurukul Kangri Collection, Haridwar

Digitized by Arya Samaj Foundation Chennai and eGangotri

...re technology is available.[20] Finally, the ME, trans-...rmed to the dielectric realm, has been found useful ...relating dielectric constant, rather than volume, to ...pplied hydrostatic pressure.[1]

DISCRIMINATION BETWEEN EQUATIONS

In the past, a decision on the adequacy of an equa-...tion of state has frequently been made on the basis of a ...sufficiently" low standard error, s_e, determined from a ...mple least-squares fitting. While this may indeed be ...n important criterion, it is by no means always un-...ambiguous or sufficient; thus, I shall here discuss and ...ustrate others which can help one decide on the ap-...licability of an equation and make a sensible choice ...etween two or more such equations.

Sometimes people have transformed equations in ...ays which allow simple linear least-squares analysis. ...Thus, the ME can be written

$$p=(n\beta_0)^{-1}[(V/V_0)^n-1], \qquad (2)$$

...e form in which it is given by Gilvarry.[3] If $(V_0/V)^n$ ...s taken as a new variable with a value of n assumed, ...$n\beta_0)^{-1}$ may be found by ordinary linear least squares. ...A similar transformation may be used with the TE.) ...Then, that n which minimizes s_e may be determined by ...ccessive least-square runs. This last step has not ...sually been applied. With the availability of nonlinear ...east-squares (NLS) computer programs which deter-...ine all parameter values simultaneously,[21] one might ...e tempted to fit p–V data directly to an equation ...uch as (2). Usually, however, relative experimental ...errors in p are considerably smaller than those in V, ...nd to good approximation one need only consider ...hose in V. But forming such a quantity as $(V_0/V)^n$ ...$n\neq -1$) may seriously bias the error distribution. If ...hat of V is originally approximately normal, it will ...ertainly not be for $V^{-n}(n\neq -1)$. Therefore, it is ...sually much preferable to fit experimental data not ...o an equation such as the ME written as in Eq. (2) ...ut instead written as in Eq. (1), involving V/V_0

TABLE I. Fitting of synthetic data. The quantity k is n for the ME and r for the TE results.

		ME	TE
ME data			
	s_e	1.74×10^{-6}	3.23×10^{-3}
	k	8.99982	12.371
	β_0	0.0999981	0.11342
	R	1.0	0.640
	Designation	M/M	M/T
TE data			
	s_e	4.27×10^{-3}	2.78×10^{-6}
	k	6.7852	9.99975
	β_0	0.086932	0.0999965
	R	1.65	1.0
	Designation	T/M	T/T

[1] A. Zeitlin, *Annotated Bibliography on High-Pressure Technology* (Butterworths, Washington, 1964).

[3] D. W. Marquardt, J. Soc. Ind. Appl. Math. **2**, 431 (1963).

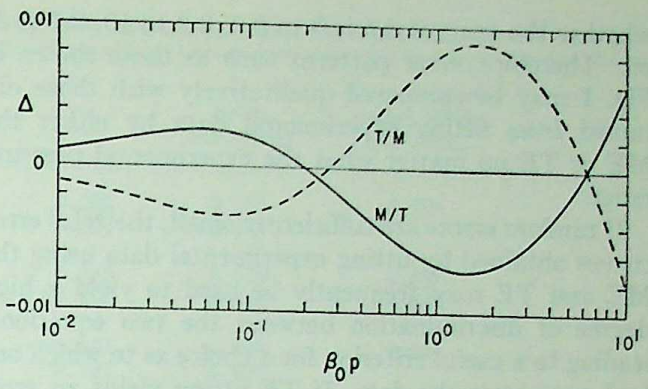

FIG. 1. The deviations, $\Delta\equiv(V/V_0)_{\rm obs}-(V/V_0)_{\rm pred}$, versus $\beta_0 p$ for fitting of TE derived data by means of the ME, T/M, and for fitting ME data by means of the TE, M/T.

directly. Nonlinear least squares can then be applied to obtain β_0 and n without biassing. In the following work, all fitting is done with the appropriate equation involving V/V_0 on the left directly. This requirement rules out the Hudleston equation,[22] which cannot be solved explicitly for V/V_0.

A useful criterion to help decide whether the TE or ME is the more applicable to given data can be developed as follows. If the ME is fitted by NLS to exact data derived from the TE, or *vice versa*, one would expect a smooth and individual curve of $\Delta\equiv(V/V_0)_{\rm obs}-(V/V_0)_{\rm pred}$. The results of such fitting with $N=45$ data pairs are shown in Table I and the distinctive deviation or error curves obtained are shown in Fig. 1. In these calculations, the "exact" data was rounded off to six decimal places, and the fitting calculations carried out with eight places. The exact values of the parameters used in calculating synthetic data from the ME and TE were $n=9$, $r=10$, $\beta_0=0.1$ and resulted in a minimum V/V_0 of about 0.54 for the TE. The quantity R in Table I is defined later. The accuracy of the NLS fitting was set to yield parameter values precise to only four to five decimal places, and it is evident from the results of fitting of each equation and its own "exact" data shown in Table I that the NLS procedure used worked correctly.

The deviation curve obtained from fitting "exact" TE data using the ME is denoted by T/M. Then, correspondingly, M/T denotes the deviation curve obtained using ME data fitted by the TE. Figure 1 shows that the T/M and M/T curves are nearly each other's negatives. Qualitatively, in terms of the general pattern of signs of the deviations alone, the two results are completely opposite in sign. This large difference in behavior is a most useful result. An extremely important property of NLS fitting as above to equations such as the ME and TE is that the deviation pattern obtained seems invariant (within wide limits) to the span of $\beta_0 p$ covered. Thus, deviation curves of the same shape and pattern are obtained, when N is sufficiently large and random errors sufficiently small,

[22] L. J. Hudleston, Trans. Faraday Soc. **33**, 97 (1937); D. M. Newitt and K. E. Weale, J. Chem. Soc. **1951**, 3092.

CC-0. In Public Domain. Gurukul Kangri Collection, Haridwar

Digitized by Arya Samaj Foundation Chennai and eGangotri

whether the span of $\beta_0 p$ is 0 to 0.2, 0.2 to 10, 0.1 to 5, etc. Therefore, error patterns such as those shown in Fig. 1 may be compared qualitatively with those obtained from fitting experimental data by either the ME or TE no matter what the experimental pressure range.

If random errors are sufficiently small, the NLS error curves obtained by fitting experimental data using the ME and TE may frequently be used to yield a high degree of discrimination between the two equations, leading to a useful criterion for a choice as to which one best represents the data. If TE fitting yields an error curve having the M/T pattern of Fig. 1 while at the same time ME fitting yields an unidentifiable or random pattern, then clearly the ME is the better choice on this criterion. Alternatively, if ME fitting yields a T/M pattern while TE fitting yields a random pattern, then the TE is the more applicable. This pattern comparison is a crude way of carrying out a cross-correlation between experimental error curves and those of Fig. 1 or equivalent. Its utility is illustrated in the next section. There are, of course, a number of distinguishable gradations in the error patterns obtained by fitting experimental data with the ME and TE which only allow less certain conclusions concerning their relative applicability. In particular, if both error curves have the same pattern, say T/M or random, then the present type of test is almost useless unless an actual, numerical cross-correlation analysis is carried out. Such similar patterns might occur when the experimental errors (systematic or random) in the data were large enough to obscure the differences between ME and TE results or when neither the ME nor TE were really applicable.

Another test which is almost certainly correlated with that above but which may be useful in its own right is described below. If the ME, for example, applies well to a given set of data, it should apply as well to any partition of that set and should yield (in the absence of experimental errors) the same parameter values. Suppose we divide a set of experimental data (preferably with $N>15$) into two parts. Let the first part (A) include all pressure values from $P=P_0$ up to some pressure, P_1, preferably sufficiently high that higher than third-order terms are necessary in the Tait or modified equation of state. This subset should then allow a reasonable determination of $n(\equiv n_A)$ and a good determination of $\beta_0(\equiv\beta_{0A})$. The second part (B) should use the same V_0 and P_0 and should include all data points with $P\geq P_1$; the resulting $n(\equiv n_B)$ should be particularly sensitive to the nonlinearity of the p–V curve.

In order to find a good criterion, the "exact" ME and TE data sets were divided into two parts, one (A) containing 23 points between $\beta_0 p=0$ and $\beta_0 p=0.2$ and the other (B) with 22 points distributed from $\beta_0 p=0.25$ to 10. The four resulting subsets were then fitted by both the ME and the TE. It was found that for the T/M situation n_A and β_{0A} both exceeded n_B and β_{0B} by approximately the same ratio, respectively. On the other hand, the M/T results yielded $r_B>r_A$ and $\beta_{0B}>\beta_{0A}$. The ratio $R\equiv k_A\beta_{0A}/k_B\beta_{0B}$, where $k\equiv n$ for fitting with the ME and $k\equiv r$ for the TE fitting, will then be a goodness-of-fit parameter and should also allow some discrimination between the ME and the TE.

In the absence of experimental error, Table I shows that R should be unity for M/M- and T/T-type fittings, should exceed unity for T/M, and should be less than unity for M/T fits. In the presence of not too large random errors, if TE and ME R's are obtained using the same experimental data, the ME would be preferred if R_M were closer to unity than R_T, and the TE preferred in the opposite case. If R_M and R_T were nearly the same, no valid discrimination could be made. Finally, the deviation of the one of these quantities closest to unity from unity should roughly indicate the importance of random or systematic errors and/or the degree to which the equation in question is a useful representation of the data. The fairly large deviations of R from unity for the M/T and T/M situations shown in Table I arise from the wide span of $n\beta_0 p$ or $r\beta_0 p$ encountered in these calculations. For the available pressure ranges of most materials, the minimum V/V_0 will be considerably greater than 0.54 and the M/T and T/M values of R (without appreciable random errors) will be closer to unity than those shown. Note that for this wide a range Table I indicates that $r\simeq n+3.3$ when both equations are used with the same data. As shown in the Appendix, $r=n+1$ in the much narrower pressure range where only second-order terms need be considered.

To summarize, four discrimination and goodness-of-fit tests are usually readily applicable. (1) If one of the s_e's obtained by ME and TE NLS fitting (with both parameters free) is substantially smaller than the other, and the smaller s_e is small enough that large random or systematic errors in the data seem unlikely, the equation yielding the smaller s_e would be preferred. (2) That equation which yields a β_0 in closer agreement with the β_0 value obtained from independent p–V measurements near $p\sim 0$ would be preferable. (3) If ME fitting yielded an unidentifiable or random error pattern and TE fitting an M/T pattern, the ME would be the more applicable. (4) Finally, if R is substantially closer to unity for one equation than the other, the one yielding the value closest to unity should be preferred.

Although these four tests are by no means entirely independent, they are each sufficiently different to be useful. Agreement of all four tests may be considered conclusive.

EXPERIMENTAL DATA FITTING RESULTS

Results of fitting experimental p–V data on water, a high molecular weight hydrocarbon liquid, and some alkali metals by the ME and TE are presented in this section. The analysis of results for these materials does not show the full range of applicability of equations like

CC-0. In Public Domain. Gurukul Kangri Collection, Haridwar

Digitized by Arya Samaj Foundation Chennai and eGangotri

TABLE II. Fitting results for some of Bridgman's water data (1–12 000 kg/cm²). ME fitting results above and TE below in each pair.

T °C	$10^4 s_e$	Error distribution	R	n r	$10^{11}\beta_0$ (cm²/dyn)	Low-pressure values $10^{11}\beta_0$ (cm²/dyn)
0	0.829	U	1.03	6.896	5.161	5.10[a]
	0.992	M/T	0.955	8.527	5.249	
20	4.53	(M/T)	0.785	6.336	4.579	4.58[b]
	5.46	(M/T)	0.755	7.893	4.644	4.64[a]
40	2.79	(M/T)	0.926	6.311	4.398	4.42[a]
	4.36	M/T	0.839	8.121	4.527	
60	2.91	U	1.06	6.290	4.420	4.43[a,b]
	2.45	(M/T)	0.935	8.102	4.551	
80	3.42	U	1.102	6.312	4.549	4.57[b]
	2.15	(M/T)	0.975	8.141	4.689	
100	6.99	T/M	1.27	6.532	4.948	4.80[b]
	4.21	(T/M)	1.11	8.416	5.116	

[a] M. D. Pena and M. L. McGlashan, Trans. Faraday Soc. **55**, 2018 (1959). Some values determined from graphical interpolation or extrapolation.
[b] D. Tyrer, J. Chem. Soc. **105**, 2534 (1914).

e ME and TE to solids and liquids and is only in-ended to be illustrative of possibilities.

A. Water

Table II shows results obtained for water using data Bridgman.[23] The maximum deviations, Δ, in these ings and those presented later generally did not ceed about $2s_e$, showing the smoothness of the data al. All s_e's calculated involved $(N-2)^{-\frac{1}{2}}$ since there two degrees of freedom involved in fitting either TE or ME. The maximum value of $n\beta_0 p$ for the ter data was of the order of 4. The symbol U in ble II indicates that the Δ deviation distribution unidentified and not of either the M/T or T/M e. Those designations in parentheses such as (M/T) one or at most two points opposite in sign to the icated error distribution type.

The very small s_e values shown in Table II indicate t either the TE or ME can represent the data well. ese values do not discriminate very well between two equations. Test 2, however, definitely suggests t the ME is superior on the whole. The experimental values of Tyrer given were obtained from directly asured adiabatic values and are likely to be less urate at the higher temperatures. Except for the °C results, which are ambiguous, Test 3 also indi-es that the ME is more applicable than the TE. The est is not very meaningful for these data since N s rather small. Like Test 1 it shows, however, a ght ME superiority for the three lower temperatures d TE superiority for the three higher ones.

Table II shows some dependence of both r and n on perature. This dependence is significant. If the 0°C ing, for example, is carried out with the following ed values: $n=6.311$, $r=7.893$, then it is found that corresponding s_e's obtained are very nearly an order of magnitude larger than those shown. Further, the ME and TE β_0 values obtained are about 4% smaller, both below the most likely value. Thus, much worse fits would be obtained if n or r were held temperature-independent. In their extensive work of applying the TE to liquids, Gibson and Loeffler[24] used a value of the TE parameter $C(\equiv J \ln 10)$ leading to the constant value $r\cong 7.31$ for water at all temperatures. This value was apparently not obtained by least squares. Since it falls outside the range of the r's given in Table II, its use with Bridgman's data would lead to much larger s_e's than those shown.

B. A Hydrocarbon Liquid

Table III shows results obtained on fitting p–V data[15] for the very compressible hydrocarbon 1-cyclopentyl-4 (3-cyclopentylpropyl) dodecane. Here, the maximum value of $n\beta_0 p$ was of the order of 9. Again, the results of applying both equations seem to be within the experimental accuracy of the data. Here, however, Tests 1, 3, and 4 all indicate that the TE is preferable to the ME. The TE β_0 values shown are therefore probably slightly closer to the (unknown) true values for this material than those following from the ME. Incidentally, the separate n, r, and β_0 values obtained from the A–B partition of each data set necessary to calculate R values generally, but not always, spanned the corresponding values shown in Table III.

Cutler, McMickle, Webb, and Schiessler[15] analyzed their dodecane data using the TE with a temperature-independent constant equivalent to the choice $r=11.2$. When this constant value is used, the resulting β_0's are 3 to 5% larger than those shown in the table. The values of s_e are only increased by 50% or less. Thus,

[23] P. W. Bridgman, J. Chem. Phys. **3**, 597 (1935).

[24] R. E. Gibson and O. H. Loeffler, J. Am. Chem. Soc. **63**, 898 (1941).

CC-0. In Public Domain. Gurukul Kangri Collection, Haridwar

Digitized by Arya Samaj Foundation Chennai and eGangotri

TABLE III. Fitting results for 1-cyclopentyl-4 (3-cyclopentylpropyl) dodecane (1–10336.5 bars). ME fitting results above and TE below in each pair.

T °C	$10^4 s_e$	Error distribution	R	n / r	$10^{11}\beta_0$ (cm²/dyn)
37.8	6.80	U	1.13	8.834	6.329
	6.07	U	1.05	10.61	6.465
60.0	8.63	T/M	1.22	8.948	7.257
	6.86	U	1.09	10.93	7.504
79.4	10.3	T/M	1.35	8.724	7.645
	7.62	T/M	1.19	10.75	7.933
98.9	12.1	T/M	1.60	8.484	8.368
	7.59	(T/M)	1.38	10.71	8.839
115.0	16.0	T/M	1.30	8.556	9.409
	10.5	T/M	1.09	10.86	10.00
135.0	9.73	T/M	1.28	8.575	10.26
	4.22	(T/M)	1.08	10.93	10.95

the appropriateness of a temperature-independent r cannot be as thoroughly ruled out here as it could be in the water case. A constant value near $r=10.8$ appears to be somewhat superior to 11.2 for this material, however.

To investigate the fitting accuracy possible with these data somewhat more, a ηp^2 term was added to both the ME and TE and the parameter η determined by NLS along with β_0, n, and r. The s_e's of both the augmented ME and TE fittings of the 98.9°C data, for example, fell to about 4.7×10^{-4} upon addition of the ηp^2 term. In spite of the reduced s_e's, the resulting error patterns were still by no means random but showed considerable regularity. The values of n, r, and β_0 obtained were all somewhat increased over those shown. The quantity η was negative for both augmented ME and TE fitting. Its magnitude was appreciably larger for the ME than the TE fitting, however, again indicating the greater applicability of the TE as compared to the ME for this material.

C. Four Alkali Metals

Tables IV and V show TE and ME fitting results using Bridgman's[25] room-temperature data for four alkali metals taken over two different overlapping pressure ranges. No very accurate independent determinations of β_0 seem available; those of Richards[26] yield for $10^{11}\beta_0$ the values 0.90, 1.56, 3.17, and 4.00 cm²/dyn for Li, Na, K, and Rb, respectively. Except for Rb, the ME β_0 values are generally closer to Richards' results than the TE β_0's. It seems likely that Richards' β_0 for Rb is too high.

All but one of the ME s_e values are appreciably smaller than those obtained from the TE fitting. Most of the s_e values are quite high, however. Many of the error patterns are the same for TE and ME fits, but they seem nevertheless to favor the ME over the TE slightly. We have not calculated R values for these data since data from two separate runs and their combination are here analyzed. Since the runs cover somewhat different pressure ranges, parameter differences for the separate runs on a given material should be significant for deciding on the applicability of the TE or ME. Tables IV and V show that the triads of s_e, n, and β_0 values obtained with the ME are appreciably more stable (less internal variation) than the corresponding triads obtained with the TE. All the tests thus seem to indicate that the ME is considerably superior to the TE for these materials and data.

As mentioned, Gombas[10] used the value $n=10/3$ in a theoretical equation of state he derived for the alkali metals which reduces to a differential form of the ME for sufficiently low pressures. Although the present pressure limits appreciably exceed his range, it is very interesting to find most of the n values in Table V quite close to 10/3.

Ginell and Quigley[12] have analyzed the Bridgman data used in obtaining the numbers in Tables IV and

TABLE IV. TE fitting results for alkali metals. Top row of each triad: 1–40 000 kg/cm², middle row: 1–100 000 kg/cm², bottom row: combined data (1–100 000 kg/cm²).

Material	$10^4 s_e$	Error distribution	r	$10^{11}\beta_0$ (cm²/dyn)
Li	2.82	M/T	4.685	0.8732
	9.90	T/M	5.441	0.9211
	16.5	U	5.469	0.9288
Na	9.89	M/T	5.116	1.540
	21.6	T/M	6.311	1.745
	41.2	(M/T)	6.273	1.751
K	12.0	M/T	5.611	3.366
	18.6	M/T	6.630	4.169
	44.3	M/T	6.302	3.802
Rb	17.3	M/T	5.429	3.607
	9.80	T/M	6.306	4.313
	44.6	M/T	6.082	4.056

[25] P. W. Bridgman, Proc. Am. Acad. Arts Sci. 76, 55–70, 71–87 (1948).

[26] T. W. Richards, J. Am. Chem. Soc. 37, 1643 (1915).

CC-0. In Public Domain. Gurukul Kangri Collection, Haridwar

Digitized by Arya Samaj Foundation Chennai and eGangotri

by means of the TE. Their results may be shown to be fairly close to those in Table IV in some cases but very far off in others. They analyzed the data by first interpolating to yield equally spaced pressure values, then numerically differentiating, and finally fitting the resulting $\partial P/\partial V$ points by linear least squares. No s_e values obtained were quoted. This fitting procedure may be expected to bias the original errors in the data and perhaps to introduce new errors. Three of their values for $L \equiv B(\cong 1/r\beta_0)$ were negative, for example. Since their corresponding V_0 and J values were positive, the associated r values must also be positive and the β_0's negative. But negative β_0's (or B's) in the TE do not then lead to the proper type of dependence of V/V_0 on p.

Two of Ginell and Quigley's negative L values were obtained from data which led to the last two K rows in Table IV. The values of r and β_0 given there lead to $1/r\beta \cong 3.62\times10^9$ and 4.17×10^9 dyn/cm² for the middle and bottom K rows, respectively. The small amount of variation suggests that the data used in the two runs is reasonably consistent and that no negative values of L should appear.

In integrating the differential form of the TE, Ginell and Quigley use V_0 (specific volume) as an additional parameter and find wide variation in it between the various alkali metals. For example, their quoted fitting results for the 0–40 000 kg/cm² Rb data lead to $L \cong 0.68$, $r \simeq 6.43$, and $\beta_0 \simeq 5.44\times10^{-11}$ cm²/dyn. If $r=6.43$ is taken fixed, and β_0 obtained by NLS using the TE with the same data, I find $s_e = 7.93\times10^{-3}$ and $\beta_0 \cong 4.40\times10^{-11}$ cm²/dyn. Alternatively, if β_0 is held fixed at 5.44×10^{-11} cm²/dyn, the TE yields $s_e = 1.49\times10^{-2}$ and $r = 7.334$. It is clear that all these results are far inferior to the Table IV NLS determination of parameters with both parameters free to vary.

D. Sodium

Beecroft and Swenson[27] (abbreviated B–S) have carried out a thorough P–V–T study for Na. It is of interest to use their results in a further test of TE and ME applicability, to investigate the temperature dependence of n and β_0 obtained from ME fitting, and to compare with the Na results in Table V.

Table V. ME fitting results for alkali metals. Top row of each pair: 1–40 000 kg/cm², middle row: 1–100 000 kg/cm², bottom row: combined data (1–100 000 kg/cm²).

Material	$10^4 s_e$	Error distribution	n	$10^{11}\beta_0$ (cm²/dyn)
Li	1.70	U	3.218	0.8589
	16.9	T/M	3.470	0.8593
	16.4	(M/T)	3.578	0.8800
Na	3.89	(M/T)	3.417	1.488
	32.8	T/M	3.875	1.519
	35.7	(M/T)	4.002	1.583
K	10.6	T/M	3.518	3.106
	13.5	(M/T)	3.522	3.048
	15.3	U	3.583	3.130
Rb	5.52	T/M	3.318	3.311
	29.3	T/M	3.212	3.115
	26.9	U	3.346	3.301

[27] R. L. Beecroft and C. A. Swenson, J. Phys. Chem. Solids **18**, 329 (1961).

Table VI. ME fitting results for Na (0–20 000 atm). Original data of Beecroft and Swenson (Ref. 27).

T °K	$10^4 s_e$	Error distribution	n	$10^5\beta_0$ (atm^{-1})	$-10^5 a_1$ (atm^{-1})
20	5.03	M/T	4.144	1.417	1.351
51	5.76	M/T	3.999	1.411	1.340
77	5.09	(M/T)	4.051	1.450	1.387
77	4.19	M/T	4.428	1.477	1.417
115	5.96	M/T	4.049	1.481	1.405
138.6	4.20	(M/T)	4.093	1.512	1.443
171	3.96	(M/T)	3.947	1.527	1.462
201	5.41	(M/T)	4.123	1.614	1.537
204	7.18	U	3.835	1.559	1.477
246	5.10	M/T	3.972	1.645	1.567
297	4.64	M/T	3.747	1.653	1.580
297	6.70	M/T	3.759	1.651	1.562
297	4.33	M/T	4.193	1.708	1.642
349	4.70	(M/T)	3.726	1.720	1.642

Table VI shows the results obtained with ME fitting. The largest value of $n\beta_0 p$ is here only about 1.4. TE fitting generally yielded somewhat larger s_e's and β_0 values one to two percent larger than those in Table VI. B–S fitted their $(V-V_0)/V_0$ results to the cubic $a_1p+a_2p^2+a_3p^3$, essentially by least squares. Slightly different values of the cubic coefficients than those given by B–S are obtained when the quoted $(V-V_0)/V_0$ data are fitted directly to the above cubic by least squares. The results obtained for $-a_1$ are shown in the last column of Table VI. They should, of course, equal corresponding β_0 values since both quantities give the initial compressibility. Although β_0 and $-a_1$ are highly correlated, the a_1 dependence on temperature is considerably more irregular than the β_0, and a_1 is generally about 5% smaller than β_0. On the other hand, the cubic fitting uses three adjustable parameters and the ME only two. It is not surprising, therefore, that the cubic s_e's found are often only about half as large as the s_e's in Table VI.

When curve fitting was carried out for the second 297°K set of data using the ME augmented with a ηp^2 term (added in with $n\beta_0 p$), the resulting s_e was appreciably smaller than that obtained with the cubic although both fittings involve three parameters. The error distribution obtained appeared random, n was reduced to about 1.5, the β_0 value found fell between the ordinary ME β_0 and $-a_1$, and η was small and positive. As a further comparison test, some of the data were analyzed by NLS using the ordinary ME but written in the form of Eq. (2). For example, the second 297°K data set led to a s_e of about 101 atm, $n \cong 3.902$, and $\beta_0 \cong 1.683\times10^{-5}$ atm^{-1}. The n and β_0 values are significantly, but not greatly, different from those shown in Table VI obtained with V/V_0 as the dependent variable.

Since it is not known that the ordinary ME is a very good approximation to the true equation of state for sodium, it is not possible to conclude unequivocally

CC-0. In Public Domain. Gurukul Kangri Collection, Haridwar

Digitized by Arya Samaj Foundation Chennai and eGangotri

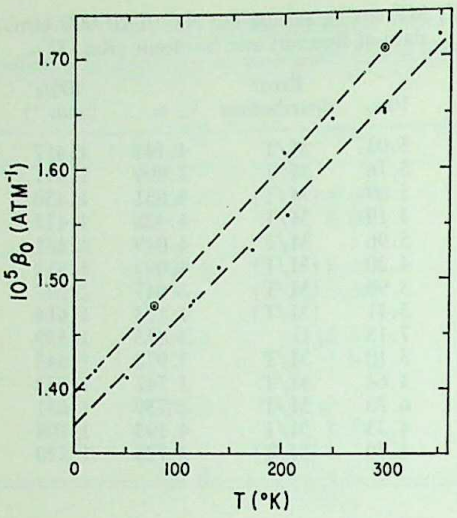

FIG. 2. Initial compressibility β_0 derived from uncorrected Na p–V–T data, versus absolute temperature.

that the β_0 values are better estimates of the true initial compressibility than the $-a_1$'s. In a paper discovered after the calculations of Table VI were carried out, Monfort and Swenson[28] state that the B–S pressure scale was in error and that all pressures given in B–S should be increased by 3%. This change results in a reduction of Table VI β_0 and a_1 values by the factor 0.971. The results in Table VI and Fig. 2 have been left unchanged, for easier comparison with the original B–S results. From now on the factor 0.971 will be applied to all quoted β_0 and a_1 values derived from the B–S data.

Richards'[26] value for β_0 at room temperature is 1.56×10^{-11} cm²/dyn while B–S have deduced a value of about 1.618×10^{-11} cm²/dyn from ultrasonic data. The first two room-temperature values of $-a_1$ in Table VI correspond to about 1.514×10^{-11} and 1.499×10^{-11} cm²/dyn, respectively. The corresponding values of β_0 are about 1.584×10^{-4} and 1.582×10^{-11} cm²/dyn, appreciably closer to the B–S ultrasonic value, and, for that matter, to Richards' result as well. In a re-analysis of his Na data, Swenson[28] quotes a value of the room-temperature bulk modulus which leads to $\beta_0\cong1.587\times10^{-11}$ cm²/dyn, in close agreement with the present β_0 results.

The above agreement plus the greater regularity of the β_0's suggest that they are indeed better estimates than the $-a_1$'s. On the other hand, the almost ubiquitous appearance of the M/T error pattern in Table VI (although it appears less strongly in Table V) suggests that unless there are systematic errors in the p–V data, there are some small, yet real, systematic deviations between the ME and the actual p–V behavior of Na. Such discrepancies might still allow β_0 to be a better estimator than $-a_1$, however. The lack of close agreement between the Na n's and β_0's of Table V and the room-temperature results in Table VI certainly still leaves the question open, however, as to whether the systematic deviations arise from experimental errors or from some failure of applicability of the ME.

Figure 2 shows the dependence of β_0 (uncorrected) on temperature. It is not immediately obvious from Table VI that the β_0 results fall so regularly into two groups. The dashed lines shown are the linear least-square fits for these groups separately. For the lower line, the result (corrected for pressure scale error) is $\beta_0=1.327\times10^{-5}(1+7.155\times10^{-4}T)$ atm^{-1}. The s_e's for the upper and lower lines were 6.77×10^{-3} and 8.44×10^{-3}, respectively. A quadratic fit only changed the s_e's to 8.09×10^{-3} and 8.40×10^{-3}. The two points indicated with circles are derived from data extending to only 12 000 atm for which a different sample holder was used. It is not known why the β_0 values should separate so clearly into two groups; random experimental error alone may be the culprit or perhaps there was some difference in the experimental procedure for the two subsets. In any event, it appears that β_0 can be well represented by a linear temperature dependence in the range here shown.

In considering the temperature dependence of n, it seems reasonable to examine the two subsets separately. The n values for temperatures of 20°, 77° (second in Table VI), 201°, 246°, and 297° (third in table) correspond to β_0 values associated with the upper line. These n's show no significant temperature dependence. On the other hand, the remaining n's show a quite regular but slight dependence. If all the low temperature values are taken as approximations to some number near 4, then n decreases down to 3.73 at 349°K. This slight dependence leads, through the use of $\gamma=\frac{1}{2}(n-\frac{1}{3})$, to smaller dependence of γ on T than may be inferred from results given by B–S. The result that the ME can represent the p–V data very well with a pressure-independent n also suggests that γ for Na varies with volume less than concluded by B–S. Nevertheless, B–S point out that the Poisson ratio is a function of volume for Na. In spite of the apparent usefulness of the ME, this result suggests that the theoretical relation $n=2\gamma+\frac{1}{3}$ should only be used with caution, if at all, and that therefore n should perhaps best be considered only a heuristic, slightly temperature-dependent fitting parameter.

Cook and Rogers[8] have suggested that for materials such as Na and H_2O, which may be expected to have significant concentrations of thermodynamic defects at room temperature and atmospheric pressure, the ME should be applied only for the high-pressure region, above about 12 kbars for Na and H_2O. Their own high-pressure analyses for these materials, when extrapolated to zero pressure, do not yield good values of β_0. On the other hand, in the present work the ME has been used over the full pressure range available (which includes many data points below 12 kbars) and has led to excellent values of β_0. It therefore appears that it can

[28] C. E. Monfort and C. A. Swenson, J. Phys. Chem. Solids 26, 291 (1965).

CC-0. In Public Domain. Gurukul Kangri Collection, Haridwar

Digitized by Arya Samaj Foundation Chennai and eGangotri

account adequately for the effects of Schottky defects and holes in liquids, when important, on the p–V relation provided NLS fitting with both parameters free is employed.

Because the present treatment is intended to illustrate possibilities rather than to be comprehensive, no detailed analysis is included here of Monfort and Swenson's K data[28] or of Swenson's recent Li results.[29] These authors have suggested that the ME (not identified or related to earlier equations of state) with $n=3.8$ will fit the Na, K, and Li p–V data extrapolated to zero degrees. Apparently, no NLS fitting with free parameters was carried out, and the value 3.8 was arrived at as a compromise between experimental values of $d(\beta^{-1})/dP$ of 3.95 for Na, 3.85 for K, and 3.6 for Li. The present results for Na suggest a value of n at $T=0$°K of 4 to 4.2.

Since Table VI shows no trend to smaller s_e values as T is reduced, the ME is apparently as applicable at nonzero temperatures as it is in the limit $T\to 0$. Further, its application for $T>0$ can yield, as has been shown above, useful information on the temperature variation of β_0 and perhaps n. Incidentally, the value $\beta_0=1.327\times 10^{-5}$ atm applying for Na at $T=0$°K and derived from the lower least-squares line in Fig. 2 is appreciably smaller than 1.369×10^{-5} atm, the value following from Swenson's[28] re-analysis of the B–S data. The former value is probably derived from a more detailed analysis of more of the data than the latter.

DISCUSSION AND CONCLUSIONS

In order to yield stringent tests of the applicability of the TE and ME and allow utmost discrimination between them, the materials analyzed thus far were picked for their relatively high compressibilities. Except for the highly compressible dodecane, the ME was found to be superior to the TE. It appears, in fact, that the ME is the most generally applicable wide-pressure-range two-parameter equation of state for liquids and solids. It should, however, be considered primarily as an empirical equation because some of the assumptions made in deriving it theoretically are often inapplicable to real materials. As such, it should be particularly useful in deriving good values of $\beta_0(T)$ from p–V–T data, in smoothing such data, and in finding experimental errors.

Although the agreement found thus far between the ME predictions obtained with NLS fitting and the original p–V data has been quite good and usually within likely experimental error limits (even when M/T or T/M behavior could be distinguished), it is worth pointing out that the ME can frequently yield, for less compressible materials, fits about an order of magnitude better than those illustrated thus far. For example, using Bridgman's[25] 0–40 000 kg/cm² zinc data, the ME yields $s_e\cong 1.41\times 10^{-6}$, $n\cong 5.663$, and $\beta_0\cong 1.652\times 10^{-12}$ cm²/dyn. The data have four significant figures (the value of V/V_0 at the highest pressure is 0.9463) and the largest fitting error found in the predicted V/V_0 was 2.1×10^{-5}! With this good a fit, the error distribution was unidentifiable and apparently random.

In addition to the fact that the theoretical assumptions made in deriving the ME and TE are not generally applicable, there is another important reason why neither the ME nor TE should be applied beyond a certain limited pressure range. The total elastic or cohesive energy (at a given temperature but excluding the energy to transform molecules to atoms, etc.) is $W(\infty)$, where

$$W(V)=-\int_{V_0}^{V} P\,dV. \tag{3}$$

$W(V)$ for the ME, for example, may be readily calculated using (2) and (3), and even with $P_0=0$ leads to $W(\infty)=\infty$, an unacceptable value. The same result follows from the TE.

Both the ME and TE predict a finite negative pressure, p_∞, at which $V\to\infty$ (see Appendix). Any equation of state yielding such a pressure must lead to an infinite $W(\infty)$. Gilvarry's three-parameter general equation,[3] which includes the one-parameter Bardeen and Birch equations, does not suffer from this defect provided his parameters n and m both exceed unity. When $m=0$, the ME is obtained. The general equation leads to a maximum absolute value of negative pressure (at $\partial P/\partial V=0$); then the negative pressure decreases in magnitude towards zero as V/V_0 increases further towards infinity. For m and $n\geq 1$, Gilvarry's equation yields

$$W(\infty)=V_0/[\beta_0(n-1)(m-1)], \tag{4}$$

a reasonable and possibly new result which could be checked against published values of $W(\infty)$ for a variety of materials after NLS fitting provided n, m, and β_0 values. Unfortunately, this three-parameter equation of state does not allow V/V_0 to be solved for explicitly in terms of pressure for general n and m. Some discussion of the applicability of several of the equations discussed in this paragraph has been given by Gilvarry,[3] without, however, mention of the $W(\infty)=\infty$ catastrophe for the ME and TE. More recent discussion of a few equations of state for solids has been presented by Knopoff.[30]

The above results suggest that although the ME (or TE) may be very useful for positive pressures, its range of applicability should not be extended very far into the negative pressure region. Briggs[31] has measured, by centrifugal force, what seems to be the largest negative pressure or tensile strength value for water, namely, -277 atm. Equation (1) together with the room-temperature ME water parameters of Table II,

[28] C. A. Swenson, J. Phys. Chem. Solids **27**, 33 (1966).

[30] L. Knopoff in *High Pressure Physics and Chemistry, I*, R. S. Bradley, Ed. (Academic Press Inc., New York, 1963).

[31] L. J. Briggs, J. Appl. Phys. **21**, 721 (1950).

CC-0. In Public Domain. Gurukul Kangri Collection, Haridwar

Digitized by Arya Samaj Foundation Chennai and eGangotri

lead to $p_\infty \cong -3410$ atm, in poor agreement with the above value. The value of -277 atm corresponds, through Eq. (1), to $V/V_0 \cong 1.0135$. For comparison, if V_0 for water is taken unity at NTP, then $V/V_0 \simeq 1.043$ at atmospheric pressure and the boiling point of water. This is not really a valid comparison, however, since thermal measurements yield results depending on both the attractive and repulsive parts of the internal potential while the results of low-temperature pressure measurements depend primarily on the repulsive part of the potential. The Bardeen and Birch equations lead to $V/V_0 \sim 1.5$ to 2 at the negative pressure for which $\partial P/\partial V = 0$.

Cook and Rogers[8] have taken an "internal pressure" in their derivation of the ME essentially given by $-p_\infty \equiv (n\beta_0)^{-1}$. They have set this equal to ϵ_0/v_0, where ϵ_0 is the cohesive energy at absolute zero and v_0 the specific volume. Since the ME cannot be used to calculate a cohesive energy, this approach seems inconsistent, although it led to β_0 values in generally good agreement with independently observed compressibilities for many metals. These β_0 values were obtained by using independent determinations of $v_0/\epsilon_0 (= n\beta_0)$ in the ME and deriving n values graphically. The resulting n's were then used in the above relation to obtain the β_0's.

The Cook–Rogers n's are not in very close agreement with those for corresponding materials derived by NLS herein. Since the present n's and β_0's are maximally consistent with the data provided the ME is applicable, and since the present β_0's agree well with independent values, the relation $v_0/\epsilon_0 = n\beta_0$ is probably rather inexact when accurate values of n and β_0 are used. It would be surprising if it were exact since while p_∞ is the negative pressure for breakup of the material according to the ME, it has been shown above that p_∞ cannot be well related theoretically to the cohesive energy. On the other hand, since $W(\infty)$ is likely to be proportional to β_0^{-1}, at least to first order [see above Gilvarry-equation result for $W(\infty)$], the Cook–Rogers relation is of a reasonable form.

The TE yields $P_\infty \equiv p_\infty + P_0 = -(r\beta_0)^{-1} + P_0 = -B$. The results in Table II for water lead to $P_\infty \cong p_\infty \cong -2690$ atm, somewhat smaller than the ME result. For comparison, values of the "internal pressure" of water quoted by Dorsey[32] are near 11 000 atm. The quantity B has been interpreted in a number of ways. It has been suggested that it is related to the cohesive energy density of the material,[13] that it is an internal pressure,[33] that B or $B+P$ is the difference between the expansive thermal pressure and the attractive cohesive pressure of the material,[18,23,34,35] and that B is a measure of the excluded volume of large particles.[18] I have suggested above, however, that $P_\infty = -B$ is not a valid measure of the tensile strength of the material, since neither the TE nor ME can yield a cohesive energy. Therefore, it seems to me that all of the above interpretations of B are inapplicable and that B, if it must be introduced, should merely be interpreted as $\backsim (r\beta_0)^{-1}$. It seems far better to use instead the normal thermodynamic quantity β_0 in the TE or ME and to investigate its temperature dependence rather than to use B, whose interpretation is uncertain and whose temperature dependence involves those of both r and β_0.

To summarize, the present results suggest that:

1. The ME is generally superior to the TE but both equations should be considered only as heuristic equations of state useful in the positive pressure range up to very high pressures.

2. Both the ME and the TE should be written in forms involving the initial compressibility parameter β_0 directly, and no interpretation then need be given to the Tait parameter B.

3. The n and r parameters should not be taken temperature independent.

4. Fitting of experimental p–V results to an equation of state should be carried out, wherever possible, with V/V_0 as the explicit dependent variable expressed directly on the left-hand side of the equation of state.

5. All fitting of the ME or TE to experimental data should be done by means of NLS directly at the p–V level, and as many of the goodness-of-fit and discrimination tests discussed herein as possible applied. Certainly, the conclusion that a material obeys the TE should not be made without such tests and without comparison with the ME and any other reasonable equation of state such as the Birch equation.

ACKNOWLEDGMENT

The computational help of Marilyn White is much appreciated.

APPENDIX: THE TAIT AND MODIFIED EQUATIONS

1. Tait Equation

The TE has been frequently written as[24,34,35]

$$V_0 - V = C \log_{10} [(P+B)/(P_0+B)], \quad \text{(A1)}$$

where $V_0 \equiv V(P_0)$, a reference volume. The parameters B and C are taken pressure-independent. Let us now write

$$J \equiv C \log_{10} e \quad \text{(A2)}$$

$$r \equiv V_0/J = V_0 \ln 10/C, \quad \text{(A3)}$$

$$\beta_0 \equiv [r(P_0+B)]^{-1}, \quad \text{(A4)}$$

and

$$p \equiv P - P_0. \quad \text{(A5)}$$

[32] N. E. Dorsey, *Properties of Ordinary Water-Substance* (Reinhold Publishing Corp., New York, 1940), p. 181.
[33] A. Wohl, Z. Physik. Chem. **99**, 234 (1921).
[34] R. E. Gibson and J. F. Kincaid, J. Am. Chem. Soc. **60**, 511 (1938).
[35] R. E. Gibson and O. H. Loeffler, J. Am. Chem. Soc. **61**, 2515 (1939).

CC-0. In Public Domain. Gurukul Kangri Collection, Haridwar

Digitized by Arya Samaj Foundation Chennai and eGangotri

The TE rewritten in terms of these new quantities becomes

$$V/V_0 = 1 - r^{-1} \ln (1 + r\beta_0 P). \tag{A6}$$

The quantity r (or C/V_0) has been taken to be essentially temperature independent for many materials[13-16,24,34,35] although some slight dependence has been reported.[18,33]

The isothermal (instantaneous) compressibility $\beta \equiv -V^{-1}(\partial V/\partial P)_T$ calculated from (A6) is

$$\beta = \beta_0 (V_0/V)[1 + r\beta_0 p]^{-1}, \tag{A7}$$

a differential form of the TE. It is clear that when $P = P_0$, $\beta = \beta_0$. If P_0 is taken as atmospheric pressure, then β_0 may be identified as the isothermal "initial" compressibility of the material considered. Since B is usually much greater than P_0, the temperature dependence of β_0, which may be appreciable, is then just the inverse of that of B, provided r is temperature-independent.

Note that (A7) is relatively complicated and that (A1) and (A6) have the disadvantage that they yield $V < 0$ above the pressure

$$p_L \equiv (r\beta_0)^{-1}(e^r - 1) = (P_0 + B)(e^r - 1) \tag{A8}$$

at which $V = 0$. There is a negative pressure, p_∞, at which $V \to \infty$. From (A6), it is

$$p_\infty \equiv -(r\beta_0)^{-1} = -(P_0 + B), \tag{A9}$$

or

$$p_\infty \equiv -B. \tag{A10}$$

2. Modified Equation

The negative volume catastrophe of the TE makes it theoretically unappealing even though p_L is usually of the order of millions of atmospheres and so beyond the range of most measurements. It is therefore desirable to modify the TE slightly in a way which will avoid this difficulty and so perhaps extend the range of applicability of the equation. One may modify Eq. (A6) as follows.[1] First, to avoid $V < 0$ behavior, write $r \equiv \ln (1 + r\beta_0 p)^{1/r}$ and replace $V/V_0 = 1 - x$ by $V_0/V = 1 + x$, the same to first order in x. This result, itself a possibly useful equation of state, may be further modified by replacing $(V_0/V) - 1$ by $\ln (V_0/V)$, again the same to first order in $(V_0/V) - 1$. On making the transformation $r \to n$ in x, one finally obtains

$$V/V_0 = (1 + n\beta_0 p)^{-1/n}. \tag{A11}$$

From (A11) it follows that

$$\beta = \beta_0[1 + n\beta_0 p]^{-1} = \beta_0 (V/V_0)^n, \tag{A12}$$

considerably simpler than (A7) yet again equal to β_0 when $p = 0$.

The transformation $r \to n$ has been made in order to distinguish between these parameters and to allow (A6) and (A11) to agree to as high order in $\beta_0 p$ as practical. Expand V_0/V in a power series in $\beta_0 p$ using first (A6) then (A11). On comparing the results term by term, one finds equalities for zero and first orders whatever the values of r and n. The second-order terms may also be made equal if we take $n = r - 1$. When this value is substituted into the third-order term of the ME, the coefficient of $(\beta_0 p)^3$ becomes $(r^2/3) - (7/6)r + 1$. That of the TE is $(r^2/3) - r + 1$, virtually the same except for a difference of $r/6$. Thus, the relation

$$n = r - 1 \tag{A13}$$

makes the ME and TE identical to second order and almost identical to third.

Bridgman and others have conventionally expressed experimental p–V results for many solids by means of

$$V/V_0 = 1 - ap + bp^2 - Cp^3 + \cdots. \tag{A14}$$

If we compare term by term with the power series expansion of (A11), we find

$$a \equiv \beta_0, \tag{A15}$$

$$b \equiv (n+1)\beta_0^2/2, \tag{A16}$$

$$c \equiv (2n^2 + 3n + 7)\beta_0^3/6, \tag{A17}$$

etc. Thus, a test of whether Bridgman's results may be well fitted in the low to medium pressure range by the modified equation is whether $b/a^2 = (n+1)/2$ and $c/a^3 = (2n^2 + 3n + 7)/6$ using the same n in both relations. This comparison is only fruitful, of course, when $n\beta_0 p$ is so small that higher than third-order terms in the expansion of (A11) may be neglected.

CC-0. In Public Domain. Gurukul Kangri Collection, Haridwar

Digitized by Arya Samaj Foundation Chennai and eGangotri

REVIEWS OF MODERN PHYSICS VOLUME 38, NUMBER 4 OCTOBER 1966

Thermodynamic Properties of an Electron Plasma*

T. J. LIE, YOSHI H. ICHIKAWA†
Department of Physics and Coordinated Science Laboratory, University of Illinois, Urbana, Illinois

The thermodynamic properties of an electron plasma are investigated on the basis of the Bogoliubov–Born–Green–Kirkwood–Yvon hierarchy equation. The correlation energy has been calculated up to the ϵ^2 term (ϵ is the standard plasma parameter) in terms of an exact solution of the binary correlation function taking into account the short-range collision effect. The contribution of ternary correlations to the correlation energy has been determined in lowest order, which turns out to be of the second order in ϵ. The total sum of the corrections due to the short-range collision effect and the ternary correlation effect is found to be in agreement with the result obtained by Abe, Bowers, and Salpeter within the regime of Gibbs' statistical thermodynamics. Although the appearance of the binary correlation function obtained in the present studies differs from those derived by Bowers–Salpeter and by O'Neil–Rostoker, it is shown that all of these expressions are essentially equivalent. According to the present analysis, however, it is proven that these expressions do not describe correctly the way in which correlation effects diminish at large distances and therefore the statement made by DeWitt saying that $g(x)\sim\frac{1}{8}(\ln 3)\epsilon^2\exp(-k_D r)$ as $r\to\infty$ is not correct.

I. INTRODUCTION

During the past years, kinetic properties of plasmas in the nonequilibrium state have been extensively examined by many authors on the basis of the Liouville equation or the Bogoliubov–Born–Green–Kirkwood–Yvon hierarchy equation,[1,2] while thermodynamic properties of plasmas have been investigated by applying Mayer's cluster expansion method within the framework of Gibbs' statistical thermodynamics.[3,4] Recently, however, several authors have attempted to investigate thermodynamic properties of plasmas by solving the BBGKY hierarchy equation for the equilibrium case.[5–7] It is worth investigating the way in which various physical effects contribute to thermodynamic properties of plasmas through the BBGKY hierarchy equation.

Guernsey[6] has solved the BBGKY hierarchy equation for the equilibrium state by a method of double series expansion and has presented a "dynamic" derivation of the equation of state for an electron plasma, which is correct through second order in the plasma parameter $\epsilon=(4\pi n\lambda_D^3)^{-1}$. n is the number density of electron and λ_D is the Debye distance. On the other hand, O'Neil and Rostoker[7] have determined a binary correlation function for an equilibrium electron plasma by solving analytically the BBGKY hierarchy equation. In obtaining the solution, they have introduced an arbitrary distance r_0 to divide the whole space into the inner region $r<r_0$ where the short-range collisions play a dominant role and the outer region $r>r_0$ where the effects of short-range collisions can be disregarded. Different expansions in the plasma parameter ϵ have been applied for the equations obtained in each region. The solutions valid in each region have been matched approximately at the distance $r=r_0$. The same authors have also obtained the correlation energy which is correct up to the ϵ^2 term, by arbitrarily defining r_0 as the mean distance between particles $n^{-1/3}$.

The present paper removes the arbitrariness inherent in the above-mentioned interpolation method for solving the BBGKY hierarchy equation for the equilibrium case. We present the fundamental equations in Sec. II. In Sec. III, ignoring the ternary correlation effect, we examine the influence of the short-range collisions on the binary correlation function in some details. Following the calculation of Lamb and Burdick,[5] we can calculate corrections to the Debye–Hückel limiting value of the correlation energy up to the second order in ϵ as follows:

$$E^{(C)}/\kappa T=-\tfrac{1}{4}\epsilon^2\ln\epsilon-\tfrac{1}{2}(\gamma-\tfrac{1}{4})\epsilon^2, \tag{1}$$

where $\gamma=0.5772$ is the Euler constant, κ is the Boltzmann constant, and T is the electron temperature. In Sec. IV, we analyze the effect of the ternary correlation on the binary correlation function in some detail. The contribution of the ternary correlation to the correlation energy is calculated as

$$E^{(T)}/\kappa T=-\tfrac{1}{4}(\ln 3-\tfrac{5}{6})\epsilon^2. \tag{2}$$

Adding up Eqs. (1) and (2) to the Debye–Hückel limiting value of the correlation energy $-\epsilon/2$, we obtain

$$E/\kappa T=-\tfrac{1}{2}\epsilon-\tfrac{1}{4}\epsilon^2\ln\epsilon-\tfrac{1}{2}(\gamma-\tfrac{2}{3}+\tfrac{1}{2}\ln 3)\epsilon^2 \tag{3}$$

which is the result obtained by Abe,[3] and by Bowers and Salpeter.[4] Thus, the present analysis demonstrates explicitly that the approach based on the method of solving the BBGKY hierarchy equation can provide such detailed information as contributions of the dynamical effect of short-range collisions and of ternary correlations to the thermodynamic properties of an electron plasma. In the last section, we discuss the present result for the binary correlation function by comparing it with that obtained by Bowers and Salpeter.

* This work was supported wholly by the Joint Services Electronic Programs (U.S. Army, U.S. Navy, and U.S. Air Force) under contract No. DA 28 043 AMC 00073(E).

† On leave of absence from the Department of Physics, College of Science and Engineering, Nihon University, Tokyo, Japan.

[1] R. Balescu, Phys. Fluids 3, 52 (1960).
[2] A. Lenard, Ann. Phys. (N. Y.) 3, 390 (1963).
[3] R. Abe, Progr. Theoret. Phys. (Kyoto) 22, 213 (1959).
[4] D. L. Bowers and E. E. Salpeter, Phys. Rev. 119, 1180 (1960).
[5] G. L. Lamb, Jr., and B. Burdick, Phys. Fluids 7, 1087 (1963).
[6] R. L. Gurnsey, Phys. Fluids 7, 792 (1963).
[7] T. O'Neil and N. Rostoker, Phys. Fluids 8, 1109 (1965).

CC-0. In Public Domain. Gurukul Kangri Collection, Haridwar

Digitized by Arya Samaj Foundation Chennai and eGangotri

II. FUNDAMENTAL EQUATIONS

We consider a system composed of N electrons imbedded in a neutralizing uniform background of ions in a large volume V. Assuming the system is spatially uniform, we have the following expressions for the BBGKY hierarchy equation:

$$\frac{\partial}{\partial t}F(v_1)=\frac{n}{m}\int d3\,\frac{\partial\varphi(r_{12})}{\partial \mathbf{r}_1}\cdot\frac{\partial}{\partial \mathbf{v}_1}G(1,2) \tag{4a}$$

$$\left\{\frac{\partial}{\partial t}+\mathbf{v}_1\cdot\frac{\partial}{\partial \mathbf{r}_1}+\mathbf{v}_2\cdot\frac{\partial}{\partial \mathbf{r}_2}\right\}G(1,2)=\frac{1}{m}\frac{\partial\varphi(r_{12})}{\partial \mathbf{r}_1}\cdot\left(\frac{\partial}{\partial \mathbf{v}_1}-\frac{\partial}{\partial \mathbf{v}_2}\right)[F(v_1)F(v_2)]+\frac{1}{m}\frac{\partial\varphi(r_{12})}{\partial \mathbf{r}_1}\cdot\left(\frac{\partial}{\partial \mathbf{v}_1}-\frac{\partial}{\partial \mathbf{v}_2}\right)G(1,2)$$
$$+\frac{n}{m}\left\{\frac{\partial F(v_1)}{\partial \mathbf{v}_1}\cdot\int\frac{\partial\varphi(r_{13})}{\partial \mathbf{r}_1}G(2,3)\,d3+\frac{\partial F(v_2)}{\partial \mathbf{v}_2}\cdot\int\frac{\partial\varphi(r_{23})}{\partial \mathbf{r}_2}G(1,3)\,d3\right\}$$
$$+\frac{n}{m}\int\left(\frac{\partial\varphi(r_{13})}{\partial \mathbf{r}_1}\cdot\frac{\partial}{\partial \mathbf{v}_1}+\frac{\partial\varphi(r_{23})}{\partial \mathbf{r}_2}\cdot\frac{\partial}{\partial \mathbf{v}_2}\right)H(1,2,3)\,d3, \tag{4b}$$

and

$$\left\{\frac{\partial}{\partial t}+\sum_{i=1}^{3}\mathbf{v}_i\cdot\frac{\partial}{\partial \mathbf{r}_i}\right\}H(1,2,3)=\frac{1}{m}\left\{G(2,3)\,\frac{\partial F(v_1)}{\partial \mathbf{v}_1}\cdot\left(\frac{\partial\varphi(r_{12})}{\partial \mathbf{r}_1}+\frac{\partial\varphi(r_{13})}{\partial \mathbf{r}_1}\right)+(1\to2,\,2\to3,\,3\to1)+(1\to3,\,2\to1,\,3\to2)\right\}$$
$$+\frac{1}{m}\left\{F(v_1)\left(\frac{\partial\varphi(r_{21})}{\partial \mathbf{r}_2}\cdot\frac{\partial}{\partial \mathbf{v}_2}+\frac{\partial\varphi(r_{31})}{\partial \mathbf{r}_3}\cdot\frac{\partial}{\partial \mathbf{v}_3}\right)G(2,3)+(1\to2,\,2\to3,\,3\to1)+(1\to3,\,2\to1,\,3\to2)\right\}$$
$$+\frac{1}{m}\left\{\frac{\partial\varphi(r_{12})}{\partial \mathbf{r}_1}\cdot\left(\frac{\partial}{\partial \mathbf{v}_1}-\frac{\partial}{\partial \mathbf{v}_2}\right)H(1,2,3)+(1\to2,\,2\to3,\,3\to1)+(1\to3,\,2\to1,\,3\to2)\right\}$$
$$+\frac{n}{m}\left\{\frac{\partial F(v_1)}{\partial \mathbf{v}_1}\cdot\frac{\partial}{\partial \mathbf{r}_1}\int\varphi(r_{14})H(2,3,4)\,d4+(1\to2,\,2\to3,\,3\to1)+(1\to3,\,2\to1,\,3\to2)\right\}$$
$$+\frac{n}{m}\left\{\int\left(\frac{\partial\varphi(r_{14})}{\partial \mathbf{r}_1}\cdot\frac{\partial}{\partial \mathbf{v}_1}+\frac{\partial\varphi(r_{24})}{\partial \mathbf{r}_2}\cdot\frac{\partial}{\partial \mathbf{v}_2}\right)G(1,2)G(3,4)\,d4\right.$$
$$\left.+(1\to2,\,2\to3,\,3\to1)+(1\to3,\,2\to1,\,3\to2)\right\}, \tag{4c}$$

---

where $F(v)$ is the one-particle distribution function. The binary correlation function $G(1,2)$ and the ternary correlation function $H(1,2,3)$ are introduced through the following decomposition of the two-particle distribution function $F(1,2)$ and the three-particle distribution function $F(1,2,3)$:

$$F(1,2)=F(v_1)F(v_2)+G(1,2), \tag{5a}$$

$$F(1,2,3)=F(v_1)F(v_2)F(v_3)+\{F(v_1)G(2,3)+(1\to2,\,2\to3,\,3\to1)+(1\to3,\,2\to1,\,3\to2)\}+H(1,2,3). \tag{5b}$$

In Eqs. (4c) and (5b), the terms denoted as $(i\to j,\ j\to1)$ represent the term obtained by applying the assigned permutation to the first term in the curly brackets of these equations. The integral over the specific number i denotes the integral over the velocities and the spatial coordinates of the ith particle. The interaction potential $\phi(r_{ij})$ is the Coulomb potential,

$$\phi(r_{ij})=e^2/|\,\mathbf{r}_i-\mathbf{r}_j\,|. \tag{6}$$

We have normalized the distribution functions as

$$1=\frac{1}{V}\int F(v_1)\,d1 \tag{7a}$$

$$F(v_1)=\frac{1}{V}\int F(1,2)\,d2 \tag{7b}$$

and have applied the limiting procedure of $N\to\infty$, $V\to\infty$, with $n=N/V$ kept finite.

In the thermal equilibrium state, the correlation functions G and H can be expressed as

$$G(1,2)=F(v_1)F(v_2)g(r_{12}) \tag{8a}$$

and

$$H(1,2,3)=F(v_1)F(v_2)F(v_3)h(r_{12},r_{23},r_{31}). \tag{8b}$$

CC-0. In Public Domain. Gurukul Kangri Collection, Haridwar

Digitized by Arya Samaj Foundation Chennai and eGangotri

Then it is straightforward to reduce Eqs. (4b) and (4c) to,

$$\frac{d^2}{dr^2}g+\left(\frac{2}{r}-\frac{b}{r^2}\right)\frac{d}{dr}g-k_D^2 g=\frac{k_D^2}{4\pi}\frac{\partial}{\partial \mathbf{r}_1}\cdot\int\frac{\hat{r}_{13}}{r_{13}^2}h(r_{12},r_{23},r_{31})\,d\mathbf{r}_3 \tag{9a}$$

and

$$\frac{\partial}{\partial r_{12}}h(r_{12},r_{23},r_{31})-\frac{k_D^2}{4\pi}\int\frac{\hat{r}_{12}\cdot\hat{r}_{14}}{r_{14}^2}h(r_{23},r_{34},r_{42})\,d\mathbf{r}_4-(b/r_{12}^2)h(r_{12},r_{23},r_{31})$$
$$=(b/r_{12}^2)[g(r_{12})+g(r_{23})]+(k_D^2/4\pi)\int\frac{\hat{r}_{12}\cdot\hat{r}_{14}}{r_{14}^2}g(r_{13})g(r_{24})\,d\mathbf{r}_4, \tag{9b}$$

where k_D is the Debye wave number $(4\pi e^2 n/\kappa T)^{1/2}$ and b is the Landau distance defined as

$$b=(e^2/\kappa T). \tag{10}$$

The vector $\hat{r}_{ij}$ is a unit vector defined as

$$\hat{r}_{ij}=(\mathbf{r}_i-\mathbf{r}_j)/|\,\mathbf{r}_i-\mathbf{r}_j\,|. \tag{11}$$

Equations (9a) and (9b) are the set of fundamental equations of the present studies. Solving Eqs. (9a) and (9b) for $g(r)$, we can calculate the correlation energy E as

$$\frac{E}{\kappa T}=\frac{1}{2}\frac{n}{\kappa T}\int d\mathbf{r}\frac{e^2}{r}g(r)=\tfrac{1}{2}k_D^2\int_0^\infty drrg(r) \tag{12}$$

and thus we can determine thermodynamic properties of the electron plasma.

In Eq. (9a), the term $-(b/r^2)dg/dr$ is due to the second term on the right-hand side of Eq. (4b). This term describes the effect of the short-range collisions. The term $-k_D^2 g$ of Eq. (9a) is due to the third term on the right-hand side of Eq. (4b). This term represents the screening effect of the long-range Coulomb potential. The right-hand side of Eq. (9a) expresses the modification of the binary correlation function resulting from ternary correlations between particles.

Neglecting contributions of short-range collisions and ternary correlations, we obtain the well-known expression for the binary correlation function as

$$g(r)=-(b/r)\exp(-k_D r). \tag{13}$$

Substituting Eq. (13) into Eq. (12), we obtain the Debye–Hückel limiting value of the correlation energy

$$E^{(D-H)}/\kappa T=-\tfrac{1}{2}\epsilon. \tag{14}$$

In the following sections, we investigate the influence of short range collisions and ternary correlations on the binary correlation function. We then determine the corresponding corrections to the Debye-Hückel limiting value of the correlation energy.

III. EFFECT OF SHORT-RANGE COLLISIONS ON THE BINARY CORRELATION FUNCTION

It is evident that the binary correlation function obtained as Eq. (13) loses its validity at small distances. Lamb and Burdick[4] succeeded in eliminating this defect by taking into account the influence of short-range collisions. Disregarding the influence of ternary correlations, Eq. (9a) reduces to the following equation:

$$(d^2/dr^2)g+[(2/r)-(b/r^2)](d/dr)g-k_D^2 g=0. \tag{15}$$

Introducing the transformations

$$g(r)=(b/r)\exp(-b/2r)U(r), \tag{16a}$$

$$x=k_D r, \tag{16b}$$

we can eliminate the first derivative term from Eq. (15), and obtain the equation for $U(x)$,

$$(d^2/dx^2)U(x)-[1+(\epsilon^2/4x^4)]U(x)=0. \tag{17}$$

With the aid of the transformation,[8]

$$x=(\epsilon/2)^{1/2}\exp(Z),\qquad U(x)=x^{1/2}Y(Z), \tag{18}$$

Eq. (17) is reduced to the associated Mathieu equation for $Y(Z)$

$$(d^2/dZ^2)Y(Z)-[\lambda+2h^2\cosh(2Z)]Y(Z)=0 \tag{19a}$$

with

$$\lambda=\tfrac{1}{4},\qquad h^2=\epsilon/2. \tag{19b}$$

The solutions of Eq. (19a) are expressed as

$$Y(Z)=\begin{cases}\displaystyle\sum_{m=-\infty}^{\infty}(a_{2m}/a_0)^{\nu}I_m(he^{-Z})I_{m+\nu}(he^{Z}) & (20a)\\ \displaystyle\sum_{m=-\infty}^{\infty}(a_{2m}/a_0)^{\nu}I_m(he^{Z})I_{m+\nu}(he^{-Z}) & (20b)\\ \displaystyle\sum_{m=-\infty}^{\infty}(-1)^m(a_{2m}/a_0)^{\nu}I_m(he^{-Z})K_{m+\nu}(he^{Z}) & (20c)\\ \displaystyle\sum_{m=-\infty}^{\infty}(-1)^m(a_{2m}/a_0)^{\nu}I_m(he^{Z})K_{m+\nu}(he^{-Z}), & (20d)\end{cases}$$

[8] The region of $x>(\epsilon/2)^{\frac{1}{2}}$ corresponds to the region of $0<Z<+\infty$, while the region of $x<(\epsilon/2)^{\frac{1}{2}}$ corresponds to the region of $-\infty<Z<0$.

CC-0. In Public Domain. Gurukul Kangri Collection, Haridwar

Digitized by Arya Samaj Foundation Chennai and eGangotri

where the coefficients a_{2m} are determined by the recurrence formula

$$a_{2m}{}^{\nu}[(2m+\nu)^2-\lambda]-h^2(a_{2m+2}{}^{\nu}+a_{2m-2}{}^{\nu})=0 \quad (21)$$

ν is related to λ via

$$\lambda=\nu^2+[2(\nu^2-1)]^{-1}h^4 +[(5\nu^2+7)/32(\nu^2-1)^3(\nu^2-4)]h^8+\cdots. \quad (22)$$

In the present problem, ν is determined from Eq. (22) for the given values of λ and h^2 as defined by Eq. (19b).

Inspection of Eq. (17) determines the following asymptotic behavior of the function $U(x)$,

$$U(x)\sim e^{\pm x} \quad \text{as} \quad x\to\infty, \quad (23a)$$

and

$$U(x)\sim(2/\epsilon)^{1/2}x\exp(\pm\epsilon/2x) \quad \text{as} \quad x\to 0. \quad (23b)$$

Therefore, two independent solutions of Eq. (19a) are chosen from the solutions Eqs. (20a)$\sim$(20d) to be in accord with the above asymptotic behavior of the function $U(x)$. For the outer region $x>(\epsilon/2)^{1/2}$, these solutions are given by

$$U_<{}^{(o)}(x)=(2\pi)^{1/2}x^{1/2}\sum_{m=-\infty}^{\infty}(a_{2m}/a_0)^{\nu}I_m(\epsilon/2x)I_{m+\nu}(x) \quad (24a)$$

$$U_>{}^{(o)}(x)=(2/\pi)^{1/2}x^{1/2}\sum_{m=-\infty}^{\infty}(-1)^m(a_{2m}/a_0)^{\nu}I_m(\epsilon/2x)K_{m+\nu}(x) \quad (24b)$$

and for the inner region $x<(\epsilon/2)^{1/2}$ by

$$U_<{}^{(i)}(x)=(2/\pi)^{1/2}x^{1/2}\sum_{m=-\infty}^{\infty}(-1)^m(a_{2m}/a_0)^{\nu}I_m(x)K_{m+\nu}(\epsilon/2x), \quad (25a)$$

$$U_>{}^{(i)}(x)=(2\pi)^{1/2}x^{1/2}\sum_{m=-\infty}^{\infty}(a_{2m}/a_0)^{\nu}I_m(x)I_{m+\nu}(\epsilon/2x). \quad (25b)$$

The superscripts (o) and (i) stand for the outer and the inner region, respectively. The above set of solutions is used to calculate the effect of ternary correlations on the binary correlation function. We notice that the solution $U(x)$ should behave as

$$U(x)\sim\exp(-x) \quad \text{for} \quad x\to\infty \quad (26a)$$

and

$$U(x)\sim-(x/\epsilon)\exp(\epsilon/2x) \quad \text{for} \quad x\to 0 \quad (26b)$$

so that the boundary conditions for the binary correlation function $g(x)$ [i.e., $g(\infty)=0$ and $g(0)=-1$] are satisfied. Therefore, the solutions of Eq. (17) which satisfy the required boundary conditions are obtained as

$$U^{(o)}(x)=B\sum_{m=-\infty}^{\infty}(-1)^m a_{2m}{}^{\nu}x^{1/2}I_m(\epsilon/2x)K_{m+\nu}(x),$$

for $x>(\epsilon/2)^{1/2}$, (27a)

and

$$U^{(i)}(x)=\sum_{m=-\infty}^{\infty}a_{2m}{}^{\nu}x^{1/2}I_m(x)I_{m+\nu}(\epsilon/2x) +C\sum_{m=-\infty}^{\infty}(-1)^m a_{2m}{}^{\nu}x^{1/2}I_m(x)K_{m+\nu}(\epsilon/2x),$$

for $x<(\epsilon/2)^{1/2}$. (27b)

In the limit of $x\to 0$, the function $U^{(i)}(x)$ behaves asymptotically as

$$U^{(i)}(x)\sim a_0{}^{\nu}(\pi\epsilon)^{-1/2}x\exp[\epsilon/(2x)], \quad (28)$$

By comparing Eq. (28) with Eq. (26b), we can determine the coefficient $a_0{}^{\nu}$ as

$$a_0{}^{\nu}=-(\pi/\epsilon)^{1/2} \quad (29)$$

Since ν is determined from Eq. (22) as

$$\nu=\tfrac{1}{2}+\tfrac{1}{6}\epsilon^2+O(\epsilon^4), \quad (30)$$

we have

$$(a_2/a_0)^{\nu}=\tfrac{1}{12}\epsilon, \quad (31a)$$

$$(a_4/a_0)^{\nu}=\tfrac{1}{480}\epsilon^2. \quad (31b)$$

The constants B and C are determined from the following boundary conditions at $x=(\epsilon/2)^{1/2}$,

$$U^{(o)}[(\epsilon/2)^{1/2}]=U^{(i)}[(\epsilon/2)^{1/2}], \quad (32a)$$

$$dU^{(o)}/dx\,|_{x=(\epsilon/2)^{1/2}}=(dU^{(i)}/dx)\,|_{x=(\epsilon/2)^{1/2}}. \quad (32b)$$

Keeping terms of the order ϵ^2, we can determine the constants B and C as,

$$B=(2/\pi)^{1/2}\epsilon^{1/2}(1+\tfrac{1}{2}\epsilon) \quad (33a)$$

and

$$C=-\pi^{-1}\epsilon. \quad (33b)$$

In order to calculate the correlation energy up to the order ϵ^2, it is sufficient to take $\nu=\frac{1}{2}$ and $m=0$. Thus Eqs. (27a) and (27b) are reduced to

$$U^{(o)}(x)=-(2/\pi)^{1/2}(1+\tfrac{1}{2}\epsilon)x^{1/2}I_0(\epsilon/2x)K_{1/2}(x) \quad (34a)$$

and

$$U^{(i)}(x)=-(\pi/\epsilon)^{1/2}x^{1/2}\{I_0(x)I_{1/2}(\epsilon/2x) -(\epsilon/\pi)I_0(x)K_{1/2}(\epsilon/2x)\}. \quad (34b)$$

CC-0. In Public Domain. Gurukul Kangri Collection, Haridwar

Digitized by Arya Samaj Foundation Chennai and eGangotri

These expressions can be simplified further by retaining leading terms to obtain the correlation energy correctly up to second order in ϵ. Finally, the binary correlation function becomes

$$g^{(o)}(x) = -\epsilon(1+\tfrac{1}{2}\epsilon)x^{-1}\exp\left[-x-(\epsilon/2x)\right] \quad x>(\epsilon/2)^{1/2} \tag{35a}$$

and

$$g^{(i)}(x) = -1+(1+\epsilon)\exp\left(-\epsilon/x\right) \quad x<(\epsilon/2)^{1/2}. \tag{35b}$$

Substituting Eqs. (35a) and (35b) into Eq. (12), we obtain

$$\frac{E^{(B)}}{\kappa T} = \frac{1}{2}\int_0^{(\epsilon/2)^{1/2}} xg^{(i)}(x)\,dx + \frac{1}{2}\int_{(\epsilon/2)^{1/2}}^{\infty} xg^{(o)}(x)\,dx$$
$$\approx -\tfrac{1}{2}\epsilon - \tfrac{1}{4}\epsilon^2\ln\epsilon - \tfrac{1}{2}(8-\tfrac{1}{4})\epsilon^2. \tag{36}$$

Comparing this result with Eq. (14), we conclude that by taking into account short-range collisions we obtain the correction to the Debye–Hückel limiting law to order $\epsilon^2\ln\epsilon$. There arise terms of order ϵ^2 as well. Since, however, the coefficients of the ϵ^2 term in Eqs. (36) and (3) do not agree, we conclude that ternary correlations must be included to calculate this term properly.

IV. CONTRIBUTION OF TERNARY CORRELATIONS ON THE BINARY CORRELATION FUNCTION

In order to investigate the effect of ternary correlation, let us write the binary correlation function as

$$g(r) = g^{(B)}(r) + g^{(T)}(r), \tag{37}$$

where the function $g^{(T)}(r)$ is presumed to be of higher order than the function $g^{(B)}(r)$. We may then decompose the set of Eqs. (9a) and (9b) into the following set of equations:

$$\frac{d^2}{dr^2}g^{(B)} + \left(\frac{2}{r}-\frac{b}{r^2}\right)\frac{d}{dr}g^{(B)} - k_D{}^2 g^{(B)} = 0 \tag{38a}$$

$$\frac{d^2}{dr^2}g^{(T)} + \left(\frac{2}{r}-\frac{b}{r^2}\right)\frac{d}{dr}g^{(T)} - k_D{}^2 g^{(T)} = \frac{k_D{}^2}{4\pi}\frac{\partial}{\partial \mathbf{r}_1}\cdot\int \frac{\hat{r}_{13}}{r_{13}{}^2}h^{(B)}(r_{12}, r_{23}, r_{31})\,d\mathbf{r}_3, \tag{38b}$$

where $h^{(B)}(r_{12}, r_{23}, r_{31})$ is determined from the following equation:

$$\frac{\partial}{\partial r_{12}}h^{(B)}(r_{12}, r_{23}, r_{31}) - \frac{k_D{}^2}{4\pi}\int \frac{\hat{r}_{12}\cdot\hat{r}_{14}}{r_{14}{}^2}h^{(B)}(r_{23}, r_{34}, r_{42})\,d\mathbf{r}_4$$
$$= \frac{b}{r_{12}{}^2}\left[g^{(B)}(r_{12})+g^{(B)}(r_{23})\right] + \frac{k_D{}^2}{4\pi}\int \frac{\hat{r}_{12}\cdot\hat{r}_{14}}{r_{14}{}^2}g^{(B)}(r_{13})g^{(B)}(r_{24})\,d\mathbf{r}_4. \tag{38c}$$

Solutions of Eq. (38a) have been discussed in detail in the preceding section. Here, we wish to solve Eqs. (38b) and (38c) and thereby calculate the contribution of ternary correlations to the correlation energy.

Eliminating the first derivative term of Eq. (38b) by a transformation defined by Eqs. (16a) and (16b), we can reduce Eq. (38b) to

$$(d^2/dx^2)U_T(x) - \left[1+(\epsilon^2/4x^4)\right]U_T(x) = \lambda(x) \tag{39a}$$

$$\lambda(x_{12}) = \frac{1}{4\pi}\exp\left(\frac{\epsilon}{2x_{12}}\right)\left[x_{12}\frac{d}{dx_{12}}+2\right]\int \frac{\hat{x}_{12}\cdot\hat{x}_{13}}{x_{12}{}^2}h(x_{12}, x_{13}, x_{23})\,d\mathbf{x}_3. \tag{39b}$$

The boundary conditions for the function $U_T(x)$ are $U_T(x)\to 0$ for $x\to\infty$ and $x\to 0$. We define the Greens function $K(x, x')$ as the solution of

$$(d^2/dx^2)K(x, x') - \left[1+(\epsilon^2/4x^4)\right]K(x, x') = \delta(x-x') \tag{40}$$

with the boundary conditions

$$K(x, x')\to 0 \quad \text{for} \quad x\to\infty \quad \text{and} \quad x\to 0, \tag{41a}$$

and

$$(dK/dx)\,|_{x=x'+\delta} - (dK/dx)\,|_{x=x'-\delta} = 1 \qquad (\delta>0). \tag{41b}$$

The solution of Eq. (39a) is then given by

$$U_T(x) = \int_0^{\infty} K(x, x')\lambda(x')\,dx'. \tag{42}$$

CC-0. In Public Domain. Gurukul Kangri Collection, Haridwar

Digitized by Arya Samaj Foundation Chennai and eGangotri

Since we have obtained the two independent solutions of the homogeneous equation, Eq. (17), as Eqs. (24a), (24b) and Eqs. (25a), (25b), we can construct the Greens function $K(x, x')$ as follows:

$$K^{(o)}(x, x') = \begin{cases} K_<^{(o)}(x, x') = -\frac{1}{2} U_<^{(o)}(x)\, U_>^{(o)}(x'), & (\epsilon/2)^{1/2} < x < x', \quad (43a) \\ K_>^{(o)}(x, x') = -\frac{1}{2} U_>^{(o)}(x)\, U_<^{(o)}(x'), & (\epsilon/2)^{1/2} < x' < x, \quad (43b) \end{cases}$$

and

$$K^{(i)}(x, x') = \begin{cases} K_<^{(i)}(x, x') = -\frac{1}{2} U_<^{(i)}(x)\, U_>^{(i)}(x'), & x < x' < (\epsilon/2)^{1/2}, \quad (44a) \\ K_>^{(i)}(x, x') = -\frac{1}{2} U_>^{(i)}(x)\, U_<^{(i)}(x'), & x' < x < (\epsilon/2)^{1/2}. \quad (44b) \end{cases}$$

The constant factor $-\frac{1}{2}$ has been determined from the boundary condition given by Eq. (41b). Substituting Eqs. (42a), (43b), (44a), and (44b) into Eq. (42), we obtain

$$U_T^{(o)}(x) = -\frac{1}{2}\left[U_>^{(o)}(x) \int_{(\epsilon/2)^{1/2}}^{x} U_<^{(o)}(x')\lambda(x')\, dx' + U_<^{(o)}(x) \int_x^{\infty} U_>^{(o)}(x')\lambda(x')\, dx' \right], \quad [x > (\epsilon/2)^{1/2}], \quad (45a)$$

and

$$U_T^{(i)}(x) = -\frac{1}{2}\left[U_>^{(i)}(x) \int_0^{x} U_<^{(i)}(x')\lambda(x')\, dx' + U_<^{(i)}(x) \int_x^{(\epsilon/2)^{1/2}} U_>^{(i)}(x')\lambda(x')\, dx' \right] \quad [x < (\epsilon/2)^{1/2}]. \quad (45b)$$

Let us proceed to calculate the function $\lambda(x)$. Since it has been confirmed that the contribution of $g^{(T)}(x)$ to the correlation energy will be in the second order of ϵ, it is sufficient to determine the function $h^{(B)}(r_{12}, r_{23}, r_{31})$ correctly up to the second order of ϵ. Examining the structure of Eq. (38c), we find that the function $g^{(B)}(x)$ can be approximated by its lowest-order expression as

$$g^{(B)}(x) \sim g^{(0)}(x) = -(\epsilon/x) \exp(-x), \quad (46)$$

Then, as shown by O'Neil and Rostoker, the ternary correlation function $h^{(B)}(x_{12}, x_{23}, x_{31})$ is obtained as a solution of Eq. (38c) as follows:

$$h^{(B)}(x_{12}, x_{23}, x_{31}) = g^{(0)}(x_{12})g^{(0)}(x_{31}) + g^{(0)}(x_{31})g^{(0)}(x_{23}) + g^{(0)}(x_{31})g^{(0)}(x_{23}) + n\int g^{(0)}(x_{14})g^{(0)}(x_{24})g^{(0)}(x_{34})\, d\mathbf{x}_4 . \quad (47)$$

This expression of the ternary correlation function is taken to be valid over the region $\infty > x > (\epsilon/2)^{1/2}$ in the lowest-order approximation, while O'Neil and Rostoker have assumed that this expression is valid only in the region $\infty > x > (4\pi\epsilon)^{1/3}$. Having determined the ternary correlation function $h^{(B)}(x_{12}, x_{23}, x_{31})$, we can proceed to calculate the function $\lambda(x)$. Details are discussed in the Appendix. Since the function $\lambda(x)$ itself is a quantity of second order in ϵ, we may evaluate the function $U_T(x)$ given by Eqs. (45a) and (45b) in the asymptotic limit of $\epsilon \to 0$. Therefore, Eq. (A17) can be approximated by

$$\lambda^{(0)}(x) = -\tfrac{1}{2}(\pi)\epsilon^2\{2(1+x)(1/x^3)\exp(-x) - (5x^2+4x+2)(1/x^3)\exp(-2x) + \tfrac{1}{2}[\ln 3 \exp(-x) + \mathrm{Ei}(-x)\exp(-x) + \mathrm{Ei}(-3x)\exp(+x)]\}. \quad (48)$$

To the lowest order in ϵ, we have simply

$$U_>^{(o)}(x) = \exp(-x), \quad (49a)$$

$$U_<^{(o)}(x) = 2\sinh(x). \quad (49b)$$

Thus, taking the asymptotic limit of $\epsilon \to 0$, we can evaluate Eqs. (45a) and (45b), and obtain

$$U_T^{(o)}(x) \simeq -e^{-x}\int_0^x \sinh(x')\lambda(x')\, dx' - \sinh(x)\int_x^{\infty} e^{-x'}\lambda(x')\, dx'$$
$$= -\tfrac{1}{8}\epsilon^2\{-\tfrac{4}{3}(2x-3)(1/x)e^{-x} - \tfrac{4}{3}(x+3)(1/x)e^{-2x} - (3+x)\,\mathrm{Ei}(-3x)e^{+x} + (3-x)[\mathrm{Ei}(-x) + \ln 3]e^{-x}\} \quad (50a)$$

and

$$U_T^{(i)}(x) \simeq 0. \quad (50b)$$

Substituting Eqs. (50a) and (50b) into Eq. (12) with the transformations Eqs. (16a) and (16b), we can calculate the correlation energy resulting from the ternary correlation effect as

$$\frac{E^{(T)}}{\kappa T} = \frac{1}{2}\int_0^{\infty} x g^{(T)}(x)\, dx \simeq \frac{1}{2}\int_0^{\infty} U_T(x)\, dx \simeq -\tfrac{1}{4}(\ln 3 - \tfrac{5}{6})\epsilon^2. \quad (51)$$

CC-0. In Public Domain. Gurukul Kangri Collection, Haridwar

Digitized by Arya Samaj Foundation Chennai and eGangotri

V. CONCLUDING DISCUSSION

In the preceding sections, we have discussed a systematic approach to solve the BBGKY hierarchy equation in the thermal equilibrium case. Summing up Eqs. (36) and (51), we obtain the correlation energy of the electron plasma correct up to the second order in ϵ.

According to the analysis in Sec. III, we have shown explicitly that the dynamic effect of short-range collisions becomes appreciable at distances of the order of

$$x_0=(\epsilon/2)^{1/2}\lambda_D=(4\pi)^{-1/3}(\epsilon/8)^{1/6}n^{-1/3}, \qquad (52)$$

which is far smaller than the mean distance between particles $n^{-1/3}$. Since the Coulomb interaction is rather weak, this is physically a reasonable result.

In Sec. IV, we have examined the contribution of ternary correlation on the binary correlation function without taking into account the effect of short-range collisions. It has been confirmed that this approximation is consistent in calculating the thermodynamic properties of the electron plasma up to the second order in ϵ. In view of Eq. (51), we can conclude that the binary correlation function due to the ternary correlation effect $g^{(T)}(x)$ is given by

$$g^{(T)}(x)=(\epsilon^2/8)x^{-1}\{\tfrac{4}{3}(2x-3)x^{-1}e^{-x}+\tfrac{4}{3}(x+3)x^{-1}e^{-2x}$$
$$+(3+x)\ \mathrm{Ei}\ (-3x)e^{x}-(3-x)[\mathrm{Ei}\ (-x)+\ln 3]e^{-x}\} \qquad 0<x<\infty \qquad (53)$$

while the binary correlation function $g^{(B)}(x)$ is obtained as

$$g^{(B)}(x)=\begin{cases}-\epsilon(1+\frac{1}{2}\epsilon)x^{-1}\exp\left[-x-(\epsilon/2x)\right], & \infty>x>(\epsilon/2)^{1/2} \qquad (54a)\\ -1+(1+\epsilon)\exp\left(-\epsilon/x\right), & (\epsilon/2)^{1/2}>x>0. \qquad (54b)\end{cases}$$

The point $x_0=(\epsilon/2)^{1/2}$ is determined from structure of the differential equation for the function $g^{(B)}(x)$, and thus the arbitrariness involved in the interpolation method of O'Neil and Rostoker has been eliminated completely in the present approach.

It would be worthwhile to discuss the relationship between the various expressions for the binary correlation function, since our expressions as given by Eqs. (53), (54a), and (54b) appear to be different from the Bowers–Salpeter expression and the O'Neil–Rostoker expression. In Ref. 4, the binary correlation function which gives rise to the correlation energy correctly up to the order of ϵ^2 is given as,[9]

$$g^{\mathrm{B-S}}(x)=\{\exp\left[-(\epsilon/x)e^{-x}\right]-1\}+w_1(x) \qquad (55a)$$

with the abbreviation

$$w_1(x)=-(\epsilon^2/8)x^{-1}\{\tfrac{4}{3}(e^{-x}-e^{-2x})+(3-x)$$
$$\times[\mathrm{Ei}(-x)+\ln 3]e^{-x}-(3+x)\ \mathrm{Ei}\ (-3x)e^{x}\}. \qquad (55b)$$

First of all, the O'Neil–Rostoker expression of the binary correlation function is essentially equivalent to the Bowers–Salpeter expression because the first two terms of the function $\phi_I(x)$, which is given in Sec. 5 of Ref. 7, are the first two terms of the expansion

$$\exp\left[-(\epsilon/x)e^{-x}\right]-1\approx-(\epsilon/x)e^{-x}+\tfrac{1}{2}(\epsilon/x)^2e^{-2x}+\cdots \qquad (56)$$

while the remaining terms of $\phi_I(x)$ are nothing but the function $w_1(x)$ of Bowers and Salpeter.[10] Turning to the present expression of the binary correlation function, we can show that our expression is also equivalent to the Bowers–Salpeter expression as follows: the function $g^{(T)}(x)$ can be rewritten as

$$g^{(T)}(x)=w_1(x)+(\epsilon^2/2x^2)\{(x-1)e^{-x}+e^{-2x}\}, \qquad (57)$$

hence the present expression of the binary correlation function can be expressed as,

$$g^{L-I}(x)=g^{*}(x)+w_1(x) \qquad (58a)$$

with the abbreviation

$$g^{*}(x)=g^{(B)}(x)+(\epsilon^2/2x^2)\{(x-1)e^{-x}+e^{-2x}\}. \qquad (58b)$$

With the expression for $g^{(B)}(x)$ as given by Eq. (54a), the function $g^{*}(x)$ reduces to

$$g^{*}(x)\approx\epsilon(1+\tfrac{1}{2}\epsilon)(1/x)e^{-x}[1-(\epsilon/2x)]$$
$$+(\epsilon^2/2x^2)\{(x-1)e^{-x}+e^{-2x}\} \qquad (59)$$
$$=-(\epsilon/x)e^{-x}+\tfrac{1}{2}(\epsilon/x)^2e^{-2x}+\cdots$$

which agrees with the expansion of Eq. (56) for large values of x. In the region for which $x<(\epsilon/2)^{1/2}$, we can

[9] Recently DeWitt (Ref. 11) has obtained the same expression as $g^{\mathrm{B-S}}(x)$ by a diagramatic method which is slightly different from that used by Bowers and Salpeter.

[10] The factor $\frac{1}{2}$ in front of $\exp(-2x)$ of $\phi_I(x)$ should be replaced by $\frac{1}{3}$. This error does not affect the correlation energy calculated by O'Neil and Rostoker, since they have used the Fourier transformation of $\phi_I(x)$ in order to calculate the correlation energy.

CC-0. In Public Domain. Gurukul Kangri Collection, Haridwar

Digitized by Arya Samaj Foundation Chennai and eGangotri

approximate the second term of Eq. (58b) by

$$(\epsilon^2/2x^2)\{(x-1)e^{-x}+e^{-2x}\}\approx-\tfrac{1}{2}\epsilon^2. \tag{60a}$$

On the other hand, Eq. (54b) can be written,

$$\begin{aligned} g^{(B)}(x) &= -1+(1+\epsilon)\exp(-\epsilon/x) \\ &\approx -1+\exp\{-(\epsilon/x)(1-x)\} \\ &\approx -1+\exp\{-(\epsilon/x)e^{-x}\}. \end{aligned} \tag{60b}$$

The contribution of Eq. (60a) to the correlation energy is of higher order than ϵ^2. Thus, the present expressions given by Eqs. (53), (54a), and (54b) are essentially equivalent to the Bowers–Salpeter expression.

Finally, let us discuss a controversial point discussed in Ref. 11. DeWitt has pointed out that when x is larger than $8/(\epsilon \ln 3)$ the correction term $z_1(x)$ dominates over the lowest-order Debye–Hückel term. Within the framework of the present approach, this means the contribution of ternary correlation on the binary correlation function dominates over the lowest order binary correlation effect at very large distances. We should remember, however, that the decomposition of Eqs. (9a) and (9b) into the set of Eqs. (38a), (38b), and (38c) is carried out by assuming the function $g^{(T)}(x)$ to be of higher order than the function $g^{(B)}(x)$ in Eq. (37). Hence, the fact that $g^{(T)}(x)$ becomes larger than $g^{(B)}(x)$ at large distances indicates simply that the above decomposition of the equations loses its validity when x becomes very large. Returning to Eq. (4b), we can see explicitly that the third term, which is essential to screen the long-range interaction, dominates over the last term in the limit of $r_{12}\to\infty$. Therefore, at very large distances, the exact binary correlation function should behave as

$$g(x)\sim-\epsilon x^{-1}\exp(-x). \tag{61}$$

If we could solve Eqs. (9a) and (9b) exactly, the asymptotic form of the binary correlation function would be

$$g(x)\sim\epsilon x^{-1}\exp\{-x-\Psi(x)\}, \tag{62a}$$

where the function $\Psi(x)$ behaves asymptotically as

$$\Psi(x)\sim\tfrac{1}{8}\epsilon\ln 3x\exp\{-\tfrac{1}{8}\epsilon\ln 3x\}. \tag{62b}$$

As long as x remains smaller than $8/(\epsilon\ln 3)$, Eqs. (62a) and (62b) can be expanded as

$$g(x)\sim-(\epsilon/x)e^{-x}+\tfrac{1}{8}\epsilon^2\ln 3e^{-x} \tag{63}$$

which agrees with the asymptotic form of $g^{B-S}(x)$. When x becomes larger than $8/(\epsilon\ln 3)$, Eq. (62a) is reduced to Eq. (57) since $\Psi(x)$ vanishes in the limit of $x\to\infty$. DeWitt has shown that the higher-order term $w_1(x)$ dominates over the lowest-order term $(\epsilon/x)\exp(-x)$ at large distances. He relates this to a similar phenomenon that occurs in the study of the dynamic behavior of a plasma, where the correlation damping can become larger than the Landau damping in the long wavelength region. (This effect has been discussed first by one of the present authors[12] on the basis of the BBGKY equations.) Our analysis shows explicitly, however that this is not the case. Furthermore, according to the above analysis, we can conclude that the partial summations of the cluster diagrams carried out by Bowers, Salpeter, and DeWitt are inadequate to determine the correct behavior of the binary correlation function at large distances.

ACKNOWLEDGMENTS

The authors are much obliged to Professor D. Pines for stimulating suggestions and valuable criticisms. They are also grateful to Professor E. A. Jackson, Professor M. Raether, and Professor K. Yamada for helpful discussion.

APPENDIX: CALCULATION OF THE FUNCTION $\lambda(x)$

Here, we describe some details of calculation of the function $\lambda(x)$. We have

$$\lambda(x)=(4\pi)^{-1}\exp[\epsilon/(2x)]\left(x\frac{d}{dx}+2\right)\int\frac{\hat{x}\cdot\hat{x}_{13}}{x^2}h(x,x_{13},x_{23})\,d\mathbf{x}_3, \tag{A1}$$

where

$$h(x,x_{13},x_{23})=g^{(0)}(x)g^{(0)}(x_{13})+g^{(0)}(x)g^{(0)}(x_{23})+g^{(0)}(x_{13})g^{(0)}(x_{23})+(4\pi\epsilon)^{-1}\int g^{(0)}(x_{14})g^{(0)}(x_{24})g^{(0)}(x_{34})\,d\mathbf{x}_4. \tag{A2}$$

In Eqs. (A1) and (A2), the relative coordinate x_{12} is denoted as x for the simplicity of notations. First, let us discuss the following integral:

$$\int\frac{\hat{x}\cdot\hat{x}_{13}}{x_{13}^2}g^{(0)}(x_{23})\,d\mathbf{x}_3=-4\pi(d/dx)\left[x^{-1}\int_0^x x_{23}^2g^{(0)}(x_{23})\,dx_{23}+\int_x^\infty x_{23}g^{(0)}(x_{23})\,dx_{23}\right]=\frac{4\pi}{x^2}\int_0^x x_{23}^2g^{(0)}(x_{23})\,dx_{23}. \tag{A3}$$

[11] H. E. DeWitt, Phys. Rev. **140**, A466 (1965).
[12] Y. H. Ichikawa, Progr. Theoret. Phys. (Kyoto) **24**, 1083 (1960).

CC-0. In Public Domain. Gurukul Kangri Collection, Haridwar

Digitized by Arya Samaj Foundation Chennai and eGangotri

The integral given by Eq. (A3) can be decomposed into two terms as follows:

$$\int_0^x x_{23}^2 g^{(0)}(x_{23})\, dx_{23} = \int_0^{(\epsilon/2)^{1/2}} x_{23}^2 g^{(0)}(x_{23})\, dx_{23} + \int_{(\epsilon/2)^{1/2}}^x x_{23}^2 g^{(0)}(x_{23})\, dx_{23}\,. \tag{A4}$$

If we evaluate the first term of Eq. (A4) by substituting Eq. (35b) for $g^{(0)}(x)$, we can confirm that the contribution of this term is of higher order than ϵ^2. The second term of Eq. (A4) can be calculated by using the approximate expression given by Eq. (46) as follows:

$$\int_{(\epsilon/2)^{1/2}}^x x_{23}^2 g^{(0)}(x_{23})\, dx_{23} = \epsilon\{(1+x)\exp(-x) - [1+(\epsilon/2)^{1/2}]\exp[-(\epsilon/2)^{1/2}]\}. \tag{A5}$$

Therefore, we have the following approximate result:

$$\int \frac{\hat{x}\cdot\hat{x}_{13}}{x_{13}^2} g^{(0)}(x_{23})\, d\mathbf{x}_3 = (4\pi\epsilon/x^2)\{(1+x)\exp(-x) - [1+(\epsilon/2)^{1/2}]\exp[-(\epsilon/2)^{1/2}]\}. \tag{A6}$$

Now, excluding the domain of $x_{ij} < (\epsilon/2)^{1/2}$ from the following calculation, we may proceed to discuss the integral

$$I(x) = \int \frac{\hat{x}\cdot\hat{x}_{13}}{x_{13}^2}\left\{g^{(0)}(x_{13})g^{(0)}(x_{23}) + (4\pi\epsilon)^{-1}\int g^{(0)}(x_{14})g^{(0)}(x_{24})g^{(0)}(x_{34})\, d\mathbf{x}_4\right\} d\mathbf{x}_3\,. \tag{A7}$$

First, we notice the following relation:

$$\int \frac{\hat{x}_{13}}{x_{13}^2} g^{(0)}(x_{34})\, d\mathbf{x}_3 = \hat{x}_{14}\frac{\partial}{\partial x_{14}}\int x_{13}^{-1} g^{(0)}(x_{34})\, d\mathbf{x}_3$$

$$= \hat{x}_{14}(4\pi\epsilon/x_{14}^2)\{(1+x_{14})\exp(-x_{14}) - [1+(\epsilon/2)^{1/2}]\exp[-(\epsilon/2)^{1/2}]\}. \tag{A8}$$

Therefore, the integral $I(x)$ is reduced to

$$I(x) = \int \frac{\hat{x}\cdot\hat{x}_{14}}{x_{14}^2} g^{(0)}(x_{13})g^{(0)}(x_{23})[1+\{(1+x_{14})\exp(-x_{14}) - [1+(\epsilon/2)^{1/2}]\exp[-(\epsilon/2)^{1/2}]\}]$$

$$= \{1-[1+(\epsilon/2)^{1/2}]\exp[-(\epsilon/2)^{1/2}]\}\int \frac{\hat{x}\cdot\hat{x}_{14}}{x_{14}^2} g^{(0)}(x_{14})g^{(0)}(x_{24})\, d\mathbf{x}_4 + \int \frac{\hat{x}\cdot\hat{x}_{14}}{x_{14}^2}(1+x_{14})\exp(-x_{14})g^{(0)}(x_{14})g^{(0)}(x_{24})\, d\mathbf{x}_4$$

$$\simeq \epsilon^2 \int (\hat{x}\cdot\hat{x}_{14})(x_{14}^2 x_{24})^{-1}(1+x_{14}^{-1})\exp(-2x_{14}-x_{24})\, d\mathbf{x}_4 \qquad x_{14} > (\epsilon/2)^{1/2},\quad x_{24} > (\epsilon/2)^{1/2}, \tag{A9}$$

where the first term of the second line has been disregarded since it is smaller than the second term by a factor ϵ^2. Integration of Eq. (A9) can be carried out by introducing prolate spherical coordinates,

$$x_{14} = (\xi+\eta)x_{12}/2 \tag{A10a}$$

$$x_{24} = (\xi-\eta)x_{12}/2. \tag{A10b}$$

The domain of variables ξ and η is given by

$$1 < \xi < +\infty, \qquad -1 < \eta + 1. \tag{A10c}$$

The allowed domain of the integral of Eq. (A9) then becomes

$$\xi - a > \eta > -\xi + a \tag{A11}$$

with the abbreviation $a = (2\epsilon)^{1/2}/x$. Equation (A9) then reduces to

$$I(x) = 2\pi \int d\xi \int d\eta \frac{1+\xi\eta}{(\xi+\eta)^2}\left(1+\frac{2}{x}\frac{1}{\xi+\eta}\right). \tag{A12}$$

CC-0. In Public Domain. Gurukul Kangri Collection, Haridwar

Digitized by Arya Samaj Foundation Chennai and eGangotri

Changing the variable η into the new variable ζ by a transformation

$$\zeta=\xi+\eta, \tag{A13}$$

we can transform Eq. (A12) as follows:

$$I(x)=2\pi\left[\int_1^{1+a}d\xi\int_a^{2\xi-a}d\zeta+\int_{1+2}^{\infty}d\xi\int_{\xi-1}^{\xi+1}d\zeta\right]\left(\frac{1-\xi^2}{\zeta}+\xi\right)\zeta^{-1}\left(1+\frac{2}{x\zeta}\right)\exp\left(-x\xi-\tfrac{1}{2}x\zeta\right), \tag{A14}$$

where the domain of integration corresponds to the case $x>(2\epsilon)^{1/2}$. Since the contribution arising from the region of $(2\epsilon)^{1/2}>x>(\epsilon/2)^{1/2}$ to the function $U_T^{(o)}(x)$ is found to be higher order than ϵ^2, this region can be disregarded in the present analysis. Performing the integration in Eq. (A14) results in,

$$I(x)=\pi\epsilon^2\{(1/x^2)(1+x)[\ln 3+\mathrm{Ei}(-x)]\exp(-x)+(1/x^2)(1-x)\,\mathrm{Ei}(-3x)\exp(x)\},\qquad x>(2\epsilon)^{1/2}. \tag{A15}$$

Combining the contributions of Eqs. (A6) and (A15), we find

$$\begin{aligned}\int\frac{\hat{x}\cdot\hat{x}_{13}}{x_{13}^2}h(x,x_{13},x_{23})\,d\mathbf{x}_3=\pi\epsilon^2[&(4/x^3)\{(1+x)\exp(-2x)-[1+(\epsilon/2)^{1/2}]\\&\times\exp[-x-(\epsilon/2)^{1/2}]\}+(1/x^2)(1+x)[\ln 3+\mathrm{Ei}(-x)]\exp(-x)\\&+(1/x^2)(1-x)\,\mathrm{Ei}(-3x)\exp(x)],\end{aligned} \tag{A16}$$

Substituting Eq. (A16) into Eq. (A1), we finally obtain the function $\lambda(x)$ as

$$\begin{aligned}\lambda(x)=-\tfrac{1}{4}\epsilon^2\exp[\epsilon/(2x)]\{&4[1+(\epsilon/2)^{1/2}](1/x^3)(1+x)\exp[-x-(\epsilon/2)^{1/2}]\\&-(2/x^3)(2+4x+3x^2)\exp(-2x)+[\ln 3+\mathrm{Ei}(-x)]\exp(-x)+\mathrm{Ei}(-3x)\exp(x)\}.\end{aligned} \tag{A17}$$

CC-0. In Public Domain. Gurukul Kangri Collection, Haridwar

Digitized by Arya Samaj Foundation Chennai and eGangotri

REVIEWS OF MODERN PHYSICS VOLUME 38, NUMBER 4 OCTOBER 1966

Evaluation of Molecular Quadrupole Moments

KRISHNAJI, VINOD PRAKASH
Physics Department, University of Allahabad, Allahabad, India

Knowledge of the molecular quadrupole moments may be used to propose a better model for the structure of the molecule and could also provide a crucial test for the accuracy of the trial wave functions that are used in other molecular calculations. A general survey of the different methods available for the evaluation of molecular quadrupole moments has been made and their relative merits and demerits have been discussed. It is suggested that the quadrupole moments determined by the microwave linewidth data are probably more reliable. The quadrupole moments of different molecules known to date have been tabulated.

CONTENTS

I. Introduction 690
II. The Molecular Orbital Method 691
III. The Induced Optical Birefringence Method 692
IV. The Second Virial Coefficient Method 694
V. The Spectral Line-Broadening Method 697
VI. Other Methods 700
VII. Discussion 702
VIII. List of Molecular Quadrupole Moments 704

I. INTRODUCTION

The way a molecule interacts with another, has long been the subject of extensive investigations. The essential problem is to find the molecular interaction potential. For this purpose a molecule can be considered as a special case of a charge distribution, the total charge of the system being zero. The interaction potential is[1] electrostatic and can be expanded in terms of a set of parameters, characteristic of the particular distribution in question. These parameters are:

1. The total charge

$$q=\sum_i e_i,$$

2. The dipole moment

$$\mu=\sum_i e_i r_i,$$

3. The quadrupole moment

$$\theta_{\alpha\beta}=\tfrac{1}{2}\sum_i e_i(3r_{i\alpha}r_{i\beta}-r_i^2\delta_{\alpha\beta}),$$

$\cdots$ etc. or, in general, 'the multipole moment of order n.' The potential expansion then has the general form

$$\phi=(q/r)+(\mu_\alpha r_\alpha/r^3)+(\theta_{\alpha\beta}/3r^5)(3r_\alpha r_\beta-r^2\delta_{\alpha\beta})+\cdots. \tag{1.1}$$

For a complete specification of the potential the parameters need be known beforehand. The total charge q, is always zero for a molecular charge distribution. The dipole moment μ can be measured fairly accurately by a number of methods.[2–5] The quadrupole moment $\theta_{\alpha\beta}$ can not be measured easily nor accurately. Most of the available methods involve certain assumptions and approximations whose validity is doubtful. A general survey of these methods is the main object of the present paper. Knowledge of molecular quadrupole moments is of interest not only because it helps in a better understanding of all the phenomena resulting from the interaction of the molecule with any other external system but also because it may be used to propose a better model for the structure of the molecule. Recently, Buckingham[6] has pointed out that if accurate values of the quadrupole moment were known, it would provide a crucial test for the accuracy of the trial wave functions that are used in other molecular calculations. All this makes the measurement of molecular quadrupole moments important in spite of the difficulties involved. The last review on Molecular Quadrupole Moments was published by Buckingham[1] in 1959. Since then a large amount of work has been done on the subject.

The molecular quadrupole moment is defined as[1]

$$\theta_{\alpha\beta}=\tfrac{1}{2}\sum_i e_i(3r_{i\alpha}r_{i\beta}-r_i^2\delta_{\alpha\beta}), \tag{1.2}$$

where $\delta_{\alpha\beta}=1$ if $\alpha=\beta$ and, $=0$ if $\alpha\neq\beta$ and where the summation is over all the charges in the molecule.

$\theta_{\alpha\beta}$ is thus a tensor having nine components. However, by a proper choice of the axes of reference all the off-diagonal terms $\theta_{\alpha\beta}(\alpha\neq\beta)$ can be made to vanish. Thus three principal axes x, y, and z are obtained such that only the following three components for which $\alpha=\beta$ survive:

$$\begin{aligned}\theta_{xx}&=\tfrac{1}{2}\sum_i e_i(3x_i^2-r_i^2),\\ \theta_{yy}&=\tfrac{1}{2}\sum_i e_i(3y_i^2-r_i^2),\\ \theta_{zz}&=\tfrac{1}{2}\sum_i e_i(3z_i^2-r_i^2).\end{aligned} \tag{1.3}$$

These are the three principal quadrupole moments of the molecule. However, Eqs. (1.2) and (1.3) show that

$$\theta_{\alpha\alpha}=\theta_{xx}+\theta_{yy}+\theta_{zz}=0$$

so that only two of these are independent.

If the distribution of the charges is considered to be continuous, the summation over discrete charges need to be replaced by an integration of the charge density $\rho(r)$ over the whole space. Thus

$$\begin{aligned}\theta_{xx}&=\tfrac{1}{2}\int(3x^2-r^2)\rho(r)\,d\tau,\\ \theta_{yy}&=\tfrac{1}{2}\int(3y^2-r^2)\rho(r)\,d\tau,\\ \theta_{zz}&=\tfrac{1}{2}\int(3z^2-r^2)\rho(r)\,d\tau.\end{aligned} \tag{1.4}$$

CC-0. In Public Domain. Gurukul Kangri Collection, Haridwar

Digitized by Arya Samaj Foundation Chennai and eGangotri

If the charge distribution is symmetrical about any axis, say z axis, then

$$\theta_{xx}=\theta_{yy}=-\tfrac{1}{2}\theta_{zz}=-\tfrac{1}{2}\theta \text{ (say)}. \quad (1.5)$$

The problem of evaluation of the molecular quadrupole moments can be attacked in many ways. A theoretical approach utilizes knowledge of the quantum-mechanical wave functions.

For experimental measurement a direct method is, in principle, possible. In this the energy of interaction of the molecule with an external electric field is measured. A simple electrostatic argument[1] shows that this energy consists of, besides other terms, a term depending only on the quadrupole moment $\theta_{\alpha\beta}$ of the molecule and the gradient $F_{\alpha\beta}'$ of the applied field at the center of the molecule. Thus if one can separate out the contribution of this term for known field-gradient values, the quadrupole moment comes out directly. But this method is not practicable because of the difficulties in producing sufficiently large field gradients over the size of the molecule. The largest gradients obtainable are of the order of 1000 esu while the quadrupole moment values are only of the order of 10^{-26} esu. Thus the contribution of the quadrupolar term is only about 10^{-23} ergs which is difficult to separate out from the rest of the interaction energy. Thus this direct method which can work well in the case of the dipole moments, fails in the present case.

However, a slight modification of this results in an elegant method, applicable to the molecules with anisotropic polarizability only. The application of an external electric field makes these molecules birefringent[7] and the amount of birefringence induced depends on the interaction of the molecule with the applied field. A method based on measuring the birefringence resulting due to the interaction proves to be practicable. This method was first suggested by Buckingham[6] in 1959 and has since been successfully applied to the case of the CO_2 molecule.[8]

The other method is to study the interaction between two molecules themselves. At a point a few angstroms from a polar molecule, the field gradient is $\sim 10^{14}$ esu whereas the field strength is only $\sim 10^{6}$ esu. Thus if a second molecule comes in this region, it will interact with the field of the first one giving rise to an interaction energy. The contribution of the quadrupolar term ($\theta_{\alpha\beta}F_{\alpha\beta}'\sim 10^{-12}$) to this energy then is of a comparable order of magnitude to the contribution of the dipolar term ($\mu F\sim 10^{-12}$). Thus molecular quadrupoles contribute significantly to intermolecular forces and this suggests that their indirect evaluation from a study of these forces should be practicable. These indirect methods are the ones that involve one or the other observable phenomenon to which the presence of a finite interaction between the gaseous molecules gives rise.

The principal methods for the evaluation of the molecular quadrupole moments can thus be listed as follows:

1. The Molecular Orbital Method.
2. The Induced Optical Birefringence Method.
3. The Second Virial Coefficient Method.
4. The Spectral Line-Broadening Method.
5. The Anisotropic Susceptibility Method.
6. The Dielectric Constant Method.
7. The Pressure-Induced Absorption Method.
8. The Bond Moments Method.

A few other methods, e.g., "the quadrupolar radiation method," "the macroscopic-quadrupole vibration method," etc. have also been proposed. But the investigations show that none of these can be regarded as practical methods for the evaluation of the molecular quadrupole moments having a wide applicability. A detailed survey of these will not be made here. For a brief discussion one may refer to the previous review.[1]

II. THE MOLECULAR ORBITAL METHOD

In the molecular orbital method one evaluates the nuclear and the electronic contributions to the molecular quadrupole moment, separately. For the nuclear contributions, a straightforward computation of the quadrupole moment components from Eqs. (1.3) is feasible because the charges in the different nuclei and their positions in reference to the origin (usually the center of mass of the molecule) are known.

For the electronic contributions, such a direct calculation is not possible because of the continually changing positions of the electrons so that their coordinates x_i, y_i, z_i, and r_i can not be uniquely defined. For such a case of a continuous charge distribution the quadrupole moment components are evaluated from Eqs. (1.4) with density $\rho(r)$ of the distribution given by

$$\rho(r)=e\sum_i |\phi_i(r)|^2, \quad (2.1)$$

where e is the electronic charge and ϕ_i is the wave function associated with the ith electron. The two center integrals, if any, involved in this evaluation may be taken from Coulson's paper.[9]

To determine the different wave functions ϕ_i use is made of the molecular orbital theory.[10,11] The self-consistent field molecular orbitals ϕ_i are usually determined in the linear combination of atomic orbitals approximation using one or more Slater-type orbitals[12] or Gaussian orbitals[13] as the basis for the linear combination.

It is sometimes more convenient and advantageous to use the method of equivalent orbitals developed by Lennard-Jones.[14,15] In this the set of molecular orbitals ϕ_i is transformed by the methods based on group theory to another set of orbitals which have the property of equivalence in the sense that they are interchangeable under the operations of the group. It is this set of equivalent orbitals which is used in Eq. (2.1) to

CC-0. In Public Domain. Gurukul Kangri Collection, Haridwar

Digitized by Arya Samaj Foundation Chennai and eGangotri

calculate the charge density[16,17] and then the quadrupole moment components[17] from Eqs. (1.4).

III. THE INDUCED OPTICAL BIREFRINGENCE METHOD

Application of an external electric field F makes a fluid optically birefringent, that is to say, the fluid becomes doubly refracting having one value (say n_x) of the refractive index for light beams with electric vector parallel to F and another value (say n_y) for light beams with electric vector perpendicular to F. The difference (n_x-n_y) is known as the optical birefringence induced by the field F and is determined by the interaction of this field with the molecules of the fluid.

If the field is uniform, the interaction is that between the strength of the field and the permanent dipole moment as well as the polarizability anisotropy of the molecules. The resulting birefringence has been identified as the normal Kerr effect and is proportional to the square of the strength of the applied field[18]

$$(n_x-n_y)_F=KF^2. \tag{3.1}$$

However, if the field is inhomogeneous, an additional interaction between the gradient of the applied field and the quadrupole moment of the molecules will come up. This will result in an additional birefringence $(n_x-n_y)_{F'}$, which is proportional to the gradient of the applied field

$$(n_x-n_y)_{F'}=QF'. \tag{3.2}$$

The proportionality factor Q, for a dilute gas of axially symmetric molecules, is given by

$$Q=(4\pi N/15)[\tfrac{1}{2}^5B+(\theta/kT)(\alpha''-\alpha')], \tag{3.3}$$

where N is the number of molecules per unit volume, B is the quadrupole polarizability of the molecules, and α'' and α' are the polarizabilities parallel and perpendicular to the symmetry axis, respectively.

Thus if the component of the birefringence due to the gradient of the field could be separated out, the quadrupole moment can be evaluated from Eqs. (3.2) and (3.3).

Theory of the Method[6]

Consider a molecule whose position and orientation are described by a variable τ and suppose it is placed in an electrostatic potential field ϕ. Then its energy $u(\tau, \phi)$ can be expressed as

$$u(\tau,\phi)=\{u^0-\mu_\alpha F_\alpha-\tfrac{1}{2}\alpha_{\alpha\beta}F_\alpha F_\beta-\tfrac{1}{6}\beta_{\alpha\beta\gamma}F_\alpha F_\beta F_\gamma-\tfrac{1}{24}\gamma_{\alpha\beta\gamma\delta}F_\alpha F_\beta F_\gamma F_\delta$$
$$-\tfrac{1}{3}\theta_{\alpha\beta}F_{\alpha\beta}'-\tfrac{1}{3}A_{\alpha:\beta\gamma}F_\alpha F_{\beta\gamma}'-\tfrac{1}{6}B_{\alpha\beta:\gamma\delta}F_\alpha F_\beta F_{\gamma\delta}'-\tfrac{1}{6}C_{\alpha\beta:\gamma\delta}F_{\alpha\beta}'F_{\gamma\delta}'-\cdots\}, \tag{3.4}$$

where u^0 is the energy of the molecule in the absence of the field, μ_α and $\theta_{\alpha\beta}$ are the permanent dipole and quadrupole moments of the molecule, F_α and $F_{\alpha\beta}'$ are the applied field strength and the field gradient, and the higher-order tensors denote the polarizabilities.

Differentiation of (3.4) with respect to F_α gives the total dipole moment $\mu_\alpha{}^T$ of the molecule as

$$\mu_\alpha{}^T=\{\mu_\alpha+\alpha_{\alpha\beta}F_\beta+\tfrac{1}{2}\beta_{\alpha\beta\gamma}F_\beta F_\gamma+\tfrac{1}{6}\gamma_{\alpha\beta\gamma\delta}F_\beta F_\gamma F_\delta+\tfrac{1}{3}A_{\alpha:\beta\gamma}F_{\beta\gamma}'+\tfrac{1}{3}B_{\alpha\beta:\gamma\delta}F_\beta F_{\gamma\delta}'+\cdots\}e_\alpha{}^{\|}, \tag{3.5}$$

where $e_\alpha{}^{\|}$, $e_\beta{}^{\|}$, $\cdots$ denote unit vectors along the α, β, $\cdots$ component directions.

Differentiating (3.5) with respect to F_β, one gets

$$\partial\mu_\alpha{}^T/\partial F_\beta=\{\alpha_{\alpha\beta}+\beta_{\alpha\beta\gamma}F_\gamma+\tfrac{1}{2}\gamma_{\alpha\beta\gamma\delta}F_\gamma F_\delta+\tfrac{1}{3}B_{\alpha\beta:\gamma\delta}F_{\gamma\delta}'+\cdots\}e_\alpha{}^{\|}e_\beta{}^{\|}=\pi_{\alpha\beta}e_\alpha{}^{\|}e_\beta{}^{\|}, \tag{3.6}$$

where $\pi_{\alpha\beta}$ stands for the quantity within brackets. The quantity on the left-hand side describes the increase in moment $\mu_\alpha{}^T$ per unit increase in the field F_β and is known as the "differential polarizability" associated with α and β directions. Similarly the differential polarizability associated with the perpendicular directions is $\pi_{\alpha\beta}e_\alpha{}^{\perp}e_\beta{}^{\perp}$, where $e_\alpha{}^{\perp}$, $e_\beta{}^{\perp}$, $\cdots$ denote the unit vectors at right angles to the α, β, $\cdots$ directions. The difference $\pi(\tau, \phi)$ between the two is

$$\pi(\tau,\phi)=[\alpha_{\alpha\beta}+\beta_{\alpha\beta\gamma}F_\gamma+\tfrac{1}{2}\gamma_{\alpha\beta\gamma\delta}F_\gamma F_\delta+\tfrac{1}{3}B_{\alpha\beta:\gamma\delta}F_{\gamma\delta}'+\cdots](e_\alpha{}^{\|}e_\beta{}^{\|}-e_\alpha{}^{\perp}e_\beta{}^{\perp}). \tag{3.7}$$

The difference (n_x-n_y) between the refractive indices for light beams with electric vectors along x and y then becomes

$$(n_x-n_y)=2\pi N\bar{\pi}, \tag{3.8}$$

where $\bar{\pi}$ is the average of $\pi(\tau, \phi)$ over all configurations τ, averaged with a Boltzmann-type weighting factor

$$\bar{\pi}=\int\pi(\tau,\phi)\exp[-u(\tau,\phi)/kT]\,d\tau\Big/\int\exp[-u(\tau,\phi)/kT]\,d\tau. \tag{3.9}$$

Since $\bar{\pi}$ depends on the applied field also, it can be expanded in terms of its value and the derivatives at $\phi=0$. Thus

$$\bar{\pi}=\left[(\bar{\pi})_{\phi=0}+\left\{\left(\frac{\partial\bar{\pi}}{\partial F}\right)_{\phi=0}F+\frac{1}{2}\left(\frac{\partial^2\bar{\pi}}{\partial F^2}\right)_{\phi=0}F^2+\cdots\right\}+\left\{\left(\frac{\partial\bar{\pi}}{\partial F_{xx}'}\right)_{\phi=0}F_{xx}'+\frac{1}{2}\left(\frac{\partial^2\bar{\pi}}{\partial F_{xx}'^2}\right)_{\phi=0}F_{xx}'^2+\cdots\right\}\right]. \tag{3.10}$$

CC-0. In Public Domain. Gurukul Kangri Collection, Haridwar

Digitized by Arya Samaj Foundation Chennai and eGangotri

Here the first term denotes the value of $\bar{\pi}$ in the absence of the applied field, the terms in the first bracket give the various order contributions from the field strength, those in the second bracket give the various order contributions from the gradient of the field and so on. In the second bracket the second-order term comes out to be zero so that for all moderate field gradients, only the first term in F_{xx}' need to be considered to describe the anisotropy due to the field gradients. Thus

$$(\bar{\pi})_{F_{xx}'} = (\partial\bar{\pi}/\partial F_{xx}')_{\phi=0} F_{xx}'. \tag{3.11}$$

Now Eq. (3.9) shows that

$$\left(\frac{\partial\bar{\pi}}{\partial F_{xx}'}\right)_{\phi=0} = \left\langle \frac{\partial\pi}{\partial F_{xx}'} \right\rangle_{\phi=0} - (kT)^{-1} \left\langle \pi \frac{\partial u}{\partial F_{xx}'} \right\rangle_{\phi=0} + (kT)^{-1} \langle\pi\rangle \left\langle \frac{\partial u}{\partial F_{xx}'} \right\rangle_{\phi=0}, \tag{3.12}$$

where $\langle\ \rangle$ indicates an average over the configurations τ, averaged with a Boltzmann-type weighting factor. Equation (3.7) shows that

$$\pi(\tau, 0) = \alpha_{\alpha\beta}(e_\alpha{}^{\parallel} e_\beta{}^{\parallel} - e_\alpha{}^{\perp} e_\beta{}^{\perp})$$

which vanishes on averaging over all directions of $e_\alpha{}^{\parallel}$. Equation (3.12) thus reduces to

$$(\partial\bar{\pi}/\partial F_{xx}')_{\phi=0} = \langle \partial\pi/\partial F_{xx}' \rangle_{\phi=0} - (kT)^{-1} \langle \pi(\partial u/\partial F_{xx}') \rangle. \tag{3.13}$$

For an applied field such that $F_{xx}' = -F_{yy}'$ and $F_{zz}' = 0$, one finds from Eq. (3.7) that

$$\langle \partial\pi/\partial F_{xx}' \rangle = \tfrac{1}{3} B_{\alpha\beta:\gamma\delta} \langle (e_\alpha{}^{\parallel} e_\beta{}^{\parallel} - e_\alpha{}^{\perp} e_\beta{}^{\perp})(e_\gamma{}^{\parallel} e_\delta{}^{\parallel} - e_\gamma{}^{\perp} e_\delta{}^{\perp}) \rangle. \tag{3.14}$$

A simple trigonometrical analysis then shows that

$$\begin{aligned} \langle e_\alpha{}^{\parallel} e_\beta{}^{\parallel} e_\gamma{}^{\parallel} e_\delta{}^{\parallel} \rangle &= \langle e_\alpha{}^{\perp} e_\beta{}^{\perp} e_\gamma{}^{\perp} e_\delta{}^{\perp} \rangle = \tfrac{1}{15}(\delta_{\alpha\beta}\delta_{\gamma\delta} + \delta_{\alpha\gamma}\delta_{\beta\delta} + \delta_{\alpha\delta}\delta_{\beta\gamma}) \\ \langle e_\alpha{}^{\parallel} e_\beta{}^{\parallel} e_\gamma{}^{\perp} e_\delta{}^{\perp} \rangle &= \langle e_\alpha{}^{\perp} e_\beta{}^{\perp} e_\gamma{}^{\parallel} e_\delta{}^{\parallel} \rangle = \tfrac{1}{30}(4\delta_{\alpha\beta}\delta_{\gamma\delta} - \delta_{\alpha\gamma}\delta_{\beta\delta} - \delta_{\alpha\delta}\delta_{\beta\gamma}), \end{aligned} \tag{3.15}$$

where $\delta_{\alpha\beta} = 1$ if $\alpha = \beta$ and, $= 0$ if $\alpha \neq \beta$. Substituting from equation (3.15) in Eq. (3.14) one finds

$$\langle \partial\pi/\partial F_{xx}' \rangle = \tfrac{1}{45} B_{\alpha\beta:\gamma\delta} [-2\delta_{\alpha\beta}\delta_{\gamma\delta} + 3\delta_{\alpha\gamma}\delta_{\beta\delta} + 3\delta_{\alpha\delta}\delta_{\beta\gamma}]. \tag{3.16}$$

From Eqs. (3.4) and (3.7) one has

$$[\pi(\partial u/\partial F_{xx}')]_{\phi=0} = -\tfrac{1}{3}\theta_{\gamma\delta}\alpha_{\alpha\beta}(e_\alpha{}^{\parallel} e_\beta{}^{\parallel} - e_\alpha{}^{\perp} e_\beta{}^{\perp})(e_\gamma{}^{\parallel} e_\delta{}^{\parallel} - e_\gamma{}^{\perp} e_\delta{}^{\perp})$$

and so

$$\langle \pi(\partial u/\partial F_{xx}') \rangle_{\phi=0} = -\tfrac{1}{45}\theta_{\gamma\delta}\alpha_{\alpha\beta}[-2\delta_{\alpha\beta}\delta_{\gamma\delta} + 3\delta_{\alpha\gamma}\delta_{\beta\delta} + 3\delta_{\alpha\delta}\delta_{\beta\gamma}]. \tag{3.17}$$

Substitution from Eqs. (3.16) and (3.17) into Eq. (3.13) then gives

$$(\partial\bar{\pi}/\partial F_{xx}')_{\phi=0} = \tfrac{2}{15}[B_{\alpha\beta:\alpha\beta} + (kT)^{-1}\theta_{\alpha\beta}\alpha_{\alpha\beta}]. \tag{3.18}$$

Equations (3.8), (3.11), and (3.18) then give the induced birefringence as

$$(n_x - n_y)_{F_{xx}'} = (4\pi N/15) F_{xx}'[B_{\alpha\beta:\alpha\beta} + (kT)^{-1}\theta_{\alpha\beta}\alpha_{\alpha\beta}]. \tag{3.19}$$

If the molecules are axially symmetric having a quadrupole moment θ and the polarizabilities α'' and α' along and at right angles to the symmetry axis, then Eq. (3.19) reduces to

$$(n_x - n_y)_{F_{xx}'} = (4\pi N/15) F_{xx}'[B_{\alpha\beta:\alpha\beta} + (\theta/kT)(\alpha'' - \alpha')]. \tag{3.20}$$

{*Note added in the proof.* Buckingham and Pariseau [A. D. Buckingham and M. Pariseau, Trans. Faraday Soc. 62, 1 (1966)] have given the quantum-mechanical derivation of an expression for $(n_x - n_y)$ and its application to diatomic molecules. This treatment introduces two distinct modifications. One takes care of the different discrete rotational states of the molecule and results in a more complex temperature dependence than the simple T^{-1} law obtained classically. The other takes care of the nuclear motions and introduces the derivatives of the equilibrium separation quadrupole moment θ_e in the expression for $(n_x - n_y)$. It may be noted that this makes the evaluation of quadrupole moment from this expression more difficult. It has also been observed that for CO_2 at room temperature these corrections are unimportant while for H_2 at room temperature they lead to a value of the birefringence about 75% of the classical value. At lower temperatures the corrections may become more important.}

For spherically symmetric molecules $B_{\alpha\beta:\alpha\beta} = \frac{1}{2}\frac{5}{}B$. For other molecules there are more than one quadrupole polarizability components and further simplification is difficult. However, for simplicity this quantity is replaced by $(15/2)B$ for the axially symmetric molecules also. Thus the birefringence due to the gradient of the field can, for the axially symmetric

CC-0. In Public Domain. Gurukul Kangri Collection, Haridwar

Digitized by Arya Samaj Foundation Chennai and eGangotri

molecules, be written as

$$(n_x-n_y)_{F'_{xx}}=(4\pi N/15)F_{xx}'[\tfrac{1}{2}^5B+(\theta/kT)(\alpha''-\alpha')]. \quad (3.21)$$

Thus if the anisotropy $(\alpha''-\alpha')$ and the quadrupole polarizability B are known, measurements of the birefringence would lead to the molecular quadrupole moments from Eq. (3.21).

The details of the experimental method of measurement of the induced birefringence may be seen elsewhere.[8]

IV. THE SECOND VIRIAL COEFFICIENT METHOD

Many gases exhibit deviation from ideal gas behavior. This deviation is expressed in terms of the virial coefficients as[19]

$$\text{Deviation}=\left(\frac{PV}{RT}-1\right)=\frac{B}{V}+\frac{C}{V^2}+\frac{D}{V^3}+\cdots. \quad (4.1)$$

If there is no mutual interaction between the molecules, the gas behavior will be ideal and the coefficients $B, C, D, \cdots$ will all vanish. However, if a finite interaction exists, the coefficients are finite. If the magnitudes of these virial coefficients are known it should be possible to draw inferences about the interactions. In particular, if the explicit expression for the second virial coefficient B in terms of the interaction potential u is known one can calculate the leading unknown parameter of this potential. In most cases the molecular quadrupole moment θ is this parameter. A trial value of θ is used for calculating the value of B from the known expression. This value of B is compared with the measured B and the value of θ is adjusted such that the two B values agree.

Theory of the Method[20–22]

Second virial coefficient B is explicitly given in terms of interaction potential energy u by the equation

$$B(T)=\frac{N}{8\pi}\int_{\text{vol}}[1-\exp(-u/kT)]\,d\tau, \quad (4.2)$$

where N is the Avogadro number, k is the Boltzmann constant, T is the temperature of the gas, and $d\tau$ is a volume element.

Suppose that the potential u can be broken up into two parts as

$$u=u^0+u'. \quad (4.3)$$

Then Eq. (4.2) yields

$$B(T)=B_0(T)+\sum_{p=1}^{\infty}B_p(T), \quad (4.4)$$

where

$$B_0(T)=\frac{N}{8\pi}\int_{\text{vol}}[1-\exp(-u^0/kT)]\,d\tau,$$

$$B_p(T)=-\frac{N}{8\pi}\int_{\text{vol}}\frac{1}{p!}\left(-\frac{u'}{kT}\right)^p\exp(-u^0/kT)\,d\tau. \quad (4.5)$$

In an actual case of two interacting molecules the interaction potential u consists of a number of terms. Each term, in general, has a separation-dependent term multiplied by certain functions of angles θ_1, ϕ_1, and θ_2, ϕ_2. For convenience the potential u is expressed[20] such that the angular functions appear in the form of spherical harmonics

$$S_{lm}=\left[(2l+1)\frac{(l-|m|)!}{(l+|m|)!}\right]^{1/2}P_l^m(\cos\theta)\exp(im\phi). \quad (4.6)$$

The interaction potential u then has the form

$$u=\sum_{l_1l_2m}\xi^{l_1l_2m}(r)S_{l_1m}(\theta_1,\phi_1)S_{l_2m}(\theta_2,\phi_2), \quad (4.7)$$

where $\xi^{l_1l_2m}(r)$ incorporates in itself the radial dependence as well as the other constants not included in S_{l_1m} and S_{l_2m}. Since $S_{00}=1$, this reduces to

$$u=u^0+u',$$

where

$$u^0=\xi^{000}(r)$$

$$u'=\sum_{l_1l_2m}{}'\xi^{l_1l_2m}(r)S_{l_1m}(\theta_1,\phi_1)S_{l_2m}(\theta_2,\phi_2) \quad (4.8)$$

a prime over the summation sign indicating that the summation is over all the terms except the one for which $l_1=l_2=m=0$.

Thus u^0 is the term independent of the orientations θ and ϕ while u' becomes the orientation-dependent term. In Eq. (4.4) then one can interpret $B_0(T)$ as the contribution to the second virial coefficient from the orientation-independent or the so-called central forces, while $B_1(T)$, $B_2(T)$, $\cdots$ can be interpreted as first-order correction, second-order correction, $\cdots$ to second virial coefficient $B_0(T)$ when noncentral forces are present in addition to the central ones. If the noncentral forces are small, (u'/kT) will be small so that $B_3(T)$ and higher-order correction terms containing the third and higher powers of (u'/kT) can safely be neglected. The virial coefficient $B(T)$ then becomes

$$B(T)=B_0(T)+B_1(T)+B_2(T), \quad (4.9)$$

where $B_0(T)$, $B_1(T)$, and $B_2(T)$ are given by Eq. (4.5).

Equation (4.5) gives

$$B_0(T)=2\pi N\int_0^{\infty}[1-\exp(-u^0/kT)]r^2\,dr.$$

If the central force potential u^0 is taken to be the Lennard-Jones (12–6) potential[23]

$$u^0=4\epsilon[(r_0/r)^{12}-(r_0/r)^6], \quad (4.10)$$

then

$$B_0(T)=\tfrac{2}{3}\pi Nr_0^3F(T^*), \quad (4.11)$$

where

$$F(T^*)=3r_0^{-3}\int_0^{\infty}[1-\exp(-u^0/kT)]r^2\,dr \quad (4.12)$$

is known as the reduced second virial coefficient and has been tabulated by Hirschfelder *et al.*[24] as a function of $T^*=kT/\epsilon$.

CC-0. In Public Domain. Gurukul Kangri Collection, Haridwar

Digitized by Arya Samaj Foundation Chennai and eGangotri

For $B_1(T)$ one has from Eq. (4.5)

$$B_1(T)=\frac{2\pi N}{kT}\int_0^\infty r^2\langle u'\rangle_{Av}\exp(-u^0/kT)\,dr,$$

where $\langle u'\rangle_{Av}$ indicates a classical average of u' over all orientations. This will evidently consist of some inverse power of the separation r multiplied by some constants. One therefore takes it to be of the form

$$\langle u'\rangle_{Av}=-4\epsilon a(r_0/r)^n, \tag{4.13}$$

where the only two unknown parameters a and n are to be adjusted appropriately in any specific case. Substituting this above one gets

$$B_1(T)=-\tfrac{2}{3}\pi N r_0^3(a/4)[H_n(y)/y^2], \tag{4.14}$$

where $y=2(\epsilon/kT)^{1/2}$ and $H_n(y)$ is the function

$$H_n(y)=12y^4r_0^{n-3}\int_0^\infty r^{-n}\exp(-u^0/kT)r^2\,dr. \tag{4.15}$$

This function has been tabulated by Buckingham and Pople.[22]

However, if several interactions are present simultaneously, $\langle u'\rangle_{Av}$ may have to be expressed as a sum of two or even more terms as

$$\langle u'\rangle_{Av}=-4\epsilon[a_1(r_0/r)^{n_1}+a_2(r_0/r)^{n_2}+\cdots]. \tag{4.16}$$

$B_1(T)$ then becomes

$$B_1(T)=-\tfrac{2}{3}\pi N r_0^3\{\tfrac{1}{4}(a_1)[H_{n_1}(y)/y^2]+\tfrac{1}{4}(a_2)[H_{n_2}(y)/y^2]+\cdots\}. \tag{4.17}$$

For $B_2(T)$ one has from Eq. (4.5)

$$B_2(T)=-(N/16\pi^2k^2T^2)\int_{vol}u'^2\exp(-u^0/kT)\,d\tau.$$

This can similarly be expressed in terms of the average of u'^2. But in this case it is more convenient to use the form of u' obtained in Eq. (4.8). Substituting this and using standard properties of spherical harmonics

$$B_2(T)=-\frac{N\pi}{k^2T^2}\sum_{l_1l_2m}'\int_0^\infty r^2\exp(-u^0/kT)[\xi^{l_1l_2m}(r)]^2\,dr.$$

The radial function $\xi^{l_1l_2m}(r)$ consists of some inverse power of r multiplied by some constants. One therefore takes it to be of the form

$$\xi^{l_1l_2m}(r)=4\epsilon b(r_0/r)^s, \tag{4.18}$$

where the two unknowns b and s are to be adjusted appropriately in any specific case. Substituting this in the above expression for $B_2(T)$

$$B_2(T)=-\tfrac{2}{3}\pi N r_0^3\,\tfrac{1}{8}\sum_{l_1l_2m}'b^2H_{2s}(y). \tag{4.19}$$

However, it is quite possible particularly when directional interactions of several types are being considered, that $\xi^{l_1l_2m}(r)$ may have to be expressed as a sum of two or even more terms as

$$\xi^{l_1l_2m}(r)=4\epsilon[b_1(r_0/r)^{s_1}+b_2(r_0/r)^{s_2}+\cdots]. \tag{4.20}$$

A substitution then gives $B_2(T)$ as

$$B_2(T)=-\tfrac{2}{3}\pi N r_0^3\cdot\tfrac{1}{8}\sum_{l_1l_2m}'[b_1^2H_{2s_1}(y)+b_2^2H_{2s_2}(y)+\cdots+2b_1b_2H_{s_1+s_2}(y)+\cdots]. \tag{4.21}$$

Substituting from Eqs. (4.11), (4.17), and (4.21) in Eq. (4.9), the complete expression for the second virial coefficient $B(T)$ to the second order for a gas having a small noncentral force in addition to central one between its molecules, is

$$B(T)=\tfrac{2}{3}\pi N r_0^3[F(T^*)-\{\tfrac{1}{4}(a_1)[H_{n_1}(y)/y^2]+\tfrac{1}{4}(a_2)[H_{n_2}(y)/y^2]+\cdots\}-\tfrac{1}{8}\sum_{l_1l_2m}'\{b_1^2H_{2s_1}(y)+b_2^2H_{2s_2}(y)+\cdots+2b_1b_2H_{s_1+s_2}(y)+\cdots\}], \tag{4.22}$$

where the central force is represented by Lennard-Jones potential [Eq. (4.10)] and the constants $a_1, n_1, b_1, s_1, \cdots$ specify noncentral forces. These constants are the only unknowns in Eq. (4.22) and need to be evaluated for noncentral forces of specific types.

Specific Cases

Dipole–Dipole Interaction

The potential for a dipole–dipole type interaction is[1]

$$u_{\mu\mu}'=(\mu^2/r^3)[2\cos\theta_1\cos\theta_2+\sin\theta_1\sin\theta_2\cos(\phi_1+\phi_2)], \tag{4.23}$$

where μ is molecular dipole moment. To assign appropriate values to the constants $a_1, a_2, \cdots$ and $n_1, n_2, \cdots$ one has to find the average value of u'

$$\langle u_{\mu\mu}'\rangle_{Av}=\frac{\mu^2}{r^3}\int_0^\pi\int_0^\pi\int_0^{2\pi}\int_0^{2\pi}u'\sin\theta_1\sin\theta_2\,d\theta_1\,d\theta_2\,d\phi_1\,d\phi_2\Big/\int_0^\pi\int_0^\pi\int_0^{2\pi}\int_0^{2\pi}\sin\theta_1\sin\theta_2\,d\theta_1\,d\theta_2\,d\phi_1\,d\phi_2=0$$

which by comparison with Eq. (4.16) gives

$$a_1=a_2=\cdots=n_1=n_2=\cdots=0. \tag{4.24}$$

Similarly, for assigning proper values to the constants $b_1, b_2, \cdots$ and $s_1, s_2, \cdots$ one has to express u' in the form

CC-0. In Public Domain. Gurukul Kangri Collection, Haridwar

Digitized by Arya Samaj Foundation Chennai and eGangotri

(4.8) and then compare the nonvanishing $\xi^{l_1 l_2 m}(r)$ with Eq. (4.20). Suppose on expressing u' in the form (4.8) the only nonzero $\xi^{l_1 l_2 m}(r)$ are

$$\xi^{100}=x_1(\mu^2/r^3), \qquad \xi^{010}=x_2(\mu^2/r^3), \qquad \xi^{110}=x_3(\mu^2/r^3), \qquad \xi^{111}=\xi^{11-1}=x_4(\mu^2/r^3).$$

Then,

$$u'=(\mu^2/r^3)[x_1\sqrt{3}\cos\theta_1+x_2\sqrt{3}\cos\theta_2+3x_3\cos\theta_1\cos\theta_2+3x_4\sin\theta_1\sin\theta_2\cos(\phi_1+\phi_2)].$$

Comparing this with Eq. (4.23)

$$x_1=x_2=0, \qquad x_3=\tfrac{2}{3}, \qquad x_4=\tfrac{1}{3}.$$

Thus the only nonzero $\xi^{l_1 l_2 m}(r)$ are

$$\xi^{110}=\tfrac{2}{3}(\mu^2/r^3), \qquad \xi^{111}=\xi^{11-1}=\tfrac{1}{3}(\mu^2/r^3). \tag{4.25}$$

In any other case also the average value of u' and the nonzero $\xi^{l_1 l_2 m}(r)$ can similarly be found out. The detailed computation for every case has not been attempted here. The results are reproduced below.

Dipole–Quadrupole Interaction

The interaction potential is[1]

$$u_{\mu\theta}'=(3\mu\theta/2r^4)[\{\cos\theta_1(3\cos^2\theta_2-1)+2\sin\theta_1\sin\theta_2\cos\theta_2\cos(\phi_1+\phi_2)\}$$
$$+\{\cos\theta_2(3\cos^2\theta_1-1)+2\sin\theta_1\sin\theta_2\cos\theta_1\cos(\phi_1+\phi_2)\}]. \tag{4.26}$$

The average of this vanishes. The nonzero $\xi^{l_1 l_2 m}(r)$ are

$$\xi^{120}=(\tfrac{3}{5})^{1/2}(\mu\theta/r^4), \qquad \xi^{210}=(\tfrac{3}{5})^{1/2}(\mu\theta/r^4), \qquad \xi^{121}=\xi^{12-1}=5^{-1/2}(\mu\theta/r^4), \qquad \xi^{211}=\xi^{21-1}=5^{-1/2}(\mu\theta/r^4). \tag{4.27}$$

Quadrupole–Quadrupole Interaction

The interaction potential is[1]

$$u_{\theta\theta}'=(3\theta^2/4r^5)[1-5\cos^2\theta_1-5\cos^2\theta_2+17\cos^2\theta_1\cos^2\theta_2+2\sin^2\theta_1\sin^2\theta_2\cos^2(\phi_1+\phi_2)$$
$$+16\sin\theta_1\sin\theta_2\cos\theta_1\cos\theta_2\cos(\phi_1+\phi_2)]. \tag{4.28}$$

The average of this is zero. The nonzero $\xi^{l_1 l_2 m}(r)$ are

$$\xi^{220}=\tfrac{6}{5}(\theta^2/r^5), \qquad \xi^{221}=\xi^{22-1}=\tfrac{4}{5}(\theta^2/r^5), \qquad \xi^{222}=\xi^{22-2}=\tfrac{1}{5}(\theta^2/r^5). \tag{4.29}$$

First-Order Induction Interaction

The potential for interaction of the dipole of one molecule with the dipole that it induces in the other is[25]

$$u_{\mu-\alpha\mu}'=-(\alpha\mu^2/2r^6)[(3\cos^2\theta_1+1)+(3\cos^2\theta_2+1)]. \tag{4.30}$$

The average of this over all orientations is

$$\langle u_{\mu-\alpha\mu}'\rangle_{\text{Av}}=-2\alpha\mu^2/r^6. \tag{4.31}$$

The nonzero $\xi^{l_1 l_2 m}(r)$ are

$$\xi^{000}=-2\alpha\mu^2/r^6, \qquad \xi^{020}=-5^{-1/2}(\alpha\mu^2/r^6), \qquad \xi^{200}=-5^{-1/2}(\alpha\mu^2/r^6). \tag{4.32}$$

Second-Order Induction Interaction

The potential for interaction of the quadrupole of one molecule with the dipole induced in the second by the dipole of the first plus that of the dipole of first molecule with the dipole induced in the second by the quadrupole of the first, is[25]

$$u'_{(\mu-\alpha\theta+\theta-\alpha\mu)}=-(12\mu\theta\alpha/r^7)(\cos^3\theta_1+\cos^3\theta_2). \tag{4.33}$$

The average value of this potential vanishes. The nonzero $\xi^{l_1 l_2 m}(r)$ are

$$\xi^{100}=\xi^{010}=-(12\sqrt{3}/5)(\mu\theta\alpha/r^7), \qquad \xi^{300}=\xi^{030}=-[24/5(7)^{1/2}](\mu\theta\alpha/r^7). \tag{4.34}$$

Third-Order Induction Interaction

The potential for interaction between the quadrupole of one molecule and the dipole induced by this quadrupole in the second molecule, is[1,25]

$$u_{\theta-\alpha\theta}'=-(9\alpha\theta^2/4r^8)[1-\cos^2\theta_1-\cos^2\theta_2+\tfrac{5}{2}\cos^4\theta_1+\tfrac{5}{2}\cos^4\theta_2]. \tag{4.35}$$

The average value of this is

$$\langle u_{\theta-\alpha\theta}'\rangle_{\text{Av}}=-3\alpha\theta^2/r^8 \tag{4.36}$$

CC-0. In Public Domain. Gurukul Kangri Collection, Haridwar

Digitized by Arya Samaj Foundation Chennai and eGangotri

The nonzero $\xi^{l_1 l_2 m}(r)$ are

$$\xi^{200}=\xi^{020}=-[12/7(5)^{1/2}](\alpha\theta^2/r^8), \qquad \xi^{400}=\xi^{040}=-\tfrac{3}{7}(\alpha\theta^2/r^8). \tag{4.37}$$

Anisotropic Dispersion Interaction

The potential for dispersion interaction is[26]

$$u_{\text{dis}}'=-(1/r^6)[\{\tfrac{2}{3}A+\tfrac{5}{3}B+B'+\tfrac{8}{3}C\}+\{(A-B-B'+C)(\sin\theta_1\sin\theta_2\cos(\phi_1+\phi_2)+2\cos\theta_1\cos\theta_2)^2+3(B-C)\cos^2\theta_1+3(B'-C)\cos^2\theta_2-\tfrac{2}{3}(A+B-2C)\}], \tag{4.38}$$

where

$$A=\tfrac{1}{4}(h)\alpha_1''\alpha_2''[\nu_1''\nu_2''/(\nu_1''+\nu_2'')], \qquad B=\tfrac{1}{4}(h)\alpha_1''\alpha_2'[\nu_1''\nu_2'/(\nu_1''+\nu_2')]$$
$$B'=\tfrac{1}{4}(h)\alpha_1'\alpha_2''[\nu_1'\nu_2''/(\nu_1'+\nu_2'')], \qquad C=\tfrac{1}{4}(h)\alpha_1'\alpha_2'[\nu_1'\nu_2'/(\nu_1'+\nu_2')], \tag{4.39}$$

where α_1'', α_1', are parallel and perpendicular components of the polarizability of first molecule and ν_1'', ν_1' are those of the fundamental frequency of oscillations for first molecule. α_2'', α_2' and ν_2'', ν_2' denote these quantities for second molecule.

For an isotropic molecule α'' and α' as well as ν'' and ν' are identical and the constants A, B, B', and C are all equal. In u_{dis}' then all the terms except those in the first curly brackets vanish. These can therefore be regarded as the isotropic part. This has already been accounted for by the inverse sixth-power term of Lennard-Jones potential.

The remaining anisotropic part of dispersion interaction potential thus becomes

$$u'_{\text{anis dis}}=-(1/r^6)[(A-B-B'+C)\{\sin\theta_1\sin\theta_2\cos(\phi_1+\phi_2)+2\cos\theta_1\cos\theta_2\}^2+3(B-C)\cos^2\theta_1+3(B'-C)\cos^2\theta_2-\tfrac{2}{3}(A+B-2C)]. \tag{4.40}$$

The average value of this is zero. The nonzero $\xi^{l_1 l_2 m}(r)$ are

$$\xi^{200}=\xi^{020}=-(4/5^{1/2})\kappa\epsilon(r_0/r)^6, \qquad \xi^{220}=-\tfrac{12}{5}\kappa^2\epsilon(r_0/r)^6$$
$$\xi^{221}=\xi^{22-1}=-\tfrac{8}{5}\kappa^2\epsilon(r_0/r)^6, \qquad \xi^{222}=\xi^{22-2}=-\tfrac{4}{5}\kappa^2\epsilon(r_0/r)^6, \tag{4.41}$$

where it has been assumed that $\nu''=\nu'=\nu$ and where use has been made of the fact that isotropic part is equal to the inverse sixth-power term of Lennard-Jones function.

In any specific case if more than one of these noncentral forces are present, the complete list of nonzero $\xi^{l_1 l_2 m}(r)$ should first be written out considering all the noncentral interactions present. It is only then that the constants b_1, b_2, $\cdots$ and s_1, s_2, $\cdots$ are evaluated by comparison with standard form [Eq. (4.20)] and substituted in Eq. (4.21) to get $B_2(T)$.

The details of experimental method of measurement of the virial coefficients may be seen elsewhere.[27–29]

V. THE SPECTRAL LINE-BROADENING METHOD

The causes of spectral linewidth are the following[30]:

1. Natural linewidth due to zero point energy.
2. Doppler broadening.
3. Wall collision broadening.
4. Saturation broadening.
5. Collision broadening.

Contributions of the first four causes in the microwave and infrared regions are either negligible or can be made extremely small by suitable choice of experimental conditions. Experimentally observed linewidths are thus due to the collisions among gas molecules. These collisions produce the interaction energy which perturbs the molecular energy levels causing the shift and the width of a spectral line. If other molecular parameters are known a suitable value of the quadrupole moment could be chosen to give the desired results.

Theory of the Method

Many theories[31–39] have been put forward to explain the linewidths in the microwave and infrared regions. But the one that has so far been most widely used is the Anderson theory. According to this the intensity $I(\omega)$ at any frequency ω in a broad line is given by[31,40]

$$I(\omega)=\text{const}\times\frac{n v\sigma_r}{(\omega-\omega_{if}+nv\sigma_i)^2+(nv\sigma_r)^2}, \tag{5.1}$$

where σ_r and σ_i are, respectively, the real and imaginary parts of the collision cross section σ, n is the number of molecules per unit volume given by

$$n=9.68\times[p(\text{mm Hg})/T(^\circ\text{K})]\times10^{18}, \tag{5.2}$$

and where v is the average relative velocity of the two molecules given by

$$v=(8RT/M\pi)^{1/2}, \tag{5.3}$$

where R is the gas constant, T the temperature, and M the reduced mass of the system of two molecules.

Equation (5.1) shows that the half-intensity half-width of the line is

$$\Delta\nu=(nv/2\pi)\sigma_r. \tag{5.4}$$

The radiating molecule interacts with a large number of molecules passing at different distances from it. The number of molecules which pass at a distance b

CC-0. In Public Domain. Gurukul Kangri Collection, Haridwar

Digitized by Arya Samaj Foundation Chennai and eGangotri

is proportional to $2\pi b\,db$. Interactions with some of these may disturb the radiation completely, with others less completely, while with still others it may not disturb at all, depending upon their separation, their energy states, and upon the types of interactions involved. It is thus convenient to define a probability function $S(b)$ which specifies the probability that the interaction with a molecule in the rotational state J_2 passing from a distance b will disturb the radiation completely. Thus the effective number of collisions that do actually disturb the radiation is only $2\pi b\,dbS(b)$. This when integrated over all b gives the cross section for collisions with the molecules in the J_2 state

$$\sigma_{J_2}=\int_0^\infty 2\pi b\,dbS(b).$$

The function $S(b)$ can be expanded as[40]

$$S(b)=S_0(b)+S_1(b)+S_2(b)+\cdots,$$

where $S_0(b)$ is zero, $S_1(b)$ is an imaginary quantity, while $S_2(b)$ is a real quantity. Since we are interested in the real part alone, the partial cross section to the first order becomes

$$\sigma_{J_2}=\int_0^\infty 2\pi bS_2(b)\,db.$$

The function $S_2(b)$ has a very small value for large b and increases as b decreases till at $b=b_0$, $S_2(b_0)=1$. But as $S_2(b)$ is a probability function, a value greater than one makes no sense. So it is assumed that for $b=b_0$ to 0, $S_2(b)=1$. σ_{J_2} then becomes

$$\sigma_{J_2}=\pi b_0^2+\int_{b_0}^\infty 2\pi bS_2(b)\,db. \tag{5.5}$$

The cross section for the molecules in different rotational states is, in general, different and an average must be found for the effective collision cross section σ_r

$$\sigma_r=\sum_{J_2}\rho_{J_2}\sigma_{J_2}, \tag{5.6}$$

where ρ_{J_2} denotes the fraction of the molecules in the rotational state J_2 which for the case of linear molecules is given by[41]

$$\rho_{J_2}=(hcB/kT)\,(2J_2+1)\,\exp\{-(hcB/kT)J_2(J_2+1)\}, \tag{5.7}$$

where B is the rotational constant of the second molecule and other symbols have their usual significance.

The probability function $S_2(b)$ has been calculated in terms of the P matrices and is expressed as[40]

$$S_2(b)=\frac{1}{2}\left[\sum_{m_im_2}\frac{(J_im_iJ_2m_2\mid P^2\mid J_im_iJ_2m_2)}{(2J_i+1)\,(2J_2+1)}+\sum_{m_fm_2}\frac{(J_fm_fJ_2m_2\mid P^2\mid J_fm_fJ_2m_2)}{(2J_f+1)\,(2J_2+1)}\right]$$
$$-\sum_{m_im_i'm_fm_f'm_2m_2'M}\sum_{J_2'}\frac{(J_f1m_fM\mid J_im_i)\,(J_f1m_f'M\mid J_im_i')}{(2J_i+1)\,(2J_2+1)}\times(J_fm_fJ_2m_2\mid P\mid J_fm_f'J_2'm_2')\,(J_im_i'J_2'm_2'\mid P\mid J_i'm_iJ_2m_2), \tag{5.8}$$

where P is a matrix with its elements

$$(m\mid P\mid n)=\hbar^{-1}\int_{-\infty}^{+\infty}\exp\,(i\omega_{mn}t)\,(m\mid H_c(t)\mid n)\,dt. \tag{5.9}$$

The matrix P and the function $S_2(b)$ thus depend on the collision interaction Hamiltonian $H_c(t)$.

The forms of $S_2(b)$ and of σ_{J_2} obtained as a result of subsequent integration [Eq. (5.5)] have been worked out for interactions of different types. A detailed derivation is not attempted here but the results are reproduced below.

In the general case of two interacting molecules, the leading interactions are of the following types: the dipole–dipole, the dipole–quadrupole, the quadrupole–dipole, and the quadrupole–quadrupole representing electrostatic forces, first-order and second-order induction interactions, the dispersion forces, and the exchange forces.

The probability function is then[42–44]

$$S_2(b)=\{S_2(b)_{\mu_1\mu_2}+S_2(b)_{\mu_1\theta_2}+S_2(b)_{\theta_1\mu_2}+S_2(b)_{\theta_1\theta_2}\}+\{S_2(b)_{\mu_1\alpha_2\mu_1}+S_2(b)_{\mu_1\theta_1\alpha_2}\}+S_2(b)_{\text{dis}}+S_2(b)_{\text{exch}}. \tag{5.10}$$

The individual contributions $S_2(b)_{\mu_1\mu_2}$, $\cdots$ are[40,44–47]

$$S_2(b)_{\mu_1\mu_2}=A^4{}_{\mu_1\mu_2}b^{-4}\{\sum_{J_i'J_2'}D_1(J_iJ_i')D_2(J_2J_2')f_1(k)+\sum_{J_f'J_2'}D_1(J_fJ_f')D_2(J_2J_2')f_1(k)\}$$
$$S_2(b)_{\mu_1\theta_2}=A^6{}_{\mu_1\theta_2}b^{-6}\{\sum_{J_i'J_2'}D_1(J_iJ_i')Q_2(J_2J_2')f_2(k)+\sum_{J_f'J_2'}D_1(J_fJ_f')Q_2(J_2J_2')f_2(k)\}$$
$$S_2(b)_{\theta_1\mu_2}=A^6{}_{\theta_1\mu_2}b^{-6}\{\sum_{J_i'J_2'}Q_1(J_iJ_i')D_2(J_2J_2')f_2(k)+\sum_{J_f'J_2'}Q_1(J_fJ_f')D_2(J_2J_2')f_2(k)+B\sum_{J_2'}D_2(J_2J_2')f_2(k)\}$$
$$S_2(b)_{\theta_1\theta_2}=A^8{}_{\theta_1\theta_2}b^{-8}\{\sum_{J_i'J_2'}Q_1(J_iJ_i')Q_2(J_2J_2')f_3(k)+\sum_{J_f'J_2'}Q_1(J_fJ_f')Q_2(J_2J_2')f_3(k)+B\sum_{J_2'}Q_2(J_2J_2')f_3(k)\}$$
$$S_2(b)_{\mu_1\alpha_2\mu_1}=A^{10}{}_{\mu_1\alpha_2\mu_1}b^{-10}\{\sum_{J_i'}Q_1(J_iJ_i')g_1(k)+\sum_{J_f'}Q_1(J_fJ_f')g_1(k)+B\}$$
$$S_2(b)_{\mu_1\theta_1\alpha_2}=A^{12}{}_{\mu_1\theta_1\alpha_2}b^{-12}\{\sum_{J_i'}D_1(J_iJ_i')g_3(k)+\sum_{J_f'}D_1(J_fJ_f')g_3(k)\}$$

CC-0. In Public Domain. Gurukul Kangri Collection, Haridwar

Digitized by Arya Samaj Foundation Chennai and eGangotri

$$S_2(b)_{\text{dis}}=S_2(b)_{\text{dis }2}+S_2(b)_{\text{dis }4}$$

$$S_2(b)_{\text{dis }2}=A^{10}{}_{\text{dis }2}b^{-10}\{\sum_{J_i'}Q_1(J_iJ_i')g_1(k)+\sum_{J_f'}Q_1(J_fJ_f')g_1(k)+B\}$$

$$S_2(b)_{\text{dis }4}=A^{10}{}_{\text{dis }4}b^{-10}\{\sum_{J_i'J_2'}Q_1(J_iJ_i')Q_2(J_2J_2')g_2(k)+\sum_{J_f'J_2'}Q_1(J_fJ_f')Q_2(J_2J_2')g_2(k)+B\sum_{J_2'}Q_2(J_2J_2')g_2(k)\}$$

$$S_2(b)_{\text{exch}}=A^{\text{exp}}{}_{\text{exch}}b[1-\tfrac{9}{4}(a/b)+\tfrac{16}{32}(a^2/b^2)]C_{J_iJ_f}\exp\{-2[(b-d/a)]\}, \tag{5.11}$$

where

$$A^4{}_{\mu_1\mu_2}=\tfrac{4}{9}(\mu_1\mu_2/\hbar v)^2, \qquad A^6{}_{\mu_1\theta_2}=\tfrac{16}{45}(\mu_1\theta_2/\hbar v)^2$$

$$A^6{}_{\theta_1\mu_2}=\tfrac{16}{45}(\theta_1\mu_2/\hbar v)^2, \qquad A^8{}_{\theta_1\theta_2}=\tfrac{16}{25}(\theta_1\theta_2/\hbar v)^2$$

$$A^{10}{}_{\mu_1\alpha_2\mu_1}=(21\pi^2/640)(\alpha_2\mu_1^2/\hbar v)^2, \qquad A^{12}{}_{\mu_1\theta_1\alpha_2}=(27\pi^2/32)(\mu_1\theta_1\alpha_2/\hbar v)^2$$

$$A^{10}{}_{\text{dis }2}=\frac{84\pi^4}{10240}\left[\frac{\epsilon_1\epsilon_2}{\epsilon_1+\epsilon_2}\cdot\frac{(\alpha_1''-\alpha_1')\alpha_2}{hv}\right]^2, \qquad A^{10}{}_{\text{dis }4}=\frac{2236\pi^4}{1228800}\left[\frac{\epsilon_1\epsilon_2}{\epsilon_1+\epsilon_2}\,\frac{(\alpha_1''-\alpha_1')(\alpha_2''-\alpha_2')}{hv}\right]^2$$

$$A^{\text{exp}}{}_{\text{exch}}=\frac{256\pi}{5}\left(\frac{\gamma}{3+\gamma}\right)^2 a\left[(hv)^{-1}\left\{kT+d^{-6}\left(\tfrac{1}{2}\pi\alpha_2\mu_1^2+\frac{3\pi}{16}\,\frac{\epsilon_1\epsilon_2}{\epsilon_1+\epsilon_2}\,(2+\tfrac{1}{3}\gamma)\alpha_1\alpha_2\right)\right\}\right]^2. \tag{5.12}$$

μ_1, μ_2, θ_1, and θ_2 are the dipole and quadrupole moments of the two molecules, ϵ_1 and ϵ_2 are their ionization energies, α_1'' and α_1' are, respectively, the parallel and perpendicular components of the polarizability of first molecule, α_2'' and α_2' are that for the second molecule, a and d are the range of exchange forces and the hardcore diameter, respectively, and $\gamma=(\alpha_1''-\alpha_1')/\alpha_1$.

$$C_{J_iJ_f}=Q_1(J_i, J_i)+Q_1(J_f, J_f)+B$$

$$B=(-1)^{J_i+J_f}2[(2J_i+1)(2J_f+1)Q_1(J_i, J_i)Q_1(J_f, J_f)]^{1/2}W(J_iJ_fJ_iJ_f, 12), \tag{5.13}$$

where W is the Racah coefficient given by

$$W(J_iJ_fJ_iJ_f, 12)=(-1)^{2J}[(2J+5)(J+2)J(2J-1)]^{1/2}/[(J+1)(2J+1)(2J+3)]. \tag{5.14}$$

D_1, D_2, Q_1, and Q_2 are the dipolar and quadrupolar transition probabilities[48] given for the case of linear molecules, by

$$D(J, J+1)=\frac{J+1}{2J+1}, \qquad D(J, J-1)=\frac{J}{2J+1}, \qquad Q(J, J+2)=\frac{3}{2}\,\frac{(J+1)(J+2)}{(2J+1)(2J+3)}$$

$$Q(J, J-2)=\frac{3}{2}\,\frac{J(J-1)}{(2J-1)(2J+1)}, \qquad Q(J, J)=\frac{J(J+1)}{(2J-1)(2J+3)}. \tag{5.15}$$

The functions $f_1(k)$, $f_2(k)$, $f_3(k)$, $g_1(k)$, $g_2(k)$, and $g_3(k)$ are functions of $k=(2\pi c/v)b\Delta E$, ΔE being the sum of transition energies of the two molecules, defined and tabulated elsewhere.[40,44]

The partial collision cross section σ_{J_2} is obtained as[44]

$$\begin{aligned}\sigma_{J_2}=\pi b_0^2\Big[&1+A^4{}_{\mu_1\mu_2}b_0^{-4}\{\sum_{J_i'J_2'}D_1(J_iJ_i')D_2(J_2J_2')F_1(k_0)+\sum_{J_f'J_2'}D_1(J_fJ_f')D_2(J_2J_2')F_1(k_0)\}\\
&+A^6{}_{\mu_1\theta_2}b_0^{-6}\{\sum_{J_i'J_2'}D_1(J_iJ_i')Q_2(J_2J_2')F_2(k_0)+\sum_{J_f'J_2'}D_1(J_fJ_f')Q_2(J_2J_2')F_2(k_0)\}\\
&+A^6{}_{\theta_1\mu_2}b_0^{-6}\{\sum_{J_i'J_2'}Q_1(J_iJ_i')D_2(J_2J_2')F_2(k_0)+\sum_{J_f'J_2'}Q_1(J_fJ_f')D_2(J_2J_2')F_2(k_0)+B\sum_{J_2'}D_2(J_2J_2')F_2(k_0)\}\\
&+A^8{}_{\theta_1\theta_2}b_0^{-8}\{\sum_{J_i'J_2'}Q_1(J_iJ_i')Q_2(J_2J_2')F_3(k_0)+\sum_{J_f'J_2'}Q_1(J_fJ_f')Q_2(J_2J_2')F_3(k_0)+B\sum_{J_2'}Q_2(J_2J_2')F_3(k_0)\}\\
&+A^{10}{}_{\mu_1\alpha_2\mu_1}b_0^{-10}\{\sum_{J_i'}Q_1(J_iJ_i')G_1(k_0)+\sum_{J_f'}Q_1(J_fJ_f')G_1(k_0)+\tfrac{1}{4}B\}\\
&+A^{12}{}_{\mu_1\theta_1\alpha_2}b_0^{-12}\{\sum_{J_i'}D_1(J_iJ_i')G_3(k_0)+\sum_{J_f'}D_1(J_fJ_f')G_3(k_0)\}\\
&+A^{10}{}_{\text{dis }2}b_0^{-10}\{\sum_{J_i'}Q_1(J_iJ_i')G_1(k_0)+\sum_{J_f'}Q_1(J_fJ_f')G_1(k_0)+\tfrac{1}{4}B\}\\
&+A^{10}{}_{\text{dis }4}b_0^{-10}\{\sum_{J_i'J_2'}Q_1(J_iJ_i')Q_2(J_2J_2')G_2(k_0)+\sum_{J_f'J_2'}Q_1(J_fJ_f')Q_2(J_2J_2')G_2(k_0)+B\sum_{J_2'}Q_2(J_2J_2')G_2(k_0)\}\\
&+A^{\text{exp}}{}_{\text{exch}}\,a^3b_0^{-2}\left(\frac{145}{32}-\frac{5}{4}\frac{b_0}{a}+\frac{b_0^2}{a^2}\right)C_{J_iJ_f}\exp\left\{-2\left(\frac{b_0-d}{a}\right)\right\}\Big],\end{aligned} \tag{5.16}$$

CC-0. In Public Domain. Gurukul Kangri Collection, Haridwar

Digitized by Arya Samaj Foundation Chennai and eGangotri

where b_0 is such that $S_2(b_0)=1$, $k_0=(2\pi c/v)b_0\Delta E$ and where the functions $F_1(k_0)$, $F_2(k_0)$, $F_3(k_0)$, $G_1(k_0)$, $G_2(k_0)$, and $G_3(k_0)$ are the functions of k_0 defined and tabulated elsewhere.[40,44]

Method of Computation[42,43]

One calculates the average relative velocity v from Eq. (5.3). With this v and other known constants of the two molecules and an assumed value for the unknown constant, if any, the different A coefficients are evaluated from Eq. (5.12). Then for a given value of J_2 a trial value of b is taken and $S_2(b)_{\mu_1\mu_2}$, etc. are calculated from Eq. (5.11). If the value of the function $S_2(b)$ comes out to be different from unity, another value of b is taken and the calculations are repeated till $S_2(b)$ becomes unity. The corresponding value of b is b_0. With this b_0 then the partial collision cross section σ_{J_2} is evaluated from Eq. (5.16) using the known values of A coefficients and transition probabilities and the values of $F_1(k_0)$, $\cdots$ from the tables.

The value of σ_{J_2} is thus found for every J_2 starting right from $J_2=0$ and upto the value say $J_2^{\max}$ after which σ_{J_2} becomes independent of J_2. In practice the calculation of σ_{J_2} at five or six values of J_2 and a subsequent graphical interpolation for intermediate values of J_2, suffices. The average collision cross section σ_r is then evaluated from Eq. (5.6) in the following manner:

$$\sigma_r=\sum_{J_2=0}^{J_2^{\max}}\rho_{J_2}\sigma_{J_2}+(1-\sum_{J_2=0}^{J_2^{\max}}\rho_{J_2})\sigma_{J_2\,\max}. \quad (5.17)$$

The values of ρ_{J_2} needed here are calculated in advance from Eq. (5.7).

The half-intensity half-width $\Delta\nu$ is then calculated from Eq. (5.4), using known value of v and that of n from Eq. (5.2).

If any one of the constants of the two molecules, particularly if the quadrupole moment of any one molecule, be unknown the width is evaluated as explained above for several values of the quadrupole moment and a curve of linewidth vs quadrupole moment is drawn. The value corresponding to the measured width gives the best value of the quadrupole moment of the molecule.

The details of experimental method of measurement of microwave spectral linewidths may be seen elsewhere.[49–52]

Lineshift Method[53,54]

An investigation of the lineshifts in the microwave or infrared regions can also lead to the molecular quadrupole moments. Following the impact theory of Anderson, Eq. (5.1) directly gives the lineshift as

$$\delta\nu=-(nv/2\pi)\sigma_i, \quad (5.18)$$

where σ_i is the imaginary part of collision cross section averaged over all the rotational states J_2 of the perturbing molecules

$$\sigma_i=\sum_{J_2}\rho_{J_2}\sigma_{J_2}. \quad (5.19)$$

Since we are now interested in the imaginary part alone, the partial collision cross section σ_{J_2} is

$$\sigma_{J_2}=\pi b_0^2+\int_{b_0}^{\infty}2\pi bS_1(b)\,db, \quad (5.20)$$

where $S_1(b)$ is the leading imaginary term in the expansion of $S(b)$ and where it has been assumed that from $b=b_0$ to 0, $S_1(b)=1$, b_0 being such that $S_1(b_0)=1$.

The function $S_1(b)$ is expressed in terms of the P matrices [Eq. (5.9)] as follows[40]:

$$S_1(b)=i\Big[\sum_{m_i,m_2}\frac{(J_im_iJ_2m_2\mid P\mid J_im_iJ_2m_2)}{(2J_i+1)(2J_2+1)}-\sum_{m_f,m_2}\frac{(J_fm_fJ_2m_2\mid P\mid J_fm_fJ_2m_2)}{(2J_f+1)(2J_2+1)}\Big]. \quad (5.21)$$

The theoretical lineshift investigations have been carried out mainly in the infrared region only by a number of workers.[53,54] But the expressions for the function $S_1(b)$ and the collision cross section have so far been worked out only for the induction and dispersion interactions in an attempt to explain the shift of a dipolar line perturbed by rare gas molecules. However, the expressions for electrostatic interactions can be derived in a similar manner. Then if θ is the only unknown parameter, its value may be suitably chosen to fit the experimental lineshift data.

Recently, Kranendonk[55–57] has investigated the broadening of Raman lines and it appears that these investigations may also lead to molecular quadrupole moments. However, as the accuracy of Raman line measurements may not be very high, the values may probably not be very reliable.

VI. OTHER METHODS

The Anisotropic Susceptibility Method

The diamagnetic susceptibility of a molecule is, in general, anisotropic. For axially symmetric molecules the susceptibility χ'' along the symmetry axis and χ' at right angles to it are given by[58]

$$\chi'=(e^2/4mc^2)\sum_i(y_i^2+z_i^2)+\chi_{HF}'$$
$$\chi''=(e^2/4mc^2)\sum_i(x_i^2+y_i^2), \quad (6.1)$$

where x_i, y_i, z_i are the coordinates of ith electron and the summation is over all the electrons in the molecule. χ_{HF}' is the contribution to χ' from the high-frequency matrix elements occurring in the theory of diamagnetic susceptibility. This contribution to χ'' is zero because of the symmetry of the Hamiltonian of the electrons about the molecular axis.

CC-0. In Public Domain. Gurukul Kangri Collection, Haridwar

Digitized by Arya Samaj Foundation Chennai and eGangotri

Equations (6.1) yield

$$e\sum_i (z_i^2 - x_i^2) = (4mc^2/e)\{(\chi' - \chi'') - \chi_{HF}'\}. \quad (6.2)$$

The left-hand side of this equation is identified as the electronic contribution to the molecular quadrupole moment and can be determined provided the anisotropy $(\chi' - \chi'')$ in diamagnetic susceptibility and the high-frequency contribution χ_{HF}' were known.

The anisotropy $(\chi' - \chi'')$ is determined[59] by studying the dependence of diamagnetic susceptibility on the orientation of molecular rotational angular momentum. Let χ_M represent the diamagnetic susceptibility of a molecule with rotational quantum number $J=1$ and with rotational magnetic quantum number equal to M. If θ be the angle between the applied field and the internuclear symmetry axis

$$\chi_M = \chi' \langle \sin^2\theta \rangle_M + \chi'' \langle \cos^2\theta \rangle_M \quad (6.3)$$

where the angular brackets indicate an average over the state concerned. These averages have been evaluated for the three possible values of M and are[59]

$$\langle \sin^2\theta \rangle_{\pm 1} = \tfrac{4}{5}, \qquad \langle \sin^2\theta \rangle_0 = \tfrac{2}{5}$$
$$\langle \cos^2\theta \rangle_{\pm 1} = \tfrac{1}{5}, \qquad \langle \cos^2\theta \rangle_0 = \tfrac{3}{5}. \quad (6.4)$$

Substituting this in Eq. (6.3) one gets

$$(\chi' - \chi'') = \tfrac{5}{2}(\chi_{\pm 1} - \chi_0). \quad (6.5)$$

The difference $(\chi_{\pm 1} - \chi_0)$ has been measured by Ramsey[60] using molecular beam experiments. This gives the anisotropy $(\chi' - \chi'')$. Its value for a number of molecules is now available in literature.[61]

The high-frequency contribution χ_{HF}' has been shown[60] to be related to the rotational magnetic moment of the molecule. This can be measured by studying the radio-frequency spectrum of a molecular beam in a strong magnetic field.[60,62]

The structure of the molecules being known from other sources, the nuclear contribution to the molecular quadrupole moment is calculated directly from Eq. (1.3).

The Dielectric Constant Method

The dielectric constant of any real gas is determined both by the properties of isolated molecules and by the effects of molecular interactions. If the interactions are small, they can be neglected completely and the dielectric behavior of the gas is represented well by the Clausius–Mossotti equation[4]

$$[(\epsilon - 1)/(\epsilon + 2)](n/v) = A, \quad (6.6)$$

where (n/v) is molar density of the gas and $A = 4\pi\alpha/3$, α being average polarizability of the molecules. However, for a real gas the effect of molecular interactions is fairly important and one has to consider the complete virial expansion of the Clausius–Mossotti function as[63]

$$\frac{\epsilon - 1}{\epsilon + 2}\frac{n}{v} = A + B\left(\frac{n}{v}\right) + C\left(\frac{n}{v}\right)^2 + \cdots, \quad (6.7)$$

where the coefficients B, C, $\cdots$ are known as second, third, $\cdots$ dielectric virial coefficients. The second coefficient B incorporates the effects of pair interactions, the third one C that of the three body interactions and so on.

The second dielectric virial coefficient B has been calculated theoretically[64–67] considering the dipole moment induced in a molecule by the quadrupolar field of a neighboring molecule at the first one. Its value for a nonpolar gas of axially symmetric molecules is

$$B = \frac{16\pi^2 N^2}{3kT}\alpha^2\theta^2(1 + \tfrac{4}{5}\kappa^2)\int_0^\infty r^{-8}\exp\{-u(r)/kT\}r^2\,dr, \quad (6.8)$$

where N is the Avogadro number, κ and θ are, respectively, the polarizability anisotropy and the quadrupole moment of the molecules of the gas, and $u(r)$ is the pair interaction potential assumed purely radial in the theory.

Using a Lennard-Jones potential [Eq. (4.10)] for $u(r)$ one has

$$B = (\pi N\alpha/3y)^2\,(1 + \tfrac{4}{5}\kappa^2)\,(\theta^2/\epsilon r_0^5)\,H_8(y), \quad (6.9)$$

where $H_n(y)$ is the function as defined in Eq. (4.15) and tabulated by Buckingham and Pople.[22]

The coefficient B may be evaluated experimentally also by[63,68] fitting the observed dielectric constant data into Eq. (6.7). Then if other molecular parameters occurring in Eq. (6.9) are known, the value of quadrupole moment θ may be chosen such that the two B values agree.

The Pressure-Induced Absorption Method

Transient dipoles may be induced in the molecules when perturbed by strong external fields or by intermolecular force fields. Thus nondipolar gases may also exhibit rotational absorption at high pressures. Such absorption has been observed in a number of gases.[69–73] The integrated intensity at moderate pressures increases as the square of the density indicating that the absorption is caused by the bimolecular force fields. The quadrupole field has a greater range than other possible force fields. In fact the pressure induced rotational absorption has so far been observed only in the quadrupolar gases such as CO_2, C_2H_4, etc. For gases like CH_4 and SF_6 having higher multipoles as their leading multipoles, the absorption is immeasurably small.[72]

Considering these quadrupole induced dipoles, Maryott and Birnbaum[71] have derived an expression for the loss factor in terms of pertinent molecular pa-

CC-0. In Public Domain. Gurukul Kangri Collection, Haridwar

Digitized by Arya Samaj Foundation Chennai and eGangotri

rameters. They obtain

$$\epsilon''=3(\epsilon_0-\epsilon_\infty)\omega\pi r_0\langle 1/v\rangle/28, \tag{6.10}$$

where $(\epsilon_0-\epsilon_\infty)$ is the total contribution to the dielectric constant arising from quadrupole induced dipoles, ω is the angular frequency, r_0 is kinetic collision diameter, and $\langle 1/v\rangle$ is the Boltzmann average of the reciprocal of the relative velocity.

On introducing the molecular parameters and rearranging, Eq. (6.10) becomes[72]

$$\theta^2=\frac{7}{3\pi^{7/2}}\left(\frac{V_{\rm STP}{}^2}{N^{3/2}}\right)\left(\frac{\epsilon''}{\omega\rho^2}\right)\frac{(kT)^{3/2}}{\alpha^2 r_0 M^{1/2}}\Big/\int_0^\infty r^{-8}\exp\{-u(r)/kT\}r^2\,dr, \tag{6.11}$$

where θ is the molecular quadrupole moment, α is the average polarizability of the molecules, N is the Avogadro number, M is the molecular weight, $V_{\rm STP}$ is the molar volume at 1 atm and 0°C, ρ is the density in Amagat units, and where $u(r)$ is the intermolecular potential assumed purely radial in the theory.

Using Lennard-Jones potential [Eq. (4.10)] for $u(r)$ one has

$$\theta^2=112\,\frac{V_{\rm STP}{}^2}{\pi^{7/2}N^{3/2}}\,\frac{\epsilon^2}{(kT)^{1/2}}\,\frac{r_0{}^4}{\alpha^2M^{1/2}}\cdot\frac{1}{H_8(y)}\left(\frac{\epsilon''}{\omega\rho^2}\right), \tag{6.12}$$

where $H_n(y)$ is the function as defined in Eq. (4.15) and tabulated by Buckingham and Pople.[22]

Thus if other molecular parameters were known, Eq. (6.12) could be used to evaluate molecular quadrupole moments from the measured absorptions at known values of the density and frequency.

The Bond Moments Method

Let us consider a molecule having several bonds with known multipole moments. Then an approximate distribution of the charges in the bonds can be obtained provided a suitable model for this is assumed. One assumes[74] a classical model in which each bond is supposed to consist of two $+e$ charges at each of the two nuclear positions and two circular charge rings each of radius r and charge $-e$ at distances say z_1 and z_2 from the center of the bond. The coordinates r, z_1, and z_2 are then to be found.

The contributions of the discrete positive charges to the bond moments are calculated directly and subtracted from the known moments to get the contributions μ, P, Ω, ϕ, $\cdots$ of the charge rings to the dipole-, quadrupole-, octopole-, hexadecapole-, $\cdots$ moments of the bond.

These are calculated directly also from Eq. (1.4). Thus

$$\begin{aligned}\mu&=r(z_1+z_2)\\ P&=e(z_1{}^2+z_2{}^2-r^2)\\ \Omega&=e[z_1{}^3+z_2{}^3-\tfrac{3}{2}r^2(z_1+z_2)].\end{aligned} \tag{6.13}$$

A simultaneous solution of these three equations gives the coordinates r, z_1, and z_2.

The contribution of the rings to the quadrupole moment θ of the molecule is then calculated from Eq. (1.4). The nuclear contribution is calculated directly from Eq. (1.3). The inner-shell electrons, if any, may be considered along with the appropriate nucleus.

VII. DISCUSSION

The Molecular Orbital Method

The molecular orbital method is, in principle, applicable to any type of molecule. There are no restrictions as regards the symmetry properties of the molecule. This makes it specially suitable and advantageous for asymmetric molecules like H_2O, NH_3, $\cdots$ for which so far it has not been possible to apply most of the other available methods. The method is a direct one starting from the microscopic standpoint of electronic charges and nuclei constituting the molecule. It has the credit of determining the magnitude as well as the sign of the molecular quadrupole moment.

This method is based on the knowledge of electronic wave functions which are determined by the considerations of energy of the molecule. But the energy of a molecule is not so sensitive to these wave functions as is the molecular quadrupole moment. The quadrupole moment values derived from these wave functions will therefore not be very reliable.

The determination of electronic wave functions involves evaluation of the multicenter Coulomb and exchange integrals between different electrons of the molecule. This becomes prohibitively tedious as the number of centers exceeds three or four. The applicability of the method is thus limited to smaller molecules only.

The Induced Optical Birefringence Method

This is a direct method determining the magnitude as well as the sign of the molecular quadrupole moment. It is applicable for the axially symmetric molecules only.

The measurement is essentially of the quantity $y=[\frac{15}{2}B+(\theta/kT)(\alpha''-\alpha')]$. Thus the values of the quadrupole polarizability B and the anisotropy $(\alpha''-\alpha')$ must be known before the quadrupole moment θ can be calculated. The value of B can be assessed by making the measurements over a range of temperatures and plotting y against $1/T$. For obtaining an appreciable range in y, a fairly large range of temperatures has to be covered. But there are practical difficulties in extending the temperature range upwards while at lower temperatures the low vapor pressure of most of the

CC-0. In Public Domain. Gurukul Kangri Collection, Haridwar

Digitized by Arya Samaj Foundation Chennai and eGangotri

gases of interest presents practical difficulties. Thus an accurate assessment of B is rather difficult. It is then seen that for many molecules it contributes at most a few per cent only. The influence of B is therefore neglected completely. This neglect is justifiable for molecules with large values of the product $\theta(\alpha''-\alpha')$ but not for those with smaller values of this product. In many molecules, as for example in the H_2 molecule, the two terms in y being of opposite signs, cancel each other and a separation of the two by measurements over a range of temperatures becomes still more difficult. Thus the complications due to the quadrupole polarizability B render the method suitable only for those molecules for which the product $\theta(\alpha''-\alpha')$ is large and a fairly high vapor pressure is obtainable.

The anisotropy $(\alpha''-\alpha')$ is known for a large number of molecules. But an examination of the data shows that there exists much uncertainty about this factor. This introduces a corresponding ambiguity in the calculated quadrupole moment and constitutes the most serious drawback of the method.

The Second Virial Coefficient Method

This is an indirect method involving molecular interactions manifested in the form of an imperfection in the gas behavior. It determines only the magnitude of the quadrupole moment and gives no idea about its sign. It is applicable to axially symmetric molecules only.

In the theoretical treatment of the method, the directional part of the intermolecular potential is assumed to be small and $B_3(T)$ and higher-order terms are neglected. However, in the case of molecules having a large dipole moment and a high polarizability, this assumption is not quite justified and one must consider up to at least the $B_3(T)$ term in the expansion of $B(T)$.

Calculations show that in many cases the sensitivity of the second virial coefficient B to the quadrupole moment is poor. Small uncertainties in the measured B lead to much larger uncertainties in the calculated quadrupole moment of the molecule.

The experimental value of $B(T)$ is found from high-pressure p–v–t data which may extend up to 100 atm or even more. At such high pressures, apart from the changes in the polarizability and its anisotropy, a distortion in the shape of the molecules takes place. The quadrupole moment being highly sensitive to the shape of the molecular charge distribution, its value at such high pressures will be different from that for the normal molecules at low pressures of the gas.

The Spectral Line-Broadening Method

This is an indirect method depending on the use of Anderson theory and the experimentally determined width of the spectral lines in the microwave or infrared regions. Only the magnitude of the quadrupole moment can be determined by this process. So far this method has been used for axially symmetric molecules only. The difficulty with the asymmetric molecules is that the quadrupole transition probabilities in them are still not known.

In many polar molecules having a large dipole moment and polarizability (for example in the linear molecule BrCN[75]), the width of the line is not quite sensitive to the quadrupole moment and it is seen that small errors in the measured width lead to quite discouraging deviations in the calculated quadrupole moment of the molecule. This means that the self-broadening method is suitable only for those molecules which have a low value of the dipole moment. For nonpolar molecules the line of some other polar molecule as broadened by this nonpolar molecule is studied. In this case a change in the quadrupole moment changes the linewidth more than in the first case.

The experimental measurement of the linewidth in the microwave region can be done with a high degree of accuracy. The measurements are made at low pressures where the molecular charge distribution is not distorted. This constitutes a great advantage of the present method.

The microwave linewidth investigations are to be preferred over the infrared lineshift and Raman linewidth investigations because of higher experimental accuracy and reliability.

The Anisotropic Susceptibility Method

This is a very elegant and accurate method determining the nuclear and the electronic contributions to the quadrupole moment separately. Thus both the magnitude as well as the sign of the quadrupole moment are determined. Like most of the other methods this also is applicable for the axially symmetric molecules only.

The evaluation is based on an accurate determination of rotational magnetic moment by the high-precision molecular-beam resonance techniques. The experimental difficulties involved in this technique limit the applicability of this method.

The Dielectric Constant Method

This also is an indirect method and determines only the magnitude of the quadrupole moment. It applies strictly to axially symmetric molecules only. However, a more general treatment applicable to the molecules of lower symmetry also could be given.

The evaluation is based on the determination of second dielectric virial coefficient B, in the theoretical treatment of which the intermolecular potential is taken to be a purely radial L-J potential. For many nonpolar gases the orientation dependent quadrupole–quadrupole interaction is of considerable importance and needs to be considered. An approximate correction for this term gives[68] an additional $+ve$ contribution to B, thereby reducing the calculated quadrupole moment. The complex angular dependence of θ–θ interaction makes a very accurate treatment rather difficult.

CC-0. In Public Domain. Gurukul Kangri Collection, Haridwar

Digitized by Arya Samaj Foundation Chennai and eGangotri

The experimental determination of B is done through the deviations from Clausius–Mossotti equation. Since this effect is small at moderate pressures, very high precision measurements of the dielectric constant are essential. Further, appreciable deviations from the C–M behavior appear only at high pressures that may extend up to 100 atm or so. Because of the distortions in the molecular charge distributions at such high pressures, the quadrupole moment is likely to be different from that for the normal molecules.

The Pressure-Induced Absorption Method

This also is an indirect method determining only the magnitude of the quadrupole moment and is applicable to axially symmetric molecules only. Since this also makes use of the high-pressure data (appreciable absorption is induced only at high pressures), the derived quadrupole moment values are expected to be erroneous.

In the sensitivity and experimental accessibility these measurements offer definite advantages over direct studies of the dielectric constants.

For a more accurate evaluation one should study the induced absorption in the quadrupolar gas–foreign nonquadrupolar gas system and not in the pure quadrupolar gas system. This is because the large quadrupole–quadrupole interaction in the latter case changes the intermolecular potential appreciably from the assumed L-J potential. It is for this reason that the quadrupole moment values calculated with this potential for the pure gas are somewhat higher than those derived from the mixtures.[73] If pure gas is used, an allowance must be made for the θ–θ interaction which will reduce the calculated quadrupole moment.

The Bond Moments Method

This method evaluates the nuclear and the electronic contributions to the molecular quadrupole moment separately and, therefore, has the credit of determining its magnitude as well as the sign. It is applicable irrespective of the symmetry properties of the molecule and does not involve any tedious computational effort even for the larger molecules having a larger number of bonds. The method, however, does not account properly for the contribution of lone-pair electrons which in some molecules do contribute significantly.[74] Further, the simple model assumed for the charge distribution in the bonds appears too crude to give accurate molecular moments.

The bond moments to be used in the calculations are obtained either by the molecular orbital calculations or from the internal rotation data. If the complete MO calculations are to be done it would be better to compute the molecular moments directly rather than to compute first the bond moments and then to derive the molecular moments by the above method. The second method[76] is to interpret the measured "barrier to internal rotation" in terms of the interactions between the members of two groups of bonds in the same molecule and hence to derive the bond moments. This would give fairly accurate bond moments provided the assumption that the barrier arises from the bond-bond interaction is justified. It may be pointed out here that because of the effects of the environments on the bonds, the moments of a bond as such do not have a very precise significance. If the same bond occurs in several molecules, the calculation of its moments has to be done for each molecule and for each of its geometrical configurations.

VIII. LIST OF MOLECULAR QUADRUPOLE MOMENTS

Serial Nos.	Molecule	Quadrupole moment[a] $\times 10^{-26}$ esu cm^2	Method	Reference
1.	H_2	0.60	Theoretical MO calculations	77
		0.78	Theoretical MO calculations	78
		0.34	Theoretical MO calculations	79
		0.626	Theoretical MO calculations	80
		0.64	Theoretical modified Schrödinger equation calculations	81
		0.95	Second virial coefficients	21
		0.52	Second virial coefficients	82
		0.3	Microwave line broadening—NH_3	83
		0.38 ± 0.02	Microwave line broadening—NH_3	84
		0.63	Anisotropic susceptibility measurements	62
		0.6	Pressure-induced absorption	85
		1.0	Pressure-induced absorption	72

CC-0. In Public Domain. Gurukul Kangri Collection, Haridwar

Digitized by Arya Samaj Foundation Chennai and eGangotri

Molecule	Quadrupole moment[a] $\times 10^{-26}$ esu cm^2	Method	Reference
	2.45	Microwave line broadening—OCS	86
	0.82±0.10	Microwave line broadening—CHF_3	86
	1.23±0.25	Microwave line broadening—N_2O	86
HD	3.25	Microwave line broadening—OCS	86
D_2	3.1	Microwave line broadening—OCS	86
	1.02±0.07	Microwave line broadening—CHF_3	86
	1.33±0.25	Microwave line broadening—N_2O	86
	−2.55	Theoretical MO calculations	87
N_2	−1.221	Theoretical MO calculations	88
	1.80	Second virial coefficients	21
	1.90	Second virial coefficients	82
	1.27	Crystal data	89
	1.2	Combined second virial coeff. and crystal data	90
	0.8	Microwave line broadening–NH_3	83
	0.80±0.02	Microwave line broadening–NH_3	84
	1.23	Microwave line broadening—H_2O	91
	1.4	Microwave line broadening—SO_2	92
	2.75±0.25	Microwave line broadening—OCS	44
	3.05	Microwave line broadening—OCS	86
	1.35±0.08	Microwave line broadening—CHF_3	86
	2.11±0.30	Microwave line broadening—N_2O	86
	1.64	Pressure-induced absorption	93
	1.0	Pressure-induced absorption	72
	1.5	Pressure-induced absorption	94
	1.5	Pressure-induced absorption	95
	0.50	Microwave line broadening—O_2	96
O_2	1.90	Second virial coefficients	21
	0.19	Microwave line broadening—O_2	97
	1.13±0.12	Microwave line broadening—O_2	98
	0.43	Microwave line broadening—NH_3	83
	0.35±0.03	Microwave line broadening—NH_3	84
	0.41	Microwave line broadening—H_2O	99
	1.0±0.1	Microwave line broadening—OCS	100
	−1.806	Theoretical MO calculations	88
CO	−1.97	Theoretical MO calculations	101
	2.81	Second virial coefficients	82
	1.71	Crystal data	89
	0.94	Microwave line broadening—NH_3	102
	1.60	Infrared line broadening	103
	2.0	Infrared line broadening	43
	−8.5	Theoretical MO calculations	104
CO_2	−4.1	Induced optical birefringence	8
	5.73	Second virial coefficients	20

CC-0. In Public Domain. Gurukul Kangri Collection, Haridwar

Digitized by Arya Samaj Foundation Chennai and eGangotri

Serial Nos.	Molecule	Quadrupole moment[a] $\times 10^{-26}$esu cm^2	Method	Reference
		5.00	Second virial coefficients	21
		4.59	Second virial coefficients	82
		3.3	Second virial coefficients	29
		5.8	Second virial coefficients	105
		4.60	Crystal data	1
		5.29	Combined second virial coeff. and crystal data	90
		3.5	Refractivity virial coefficients	106
		1.8	Microwave line broadening—NH_3	83
		1.72±0.14	Microwave line broadening—NH_3	84
		2.7	Microwave line broadening—SO_2	107
		3.95	Microwave line broadening—OCS	86
		2.81±0.16	Microwave line broadening—CHF_3	86
		2.24±0.30	Microwave line broadening—N_2O	86
		7.9±1.0	Dielectric constants	66
		5.3	Dielectric constants	68
		5.9	Pressure-induced absorption	72
		5.2	Pressure induced absorption[77] (recalculation by Johnston and Cole[73])	68
		4.4	Pressure-induced absorption	73
6.	C_2H_2	3.0	Microwave line broadening—NH_3	102
		13.06±0.11	Bond moments	74
7.	C_2H_4	3.92	Second virial coefficients	82
		1.32	Microwave line broadening—NH_3	102
		4.0	Dielectric constants	68
		2.6	Pressure-induced absorption	72
		4.24±0.04	Bond moments	74
8.	C_2H_6	0.77	Microwave line broadening—NH_3	102
		0.3	Pressure-induced absorption	72
		1.72±0.13	Bond moments	74
9.	C_6H_6	3.6	Microwave line broadening—NH_3	102
10.	OCS	1.47	Microwave line broadening—NH_3	83
		4.32	Microwave line broadening—OCS	108
		5.9	Microwave line broadening—OCS	109
		3.55	Microwave line broadening—OCS	42
		1.5±0.25	Microwave line broadening—OCS	44
		1.0	Microwave line broadening—OCS	86, 100
11.	BrCN	10.1	Microwave line broadening—BrCN	108
		6.75±4.0	Microwave line broadening—BrCN	75
12.	ClCN	3.3	Microwave line broadening—NH_3	73
13.	HCN	2.21	Microwave line broadening—NH_3	73
14.	HCl	3.96	Theoretical MO calculations	110
		3.75	Infrared line broadening	43

CC-0. In Public Domain. Gurukul Kangri Collection, Haridwar

Digitized by Arya Samaj Foundation Chennai and eGangotri

Serial Nos.	Molecule	Quadrupole moment[a] $\times 10^{-26}$ esu cm^2	Method	Reference
15.	HF	3.0	Infrared line broadening	43
16.	HI	6.0	Infrared line broadening	43
17.	BF	-4.382	Theoretical MO calculations	88
		-4.49	Theoretical MO calculations	101
18.	CH_3F	20	Dielectric studies	111
19.	NO	0.77	Microwave line broadening—NH_3	102
		2.9	Microwave line broadening—OCS	86
		0.93 ± 0.09	Microwave line broadening—CHF_3	86
		1.89 ± 0.30	Microwave line broadening—N_2O	86
20.	N_2O	1.63	Microwave line broadening—NH_3	102
		3.95 ± 0.20	Microwave line broadening—N_2O	86
21.	CH_2Cl_2	4.13	Microwave line broadening—NH_3	83
22.	CS_2	1.78	Microwave line broadening—NH_3	83
23.	SO_2	4.42	Microwave line broadening—NH_3	83
24.	H_2O	$\theta_{xx}=-0.907$ $\theta_{yy}=0.694$ $\theta_{zz}=0.213$ (Referred to Oxygen nucleus as origin)	Theoretical MO calculations (using the equivalent orbitals developed by Lennard-Jones)	17
		$\theta_{xx}=-1.149$ $\theta_{yy}=0.755$ $\theta_{zz}=0.394$	Theoretical MO calculations (using the wave function of Ellison and Shull[113])	112
		$\theta_{xx}=-1.304$ $\theta_{yy}=0.940$ $\theta_{zz}=0.364$	Theoretical MO calculations (using "bond orbital" wave function McWeeny and Ohno[114])	112
		$\theta_{xx}=-1.211$ $\theta_{yy}=0.853$ $\theta_{zz}=0.358$	Theoretical MO calculations (using McWeeny–Ohno's[114] configuration interaction bond orbital' wave functions with 7 configurations)	112
		$\theta_{xx}=-1.055$ $\theta_{yy}=0.660$ $\theta_{zz}=0.395$	Theoretical MO calculations (using McWeeny–Ohno's[114] "configuration interaction bond orbital wave functions" with 12 configurations)	112
		$\theta_{xx}=-1.228$ $\theta_{yy}=0.868$ $\theta_{zz}=0.360$	Theoretical MO calculations (using McWeeny–Ohno's[114] 'modified electron pair' wave functions)	112
		$\theta_{xx}=-1.143$ $\theta_{yy}=0.729$ $\theta_{zz}=0.414$	Theoretical MO calculations (using McWeeny–Ohno's[114] SCF LCAO wave functions)	112
		$\theta_{xx}=-1.61$ $\theta_{yy}=1.35$ $\theta_{zz}=0.26$	Theoretical MO calculations based on Rowlinson's empirical four-point-charge model[115]	112
25.	NH_3	$\theta_{xx}=\theta_{yy}=0.069$ $\theta_{zz}=-0.137$ (Referred to nitrogen nucleus as the origin)	Theoretical MO calculations (using the equivalent orbitals developed by Lennard-Jones)	17

[a] Some of the values were recalculated to conform to the definition used here.

CC-0. In Public Domain. Gurukul Kangri Collection, Haridwar

Digitized by Arya Samaj Foundation Chennai and eGangotri

ACKNOWLEDGMENTS

We are thankful to S. L. Srivastava for many helpful discussions. We are also thankful to all other workers in the Microwave Laboratory for their help and cooperation. One of us (V.P.) is indebted to the Council of Scientific and Industrial Research, India, for the award of a research fellowship. Thanks are also due to the National Bureau of Standards, U.S.A., for supporting a project "Microwave Absorption and Molecular Interaction" under the PL-480 program.

REFERENCES

[1] A. D. Buckingham, Quart. Rev. **13**, 183 (1959).
[2] R. J. W. LeFevre, *Dipole Moments* (Methuen and Co., Ltd., London, 1953).
[3] J. W. Smith, *Electric Dipole Moments* (Butterworths Scientific Publications, Ltd., London, 1955).
[4] P. Debye, *Polar Molecules* (Dover Publications, Inc., New York, 1947).
[5] C. P. Smyth, *Dielectric Behavior and Structure* (McGraw-Hill Book Co., Inc., New York, 1955).
[6] A. D. Buckingham, J. Chem. Phys. **30**, 1580 (1959).
[7] P. Debye, Physik. Z. **22**, 302 (1921).
[8] A. D. Buckingham and R. L. Disch, Proc. Roy. Soc. (London) **A273**, 275 (1963).
[9] C. A. Coulson, Proc. Cambridge Phil. Soc. **38**, 210 (1942).
[10] C. C. J. Roothaan, Rev. Mod. Phys. **23**, 69 (1951).
[11] J. C. Slater, *Quantum Theory of Molecules and Solids* (McGraw-Hill Book Co., Inc., New York, 1963), Vol. 1.
[12] R. S. Mulliken, Rev. Mod. Phys. **32**, 232 (1960).
[13] S. F. Boys, Proc. Roy. Soc. (London) **A200**, 542 (1950).
[14] J. Lennard-Jones, Proc. Roy. Soc. (London) **A198**, 14 (1949).
[15] J. Lennard-Jones and J. A. Pople, Proc. Roy. Soc. (London) **A202**, 166 (1950).
[16] J. A. Pople, Proc. Roy. Soc. (London) **A202**, 323 (1950).
[17] A. B. F. Duncan and J. A. Pople, Trans. Faraday Soc. **49**, 217 (1953).
[18] A. D. Buckingham and J. A. Pople, Proc. Phys. Soc. (London) **A68**, 905 (1955).
[19] J. O. Hirschfelder, C. F. Curtiss, and R. B. Bird, *Molecular Theory of Gases and Liquids* (John Wiley & Sons, Inc., New York, 1954), p. 131.
[20] J. A. Pople, Proc. Roy. Soc. (London) **A221**, 498 (1954); **A221**, 508 (1954).
[21] S. Kielich, Physica **28**, 511 (1962).
[22] A. D. Buckingham and J. A. Pople, Trans. Faraday Soc. **51**, 1173 (1953).
[23] J. O. Hirschfelder, C. F. Curtiss, and R. B. Bird, Ref. 24, p. 32.
[24] J. O. Hirschfelder, C. F. Curtiss, and R. B. Bird, Ref. 24, pp. 1114–1115.
[25] J. O. Hirschfelder, C. F. Curtiss, and R. B. Bird, Ref. 24, p. 984.
[26] F. London, J. Phys. Chem. **46**, 305 (1942).
[27] K. E. Maccormack and W. G. Schneider, J. Chem. Phys. **18**, 1269 (1950).
[28] A. Michels, W. De Graaff, and C. A. TenSeldam, Physica **26**, 393 (1960).
[29] E. G. Butcher and R. S. Dadson, Proc. Roy. Soc. (London) **A277**, 448 (1964).
[30] C. H. Townes and A. L. Schawlow, *Microwave Spectroscopy* (McGraw-Hill Book Co., Inc., New York, 1955), p. 336.
[31] P. W. Anderson, Ph.D. thesis, Harvard University, Cambridge, Massachusetts (1949); Phys. Rev. **76**, 647 (1949).
[32] M. Baranger, Phys. Rev. **111**, 481 (1958).
[33] M. Baranger, Phys. Rev. **111**, 494 (1958).
[34] M. Baranger, Phys. Rev. **112**, 855 (1958).
[35] A. C. Kolb and H. Griem, Phys. Rev. **111**, 514 (1958).
[36] Oldwig von Roos, *Proceedings of the Fifth International Conference on Ionization Phenomena in Gases, Munich*, 1961 (North-Holland Publ. Co., Amsterdam, 1962), pp. 913–24.
[37] A. O[illegible]no, J. Phys. Soc. Japan **16**, 2402 (1961).
[38] U. Fano, Phys. Rev. **131**, 259 (1963).
[39] A. Di Giacomo, Nuovo Cimento **34**, 473 (1964).
[40] C. J. Tsao and B. Curnutte, Jr., J. Quant. Spectry. Radiative Transfer **2**, 41 (1962).
[41] C. H. Townes and A. L. Schawlow, Ref. 35, p. 20.
[42] Krishnaji, S. Chandra, and S. L. Srivastava, J. Chem. Phys. **41**, 409 (1964).
[43] W. S. Benedict and R. Herman, J. Quant. Spectry. Radiative Transfer **3**, 265 (1963).
[44] Research Report No. 3, Microwave Laboratory, Physics Department, University of Allahabad, Allahabad, India (1964).
[45] Krishnaji and S. L. Srivastava, J. Chem. Phys. **41**, 2266 (1964).
[46] Krishnaji and S. L. Srivastava, J. Chem. Phys. **42**, 1546 (1965).
[47] Krishnaji and S. L. Srivastava, J. Chem. Phys. **43**, 1345 (1965).
[48] E. U. Condon and G. H. Shortley, *The Theory of Atomic Spectra* (Cambridge University Press, Cambridge, Mass., 1963), pp. 76–77.
[49] C. H. Townes and A. L. Schawlow, Ref. 30, Chap. 15.
[50] W. Gordy, W. V. Smith, and R. F. Trambarulo, *Microwave Spectroscopy* (John Wiley & Sons, Inc., New York, 1953).
[51] S. Chandra, D. Phil. thesis, Physics Department, University of Allahabad, Allahabad, India (1962).
[52] E. A. Rinehart and C. C. Lin, Rev. Sci. Instr. **32**, 562 (1961).
[53] A. Ben Reuven, S. Kimel, M. A. Hirschfeld, and J. H. Jaffe, J. Chem. Phys. **35**, 955 (1961).
[54] A. Ben Reuven, H. Freidmann, and J. H. Jaffe, J. Chem. Phys. **38**, 3021 (1963).
[55] J. Fiutak and J. Van Kranendonk, Can. J. Phys. **40**, 1085 (1962).
[56] J. Fiutak and J. Van Kranendonk, Can. J. Phys. **41**, 21 (1963).
[57] J. Van Kranendonk, Can. J. Phys. **41**, 433 (1963).
[58] J. H. Van Vleck, *Theory of Electric and Magnetic Susceptibilities* (Oxford University Press, New York, 1932), p. 275.
[59] N. F. Ramsey, Phys. Rev. **78**, 221 (1950).
[60] N. F. Ramsey, Phys. Rev. **58**, 226 (1940); **87**, 1075 (1952).
[61] Landolt-Bornstein, *Zahlenwerte und Functionen* (Springer-Verlag, Berlin, 1951), Band 1, Teil 3, p. 536.
[62] N. J. Harrick and N. F. Ramsey, Phys. Rev. **88**, 228 (1952).
[63] D. R. Johnston, G. J. Oudemans, and R. H. Cole, J. Chem. Phys. **33**, 1310 (1960).
[64] A. D. Buckingham and J. A. Pople, Trans. Faraday Soc. **51**, 1029 (1955).
[65] A. D. Buckingham and J. A. Pople, J. Chem. Phys. **27**, 820 (1957).
[66] R. W. Zwanzig, J. Chem. Phys. **25**, 211 (1956); **27**, 821 (1957).
[67] L. Jansen, Phys. Rev. **112**, 434 (1958).
[68] D. R. Johnston and R. H. Cole, J. Chem. Phys. **36**, 318 (1962).
[69] J. P. Colpa and J. A. A. Ketelaar, Mol. Phys. **1**, 14 (1958).
[70] Z. J. Kiss, Gush, and H. L. Welsh, Can. J. Phys. **37**, 362 (1959).
[71] A. A. Maryott and G. Birnbaum, J. Chem. Phys. **36**, 2026 (1962).
[72] G. Birnbaum and A. A. Maryott, J. Chem. Phys. **36**, 2032 (1962).
[73] A. A. Maryott and S. J. Kryder, J. Chem. Phys. **41**, 1580 (1964).
[74] G. K. Pandey (to be published).
[75] S. L. Srivastava and V. Prakash, J. Chem. Phys. **42**, 3738 (1965).
[76] E. N. Lassettre and L. B. Dean, J. Chem. Phys. **17**, 317 (1949).
[77] H. M. James and A. S. Coolidge, Astrophys. J. **87**, 438 (1938).
[78] C. A. Coulson, Proc. Cambridge Phil. Soc. **34**, 204 (1938).
[79] Massey and R. A. Buckingham, Proc. Roy. Irish Acad. **A45**, 31 (1938).
[80] W. Kolos and C. C. J. Roothaan, Rev. Mod. Phys. **32**, 219 (1960).
[81] E. Corinaldesi and G. Hurford, Phys. Letters **9**, 135 (1964).
[82] R. H. Orcutt, J. Chem. Phys. **39**, 605 (1963).
[83] W. V. Smith and R. Howard, Phys. Rev. **79**, 132 (1950) [revised according to W. V. Smith, J. Chem. Phys. **25**, 510 (1956)].

CC-0. In Public Domain. Gurukul Kangri Collection, Haridwar

Digitized by Arya Samaj Foundation Chennai and eGangotri

[84] H. Feeny, W. Madigosky, and R. Winters, J. Chem. Phys. 27, 898 (1957).
[85] J. P. Kolpa and J. A. A. Ketelaar, Mol. Phys. **1**, 343 (1958).
[86] B. Th. Berendts, Ph.D. thesis, Catholic University of Nijmegen, Denmark (1966).
[87] C. W. Scherr, J. Chem. Phys. **23**, 569 (1955).
[88] R. K. Nesbet, J. Chem. Phys. **40**, 3619 (1964).
[89] L. Jansen, A. Michels, and J. M. Lupton, Physica **20**, 1235 (1954).
[90] A. D. Buckingham, J. Chem. Phys. **23**, 412 (1955).
[91] W. S. Benedict and L. D. Kaplan, J. Chem. Phys. **30**, 388 (1959).
[92] Krishnaji and S. Chandra, J. Chem. Phys. **38**, 232 (1963).
[93] J. Van Kranendonk, Physica **24**, 347 (1958).
[94] J. D. Poll, Phys. Letters **7**, 32 (1963).
[95] J. A. A. Ketelaar and R. P. H. Rettschnick, Mol. Phys. **7**, 191 (1963–64).
[96] J. O. Artman, D. Phil. thesis, Columbia University (1953).
[97] R. S. Anderson, W. V. Smith, and W. Gordy, Phys. Rev. **82**, 264 (1951).
[98] M. Mizushima, Phys. Rev. **83**, 94 (1951).
[99] W. S. Benedict and L. D. Kaplan, J. Quant. Spectry. Radiative Transfer **4**, 453 (1964).
[100] S. L. Srivastava, D. Phil. thesis, Physics Department, University of Allahabad, India (1966).
[101] W. M. Huo, J. Chem. Phys. **43**, 624 (1965).
[102] R. M. Hill and W. V. Smith, Phys. Rev. **82**, 451 (1951) [revised according to W. V. Smith, J. Chem. Phys. **25**, 510 (1956)].
[103] D. R. Eaton and H. W. Thompson, Proc. Roy. Soc. (London) **A251**, 475 (1959).
[104] W. C. Hamilton, J. Chem. Phys. **25**, 1283 (1956).
[105] A. D. King, Jr., J. Chem. Phys. **42**, 2610 (1965).
[106] A. D. Buckingham, Trans. Faraday Soc. **52**, 747 (1956).
[107] Krishnaji and S. Chandra, J. Chem. Phys. **38**, 1019 (1963).
[108] W. V. Smith, H. A. Lackner, and A. B. Volkov, J. Chem. Phys. **23**, 389 (1955); **23**, 1559 (1955).
[109] M. L. Sage (private communication).
[110] R. K. Nesbet, J. Chem. Phys. **41**, 100 (1964).
[111] A. D. Buckingham and J. A. Pople, Trans. Faraday Soc. **51**, 1179 (1955).
[112] R. M. Glaeser and C. A. Coulson, Trans. Faraday Soc. **61**, 389 (1965).
[113] F. O. Ellison and H. Shull, J. Chem. Phys. **23**, 2348 (1955).
[114] R. McWeeny and A. Ohno, Proc. Roy. Soc. (London) **A255**, 367 (1960).
[115] J. S. Rowlinson, Trans. Faraday Soc. **47**, 120 (1951).

पुस्तकालय
गुरुकुल कांगड़ी विश्वविद्यालय
हरिद्वार

CC-0. In Public Domain. Gurukul Kangri Collection, Haridwar

112441

Digitized by Arya Samaj Foundation Chennai and eGangotri

CONTENTS

JANUARY 1966

Electron Impact Ionization Cross-Section Data for Atoms, Atomic Ions, and Diatomic Molecules: I. Experimental Data . . . . . L. J. Kieffer and Gordon H. Dunn 1

Complex Coordinates and Quantum Mechanics . . . . . F. Strocchi 3

Survey of Some Systematic Properties of the Nuclear *E*1 Transition Probability . . . . . Charles F. Perdrisat 4

Unitary Groups: Representations and Decompositions . . . . . C. Itzykson and M. Nauenberg 9

Quasi-Free Scattering and Nuclear Structure . . . . . Gerhard Jacob and Th. A. J. Maris 12

Compound Inelastic Nucleon and Gamma-Ray Angular Distributions for Even- and Odd-Mass Nuclei . . . . . Eric Sheldon and Douglas M. Van Patter 14

The Role of Boltzmann Factors in Line Shape . . . . . D. L. Huber and J. H. Van Vleck 18

Spectral Distribution of Scattered Light in a Simple Fluid . . . . . Raymond D. Mountain 20

APRIL 1966

Dynamical Symmetry in Particle Physics . . . . . A. Pais 2

Recent Work on the Interstellar Medium . . . . . Nannielou H. Dieter and W. Miller Goss 2

Considerations on the Flow of Superfluid Helium . . . . . P. W. Anderson 2

Magnetic Electron Scattering from Nuclei . . . . . J. Goldemberg and R. H. Pratt 3

Group Theory and the Hydrogen Atom (I) . . . . . M. Bander and C. Itzykson 3

Group Theory and the Hydrogen Atom (II) . . . . . M. Bander and C. Itzykson 3

Classical Noise. III. Nonlinear Markoff Processes . . . . . Melvin Lax 3

Thermal Diffusion in Isotopic Gas Mixtures and Intermolecular Forces . . . . . S. C. Saxena and B. P. Mathur 3

JULY 1966

A Survey of Fast-Neutron Reactions . . . . . N. Cindro 39

On the Problem of Hidden Variables in Quantum Mechanics . . . . . John S. Bell 4

A Proposed Solution of the Measurement Problem in Quantum Mechanics by a Hidden Variable Theory . . . . . D. Bohm and J. Bub 4

A Refutation of the Proof by Jauch and Piron that Hidden Variables Can Be Excluded in Quantum Mechanics . . . . . D. Bohm and J. Bub 4

Present Phenomenological Status of the Regge Pole Theory . . . . . E. Leader 4

Hamiltonian Path-Integral Methods . . . . . Claude Garrod 4

High-Frequency Conductivity of a Solid-State Plasma with Dynamically Screened Interactions. I. Thermal Equilibrium . . . . . D. E. McCumber 4

Atomic Fluorescence Yields . . . . . R. W. Fink, R. C. Jopson, Hans Mark, and C. D. Swift 5

Classical Noise. IV. Langevin Methods . . . . . Melvin Lax 5

OCTOBER 1966

Quantization of Macroscopic Motions and Hydrodynamics of Rotating Helium II . . . . . E. L. Andronikashvili and Yu. G. Mamaladze 5

High-Energy Electromagnetic Conversion Processes in Intense Magnetic Fields . . . . . Thomas Erber 6

Accelerator Calibration Energies . . . . . Jerry B. Marion 6

Some Simple Isothermal Equations of State . . . . . J. Ross Macdonald 6

Thermodynamic Properties of an Electron Plasma . . . . . T. J. Lie and Yoshi H. Ichikawa 6

Evaluation of Molecular Quadrupole Moments . . . . . Krishnaji and Vinod Prakash 6

112441

CC-0. In Public Domain. Gurukul Kangri Collection, Haridwar

Digitized by Arya Samaj Foundation Chennai and eGangotri

CC-0. In Public Domain. Gurukul Kangri Collection, Haridwar

Digitized by Arya Samaj Foundation Chennai and eGangotri

Compiled
1999-2000

सन्दर्भ ग्रन्थ
REFERENCE BOOK

यह पुस्तक वितरित न की जाय
NOT TO BE ISSUED

CC-0. In Public Domain. Gurukul Kangri Collection, Haridwar

Digitized by Arya Samaj Foundation Chennai and eGangotri

CC-0. In Public Domain. Gurukul Kangri Collection, Haridwar

Digitized by Arya Samaj Foundation Chennai and eGangotri